PROCEEDINGS OF THE 24th INTERNATIONAL MINING CONGRESS OF TURKEY

APRIL 14-17, 2015 Antalya/TURKEY

EDITORS

Dr. Mehtap GÜLSÜN KILIÇ Öznur ÖNEL Dr. Hakan BAŞARIR

Dr. Mehmet KARADENİZ Elif TORUN BİLGİÇ

UCTEA

THE CHAMBER OF MINING ENGİNEERS OF TURKEY

IMCET2015 / ANTALYA / TURKEY / APRIL 14-17

PROCEEDINGS OF THE 24TH INTERNATIONAL MINING CONGRESS AND EXHIBITION OF TURKEY

EDITORS
Dr. Mehtap Gülsün Kılıç
Öznur Önel
Dr. Hakan Başarır
Dr. Mehmet Karadeniz
Elif Torun Bilgiç

TMMOB
MADEN MÜHENDİSLERİ ODASI
Chamber of Mining Engineers of Turkey

This Congress is supported by TÜBİTAK
(The Scientific and Technological Research Council of Turkey)

All the papers have been selected for presentation at the congress by the Editorial Board based on the review of the paper by at least two members of the scientific committee.

The content of the papers is the responsibility of the author/s and it does not necessarily reflect any position of the Chamber of Mining Engineers Turkey.

ISBN: 978-605-01-0705-0

Published by: TMMOB Maden Mühendisleri Odası
Selanik Cad. 19/4 Kızılay-Ankara

Phone : +90 312 425 10 80
Fax : +90 312 417 52 90
www.maden.org.tr
maden@maden.org.tr

Member of Boards of the Chamber

President	: Ayhan YÜKSEL
Vice President	: Hüseyin Can DOĞAN
Secretary	: Necmi ERGİN
Treasurer	: Mehmet ÖZYURT Mehmet ZAMAN Emre DEMİR Emra Ergüzeloğlu KARATAŞ

Executive Committee of the Congress

Chairman	: Dr. Bülent TOKA
Vice Chairman	: Dr. Mehmet KARADENİZ
Secretary	: Niyazi KARADENİZ
Treasurer	: Mehmet ÖZYURT
Members	: M. Erşat AKYAZILI Nadir AVŞAROĞLU Dr. Hakan BAŞARIR Şadiye BENGÜ Elif TORUN BİLGİÇ Necmi ERGİN Pelin KERTMEN Dr. Mehtap GÜLSÜN KILIÇ Öznür ÖNEL Ali ÖNEMLİ Davut ÖZLEN Dr. Nejat TAMZOK Tuğba TOKER Muharrem TORALIOĞLU

Scientific Committee

Dr. A. Ekrem YÜCE
Dr. Abbas TAHERI
Dr. Abdülhadi Erdal ÖZDENİZ
Dr. Abdullah SEYRANKAYA
Dr. Abdurrahman DALGIÇ
Dr. Adem ERSOY
Dr. Agnieszka SUROWIAK
Dr. Agus Pulung SASMITO
Dr. Ahmet Hamdi DELİORMANLI
Ahmet Güneş YARDIMCI
Dr. Ahmet Mahmut KILIÇ
Dr. Ahmet ÖZARSLAN
Dr. Ahmet ŞENTÜRK
Dr. Alaaddin ÇAKIR
Dr. Alaettin KILIÇ
Dr. Ali Ekrem ARITAN
Dr. Ali İhsan AROL
Ali ÖNEMLİ
Dr. Ali Osman YILMAZ
Ali Rıza KILIÇ
Dr. Ali SARIIŞIK
Dr. Ali UÇAR
Dr. Andre XAVIER
Dr. Antonio NIETO
Dr. Antonio ZUCCA
Asım KUTLUATA
Dr. Askeri KARAKUŞ
Dr. Ata Utku AKÇİL
Dr. Ataç BAŞÇETİN
Dr. Atilla CEYLANOĞLU
Dr. Ayhan KESİMAL
Dr. Aykut AKGÜN
Dr. Bahri ERSOY
Dr. Bahtiyar ÜNVER
Dr. Bayram ERÇIKDI
Dr. Bayram KAHRAMAN
Dr. Bekir GENÇ
Dr. Bern KLEIN
Dr. Bülent ERDEM
Dr. Bülent TOKA
Dr. Bülent TÜTMEZ
Dr. C. Okay AKSOY
Dr. Çağatay PAMUKÇU
Dr. Carlos Hoffmann SAMPAIO
Dr. Celal KARPUZ
Dr. Cem ŞENSÖĞÜT
Dr. Cenk GÜRAY
Dr. Çetin HOŞTEN
Dr. Çiğdem KELEŞ
Dr. Jan DRYZMALA
Dr. John MEECH
Dr. John STURGUL
Dr. Jörg BENNDORF
Dr. Kaan ERARSLAN
Dr. Kadri DAĞDELEN
Dr. Kemal BARIŞ
Dr. Kemal BİLİR
Dr. Kerim AYDINER
Dr. Kerim KÜÇÜK
Dr. Kevin BROWN
Dr. Kremena DEDELYANOVA
Dr. Ljudmilla BOKÁNYI
Dr. M. Erdinç BİLİR
Dr. M. Kemal ÖZFIRAT
Dr. M. Saim SARAÇ
Dr. M.Suat DELİBALTA
Dr. Mahmut PARLAKTUNA
Dr. Malcolm SCOBLE
Dr. Maria E. HOLUSZKO
Dr. Meftuni YEKELER
Dr. Mehmet Ali HİNDİSTAN
Dr. Mehmet KARADENİZ
Mehmet KAYADELEN
Dr. Mehmet KIZIL
Dr. Mehmet SARI
Dr. Mehmet TANRIVERDİ
Dr. Mehtap Gülsün KILIÇ
Dr. Melih GENİŞ
Dr. Melih İPHAR
Dr. Metin UÇURUM
Dr. Michael A. ZHURAVKOV
Dr. Mohan YELLISHETTY
Dr. Morteza Gholi OSANLOO
Dr. Murat ERDEMOĞLU
Dr. Murat KARAKUŞ
Dr. Mustafa AYHAN
Dr. Mustafa ÇINAR
Dr. Mustafa ÇIRAK
Dr. Mustafa Kemal EMİL
Dr. Mustafa KUMRAL
Dr. Mustafa ÖNDER
Dr. N. Erhan YAŞITLI
Dr. N. Metin CAN
Dr. Naci Emre ALTUN
Nadir AVŞAROĞLU
Dr. Nazife ERARSLAN
Necati YILDIZ
Dr. Necmettin ÇETİN

Dr. Cihan DOĞRUÖZ
Dr. Cyril O'CONNOR
Dr. Dee BRADSHAW
Dr. Deniz AYDIN
Dr. Deniz TUMAÇ
Dr. Didem EREN SARICI
Dr. Doğan KARAKUŞ
Dr. E. Yener YAZICI
Dr. E.İlknur CÖCEN
Dr. Eleonora WIDZYK-CAPEHART
Dr. Elizabeth MAKHATHA
Dr. Emin Cafer ÇİLEK
Dr. Emrah Tuğcan TUZCU
Dr. Ercan EMİR
Dr. Ercüment YALÇIN
Dr. Erdoğan KAYMAKÇI
Dr. Eren Caner ORHAN
Dr. Erhan ÇETİN
Dr. Erhan TERCAN
Dr. Erkan ÖZKAN
Dr. Erkan TOPAL
Dr. Erkin NASUF
Dr. Erol KAYA
Dr. Evren ÖZBAYOĞLU
Dr. F. Deniz ÖZTÜRK
Dr. Fatih BAYRAM
Dr. Ferdi CİHANGİR
Dr. Fikri KAHRAMAN
Dr. Giorgio MASSACCI
Dr. Givemore SAKAHUNI
Dr. Gökhan AYDIN
Dr. Graeme JAMESON
Dr. Gülay BULUT
Dr. Gülhan ÖZBAYOĞLU
Dr. Gülşen TOZSİN
Dr. Güneş ERTUNÇ
Dr. Gürcan KONAK
Dr. Güzide Meltem LÜLE
Dr. Güzin Gülsev UYAR
Dr. Hacı DEVECİ
Dr. Hakan BAŞARIR
Dr. Hakan TUNÇDEMİR
Hakkı ÖKTEM
Dr. Haldun KURAMA
Dr. Halil İPEK
Dr. Halil KÖSE
Dr. Hanifi ÇOPUR
Dr. Hasan ÇİFTÇİ
Dr. Hasan HACIFAZLIOĞLU
Dr. Hasan ÖZTÜRK
Dr. Hikmet SİS
Dr. Nejat TAMZOK
Dr. Niyazi BİLİM
Dr. Nuh BİLGİN
Dr. Nural KUYUCAK
Dr. Nuray DEMİREL
Dr. Nuray KARAPINAR
Dr. Nuray TOKGÖZ
Dr. Nuri Ali AKÇIN
Dr. Okan SU
Dr. Oktay BAYAT
Dr. Olgaç M. KANGAL
Dr. Ömürden GENÇ
Dr. Önder UYSAL
Dr. Osman SİVRİKAYA
Dr. Osman Zeki HEKİMOĞLU
Dr. Özcan GÜLSOY
Dr. Özgür AKKOYUN
Dr. Özlem BIÇAK
Dr. Özlem KAYA
Dr. Paul HAGAN
Dr. Petr SOLOZHENKIN
Dr. Phillip STOTHARD
Dr. Pier Paolo MANCA
Dr. Raj SINGHAL
Dr. Richard Minnitt ECON
Dr. Rudrajit MITRA
Dr. Sabiha KOCA
Dr. Sair KAHRAMAN
Dr. Sait KIZGUT
Dr. Savaş ÖZÜN
Dr. Seher ATA
Dr. Selamet G. ERÇELEBİ
Dr. Selçuk SAMANLI
Dr. Serhat AKIN
Dr. Serkan SAYDAM
Dr. Sevgi GÜRCAN
Dr. Şevket DURUCAN
Dr. Seyfi KULAKSIZ
Dr. Seyhan ÖNDER
Dr. Sezai ŞEN
Dr. Sinan Turhan ERDOĞAN
Dr. Suphi URAL
Dr. Taki GÜLER
Dr. Tarkeshwar KUMAR
Dr. Tevfik GÜYAGÜLER
Dr. Tolga DEPÇİ
Dr. Tomasz NIEDOBA
Dr. Tuğrul ÜNLÜ
Dr. Tuncay USLU
Dr. Tuncel YEGÜLALP
Dr. Turan BATAR

Dr. Hürriyet AKDAŞ
Dr. Hüseyin ANKARA
Dr. Hüseyin YAVUZ
Dr. İ.Sedat BÜYÜKSAĞIŞ
Dr. İbrahim ALP
Dr. İbrahim ÇAVUŞOĞLU
Dr. İbrahim OCAK
Dr. İbrahim ONUR
Dr. İbrahim UĞUR
Dr. İhsan ÖZKAN
Dr. İhsan ÖZTÜRK
Dr. İlgin KURŞUN
Dr. İlkay Bengü ÇELİK
Dr. İlker ACAR
Dr. İlknur EROL
Dr. Irena GRIGOROVA
Dr. İrfan Celal ENGİN
İrfan GÜVEN
Dr. İsmail BENTLİ
Dr. Ivan NISHKOV
Dr. İzzet KARAKURT
Dr. Turgay ONARGAN
Dr. Türker HÜDAVERDİ
Dr. U. Gökhan AKKAYA
Dr. Uğur DEMİR
Dr. Uğur ÖZBAY
Dr. Uğur ULUSOY
Dr. Ümit ATALAY
Dr. Ümit ÖZER
Dr. Vedat ARSLAN
Dr. Vedat DENİZ
Dr. Vedat DİDARİ
Dr. Vladimir E VIGDERGAUZ
Dr. Volkan BOZKURT
Dr. W. Scott DUNBAR
Dr. Yadigar Vasfi MÜFTÜOĞLU
Dr. Yakup UMUCU
Dr. Yaşar KASAP
Dr. Yaşar KİBİCİ
Dr. Zekeriya DURAN
Dr. Zeki KARACA

PREFACE

For the Turkish Republic period, looking at a glance at the development of Turkish mining sector, about which the structure and problems have been always matters of debates, we see that the background of scientific organizations that must play a vital role to overcome these issues goes only back to 1960's. Those were the times when the young Republic was still passing through social and political turbulences, a period of major transitions. Significant efforts and attention were being directed towards industrialization, but the practice and the reality was far from these goals. Mining industry of the country, which should be a major driving force, was facing many faceted problems to be addressed. In addition, the mining industry was way below the desired level. It required not only powerful and ambitious moves, but also several radical, aggressive changes. This task was obviously to be undertaken by the mining people to a great extent. Being fully aware of this, the first time in 1969, a national event, the "Scientific and Technical Mining Congress of Turkey" was organized by the Chamber of Mining Engineers of Turkey of UCTEA (Union of Chambers of Turkish Engineers and Architects).

At the beginning, two major outcomes were anticipated: One for the Turkish mining industry; and one for the fore coming congresses. On one side it was aimed to increase the quality of the event and eventually to achieve international reputation and acceptance to make this event a tradition. On the other; the objective was to identify and to state issues and obstacles, to provide scientific-technical solutions to address these and, obviously to support the professional development of the young generations trained in mining.

This is how this ever-lasting journey started 46 years ago. Perhaps, the path undertaken is not too long, however, it has been a tough experience of many challenges. Since its start, even if our congress has sometimes had slight deviations, mainly on accounts of the conditions of the times, but the general tendency has always been upwards. And a further look into the details shows that significant progress has been made in such a short period. Such that, despite limited resources and several other restrictions, this congress became an internationally admitted event by 1973, thanks to the intensive and endless efforts and devotion of the amateur and volunteer staff of the Mining Engineers Chamber. Without an exception, the congress became a biannual event. To reflect this major achievement its title has been changed to "International Mining Congress and Exhibition" in 2001 when the event was organized for its 17th time.

Undoubtedly, the endeavors put forward are commendable. However, the role that technology has played should also be emphasized here. As very-well known, with the significant progress in information technologies that initiated particularly by 1990's, a broader geography became accessible. Such progress apparently contributed to increasing the scientific, sociological and cultural features as well as its international recognition. But, at the same time, these also put a pressure towards acquiring even further progress in such aspects as rapidly as possible. Within this context, the Chamber of Mining Engineers of Turkey now carries the vital responsibility to institutionalize this big mining event of Turkey and to make it one of the most reputable global mining organizations. In this respect, the 24th International Mining Congress and Exhibition of Turkey has been realized, showing that strong steps have been taken towards this major goal. This event of four days indeed became a means of gathering for academicians, scientists, engineers, managers, consultants, decision-makers, investors, industry experts, customers and suppliers from all across the world, as scientific, technical and social issues were discussed and recent mining technologies and latest products and developments in the mining industry were successfully exhibited. Further, the sessions held,

the social and cultural activities, tours and field trips have created even more opportunities for joint ventures, mutual cooperation and business relations among delegates. For this particular event, scientific contributions in the form of poster and oral presentations, broad participation raise our hopes for the future of Turkish mining industry.

As 44th Administrative Board of Turkish Mining Chamber and the Executive Committee of 24th International Mining and Exhibition of Turkey, we sincerely and initially thank to those who have carried on our chamber and congress since 1954, to those who made an effort for the organization of the congress, to the scientist who contributed the congress by their papers and presentations, to session chairs raising the scientific merits of the event and to all participating organizations and institutions.

44th Management Board of Turkish Mining Chamber of UCTEA

The Executive Committee of 24th Mining Congress and Exhibition of Turkey

TABLE OF CONTENTS

HISTORY, EDUCATION, AND POLITICS OF MINING AND ENERGY

OCCUPATIONAL HEALTH AND SAFETY

ROCK MECHANICS AND GEOTECHNICAL APPLICATIONS

MINE DESIGN, MODELLING, AND OPTIMIZATION

GIS AND TOPOGRAPHY APPLICATIONS

DRILLING AND BLASTING, DRILLING TECHNOLOGY, AND MECHANIZATION

MINE VENTILATION, METHANE, AND SHALE GAS

COAL AND COAL TECHNOLOGY

INDUSTRIAL RAW MATERIALS AND PRECIOUS METALS

DESIGN OF MINERAL PROCESSING PLANTS AND BENEFICIATION METHODS

HYDROMETALLURGY AND BIOHYDROMETALLURGY

RECYCLING

MINING AND ENVIRONMENT

History, Education, and Politics of Mining and Energy

2012 Effects In The South African Platinum Sector

B. Genc
Universitv of the Witwatersrand. Johannesbura. South Africa

ABSTRACT This paper studies the fundamentals affecting the South African platinum sector. It offers a brief overview of the current challenges faced by the platinum sector in general, and labour unrest related issues in the sector in particular. The difficulties the South African platinum producers have to deal with to plan their future production are also scrutinized. These include rising cost of labours, declining profit margins and the possibility of falling metal prices. It would be presumptuous to suggest solutions but this article nevertheless offers the reader an understanding of the challenges facing the South African platinum sector overall. In this light, where available, the financial performances of mining companies in the sector, obtained from published annual results, are also analysed, and on this bases the paper offers several recommendations.

Keywords: Platinum, cost, price, market

1 INTRODUCTION

South Africa is a mineral rich country and is the world's number one platinum producer. South Africa produced 73% (4.12 million ounces) of the annual global platinum output in 2013, up 0.7% compared to 2012 (Johnson Matthey, 2014) after the Marikana strike in South Africa in 2012. The strike was considered an important event in South African history, and was followed by similar strikes at other mining sectors such as gold and iron ore across South Africa. The mineworkers demanding better wages and improved living conditions initiated wildcat strikes in the platinum belt. These strikes led to a tragedy that took place in August 16, 2012 when 34 striking Lonmin mineworkers were shot dead by the police in Lonmin's platinum mine in Marikana. This shooting made international headlines. The strike lasted just over two months and ended in September 18, 2012.

The Marikana incident caused some production loses to the major platinum producers in South Africa. However, South Africa still managed to produce 4.09 million ounces of platinum in 2012, down 16% compared to 2011 (Johnson Matthey, 2014). Anglo American Platinum (Amplats), the number one platinum producer of the world, produced 2.32 million ounces of platinum in 2013, very similar production levels compared to 2012, which is equivalent to 40% of the world's annual platinum production. Impala Platinum (Implats), the number two platinum miner of the world, produced 1.58 million ounces of platinum in 2013, up 9.3% compared to 2012. Lonmin Plc (Lonmin), the number three platinum producer of the world, produced 0.75 million ounces of platinum in 2013, a similar figure compared to 2012. Although the South African platinum mines combined produced 72% of the world's annual platinum production in 2013, the 2014 platinum production outlook is expected to be 40% less than the 2013 figures as during 2014 the South African mining industry witnessed the five months long strike action in the platinum sector, the lengthiest strike action in the South African mining history, which ended on the 24th of June, 2014. This paper examines the reasons behind the long lasting industrial actions in the platinum belt, hence the impacts of the 2012 Marikana strike action in the South African platinum sector.

2 PLATINUM PRICES

Platinum prices are the main factors behind concluding if the platinum producers are profitable and determined by demand and supply figures. Total world supply for a

commodity is estimated by calculating the total amount of that commodity made available to the market. Mineral commodities are made available from primary production (which generates individual products, main products, co-products and by-products) and secondary production, i.e. recycling of scrap. Figures for both primary and secondary production are available in annual reports of producers, such as Amplats, Implats and Lonmin (Genc, 2008).

Platinum producers are required to publish their production results annually; they also publish their interim results as well as their quarterly reviews and production reports. This information can be obtained from the producers' internet web-sites and news reports. Once the underlying factors that affect supply and demand of a commodity have been well researched, a supply and demand balance can be calculated in such a way that analysts can determine future supply so that they can predict future platinum prices (Genc, 2008). If the supply figures come down and the demand stays the same, the platinum price should go up. Similarly if the demand drops and the supply stays the same, then the price should fall. Figure 1 shows daily platinum prices between 2010 and 2014. Platinum price averaged at USD 1 554 over the last five years (2010-2014).

While the platinum price is crucial for the South African producers, the exchange rate between the South African Rand (ZAR) and USD determines the levels of profitability. The reason behind this is that most costs associated with platinum productions are in ZAR while the revenues are wholly in USD making the USD to ZAR exchange ratio very important. This also means that a weak ZAR is good for the platinum producers. The platinum price was in the highest level during August 2011, reaching USD 1 900, in line with the global commodity price boom, mainly caused by high demand by the auto-catalyst sector in Europe.

3 CHALLENGES IN THE PLATINUM SECTOR

Since 2008, the financial market woes, hence the volatility in the global commodities markets is still continuing. Although the world's leading financial indices such as the Dow Jones Industrial Average, The NASDAQ Stock Market and The S&P 500 index are continuously breaking their all-time high records respectively in 2014, all these developments still were considered as a part of global recovery. Similar observation are also visible for the European markets too, as they are also coming out of recession. The European economy's well-being is very important for the platinum sector as it impacts on the platinum market due to auto-catalysts demand, most of which originate from Europe. This demand has a direct impact on the platinum price. Furthermore, China is the driving force behind the commodity market and platinum is no exception. The World Bank recently cut its global growth forecast sighting weaker outlooks for the U.S., Russia and China; China's economic growth was lowered to 7.6% for 2014, however it was 10% per annum in 2008. Overall, the platinum price averaged at USD 1 390 in 2014 compared to USD 1 490 in 2013, down 7%.

The above factors all contributed to uncertainty in terms of realising increased returns on investment and South Africa is no different. Companies operating in South Africa which are able to anticipate and plan for these uncertainties will undoubtedly secure a competitive advantage. A combination of challenges in the South African mining sector has had a negative impact on its mining industry. Frequent bad news headlines related to mining industry, long lasting strikes and the recent rating downgrades by Fitch, Moody's and Standard and Poor heavily impacted on this volatile industry. A similar downgrade occurred by the afore-mentioned rating agencies in 2012 preceding the illegal strike action by the Marikana miners.

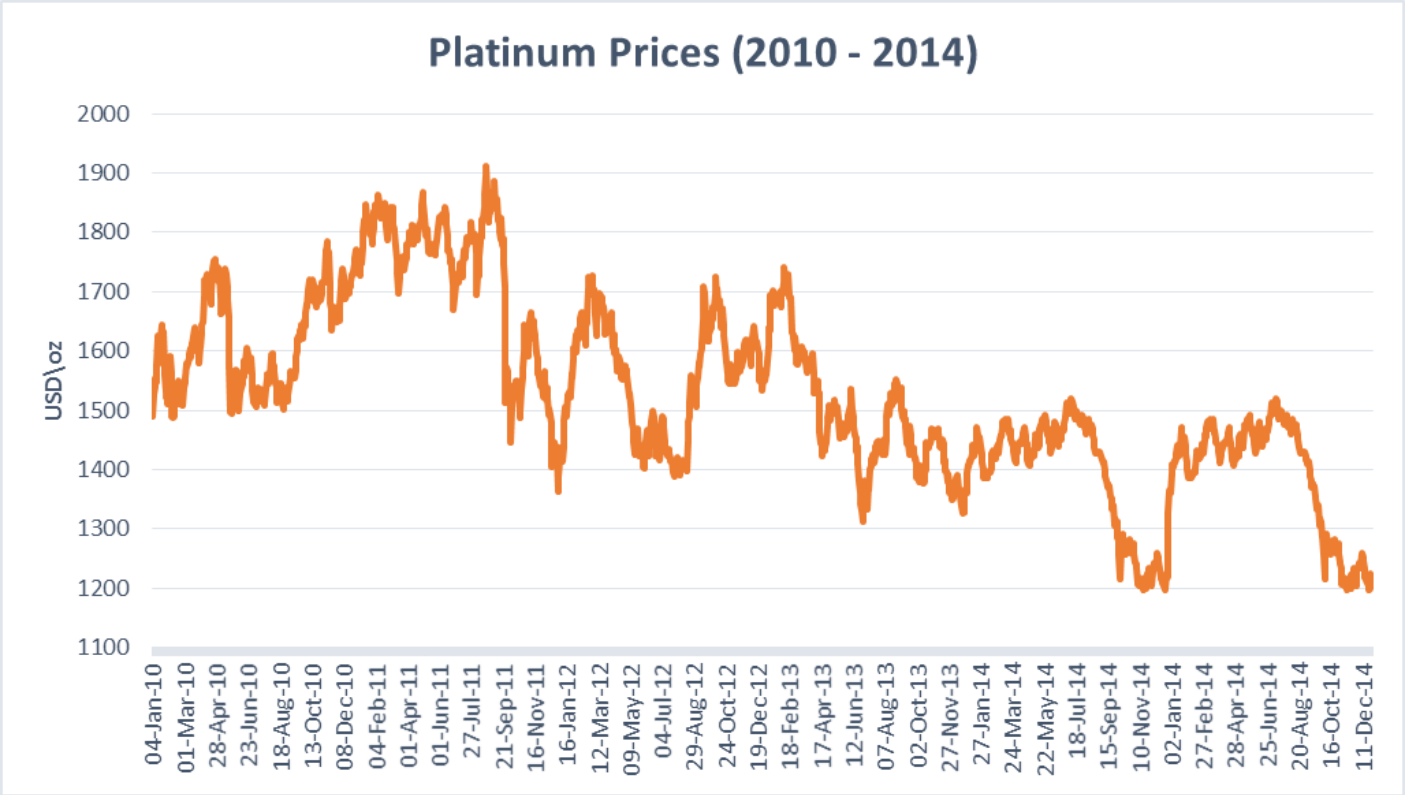

Figure 1. Platinum prices between 2010 and 2014 (adopted from Johnson Matthey, 2014)

4 POST 2012 EFFECTS IN THE PLATINUM SECTOR

As previously mentioned, the longest lasting strike action in the platinum belt ended on the 24th of June, 2014 after a five month long strike. Workers affiliated to the Association of Mineworkers and Construction Union (AMCU), which represents 70% of the work force in the platinum belt, has initiated the industrial strike action on the 23rd of January, 2014. The top three platinum companies employed around 136 000 people by the end of 2013. The AMCU workers were demanding a ZAR12 500 basic salary, an almost 30% salary increase, but employers were offering about 9%, which was higher than the inflation rate of 6.6% in June, 2014. This huge difference between what is offered and what employees' demands are could be linked to what happened in Marikana in 2012. The Marikana strike was also initiated with the same salary demand of ZAR 12 500. The strike forced all top three platinum producers to cease the operations until the strike was over as there has been some concerns about non-striking workers safety.

Post 2012, the mining sector overall became more fragile. Although no major strikes took place during 2013, workers demand for better wages continued. Wage demand related issues is only one of the challenges the platinum sector is facing; recently, the difficulties the South African platinum producers have to deal with to plan their future production are becoming very difficult to predict. These include the rising cost of labours, declining profit margins, and the possibility of falling metal prices, but the latest industrial strike action was not accounted for.

The real impacts of what happened in Marikana more than two years ago started to surface. The top three South African platinum producers have all been affected by the strikes. According to the Platinum Wage Negotiations website (2014), which was established by the platinum producing companies' revenues lost amounted to ZAR 24.1 billion while the employees' earnings lost was around ZAR 10.7 billion as of the end of the strike action on 24th of June, 2014.

In 2012, the South African supply of platinum fell to its lowest since 2001 as a result of the strikes. Failing productivity, the decline in grades, and the rapid escalating input costs also contributed to the crippling effect the mining industry experienced. Because of the rising costs of electricity and salaries, and other inputs such as the increase in fuel prices, as well as violent strikes, all three companies initiated retrenchments to become profitable again (Genc and Jerome, 2013). According to the National Union of Mineworkers (NUM) national executive committee meeting (2014) held on 24 February 2014, the after effects of major restructuring caused retrenchments of 7 450 workers at Amplats, 5 210 jobs at Implats and an estimated 3 000 jobs at Lonmin, totalling 16 660 during 2013. This was one of the expected outcomes of the 2012 strikes in the platinum belt. As the five month long strike had just ended, the consequences of the longest strike in SA's history is difficult to predict, but, similar to what followed the 2012 strike as mentioned earlier would be the most probable outcome. Figure 2 shows the strike effects on production in Lonmin's Marikana mine.

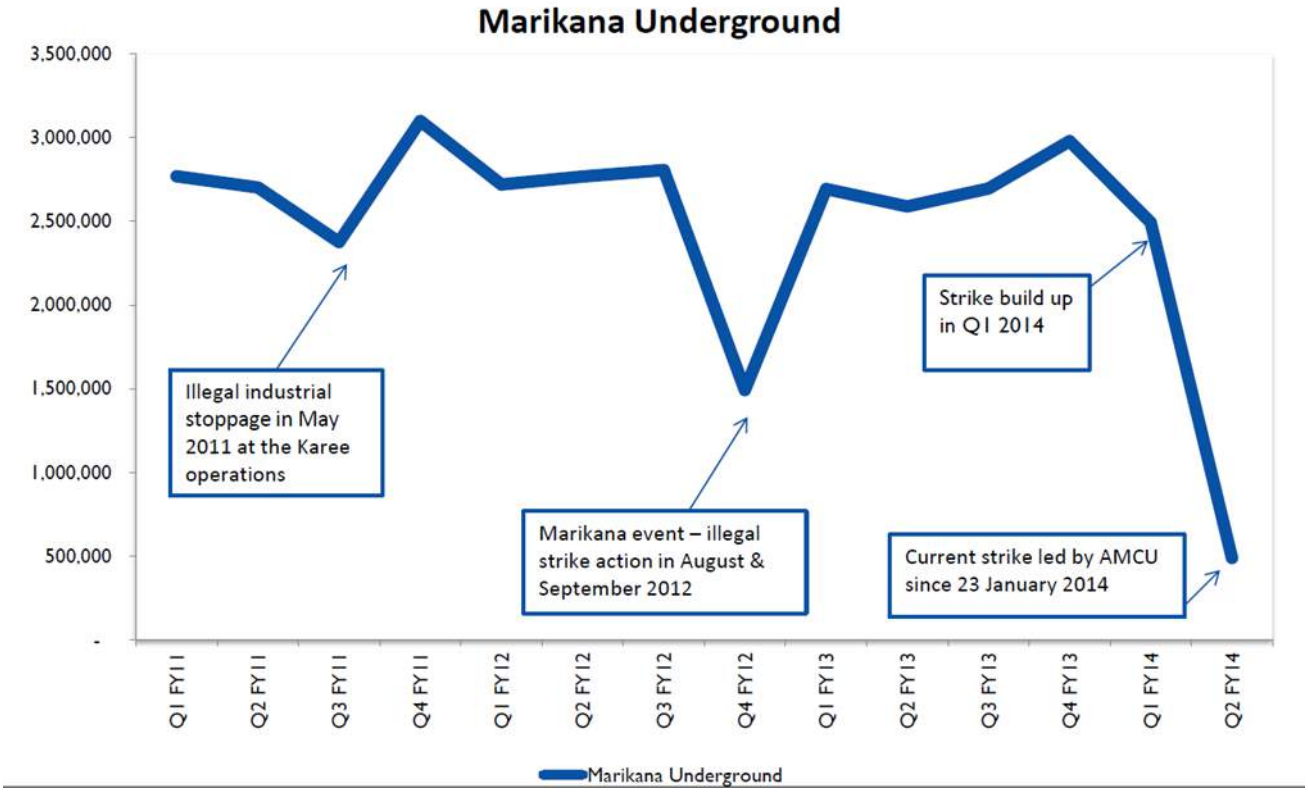

Figure 2. Strike effects in Lonmin's Marikana operations (after Magara, 2014)

The fact is that the platinum sector is in crisis as the platinum price had declined by 31% over the past five years, between 2010 and 2014. Although, at the same time, the ZAR depreciated by almost 50% against the USD, this depreciation was almost wiped away by not only the operational costs which have risen by 18%, but also above-inflation increases in fuel and electricity and annual wage increases higher than the inflation rate. One of the outcomes of the five months long strike has been the platinum price remained unchanged. The platinum price averaged at USD 1 440 during the first six months of 2014 while the strike was ongoing. Although the five months old strike was expected to have caused some platinum deficit in the market, according to World Platinum Investment Council (2014), which was established by the platinum producing companies', there are over 2.56 million ounces of platinum stockpiles at the end of the year 2014 which off-sets the supply concerns in the market. This is the reason

why the current level of platinum price is around USD 1 200 an ounce at the end of the year, 2014. In this light, it is also important to look at the financial performance of the top platinum producers.

5 FINANCIAL PERFORMANCE OF THE TOP THREE PRODUCERS IN THE PLATINUM SECTOR

In this section, the financial performance of the top three platinum producers are outlined. The financial comparisons were made using four key indicators, namely:

- Refined platinum production
- Headline earnings per share profile
- Operating profit and
- Headline profit.

The following tables (Table 1, 2, 3 and 4) show the top three platinum producers' financial performances between 2009 and 2013. As Lonmin reported its financial results in USD, an exchange rate of 7.47, 7.10, 7.36, 8.23 and 9.91 average ZAR values are used to convert the results to ZAR equivalent values, respectively.

Similar to any other business model, platinum miners also have to stay profitable to continue their core mining operations. Unforeseen circumstances such as illegal and lengthy legal industrial actions can affect profitability in a negative way. For example, the main reason behind the huge financial losses that Amplats suffered in 2012, were those illegal strikes. Figure 2 shows production related losses where the 2012 strike had a clear impact on.

Volatility in the mining industry is a well-known fact. For instance, Amplats's operating loss in the 2012 financial year amounted to ZAR 6.33 billion but in the next year, Amplats managed to turn into profit and declared ZAR 1.97 billion profit for the 2013 financial year. Similarly, Lonmin also made profit in 2013 after making a huge loss in 2012. This is a clear indication of volatility within the platinum sector. Headline earnings per share profile, operating profit and headline profit results were shown in Table 2, 3 and 4 respectively, clearly indicate the impact of the 2012 strike, hence the volatility within the platinum mining sector.

Table 1. Refined platinum production (000's) ounces

	2009	2010	2011	2012	2013
Amplats	2 464	2 484	2 410	2 219	2 320
Implats	1 704	1 741	1 836	1 448	1 582
Lonmin	683	706	720	701	751

Table 2. Headline earnings per share profile

	2009	2010	2011	2012	2013
Amplats	ZAR 2.89	ZAR 19.35	ZAR 13.65	ZAR -5.62	ZAR 5.56
Implats	ZAR 10.01	ZAR 7.86	ZAR 11.05	ZAR 6.85	ZAR 3.30
Lonmin	ZAR -10,38	ZAR 4,40	ZAR 9,99	ZAR -8,86	ZAR 3,09

Table 3. Operating profit (000 000's)

	2009	2010	2011	2012	2013
Amplats	ZAR 921	ZAR 7 253	ZAR 7 965	ZAR -6 334	ZAR 1 968
Implats	ZAR 8 823	ZAR 7 031	ZAR 10 193	ZAR 5 703	ZAR 2 376
Lonmin	ZAR -1 061	ZAR 1 441	ZAR 2 260	ZAR -5 777	ZAR 1 457

Table 4. Headline profit (000 000's)

	2009	2010	2011	2012	2013
Amplats	ZAR 705	ZAR 4 931	ZAR 3 566	ZAR -1 468	ZAR 1 451
Implats	ZAR 6 015	ZAR 4 718	ZAR 6 639	ZAR 4 151	ZAR 2 001
Lonmin	ZAR –1 808	ZAR 866	ZAR 2 009	ZAR -3 374	ZAR 1 695

When compared Table 1, 2, 3 and 4 all show that the companies' selected financial indicators were the lowest in 2012 due to the illegal strikes. Since then the metal price has not fluctuated much and the last five years (2010 to 2014) average metal price was around USD 1 554. The drop in the platinum price also affected operating profit (Table 3) negatively over the last five years. The full year earnings for all the three producers for the year 2014 is expected to be lower than the 2013 levels.

6 CONCLUSION

The post 2012 affects in the platinum sector is outlined in this paper. The platinum sector in South Africa is facing extreme pressure on the profit margins. The fact is that the platinum sector is in crisis as the platinum price has declined by 31% over the past five years. Although at the same time ZAR depreciated almost 50% against USD, this depreciation was wiped away by not only the rising operational costs by 18%, but also above-inflation increases in fuel and electricity prices and the annual wage increases higher than the inflation rate. One outstanding fact is that, although there was a five months long strike in the platinum belt in 2014, the price of platinum has not improved and ended the year 2014 at USD 1 200 level, the lowest level over the five years. As long as the current high level of stockpiles exist, the platinum prices will not improve.

The wage negotiations are a very complex and sensitive topic. While investors are always on the lookout to find better returns, on the other hand employees demand for better wages and improved working conditions needs to be addressed. This is essential to create not only a positive work environment and right balance between the employers and the mineworkers demand but also to establish the trust between the parties involved. As long as legacy issues are not resolved, there will be a possibility for even longer strikes. One of the important facts behind the 5 months long strike was that companies' revenues lost amounted to ZAR 24.1 billion while employees' earnings loss was around ZAR 10.7 billion. To avoid future confrontations, it will be in everybody's interest to find common ground to avoid long lasting strikes through dialogue and mutual understanding.

7 RECOMMENDATIONS

It is recommended that the salary negations need to continue in good faith by considering all the facts, including legacy issues. To avoid long lasting and potentially damaging impacts of the strikes, not only employers and mineworkers need to work together to resolve burning issues, but also government as a custodian of the mineral wealth of the country needs to get involved ideally before strike action becomes imminent to find solutions. Although there is no quick fix to the current labour related problems in South Africa, nevertheless it is crucial that involved parties show good leadership during the negotiations.

REFERENCES

Anglo American Platinum (2014*): Annual Results*, (2009-2013). http://www.angloplatinum.com, Accessed on 11 June 2014.

Genc, B (2008): Where is platinum heading? Proceedings of the Third International Platinum Conference - Platinum in Transformation, Southern African Institute of Mining and

Metallurgy, Sun City, South Africa, *October. Symposium Series* S52. 401-405.

Genc, B. and Jerome, J. (2013): Challenges in the South African Platinum Sector. *22nd International Symposium on Mine Planning and Equipment Selection - MPES 2013*, October 14-19, Dresden, Germany.

Impala Platinum (2014)*: Annual Results*, (2009-2013). http://www.implats.co.za/implats/index.asp. Accessed on 22 June 2014.

Johnson Matthey (2014)*: Platinum* 2013. www.platinum.matthey.com, June 2014.

Lonmin Plc (2014): *Annual Results,* (2009-2013). https://www.lonmin.co.za/ Accessed on 19 June 2014.

Magara, B (2014): *Final Results Presentation* 2014. https://www.lonmin.co.za/downloads/media_centre/news/press/2013/Final_Results_2013_presentation.pdf Accessed on 21 June 2014.

National Union of Mineworkers (2014): *NUM post NEC statement*. http://www.cosatu.org.za/docs/cosatu2day/2014/pr0224a.html. Accessed on 21 June 2014.

Platinum Wage Negotiations (2014): *Financial impact of strike*. http://platinumwagenegotiations.co.za/ Accessed on 22 December 2014.

World Platinum Investment Council (2014): *Platinum investment*. http://www.platinuminvestment.com/ Accessed on 22 December 2014

Estimating the Energy Costs of Mine Equipment Using an Information System

A. R. Sayadi, J. Khademi

Tarbiat Modares University, Theran, Iran

M. A. Rahimi,

Msc Student, Tehran University, Iran

ABSTRACT The energy cost has a significant share in the total costs of mineral production. Estimation and improving the energy costs require access to the costs of all equipments used in mining production including exploitation, transportation and mineral processing. Considering the variety and wide range of equipment in this business, to figure out the costs of energy is only possible through designing and building databases for technical and economical specifications of such equipment. In the course of this research a comprehensive database has been developed that stores various specs of these equipments, particularly the equipment powers and energy costs. With the help of such data the energy cost functions of equipment are calculated. These data can be used in estimation of energy costs, selection and improvement of equipment in mining projects. Energy requirements vary considerably for any equipment and they depend on the type and the size of equipment being operated, whether it is underground or surface. The amount of energy consumption is mainly a nonlinear function of the capacity of a machine and the amount and type of the function depend on the type of the machine. For example, the energy costs for one hour work of a loading machine in open-pit mines (shovel) is a nonlinear function of the volume of the bucket, and in cable and hydraulic shovels the power would be 0.98 and 0.60 respectively.

Keywords Energy costs, equipment, mine, mill, database

1. INTRODUCTION

Energy costs represent a significant component of the total costs of operations for mining sector. The energy use in the mining sector is also a significant contributor to the world's greenhouse gas emission. Improving energy efficiency reduces greenhouse gas emission that contributes to climate changes. There are, therefore, compelling economic and environmental reasons for mining and milling operations to examine their energy consumption and costs comprehensively.

Main part of the energy in mining sector is used for exploitation and mineral processing. Studying the amount of energy consumption and its costs requires studying and reviewing the total energy consumed by various equipment used in mines and processing factories. The main subject and target of this research paper is to study the power and energy costs of various equipment used in mining and processing operations concerning their technical specs such as capacity, power, and some other technical specs. To achieve this goal and considering the variety and wide range of capacity and the large volume of technical and economical data for mining and processing equipment, a comprehensive information system, including a database and a software package, has been developed for easy and efficient application and management of this database. This database provides the opportunity to analyze the costs of energy consumed by equipment. This paper introduces this software, and presents the some functions for estimation and prediction of the amount of energy costs.

2. THE POSITION OF ENERGY IN MINING

Energy used in mining operations accounted for approximately 3.3 percent of total industrial energy use in the U.S. in 2000. The U.S. Department of Commerce reports total energy consumption in mining to be 491 trillion Btu; however, this does not include data withheld. The US Department of Energy, Office of Industrial Technologies has estimated total industry energy consumption including data withheld to be 753 trillion Btu (US. Department of Energy, 2000). This total is reported about 1,246 Trillion Btu/year in 2007 (BCS, 2007).

Equipment-level and process-level energy consumption estimates are needed because improvements in energy efficiency will be driven by improvements in mining processes and technologies.

Extraction, materials handling and beneficiation– processing can be represent as the three main stages in mining process. As shown in Figure 1 materials handling accounts for 42 percent of the energy consumed. Diesel equipment accounts for 87 percent of energy used in materials handling. Beneficiation and processing consume 39 percent of the energy in mining. Crushing and grinding activities account for 75 percent of the energy used in beneficiation and processing. The remaining 19 percent of energy in mining is consumed by extraction activities. Pumps account for 41 percent of the energy in extraction (Mining Overview, 2010).

Surface mining may extend to depths as much as 500 m. The energy used and the cost of hauling rock from such depths become important limiting factors. The five principal energy-using units in mining are drilling, blasting, loading, hauling, and ancillary processes.

The share of hauling is important, for example, for copper, hauling by truck consumes more than 54% of the total energy required in mining (IPT Mining, 2002).

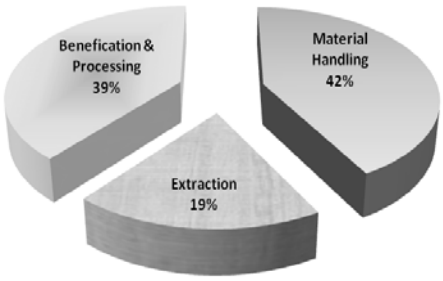

Figure 1. Estimated energy consumption by stage (percent of total energy requirements)

The total energy costs for open-pit mining for the nine operations in Canada vary from $170 per kiloton of ore mined to $3,120 per kiloton (Tab. 1) (NRC, 2005). The total cost covers drilling, blasting, excavating, hauling, pit dewatering, and mine support equipment, road maintenance and service equipment. Any in-pit crushing or re-handling of ore from stockpiles is excluded.

Table 1. The range of energy cost and efficiencies for open-pit mining in Canada

	Range High: Low
Energy cost ($/kiloton of ore mined)	3 120 : 170
Energy consumption (kWh_e/kiloton of ore mined)	42 474 : 7 006
Unit energy cost ($/$kWh_e$)	0.073 : 0.022

In processing plants, 50-70% of the energy is typically used for communication. In processing for copper, grinding and concentration consume about 45 percent of the energy used, with grinding accounting for the majority of the energy consumed.

The total energy costs for open-pit mining-Mill/Concentrator operations for seven operations in Canada vary from $105 per kiloton of ore processed to $2,367 per kiloton (Tab. 2). The total costs cover crushing, grinding, all other concentration, extraction and recovery operations, tailings treatment, process water supply, and other plant energy. Any in-pit crushing has been included with the primary crushing operations at the mill.

Table 2. The range of open-pit mining-Mill/Concentrator in Canada

	Range High : Low
Energy cost ($/kilotonne of ore processed)	2 367 : 105
Energy consumption (kWhe/kilotonne of ore processed)	35 701 : 13 144
Unit energy cost ($/kWhe)	0.083 : 0.005

Because of globalization and international competition, mineral processing plant managers seek at reducing production costs. These plants are major energy consumers and therefore energy efficiency is becoming an important objective. Other incentives are the energy cost that will probably continue to rise and the environmental and social pressures for reducing energy consumption. Using more energy efficient equipment is a first approach.

There are some general estimates of potential energy savings from attaining the performance of the most energy-efficient operations. After Natural Resource of Canada (NRC), potential annual energy savings identified with the most efficient operation for each production stage can be about one third of total energy costs. It should point out that these savings are hypothetical and may not be achievable owing to circumstances faced by each mine, i.e. the nature of the ore body, technology employed, long-term contractual obligations, etc.

In this study a database of mining and milling equipments is developed. The focus is a detailed comparison of the energy costs for open-pit mining and concentration equipments.

3. DESIGNING THE DATABASE AND SOFTWARE

Information systems and databases provide easy method for data analysis and pattern recognition. In this regard, a database related to technical and economical specs of common equipment used in mining and mineral processing along with a software package for managing this database has been designed and developed. It's needed to mention that in order to improve this software's efficiency and applicability, in addition to the costs of energy consumed by these equipment, other capital and operating costs have been taken into account as well but they are out of the framework of this paper as the main focus here is on the energy and fuel costs.

Databases are designed to support the data storage, processing, and retrieval activities related to data management in information systems (Zongin, 2006). A database is a set of files that are interrelated. It is not just a collection of files and the word "interrelated" is the keyword as these files need to be able to relate and connect to other files in the database (Whitten and Bentley, 2008). In the other word a database is an organized collection of information called data. Data are the raw numbers or basic information collected from the appropriate sources at the proper times using the correct methods to answer a question or solve a problem. These data are analyzed numerically, spatially, visually and/or statistically and converted into information (Mclemore et al., 2005). Databases are designed to support the data storage, processing, and retrieval activities related to data management in information systems (Zongin, 2006). A more rigorous definition of a database is a collection of data organized to serve many applications efficiency by centralizing the data and controlling redundant data. Rather than storing data in separate files for each application, data are stored so as to appear to users as being stored in only one location. A single database services multiple applications (Laudon and Laudon P., 2006).

Databases are handled by database management systems (DBMS) (Laudon and Laudon P., 2006). Database management systems form the foundation of most information systems. A database management is a complex multi-attribute tool that supports many types of business applications (Post and Kagan, 2001). A DBMS is simply the software that permits an organization to centralize data, manage them efficiency, and provide access to the stored data by application programs (Laudon K. and Laudon P., 2006). It is specialized computer software,

available from computer vendors, that is used to create, access, control, and manage the database. The core of the DBMS is often called database engine. The engine responds to specific commands to create database structures and then to create, read, update, and delete records in the database (Whitten and Bentley, 2008).

3.1. The Specification of Mining Equipment Database

Every database is built based on a data model. A data model is a set of tools that describe data, relations between data and meaning of data and finally is a way to describe the stages of designing the database (Silberschatz, 2006). Unified Modeling language (UML) is used to design this database. The UML Data Modeling Profile was proposed by Rational Software from IBM (Song et al.). The Unified Modeling Language has quickly become the standard language used for modeling business and software application needs (Naiburg and Maksimchuk, 2001).

Relational model is the most used data model and the most of database systems are base on this model (Silberschatz, 2006) and here in this case the relational model has been selected and considered to design this database. The equipment in this database has been categorized into four categories of surface, underground, processing and miscellaneous. In general, for each of these categories a number of technical specs are taken into account, which based on these specs the capital and operating costs data would be entered into this database. One the most important costs considered for each machine in this database is the energy and fuel costs, which based on the type of the equipment; it can be the costs of diesel, gasoline, natural gas or electricity calculated by dollar per hour of operation. Please note that a separate table is allocated for each equipment group, and a total of 309 equipment groups have been fallen into four categories mentioned above (e.g. cable shovels). Later on the expenditure data related to each type of this equipment is entered in this database. Table 3 shows a summary of the status of these groups and equipment in this database broken down by surface, underground, processing and miscellaneous. Figure 2 also shows the number of the records in each of these four categories in this database. Tables 4 and 5 display more detailed information about descriptive and expenditure data in this database.

Table 3. A summary of the status of these groups, and the types of the equipment in this database

Category	Number of Tables (Equipment Groups)	Number of Records (Equipment Types)	Number of Appendix Tables	Number of Cost Items	Number of Descriptive Items
Surface	54	349	4	4188	1396
Underground	73	503	13	6036	2012
Mineral Processing	94	1648	19	19776	6592
Miscellaneous	78	883	1	10596	3532
Total	309	3383	37	40596	13532

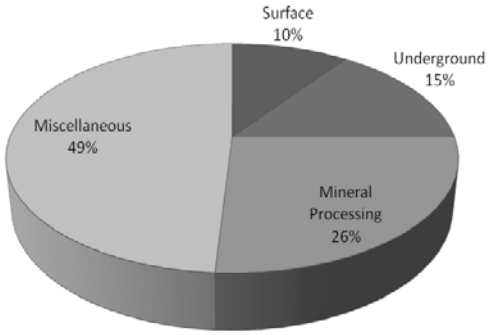

Figure 2. The number of records in each of these four categories

Table 4. Descriptive data of database

Table Names	Su_desc	Ug-desc	Milling_desc	Misc_desc
Goal	Saving Descriptive Information of Surface Equipment	Saving Descriptive Information of Underground Equipment	Saving Descriptive Information of Milling Equipment	Saving Descriptive Information of Miscellaneous Equipment
Number of Records	349	503	1648	883
Number of Fields (Column)	23	23	23	23

Table 5. Cost data of database

Table Names	Su_desc	Ug-desc	Milling_desc	Misc_desc
Goal	Saving Cost Information of Surface Equipment	Saving Cost Information of Underground Equipment	Saving Cost Information of Milling Equipment	Saving Cost Information of Miscellaneous Equipment
Number of Records	349	503	1648	883
Number of Fields (Columns)	13	13	13	13

Once the data modeling is completed and the specification of the database is defined and determined, a SQL Server platform has been used to implement the Database Management System (DBMS). Figure 3 displays a summary of the status and situation of the main tables as implemented within SQL Server.

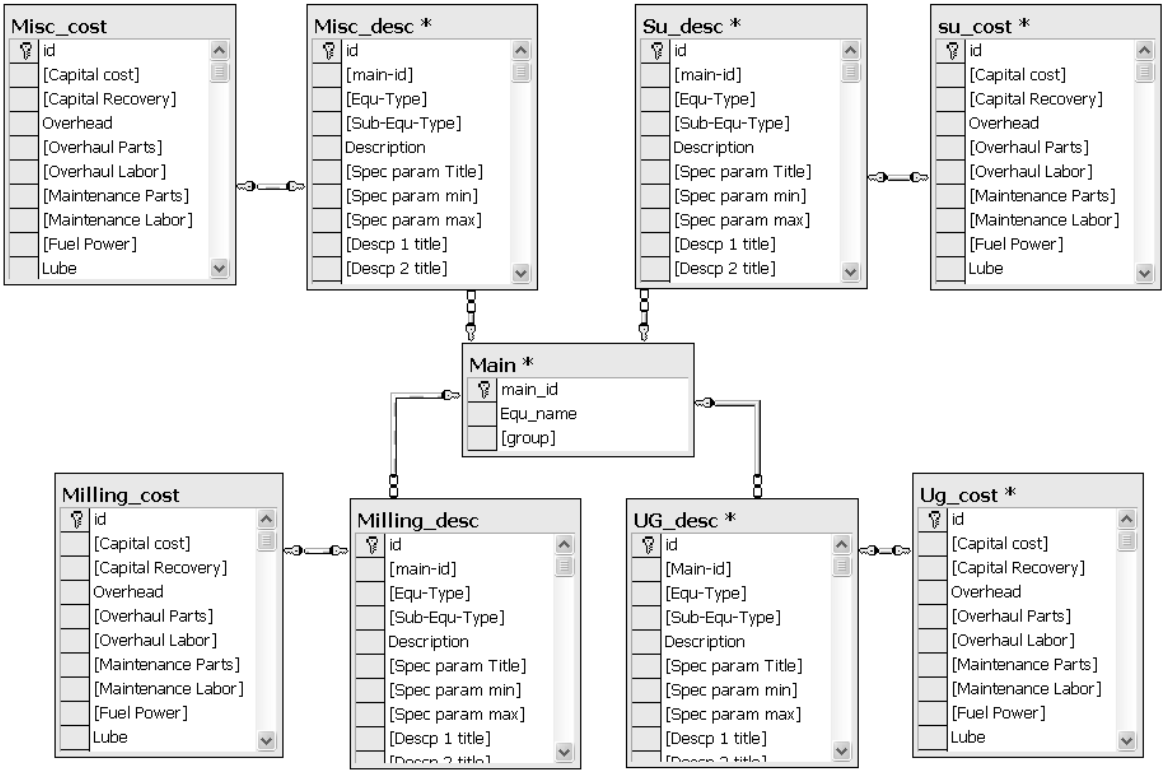

Figure 3. The relationship between the main tables in the database implemented in SQL Server

3.2. The Specification of the Cost Estimating Software

In order to improve the efficiency and capabilities of this database, an applied software package called EquipMine has been designed and installed as the front-end on the top of this database.

EquipMine is a software tool that processes, manages and provides the capital and operating costs of mining and processing equipment including the energy and fuel costs during mining operations. There are two important strong points for this front-end tool; first strong point is the great effort made in understanding the conceptual and logical models on technical and scientific basis during the course of implementation of this software, and the second one is the fact that the software has been built and implemented as simple, attractive and user-friendly as possible, and it's application is very easy yet very efficient. This software has been developed with .NET technology and the standard features in developing applied business application have also been considered in its design and implementation.

This software is designed based on 3-tiered model, which includes application layer, classes' layer and database layer. Figure 4 shows a schematic view of this model.

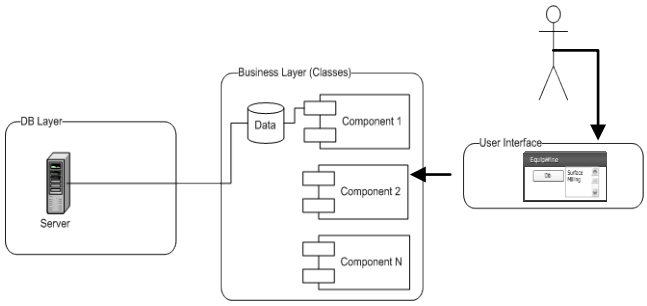

Figure 4. Architecture of EquipMine

With use and help of this software, we can assess and calculate the capital and operating costs related to each type of equipments with regards to its technical specs and data in the database. Therefore, it is possible to estimate the energy and fuel costs for all equipment working in a given mine based on dollar per hour. Figure 5 displays a sample report generated by this software in which the capital, energy and

fuel costs are displayed for selected equipment. Figure 6 also shows a sample graph created by the software in which the trend of changes in the energy and fuel costs is displayed for mill type machines based on the changes in the mill radius.

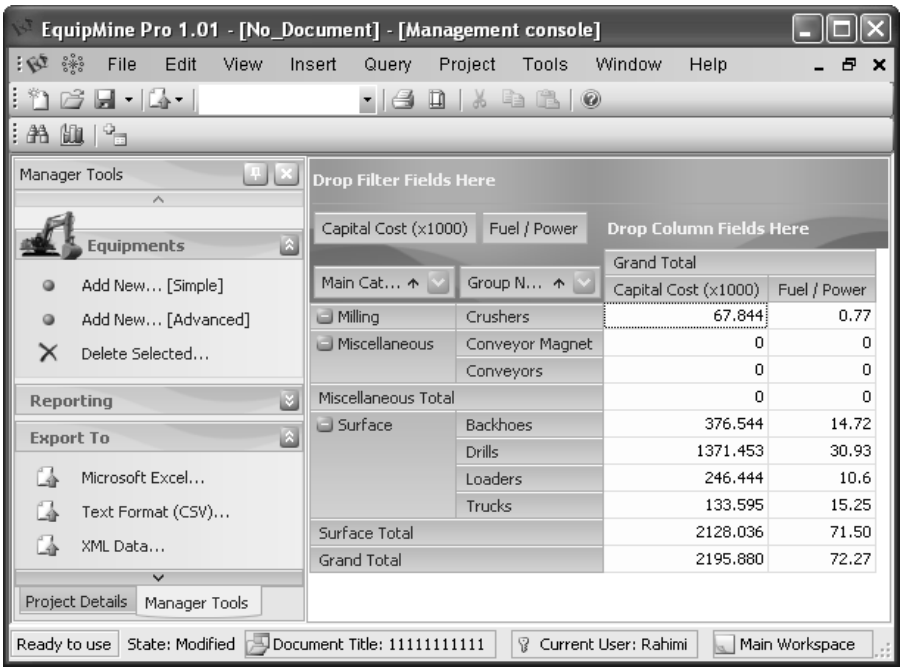

Figure 5. Sample report generated by the software

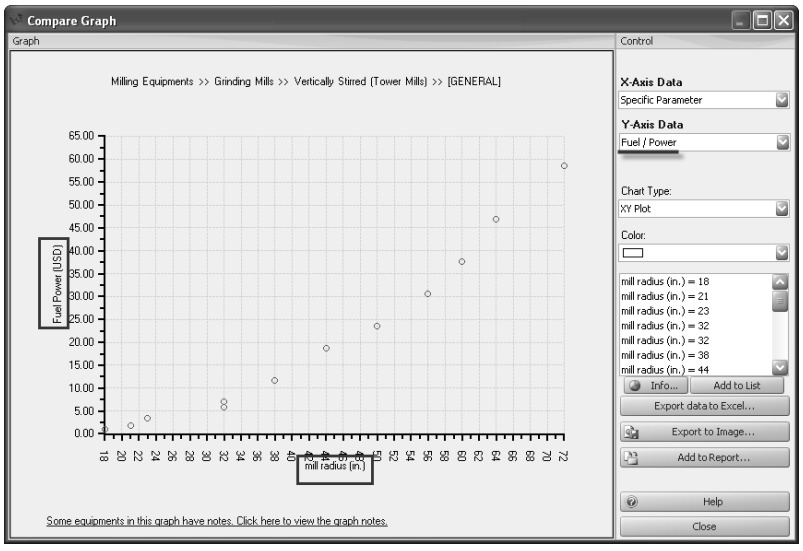

Figure 6. Sample graph created by the software (changes of hourly energy/fuel costs based on the radius of the mill)

Below is a summary of the benefits of having such software:

- Covers a wide range of mining equipment
- Few software packages exist in this area of expertise
- Multi-user capability
- Ability to adjust to the condition(s) of the country hosting the project
- Ability to update the costs using the cost indexes
- Ability to add new equipment data
- Ability to generate graphs and reports in various formats

Figure 7 also shows a summary of the main components of this software.

4. DATA ANALYZING SAMPLES

Considering the variety and multiplicity of the equipment, the energy costs for a selection of mining and processing equipment are being analyzed in this section.

4.1. Mining Equipment Shovels:

Figure 8 shows the variation of energy cost ($/h) for shovels based on the volume of their buckets broken down by cable and hydraulic shovels.

The energy cost is a nonlinear function of volume of the bucket; in cable and hydraulic shovels it would be around 0.98 and 0.60, respectively. It should be noted that the effect of rock formation property has not been considered.

Trucks:

A variety of trucks using in surface mining such as bottom-dump (mechanical), rear-dump (articulated), and read-dump (rigid frame) have been studied. The function of energy costs for rear-dump (articulated) turned out to be exponential and different from the other two (Fig. 9). Trucks using in underground mines have also been studied (Fig. 10). The energy cost is a nonlinear function of the capacity of the truck per ton and the power of 0.73.

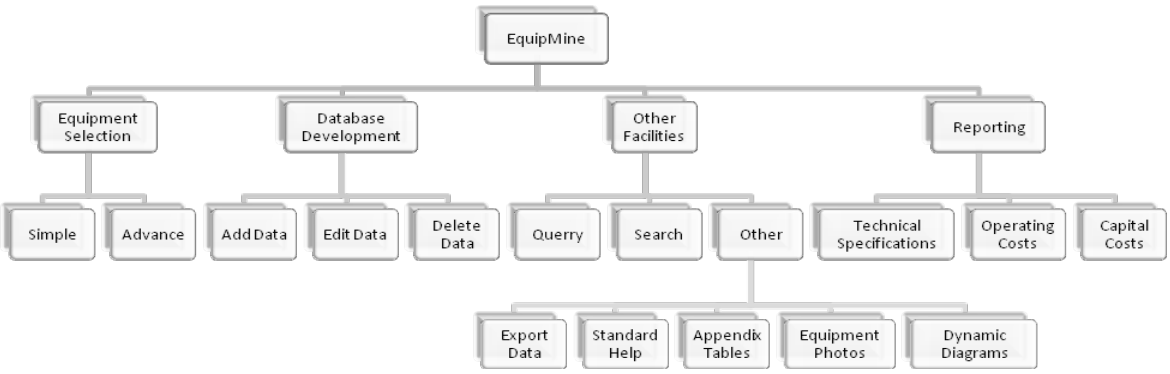

Figure 7. A schema of the main components of EquipMine software

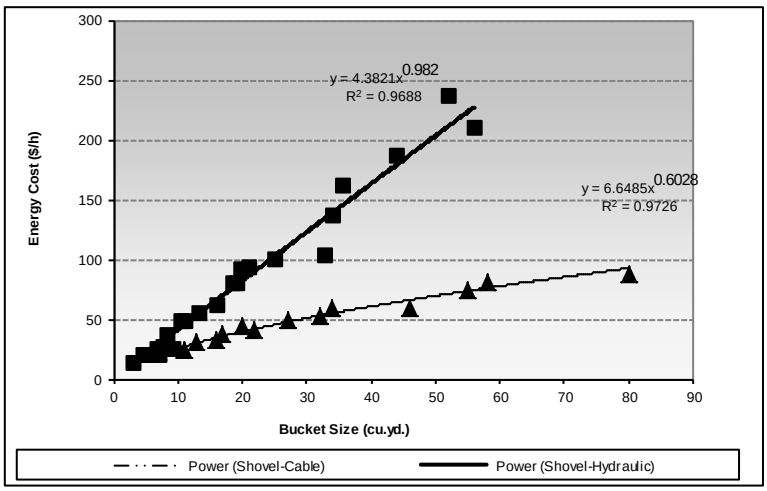

Figure 8. Energy cost vs. shovels bucket volume (cu.y.)

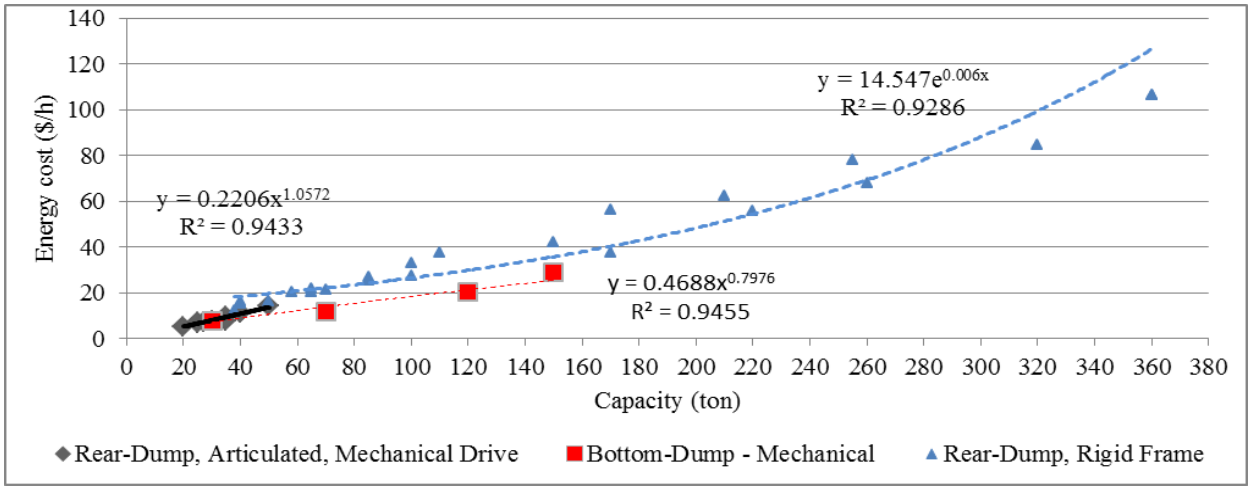

Figure 9. Energy cost vs. trucks capacity (surface mining)

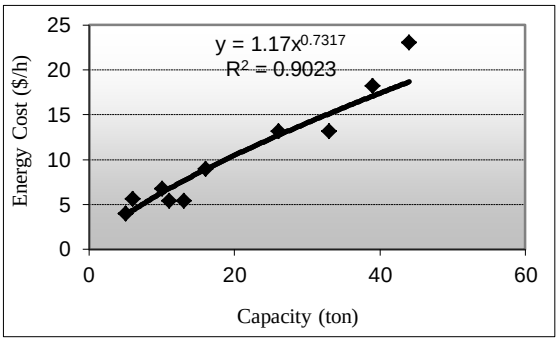

Figure10. Energy costs vs. capacity of read-dump (articulated) trucks (underground mining)

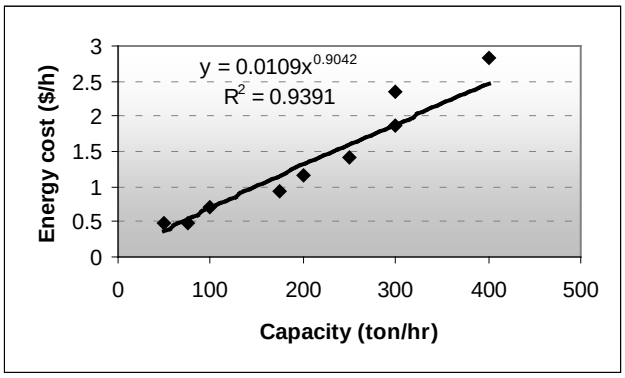

Figure 11. Energy cost vs. capacity of classifiers

4.2. The Processing Equipment

There are various and numerous equipment being used in mineral enriching processes. The energy costs of classifiers are function of their capacity (tons per hour), and it is a nonlinear function with power of 0.9 (Fig. 11). The energy costs of grinding-mill vertical machines are a function with the power of 2.8 relative to the radius of the mill (Fig. 12).

5. CONCLUSIONS

Information systems can be used as a very helpful tool in analyzing and estimating the energy costs of mining equipment. In this regard, a comprehensive database and a front-end tool have been designed and developed for technical and economical specs of mining equipment, and some functions been presented for estimation and analysis of the equipment energy costs in mining projects.

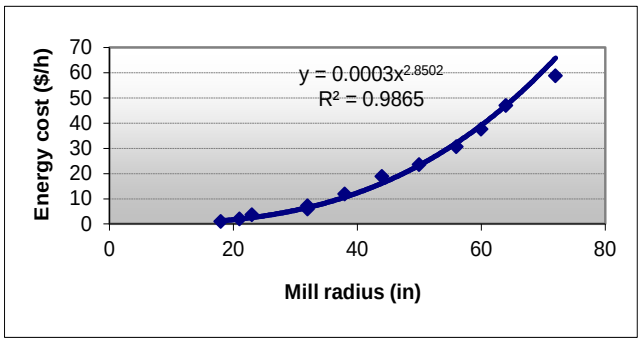

Figure 12. Energy costs vs. radius of grinding-mill vertical machines

In addition to that, this software can also be used to improve the equipment expenditures from the costs of energy point of view. The results from this study indicate that the energy costs of different equipment in relation to their capacity would show different pattern and behavior, and the cost functions clearly explain such behavior.

In this research the costs of equipment has been studied individually but it is needed to develop this software to the extent that it provides the opportunity to assess and improve the energy costs for the whole fleet of such equipment.

REFERENCES

BCS, 2007. Mining industry energy bandwidth study, U.S. Department of Energy's (DOE) Office of Energy Efficiency and Renewable Energy (EERE).

IPT Mining, 2002. Energy and Environmental Profile of the U.S. Mining Industry Energy and Environmental Profile of the U.S. Mining Industry, Copper.

Laudon K. C. and. Laudon J. P, 2006. "Management Information Systems", 9th edition, Prentice Hall.

Mclemore, V. T., Krueger, C.B., Johnson, P. Raugust, J.S, Jones, G.E, Hoffman, G.K and Wilks, M. 2005. "New Mexico Mines Database", Mining engineering Journal, Feb, PP. 42-49.

Mining Overview, 2010. Energy and Environmental Profile of the U.S. Mining Industry, available on: http://www1.eere.energy.gov/industry/mining.

Naiburg, E. J, Maksimchuk, R. A., 2001."UML for Database Design", First Edition, Addison Weseley.

NRC, 2005. Benchmarking the energy consumption of Canadian open-pit miens, http://oee.nrcan.gc.ca/

Post G. and Kagan A., 2001. "Database management systems: design considerations and attribute facilities" The Journal of Systems and Software. vol. 56, pp. 183–193.

Silberschatz, A. 2006. "Database System Concepts", McGraw Hill.

Song, E., Yin, S., Ray I., 2007. Using UML to model relational database operations", Computer Standards & Interfaces Journal, Vol. 29, pp. 343-354, 2007.

U.S. Department of Energy, 2000. Energy Efficiency and Renewable Energy, Office of Industrial Technologies.

Whitten, J. L., Bentley, L. D., 2008. "Introduction to Systems Analysis & Design", New York, McGraw Hill.

Zongin, M., 2006. "Database Modeling for Industrial Data Management," Idea Group Publishing (IPG).

Indonesian Low Rank Coal Regulation: Economic Approach

T. Winarno
Ministry of Energy and Mineral Resources of The Republic of Indonesia

C. Drebenstedt
TU Bergakademie Freiberg, Sachsen, Germany

ABSTRACT The Gross Domestic Product (GDP) of Indonesia growth in the last 5 years rose to on average of 5.5 %/y, with final energy consumption grows on an average of 2.91 % per year. Moreover, the GDP growth target of more than 6 %/y, estimated energy needs in Indonesia have significantly increased. In the last forty years, Indonesian energy consumption has been heavily depended on oil fuel, and currently, Indonesia is trying to diversify energy.

One of the energy resources that can be utilized to diversify is the Low Rank Coal (LRC). Utilizations are limited due to its low heating value and spontaneous combustibility, but has low sulfur/ash content. Solution of the LRC utilization is by value-added. The value added can be done by mixing/blending, upgrading, coal gasification, coal water mix/fuel and even by coal liquefaction. So far, the value added of LRC is limited only blending/mixing to improve market demand. However, the use of the LRC relies primarily on economic and technological considerations. This paper will discuss the economics of LRC utilization based on regulation of the Indonesian government, so as to provide an overview LRC utilization opportunities in Indonesia.

Keywords: LRC, market, economic analysis

1 INTRODUCTION

Coal is a major mining commodities Indonesia. In 2013, production reached 426 million tons, or increased three times compared to 2004 (131 Million tons). More than 70% of coal production was exported, and Indonesia became the biggest steam coal exporter in the world (worldcoal, 2014). Unfortunately, the production and utilization of the LRC was not optimal yet.

LRC Classification sometimes cause confusion/trouble. Each country with a coal industry has tended to develop its own criteria in order to classify its domestic coals, often for a particular application. These classification parameters were often chosen for historical reasons (Carpenter, 1988). In Indonesia, the LRC is intended to caloric value <5,100 kcal/kg (adb). The combination of the high moisture content and high reactivity of LRC necessitate their utilization close to the mine, unless by upgraded to value-added products to improved transport safety and economics (Allardice, 2001).

Currently, the value added is a major issue in Indonesia, as contained in the Law 4 of 2009 on Mineral and Coal Mining. This means that the mineral and coal can be more beneficial for economic growth in Indonesia. For coal especially the LRC, the government will require companies doing the added value before using, with the main target for domestic needs. Some of the reasons for the needs to improve the added value are : optimizing the use of coal (conservation), meet domestic raw materials industry, improve the national economy, lead to the development of downstream industries.

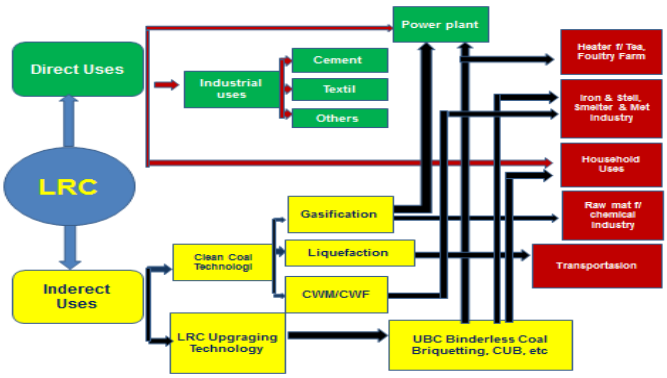

Figure 1. Indonesia LRC Management (Sihite, 2012)

In each country, the present status is that the LRC utilization technology is under development according to the situation in each country and the expected utilization in the future of low rank coal (METI, 2012). In Indonesia, LRC be used directly for the industry, cement and textile, (with or without blending), and attempted to be used indirectly as Clean Coal Technology (Gasification, Liquefaction and CWM/CWF) and LRC Upgrading or quality improvement with UBC (Upgrading Brown Coal) or CUB (Coal Upgrading Briquette Technology). The most important issue of LRC utilization in Indonesia are the economical and technology aspect itself.

With a GDP growth target of more than 6%/year, estimated energy needs in Indonesia have significantly increased and expected LRC can contribute. In order to utilize, economic calculation must be performed to assess the feasibility of the value added. Analysis and determination of the economic analysis/feasibility are done by using the criteria : *Net Present Value* (NPV), *Internal Rate of Return* (IRR), *Profitability Index* (PI), and *Discounted Pay Back Period* (PBP).

2 DOMESTIC MARKET OF THE LRC

Indonesian energy consumption increased from 764 million Barrels Oil Equivalent (BOE) in 2000 to 1,079 million BOE in 2012, a rose of an average 2.9%/y. The largest share of energy demand are industry sector (34.8%) followed by the household (30.7%), transportation (28.8%), commercial (3.3%), and other sector (2.4 %) (BPPT, 2014). While the type of energy used, the oil fuel is still dominated by 38.86%, coal 22.44%, biomass 18.36%, gas 16.87%, hydropower 2.1%, Geothermal 1.08%, and biofuel 0.29% (EMR, 2013). Expected in the future, the role of coal and gas are increasing, while the role of oil fuel decreases, as according by Presidential Instruction No. 5 of 2006 on the Energy Mix.

2.1 Direct Uses

2.1.1 Power plant

Coal is one of the primary energy for power plants. In Indonesia (2013), 52 % of the power plants using coal or about 65 million metric ton of coal burned. Coal used consist of 9 million metric tons of High Rank Coal (HRC), 31 million metric tons of Medium Rank Coal (MRC) and 25 million metric tons of LRC (3800-4500 kcal/kg GAR). Currently, the electrification ratio around 79 % or only 680 kWh/capita and Indonesia will add 60 GW additional capacity period of 2013-2022, consist of 38 GW coal fired (Nasri, 2014).

2.1.2 Cement, textile and others industries

The industrial sector is the largest energy user in Indonesia in 2012, and shows the numbers continue to rise. All industries showed a significant increase in production, although coal has not been widely used. The main industries that use coal is cement. With a production of 60 million metric tons of cement, requires about 7.8 million metric tons of coal per year, consisting of 0.55 million metric tons of HRC, 5.2 million metric tons of MRC and 2.05 million metric tons of LRC. In the last 10 years (2002-2012), the industry grows by 6%/y (Indusrty,

2012). Other industries have not used the LRC for its energy supply.

2.2 Indirect Uses

2.2.1 Upgrading

Coal upgrading technology (UBC/CUB) is one option for the utilization of LRC by reducing the moisture content so that it will directly increase the calorific value of the coal. With higher caloric value of the coal can respond to market needs, especially power plants that already exist, and others industrial sector. With growth in all industries, LRC has high utilization opportunities and coal mining industries in Indonesia will continue to grow and can be contribute as an energy supplier for the country and increase the exports in the future.

Briquetting is another option of coal upgrading. Briquetting make coal an attractive substitute fuel by converting it into compact, stable and inexpensive coal (Glenn et al, 1989). Briquettes can be substituted for firewood, even kerosene and LPG. Briquettes can be used for small industry and households, poultry farm, restaurant and others.

2.2.2 Clean coal technology

2.2.2.1 Gasification

Coal gasification is the technology for high-efficient conversion and utilization of coal (Yiman, et.al, 2013). The methods for producing gas from coal are numerous (James, et.al, 1984). Gas production in Indonesia (2012) has reached of 3,087 Billion Standard Cubic Feet (BSCF) with consumption of 1,329 BSCF (EIA, 2014). Gas distribution infrastructure constraint in Indonesia, so that utilization is not optimal yet. In general, the gasification of the LRC is not needed at this time in Indonesia

2.2.2.2 Liquefaction

The process of coal liquefaction is the process of converting coal into oil such as gasoline or diesel. This process is often termed as coal liquefaction or coal-to-liquids (CTL). There are two ways to produce oil from coal is through direct coal liquefaction (DCL) and indirect coal liquefaction (ICL), each of which has advantages and disadvantages. The results of this liquefaction process can be used as a fuel for transportation and industry. Indonesia has been cooperating with Japan in LRC liquefaction, namely Brown Coal Liquefaction.

Currently (2012), oil production amounted to 989,000 barrels oil per day (bopd), with consumption of 1,610,000 bopd. Import of oil is expected to continue to increase. Anyway, with oil production steadily declining since 2004, expected that BCL (Brown Coal Liquefaction) technology can be operated in Indonesia.

2.2.2.3 Coal water mix/coal water fuel (CWM/CWF)

CWF is a homogeneous mixture consisting of coal, water and additives, which form a slurry. CWF can not be used directly as fuel and have the nature of non-flammable, but have a flow properties such as fuel. When it will be used as a fuel must go through by another heating media (furnace). Combustion is done by using a pump to spraying the CWF furnace which has been preheated (injection system). Combustion efficiency depends on the degree of atomization of the CWF and the type used of atomization (Wall, 1987). CWM/CWF can be used as energy in several industries and even as a fuel for large ships.

Paragraph starts immediately after a heading or a gap.

3 ECONOMIC ANALYSIS

There are several models that can be used to analyze a project, e.g. the net present value, internal rate of return, profitability index and the discount payback period (Shapiro, 2005).

3.1 Net Present Value (NPV)

Net Present Value (NPV) is a method of investment appraisal, which is the present value of cash flows in the future, discounted at an appropriate cost of capital, reduced by investment cost. If there are mutually exclusive projects, the higher NPV will be accepted.

$$NPV = -Io + \sum_{t=1}^{n} \frac{CFt}{(1+r)^t} \quad (1)$$

NPV = Net Present Value
Io = investment cost
CFt = Cash flow at t period
t = the time of the cash flow
r = discount rate
n = total number of periods
Assessment Criteria :
- If NPV ≥ 0, then the project is accepted
- If NPV < 0, then the project is rejected

3.2 Internal Rate of Return (IRR)

IRR is the discount rate that results in NPV to zero or that makes the net present value of all cash flows from a particular project equal to zero.

$$0 = -Io + \sum_{t=1}^{n} \frac{CFt}{(1+IRR)^t} \quad (2)$$

Assessment Criteria :
- If the IRR is greater than the capital costs, the project is accepted.
- If the IRR is less than the capital cost, the project is rejected.

3.3 Profitability Index (PI)

Profitability Index or cost-benefit ratio is an investment appraisal technique by dividing present value of future cash flows by initial investment cost.
Assessment Criteria :
A profitability index equal to or greater than 1 is considered good. It means that the project is worth executing.

3.4 Discounted Payback Period (DPP)

The discounted payback period is the amount of time to return the initial investment cost in the form of cash flow based on total revenue minus all cost except depreciation cost.
Assessment Criteria :
If the DPP is smaller than the specified economic life of the project, the investment of the project is acceptable.

4 DISCUSSION

4.1 Coal Upgrading

With assumption of coal price US $ 24.7, investment cost US $ 133.1 million, capacity 5000 t/d, 8% of interest, operation cost US $ 10.71/t, and price of product US $ 65.7, then the economic analysis result:

No	Parameter	Result	Criteria	Decision
1	NPV	US$ 64,106,558.73	NPV > 0	Feasible
2	IRR	14.64%	IRR > 8 %	Feasible
3	PI	1.48	PI > 1	Feasible
4	DPP	8 year 10 month	DPP<15 year	Feasible

4.2 Coal Briquetting

With assumption of coal price US $ 24.7, investment cost US $ 3,125,000 million, capacity 60,000 t/d (prod : 45000 t/d) , 8% of interest,operation cost US $ 1,527,566.67, and price of product US $ 166.67/ton, then the economic analysis result:

No	Parameter	Result	Criteria	Decision
1	NPV	US$ 8,502,798.23	NPV > 0	Feasible
2	IRR	69.04%	IRR > 8 %	Feasible
3	PI	3.7	PI > 1	Feasible
4	DPP	1 year 7 month	DPP<10 year	Feasible

4.3 Coal Liquefaction

Assumption of, investment cost US $ 2,334 million, capacity 6000 t/d, 8% of interest, operation cost US $ 30.75/t (Anonymous, 2008), coal price US $ 24.7, oil price US $ 70/barrel and price of product US $ 2,122,498 (26,905 bbl/d, 234 t/d of LPG, 10 t/d of sulphur, 1.2t/d of phenol and 49 t/d ammonia) then the economic analysis result:

No	Parameter	Result	Criteria	Decision
1	NPV	US$ 1,066,677,052	NPV > 0	Feasible
2	IRR	12.48 %	IRR > 8 %	Feasible
3	PI	1.45	PI > 1	Feasible
4	DPP	13 years 1 month	DPP<25 year	Feasible

4.4 CWM/CWF

With assumption of, investment cost US $ 250 million, capacity 1,000,000 t/y, 8% of interest, price of product US $ 250 (Dedy Y, et al, 2012), operation cost US $ 65/t, and coal price US $ 24.7, then the economic analysis result :

No	Parameter	Result	Criteria	Decision
1	NPV	US$ 760,107,350.63	NPV > 0	Feasible
2	IRR	50.12 %	IRR > 8 %	Feasible
3	PI	4.04	PI > 1	Feasible
4	DPP	2 years 4 month	DPP<15 year	Feasible

5 CONCLUSION

All of increases in added value of the LRC are feasible from the results of the economic calculation. With the growth in all industries, population, and GDP growth target, making the market to increase the added value of coal is very open. However, because it involves investment and certainty of capital return, require assurance from the government to support, especially regarding the royalties (before/after the value added), market, distribution (for BCL because oil distribution is a government monopoly) and subsidies (LPG subsidies for households and small industries make briquettes difficult to growing).

REFERENCES

http://www.worldcoal.org/resources/coal-statistics/ cited on 05-11-2014

Allardice, D.J., et al, 2001, Utilization of Low Rank Coal,Australia http://www.member.melbpc.org.au/~allad/files/pi ttc111.pdf, cited on 14.05.2013

Anonymous, 2012, Study on Clean Coal Technology Project, The Institute of Energy Economics (METI), Japan.

BPPT, 2014, *Indonesia Energy Outlook 2014*, Agency for the Assessment & Application of Technology, Jakarta.

MER, 2013, Handbook of Energy and Economy Statistic of Indonesia, Ministry of Energy and Mineral Resources, Jakarta

Nasri Sebayang, 2014, Development and Accelerate Large Scale Hydropower in Indonesia, Indonesian Hydropower Association, Jakarta

Ministry of Industry, 2012, Industrial Sector Energy Demand Planning, Planning Bureau of Ministry of Industry, Jakarta

Sihite, Thamrin, 2012, Low Rank Coal Utilization in Indonesia, Clean Coal International Symposium, Tokyo

Glenn G.Steverson and Robert D. Perlack, 1989, The prospects for coal briquetting in the Third World, Butterworth & Co (Publisher) Ltd, America

Yi Man, et.al, 2013, Environmental impact and Techno-economic analysis of coal gasification process with/without CO_2 capture, Journal of Cleaner Production 71 (2014) 59-66.

EIA, *International Energy Statistic* http://www.eia.gov/countries/country-data.cfm?fips=ID, cited on 12-11-2014

Wall. T. F.. 1987. *The Combustion of Coal as Pulverized Fuel through Swirl Burners. In: Principles of Combustion Engineering for Boiler. C. J. Lawn (ed)* London. UK.

Shapiro, A.C, 2005, Capital Budgeting and Investment Analysis, First edition, New Jersey : Pearson Education.

Anonymous, 2008, FS for Brown Coal Liquefaction in Indonesia, Japan Bank for International Cooperation-Kobe Steel Ltd-Sojitz Corporation.

Dedy Y, et.al, 2012, Optimization of Process And Combustion of CWF As Boiler Fuels, Research and Development of Mineral and Coal, Bandung

A Case Study: Incongruity In Mining Laws In India

P. Kumar
Director, Ministry of Mines, Government of India

ABSTRACT The regulation of mines in India, through policy & legislation, is under a federal setup. The Constitution of India empowers the Union Government for regulation of mines and development of minerals by enacting laws expedient in the public interest. The State Governments, on the other hand, have been given powers, subject to control of the Union. Union Government has enacted the Mines and Mineral (Development & Regulation) Act, 1957 and rules thereunder, to provide for the regulation of mines and development of minerals under control of the Union. They constitute the basic laws governing the mining sector in India. The State Government has been conferred full legislative powers with regard to the minor minerals.

The mining sector in India is also required to comply with the various laws & regulations in regard to forest, environment, labour, mine safety, etc., each of them are administered by separate government agencies at Union and State level, leads to infringements, gaps, overlaps and even incongruities, in the comprehensive regulation of the mining activity.

The case study of operation of a mining lease of iron ore mines, located in the mineral rich Barbil-Barajamda belt in the Keonjhar and Sundergarh districts of the State of Odisha, will be presented to depict the interwoven laws. The case captures the interaction of the forest laws with the mining laws. The mining lease area is mostly spread over the forest, requiring the forest clearances and diversion of forest land, for the purpose of carrying out mining in the forest area.

The diversion of forest lands in India, for the non-forestry purposes (including mining), is regulated by the Union Government through the Forest (Conservation) Act, 1980, (Ministry of Environment, Forests & Climate Change), in the national interest and in the interest of future generations.

The case traverses the life cycle of the mining lease and its renewals through the various amendments in the mining laws and its incompatibilities with the compliance of the existing forest laws. The requirement of clearances and proscriptions in the mining laws lead to the impasse in mine operations.

The paper explains the problem with the help of the above case study and identifies specific points of discord. It then analytically delves to find plausible solutions by harmonizing the laws inter-se and with their field implementation.

Keywords: Mining laws, India, Concession regulations

1 INTRODUCTION

1.1 Indian Mineral Scenario

Minerals are vital raw material for development of infrastructure, capital goods and basic industries in any country. India is fortunate that it is blessed with ample resources of a number of minerals. It is globally well accepted amongst the geologists that India has the geological environment for discovery of many deep seated precious minerals. This premise is based on the assumption that India belongs to an ancient land-mass which gave many resource-rich countries like Australia, South Africa and Latin America.

1.2 Grant Of Mineral Concession And Its Regulation In India

The regulation of mines and development of minerals is undertaken in terms of the Mines and Minerals (Development and Regulation)(MMDR) Act, 1957. The MMDR Act 1957 has laid down the framework for grant of mineral concessions (Table 1, Figure 1) which have been supported by the Mineral Concessions Rules, 1960 (MCR) and Mineral Conservation and Development Rules, 1988 (MCDR), elaborating the grant procedures and the regulation of the mineral concessions

In the federal structure of India, the State Governments grant the mineral concessions for all minerals under the provisions of the MMDR Act, 1957. All minerals other than those specified in Parts 'B' and 'C' of the First Schedule to the Act are under the exclusive control of the State Governments and Ministry of Mines has no role in their grant. It is only for The 11 Atomic Minerals listed in Part 'B' and 10 Metallic and Non-Metallic Minerals listed in Part 'C' of the First Schedule to the MMDR Act (hereinafter refereed as 1st Schedule Minerals) that the State Governments require prior approval of the Central Government under Section 5 (1) of the Act for grant of mineral concession.

Table 1: Types of Mineral Concessions as per the MMDR Act, 1957

Types of Mineral Concession	Purpose
Reconnaissance Permit (RP)	For undertaking any operations for preliminary prospecting of a mineral
Prospecting License (PL)	For undertaking prospecting operations for locating or proving mineral deposit to take up mining
Mining Lease (ML)	For mining the mineral

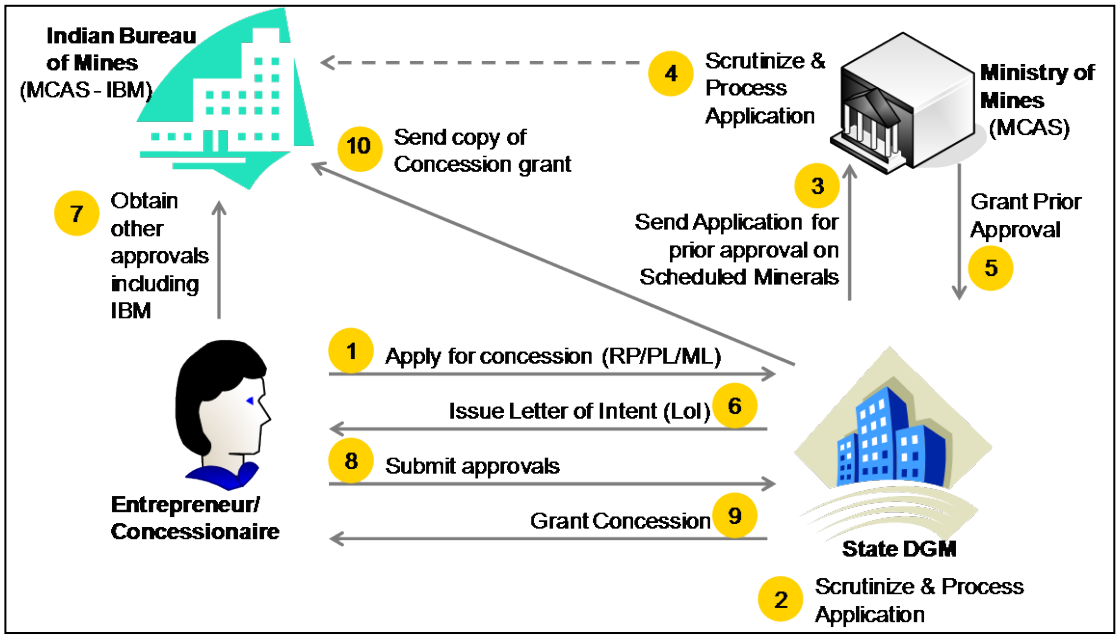

Figure 1: Process Workflow of the Grant of Mineral Concession (1st Schedule Minerals) in India

Subsequent to the prior approval of the Central Government, the State Governments grant the mineral concession, after the prospective permit holder/license/lessee has obtained necessary statutory approvals and clearances such as

- Forest Clearances, Environment Clearances, Wildlife Clearances – from the Ministry of Environment, Forest & Climate Change, Government of India governed by their respective Act and Rules.

► Approvals / clearances from other agencies like Pollution Control Board etc

1.3 CHANGES IN MINERAL CONCESSION REGULATIONS

The mineral concessions tenures are by nature have long tenures which are subject to the changing laws and legislations, governing them, in the country. The MMDR Act of 1957 has undergone several amendments, passed by the Parliament of India, of which the last one being on 12th January, 2015. The subordinate legislations - Mineral Concessions Rules, 1960 (MCR) and Mineral Conservation and Development Rules, 1988 (MCDR), are subject to continuing amendments by the Central Government from time to time, suiting the requirements for better regulation, conservation & development of the mineral sector in the country.

The changes in Mining regulations mentioned above are also subject to the associated regulations of the environment, forest, etc. as the mining sector in India is also required to comply with the various laws & regulations in regard to forest, environment, labour, mine safety, etc., each of them are administered by separate government agencies at Union and State level, leads to infringements, gaps, overlaps and even incongruities, in the comprehensive regulation of the mining activity.

The case study of operation of a mining lease of iron ore mines, located in the mineral rich Barbil-Barajamda belt in the Keonjhar and Sundergarh districts of the State of Odisha, will be presented to depict the interwoven laws. The case captures the interaction of the forest laws with the mining laws. The mining lease area is mostly spread over the forest, requiring the forest clearances and diversion of forest land, for the purpose of carrying out mining in the forest area.

The diversion of forest lands in India, for the non-forestry purposes (including mining), is regulated by the Union Government through the Forest (Conservation) Act, 1980, (Ministry of Environment, Forests & Climate Change), in the national interest and in the interest of future generations.

The case traverses the life cycle of the mining lease and its renewals through the various amendments in the mining laws and its incompatibilities with the compliance of the existing forest laws. The requirement of clearances and proscriptions in the mining laws lead to the impasse in mine operations.

The paper explains the problem with the help of the above case study and identifies specific points of discord. It then analytically delves to find plausible solutions by harmonizing the laws inter-se and with their field implementation. The problems being faced by the mining industry due the changes in

2 CASE STUDY: KASIA IRON DOLOMITE MINE

2.1 General Information

- Mine Name : KASIA
- Lessee : ESSEL MINING & INDUSTRIES LTD.
- Address : KASIA IRON DOLOMITE MINE, PO-KASIA DIST-KEONJHAR,PIN-758035, ODISHA, INDIA.
- Category : Mechanized
- Type of Working : Opencast
- First opening date : 14/09/1955
- Mineral worked : IRON ORE, DOLOMITE
- Lease area : 134.73
- Indian Bureau Of Mines, Mines Control And Conservation Of Mineral Division inspected mine on 26th July, 2011.
- IRON ORE Production in 2011: 556659 TON

2.2 Fact Sheet of Kasia Iron And Dolomite Mines

1. Original Mining Lease was granted and executed over an area of 297.444 Ha on 14.09.1955 for a period of 30 years (1955-85).

2. 1st renewal of Mining Lease application was filed on 25.07.1984 (One year prior to the expiry of the lease as prescribed by the then rules) over a reduced area of 194.196 Ha (173.039 Ha forest land + 21.157 Ha Non Forest Land) which was a part of the original lease area.
3. State Government took possession of the balance 103.248 Ha on 26.06.1986, which was not applied for renewal.
4. Ministry of Mines accorded approval on 26.10.1987 under section 8(2) of MMDR Act for grant of lease over an area of 194.196 Ha based on the recommendation of the State Government for a period of ten years (85-95).
5. State Government issued terms and conditions for grant of Mining Lease over 194.196 ha area as per approval accorded by Ministry of Mines on 16.05.1988 and Lessee accepted the same.
6. Forest Diversion proposal was applied in 1988 and recommended by State Government for diversion of total forest area of 152.229 Ha excluding the safety zone area of 20.810 ha (7.5 mtrs along the periphery of the lease which is not to be diverted as per the Forest Conservation Act Guidelines)
7. Section 8(2) of MMDR Act got amended on 25.01.1994 revising the provision of 1st renewal from two periods of ten years each to twenty years.
8. Pursuant to the revision, the Lessee applied to the State Government on 16.02.1995 prior to the expiry of the approved period of 1st renewal of Mining Lease to extend the period of renewal from 10 years to 20 years.
9. State Government recommended the request of the Lessee in October 1995 to the Government of India with a request to extend the approved lease period from 10 to 20 years.
10. Government of India in Feb 1997 returned back the proposal to State Government asking them to take action in line with the amended provisions vide notification dated 30.01.1997 authorising the State Government to grant the 1st renewal.
11. MINISTRY OF ENVIRONMENT, FOREST & CLIMATE CHANGE accorded approval over 83.88 ha of broken forest on 22.01.1998 against the approval sought over an area of 152.229 ha. On further correspondence by the State Government, the MINISTRY OF ENVIRONMENT, FOREST & CLIMATE CHANGE revised their above final approval order on 27/28.05.2004 and accorded final clearance for 83.88 ha of broken forest land and additional 30 ha of virgin forest land (total 113.88 Ha) during the 1st period.
12. The additional 30 ha land was granted considering the production rate and the balance lease period.
13. State Government issued another Terms and Conditions on 20.08.2002 for grant of Mining Lease over an area of 134.733 ha (113.88 ha forest land +20.853 ha Non forest land) which was accepted by the Lessee
14. State Government passed grant order on 09.09.2002 for grant of Mining Lease over an area of 134.733 ha. No opportunity for hearing under Rule 26(1) was given before reduction of the area.
15. The state Government also did not take over the balance area nor the lessee was asked to surrender the balance area.
16. The lessee deposited the fees for survey and demarcation of the approved area.
17. Further the lessee requested the State Government for grant of the balance area of 59.463 ha of the ML on 22.02.2003.
18. Lease Deed could not be executed during the 1st period and the Lessee continued the operations as per provision of 24 A(6) of Mineral Conservation Rules.
19. Lessee applied for diversion of forest land over entire forest area on 07.09.2004 (one

year prior to the expiry of the lease.) for the 2nd lease period.

20. Lessee has got the final Mining Plan approved over an area of 194.196 Ha area.
21. Ministry of Environment, Forest & Climate Change accorded final clearance on 18.11.2011 over the entire forest land of 173.039 ha on the recommendation of the state Government.
22. Lessee also obtained the environmental clearance for the project in March 2006 and November 2010.
23. Lessee has obtained valid consent to operate valid upto 31.03.2016.

Table 2: Chronology Of 'Mining Lease' (ML)

Date	**Activity**
14-09-55	Original ML period
19-02-83	Dolomite added over Iron Ore for the same validity of Original ML
25-07-84	Application for 1st Renewal of ML (RML) under 24(A)(1)
25-07-84	State Government (SG) forwarded to Central Government (CG) for renewal
26-06-86	SG took possession of the Lessee surrendered 103.248 ha
26-10-87	CG gave prior approval for entire area and not the reduced area but for 10 years for iron, limestone & dolomite
16-05-88	SG granted the approval area for 10 years, subject to the approval of MoEFCC (Ministry of Environment, Forest & Climate Change) for diversion of forest land
23-10-90	Company got its name changed from M/s Lal & Co to Essel Mining & Industries Ltd
18-12-94	Lessee working on the strength of SG of Odisha working permission on the forest area broken prior to 25.10.1980
25-01-94	Amendment of Section 8 read with Section 16
20-07-95	Decided to revise period of grant of 1st RML from 10 to 20 years with approval of CG
22-01-98	MoEFCC accorded final approval for mining on pre-1980 broken up forest land
17-06-99	Approval for Virgin Forest by MoEFCC
09-09-02	SG granted reduced area for for 1st RML period on the broken up forest land by MoEF and Forest Land approved by MoEFCC
13-12-02	Reduced area sent for Survey & Demarcation to Local District government unit
22-02-03	Lessee demanded for grant of entire area than the reduced area
27-02-03	Local District government unit asked for RoR & village map, which were not submitted, so the work of survey and demarcation could not be completed by the end of 1RML period, meanwhile lessee filed for 2nd RML

Table 2 (cont'd): Chronology Of 'Mining Lease' (ML)

02-09-04	Applied for 2nd RML
	Forest Land broken up in the 1st RML duration including 83.88 pre-1980 broken up forest land
02-06-08	MoEFCC granted temporary working permission on 83.88 ha for 1 year subject to 8 conditions and extended by 3 months
18-11-11	MoEFCC granted Stage II FC coterminous with the RML period
16-02-13	State DMG (Department of Mining and Geology) prepared precise area map to complete the process of 1st RML
06-09-13	State Forest Dept wrote to MoEFCC for withdrawal of FC dt. 18.11.11 & cancellation of lease as it had produced incorrect records for processing of forest diversion
10-12-13	State DMG gave memo to F&E Dept. communicating information regarding 2nd RML
28-12-13	SG wrote to MoEFCC intimated facts and asked to take necessary acion
25-01-14	SG again wrote in ref to its earlier letter to take up steps for revocation of FC
03-02-14	MoEFCC letter to SG for Map of 134.733 ha area and action taken against officials taking prior approval of 173.039 hs of forest land from GOI

3 HISTORY OF RENEWAL OF MINING LEASE REGULATIONS

The Mineral Concession Rules, 1960 which was notified vide GSR 1398 dated 11.11.1960, contained laws governing the renewal of Mining Leases, but originally did not have the provision of deemed extension. **MCR 1960 was amended on 6.5.1962** which was notified in the Gazette vide notification No. MII – 169(44)/61 dated 6.5.1963. By this amendment sub-rule (6) was inserted under Rule 28 whereby a provision of deemed extension for a period of six months was introduced. The provisions spelling out the renewal / deemed renewal status have been chronologically tabulated below-

Table 3: Chronology of Renewal / Deemed Renewal Legislations of Mining Leases

Date	**Renewal / Deemed Renewal Status**
11.11.1960	No deemed renewal
6.5.1963	sub-rule (6) was inserted under Rule 28 whereby a provision of deemed extension for a period of six months was introduced

Table 3(cont'd): Chronology of Renewal / Deemed Renewal Legislations of Mining Leases

10.2.1987	The provisions relating to renewal of mining lease which were hitherto under Rule 28 were now inserted under Rule 24A. *"… (6) If an application for first renewal of a mining lease made within the time referred to in sub rule (1) is not disposed of by the State Government before the date of expiry of the lease, the period of that lease shall be deemed to have been extended by a further period of one year or end with the date of receipt of the orders of the State Government thereon, whichever is shorter...."*
1.4.1991	The words "If an application for 1st renewal" in sub rule (6), the words "Notwithstanding the provisions of sub-rule (5), if an application for renewal" were substituted
7.01.1993	sub-rules (4) and (5) of rule 24A were omitted. This amendment also omitted the words "notwithstanding the provisions of sub-rule (5)," occurring in sub-rule (6) of the rule 24A.
27.9.1994	Amended the Sub-Rule (6) - "*(6) If an application for renewal of a mining lease made within the time referred to in sub-rule (1) is not disposed of by the State Government before the date of expiry of the lease, the period of that lease shall be deemed to have been extended by a further period till the State Government passes order thereon"* **Now provision given for Unlimited deemed renewal**
17.1.2000	The renewal of Mining Lease in Part 'C' of 1st Schedule can now be done by the state governments without prior approval of Central Government. The amendments read as *"(2) The renewal or renewals of a mining lease granted in respect of a mineral specified in Part 'A' and Part 'B' of the First Schedule to the Act may be granted by the State Government with the previous approval of the Central Government.* *(3) The renewal or renewal of a mining lease granted in respect of a mineral not specified in Part 'A' and Part 'B' of the First Schedule to the Act may be granted by the State Government."*
11.1.2002	By this amendment a proviso was inserted in sub-rule (3) which read as follows: "*Provided that before granting approval for second or subsequent renewal of a mining lease, the State Government shall seek a report from the Controller General, Indian Bureau of Mines, as to whether it would be in the interest of mineral development to grant the renewal of the mining lease.* *Provided further that in case a report is not received from Controller General, Indian Bureau of Mines in a period of three months of receipt of the communication from the State Government, it would be deemed that the Indian Bureau of Mines has no adverse comments to offer regarding the grant of the renewal of mining lease."*
18.7.2014	Rule 24A was further amended on 18.7.2014 to the effect that the provision of deemed was : (i) limited to a period of two years; and (ii) was applicable only to cases of first renewal and not to cases of second and subsequent renewal as provided for u/s 8(3) of MMDR Act.-

4 CONCLUSION

It is evident from the above discussion that the discrepancy between the area in regard to which the renewal must be granted has arisen due to incongruity of different mining laws.

Under these conditions, the lessee was claiming that taking into consideration the statutory rights of the lessee over the 1st of 194.196 ha as per the revision of the lease period from 10 to 20 years and non observance of the provisions of MINERAL CONSERVATION RULES 26 (1) while reducing the area, nor passing a reasoned order for reduction in granted area, neither taking over possession of the balance area nor asking the lessee for surrender of the balance area, the 1st period will be considered as 194.196 ha area for 20 years wef 1985 till 2005 and the Lessee is entitled to seek clearances over an area of 194.196 ha during the 2nd period.

The Rule 24A of the MCR, was further amended on 18.7.2014 to the effect that the provision of deemed was : (i) limited to a period of two years; and (ii) was applicable only to cases of first renewal and not to cases of second and subsequent renewal as provided for u/s 8(3) of MMDR Act. Thus, taking away the right of any further second renewal from the Lessee.

The Ordinance for amendment of the MMDR Act 1957 promulgated on 12th January, 2015, provides by way of its Sub-Section 5 and 6 of Section 8(a) that the Mining Leases would be deemed to be extended from the date of their last renewal to 31st March, 2030 (in the captive miners) and till 31st March, 2020 (for the merchant miners) or till the completion of the renewal already granted, if any, whichever is later. Thus, no Mining Lease holder is likely to be put into any disadvantaged condition. It is expected that this would immediately permit such closed mines to start their operations, of course, subject to the necessary clearances like forest and environment.

REFERENCES

Mines and Minerals (Development and Regulation)(MMDR) Act, 1957.

Mineral Concessions Rules, 1960 (MCR)

Mineral Conservation and Development Rules, 1988 (MCDR)

Forest (Conservation) Act, 1980

MCDR Inspection Report dated 26/07/2011, Mine File No: ORI/IRON-DOL/KJR/MCDR-34/BBS by Regional Conroller of Mines, Indian Bureau of Mines, Bhubaneshwar Regional Office.

Coal Cities: Characteristics, change and forms of intervention
Kömür Kentleri: Karakteristikler, değişim ve müdahale biçimleri

Ş. Işın
Bülent Ecevit Üniversitesi, Siyaset Bilimi ve Kamu Yönetimi Bölümü, Kentleşme ve Çevre Sorunları Anabilim Dalı, Zonguldak

ABSTRACT Coal cities comprise characteristic urban context mainly based on the relationship between production and urbanization. Apart from taking into consideration of local, geographical and social idiosyncracies, studies on coal cities bring forth some common characteristics in terms of demographic characteristics, economic characteristics, production culture, solidarity networks, social identity, all inscribed in urban space socio-spatially. Hence, coal cities remain as a subject for interdiciplinary research.

Coal cities and coal mining regions, as old industrial regions, have experienced dramatic urban and regional change due to changes in terms of production process, introduction of new technologies and new environmental legislation related to coal and also introduction of new energy sources. This conceptual paper will study the main characteristics of coal cities, the impacts of change on coal cities socio-spatially and main forms of intervention to coal cities as part of urban and regional restructuring as responses relying on an in-depth literature review.

Keywords: Coal cities, Zonguldak, socio-spatial

ÖZET Kömür kentleri temel olarak üretim ve kentleşme arasındaki ilişkiye dayalı olarak karakteristik bir kentsel bağlam içerirler. Yerel, coğrafik ve sosyal kendine özgülükler dışında, kömür kentleri üzerine olan çalışmalar, tümü sosyo-mekânsal olarak kentsel mekân içerisine kazılı olan demografik karakteristikler, ekonomik karakteristikler, üretim kültürü, dayanışma ağları, sosyal kimlik gibi bazı ortak karakteristikleri öne çıkarırlar. Dolayısıyla, kömür kentleri, disiplinler arası araştırmaya konu oluştururlar.

Kömür kentleri ve eski endüstriyel bölgeler olarak kömür madenciliğinin yapıldığı bölgeler, üretim süreci, yeni teknolojilerin ve kömüre ilişkin yeni çevresel mevzuatın ortaya çıkışı ve yeni enerji kaynaklarının da bulunması açısından ortaya çıkan değişimler nedeniyle çarpıcı kentsel ve bölgesel değişimler geçirmişlerdir. Bu kuramsal çalışma, kömür kentlerinin temel karakteristiklerini, sosyo-mekânsal olarak değişimin kömür kentleri üzerine olan etkilerini ve değişime verilen karşılıklar olarak kentsel ve bölgesel yeniden yapılanmanın bir parçası olması açısından kömür kentlerine olan temel müdahale biçimlerini derinlemesine literatür taramasına dayalı olarak inceleyecektir.

Anahtar Kelimeler: Kömür kentleri, Zonguldak, sosyo-mekân

1 SOCIO-SPATIAL CHARACTERISTICS OF COAL CITIES

Production, working practices, coal reserve or basin as resource play preliminary roles in emergence of urban set-up and urbanization process in coal cities. Coal cities or coal mining regions define an employment structure mainly based on coal mining and complementary economic activities.

The spatial division of labor and industrial production characterize the socio-spatial pattern of coal mining cities. Coal mining towns embody characteristic socio-spatial

structures in close relation to industrial production and production culture. The social structure of mining communities, excluding context-dependent and place-specific differences, comprises strong binds, an understanding of solidarity and social identity in relation with hard working conditions, labor class consciousness and trade union tradition (Massey 1984, Işın 2009).

Coal mining remained and was perceived as one of the main engines for national economic growth. It generally integrates with heavy industry, particularly iron and steel manufacturing industry and energy production via coal burned thermal power stations. Thus, the spatial and employment structure at the urban and regional scales is dominated by the main industry, such as coal mining industry and directly related complementary industries (Massey 1984, Işın 2009).

Specific structures based on economic and social relations characterize the coal mining areas and they reveal spatial division of labor (Massey 1984). Massey (1984) discusses specific social and economic structures and their characteristics on South Wales Case, in the UK. Self-conception and identification with working practices have remained characteristic to coal mining areas and they are associated with specific social relations brought by working practices (Massey 1984). Toughness of the work, masculinity, collectiveness as a basis for labour movement, labour power and solidarity have been emphasized as some of those social relations embedding in working practices.

Especially in coal mining towns where the preeminence of a single industry is evident, domination of male labor prevails (Massey 1984) and consequently, there remains shortage of both job opportunities for female labour and alternative jobs for male labour as well as the deficient number of local small firms (Massey 1984). Poor housing and lack of higher ordered services are also mentioned as other common characteristics of some coal mining localities (Spooner 1991).

As specific cases, coal-mining towns characterize social and economic insularity (Turner 2000) within a not much diversified regional economic base.

Old coal mining regions carry characteristics of nineteenth century industrial production associated with specific socio-spatial characteristics. Accordingly, spatial division of labor, relationships between industrial production and the spatial pattern exhibit the specific spatial characteristics of these localities. This type of industry shapes socio-spatial structure with respect to urban macro form, transportation network and urban land regarding industrial production and the resource, coal. Coal mining industry as complementary to iron and steel industry embeds in a relatively isolated socio-spatial structure. The citizens are miners and their families at the origin of urbanization and urban form. Therefore, changes in employment structure and also in the local economic base reveal chances to observe spatial change consistently (Işın 2009).

As engines of national growth, coal mining and complementary industries once acted as the prominent industrial activities in industrial development. Development economics and interventionist developmental states have reinforced externally driven expectations of both the local institutions and local community (Işın 2009).

In cases of coal cities, dominance of a single industry has brought forth a particular kind of social, political and community culture insular in characteristics and including a sense of community in coal mining localities within a mono structural economy (Turner 2000).

2 CHANGE IN COAL CITIES: DEINDUSTRIALIZATION AND SOCIO-SPATIAL RESTRUCTURING

Change in coal cities can be mainly discussed on the relational context of deindustrialization and socio-spatial restructuring.

Industrial change in the coal mining sector offers an opportunity to observe disintegration tendencies among geographical production clusters composed of complementary industries to coal mining industry.

Industrial change which brings socio-economic and socio-spatial change in coal mining localities have revealed impacts and responses related to their characteristics. Local restructuring in the economic, institutional and spatial dimensions interrelate with response capacity and intervention strategies which both affect and are affected by the former characteristics of old coal mining regions. A common ground to search for these impacts may show their experience of change and response capacity (Işın 2009).

Change in coal mining cities including specific socio-spatial characteristics, based on working practices and the existence of coal can bring forth deindustrialization, decline and restructuring as socio-spatial phenomena. Deindustrialization process is simply defined as the change in economic base involving decline in industrial production, hence manufacturing industry and transition to service sector with alternatives to also different forms of industrialization. Işın (2009) points out that industrial decline, deindustrialization and restructuring are interrelated and defines deindustrialization as a process of socio-economic and socio-spatial decline based on industrial decline comprising changes in local socio-spatial pattern and in old forms of development. Hence, apart from impacts of change, responses to change are also evident within deindustrialization process (Işın 2009).

2.1. Dynamics Behind Change in Coal Cities or Coal Mining Regions

As a process embodying interrelated causal processes (John and Wild 1991), deindustrialization can be examined via global economic restructuring, its repercussions at multi dimension revealing local and regional restructuring and structural changes at the national level (Işın 2009). Consistently, the dynamics behind deindustrialization can be searched through economic, social and institutional restructuring within a relational context (Castells 2005).

Old industrial regions, mainly based on traditional industries, such as coal mining, textiles, iron and steel manufacturing, vice versa witnessed industrial decline and deindustrialization and generated diverse responses to change through restructuring (Işın 2009). For the coal cities or coal mining regions, in particular, regulational change via coal content in terms of new legislation and introduction of new clean technologies, together with the rise of low carbon economies remain as evident complementary factors in their deindustrialization and restructuring processes.

2.1.1 Global economic restructuring and its repercussions: National, regional and local restructuring

Fluctuational processes within increased mobility particular to global economic restructuring (Wallerstein 1974, Jones and Wild 1991) associated with internationalization of world economy and dispersion of technological innovations (Cheshire and Hay 1989) lay behind deindustrialization process. As inseparable from economic and social restructuring, changing land use patterns and spatial division of labour are major outcomes of spatial restructuring (Massey 1984, Işın 2009). Consistently, urban decline, urban transformation and regeneration can act as components of urban change (Işın 2009). Anderson, Duncan and Hudson (1983) have stated the concept of redundant spaces relating to inner city problems, urban decline and urban decay in relation with industrial decline and deindustrialization (Işın 2009).

Different viewpoints within different theoretical approaches exist in explaining the relational bind of global restructuring with deindustrialization (Jones and Wild 1991, Işın 2009). These are the neo-

Schumpeterian approach focusing on the relationship between technical change and economic growth mainly depending on innovation and entrepreneurial activity; the Neo-Marxist approach focusing on fragmentation in the production process and change in the mode of production, accumulation and regulation and the third viewpoint revealing Castells's (2005) concept of informationalism founding on information economy and its relational context with economic and social restructuring (Jones and Wild 1991, Işın 2009).

Işın (2009) states that economic restructuring is examined in terms of three dominant theoretical frameworks, in particular the economic restructuring process in Western Europe referring to Jones and Wild (1991) and Keeble (1991). These theoretical frameworks of Neo-Schumpeterian, Neo-Marxist approaches and the one based on information economy, introduce different dimensions in evaluating deindustrialization on different scales dealing with the restructuring process. They further draw attention to the simultaneous facts taking place considering change from diverse perspectives (Işın 2009).

The first is stated to focus on the cyclic mode of industrial restructuring in relation with technical change, technological innovation and entrepreneurial activity to further reflect on either economic growth or stagnation referring to Schumpeter (1939). The second theoretical framework focuses on the mode of production, revealing transition from the Fordist mode of accumulation to the Post-Fordist/flexible mode of accumulation, as the most important dynamic behind industrial restructuring (Mandel 1975, Jones and Wild 1991). The transition has shown a shift from mass production of standardized goods in the media of assembly line and unskilled, unionized labor large in size to flexible production characterized by specialization and highly skilled labor (Jones and Wild 1991, Harvey 1999, Soja 2001). The mass production system of standardized goods and big fixed capital investments within vertically integrated large firms have characterized the Fordist mode of accumulation while collective consumption and social reproduction of labor have indicated the Fordist mode of regulation managed by the Keynesian state (Harvey 1999).

Transition from economies of scale to economies of scope is another description to inform the transition process. This process of transformation has pointed out the emergence of a new division of labor and informed the start for the deunionization process due to requisite flexible labor practices in the new industrial production process. Further, new technologies are introduced and are an important factor in the global change in organization of production and the introduction of a new division of labor (Harvey 1999).

Global change in the organization of production and technological advances have played major roles in shifts in paradigms of development and also on the social transformation process (Işın 2009). The first and second Oil Crises meant a crucial rise in energy cost in production, which could be compensated by a contraction in labor cost with high wages due to organized labor and strong trade unions (especially in the UK and the USA). Soon, low cost East and Japanese goods grounding on low cost labor invaded these markets and the need to decrease production costs as a productivity constraint has formed the main motivation behind peripherization of labor. In addition to rise in prices of energy inputs, labor unrest and wheat shortages are emphasized as other events behind deindustrialization in terms of reorganization of production (Pietrikowsky 1999). Capital has moved to areas where low cost labor is available. These events have informed the reorganization of production and a more flexible, fragmented production process is introduced (Işın 2009).

The transition to the flexible mode of accumulation has re-conceptualized the production process proliferating some sectors such as finance, production services involving insurance, advertisement, etc.,

telecommunication and research sectors while excluding some other. In this sense, traditional industries peculiar to old industrial regions such as coal mining, iron and steel manufacturing, shipbuilding and textile have declined (Castells 2005). The decline of the traditional old industries has been related to their decreasing competitiveness and the emerging new paths for competitiveness (Cooke 1995).

The third theoretical framework on the relationship between deindustrialization and restructuring is based on information economy (Jones and Wild 1991). Castells (2005) emphasizes the introduction of the universal communication system and the direct effect of information on productivity. Information, as an asset in the production process has revealed certain breaking points brought by capitalism, such as flexible management, network of firms, individualization and variety in working relations, empowerment of capital over labor--hence decline in labor movements--restructuring in global economic competitiveness in terms of capital accumulation, and management and integration of financial markets. Following these developments, he further notes that the characteristics of the new type of production are mainly based on communication and innovation transformed to a single operating system in the form of mutual dependence (Işın 2009).

Consolidations and integrations between firms are observed to act around the globe, often making investments in multi-sector business activities. Outsourcing and subcontracting type operational constraints have introduced vertical disintegration. Minimizing transaction costs has become a crucial constraint within and between firms, again referring to vertical and horizontal disintegration for further re-integration, often laying the relation of reason in formation of geographical clusters of new industrial production motivated by innovation, research and development (Scott 1986, Işın 2009).

Changes in both social organization of labour and social structure of employment are put forward in parallel to changing working process and practices as part of social restructuring. Accordingly, Castells (2005) stresses the central role of the working process for the social structure. He puts forward components of social restructuring in relation with changing working practices as the change in capability and productivity introduced by the new division of labor together with occupational variety. He further emphasizes the change in working practices and in labor beside sectoral shifts within economy in explaining social restructuring in relation to economic restructuring. Massey (1984) points out that the social composition of the workforce has changed with a tendency of increasing female labor while its distribution has preserved its importance in the changing social structure of employment (Işın 2009).

Structural changes have impacted localities in terms of their economic, social, institutional restructuring processes. In that sense, national economic restructuring and its repercussions in old industrial regions have revealed a meso-level investigation of deindustrialization and its decline impacts on the locality. On a wider scale, the repercussions of global economic restructuring have reflected on national economies as changing development policies in the context of the structural adjustment process (Işın 2009).

What has altered in national systems through transforming paths in development is a question behind the changing modes of accumulation and regulation, in particular to the role of the state in these processes. Accordingly, Castells (2005) points out the changing roles of the state in the Fordist and Post-Fordist eras through stressing that industrialization relies on a statist type of production where the state owns the surplus and aims to maximize state power while post-industrialization relies on a capitalist type of production with the aim of profit maximization. Therefore, he stresses that industrialization as a development type aims maximum industrial output and hence economic growth, and states that the main objective in industrial society is the

production and distribution of energy while for post-industrial society, it is stated to be information and information technologies in improving productivity as new dynamics.

The industrial era is pointed out to be based on the link between mass consumption and mass production and this link is outlaid by the close relationship between productivity growth and real wage income referring to Fordist mass production and the relations between capital, unions and the state referring to Fordist mass consumption (Bowles, Gordon and Weisskopf 1983, Pietrikowsky 1999 and Piore and Sabel, 1984). The weakening of the developmentalist state, hence statism, and its regulational role are stated to be undermined within an integration process with global capitalism (Castells 2005). The role of the state as the entrepreneur and the investor in industrial development has in a way come to an end (Işın 2009).

Winterton (2003) has characterized the 1980s by a period of deregulation informing the fall of the Keynesian state and its failure in managing crisis together with a crisis of investment leading to stagnating productivity in manufacturing industry in the 1980s accompanying a dominancy of neoliberal policies. The restructuring process brought by economic globalization is on the agenda since the 1980s through the changing national economic systems, organizational structure of production process, changing capacities and capabilities as well as changing tools and intervention areas for development. The extent of response to this restructuring process has remarked the existence of localities/regions/nations in the network constructing the global capitalist economy (Işın 2009).

Deindustrialization, with its relation to disinvestment and also deunionization has formed complementary developments within the national economic restructuring process. Deregulation remains as an evident part of this process in the neo-liberal climate. Transition from import substitution to export led development strategies has marked changing economic and development models especially starting with the 1980s under the influence of the neo-liberal wave. Deregulation, deindustrialization and privatization have dominated the agenda that changed regulational constraints on subsidy transfers, public spending and investment structures. Apart from distributional constraints, a decline discourse has started to be coded on old industrial regions with high production costs and organized labor, which leads to deindustrialization, disinvestment and deunionization processes (Işın 2009).

Işın (2009) denotes that deindustrialization is complementary to processes of deunionization and disinvestment at the meso-level related to impacts of global change in organization of production, the preferences of flowing capital in form of foreign direct investment and multi-national investment on national economic systems and policies. This explanation shows the impact of globalization on national economies and further provides insight into the relationship between restructuring national economies and industrial production. This relation reveals changes in the investment and subsidy structures concerning especially the public sector in industrial production. Following the dominancy of neoliberal policies in national economies, and hence deregulation, such effects like disinvestment and deunionization are evident within national industries. In addition, the downsizing, privatization, contraction in labor force or weakening of the trade unions all provide insight on such repercussions of global economic restructuring on national industries/economies and industrial production in general (Işın 2009).

Townsend (1983) sees disinvestment as one of the dynamics behind the deindustrialization process in relation with financial circumstances and national decline in competitiveness. Also, Anderson, Duncan and Hudson (1983) relate decline in both investment and profit rates with declining employment and production in manufacturing.

The free flow of capital led by deregulation in the finance system and trade has changed investment structures of

national systems. The transnational institutions like the WB and IMF are introduced to manage free flow of capital by changing and orienting weakened developmental states to adapt to this process in terms of fiscal, monetary and distributional means in national systems. Transnational capital investments and foreign direct investments have chosen geographies of low cost labor, catalyzing fragmentation in organized labor and the deunionization process in localities (Işın 2009).

Cooke (1995) comments that the multinational investments and their locational decisions have played important roles in weakening the control of the nation-states on national economies. Global localization is used to define the activities of multinational investments in localities though investing mostly in research and design both at the micro and macro regional levels (Cooke 1995).

State-owned enterprises might be pointed out as the components in industrialization that are affected most severely. Liberalization, by means of availability of cheap imported inputs, outsourcing, and possible technology transfers by partnerships with transnational firms, have disintegrated domestic industrial regions to sustain export capacity beside upcoming new regulations on product content and quality in the global market. Participating in the global commodity chain has become a constraint for firms to be included in the global market network, especially in developing countries (Işın 2009).

Deunionization remains to be a major change as part of the social restructuring process. The deunionization process is emphasized due to its complementary consequences of fragmentation, decrease in bargaining and mobilization power and exclusion of the unions from regulations related to employment (Smith 2001) . Smith stresses that the most prominent events beneath these consequences have comprised free capital flows and changing employment relations, such as sub-contracting, as well as restructuring in legislation on employment. One other consequence is stated to be the decrease in union membership accompanied by a loss of identity. Likewise, Wallerstein and Western (2001) point out degradation of union organization and strength in relation with declining centralized wage setting practices especially after 1980 in advanced industrial societies.

Wallerstein and Western (2000) put forward demolition of centralized systems of wage-setting and labor experiencing high unemployment in Europe and highlight labor market inflexibilities contra capital flight and global competition.

Işın (2009) synthesizes that deindustrialization is discussed with reference to multi-dimensional and multi-perspective criteria and is evident to have impacts at diverse levels that concern globalization of capital emphasizing free flow of capital and changing investment structures through accelerated foreign direct investment and multi-national investment in addition to the global change in organization of production and new technologies. Accordingly, the impact of globalization on national economic systems and policies via changing national investment and subsidy policies together with deregulation process are discussed. The impacts of national economic restructuring on unionized industrial workers, hence deunionization and disinvestment at the regional and local levels are emphasized in relation with deindustrialization. Furthermore, regional impacts concerning disintegration in old industrial clusters in terms of outsourcing or use of imported raw material and changing property schemes via privatization are pointed out. These evaluations have considered macro and meso levels of change and restructuring. On micro scale, impacts on locality via local population/community, local economy and local socio-spatial characteristics acting on the whole urban set-up remain.

With regard to relational context covering socio spatial restructuring at the regional and local levels and deindustrialization, Işın (2009) highlights that socio economic and socio spatial restructuring at the local and

regional levels concern local specific characteristics having impacts on how the change is experienced, on response capacity to change and restructuring on wider scales. Characteristics of urban set-up, local economy and local population, especially local labor market have been taken into consideration as major references. The impacts of change and restructuring on the local labor market, on major economic sectors, on firms and on spatial pattern reveal the change in locality and further reveal outcomes of change and bring the response problem to change. Different experiences of several cases of deindustrialization and industrial decline serve as a common ground to reveal indicators of change defined by deindustrialization and industrial decline through impacts, outcomes, phases of transformation and response capacity (Işın 2009).

The mutual relationship between socio-economic change and spatial change gives insights to industrial and spatial restructuring processes. The impacts of deindustrialization have mainly concentrated on local economy, local population in particular to local labor market and local socio-spatiality (Işın 2009).

2.1.2. Changing regulations on coal content and its polluting effects and changing technologies

The globalization process has affected coal mining industry directly through reorganization in the production process in this sector by bringing technological changes and changing market constraints on putting new content-related regulations on coal in relation with global climate change (Işın 2009). Globalization has also had impacts on the coal mining sector through introduction of the liberalization process in energy sector, on changing state policies related to (state owned) enterprises associated with their subsidy and tax systems, and on the introduction of new capacities and capabilities, thus capital for development (Işın 2009).

Global changes concerning technological changes in the coal production process accompanied by changing legislative constraints on coal content and market changes in coal exportation are crucial in restructuring of coal production and coal mining industry (Işın 2009).

Tamzok (2007) has stressed the impacts of developments and advances in communication, transportation and distribution in the world coal sector by putting forward the impact of liberalization of electricity production on coal production due to the availability of cheap coal in electricity production and the emergence of new actors in coal production, as revealing the change in management of corporations in coal production together with intensified competitiveness in the global market. Especially the liberalization process has played an important role in segregation of domestic regional production in terms of distortion of linkages between the complementary sectors of especially coal mining, iron and steel production and coal burning thermal power stations in the domestic market (Işın, 2009).

Restructuring in coal mining industry has comprised technological change in production process and compensation for new standards for product content in order to adapt to the global coal market to meet environmental concerns on carbon and sulphur emissions (Işın 2009). International and regional environmental conventions such as Kyoto Protocol, United Nations Framework Convention on Climate Change, regional Clean Air Acts as well as introduction of low carbon economics signify regulationary base for such changes. Apart from discussed direct impacts of the globalization process on the sector and on output, globaliation also affected coal mining industry in mediation of changes at the national policy level concerning structural changes in the national system led by supranational institutions such as WB and IMF. These impacts have concerned changes in subsidy structure and changes in economic models that affect trade policies and energy policies as well. On the coal

mining side, changes in investment structure and impacts on state owned enterprises can be primarily specified followed by possible mine closures, as one of the specific outcomes of deindustrialization (Işın 2009).

WEC (2007) discusses coal use and its relational background within energy use, structural changes and environmental constraints, pointing out that relative fuel prices, government policies on fuel diversification, climate change and air pollution, together with developments in clean coal technology in power generation affect the regional coal use to a larger extent.

Early domestic industrial geographical clusters have faced a distortion in their relational context due to restructuring within the coal mining sector, by mediation of liberalization in electricity production, which intensify the use of imported coal in iron and steel manufacturing and thermal power stations.

Işın (2009: 64) synthesizes that impacts of the globalization process on the coal mining sector can be briefly specified in terms of such developments (Tamzok 2007, Yılmaz and Uslu 2007):

• "Increased competitiveness in the global market for coal resulting from the introduction of new partners, such as active multinational firms

• Changes in management and organizational set-up of firms in terms of emerging consolidations, selling, buying and integration of firms by taking advantage of scale economies with an aim to decrease their production costs

• Introduction of new global regulation constraints on coal content to manage carbon and sulphur emissions which act on climate changes and introduction of new content standards for the use and export of coal in global market

• Change in technology of coal production and coal use in other industries on phases of coal excavation, coal cleaning, use of coal in thermal power station by means of modern thermal power systems that increase the productivity of coal use, increasing quality of coal and control of waste management

• Deregulation concerning changes in legislation to include the private sector and proliferating competitiveness in the domestic market

• Changes in investment structure in favor of the private sector and to the disadvantage of state owned enterprises through subsidy cuts, privatization policies accompanied by practices and closures

• Fuel transfers in electricity production through the introduction of new alternative resources to coal"

After mentioning dynamics behind change in coal cities or coal mining regions in relation with old industrial regions, indicators of deindustrialization will be discussed. Restructuring will be taken into consideration via developing response capacity to change.

2.2. Indicators of Deindustrialization and Industrial Decline

The decline impacts of deindustrialization in coal mining regions can be put forward with reference to the intensity of these impacts resulting from the specific characteristics of these regions. The fact that these regions have narrow or single base localities may lead to deeper impacts on local population. Turner (2000) points out those significant changes in local economy, such as pit closures, create demoralizing effects on local workforce; decrease in consumer demand for locally traded goods and services, and an increase in petty crime rates (Işın 2009).

From the vulnerability perspective, change in the nature of the labor process and in work practices; in skill composition of the workforce are emphasized (Massey 1984). Removal of autonomy and individual control over the labor process as major aspects of work, solidarity and organization; increasing difficulties of working class organization by heightening heterogeneity; weakening of the trade union organization by the effect of long-term unemployment are the deficiencies in the labor process and organization of labor in relation with deindustrialization in coal mining regions (Cooke 1981, Friedmann 1977, Massey

1984). Furthermore, the new spatial reorganization of labor has changed social and spatial coherence (Massey 1984). Accordingly, Barchiesi and Kenny (2002) adds that the emergence of new forms of low-wage economy as well as employment, social exclusion, employment uncertainty, vulnerable employment, loss of rights and power are evident disempowering developments, relying on their case, Coal Rim Cluster in Northern KwalaZulu-Natal in South Africa (Işın 2009).

Mine closures, as one of the specific outcomes of deindustrialization in coal mining localities, remain vital. Apart from strikes and political conflict on the labor side, the difficulties in developing ability to take action and respond to mine closures are stated as a major problem (Camagni 1991, Nel, Hill, Aitchison, and Buthelezi 2003).

Turning to a wider frame of general discussion on indicators of deindustrialization, it can be pointed out that freeing capital from space and time has affected industrial regions and their social structures leading to the deindustrialization process. Işın (2009) states that rising unemployment and decreasing real wage on the labor side and closures, privatization experiences on the firm side in an era of increased international competition are the prominent outcomes of the deindustrialization process by referring to Anderson, Duncan and Hudson (1983), Harvey (1999) and Winterton (2003). Introduction of a new division of labor with capabilities to understand, direct and manage new rationality in a complex network of knowledge, innovation and new technologies with high mobility around the globe have defined a privileged group low in numbers with high wages and high living standards (Harvey 1999, Soja 2001) while exclusion of blue-collar labor accompanied the deindustrialization process directing them to generally low cost and non-security service sector jobs, laying a foundation for the emergence of non-capable underclass (Massey 1984, Soja 2001 and Turner 2000). Additionally, Işın (2009) highlights that the feminization of labor, including female labor in temporary low-cost service sector, has come along with the deindustrialization process and the globalization process has further enabled the re-emergence of old type informal work organizations within family production, paternalistic work organization toward informationalization by referring to Soja (2001), Harvey (1999) and Turner (2000).

Işın (2009) reviews indicators of deindustrialization by focusing on impacts and outcomes of change brought by the process. Accordingly, urban economic decline and urban depopulation remain the main indicators to assess local change in terms of deindustrialization. Changes in employment structure and contraction in labor force due to job losses in the manufacturing sector are revealed as the primary impacts of deindustrialization on localities. Thus, the main indicators of deindustrialization emerge as unemployment in relation to job losses in manufacturing employment and consequently, a decline in purchasing power or real incomes (Anderson Duncan and Hudson 1983, Jones and Wild 1991). In addition, stagnation or decline in absolute manufacturing output and dislocation of manufacturing are denoted as evident components in deindustrialization (Townsend 1983). Deindustrialization is stated to also point to a decline in percentages of active workforce and decline in the total economic output of a city in general (Helmut 1991).

The deindustrialization process has revealed decline in terms of urban set-up via urban economic decline and urban depopulation. Closures, massive lay-offs of labor, and early retirement policies remain characteristic to urban economic decline while decreasing population growth rates and increasing out migration rates have indicated urban depopulation (Işın 2009). Consequently, Butzin (1991) highlights that weak endogenous potential is complementary to urban depopulation and urban economic decline due to its relation with loss of human capital and hence poor potential for creativity. He further comments that population losses are indicated to

exceed the regional average. Likewise, Jones and Wild (1991) mention problems on social and economic capital, old infrastructure, environment, and image associated with deindustrialization in old industrial regions. Vulnerable local economy has remained as a consequence of the mentioned outcomes.

Apart from economic and social consequences of deindustrialization, environmental constraints and spatial change are characteristic (Işın 2009). Abandoned industrial buildings, contaminated and derelict physical environment, smokestack landscapes describe the imagery of decline within the context of deindustrialization (Townsend 1983). Environmental deterioration is taken into consideration as an ongoing problem associated with deindustrialization (Cooke 1995) while spatial inequalities characterize declining traditional industries (Jones and Wild 1991). Rust-belt old industrial regions are characterized with limited socio-cultural infrastructure as well as physical infrastructure; outdated housing and polluted environment with complementary social characteristics of homogeneity in terms of working practices within the domination of large industrial firms and strong trade unions (Jones and Wild 1991).

Apart from economic, social, spatial and environmental consequences of decline and deindustrialization, there are psychological consequences. Integrated in its specific social context, an economic activity and the impacts on the local community are related to wider social consequences beyond loss of income and job such as loss of hope for the future, loss of the main assets to develop one's social identity and loss of value on one's capability (Işın 2009). The high levels of disempowerment in communities through discrimination and negated opportunities are remarked within this context (Nel et al. 2003). Likewise, diminishing living standards for the working class are stated as complementary (Anderson, Duncan and Hudson 1983). In addition, diverse forms of exclusion as outcomes of long term structural poverty and unemployment are some of the mentioned results of deindustrialization in the long run (Cooke 1995, Massey 1984, Nel et al. 2003).

Işın (2009) highlights that the spatial transformation, embedded in socio-economic phenomena, hides in itself the landscapes of production that once served as the motors of economic growth with its images on the production culture and the institutional context. In this regard, the dominance of a situation of becoming "out of context" has accompanied some of the old industrial regions.

The local restructuring process is embedded in the experience of consequences of deindustrialization and industrial decline (Işın 2009). Spatial restructuring can be considered as responses to complex and multi-dimensional socio-economic changes. Spatial structures of production are observed as outcomes of integrated capital, technical and organizational characteristics of an industry and change in industrial production in terms of its organization considering technology, working practices, skills, investment and vice versa lays behind changing spatial pattern (Massey 1984).

Mass unemployment, manufacturing job losses, collapsing local economies beside to plant closures, clearance and landscaping problems reveal the reflections of deindustrialization of the 1980s (Townsend 1983). The crisis of deindustrialization severely affected old industrial regions mainly based on old industries such as textile manufacturing, resource extraction such as coal mining and iron and steel manufacturing industries and further these regions have been indicated to show structural, organizational and technological weaknesses (Jones and Wild 1991)

Deindustrialization goes beyond the negative effects and the repercussions of these effects can be set as chain reactions on other sectors and on the macro-economy (Nel et al. 2003). One other dimension of deindustrialization can be set as the common ground it shares with urban decline process.

Urban demographic change in relation with deindustrialization has been remarked in terms of negative net migration rates and declining birth rates as similar indicators of

urban decline referred by Clark (1989). Furthermore, it is acknowledged that employment losses, low capacity for regeneration, urban and national economic decline are the common indicators to discuss deindustrialization and urban decline.

The relationship between national and local concern the difference that local brings in both experiencing the impacts and responding to changes brought by national policy changes (Massey 1984). According to their local characteristics and socio-spatial characteristics, localities undergo changes in diverse ways. Therefore, their responses can also be assumed to be different. The different preexisting structures create differences in experiencing of processes of change and thus reveal different impacts and responses to change (Işın 2009).

Deindustrialization and local restructuring processes are interwoven. Restructuring, as a response to change, concerns two basic discussions. The first discussion depends on response capacity in restructuring the process considering basic characteristics of old industrial regions and relationships within intra structural actors (institutions, firms, etc.) which are discussed with reference to social capital, transformative capacity leaning on lock-in and path dependency in the development literature (Işın 2009).

The second discussion approaches the restructuring process via action oriented strategies and related policies. These provide concrete experiences related to tools, actors and further impact assessment on old industrial regions after restructuring process. As a result, it is possible to assess whether the restructuring process acts on severely affected old forms of industrial production that are integrated with socio-spatial structure and with concerned local characteristics in real terms, or whether the out of context condition of the former socio-spatial structure is excluded from new paths for development within the transformation process. (Işın 2009)

3 RESPONSE CAPACITY TO CHANGE

Reactive and pro-active actions attempted to struggle with outcomes of deindustrialization on the labor and local community sides are observed in coal mining communities. Specific buffer mechanisms that introduce survival strategies for the local community, particularly labor households, remain an important component of investigation of responses to the impacts of the deindustrialization process in old coal mining regions (Işın 2009).

Generally, the economic base of coal mining regions is not much diversified. Işın (2009) states that, monostructure has repercussions on formation of strong ties between actors and the level of vulnerability in change, thus in the restructuring process in case of a too narrow local economy in a coal mining region. To an extent, these characteristics reflect the constraints these localities experience in formation of endogenous potential in giving response to change and creating strategies to cope with the crisis condition. Accordingly, this crisis condition may be either led by structural changes, such as deregulation, disinvestment and deunionization processes, or by new technologies and new demands on environmental cost minimization on coal content, both at the state and the global scale (Işın 2009).

Old industrial regions dominated by coal mining, heavy industry, shipbuilding and textiles are stated to be most severely affected by deindustrialization and industrial decline. Likewise, for the West Germany and Britain cases Jones and Wild (1991: 16) stress that “regions with a heavy dependence on resource endowments of coal and ironstone, port-linked industries or textiles, all redolent of nineteenth century patterns of industrialization, dominate the locations of decline” in Işın (2009).

The relationship between single-industry dominance and coherence in local social structure in addition to the relationship between working practices and solidarity in coal mining localities reveal greater

resistance to change on the labor side (Massey 1984, Işın 2009).

Turner (2000) stresses the single economic base of coal mining towns and the difficulties in regeneration of these localities. Due to the specific characteristics of coal mining towns, coal mining towns reveal and lead stagnancy in terms of both economic and social dimensions within a process of change, especially when indicating a single base economy. Complementarily, the underdeveloped and disadvantageously progressed small business sector peculiar to coal mining communities; the single activity based nature of many localities associated with coal have resulted in problems for any form of economic regeneration strategy due to the dominant specific skills indigenous to working practices in coal mining industry, usually intergenerational transfer of skills, and the unvaried local economic base to motivate alternative capabilities (Turner 2000, Işın 2009).

The capability of developing endogenous potential is considered important in intervention in the restructuring process (Butzin 1991). One of the burdens of developing endogenous potential may be the inability to generate bottom-up strategies collectively. One of the reasons of such a phenomenon may present a tradition of external expectation of subsidization for a long period of time. In other words, as Massey (1984: 207) states, change in coal mining areas is in fact the change in their externally directed economic control of the means of production and possession, which is what Massey calls “pre-existing economic peripherality”.

Evaluation of response problem to decline is taken into consideration to introduce a base for why and at what perspectives in dealing with and overcoming decline in relation to restructuring. After evaluating deindustrialization, industrial decline and the restructuring process at the global and national levels, restructuring processes and their repercussions on old industrial regions, local response and local restructuring become vital (Işın 2009).

The failure and success stories in local and regional restructuring provide clues in evaluations about response capacity. The decline of old industrial regions and their restructuring problems are subjects for research in school of evolutionary technical change in economic geography, in development studies and in embeddedness literature (Hassink, and Shin 2005, Hassink 2007). Işın (2009) puts forward that declining old industrial regions can be evaluated from the three mentioned perspectives. Localities dominated by steel, coal mining, and shipbuilding have characterized resource-based mono structural areas as old industrial regions (Hassink and Shin 2005), which can be taken into consideration as specific cases in evaluation of response capacity to decline and change. Declining old industrial regions, some of which can be considered as geographical production clusters, are stated to carry characteristics of insularity mostly inferior to resource-based mono structural areas and also areas specialized in consumer goods (e.g. textiles) in particular (Steiner 1985, Hassink and Shin 2005). Also, it is interpreted that declining old industrial regions, independent of whether they exist in a geographical cluster or not, are stated to indicate a loss of regional or national competitiveness which stresses organizational structure alongside the technological changes or changes at the firm level (Porter 1990, Grabher 1993, Glasmeier 1994, Enright 1995, Steiner 1998, Hassink 2005, Hassink and Shin 2005, Hassink 2007).

The two major concepts of lock-in and path-dependency are highlighted importance while evaluating response capacity to change. In a more detailed way, these two concepts are useful in understanding characteristics defining the current situation of old industrial regions, and in finding out the relations and assets in their experience of change and in their response capacity to change (Işın 2009). Pointing out that there exists no clear definition on regional lock-in concept, Martin and Sunley (2006: 395) define path dependence as being “locked

into development paths that lose dynamism" and also as the protection against danger and against "reinvention through successive new paths or phases of development". They admit that regional path creation and path-dependence are important assets for economic landscapes in this context.

Evaluation of decline in context of industrial evolution is denoted to be considered in two ways (Grunsven and Smakman 2005). One is explained to take into consideration decline as problems of adjustment in the context of path dependency and lock-ins concerning interaction patterns between economics, political and institutional actors because they affect ability to react. The second conceptualization of decline approaches decline as a natural inevitable process based on decline of the mono structure through cumulative decline in output and further damage of the local economy through negative feedback (Boschma 2003, Grunsven and Smakman 2005).

Işın (2009) stresses that the lock-in concept is used to describe decline in old industrial areas under domination of a traditional heavy industry by referring to (David 1985, Arthur 1989, Grabher 1993, Hassink, 2005, Hassink 2007). Lock-ins are explained to act as barriers to restructuring while hindering endogenous development (Hassink 2007) and also inner potential for creativity (Hassink and Shin 2005).

Responses to failure mechanisms are mentioned to arise in three forms. Hassink (2007) affirms that renewal, as the first form, expresses a tendency for diversification and innovation oriented development interrelating with weak lock-in and quiet restructuring, reflecting low resistance to change (Hassink 2007). The second form of response is stagnation or gradual decline (Chapman, McKinnon and Cumbers 2004, Hassink, 2007). The third form of overcoming failure mechanisms is presented as adjustment referring to an attempt to preserve the existing development path while only creating significant changes to sustain the prosperity of the cluster, which is related to noisy restructuring and hence a relatively high resistance to change (Hassink 2007, Işın, 2009).

These discussions provide insight to re-evaluate decline in old industrial regions in terms of new paths in development, main strategies of renewal, adjustment, reinforcement of decline and offer information on creation of potentiality in transformation through characteristics of relationships among actors in positioning to change (Işın 2009). Old coal mining regions can be highlighted here to further look into via specific characteristics of coal mining regions and coal cities.

4 INTERVENTION ON DECLINING COAL CITIES AND REGIONS: STRATEGIES AND POLICIES

When discussing intervention on coal cities there emerge contradictory consequences of restructuring concerning the former employment structure and spatial change. Massey (1984) denotes that the main strategy of restructuring following the decline of coal mining industry is diversification away from declining sectors economically and away from the region spatially. Stressing effectiveness of diversification and multinationalization on local capital and local labor, it is also added that there is a tendency of changes in regional/local capital toward supraregional integration. Moreover, the labor side preferences of multinationals of female labor in a condition faced with redundant organized male labor is saved to be prevalent in reorganization of skills in the production process and in class structure within the locality (Massey 1984, Işın 2009).

The change in the intervention of the state in industrial development has meant much for monostructural, big public firms in relation with structural changes having a tendency of market-led policies. Thus, disinvestment policies have put pressure on big public firms while affecting the whole socio-spatial structure (Işın 2009).

The regeneration and renewal efforts in the former coal mining towns experience difficulties due to the relatively low ability

to transform. This low transformation ability could be linked to homogeneous, coherent structure characterized by working practices together with social and economic relations and strong ties specific to coal mining regions (Işın 2009). This fact is emphasized by Turner (2000) who states that local economies of old coal mining localities have very limited capacity to offer local population jobs and other economic activities after pitfalls. So in a way, special characteristics of coal mining towns are considered to act as a catalyzing factor in resistance to change and are more vulnerable in a process of change and restructuring (Işın 2009).

Regarding the difficulties in taking action against and responding to mine closures, as one of the indicators of deindustrialization in coal cities, it has been indicated that the typology of local strategic responses reveal four key stages of intervention in mine closures as attempts to preserve existing economic life, finding and expanding existing alternative local jobs, development of new activities and movement into high technological sectors (Liljenas 1992, Nel et al. 2003).

It is emphasized that intervention attempts in local restructuring and responding to impacts of deindustrialization in coal mining regions are difficult compared to that of other localities. Consequently, Turner (2000) has remarked the main problems of the inability to attract inward investment as the economically unattractive local settlement, old infrastructure, challenges brought by geography, and isolation and poor accessibility in old coal mining regions. He further comments that the regeneration strategies of coalfields through job creation via enterprise zones, via proliferating small businesses and via reindustrialization attempts are rarely successful. Nonetheless, it is acknowledged in the same article that improvements in training and infrastructure are evident in attempts to attract inward investment. Local economic change which signifies the tertiarisation process is acknowledged to offer less skilled, less income service jobs for redundant skilled labor, and security remains in question (Tomaney, Pike and Conford 1999, Turner 2000, Işın 2009).

Işın (2009) discusses that industrial change and socio-spatial change processes are mutually interacting dynamics in the restructuring process. Restructuring experiences inform intervention strategies and policies in various ways which are both affected by mechanisms on a wider scale and simultaneously impact on local and regional structures. Restructuring is evaluated multi-dimensionally. Change in old forms of industrial production, hence previous paths of development lay on common ground to the deindustrialization and restructuring processes. Işın (2009: 41) indicates that restructuring can briefly be observable through such bases:

- "restructuring in regional economy comprising restructuring of urban economic base measured via changing employment structure and occupational schemes
- restructuring within the previous economic sector itself
- restructuring within the firm: changing policies on labor, property, organization, relationship with other firms, form of capital
- institutional restructuring: trade union; availability of social capital
- restructuring within spatial pattern, urban restructuring" (Işın 2009: 41)

There exist responsive attempts to the impacts of deindustrialization that create the characteristics of a restructuring process in a locality. Restructuring appeared on the agenda in the 1980s and deepened its conceptualization in the 1990s via changing global and state policies and constraints on growth and development. Local response to such a change has included various intervention bodies, tools and policies together with joining the restructuring process in terms of inner potentialities and context-dependent local characteristics.

Işın (2009: 42) puts forward that intervention facing out coming impacts of deindustrialization concern what main strategies have put on the agenda. Accordingly, three forms of reorganization are set after deindustrialization:

• “Intensification that comprises improvements in productivity across a wide range of plants without heavy new investment.

• Investment and technical change that occurs where employment decline is accompanied by heavy net capital investment providing that the new investment leads to replacement and closure but mobile employment remains there.

• Rationalization involving complete or partial plant closures due to lack of profitability and hence leading job losses and unemployment” (Massey and Meagan 1978, Townsend 1983).

Furthermore, Martin (1989) suggests six strategies for intervention in regional and local restructuring (as cited in Spooner, 1991:123 and in Işın 2009: 42):

• “reindustrialization (most often through the development of high-tech industry);

• modernization of the existing industry

• tertiarization

• reskilling and ‘flexibilization’ of the labor force;

• infrastructure renewal

• the creation of regionally- and locally-based financial markets”

Emphasizing the relationship between economic restructuring and urban restructuring, Clark (1989) states the main intervention strategies in response to urban decline. In this sense, main points of emphasis arise as below:

• “spatial consequences of changes in size and character of the manufacturing sector

• the consequences of shift of employment

• counterurbanization as a demographic response to the locational dictates of capital

• secondary consequences of sectoral policies” (Işın 2009: 42-43)

Deindustrialization, industrial and economic restructuring give insights to urban decline and urban restructuring. Clark (1989) describes this relationship by focusing on the ceasing of agglomerative forces of the former industry. He further states three main perspectives in intervention toward urban decline. Işın (2009) summarizes them. The first is reviving the cities through revival policies in order to reverse decline. The second is recapturing the cities on aims of minimizing the harmful effects of decline and re-attracting lost population and industry by expanding the boundaries of cities. While explaining this intervention strategy, the new locational choices of industry outside the city center, especially rural areas for the UK case, was stressed. The third strategy suggested is reinforcing decline which proposes to encourage decline and orient growth to somewhere other than the old industrial and spatial structure.

Intervention strategies are subject to responding to regional change. Deindustrialization, reindustrialization and tertiarization are stated to be three mutually interacting processes indicating regional economic change in this regard, (Jones and Wild 1991). Keeble (1991: 41) briefly defines these interacting processes through an evaluation of European regional economic restructuring in the 1980s as describing deindustrialization through evident manufacturing decline, especially of employment by focusing on nineteenth century ‘smokestack’ industries (steel, shipbuilding, heavy engineering, textiles) and old industrial regions; by describing reindustrialization through small firm or new firm resurgence, often in new, less-industrialized regions and rapid growth of ‘high technology’ industry, especially based on microelectronics and widespread adoption of new computer-based technologies by existing industries and by describing tertiarisation process including growth of tourism, recreation and leisure industries (Işın 2009).

Jones and Wild (1991:18) in Işın (2009: 44) attract attention to three interrelated processes of economic development, each with their characteristic location logic and spatial division:

• “.. the creation of new industrial spaces through the medium of new types of manufacturing industries”

• “.. the application of new industrial investment to foster the reindustrialization of old industrial regions”

• "..the immense pressures for change, generated by the increased tertiarisation of the economies of selected major cities" (Jones and Wild 1991: 18) in Işın (2009: 44).

The new industrial spaces, unlike the old ones, have demands on knowledge and innovation oriented resources and capital rather than demands on raw materials and transportation (Işın 2009). Also, in spatial terms, the establishment of new industrial spaces outside the old industrial regions is stressed while old industrial regions undergo underinvestment or disinvestment (Jones and Wild 1991). Likewise, Butzin (1991) states that new industries tend to choose to establish their own spatial pattern of industry in new regional locations rather than reuse the already established industrial locations.

Alongside the disintegration in production process in geographical means, the choices of the new industries for location have comprised diverse firm size and externalities via reach to information, research and development facilities, advanced service activities and advanced technology (Butzin 1991, Jones and Wild 1991). This points to cooperation of universities and new industry as observed in technopoles and science parks (Işın 2009).

Reindustrialization of old industries is confirmed to be achieved by using processes and products of the new technology as inputs into production process of old declining industries, such as iron and steel industry (Jones and Wild, 1991: 19).

The restructuring process has come to involve two bases of intervention revealing constraints on old industrial regions:

• "..inadequate rate of generation of local businesses, especially in the high tech and information spheres"

• ".. imposition of "checks upon the types of industrial enterprises, which these regions are able to attract" (Jones and Wild 1991: 23) in Işın (2009: 46).

Işın (2009) highlights that the reindustrialization process creates a contradictory situation for the employment structure and labor working in old industries. Feminization of labor, demand for unskilled and semi skilled female labor, especially for part-time, low paid service jobs remain indicative in deindustrializing old industrial regions in this context (Jones and Wild 1991, Turner 2000).

Following the discussion on employment structure change, Jones and Wild (1991: 24) clarify the tertiarisation process by defining it as "the shift in the employment structure from industry to services-from secondary to the tertiary (including quaternary) sector-which characterizes the post-industrial period". Jones and Wild (1991: 25) also point out and relate the inner-city decline by tertiarisation process revealing decentralization of economic activity and population (Işın 2009). They further emphasize the severe socio-economic impacts of tertiarisation process on local populations in terms of decline in jobs parallel to inner urban deindustrialization in the British experience. Three key factors are evident in recovery and regeneration of British inner cities:

• "the cardinal role of property-led development schemes";

• "the pivotal role of service based activities in the employment"

• "the dominance of private capital and entrepreneurship" (Jones and Wild 1991: 25 in Işın 2009: 47).

For further evaluation of the tertiarisation process and property development schemes on old economic and social structure, attention is drawn to the conflicting situation led by them through reinforcing economic, social and spatial inequalities (Jones and Wild, 1991).

Jones and Wild (1991) evaluate the British case whose regional policy comprised enterprise-led initiatives within a deregulative structural change and immense investments in constructions of recreation, leisure, consumption spaces and offices directed to tertiarisation and the West Germany Case founding on regional policy mainly on environmental problems through retrieving and rehabilitating strategies for derelict land in the Ruhr.

Regional imbalances are stressed relying on the diverse spatial impacts and demands of deindustrialization and new

industrialization (Işın 2009). Regional economic recovery is expected to come out through utilizing diversifying regional economic development policies regarding industrial restructuring (Cooke 1995).

Cooke (1995) indicates one dynamic behind regional policies on specialization as foreign direct investment by pointing out the policy responses considering the 1990s as depending on increased regional competitiveness through integration of regional and global networks of innovation and production. In this respect, Cooke emphasizes the active roles of regional production clusters and their relations with a global network of production and innovation for regional competitiveness(Işın 2009).

Işın (2009) stresses that, having fulfilled their restructuring process so as to intervene in the impacts of deindustrialization and generate new paths for development, most Anglo-American cases have various policy responses and revitalization attempts. These examples illustrate an evident shift from heavy industries to culture industries in relation with universities, arts and culture; urban renewal practices for old heavy industry towns through image renewal; development of regional technology plans by development agencies and shift from heavy industries to cultural heritage tourism as part of urban regeneration and image renewal (Cooke 1995).

Restructuring through reinforcement of decline remains one of the strategies of regional economic restructuring in old industrial regions (Işın 2009). This strategy is characterized by no direct or real effort to reverse industrial decline as Cooke (1995) points out for South Wales Case in the UK. Stagnating government expenditure accompanied by idle regional spending that assists declining old industrial areas in the 1980s and the 1990s are given as examples of some tools for reinforcement of decline strategy (Cooke 1995). Furthermore, urban policy on private property development in addition to strengthening inward investment for new jobs are denoted to be complementary strategies. The proliferation of indigenous and medium sized firms demanding female employment is set as one of the main strategies while letting the traditional industries of coal, steel, shipbuilding or textiles decline accompanied by a large group of redundant labor. Cooke has specified this also as one of the cases of external diversification externally driven by government policies. In contrast, the internal diversification strategy comprises the inclusion of previous industrial workers in the restructuring process (Cooke 1995), which may enable reemployment of the former labor in the new industrial activities through training (Işın 2009).

Training initiatives, and governmental and private sector initiatives are indicated as possible tools of diversification through reindustrialization and revitalization (Deitrick and Beauregard 1995). Regional institutions, such as non-profit organizations that support the development of advanced technology and modernization of manufacturing, may become actors of intervention in declining industrial regions in this regard (Işın 2009).

Spatial restructuring provides insight to industrial restructuring that proliferates the new socio-economic and socio-spatial structure (Massey 1984). In the urban restructuring stage, the new demands on housing and market have remained striking in relation with the new division of labor of higher incomes (Cooke 1986, Spooner 1991, Işın 2009).

Işın (2009) lastly attracts attention to household survival strategies so as to be be considered as a response and intervention on the consequences of deindustrialization. She saves that decreasing household consumption demand and purchasing power due to contraction in the labor market motivate households to create their own survival strategies, as carrying potentialities of creation of buffer mechanisms as response to socio-economic transformation in order to slow the pace of change. Işın (2009) highlights that these buffer mechanisms are embedded in place specific characteristics and local idiosyncracies and they serve as a ground to grasp the socio-economic dimension of industrial decline at the

household level in deindustrializing old industrial regions, in particular, the most directly affected households such as in lain off blue collar labor households.

5 DISCUSSION

Coal cities and coal mining regions can be taken as specific socio-spatial contexts to look into deindustrialization and restructuring processes due to strong binds between production and division of labor and urban context. In general, the homogeneous, insular and monostructural characteristics of coal mining localities play major roles in severe decline impacts of deindustrialization which are observable mostly in urban depopulation and unemployment at the first stage and further disintegrating production linkages among interrelated sectors within industrial regions at the regional level. In relation with deregulation, disinvestment, deunionization processes, deindustrialization remains all-inclusive hiding in itself economic, demographic, socio-pscyhological and environmental impacts and indicators. When it comes to giving response to change, in particular, deindustrialization and decline, and further intervention strategies, the characteristics of coal cities or coal mining regions play major roles making them more vulnerable and more limited in the sense of developing response capacity. Apart from reindustrialization and new industrialization, tertiarization reveals the dramatic transformation from production to consumption facilities in urban economy, mainly comprising leisure and recreational facities in addition to industrial cultural heritage evident in coal museums in urban context.

REFERENCES

Arthur, W. B., (1989). Competing technologies, increasing returns, and lock-in by historical events, *Economic Journal*, 99, p.116 -131.

Anderson, J., Duncan, S. and Hudson, R., (1983). Urban development, redundant spaces? An introduction. In J. Anderson, S. Duncan and R. Hudson (Eds.). *Redundant spaces in cities and regions*, Academic Press, London, p. 1-15.

Barchiesi, F. and Kenny, B., (2002). From Workshop to Wasteland: De-industrialization and Fragmentation of the Black Working Class on the East Rand (South Africa), 1990-1999. *IRSH*, 47, p.35-63.

Bowles, S., Gordon, D. M., and Weisskopf, T. E., (1983). *Beyond the waste land: a democratic alternative to economic decline.* Anchor Books.

Butzin, B., (1991). Regional life cycles and problems of revitalization in the Ruhr, In Wild, T. and Jones, P. (Eds.), *De-industrialization and new industrialization in Britain and Germany. A project of the Anglo-German Foundation for the study of industrial society*, Billing and Sons Ltd. Worcester.

Camagni, R, P., (1991). Regional de-industrialisation and revitalisation processes in Italy, In Rodwin, L & Sazanami, H. (Eds.). *Industrial change and regional economic transformation: the experience of Western Europe,* Harper Collins, London, p.136–166.

Castells, M., (2005). *Enformasyon Çağı: Ekonomi, Toplum ve Kültür: Ağ Toplumunun Yükselişi*, Cilt 1, E. Kılıç (Çev.), Bilgi Yayınları, İstanbul.

Chapman, K., MacKinnon, D., Cumbers, A., (2004). Adjustment or renewal in regional clusters? A study of diversification amongst SMEs in the Aberdeen oil complex, *Transactions of the Institute of British Geographers*, New Series, 29, p. 382 – 396.

Cheshire, P. C. and Hay, D. G., (1989). *Urban Problems in Western Europe: an Economic Analysis*, Hyman.

Clark, D. (1989). *Urban Decline*, Routledge, London.

Cooke, P. N. (1981). Inter-regional class relations and the redevelopment process, *UWIST Papers in Planning Research*, 36. Cardiff.

Cooke, P. (1986). The changing urban and regional system in the United Kingdom, *Regional Studies*, 20, p. 243-252.

Cooke, P. (1995). Introduction. Cooke, P. (Ed.), *The rise of the rustbelt*, UCL Press, London.

DEK/TMK, WEC/TNC. (2007). Kömür çalışma grubu raporu, Ankara.

David, P. A. (1985). Clio and the Economics of QWERTY. *American Economic Review*, 75, p. 332- 337.

Deitrick, S. and Beauregard, R. A., (1995). From front-runner to also –ran- the transformation of a once-dominant industrial region: Pennsylvania, USA, In P. Cooke (Ed.). *The rise of the rustbelt*, UCL Press Limited, London, p. 52-71.

Enright M. J., (1995). Regional clusters and economic development: a research agenda, *Working paper*, MA: Harvard Business School, Boston.

Friedmann, A., (1977). *Industry and Labour: Class Struggle at Work and Monopoly Capitalism*, Macmillan, London.

Grabher, G., (1993). The weakness of strong ties; the lock-in of regional development in the Ruhr area, In G Grabher (Ed.). *The Embedded Firm: On the Socioeconomics of Industrial Networks*, Routledge, London, p.255-277.

Grunsven, L. V., and Smakman, F., (2005). Industrial restructuring and early industry pathways in the Asian first-generation NICs: the Singapore garment industry, *Environment and Planning A*, 37, p. 657-680.

Harvey, D. (1999). *Postmodernliğin Durumu: Kültürel Değişimin Kökenleri*, S. Savran (Çev.), İstanbul, Metis Yayınları.

Hassink, R. and Shin, D-H., (2005). Guest Editorial. The restructuring of old industrial areas in Europe and Asia, *Environment and Planning A*, 37, p. 571 – 580.

Hassink, R., (2005). How to Unlock Regional Economies from Path Dependency? From Learning Region to Learning Cluster, *European Planning Studies*, 13, 4, p.521-535.

Hassink, R., (2007). The strength of weak lock-ins: the renewal of the Westmünsterland textile industry, *Environment and Planning A*, 39, p. 1147-1165.

Helmut, N., (1991). De-industrialization and problems of revitalization in the Hamburg port area, In Wild, T. And Jones, P. (Eds.), *De-industrialization and new industrialization in Britain and Germany. A project of the Anglo-German Foundation for the study of industrial society*. Billing and Sons Ltd., Worcester.

Glasmeier, A., (1994). Flexible districts, flexible regions? The institutional and cultural limits to districts in an era of globalization and technological paradigm shifts, In A. Amin, N Thrift, (Eds.). *Globalization, Institutions, and Regional Development in Europe*, Oxford University Press, Oxford, 118-146.

Işın, Ş., (2009). Deindustrialization, decline and restructuring in socio-spatial context: A multi-layer exploratory study on mono-centric local Economy, Zonguldak Case. ODTÜ, Ankara (Yayınlanmamış doktora tezi).

Jones, P. and Wild, T., (1991). Industrial restructuring and spatial change in Britain and West Germany. In T. Wild and P. Jones (Eds.). *De-Industrialization and New Industrialization in Britain and Germany. A project of the Anglo-German Foundation for the Study of Industrial Society*. Billing and Sons Ltd., Worcester.

Keeble, D. (1991). De-industrialisation, new industrialization processes and regional restructuring in the European Community. In T. Wild and P. Jones (Eds.), *De-Industrialization and New Industrialization in Britain and Germany. A project of the Anglo-German Foundation for the Study of Industrial Society*. Billing and Sons Ltd., Worcester.

Liljenas, I., (1992). From mine to outer space: the case of Kiruna, a town in northern Sweden. In Neil, C, Tykkylainen, M & Bradbury, J (Eds), *Coping with closure: an international comparison of mine town experiences*, Routledge, London, p. 247–64.

Mandel, E., (1978). *Late Capitalism*, Verso, London.

Martin, R., (1989). The new economics and politics of regional restructuring: the British Experience, In P. Seed and L. Albrechts, (Eds). *Regional policy at the crossroads: European perspectives*. J. Kingsley, London, p. 27-51.

Martin, R., and Sunley, P., (2006). Path dependence and regional eonomic evolution, *Journal of economic geography*, 6, p. 395-437

Massey, D., (1984). *Spatial Divisions of Labour: Social Structures and the Geography of Production*, Macmillan, Hong Kong.

Massey, D. and Meagan, (1978). Industrial restructuring versus the cities, *Urban Studies*, 15, 3.

Nel, E. L., Hill, T. R., Aitchison, K., C and Buthelezi, S., (2003). The closure of coal mines local development responses in Coal-Rim Cluster, northern KwaZulu-Natal, South Africa, *Development Southern Africa*, 20, 3, p. 369-381.

Pietrikowsky, B., (1999). Beyond The Fordist/Post-Fordist Dichotomy: Working through the second industrial divide, *Review of Social Economy*, LVII, 2.

Piore, M. J. and Sabel, C. F., (1984). *The Second Industrial Divide: Possibilities for Prosperity*, Basic Books, New York.

Porter, M. E., *(1990). The Competitive Advantage of Nations*. Macmillan, London.

Schumpeter, J. A., (1939). *Business Cycles: A Theoretical, Historical and Statistical Analysis of the Capitalist Process.* McGraw Hill Book Co., New York.

Scott, A., J., (1986). Industrialization and Urbanization: A Geographical Agenda, *Annals of the Association of American Geographers*, 76 1, p. 25-37.

Smith, P., (2001). *Unionization and union leadership: the road haulage industry*, Routledge, UK.

Soja, E. W., (2001). *Postmetropolis*, UK, Blackwell Publishers.

Spooner, D., (1991). Across the great divide: restructuring at the local scale in the eastern England, In Wild, T. And Jones, P. (Eds.), *De-industrialization and new industrialization in Britain and Germany. A project of the Anglo-German Foundation for the study of industrial society*. Billing and Sons Ltd., Worcester.

Steiner, M., (1985). Old industrial areas: a theoretical approach, *Urban Studies*, 22, p.387-398.

Steiner, M., (1998). The discreet charm of clusters: an introduction, in European Research in Regional Science,,8. M Steiner (Ed.). Clusters and Regional Specialisation: On Geography, Technology and Networks. (1-17). London: Pion.

Tamzok, N. (2007). Küreselleşme, serbestleşme ve kömür endüstrisi. *Temiz kömür Teknolojileri ve Yakma teknikleri Semineri Bildiriler Kitabı*, Kahraman Maraş-Elbistan.

Tomaney, J., Pike, A. and Conford, J., (1999). Plant Closure and the Local Economy: The Case of Swan Hunter on Tyneside, *Regional Studies*, 33, 5, p. 401-411.

Townsend, A. R., (1983). *The Impact of Recession: On Industry, Employment and the Regions, 1976-1981*, Croom Helm, Austria.

Turner, R., (2000). After Coal. In R. Turner (Ed.). *British Economy in Transition: From Old to New?*, Routledge, USA, (23-45).

Yılmaz, A. O. ve Uslu, T., (2007). The role of Coal in Energy Production-Consumption and Sustainable Development of Turkey, *Energy Policy*, 35, 2, p.1117-1128.

Wallerstein, I., (1974). The Rise and Future Demise of the World Capitalist System: Concepts for Comparative Analysis, *Comparative Studies in Society and History*, 16, p. 387-415.

Wallerstein, M. and Western, B., (2000). Unions in Decline? What has changed and Why, *Annual Review of Political Science*, 3, p. 355-377.

Winterton, G. (2003). The Limits and Use of Executive Power by Government, *Federal Law Review*, 31, 421.

Rethinking Impact Assessment of Mining Projects in the Context of Ecosystem Services

D. Damigos, M. Menegaki, D. Kaliampakos
National Technical University of Athens, Athens, Greece

V. Kazakidis
Laurentian University, Sudbury, Ontario, Canada

ABSTRACT During the last years there is an ongoing discussion among scholars, both academics and practitioners, about whether it is useful to weave the concept of Ecosystem Services into the environmental assessment framework of industrial and other activities. Although it is argued that this may introduce a new level of complexity, the concept of Ecosystem Services, i.e. the benefits generated by ecosystems for human well-being, seems to becoming an important component of mainstream environmental decision making. As such, it is more than probable that mining sector will be affected in certain ways. Towards this direction, this paper wishes to contribute to a better understanding of the role of Ecosystem Services on the mining sector by providing a brief literature review and highlighting central topics with regards to potential applications, perspectives and challenges around this issue.

Keywords: Ecosystem services, impact assessment, mining

1 INTRODUCTION

It is widely established that surface mining and quarrying activities can have significant impacts of natural and social environments. Thus, mineral works are highly regulated worldwide.

One of the most common legislative requirements and obligations related to permitting of mining operations is the preparation of an environmental impact assessment (EIA) study of the proposed mining project. Typically, EIA can be defined as "*…a process for identifying the likely consequences for the biophysical environment and for man's health and welfare of implementing particular activities, and conveying this information, at a stage when it can materially affect their decision, to those responsible for sanctioning the proposals…*" (Munn, 1979).

Just like in other sectors, the implementation of the EIA process in mining activities within different countries is inconsistent. For instance, in EU countries despite commonalities in European legislation there are no common processes owing to existing and sometimes highly bureaucratic frameworks (Telfer et al., 2009). The situation is more or less the same in the USA, since the environmental legislation is different and often conflicting depending on whether it is considered under federal, state, or county regulation requirements (ibid.). Nevertheless, and apart from the differences in the details, legislation for mining-related EIA studies encompasses some common elements, such as characterization and of the project, estimation of emissions to the water, soil and atmosphere, evaluation of landscape changes, assessment of predicted impacts on abiotic and biotic environment, monitoring and mitigation of environmental impacts, consultation with the affected community etc.

In order to enhance the environmental effectiveness of current regulatory approaches, a discussion has emerged during the last years on the potential role of Ecosystem Services within the EIA framework. Ecosystem Services (ES) are the benefits generated by ecosystems for human

well-being and are at the core of modern social-ecological research, in both academia and industry, especially after the Millennium Ecosystem Assessment adopted the ecosystem approach (MEA, 2005). Nowadays, there are a few examples of seminal work that are driving this area forward (MEA, 2005; TEEB, 2011; Haines-Young & Potschin, 2013). In addition, there are some efforts towards incorporating Ecosystem Services in international and national environmental policy and guidelines or other forms of support have been produced (e.g. CBD, 2004; DEFRA, 2007a; OECD, 2008; NER, 2010; Landsberg et al., 2011; Landsberg et al., 2014; UNEP, 2014).

As mentioned by Baker et al. (2013), from the existing guidance documents, two key conclusions are drawn regarding the inclusion of Ecosystem Services in environmental assessment:

- Using ES presents a more complete, holistic and integrated consideration of the socio-ecological system.
- The ES concept is an effective framing of the environment in terms of communicating with and influencing stakeholders and decision makers.

On the other hand, it is argued that the inclusion of ES in EIA studies may introduce a new level of complexity (e.g. Chan et al., 2012). Yet, the concept of Ecosystem Services seems to becoming an important component of mainstream environmental decision making by permitting authorities and corporations (e.g. de Groot et al., 2010; Karjalainen et al., 2013).

Taking into consideration the above-mentioned remarks, it is more than probable that mining industry will be affected in certain ways from this new trend. So far, however, the discussion within the sector has been rather limited. This paper wishes to contribute to a better understanding of the role of Ecosystem Services on the mining sector by providing a brief literature review and highlighting central topics with regards to potential applications, perspectives and challenges around this issue.

2 ECOSYSTEM SERVICES APPROACHES AND EIA

2.1 Classification Systems of ES

The concept of Ecosystem Services seems attractive because it describes some of the ways that humans are linked to, and depend on, nature. For instance, describing Ecosystem Services and how humans change their capacity to deliver benefits, could help towards mapping or valuing economically the natural capital (Young & Potschin, 2013).

So far, researchers have proposed different approaches to categorize ecosystem goods and services. For example, Boyd and Banzhaf (2007) viewed Ecosystem Services as the components of nature directly enjoyed, consumed, or used to yield human well-being. Wallace (2007) defined Ecosystem Services based only on benefits people obtain from end services of ecosystems, while Fisher et al. (2009) argued that Ecosystem Services are the aspects of ecosystems utilized (actively or passively) to produce human well-being.

Internationally three classification systems are available, as shown in Table 1, and mostly recognized towards classifying Ecosystem Services, namely MEA, TEEB and CICES, which relate to a large extent to each other (Maes et al., 2013).

The Millennium Ecosystem Assessment (MEA - http://www.maweb.org) was the first large scale ecosystem assessment. The MEA classifies Ecosystem Services into four groups, namely (MEA, 2005):

(1) provisioning services (i.e., goods or products obtained from ecosystems, such as food, timber, fiber, and freshwater);

(2) regulating services (i.e., contributions to human well-being arising from an ecosystem's control of natural processes, such as climate regulation, disease control, erosion prevention, water flow regulation, and protection from natural hazards);

(3) cultural services (i.e. recreation, spiritual values, and aesthetic enjoyment); and

(4) supporting services (i.e. natural processes, such as nutrient cycling and

primary production, that maintain the other services).

The MEA framework was adopted and was further refined by TEEB and CICES. More specifically, the Economics of Ecosystems and Biodiversity framework (TEEB - www.teeb.org) proposes a typology of 22 Ecosystem Services divided in four main categories, following mainly the MEA classification: (1) provisioning services; (2) regulating services; (3) habitat services; and (4) cultural and amenity services (TEEB, 2010 & 2011). More specifically, TEEB omits supporting services, which are seen as a subset of ecological processes, while, habitat services have been identified as a separate category to highlight the importance of ecosystems to provide habitat for species and gene-pool "protectors", such as natural habitats allowing natural selection processes to maintain the vitality of the gene pool (Maes et al., 2013).

Finally, the Common International Classification of Ecosystem Services (CICES - http://cices.eu) has been developed to help negotiate the different perspectives that have evolved around the Ecosystem Service concept. It assists in the exchange of related information and offers a structure that links with the framework of the UN System of Environmental-Economic Accounting (SEEA). Thus, CICES has refined MEA framework to reflect some of the key issues that have been discussed in the wider research literature (Haines-Young & Potschin, 2013). CICES is more explicitly hierarchical in structure. At the highest level there are three familiar services used in MEA called 'Sections', namely: (1) provisioning (i.e. all nutritional, material and energetic outputs from living systems, where a distinction is made between provisioning and material outputs arising from biological or organic materials and water); (2) regulating and maintenance (i.e., all the ways in which living organisms can affect human performance by mediating or moderating the ambient environment); and (3) cultural (i.e. all the non-material and normally non-consumptive outputs of ecosystems that affect physical and mental states of people, which can involve individual species, habitats and whole ecosystems). Below these Sections are nested a series of 'Divisions', 'Groups' and 'Classes' (Haines-Young & Potschin, 2013).

A major difference between MEA and CICES is that CICES excludes the supporting services from the classification and focuses only on the provisioning, regulating and cultural components. The reason for this was to avoid the problem of 'double counting' if ecosystem and economic accounts are to be linked. Furthermore, CICES and TEEB classifications treat 'habitat services' differently. TEEB identifies them as a distinct grouping at the highest level, while CICES regards them as part of a broader 'regulating and maintenance' section (ibid.). The correspondence between these classifications as provided by Maes et al. (2013) is illustrated in Table 1.

2.2 Ecosystem Services and EIA Studies

Environmental impact assessment (EIA) is a well established procedure in the world as a means to assess the impacts of projects that can potentially impact the environment and, consequently, the Ecosystem Services provision in multiple ways. Weaving Ecosystem Services into EIA studies could enhance the impact assessment process (Geneletti, 2011). Thus, new regulatory and financial impact assessment standards require that EIA studies systematically address impacts on Ecosystem Services (Landsberg et al., 2011). However, owing to lack of guidance on how to address Ecosystem Services, and what its added value is, EIA practitioners still are not engaged to that concept (Honrado et al., 2013). As a result, the implementation of the Ecosystem Services in the context of EIA practice is still quite immature (ibid.).

Table 1. Ecosystem Services categories in MA, TEEB and CICES

MA categories	TEEB categories		CICES v4.3
Food (fodder)	Food	**Provisioning services**	Biomass [Nutrition]
			Biomass (Materials from plants, algae and animals for agricultural use)
Fresh water	Water		Water (for drinking purposes) [Nutrition]
			Water (for non-drinking purposes) [Materials]
Fibre, timber	Raw Materials		Biomass (fibres and other materials from plants, algae and animals for direct use and processing)
Genetic resources	Genetic resources		Biomass (genetic materials from all biota)
Biochemicals	Medicinal resources		Biomass (fibres and other materials from plants, algae and animals for direct use and processing)
Ornamental resources	Ornamental resources		Biomass (fibres and other materials from plants, algae and animals for direct use and processing)
			Biomass based energy sources
			Mechanical energy (animal based)
Air quality regulation	Air quality regulation	**Regulating services (TEEB)**	[Mediation of] gaseous/air flows
Water purification and water treatment	Waste treatment (water purification)		Mediation [of waste, toxics and other nuisances] by biota
		Regulating and supporting services (MEA)	Mediation [of waste, toxics and other nuisances] by ecosystems
Water regulation	Regulation of water flows		[Mediation of] liquid flows
	Moderation of extreme events	**Regulating and maintenance services (CICES)**	
Erosion regulation	Erosion prevention		[Mediation of] mass flows
Climate regulation	Climate regulation		Atmospheric composition and climate regulation
Soil formation (supporting service)	Maintenance of soil fertility		Soil formation and composition
Pollination	Pollination		Lifecycle maintenance, habitat and gene pool protection
Pest regulation	Biological control		Pest and disease control
Disease regulation			
Primary production	Maintenance of life cycles of migratory species (incl. nursery service)		Lifecycle maintenance, habitat and gene pool protection
Nutrient cycling (supporting services)			Soil formation and composition
			[Maintenance of] water conditions
	Maintenance of genetic diversity (especially in gene pool protection)		Lifecycle maintenance, habitat and gene pool protection

Table 1. Ecosystem Services categories in MA, TEEB and CICES (Cont'd)

MA categories	TEEB categories		CICES v4.3
Spiritual and religious values	Spiritual experience	**Cultural services**	Spiritual and/or emblematic
Aesthetic values	Aesthetic information		Intellectual and representational interactions
Cultural diversity	Inspiration for culture, art and design		Intellectual and representational interactions Spiritual and/or emblematic
Recreation and ecotourism	Recreation and tourism		Physical and experiential interactions
Knowledge systems and educational values	Information for cognitive development		Intellectual and representational interactions Other cultural outputs (existence, bequest)

Source: Maes et al., 2013

There are some recent efforts to provide technical guidance to address Ecosystem Services in impact assessment. These include the Convention on Biological Diversity's voluntary guidelines on including biodiversity and Ecosystem Services in impact assessment (Slootweg et al., 2006) and the OECD's recommendations on how to include Ecosystem Services in Strategic Environmental Assessments (OECD, 2008). A more sector oriented approach regarding ecosystem service dependencies for oil and gas developments has been proposed by IPIECA/OGP (2011).

Recently, a guidance manual was released by UNEP (2014), which is the output of the GEF funded "Project for Ecosystem Services" (ProEcoServ) implemented by the Ecosystem Services Economics Unit, DEPI. The methodological approach is divided into four stages each comprising two or three specific tasks, as follows:

- Stage 1: Establish the Ecosystem Services context
- Stage 2: Determine and assess priority of Ecosystem Services
- Stage 3: Identify alternatives and assess impacts on Ecosystem Services
- Stage 4: Follow up on Ecosystem Services

This approach, as mentioned, aims at integrating Ecosystem Services in Strategic Environmental Assessment (SEA). Nevertheless, provided that the ProEcoServ project wishes to integrate ecosystem assessment, scenario development and economic valuation of Ecosystem Services into development planning even at local scale, it could be applied in EIAs, as well.

The most relevant and perhaps integrated effort to establish a detailed guidance framework for EIA practitioners, namely the "Ecosystem Services Review (ESR) for Impact Assessment (IA)", has been carried out by Landsberg et al. (2011) and was recently updated (Landsberg et al., 2014). The ESR for IA approach builds on the elements and causal relations of the original MEA framework and consists of six steps implemented in following stages:

- The Scoping stage involves one step (Step 1) and aims at identifying the key Ecosystem Services that could be impacted by, or could constrain the successful implementation of, the project.
- The Baseline and impact analysis stage includes Steps 2, 3, 4 and 5 and its aim is twofold: (a) to establish baseline for key environmental and social issues and for priority Ecosystem Services, and (b) to assess project impacts and project dependencies on key environmental and social issues and on priority Ecosystem Services. More specifically, Step 2 defines the Ecosystem Services on which to conduct the impact and dependence assessments. Step 3

establishes the geographical boundaries of the ecosystem service impact and interdependence assessments and identifies indicators of impact and dependence. Step 4 determines how priority Ecosystem Services currently contribute to affected stakeholders' livelihoods, health, safety, or culture. Finally, Step 5 assesses project impacts and dependencies on priority Ecosystem Services and identifies which of these services require mitigation or management measures.

- The Mitigation stage includes the last step (Step 6) of the methodology. It aims at identifying appropriate biophysical and/or socioeconomic measures to mitigate impacts and manage dependencies on Ecosystem Services for incorporation into environmental and social management plans. These measures should be monitored and assessed against the objectives of: (a) achieving at least no loss of Ecosystem Services benefits by global and local stakeholders, and (b) ensuring planned operational performance.

So far, there are only limited examples of the use of Ecosystem Services within environmental assessment. Baker et al. (2013) summarize five EIA and SEA case studies. These illustrate a range of approaches to using Ecosystem Services in environmental assessment from Portugal, South Africa and UK. Based on the analysis of the case studies, Baker et al. (2013) discuss the major strengths and weaknesses of encompassing Ecosystem Services in environmental assessments.

Among the benefits, the authors identfy that Ecosystem Services provide a more integrated description of the environment and emphasize on wider economic benefits of certain habitats and land cover types offering alternative information to policy and decision makers, as well as to stakeholders and communities. On the other hand, it is argued that the integrated nature of Ecosystem Services presents an inherent difficulty and requires significant primary research to be undertaken to form an effective baseline, especially for valuation purposes. In addition, it is noted that only certain types of plans, programmes or projects may be relevant for using Ecosystem Services. They conclude, however, that incorporating Ecosystem Services in environmental assessment is probably more of a help than a hindrance and may help in addressing problems with current environmental assessment practices.

3 ECOSYSTEM SERVICES AND IMPACT ASSESSMENT IN MINING SECTOR

Focusing on mining activities, two general questions pertinent to the mining sector should be addressed: (a) Why should Ecosystem Services be considered in impacts assessments of mining projects; and (b) Have Ecosystem Services been used in mining practice?

3.1 Involving ES into EIAs of Mining Projects

As regards the first question, there is a number of reasons why the mining sector should become more familiar with the concept of Ecosystem Services. Firstly, it can be inferred that the concept of Ecosystem Services is becoming mainstream at all levels of environmental decision making because it provides a new way to approach environmental management (e.g. Carpenter et al., 2009; de Groot et al., 2010; Chan et al., 2012; Karjalainen et al., 2013). Secondly, this trend is reflected at the standards and requirements of organizations that are associated with the mining sector, such as the International Finance Corporation (IFC). The IFC, founded in 1956 with 182 member countries, holds equity in over 722 companies worldwide, including 184 fund management groups.. With respect to mining industry, the IFC's Mining Group provides equity and loan financing for mining companies to build projects that reward owners, investors, and local communities. The IFC's investment

portfolio in mining was around $500 million in 2011 and included 37 mining projects of Rio Tinto, Anglo American, NewMont, Minera Escondida, Lonmin and other companies in 25 different countries (IFC, unknown). In 2012, IFC's investment portfolio in mining, oil, and gas was $2.3 billion (IFC, 2012a). In 2013 and 2014, the IFC's new commitments in the sector totaled $389 and $441 million, respectively (IFC, 2014). The IFC finances projects that meet certain criteria. In January 2012, the IFC set out the Performance Standard 6 "Biodiversity Conservation and Sustainable Management of Living Natural Resources" that requires IFC-financed projects to preserve the benefits from Ecosystem Services, reflecting this recent trend. Furthermore, the IFC requires that the environmental and social risks and impacts identification process considers a project's dependence on Ecosystem Services.

For mining companies, it is more than evident that obtaining a formal operating licence from regulating authorities is no longer enough, as it has become an increasingly insufficient means of satisfying society's expectations with regard to mining issues (Bridge, 2004). Thus, it is widely recognized that mining companies need to gain also a "social licence to operate" that includes revenue sharing, so as to avoid conflicts with local communities (Prno & Scott Slocombe, 2012; Prno, 2013; Owen & Kemp, 2013; Moffat & Zhang, 2014). There are several definitions of "social license to operate". In general, it can be said that a "social licence to operate" exists when "*a mining project is seen as having the broad, ongoing approval and acceptance of society to conduct its activities*" (Prno, 2013). Several factors may affect the "social licence to operate" outcomes. In general, it is argued that sustainability considerations, participation of the public in decision making process and securing and provisioning of local benefits are crucial elements in obtaining the "social licence to operate". All these factors are strongly anchored with the concept of Ecosystem Services either explicitly or implicitly. For example, the "Ecosystem Services Review for Impact Assessment" (Landsberg et al., 2014), as described earlier, facilitates integration of the environmental and social assessments. Thus, it is considered to be useful among others to projects that:

- may alter ecosystems on which people and communities have a high level of dependence for maintenance of their livelihoods, health, safety, or culture
- are controversial and require the project developers to be proactive in their relations with affected stakeholders to avoid legal battles or delays in project implementation or operation.

Both cases are quite relevant to mining operations. In addition, Landsberg et al. (2014) argue that integrating Ecosystem Services in environmental assessment provides significant benefits to global and local stakeholders, due to the fact that stakeholder engagement becomes more inclusive, the assessment of the impacts of the project over its life cycle is more comprehensive, and the target of mitigation measures is to maintain pre-project benefits to local communities that derive from impacted ecosystems.

Finally, Ecosystem Services concept is important to mining sector because there is a need to justify the overall impact of a mining project in the context of a social cost-benefit analysis, so as to decide whether the exploitation of mineral resources is socially desirable. in the last three decades, there has been an increasing effort in mining project appraisals to account for environmental and social impacts, apart from the traditional techno-economic valuation in the decision-making process driven by market values. For example, Resource Assessment Commission (Imber et al. 1991) used a non-market valuation approach, namely Contingent Valuation, in order to assess the environmental value of the Kakadu Conservation Zone and to decide whether or not to permit the exploitation of mining deposits found in the region. The Department of the Environment, Transport and the Regions (DETR) conducted two separate studies aiming at calculating a tax

on the output of aggregates based on the externalities generated by quarrying activity (London Economics, 1998 & 1999). In Greece, the Council of Greek State ruling on the case of TVX's investment at Olympias area, in Northern Greece with the Decision Record 613/2002 concluded that the environmental impacts (water pollution, devastation of forests, land occupation, etc. and the risk of a severe environmental accident due to the use of cyanide in the extraction process) outweighed overall economic benefits, resulting in the cassation of the mining investment (Damigos, 2006).

To this end, Ecosystem Services valuation will play an important role. According to TEEB (2010), ecosystems generate output values (e.g., food production, climate regulation and recreational value) and insurance values. The latter is closely related to the "option value". Provided that Ecosystem Services can directly and indirectly affect human well-being, they link well to taking an economic approach. Under the Total Economic Value (TEV) conceptual framework, people derive utility from the actual or potential use of ecosystems and for reasons not connected with use, i.e. create use and non-use values. Use values involve direct use (i.e. individuals make actual use of an ecosystem service), indirect use (i.e. individuals benefit from ecosystem services supported by a resource rather than directly using it) and option value (i.e. the value of ensuring the option to use a resource in the future). Non-use values derive from the knowledge that the environment is maintained and include altruistic, bequest and stewardship motivations (DEFRA, 2007b). So far, however, there are limited efforts dedicated to establishing monetary values for Ecosystem Services (e.g. Costanza et al., 1997; de Groot et al., 2012).

3.2 ES and Recent Mining Practice

Not surprisingly, there are very limited efforts in incorporating Ecosystem Services in mining sector.

Rosa & Sanchez (2013) used the "Sapo-Ferrugem" mine mining project in Minas Gerais State, Brazil, in order to test the Ecosystem Services approach (ESA) to the 'traditional' environmental impact assessment (EIA). The research steps were, as follows:

(1) Compiling a summary description of the present environment conditions with an emphasis on identifying affected ecosystems and their services from the baseline featured in the Environmental Impact Statement (EIS);

(2) Compiling from the project description featured in the EIS a list of major project activities;

(3) Identifying Ecosystem Services that could be affected by the project;

(4) Adjusting the identification of Ecosystem Services to the results of a rapid appraisal;

(5) Identifying, from the rapid appraisal, beneficiaries of Ecosystem Services;

(6) Reviewing all impacts described in the EIS and searching for possible matching with Ecosystem Services.

In order to compare the ESA with the traditional EIA approach, the impacts described in the EIS were arranged in a matrix to show the correspondence with the impacted ES. The analysis showed that the 'traditional' EIS identified 10 physical, 12 biotic and 20 social negative impacts. The biotic and nine of the ten physical negative impacts were also identified by the ESA, but only nine out of the twenty negative social impacts described by the EIS could be identified through the ESA. The conclusion was that: (i) some impacts identified in the EIS cannot be described by the ESA; (ii) some impacts are equivalent under both approaches and (iii) the ESA allowed the identification of several effects not identified by the traditional approach.

King (2013) attempted to show how ESA could offer a systematic framework to enhance, structure, and communicate the benefits offered by quarry restoration. More specifically, the findings include the types of ecosystem services that restored quarries could generate for four common habitat types (i.e., heathlands, grasslands, wetlands and farmland) and how ecosystem services

from these habitats may be valued to assess public benefits in environmental consideration. To this direction, a number of business opportunities and threats are identified in relation to ecosystem service trends and key recommendations for the sector are stipulated.

Larondelle & Haase (2012) implemented ESA to assess the impacts of mining activity over a considered 100-year period, to pre- and post-mining landscapes. Using one of the largest opencast lignite mining areas in Europe, in Eastern Germany, south of Leipzig, they recorded historical land use data from maps and outlined three future potential land use scenarios based on current planning documents in order to: (1) assess the pre-mining, mining and post-mining landscapes with respect to function and sustainability; (2) apply ESA to this assessment; and (3) evaluate the applicability of the Ecosystem Services concept to mining impact assessment and post-mining landscape patterns. Although the authors recognize that there are shortcomings related mostly to the choice of Ecosystem Services and indicators, the results indicate that it is possible to provide information for the planning process about what natural and ecosystem potential was eliminated by mining and what restoration offers.

Alcoa & CBBC (2011) applied the Corporate Ecosystem Services Review (ESR) developed by the World Resources Institute (WRI) as a complementary approach to carrying out an EIA study for the modernization of Alcoa's Baie-Comeau smelter in Quebec, Canada. The ESR process involved the following steps:

(1) Selection of the scope and boundaries of the analysis.

(2) Identification of priority ecosystems services by evaluating the degree of the facility dependence and impact on 24 ecosystem services.

(3) Assessment of the level of dependence and impact in priority ecosystem services.

(4) Identification of business risks and opportunities that may arise due to the trends in priority ecosystem services.

(5) Development of strategies that will be implemented both at the existing plant and within the modernization project to incorporate the findings of the ESR.

According to Alcoa & CBBC (2011), the ESR methodology raised certain questions, related to the determination of the scope and the boundaries of the considered industrial system, the understanding of some Ecosystem Service categories where the relationship with other ecosystem services made it difficult to discriminate impact and dependence.

Finally, Olsen et al. (2011) examined the benefits of Rio Tinto's plan to support the conservation of approximately 60,000 hectares of lowland rainforest in Madagascar in order to compensate in part for the unavoidable residual impacts of its mining mineral sands operations on the region. This plan is part of Rio Tinto's policy goal of net positive impact (NPI) on biodiversity in its operations. The analysis covered the biodiversity and ecosystem services of a large part of Tsitongambarika, the largest expanse of lowland humid forest remaining in southern Madagascar, and aimed to quantify and value changes in ecosystem services resulting from proposed interventions. The considered ecosystem benefits were: wildlife habitat, hydrological regulation and carbon storage, while the costs of conservation included up-front investment and maintenance costs of protected areas, as well as lost opportunity costs that local people bear when they lose access to land that has historically provided food and cash income, and a resource for agricultural expansion. Furthermore, the study concluded that there were significant net economic benefits associated with conservation, mainly due to carbon storage benefits.

4 DISCUSSION AND CONCLUDING REMARKS

Mining projects, like other human activities, may have significant impacts on Ecosystem Services, and, consequently, on human well-being. There are strong arguments in the

literature that support the need to incorporate Ecosystem Services in environmental assessments, at all levels of decision-making. Nevertheless, the process is still in its infancy.

There are, so far, certain weaknesses, as an accurate understanding of not only concepts such as ecological process, biodiversity or of ecosystem service itself, but also of its classification is required (Rosa and Sanchez, 2013). The literature provides different classifications of Ecosystem Services with notable differences is some cases. In addition, there are certain inconsistencies with regard to the implementation of the environmental assessment process in mining activities within different countries, which further complicate the implementation of ESA. In order to improve this situation, a more consolidated methodological framework will have to be established based more on globally standardized classifications than on the legislation and the characteristics of each country.

Due to the aforementioned reasons the applications of ESA in strategic and policy environmental assessment in general and in mining sector in particular are quite limited. Nevertheless, the mining sector should become more familiar with the concept of Ecosystem Services not only because it becomes mainstream in several standards and requirements of governmental and other organizations, but also because it may help in successful conflict management and negotiations within the permitting and social licensing processes.

REFERENCES

Alcoa and Canadian Business and Biodiveristy Council, 2011. *Ecosystem services review of an aluminum smelter in a biosphere reserve*, Canadian Business and Biodiversity Council. Available from: http://www.businessbiodiversity.ca/documents/10-Alcoa.pdf

Baker, J., Sheate, W.R., Phillips, P., and Eales, R., 2013. Ecosystem Services in environmental assessment - Help or hindrance? *Environmental Impact Assessment Review*, 40, pp. 3-13.

Boyd, J. and Banzhaf, S., 2007. What are Ecosystem Services? The need for standardized environmental accounting units, *Ecological Economics*, 63(2-3), pp. 616–626.

Bridge, G. (2004). CONTESTED TERRAIN: Mining and the Environment, *Annual Review of Environment and Resources*, 29(1), pp. 205-259.

Carpenter, S.R., Mooney, H.A., Agard, J., Capistrano, D., Defries, R.S., Díaz, S., Dietz, T., Duraiappah, A. K., Oteng-Yeboah, A., Pereira, H. M., et al. (2009). Science for managing ecosystem services: Beyond the Millennium Ecosystem Assessment, *Proceedings of the National Academy of Sciences of the United States of America*, 106(5), pp. 1305-1312.

Chan, K.M.A., Satterfield, T., and Goldstein, J., 2012. Rethinking Ecosystem Services to better address and navigate cultural values, *Ecological Economics*, 74, pp. 8-18

Convention on Biological Diversity (CBD), 2004. *The Ecosystem Approach (CDB Guidelines)*, Secretariat of the Convention on Biological Diversity, Montreal, 50 p.

Costanza, R., d'Arge, R., Groot, R. de, Farber, S., Grasso, M., Hannon, B., Limburg, K., Naeem, S., O'Neill, R. V., Paruelo, J., et al., 1997. The value of the world's ecosystem services and natural capital. *Nature*, 387(6630), pp.253-260.

Damigos, D., 2006. An overview of environmental valuation methods for the mining industry, *Journal of Cleaner Production*, 14, pp. 234-247.

de Groot, R., Brander, L., Ploeg, S. van der, Costanza, R., Bernard, F., Braat, L., Christie, M., Crossman, N., Ghermandi, A., Hein, L., et al., 2012. Global estimates of the value of ecosystems and their services in monetary units, *Ecosystem Services*, 1, pp. 50-61.

de Groot, R.S., Alkemade, R., Braat, L., Hein, L., and Willemen, L., 2010. Challenges in integrating the concept of Ecosystem Services and values in landscape planning, management and decision making. *Ecological Complexity*, 7(3), pp. 260-272.

DEFRA, 2007a. *Case study to develop tools and methodologies to deliver an ecosystems approach-Heysham to M6 link DEFRA research project nr0110*. Available from: http://randd.defra.gov.uk/Document.aspx?Document=NR0110_7329_FRA.pdf.

DEFRA, 2007b. *An introductory guide to valuing ecosystem services*. Available from: https://www.gov.uk/government/uploads/system/uploads/attachment_data/file/191502/Introductory_guide_to_valuing_ecosystem_services.pdf

Fisher, B., Turner, K.R., Morling, P.. 2009. Defining and classifying Ecosystem Services for decision making, *Ecological Economics*, 68(3), pp. 643–653.

Geneletti, D., 2011. Reasons and options for integrating Ecosystem Services in strategic environmental assessment of spatial planning.

International Journal of Biodiversity Science, Ecosystem Services & Management, 7(3), pp.143–149.

Global oil and gas industry association for environmental and social issues (IPIECA) and International Association of Oil and Gas Producers (OGP), 2011. *Ecosystem Services guidance: Biodiversity and Ecosystem Services guide and checklists*. Available from: http://www.ipieca.org/publication/ecosystemservices-guidance

Haines-Young, R. and Potschin, M., 2013. *Common International Classification of Ecosystem Services (CICES): Consultation on Version 4*, August-December 2012. EEA Framework Contract No EEA/IEA/09/003.

Honrado, J. P., Vieira, C., Soares, C., Monteiro, M. B., Marcos, B., Pereira, H. M., & Partidário, M. R., 2013. Can we infer about Ecosystem Services from EIA and SEA practice? A framework for analysis and examples from Portugal. *Environmental Impact Assessment Review*, 40, pp. 14-24.

Imber, D., Stevenson, G., and Wilks, L., 1991. *A contingent valuation survey of the Kakadu Conservation Zone*. RAC Research Paper N.3, February, Resources Assessment Commission, Canberra.

International Finance Corporation (IFC), 2012. *IFC in Oil, Gas, and Mining*. Available from: http://www.ifc.org/wps/wcm/connect/fc9093804cef7376919dd5f81ee631cc/IFC+Issue+Brief_AM12_Extractives+9.20.12.pdf?MOD=AJPERES

International Finance Corporation (IFC), 2014. Oil, Gas and Mining. Available from: http://www.ifc.org/wps/wcm/connect/corp_ext_content/ifc_external_corporate_site/annual+report/2014_online_report/global_results/industry_results/ar14_results_industry_ogmc

International Finance Corporation (IFC), unknown. *IFC Global Mining*. Available from: http://www.ifc.org/wps/wcm/connect/434c0a0049a5f8cda3d0e3a8c6a8312a/IFC+Mining+Overview.pdf?MOD=AJPERES

Karjalainen, T. P., Marttunen, M., Sarkki, S., and Rytkönen, A. M., 2013. Integrating Ecosystem Services into environmental impact assessment: An analytic-deliberative approach. *Environmental Impact Assessment Review*, 40, pp. 54-64.

King, H., 2013. *Introducing an ecosystem services approach to quarry restoration*, Cranfield University, Cranfield.

Landsberg, F., J. Treweek, M.M. Stickler, N. Henninger, and O. Venn. 2014. *Weaving Ecosystem Services Into Impact Assessment Technical Appendix (Version 1.0)*. Washington, DC: World Resources Institute. Available at: http://www.wri.org/publication/weaving-ecosystem-services-into-impactassessment

Landsberg, F., S. Ozment, M. Stickler, N. Henninger, J. Treweek, O. Venn, and G. Mock. 2011. Ecosystem Services Review for Impact Assessment: Introduction and Guide to Scoping. *WRI Working Paper*. World Resources Institute, Washington DC. Available from: http://www.wri.org/publication/ecosystemservices-review-for-impact-assessment

Larondelle, N. and Haase, D., 2012. Valuing post-mining landscapes using an ecosystem services approach-An example from Germany, *Ecological Indicators*, 18, pp. 567-574.

London Economics, 1998. *The environmental costs and benefits of the supply of aggregates*, Report to the Department of Environment, Transport and the Regions, DETR, London.

London Economics, 1999. *The environmental costs and benefits of the supply of aggregates (Phase 2)*, Report to the Department of Environment, Transport and the Regions, DETR, London.

Maes, J., Teller, A., Erhard, M., Liquete, C., Braat, L., Berry, P., Egoh, B., Puydarrieux, P., Fiorina, C., Santos, F., et al., 2013. *Mapping and Assessment of Ecosystems and their Services. An analytical framework for ecosystem assessments under action 5 of the EU biodiversity strategy to 2020*. Publications office of the European Union, Luxembourg.

Millennium Ecosystem Assessment (MEA), 2005. *Ecosystems and human well-being: our human planet-Summary for decision makers*, Island Press, Washington, DC.

Moffat, K. and Zhang, A., 2014. The paths to social licence to operate: An integrative model explaining community acceptance of mining. *Resources Policy*, 39(1), pp. 61-70.

Munn, R.E., (ed.) 1979. *Environmental impact analysis. Principles and procedures*, 2nd ed. John SCOPE Report No. 5, Wiley and Sons Chichester, 190 p.

NER, 2010. *Valuation of Ecosystem Services and strategic environmental assessment: lessons from influential cases*. Available from: https://www.cbd.int/impact/case-studies/cs-impact-nl-sea-valuation-en.pdf

OECD, 2008. Strategic environmental assessment and Ecosystem Services. DAC Network for Environment and Development Co-operation (ENVIRONET) *Strategic environmental in assessment Ecosystem Services*. Available from: http://www.oecd.org/dataoecd/24/54/41882953.pdf.

Olsen, N., Bishop, J. and Anstee, S., 2011. *Exploring Ecosystem Valuation to Move Towards Net Positive Impact on Biodiversity in the Mining Sector*, IUCN and Rio Tinto Technical Series No. 1. IUCN, Cland, vii + 41pp.

Owen, J.R. and Kemp D., 2013, Social License and Mining: A Critical Perspective, *Resource Policy*, 38, pp. 29-35

Prno, J. and Scott Slocombe, D., 2012. Exploring the origins of "social license to operate" in the mining sector: Perspectives from governance and sustainability theories, *Resources Policy*, 37(3), pp. 346-357.

Prno, J., 2013. An analysis of factors leading to the establishment of a social licence to operate in the mining industry, *Resources Policy*, 38(4), 577-590.

Rosa, J.C.S. and Sanchez, L.E., 2013 . Revisiting the EIS of a mining project using ecosystem services, *Impact Assessment the Next Generation 33rd Annual Meeting of the International Association for Impact Assessment IAIA13*, Calgary, pp. 1-5.

Slootweg, R., A. Kolhoff, R. Verheem, and R. Höft. 2006. *Biodiversity in EIA and SEA, Background Document to CBD Decision VIII/28: Voluntary Guidelines on Biodiversity-Inclusive Impact Assessment*. Netherlands Commission for Environmental Assessment. Available from: http://www.cbd.int/doc/publications/imp-bio-eia-and-sea.pdf

TEEB, 2010. *The Economics of Ecosystems and Biodiversity: Ecological and Economic Foundation*, Earthscan, London.

TEEB, 2011. *The Economics of Ecosystems and Biodiversity in National and International Policy Making*, Earthscan, London.

Telfer, T.C., Atkin, H. and Corner, R.A., 2009. Review of environmental impact assessment and monitoring in aquaculture in Europe and North America. In FAO. Environmental impact assessment and monitoring in aquaculture. *FAO Fisheries and Aquaculture Technical Paper*. No. 527. Rome, FAO. pp. 285–394.

UNEP, 2014. *Integrating Ecosystem Services in Strategic Environmental Assessment: A guide for practitioners*, Report of Proecoserv. Geneletti, D.

Wallace, K.J., 2007. Classification of Ecosystem Services: problems and solutions, *Biological Conservation*, 139(3-4), pp. 235–246.

Energy Spectrum In India

B. Prasad
CMPDIL, a subsidiary of Coal India Limited, Ranchi, India

R. Prasad
Colorado School of Mines, CO, USA

ABSTRACT This paper presents a comprehensive review of energy sources in India such as Coal, Lignite, Natural Gas, Crude Oil, Hydro Power, Nuclear Power and Renewables. First, we look at how share of each fuel in total energy production and consumption in India is varying from 2000-01 to present and their projections until 2021-22. Then, we analyse each of the different energy source by examining its reserve, historic and projected demand, consumption and production. Further, we discuss key challenges and opportunities emerging in each of these sources. Finally, we discuss implications of energy security and environmental aspects on the development of various energy sources. This comprehensive analysis of each of these major energy sources leads us to the fact that despite the need to develop renewable and alternate energy sources in view of long-run sustainability, our dependence on primary energy sources especially coal is irreversible in the long-run.

Keywords: Energy Sources, India, energy security, environmental aspects

1 INTRODUCTION

As energy consumption level is generally known to be a certain indicator of rise in living standard in context of modern industrial civilization, it is even more important for emerging economies like India, to meet the ever-increasing energy requirements to meet the development needs. With burgeoning population, particularly in emerging economies like India, it is imperative to develop energy resources to meet the energy requirements and developmental needs of the country with due emphasis of sustainability.

2 WORLD ENERGY SCENARIO

World energy consumption is expected to increase from 524 quadrillion Btu in 2010 to 630 quadrillion Btu in 2020 and 820 quadrillion Btu in 2040. The current share of coal in global power generation is over 40%. Global oil reserves are almost 60% larger today than 20 years ago, and the production of oil has gone up by 25%. If the unconventional oil resources, including oil shale, oil sands, extra heavy oil and natural bitumen are taken into account, the global oil reserves will be four times larger than the current conventional reserves.

3 INDIAN ENERGY SCENARIO

Though India is the fourth largest consumer of electricity after China, USA and Russia, its per capita energy consumption was 585 kilograms of oil equivalent (kgoe) in 2009, far lower than the global average of 1797 kgoe. Total primary commercial energy demand is expected to reach 937.26 million tons of oil equivalent (mtoe) in 2016-17 and 1219.76 mtoe by 2021-22. Coal, followed by Crude Oil and Natural Gas continue to be major fuel sources even until 2021-22 to meet this energy demand.

However, only 669.5 mtoe is expected to be met by domestic production with the remaining 267.76 mtoe by imports in 2016-17.

Table 1. Share of each fuel in total energy consumption in India

	2000-01	2006-07	2011-12	2016-17
Coal & Lignite	50.36	53.22	53.45	55.41
Crude Oil	37.45	33.41	31.51	26.04
Natural Gas	8.49	6.99	10.32	13.46
Hydro Power	2.17	2.53	2.17	1.79
Nuclear Power	1.49	1.24	1.57	2.26
Renewable Energy	0.04	0.22	0.98	1.43

3.1 Coal and Lignite

Coal (including lignite) is the mainstay of India's energy sector and accounted for over 58% of total installed electricity generation capacity of 223344 MW as on 31.03.2013 and occupies a share of 79% of total electricity capacity addition target of 118,537 MW for 12th FYP to support the targeted 9% GDP growth rate. By 2016-17, coal requirement to meet the forecasted consumption by various sectors by works out to around 980.5 MT. With increasing demand for energy and absence of coal deposits in Indian states of Tamilnadu, Gujarat, Rajasthan, Pondicherry, Jammu & Kashmir and Kerala, these states will benefit with the exploitation of their lignite reserves as they are facing high transportation costs in transporting coal from far off coal fields.

3.1.1 Reserves

The total updated geological reserves of Coal stands at 293.497 billion tonnes as on 01.04.2012 up to a depth of 1200m and that of Lignite at 40.91 billion tonne. Critical analysis reveals that reserves position in the long-term perspective is far from satisfactory. Tamilnadu has 80.41% of the Indian Lignite reserves. Also, there has been significant increase in proved Lignite reserves in recent years increasing the potential for immediate exploitation of reserves. Category-wise coal & lignite resources, as per Geological Survey of India (GSI), as on 01-04-2012, are given in Table-2.

Table 2. Coal & Lignite Reserves in India (In Billion Tonne)

	Proved	Indicated	Inferred	Total
Coal	118.15	142.17	331.84	293.5
Lignite	6.15	25.79	8.97	40.91

3.1.2 Production

During the 11th FYP (2007-12), the growth in all India coal production showed an increasing trend in the first three years. However, in 2010-11, the production growth was not the expected mainly due to delay in Forestry & Environmental Clearances (FC & EC), besides land acquisition, Rehabilitation and Resettlement (R&R) and coal evacuation. In 2013-14, all India raw coal production is 565.64 MT as against the target of 604.55 MT. Coal production is projected to increase at a Compound Annual Growth Rate (CAGR) of 7.57% during 2012-17 and reach 795 MT in 2016-17. Coal production across the terminal year of plan periods is shown in Figure-1. Lignite is projected to be 68.60 MT by 2016-17 and 104.55 MT in 2021-22.

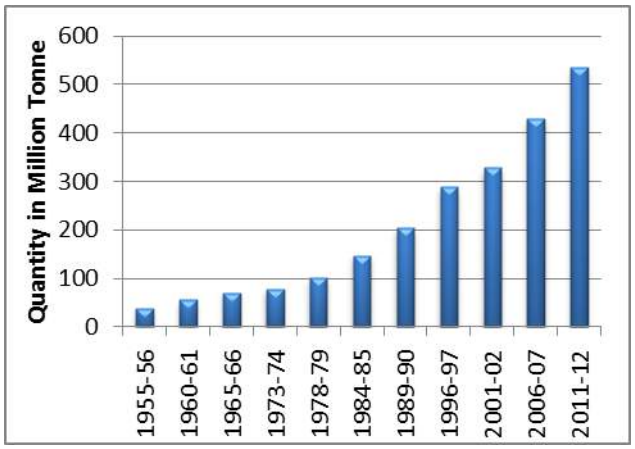

Figure 1. Coal Production

3.1.3 Demand

The demand for coal is projected to reach about 980 MT in 2016-17 Sector-wise coal demand is shown in Figure-6. Going forward, the demand projection for 2021-22 is 1373 MT. The demand for Lignite is projected to reach 71.96 MT during 2016-17 and 108.62 MT by 2021-22.

3.1.4 Demand-supply gap

In 2016-17, a supply-demand gap of 265.50 MT is projected comprising of 35.50 MT of coking coal and 230.00 MT of non-coking coal. The supply-demand position for 2016-17 is shown in Table-6. Of the total 10.14 MT shortfall in lignite production during the total twelfth plan period, Gujarat state will face a highest shortfall of 9.00 MT.

Table 3. Supply-Demand position of Coal in 2016-17 (in MT)

Source	Coking	Non-Coking	Total
Demand	67.20	913.30	**980.50**
Availability			
CIL	15.74	540.66	556.40
SCCL	0.00	57.00	57.00
Others	15.96	85.64	101.60
Indigenous	31.70	683.30	**715.00**
Gap(-)	35.50	230.00	**265.50**

3.1.5 Challenges in coal production

Although, India's coal demand increased at a CAGR of 8.5% during 2007-11, CIL's production increased at CAGR of 4.6% only. While time consuming procedures to obtain environmental clearances from MOEF and land from state governments being the primary reason for the slow growth in production, this shortage would continue to be a serious issue for the energy security of India.

a. Coal Imports

As mentioned earlier, coal imports are projected to reach 265.50 MT by 2016-17. The major import sources of thermal coal are Indonesia and South Africa. Indonesia contributes to 70% of India's thermal coal import. In the recent past, there have been regulatory changes in the nations like Indonesia. Thus coal imports from Indonesia are expected to face a hit. For coking coal import, Australia is the primary destination. It accounts to more than 80% of India's coking coal imports. Australia has recently proposed Mineral Resources Rent Tax (MRRT) which would increase cost of Australian coal. This is expected to impact Indian steel industry. Thus it is very important for India to diversify its import sources. Moreover, coal imports have concerns around limited supporting infrastructure, huge price difference between imported and domestic coal and changing regulations in the source countries.

b. Acquisition of Foreign Coal Assets

With a large number of captive coal blocks allotted being struck in obtaining various clearances for mining, companies are depending mostly on coal imports. India is facing stiff competition from other Asian economies like Japan, South Korea and China in terms of coal imports. It is therefore, necessary to secure sustainable supply of coal through available options such as long term off-take contracts with coal producers and overseas acquisition of assets

At present Coal India Ltd. has only two blocks in overseas. It is currently conducting drilling operations to assess the size and quality of the fuel in Mozambique. It has also signed an initial agreement with South Africa's Limpopo provincial government for exploring the possibility of developing coal mines. But, acquisition of coal assets in foreign countries by domestic mining players is fraught with its own set of challenges. Locating quality mines, managing supply chains, reducing financial risks and recognizing external risks are important to make an acquisition succeed.

c. Investment

Coal mining is virtually closed for private sector except for captive mining purposes. But to meet the burgeoning demand for coal, there is a need to bring in new technologies and modern mining methods to improve productivity and sustainability of operations. Competition among the players will help improve performance.

d. Infrastructure

Lack of proper road connectivity, railway wagons, 24/7 availability of power, port facilities, have put brakes on the growth of coal mining industry in India. Further, there are concerns that there are very limited

manufacturers of mining equipment and machinery in the country. Hence, there is a need for indigenous development of mining equipment with government support through R&D funding to technical institutes.

e. Policy issues

There is a pressing need for adequate regulatory interventions to ease out the various concerns plaguing the sector. Major concerns such as land acquisition and R&R, environment and forest clearances, institutionalization of coal regulator can be alleviated to a significant extent with dynamic policy framework.

f. Quality of Coal & Washing

Another major problem associated with Indian coals is its high ash content (15-45%) and low calorific value. There is an urgent need for introducing new techniques and technologies for beneficiating Indian high ash coals. Dry ash beneficiation is one of the promising areas which is now being considered by Indian coal producing companies for their adoption.

3.1.6 Challenges in lignite production

a. Technological Constraints

Currently available technology for lignite mining in India is not suitable for production below 150 meters. With 80% of lignite reserves being below 150 meters in India, there is a need for upgradation of technology to extract deeper deposits of up to 300m under tough geo-mining conditions.

b. Land Acquisition

While opencast mining being the only viable option for lignite mining and with majority of the lignite reserves in Tamil Nadu and Gujarat are under fertile agriculture land with thick population, land acquisition has become a major concern.

c. Regulatory issues

With the requirement of tariff based competitive bidding route to set up lignite based thermal projects, there is an increased difficulty in getting faster clearance for lignite projects.

3.1.7 Ways to increase coal supplies

a. Exploration is considered a risky venture. So Govt. must encourage investments in this sector through proper incentives and security of tenure.
b. Taking action on pending mining applications within a time bound manner i.e. by imposing a time limit for clearing an application.
c. At present, all related subjects such as land, water, mineral, environment and forest etc. are administered by different departments and ministries as a result of which processing of mining applications is becoming very complex. So a Single Window Clearance Agency (SWCA) could bring speed in decision-making and application processing.
d. A lot of mining leases have been granted in the past comprising of small areas to individuals. The mine owners are not able to develop them economically and would like to dispose of these areas. States may allow transferring these assets at a premium so that these dormant assets can be developed to increase supply in domestic market, leading to the utilization of dormant resources.
e. The exploration and exploitation of minerals requiring huge capital should be extended to experience the same benefits and incentives that are available to the Oil & Gas sector under the new Exploration Licensing Policy (NELP).

3.2 Natural Gas

Last decade has showed growth in Indian gas sector and has slowly emerged as one of the primary source of energy for India along with coal and oil. As on 31.03.2012, total gas-based power generation capacity of 20110 MW accounts for 9% of total installed capacity in India.

3.2.1 Reserves

Natural Gas (NG) reserves in India have grown at a CAGR of 2.63% from 1100.99 billion cubic meters in 2005 to billion cubic meters 1354.76 in 2013.

3.2.2 Production

The total domestic gas availability during is expected to increase from 124 Million Metric Standard Cubic Meter per Day (MMSCMD) in 2012-13 to 209 MMSCMD in 2016-17.

3.2.3 Demand

Demand for natural gas in India is expected to grow at a very rapid rate. Demand is expected to increase from 194 MMSCMD to 473 MMSCMD during the period 2011-2012 to 2016-2017.

3.2.4 Demand-supply gap

With increasing demand, dependence on imports is increasing steadily because of limited domestic supplies as shown in Table-4.

Table 4. Demand-Supply Gap of NG

(MMSCMD)	2012-13	2013-14	2014-15	2015-16	2016-17
Supply	124	149	170	177	209
Imports	63	87	87	129	150
Demand	**187**	**236**	**257**	**306**	**359**

3.2.5 Challenges

1. Due to a limited investment from foreign companies as evidenced in recent NELP bidding rounds, there is a delay in bringing technological expertise, diverse project experience.
2. With ambiguity over the gas pricing issues and a lack of predictive policy framework, it is getting difficult to increase participation by foreign companies.
3. Mature gas fields like PannaMukta Tapti, Bassein and Niko have declining production levels.

3.2.6 Opportunities

1. The Indian sedimentary basins and deep water areas largely remain unexplored which indicates the potential for large hydrocarbon discoveries. This creates opportunities for the investors possessing relevant technical expertise.
2. The CBM Policy devised by Government of India encourages investment and provides favourable investment climate like freedom to sell CBM in the domestic market, infrastructure status exemption from payment of customs duty on imports required for CBM operations and fiscal stability.
3. According to US Energy Information Administration in April 2011, India has technically recoverable shale gas resources of nearly 63 trillion cubic feet.
4. Underground Coal Gasification (UCG) has been notified as one of the end uses under the government captive mining policies and these projects requires technical expertise that none of the domestic companies possess at present which provides a good space for investment.
5. A decline in the domestic gas supply along with increase in the gas demand has created opportunities for developing LNG import facilities, providing opportunities to investors, service providers, equipment suppliers and Engineering, Procurement and Construction (EPC) contractors.

3.3 Crude Oil

With only 0.5% of world's proven oil reserves and 15% of world's population, pressure on increasing crude oil production to meet the exploding demand for energy has placed Crude Oil one of the sought over energy sources available in India.

3.3.1 Reserves

Crude Oil reserves in India have reduced from 786.04 Million Metric Tonne (MMT) in 2005 to 758.27 MMT in 2013 as shown in Figure-2.

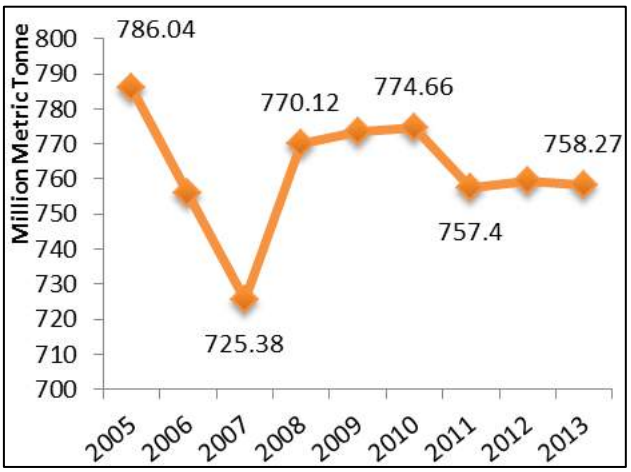

Figure 2. Crude Oil Reserves in India

3.3.2 Production

Supply of petroleum products/crude oil is likely to increase from 42.305 Million Metric Tonne Per Annum (MMTPA) in 2012-13 to 41.156 MMTPA in 2016-17.

3.3.3 Demand

Demand for petroleum products is likely to increase from 147.997 MMTPA in 2011-12 to 186.209 MMTPA in 2016-17 at a CAGR of 4.7%.

3.3.4 Demand-Supply Gap

Over the 12th Five Year Plan period, the growth in domestic production is not sufficient to meet the projected demand. This results in increasing dependence on imports, with the share of crude imports increasing from around 76.6% in 2011-12 to 77.8% in 2016-17 as shown in Table-5.

Table 5. Crude Oil Demand-Supply Gap (in MMTPA)

Year	2012-13	2013-14	2014-15	2015-16	2016-17
Supply	42.3	45.6	44.8	42.6	41.2
Demand	152.9	160.4	168.6	177.0	186.2
Gap(-)	110.6	114.8	123.8	134.4	145.0

3.3.5 Challenges

1. Upstream skills, technology and equipment shortage are some of the major issues faced by the industry. The industry is especially pressed with the shortfall of technical and experienced personnel like Reservoir engineers.
2. Only half of the country's potential basins have been explored, and large blocks offshore remain untested, especially in deep water.

3.3.6 Opportunities

1. Most of the existing refineries in India are old and need massive investment to make them complaint with the stringent fuel emissions norms introduced in India. Refinery capacity additions also will require the setting up of new pipelines in India or increasing capacities of the existing ones.
2. India offers huge opportunities for equipment supplies of Exploration and Production (E&P) industry. Companies like Oil and Natural Gas Corporation (ONGC) and Oil India Limited (OIL) are investing heavily in Increased Oil Recovery (IOR) and Enhanced Oil Recovery (EOR) techniques.

3.4 Hydro Power

Being a renewable and clean source of energy, the vast hydro-power potential can be harnessed with due consideration for ecology conservation. Moreover, given the operational flexibility of hydro-power plants, it can be used to meet peak demand scenarios.

3.4.1 Hydropower potential in India

As per the reassessment studies undertaken by the Central Electricity Authority (CEA) in 1978-87, India's total theoretical hydropower potential at 60% load factor was assessed as 301,117 MW and the economic potential at 84,044 MW.

3.4.2 Hydro-based capacity addition

During 2007-11, only 5544 MW of hydro-based power generation capacity is installed as against the target of 15,627 MW. Private companies have lagged behind the state-run

units in meeting their targets. The total installed hydro-based capacity as on 31.03.2013 is 39491 MW, occupying 18% of total all India generation capacity. India is planning to add 9204 MW Hydro capacity by 2016-17. The sector-wise break-up of this capacity addition requirement is shown in Table-6. North-East has a huge potential for hydro power of around 50,000 MW, challenges related to the evacuation of power has made the progress in this area very slow.

Table 6. Hydro Capacity Addition Target during 2012-17 (in MW)

Sector	Central	State	Private	Total
	5632	1456	2116	9204

3.4.3 Challenges

1. With significant land requirement for large plants, land Acquisition is a major constraint in undertaking various hydro-power projects.
2. Because of increasing public resistance due to relocation, R&R issues have become another major constraint.
3. Delays in EC&FC are leading to increase in already high capital expenditures.
4. Limited transmission and evacuation infrastructure in high hydro-power potential areas.

3.4.4 Opportunities

1. Nearly 95% of the hydro-potential is north-eastern states of India is untapped.
2. Given the need for robust engineering services to undertake projects in more difficult terrains, there is a great market opportunity ahead for EPC contractors and technology providers.
3. With the sector offering option of 100% foreign equity, this sector remains attractive for investors looking for higher returns over a long term of 30 to 50 years.

3.5 Nuclear Power

Nuclear power is economically competitive and therefore can provide large base load generation. It contributes to de-carbonization of power sector, being devoid of greenhouse gas emissions, with lifecycle emissions comparable with hydro and wind power.

3.5.1 Nuclear power potential in India

Though India has only 1.5% (as of 2009-Wikipedia) of global Uranium reserves, it accounts for 1/3rd of global reserves of Thorium. India's three-stage nuclear power programme formulated by Dr.Homi Bhabha considers both the Uranium and Thorium reserves. With the known uranium reserves, first-stage programme can generate about 10,000 MW based on Pressurised Heavy Water Reactors (PHWRs). This potential can be increased by another 20,000 MW in the second-stage programme based on Fast Breeder Reactors (FBRs). Utilizing Thorium in the third-stage reactors the energy potential is very high. The stage-wise Nuclear Energy Potential based on domestic resources is as given in the Table-7

Table 7. Stage-wise Nuclear Energy Potential in India

Particulars	Stage	Reserves	Electricity
			MW
Uranium Metal			
In PHWR	I	170,000-t	10,000
In FBR	II		5,00,000
Thorium-Metal		2,25,000-t	
In Breeders	III		Very Large

3.5.2 Nuclear power generation

Nuclear power generation in India has increased 18634 GWh in 2006-07 to 25471 GWh in 2013-14 (upto December 2013).

3.5.3 Capacity addition

As on 31.03.2013, India has 4780 MW of Nuclear-based generation capacity and is planning to add 2800 MW nuclear based capacity during 2012-17.

3.5.4 Challenges

1. High Capital Investment and rising compliance costs have been hindering the speedy execution of new projects.
2. Public concern about plant operations and final waste disposal is delaying the clearances issued by the government.
3. Increasing concerns by foreign equipment suppliers regarding liabilities in case of nuclear accident is delaying the procurement of equipment.
4. There is no nuclear insurance pool in India, apparently due to restrictions on inspection of facilities by international pools.

3.5.5 Opportunities

1. With increasing positive signs of international cooperation, new opportunities in the area of import and export of nuclear goods, equipment and services will open up.
2. With designs of nuclear power plants becoming more effective, cost of electricity generated is competitive.
3. Cost of nuclear fuel is low because of the use of domestic thorium.
4. Economics of nuclear power generation can be improved significantly if plants are built away from coal reserves i.e. in north-western, western and southern India.

3.6 Renewables

Renewables generally include Wind, Small Hydro, Biomass Power, Waste to Energy, Bagasse Cogeneration and Solar Power. Of these sources of energy, Wind based energy generation is occupying a major share in the country.

3.6.1 Capacity addition

During 2007-11, 14,661 MW of capacity has been added through Grid Interactive Renewable Power.

3.6.2 Cost of renewable electricity generation

Cost of solar based power generation is the highest among the renewables at around 10.39-12.46 Rs/kWh and small hydro based power generation is the lowest at 3.54-4.88 Rs/kWh. The estimated cost of electricity generation for various renewable sources is shown in the Table-8.

Table 8: Cost of Power for Various Renewable Energy Sources

Source	Estimated initial Capital Cost (Crore Rs./MW)	Estimated cost of electricity generation (Rs. /kWh)
Small Hydro Power	5.50-7.70	3.54-4.88
Wind Power	5.75	3.73-5.96
Biomass Power	4.0-4.45	5.12-5.83
Bagasse Cogeneration	4.2	4.61-5.73
Solar Power	10.00-13.00	10.39-12.46

3.6.3 Capacity addition requirement

As per the norms laid out by The National Action Plan for Climate Change (NAPCC), share of renewables in electricity mix should reach 12% by 2016-17. Given the present installed capacity of 24,503.45 MW (CEA), there is a requirement of 30,000 MW of capacity addition to meet those norms.

3.6.4 Challenges

1. Solar P.V. key challenge

a. PV technology is less amenable to very large scale and widespread grid connectivity due to bottlenecks in storage and hence the ability to have a flexible dispatch schedule.
b. The performance of the modules depends significantly on the manufacturer of the cells and the module. The ability of the developer to improve the cost & performance is limited.

2. Solar Thermal-key challenge

a. There is presently negligible indigenous manufacturing capability for Concentrated Solar Power (CSP) projects and have to be sourced from few global manufacturers.
b. Solar thermal installations, which require large amounts of dedicated land, are competing with other necessities that require land as well.
c. Presently, there are no installed CSP projects in the country. Thus, project management and installation capability are questionable.

3. Biomass key challenges

a. Unlike other Renewable Energy technologies, biomass technology requires feedstock as fuel for power plant, entailing an additional and significant cost to the project developer.
b. High and fluctuating cost of biomass is a major issue in this sector. The cost of biomass has almost doubled in the last 5 years.

4. Hydro-power challenges

Small Hydro power (SHP) projects are location specific, varying significantly in costs and feasibility depending upon topography, hydrology, geology and approachability. Despite support from government by the way of financial support and other policy incentives, SHP has not made significant progress due to the above said technical challenges as well as procedural challenges.

5 Grid integration has become a serious challenge to readily start more projects.
6 Lower subsidies and growing material input costs is another major issue in wind based power generation.

3.6.5 Opportunities

Steadily, India is looking to build a strong renewable energy portfolio in coming years. Government of India (GOI) is offering a number of incentives to accelerate investment in Renewable energy space. The renewable purchase obligations (RPO) requirements set by state regulators and REC mechanism is expected to create demand for renewable energy across solar and non-solar sources. In addition, several benefits like accelerated depreciation, preferential tariff and generation based incentives offer attractive incentives to the investors in renewable energy.

a. Solar

There is an emphasis on setting up manufacturing capacity of 2500 MW of solar cells/ modules and 2500 MW equivalent capacity of components/sub-systems of solar thermal power plants by 2016-17. With this, we can expect the cost of solar cells/modules and components of power plants to come down and thus cost of producing energy may decrease. The recent solar bids concluded are an indication that the players are becoming increasingly competitive in this space.

b. Bio-mass

The GOI has announced a proposed “biomass mission” in late 2011 which may target the installation of 1600MW of biomass power by 2020. This is likely to provide ample opportunities to investors. In light of the ever rising demand for biomass feedstock, energy plantations and captive generation can become promising business opportunities in the biomass sector.

c. Small Hydro Power (SHP)

Since SHP is an old and matured industry, there are large number of SHP units, requiring renovation and modernization.

4 ENERGY SECURITY

The policy and planning is largely controlled by the central government in India’s federal political set up. According to the Indian Energy Policy report of 2006, the country’s hydrocarbon resources will be grossly inadequate to meet its demand. The government has taken certain steps to build infrastructure for energy security.

4.1 Strategic Petroleum Reserves

GoI has set up the Indian Strategic Petroleum Reserves Ltd (ISPRL), which is building three huge underground caverns that can hold beneath the earth that can hold 14 days' worth of oil. Moreover, the new facilities will have a combined capacity of 39 million barrels.

4.2 Overseas Acquisition in O&G

India has carefully entered into cooperative relationships with several oil-producing countries in Africa and the Middle East.

The ONGC Videsh Ltd (OVL) has invested 11 billion USD abroad. In addition, a number of other investors, both public sector undertakings and private players, have also invested in 50 other projects in 19 countries. The OVL oil equity so far accounts for only 9% of India's current oil import requirements. If these assets were to meet at least 10% of the requirements in 2031-32, the investments will have to be increased six times. To import natural gas, LNG terminals have been set up at Dahej and Ratnagiri and a new one is under implementation at Kochi. Imports of 7.5 million tonne of LNG on a long-term supply basis for 25 years have been planned by Petronet LNG at Dahej under an agreement with Qatar. Another 1.5 million tonne has been planned through a tie up with Exxon Mobil for 20 years from Gorgan LNG project in Australia.

4.3 Overseas Acquisition in Coal

India will have to import large quantities of coal in the future. Though a number of private players have invested in mines in Indonesia and Australia, Coal Videsh, formed under the Ministry of Coal, has done very little business so far. Around 70% of 950,000 MW of power requirement in 2031-32 will be from coal. Thus, there is a need to give a very strong push to the mining investments abroad.

4.4 Sovereign Wealth Fund

The government proposed to set up a Sovereign Wealth Fund of 10 billion USD from the disinvestment proceeds to team- up with state-run companies for acquiring overseas raw material and energy assets including crude oil, gas and coal. The fund will be financed through the budget. Also, the budget division has proposed that large PSUs such as ONGC have reserves that can be used by this fund for acquiring energy assets aboard. This can be a second source of funding. The third source of funding can be the RBI's forex reserves. But this still needs to be debated, as the RBI may not be in favour of this.

4.5 Energy Efficiency

India's energy efficiency is the fifth-lowest in the world. Therefore, it is imperative to have a consistent energy policy, relentlessly pursue energy efficiency and conservation, maximise coal production, improve the rail and port infrastructure and develop alternative infrastructure for coal transportation such as coastal rivers.

5 ENVIRONMENTAL ASPECTS

The largest contributors of Greenhouse gases are power stations (many of which burn coal or other fossil fuels), industrial processes, transportation fuels (generally fossil fuels), and agricultural by-products (mainly methane from enteric fermentation and nitrous oxides from fertilizer use). Between 1750 and 2007, about two-thirds of anthropogenic CO_2 emissions were produced from burning fossil fuels, and about one-third of emissions from changes in land use. Rapidly advancing technologies can achieve a transition of energy generation, water and waste management, and food production towards better environmental and energy usage practices using methods of systems ecology and industrial ecology.

6 CONCLUSION

Considering the current generation capacities and future potential of various energy resources along with their associated challenges and opportunities, below mentioned are some of the issues which must be given due emphasis to meet India's energy needs and to become energy independent.

1. At the current level of coal production, proven coal reserves are estimated to last for over 100 years. Even though there is an increasing gap between demand and supply, coal-based energy is the most economic option. Thus, there is a need to quickly expand domestic production.
2. Around 35% of non-metallurgical coal reserves are occurring at a depth of 300-1200 m, to access these reserves there is a need for up gradation of technology in existing coal mines by introducing mass production technologies, particularly in underground mines with due consideration of environmental and social impacts.
3. There is a pressing need to undertake reforms in the areas of exploration, project formulation, clearances and licences.
4. With 12% of sedimentary area being unexplored and 22% being poorly explored, there is a need to increase the exploration activities to bring out more reserves. Also, deep water exploration is another important area to focus upon.
5. Strategic acquisition of foreign oil, gas and coal reserves should be given more emphasis by integrating our energy security interests into foreign policy decision through energy diplomacy.
6. Given the challenges associated with ensuring required supply of energy, there is a need to address energy demand by achieving desired level of energy efficiency.
7. There is a need to improve our regulatory framework to encourage investments in various energy sectors.
8. Unconventional energy sources must be given due priority by investing in infrastructure to facilitate the development of these sources like Coal Bed Methane, Underground Coal Gasification and Shale Gas.
9. Adoption of latest IT tools for effective utilization of human resources and machinery.
10. Highly efficient and flexible power plants with Carbon Capture and Storage Technologies have to be given due importance.
11. Thrust on nuclear energy with the use of substantial reserves of Thorium in India.
12. A clear cut policy on Coal to Liquid will help to reduce oil imports.
13. Measures to switching from oil to natural gas will lead to conservation of oil resources.
14. Strict vigilance and control over energy transmission and distribution losses will help in reducing energy imports.
15. There is an immediate need to take steps to reduce our dependence on energy imports as the imports is slated to reach $230 Billions (13.8 lakh crore rupees) in the next decade.
16. Develop smart grids and dedicated information technology to improve power supply of our now integrated national grid.
17. Absorb commercially available technologies like Integrated Gasification Combined Cycle (IGCC) to boost thermal efficiency and thereby boost generation.
18. Currently available technologies like supercritical and ultra-supercritical steam boilers must be given more emphasis than conventional pulverised coal technology.
19. There is also need for refitting and redesigning of commercially available technology, given the high ash content of our coals.

ACKNOWLEDGEMENT

The views expressed in this paper are those of the authors' and does not necessarily reflect those of the organization.

REFERENCES

- International Energy Outlook 2013
- 12th Five Year Plan Document-Planning Commission
- Geological Survey of India

- Working Group on Coal & Lignite for XII FYP
- India Energy Book 2012
- Indian Petroleum & Natural Gas Statistics (2012-13), Ministry of Petroleum & Natural Gas
- Report of the Working Group on Petroleum & Natural Gas Sector for the 12th Five Year Plan
- National Institute of Hydrology, Roorkee
- Central Electricity Authority
- Working Group on Power for 12th Five Year Plan
- World Nuclear Association
- Nuclear Power Corporation of India Ltd. (NPCIL)
- Ministry of New and Renewable Energy, GOI
- CERC (Terms and Conditions for Tariff Determination from Renewable Energy Sources) Regulations, 2012 dated 27 March 2012
- Ministry of New and Renewable Energy, GOI

Forecasting of Turkey's Coal Consumption Using Grey Prediction Technique

I. Karakurt, G. Aydin, S. Kaya
Karadeniz Technical University, Mining Engineering Department, Trabzon, Turkey

C. Hamzacebi
Karadeniz Technical University, Industrial Engineering Department, Trabzon, Turkey

ABSTRACT: Coal is by far the most plentiful energy resource in Turkey. Domestically produced coal accounts for more than half of the country's total energy production. Coal has been consumed primarily for power generation, steel manufacturing, and cement production. Due to its importance in country's energy balance, modeling and forecasting of coal consumption is an important issue for government, energy sector investors and other corporations in Turkey. In this study, therefore, coal consumption of Turkey was forecasted using a Grey modeling (1,1) technique. The data used in the study was composed of coal consumption in Turkey for the period of 1965-2013. Using these historical data, the coal consumption of Turkey was forecasted for the period of 2014-2025. Additionally, the performance of forecasting was measured using mean absolute percentage error (MAPE) and mean absolute error (MAE).

Keywords: Grey prediction technique, mean absolute percentage error, mean absolute error

1 INTRODUCTION

The world energy demand has rapidly risen as a result of social and economical growth, urbanization and economic expansion. Therefore, the uses of all kinds of energy increase over time, especially uses of fossil fuels are expected to continue supplying much of the energy used worldwide (Karakurt and Aydin, 2013).

The world benefits from a plentiful supply of coal. It has many uses critically important to economic development and poverty alleviation worldwide with the most significant being electricity generation, steel and aluminum production, cement manufacturing and use as a liquid fuel (Höök et al., 2010). Almost every country worldwide has coal reserves, however, approximately 70 of those has recoverable coal reserves. It remains abundant and broadly distributed around the world (Mason, 2007). Proved coal reserves in the world at the end of 2013 were 891531 million tons (Table 1). It is seen from Table 1 that world coal reserves can be distributed in thirds; one is located in North America (28.5 %), dominated by the United States; other is located in Europe&Eurasia (35.4%), dominated by Russia and the last is located in Asia Pacific (30.9%), dominated by China and Australia.

Turkey being a developing country with respect to population, industrialization and the economy, is growing rapidly. Its energy demand is continuously increasing with its growth. Studies on forecasting future energy requirements have shown that these requirements will continue to increase in the coming years (Kabak and Dağdeviren, 2014).

Among many energy resources, coal is by far the most plentiful energy resource in Turkey. Domestically produced coal accounts for more than half of the country's total energy production. Coal has been consumed primarily for power generation, steel manufacturing, and cement production (Karakurt and Aydin, 2013). In 2013, coal has the second place among primary energy

consumption of Turkey (see Fig.1). Due to its importance in country's energy balance, coal covers an important place for government, energy sector investors and other corporations in Turkey. Therefore, this study focused on the coal consumption of Turkey. The coal consumption was forecasted using a Grey modeling (1,1) technique based on the data composed of the period between 1965 and 2013. Using these historical data, the coal consumption of Turkey was forecasted for the period of 2014-2025. Additionally, the performance of forecasting was tested using performance measures.

Table 1. Proved coal reserves of the world at the end of 2013 (BP, 2014).

Region	Reserves (million tons)			
	Bituminous and anthracite	Sub-bituminous and Lignite	Total	Share (%)
North America	112835	132253	245088	27.5
S. & Cent. America	7282	7359	14641	1.6
Europe & Eurasia	92557	217981	310538	34.8
Middle East	1122	-	1122	0.1
Africa	31600	214	31814	3.7
Asia Pacific	157803	130525	288328	32.3
World total	**403199**	**488332**	**891531**	**100**

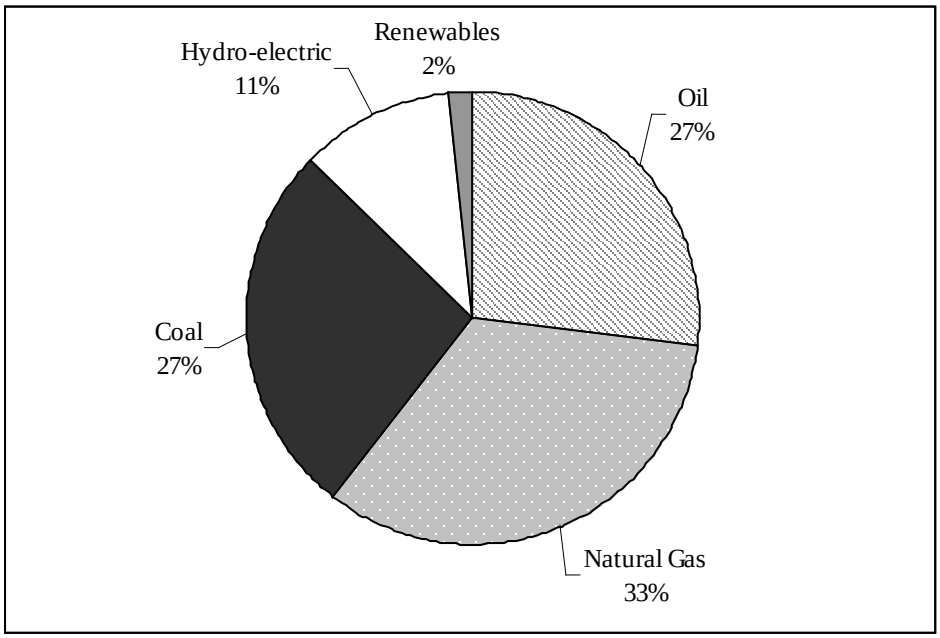

Figure 1. Primary energy consumption of Turkey by fuel type in 2013 (BP, 2014).

2 GREY PREDICTION MODELS

Grey prediction models such as GM(1,1), GM(0,N), and GM(1,N) are a part of grey systems theory (GST) proposed by Deng (1982). The GST has been successfully applied in many fields such as management, economy, engineering, finance, etc. There are three types of systems. One is called "white", other is called "black" and the last is called "grey". A system is called a white system when its information is totally clear. When a system's information is totally unknown, it is called a black system. If a system's information is partially known, then it is called a grey system (Pi et al., 2010).

In the real life, uncertain systems with small samples and poor information exist commonly (Liu et al., 2012). Grey prediction models are used both time series prediction,

and cause and effect type prediction. While GM(1,1) is used for prediction based on time series, GM(1,N) and GM(0,N) are used for prediction based on cause and effect relationships. Most widely used grey prediction model is GM(1,1).

2.1 GM(1,1)

GM(1,1) model can be used in circumstances with relatively little data, and it can use a first-order differential equation to characterize an unknown system. Therefore, GM(1,1) model is suitable for forecasting the competitive environment where decision makers can reference only limited historical data (Pi et al., 2010; Hamzacebi and Es, 2014). GM (1,1) is based on three essential steps: one is accumulated generation operation (AGO), other is grey modeling and the last is inverse accumulated generation operation (IAGO). The steps of GM (1,1) are shown below as indicated by Hamzacebi and Es (2014).

Step 1: For the initial time sequence

$$X^0=\left\{X_1^0,X_2^0,X_3^0,.....,X_n^0\right\}=(X_t^0;\quad t=1,2,3,...,n;n\geq 4) \qquad (1)$$

where X_t^0 is a non-negative sequence and n is the number of the data.

Step 2: is obtained after sequence is subjected to AGO.

$$X^1=\left\{X_1^1,X_2^1,X_3^1,.....,X_n^1\right\}=(X_t^1;\quad t=1,2,3,...,n;n\geq 4) \qquad (2)$$

where

$$X_k^1=\left\{\sum_{t=1}^{k}X_t^0,t=1,2,...,n;k=1,2,...,n\right\} \qquad (3)$$

Step 3: Setup grey modeling by establishing a first order grey differential equation

$$X_t^0+aZ_t^1=c,\quad t=2,...,n \qquad (4)$$

where

$$Z_t^1=\beta X_t^1+(1-\beta)X_{t-1}^1,\quad t=2,..,n \qquad (5)$$

β denotes a horizontal adjustment coefficient, $0<\beta<1$ and generally $\beta=0.5$. In equation (4), a is called the development coefficient and c is called driving coefficient. Applying least square method coefficients, can be estimated as

$$A=\begin{bmatrix}a\\c\end{bmatrix}=(B^TB)^{-1}B^TY_n \qquad (6)$$

where

$$B=\begin{bmatrix}-Z_2^1 & 1\\ -Z_3^1 & 1\\ .... & ...\\ -Z_n^1 & 1\end{bmatrix},\qquad Y=\begin{bmatrix}X_2^0\\X_3^0\\.....\\X_n^0\end{bmatrix} \qquad (7)$$

$$Y=BA$$

Step 4: The whitenization processes is defined as follows;

$$\frac{dX_t^1}{dt}+aX_t^1=c \qquad (8)$$

Hence, a using a and b coefficients the AGO grey prediction model can be obtained.

$$\hat{X}^1_{t+1}=\left[X_1^0-\frac{c}{a}\right]e^{-at}+\frac{c}{a},\quad t=0,1,2,.... \qquad (9)$$

Step 5: Obtain the prediction value of original sequence by IAGO operation. IAGO operation can be defined as:

$$X_{t+1}^0=X_{t+1}^1-X_t^1 \qquad (10)$$

If Eq. (9) is substituted in Eq. (10), then Eq. (11) is obtained as

$$\hat{X}^0_{t+1}=(1-e^a)\left[X_1^0-\frac{c}{a}\right]e^{-at} \qquad (11)$$

3 DATA AND METHODOLOGY

The data used in the forecasting models were obtained in an annual basis from BP (British Petroleum) Statistical Review of World Energy (BP, 2014). Figure 2 shows the used data graphically. As it is seen, the coal consumption of Turkey increased over the period of 1965 and 2013. The data from

$[a\quad c]^T$

1965 to 2008 was used for model fitting and the data from 2009 to 2013 was reserved for testing.

In order to forecast two or more future periods, iterative or direct forecasting approaches can be used. Hamzacebi and Es (2014) indicated that grey direct forecasting approach give better result over iterative approach.

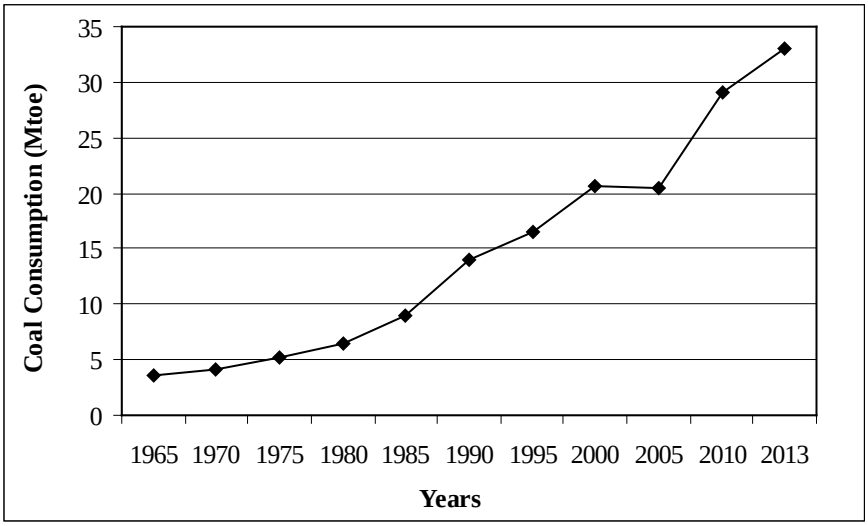

Figure 2. Coal consumption of Turkey over the period of 1965-2013 (BP, 2014).

Hence, grey direct forecasting approach was applied in current study. The following equations (Eq.12-15) illustrate how the grey direct forecasting method is applied to predict the value of p for future periods:

$$\hat{X}_{t+1} = GM(1,1)\left[X_t, X_{t-1},..., X_{t-(k-1)}\right] \quad (12)$$

$$\hat{X}_{t+2} = GM(1,1)\left[X_t, X_{t-2}, X_{t-4},..., X_{t-2(k-1)}\right] \quad (13)$$

$$\hat{X}_{t+3} = GM(1,1)\left[X_t, X_{t-3}, X_{t-6},...X_{t-3(k-1)}\right] \quad (14)$$

.....

$$\hat{X}_{t+p} = GM(1,1)\left[X_t, X_{t-p}, X_{t-2p},...X_{t-p(k-1)}\right] \quad (15)$$

The main advantage of grey direct forecasting approach is to use the past real observations as seen in Equations from 12 to 15. It selects the past observation values according to the value of *p*. For example, if *p=2*, the approach uses $\left[X_t, X_{t-2}, X_{t-4},...X_{t-2(k-1)}\right]$ subsequence to predict the next 2 periods. To forecast *p* for future periods ahead the approach selects the past observation values from the present time to *k* periods backwards by in every *p* periods. Thus, $\left[X_t, X_{t-p}, X_{t-2p},..., X_{t-p(k-1)}\right]$ subsequence is obtained to forecast $\hat{X}_{t+p}$

3.1 Performance Measures

In order to evaluate the forecasting capability of the prediction models, various performance measures are available in the literature. In this study, the mean absolute percentage error (MAPE) and , the mean absolute error (MAE) were used for evaluating the model performance. These are expressed as follows:

$$MAPE = \frac{1}{n}\sum_{i=1}^{n}\left|\frac{e_i}{Y_i}\right| * 100 \quad (16)$$

$$MAE = \frac{1}{n}\sum_{i=1}^{n}\left|e_i\right| \quad (17)$$

where e_i and Y_i are the error and observation values of the ith period. Lower values of all performance measures indicate the higher forecasting precision. Table 2 gives the reference values of the forecasting precision levels. Among these measures, Lewis (1982) interprets the MAPE results as the decisive factor since it is expressed in easy generic percentage term to judge the accuracy of the forecast.

Table 2. MAPE for model evaluation (Lewis, 1982).

MAPE (%)	Forecasting Power
>50	Weak and inaccurate forecasting
20-50	Reasonable forecasting
10-20	Good forecasting
<10	Highly accurate forecasting

4 FORECASTING RESULTS

The forecasted data, together with the actual data, were presented in Figure 3. The forecasting results showed that Turkey's coal consumption will increase in near future. The coal consumption will grow up to 47.73 Mtoe in 2025 which shows an increase of 1.31 and 0.64 growth rates when compared to that in 2000 and 2010 respectively. Additionally, the MAPE value for model fitting was found as 6.40%, while the MAPE value for testing was found as and 5.85% as given in Table 3. It is seen that both MAPE values are less than 10%. As indicated in Table 2, the GM(1,1) in this study was adequate to forecast coal consumption in Turkey with highly accurate forecasting power.

Table 3. MAPE and MAE values for model evaluation.

Criteria	Model fitting	Model testing
MAPE	6.40	5.85
MAE	1.07	1.92

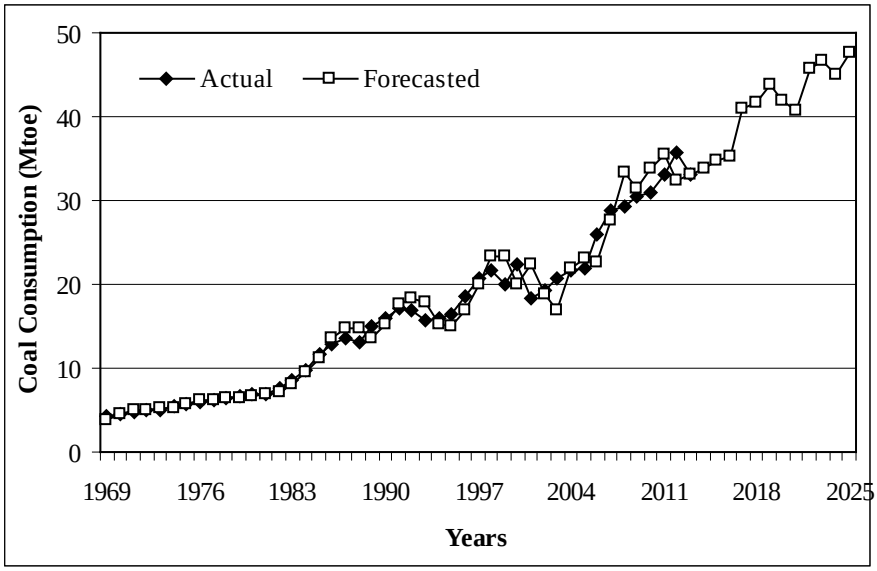

Figure 3. Actual and forecasted coal consumption of Turkey.

5 CONCLUSION

In this paper, Turkey's coal consumption was forecasted based on the grey system theory. In this regards, a GM (1,1) model was built and tested. The results indicated that grey system theory can be used to forecast the coal consumption in Turkey, and highly accurate forecasting can be obtained by the GM (1,1) model. Based on the forecasting model, the coal consumption of Turkey will grow up to 47.73 Mtoe in 2025 which shows an increase of 1.31 and 0.64 growth rates when compared to that in 2000 and 2010 respectively.

Due to the importance of forecasted values for both planning the countries' energy policy and maintain the international agreement on climate change mitigation, policy makers and related scientists should consider different forecasting techniques as well for the creation and effective implementation of energy policies in rapid growth market such as Turkey.

REFERENCES

BP., 2014. Statistical review of World energy full report by British Petroleum, available at

http://www.bp.com/en/global/corporate/about-bp/energy-economics/statistical-review-of-world-energy.html., accessed on 1 November 2014.

Deng J.L., 1982. Control problems of grey systems. System Control Letters. 1(5), 288-294.

Hamzacebi, C., and Es, H.A. 2014. Forecasting the annual electricity consumption of Turkey using an optimized grey model. Energy 70:165-171.

Höök, M., Zittel, W., Schindler, J., Aleklett, K., 2010. Global coal production outlooks based on a logistic model. Fuel 89, 3546-3558.

Kabak, M., Dağdeviren, M., 2014. Prioritization of renewable energy sources for Turkey by using a hybrid MCDM methodology. Energy Conversion and Management 79, 25-33.

Karakurt, I., Aydin, G., 2013. Fossil fuel use and related carbon dioxide emissions: A global perspective. 23rd International Mining Congress and Exhibition of Turkey, pp. 2137-2141, Antalya-Turkey.

Lewis, C.D., 1982. International and business forecasting methods. London, Butterworths.

Liu, S.F., Forrest, J., Yang, Y.J., 2012. A brief introduction to grey systems theory. Grey Systems: Theory and Application 2(2), pp. 89–104.

Mason, J.E., 2007. World energy analysis: H_2 now or later?. Energy Economics 35, pp. 1315-1329.

Pi, D., Liu, J., Qin, X., 2010. A grey prediction approach to forecasting energy demand in China. Energy Sources, Part A: Recovery, Utilization, and Environmental Effects 32, 1517–1528.

Modeling of Coal Consumption in Turkey: An Application of Trend Analysis

G. Aydin, S. Kaya, I. Karakurt
Karadeniz Technical University, Department of Mining Engineering, Trabzon, Turkey

ABSTRACT In the current modeling, trend analysis is used to model coal consumption (CC) and forecast the future coal demand in Turkey. The data is divided into two groups as the data for training the model (during the period 1970–2005) and the data for testing the model (during the period 2006–2013). The developed models are tested by the t-distribution, F-distribution and residual analysis. Additionally, the performance of the derived models are assessed using mean absolute percentage error (MAPE), root mean square error (RMSE) and means absolute error (MAE). The results show that the proposed models can be used for forecasting of future coal demand in Turkey.

Keywords: Coal, absolute percentage error, root mean square error, means absolute error

1 INTRODUCTION

A projection of future energy consumption is a vital input to many analyses of economic, energy, and environmental policies (Chang et al., 2012; Suganthi and Samuel, 2012). The decision on future energy investment requires an outlook on future energy consumption (Craig et al., 2002; O'Neill et al., 2005).

The experiences of the last five decades led to a blast in the number of energy supply/demand studies due to worries about the emissions of greenhouse gases (GHGs) from the combustion of fossil fuels (Yu et al., 2012; Aydin, 2014a; Aydin, 2014b). Therefore, since the early 1970s, various energy supply/demand studies have been carried out using various estimation methods. These methods can be classified as below.

i. Econometric approach: Linear regression (LR), partial least square regression (PLSR), and time series (ARIMA), etc.
ii. Artificial intelligence approach: Ant colony optimization (ACO), genetic algorithms (GAs), and particle swarm optimization (PSO) algorithm.
iii. Hybrid model.
iv. Grey theory forecasting model.
v. Long-range energy alternatives planning model.

In forecast modeling, various methodologies presented above can be used for energy forecasts. In the current modeling, trend analysis was used to model CC in Turkey. In the analysis, it was assumed that the future demand for coal will follow the historical trend observed in the past. The main advantage of this approach is its simplicity, and forecasts are based on whatever data are available (Kone and Buke, 2010; Aydin, 2014c; Aydin, 2015a). The study could be helpful for the energy planners and the policy makers of Turkey. They can get a general overview of future prospects for coal and its environmental affect.

2 DATA AND METHODOLOGY

The CC data for the study period were taken from British Petroleum (BP, 2014). The SPSS 17 statistical software which offers a choice of regression was used for the trend analysis. The data is divided into two groups as the data for training the model (during the period 1970–2005) and the data for testing the model (during the period 2006–2013). As can be seen from Fig. 1, the data for the CC appropriate for the linear regression

analysis (LRA). LRA is employed in two forms (Eq. 1-2) for modeling of Turkey's CC based on year.

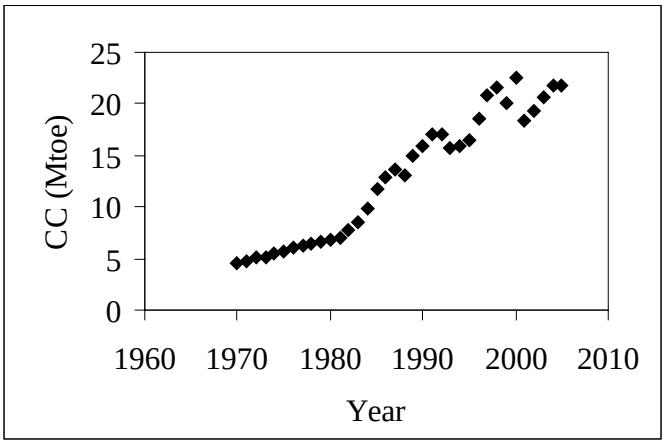

Figure 1. Turkey's CC during the period 1970-2005.

$$y = at + b \quad (1)$$

$$\ln (y) = a \ln (t) + b \quad (2)$$

where; y (*CC*), *t*: year, *b*: the intercept or the constant and *a*: the slope.

Once the model developed, confirmation of the goodness-of-fit of the models and the statistical significance of the estimated variable is done by considering the determination coefficient, F-test of the overall fit, followed by t-test of the individual variable (Mohamed and Bodger, 2005; Aydin, 2015b; Aydin, 2015c). The residual plots of the error are also studied to determine the appropriateness of the models. Moreover, the performance of the derived model for the testing data is assessed using the MAPE, RMSE and MAE.

3 MODELING OF TURKEY'S CC

Results of the trend analyses concerning the relations between Turkey's CC and the years are presented in Table 1. Statistically significant trends were indicated. As a result of analyses, following models (Eq. 3-4) were developed.

Table 1. Results of the trend analyses applied for CC modeling.

Depend. Variable	Coefficients	Unstandardized Coefficients		Stand. Coefficients	Std. Error of the Estimate
		B	Std. Error		
y	(Constant)	-1126.293	46.170		1.448
	T	0.573	0.023	0.973	
ln (y)	(Constant)	-758.670	32.848		0.136
	ln (t)	100.219	4.325	0.970	

$$y = -1126.293 + 0.573\, t \quad (3)$$

$$\ln (y) = -758.670 + 100.219 \ln (t) \quad (4)$$

The R^2 values for the models are 0.947 for Model I and 0.97 for Model II respectively, indicating a high degree of relationship between CC and t. The coefficient of determination also indicates that 0.053% of the variation in CC for Model I and 0.03% of the variation in CC for Model II is due to all causes other than the predictor. Equivalently, it can be stated that indicated variations in the models remains unexplained.

The generality and reliability of the model are further studied by examining the predicted trend versus the observed trend as shown in Fig. 2. It can be clearly seen that the predicted values of CC are very close to the actual ones for two models.

In this t test, a confidence level of 95% was chosen. As can be seen from Table 2, the computed t-values are greater than the tabulated t-values, suggesting that the developed models are statistically valid. Again at the 95% confidence level, valid for all the models, the computed F-values are greater than the tabulated F-values, indicating that the models are statistically valid (see Table 2).

The plots of the residuals against the predicted CCs by the proposed models are shown in Fig. 3. The figures indicate that the residuals appear to be scattered about x axis, confirming the accuracy of the models.

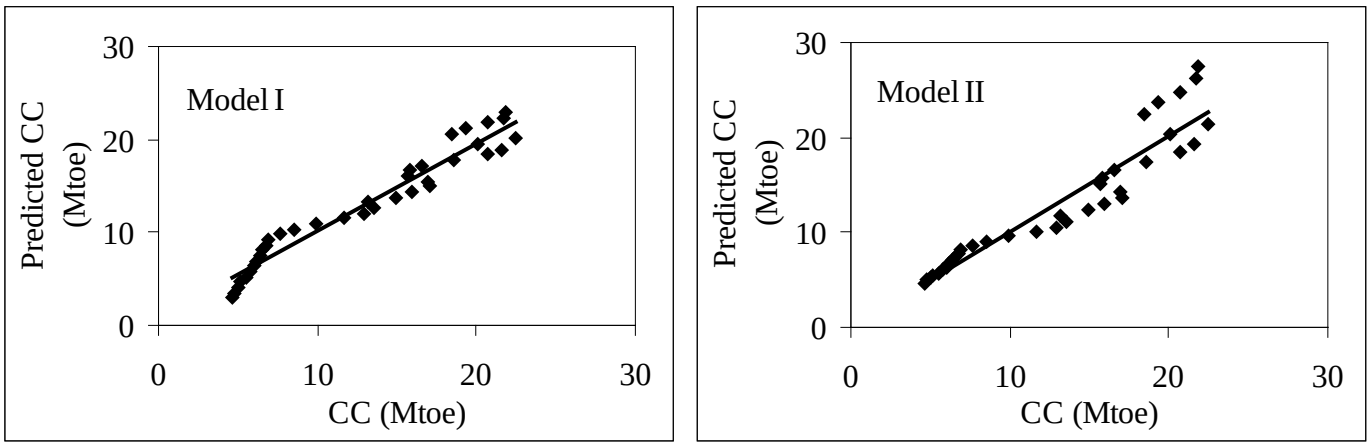

Figure 2. Comparison of the actual and predicted CC.

Table 2. Results of verification tests.

Dependent Variable	R Square	Adjusted R Square	t_{table}	t	F_{table}	F
Model I	0.947	0.946	1.690	-24.394 24.675	4.120	608.847
Model II	0.970	0.940	1.690	-23,098 23,171	4.120	536.913

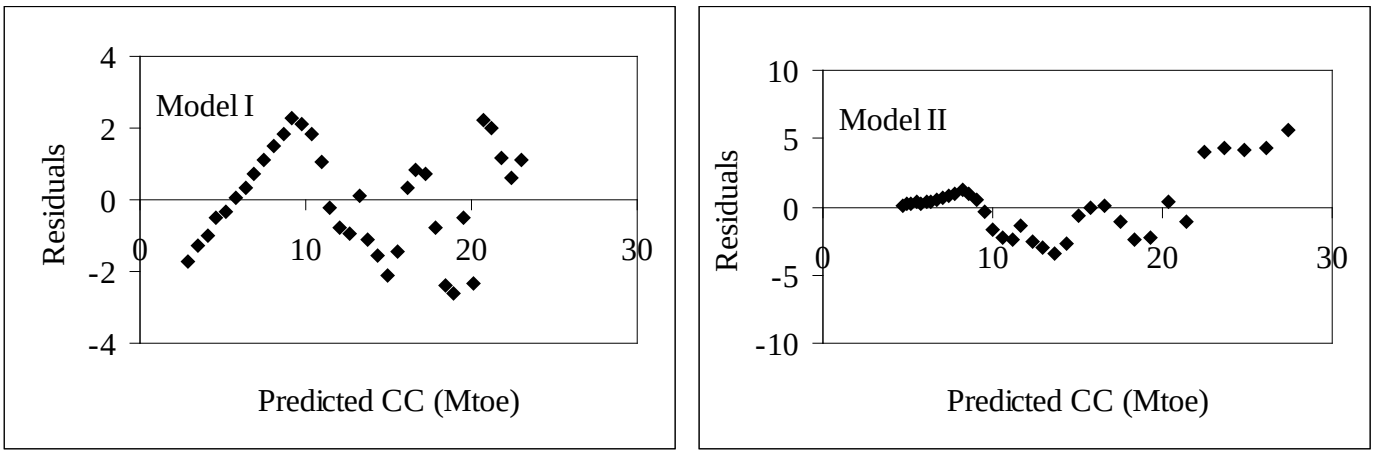

Figure 3. Residuals against the predicted CC.

The accuracy of prediction is evaluated based on the estimation of error. The smaller values of MAE, RMSE and MAPE indicate the better prediction performance. The equations of these performance criteria are given below.

$$MAPE = \frac{1}{n}\sum_{i=i}^{n}\left(\frac{|e_i|}{y_i}\right)100 \quad (5)$$

$$RMSE = \sqrt{\frac{1}{n}\sum_{i=1}^{n} e_i^2} \quad (6)$$

$$MAE = \frac{1}{n}\sum_{i=1}^{n} |e_i| \quad (7)$$

where, n is the total number of measurements, e_i is differences between actual and predicted values, y_i is actual values.

As shown in Table 3, the MAPE value was determined as 16.9% for Model I and

11.9 Model II, while the RMSE value was determined as 5.608 for Model I and 4.122 for Model II. Similarly, the MAE value was determined as 5.339 for Model I and 3.715 for Model II. These results show the superiority of Model II over the Model I.

Table 3. Performances of the models.

Model	MAPE (%)	MAE	RMSE
I	16.9	5.339	5.608
II	11.9	3.715	4.122

MAPE is the decisive factor since it is expressed in easy generic percentage term. Table 4 shows the criteria of MAPE for model evaluation based on Lewis (1982). These results showed that the derived models can give adequate forecasting for Turkey's CC. The models can be also classified as good prediction model because their MAPEs are between 10% and 20%. Additionally, it can be clearly seen from Table 5 that the predicted CC values are close to the actual ones.

Table 4. Typical MAPE values for model evaluation.

MAPE (%)	Evaluation
MAPE ≤ 10%	High accuracy prediction
10% < MAPE ≤ 20%	Good prediction
20% < MAPE ≤ 50%	Reasonable prediction
MAPE > 50%	Inaccurate prediction

Table 5. Performance of the regression models.

Year	CC (Mtoe)	Predicted CC (Mtoe)	Predicted CC (Mtoe)
		Model I	Model II
2006	25.909	23.539	28.866
2007	28.855	24.112	30.344
2008	29.182	24.686	31.897
2009	30.440	25.259	33.529
2010	30.864	25.832	35.244
2011	33.086	26.405	37.045
2012	35.749	26.978	38.938
2013	32.989	27.552	40.926

Primary energy consumption in Turkey has increased rapidly due to social and economical growth in the past two decades As a results of the increase in Turkey's PEC, CC have increased recently. Future CCs calculated from the proposed models are presented in Table 6.

Table 6. Forecasts for Turkey's CC.

Year	Predicted CC (Mtoe)	
	Model I	Model II
2014	28.125	43.015
2015	28.698	45.209
2016	29.271	47.514
2017	29.,844	49.935
2018	30.418	52.478
2019	30.991	55.149
2020	31.564	57.955

Using Model I, Turkey's CC is forecasted to decrease from 32.989 Mtoe in 2013 to 31.564 Mtoe in 2020 with an annual percentage change of 0.55%. Additionally, Model II forecast Turkey's CC as 57.955 Mtoe in 2020, 75.68% higher than 2013.

4 CONCLUSIONS

In the current study, Turkey's CC was modeled and forecasted using trend analysis. Statistically significant trends were determined. It was concluded that the proposed models are statistically valid in terms of F-test, t-test and residual analysis. The results obtained from the trend analyses showed that the developed models can be used for forecasting of Turkey's CC into the future planning.

Modeling results showed that Model II presents good performance for forecasting of Turkey's CC. However, when the trend in the last decades is investigated, it is hard to come true the values obtained by Model II. High values of CC were forecasted with

Model II due to the equation form (ln). Therefore, Model I is recommended for forecasting of Turkey's CC.

Future CC in Turkey is affected by many factors, mainly economic growth, population growth, coal prices and its availability. Technologies that improve efficiency of power plants, decreasing the energy losses, environmental and emissions regulations and standards could also affect the CC in the country. For providing more successful results, forecasts should include some evaluations of these factors.

REFERENCES

Aydin, G., 2014a. Modeling of energy consumption based on economic and demographic factors: The case of Turkey with projections. Renewable and Sustainable Energy Reviews, 35, 382-389

Aydin, G., 2014b. The modeling of coal related CO_2 emissions and projections into future planning. Energy Sources Part A: Recovery, Utilization, and Environmental Effects, 36 (2), 191-201

Aydin, G., 2014c. Production modeling in the oil and natural gas industry: An application of trend analysis. Petroleum Science and Technology, 32 (5), 555-564

Aydin, G., 2015a. The modeling and projection of primary energy consumption by the sources. Energy Sources Part B: Economics, Planning, and Policy, 10 (1), 67-74

Aydin, G., 2015b. The Application of trend analysis for coal demand modeling. Energy Sources Part B: Economics, Planning, and Policy, 10 (2), 183–191

Aydin, G., 2015c. The Development and validation of regression models to predict energy-related CO_2 emissions in Turkey. Energy Sources Part B: Economics, Planning, and Policy, 10 (2), 176–182

British Petroleum (BP). 2014. Statistical review of world energy. London: British Petroleum.

Chang, Y., Lee, J., and Yoon, H., 2012. Alternative projection of the world energy consumption in comparison with the 2010 International Energy Outlook. Energy Policy, 50, 154–160.

Craig, P., Gadgil, A., Koomey, J., 2002. What can history teach us? A retrospective examination of long-term energy forecasts for the United States. Annual Review of Energy and the Environment, 27, 83–118.

Köne, C.A., and Büke, T., 2010. Forecasting of CO_2 emissions from fuel combustion using trend analysis. Renewable and Sustainable Energy Reviews, 2906–2915.

Lewis, C.D., 1982. International and business forecasting methods. London: Butterworths.

Mohamed, Z., Bodger, P., 2005. Forecasting electricity consumption in New Zealand using economic and demographic variables. Energy 2005;30:1833–43.

O'Neilla, C.B., and Desai, M., 2005. Accuracy of past projections of US energy consumption. Energy Policy, 33, 979–993.

Suganthia, L., and Samuel, A.A., 2012. Energy models for demand forecasting—A review. Renewable and Sustainable Energy Reviews, 16, 1223–1240.

Yu, S., Zhu, K., and Zhang, X. (2012). Energy demand projection of China using a path-coefficient analysis and PSO–GA approach. Energy Conversation and Management, 53, 142–153.

Modeling of Energy Consumption Based on Population: The Case of Turkey

G. Aydin, S. Kaya, I. Karakurt
Karadeniz Technical University, Department of Mining Engineering, Trabzon, Turkey

ABSTRACT In this study, Turkey's primary energy consumption (PEC) is modeled by linear regression analysis (LRA) based on population (P). The derived models are validated through some statistical approaches such as the determination coefficient, t-test, F-test, and residual analysis. For the performance assessment of the proposed model, three performance measures such as mean absolute percentage error (MAPE), root mean square error (RMSE) and mean absolute error (MAE) are used. Three scenarios are used for forecasting Turkey's PEC in the years 2013–2020. For each scenario, various assumptions are made considering different growth rate for P. Using the proposed model, Turkey's PEC is forecasted under different scenarios. The results show that the proposed model can be affectively used for forecasting of Turkey's PEC. The scenarios show that Turkey's PEC would vary between 135.523 Mtoe and 140.745 Mtoe in 2020.

Keywords: Energy consumption, population, modeling

1 INTRODUCTION

Turkey's energy demand has rapidly increased recently as a result of social and economic development (Tunç et al., 2006). Turkey's PEC increased from 13.07 Mtoe in 1970 to 122.79 Mtoe in 2013, representing an annual growth of 5.22% (see Figure 1). Figure 2 shows the share of energy sources in Turkey's PEC for the year 2013 (BP, 2014).

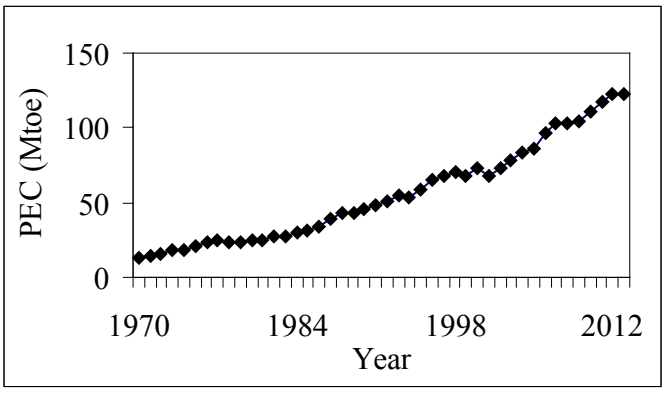

Figure 1. Turkey's PEC during 1970-2013.

The uses of all kinds of energy sources in Turkey have increased over time. The growth in global energy demand is estimated to rise over the coming years (Aydin, 2014a; Aydin 2014b). In 2013, about 90% of Turkey's PEC was supplied from fossil fuels (26.97% oil, 33.45% natural gas, and 26.87% coal), 10.92% from hydroelectric, and 1.79% from renewables (see Figure 2).

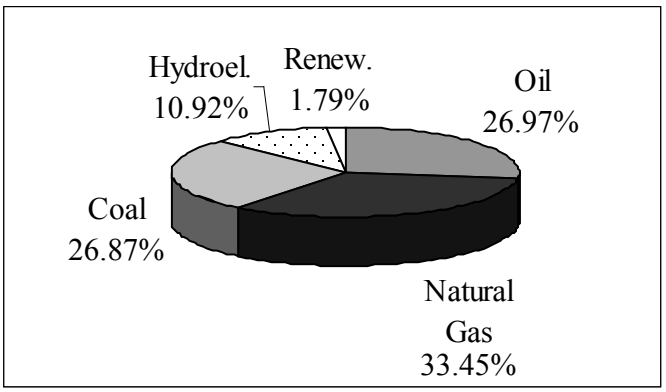

Figure 2. Share of energy sources in Turkey's PEC.

A projection of future energy consumption is a vital input to many analyses of economic, energy, and environmental policies. For example, the decision on future energy investment requires an outlook on future energy consumption (Chang et al., 2012; Suganthia and Samuel, 2012). Underestimation of the energy consumption would lead to potential greenhouse gases;

whereas overestimation would lead to unnecessary idle capacity. Therefore, it would be better to model energy consumption with a good accuracy in order to avoid the costs related to the errors (Kankal et al., 2011; Aydin, 2014c).

The scope of current study is to present a new model for forecasting of Turkey's PEC using LRA. The study is thought to be helpful for the energy planners and the policy makers in Turkey.

2 DATA AND METHODOLOGY

This study collects annual data on Turkey's PEC (Mtoe) and P for the period 1970–2013 from the British Petroleum (2014) and the World Bank (2014), respectively. The total data is used rather than per capita data as recommended by Friedl and Getzner (2003), Pao and Tsai (2011), and Aranda et al. (2012). The SPSS 17 statistical software which offers a choice of regression is used for the analysis. The data is divided into two groups as the data for training the model (during the period 1970–2005) and the data for testing the model (during the period 2006–2013). Presents the relationship between PEC and P in ln form. Figure 3 indicates that the data is appropriate for the LRA. Therefore, the LRA is employed for modeling of Turkey's PEC based on P.

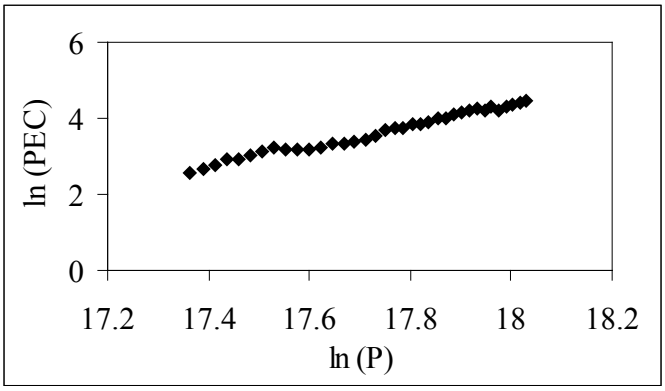

Figure 3. Relationship between ln (P) and ln (PEC).

$$ln\,(PEC) = a\,ln\,(P) + b \quad (1)$$

where; *PEC* (primary energy consumption), *P*: population, *b*: the intercept or the constant and *a*: the slope.

Once the model developed, confirmation of the goodness-of-fit of the model and the statistical significance of the estimated variables is done by considering the determination coefficient, F-test of the overall fit, followed by t-test of the individual variables (Mohamed and Bodger, 2005; Aydin, 2015a; Aydin, 2015b; Aydin, 2015c). The residual plots of the error are also studied to determine the appropriateness of the model. Moreover, the performance of the derived model for the testing data is assessed using the MAPE, RMSE and MAE.

3 MODELING OF TURKEY'S PEC

Results of the analyses concerning the relations between Turkey's PEC and the P are presented in Table 1. Statistically significant trends were indicated. As a result of analyses, the following model (Equation 2) was developed.

$$ln\,(PEC) = -44.789 + 2.730\,ln\,(P) \quad (2)$$

The R^2 value for the model is 0.984, indicating a high degree of relationship between the PEC and P (see Table 2). The coefficient of determination also indicates that 0.016 % of the variation in the PEC is due to all causes other than the predictors. In other words, it can be stated that 0.016 % variation in the PEC remains unexplained. Additionally, it can be clearly seen from Fig. 4 that the predicted PEC values are very close to the actual ones.

Table 1. Results of the trend analyses applied for modeling Turkey's PEC.

Depend. Variable	Coefficients	Unstandardized Coefficients		Stand. Coefficients	Std. Error of the Estimate
		B	Std. Error		
ln (PEC)	(Constant)	-44.789	1.053		0.071
	ln (P)	2.730	0.059	0.992	

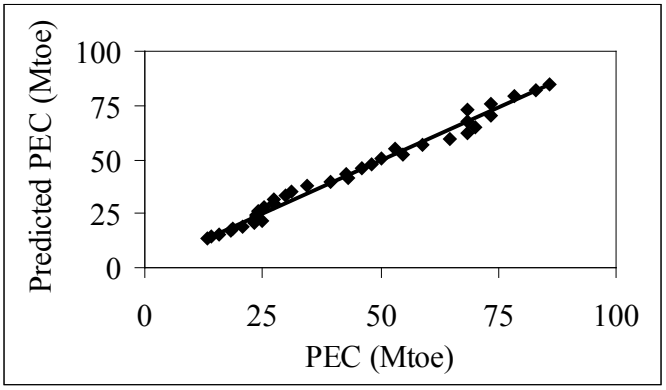

Figure 4. Comparison of the actual and predicted PEC.

As seen in Table 2, the critical value of F (4.120) is much smaller than the calculated F value. Therefore, it can be concluded that the Eq. 2 is significant at the 95 % confidence level. The t-test result for coefficient P is higher than the 95 % critical value of t (1.690). This means that P in Equation 2 is significant in its use in the model (see Table 2).

The plots of the residuals against the predicted PEC for the model case are also shown in Figure 5. The figure indicates that the residuals appear to be scattered about the x axis, confirming the accuracy of the model.

Table 2. Results of verification tests.

Dependent Variable	R Square	Adjusted R Square	t_{table}	t	F_{table}	F
PEC	0.984	0.984	1.690	$\frac{-42.542}{45.995}$	4.120	2115.498

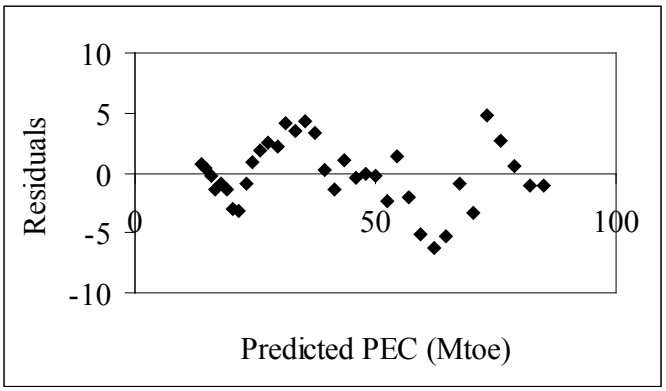

Figure 5. Residuals against the predicted PEC.

In order to assess the model performance, three performance measures such as MAPE, RMSE and MAE were used. The equations of these performance criteria are given below.

$$MAPE = \frac{1}{n}\sum_{i=i}^{n}\left(\frac{|e_i|}{y_i}\right)100 \quad (3)$$

$$RMSE = \sqrt{\frac{1}{n}\sum_{i=1}^{n} e_i^2} \quad (4)$$

$$MAE = \frac{1}{n}\sum_{i=1}^{n} |e_i| \quad (5)$$

where, n is the total number of measurements, e_i is differences between actual and predicted values, y_i is actual values.

The accuracy of prediction is evaluated based on the estimation of error, thus the smaller the value of MAE, RMSE and MAPE, the better the prediction is. The results are presented in Table 3.

Table 3. Performance of the model.

MAPE (%)	MAE	RMSE
9.2670	10.265	10.589

As shown in Table 3, the MAPE value was determined as 9.267%, while the RMSE value was determined as 10.589. Similarly, the MAE value was determined as 10.265. MAPE is the decisive factor since it is expressed in easy generic percentage term. Table 4 shows the criteria of MAPE for model evaluation based on Lewis (1982). These results showed that the derived model can give adequate forecasting for Turkey's PEC. The models can be also classified as high accuracy prediction model because its MAPE is below 10%.

Table 4. Typical MAPE values for model evaluation.

MAPE (%)	Evaluation
MAPE ≤ 10%	High accuracy prediction
10% < MAPE ≤ 20%	Good prediction
20% < MAPE ≤ 50%	Reasonable prediction
MAPE > 50%	Inaccurate prediction

Three scenarios were used for forecasting Turkey's PEC in the years 2013–2020. For each scenario, various assumptions were made considering different growth rates for P (see Table 5).

To forecast Turkey's PEC, P was initially forecasted using Equation 6. The forecasted results for P based on different growth rates are presented in Table 5.

Table 5. Forecasted P based on different growth rate.

Year	Scenario I G.R.* 1 %	Scenario II G.R.* 1.1 %	Scenario III G.R.* 1.2 %
2014	75681967	75756900	75831837
2015	76438787	76590226	76741815
2016	77203175	77432718	77662716
2017	77975207	78284478	78594669
2018	78754959	79145608	79537805
2019	79542508	80016209	80492259
2020	80337933	80896388	81458166

*G.R.: Growth Rate

$$V(t_n) = V(t_0)(1+CAGR)^n \quad (6)$$

where CAGR is compounded annual growth rate, $V(t_0)$ is start value, $V(t_n)$ is finish value and n is number of periods.

Based on these assumptions, Scenario I assumes that Turkey's PEC is projected to increase from 122.79 Mtoe in 2013 to 135.523 Mtoe in 2020, an increase of 10.37%, or 1.24% growth per year. According to Scenario II, Turkey's PEC increases to 138.110 Mtoe in 2020, 12.47% higher than 2013, and representing average growth of 1.48% per year. Turkey's PEC increases more quickly in the Scenario III, reaching 140.745 Mtoe in 2020, 14.62% higher than 2013, and representing average growth of 1.72% per year (see Table 6).

Table 6. Forecasted PEC under different scenarious.

Year	PEC (Mtoe)		
	Scenario I	Scenario II	Scenario III
2014	115.137	115.449	115.761
2015	118.308	118.950	119.593
2016	121.567	122.556	123.553
2017	124.915	126.272	127.643
2018	128.355	130.101	131.869
2019	131.890	134.046	136.235
2020	135.523	138.110	140.745

4 CONCLUSIONS

In this study, Turkey's PEC was modeled based on P. It was concluded that the derived model can be successfully used as a forecasting tool for Turkey's PEC. The results of forecasting scenarious showed Turkey's PEC would vary between 135.523 Mtoe and 140.745 Mtoe in 2020.

Forecasting of Turkey's PEC can be also investigated with other forecasting methods. The results of the different methods could be compared with the LRA to see the performance of the proposed model.

REFERENCES

Aranda, A., Ferreira, G., Mainar-Toledo, D.M., Scarpellini, S., Sastresa, L.E., 2012. Multiple regression models to predict the annual energy consumption in the Spanish banking sector. Energy and Buildings, 49, 380–387.

Aydin, G., 2014a. Modeling of energy consumption based on economic and demographic factors: The case of Turkey with projections. Renewable and Sustainable Energy Reviews, 35, 382-389

Aydin, G., 2014b. The modeling of coal related CO_2 emissions and projections into future planning. Energy Sources Part A: Recovery, Utilization, and Environmental Effects, 36 (2), 191-201

Aydin, G., 2014c. Production modeling in the oil and natural gas industry: An application of trend analysis. Petroleum Science and Technology, 32 (5), 555-564

Aydin, G., 2015a. The modeling and projection of primary energy consumption by the sources. Energy Sources Part B: Economics, Planning, and Policy, 10 (1), 67-74

Aydin, G., 2015b. The Application of trend analysis for coal demand modeling. Energy Sources Part B: Economics, Planning, and Policy, 10 (2), 183–191

Aydin, G., 2015c. The Development and validation of regression models to predict energy-related CO_2 emissions in Turkey. Energy Sources Part B: Economics, Planning, and Policy, 10 (2), 176–182

British Petroleum (BP). 2014. Statistical review of world energy. London: British Petroleum.

Chang, Y., Lee, J., and Yoon, H., 2012. Alternative projection of the world energy consumption in comparison with the 2010 International Energy Outlook. Energy Policy, 50, 154–160.

Friedl, B., Getzner, M., 2003. Determinants of CO_2 emissions in a small open economy. Ecological Economics, 45, 133-148.

Kankal, M., Akpınar, A., Komurcu, I.M., Ozşahin, S.T., 2011. Modeling and forecasting of Turkey's energy consumption using socio-economic and demographic variables. Applied Energy, 88, 1927–1939.

Lewis, C.D., 1982. International and business forecasting methods. London: Butterworths.

Mohamed, Z., Bodger, P., 2005. Forecasting electricity consumption in New Zealand using economic and demographic variables. Energy, 30, 1833–43.

Pao, H., Tsai, C., 2011. Modeling and forecasting the CO_2 emissions, energy consumption, and economic growth in Brazil. Energy, 36, 2450–2458

Suganthia, L., and Samuel, A.A., 2012. Energy models for demand forecasting—A review. Renewable and Sustainable Energy Reviews, 16, 1223–1240.

Tunç, T., Çamdali, Ü., Liman, T., Değer, A., 2006. Electrical energy consumption and production of Turkey versus world. Energy Policy, 34, 3284–3292.

World Bank. 2014. World Development Indicator. Available at: http://data.worldbank.org/

Recent Developments in Australian Mining Education

M. S. Kizil
The University of Queensland, School of Mechanical and Mining Engineering, Australia

ABSTRACT The Australian mining industry is responsible for more than 50% of the export revenues and is one of the top five largest exporters in the world. Graduating good quality engineers for such an important industry requires world-class education. Mining Education Australia (MEA) was established to deliver a common undergraduate curriculum in mining engineering across Australia. This unique initiative was developed in response to increased demand for mining industry professionals in an environment of limited funding within the traditional university environment and a critical shortage of suitably qualified academic staff. MEA is an unincorporated joint venture between The University of Queensland, The University of New South Wales and Curtin University in Western Australia. In 2009, The University of Adelaide that is the fourth biggest school of mine in Australia became a member of the MEA Program. This paper discusses the history and governance of MEA as well as the structure of the common curriculum and teaching innovations adopted.

Keywords: Australia, mining education, strategy, benefits

ÖZET Avustralya madencilik sektörü, ihracat gelirinin %50'den fazlasını karşılayan ve dünyanın en büyük beş üreticisinden biri olan önemli bir sektördür. Böyle önemli bir sektöre maden mühendisi yetiştirmek için, dünya kalitesinde bir eğitim gerekmektedir. 1996 yılında, Avustralya çapında standart bir maden mühendisliği eğitimi imkanı sunacak, orijinal adı Mining Education Australia (MEA) olan Avustralya Maden Eğitimi adı altında ulusal bir maden okulu kuruldu. MEA'ın kuruluş amacı, maden bölümlerine verilen maddi desteğin azalması, öğretim üyelerinin sayısındaki azalmaya karşın maden endüstrisinin artan mühendis ihtiyacını karşılamak ve daha kaliteli mühendis yetiştirmekti. Kurucu üyeler Queensland, New South Wales ve Curtin Üniversiteleriydi. 2009 yılında Avustralya'nın dördüncü büyük maden okulu olan Adelaide Üniversitesi de MEA'ye katıldı. Bu makale, MEA'nin kuruluş tarihçesini, oluşturulan ortak ders programını ve eğitim ve öğretimde getirilen yeni standartları ve metotları kapsamaktadır.

Anahtar Kelimeler: Avustralya, madencilik eğitimi, strateji, faydalar

1 INTRODUCTION

The global mining education institutions, especially in the developed countries, faced a number of challenges between 1985 and 2003. These included an acute shortage of talented academic staff, small number of student enrolments, high relative costs, making mining programs vulnerable to closures, when universities were under extreme cost pressures, and most importantly under-resourcing of mining departments because of their comparatively small size, making these departments incapable of delivering top class teaching in all aspects of their courses, despite being excellent in some areas. In Australia, this concern was felt more by the industry when it was realised that a number of mining departments across the world had already been closed down as shown in Figure 1 with exception of Chile, South Africa and Australia. The mining industry through its representative body, the Minerals Council of Australia (MCA) set up a task force to review the state of the

minerals education in Australia. The findings and recommendations from this review was published in a report called *"Back from the brink"* in 1998 (MCA, 1998). In response to industry's concerns the National Tertiary Education Taskforce established the following Mission.

"The Development of World-Class Education for a World-Class Minerals Industry"

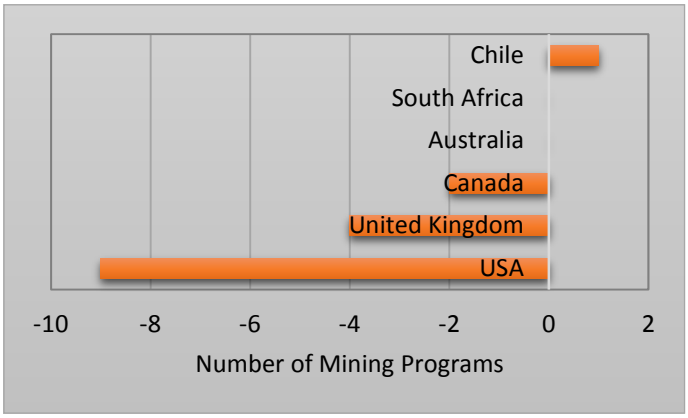

Figure 1. Change in number of mining programs between 1985 and 2003.

The Australian minerals industry's main concern was that, new industry professionals needed to be better educated to deal with emerging challenges of the industry such as globalisation, competition, and rapidly changing technologies. The industry was seeking to ensure that there were sufficient technically capable graduates available to meet its needs, that these graduates valued continuing professional development and that they had sufficient exposure to industry workplaces to ensure they were aware of broader issues such as safety, environmental care and commercial aspects of their work (MCA, 1998). This resulted in establishment of the Minerals Tertiary Education Council (MTEC) which is a division of the MCA in October 1999. Since this time MTEC has been a major driver in establishing three national higher education programs in Mining Engineering, Minerals Geoscience and Metallurgy across 15 Australian universities, which now produce the bulk of new, highly skilled technical professionals from those disciplines (MTEC, 2015). One of the MTEC initiatives was to support the establishment of Mining Education Australia (MEA).

2 MINING EDUCATION AUSTRALIA

Soon after establishing MTEC, the industry started supporting the mining schools by sponsoring two academic positions at each institution and financially supporting the key course development. While this support helped to sustain the minerals education institutions, it did not provide the kind of improvement in the education system the industry was hoping for. Therefore, the discussions for establishing a national mining school started in 2004 which resulted in the establishment of the Mining Education Australia (MEA). MEA was developed to meet the increasing demand for mining industry professionals in an environment where limited funding exists within the conventional university system and to maintain a critical mass of suitably qualified academic staff. The initiative was stimulated by support and funding from the MCA representing the Australian mining industry. The MCA remains committed to the on-going financial support of MEA to deliver a world class program of undergraduate education in mining engineering.

MEA was set up as a joint venture between three major mining education providers in Australia, namely; the University of Queensland, the University of New South Wales and Curtin University. In 2008, the University of Adelaide became a member of the MEA Program. MEA provides a common curriculum for 3rd and 4th year mining engineering students, as shown in Figure 2.

SEM	MINING ENGINEERING UNDERGRADUATE PROGRAM 2015			
1	ENGG1100 Engineering Design	MATH1051 Calculus & Linear Algebra I OR Elective	ERTH1501 Earth Processes & Geological Materials for Engineers	ENGG1400 Engineering Mechanics Statics and Dynamics OR Elective
2	ENGG1200 Introduction to Engineering Problem Solving	MATH1051 Calculus & Linear Algebra I OR Elective	MATH1052 Multivariate Calculus & ODEs	ENGG1400 Engineering Mechanics Statics and Dynamics OR Elective
3	MINE2105 Introduction to Mining	MECH2410 Fundamentals of Fluid Mechanics	STAT2201 Analysis of Eng & Sci. Data / MINE2123 Structural Mechanics in Mining	MATH2000 Calculus & Linear Algebra II
4	CIVL2210 Soil Mechanics	MINE2201 Physical & Chemical Processing of Minerals	MINE2106 Resource Geology & Surveying	ELECTIVE
5	MINE3120 Resource Estimation	MINE3121 Mining Geomechanics	MINE3122 Mining Systems	ELECTIVE
6	MINE3123 Mine Planning	MINE3124 Mine Ventilation	MINE3125 Rock Breakage	ELECTIVE
7	MINE4120 Mine Geotechnical Engineering	MINE4122 Mining Research Project I	MINE4124 Hard Rock Mine Design & Feasibility	ELECTIVE
8	MINE4121 Mine Management	MINE4123 Mining Research Project II	MINE4125 Coal Mine Design & Feasibility	ELECTIVE

Figure 2. The University of Queensland's undergraduate Mining Program showing common 3rd and 4th year MEA courses *(MEA electives includes: Surface Mining Systems, Underground Mining Systems, Mining Asset Management and Services, Socio-Environmental Aspects of Mining, Advanced Mine Geotech Eng, Mining in a Global Environment and Advanced Ventilation).*

The development of MEA was supported by a $1.3 million grant from the Federal Government through the Collaboration and Structural Reform funding scheme. Funds from a government grant have permitted new mining courses and resource materials to be developed to a world class standard. Advanced tools and systems are being applied to the management and delivery of the Joint Venture's teaching resources and innovative delivery and assessment techniques have been developed and are being adopted in all courses. The experience gained from these activities is being shared with others through an active dissemination program including publications. These achievements have been undertaken in a strong interactive environment that forms a model for future cross-university collaboration.

The following is a chronology of the development of MEA.

2004 Initial discussions for MEA started.
MEA was established.
Identified common courses.
Established a common program structure.
Identified course convener and local coordinators.

2005 Established a common program.
Established new courses at local universities.
Detailed course content.
Developed course profiles.
Identified course delivery mechanisms.
Test run of some common courses.

2006 Inclusion of details in Universities' Handbooks.
Transition run.

2007 Australian undergraduate school of mining was fully operational.

2008 MEA produced first graduates.
Adelaide University joined MEA.

3 BENEFITS OF MEA

Mining Education Australia is a first and unique educational initiative in the world which standardised the mining education across the country through industry, government and university collaboration. It has provided many benefits to the universities, students and the industry, which includes (Tuckwell, 2004):

- improved quality of graduates;
- increased quantity of graduates;
- allowed sharing academic expertise;
- provided a common education standards (across universities);
- sustained viability of programs – opportunity for growth;
- increased the quality of teaching courses and materials;
- access to marketing strategies – broad and focused;
- international market; and
- new generation academics.

The major benefits MEA program provides for mining engineering students includes:

- a nationally recognized, comprehensive educational program covering all aspects of mining engineering, technical, operational and social/community issues;
- access to national group of mining academic staff with skills in all major areas;
- exciting new and innovative teaching and learning programs, including collaborative student activity across four member university nodes;
- opportunities to undertake exchange semesters among member universities; and
- a world-class degree and industry-supported national program.

Since the setup of MEA, the number of mining graduates produced by the member universities for the mining industry has more than tripled from 72 in 2007 to 250 in 2014 as shown in Figure 3. Today, MEA provides 90% of Australia's mining engineering graduates.

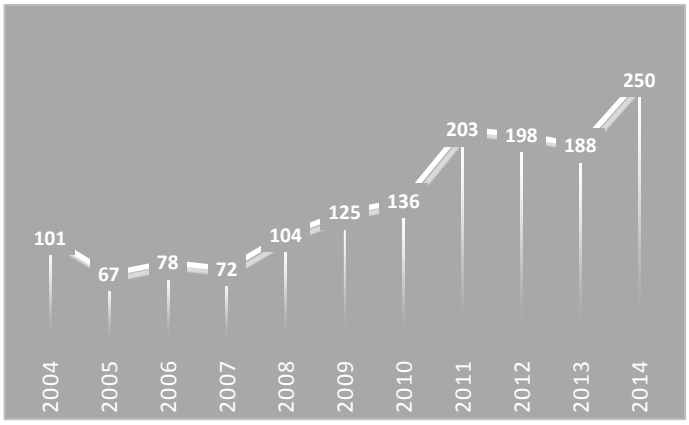

Figure 3. Total number of mining engineering graduates from the MEA member universities.

4 MAJOR CHALLENGES IN SETTING UP MEA

Mining academic staff at all four member universities played a major role in preparing for and establishing the MEA joint venture, aligning curricula among the MEA universities and developing courses to be taught at all four institutions. Major challenges and obstacles were identified and addressed during the establishment of MEA included different program structures at each university, variations in teaching styles, the need for specialised courses, the number of courses offered, course weightings, pre-requisites, time table incompatibilities, lack of commonality in delivery and assessment mechanisms, electives, and laboratory facilities. In order to overcome these challenges and develop a climate of collaboration, MEA developed and implemented a range of collaborative strategies. These include:

- a joint venture agreement between the four universities;
- collaborative course teams;
- implementation of tools to support cross university teaching and assessment;
- implementation of tools and processes for cross university student collaborative assessment, moderation and evaluation processes;

- program leaders committee, and
- twice yearly academic workshops.

5 MEA CORPORATE STRUCTURE

The corporate structure of MEA is shown in Figure 4. It has a governing board, executive committee, program leaders committee and course leaders and course coordinators.

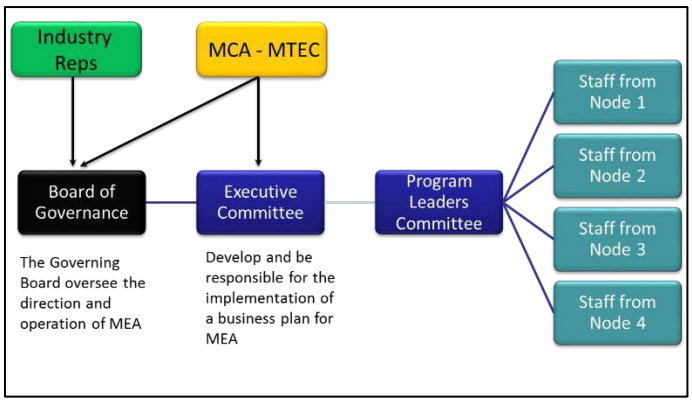

Figure 4. MEA Management Structure

5.1 Governing Board

The MEA Governing Board has a member from each member universities, three members from the industry, the MEA Director and the director of MTEC, meets once a year and oversees the direction and operation of MEA. In particular, it:

- sets the strategic direction of MEA;
- is responsible for the financial management of MEA;
- sets goals and key performance indicators for MEA;
- approves the annual operating plan and budget;
- appoints the Director;
- approves the curriculum and the program content and structure; and
- develops and oversights student recruitment.

The Governing Board appoints a Director who is a senior academic of one of the Members. As a general rule, the appointment will rotate between academics of the Member Universities. The appointment may be on a part-time basis and is for a three year term, which may be renewed.

5.2 Executive Committee

The Executive Committee is chaired by the Executive Director of MEA and comprises senior teaching nominees from each participating university and the Chairman of the Program Leaders' Committee. The committee meets at least four times a year and is responsible for implementing the business plan approved by the Board and pursuing the strategic objectives defined by the Board.

The MEA Executive Committee:

- develops and is responsible for the implementation of a business plan;
- implements the strategic directions and marketing plan;
- monitors and reports to the Board on the performance of MEA against the key performance indicators and goals set by the Governing Board; and
- considers recommendations brought forward by the Program Leaders Committee regarding academic matters.

5.3 Program Leaders Committee

Each university appoints a senior teaching academic as its Program Leader responsible for coordinating the undergraduate teaching program at that university. The Program Leaders are represented on the MEA Executive by their chairman and responsible for:

- designing and reviewing the program structure, content, delivery and resource requirements and allocation;
- approving course outlines, learning guides and assessment schedule;
- implementing and monitoring an assessment moderation process;
- approving the exchange of students between MEA partners;
- monitoring the level of collaboration within each of the course teams;
- reviewing and researching potential innovative teaching and learning technologies and encouraging their adoption in the MEA Program.

5.4 Course Leaders and Coordinators

The Program Leaders appoint Course Leaders at each university to be responsible for the development and delivery of each MEA course. For each course the Course Coordinators from each university work as a team under the leadership of the Course Leader.

6 MEA STRATEGIES/ACTIVITIES

6.1 Academic Staff Workshops

Twice yearly all academic staff of MEA come together for three day workshops. This workshop is held in Sydney, Brisbane and Perth (or Kalgoorlie) in a rotating fashion. This workshop enables all participants to discuss different aspects of the project, participate in staff development workshops, assess the progress of the project, deal with any issues that might be impeding the project and build an understanding of the common goals and values of MEA. This workshop is a major change management strategy (Andrews and Lind, 2007).

6.2 Course Development and Improvement

MEA currently supports 12 compulsory common courses during the final two years of mining engineering program at each member university complemented by a number of more specialised elective courses. Member universities continue to be responsible for the more general engineering education during the first two years of the degree.

MEA takes a collaborative approach to course development, delivery and assessment. Each course is developed by a team of academics consisting of a representative from each partner institution and includes a nominated course convenor and three node co-ordinators. Under the guidance of an educational consultant, a rigorous course development process ensuring alignment between course objectives, teaching and learning activities, graduate attributes and assessment was introduced and is an integral part of the development of all courses. This approach to course development was new to most of the academics in MEA and required them to build capacity to undertake the collaborative development essential for MEA's common curriculum and to design course that met industry requirements that specifically requested the development of workplace skills such as team work and communication.

In order to address regional differences and specialities, 80% of the content is core and 20% complimentary. Regular meetings occur between the course teams and the twice yearly workshops enable the course team members to work together to maintain high academic standards and implement any minor changes required. This rigorous approach to course design is now an integral part of MEA course development activities, with existing academics demonstrating high levels of expertise in the MEA curriculum design process and providing support in this regard to new academics coming into the program. This ensures the high standard of curriculum design implemented for the MEA course development process continues.

Course materials (learning guides, readers, slides, etc.) are professionally developed, reviewed by the industry and UQ's Teaching and Educational Development Institute (TEDI) and published for students. The materials are provided to students in the first week of each semester.

6.3 Course Evaluation and Improvement

MEA has implemented a comprehensive course evaluation and improvement process. Feedback is received from the students for every course through end of semester evaluations. Course leaders collect the survey results from all MEA universities and analyse the results to identify any issues, develop an action plan to resolve these issues and report back to the Program Leaders Committee for implementation.

6.4 Collaboration Process

MEA offers a unique opportunity for students at the partner institutions to access a

much larger pool of expertise than is available through single institution programs. Academic staff who are expert in their teaching areas are called upon by other MEA universities to give a set of lectures to share their expertise with all MEA students. Using a range of technologies, including collaborative teaching tools such as Moodle, video conferencing and SparkPlus™, staff are able to teach across the institutions providing access to a rich pool of expertise and addressing shortfalls in expertise at individual institutions. The collaboration also enables cross-institutional student projects and other learning activities.

6.5 Quality Assurance and Moderation Process

In order to ensure standardisation of assessment across the program, MEA developed standard criteria for projects, group work, presentations and assignments, with the ability to adapt for specific circumstances within the individual course. It was also recognised that is some cases course teams would need to develop criteria for specific assessment items not covered by the generic tools. This work was largely carried out by the program leaders committee with feedback from other staff. A moderation process for assignments and courses was also developed. It was decided that a sample of individual and group assessment items in three of the courses would be reviewed against the standardised assessment criteria developed for each assessment item. An individual assignment, a group assignment and an individual examination made up this process.

6.6 Student Conference

MEA holds a student conference each year which showcases the best of high quality research projects undertaken by students enrolled in MEA mining engineering programs across Australia. The location of this conference is rotated each year between members' universities.

Up to five students selected from each university who are sponsored by MEA and their home university to attend and present their paper at the conference. In addition to each student receiving a certificate of participation and their paper published in the MEA journal, the best three presentations are awarded. The judging panel comprises programme directors from each of the MEA universities for the selection of award winners.

The conference is telecast live and students at each university are encouraged to engage in the Conference. Students in Years 3 and 4 are particularly encouraged to view the telecast and participate during question time.

6.7 Journal of Research Projects Review

All papers presented at the MEA Student Conference are automatically eligible for inclusion in the journal of MEA Research Projects Review, following a peer review process. This journal is circulated to the industry and other stakeholders to highlight the quality of research projects undertaken by MEA undergraduate students by publishing a selection of only the best research papers.

The Course Convenor at each university may nominate up to two further papers for inclusion in the journal. Each submitted paper must be reviewed and co-authored by the student's supervisor.

6.8 Student Exchange Program

As 3rd and 4th year curriculum of every MEA university is the same, any student from an MEA university can study at another MEA university as an exchange student for a semester or two in their 3rd or 4th year of study program. As the offered courses are the same at each institution, students have no problems with course selections/ compatibility.

This exchange study program offers many benefits for students, including:

- spending one or two semester(s) at an MEA institution other than their home node;
- opportunity to meet and work with other student groups; and
- living and studying in different location;
- possibility to link in with summer industrial work experience.

7 CONCLUSIONS

Mining Education Australia was developed to meet the increasing demand for mining industry professionals in an environment where limited funding exists within the conventional university system and to maintain a critical mass of suitably qualified academic staff. The initiative was stimulated by support and funding from the MCA representing the Australian mining industry. The MCA remains committed to the on-going financial support of MEA to deliver a world class program of undergraduate education in mining engineering.

MEA is unique from a world-wide perspective. Approximately 30 academics across four institutions develop and deliver a common curriculum. Commonly, academics develop and deliver their programs either individually or in teams within their own institutions. Developing an environment that encouraged collaboration between the different institutions and enabled the development of an agreed curriculum has been essential to the success of MEA.

MEA has become a successful initiative with superior education outcomes, including:

- a comprehensive educational program covering all aspects of mining engineering, technical, operational and social/community issues.
- improved and enhanced student experience through access to a combined national cohort of mining academics at four institutions and alternative and innovative delivery and learning methods; and
- student access to well prepared, up-to-date and quality assured teaching materials including course profiles, learning guides, reading material, slides, videos, mining industry software packages, and laboratories.

The success of the MEA was commended in the recent Accreditation Report by Engineers Australia to the School of Engineering, citing *"Team skills, project management, sustainability and ethics are all well covered throughout the program, and the implementation of MEA has assisted in mapping graduate attributes well to course content"*. MEA provides industry with graduates equipped with professional skills, life-long learning capabilities and exposure to a standard curriculum.

REFERENCES

Andrews, T. and Lind, G. 2007. Enabling collaboration: Staff perceptions of a national mining engineering collaboration. *Proceedings of the 2007 AAEE Conference,* Melbourne.

MCA. 1998. Back from the brink, reshaping minerals tertiary education, discussion Paper. *Minerals Council of Australia, national tertiary education taskforce.* MCA, Braddon ACT, Australia.

MTEC, 2015. The Minerals Tertiary Education Council, http://www.mtec.org.au/.

Tuckwell, K. 2004. Australian Undergraduate School of Mining, AuSMin. *Internal presentation,* MCA-MTEC, Hobart, Tasmania.

Is Landfill Mining a New Prospect for the Mining Sector?

M. Menegaki, A. Benardos, D. Kaliampakos, K. Tsakalakis
National Technical University of Athens, Athens, Greece

ABSTRACT Sustaining the availability of resources is one of the major challenges that the future generations will face. Traditional mining approaches seem incapable of meeting such demands and new streams for materials need to be discovered. The utilization of municipal waste can develop into a promising solution for the recovery of valuable materials and energy while at the same time minimizing the environmental strains. The paper discusses the concept of landfill mining, analyses its characteristics and furthermore it presents the approach utilized for the pilot application of landlfill mining that is currently under way in Polygyros, Greece.

Keywords: Landfill mining, Polygyros, Greece

1 INTRODUCTION

The depletion of natural resources is one of the main challenges that the global economy in general and the mining sector in particular have to face, as the material extraction has been increased rapidly since the last century. The global extraction of material resources per year in 2007 was 60 billion metric tonnes (Gt), presenting an estimated 8-fold increase over the last century, when material extraction was less than 7 Gt per year (Krausmann et al., 2009). In the U.S.A., the material resources consumed from 1900 to 1995 have grown from 161 million metric tons to 2.8 billion metric tons respectively (Matos and Wagner, 1998). The last 25 years there has been an enormous increasing in the consumption rate. Only between the years 1970 and 1995 the worldwide consumption of raw materials (not including food and fuel) doubled (USGS, 2008). According to European Commission (EC, 2011), the use of resources at the current rate, will create the need by 2050, on aggregate, of the equivalent of more than two planets to sustain us. In the EU, each person consumes 16 t of materials annually, of which 6 t are wasted. The municipal waste generation exhibits significant fluctuations among the EU countries owing to consumption patterns, levels of economic development, and organization of municipal waste collection and management Eurostat (2011). For instance, in 2009, municipal waste generation ranged from 831 kg per capita in Denmark to 316 kg per capita in the Czech Republic. Waste generation generally increased between 1995 and 2009 for the majority of the countries, with half of the waste going to landfill (EC, 2011). Although the landfilling rate has been reduced the last twenty years due to strict regulations in order to reduce the amount of wastes, landfilling remains the prevailing solid waste disposal method in many countries (Eurostat, 2014). It is estimated that in the EU the total number of closed and active landfills ranges between 150,000 and 500,000 (Hogland et al., 2011; van Vossen, 2005).

There are several studies providing data with respect to the quantities of materials disposed of in landfills. Typically, besides organic matter municipal solid waste landfills contain significant amounts of paper, plastic, wood, rubber, glass, leather and other textiles, and earth construction materials and metals (e.g. Obermeier et al., 1997; Hogland et al., 2004; Kurian et al., 2007). For example, according to Kapur and Graedel (2006), the quantity of copper located in landfills and other waste repositories around the world is about 300 million tonnes, an amount corresponding to more than 30 percent of the remaining

reserves in known ores (Frändegård et al., 2013). These waste deposits could be the source of a significant stream of secondary materials and energy (Jones et al., 2013), that could comprise the "ore" of the future.

Besides municipal solid waste landfills, mine waste heaps may also constitute an important source of materials. This is especially the case with sites polluted with heavy metals, where on one the hand they can have a significant negative impact to the environment while on the other, materials can be recovered, proceeded and finally would re-enter the production cycle. For example, in the site of the Lavrion Technological and Cultural Park (LTCP), a special "dry tomb" landfill structure was constructed to dispose of approximately 115,000 m^3 of contaminated soil containing heavy metals and toxic metalloids, such as arsenic, lead, cadmium and zinc (Kaliampakos et al., 2007). It can be seen as a man-made orebody, which might be marginal or uneconomical to be exploited today, yet it may present a significant resource, for the future. It is estimated that approximately 17,000 t of metals are found in the repository, the value of which is estimated at around $US 41.4 million, in current prices with the most significant materials being Pd and Zn.

Under the pressure of resources deficiencies and environmental challenges, many countries have included resource productivity issues in their sustainable development strategies. To this end, they have introduced integrated waste and materials management policies such as sustainable materials management (SMM), 3R (Reduce, Reuse, Recycle) related initiatives or circular economy approaches (OECD, 2011). Materials management is a conceptual framework for systematically addressing the movement of materials through the economy and the environment from extraction to end of life (USEPA, 2009). As Jones et al. (2013) mention: "…*in a circular economy material loops need to be closed by direct recycling of pre-consumer manufacturing scrap/residues (e.g. steel slags), urban mining of post-consumer End-of-Life products (e.g. recovery rare earth metals from electronic waste), and landfill mining of historic (and future) urban waste streams*….". Figure 1 presents the different ways of closing materials loops in a circular economy.

Landfill mining is described as "*a process for extracting minerals or other solid natural resources from waste materials that previously have been disposed of by burying them in the ground*" (Krook et al., 2012). Thus, landfill mining could be the chance not only to transform landfills into the new "mines", but also to enhance the image of mining sector in society as a necessary partner in modern circular economy.

In the light of the above-mentioned remarks, this paper wishes to contribute to the discussion surrounding the landfill mining issue and the role of mining sector in supporting this concept. Towards this direction, the fundamentals of landfill mining are explored and the results from an ongoing research project carried out in Greece are discussed.

2 THE CONCEPT OF LANDFILL MINING

Technically, landfill mining (LFM) is the process of excavating from operating or closed solid waste landfills by employing the method of open cast mining, and sorting the unearthed materials for recycling, processing, or for other dispositions (Lee and Jones, 1990; Cosu et al., 1996; Hogland et al., 1997; Carius et al., 1999). The concept of LFM is not new. Examples have been cited since the early 1950s (e.g. Savage et al., 1993) and it is likely that earlier, unrecorded activities took place (Fisher, 2013).

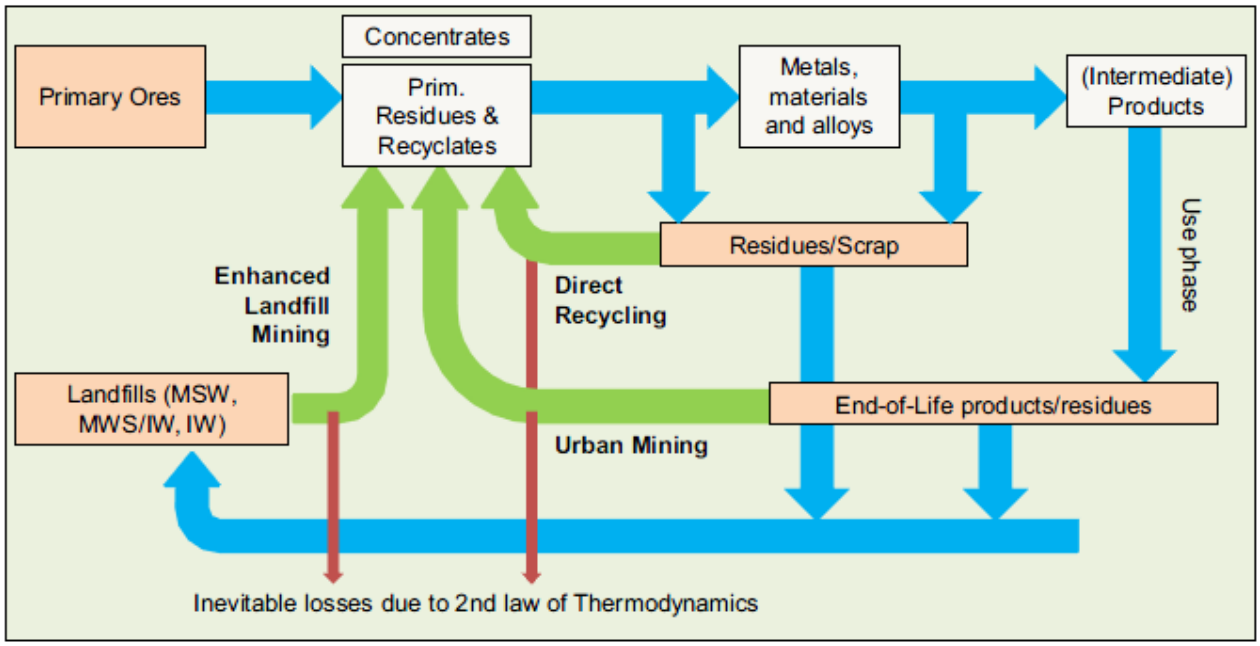

Figure 1. Different ways to close materials loops in a circular economy. Reproduced from Jones et al. (2011).

It is not a practice unique to one country, region or has any specific strategy. The initiatives for LFM are often unique to the site itself and include different objectives, such as: conservation of landfill space, reduction in landfill area, elimination of potential contamination source, rehabilitation of dump sites, energy recovery from recovered wastes, reuse of recovered materials, reduction in waste management costs (USEPA, 1997; Lee and Jones, 1990; Hogland et al., 1997; Cossu et al., 1996; Krook et al., 2012).

2.1 Considerations about Landfill Mining

There are three main strategic reasons for LFM operations, namely: (a) extraction for recycling of materials; extraction for energy recovery; and (c) extraction for the reclamation of land. These reasons may be independent drivers for LFM but may also be combined to deliver wider benefits and maximize the LFM opportunity. The third reason, however, has greater potential for considering environmental and wider sustainability drivers (Fisher, 2013).

The extraction of wastes for their recycling potential is driven by the material values in the market place. Recovered materials, such as ferrous metals, aluminum, plastic, and glass have the highest values, and are often cited as targets for LFM. Recovery of combustible materials for conversion to energy may be considered a 'renewable' energy source. Finally, landfill mining for reclamation (LFMR) for land reclamation may include one or a combination of the following:

- Landfill sites may be in locations that are ideal for other development purposes and may form a physical barrier to a development that is planned.
- Landfill sites may be a source of contamination that has to be removed.
- There may be a need to reuse the available landfill space at the site for different kinds of wastes more suitable to long-term disposal, such as non-reactive hazardous waste.

In this way, LFMR extends the life of the current landfill facility and reduces the size of the landfill "footprint". Hence, the facility operator may be able to avoid the cost and time to locate, design, permit, and construction of a new landfill; lower the cost of closing the landfill; or make land available for other uses.

So far, more than 60 LFMR projects are reported in the literature (van Vossen and Prent, 2011). Ford et. al. (2013) have

recorded 57 of them, shown in Table 1, describing also the principal project driver.

LFM, however, has certain limitations. Historic landfill sites have many unquantifiable variables and only in recent years it was made possible to assess the types of wastes a landfill site may contain (Fisher, 2013). Lack of knowledge about the nature of waste may generate safety issues. Other safety issues include physical injury from rolling stock or rotating equipment; exposure to leachate, and hazardous material or pathogens during mining or processing; subsurface fires and landfill gas emissions. Other limitations include odour and air emissions, increased traffic on roads between the landfill and resource recovery facility, extra mixing and handling of waste at the resource recovery facility, and the handling of additional inert materials.

Many of these risks are similar to traditional mining operations but are enhanced by the heterogeneous nature of the wastes in a landfill.

Table1. Principal drivers for historic and current LFMR projects worldwide

Principal project driver	Europe	North America	Asia	Total projects
Not specified	12	4	2	18
Void space recovery	3	4		7
To allow site redevelopment	5		1	6
To mitigate pollution	2	5	1	8
To improve landfill engineering (e.g. meet regulatory requirements)	4	2	1	7
Material reclamation for recycling or energy production	3	2	6	11
Total projects	29 projects across 9 countries	17 projects of which 1 in Canada and 16 in the USA	11 projects across 7 countries	57

Source: Ford et al., 2013

2.2 Landfill Mining Process

The first step in planning a LFM project involves a site survey to gather site-specific information such as its operating history, types of wastes present, dimensions, topography and physical characteristics (Salerni, 1995). Furthermore, this first step includes planning for preliminary excavation and obtaining the necessary regulatory approvals. According to Joseph et al. (2004), several factors should be addressed for planning an LFM project, e.g. proper time to begin extracting material from the landfill, taking into consideration the odour that will be produced, appropriate methodology in taking representative samples, expected quality of the recovered materials in terms of purity, variation of degradation with time, wastes and space, enhancement of waste stabilization and integration of landfill design and operation, environmental and health risks of landfill rehabilitation works, etc.

The operational phase typically consists of three primary stages: excavating, processing, and managing the excavated or processed material. The excavated waste can be processed to meet several objectives, including separating bulky materials, sorting hazardous material and other unidentified waste, screening soils from waste, and sorting materials for recycling or use as fuel. The objectives will determine at a great extent the selection of the appropriate equipment. To this end, several common mechanical processes (such as magnets for ferrous metal and eddy current separators for aluminum) can be used. Other major factors that influence the choice of processing methodology are the condition and properties of the excavated materials, as well as the cost and time for processing the

excavated material. Figure 2 presents a generalized flow chart of the process that LFM projects employed according to IWCS (2009).

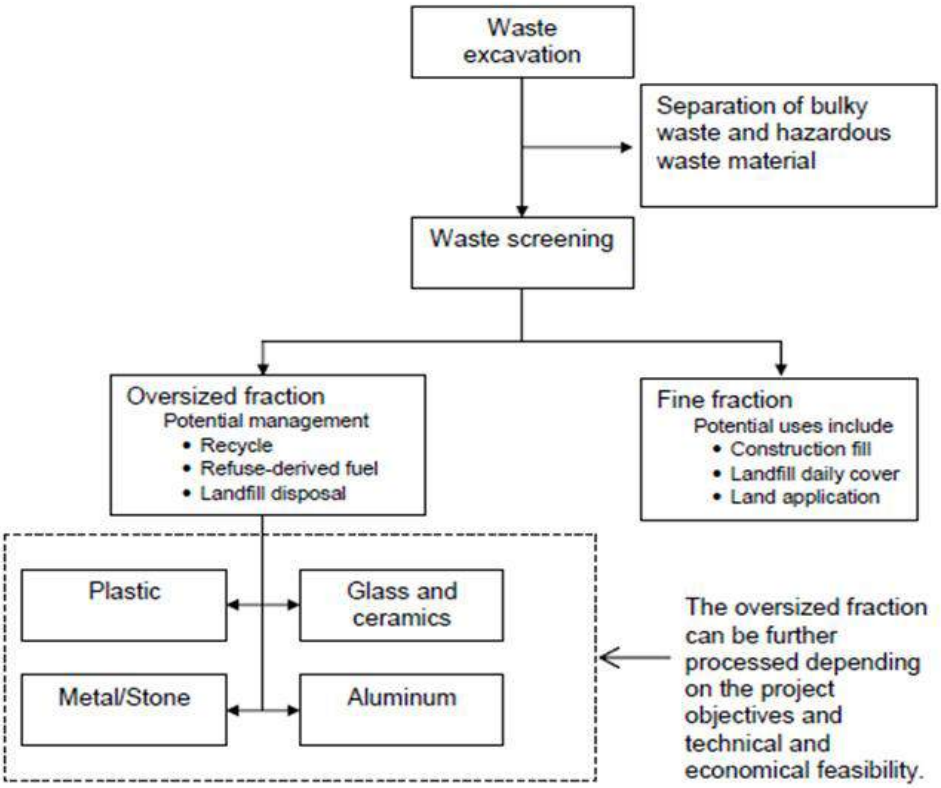

Figure 2. Landfill Mining Process (IWCS, 2009).

3 POLYGYROS LANDFILL MINING PROJECT

The mining activities in the Polygyros Landfill (PL) are part of the "LIFE-RECLAIM" research project co-funded by the EU-LIFE. The project aims at exploring both technical and social aspects of landfill mining. Thus, it will be possible to demonstrate potential environmental and economic benefits, fulfilling sustainability needs that are present not only in Greece but in many other European countries as well.

Apart from the above, the project includes the development of a demonstration waste processing and sorting unit that will serve as a pilot-scale application capable of analyzing techniques for the separation of mixed MSW.

At the current stage, the project is focused on the design of the mining scheme to be used in the facility as well as on the design of the sorting and separation unit. Also, a sampling campaign has been implemented to further analyze the nature of the waste materials in the Polygyros landfill and to provide inputs for the aforementioned design studies.

3.1 Basic Data

The Polygyros Landfill (PL) is located in Northern Greece, in the Chalkidiki area, approximately 3.5 km northwest (NW) of the Polygyros town. The PL site is developed at that hilly terrain at an elevation between +580m, at the northwestern part, and +680m, at the southern part of the area. The geology of the area is consisted mainly by phyllites and quartzites, while at places quartzite shales and quartzite sandstones are found.

The facility is operational from 2008 and covers a total area of 9.3 ha, from which the disposal area is around 2.6 ha (Figure 3).

The disposal area is developed with the use of HDPE membranes along with leachate collection pipes and pond, biological treatment plant as well as biogas active pumping.

Figure 3. General layout of the Polygyros Landfill site.

The PL is designed to hold a total of 266,000 m^3 of municipal solid waste (MSW) that will be disposed in two phases, namely A and B that have a maximum design capacity of 6,000 and 8,100 m^3 per annum, respectively. The main disposal area is located in the western part of the site and at the moment, the landfilling operations are taking place as part of the 1st phase, located at the lower part of the area.

With the maximum disposal capacity of PL set at about 8,100 m^3 per annum, its service life was estimated at around 21 years. Nevertheless, an increase in quantities of the waste brought at the PL site has been experienced in the last 2 years. This is mainly derived from the increase in the touristic volume at the area, as well as from the delays in the development of additional landfill facilities in the Chalkidiki area. Thus, the PL facility is now receiving waste streams from an area greater than initially projected, narrowing down its projected life. It is now estimated that its useful life is less than 12 years.

Thus, the development of a successful waste mining scheme apart from the recovery of materials can also lead to the extension of the service life of the facility, or in other words the recovery of valuable surface space.

3.2 Mining Plan

The mining plan provides the necessary information regarding the extraction of the HSW material from the landfill body. With respect to the project's requirements the waste materials to be mined and processed reaches a volume of approximately 1,000 m^3.

3.2.1 Sampling campaign

At first, a sampling campaign took place in order to obtain information that would be used to design the main excavation scheme. Its main purpose is to identify the type and characterization of waste in terms of content. Furthermore, it could be used to get insight regarding the physical characteristics of the waste and assess its geotechnical properties.

In the case of PL the most appropriate method is the development of sampling trenches as the depth of the landfill is relatively low. Two sampling areas were selected and their excavation took place using a typical backhoe excavator. The materials were processed using a custom made screening equipment with a sieve opening of 15 cm. The materials identified were mainly rock and soil materials (50%) while metal content (ferrous and non-ferrous) ranged from 1-1.5% and the plastics were about 4%.

3.2.2 Mining area selection

The target area for the development of the mining scheme should be (a) representative of waste content, (b) easily accessible to the equipment and (c) appropriately located in areas where the extraction works could not interfere with the daily waste disposal operations. The best possible arrangement, given the current state of the PL site, is to designate the mining area at the elevation of +620 m, at the central part of the disposal area, approximately 30 m eastern from the toe area of the current working cell.

In there, the mining could take place almost independently from the disposal operations. At the same time, the waste material found there covers a significant part of the PL's working life, from almost 2008 to 2012. Another advantage of the position is the minimization of the development works required for the setting up of the haulage road. The main internal access network of the PL will be used, while only limited new road development is required at the level of +620. The area where the processing unit will be installed is located at the entrance point of the disposal area, and thus, the total haulage length from the designated mining area to that point is almost 125 m. The proposed arrangements, the designated mining and processing areas along with the proposed haulage access road are presented in Figure 4.

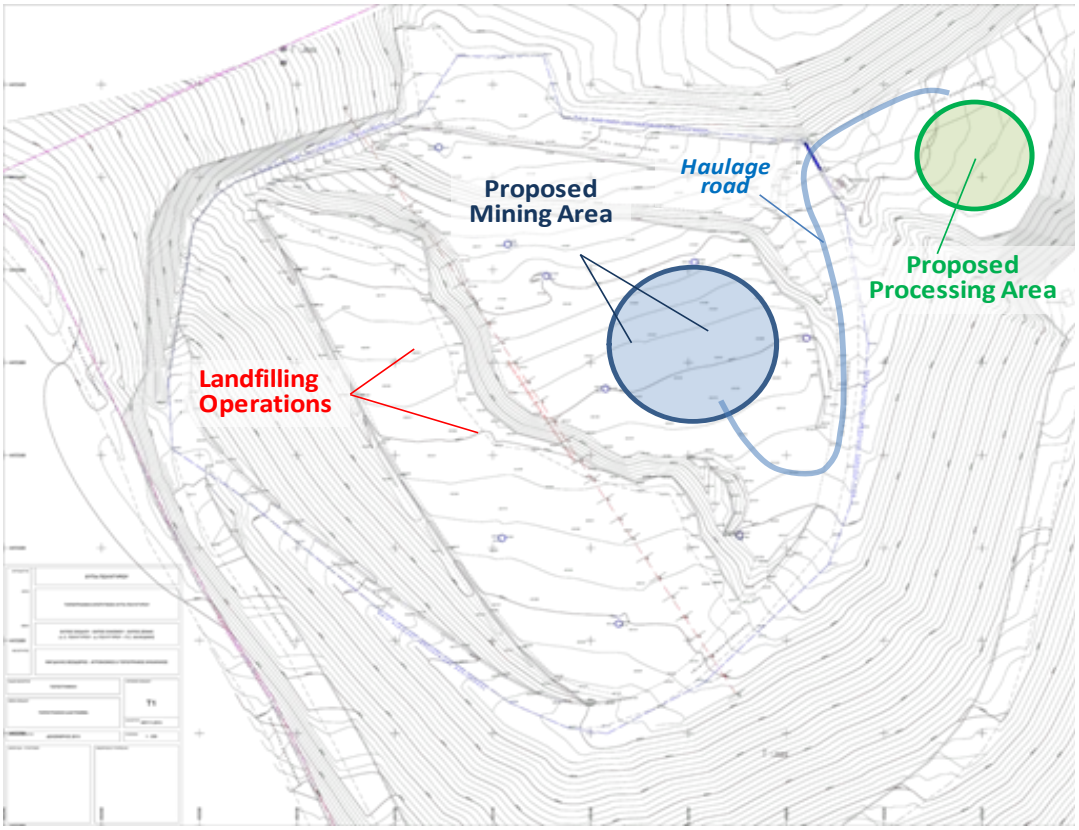

Figure 4. Proposed location of the landfill mining area, with respect to the current landfilling operations and the proposed processing area.

3.2.3 Mining process

The mining of the waste will be made with conventional surface mining equipment. At this stage the whole process is designed so that the work can commence at the start of the spring of 2015, taking advantage of the favorable weather conditions. The PL mining scheme proposes the excavation to take place from the top (+620 m level) using a hydraulic excavator at the crest area, rather than making the extraction from the toe using front-end loaders and by scraping the wastes. The excavator can perform quite well with high productivity, extracting the loose waste found below, up to a depth of 4 - 5 m. The other alternative would require the

development of an initial trench excavation and then the moving of the equipment (front loader and bulldozers) at the lower extraction level. This method could be applied successfully to a large scale mining scheme, but in the current mining application the development of the initial trench alone can provide the required waste volume. Therefore, the direct mining approach selected for the Polygyros pilot LFM is more simple, straightforward and therefore less risky and more productive.

Based on the proposed mining plan, the waste will be mined using 3 - 5 m wide and 3 - 4 m deep trenches, aligned in the NW-SE direction. Special attention will be paid to the gas extraction wells found in the area or other fixed infrastructure so as not to disturb them. The trench excavation will start from one end (the SW - or the NE one) having a length of about 20 m. At the end of the section the next cut will start. The excavation will continue to develop towards the NE (or SW) direction, until the target volume of 1,000 m^3 is reached. It is estimated that finally a "box cut" of about 20 x 20 x 4 m will be developed, at the end of the operations.

In terms of stability, the relatively shallow excavation is expected not to create strains or problems to the slope. Yet, special attention needs to be paid with a constant careful assessment of the waste condition directly below the excavator. Caution is to be paid in cases of extreme rainfalls that could deteriorate the stability conditions. In those events the possibility of the temporary suspension of the excavation will be considered.

As a general rule, the final slope of the mined area should not exceed the 1:3 limit. Furthermore, a buffer distance of around 5 to 10 m is required between the mined area and the adjacent southwestern landfilled slope. A safety distance should be kept between the loading trucks and the trench's crest, with each truck stopping at least 2 - 3 m away from the working face.

The rate of excavation will be directly linked with the feeding capacity of the processing unit, as the possible temporal stockpiling of the waste material needs to be minimized for environmental reasons. Thus, the excavation will be taking place at intervals but no apparent problems or other issues are anticipated, as long as a constant flow of materials can be maintained. However, for flexibility reasons, the possibility of developing a small stockpile near the processing unit will be considered. However, the proper design of the unit in terms of feeding rate can ensure the smooth operation in both the mining and the screening process. Based on preliminary estimations the whole mining and waste processing phase can be completed in about 25 working days.

At the start of the operation, the soil cover will be carefully removed and stockpiled for further reuse. The mining face need to be covered with soil so as to minimize odour issues, reduce windblown litter, etc. This can be done on a daily basis, at the end of the working shift. To facilitate the whole process, having also in mind the excavation rate, it is recommended that the exposed working face should be kept to a minimum. Further issues to take into account are the problems related to storm water and runoffs after heavy rainfalls. It is recommended that a surface water drainage system (e.g. diversion berms, grading of the surface adjacent to the excavation) could appropriately address such issues. For the case of the exposed face in the trench excavation a geomembrane cover will be applied, so as to minimize waste and water interference.

The haulage of the material will be performed using standard dump trucks. Their capacity is quite adequate to cover the capacity of the excavator and the processing unit, given the relatively small transport distance. The road network should be periodically inspected and properly maintained. Also in case where dust problems are expected, water spraying can be applied in the road surface with the use of tanker trucks.

Finally, the environmental monitoring of the site will take place, identifying critical

conditions and safeguarding the compliance with the environmental standards.

4 CONCLUDING REMARKS

The depletion of the mineral resources, together with the environmental footprint of former and operating mining sites, puts a lot of stress in mining companies. To deal with the challenges of the new era, a lot of discussion is being made for re-exploitation of low grade resources, underwater mining or even extraterrestrial mining. Technological evolution may allow these types of exploitation in the near future. Nevertheless, in terms of sustainability, the sector should look into the opportunities they appear today in order to continue not only to be competitive but also to respond to the increasing social requirements.

To this end, a number of individual companies have started to develop a better understanding of the full life-cycle of minerals and metal products, so as to maximize societal value and minimize impact on human health and the environment (USEPA, 2009). To this end, urban mining has become a familiar term describing different types of materials recycling potentials (i.e. electronic waste, demolition waste). As Krook and Baas (2013) mention, although landfill mining could be considered as a subcategory of urban mining, it contains features making it somewhat different, since landfill mining originates from the waste sector associated with serious problems. Moreover, there are significant uncertainties with regard to the composition of waste in each site. The objects of the majority of projects that have been carried out until today, were mainly the conservation of landfill space, the remediation or the solving of other traditional waste management issues (Frändegård et al.; 2013). There is an emerging approach, however, presented in several studies (e.g. Baas et al., 2010; Jones et al., 2010; Krook et al., 2012) of landfill mining as a strategy to recover deposited materials and energy resources by employing more advanced, up-to-date material separation and processing technologies (Krook and Baas, 2013). This approach is the result of the outcomes of a lot of studies showing that in many regions of the world massive amounts of metals have accumulated in landfills (Lifset et al., 2002; Kapur and Graedel, 2006; Müller et al., 2006; Krook et al., 2012).

In the light of the above, it is evident that the mining sector could have a key role in landfill mining, provided that it has the state of the art technology for mining and material processing. At the same time, the mining sector has an opportunity to improve its environmental performance and its poor public image. The landfill mining concept, however, is quite new in general and for the mining sector in particular. The uncertainties involved in this process are much alike the uncertainties involved in the potential exploitation of a new ore. Each potential "ore" coming from both natural resource reservoirs and landfills is unique. Composition of the extracted materials, market variability, financial, environmental and social costs and benefits should be estimated for each project individually. But, this is what the mining sector has been traditionally doing. After all it is another "dirty job but somebody has to do it".

ACKNOWLEDGEMENT

This work was supported by the LIFE+ financial instrument of the European Community in the context of LIFE RECLAIM "Landfill mining pilot application for recovery of invaluable metals, materials, land and energy" (www.reclaim.gr), Grant: LIFE12 ENV/GR/ 000427. The coordinating beneficiary is ENVECO S.A. and the associated beneficiaries are the Municipality of Polygyros, School of Mining & Metal Engineering NTUA and HELECTOR S.A.

REFERENCES

Baas, L., Krook, J., Eklund, M., Svensson, N., 2010. Industrial ecology takes a second look at landfills, *Regional Development Dialogue*, UNCHR, 31(2), pp. 169-181.

Carius, S., Hogland, W., Jilkén, L., Mathiasson, A., and Andersson, P-Å., 1999. A Hidden Waste Material Resource: Disposed Thermoplastic, *Proceedings of the 7th International Waste Management and Landfill Symposium*, 4-8 October 1999, Cagliari, Italy, pp. 229-235.

Cossu, R., Hogland, W. and Salerni, E., 1996. Landfill Mining in Europe and USA. *ISWA Year Book*, International Solid Waste Association (ed), pp. 107-114.

European Commission, 2011. *Roadmap to a Resource Efficient Europe*, COM (2011) 571. Available from: http://ec.europa.eu/environment/resource_efficiency/about/roadmap/index_en.htm

Eurostat 2014. Landfill rate of waste excluding major mineral wastes. Available from: http://ec.europa.eu/eurostat/tgm/table.do?tab=table&init=1&language=en&pcode=t2020_rt110&plugin=1

Eurostat, 2011. *Municipal waste statistics. Statistics explained*. Available from: http://ec.europa.eu/eurostat/statistics-explained/index.php/Municipal_waste_statistics

Fisher, R., 2013. Landfill Mining. ISWA Key Issue Paper. Available from: https://www.iswa.org/index.php?eID=tx_iswaknowledgebase_download&documentUid=3154

Ford, S., Warren K., Lorton, C., Smithers, R., Read, A. and Hudgins, M., 2013. *Feasibility and Viability of Landfill Mining and Reclamation in Scotland", Scoping Study*, Final Report, Zero Waste Scotland.

Frändegård, P., Krook, J., Svensson, N., Eklund, M., 2013. A novel approach for environmental evaluation of landfill mining, *Journal of Cleaner Production*, 55, pp. 24-34.

Hogland, W., Hogland, M., Marques, M., 2011. Enhanced landfill mining: material recovery, energy utilization and economics in the EU (Directive) perspective, *Proceedings International Academic Symposium on Enhanced Landfill Mining*, Houthalen-Helchteren, pp. 233-247.

Hogland, W., Marques, M. and Thörneby, L., 1997. Landfill Mining - Space Saving, Material Recovery and Energy Use, *Proceedings of Seminar on Waste Management and the Environment-Establishment of Cooperation Between Nordic Countries and Countries in the Baltic Sea Region*, 5-7 November 1997, Kalmar University, Kalmar, Sweden, pp. 339-355.

Hogland, W., Marques, M., Nimmermark, S., 2004. Landfill mining and waste characterization: a strategy for remediation of contaminated areas, *Journal of Material Cycles and Waste Management*, 6, pp. 119–124.

IWCS, 2009. *Landfill Reclamation Demonstration Project*, Innovative Waste Consulting Services, Perdido Landfill, Escambia County, Neighborhood and Community Services Bureau, Division of Solid Waste Management.

Jones, P.T., Geysen, D., Rossy, A., Binge, K., 2010. Enhanced Landfill Mining (ELFM) and Enhanced Waste Management (EWM); essential components for the transition to Sustainable Materials Management (SMM). In: Jones, P.T.,Tielemans, Y. (Eds.), *Enhanced Landfill Mining and the Transition to Sustainable Materials Management*, Haletra, Houthalen-Helchteren, pp. 19-37

Jones, P.T., Geysen, D., Tielemans, Y., Passel, S.V., Pontikes, Y., Blanpain, B., Hoekstra, N., 2013. Enhanced Landfill Mining in view of multiple resource recovery: a critical review, *Journal of Cleaner Production*, 55, pp. 45 – 55.

Jones, P.T., van Gerven, T., van Acker, K., Geysen, D., Binnemans, K., Fransaer, J., Blanpain, B., Mishra, B., Apelian, D., 2011. CR3: cornerstone to the sustainable inorganic materials management (SIM2) research program at K.U. Leuven, *Journal of Metals*, 63(12), pp. 14-15.

Joseph, K., Nagendran, R., Palanivelu, K., Thanasekaran, K. and Visvanathan, C., 2004. *Dumpsite Rehabilitation and Landfill Mining*, CES, Anna University, Chennai-600 025, India.

Kaliampakos, D., Damigos, D., Karachaliou, T. 2007. Using the "dry tomb" technique in the remediation of heavily contaminated land. *Proceedings of the 10th Int. Symposium on Environmental Issues and Waste Management in Energy and Mineral Production (SWEMP 2007)*, December 11-13, 2007, Bangkok, Thailand.

Kapur, A., Graedel, T.E., 2006. Copper mines above and below ground. Estimating the stocks of materials in ore, products, and disposal sites opens up new ways to recycle and reuse valuable resources, *Environmental Science & Technology*, 40, pp. 3135–3141.

Kapur, A., Graedel, T.E., 2006. Copper mines above and below ground. Estimating the stocks of materials in ore, products, and disposal sites opens up new ways to recycle and reuse valuable resources, *Environmental Science & Technology*, 40, pp. 3135–3141.

Krausmann, F., Gingrich, S., Eisenmenger, K., Erb, K-H., Haberl, H., Fischer-Kowalski, M., 2009. Growth in global material use, GDP and population during the 20th century, *Ecological Economics*, 68(10), pp. 2696-2705

Krook, J., Baas, L., 2013. Getting serious about mining the technosphere: a review of recent

landfill mining and urban mining research, *Journal of Cleaner Production*, 55(15), pp. 1-9.

Krook, J., Svensson, N., Eklund, M., 2012. Landfill mining: a critical review of two decades of research, *Waste Management*, 32, pp. 513-520.

Kurian, J., Esakku, S., Nagendran, R., 2007. Mining compost from dumpsites and bioreactor landfills, *International Journal of Environmental Technology and Management*, 7, pp. 317–325.

Lee, G. F. and Jones, R. A., 1990. Use of Landfill Mining in Solid Waste Management. *Water Quality Management of Landfills Conference*, Water Pollution Control Federation, Chicago, IL, pp. 9.

Lifset, R.J., Gordon, R.B., Graedel, T.E., Spatari, S., Bertram, M., 2002. Where has all the copper gone, *JOM*, 54, pp. 21–26.

Matos, G. and Wagner, L., 1998. Consumption of materials in the United States 1900–1995. Annual Review of Energy and the Environment, 23, pp. 107–122.

Müller, D., Wang, T., Duval, B., Graedel, T.E., 2006. Exploring the engine of anthropogenic iron cycles, *PNAS*, 103, pp. 16111–16116.

Obermeier, T., Hensel, J., Saure, T., 1997. Landfill mining: energy recovery from combustible fractions, *Proceedings Sardinia '97, Sixth International Landfill Symposium*, Cagliari, Italy, pp. 569–578.

OECD, 2011. *Resource Productivity in the G8 and the OECD - A Report in the Framework of the Kobe 3R Action Plan*, Organisation for Economic Co-operation and Development, Paris. Available from: http://www.oecd.org/env/waste/47944428.pdf

Salerni, E.L., 1995. Landfill Reclamation Manual, *Reclaim-95-Landfill Mining Conference*, 28-29 September 1995, SWANA Landfill Reclamation Task Group.

Savage, M.G., Golueke, C.G. and Stein, E.L., 1993. Landfill Mining – Past and Present, *Biocycle*, 34(5), pp. 58–61.

USEPA, 1997. *Landfill Reclamation*, United States Environmental Protection Agency, Solid Waste and Emergency Response (5306W), EPA530-F-97-001.

USEPA, 2009. Sustainable Materials Management: The Road Ahead, EPA 530-R-09-009. Available from: http://www.epa.gov/epawaste/conserve/smm/pdf/vision2.pdf

USGS. 2008. *Materials Flow and Sustainability*, Available from: http://pubs.usgs.gov/fs/fs-0068-98/fs-0068-98.pdf

van Vossen, W., 2005. *Aftercare of Landfills - Overview of Traditional and New Technologies*, Report prepared for the Interreg IIIC project Sufalnet4eu. Available from: http://www.sufalnet4.eu/

van Vossen, W.J and Prent, O.J, 2011. Feasibility study – Sustainable material and energy recovery from landfills in Europe", *Proceedings of the 13th International Waste Management and Landfill Symposium*, Sardinia 2011.

Occupational Health and Safety

A Review of Preconditioning and its Influence on Mining Conditions with Particular Emphasis on Health and Safety

S. Modisha and T. Zvarivadza
School of Mining Engineering, University of the Witwatersrand, Johannesburg, SA

ABSTRACT The basic premise of any mining operation is to be profitable. In light of this, there should be a balance between safety and maximum extraction. Current gold mining in the Witwatersrand occurs at depths that are in excess of 3 kilometres. At such great depths, stress conditions are increasingly high and seismicity is also widespread. The success of any operation at these depths thus depends on the efficient negotiability of these high stresses. These stresses are capable of inducing violent ejection of rock from the faces which is detrimental to the workmen in the vicinity of the face area. Preconditioning as a means to ameliorate rockburst conditions in deep level gold mining complexes was introduced and it has since proven to be beneficial at various experimental sites.

The primary objective of this research was to conduct a review of preconditioning as a means to mitigate face bursts and its influence on mining conditions with particular emphasis on the Health and Safety aspects. The investigation process to complement this review was undertaken at one of the deep hard rock underground mines in South Africa. An extensive review of the current state of preconditioning and the advances thereof was conducted to unfold the techniques and mechanisms involved in preconditioning. The detailed investigation at the South African deep hard rock mine established that preconditioning, if applied correctly as per well informed mine standards, can be used as a tool to combat face bursts.

The authors observed that the correct application of the technique is the most important factor in order to ensure the effectiveness of this tool. The research also noted that well preconditioned stopes are generally safer than those that are incorrectly preconditioned or not preconditioned at all. It also follows that incorrect preconditioning is worse than not preconditioning at all. It is a recommendation of this paper that the importance of preconditioning, its operational benefits and correct application should be reiterated to stoping crews to ensure that stopes are safe for the workmen in the vicinity.

Keywords: Preconditioning, mitigate face bursts, health and safety

1 INTRODUCTION

Mining in the Witwatersrand Basin currently occurs at depths greater than 3000 metres and at vertical virgin stress levels which are in excess of 79MPa. Relatively high mining induced stresses are also inevitable under such conditions. The mine studied in this research is located in a seismically active and geologically complex deep level mining area. At such great depths the Ventersdorp Contact Reef (VCR) and the Carbon Leader Reef (CLR), which host most of the remaining gold resources becomes prone to rock bursting conditions due to the increased stress profile which then poses a significant safety risk to the workforce in the vicinity.

A rock burst occurs when the stored strain energy is abruptly released resulting in a violent ejection of the highly stressed rock from the mine workings (Eberhardt, 2014). Rock bursts are therefore associated with mining in high stress areas which is prevalent in the current South African gold mining landscape. A violent failure of a mining face results in a faceburst. This has become a widespread problem in deep level gold mining due to the presence of the hard and brittle quartzite rocks and relatively high stress regimes imposed on the rock mass.

Fatalities, possible stope closures hence lost production time; equipment damage and loss of mineral resource are inevitable from these conditions if there are no control measures in place to mitigate the effects thereof. Owing to this, the mining industry was prompted to conduct extensive underground investigations in the 1950s which then led to the implementation of preconditioning as a tool to ameliorate face burst conditions in deep level gold mining industry.

The research investigates and reviews different issues with regards to preconditioning as a means to ameliorate rock burst damage in underground gold mining and its influence on mining conditions. The effects of incorrect or not preconditioning and the consequences thereof with regards to safety of the workers are determined and reviewed. The study also compares preconditioning as it is applied at the face with the set out preconditioning standard.

1.1 Seisimicity Challenge and the Need for Effective Preconditioning

The VCR and CLR of the Witwatersrand basin are faceburst prone and as such, this poses a significant risk to people working in the vicinity of the stope areas. Face bursts and falls of grounds are the major causes of fatalities and injuries in narrow reef mining. Rock bursts and rock related accidents reportedly account for some 25% of all reportable injuries and more than 50% of all fatalities in the gold mining industry.

Preconditioning the stope face has been implemented as a technique to alleviate these risks thereby providing a safe working environment for the workmen in the stopes. It is therefore imperative to review the application of this technique with regards to its success and associated shortcomings in order to recommend appropriate corrective measures which effectively improve current practices which are widely applied in narrow reef gold mining.

2 PRECONDITIONING BACKGROUND

2.1 The Development of Preconditioning

The management of the East Rand Proprietary Mines (ERPM) along with the Council for Scientific and Industrial Research (CSIR) introduced preconditioning, then referred to as de-stress blasting in the 1950s, as a means to mitigate the effects of face bursting conditions in deep level gold mining (Roux et al, 1957 as cited in Lightfoot et al, 1996). Since then, a wealth of knowledge on this technique has been gathered and compiled to provide guidance on how to negotiate such dangerous conditions. Between 1990 and 1996, there were 214 fatalities that were a result of 134 face burst incidents across the South African gold mining industry (Toper et al, 1998). The basic premise on which preconditioning was based at that time was that the effects of face bursts can be reduced by increasing the depth of the fracture zone. Albeit the damage resulting from face burst incidents is only local, that is, events with a magnitude less than 2, it still poses a significant risk to the workers as stopes would typically have a concentration of eight to ten workers at any one time.

This then led to the undertaking of the Gold and Platinum (GAP)030 and GAP336 projects by the Rock Engineering programme of the CSIR to develop and implement preconditioning techniques that will effectively control face ejection rock bursts to allow safer mining in seismically hazardous areas. These projects have led to some of the major developments on de-stress blasting which include two preconditioning techniques namely; face parallel and face perpendicular preconditioning both of which have practical limitations in terms of the mining environment in which they can be applied. Some of the major recommendations from these projects were to include preconditioning in the mine's code of practice so as to enable the mine's safety personnel to follow up on compliance and to also educate the production personnel and train stoping crews on implementing

preconditioning which then changed the safety landscape of deep level gold mining.

2.2 The Mechanism of Preconditioning

Pre-conditioning, previously referred to as destressing is a means of reducing the potential for rock burst damage by extending existing fractures ahead of faces and thus moving the high concentration of stresses away from the immediate face area into the solid rock. The potential for faceburst is reduced by remobilising existing fractures into the rockmass thereby preventing the accumulation of strain energy ahead of the working face (Venter, 2008). Preconditioning mitigates the effects of a seismic event by acting as a cushion between the seismic event and the working place. Figure 1 illustrates an idealised model of how preconditioning moves the peak stresses that has accumulated in the rock mass further away from the face such that the inevitable bursting that would happen could occur within the fractured zone, with fractures acting as a cushion to reduce the consequent effects of such bursting.

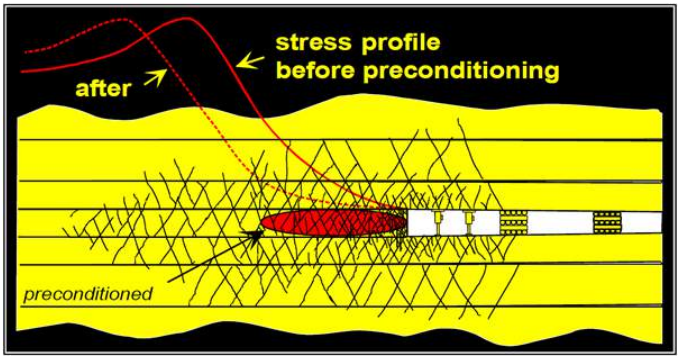

Figure 1. Stress redistribution due to preconditioning (Venter, 2008)

A preconditioning blast, after being set off, pulverises the rock in the immediate vicinity of the blast hole. This pulverisation is a result of the high compressible stresses acting on the wall of the preconditioning hole. As a result, the hole is pressurised thus generating stress waves capable of creating an intense radial fracturing zone close to the preconditioning hole (Toper *et.al*, 2003). The gases originating from the explosives in the preconditioning hole extend radially outwards from within, into the surrounding rock mass thereby extending the existing fractures by forcing apart the sides of the existing fractures to reduce any clamping stresses present in the rock. This would then encourage slip across factures and will ultimately relieve the stresses acting on the immediate face.

2.2.1 The GAP030 Project

The GAP030 project provided guidelines on optimal parameters and the actual methodology for the implementation of the various preconditioning techniques (Lightfoot et al, 1996). Some of the parameters proposed include the optimal spacing of 3m between preconditioning holes and offsetting of holes 50cm from the previous day's holes. Figure 2 illustrates the basic outline of the three day cycle preconditioning technique as was proposed in the GAP030 project report.

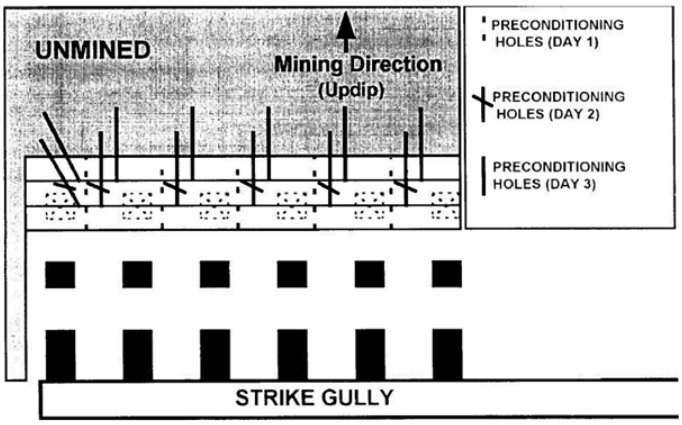

Figure 2. Layout of the three day preconditioning cycle (Lightfoot et al, 1996)

Lightfoot et al (1996) further postulated that stress transfer is a dynamic process that is a response to mining and preconditioning, as such it should be amalgamated into the mining cycle in a controlled and sequential manner. Also, based on the preconditioning experimental site, it was established that the effects of preconditioning are local and temporary in both space and time. It followed that every production blast must be carried out concurrently with a preconditioning blast to ensure maximum

face stability. The GAP030 project established that preconditioning works on the mechanism of slip on existing fractures rather than the generation of complete new fractures, the cause of slip at that stage, with the then available body of knowledge was however not known. Lightfoot et al (1996) also proposes that as an additional benefit, preconditioning can be seen to trigger larger seismic events.

2.2.2 The GAP336 Project

The GAP336 project was aimed at informing the practicing engineer about the importance of correct application of the technique chosen. The findings of this project included the specifications of conditions under which the various preconditioning techniques can be implemented i.e. face parallel preconditioning is widely used in pillar and remnant extraction. The advantages and disadvantages of each technique were also weighed out as shown in table 1.

Table 1. Comparison between face perpendicular and face parallel preconditioning techniques

Perpendicular face drilling	Parallel face drilling
Primary mining	Secondary mining
Ideal for deep level mining and up dips	Ideal for extraction of stability pillars
No special equipment required	Special equipment required
Integrated into the existing mining cycle	Requires a special production cycle
No limit on face length	Limits face length

Also, assessing the effectiveness of each technique was an important recommendation of the GAP336 project. Because this project was based on an experimental site, individual mines might have different conditions and as such practicing engineers were advised to optimise or adjust preconditioning parameters such that they would suit the specific site conditions of that particular mine.

2.2.3 The GAP811 Project

Further works done by CSIR Miningtek for the Safety in Mines Advisory Committee (SIMRAC) involved determining the criteria for preconditioning at high stoping widths in the research project GAP811 which involved the establishment of various high stoping preconditioning experimental sites. It was recommended that the preconditioning holes must be drilled at 60cm from the hanging wall to avoid over hanging faces. This project further established that training of mining personnel on the correct implementation procedures of preconditioning was an essential component of its success in mitigating the effects of rock burst damage (Toper et al, 2003).

2.2 Quantifying the Effects of Preconditioning

Research was further undertaken by Grodner (2001) to effectively establish an optimal method of preconditioning; Ground Penetrating Radar (GPR) was used to quantify the effects of preconditioning on the fracture patterns. This was an essential undertaking as it affirmed the initial hypothesis formed regarding fracturing of rock ahead of the stope face. The radial zone of influence of each preconditioning hole was also established which then allowed the optimisation of preconditioning. Assessing fracture patterns was also essential for understanding whether precondition blasts result in the development of entirely new fractures or the extension of pre-existing fractures which is essentially the framework of the mechanism by which preconditioning occurred (Grodner, 2001).

Mitri (2000) as cited in Saharan and Mitri (2011) postulates that even though preconditioning can be used to contain the effects of strain bursting, measures like using alternative methods and appropriate rock support systems such as back filling were necessary to reduce the damaging effects of excessive stresses. This is a particularly important realisation because depending on preconditioning to remedy all rock related problems underground might deem it ineffective to a certain extent. It is also worth noting that preconditioning is only a tactical measure while a change in mining layout can be incorporated in the

mine design and should therefore be planned in advance and as such it is a strategic measure.

Saharan and Mitri (2011) state that a major challenge with preconditioning is that the source that is responsible for initiating rock bursts is yet to be known. The fact that the timing of these events cannot be predicted regardless of the scientific and technological advances made in mining poses a persistent risk to future mining. This poses a significant problem such that a proactive technique which could entirely alleviate rock burst damage cannot be implemented without the understanding of the genesis thereof. This is also a challenge to researchers as rock burst might increase despite the application of preconditioning (Saharan and Mitri, 2011).

A case study done at Mponeng mine affirms that there is a decrease in the occurrence of face bursting during effective shift times and the frequency of injuries associated with seismicity (Viljoen, 2003). This is attributed to the improved hanging wall and face conditions and as such, this technique is seen as the only tool to ameliorate face bursts (Viljoen, 2003). In this case study, it was established that drilling of preconditioning holes at 60cm from the hanging wall has some practical implications such that it necessitates the establishment of two preconditioning standards for high and low stoping widths respectively. This led to a conclusion that preconditioning holes must be drilled in the middle, between the hanging and footwall to produce one preconditioning standard so as to avoid confusing the stoping crews (Viljoen, 2003).

3 RESEARCH OBSERVATIONS

3.1 Utilised preconditioning approach

Panels that are situated in highly stressed grounds are preconditioned in order to alter the behaviour of the overstressed rock and thus minimise the hazards and risks that are associated with these stress levels. The mine uses a face perpendicular preconditioning technique which was decided by weighing it against the face parallel technique which cannot be incorporated in the current mining cycle. Four underground working places were investigated

3.1.1 The Preconditioning Cycle and Drilling

Using drilling machines that are used for normal production holes, 2.4m preconditioning holes (twice the production hole length) are drilled at 90 degrees to the face, spaced 3m apart. There should thus be enough spacing between the last line of support and the face to accommodate the use of these 2.4m drill steels. These holes are drilled in the middle of the face between the bottom and top holes in the channel of the reef and must be drilled at least 60cm below the intended hanging wall so as to not compromise the stability of the hanging wall.

Lightfoot *et al* postulated that the effective area of a preconditioning hole is indeed 1.5m in radius after assessing Giltner (1992)'s assumption and as such these holes are drilled at 3m spacing. However, observations made at the study working places have shown that rock drill operators (RDOs) have a proclivity to drill these holes at distances that are either shorter or greater than the prescribed distances.

This technique is cyclic and each cycle consists of 3 days. Consistent with the findings by Toper *et al* (2003, 71-72), preconditioning holes are offset at 50cm from the sockets of the previous day's preconditioning holes along the strike of the reef. The panel face is advanced almost 2.7m (0.9m advance/day) in three days and as such the holes of the fourth day are drilled on the same position as the one for the first day. Also, with such an advance rate, there should not be sockets remaining at these positions because three production rounds would have been blasted. Figure 3 shows a typical layout of the 3 day cycle face perpendicular preconditioning technique.

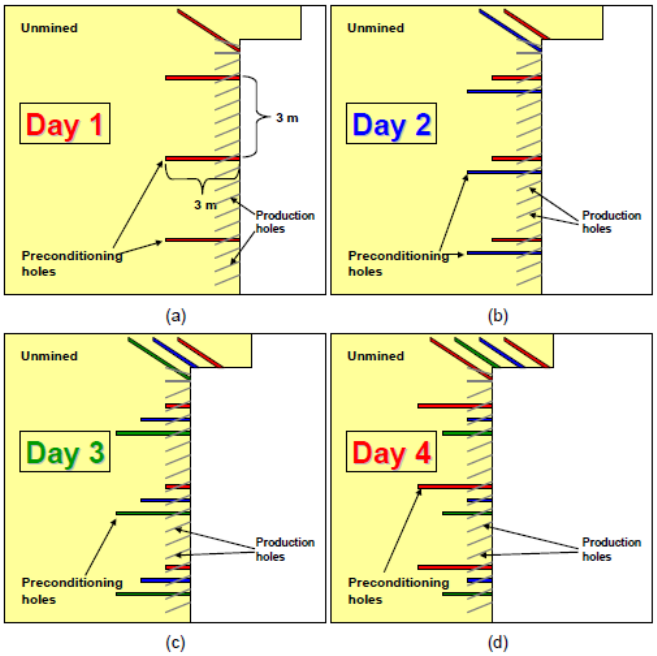

Figure 3. Layout of the three day cycle preconditioning technique (Toper *et al*, 2003)

3.1.2 Charging and timing

Preconditioning works by allowing shearing along pre-existing fractures in the rock mass so as to redistribute the stresses in the immediate face area to the solid rock ahead of the face and as such large volumes of gas are required to extend these fractures. The same explosives that are used to charge up the production round are used for preconditioning hole. The 34mm diameter preconditioning holes are charged from the bottom with a water based gel and top primed for 1.4m. The remaining 1m of the hole is stemmed with tamping clay to retain the maximum explosive energy thus achieving efficient fracturing. 2.4m long fuses are used to time the preconditioning holes. These holes are timed such that they have a four-hole burning front; this ensures that they detonate four holes before the normal production holes could detonate. An illustration of the charging up of preconditioning holes is shown in figure 4.

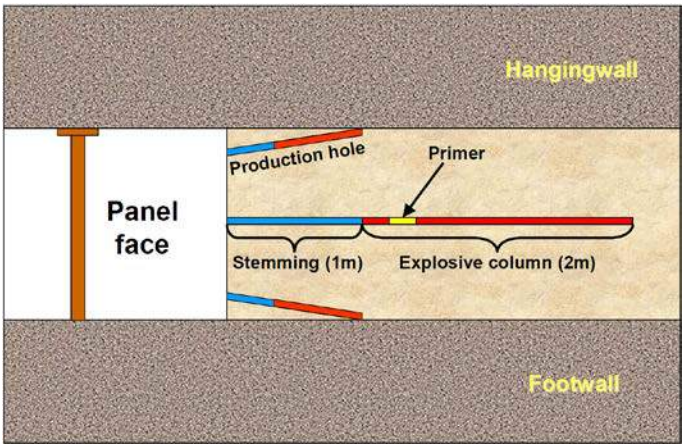

Figure 4. Illustration of charging up of preconditioning holes (Toper *et al*, 2003)

3.2 Preconditioning Human Factor Observation

Some stope crew believe that drilling preconditioning is extra work and as such, they should be paid for it. In some stopes, stoping crew believe that the night shift did not clean the panel and as such, the RDOs could only start cleaning late in the shift, production holes were therefore prioritised over preconditioning holes. It is crucial to note that pressure from management wanting production may lead production crews to focus more on drilling production blast holes. Behavioural change amongst all interested parties is needed in order to facilitate improvements in the preconditioning technique.

4 Evaluation Of Reseach Observations

4.1 Preconditioning Parameters

4.1.1 Hole length

This is sometimes not done completely to standard. This is evidenced by preconditioning holes that are shorter than the specified length of 2.4m in the preconditioning standard. Although the variance between the specified hole lengths and the ones measured is not grossly disproportionate, if the hole length is shorter or longer than 2.4m, there may be grave consequences. Drilling of short holes may render preconditioning ineffective resulting in misfires and under breaking of the face.

Excessive stresses would be placed in the rock ahead of the face should over breaking occur.

Drilling of longer holes also has detrimental consequences in that it will result in fracturing of the block too far ahead of the face. This will essentially leave a slightly fractured area between the previously fractured area and the newly preconditioned area. A highly stressed block ahead of the face will then be created leaving an area which could potentially result in face bursting.

4.1.2 Spacing

The radius of influence of each preconditioning hole was found to be 1.5m on either side which translates to spacing between preconditioning holes of 3m. Holes that are spaced at a distance greater than the prescribed spacing result in a stress amplification between these holes. The stresses become concentrated in the portion of the area between these holes that did not fall into the area defined by the radius of influence of each hole. This causes stress concentrations between holes. The increased stress levels between these holes thus increases the chances of instability.

4.1.3 Charging and Timing

Preconditioning holes should be charged as per specified mine standard. A common misconception that overcharging of holes would result in maximum stress transferal was noted, instead this gives similar effects to that of drilling short holes in that it results in under breaking of the face. This then places excessive stresses ahead of the face which can be detrimental to the workmen in the vicinity once this position of the face area is encountered. While over charging of the holes is detrimental to the safety of the workers, under charging will render preconditioning ineffective by resulting in misfires. Misfires are time consuming to clean and may potentially lead to lost blasts which are detrimental to production and the total mine productivity.

4.2 Preconditioning and seismicity

Scattered mining configuration as is practiced at the mine often necessitates creating reef and off-reef pillars for regional stability which can induce seismicity. The scattered mining configuration is largely due to the fact that the mining complex is highly faulted. Seismic events associated with these pillars do not only occur while active mining is taking place in their vicinity but after a considerable amount of time Van der Heever (1998). The relatively high frequency of seismic events in the mining complex can, in part, be attributed to the scattered mining configuration. Also, the load on these pillars increase as more areas are being stoped out; pillars also deteriorate in terms of strength and stability over time. Although preconditioning does not reduce the likelihood of a seismic event, it mitigates the effects of such an event by acting as a cushion between the seismic event and the working place, thus preventing the face from bursting and the consequent risk of injury to the people in the vicinity. Preconditioning offers protection against face bursting but it cannot influence the source of the events causing the face to burst. Also, preconditioning can be seen to induce seismicity, such that the fractures allow a controlled release of strain energy in the highly stressed areas.

4.2.1 Preconditioning Judgement

The checklist provided in Table 2 was used by the authors for an objective judgement of the preconditioning blasts that were recorded during the research. This was done for each of the four working areas investigated.

The approach takes the approximate amount of explosives used and the subsequent seismicity recorded into account so as to minimise the subjectivity in the judgement.

Table 2. Example checklist for first working area

Preconditioning Checklist	
Day 1	
Average spacing between holes	3m
Average Length of holes	2.2m
Average Inclination to the hangingwall	85°
position of the holes on the face	middle
Day 2	
Condition of the face (blocky, fractured or smooth)	fractured
How many holes detonated?	all
Are there any misfires?	no
Average Length of day 1 sockets	1.9m
Average spacing between holes	3.4m
Average length of holes	2.3m
Average inclination to the hangingwall	75°
position of the holes on the face	middle
Day 3	
Condition of the face (blocky, fractured or smooth)	smooth
How many day 2 holes detonated?	5
Are there any misfires?	Yes (3)
Average length of day 1 sockets	1.2m
Average length of day 2 sockets	1.8m
Average spacing between holes	3m
Average Length of holes	2.2m
Average Inclination to the hangingwall	80°
position of the holes on the face	middle
Day 4	
Condition of the face (blocky, fractured or smooth)	fractured
How many day 3 holes detonated?	all
Are there any misfires?	no
Average length of day 1 sockets	0.3m
Average length of day 2 sockets	0.9m
Average length of day 3 sockets	0m
Average spacing between holes	2.9m
Average Length of holes	2.1m
Average Inclination to the hangingwall	85°

4.3 Operational Benefits of Preconditioning a Stope Face

Preconditioning has certain operational benefits when done correctly. Some of the benefits observed by the authors during the study include:

- Improved ground conditions and consequently a smoother hanging wall and stope face. These conditions result in better stoping width control.
- In a less stressed face, the face advance per blast tends to increase which therefore results in greater productivity.
- Consistent and better fragmentation resulting from efficient drilling and blasting.
- Safer working environment for the workers in the vicinity of the face area due to a smoother hangingwall and a less stressed immediate face area.
- Easier cleaning (scraping) made possible by improved fragmentation.
- Reduced stoping costs due to a better stoping width control.
- As an additional benefit, preconditioning can also serve to trigger larger seismic events in that it encourages a controlled release of stored strain energy.
- The summed effect of a safer working environment, easier workload and more production resulting from improved face advances equals increased stoping team confidence due to safety and production incentives.

4.4 Strategic and Tactical Measures to Supplement Preconditioning

Preconditioning, if employed correctly can significantly alter the behaviour of overstressed rock by mobilising the fracture zone ahead of the advancing stope thus forcing it to dissipate the stored strain energy as well as reducing its load carrying capacity. This technique has proven to be effective and as such it can prevent fatalities and ore reserve abandonment due to stope closures or ultimate mine closures by the issuing of penalties from the department of mineral resources. However, to adequately improve some problems underground, a change in mining method or stope layout may be necessary and as such, it should be done rather than depending on preconditioning in its entirety to remedy all rock related problems (Toper et al, 2003). Also, efficient support systems can go a long way in supplementing preconditioning.

4.4.1 From scattered to sequential grid mining

The mining configuration employed at the mine shaft is scattered mining which involves leaving of strike pillars. In face burst prone areas, it is quite evident that strategic measures included in mine design such as a properly sequenced stoping process as opposed to the scattered mining configuration currently employed can minimise the rockburst damage. One such

strategic measure would include the switch to sequential grid mining in all the stopes which is capable of capping the Energy Release Rate (ERR) in the mining front by limiting the mining span

Sequential grid mining is characterised by leaving systematic dip pillars for regional support as opposed to strike pillars left during scattered mining and as such, this makes the mining layout more orderly due to the predetermined grid of mining. Because the current mining is occurring at a geologically complex district characterised by faults and dykes near the stopes and it is at depths in excess of 2000m where there are a lot of remnant areas left between stopes, mining induced seismicity and rock bursting pose significant risks to the workmen. Sequential grid mining method is an ideal strategy for reducing the number of remnants being formed and the associated seismicity generated on these geological features would be kept at a minimum (Handley et al, 2000).

4.4.2 Support systems

The use of elongate support and in-stope roof bolts to minimise the effects of seismicity has proven to be successful as a tactical measure to complement preconditioning and as such, the correct implementation has to be reiterated to the workforce. Back filling to fill out mined out areas reduces the occurrence and the effects of large seismic events thus reducing rock bursting conditions.

5 CONCLUSIONS

An efficient preconditioning methodology relieves stresses on the immediate face area thus providing a safe working area to the workmen in the vicinity.

To mitigate the effects of face bursts, a face perpendicular preconditioning technique is used at the mine shaft. This was on the basis that this technique does not pose any significant disruption in the mining cycle and can easily be integrated into the existing mining. The technique offers some operational benefits when carried out properly on top of the main benefit of ameliorating face bursts, this gives more impetus for the workmen to precondition the face with every blast.

Preconditioning involves stress redistribution from the immediate face area back into the solid rock ahead of the mining face, existing fractures are remobilised. It is localised in both space and time and as such it has to be carried out with every blast because its benefits are temporary. This technique is a proactive tool in combating face bursts incidences and providing a safer working environment.

The summed effect of a safer working environment and increased throughput due to improved advance rates leads to increased worker morale.

The authors recognise that there is still room for improvement in the application of this technique at the mine and give the following recommendations to facilitate the improvement.

• The importance of preconditioning has to be reiterated to the stoping crews to ensure maximum adherence to the mine standard thus achieving the desirable results. It is also worth reiterating that incorrect preconditioning can exacerbate the stress conditions on the face by inducing face bursts rather than the prevention thereof, as such, if preconditioning is to be done, it has to be done correctly.

• Regular training needs to be carried out to ensure that workers adhere to the standards. Training of newer employees and re-training older employees on the importance of preconditioning is also imperative. Preconditioning depends largely on correct application and as such, its success lies in ‘on the job’ training and coaching of employees to ensure that preconditioning standards are thoroughly adhered to.

• If maximum results are to be achieved, some sort of a compliance incentive has to be introduced. The mine can adopt the same system of incentivising the workmen for installing in-stope rock bolts. This will encourage the workers to correctly precondition the panels on a daily basis.

• Dynamic or rapid yielding support systems such as pre-stressed elongates and hydraulic props in faceburst prone areas still prove to limit the extent of rockburst damage as such, they must be installed correctly as per mine standard on support systems.
• Alleviating safety problems should be done as a holistic approach, mine design and planning strategies that can effectively reduce or expose workers to rock bursting conditions should be taken rather than the utter reliance on preconditioning to alleviate all rock bursting conditions. This would ensure that a proactive approach of risk amelioration is adopted in a bid to reach the resilience stride of the risk maturity journey model.

REFERENCES

Eberhardt, E. (2014). EOSC 547: Tunnelling & Underground Design. The University of British Colombia Geological Engineering department. Available at: http://www.eos.ubc.ca/courses/eosc547/lecture-material/Topic6-WeakRockTunnelling.pdf (Accessed on 15 April 2014).

Grodner, M. (2001). Delineation of rockburst fractures with ground penetrating radar in the Witwatersrand Basin, South Africa. International Journal of Rock Mechanics and Mining Sciences, 38(6), pp 885-891.

Giltner, S.G. (1992). Proposed method of preconditioning stope faces with small diameter blastholes. Comro internal note number 06/92.

Handley, M.F., de Lange, J.A.J., Essrich, F., and Banning, J.A. (2000). A review of the sequential grid mining method employed at Elandsrand Gold Mine. The Journal of the South African Institute of Mining and Metallurgy, vol 100 (3), May/June, pp 160 – 167.

Lightfoot, N., Kullman, D.H., Toper, A.T., Stewart, R.D., Grodner,M., Janse van Rensburg, A.L., and Longmore, P.J .(1996). Preconditioning to reduce incidence of face bursts of highly stressed faces. Safety in Mines Research Advisory Committee, GAP 030, Available at: http://researchspace.csir.co.za/dspace/handle/10204/1640 (Accessed on 27 February 2014).

Saharan, M.R, and Mitri, H. (2011). Destress Blasting as a Mines Safety Tool: Some Fundamental Challenges for Successful Applications. Procedia Engineering, vol.26,pp 37-47.

Toper, A.Z., Kullman, D.H., Lightfoot,N., Stewart, R.D., Grodner,M., Janse van Rensburg, A.L., and Longmore, P.J (1998). Develop and implement preconditioning techniques to control face ejection rockbursts for safer mining in seismically hazardous areas. Safety in Mines Research Advisory Committee, GAP336.

Toper, A. Z., Janse van Rensburg, A. L., Milev, A.M., Grodner, M.W and Noble, B.R. (2003). Criteria for preconditioning at various stoping widths in different geotechnical areas, Safety in Mines Research Advisory Committee, GAP 811, Available at: http://www.mhsc.org.za/sites/default/files/GAP811Final.pdf (Accessed on 16 March 2014).

Van der Heever, P.K. (1998). A seismic investigation of mine tremors in the Klerksdorp mining complex. The Chamber of Mines of South Africa. pp47-50.

Venter, D.P. (2008). Pre-conditioning course. Rock engineering exam preparation courses. Rock Engineering Training Institute. Available at: http://www.reti.co.za/Downloads/ (Accessed on 17 March 2014).

Viljoen, J.L. (2003). Preconditioning: A tool to combat face bursts at Mponeng. AngloGold Ashanti Available at: http://www.ammsa.org.za/admin/tech/files/pre_conditioning_mponeng_sep2003.pdf (Accessed on 20 February 2014).

A Risk Assessment Approach to Achieving Mining Safety Goals

D. Kent
Mine Site Technologies, Sydney Area, Australia

ABSTRACT Given the recent focus on mine safety in Turkey, and the role of technologies to support these initiatives this paper discusses the two differing approaches to mine safety that have developed over the years in the USA and Australia. Though the outcomes can be similar, the approaches are from two different viewpoints; one being prescriptive based (USA) and the other being risk assessment based (Australian).

A key difference is one vests the control, and hence responsibility, with the mine operator and workers, whilst the other approach vests much of the responsibility with the government authorities to police mine operators to ensure they follow the legislated rules. Focus will be placed on the outcomes that result, in that similar systems and technologies may be deployed, but the actual quality of the total safety systems can vary quite significantly.

This paper discusses these approaches to improving safety and some of the key technologies, including tracking and communication systems, that provide the engineering controls to key mining risks as well as meet stringent mine safety laws.

Keywords: Risk assesment, mining safety, tracking, communication systems, mine safety laws

1 INTRODUCTION

There is a striking difference in the approach different countries around the world take in addressing safety and management processes of their respective industries. This paper will focus on the US and Australian mining industries, as they are both well regarded internationally and represent first world mining.

Stepping back to 2006 the coal industry in the US was jolted by the tragic explosion at Sago Mine that resulted in the death of 12 miners. Mine Site Technologies was pulled into the subsequent analysis and media frenzy because some of our equipment got into the hands of government authorities and was waved around in Senate hearings.

What became apparent was a fundamental difference to how safety was managed and implemented between the US and Australia mining industries.

The difference is the one that really interested me. It was best summed up by a common question, that was almost an accusation, I was asked when discussing our communication and tracking technologies at industry forums and presentations in 2006.
When I mentioned how 90% of the underground coal mines in Australia had a certain one of our technologies installed, the common remark was: ’”Yeah, yeah that’s because *the regulations say* they must have it”.

My response was “No, our technology was installed because it was the best available device to *manage a risk they had identified*”.

Then the common comeback was along the lines of: “Yeah, yeah, that’s because the *law says they have to install it*”. As if the “it” was specified precisely.

And around it went.
These exchanges kept me thinking for a long time and have resulted in this paper.

2 WHAT WILL WORK?

Australia had their “Sago” in 1994 when 11 miners we killed in an explosion at Moura No.2 Mine in Queensland. It really stunned the industry, particularly the Queensland

industry including both the mining companies and government authorities.

Here we were in 1994, improved laws, inspections and equipment, and yet this happened again. Over the preceding 20 years there had been major explosions at Kianga, Appin and Moura No.4 mines resulting in a total of 39 deaths.

To the industry's credit the mine operators, government authorities and unions stood back and realized there had to be a better way to improve safety, just implementing new rules or regulations did not get to the heart of the problem.

Taking a lead from the chemical and the oil & gas industries, a safety system was developed around risk management principles.

As previously mentioned, up to now safety was driven by new rules and regulations, forcing miners to install better equipment, specific back-up devices, etc. But this hadn't worked as effectively as hoped.

What was needed was a change of process, and that process driven by all involved, being the unions, mining companies and government. Plus the responsibility and control rests with those directly involved in its use – the mine management and mine workers.

Basically there was a duty of care to every employee to be able to arrive at work, complete their shift and go home safely to their families. All well and good, but how to achieve it?

So over a number of years this new approach to safety was developed and the trust between parties was established that allowed the benefits of this new way of safety to be realized.

The result? The following two Figures show the dramatic reduction in Fatalities and Lost Time Injury Frequency rates (LTIFR) since 1980.

Balanced against this is another interesting statistic, Figure 3 shows the productivity of Australian coal mines over a similar period.

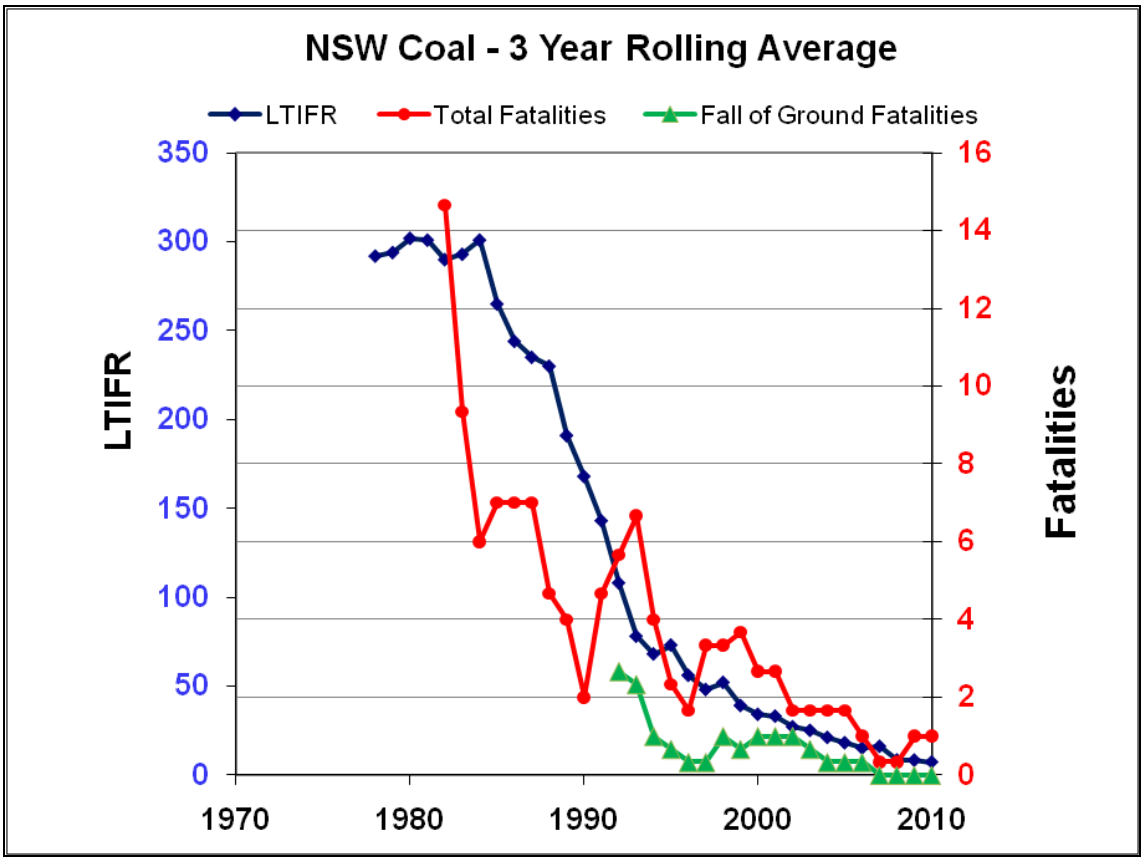

Figure 1. Fatalities & LTIFR in NSW Coal Sector (from Galvin 2011).

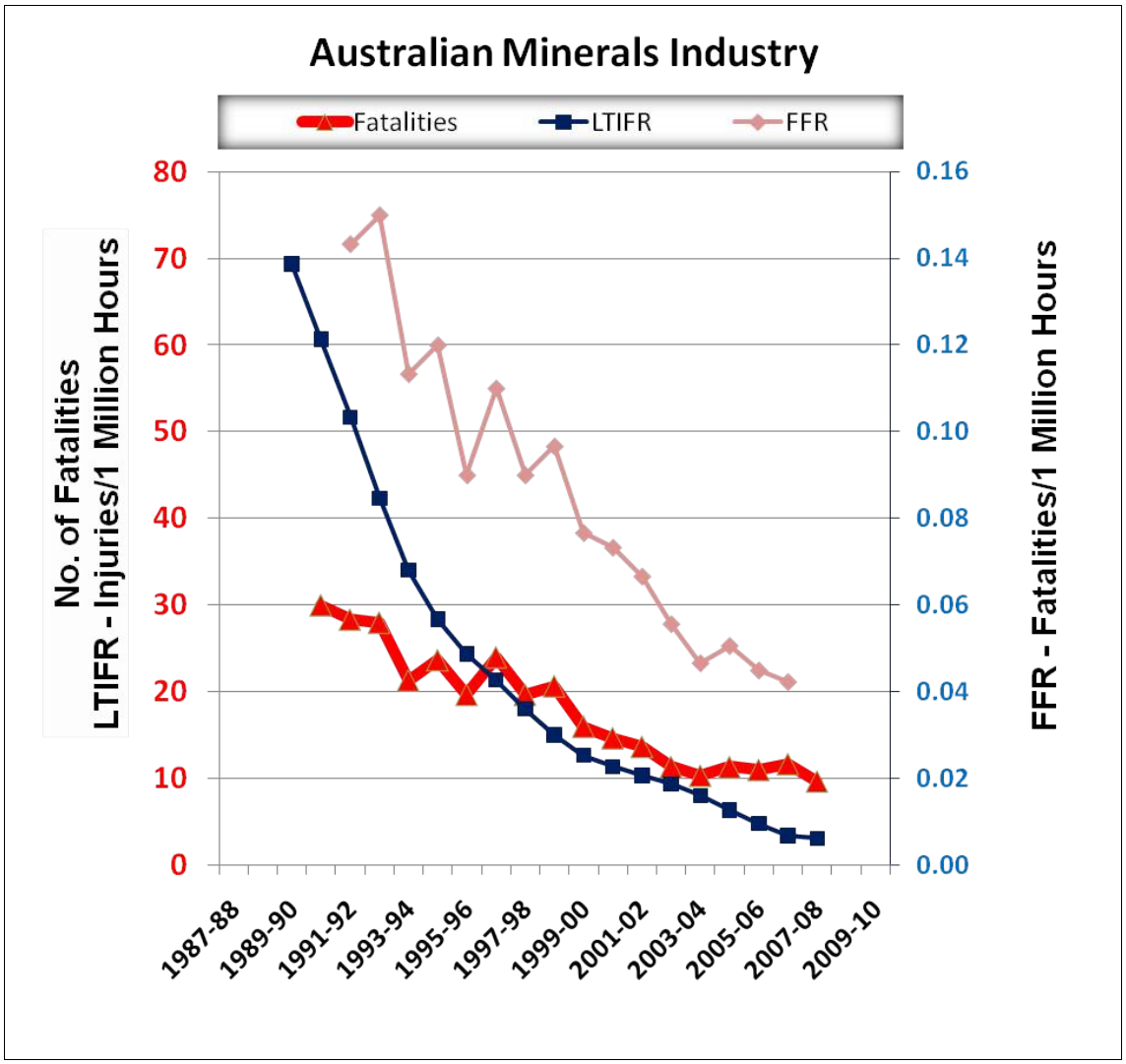

Figure 2. Fatalities & LTIFR in Australia Minerals Industry (Galvin 2011)

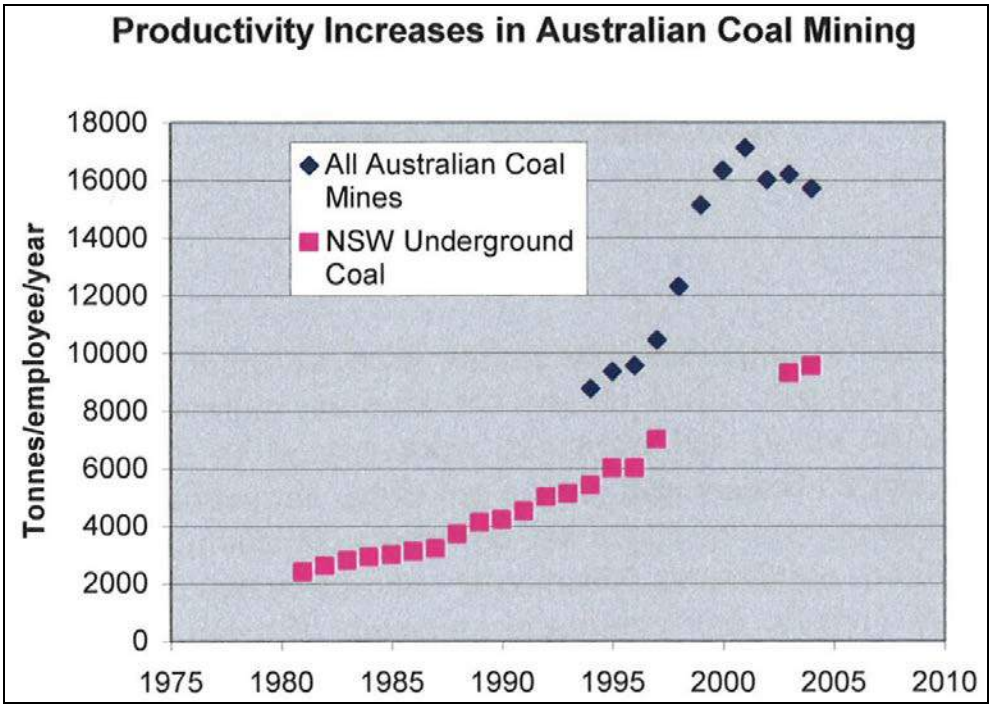

Figure 3. Productivity Increase in Australian Coal Mining since 1980 (Galvin 2005)

Over this same period there had been excellent improvements in the US industry as well, where a more traditional prescriptive approach dominates.

Though flattening over the last few years, the US industry has had major advances in mine safety, as demonstrated by the fall in the number of fatalities over the years as shown in Figure 4.

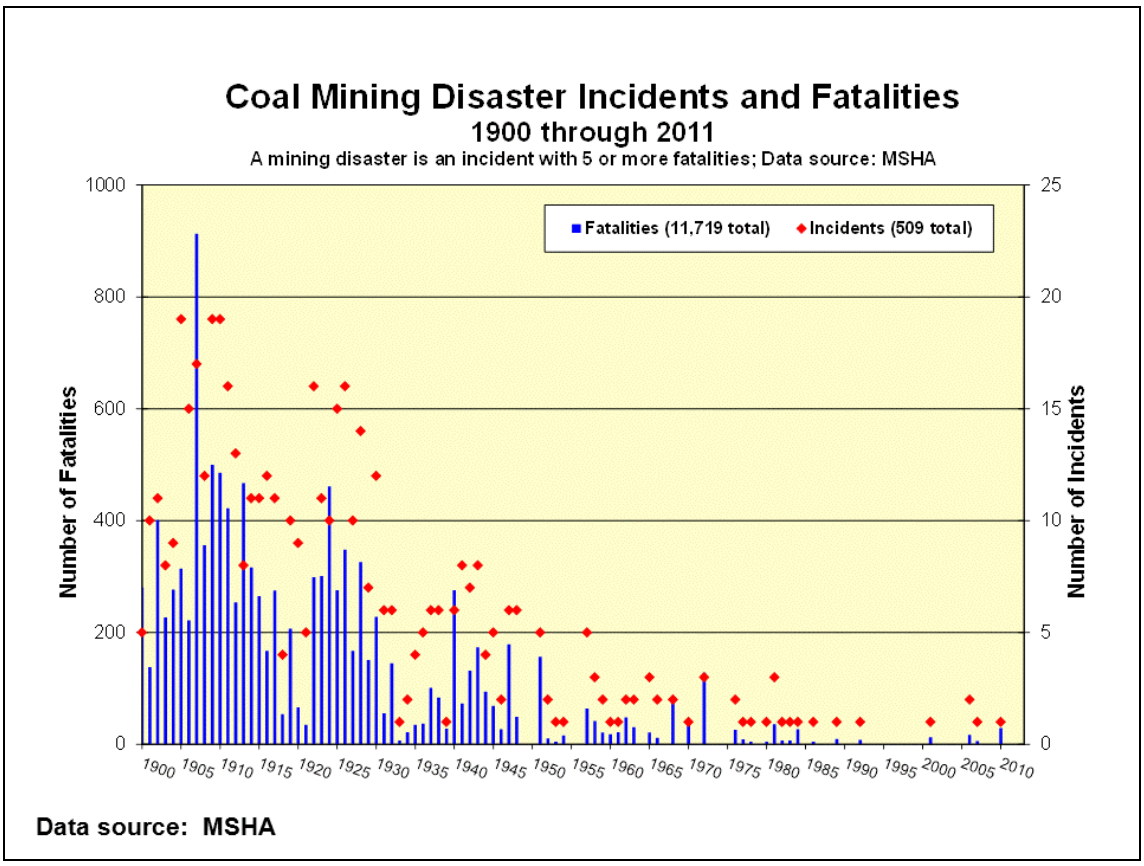

Figure 4. Coal Mining Fatalities 1900 to 2011 (MSHA)

3 THE PROCESSES BEHİND THE SAFETY IMPROVEMENT

The end result between the US prescriptive approach and the Australian risk assessed approach is often remarkably similar in what ends up being implemented at the individual mine sites.

Given the investigations and analysis that goes on after a mining disaster, this is not surprising. However, having been witness to, and involved in both industries for considerable time, I would contend the risk assessed approach is more proactive as opposed to the more reactive, prescriptive approach.

Basing your safety systems on a risk assessment approach, means that as each aspect of the operation and its safety systems are analysed in a risk assessment, there is an immediate responsibility to address the issues identified in that risk assessment. The responses being:

- Eliminate the risk if possible.
- Put engineering controls & barriers in place to minimise the risk,
- Put controls in place should an event occur to minimise the impact of the event on the people and the mining operation.
- Develop procedures to reduce risk

The classic Bowtie Diagram in Figure 5 illustrates this very well

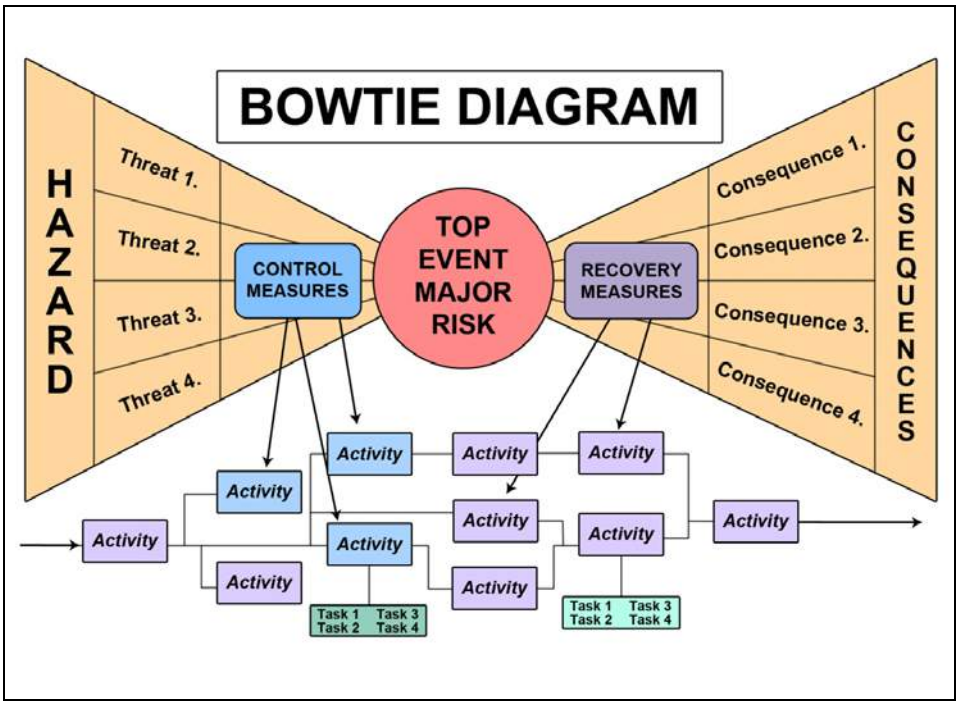

Figure 5. Bowtie Diagram

This is not new to many people, but to implement it properly throughout an operation is a significant task. Good miners anywhere have always done their own "mini risk assessments" every time they start their day at the face. When I started on the face the older, experienced miners I was with just didn't leap onto machines and start cutting coal, they spent a minute or two looking around. Basically, it was a long entrenched, albeit brief, private risk assessment process.

What the modern risk assessment processes of today are doing, is allowing the individual experience and ideas to be gathered and shared in a formalized process.

This entails the involvement of the mine workers and operators, as well as management, as a single team. This reinforces a critical element in a successful risk assessment – the shared responsibility and commitment to implement the recommendations.

And for someone who has straddled the older prescriptive system in Australia to the newer proactive approach, success can only be achieved in the latter by a cultural change in the attitude to mine safety. When I worked underground we lost about one guy every year or two at the operations, and twice it was a co-worker in the crew I worked in.

It was shattering, it was sad, BUT in some way there was a tacit assumption by everyone that it was "expected", after all "mining is a dangerous game". That attitude has completely changed and I can stand here today and say I do not believe that there is one person in the Australian or US mining industry that would consider a fatality as inevitable. That is a considerable change and it did take time.

So what are the processes behind the improvements? Apart from individual assessments on new equipment or situations, the process began with a foundation of each mine required to manage their core risks and develop Safety Management Plans for all aspects of the operation. Core Risks for underground coal mines were identified and the Safety Management Plans had to address them. The generic core risks are shown in Table 1.

Table 1. Core Risks

Core Risk	Related Risks & Items
Ground Control	Strata Stability: -Local -Regional
Ventilation	-Gas -Fires & Explosions -Dust
Spontaneous Combustion	Related to ventilation & design, but categorized separately
Water Inrush	
Failure to Isolate	-Electrical -Mechanical, including hydraulic & pneumatic
People/Vehicle Interaction	Most recent of what is a general core risk
Other Mine Specific Risks	Such as: -Lightning & extreme weather

Managing Core Risks through risk assessments can have many paths leading to the Safety Management Plans. A typical process can be seen in the development of TARPs (Trigger Action Response Plans) in Queensland, Australia.

As an example of this process a key risk is identified at a high management or Board level. This in turn leads to a risk assessment or assessments at each operation exposed to the risk, out of which a number of controls and procedures are identified to eliminate or reduce the risk and any consequences should they occur.

Then this flows into the so called TARPs for the practical implementation and management of the controls at the mine site. The TARPs are designed to allow for a simple flow of actions that can be easily followed, even under the stress of a major incident.

Diagrammatically the process is shown in Figure 6 below.

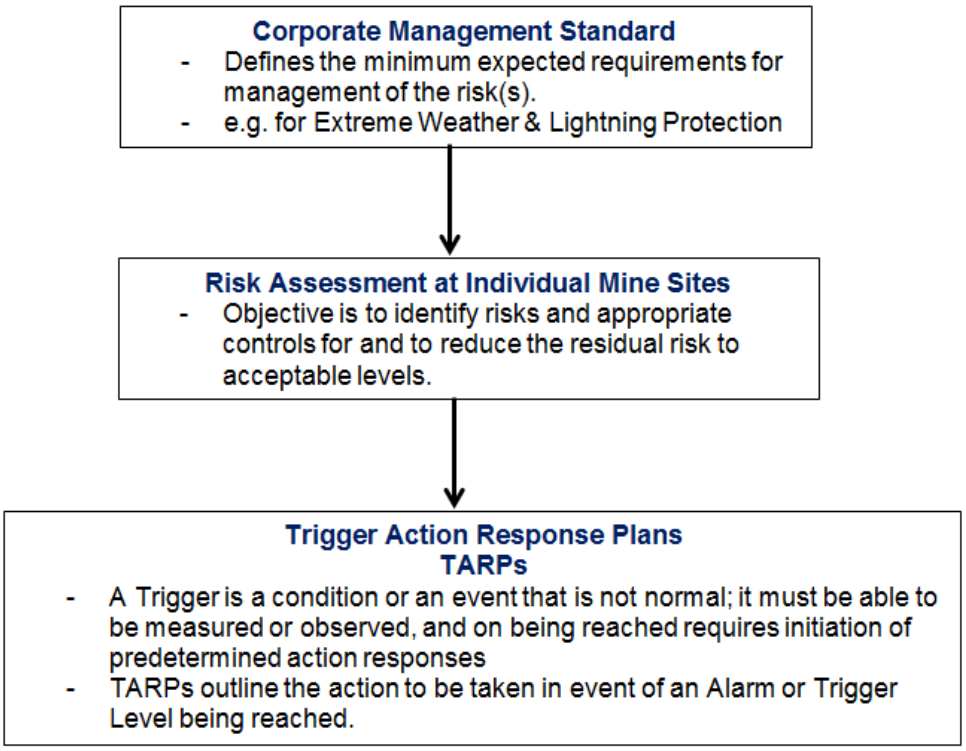

Figure 6. Simplified TARP Development Diagram

So, again, what is the difference in the end result between the two approaches adopted by the US and Australia – sometimes very little. Similar equipment and systems are in place trying to control and manage risks.

But the timing of implementation and on-going reviews and improvements do seem to vary.

For example in the area of communications in which we are closely involved, once the risk assessment methodology started to be taken up, companies identified risks in the lack of communications in emergencies, so we found from the mid to late '90's mines in Australia were equipping all miners going underground with our Personal Emergency Device (PED) pagers, rather than just 20% to 30% of the workforce.

The process to get to this decision was started with the requirements of the Safety Management Plans, one of which being the Emergency Management Plan (Emergency Preparedness Plan). The following Figure shows the overall plan structure, and in this case also shows the role of emergency exercises that are conducted in Queensland coal mines.

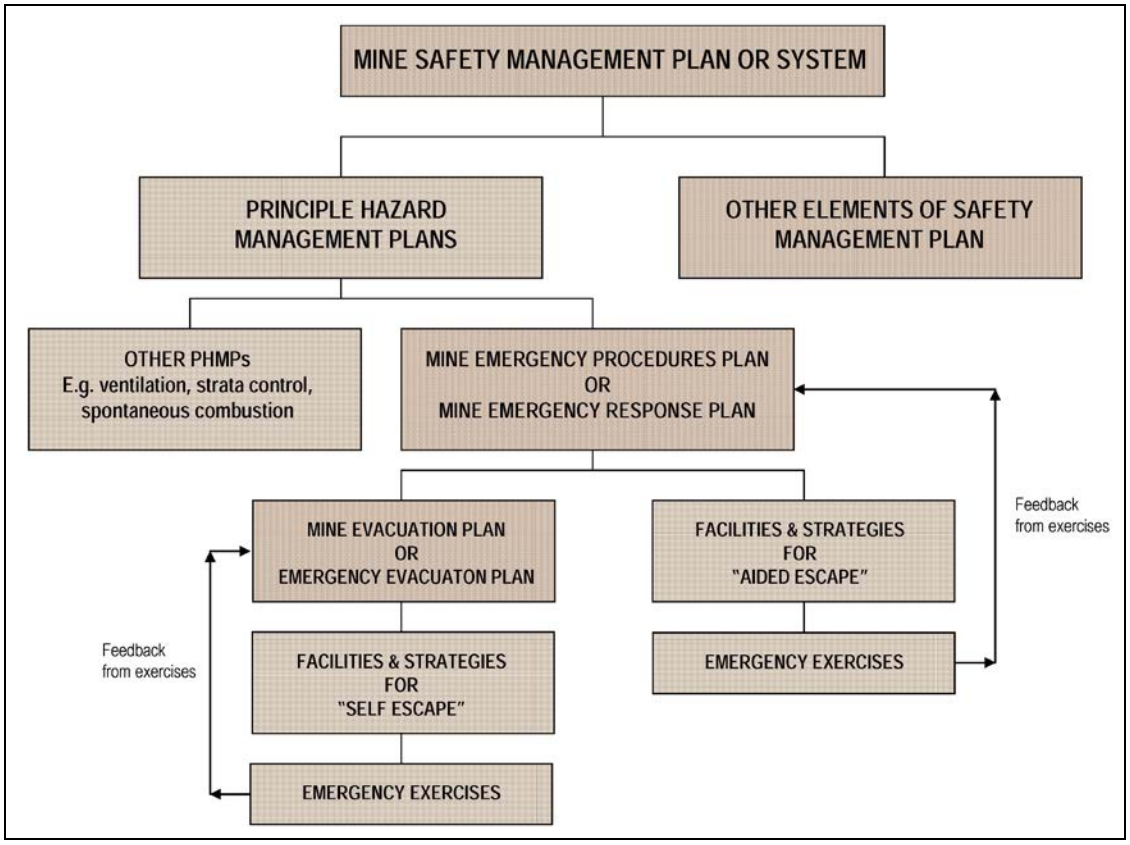

Figure 7. Emergency Management Plan

During the risk assessments for this plan it was identified that a key element was ensuring you were able to contact personnel and issue specific evacuation instructions as quickly as possible should an incident occur, such as a fire. PED was available and judged the best control for that risk at the time; in fact PED is still used in this role in about 70% of underground coal mines in Australia.

Similarly, as the importance of knowing who is underground and which areas underground they are located became identified of critical importance to managing emergency responses, our tracking systems have become widely deployed.

There was no law saying you must "install a through-the-earth emergency warning system" or "track people at a minimum of 2,000 feet spacing", or whatever. The mines had complete control in selecting what to implement. If a better solution came along, they would assess it and deploy it if it was deemed to be a better control. For example, today we see mobile, two-way communication and tracking systems, such

as the ImPact Digital Network, being installed. Mostly these are in addition to PED, to complement its functionality rather than replacing it.

This is the process I referred to earlier that many of the US miners did not understand back in 2006.

Another aspect worth noting is the Australian mining industry is overwhelmingly export driven, so they must be cost competitive on a worldwide basis. So there has been a long history of technology adoption to improve efficiencies in the mining operations, which is why high bandwidth communication systems are now integral to many operations.

One final point on this risk assessment approach is that it does require considerable commitment from all levels of an organization and more specifically, significant investment – that is, hard dollars.

This investment along with general consolidation in mine ownership has seen many of the smaller operations disappear in Australia. Inevitable, but as a person that loves mining and mining history it is not without some regret.

4 MANAGING ALL THIS

As mentioned, to establish these systems does take a considerable effort in time and money. Then there is an on-going requirement to maintain, review and improve what is inherent in the process, to deliver long term results.

All this responsibility on the mining companies does give them control over their choices, but certainly doesn't eliminate government mining authorities and regulations.

The Australian equivalents of MSHA are more about setting the safety framework in place that the mines need to work within, but the mines do have considerable flexibility in how they meet the ultimate requirements for safety at their operations.

Zeroing in on one aspect of the two countries' authorities is the role of government inspectors. Because of the prescriptive approach, MSHA inspectors could be seen more like policeman, investigating and issuing fines. In contrast the Australian inspectors are more like auditors, coming in to review the processes. Certainly fines can be issued and operations ordered to stop, but that is rare as their role is more about mentoring and ensuring the established procedures are being maintained and reviewed.

5 CONCLUSİON - WHAT NEXT?

Not over doing it! The risk assessments and documentation could be seen as getting out of control in Australia and has the potential to actually reduce the effectiveness of what is intended. So reviews are now beginning to take place into how to streamline what has become, quite a complex system.

Another aspect of the safety drive in Australia that is seen by many as hindering the progress to zero harm is the prosecution mentality, particularly in NSW. This view is shared by a number of internationally recognized mine safety experts, such as Prof Jim Galvin. No one disagrees that the blatant disregard for someone's safety, requires punishment under law, as long as it does not lead to a "guilty until proven innocent" mentality and methodology

The risk is that focus has to be given to anticipating the potential legal ramifications of any decision through to a possible reluctance to openly raising and investigating high potential incidents. The latter is a real concern, as the high potential incident is an enormous opportunity for free learning. However the risk of it potentially being used in evidence against someone in some possible, future event, may actually cause hesitation amongst some to raise such things.

But this is only one negative, in what has overwhelmingly been a successful transition in safety methodology in Australian mining from reactive to proactive.

This has taken a lot of commitment and trust from all parties involved. In particular the mining companies have invested a lot of money into implementing the recommendations from the risk assessment,

in terms of equipment, additional controls, training and personnel to manage the whole process. Compared to the personal and financial consequences of serious injuries and fatalities in this day and age, it really is a sound investment.

There is no doubt that momentum is growing in the US for a more proactive approach to safety. Like Australia, after dramatic reductions in fatalities and injuries over the decades, the accident statistics are flattening out and the difficulties associated in achieving the ultimate zero harm remain a challenge.

From "a few to zero" is the hardest, and no industry is yet to achieve it – but I'm confident that Australia and the US will be amongst the first to do so.

REFERENCES:

Galvin, JM: 2005, OH&S performance and Prosecution in the Australian Mineral Industry. The Mining Technology Publication

Galvin, JM: 2012, Towards Zero Harm. Company Director magazine.

Galvin, JM: 2011, OH&S Governance Considerations. Safety Advisory Board paper.

MSHA: 2011, Fatality Statistics 1900 to 2011

Queensland Government, Recognised Standard 08. Conduct of Emergency Exercises

Stansfield, B: 2012, Private correspondence regarding Moranbah North Coal Mine lightning safety processes and TARPs development.

Whitbourn, G: 2012, Private correspondence regarding Anglo American safety processes and Management Plans.

Analysis Factors Influence To Mining Accident Using HFACS-MI Frameworks (A Study at Underground Coal Mining of CV. ABC)

A. Yulianto, M.N. Haramaini, S.M. Siregar
Balai Diklat Tambang Bawah Tanah – Kementerian ESDM, Sawahlunto, Indonesia

ABSTRACT: Underground coal mining of CV. ABC has 14 mine tunnels. The risks of underground mine accident are high, more depth of mining will increase the amount of gasses, more complex underground mining technology is applied. Based on data from the Office of Mines, Industry, Trade, and Cooperatives (Disperindagkop) Sawahlunto, during 2010 – 2012, CV. ABC reported that there were 4 cases of mine accidents with severe injury categories. And based on data from CV. ABC, in 2013, there were 9 cases of mine accidents with minor categories. Mining accidents must be prevented and must not to be happen again. The aim of research was analyzing the factors influence mine accidents using Human Factor Analysis and Classification System in Mining Industry frameworks. This was a cross sectional analytic survey research. The method of research used mixed methods, which combine qualitative and quantitative. Analyzing quantitative data by using *Chi-square* and logistic regretion test, firstly to analyze the correlation between all independences variable with mining accidents, and then to mapping factors influence mining accidents. The logistic regretion result as multivariat that there were contextual relationship where (P<0,05) for the characteristics are unsafe acts, mining technology, communication personnel, and physical readiness before work. The result of quantitative compared with the result of qualitative to know the difference or a combination. The recommended that the efforts to control mining accidents include : providing additional knowledge and attitude improvement work to employees, conducting for analyzing and technical improving to the application of mining technology, pushing the head of the tunnel and employees to create a climate conducive communication without any distinction, providing direction to all employees as well as campaigning for quality sleep.

Keywords: HFACS-MI frameworks, CV. ABC, mine accidents, coal mine

1 INTRODUCTION

Underground mine accident risk is still high, refer to several cases of underground mine accidents in Indonesia, as example underground coal mine explotion in Sawahlunto at 2009 which caused 33 mine worker died (Disperindagkop Sawahlunto, 2009), then at May 14, 2013 the collapse of tunnel roof at underground training site of PT. Freeport Indonesia (Esdm, 2013).

Many accident theories try to analyze the factor that influence of mining accident. Theory of *Human Factor Analysis and Classification System in Mining Industry* (HFACS-MI) is developed by Jessica Marrie Patterson (2009) from the *Human Factor Analysis and Classification System* (HFACS) which is announced by Wiegmann dan Shappell (2003). This theory studies and analyzes accident at working not only from the direct cause, but also from the other factor as a latent cause. Cause factor analysed using HFACS-MI are *Unsafe Acts Factor, Precondition for Unsafe Acts Factor, Unsafe Leadership Factor, Organizational Influences Factor,* and *Outside Factor*.

According to data from Office of Mine, Industry, Trade and Cooperatives Sawahlunto, at the periode 2010 - 2012 there were 4 cases of high injuries mining accident reported by CV. ABC. That is low quantity accident, but we must aware that there are

some cases of light injuries do not reported. Studied by Franks E. Bird, Jr. (1969), from 1.753.498 accident happened at working area, that for every seriously accident reported, there were 9,8% light accident, 30,2% accident that caused properties damage, and 600 accident without financial losses. That is proven in CV. ABC, from the 2013 accident report, there were 9 case of light accident.

From that description, it is necessary doing some research to analyse what are the factor that influence mining accident in CV. ABC using HFACS-MI framework.

2 RESEARCH METODOLOGY

Observational research using *mixed methods* approach to combine or using together quantitative method with qualitative method to analyse factors that will influence mine accident in CV. ABC, so the data collected are more comprehensive, valid, reliable and objective.

Table 1. Summary of *Crosstabs* Experiment Significansy On Variabel Correlation of HFACS-MI Framework with Mine Accident in CV. ABC at 2014

Independent Variable	Dependent Variable : Mine Accident		
	p	R	OR
Layer 1 : Unsafe Action			
Unsafe Act	0,000	0,298	6,853
Layer 2 : Precondition for Unsafe Action			
Mine Working Environment	0,000	0,403	7,112
Mining Tehnology	0,000	0,499	17,175
Worker worriness	0,513	0,094	-
Worker exhaustion	0,047	0,198	-
Physical limitation before work	0,772	0,084	0,694
Personel Communication	0,802	0,040	1,256
Physical readiness before work	0,000	0,326	4,737
Layer 3 : Unsafe Leadership			
Tunnel Chief leadership	0,000	0,369	6,008
Mine operation planning	0,000	0,386	6,561
Problem Solving abilities	0,000	0,386	6,561
Kepatuhan Kepala Terowongan	0,000	0,396	7,034
Layer 4 : Organizational Influences			
Management Commitment	0,000	0,409	7,624
Organization Working Environment	0,000	0,409	7,624
Application Safety Procedure	0,000	0,362	5,670

(Source : Data Primer, 2014)

3 RESULT AND DATA ANALIZATION

Table 1 shown about Summary of *Crosstabs* Experiment Significansy On Variabel Correlation of HFACS-MI Framework with Mine Accident in CV. ABC at 2014.

3.1. Factor Influenced Mine Accident In CV. ABC

3.1.1. Correlation of Unsafe Acts with Mine Accident

According to statistical experiment, unsafe acts variable had value , p = 0,000. This is indicated a significant correlation of unsafe act variable with mine accident.

From interview with mine workers, some examples of unsafe acts done :

a) Don not follow procedure, as if do not install temporary roof support after develop tunnel as far 1 m, or do not install permanent support after 1,5 m development, or do not *scalling* (clearing of hanging coal).
b) Do not use personel safety device, like helm, or do not use helm properly.
c) Use uncorrect equipment, like using axe or crowbar for digging.

3.1.2. Correlation of Precondition for Unsafe Action Factor with Mine Accident

According to statistical experiment, variable of mine working environment, mining tehnologies, worker exhaustion, and physical readiness had value p < 0,05. This is indicated a significant correlation of that variables with mine accident.

Observation show that all mine tunnels of selected sample *culster* already do effort to control physical mine working environment, that is to measure mine gases as monitoring to anticipate the increase of mine gas that could triggering mine explotion and to neutralize methan gas detected.

For mining technologies, observation show that all mine tunnel of selected sample *culster* already try to improvised technologies used, like as maintening the rotten and broken support, or repairing damage electrical installation. But at the field observation, still found supporting system, or electrical equipment, and ventilation system that not conform with standard regulated by government.

Interview with mine workers, the management in all mine tunnel of selected sample *culster* are already do some persuasive talk with modest spirit worker, caused by individual problem..

Interview result also show that all mine workers of all mine tunnel of selected sample *culster* already got health treatment for sick worker. And for physical disabilities, there are some worker had decreasing of sighting fuction because of age condition.

Interview result also pointed that there some efforts to give communication opportunity for all workers, if they have problem with mining operation.

For physical readiness, from health examination of all workers, resulted that almost all worker of mine tunnel of selected sample *culster* do not have physical disabilities.

3.1.3. Correlation of Unsafe Leadership Factor with Mine Accident

According to statistical experiment, variables of Tunnel Chief leadership, mining operation planning, problem solving abilities, and obedience of Tunnel Chief had value p < 0,05. That is indicated significant correlation of that variables with mine accident.

From the interview with Tunnel chief, got explaination that in all tunnel of selected sample cluster, the chief has responsibilities to all mining operation, from mine planning, equipping mining and supporting equipment, completing self protection devices of miner, and fulfilling production target. Tunnel chief alsao communicated the daily development plan with miner everyday at the safety talk time.

Tunnel chief also explained that they all have abilities in problem solving of mining operation, and they all obedience to mining operation procedure.

3.1.4. Correlation of Organizational Influences Factor with Mine Accident

According to statistical experiment, variable of management commitment, organizational working environment, application of safety procedure had value p < 0,05. That is indicated significant correlation of that variables with mine accident.

Interview with tunnel chief, understood that duty to equipped miner tools for running of mining operation already done by management dengan kepala terowongan. That is agree with the result of field observation, That the company equipped all resources, like gas measurement instrument, supporting material, ventilation equipment, electrical equipment, self protecting devices, miner tools, and health care in company clinic.

Interview result also so that all tunnel chief of selected sample cluster, give wide opportunities to miner to create in working and discussion.

Observation show that CV. ABC already have some work procedure regulated to all tunnel without exception. The chief said that all operation activities must refered to the safety procedures.

3.1.5. The Influence of Mine Inspector Report to the Organization role on Mine Safety

Layer number-5 on HFACS-MI are *outer factors*, that is influence from outside that influences organization on the application of mining safety. Inspection doing by mine inspector from the government expected to improve safety in mining industry. There are some excerpt from the interview with mine inspector according to the purpose of inspection.

"The principle things of our inspection in underground mine are to observe support.... then... electricity.... and ventilation..." (Informan AW, Mine Inspector)

"Because the risk of underground coal mine are the collapse of tunnel roof.... danger of gas.... and explotion cased by electric spark..." (Informan AW, Mine Inspector)

According to that excerpt concluded that some purpose of mine inspection are to develop safety in coal underground mine operation.

Inspection by mine inspector has an object. To understand the object of the inspection, there are some interview excerpt like below.

"One of our inspection object is mine safety...." (Informan AW, Mine Inspector)

"That is regulated in Minister Mining and Energy Act No : 2555 year 1993 and Act No : 555 year 1995" (Informan AW, Mine Inspector)

"All of object in details are.... inspection to the suitable of infrastructure, installation infratructure, and mining equipment.... and then tehe competence of mine worker.... then.... the evaluation of technical studies of mining operation...." (Informan AW, Mine Inspector)

So can summarized that the inspection object already regulated by the government.

The result of their inspection to the company are descripted as below.

"For CV. ABC the most crusial note are the concentration og methane gas...." (Informan AW, Mine Inspector)

"The measurement approximately 0 LEL – 3 LEL.... this value is below the limitation regulated... but if we don't continuely monitoring the accumulation will increase very fast....." (Informan AW, Mine Inspector)

According to that excerpt concluded that the result of inspection are based on field observation and report from the companies to the mine office.

Below the explanation of the result found by mine inspector.

"From several inspection by mine inspector since my carrer here.... I as myself and also as person who have responsibilities of mining operation in this CV. ABC... there are many benefit we got..." (Informan AA, KTT)

"Some of inspection found all are carryon to us....." (Informan AA, KTT)

"Explaining all found in inspection... then discussing with us.... many valuable suggestion to us." (Informan AA, KTT)

According to that excerpt above, can concluded that the result of the inspection are for the safety f mining operation so they must be presented and discused.

Below are description of the benefit obtained by the company on the result of the mine inspection.

"That time...when mine inspection... on one of our tunnel there are very much water leakage on the wall and roof of tunnel... that water makes the floor muddy... and slipery... The report recommended to make drainage, and then the watershould be pump to outsite the tunnel" (Informan AA, KTT)

"We get benefit directly.... after proposed to the mine director.... he is very responsive... and then the tunnel where the water leak already not muudy and slippery..." (Informan AA, KTT)

According to that interview can conclude that the report of inspection by mine inspector have benefit directly to underground coal mine operation safety.

3.2. *The Mapping of Factors that Influence Mine Accident in CV. ABC*

To mapping the factor that influence mine accident in CV. ABC, we must conduct statistical analysis using statistical experiment logistic regretion to find the influence of several variables on the HFACS-MI frameworks simultanously.

The result of analysis Logistic regretion on tabel show that from all variables of HFACS-MI frameworks, only variable of unsafe acts, mining technologies, personel communication, and physical readiness before works that has influence to mine accident ($p < 0,05$). Value R square (correlation coefisien) obtained is 0,678, That means variables of unsafe acts, mining technologies, personel communication, and physical readiness before works could explained or predicted Value of **variabel terikat,** that is mine accident in the value of 67,8% and the remaining 32,2% influenced by the other factor.

The Probability of mine accident happened could counted by test the logistic regretion model using equation below :

$$Prob.(Y = 1) = \frac{1}{1 + e^{-(\beta 0 + \beta 1 X1 + \beta 2 B2)}}$$

That means the probability of mine accident is caused by worker do unsafe acts, the worst personel communication, and physical unreadiness before works is valued P (Ever Accident).

Table 2. Final Result of Logistic Regretion Experiment on The Factors Influenced to Mine Worker Accidents in CV. ABC Year 2014

Variable	β	Df	P	OR	R
Unsafe Acts	-2,710	1	0,010	0,067	0,678
Mine Physical Environment	-1,151	1	0,141	0,316	
Mining Technologies	-3,699	1	0,000	0,025	
Worker worriness	-1,710	1	0,217	0,172	
Worker exhaustion	0,141	1	0,931	1,152	
Worker Physical limitation	25,147	1	0,999	8,34E10	
Personil Communication	2,300	1	0,015	9,971	
Physical Readiness Before Works	-1,492	1	0,019	0,225	
Tunnel Chief leadership	36,228	1	0,999	5,41E15	
Mine Operation planning	-19,749	1	0,999	0,000	

Table 2. (cont'd) Final Result of Logistic Regretion Experiment on The Factors Influenced to Mine Worker Accidents in CV. ABC Year 2014

Variable	β	Df	P	OR	R
Problem Solving Abilities	2,323	1	0,309	10,203	0,678
Tunnel Chief Obedience	9,410	1	1,000	1,22E4	
Management Commitment	-1,755	1	0,336	0,173	
Organization Works Environment	-62,414	1	0,999	0,000	
Aplication of Safety Procedures	36,381	1	0,999	6,31E15	
Constant	-22,008	1	0,999	0,000	

(Source : Prime Data, 2014)

4 DISCUSSION

4.1. Correlation of Variable on HFACS-MI Frameworks with Mine Accident

4.1.1. Correlation of Unsafe Acts with Mine Accident

The significant correlation among unsafe acts with mine accident are indicated by some mine workers of CV. ABC still doing unsafe action because of carelessness, as like forgetting self protection device (safety shoes, helmet), using unproper tools, not installing temporary roof support after 1 m development or not installing permanent roof support after 1,5 m development. According to Kletz (2001) on Fikie (2004), one of classification human error that influence ansafe cation is forget, this error happens to sameone that already understand, able and want to do rightly and safely and already customary practiced.

4.1.2. Correlation of Precondition for Unsafe Act Factor with Mine Accident

The significant correlation among mine physical environment with mine accident indicated by the worker are not allowed enter the mine tunnel when daily measurement show that the consentration of mine gas are high or some of roof supporting are broken so could trapped the miner. According to Wignjosoebroto (1995), one of outside factor is physical condition of working environment, that are including temperature, humidity, air circulation, lighting, noise, mechanical vibration and the others. They could influence significantly to the human work result.

The technologies of underground coal mine are very complex, so the proper technologies used are useful to do the works, but also could cause failure to the works. Although already use the right technologies, the danger from nature of underground coal mine could sometime influence the worker. Coal underground mining activities, according to Saepulloh (2011), could not liberated from tunneling on the earth, and the rock will expanded because of earth pressure make some fault and *stress relief* zone which could cause the rock fall or callapse, so that tunnel developed must supported.

No significant correlation among worker worrieness with mine accident are explained by some low spirit (bad mood) workers, Directly persuaded by tunnel chief. According to Geller (2001) descripted that individual personel, behaviour and environment lingkungan are have interaction to build what called by *The safety triad* that consist of safety culture inside.

The significant correlation among worker exhaustion with mine accident is explained by some medical treatment to exhausted or unhealthy mine workers from company medic representative. Nurmianto (1998) said that basically all works produce exhaustion or fatigue. Exhaustion will decrease productivity and increase works error. The increasing error could product opportunity of work accident in industries.

No significant correlation among worker's physical limitation with mine accident show that there were no workers wit physical disabilities. Budijanto (2003) said that physical limitation (disabilitas) is the lack of abilities or deterioration or decreased

individual function to do daily activities which preceding by condition of impairment, that the activities previously could done without difficulties or with the others help..

No significant correlation among personel communication with mine accident could explained by the giving of daily works plan every morning at the time of safety talk, so the personel communication become very friendly. That is not appropriate with the research by Senjaya (2011) in Plantation PT. Gunung Sejahtera Dua Indah Astra Group Kalimantan, the conclution is there were correlation among information from supervisor to worker with level work accident with significant value p = 0,000.

The significant correlation among physical readiness with mine accident explained by majority of mine worker do not have physical disablities according to montly examination at campany clinic. According to widodo (2009), the work readiness is readiness of all person condition to preparing himself physically, mental, and experience to do some works.

4.1.3. Correlation of Unsafe Leadership Factor with Mine Accident

The significant correlation among tunnel chief leadership with mine accident is explained by the responsibilities of tunnel chief to plan mine operation and to fullfil the safety equipment of all worker. That is match with Mabruri (2010), on his research in Machine workshop PT. DOK and Shipyard of Surabaya at 2010, achieved that there were correlation among leadership style with works accident with significancy value p = 0,041.

The significant correlation among mine operation planning with mine accident is explained by the full responsibilities of planning by tunnel chief. According to Sudrajat (2010), Mining operation is activities that against nature, which makes destruction, caused soil or rock movement and environmental pollution. So the mining activities have opportunity produce danger without carefully planned.

The significant correlation among problem solving abilities with mine accident is explained by the abilities of tunnel chief to solve problem on mining operation, like like handling rock fault, or the increasing of methane concentration. Levine on Prihartini (1994) said that somebody could have good *problem solving* ability, if that person could solve problem efectively , that means affected the target and minimalize negative effect, for himself and other person.

The significant correlation among obedience of tunnel chief with mine accident explained by the responsibilities of tunnel chief to make sure the condition of tunnel are safe enough for the workers and operations. According to Suma'mur (1985), the leader must make every effort seriously on safety because he would become example of safety act by his workers on his responsibilities.

4.1.4. Correlation of Organizational Influences Factor with Mine Accident

The significant correlation of management commitment with mine accident is showed by fullfiled of gas measurement equipment, ventilation machine, medical clinic, etc. Reason (1997) said safety work program must start from begin, at this case from company top management.

The significant correlation of organization working environment with mine accident is showed by management effort to create good environment for worker to do the work creatively. Working environment begin with daily practice on organization and influence behavior of members positively like productivity, satisfaction, and motivation, or negatively like absent, turnover and work accidents (Furnham, 2003; Gillies, Franks, & Child, 1990; Runtu & Widyarini; 2009).

The significant correlation of application of safety procedures with mine accident is explained by applied safety procedures appropriate to company standard. Sitrisni and Kusmawan (2007) said that the procedures to works safely and orderly are regulated on every industries, usually on the form like regulation or behavior act.

4.1.5. Influence of the Report of Mine Inspector to Organization participation on Mine Safety

On Ministry of Energy and Mineral Resources Act No. 02 Tahun 2013, the responsible to inspect of mine industries are minister, governor, and city or municipal major helped by functional officer of mine inspector. The job of mine inspector basically to inspect mining industrial safety.

Consequence of publication of Mine Permit is inspection. Inspection on mining sector principally to make sure the holder of mine permits are more directed on their mining activities, so will not deviate from the regulation. Theoritical George R. Terry (2001) have opinion that the inspection are aimed to definite what are want to achieve, evaluate and do corrective effort if necessary, to make sure the result as needed.

4.2. Mapping the Faktor that Influence Mine Accident in CV. ABC

Mapping the factor that influenced mine accident in CV. ABC doing by statistical analysis using logistic regretion statistical experiment with the purpose to found influence of several variables on HFACS-MI frameworks Simultanously.

The result of the mapping concluded that the independent variables which had influence to the mine accident are :

4.2.1. Unsafe Actions

Unsafe action example doing by underground coal mine worker of CV. ABC are forget using self protection device (safety shoes, helmet), using unproper tools, not installing temporary roof support after 1 m development or not installing permanent roof support after 1,5 m development. According to Kletz (2001) on Fikie (2004), one of classification human error that influence ansafe cation is forget, this error happens to sameone that already understand, able and want to do rightly and safely and already customary practiced.

4.2.2. Mining Technologies

The Effect of tunneling on earth, according to Hartman (1987), there are some pollutant gases on the mine, as the result of mining process or from the rock or mineral mined. So Prata (2006) said underground mine should use ventilation system to supplying fresh air, good enough in quantities and quality, then supply it and devide it to the mine tunnels so there is safe working condition for the miner and mining proceses.

4.2.3. Personel Communications

Daily works plan of the mine operation are communicated from the tunnel chief to the workers, supported by newest physical condition of tunnel give certainity to the workers that they could work safely and comfortable. Comfortable working evidence worker satisfaction because the good communication are the activity that integrated worker by the behavior.

If the working condition uncomfortable, like difference treatment among the workers, unfulfilled equipment to work, that will make uncomfortable conditions that make the worker anxious and stressed. That is appropriate with judgement of t Chen et al., (2006) on (Wahyuni, 2009) that said the organization communication have positive correlation with organization commitment and productivity , and have negative correlation with working stress.

4.2.4. Physical Readiness Before Works

Mine worker who are not ready physically will not allowed to do works, because that will be dangerous to them. According to Robbins (2006), he said that abbilities of individu basically consist of two factor : intelectual ability nad physical ability. Physical ability is his ability to do work that wants stamina, adroitsness, strength and skill.

5 CONCLUSION

According to research result and discussion, can conclude as:

1. There is correlation of *unsafe* actions with mine accident.
2. *Precondition for unsafe acts* factors which has correlation with mine accident are : mine physical environment, mining technologies, exhaustion of workers, and physical readiness before works.
3. *Unsafe leadership* factors which has correlation with mine accident are: tunnel chief leadership, mine operation planning, abilities of problem siolving, and obedience of tunnel chief.
4. *Organizational influences* factor which has correlation with mine accidents are : management commitment, organization working environment, and application of safety procedures.
5. *Outside factor* which has influenced organization partipation to the mine accident is the report of mine inspector.
6. The result of mapping to the factors that influenced mine accident are: unsafe acts variable, mining technologies variable, personel communications variable and physical readiness variable.

6 SUGGESTION

Suggest to the company from this research are :

1. To increase the awareness and discipline, and to improve mine worker to do safe acts during work, the company should do education and training about safety operation and supporting system of underground mine.
2. To increase communication on the work, the company should do education nad training about effective communication.
3. To anticipate risk cause by roof tunnel collapse, the company should studies and maintenances the supporting system.
4. To decrease the risk of gas pollution on mining which danger to the miner, the company should studies and repairs ventilation system of underground mine.
5. To decrease the risk of mine explotion by spark of electrical equipment, the company should studies and repairs the electrical system of underground mine.
6. To increase the awareness and readiness of mine worker according to the the physical readiness before work, the campany should campaign program of the benefit of quality rest**.**

REFERENCES

Ariani, Diah. 2009. Tinjauan Faktor Yang Mempengaruhi Tingkat Kelelahan (*Fatigue*) Pada Pengemudi *Bulk Truck* PT. BCS Subkontraktor PT. Holcim Indonesia TBK Plant Narogong Tahun 2009. *Skripsi*. FKM UI.

Bird, Frank E. Jr. 1982. *Loss Control Management*. Published by Institute Press. Louanville. Georgia. USA

Bird, Frank E. & Germain, George L. 1990. *Practical Loss Control Leadership*. Georgia: International Loss Control Leadership

Cheyne, A., Sue, C., Oliver, A., and Tomas, J.M., 1998, "*Modeling Safety Climate in the Prediction of Levels of Safety Activity*", Work & Stress, 12, 3, 255-271.

Colling, David. 1990. *Industrial Safety Management and Technology*. Pentice Hall Inc.

Fikie, Eliantho. 2004. Faktor-Faktor yang Mempengaruhi Perilaku Aman Awak Kapal Tunda PT. X yang Beroperasi di Anjunan Lepas Pantai Area Balikpapan. *Tesis.* FKM UI.

Geller, E.S. 2001. *Working safe: how to help people actively care for health and safety*. Lewis Publisher.

Heinrich, H. W. 1980. *Industrial Accident Prevention*. McGraw-Hill Book Company. New York.

Howard L. Hartman. 1987. *Introductory Mining Engineering*. John Wiley & Sons, New York.

Mok, E. & Au-Yeung, B. 2002. *Relationship between organizational climate & empowerment of nurses in Hong Kong*. Journal of nursing management, 10, 129-137.

Nedo. 2004. *Bahan Pelajaran Pelatihan Umum Teknik Pertambangan Batubara*. Proyek Alih Teknologi Pertambangan Batubara, Japan, 2004

Notoatmodjo, S. dan Sawono S. 1985. *Pengantar Ilmu Perilaku Kesehatan*. Badan Penerbit Kesehatan Masyarakat, Fakultas Kesehatan Masyarakat, Universitas Indonesia.

Patterson and Shappel. 2008. *Analysis of mining incidents and accidents in Queensland, Australia from 2004–2008 using the HFACS-MI framework. Sumarry of* Queensland Mines and Energy (QME) Project.

Patterson, Jessica Marrie. 2009. *Human Error in Mining: A Multivariable Analysis of Mining Accident/Incidents in Queensland, Australia and*

The United States of America Using The Human Factors Analysis and Classification System Framework. *Dissertation.* Philosophy Clemson University.

Prata, Darius Agung. 2006. Ventilasi Tambang. *Bahan Pelajaran Pendidikan dan Pelatihan Teknisi Keselamatan Tambang Bawah Tanah*. Balai Diklat Tambang Bawah Tanah. Sawahlunto.

Pratama, Ade Cipta. 2012. Analisis Insiden Unsafe Act Berdasarkan Faktor Prakondisi Di PT. Bukit Makmur Mandiri Utama Jobsite Lanna Harita Indonesia Tahun 2011. *Skripsi*. FKM UI.

Reason, J. 1997. *Managing the Risks of Organizational Accidents*. Ashgate Publishing Company.

Robbins, Stephen P. 2001. *Organizational Behavior*. 9 edition, New Jersey: Prentice Hall, inc.

Runtu, D.Y.N., & Widyarini, M.M.N. 2009. Iklim organisasi, stress kerja, & kepuasan pada perata. *Jurnal psikologi*, 2 (2), 107-112.

Saepulloh, Ahmad. 2011. Penyanggaan Tambang Bawah Tanah. *Bahan Pelajaran Pendidikan dan Pelatihan Sistem Penyanggaan Tambang Bawah Tanah*. Balai Diklat Tambang Bawah Tanah. Sawahlunto.

Sanders, M.S., & McCormick, E. J. 1993. *Human Factors In Engineering and Design (7th edition)*. New York : McGraw-Hill.

Sarwono, Sarlito Wirawan. 1999. *Teori-teori Psikologi Sosial*. Jakarta: PT. Raja Grafindo Persada.

Siregar, Sihar. 2012. Sistem Penambangan Batubara Bawah Tanah. *Bahan Pelajaran Pendidikan dan Pelatihan Teknik Pertambangan Batubara Bawah Tanah*. Balai Diklat Tambang Bawah Tanah. Sawahlunto.

Suma'mur. 2009. *Higiene Perusahaan dan Kesehatan Kerja*. Jakarta: CV. Mas Agung Seto.

Wiegman, Douglas A, et al. 2007. *Human Error and General activation accident: A Comprehensive, Fine-Grained Analysis using HFACS*. Available from http://www.humanfactors.uiuc.edu. (Sitasi 17 November 2013)

Winarsunu, Tulus. 2008. *Psikologi Keselamatan Kerja*. Malang : UMM Press.

Investigation on Dust Generated During Rock Cutting by Ansys Software

V.Raghavan
Assistant Professor, Department of Mining Engineering, Dr.T.Thimmaiah Institute of Technology, Kolar Gold Fields-563120, India

Ch.S.N.Murthy, V.R.Sastry.
Professors, Department of Mining Engineering, NITK, Surathkal-575025, India

ABSTRACT: Underground coal mining operations continue to increase production as mining equipment and practices are improved. Unfortunately, increased production also results in the potential for increased Respirable dust generation and worker exposure. In response, operations are applying basic controls at elevated levels and looking to emerging technologies in an effort to better control Respirable dust levels. Ventilating air and water sprays remain the basis of dust control strategies for both longwall and continuous mining operations, and the level of application for these controls continued to increase. In addition, new technologies are emerging that have the potential to further reduce dust levels. In this Paper an attempt is made to study the Stresses Produced and its Influence on Dust generation at different Attack angle and force applied on the cutting material.

Keywords: Dust generation, rock cutting, sieve analysis, finite element analysis

1 INTRODUCTION

The high demand for coal production has increased the need for mechanical coal cutting in underground coal mines. On the other hand our coal reserves are shrinking, forcing operators to mine thin coal seams and subsequently to cut roof/floor rocks in order to maintain sufficient clearance for equipment. Enormous miles of entries are developed by these continuous miners for long wall operations as well as bord & pillar mining [12]. The amount of repairable dust generated by excavating coal and cutting roofs with continuous mining machines is the major concern to the mining industry. Dust is an inevitable product of mining, given by the nature of mining operations such as cutting/drilling, loading and transportation of coal. It is dispersed into the mine atmosphere by the ventilating air current, and travels downwind. Once airborne, the Respirable dust particles are difficult to capture and remove as they fall very slowly because of associated aerodynamic properties. As a result, miners are exposed to high Respirable dust concentration levels. Respirable dust is a continuing problem in the mine environment, where it adversely affects the safety and productivity of a miner. In underground coal mining, dust particles ranging from 1to10 micron sizes (Respirable particulate matter ranges from 1-5µm & greater than 5µm are suspended particulate matter as per ISO 7708, 1995), In addition, dust also results in obscuring visibility and affects general mobility of the miners, and may also lead to sudden catastrophic incidences of explosion. During last three decades with the introduction of the mechanization, i.e. Road header, Continuous Miner and Double Ended Ranging Drum Shearer in the underground coal mining, it has become a greater menace than ever posing threat to the health and safety of miners. The majority of Respirable dust generated by mechanical miners is the result of material that is crushed directly under the individual bits/cutters on the cutter head. Figure .1 shows the crushed zone underneath a bit and the resulting fractures in the rock

that lead to production of Respirable dust. Reducing the amount of dust produced will reduce the risk of dust getting airborne in the working area [2].

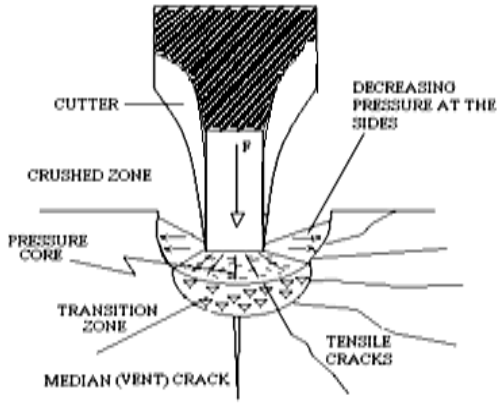

Figure 1. Crushed zone where dust is generated [2].

The main machine parameters that influence the cutting efficiency of a continuous mining machine include bit spacing, depth of cut and bit geometry. Through a correct combination of bit spacing and depth of cut, two adjacent grooves start interacting and the land/ridge between the two cuts can be removed which will result in large chip formation and less dust generation.

1.1 Objectives

The main objectives of this research study are:

- Fabrication of experimental set up of rock cutting machine with necessary arrangement like holding the rock specimen, for changing Cutting drum, RPM and thrust applied and the effect of Physico-Mechanical properties and mineralogical composition of samples on cutting rate and dust generation and also the effect of operational parameters of RPM and thrust and torque on cutting rate and dust generation

1.2 Literature Survey

The mining industry has centered its attention on mastering the goal in decreasing the amount of respirable dust generated during the cutting process. A better understanding of the influence of several parameters, including both machine-controlled and operator-controlled, during the rock cutting process is required. Important parameters affecting coal cuttability rate are physical and mechanical properties of coal/rock such as: density, uniaxial compressive strength, tensile strength and shear strength etc. Chemical composition of coals may directly or indirectly affect the coal cuttability. Increasing of 27% and 22% in moisture and volatile material respectively in coals may cause decrease in strength of coal, but less than these values, coal strength may increase [18]. Some of the minerals like Quartz can play a major role on erosion of cutter of coal winning machines, affecting the cutter life considerably. In the past, much research has been carried out to select the design parameters for cutting tools on a trial and error basis. The mining industry is yet to receive a solution, which could provide optimum parameters like type of bit, bit angle and angle of attack etc, for coal/rock cutting in underground coal mines. [17].

While mechanical coal cutting is a relatively well-understood topic, the technique has changed little in recent years. Primary enhancements have tended to centre on metallurgical improvements and advancements in the manner in which the tools engage the face. This, as a general observation, indicates that the understanding of the involved mechanics and technology is optimal, although a cautionary note must be sounded from the preceding section, which examined the generic or petro graphic content related mechanical properties of South African coal. In general, it can be concluded that several authors [14], [15] and [16] have alluded to differences between South African coals and those of Europe or America, that inherently make South African coal more difficult to cut.

Mechanized coal cutting traditionally makes use of tools that are dragged across the face, typically driven by a rotary drum, in order to liberate the coal. These tools are commonly described as either point attack or radial drag bits, so named as these terms best describe their generic method of engaging

the coal. The mechanisms of cutting using drag bits are well understood, and whilst there have been advances in cutting methods in recent years, the generic tool shapes have changed little.

2 CUTTING PARAMETERS

The influence of common parameters on drag tool cutting, such as geometry and speed, is depicted in Figure.2 and Figure.3 which graphically summarizes the different cutting parameter.

The following parameters commonly influence the cutting tool operations

2.1 Rake Angle

The angle of the cutting face relative to the work. There are two rake angles, namely the back rake angle and side rake angle, both of which help to guide chip flow.

2.2 Back Clearance Angle

The angle between a plane containing the end surface of a cutting tool and a plane passing through the cutting edge in the direction of cutting motion. The back clearance angle should not be less than 5° and not greater than 10°.

2.3 Attack Angle

The attack angle is the angle between the axis of the tool and the surface being cut. The attack angle is usually between 45° and 55° for rocks of lower strength. The most common tip angle is 75°. The preferred rake and back clearance angles should not be less than 25° and not more than 10° for conical bits.

2.4 Cutting Speed

Cutting speed has no significant influence on the magnitude of the pick forces provided the wear effect has been discounted.

2.5 Line Spacing

Line spacing is the distance between adjacent tools or picks in the axial direction, on the cutter or shearer drum. If the line spacing is too close, the cutting is inefficient due to over-crushing of the rock, and if it is too wide, the tool cuts in an unrelieved mode (tensile fractures from adjacent cut cannot reach each other to form a chip), creating a groove-deepening situation, resulting in the formation of a rib between cuts.

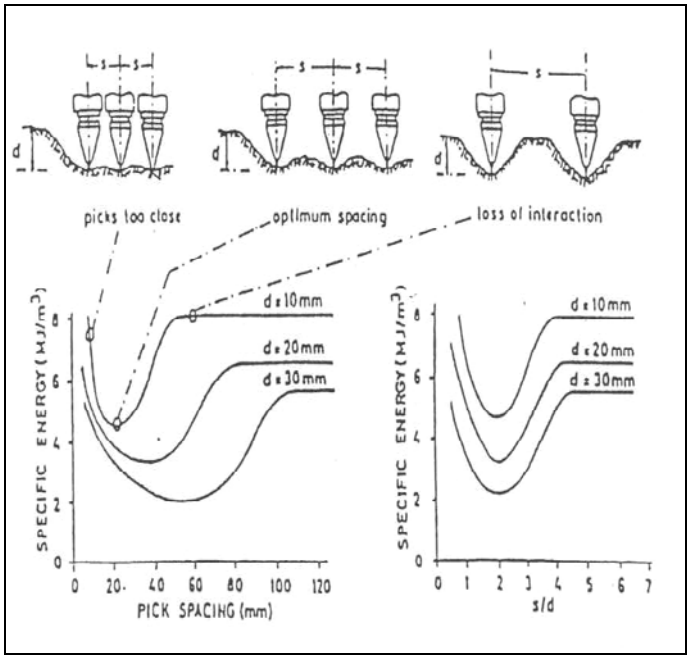

Figure 2. Line spacing is the distance between adjacent tools or picks [10].

The minimum specific energy is obtained with an optimum spacing to depth ratio has indicated to be in the region of 2:1.

2.6 Depth of Cut

It is the thickness of material removed by one pass of the cutting tool. It can be seen that the Specific energy improves substantially as the depth of cut is increased. This result has been proved both in the laboratory and by in-situ testing of an instrumented continuous miner

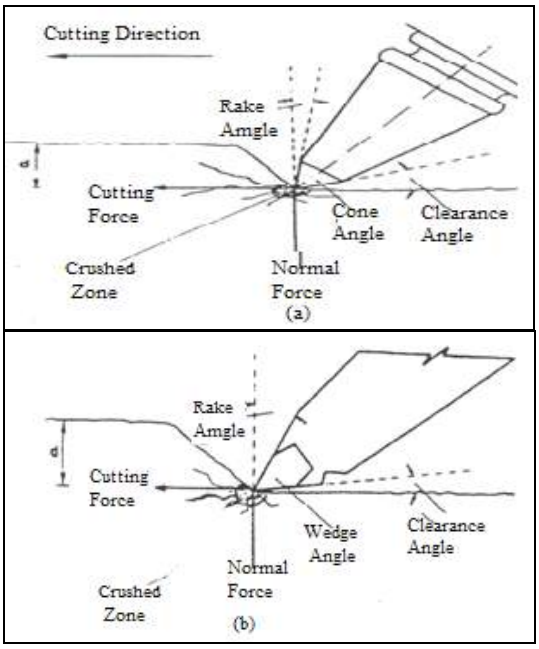

Figure 3. Interaction of bit with rock and bit geometry [10]

3 MECHANICAL PROPERTIES

3.1 Uniaxial Compressive Strength

Compressive strength is the capacity of a material to withstand axially directed compressive forces. The most common measure of compressive strength is the uniaxial compressive strength or unconfined compressive strength. Usually compressive strength of rock is defined by the ultimate stress. It is one of the most important mechanical properties of rock material, used in design, analysis and modeling.

3.2 Young's Modulus

Young's Modulus is modulus of elasticity measuring of the stiffness of a rock material. It is defined as the ratio, for small strains, of the rate of change of stress with strain. This can be experimentally determined from the slope of a stress-strain curve obtained during compression or tensile tests conducted on a rock sample.

3.3 Poisson's Ratio

Poisson's ratio measures the ratio of lateral strain to axial strain, at linearly-elastic region. For most rocks, the Poisson's ratio is between 0.15 and 0.4. As seen from early section, at later stage of loading beyond linearly elastic region, lateral strain increase fast than the axial strain and hence lead to a higher-ratio.

Table 1. Mechanical properties of Rocks (10 rock samples)

Rock	**Sample Collected**	Density (Kg/cm^2)	Compressive strength (MPa)	Young's Modulus (GPa)	Poisson's Ratio
Coal	5 Incline Mines, SCCL,AP	2.2	23-60	2.65-3.63	0.32
Sand Stone	MOCP 1, SCCL,AP	2.5	27 – 170	9-15	0.26
Limestone	JK cements, Mudhapur, Bagalkot	2.3	30 – 200	20-55	0.30

3.4 Description of Rock Cutting Machine

Figure 4. Rock cutting machine

Rock cutting machine is a prototype model of a Road header, Continuous Miner or Coal Shearer used for cutting coal/ rock in underground mines/tunneling which is installed at NITK, Suatkal as shown in Figure 4.

Rock cutting machine consists of a firm base with two parts protruding: one of the part has a prime mover (motor) mounted on it. A base plate attached to the motor has guide ways, which helps in moving to and fro movement and sideways also. A Motor is in turn is attached to a shaft pulley by belt drive. The cutter head will be attached to the shaft by a flange. Cutter head consists of a drum head with number of bits mounted on it.The other part of rock cutting machine has firm sample holder, in turn connected to a hydraulic cylinder, which can provide sideways movement during cutting operation and a dust collecting bin.

3.5 Sieve analysis

A **sieve analysis** (**gradation test**) is a practice or procedure used (commonly used in civil engineering) to assess the particle size distribution of a granular material. The size distribution is often of critical importance to the way the material performs in use. A sieve analysis can be performed on any type of non-organic or organic granular materials including sands, crushed rock, clays, granite, feldspars, coal, and soil, a wide range of manufactured powders, grain and seeds, down to a minimum size depending on the exact method. Being such a simple technique of particle sizing, it is probably the most common.

Procedure:

1. Arrange the nest of Sieves starting from 0.3, 0.212, 0.18, 0.15, 0.106 mm (0.3 mm sieve at the top and 0.106 mm sieve at bottom),
2. Place the sample material at the top most sieves that is on 0.3 mm sieve.
3. Place the sieve set on the sieve shaker and allows the machine to run for 5 min.
4. Weigh the material which is retained in each sieve and the bottom most pan to the most nearest of 0.1 gm. Tabulate the results in the standard form of sieve analysis shown in Table 2 and Table 3.

Table 2. Sieve Analysis data for 45°

Sample	Coarse (gms)	Medium (gms)	Fine (gms)	TOTAL (gms)
Coal	239.4	2.4	1.7	243.5
Sand Stone	19.3	4.6	4.1	28
Limestone	29.7	10.9	17	57.6

Table 3. Sieve Analysis data for 55°

Sample	Coarse (gms)	Medium (gms)	Fine (gms)	TOTAL (gms)
Coal	187.8	1.9	1.4	191.1
Sand Stone	17.2	3.2	3.4	23.8
Limestone	27.1	9.5	16.5	53.1

4. DISPLACEMENT OF ROCK

Figure 5. Displacement Occurred during Cutting of Coal with Cutting angle at 45°

Figure 6. Displacement Occurred during Cutting of Coal with Cutting angle at 55°

Figure 7. Displacement Occurred during Cutting of Sand Stone with Cutting angle at 45°

Figure 8. Displacement Occurred during Cutting of Sand Stone with Cutting angle at 55°

Figure 9. Displacement Occurred during Cutting of LimeStone with Cutting angle at 45°

Figure 10. Displacement Occurred during Cutting of Lime Stone with Cutting angle at 55°

4.1 Von Mises stress of rock

Figure 11. Von Mises Stress occurred during cutting coal with Cutting angle at 45°

Figure 12. Von Mises Stress occurred during cutting coal with Cutting angle at 55°

Figure 13. Von Mises Stress occurred during cutting Sand Stone with Cutting angle at 45°

Figure 14. Von Mises Stress occurred during cutting Sand Stone with Cutting angle at 55°

Figure 15. Von Mises Stress occurred during cutting Lime Stone with Cutting angle at 45°

Figure 16. Von Mises Stress occurred during cutting Lime Stone with Cutting angle at 55°

5. RESULT

5.1 Displacement Occurred during Cutting of Rocks

Table 4. Displacement occurred in Rocks at an attack angle of 45°

Rock Name	Attack Angle	For First Cut			For Second Cut		
		DMX	SMN	SMX	DMX	SMN	SMX
Coal	45°	0.904E-03	-0.834E-03	0.303E-05	0.001254	-0.001138	---------
Sand Stone		0.100E-03	-0.938E-04	0.209E-06	0.138E-03	-0.128E-03	---------
Lime Stone		0.945E-04	-0.878E-04	0.541E-06	0.128E-03	-0.119E-03	0.278E-06

Table 5: Displacement occurred in Rocks at an attack angle of 55°

Rock Name	Attack Angle	For First Cut			For Second Cut		
		DMX	SMN	SMX	DMX	SMN	SMX
Coal	55°	0.00128	-0.00118	0.428E-05	0.001774	-0.00161	----------
Sand Stone		0.182E-03	-0.168E-03	0.291E-06	0.253E-03	-0.231E-03	----------
Lime Stone		0.108E-03	-0.934E-04	0.518E-06	0.141E-03	-0.112E-03	0.102E-06

5.2 Von Mises stresses occurred during cutting of rocks

Table 6. Von Mises Stresses occurred in Rocks at an attack angle of 45°

Rock Name	Attack Angle	For First Cut			For Second Cut		
		DMX	SMN	SMX	DMX	SMN	SMX
Coal	45°	0.904E-03	0.206E-04	0.044964	0.001254	0.751E-04	0.04809
Sand Stone		0.100E-03	0.288E-04	0.077877	0.138E-03	0.212E-03	0.078832
Limestone		0.945E-04	0.172E-04	0.36808	0.128E-03	0.142E-03	0.037284

Table 7. Von Mises Stresses occurred in Rocks at attack angle of 55°

Rock Name	Attack Angle	For First Cut			For Second Cut		
		DMX	SMN	SMX	DMX	SMN	SMX
Coal	55°	0.00128	0.292E-04	0.63628	0.001774	0.106E-03	0.068052
Sand Stone		0.128E-03	0.493E-04	0.105749	0.105749	0.142E-03	0.112322
Limestone		0.102E-03	0.249E-04	0.053472	0.053472	0.973E-04	0.057367

When the rock was cut with a cutting angle of 45°, the stresses induced is less and the dust generated is more. But, when the rock was cut with a cutting angle of 55°, the stresses induced is more and the dust generated is less. Hence, we got good results. At an angle of 55°, it is very effective and best suited for Rock Cutting.

6 CONCLUSION

1. The Experiment was conducted on 45° & 55° Attack angles and the results were found good in **55°**. Both the strength implied is more and dust generated is less.
2. By using this method, we are able to reduce the dust generation in coal mine, experiment was conducted on Sand Stone and Lime Stone also, the results are positive and the dust generation is less.
3. Due to the less dust generated, workers efficiency will increase and can reduce the occupational health diseases..

REFERENCES

1. Achanti, V. B. and Khair, A. W (2000), "Bit Geometry effects on Failure Characteristics of Rock." SME Mining Engineering Journal, June, pp 101-107.
2. Asbury, M. Cigla. (2002), "Design Methodology, Field Testing and Evaluation of a Continuous Miner Cutterhead for Dust Reduction in Underground Coal Mines", Society for Mining, Metallurgy and Exploration (SME) Annual Meeting, .
3. Black, S. and Round, J. (1977), "Deep cutting conditions miner – effect of drum rotational speed and depth of cut on Airborne respirable dust and specific energy." US dept. of commerce, NTIS.
4. Brooker, C. M, (1979), "Theoretical and practical aspects of cutting and loading by shearer drums." Colliery Guardian, April, Pp 41-50.
5. Dimla E. Dimla Snr (2000) "Sensor signals for tool-wear monitoring in metal cutting operations—a review of methods" Department of Mechanical and Manufacturing Engineering, De Montfort University, The Gateway, Leicester LE1 9BH, UK, 40(8), June, pp 1073–1098
6. Evenden, M. P. and Edward, J. S. (1985), "Cutting theory and coal seam assessment techniques and their application to shearer design." Mining Science and Technology, 2, 253 – 270.
7. Hamilton, R. J., French, A. G. and Spence, A. C. (1976), "Development in dust control in coal mines." Society of Mining Engineer, March, pp 317-326.
8. Hekimoglu, O. Z. (1995), "Investigation into performance of point attack and radial type rock and coal cutting picks." Transaction of the Institute of Mining and Metallurgy, 107, pp 55-59.
9. Hurt, K.G., Morris, C. J. and Mullins, R. (1988), "Development in coal cutting techniques." Society of Mining Engineer, pp 467-477.
10. Ismail, and TM O'Brien (2002), "Audit of coal cutting technologies." CSIR, miningtek, CoalTech 2020.
11. Khair, (2001). "Research and Innovations for Continuous Miner's Cutting Head, for Efficient Cutting Process of Rock/Coal" 17th International Mining Congress and Exhibition of Turkey- IMCET, pp 45-55
12. Khair, (1984), "Design and fabrication of a rotary coal cutting simulator." Proceeding of the Coal Mine Dust Conference, West Virginia University, Morgantown, pp 190-197.
13. Rizwan.A.Qayyum, (2003)." Effects of Bit Geometry in Multiple Bit-Rock Interaction" Thesis (Master of Science in Mining Engineering), College of Engineering and Mineral Resource at West Virginia University, Morgantown, West Virginia.
14. Shahriar.K, Bakhtavar, Moeinizadeh.A. (2009). "Some experiments *in-situ* and in laboratory to determine the physico-mechanical properties of coal" www.academia.edu.

Determination of ^{222}Rn, ^{220}Rn and Their Decay Products in Natural Ancient Mine Measured with Nuclear Track Detectors: Radiation Dose Assessment

L. Oufni, M. Amrane
Department of physics, Faculty of Sciences and Techniques (LPM-EIRM), University Sultan Moulay Slimane, B.P. 523, 23000 Beni-Mellal. Morocco.

ABSTRACT Radon (and thoron) is a naturally occurring radioactive noble gas, having variable distribution in the geological environment. The exposure of human beings to ionizing radiation from natural sources is a continuing and inescapable feature of life on earth. Radon, thoron and their short-lived decay products in the atmosphere are the most important contributors to human exposure from natural sources. The aim of this study is to determine alpha-and beta-activities per unit volume of air due to radon (^{222}Rn), thoron (^{220}Rn) and their progenies in the air of ancient mine of Aouli in which there is no working activity is situated at approximately 25 km north of the city of Midelt (Morocco), by using LR-115 type II and CR-39 solid state nuclear track detectors (SSNTDs). Equilibrium factors between radon and its daughters and between thoron and its progeny were evaluated in the studied atmospheres. The committed equivalent doses due to the ^{218}Po and ^{214}Po radon short-lived progeny were evaluated in different tissues of the respiratory tract of the visitors of the considered ancient mine.

Keywords: Radioactive noble gas, radon, thoron, alpha- and beta- activities in air

1 INTRODUCTION

Due to its long half-life time relative to other isotopes, radon (^{222}Rn, $T_{1/2}$ = 3.82 d) which is a descendent of uranium-238 (^{238}U, $T_{1/2}$ = 4.5×10^{9} y) is considered to be the most significant isotope of radon problem in the environmental studies. It's well known that the radiations emitted from the primordial radionuclide originating from the Earth's crust are the major contributors to the total background exposures to the human populations. The include external gamma exposures and inhalation exposures, approximately in equal measure, the latter being due to radon (^{222}Rn), thoron (^{220}Rn) and their progenies in the indoor environment. ^{222}Rn, a progeny of uranium-238 (^{238}U), is a colorless, odorless, noble and radioactive gas. Its half-life is 3.82 days and its decay with the emission of 5.48MeV α particles. Radon and its short-lived decay products in dwellings present the main source of public exposure from the natural contributing to nearly 50% of the global effective dose to population.[1] Lung cancer pathologies caused by inhalation exposure to radon is due to alpha-dose deposited by short-lived radon decay products. It's well known that exposure of population to high concentrations of radon and its daughters for a long period leads to some pathological effects like the respiratory functional changes and the high occurrence of lung cancer.[2] Radon appears mainly by diffusion processes from the point origin following α-decay of ^{226}Ra in underground soil. Radon diffusion and transport through different media is a complex process and is affected by several factors.[3,4] It is well known that for material medium, the porosity, permeability and the diffusion coefficient are the parameters which can affect directly the capacity to hinder the flow of radon soil gas.

In the present work, we used a technique based on using CR-39 and LR-115 type II SSNTDs for measuring the concentration of radon, thoron and their progenies in different ancient mines. We also determined annual committed equivalent doses due to the inhalation of radon short- lived daughters by

the members of the public. This technique has been previously used to study the indoor radon level in different dwellings [1-3].

2 MATERIALS AND METHODS

2.1 Studied Area

Morocco with its large number of metalliferous sites is considered a traditional mining region since antiquity. One of these sites is the Upper Moulouya lead district which contained one of the largest concentrations of lead in Morocco. The former lead mine of Aouli is located about 26 km north of Midelt, at the junction of chains of medium and upper eastern Atlas (Figures 1 and 2).

2.2 Determination of Alpha Activities per Unit Volume due to Radon, Thoron and Their Decay Products in the Air of Ancient Mine

Square shaped Pershore Mouldings CR-39 (500µm thickness) and Kodak LR-115 type II (12µm cellulose nitrate on 100 µm polyester base) solid state nuclear track detectors (SSNTDs) of surface equal to 9 cm^2 have been placed in different locations inside t ancient mines for one month. During the exposure time, a-particles emitted by radon, thoron and their progenies bombarded the SSNTD films. After the irradiation, the exposed films were etched in two NaOH solutions at optimal conditions of etching, ensuring good sensitivities of the SSNTDs and a good reproducibility of the registered track density rates: the first solution of 2.5 mol L^{-1} normality at 60°C for 120 minutes for the LR-115 II films and the second solution of 6.25 mol L^{-1} normality at 70°C for 7 hours for the CR-39 detectors. After this etching treatment the track densities registered on the CR-39 and LR-115 II SSNTDs were determined by means of an optical microscope of magnitude 40x. For our experimental etching conditions, the residual thickness of the LR-115 type II SSNTD is 5 µm which corresponds to the lower (E_{min} = 1.6 MeV) and upper (E_{max} = 4.7 MeV) energy limits for the registration of tracks of alpha-particles in the LR-115 II films [4]. All a-particles emitted by the radon and thoron series that reach the LR-115 II detector surface under an angle lower than its critical angle of etching, with a residual energy between 1.6 MeV and 4.7 MeV are registered as bright track-holes. The CR-39 detector is sensitive to all a-particles reaching its surface under an angle smaller than its critical angle of etching.

The rate of track density (tracks cm^{-2} s^{-1}), due to α-particles emitted by the radon, thoron and their decay products in the outdoor air of a location, registered on the LR-115 II and CR-39 detectors, after subtracting the corresponding backgrounds, are given by :

$$D(LR) = \frac{\Delta R}{4}\sin^2\theta_c\left[\sum_{i=1}^{3} A_c(i)K_i + \sum_{i=1}^{4} Ac(i)K_i'\right] \quad (1)$$

$$D(CR) = \frac{1}{4}\sin^2\theta'_c\left[\sum_{i=1}^{3} A_c(i)K_iR_i + \sum_{i=1}^{4} Ac(i)K_i'R_i'\right] \quad (2)$$

where:

A_i ($Bq.cm^{-3}$) is the α-activity of the i^{th} α-emitter, and are the ranges in air of an α-particle of index i and initial energy E_i emitted by the nuclei of the radon and thoron series in the outdoor air of a location, respectively,

K_i and K'_i are respectively the branching ratios corresponding to the disintegration of the nuclei of the radon and thoron groups and,

R_i and R'_i are the α particles ranges in air which correspond to the lower (E_{min}) and upper (E_{max}) ends of the energy window. The ranges of the alpha-particles emitted by the radon and thoron series in air were calculated by using a TRIM program [5].

θ_c, θ'_c are the critical angles of etching for LR-115-II and CR-39, respectively. (the critical angle for a detector is defined as the angle between the direction of the projectile and the normal to the detector surface under which no track can be revealed by etching).

The activities of a i^{th} nucleus $A_c(i)$ and its (i + 1)th daughter $A_c(i + 1)$ of the radon and thoron series are related by Jacobi, 1972 [6]:

$$\frac{D_T}{\lambda_i}\frac{\partial^2}{\partial z^2}A_i(z)+A_{i-1}(z)-A_i(z)=0 \qquad (3)$$

$A_i(z=0)=0$ for i= 1, 2, 3 and 4 and $A_i(z=+\infty)=0$ for i = 0, 1, 2, 3 and 4, that is, far from the ground.

2.3 Evaluation of Annual Committed Equivalent Doses due to the Inhalation of Radon Decay Alpha Products in the Respiratory Tract of the Members of the Public in Ancient Mines

By using the ICRP model [7] the human respiratory tract is divided into two major regions: the thoracic TH and extrathoracic ET regions.

The thoracic region is divided into four sub-regions (alveolar interstitium AI, Bronchioles bb, bronchi BB and Lymphatics LN_{TH}) and the extrathoracic region is divided into three sub-regions (anterior nasal ET_1, posterior nasal passage, larynx, pharynx and mouth ET_2 and lymphatics LN_{ET}).

There are ten compartments in the thoracic region respectively numbered from 1 to 10: AI_1, AI_2, AI_3, bb_1, bb_2, bb_{seq}, BB_1, BB_2, BB_{seq} and LN_{TH}. The extrathoracic region contains four compartments respectively numbered from 11 to 14: ET_2, ET_{seq}, LN_{ET} and ET_1.

The rate of change of a j'th radon decay product α-activity in a compartment i of the respiratory tract (ICRP, 1994) at any time is given by:

$$\frac{dA_c^i(j')}{dt}=F_d(i)I_0(j')+\sum_n \lambda_{n,i}A_c^n(j')-\left(\sum_n \lambda_{i,n}+\lambda_{j'}\right)A_c^i(j') \qquad (4)$$

where F_d (i) is the fractional deposition in the compartment i of the respiratory tract of different members of the public (ICRP, 1994), $I_0(j')=BA_C(j')$. B is the average breathing rate for different members of the public. $A_c(j')$ ($Bq.m^{-3}$) is the α-activity of the j' th radon decay product in the atmosphere ancient mine, $\lambda_{n,i} = m_{n,i} + S_s$ where $m_{n,i}$ is the clearance rate from region n to region i due to particle transport and S_s is the clearance rate due to particle absorption into blood (ICRP, 1994). The rate of absorption of a material into blood is the same in all regions of the respiratory tract, except in the anterior nasal passages (ET_1), where no absorption occurs (ICRP, 1994). $\lambda_{n,i}=0$ for i=1,2,3,5,6,8,9,12 and 14 (ICRP, 1994), $\lambda_{i,n} = m_{i,n} + S_s$ where $m_{i,n}$ is the clearance rate from region i to region n due to particle transport [7] and $\lambda_{j'}$ is the radioactive constant of the j'th radon decay product.

Alpha activities corresponding to the j' radon decay product in each of the 1-14 compartments of the respiratory tract as functions of time are obtained by solving Eq.(4).

3 RESULTS AND DISCUSSION

The activities per unit volume air due to the radon and their progenies have been measured in different locations of the studied ancient mine. Data obtained are shown in Table 1. From the statistical error on track counting one can determine the error on track density rate and then evaluate the relative uncertainty of the radon and their progenies determination which is about 8%. The radon alpha-activity per unit volume increases with the distance from the entrance of the studied ancient mines. This is due to the fact that the ventilation rate decreases when penetrating inside the ancient mine studied. Values obtained for the alpha-activity per unit volume due to radon P7 and P8 places of the Aouli ancient mine (Table 1) are clearly higher than the 400 Bq.m-3 concentration limits for the members of the public. We notice that alpha activities due to radon and its decay products are higher than those due to thoron (Table 2) and its daughters for the ancient mine which is the subject of our study. This is due to the fact that thoron (^{220}Rn) half-life is too short (55s) compared to the exposure time (30 days) of the SSNTD films inside the ancient mine whereas radon (^{222}Rn) has a half-life of 3.82d. The average values of the alpha-activity due to ^{218}Po and ^{214}Po were found to be (190.60±12.86) Bq.m-3 and (121.30±8.47) Bq.m-3. Equilibrium factors between radon and its progeny F^{222} and between thoron and its daughters F^{220} were

evaluated for the studied ancient mine (Tables 1-2). The F^{222} and F^{220} factors decrease when the ventilation rate V increases. These factors do not depend on the nature of the rocks forming the studied ancient mine.

Annual committed equivalent doses per hour of exposure due to the ^{218}Po ($H_T(^{218}Po)$) and ^{214}Po ($H_T(^{214}Po)$) radon short-lived alpha emitting daughters have been evaluated in the respiratory tract of male and female adult from the inhalation of air in the studied ancient mine. Data obtained are shown in Table3. After inhalating air, amounts of ^{218}Po and ^{214}Po are deposited in the extrathoracic region ET and thoracic region TH. According to the ICRP compartmental model (ICRP, 1994) a quantity of ^{218}Po is transferred from the TH region to the ET region. As a consequence, we found that annual committed equivalent dose due to ^{218}Po is higher in the ET region than in the TH region. We notice that annual committed equivalent doses due to the ^{214}Po are smaller than those due to ^{218}Po in both ET and TH regions. This is due to fact that ^{214}Po has a very short half-life ($1.64.10^{-4}$s) compared to the exposure time of the tissues. Annual committed equivalent doses due to ^{218}Po and ^{214}Po in the respiratory tract of the members of the public increase when alpha-activity due to radon increases in the air of the studied ancient mine.

4 CONCLUSION

Using CR-39 and LR-115 type II SSNTDs we can evaluate the concentration of radon, thoron and their progenies in the environment air in the studied ancient mine. Alpha activities per unit volume air due to the radon and thoron inside the studied ancient mine depend on the ventilation rate. It has been shown that annual committed equivalent doses due to the radon alpha – emitting short- lived decay products (^{214}Po and ^{218}Po) increase when the radon concentration inside the considered ancient mine increase. We noted that the annual committed equivalent doses due to ^{218}Po and ^{214}Po in the bb and BB tissues is significantly higher than doses in the thoracic region. Similarly, we note that the dose in the ET_2 tissue is much higher than that calculated in the extrathoracic region

REFERENCES

[1] Singh. S, Kumar. A, Singh .B, 2002. Radon level in dwellings and its correlation with uranium and radium content in some areas of Himachal Pradesh, India. Environ. Int., 28(1-2), pp.97-101.

[2] Barooah .D, Laskar. I, Goswami .A.K, Ramachandran. T.V, Nambi. K.S.V, 2003. Estimation of indoor radon, thoron and their progeny using twin cup dosemeters with solid-state nuclear track detectors in Digboi of Upper Assam. Radiat. Measur., 36(1–6), pp:461-463.

[3] Oufni. L, Misdaq. M.A, Amrane. M, 2005. Radon level and radon effective dose rate determination in Moroccan dwellings using SSNTDs. Radiat. Measur., 40(1), pp:118-123.

[4] Hafez. A.F, Naim.M.A, 1992. Plastic nuclear track detection methodes for estimation of thorium and uranium ratio in thick natural materials. Nucl. Instr. Meth. Phys. Res., B 69, pp: 373-381.

[5] Biersack. J.P, Ziegler. J.F, 1998. IBM Research, TRIM, Version 98. New York: IBM.

[6] Jacobi. W, André. K, 1963. The vertical distribution of radon 222, radon 220, and their decay products in the atmosphere. J. Geophys.Res. 68 (13), pp: 3799-3814.

[7] ICRP, 1994. Human respiratory tract model for radiological protection. Ann. ICRP 24 (1-3), ICRP Publication 66.

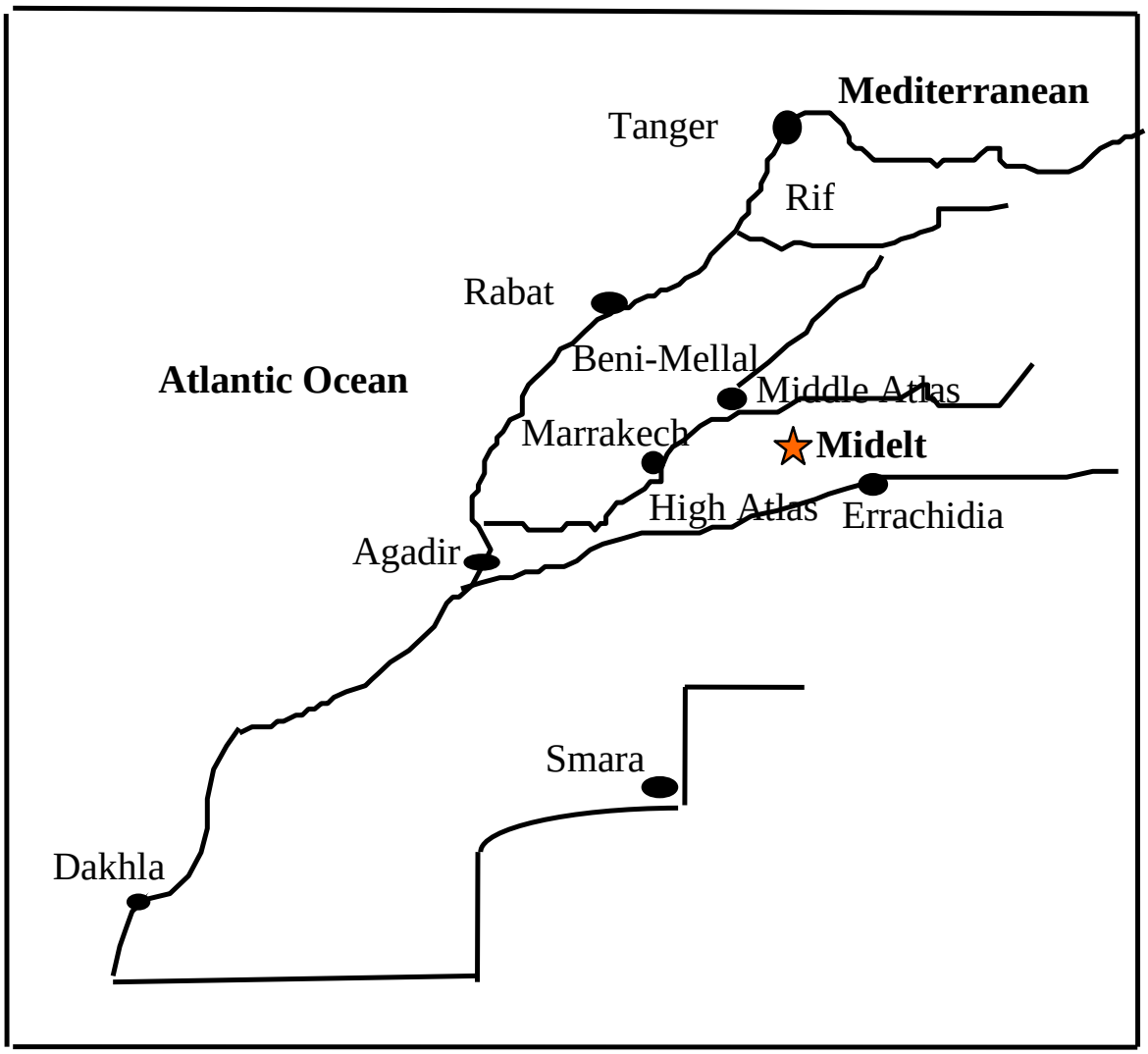

Figure1. Map showing the localization of the studied mine in the Midelt region (Morocco).

Figure2. The entrance of the studied mine in the Midelt region (Morocco).

Table 1. Ventilation rate (V) and alpha activities per unit volume of air due to the radon alpha emitters inside the Aouli ancient mine.

Place	V (h^{-1})	$A_C(^{222}Rn)$ (Bq m^{-3})	$A_C(^{218}Po)$ (Bq m^{-3})	$A_C(^{214}Po)$ (Bq m^{-3})	F^{222}
P_1	0.27	200±16	103±8	27±2	0.20
P_2	0.25	230±18	116±9	34±2	0.20
P_3	0.24	244±19	122±10	37±2	0.20
P_4	0.22	272±21	143±11	41±3	0.20
P_5	0.20	316±25	161±12	48±3	0.20
P_6	0.18	350±27	183±14	53±4	0.21
P_7	0.16	411±32	208±16	65±5	0.21
P_8	0.15	437±34	223±17	68±5	0.21
P_9	0.14	484±38	250±19	76±6	0.21
P_{10}	0.13	525±41	272±21	85±6	0.21

Table 2. Ventilation rate (V) and alpha activities per unit volume of air due to the thoron alpha emitters inside the Aouli ancient mine.

Place	V (h^{-1})	$A_C(^{220}Rn)$ (Bq m^{-3})	$A_C(^{216}Po)$ (Bq m^{-3})	$A_C(^{212}Po)$ (Bq m^{-3})	F^{220}
P_1	0.27	20.5±1.4	20.2±1.3	0.4±0.03	0.04
P_2	0.25	24.1±1.8	24.3±1.9	0.6±0.04	0.04
P_3	0.24	26.1±2.0	25.6±2.0	0.6±0.04	0.04
P_4	0.22	28.0±2.2	27.9±2.2	0.7±0.05	0.04
P_5	0.20	30.8±2.5	30.6±2.4	0.8±0.06	0.04
P_6	0.18	34.0±2.4	32.9±2.3	0.9±0.07	0.04
P_7	0.16	39.2±3.1	38.5±3.0	1.2±0.09	0.05
P_8	0.15	43.7±3.5	43.3±3.4	1.4±0.1	0.05
P_9	0.14	46.8±3.6	46.6±3.7	1.5±0.1	0.05
P_{10}	0.13	49.7±3.9	49.3±3.9	1.7±0.1	0.05

Table 3. Data of annual committed equivalent dose due to the ^{218}Po and ^{214}Po in the tissues of adult male and adult female from the inhalation of air in the Aouli ancient mine.

Respiratory Tract region	Tissue	Committed equivalent dose (Sv y^{-1} per hour exposure)			
		Adult male (^{218}Po)	Adult female (^{218}Po)	Adult male (^{214}Po)	Adult female (^{214}Po)
Thoracic	AI	$(1.41\pm0.08)10^{-8}$	$(1.02\pm0.05)10^{-8}$	$(4.02\pm0.24)10^{-15}$	$(2.86\pm0.17)10^{-15}$
	bb	$(2.05\pm0.12)10^{-6}$	$(1.71\pm0.12)10^{-6}$	$(5.86\pm0.37)10^{-13}$	$(4.83\pm0.32)10^{-13}$
	BB	$(5.90\pm0.37)10^{-7}$	$(5.36\pm0.32)10^{-7}$	$(1.63\pm0.09)10^{-13}$	$(1.42\pm0.10)10^{-13}$
	LN_{TH}	$(2.84\pm0.16)10^{-16}$	$(2.66\pm0.16)10^{-16}$	$(8.10\pm0.51)10^{-29}$	$(7.40\pm0.46)10^{-29}$
Extrathoracic	ET1	$(6.47\pm0.44)10^{-7}$	$(5.22\pm0.35)10^{-7}$	$(1.84\pm0.14)10^{-13}$	$(1.47\pm0.10)10^{-13}$
	ET2	$(2.41\pm0.17)10^{-5}$	$(1.92\pm0.11)10^{-5}$	$(8.69\pm0.55)10^{-12}$	$(6.93\pm0.44)10^{-12}$
	LN_{ET}	$(1.40\pm0.09)10^{-18}$	$(1.18\pm0.05)10^{-18}$	$(3.91\pm0.23)10^{-31}$	$(3.40\pm0.20)10^{-31}$

Physiological Effects of Dust on the Human Body

B. Plush
PM_{10} Laboratories - Particulate Matter Management, Somersby, NSW, Australia

ABSTRACT Lung diseases such as Coal Workers' Pneumoconiosis (CWP), also called black lung disease, develop when respirable coal mine dust (PM10 – 10 micron or smaller sized particles) is inhaled during the normal mining operation. Once inhaled, PM10 sized particles deposit and remain in the lungs forming the foundation for this deadly disease. It is a chronic, fibrotic, and irreversible disease that robs miners of their breath and eventually their life. CWP is a wholly preventable disease with the diligent use of best practice dust control measures including adequate ventilation, water sprays, water pressure and water flow, dust collectors and scrubbers and a quantifiable process for dust measurement to ensure compliance to statutory requirements (Davitt, 2011).

Keywords: Lung disease, dust classification, physiological effect

1 INTRODUCTION

The Upper Big Branch (UBB) disaster in April 2010, a mine owned by Massey Energy, in Raleigh County West Virginia, killed 29 men as a result of a massive dust explosion. It was subsequently found that 17 of the 24 victims' autopsied (71%) had CWP. This compares with the national prevalence rate for CWP among active underground miners in the U.S. of 3.2%, and the rate in West Virginia of 7.6%. The ages of the UBB victims with CWP ranged from 25 to 61 years (Davitt, 2011).

According to Davitt, of the 17 UBB victims with CWP, five of them had less than 10 years of experience as coal miners, while nine had more than 30 years of mining experience. At least four of the 17 worked almost exclusively at UBB. All but one of the 17 victims with CWP began working in the mines after the 2.0 milligram coal mine dust limit was put in affect in 1973. This was an exposure limit that was believed at the time sufficient to prevent black lung disease. It has since been determined ineffective to protecting miners' health and recommendations have been made to lower the exposure level for workers (Davitt, 2011).

Further, the victims of the UBB disaster constitute a random sample of miners on which autopsies were carried out. The fact that 71% of them show evidence of CWP has been seen as an alarming finding given the ages and work history of these men, and the fact that the disease was far more advanced than industry average indicated it should have been (Davitt, 2011).

Respiratory problems caused by exposure to dust are among the oldest identified industrial diseases. Early medical opinions in the 1920's, suggested that only hardrock workers were exposed to potential lung diseases from dust. It was identified at the time that silicosis from hardrock mining led to tuberculosis and eventual death (McPherson, 2009). During that time coal dust was not regarded as particularly harmful. However, during the 1930's, the number of recognized cases of pneumoconiosis increased dramatically resulting in the British Medical Research Council initiating an investigation into respirable disease within the black coal workers of South Wales. Europe and the United States had previously identified the hazards of dust in coal mines and by 1950 it was confirmed that workers in bituminous coal mines were also exposed to potential dust diseases, particularly pneumoconiosis (McPherson, 2009).

However, it took many years for a definitive association to be established between the atmospheric contaminants in an operating coal mine and respiratory dysfunction of coal workers exposed to these atmospheric contaminants. McPherson suggests that there were three reasons for this delay in recognising the association between airborne contaminants and lung disease. Firstly, it takes years of exposure to coal dust before the coal mine worker shows signs of lung disease and suffers significant breathing impairment whilst performing normal activities. Secondly, the onset of lung disease often presents symptoms similar to those of naturally occurring ailments such as coughing, wheezing, shortness of breath and flu like symptoms. Thirdly, at the time, the commonly used method for determining the dust concentration level in the atmosphere was to measure the number of particles in a unit volume of air. However, the relationship between dust levels measured as a particle count in a unit volume of air and the incidence of pneumoconiosis in coal workers was not completely understood (McPherson, 2009).

During the International Pneumoconiosis Conference held in Johannesburg, South Africa in 1959, a re-direction of pneumoconiosis studies was recommended, with particular focus being directed at the limitations to the existing methods of dust sampling. Studies had identified that those particles of equivalent diameter less than 5μm were the particles most likely to be retained within the lungs and create lung disease in coal mine workers. These size particle fractions were named respirable dust. Studies further established that the mass concentration of respirable dust in any given atmosphere, over the period of a shift (usually 8 hours) was a much better measure of the potential health hazard to a coal mine worker than the existing particle count methods. (McPherson, 2009).

It was from this point forward that the TWA method of determining exposure levels was implemented and statutorily enforced. It was also at this time that equipment capable of measuring TWA's in the atmosphere was developed.

2 LUNG DISEASE

Lung diseases caused by the inhalation of coal dust are known by the general term pneumoconiosis. This is often referred to as dusted or black lung.

The changes which occur in the lungs vary with the deposition of the different dust fractions. For example, the inhalation and subsequent deposition of coal dust in the lungs can initially cause symptoms such as:

- coughing;
- wheeze, or worsening of asthma;
- increased need for medications (eg: puffers, antibiotics);
- increased breathlessness; and
- flu like symptoms.

Continued exposure and inhalation of coal dust can then lead to pneumoconiosis, Coal Workers Pneumoconiosis (CWP) and Progressive Massive Fibrosis (PMF).

In contrast, lung disease caused by exposure to silica is much more severe and identified by areas of scar tissue surrounded by normal lung tissue. Because the injured areas are separated from each other by normal tissue, the lungs do not completely lose their elasticity. Some particles are dissolved in the blood stream and then carried around the body where it may affect the brain, kidneys and other organs (CCOHS, 2012).

Health effects resulting from exposure to pneumoconiosis may not appear for many years and may in fact only appear after exposure has ceased. This delay in the production of symptoms from this exposure may then be mistakenly attributed to non-occupational conditions such as smoking. Another more serious example is the identification of the fatal lung disease mesothelioma. Mesothelioma results from exposure to asbestos fibres and cases of the disease have appeared over 40 years after actual exposure to the asbestos have occurred. It is important for hygienists, and other professionals in this field, to consider the fact that although exposed workers may

not display any symptoms of lung disease, it should not be assumed that significant lung damage has not already occurred. It is now recognised that shorter exposures to higher concentrations of pneumoconiosis-producing dusts, has produced cases of acute lung disease. (WHO 1999, USDOL, 2010).

2.1 Dust Classifications

Within the alveoli are cells called *macrophages* (i.e., scavenger cells*)* that are released by the stimulus of foreign bodies, such as dust. The macrophages engulf the dust particles deposited in the lung. Some of the dust-laden macrophages, which have the ability to move freely within the air spaces of the lung and alveoli, are removed from the lung by two different pathways (WHO 1999, McPherson, 2009, USDOL, 2010).

2.1.1Mucociliary escalator

The dust-laden macrophages move to the finer bronchioles, from which further clearance takes place by mucociliary action, as described above. Eventually these cells, along with the coarser particles initially deposited within the upper respiratory tract, reach the mouth and are swallowed or expelled via spiting or coughing. Most of the dust deposited in the alveolar spaces is removed in this manner (WHO 1999, McPherson, 2009, USDOL, 2010).

2.1.2 Lymphatic system

Dust-laden macrophage cells may pass through the alveolar walls of the lungs into the lymphatic system, which starts as a mesh of fine vessels and drains the tissue spaces. These vessels come together to form larger and larger vessels that eventually discharge the lymph into the bloodstream. At the various branching points (bifurcations) of the trachea and the bronchi, the lymph passes through glands termed lymph nodes, one of whose functions is the filtration of foreign bodies. Hence, a great deal of particulate matter is deposited by the macrophages at the lymph nodes, and it is here that fibrosis of healthy tissue often starts. Other dust-laden cells may be deposited and remain on the alveolar walls where, again, fibrosis can be initiated (USDOL, 2008).

According to the US Department of Labor, a classification of dusts with respect to potential hazard to the health and safety of industrial workers may be divided into five categories (USDOL, 2008).

2.2 Toxic Dusts

These can cause chemical reactions within the respiratory system or allow toxic compounds to be absorbed into the bloodstream through the alveolar walls. They are poisonous to body tissue or to specific organs. Coal dust is not typically classified as a toxic dust (USDOL, 2008).

2.3 Carcinogenic (cancer causing) Dusts

A combination of abrasion of lung tissue and surface chemical action can result in tumour formation from freshly produced quartz particles. Studies have identified that an excessive risk for lung cancer in certain dust producing occupations exists. These included dust producing occupations such as mining, although coal-mine workers were not specifically identified. Increased lung cancer risk among coal-mine workers appears to be found only in those with exposure to high levels of crystalline silica (AIOH, 2008, WHO 1997).

2.4 Fibrogenic Dusts

The scouring action of many dusts causes microscopic scarring of lung tissue. If continued over long periods this can produce a fibrous growth of tissue resulting in loss of lung elasticity and a greatly reduced area for gas exchange and lead to pneumoconiosis and CWP (AIOH, 2008, WHO 1997).

2.5 Explosive Dusts

These are a concern of safety rather than health. Coal dust becomes explosive when small particles become and remain airborne. If an ignition source is encountered with

sufficient methane in the area, then the ensuing methane ignition can lead to a catastrophic dust explosion (AIOH, 2008, WHO, 1997).

2.6 Nuisance Dusts

Nuisance dust can be defined as dust that contains less than 1% quartz. Because of its low content of silicates, nuisance dust has been shown to have little adverse effect on the lungs. Any reaction that may occur from nuisance dust is potentially reversible. However, excessive concentrations of nuisance dust in the workplace may reduce visibility potentially causing accidents or injury, may cause unpleasant deposits in eyes, ears, and nasal passages, and may cause injury to the skin or mucous membranes by chemical or mechanical action (USDOL, 2008, McPherson, 2009).

3 TYPES OF LUNG DISEASE

3.1 Pneumoconiosis (Black Lung)

In general, the human respiratory system's physiological reaction to any inhaled particulate depends on many factors, with particle aerodynamic diameter being the main consideration relative to coal dust. Pneumoconiosis is the primary concern with coal dust (USDOL, 2008).

The term pneumoconiosis is a generic term for damage to cardio-respiratory organs caused by the inhalation of dust and effectively means dust in the lungs. It is defined by the International Labor Organization (ILO) as the accumulation of dust in the lungs and the tissue's reaction to its presence. The inhalation of coal dust, over a long period and at sufficient concentrations, can result in the formation of scar tissue and loss of elasticity, referred to as fibrosis. This reaction is termed pneumoconiosis when linked to coal dust exposure (USDOL, 2008).

Pneumoconiosis occurs in two forms: simple Coal Workers Pneumoconiosis (CWP) and complicated CWP which leads to the condition of Progressive Massive Fibrosis (PMF). Over sufficiently long periods of exposure a build-up of retained dust occurs in the lung tissue in the form of soft plaques within the lung tissue. These can be observed as a small spot on chest x-rays (NCBI, 2012). Figure 1 shows a chest x-ray of simple pneumoconiosis in a coal workers lung. There are diffuse, small (2 to 4 mm each), light areas throughout both lungs. In the right upper lung (seen on the left side of the picture), there is a light area (measuring approximately 2 cm by 4 cm) with poorly defined borders, representing coalescence (merging together) of previously distinct light areas (NCBI, 2012).

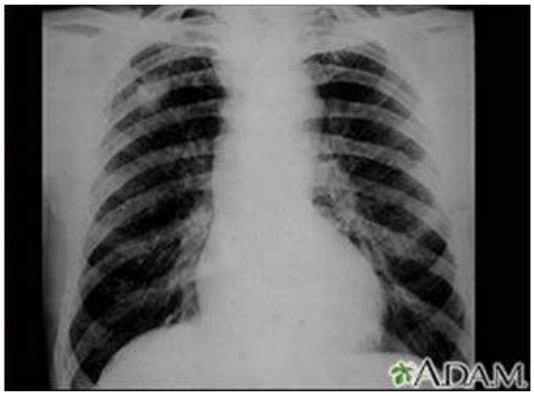

Figure 1. X-ray Showing Simple Pneumoconiosis

Figure 2 shows an X-ray of complicated pneumoconiosis. There are diffuse, massive light areas that run together in the upper and middle parts of both lungs.

These are superimposed on a background of small and poorly distinguishable light areas that are diffuse and located in both lungs (NCBI, 2012).

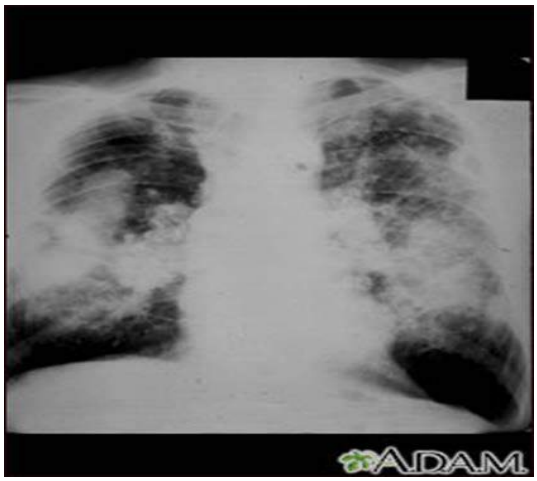

Figure 2. X-ray Showing Complicated Pneumoconiosis

Indications of CWP may not be revealed for some 10 to 15 years after initial exposure from employment in coal mines. Furthermore, the subjects may not be aware of any incapacity, or restrictions on lung function during that time. In more advanced cases, the opacities grow in size and number until they coalesce as seen in Figure 2. This is likely to be accompanied by fibrosis as shown in Figure 3 (McPherson, 2009).

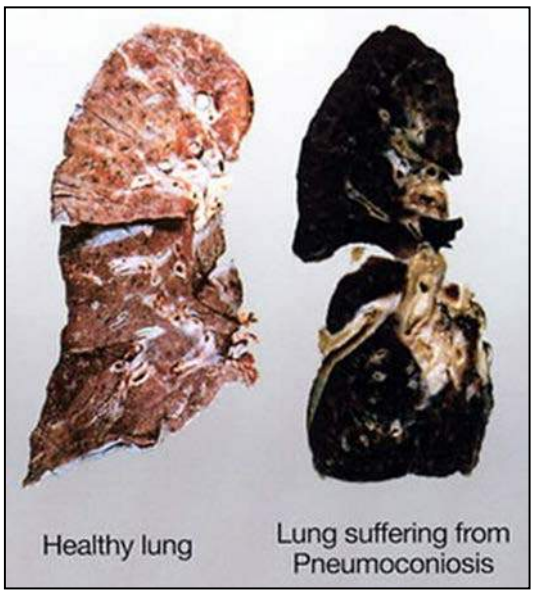

Figure 3. Healthy Lung and Lung with CWP

3.2 Silicosis

Silicosis is a fibrosing disease of the lungs caused by the inhalation and retention of respirable crystalline silica (RCS) produced during the cutting cycle of mining operations (Organiscak, et.al, 2003). The early stages of the disease produce lung accumulations that may be observed on x-ray films similar to that seen in identified cases of pneumoconiosis detailed in 2.5.1 (McPherson, 2009). Silicosis is irreversible, progressive, incurable and at later stages disabling and eventually fatal (WHO, 1999).

Four clinical types or presentations of silicosis that can be produced from the inhalation and deposition of dusts containing respirable crystalline silica have been defined as:

- simple silicosis;
- complicated silicosis
- accelerated silicosis; and
- acute silicosis.

Once these conditions have developed, no known cure or medical treatment is available, no reversal of the condition will occur over time, and it has been identified that the effects worsen even though no further exposure to silica is experienced (USDOL, 2008, McPherson, 2009, WHO, 1999).

3.2.1 Simple silicosis

Simple silicosis is the most common clinical presentation of the disease and results in fibrotic changes in the air exchange region of the lung that may occur after 10 to 30 years of inhalation of RCS. The fibrotic changes (like scars) are called silicotic lesions which are of a nodular appearance and these lesions increasingly affect the ability of the lung to exchange gases. Those changes in turn place extra stress on the cardiovascular system and reduce the body's ability to combat respiratory infections (USDOL, 2008, McPherson, 2009, WHO 1999).

Determining the exposure limit at which workers are at risk of developing simple silicosis is an extremely difficult task for a variety of reasons. These reasons include but are not limited to:

- lack of reliable past dust exposure information;
- insufficient medical surveillance information;
- individual susceptibility; and
- the role of other exposures such as smoking.

It is generally believed, however, that daily workplace exposures that exceed established exposure standards as detailed in this document can result in simple silicosis (USDOL, 2008).

The first symptom of silicosis is dyspnoea (difficult or laboured breathing and/or shortness of breath). This is first observed within the normal work activity or exercise and later as the lung function deteriorates, may be observed whilst resting or during periods of no activity. Workers with simple silicosis are usually without any symptoms. If symptoms occur, they are typically limited

to a chronic cough with phlegm (mucus) production and often get misdiagnosed as other ailments. It is also possible that there may be no shortness of breath or other symptoms and the disease may first be detected through an abnormal chest x-ray. The x-ray may show quite advanced silicosis with only minimal symptoms (USDOL, 2008).

The fibrosis in simple silicosis occurs predominantly in the upper lung zones and appears on the chest x-ray as small discrete nodules (lesions) arranged in a birdshot pattern (USDOL, 2008). Figures 4 and 5 below show a basically normal lung and a lung with simple silicosis.

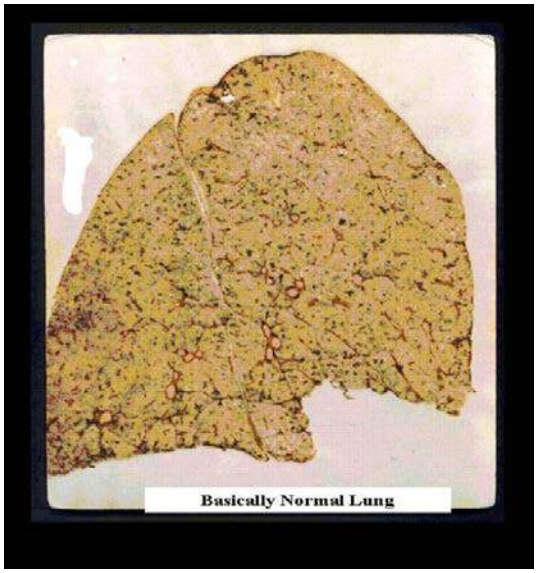

Figure 4. Normal Lung

Figure 5. Simple Silicosis

3.2.2 Complicated silicosis

Complicated silicosis usually occurs after 10 or more years of exposure at relatively low concentrations of silica dust. The silicosis nodules increase in size and coalesce into large lesions usually greater than 1 cm in diameter. The conglomerate lesions may obliterate bronchi and vessels and cause marked distortion of lung structure and function. The disease results in progressive massive fibrosis (PMF).

When progressive massive fibrosis occurs, the patient develops progressive respiratory symptoms from reduction in lung volume, distortion of bronchi, and bullous emphysema. The main symptom is shortness of breath which is related to a loss in lung volume as can be clearly seen in figure 7 below. Figure 6 shows a healthy lung.

Complicated silicosis is progressive and ultimately disabling, potentially leading to cardio respiratory failure and possible death (AIOH, 2009, USDOL, 2008).

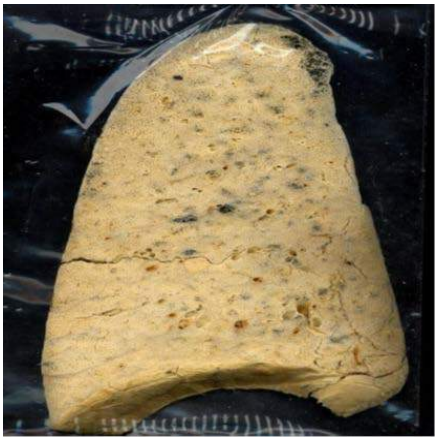

Figure 6. Healthy Lung

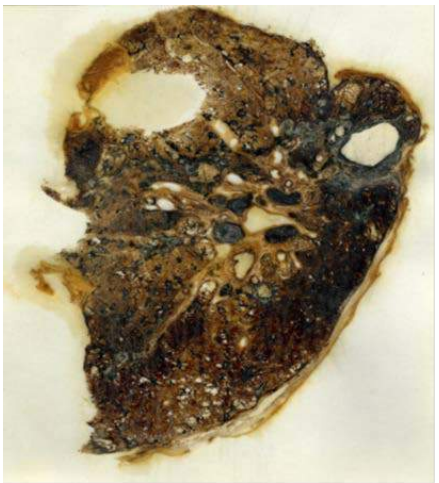

Figure 7. Complicated Silicosis

3.2.3 Accelerated silicosis

Accelerated silicosis results from the inhalation of very high concentrations of respirable crystalline silica over a relatively short period, in the order of 5 to 10 years, whereas complicated silicosis may take 10 to 30 years to develop. Although accelerated silicosis develops in a pattern similar to that of complicated silicosis, the time from initial exposure to the onset of the disease is significantly shorter and the progression to complicated silicosis is more rapid. This form of the disease is life-threatening, and death may occur as a result of insufficient levels of oxygen in the blood in as little as 10 years after exposure has occurred (USDOL, 2008, AIOH, 2009).

It has been reported that the onset of silicosis has occurred amongst drill operators within a year of being exposed to air concentrations of silica 2000 times the accepted statutory exposure level (WHO, 1999).

3.2.4 Acute silicosis

Acute Silicosis develops from the inhalation of high concentrations of RCS and is the most aggressive of the silicotic diseases. Acute silicosis develops over a very short period ranging from as little as a month to 4 or 5 years.

Acute silicosis differs from complicated and accelerated silicosis in that the characteristic nodular pattern in the upper lung is absent with the x-ray's appearance instead being similar to that of diffuse ground glass.

Symptoms of acute silicosis include cough, weight loss, and fatigue. This may progress rapidly to respiratory failure over a period of several months. Death occurs after a few months (USDOL, 2008, AIOH, 2009).

3.3 Silica and Lung Cancer

In 1997, after re-evaluating the scientific literature on respirable crystalline silica, the International Agency for Research on Cancer (IARC) published a monograph that concluded that there is now sufficient evidence in humans that inhaled crystalline silica in the form of quartz from occupational sources can cause cancer (IARC, 1997).

An IARC working group on the question of silica exposure and cancer risk in humans found that several studies among the many reviewed, were negative or equivocal. The studies also identified that the carcinogenicity of silica was not detected in all industrial operations.

However, nine studies did identify an excessive risk for lung cancer in certain dust producing occupations. These dust producing occupations included mine workers, although coal-mine workers were not specifically identified. Increased lung cancer risk among these groups appears to be found only in those with exposure to high levels of crystalline silica (IARC, 1997, AIOH, 2008, WHO 1994).

4 CONCLUSION

Particulate matter smaller than 10 micron can remain deposited in the lungs of workers exposed to these particles. Coal miners are particularly at risk of lung disease by simply performing their everyday duties.

The UBB disaster has identified that the deaths of these 29 miners may have been averted if more stringent attention had been paid to the management of dust produced during the mining cycle.

It has also been identified through detailed analysis that 71% (17 of the 24 autopsies performed) of the men that died in this disaster had advance lung disease. The fact that 71% of them showed evidence of CWP is an alarming finding given the ages and work history of these men.

With the alarming findings of lung disease from the UBB disaster, and the finding that the disaster may have been averted with greater dust control practices, all persons involved in the coal mining industry, in fact, in any dust producing industry, should place dust mitigation and control at the top of their HSE policies and planning, to prevent future disasters occurring and more importantly, to

protect all workers in any industry from this insidious and fatal disease.

REFERENCES

Australian Institute of Occupational Hygienists Inc., *Respirable Crystalline Silica and Occupational Health Issues*, prepared by AIOH Exposure Standards Committee, February 2009

Canadian Centre for Occupational Health and Safety (CCOHS), *What are the Effects of Dust on the Lungs?*, OSH Answers, Chemicals and Materials, http://www.ccohs.ca/oshanswers/chemicals/lungdust.html accessed 17.10.2012

Davitt McAteer, J,. *Upper Big Branch The April 5, 2010, explosion: a failure of basic coal mine safety practices,* Report to the Governor, Governor's Independent Investigation Panel, May 2011

International Agency for Research on Cancer (IARC) *Silica, Some Silicates, Coal Dust and para-Aramid Fibrils,* Monographs on the Evaluation of Carcinogenic Risks to Humans, Volume 68, 1997

McPherson, Malcolm J., *Subsurface Ventilation and Environmental Engineering*, Part 5 Dust, Chapter 19, The Hazardous Nature of Dusts, 2nd ed, Chapman & Hall, 2009.

National Center for Biotechnology Information (NCBI), *Coal Worker's Pneumoconiosis*, U.S. National Library of Medicine 8600 Rockville Pike, Bethesda MD, 20894 USA, http://www.ncbi.nlm.nih.gov/pubmedhealth/PMH0001187/ accessed 17.10.2012

Organiscak JA, Page SJ, Cecala AB, Kissell FN [2003]. Surface mine dust control. In: Kissell FN, ed. Handbook for dust control in mining. Pittsburgh, PA: U.S. Department of Health and Human Services, Centers for Disease Control and Prevention, National Institute for Occupational Safety and Health, DHHS (NIOSH) Publication No. 2003-147, IC 9465, pp. 73–81

World Health Organization International Agency for Research on Cancer, *IARC Monographs on the Evaluation of Carcinogenic Risks to Humans*, Volume 68, Silica, 20th May 1997

World Health Organisation, *Hazard Prevention and Control in the Work Environment: Airborne Dust*, WHO/SDE/OEH/99.14

U.S. Department of Labor, Mine Safety and Health Administration, *A Practical Guide to an Occupational Health Program for Respirable Crystalline Silica*, Instruction Guide Series IG 103, Jan 25, 2008

U.S. Department of Labor, Mine Safety and Health Administration, *Lowering Miners' Exposure to Respirable Coal Mine Dust, Including Continuous Personal Dust Monitors; Proposed Rule, 30 CFR Parts 70, 71, 72, et al.,* October 19, 2010

Preparation of Anti-Explosive Materials by Hydrophobization Technique

E. Vogt
AGH - University of Science and Technology, Faculty of Energy and Fuels
Cracow, Poland

ABSTRACT In the work are presented new methods of manufacturing of anti-explosive materials for coal mining industry on the example of hydrophobization of limestone powder. The techniques of limestone powder hydrophobization were carried out in apparatuses of own design. The evaluation of the usability of commercial modifiers (stearic acid, silicone preparation) for hydrophobization of limestone powders was made. The degree of hydrophobization of modified materials was determined. Additionally the densimetric properties of raw and hydrophobized materials were measured in order to evaluate the effect of commercial modifier on flow properties of these materials. The suitable values of floodability and flowability indexes were assigned for tested materials. The thermal decomposition of materials was also made. It was stated that hydrophobization process improves not only water-proof properties of modified materials but also reduces their cohesion properties and improves flow qualities.

Keywords: Coal mining, anti-explosive material, hydrophobization, limestone powder

1 INTRODUCTION

Limestone powder characterized by hydrophobic properties is used as an anti-explosive agent in coal mining industry. Especially fine dispersional limestone, which grain diameter equals less than 80 μm (limestone meal) is useful for this purpose. In many works one can read that this powder (water-proof hydrophobized limestone meal) barriers very effective interrupt the flame propagation. Cybulski (2004), Lebecki (1993), Man & Teacoach (2009), Polish Standard (1994). As a precaution against coal dust explosions, limestone powder is spread within mine barriers (Figure 1).

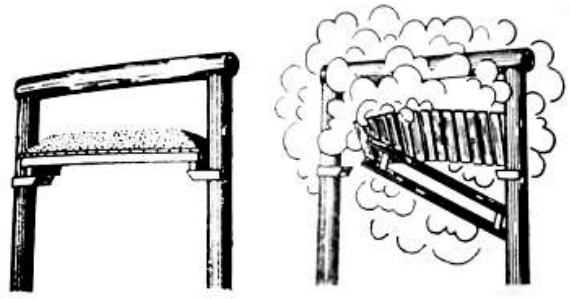

Figure1. Dust barrier activation process Cybulski (1973).

During an explosion the limestone powder disperses, mixes with the coal dust and prevents flame propagation, acting as an inhibitor. Limestone powder reduces the flame temperature to a point where devolatilization of the coal dust can no longer occur; starved of fuel, the explosion is inhibited.

The water-proof hydrophobized limestone powder nowadays is produced by milling raw limestone with stearic acid. In the consequence of modernization of quarries the quantity of possible producers of such powder could be reduce. For this reason new methods of manufacture of water-proof limestone meal should be searched. This new product protects human life so its properties are very important and should be well-known.

Hydrophobization is a beneficial process from the economic point of view since, as it is commonly known, hydrophobic materials are sensitive to the harmful effect of humidity to a much lower degree than solids with similar applications but not possessing this characteristic. In general terms, methods

of hydrophobisation can be divided into protection of material surface by substances characterised by hydrophobic properties or modification of properties inside material volume Vogt (2008). In the case of fine dispersional materials such as limestone meal the layer hydrophobisation (protection of material surface) is the most often used. This process guarantee good contacting of each fine dyspersional materials grains with a hydrophobizing preparation.

2 EXPRIMENTAL

2.1 Limestone Material

In this work limestone powder (meal) from the Czatkowice Lime Quarry Buczek & Vogt (2007) with the particle diameter less than 80 µm was used as a raw material during researches. This powder is, among others, used in the coal mining industry as one of the elements of the anti-explosive safety system (raw anti-explosive limestone powder) Polish Standard (1994), Lebecki (1993), Skalski (2005), Man & Teacoach (2009), Lebecki & Małachowski (2012). The average chemical composition of limestone meal in accordance with the manufacturer's data is presented in Table 1.

Table 1. Chemical composition of limestone meal – manufacturer's data.

Component	(% w/w)
$CaCO_3$	96.00
SiO_2+NR	1.50
$MgCO_3$	1.50
Fe_2O_3	0.11
Al_2O_3	0.08
Na_2O	0.023
K_2O	0.037
Heavy metals	In trace amounts

The real density of the limestone meal, marked with the method of helium picnometry with the use of the AccuPyc 1330 apparatus, amounts to 2.7642 g/cm^3.

2.2 Modifiers

Due to extensive pulverization of limestone meal and its cohesive properties, industrial modifiers were chosen for research as they, according to the author, guarantee good contacting of powder grains with a hydrophobizing preparation. Stearic acid is used in mining production plants for the production of anti-explosive powder with the traditional method. Another preparation used in the researches include existing on the market representatives of groups of compounds often quoted in literature and applied for the hydrophobization processes of mineral bulk materials; these are: a silicone preparation with the marketing name SARSIL® H-15 produced by the Chemical Plant "Polish Silicones" Ltd in Nowa Sarzyna. The second mentioned preparation is a solution of methyl salicylate resin in isoparaffin solvent - has got the density of 0.78 kg/m^3 and is applied for protecting building materials such as brick, concrete, gypsum, plasters.

2.3 Applied Hydrophobization Techniques

2.3.1 Selection of a modification technique

The densimetric characteristic of limestone meal was the basis for the proposed methodology of conducting the hydrophobization process. Processes enabling the dispersion of powdr to a degree which allows for the contact of single grains with the modifier were taken into account. It was assumed that the modifier should be introduced into the process in such a form which would build a monomolecular layer on the surface of single limestone powder grains. Although limestone powder is characterized by a low porosity level, it was assumed that due to its vulnerability to moisture the modifier should also block the entrances of the pores inside powder particles or coat the pores' surface with a protective layer against moisture. Both modifications were conducted on the air-dry limestone meal.

2.3.2 Hydrophobization with the use of stearic acid

In the work two techniques of applying the modifier (stearic acid) on a powder surface were proposed, which are different from the classical milling limestone with stearic acid technique.

The first proposed method of powder modification was the hydrophobization by ether solutions of stearic acid (diethyl ether, petroleum ether). It was assumed that stearic acid particles dispersed in the solution should have an easy access to the powder grains surface and easily settle on it. The concentration of the solutions used during modification was determined on the basis of the Polish Standard (1994) in such a way that the content of stearic acid in the modified powder was within the range 0.15-0.30%. Hydrophobization from solution was carried out with two methods: mixing solutions with the powder in a beaker at room temperature, and contacting the powder with the modifier in a laboratory evaporator, at an increased temperature.

The other proposed method of limestone meal hydrophobization (with the use of stearic acid) was carried out in an installation of own design, and it consisted in free sedimentation of the powder layer dispersed by stearic acid vapour in powder countercurrent flow (Figure 2). The method guarantees the fulfillment of earlier expressed expectations regarding the modification technique. Falling in a straight line and not meeting any obstacles, the powder was dispersed, and the stearic acid converted into the vapour state may freely settle on its outer surface and penetrate inside pores. The contacting time of both media was extended in relation to the time of hydrophobization from solutions, and volatile organic solvents were eliminated from the process. The author, after characterisation of material hydrophobized with the use of stearic acid, stated that second methods of hydrophobization (Figure 2) is more profitable. So sample S_18, obtained in this way, was find as a main hydrophobized by stearic acid material and its properties were studied in the work.

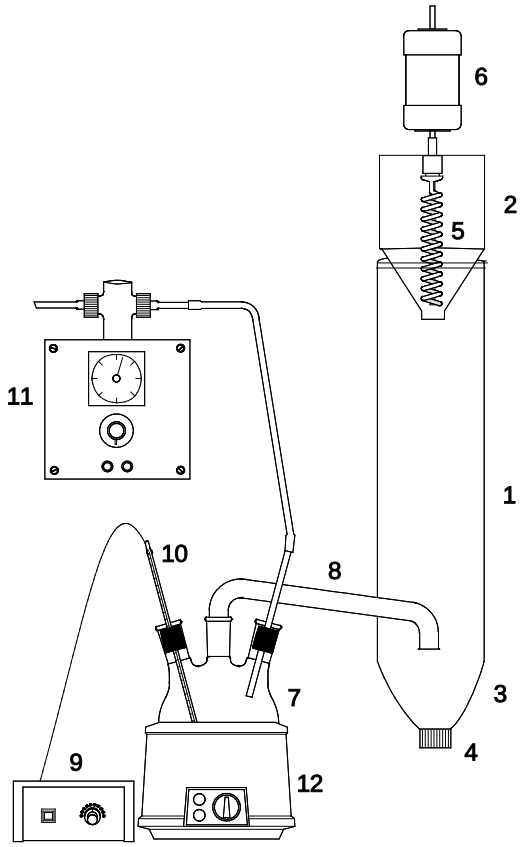

Figure 2. The hydrophobisation installation: 1 – hydrophobisation column, 2, 3 - hoppers, 4 - lock of hopper, 5 - batcher, 6 - electric drive, 7 – boiler, 8 - ting up pipe, 9 – thermoregulator, 10 – thermocouple, 11 – compressor, 12 – heater.

2.3.3 Hydrophobization with the use of silicone preparation

According to the manufacturer's instructions, the SARSIL® H-15 silicone preparation may be applied onto a dry surface of the building material by spraying or painting.

The moisture content in limestone meal (on the modification day) was established with the drier method Polish Standard (1980) and amounted to 0.04%, which is such a low value that the powder was considered as dry.

The initial research determined the preparation volume that should be added to the limestone powder in order to obtain optimal conditions for the contact of the preparation with the powder. The first experiments with a large excess of the modifier guaranteed easy and thorough mixing of reagents, but the achieved time of meal drying was too long. As a result, the limestone meal underwent the process of irreversible lumping. Further experiments

allowed to determine the optimal modifier quantity. The material obtained after modification (S_SH15 sample) was lumped only to a slight degree, and its total disintegration was achieved by sieving the meal with the use of a brush Buczek & Vogt (2013).

2.4 Hydrophobic properties obtained materials

The conducted literature analyses indicate that, although there are a large number of works on hydrophobization processes, no uniform techniques of determining the hydrophobization degree have been developed for materials modified with the use of various modifiers Vogt & Hołownia (2010). This problem is particularly visible in the case of powder materials. Both the modification process itself and the examination of hydrophobic properties of fine-dispersional materials are not as simple as analyzing the same properties for solids with large surfaces. There indeed are methods which may be applied for this purpose, but some of them are so specific that they may be applied only in an exceptional case, as it is the case, e. g. while determining the content of stearic acid in anti-explosive limestone powder Polish Standard (1994), Dang-Vu & Hupka (2005), Fuerstenau & Williams (1987). It is difficult to find a single research method which could be applied to determine the hydrophobization degree of powder materials modified with the use of various modifiers. In the presented research, it turned out that conducting it with the limestone powder helped to search for the method of examining the hydrophobization degree. This fact makes it possible to compare the hydrophobic properties of lime meal modified in the work with the properties of industrial hydrophobic anti-explosive powder available on the market, produced by limestone and margiel quarry of cement plant in Małogoszcz (PH).

2.4.1 Methods measurement of hydrophobic limestone meal properties

A relative evaluation of the hydrophobization degree of the analyzed materials was based on a very simple experiment, the so-called „floating on water" test. The experiment consisted in placing a small amount of powder on the surface of water in a beaker. The following were accepted as reference materials: raw limestone meal and hydrophobic limestone meal (limestone and margiel quarry of cement plant in Małogoszcz – PH sample). Immediately on contact with the water surface, the raw limestone powder became moist and fell onto the beaker bottom. This effect was assumed as the zero hydrophobization degree. By contrast, the complete portion of the industrial hydrophobic material PH remained on the water surface until it evaporated (within approximately three weeks). The hydrophobization degree of materials modified in the work was evaluated on the basis of the limestone meal amount floating on the water surface for a specified period of time.

On the basis of the observations, it can be concluded that the all of materials after modification acquired hydrophobic properties at the level of the hydrophobic properties of the standard material (PH). Both the powder modified with stearic acid from ether solutions, at an increased temperature, and from the vapour phase as well as the powder modified by the method of mixing with the SARSIL® H-15 preparation remained on the water surface for the period of three weeks, just as it was in the case with the commercial material (PH).

It is easy to determine the hydrophobization degree (not only as a relative evaluation but also as a number manner) of material when stearic acid is used as a modifier, because there is a standard, which defines this measurement. The manufactured sample (S_18) contains 0.18 % of stearic acid, being an acceptable level according to the Polish Standard (1994). Unfortunately the contain of stearic acid

can't be measured for meal modified with the use silicone preparation.

In the case of the SARSIL® H-15 silicone modifier the author had to work out the method for determination of hydrophobization C coefficient. The film flotation method could be used if the standard material PH was used as a comparative sample Fuerstenau & Williams (1987), Diao & Feuerstenau (1991). The C coefficient defining to what extent the hydrophobic properties of the S_SH15 sample are different from the hydrophobic properties of the PH sample on contact with a suitable methanol solution was calculated from the equation:

$$C\ [\%] = \frac{f_{pi} \cdot 100}{f_p}$$

Where f_{pi} and f_p are mass percentage of S_SH15 sample and PH sample floating on a selected (10, 20, and 60 % (w/w)) methanol solution surface respectively.

The average value of the C = 84 % coefficient shows that the S_SH15 sample obtained sufficient hydrophobic properties.

It was also measured the water wetting angle. The average values of obtained results are presented in Table 2.

Table 2. Water wetting angle.

Modifier	Wetting angle [degree]
Limestone meal from Czatkowice Quarry	
Lack	33,7 ± 6,04
Stearic acid	125,5 ± 5,77
SARSIL® H-15	101,6 ± 9,96
Standard (limestone meal) material from Małogoszcz	
Stearic acid	76,5 ± 3,99

The obtained values of wetting angle show that both modified materials have achieved the better hydrophobic properties than the commercial anti-explosive powder (PH)

2.5 Thermal Decomposition

The thermal decomposition of the hydrophobized limestone powders was studied. One of the role of limestone powder in the system of protection against explosions brings to the increasing of content of non-combustible parts in coal dust and physical prevention of the flame propagation. Under the influence of the flames temperature comes to the thermal decomposition of limestone powder and both calcium oxide and carbon oxide (IV) are emitted. This endothermic process consumes some of the flame energy. The gases mixture is enriching in non-flammable CO_2. It causes the reduction of the system's explosion.

The thermo balance TA Instruments 2960 SDT was used during researches. DTA curves and the composition of obtained gasses (EGA) were measured. The results are showed at the Figures 3-4. The continuous line (Figures 3-4) represents the course of TG, DTG and DTA curves for the raw material. The dashed lines were obtained for limestone powder modified by stearic acid (Figure 3) and silicone preparation (Figure 4).

The CO_2 contents in emitted gasses showed in the Figure 5 (EGA). The curves obtained for modified meal overlaps with this one obtained for the raw material.

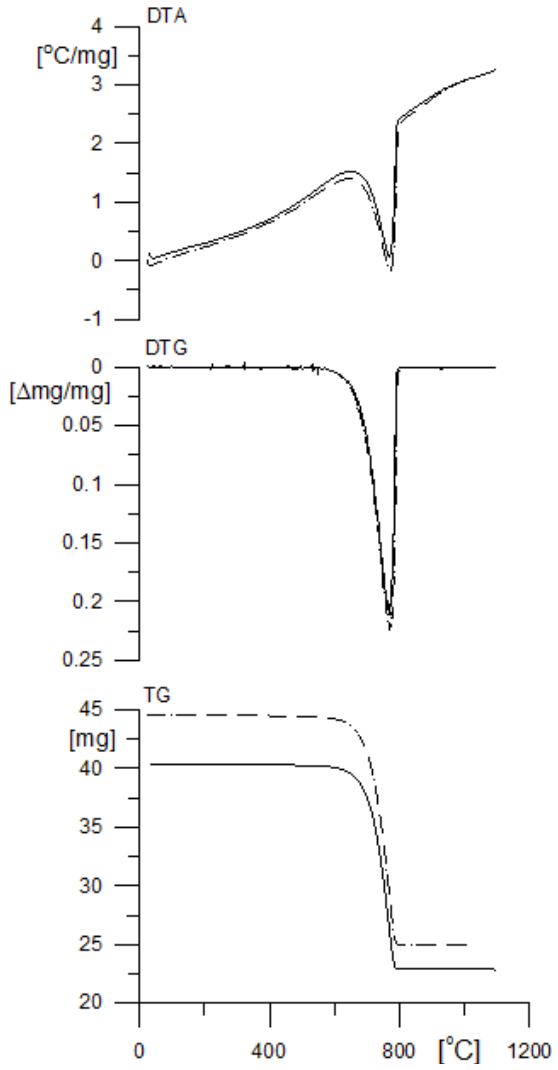

Figure 3. TG, DTG and DTA curves for limestone powder: raw – continuous line, modified by stearic acid – dashed line Buczek &Vogt (2014).

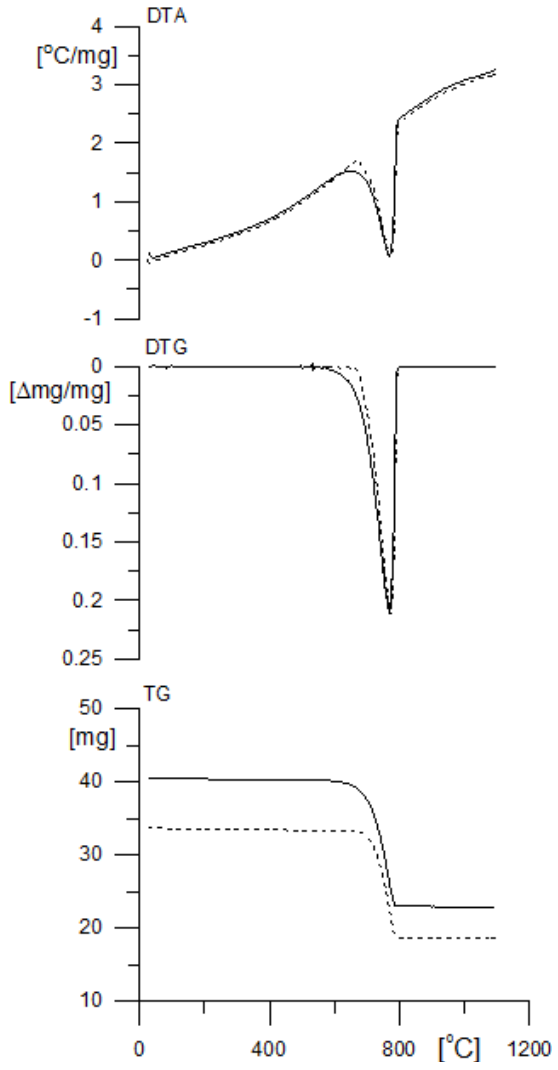

Figure 4. TG, DTG and DTA curves for limestone powder: raw – continuous line, modified by silicone preparation – dashed line Buczek &Vogt (2014).

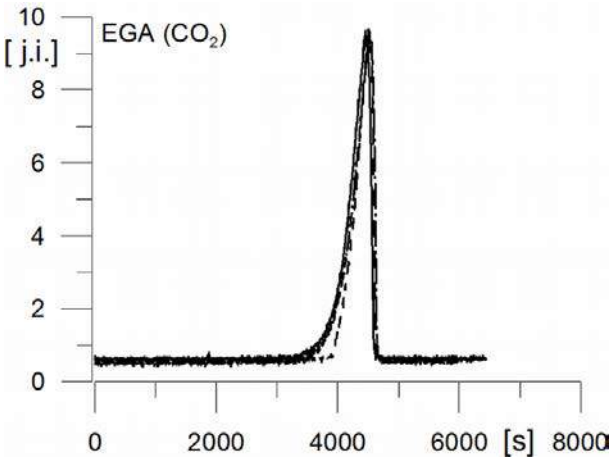

Figure 5. EGA curves for limestone powder: raw –continuous line modified by stearic acid or modified by silicone preparation – dashed line Buczek & Vogt (2014).

The little differences between of courses of TG, DTG or DTA curves for all investigated materials were stated. The obtained results show that the character of the thermal decomposition of modified samples is the same as this one for raw limestone meal, what is profitable for application of hydrophobized meal as an anti-explosive agent.

2.6 Flowability (F_1) and floodability (F_2) indexes

The densimetric parameters (obtained with the use of the Powder Characteristic Tester (PChT), type PT-E, Ser. No. 90133 enable us to estimate the flowability and volatility of powders. These parameters characterised the cohesion properties of limestone meal that are very important during storage and manufacturing of fine dispersional materials. The obtained results may be used also to assess the direction of changes of flow properties of limestone meal, which were caused by the hydrophobization process. There are special tables available which make it possible for the measured parameters to be assigned appropriate ranges of the flowability (F_1) and floodability (F_2) index values Carr (1965), Index Tables (1965), Thomas (2005). Table 3 presents the compressibility (C) and dispersibility (D) values calculated for raw and modified powders and their corresponding ranges of flowability and floodability index values.

Table 3. Values of compressibility and dispersibility calculated for raw and modified limestone meal (Czatkowice Quarry) and their corresponding ranges of flowability and floodability index values Vogt (2008).

Parameters	Material		
	Raw	S_18	S_SH15
C (%)	50.9	39.8	44.1
F_1	0-19	0-19	0-19
D	20	42	16
F_2	60-79	80-100	40-59

It can be observed that the modification process resulted in reduced compressibility of all materials. In spite of this fact the modified materials may be assigned the same range of the flowability index and they constitute the same group of materials as raw limestone meal Carr (1965), Index Tables (1965), Thomas (2005). Such a qualification suggests that during the flow, the materials have a tendency to settle in pipe elbows and clog their outlets. However, it may be assumed that in the case of modified powders flow disturbances upon storage and conveying will be present on a smaller scale than in the case of a raw material.

The meal modified with stearic acid (S_18) is characterized by dispersibility allowing assigning the highest range of floodability index values to these materials (Table 3). In the case of this material, the necessity may arise to implement special precise seals of apparatuses suitable for use with powders. The determined dispersibility of the S_SH15 material is generally comparable for raw powder.

3 CONCLUSION

The presented work is a short summary of the author's research works regarding the hydrophobization of limestone meal. The selection of the presented content was made from the point of view of the evaluation of the usability of industrial modifiers for limestone meal hydrophobization. It was taken into account that the obtained water-proof product should be useful as an anti-explosive limestone powder. The evaluation of the hydrophobization degree of modified materials were made on the basis of the results obtained with the simple method – the test of „floating on water", and special methods suitable for used modifiers. The first measurement enable us to illustrate the relative difference in hydrophobic properties of materials modified with various modifiers. The measurement of stearic acid contents for S_18 sample is suitable when this modifier is used but isn't possible to obtained the same parameter for S_SH_15 sample. The "film flotation" method is an interesting method of

testing the hydrophobization degree for limestone powders modified in different ways. On the basis of the obtained results it may be concluded that all the applied modifiers change the characteristics of limestone meal towards the hydrophobic character. Materials may be useful as an anti-explosive powders in mining.

For all investigated materials was stated that the character of the thermal decomposition of modified samples is the same as this one for raw limestone powder (TG, DTG or DTA and EGA curves). In the case of application of hydrophobized powders as an anti-explosive agent this fact is very profitable.

The densimetric measurements were used to assess the direction of changes of flow properties of limestone powders, which were caused by the hydrophobization process. Familiarity with such characteristics is useful for the designing of devices and apparatuses suitable for use with powder materials or for the proper conducting of such processes.

It was also established that the hydrophobization processes with the use of stearic acid and the silicone preparation as modifiers had the most beneficial effect as far as flow properties of limestone meal are concerned. The modification process maintained the meal powders flow abilities. The application of the water-proof limestone meal is more profitable than use of the raw limestone material.

ACKNOWLEDGEMENTS

The authors are grateful to the AGH University of Science &Technology (Project No. 11.11.210.244) for financial support of this work.

REFERENCES

Buczek B., Vogt E., 2007. A new method of production of non-explosive stone dusts, *Twenty - Fourth Annual International Pittsburgh Coal Conference: Coal - Energy, Environment and Sustainable Development*: September 10–14, Johannesburg, South Africa, Pittsburgh Coal Conference PCC, pp. 51.

Buczek B., Vogt E., 2013. Aplication of silicone modifiers for hydrophobization of lime dust, Polish patent 217493 B1.

Buczek B., Vogt E., 2014. Waterproof anti-explosive powders for coal mines, *Archives of Mining Sciences*, 59, 1, pp. 169–178.

Carr R., 1965. Classifying flow properties of solids. *Chemical Engineering* 72, pp. 163-168.

Cybulski W., 1973. *Wybuchy pyłu węglowego i ich zwalczanie*, Publisher Śląsk, Katowice (In Polish).

Cybulski K., 2004. Assessment criteria of protective zones against coal dust explosions, *Archives of Mining Sciences*, 49, 4, pp. 477–494.

Diao I., Feuerstenau D.W., 1991. Characterization of the wettability of solid particles by film flotation. Part II Theorectical analysis. *Colloids and Surfaces*, 60, pp. 127-144.

Fuerstenau D. W., Williams M. C., 1987. Characterization of hydrophobicity of particles by film flotation, *Colloids and Surfaces*, 22, pp. 87-91.

Dang-Vu T., Hupka J., 2005. Characterization of porous materials by capillary rise method, *Physicochemical Problems of Mineral Processing*, 39, pp. 47-65.

Index Tables. *Handbook of powder characteristics tester*. Hosokawa Micron Corporation. Reprinted from Carr R.,. 1965 Chemical Engenering, 18, pp. 166-167, with approval of Mr. R. Carr and the copyright owner McGraw-Hill Incorporated, New York, 10036, U.S.A.

Lebecki K., 1993. Neutralizacja osiadłego pyłu węglowego jako zabezpieczenie przed przenoszeniem wybuchu, *Prace Naukowe Główny Instytut Górniczy* 784 (In Polish).

Lebecki K., Małachowski M., 2012. Optical method for continuous monitoring of dust deposition In mine's entry, *Archives of Mining Sciences*, 57, 3, pp. 517–534.

Man C.K., Teacoach K.A., 2009. How does limestone rock dust prevent coal dust explosion in coal mines?, *Mining Engineering*, 61, 9, pp. 69-73.

Polish Standard PN-80/G-04511, 1980. Solid fuels. Moisture measurement.

Polish Standard PN-G-11020. 1994, Mining-Anti-explosive stone powder.

Skalski Z., 2005. Workowe zapory pyłowe dla podziemnych wyrobisk kopalń węgla kamiennego, *Wiadomości Górnicze*, 12, pp. 612-619 (In Polish).

Thomas M.A., 2005. Tablets & Capsules: Powder Density in Solid Dosage Forms, Quanta-chrome Corporation.

Vogt E., 2008. Hydrophobization of fine solids presented on the example of limestone powder, *Polish Journal of Chemical Technology*, 10, 1, pp. 49-51.

Vogt E., 2011. Hydrophobized limestone powder as an anti-explosive agent, *Polish Journal of Environmental Studies*, 20, 3, pp. 801-804.

Vogt E., Buczek B., 2007. Rola i znaczenie pyłu wapiennego w systemie zabezpieczeń przeciwwybuchowych w kopalniach węgla kamiennego, *Gospodarka Surowcami Mineralnymi*, 23, 3, pp. 235-242 (In Polish).

Vogt E., Hołownia D., 2010. Badanie właściwości hydrofobowych modyfikowanych pyłów wapiennych, *Gospodarka Surowcami Mineralnymi*, 26, 2, pp. 41-56 (In Polish).

Systematical and Radical Precautions in the Prevention of Mine Accidents and Professional Diseases

T. Güyagüler
Mining Engineering Department, METU, Ankara

ABSTRACT The increasing demand for energy raw materials and various industrial minerals increased the importance of mining. It is obvious that this demand will be rising in the near future. Mining, due to the risks it involves, requires specific knowledge, experience and continuous technical inspection.

It has been observed that recently the number of mine accidents and professional diseases are increasing in Turkey. This trend can only be reversed by the application of systematical arrangements and radical reconstructions.

In this paper, the importance of technical inspection, application of accident preventing methods, approval of mining projects and the responsibilities in the occurrence of accidents and the related recommendation for the improvement will be discussed. In addition, the importance of developing a consistent health and safety policy, responsibilities of employers and employee, recommendations regarding inspection institutions and description of procedures to ensure that the inspections are fully carried out, will also be discussed.

Keywords: Health and safety, accident prevention, environment, ergonomics

1 INTRODUCTION

Accidents and professional diseases results high number of fatalities, injuries and illnesses together with huge money losses. Recently, it has been observed that the number of fatal accidents and professional diseases are increasing in mining industry.

Labor protection is defined as a system of legal acts and relevant socio-economic, technological and organizational measures ensuring safety and health, accident prevention and industrial hygiene and fitness to work

It is the duty of **government, management and workers (unions)** to provide healthy and safe working place and minimize the frequency of accidents and occupational diseases.

2 ASPECTS OF LABOR PROTECTION

2.1 Legal Provisions

The basic statutes on labor protection are **laws, regulations, directives, instructions and standards.** Revising existing statutes and bring them to EU standards is important. It is a known fact that even perfect legal provisions are useless unless effective inspection and control exist. Safety legislation oblige management to ensure safe and healthy working conditions in industry, promote safety layouts and devices that prevent accidents, provide sanitary and hygienic conditions that reduce the incidents of occupational diseases and observe safety and hygienic requirements during the operation.

Governmental inspection is necessary to prevent the violation of health and safety rules and regulation. Controlling should start at the project acceptance stage. Determining suitable mining method, ventilation, transportation and supporting system has vital importance to operate the mine. It can be said that majority of accidents occur due to the mistakes involved in above mentioned factors. The group of engineers who are employed by an institute (MİGEM) as a part of the Ministry of Energy and Natural

Resources, controls the project whether it is prepared according to the mining principles and technology or not. This control should go on throughout the mine life. Therefore the engineers employed by MİGEM should have enough knowledge and experience to do the job properly.

It has been realized that safety legislation would be ineffective or useless unless understood, obeyed and complied with. The inspectors who are employed by The Ministry of Labor and Social Security inspect the companies whether they obey to safety regulation or not. Recently, severe accidents happened in coal mines in Turkey. For this reason inspectors should be capable to find the causes leading to fatal accidents in gassy mines for gas explosion (as seen in Zonguldak) and mine fires, especially spontaneous combustion (as seen in Soma). Here, it may be suggested that an expert group of inspector can reduce the severe accidents.

If safety rules and regulations are ignored, there is an apparent need to enforce and supervise their compliance and observance.

2.2 Environment and Human Factors

In modern mining, psychological overload during working hours has greatly intensified. Therefore, new concepts such as **ergonomics, human behavior, social environment and fatigue management** should be considered in the accident prevention programs.

Ergonomics is defined as the scientific study of the relationship between man, machine and environment.

Man at work is liable to make mistake, particularly if working under stress. These mistakes may cause accidents. The incidence of such mistakes can be reduced by the application of the ergonomics.

In accident prevention programs the main emphasis is generally given on machine guards and accident preventing equipment instead of human mistakes. Most of the machines are designed neglecting to consider the natural behavior of the human being.

Human factors that may cause to accidents are short term memory, expectation, information handling capacity, underestimating the risk, failure to judgment, perceptual limitation and physical limitation (Güyagüler et. al., 2005). These factors should also be considered in accident preventing programs.

Besides the physical environment (gas and dust content, illumination, noise, temperature and humidity etc.), social environment plays an important role in the occurrence of accidents. The important factors involved in social environment are communication, management, family, friends, economics, government, unions and associates. It is very important to consider these factors to minimize the accidents (Murrel, 1979).

2.3 Other Factors

Another important factor, fatigue which is a general term used to describe the feeling of being tired, drained or exhausted should be considered in fighting against accidents. Sign of fatigue are loss of attention, increased impatience and irritability, increased risk taking, short unplanned naps, poor decision making, increased reaction time, lowered ability to think logically, feeling lethargic and inability to anticipate danger

2 APPLYING THE ACCIDENT PREVENTING TECHNIQUES

Data in accident report form can be used to evaluate hazards, prepare job safety guides, formulate new policies, redesign equipment, modify operating procedures, develop training programs etc. The detailed analysis of an accident requires the knowledge of many factors such as location, time, type of accident, profession victim, nature of the injury, personal and environmental factors etc. Detailed information is necessary to analyze the accidents end minimize the accidents, proper Accident Report Form is needed. Analyses of accidents can be done in

a minutes by computer programs using these forms.

The priority and the urgency for correcting a hazard should be determined on the basis of severity, frequency and exposure. In this context, risk levels can be determined using qualitative or semi-quantitative methods. First rating calls for immediate shutdown of the system and eliminating the causes of the hazard leading accident.

General methods of accident prevention and labor protection should be realized by applying officially accepted modern accident prevention methods such as Job Safety Analysis (JSA) and Fault Tree Analysis (FTA) (???).

Accidents can be prevented by simply eliminating one or more of the accident causes. By identifying and correcting the sources of failure, a system can be made safer and more efficient.

3 CONCLUSIONS

As a conclusion the followings can be recommended to minimize accidents and occupational disease

- Proper accident report form and coding system is necessary to analyze and to prevent the accidents. In this context the validity and accuracy of the accident report has vital importance.
- To determine the level of health and safety, legally accepted indicators should be used. It will be helpful for the further accident analysis of and accident prevention.
- Proper risk analysis should be conducted to the mines and its applicability should be controlled.
- After statistical analysis, order the type of the accidents according to their criticality (risk levels).
- Officially one of the accident preventing techniques such as job safety analysis and/or fault tree analysis should be accepted.
- Mining method, ventilation, transportation and supporting system should be suitable to the operation. The control of these should be done during the license acceptance stage and control should continue throughout the mine life.
- Inspectors sent to control the mine should be expert and certified on mine workings.
- Insufficient expenditure creates health and safety problems. Therefore, sufficient money should be spared for the health and safety. It is a known fact that the money spent after accident is always higher than the money spent to prevent the accident. In this context, legally non-fatal and fatal cost models should be prepared.
- Fatal accidents should be analyzed and related precautions should be taken immediately. There are common characteristics causing to firedamp explosions occurred in the coal mines. If the main causes are eliminated, most explosions can be prevented. The similar precautions should be taken to prevent fires resulting spontaneous combustion.
- Principles of ergonomics, fatigue management and social environment concepts should be included into the accident preventing programs.
- Management should provide education and training to the employee and give them information about the risks involved in the working area.
- Punishments given to the employer due to the wrong application of health and safety principles should be high enough to correct mistakes immediately.

As a final conclusion, all types of accidents can be prevented if required precautions are taken.

REFERENCES

Güyagüler, T., Karakaş A., Güngör, A. Occupational Health and Safety in Mining Industry, page 10-16, 2005

Health and Safety Documents, Safety Rules and Regulations in Turkey and USA.

K.F.H.Murrel, Ergonomics, Man in his Working Environment, John Wiley and sons, New York,1979

Wireless Health Monitoring System for Miners

A. Anas
Assistant Manager (E&M), Coal India Ltd., Ranchi, India

ABSTRACT The aim of this Project is to create an easy and effective Health Monitoring System for Miners working in Underground or Open cast Mines. Being exposed to dust, metals and large no. of harmful substances, Miners usually come across many health problems which are not cured on time because of lack of diagnosis and ultimately leads to disastrous results for them and their families. The Wireless Health Monitoring System for Miners speaks about an effective and user friendly system. It comprises of a server terminal and a portable terminal. The server terminal is connected to a central server and portable terminal can be installed in the mines which can periodically be used by miners to provide their body parameters to Health and Safety Officer of the respective mine. The body parameter such as Blood pressure, Pulse rate/Heartbeat, Body temperature etc. may be recorded with the help of portable terminal. A finger print based identity system may be used to save the body parameters of different individuals. These data of different individuals working in mine will be taken and transferred time to time daily, automatically to the server terminal with the help of a Zigbee (XBee) module. The data received at the server terminal will automatically be saved in the specified files in specific formats on server. These files are part of database of a Website which is accessible to appointed doctors. The data collected time to time from miners may be checked on regular basis by doctors and if any disturbance from normal in the body parameters of an individual is detected or noted, doctors may immediately call him/her.

Keywords: Health monitoring system, wireless, record of body parameters

1 INTRODUCTION

1.1 Rationale

Human health is an increasingly popular public concern. People spend lot of money on it because if one gets severely sick or dead, everything else becomes meaningless for them. Unfortunately, millions of people get their disease diagnosed when it becomes too late to receive medical treatment and care. In many of the cases it is observed that if an early action was taken, disease could have been cured. This early action needs proper examination and reports of body parameters of the concerned patient which is not feasible with the current system, as frequent access to medical examining equipment is inconvenient and expensive.

Among the most important indexes of human health, Heart beat/Pulse Rate, Blood Pressure and Body temperature are the most vital ones and they have the advantage of easy access. Unlike X-ray and MRI, the measurement of Heart beat/Pulse Rate, Blood Pressure and Body temperature is an easy conduct and does not cause much harm to human body tissues.

In current market, however there are some measurement devices available which can be used by the patients, but due to non-medical background of majority of patients, and restricted information provided by the instruments, meaningful medical diagnosis on their part is not possible. As far as Miners in particular concerned, majority are either illiterate or very less educated. All the miners are subjected to very high exposure to harmful substances such as dust and other mine gases. Unfortunately till now there is no effective working health monitoring system arranged for them.

In view of the above facts, it is need of hour to design an efficient, convenient inexpensive and user friendly system to read, record, interpret, transfer, save and display the important human body parameters which

can be made available to a doctors through Internet.

1.2 Objectives

- The device and system should be very user friendly so that patients with zero medical and technical background can also use it.
- The device should be power efficient, less costly and reliable.
- The system should be such that it can be easily integrated with present network technologies.

1.3 Functional Structure

The system consists of two parts:

1. Portable Terminal
2. Server Terminal

1.3.1 Portable terminal

It consist of the main measurement circuit, processing unit, small memory and a wireless transmitter. Measurement circuit consist of a temperature detecting sensor and a pulse detection circuit. The data from circuit is given to Analog to Digital Converter (ADC) of Micro-controller Unit (MCU). This Micro-controller Unit is employed for the conversion and processing of data. Then the processed data is taken out from UART (Universal Asynchronous Receiver Transmitter) serial channel of MCU to the Transmitter.

1.3.2 Server terminal

It consists of a wireless receiver, a server and a COM port to interface with. The data generated at the Portable Terminal is received at the server side with the help of a wireless receiver, processed and saved in the form of different files on the server and can be accessed from Internet or intra-net by the doctor through a web based portal hosted on the server.

2 HARDWARE REQUIREMENTS

2.1 Temperature Transducer / Sensor

A temperature Transducer/Sensor is required in designing this device as body temperature is a very important parameters as far as diagnosis is concerned. A simple temperature transducer that can be used here is LM35, which is an integrated circuit based temperature sensor. It converts the temperature into a proportional electric signal which can be easily converted into equivalent temperature through calibration.

LM35 temperature transducer is a precise integrated circuit based sensor, whose output voltage is linearly proportional to input temperature. It provide typical accuracies of $\pm 0.25\ ^{\circ}$C at room temperature and ±0.75 °C at over a full -55 to +150 °C temperature range. LM35 is a low output impedance, linear output and precise inherent calibration interface device. It can be used with a single power supply. As it draws only 60 μA from its supply, it has very low self-heating, i.e. less than 0.1 ^{O}C in still air.

The fabrication of a temperature sensor depends upon exploiting a property of some material which is a changing function of temperature. A silicon NPN transistor can be used for such a requirement. The base-emitter voltage (V_{BE}) of such a transistor has a temperature dependence over smaller range of temperatures. The approach developed is one where the difference in the base-emitter voltage of two transistors operated at different current densities is used as a measure of temperature.

2.2 Infra – Red Led

An Infra-Red Light Emitting Diode is required to generate an electrical signal proportional to the pulse rate of a person. A simple Infra-Red LED which can be used here is LTE4208. Some of its important parameters are:

PARAMETER	MAXIMUM RATING
Power Dissipation	100 mW
Peak Forward Current	3A
Continuous Forward Current	50 mA
Reverse Voltage	5V
Operating Temperature Range	-40 ^{O}C to + 85 ^{O}C
Storage Temperature Range	-55 ^{O}C to +100 ^{O}C
Lead Soldering Temperature	260 ^{O}C for 5 sec

2.3 Infra-Red Phototransistor / Sensor

The Infra-Red (IR) Photo-transistor can be used in the design of portable terminal for providing the complementary role of detecting the signal produced by IR – LED and reflected after striking on the finger of patient or concerned person. It consist of a NPN silicon transistor mounted in a lensed, clear plastic end looking package. Some of its important parameters are:

PARAMETERS	MAXIMUM RATING (25 ^{O}C)
Power dissipation	100 mW
Collector – Emitter Voltage	30V
Operating Temperature Range	-40 ^{O}C to + 85 ^{O}C
Storage Temperature Range	-55 ^{O}C to +100 ^{O}C
Lead Soldering Temperature	260 ^{O}C for 5 sec

2.4 Operational Amplifier (OpAmp)

An Operational Amplifier (OpAmp) can be used in the design of measurement circuit to provide voltage gain and work in the filter for obtaining desired range of frequency of the signal obtained from the Infra-Red Photo-transistor. A simple OpAmp that can be used here is LM358. It consist of two independent, high gain, internally frequency compensated OpAmps designed to operate from a single power supply over a wide range of voltages.

2.5 Micro-Controller

A Micro-controller can be used in the design of Portable Terminal for converting the filtered out analog signal to digital form with the help of its Analog to Digital Converter (ADC) and then processing it to transfer the desired result by sending it to the RF wireless transmitter. A Micro-controller is a computer-on-a-chip. It is a type of microprocessor emphasizing self-sufficiency and cost-effectiveness, in contrast to a general-purpose microprocessor. The only difference between a micro-controller and a microprocessor is that a microprocessor has three parts – ALU, Control Unit and Registers, while a micro-controller has additional elements like ROM, RAM etc.

A simple Micro-controller that can be used here is ATmega32L. ATmega32L is a low power CMOS 8-bit Micro-controller based on the AVR enhanced RISC Architecture. By executing powerful instructions in a single clock cycle, the ATmega32L achieves throughputs approaching 1 MIPS per MHz allowing the system designer to optimize power consumption with processing speed.

2.6 Wireless Transceiver (ZIGBEE)

In order to transfer the data received and processed by the Micro-controller to the server terminal wirelessly, a Radio Frequency Wireless Transmitter can be used here. Such most convenient device that can be used here is a ZIGBEE Module. Zigbee is a kind of wireless communication device which owns the lowest power consumption and cost in its field. As far as radio frequency bands are concerned Zigbee can operate in the industrial, scientific and medical radio frequency bands. Zigbee is considered to be the most appropriate device for this role in the current scenario because of the following reasons:

- Low Cost
- Secure
- Reliable and Self-Healing
- Flexible and Extend-able
- Low power consumption
- Can be globally used in the non-license requiring radio bands.
- Integrated intelligence for network setup and message routing.

Zigbee is the only standards-based technology that addresses the unique needs of most remote monitoring and control sensory network applications.

2.7 Miscellaneous

There are a many more small components which are to be used in the design of Portable terminal of the device. Some of these are:

- Resistors
- Capacitors
- Trimpot
- Battery or any other power source.
- GP Board
- 2 pin Jumper wires
- IC 7805 Voltage Regulator

Resistors and Capacitors of different value as per the requirement of circuit may be used to design both measuring as well as filter circuits. A trimpot (or rheostat) is a device used to get a variable voltage gain by changing its variable resistance. IC7805 voltage regulator is an integrated circuit based voltage regulator for a regulated D.C. Power supply of +5V. Since Micro-controller ATmega32 as well as OpAmp LM358 cannot withstand voltages more than +5V this regulated D.C. Power Supply is necessary for this design.

3 SOFTWARE REQUIREMENTS

3.1 Real-Time Operating System

3.1.1 System overview

On the system level, two sensing tasks, heart rate sensing and temperature sensing, needs to be done. Another task is needed for communication between the MCU and web-server. The temperature sensing task just needs ADC conversion so this can be done in interrupt handlers. The other two tasks need separate functions to perform. The behavior of the system should be predictable and the time when the measurements are performed needs to be recorded. In this scenario, a real time system is used to schedule the tasks.

3.1.2 Real-time OS configuration

A customized real-time OS UART library trtUart.c can be used in the program with a creation of two semaphores, SEM_RX_ISR_SIGNAL and SEM_STRING_DONE. The variable of heart rate is a shared variable between the task of communication (task 1) and the task of heart rate measurement (task 2). The semaphore HEART_OUTPUT is created to protect this variable. Also, the task of measuring heart rate is only allowed to run after a new data point is ready. Therefore, another semaphore, DATA_READY is created to control the execution of task2. Semaphore HEART_OUTPUT is initialized as unblocked and all the others are initialized as unblocked.

3.1.3 Tasks description

Task 1 communicates with the web-server and it is desirable to guarantee that the information is received or transmitted. Therefore, task 1 is assigned higher priority over task 2. The priority is assigned by giving task 1 an earlier deadline than task 2 when the two tasks are created and their deadlines are kept fixed.

In the communication between the MCU and the web-server, all the communications are initiated by the web-server. Therefore, task 1 keeps receiving instruction from the server and it is blocked until a "\r\n" is received. Once task 1 receives a "\r\n", it will perform different things according to the instructions received.

Task 2 is the heart rate detection algorithm and it is executed after a data point of the heart pressure wave is ready and it must be done before the next data point of the heart

pressure wave is ready. So at the end of the task 2, the process waits for the next data point to be ready. And when the next data point is ready in the ISR (Interrupt Service Routine), the ISR will signal task 2 to go. Task 2 is also in charge of saving data for the most recent 5 stable pulses. Two buffers are used to do this task. Once one buffer successfully records the data for 5 successive stable pulses, this buffer becomes the ready buffer and the other buffer will be in charge of recording data for the next 5 stable pulses. This guarantees that 5 successive stable pulses are recorded and the recorded data are up to date.

The data sampling of the heart wave needs to be accurate. Data points must be sampled at 5ms intervals to ensure correct calculation. Since interrupts have highest priority in a real time system, the sampling of data is controlled by the ISR. Timer 0 is used for the interrupt and the ISR is called every 1ms. In the 5ms interval, 2 milliseconds are assigned to the ADC conversion of the heart wave and the rest 3 milliseconds are assigned to the ADC conversion of the temperature. So at the end of the first two milliseconds, the ADC result is taken as a data point for the heart wave and the ISR signals task 2 to run. Then the ADC channel is switched and the conversion of temperature starts. At the end of the last 3 milliseconds, the ADC result is taken as a data point for the temperature. Then ADC channel is switched back and another conversion of the heart wave starts. In this way, both heart rate sensing and temperature sensing go well and the data points for the heart wave are sampled at 5ms intervals accurately.

3.2 Data Logger Software

As required a data logger program can be created to attempt to log the data periodically. The design theory behind its creation can be stated as:

3.2.1 Program Overview

The data-logger has several fields. Both the temperature and the heart rate have to be saved in different files. In the text box where it says heart Rate File Name, one has to enter the appropriate location of the heart rate file. The same is true of the temperature file name. The Com port field allows one to choose from 9 COM ports. And the baud rate field allows one to choose from the following baud rates: 9600, 2400, 4800, 9600, 19200, 38400. Once one has selected the baud rates, the com port and the file locations and names, one has to click communicate in order to activate the communication.

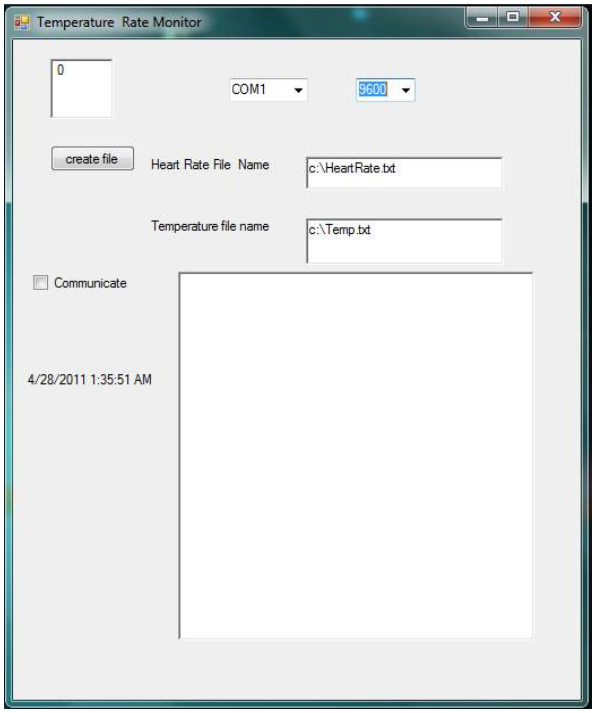

3.2.2 Code description

A quick description about how windows operating system works is necessary in order to explain how the code was written. Windows operating system is very much based on the idea of an interrupt event driven operating system. It has these things called event handlers. For example when you click, the communicate check box, windows will call the following event handler in your visual basic code

Private Sub cbCommunicate_CheckedChanged (ByVal sender As System.Object, ByVal e As System.EventArgs) Handles cbCommunicate. CheckedChanged

So when the status of the check box changes (which happens whenever the user clicks on the checkbox), the event handler will get called. Once this event handler gets called, the code will check to see if the box is checked or not. If the box is checked, it will disable the com port box, the baud rate box and the file name boxes. The code also enables the timer if the box is checked. However, if the box is unchecked, all of this is undone.
Once the timer is enabled, the event

Private Sub Timer1_Tick1(ByVal sender As Object, ByVal e As System.EventArgs) Handles Timer1.Tick
Dim heartRate As String

is called once every 15 milliseconds. Basically what happens in this events is that the Serial Port is opened. Next by using the write (String message) function in the serial port object that comes as one of the VB.NET libraries, we send the MCU a request for the heart rate using the string "H\r\n" or a request for the temperature using the string "T\r\n". When such a request is sent out, the program then waits until a byte is received in the serial port buffer. Whenever this happens, another event called

Private Sub serialPort_DataReceived(ByVal sender As Object, ByVal e As System.IO.Ports.SerialDataReceivedEventArgs) Handles serialPort.DataReceived

is called. Whenever this gets called, we use the ReadExisting() function in the serial Port library, to store both the current heart rate and the current temperature in two global variables. Since we are expecting the heart rate and the temperature to be received from the data-logger, this event Handler also ends up closing the serial port after the temperature is received in order to allow the Web-Server to access the com port whenever it needs to. In order to differentiate between the temperature and the heart rate, the event handler has a static variable that keeps track of the number of times the event is called. Every even number of times the event is called, the software assumes that the heart rate is received from the MCU. Every odd number of times this event gets called, the data that is received will be the temperature. The reason why we can make this assumption is because the data logger is always sending out both requests for the heart rate and the temperature one right after the other, and when the MCU sends the data, this event gets called once for the temperature and once for the heart rate. Next, this event handler will store the temperature and the heart rate in their corresponding files. But before it can do this, it will of course have to open it. Please note that since two programs cannot access the same file at once, the program will wait until the files are accessible in order to access them. Once the data has been written to the appropriate files, the data logger will then close the files so as to give access to the web-server.

3.3. MCU Programming Software

In order to program the micro-controller as per our requirements to set its ports, a micro-controller programming software is required. A simple software that can be used for such a programming is Code Vision AVR (CVAVR).

CVAVR is a C-program language compiler which is used to program the micro-controller. CVAVR is a highly versatile software which offers “High Performance ANSI C Compiler, Integrated Development Environment, Automatic Program Generator and In-System Programmer for the Atmel AVR family of micro-controllers.

4 IMPLEMENTATION

4.1 Measurement Circuit

4.1.1Temperature measurement

Temperature measurement in this design is done by LM35 temperature transducer. This semiconductor based temperature transducer has got three terminals. One terminal is the ground. Other is the +Vs which should be from 4V to 20V. The third terminal gives us output voltage proportional to temperature with 10mV/ ºC. The output pin of this device

is connected to channel of ADC of the micro-controller.

4.1.2Heart Rate / Pulse Rate Detection

Heart rate or pulse rate detection can be done by a technique known as **Plethysmography**. Plethysmography is a non-invasive technique of measuring blood flow in the human body. In this method, a part of human body is which is under consideration, is illuminated by an Infra-Red light generating source such as Infra-Red LED. As the blood volume inside the organ pulsates due to variation in blood pressure, the IR rays reflected from and transmitted through the organ pulsates. This pulsation can be converted into electrical signals using an IR phototransistor.

As the blood volume changes in the arteries of organs due to varying blood pressure whose frequency of variation is same as that of heart beat, by detecting the variation of reflected and transmitted IR rays using photo-transistor, the Heart rate/Pulse rate can be deduced. In the design of this project, finger Plethysmography can be used. Hence finger of the concerned person, which may be a miner in our case can be used to detect the heart rate / pulse rate using this method.

4.1.3Filtering and Amplifying

The signal extracted from the finger using IR sensor needs to be filtered and amplified first to make it suitable for interpretation use. For this two stage band pass filters are used. Each band pass filter consists of a passive high pass filter (HPF), and an active low pass filter (LPF). This active low pass filter provides us with suitable amplification in our signal.

High Pass Filter (HPF) – The high pass filter we can use, is having a single pole RC circuit as shown below. This is a passive HPF.

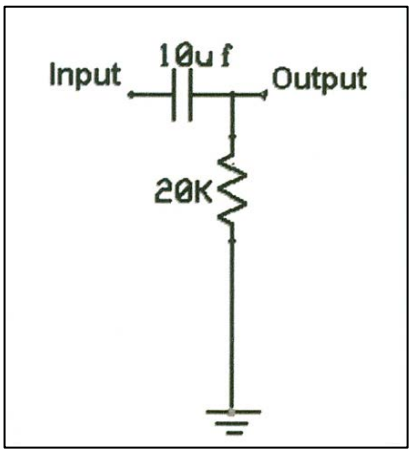

As this contains a capacitor in between input and output so it blocks dc signal. Further the capacitance offer high impedance to the low frequency signal and vice – versa thus implementing high pass characteristics. The cut-off frequency is given as:

$f = 1/2\pi RC$

Where R = Resistance of Circuit
C = Capacitance of Circuit

Here R = 20K, C = 10μF

Hence f = 0.8 Hz

Low Pass Filter (LPF)

The low pass filter which can be used in this project is non-inverting OpAmp based active low pass filter.

It consists of two resistors of 1K & 100K values, which gives a non-inverting dc gain of 1+R2/R1. The capacitor C is used to make it low pass filter with cut-off frequency $f = 1/2\pi CR2$.

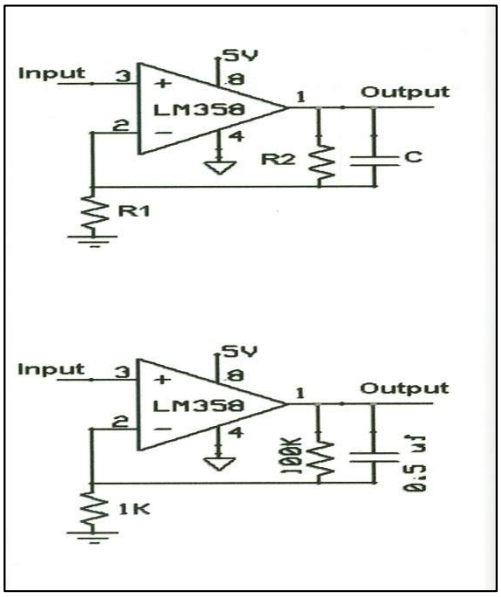

Shown above is the actual circuit with the values of capacitance and resistances. It's non-inverting dc gain is 101 and it's cut-off frequency is 3.18 Hz.

The overall filtering circuit is as follows:

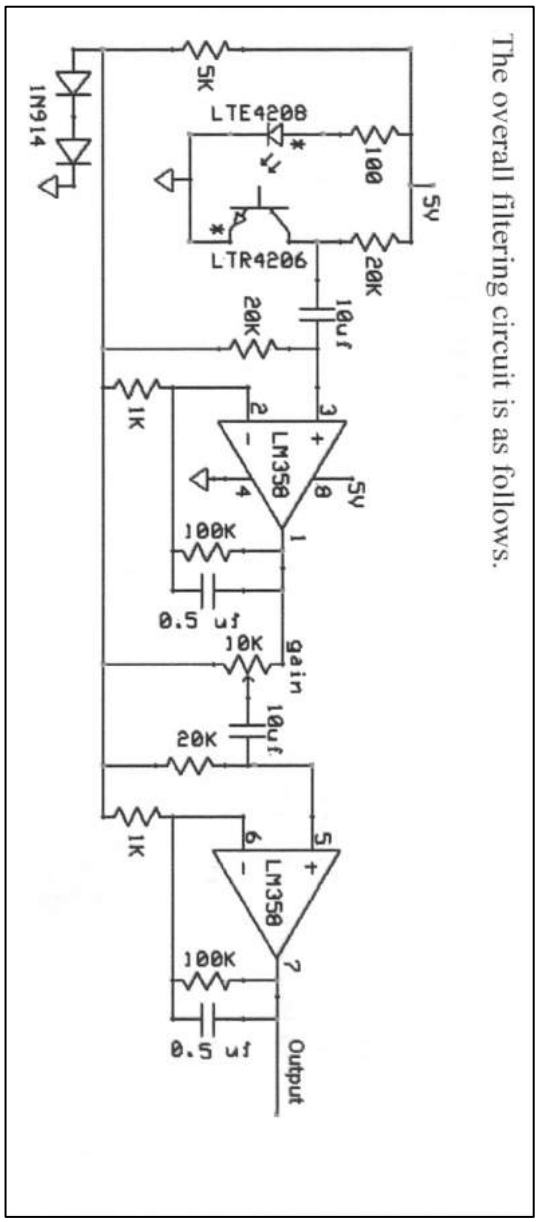

4.2 XBEE – ATmega Interface

This interface will be on the portable terminal side, where slave XBEE should be connected to ATmega32 micro-controller. This interface is designed using UART of the ATmega32. Pin 14 can be the RXD (Receiving) pin of micro-controller which is to be connected to pin 2, the D_{OUT} pin of the Zigbee. Pin 15 i.e. TXD (Transmission) pin is connected to pin 3 of the Zigbee i.e. D_{IN} pin. As both the ICs have CMOS level logic, they can be directly connected.

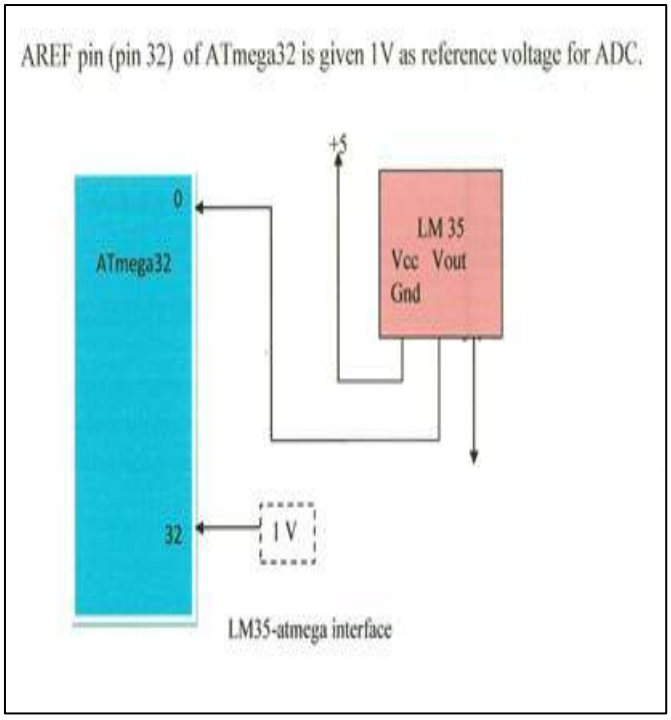

4.3 LM35 – ATmega Interface

As LM35 is a 3 pin device which gives voltage as output corresponding to the temperature in its surrounding, the output pin of LM35 is connected to ADC pin(pin A.0) on the micro-controller. Pin 32 of ATmega32 is given 1V as reference voltage for ADC.

4.4 The Portable Terminal Realization

This terminal consists of the two measurement circuits, i.e. the pulse rate detection circuit and the temperature measurement, the micro-controller board and the RF Transmitter Zigbee module. The pulse rate measurement circuit is realized on a General Purpose board and the output is connected to ADC of the Micro-controller unit. Similarly the output of temperature measurement circuit is also given to ADC of the micro-controller unit. The Micro-controller converts the signal into digital form and the values as according to the micro-controller program are transferred to the Zigbee transmitter module. Zigbee transmits these values wirelessly to the server terminal. The manually realized portable terminal can be seen as below:

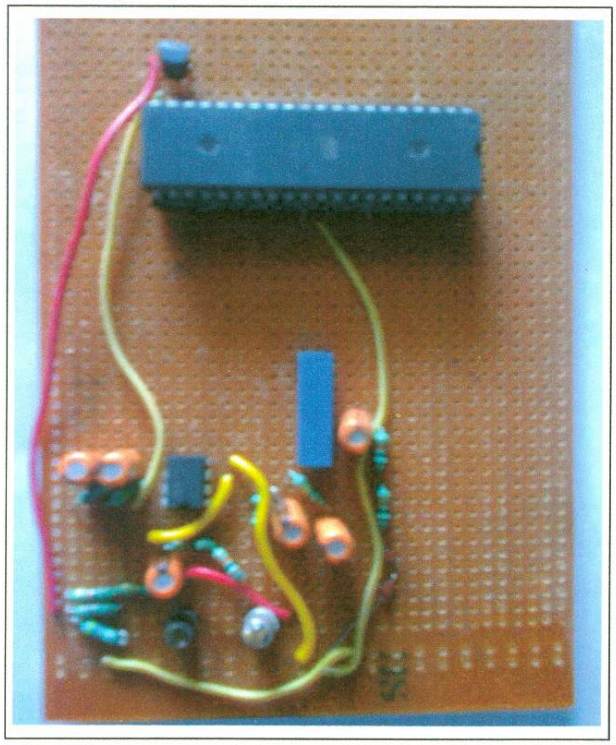

In this part a Biometrics based Identification and storage system can be attached which according to the identity of a concerned person saves the desired body parameters in his/her name in the memory, from where it gets transferred to the server terminal and gets saved with specific file name and format.

4.5 The Server Terminal Realization

The server terminal consist of Zigbee RF receiver module with a MAX233 level shifter. Zigbee module receives the data sent by zigbee transmitter. This zigbee module is connected to server through a COM port directly or through a COM to USB converter via MAX233. The data received is converted to the required specific format and gets saved as files in a specific folder in the system from where the data can be accessed as and when required.

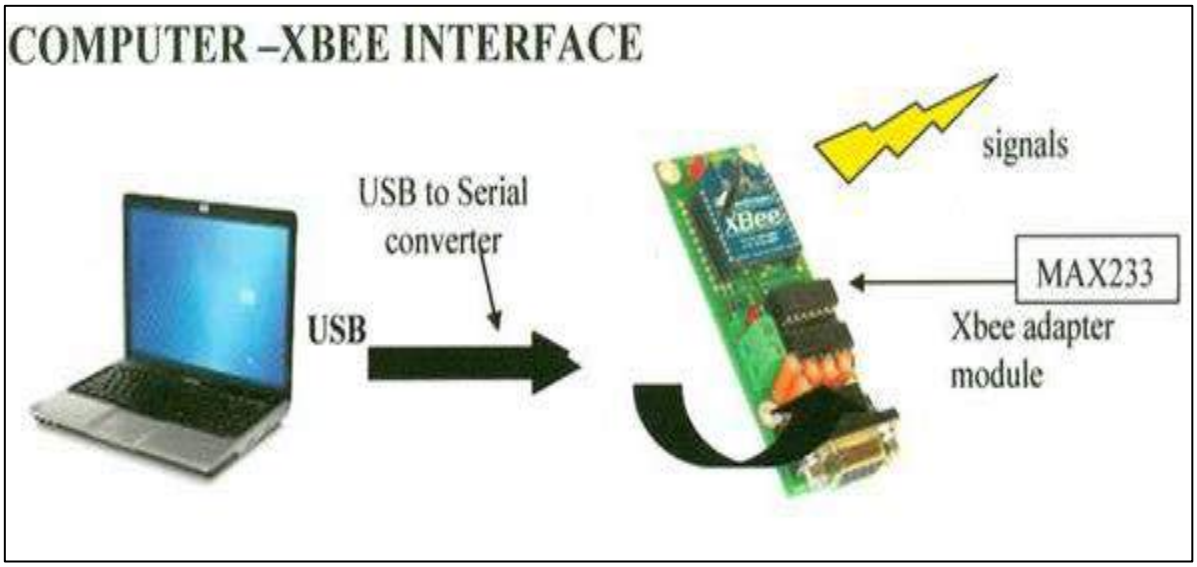

5 CONCLUSION

To conclude, we can say that by this method of designing a Wireless Health Monitoring System for Miners we can implement a cheap, portable and easy to use system. The use can be as simple as installing the portable terminal part at the entrance gate of Mining areas. Each and every personnel involved in the mining activities in that particular area may get themselves registered in the Medical Incharge's office and by providing personal details, medical history and biometrics. The same may be updated in the server and the memory of portable terminal. As soon as the person gives his biometrics by giving thumb impression (or any other method suitable) on the biometrics system attached to the portable terminal, all the body parameters taken by the portable terminal will be transferred to the server and get saved in a designated for him. Thus it will be very easy for doctors to check periodically required body parameters of concerned person periodically. This has special importance for people who are prone to cardiac problems.

For Primary objective, measurement of only two important body parameters is explained here. Further enhancement can be

done as and when required to fulfill the need of Medical Officers and the patients accordingly.

REFERENCES

Sehgal V.K., Durg S. Chauhan, *"Smart Wireless Temperature Data Logger Using IEEE 802.15.4/Zigbee Protocol", TENCON 2008 – 2008 IEEE Region 10 Conference,* Hyderabad India.

Kazem Sohraby, Daniel Minoli and Taieb Znati *"Wireless Sensor Networks: Technology, Protocols and Application"* (Hardcover – April 6, 2007)

Jan Axelson, c1998, 1999, 2000 *"Serial Port: Complete Programming and Circuits for RS-232 and RS – 485 Links and Networks",* Published by *Lakeview Research*, ISBN 0-9650819-2-3

S. Josephine Selvarani, *"Online Health Monitoring System Using Zigbee", International Journal on Computer Science and Engineering (IJCSE),* Apr 2011, Vol. 3 No. 4, ISSN : 0975-3397

Hashem, M.M.A. Shams, R. Kader, M. A., *"Design And Development of A Heart Rate Measuring Device Using Fingertip", International Conference on Computer and Communication Engineering,* 2010 issue : 11 – 12 May 2010, Page (1-5).

Risk Assessment and Management in Mining

A Comparison: Empirical Methods or Artificial Neural Network for Peak Particle Velocity prediction in DOZ Underground Mine

S. Prahastudhi, E. Riyanto, D. Napitupulu
Microseismic Section – UG Geotech & Hydrology, Geoservices DivisionPT Freeport Indonesia, Papua – Indonesia

ABSTRACT Artificial neural network is an algorithm for data pattern recognition analysis which is basically similar with the human neural system. The application of neural network has been widely used in all of kind of studies, such as economics, earth science, medic and etc. In a case of underground mine, blasting operation is one of the most important part in the mine production and operation, then, a study regarding blasting operation and its impact in the underground mine environment, such as pillar/tunnel stability is a must. One of the blasting impacts that can be quantified is the peak particle velocity (PPV, unit mm/s). There are many ways to forecast the peak particle velocity, most of them are using empirical equation which is derived from data samples and laboratory scale analysis and it also produce a linear relation between the blasting component (such as charging and distance) and the peak particle velocity. Using artificial neural network, the data pattern of blasting operation and the resulting peak particle velocity can be analysed, then, it can be used as peak particle velocity prediction. Supervised neural network, with one hidden layer and two inputs is the neural architecture which is used in this research. The blasting monitoring data was collected during August until December 2013 in the Deep Ore Zone (DOZ) mine. Compared with another empirical method, USBM (United States Bureau of Mine, Langeford-Kihlstrom and Ambreseys Hendron, artificial neural network has the best correlation coefficient.

Keywords: Neural network, particle velocity, blasting

1 INTRODUCTION

In the underground mine, blasting operation is one of the most important part in the production process. The safety factor and the impact of the blasting is another concern beside the production target. One of the quantified parameter which can describe the blasting impact in the underground mine is peak particle velocity (PPV, unit mm/s). Peak Particle Velocity is defined as the highest speed at which individual earth particle moves or vibrates as the waves pass a particular sites (Kujur, 2010). To come out with proper amounts of maximum charging per delay (explosive) which produces limited ground vibration, several equation are available, such as Ambreseys-Hendron, USBM and Langeford-Kihlstrom (Alipour et all, 2012). According to the existing empirical predictors equations, the PPV is function of distance and maximum charging per delay (Rai et all, 2005). Use these empirical equations. Rai et all (2005) showed that using the empirical predictors, the very accurate value of charge per delay will not be obtained.

Neural network have emerge in the last decade as a promising computing technique which enable computer system to exhibit some of the desirable brain properties. Various types of networks have been applied successfully in a variety of scientific and technological fields. Examples are application in industrial process modelling and control, ecological and biological modelling, sociological and economical sciences, as well as medicine (Kavli, 1992). Within the exploration and production world, neural network technology is now being applied to geological analysis (Doveton, 1994) and seismic attribute analysis (Schultz, 1994).

Neural network research started in forties. McCulloh and Pitts (1943) describe the logical function of a biological neuron. They describe that the transmission of the neuron signal is an all-or-nothing situation. A neuron fires only if the cell has been stimulated above a certain threshold. The output signal will, in general, have constant length. McCulloh and Pitts describe that network consisting of many neurons might be used to develop the universal Turing Machine (a kind of computer described by Turing (1937) that could solve all mathematical problems.

In recent years, the neural network application has emerged as a powerful tool for analyzing of rock engineering problems. Several studies have recently been proposed to predict the environmental effects of blasting in terms of peak particle velocity on the basis of artificial intelligence (Alipour et al, 2012). As an artificial intelligence method, the sigmoid function of neural network had an ability to calculate the non-linear relationship between input and the output data. In this research, we compared the ability of empirical equations and neural network to predict the peak particle velocity produced by blasting operation in the underground gold mine in DOZ (Deep Ore Zone) mine, Papua, Indonesia.

2 SITE DESCRIPTIONS

Generally, the geological condition in the DOZ mine is in the infiltration zone. Those area located in the edge of the subduction zone between Australian and Indo-Pacific plates. The result of the infiltration make the sediment rock above the plates (carbonate) upraised then the magma intrusion was filling the edges of the plates. Those intrusions resulted a complex system of igneous rock which is had intermediate (dioritic) composition. Finally this geological process creates a complex mineralization (skarn).

The DOZ ore deposit is a part of the Ertsberg East Skarn System which is include in the carbonate tersier altered with silicate calcium-magnesium. Ertsberg East Skarn System (ESSS) is a vertical deposit with reach 1200m high and the length of the strike is more than 1000m and the average wide is 2000m. Several deposit which is occur in the DOZ mine are diorite, dolomite marble, calcite marble, limestone and skarn (forsterite skarn, forsterite magnetite skarn and magnetit skarn).

3 THEORIES AND METHOD

3.1 Empirical Predictor

In the prediction of the peak particle velocity, there are several equations which usually used. They are, USBM, Langeford-Kihlstorm and Ambreseys-Hendron. USBM assume the cylindrical charges. They conclude that any linear dimension should be scaled with the square root of the explosive charge weight based on dimensional analysis (Kujur, 2010). The equation proposed by USBM is:

$$v = K\left[\frac{R}{\sqrt{Q}}\right]^{-B} \qquad [1]$$

Any other empirical predictor is Langefors and Kihlstorm predictor (1963). They proposed the following relationship for various charging levels to estimate the peak particle velocity. The equation is:

$$v = K\left[\frac{\sqrt{Q}}{R^{2/3}}\right]^{B} \qquad [2]$$

In 1968, Ambreseys-Hendron are also derived an empirical equation to predict peak particle velocity. If the USBM investigator suggested that any linear dimension should be scaled the cubic root of the explosive charge weight for spherical geometry. An inverse power law was suggested to related amplitude of seismic waves and scaled distance to obtain the following relationship:

$$v = K\left[\frac{R}{Q^{1/3}}\right]^{-B} \qquad [3]$$

Where,
V: peak particle velocity (mm/s)

R: distance between blast face and monitoring point/sensor (m)
Q: maximum explosive charge used per delay (kg), and
K, B: site constant which can be determined by multiple regression analysis.

3.2 Artificial Neural Network

The artificial neural network divided into two major types, supervised and unsupervised. The different between them is that the supervised neural network need the data result from measurement to supervise the network training.

Back propagation neural network is one of supervised neural network type. It has an input, output and in the most application, have one hidden layer (Sutrisno et al, 2013). The number of inputs and outputs of the neural networks are determined by considering the characteristic of the application. In most of the cases, one hidden layer is satisfactory (Saemi, 2007).

Each neuron of a layer is generally connected to the neurons in the proceeding layer. Repeating forward-propagation and backward propagating steps performs the required learning. When a pattern is given to the input pattern, the forward propagation step begins. The activation levels are calculated and the results are propagated forward through the following hidden layers until reach the output layer. Every processing unit sums its respective inputs and then applies a function to compute its output. Sigmoid is the most commonly used function (Bean and Jutten, 2000).

The algorithm of multilayer perceptron neural network with back propagation type consist of three layers, there are input layer, hidden layer and output layer. Input layer and hidden layer associated with “X”, as a weighting. This process started from inputting the parameter in input layer. Activation levels are calculated and the results are sent through the hidden layer until it reaches the output layer. Each processing unit summing each input is the used to calculate a sigmoid function output (Saemi, 2007).

Sigmoid function is used in neural network with interval output value between 0 and 1 is a binary sigmoid function which is defined as

$$y = f(x) = \frac{1}{1 + e^{-x}} \qquad [4]$$

Backward propagation phase starting from the output layer, re-input layer through hidden layer. Various networks are trained by minimization of an appropriate error function defined with respect to the training set. Performance of the networks is then compared by evaluating the error function using the training validation set, and the network which have the smallest error with respect to the training validation set is selected (Niculescu, 2003).

The difference error of this result is given by:

$$\text{Error} = \frac{\sum_{i=1}(O_i - T_i)^2}{n} \qquad [5]$$

Where,

O: expected output (target)

Q: output of the forward propagation

n: total calculated data

4 APPLICATIONS

DOZ mine, is a kind of underground mine with block caving type which is operated by PT Freeport Indonesia and it located in the Papua island. Due to block caving operation (production), there were so many blasting perform in this mine, more precisely in the undercut level.

During August 2013 to December 2013, the blasting data was compiled for this research. The data consists of peak particle velocity (PPV) in mm/s unit, distance in m unit and charge/delay in kg unit. Based on the empirical relation (USBM, Langefors and Kihlstorm, Ambreseys-Hendron), the data can be used to determine the ability of those empirical relation to predict the peak particle velocity using equation 1, 2, 3.

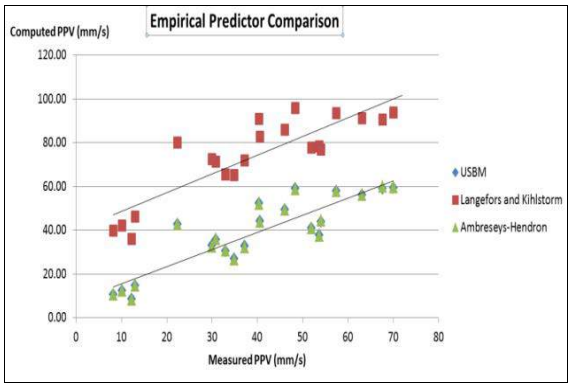

Figure1. Empirical predictor comparison for PPV prediction

The result shows that the correlation coefficient (R) for USBM is 0.7802, Langefors and Kihlstrom 0.7465 and 0.7848 for Ambreseys-Hendron. Then, the Ambreseys-Hendron has the best correlation coefficient value among those other empirical predictors.

A back propagation neural network method has been performed to analyze the blasting data to make a forecasting method. The neural architecture that used in this research is multilayer perceptron with 2 inputs and one hidden layer, the hidden layer consist of 3 nodes.

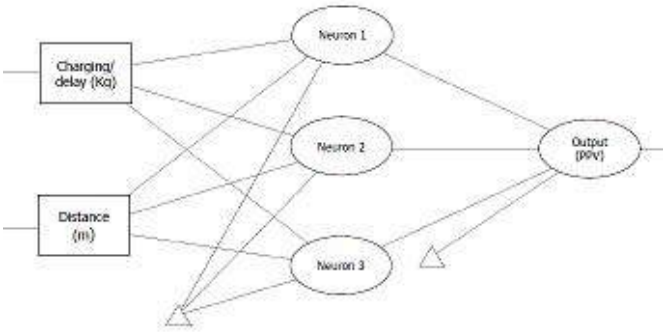

Figure2. Neural Architecture

The charging per delay (Q) and distance between blast point and sensors (r) are become the input that fill the input nodes, and the PPV fill the output layer. Sigmoid binary function has been used as the transfer function in both connected layer (input to hidden layer and hidden layer to output).

To make the iteration faster, data normalization must be perform in the input data. The charge per delay had been conditioned into tons unit. Then, the data divide into two types with proportion 60% for train data and 40% for test data.

An optimized in neural network called momentum has been used to prevent the significant change in the weights due to back propagation process. With the additional momentums the new weight at (T+1), based on the weight at (T) and (T-1).

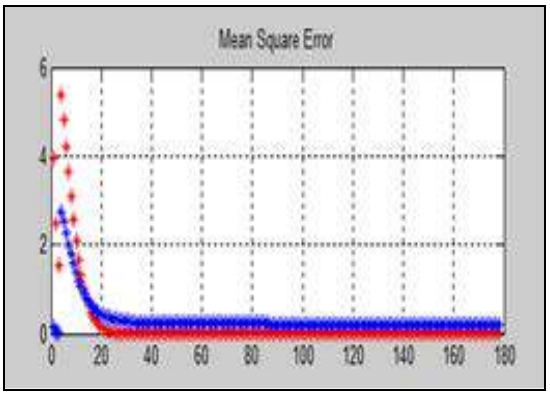

Figure3. Iteration in the back propagation process, the red line indicated the test data and the blue line indicate the train data.

From the figure above (figure 3), we can see that the system reach the convergence function after iterated 20 times.

The iteration result shows that train and test data have correlation coefficient 0.89, which is better than any other empirical relation, in this case is Ambreseys-Hendron, USBM and Langefors-Kihlstorm.

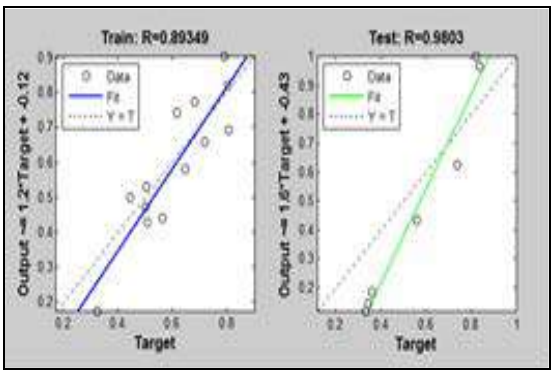

Figure4. The correlation coefficien of the neural network prediction and the real data

5 CONCLUSIONS

Compared with the empirical methods (Ambreseys-Hendron, USBM and Langefors-Kihlstrom), supervised back propagation neural network have a better correlation coefficient to predict the peak

particle velocity from blasting operation in an underground mine. The advantage of using neural network that it can recognize the pattern of the blasting data and accommodate the nonlinear relation between charging per delay, distance and the peak particle velocity which is the empirical relation cannot be done because their linear relation.

Future research by adding another parameters such the influence of ground support, tunnel geometry and any other discipline must be included so it can be compared with the damage classification in underground mine

REFERENCES

Alipour et.al., 2012. Artificial neural network or empirical criteria? A comparative approach in evaluating maximum charge per delay in surface mining – Sungun copper mine. *Journal Geological Society of India Vol 79*, June 2012, pp.652-658.

Bean, Mirko., and Jutten, Christian., 2000. Neural network in geophysics application, *Journal of Geophysics, Vol 65*, No 4, pp.1032:1047.

Doveton, J.H., 1994. *Geologic log analysis using computer methods*. AAPG computer applications in Geology, No 2. AAPG.

Ambreseys, NR., Hendron, AJ., 1968. Dynamic behaviour of rock masses. Rock Mechanics in engineering practices. London: Wiley; p.203-207.

Kavli, T.O., 1992. *Learning principle in dynamics control*. PhD Thesis University of Oslo, ISBN no. 82-411-0394-8.

Kujur, Badal Kumal., 2010. *Blast vibration studies in surface mine*. Bachelor thesis, Rourkela Institute of Technology India.

Langefors, U., Kihlstrom, B., 1963. *The modern technique of rock blasting*. Almqvist & Wiksell/Gebergs Forlag, Stockholm.

McCulloh, W.S. and Pitts, W., 1943, A logical calculus of idea's immanent in nervous activity. *Bulletin of Mathematical Biophysicsc 5*, p115-133. Reprinted in Anderson, J.A. and Rosenfield, E., 1988. *Neurocomputing: Foundation of Research*, Cambridge MIT Press.

Niculescu, Stefan., 2003. Artificial neural network and genetic algorithm in QSAR. *Journal of molecular structure (Theochem)* pp.622, 71-83.

Rai et,al., 2012. Prediction of maximum safe charge per delay in surface mining. *Mining technology (Trans. Inst. Min. Metall. –A)*, v.114, A, pp.227-231.

Saemi, Mohsen., 2007. Design of artificial neural network and genetic algorithm for permeability estimation of the reservoir. *Journal of International Petroleum Science and Engineering 59*, Tabiat Modaret University, 97-105.

Schultz et.al., 1994. Seismic-guided estimation of log properties, Part1: A data-driven interpretation methodology. *The Leading Edge, May 1994; Part2: Using artificial neural networks for nonlinear attribute calibration. The Leading Edge*, June 1994.

Sutrisno, Wahyu., Prahastudhi, Septian., Bahri, Syaeful., Wulandari, Yulia Putri., 2013. Application of common contour binning and back propagation neural network for oil water contact prediction in carbonate reservoir. *Proc. 37th IPA Convention & Exhibition*

Turing A.M., 1937. On computable numbers, with an application to the Entscheidungsproblem. *Proc. Lond. Math. Soc (ser.2)*, 42, pp.230-65

Environmental Effects and Importance of the Risk Assessments for Mining Wastewater

A. Celebi
Department of Environmental Engineering, Sakarya University, 54187, Sakarya, Turkey, Water and Environmental Engineering Group, Faculty of Technology, University of Oulu, 90014, Oulu, Finland

S. Özdemir
Department of Environmental Engineering, Sakarya University, 54187, Sakarya, Turkey,

ABSTRACT Every scale of mining activities have huge impact to environment. Monitoring and assessing of the size of the effect and take measure is vital. In this present study risk assessment studies in mining areas and their effect to especially groundwater and ecosystem was investigated. Risk assessment steps were determined, explained detailed especially for huge amount of mining wastewater. Tailings are fine-grained waste material from the mining industry and main source of pollutant. Pollution risks of the groundwater, and after its reaching to human are crucial. Our study showed that management of mining wastewater is vital. Results show that Environmental impact assessment and monitoring studies must be carefully done before and closure time. Relevant policies must be ready and applicable. Factors of climate, geology and human health must be considered for long time period. International assumption, standards and health risk assessments should be done as mandatory.

Keywords: Risk assessment, mining wastewater, pollution risk

1 INTRODUCTION

Mining operations and the pollutant sources of concern can affect water (surface and groundwater) quality in terms of many parameters, create hydrologic impacts, decrease air quality, contaminate soils, and diminish ecosystem quality. The major categories of environmental problems arised from mining are water pollution and its reaching to human (EPA, 1997; Celebi and Özdemir 2014).

Mining industry is one of the emerging sectors in the world. For instance in Turkey, only overall 2011 gold production is expected to reach 25 mt/y, compared to 17 mt/y in 2010. In the long-term, analysts expect it to stabilize around 60 mt/y. But preparing the mining waste policy and applications can acceptable quite new in Turkey (GBR, 2012).

Tailings are fine-grained waste material from the mining industry, contain all other constituents of the ore but the extracted metal, among them heavy metals and other toxic substances. Moreover, the tailings also contain chemicals added during the milling process (Ganesh, 2006). The quality of the drainage is, nevertheless, controlled by a series of mineralogical and geochemical reactions in the waste area, and the outcome of these reactions is reflected in the seepage waters surfacing through tailings dams (Blowes, 2003; Lottermoser 2007; Heikkinen, 2009). The seepage quality additionally changes due to precipitation and dilution during transport to the receiving water body (Chapman, 1983; Räisänen, 2005). The leak to groundwater during mining operation and even after the closure period is typical huge environmental risk factor.

Abandoned mine sites also generate chronic environmental hazards. Contaminated runoff from abandoned mines impacts land, groundwater, streams, rivers,

and lakes. Principal environmental pollutants from abandoned mines are arsenic, lead, and other heavy metals associated with acid rock drainage. The degree of potential contamination depends on many factors which the commodity being mined (gold, copper, chromium, etc.), mining methods, ore processing methods and disposal methods. Other contaminants can include chemicals used to process ore and fuel, lubricants, and solvents used to operate and maintain equipment (The Sierra Fund, 2008).

Main objective of the present study is to attract and show best mining management issues in the mining operation and how size potential risks are in the mining areas to water and water related pollution.

2 GROUNDWATER POLLUTION RISK IN MINING AREAS

Groundwater is vital part of ecosystem and also direct or indirect effective to human. İts contamination is extremely difficult to remedy if we compare with surface water, once it occurs makes it a serious concern. Mining operations may affect groundwater quality in many ways. The most obvious occurs in mining below the water table, either in underground workings or open pits. This provides a direct conduit to aquifers. Groundwater quality is also affected when waters (natural or process waters or wastewaters) infiltrate through surface materials (including overlying wastes or other material) into groundwater. Contamination may also occur when there is a hydraulic connection between surface and groundwater. Any of these could cause elevated pollutant levels and contamination in groundwater. Further, disturbance in the groundwater flow regime can affect the quantities of water available for other local uses. Eventually, the groundwater may recharge surface water down gradient of the mine, through contributions to base flow in a stream channel or springs.

Figure 1. The seepage water points at showing the upper area at the toe of the upper section of a dam (Heikkinen, 2009).

The ability of pollutants to dissolve and migrate from materials to groundwater varies significantly depending on the constituent of concern, the nature of the material/waste, the design of the management, soil characteristics and local hydrogeology (including depth, flows, and geochemistry of the underlying aquifers). An example of mining area is showing on Figure 2. Risks to human health and the environment from contaminated groundwater usage vary with the types and distance to local people. Besides, impacts on groundwater may also indirectly affect surface water quality (through recharge and/or seepage) (EPA, 1997). Sustainable groundwater management is vital. The Dutch Intervention Value for groundwater is based on the serious risk level for humans and the ecosystem, including direct consumption of groundwater as drinking water. The value is a trigger for further investigation and a decision about the urgency for remediation of historical groundwater contamination (Lijzen et al., 2014).

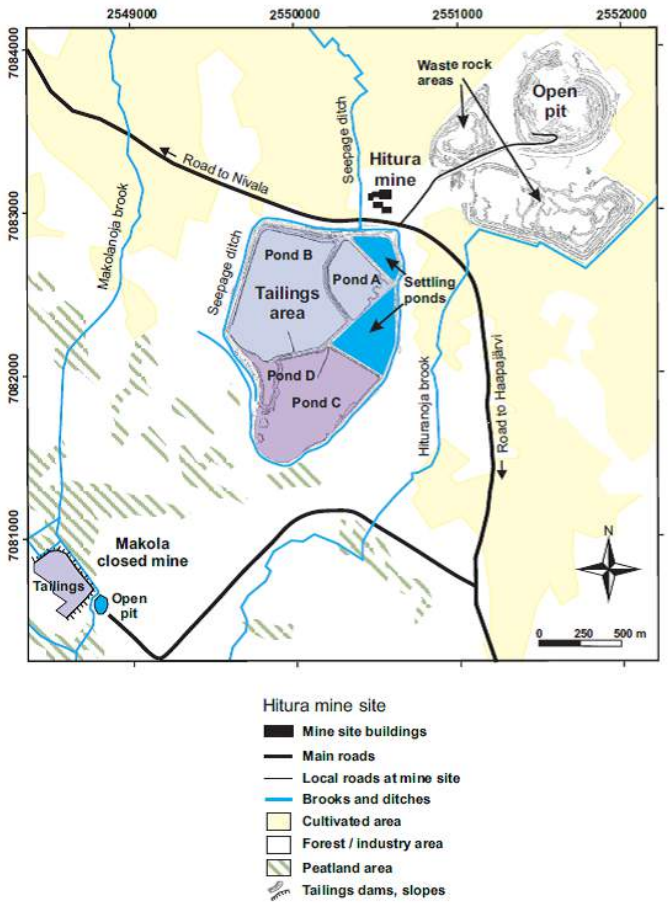

Fig. 2. Overall setting of the Hitura mine and the tailings area in Finland (Heikkinen 2009).

Recent studies revealed about mining area groundwater contamination. It is used to characterize pollutant sources and to quantify the resulting current and future effects on both groundwater and river water quality in a study in many location and Germany as well. The reactive transport simulations illustrate the long-term fate of sulfate from the mining dumps into groundwater and from groundwater into surface water. The simulations indicated that groundwater borne diffuse input of sulfate into the rivers is 2200 t/years and could increase till 11000t/years in the next 40 years. The results for the River compare well with the observed increase of sulfate concentrations before and after passing the mining area (Graupner et al. 2014). Arsenic is a common constituent in groundwater that affects human health adversely at levels as low as 10 lg/L (WHO, 1993; Bhattacharya, 2002). In a mine area of western Turkey, arsenic showed high spatial variation ranged from 33 to 911 lg/L in the groundwater samples. Arsenic concentration values increased close to the mines, reaching 305 lg/L and decreased to the south of the study area (Gemici et al., 2008). A wide variety of adverse health effects, including skin and internal cancers and cardiovascular and neurological effects, has been attributed to chronic as exposure, primarily from drinking water (NRC, 1999).

3 ASSESSMENTS OF ENVIRONMENTAL EFFECTS AND ECOLOGICAL RISK FOR MINING ACTIVITIES

Mining causes land disturbances naturally. These disturbances affect aquatic resources, wildlife, and vegetation and can lead to habitat destruction. Surface mining activities directly destroy habitat as a result of removal of overburden to expose ore bodies, deposition of waste and other materials on the ground, surface the construction of roads, buildings and other facilities.

Two major types of impacts on aquatic resources occur in mining operation and aquatic life. The first type of impact results from the contribution of eroded soil and material to water bodies and from the release of pollutants from ore, waste rock or other sources. The second results from the direct disruption of ephemeral, intermittent perennial streams, wetlands or other water bodies. Disruptions occur from road construction and similar activities. Permanent impacts are caused by actual mining of the area or by placement of refuse, tailings or waste rock directly in the drainage way. In addition, lowering of area surface water and groundwater caused by mine dewatering could affect sensitive environments and associated aquatic life. The impacts of mining operations on aquatic resources can be also beneficial. Potential impacts also vary significantly with the affected biota. For example, increases in

stream flow may preclude habitation of certain species of fauna and/or flora but may also provide new habitat for other species of aquatic life. Mining negative effects are also visible. A good example of visible effect to environment are shown Figure 3.

Figure 3. An open pit of copper mining area in Romania (VQR, 2012)

The impacts of mines on aquatic resources have been well documented. Mineral Creek fisheries and habitat survey conducted by the Arizona Game & Fish and the U.S. Fish & Wildlife Service showed that significant damage was caused by an active mining activity on the shores of Mineral Creek. The upstream control station showed an overhead cover (undercut bank, vegetation, etc.) of 50% to 75%. The dominant substrate was small gravel and in stream cover consisted of aquatic vegetation. Five species of fish were observed for a total of 309 individual fish. In another side, the downstream station showed an overhead cover of less than 25%. The dominant substrate was small boulders and in stream cover consisted of only interstitial spaces and very little aquatic vegetation. No species of fish and very few aquatic insects were observed or captured. This Mineral Creek survey proves a significant degradation of habitat below the mine. In another study and area, which received a massive discharge of tailings and pregnant leach solution from an active copper mine, was also surveyed (EPA, 1994 and 1997). The tailings had a smothering, scouring effect on the stream (Kauppila et al. 2011).

Mining operations can have substantial impacts on terrestrial wildlife, ranging from temporary noise disturbances to destruction of food resources and breeding habitat. Unless closure and reclamation return the land essentially to its pre-mining state, certain impacts to some individuals or species will be permanent. Biological diversity is often viewed as a way to measure the health of an ecosystem. Noise during the construction phase or during operations, for example, can displace local wildlife populations from otherwise undisturbed areas surrounding the site. Some individuals or species may rapidly acclimate to such disturbances and return while others may return during less disruptive operational activities. Still other individuals may be displaced for the life of the project. Other wildlife impacts include habitat loss, degradation or alteration. Wildlife may be displaced into poorer quality habitat and therefore may experience a decrease in productivity or other adverse impact. Habitat loss may be temporary (e.g., construction-related impacts), long-term (e.g., over the life of a mine), or essentially permanent. Vegetation strongly related to the diversity of wildlife. All vegetation is removed before and during mine development and operation in the area. Vegetation immediately adjacent could be affected by the roads, water diversions or other development. Vegetation further removed from activities may be affected by sediment carried by overland flow and by fugitive dust (EPA, 1997).

West African rainforest birds were observed most strongly affected by adjacent mining whether the mining was immediately adjacent or >500m away, irrespective of distance to forest edge in Ghana. Even no

additional forest loss, increased surface mining is likely to result in declines of forest birds (Deikumah et al., 2014).

In general, risk management tools are not designed specifically for the mining industry. They are usually borrowed from other areas such as the nuclear, petrochemical or construction industries or from military structures. Risk management practices, standards, tools and approaches used both in the mining industry and in other industrial sectors. Catalogued risk evaluation standards and guides (e.g. ANSI/AAMI/ISO 14971: 2000; ISO-17776: 2000 and DOE-DP-STD-3023-98: 1998) and risk analysis techniques (e.g. NASA: 2002 and DOE Guidelines: 1992) Komljenovic & Kecojevic, 2007; Badri et al. 2013).

Risk assessment is important part of environmental protection issue and should apply latest standards for all mining operations. Basically we can use table x for pre assessment. Firstly we should Determine the consequences; the most probable consequence in terms of harm should an event occurs with existing risk controls. For example Catastrophic: Long term environmental damage (5 years or longer), Insignificant; Negligible environmental impact, managed within operating budgets. Secondly we should Determine the likelihood; the most probable likelihood of the determined consequence occurring. Almost certain Is expected to occur in most circumstances and has a history of occurrence, Once a year or more frequent; Rare: May occur only in exceptional circumstances, Once in 100 years or more. Then we can use the table for each identified hazard.

Table 1. Risk Matrix

Likelihood	**Consequences**				
	Catastrophic 1	Major 2	Moderate 3	Minor 4	Insignificant 5
Almost certain A	Extreme	Extreme	High	High	Medium
Likely B	Extreme	Extreme	High	Medium	Low
Possible C	Extreme	High	Medium	Medium	Low
Unlikely D	High	Medium	Medium	Low	Low
Rare E	High	Medium	Low	Low	Low

Environmental risk assessment studies are one of the risk assessment study and they are in same base. In Figure 4 showing a good example of Environmental risk management standard and the process with steps.

With respect to the overall framework in risk management (Figure 4), steps 1 to 3 above represent that first step (before risk assessment) is the 'establish the context' phase, step 2nd represents the Risk assessment (identify risks, analyses risks, evaluate risks) and step 3rd (after risk assessment) represents the 'treat the risks' phases.

ESTABLISH THE CONTEXT; All external, internal, risk management context along with clear evaluation criteria and descriptions must be prepared before the Risk Assessment step.

RISK ASSESSMENT*; Identify risks* involves the use of risk assessment "tools" appropriate for identifying potential loss scenarios associated with the Project. The tools consist of:

- Introduction – Before the potential issues are brainstormed, it is important that the whole team had a good understanding of the Project. This is confirmed by the facilitator.
- Brainstorming –Used to draw out the main issues using the understanding, relevant experience and knowledge of the team.

This session also use prompt words to build on the experience base of the team and identify any potential environmental issues and potential loss scenarios.

- Modified Hazard and Operability Analysis – This involve the review of key words drawn from the Project and aerial photographs and environmental issues at each location during each phase of operation (Stratford Coal 2012).

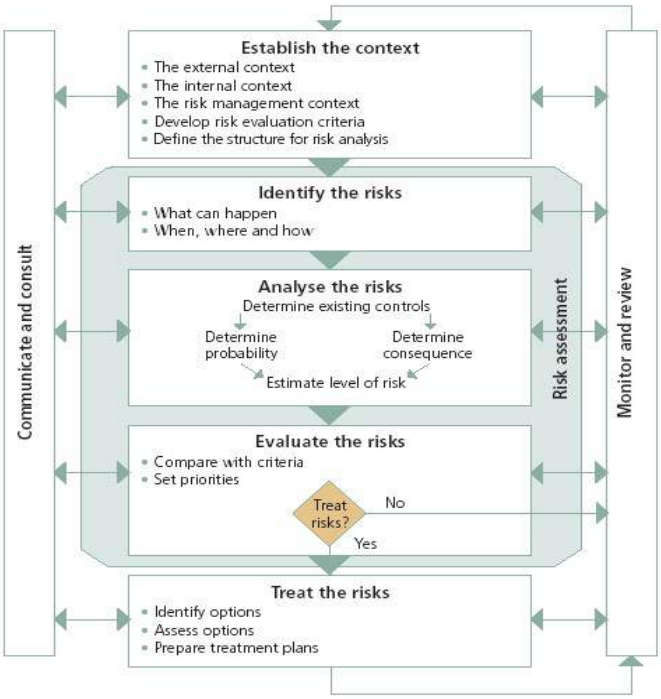

Figure 4. Risk Management Process (AS/NZS ISO 31000:2009)

Risk identification must be conducted at the level of the mining enterprise building. Besides, all the enterprise stakeholders should participate in this activity: employees, ecologists, and representatives of local, regional and national authorities (Buysse and Verbeke, 2003; Delmas and Toffel, 2004). Only such sustainable cooperation enables construction of complete risks. The selection of instruments of environmental and social risk assessment in all stages should include new conceptions according to a management paradigm (Kowalska, 2014).

4 CONCLUSION

Big environmental effects, especially disasters from mining areas are certainly preventable, barring unpredictable scenarios. Today's technologies are available to ensure safe containment of hazardous material. Environmental Risk Assessment studies should be done detailed for all size mining activity. This assessment should be done qualitative and quantitative as taking into account all necessary parameters and long time. Especially groundwater pollution should be monitored well and should not use as drinking water by local inhabitant people. Effect to ecosystem and natural life could be very negative, irreversible. Relatively small investments today can prevent future liabilities and environmental losses. Further researches about groundwater contamination and Environmental Risk Assessments are crucial for sustainable management of mining sites. Besides each large mining area may have specific conditions and they must be considered individually.

REFERENCES

Badri, A., Nadeau, S., Gbodossou, A. 2013, A new practical approach to risk management for underground mining project in Quebec, Journal of Loss Prevention in the Process Industries 26, 1145-1158.

Bhattacharya, P., Jacks, G., Ahmed, K.M., Routh, J. and Khan, A.A. 2002 Arsenic in groundwater of the Bengal Delta Plain Aquifers in Bangladesh. Bull. Environ. Contam. Toxicol. **69**, 538–545.

Blowes, D. W., Ptacek, C. J. and Jurjovec, J. 2003 Mill tailings: hydrogeology and geochemistry. In: Jambor, J. L., Blowes, D. W. & Ritchie, A. I. M. (eds.) Environmental aspects of mine wastes. Mineralogical Association of Canada, Short Course Series, Vol. 31, 95–116.

Buysse, K., Verbeke, A., 2003. Proactive environmental strategies : a stakeholder management perspective. Strat.Manage.J.24, 453–470.

Celebi A. and Özdemir S. 2014, Mining wastewater management and its effects on groundwater and ecosystems, Water Science & Technology, 70.9, 1481-87.

Chapman, B. M., Jones, D. R. & Jung, R. F. 1983 Processes controlling metal ion attenuation in

acid mine drainage streams. Geochimica et Cosmochimica Acta **47**, 1957–1973.

Delmas, M., Toffel, M., 2004. Stake holders and environmental management practices: an institutional framework. Bus. Strat. Environ. 13,209–222.

Deikumah, J.P., McAlpinea, C. A. Maron, M. 2014, Mining matrix effects on West African rainforest birds, Biological Conservation 169, 334–343.

EPA 1997 Potential environmental impacts of hardrock mining, Appendix B. Washington, DC

EPA 1994 *Copper - Extraction and Beneficiation of Ores and Minerals, Volume 4*, EPA/530-R-94-031, NTIS/PB94-200 979, Washington, D.C.

Ganesh, M. 2006 Monitoring of Tailings Dams with Geophysical Methods, Luleå University of Technology-Sweden.

GBR 2012 *Mining in Turkey*, Global Business report, E&MJ, 28p..

Gemici U., Tarcan G., Helvacı C. and Somay A. M. 2008 High arsenic and boron concentrations in groundwaters related to the mining activity in the Bigadiç Borate Deposits (Western Turkey) Applied Geochemistry 23, 2462–2476. DOI: 10.1016/j.apgeochem.2008.02.013

Graupner, B.J., Koch, C. and Prommer, H. 2014 Prediction of diffuse sulfate emissions from a former mining district and associated groundwater discharges to surface waters, Journal of Hydrology 513, 169–178.

Heikkinen, P. M. 2009 Active sulphide mine tailings impoundments as sources of contaminated drainage. Espoo: Geological Survey of Finland. 38 p.

Kauppila, P. M., Kauppila, T., Mäkinen, J., Kihlman, S. and Räisänen, M. L. 2011 Geochemistry in the characterisation and management of environmental impacts of sulfide mine sites. *Geological Survey of Finland, Special Paper* 49, 91–102.

Kowalska , I.J. 2014, Risk management in the hard coal mining industry : Social and environmental aspects of collieries' liquidation, Resources Policy 41, 124–134.

Komljenovic, D., & Kecojevic, V. (2007). Risk management programme for occupational safety and health in surface mining operations. International Journal of Risk Assessment & Management, 7(5), 620-638.

Lijzen, J.P.A., Otte, P., Dreumel, M. 2014, Towards sustainable management of groundwater: Policy developments in The Netherlands, Science of the Total Environment 485–486, 804–809.

Lottermoser, B.G. 2007 Mine Wastes. Characterization, Treatment, Environmental Impacts. Second edition. Berlin–Heidelberg: Springer-Verlag. 304 p.

NRC, 1999 Arsenic in Drinking Waters: Subcommittee on Arsenic in Drinking Water. National Research Council. National Academy Press, Washington DC.

Räisänen, M. L., Heikkinen, P., Pulkkinen, K., Korkka-Niemi, K. and Salonen, V. P. 2005 Finland – Mine Water Quality in some Abandoned and Active Finnish Metal Sulphide Mines. In: Wolkersdorfer, C. & Bowell, R. (eds.) Contemporary Reviews of Mine Water Studies in Europe, Part 2. Mine Water and the Environment 24, 5–7.

Standards Australia, Risk management— Principles and guidelines, AS/NZS ISO 31000:2009, Australia

Stratford Coal 2012 Stratford Extension Project, Environmental Risk Assessment, NSW, Australia.

The Sierra Fund 2008 Mining's Toxic Legacy an Initiative to Address Mining Toxins in the Sierra Nevada.

WHO (World Health Organization) 1993 Guidelines for Drinking Water Quality. Health Criteria and Other Supporting Information, vol. 2. WHO, Geneva.

VQR 2012, Mountains of Gold, A National Journal of Literature & Discussion, http://www.vqronline.org/articles/mountains-gold

Magner A., Sarfraz A. 2010, Environmental Risk Rating Procedure, Version: 1.0. Effective, Protection of Environmental Operations Act 1997, UNSW Environmental Policy.

Firefighting a Hidden Fire at TTT´s Amasra Coalmine with the Innovative One Seven System

M.T. Stöttner
One Seven of Germany, Luckenwalde, Germany

B. Inan
TTK, Zonguldak, Turkey

E. Erbay
TTK, Amasra, Turkey

R. Karaaslan
TTK, Zonguldak, Turkey

G. Beyer
ISSA mining, Bochum, Germany

ABSTRACT In a 20 days continuous engagement (07/16 – 08/03 2014) a covered mine fire in the Kalın Damar seam, whose development 5.5 months lagged, could be extinguished by using a One Seven MINING 6000 machine and the Class A foam-concentrate AM. This system is capable to produce compressed air foam, also known as CAF. A total amount of about 91,000 m³ wet and dry foam was brought into the dammed fire area. The water consumption was 4,200 m³; the foam-concentrate consumption was 6,320 liters.

Finally, it was found that by use of the OS MINING 6000 and the foam-concentrate One Seven AM a fire area could be regained which had to be abandoned using the conventional method (nitrogen inerting).The equipment was recovered and the excavation of the Kalın Damar seam could be continued.

Keywords: Firefighting, One Seven MINING 6000, the Class A foam-concentrate AM, Amasya

1 HISTORY OF THE FIRE

The fire suffered in a geological fault area of the Kalın Damar seam on 02/05/2014 either as spontaneous combustion of coal or an over the shield column placed phenolic foam, in the goaf of the langwall face.

The fire escalated in the course of 02/08. There was a lot of smoke and an upcoming CO-production, at least the mining area was evacuated and dammed off. The gas values measured in the evening of 02/08 were: CO 115 ppm, CH4 0.70 %, O2 20.4 % and CO2 0.002 % at a ventilation rate of 500 m³/min. The gas values measured at the head gate dam were on 02/10: CO 665 ppm, CH4 1.38 %, O2 19.5 % and CO2 0.44 %. The fire obviously had been escalated further!

At 03/09 nitrogen inerting of the abandoned area was started. Within five days of inerting an extinguishing could not be achieved, the inerting was terminated on 03/16. The overall nitrogen consumption was 49,300 m³.

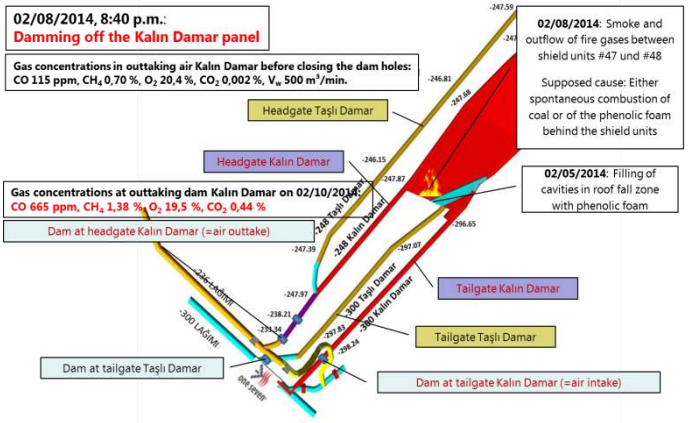

Figure 1. Amasra mine, southeastern working section

.

2 THE ONE SEVEN SYSTEM

2.1 Where Does the Name Come From?

By adding a special foam-concentrate and compressed gas (air or nitrogen) to the water, the volume of one drop of water expands into seven foam bubbles.

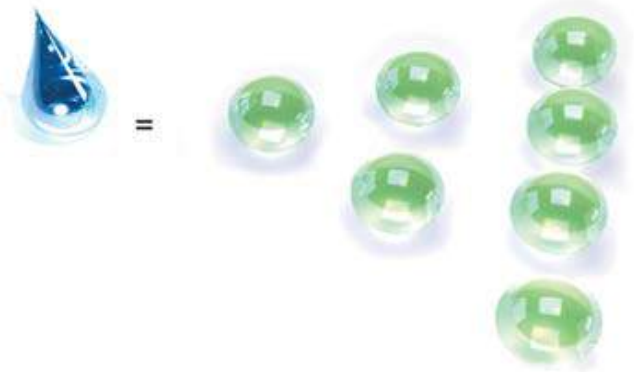

Figure 2. The seven times expansion of a water drop

At the end you get a CAF: Compressed Air Foam.

2.2 The MINING 6000 Machine and Its Properties

The MINING system was developed for use in mines with a ruggedized design for tough job. It´s an explosion proof system (ATEX I).The water and gas (air or nitrogen) has to be supplied by installations in the mine. The operational pressure for both is from 2 bar (29 psi) up to 10 bar (145 psi). The machine flows up to 6.000 l (1.585 gal US) of foam per minute.

Figure 3. The One Seven MINING 6000

The technical data are as follows:

- Dimensions (LxWxH): 2.550 x 990 x 1.420 mm
- Weight (dry): 1.550 kg
- Weight (operational): 1.750 kg
- Water consumption: max. 300 l/min @ min. 2 bar (29 psi) and max. 10 bar (145 psi)
- Gas consumption: max. 6.000 l/min @ min 2 bar (29 psi) (Nitrogen/Air) and max. 10 bar (145 psi)
- Foam-concentrate: One Seven® Foam Class AM (0.3%)
- Foam-concentrate tank: 150 l (build-in)
- Foam quality: free adjustable for firefighting (wet) to preventive (dry)
- Life-time of dry foam: about 5 h

The One Seven MINING system is usable for prevention as well as for firefighting!

3 STARTING THE MISSION

Because the matter is that the longwall face working is in the steep formation, the fire-fighting operations have been carried out in three phases:

Phase A: From 07/16 until 07/20 the tail gate gallery was backfilled with foam, which was also the intake airway at the

same time, to completely cut off the fire area of the air supply.

Phase B: After the machine´s removal to the head gate dam the fire area was completely inundated with foam over the head gate gallery from 07/20 until 08/02, so that…
Phase C: …from 08/03 the mine rescue brigade was able to penetrate under auxiliary ventilation and continuous carrying of foam into the fire area.

With our arrival at the mine site on 07/14 we got the first up-to-date information, the gas concentrations at the outtake dam at head gate Kalın Damar were:
CO 4-6 ppm, CO2 2,4 %, CH4 14-16 % und O2 11 %
This gas mixture becomes explosive at 17 % O2 and up!
Due to the fact that there was no pressurized nitrogen with 2 bar (minimum required pressure for the machine) available on mine site the machine was operated with compressed air.

On 07/15 the machine was placed in an old gate road of the Tavan Damar seam. There the coal mine has a parallel road to the head gate of the affected mining panel. From there two holes were drilled into the Kalın Damar goaf (= suspected hot spot), see figure 6. About these holes the foam should be placed from above onto the suspected source of fire. This test had to be terminated uncompleted due to the insufficient swallow capacity of the boreholes. Supposedly foaming of the head gate as the next step - thus with gravity - would certainly be most effective and would probably lead to fast success, but this wasn't debatable, because we were "up" on the return air side of the fire, and so that we were in toxic and explosive gases.

4 FIREFIGHTING WORKS

4.1 Phase A

The machine was situated about 60 m west of the tail gate dam (see figure 1, below left). It was connected via a hose line to the 75mm diam. pipe in the dam. With the beginning of the foaming works on 16th air samples were taken at the head gate dam Kalın Damar (outtaking air) every three hours and were evaluated in the laboratory. The graphic figures of trends in the concentrations of CO, CO2, CH4 and O2 during the operation are shown in figure 4. The foaming work was commenced with wet foam, later conversion to dry foam. Continuation of the foaming work until 07/20, at 0:00 a.m.: Opening the dams headgate Kalın Damar and tailgate Taşlı Damar while maintaining the foaming in the tail gate Kalın Damar. After about 20 minutes the CO-concentration at borehole #1 increased rapidly up to 80 ppm. A reignition had to be assumed, the fire hadn't been extinguished! In the morning hours of 07/21 the team leader decided to close the two dams again. During this works a pressure hose DN 75 was put through the dam at the head gate Kalın Damar to keep the opportunity open for foaming in this way.

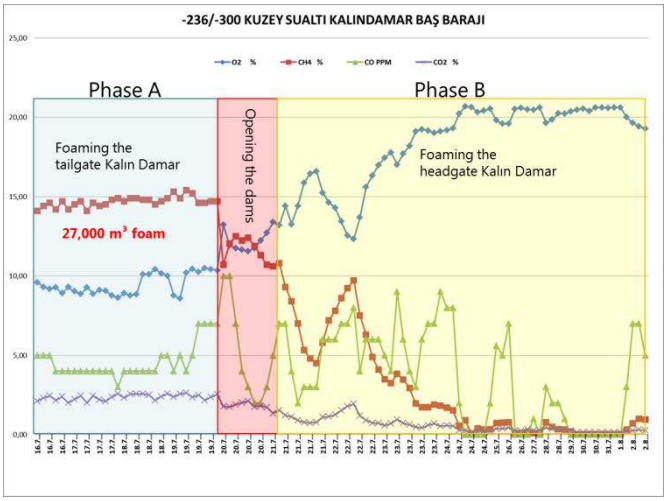

Figure 4. Gas development during phases A and B at outtaking dam Kalın Damar

Termination of phase A and begin of phase B. During phase A 27,000 m³ foam have been discharged into the tailgate.

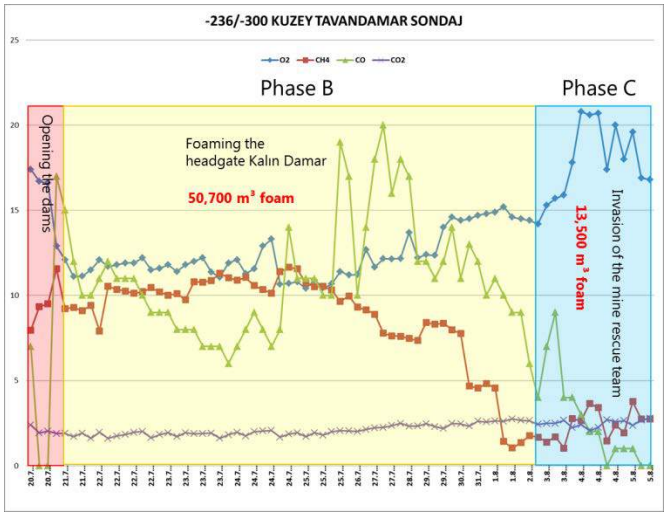

Figure 5. Gas development during phases B and C at borehole #2 in Tavan Damar

4.2 Phase B

With the beginning of Phase B on 07/20 – foaming the headgate – measurements of the gases CO, CO2, CH4 and O2 were carried out through the borehole #2 in Tavan Damar, the courses can be read in the graphic, figure 5. From 07/24 a measuring station was set at the tailgate dam in Kalın Damar (air intake!), for values see subsequent table 1. Parallel to the foaming through the headgate dam the borehole #1 in Tavan Damar was ready for foaming. Also here the foaming work was commenced with wet foam, later conversion to dry foam. On 08/02 end of phase B, newly opening the dams. During phase B 50,700 m³ foam have been discharged into the headgate and borehole #1. Begin of phase C.

Table 1. Gas development during phase B at intaking dam Kalın Damar

A.T.İ.M. MÜDÜRLÜĞÜ

-300 KUZEY SUALTI KALINDAMAR DİP BARAJ

TARİH	SAAT	ÖLÇÜLEN DEĞERLER			
		CO	CH_4	O_2	CO_2
24.7	20:00	98	8,6	15,11	1,01
25.7	04:30	89	8,98	14,34	1,08
25.7	11:00	70	10,34	11,97	1,52
25.7	14:00	66	10,27	11,88	1,52
25.7	18:35	58	9,87	12,19	1,36
26.7	02:00	49	8,45	13,64	1,13
26.7	11:45	51	7,09	15,21	0,93
26.7	18:20	49	7,01	15,13	0,84
27.7	01:00	24	3,01	18,66	0,36
27.7	11:15	21	2,35	19,1	0,29
27.7	16:30	17	2,25	19,1	0,29
28.7	00:25	13	1,69	18,4	0,22
28.7	09:15	9	1,46	19,19	0,18
28.7	14:30	7	1,26	19,22	0,17
28.7	17:30	9	1,34	19,56	0,2
29.7	baraj su ile dolduğundan numune alınamıyor				

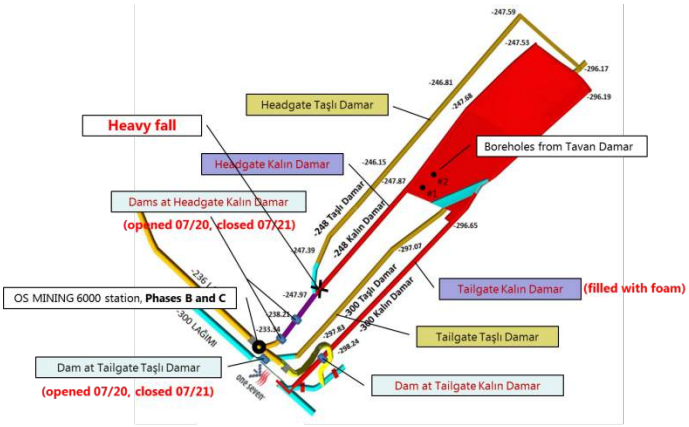

Figure 6. Situation in phases B and C

4.3 Phase C

On 08/03 0:00 a.m. reopening of the head gate dam Kalin Damar while maintaining the foaming (dry foam), approach of the mine rescue brigade under auxiliary ventilation, see subsequent photo, fig. 7. Begin of phase C: Proceeding of the mine rescue brigade into the affected mining area encountering a heavy fall east of the junction headgates Kalın Damar and Taşlı Damar, see figure 6. This had to be worked over for further action. Beginning the removal of the heavy fall under auxiliary ventilation and under protection of the foam dam. After the workover of the heavy fall the crews went section by section in the direction of the longwall face, in which they placed repeatedly dry foam as a new protection barrier and tracking the auxiliary

ventilation. With this approach longwall access had been reached at the end of the 32nd week. This action was carried out in the longwall face according to the same pattern in the 33rd week.

End of Phase C and completing the mission.

The equipment could be recovered and prepared for continuing the excavation of Kalın Damar seam.

Figure 7. Auxiliary ventilation through the head gate dam Kalin Damar, the smaller foaming hose (DN 75) is also visible

Figure 8. Result of phase B: The head gates Kalin Damar and Taşlı Damar are totally inundated with foam (in front: ventilation engineer and assistant)

5 SUMMARY & INTERPRETATION

The One Seven MINING 6000 machine can be operated with both nitrogen and air as the gas pressure medium. Due to the fact that there was no pressurized nitrogen with 2 bar (minimum required pressure for the machine) on site available the machine was operated with compressed air. At the first sight it is a disadvantage that air oxygen was brought into the fire area with the foam. It had to be assumed that a successful extinguishing only could be achieved by direct contact of the foam with the source of the fire.

Accordingly, the gas values in phase A did not indicate the successful extinguishing of the fire. These changed with the start of the 2nd phase to good and to the final fire extinguishing. We interpreted the CO-course in the borehole #2, and then we might expect a slight decay of the fire until 07/24. However, from 07/25 the CO production increased up to 07/31 recognizable again and then fell relatively quickly to zero (finally on 08/04). The interim CO-increases during phase B could be explained with methane fires while switching the O2/CH4-mixture between inside and outside the flammability-triangle. The sudden decline of CO and CH4 could be affected by the displacement of the fire gases through the foam. To this interpretation fits the development of the gas values at the tail gate dam Kalın Damar. Especially the CO and CH4 values led us to suppose, that the foam replaced the gases literally in front of them and simultaneously increased O2 content constantly.

Finally, it was found that by use of the OS MINING 6000 and the foam concentrate One Seven AM a fire area could be regained for extraction, with the conventional method (nitrogen inerting) this fire area would have to be abandoned.

The key finding is that the opening of the fire area and the safely entrance of the mine rescue brigade in the fire area was possible just under the protection of the

previously placed foam and the carriage of the new mined out foam.

A critical evaluation must be said that a foaming of probably with nitrogen foam would have been more efficient and would have led to a faster successful extinguishing. The experiences from this application show us that the gas composition in the fire area can be in the explosive range with compressed air foam over a longer period, possibly this state can be first produced by the air entrance even. This firefighting can be seen as uncritical, if it is dammed up with an explosion-proof dam. The conclusion is that with unavailable pressurized nitrogen it isn't necessary to waive the using of the One Seven MINING technology, when the fire area is dammed explosion-proof!

The practiced scheme can be briefly described as follows:

a) In the dammed state the cut off of the fire area from any ventilation and the displacement of all gases are to bring about by complete foaming of the fire area.

b) After opening of the fire area: section-by-section approach under the auxiliary ventilation by constantly reciting a foam dam, which worked almost like a drift face and protect the work area against the ingress of toxic and explosive gases.

All potentially flammable materials such as coal, wood, etc. were wetted by the first foaming and at the moment nonflammable (antipyrogenic effect of the One Seven AM foam).

c) Restoration of continuous ventilation.

6 CONCLUSION

In a 20 days continuous engagement (07/16 – 08/03) a covered mine fire, whose development 5.5 months lagged, could be extinguished by using a One Seven MINING 6000 machine and the Class A foam- concentrate One Seven AM.

A total amount of about 91,000 m³ wet and dry foam was brought into the dammed fire area. The water consumption was 4,200 m³; the consumption of foam concentrate was 6,320 liters.

A comparable safety by opening and inspecting a fire area has never been seen in the coal mining industry before. The longwall equipment was found largely undamaged, which is suggestive of a limiting of the fire in the goaf. The equipment was recovered and prepared for continuing the excavation of Kalın Damar seam

Early Detection of Spontaneous Combustion Using Laboratory Gas Evolution Tests

T. Levi
CRL Energy Ltd, Lower Hutt, New Zealand

B. Beamish
CB3 Mine Services Pty Ltd, Brisbane, Australia

R. Brown
CRL Energy Ltd, Lower Hutt, New Zealand

J. Theiler
CB3 Mine Services Pty Ltd, Brisbane, Australia

J. Pope
CRL Energy Ltd, Christchuch, New Zealand

ABSTRACT A laboratory gas evolution test has been developed to assist with identifying the most relevant gases and gas ratios for trending and setting trigger levels as part of the Principal Hazard Management Plan for Spontaneous Combustion. The purpose of this paper is to present case study results of gas trends for a high volatile A bituminous coal where the results show differences in gas evolution trends with increasing coal temperature. Carbon monoxide evolution progressively increases from ambient to the advanced stages of heating, whereas ethylene only appears in significant concentration during the advanced stages.

Keywords: Spontaneous combustion, early detection, principal hazard management plan

1 INTRODUCTION

Underground coal mines use gas monitoring systems to detect the presence of seam gas emissions and signs of coal self-heating. Additional gas analysis is performed using gas chromatography to detect the presence of higher hydrocarbons (ethane and ethylene) and hydrogen.

The site-specific nature of coal has a major effect on the gas evolution trends that occur during self-heating. For example, the presence of seam gas such as CO_2 can distort the CO/ CO_2 to the extent that it is unreliable as an indicator of heating development. Conversely, the presence of ethane as a seam gas may provide an early indication of coal temperature increase due to increased ethane desorption, but only if other gas indicators are showing a similar trend. Instances of localised high ethane seam gas content can create misleading interpretations in terms of spontaneous combustion indication (Claassen and Beamish, 2010).

The Principal Hazard Management Plan (PHMP) for spontaneous combustion at the mine can use the gas analysis information to provide trigger levels for actions to be taken in response to stages of a heating development. This is formally known as a Trigger Action Response Plan (TARP) and various trigger levels are set in the TARP, which range from “normal” up to “evacuate the mine” based on the gas levels present.

It is therefore important that appropriate gas indicators are identified for each mine to assist with gas trending analysis and interpretation.

This paper presents results from laboratory testing of a high volatile A

bituminous coal sample that demonstrates the process used to identify site-specific gas indicators, which can be used to support the setting of trigger levels in the TARP.

The testing also highlights the complications that can occur from the presence of seam gas.

2 COAL SAMPLE AND GAS EVOLUTION TESTING

A summary of the coal quality analysis for the coal used in these tests is shown in Table 1. The ASTM rank of the sample is high volatile A bituminous and the coal type is inertinite-rich, as shown on the Suggate rank plot (Suggate, 2000) in Figure 1.

The seam has a very low gas content (<0.5 m^3/t) which was determined from standard gas content measurements. The R_{70} value for this coal is 2.44°C/h, which rates the coal as having a medium intrinsic spontaneous combustion propensity.

Table 1. Summary of coal quality analysis.

Moisture (%)	(air-dried basis)	2.2
Ash (%)	(air-dried basis)	13.5
VM (%, dmmf)		25.3
CV (Btu/lb, mmf)		14 466
ASTM rank		hvAb

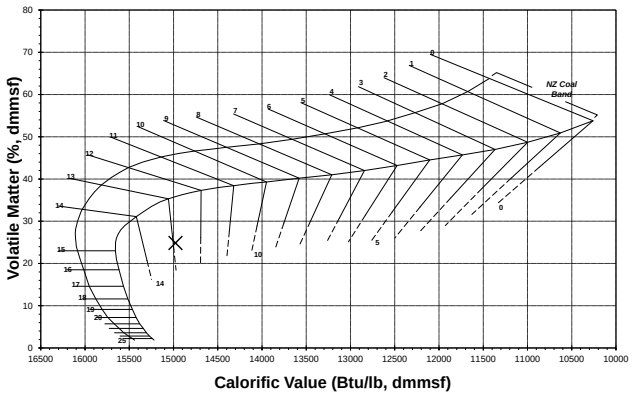

Figure 1. Suggate rank plot of coal sample used for gas evolution testing.

3 EXPERIMENTAL

Fresh coal samples are crushed, placed in a sealed flask in an oven and left to equilibrate at the pre-set start temperature. A flow of dry air is passed through the sample and the oven set to heat the sample to approximately 200ºC.

A Micro Gas Chromatograph determines the concentrations of oxygen, nitrogen, methane, carbon dioxide, carbon monoxide, hydrogen, ethane and ethylene at regular temperature increments. This information is used to evaluate the gas evolution trend of the coal in response to increasing temperature. In addition, established gas indicator ratios such as Young's, Graham's, Jones-Trickett and CO/CO_2 are calculated to establish the most reliable gas ratios for trending the development of a heating event.

4 RESULTS

1.1 Evolution of Individual Gases With Increasing Coal Temperature

The gas evolution results for individual gases are shown in Figures 2 -7 and the following trends are apparent:

The carbon monoxide (CO) evolution, shown in Figure 2, progressively increases with coal temperature, which makes it a reliable indicator of the stages of coal self-heating.

The trend for carbon dioxide (CO_2) evolution shown in Figure 3 is similar to that for CO. When these readings are obtained at the mine the presence of seam gas must be considered.

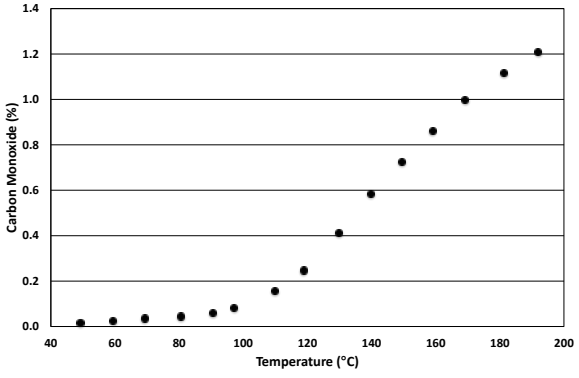

Figure 2. Carbon Monoxide evolution in response to increasing coal temperature.

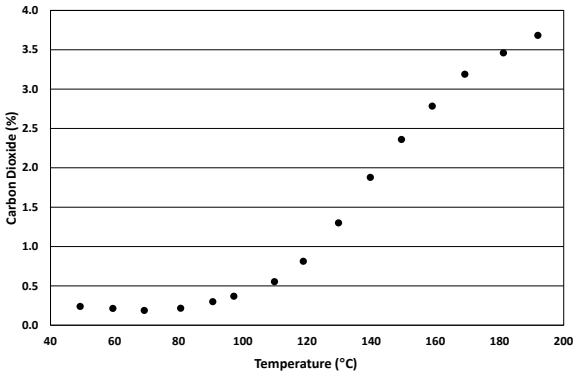

Figure 3. Carbon Dioxide evolution in response to increasing coal temperature.

Hydrogen (H_2) evolution, Figure 4, is measureable even at low temperatures and progressively increases with coal temperature and it is clear from Figure 4 that significant H_2 is evolved at the elevated temperatures of an advanced heating.

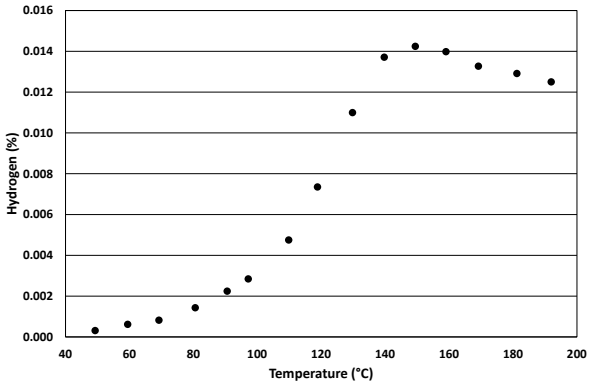

Figure 4. Hydrogen evolution in response to increasing coal temperature.

Methane (CH_4) evolution, Figure 5, for this coal does not reach significant levels until the coal exceeds 120ºC. There are only traces of methane as seam gas in this case.

The ethane (C_2H_6) evolution presented in Figure 6 shows a strong decreasing trend at low temperatures and then increases again once the coal exceeds 130ºC. The initial ethane evolution is associated with residual ethane present as seam gas and the subsequent increase in ethane evolution is due to coal oxidation. The desorption of the ethane as the coal warms may be an early detection indicator of self-heating and this feature has been used previously at the Spring Creek Mine in New Zealand (Beamish and Hughes, 2009).

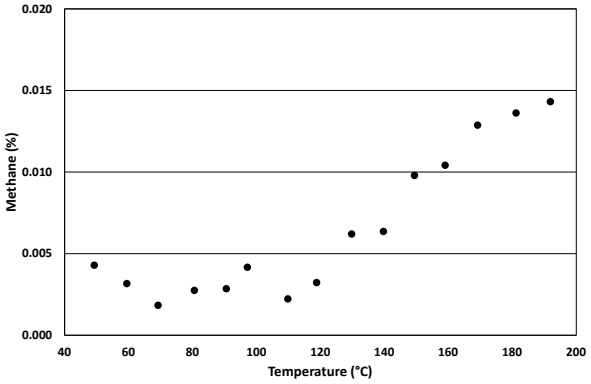

Figure 5. Methane evolution in response to increasing coal temperature.

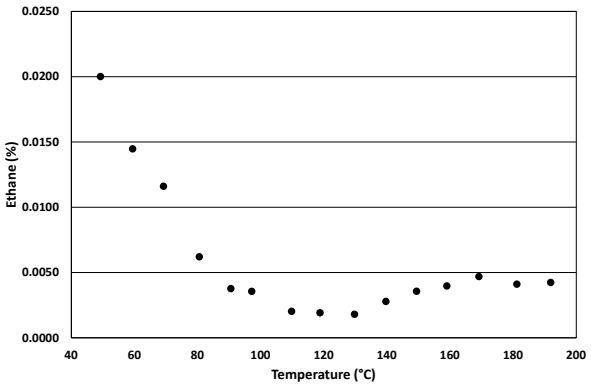

Figure 6. Ethane evolution in response to increasing coal temperature.

Ethylene (C_2H_4) evolution, Figure 7, does not occur for this coal until the temperature exceeds 140ºC. It is a clear marker of advanced coal self-heating for this particular coal and could be used for setting the upper trigger levels of the TARP.

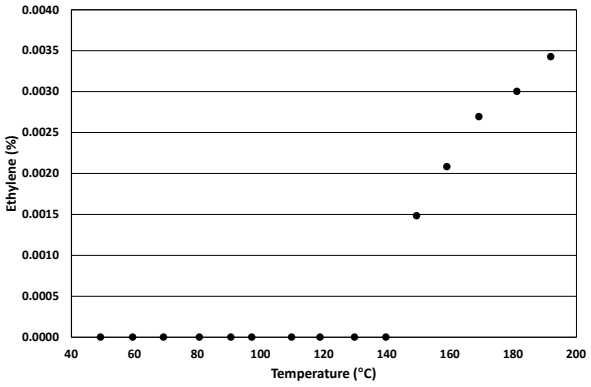

Figure 7. Ethylene evolution in response to increasing coal temperature.

1.2 Gas Ratio Response with Increasing Coal Temperature

One of the most common gas ratios used by the coal industry as an indicator of spontaneous combustion is Graham's Ratio (GR). This is calculated as the ratio of carbon monoxide produced to oxygen consumed (oxygen deficiency) using the following equation:

GR = (CO × 100)/(oxygen deficiency)

Where, for fresh air:

Oxygen deficiency = $(20.93/78.11 \times N_2 - O_2)$

A factor of 100 is applied to the ratio to produce meaningful numbers for comparison as CO is generally in concentrations of parts per million, whereas the other major gases are in units of per cent. It should be noted that the GR value is very sensitive to low levels of oxygen deficiency and may produce anomalous results due to this sensitivity (Brady, 2008).

An example of how the GR value can be related to the stages of a heating is reported by Moreby and Chalmers (2009) Table 2, but it should be noted that these values can vary for individual coals:

Table 2. GR value related to heating stages.

GR ≤ 0.4	Indicates normal value
0.4 ≤ GR ≤1.0	Indicates possible early stages of heating
1.0 ≤ GR < 2.0	Indicates event almost certain
2.0 ≤ GR < 3.0	Indicates serious event
GR ≥ 3.0	Indicates active fire

For the coal tested in this study, the GR values show a strong positive correlation with increasing coal temperature, Figure 8, and there is a noticeable change in slope once the coal exceeds 100ºC, which may be due to moisture removal from the coal freeing up easier access to reactive sites. Based on the trend of the GR values in Figure 8, the normal background is expected to be 0.20 assuming an ambient temperature of 30ºC. This would need to be confirmed with current on-site measurements to set a baseline value for normal conditions in the TARP. Subsequent trigger levels could be defined using a doubling of the GR value for example.

Young's Ratio (YR) uses CO_2 instead of CO as the indicator of oxidation according to the equation:

YR = CO_2 / (Oxygen deficiency)

Where for fresh air:

Oxygen deficiency = $(20.93/78.11 x N_2 - O_2)$

$CO_2 = CO_2 - 0.035/78.11 x N_2$

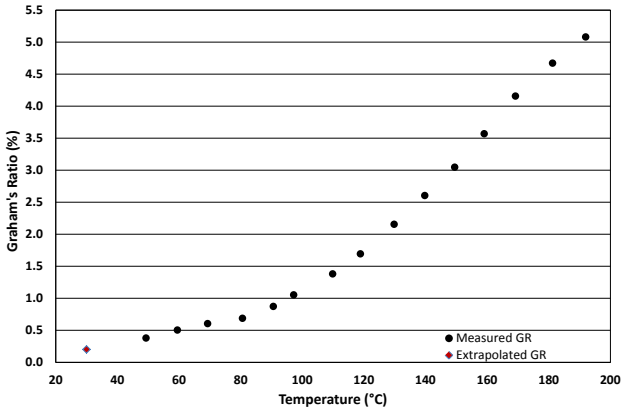

Figure 8. Graham's Ratio in response to increasing coal temperature.

The initial trend in the YR values shows a decrease followed by an increasing trend above 70ºC (Figure 9) and shows a similar trend to the GR values. The initial decreasing trend is in response to seam gas desorption. As such, for this coal the YR values would not provide a reliable early indication of coal self-heating at low temperatures, but could be used to confirm heating development at higher temperatures.

The Morris ratio (MR) is a measure of the amount of oxygen absorbed in relation to the amount of the major oxidation products (CO and CO_2) generated by the coal:

MR = (Nitrogen excess) / (CO + CO_2)

Where, for fresh air:

Nitrogen excess = $(N_2 - 78.11/20.93 \times O_2)$

$CO_2 = CO_2 - 0.035/78.11 x N_2$

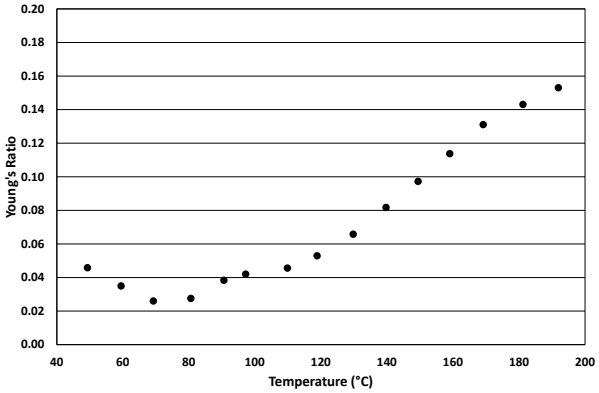

Figure 9. Young's Ratio in response to increasing coal temperature.

Again, for this coal the low temperature region shown in Figure 10 indicates an influence of CO_2 seam gas desorption as the MR values increase initially and then consistently decrease in excess of 70ºC.

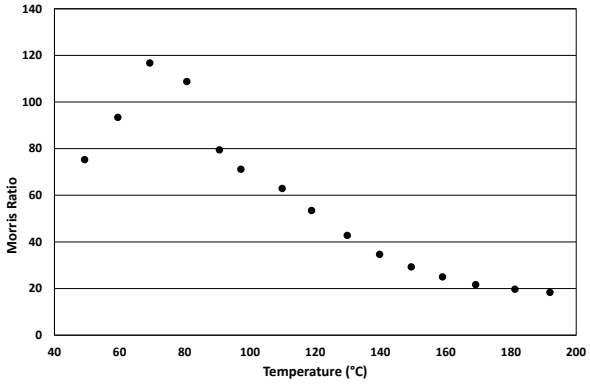

Figure 10. Morris Ratio in response to increasing coal temperature.

The CO/CO_2 and H_2/CO ratios are independent of oxygen deficiency and are therefore valuable in supporting confirmation of heating progression shown by other gas indicator ratios that rely on accurate oxygen deficiency results. The trends obtained for the coal (Figures 11 and 12) show differences in the nature of the gas evolution of these oxidation products as the CO/CO_2 ratio provides a consistent increasing trend up to approximately 130ºC compared to the H_2/CO ratio, which shows a maximum value at 90ºC before consistently decreasing. The absolute value of the CO/CO_2 ratio obtained from laboratory testing should not be considered to apply at the mine site as due to the presence of seam gas desorption from pillars, caved coal and other strata the actual ratio can be up to two orders of magnitude lower. However, the trending would be the same as the coal temperature increases.

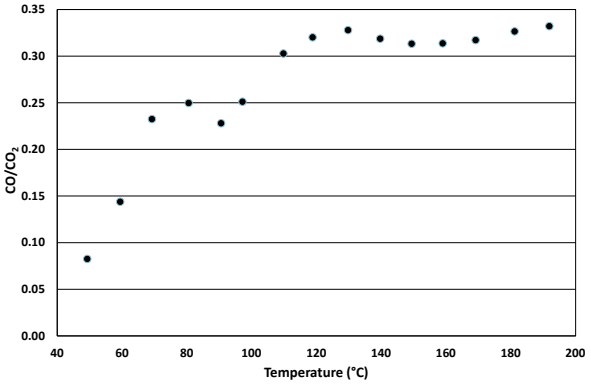

Figure 11. CO/CO2 Ratio in response to increasing coal temperature.

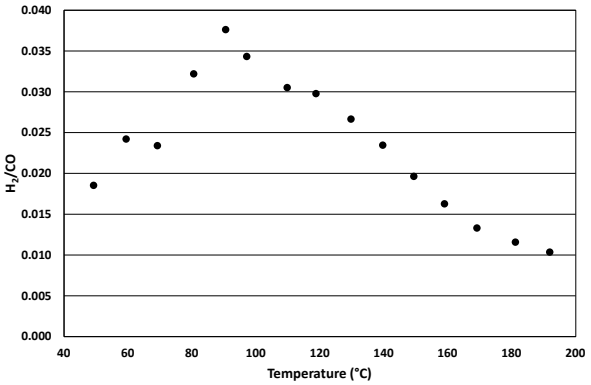

Figure 12. H2/CO Ratio in response to increasing coal temperature.

5 CONCLUSIONS

For the high volatile A bituminous coal tested in this study there are clear trends shown by most of the normal gas indicators used for spontaneous combustion detection. CO evolution provides a continuous record of heating development, which is supported by the Graham's ratio.

The coal has a unique ethane desorption signature at low temperature that may provide an early indication of the coal self-heating.

Advanced stages of self-heating are indicated by the evolution of ethylene and confirmation is provided by gas ratios such as Young's ratio and Morris ratio.

REFERENCES

Beamish, B and Hughes, R, 2009. Comparison of laboratory bulk coal spontaneous combustion testing and site experience – A case study from Spring Creek Mine, *Proceedings 9th Coal Operator's Conference COAL 2009*, pp 287-295.

Brady, D, 2008. Problems with determining oxygen deficiencies in ratios used for assessing spontaneous combustion activity, *Proceedings 8th Coal Operators' Conference COAL 2008*, pp 209-216.

Claassen, C and Beamish, B, 2010. Case study of ethane emissions at Mandalong Mine, *Proceedings 10th Coal Operator's Conference COAL 2010*, pp 274-280.

Moreby, R and Chalmers, D, 2009. Mine ventilation, Mining Education Australia course notes (CD ROM).

Suggate, R P, 2000, Rank (Rs) scale: it basis and its applicability as a maturity index for all coals, *New Zealand Journal of Geology and Geophysics*, Vol 4, pp521-553.

Providing a Risk Model for Iran's Mines Based on Extreme Value Theory

R.Noori, M. Ahmad Sherbafi
Iran's Mining Investment Insurance Corporation, Tehran ,Iran

ABSTRACT Lack of proper knowledge about the risk already exists in the credit insurance of the miners has led to a poor market to issue mine's credit policy. In Iran, as a country with a huge potential in its minting sector, this has also been one of the main reasons why investors are generally reluctant to run projects in the sector.

Credit risk of miners has been tried to be analyzed with the usage of Extreme Value Theory as one of the risk management's tool in this current paper. This theory works based on the Generalized Extreme Value and the Generalized Pareto distribution methods to estimate distribution function of the losses in credit risk.

The analytic data has been collected from Iran's mines. As a result, we model extreme historical losses of Iran's mines credit risk and find an optimum threshold for them.

Keywords: Extreme Value Theory, risk model

1 INTRODUCTION

After oil, mining is the second important sector that the Iranian economy relies on, playing a very important role in the economic development of the country. However the mining sector hasn't achieved the real position in the economy yet due to lack of necessary investments are caused by management which is not eligible at the micro and macro level especially risk management. Investment in the mining sector, which is regarded very risky, needs proper insurance covering such as the credit risk which is normally covered through insurance services. However, insurance companies seem to have no proper knowledge about the level and intensity of risks associated with mining operations, which is mainly due to the fluctuations in the economic, cultural, technical, environmental, legal and management conditions in the country. The current paper analyzes the losses associated with the credit risk in Iran's mining activities using the Extreme Value Theory which can offer a proper model in risk analysis in the sector.

The Extreme Value Theory is one of the major tools for analysis and modeling of risks which is mainly conducted in two manners, namely the Generalized Pareto Distribution (GPD) and Generalized Extreme Value (GEV). The method has been used in a wide range of applications in various sciences including credit risk measurement, Gillli and Kellezi (2006); Paul and Barnes (2010); Manchini and Trojani (2010), risk management in insurance industry, Embrechts and I.Resnick (1999), climate and natural hazard, Das, et al (2012) and risks in stock and share market, Karmakar and Shukla (2014); L.c.dasilva and V.de melomendes (2003).

However, the EVT has been rarely used in measurement of risks in the mining industry with exceptions like the recent study in South Africa in which the method was applied to the mining sector, CHinhuang et al (2014). The study was conducted on mining companies' indicators in Johannesburg mining stock market. The EVT model was also used in oil industry in Thailand in 2014 that the price of crude oil was predicted based on GPD and GEV models, Taveeapiradeecharoen et al (2014). In the Iranian literature of research however, there has been no case of the method being used in the mining sector.

The current study is based on the data provided by the exclusive insurer of the mining activities in Iran and the sole excusive lender in the sector. The results identify the main obstacles for the insurers, banks and credit institutions in engaging in mining activities and provide projections on the potential losses that may arise in the sector. It also provides the banks and insurance companies with this knowledge to decide on the issue better.

2 MINING AND THE NEED FOR A CREDIT RISK, A CASE STUDY ON IRAN

Mining is a very risky, adventurous operation with many threats for the investors who are active in the sector. Depending on the value of the mining project and the risk could be a function of many economical and physical uncertainties like the price of the mineral and its quality, expenditures, planning and other environmental conditions that most of them still are unidentified, Martinez (2009).

The investment in mines is either in direct form by the investor or through the loans and credits provided by the banks. In the former case, any potential loss in the benefits of the project and the return of investment is totally inflicted on the investor and his partners. However, if banks invest in mining projects, it will be their assets and possessions that would suffer most from the credit risks in the mining activities. This is one of the main reasons why banks are reluctant to invest in mining projects. The current amount of unpaid loans or loans that may not be returned show how much the operation could be risky for the banks. The weak management of the portfolio risk, little attention to economic changes or other conditions that may risk the credit position of the banks also contributes to the situation. This could be more evident in the work of those mining companies that are closely dependent on the technical and economic conditions and especially the government's policies. In other words, banks should not only take into account the investment needed for compensating the risks, they should also have the required knowledge and expertise about the identification, measurement, protection and control of credit risk in the mining sector.

Better management of the risks associated with the losses in the mining operation or mining companies' delay in reimbursement of loans needs a proper system of insurance cover. Iran’s Mining Investment Insurance Corporation (MICO), which is run by the government, is the sole and exclusive insurer of the sector in the country which was established based on article 31 of Iran's Mining Law, IRI Parliament Research Center (2014). All mining companies are referred to this fund for receiving credits and loans.

The fund takes the mines' license as the principal collateral and uses it to compensate the potential losses brought about by the negligence of the mining companies. During the process of issuing the insuring policy which is used by miners for receiving loans from the banks, the experts are working for the fund study the mining project and if it justified economically, the current investment and the potential investments would be estimated.

The management of the risks associated with the negligence of the miners is through taking strong collaterals and guarantees from the insured. The banks and credit institution then accept the policies issued by the fund as the collateral to grant loans to the miners.

If the loans are not reimbursed during the operation of the mines, the banks will inform the fund through a notice so the fund compensates the losses for the bank. The portfolio management of the fund is done through selling the collaterals unless the insured pays the amounts he owes.

Now that we have studied the prevalent mechanism for credit insurance of the mines in Iran, we can present and analyze the loss model.

3 THE EXTREME VALUE THEORY

The management of risks has become a must for many businesses. The measurement and management of risks triggered by

uncertainties have created a necessity for owners of businesses to look for a proper system for measurement of the risks associated with their assets and possessions and this naturally applies to all fields of business including the financial, engineering and insurance markets. The significance of such necessity has been doubled over the past two decades in which markets have experienced a meaningful instability, proving the huge and infinite dimensions of the losses. This has forced the financial institutions to look for more thorough and robust methodologies for modeling large-scale, extreme losses, Paul and Barnes (2010).

The Extreme Value Theory is one the most distinguished tools for risk managers in the loss modeling. The theory has proved to be very effective in the most advanced areas of science, engineering and insurance. Used as a statistical tool, the theory has a wide range of applications in various field including insurance, McNeil (1997), financial risk estimate, Gilli and Kellezi (2006); Mancini (2010); Paul and Barnes (2010), hydrology and meteorology, L.Smith (1986); A.Tawn (1988);, stock market, K.Singh, et al (2012); L.C.dasilva (2003); Karmakar and Shukla (2014); Taveeapiradeecharoen, et al (2014), communication, geology and seismic studies, biology and public health. Penalva, et al (2013) have classified these applications in two major groups:

- Environmental area such as the study of sea levels, wind speed, water flow in rivers, etc.
- Reliability and structural safety area like measurement of credit risk in risk management.

The quantification of the most extreme losses in financial markets is a necessity in the current situation of the global economy and the extreme value theory is the best method to perform such a mission.

Banks normally look for the best statistical method for protecting their giant reserves against any potential losses. For example, the Swiss Bank Corporation has introduced a statistical model for calculation of risks (ACRA) in which the measurement is defined based on the Expected loss, the Unexpected loss and the Stress loss, Embrechts, et al (1999).

The current paper uses the EVT in modeling the credit risk loss of the mining projects in Iran for the first time. The study is conducted based on the data provided by the sole specialized insurer of the mining sector in the country. The results are then used to analyze the mining credit risk cover provided in the sector which can further be applied by other insurers, banks and credit institutors. The credits and loans granted to the mining sector in Iran are only provided by this insurer. The data used in the study is only those provided by this fund that is related to all mines in Iran.

The Extreme Value Theory's use in insurance leads to a modeling for positive random variable which shows the amount of money that the insurer should pay the insured due to the loss occurred. The variable is in fact the maximum loss or the extreme loss. The finite behavior of these maximums is studied in the Extreme Value Theory and heavy-tail distributions are used for their modeling.

The choice of loss random variable is based on GEV(Generalized Extreme Value Distribution) and GPD(Generalized Pareto Distribution)methods. The GEV uses similar blocks of observation like fixed periods or monthly or yearly periods. These observations are called Block Maxima and they can be modeled through finding their distribution function which is then extended to the Extreme Value Distribution function. The GPD has nothing to do with observations in fixed periods but it considers the maximums that are beyond a limited threshold. These observations are then called Peaks-Over Threshold (POT). These maximums are modeled and estimated through General Pareto Distribution, Gilli and Kellezi (2006), Gencay and Selcuk (2001).

4 THE MATHEMATICAL MODEL FOR EXTREME VALUE THEORY

4.1 The Generalized Extreme Value Distribution

4.1.1 Block maxima

In this method, the random variables are selected from observations in a fixed period of time which are called the block maxima. - Assume a sample $X_1,X_2,\ldots,X_N$ of independent and identically distributed data drawn from an unknown distribution F.

We divide the sample into m non-overlapping subsamples of n observations each (n-blocks), for given integer m ,n (0<m ,n<N) and denote $M_{n,j}$ are the maximum of the j^{th} subsample. Assume that F belongs to the maximum domain of attraction of $G_{\xi,\mu,\delta}$ for some $\xi,\mu,\delta \in \Re$ with$\delta > 0$.

The GEV method fits distribution function $G_{\xi,\mu,\delta}$ to the sequence of block maxima $M_{n,1}$,…, $M_{n,m}$ with estimated parameters $\hat{\xi},\hat{\mu},\hat{\delta}$.

4.1.2*Theorem1, Fisher and Tippett (1928); Gnedenko (1943)*

Let X_n be a sequence of independent and identically random variables. If there exist constants $c_n>0$, $d_n\in \mathbb{R}$ and some non-degenerate distribution function H such that $\frac{M_n - d_n}{c_n} \xrightarrow{d} H$.Then H belongs to one of the three standard extreme value distributions 1, 2 or 3:

Fréchet: $\phi_\alpha(x)=\begin{cases}0, & x\le 0\\ e^{-x^{-\alpha}}, & x>0\end{cases}$ $\alpha > 0$ (1)

Weibull: $\psi_\alpha(x)=\begin{cases}e^{-(-x)^{\alpha}}, & x\le 0\\ 1, & x>0\end{cases}$ $\alpha>0$ (2)

Gumbel: $\Delta(x)=e^{-e^{-x}}$,$x\in R$ (3)

Jenkinson (1955) and vonMises (1954) have proposed that the above mentioned functions be showed as a one-variable function in which $1+\xi x > 0$,

$$H_\xi(x)=\begin{cases}e^{-(1+\xi x)^{-\frac{1}{\xi}}} & \text{if } \xi\neq 0\\ e^{-e^{-x}} & \text{if } \xi=0\end{cases} \quad (4)$$

This generalization is known as the Generalized Extreme Value distribution (GEV).

4.2The Generalized Pareto Distribution

4.2.1Peak-Over –Threshold (POT)

This approach is to consider the distribution of exceedances over a certain threshold like u. We are interested in estimating the distribution function F_u of values of x above a certain threshold u. The distribution function F_u is called the conditional excess distribution function and is defined as

$F_u(y)=P(X-u\le y|X>u)$, $0\le y\le x_F-u$ (5)

In which X is the random variable, u is a given threshold and y=x-u are the excesses and $x_F \le \infty$ is the right endpoint of F.

4.2.2*Theorem2, Pickands (1975), Balkema and de Haan (1974)*

For a larger class of distribution functions F, the conditional excess distribution function $F_u(y)$, for u large, is well approximated by

$F_u(y)\approx G_{\xi,\sigma}(y)$, $u\to\infty$ (6)

Where

$$G_{\xi,\sigma}(y)=\begin{cases}1-\left(1+\frac{\xi}{\sigma}y\right)^{-\frac{1}{\xi}} & \text{if } \xi\neq 0\\ 1-e^{-\frac{y}{\sigma}} & \text{if } \xi=0\end{cases} \quad (7)$$

For $y\in[0,(x-u)]$if $\xi\ge 0$,$y\in\left[0,-\frac{\sigma}{\xi}\right]$ if $\xi<0$

$G_{\xi,\sigma}(y)$ is the so called Generalized Pareto Distribution (GPD).

5 DATA AND SELECTION OF VARIABLES FOR STARTING ANALYSIS

The data used in this paper covers the losses aggregated in Iran's mining insurance corporation for all mines across the country which was paid between 2006 till August 2014. The insurer has a 12-year experience in the mining sector and the data used in the paper is about the period after 2006. The analysis and modeling of the data are conducted using R 2.15.1. Figures1 and 2 show the time series and histogram for losses of credit insurance of the mining activities in Iran between 2006 till August 2014 respectively.

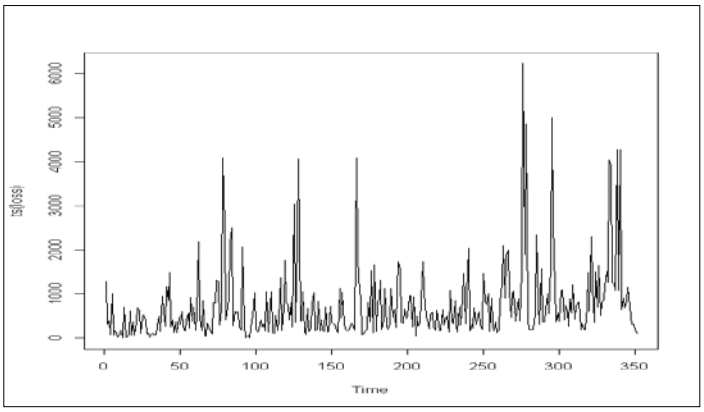

Figure 1. Time series plot of losses.

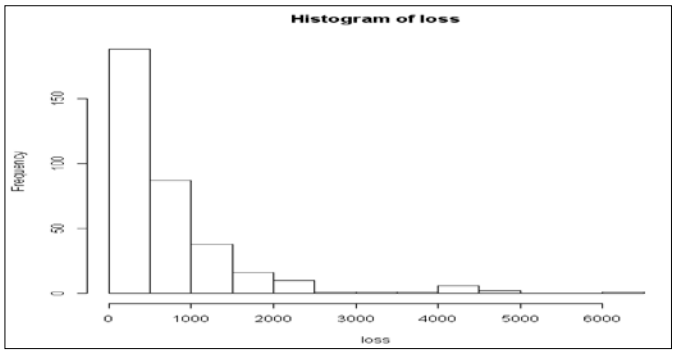

Figure 2. Histogram of losses.

Table 1 shows that the normality assumption of the data distribution is rejected at all levels of significant. The probability plot indicates the empirical distribution of the data is exponential distribution with an average 728.15 million Rial (IRR). Considering the loss data that is usually heavy-tail, so this result isn't beyond the fact (Figure 3).

Table 1- Descriptive statistics summary

n	Min	Max	Mean	Stdev	Kolmogorov -Smirnov (P-value)	Skewness	Kurtosis
351	1.82	6226	728.14709	844.86	0.2997(0.00)	2.99	11.45

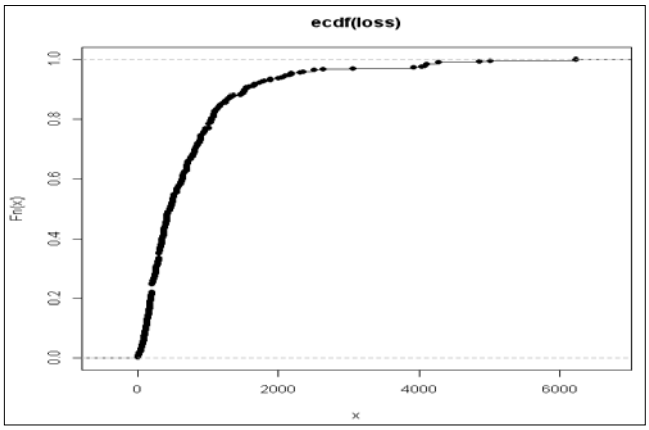

Figure 3. Emprical function of losses.

5.1 Estimating the Generalized Extreme Value distribution

In order to show the distribution function based on GEV model, we should first block the data. Seasonal blocks are used in the current paper due to the fact the Iran's mining insurance corporation is almost young. It is also because of the lack of the data in each year so we decided to use the seasonal data and then select their maximums. The estimate of the model parameters for seasonal blocks of the loss can be seen in Table 2.

Table 2 shows that the Maximum Likelihood Estimation (MLE) for shape parameter ξ of model is positive. This means that the block maxima of the credit insurance loss in Iranian mining industry follow the $Fréchet$ model with $\xi = 0.3615$. Diagnostic plots for assessing the accuracy of the EVT model for this data are shown in Figure 5. These plots show the $Fréchet$ model as being adequate for modeling this data. A 95 % confidence interval for parameter ξ shows that is always positive (Figure 4).

Thus, using the block maxima method, the loss model for credit insurance in Iran's mines based on the distribution function is estimated as following

$$H_{\xi}(x) = e^{-(1+0.3615x)^{-2.7}} \qquad \xi>0 \qquad (8)$$

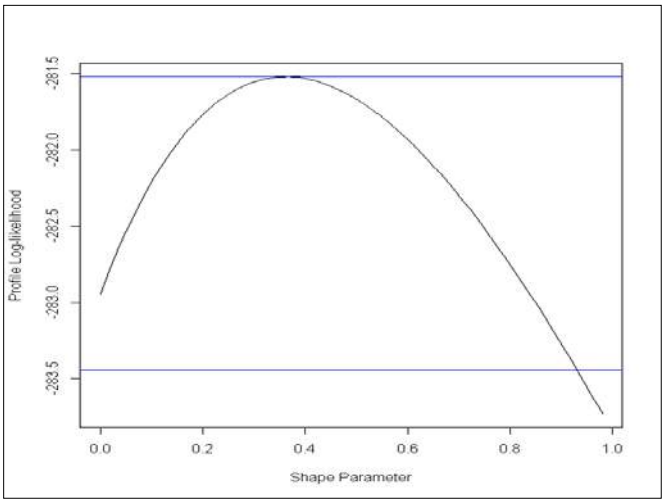

Figure 4. 95 % confidence interval for ξ.

Having the loss distribution function of x, we can now expand our study for each x in range of variable and obtain the probability of various losses. The assessment and discovery of the central tendencies and scattering measurements in the portfolio losses of the credit insurance is conducted through using the model. For example, the average maximum of occurred losses based on the seasonal blocks which is viewed as one of the main central tendencies is estimated to be $\mu = 1551.68$ million Rial (IRR).

Table 2. GEV outputs for losses

Block size	Maxima	Estimated parameters and standard errors					
		ξ	s.e(ξ)	δ	s.e(δ)	μ	s.e(μ)
4	31	0.3615	0.243	1482.5	297.3	1551.68	337.1

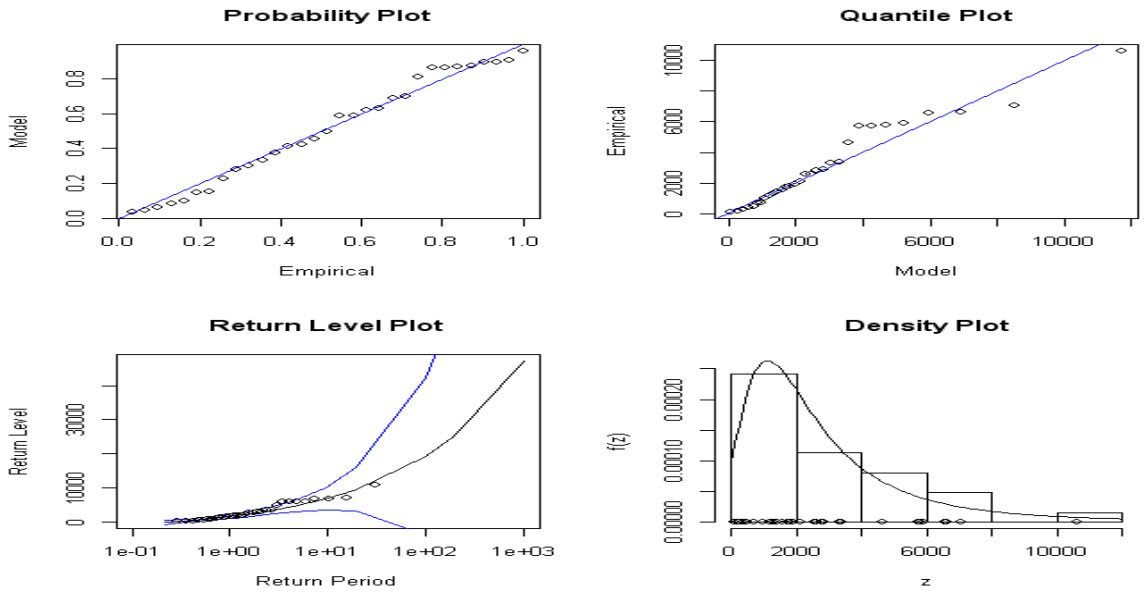

Figure 5-Diagnostic plots for GEV fit to the losses.

5.2Estimation of loss through the Generalized Pareto Distribution (GPD)

The main objective in the GPD model is to estimate a proper threshold u so that the distribution function of exceedances over u would include Generalized Pareto Distribution model. The Mean Excess and the empirical distribution of loss are used for the assessment of the threshold (Fig 6, 7). Figure 6 shows that the u threshold which is between 1246 and 1538 million Rial (IRR) is a logical and acceptable threshold, because at least 85 percent of data is smaller than the current threshold. The selected values are used for the estimation of the thresholds that

are coincidence with 85% to 90% quantiles of the data. Table 3 shows the estimation for parameters of Generalized Pareto Distribution for threshold between 1246 to 1538.

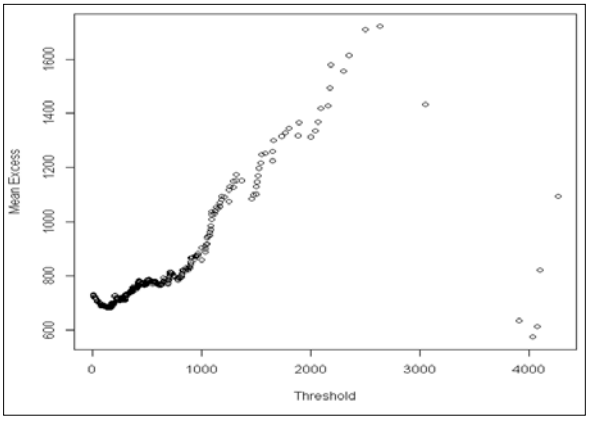

Figure 6- Mean excess function of losses

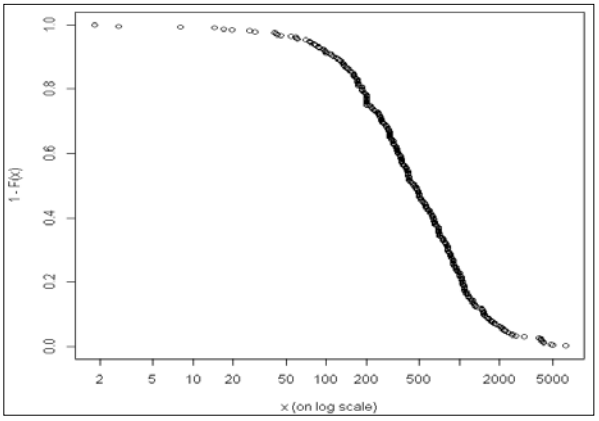

Figure 7- Empirical function of losses

Table3-GPD outputs for losses

Threshold	Extremes	Method	Estimated parameters and standard errors			
P	u	n		ξ	s.e(ξ)	σ	s.e(σ)
0.85	1246.5	50	MLE	0.200	0.218	870.3	225.1
0.87	1311.2	45	MLE	0.118	0.223	998.3	267.2
0.89	1510	37	MLE	0.150	0.291	982.5	328.0
0.90	1538.4	35	MLE	0.067	0.290	1105.8	370.7

The Maximum likelihood Estimation method (MLE) is again used for the estimation of the variables. It can be seen from Table 3 that the standard errors of the estimated parameters increase as the threshold increases. In order to select the optimum threshold, one should use the validity plots like the following chart (Fig 8) in which the value of u=1246.5 is viewed as a desired threshold for the data of the losses in the threshold.

The Generalized Pareto Distribution model would be as following:

$$G_{\xi,\sigma}(y)=1-(1+0.000231\,y)^{-4.980}\ ,\xi>0 \quad (9)$$

This model indicates that the threshold of loss in an insurer's portfolio of credit insurance is 1246.5 for one policy. This can inform the insurer about the loss threshold in a credit policy issued for mining projects which is equal to 1246.5 in the portfolio and the insurer must take reserves for losses more than threshold.

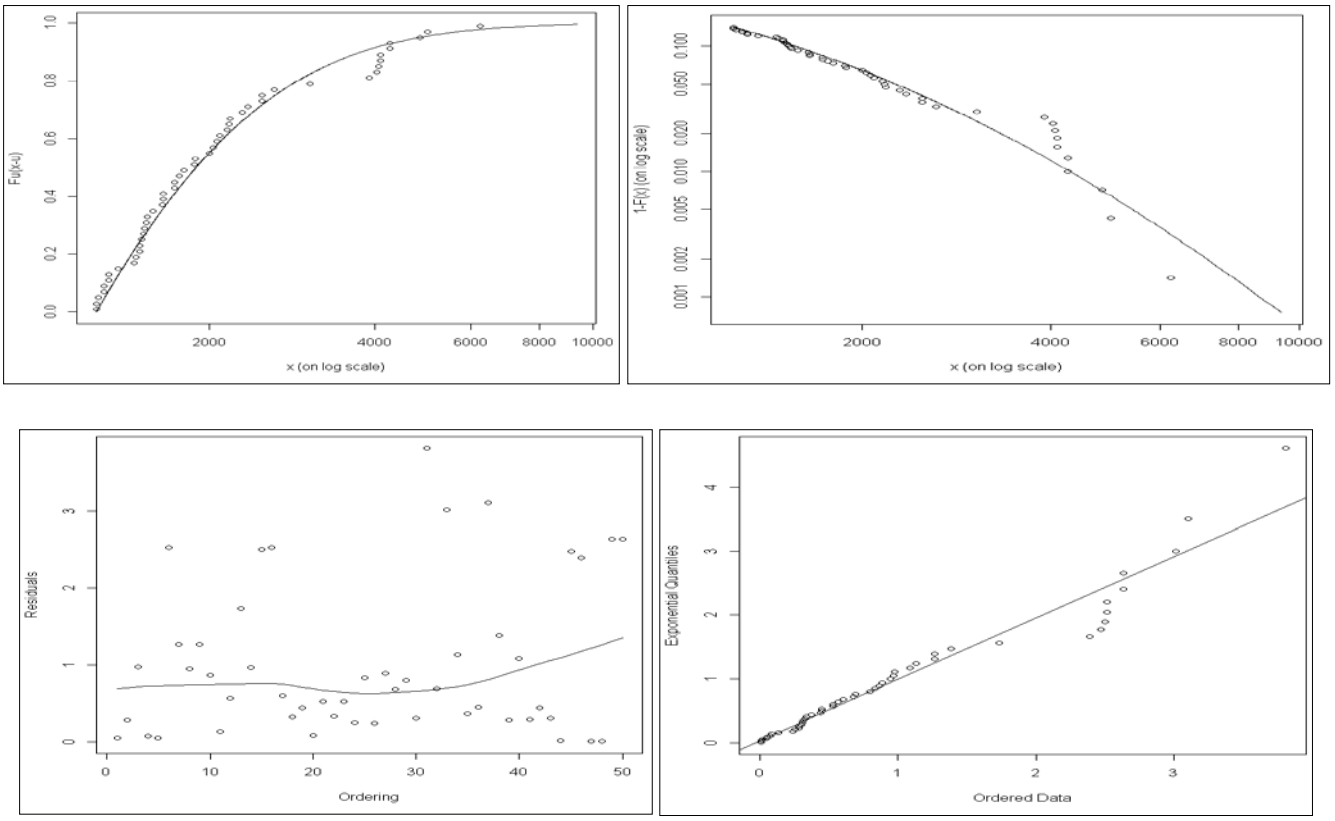

Figure 8- Excess distribution(top left),tail the underlying distribution(top right), a scatter plot of residuals(bottom left) and Q-Q plot(bottom right)for losses.

6 CONCLUSION

The aim of this paper has been to consider two alternative models, namely GEV and GPD for the loss of mining credit risk. These models provided better fit that the classical normality assumption due to the kurtosis and skewness of the loss data in mining credit risk. In addition, Extreme Value models are able to capture the probabilities of the extreme events in mining credit risk.

The financial loss data in mining credit risk was fitted with GEV the using block maxima approach and GPD using the POT method at various threshold values. Graphical analysis, such as diagnostic plots, Mean Excess plot and Q-Q plot have revealed that these models provide good depiction of our data and result quantifies the loss latent information in the portfolio of the credit section of a mining insurance company clearly.

It is hoped that the outcomes could benefit all stakeholders and principal decision makers in Iran's mining sector so that they can conduct more optimized management in their risk coverage operations.

REFERENCES

A.Tawn, J, 1987, An extreme–value theory model for dependent observations, *Journal of hydrology*, 101, pp.227-250.

Chinhamu, K, Huang, C-K, Huang, C-S, Hammujuddy, J, 2014. *South African journal of economics* (10.111/saj.12051), pp1-15.

Das, D, Kodra, E, R.Ganguly, A, Obradovic, Z, 2012. Mining Extreme Values: Climate and natural hazards.

Embrechts, P, I.Resnick, S, Samorodnitsky, G, 1999. Extreme value theory as a risk management tool, *North American actuarial journal*, 3, pp.30-41.

Gencay, R, Selcuk, F, 2001. EVIM: a software package for extreme value analysis in Matlab , *Studies in nonlinear dynamics and economics*, 5, 3, pp.213-239.

Gilli, M, Kellezi, E, 2006. An application of extreme value theory for measuring financial risk, *Computational Economics*, 27, pp.207-228.

< http://rc.majlis.ir/fa/law/show/99669>, viewed 2014.

L.c.da silva, A, V.de melomendes, B, 2003. Value-at-risk and extreme returns in Asian stock markets, *International journal of business*, 8, 1, pp.17-40.

L.Smith, 1986, Extreme value theory based on the r largest annual events, *Journal of Hydrology*, 86, pp.27-43.

Karmakar, M, Shukla, G, 2014. Managing extreme risk in some major stock markets: An extreme

value approach, *International review of economics and finance*, 35, pp.1-25.

K.singh, A, E.allen, D, J.Rober, P, 2013. Extreme market risk and extreme value theory, *Mathematics and computers in simulation*, 94, pp.310-328.

Manchini, L, Trojani, F, 2010. Robust value at risk prediction: Appendix, *Swiss Finance Institute Research*, pp.7-31

Martinez, L, 2009. Why accounting for uncertainty and risk can improve final decision-making in strategic open pit mine evaluation, *Project Evaluation Conference*, pp113-124.

Mcneil, A, 1997. Estimatin the tails of loss severity distributions using extreme value theory, *Astin Bulletin*, 27, pp.117-137.

Paul, S, Barnes, A, 2010. Application of extreme value theory to economic capital estimation, *Statistics for industry and technology*, 27, pp.329-336.

Penalva, H, Neves, M, Nunes, S, 2013. Topics in data analysis using R in extreme value theory, *Metodoloski zvezki*, 10, 1, pp.17-29.

Taveeapiradeecharoen, P, Chaitip, P, Chaiboonsri, C, Saosaovaphak, A, Chokethaworn, K, Sriboonchitta, S, 2014. The study of stock price return of petroleum and other liquids using extreme value theory based decision on belief function theory, *Procedia economics and finance*, 14, pp.595-604.

Risk Analysis in Mining Projects by using Fuzzy Synthetic Evaluation Technique

M. H. Basiri, A. Azad
Department of Mining, Faculty of Engineering, Tarbiat Modares University, Tehran, Iran

ABSTRACT Uncertainty is one of the most important features in mining projects. The extractive industries encounter with a high level of risk associated. Risk management plays a central role in this regards. Risk ranking, particularly when the number of risk factors increases, is an important part of the risk assessment process. In this research, the Multiple Attribute Decision Making (MADM) methods accompanied with the Fuzzy technique have been implemented for ranking the risks. A Fuzzy Synthetic Evaluation (FSE) approach is proposed as a new tool for this purpose. This method, as a tool in the multi-criteria decision making, has been adopted in many fields, including evaluating of reservoir water quality, health risk assessment, etc. This paper measures the risk index for each particular risk and evaluates the overall risk indices of mining projects.

Key words: Risk analysis, mining project, MADM, fuzzy synthetic evaluation

1 INTRODUCTION

Mining industry makes a major contribution to the world's economy as well as to the well-being of society as a whole. Uncertainty is one of the most important features of the mining projects. The investment in the project is heavily influenced by risk factors. Therefore the decision making for financing the projects needs to consider the risk management techniques.

The purpose of risk management is to reduce the impacts of these kinds of risks. Mining industry are accompanied with inherent potential of major accidents that may lead to injure or kill many people, damage the environment, cause serious loss of production and profit. Therefore it needs a particular consideration to implement the risk management.

Risk assessment aims to employ the effective management of risks, by identifying the followings:

- Which risks have more priority to be reduced, and the procedures to achieve this matter?
- Which risks need careful on-going management, and the nature of that on-going attention?

Risk management is the identification of project risks, assessing and prioritization of them, and adopt appropriate.

One of the central methods to identify and classify risks is the Risk Breakdown Structure (RBS).

Various risk assessment techniques are different in the way of combining the suitable aspects into one value. In mining industry many risk assessment techniques are performed, various risk assessment techniques are different in the way of combining the different aspects into one value.

In the mining industry, many risk assessment techniques are performed, such as; Using simulation analysis for mining project risk management (Chinbat, 2011, Takakuwa, 2009).

Risk assessment in the mining industry: Apply Management (Radosavljević and Radosavljević, 2009) and etc.

The complexity of mining projects is characteristic of these projects. Therefore, for risk assessment we need high quality data.

One of the researches done to risk analysis in ultra-deep scientific drilling project (Liu, Li, Wang, 2013), to overcome the

difficulties mentioned above proposes an analytic hierarchy process / analytic network process, AHP/ANP, based fuzzy synthetic evaluation (FSE) approach to evaluate risks in deep scientific drilling project.

Therefore, in this study, because access to high-quality data in the mining industry is problem, after pointing out the risks of the mining industry, we refer to fuzzy synthetic evaluation method.

2 IDENTIFYING RISKS

Identifying risks are the process of determining which risks may affect the project and documenting their characteristics (PMI, 2008).

This is perhaps the critical step of a risk assessment. A risk which is not identified cannot be actively managed. There are many techniques available for identifying risks, but none of them can be expected to identify all the risks.

In the mining industry, identifying risks are very difficult, because these projects have different situation from mine to other mine. When undertaking the first study of a mine in which there has been no previous formal risk assessment, any attempt to identify all risks in detail would result in an extremely long list, of which only the most severe could be analyzed, assessed and treated in the foreseeable future. The degree of detail in risk identifications should be appropriate to the objectives of the investigation.

The following sections are some of the major risks of the mining industry, the impact of each on the outcome of the project is important.

2 RISKS IN MINING PROJECTS

Due to uncertainties in the mining industry, this industry is constantly exposed to the critical state. One of the reasons is the lack of sufficient knowledge of the land situation.

On the other hand, external factors affecting the project are too risky. One of those factors is condition price and the market. Thus the conditions for the project will be positive or negative, if the conditions are good or poor. Risks of the mining industry are very important. If you do not pay attention to these risks, the failure of the project and will lose both time and money for companies. Therefore, for the readers understanding of the key risks in the mining industry are listed below.

Figure 1. Risks in mining projects

2.1 Risks in Exploration

Exploration is the initial stages of mining projects. At this stage of mining, there is a proven source of minerals and if to be valuable mineral, the output of this stage quantity and grade of mineral reserve and the distribution of grades in the region.

Thus it can be seen that the stage sensitivity is high. Because if done carefully down the steps, the other steps are will problem.

With incorrect exploration information, mining companies are suffered very high financial losses. Therefore, the exploration risks are component of major risk in mining projects.

2.2 Market Prices

One of the most important economic risks of the mining industry is the market prices risk.

Profitability of the company is variable with increase or decrease the price of products.

Profitability of the company is dependent to many factors; they are which most sensitive to price.

Thus, we can reduce the impact of this risk with forecast market conditions.

2.3 Political Risks

Mining companies operate in different countries with varying regulations on mining claims.

The regulations in some countries rarely change, but others have more volatile legal system.

So, even if a mining company has a great deposit, the capital to develop it and a favorable market, a change in the political environment where the deposit is located can throw a wrench in successfully getting the minerals to market.

Mining companies that operate in stable countries are preferable from a risk perspective, but mining companies go where the minerals are, so it is often a question of how much political risk an investor is reasonable.

2.4 Environment Risks

Where material is excavated from an open pit, is one of the most common forms of mining for strategic minerals. This type of mining is particularly damaging to the environment because strategic minerals are often only available in small concentrations, which increases the amount of ore needed to be mined.

Environmental risk is very important, in many cases; this risk is to stop the project.

2.5 Societal Risks

This risk depends on the social component, such as: Social conditions in the region, Social satisfaction of project activity, Increase or decrease in demand in the industry, Population growth rate, Rate of unemployment, Social stresses, etc.

2.6 Financial Risks

Financial risk is rooted in economic factors and the impact of these risks on the project is undeniable.

Some of them factors include: Inflation rate, Interest rate, Tax Law, Economic sanctions, World prices, Market conditions, Government subsidies, Energy and fuel prices, etc.

2.7 Management Risks

Due to extensive mining projects, the management of these projects is difficult.

In case of poor management, projects face many risks, projects which are likely to fail.

2.8 Workforce

With efficient manpower productivity in industry will progress. In this respect, it is important to identify the workforce risks for project success.

This risk depends on many parameters such as: motivating work, appropriate wage, good working condition, etc.

2.9 Technical

Due to the uncertainty existing in the mining projects, the design of each project is different from other projects. Therefore, requires a unique design. The design should be carried out optimized and economically, which depends on the ability of the design team.

3 ANALYSES RISKS

Risk analysis is “A systematic use of available information to determine how often specified events may occur and the magnitude of their likely consequences” (McKensey, 1979).

The complexity of mining projects is characteristic of these projects. Therefore, for Risk assessment we need high quality data.

One of the researches done to risk analysis in ultra-deep scientific drilling project (Liu, Li, Wang, 2013), To overcome the difficulties mentioned above proposes an

AHP/ANP based FSE approach to evaluate risks in deep scientific drilling project.

A FSE approach, as a tool in the multi-criteria decision making, has been adopted in many fields, including evaluating of reservoir water quality, health risk assessment, public–private partnership PPP project risk analysis, deep scientific drilling project, etc.

Therefore, in this study, because access to high-quality data in the mining industry problems, we refer to fuzzy synthetic evaluation method.

3.1 Fuzzy Synthetic Evaluation Approach

The procedures of fuzzy synthetic evaluation approach are as follows (Liu, Li, Wang, 2013):

(1) Determine the set of basic criteria/factors π= {f1, f2, ⋯, fm},
where (m) is the number of criteria.

(2) Determine the set of grade alternatives E= {e1, e2, ⋯, en},

where n is the number of alternatives. For example, e1=very low; e2 =low;
e3 =moderate; e4=high; and e5= very high. Grades will be given for each alternative, such as 1=very low; 2=low; 3=moderate; 4=high; and 5=very high.

(3) Determine weight for each criterion or factor W= {w1, w2, ⋯, wm}.

The weight of each criterion can be obtained by various approaches, for example, AHP/ANP, etc.

(4) For each criterion, an evaluation is a fuzzy subset of grade set, whose membership function can be established by the risk assessment group.

All the evaluations form a fuzzy $R = (rij)m * n$ evaluation matrix where rij is the

degree to which alternative ej satisfies the criterion fi.

(5) Fuzzy synthetic evaluation. The results of the evaluation are obtained by calculating the fuzzy composition of the weighting vector and the fuzzy evaluation matrix, where ° is a fuzzy composition operator.

D= R ° W

$$\mathrm{dj} = \min\left(1, \sum_{i=1}^{m} wi * rij\right), \quad dj \in D$$

The final evaluation denoted by D is also a fuzzy subset of the alternative set.

(6) Normalize the fuzzy evaluation vector and calculate the risk index according to

$$\mathrm{RI} = \sum_{k=1}^{n} dk * ek$$

The evaluation of each risk has been done now, and the risks can be rated by the numerical value of their risk index.

4 CONCLUSIONS

In the mining industry, many risk assessment techniques are performed; uncertainty is one of the most important features of the mining projects. In mining industry, identifying risks are very difficult, because these projects have different situation from mine to other mine.

The complexity of mining projects is characteristic of these projects. Therefore, for Risk assessment we need high quality data. FSE approach, as a tool in the multi-criteria decision making, has been adopted in many fields, Therefore, in this study because access to high-quality data in the mining industry problems, we refer to fuzzy synthetic evaluation method.

REFERENCES

B. R. McKensey, 1997. Risk Management Handbook for the Mining Industry, NSW ministry of industries Publitions.

Project Management Institute, 2008. A Guide to the Project Management Body of Knowledge (PMBOK).

Jialin Liu, Quanxi Li, Yuhan Wang, 2013.. Risk analysis in ultra deep scientific drilling project- A fuzzy synthetic evaluation approach, *International Journal of Project Management* , *31*, (*449–458*).

Undram Chinbat, 2011. Risk Analysis in the Mining Industry, Risk Management in Environment, Production and Economy, Dr. Matteo Savino (Ed.), ISBN: 978-953-307-313-2,

S. Radosavljević, M. Radosavljević, 2009. Rısk Assessment in Mining Industry: Apply Management, *Serbian Journal of Management 4*, 1, (91-104).

Andrew Beattie, 2015. The Biggest Risks Mining Stocks Face, © 2015, Investopedia, LLC.

http://web.mit.edu/12.000/www/m2016/finalwebsite/problems/mining.html

Soemon Takakuwa, Undram Chinbat, 2009. USING SIMULATION ANALYSIS FOR MINING PROJECT RISK MANAGEMENT, *Proceedings of the 2009 Winter Simulation Conference*

Risk Reduction of Minerals' Revenue in the Economy of Resource Rich Countries

N. Adibee, M. Ataee-pour
Department of Mining and Metallurgical Engineering, Amirkabir University of Technology, Tehran, Iran

ABSTRACT Some countries have a variety of mineral products and commodities which is the source of government revenue and foreign exchange. These revenues are essential for development of mineral countries. Because of some local and international changes in mineral markets, the revenue gained from minerals may be very variable. In order to plan for mineral revenue by governments, the risk of mineral revenue should be decreased. In this paper, minerals are considered as risky assets to apply the Modern Portfolio Theory (MPT). This method is able to decrease the risk of minerals' revenue by optimum diversification. As a case study, minerals production of Iran mining sector is studied. The non-linear model is solved by quadratic programming. To achieve the country's expected revenue the model determines the type and quantity of minerals to be produced. The findings show that the MPT model has an adequate potential to reduce the risk of government's minerals revenue compared with the current situation.

Keywords: Modern Portfolio Theory, risk reduction

1. INTRODUCTION

Some of the world's countries are rich in mineral resources. Mineral and energy commodities play an important role in national economic development (Dorian and Humphreys, 1994). Mineral resources are a gift of nature available to be developed, sold, and used to better the lot of a nation's citizens. Mineral production generates income and foreign exchange (if exported), can stimulate local economies through the local purchase of inputs, and can be the basis for downstream processing and manufacturing industries. Mining companies employ workers, who earn income, some of which they spend on domestically produced goods and services. Governments receive tax revenues from mineral production, which are available to fund education, health care, roads, electric-power supplies, and other forms of infrastructure (Eggert, 2001 and Power, 2007). Foreign direct investment, Balance of payments, Human capital development and social investment are other benefits of mineral industry. The mining industry makes a major contribution to the economy of mineral rich countries. It is a very important force in the global economy, occupying a primary position in the supply chain resources. Despite this fact, its role varies and greatly differs at national level from an economy to another (Dorin et al., 2014).

Minerals are essential in a large number of industries such as constructions, electronics, glasses, and metals. Mining is economically critical for millions of the world's poorest people with some 50 countries being significantly dependent on mining (ICMM, 2014). The Contributions of mining to economic of countries with low or middle national income, where mining brings significant direct economic benefits, are presented in Table 1.

Table 1. Contributions of mining to low and middle income economies in resource rich countries (ICMM, 2012).

Mining benefits	Share in the contries
Foreign direct investment (FDI)	60–90% of total FDI
Government revenue	30–60% of total exports
Government revenue	3–20% of government revenues
National income (GDP*)	3–10% of total national income
Employment	1–2% of total employment

*. Gross Domestic Product

Mineral market has uncertainty because more of them are trading in global markets. These lead to some fluctuations that are harmful effects on countries whose economies are based on mineral production. The volatility of mineral earnings makes it difficult for developing countries to plan investment because of the tendency to induce sudden swings in mineral revenues from the mineral sector. The aim of this paper is providing a method for achieving sustainable revenue for these mineral countries. The proposed method is based on Markowitz's modern portfolio theory that introduced in 1952.

This paper demonstrates how governments can use portfolio-optimization methods to determine a set of mineral productions that provides the minimum risk for a given level of revenue.

2. MODERN PORTFOLIO THEORY

The mean–variance framework pioneered by Markowitz (1952) has long been recognized as the cornerstone of Modern Portfolio Theory (MPT) and has been widely adopted and applied in both academia and industry (Yao et al., 2014). In the portfolio selection problem, given a set of available securities or assets, one want to find out the optimum way of investing a particular amount of money in these assets. Each one of the different ways to diversify this money between the several assets is called a portfolio. For solving this portfolio selection problem, Markowitz (1952) presented the mean-variance model, which assumes that the total return of a portfolio can be described using the mean return of the assets and the variance of return (risk) between these assets. The portfolios that offer the minimum risk for a given level of return form what it is called the efficient frontier. For every level of desired mean return, this efficient frontier gives us the best way of investing our money (Fernández and Gómez, 2007). MPT is a mathematical problem. According to Markowitz, investors could virtually eliminate their exposure to the risks unique to individual securities by choosing stocks that do not move precisely together. An investor is supposed to be risk-averse, hence he/she wants a small variance of the return (i.e. a small risk) and a high expected return (West, 2006). MPT is typically applied to common stocks. However, it can also be applied to bonds if there are risks with respect to default, exchange rates, inflation, etc. (Muller, 1987)
When assets are combined in a portfolio, the expected return is a weighted average of the individual asset's expected return. The weights are the proportions of these assets held in the portfolio. The portfolio risk is however more complex. The portfolio risk depends not only on the weights and the individual risks but also on the correlation between assets. The correlation coefficient, ρ, (also written as R^2) measures joint movements between the two variables, how they fluctuate together. The value can vary from –1.0 to +1.0 as illustrated in Figure 1. Although for most variables, the correlation coefficient falls somewhere between these two values. The risk is at its maximum when all correlations are perfectly correlated (+1). In this case, assets are substitutes for each other, which mean that as one of the variables increase or decrease in value, so does the other in exact proportions. When the correlation is -1.0, the return are perfectly negative correlated meaning that as one of the variables increase or decrease in value, so does the other in opposite proportions. The correlation coefficient for assets without any correlation at all is zero (Sandberg, 2005). Effective diversification is finding risky assets with as low correlation as possible. Zero correlation results in that the assets interact independently of each other. One asset's movement does not affect another asset's direction, consequently efficient diversification is accomplished. A compounded portfolio with an overall low

correlation is crucial for investors' that aims to diversify in order to eliminate the risk (Sharpe, 2000).

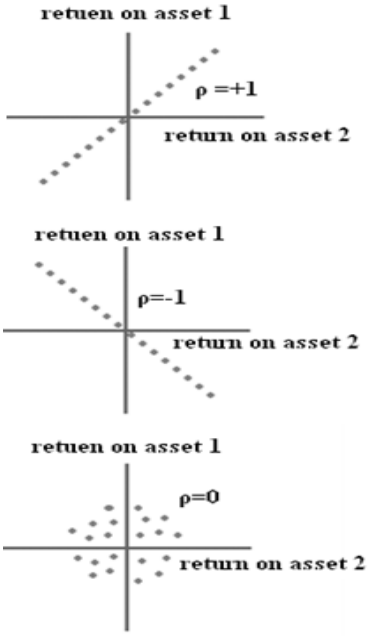

Figure 1. Correlation analysis of two assets' returns (Sandberg, 2005).

Figure 2 illustrates four concepts of portfolio. A feasible portfolio is any portfolio whose proportions sum to one. The feasible set is the set of portfolio means and standard deviations generated by the feasible portfolios; this feasible set is the area inside and to the right of the curved line. A feasible portfolio is on the envelope of the feasible set if for a given mean return it has minimum variance. Finally, a portfolio is efficient if it maximizes the return given the portfolio variance (or standard deviation). The set of all efficient portfolios is called the efficient frontier; this frontier is the heavier line in the graph (Benninga, 2008).

The mathematical form of standard Markowitz mean-variance model for the portfolio selection problem is as follows (Markowitz 1952):

$$\text{minimize} \sum_{i=1}^{N} \sum_{j=1}^{N} x_i \, \sigma_{ij} \, x_j \qquad (1)$$

Subject to:

$$\sum_{i=1}^{N} \mu_i x_i = R \qquad (2)$$

$$\sum_{i=1}^{N} x_i = 1 \qquad (3)$$

$$0 \leq x_i \leq 1 \ , i = 1, \ldots, N \qquad (4)$$

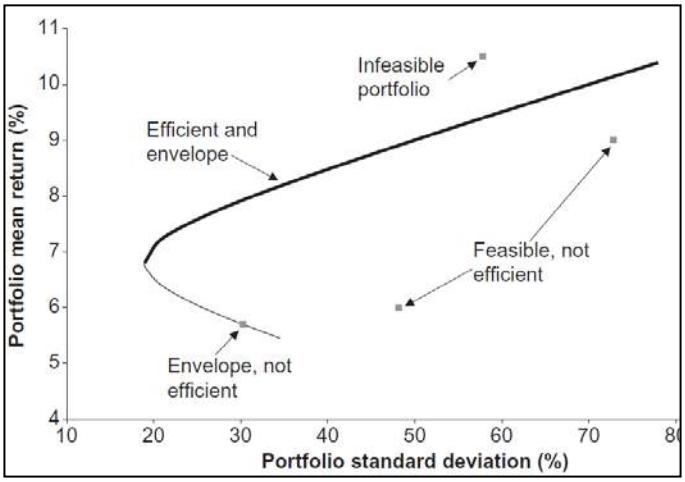

Figure 2. Efficient frontier and feasible portfolios (Benninga, 2008).

where N is the number of assets available; μ_i is the mean return of asset *i*; σ_{ij} is the covariance between returns of assets *i* and *j*; *R* is expected return of portfolio and x_i is the decision variable that represents the proportion of capital to be invested in asset *i*.

Equation 1 minimizes the total variance (risk) associated with the portfolio while Equation 2 ensures that the portfolio has an expected return of *R*. Equation 3 ensures that the proportions add to one. In Equation 4 the proportion held in each asset is between zero (minimum amount) and one (maximum amount). This formulation (Equation 1-4) is a quadratic programming problem and nowadays it can be solved optimally using available software tool. By solving the above optimization problem continuously with a different *R* each time, a set of efficient points is traced out. This efficient set called the efficient frontier and is a curve that lies between the global minimum risk portfolio and the maximum return portfolio. In other words, the portfolio selection problem is to find all the efficient portfolios along this frontier (Chang et al. 2009).

The portfolio's variance in matrix notation, can be written as

$$Var(r_p) = X.S.X^T \qquad (5)$$

$$X = [x_1, x_2, \dots, x_n], \quad X^T = \begin{bmatrix} x_1 \\ x_2 \\ \vdots \\ x_n \end{bmatrix},$$

$$S = \begin{bmatrix} \delta_{11} & \delta_{12} & \delta_{13} & \cdots & \delta_{1n} \\ \delta_{21} & \delta_{22} & \delta_{23} & \cdots & \delta_{2n} \\ \delta_{31} & \delta_{32} & \delta_{33} & \cdots & \delta_{3n} \\ \vdots & & & & \\ \delta_{n1} & \delta_{n2} & \delta_{n3} & & \delta_{nn} \end{bmatrix} \qquad (6)$$

3. METHODOLOGY

The proposed method includes a number of steps as follows:

- Identifying of mineral resources of the country
- Calculating of mineral returns and their variance-covariance matrix and mean
- Modeling of problem as a portfolio optimization problem
- Solving the model under quadratic programming
- Finding the optimize portfolio (minerals that should produce)

4. APPLYING MPT TO IRAN MINERALS MARKET

To evaluate the performance of the MPT model in minerals market, Iran mineral sector is selected as a case study. Iran produces a wide variety of minerals therefore its mineral sector has enough potential for using the proposed model.

Iran has more than 68 kind of mineral and total country reserve is 43 Billion MT, with an estimated value of 700 B US$. Iran Export of mines and mining industries was around 8 Billion US$ last year. The mines and mining industries employed more than 620000 employees in Iran. Market Share of mine and mining industries in Tehran Stock Exchange is more than 25% of the total value equal to 30 B US$ (IMIDRO, 2014)

The country was estimated to account for about 9% of the world's output of gypsum and pumice; more than 2% of the world's output of barite, feldspar, and sulfur; and more than 1% of the world's output of cement, industrial (or glass) sand, molybdenum, and nitrogen (USGS, 2012).

In accordance with the result of "WORLD-MINING-DATA" (Reichl et al., 2013), Iran is one of the most important mineral producers in the world, ranked among 15 major mineral-rich countries (Fig. 3).

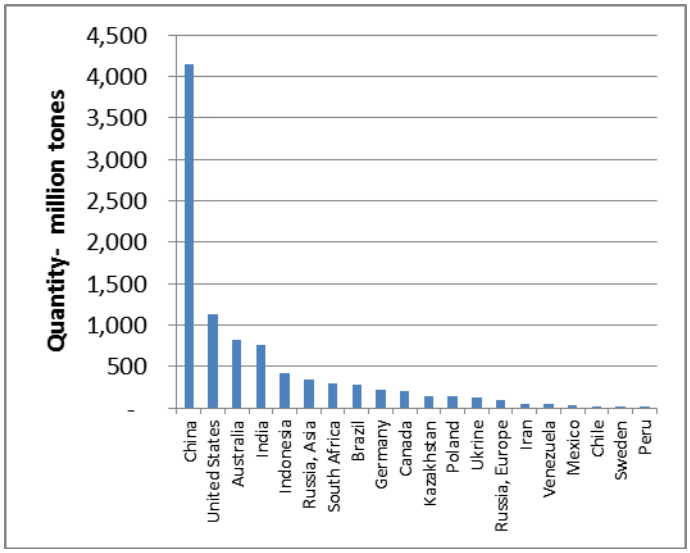

Figure 3. 20 largest producer countries 2011 (without oil, gas and construction minerals).

The mining sector's (includes exploitation and mineral processing) contribution to the Iran economy is only about 1% and employ 0.38% of the country's workforce with 84922 employees. Iran mineral production's value is presented in Figure 4.

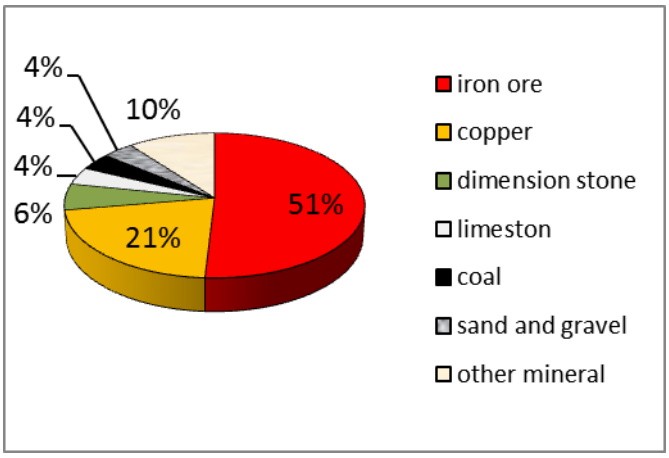

Figure 4. Iran mineral production's value in 2012.

According to the Figure 5, productions of six mineral that have highest value in Iran are include: iron ore, copper, dimension stone, limestone, coal, sand and gravel. The share of other minerals is about ten percent of the country's mineral production. A detail information of Iran minerals product

between 2012 and 2013 is presented in Table 2.

Table 2. Detail information of Iran minerals market in 2012-2013.

Mineral	Production of current year ton	Unit price 1000IRR/ton	Value of current year Production 1000000IRR/ton	Share in mineral production's value in current year- %
Co	2819792	1372	3867558	3.8
IO	39783479	1295	51536843	50.9
Cp	2022033	10719	21674794	21.4
S-G	94618407	40	3758876	3.7
DS	14276579	416	5935942	5.9
Ls	123116152	32	3926086	3.9
OM	63824875	165	10509737	10.4
Total	340461317		101209836	100

4.1. APPLICATION OF MPT

The MPT has been applied to the Iran mineral market for reducing of mineral revenue risk in national level. Iran mineral sector's historical data (related to Production and revenue) is collected from 2005 to 2012. This information was gathered from Iran Statistical Yearbooks. Then the minerals unit price is calculated from its annual income divide by production tonnage. Based on unit prices and using Equation 8, the minerals return is calculated (Table 3).

$$r_{i,t} = \frac{p_{i,t}}{p_{i,t-1}} - 1 \qquad (8)$$

where, $r_{i,t}$ is yearly returns of the mineral and metal i at the year t; $p_{i,t}$ is the price of mineral and metal i at the year t and $p_{i,t-1}$ is the price value of mineral and metal i at the year t-1.

The mean and standard deviation of minerals return are presented in two last row of Table 3. Covariance matrix also is presented in Table 4.

Table 3. Annual returns of Iran's mineral value per ton.

Year	Co	IO	Cp	Cr	S-G	DS	Ls	OM
2006	-0.05	-0.07	-0.10	-0.07	0.14	-0.13	0.51	-0.05
2007	0.35	0.66	0.07	0.62	0.51	0.24	-0.06	0.35
2008	0.27	0.16	-0.13	0.17	0.05	0.07	-0.06	0.27
2009	0.03	-0.11	0.15	0.12	0.03	-0.05	-0.01	0.03
2010	0.03	0.39	-0.05	0.05	0.13	0.31	0.14	0.03
2011	0.20	0.36	-0.13	0.47	0.11	0.08	0.21	0.20
2012	0.46	0.70	0.45	0.16	0.10	0.05	0.45	0.46
Mean (μ_i)	0.19	0.30	0.04	0.22	0.15	0.08	0.17	0.19
Standard Deviation	0.17	0.30	0.20	0.22	0.15	0.14	0.22	0.17

Co: Coal; IO: Iron ore; Cp: Copper; Sand and Gravel; DS: Dimension Stone; LS: Limestone; O M. Other Mineral

Table 4. Covariance matrix of the returns data (σ_{ij}).

	Co	IO	Cp	S-G	DS	Ls	OM
Co	0.031	0.043	0.019	0.022	0.009	0.007	0.003
IO	0.043	0.091	0.028	0.039	0.026	0.028	0.001
Cp	0.019	0.028	0.039	0.000	0.001	-0.001	0.011
S-G	0.022	0.039	0.000	0.050	0.023	0.014	-0.023
DS	0.009	0.026	0.001	0.023	0.023	0.011	-0.008
Ls	0.007	0.028	-0.001	0.014	0.011	0.020	-0.014
OM	-0.003	0.001	0.011	-0.023	-0.008	-0.014	0.048

The MPT model was solved using Matlab software. The efficient frontier curve and share of mineral in optimal portfolio are shown in Figures 5 and 6 respectively. Figure 5 explains the risk value of efficient portfolio in a given return. for example, if the portfolio return is 20%, then corresponding risk is 12%. Figure 6 describes that what kind of minerals are in the portfolio and how much are their shares. for example in the return of 20% , the share of coal, iron ore, copper, sand and gravel, dimension stone, limestone and other minerals are 1, 7, 0, 47, 0, 0, 45 respectively.

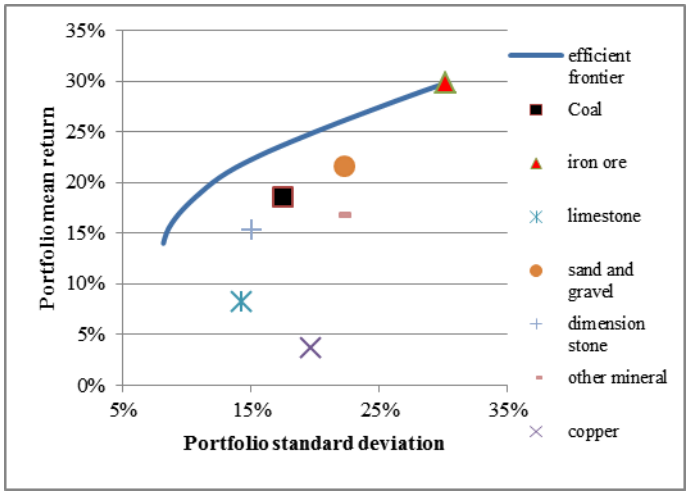

Figure 5. Efficient frontier of Iran mineral market

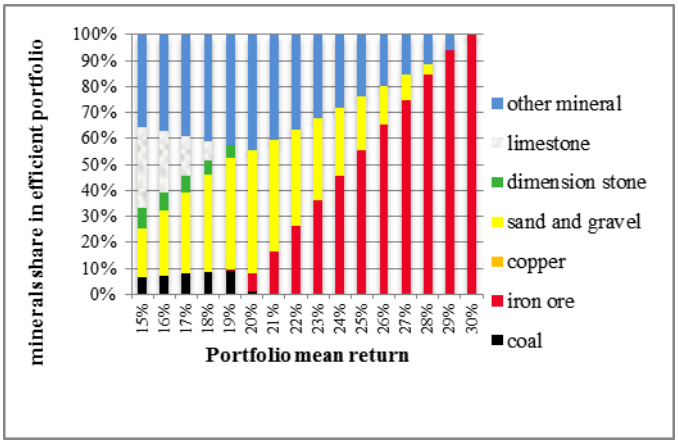

Figure 6. Share of mineral in optimal portfolios

5. DISCUSSION

Based on efficient frontier (Fig. 5), the efficient portfolios' return varies between 3.7% (as a minimum) and 29.8% (as a maximum) that is related to copper and iron ore return respectively. It means that the optimal portfolio returns (in terms of no short-selling ($x_i \geq 0$), which was applied in the model) is between the minimum and the maximum returns of minerals. On the other hand, the corresponding risk of the efficient portfolios varies between 8% and 30%. According to Table 3, the minimum risk of mineral is 14.3% that is related to limestone. Therefore, the risk of optimal portfolios can be less than the minimum risk of minerals.

To achieve the higher return in mineral market, one need to borne more risk. In low return (for example 12% in Fig. 5) risk is low (8%) but in higher return (for example 24%) risk is higher (18%). Generally, minerals with higher risk are contributed highly in the efficient portfolio. For example iron ore in Figure 6, with a risk of about 30% has the largest share in the optimal portfolios that their returns are more than 23%.

Figure 6 shows the share of minerals in efficient portfolio. According to the Figure 6, there is not any comprehensive efficient portfolio that contains all the minerals. For example in return of 24%, the share of mineral is presented in Table 5. The quantity of mineral in this return also, is presented in Table 5.

Table 5. Optimum portfolio of mineral production based on MPT – return 24 %.

Description	Ls	DS	S-G	Cr	Cp	IO	Co
Share in portfolio-%	0	46	0	26	0	0	28
Current year revenue - 1000000 IRR	101209836						
Share in portfolio-1000000 IRR	0	46327545	0	26344320	0	0	28537971
Unit price- 1000 IRR/ton	1372	1295	10719	40	416	32	165
Production - ton	0	35774000	0	658608000	0	0	172967400
Sum of productions-ton	867349400						

If the decision maker (government) decides to select the optimum portfolio in return of 24%, the mineral production in future year will be increase from 340461317 ton (Table 2) to 867349400 ton (Table 5). This is an inaccessible production because there is not enough capacity in the country for Multiplier production of some minerals. For example in this case (optimum portfolio in 20% return) the production of sand and gravel should be extended more than 10 times. It needs to capacity building that it takes time. Additional production of mineral also, may not use in the country or for export market. There another problem in the result o MPT model. Production of some mineral is stopped that it leads to the closure of mines and related factories. In this case (optimum portfolio in 20% return) production of coal, copper, dimension stone and limestone should be stopped.

For solving the issue, the minimum and maximum limits of production should be added to the model. Therefore the decision maker needs to study each mineral market and identify the upper and lower bound of each mineral's production level in the country.

To evaluate the performance of the MPT model in the Iran mineral market, we want to evaluate that how much MPT models reduce the mineral's portfolio risk. Based on information that is presented in Table 2, the expected return of Iran mineral market portfolio is:

$$E(r_p) = \sum_{i=1}^{N} \mu_i x_i = (0.185 \times 0.038 + 0.298 \times 0.509 + 0.037 \times 0.214 + 0.216 \times 0.037 +$$

$0.153 \times 0.059 + 0.082 \times 0.039 + 0.168 \times 0.104 = 20.44\%$

The variance is calculated based on given data and Equations (11-13):

$$[0.0382 \quad 0.5092 \quad 0.2142 \quad 0.0371 \quad 0.0586 \quad 0.0388 \quad 0.1038] \times$$

$$\begin{pmatrix} 0.0306 & 0.0429 & 0.0190 & 0.0224 & 0.0092 & 0.0070 & -0.0031 \\ 0.0429 & 0.0911 & 0.0276 & 0.0394 & 0.0255 & 0.0285 & 0.0013 \\ 0.0190 & 0.0276 & 0.0387 & -0.0003 & 0.0010 & -0.0013 & 0.0111 \\ 0.0224 & 0.0394 & -0.0003 & 0.0498 & 0.0231 & 0.0143 & -0.0232 \\ 0.0092 & 0.0255 & 0.0010 & 0.0231 & 0.0228 & 0.0105 & -0.0082 \\ 0.0070 & 0.0285 & -0.0013 & 0.0143 & 0.0105 & 0.0204 & -0.0144 \\ -0.0031 & 0.0013 & 0.0111 & -0.0232 & -0.0082 & -0.0144 & 0.0483 \end{pmatrix} \times \begin{pmatrix} 0.0382 \\ 0.5092 \\ 0.2142 \\ 0.0371 \\ 0.0586 \\ 0.0388 \\ 0.1038 \end{pmatrix} = 0.039$$

Its value is $var(r_p)= 0.039$ and standard deviation (risk of portfolio) is 0.197. The risk of portfolio at certain return (20.44%) is show in Table 6.

Table 6. risk reduction value in Iran's mineral market using MPT models.

	Return	Standard deviation (Risk)	Risk reduction
Current portfolio	20.44%	19.70%	
Optimum portfolio	20.44%	12.50%	36.54%

According to Table 6, the risk reduction value of minerals portfolio in MPT model is 36.54%. With accordance to the result, a significant amount of risk reduction shows the efficiency of this method.

6. CONCLUSIONS

There is a portfolio of minerals production in the mineral rich countries with variety of minerals that is sometimes necessary for governments' revenue. Because of some changes in the mineral market, achieving to the certain revenue may not feasible. The main objective of this paper is reduction of such risk with using diversification via MPT model. In this regard, the MPT model was used. This model was applied in Iran minerals market as a case study. Some important minerals with share more than 4% of total mineral income of Iran were selected. Remained minerals with less than 4% share are considered as "Other mineral" in the assets list. The result of MPT model was plotted in the efficient frontiers. In a certain return, the risk value of optimal portfolio was obtained from the model and compared with Iran's current mineral market portfolio. The result showed that using the MPT model might lead to decrease of government's return risk around 37% then to current situation. Because of limitation in the mineral production capacity in each country, the result of MPT is acceptable when the decision maker consider the mineral minimum production level. Using the MPT model, governments would be able to select an optimal portfolio of minerals to meet their requested revenue while complying with production restrictions. At the same time, governments seek to control the overall risk of the portfolio. The application of portfolio optimization problem is attractive because it is able to show the result of the mineral production strategy. The proposed method can provide an efficient and convenient tool for investors (governments or mineral international companies). With different risks, investors are able to find efficient portfolio based on a fixed amount of assets.

REFERENCE

Benninga S.,2008, Financial Modeling, Third Edition, Massachusetts Institute of Technology, London

Chang T.J., Yang S.C. and Chang K.J., 2009, Portfolio optimization problems in different risk measures using genetic algorithm, Expert Systems with Applications, 36: 10529–10537

Chang T.J., Meade N., Beasley J. and Sharaiha Y., 2000, Heuristics for cardinality constrained portfolio optimization. Computers & Operations Research, 27:1271–302

Dorin I., Diaconescu C. and Topor D.I., 2014, The role of mining in national economies, International Journal of Academic Research in Accounting, Finance and Management Sciences 4 (3): 155–160

Dorian J. P. and Humphreys H. B., 1994, Economic impacts of mining: A changing role in the transitional economies, Natural Resources Forum, 18 (1): 17-29

Eggert, 2001, Mining and economic sustainability: national economies and local communities, Mining, Minerals and Sustainable Development

(MMSD) project of IIED, Colorado School of Mines, US
Fernández A., Gómez S., 2007, Portfolio selection using neural networks, Computers & Operations Research, 34: 1177–1191.
IMIDRO (Iran Mine and Mining Industrial Development Organization), 2014, iran-mining-industry, www.numov.org/en/wirtschaftsforum-nah-und-mittelost/doc_download/1301-iran-mining-industry
International Council on Mining and Metals (ICMM), 2012, "The role of mining in national economies: mining's contribution to sustainable development", In brief, Accessed online: http://icmm.com/document/4440
International Council on Mining and Metals (ICMM), 2014, "Enhancing mining's contribution to the Zambian- Mining: Partnerships for Development", Chamber of mine of Zambia, Accessed online: http://icmm.com/document/7065
Jobst N, Horniman M., Lucas C. and Mitra G., 2001, Computational aspects of alternative portfolio selection models in the presence of discrete asset choice constraints. Quantitative Finance, 1: 1–13.
Markowitz, H., 1952, Portfolio Selection, The Journal of Finance, 7(1): 77-91
Muller H.H., 1987, Modern portfolio Theory: Some main Results, , Astin Bulletin, 8(2): 9-27
Reichl C., Schatz M. and Zsak G.., 2013, WORLD-MINING-DATA, International Organizing Committee for the World Mining Congresses, Volume / Heft 28 Vienna
Sharpe W. F., 2000, Portfolio Theory and Capital Markets, McGraw-Hill, New York.
Sandberg P., 2005, How Modern is Modern Portfolio Theory - A study of the approach to portfolio theory within recent real estate research, Master Thesis Number: 304, Department of Real Estate and Construction Management Section for Building and Real Estate Economics, Royal Institute of Technology
USGS, 2014, Historical Statistics for Mineral and Material Commodities in the United States http://minerals.usgs.gov/minerals/pubs/historical-statistics/
West G., 2006, An Introduction to Modern Portfolio Theory: Markowitz, CAP-M, APT and Black-Litterman, Financial Modeling Agency, http://www._nmod.co.za/MPT.pdf.
Yao H., Li Z., Chen S., 2014, Continuous-time mean–variance portfolio selection with only risky assets, Economic Modeling, 36: 244–251

Exploration Studies, Mining Geology and Geostatistics

3D Ore Model and Resource Estimation of Garpenberg North, Garpenberg Mine, Sweden

N. Fjellström
M.Sc Mining Engineer,Boliden, Skelleftea, Sweden

ABSTRACT This paper presents Boliden's methodology upon preforming modeling and resource estimation of the North ore body of Garpenberg mine. Programs used in the evaluation are Leapfrog Geo, Snowden Supervisor and Datamine. In 1997 the first drill hole for the North ore body was made and it intersected a Zn-Pb-Ag mineralization. The finding was hosted within a dolomitic marble in an area where barren hanging wall lithologies were expected. Follow-up drilling showed the Kaspersbo ore body to be a silicified dome like sub structure slightly offset from the northern limb of Garpenberg syncline; most likely structurally controlled. The mineralization within the dome structure is hosted within dolomitized marbles, pyroxene and amphibole skarns and altered footwall volcaniclastics. In 2013, as drilling progressed along strike to the east, it became apparent that what had initially been referred to as the northern extent of the Kaspersbo deposit is essentially the depth extension of the main North ore deposit.

Keywords: 3D modelling, resource estimation

1 INTRODUCTION

Mining of the deposits at Garpenberg, Central Sweden, began way back in the 13th century and the oldest letters patent still in existence for mining operations at Garpenberg were issued in 1354 by Swedish King Magnus Eriksson. This means that Garpenberg is one of the oldest mining areas in the world that is still operational. Boliden acquired Garpenberg in 1957 and exploration work has since resulted in a substantial increase in its ore reserves.

Garpenberg mine (Figure 1) is located near Hedemora, 157 km north-west of Stockholm, Sweden.

Today, Garpenberg mine produces complex ores containing zinc, lead, silver, copper, and gold, and it is this metal mix that has contributed to the areas favorable cost position. Successful exploration, coupled with modern technological development, has enabled an expansion of the Garpenberg mine. Thus, production will increase from 1.4 to 2.5 million tonnes of ore per year in 2015 and make Garpenberg one of the world's most cost-effective and modern underground mines.

Ore Reserves and Project Evaluation Division within Boliden has been assigned to create a resource block model for the North part.

The aim of the paper is to present the resource estimation methodology that Ore Reserves Division within Boliden applies for the resource estimates of Boliden mines and resources.

Figure 1. Location of the Garpenberg Mine

2 GEOLOGY

Regional setting; the geology of the Bergslagen region is characterized by successive generations of intrusive rocks that surround multiple inliers, the latter consisting primarily of felsic metavolcanics and metasedimentary rocks formed ca. 1.89 – 1.91 Ga. These supracrustal inliers can extend to 2km in depth and are often highly deformed and metamorphosed. Importantly; the majority of the many mineral prospects in Bergslagen are associated with these volcaniclastic successions, including Garpenberg (Figure 2) (Stephens *et al*., 2009).

The Garpenberg mine exploits a series of polymetallic deposits hosted within a NE-SW trending syncline which is *ca.* 15 km long and 7 km wide (Vivallo, 1985). The deposits are, for the most part, hosted along the same stratigraphic level within the predominantly rhyolitic sequence. This succession is considered to have been originally formed within a large, shallow marine depositional environment where pyroclastic flow material was abundant during multiple periods of volcanic activity. Bedforms and facies associations indicate that the thick footwall succession accumulated mainly below the wave base prior to a change in conditions that enabled the formation of the limestone unit that is intrinsically linked to all of the Garpenberg sulphide deposits (Allen, 1999).

This limestone unit is thought to represent a volcanic hiatus during which relatively stable and shallow sub-wave base marine conditions prevailed; facilitating the development of an extensive stromatolitic reef. The overlying lower hanging-wall stratigraphic package represents a later depositional environment characterized by uplift, exposure, erosion and shallow water environments, followed by subsidence to deep water conditions (Allen *et al*., 2003).

The Garpenberg ore deposits vary somewhat in style depending on their origin and subsequent location within the sequence, from massive in-situ mineralization associated with the altered Limestone unit found along the footwall – hanging wall contact, to tectonically remobilized ‘bands’ of ore that run sub-parallel to the dominant footwall foliation.

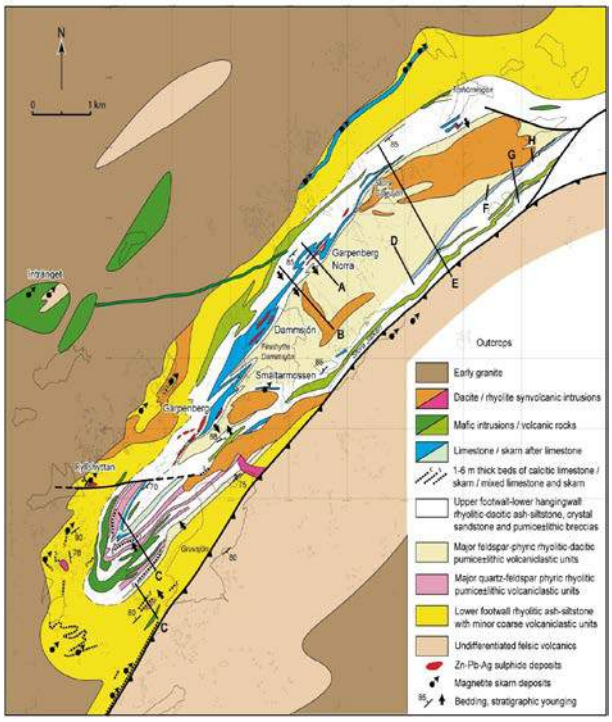

Figure 2. Geological map of Garpenberg region (Allen *et al.* 2003)

3 STRUCTURE

Regionally, the Garpenberg syncline has a complex geometry and it has been generalized (Allen, 1999) that the entire down dip extent of the Garpenberg North deposit is characterized by a series of doubly plunging to locally flat-lying parasitic folds.

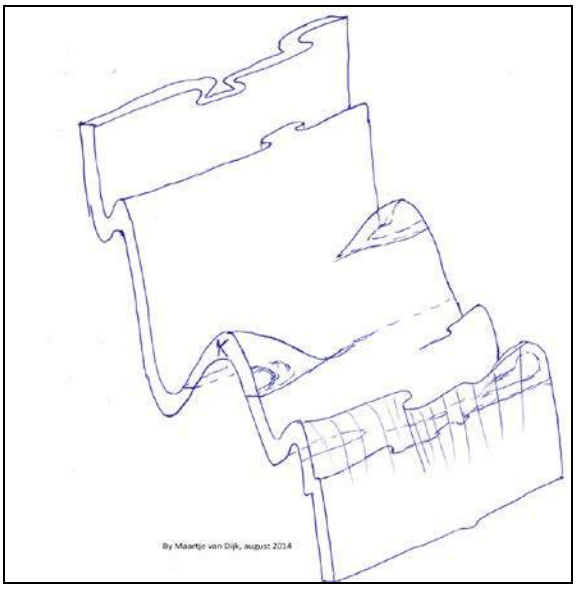

Figure 3. Sketch of the Kaspersbo structure (“K”) within northern limb of Garpenberg syncline (Maartje van Dijk, 2014)

One such structure is the Kaspersbo deposit structure is located immediately west of the Garpenberg North deposit between the 900m and 1150m level and is understood to be a dome-like antiform structure, stemming from the main northern limb of the syncline. (Figure 3) Accordingly, ore zones are broader on the upper reaches of the antiform where they are compressed and the 'double dipping' dome like structure results in significant thickening of the mineralized sequence along the lateral extent (Allen et al. 2003), making it an attractive prospect. Due to the proximity of Kaspersbo deposit to the western extent of the target 'Garpenberg North towards depth' mineralization, the two deposits are structurally interconnected between 990 – 1250m levels, which are difficult to interpret or define. In this study, the working 'boundary' between Kaspersbo deposit and north lenses was set at the eastern extent of the dome structure. This 'boundary' is evident in grade modelling whereby the altered limestone hosted 'in-situ' style mineralization that characterizes the Kaspersbo deposit has a consistently higher Ag grade than the Garpenberg north lenses (Figure 4).

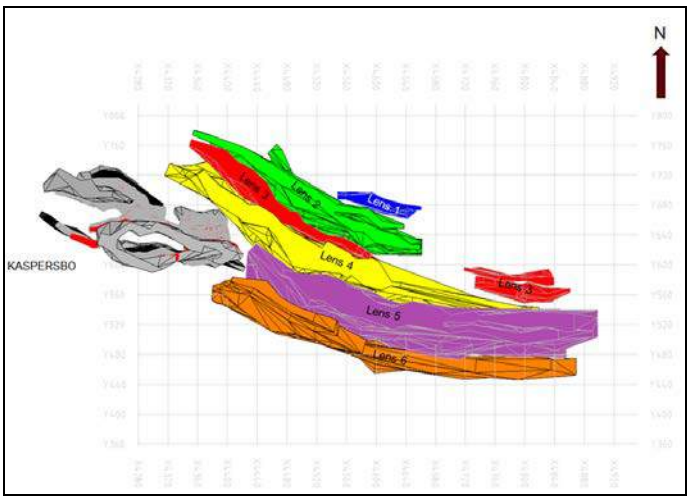

Figure 4. Garpenberg North lenses between 990-1250 z in top view

4 EXPLORATION DATA

4.1 Drilling

The majority of the drilling data utilized in this calculation was carried out by Near-Mine exploration during 2013 and 2014. The aim of this programme was to extend the 50 m by 50 m resource drilling of 'Main ore' ore deposit to the east of Kaspersbo from 4400Y to 4850 Y between 1000-1250Z from the 1080 exploration drift (Figure 4). The exploration programme consisted of 45 drill holes drilled during 2013, followed by further 16 drill holes in 2014, totalling 16600 meters of drilling over 10 profiles with a N-S orientation (local mine grid). This programme also included complimentary drilling on profiles 4400 Y, 4500 Y and 4550 Y with two oblique (local grid west) profiles from 4650 Y where further 'in-fill' data was required (Figure 4). The interpretation and digitization of geological sections and preliminary ore calculations were carried out in conjunction with core logging.

The recent programme of resource drilling was a structured follow-up of earlier drill testing that began in 1997 when the target area was tentatively explored from, 870 Z, 900 Z and 990 Z respectively. Latterly, in 2007 the western extent of the mineralization was tested from the 1080 Z exploration drift.

All cores have been drilled with T56 drill rods (hole diameter 56.3mm) except on the rare occasion where technical issues have required that smaller diameter rods be utilized over short intervals of perhaps 2-3 meters.

4.2 Sampling Data

All drillcore has been logged using WellCAD logging software. Core has been sampled so that any interval featuring visible sulphides or potential to host mineralization (based on lithological and / or mineralogical parameters) has been assayed. During the 2013 and 2014 exploration programme, ca. 83% of all core drilled was assayed. Core that remained unsampled was, for the most part, either barren footwall intersected prior to mineralization or barren hanging wall intersected when drilling had exited the system.

4.3 Surveying of Drill Holes

All drill holes that are longer than 100 m are surveyed with Reflex Maxibor. Maxibor is an optical method to measure changes in slope and direction.

4.4 Geophysical Surveys

No downhole geophysical surveys have been carried out on this drilling.

4.5 Logging and Coding

Logging was carried out digitally on WellCAD software. Prior to logging all core is measured to check for correct core length and any possible core loss. For a list of lithologies used in logging see under stratigraphy in chapter seven. Rock quality is recorded during logging by noting attributes which are known to affect operations at Garpenberg. Attributes found most to affect rock stability here include structure, mineral and rocktype. Primarily, logging of structural attributes with respect to delineating rock quality aims to record instances of crushed rock and schistocity, quantified by intensity. Any schistose rock type is per automatic included in this classification. Perhaps most importantly, certain minerals must be recorded as they are known to cause instability during drifting and mining operations; specifically talc and chlorite.

4.6 Sampling and Sample Preparation

During 2013 & 2014, *ca*. 5850 core samples were taken from diamond drill core that had intersected the study area. Sample intervals do not exceed 3.5 meters (minimum length of 0.85 m) and are determined by key geological factors such as lithological boundaries, alteration zones (where deemed relevant) and observed variations in sulphide content. If for example a barren dyke is intersected within a mineralized zone then it too is sampled so as to maintain data availability for subsequent modeling of the ore zone. Drill core is cut on site in Garpenberg and half core samples are sent for preparation, including drying, crushing, splitting and pulverizing. Pulps are sent for assay in Vancouver where they are analyzed for Au, Ag, Cu, Zn, Pb and S utilizing aqua regia digestion followed by atomic absorption spectrometry (Zn, Cu, Pb), leco furnace and Infrared Spectroscopy (S) and fire assay (Au and Ag).

4.7 QAQC System and Results

Check assays (on average one duplicate every 20^{th} sample) were analysed at laboratory for QAQC. The two assay results from a single pulp sample are monitored over time to identify for any variation in results. Blanks and Boliden in-house standards (reference) samples are also used as part of the QAQC routine. The assays from standards and blanks are regularly monitored for inconsistencies that may represent poor quality control at the laboratory, such as sample ‘mix up’ or contamination. The QAQC system has been developed to ensure that a proportional number of blank samples, standards are sent relative to the actual number of samples from each drill hole.

5 RESOURCE MODEL

5.1 Geological Interpretations and Mineralization

Geological Interpretations are based on geological knowledge over the area and geological logging data which has been gathered through underground diamond drillings.

Mineralised boundaries were drawn within the massive and semi massive sulphide.

In accordance with existing understanding of the ‘Main ore’ deposit, drilling has shown that it is dominated by tectonically controlled remobilized Zn-Pb-Ag (with weak inconsistent Cu-Au) stringer style mineralization. These stringers are often sub-parallel to dominant cleavage and lithological boundaries, and can therefore appear to be beds of sulphides (and have historically been interpreted as such). They

are understood to have been tectonically emplaced (Allen, 1999) after or late in the main F2 folding and as such; these zones are essentially mechanically remobilized from primary ore zones.

The 3-4 key mineralized zones run parallel to the dominant structural trends (WNW-ESE in the mine grid) and are sub-parallel to stratigraphy of the footwall volcaniclastics (modelled as Lens 1 – Lens 3). These lower footwall lenses are somewhat discontinuous 'along strike'. The most continuous and indeed broadest of the ore lenses are hosted within the upper footwall along the hanging wall contact (modelled as Lens 4 - Lens 6). In the west of the study area where these lenses boarder the Kaspersbo deposit, improved grades are observed. This is likely influenced by the increased occurrence of higher grade (increased Ag) in-situ style mineralization common along the boundary between the Kaspersbo anti-form structure and the adjacent footwall.

Generally, the footwall hosted remobilized mineralized zones are associated with strong silicification; however less common skarn associations have been observed (possibly a result of local reaction between the remobilizing fluids and localized carbonate occurrences). In the study area, structurally controlled zones of remobilized mineralization are observed to be broader and richer the nearer they are to footwall-hanging wall contact and associated altered carbonate hosted in-situ mineralization. Conversely, zones of remobilized mineralization located lower down in the footwall sequence are weaker and more inconsistent 'along strike'. Especially (and this may be significant) the further east they are from the Kaspersbo anti-form, it is of course unclear what influence the Kaspersbo structure has had (if any) on these remobilized stringers.

This has created a slight paradox in the study area whereby grades and thicknesses of the footwall hosted stringer zones become more prospective at depth (especially in the upper footwall lenses (Lens 5 – Lens 6). However, considering the geometry of the steeply dipping, undulating northern limb of the anticline, these remobilized zones have been assumed to have come from above (Z as opposed to stratigraphy) and would therefore become weaker at depth. That the most prospective lenses are those located within the upper footwall, nearest to or indeed on the actual footwall – hanging wall contact at depth may raise the possibility of an additional source / structure at depth (as yet untested by drilling).

East of Kaspersbo, the altered limestone horizon extends along strike from silicified dome at 4400-4500 Y (Figure 3 and Figure 4) and progressively diminishes as it is replaced by a skarn horizon which also follows the hanging wall-footwall contact. This continuous skarn horizon subsequently tapers out until 4600 Y where it essentially disappears. There are however, discontinuous relatively small skarn lenses at this stratigraphic level at 4800-4850 Y. This discontinuity along the contact could be a result of structural deformation and /or extreme alteration that has overprinted original lithologies. Generally, mineralized zones follow this diminishing trend eastwards, especially between 1000 – 1150 Z. East of 4700 Y the most prospective target is the upper footwall lenses Lens 5 and Lens 6 at depth (below 1150 Z); these are currently open along strike east of 4900 Y and at depth below 1250 Z.

Interpreting the ore distribution is not straightforward; although footwall hosted remobilized ore is a common feature of the Garpenberg mine, at the Garpenberg North main ore zone between 990 and 1250 Z it is evident that the most prospective zones are those located in the upper footwall nearest hanging wall contact. That these remain open along strike to the east of recent drilling and towards depth below 1250 Z suggests that the ore distribution is not controlled by stratigraphy alone, it is also possible the lenses are off-set along strike by lateral shearing. Observations along the stratigraphic contact show that host lithology does not appear to affect the presence/absence of the ore in any significant way.

In addition, occurrences of disseminated Willemite (Zn2SiO4) have been observed within the footwall sequence; such disseminations are however inconsistent and do not appear to be directly associated with the remobilized massive sulphide mineralization.

5.2 Estimation and Modeling Methodology

5.2.1 Zn – Ag grade shells

Ore boundaries have been interpreted based on massive and semi massive sulphides in combination with Zn and Ag analyses. Zn and Ag grade shells (Figure 5 and Figure 6) have been created in Leapfrog Geo software to understand the difference in different domains visually. Before interpretation, each domain has been checked against geological consistency, single grade population and single continuity orientation. Domains have been further studied statistically in Snowden Supervisor.

Based on geology and grade shells, 6 different mineralized domains have been interpreted.

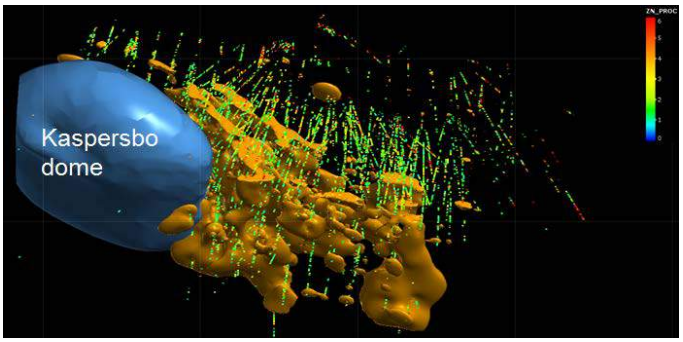

Figure 5. Zn grade shells (Zn>2%) in isometric view, Leapfrog Geo

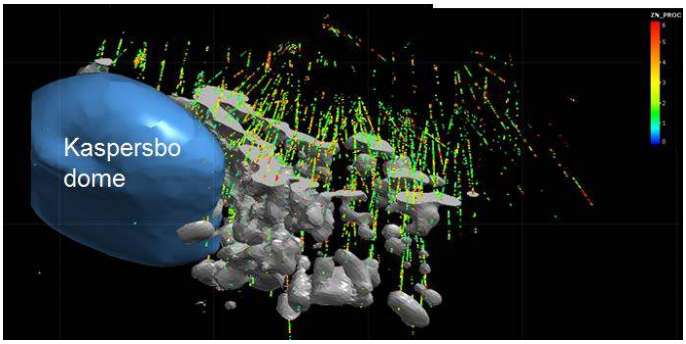

Figure 6. Ag grade shells (Ag>70ppm) in isometric view, Leapfrog Geo

5.2.2 Assay statistics

Geostatistical studies have been completed in Snowden Supervisor in order to understand the high and low grade tendencies and relation between geology and the data in Main ore region.

In addition, composite length analysis, top-capping and variogram parameters for Kriging were also analyzed in Snowden supervisor.

5.2.1.1 Composite length analysis

To be sure about the coverage of the sampling, a log histogram over different analyzed section lengths has been plotted. In the histogram, dominating length was observed around 3m which was corresponding 90% of the analyze lengths. The effect of change in composite length on zinc and silver grades has also been studied.

Assay mean and variance for each element has been calculated in Datamine and plotted in Excel. Later on, the compositing has been performed by using 10 different composite lengths and length weighted means and variances have been calculated for each analyzed section length and added on the graphs.

5.2.1.2 Declustering and compositing

For declustering, decluster by cell weighting technique has been used. By this technique, the data is covered by a grid and each sample in the data has a weight according to number of samples within each cell in the grid. This technique is used to decrease the effect of a high grade sample on mean grade.

By compositing, sample grades have been weighted in every 3m.

5.2.1.3 Box-and-whisker plot

6 different domains within the Main ore zone have been compared with Box-and-whisker plot in order to see the grade trends by compared to each other.

5.2.1.4 Top-capping

Extreme grades in a data set can cause wrong grade calculation. Since high grades of Au, Ag and Pb have been observed in North lenses, these high values have been re-set to the top capping values. Top capping values for Au, Ag and Pb have been decided according to as follows:

1. Data has been declustered.
2. All data has been plotted for each domain in a log-scale histogram
3. The points where the high grade tail starts in log scale histogram has been selected as top capping values.
4. The selected values have been compared with previous production grades of the mined out areas in the same ore body.

5.2.1.5 Variography

The North ore body consists of 6 lenses. Before the evaluation of the continuity in the domains, hangingwall and footwall lenses have been grouped. With the variography the direction of the lowest difference in grades for the longest distance is set for strike, dip and plunge.

In this study, the grade continuity of the all grades (Au, Ag, Cu, Zn, Pb, S) within ore body have been analyzed. The directions of maximum continuity for Lens 1, 2 and 3 have been chosen according to Lens 4 and zinc element as a reference. For Lens 5 and 6, different continuity parameters have been chosen due to the change in continuity.

5.2.1.6 Kriging neighbourhood analysis

KNA calculations have been carried out in Snowden Supervisor to decide the block size, minimum and maximum number of closest samples, the size of search ellipse and block discretization.

In Supervisor, many different block sizes have been tested and the one which gave the highest kriging efficiency and slope of regression has been selected. The same procedure is also applied for the other parameters.

It has been checked that the block size is neither too small nor not too big for the model. As a rule of thumb, the block size should not be smaller than half of the drill spacing.

Orientation of the search ellipse has been arranged according to variography. The continuity and the geology have been taken into consideration for both the orientation and the size of the search ellipse.

In addition to minimum and maximum number of nearest samples, maximum number of samples per drill hole has been set as a controlling parameter to avoid too many samples from a same drill hole come into the estimation of a block.

Model has been estimated by ordinary Kriging.

5.3 Model Validation

Model has been verified by visual and statistical validation methods. Model validation has been made to understand if the created model is a reflection of a drill hole data.

5.3.1 Visual controls

Visual validation for Zn, Ag and ore value of the blocks have been done in Datamine by comparing the grade of composites with block grades section by section in every 6m. Zn grades comparison is shown in Figure 7.

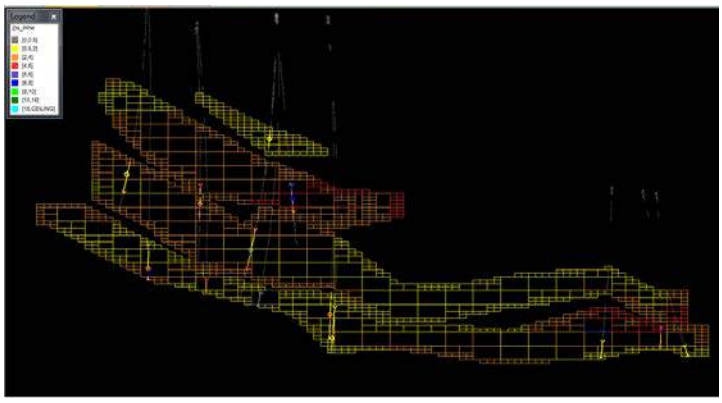

Figure 7. Comparison of Zn grades in block model and composites at level 1230z, Datamine Studio3.

5.3.2 Statistical controls

Statistical controls have been carried out in Snowden Supervisor software. First of all, trend plots have been created for each direction as Easting(x), Northing (y), and RL (z) for Ag and Zn (dominating grades within the ore body) grades in block model and composites. The block and composite grades have been compared to see whether both of them are following the same trend in easting, northing and depth.

In Figure 8, validation of Zn grades by Easting is shown.

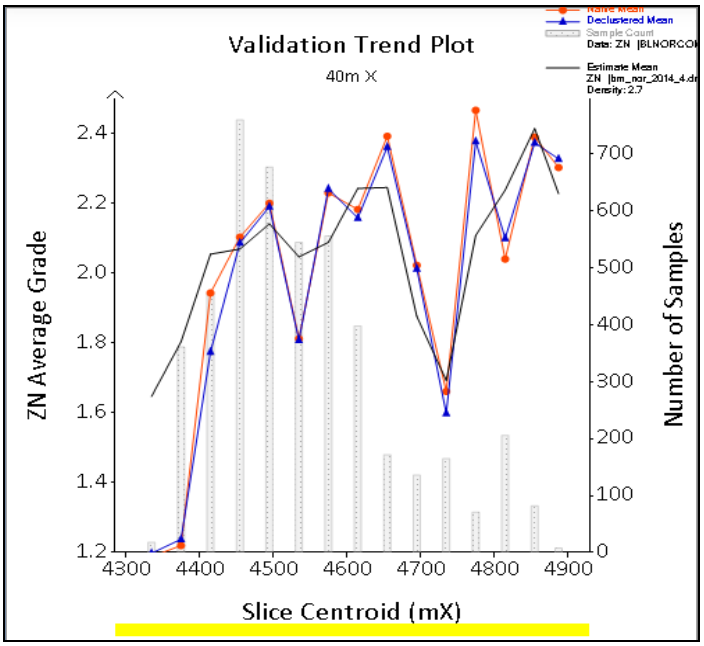

Figure 8. Validation plot for Zn by Easting (X)

Top capping has also been checked if it was too hard on the estimated grades.

The average block grade and the average grade of the drill hole data set has been compared for each domain.

In the analysis the following has been observed:

Excessive peaks in drill hole/composite grades have been smoothed out in the block model. Areas with a limited number of composites show less correlation between the composite grades and the block model grades. In some areas, the block model grades seem high due to a small number of high grade composites affecting a relatively large number of blocks. Moreover, Zn and Ag grade of estimates have been compared with composite grades in Statistical comparison table in Snowden Supervisor and it has been verified that the difference was below 5% (Figure 9)

Statistic	SampleData	DeclusteredSampleData	BlockData1(TonnageWeighted)	BlockData1VsSample%Diff	BlockData1VsDeclustered%Diff
Points	4610.00	4610.00	205251.00	4352.30	4352.30
Mean	2.02	2.04	2.09	3.46	2.33
Std Dev	1.83	1.85	0.94	-48.66	-49.28
Variance	3.35	3.43	0.88	-73.64	-74.28
CV	0.91	0.91	0.45	-50.38	-50.44
Skewness	2.39	2.97	21.93	818.77	638.98
Kurtosis	14.06	24.80	4637.18	32888.79	18597.62
Log Mean	0.41	0.39	0.62	49.91	57.34
Log Variance	1.05	0.95	0.28	-73.57	-70.91
Geom. Mean	1.51	1.48	1.86	22.92	25.34
Log-Est. Mean	2.55	2.39	2.13	-16.43	-10.59
Maximum	24.94	24.94	10.96	-56.05	-56.05
75%	2.79	2.79	2.65	-5.02	-5.02
50%	1.66	1.67	1.99	19.88	19.16
25%	0.74	0.79	1.43	93.24	81.01
Minimum	0.00	0.00	0.00	0.00	0.00

Figure 9. Snowden Supervisor statistical comparison table for Zn

6 CONCLUSION

In this paper, the methodology of resource estimation that Boliden follows has been described and Garpenberg mine has been selected as an example for this study. Modelling is maybe the most important step to interpret the geology in numbers. New tools and technologies contribute a lot for the accuracy of resource estimation as soon

as the geology and the input data are understood and used together properly.

REFERENCES

Allen, R. (1999) *Garpenberg Norra Zn-Pb- Ag deposit, Bergslagen, Sweden: Construction and Interpretation of a Geological Cross Section at 4540 Y*. Internal Report Boliden, *GP 99 033*

Stephens, M.B., Ripa, M., Lundström, I., Persson, L., Bergman, T., Ahl, M., Wahlgren, C., Persson, P. and Wickström, L. (2009) *Synthesis of the bedrock geology of the Bergslagen region, Fennoscandian Shield, south-central Sweden*. Sveriges Geollogiska Undersökning, *Ba 58, 260pp.*

Allen, R., Bull, S., Ripa, M. and Jonsson, R. (2003) *Regional stratigraphy, basin evolution, and the setting of stratabound Zn-Pb-Cu-Ag-Au deposits in Bergslagen, Sweden*: Final report for SGU-FoU project 03-1203/99, 80 pp.

Advancing Exploration Projects to Production: Critical Inputs for Success

A. Ebrahimi
Principal Consultant at SRK and Adjunct Professor at UBC, Vancouver, Canada

J.P. Siddorn
President, SRK Consulting (Canada) Inc

ABSTRACT "Easy mining" doesn't exist anymore. It takes years to build a mine. A mining project goes through a series of expensive phases before generating a positive cash flow. Exploration is the most uncertain and risky phase of developing a mine. Having a well-defined plan (road map) will increase the success rate of exploration companies. In modern exploration activities goals goes beyond defining only resources. Geotechnical, metallurgical, environmental, water, power, logistics, community and political issues are all examples of additional data collection and assessments that exploration companies need to cover. These are the pieces that must be put together to have a clear picture of potential mine.

Not all exploration activities lead to constructing a mine. Early diagnosis of major problems helps to reduce the general risk of investment as well as reducing the time of developing a mine. This paper highlights the issues and information important to advancing exploration projects to production.

Keywords: Exploration, schedule , planning

1 INTRODUCTION

Mining is a temporary use of land. It starts with a green field, extracts the good materials from the ground and leaves behind a reclaimed land that can be used again. As it can be seen in Figure 1 during its "life" a mining project evolves by going through a number of lengthy development stages: exploration, evaluation, construction, operation, and closure. Although in consequences, exploration, evaluation and construction activities have many overlapping areas.

Mining, in general, is a risky business because it deals with unknowns and uncertainties to the end of its life. This most often produce complications. As the first segment in the chain of mining activities, exploration companies take most of the risks. Deposits are mostly buried, generally of unknown shapes and have to be sampled by expensive methods such as drilling. There are many other uncertainties and unknowns such as marketing, environmental and political issue that affect the destiny of a project. In addition to geology these types of risks are also need to be measured in exploration stage.

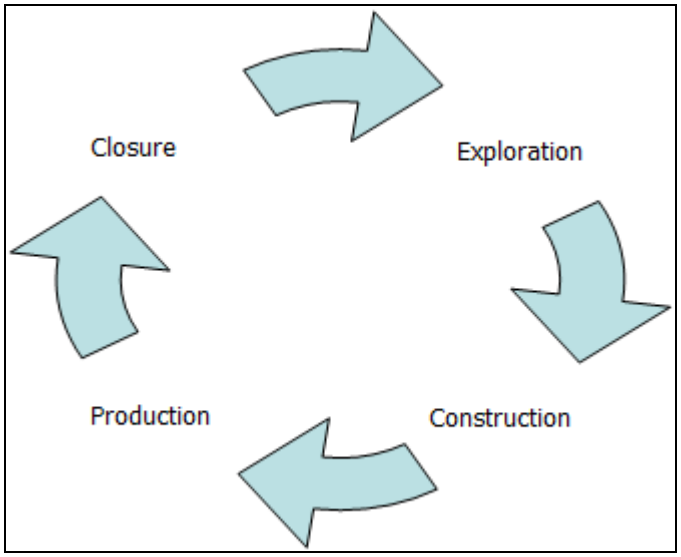

Figure 1. Mine development stages.

Exploration is art and science of collecting, analyzing and interpreting data. It is a business. Like any other business it spends

time and money and it is expected to return profit.

Not all exploration activities lead to constructing a mine. The success rate for exploration projects vary for different fields and operators. It is between 1 for each 200 in brownfield to 1 for more than 3000 in greenfield projects (Lord, et al.). In past several researches tried to explain the low success rate in mineral exploration and finding a way to improve it. For example Natural Sciences and Engineering Research Council (NSERC) of Canada in 2013 granted $5.1M the initiative researches aiming to increase the success rate of exploration projects in Canada.

Many researchers used statistics and probability distributions to understand and explain the exploration success rate (Kreuzer, et al.). Although exploration activities are associated with uncertainties however it is not entirely a game of cards. There are not many researches and studies that are focused on exploration planning (Mackenzie B.). Exploration planning can improve the economics of exploration activities. If implemented well, collectively, it can increase the success rate of exploration companies.

This paper tries to emphasize on the importance of exploration planning. It presents a generic work flow for activities in development stages and also discusses the importance of having an exit strategy for every exploration project.

2 MANAGING EXPLORATION COSTS

To be successful, every exploration company must overcome several challenges including financial, permitting, community relations, environmental, staffing and logistics. Among these hurdles funding a project can become the biggest challenge for most exploration companies. In addition sometimes exploration companies have limited access to skilled workers, expertise and equipment. For these reasons, managing the limited resources available is one of the most important keys exploration companies need for success.

A common approach to managing exploration costs is to do the work in sequences. The usual steps involved in developing mining projects are: scoping study/preliminary economic assessment (PEA), preliminary feasibility study (PFS), feasibility study (FS), and engineering/procurement (EP). As work progresses, the cost of development increases which usually results in a better understanding of the project. Due to knowledge improvements at every step of development, more accurate decisions can be made about the future of the project. It is expected that the results of a feasibility study will be more reliable than the results of a scoping study.

Although the sequencing of mine development is well accepted among the industry, its details and dynamics (exploration planning) are still not well defined and formulized. The main reason for this is the complexity of mining projects. It is impossible to copy the development plan of a mining project and simply apply it to any other deposit, even if they both look similar. Every project needs a well-defined and detailed individual development plan.

The main goal of sequencing exploration and mine development into stages is to control costs and lower the investment risk. Only the few projects that demonstrate positive outcomes at each stage can go through all these stages. Most projects will be stopped after showing signs of negative outcome or weaknesses. In the early stages of work, such as the scoping study when information is limited, it is difficult to make an accurate project evaluation hence using people that have both extensive experience and general business vision helps to reduce unnecessary iterations. Figure 2 shows the development stages of a mining project and the expected accuracy for each stage. Accuracy of studies varies from +/- 50% in scoping level to +/-10% for feasibility studies.

Based on the success rate of exploration projects figure 2 also suggests the minimum number of projects that exploration companies need to undertake to get to a

producing mine. A company sometimes may need to investigate 100s of grass root projects before it decides to spend millions of dollars in some of the promising ones. A project should NOT advance to higher stage if it doesn't demonstrate reasonable prospects for success. Advancing a project to higher level requires an honest internal due diligence and evaluation.

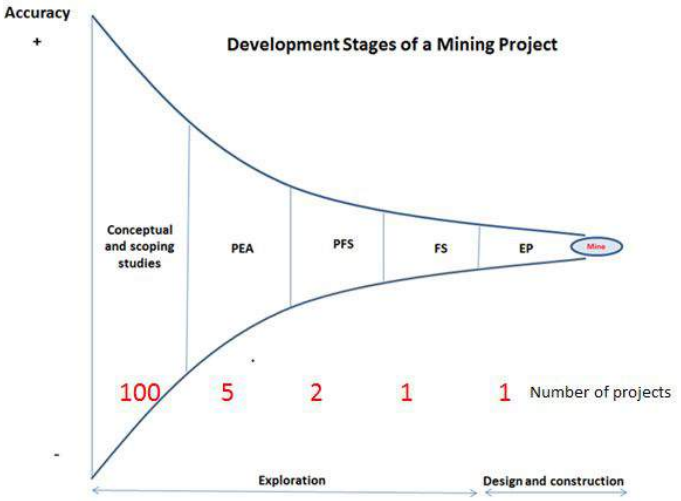

Figure 2. Development stages of a mining project

Exploration costs can vary a lot based on the location of the site, topography, complexity of geology and mineralogy. Therefore it is hard to formulize a budget that can be fit to all projects. To start an exploration project (prospect stage) probably less than a million dollar would be enough however to get the project to a PEA level at least several millions of dollars need to be spent including some initial drilling. Sometimes this may exceeds 10 million dollar. To reach to a PFS/FS level tens of millions of dollars need to be spent for drilling, tests and studies. Figure 3 shows approximate expected costs of developing a medium size base metal mine in today's market and in a well-developed mining region. As it can be seen by the cost of a FS one can cover at least 4 PEA. To reduce the risk of investment exploration companies need to adequately justify advancing each project to higher level.

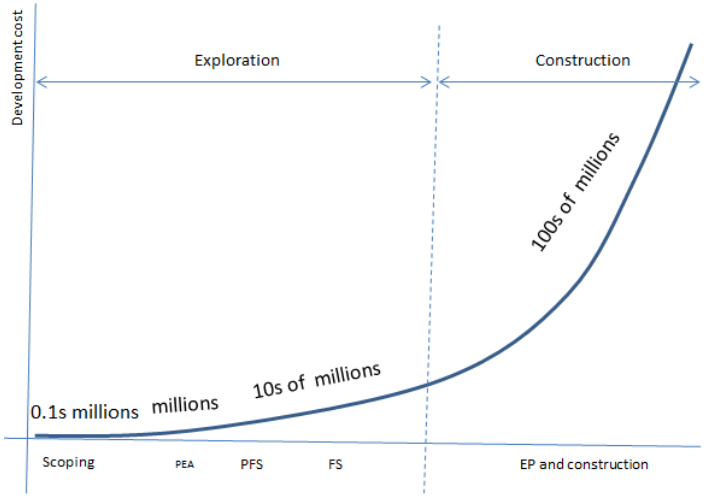

Figure 3. Approximate expected expenditure of a developing mining project

3 DATA COLLECTION CHECK LIST

To properly assess the value of a project a mineral exploration company needs to gather different pieces of data and information over stages of exploration. These fairly diverse pieces of information are collected not only from the ground but also from sources such as local communities, government and market.

Collecting data and information takes time and is costly. To control the cost and to be more efficient information should be collected according to a plan and in a sequence. Not all the information needs to be collected in first stage. Each step must be based on a thorough analysis of data collected in previous stage. For example it is just after geophysics and surface geology that a diamond drilling program should be developed. Even then drilling should start in large grids and in certain areas. Afterward based on the results of the first round of drilling, exploration can be followed with denser drilling and only in a few targeted zones.

Another example is geotechnical drilling that is usually done in more advanced phases when dimensions of the pit and the deposit are relatively known. Or it is premature to perform detailed tailing storage or waste dump design when the scale of mill operation is not known.

For every exploration project it is helpful to develop a check list of the information that is required to be collected in different

phases. Table 1 shows a simple example for data collection check list. In many exploration projects this table can become very sophisticated.

Table 1. Data collection check list,

Data collection task / studies	PEA	PFS	FS
Diamond drilling	✓		
In-fill diamond drilling		✓	✓
Geotehcncial drilling			✓
Metallurgical sampling and tests		✓	✓
Water sampling		✓	✓
Comunity engagement	✓	✓	✓
Strategic planning	✓	✓	✓
…			

4 MINING STUDIES WORK FLOW

Instead of focusing on a single project, exploration companies can be more successful if they work on a number of properties or interests. The properties must be prioritized in order to get investment funds, but the priority list must be dynamic and responsive as the values of the properties will change over time as exploration expenses are incurred and project data is collected.

As mentioned before it is important to realize that most properties have little chance of being developed as a producing mine in the near future. Besides the quality and quantity of the deposit itself, there are many other factors, such as environmental or community issues and poor infrastructure, that could bring a project to a halt. When project studies are planned and managed well, such issues can be detected in the early stages of development. This can help exploration companies allocate their limited resources better and focus on projects that have a better chance of progressing further into development. Making decisions about whether to continue working on a property, or to stop working and shift the focus to other projects, should be the top priority for management team of exploration companies. Shutting down work at a particular property doesn't mean the end for an exploration company.

Every exploration company has the potential to own a mineable deposit, or even to become a producing mining company, if it learns how to plan for it. In order to get there, a well-defined road map must be developed right from the initial step. Figure 4 shows the generic work flow for development stage of a mine. As it is implied from model in Figure 4 an exploration project goes through similar round of activities but in different level in its life. In each level the time and money we spent on the project increases. As a result it is expected to have higher level of accuracy (lower risk) in assessing the project as it goes forward.

Planning is the first and essential activity in all levels of exploration. In its core, an exploration road map includes three components: a work plan (budget and schedule), data collection (execution), and assessment.

The budget must be focused on only one phase and be as detailed as possible. Every expenditure must be well justified. Where, why, and when to spend the money, are the questions that need to be systematically investigated and answered. Every expense must help the company get closer to its target otherwise, the spending is a waste. In exploration planning we must keep in mind that the biggest question in early stages of exploration is whether to proceed to next phase or not.

The schedule must be practical and include all realistic parameters such as logistics, weather delays, and third parties' schedules (such as the availability of mineralogy laboratory). The tasks in a mining project need to be prioritized, because advancing in one task without completing its prerequisites may waste time and money. For example and as mentioned before, it is important to understand when is the right time to start geotechnical drilling or taking metallurgical samples.

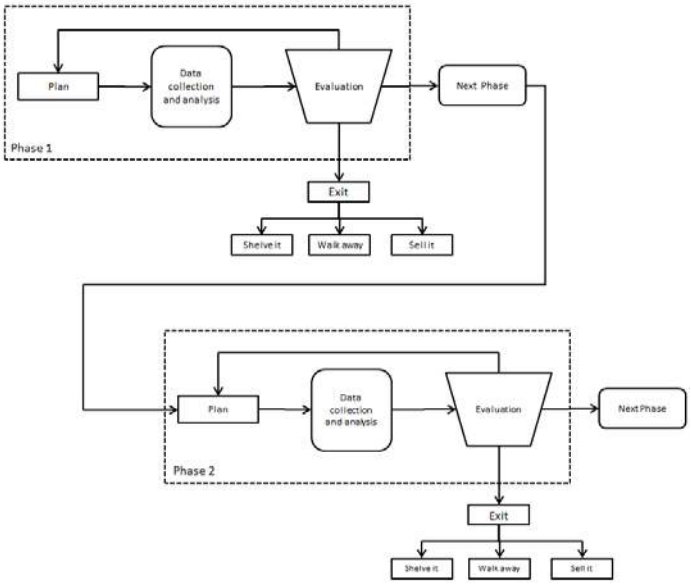

Figure 4. Generic work flow for a mine development phase

At the end of every phase, the project must go through an intensive evaluation. The evaluation must answer the crucial question: should the project be stopped or can it move forward to next phase? Based on the results of the evaluation there are three possibilities for the project:

a) Progress to the next phase
b) Redo the current phase
c) Stop the project

A positive result requires a more advanced investigation into the property. Every phase will point to a list of more specific questions that must be addressed in subsequent phases, where the evaluation process will be applied to a higher level of accuracy. However, until a project reaches the feasibility study phase, its chances of being halted remain high. Therefore, expenses must be carefully controlled to the end. The new plan and budget for each next phase must reflect the specific questions that have been raised in the previous phase(s).

In early stages project assessment or evaluation doesn't need to be complicated and expensive but rather should be robust and comprehensive. The project should be evaluated frequently—usually after major progress in data collection or when a new market outlook is adopted. Data should be collected under standardized procedures and adequate supervision. It is crucial to analyze data as they are being collected. After collection, the data must be well organized and converted into a meaningful format.

In many cases, especially in earlier stages of development, the studies may need to be updated. In such cases, it is necessary to revisit the study plan before making final conclusion for that phase. There are many reasons to do this, including changes in market outlook or company strategy. For example, a common occurrence at the scoping level is the discovery of better drilling targets. Therefore, before making a final decision about the property based on the old plan, it may be more appropriate to change the plan and wait for new drill results. When updating a study it is important to include all the information collected up to that point.

5 EXIT STRATEGY

If project evaluation shows weak result then the possibility of having to abandon the project should be considered. A key to success for exploration companies is often finding the right time to exit from a weak project as well as to find a right project to pursue.

A company's strategy and vision must be well understood and its team needs to be realistic about the company's capacities when a project is being evaluated.

When exiting a project, all possibilities for the property need to be considered. Some projects have the potential to be re-activated in near future, for example, in cases where the prices are higher or community relations are improved. In such a case, the company must understand in detail the costs of keeping all the licenses up-to-date for the shelving period, and be aware of other consequences of staying on the property. In other cases, the scale of project may be too big for the size of the company and the exploration company may consider selling the project or calling for a partner. In the worst case scenario, if there is no promising opportunity available for the project, it is better to walk away from the field as early as possible.

Exploration companies should focus on adding value to a project rather than advancing it at any cost. The value of an exploration property is related to the quality and quantity of knowledge that has been acquired about it. When it comes to an exploration project, “How much is it worth?” is equal to “How much do you know about it?”

6 STRATEGIC MINE PLANNING CAN HELP

Mine evaluation helps for early assessment of exploration projects. This can be done using strategic mine planning method. Strategic mine planning is mine simulation and economic analysis combined. For every phase of development, using knowledge that have been developed it is possible to simulate options that are conceivable for the project. Strategic mine planning is a technique that can help to make fundamental decisions. It is efficient way to guide an exploration or mining company through its development stages. Strategic mine planning can answer basic but fundamental questions such as:

-What should be the mining method?
-What is the optimum range for scale of operation?
-What are the sensitive and insensitive parameters?
-What are the weaknesses and strengths of the project?

In strategic mine planning, once enough information is collected, different production scenarios are simulated so that all the possibilities can be explored. Mine simulation studies the strengths and weaknesses of a project and provides practical advice for improvement. To be effective, strategic mine planning needs a thorough analysis of not only the mineral resources, but also of the company’s whole business and, therefore, requires the input of expertise from different fields.

7 CONCLUSION

The success of exploration companies are related to the amount of planning and evaluation efforts they put in projects. For every exploration project a road map is required to be developed in early stages. Road maps must include details about the data collection, budgets, schedules and evaluation systems. In order to stay on right track, evaluation must be done frequently and before proceeding to a higher level. While focusing on advancing the project to the higher levels, road maps must clearly mark the safe exit doors for every stage of the work.

ACKNOWLEDGMENT

Author(s) acknowledges the time and efforts and put to review the paper. SRK consulting’s support to develop this paper is also highly appreciated.

REFERENCES

Lord D. Etheridge, M.A., Willson, M. Hall, G. & Uttley, P.J. 2001, Measuring exploration success: an alternative to the discovery-per-ounce method of qualifying exploration success, *SEG newsletter 45, 1 & 10-16.*

Kreuzer, O.P., 2007. Risk modeling – increasing the effectiveness of our exploration investment, *Geoconference (WA) Inc. Kalgooorlie 07 conference*.

Kreuzer, O.P., Etheridge, M. A., 2010. Risk and Uncertainty in Mineral Exploration: Implications For Valuing Mineral Exploration Properties, *AIG NEWS No 100,*.

McIlroy, A. R. 1999, The return from exploration success: relating economic quality to geological quality, *A Ph.D. thesis submitted to department of geological science, Queen’s University,* Kingston, Ontario, Canada

Mackenzie, B, 1987, mineral exploration economics: focusing to encourage success, *Exploration 1987, Toronto*

An Alternative Multivariate Kriging Technique: Covariance Matching Constrained CoKriging

G. Ertunç, A.E. Tercan, F. Atalay
Hacettepe University, Mining Engineering Department, Ankara

ABSTRACT In predicting second-order stationary vector random fields, simple and ordinary cokriging techniques are widely used. In this study, an alternative multivariate kriging technique Covariance Matching Constrained CoKriging (CMCoK) is introduced and compared with ordinary kriging (OK) and its multivariate counterpart ordinary cokriging (CoK). For comparison, Meuse River data are used and results are discussed by means of local accuracy and spatial variability. From the results, it is seen that error variance for CMCoK is considerably less than CoK and OK.

Keywords: Kriging, CMCoK, OK, CoK

1 INTRODUCTION

Cokriging is the extension of kriging to more than one variable. The system is beneficial when the primary variable is under sampled with respect to the secondary variable(s) that are assumed to be correlated with the primary variable. In some applications there are only a few measurements of the samples of interest; the resultant predicated maps have poor resolution and the corresponding uncertainty may bevery large. In such situation it is critical to account for secondary, indirect information that may be more densely sampled (Goovaerts, 1997). If the two variables are spatially cross-correlated , this information can be used to make predictions of the primary variable (Bivand R.S. et al., 2008). Isotopic cokriging requires that the data for the primary and auxiliary variables be measured at all sampling locations. Heterotropic cokriging requires that only some of the sample points contain measurements of both primary and secondary variables (Wackernagel, 2003).

Depending on whether or not the mean of the vector random field is assumed to be known, estimation of a second-order stationary vector random field, i.e kriging, includes two alternatives namely simple and ordinary cokriging (Myers, 1982; Ver Hoef and Cressie, 1993; Wackernagel, 2003). Detailed derivation of cokriging equation systems is given in numerous publications such as Bishop, T.F.A. and Lark, R.M. (2006), Papritz, A. (2008) and Emery, X., (2012)

Multivariate geostatistical estimations are applied in wide range such as mineral resources evaluation (Journel and Huijbregts, 1978; Pan et al., 1993), environmental studies (Singh, V., 2011), remote sensing (Pardo-Iguzquiza, E., 2011), and geochemistry (Wackernagel, 1988; Lark, L.M. et al., 2014).

In this study, Covariance Matching Constrained CoKriging (abbreviated CMCoK in the sequel) is introduced and its performance is tested by means of spatial variability and accuracy. In previous studies, univariate case of covariance matching process based kriging showed promising tool and by this study the multivariate case of the method is compared with ordinary kriging (OK) and its multivariate counterpart ordinary cokriging (as CoK). Covariance Matching Constrained Kriging (CMCK) is an hybrid method that considers local accuracy property in kriging and preservation of spatial variability in stochastic simulation. The method estimates the unknown vector by adding the constraint to match the variance–covariance matrix of estimated values with the variance–covariance matrix of actual values under

unbiasedness constraint, introduced by Cressie and Johannesson, (2001). Various researchers made contributions to this method. Tercan (2004) applied CMCK to a lignite deposit in order to estimate the global recoverable reserve. The study also covers a comparison of CMCK with OK on estimation of quality tonnage curves. Hofer and Hofer and Papritz (2010, 2011) examined the performances of various techniques such as universal kriging (UK), conditional simulation (CS), constrained kriging (CK) and CMCK. Ertunç et. al., (2013) made a comprehensive comparison of techniques used in estimation of coal quality variables in 3D, including CMCK, OK, and CS.

2 METHODOLOGY

Multivariate estimation is useful when primary variable of interest is under sampled, compared with the cross correlated secondary variable. Thus, the cokriging estimate is a linear combination of both primary and secondary data values,

$$Z^*(x_0) = \sum_{i=1}^{n} a_i U(x_i) + \sum_{j=1}^{m} b_j V(x_j) \qquad (1)$$

Where $Z^*(x_o)$ is the predictor of $Z(x_0)$ at location x_0,

$U(x_i)$: a vector with elements of the measured values at location x_i, i=1,…,n,

$V(x_j)$: a vector with elements of the measured values at location x_i, i=1,…,m,

a_i: vector of kriging weights of primary variable, and

b_i: vector of kriging weights of secondary variable.

Exact formulas for cokriging are derived from unbiasedness condition Eq. (2) and minimization of error variance as given in Journel and Huijbregts (1978), Isaaks and Srivastava (1989), Cressie (1991), Goovaerts (1997) and Chiles and Delfiner (2012)

$$\begin{aligned} E\{\hat{U}_0\} &= E\left\{\sum_{i=1}^{n} a_i U_i + \sum_{j=1}^{m} b_j V_j\right\} \\ &= \sum_{i=1}^{n} a_i E\{U_i\} + \sum_{j=1}^{m} b_j E\{V_j\} \\ &= \tilde{m}_U \sum_{i=1}^{n} a_i + \tilde{m}_V \sum_{i=1}^{n} b_j \\ \sum_{i=1}^{n} a_i &= 1, \sum_{i=1}^{n} b_j = 0 \end{aligned} \qquad (2)$$

Minimizing error variance will lead the matrix form of cokriging Eq.(3) as follows:

$$\begin{bmatrix} \Sigma_z & 1 \\ 1' & 0 \end{bmatrix} \begin{bmatrix} \lambda \\ \mu \end{bmatrix} = \begin{bmatrix} C \\ 1 \end{bmatrix} \qquad (3)$$

Where

$$\Sigma_z = \begin{bmatrix} \Sigma_{11} & \Sigma_{12} \\ \Sigma_{21} & \Sigma_{22} \end{bmatrix}, \mu = \begin{bmatrix} \mu_1 \\ \mu_2 \end{bmatrix}, \lambda = \begin{bmatrix} a_i \\ b_j \end{bmatrix}, C = \begin{bmatrix} \Sigma_{10} \\ \Sigma_{20} \end{bmatrix},$$

Σ_{11}, Σ_{22}, Σ_{12}, Σ_{21} are covariance matrices for the primary, secondary data and between them respectively.

Σ_{10}, Σ_{20}: Covariance matrices among the primary, secondary data and target locations.

λ: the weights of primary and secondary variable;

μ: vector of Lagrange multipliers.

Solving for the weights yields,

$$\lambda = \Sigma_z^{-1}(C - 1\mu), \qquad (4)$$

Where,

$$\mu = (1'\Sigma_z^{-1}1)^{-1}(1'\Sigma_z^{-1}C - 1)$$

1, ‘, and $(.)^{-1}$ denote unity matrix, transpose and inverse of matrix respectively.

The CMCK method estimates unknown values such that the variance–covariance matrix of estimated values is matched with the variance–covariance matrix of actual values under unbiasedness constraint. The matching process is achieved by controlling K matrix (Tercan, 2004; Kukush, A. and Fazekas, I., 2005; Ertunç et. al. 2013).

By adding K matrix into multivariate case, the kriging weights can be calculated as follows:

$$\lambda = \Sigma_z^{-1}\left(C - \mathrm{K}(1'\Sigma_z^{-1}1)^{-1}(1'\Sigma_z^{-1}C - 1)\right) \qquad (5)$$

3 CASE STUDY

In this study, very well known Meuse river data is used for testing the performance of CMCoK. For the comparison, besides CMCoK, estimation is made by univariate ordinary kriging and multivariate variant, cokriging. The results are compared on the base of estimation map and prediction error map, more specifically, minimum squared prediction errors (MSPE) so that both spatial variability and local accuracy can be compared.

The meuse data is a set of data comprising of four heavy metals measured in the top soil in a flood plain along the river Meuse (Fig.1). This set is available with R Software package called gstat (Pebesma, E., 2004).

Two metal concentrations, having high correlation (Fig.2), Zn and Pb are used out of four available metals. Zn concentrations are used as primary variable and in order to create heterotopic case, 25 Zn samples are randomly discarded from total 155 sample locations (Fig. 2).

Prior to the estimations, both data are standardized and the Linear Model of Corregionalization (LMC) is fitted. Experimental and model direct and cross variograms variograms are presented in Figure 3. The LMC model includes a nugget effect and two spherical structures with the corresponding ranges 150 m and 1200 m respectively.

$$\begin{bmatrix} \gamma_{Zn} & \gamma_{Zn\text{-}Pb} \\ \gamma_{Zn\text{-}Pb} & \gamma_{Pb} \end{bmatrix} = \begin{bmatrix} 0.113 & 0.087 \\ 0.087 & 0.076 \end{bmatrix} nug + \begin{bmatrix} 0.062 & 0.048 \\ 0.048 & 0.049 \end{bmatrix} Sph_{150m} + \begin{bmatrix} 0.231 & 0.101 \\ 0.101 & 0.067 \end{bmatrix} Sph_{1200m}$$

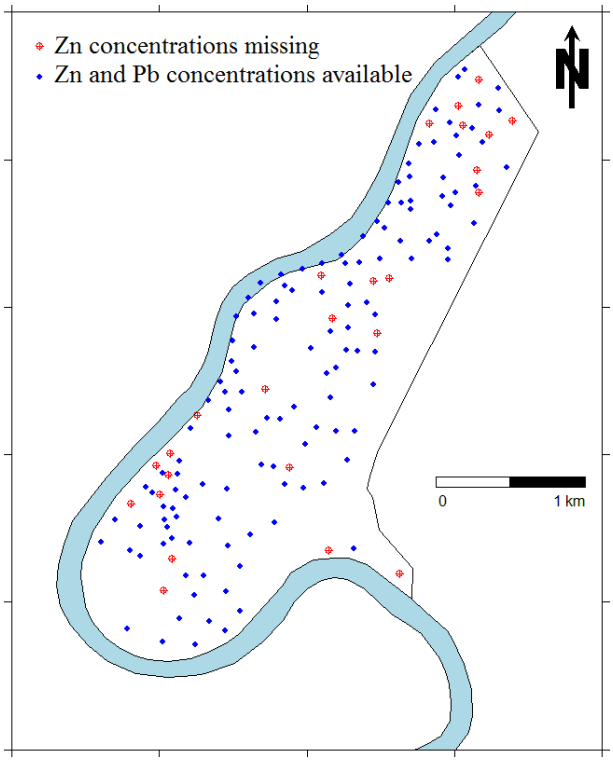

Figure 1. Meuse river and study area, sample locations.

Descriptive statistics of Zn and Pb concentrations are given in Table 1.

Table 1. Descriptive statistics of primary and secondary data.

	Pb	Zn
Count	155	130
Minimum	-0.902	-1.509
Maximum	1.084	1.368
Mean	0.000	-0.019
Variance	0.171	0.338

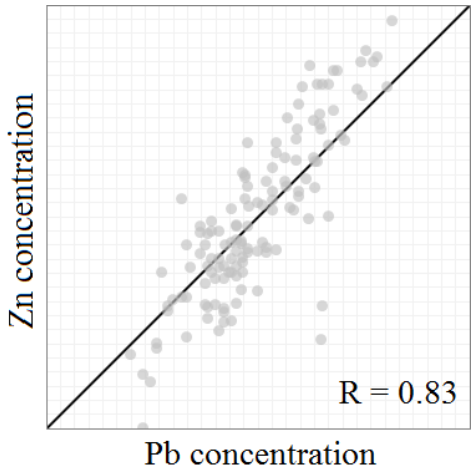

Figure 2. Scatter diagram of Zn and Pb concentrations.

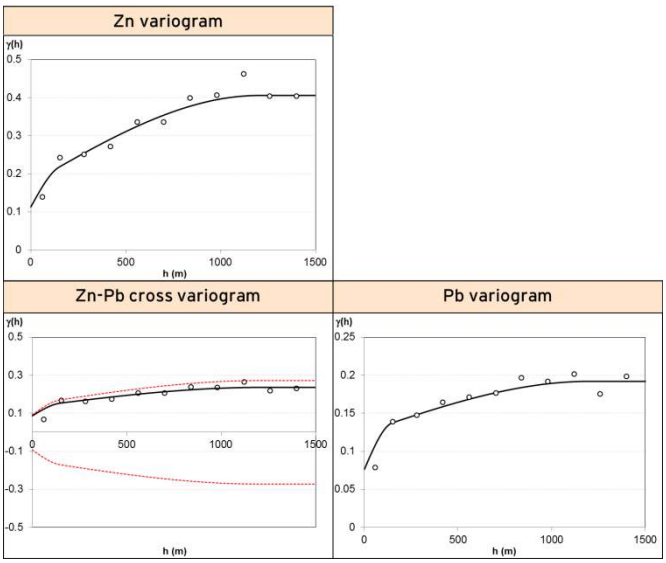

Figure 3. Model direct and cross variograms of Zn, Pb cocentrations. (Red dot line forms the hull of perfect positive and negative spatial correlation.)

In kriging with a moving neighborhood, each target point is estimated from a subset of data that varies with the target. In this study, moving neighborhood with a radius of 1500 m with nearest 8 points subsets are used. Results are given in next section by means of comparison of image maps, MSPE map, and swath plots.

4 RESULTS AND DISCUSSION

Image maps produced by three methods, OK, CoK, and CMCoK is given in the Figure 4. It is seen that, when compared with OK results Fig.4a, highly correlated secondary variable in the case of CoK Fig.4b slightly improved the spatial variability.

Covariance-matching based multivariate case CMCoK in Fig.4c is more sensible to low and high variation of attribute of interest, and this variation reflect as less smooth image map when compared to the OK and CoK. Since the most unavoidable phenomenon of kriging estimations is smoothing, the less smoothing behavior of constrained kriging can be used in further studies as an alternative.

As an other comparison tool, MSPE maps are used in comparison among three estimations (Fig. 5). CMCoK estimates MSPE map (Fig. 5c) shows that, points used in data are distinguishable rather than other methods. Although CoK produced image map almost same variability with OK; CoK MSPE map shows that, prediction errors are slightly lowered when compared to the univariate case OK. This is an indication of contribution of highly correlated secondary variable.

A swath plot is a graphical display of the attribute in interest from a series of slices, or swaths, generated in several directions through the study area. In this study, the slices are selected with same orientation with data, since regular Easting and Northing selecting might led misjudgement of results because of the irregular spread of data. The study area is divided into slices along with the direction under consideration and the weighted average of each slice for the respective attribute is calculated. The averages are plotted against the slice number. Swath plots are drawn for the target points and data in for three estimation methods. Results are represented in Figure 6.

From Figure 6, it is seen that OK estimates are locally much more accurate than multivariate estimations CoK, and CMCoK. When multivariate cases compared, CoK produced more accurate results than the covariance-matching processed variant.

Table 2. Descriptive statistics of results.

	OK	CoK	CMCoK
Count	3103	3103	3103
Minimum	-1.543	-1.629	-2.137
Maximum	1.482	1.530	2.240
Mean	-0.091	-0.096	-0.097
Variance	0.411	0.464	0.711

Table 2 gives the descriptive statistics of results of univariate OK, and multivariate cases CoK and CMCoK. From results, it is seen that CMCoK results lie in largest interval [-2.137, 2.240] when compared to ordinary kriging estimations. CoK results seem same characteristics with univariate case by means of similar interval, mean and variance, while CMCoK produced higher variance result.

It can be concluded that, covariance matching process is successfully adapted into multivariate case of kriging and seems promising tool since the technique is more effective to predict low and high values than univariate and multivariate ordinary kriging. Since the ordinary cokriging is an special case of an universal kriging (UK), the study shows that covariance-matching constrained equation and matrice systems can easily be adapted into cases which UK estimation is an altenative.

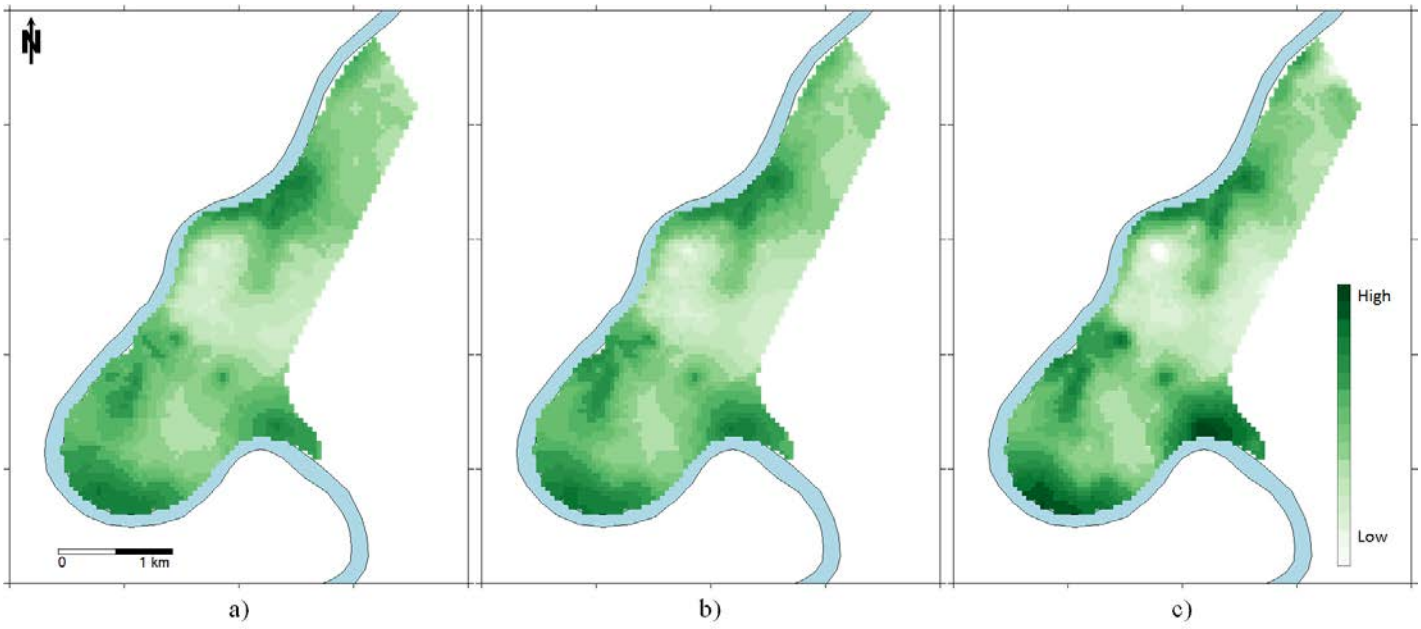

Figure 4. Image map of estimations by a) OK, b) CoK, and c) CMCoK.

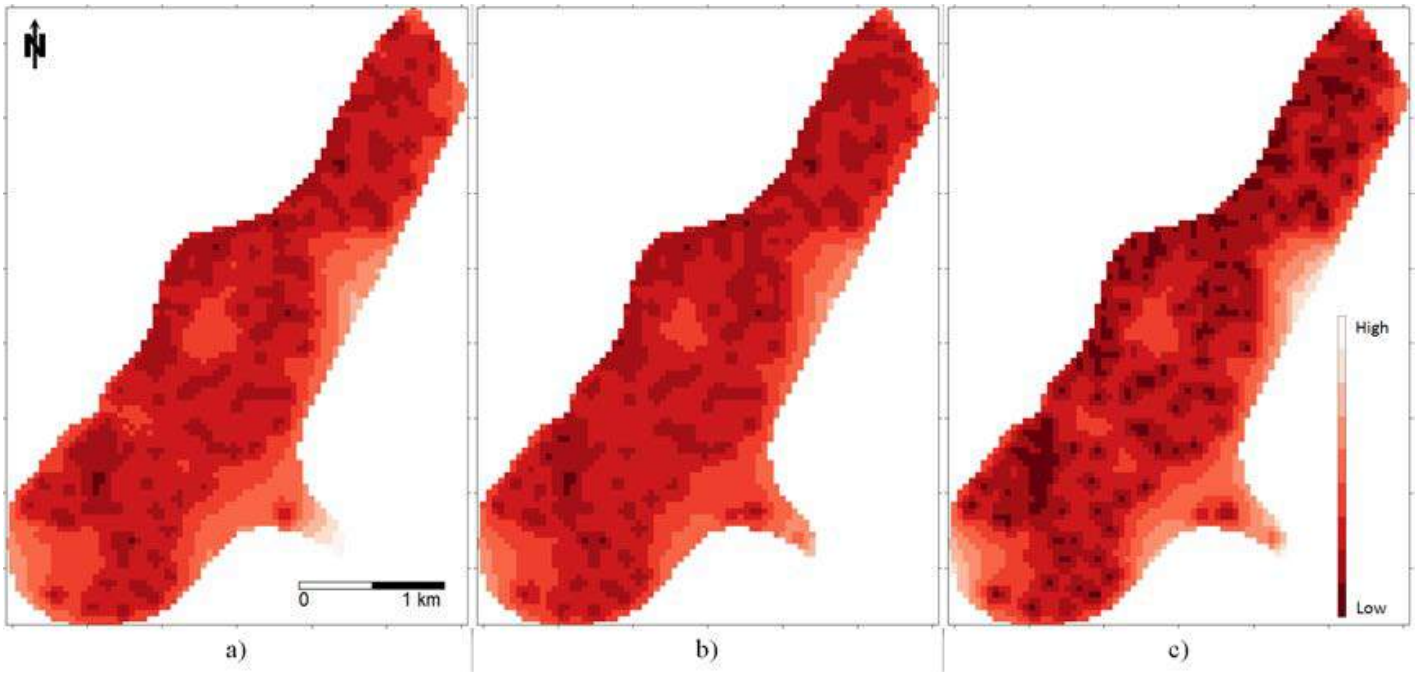

Figure 5. Image map of estimations by a) OK, b) CoK, and c) CMCoK.

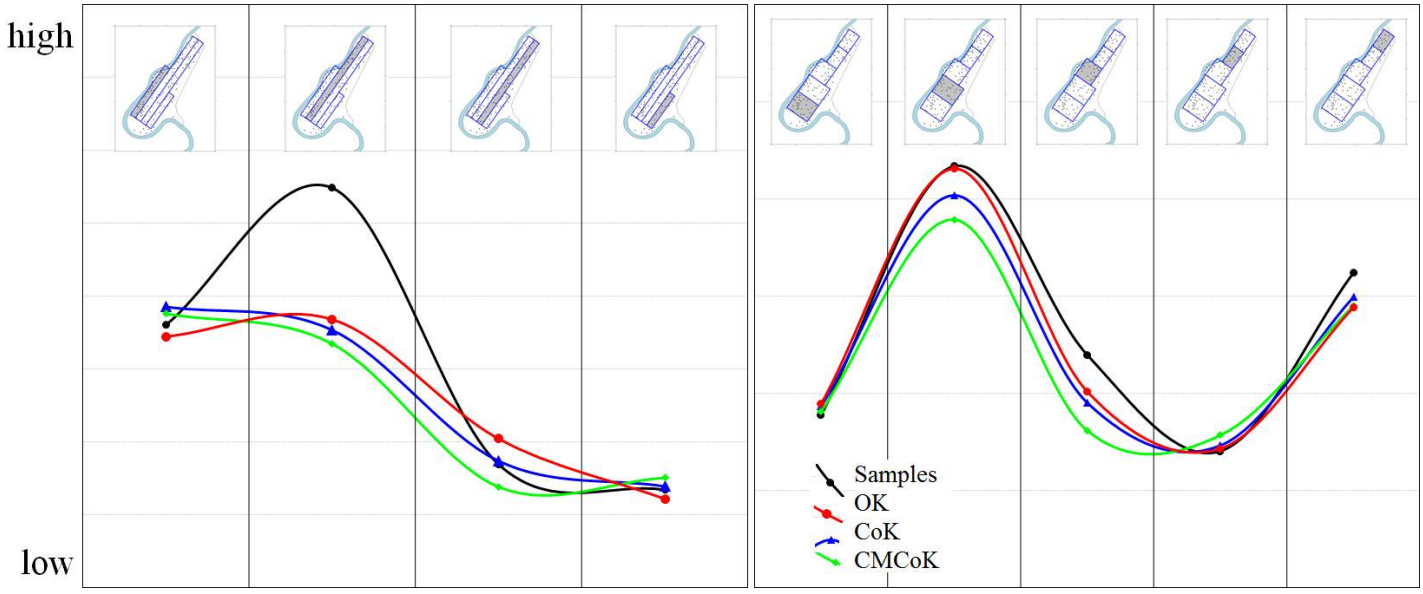

Figure 6. Image map of estimations by a) OK, b) CoK, and c) CMCoK.

REFERENCES

Bishop, T.F.A. and Lark, R.M., 2006, The geostatistical analysis of experiments at the landscape-scale, *Geoderma*, 133,1-2.

Bivand, R.S., Pebesma, E., Gómez-Rubio V., 2008, *Applied Spatial Data Analysis with R*, Springer.

Chiles, J.P., Delfiner, P., 2012, *Geostatistics: Modeling Spatial Uncertainty, 2nd Edition,* John Wiley and Sons Ltd, United Kingdom.

Cressie, N., Johannesson, G., 2001. Kriging for cut-offs and other difficult problems. *In: Monestiez, P., Allard, D., Froidevaux, R. (Eds.), geoENV III Geostatistics for Environmental Applications.*

Cressie, N.A.C., 1991, *Statistics for spatial data*, John Wiley & Sons, New York.

Emery, X., 2012, Cokriging random fields with means related by known linear combinations, *Computers & Geosciences*, 38.

Ertunç, G., Tercan, A.E., Hindistan, M.A., Ünver, M.A., Ünal, S., Atalay, F., Kıllıoğlu S.Y., 2013, Geostatistical estimation of coal quality variables by using covariance matching constrained kriging. *International Journal of Coal Geology*, 112.

Goovaerts, P., 1997. *Geostatistics for Natural Resources Evaluation*. Oxford University Press, New York.

Hofer, C., Papritz, A., 2010. Predicting threshold exceedance by local block means in soil pollution surveys. *Mathematical Geosciences* 42.

Hofer, C., Papritz, A.,2011. constrainedKriging: anR-package for customary, constrained and covariance-matching constrained point or block kriging. *Computers and Geosciences* 37.

Isaaks, E.H., Srivastava, R.M., 1989. *An Introduction to Applied Geostatistics*. Oxford University Press, New York.

Journel, A.G., Huijbregts, C.J., 1978. *Mining Geostatistics*. Academic Press, London.

Kukush, A., Fazekas, I., 2005. Kriging and prediction of nonlinear functionals. *Austrian Journal of Statistics* 34, 2.

Lark, R.M., Ander, E.L., Cave, M.R., Knights, K.V., Glennon, M.M., Scanlon R.P., 2014, Mapping trace element deficiency by cokriging from regional geochemical soil data: A case study on cobalt for grazing sheep in Ireland, *Geoderma*, 226–227.

Myers, D.E., 1982. Matrix formulation of co-kriging. *Mathematical Geology* 14 (3), 249–257.

Pan, G., Gaard, D., Moss, K., Heiner, T., 1993. A comparison between cokriging and ordinary kriging: case study with a polymetallic deposit. *Mathematical Geology* 25 (3), 377–398.

Papritz, A., 2008, Standardized vs. customary ordinary cokriging: Some comments on the article "The geostatistical analysis of experiments at the landscape-scale" by T.F.A. Bishop and R.M. Lark, *Geoderma*, 146, 1-2.

Pardo-Iguzquiza, E., Rodríguez-Galiano, V.F., Chica-Olmo, M., Atkinson P.M., 2011, Image fusion by spatially adaptive filtering using downscaling cokriging, *ISPRS Journal of Photogrammetry and Remote Sensing*, 66, 3.

Pebesma, E.J., 2004. Multivariable geostatistics in S: the gstat package. *Computers & Geosciences* 30, 683-691.

Tercan, A.E., 2004. Global recoverable reserve estimation by covariance-matching constrained kriging. *Energy Sources* 26.

Ver Hoef, J.M., Cressie, N., 1993. Multivariable spatial prediction. *Mathematical Geology* 25 (2), 219–240.

Vikas Singh V., Carnevale, C., Finzi, G., Pisoni E., Volta M., 2011, A cokriging based approach to reconstruct air pollution maps, processing measurement station concentrations and deterministic model simulations. *Environmental Modelling & Software*, 26, 6.

Wackernagel, H., 1988. Geostatistical techniques for interpreting multivariate spatial information. In: Chung, C.F., Fabbri, A.G., Sinding-Larsen, R. (Eds.), *Quantitative Analysis of Mineral and Energy Resources*. Reidel, Dordrecht.

Wackernagel, H., 2003. *Multivariate Geostatistics: An Introduction with Applications*. Springer, Berlin, 387pp.

The Integration of Artificial Neural Networks and Geostatistical 3D Geological Block Modelling- a Case Study on a Mineral Sand Deposit

A.B. Jalloh
Kyushu University, Fukuoka, Japan

K. Sasaki
Kyushu University, Fukuoka, Japan

Y. Jalloh
London Mining Company, Freetown, Sierra Leone

ABSTRACT In this research, an Artificial Neural Network model was developed to predict metal content from drillhole data using the back propagation algorithm. For validation purposes, results between the actual and predicted mineral grades were compared, and regression analysis of the compared results indicate that the predicted mineral grades were in close proximity to the actual grades. The validated model was used to predict mineral grades at unsampled locations in order to determine the feasibility of drilling in those areas. The optimum results obtained from the neural network were fed to geostatistical techniques for developing a geological 3D block model for mine design. The generalized data from the Neural Network show that Artificial Neural Networks can be used to complement exploration activities and is an effective approach for mineral reserve estimation without worrying about spatial variability or other assumptions.

Keywords: Geostatistics, Artificial Neural Network, Geological block modelling

1 INTRODUCTION

Mineral deposits are very complex structures due to the geological processes involved in their deposition. The most important factor in reserve estimation is the distribution of the ore grades (Sathit, and Shigeru, 2013). The distribution of ore grades must be determined to enable the estimation of ore reserves. For the last five decades the mining industry has adopted and applied geostatistics (Kriging and Conditional Simulation) as an ideal and optimal tool for mineral reserve estimation. This is because geostatistics provide powerful tools for modelling most of the aspects of an ore deposit. The main steps involved mineral reserve estimation are as follows: (1) obtain the variogram model of the deposit, (2) fit a standard model to the variogram and (3) finally produce block estimates. However, geostatistics only considered spatial continuity as the main factor (Sathit, and Shigeru, 2013). There are other factors like mineral deposition environment, geological structure and deposit type which are not considered. To date, the biggest challenges on using geostatistics lie in the failure in variogram modelling, nonstationarity and normality of the data.

Developments in computing technologies have produced several machine learning algorithms, like, Artificial Neural Networks (ANNs) which have the ability to operate nonlinearly. With this technique, no assumptions are made about any factor or relationship. The ANNs learn the underlying functional relationship present in the data from the samples that are made available to them (Sathit, and Shigeru, 2013). Recently, despite the efficacy of geostatistics to reserve estimation, several researchers have opted for a neural network modelling approach for ore grade estimations, and the

utility and performance of this model in many practical applications have been demonstrated.

In this research, a neural network model is trained on the available drillhole data. The model was used to generalize in unsampled areas. The predicted and drillhole data were fed into geostatistics (OK) to produce gridded 3D geological block model. Figure 1 shows the schematic illustration of the research.

The data used in this study for training, testing and validating the model consist of 2880 composite samples. The samples include sample co-ordinates (easting, northing, and elevation), sample length and the rutile ore grade. The network is presented with this data for training, testing and validation. It is taught to recognize the relationship patterns between input and target and then generalize to interpolate ore grades. The performance of the neural network model was assessed by two estimation errors, namely, the mean squared error (MSE) and correlation coefficient (R^2). The performance of the ANN model is validated by comparing results with the traditional geostatitical techniques of ordinary kriging (OK).

2 CASE STUDY: GENERAL GEOLOGY AND DEPOSIT DESCRIPTION

The study area is located on the south Western part of Sierra Leone roughly at latitude 7°40'N and longitude 12°20'W. Figure 2 shows the location of the deposit overlain with some of the drillholes used in this study and the drillhole map.

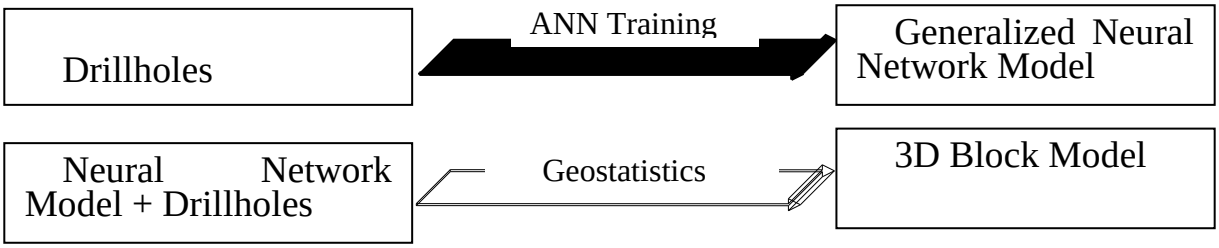

Figure 1. Schematic Illustration of the research outline.

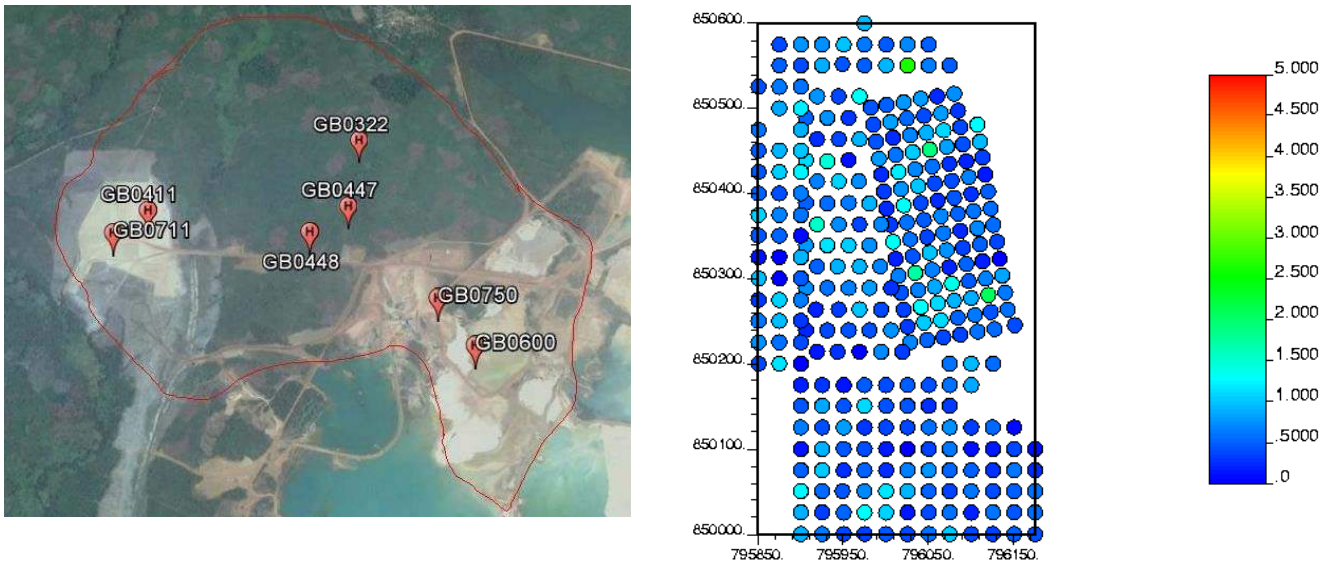

Figure 2. Location Map of drillholes in the studied Area

The deposit is one of the four largest developed in the area. The deposition is as a result of the rivers' tributaries crisscrossing all over the area stripping off materials from adjacent hills. The mineral distribution pattern comes in two folds and is mostly observed within the interfluves. The deposit show secondary surface enrichment averaging 1.99%HM, %RR of 0.81 with thickness being 8.9m.

2.1Data Analysis and Spatial Modeling

The assays include sample co-ordinates (easting, northing, and elevation), length of sample, and the rutile ore grade. The sampling was done at a regular grid interval. Preliminary statistical analysis conducted on drillhole composites from displayed a significantly large grade variation, with a mean and standard deviation of 0.84% and 0.43, respectively. The coefficient of variation is, however, less than one. For the sake of simulation, and network training, the grade was normal score transformed. Figure 3 shows the histogram plot and the normalized plot of the rutile grades. Table 1 shows the summary statistics.

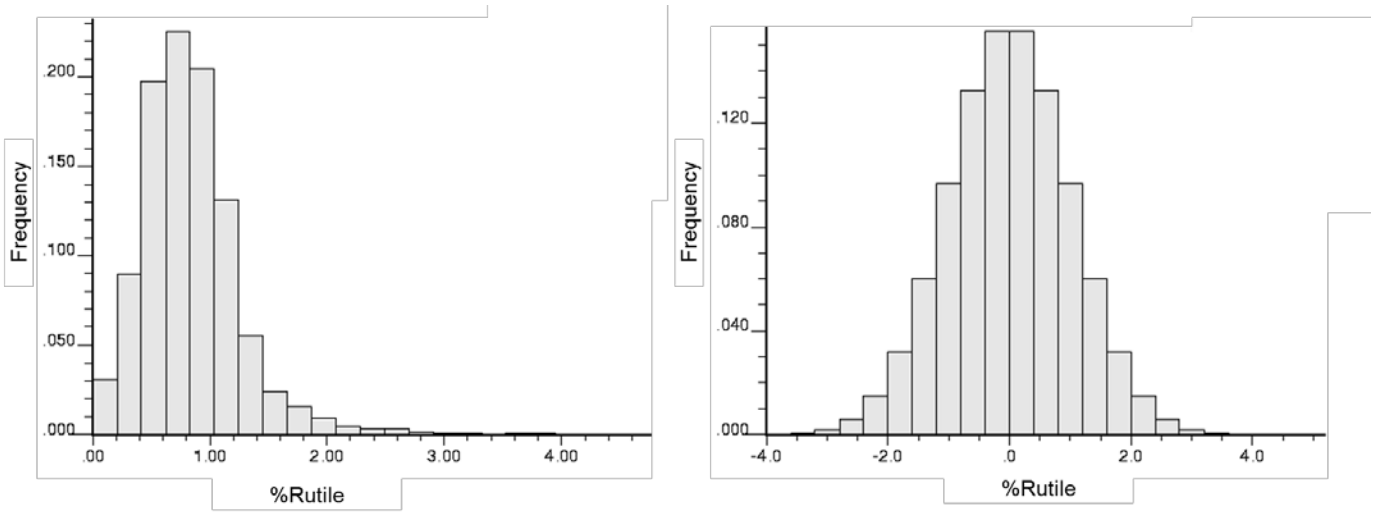

Figure 3. Histogram plot of raw data and normalized data respectively

Visual observation of the histogram plot reveals that the drill data is composed of a large proportion of low values and a minute proportion of extremely high grade values. For geostatistical estimation purposes and after preliminary analysis of the data, the spatial continuity of the data was explored by preparing the variogram models both directional and Omni-directional of the data. Spatial studies of the deposit show that the variograms reveal significant contribution from the nugget, thereby indicating difficult modelling conditions. The directional variogram model provided a better understanding and enabled to check for anisotropies in the deposit. Table 2 shows the parameters from which the directional variogram was constructed..

Large proportions of spatial variability occur from the nugget effect, indicating the presence of a poor spatial correlation structure in the deposit over the study area, and the variogram figure also indicate zonal anisotropy of the deposit. This anisotropy was taken into account during ordinary kriging.

Table 1. Summary statistics

Statistics	Values
Mean	0.84
Standard Deviation	0.43
Coefficient of Variation	0.51
Median	0.79
Minimum	0.00
Maximum	4.12
Upper Quantile	1.04
Lower Quantile	0.56

Table 2. Variogram parameters

Parameters	Value
Direction/Azimuth	135°
Nugget effect	0.0
Sill	0.335
Effective Range (m)	25
Zonal Anisotropy	1 and 0
Model Type	Exponential

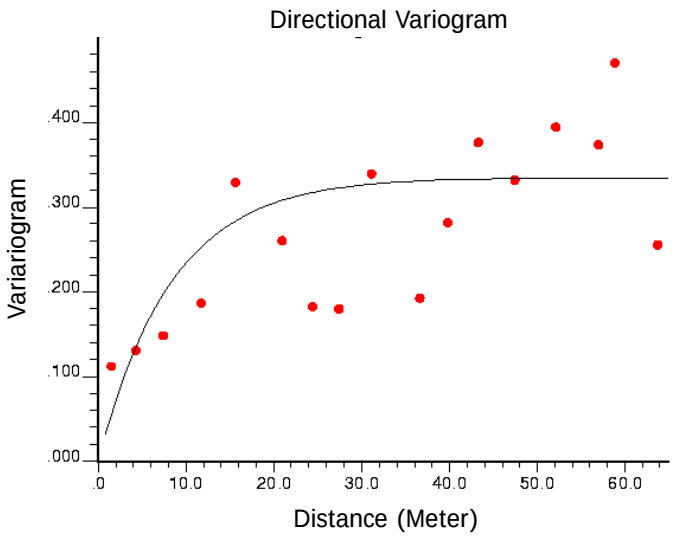

Figure 4. Variogram plot

3 PRICIPLES OF ARTIFICIAL NEURAL NETWORK USING BACKPROPAGATION

In 1986 David Rumelhart, Geoffrey Hinton, and Ronald Williams wrote a paper describing the use of several neural networks where the backpropagation algorithm works far faster than earlier approaches to learning, making it possible to use neural network applications to many areas. The attraction of neural networks is that they are best suited to solving problems that are the most difficult to solve by traditional computational methods.

Figure 5 explains the principle of the backpropagation technique in which each neuron receives a signal from the neurons in the previous layer, and each of those signals is multiplied by a separate weight value. The weighted inputs are summed, and passed through a limiting function (Sigmoid function) which scales the output to a fixed range of values. The output of the sigmoid function is then broadcast to all of the neurons in the next layer. So, to use the network to solve a problem, we apply the input values to the inputs of the first layer, allow the signals to propagate through the network, and read the output values.

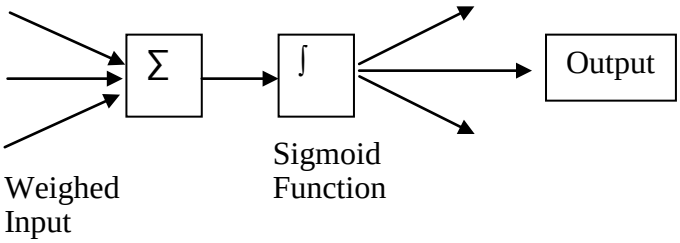

Figure 5. The structure of a neuron

The propagation error is calculated using the sigma transfer function. This function is derived as follows:

$$\frac{dx}{dy}\sigma(x)=\frac{d}{dx}\left(\frac{1}{1+e^{-x}}\right)$$

$$=\frac{e^{-x}}{(1+e^{-x})^2}=\frac{(1+e^{-x})-1}{(1+e^{-x})^2}$$

$$=\frac{1+e^{-x}}{(1+e^{-x})^2}-\left(\frac{1}{1+e^{-x}}\right)^2$$

$$=\sigma(x)-\sigma(x)^2$$

$$\sigma'=\sigma(1-\sigma)$$

To generate network output, elements in the input layer and the hidden layer of the neural network are manipulated by a weighing function as illustrated below.

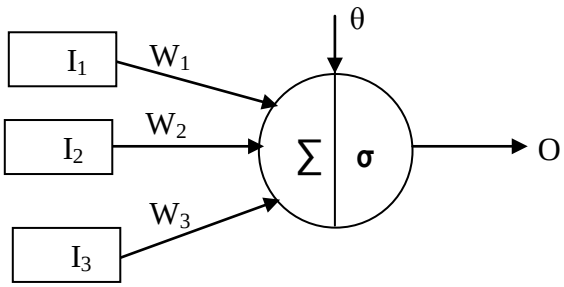

$$O = \sigma\,(W_1I_1+W_2I_2+W_3I_3+\theta)$$

Where σ’ = the sigmoid transfer function
W = weight of input neurons
I = Input to the neurons

O = output

θ = Bias term

Given a set of training and target output data, also, and assuming that K= output layer, O_j =output node and T_j= target, then the error can be calculated thus:

$$E= ½ \sum (O_j-T_j)^2$$

The process of determining the weights is called training, and depending upon the output, the network adjust weights iteratively based on their contribution to the error. This process of propagating the effect of the error onto all the weights is called backpropagation (Dutta et. al, 2010).

The general architecture of neural network is made of an input layer consisting of inputs, two or more hidden layers consisting of a number of neurons, and the output layer consisting of outputs (Dutta et. al, 2010).

3.1 Model Training, Testing and Validation

Our neural network model for training, testing and validation is a two layer feedforward network with sigmoid hidden neurons. This network is presented with four input neurons which are X, Y, and Z coordinates, and sample length, consisting of two hidden layers with 20 neurons and one output layer, grade (%Rutile). Like (Dutta et. al, 2010), the number of hidden neurons chosen was based on the minimum generalization errors of the Neural Network model while experimenting with a different number of hidden nodes in the hidden layers. The network was trained using the Levenberg-Marquardt backpropagation algorithm. A MATLAB code was developed for the Neural Network modeling. Figure 6 shows the architecture of the feedforward neural network model.

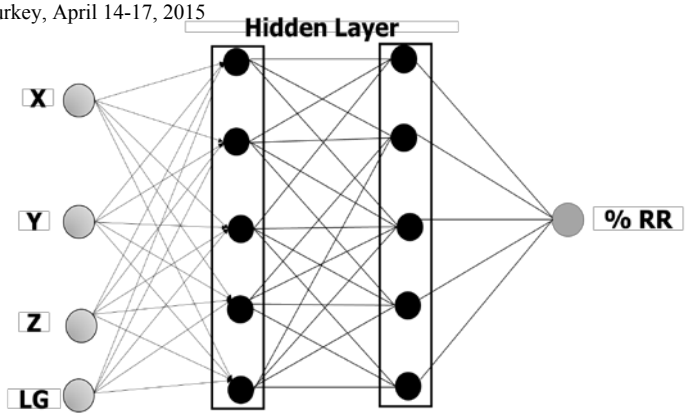

Figure 6. Architecture of the feedforward Neural Network Model

As mentioned earlier, to reach generalization, the data is split into three parts. Table 3 shows the data comprising each set for training, testing and validation of the model with their respective correlations.

The training data was used to train the neural net, the validation data was used to determine the performance of the network on the data that were excluded during training, and the test data was used for checking the overall performance of the neural net model.

Table 3. Data and model correlation results

Data	Samples	R^2	MSE
Training	2016	0.8925	0.2044
Validation	432	0.8805	0.2090
Testing	432	0.8807	0.2087

The predictions from the trained model were in agreement with the actual data with overall R^2 regression value of 0.889. This means that for the drillhole data used 88.9% of the variability can be explained by the neural net model. Figures 7 and 8 shows the regression plot for the training and validation, and overall regression R^2 plots of the model.

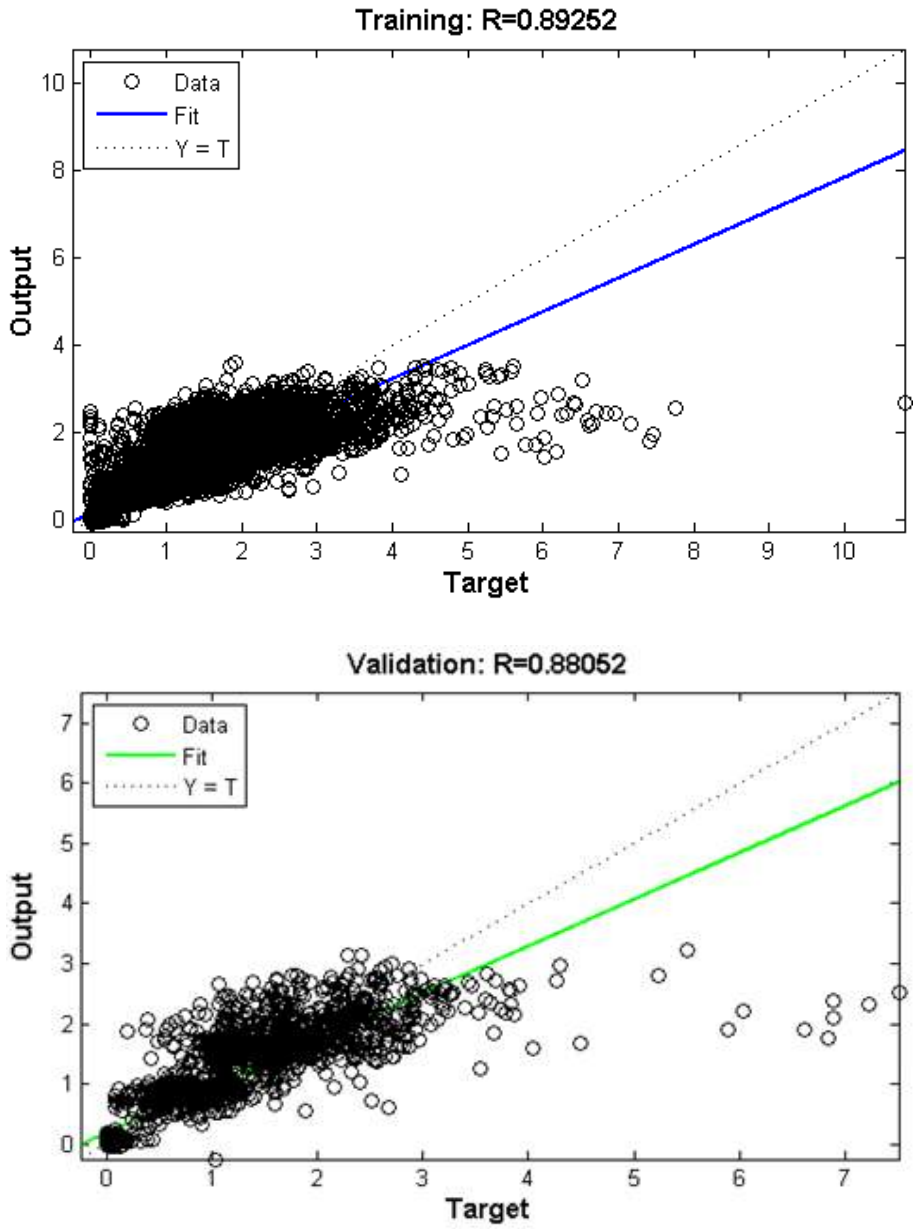

Figure 7. Output vs target for the training and validation data

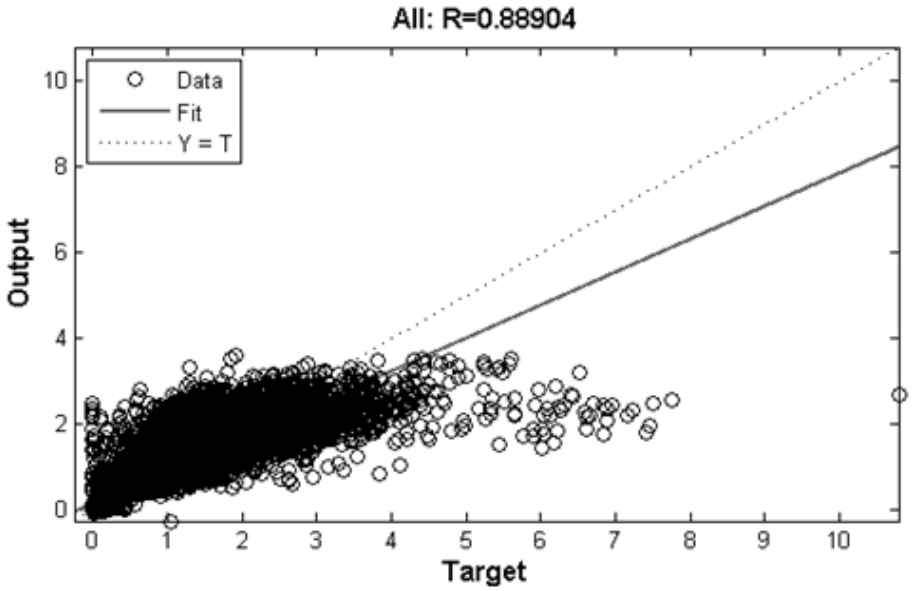

Figure 8. The correlation between outputs and targets of the Neural Network Model

4 GEOSTATISTICAL BLOCK MODELING

Appropriate dimensions were selected to construct 3D geological modeling grids from the neural network model. The dimensions were 60 m by 60 m by 5 m. GSLIB was used for variogram modelling and ordinary kriging.

Previously, (Wu and Zhou, 1993), estimated grades based on drillhole composite for a level in a surface mine with an assumed bench height of 12 m. In this study, the entire mineral deposit was estimated using composited drillhole data with a 1.5 m sample interval. After generating the optimum results from the neural net model, these results were fed in to the kriging algorithm for block grade gridding. Table show the results obtained from the kriging and neural net block grades.

Table 3. Data and model correlation results

	Neural Net	**Kriging**
Blocks	18000	18000
Variance	0.0121	0.0338
%Average	0.8039	0.7995

5 CONCLUSION

This study investigated ore reserve estimation capabilities of Artificial Neural Networks and applied it on a mineral sand deposit located in Sierra Leone.

The results show that the neural network can make accurate predictions of the grade and this is true within the zones of mineralization more than the edges. The artificial neural network tool can be used to assess grade distribution based on few available drillhole data. This techniques helps in determining the feasibility of the drilling program. When integrated with geostatiscs, the model produced provides realistic models take into account the available geological information at the time of modelling.

REFERENCES

Dowd, P., A., and Saraq, C.: A Neural Network Approach to Geostatistical Simulation: *Mathematical Geology, 1994, vol. 26, no. 4, pp. 491–503.*

Dutta, S., Bandopadhyay, S., Ganguli R., and Misra, D.: Machine Learning Algorithms and Their Application to Ore Reserve Estimation of Sparse and Imprecise Data, 2010.

Kapageridis, I., K., and Demby, B.: Integration of a Neural Ore Grade Estimation Tool in a 3D Resource Modeling Package.

Kapageridis, I., K., and Demby, B.: Neural Network Modelling of Ore Grade Spatial Variability.

Li, Z., Rizzo, D., Hayden, N., and Stevens, L.: Using Geostatistics and Artificial Neural Networks to Determine the Location of a Containment Source: *GeoCongress 2006.*

Pejman T. and Ardeshir H.: Application of a Modular Feedforward Neural Network for Grade Estimation: *Natural Resources Research, Vol. 20, No. 1, March 2011 (2011) DOI: 10.1007/s11053-011-9135-3.*

Saleh, M., A., and Tawo, E., E.: Application of Artificial Neural Networks in Mineral Resource Evaluation: *J. King Saud Univ., Vol. 10, Eng. Sci. (1), pp 127-139 (A.II.1418/1998).*

Sathit P., and Shigeru M.: Generating Prediction Map for Geostatistical Data Based on an Adaptive Neural Network Using only Nearest Neighbors: *International Journal of Machine Learning and Computing, Vol. 3, No. 1, February 2013.*

Samantha, B., Ganguli R., and Bandopadhyay, S.: Comparing the Predictive Performance of Neural Networks with Ordinary Kriging in a Bauxite Deposit: *Transactions of Institute of Mining and Metallurgy, Section A, Mining Technology, Vol. 114, No. 3, 2005b, pp. 129-139.*

Wu, X and Zhou, Y: Reserve Estimation Using Neural Network: *Computers & Geosciences, Vol. 19, No. 4, pp. 567-575, Pergamon Press, 1993.*

Application of Plurigaussian Simulation Technique to a Cement Raw Material Deposit

T.Y. Yunsel, A.Ersoy
Adana Science and Technology University, Adana, TURKEY

ABSTRACT The traditional simulation methods have serious limitations for applications to large numbers of domains, which have complex contact relations. Plurigaussian simulation is an effective method which can be applied to any number of domains, using both local and global geological information to infer the distributions of rock types. This study presents the application of the plurigaussian simulation method to the cement raw material deposit of Adana Cement Factory and assesses the spatially varying rock type proportions, and accounts for uncertainties between them. The method is able to incorporate cement quality parameters and geological logging from drill hole samples as well as prior geological knowledge as conditioning information for the realisations of rock types. The results indicate that the plurigaussian method correctly reproduces the different orientations of the individual rock types.

Keywords: Plurigaussian simulation, cement raw material

1 INTRODUCTION

Determination of uncertainty related to reserve classification plays an important role in mining applications especially raw material production in cement factories. Inability to construct a realistic geological model or insufficient geoinfomation generally results in high uncertainty. Main objective of this study is to reveal the underground rock type distribution to be used as raw material and fed to cement factory.

Geostatistical simulation procedures provide a solution for this uncertainty by incorporating multiple simulations at once for the mineral grades (Emery et al., 2008). Although the main concepts for the simulations include a single variable application, extended usage of the algorithm allow realizations of multiple variables simultaneously. This kind of application of simulations deals with geological domains and it requires an exhaustive simulation procedure. Here, geological domains stand for the preciously defined mineralisation zones. Dealing with the geological domains by simulation techniques requires categorical variables called rock types. There are several types of the simulations applied to characterize the geological domains. However, Gaussian based methods are well developed techniques and they include the advanced use of the old Truncated Gaussian simulations (LeLoc'h and Galli, 1996; De Almeida, 2010). Plurigaussian simulations exhibit better results in domains having complex transitive rock types and are becoming popular in recent years. Applications of plurigaussian simulations have found wide acceptance in the literature (Vargas-Guzman and Al-Qassab, 2006; Deraisme and Farrow, 2005; Yünsel, 2012). Complications and processes in dealing with geological domains to create the realistic geological structure as taking into account the proportions among related rock-types have been presented here. In this study especially a cement raw material field were chosen for application of the Plurigaussian Simulations. The case study aims to assess the spatial structure of the distributions of rock types for cement raw materials.

2 STUDY AREA AND GEOLOGICAL SETTINGS

Study area is located near to Adana City. The distance between the city centre and study area is approximately 10km (Figure 1). The cement factory is located next to the study area to avoid unnecessary transportation costs. Adana Cement Industry is the biggest cement producer of the Turkey. The factory has a wide range of cement production changing from Portland to pozzolanic cement. The majority of the production is put up on domestic market while remainder is exported to European and Middle-Eastern countries.

Geology of the study area exhibits a sedimentary lithology aged in Upper Miocene. Lithology consists of marl and limestone originated materials. Limestone covers the majority of the region and dominates the other formations. Thickness is relatively variable and gradually changing into related formations such as clayey limestone, marl may be observed. The rock is observed in different forms including microcrystalline calcite, clay minerals, microcrystalline quartz and fossil fragments. Geologically marls are formed by sedimentation of clay minerals and carbonate rocks at the same time. Marls are the most demanded formations by the factory since it naturally has the optimum mixture content and ready to process directly. Also, quartz carrying formations take place northern parts of the study area and related sandstone contains large amount of fossils. Raw material is removed by open pit mining methods in the field.

3 THE DATA

There are 43 drilling boreholes in the field and average depth is about 25m (Figure 2). All boreholes were drilled to 40m altitudes, because of problems with groundwater which is costly to drain. Different length of cores are logged and stamped at different sampling depths. Core logs include chemical analysis, sample length, coordinates, and rock type definitions. A representative 195 core samples were collected for the analysis. Although the boreholes have different variables, only rock types are used in the simulations.

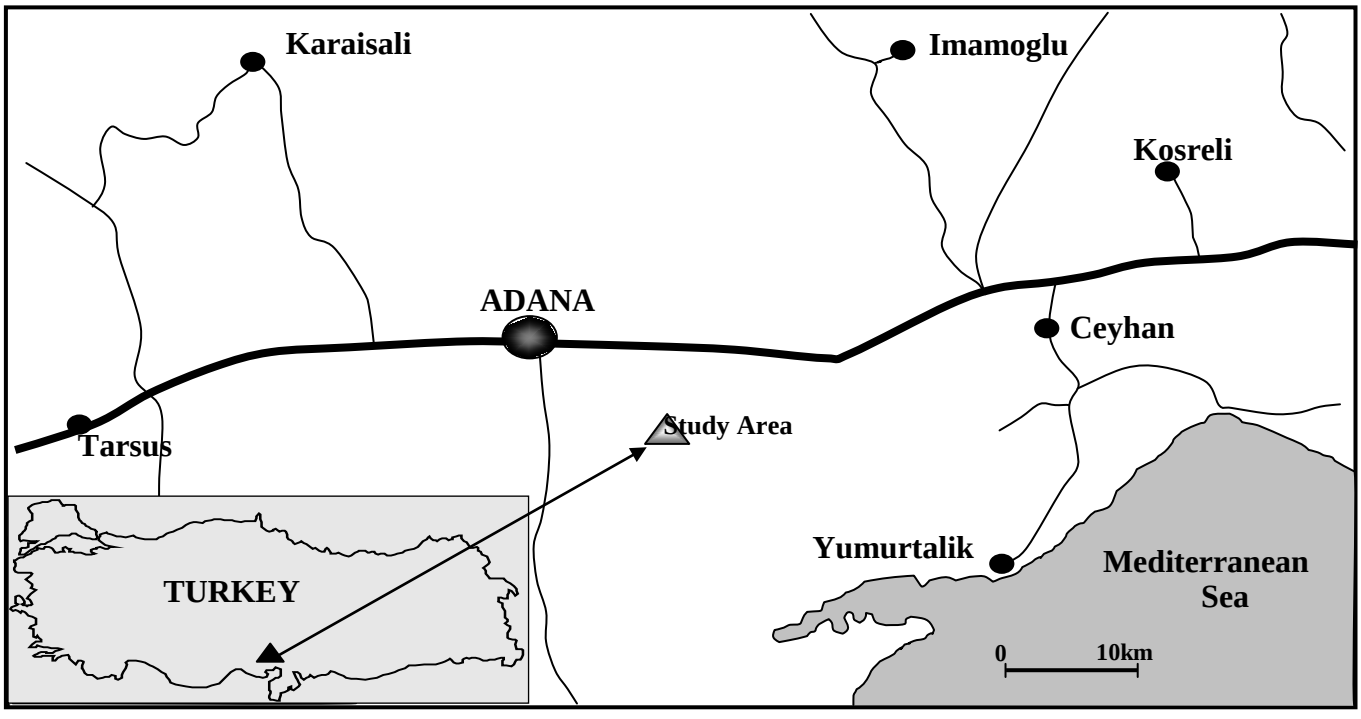

Figure 1. Location map of study area.

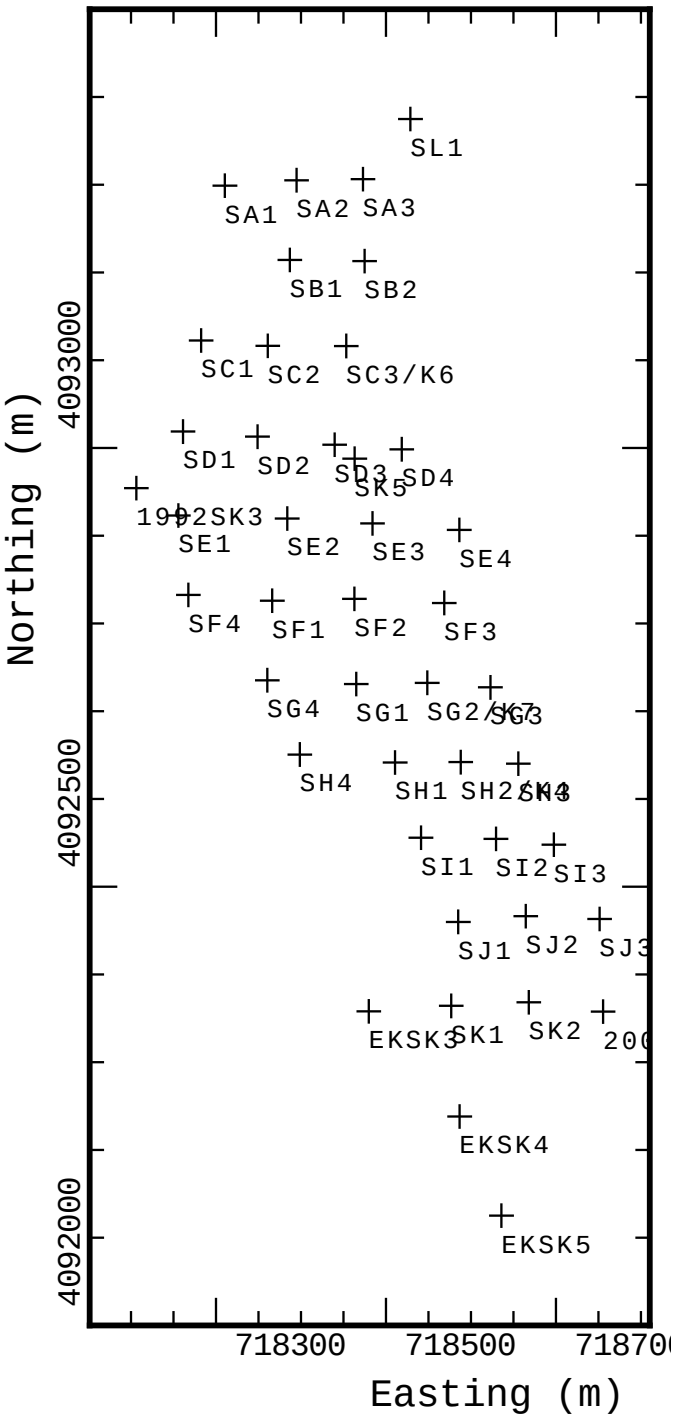

Figure 2. Drilling locations in the study area.

Chemical analyses include different oxides such as CaO, SiO_2, Al_2O_3, Fe_2O_3. These chemical compounds are used in calculation of the main cement modulus's including "Lime Standard", "Aluminium Modulus" and "Silica Modulus".

These standards play a vital role on optimal clinker production process by adjusting the chemical mixture content. The main rock types strongly affect the chemical contents of the samples. Thus, a correct characterisation of the field in terms of the rock types directly affect the clinker or cement production.

The rock types in the field are divided into three rock types. They are "Limestone", "Marl" and "Sandstone". In addition, limestone is divided into two groups according to their CaO contents. Limestones including lover than 45% CaO assigned as "Clayey Limestone". Finally, four rock types were used for the raw material deposits characterisation.

4 PLURIGAUSSIAN SIMULATIONS

Although it is similar in many aspects, Plurigaussian simulations is a different form of the Truncated Gaussian Simulations to be used for multiple realisations of the rock types. Detailed review of the methods can be found in relevant literature (Yünsel and Ersoy, 2013; Deraisme and Forrow, 2004; Armstrong et al., 2011). The basic procedure may be described under four steps:

1. Discretization and flattening is used to describe variables and the working grid system. Available data coordinates migrated to a working grid system to get better correlations between different rock types.

2. Vertical proportion curves are calculated for individual polygons created on the study field covering whole drilling boreholes. Each proportion curve is processed to get a representative geological structure in related polygon areas.

3. The following step includes the Plurigaussian variogram analyses. In this process, relations among rock types are modelled according to the described lithotype rules and correlation between Gaussian random functions and their variogram models.

4. The final step covers simply employing Plurigaussian Simulations and transferring the simulation results to its original space.

The rock types in the study are described as follows:

(1) Blue : Marl
(2) Yellow : Clayey Limestone
(3) Green : Limestone
(4) Red : Sandstone

According to the described colour, the positions of the rock types in 3D across the study area can be seen in Figure 3 (Z axis expanded by 10x).

A total of 20 polygons were created for the individual vertical proportion curves (VPC) (Figure 4). As it can be seen in the Figure 4, each polygon area has its own VPC to combine the related boreholes. Averaged within polygons designed to take into account lateral rock type changes. The vertical proportion curve counts the number of occurrences of each rock type distribution, and in validating the sedimentology interpretation. The data for the proportion curve are obviously related to the choice of the reference level used for the flattening step.

Next step includes the Plurigaussian variogram analysis of the categorical rock types to model the relation among them. The determination of the lithotype rule to identify the relation among rock types takes place at this stage. Multiple variogram analysis is carried out for each rock type at the same time in horizontal planes (X-Y) and vertical plane. This is the most important and time consuming phase of the process. Figure 5 shows the lithological rules defined from the transitions probabilities of the rock types, measured with the input dataset, and geological information about the rock type. In this diagram, the horizontal axis for the first Gaussian random function, including, marl. The vertical axis stands for the second Gaussian random function, including limestone, clayey limestone and sandstone. The application also produces a set of histograms showing the frequency of transitions between rock types along the wells. In the lithotype rule, the ore contact all rock types, have been imposed, according to the transitions probabilities. This is consistent with the real geology (borehole logs). Indicator vertical variograms for the rock types are presented in Figure 6. In the variogram graph, the thin continuous lines and thick continuous lines represent the experimental and modelled variograms respectively in a multigaussian frame.

Final process is the operating the Plurigaussian Simulation process using previously determined models and rules. As a post processing, low pass filtering and the median filtering methods are used to get a smoother rock type transitions as naturally should be in the field. In Figure 7 and 8 the distribution of the each rock type is presented. In these maps, the transitions, distributions, contacts and geometric positions of the rock types can easily be followed. Also rock type distribution in the field can be visualised in required lateral or vertical plane. This feature of the result provide invaluable information and flexibility for production planning and the process control in the study field.

Figure 7 is the vertical section of the field across the Y-Axis plane at the intersection of 718294th meter with the X-axis. Figure 8 shows the cross-section of the field taken at the level of 44m in horizontal plane. The following points may be drawn from an examination and interpretation of Figure 7 and 8.

- Marl is more abundant than the other rock types.
- Limestone proportions increases with depth.
- Approximately 10% of the cross sections area is covered by sandstone
- Limestone occurs in the northern part of the study area.
- There are contacts between all rock types. This is consistent with borehole logs.

Success of the simulation results can be validated by checking the input and the output information. The statistics of the simulated rock types are nearly the same as the input data statistics (Figure 9). Clearly, the plurigaussian simulations have been successful in reproducing the statistical and spatial character of the original data.

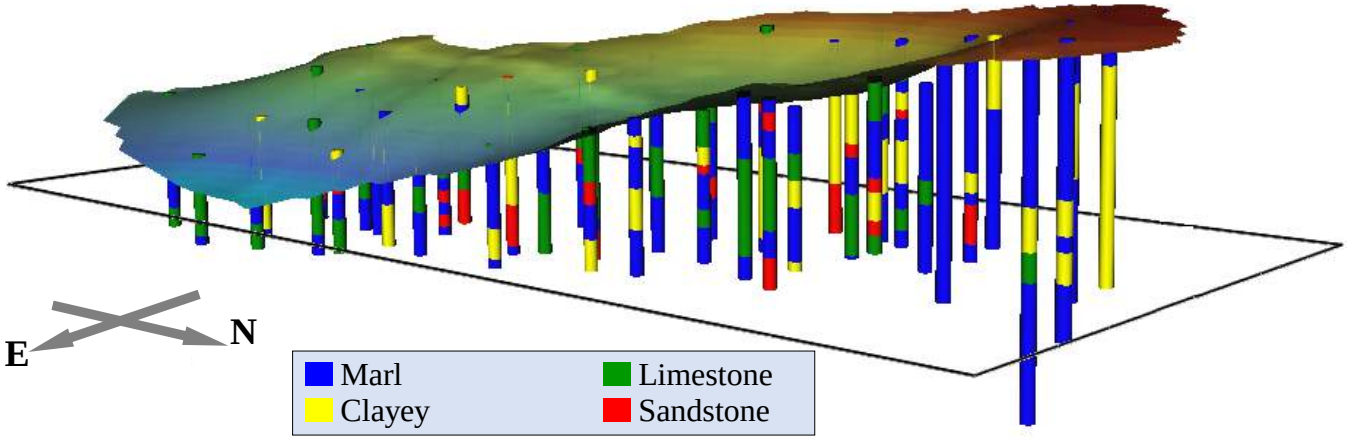

Figure 3. Rock type distribution along boreholes in the field.

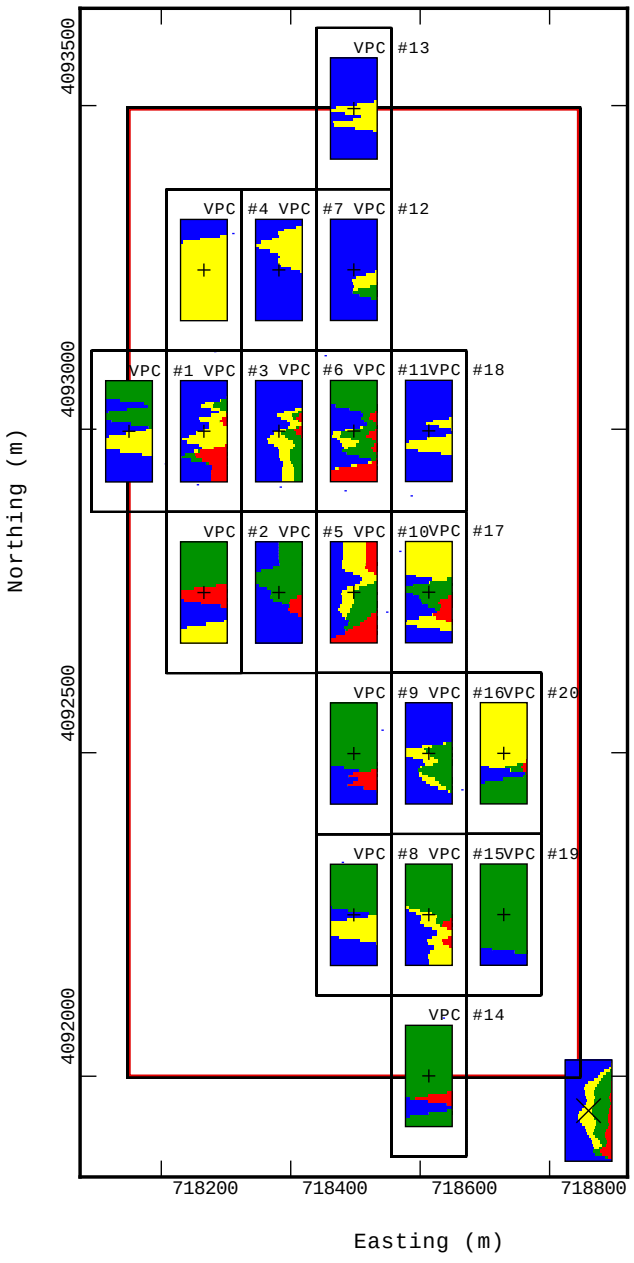

Figure 4. Vertical proportion curves.

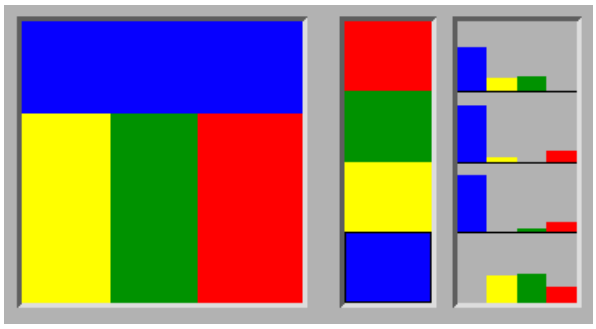

Figure 5. Lithotype rule for rock types.

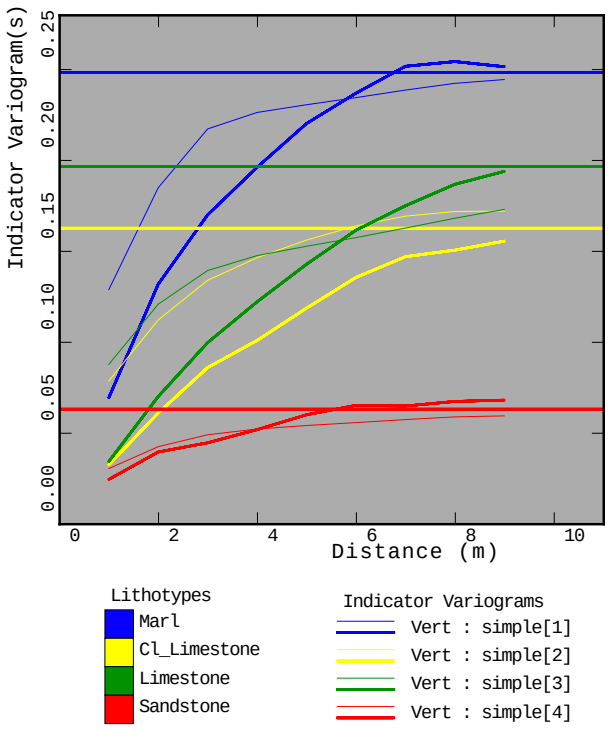

Figure 6. Simultaneous vertical variogram modelling of rock types.

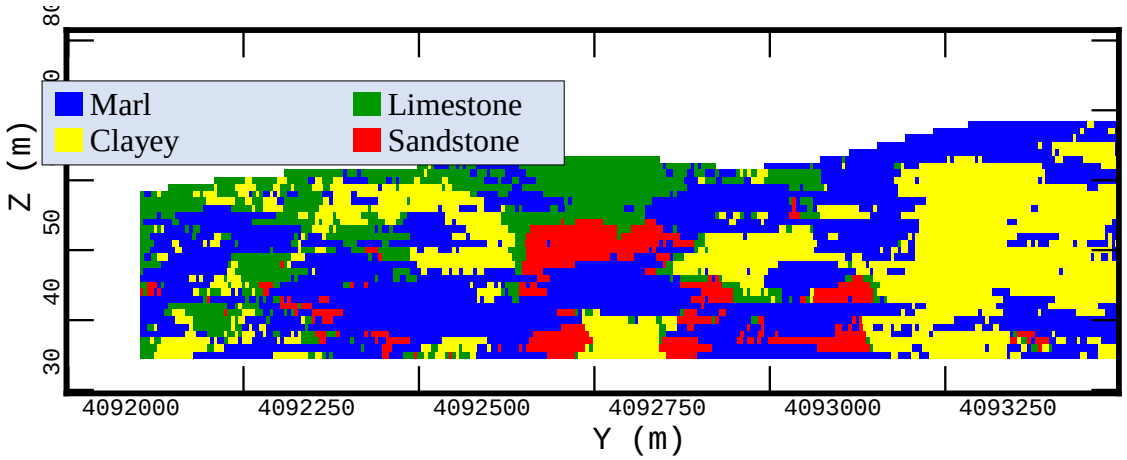

Figure 7. Vertical view at 718294th m in X-Axis.

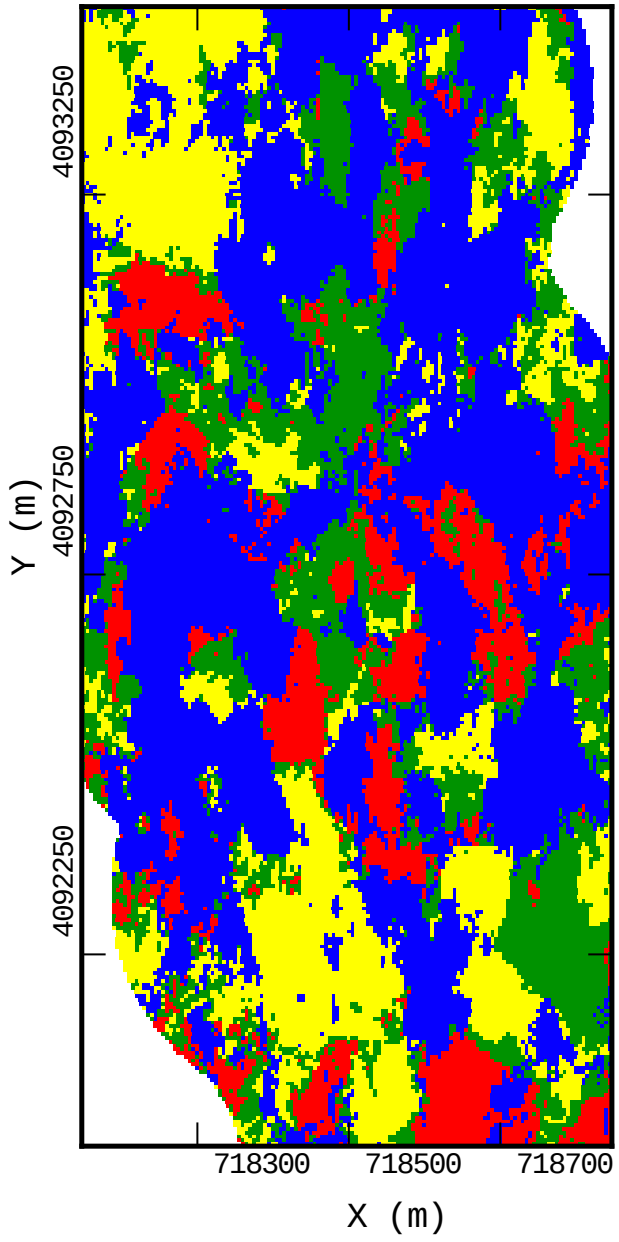

Figure 8. Horizontal view at 44m level.

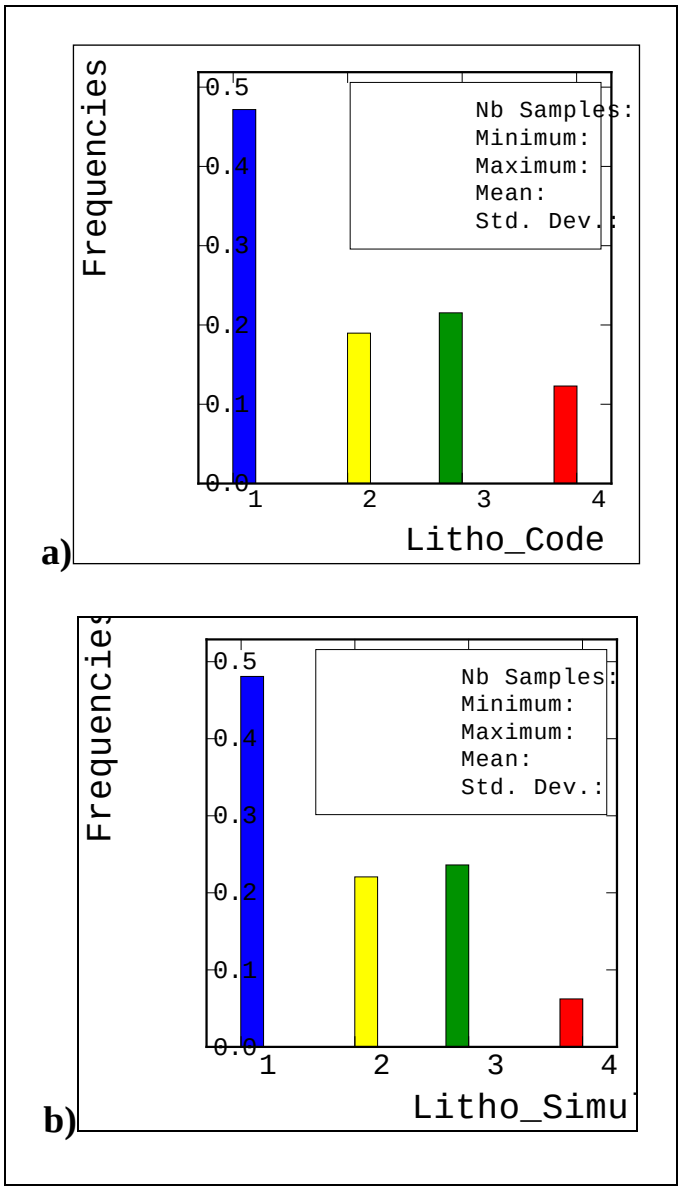

Figure 9. Rock type statistics: **a)** Input data, **b)** Simulated data.

5 CONCLUSIONS

Plurigaussian simulation was shown to be effective in reproducing the characteristics of the different rock types and the main features of the geology at the cement raw material deposit. Such modelling is the basis of resource estimation for the raw material deposit. This may be explored in an operational context. Therefore, the work will help raw material operation, production planning, and economic decision making. Plurigaussian simulation relies hardly on the effective integration of geostatistical knowledge and geological experience. The case study was focused on geological models of a cement raw material deposit. The results of the analysis are likely to be potentially useful for a wide range of users, such as mining-resource researchers, practitioners, technologists, and decision makers for deposit planning and scheduling.

This kind of geostatistical simulation methods are very important in terms of geological understanding of the interested rock type domains. Result of the study revealed the distribution and the complex relation of the rock-type domains in the area. This is basic information for the particular industries such as cement factory. Identification of such domains play a key role for future production planning and used in decision making. Results of this study may be used in mining, petroleum, geological and other earth-related sciences.

ACKNOWLEDGEMENT

Authors extent their thanks to Adana Cement Industry for providing the data set for this study.

REFERENCES

Armstrong M., Galli A., Beucher H., Loc'h G., Renard D., Doligez B., Eschard R., Geffroy F., 2011, *Plurigaussian Simulations in Geosciences (2nd Edition).* Springer, Berlin.

De Almeida J.A.,2010, Stochastic simulation methods for characterization of lithoclasses in carbonate reservoirs. *Earth-Science Reviews*, 101, 250-270.

Deraisme J., Farrow D., 2005, Geostatistical simulation techniques applied to kimberlite orebodies and risk assessment of sampling strategies. In: Leuangthong O., Deutsch C.V. (Eds.), *Geostatistics Banff 200*4, Springer, 14, 429-438

Deutsch C.V., 2006, A sequential indicator simulation program for categorical variables with point and block data: BlockSIS. *Computers & Geosciences*, 32, 1669-1681

Emery X., Lantuéjoul C., 2006, TBSIM: A computer program for conditional simulation of three-dimensional Gaussian random fields via the turning bands method, *International Journal of Coal Geology*, 32, 1615-1628

Emery X., Ortiz J.M., Cáceres A.M., 2008, Geostatistical modeling of rock type domains with spatially varying proportions: Application to a porphyry copper deposit, *Journal of the South African Institute of Mining and Metallurgy*, 108, 285-292

Geovariances, 2014. *Isatis Software Manual*, Fontainebleau, France.

Le Loc'h G., Galli A., 1996, Truncated plurigaussian method: theoretical and practical points of view. In: Baafi E.Y., Schofield N.A. (Eds.), *Geostatistics Wollongong '96*, Dordrecht, 211-222

Vargas-Guzman J.A., Al-Qassab H., 2006, Spatial conditional simulation of facies objects for modeling complex clastic reservoirs. Journal of Petroleum Science and Engineering, 54, 1-9

Yünsel, T.Y, 2012, A Practical Application of Geostatistical Methods to Quality and Mineral Reserve Modelling of Cement Raw Materials, *The Southern African Institute of Mining and Metallurgy*, 112, 239-249

Yünsel, T.Y, 2012, Risk quantification in grade variability of gold deposits using sequential gaussian simulation, Journal of Central South University, 19, 324-3255

Yünsel, T.Y, Ersoy, A., 2013, Geological Modeling of Rock Type Domains in the Balya (Turkey) Lead-Zinc Deposit Using Plurigaussian Simulation, *Central European Journal of Geosciences*, 1, 77-89

Characterization and Monitoring of Underground Cavities and Associated Disorders by Electrical Tomography

K. Hebbache, D. Benmeddour, M. Mellas, A. Mabrouki
Civil Engineering Laboratory, Biskra University, BP 145 Biskra 07000 Algeria

ABSTRACT The electrical tomography method is considered one of the best non-destructive geophysical methods for the detection, characterization and monitoring of underground cavities and associated disorders. The detection of cavities in urban areas is a very important tool to prevent different causes of accidents related to possible collapse. This study focuses on the assessment carried out in the framework of the construction of a project of buildings in the town of Tolga, Biskra province of southeastern Algeria. This field contains a plurality of cavities that are essentially of natural type, also of different dimensions and different depths. The procedures, using the electrical Tomography Wenner device to detect the cavities, are performed for depths ranging from 2m to 4m. These cavities result for most of the natural phenomenon of dissolution of carbonate material grounds. The electrical tomography results are calibrated, by the mechanical tests and trials dynamic penetrometer.

Keywords: Electrical tomography, underground cavities

1 INTRODUCTION

The methods of geophysical prospecting are used in the preliminary studies, for projects of construction that cover large surfaces. They can quickly and inexpensively obtain an overall assessment of the subsurface. Practically, there are several methods such as the electrical, gravimetrical, seismically, and the electromagnetically methods. The electrical method is the most commonly used to resolve geological and geotechnical problems. Many works have been made by this technique to present, applications of underground cavities detection (El Khammari *et al*, 2007; Emin and Irfan, 2006; Fehri *et al*, 2011; Metwaly and Alfouzan, 2013; Van schoor, 2002), the archaeological investigation (Muztasa *et al*, 2012) and environmental and hydrogeologically studies (Martinez *et al*, 2009; Sumanovac, 2006). This technique is not the only one used to discover the subterranean cavities. Gravimetrical and electromagnetically methods for geological radar are also used, to obtain a good recognition of the subsurface (Park *et al*, 2010; El Khammari *et al*, 2007; El-qadi *et al*, 2005).

In the present study, the technique of electrical panels is implemented for the detection and delimitation of underground cavities within foundation soil layers. The electrical tomography is non destructive method. Spatially integrative technique has recently been introduced into the geotechnical studies. The mechanical tests and trials dynamic penetration tests are used to confirm the geophysical measurements.

In the town of Tolga, willaya of Biskra situated in South east Algeria, there are underground cavities of natural origin, that are formed by the process of dissolution of limestone. The presence of these cavities influences the stability of constructions.

The objective of this work is to analyse the subsoil resistivity in the city of Tolga, to assess the potentiality of the geo-electric method to detect underground cavities.

2 PROCEDURE OF INVESTIGATION

Electrical tomography makes use of a multi-electrode device that enables acquiring a large number of measurements corresponding to the various four-electrode combinations. The principle of the electrical

resistivity panels is to inject in the ground an electric current of intensity (I) between two electrodes C1 and C2 and measuring the difference of potential (V) induced between another pair of electrodes P1 and P2 (Fig. 1).

From the value of the injected current (I) measuring the potential difference (V) and the spacing between the different electrodes. The apparent electrical resistivity of the subsurface can bee determined by the Ohm's law:

$$\rho_{app} = \frac{\Delta V}{I}.K \qquad [1]$$

K: Factor of geometry depends on the distance between electrodes.

ΔV : Difference of potential

I: Intensity of current

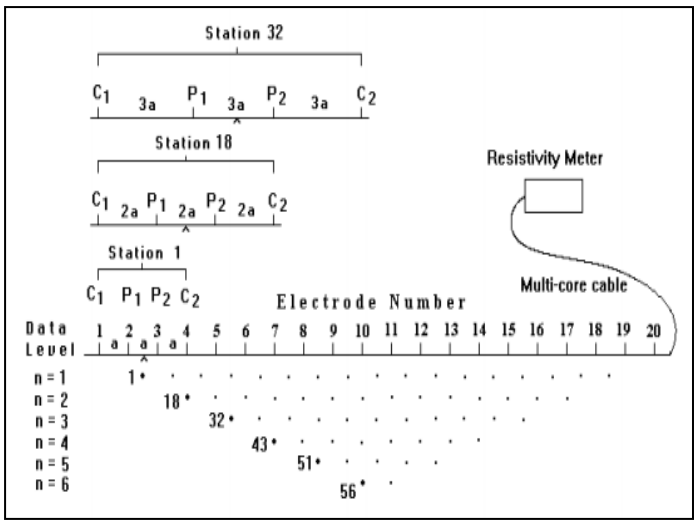

Figure 1. Classification of electrodes according to Wenner's method (*manual RES2Dinv*).

3 METHODOLOGY

The main objective of the present study is to implement the technique of tomography for the detection and delimitation of underground cavities, within urban area.

In the present study, series of two dimensional tests (resistivity measurement of the ground) have been carried out with the apparatus of resistivity meter SARIS (Scintrex Automated Resistivity Imaging System) of the company (Scintrex Ltd).

The program of geophysical recognition contains eight (8) electrical panels; their characteristics are represented in the Table 1.

Table 1. Electrical profiles characteristics.

N° of profiles	Number of electrodes	spacement (m)	Direction
1	30	2	W-S
2	29	2	N-S
3	30	2	W-E
4	25	1	W-E
5	25	1	W-E
6	25	1	W-E
7	25	0.5	N-S
8	24	0.5	N-S

The optimal disposal of profiles allows collecting maximum of information about the experimented zone (Fig. 2). The Wenner configuration was adopted for all the electrical profiles (Dahlin and Loke, 1998). This configuration has a horizontal sensibility, and it is recommended to discover horizontal structures; however, it is misadvised for vertical structures (Dahlin and Zhou, 2004). After the collection of data, the following stage concerns the inversion of data.

Figure 2. Disposal of the group of the electrical panels.

The inversion of data obtained from the electrical imaging is made by the code of inversion RES2Dinv (Loke and Barker, 1996), which determines automatically in two dimensions: the model of resistivity and the polarization provoked by the subsoil (Grifiths and Barker, 1993). The inversion

code is able to calculate the values of apparent resistivity by the technical optimization of nonlinear least squares (DeGrout and Constable, 1990; Loke and Barker, 1996; Sasaki, 1992). For the modelling, the RES2Dinv program distributes data by considering rectangular meshes on all the investigation depth (Edwards, 1977).

4 RESULTS AND DISCUSSIONS

4.1 Geophysical Investigations

The electrical tomography results are presented as pseudo-sections or electrical panels. The apparent resistivities values obtained for all electrical panels vary between 10 to 500 ohms - m, and indicate that the subsurface is very heterogeneous. The inversion code RES2Dinv represents three pseudo-sections, the first is the apparent resistivity measured, the second is the calculated apparent resistivity and the last is the proposed inversion model.

In this study, only the inversion models are shown in figures (3, 4, 5, and 6) for illustrative purposes. Figure 3 shows three electrical panels corresponding to the profiles P1, P2 and P3. The electrical panel P1 shows that the ground consists of a layer clay measured approximately 16m in length and 1.3m in width, with an apparent resistivity ranging from 35 to 40 ohms - m. Also, below the upper layer clay, there are carbonate formations, corresponding to limestone characterised by high resistivities of the order of 200 ohms - m, which are located at 3m in depth. The first and the second panels contain approximately similar characteristics (clay, clayey carbonates, and carbonate formation).

The electrical panel P3 indicates the presence of three formations in the subsoil, which are clay layer near the surface, clay carbonates layer at a depth of 3m and carbonate formation presents the deep layer.

The profiles P4, P5 and P6 were performed in the longitudinal direction at the excavation bottom. The results are shown in Figure 4. The panel P4 shows a carbonate formation covering the entire study parcel, and the resistivity is of the order of 200 ohm - m. Also, there is a highly conductive clay laver of resistivitv 20 ohm - m.

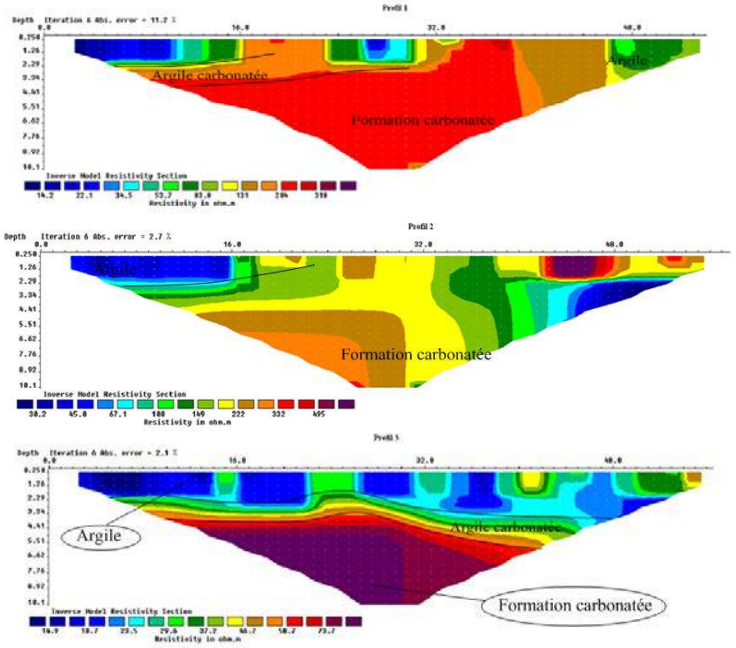

Figure 3. Geophysics measurement results of profiles P1, P2 and P3.

The electrical panel P5 shows the existence of a highly resistive region, that reveal a resistant body whose core is located at approximately 1.5 m; this can be explained by the presence of a horizontally elongated cavity. Both P4 and P5 profiles have similar characteristics, corresponding to carbonate formations. However, the electrical panel P6 is characterized by carbonate formations; in addition, there is a conductive area in the center of the panel, and its apparent resistivity equals to 20 ohm-m. This area corresponds to a clay formation.

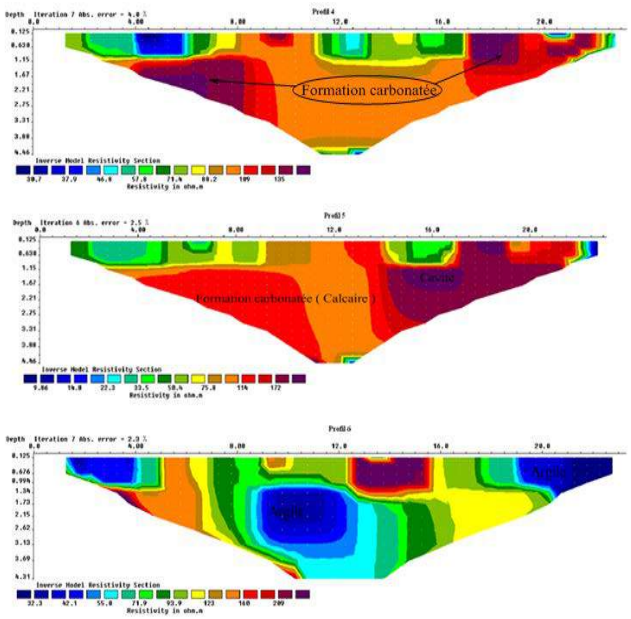

Figure 4. Geophysics measurement results of profiles P4, P5 and P6.

Figure 5 shows the Geophysical measurement resulting of profiles P7 and P8. These profiles are performed in the transverse direction at the excavation bottom. These electrical panels show that the foundation soil contains carbonate formations (limestone) that spreads in depth and the soil surface. The results clearly show an electrically resistive basement; moreover, it can be concluded that the electrical tomography method allows characterizing the existing formations in the study site.

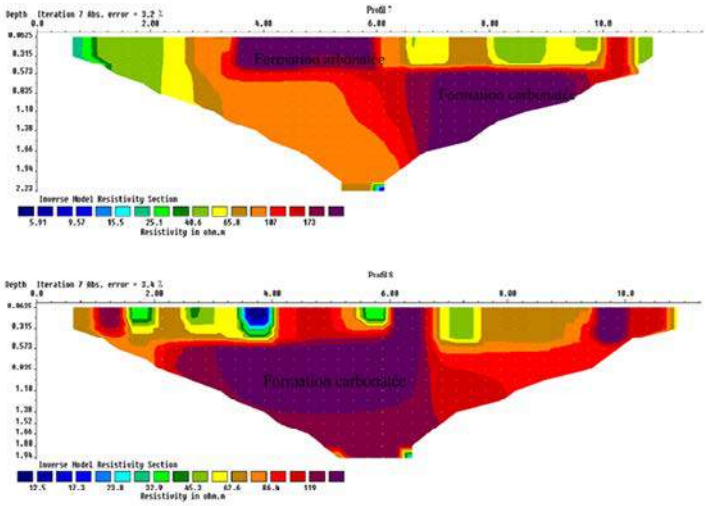

Figure 5. Geophysical measurement results of profiles P7 and P8.

4.2 Geotechnical investigations

To confirm the existence of the subterranean cavities and assess the performance of the geo-electrical method, the mechanical tests, and dynamic penetration tests were conducted. The excavation confirms that, within this geological context, for the most part can be classified as carbonate, dissolution phenomena have engendered the appearance of a complex system of underground cavities of variable size and highly irregular shape. Figure 6 illustrates the type of subterranean cavities encountered after excavation of 2.5m in depth.

The results of mechanical tests clearly show the continuity of carbonate formation of the ground. Finally, the site contained a white porous limestone, silty clays, clays highly carbonates, gravelly and stony tuffs with sandy silt passages.

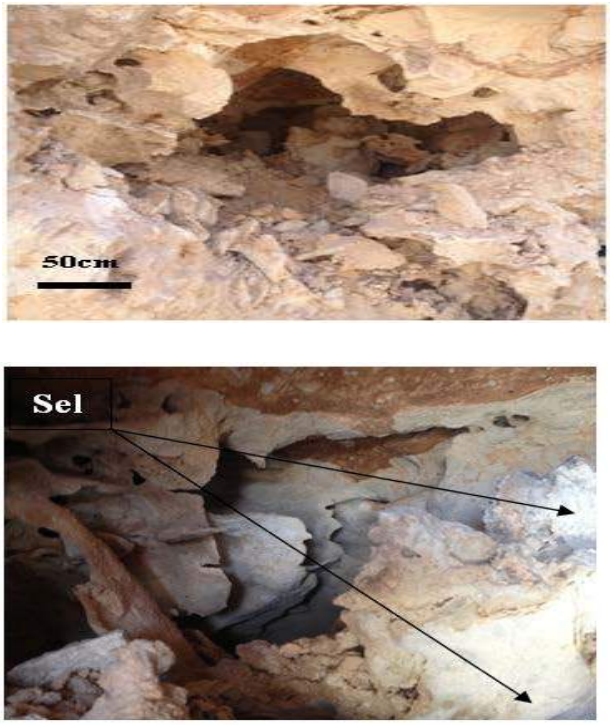

Figure 6. Illustration of subterranean cavities (city of Tolga)

5 CONCLUSION

The geophysical prospecting by electrical tomography allows detecting the subterranean cavities and their extension. The presence of cavities in the Tolga region

is mainly due to the dissolution of the material in the limestone. The electrical panels gave vertical section below realized profiles; these panels contain information necessary for correct interpretations.

The applicability of the present technique is illustrated by a comparison with the results from mechanical tests. Tests performed by dynamic penetration gave very satisfactory resistances of the foundation soil.

The solution proposed to realize the infrastructure, is a total excavation and reconstruction of the soil foundation, treated with a hydraulic binder, for example 15% cement, and compacted layer by layer of depth of 20 to 30 cm. Cavities and voids localized according to their dimensions can be filled with mortar of cement or concrete.

REFERENCES

Dahlin, T., Zhou, B., (2004). A numerical comparison of 2-D resistivity imaging with 10 electrode arrays. *Geophysical Prospecting* 52, 379-398.

Dahlin, T., and Loke, M., (1998). Resolution of 2d wenner resistivity imaging as assessed by numerical modeling*: Journal of Applied Geophysics*., **38**, 237 24.

DEGroot-Hedlin, C., Constable, S., (1990). Occam's inversion to generate smooth, two dimensional models form magnetotelluric data. *Geophysics* 55, 1613–1624.

Edwards L.S., (1977). A modified pseudosection for resistivity and induced-polarization. Geophysics, 42 (5), 1020-1036.

EL Khammari, K., Najine, A., Jaffal, M., Aifa, T., Himi, M., Vàsquez, D., Casas,A., and Andrieux, P., (2007). Imagerie combinée géoelectrique-radar géologique des cavités souterraines de la ville de zaouit ech cheick (maroc) : *comptes rendus Geoscience* 339,no. 7, pp.460-467.

EL-Qady, G., Hafez, M., Abdalla, M.A., Ushijima, K., (2005). Imaging subsurface cavities using geoelectric tomography and ground-penetrating radar. *Journal of Cave and Karst Studies* 67 (3), pp. 174–181.

Emin U. U., and Irfan A., (2006). Detection of cavities in gypsum. *Journal on the Balkan. Geophyscal Society*, Vol. 9, No. 1, pp. 8-19.

Fehdi CH, Baali F, Boubaya D, Rouabhia A., (2011). Detection of sinkholes using 2D electrical resistivity imaging in the Cheria Basin (north-east of Algeria). *Arab J Geosci* 4:181–187.

Grifiths, D.H., Barker, R.D., (1993).Two-dimensional resistivity and modelling in areas of complex geology. *Journal of Applied Geophysics* 29, 211–226.

Loke, M.H., Barker, R.D., (1996). Rapid least-squares inversion of apparent resistivity pseudo sections by a quasi-Newton method. *Geophysical Prospecting*, 42, 813-824.

Martinez, J., Benavente, J., Garcia-Arostegui, J.L., Hidalg M.C., and Rey, J., (2009), Contribution of electrical resistivity tomography to the study of detrital aquifers affected by seawater intrusion-extrusion effects: The River Vélez delta (Vélez-Malaga, southern Spain):*Engineering Geology*,v.108,p.161 168doi:10.1016/j.enggeo.2009.07.004.

Metwaly, M., Alfouzan, F., (2013). Application of 2-D geoelectrical resistivity tomography for subsurface cavity detection in the eastern part of Saudi Arabia. *journal of geoscience frontriers* 4,469-476. doi.org/10.1016/j.gsf.2012.12.005.

Muztaza, N., Mokhtar Saidin, M., Saad, R., Nordiana, M.M., (2012). 2D Resistivity Method to investigate an Archaeological Structure in Jeniang, Kedah, *Electronic journal of Geotechnical Engineering*, Vol. 17, Bund C, pp 353-360.

Park, G , Park, S , YI, M J , Rim, H , Cho, S J , and Kim, J H., (2010). Geostatistical integration using 2-D electrical resistivity and 3-D gravity methods for detecting cavities in a Karst area, *Environmental Earth Sciences* 60, 965-974.

Sumanovac, F., (2006). Mapping of thin sandy aquifers by using high resolution reflection seismics and 2-D electrical tomography: *Journal of Applied Geophysics*, v. 58, p. 345– 346. doi:10.1016/j.jappgeo.2005. 06.005.

Sasaki, Y., (1992). Resolution of resistivity tomography inferred from numerical simulation.*Geophysical Prospecting* 40, 453–464.

Van Schoor, M., 2002. Detection of sinkholes using 2D electrical resistivity imaging. *Journal of Applied Geophysics* 50 (4), 393–399.

Comparative Study of Systemic Methods in Geochemical Data Optimization, for Cu-Mo Prospecting in Gulan Area, E-Azerbaijan, Iran

A. Nasseri
Department of Mining Engineering, Tehran Science and Research Branch, Islamic Azad University, Tehran, Iran

M.J. Mohammadzadeh
Associate Professor in Faculty of Mining Engineering, Sahand University of Technology, Tabriz, Iran

S.H. Tabatabaei
Head Department of Geophysics, Exploration Directorate of National Iranian Oil Company (N.I.O.C), Tehran, Iran

ABSTRACT: Detection of optimized geochemical pattern requires Orientation Survey (O.S.) in which one of its important layers is selecting an effective data analysis method. In order to detect favorable potentials in Gulan area, discrimination of mineralized and blind ore zones using advanced techniques with presenting a suitable geochemical pattern and relative pathfinders is the scope of this study. In this respect 233 stream sediment samples were collected from the area and analyzed for base metals (Cu, Mo, Cr, Co, Ni, Pb, Zn, As, Y …) and their indicator elements.

The anomalous zones in the area were detected using two systemic methods such as principle component analysis (PCA) and Fractal (F) methods. Application of F method on geochemical data leads to detection of two anomalous zones of Cu in Gharachilar and west of Loutkeh, with Mo appearance in Namnigh. The separation of these two anomalous zones (Cu& Mo) probably is due to acidity of area formed by solubility of sulphides from outcrops and migration of Mo in the form of Molibdat which caused the precipitation of Cu and Mo in two different zones.

Results shows in spite that both the methods (F& PCA) have similar detection zones but the capability of PCA in enhancement of halos and detection of blind ore zones is more effective than F method. As in this case it could detect strong blind anomalous zone of Mo in Namnigh in addition to Cu & Mo trend. Overall the characterization of methods also revealed that the PCA is more reliable in rejecting the syngenetic effects and the results can be more precisely used in the area.

Keywords: Geochemical pattern, favorable potentials, PCA and Fractal method, Gulan area

1 INTRODUCTION

Mineral exploration is a multidisciplinary task that requires the simultaneous consideration of numerous disparate geophysical, geological, and geochemical datasets (Knox-Robinson, 2000). Furthermore, it needs spatial modeling using observations regarding the association of mineral occurrences with various geological features in a qualitative manner.

In exploratory studies, singular geological processes result in elemental enrichments (or depletions) and geochemical distribution patterns representing mineralized zones.

Therefore, in order to identify promising areas, assessment of the elements distribution pattern in different environments is essential.

One of the most important fundamental issues in exploration geochemistry is the separation of anomalies that are associated with mineralization from background concentrations of elements which results from geological processes (Gałuszka, 2007; Hawkes and Webb, 1962). The relationship between anomalies and background concentrations especially for ore-forming elements is an important issue in spatial data analysis(Hawkes and Webb, 1962).

In exploratory data analysis it is well known that geochemical data are characterized by their spatial positions, which means that the element concentration varies spatially. Thus, the traditional methods emphasize only the frequency distribution of the element concentration and ignore spatial variability. In addition, these methods are only applicable to situations where geochemical data follow a normal distribution(Ahrens, 1954a; Ahrens, 1954b). Many statistical methods that have used to enhance geochemical anomalies include probability graphs, univariate and multivariate analysis, moving averages, fractals methods (Cheng, 1999; Govett et al., 1975; Miesch, 1981; Sinclair, 1974, 1991; Sinclair, 1976; Stanley and Sinclair, 1989). Various characteristics of geochemical data are considered in these statistical methods: 1) The frequency distribution of elements is applied in most methods; 2) Both the content and spatial position of samples are considered in moving average, kriging and spatial factor methods and 3) in addition to element contents and spatial position of samples, the geometrical characteristics of anomalous areas are used in fractal and multifractal methods (Changjiang et al., 2002; Changjiang et al., 1995; Cheng, 1995; Cheng et al., 1994; Cox and Wang, 1993; Sun et al., 2006; Xu and Cheng, 2001; Yuhua, 1994; Zhangdong et al., 1998). Due to the natural uncertainty and nonlinear behavior of elements in this study, it was attempted to apply a comparative optimization based on multivariate statistical method (PCA[1]) and spatial analysis method (fractal) for quantify spatial relationships of elements and discriminating anomaly from background in order to enhance mineralization zone in the Gulan area.

1.1 Geological Settings

Gulan area is located between ($46^{\circ}15'-46^{\circ}30'$) longitude and ($38^{\circ}45'-39^{\circ}$) attitude in 50 km north of Tabriz,70 km from W-Ahar city in Azerbaijan province, NW of Iran (Figure 1). Geochemical exploration background in the area represents the Gharahchilar area as a promising area for Cu-Mo mineralization (Alavi, 1991).

Based on the Siahrood geological map (Figure 1), the oldest rock unit is disrupted collection of metamorphic rocks and its main outcrop is visible in the NE of the area. Further, it consists of alternating layers of slate, mica schist, metatuff, metaandesite, calcschist and quartzite. These rocks have also undergone a further change under the intrusion of igneous masses. During the Upper Cretaceous, activation of sedimentary basins has led to form the variety of volcanoclastic facies which are transformed into each other laterally. Moreover, Oligocene magmatic activities have the important role in the geology of the area. Middle Alpine tectonic activities could also appear as faults and folds by influencing in the sedimentary and igneous deposits and the related outcrops are visible in the southern part of geological map. The main faults trend is in NW-SE and E-W directions. Paleogene volcanic series which is known as a process of Alpine tectono-magmatic cycle, is able to host significant mineralization of Cu, Mo, Pb, Au and Ag around the Ahar city, NW of Iran. It seems that this mineralization is accordance with the Alp- Himalaya copper belt and faulting of the area is continued from NW to SE towards Sungun copper deposit.

1 - Principal Component Analysis(PCA)

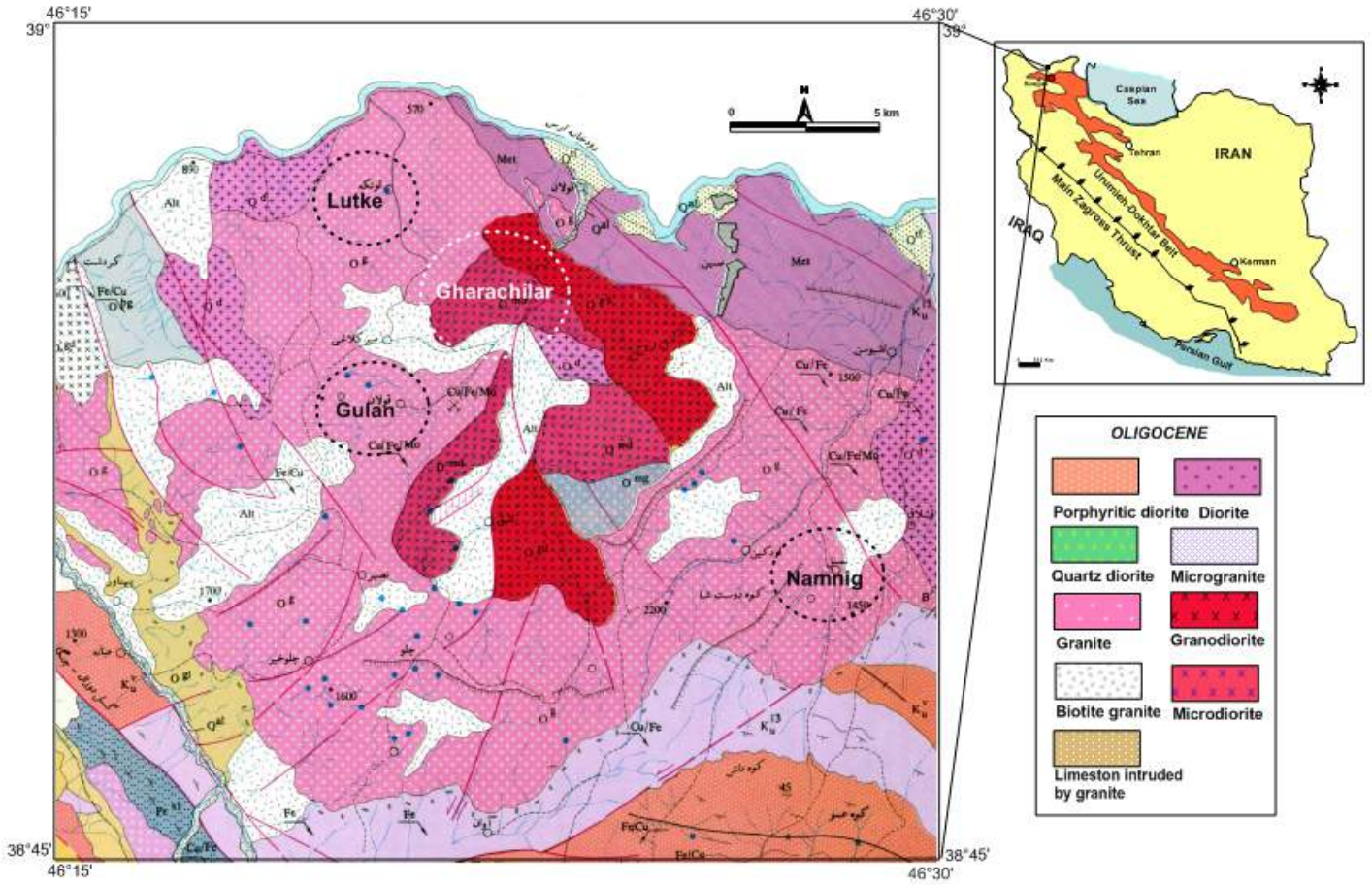

Figure 1. Modified and simplified geology map showing the location of study area

Stream sediments sampling was attempted in the area with the aim of detecting promising area for Cu mineralization by employing the systemic optimized methods.

2 MATERIALS AND METHODS

2.1 Sampling

Sampling operations were performed by three expert teams and total of 233 stream sediments were collected from the area. Each sample covers approximately an area of 1-2 kilometers square based on streams density in the catchments and had maximum compatibility with topology center method. The higher density of sampling was carried out for important zones such as intrusive and extrusive bodies, alteration zones, vicinity of faults and their intersections.

After preprocessing, the samples were converted to -200 mesh and analyzed for Cu, Mo, Cr, Co, Ni, Pb, Zn, As and Y by different analytical methods specially XRF-Sequential method. Figure 2 presents the stream sediments sample location map in Gulan area.

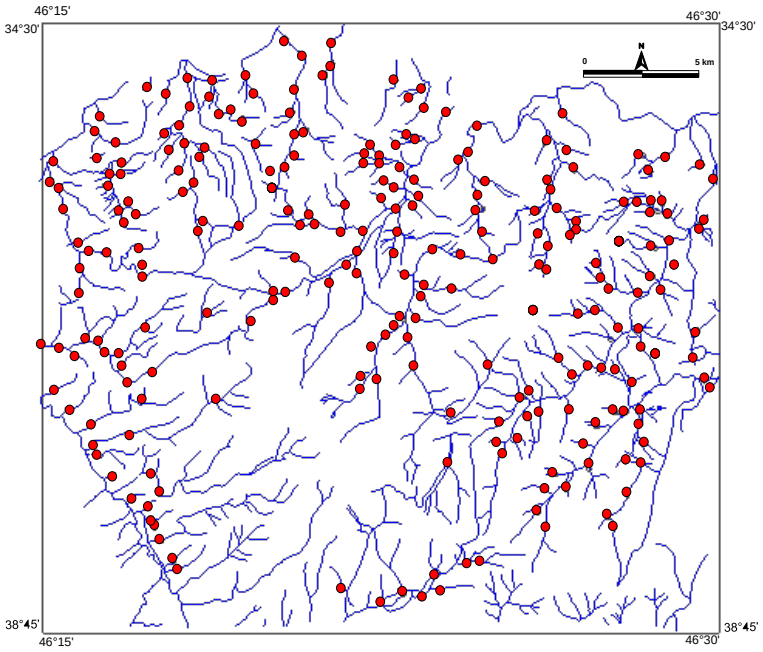

Figure 2. Stream sediments sample location map in Gulan area

2.2 Data Analysis

2.2.1 Principal Component Analysis(PCA)

Multivariate analysis methods have been used in mineral exploration for characterizing interrelationships occurring in large multi-element geochemistry datasets. Large datasets simplifying and analyzing process often becomes complicated and difficult when dealing with more variables. Therefore it is essential to apply dimension reduction methods in multivariate analysis. Principal component analysis (PCA) - as a multivariate statistical method- is a well mathematical method to reduce the dimensionality of the variable space based on the reduced factor solution. In the present study, PCA proceed in four steps: 1) computing the correlation matrix for all variables, 2) extracting factors, 3) rotating factors and 4) calculating scores between the original values and the extracted factors.

During this process, the obtained factors were subjected to orthogonal rotation by the varimax method to minimize the medium loaded elements in the extracted factors and to maximize low and high loadings of the elements. Since PCA with varimax normalized rotation was performed, each PC score contains information on all of the metal elements combined into a single number, while the loadings indicate the relative contribution of each element makes to that score. The PC loadings were plotted and accordingly the anomalous zones were detected (Figures 4& 5).

In order to assess the performance of the PCA for anomaly detection, we made a comparison of the results obtained from PCA with that of Fractal (F) over the same data.

2.2.1 Fractal method

This section contains a description of the Fractal construction and its application in discriminating anomaly from background in Gulan area. In this regard, the spatial distribution of elements values in a frequency domain was characterized and distinct patterns were separated using the concentration-area fractal method, which has been developed originally for anomaly separation in a spatial domain (Cheng, Agterberg, and Ballantyne, 1994; Cheng, 1999 asfollows:

$$A(\rho \le \upsilon)\alpha\rho^{-\alpha_1} \; ; \quad A(\rho \ge \upsilon)\alpha\rho^{-\alpha_2} \qquad (1)$$

Where $A(\rho)$ denotes the area with concentration values greater than the contour value ρ; υ represents the threshold; and α_1 and α_2 are characteristic exponents (fractal dimension).

All the resulting data from 233 stream sediment samples of the study area were analyzed using the aforementioned model for enhancing for enhancing and separating the anomalies from background, especially those week anomalies with relatively low concentration values.

The most important issue for calculating the fractal dimension in the studied area is to calculate concentration and grid area in gridded system. In this regard, there are several methods for interpolatingof data depending on the type of data. Due to the nature of the stream sediments data and considering the fact that each sample is only representative of its upstream thus radial estimation method was employed. After preparing gridded map(1000*1000 m^2), it was attempted to consider the area and concentration(C & A) for each cell. Ultimately, concentration-area log–log plot was constructed and then the threshold value was estimated based on the plot.

3 RESULTS AND DISCUSSION

Since multivariate techniques are sensitive to non-representative data, such as censored data, missing values and outliers, which impart strong variations in a dataset therefore prior to application of these techniques, a careful univariate analysis of the data set is required (Reimann et al., 2002). Accordingly, outliers were detected and replaced with Q method prior to data normalization and entering to PCA.

3.1 PCA Results

After pre-processing, univariate and bivariate statistical methods such as correlation coefficient was applied on the data. Considering the appropriate association of elements, PCA was conducted and the relevant maps were shown in Figures 4& 5 with their statistical parameters in Table1. This table shows the major loading of variables on each component in Gulan area. Further, a number of statistical parameters such as cumulative variance of each PC presented in the table, which can be used to judge the quality of a principal components analysis. Figure 3 a scree plot of the eigen values against their indices for different principal components (PC1 to PC8) indicating the importance of each component. The principal components calculated from a correlation matrix and only the first three components have eigen values above 1. These three components altogether account for 88.12% of the total variation in the original variables. The first principal component accounts for 38.88% of the variance including most of the variation in Zn,CO,Cu and Ni.

Table 1. Total variance and component matrixes for stream sediments samples in Gulan area

Element	PC_1	PC_2	PC_3
Cu	0.577	0.391	-0.486
Mo	-0.309	0.773	-0.341
Co	0.846	-0.328	0.143
Zn	0.817	-0.11	0.252
pb	-0.082	0.816	0.264
As	0.242	0.557	-0.015
Ni	0.632	0.335	-0.065
Zr	0.189	0.103	0.847
Cumulative (%) Variance	38.88	68.5	88.12

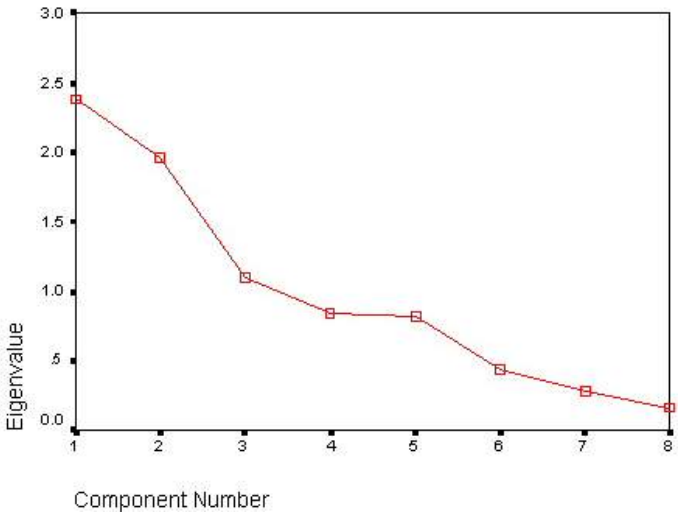

Figure 3. Diagram shows a scree plot of the eigen values against their indices for different principal components (PC1 to PC8) in Gulan area

Figure 4 shows a map of PC1 loading factor which indicates equal distribution of the elements in the area. Geochemically, it can be said that this distribution is the result of the weathering process. During this process, the elements have high mobility in aqueous solutions and can migrate for a long distances with relatively high stability. Depletion of Pb mobility in the area has been marked with intensity of Mo with extended secondary halos. In contrast positive correlation between Mo, Pb was observed in PC2 (with 29.62% of the total variance) that's why PC2 can not be used in geochemical interpretation of elements and determination of Mo and Pb anomalies. The third principal component (PC3) accounts for 19.62% and has high negative loadings score on Cu and Mo. Figure 4 shows the geochemical distribution map of (-PC3) which indicates high correlation between Cu, Mo in Namnig and Garehchiler zones. But the concentration of Cu, Mo in Namnig is more prominent compare to Garahchilar.

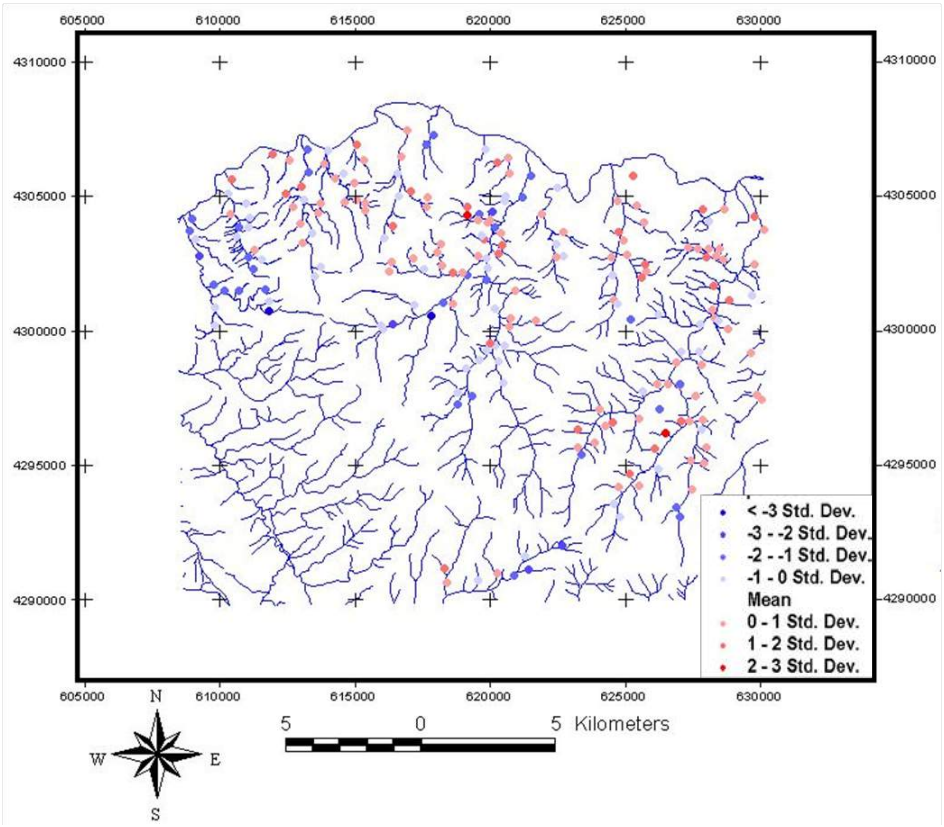

Figure 4. Mapping of the first (PC1) principal component in Gulan area.

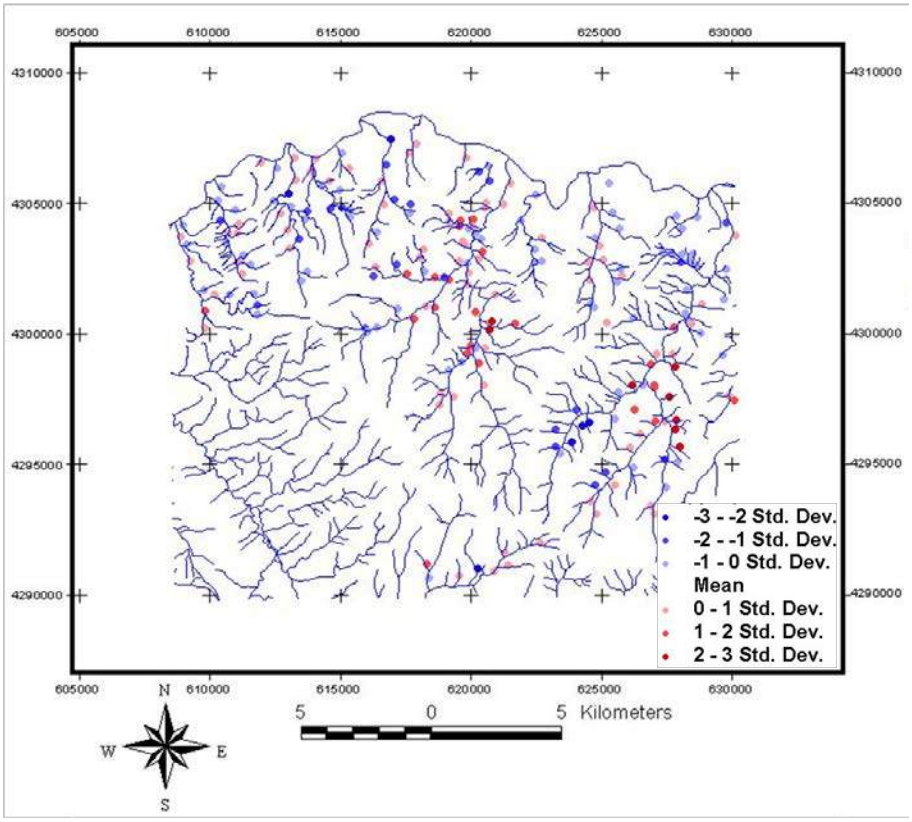

Figure 5. Distribution pattern map of (-PC3) showing high correlation between Cu and Mo in Namnig and Garahchilar.

3.2 Fractal Results

Figure 6 shows the grid pattern and catchment basin boundaries in Gulan area. Accordingly, most of catchments are overlapping in a cell. This issue was considered in calculating the final grade of each cell. After calculating the final grade for each cell, all log–log graphs were plotted (Figures 7& 8). To achieve this goal, the concentration-area fractal method was implemented for separating geochemical anomaly from background in the studied area. Distinct patterns separated by different straight-line segments with different slopes fitted to the elements values. Two line segments were fitted to the Cu and Mo values in Figures 7& 8, yielding a threshold value of 70ppm for Cu and 26 ppm for Mo respectively.

It can be seen that the areas with Cu values greater than 70ppm represent the Cu anomalies and the areas with 30 ppm for Cu as background value which may correspond to the average concentration of Cu in granodiorite and the effects of Cu mineralization. Figure 9 represents the geochemical distribution pattern of Cu anomaly population in the area. Based on this figure, three zones of West of Lutkeh, Gharachilar and Namnig were detected as promising areas for Cu mineralization. Similarly, figure 10 shows the anomaleous geochemical distribution pattern of Mo trending NW-SE of Gharachilar. This element manifested as molybdenite in the area and due to its high mobility, the corresponding secondary halos have expanded in the area. Therefore it can be used regional guide for prospecting. The lack of overlapping between secondary halos of Cu and Mo in Namnig and W of Lutkeh probably is due to acidification of the area by pyrite and Chalcopyrite presence from the outcrops. Thereby causing Mo to be transported in the form of molibdates in acidic environment concentrate its halo in Garachilar somehow discriminated from the Cu halos located in Namnig.

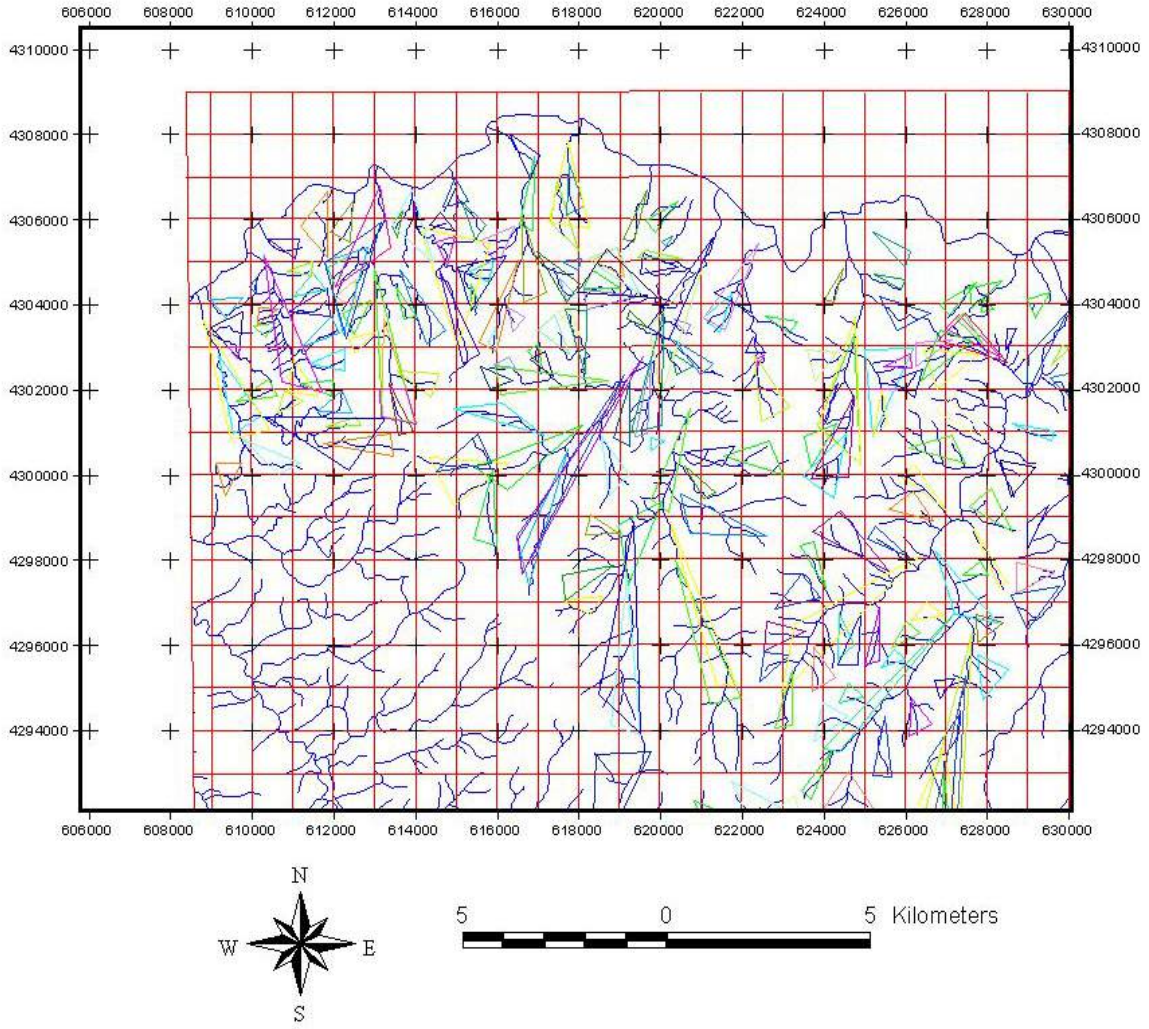

Figure 6. Ilustrating stream sediment samples grid and related catchment basin for fractal modeling in Gulan area

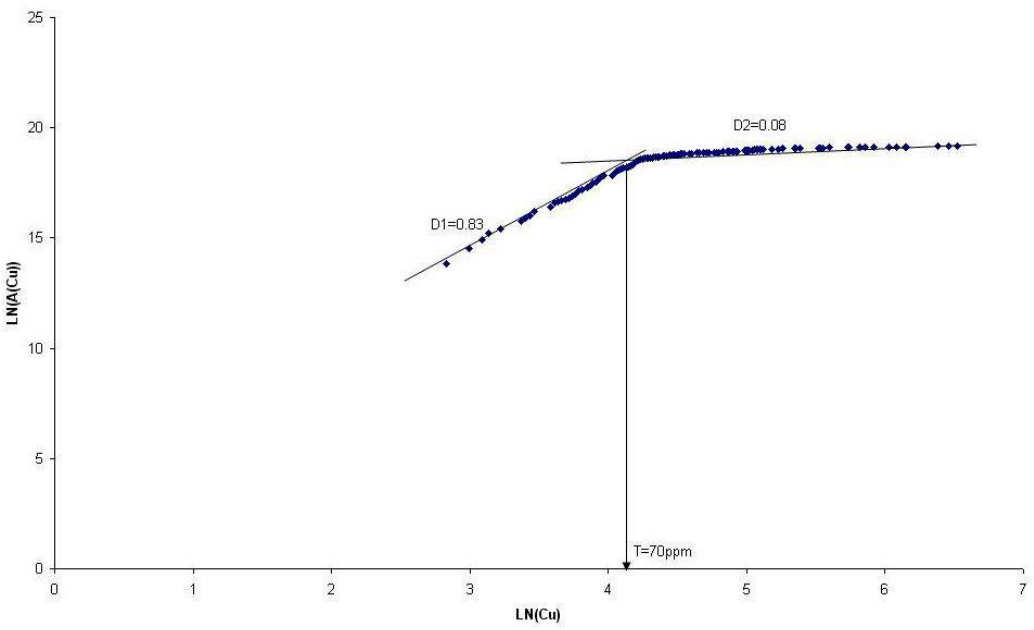

Figure 7. Log-log plot showing the relationship between frequency and Cu threshold value in Gulan area.

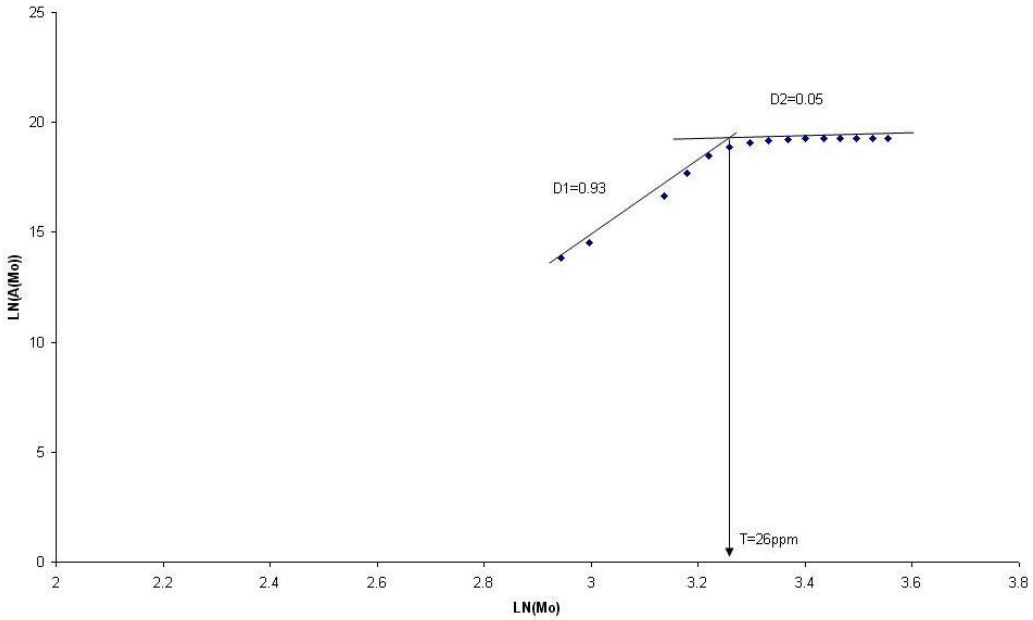

Figure 8. Log-log plot showing the relationship between frequency and Mo threshold value in Gulan area.

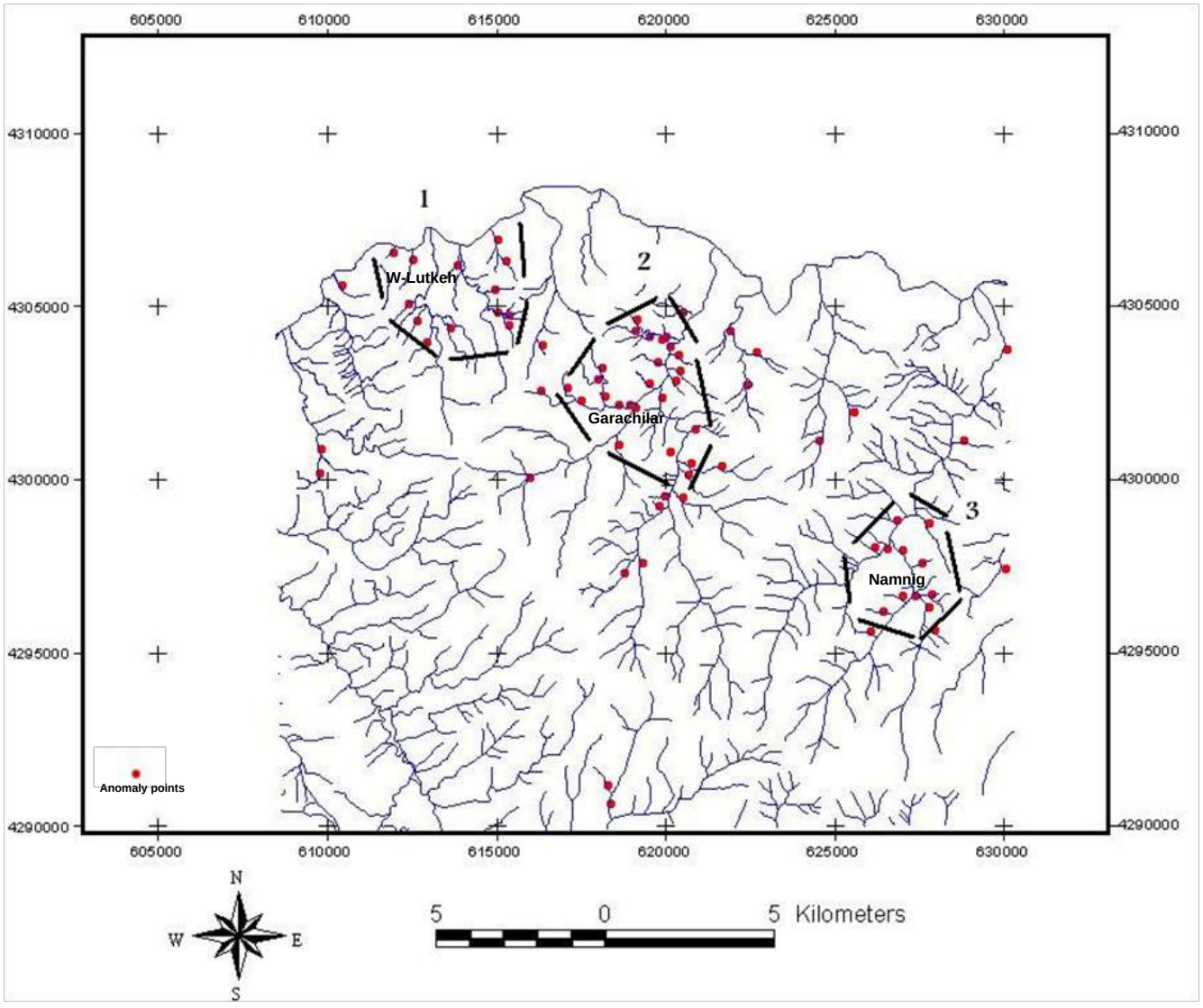

Figure 9. Cu anomaly delineation based on C–A model

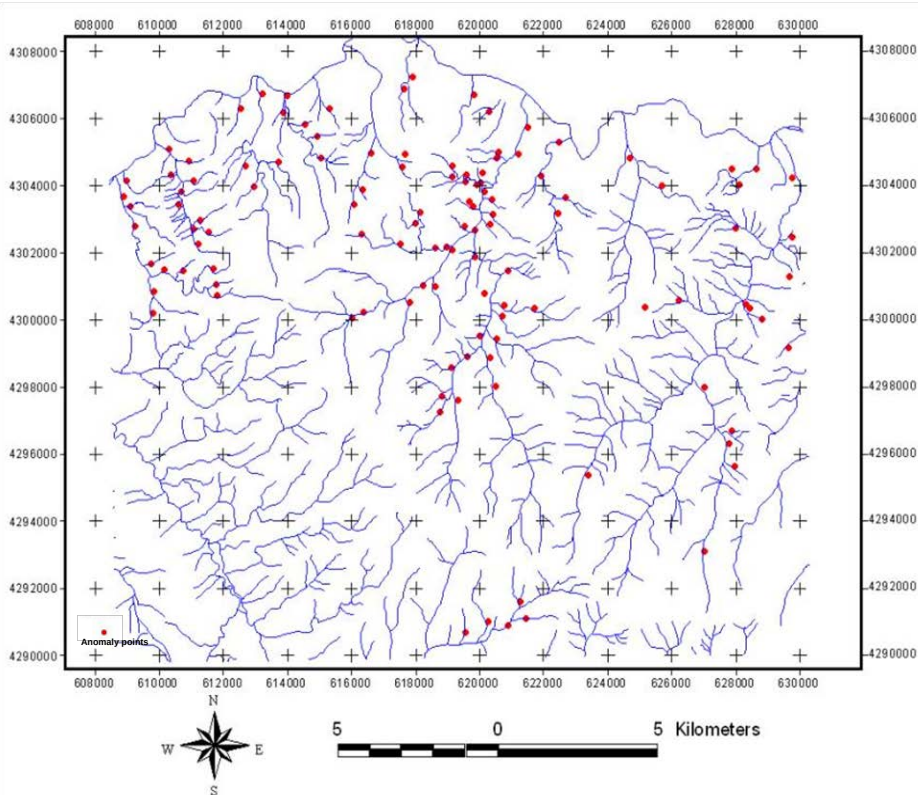

Figure 10. Mo anomaly detection based on C–A model

4 CONCLUSION

1) The results from PCA implementation in Gulan area reveals three parts of studied area as potentially promising zones for Cu- Mo prospecting in NW-SE direction. Application of this method enabled to detect more prominent anomalous zone in Namnig with higher intensity compared to Garachilar ad west of Lutkeh.

2) The intensity of Cu-Mo mineralization in the study area influenced by Caucasus tectonics and volcano-plutonic system of Shiyvar - Shahjahan-Ordubad orogeny trending with higher intensity toward NW-SE part of the area. This mineralization zone complying Alp-Hymalian Cu metalogenic belt trending toward famous Sungun copper mine –Anjerd and Kighal area.

3) Application of C-A fractal model in Gulan area indicate western part of Lutkeh, Gharachilar and Namnig for Cu prospecting while it proposed Gharachilar area for prospecting of Mo blind anomalous zone.

4) Results shows in spite that both the methods (PCA& F) have similar detection zones (western part of Lutkeh, Gharachilar and Namnig) but the capability of PCA in enhancement of halos and detection of blind ore zones is more effective than F method in this region. As in this case it could detect strong blind anomalous zone of Mo in Namnigh in addition to Cu – Mo general trend of mineralization. Overall the characterization of methods introduce PCA as a reliable method in rejecting the syngenetic effects and detecting anomalous zones with more accuracy and precision in Gulan area.

ACKNOWLEDGEMENT

Senior exploration engineer Hadi Fathi is hereby appreciated for his useful discussions and constructive advises in fractal data analysis. Furthermore, the authors also would like to acknowledge their sincere thanks to anonymous reviewers for their precious time and comments including all the organizers of the conference and other well wishers of the program

REFERENCES

Ahrens, L., 1954a, The lognormal distribution of the elements (2): Geochimica et cosmochimica acta, v. 6, no. 2, p. 121-131.

Ahrens, L. H., 1954b, The lognormal distribution of the elements (a fundamental law of geochemistry and its subsidiary): Geochimica et Cosmochimica Acta, v. 5, no. 2, p. 49-73.

Alavi, H., 1991, Siahrood 1:100000 sheet geological report. Geological survey of Iran. p. 100.

Changjiang, L., Nailiang, Z., and Tuhua, M., 2002, Fractal reconstruction with unorganized geochemical data: Mathematical geology, v. 34, no. 7, p. 809-829.

Changjiang, L., Tuhua, M., and Youlang, X., 1995, GEOCHEMICAL LANDSCAPE ATTRACTOR AND ITS IMPLICATIONS [J]: Geology of Zhejiang, v. 1.

Cheng, Q., 1995, The perimeter-area fractal model and its application to geology: Mathematical Geology, v. 27, no. 1, p. 69-82.

Cheng, Q., 1999, Spatial and scaling modelling for geochemical anomaly separation: Journal of Geochemical exploration, v. 65, no. 3, p. 175-194.

Cheng, Q., Agterberg, F., and Ballantyne, S., 1994, The separation of geochemical anomalies from background by fractal methods: Journal of Geochemical Exploration, v. 51, no. 2, p. 109-130.

Cox, B. L., and Wang, J., 1993, Fractal surfaces: measurement and applications in the earth sciences: Fractals, v. 1, no. 01, p. 87-115.

Gałuszka, A., 2007, Different approaches in using and understanding the term “geochemical background”–practical implications for environmental studies: Polish Journal of Environmental Studies, v. 16, no. 3, p. 389-395.

Govett, G., Goodfellow, W., Chapman, R., and Chork, C., 1975, Exploration geochemistry—distribution of elements and recognition of anomalies: Journal of the International Association for Mathematical Geology, v. 7, no. 5-6, p. 415-446.

Hawkes, H. E., and Webb, J. S., 1962, Geochemistry in mineral exploration.

Miesch, A., 1981, Estimation of the geochemical threshold and its statistical significance: Journal of Geochemical Exploration, v. 16, no. 1, p. 49-76.

Sinclair, A., 1974, Selection of threshold values in geochemical data using probability graphs: Journal of Geochemical Exploration, v. 3, no. 2, p. 129-149.

Sinclair, A., 1991, A fundamental approach to threshold estimation in exploration geochemistry: probability plots revisited: Journal of Geochemical Exploration, v. 41, no. 1, p. 1-22.

Sinclair, A. J., 1976, Applications of probability graphs in mineral exploration, Association of Exploration Geochemists Rexdale, Ontario, v. 4.

Stanley, C. R., and Sinclair, A. J., 1989, Comparison of probability plots and the gap statistic in the selection of thresholds for exploration geochemistry data: Journal of Geochemical Exploration, v. 32, no. 1, p. 355-357.

Sun, W., Xu, G., Gong, P., and Liang, S., 2006, Fractal analysis of remotely sensed images: A review of methods and applications: International Journal of Remote Sensing, v. 27, no. 22, p. 4963-4990.

Xu, Y., and Cheng, Q., 2001, A fractal filtering technique for processing regional geochemical maps for mineral exploration: Geochemistry: Exploration, environment, analysis, v. 1, no. 2, p. 147-156.

Yuhua, F., 1994, Improvement of fractal technique on the application in oil and gas prospecting: variable dimension fractal technique: China Offshore Oil and Gas (Geology), v. 3, p. 210-214.

Zhangdong, J., Xinwei, L., and Chuanlin, Z., 1998, A Study of Fractal Dimension of the Fracture System in the Dexing Porphyry Copper Orefield, Jiangxi [J]: Geological Review, v. 1, p. 009.

Digital Borehole Camera Technology and Its Applications in Mining Geology Exploration

H. Zengqiang, W. Chuanying, H. Sheng
State Key Laboratory of Geomechanics and Geotechnical Engineering, Institute of Rock and Soil Mechanics, Chinese Academy of Sciences, Wuhan 430071, CHINA

ABSTRACT Taking geological engineering exploration in Tangshan mining area of Kailuan Coal Mine as the engineering background, Digital Borehole Camera Technology is used to obtain discontinuities characteristics of rock mass in borehole. Further, a new method, rock mass integrity index (RMDI), is proposed to describe rock mass integrity. This article put forward a new technique and analysis method for geological survey of mining area. The research shows that: (1) The high resolution borehole image gives superior discontinuities information for geological survey of mining area; (2) The use of rock mass integrity index (RMDI) to evaluate rock mass quality is feasible, accurate and effective.

Keywords: Borehole camera technology, rock mass integrity, integrity index, geological survey

1 INTRODUCTION

With the rapid development of economy, the exploitation of mineral resources has entered a new stage with the increasing scale and strength of mining. However, this development also brings a series of problems to the geological disasters in mining area, making detailed geological survey of mining area become the main task of the mining work. For a long time, drilling core has become an important method of all kinds of geological survey work, which plays a huge role in the engineering geological survey. However, because of the complexity and particularity of the geological conditions of mining area such as the weak bedding, fault, fracture zone, the void region etc. and limitations of drilling technique such as low or zero rate of core caused by mechanical disturbance, this method loses its accuracy and sometimes even leads to wrong results.

It's one of the basic engineering geological survey works to collection of joints information, statistical analysis and assessment of the integrity of rock mass in mining area. At present, collection information on are mainly carried out in the outcrops of rock mass, and various geometric parameters of joints are artificially observed and measured with a huge workload and inaccurate results. On evaluation methods of rock mass integrity, RQD (rock quality index) method proposed by American Deere is the most widely used, however, this method also exist many problems in the process of actual application. In view of the above insufficiency, based on digital borehole camera technology, this article focuses on collecting and analyzing joints information and presents a new method for evaluation of rock mass quality—RMDI. Then, this research applies to geological engineering of Kailuan coal mine in Tangshan mining area survey work and has been achieved good results.

2 DIGITAL BOREHOLE CAMERA TECNOLOGY

Digital borehole camera technique is an advanced exploration method with a set of electronic technology, video technology and digital image technology which can realize 360° continuous panoramic imaging of borehole wall. Moreover, the borehole images superimpose on the range and depth of information that geological conditions of the whole drilling can be judge initially.

Problems which engineering geology concerned such as broken belt, joints can implement measurement, calculation and analysis. This technique has been successfully applied in water conservancy, civil engineering, energy, mining and other fields.

Figure 1. Digital panoramic borehole camera system

3 INVESTIGATION AND STATISTICAL ANALYSIS OF JOINTS

3.1 Calculation Of Joint Parameters

Assuming the relationship of joint and borehole is completely cutting, the geometric shape of joint in expansion graph is a sine curve as shown in Fig.2.

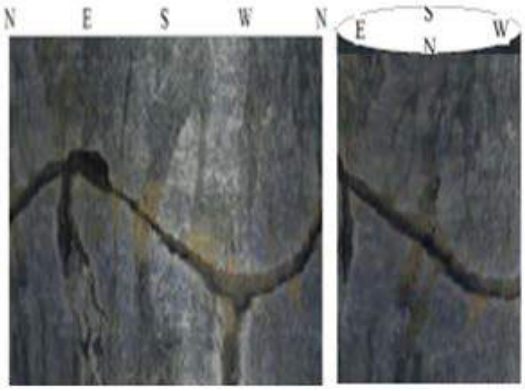

Figure 2. The expansion graph and three dimensional core graph of borehole wall

Through the calculation of the sine curve in the setting coordinate, multiple joint parameters can be obtained. In a borehole image, joint parameters mainly include: (1) Position depth. Joint position along the direction of borehole; refer to the distance from ellipse center point which formed by joint and borehole intersection to the orifice center point. (2) Dip direction. The angle between the line's drop shadow on the horizontal plane and the geomagnetic north direction; the line refers to link the highest point and the lowest point in joint cutting borehole. (3) Dip angle. The angle between the line and the horizontal plane; the line refers to link the highest point and the lowest point in joint cutting borehole. (4) Width. The vertical distance from the upside to underside of joint; mean values of multiple points when the two interfaces are not parallel.

3.2 Statistical Analysis Of Joints

Kailuan coal mine of Tangshan mining area has been 120 years of mining history with an annual output of raw coal 4×106t. Because of the large thickness of exploitation coal seam, repeated mining in multiple coal seams produce large surface subsidence and cause many social and environmental problems. For this reason, the group starts processing the subsidence caused by mining. For the further investigation into the engineering geological conditions of mining area, digital borehole camera technology is used to investigate joints, structural indications, the main discontinuities and fault structural fracture zone.

Twelve boreholes were arranged in the survey area, and with the imaging survey from top to bottom of the borehole wall, joints parameters can be obtained such as depth, occurrence and width. Through reasonable statistical methods to analyze these parameters, we can obtain some statistical rules. In No. ZK2 borehole as example, we get the following statistical results: First, drawing the whole joints occurrence distribution graph as shown on Fig.3, All joints can be divided into three groups according to the occurrence with the dominant occurrence are respectively N28° E∠37° , S24° W∠62° and N82° W∠78° .

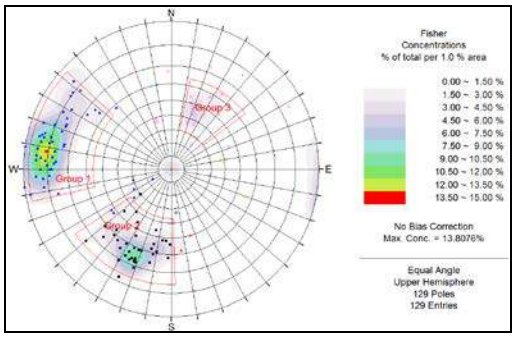

Figure 3. Occurrence distribution graph

Second, making classification statistic according to the different joint width as shown in Fig.4, the results show that joints with width of 5-10mm are in the largest number.

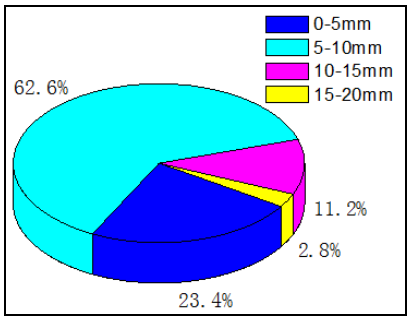

Figure 4. Width distribution graph

Third, making summary statistics of abnormal zones such as broken zone and cavity zone as shown in Fig.5, the results show that there are three abnormal zones should pay attention to.

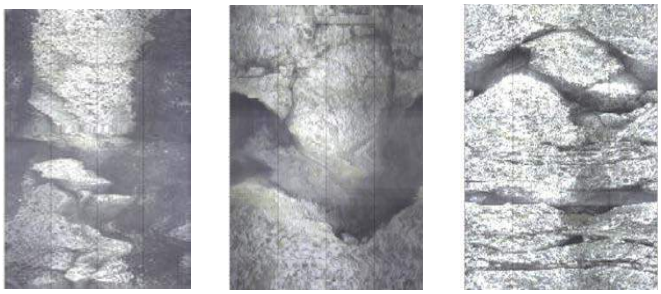

183.4-183.8m 202.5-202.8m 226.7-227.2m

Figure 5. Abnormal zones

4 INTEGRITY EVALUATION OF BOREHOLE WALL ROCK MASS

4.1 The Evaluation Method

In order to realize the accurate evaluation on the borehole wall rock integrity, an integrity index density function is established. In this function, the concept of integrity and broken are defined based on digital borehole image with the reason that there is a direct relationship between the geological structure and integrity or broken in borehole image. For example, all kinds of closed interface have very little effect of rock integrity and the color, texture of borehole image is well-distributed, showing integrity characteristics; open joints and fault fracture zones make the rock mass break and the color, texture of borehole image is varies greatly, showing broken characteristics. Therefore, we can define two rock mass characteristics reflected in the borehole image: broken and non-broken.

Integrity index density function (DIDF) is a single variable function changing along the borehole axial, expressing as f(z) which z represents the depth. The function is shown as follows:

$$f(z)=\begin{cases} 0 & \text{Fractured Rock Mass} \\ \alpha\times 1 & \text{Non Fractured Rock Mass} \end{cases}$$

In the formula, α is the size reflection of rock block. About the determination of rock integrity block size reflection coefficient, based on grading standard of joints spacing ISRM recommended, α is defined as shown in Table 1.

Table 1 Rock mass size and corresponding size effect coefficients

Standard	Structure Types				
	Integrity	Block	Lamellar	Fracture	Granular
ISO/WC 182/WGI/SC	>0.6m		0.2-0.6m	<0.2m	
Block size as α	>1.0m	0.6-1.0m	0.3-0.6m	0.1-0.3m	<0.1m
α	1.0	0.8	0.5	0.2	0.1

On the basis of integrity index density function (DIDF), rock mass integrity index (RMDI) is proposed to evaluate the integrity of rock mass. Rock mass integrity index (RMDI) means scale complete rock block degree occupies within a given range expressed as a percent. If the depth range is given as [h1, h2], RMDI can be indicated by

the definite integral of DIDF in the range. The expression is shown as follows:

$$\mathrm{RMDI} = \frac{\int_{h_1}^{h_2} f(z)dz}{\int_{h_1}^{h_2} 1dz}$$

4.2 Case Analysis

Taking borehole No.ZK2 for example, borehole wall rock integrity is evaluated combined with the joints statistical analysis. The test range of borehole No.ZK2 is 175.5～245.5m. By dividing structure types and determining the effect coefficient, integrity index density function (DIDF) is established. Based on DIDF, RMDI in different deep range is analyzed. Results are shown in Table 2.

Table 2 Results of RQD and RMDI

Depth/m	RQD/%	RMDI/%
175.5-185.5	97.94	92.58
185.5-195.5	95.43	91.87
195.5-205.5	92.65	90.53
205.5-215.5	88.56	87.49
215.5-225.5	99.91	97.36
225.5-235.5	91.69	86.79
235.5-245.5	98.73	79.39

Through the above analysis and calculation, the value of RQD is generally bigger than the value of RMDI. This result mainly because RQD is only the cumulative length, however, RMDI is the definite integral of DIDF which considers the effect of size effect of rock block.

5 CONCLUSION

The article researches the application of borehole camera technology in geological survey of mining area, combined a project case to show how this research to carry out. The results show that: (1) Borehole camera technology makes up for the lack of core drilling; (2) The high resolution borehole image gives superior discontinuities information for geological survey of mining area; (3) Using RMDI method for the evaluation of rock mass integrity is feasible.

REFERENCES

Prensky S E. Advances in borehole imaging technology and application[C]//*Borehole Imaging: Applications and Case Histories.* London: Geological Society, 1999: 1-43

Wang Chuan-ying, LAW KTIM. Review of borehole camera technology[J]. *Chinese Journal of Rock Mechanics and Engineering*, 2005, 24(19): 3440-3448.

Wang Chuan-ying, ZHONG Sheng, SUN Wei-chun. Study of connectivity of discontinuities of borehole based on digital borehole images[J]. *Chinese Journal of Rock Mechanics and Engineering*, 2009, 28(12): 2405-2410.

John Kemeny, Randy Post. Estimating three-dimensional rock discontinuity orientation from digital images of fracture traces[J]. *Computers & Geosciences*, 2003, 9: 65-77.

Chen Jian-ping, SHI Bing-feng, WANG Qing. Study of the dominant orientations of random fractures of fractured rock masses[J]. *Chinese Journal of Rock Mechanics and Engineering*, 2005, 24(12): 241-245.

Hu Wen-tao, ZHANG Xian-zhi. Methods for evaluating engineering rock mass integrity[J]. *Journal of Xi'an Engineering University*, 2001, 23(3): 50－54.

Estimating the Reserve of Chelkureh Copper Deposit Using Ordinary Kriging Method

A. A. Daya
Department of Mining Engineering, University of Sistan and Baluchestan, Zahedan, Iran

ABSTRACT This paper presents a reserve estimation of Chehelkureh copper mine by ordinary kriging method. The case study consists of borehole samples measuring the Cu concentration. This deposit was explored principally by 48 boreholes totaling to 2976.7 m of drilling. In order to estimate the deposit, 1351 input data gained from 48 boreholes were used. To estimate the Cu grade, ordinary kriging was used. For application of ordinary kriging, a spherical model was fitted over empirical variogram. Then the model was verified through cross validation method and proved to be valid with a very good coherence coefficient between the estimated and real data. Plotting the empirical variogram in different directions showed geometric anisotropy for the deposit. Results showed that ordinary kriging can be used for estimating and modelling the Cu concentration in the Chelkureh mine.

Keywords: Ordinary krigging method, Chelkureh copper mine, reserve estimation

1 INTRODUCTION

Geostatistics provides a coherent framework for spatial prediction and uncertainty assessment spatial prediction or interpolation is concerned with how to estimate the variable under study at an un-sampled location, given sample observations at nearby locations. This question aims at finding a single number, termed the 'estimate', at the un-sampled location. Estimation is possible due to spatial correlation, i.e. the underlying biophysical phenomenon causes observations that are measured closely to be dependent on one and another (Zhang and Yao 2008). If the unknown values at the un-sampled location were dependent on the known sample value at another location, then those sample values carry information about the unknown (Zhang and Yao 2008).

An important problem in mineral exploration is the estimation of two- or three-dimensional regional variables in a studied area, especially ore grade distribution. According to this problem, which is known as spatial interpolation, several methods were proposed which consist of linear and non-linear kriging methods, inverse distance weighted (IDW), interpolating polynomials, splines, and power and Fourier series fitting (Shahbeik et al. 2013). Ordinary kriging is now well accepted method in mining grade control and mine reserve estimation.

The aim of this study is to evaluate the potential and applicability of ordinary kriging method, as a tool for estimating the reserve of Chelkureh copper deposit. To estimate, all of the exploitable blocks with dimensions 20 m * 20 m * 10 m were block estimated within the estimation space. Ordinary kriging was used to estimate the regionalized variable (Cu Concentration) at unsampled locations. After that a three dimensional model of estimated value is presented by ordinary kriging. The study shows that ordinary kriging can be applied successfully for modeling the grade of an ore deposit. Results showed that the correlation between the estimated value and the real value at locations is 82.9%.

2 GEOLOGICAL SETTING OF CHELKUREH DEPOSIT

The Chehelkureh deposit is located in the Nehbandan- Khash zone (eastern Iran) between the Afghan block to the east, the Neh Fault to the west, and the Bashagard Fault to the south (Stocklin et al. 1972). This

zone, also known as the Sistan suture zone of eastern Iran (Tirrul et al. 1983), represents a narrow, short-lived strip of oceanic lithosphere that was consumed in the Sennonian and Paleogene and, in part, obducted during the Eocene continental collision (Tirrul et al. 1983).

Dikes and lavas from the Chehelkureh ophiolitic mélange are plagioclase-phyric basalts with chemical compositions that indicate that they were mid-ocean ridge and marginal basin tholeiites (Desmons and Beccaluva 1983). There is no metasedimentary rock older than Cretaceous in the Sistan suture zone (Maanijou et al. 2012). The Cretaceous facies consists of flysch (turbidite) sediments and volcanic rocks (Stocklin et al. 1972) up to 3 km thick. The turbidites are strongly tectonized and underwent low-grade metamorphism (e.g., zeolite-subgreenschist facies) during the Cretaceous, which converted them to slate, phyllite, and schist. The N-S–trending Lunka-Malusan Mountain Range is the highest in the region, with Kuh-e-Lunka (2,300-m elevation) comprising metaturbidites (Fig.1) and Kuh-e-Malusan (2,425-m elevation) comprising gabbro (Maanijou et al. 2012). The study area is divided into three lithotypes on the basis of rock components: igneous rocks (younger than ophiolites), sedimentary rocks, and the ophiolitic mélange (Fig. 1). Each of these lithotypes is described below, relative to its age (i.e., from the oldest to the youngest unit). Sedimentary layers, which consist of graywacke, shale, and limestone, are tightly folded, steeply dipping, and faulted (Maanijou et al. 2012). Cretaceous turbidites have faulted contacts with the ophiolitic complex and are composed of phyllite and small lenses of marble (Maanijou et al. 2012). Paleocene turbidites are composed of shale and sandstone with rare limestone layers (Fig.1). Eocene turbidites are up to 1 km thick and widespread. In metamorphosed turbidites the basal conglomerate is the oldest unit. The western turbidites, which are altered, host the Chehelkureh ore deposits (Maanijou et al. 2012). Several granitoid stocks and dikes intruded the sedimentary sequence where they are oriented parallel to the major NWSE– trending fault set (Fig.1). Plutonic rocks crop out mostly to the west of the Chehelkureh Fault in the Lunka-Malusan Mountain Range (Valeh and Saeedi 1989).

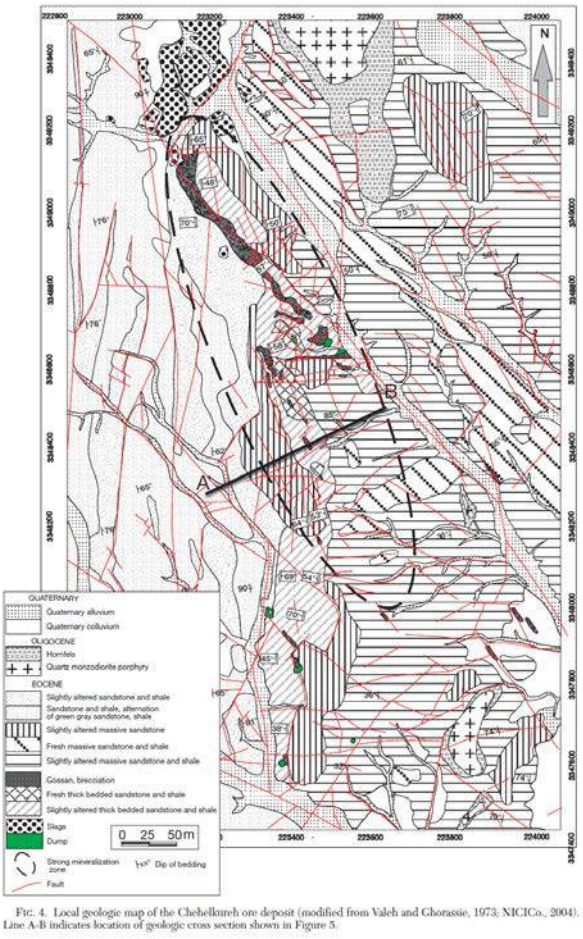

FIG. 4. Local geologic map of the Chehelkureh ore deposit (modified from Valeh and Ghorassie, 1973; NICICo., 2004). Line A-B indicates location of geologic cross section shown in Figure 5.

Figure 1. Regional geologic map of the Chehelkureh ore deposit (Maanijou et al. 2012)

Intrusive bodies consist of quartzmonzodiorite and granodiorite at the Chehelkureh deposit. Exposures of rock in the vicinity of the Chehelkureh deposit are controlled by major N-S– and NW-SE–trending faults, based on air photo lineaments, surface traces, and offsets of geologic features (Maanijou et al. 2012). The strata in the western part of the area, as well as the enclosing faults belonging to the Neh fault system, have an N-S trend. The Neh fault system is a dominantly right-lateral strike-slip set of faults that have been recently active. The N-S–trending Khanibeyk Fault (the eastern branch of Neh Fault) and northwest-southeast Chehelkureh

Fault are the most important faults in the area (Maanijou et al. 2012).

The Chehelkureh deposit comprises numerous lenses and veins. There were two stages of mineralization, the first of which consists of metallic mineralization concentrated along the brittle, finely fractured parts of the beds of sandstone, siltstone, and shale. The second stage of mineralization formed along fractures that crosscut sandstone, siltstone, and shale, displacing them by several millimeters.

3 STATISTICAL ANALYSIS ON DATA

This deposit was explored principally by 48 boreholes (Fig. 2) totaling to 2976 m of drilling. In general, the drilling grid is irregular; the distance between two boreholes varies from 50m to 100m (Fig. 2). Borehole samples were analyzed by ICPMS method. They were of unequal length. It is very important in estimation to work with equal support (volume) samples. This is why the data were composited to equal lengths (Daya 2013; Daya and Bejari 2014).

Statistical studies were performed on the raw data, the results of which are shown in Fig. 3 for Cu concentration values more than 0.20 %. The histogram of the raw data (Fig. 4) was generated by GSLIB Software (Deutsch and Journel. 1998). This regionalized variable (Cu %) can be modeled using a second- order stationary random function. There is no trend of Cu concentration in any directions; it means that Cu concentration does not depend on the coordinates of samples (Fig 4, 5, 6). Assumptions of stationary thus appear to be tenable (Daya 2014). Since the Gaussian kriging method was not used in this study, the data were therefore not normalized and raw data can be utilized (Shahbeik et al. 2013).

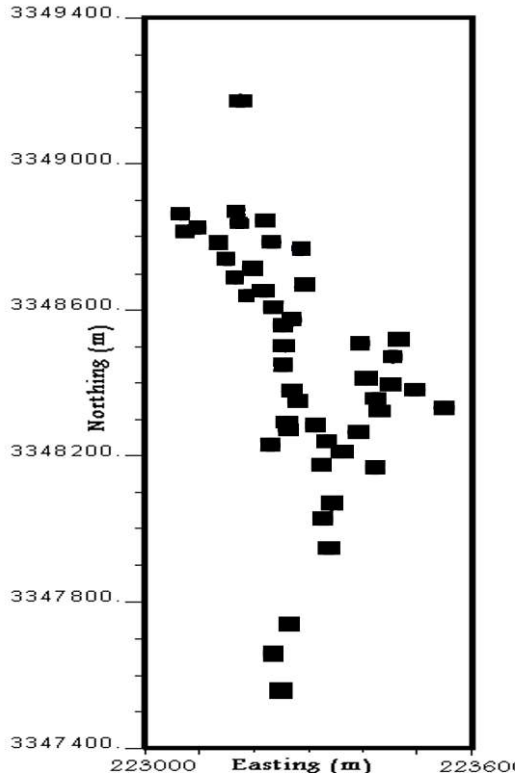

Figure.2. Borehole location map of Chelkureh deposit

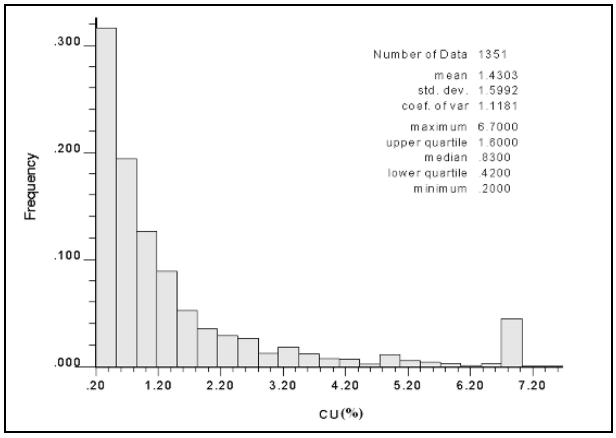

Figure 3. Histogram of the data for Chehlkureh deposit

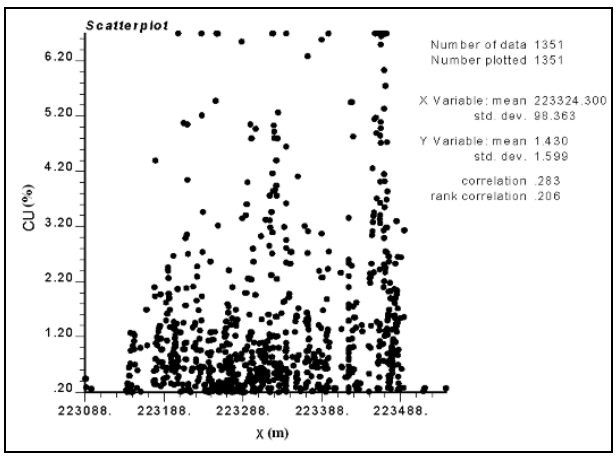

Figure 4. Variability of Cu concentration in east–west direction for Chehlkureh deposit

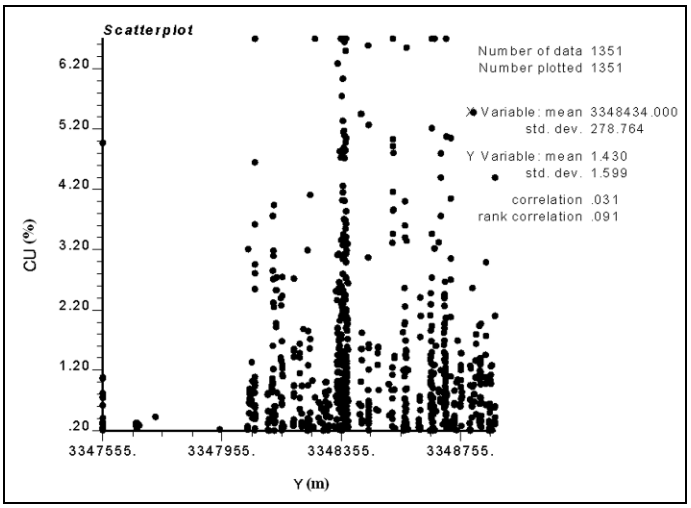

Figure 5. Variability of Cu concentration in north–south direction for Chehlkureh deposit

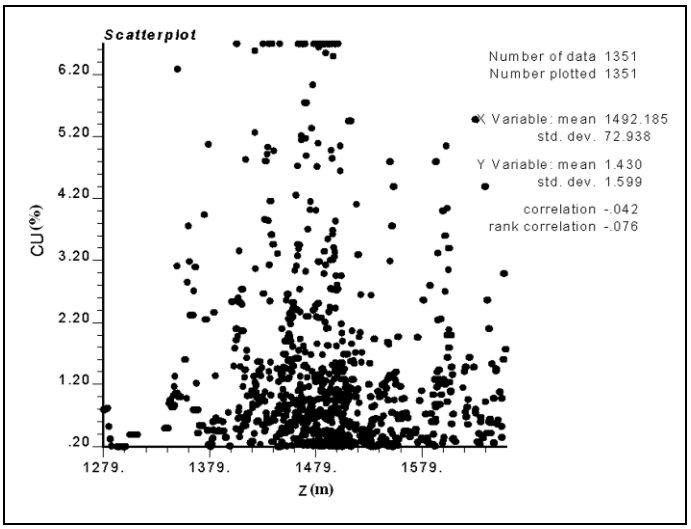

Figure 6. Variability of Fe Cu concentration in depth for Chehlkureh deposit

4 DISCUSSION

Variogram modelling and estimation is extremely important for structural analysis and spatial interpolation (Burrough and McDonnell 1998). They are widely used tools for spatial interpolation, which are the fundamental parameters for geostatistical modeling (Shahbeik et al. 2013; VerHoef and Cressie1993; Calder and Cressie 2009). The experimental variogram displays several important features (Burrough and McDonnell, 1998). The variogram models may consist of simple models, including: Nugget, Exponential, Spherical, Gaussian, Linear, and Power model or the nested sum of one or more simple models (Burrough and McDonnell 1998; Pebesma 2004; Webster and Oliver 2001). The most commonly used model in mining industry is spherical model. In the current study the spherical model was used. In this study, the non-directional and directional variograms were generated by GSLIB Software (Deutsch and Journel. 1998) in the Chelkureh deposit, as shown in Fig. 7.

After studying of variograms in different direction (Fig 7: B, C, D) it was found out that the ore deposit has no anisotropy, because in most of the variograms same ranges were obtained. The best fitted variogram model (Fig. 7 D) is considered for ordinary kriging estimation. Cross-validation was used to evaluate the accuracy of the variogram model for kriging (Fig. 8). In this procedure, every known point is estimated using the values at the neighborhood around it, but not itself (Isaaks and Srivastava 1989). After trial and error process of the cross validation a variogram with the best summary statistics is chosen. Model consists of a pure nugget effect with 0.30 plus a spherical scheme with sill 1.10 and range 30 m. This model is required since ordinary kriging estimation will be based on.

To estimate the Cu %, the ordinary kriging method was used to get estimates at points on a grid 20m x

20m x 10m. These points may be taken as the center-points of cubes of dimension 20m x 20mx 10m. The estimation and 3-D modelling process commenced from the elevation of 1280m above the sea level to 1670m above the sea level in the mine. It also began from 223075m to 223575m in the east direction and from 334755m to 3348850m in the north direction (Fig 9, 10). For the application of OK, GSLIB Software (Deutsch and Journel. 1998) has been used. Fig.9 and Fig.10, respectively, show estimates and kriging errors of Cu concentration in different elevations above sea level computed by OK.

Three dimensional modeling of grade in an ore deposit has a lot of advantageous. Therefore if this process is done carefully, evaluations and judgments about different parts of ore deposit would be better.

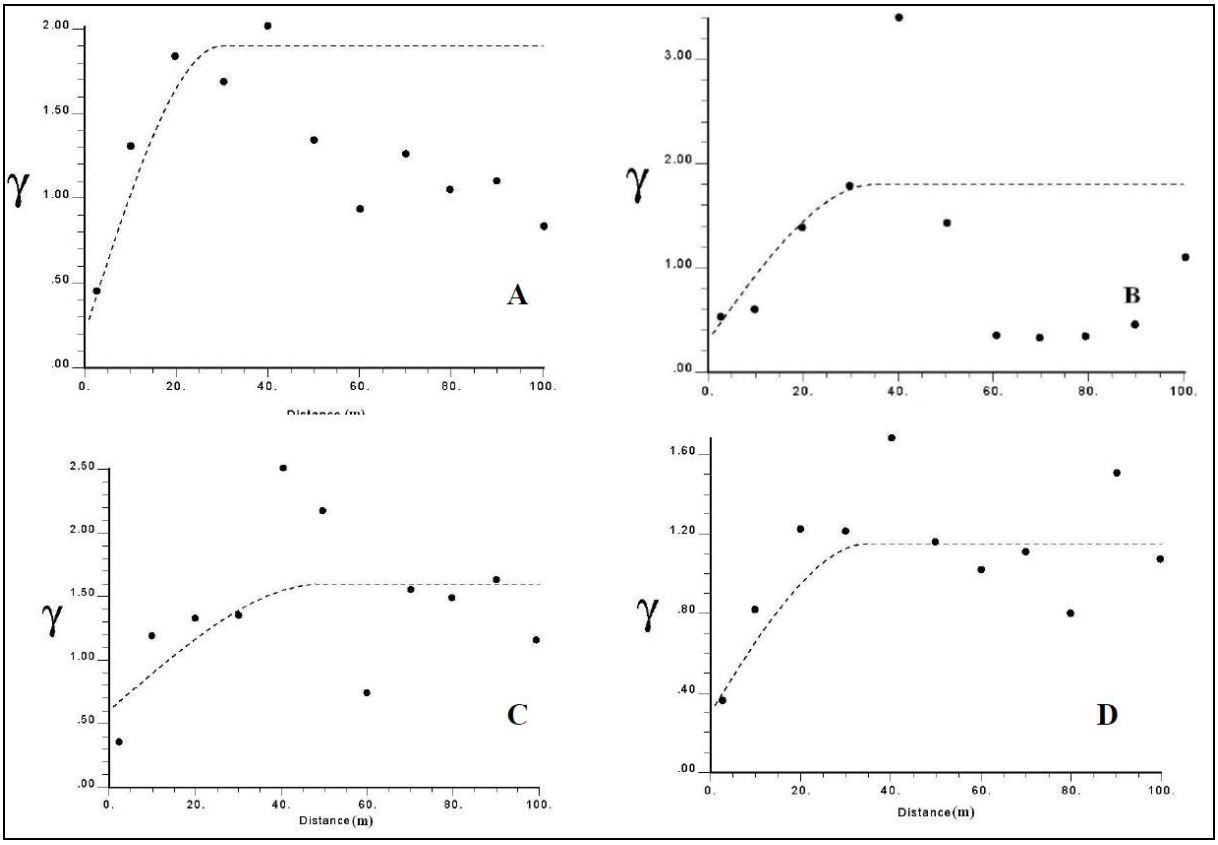

Figure 7. Non-directional and directional variograms: A non-directional, B North-South direction, C East-West direction, and D Vertical direction

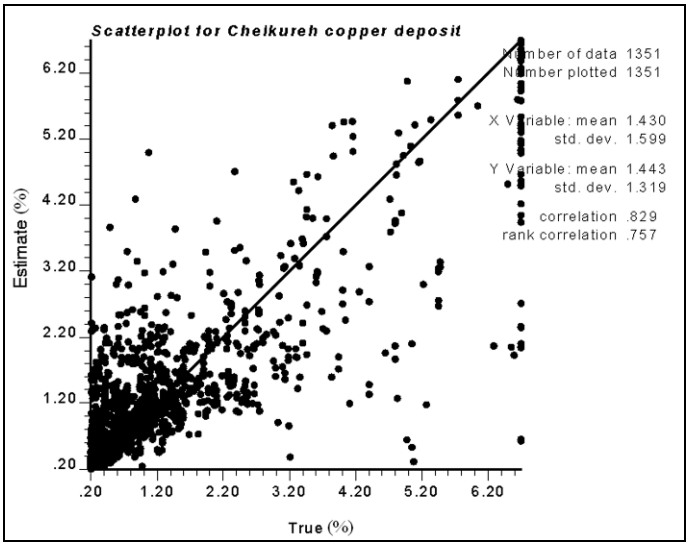

Figure 8. Cross validation diagram for real and estimated values of Cu in Chelkureh copper ore deposit.

In ore estimation it is necessary to calculate the error of each voxel and the classification of reserves. The following formula for calculation of the estimation error is used (Noppé 1994):

$$\% \text{ Error} = ((Z.S)/ (X.\sqrt{N})) \times 100 \quad (1)$$

(1)

S, X and V are the standard deviation of each voxel, assay of each voxel and the number of samples that are participating in the grade estimation, respectively. Z is the integer constant, which is 1.96 if the confidence level is 95% or 1.64 if the confidence level is 90%. In this study, the confidence level assigned to Z was 90% hence a Z of 1.64 was used.

The reserve estimated by OK method was classified based on error estimation. The JORC (2012) method was selected to classify the reserve, as shown in Table 1. The classification framework based on the prepared code by the Joint Ore Reserves Committee of the Australasian Institute of Mining and Metallurgy, Australian Institute of Geoscientists and Minerals Council of Australia (JORC code), which is one of the international standards for mineral resource and ore reserve reporting, provides a template system that conforms to

international society requirements (Li et al. 2008; Asghari and Madani 2013).

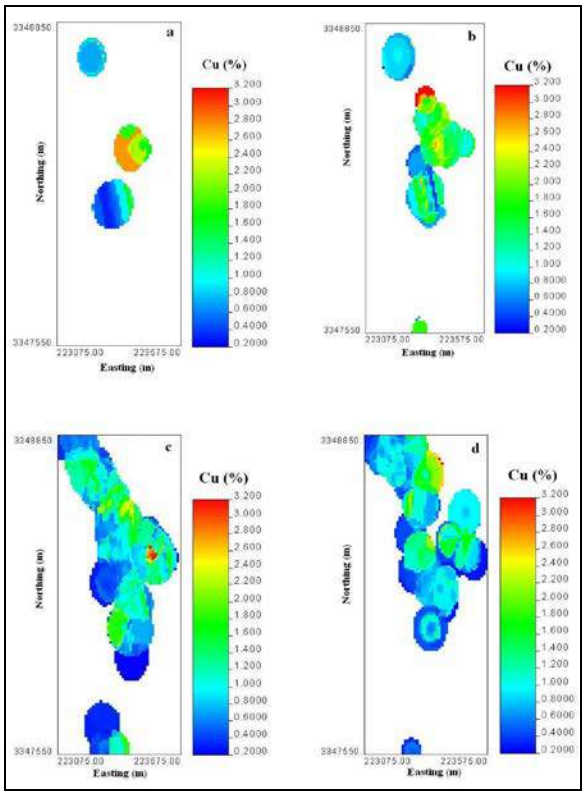

Figure 9. Estimates of Cu concentration by ordinary kriging in different elevations (a=1330m, b=1380m, c=1480m, d=1580m above the sea level) in Chehelkureh deposit

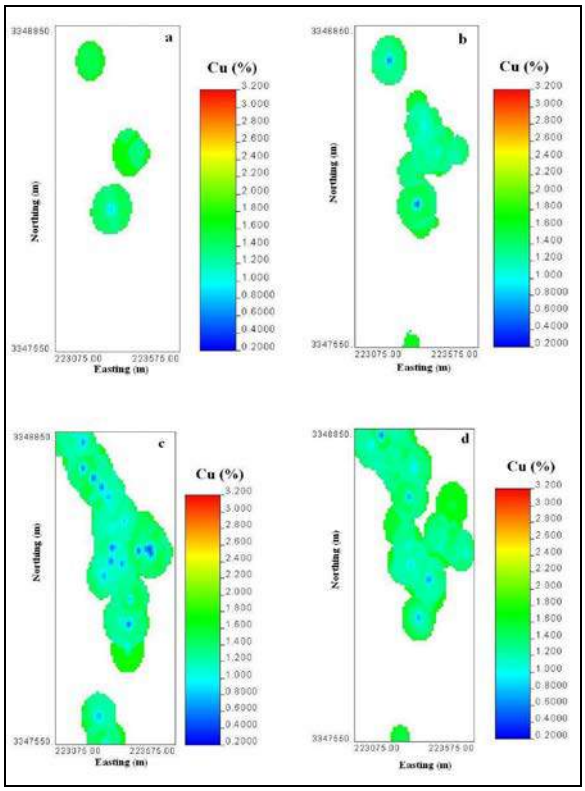

Figure 10. Ordinary kriging errors of Cu concentration in different elevations (a=1330m, b=1380m, c=1480m, d=1580m above the sea level) in Chehelkureh deposit increasing the cut-off grade the amount of deposit decreases.

Most parts of the estimated block model derived via the OK method (higher than 92.66%) were classified in the A category based on JORC standard (Table 1). And, 7.34 % of the estimated tonnages by the OK method were categorized in the B class (Table 1).

Grade-tonnage curves are one of the tools which enable the mine managers to determine the correct long-time, mean-time and short-time parameters for ore producing. Drawing grade-tonnage curves needs to finding the tonnage of different grades. To find the tonnage of each block, the specific gravity of ore and core recovery percent is required. So according to this data, we could calculate the deposit based on different cut-off grades. Fig. 11 shows the grade-tonnage curve of Choghart north anomaly copper ore deposit. It could be seen that with reducing the cut-off grade of copper the amount of deposit increases and with

Table 1. Reserves classification based on JORC standard

Error (%)	Average Grade (%)	Tonnage (%)	Class
0-20	1.12	92.66	A
20-40	0.41	7.34	B
40-60	-	-	C
>60	-	-	Possible
Total	1.054	100	

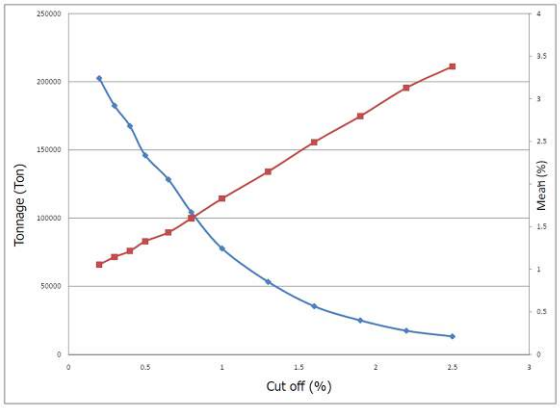

Figure 11. Tonnage grade curve of Choghart north anomaly iron copper ore deposit.

5 CONCLUSION

Choosing the proper method for estimation of reserve with a minimum error is very important in geostatistical operations in mining engineering. The case study presented in this paper shows that ordinary kriging is a useful method in the estimation of reserves or resources of vein type deposits, such as in Chelkureh copper deposit. After trial and error a variogram with the best summary statistics was chosen. Model consists of a pure nugget effect with 0.30 plus a spherical scheme with sill 1.10 and range 30 m. The cross validation results show that the correlation coefficient between estimated and real data is 0.829. The total tonnage of the ore deposit based on various cut-off grades is different and with 0.20% cut-off grade are 200,000 tones, with 0.5% cut-off grade are 150,000 tones and with 0.80% cut-off grade are 100,000 tones. Classification of reserve has been carried out successfully by JORC standard. High-grade reserves including 92.66 % of reserve have errors less than 20 % based on estimation by OK technique. Based on results obtained by OK method, parts of the high-grade reserves that include 7.34 % of reserve have an error between 20 to 40 %. It is hoped that this example taken from very different application fields will encourage practitioners in applying ordinary kriging with variety of ore deposits.

REFERENCES

Burrough, P.A., McDonnell, R.A., 1998. Principles of Geographical Information Systems. Oxford University Press, Oxford, 333 pp.

Calder CA, Cressie N (2009) Kriging and variogram models. Elsevier, Oxford, pp. 49–55.

Daya, A.A., 2013. Application of median indicator kriging in the analysis of an iron mineralization. Arabian journal of Geosciences, In press.

Daya, A.A., 2014. Application of disjunctive kriging for estimating economic grade distribution in an iron ore deposit: a case study of the Choghart North Anomaly, Iran. J Geol Soc India 83:567–576.

Daya, A.A., Bejari H 2014. A comparative study between simple kriging and ordinary kriging for estimating and modeling the Cu concentration in Chehlkureh deposit, SE Iran. Arabian journal of Geosciences, In press.

Desmons, J., Beccaluva, L., 1983. Mid-oceanic ridge and island arc affinities in ophiolites from Iran: Paleogeographic implication. Chemical Geology, 39 39–63.

Deutsch, C.V., Journel, A.G., 1998. GSLIB: Geostatistical software library and user's guide, second ed. Oxford University Press, New York, NY, p 369.

Isaaks, E.H., Srivastava, R.M., 1989. Applied Geostatistics. Oxford University Press, New York, 561 pp.

JORC 2012. Australasian Code for Reporting of Identified Mineral Resources and Ore Reserves (The JORC Code), The Joint Ore Reserves Committee of the Australasian Institute of Mining and Metallurgy, Australian Institute of Geoscientists, and MineralsCouncil of Australia.

Journel, A.G., Huijbregts, C.J., 1978. Mining Geostatistics. Academic Press, London, 600 pp.

Li, J., Heap, A.D. 2008. A Review of Spatial Interpolation Methods for Environmental Scientists.Geoscience Australia, GPO Box 378, Canberra, ACT 2601, Australia.

Maanijou, M., Rasa, I., Lentz, R.D., 2012. Petrology, geochemistry, and stable isotope studies of the Chehelkureh Cu-Zn-Pb deposit, Zahedan, Iran. Economic Geology 107,683–712

Noppé, M.A., 1994. Practical Geostatistics for on-Site Analysis - A Coal Example. Mining Geostatistics Conference, Geostatistical Association of South Africa, Kruger National Park, South Africa

Shahbeik, Sh., Afzal P, Moarefvand P (2013) Ordinary kriging (OK) and inverse distanceweighted (IDW) based on estimation error case study: in Dardevey iron ore deposit, NE Iran. Arab J Geosci (In press).

Stocklin, J., Eftekhar-Nezhad, J., Hushmand-Zadeh, A. 1972. Central Lut reconnaissance, east Iran. Geological Survey of Iran, Report 22, 62 p.

Tirrul, R., Bell, I.R., Griffis, R.J., Camp, V.E. 1983. The Sistan suture zone of eastern Iran. Geological Society of America Bulletin 94, 134–150.

VerHoef, J.M., Cressie, N., 1993. Multivariable spatial prediction. Math Geol 252:219–239.

Fuzzy Analytical Hierarchy Process for Mineral Exploration Potential Mapping: a Case Study in Kamoshgaran Region (NW, Iran)

A.A. Daya, H. Bejari
Department of Mining Engineering, University of Sistan and Baluchestan, Zahedan, Iran

ABSTRACT: Selection of potential areas for mineral exploration needs many diverse criteria. Analytic hierarchy process (AHP) modeling provides an effective means for studies of mineral potential mapping evaluation. Fuzzy AHP is an extension of conventional AHP and by using fuzzy theory is obtained the advantage rather AHP method. In this paper to provide, potential mapping for elemental mineralization used fuzzy AHP in the Kamoshgaran region, several criteria, such as geology, geochemical, alteration, and faults were used. Each criterion was evaluated with the aid of fuzzy AHP. The method allowed a mixture of quantitative and qualitative information with group decision. The results and its validation demonstrate the acceptable outcomes for mineral exploration.

Keywords: Fuzzy, Analytic hierarchy process (AHP), Kamoshgaran

1 INTRODUCTION

Localization is one of the spatial analyses that have great effect on reducing the costs of creating and construction of various activities. Today, finding a suitable place or places for the creation of an activity in a specific geochemical field is an important step. Over the past decades, many methods such as simple additive weighting (Hwang and Yoon 1981), the technique for order preference by similarity to ideal solution (Hwang and Yoon 1981), analytical hierarchy process (Saaty 1980), data envelopment analysis (Cooper et al. 2000), and so on have been developed to deal with a multiple decision making problem. One of the most powerful and flexible method of decision-making means is analytical hierarchy process (AHP) method which was initially presented by Saaty (1980) for use in solving multiple criteria decision problems. Analytic hierarchy process (AHP) is one of the most commonly used multi-criteria decision-making (MCDM) methods, which integrates subjective and personal preferences in performing analyses. Fuzzy logic, resembling human reasoning in its use of approximate information and certainty to generate decisions, is a better approach to convert linguistic variables to fuzzy numbers under ambiguous assessments. This method under fuzzy environment has been used for a variety of specific application in decision making problem (Önüt and Soner 2008; Torfi et al. 2010; Erensal et al. 2006; Dağdeviren et al. 2009; Khademi Hamidi et al. 2010; Bejari et al. 2010; Aalianvari et al. 2012; Ataei et al. 2012; Rafiee et al. 2013; Fattahi et al. 2014 and Pazand et al. 2014), nevertheless its application in selecting the best geochemical fractal anomalies has not been reported yet.

Fractal theory has been established and developed by Mandelbrot (1983), as an important branch of nonlinear mathematical sciences has been applied in different fields of geosciences since 1980s. Cheng et al. (1994)'s studies show that geochemical dispersion patterns of different elements are fractals. Several fractal models have been developed and applied to geochemical exploration for separate anomalies from background. One of the most important method for separating anomaly from background is the number–size model (N–S model) proposed by Mandelbrot (1983), which has been widely used by many

geoscientists (e.g., Agterberg, 1995; Turcotte, 2002; Zuo et al., 2009c; Wang et al., 2010).

In this paper, first Cu, Au, As, and Mo anomalies were delineated by number–size fractal model and then selecting the best anomalies was done using fuzzy-AHP method.

2 NUMBER-SIZE (N-S) MODEL

Number–size (N-S) method proposed by Mandelbrot (1983) can be utilized to describe the distribution of geochemical populations (Sadeghi et al., 2012). In this method, geochemical data do not undergo any pre-processing (Mao et al., 2004). This model shows a relationship between desirable attributes (e.g. elemental concentration in this study) and their cumulative numbers of samples (Sadeghi et al., 2012). A power-law frequency model has been proposed to explain the N–S relationship according to the frequency distribution of elemental concentrations and cumulative number of samples with those attributes (e.g., Li et al., 1994; Sanderson et al., 1994; Shi and Wang, 1998; Turcotte, 1996; Zuo et al., 2009a; Sadeghi et al., 2012). The model is expressed by the following equation (Deng et al., 2010; Mandelbrot, 1983):

$$N(\geq \rho) = K\rho^{-D}$$

where ρ denotes elemental concentration, N(≥ρ) denotes the cumulative number of samples with concentration values greater than or equal to ρ, *K* is constant, and *D* is the fractal dimension of the distribution of elemental concentrations. According to Mandelbrot (1983) and Deng et al. (2010), log–log plots of *N* (≥*ρ*) versus ρ show straight line segments with different slopes – *D* corresponding to different concentration intervals (Sadeghi et al., 2012).

3 FUZZY ANALYTIC HIERARCHY PROCESS (F-AHP)

Analytic hierarchy process (AHP) is a useful approach for evaluating complex multiple criteria alternatives involving subjective judgment. The AHP structures the decision problem in levels which correspond to one understands of the situation: goals, criterion, sub-criterion, and alternatives. By breaking the problem into levels, the decision-maker can focus on smaller sets of decisions. In AHP technique, the elements of each level compared to its related element in upper level by pairwise comparison method. Though the aim of AHP is to capture a decision maker's knowledge, the conventional AHP cannot fully reflect the human thinking style. Linguistic and vague descriptions could not be solved easily by AHP until the recent development in fuzzy decision-making (Cheng 1999). Fuzzy set theory first proposed by Zadeh (1965) as a means representing uncertainty using set theory.

The traditional AHP employs exact numbers such as 1–9 to score. However, much decision-making involves some uncertainty. The traditional AHP does not take into account the uncertainty associated with the mapping of one's perception (or judgment) to a number (Cheng 1996).

Fuzzy set theory, resembling human reasoning in its use of approximate information and certainty to generate decisions, is a better approach to convert linguistic variables to fuzzy numbers under ambiguous assessments (Zadeh 1975). By incorporating fuzzy set theory with AHP, fuzzy AHP allows a more accurate description of the decision-making process. So, the use of fuzzy numbers and linguistic terms is more suitable since the traditional AHP approach is somewhat arbitrary. A fuzzy number describes the relationship between an uncertain quantity x and a membership function μ_x, which ranges between 0 and 1. A fuzzy set is an extension of the classical set theory (in which x is either a member of set A or not) in which an x can be a member of set A with a certain membership function μ_x. Different shapes of fuzzy numbers are possible (e.g., bell, triangular, trapezoidal, Gaussian, etc.). In order to simplify the implementation, in this

paper, triangular fuzzy numbers (TFNs) are used. TFN is represented by three points (a, b, c) on the universe of discourse (scale X on which criterion is defined), representing the minimum, most likely, and maximum values, respectively. Figureure 1 illustrates a triangular fuzzy number (TFN).

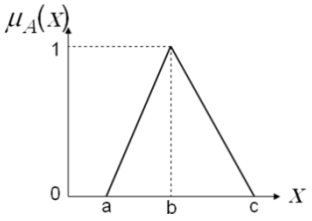

$$\mu_A(x) = \begin{cases} 0 & if\ x \le a \\ \dfrac{x-a}{b-a} & if\ a < x \le b \\ \dfrac{c-x}{c-b} & if\ b < x \le c \\ 0 & if\ x > c \end{cases}$$

Figure 1. A triangular fuzzy number

This paper proposes a seven-step procedure for F-AHP which is schematically given in Figure. 2. These seven steps are followed through a simple hierarchical structure example shown in Figure. 3. A step-by-step description of the methodology is presented as following.

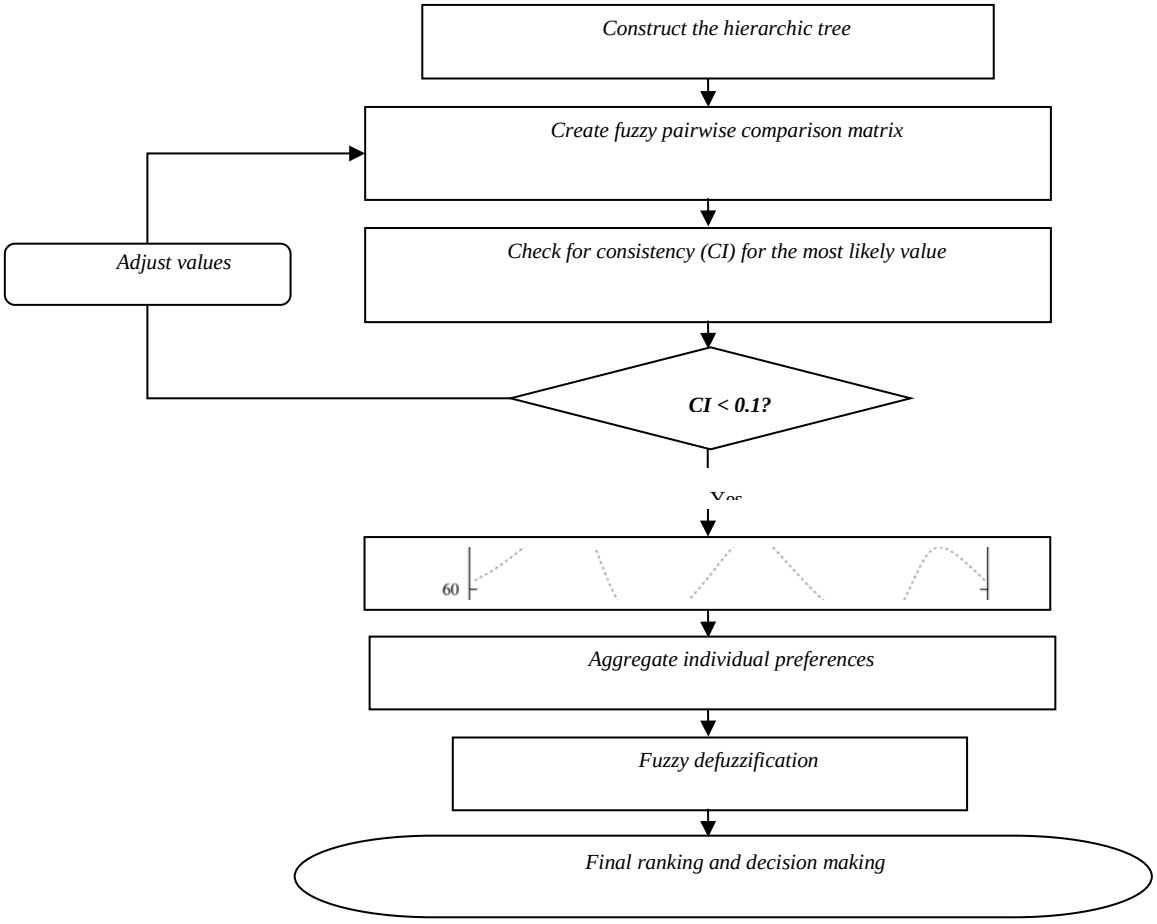

Figure 2. Proposed methodology for fuzzy AHP

3.1 Construction Of Hierarchical Structures

Constructing the hierarchical model includes the decomposition of a complex decision problem into smaller manageable elements of different hierarchical levels. The first level of the hierarchy corresponds to objective or goal, and the last level corresponds to the evaluation alternatives (options), whereas the intermediate levels correspond to criteria and sub-criteria.

Development Of Fuzzy Judgment Matrix Using Pairwise Comparisons

Within a hierarchical structure, the elements of a particular level are compared pairwise with a specific element of an upper level. A fuzzy judgment matrix ($\tilde{J}$) is generated using fuzzy pairwise comparison index ($\tilde{j}_{ij}$).A relative importance of the pairwise comparison is assigned using a scale of 1–9 (Saaty 1977, 1980), which are fuzzified to capture vagueness in perception and meaning (Table 1). For *n* number of comparison items, the fuzzy judgment matrix $\tilde{J}$ is:

$$\tilde{\mathrm{J}} = \begin{bmatrix} \tilde{j}_{11} & \tilde{j}_{12} & \cdots & \tilde{j}_{1n} \\ \tilde{j}_{21} & \ddots & & \tilde{j}_{2n} \\ \vdots & & \ddots & \vdots \\ \tilde{j}_{n1} & \tilde{j}_{n2} & \cdots & \tilde{j}_{nn} \end{bmatrix} \quad (1)$$

Table 1. Fuzzy scales for pairwise comparisons

For diagonal entries, i.e., i = j, $\tilde{j}_{ij} = 1$. Upper right-hand triangle entries $\tilde{j}_{ij}$ are comparison items needs to be defined by decision maker, whereas for lower left-hand triangle entries are derived by taking reciprocals, i.e., $\tilde{j}_{ji} = 1/\tilde{j}_{ij}$. For illustration purpose, a comparison is performed between three items in Figure. 3, C31, C32 and C33, using the relative importance given in Table 1; let the level of importance of C31 to C32 is a fuzzy number $\bar{3}$; C31 to C33 is $\bar{5}$ and C32 to C33 is $\bar{4}$. Hence the judgment matrix is populated as:

$$\tilde{\mathrm{J}} = \begin{bmatrix} \bar{1} & \bar{3} & \bar{5} \\ 1/\bar{3} & \bar{1} & \bar{4} \\ 1/\bar{5} & 1/\bar{4} & \bar{1} \end{bmatrix}$$

The concept of fuzzification factor δ is introduced in Table 1. For this example, the value of fuzzification factor δ is assumed "1", i.e., $\bar{3}$ meaning a TFN (2, 3, 4).

3.2 Check For Consistency

Consistency is important in human thinking, which enables us to order the world according to dominance (Saaty 2005). It is important to ensure that there is consistency in the pairwise comparisons. Therefore, it would be useful to have a measure of inconsistency associated with the pairwise comparison matrix J. In order to measure the degree of consistency, one can calculate the Consistency Index (CI). Consistency index therefore, indicates whether a decision maker provides consistent values (comparisons) in a set of evaluation. The CI is calculated as:

$$\mathrm{CI} = (\lambda_{\max} - \mathrm{n})/(\mathrm{n} - 1) \quad (2)$$

where $\lambda_{\max}$ is the maximum eigenvalue and n is dimension of the judgment matrix.

The final inconsistency in the pairwise comparisons is solved using consistency ratio $CR = CI/RI$ where RI is the random index, which is obtained by averaging the CI of a randomly generated reciprocal matrix (Saaty

1980). The values of RI are tabulated in Table 2. The threshold of the CR is 0.1, and in case of exceedance a three-step procedure should be followed (Saaty 2005): (1) identify the most inconsistent judgment in the decision matrix, (2) determine a range of values the inconsistent judgment can be changed to so that would reduce the associated inconsistency, and (3) ask the decision maker to reconsider the judgment to a 'reasonable value'. In this paper, though the pairwise comparison indices of the judgment matrix are TFNs, however, the CI is evaluated for the most likely value.

Table 2. Random inconsistency indices (RI)

No. of criteria	**1-2**	**3**	**4**	**5**	**6**	**7**	**8**	**9**	**10**
RI	0	0.58	0.9	1.12	1.24	1.32	1.41	1.45	1.49

Following the example of the judgment matrix illustrated in Step 2, the CI is computed. The maximum eigenvalue evaluated is ($\lambda_{max} = 3.086$). Thus, for n=3, the CI from Eq. 2 is (CI=0.043) and the random index from Table 2, RI=0.52. Finally, the consistency ratio CR is computed to be 8%.

3.3 Calculation Of The Fuzzy Weights

Various techniques are used to compute the final fuzzy weights, such as, computation of the eigenvector (as described in Step 3), arithmetic mean, geometric mean, etc. In this paper, for the ease of implementation the geometric mean is adopted to estimate the weights. Some commonly used fuzzy arithmetic operations are listed in Table 3.

Table 3. Common fuzzy arithmetical operations by two TFNs

Operators	***Formulae**	**Results**
Summation	A + B	$(a_1 + b_1, a_2 + b_2, a_3 + b_3)$
Subtraction	A – B	$(a_1 – b_3, a_2 – b_2, a_3 – b_1)$
Multiplication	A * B	$(a_1 * b_1, a_2 * b_2, a_3 * b_3)$
Division	A/B	$(a_1/b_3, a_2/b_2, a_3/b_1)$
Scalar product	Q·B	$(Q*b_1, Q*b_2, Q*b_3)$

* A= (a_1, a_2, a_3); B= (b_1, b_2, b_3)

Fuzzy arithmetic operations are utilized over matrix $\tilde{J}$ to compute the fuzzy weights. Following the previous example for $\tilde{J}$, the geometric mean is computed for each row $\tilde{J}_i$. Given $\tilde{J}$ from Eq. 1, the corresponding fuzzy weights are computed as:

$$\tilde{J}_i = (\tilde{j}_{i1} \otimes \cdots \otimes \tilde{j}_{in})^{\frac{1}{n}} \quad (3)$$

$$\tilde{w}_i = \tilde{J}_i \otimes (\tilde{J}_1 \oplus \cdots \oplus \tilde{J}_n)^{-1} \quad (4)$$

where $\tilde{w}_i$ is the fuzzy weight (where i =1 to n). Therefore, for C31, C32 and C33, the fuzzy weights are computed as:

$$\tilde{J}_1 = (\bar{1} \otimes \bar{3} \otimes \bar{5})^{\frac{1}{3}} = [(1,1,1) \otimes (2,3,4) \otimes (4,5,6)]^{\frac{1}{3}} = (2.0, 2.5, 2.9)$$
$$\Rightarrow \tilde{w}_1 = \tilde{J}_1 \otimes (\tilde{J}_1 \oplus \tilde{J}_2 \oplus \tilde{J}_3)^{-1} = (0.43, 0.63, 0.89)$$

similarly

$$\tilde{J}_2 = (1/\bar{3} \otimes \bar{1} \otimes \bar{4})^{\frac{1}{3}} = [(1/4, 1/3, 1/2) \otimes (1,1,1) \otimes (6,4,5)]^{\frac{1}{3}} = (0.32, 0.37, 0.44)$$
$$\Rightarrow \tilde{w}_2 = (0.19, 0.28, 0.42)$$

and

$$\tilde{J}_3 = (1/\bar{5} \otimes 1/\bar{4} \otimes \bar{1})^{\frac{1}{3}} = [(1/6, 1/5, 1/4) \otimes (1/5, 1/4, 1/3) \otimes (1,1,1)]^{\frac{1}{3}} = (1.58, 1.73, 1.87)$$
$$\Rightarrow \tilde{w}_3 = (0.07, 0.09, 0.14)$$

Sum of the most likely values of weights $\tilde{w}_i$, i = 1, 2, 3, equals to 1 (=0.63+0.28+0.09), which is the basic axiom of AHP. Therefore, crisp AHP is a special case of F-AHP, when fuzzification factor reduces to zero.

3.4 Establishment of Global Preference Weights

The local priorities at each level are aggregated to obtain final preferences of the alternative. This computation is carried out from the evaluation alternatives to the top level (Goal). As depicted in Figure. 3, each of the three alternatives (level 4), A_i, i = 1, 2, 3 are aggregated through level 3, level 2 and finally to level 1 (Goal). Therefore, following Figure. 3 at each level k of hierarchical tree, the fuzzy global preference weights ($\tilde{G}_k$) are computed as:

$$\tilde{G}_k = \tilde{w}_k \cdot \tilde{G}_{k-1} \quad (5)$$

The final fuzzy AHP score ($\tilde{F}_{Ai}$) for each alternative A_i is obtained by carrying out fuzzy arithmetic sum over each global preference weights:

$$\tilde{F}_{Ai} = \sum_{k=1}^{n} \tilde{G}_k \text{ for each alternative Ai.} \quad (6)$$

3.5 Ordering the Alternatives Using Fuzzy Ranking Methods

The defuzzification entails converting the final fuzzy AHP score $\tilde{F}_{Ai}$ into a crisp value. Once the final fuzzy AHP score ($\tilde{F}_{Ai}$) of each alternative is defuzzified, the crisp numbers are compared and ranked accordingly. In this paper the most common centroid index method developed by Yager (1980) is employed. The index is a geometric center $x_O(A_i)$ of the fuzzy number of alternative A_i, where for a given TFN (a_1, b_1, c_1) is formulated as follows:

$$x_O(A_i) = \frac{\int_0^1 A_i \mu_{Ai}(x)dx}{\int_0^1 \mu_{Ai}(x)dx} = \frac{(b_1 - a_1)(a_1 + \frac{2}{3}(b_1 - a_1)) + (c_1 - b_1)(b_1 + \frac{1}{3}(c_1 - b_1))}{(b_1 - a_1) + (c_1 - b_1)} \quad (7)$$

Where A_i is treated as a moment arm (weight function) measuring the importance of the value *x*. The value of $x_O(A_i)$ may be seen as the weighted mean value of the fuzzy number A_i. Hence, the bigger the $x_O(A_i)$ values are, better will be the ranking of an alternative.

4 STUDY AREA

Kamoshgaran region is located in the southwest of Ghorveh, east of Kurdestan province, northwest of Iran, in the Sanandaj-Sirjan zone (Figure. 1) and covers the area of about 600 km^2. The studied area has been important for Au mineralization occurring in the fault zones. Most of the large and known Iranian Au deposits are located along the Sanandaj–Sirjan metamorphic-structural zone, which hosts upper Paleozoic to upper Mesozoic volcano-sedimentary sequences of lower green schist to lower amphibolite metamorphic facies (Aliyari et al., 2012).

Sanandaj–Sirjan zone (SSZ) is a track from the southwest of central Iran, which is located immediately on the northeast of the main thrust of Zagros. Structural and rock features of SSZ indicate a deep valley between Arabian-Iranian Precambrial Shield. Thus, its geological features are clearly different from those of the adjacent zones (Aghanabati, 2004). Agreement of structural trend, equality of structural pattern, and dominance of thrusts, especially admitting the standard pattern of orogenic areas in collision zones, have led geologists like Falcon (1961), Farhoudi (1978), and Alavi (1994) to consider SSZ as a subzone of Zagros Orogen. Thiele et al. (1968) believed that Hercynian phase in this zone was accompanied by metamorphism. Except in rare cases, Permian rocks are covered by Upper Triassic-Jurassic Schist and the available evidence indicates that metamorphism has occurred in the Middle Triassic, as a result of which SSZ rocks have undergone dynothermal metamorphism (Aghanabati, 2004). According to the available information, it can be acknowledged that SSZ has a main structural field, starting from Late Precambrian by rifting and ending in Early Cimmerian orogeny by tectonic inversion.

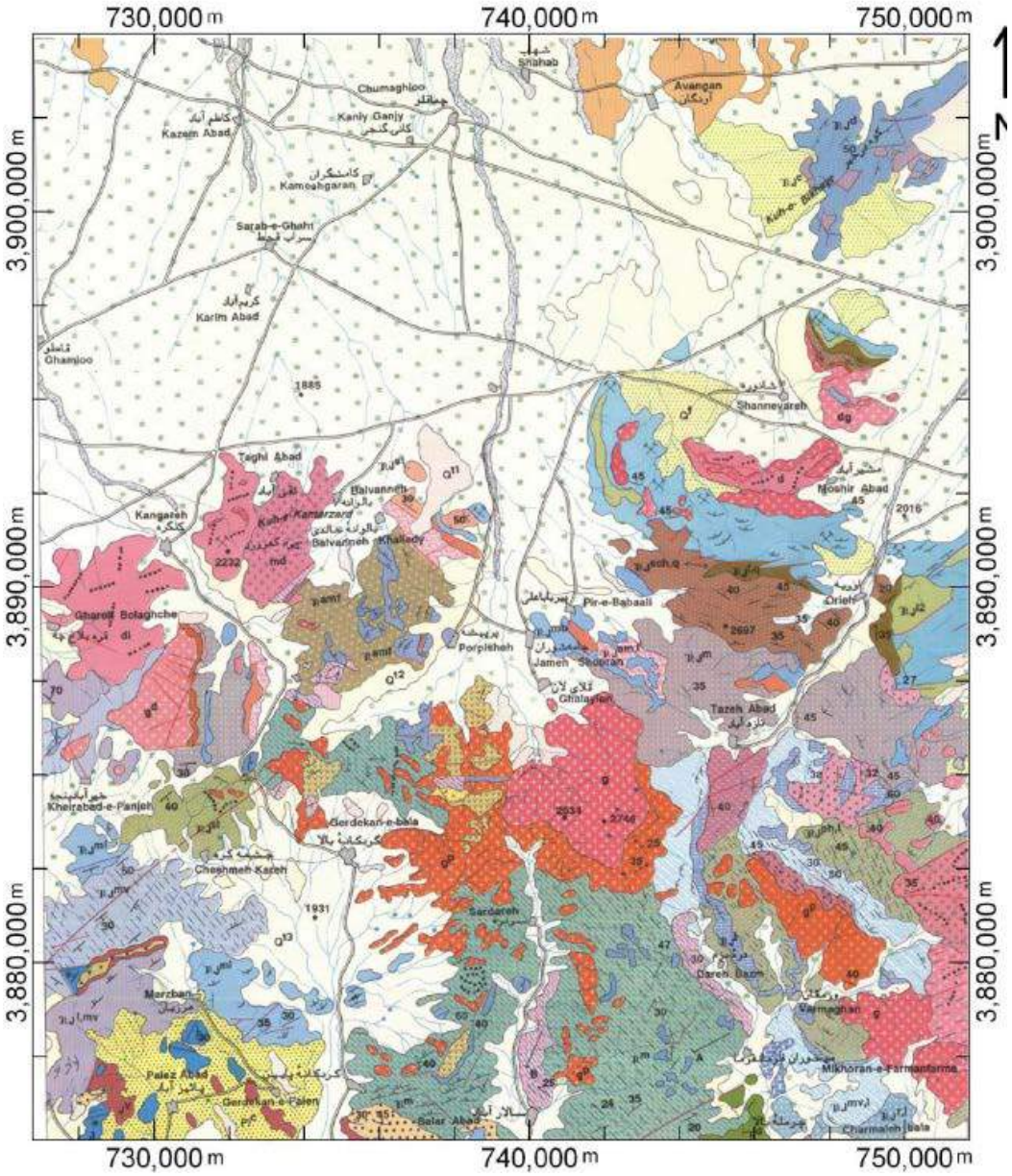

Figure 3. Geological map of Kamoshgaran region (based on the 1:100,000 geological map of Qorveh) and geology of Iran showing the location of the studied area in metamorphic–magmatic Sanandaj–Sirjan zone (compiled and simplified by Sahandi et al. (2005) based on the 1:2,500,000 geologic map of Iran)

The studied area consisted of metamorphic rocks including sch;ist, marble, amphibolites, and gneiss along with massive intrusive rocks with different chemical compositions. A geology map of Kamoshgaran region is shown in Figure. 1. Lithological sequences include Triassic, Triassic-Jurassic, Jurassic metamorphic, and Eocene non-metamorphic rocks, respectively (Hosseiny, 1999). There are also massive intrusive rocks with the compositions of gabbrodiorite, diorite, granodiorite, and granite in the region.

5 DISCUSSION

Four elements (As, Au, Cu, and Mo) from 317 stream sediment samples were used to identify number-size geochemical anomalies. Stream sediment samples of the −80 mesh (0.18mm) fraction were collected from the center of the streams. Kamoshgaran region was modeled using 10,323 cells. The area was gridded by 250×250 m cells, which were determined based on the geometrical properties of the studied area and sampling spacing (David, 1977). Arsenic, Au, Cu, and Mo distribution models were obtained via ordinary kriging (Ok) method using GSLIB software (Deutsch and Journel, 1998). The elemental concentrations were sorted based on decreasing concentrations and cumulative numbers were calculated for the concentrations. Finally, N-S log-log plots were generated for As, Au, Cu, and Mo (Figure. 4). Based on the N-S plots, there were five enrichment steps for As, four enrichment steps for Au and Cu and three enrichment steps for Mo (Figure. 4). Various enrichment steps derived by N–S method represented different geological factors and lithological differences.

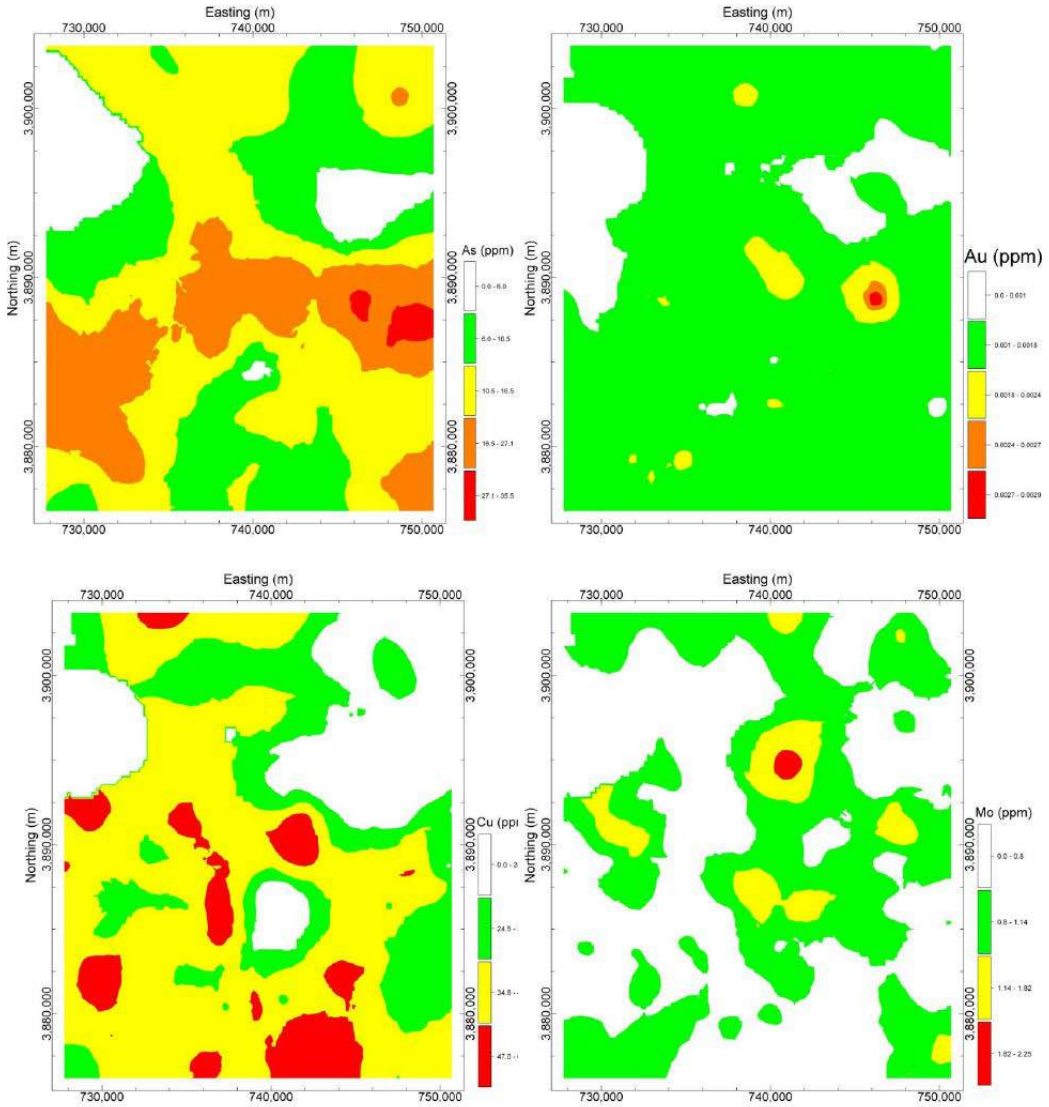

Figure 4. N-S log–log plots of As, Au, Cu, and Mo

Geochemical maps of the elements were obtained using RockWorks 15 software package. Based on the results of the N-S method, As, Au, Cu, and Mo anomalous maps were drawn (Figure. 5). According to the elemental anomaly map resulted from N-S plot, the high intensity of As values existed in the eastern part of the area and correlated with Au anomalous location (Figure. 5). Most of the Au anomalies were located in the eastern and central parts of the area, especially very high-intensity Au anomalies (> 0.0024 ppm). Few parts of these anomalies were also located in the southwestern and northern parts of the studied area. From Figure.5 it can been seen that there are a lot of anomalous area. It is very difficult to visually select the best anomalous areas. This process was done using fuzzy-AHP method. The data used in this study were selected based on the relevance with respect to Au exploration criteria. The five main criteria as input map layers including rocks, stream sediment geochemical data, altered units, structural data, and mining index were used. At the first step, the criteria for Au potential were determined and placed in a hierarchic structure. Each layer in this hierarchic structure was evaluated in pairwise comparisons related to each of the elements at the level directly above. The level of the structure was established by analyzing the relationship of each index.

Relative importance of the criteria was analyzed by called Expert Judgment System. In this research, we invited experts with Au backgrounds to give the corresponding relative importance of each factor and then analyzed all the opinions, and finally, gained the rank of relative importance for each factor by nine basic terms as shown in Table 4.

Table 4. Membership function of linguistic scale (example)

Fuzzy number	Definition	Scale of fuzzy member
9	Perfect	(8, 9, 10)
8	Absolute	(7, 8, 9)
7	Very good	(6, 7, 8)
6	Fairly good	(5, 6, 7)
5	Good	(4, 5, 6)
4	Preferable	(3, 4, 5)
3	Not bad	(2, 3, 4)
2	Weak Advantage	(1, 2, 3)
1	Equal	

In this paper, the computational technique is based on the following fuzzy numbers defined by Gumus (2009) in Table 4. Here, each membership function (scale of fuzzy number) is defined by three parameters of a symmetric triangular function of fuzzy numbers, the left point, middle point, and right point of the range over which the function is defined. Pairwise comparisons of all the related attribute values were used for establishing the relative importance of hierarchical elements. Pairwise comparison matrices were calculated. These matrices are shown for rocks (e.g. Table 5), stream sediment geochemical data, altered units, structural data, mining index and main criteria.

Table 5. Pairwise comparison among rocks

	C11	C12	C13	C14
C11*	(1 1 1)	(2 3 4)	(6 7 8)	(8 9 9)
C12*	(1/4 1/3 ½)	(1 1 1)	(2 3 4)	(5 6 7)
C13*	(1/8 1/7 1/6)	(1/4 1/3 ½)	(1 1 1)	(3 4 5)
C14*	(1/9 1/9 1/8)	(1/5 1/6 1/7)	(1/3 1/4 1/5)	(1 1 1)

*C11= Methamorphosed Igneous Rocks, *C12= Contact Methamorphic Rocks, *C13= Intrusive Rocks, *C14= Others

To determine the final score, Saaty (1980) uses the hierarchic composition principle; this results in the production of the vector regarding all the decisions at every level of the hierarchic structure. The final potential map for Au mineralization, using the obtained score, indicates appropriate areas for Au mineralization (Figure. 5).

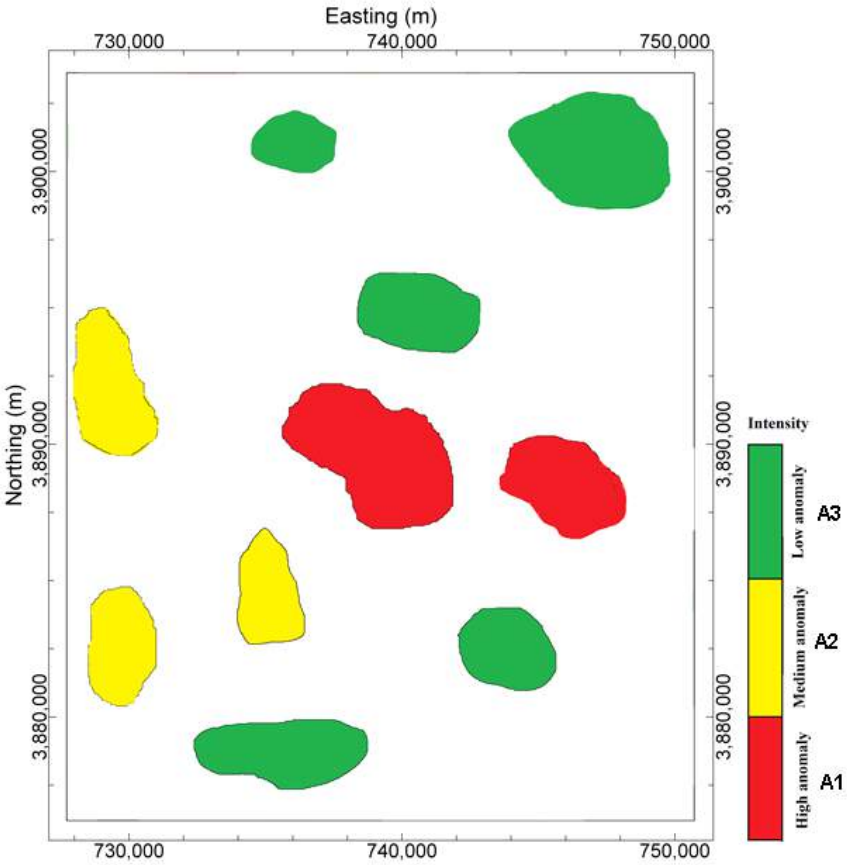

Figure 5. The final potential map for Au mineralization, using the obtained score.

6 CONCLUSIONS

Exploration strategies for nonrenewable resources have been changing rapidly along with the accelerating innovations in information processing technology. The aim of this research was to construct a fuzzy AHP model to select the best anomalies. This methodology allowed us to have a deeper understanding of the problem and helped us follow a systematic approach to evaluate the potential alternatives. The application of the AHP method for selecting the best anomalies provides a strong theoretical framework for handling the complexity of modeling multiclass anomalies maps in a scattered and widespread anomalies areas.

REFERENCES

Aghanabati, A., 2004. Geology of Iran. Geological Survey of Iran publication.

Agterberg, F.P., 1995. Multifractal modeling of the sizes and grades of giant and supergiant deposits. International Geology Review 37, 1–8.

Alianvari A, Katibeh H, Sharifzadeh M (2012) Application of fuzzy Delphi AHP method for the estimation and classification of Ghomrud tunnel from groundwater flow hazard. Arabian Journal of Geosciences. 5:275–284

Aliyari, F., Rastad, E., Mohajjel, M., 2012. Gold Deposits in the Sanandaj–Sirjan Zone: Orogenic Gold Deposits or Intrusion-Related Gold Systems? Resource Geology 62, 296–315.

Ataei M, Mikaeil R, Hosseinie S H, Hosseini S M (2012) Fuzzy analytical hierarchy process approach for ranking the sawability of carbonate rock. International Journal of Rock Mechanics and Mining Sciences. 50:83-93

Bejari H, Shahriar K, Akbarpour Shirazi M, Khademi Hamidi J (2010) Optimal tunneling method selection using fuzzy multiple attribute decision making technique. ISRM International Symposium 2010 and 6th Asian Rock Mechanics Symposium - Advances in Rock Engineering, New Delhi, India. pp 240-247

Cheng, Q., 1999. Spatial and scaling modelling for geochemical anomaly separation. Journal of Geochemical Exploration 65,175–194.

Cheng, Q., Agterberg, F.P., Ballantyne, S.B., 1994. The separation of geochemical anomalies from background by fractal methods. Journal of Geochemical Exploration 51, 109–130.

Cooper W W, Sieford L M, Tone K (2000) Data Envelopment Analysis: A Comprehensive Text with Models, Applications, References and DEA Solver Software, Kluwer Academic Publishers

Dağdeviren M, Yavuz S, Kılınç N (2009) Weapon selection using the AHP and TOPSIS methods under fuzzy environment. Expert Syst Appl. 36(4):8143–8151

David, M., 1977. Geostatistical Ore Reserve Estimation. Elsevier, Amsterdam.

Deng, J., Wang, Q., Yang, L., Wang, Y., Gong, Q., Liu, H., 2010. Delineation and explanation of geochemical anomalies using fractal models in the Heqing area, Yunnan Province, China. Journal of Geochemical Exploration 105, 95–105.

Deutsch, C.V., Journel, A.G., 1998. GSLIB: Geostatistical software library and user's guide, second ed. Oxford University Press, New York.

Erensal YC, Öncan T, Demircan M L (2006) Determining key capabilities in technology management using fuzzy analytic hierarchy process: a case study of Turkey. Inf Sci. 176(18):2755–2770

Falcon, N.L., 1961. Major earth – flexturing in the Zagros Mountain of southwest Iran. Journal of the Geological Society of London 117, 367 – 376.

Farhoudi, G., 1978. A Comparison of Zagros Geology to Island Arcs. Journal of Geology 86, 325- 334.

Fattahi H, Ebrahimi Farsangi M A, Shojaee S, Mansouri H (2014) Selection of a suitable method for the assessment of excavation damage zone using fuzzy AHP in Aba Saleh Almahdi tunnel, Iran. Arab J Geosci. DOI: 10.1007/s12517-014-1280

Khademi Hamidi J, Shahriar K, Rezai B, Rostami J, Bejari H (2010) Risk assessment based selection of rock TBM for adverse geological conditions using Fuzzy-AHP. Bulletin of Engineering Geology and the Environment. 69:523-532

Li, C., Ma, T., Shi, J., 2003. Application of a fractal method relating concentrations and distances for separation of geochemical anomalies from background. Journal of Geochemical Exploration 77, 167–175.

Mandelbrot, B.B., 1983. The Fractal Geometry of Nature. Freeman, San Francisco.

Mao, Z., Peng, S., Lai, J., Shao, Y., Yang, B., 2004. Fractal study of geochemical prospecting data in south area of Fenghuanshan copper deposit, Tongling Anhui. Journal of Earth Sciences and Environment 26, 11–14.

Önüt S, Soner S (2008) Transshipment site selection using the AHP and TOPSIS approaches under fuzzy environment. Waste Manage. 28:1552–1559

Pazand K, Hezarkhani A, Ghanbari Y (2014) Fuzzy analytical hierarchy process and GIS for predictive Cu porphyry potential mapping: a case study in Ahar–Arasbaran Zone (NW, Iran). Arabian Journal of Geosciences. 7(1):241-251

Rafiee R, Ataei M, Jalali SME (2013) The optimum support selection by using fuzzy analytical hierarchy process method for Beheshtabad water transporting tunnel in Naien, Iranian Journal of Fuzzy System. 10(6):39-51

Saaty TL (1980) The analytic hierarchy process: planning, priority setting and resource allocation. McGraw-Hill, New York

Sadeghi, B., Moarefvand, P., Afzal, P., Yasrebi, A., Saein, L., 2012. Application of fractal models to outline mineralized zones in the Zaghia iron ore deposit, Central Iran. Journal of Geochemical Exploration 122, 9–19.

Sanderson, D.J., Roberts, S., Gumiel, P., 1994. A Fractal relationship between vein thickness and gold grade in drill core from La Codosera, Spain. Economic Geology 89, 168–173.

Shi, J., Wang, C., 1998. Fractal analysis of gold deposits in China: implication for giant deposit exploration. Earth Sciences-Journal of China University of Geosciences 23, 616–618 (In Chinese with English abstract).

Torfi F, Zanjirani Farahani R and Rezapour S (2010) Fuzzy AHP to determine the relative weights of evaluation criteria and Fuzzy TOPSIS to rank the alternatives, Applied Soft Computing. 10(2):520-528

Turcotte, D.L., 1996. Fractals and Chaos in Geophysics, second ed. Cambridge University Press, Cambridge UK, pp. 81–99.

Turcotte, D.L., 2002. Fractals in petrology. Lithos 65, 261–271.

Geochemical Anomaly Separation by Number-Size (N-S) Fractal Model in Nakhilab Region, SE Iran

N. Mazraee
Department of Geosciences, University of Sistan and Baluchestan, Zahedan, Iran

A. A. Daya
Department of Mining Engineering, University of Sistan and Baluchestan, Zahedan, Iran

M. Boomeri
Department of Geosciences, University of Sistan and Baluchestan, Zahedan, Iran

ABSTRACT Separation anomaly from background is one of the most important purposes of geochemical exploration studies. Many methods have been used for this purpose. Methods based on fractal geometry are common for separation anomaly from background. Geochemical anomaly separation using the number-size (N-S) method at Nakhilab region, SE Iran, is studied in this paper. Stream sediments data sets were used in this geochemical survey which was conducted for the exploration for Au and Cu mineralization in Nakhilab region. The study shows threshold values for elements are being a consequence of the occurrence of anomalous accumulations of silicification and alterations rocks. The obtained results were compared with lithological unit patterns reveals a positive direct correlation between mineralization in anomalous areas and the related lithological units present in the region.

Keywords: Anomaly separation, Number-size (N-S) fractal model, Nakhilab

1 INTRODUCTION

Identification and recognition of anomalies from background is an essential issue in geochemical exploration. In the last century, customized statistical methods usually assumed that the concentration of chemical elements in the crust follow a normal or log-normal distribution. A geochemical anomaly as defined is a region where the concentration of a specific element is greater than a certain threshold value by statistical parameters, such as mean, median, mode, and standard deviation (Li et al. 2003; Daya 2014a,b). But, statistical methods, e.g., by histogram analysis or Q–Q plots assuming normality or log-normality, do not consider the shape, extent, and magnitude of anomalous areas and disregard spatial distribution (Cheng et al. 1994; Agterberg 1995).

Fractal theory has been established and developed by Mandelbrot (1983), as an important branch of nonlinear mathematical sciences has been applied in different fields of geosciences since 1980s. Bolviken et al. (1992) and Cheng et al. (1994)'s studies show that geochemical dispersion patterns of different elements are fractals. Several fractal models have been developed and applied to geochemical exploration for separate anomalies from background. One of the most important method for separating anomaly from background is the number–size model (N–S model) proposed by Mandelbrot (1983), which has been widely used by many geoscientists (e.g., Agterberg, 1995; Turcotte, 2002; Zuo et al., 2009c; Wang et al., 2010).

In this paper, Cu, Au, As, and Ag anomalies are studied and delineated by number–size model in Nakhilab area, SE Iran. Consequently, a general discussion is argued whereby the anomalous threshold values are correlated to the relevant structural and lithological units.

2 NUMBER-SIZE (N-S) MODEL

Number–size (N-S) method proposed by Mandelbrot (1983) can be utilized to describe the distribution of geochemical populations (Sadeghi et al., 2012). In this method, geochemical data do not undergo any pre-processing (Mao et al., 2004). This model shows a relationship between desirable attributes (e.g. elemental concentration in this study) and their cumulative numbers of samples (Sadeghi et al., 2012). A power-law frequency model has been proposed to explain the N–S relationship according to the frequency distribution of elemental concentrations and cumulative number of samples with those attributes (e.g., Li et al., 1994; Sanderson et al., 1994; Shi and Wang, 1998; Turcotte, 1996; Zuo et al., 2009a; Sadeghi et al., 2012). The model is expressed by the following equation (Deng et al., 2010; Mandelbrot, 1983):

$$N(\geq \rho) = K\rho^{-D} \qquad (1)$$

where ρ denotes elemental concentration, N(≥ρ) denotes the cumulative number of samples with concentration values greater than or equal to ρ, K is constant, and D is the fractal dimension of the distribution of elemental concentrations. According to Mandelbrot (1983) and Deng et al. (2010), log–log plots of N (≥ρ) versus ρ show straight line segments with different slopes –D corresponding to different concentration intervals (Sadeghi et al., 2012).

3 GEOLOGICAL SETTING OF THE NAKHILAB REGION

The study area is located in northwestern of Zahedan city, SE of Iran. The study area is located in boundary of Loot Block and eastern flitch zone In Iran. It is probably a part of Iran's eastern flitch zone. Loot Block in contact with Iran's eastern flitch zone occurred in a very metamorphosed, faulted, sheared, and brecciated zone. From the upper cretaceous to quaternary the study area experienced different mountainous phases including Laramide and Alpine. These mountainous phases have an effective impact in developing the geological setting of the study area. Another important feature of the study area is that it is near the active Nehbandan fault system. Loot Block is more dynamic in its eastern part where the study area is located. The study area is highly brecciated and has faults with general trend of NS and NE-SW. The folding systems in the study area are normal anticline and normal syncline. Their trend is NW-SE to NS.

In the study area lithological units comes from upper cretaceous to quaternary ages. The study area occurred in a tectonic regime that Ophiolites complex was present. The lithological units according to 1:250,000 geological map of Nakhilab sheet divide into three parts which are metamorphic, sedimentary and igneous rocks (Fig 1). Metamorphic unit itself divides into three parts. The first consists of serpentine and harzburgite. Their trend is NS and generally occurred in a folded, fractured, and transformed units. The second group consists of marble, phyllite, serisite, and schist. Theses metamorphic rocks are widespread and its strike in the study area is NS. The last (third) group of metamorphic rocks consists of chlorite, epidote, schist, and mica schist. Their strike in the region is NS. This unit is affected by tectonic activity and as a result is highly fractured. Sedimentary rocks are very widespread in the study area. The most abundant of them are shale, sandstone, limestone, marl, and conglomerate (Fig 1). There are many igneous rocks in the study area. The most important of them comes from Oligocene. It consists of granite, granodiorite, and monzonite. Alteration phenomena are obvious in the igneous rocks and these rocks are much altered (Fig 1).

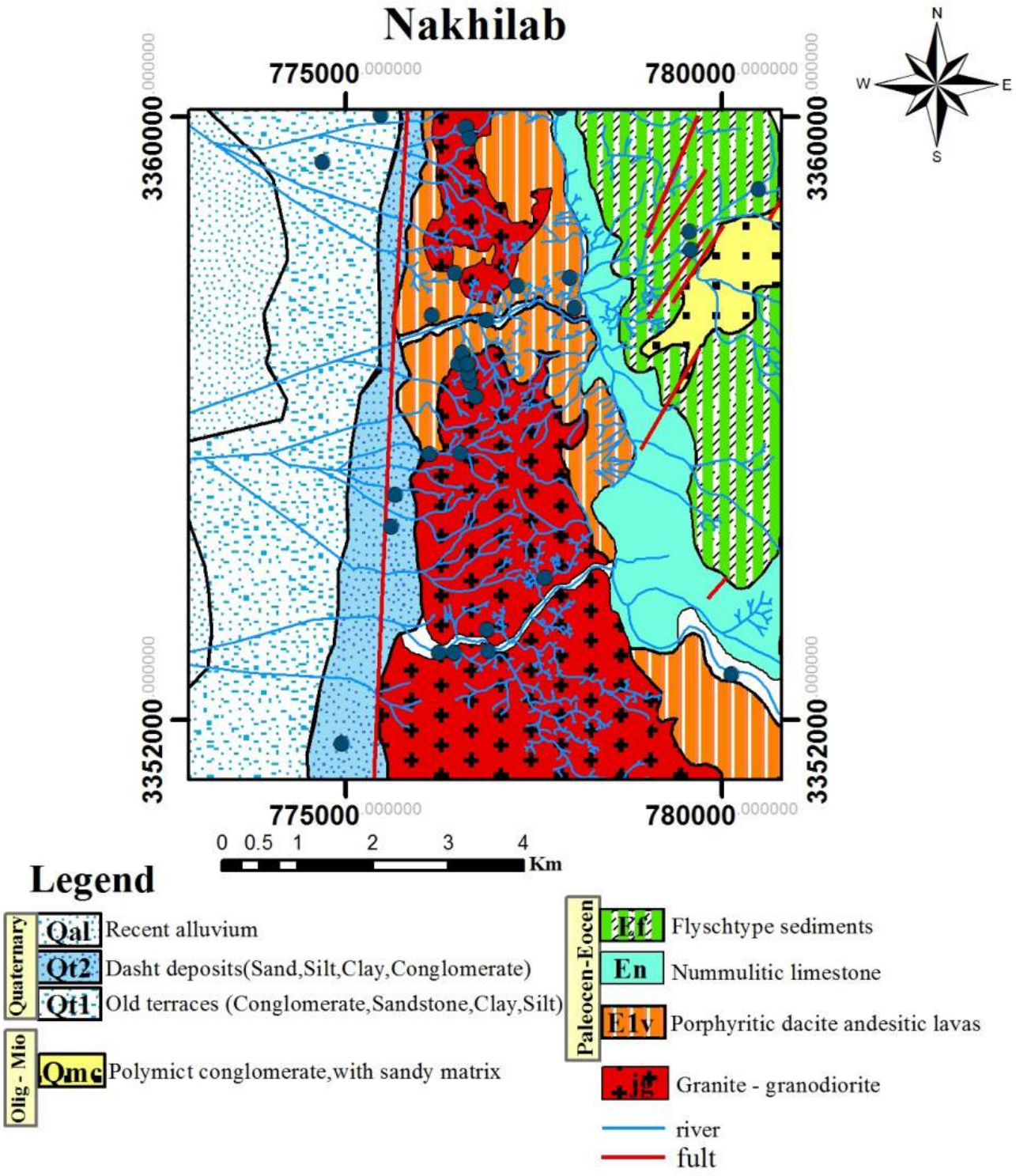

Figure 1. Geological map of Nakhilab region

4 GEOCHEMISTRY AND DATA ANALYSIS

A total of 213 collected stream sediments samples were analyzed by ICP-MS for elements which relate to Au and Cu mineralization and are of interest; As and Ag concentrations were of no significance.

Statistical results show that Cu, As, Ag and Au mean values are 2.8812, 1.1838, 0.1482 ppm and 0.0012 ppb, respectively (Table 1). Their distributions are not normal and variation between maximum and minimum for these data show a wide range (Fig. 2).

Table 1. Statistical parameters of raw data based on stream sediments geochemical samples analysis

Parameters	Au (ppb)	As (ppm)	Cu (ppm)	Ag (ppm)
Mean	0.0012	1.1838	2.8812	0.1482
Median	0.0010	1.1000	2.7600	0.0950
Variance	0.000001	97.788	89.438	0.558
Max	0.017	1.32	1.431	11.00
Min	0.0010	3	2.080	0.0800
Standard Deviation	0.0016	9.8634	9.547	0.7471

The elemental grades were sorted out based on decreasing grades and their cumulative numbers. Finally, elemental log–log plots were generated for Au, Cu, As, and Ag, as illustrated in Fig. 3. Based on this procedure, there are four geochemical populations for Au, and three geochemical populations for Cu, As, and Ag (Fig.3). Cu anomalous threshold is 25 ppm and its high-intensity anomaly is 40 ppm. Also, it is obvious that there are three steps of Cu enrichments based on log–log plot, as shown in Fig. 3. The various events derived by N–S model represent different geological factors, such as lithological differences and geochemical processes. Factors such as mineralizing events, surficial geochemical element concentrations, and surficial weathering are of considerable importance (Cheng et al. 1994).

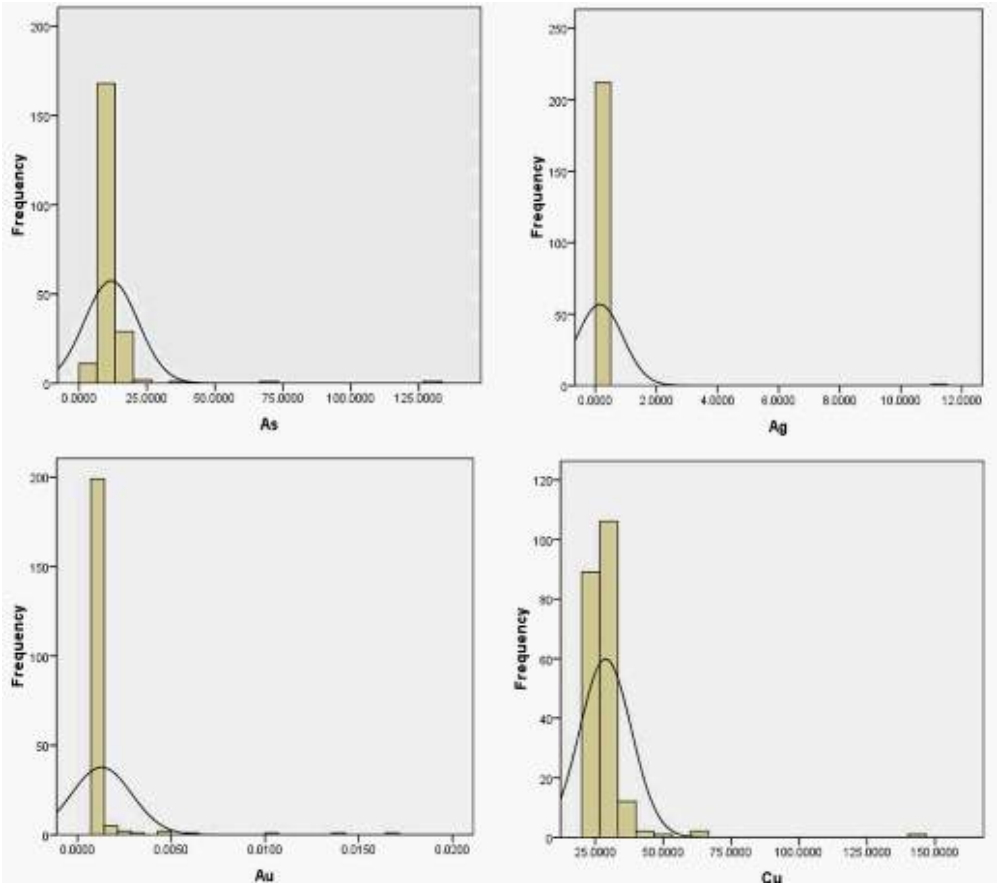

Figure 2. As, Ag, Au and Cu histograms

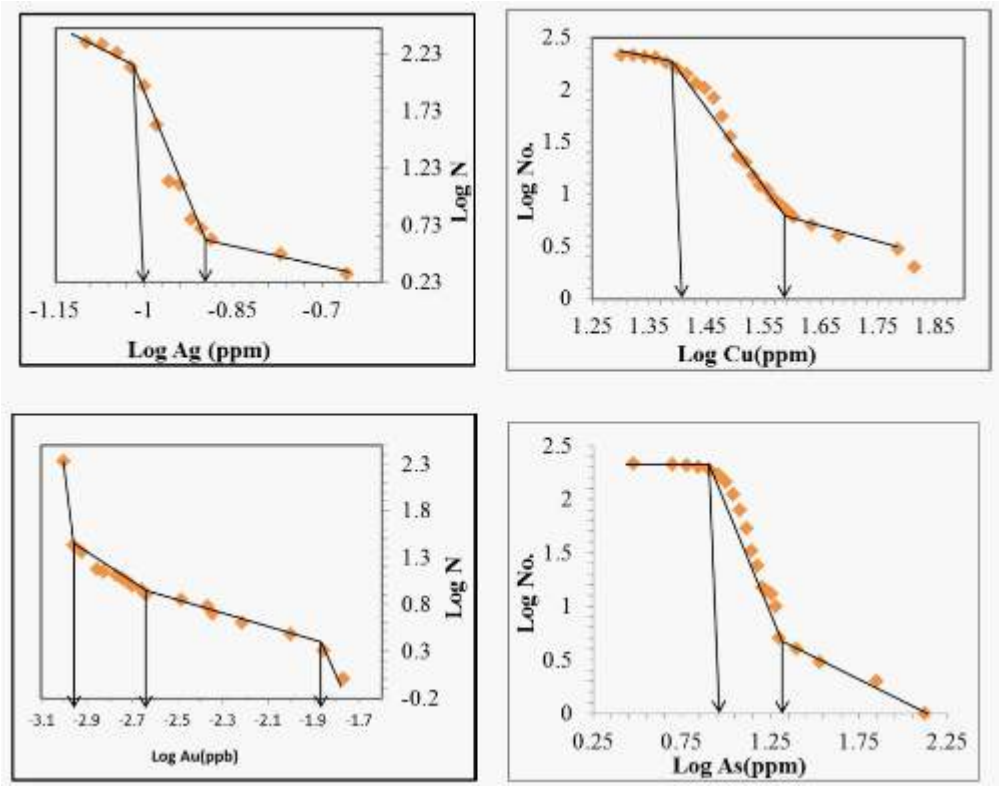

Figure 3. Log–log plots resulted from N–S model for Au, Ag, Cu, and As

Geochemical maps were constructed with inverse distance squared method by Rock Works™ v. 15 software package. The area was gridded by 250m×250m cells. Obviously, situations of Au anomalies are in northern parts of the area and the high-intensity anomalies are situated in NE parts as depicted in Fig. 4. Moreover, Cu anomalies are situated in northern, central parts of the area also high-intensity Cu anomalies were situated in central part of the study area (Fig. 4). Main Ag and Cu anomalies exist in the northern part of the area and correlated with Au anomalies location, as depicted in Fig. 4.

5 COMPARISON WITH GEOLOGICAL PARTICULARS

Threshold values of elements obtained from N–S model are compared and correlated to specific geological particulars of the area including considering nature of lithological units and faults. The anomalous parts visibly show the main identified faults especially in NE, and central parts of the area. Comparison between faults positions and elemental anomalies shows that faults intersect the anomalies situated near those structures. Moreover, faults and elemental anomalies have a proportional relationship. High-grade elemental anomalies occurred inside and within the fault zones or situated on faults intersection areas. This is a positive parameter because silicified and quartz-sulfide veins occurred along these faults and Au particles existed in these veins and veinlets. In the area, based on results of the N–S model, the elemental anomalies correlated with different rock types. High amounts of Cu, over 40 ppm, are highest in sand, silt, clay, and conglomerate. There are sulfide mineralization especially chalcopyrite. The Au high-intensity anomalous parts, higher than 0.

0.002 ppb, are situated in sand, silt, clay, conglomerate, and limestone. Also, there are quartz-sulfide veins and veinlets. An epithermal system is existed in this area and correlated within main Au, Cu, and Ag anomalies. Also, the main step, As mineralization, higher than 20 ppm, is

correlated within granitic and granodioritic units.

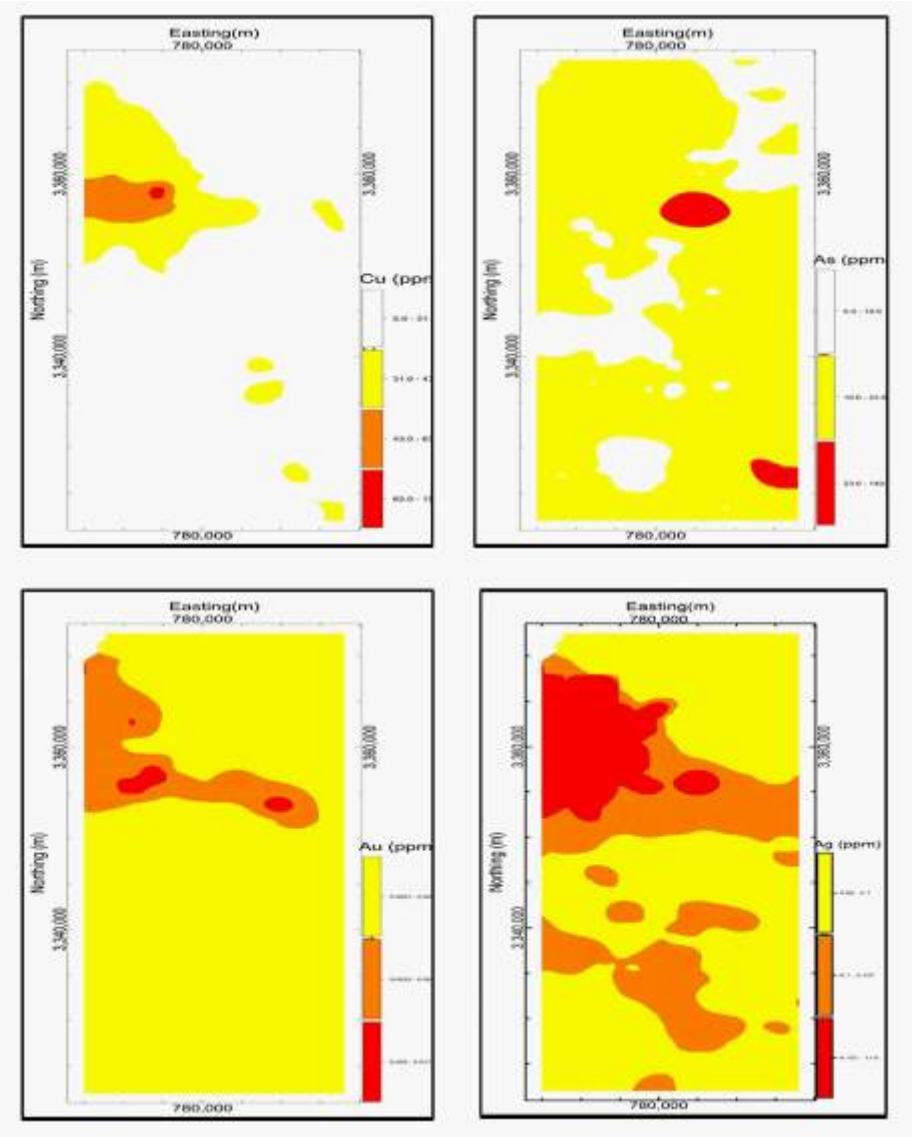

Figure 4 Au, Ag, Cu, and As geochemical population distribution maps based on N–S model

6 CONCLUSIONS

The study on Nakhilab area indicates the potential use of the N–S model for geochemical anomaly separation as a useful tool for geochemical exploration, commonly used in stream sediment geochemistry. The advantages of the model relies fundamentally on its straightforwardness, and easy computational achievement, as well as the possibility to compute the anomalous threshold values for different elements, which is the most useful criteria for cross examination of information with numerical data from different sources. There exists a proper correlation between the calculated anomalous threshold values and the geological specifics in the Nakhilab area. These results may also be interpreted differently according to their multifractal curves in log–log plots. Cu, Au, and Ag concentrations in the area may be a result of the three steps of enrichment, i.e., mineralization and later dispersions. Au and Cu log–log plots were shown that there are three steps for their enrichment and dispersion. Major Au mineralization occurred in sedimentary units in NW parts of the area. Au particles occurred in quartz-sulfide veins and veinlets. Main anomalies

of Ag and Cu are situated in the NW part of the area and correlated with main Au anomalies. It can be interpreted that there is an Au epithermal system. The occurrence of Cu higher than 40 ppm in sedimentary rocks (sandstones and conglomerate) in western parts of the area has been actually realized in the samples collected from the field. The studied elements anomalies have proper and direct relationships with faults in Nakhilab area. High intensity elemental anomalies are mostly located at fault intersections or near fault zones. It is important because quartz-sulfide veins and veinlets occurred along these faults.

REFERENCES

Agterberg, F.P., 1995. Multifractal modeling of the sizes and grades of giant and supergiant deposits. International Geology Review 37, 1–8.

Bolviken, B., Stokke, P.R., Feder, J., Jossang, T., 1992. The fractal nature of geochemical

landscapes. Journal of Geochemical Exploration 43, 91–109.

Cheng, Q., Agterberg, F.P., Ballantyne, S.B., 1994. The separation of geochemical anomalies from background by fractal methods. Journal of Geochemical Exploration 51, 109–130.

Daya A.A., 2014a. Application of concentration-area fractal method for separation of anomaly from background; A case study in Shorabhaji region, Arabian journal of geosciences. In press.

Daya A.A., 2104 b. Comparative study of C-A, C-P , and N-S fractal method for separating anomaly from background; A case study in Kamoshgaran region. Journal of geochemical exploration. In press.

Deng, J., Wang, Q., Yang, L., Wang, Y., Gong, Q., Liu, H., 2010. Delineation and explanation of geochemical anomalies using fractal models in the Heqing area, Yunnan Province, China. Journal of Geochemical Exploration 105, 95–105.

Li, C., Xu, Y., Jiang, X., 1994. The fractal model of mineral deposits. Geology of Zhejiang 10, 25–32 (In Chinese with English Abstract).

Li, C., Ma, T., Shi, J., 2003. Application of a fractal method relating concentrations and distances for separation of geochemical anomalies from background. Journal of Geochemical Exploration 77, 167–175.

Mandelbrot, B.B., 1983. The Fractal Geometry of Nature. Freeman, San Francisco.

Sadeghi, B., Moarefvand, P., Afzal, P., Yasrebi, A., Saein, L., 2012. Application of fractal models to outline mineralized zones in the Zaghia iron ore deposit, Central Iran. Journal of Geochemical Exploration 122, 9–19.

Sanderson, D.J., Roberts, S., Gumiel, P., 1994. A Fractal relationship between vein thickness and gold grade in drill core from La Codosera, Spain. Economic Geology 89, 168–173.

Shi, J., Wang, C., 1998. Fractal analysis of gold deposits in China: implication for giant deposit exploration. Earth Sciences-Journal of China University of Geosciences 23, 616–618 (In Chinese with English abstract).

Turcotte, D.L., 1996. Fractals and Chaos in Geophysics, second ed. Cambridge University Press, Cambridge UK, pp. 81–99.

Turcotte, D.L., 2002. Fractals in petrology. Lithos 65, 261–271.

Wang, Q., Deng, J., Liu, H., Yang, L., Wan, L., Zhang, R., 2010. Fractal models for ore reserve estimation. Ore Geology Reviews 37, 2–14.

Zuo, R., Cheng, Q., Xia, Q., 2009a. Application of fractal models to characterization of vertical distribution of geochemical element concentration. Journal of Geochemical Exploration 102, 37–43.

Zuo, R., Cheng, Q., Xia, Q., Agterberg, F.P., 2009c. Application of fractal models to distinguishing between different mineral phases. Mathematical Geosciences41, 71–80.

Geophysical Contribution to the Geological Study of the North Numidian Mercurial Zone (North-East of Algeria)

D.Boubaya
Laboratoire Eau et Environnement, Université de Tébessa, Tébessa 12000, Algeria

K.Allek
Laboratoire Physique de la Terre, Université M'Hamed Bougara, Boumerdes, Algeria

M.Hamoudi
Laboratoire de Géophysique, USTHB, BP32, El Alia, 16111 Dar El Beida, Algiers, Algeria

C.Fehdi
Laboratoire Eau et Environnement, Université de Tébessa, Tébessa 12000, Algeria

ABSTRACT From 1977 to 1981, The National Geological Survey and Mining Company of Algeria (ORGM) tested various geophysical methods at the North Numidian Mercurial Zone. The study included: gravity, magnetic, VES-IP, gradient array IP and a mercury vapour soil gas test. This paper presents the results of a case history from the Mra-Sma site, which is located near the city of Azzaba. The objective of the ground based geophysical survey were the mapping of the lithology and tectonic structure, as well as the study of the extension of the mineralized area. The geology of the study area is very complicated by the presence of several allochthonous units. In the majority of the cases, these allochthonous units and nappes are superimposed and strongly brought closer by tectonic movements.

The results of the present study illustrate that; an integrated geophysical strategy can assist and enhance the exploration for mineralization in a region of complicated geology such as the north Numidian Mercurial zone.

Keywords: North Numidian, gravity, magnetic, VES-IP, mercury

1 INTRODUCTION

The deposits of lead and mercury of the Northern Numidic zone are known since antiquity. The beginnings of the geological investigations go back to the middle of 19th century, when the Baryto-polymetallic deposit of Mra-Sma (1850) and that of Mercury of Ras El Ma (1853) were discovered.

During the later period up to 1966, the geological investigations could not highlight new deposits. Geological investigations were concentrated around the known sites cited above.

In 1967, following work of evaluation on the Grayer Baryto-Polymetallic deposit, a thrust slice of Palaeozoic rocks was discovered in the northern part of the mineral-bearing zone. Further studies of the frontal thrust by trenches according to the dip brought to the discovery of the Mra-Sma deposit.

In 1967-1968, on the basis of the study of the Mra-Sma and Ismail deposits, it was given the principal criteria for exploration of mercury deposits in the North Numidian Zone: The presence of structural highs(domes) covered by thrusting in combination with the feeder faults.

The large volume of exploration data and its high success within a rather short time (1966-1970) made it possible to discover 3 mercury ore deposits and 27 mineral showings of mercury, polymetallic and copper. 19 cinnabar aureoles were the subject of detailed prospection.

The Mra-Sma deposit is located 2 km in the south–east of the city of Azzaba. It is composed of two orebodies: Mra-Sma I and Mra-Sma II. They have a length of 600 m and a width of 150 m. The mineralized zone has a width ranging from 2 to 35 m.

The deposit was discovered in 1971 by Titov and Pikhota (Oblentsev et al, 1985)

The implementation of the geophysical methods (gravity, magnetics, geoelectric prospection) as well as the geochemical survey in the experiment of the studies of the Northern Numidic Zone made it possible to distinguish the positive morphological structures below thrusting and to highlight the geochemical anomalies.

One could manage to say that the deposits of Ismail and Guenicha are characterized by positive gravimetric anomalies.

The purpose of this study was to use a complex of geophysical methods. This includes: gravity, magnetic, gradient array IP and a mercury vapour soil gas test. These geophysical methods seeks to: (1) bring out the structural highs (domes) under the frontal thrust (2) mapping of grinding area and (3) mapping of the hydrothermal alteration zones enriched with sulphide mineralization.

2 GEOLOGY OF THE STUDY AREA

The Maghrebides chain is part of the peri-Mediterranean belt of Tertiary age that delimits the African from European plates and runs from the Betico-Rifan arc to Calabria (Caby, 2001)

The study area (fg.1) belongs to the lesser Kabylia which has a very complex geological structure. Lesser Kabylia belongs to the Alboran–Kabylias–Peloritan–Calabria (AlKaPeCa; Bouillin, 1986). AlKaPeCa domain is of European origin and corresponds to the former northern margin of the Alpine Tethys now included in the so called Tell-Rif, whose it forms the internal domain(Frizon de Lamotte et al, 2009). The geological structure of the area is determined by the presence of some complexes represented by the formation of various structuro-facial zones which in the majority of the cases are tectonically superimposed the ones on the others or strongly brought closer. The lower structural position is occupied by the para-autochtonous complex of the Mount Djebel Safia composed of carbonate rocks of Jurassic and of Neocomian age.

In the higher position, one notes a whole series of allochtonous complexes. Among these complexes, the lower position is occupied by the Kabylie complex consisting of a basement of metamorphic schist and sandstones of Oligocene covering the latter. Higher, one notes the complexes of flysch of Penthièvre and Guerrouch (Tithonic with Oligocene included).

The complex of the so called limestone ridge (la dorsale calcaire), usually thrusted on the complexes of flysch consisting of terrigenous and carbonate rocks of Jurassic, Cretaceous and Paleogene age.

The higher structural position is occupied by the complex of the flysch «with microbreccia» and the Numidian complex, the topmost of the allochtonous complexes.

The formations of Miocene and Quaternary form the post-nappe autochthonous complex.

3 MATERIALS AND METHODS

3.1 Aeromagnetic Survey

The aeromagnetic data used in this study were extracted from a regional-scale aeromagnetic survey of northern Algeria conducted by Aeroservice Corporation for the Société Nationale de Recherches et d'Exploitations Minières (SONAREM) from 1971 to 1974 as a part of the latter's mineral exploration program. The survey was conducted with NNW–SSE profiles perpendicular to the general geologic strike of the study area. . The survey was flown in drape mode using Doppler-assisted navigation at an average ground clearance of 150 m and a line spacing of 2 km for traverses and 10 km for tie lines. The data were collected at a sampling interval of 46 m using a high resolution cesium magnetometer.

Aeroservice Corporation performed standard levelling corrections; however the aeromagnetic map gridded from flight line data suffered from levelling errors appearing as stripes along the flight line direction. To provide the highest quality data possible, most rigorous procedures were performed during the re-processing of the aeromagnetic data. This included the application of a de-spiking filter and microlevelling (Boubaya et al, 2011).

3.2 Ground Geophysical Data

An integrated ground based geophysical study (Oblentsev et al, 1985) comprising gravity, magnetic, VES-IP, gradient array IP and a mercury vapour soil gas test was conducted between 1977 and 1981 to study the possible extension of the mineralization near the known Mra-Sma deposit.

The gravity data were collected on north-south lines with a grid of (100 x 50). The gravity measurements were carried out with a Scintrex CG-1 gravimeter. A reduction density of 2500 kg/m^3 was used for the Bouguer correction. The error on the Bouguer anomaly is estimated to be better than 0.05 mGal.

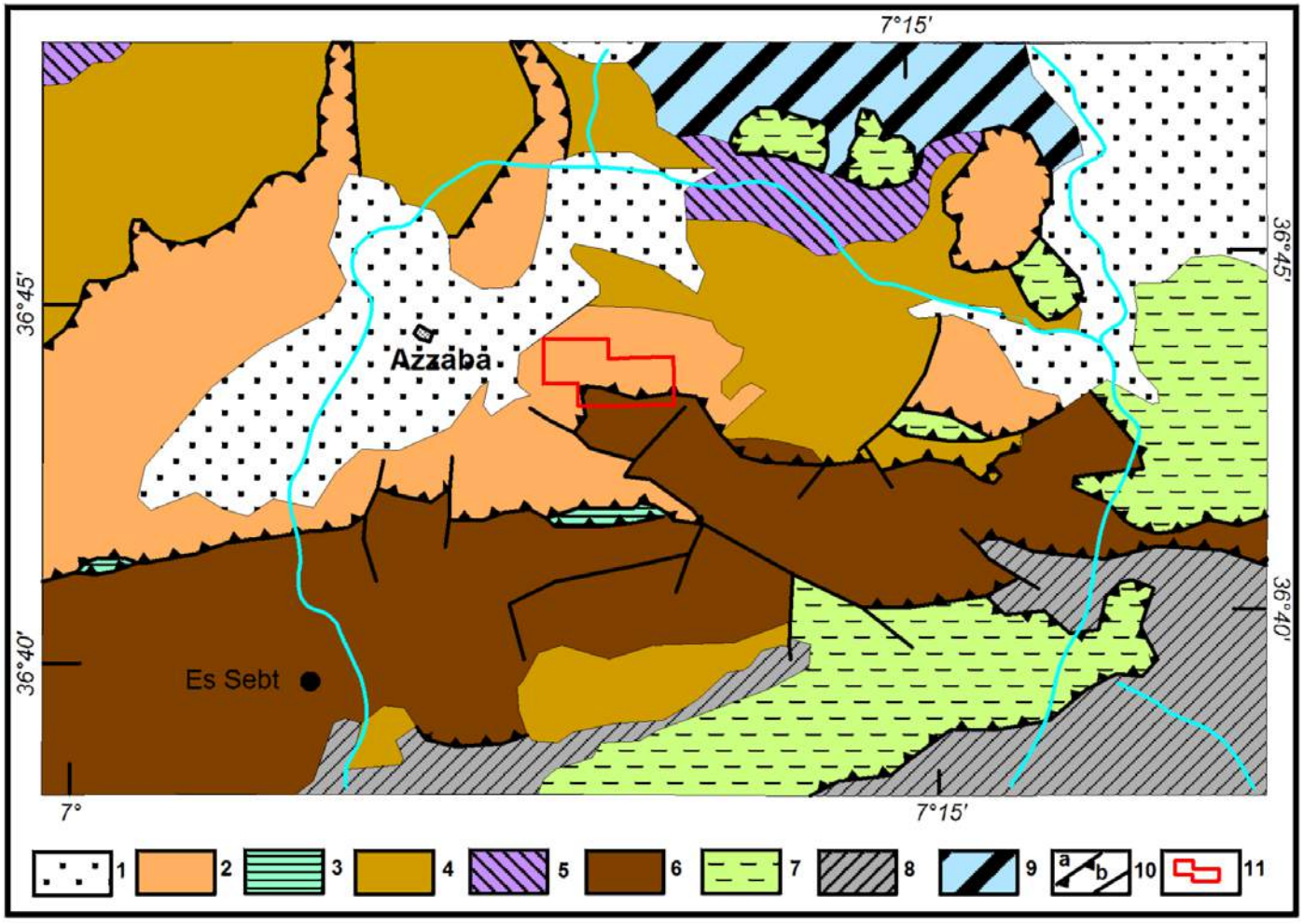

Figure 1. Structural geologic map of the study area (after Tchekhovitch, V. 1971)
Legend: 1- Post nappe complex 2- Numidian nappe 3- Flysch with Microbrecchia unit, 4- neoautochtone Oligocene 5- Kabylie unit 6- The limestone ridge (la dorsale) 7- Guerrouch unit 8- Penthievre unit 9- Parautochtone complex 10- a- thrust, b- fault, 11- study area

Magnetic data were also collected in the same gravity grid with an MF-2 magnetometer measuring the vertical intensity of the earth geomagnetic field. The error on the measured vertical intensity of the geomagnetic field is estimated to be around 10 nT.

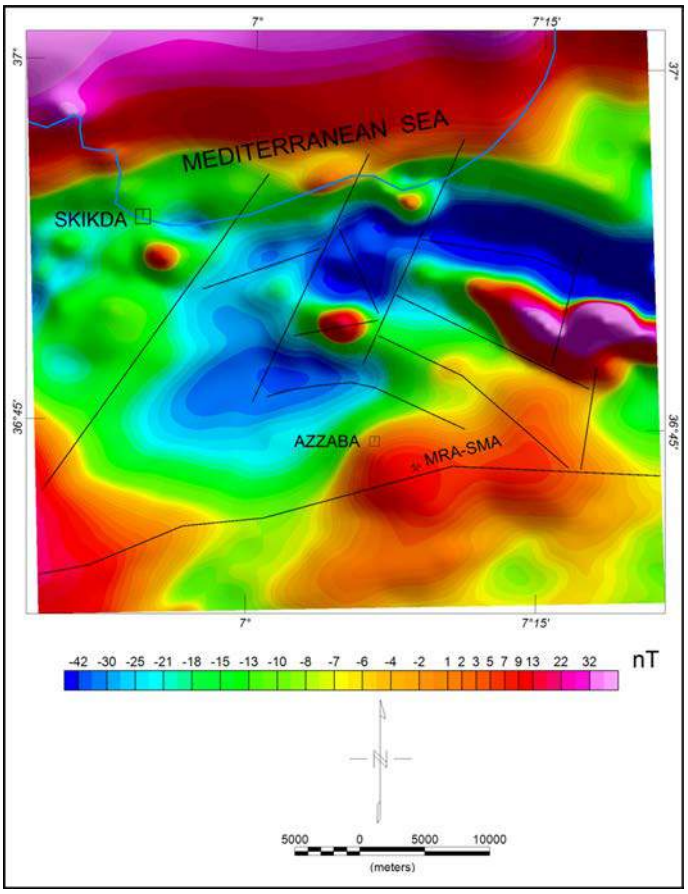

Figure 2. Shaded residual aeromagnetic map of the study area and adjacent regions

Resistivity and Induced polarization (Gradient-IP and VES-IP) data were acquired in the time domain, using a 2S square wave signal with resistivity values calculated during the on times, and IP decay amplitudes were measured in 6 windows during the off times. The resistivity survey was carried out using a Scintrex system operating in the time domain consisting of an IPR-8 receiver and a TSQ-2E transmitter.

4 RESULTS

4.1 Analysis of the Aeromagnetic Data

A shaded residual aeromagnetic map of the Azzaba region and surrounding area is shown in figure. 2. The magnetic field varies between a minimum of -45 nT and a maximum of 40 nT.

The Mra-Sma deposit lies on a broad positive magnetic anomaly.

Short wavelength magnetic anomalies north to the city of Azzaba correlate with the location of small iron ore deposits.

Magnetic basement faults are drawn in the total magnetic intensity (TMI) map. Parts of these basement faults were interpreted by Aeroservice Corporation (AeroService, 1975).

The most prominent geophysical lineament is situated in the south of Azzaba and trends in E-W direction. This linear feature is probably the principal feeder for Mercury mineralization of the North Numidic Mercurial Zone.

4.2 Analysis of the Ground Geophysical Data

In this part, we will deal only with the gravity and VES-IP data.

Figure.3 shows the map of the detailed gravity survey over the Mra-Sma region.

The Bouguer gravity data compiled with a density of 2500 kg/m^3 varies between a minimum of 28 mGal and a maximum of 32 mGal.

The steep gradient in the SW of the map correlate with the Mra-Sma fault which has a total length of 10 km. The Mra-Sma deposit itself lies on a moderate gravity high.

The interpretations of nine (9) VES-IP points conducted in the vicinity of the Mra-Sma deposit along line 08 are presented in figure.4. The section outlines 3 geoelctric layers:

(1) The first layer corresponds to the cover is characterized by low resistivities and low chageabilities

(2) The middle layer corresponds to the mineralized zone and has a moderate high resistivities and high chargeabilities. The rise of chargeability is probably caused by the presence of sulfides

(3) The last layer corresponds to the basement. This layer is characterized by low resistivities and low chargeabilities.

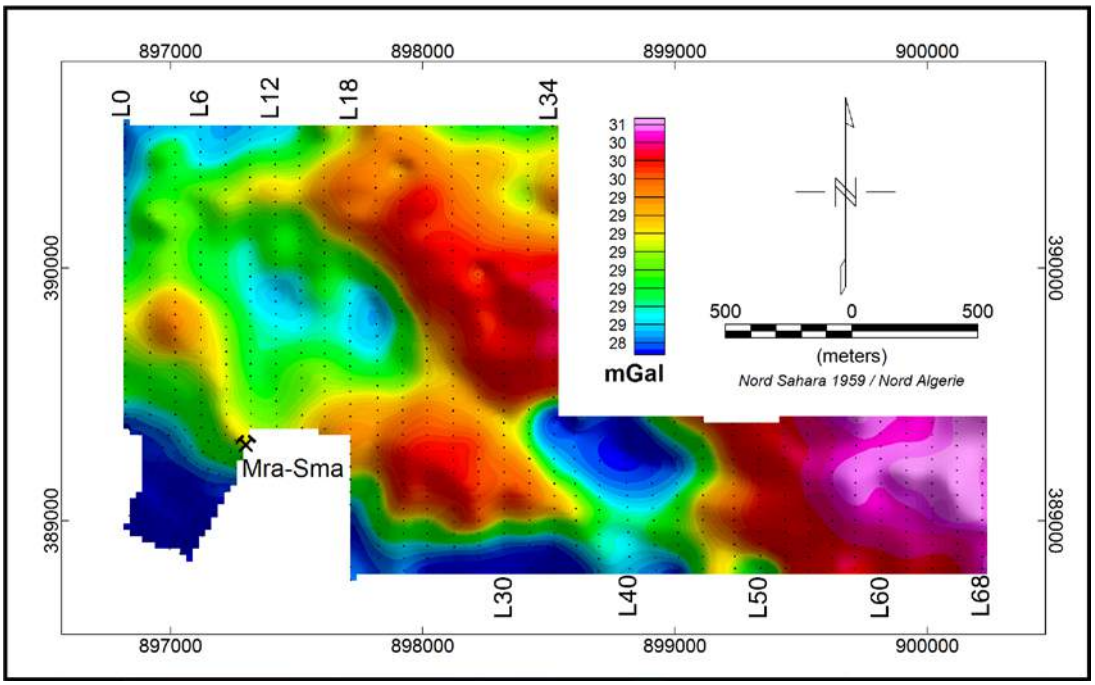

Figure 3. The Bouguer gravity map of Mra-Sma

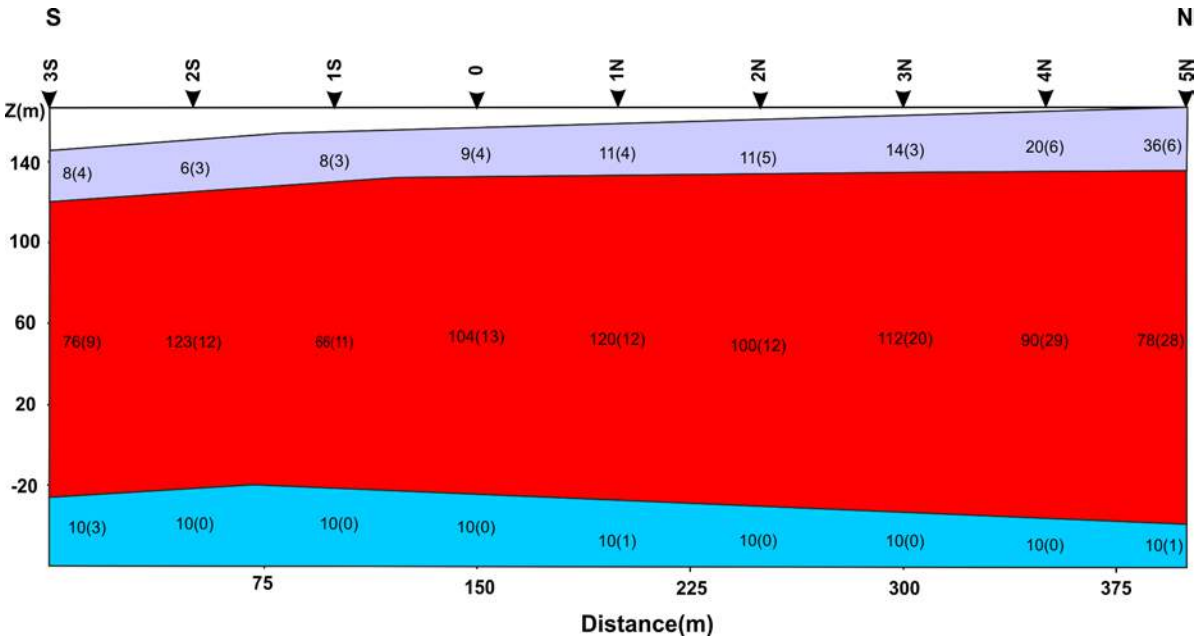

Figure 4. VES Geoelectric section along line 08 of Mra-Sma
10(0): values of resistivity and chargeabity

5 CONCLUSION

The integrated geophysical study conducted in the vicinity of the Mra-Sma deposit of Mercury helps us to study the extension of the mineralized area further to the east and to the north of the known deposit.

The mineralized area has a moderate resistivity and a high chargeability.

The VES-IP data provide important information about the deeper parts of the survey area.

REFERENCES

Aeroservice, Corporation, 1975. Aero-magneto-spectrometric Survey of Algeria, Final Report, 3 Volumes, Houston, Philadelphia

Boubaya, D, Allek, K and Hamoudi,M. 2011. Is there a hidden near surface salt diapir in the Guelma Basin, north-east of Algeria? Journal of Applied Geophysics, 73, 348-356

Bouillin, J.P., 1986. Le “bassin maghrébin”: une ancienne limite entre l'Europe et l'Afrique à l'Ouest des Alpes. Bull. Soc. Geol. Fr. 8 (II), 547–558.

Caby, R., Hamor, D., Delor, C. 2001. Metamorphic evolution, partial melting and Miocene exhumation of lower crust in the Edough metamorphic core complex, west Mediterranean orogen, eastern Algeria, Tectonophysics, 239–273

Frizon De Lamotte,D., Leturmy,P., Missenard,Y., Khomsi, S. 2009. Mesozoic and Cenozoic vertical movements in the Atlas system (Algeria, Morocco, Tunisia): an overview, Tectonophysics, 9-28

Oblentsev,A., Ivonine,I., Kalinine, A.1985. Rapport sur les résultats des travaux de recherches sur les champs miniers de Mra-Sma et ismail(Zone Nord Numidique) durant la période 1977-1981, ORGM, internal report

Tchekhovitch, V.1971. Carte géologique de la feuille Azzaba au 1: 50 000 et Notice explicative SONAREM, Département Recherches

Geostatistics As a Tool to Estimate Undiscovered Deposits of Coal

F. Atalay, A. E. Tercan, G. Ertunç
Hacettepe University, Mining Engineering Department, Ankara

ABSTRACT The key of sustainable electricity production is directly related to coal. In order to satisfy sustainability, coal presence and undiscovered coal potential have to be studied carefully. The aim of this study is to examine potential coalfields in Turkey by using geostatistical tools such estimation and simulation. For this purpose, kriged and simulated maps for lower calorific value are produced using the coal data collected in the Tertiary fields of Turkey. Then locations for which the kriged values do not fall in symmetric 95% probability intervals of simulated values are determined and these locations are considered as highly uncertain and target areas for potential coal resources. This study experimentally shows that geostatistical tools such as kriging and simulations have a great potential to predict and analyze coal resources.

Keywords: Geostatistic, coal, kriging, simulation

1 INTRODUCTION

In Turkey, 73 % of the electricity is produced by the thermal power stations (T.E.T.C, 2013) where coal is the feeding source. Coals in Turkey mostly occurred in the Tertiary period with some exceptions. Therefore, sustainability of the electric production is directly related to the presence and discovery of the Tertiary coal resources.

Tertiary fields are studied by the Paşamehmetoğlu et al. (1983), Görür et al. (1996), Temur et al. (2008) from the view point of coal potential and discovery. Paşamehmetoğlu et al. carried out coal prospecting studies in various sites and determined target locations for coal. Görür et al. made an attempt to classify tertiary basins into seven categories according to their tectonic characteristics and discussed the geological evolution and coal potential of each basin. Tuncalı et al. (2002) studied the chemical and technological properties of the tertiary coals. In these studies, main method for the discovery of coal was surveying. Neither mathematical models nor sophisticated estimation methods were used in these studies to predict the location of the undiscovered coal resources.

In this study, geostatistical methods are used to predict the locations of the undiscovered coal resources. Using the data collected from Tertiary coal fields, lower calorific value (LCV) distribution over the Tertiary fields is estimated by using ordinary kriging . To asses the uncertainty of the LCV distribution multiple realizations of LCV are generated using sequential gaussian simulation. Then locations for which the kriged values do not fall in symmetric 95% probability intervals of simulated values are determined and these locations are considered as highly uncertain and target areas for potential coal resources. This experimental study shows that geostatistical tools such as kriging and simulations have a great potential to predict the location of the undiscovered coal resources.

2 MATERIALS and METHODS

Data used in this study is based on Tuncalı et al. (2002) who collected data primarily from both government and private owned coal fields. Descriptive statistics of LCV is given in Table 1.

Table 1. Descriptive statistics of LCV

	LCV (kCal/kg)
Number of data	187
Minimum	1185
Maximum	5574
Average	3186
Median	3103
Standard Deviation(σ)	921
Skewness	0.30
Kurtosis	-0.21

For the purpose of estimation and simulation a block model of the Tertiary fields is created with individual block dimensions of 4000 X 4000 m. LCV is estimated by using ordinary kriging and then simulated using Sequential Gaussian Simulation.

Experimental variogram for LCV is calculated and modelled. The parameters of the model variogram are shown in in Table 2.

Table 2. Variogram model parameters of LCV

	LCV (kCal/kg)
C0 (Nugget)	187
C (Sill)	1185
Range (m)	5574
Model	Spherical

In order to assess the validity of the variogram model cross validation is performed. Table 3 presents the cross validation results. For a reasonable variogram model, the average of errors should be near to zero, error variance and kriging variance should be close to each other and percentage of error within two standard deviation should be around 95. Table 3 shows that model parameters are acceptable in terms of these criteria.

Table 3 Cross validation results

	LCV
Number of Data	187
Average Error	39
Error variance	811
Kriging error variance	770
Error % in ±1.96 σ	93.5

Using the variogram model given in Table 2. lower calorific value of the Tertiary fields is estimated. In estimation a maximum of 16 samples and a minimum of 3 samples are used. The distance of one and half times of the range is considered as a size of search neighborhood. Estimation only gives a single estimate in an un-sampled location. In order to characterize the uncertainty of the estimates simulation is widely used.

To characterize the uncertainty of the estimation results, direct sequential simulation is used. This simulation method is first introduced by Soares (1998) based on the principle introduced by Journel (1994). The LCV distribution of the tertiary fields is simulated fifty times in order to capture the uncertainty associated with the tertiary fields

3 RESULTS and DISCUSSION

Figure 1 shows the kriged map of LCV over Tertiary fields while Figures 2, 3 and 4 present 1st, 25th and 50th realizations of the simulations respectively.

To determine the high uncertainty areas kriging and simulation results are compared. The areas where the kriging result falls beyond the 95% confidence interval are considered as the high uncertainty areas. These areas are shown in the Figure 5.

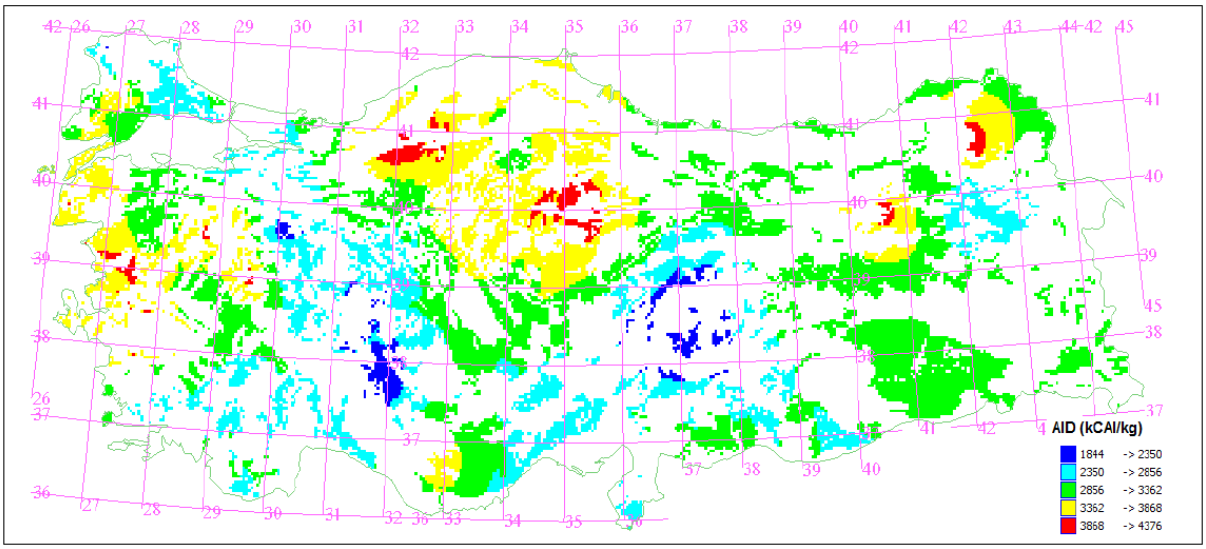

Figure 1 Spatial distribution of LCV over Tertiary fields

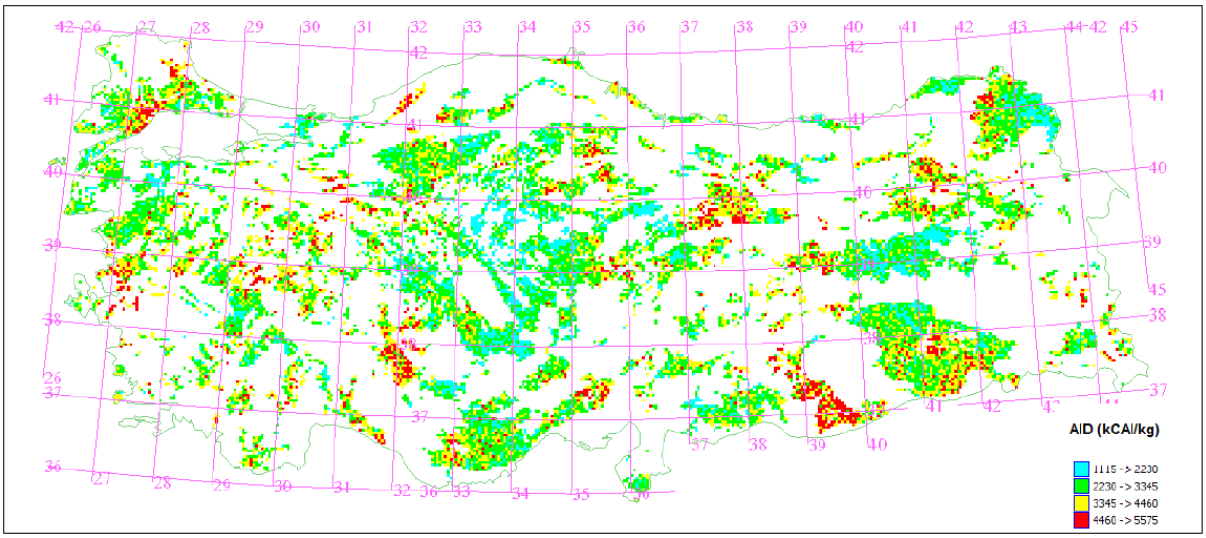

Figure 2. 1st realization of the LCV distribution of the Tertiary Fields

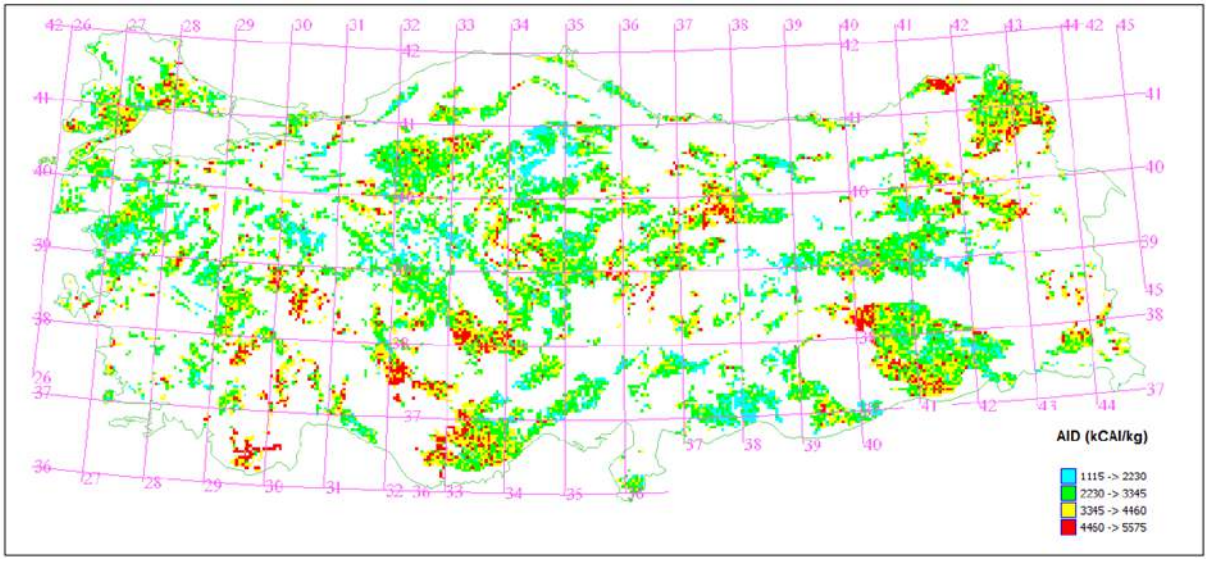

Figure 3. 25th realization of the LCV distribution of the Tertiary Fields

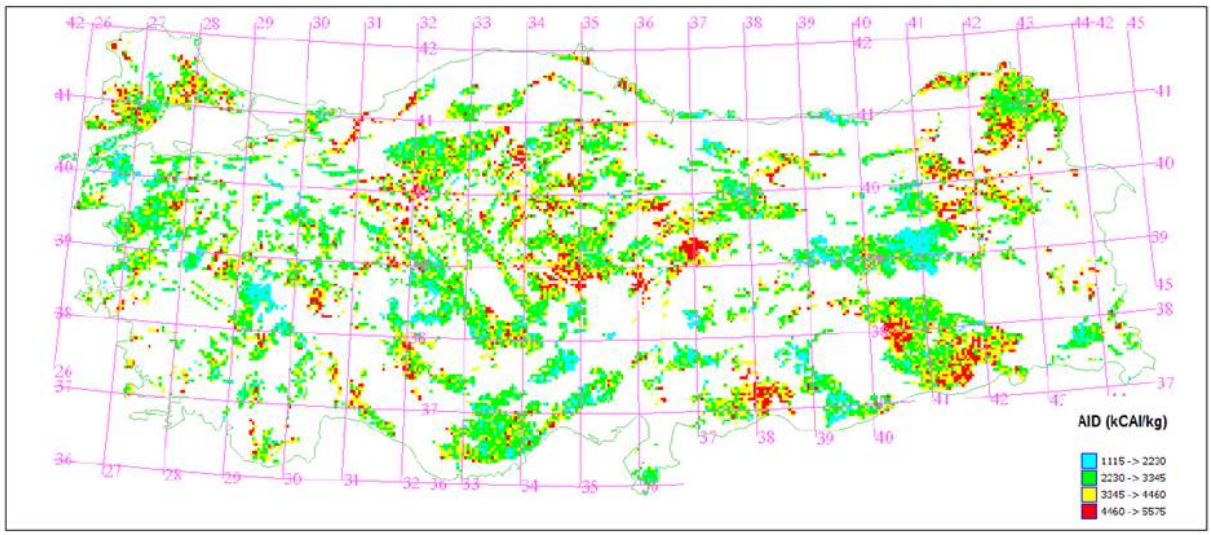

Figure 4. Figure 3. 50th realization of the LCV distribution of the Tertiary fields

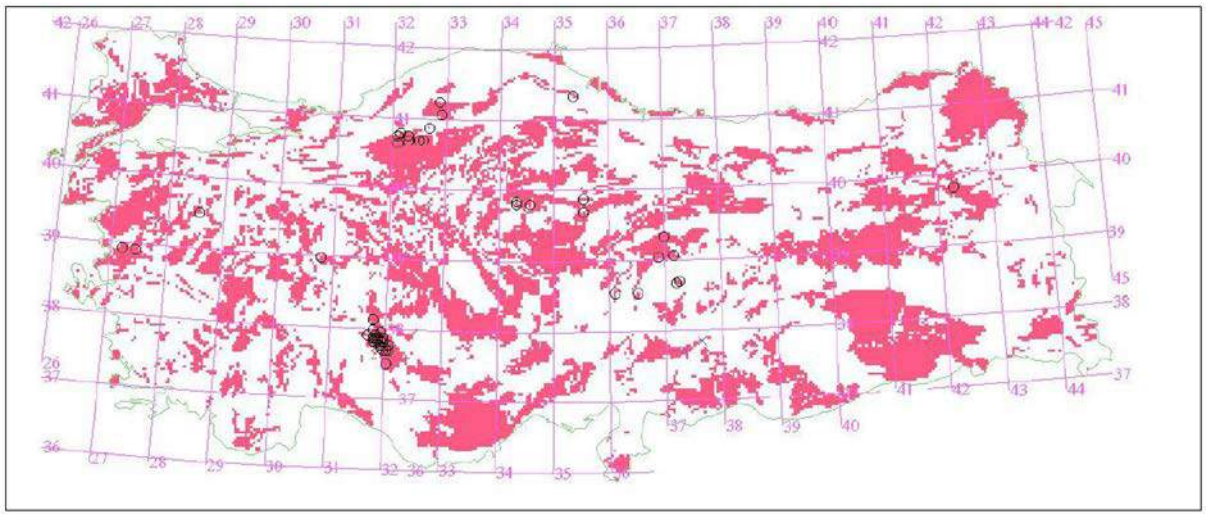

Figure 5. Locations of the high uncertainty areas in black circles

High uncertainty areas are located at Ağrı, Bolu – Gerede, Sivas Gürün and Kangal districts,Sinop-Nezir Köprü, İzmir-Kırkağaç, and especially at Konya regions. At the time of this study is made no data was available from the Konya region. Recently a big coal resource discovered by the General Directorate of Mineral Research and Exploration (MTA) which is close to the uncertainty areas found by this research. This shows that high uncertainty areas has great potential to discover the yet undiscovered coal resources.

4 CONCLUSIONS

From global perspective to assess the coal fields geostatistical estimation and simulation can be used. Using simulation high uncertainty areas can be determined and additional sampling should be carried out at this areas in order to better understanding of the field. This high uncertainty areas can reveal the coal occurrence which is not discovered yet. So geostatistics potentially can be used to estimate the undiscovered coal resources.

REFERENCES

Görür N., Akkök R., Sakınç M., Ünalan G., & Yaltırak C., (1996), *Türkiye Tersiyer Havzaları ve Kömür potansiyeli, Türkiye kömür arama hedeflerinin belirlenmesi ve arama yöntemlerinin saptanması*, (Editorials: Önal G., Kurşun İ., Yazıcı H.) , Yurt Madenciliğini Geliştirme Vakfı, İstanbul, 130p.

Journel, A. G., (1994), *Modeling uncertainty: some conceptual thoughts in Geostatistics* Dimitrakopoulos, R., ed.,Geostatistics for the Next Century: Kluwer Academic Pub., Dordrecht, The Netherlands, p. 30–43.

Paşamehmetoğlu A.G., Oskay M., Erler A., Lünel T., Güleç N., Dirik K., et al. (1983), *Turkey coal master plan, Turkey Coal Potential and Researches*, 4, 285p, TKE.

Soares, A., (1998), *Direct Sequential Simulation and Cosimulation*, Mathematical Geology, Vol. 33, No. 8, p. 911–925.

Temur S., Orhan H., & Deli A. (2008), *Statistical interpretation of some physical and chemical data of the tertiary coal deposits in Turkey*. Geochemistry International, 46(4), p. 407-4022. Pleiades Publishing.

Tuncalı E., Bilgin Ç., Yavuz N., Toprak S., Köker A., Gencer Z., et al. (2002), *Türkiye Tersiyer Kömürlerinin Kimyasal ve Teknolojik Özellikleri, Maden Tetkik ve Arama Genel Müdürlüğü*, Ankara, 401 p.

Türkiye Elektrik İletim A.Ş. Genel Müdürlüğü, Apk Dairesi Başkanlığı, (2013), *Türkiye Elektrik Enerjisi 5 Yıllık Üretim Kapasite Projeksiyonu* (2013 – 2017), 106p.

Identification of Geochemical Anomalies by Using of Concentration-Area (C-A) Fractal Model in Nakhilab Region, SE Iran

N. Mazraee
Department of Geosciences, University of Sistan and Baluchestan, Zahedan, Iran

A. A. Daya
Department of Mining Engineering, University of Sistan and Baluchestan, Zahedan, Iran

M. Boomeri
Department of Geosciences, University of Sistan and Baluchestan, Zahedan, Iran

ABSTRACT Delineating the geochemical anomalies from background is a fundamental task in geochemical exploration. Fractal methods are very useful methods for such purposes. This paper is devoted to separate geochemical anomalies from background based on stream sediments data by utilizing the Concentration-Area (C-A) fractal model in Nakhilab region, southeast of Iran. Stream sediments data were used in this study which was conducted for the primary regional exploration for 4 elements (Au, As, Ag, Cu) in Nakhilab region. Log-log plots for the mentioned elements were drawn. Threshold values for the region were computed based on these log-log plots. The thresholds were identified for elements. Based on the thresholds of the C–A model, the anomaly maps of elements were drawn. Results showed that C-A method was capable for separation anomaly from background.

Keywords: Anomaly identification, Concentration-area (C-A) fractal model, Nakhilab

1 INTRODUCTION

Separation anomaly from background is a fundamental issue in mineral exploration (Daya 2014a, b). The methods and techniques for separation of anomalies from background have been the subject of research for many years (Cheng et al., 1994). For the past two decades, the traditional statistical methods assumed that the concentration of chemical elements follows a normal or log-normal distribution. A geochemical anomaly is defined as a region where the concentration of the element of interest is greater than a certain threshold value.

Various quantitative methods have been developed in this field, and among them, statistical methods have played an important role. Conventional statistical methods used for geochemical anomaly separation such as moving-averages, Kriging, probability graphs, univariate and multivariate analysis methods are primarily concerned with the frequency distributions of element concentration values and correlation coefficients among multiple variables. Spatial statistical methods such as moving average techniques, Kriging and spatial factor analysis can take into account spatial correlation and variability within neighboring samples in addition to concentration value frequency distributions and correlation coefficients.

Fractals is a natural consequence for geological phenomena that display self-similarity resulting from scale-independence properties, such as the frequency-size distributions of sediments and porosity, faults, earthquakes, volcanic eruptions, mineral deposits and oil fields. Fractal is more or less important in nearly all geoscientic disciplines. Scientists interested in fractal applications come from widely deferent backgrounds both inside and

outside the earth sciences. Fractal geometry established by Mandelbrot (1983) is a non-linear geometry based on the Latin word ‘‘fractus’’ and has been widely applied in geosciences (e.g., Turcotte, 1986; Sim et al., 1999; Ali et al., 2007; Zuo et al., 2009a,b,c; Afzal et al., 2010). Cheng et al. (1994) proposed the Concentration–Area (C–A) fractal method for separating different geochemical populations. This method has been an evolution in geochemical studies for recognition of different grade anomalies and related mineralization from background. Fractal dimensions in geological and geochemical processes correspond to variations in physical attributes such as rock type, vein density or orientation, fluid phase, alteration phenomena, structural feature or dominant mineralogy, and so on (Sim et al., 1999). The concentration–area model (C–A model) proposed by Cheng et al. (1994) has been developed and applied by many geoscientists (e.g., Sim et al., 1999; Ali et al., 2007; Wang et al., 2012).

The aim of current study is to separate geochemical anomalies from background based on stream sediments data by utilizing the concentration–area (C–A) fractal model in Nakhilab region, northwest of Iran. Stream sediments data were used in this study which was conducted for the primary regional exploration for eight elements (Au, Ag, Cu, As) in Nakhilab region.

2 CONCENTRATION-AREA (C–A) MODEL

Cheng et al. (1994) proposed the concentration–area (C–A) method, which can be used for separating geochemical anomalies from background. Concentration-area (C–A) method has the general form of:

$$A(\rho \leq v) \propto \rho^{-a1};\ A(\rho \geq v) \propto \rho^{-a2} \quad (1)$$

where A(ρ) denotes the area with the concentration values greater than contour value ρ, v represents the threshold, and $-a1$ and $-a2$ are fractal dimensions. Two approaches that were used by Cheng et al. (1994) to calculate A(ρ) include: (1) A(ρ) is the area enclosed by contour value ρ on a geochemical contour map resulting from the interpolation of the original data by weighted moving average method, and (2) A(ρ) is the value obtained by the box-counting of original elemental concentration values. By box-counting, one superimposes the grid with cells on the studied region. The area A(ρ) for a given ρ is equal to the number of cells multiplied by the cell area with the values of greater than ρ (Cheng et al., 1994). Area–concentration [A(ρ)] with the elemental concentrations greater than ρ usually shows a power–law relation (Cheng et al., 1994). The breaks between straight-line segments on this log–log plot and the corresponding values of ρ have been used as thresholds to separate geochemical values into different components (Afzal et al., 2010).

3 GEOLOGICAL SETTING OF THE NAKHILAB REGION

The study area is located in northwestern of Zahedan city, SE of Iran. The study area is located in boundary of Loot Block and eastern flitch zone In Iran. It is probably a part of Iran’s eastern flitch zone. Loot Block in contact with Iran’s eastern flitch zone occurred in a very metamorphosed, faulted, sheared, and brecciated zone. From the upper cretaceous to quaternary the study area experienced different mountainous phases including Laramide and Alpine. These mountainous phases have an effective impact in developing the geological setting of the study area. Another important feature of the study area is that it is near the active Nehbandan fault system. Loot Block is more dynamic in its eastern part where the study area is located. The study area is highly brecciated and has faults with general trend of NS and NE-SW. The folding systems in the study area are normal anticline and normal syncline. Their trend is NW-SE to NS.

In the study area lithological units comes from upper cretaceous to quaternary ages. The study area occurred in a tectonic regime that Ophiolites complex was present. The lithological units according to 1:250,000

geological map of Nakhilab sheet divide into three parts which are metamorphic, sedimentary and igneous rocks (Fig 1). Metamorphic unit itself divides into three parts. The first consists of serpentine and harzburgite. Their trend is NS and generally occurred in a folded, fractured, and transformed units. The second group consists of marble, phyllite, serisite, and schist. Theses metamorphic rocks are widespread and its strike in the study area is NS. The last (third) group of metamorphic rocks consists of chlorite, epidote, schist, and mica schist. Their strike in the region is NS. This unit is affected by tectonic activity and as a result is highly fractured. Sedimentary rocks are very widespread in the study area. The most abundant of them are shale, sandstone, limestone, marl, and conglomerate (Fig 1). There are many igneous rocks in the study area. The most important of them comes from Oligocene. It consists of granite, granodiorite, and monzonite. Alteration phenomena are obvious in the igneous rocks and these rocks are much altered (Fig 1).

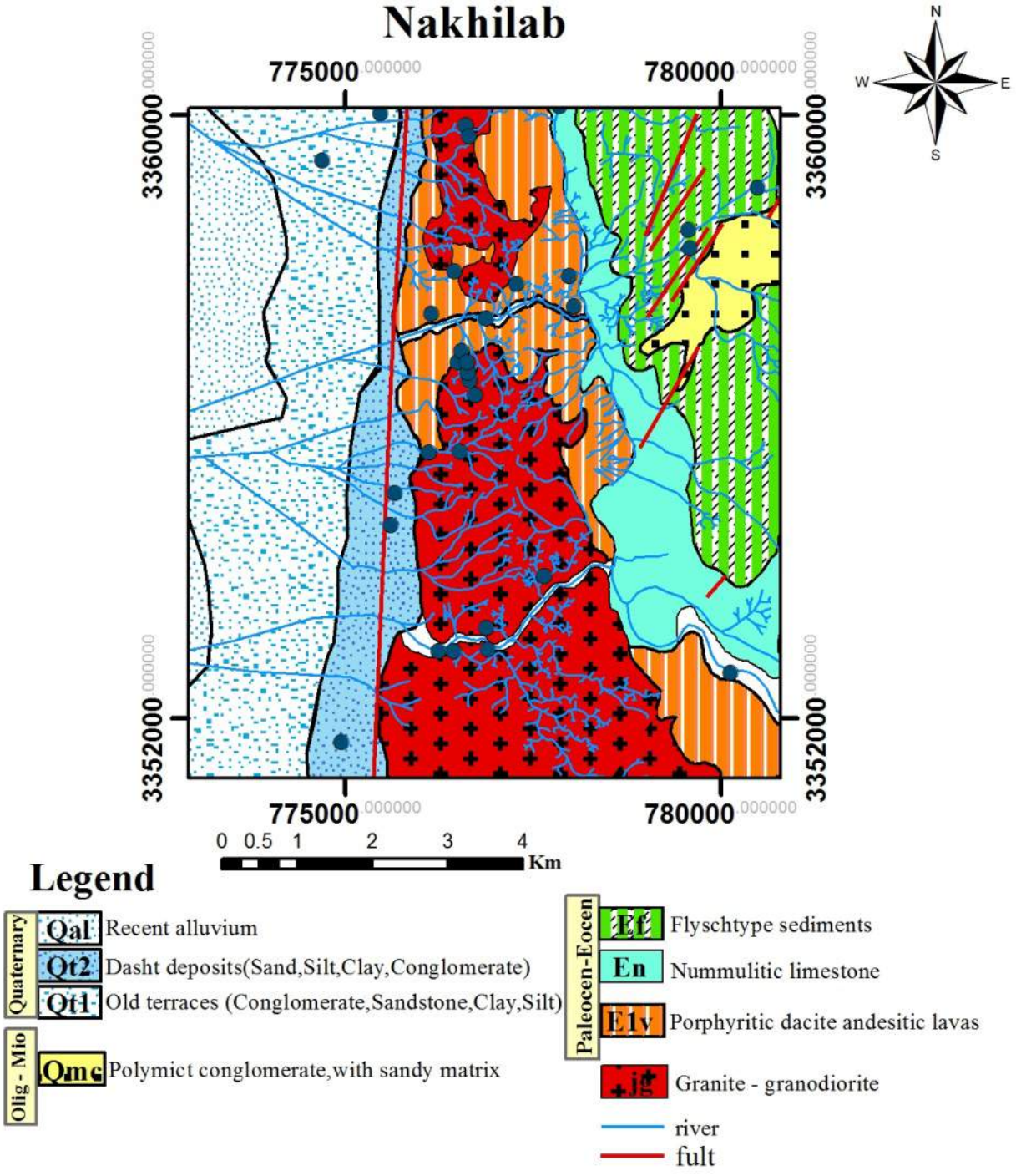

Figure 1. Geological map of Nakhilab region

4 STREAM SEDIMENTS GEOCHEMISTRY

A total of 213 collected stream sediments geochemical samples were analyzed by ICP-MS for elements which relate to Au mineralization and are of interest. Statistical results show that Cu, As, Ag and Au mean values are 2.8812, 1.1838, 0.1482 ppm and 0.0012 ppb, respectively presented in Table 1. Their distributions are as shown in Fig. 2 and are not normal. Variation between maximum and minimum for these data shows a wide range. If median is assumed to be equal to threshold values. The obtained statistical results are 2.76 ppm for Cu, 1.100 ppm for As, 0.095 ppm for Ag and 0.001 ppb for Au.

Table 1: Statistical parameters of raw data based on stream sediments geochemical samples analysis

Parameters	Au (ppb)	As (ppm)	Cu (ppm)	Ag (ppm)
Mean	0.0012	1.1838	2.8812	0.1482
Median	0.0010	1.1000	2.7600	0.0950
Variance	0.000001	97.788	89.438	0.558
Max	0.017	1.32	1.431	11.00
Min	0.0010	3	2.080	0.0800
Standard Deviation	0.0016	9.8634	9.547	0.7471

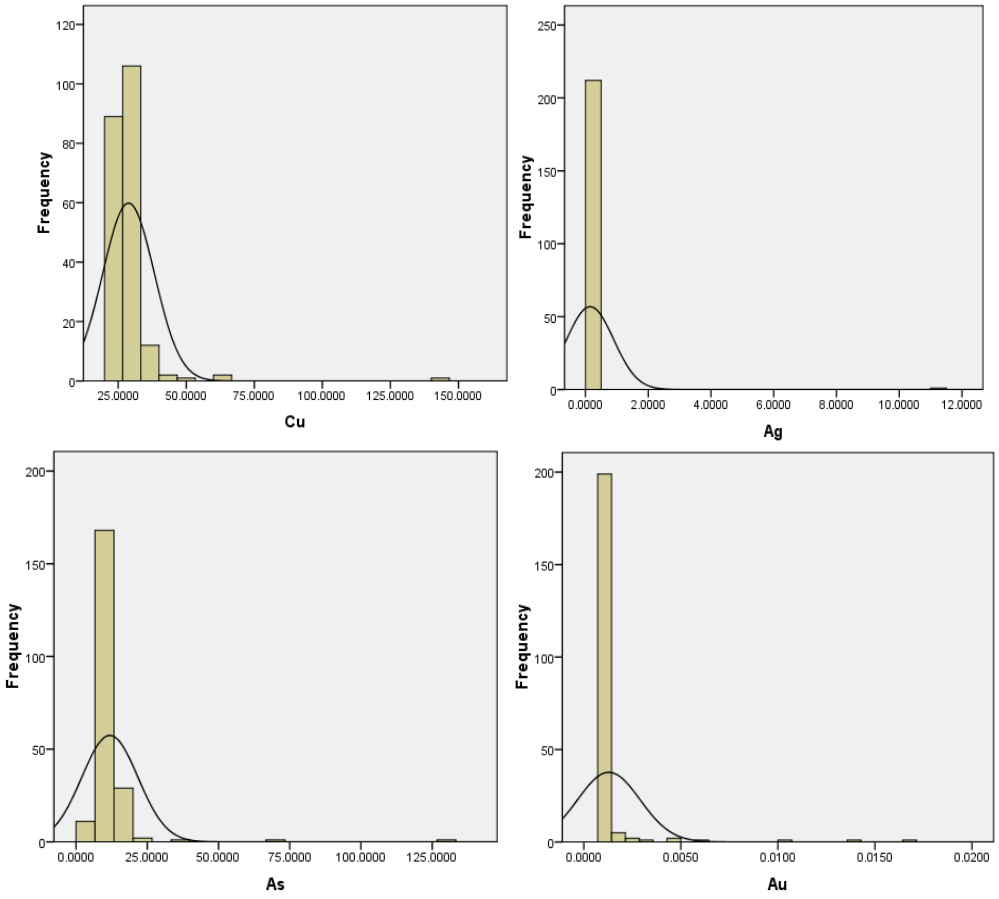

Figure 2. As, Ag, Au and Cu histograms

Geochemical maps were generated with IDS (Inverse Distance Squared) method by RockWorks™ v. 2006 software package. This procedure is suggested because it eliminates the undesired smoothing effects caused by the usage of Kriging method. Since the IDS method clarifies the ore grade boundaries and ore concentration values, it is more desirable to use IDS method instead of Kriging which inherently has rather high amounts of truncation errors for the upper and lower boundaries of ore grades. The area was gridded by 250 m×250 m cells.

The proposed gridding pattern is put to use because the fundamentals of C–A fractal method is based on the existence of partition function, and the sampled data cannot be utilized effectively; also, since one cannot sample the entire study area, and for evaluation and estimation of any parameter, i.e., ore grade, gridding of the area is inevitably a desired mandate and one cannot do otherwise. The necessary and the needed partition function to be used in fractal methods are based upon assumption of having a cell characterization in the area in order to find and calculate the area which has a certain ore grade. By this method the problem of over sampling will not enter into picture because the C–A fractal method will automatically eliminate any probable grid related problem in division of the area into smaller elements and the original fractal character is preserved (Cheng et al., 1994).

Concentration–area relations were computed by assigning an area of influence to each sampled point and summing all elemental areas whose concentration lies below a given value. This procedure was repeated for different elemental concentrations. Carrying on this procedure is not cumbersome because there is a regular gridding of 250 m×250 m cells. The evaluated grades in cells were sorted out based on decreasing grades and cumulative areas were calculated for grades.

Finally, log–log plots were constructed for Cu, Ag, As and Au (Fig. 3). Geochemical populations are delineated in these plots of Cu, Ag, As and Au. On the basis of this procedure, there are 3, 3, 4 and 3 populations for Cu, Ag, As and Au, respectively as shown in Fig. 3. Cu anomalous threshold is 49 ppm and its high intensity anomaly is 101 ppm. Also, it is clear that there are three stages of Cu enrichments based on log–log plot as depicted in Fig. 3. The first event for Cu C–A variations occurred at grades below 49 ppm. The second event shows up between grades 49 ppm and 101 ppm. The final event included major Cu mineralization which occurred and interpreted in grades higher than 101 ppm. Ag threshold and high intensity anomalies are 2.28 ppm, and 7.28 ppm (Fig. 4). As log–log plot shows that major As enrichment occurred at 24 ppm and higher. Au anomalous threshold is about 0.0024 ppb. There are three enrichment steps interpreted as seen in C–A log–log plot of Au in Fig. 3. Major Au enrichment started from 0.0024 ppb, and, 0.013 ppb concentration is beginning of high intensity Au anomaly. Each geochemical population in this study was assumed to have various kinds of distributions, and its various components, such as individual chemical elements and their concentrations could be fitted into a straight line on log–log plot.

Obviously due to non-uniform behavior of the elements, if plotted on log–log co-ordinates, the plot will have different slopes and various straight-line segments which connects them at them an angle or with breaks on the plot. Breaks between the straight-line segments and the corresponding values of As, Ag, Au and Cu have been used as cut-offs to reclassify cell values in the IDS interpolated maps and are presented in Fig. 4. Based on these results, elemental grade distribution maps were drawn as Fig. 4. Clearly most of Cu anomalies are located in central parts of the area, especially high intensity Cu anomalies. As anomalies were situated in central and southeastern parts and they are small.

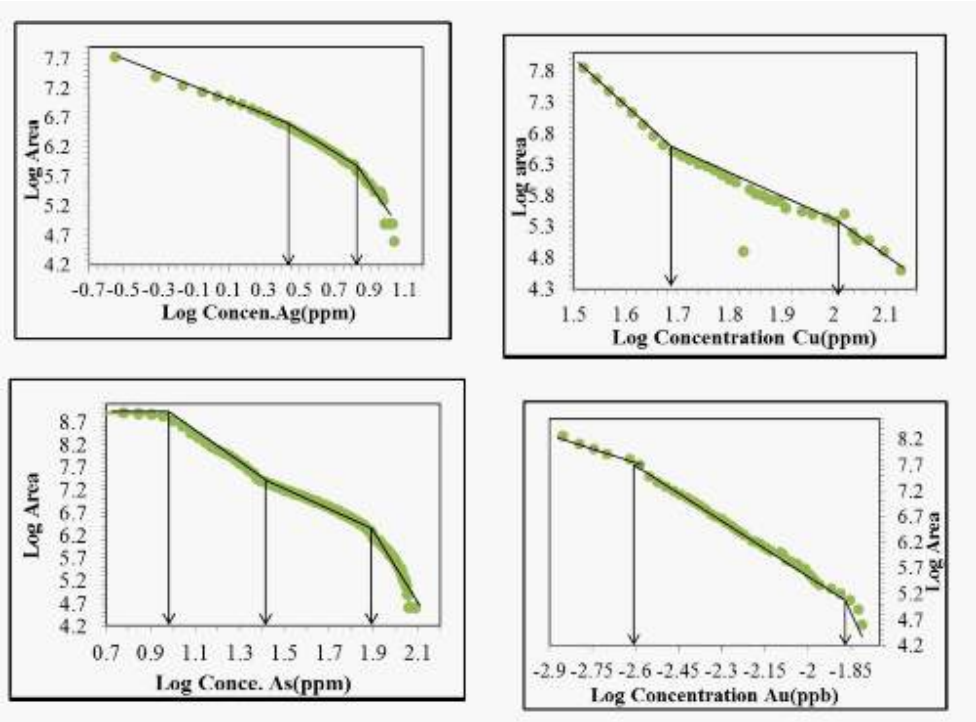

Figure 3. Log–log plots (C–A method) for As, Ag, Au and Cu. The vertical axis represents cumulative cell areas A(ρ), with elemental concentration values greater than ρ, and the horizontal axis is the actual value (ρ).

Locations of Au anomalies are in central parts of the area and the high intensive anomalies are very small located in western and central parts. Based on these maps, potential presence of these elements are located in central and western parts as shown in Fig. 4. Also, several small Ag anomalies are interpreted in northwestern part of the area as delineated in Fig. 4.

5 COMPARISON WITH GEOLOGICAL PARTICULARS

Thresholds and cut-off results from C–A method are compared and correlated to specific geological particulars of the region including considering nature of lithological units and faults.

Lithological unit's positions were correlated with elemental distribution maps. There exists astrong relationship between Cu concentration values higher than 101 ppm and Au higher than 0.013 ppb in high intensive anomalous parts with sand, silt, and conglomerate based on this correlation. It shows that sand, silt, and conglomerate host high intensive Cu enrichment and Au anomalies. In other words, major Cu and Au mineralization occurred concurrent with sand, silt, and conglomerate in final stage of Cu and Au enrichments. But, As high intensive anomalous parts (higher than 71 ppm) in central parts of the area are hosted by granite and graniodiorite units. In western parts of the area sedimentary rocks hosts high intensive Ag and Au and high intensity Cu anomalous parts as illustrated in Fig. 4. Also, faults have caused the increase in porosity or void volume in sedimentary rocks. Granite and granodiorite units contain low amounts of Cu, having the maximum values of 49 ppm and Ag and Au values are about the same as background values, lower than 8 ppm and 0.0024 ppb, respectively. Granite units have low amounts of Cu, Ag and Au that they host low intensity Cu anomalous amounts in western part of the study area, lower than 49 ppm concentration. Granitic unit present in central part of the area is barren and does not host these elements. Its elemental contents are equal to background, but in western part, sedimentary units show low values of As, between 8 ppm and 24 ppm. Results from C–A method are correlated with elements' median values in rock types. These concentrations show a good relationship with intrusions.

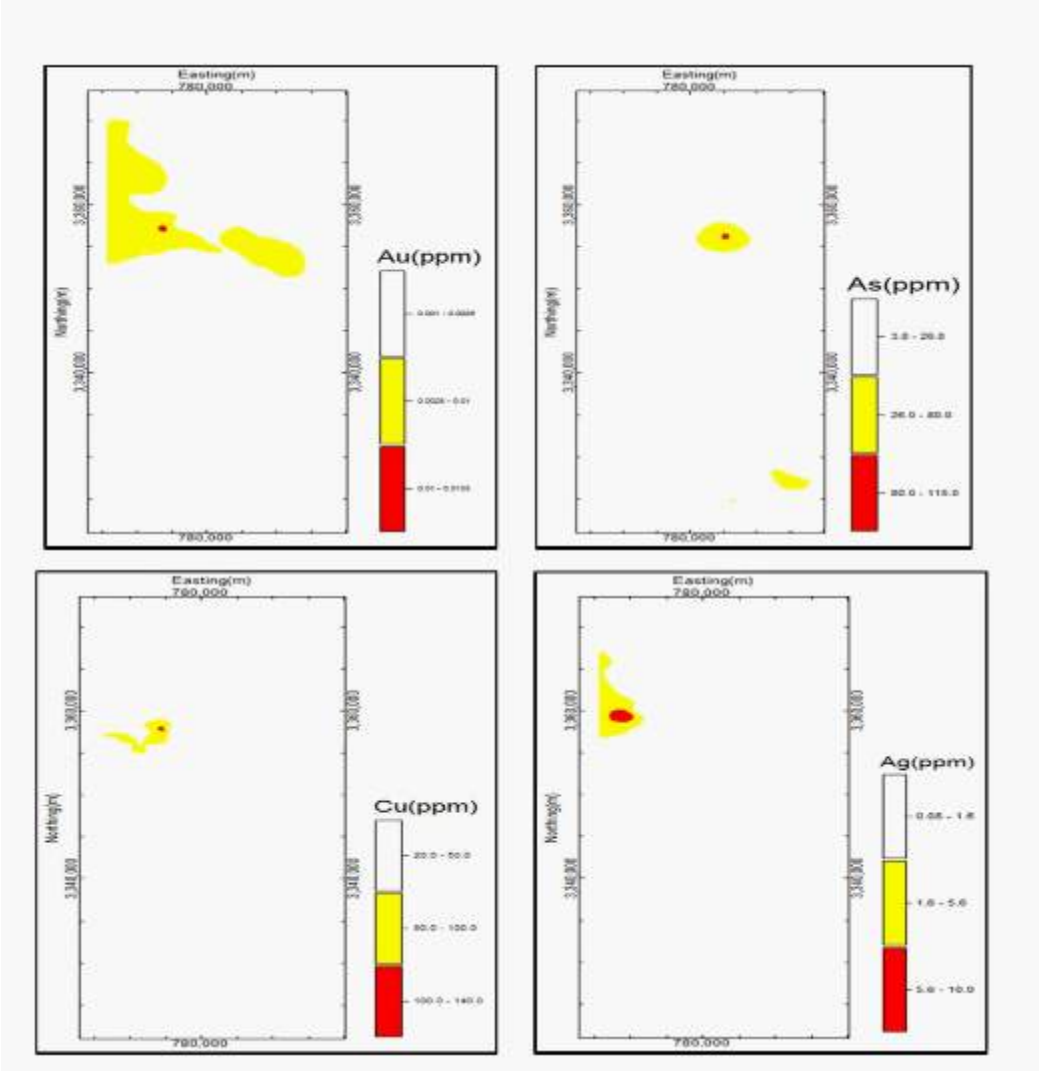

Figure 4. As, Ag, Au and Cu geochemical population distribution maps based on C–A method

6 CONCLUSIONS

Study on Nakhilab region reveals the potential use of the C–A method for geochemical anomaly separation as a useful tool for geochemical and mineral exploration. The advantages of this method rely essentially on its simplicity, and easy computational implementation, as well as the possibility to compute a numerical value of concentrations, i.e., the anomalous threshold, which is the most useful criteria for cross examination of information with numerical data from different sources, commonly used in stream sediment geochemistry. There exists a very good correlation between the calculated anomalous threshold values and the range of concentrations obtained in the rocks, especially for Cu in the Nakhilab area. Such correlation is also valid for other elements, but, the range of values is clearly different. These results may also be interpreted differently according to their nature, especially multifractal curves in log–log plots. Cu concentration in the area may be a result of the three steps of enrichment. Major Cu and Au mineralization occurred by the sedimentation of sand, silt and conglomerate in this area. But, for Ag and Au in Nakhilab area this may be explained by three enrichment steps that the major step occurred in sand, silt, and conglomerate units.

The occurrence of Cu and Au high enrichments in sand, silt, and conglomerate in western parts of the area has been actually realized in the samples collected from the field. As high intensive anomalies was found within granitic units. Statistical analysis also confirms these results. Elemental anomalies in western parts of the area are associated

with sand, silt and conglomerate. Granitic units in central parts host As in high intensive anomalies. It can be concluded that lower grade enrichment of Cu has occurred in granitic and granodioritic units. Also, data analysis shows that major Cu and Au enrichment steps are concurrent with that of sand, silt and conglomerate. The process for As enrichment is synchronized with granitic rocks and their subsequent changes. Cu, Ag and Au enrichment processes are correlated with lithological units and their time table emplacement. Granitic and granodioritic units were last emplacements in this area and these units host high grade As anomalies. Ag anomalies in western part of the area are located in sedimentary units that show Ag enrichment may have occurred in primary and secondary emplaced sedimentary rocks. Low Ag grade is proper evidence in this area. Although it may be easier to study geochemical anomalies with the C–A method, multifractal nature of C–A log–log curves could be of essential help to geoscientists for interpreting the stages which an element is enriched. The developments in multifractal theory and their usage could provide a favorable ground for the stochastic simulation of geochemical distributions, and their understanding and interpretations.

REFERENCES

Afzal, P., Khakzad, A., Moarefvand, P., RashidnejadOmran, N., Esfandiari, B., FadakarAlghalandis, Y., 2010. Geochemical anomaly separation by multifractal modeling in Kahang (GorGor) porphyry system, Central Iran. Journal of Geochemical Exploration 104, 34–46.

Ali, K., Cheng, Q., Chen, Z., 2007. Multifractal power spectrum and singularity analysis for modelling stream sediment geochemical distribution patterns to identify anomalies related to gold mineralization in Yunnan Province, South China. Geochemistry: Exploration, Environment, Analysis 7, 293–301.

Cheng, Q., Agterberg, F.P., Ballantyne, S.B., 1994. The separation of geochemical anomalies from background by fractal methods. Journal of Geochemical Exploration 51, 109–130.

Daya A.A., 2014a. Application of concentration–area method for separating geochemical anomalies from background: a case study of Shorabhaji region, northwest of Iran. Arabian journal of geosciences, In press.

Daya A.A., 2014b. Comparative study of C–A, C-P, and N-S fractal methods for separating geochemical anomalies from background: A case study of Kamoshgaran region, northwest of Iran. Journal of geochemical exploration, In press.

Mandelbrot, B.B., 1983. The Fractal Geometry of Nature. Freeman, San Francisco.

Sim, B.L., Agterberg, F.P., Beaudry, C., 1999. Determining the cutoff between background and relative base metal contamination levels using multifractal methods. Computers & Geosciences 25, 1023–1041.

Turcotte, D.L., 1986. A fractal approach to the relationship between ore grade and tonnage. Economic Geology 18, 1525–1532.

Wang, G., Carranza, E.M.J., Zuo, R., Hao, Y., Du, Y., Pang, Z., Sun, Y., Qu, J., 2012. Mapping of district-scale potential targets using fractal models. Journal of Geochemical Exploration 122, 34–46.

Zuo, R., Cheng, Q., Xia, Q., 2009a. Application of fractal models to characterization of vertical distribution of geochemical element concentration. Journal of Geochemical Exploration 102, 37–43.

Zuo, R., Cheng, Q., Agterberg, F., Xia, Q., 2009b. Application of singularity mapping technique to identify local anomalies using stream sediment geochemical data, a case study from Gangdese, Tibet, western China. Journal of Geochemical Exploration 101, 225–235.

Zuo, R., Cheng, Q., Xia, Q., Agterberg, F.P., 2009c. Application of fractal models to distinguishing between different mineral phases. Mathematical Geosciences41, 71–80.

Improving Mineral Resource Estimation Using Domaining: A Case Study

S. Al-Hassan
University of Mines and Technology, Tarkwa, Ghana

W. A. Anandorah
AngloGold Ashanti, Obuasi, Ghana

ABSTRACT The Obuasi Mine gold orebody is structurally controlled exhibiting dextral strike-slip duplex structures with numerous faulting and fissures. Various geologically homogeneous lithological and structural zones are identifiable on the mine. Structurally, straight faults, points of inflection, metavolcanic-caps and fissure junctions do occur. The mineralization is either free milling gold in quartz veins or gold in sulphide ore. Historically, Obuasi resource evaluation was done across heterogeneous zones (domains): free milling gold in quartz veins and gold bearing sulphide zones. This practice did not recognize the different styles of the mineralization in these domains; thereby resulting in unsatisfactory reconciliation between estimated grades and mined grades.

This paper presents the study that reviewed the resource estimation methodology taking into account the two important domains (free milling gold in quartz veins and gold bearing sulphide zones). The new model improved reconciliation between estimated and mined grades.

Keywords: Reconciliation, variography, wireframe, grades, domaining

1 INTRODUCTION

Obuasi Gold Mine is situated within the Obuasi mining district approximately 320km north-west of Accra, the capital of Ghana in West Africa (Figure 1). The Obuasi concession is located on a north-easterly striking Ashanti belt, the most prominent of the five Birimian Supergroup gold belts found in Ghana (c.f. Figure 1). Two broad styles of gold mineralization are present at the Obuasi mine. The free milling quartz vein gold in shear zones and sulphide-rich (arsenopyrite) disseminated refractory gold lodes which form alteration haloes around the quartz vein lodes (Anon, 2011; Kesse, 1985). The study area covers Blocks 9 and 10 in the southern part of the mine.

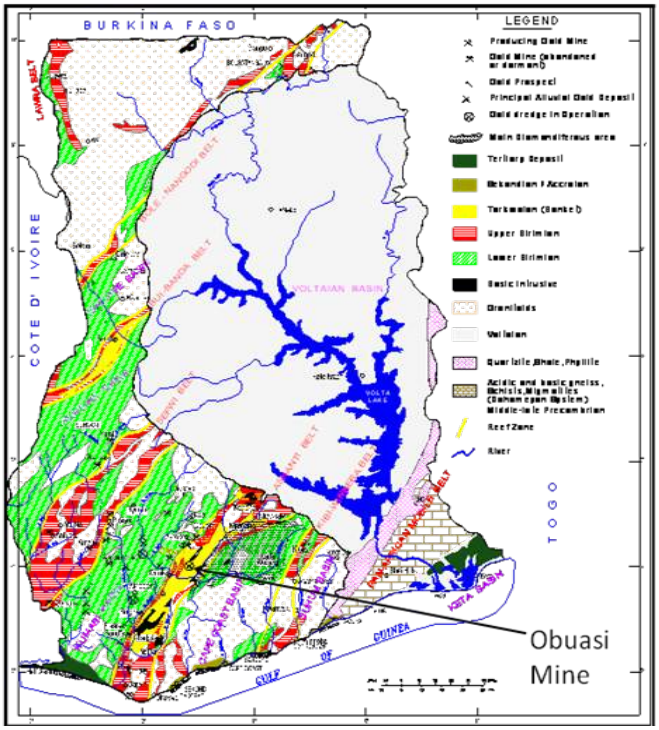

Figure 1. Location of Obuasi in Ghana (Modified after Kesse, 1985)

Historically, Obuasi Resource evaluation was done across heterogeneous zones

(domains): free milling gold in quartz veins and gold bearing sulphide zones. This did not recognize the different styles of the mineralization in these domains and this resulted in significant smearing effects resulting in poor reconciliation between resource grades and milled grades. This study takes into account these domaining and estimates the quartz and sulphides differently. It improves reconciliation considerably from 71% to 103%.

2 LOCAL GEOLOGY

Obuasi concession is located on a north easterly striking Ashanti volcanic belt which predominantly comprises sedimentary and mafic volcanic rocks, and is the most prominent of the five Birimian Supergroup gold belts found in Ghana (Kesse, 1985).

The Obuasi deposit is also characterised by the development of strong pinch and swell structures, as shown in Figure 2. It is often associated with mineralized lodes. In some areas, this is spectacularly demonstrated with abrupt termination of massive quartz material at an inter-nodal or necking point. Periodicity of these structures is variable, ranging from a few tens of meters to less than a meter.

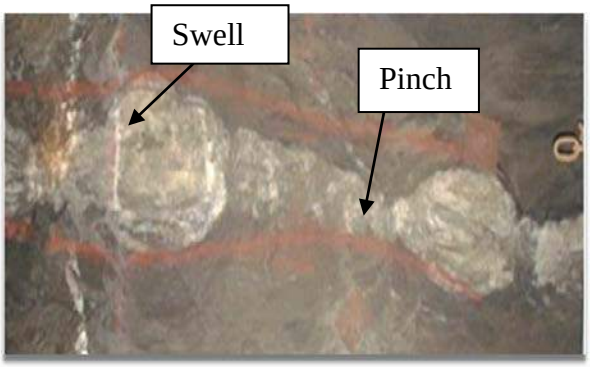

Figure 2. Underground Exposure of Pitch and Swell Structures

There are two basic ore types at the mine (Anon, 2011):

i. Free milling gold in quartz veins (QVs) which are found in the shear zones. These zones are responsible for the highest grades recorded at Obuasi Mine. It is characterised by free gold sometimes visible to the naked eye and as nuggets. The quartz veins may range from a few centimetres to over 2 m wide and from a meter to over 300 m long in strike and along dip.

ii. Sulphide-rich (arsenopyrite) disseminated refractory gold lodes which form alteration haloes around the quartz vein lodes that may be much wider and longer than the quartz veins.

These can be modelled as separate domains since they have different styles of mineralisation. The grades in the quartz veins, averaging over 12 g/t, are normally much higher than those of the sulphides which average about 7g/t. These are very common in the project area and in many ore blocks in the Obuasi Mine.

3 DATA COLLECTION AND VALIDATION

The project area covers Blocks 9 & 10. The data collected in the project area consisted of 4212 sulphide samples and 1077 quartz samples. Core sample lengths varied between 0.3 and 1.5 m. These were validated to correct for duplicates, missing data, inconsistent coordinates, etc. Various parameters of drill holes that were collected included Borehole identification (BHID), Collar coordinates, Surveys, Lithological units, Assays and Recoveries. These were entered into a Century Database and then imported into Datamine and *desurveyed*.

The orebody geology was modelled by digitizing around quartz ore (red line) and the sulphide ore (green line) at various elevations as exemplified in Figure 3.

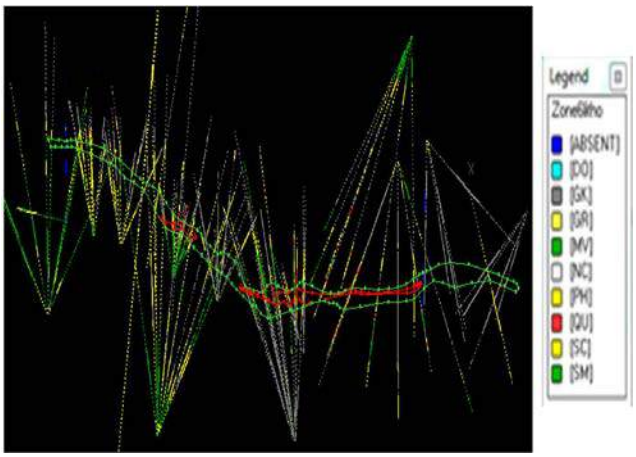

Figure 3. Digitized plan- view at -930 m elevation.

The digitized strings were linked into 3-D wireframe volumes with the quartz volumes occurring in the sulphide volumes as quartz veins, though some portions of the quartz veins do protrude to the outside of the sulphides. Figure 4 shows the quartz and sulphide domains.

4 DATA ANALYSIS

Samples within each wireframe were retrieved. There were 4212 sulphide samples and 1077 quartz samples. The two sample types were subjected to further validation processes which included:

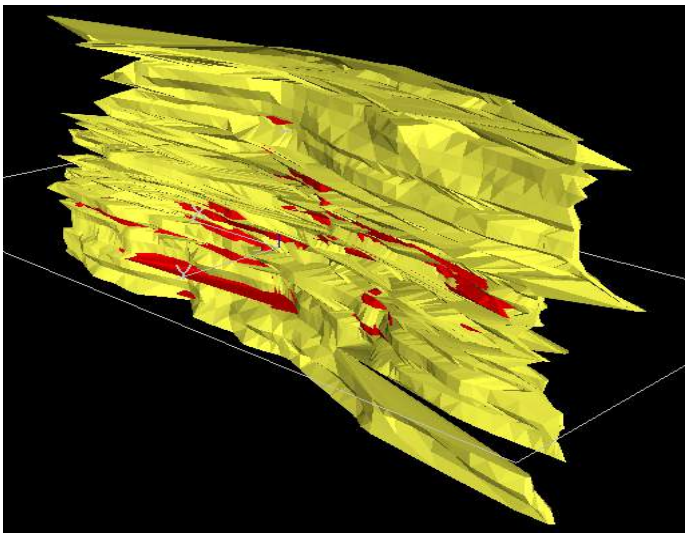

Figure 4. Wireframe showing quartz (red) sandwiched in Sulphides (yellow).

- Compositing over 0.9m so as to make their statistics meaningful with equal support (Dowd & Milton, 1987; Reedman, 1979).
- Removing unrealistic sample lengths.

Classical statistical analysis on the composite was done. Table 1 shows the summary statistics for each ore type. Both F- and t-tests at 5% level of significance failed, indicating that the quartz and sulphide samples did not come from identical populations (Davis, 1986) and this further justified their being modelled separately.

Table1. Statistics of the composited samples

Sample statistic	**Sulphide samples**	**Quartz samples**
Number of samples	3981	961
Maximum (g/t)	29.75	59.09
Minimum(g/t)	0.01	0.01
Mean(g/t)	4.41	9.22
Variance	24.18	55.54
Skewness	1.70	0.73
Kurtosis	2.93	0.37

Various methods are available for identifying and handling outliers (Anderson et al., 2003; Bluman, 2004; Bowerman, B. L. & O'Connell, R. T., 2003). Top cutting was used to minimise the impact of outliers. Cumulative frequency graphs of the composites shown in Figures 5 and 6 for quartz and sulphide respectively, using the 95% (Annels, 1991) were used. Thresholds of 35 g/t and 13 g/t for quartz and sulphide respectively were obtained.

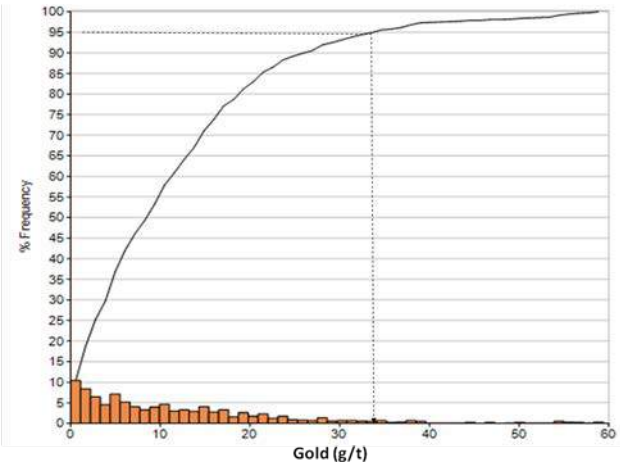

Figure 5. Cumulative frequency plot of quartz samples

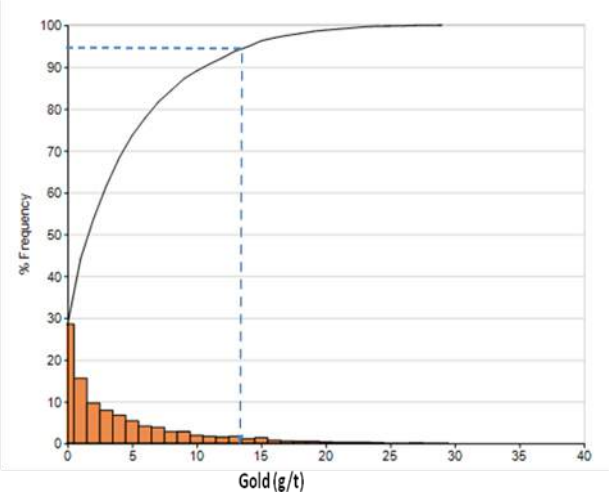

Figure 6. Cumulative frequency plot of Sulphide samples

5 VARIOGRAPHY

Semi-variograms were calculated for both quartz and sulphide samples vertically and along 0°, 45°, 90° and 135°. The directional experimental semi-variograms for the sulphide samples had discernible simple isotropic structures and were modelled with a simple spherical model. Figures 7 and 8 show examples of semi-variograms in 045° and 135° respectively.

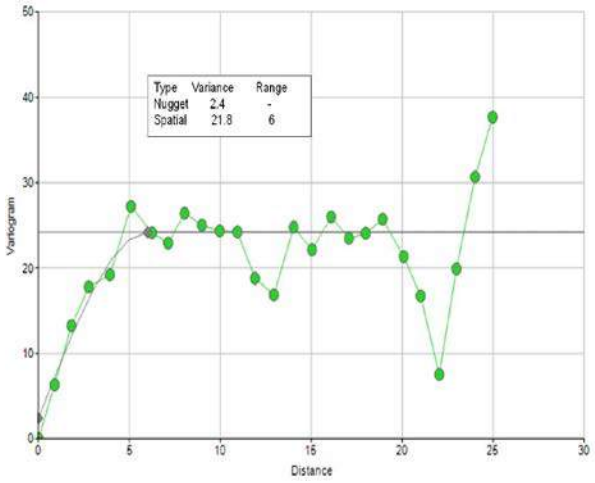

Figure7. Experimental and model semi-variograms for Sulphide samples (045º)

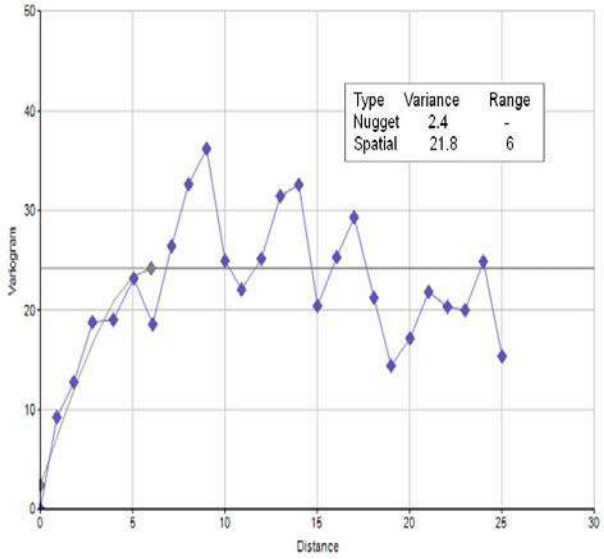

Figure 8. Experimental and model semi-variograms for Sulphide samples (135º).

However, the experimental semi-variograms for the quartz samples were so erratic that there were no discernible structures. Hence they could not be modelled. Inverse distance weighting was used instead as there have been instances when IDW has given acceptable results (Royle, 1978).

6 RESOURCE BLOCK MODEL

Block modelling was done with block dimensions of 5x5x5m that corresponds with the typical mine stope size. Other stopes are multiples of this parental cell size. Details of the model are shown in Table 2.

Table 2. Details of the block Model

	Coordinate Limits		Cell Sizes	
	Min.	Max.	Min.	Max. (Parent)
X	13350	14600	2.5	5
Y	10775	11025	2.5	5
Z	-1125	-575	2.5	5

7 RESOURCE ESTIMATION

Grades of the Sulphide orebody (zone 1) were estimated using ordinary kriging whilst those of the quartz orebody (zone 2) were estimated using Inverse Distance Weighting (IDW) method (established through cross

validation). In both cases a minimum of 3 and maximum of 20 samples were used.

The resource model was validated by visual inspections. For a good and well optimized model, all model cells within the quartz wireframe should have Zone 2. The Sulphide should have Zone 1 while the Waste Zone should have Zone 0. Grade estimates into the geology block model cells at -830m elevation are shown in Figure. 9. The quartz zone (Zone 2) wireframe is shown as red outline and that of the sulphide as green.

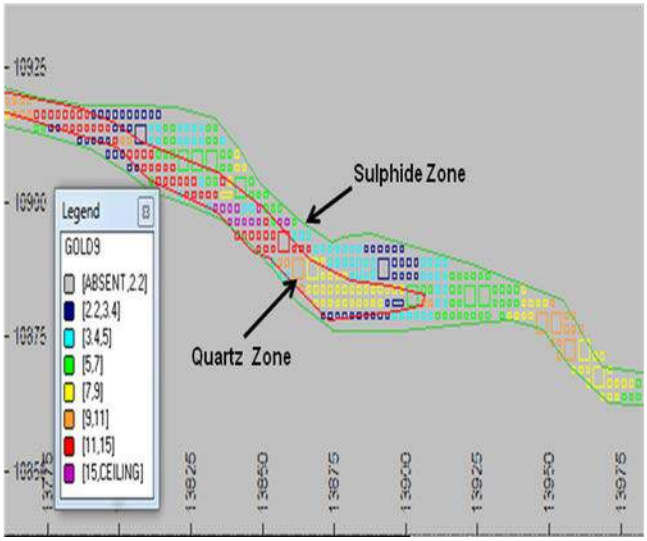

Figure. 9. Grade estimates into the geology block model at -830m RL

8 COMPARISON OF THE NEW MODEL WITH THE OLD MODEL

A portion of the new model has been mined out and a cavity monitoring survey (CMS) was carried out to measure the void created. The CMS wireframe generated was used to evaluate the new model and old models. The new model, together with the CMS wireframe, is shown in Figure. 10. Since the zonal constraining process was applied, there was no significant smearing of grades.

Figure 11 also shows the old model with the same CMS wireframe. There was no quartz and sulphide domaining for the old model, but just one wireframe which lumped together the quartz and sulphides; thereby, resulting in severe smearing of grades.

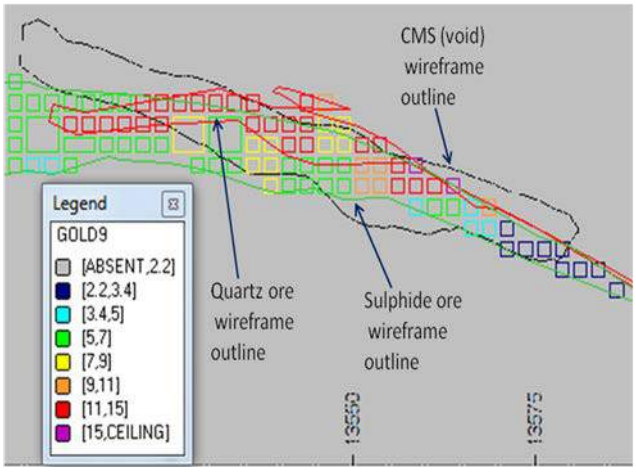

Figure 10. New model with quartz, sulphide and CMS wireframe

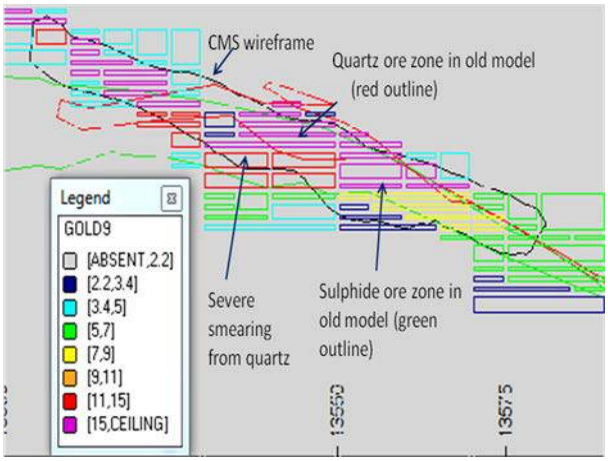

Figure 11. Old model with the CMS and Ore Wireframe

Tonnage and grade calculations within the CMS wireframe for both models were done. Table 3 shows a comparison of the volumes of the new and old models that were contained in this CMS void. Also, Table 3 shows the calculated tonnes and grades of the two models within the void.

There is smearing of high grades from the quartz into the sulphides such that grades in some of the sulphides are bloated up to the level of grades usually found in the quartz and makes them appear as quartz zones. Also the same density (2.89) was used for both quartz and sulphides in the old model.

9 RECONCILIATION OF THE NEW AND OLD MODEL GRADES WITH ACTUAL PRODUCTION GRADES

Table 4 shows the reconciliation of the estimated grade from both models and the actual mined grade from within the CSM.

Table 3. A summary of the calculation results and comments

	New model				Old model			
Category	Tonnes	Grade	Oz	Zone	Tonnes	Grade	Oz	**Comments**
[< 2.2]	50653	1.64	2671	0	35631	0.87	997	Smearing of grade from quartz improved some waste and low grades material
[2.2 ,3.4]	7143	2.84	652	1	4620	2.62	389	
[3.4, 5]	9222	4.08	1210	1.	3210	4.06	419	Sulphide tonnes constrained in their zones in the new model
[5, 7]	12130	5.87	2289	1	2209	5.93	421	
[7, 9]	4665	7.94	1191	1.6	8113	8.12	2118	High grades in quartz smeared the sulphides in the old model
[9, 11]	9071	10.19	2972	2	9213	9.80	2903	Similar
[11, 15]	13132	12.39	5231	2	11690	13.23	4972	Similar
[≥ 15]	4003	16.48	2121	2	41386	22.76	30284	Grades in some sulphides bloated up by smearing in old model, such amount of tonnes (41385.9) of quartz as in the old model do not really exist in the block
Total	110018	7.87	27837		116072	11.39	42505	

Table 4. Reconciliation of the new and old model mined grades to actual mined grades

	New Model	**Old Model**
Actual (g/t): (a)	8.11	8.11
Estimate (g/t): (b)	7.87	11.39
Reconciliation (%): (a/b)x100%	103	71

It can be observed that the new model has better reconciliation. The old model causes more smearing effects.

10 DISCUSSION

It is well known that in the Block 9 & 10 when the quartz pinches off the sulphides grades become very low (experience of the second author). This can be observed in the drill holes and channels in the mine. There is therefore smearing of high grades from the quartz into the sulphide zones in the old estimation model.

The comparison of the results in Table 3 indicates that the smearing effect of high grades from the quartz causes two significant adverse consequences:

- Low grade materials, that could have been considered waste, may be brought up to ore category.
- The low grades in the sulphides can be bloated up to very high grade levels found in the quartz.

This poses a problem of poor reconciliation between estimated grades and mined grades.

With the new model, it is possible to know the amounts of quartz and sulphide ores, with their respective grades and

ounces, in any piece of block planned to be mined. A prediction of what ounces will be contained when the quartz should pinch off unexpectedly can also be made.

11 CONCLUSIONS

The following conclusions may be made:

- The old model did not recognize the different styles of the mineralization in the deposit; thereby resulting in significant smearing effects of the high grades from the quartz. This causes two significant adverse results: sub-grade material can be brought up to economic values, and the grades in the sulphides can be bloated up to very high grade levels. Hence the problem of poor reconciliation between estimated grades and mined grades.
- From the variography, there appears to be a structure in the sulphides but not in the quartz; a simple isotropic spherical model semi-variogram of a range of 6 m in the x, y and z-directions respectively was established for the sulphides.
- A prediction of what ounces may be produced in case quartz pinches off unexpectedly can be made.
- Ordinary Kriging and Inverse Distance Weighting may be used to estimate the quartz and sulphides resources respectively. The resource estimates using domaining are shown in Table 5, which is a summary of Table 3.

  Thus, the resources in the block are estimated as 10,760 000t @ 5.4g/t for the sulphide ore, 592 000 t @ 12.75g/t for the quartz ore and 783 000t @ 9.95g/t of sulphide and quartz mix.

Table 5. Resource Estimates using the new model

Grade Category (g/t)	Tonnes (t)	Ore Type	Grade (g/t)	Totals
[3.4 - 5]	5, 375442	Sulphides	4.19	
[5 - 7]	3,543,210	Sulphides	5.85	
[7 - 9]	1,841,741	Sulphides	7.92	10760393t @ 5.38g/t
[9 - 11]	783738	Sulp/Quartz	9.95	783738t @ 9.95g/t
[11-15]	547251	Quartz	12.49	
[>15]	44795	Quartz	15.91	592046t @ 12.75g/t

12 RECOMMENDATIONS

It may be recommended from the study that:

- Ore shoots in the Obuasi Mine that have considerable quartz veins in strike and width must be domianed into quartz and sulphide zones and the estimates constrained within each zone in order to improve upon reconciliation.
- A major research work on the structural controls of gold localisation in the major ore shoots of the Obuasi Mine is highly recommended, since geological structures like straight faults zones, points of inflection in the fault planes, the shear morphologies, metavolcanic-caps in the shear zones and fissure junctions occur and play significant roles in the gold.

REFERENCES

Anderson, D. R., Sweeney, D. J. & Williams T. A., 2003.*Modern Business Statistics with Microsoft Excel*, Melissa Acuna Publishers, USA,pp.625 – 627.

Annels, A. E., 1991.*Mineral Deposit Evaluation – A Practical Approach*, Chapman & Hall, London, 436 p.

Anon., 2011, *Technical Report on the Fakiakoba Gold Project, Ghana, West Africa*, www.asantefold.com/.../ 43101_ fakiakob Oct 24.2011 -23.2.3, p.43.

Anon., 2012.*The Obuasi Mine Geology Department Competent Person's Report*, December, 2012 (Unpublished).

Ortiz, J. M. & Emery, X., 2015. *Geostatistical estimation of mineral resources with soft geological boundaries: a comparative study*, www.captura.uchile.cl/bitstream/handle/2250/6088/Ortiz_JM.pdf;jsessionid=582DCAB26AB1C4E7F885C008C164CADE?sequence=1 2/1/15

Bluman, A. G. 2004.*Elementary Statistics: A Step by Step Approach*, McGraw Hill, London, pp.130 – 141.

Bowerman, B. L. & O'Connell, R. T., 2003.*Business Statistics in Practice*, McGraw-Hill, Irwin, London, pp.78-79.

Davis, J. C., 1986.*Statistics and Data Analysis in Geology*, John Wiley & Sons, New York, p.646 .

Dowd, P. A.& Milton, D. W.,(Matheron, G. &Armstrong, M. J., ed.), 1987.Geostatistical Estimation of a Section of the Perseverance Nickel Deposit, in *Geostatistical Case Studies*, Reindol, D. Publishing Company, Dordsecht, pp.39-67.

Kesse, G. O. 1985.*The Mineral and Rock Resource of Ghana*. A. A. Balkema, Rotterdam, Boston, pp.378 – 384.

Reedman, J. H.1979.*Techniques in Mineral Exploration. Applied Science*, (London), and pp.322– 480.

Royle, A. G., 1978. Bias and its effects in Ore-reserve estimation, *Trans. Inst. Min. Metall. (Sect. A: Min. industry)*, 87, A8-A12.

Interpretation of Environmental Data from an Exploration Perspective at the Adenac Molybdenum Corporation, Ruby Creek Molybdenum Project, BC, Canada and its Implications for Geochemical Exploration in Turkey

Ruby Creek Molibden Projesi, Kanada, BC, Çevresel Verisinin Arama Bakış Açısından Yorumlanması ve Bu Çalışmanın Türkiye'deki Bir Jeokimyasal Arama İçin Uygulanması

D.R. Gladwell, S. Caner
Jeoband A. S., Ankara, Turkey

E. Duran
AECOM Turkey Danışmanlık ve Mühendislik Ltd. Şti., Ankara, Turkey

ABSTRACT Geochemical prospecting/ mineral exploration and environmental geochemistry are typically not carried out in tandem despite the fact that some survey data and data requirements are common to both tasks. This paper examines the potential for using groundwater and surface water geochemistry data collected for environmental purposes in combination with knowledge of geology, mineralogy and basic hydrogeology to enhance understanding of processes that may be exploited by the exploration geochemist.

The novel approach in this paper can be used for maximising the value of environmental data by combining mineralogy, aqueous geochemistry and kinetic test data to design ground and surface water exploration programs to detect buried mineralization. The approach is tested on environmental data, available in the public domain, collected by Adanac Molybdenum Corporation at the Ruby Creek Molybdenum project, Atlin, BC, Canada. Implications of this approach for geochemical detection of buried mineral deposits in the Menderes Massif, Turkey are discussed.

Keywords: Molybdenum, geochemical exploration

ÖZET Jeokimyasal maden arama ve çevresel jeokimya çalışmalarının ortak etüt ve veri gereksinimleri olmasına rağmen, genelde bu iki süreç birlikte ele alınmaz. Bu makale, çevresel çalışmalar sırasında toplanmış yeraltı ve yerüstü sularından elde edilen jeokimyasal verilerin, saha hakkındaki jeoloji, mineraloji ve temel hidrojeolojik bilgiler ile birleştirilerek jeokimyasal etütlerde kullanılma potansiyelini incelemektedir.

Bu makalede ele alınan yeni teknik, çevresel verilerden elde edilen yararın, mineraloji, su jeokimyası ve kinetik test verileri yardımıyla artırılması ve gömülü mineralizasyonların bulunmasına yönelik yeraltı ve yerüstü suyu etütlerinin tasarlanmasında kullanılabilir. Bu yeni teknik, Adanac Molybdenum Şirketi tarafından Atlin, BC, Kanada'da bulunan Ruby Creek Molibden projesinde toplanmış erişime açık çevresel veriler üzerinde denenmiş ve uygulanabilirliği gösterilmiştir. Ayrıca, bu yöntemin Türkiye Menderes Masifi'nde yer alan gömülü mineral yataklarının tespitinde kullanılması konusu da tartışılmıştır.

Anahtar Kelimeler: Molibden, jeokimyasal arama

1 CONCEPTUAL MODEL

This paper describes the results of research carried out to investigate the potential of multi-parameter ground and surface water data, typically collected during environmental studies, for the detection of partially or completely buried mineralization. An initial conceptual model was proposed (Figure 1) in which precipitation percolates through surface rocks, gradually equilibrating with the minerals present in the rocks dependent on their relative solubility. It was theorized that if such percolating water were to pass through mineralized rocks it would perhaps alter the groundwater, especially if sulphidic minerals were slowly oxidizing with oxygen supplied by advective flow. Groundwater passing through fissures or cracks in the mineral deposit would at some point migrate beyond the mineral deposit and gradually slowly re-equilibrate as it encountered additional lithologies depending on reaction kinetics. Eventually the partially re-equilibrated groundwater may reach the surface at a spring or seep and contribute to surface water flow, becoming increasingly diluted in the process. It was considered that if the increasing dilution of groundwater could somehow be detected it may provide a very useful guide to buried mineralization.

The Ruby Creek Molybdenum Project was selected for study for a number of reasons: multi-parameter ground and surface water environmental data was available in the public domain; one of the authors was familiar with the project; except for a small exposure in the stream bed the deposit was buried beneath barren basalts and quartz monzonites; pyrite was known to be present above the mineralization giving rise to ‘natural Acid Rock Drainage /Metal Leach (ARD/ML)’ (Lett and Jackaman, 1995); and a zone of groundwater flow into surface water from beneath the basalts was known to exist.

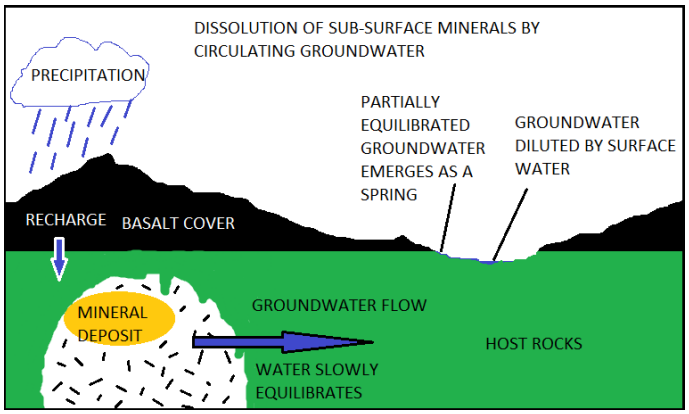

Figure 1. Conceptual model of Groundwater equilibration.

2 RUBY CREEK MOLYBDENUM PROJECT

The Ruby Creek Molybdenum project is located east of Atlin, British Columbia (BC), Canada; Figure 2. Molybdenum mineralization underlies the valley floor near the headwaters of Ruby Creek, (MacLeod, 2007). The host plutonic rocks are generally classified as quartz monzonites although sufficient variation exists to distinguish three phases of magma intrusion (Figure 3). The host intrusion, which includes the contact phase between the Cretaceous Fourth of July and Surprise Lake batholiths consists of a highly variably textured unit that grades from “coarse-grained quartz monzonite” (CGQM) south of the Adera fault through a number of texturally transitional phases. North of the molybdenum deposit’s bounding fault (Adera fault) is a quartz monzonite with fewer quartz and feldspar pheoncrysts (SQFP or “sparse quartz feldspar porphyry”), containing a higher proportion of pyrite leading to local gossan development at surface. The Mo mineralization is generally confined to fractures in quartz monzonite south of the Adera fault and except for a small exposure in the valley floor is almost completely buried under barren rocks. The quartz monzonites are overlain by a sequence of basalts and the surficial deposits include extensive scree on valley slopes as well as

alluvium in the valley bottoms and small ponds.

Figure 2. Location of study areas.

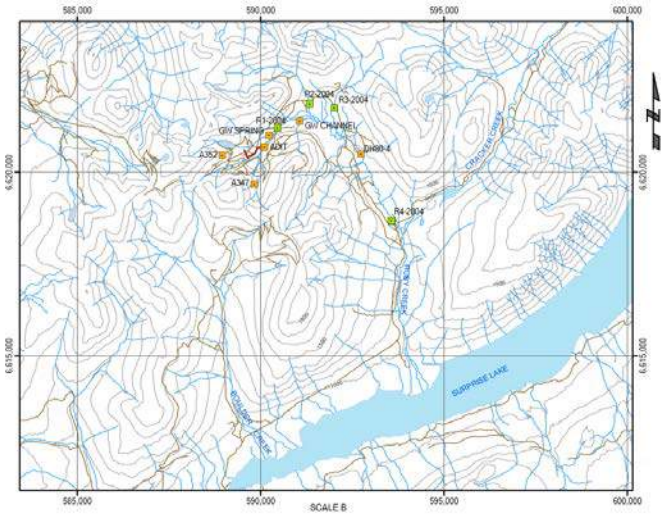

Figure 2. Ruby Creek Project study area location, also showing ground (orange) and surface water (green) sample sites.

2.1 Mineralogy / Petrography

The mineral assemblages were determined using standard X Ray Diffraction (XRD) (with Reitveld refinement) and petrographic procedures (MacLeod, 2007). SQFP was found to contain quartz (35%), orthoclase (50%), anorthitic plagioclase (12%), muscovite/sericite (1.5%), kaolinite (0.3%) and pyrophyllite (0.9%) together with trace quantities of pyrite, chalcopyrite, marcasite and minor kaolinite and limonite. CGQM was found to contain quartz (45%), orthoclase (33%), anorthitic plagioclase (15%), muscovite/sericite (6.6%) with trace magnetite. Petrographic and XRD studies did not find any molybdenite in CGQM although three repeat analyses yielded 180, 7.3 and 7.9 mg/kg Mo, illustrating a typical nugget effect. Carbonate minerals were found by acid digestion and ICP-MS analysis to typically be very low or absent in these lithologies. Gladwell and Ziten (2009) report that alkalinity and Mo are the only parameters which are statistically higher in leachate from molybdenite bearing samples.

2.2 Hydrogeology and Hydrology at Ruby Creek

Surface drainage at Ruby Creek consists primarily of a single (though in places braided) channel with a number of tributaries entering it (Figure 4). An adit was driven into the mineralized quartz monzonite in the early 1970's by Kerr Addison along which there is a low flow of groundwater into Ruby Creek. In addition, groundwater was observed flowing into Ruby Creek between the most southerly drill hole (DH-80-4) and the most southerly water sample site (R4). The hypothesized distribution of surface and groundwater, based on these observations is presented as Figure 5. It was considered that the hypothesized zone of groundwater inflow into the stream channel could contribute water into the stream that had at some point equilibrated with the mineral deposit.

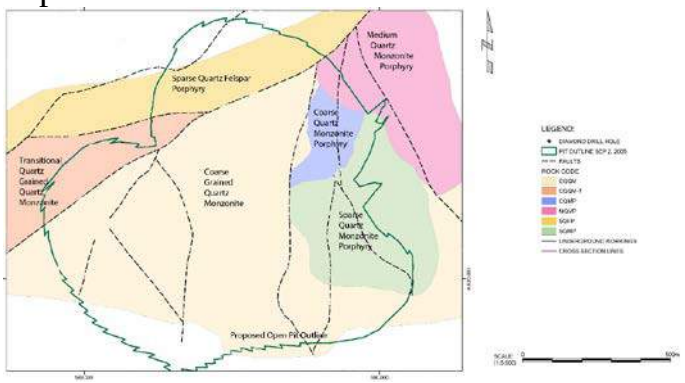

Figure 3. Ruby Creek Project study area showing simplified igneous geology.

MacLeod (2007) reports that five groundwater samples were collected at a series of groundwater springs and artesian wells in the project area through 2004 and 2005 together with five surface water samples (Figure 4). Water sampling was carried out at several dates; the earliest (2004) data was used for this study. The

water samples were analysed for a suite of cations and anions as well as general parameters such as pH, conductivity etc. PHREEQC aqueous modelling software was used to assist interpretation of the ground and surface water data (Apelo and Postma, 2007). PHREEQC, among numerous other features, facilitates charge balancing of aqueous solutions as well as calculation of the saturation index (SI). SI is defined by PHREEQC as the log of the ion activity product less the thermodynamic constant, Kt for a given mineral phase. A negative value of SI for a mineral phase implies the aqueous solution in question is thermodynamically capable of dissolving more of that phase, a SI value of zero implies the aqueous solution would be in equilibrium with that phase and a positive SI value implies the aqueous solution is thermodynamically capable of precipitating that phase. It is important to note that PHREEQC does not take account of kinetic constraints. This means, for example, that a mineral such as silica may be predicted to precipitate from the aqueous solution, based on its SI, however silica is kinetically very slow to precipitate from solution (Apelo and Postma, 2007) and these authors note that water saturated with respect to silica is quite common in the surface environment. This fact allows the silica SI to be used under certain circumstances as a 'geothermometer' (Tarcan et al., 2000).

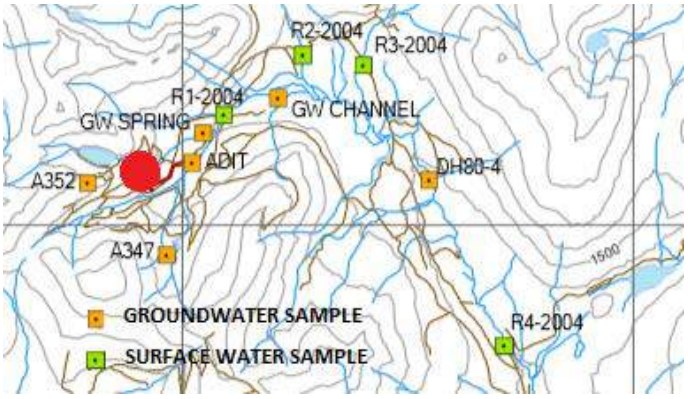

Figure 4. Ruby Creek study area showing location of surface and ground water environmental sample sites.

The authors considered, based on the conceptual model advanced above, that water samples showing high (but not necessarily positive) SI values for a number of mineral phases would tend to have a higher groundwater component than water samples dominantly comprised of surface runoff. A conceptual map of the study area showing groundwater versus surface water inflows is shown in Figure 6. Water sample site R3 is located on a tributary that drains a watershed northeast of the mineralization and therefore the water is not expected to come into contact with mineralization; it was selected as a background sample site for the purposes of this study.

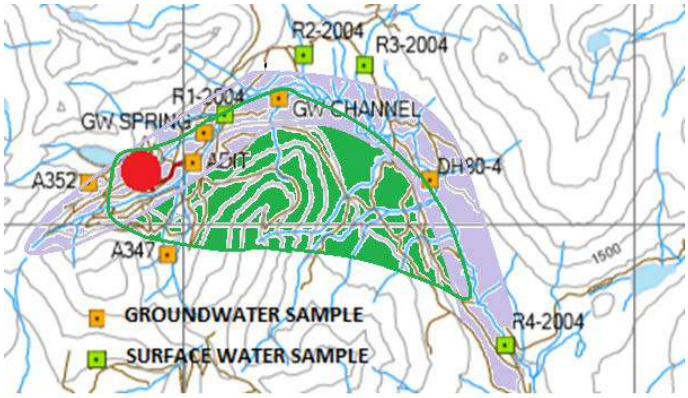

Figure 5. Ruby Creek Project study area showing hypothesized inflow of groundwater (green shading) compared to surface water (blue shading).

2.3 Geochemical PHREEQC Interpretation of Ground and Surface Water Data at Ruby Creek

The only raw geochemical parameter that clearly delineates the mineralization is Mo (Figure 7) although the only clearly anomalous value is at the mouth of the adit at 4.1 times background (R3) at 0.079 mg/L (red circles in Figure 7). Seven other water samples (orange circles on Figure 7) exceeded 0.00034 mg/L Mo. F shows lower concentrations over the mineralization. Cd also shows slight enrichment but appears to be generally associated with the monzonite (i.e. high values are observed upstream of the mineralization).

It might be expected (as noted above) that the SI for silica would be higher in groundwater samples than in surface water samples. Figure 8 shows that this is indeed the case.

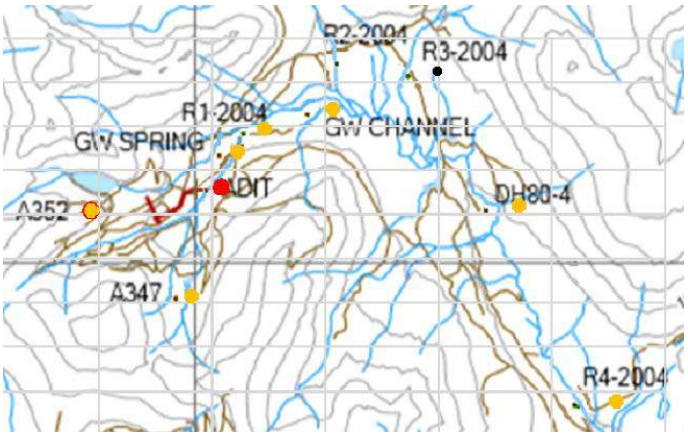

Figure 6. Ruby Creek Project study, distribution of Mo concentrations (Values as red circles exceed 0.079 mg/L and values as orange circles exceed 0.00034 mg/L).

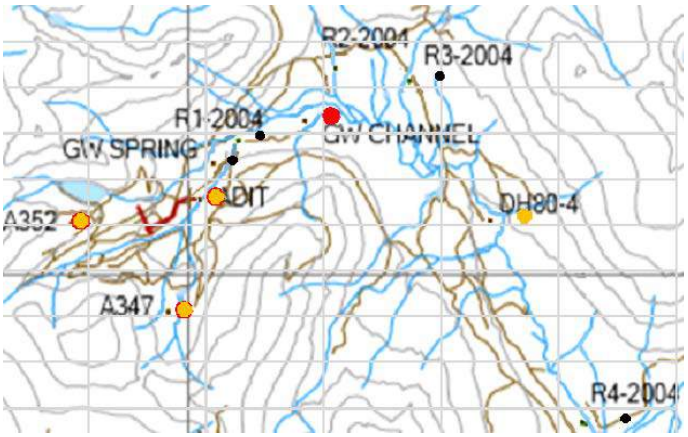

Figure 7. Ruby Creek Project study, distribution of silica SI values in ground and surface water samples (Red circles show SI values exceeding 0 and orange circles show SI values exceeding -0.47).

All of the drill hole water samples show high silica SI, as does the GW (groundwater) channel sample. R4 also shows a higher than expected silica SI sample confirming the observed groundwater input emanating from exposed basalts into the stream upstream of this site. The silica SI appears to indicate the presence of groundwater at Ruby Creek satisfactorily, as was expected from its slow reaction kinetics.

When precipitation kinetics for a particular mineral phase are slow then the SI value for that mineral may show a gradual decrease in value as the groundwater in increasingly diluted with surface runoff and as precipitation gradually occurs (if SI values are above zero). Such is the case for the fluorite SI (Figure 9), which exceeds the background (R3) SI value for over 3 km downstream. The PbMoO4 SI shows similar downstream dilution (Figure 10). Interestingly, the SI for Halloysite also shows downstream dilution (Figure 11), although the background value is reached at between 1000 and 2000 m downstream. Halloysite is most probably produced by plagioclase buffering of acidic groundwater produced by natural ARD produced by accessory pyrite in the quartz monzonite north of the Adera Fault (Gladwell and Ziten, 2009).

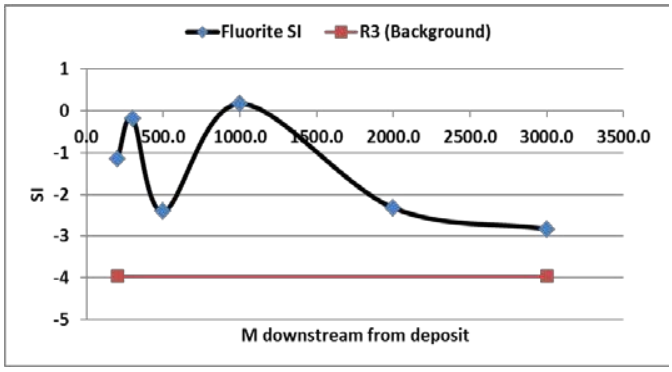

Figure 8. Ruby Creek Project, downstream dilution of the fluorite SI.

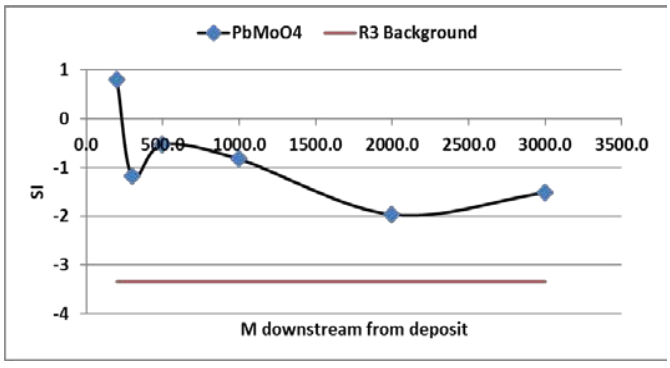

Figure 9. Ruby Creek Project, downstream dilution of the $PbMoO_4$ SI.

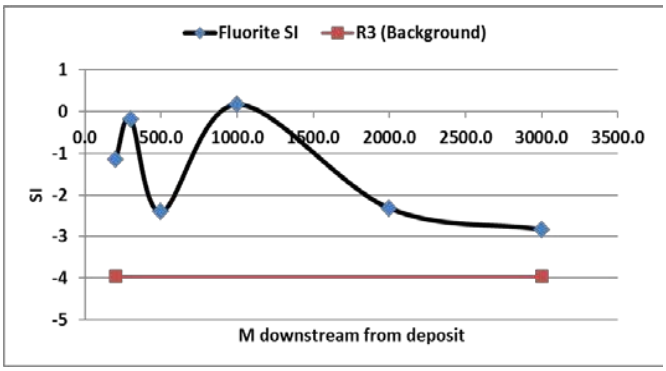

Figure 10. Ruby Creek Project, downstream dilution of the fluorite SI.

The results of the Ruby Creek Project study show that: the silica SI may be used to identify influx of groundwater into surficial drainage; dilution of SI values for mineral phases with slow precipitation kinetics may clearly indicate mineralization, and; the conceptual model for groundwater equilibration with mineral phases present in buried mineralization is corroborated. The conceptual model was subsequently applied to a reconnaissance exploration survey in the Menderes Massif, Turkey.

3 MENDERES MASSIF STUDY AREA

The Menderes study area is located near Alasehir, Western Turkey (Figure 2). The study area is on the Menders massif and close to Alasehir detachment, which is one of several detachment faults and/or related shear zones of exhumation Menderes massif (Seyioglu et al., 2014). The geology of the area comprises basement rocks of high to low grade metamorphics (gneiss, mica schists, marbles) and granodiorite of Early Triassic to Upper Cretaceous age. The basement is unconformably overlain by Neogene sedimentary rocks and basaltic lavas (Holocene Kula volcanics). Permeability is highly variable and is mainly controlled by fractures and fissures (Tarcan et al., 2000). The study area is located on the Salihli-Alaşehir part of Gediz Basin, which is the second biggest basin in Aegean Region. The important tributaries of Gediz River around the study area are Alaşehir and Nif creeks. There are two main aquifer systems namely Quaternary and Neogene in the study area (Ağartan, 2010). Natural springs are confined to fault and fracture zones.

3.1 Menderes Study Area – Water Quality Results

Twenty six groundwater samples were taken from drinking water wells along a trend of over 30 km and their multi-element cation chemistry was determined by ICP-MS and ion chromatography for anions. Sample sites are shown on Figure 12, which also shows the MTA metallogeny base map for the area. A known gold occurrence is present in the northwest of the sampled area. The multi-element chemistry was processed using PHREEQC and the SI values for minerals likely to be present were calculated.

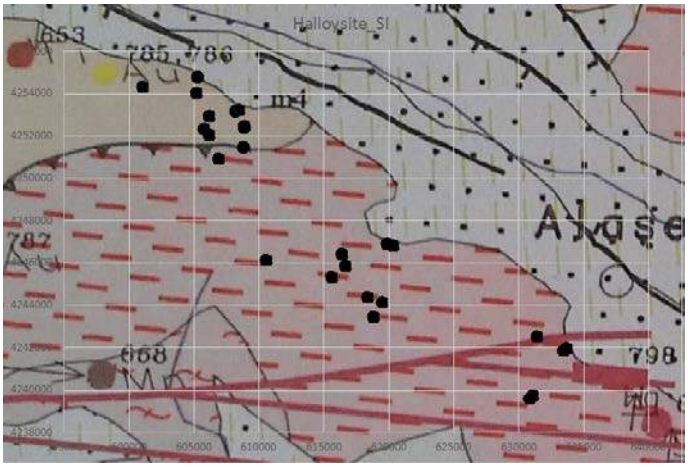

Figure 11. Menderes study area, distribution of groundwater samples superimposed on the MTA metallogeny basemap.

The distribution of positive SI values for halloysite is shown as Figure 13. The anomalous halloysite SI values form a cluster along strike from the known gold occurrence. The cluster of anomalous SI values for Halloysite is also associated with a very low level Cu anomaly (Figure 14 shows Cu concentrations above 0.0006 mg/L as red circles), which is reflected in high SI values in these samples for copper bearing minerals.

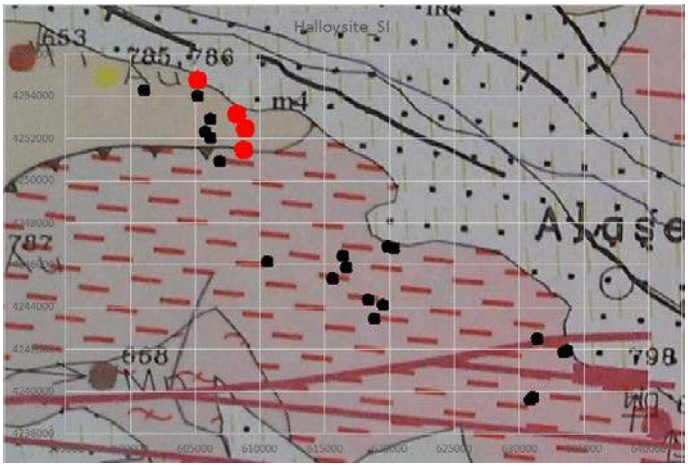

Figure 12. Menderes study area, distribution of halloysite SI values, red circles indicate SI values above zero.

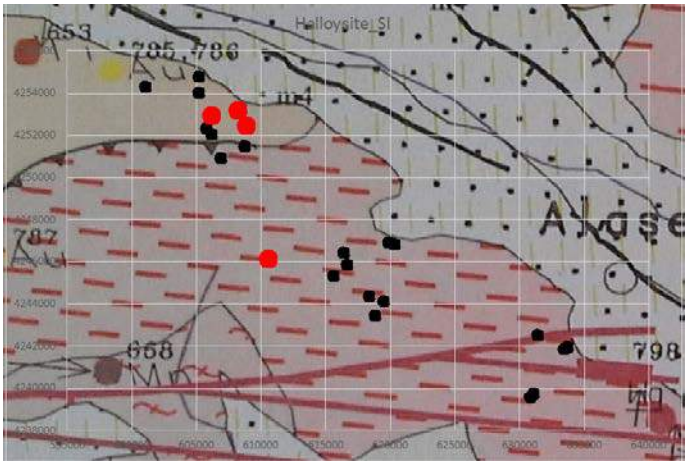

Figure 13. Menderes study area, distribution of Cu concentrations in groundwater (red circles indicate Cu concentrations above 0.0006 mg/L).

The study area is geothermally active and this is corroborated by the positive SI values for silica, which are clustered in three groups, probably reflecting movement of silica laden warm water travelling through faults and fractures (Figure 15). The observed distribution of high silica SI values suggests that the observed halloysite/Cu anomaly is of geothermal origin and may reflect mineralization along strike from the known gold occurrence.

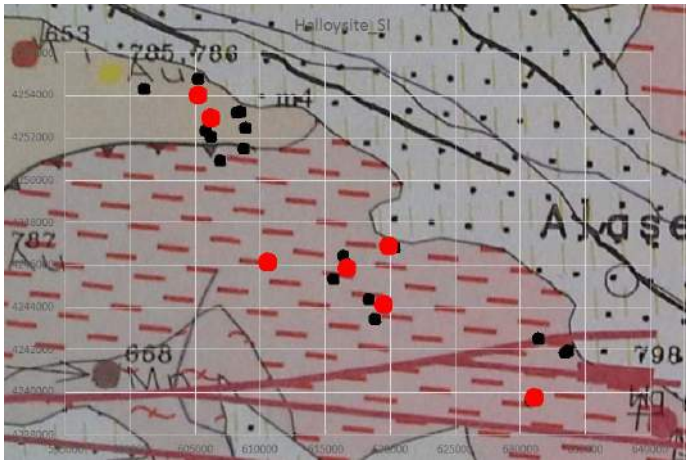

Figure 14. Menderes study area, distribution of silica SI values (red circles indicate SI values above 0.17).

4 CONCLUSION

The detailed interpretation of ground and surface water data collected for environmental purposes has allowed corroboration of a groundwater equilibration model that enhances geochemical exploration for buried mineral deposits, both on a local and reconnaissance scale. High silica saturation index values were shown to indicate groundwater entering surface drainage. In addition, dilution of ore and gangue mineral phases with slow reaction kinetics was observed and shown at the Ruby Creek (BC, Canada) and Menderes Massif (Turkey) study areas to delineate molybdenum and copper/gold mineralization respectively. The conceptual model appears to be applicable to both local (< 3 km) surveys as well as reconnaissance (> 30 km) surveys. Collection and analysis of environmental data is very expensive and careful use of the acquired data in geochemical exploration adds considerable value to the investment.

ACKNOWLEDGEMENTS

The authors are indebted to Jeoband A.S. for supporting their research and to Asia Minor Mining A.S. for permitting publication of the Menderes Study Area water quality data.

REFERENCES

Agartan, E. 2010. *Assessment of Water Supply Impact for a Mine Site in Western Turkey,* Master Thesis, Middle East Technical University, Ankara, Turkey

Appelo, C.A.J and Postma, D., 2007. *Geochemistry, Groundwater and Pollution, 2nd Ed.*, A.A. Balkema, Leiden, London, New York, Philadelphia, Singapore

Gladwell, D. R. and Ziten, C., 2009. Adding Value to Kinetic Testing Data II -Interpretation of Waste Rock Humidity Cell Data from an Exploration Perspective at the Adenac Molybdenum Corporation, Ruby Creek Molybdenum Project, BC, Canada. *In: 24th International Applied Geochemistry Symposium. Fredericton*.

MacLeod, M. 2007. Ruby Creek Molybdenum Project "Environmental Assessment Certification Application" http://a100.gov.bc.ca/appsdata/epic/html/deploy/epic_document_258_22610.html

Lett, R.E. & Jackaman, W. 1995. Application of spring-water chemistry to exploration in the Driftpile Creek area, North-eastern British Columbia. British Columbia Ministry of Energy, Mines and Petroleum Resources, *Geological Fieldwork,* 1994. 1995-1. 269-275.

Seyitoğlu, G., Işık V., Esat K., 2014. Turkish Journal of Earth Sciences, Kongre, Sempozyum vb. Kitabının adı (varsa seri numarası), 23, 479-494, Ankara.

Tarcan, G., Filiz, S, and Gemici, U., 2000. Geology and geochemistry of the Salihli Geothermal Fields, Turkey.

Mapping Curie Point Depth of the West African Craton from Satellite Magnetic Data and its Implication for Diamond Exploration

A. Bouguern, K. Allek, M. Khalifa
Laboratory of Earth Physics, University of Boumerdes, Algeria

F. Bendiab
ENAGEO, Hassi Messaoud, Algeria

D. Boubaya
University of Tebessa, Algeria

ABSTRACT The main objective of this work is to map the Curie depth of the West African Craton (WAC) using satellite magnetic data with the aim to provide first order evaluation, within this vast territory, for the spatial association between Curie-depth surface and known kimberlite locations. Taking into account Clifford's rule, the first and foremost exploration guideline for diamond exploration is the existence of a sufficiently thick lithosphere that expected to have a low surface heat flow. The Curie depth is closely related to the surface heat-flow conditions and lithosphere thickness. In actual fact, the only few regions that have sufficient density of surface heat flow measurements corroborate the association of these conditions with the diamond resources. To better explore in an efficient way the spatial relationship between the Curie depth and known diamondiferous primary sources within the WAC, we used GIS-based weights of evidence method to provide a quantitative analysis.

Keywords: Mapping, Clifford's rule, WAC, GIS, diamond exploration

1 INTRODUCTION

The diamonds form from carbon within the high-pressure environment present in nature at depths of over 150 km. In most parts of the Earth, at such depths we are right in the asthenosphere and the temperatures at this depth are too high to allow the crystallization of diamonds. However ancient cratonic blocks have a sufficiently thick (150-250 km) and relatively cool lithosphere (less than about 1200° C) in which diamonds can form and be preserved. The diamondiferous kimberlites are confined to these Precambrian cratons, particularly on those of Archean age. This empirical association is known as Clifford's rule (Clifford, 1966).

Thick and cool lithosphere potentially has a regional signature in almost all geophysical techniques. Teleseismic and magnetotelluric methods are the only methods able to directly ''look" into the mantle. However, magnetic method may predict the presence of lithospheric root (thick lithosphere) rather than direct detection. Surface heat flow measurements may be the first predictive approach for identifying conditions favorable for primary diamond deposits, as temperature at depth is the primary controlling parameter in diamond genesis. Exploration targets for diamond genesis are expected to have a low heat flow of 40–45 mW m^{-2} (Morgan, 1995). Several studies have shown a strong correlation between heat flow measured at the surface and the thickness of the magnetized crust. As is known, crustal rocks lose their magnetization at the Curie point temperature (about 525 ± 25° C). At this temperature, ferromagnetic rocks become paramagnetic, and their ability to generate

detectable magnetic anomalies disappears. The depth to the Curie isotherm surface may be at mid-crustal levels in regions of high heat flow, and at or close to the Moho in stable, low heat-flow regions. Therefore, the maximum magnetic source-depth is closely related to the surface heat-flow conditions.

The objective of this study is to assess the spatial relationship between the mapped Curie depth, and the known kimberlites locations, to answer the question whether the spatial distribution of these kimberlites is controlled by Curie-depth in the WAC assumed to be closely related to Heat-flow conditions. A geospatial quantitative assessment based on Bayesian statistical approach, in a log-linear form know as Weights of Evidence modeling technique (Bonham-Carter, 1994), was used to quantitatively analyze the spatial association between the Curie-depth surface and kimberlites locations. This method has been applied previously by Paganilli et al (2002) to determine the spatial relationship of various direction lineaments to known kimberlite locations in the Canadian Buffalo Head Hills.

2 STUDY AREA AND DATA SETS

The vast extent (4.5 million km^2) Western African Craton (WAC) considered in this study covers many countries. It lies at the North-Western part of Africa, between 17°30' W - 3°30'E longitudes and 4°10'N - 30°40'N latitudes. The geological map of west Africa (Fig. 1) shows two shields of Precambrian rocks exposed in the Reguibat and Man uplifts, separated by the Taoudeni Basin. The southern Precambrian core covers most of Sierra Leone, Liberia and southeast Guinea. In this core are located the diamond-bearing kimberlites of Sierra Leone, Liberia and Guinea. The Reguibat shield is the northern core, almost the mirror image of the southern core. Kimberlite eruptions have been rare through geological ages with an important episode during Cretaceous times. The basement of the WAC, stable since 2000 MA, is dominated by the occurrence of Archean nuclei surrounded by low-grade volcanoclastic Birrimian formations, which were affected by the Eburnean orogeny (at about 2 billion years) and intruded by numerous lower Proterozoic granitoids.

The data used in this study are extracted from satellite magnetic field model MF7 developed from CHAMP mission using measurements collected from May 2007 to April 2010. The original data set was compiled at 1.5 arc minute ascii grid of the anomaly of total intensity at 2.5 km altitude above the WGS84 ellipsoid. It is intended for use in the World Digital Magnetic Anomaly Map project for the 2011 revision. These data provide the most effective means of mapping the long wavelengths of the magnetic field caused by the magnetization of the Earth's crust. The CHAMP satellite, active until 2010, was launched in July 2000 into a lower orbit, initially at 450 km altitude. It has been providing excellent quality data at solar minimum conditions and at steadily decreasing altitudes. Using a field model instead of raw satellite magnetic field observations is highly productive as the magnetic field measured by a satellite contains contributions from several different sources: the core, the crust, the ionosphere, and the magnetosphere. Field modeling allows separation of various sources, thus allowing the crustal field to be isolated.

The crustal magnetic field of the WAC derived from world digital magnetic anomaly map was resample at a 4-km grid spacing resolution using Minimum Curvature interpolation method (Fig. 1). The main characteristics observable in the magnetic field are the NE-SW trends apparent in the central portion of the study area which seem affected by NW to WNW direction particularly in the northern part of the region. The most intense anomaly appears to be localized in the NE of Mauritania on the border with the Western Sahara. This large sub-latitudinal bipolar anomaly present an amplitude of more than 500 nT, and most of the known kimberlite occurrences discovered in Mauritania are within this zone. To the southwestward termination, a magnetic low characterizes a E-W trend within a region on horseback between Guinea, Liberia and

Sierra Leone, where all of the known diamond-bearing lithologies lie within this area.

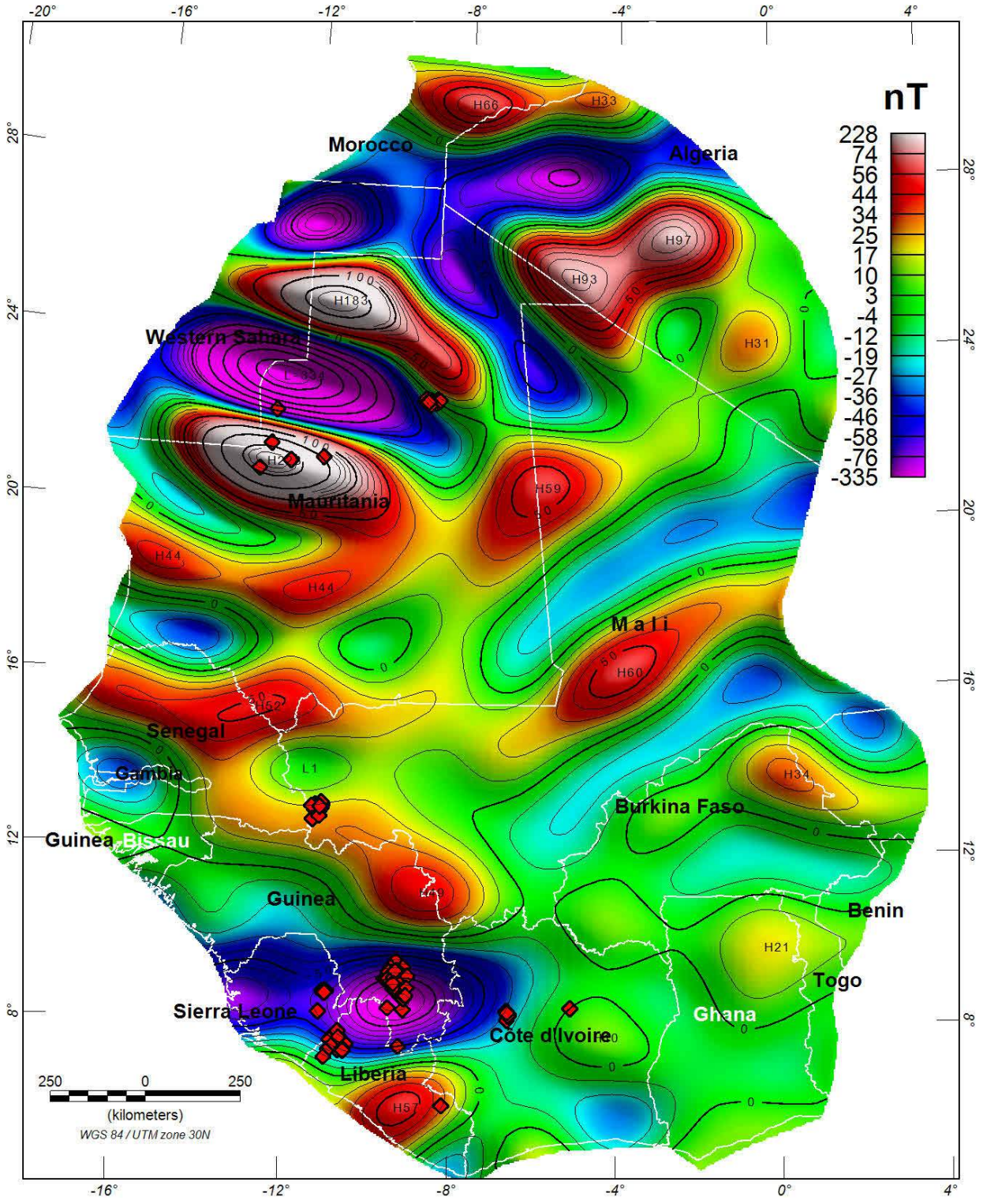

Figure 1. West African Craton crustal magnetic field and kimberlites locations

3 METHODOLOGY

3.1 Curie point depth estimation

The basic physical phenomenon that governs the investigation's of magnetic depth method is the Curie temperature by which the detection of magnetic bodies is limited by the depth of the Curie isotherm. Using magnetic data to infer heat flow is possible because the magnetic properties of rocks are temperature dependent, and at the Curie temperature rocks lose their magnetism. Negi *et al.* (1987) have elaborated empirical relationships which may

be readily used in converting Curie depth into the corresponding surface heat flow density values and lithosphere thickness.

The geothermal heat flow is an important factor in the area selection for diamond exploration. The estimation of the depth to magnetic bottom, assumed to be at the Curie temperature, can be realized using spectral analysis. However, this approach depends upon many assumptions and therefore has limitations. It requires that the depth to the bottom of magnetic sources be large relative to the depth of the top, essential to spectral separation.

Magnetic data have been used in various parts of the world in order to estimate Curie Point Depths (CPDs). Two approaches have been usually used for the computation of the CPDs; the spectral peak and the centroid depths. The spectral peak approach originally is given by Spector and Grant (1970), and the centroid approach originally presented by Bhattacharyya and Leu (1977) and was developed by Okubo et al. (1985). As part of the work presented here, we used the first one.

Spector and Grant (1970) derived an expression for the power spectrum of the total magnetic field intensity by assuming that the anomalies are due to an ensemble of vertical prisms. The method treats the observed magnetic field anomalies as a statistical population. They demonstrated that contributions from the depth, width and thickness of a magnetic source ensemble could affect the shape of the energy spectrum.

The dominant term, which controls this shape, is depth factor. The depth estimates could be made using the equation,

$$E(r) = e^{-2hr} \qquad (1)\ ;$$

where E(r), h and r are the spectral energy, depth and frequency respectively. The thickness factor $(1 - e^{-tr})^2$ plays an interesting role in shaping the power spectrum. When combined with the depth factor (e^{-2hr}) (for not too large values of r), its effect is to produce a peak in the spectrum whose position shifts towards smaller wavenumbers with increasing values of '*t*' (thickness). When this peak occurs (significant maximum), it indicates that the source bottoms are detectable. The frequency f_{max} of the spectral peak, the mean depth '*h*' to the source tops (depth to deep-seated causative bodies) and the mean depth '*d*' to the source bottom (Curie depth) are related by the equation (Boler 1978).

$$f_{max} = \frac{1}{2\pi(d-h)} ln\left(\frac{d}{h}\right) \qquad (2)$$

where d = h + t. Whether the sources appear to be depth limited or not depends very much on the size of the map. If there were no restrictions upon either the size of the map, then presumably the Curie-point depth isotherm could be observed. Therefore, large-scale magnetic maps are useful for understanding and characterization of crustal temperatures.

The WAC was subdivided in 209 square subregions (windows). The dimensions of these windows were initially set at 100 x 100 km²; in numerous cases this size was insufficient to allow the observation of spectral peak presumably related to the CPD because it occurs at frequency lower than the fundamental frequency for the subregion. This led us to increase the size of the windows gradually by steps of 10 km until reaching a size of 150 x 150 km^2 which seems suitable for CPD determination.

The radially averaged power spectra were computed for each subregion. the Curie depth estimate is derived using equation (2). Graphs of the logarithms of the spectral energies against frequencies for the various blocks were obtained. Linear segment from the low frequency portion of the spectra, representing contributions from the deep-seated causative bodies could be drawn from each graph. The slope of the linear segment can be used to calculate the depth to the ensemble of causative bodies from the equation (1). An example of spectra for one subregion is given in Figure 2.

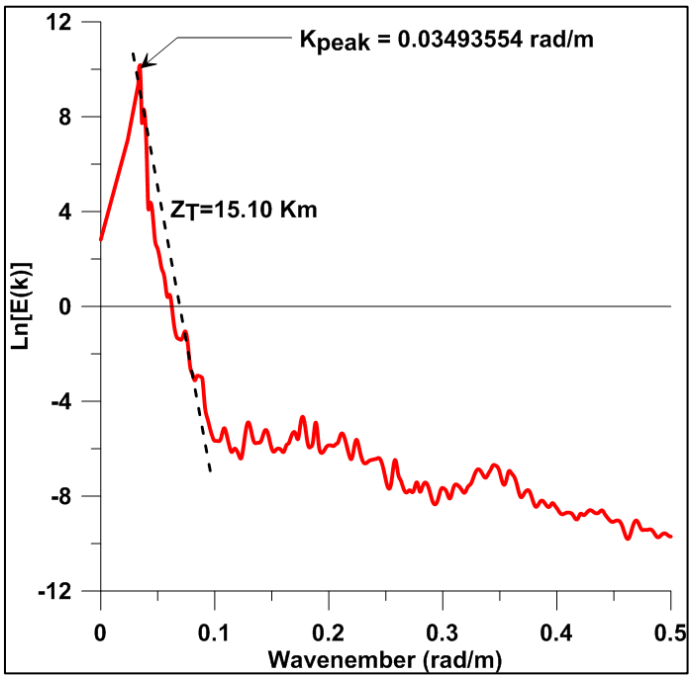

Figure 2. Example of spectrum for the estimation of the depth to Curie point using spectral peak approach.

The calculated Curie point depths were interpolated onto a regularly spaced grid using a minimum curvature technique (Briggs 1974). A grid with a cell size of 41 km was designed according to the known Rule applicable to data evenly distributed where the nominal cell size is = ¼ (sqrt (grid area / number of data points)). The data set was resampled to a 4-km grid spacing resolution in order to have more precision in the location of favorable or unfavorable evidential zones (Fig. 3). Curie point depths (CPDs) of WAC vary between 18.5 and 51.5 km.

3.2 Weights of Evidence Approach

Weights of evidence (*WofE*) is a Bayesian statistical method for assessing the degree of spatial association and for combining evidence to test a hypothesis. It determines the probability of an event to occur under certain conditions. The method was originally developed for a non-spatial application in medical diagnosis, later it was extensively used for mineral potential mapping in a GIS environment (Bonham-Carter, 1994), and soon after adapted for landslide susceptibility analysis, hazard modeling, fires and so on. The WofE method is applied here to investigate the spatial associations between Curie point depths and known kimberlite occurences within the WAC. The importance of the weights depends on the measured association and permits to provide an insight into the thermal flow condition of the WAC. This method could be used as spatial evidence in diamond prospectivity mapping.

A detailed explanation of the mathematical formulation of the WofE modeling method is available in Bonham-Carter (1994). The method uses a log-linear of the Bayesian probability model to estimate the importance of evidences by a pair of weights, one (positive weight W^+) for presence of the evidence H, and negative weight (W^-) for absence of the evidence H.

$$W^+ = ln\left(\frac{P(C|K)}{P(C|\bar{K})}\right) \quad (3)$$

$$W^- = ln\left(\frac{P(\bar{C}|K)}{P(\bar{C}|\bar{K})}\right) \quad (4)$$

where P() denotes probability, C is the presence of predictive pattern (it corresponds to area occupied by class of CPDs), $\bar{C}$ is the absence of predictive pattern, K is the presence of training points of interest corresponds to kimberlite occurrences), $\bar{K}$ is the absence of kimberlite occurrence.

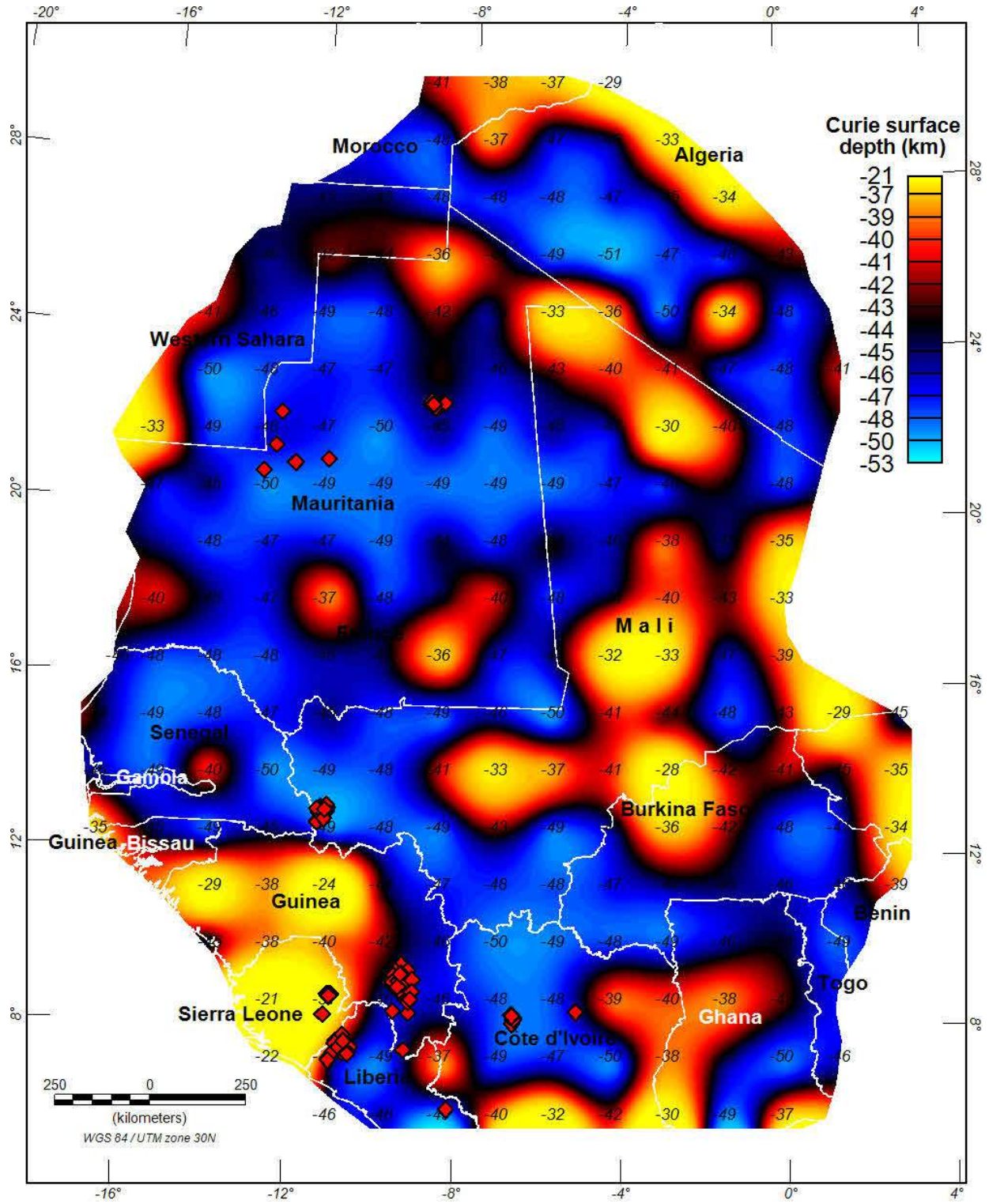

Figure 3. Curie-point isotherm map of the study area and kimberlite locations. CPDs of each subregion are reported on the map

The weights (W^+ *and* W^-) provide a measure of spatial association between the training points K and the binary theme C. The value of the weight W^+ is positive, whereas W^- is negative, indicates that there are more kimberlite occurrences on theme class C than would occur due to chance. Conversely W^+ would be negative and W^- positive for the case where fewer points occur than expected. If the kimberlite occurrences K are distributed randomly with respect to the binary theme C, then both of weights will have a value of zero, or very close to zero. The difference between the weights is known as the contrast, C. Thus:

$$C = W^+ - W^- \qquad (5)$$

The contrast is an overall measure of spatial association between the set of points K and

the theme C, combining the effects of the two weights. It is the best estimator in a large area and when a large number of points occurrences are considered (Bonham-Carter, 1994). Hence, for a positive correlation, C is positive; C is negative in the case of negative spatial correlation.

The studentized confidence value *s(C)*, defined as the contrast *C* divided by its standard deviation, corresponds approximately to the statistical level of significance defined by standard z-tests, and provides a useful measure of the significance of the contrast (Raines, 1999). The standard deviation of C is calculated as:

$$s(C) = \sqrt{s^2(W^+) + s^2(W^-)} \quad (6)$$

In the spatial analysis, as applied in this work, a simplified and intuitive approach similar to that suggested by Turner (1997), was adopted. The surface of the study area and the predictive pattern C are expressed in number of unit cells, and each training point is assumed to occupy a single unit cell. That way, the weights W^+ and W^- can be calculated by means of map crossing functions as follows:

$$W^+ = ln\left(\frac{\frac{Number\ of\ training\ points\ K\ (kimberlites)\ \boldsymbol{inside}\ the\ pattern\ C}{Total\ number\ of\ \ points\ K}}{\frac{Number\ of\ unit\ cells\ \boldsymbol{inside}\ pattern\ C\ not\ occupied\ by\ points\ K}{Total\ number\ of\ unit\ cells\ of\ the\ study\ area\ not\ occupied\ by\ points\ K}}\right) \quad (7)$$

$$W^- = ln\left(\frac{\frac{Number\ of\ training\ points\ K\ \boldsymbol{outside}\ the\ pattern\ C}{Total\ number\ of\ points\ K}}{\frac{Number\ of\ unit\ cells\ \boldsymbol{outside}\ pattern\ C\ not\ occupied\ by\ points\ K}{Total\ number\ of\ unit\ cells\ of\ the\ study\ area\ not\ occupied\ by\ points\ K}}\right) \quad (8)$$

A unit cell of 4 km x 4 km was used. The total number of unit cells area (16 km²) in the study area map is 289 181 cells. The training points used for the spatial association analysis are all diamond-bearing lithologies, namely: mafic lamprophyres, lamproites, and kimberlites from Côte d'Ivoire, Guinea, Mali, Sierra Leone, Liberia, and Mauritania publically available from World kimberlites CONSOREM database (Faure 2010).

4 SPATIAL ASSOCIATION ANALYSIS

The locations of 141 known diamondiferous primary sources (mainly kimberlites) have been used as training points to quantitatively analyze the spatial association with Curie point depths. Each training point/kimberlite is assumed to occupy a small unit area, defining the 'unit cell area'. Given that some kimberlite occurrences are very close to each other, we used a systematic reduction in the number of training points by geographic *weeding* - removing training points that are too close together. The minimum spacing is taken as the unit cell size specified when defining the study area, i.e. 4 km. After removing the undesirable items, we lead to 109 training points.

A multiclass Curie Point Depths (CPDs) map was produced from the reclassification of the original continuous grid into ten classes to create the Curie surface depth theme as shown in Figure 4. This multiclass predictor theme provides a representation of heat flow conditions in relation to kimberlite occurrences. For the weights calculations, we have initially calculated the weights for each class (table 1). Because some of the classes may have a very small number of kimberlite occurring in them and this is particularly critical for the weights calculated in this case, we experiment the computation of weights for cumulative Curie point depths, and to examine the variation of the weights and contrast at successive cumulative CPDs intervals (Table 2). The relative weights and contrasts values of the CPDs theme are shown in Table 1 and 2. As indicated by contrasts C, they clearly outline a strong spatial correlation with CPDs class interval (53 to 49 km) in which 19 kimberlite occurrences are present. A less important

spatial correlation seems to be present with the CPDs class (46 to 43 km), despite the occurrence of 49 kimberlite occurrences, resulting from the large area units proportion covered by this Curie depth class, with respect to the number of kimberlite occurrences. This spatial association between kimberlite occurrences and deepest Curie-points is due to the role of low heat flow as the primary controlling parameter in diamond genesis. This result is supported by some studies have shown a strong correlation between heat flow measured at the surface and the thickness of the magnetized crust. which reveals favourable lithospheric conditions

In general the surface heat flow reflects the tectonic stabilization of the crust, i.e. the stable old structures are characterized by low heat flow, and the young geologically active areas presumably have to display relatively high Moho heat flow. It can be concluded, from Figs. 12 and 13, that the heat flow decreases with an increase in Curie depth, as suggested by Negi et al. (1987).

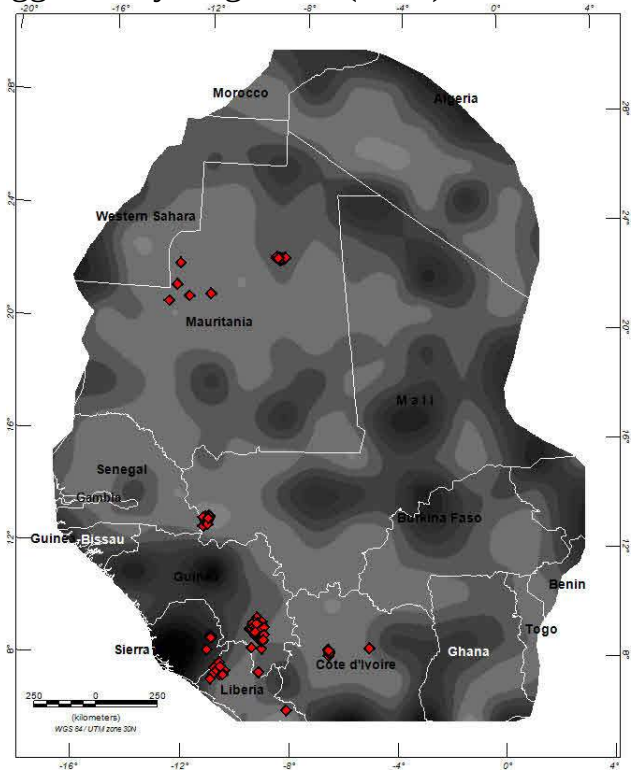

Figure 4. Classified Curie point depths map and kimberlite locations

Table1. Summary of weights for each class of CPDs

Class CPD (km)	Area (km²)	Area (units)	No. Points	W+	W-	Contrast	Confidence
-53 to -49	45600	2850	19	2.858	-0.181	3.040	12.006
-49 to -46	1704976	106561	20	0.718	0.269	-0.988	-3.991
-46 to -43	1262768	78923	49	0.478	-0.270	0.749	3.888
-43 to -40	694816	43426	13	0.251	0.039	-0.291	-0.984
-40 to -37	450288	28143	0				
-37 to -33	226592	14162	0				
-33 to -30	95760	5985	8	1.246	-0.055	1.301	3.539
-30 to -27	21520	1345	0				
-27 to -24	12752	797	0				
-24 to -20	16048	1003	0				

Table 2: Summary of weights for cumulative classes of CPDs

Class CPD (km)	Area (km²)	Area (units)	No. Points	W+	W-	Contrast	Confidence
-53 to -49	45600	2850	19	2.858	-0.181	3.040	12.006
-49 to -46	1750576	109411	39	0.077	0.045	-0.122	-0.612
-46 to -43	3013344	188334	88	0.194	-0.553	0.747	3.077
-43 to -40	3708160	231760	101	0.124	-0.906	1.031	2.806
-40 to -37	4158448	259903	101	0.010	-0.114	0.124	0.337
-37 to -33	4385040	274065	101	0.043	0.823	-0.866	-2.357
-33 to -30	4480800	280050	109	0.011	0.000	0.011	0.000
-30 to -27	4502320	281395	109				
-27 to -24	4515072	282192	109				
-24 to -20	4531120	283195	109				

5 CONCLUSION

Although the formulation of a kimberlite prospectivity mapping is not the objective of this study, the spatial association between kimberlite occurrences and deepest Curie-points is of potential importance for diamond exploration, as it may enable us to predict the diamond potential of target areas within craton on the basis of the mapped Curie point isotherm.

After these quantifications of spatial analysis, it could be implied that zones of deepest Curie-points can be fertile for diamond-bearing lithologies emplacements. This condition is most commonly found in regions of thick and cold lithosphere, and are consistent with Clifford's Rule, an empirical diamond exploration strategy.

REFERENCES

Bhattacharyya, B.K., Leu, L.K., 1977. Spectral analysis of gravity and magnetic anomalies due to rectangular prismatic bodies. *Geophysics 42, 41–50.*

Boler, F. M., 1978. Aeromagnetic measurements, magnetic source depths and the curie point isotherm in the Vale-Owyhee, Oregon, *M.Sc thesis, Oregon State University, Corvallis.*

Bonham-Carter, G.F., 1994. Geographic Information Systems for Geoscientists; Modelling with GIS *Pergamon. United Kingdom, 398 p.*

Briggs, I.C., 1974. Machine contouring using minimum curvature. *Geophysics 39, 39–48.*

Clifford, T.N., 1966. Tectono-metallogenic units and metallogenic provinces of Africa. *Earth Planet. Sci. Lett. 1, 421–434.*

Faure, S, 2010, World Kimberlites Database (Version 3), *Consortium de Recherche en Exploration Minérale CONSOREM, Université du Québec à Montréal, Numerical Database on www,consorem,ca,*

Hojat A., Guya N. H.,, and Maule C. F., 2010. A new method to determine geothermal potential sites using satellite magnetic field models, *Iranian Journal of Geophysics, 4 (1) 33-43.*

Mayhew, M.A., 1985. Curie isotherm surfaces inferred from high-altitude magnetic anomaly data. *J. Geophys. Res. 90 (B3), 2647–2654.*

Morgan, P., 1995. Diamond exploration from bottom up: regional geophysical signatures of lithosphere conditions favourable for diamond exploration. *J.Geochem.Explor. 53, 145–165.*

Negi, J.G., Agrawal, P.K., Pandey, O.P., 1987. Large variation of curie depth and lithospheric thickness beneath the Indian Subcontinent and a case for magnetothermometry. *Geophys. J. R. Astr. Soc. 88, 763–775.*

Okubo, Y., Graf, R.J., Hansen, R.O., Ogawa, K., Tsu, H., 1985. Curie point depths of the island of Kyushu and surrounding areas, Japan. *Geophysics 50, 481–494.*

Raines, G.L., 1999. Evaluation of weights of evidence to predict epithermal-gold deposits in the great basin of the Western United States. *Natural Resources Research 8, 257–276*

Spector A., and Grant F. S. 1970, Statistical Models for Interpreting Aeromagnetic Data, *Geophysics. 35, 293–302.*

Optimization of Geochemical Patterns Based on Multivariate Methods in the Duzduzan Area, E-Azerbaijan

F. Javid
Department of Mining Engineering, Ahar Islamic Azad University, Ahar, Iran.

M. J. Mohammadzadeh
Faculty of Mining Engineering, Sahand University of Technology, Tabriz, Iran

A. Nasseri
Department of Mining Engineering, Ahar Islamic Azad University, Ahar, Iran.

ABSTRACT Duzduzan area is located at 45 km of Tabriz in the NW of Iran. The main objective of the study is to recognize the distribution patterns of elements in the area in order to establish an optimized pattern in regional and semi-regional exploration programs and ultimately to detect the promising potentials in the area. In this regard 384 stream sediments samples were collected at non-regular pattern. The samples were preprocessed to (-200) meshes and analyzed for 19 elements by ICP method.

The data processing by different methods with the aim of estimating the distribution parameters were carried out. During data analysis, detecting censored and probable outliers data and data normal testing were carried out. Then to demonstrate the correlation between elements concentrations and to extract the paragenetic sequence of elements, hierarchical clustering analysis (CA) method was used. Subsequently to reduce the variant and determine relative contributions of each component in elemental distribution, the Principal Components Analysis was employed.

CA based results indicated that only elements such as Cu, Pb, Zn, Mo, and Au are major elements some extend paragenetically and geochemically are important in the ore bearing solution. Also, PCA results revealed that only 7 components are important and have maximum variations in the area. Interpreting the components showed that PC_1, PC_2, PC_3 and PC_4 indicated the major elements and syngeneic effect variations. Whereas components7, and 5 indicate epygenetic effect of mineralization and show anomalous localization of oxides and sulphides in the region. The overall results also depict that probably the area have subjected to multi-phase mineralization.

Keywords: Geochemical pattern,anomalous region,PCA and CA method and Duzduzan area

1 INTRODUCTION

Understanding the pattern of distribution of elements in the various zone in order to intensify for the anomalies and detection the false anomalies of special importance. So in every exploration, the application of the ideal method is important for mineralization zone identifying accurately detection of the mineralization zone (Sandjivy, L., 1984. Sousa, A.J., 1989. JimeÂnez-Espinosa, R., et al, 1993. Bellehumeur, C., et al, 1994).

The application of the ideal method for processing geochemical data and providing more accurate distribution maps, requires appropriate methods for optimization the geochemical anomalies and recording the real anomalies , has finally by introduced an optimize method is possible to the separation zone and more accurate detection of them.

The present study is part of a systematic geochemical exploration, which is performed Garachaman area in 1:100000 scale. In order to obtain mineral index, the results and maps

from geochemical data, were compared with the original data (Javid, F., 2014).

Necessity if existence of ways to optimize the geochemical projects and record the original anomalies is important (Govett, G.J.S., et al., 1975). Of the methods that are frequently used in the field of science, discovery studies and detection of potential minerals, are included multivariate methods (Howarth, R.J., et al., 1983). As can be used for detection of geochemical anomalies (Loska, K. et al., 2003), remote sensing (Fresman, A.E., 1939., Loughlin, W.P.G., 1991), environmental (Loska, K., et al., 2003), geophysical researches to oil and gas (Pasadakis, N., et al., 2004., Prinzhofer, A., 2000., Sabeti, H., et al., 2007). Because of the importance of the Multivariaty method for identification the anomalies and area requirement for more accurate detection and reconnaissance geochemical halos, using a two Cluster Analysis way and Principal Component Analysis way, the detection and identification of anomalies was done.

A multivariate method, for identifying of parageners and simultaneous of materials using clustering (CA). Cluster Analysis aims to achieve a more appropriate criterion for the classification of the variables or samples based on the more similarity of in-group and every greater difference between-groups. This feature helps to data and samples to classification as clusters which had maximum possible similarity betweem themselves and maximum difference between their own. Hierarchical clustering, which its very similar continuous and repeated observations that are linked together, is the most common method. So the data simply inserted in groups, on the basis of similarity that they have with each other. Hierarchical Cluster Analysis can be very helpful when the data are available and when they are following of a completely clear model. For this, in recent years, the CA method is applied to detect the region anomalies in, isolation anomalies from the geochemical field (Ji Hongjin, et al., 1995., Collyer, P.L., et al., 1973., Julian., K., 1976). So according to application ability and resolution of simultaneous and parageners separation, the elements clustering and identification of parageners for different types of raw and normalized data in the area was done.

To identify the direction and type of minerals, there is another method called Principle Component Analysis. This method is based on that in Scree Plot the variables that are correlated with each other, considered a line with the highest variability and also plot a vertical line to it, and considering the dispersion in the new coordinate system. should always be considered a direction which has explained the most diffraction. Thus, this procedure was repeated for each series, so the best direction which express the greatest variability was considered as the main direction and mineralization, and other factors to anomalous behavior. Principal Component Analysis method is briefly called (PCA). The main problem in this way, was the expression principle of correlations between the concentration of elements values in order to display their simultaneously change pattern in the region. In recent decades, towards the geochemical regional researchs in the area of stream sediment, to identify potential areas, and the prone areas to minerals (Govett, G.J.S., et al., 1975. Jun deng., et al., 2010. Xiang Sun., et al., 2010), separation anomaly distribution (Jun deng., et al., 2010. Xiang Sun., et al., 2010), identify the source of pollution of soil (Facchinelli, A., et al, 2001. Boruvka, L., et al., 2005), and identify the results based on detection of regional anomalies and identify some results based on hydrothermal activities and leads to regional mineralogy in the area (Al Hakimi, A., et al., 2009), identify the geochemical patterns (Sulistijo. B., 2012) and identify the relationship between the type of deposit and integrate them with the alterations (Grunsky E.C., et al., 2003. Groves, D.I., et al., 1998), all were done by PCA.

2 GEOLOGY

Duzduzan area is located in East Azerbaijan province of North West of Iran and on the Metallogenic Belt of Alps – Himalaya. That

due to the having the reserves of Copper and possibly "in some parts points of parageneric polimetal, it is important. The study area is located between 47° 46° 30' east longitude and 38° 37° 30' north latitude (Figure 1).

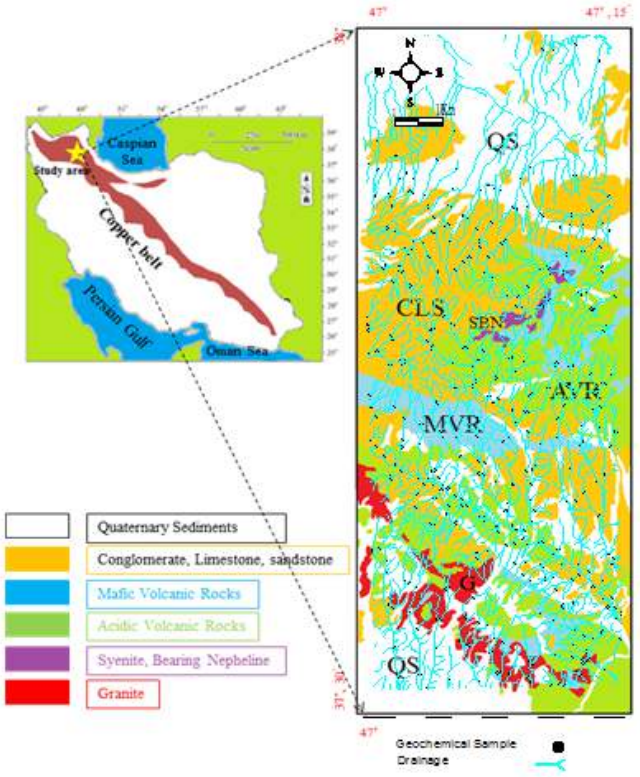

Figure 1. Geological and stream sediment sample location map of the Duzduzan area, E.Azerbaijan, Iran.

The study area is divided into two zones (Bozgush zone and zone of Shaharchayi-Gharachaman). Bozgush Eocene zone, is located in the northern region, And is mostly included of volcanic and sedimentary series.

Oligocene related rocks in this zone, are widespread both in intrusive - semi-intrusive, volcanic and sedimentary rocks. Shaharchayi-Gharachaman unit, is located in the southern region. It's Eocene and Oligocene units are mostly of volcanic rocks, intrusive masses and in small quantities of Sedimentary series. Oligo-Miocene unit of this zone, mostly composed of Sedimentary Rocks. Sediments of the present age cover a large area of that area. Area in the point view of geological structures classification, according to the Eocene Volcano Sediment sediments, is related to Urumie-Dokhtar zone. Area is from the Volcanic Rocks exhausting and existence of intrusive masses is important, which have a key role in the mineralization (Javid, F., 2014).

Metallogenic zone of the area suggest that older units of the Eocene, has not been observed the region. Geochemical analysis of the Oligocene Volcanic Rocks of this area, shows their Alkaline Magmatic origin. In the Paleogene Tectonic phase, a large Magmatic activity (Pyrenees phase) led to intrusive Igneous Rock reach the earth's surface with a wide volume, which many of these intrusive masses of Iran have been created in this phase and most Metallic minerals, especially Copper, Lead and Zinc are related of this phase. This subject have been detected in the area of Duzduzan mostly in the form of large intrusive masses of Granite and Syenite. Duzduzan area is of high mineral potential because the Magmatic origin exhausting Volcanic Rocks And the impact of intrusive Igneous masses and reactivity of Hydrothermal solutions. the Pyrite and Chalcopyrite traces in Volcanic Rocks, are sulfidized under the influence of hydrothermal solutions from the locally granite and syenite masses. Influence of acidity hydrothermal solution lead to alteration of related rocks and mineral, So then the hydrolysis of iron and magnesium silicates in the early stages and then later in the Feldspath alteration have been occurred. which lead to the kaolinite and then sericitic products in the study zone.

3 MATERIALS AND METHODS:

Regional geochemical exploration with the aims to prospecting the Duzduzan base-metals and gold were done with providing 384 stream sediments (Figure 1), which has the maximum compatibility with the center of gravity method and send to the Australia AMDEL company for analysis the 19 elements by the ICP-MS and gold element by the Fire Assay method.

For data analysis, the pre-processing stage of the data analysis was conducted Censored data and Outlier data. So outlier data with the Q method were identified and replaced.

$$Q = (x_i - x_{i+1}) / (x_{Max} - x_{Min}) \quad (1)$$

$$\overline{Q} - 2\delta_Q < Q < \overline{Q} + 2\delta_Q \quad (2)$$

The results of this study were presented in the below table (Table1).

Table 1. Determination of outlier data by Q method in Duzduzan area

	Sample.No	Natural (ppm)	Replacemant (ppm)
Mg	63	2630	2880
K	105	2950	4920
Ag	231	0.04	0.05
Cu	98-229	16.2-17.3	20
Mo	193-253-325-370	6.4-11.2-10.9-11.2	6.3
Zn	113-255-322	303-303-295	257
W	36-48-49-244-265	8.1-8.1-8.1-7.1-0.1	7-7-7-7-0.7
Nb	105-107-109	4.3-4.5-5	5.7
Ce	40-41-105-9-138-201-206	26.3-26.9-25-93.9-94.9-94.9-94.9	29.8-29.8-29.8-93.2-93.2-93.2-93.2

Table 2. Descriptive statistics of original and normal stream sediment geochemical data.

Pb	Mo	Cu	As	S	Au	Normal / Raw	Au	S	As	Cu	Mo	Pb
384	384	384	384	384	384	N	384	384	384	384	384	384
2.99	.76	3.87	3.1	5.95	.84	Mean	3.31	572.3	27.33	51.1	2.4	23.3
2.96	.74	3.85	3.1	5.85	.69	Median	2	350	22.55	47.4	2.1	19.4
2.7	.53	3.69	3	5.34	.69	Mode	2	210	20.6	40.2	1.7	16
.583	.44	.343	.57	.825	.78	Std. D	4.01	728.1	19.16	19.51	1.1	15.8
-1.2	.03	.413	.09	.509	.3	Skewness	4.52	4.317	3.092	1.573	1.3	3.35
11.3	.37	.432	1	.563	.81	Kurtosis	24.4	22.6	13.8	3.01	1.8	15.4

The statistical parameters were calculated(Table 2). Because of skewness and existence of abnormalities in elements such as Au, Cd, Pb, S, Cu, Mo, As, Hg, Bi attempts to normalization, which Figure.2 is illustrated an example of a histogram of the geochemical data for Au, Pb, Cu, S, Mo, As.

Multivariate statistical methods, provide simultaneously statistical analysis of many variables. Sometimes, in the explorational problems we are faced with N dimensional space, which makes it difficult to evaluate the relationship between them.

In such cases it is necessary, using multivariate statistical methods, reduce the number of dimensions in the study space, where, the results of this new dimension, with the number far less than previous state can explain much of the variability of the data. Thus, it was attemped to apply comparative study based on PCA and along with CA. In order to discriminate anomaly from background in the area.

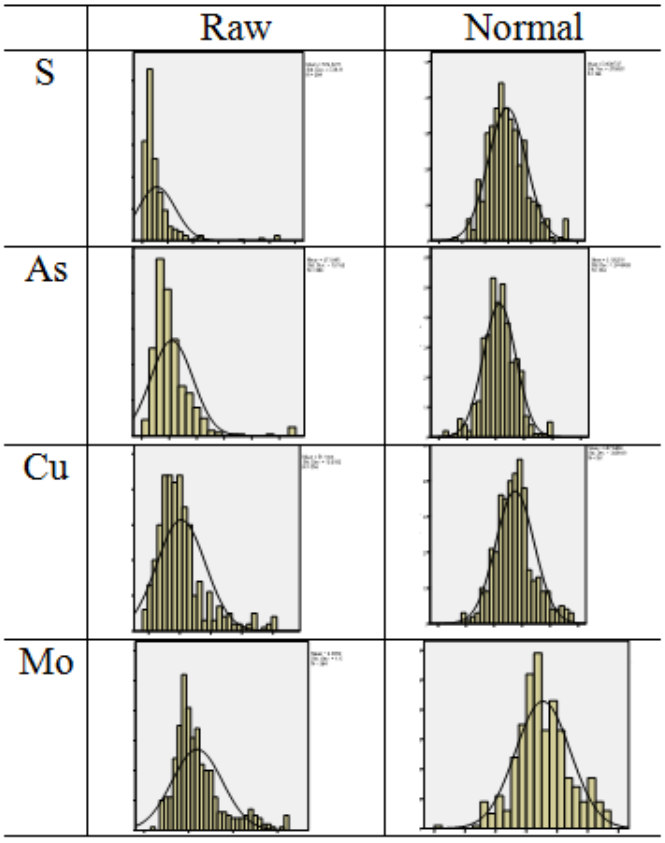

Figure 2. Histograms of As, Cu, Mo, S concentrations.

3.1 CA

Clustering is the classification of objects into different groups, or more precisely, the partitioning of a data set into subjects or clusters, so that the data in each subject share some common trait often proximity according to some defined distance measures. Data clustering is a common technique for statistical data analysis and used in many fields (MacQueen, 1967). The computational tasks of classifying the data set into different clusters include the k-clustering method, tree-clustering and two-way joining. With agglomerative algorithms on the basis of weighted pair-group average rule and Manhattan distances.

3.2 PCA

Principal Component Analysis method has has been widely used in geochemical applications to identify mineral sources and to apportion natural anthropic contribution. Application of this method to sediments (Tuncer et al., 1993; Fernandez et al., 1996), soils (Ratha and Sahu, 1993; Garcia et al., 1996), and waters (Cave and Reeder, 1995) have been carried out.

4 RESULTS

4.1 CA

Clustering states the treatment of relationship between the elements under the correlation maximum expression. The goal of this way is achievement to a criterion for the more appropriate classification of the variables or classification of the samples based on how more similarity within groups, the differences between the parties and offer paragenesis of elements (Hassani Pak, A.A. et al., 2002). With regard to functionality, resolution power in the simultaneous and paragenesis separation, attempt to the clustering of the area. the drawn dendrogram to the area elements, was significant and interpretable (Figure 3).

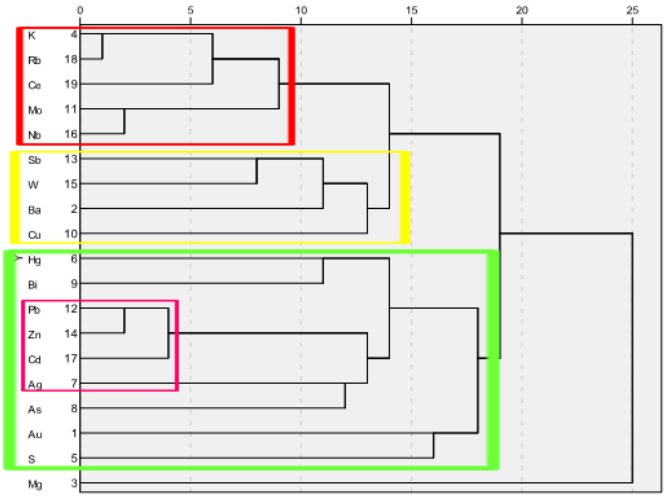

Figure 3. The horizontal cluster dendrogram of elements concentrations.

1) Mo-Rb-K-Nb-Ce
2) Bi-Cd-Zn-Pb
3) S-Hg-Ag-As-Bi-Zn-Au-Pb-Cd
4) Sb-W-Ba-Cu

Bi-Cd association with Zn-Pb elements is suggests of the detector nature of these elements for Pb-Zn sulphide deposits. Since the evidence shows that the deposits of Zn-Pb elements are volcanic, So these elements were can be used as detectors for these deposits. Due to the Simultaneous No.3, the association of these elements with gold

represents that these elements are detectors for Au, And this could be said that Au anomalies derived from Subvolcanic-hydrothermal processes in region.

4.2 PCA

This method is a technique for finding linear combinations of the original variables. The PCA method is indeed reduced the dimension of problem, which can, in fact, determine the separation of anomaly communities of context and epigenetic and syngenetic effects more precisely. With this method some directions are identified with the maximum of variability, then with define the new variables which are the linear combinations of the original variables, the number of dimensions (variables) declined and the role of each variable in the linear combination has been determined.

The main step in describing the PCA analysis results, is the describing the total variance. The proper interpretation of this table, has an important role in PCA. As one of the main criteria for the selection of components number, is the variability of the data. The new data must have a minimum number of dimension and could explain the maximum variability of all of data. The number of new dimensions, determined about 7 component (Table 3).

Table 3. Total variance explained (Seven factors selected).

Component	Initial Eigenvalues			Rotation Sums of Squared Loadings		
	Total	% of Variance	Cumulative %	Total	% of Variance	Cumulative %
1	4.44	23.37	23.37	2.93	**15.406**	**15.406**
2	2.78	14.6	37.98	1.92	**10.111**	**25.517**
3	1.88	9.88	47.86	1.89	**9.955**	**35.471**
4	1.37	7.2	55	1.86	**9.806**	**45.277**
5	1.23	6.5	61.5	1.83	**9.628**	**54.906**
6	1.13	5.97	67.5	1.75	**9.183**	**64.089**
7	1	5.3	72.8	1.66	**8.735**	**72.823**
8	.86	4.5	77.34			
9	.68	3.58	80.9			
10	.62	3.25	84.17			
11	.59	3.1	87.27			
12	.48	2.5	89.8			
13	.43	2.28	92.09			
14	.39	2.04	94.12			
15	.32	1.67	95.8			
16	.26	1.4	97.19			
17	.22	1.14	98.33			
18	.19	1.02	99.35			
19	.12	.65	100			

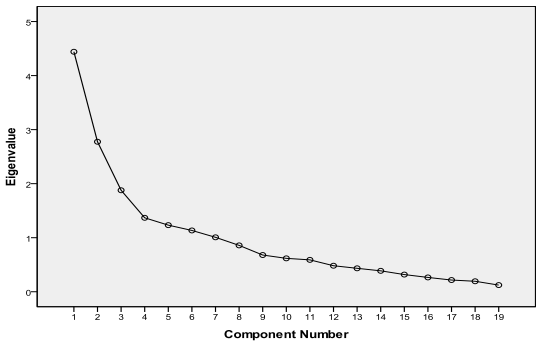

Figure 4. Scree plot of Duzduzan area

In this table the values of the statistical parameters include of spatial values, variance and the comulative variance of each component with the participation values of each component was calculated.

Based on table.3 about 7 component with 73% of the variability factor could be explain the significant changes in the region ,these results are shown graphically (Figure 4).

According to Table 3, the first component in the 19 component, explained the 15.406% of the total variability, after it, the second component has a greater role. Given the importance of the separation of paragenesis, using PCA method, obtained results are presented (Table 4). Table 4 shows existence simultaneous in the region based on the above technique.

Table 4. Component matrixes.

	Component						
	1	2	3	4	5	6	7
Au	.122	-.03	.167	.034	.098	-.02	**.783**
Ba	.482	.075	.229	.444	.408	-.14	-.28
Mg	-.23	**-.76**	-.03	.040	-.07	-.28	.066
K	**.854**	.153	.166	.137	-.03	.00	-.07
S	.241	.109	**-.52**	**.563**	-.11	.03	.225
Hg	.066	.112	-.03	.071	.071	**.85**	.011
Ag	.070	-.46	.103	**.566**	.222	.14	.153
As	-.18	.092	.170	**.780**	.100	.15	.056
Bi	.147	.172	-.2	.161	.199	.32	**.667**
Cu	.177	-.15	**.753**	.044	-.09	-.13	-.01
Mo	.381	**.607**	.047	.326	-.02	-.14	.319
Pb	.039	.146	-.07	.066	**.830**	.12	.056
Sb	-.06	.384	**.641**	.374	.114	.34	.064
Zn	.022	-.1	.091	.077	**.848**	.08	.207
W	.325	.277	**.631**	.090	.097	-.12	.137
Nb	**.540**	**.572**	.146	-.01	.134	-.35	.118
Cd	.004	-.18	-.13	.223	.249	**.61**	.402
Rb	**.775**	.134	.017	.000	-.03	.28	.220
Ce	**.773**	.104	.065	-.23	.114	-.03	.208

Whereas, an application of principal component analysis in the exploration, is drawing maps of the main components, In the studied region, these maps are communicating between the focus of its deposit with its controller component (lithology, structural, climate, geomorphology). According to the drawn plans, you can separate the elements of each main component (Table 5).
Thus The elements in each component, which have a high score gain, could be considered as an indicator element.

Table 5. Pathfinder elements.

Component	Indicator Element
PC1	K-Nb-Rb-Ce
PC2	Mg-Mo-Nb
PC3	S-Cu-Sb-W
PC4	S-Ag-As
PC5	Pb-Zn
PC6	Hg-Cd
PC7	Au-Bi

Corresponding map to the first component, shows the syngenetic mineralization (Figure 5). The second component, shows the REE (Rare Earth Elements) anomaly map (Figure 5). Fifth, sixth and seventh component shows the oxides and sulfides implied in the area and states the effects of the fluid, these three factors may be implicated on several phases of mineralization in the region which is acted in the various sequences and lead to assembly of these three components in the region (Figure 5). Second, third and fourth components derived from the properties of the rock building of the study area and has no significant relationship to the mineralizing fluids.

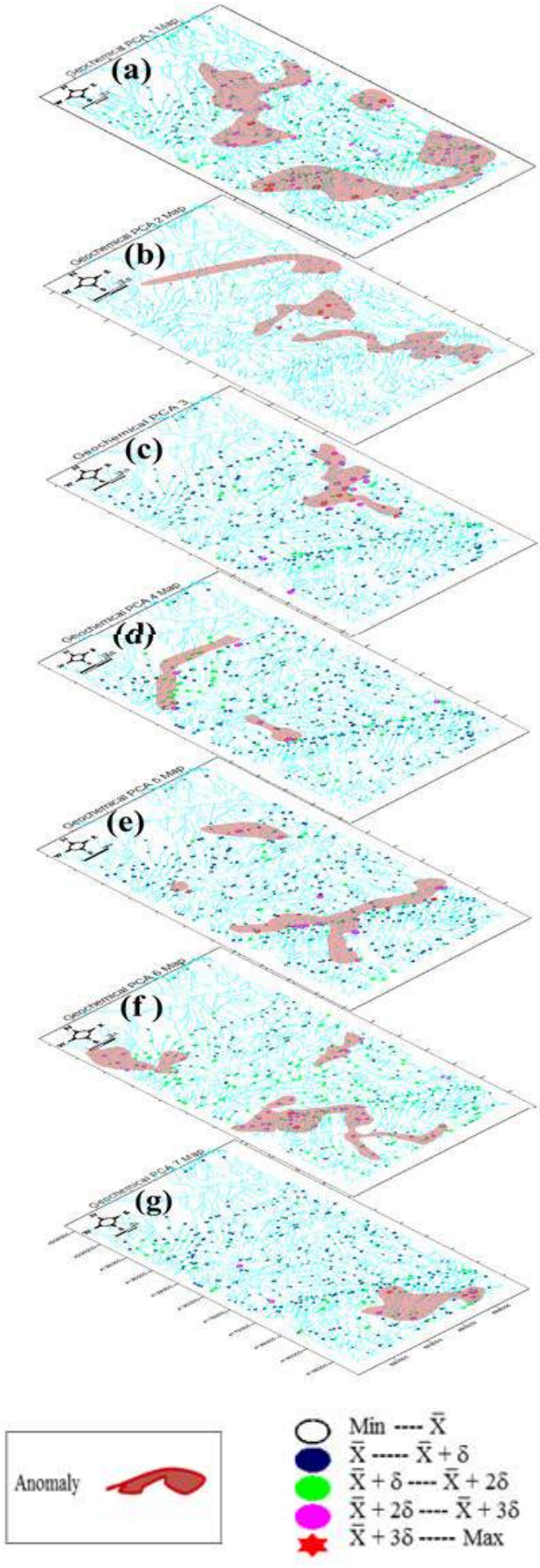

Figure 5. The results of the distributions of the PCA maps: (a): PC1 map, (b): PC2 map, (c): PC3 map, (d): PC4 map, (e): PC5 map, (f): PC6 map, (g): PC7 map.

The results show the pathfinder and potential elements of Ba, Cu, Sb, As, Au, Zn, Pb in the area. Sulphidation outcrops and the whole area was fully observed of S element distribution, correlation Mo, Cu up to more than 50 percent has been associated with causing mineral solutions, but the nature of these elements and porphyrite or other formats of these deposits including closer alteration study in this area is needed.

Association of Pb, Cu, Mo, Zn was more evident based on various studies. Study and review was conducted in the area of maximum variability of the PCA, and The results show the seven most important related component, in this study the 1, 2, 3, 4 components denote to the stone formation components (Syngenetic), and 5, 6, 7 component indicate concentration the significant anomalies associated with mineralization (Epigenetic). In principle, the more important aim of this study was to identify behavior patterns of Au, Cu, Zn, Pb elements in the Duzduzan region, and detect their pathfinders in the region. Small distance between Cu, Au was exist in the region. This area is more likely to involve several mineralization phases, because The deposition of Au, Cu probably not in the same phase.

Finally, with considering our need to very detailed record of the anomalies and separation of communities and achieving to the optimal geochemical network, multivariable methods are used, and the results indicate the severity of the anomaly intensity and revealed some anomalies which are masked in the region.

The comparison of these maps shows with the main component, shows that these two methods have an overlap with each other. The component maps can communicate between the deposit concentration with its controler factors, e.g. the lithology of building, climate, geomorphology, etc.

5 CONCLUSION

According to recent studies, the results of this study can be summarized as follows: to

be used as a key, in other parts of this region and continue of this study the detectors and concluded indicators.

In this paper, the PCA and CA model are used to identify geochemical anomalies associated with Cu and Au mineralization. The following conclusions are obtained:

(1) The multivariate statistical method PCA and CA modeling is

a useful tool to identify geochemical anomalies. The former is used to integrate multi-element concentration values, and the later is used to decompose mixed geochemical paragenesis in a complex geological setting

(2) The anomalies of Ba, Cu, Sb, As, Au, Zn, Pb occurring in the area should be further investigated in the next phase of mineral exploration.

ACKNOWLEDGEMENTS

The authors to place their thanks to Mr. Hosein Hematiyan and Geological Survey of Iran for their attentions in this respect. We would like to acknowledge our sincere thanks to reviewers for their constructive comments.

REFERENCES

Al Hakimi, A. Budi Sulistijo., 2012, "Integrated Exploration Method to Determine Cu Prospect in Seweden District, Blitar, East Java". Elsevier. 6: 64-69.

Bellehumeur, C., Marcotte, D, JeÂbrak, M., 1994. "Multi-element relationships and spatial structures of regional geochemical data from stream sediments, southwestern Quebec, Canada". J. Geochem. Explor. 51, 11-35.

Boruvka, L., et al., 2005, "Principal component analysis as a tool to indicate the origin of potentially toxic elements in soils", Geoderma, 128(3-4), P. 289-300.

Cave, M., Reeder, S., 1995. "Reconstruction of in-site compositions obtained by aqueous leaching of drill core: an evaluation using multivariate statistical deconvolation" , The Analyst 120, 1341-1351.

Collyer, P.L. and Merrian, D.F., 1973, "An application of cluster analysis in mineral exploration", Mathematical Geology, Vol. 5, No. 3, P. 213-224.

Facchinelli. A., et al, 2001, "Multivariate statistical and GIS-based approach to identify heavy metal source in soils". Elsevier. 114: P. 313-324

Fernandez, H.M., Conti, L.F.C., Patchineelam, S.R., 1994. An assessment of the pollution of heavy metals in the Jacarepagua Basin, Rio de janeiro, Brazil- a statistical approach. Environmental Technology 15(1), P: 87-94.

Fresman, A.E., 1939. "Geochemical and mineralgical methods of prospecting for useful minerals"., In: U.S. Geol. surv. Circ. P. 127-37.

Garcia, R., Maiz, I., Millan, E., 1996. Heavy metal contamination analysis of roadsoils and grasses from Gipuzkoa (Spain). Environmental Technology 17 (7), p: 763-770.

Govett, G.J.S., Goodfellow, W.D., Chapman, R.P. and Chork, C.Y., 1975. "Exploration geochemistry- distribution of elements and recognition of anomalies". Mathematical geology., P. 415-446.

Groves, D.I., et al., 1998, "Orogenic gold deposits: a proposed classification in the context of their crustal distribution and relationship to other gold deposit types". Ore geology reviews, Vol.13(1), P.7-27.

Grunsky E.C.; Smee, B.W., 2003, "Enhancements in the Interpretation of Geochemical Data using Multivariate Methods and Digital Topography", Explore - Association of Exploration Geochemists Newsletter.

Hassani Pak, A.A. et al., 2002., "Exploration Data Analysis", Tehran University Press 2536., ISBN: 964-03-4459-1., P: 1000.

Howarth, R.J., Sinding-Larson, R., 1983. "Statistic and Data Analysis in Geochemical prospecting". Handbook of exploration Geochemistry, vol. 2, Elsevier, Amesterdam, P: 207-289.

Javid, Farhad., 2014, "Geostatistical Modeling of Geochemical Anomalies in Duzduzan Area, E.Azerbaijan". M.Sc thesis, Ahar Azad Islamic Azad University., P: 250.

Ji Hongjin, Zhu Yongzheng, Wu Xisheng. 1995, " Correspondence cluster analysis and its application in exploration Geochemistry", Journal of Geochemical Exploration, Vol. 55, P. 137-144.

Jime Ânez-Espinosa,R.,Sousa, A.J., Chica-Olmo, M., 1993. "Identication of geochemical anomalies using principal component analysis and factorial kriging analysis". J.Geochem. Explor. 46, 245-256.

Julian K. Orford. 1976, "Implementation of criteria for partitioning a dendrogram", Mathematical Geology, Vol. 8, No. 1 P. 75-84.

Jun deng., et al., 2010, "Delineation and explanation of geochemical anomalies using models in the

Heqing area, Yunnan Province, China", Elsevier. 105: 95-105

Loska, K. and Wiechuła, D. 2003. "Application of principal component analysis for the estimation of source of heavy metal contamination in surface sediments from the Rybnik Reservoir", Journal of Chemosphere., 51: 723–733

Loughlin, W.P.G, 1991. "Principal Component Analysis Alteration Mapping". Photogram. Eng. Remote Sensing.

MacQueen, J. B., 1967. "Some Methods for Classification and Analysis of Multivariate Observations" , Procceding of 5-th Berkeley Symposium on Mathematical Statistics and Probability. University of California Press, Berkeley. P: 281-297.

Pasadakis, N. Obermajer, M.and Osadetz,K.G, 2004. "Definition and characterization of petroleum compositional families in Williston Basin, North America using principal component analysis". Journal of Organic Geochemistry., No. 35. P. 453–468.

Prinzhofer, A., Mello, M.R., Da Sila Freitas, L.C.& Takaki, T., 2000. "A new geochemical characterization of natural gas and its use in oil and gas evaluation". In Mello M.R. and Katz, B.J.(Eds.), Petroleum systems and south Atlantic Margins.American Association of Petroleum Geologists Bulletin, Memoir 70:107-119.

Ratha, D.S., Sahu, B.K., 1993. "Source and distribution of metals in urban soils of Bombay, India, using multivariate statistical techniques", Enviromental Geology 22 (3), p: 276-285.

Sabeti, H., Javaherian, A. and Araabi, N.D, 2007, "Principal component analysis applied to seismic horizon interpretations" .International congress of Petroleum Geostatistics, Cascais, Portugal, 10-14 September 2007.

Sandjivy, L., 1984. "The factorial kriging analysis of regiona- lized data. Its application to geochemical prospecting". In:Verly, G., David, M., Journel, A.G., Marechal, A.M. (Eds.), Geostatistics for natural resources characterization, part 1: 559±571. Reidel Publishing Company.

Sousa, A.J., 1989. "Geostatistical data analysis dan application to ore body typology". In: Armstrong, M. (Ed.), Vol 2, pp.851-860. Kluwer Academic Publishers.

Sun, X., et al., 2009, "Kohonen neural network and factor analysis based approach to geochemical data pattern recognition", Journal of Geochemical Exploration, Vol. 103, P. 6–16.

Tuncer, G.T., Tuncel, S.G., Tuncel, G., Balkas, T.I., 1993. "Metal pollution in the Golden Horn, Turkey-contribution of natural and anthropogenic components since 1913. Water Science and Technology 28 (8-9), p: 59-64.

Xiang Sun., et al., 2010, "Application of local singularity model to delineate geochemical anomalies in Xiongershan gold and molybdenum ore district, Western Henan Province, China". Elsevier., 107: 21-29.

Providing Zinc and Lead Anomaly Maps Using U Statistic, Khooni District (Esfahan Province)

N. Mahvash Mohammadi
PhD student, Department of Mining & Metallurgical Engineering, Amirkabir University of Technology,Tehran, Iran.

A.Hezarkhani
Professor, Department of Mining & Metallurgical Engineering, Amirkabir University of Technology, Tehran, Iran.

ABSTRACT Khooni area is located in 60 kilometers of North East of Anarak and 270 kilometers of Esfahan, and belongs to Central Iran geological zone. According to existence of Zinc and Lead mineralization evidences in this area, identification of favorable area and preparation of Pb and Zn mineralization potential maps is necessary, in order to separate the anomaly from geochemical background in the data which are obtained from surface sampling, initially, corrections on the data includes the estimation and replacement of censored data and adjustment of row sets were done. Then, some statistical parameters were calculated and histograms were plotted and the data were normalized. Therefore, structural method for separation of anomaly from background on the results was used. U statistic method as a highly effective method for separation the anomaly from background of the data was used. Finally, with separated anomaly values from background, the anomaly map of the promising area for elements such as lead and zinc was plotted. By studying geochemical maps, we saw that there is Lead and Zinc anomaly area in southwest and northwest of khooni mountain.

Keywords: Zinc, lead, anomaly map, U statistic

1 INTRODUCTION

Data frequency in the exploratory samples are often Lognormal due to high skewness (Graybill, et al 1965). large amounts in the samples are constitute of anomalies distribution function. The values are inseparable from other data (background) to appearance promising areas for economic mineralization. Different statistical methods are presented to distinguish anomaly areas from background. These methods are changing from simple kinds (based on distribution statistical parameters) to complicated ones (based on data spatial distribution). Second kind includes methods which consider sampling point coordination and their spatial relation in estimation of anomaly areas. The anomaly separation methods of background can be divided into two groups which includes structural and non-structural methods (Hassani pak et al 2005).

One purpose of using statistical methods in exploration geochemistry is to assist exploration geologists in separating anomalies from background. This always involves two types of negatively associated errors of misclassification: type I errors occur when samples with background levels are rejected as background; and type II errors occur when samples with anomalous values are accepted as background. U spatial statistics method is proposed to minimize errors of total misclassification using a moving average technique with variable window radius. The idea of this method was applied for the first time in 1331 by Cheng et al. In fact, this method as a strong method is proposed in the separation anomaly of background (Cheng 1999) (Sinclair 1991). The only factor controller in this method is

the number of samples for type I and II errors (errors of separating anomalies from background). Increasing the number of samples obtained better results.

1.1 Geological Setting

Khooni area is located at 60 kilometers of North East of Anarak and 270 kilometers of Esfahan, and belongs to Central Iran geological zone. According to some instances expressing Lead and Zinc minerals forming in this area, make reconnaissance of favorable area and forming potential maps of these minerals preparation as an essential fact.

Stratigraphy of the study area is from Pre-Cambrian to Quaternary. Outcrops in western area, mainly consisting of units of Cambrian metamorphic and in the eastern part are volcanic and pyroclastic of Eocene units with dominant composition of andesite and trakey andesite which have been cut by monzonite dikes. There are outcrops of Cretaceous limestones at the northwest end of the area that unconformity have been laid on the older units. Low altitude and lowland areas is covered by old alluvial terraces, sediments of plains and young and river formed alluvial. In general, the Lithology of the study area is formed from lithological units, including units of metamorphic schists to Quaternary young sediments (Fig. 1), (Heydarian dehkordi et al 2014)

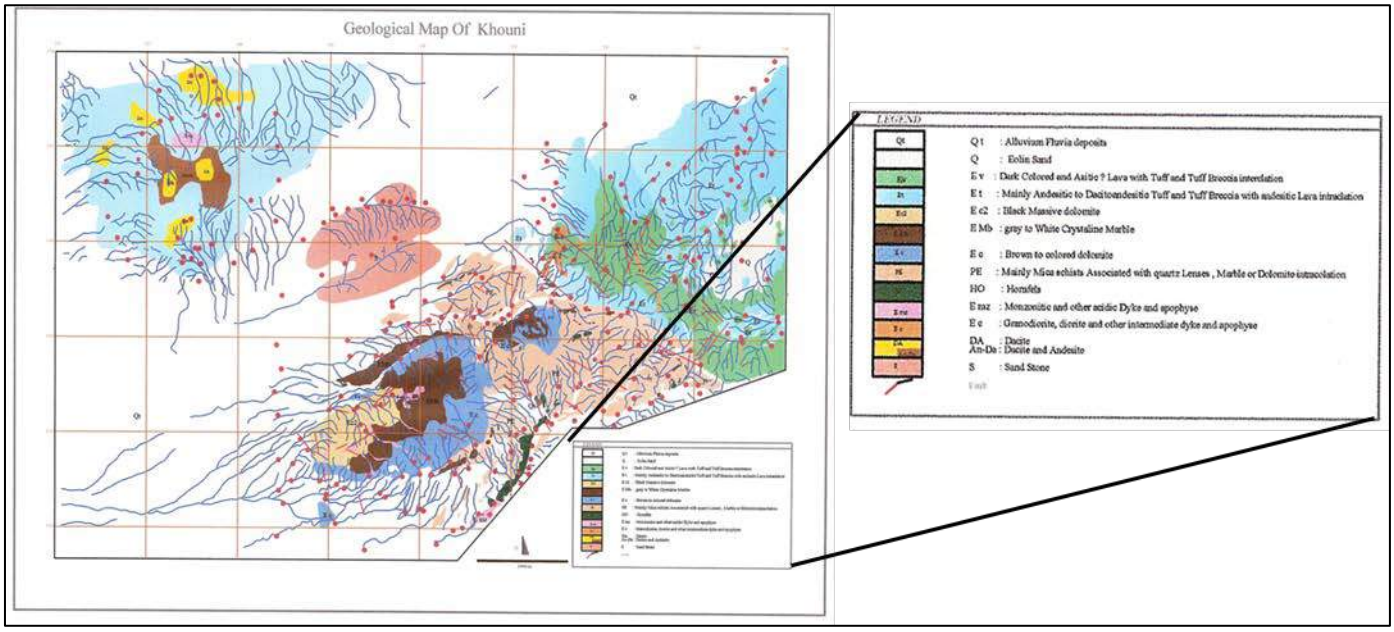

Figure 1. Geological map of khooni district(Pourjabar 2005)

2 SEPARATION ANOMALY FROM THE BACKGROUND

Investigating data are from geochemical analysis of stream sediments for 22 elements in Khooni area which are processed for separating anomaly from background., initially, corrections on the data includes the estimation and replacement of censored data and adjustment of row sets were done. Then, some statistical parameters were calculated and histograms were plotted and the data were normalized for Pb and Zn elements.

Initial investigation of the raw data showed that all elements followed an un-normal distribution with positive skewness (Fig. 2), and therefore the logarithmic conversion was used for converting all data to a normal distribution. Figure 3 showing histograms of normal distribution of lead and zinc elements.

2.1 Spatial U Statistics

Suppose that two populations (A and B) have normal distributions with means of μ_A

and μ_B, and variances σ_A^2 and σ_B^2 respectively. Independent random samples $(x_1,\ldots, x_n)$ are collected, and the aim is to distinguish between the populations A and B. A new random variable

$$U = \frac{1}{n}\sum x_i \quad (1)$$

can be constructed (U-statistic) with the following properties: $\sigma^2(U)\frac{1}{n}\sigma_A^2, E(U) = \mu_A$ if all samples are from population A, and $\sigma^2(U)\frac{1}{n}\sigma_B^2, E(U) = \mu_B$ if all samples are from B. Thus the means of U for samples from A or B are the same as means of X for A or B. but the variances of U for A or B are different from the variances of X for A or B by the factor (l/n). This factor depends only on sample size n. More generally, instead of an arithmetic average, a weighted average U is used with:

$$U = \sum_{i=1}^{n} W_i x_i \quad (2)$$

Where $\sum W_i = 1,\ 0 \le W_i \le 1$ Then $\sigma^2(U) = \sum W_i^2\sigma_A^2, E(U) = \mu_A$ if all samples are collected from population A, and $\sigma^2(U) = \sum W_i^2\sigma_B^2, E(U) = \mu_B$ if all samples come from B. In general, $\frac{1}{n} \le \sum W_i^2 \le 1$, $\sum W_i^2 = 1$ if and only if $i = k$ with W_k=1 (and W_k=0, when $i \ne k$) which implies that U= x_k; $\sum w^2 = 1/n$ if and only if W_i = 1/n, i=1,...,n, for the arithmetic average. Different types of weighting in Eq. (2) may result in a different variance $\sigma^2(U)$ depending on the factor $\sum W_i^2$. but the smallest variance is achieved for the arithmetic average (Cheng 1999).

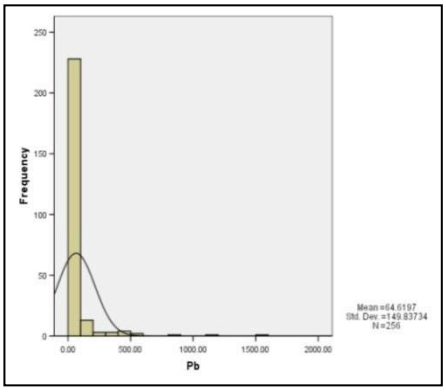

Histogram of Pb- Raw Data

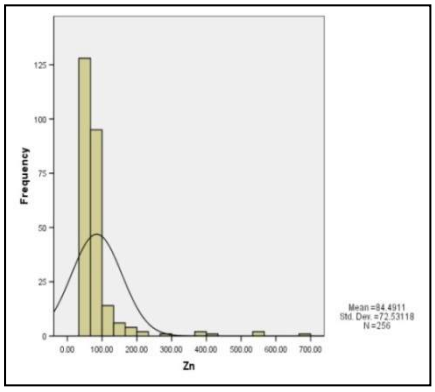

Histogram of Zn- Raw Data

Figure 2. Histograms of raw data

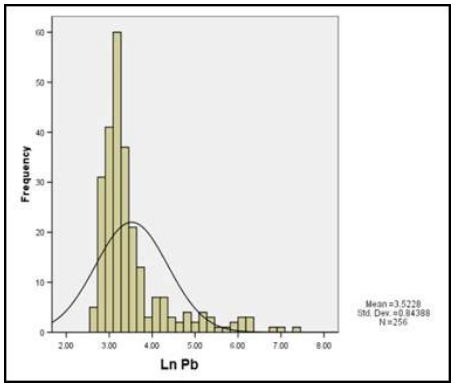

Histogram of Pb- Normal Data

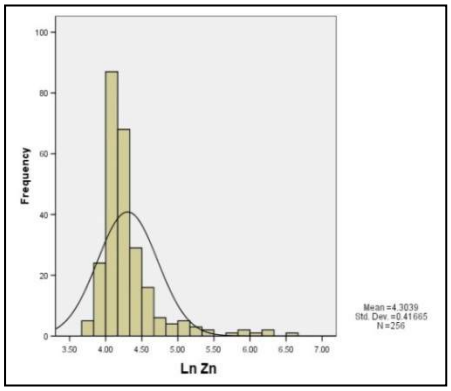

Histogram of Zn Normal Data

Figure 3. Histograms of normal data..

In the preceding discussion, all values were assumed to originate from a single population (A or B). In general, we do not know from which population the values come. However, by inspecting the geometrical characteristics of the

geochemical anomalies (the element concentrations and spatial arrangements of samples), we may notice that anomalous samples often occur in groups which correspond to geographically distinct areas. Values of samples and the geometry of anomalous areas have been considered in anomaly separation by previous authors for example by Sinclair (1991). An experimental study of average values of samples was presented by Govett et al (1975). These authors reported that for systematic sampling (grid sampling), averaging values of samples is useful for separating populations. The idea can be generalized as follows (Cheng 1999).

Suppose that a given area consists of two subareas shown schematically as A and B (Fig. 4) representing anomaly and background respectively. The anomalous area A could be circular, elliptical or belt-like in shape.

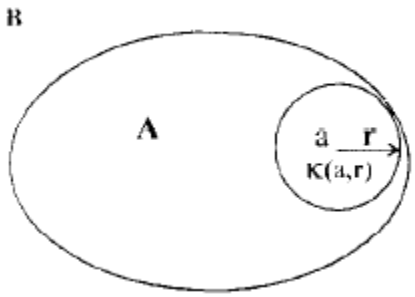

Figure 4. Circular moving window with variable radius. A is anomalous area. and B is background area. k(a,r) is circular vicinity around sample location a with radius r. Samples in k(a,r) are weighted and averaged to generate U values (Cheng 1999).

A new statistic, U is constructed that considers a spatial zone of influence. Let α_i, indicate the location of the ith sample in the study area and X_i, the element content or value of this sample; choose any sample, say α_i, from the set of samples and create a circular neighbourhood around it denoted as $k(\alpha_i,r)$ with the radius r ($0 \le r \le r_{max}$). The value of r can be assigned in such a way that $k(\alpha_i,r) \subset A$ if $\alpha_i \in A$ $k(\alpha_i,r) \subset B$ if $\alpha_i \in B$. A function for $k(\alpha_i,r)$ can be defined as follows: (Cheng 1999).

$$\mu_{k(\alpha_i,r)}(\alpha_j) = \frac{r-d(\alpha_i,\alpha_j)}{r} \quad (3)$$

Where $d(\alpha_i, \alpha_j) \le r$ represents distance from sample location α_j to α_i.This function has the properties: $0 \le \mu_{k(\alpha_i,r)}(\alpha_j) \le 1$, $\mu_{k(\alpha_i,r)}(\alpha_j) = 1$ if $\alpha_i = \alpha_j$, and $\mu_{k(\alpha_i,r)}(\alpha_j) = 0$ if $\alpha_j \neq k(\alpha_i,r)$,where $\notin$ indicates "does not belong to". A new value $U_i(r)$ for sample α_i can then be defined as a linear combination of $x_{i:}$ (Cheng 1999).

$$\mu_{k(\alpha_i,r)}(\alpha_j) = \frac{r-d(\alpha_i,\alpha_j)}{r} \quad (4)$$

With

$$\bar{X}_i(r) = \sum_{j=1}^{n} w_j(r) X_j \quad (5)$$

$$S_i(r) = \sqrt{\sum_{j=1}^{n} w_j^2(r)} \quad (6)$$

$$w_j(r) = \frac{\mu_{k(\alpha_i,r)}(\alpha_j)}{\sum_{j=1}^{n} \mu_{k(\alpha_i,r)}(\alpha_j)} \quad (7)$$

where μ and σ are the mean and standard deviation of X_i in the whole area. A new statistic $U_i^* = U_i(r_0)$ can then be defined where r_0 is the value yielding: (Cheng 1999).

$$|U_i(r_0)| = max_{\ 0 \le r \le r_{max}} |U_i(r)| \quad (8)$$

The value of U_i^* for sample α_i, has the following normal distribution: If $\alpha_i \in A$: (Cheng 1999).

$$U_i \sim N\left(\frac{\mu_A - \mu}{S_i(r_0)}, \frac{\sigma_A}{\sigma}\right) \quad (9)$$

and, if $\alpha_i \in B$:

$$U_i \sim N\left(\frac{\mu_B - \mu}{S_i(r_0)}, \frac{\sigma_B}{\sigma}\right) \quad (10)$$

Where $\mu_B \le \mu \le \mu_A$, so that $U_i^*(r_0)$ has a mean equal to $(\mu_A - \mu)/(S_i(r_0)) > (\mu_A - \mu)/(\sigma) > 0$ if α_i belongs to A and $U_i^*(r_0)$ has a mean equal to $(\mu_B - \mu)/(S_i(r_0)) < (\mu_B - \mu)/(\sigma) < 0$ if α_i belongs to *B*. If α_i is located on the boundary between A and B then r_0 should be close to zero and therefore $U_i^*(r_0)$ is reduced to $(X_i - \mu)/(\sigma)$ which is

equal to the original standardized value of X_i. The value $U^*(r_0)$ can be easily classified. The value of $U_i^*(r_0)$depends on the total number of samples within $k(\alpha_i, r)$. It is also associated with the location of α_i. Thus if α_i is located near the boundary between A and B, there can only be relatively few samples in $k(\alpha_i, r)$ and the value of $U_i^*(r_0)$ will be close to the original standardized value of X_i. of course, the value of $U_i^*(r_0)$ also depends on the density of samples collected in the area. The sampling density may influence the ability of the method to distinguish between geochemical populations (Cheng 1999).

3 DISCUSSION

This section, discussed the separation of Pb and Zn anomalies with regard to location of the samples, Radius is 18 meter. After determining the value of U for each sampling point, were Plotted the graph of the frequency distribution of U values for Zn and Pb elements with circular neighborhood with shape circular neighborhood of study area that was shown in Figure 5.

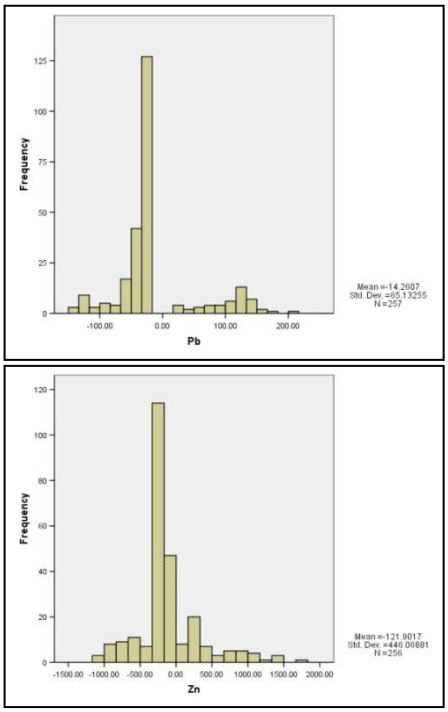

Figure 5. The frequency distribution graph of U values for Pb and Zn elements with circular shape neighborhood.

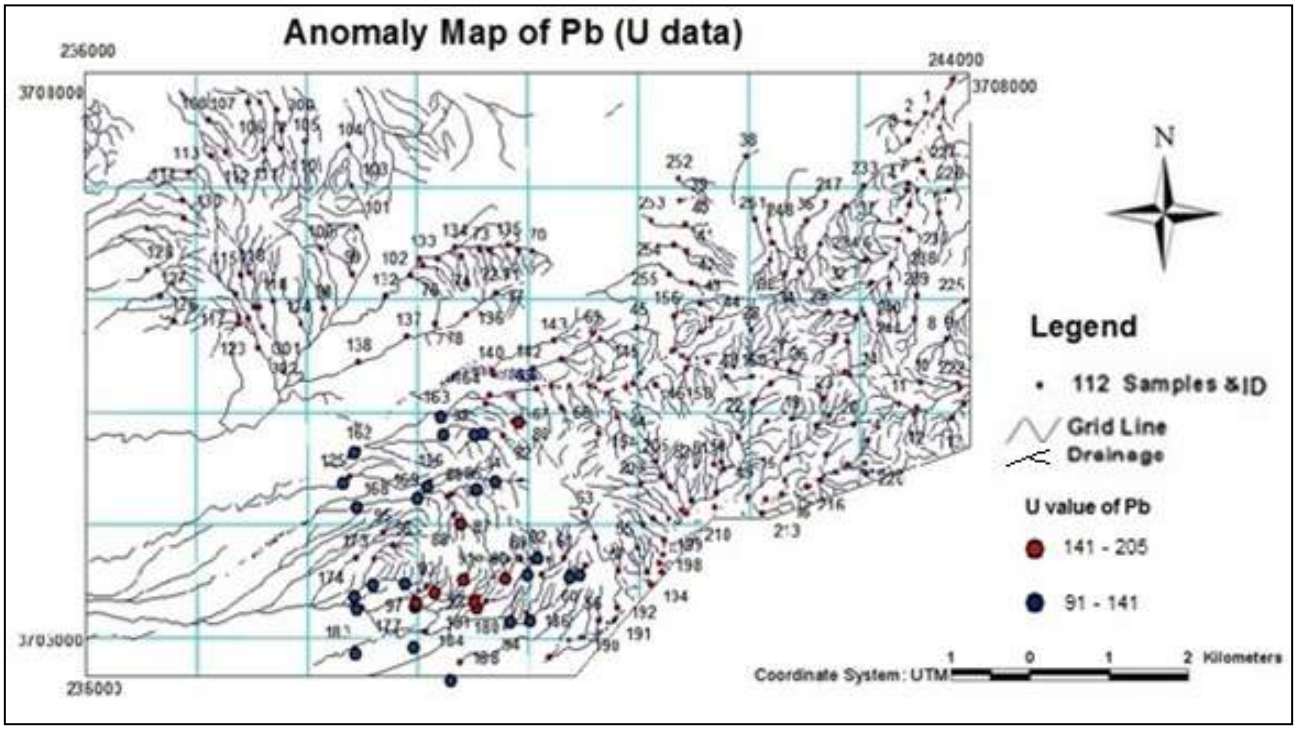

Figure 6. Lead anomaly map using $\overline{U} + 2S$ and $\overline{U} + 3S$ criteria to show probable and absolute anomalies samples

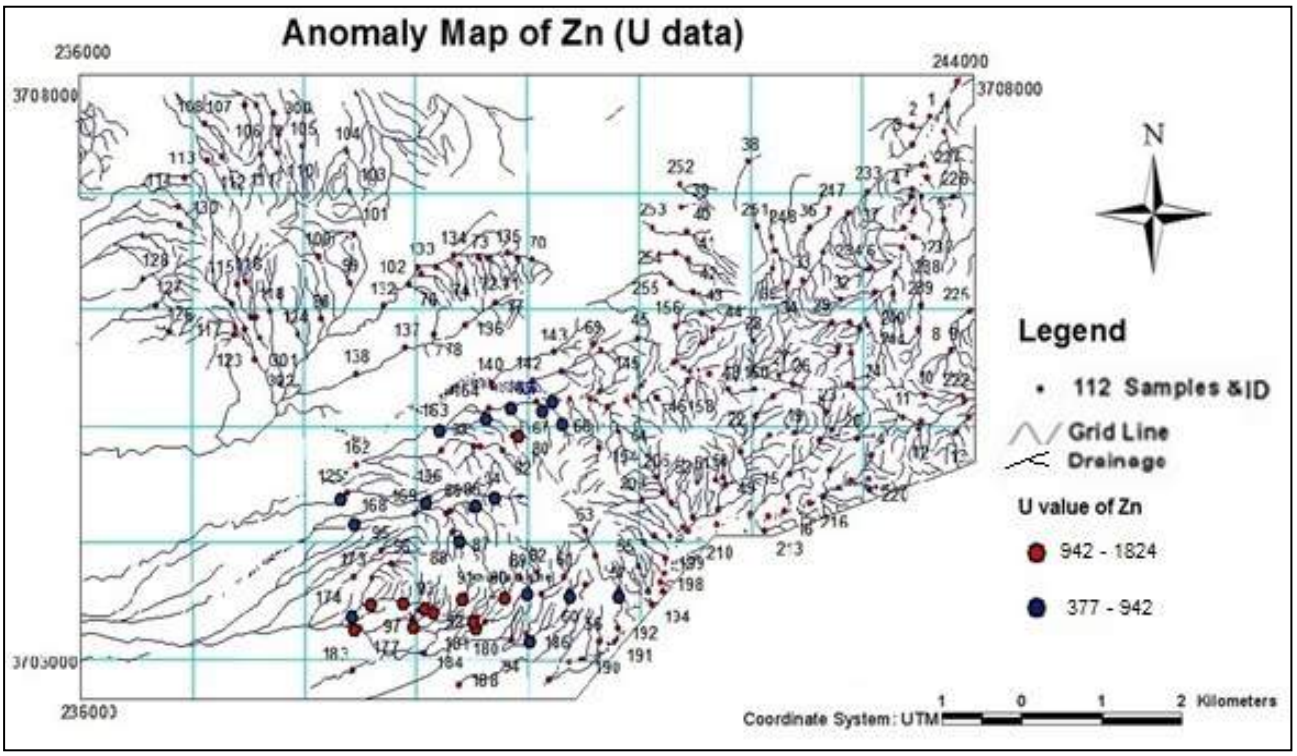

Figure 7. Zinc anomaly map using $\bar{U} + 2S$ and $\bar{U} + 3S$ criteria to show probable and absolute anomalies samples

As shown in figure 5, data have been divided to the anomalous (positive) and background (negative) values. In order to separating probable and absolute anomaly using U values, $\bar{U}+2S$ and $\bar{U}+3S$ thresholds are used respectively. The calculated results for Pb and Zn were shown on Geochemical map (Fig. 6,7). According to the Figure 6 and 7, the blue and red points represents the samples of Probable and absolute anomalies respectively. Results show that specified samples as anomaly samples include high regularity and less dispersion, also in comparison of $\bar{U}+2S$ and$\bar{U}+3S$, $\bar{U}+2S$ criterion provides larger halos and $\bar{U}+3S$ criterion refer to absolute anomalies. Considering geochemical maps of the study area, northwest and southwest districts of the Khooni Mountain are introduced as Pb and Zn anomaly areas.

4 CONCLUSION

Separation anomaly of background is one of the most important steps in geochemical studies**.** U spatial statistic method is a weighted mean, which consider sampling point coordination and their spatial relation in estimation of anomaly areas. The aim of this study is to separate anomaly area of Pb and Zn elements and providing anomaly map for these elements, in khooni area that is located in Isfahan province. The first is done correction data of 256 samples from the area and finally anomaly maps of elements was plotted based on U spatial statistic to study geochemical maps, were identified southwest and northwest of khooni mountain as Lead and Zinc
anomaly area. Also specified samples as anomaly samples, by using U-statistics, consists of high regularity and less dispersion.

REFERENCES

Cheng, Q. 1999, Spatial and scaling modelling for geochemical anomaly separation, *Journal of Geochemical Exploration*, V. 65, PP.175-194.

Govett. G. J. S., 1983, *Statistical Data Analysis in Geochemical Prospecting*, Handbook of Exploration Geochemistry, Amsterdam, Elsevior Vol. 2.

Graybill. F. A., Krumbein. W. C., 1965, *An Introduction to Statistical Models in Geology*, McGraw – Hill, New York, P. 473.

Hassanipak, A. A., Sharafeddin, M., 2005, *Exploration Data Analysis*, Tehran university press, Tehran, p. 977.

Heydarian, N., Rassa, A., 2012, Characteristics and genesis of gold mineralization in Eocene volcanic units of khooni fountain, Anarak, the nature of mineralizing fluids and comparison with other types of gold deposits, *Journal of Geology of Iran*, pp. 85-73.

Pourjabar, A., 2005, *Geochemical investigations on the polymetalic vein in Khouni (Esfahan Province)*, MSc Thesis, Amirkabir University of Technology, tehran, p.217.

Sinclair, A.J., 1991. A fundamental approach to threshold estimation in exploration geochemistry, Probability plots revisited. *Journal of Geochemical Exploration*, V. 41, pp.1-22.

Separation of Anomaly from Background Using Concentration-Perimeter (C-P) Method in Nakhilab Region, Northwestern Of Zahedan

N. Mazraee
Department of Geosciences, University of Sistan and Baluchestan, Zahedan, Iran

A. A. Daya
Department of Mining Engineering, University of Sistan and Baluchestan, Zahedan, Iran

M. Boomeri
Department of Geosciences, University of Sistan and Baluchestan, Zahedan, Iran

ABSTRACT Separation of anomaly from background is a fundamental task in geochemical exploration. There are many methods for this purpose. These methods are varies from simple statistical methods to complex fractal methods. In the current study concentration-perimeter (C-P) method was used for separation of anomaly from background. The concentration-perimeter method applied to stream sediments data (N=213) in Nakhilab region, northwestern of Zahedan. As, Ag, Cu, Au elemental concentrations were used in the current study for finding thresholds values. Based on these threshold values different population defined.

Keywords: Concentration-perimeter (C-P) approach, anomaly separation, Nakhilab region

1 INTRODUCTION

The determination of geochemical anomalies from backgrounds is fundamentally crucial for interpretation of geological evolution and the ore-forming processes. Mineral exploration based on stream sediment data has been widely used for different types of ore deposits; in this regard, separation of geochemical anomaly classes based on stream sediment data is an important stage to delineate potential areas for mineral exploration (Deng et al. 2010; Zuo 2011). Determination of elemental thresholds is important for mapping of ore deposit prospecting and reconnaissance (Carranza 2008). There have been some classical statistics methods for delineation of anomalies from background such as histogram analysis, box plot, summation of mean, and standard deviation coefficients and median (Tukey1997). The statistical methods consider only the frequency distribution of the elemental concentration paying no attention to spatial variability; the information about the spatial correlation is not always available (Daya 2014a). In addition, these methods are only applicable to cases where geochemical data follow a normal distribution (Afzal et al. 2012; Daya 2014 a,b; Bai et al. 2010; Carranza 2008; Davis 2002). Fractal and multifractal models, established by Mandelbrot (1983), have been widely applied in different branches of geosciences since 1980s, e.g., Agterberg et al. (1993), Cheng et al. (1994), Turcotte (1986)), and Meng and Zhao (1991), Daya (2014a ,b).. Bolviken et al. (1992) and Cheng et al. (1994) proved that geochemical patterns of various elements have fractal dimensions. Several fractal models have been proposed in geochemical data analysis including concentration–area (C– A) by Cheng et al. (1994), number–size (N–S) by Mandelbrot (1983), and concentration-perimeter (C-P) by Daya (2014b). The concentration-perimeter (C-P) fractal model is related to the C-A and perimeter-area (P-A) fractal models (Daya, 2014b).

The aim of this study was to use the application of C–P fractal model to distinguish geochemical anomalies in terms

of Cu, Au, As and Ag for further mineral exploration in Nakhilab sheet, southeastern of Iran. The elemental anomalies are correlated with geological particulars of the sheet.

2 CONCENTRATION-PERIMETER (C–P) MODEL

Concentration-perimeter (C-P) model is very similar to C-A fractal method and can be deduced from C-A and P-A (Cheng, 1995) fractal models. C–P fractal model has the general form of:

$$P(\rho \leq v) \propto \rho^{-a1} \; ; \; P(\rho \geq v) \propto \rho^{-a2} \quad (1)$$

where P(ρ) denotes the perimeter with the concentration values greater than the contour value ρ, υ represents the threshold, $-a1$ and $-a2$ are fractal dimensions, and P(ρ) is the perimeter enclosed by the contour value ρ on a geochemical contour map resulting from the interpolation of the original data by weighted moving average method (Daya, 2014b).

3 GEOLOGICAL SETTING OF THE NAKHILAB REGION

The study area is located in northwestern of Zahedan city, SE of Iran. The study area is located in boundary of Loot Block and eastern flitch zone In Iran. It is probably a part of Iran's eastern flitch zone. Loot Block in contact with Iran's eastern flitch zone occurred in a very metamorphosed, faulted, sheared, and brecciated zone. From the upper cretaceous to quaternary the study area experienced different mountainous phases including Laramide and Alpine. These mountainous phases have an effective impact in developing the geological setting of the study area. Another important feature of the study area is that it is near the active Nehbandan fault system. Loot Block is more dynamic in its eastern part where the study area is located. The study area is highly brecciated and has faults with general trend of NS and NE-SW. The folding systems in the study area are normal anticline and normal syncline. Their trend is NW-SE to NS.

In the study area lithological units comes from upper cretaceous to quaternary ages. The study area occurred in a tectonic regime that Ophiolites complex was present. The lithological units according to 1:250,000 geological map of Nakhilab sheet divide into three parts which are metamorphic, sedimentary and igneous rocks (Fig 1). Metamorphic unit itself divides into three parts. The first consists of serpentine and harzburgite. Their trend is NS and generally occurred in a folded, fractured, and transformed units. The second group consists of marble, phyllite, serisite, and schist. Theses metamorphic rocks are widespread and its strike in the study area is NS. The last (third) group of metamorphic rocks consists of chlorite, epidote, schist, and mica schist. Their strike in the region is NS. This unit is affected by tectonic activity and as a result is highly fractured. Sedimentary rocks are very widespread in the study area. The most abundant of them are shale, sandstone, limestone, marl, and conglomerate (Fig 1). There are many igneous rocks in the study area. The most important of them comes from Oligocene. It consists of granite, granodiorite, and monzonite. Alteration phenomena are obvious in the igneous rocks and these rocks are much altered (Fig 1).

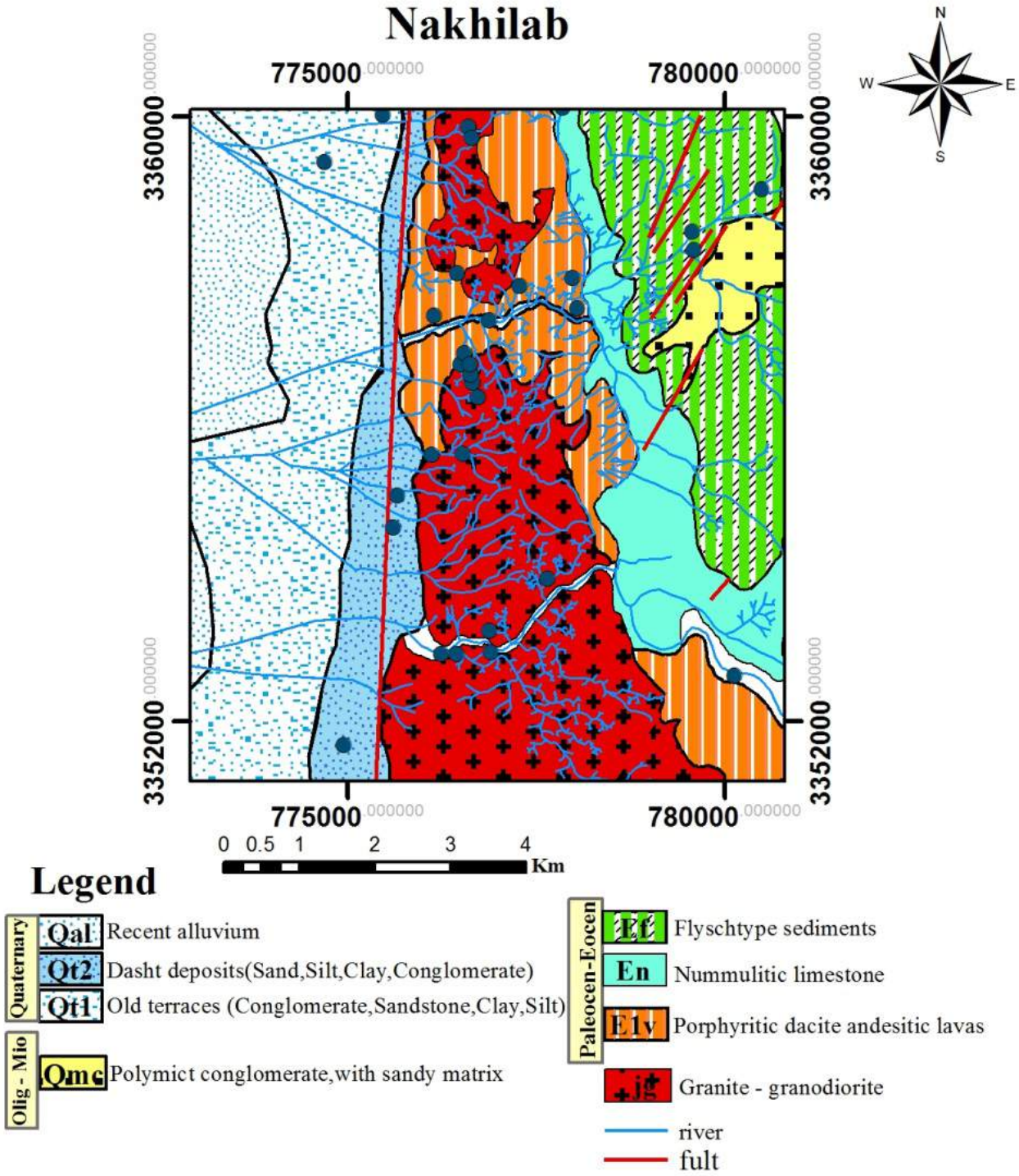

Figure 1. Geological map of Nakhilab region

4 GEOCHEMICAL DATA

Four elements (As, Au, Cu, and Ag) from 213 stream sediment samples were used to identify geochemical anomalies. Stream sediment samples of the −80 mesh (0.18mm) fraction were collected from the center of the streams. Concentrations of the elements were determined by X-Ray fluorescence spectrometry (XRF) and atomic absorption spectrometry (AAS). International standard samples (JSD1, JSD2) and replicates were analyzed after every 10 samples for checking accuracy and precision. Mean deviations between the measured concentrations and reference values were less than 10%.

Statistical analysis was carried out by SPSS 16 software. Statistical results revealed that mean values of Cu, As, Ag and Au mean values are 2.8812, 1.1838, 0.1482 ppm and 0.0012 ppb, respectively. Their distributions are as shown in Fig. 2. Table 1 lists the statistical parameters of As, Au, Cu, and Ag.

Table 1. Statistical parameters of raw data based on stream sediments geochemical samples analysis

Parameters	Au (ppb)	As (ppm)	Cu (ppm)	Ag (ppm)
Mean	0.0012	1.1838	2.8812	0.1482
Median	0.0010	1.1000	2.7600	0.0950
Variance	0.000001	97.788	89.438	0.558
Max	0.017	1.32	1.431	11.00
Min	0.0010	3	2.080	0.0800
Standard Deviation	0.0016	9.8634	9.547	0.7471

Nakhilab region was modeled using 12450 cells. The area was gridded by 250×250 m cells, which were determined based on the geometrical properties of the studied area and sampling spacing (David, 1977). Arsenic, Au, Cu, and Ag distribution models were obtained via Inverse Distance Squared (IDS) method using Rockworks software. This procedure is suggested because it eliminates the undesired smoothing effects caused by the usage of Kriging method. Since the IDS method clarifies the ore grade boundaries and ore concentration values, it is more desirable to use IDS method instead of Kriging which inherently has rather high amounts of truncation errors for the upper and lower boundaries of ore grades.

The proposed gridding pattern is put to use because the fundamentals of C–P fractal method is based on the existence of partition function, and the sampled data cannot be utilized effectively; also, since one cannot sample the entire study area, and for evaluation and estimation of any parameter, i.e., ore grade, gridding of the area is inevitably a desired mandate. By this method the problem of over sampling will not enter into picture because the C–P fractal method will automatically eliminate any probable grid related problem in division of the area into smaller elements and the original fractal character is preserved. Concentration–Perimeter relations were computed by assigning an area of influence to each sampled point and summing all elemental perimeters whose concentration lies below a given value. This procedure was repeated for different elemental concentrations. Carrying on this procedure is not cumbersome because there is a regular gridding of 250 m×250 m cells. The evaluated grades in cells were sorted out based on decreasing grades and cumulative areas.

The grid models derived from IDS method for As, Au, Cu, and Ag were used as inputs to Rockworks software package. The C–P plots consisting of the concentrations of As, Au, Cu, and Ag (ρ) versus the perimeters with the concentrations of As, Au, Cu, and Ag which were greater than or equal to ρ were obtained. There were three enrichment steps for Au, Cu, and Ag and four enrichment steps for As (Fig. 3). Based on the C-P log–log plot, there were four enrichment steps for As within the threshold values of 10, 25, and 80 ppm. The population below 10 ppm and between 10 and 25 ppm was the low and moderate enrichment steps of As, respectively. Furthermore, the population higher than 80 ppm had the high enrichment step of As in the studied area. Moreover, C–A log–log plot of Cu demonstrated three enrichment steps for this element with the threshold values of 27, 53 ppm. Low and moderate Cu enrichment steps were below 27 ppm and between 27 and 53 ppm; but, high enrichment step had a high value of As, which was higher than 53 ppm. Gold had three enrichment steps in the studied area

based on Au C–P log–log plot (Fig. 3). Their threshold values were equal to 0.0024 and 0.013 ppb. Lower than 0.0024 ppb was a low Au enrichment step in this area, the moderate one occurred between 0.0024 and 0.013 ppb, and population of higher than 0.013 ppb had high enrichment step of Au.

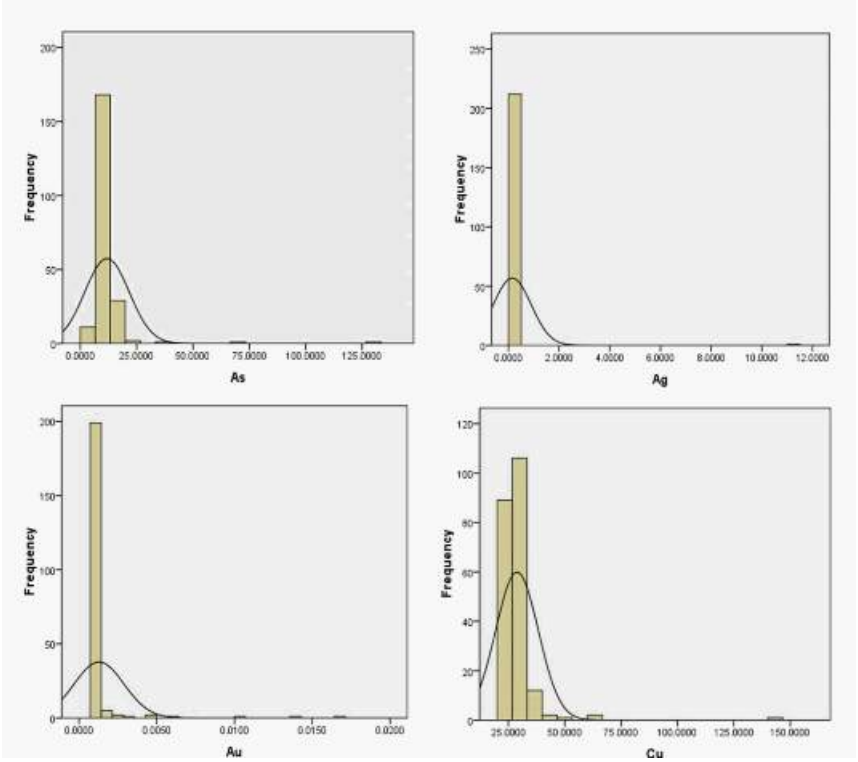

Figure 2. As, Ag, Au and Cu histograms

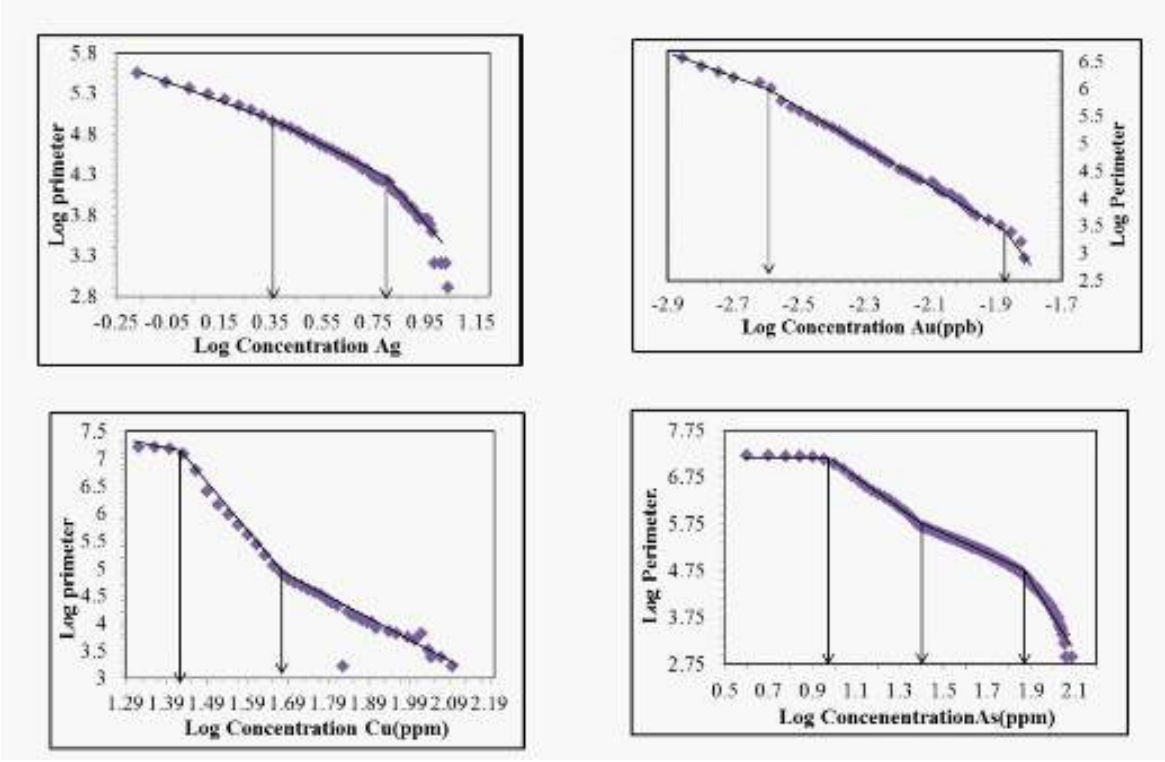

Figure 3. C-P log–log plot of Ag, Au, Cu, and As

Geochemical maps of the elements were obtained using Rockworks software package. Based on the results of the C-P method, As, Au, Cu, and Ag anomalous maps were drawn (Figs. 4). According to the elemental anomaly maps resulted from C-P

plots, the high intensity of As values existed in the central part of the area and correlated with moderate Au anomalous location (Figs. 3). Most of the Au anomalies were located in the western and central parts of the area, especially very high-intensity Au anomalies. Cu anomalies were located in the western parts of the area (Figs. 3). According to the anomaly maps, it can be concluded that Cu and Ag anomalies were simultaneously located in the western part of the studied area and corresponded to Au anomaly. From this point of view, it can be said that the studied area could be very important for Au mineralization and its western part can be the target of future exploration.

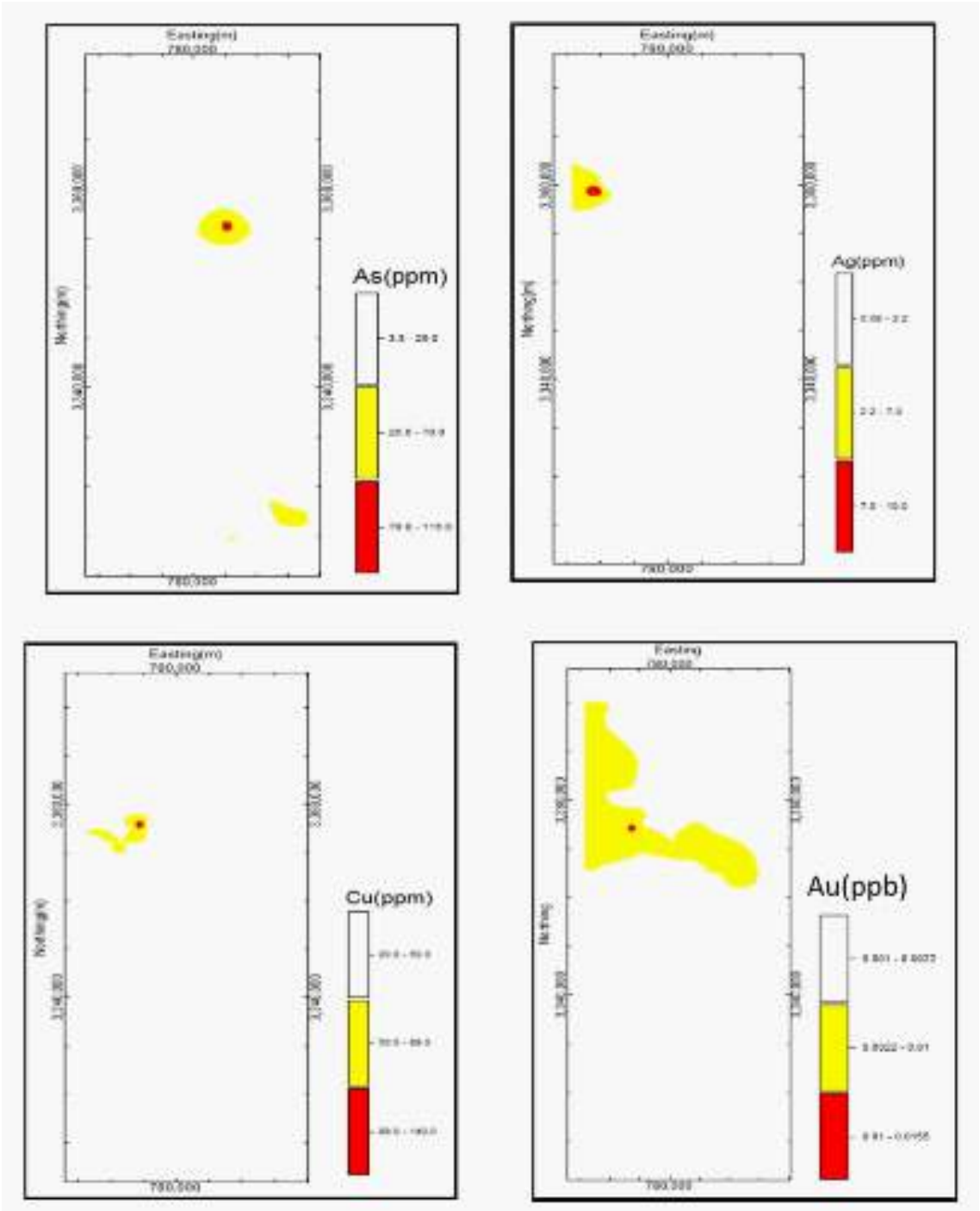

Figure 4. As, Au, Cu, and Ag anomalies obtained from the C–P plot

5 CORRELATION OF C–P MODEL WITH GEOLOGICAL SETTING

The resulting threshold values obtained from the C-P method was compared and correlated to specific lithological units. High enrichment step of Au resulting from the C–P method was situated in the western part of the studied area and correlated to the

conglomerate, sand, clay, , and silt. There was also moderate enrichment step of Au in the northwestern and central parts of the studied area which correlated to granite and granodiorite, and porphyritic dacite andesitic lava. In addition, there was a good relationship between the positions of faults and Au anomalies in the central parts of this area, which was a positive parameter, because silicified and quartz-sulfide veins occurred along these faults and Au particles existed in these veins and veinlets (Hashemi and Afzal , 2013). High enrichment step of As resulting from the C-P method was located in the central part of the studied area and correlated to the granite and granodiorite. It was also located near the faults in the central part. There were moderate As anomalous areas in the southeastern parts. In the southeast, As anomalies correlated to porphyritic dacite andesitic lava. It can be deduced that Ag element can be a very good element for tracing Au mineralization in the studied area. Based on the C-P method, very high concentration of Cu was located in the western part of the region, intersected the faults, and correlated to conglomerate, sand, clay, and recent alluvial. There were high intensive anomalies for Cu in the western part of the area based on the C-P method, which correlated to Au anomalies and sedimentary rocks according to the geological map.

6 CONCLUSIONS

Study on Nakhilab region reveals the potential use of the C–P method for geochemical anomaly separation as a useful tool for geochemical and mineral exploration. The advantages of this method rely essentially on its simplicity, and easy computational implementation. Based on the C-P method, there were three geochemical enrichment steps for Cu, Au, and Ag and four geochemical enrichment steps for As. According to the maps of anomalies by the C-P model, positions of high concentrations of Ag and Au values were the same, located in the western part of the studied area, and correlated to conglomerate, sand, clay, and silt. It can be deduced that Ag can be a good geochemical indicator for tracing Au mineralization in this area. From the maps of anomalies, Au, Cu, and Ag anomalies were simultaneously located in the western part of the studied area. From this point of view, the studied area could be beneficial for the formation of Au mineralization and its western part can be the target for future exploration. There was also a good relationship between locations of faults and Au, Ag, and Cu anomalies in the central parts of the studied area, because silicified and quartz-sulfide veins occurred along these faults and Au particles existed in these veins and veinlets. The western and central parts of the studied area were the most important parts and future, more detailed explorations including lithogeochemical sampling must be focused on these sectors.

REFERENCES

Agterberg, F.P., Cheng, Q., Wright, D.F., 1993. Fractal modeling of mineral deposits. In: Elbrond, J., Tang, X. (Eds.), 24th APCOM symposium proceeding, Montreal, Canada, pp. 43–53.

Bai J., Porwal A., Hart C., Ford A., Yu L., 2010. Mapping geochemical singularity using multifractal analysis: Applicationto anomaly definition on stream sediments data from Funin Sheet, Yunnan, China. Journal of Geochernical Exploration 104, 1-11.

Bolviken, B., Stokke, P.R., Feder, J., Jossang, T., 1992. The fractal nature of geochemical landscapes. Journal of Geochemical Exploration 43, 91–109.

Carranza, E.J.M., 2008. Geochemical Anomaly and Mineral Prospectivity Mapping in GIS. Handbook of Exploration and Environmental Geochemistry, Vol. 11. Elsevier, Amsterdam. 351 pp.

Cheng, Q., Agterberg, F.P., Ballantyne, S.B., 1994. The separation of geochemical anomalies from background by fractal methods. Journal of Geochemical Exploration 51, 109–130.

Cheng, Q., 1995. The perimeter-area fractal model and its application to geology. Mathematical Geology 27, 69–82.

Daya A.A., 2014a. Application of concentration-area fractal method for separation of anomaly from background; A case study in Shorabhaji region, Arabian journal of geosciences. In press.

Daya A.A., 2104 b. Comparative study of C-A, C-P , and N-S fractal method for separating anomaly from background; A case study in Kamoshgaran

region. Journal of geochemical exploration. In press.
Deng, J., Wang, Q., Yang, L., Wang, Y., Gong, Q., Liu, H., 2010. Delineation and explanation of geochemical anomalies using fractal models in the Heqing area, Yunnan Province, China. Journal of Geochemical Exploration 105, 95–105.
David, M., 1977. Geostatistical Ore Reserve Estimation. Elsevier, Amsterdam.
Davis, J.C., 2002. Statistics and data analysis in geology, third ed. Wiley, New York.
Hashemi, M., Afzal, P., 2013. Identification of geochemical anomalies by using of number–size (N–S) fractal model in Bardaskan area, NE Iran. Arabian Journal of Geosciences 6, 4785-4794.
Hosseiny, M., 1999. 1:100000 Qorveh Geological Map. Geological Survey of Iran.
Mandelbrot B.B., 1983. The Fractal Geometry of Nature: W. H. Freeman. San Fransisco, 468 pp.
Meng, X., Zhao, P., 1991. Fractal method for statistical analysis of geological data. Chinese Journal of Geosciences 2, 207–211.
Tukey J. W., 1977. Exploratory Data Analysis. Addison-Wesley, Reading, MA, 688 p.
Turcotte, D.L., 1986. A fractal approach to the relationship between ore grade and tonnage. Economic Geology 18, 1525–1532.
Zuo, R., 2011. Decomposing of mixed pattern of arsenic using fractal model in Gangdese belt, Tibet, China. Applied Geochemistry 26, S271–S273.

Spatial Association Analysis Between Hydrocarbon Fields and Sedimentary Résidual Magnetic Anomalies: A Case Study from the Algerian Triassic Province

K. Allek, A. Bouguern
Laboratory of Earth Physics, University of Boumerdes, Algeria

D. Boubaya
University of Tebessa, Algeria

M. Hamoudi
USTHB University, Algiers, Algeria

ABSTRACT The presence of Sedimentary Residual Magnetic (SRM) anomalies over hydrocarbon accumulations and their contribution to exploration remain somewhat controversial despite encouraging results and an improved understanding of genetic links between hydrocarbon seepage-induced alterations and near-surface magnetic minerals. These uncertainties still exist because shallow-sourced SRM anomalies are not associated exclusively with hydrocarbon. The cause of these anomalies may well be microseepage related, *but* could also *result* from others sources such as cultural features or detrital magnetite. To deal with this particular purpose, we explore the spatial association between known hydrocarbon fields within the Algerian Triassic province basin and SRM anomalies using GIS-based weights of evidence statistical approach. The results indicate that the known hydrocarbon fields are strongly associated with particular classes of anomalies. These results are significantly useful for further exploration in the case of the study region, and can also be extended to regions with similar characteristics.

Keywords: Sedimentary residual magnetic, hydrocarbon fields, spatial association analysis

1 INTRODUCTION

Airborne magnetic surveying has been used in oil exploration for many decades. It traditionally applied to quickly and economically screen large areas for mapping depths to basement and bedrock structures that control emplacement of hydrocarbon in overlying sedimentary basins. Recent years have seen a surge in interest for the application of magnetic data to the detection of intra-sedimentary shallow-sourced anomalies associated with hydrocarbon microseepages. It has been well documented that most oil and gas accumulations leak hydrocarbons, creating alteration features close to the surface that can be identified using geochemical methods as well as any of geophysical techniques such as gamma-ray spectrometry, induced polarization and magnetic (Saunders et al., 1993; Foote, 1996; Schumacher, 2000; Peres-Peres 2011; Curto et al., 2012; Flekkoy et al., 2013).

The first time that has been shown the presence of magnetic anomalies in levels near surface, associated with the presence of underlying hydrocarbon deposits was in late seventies. It was made independently by Donovan et al. (1979) and by Berezkin et al. (1978). Advances made in processing aeromagnetic data and an improved understanding of seep mechanisms and alteration processes that could result in formation of authigenic (formed in place) magnetic minerals has promoted the magnetic method from a reconnaissance tool to a valuable exploration technique for detecting hydrocarbon by mapping short wavelength magnetic anomalies assumed to

be in relationship with hydrocarbon seep-induced near-surface magnetic minerals, either in onshore or offshore basins (Foote, 1996; Burazer et al., 2001; Stone et al., 2004; Curto et al., 2012; Schumacher and Foote, 2014; Menshov et al., 2014). This seep-induced magnetic minerals has led to some development of analytical methods that allow subtle anomaly identification. Foote (1996) developed a method referred to as "Magnetic Bright Spots (MBS)" - which provide valuable clues to an underlying oil or gas accumulation. Studies from onshore and offshore examples (Schumacher and Foote, 2006; 2014) reveal stunning results. The exploration leads and prospects associated with a MBS anomaly are 4 to 6 times more likely to result in a commercial oil or gas discovery than a similar prospect without such an anomaly. Stone et al. (2004) described a simple micromagnetic aureole search methodology which is intended to the recognition of annular/aureole-shaped anomalies. The test study from a high-resolution aeromagnetic survey performed over Muglad Basin of southern Sudan has successfully revealed an annular anomaly correlating directly with the Jarayan oil field.

Despite the good consistency of results obtained from published studies, this method did not penetrate into subconsciousness of practicing geophysicists from industry. If data processing techniques can often remove the influence of deep magnetic basement rocks, this is not always the case when it comes to discriminate between the effects of shorter wavelengths anomalies which can result both from authigenic ferromagnetic minerals than possible syngenetic magnetic sources. Gay and Hawley (1991) and Gay (1992) remained skeptical about the origin of near-surface intra-sedimentary magnetic anomalies supposedly caused by hydrocarbon microssepages. They cite examples of many false anomalies caused by detrital magnetite, tuffs, "black sands" in stream channels and cultural contamination from surface and near-surface iron. It is this skepticism that appears to deter many petroleum geophysicists.

Because of this controversy about the presence, origin, and exploration significance of magnetic mineralization associated with hydrocarbon accumulations, we decide to carry out a more analytical and more objective methodology, using GIS-based Weights of Evidence (WofE) approach to verify the genetic links between SRM anomalies and hydrocarbon seepage environments. This method has been extensively applied for mineral potential mapping; however, the present study represents its first application to hydrocarbons exploration. The Oued Mya Basin which contains numerous oil and gas producing fields as well as the giant gas-deposit of Hassi R'mel provides an ideal case study.

Our aim was to investigate the spatial association between SRM anomalies and the known hydrocarbon fields within the study area to answer the question whether the spatial distribution of these magnetic anomalies is controlled by the underlying oil/gas fields. First, we use the WofE technique to establish a quantitative characterization of the spatial relationship. Next, we reveal the characteristics (wavelengths and amplitudes) of the type of anomalies assumed to be induced by hydrocarbon microseepages. Finally, we show evidence of the convenience of large-scale aeromagnetic data for such tasks when acquired at relatively low altitude and at suitable accuracy.

2 HYDROCARBON SEEPS

It has long been recognized that most oil and gas accumulations leak hydrocarbons due to high pressures at depth. This leakage occurs vertically or near-vertically from the reservoir to the surface through fractures in rocks and planes of weakness between geological layers or along fault discontinuities (Schumacher, 2010, Salati, 2014). Except some macro-seeps encountered sometimes in certain regions, that manifest themselves as the visible presence of oil and gas seeping to the surface, most of hydrocarbon seeps have no

visible and direct evidences of their presence (microseeps), but cause several chemical reactions and microbial oxidation in the rocks and soils and also cause changes in Eh and pH. Such changes in the near-surface soils destabilize many compounds, increase the solubility of the elements and induce mineralogical alterations such as red beds bleaching, clays formation, and creation of secondary carbonates, sulfides, and magnetic minerals (Schumacher, 1996; 2014; Srinivasan et al. 2014; Salati, 2014).

Eventov (1997) have reviewed some of the most documented theories concerning the formation of the diagenetic magnetite, caused by hydrocarbon seepages. According to these theories, the hydrocarbon-induced reducing environment can lead to the precipitation of a variety of magnetic iron oxides and sulfides, including magnetite (Fe_3O_4), maghemite (γ-Fe_2O_3), pyrrhotite (Fe_7S_8), and greigite (Fe_3S_4). Schumacher (1996) provided a model for hydrocarbon-induced magnetic minerals. In accordance with this model, upward-migrating light hydrocarbons reach near-surface oxidizing conditions, aerobic hydrocarbon-oxidizing bacteria consume methane (and other light hydrocarbons) and decrease oxygen in pore waters. With development of anaerobic conditions, the activity of sulfate-reducing bacteria results in

Sulfate ion reduction and oxidation of organic carbon to produce bicarbonate ion and reduced sulfur species which in turn combine with available iron to form iron sulfides and oxides. For their part, Machel and Burton (1991) suggested that magnetic minerals could be either produced or destroyed under the influence of hydrocarbons seeps. On the basis of extensive investigations conducted in major oil fields of several basins in China, the results of mineralogical analysis reveal that the enhanced magnetic susceptibility relating to the hydrocarbon microssepages are caused by secondary magnetite and the subsequent low-temperature oxidation products (maghemite) (Liu et al., 2004).

Diagenetic magnetic minerals created by hydrocarbon microseepage has been reported to occur over a wide range in *depth*, from surface soils to strata as deep as 1500 m (LeSchack and Van Alstine, 2002). The identification of anomalous magnetic minerals over oil and gas accumulations has been established by magnetic susceptibility measurements and magnetic mineralogy analysis of surface soils, drill cuttings and cores from oil wells. Saunders et al. (1991) documented increases in magnetic susceptibility that were caused by high concentrations of authigenic magnetic minerals (magnetite and probably maghemite) occurring just below the grass roots. Foote (1996) reported that most magnetically enhanced zones detected in high resolution ground and airborne magnetic surveys over hydrocarbon reservoirs are thought to occur at depths of 60–600 m. Peres-Peres et al. (2011) revealed the presence of authigenic magnetite at a depth of about 600 m by analyzing drill cuttings from Venezuelan and Colombian oil fields.

3 MATERIALS AND METHODS

3.1 Study area

This study was developed in a region within the Triassic province of Algeria, in fact a large basin located on the northern-central part of the Saharan Platform. It lies at the Northern part of the Oued Mya depression, between 0° 40' - 4° 48'E longitudes and 31° 06' - 33° 55'N latitudes. This study region as a whole consists of a number of structural units: Djorfa saddle, Tilrhemt dome, and parts of the Benoud trough and Touggourt saddle (Fig. 1).

The current structural scheme is the result of several tectonic phases which the most important are the Panafrican, the Hercynian, the Triassic-Jurassic extension, the Austrian, and the major Alpine phase. The Tilrhemt dome is the most important anticline structure in the region with ENE-WSW direction, and probably Hercynian age. According to the geological map, mostly Cretaceous formations outcrop in this area, whereas Neogene-Oligocene and sand dunes dominate in the rest of the region (Fig. 2).

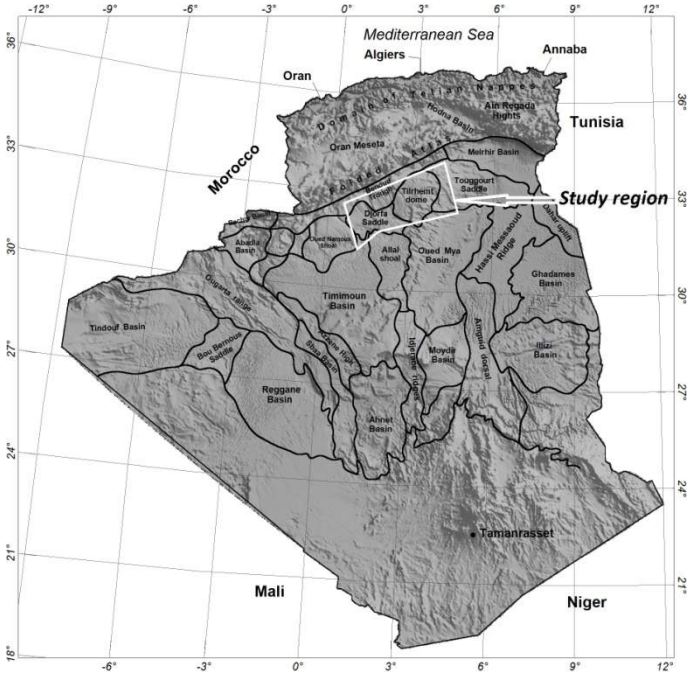

Figure 1. Algerian territory, showing defined structural units and the study area location.

The study area contains the giant Hassi R'mel gas field and numerous oil and gas deposits exploited at the Triassic and Cambrian-Ordovician levels. The Saharan Triassic which is the main petroleum objective, consists of sediments of varied continental environments; namely, fluvial, floodplain, lake, sebkha, and wind (Baouche et al., 2009). The region was first investigated in 1951 which led to the drilling of the first well south of Berriane. The encouraging results led to the discovery of the Hassi R'mel field in 1956, which was put on production in 1961 and proved to be one of the world's largest gas fields. The Field extends 70 km from north to south and 50 km from east to west (Bencherif, 2003). Exploration increased the subsequent decades leading to the discovery of several oil and gas fields in the region.

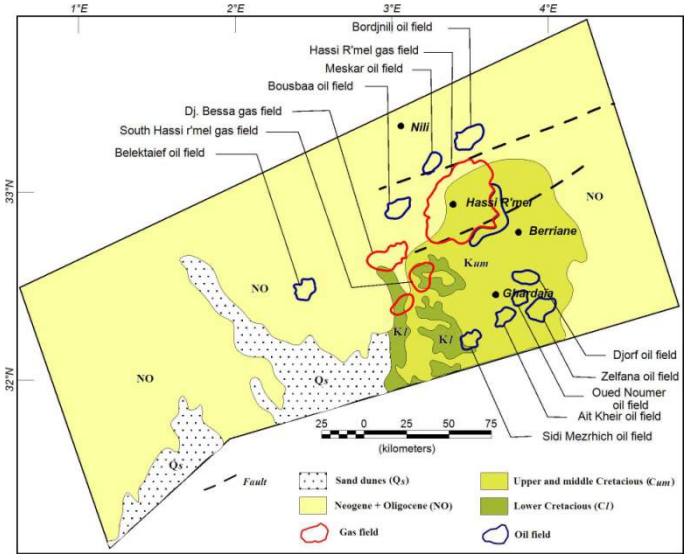

Figure 2. Simplified geological map and oil-gas fields location

3.2 Survey

The regional airborne magnetic survey over the Oued Mya region was part of the nationwide aeromagnetic survey of Algeria. The survey was completed by Aeroservices Limited in 1974 on behalf of the *SONAREM* (*Société Nationale de la Recherche et d'Exploitation Minière*). The aeromagnetic data were acquired with a nominal terrain clearance of 150 meters using a high resolution (0.02 nT) optically pumped cesium vapor magnetometer. Traverse lines were oriented N160° (NNW-SSE), with a spacing of 5 km. Tie-lines (Control-lines) were oriented perpendicular to traverse lines with a spacing of 25 km. Tie-lines were also flown along the survey boundary when not parallel to the traverse line direction. Readings were taken at one-second intervals, yielding at an average aircraft speed of 165 km/h a magnetic measurement about every 46 m along the flight path. The survey contains 13,980 line-kilometers, and covers surface of 56,900 km². Variations in the magnetic field resulting from different aircraft induced noise were electronically compensated.

In order to ensure the *quality* of measurements, the maximum diurnal change allowed was less than 3 nT for any 3-minute chord (period) of time. Data were re-acquired when this condition is exceeded, with any re-flown line segment crossing a

minimum of two control lines. Several data processing procedures: such as tie-line leveling, IGRF calculation and removal, lag effect correction and microlevelling, were carefully achieved to get the most out of the detection of subtle anomalies. Although this survey is very widely spaced, it is acquired at a relatively low height, and there are sufficient reading along each flight line such that micromagnetic anomalies close to flight lines are well identified.

3.3 Enhancement of SRM anomalies

It should be noted that for airborne magnetic data, the flight altitude, sample spacing along flight lines and line spacing play an important role in the detection of high wavenumber weak magnetic anomalies. In Algeria, most available aeromagnetic surveys were accomplished at the reconnaissance scale and, thus far they have been mostly used to define the main basin structural features. On the other hand, They are at an accuracy and at a height that makes them suitable for the detection of subtle anomalies when they are close to a flight line. However, processing the survey as grided data would tend to obscure any isolated narrow anomalies. That's why all filtering computations, performed in this study to isolate subtle anoamlies, were carried out on profile data.

To highlight Sedimentary Residual Magnetic (SRM) anomalies, the most contentious problems are to remove cultural influence and basement magnetic signal. These SRM anomalies are often masked by much stronger magnetic anomalies caused by underlying magnetic formations and/or by cultural features. However, if the basement magnetic sources generally can be distinguished by their large wavelenghts, this is not always the case when one has to do with the cultural sources. Randomly scattered oil well casings, metal storage tanks, pipelines, and other cultural features on or near the ground surface alters magnetic data acquired for hydrocarbon microseepage purposes. These sources create short-wavelength high-amplitude signatures in total field magnetic intensity maps and they can mask the effect of seep-induced anomalies and sometimes even confused with them.

We used the radial power spectra of the anomalous field (Spector and Grant 1970) to help distinguish anomalies caused by near-surface intrasedimentary sources from anomalies caused by cultural sources and those from basement rocks. The diagenetic magnetic signal is generally recognized by its longer “wavelength” (compared to cultural features and background noise). The very long basement effects and very short cultural sources were removed by applying a selective band-pass filter. Afterward, amplitudes of the Analytic Signal of the isolated Sedimentary Residual Magnetic (AS-SRM) anomalies were calculated to deal with distortion and polarity effects of anomalies so that they can be more easier studied and categorized.

4 SPATIAL ANALYSIS APPROACH

4.1 Weights of Evidence method

Weights of evidence (*WofE*) is a Bayesian statistical method for assessing the degree of spatial association and for combining evidence to test a hypothesis. It determines the probability of an event to occur under certain conditions. The method was originally developed for a non-spatial application in medical diagnosis, later it was extensively used for mineral potential mapping in a GIS environment (Bonham-Carter, 1994), and soon after adapted for landslide susceptibility analysis, hazard modeling, fires and so on. The WofE method is applied here to investigate the spatial associations between interpreted Sedimentary Residual Magnetic (SRM) anomalies and mapped hydrocarbon fields within the Oued Mya Basin. The importance of the weights depends on the measured association and permits to provide an insight into the characteristics of the SRM anomalies related to seep-induced magnetic minerals. This method could be used as spatial evidence in hydrocarbon prospectivity mapping.

A detailed explanation of the mathematical formulation of the WofE modeling method is available in Bonham-Carter (1994). The method uses a log-linear of the Bayesian probability model to estimate the importance of evidences by a pair of weights, one (positive weight W^+) for presence of the evidence H, and negative weight (W^-) for absence of the evidence H.

$$W^+ = ln\left(\frac{P(H|A)}{P(H|\bar{A})}\right) \quad (1)$$

$$W^- = ln\left(\frac{P(\bar{H}|A)}{P(\bar{H}|\bar{A})}\right) \quad (2)$$

where P() denotes probability, H is the presence of hydrocarbon pattern (it corresponds to area occupied by hydrocarbon field), $\bar{H}$ is the absence of hydrocarbon pattern, A is the presence of points of interest (corresponds to center-points of picked SRM anomalies), $\bar{A}$ is the absence of points occurrence.

The weights (W^+ *and* W^-) provide a measure of spatial association between the training points and the binary theme H. They are calculated for each class of the picked SRM anomalies. The value of the weight W^+ is positive, whereas W^- is negative, indicates that there are more SRM anomalies on binary theme H than would occur due to chance. Conversely W^+ would be negative and W^- positive for the case where fewer points occur than expected. If the picked anomalies A are distributed randomly with respect to the binary theme H, then both of weights will have a value of zero, or very close to zero.

The difference between the weights is known as the contrast, C. Thus:

$$C = W^+ - W^- \quad (3)$$

The contrast is an overall measure of spatial association between the set of points A and the binary theme H, combining the effects of the two weights. It is the best estimator in a large area and when a large number of points occurences are considered (Bonham-Carter, 1994). Hence, for a positive correlation, C is positive; C is negative in the case of negative spatial correlation.

The studentized confidence value *s(C)*, defined as the contrast *C* divided by its standard deviation, corresponds approximately to the statistical level of significance defined by standard z-tests, and provides a useful measure of the significance of the contrast (Raines, 1999). The standard deviation of C is calculated as:

$$s(C) = \sqrt{s^2(W^+) + s^2(W^-)} \quad (4)$$

In the spatial analysis, as applied in this work, a simplified and intuitive approach similar to that suggested by Turner (1997), was adopted. The surface of the study area and the binary pattern H are expressed in number of unit cells, and each training point is assumed to occupy a single unit cell. That way, the weights W^+ and W^- can be calculated by means of map crossing functions as follows:

$$W^+ = ln\left(\frac{\frac{Number\ of\ points\ A\ (picked\ anomalies)\ \boldsymbol{inside}\ the\ pattern\ H}{Total\ number\ of\ \ points\ A}}{\frac{Number\ of\ unit\ cells\ \boldsymbol{inside}\ pattern\ H\ not\ occupied\ by\ points\ A}{Total\ number\ of\ unit\ cells\ of\ the\ study\ area\ not\ occupied\ by\ points\ A}}\right) \quad (5)$$

$$W^- = ln\left(\frac{\frac{Number\ of\ points\ A\ \boldsymbol{outside}\ the\ pattern\ H}{Total\ number\ of\ points\ A}}{\frac{Number\ of\ unit\ cells\ \boldsymbol{outside}\ pattern\ H\ not\ occupied\ by\ points\ A}{Total\ number\ of\ unit\ cells\ of\ the\ study\ area\ not\ occupied\ by\ points\ A}}\right) \quad (6)$$

A unit cell of 1 km x 1 km was used. This was chosen for two reasons: the scale of the present aeromagnetic survey, and expected dimensions of SRM anomalies so that each cell can contain only one training point. The total number of unit cells area (1 km²) in the study area map is 56900 cells, while the surface occupied by the hydrocarbon fields represents 3120 cells, i.e. a little more than 5% of the total area. Thus, the areas occupied by oil and gas fields represent 2 and 3% respectively.

4.2 Application of the method

To the authors' best knowledge no study has investigated quantitatively the spatial association between known oil and gas accumulations and magnetic anomalies arising from shallow sedimentary section. In the most literature reviewed the characterization of this spatial correlation results from visual analysis (Burazer et al. 2001; Stone et al., 2004; Curto et al., 2012; Menshov et al., 2014).

In the application of the WofE method, hydrocarbon-related thematic map was overlapped with all 342 picked AS-SRM anomalies (Fig.3). The Weights of the Hydrocarbon-related theme in the model was calculated by using the relationship of the area covered by the oil and gas fields and the number of picked anomaly points that fall onto it. On the basis of this intersection, weights, contrasts and Studentized confidence values were calculated using equations (3, 4, 5, and 6).

Initially all 342 picked anomalies are treated as being either present or absent in the model, and are not weighted by characteristics such as anomaly size or amplitude. The results show relatively low values of contrast 'C' (0.6 - 0.7) for oil and gas fields whether taken separately or together (Tab. 1). This indicates that the picked AS-SRM anomalies are practically *uncorrelated* with known hydrocarbon fields within the study area because of a somewhat random distribution of these anomalies as shown in figure 3.

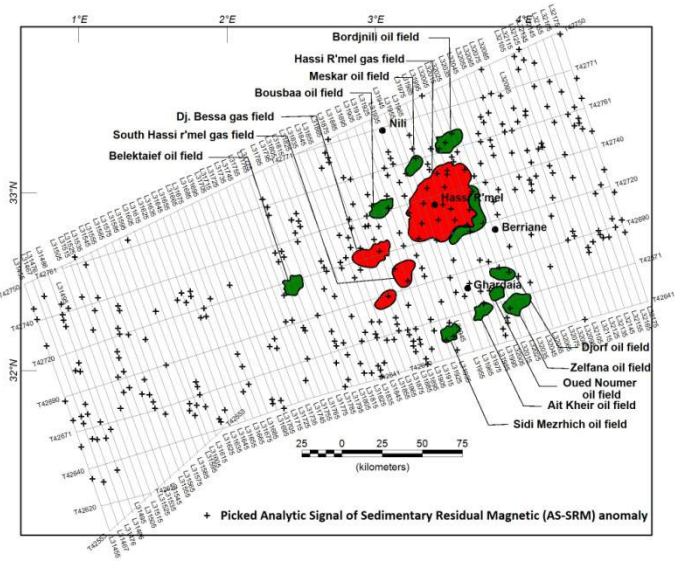

Figure 3. Location of picked AS-SRM anomalies

Table 1. Summary of spatial association defined by weights of evidence model

Theme	W-	W+	C	St(c)
Oil	-0.01	0.58	0.59	2.0
Gas	-0.03	0.60	0.63	2.7
Oil+gas	-0.05	0.68	0.73	4.1

The magnitude of the analytic signal of picked anomalies ranges from 1.5 to 13.7 nT/km with an arithmetic mean of 2.8 nT/km and standard deviation of 1.8 nT/km. Their width ranges between 1.38 and 8.8 km with an average value of 3.27 km and standard deviation of 1.2 km. To give a quick visual summary of the picked anomalies, they were divided into ten class intervals (bins) according to their wavelengths and their magnitude values (Fig. 4). The number of ten bins is chosen according to Sturges' rule, which suggests that the number of intervals should be as close as possible to $1+log_2(N)$, where N is the number of anomalies. Magnitude of AS-SRM (Fig. 4a) shows a skewed distribution to the right with a large number of anomalies (nearly 65% of all anomalies) in the lower value class (leftmost side). An almost similar shape is obtained for the width of the anomalies (Fig. 4b), which exhibits some right-skew.

The problem with this distribution of anomaly classes is that some of the classes have a very small number occurring in them. This gives rise to a very noisy and unreliable

weights, with poor estimates. The alternative is to calculate weights for classes whose intervals are selected so that each bin holds the same number of picked anomalies, and to examine the variation of the weights and contrast at each amplitude and wavelengths intervals.

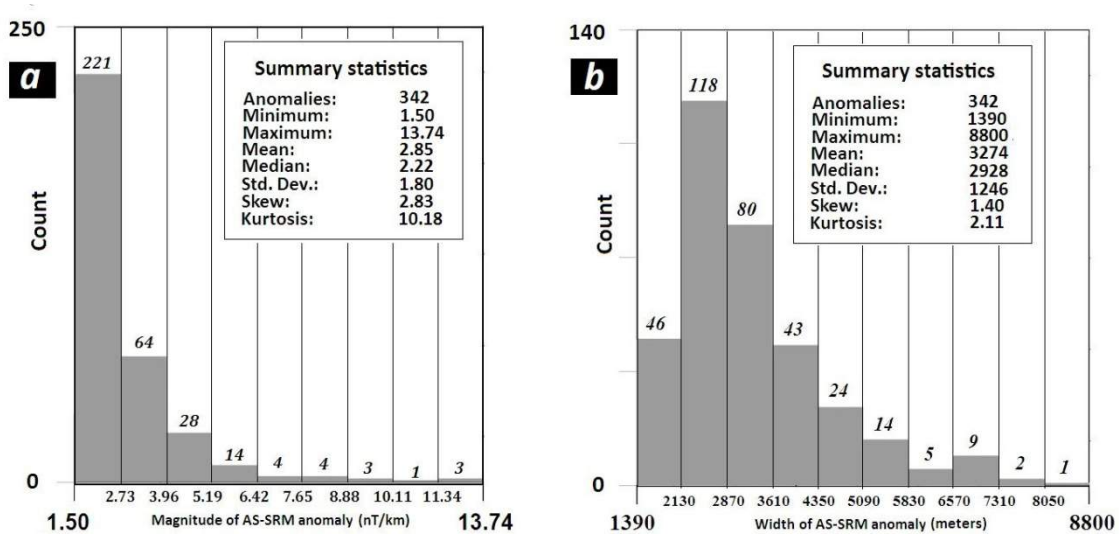

Figure 4. Frequency histogram of AS-SRM anomalies according to: (a) amplitude, (b) width.

5 RESULTS AND DISCUSSION

This study synthesizes results of the research work to develop and demonstrate the existence of relationship between oil and gas reservoirs distribution and Hydrocarbon Seepage-Induced Magnetic anomalies. Both gas and oil fields were alternately used as binary patterns in the weights of evidence (WofE) modeling for assessing their spatial association with AS-SRM anomalies, and to distinguish them from any other shallow-sourced magnetic signatures.

All picked anomalies were classified into 10 bins with varied width such that each bin contains 10% of the total of anomalies (i.e. about 34). The set of picked anomalies that fall into a defined class is used to calculate the weights for both oil and gas fields binary patterns, one weight per class, using the overlap relationships between the hydrocarbon fields and the various classes on the anomalies. Tables 2 and 3 report summary of weights, contrast and Studentized (*Confidence* C_S) for amplitude (nT/km) and size (km) for each class of AS-SRM anomalies respectively.

Table 2. Variation of weights for different amplitudes (nT/km) of AS-SRM anomalies with respect to hydrocarbon (gas and oil) fields

Class amp. (nT/km)	No. of anom.	W^+	W^-	Contrast (C)	Confidence
< 1.6	1	-0.630806	0.027001	-0.657808	-0.647955
1.6 – 1.7	0				
1.7 – 1.8	0				
1.8 – 2.0	0				
2.2 – 2.2	2	0.123321	-0.007705	0.131026	0.179358
2.2 – 2.6	1	-0.53838	0.024061	-0.562441	-0.553204
2.6 – 3.0	4	0.75645	-0.068365	0.824815	1.54863
3.0 – 3.5	**7**	**1.317028**	**-0.173782**	**1.490809**	**3.511591**
3.5 – 4.9	4	0.78632	-0.072415	0.858735	1.60906

Table 3. Variation of weights for different anomaly widths of analytic signal with respect to hydrocarbon fields.

Class width (km)	No. of points	W^+	W^-	Contrast (C)	Confidence
< 2 km	1	-0.659811	0.027868	-0.687679	-0.677672
2 – 2.3	2	0.092532	-0.005686	0.098218	0.134583
2.3 – 2.5	2	0.062661	-0.003789	0.06645	0.09114
2.5 – 2.7	1	-0.630806	0.027001	-0.657808	-0.647955
2.7 – 2.9	3	0.498318	-0.038494	0.536812	0.886106
2.9 – 3.3	1	-0.570146	0.025104	-0.59525	-0.585779
3.3 – 3.6	**7**	**1.346898**	**-0.18167**	**1.528568**	**3.586388**
3.6 – 4.1	4	0.727444	-0.064562	0.792006	1.489856
4.1 – 5.0	**8**	**1.480751**	**-0.22091**	**1.70166**	**4.184892**
>5 km	4	0.848876	-0.081355	0.930231	1.735263

It can be observed that the strongest spatial correlations are related to certain class of anomalies. They are defined by contrasts C > 1.5, and confidence C_S > 3.5 implying statistically significant for the classes of AS-SRM anomalies believed to result from near-surface sources induced by hydrocarbon microseepages have wavelengths in the intervals 3.3 - 3.6 km and 4.1 - 5.0 km and amplitudes ranging from 3.0 to 3.5 nT/km.

Plot of data over flight line No. 31905 located in the central part of the study area is presented in Figure 5. The analytic signal profile shows two anomalies with amplitude values of 2.9 and 3.5 nT/km and width of 4.9 and 3.8 km, which occur above Bousbaa oil field and South Hassi Rmel gas field respectively.

The identified near-surface anomalies in the Algerian Triassic basin suggests a possible relationship between certain type of sedimentary residual anomalies and hydrocarbon fields emplacement. This hypothesis has been supported by the statistical model which enabled the quantitatively characterization of the degree of spatial relationship.

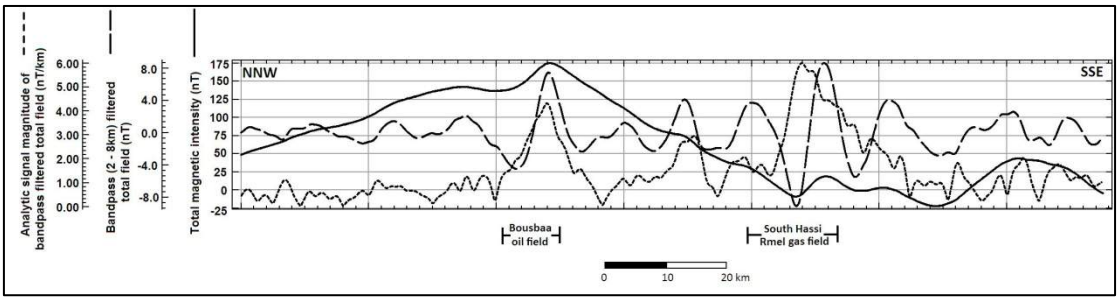

Figure 5. Aeromagnetic flight line profile L31905 across the Bousbaa oil field and the South Hassi Rmel gas field

6 CONCLUSION

Despite the availability of a large aeromagnetic coverage, these data were not always exploited in an optimal and rigorous way. In fact, they were only related, in the best of cases, to screen large areas for mapping depths to basement and bedrock structures. the results obtained from GIS-based weights of evidence analysis demonstrate that regional aeromagnetic data when acquired at relatively low altitude and at suitable accuracy can provide important information about intra-sedimentary features and residual anomalies attributed to long-term hydrocarbon microseepages. The application of spatial association analysis using GIS-based weights of evidence technique has successfully identified a particular class of sedimentary residual magnetic anomalies correlating directly with known underlying oil and gas accumulations within the Algerian Triassic basin. Even

though this approach is empirical, it nonetheless provides support for determining successful and cost effective exploration strategies in predicting areas of high hydrocarbon potential where little or no exploration activity exists.

High resolution aeromagnetic surveys are certainly more suitable for this venture allowing to improve the definition of the observed aeromagnetic field so that small seep-induced effects can be better defined in order to detect more of them and to interpret them more accurately.

REFERENCES

Baouche R., Nedjari A., Eladj S. and Chaouchi R. 2009. Analysis and interpretation of environment sequence models in Hassi R'Mel Field in Algeria. *Energy problems and environmental engineering, p. 38-48.*

Bencherif, D., 2003. Giant Hassi R'Mel gas field. *AAPG Hedberg Conference, "Paleozoic and Triassic Petroleum Systems in North Africa", Algiers, Algeria.*

Berezkin V.M., Kiritchek M.A. and Kunarev A.A. 1978. Application of geophysical exploration methods for direct exploration of oil and gas, (*in russian*). *Nedra, 223 p*.

Burazer M., Grbović M., and Žitko V. 2001. Magnetic data processing for hydrocarbon exploration in the Pannonian Basin, Yugoslavia. *Geophysics, vol. 66, n°6, p. 1669-1679.*

Curto J.B., Pires A.C.B., Silva A.M., and Crósta A.P. 2012. The role of airborne geophysics for detecting hydrocarbon microseepages and related structural features: The case of Remanso do Fogo, Brazil. *Geophysics, vol. 77, no. 2, p. B35–B41.*

Donovan T.J., Forgey R. and Roberts A., 1979. Aeromagnetic detection of diagenetic magnetite over oil fields. *AAPG Bull., 63, 245−248.*

Flekkoy E.G. ; Legeydo, P. ; Haland, E. ; Drivenes, G. ; Kjerstad, J., 2013. Hydrocarbon detection through induced polarization: Case study from the Frigg area. *Annual International Meeting - Society of Exploration Geophysicists. 2, p.800-804, SEG Houston 2013.*

Foote R. S., 1996. Relationship of near-surface magnetic anomalies to oil- and gas-producing area, in D. Schumacher and M. A. Abrams, eds., Hydrocarbon migration and its near-surface expression: *AAPG Memoir 66, p. 111-126.*

Gay, Jr., S. P., 1992. Epigenetic versus syngenetic magnetite as a cause of magnetic anomalies: *Geophysics, v. 57, p. 60–68.*

Gay, Jr., S.P., and Hawley B.W., 1991. Syngenetic magnetic anomaly sources: three examples: *Geophysics, v. 56, p. 902–913.*

Klett, T.R., 2000. Total Petroleum Systems of the Trias/Ghadames Province, Algeria, Tunisia, and Libya -The Tanezzuft-Oued Mya, Tanezzuft-Melrhir, and Tanezzuft-Ghadames. *U.S. Geological Survey Bulletin 2202-C, http://greenwood.cr.usgs.gov/pub/bulletins/b2202-c/*

LeSchack, L. A., and Van Alstine, D.R. 2002. High-resolution ground-magnetic (HRGM) and radiometric surveys for hydrocarbon exploration: Six case histories in western Canada, *in Surface exploration case histories: Applications of geochemistry, magnetics, and remote sensing, D. Schumacher and L. A. LeSchack, eds., AAPG Studies in Geology 48, SEG Geophysical References Series 11, p. 67– 156.*

Machel, H.G., and Burton E.A., 1991. Causes and spatial distribution of anomalous magnetization in hydrocarbon seepage environments: *AAPG Bulletin, v. 75, p. 1864– 1876.*

Menshov O., Kuderavets R., Chobotok I., 2014. Magnetic investigations in Carpathian Foredeep of Ukraine. *Castle Meeting; New trends on Paleo, Rock and Environmental Magnetism; Evora, 2014.*

Perez-Perez A., D'Onofrio L., Bosch M., and Zapata E. 2011. Association between magnetic susceptibilities and hydrocarbon deposits in the Barinas-Apure Basin, Venezuela, *Geophysics. vol. 76, no. 6, p. L35–L41.*

Raines, G.L., 1999. Evaluation of weights of evidence to predict epithermal-gold deposits in the great basin of the Western United States. *Natural Resources Research 8, 257–276.*

Salati S. 2014. Characterization and remote detection of onshore hydrocarbon seep-induced alteration. *PhD dissertation thesis. Univesity of Twente, Faculty of Geo-Information science and Earth observation, ITS, Enschede, The Netherlands, 162 p.*

Saunders D.F., Burson K.R., Branch J.F., Thompson C.K., 1993. Relation of thorium normalized surface and aerial radiometric data to subsurface petroleum accumulations. *Geophysics, v. 58. p. 1417–1427.*

Saunders, D. F., K. R. Burson, and C. K. Thompson, 1991. Observed relation of soil magnetic susceptibility and soil gas hydrocarbon analysis to subsurface petroleum accumulations: *AAPG Bulletin, v. 75, p. 389–408.*

Schumacher D. and Foote R.S., 2014. Seepage-Induced Magnetic Anomalies Associated with Oil and Gas Fields: Onshore and Offshore Examples.

AAPG International Conference & Exhibition, Istanbul, Turkey, September 14-17, 2014.

Schumacher D., 1996. Hydrocarbon-induced alteration of soils and sediments, *in* D. Schumacher and M. A. Abrams, eds., Hydrocarbon migration and its near-surface expression: *AAPG Memoir 66, p. 71–89.*

Schumacher D., 2000. Surface geochemical exploration for oil and gas: New life for an old technology. *The Leading Edge. p.258-261.*

Schumacher D., 2010. Integrating hydrocarbon microseepage data with seismic data doubles exploration success. *Proceedings, Indonesian petroleum association 34th annual conference and exhibition, may 2010*

Schumacher D., 2014. Minimizing Exploration Risk: The Impact of Hydrocarbon Detection Surveys for Distinguishing Traps with Hydrocarbons from Uncharged Traps. *GeoConvention 2014 CSEG CSPG CWLS Conference: FOCUS*

Spector A., and Grant F. S. 1970, Statistical Models for Interpreting Aeromagnetic Data, *Geophysics. 35, 293–302.*

Stone V.C.A., Fairhead D. J. and Oterdoom W.H., 2004. Micromagnetic seep detection in Sudan, *The Leading Edge; v. 23; n°. 8; p. 734-737.*

Structural Controls of Gold Deposit Mineralization in Zarshouran Mine, Takab, Iran

H. Hassani, V. Farahani
Faculty of Mining and Metallurgical Engineering, Amirkabir University of Technology, Tehran, IRAN

ABSTRACT Zarshuran gold deposit is located in northenwest Iran at Takab region. Zarshuran gold deposit has reserve of 6.74 million tons with 1 gram per ton cut off grade and 4.01 grams per ton average gradeZarshuran gold mineralization is similar in many ways to scattered epithermal deposit in sedimentary rocks, especially carbonates (carlin type). Deposit contains very fine grained scattered gold and high content of arsenic and sulfide. The hosted rocks for mineralization are Black shale and Chaldagh limestone. Silicification, argilic-seserisitic and alunitealteration are the most important alteration in this region. The studied area of Zarshuran is a part of Tabriz-Bazman igneous sub-zone and it is part of Imankhan anticline. The main faults of this region (Tabriz-Bazman) form a network which is dependent on a riedel type shear zone. In this work, first ,the DataMine and Rockworks software has been used to study the structure of regional faults and folds (like determining fold axis, fold dependent fractures, etc.), then faults and fold dependent joints are divided into groups. Geological dependency of different structural elements of the region has been matched on third order branched fractures mechanism of clockwise shear area with final trend of N130 and N155 and mineralization is occurred along extension of these trends. Field surveys, fractures and boreholes investigations showed that mineralization and ore deposition is consistent with the area fractures.

Keywords: Gold, structural, fault, fold

1 INTRODUCTION

Zarshouran gold deposit is located in southeast of West Azerbaijan Province with 5 kilometer distance from north to northeast of Zarshouran village and 25 kilometer distance from north of Takab City (Ojaghi, 1996). This area is among deposits with priority which was the subject of various geological and mineral activities. According to 47 drilling wells by Iranian and foreign companies, the estimated deposit of this area is 11.04 million tons with average fineness of 7.72 gr/ton with limit of 1 gr/ton (Minerals Production, 2004).

Gold mineralization in Zarshouran deposit is considerably similar to disseminated epithermal deposit in sedimentary rocks specially carbonated ones (carlin type). Gold is either scattered in a deposit in very fine-grained form with high levels of Arsenic and Sulphide or mixed with organic carbon in Zarshouran area and formed organic gold-carbon complex with high purity (Ojaghi, 1996). Studied area is geologically located at Iran central zone and is part of Sahand – Bazman (Orumiyeh – Dokhtar) magmatic sub-zone that central Iran transitional zone (Sanandaj-Sirjan) is in its southward (Alavi et al, 1982).

Sahand – Bazman main faults are forming a network which depends on a riddle zone (Alavi, 1994). Here we segregate joints of folds and faults and calculate fractures of mineralization in related district.

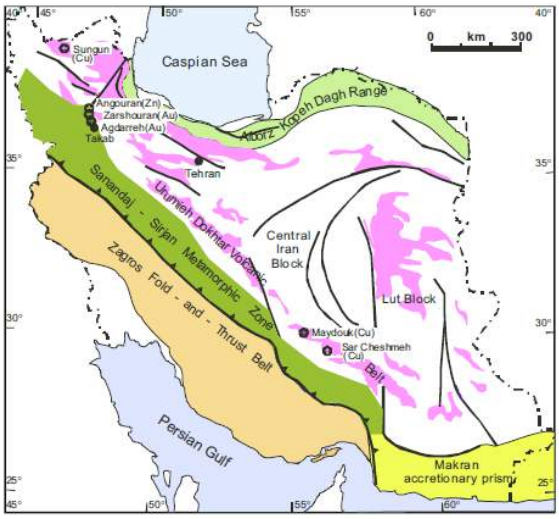

Figure 1. Takab district and Zarshouran epithermal deposit in approximation with Cenozoic –Quaternary magmatic belt, Orumiyeh – Dokhtar which is parallel with Zagros trust and Sanandaj – Sirjan transitional zone (Minerals Production, 2004).

2 REGIONAL GEOLOGY

Zarshouran deposit is located in center of Takab-Shahindezh area that according to Iran's Geological-Structural divisions is part of Orumiyeh – Dokhtar Zone. The most part of this zone includes metamorphic rocks such as Schist, Marble, Ganeiss and Amphibolites that construct the highest mountains (Bolgheis Mountain with height of 3330 and Ghebleh Dagh Mountain with height of 3208 m) at the middle of this area in northwest-southeast direction (Alavi et al. 1982).

Stratum layers in Takab region respectively includes Precambrian metamorphic rocks, late Precambrian – pre-Cambrian and Cambrian – Ordovician sedimentary rocks, Paleozoic metamorphic rocks, diorites, granodiorites and granites, sedimentary rocks, Oligo-Miocene igneous rocks, Pliocene beds and quaternary rocks (Ojaghi, 1996).

Gold sources are located in Ophiolite rock foundations and greenschists of these deposits but mineralization and centralization are performed by magmatic processes such as Tertiary-Quaternary magmatism processes and related hydrothermal solutions which resulted in enrichment of younger rocks (Daliran, 2008).

2.1 Main Structural Procedures in Sahand – Bazman Magmatic Zone

As studied region is part of Sahand – Bazman Magmatic Zone, it is required to review the results of some structural analyses about this magmatic belt and geometrical relation of its main elements.

Sahand-Bazman main faults are constructing a network which depends upon a shear zone that its fractures are developed up to third rank. Primary thrust of right-lateral shear zone which is N125-130 will move in ladder form on the basis of performance of second grade faults and its final and current thrust will be N140. This recommended pattern is extended in all districts of Iran and represents that deformation of every structural zone may depend upon its main thrust and movement of adjacent blocks. Figure 2 is indicating geometrical relations of fractures (Monfared, 2011).

3 Zone Geology

3.1 Rock Units and Present Minerals

Zarshouran deposit is part of southwest crest of anticline in 1:100000 Takhte Soleyman form which generally includes sequential mountains adjacent with deep V valleys. As indicated in figure 3, main rock units in this deposit are as follows:

1. Chlorite Schist Mylonites
2. Serpentine Schist
3. Chal Dagh Crystallized Lime
4. Carbonated Black Shale
5. Recrystallized Lime
6. Porphyry Quartz

And other units.

Gold mineralization in Zarshouran deposit is considerably similar to disseminated epithermal deposit in sedimentary rocks specially carbonated ones (carlin type) (Monfared, 2011).

Some minerals which may be deposited with gold are Orpiment, Realgar, Stibnite, Sphalerite, Galena, Getchellite, Cinnabar, and copper minerals which may be used to

extract Hg, zn, pb, Ascu, and sb. Gangue of this deposit includes quartz, fluorine, barite, and calcite. Paragenetic sequence of Zarshouran deposit is similar to type of carlin and both includes gold, mercury, arsenic, etc. that are formed in late hydrothermal stages (Mehrabi et al, 2003).

It can be concluded that Imankhan schists, Ghal Dagh limes and zarshouran black shale are for Precambrian period which are uplifted by an specific force and being covered with Neogene young units and a long-term fold layer (Monfared, 2011).

3.2 Structural Geology and Region's Tectonics

Structural elements were investigated in 70 Km^2 around of Zarshouran deposit. The studied zone is located in middle part of southwest crest of Imankhan anticline with high protozoic core. This anticline has bilateral plunge with NW-SE (N 125) direction and ellipse form which length and width are respectively about 8 km and 2 km. Imankhan metamorphic complex in located at center of this anticline (Monfared, 2011). Main faults of this area which are affecting deposit's faults and fractures are as follows (figure 4):

1. Tabriz – Zanjan structural line: this line (Zanjan and Mianeh faults) are among the main and basic faults that are located in 70 kilometer of deposit with general direction of northwest – south east (N 130). This is one of the most important structures of northern zone (Monfared, 2011).
2. Shavand fault and parallel faults systems: this is a reverse and right-lateral fault with eastward inclination and N 155-160 direction which is about 65 to 70 kilometer. This thrust with nearest distance of 5 kilometer from studies zone is very important because of its specific role in reformation and generation of mine joints system.
3. Structural Thrust of Ghezel Ozan River: this is located in west of Takab or Ghezel Ozan (more than 200 kilometer width) which is in east of Takhte Soleyman block and has more than 80 kilometer of coincidence with Ghezel Ozan River (Monfared, 2011).
4. N 45 Rock Foundation Thrusts: width thrusts with 42 to 48 direction and staple on main Zagros thrust and Sahand-Zanjan fault. Main thrusts of this field are Sefidroud thrust system (left handed), Talesh-Mianeh thrust (right handed), Aras-Marand (left handed) and eastwart Sahand Block thrust. These have significant role in structural genesis of Iran. This system has considerably affect Imankhan anticline and deposit zone. Frequency of related joints had specific role in mineralization of investigated zone (Monfared, 2011).

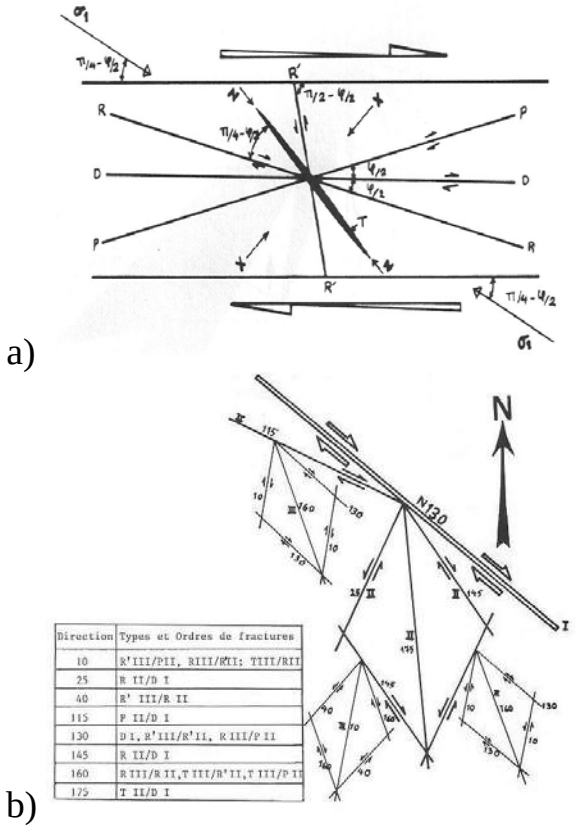

Figure 2. a) Sahand – Bazman faults' system to third grade; b) geometrical relations of 1 and 2 grade fractures (Monfared, 2011)

4 REVIEW OF STRUCTURAL ELEMENTS AND FRACTURES IN STUDIED ZONE

As indicated in figure 3, layers and joints systems were investigated in 4 main structural survey routes, 54 main structural stations, 5 subsidiary structural stations and sampling from 789 joints. 613 items of total

sampled joints were related to Precambrian units, 176 items were related to neogene units that 77 joints were measured in quartz porphyry mass and the others were measured in Oligomiocen sedimentary layer. This progress was performed through analytical methods on Wolf three-dimensional diagrams and Rock Work software diagrams to provide geometrical relations between joints and folds.

4.1 Joints Between Folds

Mentioned joints were formed immediately after impacts of tectonic tensions during various stages of folds formation and their subsequent developments affected by shear deformations, rotary displacements and etc. Four joint systems shall be determined in accordance with folds which are 1) right handed inclined joints (Dd); 2) left handed inclined joints (Dg); 3) longitudinal joints (L); 4) transversal joints (T) (Monfared, 2011). Considering rotation of joints systems of this group around folds, it will be beneficial to understand fold's geometry for realizing better special relation between fractures distribution.

Calculation of bedding of anticline's crest by RockWork software revealed that their transversal rotation will be conical (Figure 5a).

As major part of our study is located in Imankhan anticline's southward crest, local investigations are required for assessing changes of related reformations and may result from transversal shear faults system's performance specifically N 25 system (shear west-east faults). According to figure 5 (a), conical fold's axis is N205/33 which is approximate to anticline's crest incline. Aforesaid processes will develop Z form folds in investigated zone (figure 6). Considering related thrust and direction of southwest crest (N 125) of Imankhan anticline in westward structural survey, there are various joints in this area with average conditions of 004.70, 125.31, 241.76 and 303.57 which are main joints' system depending upon folds in this region (figure 5 b).

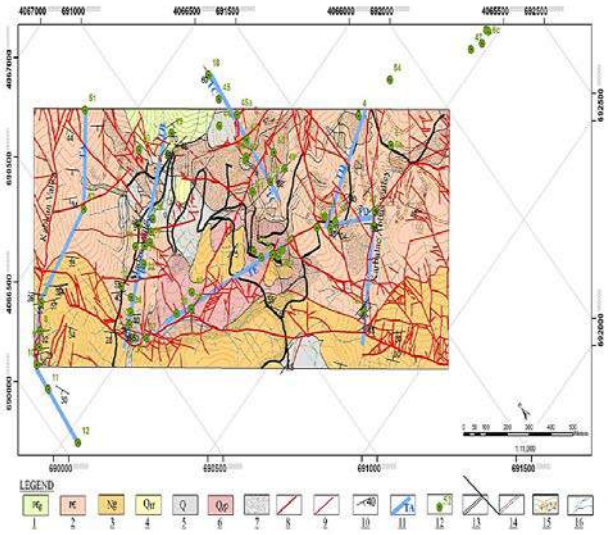

Figure 3. Geology/structural map of Zarshouran gold deposit, structural surveys and sampling stations:
1) Precambrian (Imankhan Schist); 2) Precambrian (Chal Dagh & Ghare Dash Units); 3) Neogene sedimentary – magmatic layer; 4) travertine; 5) alluvium and embankments; 6) quartz porphyry; 7) mineral and diverse units; 8) main fault; 9) subsidiary fracture; 10) bedding; 11) structural survey; 12) structural sampling stations; 13) access road; 14) exploration trench; 15) topography; 16) channel.

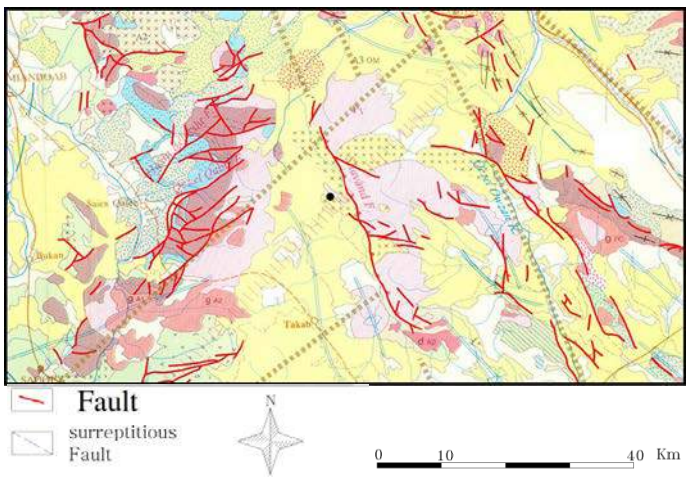

Figure 4. Structural units and elements of current study (SH: Shavand Fault; TB: Takab-Bojar fault thrust; QO: Ghezel Ozan fault thrust (or Takab Eastward Fault); TM: Talesh – Mianeh fault thrust; ZF: Zanjan fault from Zanjan – Tabriz structural line (Monfared, 2011).

4.2 Joints Which Depend Upon Shear Movements

These joints which are relating to shear tectonics are developed in studied area and had formed in latest periods of transition (Monfared, 2011). Shavand reverse dip-slip and right handed fault with 5 kilometers distance from the deposit is located in Shavand and Kouh Ghebleh foothills (figure 4). Its direction is N155 and its length in outcrop is 65 kilometer. Fractures of this shear field have considerable impacts on development of region's fractures and may result in formation of related systems up to 3rd grade in rock units. Expected direction of these joints shall be in accordance with figure 2. Obviously, development of shear faults may require formation of different T, P, D, R, R fractures (figure 2). Distribution of different fractures of a right handed fault with N130 tension is indicated in figure 2 (b) which can be generalized to thrust of Shavand fault (N155). Assuming that Ø = 30 (angle of internal friction), fractures tension will be calculated up to third grade and mean of probable tensions in eight main systems are summarized in table 1.

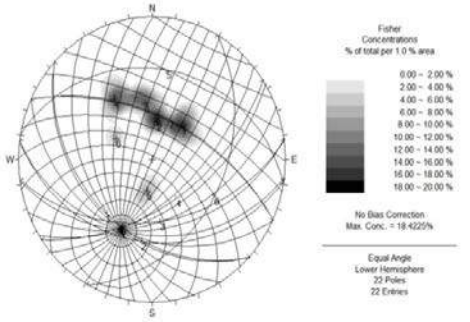

a)

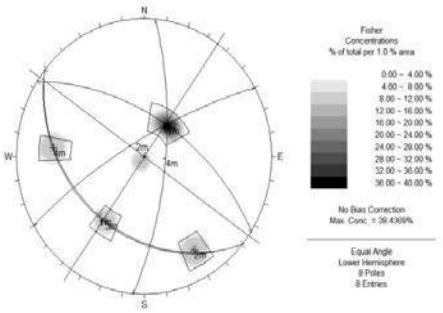

b)

Figure 5. a) Conical fold in southward crest of Imankhan anticline considering performance of right slip transversal fault. b) Bedding and fractures of folds in west survey (AB) of studied zone.

(a) (b)

Figure 6. a) Z form micro fold in lime layer of black carbonated schist of Ghaldagh lime field in eastern side and out of the area between Karbalaei Abbas Valley and Maldarasi. b) Z form subsidiary fold in border of Chaldagh greenschist and lime which indicates normal conditions of anticline crest. This fold is located in northwest corner and entrance of deposit's valley.

According to aforesaid information, it will be possible to analyze joints distribution of shear tectonics and distinguish them from other joints which are related to folds. Moreover, considering the importance of rotary movement in shear tectonics, it will be easy to recognize reasons of consequent changes of fractures' tension. Summary of main faults' thrust in Zarshouran district and related fractures (up to third stage) are presented in tables 1 and 2. Considering results of geometrical analysis, reformation in a right handed shear area may justify current structural relations. Structural curve of folds and fractures which are resulted from rotary movement and their relation with main regional faults can be analyzed in this pattern. Accuracy of this pattern is confirmed on the basis of structural analyses of Sahand-Bazman magmatic zone (figure 2) and related data.

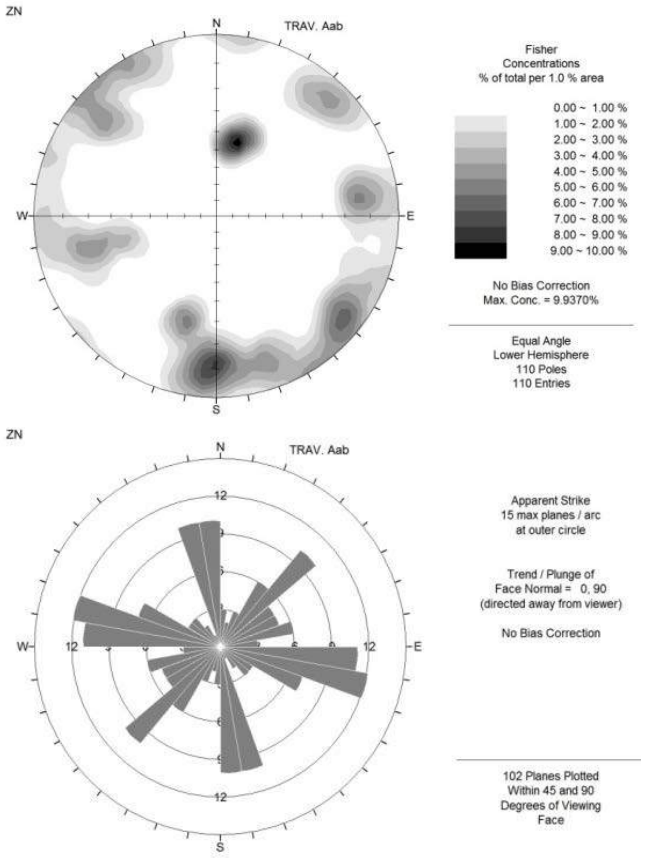

Figure 7. Fractures distribution in structural survey A in Fig. 3

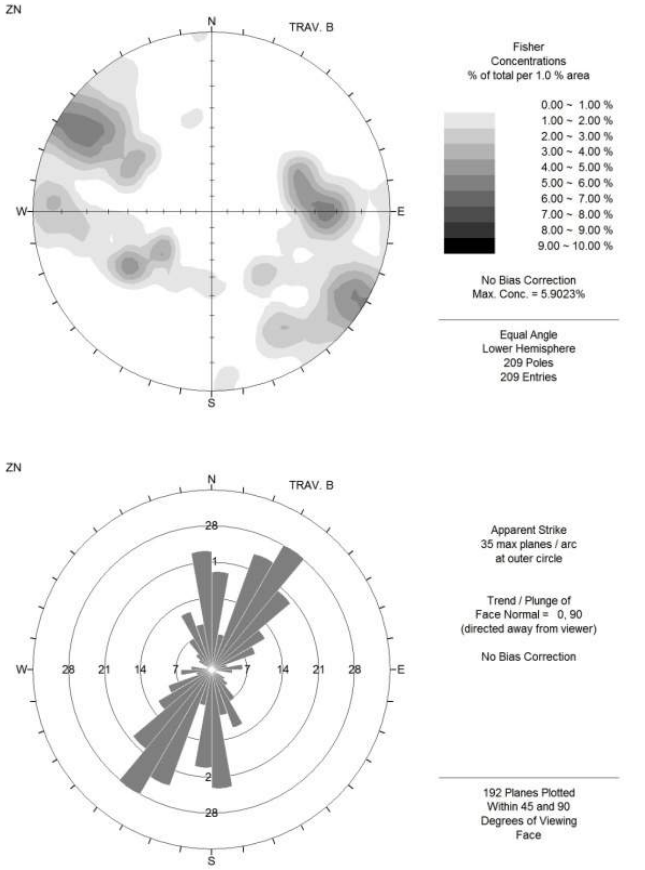

Figure 8. Fractures distribution in structural survey B in Fig. 3

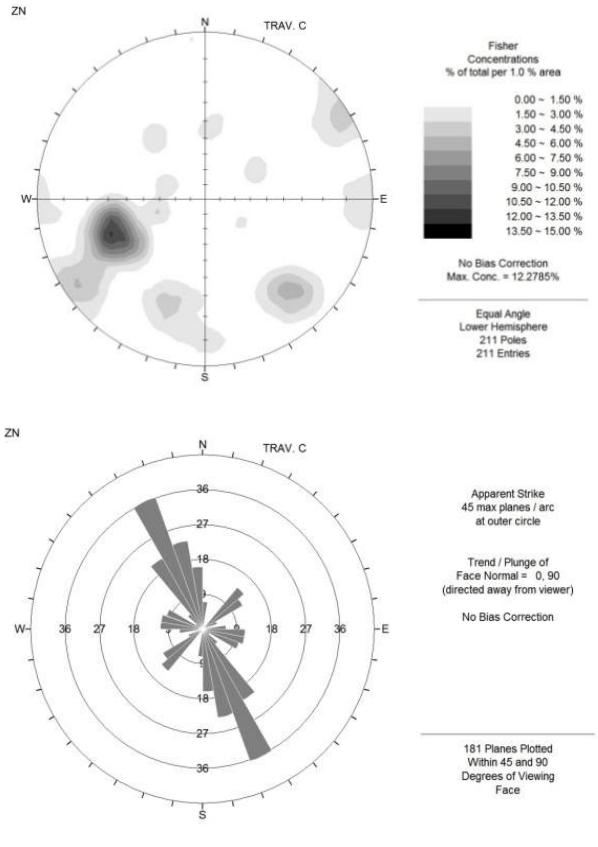

Figure 9. Fractures distribution in structural survey C in Fig. 3

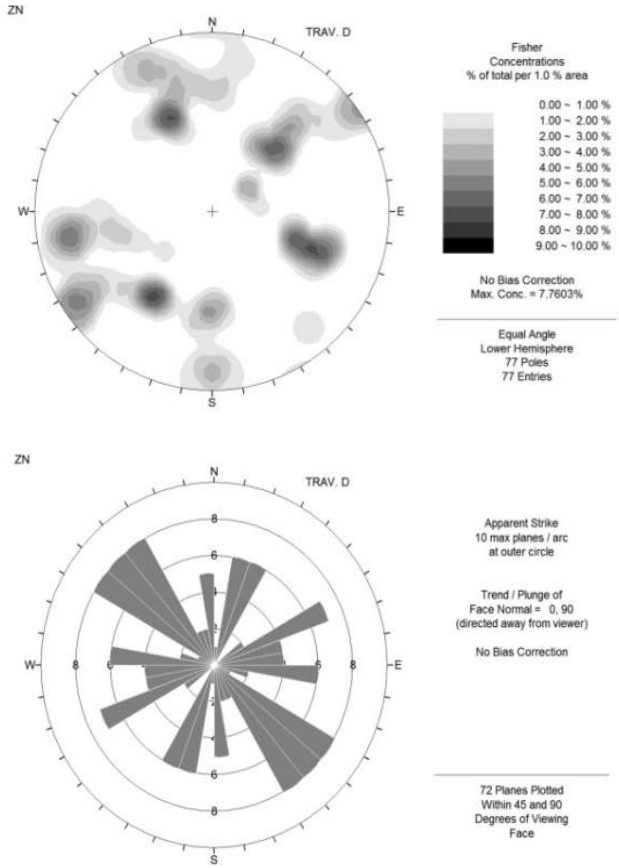

Figure 10. Fractures distribution in structural survey D in Fig. 3

Table 1. Summary of thrust of main fault field's joints (130 & 150). Type and grade of fractures are represented by different colors and letters. (Yellow thrust: N130 system; White thrusts: N155 system). Bold figures are indicating main and common fault thrusts in deposit Zone

	N130	N155	N145	N170	N25	N60	N115	N140
D	130	**155**	145	170	**25**	**60**	115	**140**
R	115	**140**	160	5	10	**45**	130	155
R`	145	170	**40**	**25**	130	165	10	**35**
P	**25**	**60**	130	**155**	**40**	75	100	125
T	175	**30**	10	**35**	160	**15**	160	5
F	85	110	100	125	70	110	70	75
	DI	**DI**	**RII / DI**	**RII / DI**	**R`II / DI**	**R`II / DI**	**PII / DI**	**PII / DI**
	N130	**N155**	**N145**	**N170**	**N25**	**N60**	**N115**	**N140**
D	130	**155**	145	170	**25**	**60**	115	**140**
R	115	**140**	160	5	10	**45**	130	155
R`	145	170	**40**	**25**	130	165	10	**35**
P	**25**	**60**	130	**155**	**40**	75	100	125
T	175	**30**	10	**35**	160	**15**	160	5
F	85	110	100	125	70	110	70	75

1st order
2nd order
3rd order

Right handed

Left handed

Tension Fault
Reverse Fault

Table 2. Summary of 25 probable fractures and their genesis different in a single system. Total fractures of shear field and fold's structure are indicated in this table. Red cells represent main and common fault thrust in deposit zone.

STR	RH	LH	TF	CF	FOLD	
5					Dd	R /T &Dd
10						R` / T
15						T
25						R / R`
30						T
35					Tf	R` /T &Tf
40						R`
45						R`
60						R / R`
65					Dg	Dg
70						F
75						R` / F
85						F
100						F
110						R / F
115						R
125					Lf	R / F &Lf
130						R
140						R
145						R / R`
155						R
160						R / T
165						R
170						R`
175						T

EXPLANATION

Shear Zone:

	Right handed
	Left handed
	Tension Fault
	Reverse Fault

Fold Related :

Lf	Longitudinal
Tf	Transversal
Dd	Diagonal,Right handed
Dg	Diagonal,Left handed

5 MINERALIZATION AND ITS RELATION WITH STRUCTURAL FACTORS

Structural factors and fractures have important role which made researchers to investigate them as a positive sign for exploration of new mineral deposits. Faults, crushed zones and fractures which are relating with folds are appropriate places for upward movements of mineral solutions and their sedimentation in upper zones. Chemical actions and reactions of these hot fluids with subsidiary stones in their flow may result in separation of some metals and replacement of other ones. Accordingly, sedimentation may occur in different stages and on the basis of various environmental conditions such as Eh, PH, thermodynamic conditions and physical and chemical specifications of elements in different stages which may result in formation of an economical deposit.

Data resulted from explorative holes, analysis of samples, and field observations revealed that primary source of mineralization is in Zarshouran carbonated black shale units and Chaldagh lime units which had formed an economical deposit near surface by the impacts of various volcanic and tectonic elements. Comparing structural map of investigated zone (figure 3) and position of drilled holes (figure 11) indicate direct relation between increase of gold carat and purity of other metals in fault and fracture zones. For example, hole no. 1 of F11 fault (figure 3) was stopped in 30 meter dept and 25ppm and 24ppm purity was recorded respectively for gold and silver. Investigating log of hole no. 3 revealed that this hole had broke F1 fault in 45 meter dept and indicated respective purity of 18ppm and 13ppm for gold and silver. These were highest purity in mentioned holes that had recorded in junction of faults. Figure 12 is indicating one of the faults in studied zone. Plants, erosion of rocks and formation of soil had hide deformation and layers of mineralization resources. Surface adjustments provided required conditions for observing conditions of this layer.

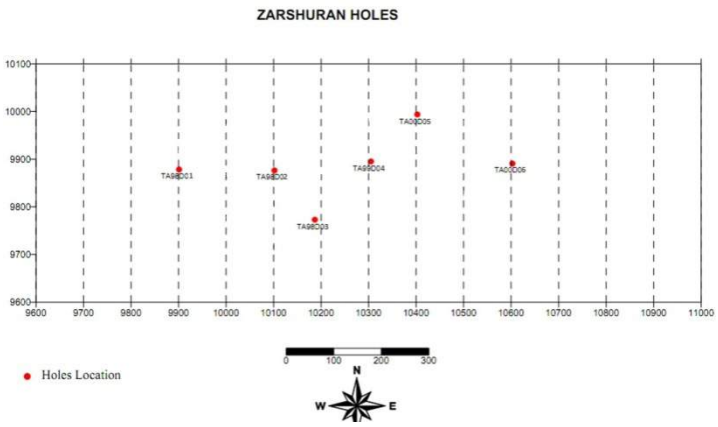

Figure 11. Some Of Drilled Holes In Investigated Zone.

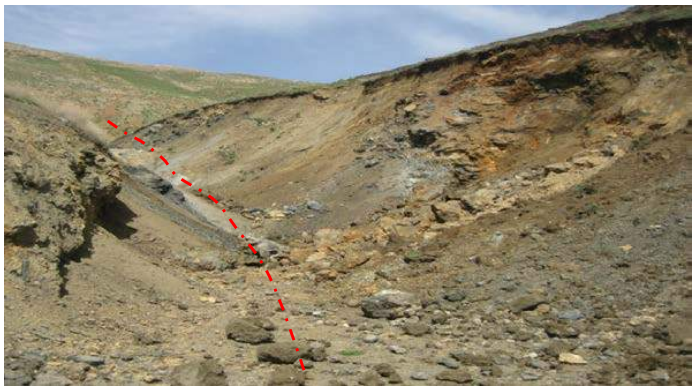

Figure 12. Faults of the investigated zone. Black shale and intense deformation of wall rocks (eastward) are recognizable.

6 RESULTS

Results of geological, field and structural studies, and analysis of samples are as follows:

1. Geometrical dependence of various structural elements in investigated zone (figure 2) are in accordance with combined performance of right handed shear fields with total thrust of N130 and N155.
2. Shear movement is indicating density and significance of regional fractures and development of magmatic phenomena in cenozoic era. These movements and related results (deformation and magmatism) had started in late of upper cretaceous and intensified in third era. The main faults which had affected Eocene rocks can be used as an example.
3. All faults in magmatic belt are relevant with fractures in right handed shear (inclined) zone which at least had developed up to third grade.
4. Basic thrust of N 40-45 is very important for structure of this area. Regional faults of investigated area and even morphology of valleys and channels are affected by this system.
5. It seems that uplifting of lower layers and formation of Imankhan anticline in north of mineralization zone had resulted in genesis of some tension faults and a crushed zone in Shaldagh and Zarshouran rock units which commonly includes lime and shale formations. Removal or decrease of pressure

will provide required conditions for injection and activity of mineralization solutions.

6. Undersurface data and log of drilled holes were reviewed to recognize mineralization host rocks and their development in Zarshouran deposit. The result revealed that host rock of Zarshouran gold deposit is Chaldagh lime unit together with Zarshouran unit.

7. According to data gathered from drilled holes and their logs, it can be concluded that lower schist units (Imankhan) had not affected by mineralization while mineralization solution had respectively penetrate from these schist layers to Chaldagh lime unit and Zarshouran unit.

8. According to performed studies, it is recommended to drill more systematic holes with less distance in Chaldagh lime unit.

REFERENCES

Ojaghi B., 1997, *Economic Geology of Zarshouran Gold Mine*, Pars Kani Company, Iran.

Zandmonfared M., 2012, Geology of Zarshouran Area, Development Organization of Ministry of Trade and Mine, Iran.

Production of Mineral Materials Company, 2005, *Instruction of Representative Samples for Laboratory Tests*, Iran.

Alavi M., 1994, Tectonics of the Zagros orogenic belt of Iran, *New Data And Interpretations. Tectonophysics*, pp211–238

Alavi M, Hajian J, Amidi M, Bolourchi H., 1982, *Geology of Takab-Saein-Qal'eh. GeolSurvIran , R*pt 50, 99p.

Anglo Exploration Gmbh- Final Technical Report – November 2001 -ZarshuranGold Project.

Calcagno P, Chilès JP, Courrioux G, Guillen, A., 2008, Geological Modelling From Field Dataandgeologica Knowledge, Part I. Modelling method coupling 3D potential-field interpolation and geological rules*".Journal Of Physearthplanet Inter* ,pp147–157.

Daliran F., 2008, The carbonate rock-hosted epithermal gold deposit of Agdarreh, Takab geothermal field, NW Iran—hydrothermal alterationand mineralization" .*Miner Deposita*, 43:383–404.

Datamine manual, version 2.1, Datamine Corporate Limited, 30 High Street, Beckenham, Kent BR3 1AY, United Kingdom, http://www.datamine.co.uk/

Rock Mechanics and Geotechnical Applications

A Numerical Study on Deformation Measurement of Rock Materials using Electrical Resistance Strain Gauges

Elektrik Dirençli Gerinim Ölçer kullanarak Kaya Malzemesi Deformasyonu Ölçümü üzerine Sayısal bir Çalışma

E. Komurlu, F. Cihangir, A. Kesimal
Karadeniz Technical University Mining Engineering Department, Trabzon, Turkey

S. Demir
Karadeniz Technical University Civil Engineering Department, Trabzon, Turkey

ABSTRACT This study aims to point out the importance of adhesive type on strain measurement and examine the accuracy of the elasticity modulus determination using the electrical resistance strain gauges glued on solid materials. For this purpose, numerical analysis via finite element method was carried out to examine the adhesive type and thickness considering mechanical properties of adhesives. Numerical studies indicated that deformation levels significantly changed for different models of adhesive types widely used in strain gauge applications. Up to 51% strain loss was obtained through the numerical model for the adhesive interlayer. According to the obtained results from numerical analyses, thin adhesive layers with low elasticity modulus suggested the most proper results. These findings pointed out that adhesive type must be taken into account for electrical resistance strain gauge usage since there is no adhesive guide for users in standards.

Keywords: Deformation, electrical resistance strain gauge**,** strain

ÖZET Bu çalışma elektrik dirençli gerinim ölçer metodu ile deformasyon ölçümü üzerindeki yapıştırıcı etkisine dikkat çekmeyi ve bu yöntemin güvenilirliğinin test edilmesini amaçlamaktadır. Bu kapsamda, yapıştırıcıların mekanik özellikleri dikkate alınarak sonlu elemanlar yöntemi ile yapıştırıcı türü ve kalınlığının etkilerinin incelenmesi için sayısal analizler gerçekleştirilmiştir. Sayısal modelleme çalışmaları yapıştırıcı türüne bağlı olarak ölçülen deformasyon miktarlarının önemli ölçüde değiştiğini göstermiştir. Yapıştırıcı modellerinin %51 oranına kadar birim deformasyon kayıbına yol açmış olduğu sonucu elde edilmiştir. Bu çalışmanın sonuçlarına gore, ince ve düşük elastisite modulü değerlerine sahip yapıştırıcı katmanların daha doğru değerler ölçülmesine olanak sağladığı görülmüştür. Bu bulgular ışığında, elektrik dirençli gerinim ölçer ile birlikte kullanılan yapıştırıcı türünün ilgili standartlarda yer alması gerekliliği görülmüştür.

Anahtar Kelimeler: Deformasyon, elektrik dirençli gerinim ölçer, gerinim

1 INTRODUCTION

One of the ways of measuring rock material deformation is the use of electrical resistance strain gauge which is also applied to measure deformation of other solid materials such as concrete, steel and glass (Hoek, 1965; Ozdogan, 1985; Kahraman, 2003; Komurlu, 2012; Brotons at al., 2014).

It is widely known that the electrical resistance strain gauge was invented by American engineers Edward E. Simmons and Arthur C. Ruge in 1938. First application of the strain gauges was the measurement of the water tank wall deformation to define applied stress. In this first experience, ordinary cigarette paper was

glued on the tank, and a small wire with end-connections glued on the paper was used. Then, Ruge and his team developed the strain gauge devices (Feder, 2000).

The place of deformation measurement via the electrical resistance strain gauge can change the results for rock core specimens tested (Ulusay et al., 2005; Komurlu and Kesimal, 2014; Ocak, 2008; Ocak and Seker, 2012; Roberts, 2013; Howarth, 1984). Additionally, undesired results can be obtained as a consequence of non-homogenous distribution of mineral particles through rock materials. According to the ISRM suggestions, strain gauges should not encroach within half of specimen diameter of specimen ends. In addition, strain gauge lengths should be greater than ten times of the maximum mineral particle size of rock material (ISRM, 2007). However, the effect of adhesive interlayer between strain gauge and rock specimen is omitted on deformation measurements, here.

There is also no definite strain gauge adhesive type in standards (ASTM D7012-10; TS 2030; AS 1012.17-1997). Strain gauges are very sensitive to any strain case and transition from the adhesive interlayer. However, these devices can not directly measure the rock deformations. Since the adhesive interlayer transfers the deformation of rock sample onto the strain gauges, it has influential effect on deformation measurements of rock materials. Physico-mechanical parameters i.e. surface shape, porosity, polymerization, thickness and stiffness are also some important variables to affect the strain transfer ability of the interlayer (Lorenzis et al., 2001). Rock strain is transmitted through a stress field varying with the change of adhesive type. Therefore, a portion of the rock strain can also be absorbed by adhesive material (Ansari and Libo, 1998).

In addition, stress transition through intersurfaces has an important role on the sense of deformation by strain gauge and reversible work of adhesive induced by deformation on adhesive interlayer (Cammarata, 1994). Adhesive solidification time shouldn’t be denied as well, since it significantly affects the properties of the intersurface between adhesive and adherends of rock and strain gauges. Waiting time to place strain gauge after the surface treatment with adhesive is critical especially for fast setting glue products. Temperature increases due to exothermic reactions of adhesive polymerization, hence stress at intersurfaces also varies in accordance with the thermal specification of adhesive type (Jiang et al., 2001). Initial stress on strain gauges before loading the rock samples can vary with strain of adhesives during the solidification reactions. The intrinsic stress applied on rock surface due to adhesive polymerization can also change the rock surface stress field underneath the strain gauge (Hutchinson, 1996). With respect to micro-mechanical framework, lacking of guidance about adhesive details can cause some inaccuracy in measurements of strain-stress.

The most commonly used strain gauge adhesives for solid specimens i.e. rocks, concretes are single component cyanoacrylate, two component epoxy and two component polyester based adhesives (TML Co., 2013). Physical properties of adhesive, curing temperature, clamping pressure, duration and thickness are thought to effect the sensitivity of the interlayer. Pore development during polymerization have also an important role on the stress-strain transition via adhesive interlayer material (Lorenzis et al., 2001; Cammarata, 1994; Ansari and Libo, 1998; Park and Eagar, 2004).

Thin cyanoacrylate layers can be easily set by clamping gently at the room temperature, whereas epoxy based adhesives need to be applied with high temperature, high clamping pressure and time. Quick curing time of cyanoacrylate is a significant advantage having also better/thin interlayer when manually bonded. Cyanoacrylate has the fastest setting among all adhesives since it can almost reach its maximum strength within several minutes (Becker, 2010; Senchenya et al., 2007). Therefore, the application process of strain gauge should be as fast as possible due to the fast

solidification characteristics of such adhesives.

Since two components of epoxy or polyester type adhesives must be consumed with ideal proportions for well polymerization, one component cyanoacrylate has an important advantage to increase the application practicality. There are various types of cyanoacrylate adhesives whose viscosities can change within a large range. Cyanoacrylates with high viscosities can be cured having thick layers under gently applied clamping pressures. On the other hand, low viscous cyanoacrylates can easily flow down and decrease the bonding efficiency between rock and strain gauge.

2 METHODS & MATERIAL MODELS

To investigate the effect of adhesive material type and the thickness of interlayer on strain measurements, a series of finite element analyses were carried out using ANSYS software. Eight node solid brick elements (Solid65) were used for three dimensional modeling of rock which has capability of three degrees of freedom at each nodes: transition in the nodal x, y and z directions, cracking under tension and crushing under compression. Rock material was modeled considering the linear elastic material properties that define behavior of the elements. This model predicts the failure of brittle materials in accordance with the Willam Warnke failure criteria used for concrete, rock and other cohesive-frictional materials such as ceramics (William and Warnke, 1974). Material of loading platens was modeled with Solid185 as a rigid steel having a 400 GPa Elasticity Modulus. Contact surface between rock and loading platens were simulated with Conta174 and Targe170 contact pair. Friction coefficient between rock and steel of loading apparatus was taken as 0.3 for all analysis. Two types of adhesive materials were modeled with different thicknesses to compare deformation measurements obtained. One of the adhesives in finite element analysis (adhesive 1) was modeled in accordance with a data sheet of epoxy adhesive (Akfix, 2013a). Model of adhesive 2 was created considering a technical data sheet of another adhesive which is cyanoacrylate based widely used type in strain gauge applications (Akfix, 2013b). Input parameters of adhesives and rock material models are given in Table 1.

Table 1. Input data for numerical models

Input Parameter	Rock	Adhesive 1	Adhesive 2
Poisson ratio	0.25	0.35	0.40
Elast. Modulus (GPa)	20	2.56	1.33
σ_t (MPa)	4	21.86	9.70
σ_c (MPa)	40	-	-

To investigate the effects of thickness differences arisen from personal application details or adhesive type, adhesive layers with length of 30 mm (same with strain gauge length) were modeled with two different thicknesses of 0.5 mm and 1.0 mm. Cylindrical rock samples with the diameter of NX core size and height to diameter ratio of 2 were modeled as stated in ISRM suggestions (ISRM 2007). Mesh dimensions for rock cylinders and adhesive layers were selected as 2x2x2 mm and 2x2x0.25 mm, respectively. A figure for the model of strain gauge on rock specimen and loading platens is given in Figure 1.

3. RESULTS AND DISCUSSIONS

According to the numerical analysis performed for each of the models, the failure load was achieved at the strain level of 2.26×10^{-3}. To assess the sensitivity of adhesive interlayer, inner and outer surface strains were separately obtained (Table 2). For all conditions, there was a significant difference between the strains of rock (inner) and gauge (outer) sides of adhesive layer. Table 3 shows the ratio between the measured (from the adhesive model) and input elasticity modulus values for the rock models. These findings suggest that significant amount of changes can be encountered in elasticity modulus values due to the differences in adhesive strains between rock and gauge sides.

Table 2. Strains of inner and outer adhesive surfaces

Adhesive type - thickness (mm)	*Inner Strain ($x10^{-3}$)*	*Outer Strain ($x10^{-3}$)*
Adhesive 1-0.5	2.14	1.95
Adhesive 1-1.0	2.03	1.50
Adhesive 2-0.5	2.17	2.00
Adhesive 2-1.0	2.09	1.59

Table 3. Ratio between measured and real elasticity modules

Adhesive	Elasticity Modulus (E_{rock})
Adhesive 1-0.5	1.16
Adhesive 1-1.0	1.51
Adhesive 2-0.5	1.13
Adhesive 2-1.0	1.42

Figure 1 and Figure 2 demonstrate the strain variations through the adhesive. Adhesive types and thickness were seen to significantly affect the measured deformations considering the obtained results from the numerical studies. The results confirmed that stress-strain curves become more representative for the rock surface strain as the adhesive interlayer thickness decreases (Jones, 2009; Liao et al., 2013; Kinloch, 1987). There was significant strain loss through the adhesive interlayer especially for the condition of higher interlayer thickness. It is evident here that the characteristics of adhesives and handling of gluing have an important role on deformation measurements since both mechanical and physical properties of the adhesive interlayer vary with application details (TML Co., 2013).

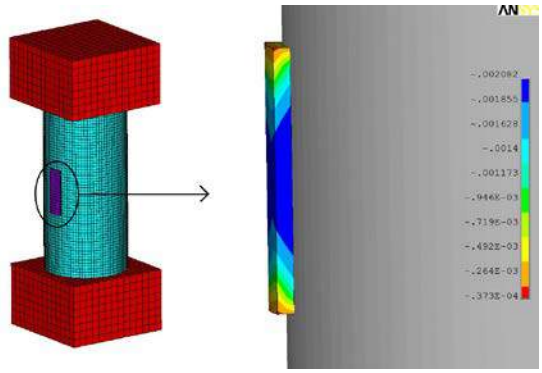

Figure 1. Numerical models of strain gauge and rock

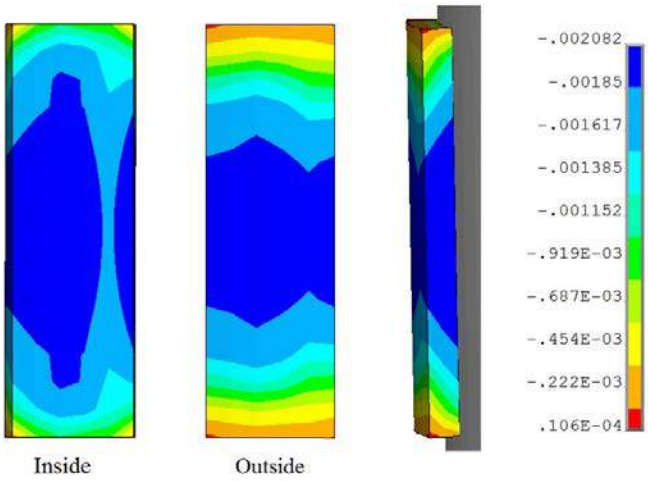

Figure 2. Strain difference between inner and outer surfaces of adhesive layer

Even though the numerical models consider ideal conditions such as perfect adhesion on rock surface and neglect some personal details, 1.51 times greater elasticity modulus than those of rock material was obtained considering the outer surface of the model for epoxy based adhesive.

Considering the adhesive strain which is always known to be less than the strain of rock surface, adhesive giving maximum deformation can be appraised as the most idoneous to be used. It was observed from the analyses that the ratio between predicted (real) and measured elasticity modulus of the models increased with a decrease in the elasticity modulus of adhesive. This data confirms the increase of the deformation sensitivity of adhesive interlayers with a decrease in the elasticity modulus (Paul et al., 2004; Turusov and Kuperman, 2014; Komurlu et al., 2014).

4. CONCLUSION

In this study, different strains up to 1.51 fold were obtained from rock surface and adhesive surface of strain gauge side. Lack of knowledge about standard strain gauge adhesive and acceptance of strain measured with any adhesive may cause important misleading in determination of deformation modulus. Also, ideal gluing application details should be taken into account through the studies to eliminate inaccuracies originating from personal details. For more accurate results, the thickness of the adhesive interlayer should be as thin as possible. This study also showed that increase in elasticity modulus was found to increase the strain loss through the interlayer of adhesive.

REFERENCES

Akfix, 2013a. E334 Epoxy adhesive technical data sheet, Akfix Chemical Co., İstanbul, Turkey

Akfix, 2013b. C709 Super glue technical data sheet. Akfix Chemical Co., İstanbul, Turkey

Ansari, F., Libo, Y., 1998. Mechanics of Bond and Interface Shear Transfer in Optical Fiber Sensors. *J Eng Mech*, 124(4), 385–394.

AS 1012.17-1997. Determination of the static chord modulus of elasticity and Poisson's ratio of concrete specimens, Standards Australia, Sydney

ASTM D7012-10, 2010. Standard test method for compressive strength and elasticity moduli of intact rock core specimens under varying states of stress and temperatures, ASTM International, West Conshohocken, PA.

Becker, M., 2010. Cyanoacrylate: Everything You Need to Know. Woodworker's Journal web article. www.woodworkersjournal.com/

Brotons, V., Toma´s. R., Ivorra, S., Grediaga, A., 2014. Relationship between static and dynamic elastic modulus of calcarenite heated at different temperatures: the San Julia´n's stone, *Bulletin of Engineering Geology and the Environment*, 73, 791–799.

Cammarata, R.C., 1994. Surface and interface stress effects in thin films, *Progress in Surface Science*, 46, 1-38.

Feder, B.J., 2000. Arthur C Ruge, Inventor of Vital stress gauge, dies at 94, *The New York Times*, 4 April.

Halliday, D., Resnick, R., Walker, J., 2005. *Fundamentals of Physics*, John Wiley & Sons, Hoboken

Hoek, E., 1965. *Rock mechanics – an introduction for the practical engineer*, Lecture notes, Imperial College of Science and Technology, London.

Howarth, D.F., 1984. Apparatus to determine static and dynamic elastic moduli, *Rock Mechanics and Rock Engineering*, 17, 255-264.

Hutchinson, W., 1996. *Stress and failure modes in thin films and multilayers*, Notes for a Danish center for applied mathemathics course, Technical University of Denmark, Copenhagen.

ISRM, 1978. Suggested methods for determining the uniaxial compressive strength and deformability of rock materials, *Int J Rock Mech Min Sci Geomech Abstr*, 16, 135–140

ISRM, 2007. *The blue book - the complete ISRM suggested methods for rock characterisation, testing and monitoring: 1974-2006.* Ulusay R, Hudson JA (eds), Turkish National Group of ISRM, Ankara

Jiang, Q., Zhao, D.S., Zhao, M., 2001. Size-dependent interface energy and related interface stress, *Acta Material*, 49, 3143-3147

Jones, M.R., 2009. *Deformation Theory of Plasticity*, Bull Ridge Publishing, Blacksburg, Virginia

Kahraman, S., 2003. Performance analysis of drilling machines using rock modulus ratio, *The Journal of Southern African Institude of Mining and Metallurgy*, 103, 515-522.

Kinloch, A.J., 1987. *Adhesion and Adhesives*, Cambridge University Press, Great Britain

Komurlu, E., 2012. Effects of rock and granular material horizontal stresses on support design (in Turkish), MSc thesis, Karadeniz Technical University Mining Engineering Department, Trabzon, Turkey

Komurlu, E., Kesimal, A., 2014. Evaluation of Indirect Tensile Strength of Rocks using Different Types of Jaws, *Rock Mechanics and Rock Engineering* (Published online: 5 September 2014), DOI 10.1007/s00603-014-0644-3

Komurlu, E., Kesimal, A., Colak, U., 2014. Polyurea type Thin Spray-on Liner Coating to Prevent Rock Bolt Corrosion, *Proceedings of 8th Asian Rock Mechanics Symposium*, Sapporo, Japan, pp. 1389-1397

Liao, L., Huang, C., Sawa, T., 2013. Effect of adhesive thickness, adhesive type and scarf angle on the mechanical properties of scarf adhesive joints, *International Journal of Solids and Structures*, 50, 4333-4340.

Lorenzis, L.D., Miller, B., Nanni, A., 2001. Bond of FRP laminates to concrete, *ACI Materials Journal*, 98(3), 256-264.

Ozdogan, M., 1985. Determination of elastic constants of rock and classification of intact and in-situ rock, *The Journal of the Chamber of Mining Engineers of Turkey*, 24, 41- 48.

Ocak, I., 2008. Estimating the Modulus of Elasticity of the Rock Material from Compressive Strength and Unit Weight, *The Journal of Southern African Institude of Mining and Metallurgy*, 108, 621-626.

Ocak, I., Seker, S.E., 2012. Estimation of elastic modulus of intact rocks by artificial neural network, *Rock Mechanics and Rock Engineering*, 45, 1045-1057.

Park, J.W., Eagar, T.W., 2004. Strain Energy Release in Ceramic-to-Metal Joints with Patterned Interlayers, *Scripta Materialia*, 50, 555-559.

Paul, K.C., Pal, A.K., Ghosh, A.K., Chakraborty, N.R., 2004. Measurements of elastic properties of some coating materials, *Surface Coatings Internationals Part B*, 87(1), 47-50.

Roberts, D.P., 2013. Numerical Simulation of Shear Fracture Evolution in Laboratory Scale Specimens, *The Journal of Southern African Institude of Mining and Metallurgy*, 112, 685-695.

Senchenya, N.G., Guseva, T.I., Golobov, Y.G., 2007. Cyanoacrylate based adhesives, *Polymer Science series C*, 49(3), 235-239.

TML Co., 2013. Adhesive products list: www.tml.jp/e/product/strain_gauge/adhesives_list/#a1

TS 2030 (1975) Turkish Standard for determination of elastic module and Poissons ratio of rocks in uniaxial compression, Turkish Standard Institution, Ankara

Turusov, R.A., Kuperman, A.M., 2014. Elastic Properties of Thin Adhesive Interlayers, *Polymer Science, Series D*, 7(1), 1–8

Ulusay, R., Gokceoglu, C., Binal, A., 2001. *Rock Mechanics Laboratory Experiments* (In Turkish: Kaya Mekaniği Laboratuvarı Deneyleri), JMO, Ankara

Zhao, Y., 2007. Analytical Modeling for Stress-Strain Curve of a Porous NiTi, *Journal of Applied Mechanics*, 74, 291-297.

A Review of the Properties of Foam Mine Fill

M. Hefni, F. Hassani
McGill University, Montreal, Canada

ABSTRACT Foam mine fill is the new material proposed for backfilling mines, and is fabricated by mixing stable foam into a mixture of tailings, binders, and water. This paper investigates the effects of both binder dosage and the amount of foam used upon the mechanical and physical properties of foam fill, mainly in regards to compressive strength, porosity and density.

Samples were prepared using tailings from a copper mine as the inert material, Normal Portland Cement as the main binding agent, and a foaming agent with a foam generator. Samples were cured for 7, 14 and 28 days and were then subjected to unconfined compressive strength (UCS) testing. Select samples were subjected to mercury intrusion porosimetry, so as to study the microstructural properties. An empirical model was then developed, using a response surface methodology to establish a relationship between the investigated parameters.

Keywords: Foam mine fill, binder dosage, compressive strength, porosity, density

1 INTRODUCTION

The disposal of mine tailings is a significant issue in the mining industry, particularly as mine production increases. Many mines re-use mine tailings for backfilling, which is a method for reducing environmental exposure to tailings, maintaining underground stability, and increasing ore recovery (Benzaazoua, Belem & Bussière, 2002).

This paper introduces a new type of backfill called 'foam mine fill' (FMF). This proposed backfill material is similar to cellular concrete, as air bubbles are entrained in cement or lime mortar, resulting in a cellular structure (Narayanan & Ramamurthy, 2000). Air voids can occupy up to 70% of the volume of concrete, which makes it light- weight, and thus can be used for a wide range of civil applications, including backfilling (Tarasov et al. 2010; Panesar, 2013). Unlike cellular concrete, the incorporation of air bubbles into a mixture of tailings, binder and water makes foam fill a potential new backfilling material. Furthermore, a preliminary investigation on foam fill samples found that pulp densities should be optimized before adding the foam, in order to produce consistent samples without foam segregation or losses (Hefni et al., 2014).

This new lightweight material would provide safer working conditions for miners, especially in underhand cut and fill mining where miners work beneath backfilled stopes. Some claim that the new material has many advantages, especially in terms of weight reduction, rheology improvement and cost minimisation (Cellcrete Technologies Inc., 2013).

This research carries out an in-depth study of foam mine fill by investigating its mechanical and physical properties, and ultimately exploring its potential applications and advantages. The paper presents the results of a laboratory experimental study, in which foam fill samples were prepared and tested for UCS after 7, 14, and 28 days of curing. Furthermore, it adopts response surface methodology (RSM) in order to establish a relationship between the parameters investigated and the response observed.

2 EXPERIMENTAL PROGRAM

2.1 Materials

2.1.1 Tailing

In this research, a copper tailing with the specific gravity of 2.9 g/cm^3 was used to prepare the foam mine fill samples. The tailing primarily consisted of quartz and albite, as well as small amounts of calcite, muscovite, actinolite, rhodoch anorthite, chalcopyrite, biotite, pyrrhotite, epidote, and chlorite. The particle size distribution of the tailing, as shown in Figure 1, was determined using sieve analysis, in accordance with ASTM C136-06 (ASTM International, 2006a).

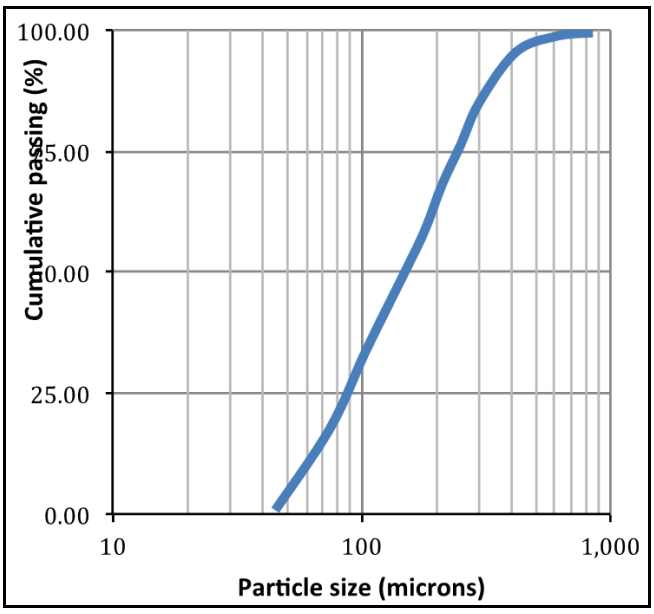

Figure 1. Particle size distribution of copper tailing

2.1.2 Binder

The use of a binder is the most costly component of backfill material, as it represents 75% of the total backfill costs (Hassani & Archibald 1998). This study used normal Portland cement, provided by Lafarge Canada, and with a specific gravity of 3.15 g/cm3, as the binder, since it is used in most Canadian mines. However, other binders, such as slag, fly ash or a blend of different binders are also being considered for further investigation.

2.1.3 Foaming agent and foam generator

Within this research it was essential to use both a high quality foaming agent and an aerator machine in order to ensure foam consistency. Based on previous experimental investigations, inconsistent foam yields samples with different physical and mechanical properties, despite their having the same mixture design (Marquez & Hassani, 2010). These problems were resolved by using the Stable Air® system, which uses Stable Air admixture (complies with ASTM C260 standard) and the Stable Air M100 aerator (ASTM International, 2010a). The foaming agent is a liquid air−entraining admixture consisting of a unique blend of synthetic materials (Cellular Concrete Technologies, Inc. 2013). Admixture is diluted with water to a ratio of 1:120, combined with compressed air, and processed through a patented foam generator in order to output Stable Air foam with a consistent density of 69 kg/m3.

2.1.4Sample preparation and curing

FMF samples were prepared using cylindrical, polyvinyl moulds, with dimensions of 4 inch high and an internal diameter of 2 inches. Samples were cured for 28 days inside a curing chamber, where the relative humidity was kept constant at 90% ± 2%, and temperature was controlled at 25°C ± 2°C to simulate underground conditions. Furthermore, grinding was used to flatten the surface of the samples, in order to make them suitable for the UCS test.

2.2 Methodology

2.2.1Experimental design

Foam fill samples were prepared using three different levels of both binder dosage and amounts of entrained air (Table 1). Pulp density was optimized to 78% to avoid foam loss or segregation. Equation 1 and 2 display the formula used to calculate the binder dosage and mass of foam in the foam fill base mix.

Table 1. Levels of factors tested

Factor	Level 1	Level 2	Level 3
Binder (%)	5	7	9
Air volume (%)	0	10	20

$$\text{Binder (\%)} = [M_b / (M_b + M_t)] \times 100 \quad (1)$$

$$\text{Mass of foam (kg)} = \text{fill vol.} \times \text{air \%} \times \rho_f \quad (2)$$

Where:
M_b = Mass of cement (kg).
M_t = Mass of tailing (kg).
ρ_f = foam density (kg/m^3)

Furthermore, face centred central composite design (FCD), a type of RSM design, was adopted to analyse the experimental results, as well as to develop an empirical model through a statistically designed experiment (Anderson & Whitcomb, 2005). The design establishes a relationship between the factors studied and the response observed, via first-degree or second-degree polynomial models.

Therefore, nine total numbers of runs were required, and Table 2 shows the mixture characteristics of the foam fill samples that were prepared. The response analysed the UCS values after 28 days of curing. DOE PRO® software (SigmaZone, 2013), which calculates the main effect of each factor, and finds which factor has the biggest influence on the UCS values, was used to analyse the results. Furthermore, this software can detect any interactions between these factors. Finally, mercury intrusion porosimetry (MIP) was conducted to investigate the microstructural properties for two selected samples.

Table 2. Mixture characteristics of the samples prepared

Run#	Binder %	Air%
1	5	0
2	5	10
3	5	20
4	7	0
5	7	10
6	7	20
7	9	0
8	9	10
9	9	20

2.2.2 UCS test

UCS tests were conducted in accordance with ASTM D2166-91 (ASTM International, 2006b) on triplicate foam fill samples after 7, 14, and 28 days of curing, from which the overall average was taken. The tests were conducted immediately after removing the samples from the humidity chamber.

3 RESULTS AND DISCUSSION

3.1 Strength Development of Foam Fill

The UCS results displayed in Figures 2, 3, and 4 show the strength development of foam fill samples at different amount of entrained air and with different curing days. In average, 60-80% of the compressive strength is achieved after seven days of curing. This can be explained by the use of Portland cement as the main binding agent, since it has a higher hydration rate than any other binders.

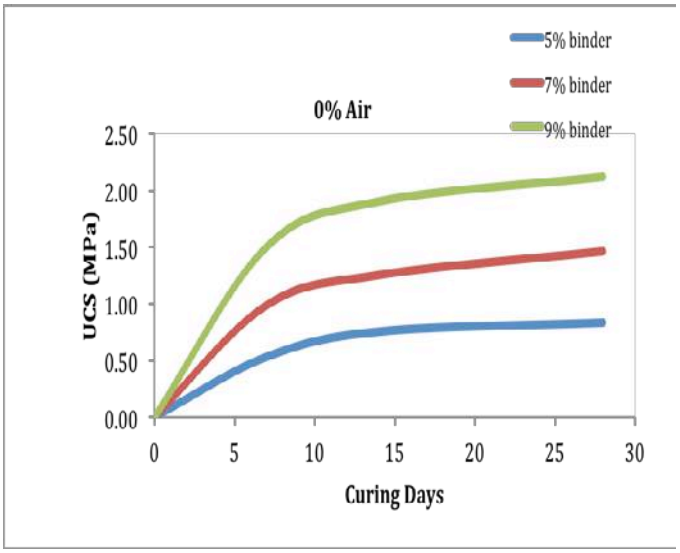

Figure 2. Effect of curing age on UCS at 0% air

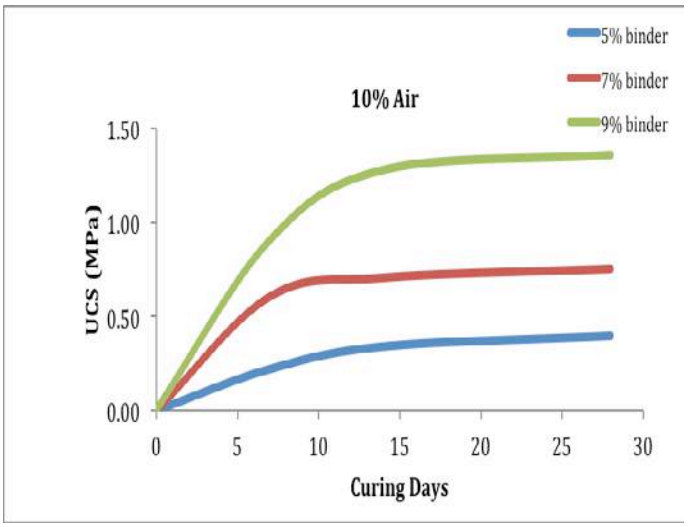

Figure 3. Effect of curing age on UCS at 10% air

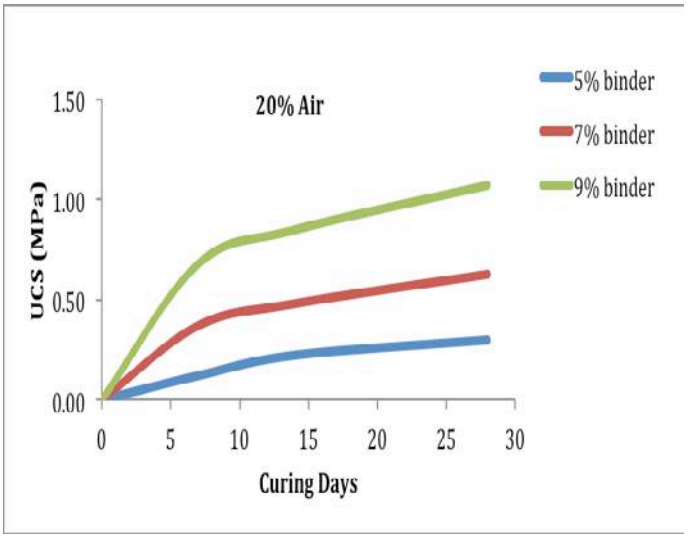

Figure 4. Effect of curing age on UCS at 20% air

3.2 Effect of Binder Dosage and Amount of Air Entrained Upon Foam Fill Properties

The relative effects of both the investigated factors and the interactions between them, in terms of compressive strength, can be graphically represented in ordered horizontal bars by a Pareto chart (Figure 5). This chart clearly shows that the main factors responsible for strength development in foam fill compressive strength, in order, are binder dosage, air volume, quadratic effect of air volume, interaction between binder dosage, and air volume, and finally quadratic effect of binder dosage. Furthermore, they were all found to be statistically significant with a p-value < 0.05.

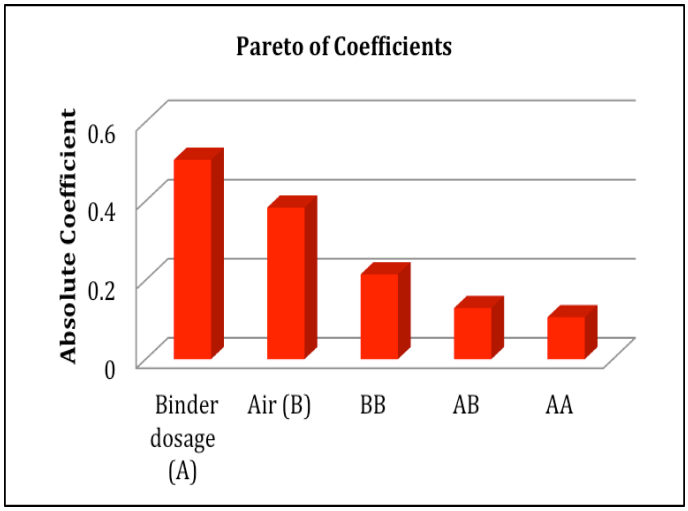

Figure 5. Pareto chart of the relative effects of FMF compressive strength

An empirical model was developed after analysing the data with DOE PRO® software (Equation (3)). Based on this model, measured UCS values were plotted against predicted values in the residual plot shown in Figure 6. The experimental and predicted data can be fitted in a straight line with a R^2 value of 0.9939

$$USC_{28days}\ (MPa) = 0.45 - 0.055A - 0.036B - 0.0065\ AB + 0.027A^2 + 0.0021B^2 \quad (3)$$

Where:
A = Binder dosage in %
B = Air volume in %

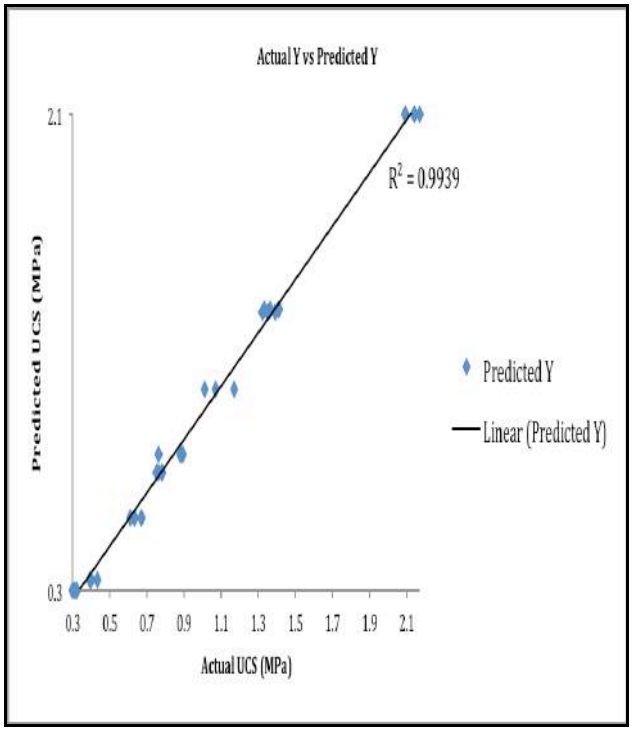

Figure 6. Residual plot of measured and predicted results

The surface response obtained is graphically represented in Figure 7, while Figure 8 shows the top view of this surface.

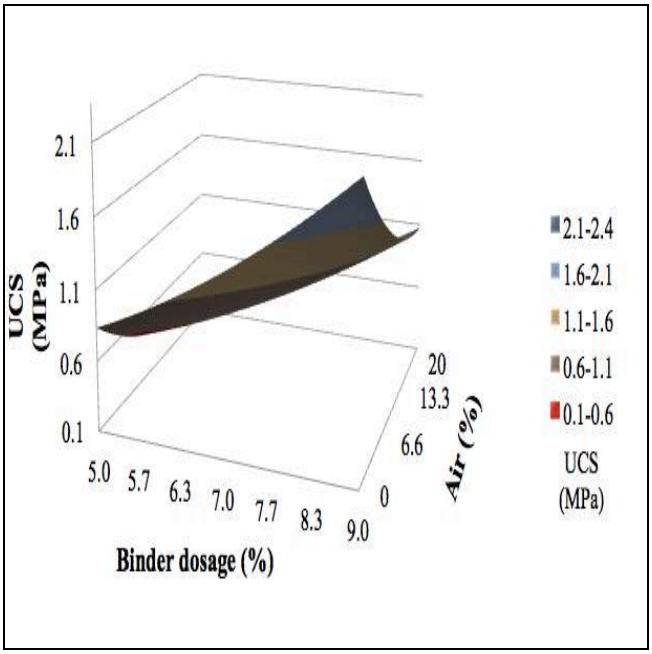

Figure 7. Response Surface of 28 day UCS in 3D view

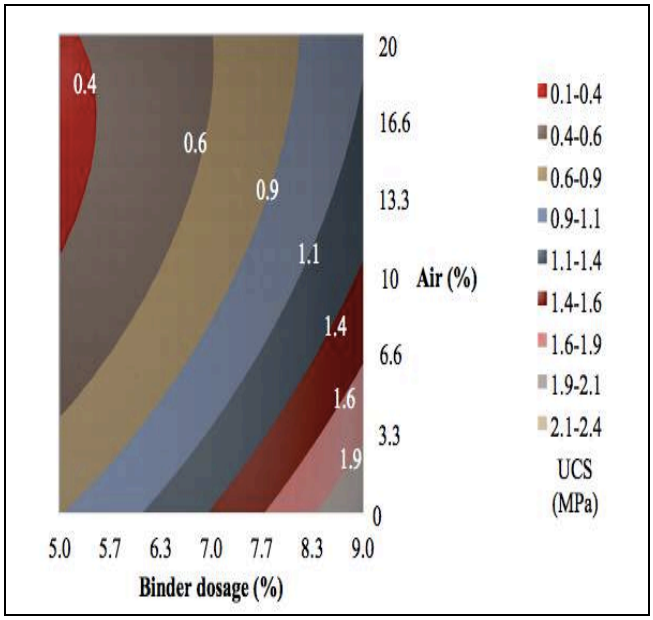

Figure 8. Contour map of 28 day UCS in 2D

The contour map in Figure 8 is used to predict the UCS value for any given binder dosage and air volume. Moreover, it displays an inverse relationship between the amount of air entrained and UCS. On the other hand, there is a direct relationship between binder dosage and UCS. This can be explained by the addition of air in a more porous sample, and hence its decrease in UCS value. This can also be illustrated in Figure 9, in which fill density decreases with the addition of more air.

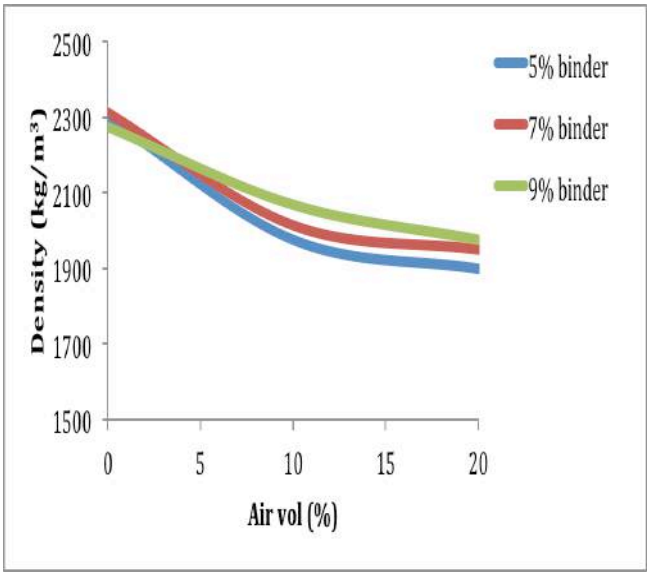

Figure 9. Effect of air volume in 28 day fill density

Finally, the decreases in UCS values are not linear. UCS drops dramatically by 5% for every 1% of additional air. This has been observed when air volume is increased from 0% to 10%. However, when air volume increases from 10% to 20%, UCS drops by 3% for every 1% of additional air. This explains the non-linearity of the empirical model obtained.

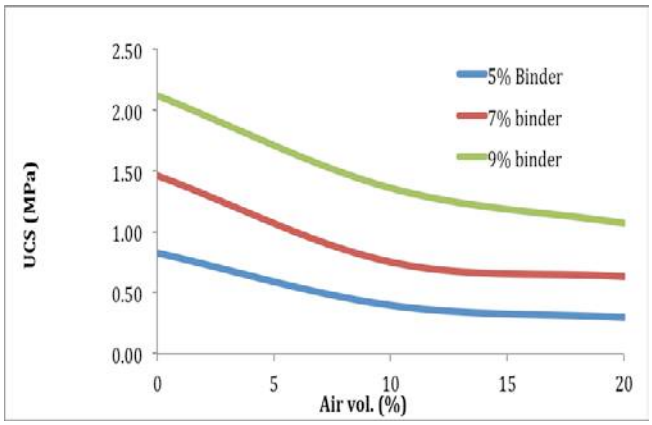

Figure 10. Effect of air volume in 28 day UCS

3.3 Foam Fill Microstructural Properties

In order to investigate the microstructural properties of FMF and its influence upon UCS results, MIP was conducted on two selected samples after being cured for 28 days, one of which had 0% air while the other had 20% air. Binder dosage and pulp density were kept constant at 9% and 78%, respectively.

Figure 11 displays the differential pore size distribution of the FMF samples, where the size of pores can range between 200 and 0.006 µm. Morover, at 0% air most of the pores are in the 1 to 10 micron range, while at 20% air most pores are in the range of 1 to 50 microns. Therefore, those samples with a higher air volume contain a notable increase in pores sizes and frequency. The total porosity of foam fill samples at 10% air and 20% air were 32.66% and 40.57%, respectively (Figure 12). This explains the higher UCS value obtained from the sample with 0% air at 2.13 MPa, in comparison to the sample with 20% air at 1.06 MPa.

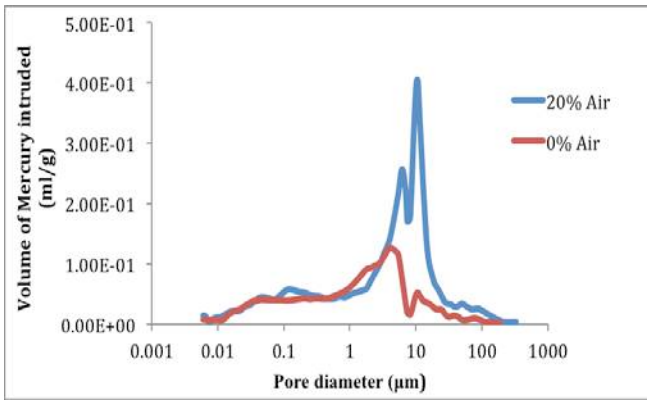

Figure 11. Differential pore size distributions of foam fill samples

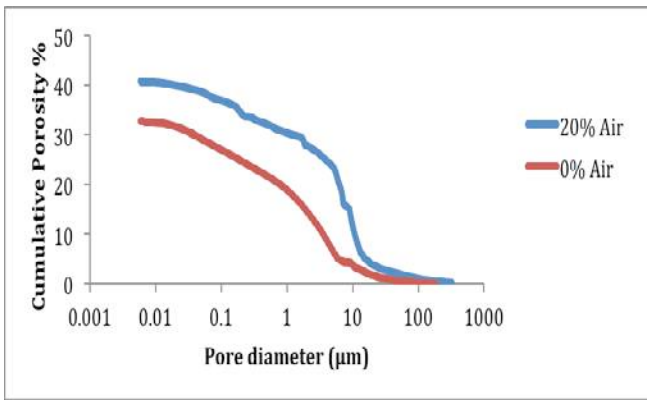

Figure 12. Pore size distributions of foam fill samples

4 CONCLUSION

An empirical model using RSM was developed in order to investigate the properties of foam fill, and it found that UCS values decrease non-linearly in relation to an increase in the amount of entrained air. Moreover, fill density decreases with the increase of the amount of entrained air, which was demonstrated by investigating the microstructural properties, and particularly the increase in porosity at 20% air. This results in a lighter filling material, which can provide a safer working environment for miners. However, the use of foam fill might be restricted, due to its high consumption of binders for maintaining an equivalent strength. There is the potential for foam fill to be used in mines where there is a shortage of tailings. The addition of air can complete the void in fillings, and reduce mining costs of buying sand or tailings from other mines for backfilling purposes.

REFERENCES

Anderson, M.J. & Whitcomb, P.J. (2005), *RSM Simplified*, Productivity Press, New York, New York.

ASTM International (2010a), *ASTM C260: Standard Specification for Air-Entraining Admixtures for Concrete*, ASTM International, West Conshohocken.

ASTM International (2006a), *ASTM C136-06: The Standard Test Method for Sieve Analysis of Fine and Coarse Aggregates*, ASTM International, West Conshohocken.

ASTM International (2006b), *ASTM D2166-06: Standard Test Method for Unconfined Compressive Strength of Cohesive Soil*, ASTM International, West Conshohocken.

Benzaazoua, M., Belem, T. & Bussière, B. (2002), 'Chemical factors that influence the performance of mine sulphidic paste backfill', *Cement and Concrete Research*, vol. 32, no. 7, pp. 1133-44.

Cellcrete Technologies Inc. (2013), *Cellcrete Technologies Inc: Cellular Paste Backfill*, Cellcrete Technologies Inc., Blaine, viewed 27 November 2013, http://www.cellcrete.com/cellularPasteBackfill.htm.

Cellular Concrete Technologies, Inc. (2013), *Stable Air® Foaming Agent*, Cellular Concrete Technologies, Inc., Irvine, viewed 27 November 2013, http://www.cellularconcretetechnologies.com/sa_foaming_agent.html.

Hassani, F.P. & Archibald, J.F. (1998), *Mine Backfill*, Canadian Institute of Mining, Metallurgy and Petroleum, Westmount.

Hefni, M., Hassani, F., Nokken, M., Kermani, M. and Vatne, D. (n.d.). Investigation into the development of foam mine fill.

Marquez, G. and Hassani, F. (2010). An Investigation into Foam Backfill. [report] McGill University.

Narayanan, N. & Ramamurthy, K. (2000), 'Structure and properties of aerated concrete: a review', *Cement and Concrete Composites*, vol. 22, no. 5, pp. 321-9.

Panesar, D. (2013), 'Cellular concrete properties and the effect of synthetic and protein foaming agents', *Construction and Building Materials*, vol. 44, pp. 575-84.

SigmaZone (2013), DOE PRO, http://sigmazone.com/doepro.htm.

Tarasov, A., Kearsley, E., Kolomatskiy, A. & Mostert, H. (2010), 'Heat evolution due to cement hydration in foamed concrete', *Magazine of Concrete Research*, vol. 62, no. 12, pp. 895-906.

Advanced Data Processing of Ground-Based Synthetic Aperture Radar for Slope Monitoring in Open Pit Mines

A. Michelini, N. Coli, F. Coppi, P. Farina, L. Leoni
IDS Ingegneria dei Sistemi SpA, Pisa, Italy

F. Costa
IDS Brasil, Belo Horizonte, Brazil

T. A. Costa, T. Costa, G. Funaioli
Vale S.A., Belo Horizonte, Brazil

ABSTRACT Nowadays ground-based Synthetic Aperture Radar Interferometry (GBInSAR) is used internationally as a leading edge tool for the near real time monitoring of slope movements on landslides and open pit mines for either safety-critical and background monitoring purposes. The success of the technology relies mainly on its ability to rapidly measure slope movements with sub-millimetric accuracy over wide areas and in almost any weather conditions. In recent years, GBInSAR has experienced significant improvements in its performances, thanks to the development of more advanced radar techniques on both data processing and sensor performances. In this paper an advanced data processing chain able to simultaneously measure a wide range of deformation rates, across four orders of magnitudes, from very fast movements (up to 150 mm/hour) to extremely low displacements (few mm/month), is presented. The new processing may result in an early detection of slow movements making possible to support mine planning activities, to review extraction methods, mine design, ground support and monitoring practices before movements start to interfere with operations and any problem become difficult or too expensive to be managed. The processing method is presented along with recent successful studies in several Brazilian iron ore mines with different characteristics, owned by Vale S.A. In the sites radar data have been integrated and compared to displacement measurements acquired by radar images and total stations over tens of prisms, in order to improve the interpretation of the local slope movements. This technique could be applied to support long term monitoring in extensive areas adding to the traditional systems and also to define target areas for deeper investigations.

Keywords: Slope monitoring, Open pit, Synthetic aperture radar interferometry (GBInSAR)

1 INTRODUCTION

In the surface mining industry a comprehensive slope monitoring program, aimed at managing potential large-scale instabilities and able to detect at the same time local scale movements, should represent an integral part of every effective slope management system. Among all the parameters to be considered and included in an effective slope monitoring program displacements, either surface or sub-surface components, play a crucial role. In fact, in open pit mines large failures are usually preceded by small scale slope movements, sometimes limited to few centimeters of total displacement and typically characterized by temporal evolutions ranging from several hours to several weeks or months.

The capability of providing advanced notice over the whole slope of impending instability conditions, through the accurate and timely measurement of precursors to slope collapses clearly represents an outstanding benefit for the staff of the pit

involved in the management of geotechnical risk.

The use of ground-based Synthetic Aperture Radar (GBInSAR) in open pit mines is today a standard practice for safety critical monitoring of the pit walls. SAR radar units are effectively used to get a better understanding of the spatial distribution of slope movements and for the provision of alerts in the event of progressive movements that can potentially lead to slope failure, thus aimed at assessing the safety of workers and increase the mine productivity.

Early detection of ground failure allows mine operators to plan and implement appropriate actions (evacuation plans) with sufficient notice to minimize the effect of the failure on personnel safety and mine productivity. GBInSAR radar technology presents the advantages of high accuracy of the measurements, long-range capabilities, limited impact of atmospheric artifacts on the measurement performances, and possibility to simultaneously acquire the response over a large area of the slope without reducing the acquisition time (Antonello et al., 2004; Bozzano et al., 2011; Farina et al, 2011, 2013; Pieraccini, 2013).

The long datasets typically acquired by GBInSAR systems installed in open pit mines (years of continuous data) thanks to the long range and the resulting possibility to monitor the pit slopes without relocating the radar during blasting as it often happens with real aperture radar characterized by shorter working range, have recently made it possible to measure very slow movements over long time periods. Such a possibility makes possible to use slope monitoring radar not only to measure fast movements potentially leading to failures of the slope but also slow movements over years. Here we present the results of advanced data processing algorithms for GBInSAR data developed by the authors able simultaneously to measure a wide range of displacement rates, across four orders of magnitudes, from very fast movements (up to 150 mm/hour) to extremely low displacements (few mm/month), with very high accuracy level (1/10 mm). These advanced capabilities open the doors of a new concept of radar monitoring, where radar also becomes a valuable source of information to better understand the slope behavior before movements start interacting with mining operations. In fact, early recognition of ground movements allows reviewing extraction techniques, mine design and ground support before the instability become difficult or expensive to mitigate. Vale's iron ore geotechnical team, have successfully implemented the advanced monitoring based on the IBIS radar GBInSAR, not only for fast movements but also develop a robust geotechnical model of the slope by taking advantage of the possibility to monitor very slow deformations over a time period of several months. In these sites radar data have been integrated and compared to displacement measurements acquired by total stations over tens of prisms and satellite images in order to improve the interpretation of the on-going ground instability issues. Text is typed in this field as justified.

2 GBINSAR FOR SAFETY-CRITICAL AND LONG TERM SLOPE MONITORING

A ground-based SAR system with Interferometric capabilities is characterized by a limited number of moving parts, being composed by a radar sensor with a couple of small horn antennas that illuminate the monitored area while sliding along a long linear scanner (Pieraccini, 2013). Modern GBInSAR systems perform a full resolution scan of the observed area in a short time (e.g. less than 3 minutes). Fast scan time means reduced impact of atmosphere on radar data and higher sensitivity to the onset of potential failure thanks to the higher sampling rate. The radar used in the two Vale mines described in this paper, are IBIS units. IBIS radar is produced by the Italian company IDS (Farina et al., 2011).

Slope monitoring radar based on real aperture radar technology (typically large dish antennas used to scan the observed scenario) were originally introduced into the

surface mining industry for near real time monitoring of specific “critical” areas of the pit, providing alarms in case of fast movements potentially leading to the failure of a portion of the slope. Due to the constraints induced by the spatial resolution achievable using real aperture radar, by their consequent limited working ranges and the significant time needed to acquire a single radar image those areas have been limited to small sectors of the pit where movements were first detected by conventional monitoring systems such as total stations or geotechnical sensors. The introduction of GBInSAR systems into the mining industry from 2010, thanks to its longer working range (resulting in wider spatial coverage) combined with its fast acquisition, made possible to revolutionize the typical application of slope monitoring radar, passing from a “tactical” use focused on critical areas to a combined and joint “strategic” and “tactical” use. GBInSAR systems in fact are effective used to either cover every few minutes large areas detecting movements over the entire pit slopes and at the same time to follow fast movements in specific sector of the pit, providing alarms in case of fast acceleration.

A further recent advance in the use of slope monitoring radar is associated with the capabilities of GBInSAR to acquire long datasets in combination with innovative processing algorithms to extend the measurable velocity by those systems, including not only fast movements (e.g. mm/day, cm/ day) but also very slow movements (mm/month, mm/year). Any device aimed at measuring displacement can measure it only when the total displacement occurred between the acquisitions used to measure it is substantially over the noise level of the instrument. Considering the typical accuracy of GBInSAR systems (up to 1/10 mm), it follows that in order to detect slow movements such us mm/month or mm/year it is necessary to consider long time intervals in order to give enough time to the movement to exceed the measurement noise. This concept can be easily explained by referring to the interferograms (the maps showing the raw phase variation, proportional to the total displacement) extracted from a radar dataset (Fig.1).

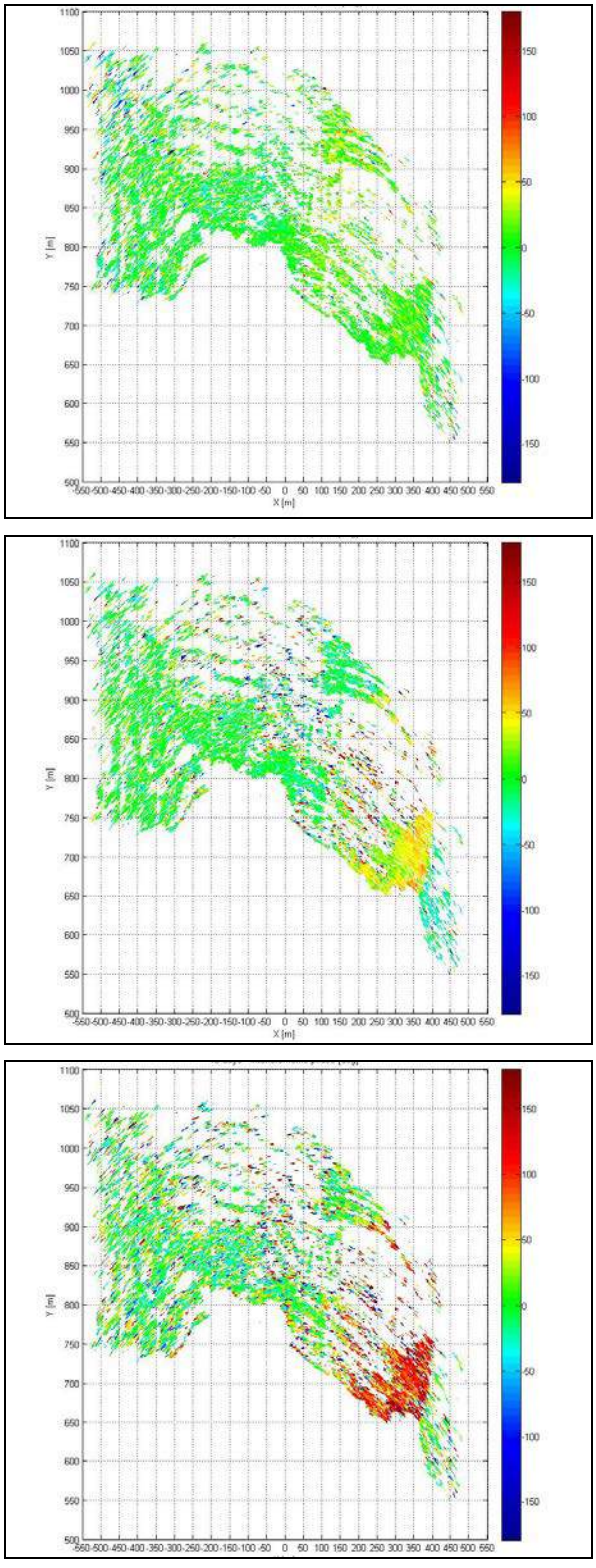

Figure 1. Interferometric phase over 5 minutes, 10 days and 15 days.

From those maps it is clear that the moving areas (yellow and red pixels) can be detected only starting from the interferograms covering a time interval of about 10 days. Unfortunately, since GBInSAR data are

based on the measurement of the signal phase, thus being affected by the phase-wrapping phenomenon, computing the interferomatric phase on a longer time interval leads to possible missing detection of faster movements. Moreover, long time interval between consecutive images typically introduces temnporal de-correlation of the radar signal, thus increasing the noise of the displacement measurement. The only way to detect fast and slow movements in a unique real-time processing chain relies in the combination of parallel processing done at different temporal scales.

The authors have developed an algorithm able to process in real time data at different temporal scales (e.g. for fast movements by processing every consecutive image acquired every 3 minutes, then by processing data every 12 hours, 24 hours, etc. for slower movements). This new processing chain, called “multiscale”, allows to automatically and accurately measure displacements across four orders of magnitudes (from up to 150 mm/h to few mm/month). The algorithm combines the standard high-performance real-time processing routines for safety critical purposes, with an advanced routine able to track slow moving areas with average velocities below a few mm/month.

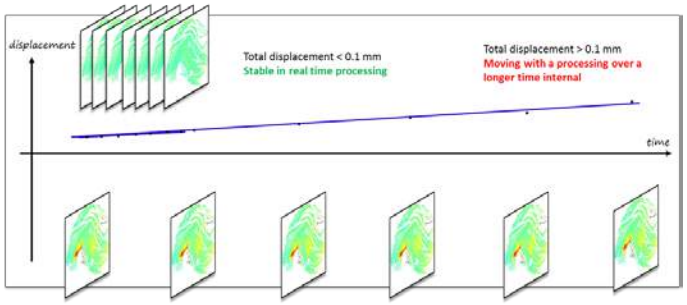

Figure 2. Conceptual scheme of the multi-scale approach.

To simplify the concept of the proposed new processing method, let’s consider an area with slow movements, e.g. 2 mm/month. By processing data every 3 minutes in real time, the movement will not be detected (and the area will be considered stable) until it will exceed the minimum sensitivity to movement of the radar. Considering that 2 mm/month corresponds to 0.06 mm/day and that the minimum sensitivity to movement of the radar is 0.1 mm, this means that before the radar will be able to detect some movement it will take at least a couple of days. If in parallel to the real time processing another processing is run with data under-sampling (e.g. by processing one radar image every 12 hours), after a couple of days that movement will be detected. The multi-scale approach simultaneously analyses the data at different temporal scales and select from each temporal scale the most reliable displacement measurement. The multi-scale approach is composed of following two main steps:

–parallel displacement analysis at different time scales

– merging of the multi-scale analysis into a single multi-scale displacement map

The merging process merges all the single-scale measurements into a single overall displacement map. The merging is performed by dividing the observed displacement velocities into independent (zero-intersection) ranges. Each velocity range is estimated by a correspondent single-scale analysis.

The result of the multi-scale processing is the extension of the velocity range measurable with a slope monitoring radar. By referring to the landslide velocity scale proposed by Cuden and Varnes (1996) slope monitoring radar, thanks to the new proposed processing approach can extend the range of velocity covered adding to moderate and slow landslides very slow (below 1.6 m/year) and extremely slow (below 16 mm/year) events.

In the following sections the results of the multi-scale algorithm used in two test sites in Brazil are presented.

3 GEOLOGICAL AND GEOTECHNICAL OVERVIEW OF VALE’S IRON ORE MINES IN IRON QUADRANGLE – BRAZIL

Vale´s iron south division mines (DIFL), are located in the west part of the Iron Quadrangle (IQ). on the Moeda and Don

Bosco Synclines and Curral Homocline ranges as presented in Figure 3.

The Iron Quadrangle , located in Minas Gerais State (Brazil), in the southern border of São Francisco Craton is one of the most important mineral provinces of the world and concentrates world class mines of gold, iron and manganese mostly. The structure is delineated by the roughly quadrangular arrangement, with Paleoproterozoic Banded iron Formations (BIF) of the Minas Supergroup, as proposed by Dorr (1969).

The iron ore host is composed of hundreds of metres of iron ore rich, banded and heterogeneous metamorphic rocks belonging to the Itabira group/Caue Formation, which constitutes the intermediate chemical member of the Minas Supergroup, a meta-sedimentary sequence. These rocks were submitted to greenshist metamorphism at west and reached amphibolite facies in the east portion (Door, 1969).

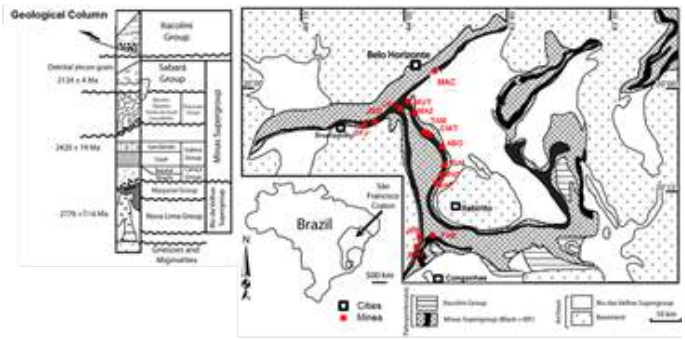

Figure 3. Vale - DIFL mines locations and Iron Quadrangle geological settings

The iron ore deposits present a millimeter to centimeter rhythmic alternation banding of ferrous minerals (hematite, martite and goethite), and no ferrous minerals (quartz, dolomite or amphibolite). Originally called Itabirites as defined by Dorr (1969), these iron deposits are classified as Superior Type according to Gross (1980). The main ore lithologies are: hematite (Fe ≥62%), and itabirite (30< Fe<62%). The main waste rocks are: phyllite, quartzite and intrusive metabasic rocks.

Banding is the most typical characteristic that defines a strong heterogeneity and anisotropy. This variation could be controlled by the original sedimentary bedding, tectonic setting, metamorphic grade, hydrothermal or supergene processes. However, the superposition of these processes causes partial or total mineralogical and textural changes. Usually the mines vary from 200 m to 500 m in depth, covering all set of possible weathering profile from completely weathered to the fresh rocks. As the depth weathered profile, generally seen in tropical countries, many mines presents high percentage of low intact rock strength. These rocks, described as weak are invariably the result of weathering of the original compact prototype imposed by leaching, alteration and/ or dissolution process.

In these mines, more than 70% of exposed slope rocks are weak and the failure mechanisms are conditioned by rock mass strength. However, this proportion can be lower for deeper mines increasing hard rocks percentage to 50%.

Figure 4 presents a typical cross section showing the main rock types and the slope geometry.

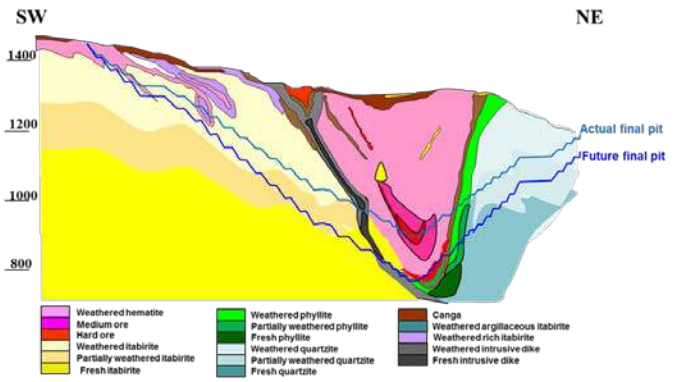

Figure 4. Typical geological cross section presenting the main rocks and weathered profile for Vale iron ore mines.

The weak rocks are more susceptible to instability under shear stress mechanism on intact mass strength due to the reduced rock strength values and secondary over high stress conditions in the slope toe. On the other hand, the hard rocks present failure mechanisms commonly associated with discontinue issues and associated characteristics.

Therefore, due to the dual slope behaviour it`s possible to find all sort of soil and rock

failure mechanisms, that can vary in geometry and velocity.. The deformation velocity observed in hard rocks are generally fast (mm/day), and for weak rocks are considered very low (mm/month) and directly associated with the rain season

For slope instabilities an ideal data acquisition interval is as closer to the continuous monitoring as possible to offer more information in shorter period and increase the ability to detect slow as well rapid and unexpected failures. In addition, high accuracy is essential to detect the early stages of movements and increase the efficiency to detect small failures as described by Osasan & Afeni (2010).

Regarding this issue Kayesa (2006), cited that an efficient monitoring program has to provide the necessary information to the geotechnical team to identify the security levels, record rock and slope deformation, and involve an accurate timing and precision survey necessary to evaluate and support mining operations to manage slope stability. In relation to time data collection an efficient slope monitoring system needs to be able to detect failure, even the small one, in the early stages to prevent failure with a considerable time advantage to avoid it. Girard (2001), pointing out that for safety in mining operations deformation signals must be detected and treated in proper time.

Monitoring these movements is the main challenge for the slope stability team and the GBInSAR technology represent an important assistance to characterize and understand the slope deformations

4. RADAR MONITORING AT VALE MINE SITES WITH GBINSAR

In one of the Vale mine located in the Iron Quadrangle until 2011 Vale's geotechnical team implemented a conventional slope monitoring network using conventional sensors like extensometers and prisms measured by a total station. The data acquired by these sensors until 2011 were limited in space and time thus providing uncertain results on the slope movements occurring on the slope.

For this reason in 2011 Vale included in the slope monitoring program an IBIS slope monitoring radar together with an improve in the prism monitoring. First results, thanks to the real time processing of data acquired every 5 minutes, allowed to exclude the presence of acceleration in the 10 months covered by the radar monitoring. The multi-scale algorithm, thanks to the longer temporal scale processing, at the same time allowed to clearly detect the presence of a moving areas. The average cumulative displacement recorded by the radar for specifically area was 25 mm over 10 months, thus showing a very slow average displacement rate of 0,10 – 0,15 mm/day. The maximum velocity within the same area recorded by the radar on some specific points in the lower part of the wall was of 0.20 – 0.25 mm/day, corresponding to a total cumulative displacement of almost 60-70 mm during the 10 months. Other minor and very localized movements were detected as well (Figure 5).

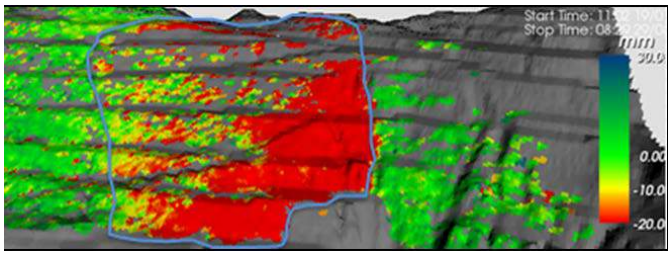

Figure 5. Radar image indicating the movement in the main slope of the closed mine.

Vegetation represents one of the problems of using the radar technology, because it increases the noise level of the radar data. Despite the presence of vegetation in the mine, the IBIS results were very good and able to clarify the temporal and spatial displacement pattern on the pit slopes while subject to a very slow movements.

Another example came from a mine with a network of 100 prisms. Initially an IBIS-FMT mobile radar unit was installed in a frontal position at an average distance of 1.000 m from the wall. Since the vegetation on the slope was introducing some noise in the radar data, IDS developed a dedicated processing tool that improved the quality of

the radar results, reducing the amount of noise thus reaching the expected results.

While the radar was installed in the first position, from July to September (dry season), by using this new processing methodology it was possible to correlate the spatial distribution of the slope movements detected by the radar to the point-wise measurements of the prisms confirming the average velocity of 1 mm/day for the upper part of the wall.

In September the radar was moved to a farther distance (1.250 from the main wall) because the operations in the pit where starting to cover the view to the lower part of the main wall from the original installation site. However, because of the first rainfall occurred in November, the area where the radar was installed started to move thus resulting in the need to move the radar again in early December. The monitoring restarted from a new location at 1.900 m of distance from the wall. From this new location it was possible to cover even the fast movements occurring on the west wall in addition to the slow movements still visible in the upper part of the south wall.

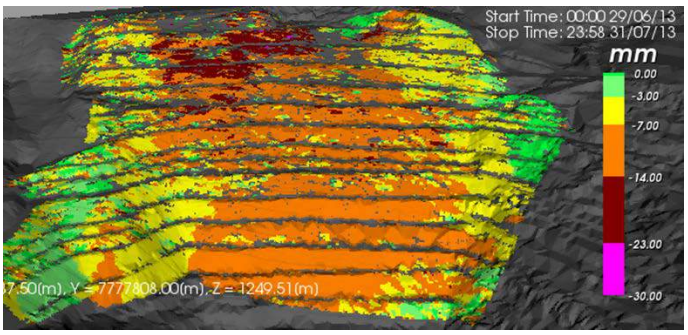

Figure 6. Radar map from position 1 covering a period of 30 days.

At the apex of the rainy season, with rainfall up to 80 mm/day, the displacement accelerated in some specific points both walls up to values of 30-40 mm/day. The rainfall reached peaks of 300 mm/day during this season. In this period the radar data resulted more reliable in comparison with the data acquired by the total station over the prisms (that was almost unable to operate during the heavy rainfalls) and provided more precise information. After the peak of the rainy season, the velocity returned to expected rate, between 0.5 to 3 mm/day.

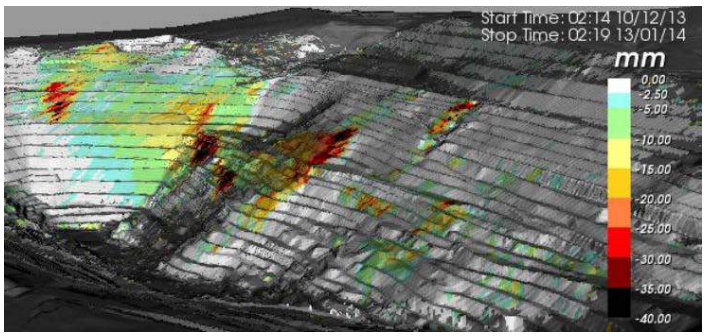

Figure 7. Radar map from position 3.

In the first very moment the radar monitoring was used to define the velocity of the global slope movements and then the radar data supported the definition of the velocities compatible with the operations at the toe and on the wall.

The monitoring results from prisms and radar were then used to calibrate a 2 D, Phase 2 and 3D, Abacus models.

5. CONCLUSIONS

The paper presents the results of advanced data processing algorithms developed by the authors for GBInSAR systems able simultaneously to measure a wide range of displacement rates. Those algorithms have been successfully applied to radar data acquired in some of the iron mines owned by Vale S.A. Brazil.

In the presented case studies radar data have been integrated and compared to displacement measurements acquired by satellite images, total stations over tens of prisms, in order to improve the interpretation of the on-going deformations. The use of integrated approaches combining the capabilities of detecting fast and slow movement supported by prism and field inspections can lead to the timely detection of slope movements in iron ore mines such as showed in the present paper.

The capability to detect at the same time fast movements and slow movements over large areas open the doors of a new concept of radar monitoring, where does not only represent a valuable tool for safety critical monitoring of the pit slopes, but also

becomes a valuable source of information to better understand the slope behaviour before movements start interacting with mining operations. In fact, early recognition of ground movements allows reviewing extraction techniques, mine design and ground support before the instability become difficult or expensive to mitigate.

REFERENCES

Antonello, G., Casagli, N., Farina, P., Leva, D., Nico, G., Sieber, A.J., Tarchi, D. (2004). Ground based SAR interferometry for monitoring mass movements. Landslides 1, pp. 21-28.

Bozzano F, Cipriani I, Mazzanti P, Prestininzi A (2011) Displacement patterns of a landslide affected by human activities: insights from ground-based InSAR monitoring. Natural Hazards 59(3): 1377-1396.Corsini et al., 2006;

Cruden, D.M. and Varnes, D.J. (1996). Landslide types and processes. In Landslides, Investigation and Mitigation. Special Report 247, Transportation Research Board, Washington, pp. 36-75.

Dorr, J. V. N. II. (1969). Physiographic, stratigraphic and structural development of the Quadrilátero Ferrífero, Minas Gerais, U. S. Geological Survey Professional Paper, 641 A: 110

Osasan, K. S., & Afeni, T. B. (2010). Review of Surface Mine Slope Monitoring Techniques. Journal of Mining Science, 46 (2), 177-186.

Farina P, Leoni L, Babboni F, Coppi F, Mayer L, Ricci P (2011) IBIS-M, an Innovative Radar for Monitoring Slopes in Open-Pit Mines. In: Slope Stability 2011: International Symposium on Rock Slope Stability in Open Pit Mining and Civil Engineering, 18-21 September 2011, Vancouver, Canada.

Farina P, Coli N, Yön R, Eken G, Ketizmen H (2013) Efficient Real Time Stability Monitoring of Mine Walls: The Çöllolar Mine Case Study. In: International Mining Congress and Exhibition of Turkey, 16-19 April 2013, Antalya, Turkey, pp. 11-117.

Girard, J. M. (2001) Assessing and monitoring open pit mine highwalls.32nd Annual Institute of Mining Health, Safety and Research, Roanoke.

Gross, G. A. (1980). A classification of iron formation based on depositional environments, The Canadian mineralogist, (18): pp.215-222.

Kayesa, G. (2006). Prediction of slope failure at Letlhakane Mine with the Geomos Slope Monitoring System. International Symposium on Stability of Rock Slopes in Open Pit Mining and Civil Engineering Situations, Series S44, South Africa pp.

Pieraccini M, (2013). Real Beam vs. Synthetic Aperture Radar for Slope Monitoring. Proceedings of PIERS 20013.

Analysis of the Effects of Stoping Overbreak/Underbreak on the Effectiveness of Support Systems for Hard Rock Mining

B. S. Lukhele, T. Zvarivadza
School of Mining Engineering, University of the Witwatersrand, Johannesburg, SA

ABSTRACT Underground support systems are essential in all underground excavations. Support systems ensure that excavations are kept stable and safe for people to work in. There are different types of excavation techniques used to excavate underground excavations but the mining industry mainly uses the drilling and blasting technique to excavate in hard rocks. In the underground drilling and blasting excavation method, drilling is an essential component. Inaccurate drilling can lead to stoping overbreak/underbreak which has potential to affect the effectiveness of the support systems used.

One of the objectives of this research was to determine in detail the factors contributing to stoping overbreak/underbreak in hard rock mining. An extensive investigation done at one of the hard rock mines in South Africa using data acquired and analysed, pointed out that factors such as geological structures and general excavation conditions prior to face preparation and drilling contribute to stoping overbreak/underbreak. This research also analysed the effects of stoping overbreak/underbreak on pillar support and the overall support systems at the mine. It was found that significant impact on pillar support is only evident should the overbreak or underbreak be concentrated to pillars which are of close proximity to each other. Pillars that have a pillar width of 7 m and less are at risk of failing as Factor of Safety (FOS) decreases to below 1.5. This is due to the changes that occur to the tributary area supported by one pillar which expands half way to the previous and next pillar. Should two consecutive pillars be affected by overbreak or underbreak, then the stability of the pillars decreases significantly.

This research noted that the overall support systems utilised at the investigated mine are effective and that stoping overbreak/underbreak does not affect the overall stability because there are numerous factors that have to interact in order for the effects of overbreak or underbreak to be substantial.

Keywords: Support systems, stoping overbreak/underbreak, pillar support

1 INTRODUCTION

Rock engineering is concerned with safe design of excavations in in-situ rock masses and the evaluation of rocks behaviour. The rock engineering department at a mine is responsible for ensuring that all the underground excavations are adequately supported and that they are excavated according to design standards. Safety of the workers is the main priority of the rock engineering department. Rock support is considered a system because it combines different components to ensure that excavations are kept stable by means of adequate support. Underground excavations tend to disturb the virgin stresses of an in-situ rock mass and in return the rock mass reacts by opposing the disturbance in order to balance out the stresses.

This paper presents a study on the effects of stoping overbreak/underbreak on the effectiveness of support systems for hard rock mining. Factors contributing to stoping overbreak/underbreak are determined and strategies which can be applied in order to minimise stoping overbreak/underbreak are put forward.

Underground excavations support is considered an important parameter when it comes to design and safety of excavations. Properly supported underground excavations

provides safe working environment, hence the need to address challenges posed by stoping overbreak/underbreak on the effectiveness of support systems.

1.1 The Stoping Overbreak/Underbreak Challenge

Hard rock mining underground excavations encounter occasional stoping overbreak/underbreak which have an impact on the overall support systems utilised. Stoping overbreak is due to excessive fracturing of peripheral blast-holes and results in greater excavated dimensions as compared to planned dimensions while stoping underbreak refers to the volume of intact rock material left unexcavated as compared to the planned excavation dimensions. Geological structures also affect underground excavations especially if the geological structures are intersected by the excavations. Stoping overbreak/underbreak tends to have an effect on pillar dimensions which in turns affects the pillar strength and also the effectiveness of the secondary support systems such as rockbolts.

A geology complex that is highly faulted and intersected by geological structures presents geotechnical challenges on the stability of underground excavations established in it.

1.2 Support of Underground Excavations in Hard Rock Mining

Underground support systems are regarded as one of the key components in ensuring safety and stability of underground excavations. Support systems designs have to account for the different types of excavations and their dimensions. Competent support systems are developed by geotechnical engineers with solid knowledge of rock behavior and factors contributing to the behavior. The installation of different types of support has to undergo strict quality control in order to ensure that adequate support is provided at all times.

There are a number of objectives that support systems tend to achieve. The objectives are related to the application of the support systems and the reinforcement provided by these support systems. The objectives are as follows (De Vries, et al., 2011):

- Ensuring that there is “zero displacement” of the rock mass by applying support that has sufficient stiffness to withstand movement.
- Maximise the support elements mechanical properties by controlling displacement of the surrounding rock with a combination of support systems.

2 RESEARCH APPROACH

Data were collected based on the parameters that were required to analyse the effects of stoping overbreak/underbreak on the effectiveness of the support systems. The data was collected using a routine underground inspection sheet which ensures that all the appropriate parameters are captured during inspection. The dimensions were measured using a digital measuring laser tape.

This information was necessary in analysing the condition of the excavations after blasting prior to drilling of new blast holes. The excavations dimensions were also collected in order to determine the extent of the overbreak/underbreak.

2.1 General Information

The research focussed on the geological structures intersected by excavations and their influence on excavation. Geological information was gathered during daily inspections. From each of the bords and splits ends, the following geotechnical information was gathered:

- rock type
- fault/shear zone
- dykes/sills/contacts
- joints
- brows
- blast induced damage
- weathered zone

2.2 General Excavation Conditions

The data collected under general face conditions were gathered after each advance of the face and were categorised into the categories given in table 1.

Table 1. General excavation conditions

Face conditions	Hangingwall conditions	Sidewalls conditions
• Face barred • Loose slabs on the face • Sockets on the face • Water seeping on the face	• Hangingwall barred • Loose slabs on hanging wall • Support installed to face • Support adequate	• Sidewalls barred • Loose slabs on the sidewalls • Water seeping from the sidewalls • Sidewalls Support required

2.3 Face Preparation and Drilling Accuracy

It is important to drill blast holes in their optimal position to ensure that there is interaction between the blast holes for good fragmentation and also to avoid stoping overbreak/underbreak. Data was collected from stoping faces and it was organised into marking data and drilling data. The face marking data was collected during face preparation while the drilling data was collected during drilling and after the drilling operation was ceased.

Table 2. Face preparation and drilling accuracy

Face marking data collected	Drilling data collected
• Face centre line not straight • Face horizontal lines not straight • Face vertical lines not straight	• Holes drilled off position • Holes less than 1m apart • Holes drilled on an uneven face

2.4 Pillar, Bords and Splits Dimensions

Data of pillars, bords and splits dimensions was collected to determine the extent of the overbreak/underbreak and analysed to check its potential impact on support. The data collected was from the pillars, bords and splits and categorised under excavation data as follows:

- mining height(m)
- bord width(m)
- pillar width(m)
- depth of reef(m)

2.5 Support Installation

The data for support installation was collected and organised into the following categories.

- last row of support from the face
- rockbolts face plate not firmly against hangingwall
- rockbolts per row
- rockbolts spacing

3 STOPING OVERBREAK/UNDERBREAK DATA

Data related to stoping overbreak/underbreak was gathered and grouped according to geotechnical conditions. The geotechnical conditions were necessary in identifying the extent that geological structures have on underground excavations. General excavation condition data was necessary in determining the potential causes of stoping overbreak/underbreak of mining underground excavations.

Stoping overbreak/underbreak has a direct influence on the effectiveness of the support

system especially in bord and pillar mining. Pillar robbing and excessive damage to hangingwall, sidewalls and stope face resulting from stoping overbreak/underbreak affects the overall effectiveness of the support systems. Factors contributing to stoping overbreak/underbreak were determined and their effect on the effectiveness of support systems was analysed. The following factors were found to be amongst contributors to stoping overbreak/underbreak:

- Geological structures
- Drilling accuracy
- Blast-hole pattern
- Blast timing
- Charging-up procedure

These factors were investigated to determine their impact on underground mining operation, stoping overbreak/underbreak and on hard rock mining support systems.

3.1 Geological Conditions Data

The geotechnical data indicated the different geotechnical parameters that are likely to contribute to stoping overbreak/underbreak. The geotechnical parameters were used to determine the effects of geological structures on the excavations at the mine. Pyroxenite is the main rock type and one of the entire inspected panel had Pyroxenite either on the hangingwall or sidewalls.

3.2 General Excavation Conditions Data

General excavation conditions evaluation involved inspecting face, hangingwall, sidewalls and backends conditions. Most common in all the inspected areas was loose slabs that required barring down because of the hazards that they pose and the likelihood of Fall of Ground (FOG). Table 3 show the parameters evaluated for the face, hangingwall and sidewalls conditions.

Table 3. Aspects considered and corresponding parameters investigated

Aspect	**Investigated parameters**			
Face conditions	Face barred or not	Presence of loose slabs on the face	Presence of sockets on the face	Water seeping on the face or not
Hangingwall conditions	Hangingwall barred or not	Presence of loose slabs on hangingwall	Support installed to face or not	Adequacy of support
Sidewall conditions	Sidewalls barred or not	Presence of loose slabs on sidewalls	Water seeping from the sidewalls or not	Sidewalls support required or not

3.3 Face preparation and drilling accuracy data

Proper face preparation and accurate marking of blast holes positions on the face has an influence on the drilling accuracy. Face preparation involves barring of face, marking of centre lines both on the face and hangingwall to ensure that mining is kept within the required mining directions. Drilling direction lines are marked on the sidewalls and hanging wall based on the survey notes issued by the survey department and it includes the required dip and excavation direction.

Table 4 shows the different parameters measured during face preparation. The parameters are recorded based on the percentage off from the correct position.

Table 4. Face preparation and drilling accuracy

	Percentages (%)				
	Face centre line not straight	Face horizontal lines not straight	Face vertical lines not straight	Blast holes drilled off marked position	Blast holes less than 1m apart
Bord 8 Split 15 South	0	5	5	0	0
Bord 10 South	10	10	15	10	25
Bord 12 South	15	10	5	5	10
Bord 12 Split 18 South	20	10	10	15	15
Bord 14 South	10	15	15	20	15
Bord 14 Split 18 South	0	5	5	5	0
Bord 16 South	0	0	5	5	5
Bord 20 South	15	15	10	10	10
Bord 20 Split 17 South	5	5	10	15	10
Bord 24 South	10	10	10	15	15
Bord 24 Split 15 North	0	5	5	0	5
Bord 26 North	5	5	5	5	5
Bord 26 Split 11 North	10	5	5	0	5

3.4 Excavation Dimensions Data

The excavation dimensions data was categories according to pillar, bords and splits dimensions. The excavation dimensions are an indication of the extent of the stoping overbreak/underbreak and they are also an indication of how pillars are affected due to the stoping overbreak/underbreak. Table 5 shows the different excavation parameters that were recorded during data capturing.

Table 5. Excavation dimensions

	Mining Height (m)	Bord Width (m)	Pillar width (m)	Depth of reef (m)
Bord 8 Split 15 South	6.8	5.9	8.2	480
Bord 10 South	5.6	7	7.9	480
Bord 12 South	4.8	6.4	8.0	480
Bord 12 Split 18 South	5.8	6.8	8.1	480
Bord 14 South	6.6	7	7.6	480
Bord 14 Split 18 South	5.2	6.4	8.1	480
Bord 16 South	6.3	6.4	8.2	480
Bord 20 South	7.4	6.2	7.8	480
Bord 20 Split 17 South	6.5	7.2	8.0	480
Bord 24 South	5.2	7	8.0	480
Bord 24 Split 15 North	6.1	6.3	8.1	480
Bord 26 North	5.2	7.5	8.2	480
Bord 26 Split 11 North	5.2	6.5	8.0	480

4 SUPPORT SYSTEMS DATA

4.1 Support Installation Data

For each of the mining area studies, the support properties necessary for evaluating support effectiveness were collected. The properties for bolts included: Bolt type, Bolt length (m), Bolt diameter (mm), Hole diameter (mm), Annulus (mm) and Washer type as well as the resin properties where applicable.

It is essential that support is installed according to the standard operating procedure to ensure effectiveness and efficiency of the support systems.

4.2 Roof Bolter Evaluation Data

The use of effective and efficient support installation equipment is also an important factor in effective support systems. Evaluation of the roof bolter was used to determine its effectiveness in the installation of support. The following are the parameters recorded during the evolution of the roof bolter: Roof bolter boom type, Cycle time (bolts per hours/shift), Drill bit type, Drill bit diameter (mm), Bolt type, Type of pin/nut, Drilling method, Free Rotation speed (rpm), Drill speed (rpm), Resin spinning speed (rpm), Torque (Nm) and Thrust (kN).

5 STOPING OVERBREAK/UNDERBREAK DATA ANALYSIS

5.1 Stoping Overbreak/ Underbreak Challenges

There are a number of challenges which are encountered due to stoping overbreak/underbreak. These challenges have been identified and categories into three groups, namely, production challenges, safety challenges and financial challenges. Each of the challenges was analysed and its practical implications on day to day mining operation expressed.

5.1.1 Production challenges

- Due to stoping underbreak, the required tonnages expected per blast are reduced. The reduction in tonnages coupled with loss in tonnage combines to affect the overall production figures.
- Due to stoping overbreak, ore dilution tends to occur in places were the excavations are advancing close to waste material. The dilution of the ore material reduces the ore tonnage expected from the blast and effect the processing of the ore.

5.1.2 Safety challenges

- Due to stoping overbreak, pillar dimensions are reduced resulting in pillar robbing. Pillar robbing is a safety challenge as it affects pillar strength which in turn affects the interaction

between adjacent pillars thereby reducing pillar stability. Pillar robbing also causes pillar failure due to the weight of the overburden as the pillar sizes are reduced below design dimensions which results in reduced pillar strength.
- Stoping overbreak/underbreak damages the hanging wall, sidewalls and face and results in uneven surfaces which increase the likelihood of scaling and can result in FOG. FOG is regarded as the major contributing factor in most fatalities in underground mines in South Africa.

5.1.3 Financial challenges

- The loss in production is financially challenging as production generates revenue and if production figure are not met, the mine operates at a loss.
- Stoping underbreak results in fewer tonnages produced which affects daily production figures which in turn affects cost per ton figures.
- Stoping overbreak results in larger excavation dimensions which require additional support which means more money than necessary has to be spent on support.

5.2 Geological Condition Analysis

Geological structures intersected by excavations cause major stability problem to underground excavations. These geological structures have the potential to cause blocks and wedges around the excavation. The following analyses was done:

- Fault/Shear Zones

From the 13 panels that were inspected, 9 panels intersected either a fault or a shear zone. This is a total of 69% of the panels inspected.

- Dykes/Sills

From the 13 panels that were inspected, none of them intersected a dyke or a sill.

- Joints

From the 13 panels that were inspected, all of the panels intersected joints. This means that 100% of all the panels intersected joints. Joints have different effects on the stability of an excavation based on the number of factors such as, the joint set number, the joint roughness number, the joint alteration number and the joint water reduction factor.

- Blast Induced Damage

From the 13 panels that were inspected, 1 panel showed blast induced damage. This is 7 % of the total panels and it can be concluded that blast induced damage does not have that much of an effect on the geological structures.

- Weathered

From the 13 panels that were inspected, none of the panels showed signs of being weathered which reduces the effects of joint water reduction factor from the joints intersected by the excavations.

From the geological condition analysis, it can be observed that most of the panels are being intersected either by a fault or a shear zone. The high percentage of panels intersecting either a fault or shear zone means that the underground excavations are prone to stability problems if not properly supported.

There is minimal number of dykes and sills intersected based on the data. The reason for this may be due to the fact that dykes and sills are rare geological structures in the geological complex in which the mine is situated but they have an effect on the stability of an excavation which is why they must be captured if encountered.

5.3 General Excavation Condition Analysis

The general excavation conditions were used to identify the factors that influence stability of the excavation and hence safety of the miners. The general conditions were categorised according to face condition, hangingwall condition and sidewalls conditions. Table 6 shows aspect conditions and the investigated parameters and results for 13 panels.

Table 6. Investigated parameters and results for the 13 panels considering different aspects

Aspect	Investigated parameters and results for the 13 panels			
Face conditions	Face barred or not	Presence of loose slabs on the face	Presence of sockets on the face	Water seeping on the face or not
	3 (23%) not	4 (31%) had	none	none
Hangingwall conditions	Hangingwall barred or not	Presence of loose slabs on hangingwall	Support installed to face or not	Adequacy of support
	5 (38%) not	2 (15%) had	7 (54%) not	6 (46%) not
Sidewall conditions	Sidewalls barred or not	Presence of loose slabs on sidewalls	Water seeping from the sidewalls or not	Sidewalls support required or not
	5 (38%) not	4 (31%) had	1 (7%) had	2 (15%) required

Figure 1 shows analysis results for face preparation and drilling accuracy of the panels inspected. From the 13 panels that were inspected, the average face centre line drawn not straight was 7.7%. The average horizontal lines drawn not straight were also 7.7%. The average face vertical lines drawn not straight were 8.1%. The average blast holes drilled off marked position were 8.1% and the average blast holes less than 1m apart was 9.2%. The number of centre lines, horizontal lines and vertical lines not drawn straight during face preparation affects the blast hole position which affects the holes interaction. The blast hole interaction is essential to ensure that the correct panel dimension are kept after each blast hence reducing stoping overbreak/underbreak.

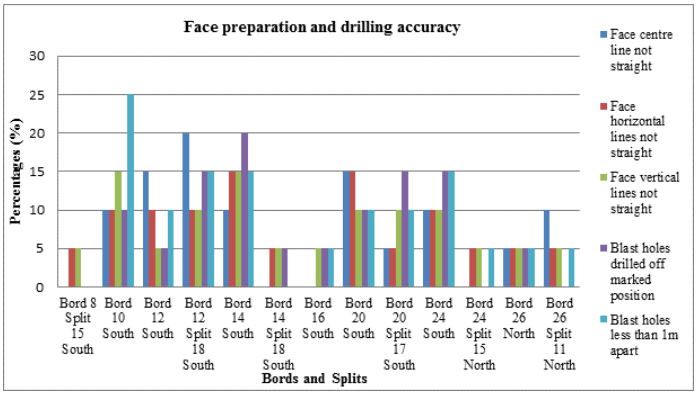

Figure 1. Face preparation and drilling.

Table 5 shows excavation dimensions of the panels inspected and from the table the following analysis in figure 2 was done. Figure 2 shows that 43% of the panels inspected had mining height greater than the designed mining height and 57% of the panels had mining height less than the designed mining height.

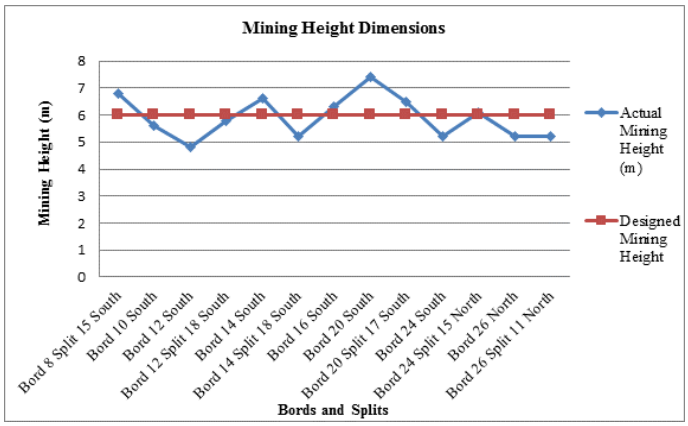

Figure 2. Mining height dimensions

Figure 3 shows 62% of the panels inspected had bord width less than the designed bord width. 23% had the same bord with as the designed bord width while 15% had bord width above the designed bord with dimensions.

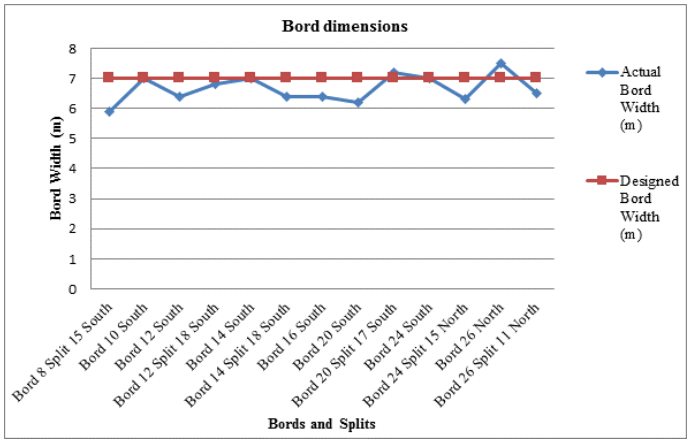

Figure 3. Bord width dimensions

Pillar design calculations were done to analyse the influence of stoping overbreak/underbreak on pillar stability. Figure 4 shows that 23% of the pillar widths were less than the designed pillar width. 31% of the pillar widths were approximately the same as the designed pillar width while 46% were above the designed pillar width. From the pillar strength formula, pillar width is an important design parameter. If the pillar width is less than the required width there is a chance that the pillar will not be able to provide the required stability hence reducing the effectiveness of the support provided by the pillar.

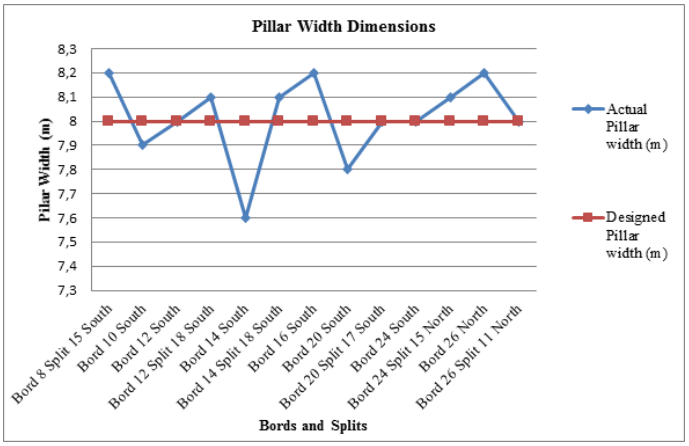

Figure 4. Pillar width dimensions

The rock engineering department monitors all the pillars. In cases where there is a robbed pillar, the adjacent pillar dimensions were increase to provide support for the robbed pillar. Pillar bolting is also done as a precaution to keep the robbed pillar safe.

6 SUPPORT SYSTEMS DATA ANALYSIS

6.1 Support Systems Challenges

Underground support systems encounter a lot of challenges depending on the rock conditions and on the installation of the support. Underground hard rock mining has a number of challenges relating to primary and secondary support. These challenges have been identified and categories into three groups, namely, production challenges, safety challenges and financial challenges. These challenges are discussed as follows:

6.1.1 Production challenges

- Incorrect installation of support leads to additional support which affects the mining cycle and hence production.
- Failing pillars, this requires the section to be closed until the pillars are supported. Production is affected, especially if most of the production is planned from that particular section.

6.1.2 Safety challenges

- Incorrect installation of roof bolts creates unsafe working conditions increasing the likelihood of scaling and FOG.
- Robbed pillars are a safety hazard as the pillars are likely to fail overtime causing the roof to collapse.

6.1.3 Financial challenges

- Re-support requires additional roof bolts which require additional cost outside of the budget.
- Any support concerns which lead to temporal closing of a section is a financial loss as no production will be achieved during the closing off period.

6.2 Support System Installation Analysis

The support systems parameters of the panels inspected were analysed and some of the results are as presented in figure 5. According to safe support standards, the last row of rockbolts must not be more than 1.5m from the face. Figure 5 shows 50% of the last row of rockbolts is more than 1.5m away from the face.

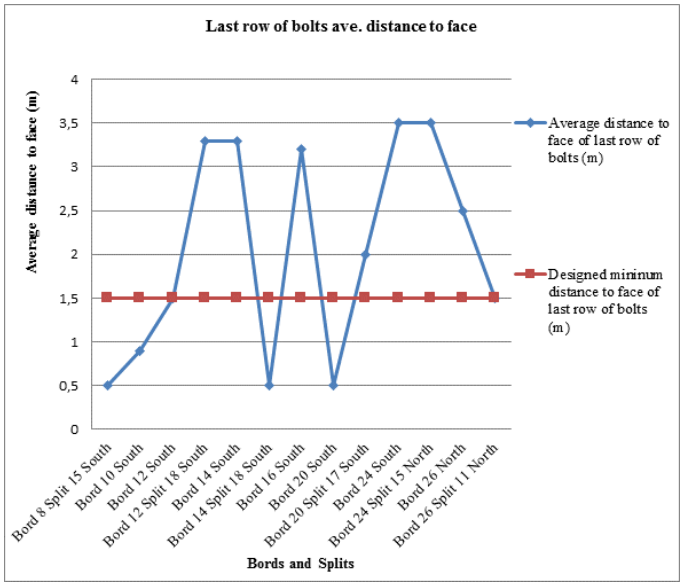

Figure 5. Distance of last row of bolts

From figure 6, it can be noted that 23% of the installed bolts had bolt spacing greater than the designed bolt spacing and 15% of the row spacing was greater than the designed row spacing.

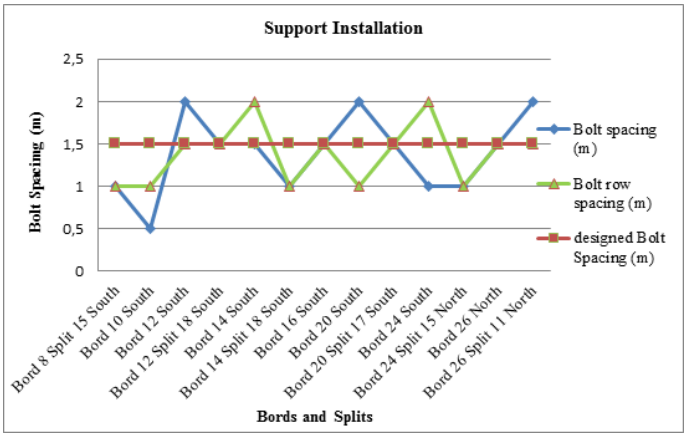

Figure 6. Support installation

The greater bolt and row spacing affects the total area required to be covered by a roof bolt hence affecting the effectiveness of the rockbolts. The optimum ratio of bolt length to bolt spacing is 1.5 (Canbulat, 2008). The mine uses 2.2m long bolts and the minimum spacing that satisfies the optimum ratio is 1.5m and less. In cases were the spacing exceed 1.5m there are chances that the rockbolts are not providing the sufficient stability.

The effectiveness of the roof bolt system is dependent on the density of the bolt pattern. The density of the rockbolts pattern depends on the number of bolts per row and the spacing between rows (Mark, et al., n.d.). This means that if the bolt pattern is not maintained there is a chance that the rockbolts will not be as effective. The number of rockbolts/row less than the required number suggests that at certain locations the support system is not as effective as it should be.

6.3 Roofbolter Analysis

The quality of installation of a support system is directly related to the performance of the equipment that is used to install the support. The relationship between support holes profile, speed, torque and thrust must be inspected as part of quality control and quality assurance of the roofbolter. The recommended roofbolter parameters for optimally producing rough walled holes in South African underground mines are as given in table 7.

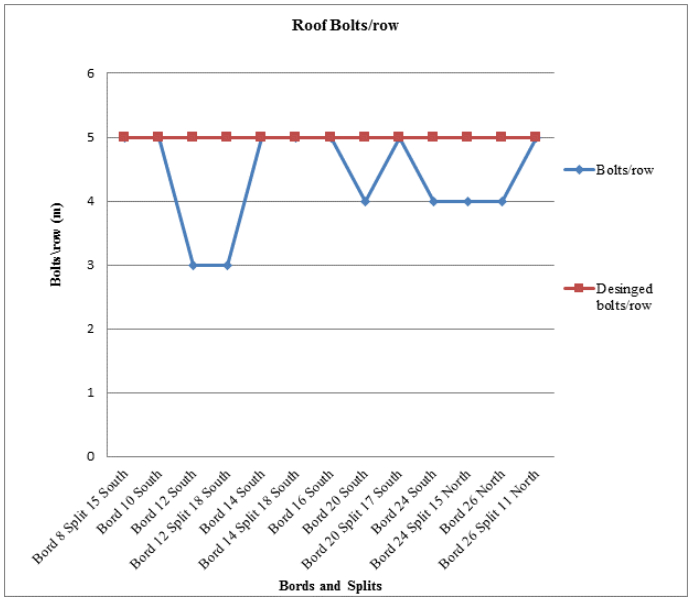

Figure 7. Roof bolts/row.

Table 7. Roofbolter parameters (Canbulat, 2008)

Spinning speed	450 rpm
Torque	240 Nm
Thrust	15 kN

Form table 7, the following observations were noted:

- The free rotation speed, drill speed and resin spinning speed of the roofbolter evaluated exceed the recommended rotation speed of 450 rpm.
- The thrust of the roofbolter far exceeds the recommended thrust of 15 kN.
- The torque of the roofbolter also exceeds the recommended torque of 240 Nm.

7 CONCLUSION AND RECOMMENDATIONS

Safety of underground excavations depends on proper excavation techniques and on proper and adequate support systems including installation. One of the research objectives was to establish and understand all factors that contribute to stoping overbreak/underbreak using the underground hard rock mining data. It is evident that geological features play a major role in stoping overbreak/underbreak. Apart from geological features, the general excavation

conditions prior to face preparation and drilling also contribute to stoping overbreak/underbreak.

Determining the actual impact of stoping overbreak/underbreak on pillar support and support systems was also crucial in this study. The data analysed show that only a few pillars dimensions were not up to the required dimensions. The impact of the reduced pillar dimensions was determined to be minimal as the pillars investigated were not in close proximity to each other and their surrounding pillars were able to maintain the overall stability around the robbed pillars. The FOS of the most robbed pillars was determined to be within the set safe standards due to initial overdesign. Support is considered to be adequate based on the analysed data and on the roof bolter analysis.

The research noted that stoping overbreak/underbreak does play a role in the overall stability but there are numerous factors that have to be combined in order for the effect of stoping overbreak/underbreak to be reliably accounted for.

This research noted that the practice of the following aspects increase stability by minimising stopping overbreak/underbreak:

- accurate marking and drilling of the panel
- accurate barring and marking of the hangingwall so that support installation is done correctly.
- accurate drilling and charging leading to accurate implementation of stoping dimensions design.
- incorporation of smooth wall blasting minimising excavation damage.

REFERENCES

Canbulat, 2008. Evaluation of roof bolting systems in South Africa.Pretoria, University of Pretoria.

De Vries, B., Ozturk, H., Foo, B. & Lima, A. D. A., 2011. Practical application of support systems to adress weak rock mass in underground mines. *Studia Geotechnica et Mechanica*, XXXIII(3).

Mark, C., Molinda, G. M. and Dolinar, D. R., n.d. *Analysis of Roof Bolt Systems,* Pennsylvania USA: Pittsburg Research Laboratory.

Behavior of FPZ and Pre-existing Cracks in an Intact Rock Specimen Subjected to Uniaxial Loading

F. Küçüköztaş, N. Erarslan
Adana Science and Technology University, Department of Mining Engineering and Mineral Processing, Adana, Turkey

ABSTRACT Rock fracture mechanics is concerned with the initiation and growth of fractures in the Earth's crust, rock mass and intact rock at scales ranging from microns to kilometers. This includes the initiation of new cracks from the heterogeneous rock fabric; the opening, closing, sliding, and growth of pre-existing cracks under tension and compression. In rocks, the crack tip non-linear process zone is caused by the initiation and propagation of the microcracks in the immediate vicinity of a crack tip and it is described as the crack tip microcracking zone or Fracture Process Zone (FPZ).This research is a numerical study and focuses on behavior of crack tips in a cylindrical intact rock sample under triaxial stress conditions. All simulations are done by using FRANC2D fracture mechanics program. Results obtained with this study show the behavior of FPZ and fracturing of the pre-existing cracks are found dependent on geometry and position of cracks in the specimen. Some fracture mechanics principles such as fracturing modes mode I (tensile) and mixed mode (tensile-shear) were considered in this research as well.

Keywords: Rock fracture mechanics, Fracture Process Zone (FPZ), FRANC2D, pre-existing crack, mode I, mixed mode

1 INTRODUCTION

Fracture mechanics is the study of propagation of cracks in materials. In general, materials can be classified into two classes, brittle or ductile (Whittaker et al., 1992). The classification can be easily described on the stress-strain curve where the elastic and plastic region could be identified. For brittle materials, plastic deformation areas are significantly smaller than those of materials of high ductility. In simple terms, brittle materials display little deformation followed by a catastrophic failure while ductile materials strains significantly before failure. This paper primarily considers the crack initiation, propagation and coalescence in brittle materials such as rocks and concrete. According to the researches, the brittle materials always have an ultimate fracture point of much greater in compression than in tension as an example of that of concrete which has four times in difference in strength (Whittaker et al., 1992 Erarslan 2011)

In numerical models, all simulations are done by using FRANC2D fracture mechanics program by considering ductility and brittleness and the geometry of the sample has been assumed as a continuous, isotropic and homogeneous elastic body with the cylindrical shape concrete block with two internal flaws are used. The simulations are modelled with the flaw angle of 30°. Since the flaw angle is constant, the simulations are done by increasing ligament length by every 6 mm in both c and s direction.

The critical issue in this research is that once the crack is started in specimen, stress distribution near the crack tip changes very much. In most cases, the crack started from the internal flaw tip due to tension stress concentration but in some cases some stress-induced cracks start around Fracture Process Zone (FPZ). According to this fact, the assumption is made to predict the crack propagation and its orientation.

According to the Linear Elastic Fracture Mechanics (LEFM), crack propagation will start when stress intensity reaches a critical

value, which is called fracture toughness. Therefore, stress intensity factor is having great role in the crack propagation and mainly depends on the fracture displacement modes and crack geometry (Whittaker, et al., 1992).

1.1 Background

When a rock sample is under an increasing load, a dominant internal stress is also increased until it reaches a critical stress level, so called rock strength. Similarly, when a cracked rock sample is under an increasing load with the effect of opening or shearing the crack, a dominant internal stress across the crack tip forms causing an increase in the crack length until it reaches an ultimate crack resistance state, called fracture toughness. Inglis (Inglis, 1913) provided a mathematical solution to the stress magnitudes around an elliptical hole in a stressed thin plate. Based on Inlis's (Inglis, 1913) stress analysis, Griffith (Griffith, 1924) established a relation between the fracture causing stress and the crack size.Griffith states that "brittle solids fail by incremental propagation of a multitude of randomly oriented, small pre-existing cracks." (Griffith 1924) The theory not only applies to microscopic fractures but also macroscopic cracks existing in brittle materials such as concrete. Griffith's theory also states that the total energy on a crack plate is equal to the summation of the boundary applied work, strain potential energy and free surface energy in the free faces of Griffith's crack and facture occurs when the tensile stress at some crack tip exceeds theoretical cohesive strength of the material (Griffith 1924).

1.2 Linear Elastic Fracture Mechanics

Linear Elastic Fracture Mechanics (LEFM) is used to determine the initiation and propagation of cracks in brittle materials. The assumptions of this method assumes material is isotropic and linear elastic. Given this, the stress field around the tip of crack can be analyzed with the theory of elasticity. The fundamentals of LEFM are generally derived from plane strains which are all associated with the three modes of failure: Mode I (tensile), Mode II (shear) and Mode III (tearing). To note, LEFM can only be used when the plastic deformation are small compared to the size of the crack known as the small-scale yielding (Whittakker et al., 1992).

Three basics fracture displacement modes in fracture mechanics are tensile (Mode I), shearing (Mode II) and tearing (Mode III). In opening mode (Mode I), the tensile stress is applied normal to the plane of crack which causes the two crack surfaces to open up and separate from each other. In sliding mode (Mode II), shear stress acting parallel to the plane of the crack which is perpendicular to the crack front. Therefore, the one crack surface slides relative to the other parallel to the crack extension direction. In tearing mode (Mode III), a shear stress acting parallel to the plane of the crack and parallel to the crack front. Figure 1 provides a visual diagram of what the types of fracture displacement modes are.

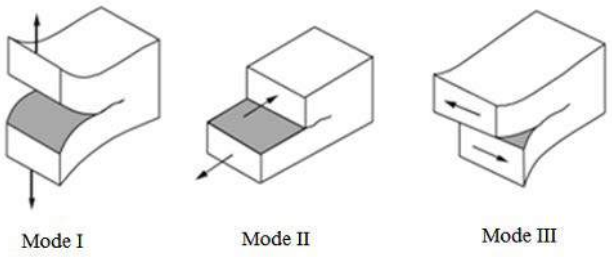

Figure 1. Fracture Displacement Modes

1.2.1 Stress Intensity Factor (SIF)

LEFM states that a crack will propagate when its stress intensity factor (KI) reaches a critical value (KIC). KI is the driving force for fracture and KIC is a measure of material resistance. Additionally, crack initiation started when the value of KI is equal to KIC. Additionally, it is corresponding to the critical state of the stress intensity factor and it is also required for crack initiation and subsequent propagation (Eraslan & Williams 2011)

In numerical modelling, it is expected to evaluate the K value (stress intensity factor)

versus new crack lengths and they are recalculated for each step of the crack length. During each crack length increment, an accurate evaluation of mode I and mode II are foreseeable for the prediction of load and angle change necessary for the corresponding length configuration for the next iteration (Whittaker et al., 1992). The following equation is used to determine the stress intensity factor

The mode I (tensile) stress intensity factor K_I itself is dependent on the crack length, C, the applied stress, σ_A, and a geometry factor, ψ (Whittaker et all. 1992).

$$K_I = \psi \sigma_A \sqrt{\pi C} \quad (1)$$

1.3 Crack Initiation under Compression

Crack initiation under compressive loading forms a much more complicated issue than in tension. Griffith (1924) postulated that crack forms under compression are a direct result from the crack tip of local tensile stresses. Significant differences in failure crack pattern can be observed for both tension and compression. (Whittaker, et al., 1992, Nasser 1995). The equations given by the linear elastic fracture mechanics (LEFM) to calculate stresses and stress intensity factors (SIF) for a crack under tensile loading, are also applicable for a crack under compressive loading, but using opposite signs, i.e. signs of KI and KII become negative. A negative KI means compressive stress acting at the crack tip and a negative KII just indicates an opposite direction of the shear stress acting parallel to the crack plane. As shown in Figure 2, inclination angle (θ) of a compressively loaded crack is such that the crack extension occurs parallel to the major principal compressive stress (Figure 2a), while it is parallel to the minor principal tensile stress in the case of a crack loaded by a tensile load (Figure 2b).

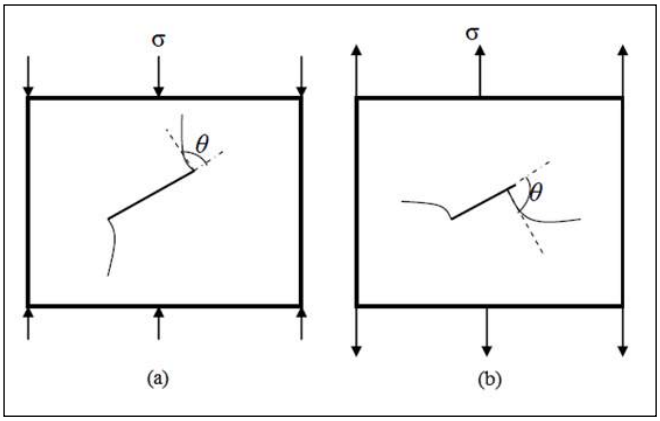

Figure 2. Crack propagation paths under compression (a) and tension (b)

1.4 Maximum Tensile Stress Criterion

The maximum circumferential tensile stress governs the crack initiation and propagation. The theory states:

- Crack propagation will initiate in a radial direction at the crack tip.
- The plane of propagation is normal to the direction of maximum tensile stress.
- Crack propagation occurs if the circumferential tensile stress reaches a critical value which is material dependent.

$$\cos\frac{\theta_0}{2}[K_1 \sin\theta_0 + K_{II}(3\cos\theta_0 - 1)] = 0 \quad (2)$$

The above equation forms a fracture initiation locus. To check whether or not a crack propagates the KI and KII factors, corresponding to the present geometry and given load configuration is substituted into equation to find the direction of probable crack propagation, θ. Then these three parameters KI, KII and θ are substituted into the left hand side of equation. If the less hand side of the equation is in unity, then the crack is stable, otherwise it will propagate Whittaker et al., 1992).

2 METHODOLOGY

The objective of this research is to investigate the relationship between ligament length (a) and stress distribution of the modelled specimen. The three main parameters flaw angle (β), 'c' (continuity) and 's' (spacing) are the main geometrical

parameters in the numerical simulations (Figure 3). Series of finite element modellings were conducted to model notch crack initiation and propagation under monotonic diametral loading. The stress distribution and crack propagation analysis in the specimens were conducted using the finite element program, FRANC2D (FRacture ANalysis Code). The right hand side of Figure 3 shows that, the internal flaws are parallel to each other and they have the length of '2a' or 12 mm. Therefore, 'a' has a value of 6 mm. And the internal flaws have 1mm in width. The ligament length are defined by two directions which include 'c' and's' direction. As shown in Figure 3, this block has the cross-section of 30 mm x 96mm with the height of the 156 mm.

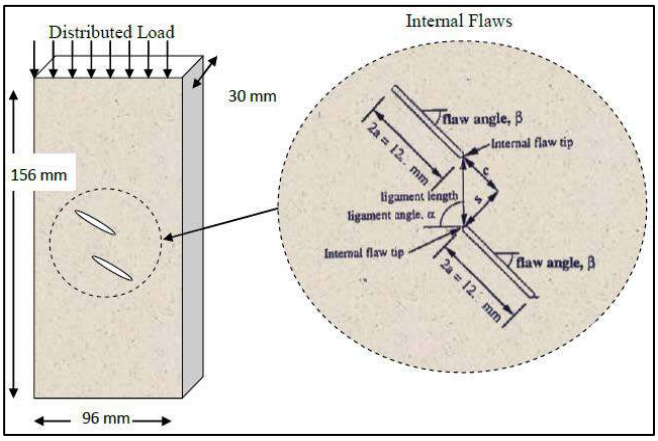

Figure 3. Specimen model and simulation parameters

The first step in modelling was to predetermine the specifications of the models that were to be created on Casca. Casca was the meshing software used to construct every mesh and is relatively simple to use, consisting of three main steps to complete a mesh: 1. Outline the shape with the geometry tools, 2. Add nodes along the boundaries of the constructed shape and 3.Mesh the parts of the constructed shape that were meant to be solid.

Before the completed mesh was imported into the testing software, called Franc2D, specifications were devised for the numerous other factors required for the pre-process.

In simulations, the rock has a Young's modulus of 59, 000 MPa and a Poisson's ratio of 0.15. Load is expressed as traction pressure, which corresponds to a projected width of the loaded section of the rectangular surface and distributed load of 2000, 000 N were applied from the top of block. In all simulations, the bottom of the surface was fixed in both x and y directions. It should be noted that the loading traction of this specimen block is not point load because the load was applied as distributed load even very small area is considered. Subsequently Franc2D can display the normal and shear stress distributions in the modelled specimen; these were observed to identify possible crack locations.

After the stress distributions had been observed and the possible crack locations identified initial cracks were made into the specimen. This was followed by a defined automatic propagation of them and an analysis of the stress intensity factors history.

Since the middle part is the most critical section, higher numbers of segments are used Sub Divide function, whereas lower numbers of segments are used for top and bottom parts of the concrete model. Therefore, in final step of meshing, Bilinear 4 method is used for top and bottom part of the concrete block whereas the middle part used Automatic meshing method. In addition, Automatic meshing method give better mesh generation then Bilinear 4 method and this will give the more exact contour data than Bilinear 4 method. The main objective of using both Bilinear 4 method for top and bottom part is to safe time from model simulation by reducing the number of mesh. After using mesh designing, FRANC2D is used for crack propagation (Figure 4).

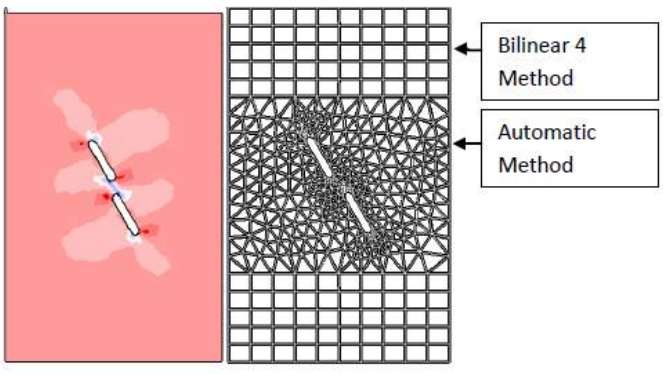

Figuıre 4. Meshing configuration

3 RESULTS

3.1 Simulations for θ=30°

In general, it was found that the full range of mixed mode loading conditions, including pure Mode I and pure Mode II loading, could be created using an inclined crack with inclination angles (β) between 0° and 90°. Figures 5 and 6 show the coloured contour diagrams for maximum principal stress (Tensile) distribution and shear stress distribution respectively with different parameters for 'c' and 's' values. There are two different sections in these figures and the top four diagrams are the stress distribution due to the variance of 's' parameter with the constant value of 'c' whereas the bottom diagrams are the stress distribution results from varying 'c' parameter with the constant value of 's'. The diagram in the top right corner of the figure shows the colour legend of the stress distribution. Pozitive numbers represent tension and negatives are for the compression.

The loading situations for various inclination angles were simulated properly without any new crack initiation or propagation. In general, the region of tensile stress distribution extended closer to the centre of the chevron notch crack, with increasing crack inclination angles. The maximum tensile stress was obtained along the crack plane at the tip of the β = 0° inclined chevron notch. Increment of 's' and 'c' value was found decreasing the maximum principal stress and shear stress for both before and after crack propagation. Additionally, there are more significant decreases on maximum principal stresses than shear stresses when the ligament length was increased. And also the increment of 's' value have greater impact on decreasing maximum principal stresses than increment of 'c' value.

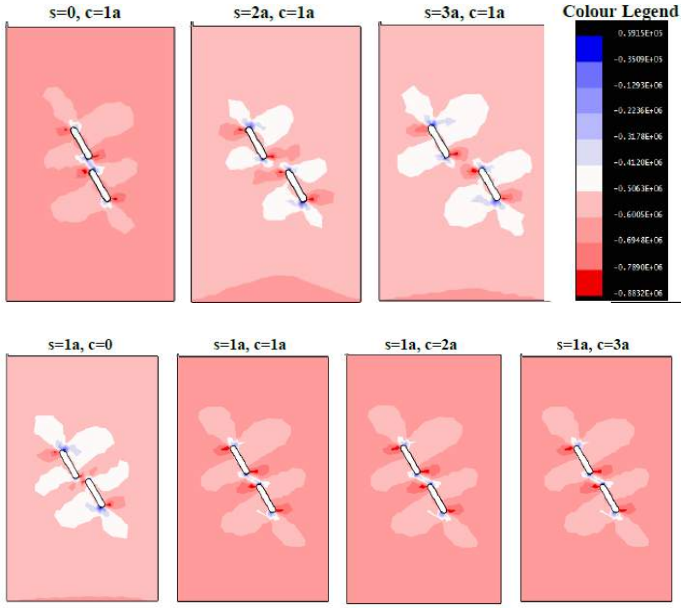

Figure 5. Maximum Principal Stress Distribution before crack initiation

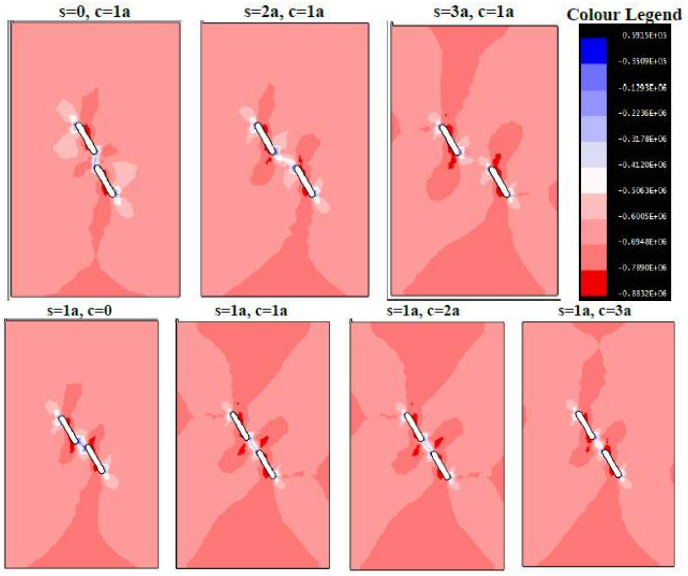

Figure 6. Shear Stress Distribution before crack initiation

After the stress distribution analysis, crack propagation analyses were conducted to investigate the crack displacements depending on the crack inclination angles. The automatic re-meshing strategy adopted in FRANC2D was to delete the elements in the vicinity of the crack tip, move the crack tip and then insert a trial mesh to connect the new crack to the existing mesh (Figure 7a). The crack propagation simulation results are shown in Figure 7. It was found that the crack initiation angle was strongly dependent on the notch crack inclination angle. Moreover, the direction of crack propagation

was found to be parallel to the loading direction and was in good agreement with experimental findings (Figure 7b). The problem type for crack simulations was plain stress and the crack propagation was conducted using the 'automatic noncohesive crack propagation' option of FRANC2D. However, the cohesive crack model implemented in FRANC2D is for Mode I fracturing only. Hence, noncohesive crack propagation was used in our models for the sake of accuracy of the inclined crack propagation simulations.

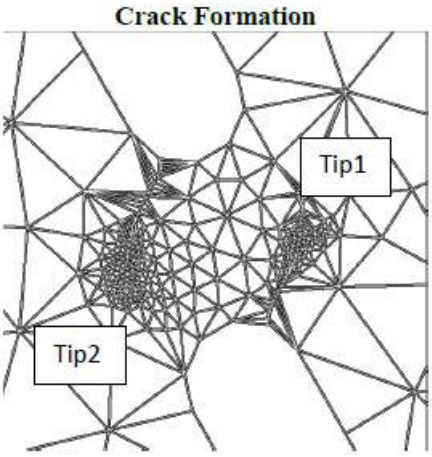

(a)

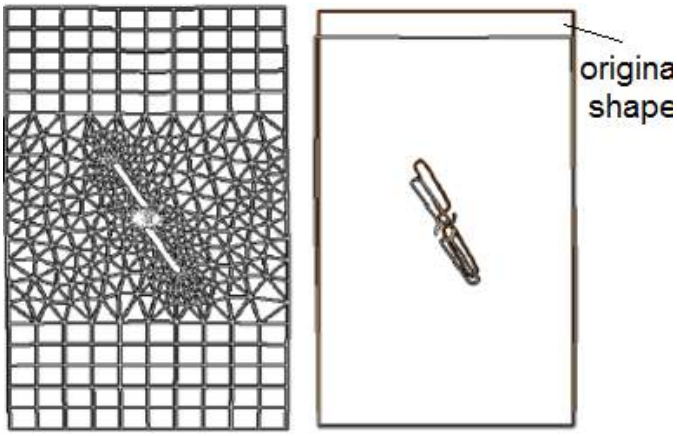

(b)

Figure 7. Crack initiation and propagation simulations (a) re-meshing at the tip (b) stress-induced crack coalescence

Figure 8 shows the stress tracks around the pre-existing cracks. As shown in Figure 8 (left), the compressive stress is quite high around the tip of cracks, it means there are possible FPZ zones around the tips of pre-existing cracks. Although the compressive zone is effective at the tips, there are also effective tensile stresses around the tips for stress-induced crack initiation and propagation.

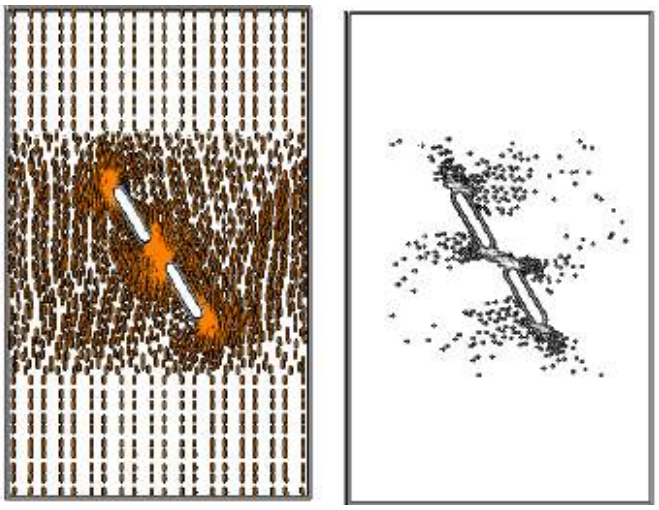

Figure 8. Stress tractions around pre-existing cracks (a) compressive (b) tension

Both the experimental and numerical results were in agreement with the findings in literature (Ingraffea 1981; Al-Shayea 2005; Lin et al. 2009).

4 CONCLUSIONS

In general, the results of the numerical stress distribution analyses showed that it was not possible to obtain pure Mode I and pure Mode II fracturing modes with uniform diametral compressive loading on to the specimen geometry. Both tensile stress and shear stress were found to be effective with all inclination angles and 's' and 'c' values.

In order to check the validity of our numerical modelling, a comparison of numerical results and experimental findings regarding crack extension (θ), crack inclination (β) angle and spacing between pre-existing cracks was made. A good agreement was found between numerical and experimental findings regarding crack extension (θ) and crack inclination (β) angles. The crack initiation angle was found to increase with increasing crack inclination angles and spacing. As the high tensile stress zone extended along the centre of the notch crack instead of the tip, with an increasing inclination angle in the stress distribution analysis in the previous section, crack

initiation in crack simulations started from a region closer to the centre of the notch crack when the β increased.

Although all crack propagations were mixed mode I-II, maximum KI value was always found higher than KII value which means that all these cracks are mainly initiated due to the tensile stress. The KI value also decreased with the increase of 's' and 'c' whereas there were no significance changes for KIIC values.

REFERENCES

Al-Shayea, N.A. (2005). Crack propagation trajectories for rocks under mixed mode I–II fracture. *Eng. Geol.*, 81, 84–97.

Erarslan, N. 2011, Static and cyclic laboratory testing of Brisbane rocks, *PhD thesis*, The University of Queensland, Brisbane.

Erarslan, N., Williams D. J. (2011). Experimental, numerical and analytical. studies on tensile strength of rocks, *International Journal of Rock Mech. & Mining Sciences*, Elsevier.

Griffith, A.A. (1924). The theory of rupture. *In Proceedings of the First International Congress for Applied Mechanics (pp.55-63)*, Biezeno, Delft. C.B., Burgers, J.M. & Waltman, J. (Eds.).

Inglis, C.E. (1913). Stresses in a plate due to the presence of cracks and sharp corners. *Trans. Inst. Naval Archit.*, 55, 219.

Ingraffea, A.R. (1981). Mixed Mode fracture initiation in Indiana limestone and Westerly granite. *Proc. 22nd US Symp. Rock Mech. (pp.186–191*, Cambridge, MA.

Lin, Q., Fakhimi, A., Haggerty, M. & Labuz, J.F. (2009). Initiation of tensile and mixed-mode fracture in sandstone. *Int. J. Rock Mech. Min. Sci.* 46, 489–497.

Nasser, N., Horii, H. (1985). Compression-induced microcrack growth in brittle solids: axial splitting and shear failure, *J. Geophys. Res., 90:B34, 3105-3215.*

Whittaker, B.N., Singh R.N., & Sun, G. (1992). *Rock Fracture Mechanics-Principles, Design and Applications*. Amsterdam: Elsevier.

Comparison of Mechanical Behaviour of G Class Cements for different Curing Time

G Sınıfı Çimentoların Mekanik Davranışlarının Farklı Kür Süresine Göre Karşılaştırılması

D. Guner, H. Ozturk
Middle East Technical University, Mining Engineering Department, Ankara, Turkey

ABSTRACT Since 1900's, well cementing is one of the most substantial method in casing application of oil, gas and geothermal. The American Petroleum Institute (API) identifies well cements in 8 classes with respect to pressure, temperature and the depth of the well. G class cement is the most commonly used cement type for well casing purpose due to its sulphate resistance ability. High sulphate-resistant (HSR) G class cements are often used in well cementing industry. API Standards mainly focus on uniaxial compressive strength (UCS) value of cements cured for 8 and 24 hours. There is no any available research on the long term (14 days) properties of G class cement in the literature. This study presents the comparison of UCS and Elastic modulus (E) growth of 3 different G class cements (2 domestic, 1 foreign products) over 14 days curing time. During the laboratory studies, samples prepared in the laboratory conditions with different curing times (2, 7 and 14 days) are tested based on ASTM standards. It is concluded that the increase in the curing time improves the UCS and E of cements 2-3 times. Logarithmic relationships exist between curing time and UCS, E. Moreover, mechanical properties of these products show significant differences between each other. The UCS and E values of G class cement produced in Turkey have values incontrovertibly lower than that of an equivalent foreign product.

Keywords: G class cement, curing time, uniaxial compressive strength, elastic modulus, high sulphate resistant (HSR), cement mechanical properties, casing

ÖZET 1900'lü yıllardan beri kuyu çimentolaması petrol, doğalgaz ve jeotermal kuyuların muhafazalanmasında kullanılan önemli bir yöntemdir. Amerikan Petrol enstitüsü (API) kuyu çimentolarını kullanılabildikleri basınç, sıcaklık ve kuyu derinliklerini esas alarak 8 farklı sınıfa ayırmıştır. G sınıfı çimento yüksek sülfat direnci nedeniyle bu çimentolar arasında kuyu muhafazası amacıyla yaygın olarak kullanılan bir çimento türüdür. API standartlarında bu çimentolar için genel olarak 8 ve 24 saatlik kür sürelerine bağlı tek eksenli basma dayanımı (TEBD) ve Elastik Modül (E) değerleri üzerinde durulmuştur. Literatürde bu çimentoların uzun vadede (14 gün) ulaştıkları TEBD değerleri bulunmamaktadır. Bu çalışmada 3 farklı firmanın ürettiği (2 yerli 1 yabancı) G sınıfı çimentoların kür süresine bağlı olarak TEBD ve E değerlerindeki artışlar sunulmuştur. Laboratuvar çalışmalarında, numuneler belirli standartlar ölçüsünde hazırlanıp farklı kür süreleri (2, 7 ve 14 gün) için deformabilite testine tabii tutulmuştur. Sonuç olarak çimentoların kür süresindeki artışın TEBD ve E değerlerini 2-3 kat arttırdığı görülmüş ve bu ilişki logaritmik eşitliklerle açıklanmıştır. Ayrıca tüm deney koşulları sabit tutulmasına karşın test edilen 3 ürünün mekanik özellikleri arasında önemli farklar gözlemlenmiştir. Yerli ürünlerin TEBD ve E değerleri eşdeğer yabancı ürüne göre yadsınamayacak şekilde düşüktür bulunmuştur.

Anahtar Kelimeler: G sınıfı çimento, kür süresi, tek eksenli basma dayanımı, elastik modül, yüksek sülfat direnci, çimento mekanik özellik, kuyu muhafazalama.

1 INTRODUCTION

Well casing has always been primary concerns for various different drilling purposes. Although generally the petroleum industry is well known for its casing system applications, there are many other fields; such as geothermal, natural gas and solution mining industries also use well casing applications. The primary purpose of cementing is to keep the casing in place, to provide stability and zonal isolation of the well, to prevent corrosion and to avoid the influx of fluids or gases into the annular space of the well.

American Petroleum Institute (API) is the only authorized standardization committee in this area. This institute classifies eight categories of cements depending of the well condition and use of well cementing purposes (API, 2005). These categories are listed in Table.1 for different depth and temperature ranges.

Table 1. API Well Cement Classification

Class	Depth Range (m)	Temperature Range (ºC)
A	0-1830	0-77
B	0-1830	0-77
C	0-1830	0-77
D	1830-3050	77-127
E	3050-4270	77-127
F	3050-4880	110-160
G	0-2440	0-93
H	3660-4880	0-93

Among these cement classes, more than 80% of the companies prefer class H & G cements for well cementing in the United States. On the other hand, the rest of the world (more than 95%) uses class G cement (SPE, 2009).
The general properties of class G cements are;

- Obtained by grinding Portland cement clinker,
- Consist of hydraulic Ca_2SiO_4,
- Generally contains one or more forms of $CaSO_4$ as an interground additive,
- No more additives other than $CaSO_4$ and H_2O.

Two different forms of class G cements are available on the market, namely medium and high sulphate-resistant (MSR, HSR). HSR type cement is more commonly used cement type in petroleum, natural gas and solution mining industry.

Although API standards give fine details of specification of class G cements, according to these standards there is no any requirement of minimum uniaxial compressive strength (UCS) value at the end of 24hours curing time. However, early or late UCS and Elastic Modulus (E) of casing might be very crucial for preventing influx of fluids or gases from neighbour rock to a well or from well to the neighbour rock.

There are many different class G suppliers in the world. In this study, three different HSR class G cements are tested (two are from local, one is from international) in accordance with test standards and the relationships between UCS, E vs. curing time is found.

2 PREVIOUS TESTS

Although the long term performance of the stated cement is not indicated in production standards, some researchers performed laboratory test with different conditions; such as different curing temperature and pressure to investigate the performances of them. In the last decade, various research studies were performed UCS and E tests on the performance of cements. The obtained results are tabulated in Table 2.

In the literature, there is only one study about the investigation of long term performance of class G cements: Teodouri et.al. (2013) performed UCS test with 5cm length cubic specimens. They stated that one day cured UCS of the specimen is about 6MPa, and this value increased substantially to 56MPa for 20 day curing. In this study, Class G cement composition had a water cement (w/c) ratio of 0.45 without any additives and the density of the slurry was given as 1.89 g/cm^3.

Table 2. UCS & E Values of Class G Cements from the Literature

Ref.	UCS (MPa)	E (GPa)	Test Conditions
Le Roy et al. (2000)	37	6.6	Cured at 77°C, 27 MPa p. for 3 days
Morris et al. (2003)	40	5.4	Cured at 84°C, 27 MPa p. for 2 days.
Wehling (2008)	49	8.7	Cured ambient temperature and p. 3 days
Teodouri et al. (2012)	48	12.0	Cured ambient temperature and p. 3 days.
Nasvi et al. (2013)	53	-	Cured at 60°C, for 3 days
Nasvi et al. (2013)	27	-	Cured ambient temperature and p. 3 days

3 LABORATORY STUDIES

Three different Class G cement products are tested in the laboratory for UCS and E determination.

3.1 Sample Preparation

Sample preparation is the most laborsome part of the laboratory testing. In order to obtain homogenous test specimens, all test specimens for each product were prepared in a single mixing process.

In mixing process, electric mixer is used at 120rpm level for all products. The samples are prepared at a constant water - cement (w/c) ratio of 0.5 (Figure 1.)

Figure 1. Slurry Agitation Stage

At the end of the mixing, density of the each slurry was measured as 1.81g/cm^3. After mixing of cement and water, slurry is poured into cylindrical 50mm diameter PVC moulds. Sometimes, it is hard to remove test specimen from the moulds, to prevent this problem and not to damage the specimen, releasing agent is sprayed into mould before casting. Prepared moulds are presented in Figure 2. PVC moulds were prepared 2-3cm longer than the aimed sample length to account for shrinkage in length during curing.

Figure 2. Moulded Test Specimens

After moulding progress PVC moulded concrete samples are submerged into water bath during curing at 25-29ºC ambient room temperature and 30-40% humidity of laboratory environment. At the end of curing time, test specimens were removed by using special removing device (Figure 3.). Finally, top and bottom surface of the specimen was smoothed out by a chainsaw for the standardized length to diameter ratio of 2.

Figure 3. Removing of Test Specimen

3.2 Testing Apparatus

Laboratory tests are carried out with a displacement controlled with a universal testing machine which has a 500kN load capacity. Since MTS machine does not enable to visualize load displacement curve during tests, a data acquisition system is attached to the test set up. Moreover, this system can record eight data reading per second; it helps to obtain more sensitive test results.

In order to record axial displacement on the specimen, two strain gauge based transducer are attached to the rigid plate and for lateral displacement recording, circumferential extensometer is attached to the middle of the specimen as shown in Figure 4.

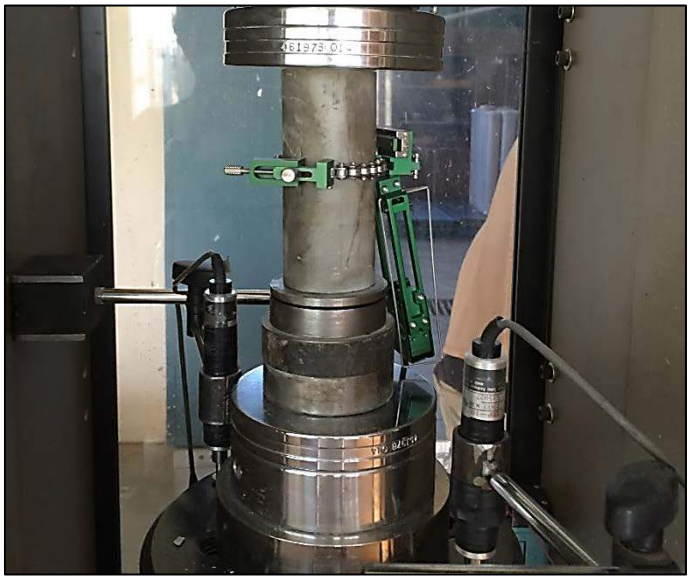

Figure 4. Laboratory Test Apparatus

3.3 Laboratory Testing

Deformability tests are conducted for 2, 7 and 14 days of curing time. Three valid test results of 2 and 7 days cured specimens for each product are obtained. For 14 day curing time, since expected UCS and E values are much higher than 2 and 7 days, six valid tests are conducted. Table 3 presents the number of tests for each curing time and the product type.

Table 3. Conducted Test Numbers in Laboratory Studies

Product Code	Curing Time (Days)		
	2	7	14
D1	3	3	6
D2	3	3	6
F	3	3	6

Product names were used as for the local products 1 and 2, international product as D1, D2 and F respectively. A total number of 36 valid tests are conducted.

Laboratory studies are carried out in accordance with the standards suggested by International Society for Rock Mechanics (ISRM) and (ASTM D7012). During laboratory studies, test are conducted under constant strain rate of 0.50 mm/min. and the specimens failed in 4 to 6 minutes.

4 TEST RESULTS

At the end of laboratory tests, stress vs. axial strain curves are plotted. Figure 5 shows a representative stress-axial strain curves of 2 days cured for three products.

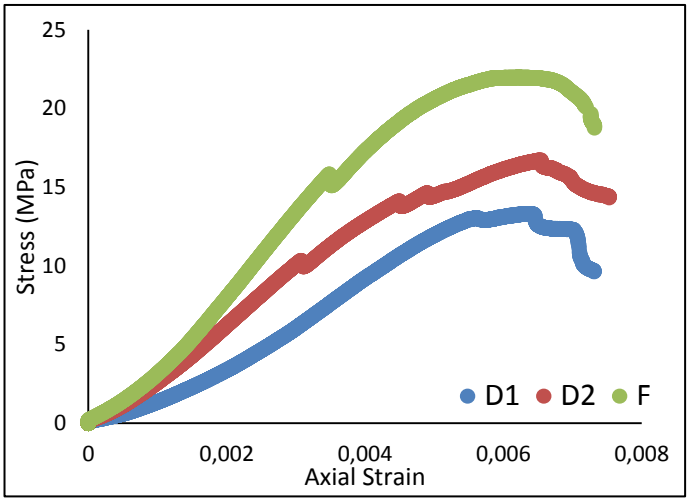

Figure 5. 2 Days Cured Representative Stress-strain Curves

According to the given curves, product F is stronger and stiffer than the other two products. At the end of the test evaluation part, UCS and E values are calculated. Figure 6 shows the relationship between UCS and curing time. The UCS values strongly depend on the curing time for the cement samples, the relationships can be expressed using a logarithmic trend line.

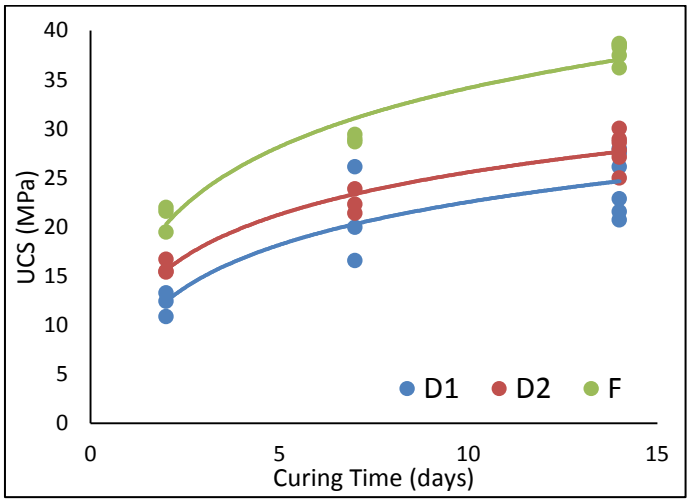

Figure 6. UCS versus Curing Time Relationships of Three Products

It should be noted that all the testing and curing conditions are kept constant for all products. Relationship between the UCS and curing time is very similar for D1 and D2 products. UCS test results, the related logarithmic relationships and correlation coefficients are presented in Table 4.

Table 4. UCS Test Results

Sample D1			
Curing Time	2 Days	7 Days	14 Days
UCS (MPa)	12.20 ± 1.23	20.89 ± 4.85	24.47 ± 3.15
Logarithmic Relationship	UCS = 6.2933ln(Days) + 8.0528		
R^2	0.75		
Sample D2			
Curing Time	2 Days	7 Days	14 Days
UCS (MPa)	15.88 ± 0.72	22.54 ± 1.27	27.92 ± 1.74
Logarithmic Relationship	UCS= 6.2035ln(Days) + 11.287		
R^2	0.93		
Sample F			
Curing Time	2 Days	7 Days	14 Days
UCS (MPa)	21.01 ± 1.35	29.02 ± 0.38	37.49 ± 1.02
Logarithmic Relationship	UCS = 8.6195ln(Days) + 14.305		
R^2	0.95		

The compressive strength increased substantially with increase in curing time from 2 to 14 days for all products. At the end of 2 weeks, Product F has more than 37MPa UCS, on the other hand corresponding UCS value for the given time of the product D2 is less than 25MPa.

Similar growth is also observed on Elastic modulus values for the three products. Figure 7 shows the relationship between elastic modulus and curing time.

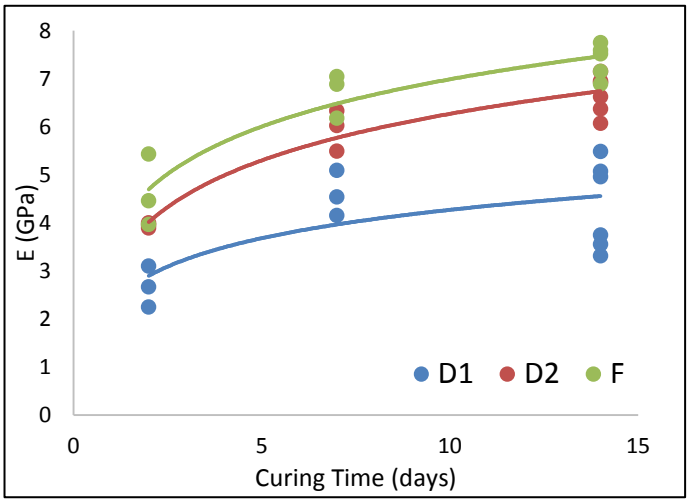

Figure 7. Elastic Modulus versus Curing Time Relationships of Three Products

As a result of the deformability tests, notable difference is observed for three different products as seen in UCS test results. Obtained Elastic modulus values, the related logarithmic relationships and correlation coefficients are presented in Table 5.

Elastic modulus values are almost doubled between the 2nd and 14th days curing time tests. At the end of the 2 weeks curing time, product F has more than 7GPa Elastic modulus value. Although similar Elastic modulus growths are observed in the other products, notable difference is obtained.

As expected, the uniaxial compressive strength and elastic modulus for three products are directly related with curing time.

Table 5. Elastic Modulus Results

Sample D1			
Curing Time	2 Days	7 Days	14Days
E (GPa)	2.25 ± 0.43	4.60 ± 0.47	4.36 ± 0.92
Logarithmic Relationship	E = 0.8528ln(Days) + 2.307		
R^2	0.45		
Sample D2			
Curing Time	2 Days	7 Days	14Days
E (GPa)	3.95 ± 0.05	5.95 ± 0.43	6.68 ± 0.41
Logarithmic Relationship	E = 1.4017ln(Days) + 3.0423		
R^2	0.92		
Sample F			
Curing Time	2 Days	7 Days	14Days
E (GPa)	4.62 ± 0.74	6.70 ± 0.46	7.38 ± 0.35
Logarithmic Relationship	E = 1.4227ln(Days) + 3.7129		
R^2	0.87		

5 CONCLUSIONS & RECOMMENDATIONS

In this study, uniaxial compressive strength and the elastic modulus of the 3 different class G cements are investigated based on the curing time. For this purpose two local and one international class G cements were tested in accordance with related test standards.

Main conclusions of this study is as follows;

- As expected, the uniaxial compressive strength and elastic modulus for class G cements are directly related with curing time. As curing time increased UCS and E values also increased. A logarithmic relationship exists between the curing time and UCS or between E and the curing time.
- Elastic modulus and UCS values almost doubled between the 2nd and 14th days. Although all the test parameters and laboratory conditions were kept constant, notably differences were observed for each product.
- The UCS and E values of G class cement produced in Turkey had values incontrovertibly lower than that of an equivalent international product.

According to the given conclusions, suggested recommendations and future works are listed as follows;

- in order to investigate the long term performance of class G cements, it may better to carry out longer curing time tests, like 28 days.
- different water-cement ratio tests might be useful.
- curing temperature, pressure and humidity are also significant parameters for cements, detailed tests considering these parameters may give important results.
- domestic class G cement suppliers may review their products by considering these obtained results.

REFERENCES

American Petroleum Institute (API), 2005. *Specification for Cement and Materials for Well Cementing, 23rd Edition. API, Washington*, 271p.

ASTM Standard D7012 - 2014, *Standard Test Methods for Compressive Strength and Elastic Moduli of Intact Rock Core Specimens under Varying States of Stress and Temperatures* ASTM International, West Conshohocken, PA, 2014, DOI: 10.1520/D7012-14, 18p.

Le Roy S., Baumgarte C., Thiercelin M., Vidick B, 2000 *New Cement Systems for Durable Zonal Isolation*, IADC/SPE Drilling Conference 59132, 10p.

Morris W., Marcelo A., Robles J., Bianchi G., 2003 *Design of High Toughness Cement for Effective Long Lasting Well Isolations*, SPE 81001.

Nasvi M., Ranjith P., Sanjayan J. 2013, *Comparison of Mechanical Behaviors of Geopolymer and Class G Cement as Well Cement at Different Curing Temperatures for Geological*

Sequestration of Carbon Dioxide, American Rock Mechanics Association, the 46th US Rock Mechanics / Geomechanics Symposium, Chicago

Teoruri C., Amani M., Yuan Z., Schubert J., Kosinowsli C., 2012. *Investigation of the Mechanical Properties of Class G Cement and Their Effect on Well Integrity.*ISSN2305-8269, 7p.

Wehling, P., 2008. *Wellbore Cement Integrity Testing,* Master Thesis, TU-Clausthal.

Correlation of Linear and Volumetric Fracture Densities in Jointed Rock Mass

H. Mirzaei
Faculty of Mining, Petroleum and Geophysics, Shahrood University, Iran

ABSTRACT In this paper the relation between linear and volumetric fracture densities is investigated with the use of synthetic discrete fracture networks. A synthetic rock mass containing one joint set with known geometrical parameters is considered and various discrete fracture network models for different amount of volumetric fracture densities were generated. For each fracture network, a set of boreholes were simulated to determine linear fracture density. Then correlation of known volumetric densities and corresponding calculated linear densities is studied. Results show that the currently used relation to obtain volumetric density is not valid.

Keywords: Linear fracture density, volumetric fracture density, Monte Carlo simulation

1 INTRODUCTION

In different mining and civil engineering activities such as stability analysis of underground mining spaces (Fekete & Diederichs 2013), slope stability in open pit mines, prediction of dilution potential in block caving method (Katherine et al. 2008), hydraulic behavior of rock mass (Lee & Moon 2004), hot dry rock geothermal energy systems (Tran & Rahman 2007) etc., geometrical modeling of jointed rock mass is essential task.

In general, in these applications, extensive sampling is difficult or expensive and the data available at the time of decision-making are scarce. For these reasons, the only feasible approach is via stochastic models based on the limited available data (Dowd et al. 2007).

The Discrete Fracture Network (DFN) analysis is a widely applied modeling approach to stochastic simulation of rock fracture network. The DFN approach relies on stochastic realizations of fracture systems using Monte Carlo simulations (Jing & Stephansson 2007).

Density is a parameter which describes the amount of fracturing of rock mass. Linear, areal and volumetric fracture densities are defined as Number of fractures per unit length, Number of fractures per unit area and Number of fractures per unit volume, respectively.

Volumetric fracture density (D_3) is one of key parameters required to simulate the geometry of jointed rock mass. Since dismantle of rock mass is not imaginable, direct measurement of D_3 is not possible. In practice, D_3 is estimated from calculated linear (D_1) or areal (D_2) fracture densities obtained from scanline, borehole or window sampling methods (Priest 1993).

In this paper the relation between linear and volumetric densities is investigated with the use of synthetic discrete fracture network models.

2 DISCRETE FRACTURE NETWORK MODELS

A large degree of uncertainty is associated with the geometric properties of fractures, especially their locations, shapes and sizes. These uncertainties are the reasons for using stochastic distributions as their mathematical representations, rather than explicit and deterministic representations.

For rock mass characterization, the field mapping data from scanlines, windows or boreholes are processed to identify the fracture sets. After identification of the sets, the fractures should be regrouped into their

corresponding sets for further statistical analysis to determine the mean values for dip direction and dip angle and their probabilistic density functions. One of the common types of distribution functions for orientation is the Fisher distribution (Jing & Stephansson 2007). With the identification of the sets complete, the rest of the parameters, i.e., the density, spacing, fracture size (trace length) and aperture are analyzed to produce the respective probability density functions (PDFs). According to the literature the negative exponential, log normal and power law probability distribution functions govern on trace length and therefore fracture size (Jing & Stephansson 2007).

To take into account the uncertainties associated with rock fracture geometrical properties, discrete fracture network concept is employed to model rock mass geometry which is based on the Monte Carlo simulation technique.

2.1 Monte Carlo Simulation

Monte Carlo simulation is a stochastic process which addresses the 'randomness' of the fracture network geometry, by representing the fracture properties of location, size, orientation and aperture as random variables following their own specific PDFs, after assuming the shapes of fractures (commonly disk shape) and calculating the volumetric densities of all sets of fractures. The aim of the simulation is to generate a large number of realizations of a fracture system, each of which corresponds to a particular set of individual random variables for the locations (of fracture geometric centers), orientations, size and apertures, generated according to their specific PDFs. In this process the number of simulated fractures in each realization is depend on volumetric density and model volume.

The procedure of Monte Carlo technique to stochastic simulation of rock fracture system is illustrated schematically in Figure 1.

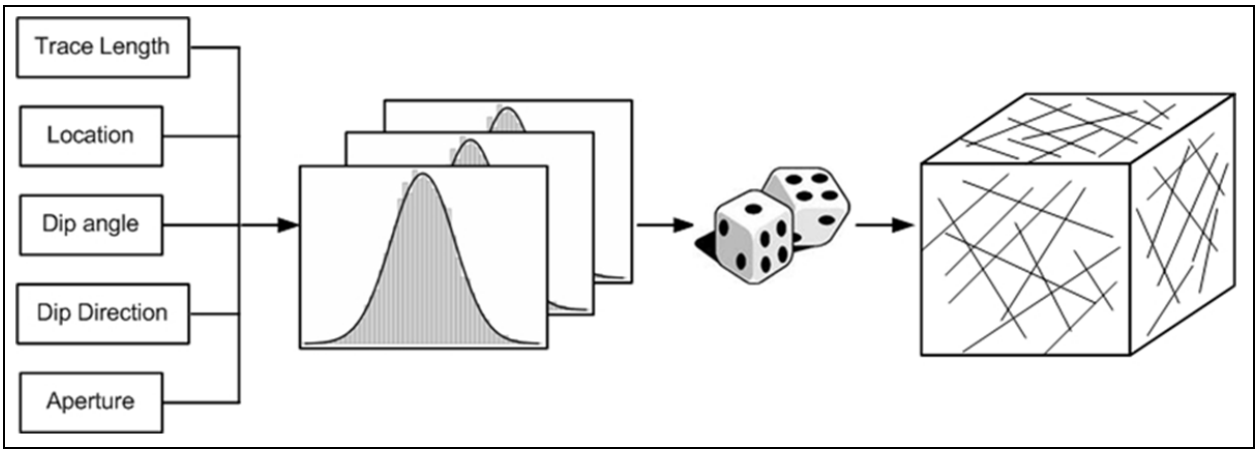

Figure 1. Monte Carlo simulation to generate rock fracture system.

2.2 Discrete Fracture Network Generation

Generation of a realization of a fracture network system can be achieved by different methods. The one described below is one of the simple cases (Jing & Stephansson 2007). It involves the following multiple steps:

a) Choosing a generation domain in 2D or 3D space within which a realization of a fracture network system is to be generated;

b) Starting from fracture set 1, calculating the number, N, of fractures to be generated according to the density values (D_2 or D_3) and spacing;

c) Generating the locations of N fracture centers as a Poisson process;

d) At each fracture center, generate two random numbers representing its values of dip direction and dip angle according to its Fisher PDF;

e) Generating a random number representing its size, according to its fracture size PDF, and generating a string of vertex coordinates defining its outer boundaries according to the shape assumptions (circular disks or rectangles, etc.);

f) Generating a random number representing its aperture according to the respective PDF;

g) Repeat steps (a) to (f) for all sets of fractures;

The above steps can establish one fracture network realization. They must be repeated to generate the desired number of fracture network realizations for a proper stochastic simulation, usually by using different seed numbers (used for initializing the random number generation process).

The probability distribution functions assumed in this sturdy for geometrical parameters are summarized in Table 1.

Table 1. Assumed probability distribution function for fracture geometrical properties.

Parameter	Probability density function
Location	Poisson process
Orientation	Fisher distribution
Size	Negative exponential

3 RESEARCH PROCEDURE

To investigate the relation between linear and volumetric fracture densities, a synthetic rock mass containing one joint set with known geometrical parameters were considered.

For various amounts of volumetric fracture density (D_3) with same geometrical properties, different DFN models were simulated. For each amount of D_3, various realizations are generated.

To calculate linear fracture density (D_1) of simulated DFN models, a set of boreholes with regular pattern were used for sampling the fractures (intersected fractures).

D_1 is dependent on the orientations of the boreholes, and is therefore termed apparent fracture density (Jing & Stephansson 2007). The apparent linear density is calculated as follow:

$$D_1 = \frac{N}{L} \quad (1)$$

where N is number of intersected fractures by borehole and L is length of borehole. To remove the orientation bias and obtain true linear density, the calculated apparent density must be corrected by the cosine of the acute angle θ of the fracture set normal and borehole direction (Zeeb et al. 2013, Lacazette 1991):

$$D_1^* = \frac{N}{L\cos\theta} \quad (2)$$

The mean of linear densities determined from different boreholes is calculated as corresponding linear density for known volumetric fracture density of current synthetic DFN model.

Once the linear densities related to different known volumetric densities were calculated from various synthetic DFN models, the relation between D_1 and D_3 could be investigated.

To produce synthetic DFN models, carry out the explained simulations and perform the above mentioned procedure, a set of computer programs were prepared in MATLAB software and used in this study.

4 CORRELATION OF LINEAR AND VOLUMETRIC DENSITIES

To investigate the relation between linear and volumetric fracture densities based on described procedure, a synthetic rock mass containing one joint set with known geometrical parameters as presented in Table 2 was considered.

Table 2. Parameters for simulation of rock mass.

Model Volume (m^3)	$10\times10\times10$
Joint set orientation (Dip/Dip Direction)	$60^\circ/180^\circ$
Fisher constant	100
Mean fracture size (m)	1

A realization of the synthetic rock mass (sample DFN model) with volumetric density of 1 ($1/m^3$) is shown in Figure 2.

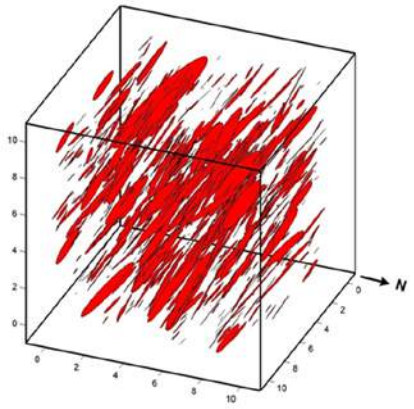

Figure 2. A realization of synthetic rock mass.

For various amounts of D_3 from interval [0.2-2.4] with same geometrical properties of Table 1, different DFN models were simulated. For each amount of D_3, five realizations of rock mass were generated.

To calculate linear fracture density (D_1) a set of boreholes (16 boreholes) with 10 m length and with regular pattern as shown in Figure 3 were used for sampling the fractures (intersected fractures).

For each borehole the number of intersected fractures was counted and apparent and corrected linear density was calculated using relations 1 and 2.

For instance for known D_3 of 1 ($1/m^3$), the values of corrected amount of D_1 determined from five boreholes for three realizations are given in Table 3.

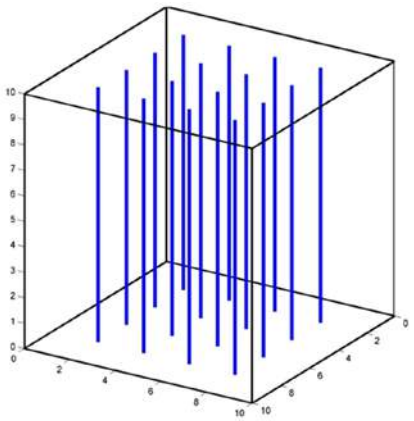

Figure 3. Pattern of simulated boreholes.

Table 3. Values of D_1 correspond to D_3 = 1 ($1/m^3$).

Borehole	Realization		
	1	2	3
1	2.2	1.6	1.4
2	1	1.4	1
3	1.4	1.2	0.8
4	1.6	0.8	1.2
5	1.4	1.4	1.2

The mean of apparent and corrected D_1 determined from 16 boreholes for five realizations of simulated rock mass are plotted with respect to D_3 in Figures 4 and 5 respectively.

Then the average of apparent and corrected D_1 values for various realizations of rock mass are determined and plotted with respect to D_3 in Figures 6 and 7 respectively.

According to Figures 6 and 7, D_3 and D_1 show linear relation. Therefore a line was fitted to these data as shown in Figures 6 and 7. Fitted line equations indicate that volumetric density is approximately equal to 0.7 of corrected linear density and 1.4 of apparent linear density.

The obtained results were compared with the relation argued in (Jing & Stephansson 2007) in Figures 6 and 7. According to this reference, D_1 and D_3 relate with together as follow:

$$D_3 = 2 D_1 \qquad (3)$$

The results of this study indicate that the currently used relation (3) is not valid.

As discussed the number of fractures to be generated during DFN construction process is depend on volumetric fracture density amount. Therefore incorrect D_3 value led to production of improper rock mass geometrical model which is the fundamental of further mechanical and hydraulic studies.

Consequently based on the results of this study, to model geometry of rock mass, first the corrected or true linear density must be calculated from borehole data or scanline method and then volumetric density must be assumed 0.7 of corrected linear density.

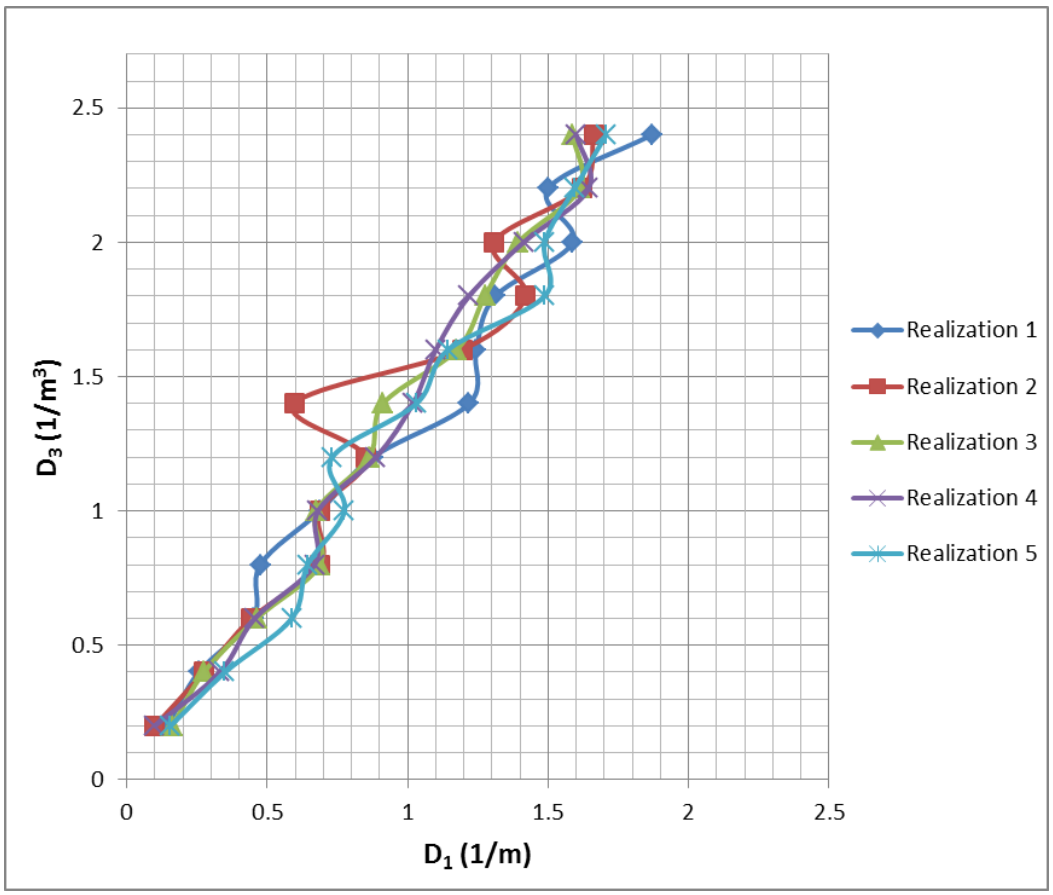

Figure 4. Apparent linear density versus volumetric density for various realizations.

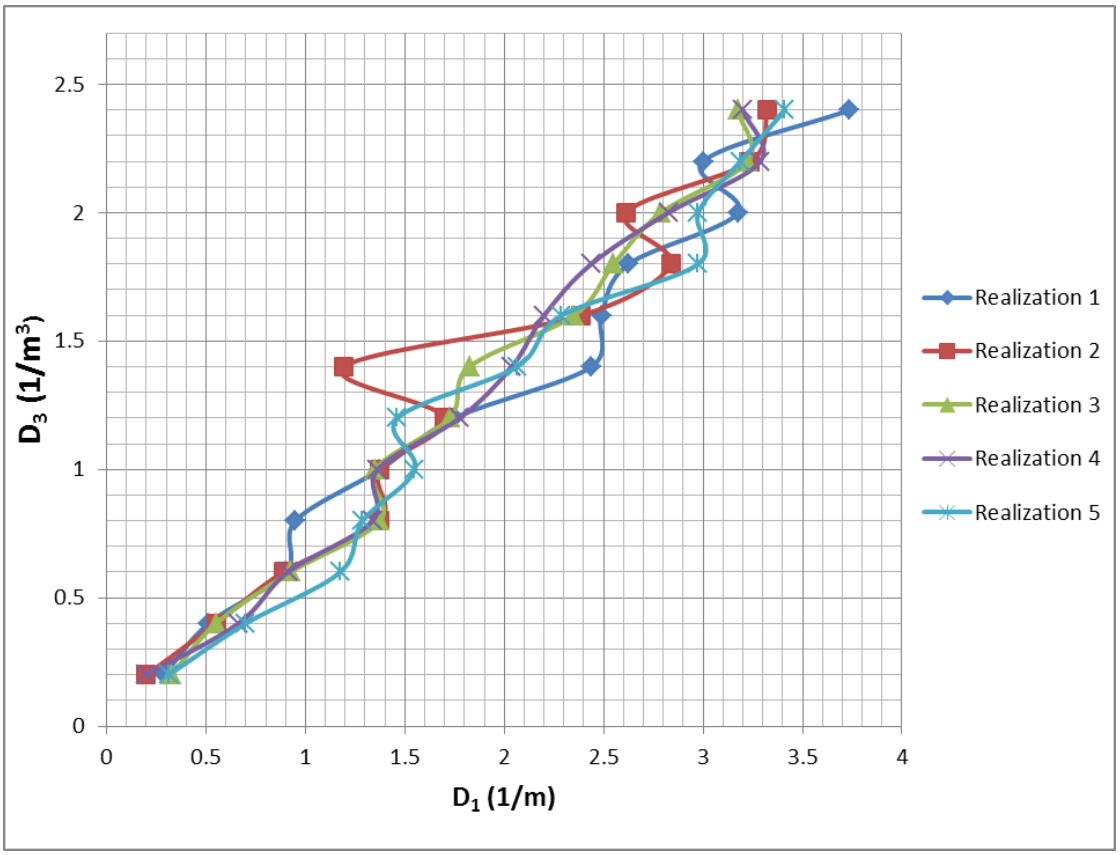

Figure 5. Corrected linear density versus volumetric density for various realizations.

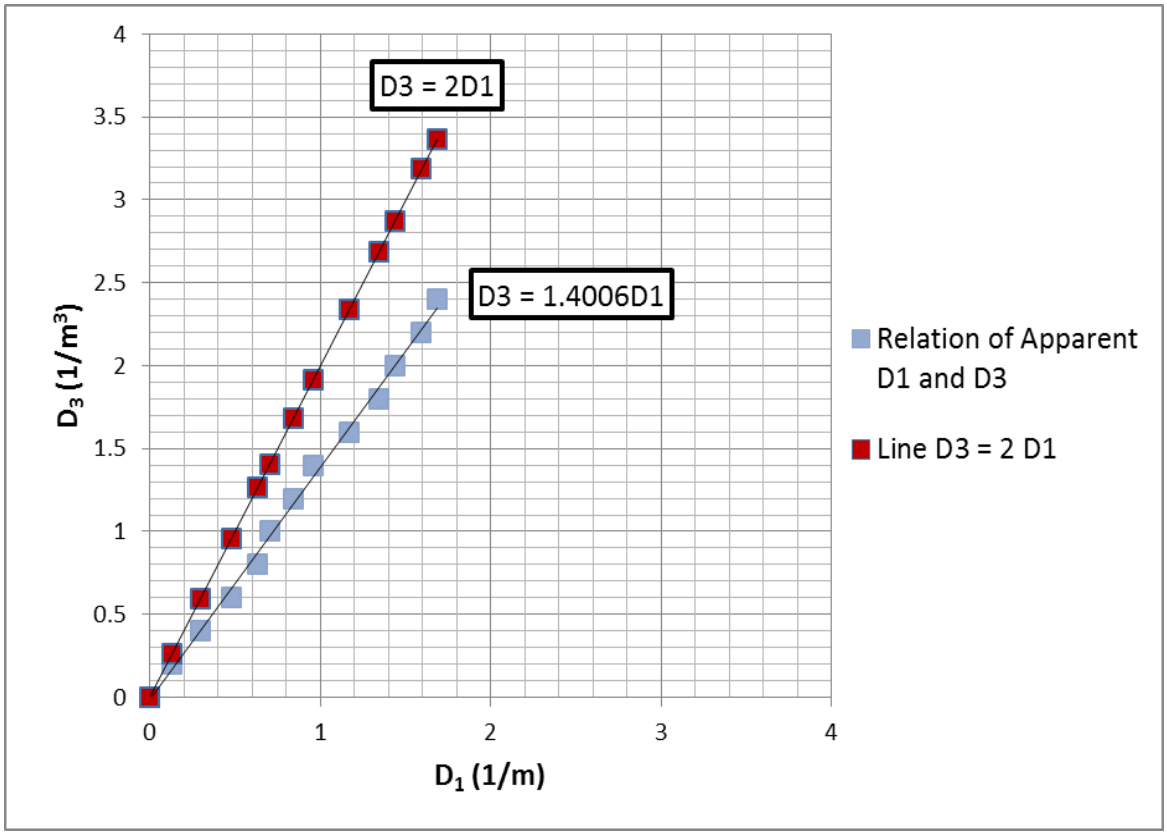

Figure 6. Relation of average apparent linear and volumetric densities in comparison with the relation $D_3 = 2\ D_1$.

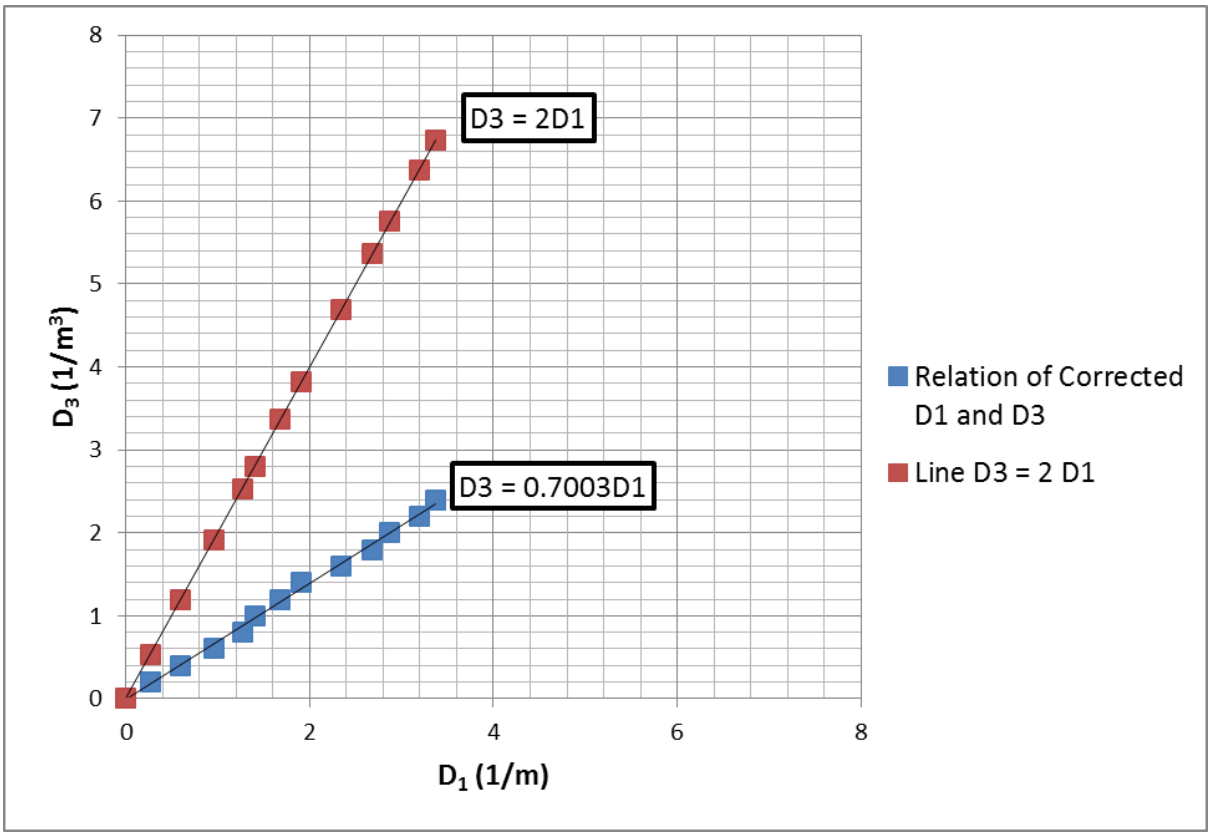

Figure 7. Relation of average Corrected linear and volumetric densities in comparison with the relation $D_3 = 2\ D_1$.

5 CONCLUSION

In this study a synthetic rock mass containing one joint set with known geometrical parameters is considered and various DFN models for different amounts of volumetric fracture densities were generated to investigate the relation between linear and volumetric densities. For each fracture network, a set of boreholes were simulated to determine linear fracture density correspond to known volumetric density. Obtained results show the currently used relation between linear and volumetric densities is not valid.

Finally this study propose that to model the geometry of rock mass, first the corrected or true linear density must be calculated from borehole or scanline data and then volumetric density must be considered equal to 0.7 of corrected linear density.

REFERENCES

Dowd, P. A., Xu, C., Mardia, K. V., Fowell, R. J., 2007. A Comparison of Methods for the Stochastic Simulation of Rock Fractures, Mathematical Geology, 39, pp. 697–714.

Fekete, S., Diederichs, M., 2013. Integration of three-dimensional laser scanning with discontinuum modelling for stability analysis of tunnels in blocky rockmasses, International Journal of Rock Mechanics & Mining Sciences, 57, pp. 11-23.

Jing, L.; Stephansson, O., 2007. Fundamentals of Discrete Element Methods, Theory and Applications, 1nd Edition, 545 p.

Kalenchuk, K. S., McKinnon, S Diederichs M. S., 2008. Block geometry and rockmass characterization for prediction of dilution potential into sub-level cave mine voids, International Journal of Rock Mechanics & Mining Sciences, 45, pp. 929-940.

LaPointe, P. R., 2002. Derivation of parent population statistics from trace length measurements of fractal populations, International Journal of Rock Mechanics and Mining Sciences, v. 39, p. 381–388.

Lee, S. D., Moon, H.K., 2004. Hydro-mechanical modelling of tunnel excavation in fractured rock massesby a 3D discrete fracture network approach, SINOROCK2004 Symposium, pp. 1-6.

Priest, S. D., 1993. Discontinuity analysis for rock engineering. Chapman and Hall, London, 473 p.

Tran, N.H., Rahman, S.S., 2007. Development of hot dry rocks by hydraulic stimulation: Natural fracture network simulation, Theoretical and Applied Fracture Mechanics, 47, pp. 77–85.

Zeeb, C., Gomez-Rivas, E., Bons, P. D., Blum, P., 2013. Evaluation of sampling methods for fracture network characterization using outcrops, AAPG Bulletin, v. 97, No. 9, pp. 1545–1566.

Earthzyme – Paving a New Way for Haul Road Construction

T. Burns
Cypher Environmental Ltd. 1149 St Matthews Ave Winnipeg, Canada R3G 0J8

ABSTRACT - The following is a technical summary of some examples of the past 15 years of Cypher Environmental Ltd.'s work with EarthZyme soil stabilizer.

The use of environmentally friendly EarthZyme soil stabilizer can dramatically reduce costs associated with the construction and maintenance of new haul roads and the stabilization of existing haul roads. EarthZyme is a concentrated blend of enzymes, electrolytes and surfactants that produce fantastic results on suitable soils. After an application of EarthZyme, treated soils have shown to yield higher densities, increase California bearing ratio (CBR) values, and reduce permeability and swell. EarthZyme works on clay based soils, stabilizing them to comparable strengths of traditional aggregate haul roads. This results in a significant cost savings in expensive raw material inputs such as coarse sand and gravel, which are not required when a soil is stabilized with EarthZyme. EarthZyme soil stabilization has been successfully used in a variety of road construction projects. Specifically in a thoroughly studied project in Ecuador, EarthZyme treated soils were determined to yield a significant reduction in swell (170 %) and an increase in CBR (51 %). These modifications in soil properties, due to stabilization with EarthZyme, are consistently reported and long-lasting even though the product biodegrades (> 90 %) within 28 days. This report will go into greater detail regarding the advantages that EarthZyme can provide when introduced to any mine site. Further to the cost savings in raw materials, emphasis will be placed on the reduced maintenance requirements and costs that introducing EarthZyme to a road construction project exhibits through the long term stabilization and improved engineering characteristics of a stabilized soil. EarthZyme has a diverse application history; from humid climates like Southern China, and tropical Latin America to the arid Gobi Desert of Mongolia, or the extreme climates of West Africa, and Northern Alberta, Canada. The most challenging of these, in terms of climate and road requirements, has been the Athabasca oil deposits of Northern Alberta, Canada. The consistently low temperatures and high levels of precipitation combined with the extreme weight of haul trucks, 400-700 tonne loaded weights, required to mine the deposit was put to Cypher Environmental Ltd. as a challenge in 2009. Cypher Environmental Ltd. eagerly met this challenge and together with our Western Canadian distributor, Frontline Integrated Services Limited, and our other industry partners, have successfully reduced the cost of all-weather haul road construction while exceeding industry standards in the Athabasca Oil Sands and around the world.

Keywords: EarthZyme, road construction, stabilized road

1 INTRODUCTION

Cypher Environmental Ltd. has been developing and applying EarthZyme liquid soil stabilizer for over a decade. In our extended time applying and developing EarthZyme we have successfully utilized the product in diverse projects and global settings. For the past 5 years Cypher Environmental Ltd. has been working closely with the mining industry in the Athabasca oil sands to construct haul roads that outperform dated and costly aggregate construction methods. These EarthZyme stabilized road s have displayed both short and long term cost savings. Due to the competitive nature of the mining industry this summation of works completed will not specifically reference our

clients or their projects. Differentiation will be made between road type a project location

2 ECONOMIC BENEFITS OF EARTHZYME CONSTRUCTION PROJECTS

Currently aggregate material is becoming scarce on many mine sites, particularly in the Athabasca oil sands. Typically haul road construction requires a well graded aggregate to achieve desired characteristics: high load bearing capacity, wear resistance, and weather resistance. Constructing haul roads with EarthZyme utilizes fine grain clayey soils and standard equipment. These clayey soils are traditionally considered mine waste or over burden. EarthZyme haul roads in the Athabasca oil sands have been studied in comparison to aggregate all-weather haul roads and have consistently produced comparative, if not superior results. These haul roads have shown to be faster to build, exhibit reduced rolling resistance and rack events, and cost less to construct.

EarthZyme road construction methods, whether for heavy mining trucks or municipal traffic, are quite similar. The difference between constructing a haul road (40 metre width) or a municipal road (7 metre width) is equipment selection. For haul road construction Cypher Environmental Ltd. recommends utilizing 1-2 large haul trucks (ex. Caterpillar 793) or steel drum rollers (ex. Caterpillar CS64) depending on availability, to compact the soil, 1-2 large water trucks (40-100 tonnes), a large grader (ex. Caterpillar 16M or 24M), and 2 reclaimers (ex. Caterpillar RM500 Reclaimer). For municipal road construction Cypher Environmental Ltd. recommends utilizing 1 steel drum vibratory compactor and a pneumatic roller (ex. Caterpillar CS64, Caterpillar PS360C), 1-2 graders (ex. Caterpillar 14M) or 1 grader and 1 reclaimer (ex. Caterpillar RM300), and a 10-20 tonne water truck. A major similarity between EarthZyme road construction projects in different industry settings is the associated short and long term cost savings.

As a result of the similarities in construction techniques and effort, and the competitive nature of the mining industry, a well-studied comparative municipal construction project will be utilized to display the short term cost saving nature of EarthZyme road construction.

2.1 Short Term Economic Benefits of EarthZyme

An empirical review of a municipal road construction project in Ecuador was conducted by Eco-Road Solutions, Quito, Ecuador (Helberth, 2012, June). This review encompassed several aspects of the project, including a cost comparison between two equal sections of road; one constructed with standard aggregates, the other using clayey soil and EarthZyme. This study determined that the EarthZyme stabilized road was completed more efficiently on all measurement criteria (Table I).

Table I - Economic savings of EarthZyme municipal road construction, Quito Ecuador

Action	Savings with EarthZyme
Material transported	95 %
Use of machinery	59 %
Material	27 %
Labour	33 %
Total Project Savings	**47 %**

The largest saving resulting from this study was in material transportation. Material and transportation cost savings result from EarthZyme projects because raw material inputs for EarthZyme road construction are considered waste by many industries and therefore inexpensive to acquire. It is worth noting that prior to this project the contractor had not previously worked with EarthZyme, but they had received mandatory training from a Cypher Environmental Ltd. representative. Also, constructing roads with EarthZyme reduces machine hours and labour, which results in increased contractor capacity.

2.2 Long Term Economic Benefits of EarthZyme

2.2.1 Reduced rolling resistance

Reducing the rolling resistance of a haul road directly results in reduced fuel cost and increases haul fleet productivity of a road segment (Regensburg & Tannant, 2001). Using EarthZyme to construct fine grain clayey haul roads has shown to reduce rolling resistance. A rolling resistance study conducted in the Athabasca oil sands determined the average rolling resistance of an EarthZyme treated haul road constructed with Clearwater Clay Shale overburden of medium to high plasticity. This study determined that the average rolling resistance was 2.7 % with a standard deviation of 0.5 %. This is well within the boundary requirements of many Athabasca oil sands companies, 3-5 % for permanent road surfaces (Regensburg & Tannant, 2001).

Haul roads constructed with similar material and not stabilized with EarthZyme exhibit considerably different characteristics than an EarthZyme stabilized haul road. Common rolling resistance values for similar material, in-situ benonitic clay shale of medium to high plasticity, range from 7-13 % with an addition of 1.5 % for every inch (2.54 cm) of penetration (Dionne 1987). Increased rolling resistance directly relates to increased fuel consumption and reduced haul fleet productivity (Figure I).

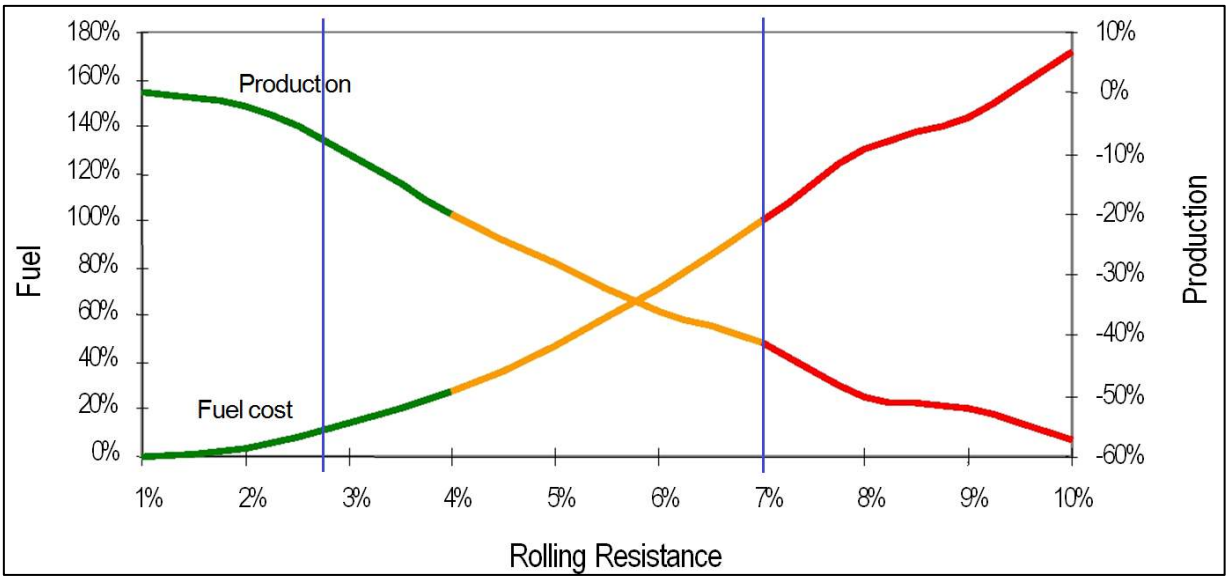

Figure I - Relationship between rolling resistance and increased fuel consumption and decreased haul fleet productivity (Holman, 2006)

Figure I was used to forecast potential economic benefit of reducing rolling resistance on a mine site. It was determined that reducing rolling resistance of a haul road from 7 % to 2.7 %, 1 deviation above average was determined to be 3.2, will increase haul fleet productivity by 35 % and decrease fuel cost by 90 % percent (Table II).

Table II - Potential savings resulting from reduced rolling resistance

Rolling Resistance (%)	Production (%)	Fuel Cost (%)
Clay Shale; 7.0	- 47	100
Clay Shale + EarthZyme 3.2	- 7	10
Savings (%)	**35**	**90**

From Table II and Figure I it is evident that reducing rolling resistance on haul roads using EarthZyme can yield extensive savings in fuel consumption and significantly

increase the productivity of a mining operation.

2.2.2 Reduced/eliminated racking events

To date the cost reductions associated with the reduced maintenance and racking events on EarthZyme haul roads has not been quantified. This is an area Cypher Environmental Ltd. plans to focus on in the future to further display the economic benefits of EarthZyme haul roads. The study previously referred to with respect to rolling resistance also determined that no trucks passing over the EarthZyme stabilized haul roads exhibited racking events. RAC events as defined by Caterpillar Inc. (2012), "RAC measures the frame's rack and pitch. Rack is the lateral twisting of the frame due to uneven loading on the diagonal tires. Pitch is the force on the frame from front to rear which occurs when the truck crosses a bump or dip perpendicular to the line of travel, hard braking or turns." (para. 2). These trucks were monitored daily. Traffic was considered high for an average mine in the Athabasca oil sands and travel speeds were consistently greater than 40 km/hr.

Although not quantified, reduced maintenance requirements have been consistently reported on EarthZyme soil stabilization projects in diverse work site application settings. The cohesive nature of the fine particles, and the improved binding and strengthened clay bonds facilitated by EarthZyme makes possible the reduced maintenance of the haul roads. To ensure that the wear surface of an EarthZyme haul road achieves the required level of water and wear resistance, a slurry coat is applied to the final lift during construction. A slurry coat is applied using approximately 1:1000 ratio of EarthZyme to water, with an application rate of 1 litre of EarthZyme to 1000 square metres of compacted surface. Contractors apply this mixture topically to the road and allow it to soak into the compacted surface. Once the moistened surface is no longer tacky, fully loaded haul truck(s) compact the surface. They make several passes until the road dries and requires rewetting or until the surface seals. This process forces the larger granular particles down and the cohesive fines to the surface, creating a tightly sealed road that effectively repels and sheds water (Figure II, A., B.).

2.2.3 Reduced maintenance

Quantifying reductions in maintenance of roads is a costly task, in both time and funds. Further complicating this task is the competitive nature of the mining industry. Through experience in road construction, Cypher Environmental Ltd. determined that reduced maintenance on haul roads can be objectively measured in grading requirements. To date EarthZyme haul roads require minimal grading, generally only to clear spillage from haul trucks. Furthermore, the high volume of traffic and loading subjected to EarthZyme treated haul roads enables the roads to maintain the high levels of density achieved during the initial compaction process carried out during construction. Due to the homogeneous nature of the soil structure, EarthZyme haul roads exhibit negligible rutting and remarkable reductions in common maintenance issues. These issues frequently result from imperfections in road surfaces or bearing layers: wash boarding, rutting, potholing.

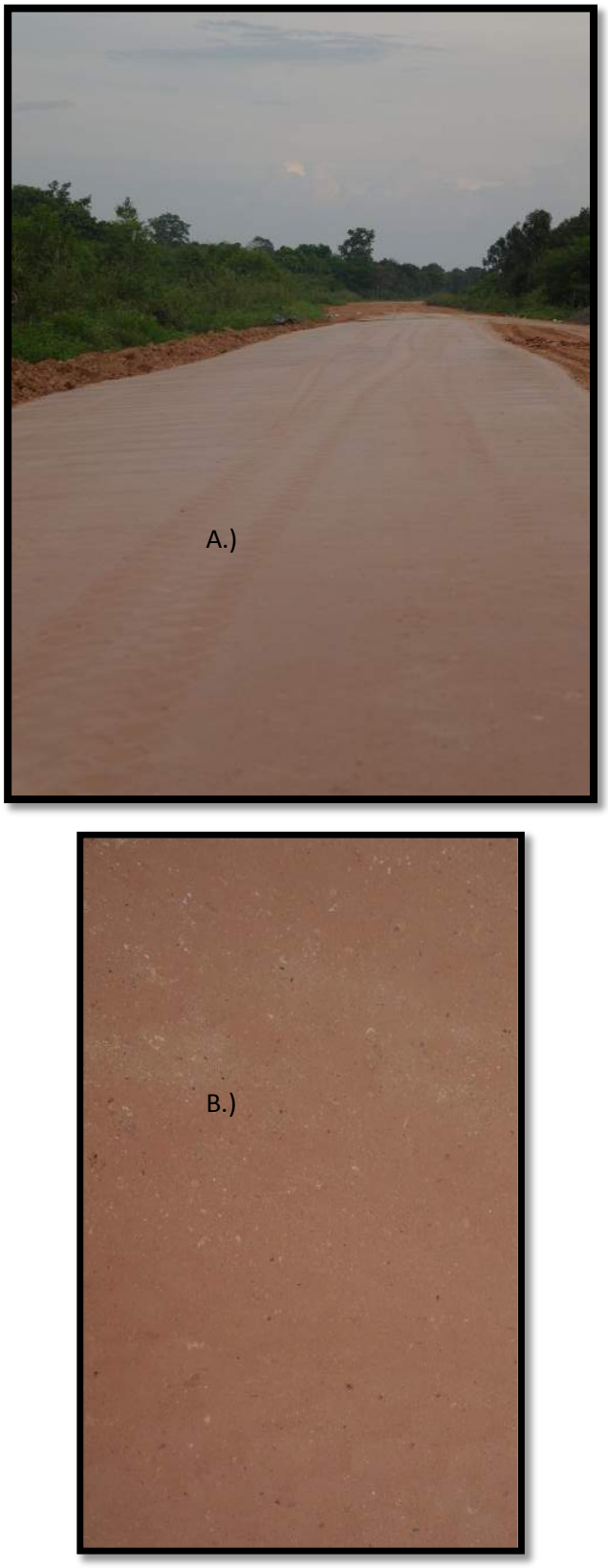

Figure II - Coal mine haul road; Indonesia

A. Sealed surface after slurry coat is finished

B. Close-up of haul road surface

It should be noted that tightly bound surface of EarthZyme treated haul roads have significantly reduced dust production. Reduced fugitive dust is of high value to mine sites as increased dust levels can result in reduced haul fleet productivity. The reduced productivity results from reduced visibility due to fugitive dust. Reduced visibility by dust is a safety hazard and requires haul trucks to slow down and in some cases stop to prevent accidents. Reducing dust caused by haul truck traffic on EarthZyme treated haul roads can allow for faster operating speed and increased efficiencies of haul fleet operations. Reducing dust can also help to reduce wear caused by dust particulates to the moving parts of haul trucks, extending part life. The overall reduction in dust also provides cleaner air for workers.

These reductions in common maintenance issues directly result from an increased homogeneity of a bearing layer and surface with increased strength and durability. These reductions in overall maintenance have been reported as a result of EarthZyme stabilization in a diverse climate setting from Northern Alberta, Canada to Columbia and Indonesia. Other examples of diverse climates that achieve similar results include: West Africa, Southern China, Dominican Republic, Ecuador, Mongolia, Peru, Romania, South Korea, Turkey, and the Southern United States.

To achieve these desirable cost savings, a client must first test the soil for compatibility with EarthZyme.

3 SOIL REQUIREMENTS

EarthZyme is not effective at stabilizing all soils. Before treating a soil with EarthZyme, Cypher Environmental Ltd. recommends several standard soil tests be conducted: Particle Size Distribution-ASTM D422, Atterberg Limits liquid and plastic-ASTM D4318.

This testing verifies that the soil contains fines in excess of 20 % by weight passing the 75 micron sieve (# 200 sieve), and a plasticity index above 8. The A-line on the Casagrande Chart determines soil acceptability for treatment. A soil that plots on or above the A-line is considered acceptable and exhibits the short and long-

term gains in engineering properties associated with EarthZyme stabilization. A soil that plots below the A-line can still be treated with EarthZyme, but will exhibit only short term gains in engineering properties. The difference in the length of effective treatment relates to the non-organic clay content and chemistry of the soil. The long-lasting stabilization of EarthZyme directly relates to the use of clay as the binding agent. This is because the clay is indigenous to the soil and not an additive that will leach out of the soil or degrade through soil microbes and soil chemistry. This combined with the increased cohesive nature of the treated clay and the permanent alteration of the chemistry of the soil, results in haul roads that exhibit minimal maintenance and increased load carrying capacity for many years.

4 EARTHZYME

4.1 What it is

EarthZyme is added to clay-mineral soils to increase compactability and decrease the mobility of water in the compacted soil matrix. EarthZyme consists of these three primary elements:

1. An ionic solution that interacts with the clay minerals in the fill to reduce the proportion of water that is weakly bonded to the clay particles. The ionic solutions serve to reduce the diffuse double-layer, which allows greater densities to be achieved under a constant compaction force.
2. A strong surfactant that serves to reduce the viscosity of the water, increasing the lubricating effect of the water during compaction. This ultimately achieves greater densities at lower moisture contents while enhancing alignment of the clay particles, which reduces the permeability of the compacted mass. The surfactant also serves as a carrier fluid for the enzymes and ionic solution.
3. A combination of enzymes that facilitate ion exchange between clay particles and the ionic solution.

These three compounds work in harmony during haul road construction enabling conventional construction equipment to achieve higher densities than with untreated compacted clay fill. The higher densities, in turn, create a compacted mass with greater clay particle alignment and binding. This results in significantly higher strength, durability, and bearing resistance. The combined affect renders the treated compacted fill hard, improving water replant characteristics, making it suitable for road surface and base construction.

4.2 How it works

Clay minerals are negatively charged. As a result, the positively charged portions of the polar water molecules are attracted to the negatively charged surfaces of the clay particles, forming weak ionic bonds between the clay minerals and the polar water. Soil scientists referred to this as the diffuse double layer, and is the mechanism that causes clay soils to swell and lose strength in the presence of free water (Das, 2008, Ch. 4). The thickness of the diffuse double layer depends on the chemistry of the clay minerals and the pore water (Michael & Soga, 2005, P. 158). The diffuse double layer thickness can be reduced by altering the clay and pore water chemistry (Michael & Soga, 2005, P. 158). EarthZyme utilizes an enormous ionic exchange potential to shrink the diffuse double layer, which reduces the soils ability to adsorb water, reducing the optimum moisture content of the treated clay soil, and allowing higher compaction densities. Surfactants enhance this ion exchange by increasing the penetration of the ion solution into the capillary structure of the soil. The surfactants also serve as a carrier fluid for the enzymes. These enzymes facilitate increased ion exchange between different clay mineralogy; enabling EarthZyme to be diversely effective. These combined effects permanently reduce the clays affinity to water.

The EarthZyme surfactants have a dual purpose during the soil stabilization process.

The EarthZyme surfactants have the temporary effect of decreasing surface tension and water viscosity, acting to encourage compaction. This lubrication results in achieving a dispersed soil structure and reduced pore spacing. This reduction in surface tension further reduces the moisture requirements of the soil for optimal compaction. The combined effect of the shrunken diffuse double layer and reduction in surface tension reduces the optimum moisture content of the soil in combination by approximately 1-2 %. This process creates a fine grained soil structure with significantly reduced pore space and increased platelet to platelet contact.

The combination of the high degree of compaction (reduced pore space and capillary structure) and dispersed (parallel) soil structure vastly reduces the permeability of the soil and vastly increases the strength (bearing capacity). As EarthZyme biodegrades the surfactants breakdown, and re-establish the surface tension of the water. This triggers the bound water (liquid bridges) to tighten, creating greater internal compression forces. These results in increased suction and skeletal forces in the soil matrix, further reducing space between cohesive clay particles, and increasing covalent and ionic bonding. Ultimately, this causes the hardening or curing of the compacted clay fill, resulting in the completed surface exhibiting increasing strength overtime. The majority of this process happens in the first 5-7 days, continuing until day 28.

The reduced void ratio also facilitates increased natural binding via chemical bonding, and Van Der Waals bonding between clay structures (Michael & Soga, 2005, Ch. 7). The increased density and subsequent increased bonding of clay fabric in combination with their parallel orientation works to create a bearing surface that exhibits not only increased strength properties, but, increased homogeneity. Combined, the effect is to resist re-adsorption of water that would otherwise reduce strength. The dispersed nature of the soil matrix further increases this effect. This dispersed soil structure also assists to reduce permeability, a result of a reduction in interconnected pores that otherwise aid in water transmission and a reduced inclination for the compacted soil to exhibit brittle failures (Bowles, 1992). This creates a strong more durable road, with a reduced inclination to water and increased uniformity of strength gains.

5 PAST PROJECTS

The diversely applicable design of EarthZyme enabled Cypher Environmental Ltd. to effectively stabilize road construction projects around the world and across the industrial/municipal sectors. EarthZyme's highly concentrated design, 1 liter of EarthZyme required to treat 33 cubic metres of compacted soil, makes EarthZyme cost effective on a global scale. Common links between all of these projects include increased bearing capacities and reduced susceptibility to water permeation and degradation. Cypher Environmental Ltd. developed alterations to the CBR test to predict the effectiveness of EarthZyme on particular soil types. Traditionally determining road design requirements utilizes the CBR test (Bowles, 1992). The CBR test is a well-known test that can be conducted in the majority of soils laboratories in both developed and developing countries. Because of this Cypher Environmental Ltd. utilized the CBR test for years to predict the strength gains and stability of foundations stabilized with EarthZyme. Reduced infiltration of and affinity to water is an important aspect of road construction with fine grained, traditionally highly expansive soils. EarthZyme effectively reduces the expansive characteristic of normally expansive soils yielding a low cost, stable construction material (Table III).

Table III - Swell reduction of fine grain soils treated with EarthZyme; 96 hour test

Project Type	Location	EarthZyme*	Untreated*	Swell (% Reduction)
Municipal Paved Road	Caupicho Quito Ecuador	0.3	0.81	**63%**
Secondary Unpaved Road	Hainan Province China	0.08	0.26	**69%**
Primary Unpaved Road	Hainan Province China	0.06	0.28	**79%**
Municipal Paved Road	Metropolitan District of Quito Ecuador	0.01	0.32	**97%**
Highway	Cajamarca Peru	0.88	1.8	**51%**

*(percentage; vertical deflection divided by initial thickness/height of compacted soil)

The significant strength gains exhibited as a result of compacting soils with EarthZyme is an important added benefit of constructing haul roads with EarthZyme and fine grained soils (Table IV).

Table IV - Increased bearing capacity of fine grained soils compacted with EarthZyme

Project Type	Location	CBR No EZ	CBR With EZ	Increase in CBR (Avg. % Change)
Primary Unpaved Road	Puerto Plata Dominican Republic	43	196	**353%**
Primary Unpaved Road	Peru	12	37	**208%**
Secondary Unpaved Road	Huiyang District China	37	135	**265%**
Haul Road	Pallancata Silver Mine, Peru	55	102	**85%**
Municipal Road	Ghana	69	296	**328%**
Highway	Cajamarca Peru	14	41	**192%**
Paved Parking Lot	Guangdong Province China	64	286	**347%**
Municipal Paved Road	Metropolitan District of Quito Ecuador	61	92	**51%**

These strength gains are a result of EarthZyme's unique ability to increase the bonding of the parallel oriented clay platelets while reducing the void ratio in fine grained soil at a moisture content below optimum (OMC). This is important in both increasing the overall strength of the soil and the uniformity of the engineering properties of a haul road. This bound particle orientation causes the soil to behave in a consolidated, sheet like elastic fashion; enabling the fine grained soils to tolerate higher loads with minimal breakdown of the consolidated soil structures. Generally, a haul road behaving in an elastic fashion is not beneficial to mine economics because it results in increased rolling resistance. The constant deflection of the haul road causes this increased rolling resistance resulting in a constant up-hill effect. This increased rolling resistance is due to the constant deflection of the haul road, which produces the constant up-hill effect previously mentioned (Regensburg & Tannant, 2001). This constant up-hill effect is not exhibited on fine grain EarthZyme stabilized haul roads because of large increases in CBR number. The combined strength gains and dispersed particle orientation of EarthZyme stabilized soils greatly increases their durability and bearing capacities. This creates a superior haul road using economical material inputs that can withstand repeated substantial loading with minimal maintenance or resurfacing.

5.1 Results from a recent Mining Haul Road Project in Mali, Africa (November 2013):

A stabilization project was carried out at the Randgold Somilo site on the haul road connecting the Gounkoto and Loulo mines. EarthZyme was used to stabilize the road to a 20 cm depth, treating the in-situ soil. On an

average month, 4200 trucks weighing 65 tons each use the haul road and after one month of operation, Randgold reported the following test results. CBR data from the road was collected before and after treatment with EarthZyme (Table V and Figure III). Samples were taken from both lanes of the road, lane "A" being the lane the empty trucks travel on and lane "B" the one the loaded trucks travel on. As shown below there was a combined CBR improvement of 159.91%.

Table V – CBR Data from EZ treated mining road in Mali, Africa

Test #	CBR% No EZ		CBR% With EZ	
	Lane A	Lane B	Lane A	Lane B
1	48.00	75.00	125.62	140.96
2	55.11	51.43	160.61	102.15
3	53.00	44.06	129.33	162.35
4	55.00	42.67	147.42	119.16
5	53.44	68.44	126.33	109.94
6			182.09	107.04
7			182.09	186.35
Mean	**52.91**	**56.32**	**150.50**	**132.56**
Var.	6.72	171.33	537.02	874.12
Std Dev.	2.59	13.09	23.17	29.57
Improvement in CBR			**184.45%**	**135.38%**
Combine CBR Improvement			**159.91%**	

**Lane A: Empty trucks lane*

Lane B: Loaded trucks lane

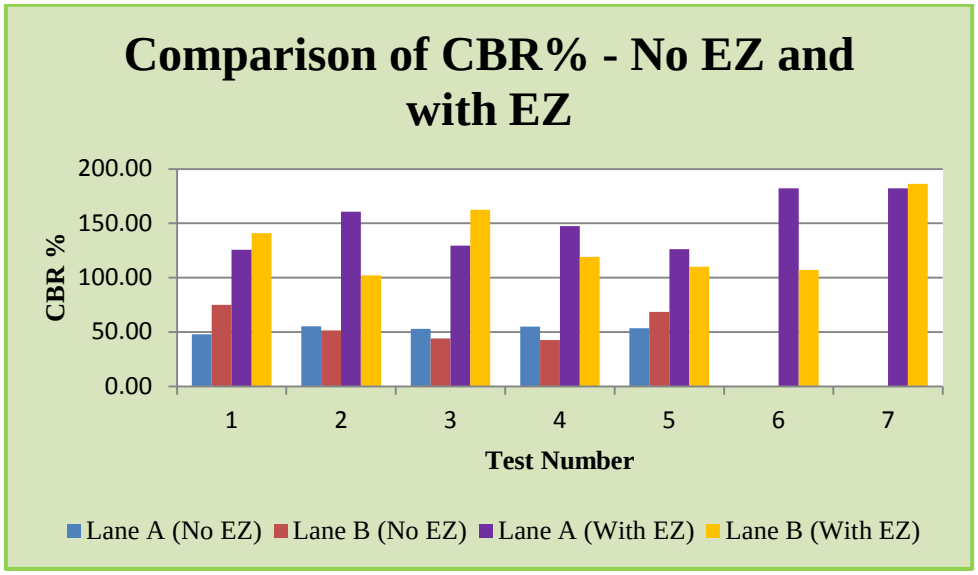

Figure III – Comparison of treated and untreated CBR in Mali, Africa

Figure IV - Gold mine haul road; Mali
A. Surface after one month of traffic
B. Close-up of haul road surface

6 SUMMARY OF BENEFITS

As a result of Cypher Environmental Ltd.'s commitment to providing the most cost effective, highly functional and environmentally friendly solution, Cypher Environmental Ltd. has been able to reduce the industrial foot print of road construction, while simultaneously reducing project costs. These reductions in cost are seen not only as a result of reduced costly raw material inputs, labour and machine hours, but throughout the extended life of the road. In the past 5 years EarthZyme has been integrated more and more into the mining industry as an effective additive to all-weather road construction projects. Studies of these all-weather haul roads have determined that EarthZyme stabilized haul roads exhibit reduced rolling resistance, racking events, and reduced grading requirements. This results in increased productivity and reduced fixed costs of road networks, increasing overall efficiencies at mine sites utilizing the EarthZyme product

REFERENCES

Bowles, J. (4th ed.), 1992. *Engineering properties of soils and their measurement*, New York, NY: Tata McGraw-Hill Education Private Limited.

Caterpillar Inc. (2012). *Road analysis control*, Retrieved from: http://www.cat.com/technology/fleet-management-solutions/road-analysis-control

Caterpillar Inc. (2006). *Haul Road Design and Management*, Retrieved from: http://www.directminingservices.com/wp-content/uploads/2010/06/CAT-Haul-Road-Design.pdf

Das, B. (3rd ed.), 2008. *Fundamentals of Geotechnical Engineering*. Stamford, CT: Cengage Learning Incorporated.

Helberth, R. (2012, June). *Report of laboratory tests and comparative analysis of cost between conventional technologies "EarthZyme" for road construction by multienzyme compounds*. REVAS & A: Technology Eco-Road Solutions, Quito, Ecuador.

Mitchell, J. & Soga, K. (3rd ed.), 2005. *Fundamentals of Soil Behavior*. New Jersey, NY: John Wiley & sons, Incorporated.

Syncrude Canada Limited (1987). *Significant development in overburden removal at Syncrude Canada Ltd. Proc. CIM District 5 Meeting*. Fort McMurray, Alberta: Dionne E.A.

Tannant, D., & Regensburg, B. (2001). *Guidelines for mine haul road design.* School of Mining and Petroleum Engineering, Dept. of Civil and Environmental Engineering, University of Alberta, [Edmonton].

Effect of Placement Configurations on Strength Behaviour of Cemented Paste Backfill

E. Yilmaz
University of Quebec in Abitibi-Témiscamingue (UQAT), Department of Applied Sciences, 445 Boul. de l'Université, Rouyn-Noranda (Québec) J9X 5E4 Canada

ABSTRACT This paper presents the effects of placement conditions on strength properties of cemented paste backfill CPB cast in different size moulds ($D \times H$ = 10 × 20 cm, 7.5 × 15 cm, and 5 × 10 cm) and prepared at binder contents of 3 wt%, 4.5 wt%, and 7 wt%. CPB samples were subjected to four placement conditions: capped-drained C-D; uncapped-drained U-D; capped-undrained C-U; and uncapped-undrained U-U. Results show that the highest strengths were obtained from C-D samples, followed by U-D, C-U and U-U samples, respectively. This may be explained by the drainage of free water within CPB at early ages, which offers higher strengths. The CPB's strength increased with a decrease in mould size in all cases for all the samples. The moulds 5 × 10 cm gave the best strengths due to a more homogenous matrix and the decreased number of micro-cracks in grains.

Keywords: Cemented paste backfill, strength parameters, placement conditions

1 INTRODUCTION

Cemented paste backfill (CPB) is a relatively high density (typically with more than 70% solids) engineered material which is made up of mill tailings mixed with hydraulic binders, and process water. CPB is being increasingly used underground as a result of increasingly stringent environmental regulations. Its main benefits include lower operating costs and a reduction of the amount of water sent to the tailings impoundments for surface disposal. The decrease of the amount of mine tailings reduces the environmental impact and offers major cost benefits for most modern mines (Benzaazoua et al., 2004; Bussière, 2007; Yilmaz, 2011; Yilmaz et al., 2014a).

The CPB mix ingredients (tailings, binder and water) greatly affect the performance of the backfill during its transportation, delivery and strength development. Mix designs must be considered for both placement and curing properties of in situ paste backfill materials. As mining operations go ever deeper, CPB is placed into stopes to provide a stable stage for miners to work on and ground support for the walls of the adjacent adits. Depending on its specific application, CPB must encompass desirable strength properties to better endure underground stresses. Overall, a sufficient unconfined compressive strength (UCS) for a CPB with binder contents of 3-7 wt% varies between 700 and 2000 kPa (Brackebusch, 1994). However, the condition for minimum strength acquisition should be determined from the design loads to which the material may be subjected. For example, when CPB is employed for underground disposal, a UCS between 150 and 300 kPa is required to remove the liquefaction at early ages (Bloss, 2002). In open stoping operations, when free-standing wall faces are exposed during pillar recovery, strengths higher than 1 MPa after curing of 28 days are desired to retain the strength and durability of CPB (Belem and Benzaazoua, 2008). When CPB is used for roof support, a UCS of higher than 4 MPa is required essentially (Grice, 1998).

Most experimental works have been done so far on CPB' intrinsic and extrinsic factors (Kesimal et al., 2004, 2005; Fall et al., 2010; Ercikdi et al., 2009, 2010; Yilmaz et al., 2009, 2011, 2014b, 2015; Benzaazoua et al., 2010; Cihangir et al., 2012; Ghirian and Fall, 2013, 2014; Belem et al., 2013). To assess the CPB's strength, unconsolidated backfills with dimensions of 10 cm in diameter and 20

cm in height are typically utilised in the laboratory studies. Handling huge volumes of tailings to be used during testing is time-consuming and costly. To end this, a number of researchers (Benzaazoua et al., 2004; Yilmaz, 2010; Pokharel and Fall, 2013) have used 5 × 10 cm plastic moulds for UCS tests. Additionally, these moulds do not often have drainage holes at the bottom and are used as their top is capped. Although the final CPB design is based on the strength properties derived from lab-prepared CPB samples using these plastic moulds, these lab studies are not mostly representative of the in situ placement and curing properties. There are in fact some problems with scaling up lab-prepared CPB samples' strength results to determine the field strength properties. The difficulties often lie in the selection of suitable specimen size and shape for lab tests (Consoli et al. 2006; Fourie et al., 2006; Hassani et al., 2007; Belem et al., 2007; Darlington et al., 2011; Thomson et al., 2012; Festugato et al., 2013; Ercikdi et al., 2014; Snyman et al., 2014). There is no standard specimen size and shape for the UCS testing of CPBs. Revell (2004) has shown that specimen size plays a key role on strength behaviour of CPB. The researcher found that, based on a height-to-diameter ratio of 2, small size cylinders (4 cm in diameter) gave 6-10% higher strengths than large size ones (10 cm in diameter).

In this paper, an investigation was done to assess the effect of placement conditions on CPB's strength. CPBs were cast in different mould sizes and subjected to four placement conditions: capped-drained C-D; uncapped-drained U-D; capped-undrained C-U; and uncapped-undrained U-U. A tool (CUAPS: curing under applied pressure system) was used for tests (Benzaazoua et al, 2006).

2 MATERIALS AND METHODS

2.1 Materials

Paste tailings were sampled as representative from the discharge of the rotary vacuum disc filter at the LaRonde Mine's paste fill plant (Quebec, Canada). To avoid any oxidation and prevent evaporation, tailings samples were stored in sealed plastic containers until their utilization for tests. The following lab tests were conducted according to American Society of Testing Materials standard testing procedures. Tests were done in triplicate and their average values are reported. Further details on material properties can be found in more detail in Yilmaz (2010).

2.1.1 Physical properties

Grain size distribution (GSD) of the tailings was analyzed using a Malvern Mastersizer laser diffraction particle size analyzer and the obtained GSD curve was compared fairly well with those of the tailings used in Canadian mines (Fig. 1). Table 1 lists the physical properties of the tailings. Tailings were found to have a 44 wt% fraction finer than 20 µm, hence classifying as a medium size tailings. The sample was well-graded with a coefficient of uniformity, C_u, of 7.9 and a coefficient of curvature, C_c, of 1.1. Based on the Unified Soil Classification System (ASTM D2487, 2011), the tailings sample was identified as low plasticity silt.

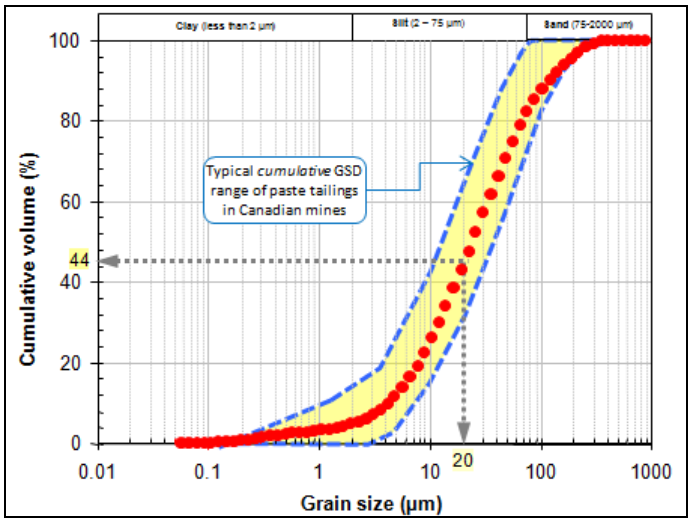

Figure 1. Grain size distribution curve of the paste tailings studied

Table 1. Physical properties of tailings

	Tailings
Specific gravity G_s	3.7
Specific surface area S_s (m^2/g)	2.2
Fines content (< 20 μm; %)	44
D_{10} (effective particle size; μm)	4.3
D_{30} (μm)	12.2
D_{50} (average particle size; μm)	24.3
D_{60} (μm)	33.6
D_{90} (μm)	119.2
Coefficient of uniformity $C_u = D_{60}/D_{10}$	7.9
Coefficient of curvature $C_c = D_{30}^2/(D_{60}xD_{10})$	1.1
Uniformity of graduation $U = (D_{90}-D_{60})/D_{50}$	4.7
Maximum dry unit weight γ_d (kN/m^3)	24.9
Optimum water content w_{opt} (%)	12.5
Void ratio at optimum condition e_{opt}	0.5

The compaction tests, based on the ASTM standard (ASTM D1557, 2012), were also performed in the laboratory as shown in Fig. 2. This method covers laboratory compaction methods used to determine the relationship between molding water content and dry unit weight of soils compacted in a 102- or 152-mm) diameter mold with a 44.48-N rammer dropped from a height of 457 mm producing a compactive effort of 2700 kN-m/m^3. The main parameters were also tabulated in Table 1. For the tailings sample, the optimum water content, w_{opt}, for the modified Proctor test was about 12.5 wt%. The corresponding dry unit weight was 24.9 kN/m^3. The calculated void ratio for the optimum condition was nearly close to 0.5.

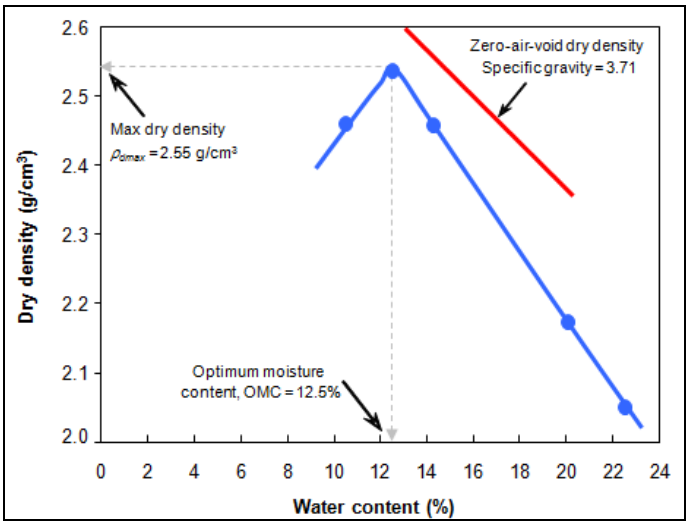

Figure 2. Moisture-dry density curve of paste tailings

2.1.2 Chemical composition

Chemical composition of the samples was determined by a Perkin–Elmer Optima 3100 RL ICP–AES (inductively coupled plasma–atomic emission spectroscopy) after sample digestion (Table 2). The tested mine tailings contained 39.2% Fe_2O_3 and 51.3% total sulfur as determined by major oxide and elemental analysis, respectively. Samples' hydraulic index ratio of unhydrated cement product ($[SiO_2+Al_2O_3]/[CaO+MgO]$) was calculated to be 0.8.

Table 2. Chemical composition of tailings, mixing waters and binders

	Tailings (wt %)	Water (mg/L)	Binder (%)
Al_2O_3	5.29	0.40	8.39
B_2O_3	0.61	0.14	0.13
BaO	0.01	0.05	0.03
CaO	0.79	782.16	42.82
Fe_2O_3	39.20	0.02	0.64
K_2O	0.24	2.77	0.55
MgO	0.16	3.03	6.19
MnO	0.02	0.01	0.18
Na_2O	0.40	455.61	2.03
S*	51.34	4069.88	3.35
SiO_2	1.07	1.91	30.91
TiO_2	0.07	n/a	0.48
ZnO	0.44	0.13	n/a

*Total sulfur was assumed expressed exclusively as SO_4^{2-} (= 2.9956 × S, based on stochiometric conversion)

2.1.3 Mineralogical properties

The Bruker AXS D8 Advance X-ray diffractometer equipped with a Co anticathode was also used to determine the mineralogy of the mine tailings tested in this study. The quantitative mineralogical analysis was also evaluated using Rietveld full-pattern fitting method equipped with the TOPAS software. The X-ray diffraction and semi-quantitative analyses revealed that the most abundant mineral within the mine tailings studied was pyrite (47%), followed by quartz (32%), chlorite (9%), paragonite (7%), muscovite (3%), talc (1%) and gypsum (1%). More information on the complete characterization of mine tailings, hydraulic binder and mixing water used in the experiments can be found in more detail in Yilmaz (2010).

2.2 Methods

2.2.1 Sample preparation

A total of 216 CPB samples were prepared by blending homogenously tailings, binder and water in an electrical Hobart D300-1 mixer until a flat consistency was achieved. Depending on the viscosity of matrix, additional water was added to set the resulting CPB solid concentration percentage to 78 wt%. Paste material was tested using the Abrams cone (ASTM C143, 2013) to achieve 7" slump for all samples (Fig. 4). To study the effect of placement conditions in the lab, samples were poured into different size moulds ($D \times H$ = 10 × 20 cm, 7.5 × 15 cm, and 5 × 10 cm) and different placement conditions (capped-drained C-D, uncapped–drained U-D, capped-undrained C-U, and uncapped–undrained U-U) for UCS testing. The capped-drained condition represents the placement of sample into the mould, which has drainage holes at the bottom and a cover on the top while the uncapped-drained condition refers to the placement of sample in the bottom-perforated mould without cover on the top. The capped-undrained placement condition, frequently used for quality control tests at both laboratory and mine sites, represents the capped mould with no drainage holes at the bottom. The uncapped-undrained placement condition represents the open-top mould with drainage holes at the bottom (Fig. 3).

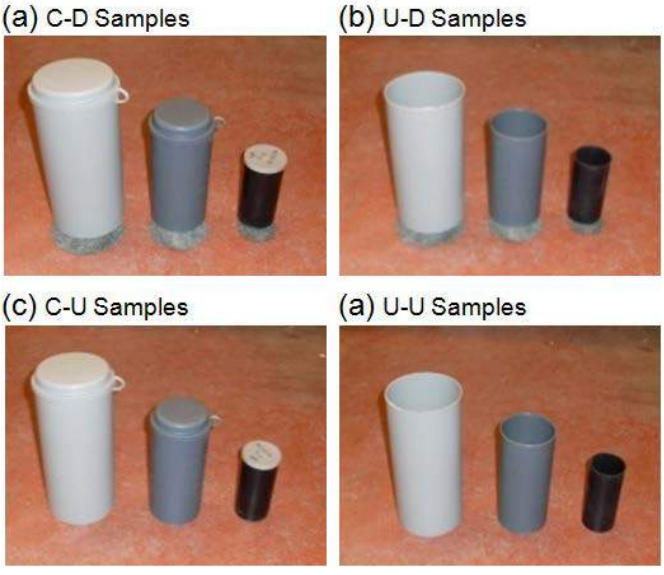

Figure 3. The drainage scenarios of paste fill

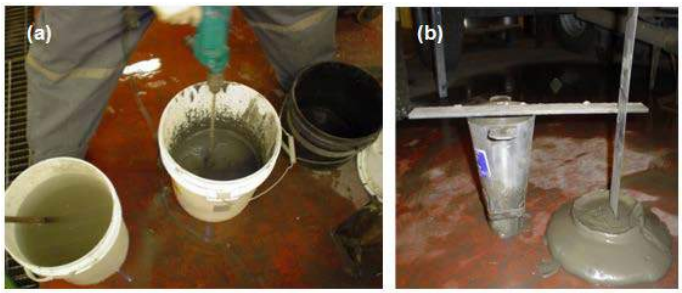

Figure 4. Photos of (a) a driller with a mixer bit in a 20-L pail, and (b) the slump test

In comparison with the unconsolidated samples a total of 108 CUAPS-consolidated samples were prepared for the prescribed curing times of 7, 14, and 28 days and binder contents of 3, 4.5, and 7 wt% (Fig. 5). For the drained scenarios, 2-mm diameter holes were drilled at the bottom of each mould, 31 holes for the 10 × 20 cm mould, 9 holes for the 7.5 × 15 cm mould, and 2 holes for the 5 × 10 cm. The geotextile filter was placed at the bottom to allow bleed water drainage. Paste samples were cast into the moulds in one-third increments. After the mould was filled, the paste was rammed in 25 blows using a small steel rod in order to eliminate any large trapped air bubbles within CPB, as described in the ASTM C143 standard. After sealing, the moulds were stored in a foggy room set at 80% relative humidity and 25°C temperature (replicates underground mine conditions) over the desired curing times.

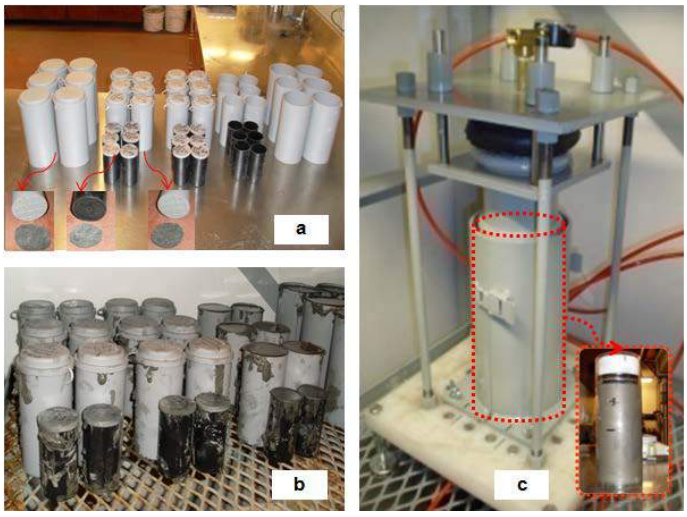

Figure 5. Photos illustrating the different size plastic moulds and test conditions: (a) empty moulds, (b) CPB-filled moulds, (c) capped-drained sample cured within CUAPS

2.2.2 Mechanical strength tests

Following the curing periods of up to 28 days, the unconsolidated paste backfills were well extracted from the drained-, undrained-, capped-, and uncapped plastic moulds using compressed air while CUAPS-consolidated paste backfill samples were extruded from the Perspex mould using an enough manual push sample extruder (Fig. 6).

Figure 6. The sample extraction methods

To determine the strength properties, the extracted CPB samples were subjected to unconfined compression tests (ASTM C39, 2012). A full automatic press (MTS Sintech 10/GL) having a loading capacity of 50 kN and a loading rate of 1 mm/min was used. Axial deformations were digitally recorded by a real-time data acquisition system. The observed UCS corresponds to the highest stress reached during the compression test. Prior to UCS testing, the samples' two ends were rectified using cutter (Fig. 7). The mean values from triplicate tests were presented in the results.

Figure 7. Photos of (a) a sample rectification and (B) CPB samples under MTS Sintech 10/GL mechanical press

2.2.3 Geotechnical index parameter tests

Some physical properties such as gravimetric water content w_g, degree of saturation S_r, dry density γ_d and void ratio e were also determined on representative CPB samples after UCS testing. A required portion of each specimen was oven-dried for about 3 days at 45 ºC in order to determine the water content of the CPB sample. Solids' specific gravity was determined by a Micromeritics AccuPyc 1330 helium pycnometer. Using these data (e.g. w_g, γ_d and G_s), the remaining physical parameters, including void ratio and degree of saturation were calculated from the mass-volume relationships. Physical properties were evaluated only on the specimen size which gave the highest mechanical strengths.

2.2.4 Mercury intrusion porosimeter tests

The CPB's microstructural properties was determined using a Micromeritics Autopore III 9420), which allows measurement of a minimum accessible radius of 0.003 µm (Fig. 8). After UCS tests, representative CPB samples ($D \times H$: 12 × 24 mm) were taken from the middle part of CPB specimen which avoids stress concentration effects. Samples were oven-dried at 45ºC for at least 96 h and then stored in a desiccator over silica gel to minimize pore alteration due to hydration product destruction and moisture ingress. For each sample, at least two MIP analyses were performed to obtain an average value.

Figure 8. Micromeritics Autopore III Model 9420 mercury intrusion porosimetry

3 RESULTS AND DISCUSSION

3.1 Effects of Placement Conditions on Strength Development of CPB

Fig. 9 shows the development of UCS with time for different CPB samples cast in a mould size of $D \times H$ = 10 × 20 cm, 7.5 × 15 cm, and 5 × 10 cm, and prepared at 3, 4.5 and 7 wt% binder dosages. These different drainage configurations appeared to affect the strength and stability, but the specimen size also played a key role in the strength development of CPB.

It can be seen from Fig. 9 that drained paste backfills generate better strengths than undrained paste backfills for a given CPB recipe and curing time. This is due the fact that the drained backfills have less water-to-cement *w/c* ratios, which favour the acceleration of cement hydration reactions with higher strengths. The results indicated are also confirmed for paste backfill samples cast in the mould sizes $D \times H$ = 7.5 × 15 cm and $D \times H$ = 10 × 20 cm (Fig. 9). It is fairly apparent that the highest strengths were obtained from the C–D samples. These samples are compared in percent with the other samples. It can be inferred from these findings that the drained CPB samples have a lesser amount of porosity. This is most often due to the fact that the water loss by drainage gives rise to the settling of the backfill and the resultant reduction of the CPB void ratio. Consequently, higher strengths are achieved when compared with the undrained paste backfills.

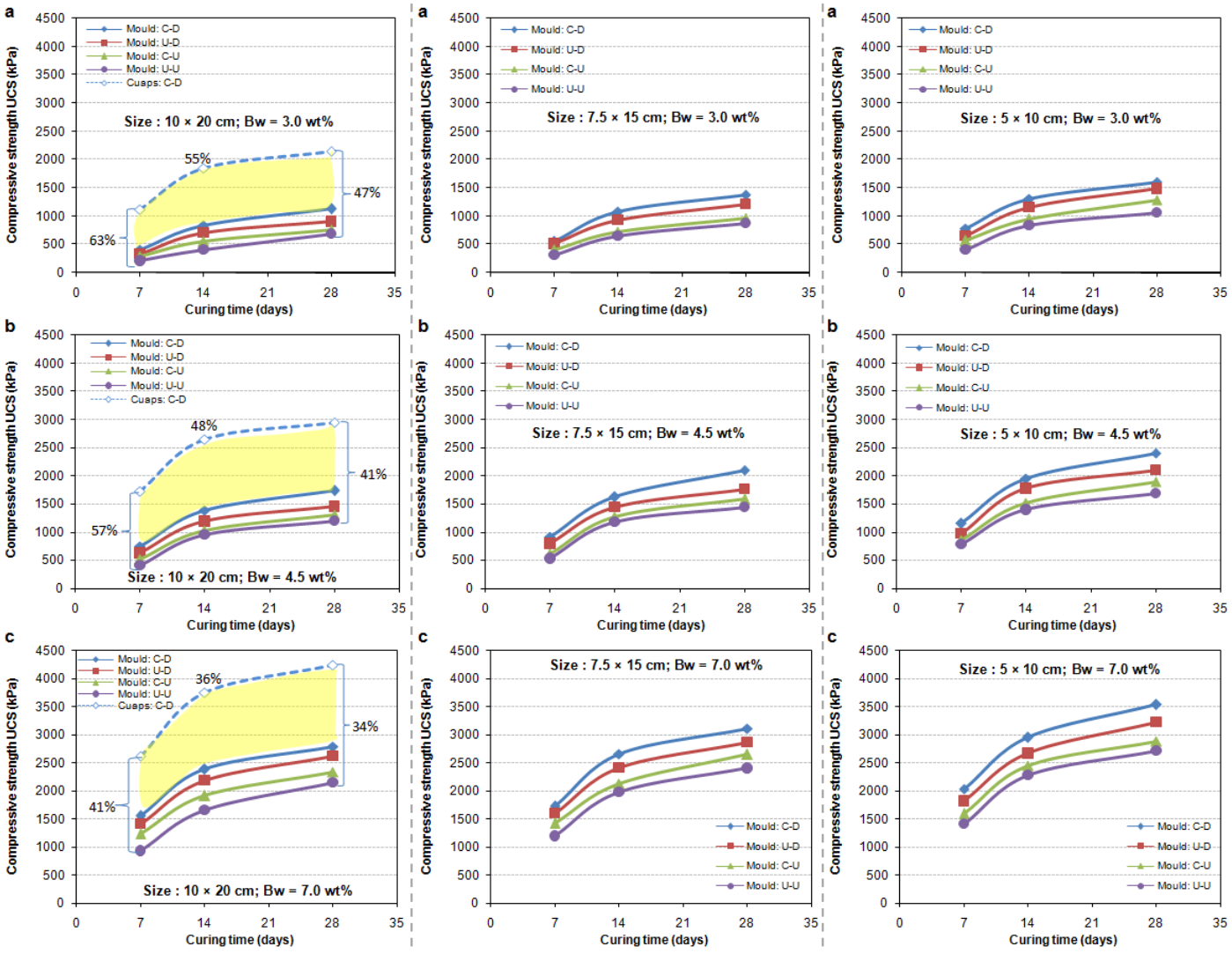

Figure 9. Change in compressive strength with curing time for different CPB samples cast in a mould size of $D \times H$ = 10 × 20 cm, 7.5 × 15 cm, and 5 × 10 cm, and prepared at binder contents of (a) 3 wt%, (b) 4.5 wt%, and (c) 7 wt%

Fig. 10 presents the evolution of the mechanical strengths of CPB prepared with 4.5 wt% of the binder type GU-Slag@20:80wt% for different curing times. It should be noted that the curing condition used in most laboratories is the C–U condition. From Fig. 7, it can be seen that the higher mechanical strengths were obtained from the small size specimen (d = 5 cm), regardless of curing condition, binder content and curing time. These findings clearly suggest the existence of specimen size effect on the resultant strength gain of CPB samples.

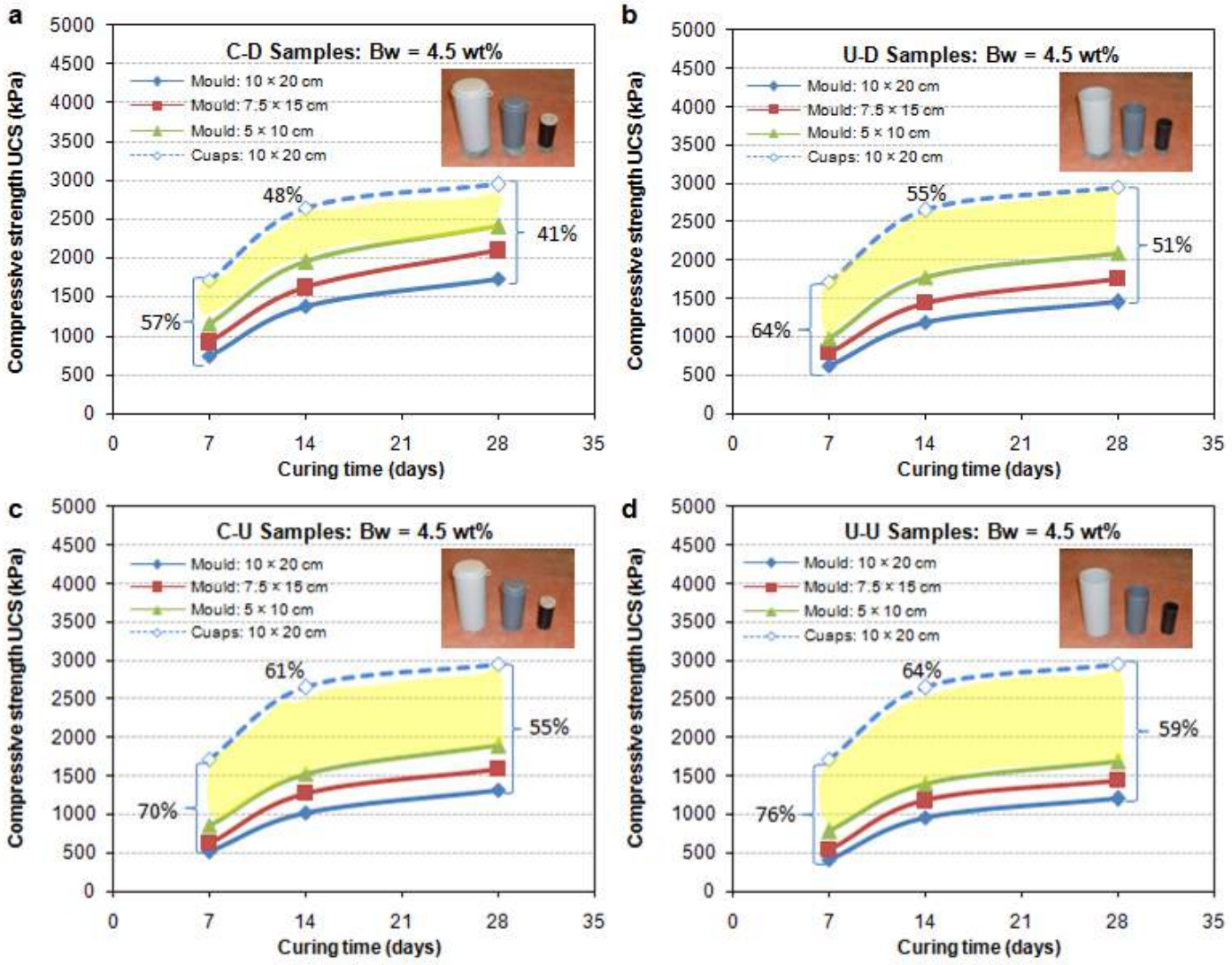

Figure 10. Specimen size effect on the UCS of CPB prepared with 4.5% of GU-Slag@20:80 wt% cured in four different placement conditions: a) capped and drained C–D; b) uncapped and drained U–D; c) capped and undrained C–U; d) uncapped and undrained U–U

3.2 Assessment of Geotechnical Index Parameters of Optimal CPB recipe

The mechanical strength properties of any CPB material are affected by its geotechnical index parameters, such as water content, void ratio, wet unit weight or specific gravity, and degree of saturation. It is well known that the physical properties that develop within CPB are greatly affected by a combination of *i*) the physical, chemical, mineralogical and micro-structural properties of paste backfill ingredients; *ii*) binder type and content; *iii*) curing conditions (with or without effective stress) including curing temperature and time; *iv*) paste mixing and placement techniques; and *v*) the internal stresses occurred in the CPB based on self-weight or time-dependent consolidation loadings.

In this study, the evaluation of physical property is made only on the most ideal CPB recipe cast in the mould 5 × 10 cm, which always gives higher strengths than other mould sizes. Fig. 11 shows the change in gravimetric water content w_g of CPB. The overall observation is that the water contents of the drained backfills is slightly lower than the undrained ones. When the binder dosage increased from 3 to 7 wt%, the water content was reduced mainly due to the initial *w/c* ratios and amounts of water required for cement hydration. This suggests that, the higher the cement content, the lower the water content is.

Fig. 11 shows the change in the void ratio *e* of different CPB samples as a function of binder content and curing time. The drained CPB samples showed smaller void ratios than the undrained ones because the water loss by drainage would give rise to the settling of paste backfill and the resulting reduction of the void ratio within backfill. Moreover, Fig. 11 illustrates that the drained CPB samples were less saturated than the undrained ones at a given binder content and/or curing time. The range of variation of degree of saturation S_r for the undrained backfills was relatively low (99.5 – 94% for the U–U samples and 99 – 92.5% for the C–U samples). After curing of 28 days, the S_r of backfill samples at 3, 4.5 and 7 wt% binder contents was determined to be 96.5%, 94.5% and 90.5%, respectively, demonstrating the decrease in the degree-of-saturation with increasing the binder content.

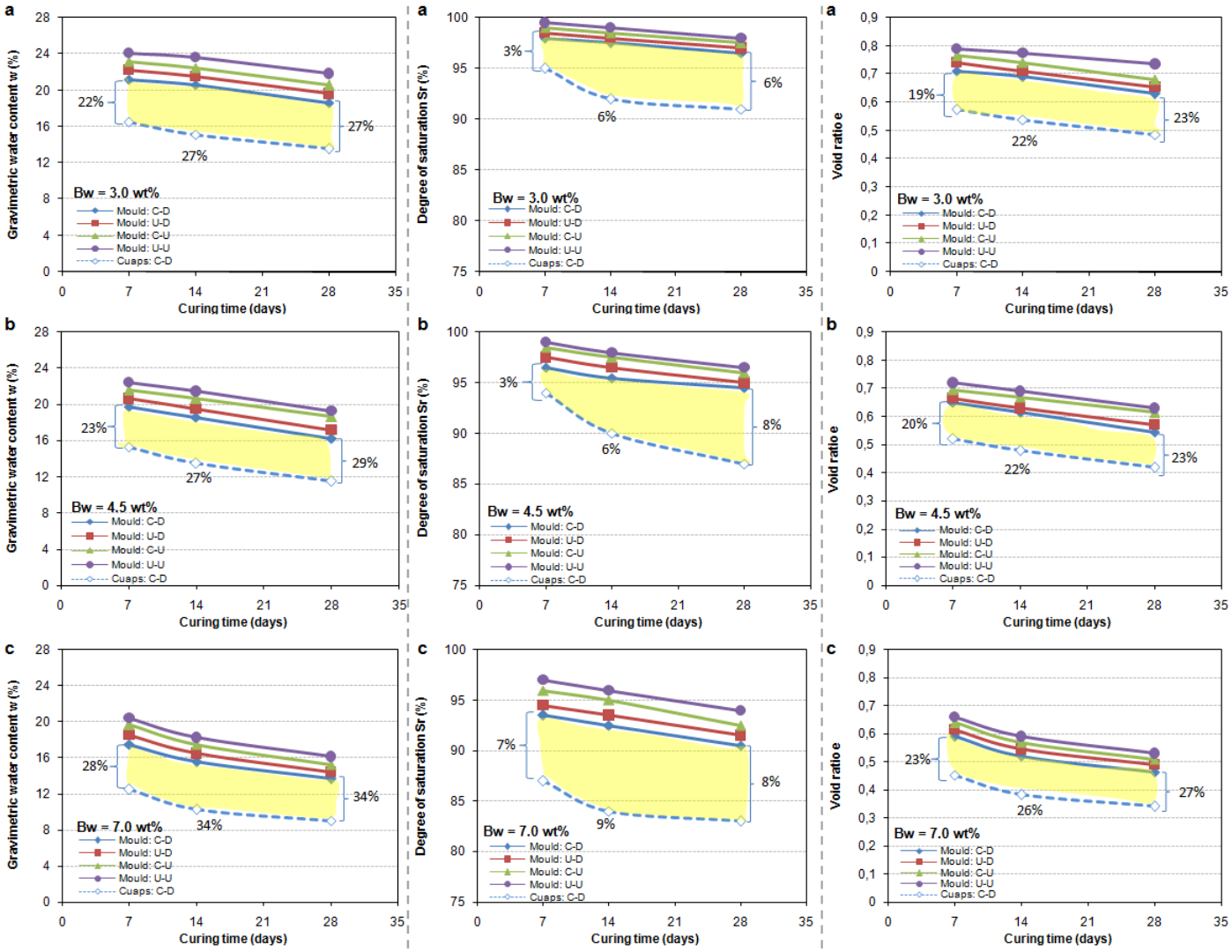

Figure 11. Change in gravimetric water content, void ratio, and degree of saturation with curing time for CPB samples cast in a mould size of $D \times H$ = 5 × 10 cm and prepared at binder contents of (a) 3 wt%, (b) 4.5 wt%, and (c) 7 wt%

Fig. 12 demonstrates the cumulative and incremental pore size distribution of the 28-day cured CPB samples prepared with the 4.5 wt% binder. The mercury intrusion porosity of CUAPS-consolidated backfills was lower (38.2%) than that of the samples consolidated in any other plastic moulds (44.8% for C-D samples, 45.8% for U-D samples, 46.2% for C-U samples, and 47.4% for U-U samples). Mercury porosimeter results indicate that the total porosity of the undrained paste backfills was greater than that of the CPB samples consolidated under effective stress due to the fact that the hydration-precipitation appears to occur to a lesser extent in the undrained samples. Application of effective stress during curing improves CPB's pore structure, and causes lower porosities in comparison with other unconsolidated samples.

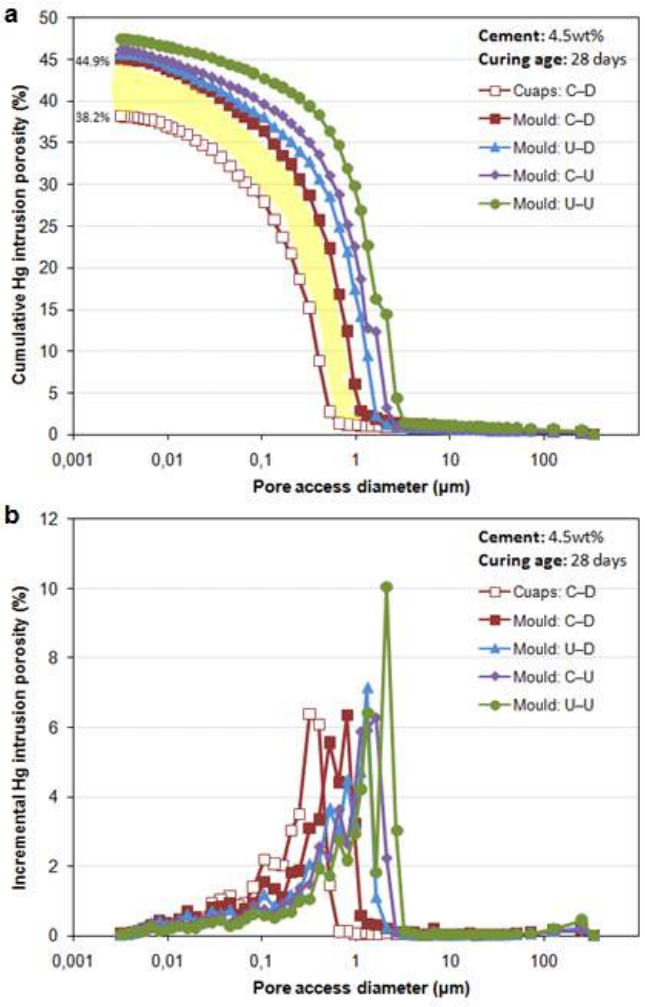

Figure 12. Cumulative (a) and incremental (b) pore size distribution of 28-day cured samples with cement content of 4.5wt%

4 CONCLUSIONS

This paper presents the results of an experimental study aimed at examining the effects of specimen sizes and placement conditions on mechanical (i.e. unconfined compressive strength) and physical (i.e. water content, degree of saturation and void ratio) properties of the CPB materials prepared using a slag blend binder consisting of 20 wt% general use Portland cement and 80 wt% blast furnace slag. A total of 432 CPB samples were produced at a binder content of 3, 4.5 and 7 wt% in different placement conditions: capped-drained C-D; uncapped-drained U-D; capped-undrained C-U; and uncapped-undrained U-U, and cast in three different size plastic moulds ($D \times H$: 5 × 10 cm, 7.5 × 15 cm, and 10 × 20 cm) over three curing times (7, 14 and 28 days).

The results from the experiments have shown that the diameter of the specimen greatly affects the overall mechanical strength for a constant height-to-diameter ratio. The most suitable specimen size with regards to the rate of strength development and the ultimate strengths was found to be $D \times H$ = 5×10 cm, which constantly provided higher strength, regardless of the placement conditions, compared to the other specimen sizes 7.5 × 10 cm and 10 × 20 cm. This is expected owing to the small volume of specimen which provides the decreased number of micro-cracks and pores in the homogenous matrix as compared with the larger specimen sizes. One of the major factors affecting the strength and stability of CPB is the placement and curing conditions entreated right after pouring the paste into the moulds. The test work has confirmed that the drained paste backfills always produce higher strengths than the undrained ones as a result of the removal of excess water within CPB, which helps accelerating binder hydration. Since in situ backfill conditions are different from those of lab-prepared backfills, the best placement condition out of different placement regimes (e.g., C-D, U-D, C-U and U-U conditions) can be determined consistent with the achieved UCS results. It is generally expected from a paste-backfilled stope condition that the porosity decreases

and the strength increases with increasing depth into the placed paste backfills. This is principally due to drainage and consolidation occurred during backfilling. The acquisition of strength for paste backfills becomes lower under the conditions of no drainage than drainage, as shown by the test results.

There is no standard backfill recipe and specimen size for the determination of the UCS of paste backfills. This work shows the prime importance of both specimen size and placement conditions for the mechanical strength development of paste backfill and hence for designing the most ideal paste backfill mixtures in the laboratory and operating a paste backfill plant in the field. Notwithstanding this, further testing is still required in order to acquire more consistent results for specimen size for determination of unconfined compressive strength of paste backfill samples, principally on the paste cored samples from paste-filled stopes. This experimental work will provide evaluation of the in situ mechanical strengths on which the field paste backfill samples are based.

ACKNOWLEDGEMENTS

The author would like to express his sincere thanks to the Natural Sciences and Engineering Research Council of Canada NSERC Discovery Grant Program, Industrial NSERC-Poly-UQAT Chair on the Environment and Mine Wastes Management and Canadian Research Chair on Integrated Management of Mine Wastes for their generous financial support. Special thanks are extended to Denis Bois, Tikou Belem, Bruno Bussière, Mostafa Benzaazoua, Nil Gaudet, David Bouchard, Yvan Poirier and Alain Perreault of the URSTM (Unité de Recherche et de Service en Technologie Minérale) Laboratory for their technical support in conducting several physical, mechanical and microstructural tests, to Nathan Mutch of Lafarge North America Inc. for providing the cement materials.

REFERENCES

ASTM Standard C143/C143M, 2013. Standard test method for slump of hydraulic cement concrete. In: *Annual Book of ASTM Standards*, 04.02, West Conshohocken, PA, United States of America, DOI: 10.1520/C0192_C0192M.

ASTM Standard C39/C39M, 2012. Standard test method for compressive strength of cylindrical concrete specimens. In: *Annual Book of ASTM Standards*, 04.02, West Conshohocken, PA, DOI: 10.1520/C0039_C0039M-12A.

ASTM Standard D1557, 2012. Standard test methods for laboratory compaction characteristics of soil using modified effort (56,000 ft-lbf/ft^3 (2,700 kN-m/m^3)) In: *Annual Book of ASTM Standards*, 04.08, West Conshohocken, PA, DOI: 10.1520/D1557-12.

ASTM Standard D2487-11, 2011. Standard practice for classification of soils for engineering purposes. In: *Annual Book of ASTM Standards*, 04.08, West Conshohocken, PA, DOI: 10.1520/D2487-11.

Belem, T., Benzaazoua M., El Aatar, O., Yilmaz, E., 2013. Effect of drainage and the pore water pressure dissipation on the backfilling sequencing. In: *23rd World Mining Congress, Canada*, August 11-15, pp. 1-10.

Belem, T., El Atar, O., Benzaazoua, M., Bussière, B., Yilmaz, E., 2007. Hydrogeotechnical and geochemical characterization of column consolidated cemented paste fill. In: *Proceedings of the 9th International Symposium in Mining with Backfill*, Montreal, Quebec, Canada, April 29 – May 2, pp. 1-10.

Belem, T., Benzaazoua, M., 2008. Design and application of underground mine paste backfill technology. *Geotechnical and Geological Engineering*, Vol. 26, No. 2, pp. 147-174.

Benzaazoua, M., Fall, M., Belem, T., 2004. A contribution to understanding the hardening process of cemented paste backfill. *Minerals Engineering*, Vol. 17, No. 2, pp. 141-152.

Benzaazoua, M., Belem, T., Yilmaz, E., 2006. Novel lab tool for paste backfill. *Canadian Mining Journal*, Vol. 127, No. 3, pp. 31-32.

Benzaazoua, M., Peyronnard, O., Belem, T., Fried, E., Stephant, D., Dublet G., 2010. Key issues related to behavior of binders in cemented paste fill. In: *The 13th Paste and Thickened Tailings*, Toronto, Ontario, Canada, pp. 345-364.

Bloss, M., 2002. Below ground disposal, In: *Paste and Thickened Tailings: A Guide* (R.J. Jewell, A.B. Fourie, and E.R. Lord, eds.), University of Western Australia, Nedlands, pp. 103-126.

Brackebusch, F.W., 1994. Basics of paste backfill systems. *Mining Eng.* Vol. 46, pp. 1175-1178.

Bussière, B., 2007. Hydrogeotechnical properties of underground hard rock tailings from metal mines and emerging environmental disposal approaches. *Can. Geotech. J.*, Vol. 44, No. 9, pp. 1019-1052.

Cihangir, F., Ercikdi, B., Kesimal, A., Turan, A., Deveci, H., 2012. Utilisation of alkali-activated

blast furnace slag in paste backfill of sulphide mill tailings: Effect of binder type and dosage. *Minerals Engineering*, Vol. 30, pp. 33-43.

Consoli, N.C., Rotta, G.V., Prietto, P.D.M., 2006. Yielding-compressibility-strength relationship for an artificially cemented soil cured under stress. *Géotechnique*, Vol. 56, No. 1, pp. 69-72.

Darlignton, W.J., Ranjith, P.G., Choi, S.K., 2011. The effect of specimen size on strength and other properties in lab testing of rock and rock-like cementitious brittle materials. *Rock Mech. Rock Eng.*, Vol. 44, pp. 513-529.

Ercikdi, B., Yilmaz, T., Kulekci, G., 2014. Strength and ultrasonic properties of cemented paste backfill. *Ultrasonics*, Vol. 54, No. 1, pp. 195-204.

Ercikdi, B., Kesimal, A., Cihangir, F., Deveci, F., Alp, I., 2009. Cemented paste backfill of sulphide-rich tailings: Importance of binder type and dosage. *Cem. Concr. Comp.*, Vol. 31, No. 4, pp. 268-274.

Ercikdi, B., Cihangir, F., Kesimal, A., Deveci, F., Alp, I., 2010. Use of water-reducing admixtures in cemented paste backfill of sulphide-rich mill tailings. *Journal of Hazardous Materials*, Vol. 179, pp. 940-946.

Fall, M., Célestin, J., Pokharel, M., Touré, M., 2010. A contribution to understanding the effect of curing temperature on mechanical properties of tailings fill. *Eng. Geol.*, Vol. 114, pp. 397-413.

Festugato, L., Fourie, A., Consoli, N., 2013. Cyclic shear response of fibre-reinforced cemented paste fill. *Géotechnique Letters*, Vol. 3, pp. 5-12.

Fourie, A., Helinski, M., Fahey, M., 2006. Filling the gap - A geomechanics perspective. *ACG Newsletter*, Vol. 26, pp. 18-24.

Ghirian, A., Fall, M., 2013. Coupled thermo-hydro-mechanical-chemical behavior of cemented paste backfill in column experiments. Part I: Physical and thermal processes and characteristics. *Eng. Geol.*, Vol. 164, pp. 195-207.

Ghirian, A., Fall, M., 2014. Coupled thermo-hydro-mechanical chemical behaviour of cemented paste backfill in column experiments. Part II: Mechanical and microstructural processes and characteristics. *Eng. Geol.*, Vol. 170, pp. 11-23.

Grice, T., 1998. Underground mining with backfill. In: T*he 2nd Annual Summit on Mine Tailings Disposal Systems*, Brisbane, Australia, November 24–25, pp. 1-14.

Hassani, F.P., Nokken, M.R., Annor, A., 2007. Physical and mechanical behavior of various combinations of mine fill materials. *CIM Bulletin*, Vol. 100, No. 1101, pp. 18-26.

Kesimal, A., Yilmaz, E., Ercikdi, B., Alp, I., Deveci, H., 2005. Effect of properties of tailings and binder on the short and long terms strength and stability of cemented paste backfill. *Mat. Letters*, Vol. 59, No. 28, pp. 3703-3709

Kesimal, A., Yilmaz, E., Ercikdi, B., 2004. Evaluation of paste backfill mixtures consisting of sulphide-rich mill tailings and varying cement contents. *Cement and Concrete Research*, Vol. 34, No. 10, pp. 1817-1822.

Pokharel, M., Fall, M., 2013. Combined influence of sulphate and temperature on the saturated hydraulic conductivity of cemented paste backfill. *Cem. Concr. Comp.*, Vol. 38, pp. 21-28.

Revell, M.B., 2004. Paste – How strong is it? In: *The 8th International Symposium on Mining with Backfill*, Beijing, China, September 19-21, pp. 286-294.

Snyman, B.J., van der Spuy, B., Correia, L.D.C., 2014. A critical look at uniaxial test procedures applied in the backfill industry. In: *The 11th International Symposium on Mining with Backfill*, Australia, May 20–22, pp. 161-174.

Thompson, B.D., Grabinsky, M.W., Bawden, W.F., 2012. In-situ measurements of cemented paste backfill at Cayeli Mine. *Canadian Geotechnical Journal*, Vol. 49, No. 7, pp. 755-772.

Yilmaz, E., 2010. Investigating the hydrogeo-technical and microstructural properties of cemented paste backfills using the versatile CUAPS apparatus. In: *Ph.D. Thesis*, Université du Québec en Abitibi-Témiscamingue UQAT, Rouyn-Noranda, Québec, Canada.

Yilmaz, E., 2011. Advances in reducing large volumes of environmentally harmful mine waste rocks and tailings. *Mineral Resources Management*, Vol. 27, No. 2, pp. 89-112.

Yilmaz, E., Benzaazoua, M., Belem, T., Bussière, B., 2009. Effect of curing under pressure on compressive strength development of cemented paste backfill. *Minerals Engineering*, Vol. 22, No. 9-10, pp. 772-785.

Yilmaz, E., Belem, T., Benzaazoua, M., Bussière, B., 2010. Assessment of the modified CUAPS apparatus to estimate in situ properties of cemented paste backfill. *Geotechnical Testing Journal*, Vol. 33, No. 5, pp. 351-362.

Yilmaz, E., Belem, T., Bussière, B., Benzaazoua, M., 2011. Relationships between microstructural properties and strength of consolidated and unconsolidated cemented paste backfill. *Cem. Concr. Comp.*, Vol. 33, No. 6, pp. 702-715.

Yilmaz, E., Benzaazoua, M., Bussière, B., Pouliot, S., 2014a. Influence of disposal configurations on hydrogeological behaviour of sulphidic paste tailings: A field experimental study. *Int. J. Miner. Proces.*, Vol. 131, pp. 12-25.

Yilmaz, E., Belem, T., Benzaazoua, M., 2014b. Effects of curing and stress conditions on hydromechanical, geotechnical and geochemical properties of cemented paste fill. *Engineering Geology*, Vol. 168, pp. 23-37.

Yilmaz, E., Belem, T., Bussière, B., Mbonimpa, M., Benzaazoua, M., 2015. Curing time effect on

consolidation behaviour of cemented paste backfill containing different cement types and contents. *Construction and Building Materials*, Vol. 75, pp. 99-111.

Effect of Poisson's Ratio on Stress/Strain Concentration at Circular Holes in Elastic Plates Subjected to Biaxial Loading-Three Dimensional Finite Element Analysis

A.A. Abd-Elhady
Mechanical Engineering Dept., Jazan Univ., Jazan 706, Kingdom of Saudi Arabia; on sabbatical leave from Mechanical Design Department, Faculty of Engineering, Helwan University, Cairo, Egypt.

M.N.H. AL-Maghrabi
Mining Engineering Department, Faculty of Engineering, King Abdulaziz University, Jeddah, Saudi Arabia.

ABSTRACT The influence of Poisson's ratio (ν) on stress and strain concentration factors of plate contains a circular notch and subjects to biaxial loading have been systematically analyzed by using three dimensional finite element (3DFE) method. It is necessary to determine stress and strain concentration factors around the circular notch in order to determine the site of crack initiation. The numerical results of the stress and strain concentration factors are traced through the plate thickness. A plate under elastic state has been used in the present work. Four values of Poisson's ratio (ν) were studied numerically, varied from 0.1 to 0.4.

It is found that the maximum stress and strain concentration factors increase with increasing the Poisson's ratio (ν). The stress and strain concentration factors increase with decrease the biaxial ratio. Furthermore, the effect of Poisson's ratio (ν) on stress and strain concentration factor decreases with increasing the biaxial ratio.

Keywords: Stress concentration factor, SCF, strain concentration factor, circular notch, biaxial load, three dimension finite element

1 INTRODUCTION

Structures with circular holes have been widely used in engineering designs. This circular notch will create stress or strain concentrations. When stress concentrations exit in a structure, its strength is often different from that measured using specimens under uniaxial loading. It is necessary to determine stress or strain concentrations around the circular notch in order to determine the site of crack initiation, which can severely reduce the overall strength of the structure.

The actual 3D stress fields in the neighborhood of the notch root or circular hole are very complex (Li & Guo, 2001). The SCF or strain concentration factor in the interior of a plate with a hole or notch is significantly higher than the value on the free surface or the corresponding planar solution (Li & Guo, 2001), (Nakamura & Parks, 1990), (Wang, 2003), (Li et al., 2000), (Yang et al., 2003), (She & Gue, 2006), (Abd-Elhady, 2010). On the other hand, in engineering practice, SCF and strain concentration factor measurement are always made on the free surfaces. This may cause danger in engineering applications without proper consideration of the 3D stress distributions. She and Guo (She & Guo, 2007) show that through thickness variation of stress concentration factor, K_σ, for elliptic holes subjected to tensile stress is very slight in the thin plate and increases with increasing the plate thickness. The corresponding peak value (K_σ) max is located at the center of thickness for thinner plate but shifts to the free surface in thick

plate. Recently, She and Guo (She & Guo, 2006), (She & Guo, 2007) have already demonstrated that the SCF changes along the hole front in the thickness direction. However, the influence of Poisson's ratio has not been considered in their works.

Kotousov and Wang (Kotousov & Wang, 2002) have studied the effect of thickness and Poisson's ratio on stress concentration based on some theoretical methods which showed that the 3D stress concentration is a function of thickness and Poisson's ratio. However, these existed theoretical methods often give the SCF as a mean value view, cannot solve the distribution of SCF along the notch front in the thickness direction and so cannot obtain the maximum SCF along the notch front. Furthermore, Peishi et al. (Peishi et al., 2008) found that the thickness-dependent maximum of SCF, increases significantly with increasing the Poisson's ratio in the elliptic holes which subjected to tensile loading. Tlilan (Tlilan, 2010) studied the influences of Poisson's ratio and the geometric configuration upon the strain concentration factor, defined under triaxial stress state, of notched bars with U-notch. Tlilan show that, the Poisson's ratio has a significant effect on the strain concentration factor, especially for deep and intermediate notch depths.

The main objective of the present work is to study the influence of Poisson's ratio (ν) and biaxial ratio on the stress and strain concentration factors and their relations of elastic finite thickness plate containing a circular subjected to far end uniform biaxial loading using 3D finite element method.

2. NUMERICAL MODEL

2.1. Definitions of the geometrical parameters

The plate containing a circular hole subjected to biaxial loading is illustrated in Fig. 1. The notch diameter is 2*D* and the radius of the notch is ρ. The thickness, width and the height of the plate are 2*B*, 2*W* and 2*H*, respectively. The plane *x-y* (plane *z* = 0) is the mid plane of plate and two plate surface are *z* = *B* and *z* = -*B*, respectively. The geometrical parameters of specimens are chosen as follows:

D = 1 mm;
B/D = 2.5 ;
ν = 0.1, 0.2, 0.3 and 0.4;
The biaxial ratio, λ, = -1, -0.5, 0, 0.5 and 1;
Young's modulus *E* = 200 GPa;
W/D = *H/D* = 100;

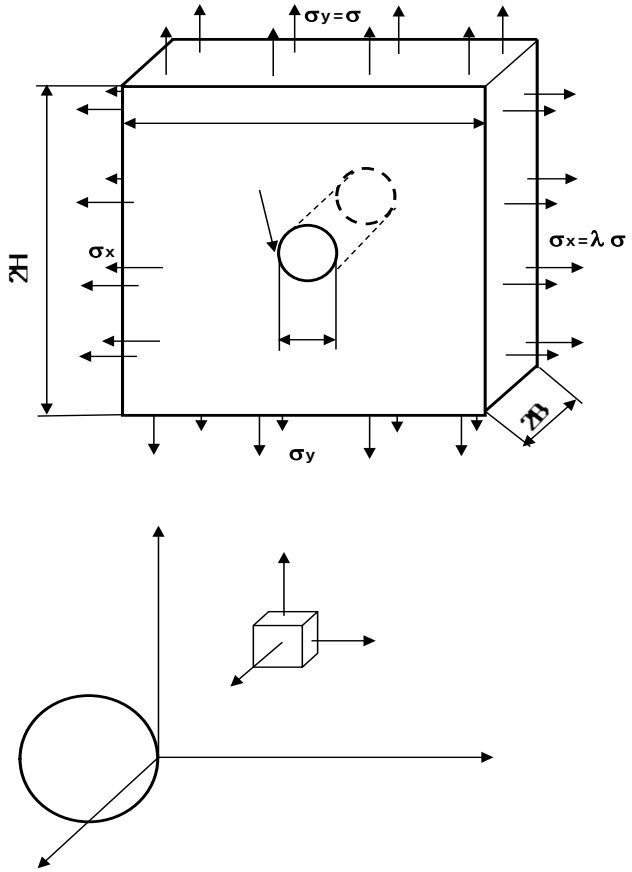

Figure 1. The geometry of the plate with circular hole under biaxial loading.

2.2. Definitions of the stress and strain concentration factor

In this paper, the stress and strain concentration factor is denoted as K_σ and K_ε respectively and the stress and strain concentration factor at the mid point of the plate is $K_{\sigma mp}$ and $K_{\varepsilon mp}$ respectively.

$$K_\sigma = \frac{\sigma_{NR}}{\sigma_{net}}; \quad (1)$$

$$K_{\sigma mp} = K_\sigma \qquad \text{at z = 0}$$

$$K_\varepsilon = \frac{\varepsilon_{NR}}{\varepsilon_{net}} \quad (2)$$

$K_{\varepsilon mp} = K_{\varepsilon}$ at z = 0

Where:

$$\sigma_{net} = \frac{\sigma_y W}{W - D} \quad (3)$$

$$\varepsilon_{net} = \frac{\sigma_y W}{E(W - D)} \quad (4)$$

Here, σ_{NR} and ε_{NR} are the longitudinal stress and strain in Y direction of plate at the notch root; σ_{net} and ε_{net} are the mean stress and strain of net section on the ligament, respectively. The K is meaning stress or strain concentration factor.

2.3. Finite Element Analysis

ABAQUS (ABAQUS, 2002) was selected to perform the numerical analysis owing to its powerful and comprehensive functions and precision. Therefore, a three-dimensional (3D) finite element model has been developed to account for geometric and material behavior of isotropic plate. A uniform, $\sigma_y = \sigma$, stress of 50 MPa is applied on the above and down boundary of the plate and $\sigma_x = \lambda\sigma$, in other hand side as shown in figure 1. The finite element meshes constructed with hexagonal structural mesh, C3D8 (An 8-node linear brick) elements, are used for a plate under Standard/static analysis.

Around 30 planar layers are divided through the thickness of the plate. The mesh refinement process is carried out to assure that results are not dependent upon the element size. So that, the size of element decreases gradually with distance from the open hole decreasing (as shown in Fig. 2). This means that the finite element (FE) meshes in the neighborhood of the hole are much denser. The plate are modeled with around 45000 elements.

2.4 Model Verification

To verify the accuracy of the present result, the values of normalized stress, $K_{\sigma}/K_{\sigma mp}$, and strain, $K_{\varepsilon}/K_{\varepsilon mp}$, concentration factor (normalized by each value of mid plane) for $\nu = 0.3$ and uniaxial loading ($\lambda = 0$) are compared with the previous numerical results using 3-D analysis found in the literature, B/D = 2.5, W/D = 100 and H/D = 100, (Zheng et al., 2008), as shown in Figures 3. Figure 3 shows An excellent agreement between present model result and data in literature (Zheng et al., 2008).

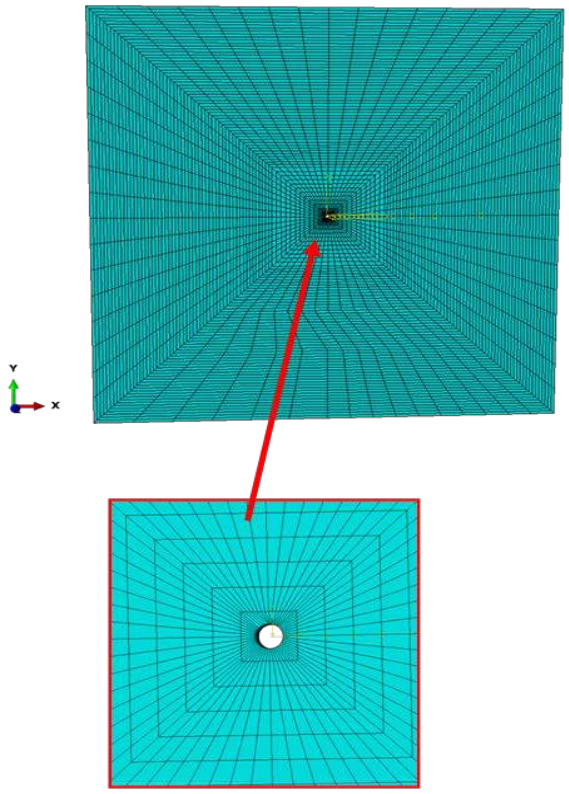

Figure 2. Finite element model mesh.

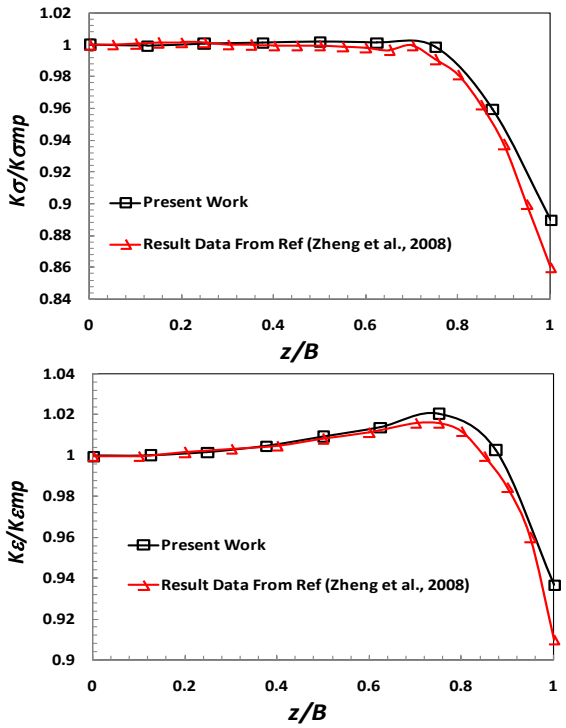

Figure 3. The distributions of the stress and strain concentration factor through-thickness of notch root for present work and numerical result in literature (Zheng et al., 2008).

3. RESULTS AND DISCUSSION

Fig. 4 illustrates the variation of normalized stress concentration factor, $K_\sigma/K_{\sigma mp}$, (the stress is normalized by each value of mid plane) versus *z/B* for different ν and λ. At different value of λ the normalized stress concentration factor has constant value equal 1 until *z/B* reach to 0.8 then decrease by increasing the dimensionless *z/B.* The obtained results for D = 1 mm, are compared with the result for D = 0.5 with the same ratio of *B/D, W/D* and *H/D* (only for $\nu = 0.1$, 0.4 and $\lambda = -0.5, 0.5$) to validate the proposed value. the values of $K_\sigma/K_{\sigma mp}$ for D = 1 is identical to this obtained for D = 0.5 with the same ratio of *B/D, W/D* and *H/D*.

Fig. 5 represents the variation of normalized strain concentration factor, $K_\varepsilon/K_{\varepsilon mp}$, (also, the strain is normalized by each value of mid plane) versus *z/B* for different ν and λ. At different value of λ the normalized stain concentration factor increase to reach to it's a peak value and then decrease by increasing the dimensionless *z/B*

The previous curves represent the variation of either the normalized $K_\sigma/K_{\sigma mp}$ or $K_\varepsilon/K_{\varepsilon mp,}$ for $\lambda \neq 1$, can be divided to three regions. In the first region $K_\sigma/K_{\sigma mp}$ or $K_\varepsilon/K_{\varepsilon mp}$ increased with increasing *z/B* to reach its peak value. In this region, the $K_\sigma/K_{\sigma mp}$ or $K_\varepsilon/K_{\varepsilon mp}$ increase with increasing ν for the same *z/B.* in the second region, all values of $K_\sigma/K_{\sigma mp}$ or $K_\varepsilon/K_{\varepsilon mp}$ decrease with increasing *z/B* by different values of decrement to intersect at one point ($z/B \approx 0.8$ in case of $K_\sigma/K_{\sigma mp}$ and $z/B \approx 0.9$ in case of $K_\varepsilon/K_{\varepsilon mp}$). In the third region ($K < K_{mp}$), the previous decrement continued to get opposite trend on the surfaces. The $K_\sigma/K_{\sigma mp}$ or $K_\varepsilon/K_{\varepsilon mp}$ decreases with increasing ν for the same *z/B*. Therefore, it can be concluded that the peak value of K_σ and K_ε locate at the interior of the plate and this value increases by increasing the value of Poisson's ratio. While, the minimum values of K_σ and K_ε locate at free surface of the plate and this value decrease by increasing the Poisson's ratio. But, for $\lambda = 1$, the normalized $K_\sigma/K_{\sigma mp}$ or $K_\varepsilon/K_{\varepsilon mp}$ are not changed by increasing the values of *z/B* and are equal 1.

Figure 6 presents the variation of mid plane stress and strain concentration factor with λ for different dimensionless ν. For $\lambda \neq 1$, the stress and strain concentration factor increase by increasing ν. $K_{\sigma mp}$ and $K_{\varepsilon mp}$ decrease with an increase in λ. This may be due to increasing the compression stress in the notch root by increasing the biaxial ratio, λ. It was found also that the $K_{\sigma mp}$ and $K_{\varepsilon mp}$ is close to that given by Peterson (Peterson, 1997) when λ is equal zero. Furthermore, the effect of Poisson's ratio (ν) on stress and strain concentration factor decreases with increasing the biaxial ratio. For $\lambda = 1$, the stress and strain concentration factor are not affected by change the values of Poisson's ratio. Furthermore, the relation between stress or strain concentration factor and biaxial ration, λ is linear as shown in the figure 6 which is agreement with derived by Peterson (Peterson, 1997).

Figures 7 and 8 show the contours of the resulted Von Mises stress and longitudinal stress (σ_{yy}) around the open hole for $\nu = 0.3$. It is observed that, the values of Von Mises stress and σ_{yy} decrease by increasing the values of the biaxial ratio λ. The value of σ_{yy} around the second notch root at the upper and lower hole transform from the compression to tension by increasing the values of the biaxial ratio λ as shown in figure 8.

4. CONCLUSIONS

It can be concluded from the present numerical work that:

The maximum stress and strain concentration factors increase with increasing the Poisson's ratio (ν) inside the plate thickness while, it have the opposite trend at the free surface.

The stress and strain concentration factors increase with decrease the biaxial ratio.

The effect of ν on stress and strain concentration factor decreases with increasing the λ. Furthermore the stress and strain concentration factor are not affected by change the values of Poisson's ratio for $\lambda = 1$.

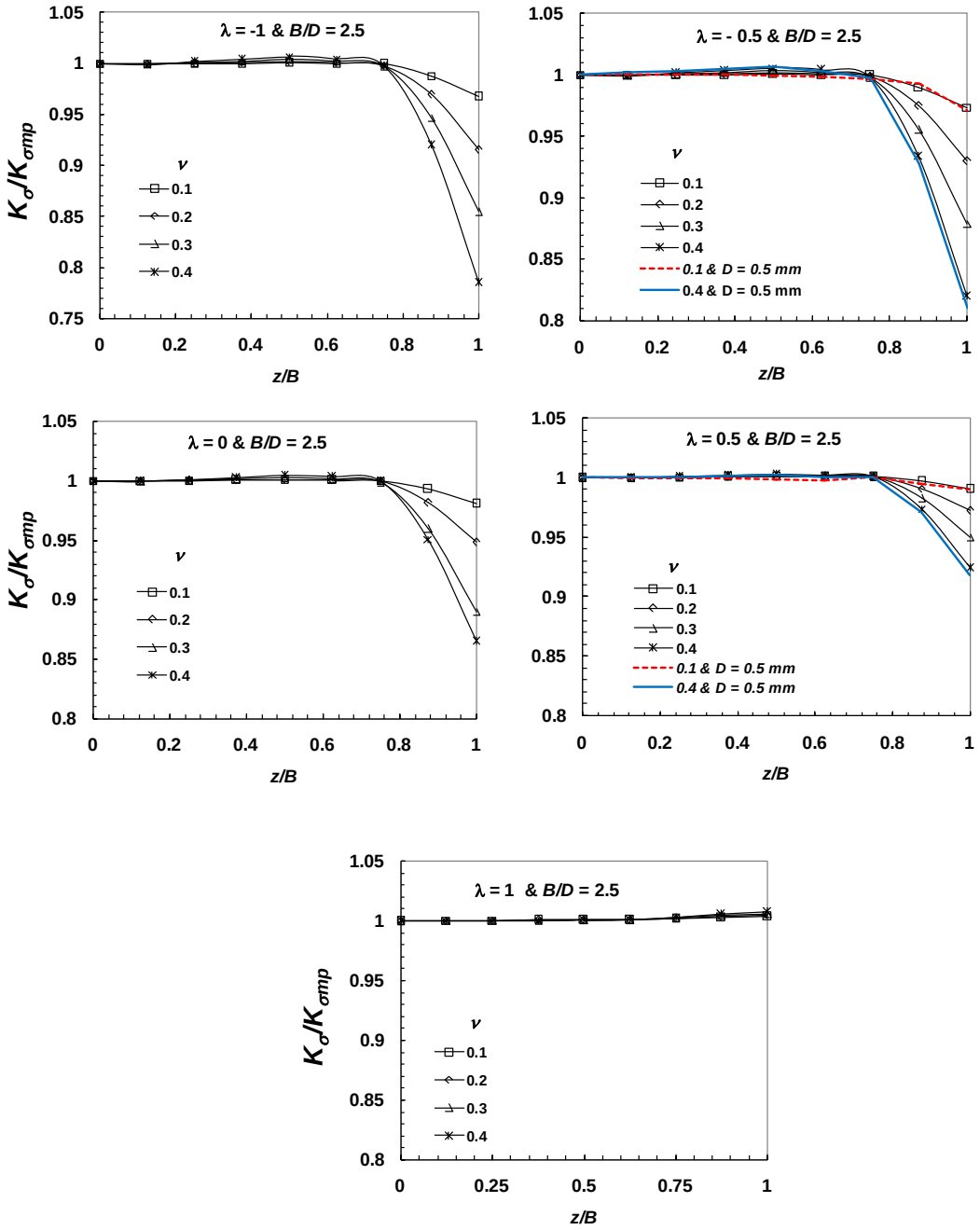

Figure 4. The distributions of the stress concentration factor through-thickness of notch root for different biaxiality ratio λ and different Poisson's ratio (ν).

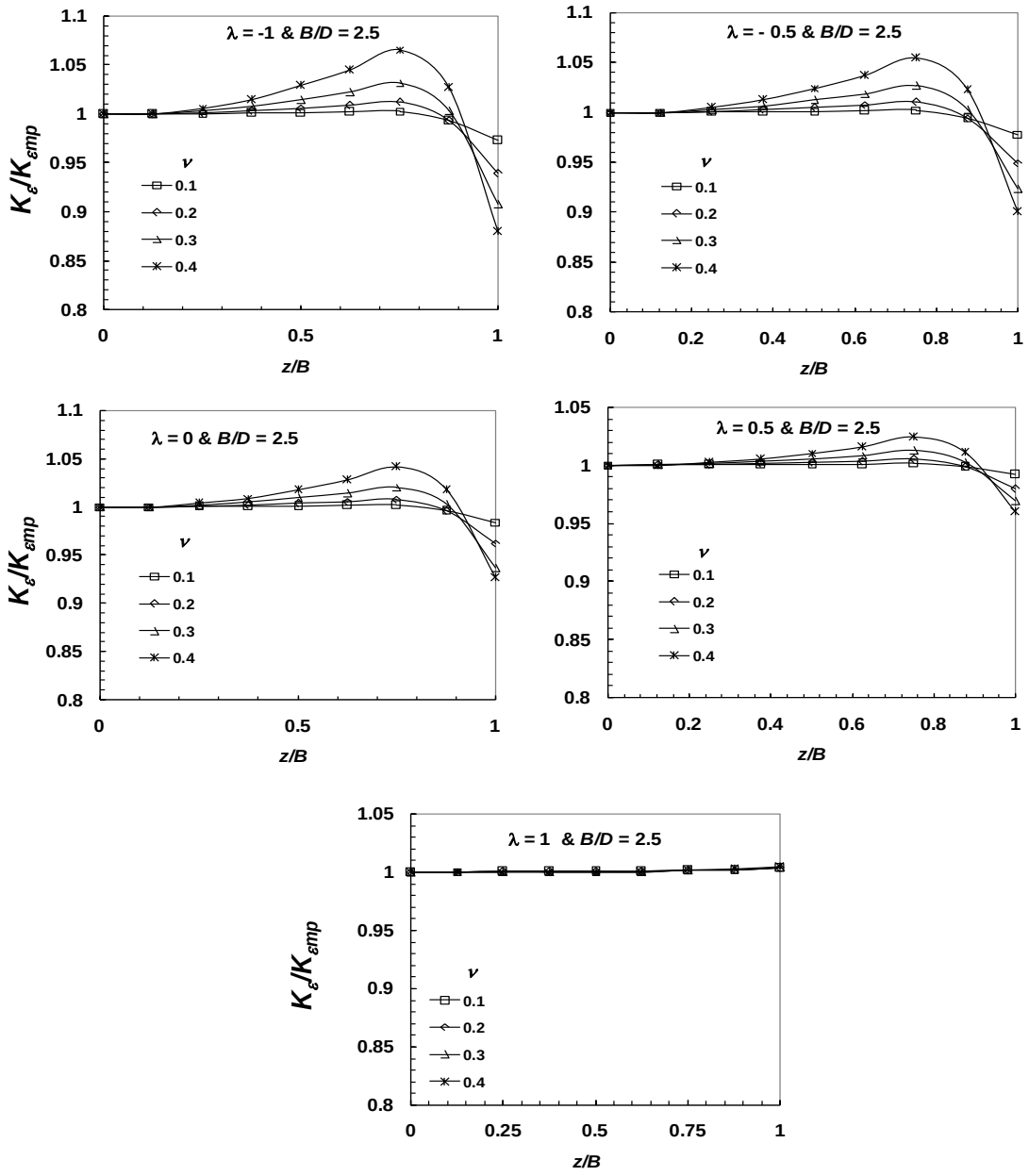

Figure 5. The distributions of the strain concentration factor through-thickness of notch root for different biaxiality ratio λ and different Poisson's ratio (ν).

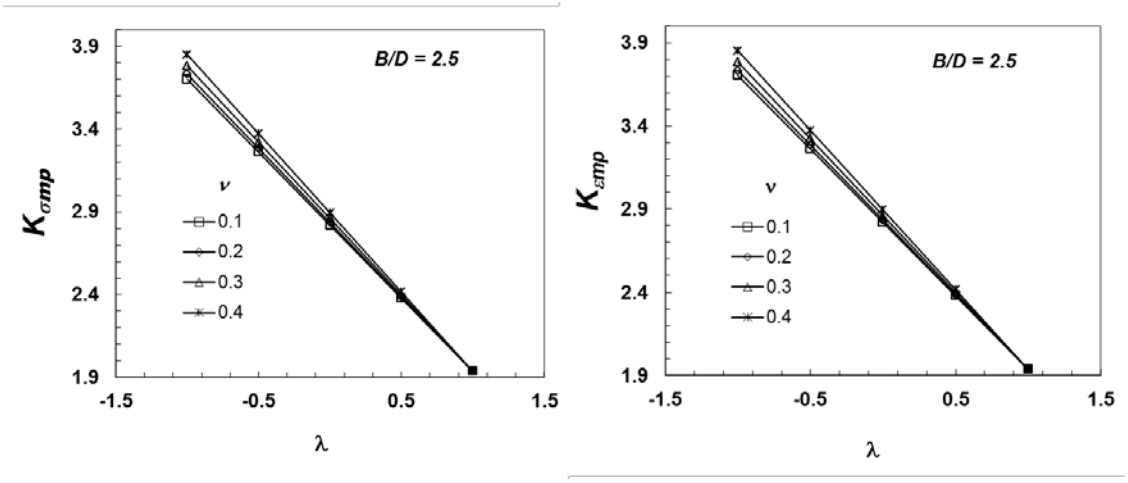

Figure 6. The stress and, strain concentration factor at the mid point of the notch versus to biaxiality ratio λ for different ν.

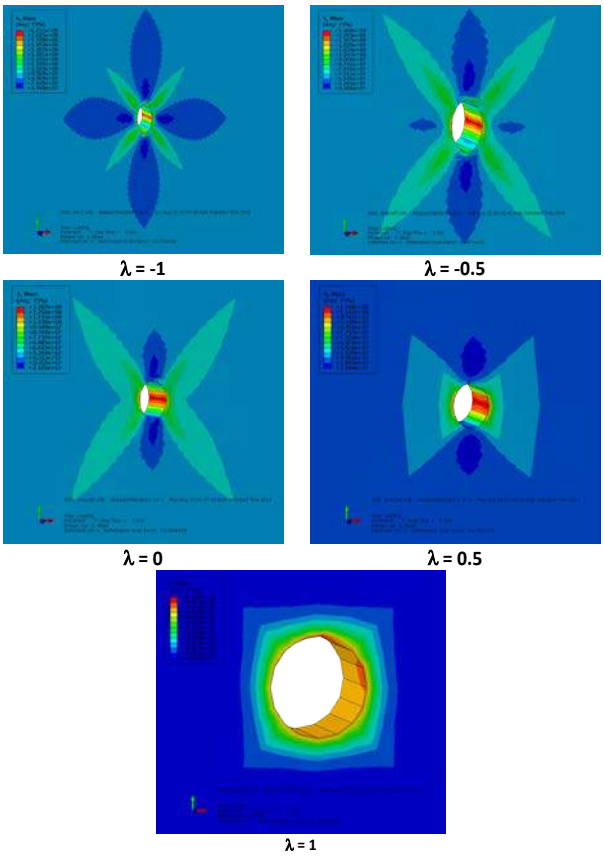

Figure 7 Von Mises contours around the open hole.

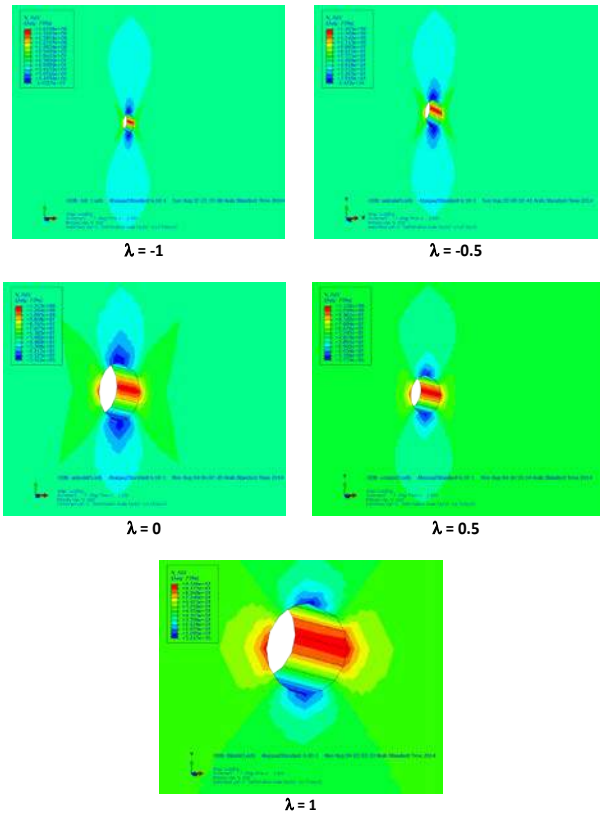

Figure 8 longitudinal stress, σ_{yy}, contours around the open hole.

REFERENCES

ABAQUS, 2002. user's manual version 6.3. Pawtucket, RI: Hibbitt, Karlsson and Sorensen Inc.

Abd-Elhady, Amr, 2010. Stress and strain concentration factors for plate with small notch subjected to biaxial loading – Three dimensional finite element analysis, Ain Shams Engineering Journal, 1, 139–145

Kotousov, A, Wang, CH, 2002. Three-dimensional stress constraint in an elastic plate with a notch, Int J Solids Struct, 39:4311–26.

Li, ZH, Guo, WL., 2001. Three-dimensional elastic stress fields ahead of blunt V-notches in finite thickness plates, Int J Fracture, 107: 53–71.

Li, ZH, Guo, WL, Kuang, ZB., 2000. Three-dimensional elastic stress fields near notches in finite thickness plates, Int J Solids Struct., 37: 7617–31.

Nakamura, T, Parks, DM., 1990. Three-dimensional crack front fields in a thin ductile plate, J Mech Phys Solids, 38:787–812.

Peterson, RE., 1997. Stress concentration factors, New York: John Wiley and Sons.

Peishi, Yu, Wanlin, Guo, Chongmin, She, Junhua, Zhao, 2008. The influence of Poisson's ratio on thickness-dependent stress concentration at elliptic holes in elastic plates, International Journal of Fatigue, 30:165–171.

She, CM, Guo, WL., 2006. Numerical investigations of maximum stress concentration at elliptic holes in finite thickness piezoelectric plates, Int J Fatigue, 28:438–45.

She, CM, Guo, WL., 2007. Three-dimensional stress concentrations at elliptic holes in elastic isotropic plates subjected to tensile stress, Int J Fatigue, 29:330–335.

Tlilan, H. M., 2010. Effect of Poisson's Ratio on the Elastic Strain Concentration Factor of Notched Bars under Static Tension and under Pure Bending, Jordan Journal of Mechanical and Industrial Engineering Volume 4, Number 6, December

Wang, X., 2003. Elastic T-stress solutions for semi-elliptical surface cracks in finite thickness plates, Eng Fract Mech, 731–56.

Yang, Z, Guo, WL, Xu, X., 2003. Three-dimensional elastic stress fields near notches in finite thickness bimaterial plates, J Mech Strength, 25:90–4.

Zheng, Yang, Chang-Boo, Kim, Chongdu, Cho, Hyeon, Gyu, Beom, 2008. The concentration of stress and strain in finite thickness elastic plate containing a circular hole, International Journal of solid and Structures, 45: 713-731.

Estimating of Hoek-Brown m_i Using Internal Friction Angle

S. Mehrishal,
Amirkabir University of Technology, Tehran, Iran

M. Sharifzadeh,
Curtin University, Australia

K.Shahryar
Amirkabir University of Technology, Tehran, Iran

ABSTRACT Application of Hoek-Brown failure criterion in rock mechanics is more common and is verified well. In this criterion, the m_i is an important factor which controls trend of failure curve. Based on rock type and triaxial test data, the method of m_i estimation for different rocks is provided by Hoek-Brown. Indeed, this parameter is a frictional property and it depends on rock type, mineralogy and granular interlocking of rocks. In addition, it can be approximately predicted from the ratio between the uniaxial compressive strength and tensile strength of brittle intact rocks. But, because of tension strength estimation difficulties, this method is not applicable well. In this paper, correlation of m_i and internal friction angle (φ) of intact rocks is investigated and based on this correlation; a comprehensible physical concept is introduced for this parameter. Therefore, using this concept, a simple and exact estimation method is developed for m_i and H-B failure criterion calculation. The results predicted by new method are well verified by comparison with experimental test results.

Keywords: Internal friction angle, Hoek – Brown failure criterion, rock mechanics

1 INTRODUCTION

The Hoek-Brown failure criterion for intact rock and rock mass was developed in 1980 and modified over the years in order to meet the needs of users. Although, A great number of rock strength criteria have been proposed over the past three decades, but the Hoek-Brown failure criterion has been the most well-known and most frequently used one, because: (a) it was developed specifically for rock materials and rock masses; (b) it's input parameters can be determined from routine unconfined compression tests, mineralogical examination, and discontinuity characterization; and (c) it has been applied for over 34 years by practitioners in rock engineering, and has been applied successfully to a wide range of intact and fractured rock types (Sari 2010).

Hoek and Brown (1980) proposed a method for obtaining estimates of the strength of jointed rock masses, based upon an assessment of the interlocking of rock blocks and the condition of the surfaces between these blocks (Hoek 2007). According to Hoek-Brown (1980), incept of this concept is rooted in Griffith criterion. Consequently, the original criterion and general criterion for intact rock and rock mass were developed as follow:

$$\sigma_1' = \sigma_3' + \sigma_{ci}\left(m_b \frac{\sigma_3'}{\sigma_{ci}} + s\right)^a \quad (1)$$

$$\sigma_1' = \sigma_3' + \sigma_{ci}\left(m_i \frac{\sigma_3'}{\sigma_{ci}} + 1\right)^{0.5} \quad (2)$$

Where σ'_1 and σ'_3 are the maximum and minimum effective principal stresses at failure, m_i and m_b are the value of the Hoek-Brown constant respectively for the intact and rock mass. s and a are constants which depend upon the rock mass characteristics and σ_{ci} is the uniaxial compressive strength of the intact rock pieces.

The relationship between the principal stresses at failure for a given rock is defined by two constants, the uniaxial compressive strength σ_{ci} and m_i. Wherever possible the values of these constants should be determined by statistical analysis of the results of a set of triaxial tests on carefully prepared core samples. For this purpose, once the five or more triaxial test results have been obtained, they can be analyzed to determine the uniaxial compressive strength σ_{ci} and the Hoek-Brown constant m_i as described by Hoek and Brown (1983). In this analysis, equation (2) is re-written in the form:

$$y = m\sigma_{ci}x + s\sigma_{ci} \tag{3}$$

Where $x = \sigma'_3$ and $y = (\sigma'_1 - \sigma'_3)^2$, for n specimens the uniaxial compressive strength σ_{ci}, the constant m_i and the coefficient of determination r^2 are calculated using linear regression. In the absence of laboratory tests, a guideline table can be used to obtain estimate of mi and σ_{ci}. Of course, it should be noted that the simple relationship between mi and rock type as envisaged by Hoek & Brown has not proven to be appropriate with the benefit of a much greater data set than was available at that time. The most accurate method of assessing m_i values remains as statistical analysis of data from a full set of laboratory test results. In the absence of a full suite of laboratory tests, R, the ratio of unconfined compressive strength to tensile strength, is a useful indicator of m_i values (Richard and Read 2011).

This paper first summarizes procedures used to calculate m_i and then introduce a new m_i estimation method based on rock's internal friction angle and finally, compares the m_i results obtained from Hoek-Brown's linear regression method and new internal friction angle method.

2 CALCULATION OF m_i VALUE

In the m_i calculation using statistical analysis, method of data analyzing can mainly affect the obtained value of m_i. In order this, Hoek-Brown used Linear Regression but the nonlinear Levenberg-Marquardt Least Squares (Madsen et al. 2004) is default analyzing method in RocData and Simplex Reflection method (Shah, and Hoek 1992) and Linear Regression are also selectable. Applicability of this different analyzing method is investigated by Douglas (2002).

In the case of intact rock material where s = 1, Hoek-Brown noted that $m \approx \sigma_{ci}/|\sigma_t|$ where σ_t is the uniaxial tensile strength of the intact rock. However, for general criterion use, they preferred to estimate m simply as a statistical curve-fitting parameter because of the difficulty in adopting the uniaxial tensile strength as a fundamental rock property (Richard and Read 2011).

Hoek & Brown suggested that m for intact rock (m_i) reflects rock type and its value increase with coarser grain size. According to this, they established guideline tables to estimate the m_i. But, study shows that calculated values for m_i are different from those in guideline tables and this difference is more specific in igneous rocks (Richard and Read 2011). Mostyn and Douglas (2000) showed that usually the calculated values are smaller than guideline values. For example, of individual lithology, sandstone has the most extensive set of test data. The frequency distribution of m_i values for this rock type from the Douglas database shows that compared with the Hoek guideline range of 13 to 21, 35 out of the 55 data points lay outside the indicated range based on lithology (Richard and Read 2011).

Correlations of m_i with unconfined compressive strength and Deere - Miller modulus ratio (intact elastic modulus E_i divided by unconfined compressive strength σ_c) and other rock parameters are mostly very poor (Richard and Read 2011). The only rock material parameter with which m_i has any reasonable correlation is the ratio of the unconfined compressive strength (σ_c) to the tensile strength (σ_t). Sheorey (1997) defined this ratio as $R = \sigma_c/|\sigma_t|$.

Tensile strength usually is determined by two, direct and indirect, methods. The results of direct (pulling) tests are not more valid,

largely due to gripping techniques and alignment of the test specimen. The indirect (Brazilian) test is a simple procedure, with many practical advantages over direct tensile tests. However in both cases the testing procedures used can have a great deal of influence on the results. Pells notes that the correspondence between direct and Brazilian type tests is usually very good if similar size specimens are used (Pells 1993). Data from Inada & Kinoshota indicate that the values obtained from the Brazilian tests are about 1.1 to 1.2 times larger than those from the uniaxial tension test (Inada and Kinoshita 2001). The results of 20 direct and 40 Brazilian tensile strength tests from Gorski &Conlon show that the Brazilian tests results were about twice those of the direct tests (Gorski and Conlon 2007). However, there appear to be few comparative studies between the two techniques in the literature.

The laboratory tensile data in the Douglas database comprised results from both direct uniaxial tension and indirect (Brazilian) testing. Using these data, the intact rock parameter mi has been calculated in overall accordance with the Hoek guidelines (≥ 5 data sets with the maximum σ3′ ranging from 0.4 to 0.6 σci). The calculations have been done with the RocLab program using the Levenberg-Marquardt technique, discarding any results with obviously poor correlation. Figure 1 shows the relationship between R and mi. There is a fairly good relationship between R and mi. Although most of the data sets involve only a single uniaxial compressive and/or tensile test, the scatter of points is also fairly uniformly distributed about the 1:1 correlation line for both test types. Therefore, it can be conclude that the value of R is a good representative for mi.

Although, tensile strength is an important element of the failure criterion, but, Hoek-Brown do not include it in mi calculation guidelines. Though not clear, this may be related to the earlier-stated difficulties with the tensile tests. While the direct tensile test is not readily available as a standard procedure in many rock testing laboratories, the Brazilian test is simple with regard to both specimen preparation and testing procedure. Therefore, inclusion of tensile testing, as advocated by Sheorey (Sheorey 1997), into a full suite of testing for mi determination is straightforward, as also practiced in some of earlier testing investigations such as Read et al. (2005). It has been proven that R provides a simple basis for estimating mi. R has also been utilized by Cai (1983) in his investigation of tensile strength determination from acoustic emission during compression testing.

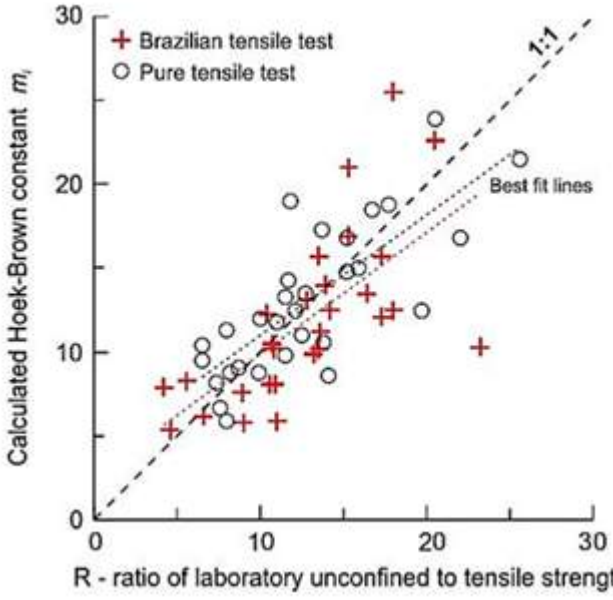

Figure 1. Plot of laboratory compressive strength to tensile strength ratio with Hoek-Brown constant m_i using data from Douglas 2002.

3 m_i ESTIMATION USING INTERNAL FRICTION ANGLE (Φ)

For each series of triaxial test data, the normal (σ_n) and shear stresses (τ) could be calculated and the Mohr circle fitting curve easily could be drawn using the equations published by Balmer (1952). Drawing Mohr fitting curve for different series of test data showed that under the low normal stress, the large and small value of m_i respectively leads to increase and decrease of instantaneous friction angles. Large values for m_i from 15 to 25 usually are associated with brittle igneous and metamorphic rocks such as andesite, gneisses and granites. And low value of m_i from 3 to 7, most are associated with ductile carbonate rocks such

as limestone and dolomite (Hoek 1983). It can be concluded that the constant m_i is related to the frictional properties of the rock and changes with the type of rock, its mineral composition, interlocking of grains, grain size and etc.

As stated previously, ratio of the unconfined compressive strength (σ_c) to the tensile strength (σ_t) has reasonable correlation with m_i and this ratio is defined as R ($R = \sigma_c/|\sigma_t|$). But, usually measuring tensile strength of rocks is difficult and the testing procedures used can have a great deal of influence on the results. In order to improve this concept, relations of Coulomb's failure theory are used in this paper. According this theory, uniaxial strength (σ_c) and tension strength (σ_t) can be written as:

$$\sigma_c = 2C \cos\varphi / (1-\sin\varphi)$$

$$\sigma_t = 2C \cos\varphi / (1+\sin\varphi)$$

Where φ is internal friction angle of intact rock and C is inherent cohesion of rock material. It is experimentally proved that rock materials usually deviate from Coulomb's failure theory in tension conditions and tension strength is about half of its theoretical value. Therefore it's assuming that:

$$\sigma_t \approx C \cos\varphi / (1+\sin\varphi)$$

Then the ratio of σ_c on σ_t (or R) is equal to:

$$\sigma_c/\sigma_t = 2(1+\sin\varphi)/(1-\sin\varphi)$$

$$R = 2(1+\sin\varphi)/(1-\sin\varphi)$$

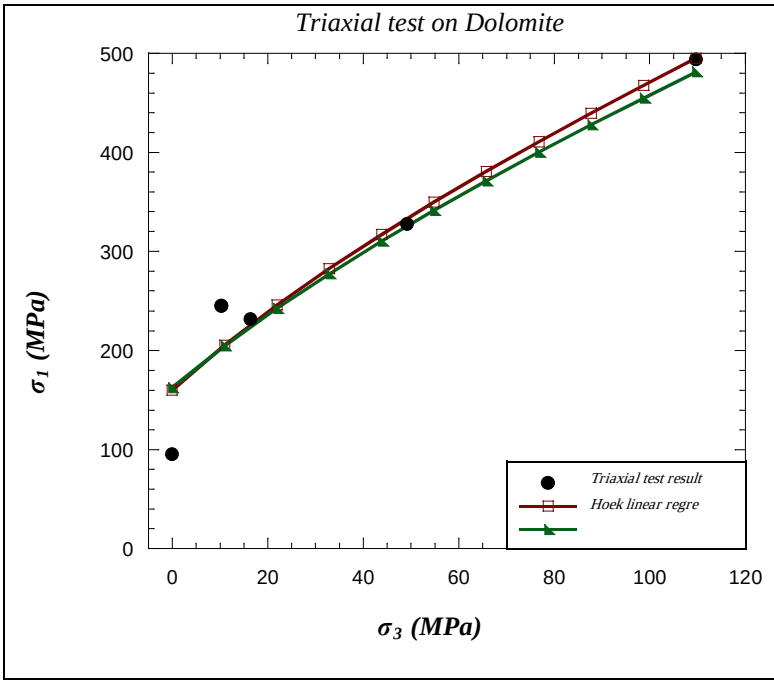

σ_c	160.12	**Hoek-Brown linear regression**
m_i	6.99	
σ_c	162.31	**Proposed Method**
m_i	6.28	
σ_1	σ_3	**Results of Triaxial test Data**
95.255	0	
244.963	10.3142	
231.615	16.3814	
327.932	49.1443	
494.022	109.665	
$\varphi=31.12^\circ$ C=45.79 MPa $\sigma_1=162.31+3.14\,\sigma_3$		

(a)

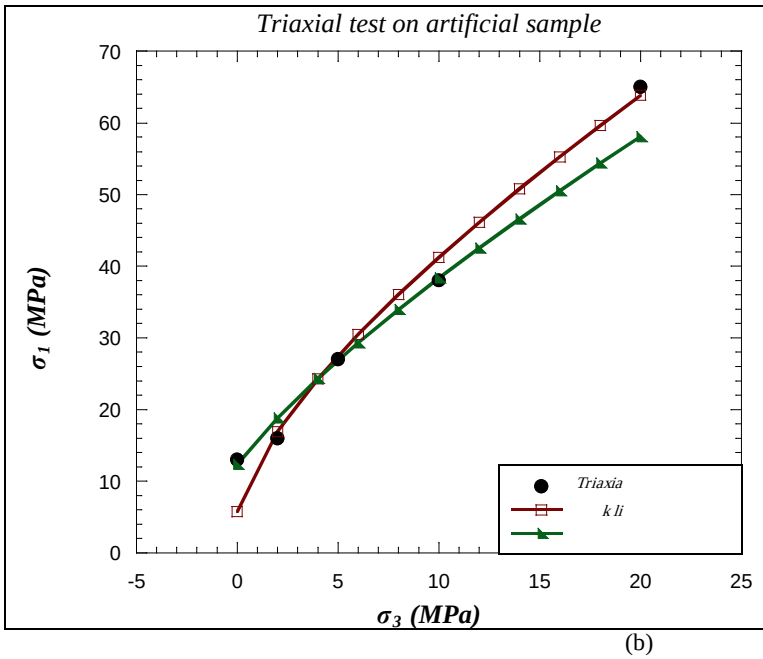

σ_c	16.35	**Hoek-Brown linear regression**
m_i	5.76	
σ_c	12.36	**Proposed Method**
m_i	5.24	
σ_1	σ_3	**Results of Triaxial test Data**
13	0	
16	2	
27	5	
38	10	
65	20	
$\varphi=26.58^\circ$ C=3.81 MPa $\sigma_1=12.36+2.62\,\sigma_3$		

(b)

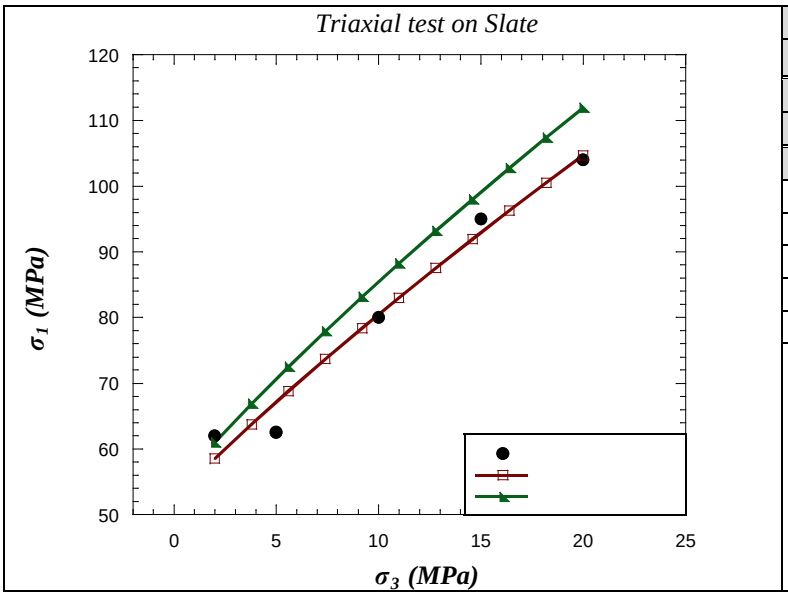

σ_c	52.4	**Hoek-Brown linear regression**
m_i	4.21	
σ_c	54.11	**Proposed Method**
m_i	5.1	

σ_1	σ_3
62	2
62.5	5
80	10
95	15
104	20

Results of Triaxial test Data

$\varphi=25.89^\circ$
$C=16.94$ MPa

$\sigma_1=54.11+2.55\ \sigma_3$

(c)

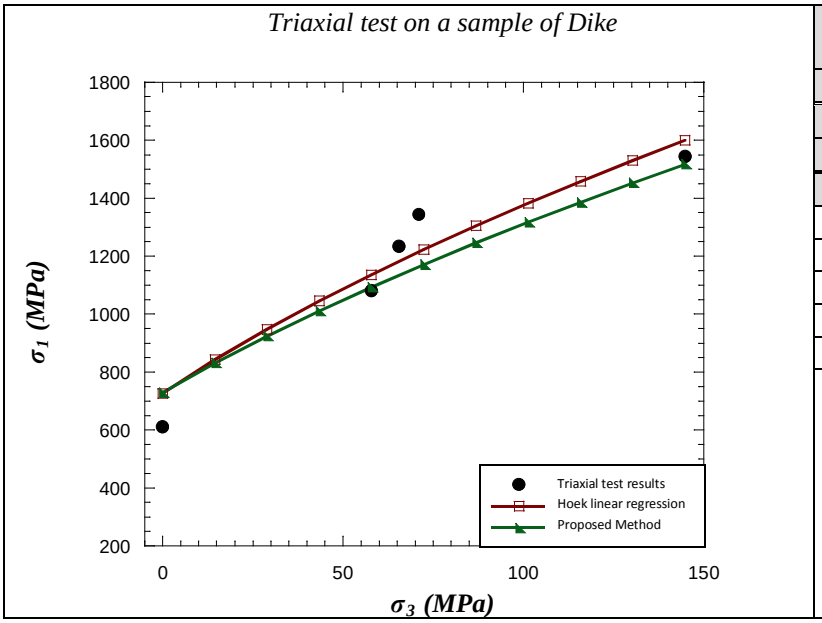

σ_c	725.77	**Hoek-Brown linear regression**
m_i	15.15	
σ_c	728.9	**Proposed Method**
m_i	12.8	

σ_1	σ_3
610.9	0
1080.4	57.9
1233.5	65.5
1344.5	71
1544.5	144.8

Results of Triaxial test Data

$\varphi=25.89^\circ$
$C=16.94$ MPa

$\sigma_1=728.9+6.4\ \sigma_3$

(d)

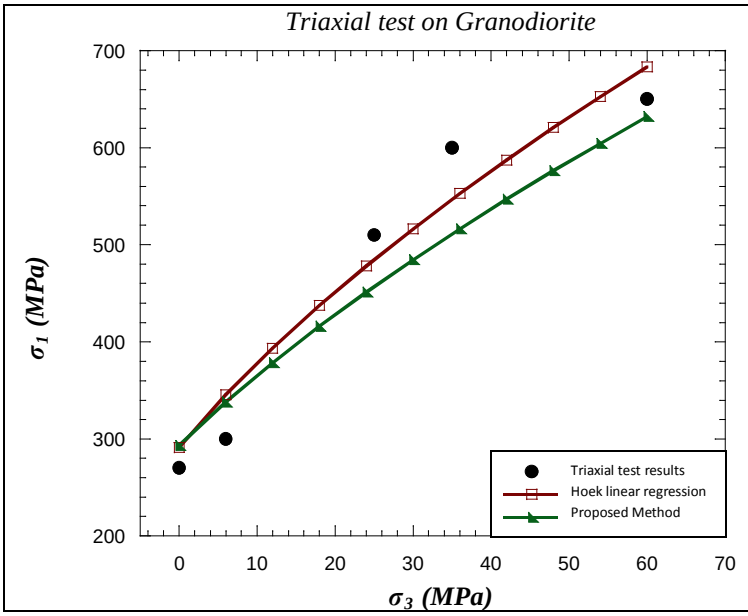

σ_c	291.2	**Hoek-Brown linear regression**
m_i	17.38	
σ_c	293.33	**Proposed Method**
m_i	13.7	

σ_1	σ_3
270	0
300	6
510	25
600	35
650	60

Results of Triaxial test Data

$\varphi=48.18^\circ$
$c=56$ MPa

$\sigma_1=293.33+6.85\ \sigma_3$

(e)

Figure 2. Comparison of Failure criterion curves obtained from H-B linear regression and new proposed method.

Finally by replacing m_i to R and tan ψ to $(1+\sin \varphi)/(1-\sin \varphi)$, a simple equation can be obtain for m_i calculation:

$$m_i \approx 2 \, tg\psi$$

Now it is simple to understand whether the constant of m_i is related to the frictional properties of the rocks and using this equation, it is possible to introduce a simple physical concept to definition of m_i. Using this approach the values of m_i and σ_c could be estimated accurately by a simple way.

In order to investigate the validation of this approach, Hoek-Brown criterion is written for several triaxial test data using linear regression method and using new internal friction approach. Comparison the results from both methods showed that the criterion calculated from internal friction angle has a good conformity by criterion from linear regression. Figures 2 (a to e) illustrate this coincidence.

4 DISCUSSION

Researches show that the large values of m_i give steeply inclined Mohr envelopes and high instantaneous friction angles at low effective normal stress levels. Therefore it can be suggested that the constant of m_i is related to the frictional properties of the rocks. In this paper, using theoretical equations and some empirical suggestions a simple relation is introduced which make possible to estimate m_i of intact rocks using internal friction angle value. This approach introduces a simple physical concept for m_i, improves the knowledge about this parameter and makes more apparent relation between rock types and Hoek-Brown criterion. Also Calculations in this method is much simpler than other previously proposed methods.

REFERENCES

Cai, M. 2010. Practical estimates of tensile strength and Hoek-Brown parameter mi of brittle rocks. *Rock Mech. & Rock Eng*. 43(2): 167-184.

Douglas, K.J. 2002. The Shear Strength of Rock Masses. Phd Thesis, School of Civil and Environmental Engineering, University of New South Wales, Sydney, Australia.

Gorski, B. Conlon, B. 2007. Determination of The Direct and Indirect Tensile Strength on Cores From Borehole. Report P-07-76, Canmet-Mmsl, Natural Resources Canada.

Hoek, E. 2007. Practical Rock Engineering. Course Notes,Hoek.Corner.Http://Www.Rocscience.Com

Hoek, E. 1983. Strength of Jointed Rock Masses. *Ge´Otechnique*; 23(3):187–223.

Inada, Y.H. Kinoshita, N. 2001. A Few Remarks on Thermal Behavior of Rock Mass Around Opening Due To Low Temperature Materials Storage. In *Proceedings of Isrm Regional Conference* "Rock Mechanics: A Challenge For Society", Eds. P Särkkä & P. Eloranta 345-349.

Madsen, K. Nielsen, H.B. Tingleff, O. 2004. Methods For Non-Linear Least Squares Problems. Informatics and Mathematical Modelling, Technical University of Denmark (Available As Http://Www2.Imm.Dtu.Dk/Pubdb/Views/Edoc_Downloa D/Imm3215.Pdf).

Mostyn, G. & Douglas, K. 2000. Strength of intact rock and rock masses. In *Proceedings International Conference on Geotechnical & Geological Engineering* Melbourne, Australia, 1389-1421. Lancaster: Technomic Publishing Company.

Pells, P.J. 1993. Uniaxial strength testing. In Comprehensive *Rock Engineering*, Vol 3 Rock testing and site characterization, ed. J.A. Hudson, 67-85.

Read, S.A.L., Perrin, N.D. & Richards, L. 2005. Evaluation of the intact properties of weak rocks for use in the Hoek-Brown failure criterion. In *Proceedings 40th US Rock Mechanics Symposium, Anchorage, Alaska*, USA, eds. G Chenn et al., paper ARMA/USRMS 05-694. Alexandria: ARMA.

Richards, L.R. Read, S.A.L. 2011. A Comparison of Methods for Determining m_i, The Hoek-Brown Parameter For Intact Rock Material. *45TH Us Rock Mechanics / Geomechanics Symposium Held In San Francisco*, Ca, Arma 11-246.

Sari, M. 2010. A Simple Approximation to Estimate The Hoek-Brown Parameter 'm_i' For Intact Rocks. Eurock, *Isrm International Symposium*, Volume: 1.

Shah, S. Hoek, E. "Simplex Reflection Analysis of Laboratory Strength Data." Can. Geotech. J., 29: 278-287. 1992.

Sheorey, P.R. 1997. "Empirical Rock Failure Criteria." *A.A.Balkema*, PP. 200.

Estimating Mechanical Properties from In-Situ Rebound Values of Some Nigerian Rocks

B. Adebayo
Department of Mining Engineering, Federal University of Technology, Akure

ABSTRACT This paper deals with the estimation of rock strength parameters using values of rebound hardness of in-situ intact rocks within South Western Nigeria basement complex. This was achieved by using L-Type hammer and the results of the rebound were obtained while holding the Schmidt hammer horizontally against the surface of the rock. The rebounds value of hardness recorded were subjected to three most accepted methods to make the data reliable. The uniaxial compressive strength and young modulus of elasticity were estimated from the equations proposed by different researchers. The result obtained showed that the compressive strength varied from 39.19 MPa to 49.38 MPa and 88.40 MPa to 101.60 MPa while the young modulus of elasticity varied from 17.55 GPa to 21.39 GPa. Strong correlation exists between uniaxial compressive strength and rebounds hardness value with multiple correlation coefficient of 0.9985.

Keywords: Schmidt hammer, rebounds, hardness, in-situ, rock

1 INTRODUCTION

The Schmidt hammer was originally designed in 1940s as an index for non-destructive testing of concrete compare to its surface rebound hardness Kahraman *et al*, (2002). The use of this instrument in rock mechanics practice was dated back to early 1960s. It has been increasingly used worldwide due to its simplicity, rapidity and portability. Also, taking the long history as well as wide spread use the standard methods of hammer rebound test by (ISRM, 1978; ASTM, 2001) might be expected to ensure consistent and reliable values for a given rock type. Aydin and Basu, (2005) in their work identified ways of reducing scatter values and thereby improving the reliability of the Schmidt hammer as a rock material characterization tool. Ayday and Goktan, (1992) found reliable correlations between L-type and N-type hammer rebounds values obtained during field testing.

Schmidt hammer models are designed at different levels of impact energy but type L and N are often use for determination of rock hardness. Type L – hammer has impact energy of 0.735 Nm while that of type N – hammer is 2.207 Nm. When the Schmidt hammer (Consist of spring-loaded piston) is pressed orthogonally against the rock surface, the piston is automatically released on to the plunger and the rebound height of the piston is considered to be an index of surface hardness (Basu and Aydin, 2004).

In the horizontal direction, energy released by the key spring is equal to the Kinetic energy of the piston with which it is released on to the plunger

$$0.5kx_1^2 = 0.5MV_1^2 \quad (1)$$

k = spring constant

x_1 = maximum stretch of the spring (when it is fully loaded)

V_1 = the velocity of the piston when it touches the plunger (while firing)

M = the mass of the piston

Similarly Basu and Adyin (2004) said that the kinetic energy of it piston at the instant of rebound starts must be equal to the energy of the key spring stretched by x_2 at maximum rebound position expressed by equation 2.

$$0.5MV_2^2 = 0.5\ k\ x_2^2 \quad (2)$$

V_2 = the initial rebound velocity of the piston

Combining Equations (1) and (2)

$$\frac{x_2}{x_1} = \frac{V_2}{V_1} \quad (3)$$

They also expressed the ratio of $\frac{x_2}{x_1}$ in percentage form called the rebound number given by equation (4)

$$R_h = \frac{x_2}{x_1} \times 100 \quad (4)$$

However, several methods of concluding Schmidt hammer test have been proposed, as described by Poole and Farmer (1978). Ayday and Goktan, (1993) statistically compared the three most accepted methods of (Hucka, 1965; Poole and Farmer, 1978; ISRM, 1981) and concluded that the ISRM method was different from other methods.

Some researchers proved that Schmidt hammer test is an important index test for rock material characterization. It was observed that during feasibility studies of mining project data on the rock properties are not readily available and the Schmidt hammer test is very cheap and quick to conduct. The objectives of this study therefore, are to estimate some rock properties from Schmidt hammer rebound values and used the data established to characterize the rock. Ultimately, this will serve as a preliminary data for investors in Solid Mineral as guide them in the selection of mine machinery as well as to be able to prepare functional feasibility studies.

1.2 Descriptions of the Study Area

The study area covers Oyo, Ogun, Osun Ondo and Ekiti State. All these states fall within the Precambrian of south western Nigeria, which is a part of Nigerian Basement Complex. Five groups of rocks could be identified in the basement complex (Rahaman, 1988). These rocks are: (i) migmatite gneiss-quartzite complex; (ii) slightly migmatised to unmigmatised meta-sediment; (iii) charnokite rocks; (iv) older granite and (v) unmetamorphosed dolerite dykes. The number of outcrops in this region varies from isolated boulders to large exfoliated domes and inserlberg. The location of the study areas are presented in Table1.

2 MATERIAL AND METHODS

2.1 Material

In-Situ hammer tests were performed on six different rock types; the test sites included operating quarries, abandoned quarries as well as natural outcrops within the South Western Nigeria Basement Complex. In addition, tests were carried out with L-type hammer having impact energy of 0.735 Nm. The tests were carried out with the hammer held horizontally against the surface of in-situ rock.

2.2 Methods

The three most accepted methods were selected among different Schmidt hammer rebound techniques and these methods are described below:

2.2.1 Test method 1

Hucka,(1965) Suggested that the peak value from ten continuous impacts at a point should be selected as presented in Table 2

2.2.2 Test method 2

ISRM, (1981) recommended that 20 rebounds values from single impacts separated by at a plunger diameter should be recorded and averaged the ten upper values as presented in Table 2.

2.2.3 Test method 3

Poole and Farmer, (1980) advised that the peak value from at least five continuous impacts at a point should be selected as presented in Table 2.

2.3 Estimating Some Rock Properties Using Mean Rebounds Values.

The uniaxial compressive strength and young Modulus of the rock samples were estimated from equation (5) and (6) proposed by Aydin and Basu, (2005) respectively and the results are presented in Table 3.

$$\sigma_{ucs} = 1.45 * e^{(0.07 \times RL)} \quad (5)$$

σ_{ucs} = estimated uniaxial compressive strength

R_L = Rebound Value of L-type hammer

$$E_t = 1.04 \times e^{0.06xRL} \quad (6)$$

Where E_t = the estimated young modulus. In addition, the limestone sample's uniaxal compressive strength and young modulus was determined from equation (7) and (8) proposed by Sachpazis, (1990).

$\sigma_{ucs} = 4.29. R_L - 67.52$ (7)

$E_t = 1.94*R_L - 33.93$ (8)

Decree and Millers, (1966) proposed equation 9 and 10 for estimation of uniaxial compressive strength these equations were used to obtained another set of values and the results are presented in Table 3

$\sigma_{ucs} = 4 (R - 25)$ (9)

For R up to 50

$\sigma_{ucs} = 20 (R - 45)$ - (10)

For R over 50

σ_{ucs} = Uniaxial Compressive strength in (MPa).

R = Hardness Rebound value

3. RESULTS AND DISCUSSION

Furthermore, the field test results of the of the rebound hardness values from six different locations are presented in Table 1. The rebounds values of hardness vary from 24 to 52, 20.6 to 50.4, 26 – 52 for test method 1, method 2 and methods 3 respectively. The sample from Ewekoro (limestone) has the least rebound value of hardness and the sample from Ikole-Ekiti (Granite) has the highest rebound value of hardness. The standard deviation of rebound values are 0.85, 1.73, 1.2 2.73 2.33 and 1.48 for samples IK0l, AW02, IB03, EW04, IG05 and OR06 respectively.

Table 1. Field Test of Rock Samples Using L- Type Hammer

Rock Code No.	Procedure Test 1	Procedure Test 2	Procedure Test 3	Standard Deviation
IK01	52.00	50.40	52.00	0.85
AW02	52.00	49.00	52.00	1.73
IB03	52.00	49.80	50.00	1.21
EW04	24.00	20.60	26.00	2.73
GA05	52.00	48.80	52.00	2.33
OR06	50.00	47.10	48.00	1.48

Table 2 presents the estimated strength parameter from equation proposed by different researchers. The Uniaxial compressive for strength and young modulus estimated from equation proposed by Aydin and Basu, (2005) ranges from 39.19 MPa to 49.38 MPa, 17.55 MPa to 21.39 MPa respectively. The uniaxial compressive strength obtained appear to be low for granite Moreso, the values of compressive strength determined from Deere and Millier, (1966) equations ranges from 88.40 MPa to 101.60 MPa these values are a bit reasonable but the equation can be used to compute rocks of low rebounds hardness values. Sachpazis, (1990) proposed equations were used to determined value of compressive strength and young modulus of elasticity for limestone of 20.85 MPa and 6.03 GPa respectively as presented in Table 2.

Table 2. Estimate of Some Mechanical Properties from In-situ Rebounds Value

Rock Code No.	Aydin and Basu,(2005)	Aydin and Basu,(2005)	Sachpazis, (1990)	Sachpazis, (1990)	Deere and Miller,(1966)	Mean Rebound Values from Test Procedure 2
	σ_{ucs} (MPa)	E_t (GPa)	σ_{ucs} (MPa)	E_t (GPa)	σ_{ucs} (MPa)	
IK01	49.38	21.39	-	-	101.60	50.40
AW02	44.77	19.67	-	-	96.00	49.00
IB03	47.34	20.63	-	-	99.20	49.80
EW04	-	-	20.85	6.03	-	20.60
GA05	44.14	19.43	-	-	95.20	48.80
OR06	39.19	17.55	-	-	88.40	47.10

Figure 1 presents the relationship between compressive strength, young modulus of elasticity and rebounds hardness values from test procedure 2, the results showed that strong linear relationship exist between the Compressive, young modulus and rebounds hardness values of test procedure 2 and these are expressed by Equation 11 and 12.

$\sigma_{ucs} = 3.076R_L - 105.82$ (11)

$E_t = 1.1597R_L - 37.113$ (12)

Where,

σ_{ucs} is the uniaxial Compressive Strength (MPa)

E_t is the young modulus of Elasticity (GPa)

R_L is the rebounds hardness value from test procedure 2

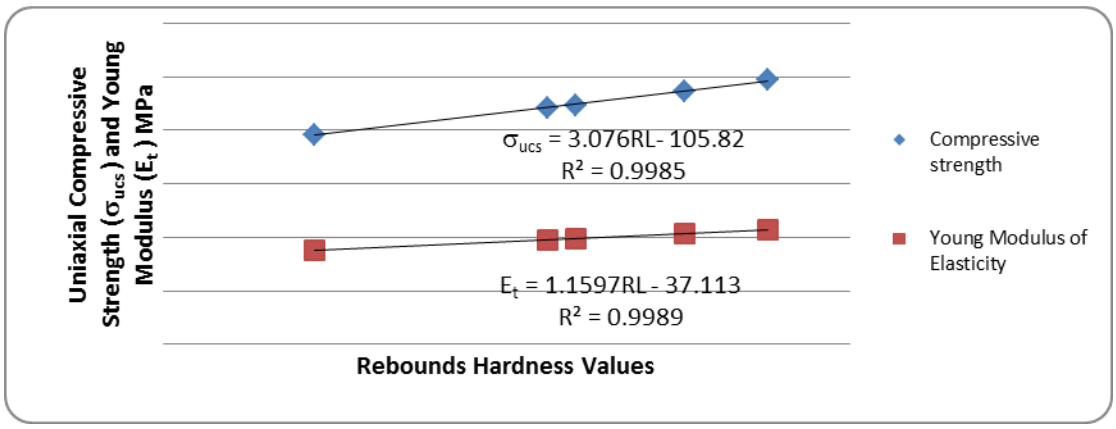

Figure 1. Compressive Strength and Young modulus of Elasticity against Rebounds Hardness Values from Test Procedure 2

4. CONCLUSION

This paper had investigated estimation of strength parameters from in-situ rebound hardness values. The result obtained showed that uniaxial compressive strength obtained from Aydin and Basu, (2005) proposed equations which ranges from 39.19 MPa to 49.38 MPa are lower than the values of strength obtained from Deere and Miller, (1966) proposed equation which ranges from 88.40 MPa –101.60 MPa. Ultimately, strong correlations exist between uniaxial compressive strength, young modulus of elasticity and rebounds hardness value from test procedure 2.

REFERENCES:

Ayday, C., and Goktan, R.M. (1992): Correlation between L and N – Type Hammer Rebound Values Obtained During Field – Testing, In: Hudson, J.A. Editor, International ISRM Symposium on Rock Characterization. Chester, pp. 47-50

Ayday, C., and Goktan, R.M. (1993): The Statistical Comparison of the Schmidt Hammer Recording Techniques, Bull Rock Mechanics (The Publication of the Turkish National Society of Rock Mechanics), 9: pp. 25 -35.

Adyin, A., and Basu, A. (2005): The Schmidt Hammer in Rock Material Characterization, Engineering Geology, 81, pp 1-14.

ASTM, (2001): Standard Test Method for Determination of Rock Hardness by Rebound Hammer, Designation D 5873.

Basu, A., and Aydin, A. (2004): A Method for Normalization of Schmidt Hammer Rebound Values, International Journal of Rock Mechanics and Mining Sciences, 41: pp. 1211-1214.

Deere, D.V., and Miller, R.P. (1966): Engineering Classification and Index Properties for Intact Rock, University of Illinois, U.S. Department of Commerce National, Technical Information Service.

Hucka, V.A. (1995): A Rapid Method Determining the Strength of Rocks In-situ, International Journal of Rock Mechanics and Mining Sciences, 2: pp. 127-134.

ISRM, (1978): Suggested Method for Determining Hardness and Abrasiveness of Rocks, International Journal of Mining Sciences Geomechanics Abstr., 15: pp. 89.

ISRM, (1981): Suggested Method, In: Brown E.T., Editor Rock Characterization Testing and Monitoring, Oxford Pergamon Press.

Kaharaman, S. (2001): Evaluation of Simple Methods for Assessing the Uniaxial Compressive Strength of Rock, International Journal of Rock Mechanics and Mining Sciences, 37: pp. 981-994.

Kaharaman, S., Ferner, M., and Gunaydin, O. (2002): Predicting the Schmidt Hammer Values of In-situ Intact Rock from Core Samples Values (Technical Note) , International Journal of Rock Mechanics and Mining Sciences, 37: pp. 395-399.

Poole, R.W., and Farmer, I.W. (1978): Geotechnical Factors Affecting Tunneling Machine Performance in Coal Measure Rocks, Tunnels Tunneling, Vol.10, pp. 27-30.

Poole, R.W., and Farmer, I.W. (1980): Consistency and Repeatability of Schmidt Hammer Rebound Data, During Field Testing, (Technical Note), International Journal of Rock Mechanics and Mining Sciences, 17: pp. 167-171.

Rahaman, M.A. (1988): Recent Advances in the study of the Basement Complex of Nigeria, In: Oluyide,P.O., Mbonu, W.C. Ogezi (editors) Precambian Geology of Nigeria, GSN Publications.

Sachpazis, C.I. (1990): Correlating Schmidt Hardness with Compressive Strength, and Young Modulus of Carbonate Rocks. Bull International Society Association, Engineering Geology, 42: pp 75-83.

Haulage Drift Stability Analysis- A Sensitivity Approach

W. Abdellah
University of Assiut, Assiut, Egypt

ABSTRACT Haulage drifts are the primary access to the mining blocks of an ore body in a multi-level mining system of a tabular ore deposit. Drift instability could lead to serious consequences such as injuries, production delays and higher operational cost. Rockmass properties are significant geotechnical design input parameters. These parameters are never known precisely and always uncertainties associated with them.

The stability of the haulage drift is examined through parametric study of a nonlinear, elastoplastic, two-dimensional finite element model representing typical mining layout most commonly adopted in Canadian underground metal mines. The parametric study examines the influence of footwall rockmass geomechanical properties (e.g., cohesion, friction angle, dilation angle and Young's Modulus) and the mining depth (e.g., horizontal-to-vertical stress ratio). Stability indicators are defined in terms of displacement, stress and the extent of yield zones, which adopt as a basis for assessing the effect of different parameter on the stability of haulage drift.

Keywords: Stability, haulage drift, rockmass properties

1 INTRODUCTION

Drifts are the arteries of mines, e.g. they are used to transport the blasted ore (valuable minerals) out of mining zone. Drift instability causes ground caving, thus can be a serious problem e.g. injuries, production delay and increase in operation costs. As the mine haulage drifts are the only access where loaders and/or trucks travel through, they must remain stable during their service life (Abdellah et al., 2013 and 2014, Wei et al., 2012, Zhang and Mitri, 2008).

Rockmass properties are significant geotechnical design input parameters. These parameters are never known precisely. There are always uncertainties associated with them. Some of these uncertainties are due to lack of knowledge, limited collected data, errors in testing and random data collection. Therefore, a one should use a tool, such as sensitivity analysis to tackle these inherent uncertainties associated with the rockmass properties.

1.1 Problem Definition

To evaluate the stability of mine haulage drift, A two-dimensional, elastoplastic, finite element model (Phase 2D) is created as shown in Figure 1. The study zone is divided into three zones; hanging wall, orebody and footwall. The orebody consists of massive sulphide rock (MASU). The hanging wall contains Metasediments (MTSD) and the footwall comprises of Norite rock (NR). Three stopes are modelled to simulate the ore extraction with respect to mining step. The haulage drift is driven in the footwall and its dimensions are 4.5 m by 4.5 m and at a distance of 15 m from the nearest orebody (e.g., stope 3).

The physical and geomechanical properties for the different rockmass units included in this study are presented in Table 1 (Abdellah et al., 2012).

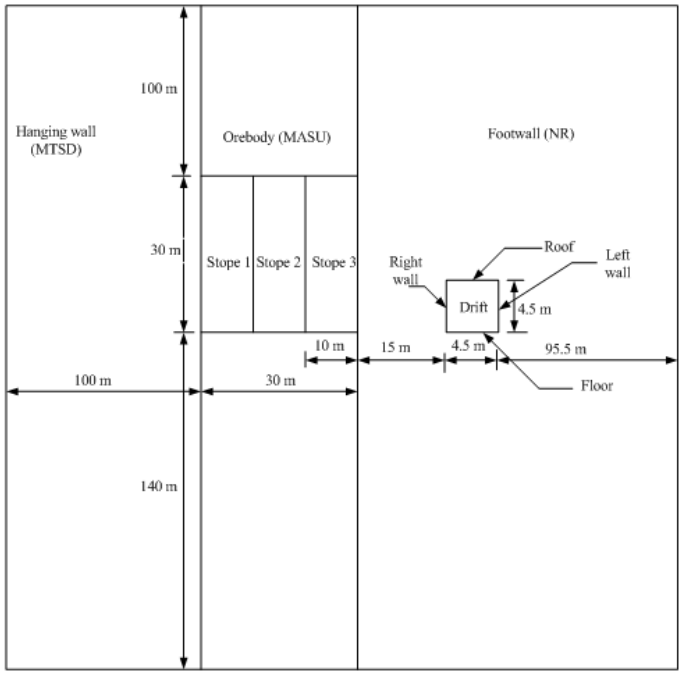

Figure 1. Model geometry and its dimensions

Table 1. Rockmass properties (Abdellah et al., 2012)

Rockmass Property	Hanging Wall	Orebody	Footwall	Backfill
Density, MN/m^3	0.027	0.030	0.029	0.023
E, GPa	40	10	24	2.5
Poisson's ratio, υ	0.18	0.22	0.15	0.35
Cohesion, C (MPa)	4.8	10.2	11.2	0.1
Tensile strength, τ (MPa)	1.52	1.80	0.99	0.075
Friction Angle, Φ (deg)	38	43	35	35
Dilation Angle, ψ (deg)	ϕ/4	ϕ/4	ϕ/4	0

1.2 Dealing with Uncertainty

As mentioned before, due to the heterogeneity of the rockmass, data from underground excavations are limited. Therefore, a great deal of uncertainty is inherent in the design of underground excavations. In order to develop a reliable design approach, one must use methods that incorporate the statistical variation of the numerical model input parameters representing the rockmass properties, i.e. mean, variance and standard deviation, as well as the design of rock failure criteria (Kwangho et al., 2005).

To quantify the uncertainty related to the model input parameters, three possible ways exist: deterministic analysis, sensitivity analysis, and simulation approach. This paper focuses on the parametric (sensitivity) analysis which will be discussed in the next section.

2 SENSITIVITY ANALYSIS

Numerical models are known to be deterministic by nature, i.e. a set of model input parameters will produce a unique set of results in terms of stress, deformation, and yield pattern. It is for this reason, model parametric study adopting sensitivity analyses is often carried out to allow for the better understanding of the problem, e.g. stability of mine openings, as a result of changing in some of critical model input parameters (e.g. Cohesion, Young's modulus, angle of internal friction, horizontal-to- vertical stress ratio) (Musunuri et al., 2009).

In a sensitivity analysis, a single parameter is systematically varied while all the other parameters are kept constant. The sensitivity analysis provides an understanding of the effect of each parameter on the overall behavior of the model. However, no distribution is obtained for the output parameters (random variables). It can be carried out by varying single parameter (random variable), at each run, based on specified coefficient of variation (COV) and monitoring the effect of this variation on the applied performance criterion. The variable, at each run, has one value of [(μ-σ), μ and (μ+σ)] while keeping all other parameters is constant (no change in their average values).

Five footwall rockmass parameters namely: cohesion, friction angle, dilation angle, Young's Modulus and horizontal-to-vertical stress ratio are varied to evaluate their effects on the stability of haulage drift with respect to mining step, as listed in Table 2.

Table 2. Footwall model input parameters at each run

Run / parameter	k	C, MPa	E, GPa	ϕ, degree	ψ, degree
Run 1	1.65	11.2	24	35	7.5
Run 2	1.98	11.2	24	35	7.5
Run 3	1.32	11.2	24	35	7.5
Run 4	1.65	13.44	24	35	7.5
Run 5	1.65	8.96	24	35	7.5
Run 6	1.65	11.2	28.8	35	7.5
Run 7	1.65	11.2	20.8	35	7.5
Run 8	1.65	11.2	24	42	7.5
Run 9	1.65	11.2	24	28	7.5
Run 10	1.65	11.2	24	35	10.5
Run 11	1.65	11.2	24	35	7

3 DRIFT STABILITY EVALUATION CRITERION

In the following section, three evaluation criteria are described, which are used as a basis for the interpretation of numerical model results for the assessment of the stability of the mine haulage drift with respect to mining step.

3.1 Extent Of Yield Zone

Yielding is the most common criterion used in numerical modelling when elastoplastic model is employed. This condition occurs when the stress state reaches the surface of the yield function, which is when the rock is loaded beyond its elastic limit. In this study, Mohr-Coulomb yield function is adopted as a measure for "drift satisfactory or /and unsatisfactory performance".

3.2 Displacement/Convergence Criteria

Displacement/convergence criteria depend on the stiffness of the rockmass properties and the purpose of underground opening. In the following, three displacement-based criteria are introduced.

3.2.1 Wall convergence ratio (WCR)

WCR is defined as the ratio of the total magnitude of the wall closure to the span of the initial drift as shown in Equation (1):

$$WCR = \left(\frac{W_0 - W_d}{W_0}\right) \times 100 \quad (1)$$

Where: W_0 is the original span of the drift and W_d: is the span of the drift after deformation.

3.2.2 Roof sag ratio (RSR)

RSR is defined as the ratio of the roof sag (ΔS) to the span of the drift as given in Equation (2):

$$RSR = \left(\frac{\Delta S}{W_0}\right) \times 100 \quad (2)$$

3.2.3 Floor heave ratio (FHR)

FHR is defined as the ratio of the floor heave (Δh) to the span of the drift, Equation (3):

$$FHR = \left(\frac{\Delta h}{W_0}\right) \times 100 \quad (3)$$

3.3 Mining-Induced Major Principal Stress (σ_1)

It defines the location of high stresses areas due to mining activity.

4 RESULT AND DISCUSSION

In the following section, the effect of each varied parameter will be demonstrated to show its effect on the stability of mine haulage drift based on the previous stability indicators.

4.1 Effect Of The Horizontal-To-Vertical Stress Ratio "K" On The Evaluation Criteria

The ratio, k, is defined as the average horizontal stress σ_h to the vertical stress σ_v as given in Equation (4):

$$K = \frac{\sigma_h}{\sigma_v} \quad (4)$$

The effect of "K" on the stability indicators is discussed below.

4.1.1 Effect of "K" on the stress

In the Canadian Shield, k varies nonlinearly with the depth. At shallow depth, k tends to be larger than it is in deeper mines. As shown in Figure 2, the increase of "K" (e.g., increase horizontal stress due to increase in depth) results in increase of major induced-mining principal stress at drift roof and floor. On the other hand decrease in the major induced-mining stress at the drift walls.

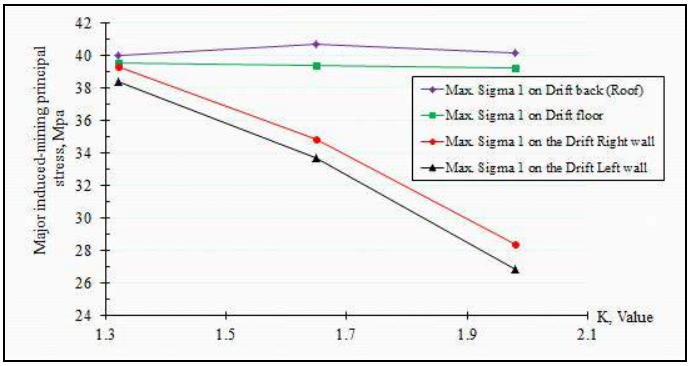

Figure. 2. K- value versus Major induced-mining principal stress.

4.1.2 Effect of "K" on the displacement

Displacement convergence criteria are generally site specific; they depend not only on the rock mass stiffness characteristics but also on the intended use of the underground opening as well as the design and code requirements. As illustrated in Figure 3, the increase of "K" value results in increase in the displacement/convergence criteria around mine haulage drift. The more effect occurs in the roof of the drift (e.g., shown by increase of the roof sag ratio "RSR") followed by right wall of the drift. The less effect appears in the drift left wall.

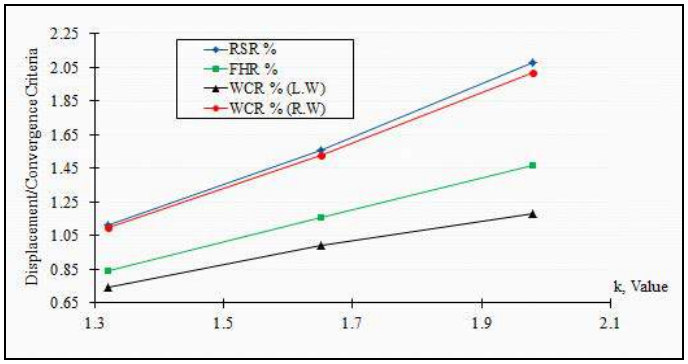

Figure. 3. K- value versus displacement/convergence criteria.

4.1.3 Effect of "K" on the extent of yielding zones

Yielding criterion is widely used in numerical modeling when elastoplastic model is adopted. Thus yielding may be considered as an important factor contributing to instability. As shown in Figure 4 below, the extent of yield zones increases as "K" increases. It can also be seen that the yielding zone extends around haulage drift as mining progresses. The maximum length of the yielding zone exceeds 15m in the left sidewall (LW) of haulage drift.

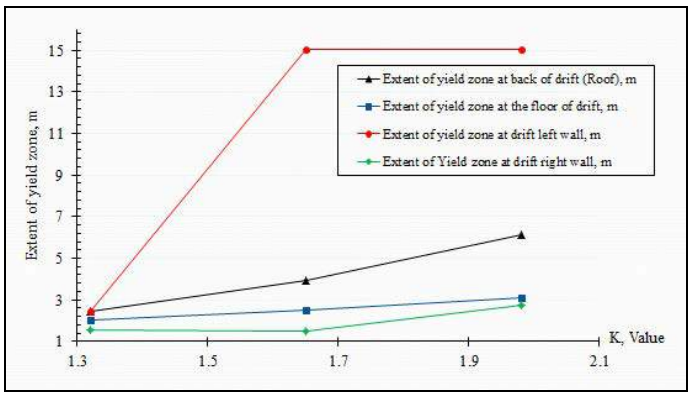

Figure. 4. K- value versus extent of yielding zones.

The development of yield zones with modelling mining steps based on Mohr-Coulomb criterion and average "K-value" of 1.65 is shown in Figure 5(a-d). It is obvious that the yielding zones increases as mining advances.

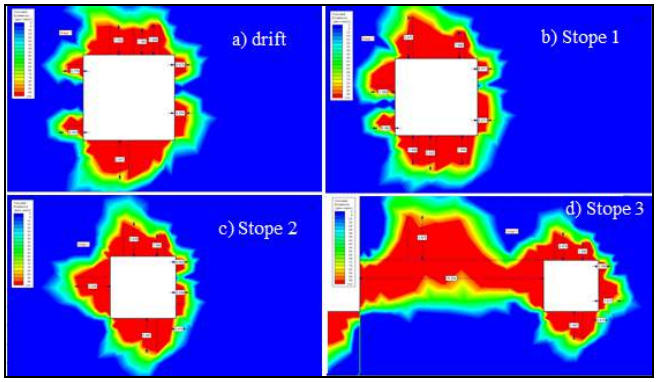

Figure 5. Development of yield zones with modelling mining steps at average "K-value" of 1.65.

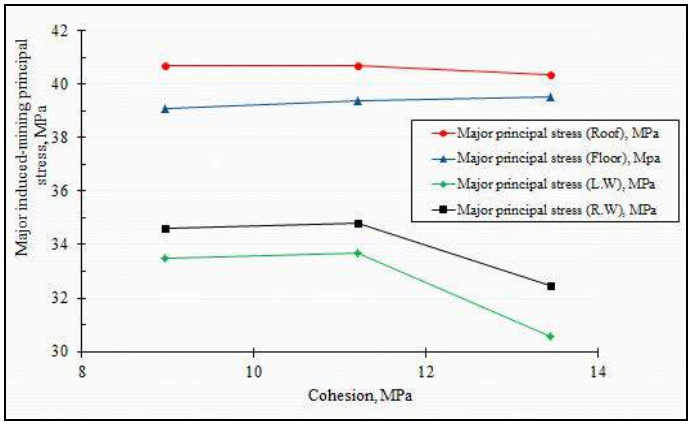

Figure 6. Cohesion versus major induced-mining principal stress

4.2 Effect Of Cohesion

Cohesion is a measure of internal bonding of the rock material. For example, if a shear force is applied to a cube of muddy soil or rock at zero normal pressure, the resulting shear deformation is accompanied by a measurable resistance. The resistance force per unit area is termed cohesion.

4.2.1 Effect of cohesion on the stress

In natural soils, cohesion results from electrostatic bonds between clay and silt particles. Thus, soils devoid of clay or silt are not cohesive except for capillary forces arising when little water forms bridges between sand grains, resulting in negative pore pressure (suction). In contrast, rocks normally exhibit much greater cohesion, thousands of times larger than soils. Figure 6 generally depicts that, as cohesion of rockmass increases the major induced-mining stress decreases. The most decrease occurs in the sidewalls of the haulage drift (e.g., left wall (LW) and right wall (RW)).

4.2.2 Effect of cohesion on the displacement/convergence criteria

Increase of cohesion results in decrease in the displacement (e.g., deformation) as shown in Figure 7.

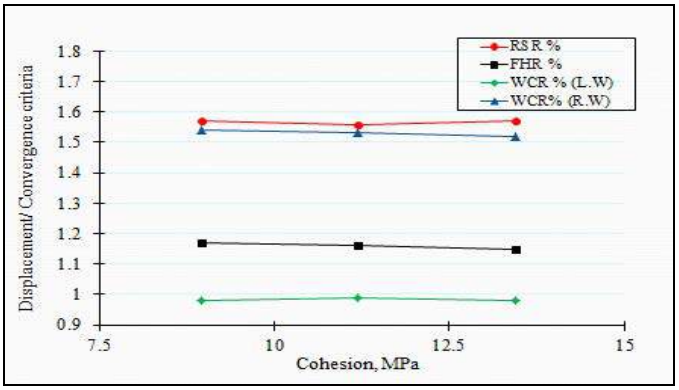

Figure 7. Cohesion versus displacement/convergence criteria.

4.2.3 Effect of cohesion on the extent of yielding zone

Figure 8 shows that, as cohesion increases, the yielding zones decreases.

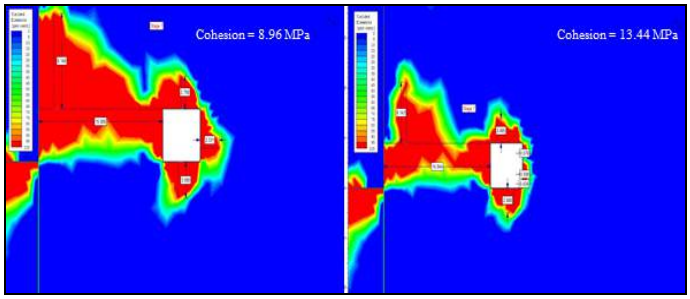

Figure 8. Extents of yield zones around haulage drift at two different cohesion values (final mining step).

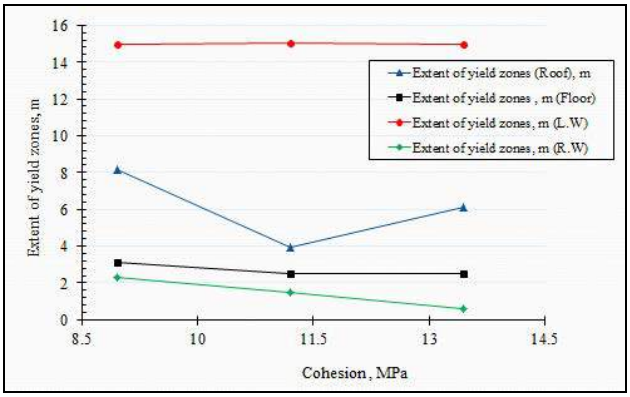

Figure 9. Cohesion versus extent of yielding zones

As shown in Figure 9 above, the increase in cohesion results in reduction in the extent of yielding or failure zones.

4.3 Effect of Young's Modulus

Young's Modulus is modulus of elasticity measuring of the stiffness of a rock material. It is defined as the ratio, for small strains, of the rate of change of stress with strain. This can be experimentally determined from the slope of a stress-strain curve obtained during compression or tensile tests conducted on a rock sample. Similar to strength, Young's Modulus of rock materials varies widely with rock type. For extremely hard and strong rocks, Young's Modulus can be as high as 100 GPa. There is some correlation between compressive strength and Young's Modulus.

4.3.1 Effect of stiffness on the stress

The increase of Young's Modulus (E) means increase the stiffness of the rockmass. The induced-mining principal stress decreases as stiffness increases, as shown in Figure 10. It can be seen that, the biggest drop in the major induced mining stress occurs in the drift left wall (LW), while the smallest decrease occurs in the drift back (roof).

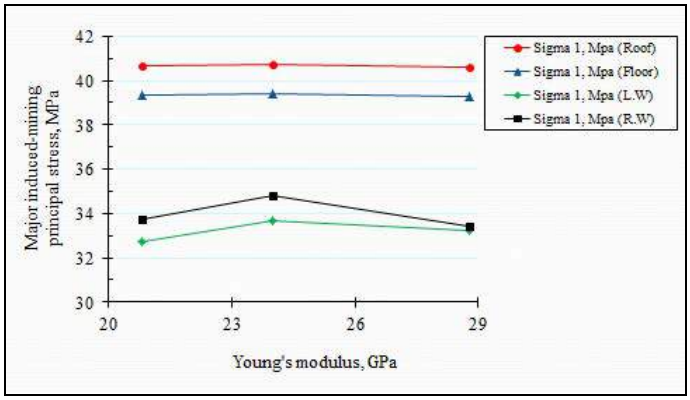

Figure 10. Young's Modulus versus major induced-mining principal stress.

4.3.2 Effect of stiffness on the displacement/convergence criteria

Figure 11 shows that, as stiffness (e.g., Young's Modulus) increases the displacement/convergence of haulage drift due to mining activity reduces. Thus means more stable condition.

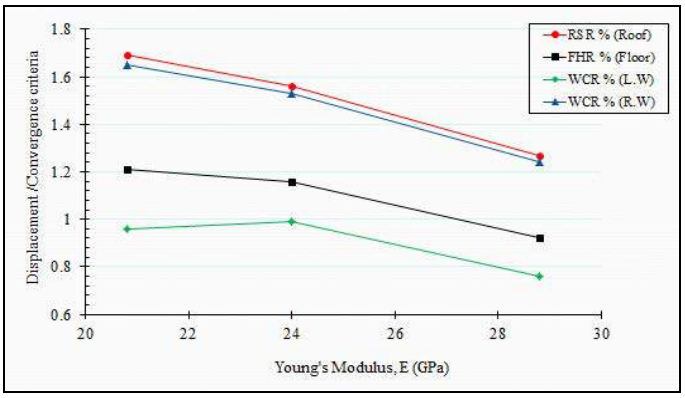

Figure 11.Young's Modulus versus displacement/convergence criteria.

4.3.3 Effect of stiffness on the extent of yielding zones

Figures 12 and 13 illustrate the decrease of the yielding zone extension as stiffness increases. The maximum decrease in the extension of yielding zones happens in the drift sidewalls.

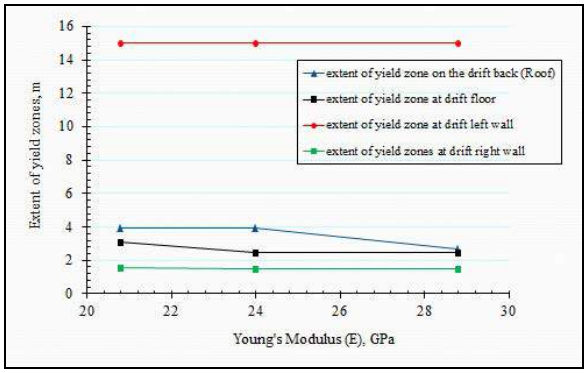

Figure 12. Young's Modulus versus extent of yielding zones.

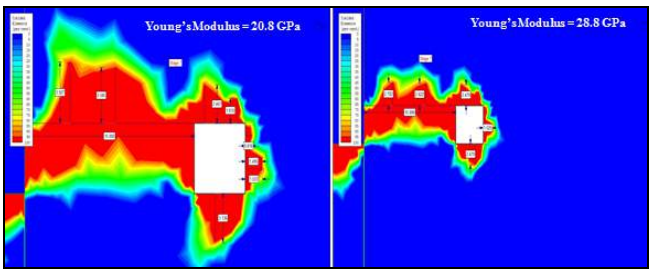

Figure 13. Extents of yield zones around haulage drift at two different stiffness values (final mining step).

4.4 Effect of Friction Angle

Internal friction is caused by contact between particles, and is defined by the internal friction angle; φ. Different rocks have different friction angles.

4.4.1 Effect of friction angle on the stress

As depicted in Figure 14 below, the increase of friction angle of rockmass results in the decrease of major induced-mining principal stress except for the floor of the drift.

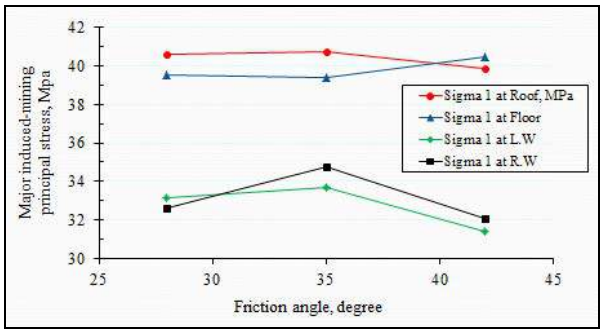

Figure 14. Friction angle versus major induced-mining principal stress

4.4.2 Effect of friction angle on the displacement/convergence criteria

Figure 15 shows that, displacement/ convergence decreases as friction angle increases.

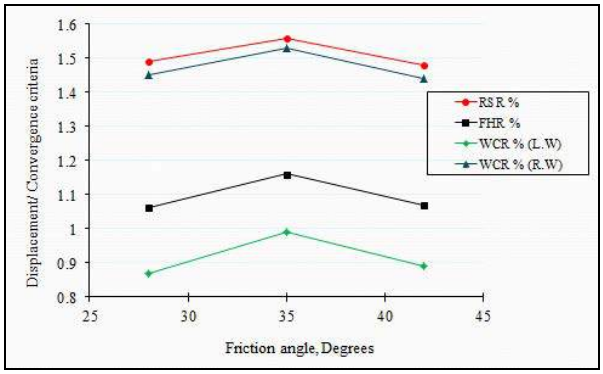

Figure 15. Friction angle versus displacement/convergence criteria.

4.4.3 Effect of friction angle on the extent of yielding zones

As shown in Figures 16 and 17, increase of friction angle produces decrease in the extent of yielding zones around haulage drift.

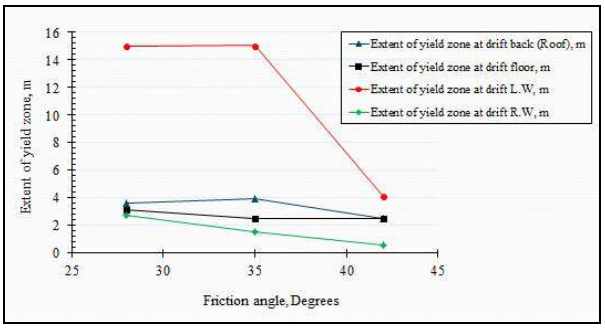

Figure 16. Friction angle versus extent of yielding zones.

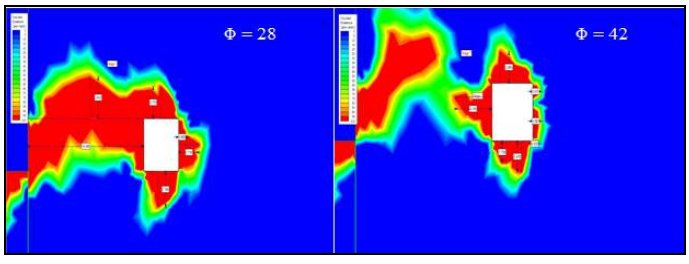

Figure 17. Extents of yield zones around haulage drift at two different friction angle values (final mining step).

4.5 Effect Of Dilation Angle

Dilation angle is one of the parameters that are not easily obtained for elastoplastic simulation of rock materials. The following section presents discussion of the sensitivity of results to the dilation angle and how this may affect the stability of haulage drift in terms of stress distribution pattern, displacements in the rockmass, and extent of yield zone.

4.5.1 Effect of dilation angle on the stress

The dilation angle has practically no effect on the stress distribution pattern and overall magnitude at locations sufficiently far from the drift, i.e. outside the stress relaxation zone. But, it affects the final magnitude of the principal stress inside the stress relaxation zone. Figure 18 illustrates that, major induced-mining principal stress decreases with the increase of dilation angle.

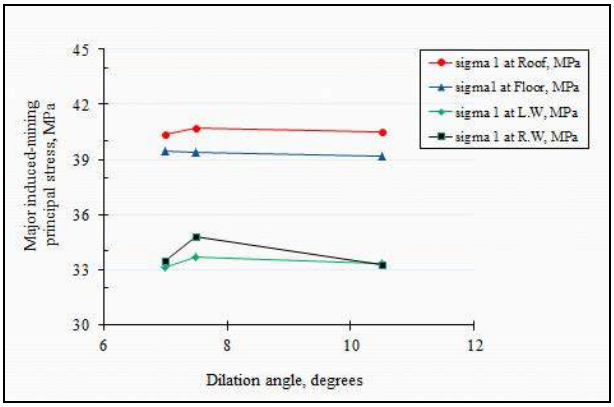

Figure 18. Dilation angle versus major induced-mining principal stress

4.5.2 Effect of dilation angle on the displacement/convergence criteria

The dilation angle is directly increases when friction angle increases (e.g., dilation angle equals one-fourth friction angle ($\Psi = \phi/4$). Thus produces the same effect on the displacement/convergence as the friction angle. Figure 19 shows the effect of dilation angle on the displacement/convergence criteria. As shown, the increase of dilation angle produces decrease in displacement.

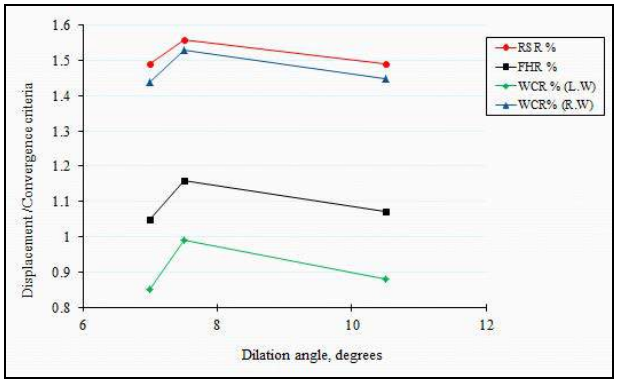

Figure 19. Dilation angle versus displacement/convergence criteria.

4.5.3 Effect of dilation angle on the extent of yielding zones

Dilation angle affects the final yield zones inside the stress relaxation zone. As the dilation increases, the final yield zone decreases. Figure 20 shows the decrease of the length of yielding zones as dilation angle increases.

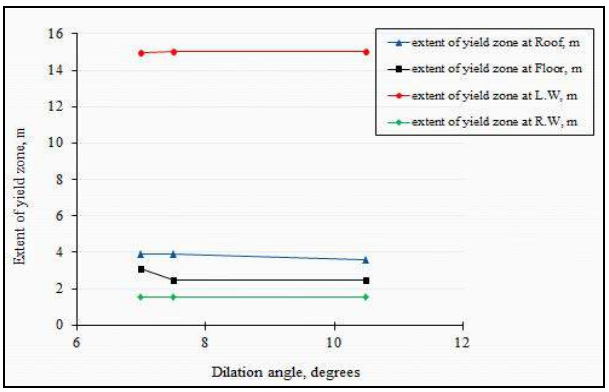

Figure 20. Dilation angle versus extent of yielding zones

5 CONCLUSION

This paper presents a sensitivity analysis to evaluate the stability of a mine haulage drift due to the heterogeneity associated with rockmass geotechnical input parameters. In this method, a single parameter is systematically varied, based on coefficient of variation, while all the other parameters are kept constant. Thus provides better understanding of the effect of each parameter on the overall behavior of the model. The stability of the haulage drift is examined through parametric study of a

nonlinear, elastoplastic, two-dimensional finite element model representing typical mining layout most commonly adopted in Canadian underground metal mines. Stability indicators are defined in terms of displacement, stress and the extent of yield zones, which adopt as a basis for assessing the effect of different parameter on the stability of the haulage drift. Five parameters have been used in this study to check their effect on the stability of haulage drift are: horizontal-to- vertical stress ratio (K), cohesion (C), Young's modulus (E), friction angle and dilation angle (ψ).

6 RECOMMENDATIONS

There are other parameters are not included in this study, e.g. mining depth, distance between haulage drift and stopes and mining sequences. Three-dimensional modelling is required to simulate the real geometry of the case study. Once the model is constructed, in-situ stress measurements should be used to calibrate the numerical model. Rock failure criteria such as Mohr-Coulomb must be calibrated based on underground measurements such as deformations (Multi-Point Borehole Extensometer or MPBX) and rockbolt loads. Although sensitivity gives good understanding of the effect of certain parameter on the overall behaviour of the model, there is not distribution or probability of failure obtained. Therefore, probabilistic analysis should be invoked to study the probability of unsatisfactory performance of the haulage drift.

REFERENCES

Abdellah, W., Mitri, H. S., Thibodeau, D. and Moreau-Verlaan, L., (2014). "Geotechnical Risk Assessment of Mine Development Intersections with respect to Mining Sequence" *Journal of Geotechnical and Geological Engineering* (JGGE). Received: 13 August 2013/Accepted: 6 March, 2014© Springer International Publishing Switzerland 2014.

Abdellah, W., Raju, D., Mitri, H. S., and Thibodeau, D. (2013). "Stability of underground mine development intersections during the life of a mine plan". *International Journal of Rock Mechanics and Mining Sciences (IJRMMS*) (Accepted -In press).

Abdellah, W., Mitri, H. S., Thibodeau, D., and Moreau-Verlaan, L. (2012). Stochastic evaluation of haulage drift unsatisfactory performance using random Monte-Carlo simulation, *Int. J. Mining and Mineral Engineering.* Vol.4 No.1.2012 pp. 63-87.

Kwangho Y., Yeonjun P., and JUN L. S. (2005), "Risk analysis for determination of a tunnel support pattern", *Tunnelling and Underground Space Technology 20* (2005) 479-486.

Musunuri, A., Wei, W., Mitri, H.S., and Thibodeau, D. 2009. Assessment of drift stability using probability of failure. *In Proceeding of Eighteenth International Symposium on Mine Planning and Equipment Selection*, Singhal, R.K., Mehrotra, A., Fytas K., and Hao G eds Banff, AB, 16-18 November, pp. 987-996.

Wei, W., Mitri, H. S., and Kelly, C. 2012. Evaluating Immediate Mining Induced Ground Movement the Performance of the Primary Support System. *In Proceedings of 21st Canadian Rock Mechanics Symposium*, RockEng12, Edmonton, AB, Canada, Editor Chris Hawkes, Associate Editors, Derek Kinakin, Sam Proskin, Denis Thibodeau, 5-9 May, pp. 61-70.

Zhang, Y., and Mitri, H. S., (2008), "Elastoplastic stability analysis of mine haulage drift in the vicinity of mined stopes", *International Journal of Rock Mechanics and Mining Sciences*, 45 (2008) 574-593.

Geodynamic Zoning for Isolation of Radioactive Waste

V. Tatarinov, V. Morozov, I. Kolesnikov, A. Kagan, T. Tatarinova
Geophysical Center of the Russian Academy of Sciences. Molodezhnaya St. 3, 119296 Moscow, Russia.

ABSTRACT The problem of the selection of the site for underground isolation of radioactive waste is acute for all countries using nuclear power. The paper presents the results of modeling the stress-deformation state of Nizhnekanskiy granitite massif. Shown is the possibility of using such simulations for the geodynamic zoning of areas. The most probable directions of groundwater filtration, which is one of the main threats to the nuclear waste repository, are present.

Keywords: Geodynamic zone, radioactive waste, granite, groundwater filtration

1. INTRODUCTION

Development of nuclear power in Russia is impossible without the resolution of the problem of burial high-level radioactive waste (HLRW) in deep geological formations. The selection of the sites for the environmentally safe underground isolation of high-level radioactive solidified waste remains a major problem for states that use nuclear energy, like Russia.

Methodologically, the choice of site for HLRW disposal is based on the finding in the relatively stable areas of the least disturbed structurally tectonic blocks (STB), which have maximum size [1, 2].

Expert assessments of the current "quality" of the site where the HLRW repository will be built, do not answer the fundamental question: how tectonics will effect of the rock mass safety for 100 thousand years and more, until there will be an environmental hazard of radionuclide. The greatest threat is the formation of new faults or intensifies existing tectonic faults and infiltration of surface water and groundwater to containers with high-level radioactive waste, followed by removal of the radionuclide in the human environment. The basic principle of ensuring safe disposal of nuclear waste is to prevent the formation of zones of dangerous concentrations of stress at the design phase spent nuclear fuel (SNF) repository on the basis of geodynamic zoning. Prediction of the evolution of the stress-deformation state (SDS) of the geological environment is very important.

The main purpose of this paper show the most likely scenario of the development of a tectonic process in Niznekansky granitoid massif. The scenario was generated on the basis of analyses of the structural-tectonic model and the calculation of stress-deformation state of the local. The simulation of the most probable direction of groundwater filtration under the influence of tectonic stress are present too.

2. RESULT AND RESEARCHES

Niznekansky granitoid massif (NKM) is located in a few kilometers to the north-east of Krasnoyarsk. According to geological and geophysical, structural, and geomorphologic studies in the western part of the massif, and partly in the surrounding rocks, three sites for HLRW disposal were pre-selected: «Kamenniy», «Itatskiy» and «Eniseiskiy» [3].

Analysis of geological data displayed [3] that SDS of the massif is determined mainly the compressive forces oriented in the south-west — north-easterly direction. It is used an elastic model of generalized plane stress to simulate the stress-deformation state. As a method of calculation it is used finite element method in the form of movements based on isoperimetric quadrilateral finite elements.

Empowering different finite element the different mechanical properties one can generate a heterogeneous finite element model, which reflects the real properties of rock massif. Fig. 1 displays a structural model of NKM to simulate the distribution of stress fields by finite element method.

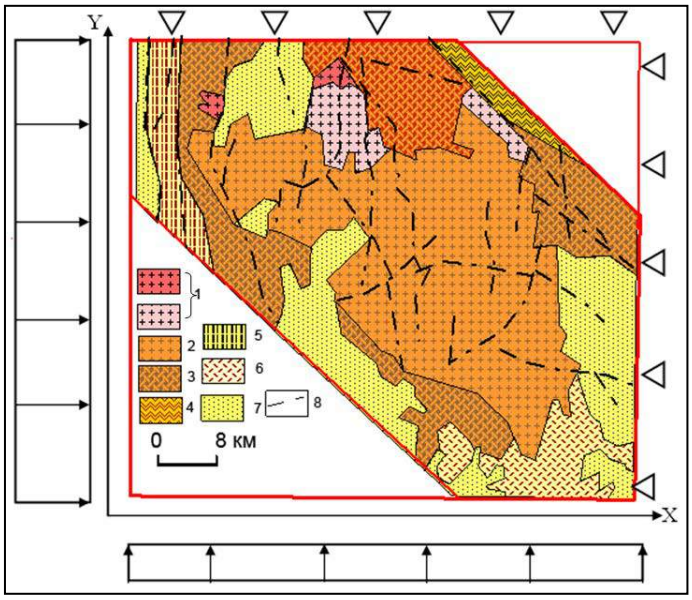

Figure 1. Structural model for simulate the distribution of stress fields by FEM. 1, 2 - contour of NKM granitiods differ in their elastic-strength properties, 3 - gneiss complex (AR); 4 - mylonite areas, 5 - amphibolite, quartzite and marble (AR-PR); 6 terrigenous-volcanic deposits (PZ_2); 7 - terrigenous deposits (J); 8 - main faults

In the model adopted the following values of the projections on the *X* and *Y* axis of the tectonic stresses: sub latitudinal N_x = 30 MPa and submeredian N_y = 10 MPa. These values are close to the stresses in the undisturbed rocks measured in the underground workings [4] at depths of up to 400 m. Detailed program of the stress calculation is presented in [5].

It is used the stress intensity σ_i for analyses the results of simulation, because σ_i is a generalized criterion of the level of SDS. Fig. 2 and Fig. 3 display the contour map of stress intensity and 3-D model of stress intensity respectively in the local area NKM.

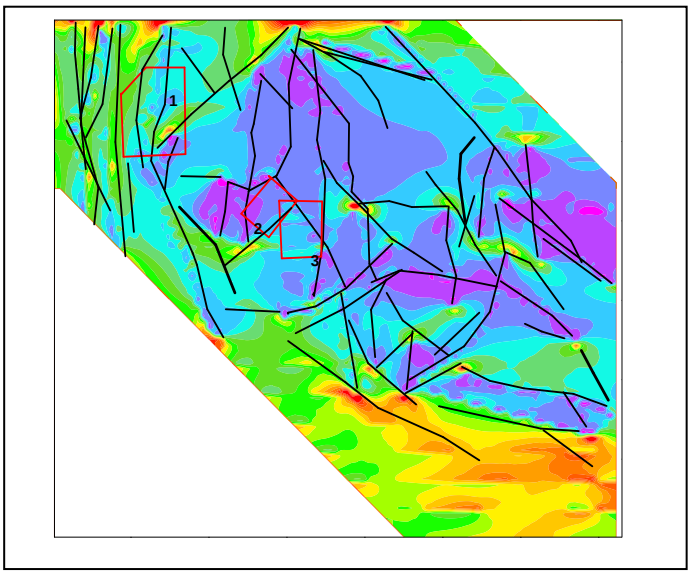

Figure 2. Distribution of stress intensity in the NKM according to calculations by finite element method. Lines indicate faults. The rectangles marked areas of detailed studies: 1– «Eniseiskiy», 2 - «Itatskiy», 3 – «Kamenniy».

The high-level differentiation of the stress intensity σ_i within the model NKM make possible for the selection of potentially dangerous areas (not suitable for isolation of HLRW). 3-D model is the basis for virtually geodynamic zoning in the purpose of the selection of the areas for the geoenvironmental secure underground isolation of HLRW in geological formations.

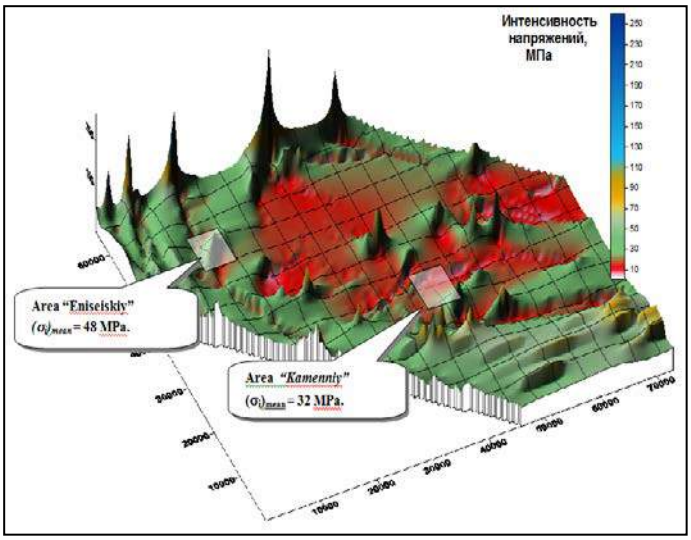

Figure 3. 3D model of the distribution of stress intensity in the NKM

We can confidently assert that the zones of concentration of stress intensity are possible sources of large-scale destruction

of the geological environment under the action of tectonic stress fields.

One of the major threats for the reliability of HLRW repository is the penetration of ground water to the containers [5, 6].

Filtration through an environment is described by Darcy's law:

$$Q = \omega K \frac{dy}{dx},$$

where Q – the flow discharge;

ω – cross section flow area;

$\frac{dy}{dx}$ – pressure gradient of flow;

K – coefficient of filtration.

Just Darcy's law can be written as:

$$V_x = -\frac{k}{\mu}\frac{\partial P}{\partial x},$$

where V – value of the filtration rate through a porous environment;

k – permeability of the medium;

μ – dynamic viscosity of fluid;

P – pressure.

The dimension Coefficient k is a velocity and it depends on the geometry of the porous space (such as the type of environment and the characteristics of pores), as well as it depends on the specific gravity and liquid viscosity. It is constant for a given liquid, if the porous environment is incompressible and isotropic.

For an isotropic environment as for an environment which has the same constant in all directions one can get:

$$V_x = -\frac{k_0}{\mu}\frac{\partial P}{\partial x}, \qquad V_y = -\frac{k_0}{\mu}\frac{\partial P}{\partial y}, \qquad V_z = -\frac{k_0}{\mu}\frac{\partial P}{\partial z};$$

or

$$V = -\frac{k_0}{\mu}\nabla(P) \qquad (1)$$

where V – velocity vector of the filtration.

Applying the divergence operation to the previous equation and using the equation

$$\nabla \cdot V = \frac{\partial V_x}{\partial x} + \frac{\partial V_y}{\partial y} + \frac{\partial V_z}{\partial z} = 0,$$

yield:

$$-\frac{k_0}{\mu}\nabla^2(P) = 0.$$

Thus, filtration through the isotropic environment can be reduced to solving the Laplace equation with appropriate boundary conditions. If the distribution P is known, then the filtration rate can be obtained from Darcy's law in the form (1).

In many cases, the porous environment is anisotropic and the permeability depends on the direction of flow. In this case, the components of the filtration velocity can be written as:

$$V_x = \frac{k_x}{\mu}\frac{\partial P}{\partial x};$$

$$V_y = \frac{k_y}{\mu}\frac{\partial P}{\partial y};$$

$$V_z = \frac{k_z}{\mu}\frac{\partial P}{\partial z}.$$

Turning to the vector form and calculating the divergence, we obtain:

$$\nabla \cdot V = -\frac{k_{0x}}{\mu}\frac{\partial^2 P}{\partial x^2} - \frac{k_{0y}}{\mu}\frac{\partial^2 P}{\partial y^2} - \frac{k_{0z}}{\mu}\frac{\partial^2 P}{\partial z^2}.$$

The previous equation can be written in next form:

$$\frac{\partial^2 P}{\partial x^2} + \frac{\partial^2 P}{\partial y^2} + \frac{\partial^2 P}{\partial z^2} = 0.$$

Thus, we have the Laplace equation again. Consequently, the true physical meaning can be represented as a fictitious isotropic in the transformed coordinates.

Communication between the components of the deformation and the displacement in a plane medium has the form:

$$\varepsilon = \begin{bmatrix} \varepsilon_x \\ \varepsilon_y \\ \varepsilon_{xy} \end{bmatrix} = \begin{bmatrix} \frac{\partial U}{\partial x} \\ \frac{\partial V}{\partial y} \\ \frac{\partial U}{\partial x} + \frac{\partial V}{\partial y} \end{bmatrix}.$$

In accordance with Darcy's law, we proceed from the assumption that the filtration velocity in the gradient field tectonic stress is proportional to the gradient of the effective stress:

$$\vec{V}_f = \begin{bmatrix} \vec{V}_x \\ \vec{V}_y \end{bmatrix} \sim \begin{bmatrix} \nabla\left(kE \dfrac{\partial U}{\partial x} \right) \\ \nabla\left(kE \dfrac{\partial V}{\partial y} \right) \end{bmatrix}$$

or

$$\vec{V}_f = \begin{bmatrix} \vec{V}_x \\ \vec{V}_y \end{bmatrix} \sim \begin{bmatrix} kE\nabla^2 U \\ kE\nabla^2 V \end{bmatrix}$$

assumption a constant filtration coefficient.

Filtration velocity, expressed in terms of stress components, in a plane-stressed state:

$$\vec{V}_f = \vec{V}_x + \vec{V}_y \sim kE\left(\sigma_{xx} + \sigma_{yy}\right)$$

If the rock massif has the anisotropic permeability $\left(k_x \neq k_y\right)$

$$\vec{V}_f = \vec{V}_x + \vec{V}_y \sim E\left(k_x\sigma_{xx} + k_y\sigma_{yy}\right).$$

Then, using these equations, it is possible to calculate and predict the development of hydrogeological conditions in the area of hypothetically construction of nuclear waste repository at the change of SDS rock mass as a result of the predicted tectonic destruction of the rock mass.

The level of the stress state of the rock massif in the local zones determined the value of stress intensity. Transfer to the stress intensity allows one to generate the model of liquid filtration independent on that particular system of coordinates. Based on the assumption that the filtration rate is determined by this integral assessment of the level of working stress in the volume element of rock massif, we have:

$$\vec{V}_f \sim \operatorname{grad}\left(\sigma_i\right). \qquad (*)$$

This simplifies the calculations of the first approximation, since the problem of estimating the stress state and filtration are solved separately. If we knew (from experimental data) the rate of change of tectonic stress in space and time, then the expression (*) reduces to:

$$\vec{V}_f(t) \sim kE\nabla\left(\frac{\partial \sigma_i}{\partial t}\right).$$

In this case, the filtration rate as a function of space and time $V(x,y,t)$, makes it possible to count water inflows in the weakened zones of tectonic fractures as a basis for further calculations of the migration rate and the predicted migration of radionuclide in the mass transfer process. In fact, the possibility of separate solutions of the elastic problem and the filtration process under the influence of local gradients of tectonic stress (i.e., without taking into account the deformation of the pore skeleton of rocks) greatly simplifies the algorithm for calculating of the possible direction of filtration flows.

Algorithm for calculating the stress gradient is introduced into the program of calculation of SDS of the massif. Figure 4 displays the result of calculation of the gradients vectors $\vec{G} \sim \left\langle \operatorname{grad}\frac{\sigma_i}{2} \right\rangle$.

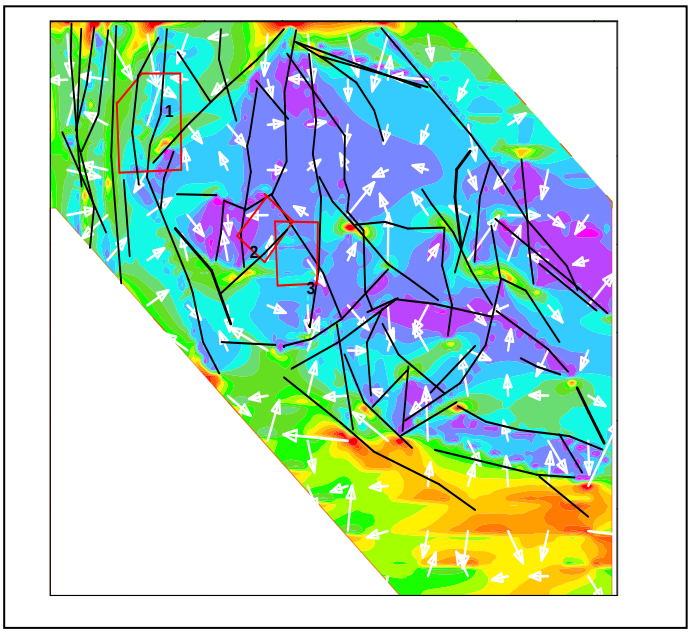

Figure 4. Vectors of filtration velocity in NKM

At the present time, area «Eniseiskiy» is the most promising in terms of creating a repository for HLRW. On this basis, we simulated the stress-deformation state of rock massif within the area «Eniseiskiy». The boundary conditions for this simulation were taken from the model for NKM.

Figure 5 displays the vectors of filtration velocity for «Eniseiskiy» area. Vectors indicate the most probable direction of groundwater filtration under the action of the tectonic stress.

Fig. 6 displays the distribution of the shear stress for area «Eniseiskiy». The

areas with maximum level of shear stress are potentially dangerous from the position of the formation of tectonic movements, i.e. formation of tectonic faults containing the shear component.

On this basis, we have identified the two most probable directions of the development of new active geodynamic zones affecting of «Eniseiskiy» area. They are displayed in Fig. 7 by dotted black lines. These are new the most probable faults in the area of «Eniseiskiy». They should be considered when assessing the environmental safety of HLRW repository.

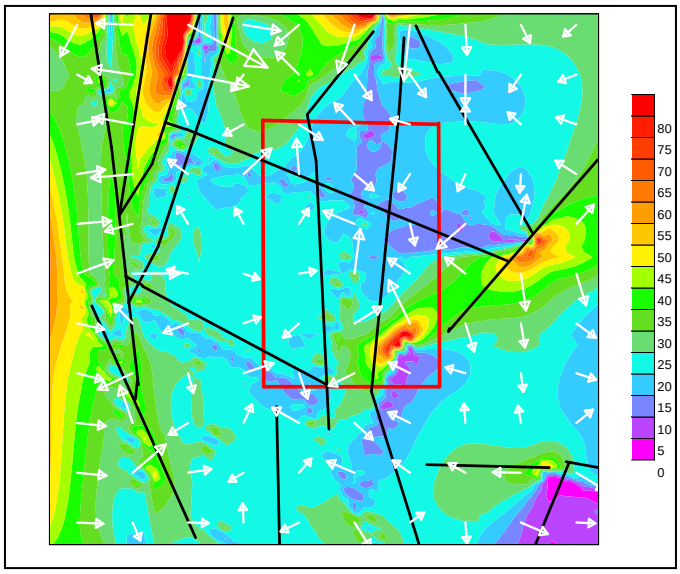

Figure 5. Vectors of filtration velocity in area «Eniseiskiy»

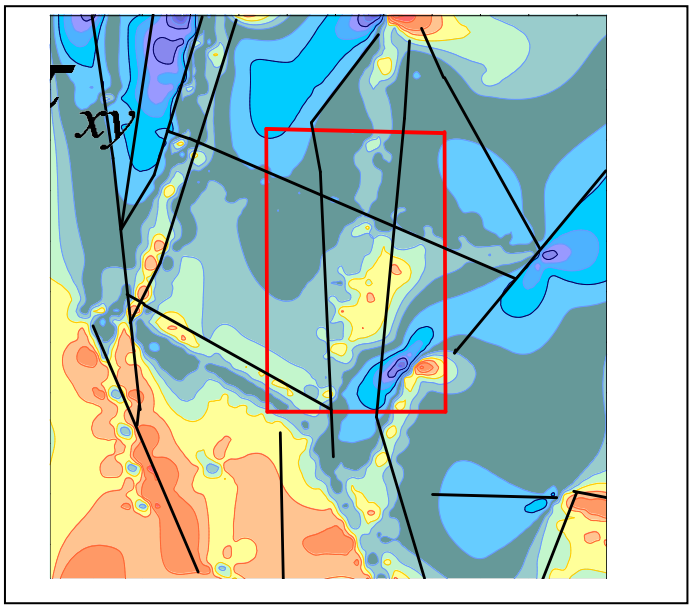

Figure 6. Distribution of shear stress τ_{xy} in «Eniseiskiy»

Directions of the vectors correspond to the movement of groundwater in the weakened zone. Vectors of gradients working stresses are directed into the zones of tectonic disturbances (Fig 7). Thus, these zones are reservoirs for groundwater flow. Filtration of water can also be caused by activation of faults, i.e. run trigger mechanism" tectonic activity.

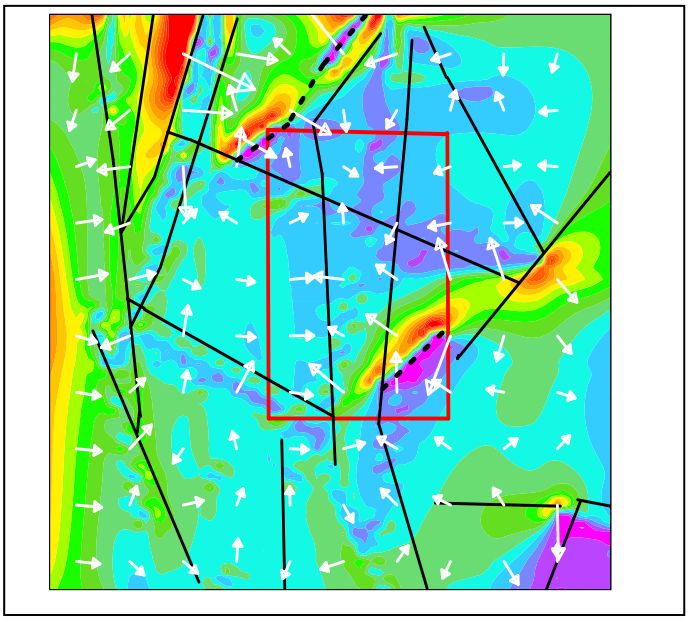

Figure 7. The distribution of stress intensity in the area «Eniseiskiy» and vectors of filtration velocity

The faults are the channels of the intensive filtering groundwater, contributing to extensive migration of radionuclide in the geological environment.

REFERENCES

[1]Morozov V.N., Tatarinov V.N. Tectonic processes development with time in the areas of HLRW disposal from expert assessment to prognosis. *Int. Nuclear Energy science and Technology*, Vol. 2 . Issue 1/2. 2006, pp. 65-74.

[2]Morozov V.N., Tatarinov V.N. Methods of selecting areas of the earth's crust to accommodate the environmentally hazardous waste. *Geoecology*. M. 1996, Issue 6, pp. 109-120.

[3]Belov S.V., Morozov V.N., Tatarinov V.N., Kamnev E.N., Hammer I. Study of the structure and geodynamic evolution of Niznekansky granitoid massif in connection with the disposal of high level radioactive waste. *Geoecology*. M. 2007, Issue 4, pp. 227-238.

[4]Morozov V.N., Gupalo T.A., Tatarinov V.N. Forecast insulating properties of the rock mass in the placement of radioactive materials in mines. *Mountain Gazette.* 1999, Issue 6, pp. 99-105.

[5]Morozov V.N., Kolesnikov I., Belov S.V., Tatarinov V.N., Stress-deformed state of Niznekansky granitoid massif – as the area of possible disposal of radioactive waste. *Geoecology.* M. 2008, Vol. 3, pp. 232-243.

[6]Morozov V. N., Kolesnikov I. Y., and Tatarinov V. N. Modeling the Hazard Levels of Stress-Strain State in Structural Blocks in Nizhnekanskii Granitoid Massif for Selecting Nuclear Waste Disposal Sites. *Water Resources.* Vol. 39, Issue 7. 2012, pp. 756–769. doi:10.1134/s009780781207007x.

Improving Utilization of Face Rigs in Bord and Pillar Mining: A Zimbabwean Case Study

J. Kwiri, T. Zvarivadza
School of Mining Engineering, University of the Witwatersrand, Johannesburg, SA

ABSTRACT The introduction of mechanized equipment within a mine is an important strategy to improve safety and minimize the cost of mining operations. This research evaluates the performance of face rigs at one of Zimbabwe's hard rock bord and pillar mines and puts forward strategies to improve mine production. In the research, the face rig is considered to be a small business unit which forms but an integral part in the functioning of the mine. The analysis focuses on the cycle of the face rigs and the mine's organizational systems and resources that are related to face drilling rigs. By considering face drilling rigs as an integral part of the mine, the research ensures that a proper insight is obtained in terms of the mine's mining cycle and that face drilling is not just considered as an isolated system.

Making use of an extensive range of mining engineering tools and techniques, a solution has been designed for the problems experienced with the use of face rigs. The solution entails the restoration of the mining cycle, a more disciplined approach to maintenance and pre-development and reducing losses due to idling by having good face preparation. Should this solution be implemented, it will enable the face rigs at the mine to perform to their potential. The mine will be able to extend the introduction of mechanized drilling equipment to other mines, recognizing that the modernization of their mining operations improves production, safety and cost-effectiveness.

Keywords: Face rigs, board and pillar mining, hard rock

1 INTRODUCTION

On a world wide scale, production costs are ever increasing and for the mining industry to be financially viable, efficient technologies are continuously being explored and implemented to ensure the industry's sustainability now and in the future. As a move to improve safety and productivity, several bord and pillar mines in Zimbabwe mechanized their face drilling and support drilling processes by the introduction of face rigs and roof bolters respectively. This research evaluates one of the mines and puts forward practical solutions in resolving challenges related to the utilization of face rigs in mechanised mines. The mine in question experiences challenges in attaining optimum utilization. Looking into the merits the face drilling rigs have brought on one hand and the procurement cost, operating and maintaining the machine, it is very important to assess the performance of these drill rigs on the other hand. Increased mining (drilling, blasting and haulage) costs and reduced throughput are also some of the major constraints in the production system of the mine.

1.1 Research Scope

The research analyses and improves the utilization of face rigs at the mine shaft by providing economically and technically sound solutions without compromising safety and quality. The following were undertaken:

- Measurement of the current utilization of face rigs.
- Identification of the limitations and underlying problems facing the mine in achieving the required utilization target.

- Determination of how the major mining delays and utilization can be optimized.

The analysis and design was predominantly from an operational perspective. The way the face rigs measure up to the expected production performance levels was evaluated. The strategic business goals, systems and resources supporting the face rigs were investigated to optimize the system for higher production performance and reduced operating cost. The face rigs form a small but integral part of the mining system at the mine. While this research has more focus on face rigs, the effect of the rest of the mining system on face rigs was also taken into consideration.

1.1 The Utilization Challenge

An operation's productivity can be verified through the assessment of its equipment utilization. This way, the mine's business model effectiveness can be ascertained. This study indicated that; measured over the last few months, year on year, the average utilization of face rigs has remained low having an average of 44%. This to some extent, resulted in a loss of production for the few months cumulative. In 2003, after the first introduction of face rigs, the mining department improved its blasted tonnage and safety record. The other key performance indicators (KPI's) were also met and the face rigs proved to be reliable and able to perform to expectations. The planning department at the mine declared the project a success. Inexplicably, over the past months, the face rigs started to perform very poorly. All the KPI's were down, in particular face rig utilization. This study investigated the factors that influenced the drop in performance. All the KPI's, the mine's organizational systems and resources associated with the face rigs were examined to optimize the system for higher productivity and reduced operating cost.

Several parameters affect the actual utilization. These parameters include operator performance and proximity of workings to each other. From the data obtained at the mine, the main problem of face rig utilization was the availability hours to drill. A number of face rigs were always under maintenance and there have been a lot of on the job break downs. Availability improved since the implementation of good maintenance program. Utilization on the other hand, did not follow the profile of availability. Utilization still decreased and this prompted the study in an attempt to find the reasons why there was continual decrease in face rig utilization.

2 THE NEED FOR EFFECTIVE FACE RIGS UTILIZATION

The mine is highly mechanized. Mining being the core process, involves four processes which make up a cycle. The processes include lashing, face preparation and drilling, charging and blasting. With the production targets that have been set, 2.5 Load Haul Dumpers (LHDs) with a capacity of 3.3 tons, are required per section but practically each section has got three. This reduces lashing problems and makes it easier for lashing teams to achieve their targets. Charging and blasting follow face preparation and face drilling and these processes do not pose a great challenge. As production targets are dependent on face preparation and face drilling a detailed analysis was done, in particular, face drilling as a large percentage of face preparation depends on the efficiency of face drilling. One of the major challenges resulting in failure to meet the mine call is face rig utilization. Figures 1, 2 and 3 show the planned and actual availability, utilization and blasted tonnages in 2012.

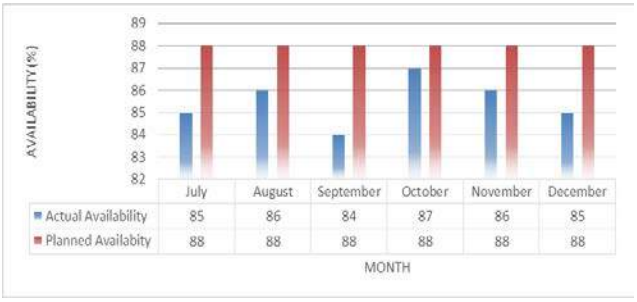

Figure 1. A bar graph showing the planned and actual availability

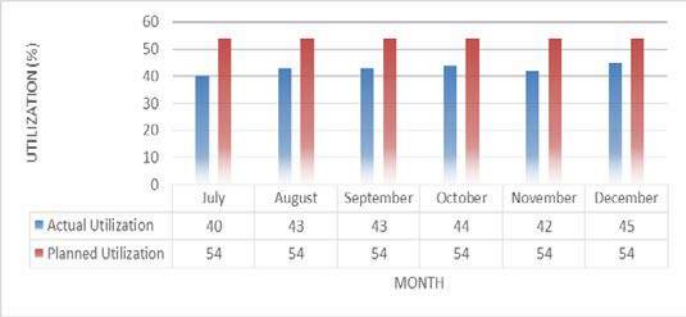

Figure 2. A bar graph showing the planned and actual utilization

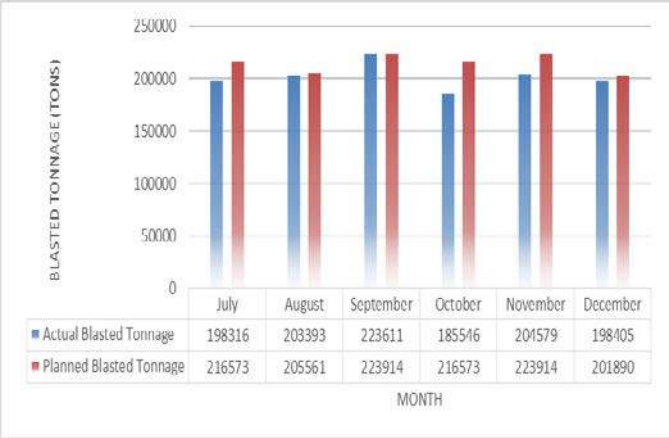

Figure 3. A bar graph showing the planned and actual blasted tonnages

From the bar graphs it can be concluded that low utilization values result in decreased production output. The month of September shows an anomaly and gives the question, "If a section or a mine can still meet its production targets, what is then the reason to worry about utilization?" Looking at one month figure gives a wrong perception and utilization is not only about meeting targets but it is also about making sure that the return on investment, that is buying the drill rigs is obtained. Looking at the financial year of 2012-2013, utilization was very low and the average production was also low. Currently the actual average utilization is 44% against the planned utilization of 54% as shown in Table 1.

Table 1. Availability and utilization of face rigs for Financial Year 2012 -2013

FY 2012 -2013			
KPI	Actual	Plan	% Variance
Face Rig Availabity	86	84	1.9
Face Rig Utilization	44	54	-5.3

From the available time per shift of 7.58 hours, 10 % (which is the difference between planned and actual utilization) is 1. 4 hours. Taking time to drill a blast hole to be 2 minutes, the number of blast holes that can be drilled in 1.4 hours is 42. From a 6m gulley with 51 blast holes, this represents approximately 80% of a production end. A fully blasted end having a capacity to produce 106 tons, 85 tons is lost in each blast. Any mining operation cannot afford the cost of such continuous loss of ore but this is happening and the cost of material loss continues to escalate unabated. As mentioned, with utilization being a factor that affects production the appropriate understanding and mitigation of underutilization of equipment cannot be overemphasized. With the mine having heavily invested in mechanizing most sections, reducing delays and fully utilising the machines is paramount to the success of its mining business.

3 MINING BACKGROUND

It is central to the goals of the mine to have a balanced mix in the extraction of high and low grade ore and move much tonnage while maintaining continuity of ore drilling in a safe and internationally acceptable manner at the lowest possible costs. Flat room and pillar mining method is used to extract the ore. Production and development occur at the same time. Entry of employees and equipment is through a decline shaft and ore is hoisted out through a different decline shaft by a series of connected conveyor belts.

Stope areas vary with class of ground. Classes C and D, stoping is done creating 6m or 9m twin gullies. Pillars separating the gullies are 10m by 3m and 3m by 3m.

Ventilation holings are punched on continuous pillars to allow smooth flow of air. For classes A and B, stoping is done on 15m panels leaving 10m by 3m insitu pillars. A 6m gulley advances at 2.8m and the 9m burden slipes in the advance gulley. Stope heights are 2m to 2.4m and the rooms are 15m wide for Class A and B ground whereas for Class C and D either 6m or 9m twin gullies are employed. Figure 4 shows the mining plan for 6m twin gulleys.

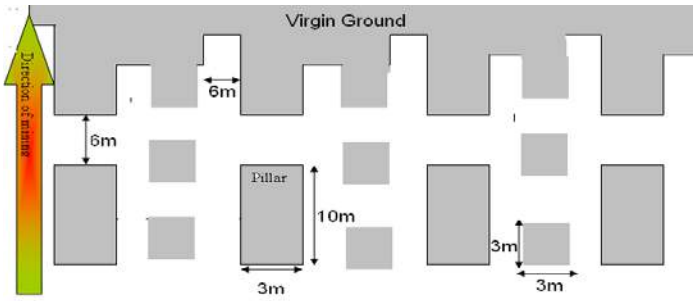

Figure 4. Mining plan for 6m twin gulleys (not drawn to scale)

3.1 Stope Development

Mining is done in two directions, the north and south along the strike direction of the ore body. A 6m gulley is always mined at most 6m in advance of the panel to create a blasting face; the rest of the panel will be slipped into the gulley. After every 10m advance of the panel a ventilation holing is mined perpendicular to the panel advance to create free air circulation.

3.2 Mining Cycle

3.2.1 Stope face drilling and blasting

Stope face drilling is done by low profile (LP) drill rigs. The face is drilled at an angle parallel to the reef dip to allow for highest grade extraction but also ensuring throw blasting of at least 40% of the ore into the advance strike drive (ASD) for easy mucking and lashing. Shock tubes and ammonium nitrate fuel oil (ANFO) explosives are used for charging up after drilling is complete. The drill holes are 3.2m in length and there is an expected advance rate of 2.88m/blast at the stope face. Blasting takes place twice a day on the day shifts at 18:30 and night shifts at 06:30.

3.2.2 Ore lashing and loading

Stope face cleaning and lashing is done by LP load-haul-dumpers (LP LHDs). Ore is collected in the ASD by the LHDs where it is then hauled to the tipping point. The LHDs access the strike conveyor through grizzlies spaced 80m apart. The strike conveyor belt is maintained at a maximum of 80m from the face.

3.2.3 Stope ground control

Roof bolt support is put in place by the use of LP roof bolters and jackhammers. For safety of personnel, jack hammers are gradually being phased out. The way the stope face is supported is based on the rock quality structures, joint angle and spacing, the filling condition and the hanging wall stratigraphy of the specific site.

3.2.4 Mining teams targets

Mining targets are set depending on the condition of ground in which a section is operating so that safety is not compromised. Sections in bad ground (classes C and D) are supposed to prepare, drill, charge and muck blasted rock from three 6m gullies or 18 face metres for each process. For classes A and B the target is 21 face metres. This implies that the daily drilling (or lashing or charging or preparing the face) target is 42 face metres for classes A and B and 36 face metres for classes C and D since there are two shifts per day. With the mining height set to be 1.95m (for design purposes) and the face expected to be blasted to an advance of 2.88m and insitu rock density to be 3.15 tons per cubic meter, Table 2 shows the daily targets for good and bad ground sections. NB: Hoisted tonnage = 0.95*Blasted tonnage to accommodate the losses incurred during the transportation of ore from underground to surface.

Table 2. Production Targets

	Mechanized Bad Ground	Mechanized Good Ground
	6m gully	15m panels
Advance per blast (m)	2.88	2.88
Drilled face meters (m)	36	42
Prepared ends	3	3
Blasted tonnage (t)	636	743
Hoisted tonnage (t)	604	706

4 UTILIZATION CHALLENGES FACED IN THE MINING INDUSTRY

In spite of the tremendous amount of research conducted in the last few decades, no single theory has been developed and accepted that adequately explains the utilization of mining equipment. There is yet no consistent and widely applicable theory but only a number of limited theories, many of which are empirical in nature and based on ideal situations. There are many schools of thought on how utilization and availability should be measured. In this research utilization is obtained as a ratio of drilling time to available time. Availability is the ratio of the difference between planned time and engineering downtime to planned time.

Utilization affects not only the local productivity of the mining department; it even influences the performance of the subsequent combination steps. The stope face, the area where drilling occurs has got the largest number of injuries in narrow reef mining. To improve safety, mining equipment manufacturers and mining companies have realized the need to develop new mining technologies that will improve safety. One of the new technologies currently being employed is the mechanization of underground mining operations. According to Croll (2004), mechanization is the use of powered machinery to replace manual labour. Within the mining context, mechanization refers to human operators being given machines to assist them with stoping functions. However, it does not refer to the use of hand powered tools such as hand held rock drills.

4.1 Mining Benefits for Using Face Rigs

According to Harrison (2008) mining using face rigs has the following benefits:

- Safety is improved because the operator is removed from the sharp end of the face.
- There is an improvement in productivity by more accurate drilling, higher face advance and production rate per employee due to the fully mechanized stoping and development.
- It is more profitable than conventional mining.
- It has the potential to mechanize at stope widths of <1,0m and at reef dips of 18 - 22° gradient.

4.2 Ergonomics of Using Low Profile (LP) Mining Equipment

Underground evaluations were performed to examine the working conditions of the LP equipment operators. The following ergonomic risk factors were identified:

- The operators experience discomfort in the lower back during all the process steps where LP equipment are used. This can be attributed to the operators having to work sitting on a very small seat.
- Discomfort is also experienced in the shoulder regions due to the pulling of the heavy power cable of the LP equipment. This usually occurs when the operator does not have an assistant.
- The control panel used by the operators and dial gauges are not clearly marked and they are frequently covered in dirt. This makes it very difficult to read the labelling on the control and increase the possibility of errors.
- Operators are concerned about the viewing angles and line of sight around the LP machines. During drilling operations the operators are required to move closer to the face machine to ensure that the drill bit are correctly positioned. This provides a potential risk if the operator moves too close to the working mechanisms of the drill rig.

The main objective of face drilling is to get holes for charging up so that rock can be

fragmented to the required size at the lowest possible cost and at the same time complying with the technical specifications and the safety conditions required. Though there are several challenges that are associated with the use of equipment, the advantages that come with efficient equipment utilization cannot be overemphasized. Efficiency in equipment utilization affects productivity and production. Face drilling on its own, is an important parameter in achieving the required targets. High face rig utilization results in more face being prepared for charging and blasting, and as a result it gives more tonnage output of fragmented rock. On the other hand, low face rig utilization results in low production output.

4.3 Losses Related to Face Rig Utilization

There are several types of losses that affect face rig utilization and these include:

4.3.1 Loss due to breakdowns

Time and quantity are two types of losses that result from breakdown losses. Unexpected, sudden or dramatic breakdowns get quick attention and they are easily predictable. Chronic breakdowns are not very common and as such they are often ignored when attempts to solve them do not prove to be successful. Many of the breakdowns that happened at the mine got attention but some were neglected and this resulted in severe problems in the mining cycle.

4.3.2 Loss due to setting up and adjusting

When production equipment is stopped due to changing of parts of equipment, the result is loss due to setting up and adjusting. There were few to none losses due to setting up or adjusting as all equipment is schedule for maintenance every week.

4.3.3 Loss due to minor stoppages and idling

Minor stoppages occur as a result of a small temporary malfunction that results in stoppage of drilling. For example the drill steel might get blocked in the drill hole which may cause the drill rig to idle. Such problems in most cases are overlooked and they result in major delays in future as solving them becomes complex and complicated.

4.3.4 Loss due to reduced penetration rates

Drilling machines are designed to operate at a specific drilling rate. When they operate at a lower rate there is reduced production. This can be a result of unsolved problems within the machine.

4.3.5 Loss due to starting up the drilling

When a machine starts up during the early stages of drilling until it stabilizes, there are losses that occur during this stability ramp up.

5 RESEARCH APPROACH

Two sections of the mine were investigated. One section from the north side and another from the southern side. The section from the northern side had its support installed by roof bolters. The one for the southern side had its roof support installed by using jack hammers.

A theoretical investigation of the required parameters required for full ideal utilization was done. Results were compared to results obtained from actual utilization measured during the course of the research. Measurement of the drilling times and determination of delays was done for the two sections.

5.1 Observations

Observations were made as the face rig was operating and the following parameters were measured.

- Rig Availability
- Rig Utilization
- Cycle Time
- Down Time

5.1.1 Rig availability

Availability is defined as a percentage of time that a machine is able to operate and is in a committable state when it is needed at any time (Memidex, 2014). The availability of the face rigs was measured and compared to the one captured by data capturing clerks.

5.1.2 Rig utilization

Face rig utilization is a key performance indicator (KPI) that reflects on the usage of the machine within its available time. Utilization was determined from the cycle time.

5.1.3 Rig cycle time

This includes time for collaring, penetration rate (drilling), inter-hole delay and time for reaming. All these times were recorded as the machine was being operated.

5.1.4 Down times

A minor stoppage is when the production stops for a temporary malfunction, or the equipment is idling. This includes non-productive time due to travelling, tramming, blasting, re-entry and no face to drill. These times were also measured during the course of the shift.

6 RESULTS AND ANALYSIS

After the identification of the status quo, practical solutions in mitigating the identified challenges were proposed as a means of bridging the gap between the actual utilization and the planned utilization.

6.1 Time Distribution Models

Table 3 shows the time distribution model for an operator during a shift.

Table 1. Drill Rig Time Distribution Model A

DRILL RIG TIME DISTRIBUTION MODEL			
Activity	From	To	Fraction of the Time
Travelling to Waiting place	8:00:00 AM	8:35:00 AM	0.583
Waiting place Procedure	8:35:00 AM	8:50:00 AM	0.250
Travelling to Workplace	8:50:00 AM	9:05:00 AM	0.250
Setting Up	9:05:00 AM	9:15:00 AM	0.167
Drilling	9:15:00 PM	17:05:00 PM	7.833
Engineering Down Time			1.480
Travelling to Waiting place	17:05:00 PM	17:25:00 PM	0.333
Travelling to Surface	17:25:00 PM	18:00:00 PM	0.583
Blasting And Re-entry	18:00:00 PM	20:00:00 PM	2.000
Total			12.00

Table 4 gives the fraction of time that is spent on each task during a shift.

Table 4. Drill Rig Time Distribution Model B

DRILL RIG TIME DISTRIBUTION MODEL			
Activity	Without Maintenance	With Maintenance	Weekly Calculations
Travelling (op)	2.33	1.75	15.75
Tramming	1.17	0.92	7.92
Setting Up	1.67	0.83	10.83
Drilling	11.37	6.77	75.01
Eng D/Time	2.96	9.48	27.24
Blasting & Re-entry	4.50	4.25	31.25
Total	24.00	24.00	168.00
Available	0.88	0.61	0.84
Total hours	21.04	14.52	140.76
Effective Utilization	0.54	0.47	0.53
Overall Utilization	0.62	0.52	0.61

Face rig utilization is a KPI that reflects on machine usage against its availability. Rig availability is measured against planned shift time of 24 hours. Availability was determined for situations with and without maintenance (mtce).

Availability (%) (without mtce)
= (planned time – engineering downtime)/planned time
= [(24 – 2.96)/24]*100%
= [21.04/24] * 100%
= 88%

Availability (%) (with mtce)
= (planned time – engineering downtime)/planned time
= [(24 – 9.48)/24] * 100%
= [14.52/24]*100%
= 61%

Maintenance is done once per week. Therefore the weighted average availability per week is;

Availability (%) (weighted average per week)
= {[(0.88 * 6) + (0.61 * 1)]/7}*100%
= 84%

Actual Rig Availability (%)
= Possible working hours – engineering downtimes

Engineering down times include mechanical and electrical breakdowns, over-run services and low penetration i.e. penetration rate > 2 minutes

Rig utilization is measured within the available time.

Effective rig utilization (%) (without mtce)
= (drilling time/available time)*100%
= (11.37/21.04)*100%
= 54%

Effective rig utilization (%) (with mtce)
= (6.77/21.04)*100%
= 47%

Effective rig utilization (%) (weighted average/week)
= {[(0.54 * 6) + (0.47* 1)]/7}*100%
= 53%

Actual rig utilization = available hours – mining downtimes/available hours

Where available hours = possible working hours – engineering down time

Mining downtime is a result of re-entry, travelling, tramming, setting up time, idle time, preparation time, no drilling tools, water - hose bursts and no power.

6.2 Observations

Table 5 shows the results of rig 16 which operated in a section that had its support system installed by hand held rock drills (jackhammers).

Table 2. Observations from face rig with jackhammers being used to install support

RIG 16								
Date	AVAIL%	UTIL%	Start	End	Traveling	Others/Idle	Tramming	Prep
05-Dec-12	95%	51%	10:20	17:00	1.00	1.50	0.75	0.00
06-Dec-12	93%	52%	9:55	17:08	1.00	1.00	1.00	0.50
07-Dec-12	92%	54%	9:50	17:30	1.00	2.00	0.50	0.00
09-Dec-12	89%	40%	10:00	17:30	1.00	1.50	1.00	1.00
10-Dec-12	96%	53%	10:10	16:35	1.00	0.50	1.50	0.00
12-Dec-12	95%	54%	9:40	16:45	0.75	0.75	1.50	0.25
13-Dec-12	82%	47%	10:10	17:15	1.00	1.50	0.50	0.75
14-Dec-12	93%	42%	12:55	17:15	0.75	0.50	0.25	1.00
16-Dec-12	96%	50%	9:50	17:20	0.75	1.50	1.25	0.25
17-Dec-12	90%	49%	9:40	16:00	0.75	1.00	0.75	0.75
19-Dec-12	97%	55%	12:35	17:00	1.00	0.50	0.00	0.50
20-Dec-12	87%	52%	10:15	17:00	1.00	1.00	0.50	0.75
21-Dec-12	90%	52%	10:10	17:00	1.00	0.50	1.25	0.50

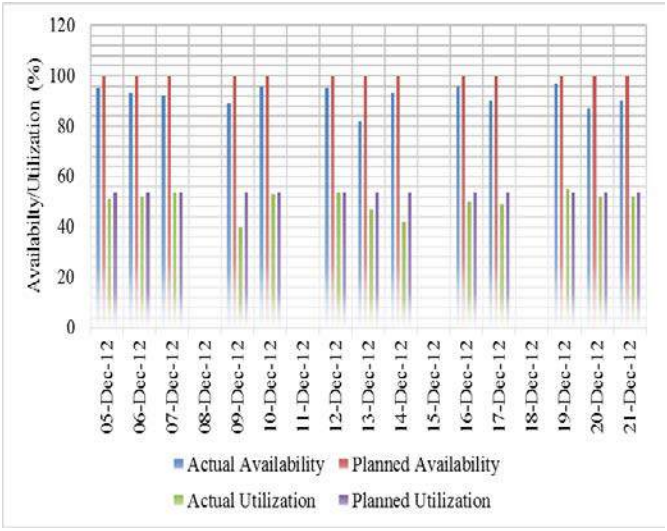

Figure 5. Bar graph showing planned and actual availability and utilization for a section that uses jackhammers to install support

Table 6 shows the results from rig 31 which was being used in a section that had a roof bolter instead of jackhammers.

Table 3. Observations from face rig with bolters being used to install support

RIG 31								
Date	AVAIL%	UTIL%	Start	End	Traveling	Others/Idle	Tramming	Prep
02-Jan-13	96%	41%	9:45	16:30	0.50	1.00	0.75	1.75
03-Jan-13	98%	31%	11:05	16:30	0.75	0.00	0.75	2.25
04-Jan-13	95%	44%	9:30	17:30	0.75	0.00	1.50	2.25
06-Jan-13	95%	48%	10:45	17:30	0.50	1.00	0.50	1.50
08-Jan-13	97%	48%	10:00	15:15	0.75	1.00	0.25	0.75
09-Jan-13	97%	29%	13:50	17:00	0.50	0.50	0.25	1.00
10-Jan-13	95%	41%	10:35	16:30	1.00	0.00	1.00	1.50
11-Jan-13	91%	40%	13:10	16:30	0.50	0.00	0.25	1.25
13-Jan-13	96%	39%	10:20	16:30	1.00	0.50	1.00	1.25
15-Jan-13	99%	37%	10:33	17:20	1.25	0.50	0.50	2.00
16-Jan-13	95%	45%	9:55	17:08	0.75	0.50	1.00	1.75
17-Jan-13	97%	35%	9:50	17:30	1.00	0.00	2.00	2.00
18-Jan-13	96%	40%	10:00	17:30	1.00	2.00	1.25	0.25

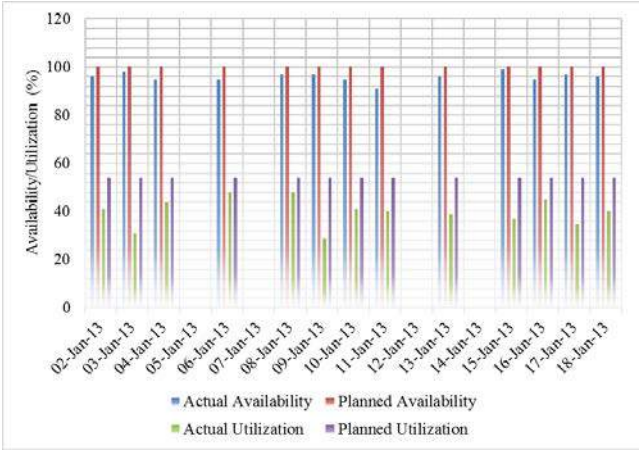

Figure 6. Bar graph showing planned and actual availability and utilization for a section that uses roof bolters to install support

6.3 Analysis of Results

Figure 7 shows the major delays for the face rig from a section that uses roof bolters to install support.

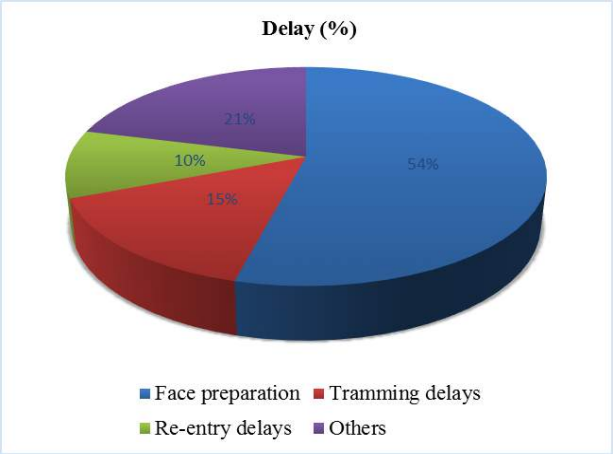

Figure 7. Pie chart showing the major delays for face rig 31 with bolters being used to install support

Figure 8 shows the major delays for the face rig from a section that uses jackhammers to install support.

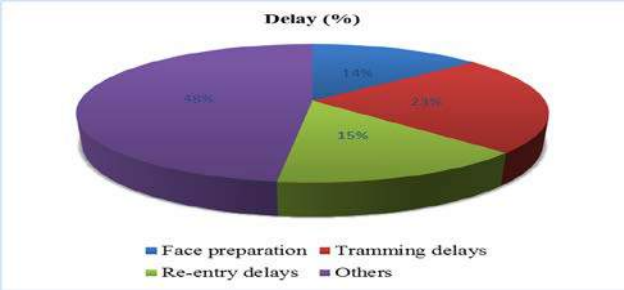

Figure 8. Pie chart showing the major delays for face rig 16 with jackhammers being used to install support

6.3.1 Major delays

Preparation delays – Figures 9 and 10 show that face preparation contributes more to major delays in sections that uses bolters to install roof support compared to the sections that uses jackhammers. This is attributed to the fact that bolter operators are relatively inexperienced and other mining delays cause failure to meet target. Jackhammers have been in operation since the beginning of mining at the mine therefore operators are more experienced in using jackhammers. A large percentage of delays due to face preparation affects face rig utilization by increasing idle time for face rigs due to non-availability of ends for drilling. Time lost in face preparation delay on average is 1. 75 hours per shift and this converts 105 tons of ore. For each day, 310 tons of ore are lost due to delay in face preparation. On the other hand, the face rig has no allowance made in its schedule for the operator to make safe the end before drilling but rather for inspection of an end that should have been made safe by team leaders or assistant miner. Making safe consumes around 40minutes; Watering down – 15 minutes; barring down – 20 minutes; Cleaning of sockets and plugging = 5 minutes.

For the ends available for drilling, making safe will consume 135 minutes ~ 68 holes at 2 minutes per hole ~ 1.33 ends lost per shift due to making safe.

Tramming delays- Due to distorted cluster of operations there is an increase in tramming times. Though this is a challenge due to ground conditions where geology can recommend ends to be stopped, failure to stick to the 3 ends per cluster result in spaced ends which increase tramming delays and setting up times compromising on the actual rig utilization. On average, tramming delays consumes 30 minutes. This is equivalent to 15 blast holes or a quarter of an end (26 tons of ore)

Other delays- Unavailability of drilling tools (rods and bits) and water due to water hose bursts and failure of boom to fit in gulley. If water hoses are damaged by being run over by mobile equipment (LHDs, Utility Vehicles (UVs) and rigs) or they have corroded due to wear and tear, they fail easily and disrupt drilling causing time losses during mending time. The average time that is lost is 40 minutes which is equivalent to 20 blast holes (~40 tons).

Rig effectiveness- The product of rig availability and utilization is called drill rig effectiveness that is:

Rig Effectiveness (%) = availability * utilization. Planned rig effectiveness
= 0.84 * 0.54 = 0.45 = 45%

Drill rig effectiveness focuses on business efficiency and reflects on the overall benefit of the machine to the organization and

therefore has a bearing on investment decision making by the company. For instance, a rig machine with low availability due to heavy maintenance schedules and breakdowns yet capital intensive cannot be a suitable investment because it will have low utilization and impact negatively on the Return on Investment (ROI). Figures 9 and 10 show the planned and actual rig effectiveness for rig 16 and rig 31 respectively.

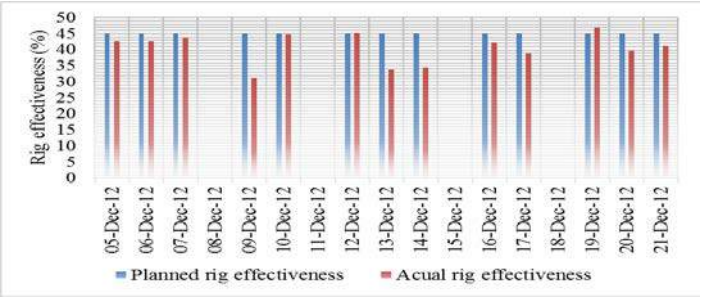

Figure 9. Bar graph showing planned and actual rig effectiveness for rig 16

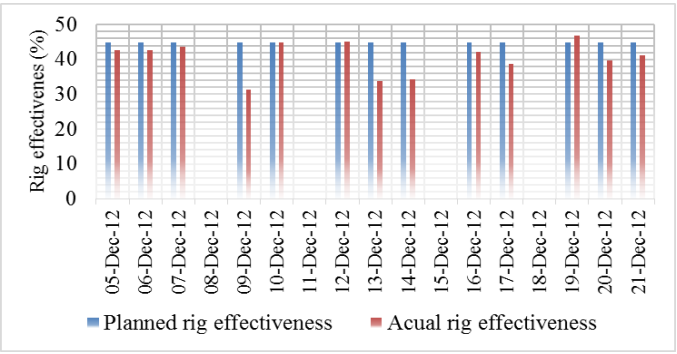

Figure 10. Bar graph showing planned and actual rig effectiveness for rig 31

6.3.2 Effect of down times and breakdowns

The effect of engineering down times is lower rig availability and mining down times represent reduced drill rig utilization and result in low rig efficiency. Rigs operating at low efficiency affect achievement of target face meters per day.

7 CONCLUSIONS

Utilization is a key performance indicator that is used to assess asset performance and production performance. From the study, the main problems that were found include dispersed workings, mechanical breakdowns, poor operator performance, and longer travelling times from surface. Improving utilization by clustering the workings will reduce the time needed for tramming and setting up. A single blast initiative has also been proposed as it will increase the available hours as well as utilization of face rigs. In order to improve operator efficiency, blending of operators proves to be effective as it provides the unskilled operator more time to get skilled. Full rig utilization for maximum production has shown that unified and mutual coordination between operators is very important as it gives the operators a way to communicate to each other through a communications log book.

REFERENCES

Croll, A.M. 2004. Mechanization—an Anglo Platinum perspective. International Platinum Conference ‘Platinum Adding Value’. The South African Institute of Mining and Metallurgy, pp. 125-142.

Harrison, G.A. 2008. Anglo Platinum Extra Low Profile (XLP) Mechanized Equipment Implementation – an update. Narrow Vein and Reef 2008 Symposium. The Southern African Institute of Mining and Metallurgy, pp.1-11, Johannesburg, 6-7 May.

Memidex Online Dictionary. 2014. Definition of availability. Internet. http://www.memidex.com/availability. Accessed on 28 July 2014.

In-situ Stress Measurements From Oriented Sub-cores Using Kaiser Effect

M. Karakus, S. Perez
School of Civil, Environmental & Mining Engineering, The University of Adelaide, SA 5005 Australia

D. Goodchild
OZ Minerals, Parkside, SA 5063, Australia

ABSTRACT Measuring in-situ stress in areas at great depth in which access is only available by exploration boreholes is a challenging task. This paper aims to investigate magnitude and orientation of in-situ stresses from cored rocks using acoustic emission (AE) and deformation rate analysis (DRA) at the exploration-drilling site in South Australia. Six independent sub-cores having different orientations for different depths of 640 m and 915 m were extracted from the original core whose dip and azimuth in mine grid are 64.4° and 186.06° respectively. Each sub-core was subjected to three cycles of loading. As the take-off point at first cycle is more pronounced than other successive cycles, calculation of stresses is based on first cycle data. Different threshold values were also tested to investigate their influence on locating take-off point. It was observed that threshold values lower than 15 mV tend to conceal point of inflexion. In AE analysis, locating point of inflexion was found to be difficult in some samples for which we also used DRA for cross checking. Therefore, we suggest that DRA should be used along with AE to ensure that the correct point of inflexion is located.

Keywords: Acoustic emission, deformation rate analysis

1 INTRODUCTION

Magnitude and orientation of in-situ stress in rock masses has to be estimated or measured before designing any underground structures or implementing a mine layout as the principal stresses will influence the overall stability of these structures. However, stress measurement, in principle, faces with an obstacle as such that stress is not a physical phenomenon than can be measured directly. Therefore, in order to determine stress in a finite body, a relation in the form of stress-strain is required (Fairhurst 2003). Seto et al. (1998, 1999) reported that common stress measurement techniques suffer from deficiencies and limitations. For example, overcoring and hydraulic fracturing are usually expensive and require highly skilled technical staff as well as being time consuming. Measuring in-situ stress in remote areas at great depth in which access from large boreholes and mine workings are hard is one of the deficiencies of these techniques.

Non-Destructive Techniques (NDTs) have been proposed to estimate in-situ stresses from cored rocks recovered at depths in order to remove limitations and deficiencies with the conventional stress measurement techniques. Kaiser effect involving acoustic emission (Kaiser 1953), and deformation rate analysis (Seto et al. 1999) are amongst the most popular unconventional stress estimation techniques. These techniques basically utilize irreversible damage process to estimate in-situ stresses.

This paper aims to analyse the results of AE and DRA to calculate in-situ stresses from cored rocks obtained from Carrapateena drilling site, SA. For this purpose, AE monitoring systems, which was developed by the first author in the school of Civil, Environmental and Mining Engineering (CEME), was used.

Six independent subcores from different orientations for depths of 640 m and 915 m have been extracted from oriented core whose dip and azimuth in mine grid are -64.4° and 186.06° respectively. Each sub-core was subjected to cyclic loading up to 52 MPa, which exceeds stress level at level 640m and 915m. Normal stresses found from AE were used to calculate stresses tensor according to Mine X=north, Y=east and Z=vertical directions. In the next stage Eigenvalue analysis is applied to calculate the principal stresses and their directions according to mine grid.

2 AE AND DRA ANALYSES

2.1 Acoustic Emission

Irreversible damage occurs in the rock when rock material subjected to loading exceeds the previously applied stress. Manifestation of micro-cracks can be observed by acoustic signals at this peak stress value where the number of acoustic hits or signals significantly increases. This effect known as Kaiser Effect (KE) is the signature of a memory of the maximum previously applied stress in a material, which was first discovered by Joseph Kaiser in 1950s. The KE is the absence of detectable AE events until the load imposed on the material exceeds the previously applied stress level (Yuan and Li, 2008).

The KE can be recognised as an inflexion (change of slope) in the dependency ‘‘cumulative AE hits versus stress’’. In order to determine the value of in situ stress (σ_m) more accurately, the curve may be approximated by two straight lines (bilinear regression). The point of their intersection projected onto the stress axis indicates the KE stress level (Lavrov 2003).

As reported by Seto et al. (1998), AE activity that occurs on the interface between the sample and loading end-platens during testing granular materials is a serious problem. In order to eliminate this AE activity, they used a 0.15 mm thick sheet of polyethylene placed between the sample and each end, while Mori et al. (2009) used stiff paper. A 10-mm thick plate of Bakelite was inserted by Li and Nordlund (1993) at each end of the specimen to block the noise from the hydraulic system of the testing machine. In order to eliminate the noise in our tests we used pre-stressed MDF material, which reduce the contact noises significantly.

2.2 Deformation Rate Analysis

In-situ stress estimation by Deformation Rate Analysis (DRA) was initiated by Yamamoto et al. in 1990. Earlier work that laid the foundation of this method was a method called differential strain curve analysis (DSCA) by Strickland and Ren (1980) that is also extension of differential strain analysis (DSA) introduced by Simmons et al. (1974). DRA uses the principles of the KE where strain is recorded under uniaxial cyclic loading. The difference in inelastic deformation in a specimen between two successive loading cycles was used to determine the previously applied stress. The strain difference function $\Delta\varepsilon_{j,i}(\sigma)$ is defined as:

$$\Delta\varepsilon_{j,i}(\sigma) = \varepsilon_j(\sigma) - \varepsilon_i(\sigma); \quad j > i \tag{1}$$

where σ is the applied axial stress and $\varepsilon_i(\sigma)$ is the reduced axial strain for the ith loading. $\Delta\varepsilon_{j,i}(\sigma)$ is approximated by a straight line with a positive gradient at stresses less than the previous peak stress that rapidly bends at or near the previous peak stress to have a negative gradient. Yamamoto et al. (2009) states that this negative gradient at applied stresses is higher than the previous peak stress indicates that the rock specimen can be easily deformed in the first loading than in the second one of two successive loading cycles. This is due to the specimen enlarging pre-existing cracks and/or to create new cracks at its first experience of a higher stress being applied. Considering what the Kaiser effect implies, this should happen especially when the applied stress exceeds the peak value of previous stress. The strain resulting from this phenomenon is irreversible for two successive cycles and not cancelled in the strain difference function defined by Eq. 1.

Many other researchers also reported that DRA is practically effective method to

estimate in-situ stress (Yamamoto et al. 1990; Hsieh et al. 2013; Wang et al. 2011; Karakus 2014). Therefore, we utilised DRA to cross validate AE results before calculating stress tensor at the drilling site.

3 EXPERIMENTAL METHODOLOGY

In order to construct stress tensor at the site, minimum six subcores are needed. Therefore six subcores were drilled from field core (master core). Orientation of the subcore samples relative to master core orientation has been converted to real mine grid (See Fig. 1).

Rock samples were prepared according to ISRM compressive testing standards. Height to diameter ratio for subcores was kept within approximately 2.

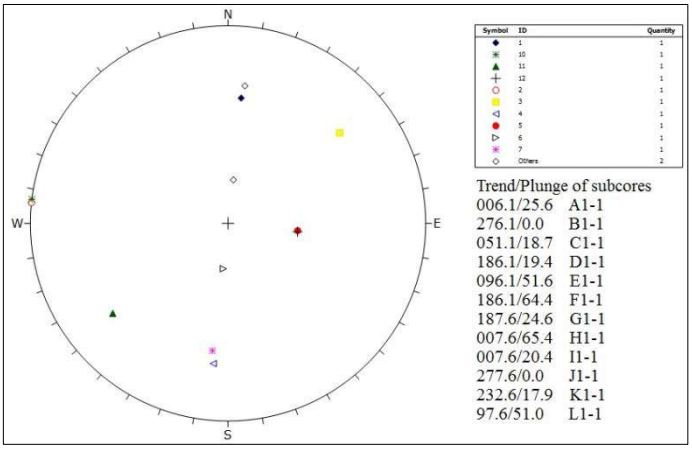

Figure 1. Pole plots for Subcore orientations (Lower Hemisphere – Equal area projection).

AE and DRA tests were carried out using Instron 1342 servo controlled hydraulic testing machine with 300 kN load capacity. The Instron controller consists of hardware components and software applications that provide closed-loop control of servo-hydraulic test equipment. This machine consists of a compression loading frame, an axial dynamic loading system and a data acquisition system. The data acquisition system consists of a signal conditioning, and an acquisition unit interfaced with a computer. Multiple or single data acquisition processes can collect data on all channels. This machine is able to perform cyclic test in both load and displacement control modes.

The AE monitoring system (see Fig. 2) consisted of AE sensors with pre-amplifiers, which were connected to a trigger signal generator with a NI PCI-6133 data acquisition unit. Frequency bandwidth of AE pico sensors is 200-800 kHz. Recording and visualisation of signals were done using a signal processing software developed in house using Labview. A set of 2/4/6 series filters with 20/40/60 dB gain single ended differential preamplifier was used to amplify signals 60dB.

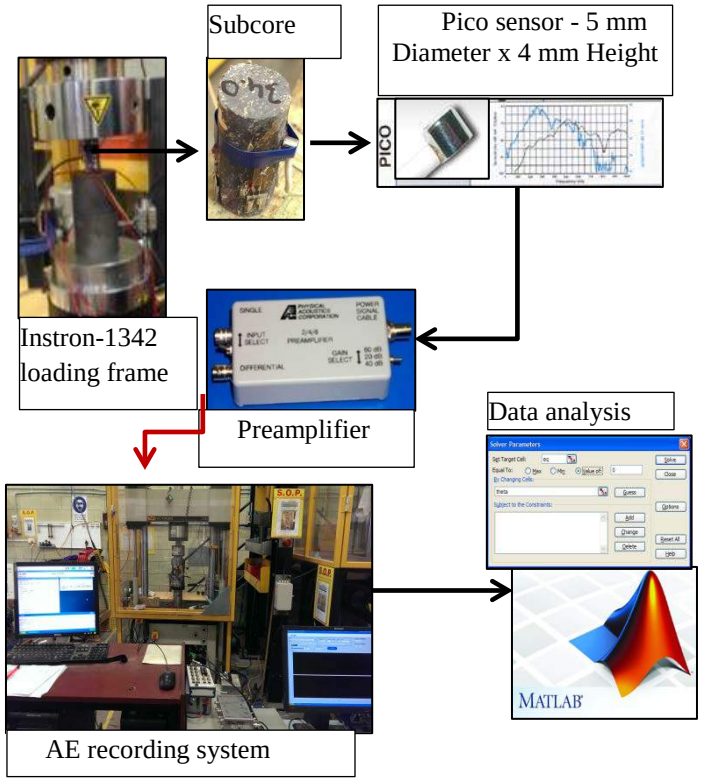

Figure 2. Schematic view of AE monitoring system.

Recent publication by Hsieh et al. (2013) on the influence of sample bending on deformation rate analysis suggests that use of four strain gauges can eliminate and reduce any errors when locating bending point for in-situ stress estimation. Therefore, each subcore was instrumented with four strain gauges and their average values were used to calculate overall strain for DRA. At the same time an acoustic sensor was attached to each sample to achieve simultaneous measurements. Acoustic pulses and axial strain during loading cycles (approx. 20 kN max. load) were continuously recorded leading to very large amount of data (approx.

12 GB). The dominant frequency for outside noise was found to be 320kHz. We, then applied digital filtering to remove outside noises so that all AE activities can be captured. When processing filtered data, we were able to apply as small as 5-10mV threshold values for AE hits. However, we found that less than 15 mV threshold value, locating point of inflexion is becoming very difficult. Therefore use of threshold limits ranging from 15mV to 150mV is suggested for AE tests.

4 EVALUATION OF THE RESULTS

In this section, firstly examples of graphical results from AE and DRA will be given to illustrate point of inflexions found in both analyses.

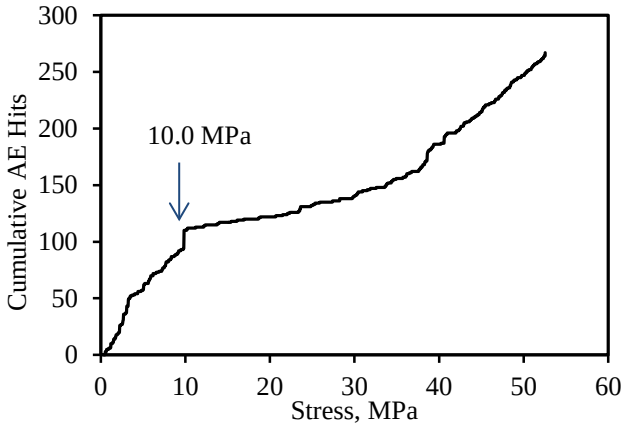

Figure 3. Cumulative AE hits versus stress for subcore D1-1.

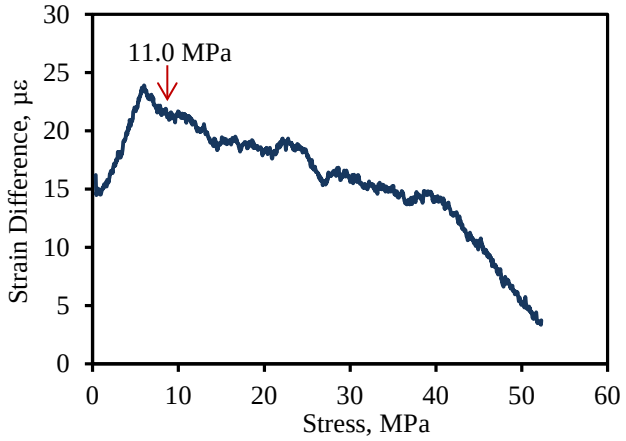

Figure 4. DRA result for subcore D1-1.

A clear take-off point at 10.0 MPa can be seen in Fig. 3 along with few other small sudden jumps which is due to the stress history that rock mass was subjected in the drilling site. Similar results as in the manifestation of strain differences can be seen in Fig. 4 where we found in situ stress is 11.0 MPa. Table 1 summarises the results from AE and DRA analysis.

4.1 Stress Tensor Calculations

Each subcore orientations were converted to real mine grid using the relations between field core orientations and relative subcore orientations. For this transformation the following equation is used:

$$cos\theta_{uv} = [\cos(\alpha_u - \alpha_v)cos\beta_u cos\beta_v] + [sin\beta_u sin\beta_v] \quad (2)$$

Where θ_{uv} is the angle between field core trend/plunge α_u/β_u and subcore trend and plunge α_v/β_v. As the angle θ_{uv} is known, using the Eq. 2 and solver in excel, orientations of the each subcore was calculated and given in Table 1. The average values of AE and DRA results were used to calculate stress tensor at the corresponding depths where the subcores were recovered.

Table 1. Orientations and locations of subcores along the master core and estimated stresses.

ID	Location (m)	Orientation (Degrees)		Stress (MPa)	
		α	β	AE	DRA
A1-1	642.0	6.1	25.6	17.0	13.9
B1-1	643.2	276.1	0.0	19.1	19.5
C1-1	642.7	51.1	18.7	25.7	25.5
D1-1	644.0	186.1	19.4	10.0	11.0
E1-1	643.6	96.1	51.6	16.8	12.2
F1-1	643.3	186.1	64.4	12.7	12.1
G1-1	915.9	187.6	24.6	21.6	17.8
H1-1	916.4	7.6	65.4	31.9	31.6
I1-1	916.7	7.6	20.4	33.3	32.1
J1-1	918.7	277.6	0.0	12.0	14.2
K1-1	919.5	232.6	17.9	14.0	18.5
L1-1	920.2	97.6	51.0	28.9	21.6

In order to obtain stress tensor for principal stress calculation, 6 independent normal stresses from subcores were used. (X=mine north, Y=mine east and N= Vertical – right handed coordinate system).

Based on the average of six normal stresses from AE and DRA results for depths of 640m and 915m, stress tensor [$\boldsymbol{\sigma}$] in the mine grid (X, Y, Z) was calculated using the following equation:

$$[\boldsymbol{\sigma}^*] = [\boldsymbol{R}][\boldsymbol{\sigma}][\boldsymbol{R}]^T \quad (3)$$

Where, $\boldsymbol{\sigma}^*$ is the stress matrix relative to the subcore axis (*l*, *m*, *n*) and [$\boldsymbol{R}$] is the rotation matrix. In an explicit form, Eq. 3 can be written as:

$$\sigma_{ll} = l_x^2\sigma_{xx} + l_y^2\sigma_{yy} + l_z^2\sigma_{zz} + 2l_xl_y\sigma_{xy} + 2l_yl_z\sigma_{yz} + 2l_xl_z\sigma_{xz} \quad (4)$$

Where, σ_{ll} is the normal stress measured in the direction of *l* in AE tests and l_x, l_y *and* l_z are the direction cosines local coordinate system and Cartesian coordinate system. Eq. 4 yields six simultaneous equations that are used to calculate stress tensor in the mine grid. For this purpose solver in excel were used to calculate stress tensor by minimizing the sum of squared errors between stresses calculated by solver and measured average normal stresses from AE and DRA analysis. The stress tensor calculated for depth of 640m is given below (in MPa):

$$\begin{bmatrix}\sigma_{xx} & \sigma_{xy} & \sigma_{xz}\\ \sigma_{yx} & \sigma_{yy} & \sigma_{yz}\\ \sigma_{zx} & \sigma_{zy} & \sigma_{zz}\end{bmatrix} = \begin{bmatrix}10.03 & 9.66 & 3.60\\ 9.66 & 21.47 & -2.26\\ 3.60 & -2.26 & 15.67\end{bmatrix}$$

We can see that normal stress at N-S direction is 10.03 MPa, E-W is 21.47 MPa and Vertical direction is 15.67 MPa.

Shear stresses found in the direction of N-S/E-W are 9.66 MPa and N-Vertical 3.60 MPa and E-Vertical is -2.26 MPa.

In the same manner, stress tensor is calculated for 915m depth as (in MPa):

$$\begin{bmatrix}\sigma_{xx} & \sigma_{xy} & \sigma_{xz}\\ \sigma_{yx} & \sigma_{yy} & \sigma_{yz}\\ \sigma_{zx} & \sigma_{zy} & \sigma_{zz}\end{bmatrix} = \begin{bmatrix}26.30 & 3.73 & 8.33\\ 3.73 & 13.87 & 6.60\\ 8.33 & 6.60 & 24.39\end{bmatrix}$$

4.2 Principal Stresses Calculations

Having calculated stress tensor, principal stress components can be calculated by Eigenvalue analysis. Using Matlab, principal stress components can easily be calculated. As described by Brady and Brown (1994), characteristic equation also known as cubic equation in principal stress (σ_p) calculation is given by:

$$\sigma_p^3 - I_1\sigma_p^2 + I_2\sigma_p - I_3 = 0 \quad (5)$$

where, the quantities I_1, I_2 and I_3 are first, second and third stress invariants given as:

$$I_1 = \sigma_{xx} + \sigma_{yy} + \sigma_{zz} \quad (6)$$

$$I_2 = \sigma_{xx}\sigma_{yy} + \sigma_{yy}\sigma_{zz} + \sigma_{xx}\sigma_{zz} - (\sigma_{xy}^2 + \sigma_{yz}^2 + \sigma_{zx}^2) \quad (7)$$

$$I_3 = \sigma_{xx}\sigma_{yy}\sigma_{zz} + 2\sigma_{xy}\sigma_{yz}\sigma_{zx} - (\sigma_{zz}\sigma_{xy}^2 + \sigma_{xx}\sigma_{yz}^2 + \sigma_{yy}\sigma_{zx}^2 \quad (8)$$

There are three distinct values of σ_p (principal stress) that provide solutions of the characteristic Eq. 5 by some general method. Three distinct values of the principal stresses; σ_1, σ_2, σ_3 are identified as major, intermediate and minor principal stresses respectively (Brady and Brown 1994). Similar procedures to calculate principal stresses are also described by Villaescusa et al. (2002).

Table 2. Principal stress magnitude and their directions in the mine grid.

Principal stresses	Depth, m	Magnitude MPa	Trend (°)	Plunge (°)*
σ_1	640	26.97	240.5	1.0
σ_2		17.10	333.4	71.3
σ_3		3.08	150.2	18.7
σ_1	915	36.08	24.5	41.4
σ_2		17.79	156.4	37.1
σ_3		10.68	268.5	26.5

Based on the assumptions described earlier, Table 2 summarizes the principal stresses at

640m and 915m depths. As can be seen from these results principal stresses are orthogonal to each other indicating correct calculations.

5 CONCLUDING REMARKS

Unconventional AE and DRA are proven to be practical, effective and low cost methods in estimation of in-situ stresses from cored rocks. These techniques are very efficient for the cases where there is no access to underground. Main difficulty arises when the cumulative acoustic emission curve does not include a clear take-off point where the use of DRA will be required to cross validate AE results. It was also found that filtering the outside noise is the imperative stage in AE analysis. Threshold values in the range of 15mV and 150mV were found to be the best range to locate point of inflexion in AE analysis. Threshold values less than 15mV and above 150mV will conceal the point of inflexion leading to inaccurate estimation of stresses. It is observed that use of four axial strain gauges also improved the results of DRA which supports the argument postulated by Hsieh et al. (2013).

Lastly, when calculating stress tensor, particular attention should be given to conversion of sub-core orientations to mine grid as this will influence the principal stress calculations.

ACKNOWLEDGEMENTS

Brett Triffett, Technical Manager, and Robert Bluff, Study Manager from OZ Minerals are gratefully acknowledged for their supports for the project. Lab technicians Adam Ryntjes and Simon Golding are also thanked for their time and effort in the preparation and testing of the core samples.

REFERENCES

Fairhurst, C., 2003. Stress estimation in rock: a brief history and review, *International Journal of Rock Mechanics & Mining Sciences* 40; 957–973.

Hsieh, A., Dyskin, A.V., Dight, P.M. 2013. The influence of sample bending on deformation rate analysis stress reconstruction, *International Journal of Rock Mechanics and Mining Sciences* 64; 90-95.

Kaiser, E.J., 1953. A Study of Acoustic Phenomena in Tensile Test. *Technische Hochschule München*, Munich, pp. 43.

Karakus, M, 2014. Quantifying the Discrepancy in pre-loads Estimated by Acoustic Emission and Deformation Rate Analysis, *International Society for Rock Mechanics, European Rock Mechanics Symposium*, Vigo, Spain.

Lavrov, A., 2003. The Kaiser effect in rocks: principles and stress estimation techniques. *International Journal of Rock Mechanics and Mining Sciences* 40; 151–171.

Li, C. and Nordlund, E.,1993. Experimental Verification of the Kaiser Effect in Rocks, Rock *Mech. Rock Engng.* 26 (4); 333-351.

Mori, Y., Obata, Y., Sikula, J., 2009. Acoustic and electromagnetic emission from crack created in rock sample under deformation, *Journal of Acoustic Emission* 27; 157-166.

Seto, M., Utagawa, M., Katsuyama, K., Kiyama, T., 1998. In Situ Stress determination using AE and DRA techniques, *International Journal of Rock Mechanics and Mining Sciences*,35(4-5); 458-459.

Seto, M., Nag, D.K., Vutukuri, V.S., 1999. In-situ rock stress measurement from rock cores using the acoustic emission method and deformation rate analysis. *Geotechnical and Geological Engineering* 17; 241–266.

Simmons, G., Siegfried, R.W. II, Feves, M., 1974. Differential strain analysis: new method for examining cracks in rocks. *J. Geophys.* Res. 79; 4383-4385.

Strickland, F.G., Ren, N.K., 1980. Use of differential strain curve analysis in predicting in-situ stress state in deep wells. Proc. 21st. *U. S. Symposium on Rock Mechanics.* pp.523-532.

Villaescusa, E., Seto, M., Baird, G., 2002. Stress measurements from oriented core, *International Journal of Rock Mechanics and Mining Sciences* 39; 603-615.

Yamamoto, K., Kuwahara, Y., Kato, N., Hirasawa, T., 1990. Deformation rate analysis: A new method for in situ stress estimation from inelastic deformation of rock samples under uniaxial compressions. *Tohoku Geophys. J.* (Sci. Rep. Tohoku Univ., Ser. 5), 33; 127–147.

Yamamoto, K., 2009. A theory of rock core-based methods for in-situ stress measurement, Earth Planets Space, 61:1143-1161.

Yuan, R.F., Li, Y.H., 2008. Theoretical and experimental analysis on the mechanism of the Kaiser effect of acoustic emission in brittle rocks, *Journal of University of Science and Technology Beijing*, 15(1); 1-4.

Assessment of In Situ Behaviour and Properties of Cemented Paste Backfill: Influence of Stope Height

E. Yilmaz
University of Quebec in Abitibi-Témiscamingue (UQAT), Department of Applied Sciences, 445 Boul. de l'Université, Rouyn-Noranda (Québec) J9X 5E4 Canada

ABSTRACT This paper presents key results from an experimental study aimed at examining the effect of stope depths (i.e. 0 m that imitates near the top of a given stope, 5 m, 10 m, 15 m and 20 m that imitates near the bottom of a given stope) on in situ behaviour and properties of cemented paste backfill CPB. Based on a new laboratory tool (CUAPS: curing under applied pressure system), all samples were prepared using the binder contents of 3, 4.5 and 7 wt% and tested after curing of 7, 14 and 28 days. One can state that as the stope depth increases, the CPB's strength increases. This may be explained by lower porosity and higher solid contents at the bottom of the stope (20 m) than higher porosity and lower solid content at the top of the stope (0 m). An evolution of CPB's geotechnical and chemical properties were also presented.

Keywords: Cemented paste backfill, Stope height, In situ properties, In situ behaviour

1 INTRODUCTION

Mine wastes generated and disposed at mine sites are problematic, because they contain harmful substances and require monitoring, treatment and safe disposal. Some techniques have been developed in the mining industry in order to prevent, rectify, lessen or remove the potential environmental impacts of mine wastes (Grice, 2001; Potvin et al., 2005; Bussière, 2007; Yilmaz, 2011). One practical tailings management system for underground mines involves refilling detrimental wastes as paste backfill into underground stopes created by ore extraction (Archibald et al., 2001; Kump, 2001; Landriault et al., 2001; Henderson et al., 1998; Benzaazoua et al., 1999; Ercikdi et al., 2012).

Cemented paste backfill CPB has become an increasingly popular system of optimizing underground mine excavations and tailings management systems to obtain a number of operational, economic and environmental benefits (Landriault, 2006). CPB is basically defined as a complex mixture of fine tailings (having 70-85 wt% solids), single or binary binder (usually 2-7 wt%) and sufficient water (required for reaching 15-25cm slump). Most investigations to date have been done on the backfill quality, and have focused on effect of tailings, binder and water (Benzaazoua et al., 2002, 2004; Kesimal et al., 2003, 2004, 2005; Fall et al., 2005, 2010; Cihangir et al., 2008; 2012; Ercikdi et al., 2009, 2010, 2014; Yilmaz et al., 2009, 2011; Ouattara et al., 2010; Fall and Pokharel, 2011; Abdul-Husain and Fall, 2012; Wu et al., 2013). But, CPB presents some difficulties with regard to the representativeness of laboratory samples and data to actual in situ materials. In fact, replicating field CPB placement and curing conditions at laboratory using plastic moulds is a challenging task, first, because it is not possible to exactly duplicate field conditions, and second, due to the absence of appropriate lab equipment and methods (Ouellet et al., 1998; le Roux et al., 2005; Orejarena and Fall, 2011; Pokharel and Fall, 2013).

The behaviour and properties of field CPB material vary principally depending on the method of preparation, placement method and particular mine conditions. Once CPB is prepared at paste plant, it is delivered (via pump or gravity) into mined-out stopes at a proper filling rate. The quicker filling rate may lead to a failure of the barricade formed. CPB is usually held in place by barricades, built across the access drift near the bottom of the stope. It is vital the pressures induced

by paste backfill do not surpass the barricade strength as costs and safety hazards linked with their failure are considerable (Bloss and Mathew, 2001; Cayoutte, 2003; Belem et al., 2004, 2010; Revell and Sainsbury, 2007; Yumlu and Guresci, 2007; Dehn et al., 2007; Grabinsky and Thompson, 2009; Thompson et al., 2010; Hughes et al., 2010). In order to design an efficient backfilling strategy, it is indispensable to assess the stress state within CPB, which often evolves over hydration. As the paste backfill's stiffness is weaker than the surrounding rock walls, it tends to settle under self-weight upon placement and create shear stresses along the rough wall surfaces. This can induce an arching effect that affects the stress distribution in stope (Hassani et al., 1998; Belem et al., 2004; Fourie et al., 2007; Pirapakaran and Sivakugan, 2007; Li et al., 2005; Li and Aubertin, 2010; Grabinsky, 2010; Thompson et al., 2012; Emad et al., 2013; El Mkadmi et al., 2014).

In current practice, the performance and properties of CPB samples are assessed by unconfined compression testing undertaken on laboratory-prepared samples with plastic moulds. But, this test does not allow backfill designers to consider how consolidation and hydration mechanisms influence the strength and stress distribution in the stope (Ouellet et al., 2005, 2006; Belem et al., 2007; Helinski et al., 2007, 2011; Yilmaz et al., 2011, 2012; Veenstra et al., 2011). A number of works have shown that, for a given backfill recipe, there are the huge differences between lab and in situ samples, whose performance are known to be underestimated. The observed differences between samples are attributable to specimen size effects, placement methods and field curing conditions (Cayoutte, 2003; Belem et al., 2007; Fourie et al., 2007; Fahey et al., 2011; Helinski et al., 2011; Yilmaz et al., 2014, 2015a,b).

It should be however confessed that more info is needed to have a better understanding of field paste backfill properties. In situ testing is crucial to obtain a real mechanical CPB response in order to improve the design of the backfilled stopes, and thus to improve safety and cut costs involved. Fortunately, these properties can be well simulated in the laboratory using a modified apparatus called the CUAPS (curing under applied pressure system; Benzaazoua et al., 2006; Yilmaz et al., 2010) which allows for the application of different pressure increments to the backfill samples during curing. As a result, aspects linked to in situ properties and conditions of CPB samples that affect greatly its strength and durability performance need to be further investigated experimentally.

The originality of this paper consists in the assessment of the influence of different stope heights and stope filling rates on behaviour and properties of CPB samples, employing sing the CUAPS apparatus. A number of the backfilled stope height scenarios, namely, 0 m (often used as control samples or mould-poured sample cured under zero pressure), 5 m, 10 m, 15 m, and 20 m were considered. In this case, 0 m simulates near the top of a given backfilled stope while 20 m simulates near the bottom of a given backfilled stope). An evolution of mechanical and geotechnical properties of paste backfills were made using different binder contents (3, 4.5 and 7 wt%) and curing times (7, 14 and 28 days).

2 MATERIALS AND METHODS

2.1 Materials

Tailings samples were taken representatively from a hard rock polymetallic mine located in Eastern Canada for laboratory preparation of paste backfill mixtures. A small portion of paste samples were air dried to conduct a set of experimental tests needed for the material characterization. All the tests were conducted consistent with American Society of Testing Materials standards and testing procedures. The entire tests were done in triplicate and their average results are reported. Additional knowledge on material characterization tests can be found in Yilmaz (2010).

2.1.1 Physical characterization testing of tailings and binders

The particle size distribution of the tailings used was analysed by a Malvern Mastersizer laser diffraction particle size analyser and shown in Figure 1. Besides, Tables 1 lists the

physical properties of tailings and binders. It can be observed that tailings were found to have a 45% fraction finer than 20 µm and more broadly graded with a coefficient of uniformity C_u (D_{60}/D_{10}; D_{60}: grain diameter at which 60% of the material passes, µm; D_{10}: particle diameter at which 10% of the material passes, µm) of ~8.

Specific gravity G_s and specific surface S_s of tailings and binders used in the study was measured using a Micromeritics AccuPyc 1330 helium pycnometry to be 3.7 and 2.9, and a Micromeritics Gemini surface analyzer to be 2.2 and 3.2 for tailings and binder, respectively. The relatively-high G_s value of tailings can be explained by their sulphide content (note that higher sulphide content implies higher density). The S_s of the tailings augments with increasing fine contents.

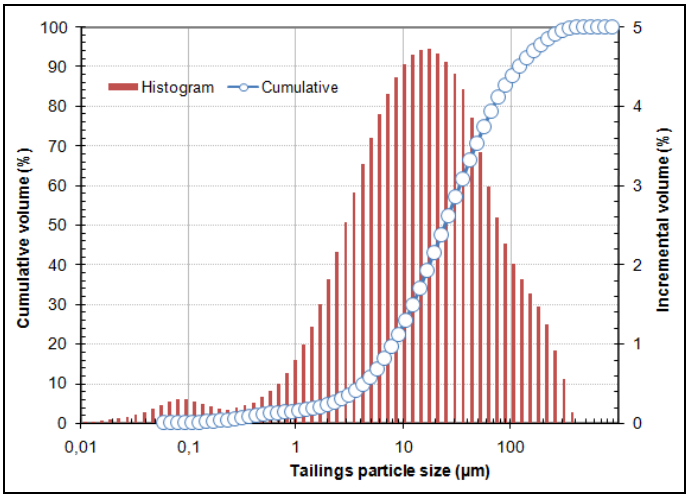

Figure 1. Cumulative and incremental grain size distribution of the studied tailings

2.1.2 Chemical and mineralogical testing of tailings and binders

The chemical composition of the tailings and binders used in this study was determined by a Perkin-Elmer Optima 3100 RL ICP-AES (inductively coupled plasma-atomic emission spectroscopy) and the obtained results were recorded in Table 2. The tailings contained 39.2% Fe_2O_3 and 51.3% total sulphur as determined by major oxide and elemental analysis, respectively. The slag-based binder contained 42.8% CaO, 30.9% SiO_2, 8.4% Al_2O_3 and 6.2% MgO.

Table 2. Chemical characterization testing of tailings and binders

Mineral (wt%)	Tailings (100%)	PCI-Slag (20-80%)	PCI (100%)	Slag (100%)
Al_2O_3	5.29	8.39	4.86	10.24
B_2O_3	0.61	0.13	0.03	0.48
CaO	0.79	42.82	65.76	31.41
Fe_2O_3	39.2	0.64	2.44	0.55
K_2O	0.24	0.55	0.83	0.51
MgO	0.16	6.19	2.21	11.29
Na_2O	0.40	2.03	2.11	2.01
SO_3	51.34	3.35	3.67	3.27
SiO_2	1.07	30.91	19.51	36.22
TiO_2	0.07	0.48	0.26	0.61
ZnO	0.44	0.00	0.03	0.00

The mineralogy of tailings was determined using the Bruker AXS D8 Advance X-ray diffractometer and evaluated using Rietveld full-pattern fitting method equipped with the TOPAS software. The X-ray diffraction and semi quantitative analyses revealed that the most abundant mineral within paste tailings was pyrite (47%), followed by quartz (32%), chlorite (9%), paragonite (7%), muscovite (3%), talc (1%) and gypsum (1%).

Table 1. Physical properties of paste tailings and hydraulic binders used in the experiments

Element (unit)	S_s (m^2/g)	G_s (-)	D_{10} (µm)	D_{30} (µm)	D_{50} (µm)	D_{60} (µm)	D_{90} (µm)	C_u (-)	C_c (-)	U (-)
Paste tailings	2.17	3.71	4.26	12.2	24.3	33.6	119.2	7.88	1.04	4.73
PCI-Slag / 20-80%	3.15	2.93	0.55	3.6	8.1	10.9	27.4	19.7	2.15	3.30
PCI (100%)	1.59	3.08	3.8	3.8	8.2	11.1	33.4	27.0	3.07	4.02
Slag (100%)	3.55	2.89	0.5	3.1	7.3	9.8	22.9	19.4	2.01	3.07

Note: S_s: specific surface area; G_s: specific gravity; C_u: Coefficient of uniformity (D_{60}/D_{10}); C_c: Coefficient of curvature ($D_{30}^2/D_{60}\times D_{10}$); U: Uniformity of graduation (D_{90}-D_{10})/D_{50}).

2.1.3 Geochemical testing of mixing water

The two types of mixing water: namely, as-received tailings interstitial water and added tap water were used for the preparation of CPB mixes. The concentrations of species in the mixing water were chemically analyzed using the ICP-AES method. Table 3 lists the results of chemical and geochemical testing. It can be observed clearly that the tailings interstitial water is highly aggressive in terms of sulphate content (SO_4^{2-} content around 4880 ppm) but also contains calcium (Ca content about 560 ppm). The origin of the sulphate was likely ferrous and/or copper sulphate that was added for cyanide removal (tailings are treated before mine backfilling), precipitating iron/copper cyanide complexes. Besides, the origin of calcium was likely the lime added during ore processing plant (often used as pH modifier).

Table 3. Geochemical analysis of tailings interstitial water and additional tap water

Relevant parameters	Tailings interstitial water	Added tap water
Al (mg/L)	0.21	0.01
Ca (mg/L)	560	40.9
Cu (mg/L)	0.29	0.84
Mg (mg/L)	1.83	2.27
SO_4^{2-} (mg/L)	4880	120
Si (mg/L)	0.89	0.90
K+ (mg/L)	32	0.71
pH	9.41	7.82
ORP (volt)	0.15	0.43
EC (mS/cm)	7.42	0.27

ORP: Oxidation-reduction potential; EC: Electrical conductivity

A Benchtop pH/ISE meter Orion Model 920A coupled with a Thermo Orion Triode combination electrode was employed for the pH, oxidation-reduction potential (ORP) and electrical conductivity (EC) measurements and the results obtained were tabulated in Table 3. The pH, ORP and EC of tailings interstitial and tap water were 9.4, 0.15 volt and 7.42 mS/cm, and 7.82, 0.43 volt and 0.27 mS/cm, respectively. The relatively high EC observed within interstitial water shows the presence of dissolved conducting ions.

2.1.4 Mixing and curing of paste backfills

The paste ingredients (that contain a range of proportions of different hydraulic binders, a predetermined amount of tailings and mixing water) were weighed. The constituents were then mixed homogenously for 10-15 minutes using an electrical Hobart A200 model mixer until the paste having a fixed slump content of ~18 cm was achieved. Slump is a measure of paste consistency and obtained using the standard 12-inch-high concrete industry cone slump apparatus. The samples were prepared using three different binder contents: 3, 4.5 and 7 wt% for slag-based binder (note that only 4.5 wt% binder proportion was used for both general use Portland cement (PCI) alone and fly ash-based binders. The backfill mixes produced were then poured into the Perspex moulds of 10 cm in diameter and 20 cm high. The prepared moulds were then sealed to keep away from evaporation and oxidization and cured in the newly-developed laboratory apparatus (CUAPS: curing under applied pressure system) for curing of 7, 14 and 28 days. Samples were left to cure in the foggy room maintained at 70% relative humidity and 25°C temperature to repeat underground mine conditions until compression testing. Figure 2 demonstrates a number of CUAPS apparatuses filled with paste backfill mixes and cured in the humidity chamber.

Figure 2. Photo showing the backfill samples cured within the CUAPS apparatus

2.2 Methods

2.2.1 Developed experimental setup

A schematic representation of the laboratory setup developed to simulate different in situ and curing conditions is shown in Figure 3. The setup consists mainly of three parts: *i*) a top loading device intended to apply vertical stress to the CPB sample at air pressures up to 600 kPa (with an LVDT for measuring vertical deformation and a loading piston), *ii*) a Perspex mould to hold CPB sample in the middle part ($D \times H$: 102 × 204 mm) covered by metal cylinder and *iii*) a bottom drainage hole (equipped with a pore water pressure transducer) to drain free water from sample. A full description of the CUAPS apparatus is beyond the scope of this paper. However, ordetailed information on its features can be found elsewhere (Benzaazoua et al., 2006; Yilmaz et al., 2010; Yilmaz, 2010).

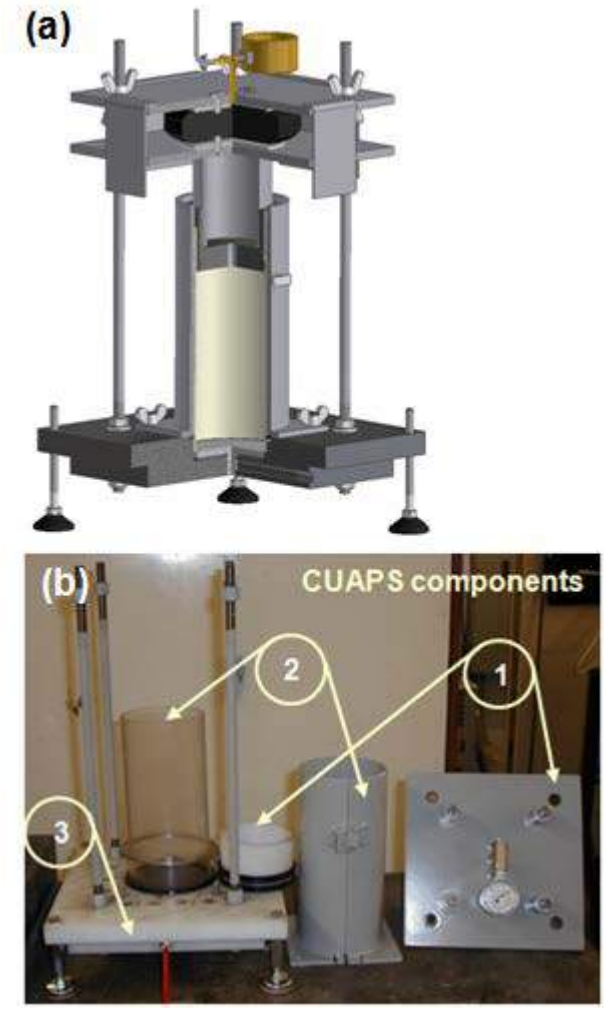

Figure 3. The developed experimental set-up: a) schematic illustration, and b) the essential components of the CUAPS apparatus

2.2.2 Backfilled stope height tests

These tests aimed to reproduce the influence of different stope filling rates and backfilled stope heights on the resultant properties of CPB samples. A number of the test scenarios that consider the four different stope heights h of 5, 10, 15 and 20 m were implemented to CPB samples. The scenarios experimented were based on the applied vertical pressure which can be taken as overburden pressure, as shown in Eq. [1] below.

$$p_v = \rho \times g \times h = \gamma_{wet} \times h \qquad [1]$$

Where, p_v is the ultimate applied vertical pressure (kPa); ρ is the density of the fluid paste backfill mixtures; γ_{wet} is the hydrostatic or pressure; h is the height of the backfilled stope; g is the gravitational constant.

Table 4 and Figure 4 provide a number of pressure application scenarios during testing simulating the underground backfilled stope heights. One can state that during the first 12 hours after the CPB's placement, no pressure was applied vertically.

Table 4. The different pressure scenarios for simulating the backfilled stope heights

Elapsed time (hours)	Applied vertical pressure p_v (kPa)	Equivalent height h (m)	Equivalent filling rate (m/h)
Scenario A (stope height = 5 m)			
12	28	1.3	0.10
24	57	2.5	0.10
48	*113*	*5.0*	*0.10*
Scenario A (stope height = 10 m)			
12	57	2.5	0.21
24	113	5.0	0.21
48	*227*	*10.0*	*0.21*
Scenario C (stope height = 15 m)			
12	85	12.3	1.03
24	170	24.6	1.03
48	*340*	*49.3*	*1.03*
Scenario D (stope height = 20 m)			
12	113	16.4	1.37
24	227	32.9	1.37
48	*453*	*65.7*	*1.37*

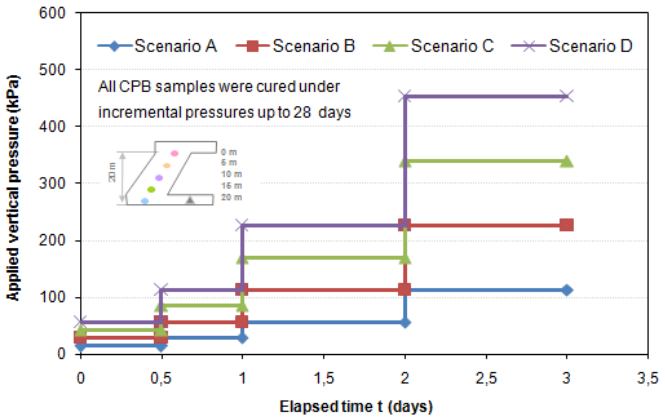

Figure 4. Plot of the four different backfilled stope heights based on applied pressure

After that, pressures were progressively increased up to the final pressure of 113 kPa (scenario A: stope height = 5 m), 227 kPa (scenario B: stope height = 10 m), 340 kPa (scenario C: stope height = 15 m) and 453 kPa (scenario D: stope height = 20 m) for a total duration of 48 hours, corresponding to a filling rate sequence of 0.1, 0.21, 1.03, and 1.37 m/h. Each sample was then left to cure for 7, 14 and 28 days (see Table 4). These tests were run to consider the quality and behaviour of in situ cemented paste backfills and compare it to that of CPB samples in the laboratory conditions. All pressures were applied to paste backfill samples within a curing period of 48 hours and left to cure for 7, 14, and 28 days.

2.2.3 Unconfined compression tests

Following the prescribed curing times of 7, 14, and 28 days, all the CPB samples were extracted gently from their Perspex moulds using a manual push specimen extruder. The two ends of the Perspex mould filled up with paste backfill samples were open and the two porous discs (both at the bottom and the top of Perspex mould) were placed at these ends for better practising the pressures to samples without having any significant damage. After paste backfill cylinder faces were rectified in order to provide a flat surface, the length and weight of the samples were measured and recorded. CPB samples were subsequently subjected to unconfined compression testing (UCS) in order to determine their mechanical strength acquisitions.

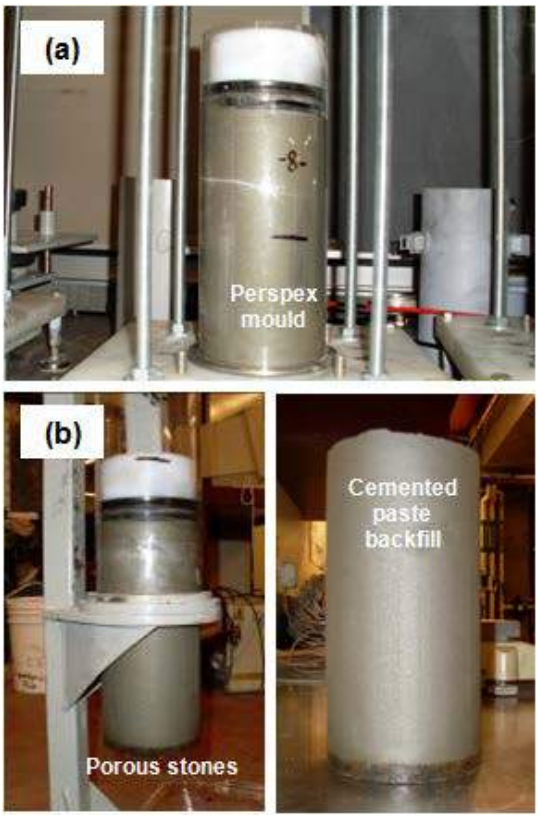

Figure 5. Photos of a) a Perspex cylinder filled with paste backfill and b) sample extractor and extracted CPB sample

The UCS tests of CPB samples were done using an automatic mechanical press (MTS 10/GL; Figure 6). The press has a nominal loading capacity of 50 kN. The compression tests were performed at a stable deformation rate of 1 mm/min. Axial deformations were automatically recorded by an electronic data acquisition system. The observed UCS value corresponds to the maximum stress (failure peak) reached during the compression test. The average values from triplicate tests were presented in the results.

Figure 6. CPB sample subjected to UCS test

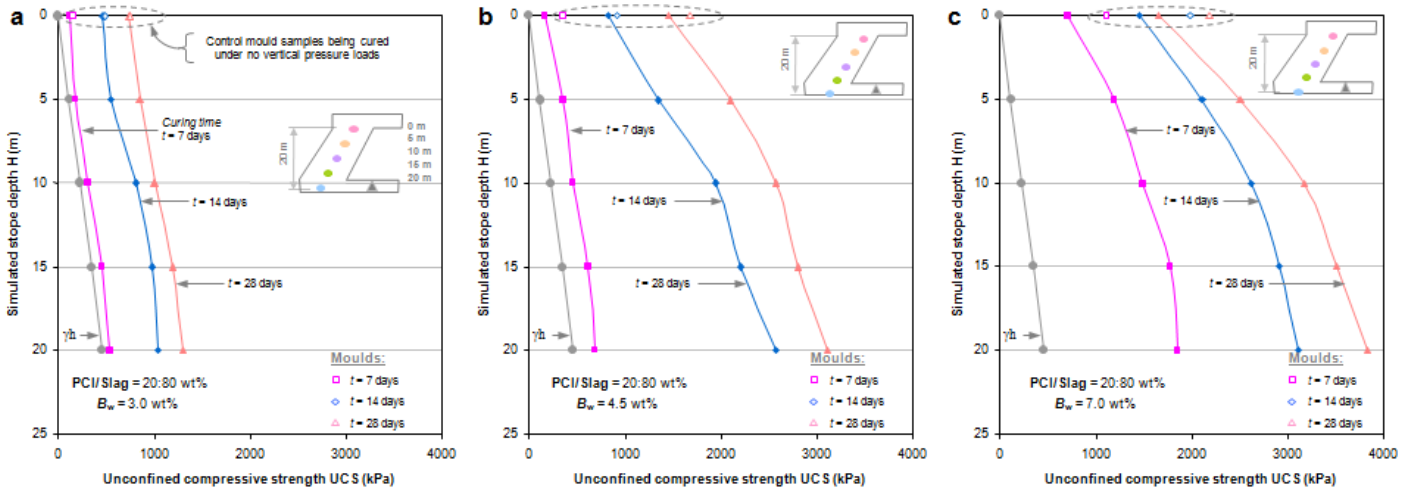

Figure 7. Variation in compressive strength with simulated stope heights for CPB samples containing slag-based binder: a) 3wt% binder, b) 4.5 wt% binder, and c) 7wt% binder.

3 RESULTS AND DISCUSSION

3.1 Effects of Simulated Stope Heights on Compressive Strength of Paste Backfill

Figure 7 shows an evolution of compressive strength with the simulated stope height for the paste backfills placed in a "virtual" stope. Note that the stope depth is taken as the dept from the top of the newly added paste fill layer. As expected, CPB's strength increases with increasing depth for a given curing time, following the same trend as overburden pressure ($\sigma_v = \gamma \times h$). After curing of 28 days, a compressive strength of 1.5, 2.1, 2.6 and 3.1 MPa were obtained from CPB samples containing 4.5wt% of slag-based binder at stope depths of 0, 5, 10, 15 and 20 m, respectively. This confirms that compressive strength of the backfilled stopes increases from the top to the bottom due to self-weight consolidation effect. In fact there are others which may greatly affect the reason why the lower part of stope produce higher strengths than the upper part of the stope. These are self-desiccation (improved effective stress) and backfilling rate (void ratio reduction and increased solid content).

Figure 8 also shows paste backfill strength with the stope dept. Samples were prepared at 4.5wt% of three different binding agents as a function of 7, 14 and 28 days. Results indicate that, at 14 and 28 days, slag-based binders create much more strengths than both general use Portland cement alone and fly ash-based binders because of their included additive amount and chemical composition. This strength difference observed remained the same during the course of 7 days.

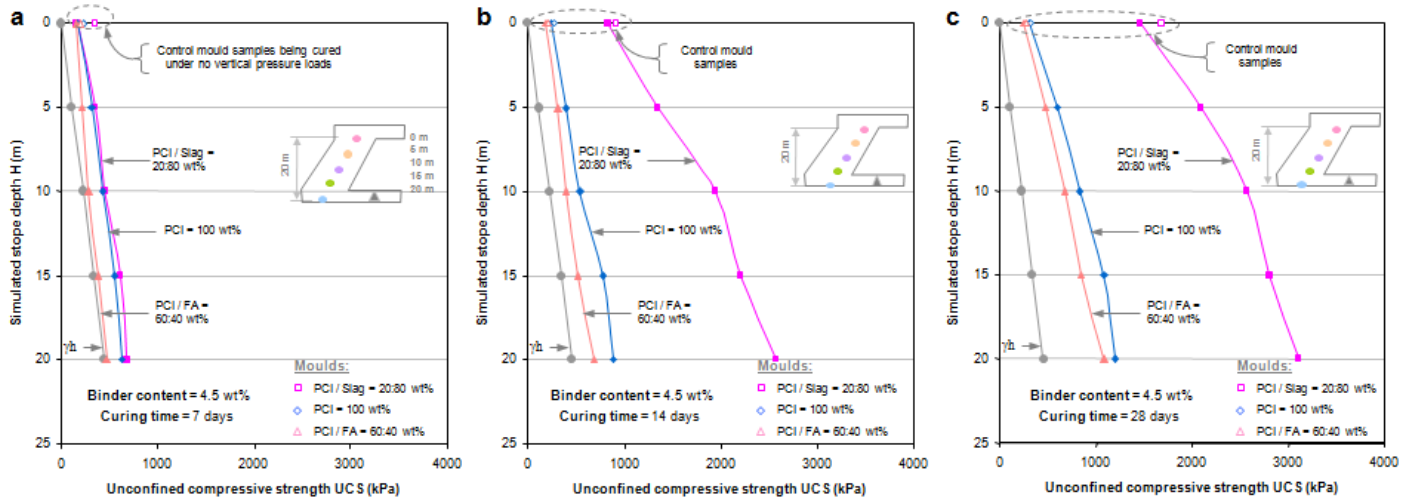

Figure 8. Variation in compressive strength with simulated stope heights for CPB samples containing different binder agents: a) 7 days, b) 14 days, and c) 28 days.

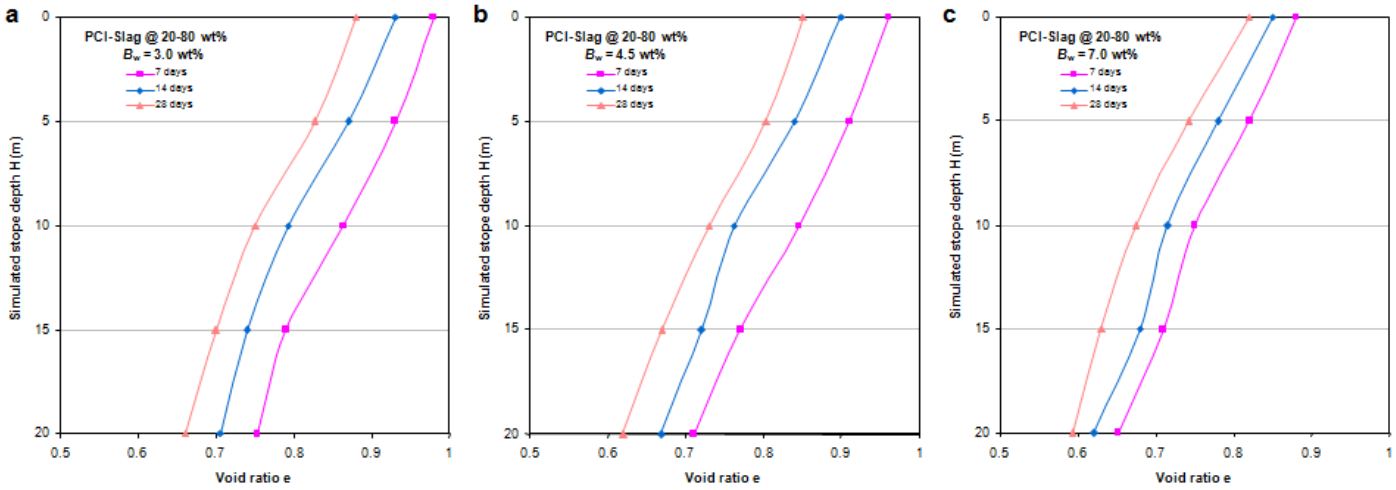

Figure 9. Variation in void ratio (porosity) with simulated stope heights for CPB samples containing slag-based binder: a) 3wt% binder, b) 4.5 wt% binder, and c) 7wt% binder.

3.2 Effects of Simulated Stope Heights on Void Ratio (Porosity) of Paste Backfill

Figure 9 illustrates an evolution of void ratio with the simulated stope heights for CPB samples having slag-based binder. Overall, the void ratio ranges between 0.6 and 1 for all samples. It can be inferred from Figs. 9 and 10 that the void ratio or porosity reduces with increasing backfilled stope depth since the corresponding relative density increases as a result of applied consolidation pressure (newly-added layer with 5 m height creates extra pressure over the already-added layer) during curing. One can say that void ratio of the backfill samples near the top of the stope changes between 0.85 and 0.95 while the void ratio of samples near the bottom of the stope changes between 0.65 and 0.85.

This is because the lower the void ratio, the closer the paste backfill particle packing, and accordingly, the lower the friction angle that develops and the stronger the material (corresponding to high cohesion). Figure 10 shows an evolution of porosity with different paste backfilled stope depths as a function of different binding agents. Observation can make clearly that CPB containing slag-based binder gives less porosity than those obtained from samples with fly ash-based binder and general use Portland cement. After curing of 7 days, there are no big differences between samples due to the fact that cement hydration products could not get well being filled with the gaps between solid particles. However, as curing time increases from 7 days to 28 days, the related porosity decreases notably.

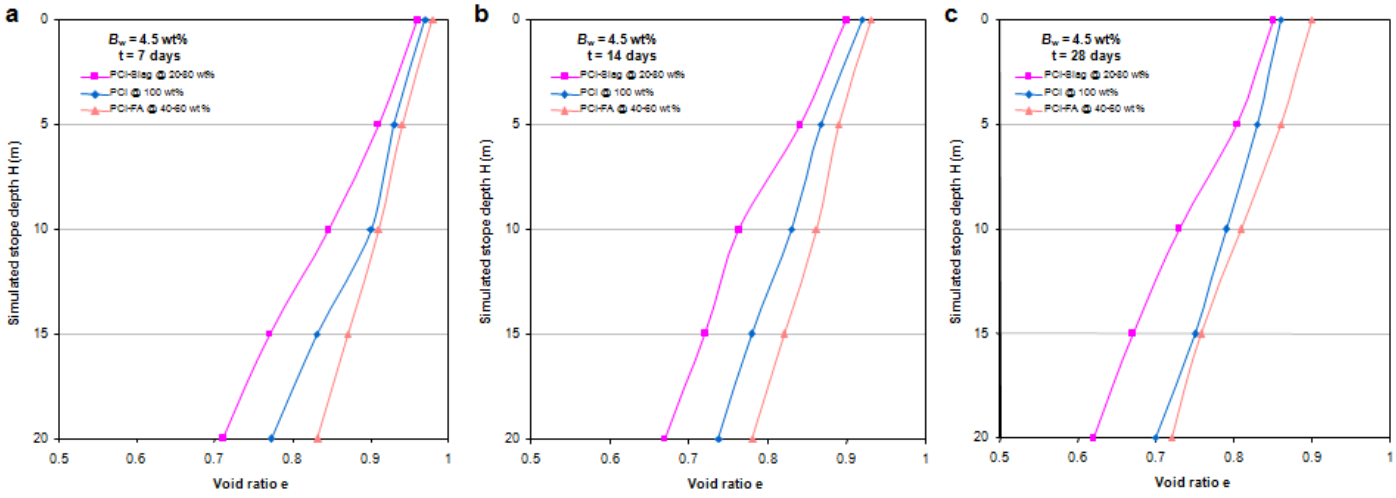

Figure 10. Variation in void ratio (porosity) with simulated stope heights for CPB samples containing different binder agents: a) 7 days, b) 14 days, and c) 28 days.

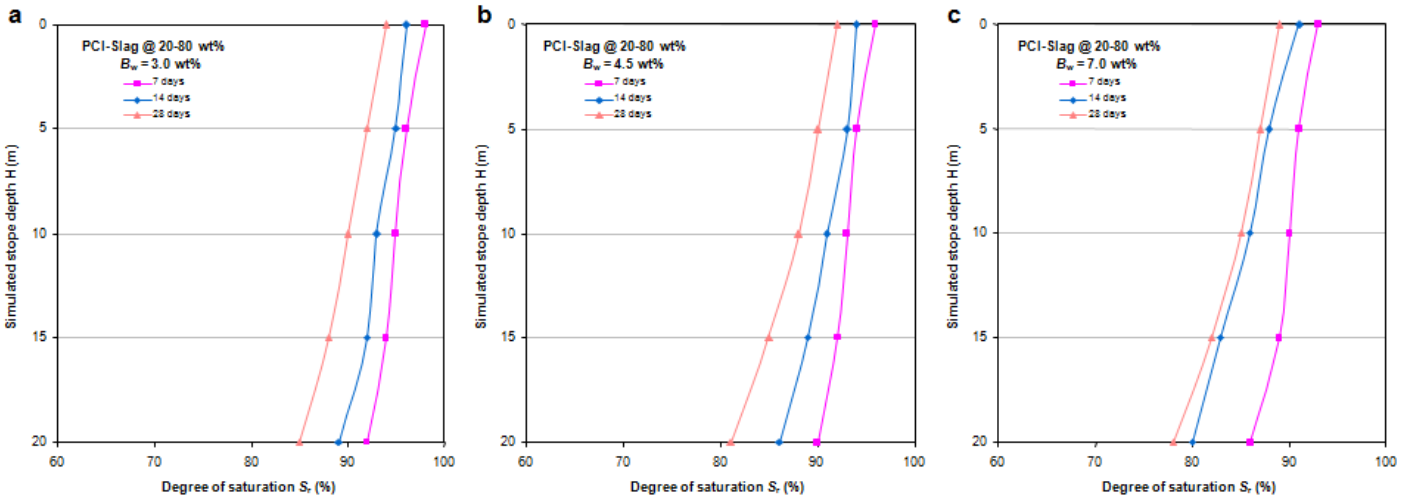

Figure 11. Variation in degree of saturation with simulated stope heights for CPB samples containing slag-based binder: a) 3wt% binder, b) 4.5 wt% binder, and c) 7wt% binder.

3.3 Effects of Simulated Stope Heights on Degree-Of-Saturation of Paste Backfill

Figure 11 presents the variation in degree of saturation with the simulated stope depth for CPB samples containing slag-based binder. The overall trend is that degree-of-saturation reduces slightly with increasing curing time and binder content for the whole samples. In general, the degree of saturation ranges 85-98% for 7 days, 81-95% for 14 days, and 78-92% for 28 days. The amount of the binder added to the paste backfill mxiture is directly related to their saturation index value. This means that the higher are the binder contents and curing times, the greater are the cement hydration products, thereby reduced degree of saturation for a given CPB material.

Figure 12 demonstrates an evolution of the degree of saturation with stope depth for the samples with three different binding agents. After 7 days, the degree of saturation for all samples remains 90-99% while, the samples cured after 28 days, the degree of saturation decreases remarkably up to 80%. Moreover, the degree of saturation is highly affected by the drainage or consolidation of cemented paste backfills. It is quite apparent that the CPB samples containing the highest binder content (7 wt%) exhibits the lowest degree of saturation, when compared to the remaining binder contents (3 and 4.5 wt%). This could be explained readily by the different water-to-cement ratios and the amounts of water required for binder hydration.

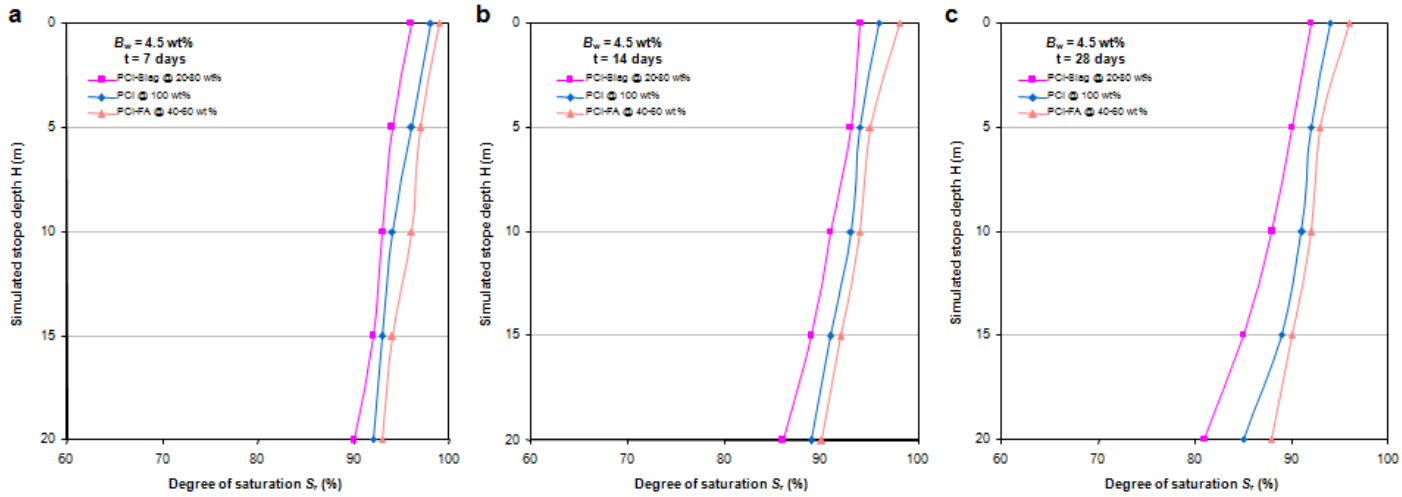

Figure 12. Variation in degree of saturation with simulated stope heights for CPB samples containing different binder agents: a) 7 days, b) 14 days, and c) 28 days.

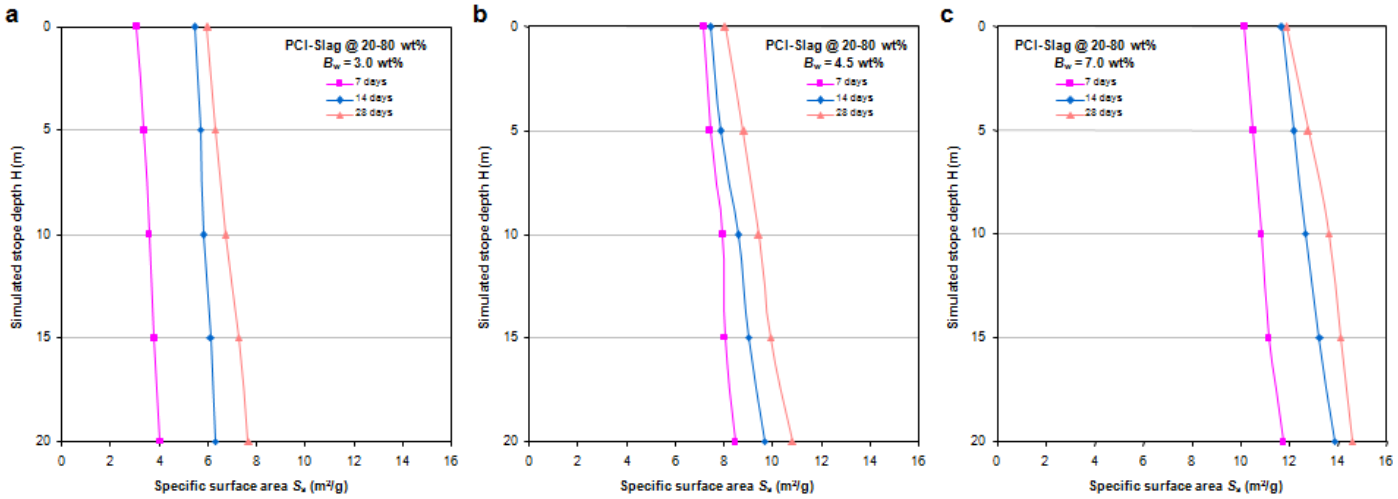

Figure 13. Variation in specific surface area with simulated stope heights for CPB samples containing slag-based binder: a) 3wt% binder, b) 4.5 wt% binder, and c) 7wt% binder.

3.4 Effects of Simulated Stope Heights on Specific Surface of Paste Backfill

Figure 13 presents the evolution of specific surface area with simulated stope depth for CPB samples with slag-based binder. Note that specific surface is directly related to the hardening phase formation during curing. The higher the binder ratio used, the higher the specific surface of CPB becomes due to the growth of hydration products. In general, the specific surface of paste backfill ranges 4-8 m^2/g for 7 days, 8-11 m^2/g for 14 days, and 12-15 m^2/g. Specific surface increases with the increasing stope depth and curing time for a given binder content. The highest specific surfaces were obtained from CPBs near the bottom of the stope ($\leq$ 11 m^2/g).

One can remark that the change in specific surface area has remained limited since all the CPB samples were consolidated under progressively-increased pressures or stresses during curing. Figure 14 shows an evolution of specific surface area with stope depths for the backfills containing the 4.5wt% of three different binding agents. The lowest specific surface area values were obtained from CPB samples with fly ash based binders (6, 7, and 8 m^2/g for 7, 14, and 28 days, respectively). The greatest specific surfaces were obtained from CPB samples with slag-based binders (9, 10, and 11 m^2/g for 7, 14, and 28 days, respectively). Note that the increased specific surface may be explained by formation and contribution of precipitated hydrates.

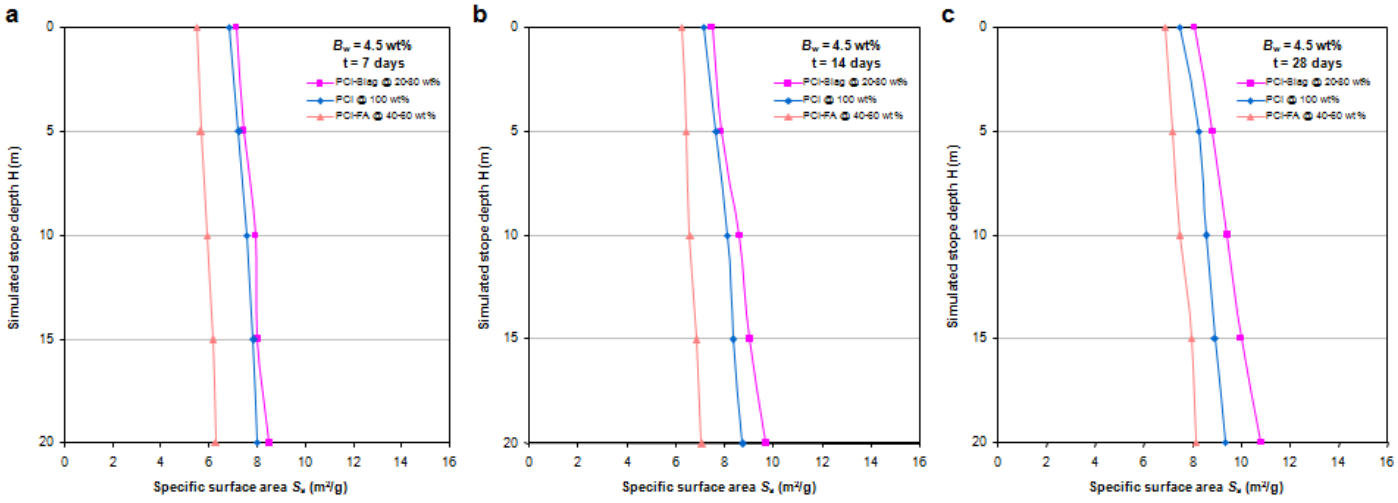

Figure 14. Variation in specific surface area with simulated stope heights for CPB samples containing different binder agents: a) 7 days, b) 14 days, and c) 28 days.

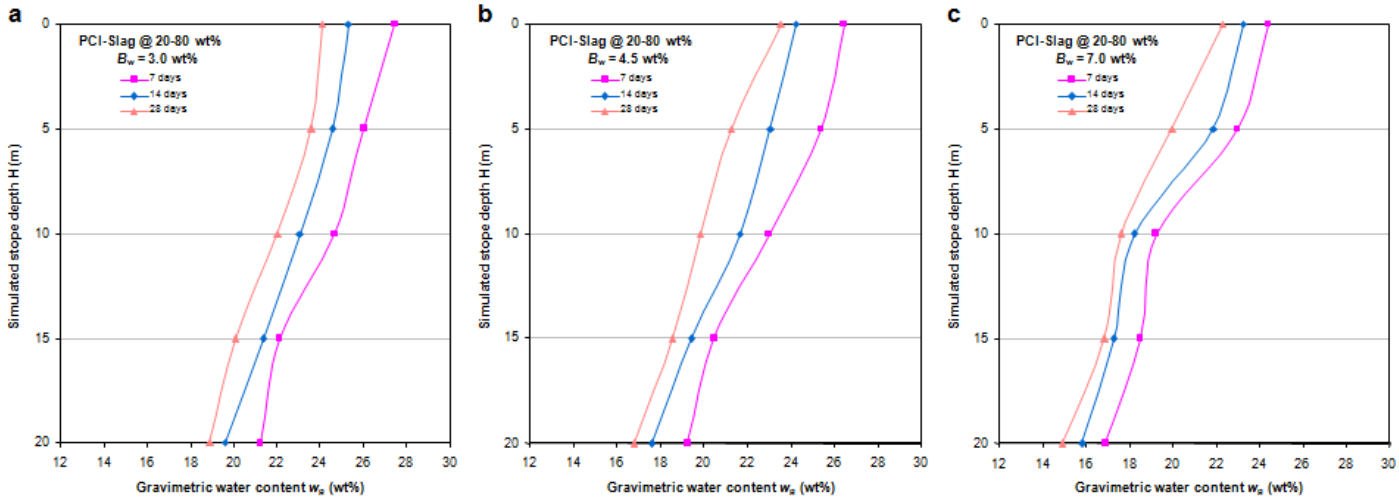

Figure 15. Change in gravimetric water content with simulated stope heights for CPB samples containing slag-based binder: a) 3wt% binder, b) 4.5 wt% binder, and c) 7wt% binder.

3.5 Effects of Simulated Stope Heights on Water Content of Paste Backfill

Figure 15 shows the evolution of gravimetric water content with simulated stope depth for CPB samples containing slag-based binder. For a given binder content, the lowest water contents (15-21 wt%) were obtained from 28-day cured CPB samples near the bottom of the stope. For CPB samples near the top of the stope (5-10 m height), the water content decreased from 23-27 wt% to 18-20 wt% when the corresponding binder content of the backfill samples increased from 3 to 7 wt%. The final water content is mainly controlled by the newly-added layer of cemented paste backfills and the amounts of excessive water required for cement hydration.

In general, the CPB samples placed at the base of the stope (subjected to overburden or hydrostatic pressure coming from each paste backfill layer having each 5 m) keep less free water in their structures, compared to CPB materials near the top of the stope where no stress is applied during the course of curing. Figure 16 shows the evolution of gravimetric water content of the simulated stope depths for CPB samples containing the 4.5 wt% of three different binding agents. As expected, the lowest water contents came from CPB samples located at the base of the stope (19-21 wt% for 7 days, 18-20.5% for 14 days, and 16.5-20 wt% for 28 days. In addition, the samples with slag-based binder exhibited the lowest water contents among others.

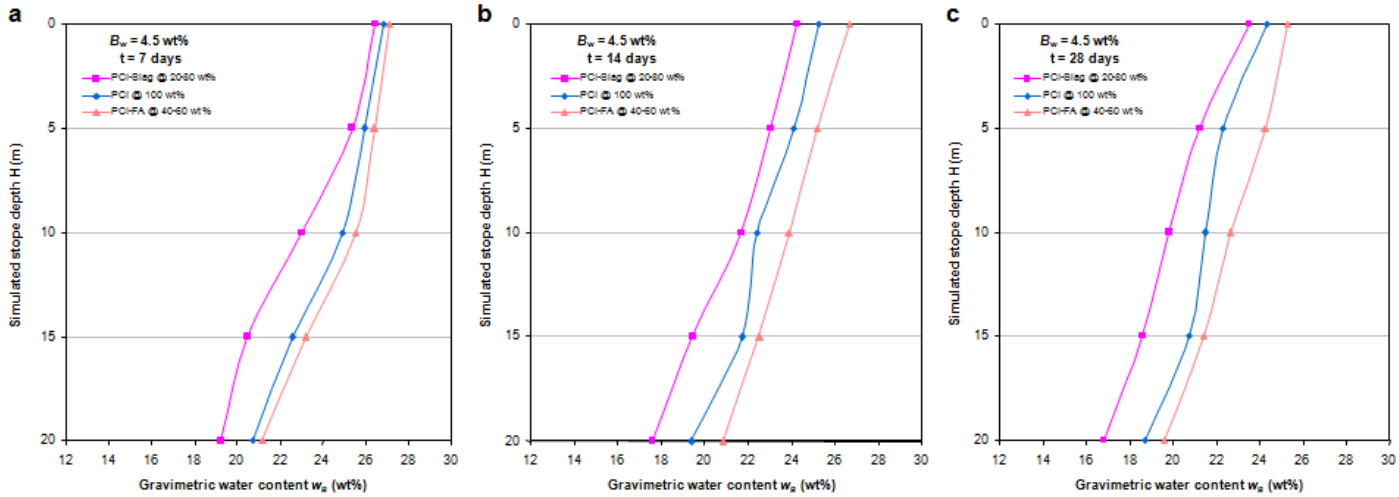

Figure 16. Change in gravimetric water content with simulated stope heights for CPB samples containing different binder agents: a) 7 days, b) 14 days, and c) 28 days.

4 CONCLUSIONS

This paper presents the promising results of a laboratory study undertaken for assessment of in situ behaviour and properties of CPB samples. The effect of stope height on paste backfill performance was investigated using an improved laboratory apparatus (CUAPS: curing under applied pressure system). A variety of CPB samples were prepared using the 3, 4.5 and 7 wt% binder contents of slag-based, fly ash-based and general use Portland cement alone and subjected to a number of pressure sequences which may simulate the different stope depths of 0 (reflects the CPB material near the top of the stope), 5, 10, 15, and 20 m (reflects the CPB material near the bottom of the stope). Results indicate that this investigation has not only presented a better understanding of in situ performance and quality of laboratory-prepared backfill samples but also identified procedures and (or) techniques that can be used to conduct field paste backfill testing in the laboratory. It is a well-known fact that conducting field testing is a challenging task because modern mines usually do not want to risk the safety of personnel or cause property damage or production losses and delays. Consequently, it is strongly believed that the results of this research work will bring a new light to paste backfill planners, practitioners, operating and regulatory professionals and researchers. It will be also a valuable tool for mines in order to characterize in situ behaviour of their CPB materials in the laboratory, saving time and money on quality control tests.

ACKNOWLEDGEMENTS

The author acknowledges the financial support from Canada Research Chair on the Integrated Management of Sulphidic Tailings using Mine Backfill Technology and the Industrial NSERC-Polytechnique-UQAT Chair on the Environment and Wastes Management. Canada Foundation for Innovation (CFI) is gratefully acknowledged for manufacturing CUAPS tools. Special thanks are extended to Denis Bois, Tikou Belem, Bruno Bussière and Mostafa Benzaazoua for UQAT-URSTM lab facilities, to URSTM expert people for their technical assistance during testing.

REFERENCES

Abdul-Hussain, N., Fall, M., 2012. Thermo-hydro-mechanical behavior of sodium silicate cemented backfill in column tests. *Tunnelling and Underground Space Technology,* Vol. 29, pp. 85-93.

Archibald, J.F., Souza, E.M., Beauchamp, L., 2001. Safe Canadian practices in mine fill operations. In: *The 10th Int. Symp. on Mining with Backfill,* Seatle, USA, pp. 249-256.

Belem, T., Harvey, A., Simon, R., and Aubertin, M. 2004. Measurement and prediction of internal stresses in an underground stope during its filling with cemented backfill. In: *The 5th Int. Symp. on Ground Support in Mining and Underground Construction*, Perth, Australia, pp. 619-630.

Belem, T., El Aatar, O., Benzaazoua, N., Bussiere, B., Yilmaz, E. 2007. Hydrogeotechnical and chemical characterization of column consolidated cemented paste backfill. In: *The 9th International Symposium in Mining with Backfill,* Montréal, Quebec, Canada, pp. 162-171.

Belem, T., Fourie, A., Fahey, M., 2010. Time-dependent failure criterion for cemented backfills. In: *The 12th Int. Seminar on Paste and Thickened Tailings*, Toronto, Canada, pp. 147-162.

Benzaazoua, M., Ouellet, J., Servant, S., Newman, P., Verburg, R., 1999. Cementitious backfill with high sulfur content: physical, chemical and mineralogical characterization. *Cem. Concr. Res.*, Vol. 29, No. 5, pp. 719-725.

Benzaazoua, M., Belem, T., Bussière, B., 2002. Chemical factors that influence the performance of mine sulphidic paste fill. *Cement and Concrete Research*, Vol. 32, No. 7, pp. 1133-1144.

Benzaazoua, M., Fall, M., Belem, T., 2004. A contibution to understanding the hardening process of cemented paste backfill. *Miner. Eng.*, Vol. 17, pp. 141-152.

Benzaazoua, M., Belem, T., Yilmaz, E., 2006. Novel laboratory tool for paste backfill. *Canadian Mining Journal*, Vol. 127, No. 3, pp. 31-32.

Bloss, M.L, Mathew, R.B., 2001. Mining with paste fill at BHP Cannington. In: *The 7th International Symposium on Mining with Backfill,* Seatle, United States, pp. 209-221.

Bussière, B., 2007. Colloquium 2004: Hydrogeotechnical properties of hard rock tailings from metal mines and emerging geoenvironmental disposal approaches. *Canadian Geotechnical Journal,* Vol. 44, No. 9, pp. 1019-1052.

Cayouette J. 2003. Optimization of the paste backfill plant at Louvicourt mine. *CIM Bulletin,* Vol. 96, Vol. 1075, pp. 51-57.

Cihangir, F., Yilmaz, E., Ercikdi, B., Kesimal, A., 2008. The effect of tailings particle size on the strength and microstructure of paste fill. In: *The 9th Regional Rock Mechanics Symposium,* Izmir, Turkey, pp. 108-115.

Cihangir, F., Ercikdi, B., Kesimal, A., Turan, A. and Deveci, H., 2012. Utilisation of alkali-activated blast furnace slag in paste fill of high-sulphide mill tailings: effect of binder type and dosage. *Miner. Eng.*, Vol. 30, pp. 33-43.

Dehn, K., Pakalnis, R., Corey, G, 2007. Determining fill fence stability during increased backfill rates at an underground hard rock mine. In: *The 9th International Symposium in Mining with Backfill,* Montréal, Quebec, Canada, pp. 150-162.

Emad, M.Z., Vennes, I., Mitri, H., Kelly, C., 2013. Backfill practices for sublevel stoping system. In: *The 22nd Int. Conference on Mine Planning and Equipment Selection,* Germany, pp. 391-402.

Ercikdi, B., Kesimal, A., Cihangir, F., Deveci, H., Alp, İ., 2009. Cemented paste backfill of sulphide-rich tailings: importance of binder type and dosage. *Cement and Concrete Composites*, Vol. 31, No. 4, pp. 268-274.

Ercikdi, B., Cihangir, F., Kesimal, A., Deveci, H., Alp, İ., 2010. Use of water-reducing admixtures in cemented paste backfill of sulphide-rich mill tailings. *Journal of Hazardous Materials,* Vol. 179, pp. 940-946.

Ercikdi, B., Cihangir, F., Kesimal, A. and Deveci, H., 2012. Waste management method for mill tailings:paste backfill technology. *Turkish Mining Journal*, Vol. 24, pp. 70-75.

Ercikdi, B., Yilmaz, T., Külekçi, G., 2014. Strength and ultrasonic properties of cemented paste fill. *Ultrasonics,* Vol. 54, pp. 195-204.

Fahey, M., Helinski, M., Fourie, A., 2011. Development of specimen curing procedures that account for the effect of effective stress during curing on the strength of cemented mine backfill. *Geotechnical and Geological Engineering,* Vol. 29, No. 5, pp. 709-723.

Fall, M., Benzaazoua, M., Ouellet, S., 2005. Experimental characterization of the effect of tailings fineness and density on the quality of cemented paste backfill. *Minerals Engineering*, Vol. 18, No. 1, pp. 41-44.

Fall, M., Célestin, J.C., Pokharel, M., Touré, M., 2010. A contribution to understanding the effects of temperature on the mechanical properties of cemented mine backfill. *Engineering Geology*, Vol. 14, No. 3-4, pp. 397-413.

Fall, M., Pokharel, M., 2011. Strength development and sorptvitiy of tailings shotcrete under various thermal and chemical loads. *Canadian Journal of Civil Engineering*, Vol. 38, No. 7, pp. 772-784.

Fourie, A., Helinski, M., Fahey, M. 2007. Using effective stress theory to characterize the quality and behaviour of paste backfill. *CIM Bulletin*, Vol. 100, pp. 15-25.

Grabinsky, M., Thompson, B.D., 2009. Thermally induced stresses in cemented paste backfill. *International Journal of Geotechnical News,* Vol. 27, No. 3, pp. 36-40.

Grabinsky, M., 2010. In situ monitoring for ground truthing paste backfill designs. In: *The 13th Int. Sem. on Paste and Thickened Tailings*, Toronto, Ontario, Canada, pp. 85-98.

Grice, T., 2001. Recent mine developments in Australia. In: *The 10th Int. Symp. on Mining with Backfill,* Seatle, USA, pp. 351-357.

Hassani, F.P., Fotoohi, K., Doucet, C., 1998. Instrumentation and backfill performance in a narrow vein gold mine. *Int. J. Rock Mechanics and Mining Sciences,* Vol. 35, No. 4-5, pp. 392-405.

Helinski, M., Fahey, M., Fourie, A, 2007. Numerical modelling of cemented mine backfill deposition. *Journal of Geotechnical and Geoenvironmental Engineering*, Vol. 133, No. 10, pp. 1308-1319.

Helinski, M., Fahey, M., Fourie, A, 2011. Behaviour of cemented paste backfill in two mine stopes: measurements and modeling. *J. Geotechnical and Geoenviron. Eng.*, Vol. 137, No. 2, pp. 171-182.

Henderson, A., Jardine, G., Woodall, C, 1998. The implementation of paste fill at Henty gold mine. In: *The 6th International Symposium on Mining with Backfill*, Brisbane, Australia, pp. 299-304.

Hughes, P.B., Pakalnis, R., Hitch, M., Corey, G., 2010. Composite paste barricade performance at Goldcorp Inc. Red Lake Mine, Ontario, Canada. *Int. J. Min. Recl. Envir.*, Vol. 24, pp. 138-150.

Kesimal, A., Ercikdi, B., Yilmaz, E., 2003. Effect of desliming by sedimentation on paste backfill performance. *Min. Eng.*, Vol. 16, pp. 1009-1011.

Kesimal, A, Yilmaz, E, Ercikdi, B, 2004. Evaluation of paste backfill mixtures consisting of sulphide-rich mill tailings and varying cement contents. *Cem. Concr. Res.,* Vol. 34, pp. 1817-1822.

Kesimal, A., Yilmaz, E., Ercikdi, B., Alp, I., Deveci, H., 2005. Effect of properties of tailings and binder on the short and long terms strength and stability of cemented paste backfill. *Materials Letters,* Vol. 59, No. 28, pp. 3703-3709.

Kump, D., 2001. Backfill: whatever it takes. *Mining Engineering,* Vol. 53, No. 1, pp. 50-52.

Landriault, D. 2006. Keynote Address: They said 'It will never work'- 25 years of paste backfill 1981-2006. In: *The 9th International Seminar on Paste and Thickened Tailings*, Ireland. pp. 277-292.

Landriault, D.A., Welch, D., Frostiak, J., Evans, D., 2001. Bulyanhulu Mine: blended paste backfill and surface paste deposition: the state of the art in paste technology. In: *The 7th Int. Symposium on Mining with Backfill,* Seattle, USA, pp. 1-14.

le Roux, K.-A., Bawden, W.F., Grabinsky, M. 2005. Field properties of cemented paste backfill at the Golden Giant Mine. *Min. Technol. IMM Trans. Sec. A*, Vol. 114, No. 2, pp. 65-80.

Li, L., Aubertin, M., Belem, T., 2005. Formulation of a three dimensional analytical solution to evaluate stresses in backfilled vertical narrow openings. *Canadian Geotechnical Journal,* Vol. 42, pp. 1705-1717.

Li, L., Aubertin, M., 2010. An analytical solution for the nonlinear distribution of effective and total stresses in vertical backfiled stopes. *International Journal of Geomechanics and Geoengineering*, Vol. 5, No. 4, pp. 237-245.

El Mkadmi, N., Aubertin, M., Li, L., 2014. Effect of drainage and sequential filling on the behavior of backfill in mine stopes. *Canadian Geotechnical Journal*, Vol. 51, pp. 1-15.

Orejarena, L., Fall, M., 2011. Artificial neural network based modelling of the coupled effects so sulphate and temperature on the strength of cemented paste backfill. *Canadian Journal of Civil Engineering*, Vol. 38, pp. 100-109.

Ouattara, D., Mbonimpa, M., Belem, T., 2010. Rheological properties of thickened tailings and cemented paste tailings and the effects of mixture characteristics on shear behavior. In: *The 63th Canadian Geotechnical Conference*, Calgary, Alberta, Canada, pp. 1178-1185.

Ouellet, J., Bidwell, T.J., Servant, S., 1998. Physical and mechanical characterization of paste backfill by laboratory and in-situ testing. In: *The 6th International Symposium in Mining with Backfill*, Brisbane, Australia, pp. 249-254.

Ouellet, J., Hassani, F., Zhu, Z. 2005. Study of the cemented paste backfill and rock mass interaction and behaviour in backfilled stopes. In: *The 40th US Symposium on Rock Mechanics*, Anchorage, Alaska, United States, Paper 801.

Ouellet, S., Bussière, B., Monimpa, M., Benzaazoua, M., Aubertin, M., 2006. Reactivity of an underground mine sulphidic cemented paste backfill. *Miner. Eng*, Vol. 19, No. 5, pp. 407-419.

Pirapakaran, K, Sivakugan, N, 2007. Arching within hydraulic fill stopes. Geotechnical and Geological Engineering, Vol. 25, No. 1, pp. 25-35.

Pokharel, M., Fall, M., 2013. Combined influence of sulphate and temperature on saturated hydraulic conductivity of cemented paste backfill. *Cement and Concrete Composites*, Vol. 38, pp. 21-28.

Potvin, Y., Thomas, E., Fourie, A., 2005. Handbook on mine fill. Australian Centre of Geomechanics, The University of Western Australia, Nedlands, Australia. ISBN 0-9756756-2-1.

Revell, M.B., Sainsbury, D., 2007. Advancing cemented paste backfill bulkhead design using numerical modeling. In: *The 9th International Symposium in Mining with Backfill*, Montréal, Quebec, Canada, pp. 185-195.

Thompson, B.D., Bawden, W.F., Grabinsky, M.W., Karaoglu, K., 2010. Monitoring barricade performance in a cemented baste fill operation. In: *The 13th Int. Sem. on Paste and Thickened Tailings*, Toronto, Ontario, Canada, pp. 85-98.

Thompson, B.D., Grabinsky, M.W., Bawden, W.F., 2012. In-situ measurements of cemented paste backfill at Cayeli Mine. *Canadian Geotechnical Journal*, Vol. 49, No. 7, pp. 755-772.

Veenstra, R.L., Bawden, W.F., Grabinsky, M.W., Thompson, B.D, 2011. Matching stope scale numerical modelling results of early age cemented paste backfill to in-situ instrumentation results. In: *The 64th Canadian Geotechnical Conference*, Toronto, Ontario, Canada, pp. 1-8.

Wu, D., Fall, M., Cai, S.-J., 2013. Coupling temperature, cement hydration and rheological behaviour of cemented paste backfill structures. *Minerals Engineering*, Vol. 42, pp. 76-87.

Yilmaz, E., 2010. Investigating the hydrogeotechnical and microstructural properties of cemented paste backfills using the versatile CUAPS apparatus. In: *PhD Thesis*, Université du Québec en Abitibi-Témiscamingue, Rouyn, Que., Canada (http://depositum.uqat.ca/34/1/erolyilmaz.pdf).

Yilmaz, E., 2011. Advances in reducing large volumes of environmentally harmful mine waste rocks and tailings. *Mineral Resources Management*, Vol. 27, Vol. 2, pp. 89-112.

Yilmaz, E., Benzaazoua, M., Belem, T., Bussière, B., 2009. Effect of curing under pressure on compressive strength development of cemented paste backfill. *Minerals Engineering*, Vol. 22, No. 9-10, pp. 772-785.

Yilmaz, E., Belem, T., Benzaazoua, M., Bussière, B., 2010. Assessment of the modified CUAPS apparatus to estimate in situ properties of cemented paste backfill. *Geotechnical Testing Journal*, Vol. 33, No. 5, pp. 351-362.

Yilmaz, E., Belem, T., Bussière, B., Benzaazoua, M., 2011. Relationships between microstructural properties and compressive strength of consolidated and unconsolidated cemented paste backfill. *Cement and Concrete Composites*, Vol. 33, No. 6, pp. 702-715.

Yilmaz, E., Belem, T., Benzaazoua, M., 2012. One-dimensional consolidation parameters of cemented paste backfills. *Mineral Resources Management*, Vol. 28, No. 4, pp. 29-45.

Yilmaz, E., Belem, T., Benzaazoua, M., 2014. Effect of curing and stress conditions on hydromechanical, geotechnical and geochemical properties of cemented paste backfill. *Engineering Geology*, Vol. 168, pp. 23-37.

Yilmaz, E., Belem, T., Bussière, B., Mbonimpa, M., Benzaazoua, M., 2015a. Curing time effect on consolidation behaviour of cemented paste fill containing different cement types and contents. *Constr. Build. Mater.*, Vol. 75, pp. 99-111.

Yilmaz, E., Belem, T., Benzaazoua, M., 2015b. Specimen size effect on strength behavior of cemented paste backfills subjected to different placement conditions. *Engineering Geology*, Vol. 185, pp. 52-62.

Yumlu, M., Guresci, M., 2007. Paste backfill bulkhead monitoring: A case study from Inmet's Cayeli Mine, Turkey. *CIM Bulletin*, Vol. 100, No. 1103, pp. 1-10.

Investigation of Strength Properties of a Sandstone Rock

A.Boutrid, M.Chettibi, S.Bensehamdi and K.Talhi
Annaba University, BP12- Algeria, Faculty of Earth Sciences, Mining Department, Annaba 23000

ABSTRACT This research aim to assess the effect of water saturation on the mechanical properties of sandstone rocks using a servo-controlled testing machine. Stress-strain curves were obtained from which the uni-axial compressive strength, Young's Modulus and the brittleness index were measured for specimens prepared from a single block of Sandstone from the Hassi Messaoud site investigation , Algeria. To see how the strength properties were affected by changes in saturation level (likely to occur on site), the specimens were divided into three groups which were prepared for testing under different conditions of saturation content.

Keywords: saturation; mechanical properties uni-axial compressive strength, Young's Modulus , brittleness index

1 INTRODUCTION

Estimation of rock mechanis properties of rocks to be is considered the most important components in any engineering project. In this regard, one of the most commonly used fundamental mechanical parameter is the uniaxial compressive strength (UCS) (Bruno et al. 2012; Minaeian and Ahangari 2011).

For both excavation and stability problems, knowledge of ground properties is essential so that excavation and stability system can be matched to the ground (Bhasim, and al.1996) . The UCS strength is one of the most widely used test for determination these properties and the purpose of this research was to study the variation in the UCS with saturation content.

Aqueous pore fluids exert significant mechanical and chemical effects on rocks. Previous studies have shown that the brittle strength of a rock is generally reduced in the presence of water (Yang et al, 2000). The water-weakening effect may arise from two mechanisms. The mechanical role of pressurized pore fluid tends to weaken rocks, and the chemical influence of pore fluids is to further weaken the rock through a reduction of surface free energy (Paterson, 1978), subcritical cracking mechanism such as stress corrosion (Atkinson and Meredith, 1987), or both combined.

Using a servo-controlled testing machine, complete stress-strain curves were obtained for specimens. Because specimen failure was controlled, brittleness of the sandstone could be studied from the form of the stress-strain relation after the peak load has been reached. Specimen preparation and the testing technique are described and stress-strain results are presented.

The UCS and Young Modulus , brittleness values are then correlated with saturation contents.

2 SITE AND SAMPLE DETAILS

A large, intact block of sandstone was obtained from the Hassi Messaoud site investigation which is situated 850 kilometers a way of Algeria. Lithologically, the rock is grey, medium-grained, weakly cemented sandstone. A sample of the rock was disaggregated by gentle pressure with a pestle and mortar, taking care not to crush individual grains. The particle size distribution and specifie gravity of the sample were determined. It was found that 85 % of the particles fell in the medium sand range (0.2-0.6mm) and 10% in the fine sand range (0.06-0.2mm) and that the particle specific gravity was 2.66.

3 EXPERIMENTAL PROCEDURE

3.1. Specimen Preparation and Testing

The representative cores for use in the experimental work are obtained from block sample. Coring of the block samples was accomplished by a diamond core drill. The original core of 95 mm was plugged with a diamond cores drill having 38 mm as nominal diameter. All core samples were cut to length/diameter ratio of 2.5:1. The ends of cores were flat and parallel (see Figure 1). The diameter and length of each specimen were measured with a vernier to the mearsest 0. 01 mm.

The specimen were divided into three groups, one group was saturated by using a vacuum –saturation process, similar to that suggested by the U.S. Bureau of reclamation (1953),this process consists of :

1. Oven- drying the specimen for a period of 24 hours at 105°C,
2. Placing the specimen in a bell joir under a vacuum exceeding 50. 80 cm for 24 hours.
3. Immersing, the specimen in water while continuing with vacuum for another 24 hours.
4. Removing the vacuum and exporing the water containing the immersed specimen to the atmosphere for at least 48 hours.

Figure 1. Cylindrical sandstone specimen

This procedure eliminates air entering in rock pores and de–airs the water. It drives water into the rock, thus assuming a complete in saturation 5 day cycle, the specimen is removed from the water surface dried, and then weighed. The saturation content is computed. The second group of specimens was immersed in water. The third group was allowed to air dry because the oven-drying may sometimes cause erratic changes in the physical property. The mass of each specimen was determined immediately before testing, and the saturation content is calculated immediately after. The affixing to the specimens of two axially oriented foil strain gauge are aixed on the sample. These pairs are placed diametrically opposite each other and located centrally on the specimen. During testing the pairs are connected up with pairs of gauges. on dummy sample away from the machine to give temperature variation compensation. This wheastone bridge is formed and strain changes are monitored by changes in the voltage across the bridge. The testing procedure was essentially the same as that described by (Hudson and Morgan1975) and the following account, slightly modified. The compression tests were carried out in a response, closed-loop, programmable testing machine (Figure.2). This type of machine was used because a constant displacement rate can be achieved throughout the test- i.e. failure is controlled after the maximum load bearing capacity of the specimen has been reached; and because it is programmable and automatic. The closed-loop, servo-control principle is shown in Fig.3. A feedback signal (f) representing the actual condition of an experimental variable, in this case the axial displacement, is continually compared with a program signal (p) representing the required experimental condition. The feedback signal corresponding to the displacement between the specimen ends was generated by four displacements transducers located at 90 degree intervals around the specimen. The individual transducer outputs were summed to provide a voltage equivalent to the average specimen displacement. This feedback signal was compared with the program signal produced by a function generator. The program signal increased linearly with tune enabling a constant displacement or strain rate to be achieved. An error signal (e) occurred if there was any difference between the feedback and program signals; this activated a servo-valve causing the hydraulic pressure in the loading ram to be adjusted and the

error signal to be reduced. Feedback and program signals were frequently compared and high speed adjustments made so that the experimental condition followed the programmed condition. The control mechanism and advantages are explained further by (Hudson, et all 1972). To carry out a test, the specimen was inserted in the testing machine between platens having the same diameter as the specimen. The program was switched on and the specimen was then displaced at a constant rate of 2x10-3 mm/sec, corresponding to an axial strain rate of about 3x10-3 per cent/sec. Displacement was thus the independent variable and force was the dependent variable. Failure was then controlled beyond the peak force because the displacement was programmed to increase at a constant rate regardless of whether this necessitated a rise or fall in applied force. The load was monitored with a pressure transducer and a complete force-displacement curve obtained for each specimen on an X-Y recorder. Axial load was additionally monitored by a remote X-Y chart recorder which was used to monitor the axial displacement detected by the strain.

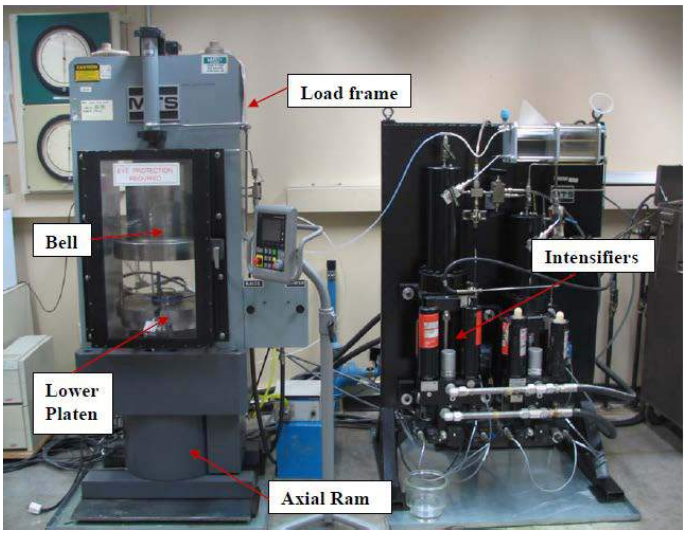

Figure.2. Machine with tests servo controlled on the test sample**.**

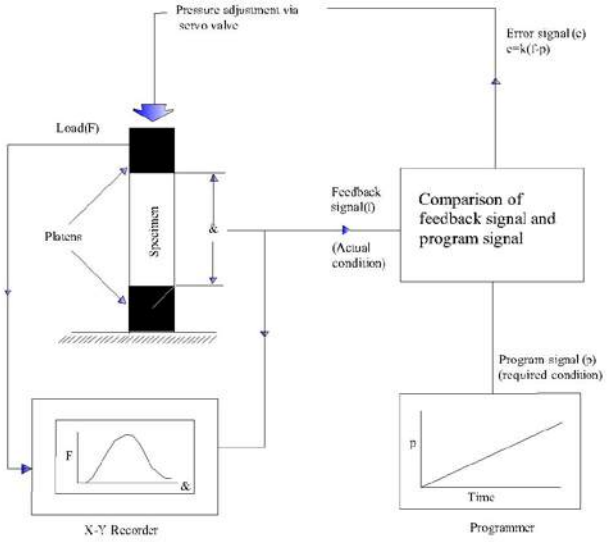

Figure 3. Closed –loop programmable testing machine control system

4 RESULTS

Load displacement curves obtained from the X-Y recorder were converted to stress-strain curves by dividing the load by the original cross- sectional area of the specimen to give stress and by dividing the displacement by the original length of the specimen to give strain; a typical result is shown in Fig.4. The brittleness index (B) defined by Hudson and Morgan (1975)as

$$B = AE/ (AE + Ap) \qquad (1)$$

Where AE is the area beneath the stress-strain curve before the peak stress and Ap is the area beneath the stress-strain curve after the peak stress (see Fig.4) was obtained for each curve by Tamaya Digital Planimeter measurements. The value of B can range from 0 to 1, for perfectly brittle rock with a post-failure curve descending vertically, B is unity since Ap is zero; for perfectly ductile rock with a horizontal post-failure curve, Ap is infinite and B becomes zero.Areas under the wves mere measured by Tamaya digital planimeter.

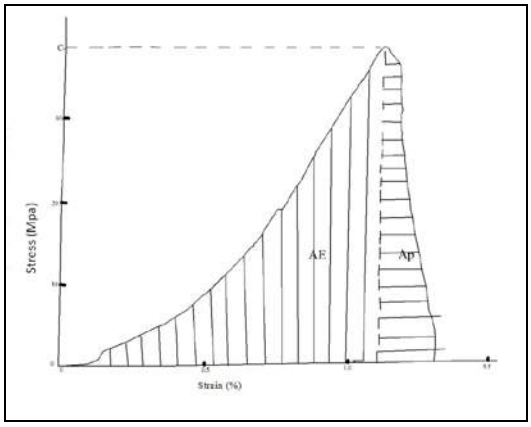

Figure 4. The stress-strain curve by Tamaya

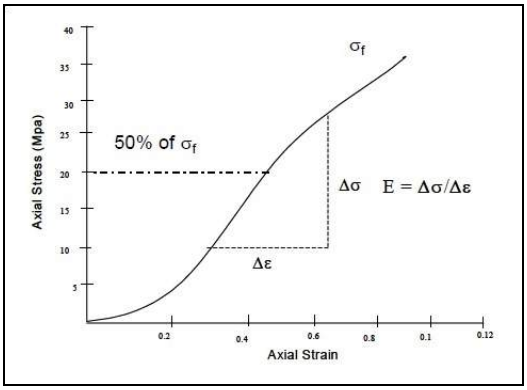

Figure 5. Calculation of Young's Modulus at 50 % of peak strength.

The uniaxial compressive strength (Co) was obtained from the peak of each curve. Young's Modulus (E) and Poisson's Ratio (μ) was obtained from the stress-strain curve (see Fig.5 and 6). Young's modulus and Poisson's ratio, are determined from the stress strain relationships for each stage. Young's Modulus is equal to the ratio of axial stress to axial strain50% of the failure load. Poisson's ratio is equal to the ratio of lateral strain to axial strain at50% of the failure load. As shown in (Fig .5), the Young's modulus is calculated from the slope of the straight-line portion of the stress-axial strain curve. Poisson's ratio can be calculated using the average slope of the straight-line portion of the stress-radial strain curve and the average slope of the axial curve.

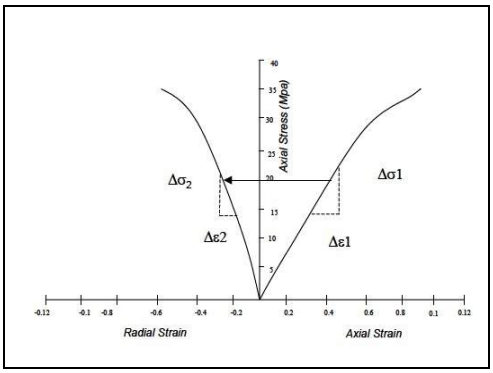

Figure 6. Calculation of Poisson's ratio from stress-strain data.

The results are summarised in Table1. To study the effect of saturation level on the strength properties, individual values of uniaxial compressive strength, Young's Modules and brittleness index have been plotted against individual values of saturation for each specimen in Figures 7,8 and 9

Table 1. Mechanical property test results

Statistical characteristics properities	Number of specimens	State	Mean	Standard deviation
Uniaxial compressive strenghth (C_0) Mpa	30	Dried	36.78	2.64
	30	Immersed in water	30.01	3.78
	30	Saturated	29.68	4.73
Young's Moudulus (E) Gpa	15	Dried	16.42	2
Poisson's ratio (μ)	15	Dried	0.25	0.05
Brittleness index (B)	15	Dried	0.65	0.09
	15	Saturated	0.68	0.08
Saturation (%)	20	Remaining 2 Weeks in Lab	0.02	0.08
	20	Immersed in water	4.57	0.82
	15	Saturated	6.90	0.55
Unit weight g/cm3	30	Dried	2.19	0.045

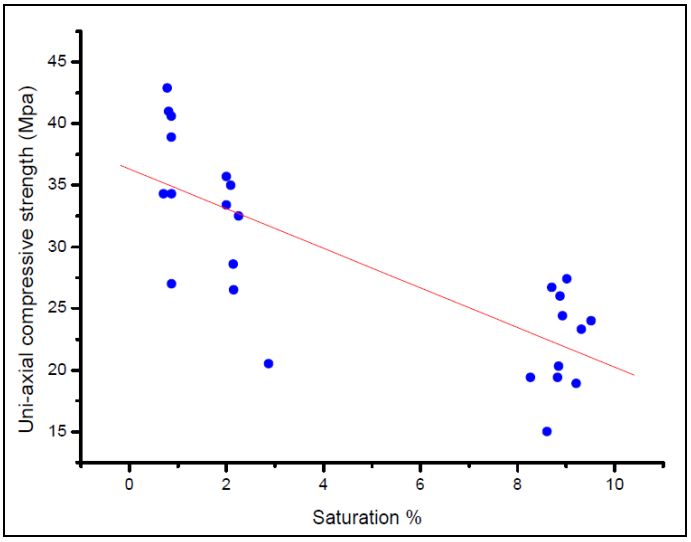

Figure 7. Effect of saturation on uniaxail compressive strength

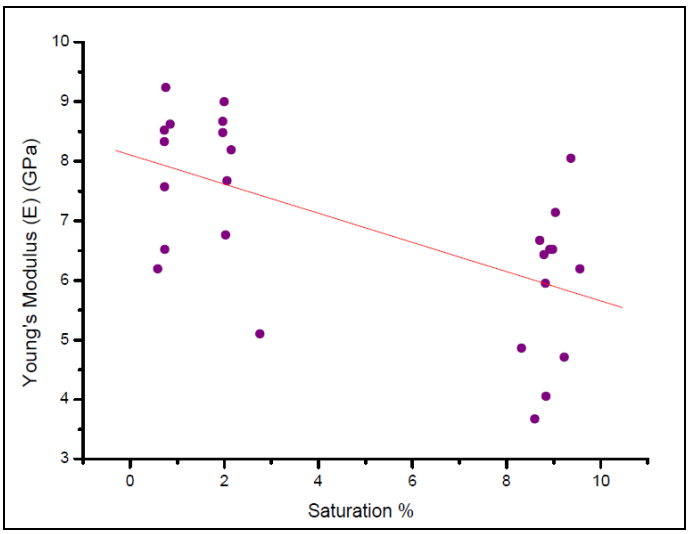

Figure 8. Effect of saturation on Young's Modulus

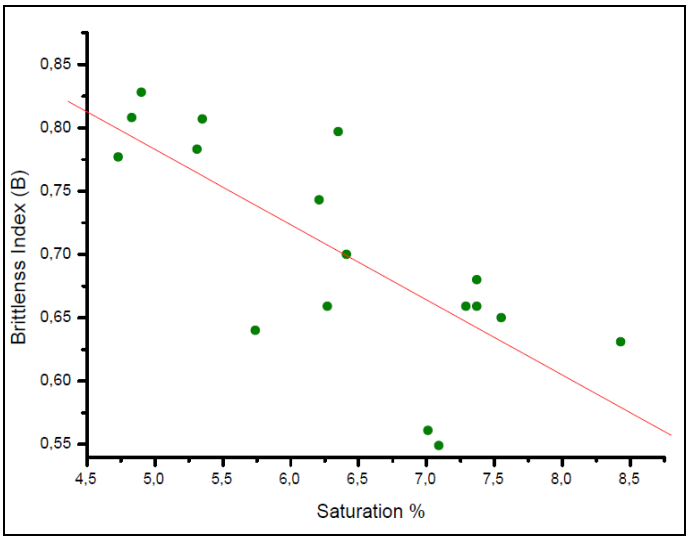

Figure 9. Effect of saturation brittlenss index

5 DISCUSSION AND CONCLUSION

Figures 7,8 and 9 show the effect of saturation content on the uni-axial compressive strength, Young's Modulus and brittleness index of the sandstone, respectively. There is a general tendency for both the uni-axial compressive strength and Young's Modulus to decrease with increasing saturation level. For the brittleness index the trend is not clear and it is not possible from these data to see whether the index is unaffected by absorption content or it has a maximum at some intermediate saturation level. On each of the figures a least square regression line for the data is shown together with the value of the computed correlation coefficient (r). A value of $r^2 \geq 0.6$ has been considered in rock mechanics as indicating a reasonable correlation . Judged by this criterion, Figures 8 and 9 show that Young's modulus and brittleness index of the sandstone are not significantly affected by saturation changes over the range from air dry to saturation. However, . Fig.7 shows that the effect of saturation on uniaxial compressive strength is just significant, the strength of the sandstone decreasing with increasing saturation . The mean uni-axial compressive strength of the air-dry sandstone 37 MPa (see Table 1. However, while the mean strength of the saturated sandstone had fallen to 23 MN/m2 that of the saturated chalk marl had fallen to 2 MPa, showing a very different response to increasing absorption content. The mean Young's modulus of the Sandstone varied from 7.2 GN/ m2 for air dried rock to 5.5 GN/ m2 for saturated rock (see Table 1). Even the lower of these values is higher than the maximum value of 3 GN/ m2 reported for the chalk and shows the sandstone is the stiffer of the two rocks. The mean brittleness index of the Sandstone varied from 0.61 to 0.77 (see Table 1). These values are lower than the values of 0.83 to 0.85 reported for the chalk and, shows the sandstone is the less brittle of the two rocks when judged by the criterion of brittleness index.

REFERENCES

G Bruno, G Vessia, L Bobbo ;2012 , Statistical method for assessing the uniaxial compressive strength of carbonate rock by Schmidt hammer tests performed on core samples. *Rock Mech Rock Eng*.

B Minaeian, K Ahangari ; 2011, Estimation of uniaxial compressive strength based on P-wave and Schmidt hammer rebound using statistical method. *Arab J Geosci*.

B. hasim and E. Grinstad.,1996 The use of stress-strain relationships in the assessement of tunnel stability‘, *Tunnelling and Underground Space Technology*, (11) 93-98,.

X Yang., P Baud,. and T Wong,. 2000, “Micromechanics of Compressive Failure and Spatial Evolution of Anisotropic Damage in Darley Dale Sandstone” *International Journal of Rock Mechanics and Mining Sciences*, 37 143-160.

M.S, Paterson., 1978. Experimental rock deformation-the brittle field, *Springer-Verlag*, New York, 262, p.3-30.

B.K Atkianson and P.G Meredith,; 1987. Experimental Fracture Mechanics Data For Rocks And Minerals, *Fracture Mechanics Of Rocks*, Edited by Atkinson B.K pp 477-525 Academic, San diego, Calif.,

M. Jafarpour, H. Rahmati, S. Azadbakht, A. Nouri, D.Chan, H.Vaziri: 2012. *Determination Of Mobilized Strength Properties Of Degrading Sandstone*‘. 52, 4, 658–667,.

U.S. Bureau of Reclamation: 1953. Physical Properties Of Some Typical Foundation Rocks‘, U.S, *Bureau Of Reclamation Comeite Lab.* Report N° SP.39.

J. A. Hudson, and J. M. Morgan,; 1975. Compressive Failure Of Chalk. Department of the Environment *TRRL Report LR 681*, Crowthorne‘ , (Transport and Road Research laboratory).

J. A. Hudson, S. L. Crouch, and C. Fairhurst,.1972.Soft Stiff And Servo-Controlled Testing Machines‘ A Review With Reference To Rock Failure. *Engineering Geology*, 6, 155 89,.

WR. Judd; 1971.Strain Distribution Around Underground Openings*: Technical Report N°6. Statistical Relationships For Certain Rock Properties*‘. USA, (Advanced Research Projects Agency, Department Of Defence,.

Determination of Slake Durability Index on Spherical Samples with Lime-Water Treatment

Kireç Banyosu Uygulanan Küre Örnekler Üzerinde Suda Dağılmaya Karşı Duraylılık Indeksinin Belirlenmesi

H. Ankara, G. Bayar, M. Aksoy
Eskişehir Osmangazi Üniversitesi, Maden Mühendisliği Bölümü, Eskişehir

ÖZET Bu çalışma Eskişehir-Derbent beyaz tüf örnekleri üzerinde kireçli su banyosu sonrası suda dağılmaya karşı duraylılık indeksini belirlemek için yapılmıştır. Önce suda dağılmaya karşı duraylılık testi için önerilen yeni örnek hazırlama yöntemi (Paşa yöntemi) ile eşit boyutlu küre örnekler hazırlanmıştır. Bu küreler 7 gün süresince kireçli suda bekletilmiştir. Daha sonra kireçli suda bekletilen örnekler ile normal küre örneklerin ikinci çevrim indeks değerleri kıyaslanmıştır. Orijinal küre örneklerinin indeks değerleri % 94,89-95,56 iken kireçli su ile muameleye tutulan küre örneklerin indeks değerleri % 95,02-96,64 olarak bulunmuştur. Bu çalışmanın sonuçlarına göre, kireçli su ile muamele edilen tüfler ile herhangi bir işlem yapılmayan tüflerin indeks değerlerine göre, kireçli su banyosunun suda dağılmaya karşı duraklılık indeks değerinin iyileşmesinde bir etkisi olmadığı görülmüştür.

Anahtar Kelimeler: Kireç banyosu, Suda dağılmaya duyarlılık, Beyaz tüf

ABSTRACT In this study, white tuff samples at the tuff quarries located at the Eskisehir/Derbent region in Turkey were treated with lime-water bath to determine the slake durability index. Firstly, Equal-sized spherical samples are prepared according to the new method, Pasha Method. Then, slake durability index tests have been applied on spherical samples kept for 7-day in lime-water bath. The second cycle index values of spherical samples subjected to lime-water bath have been compared with the index values of original spherical samples. Although the index values of original spherical samples were found as 94.89-95.56 %, the index values of spherical sample sets treated with lime-water bath were found to be in 95.02 and 96,64 %, respectively. According to the results of this study, it can be concluded that lime-water treatment has no effect on enhancement of the slake durability index values of spherical samples when compared to those of spherical samples with no treatment.

Keywords: Lime-water treatment, Slake durability index, White tuff

1 INTRODUCTION

Slake durability Index test (SDI) is widely used to provide an Index value that is related to resistance of rocks against degradation when they are subjected to two standard cycles of wetting and drying. This test was originally developed by Chandra in 1970, and improved by Franklin and Chandra (1972). After 1972, the test has been widely accepted and applied in rock mechanics. As a result of this acceptance and usage, the test was standardized and suggested as a standard test for rocks by the International Society for Rock Mechanics (ISRM, 2006). The test was also accepted by American Society for Testing and Materials, and standardized as ASTM D4644 (ASTM, 1990).

It can be said that Slake durability Index has become an important engineering parameter, and has been used extensively in literature in order to determine the durability of the rocks, especially weak and clay

bearing rocks (Bella et al 1997; Çetin et al 2000;Gemici 2001;Dhakal et al 2002; Viterbo et al 2007 ve Erguler ve Ulusay 2009).

Lime stabilization is one of the methods widely used to improve the mechanical properties of soil (Yong and Ouhadi, 2007, Fresno et al, 2011, Hejazi et al, 2012). The interaction between lime and soil in this method has been investigated by several authors and it is stated that lime stabilization enhances the strength, stiffness, plasticity and water adsorption of raw soil (Ciancio et al, 2014). In this study, it is also stated that the lime-soil reaction can be described by three general phenomena: cation exchange, pozzolanic reaction and carbonation.

This method is also applied to improve the strength of white tuff of Eskisehir Derbent region by Emir et al (2011) and they have claimed that lime treatment enhanced the uniaxial compressive strength of this tuff about 64-105 %.

The aim of this study is to investigate the effect of lime-water treatment on the slake durability index values of white tuff of Eskisehir Derbent region.

2 MATERIALS AND METHODS

2.1 White Tuff Samples

Tuff and ignimbirites type rocks were used to build historical monuments, and are being used as decorative material, nowadays in Turkey because of their softness and easy processability. For example, some important natural and historical monuments of Turkey such as Phrygian valley, Phrygian monument and chimneys of Cappadocia were formed of these type rocks. The tuffs on other regions are produced as decorative material. One of the tuff production places is near to Derbent village of Eskisehir province. Tuff bloks collected in this place is called as Derbent white tuff. The mineralogical structure of white tuff consists of Quartz, K-Feldspar, biotite and phenomenon crystals of opaque minerals. Besides, various metamorphic rock and white pumice pieces can be observed. Phenomenon crystals, rock pieces and white pumice are buried in the structure of slightly decayed tuff. In tuffs, the existence of volcanic glass pieces is very common (Sözmen, 2000). The samples used in this study were collected from Derbent white tuff quarry.

2.2 Experimental Study

The preparation of equal-sized spherical test samples consists of three stages. First stage is to cut cubes whose size is accordance with final spherical sample diameter from collected rock samples. At this stage, the length of cube edge is calculated as follows; the final sample weight is required to be 50 g by standards. Therefore, the diameter of the spherical sample is calculated from volume and dry density of the rock. After the determination of diameter, the edge length of the cube is set to be the diameter plus 2 mm (Ankara et al, 2013a,b).

Second stage is to cut cubes to form a pre-spherical shape which is called as Pasha Cut. Pasha cut is performed in two steps. The first step is to cut the edges of cube (Ankara et al, 2013a,b). This shape is shown in Figure 1-a. Second step is to cut the corners of the samples after first step. It is shown in Figure 1-b.

The final stage is to obtain equal sized spherical samples from Pasha Cut by means of an instrument modified for this purpose. After pasha cut step, samples are placed into sphere preparation machine (Covington brand). Special cutter cups having a diameter of 35 and 40 mm were designed and manufactured. Abrasive type used in these cups is diamond. This whole sample preparation process is called as Pasha Method (Ankara et al, 2013a,b).

Total of 20 spherical samples was prepared for lime-water bath and slake durability test. Firstly 20 spherical samples kept for 7 days were taken into lime-water bath. After 7 days, oven-dried samples as two sets were placed in drums mounted in the respective troughs filled with water. The drums were rotated at 20 rpm for a period of 10 min. All samples retained in the drums were carefully removed and put in the oven

for a period suggested by ISRM and ASTM standards, and the oven-dried weight was taken. The samples were again put in the drums and the whole process repeated four times. The data were used to calculate the Slake Durability Index after each cycles.

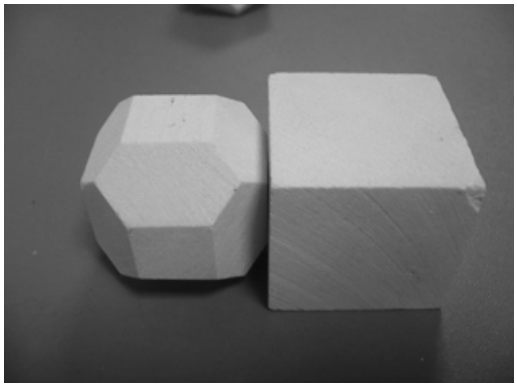

a

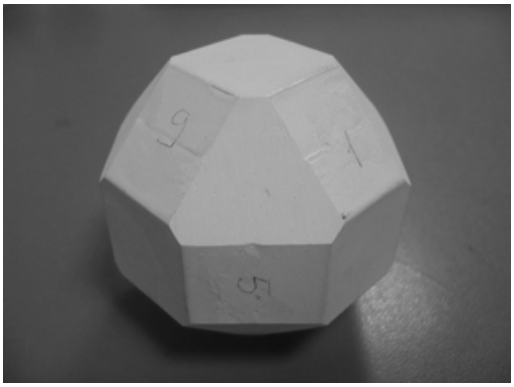

b

Figure 1. Pasha Cut; first step, edge cut (a) and second step corner cut (b)

The equal sized spherical samples shown in Figure 2 a and rounded were subjected to the slake durability test according to ISRM standard and results are given in Table 1. The condition of samples after the test for spherical samples also is shown in Figure 2 b.

Table 1. The results of slake durability index test

Index	Set-1 %	Set-2 %
I_{d1}	98.88	97.85
I_{d2}	96.64	95.02
I_{d3}	94.56	92.50
I_{d4}	92.78	90.02

a

b

Figure 2. Samples before test (a) and after the tests (b).

3 CONCLUSIONS AND DISCUSSIONS

In this study, slake durability tests were carried out on the equal sized spherical samples taken from Eskisehir Derbent white tuff quarry. Index values after fourth cycle for equal sized spherical samples kept for lime-water bath were found to be 90.02 and 92.78 %. Index values after Second cycle for spherical samples were found to be 95.02 and 96.64 %. Preliminary researches for index values of spherical samples after second cycle were determined between 94.89 and 95.56 % (Ankara et al, 2011). Index values of rounded samples after second cycle were found to be 91 and 93.8 %, being not to close each other when compared to spherical sample results (Sözmen 2000; Daloğlu 2008).

White tuff can be classified as strong according to the results of equal sized spherical sample tests. However, it can be classified as moderately strong according to the results of rounded sample tests. Second

results, index values for samples kept for lime-water bath are close each other when compared to no-treatment spherical sample results. Enhancement of slake durability index of samples kept for lime-water bath has been not observed according to no-treatment samples.

REFERENCES

Ankara, H., Aksoy, M. ve Yerel, S. 2013a. "Suda Dağılmaya Karşı Duraylılık Testi için Kayaçlardan Eş Boyutlu Küresel Örneklerin Hazırlanması", 2'nci Proje Gelişme Raporu, Proje No: 201015013, Eskişehir Osmangazi Üniversitesi BAP.

Ankara, H., Aksoy, M., Yerel, S. and Keser, Y. 2011. "A New Sample Preparation Method for Slake Durability Index Test", 4th Balkan Mining Congress, Ljubljana-Slovenia, 571-575.

Ankara, H., Aksoy, M. ve Yerel, S. 2013b. "Suda Dağılmaya Karşı Duraylılık Testi için Kayaçlardan Eş Boyutlu Küresel Örneklerin Hazırlanması", 3'ncü Proje Gelişme Raporu, Proje No: 201015013, Eskişehir Osmangazi Üniversitesi BAP.

ASTM. Standard test method for slake durability of shales and similar weak rocks (D4644). Annual book of ASTM standards, ASTM, Philadelphia, 1990; 4. 08: 863–865.

Bella FG, Entwisle DC, Culshaw MG. A geotechnical survey of some British Coal Measures mudstones, with particular emphasis on durability. Engineering Geology 1997; 46: 115-129.

Cetin H, Laman M, Ertunc A.Settlement and slaking problems in the world's fourth largest rock-fill dam, the Ataturk Dam in Turkey. Engineering Geology 2000; 56: 225–242

Ciancio D., Beckett C. T. S., Carraro J. A. H. Optimum lime content identification for lime-stabilised rammed earth. Construction and Building Materials 2014: 53, 59–65

Daloglu G., Assessment of Eskisehir-Derbent tuffs as a natural building stone material, MSc Thesis, Eskisehir Osmangazi University, Eskisehir, Turkey, 2008.

Dhakal G, Yoneda T, Kato M, Kaneko K. Slake durability and mineralogical properties of some pyroclastic and sedimentary rocks. Engineering Geology 2002; 65: 31–45.

Emir E., Konuk A., Daloglu G. Strength enhancement of Eskisehir tuff ashlars in Turkey. Construction and Building Materials 2011: 25, 3014–3019

Erguler ZA, Ulusay R. Assessment of physical disintegration characteristics of clay-bearing rocks: Disintegration index test and a new durability classification chart. Engineering Geology 2009; 105: 11–19.

Franklin JA and Chandra R. The Slake Durability Test. International Journal of Rock Mechanics and Mining Sciences 1972; 9: 325-341.

Fresno C. D.,Quesada M. D., Zamanillo V. A., Perez C. A. M. Lime Stabilization of bentonite sludge from tunnel boring. Applied Clay Science 2011: 51, 250–257

Gemici Ü. Durability of shales in narlıdere, İzmir, Turkey, with an emphasis on the impact of water on slaking behavior. Environmental Geology 2001; 41: 430-439.

Hejazi M. S., Sheikhzadeh M., Abtahi M. S., Zadhoush A. A simple review of soil reinforcement by using natural and synthetic fibers. Construction and Building Materials 2012: 30, 100–116

Sozmen B, Investigation of detoration mechanism of Yazilikaya Tuffs in Midas Monument, MSc. Thesis, METU, Ankara, Turkey, 2000.

Ulusay R., Hudson J.A. (Editors). The Complete ISRM Suggested Methods for Rock Characterization, Testing and Monitoring; 1974–2006, prepared by the Commission on Testing Methods, International Society for Rock Mechanics: ISRM Turkish National Group Ankara, Turkey, 628 ISBN 978-975-93675-4-1. 2007.

Viterbo V, McLemore V, Donahue K, Aimone-Martin C, Fakhimi A, Sweeney D. Effects of Chemistry, Mineralogy, Petrography and Alteration on Rock Engineering Properties of The Goathill North Rock Pile at The Molycorp Questa Mine, New Mexico, SME Annual Meeting Feb. 25-Feb. 28, 2007, Denver, CO.

Yong N. R. and Ouhadi R. V. Experimental study on instability of bases on natural and lime/cement-stabilized clayey soils. Applied Clay Science 2007: 35, 238–249

Micro-Mechanical and Micro-Structural Aspects of Strength Variation in Rocks under Various Loading Conditions

N. Erarslan
Adana Science and Technology University, Turkey
The University of Queensland, Australia

M. Ghamgoshar, D.J. Williams
The University of Queensland, Australia

ABSTRACT This research focuses on the micro-mechanical and micro-structural aspects of strength variation in macro-scale rock structures, because final failure of rocks comes about through a process of interaction/coalescence among the many load-parallel or load-inclined tensile fractures that are generated by micro pre-existing cracks. Provide major contributions to the understanding of stress-induced micro-fracturing of rock under various loading conditions, static and dynamic, resulting in the degradation of macro-scale rock strength, or possibly strain-hardening, of rocks. The outcome of this research is expected to provide rock cutting, civil-geotechnical and mining design engineers with access to new, more accurate rock strength estimation methods, of high value for minimising the risks associated with rock strength uncertainty.

A brittle rock type Brisbane tuff specimens were tested. Through the combined use of laboratory tests, Scanning Electron Microscope (SEM) techniques, and Computed Tomography (CT) scan technique, the damage mechanism of rocks under various loading conditions, including static and cyclic, were examined in nano-scale and the results were compared with each other for the first time in literature. Moreover, the sub-critical crack propagation phenomena , which is used to explain the premature failure of ceramics and metals and Fracture Process Zone (FPZ) phenomena, are explained in this research in terms of micro-mechanical strength reduction due to rock fatigue. Thus, modelling and understanding the crack propagation behaviour depending on different amplitude and frequencies are believed very important for the dynamic rock cutting researches and rock cutting machine manufacturers.

Keywords: Rock strength, Micro-mechanical, Micro-structural, Damage mechanism

1 INTRODUCTION

1.1 Background

Rock strength is the key parameter for the design of many rock structures and applications; in building-stone, rock cutting, civil and mining underground openings, e.g. tunnels, radioactive repositories, drilling and blasting, oil and gas reservoirs, etc. Its variation is explained by a number of factors, including mineral composition, density, porosity, fabric, moisture content, state of alteration or changes due to weathering, shape and size of the test specimen, and test conditions such as temperature, strain rate, etc. Surprisingly, the effect of micro-mechanical features (including the existence of micro-scale pre-existing cracks and their orientation in the rock, pre-existing and/or stress-induced intra-granular and/or inter-granular micro-cracks) and micro-structural parameters (such as grain size, grain shape, micro-lithologies, and petrography) on the strength of rocks continue to receive little attention due to absence of the application of laboratory techniques such as nano-scale imaging and stiff testing frames with dynamic testing capability.

It has been postulated that the final failure of rocks comes about through a process of interaction/coalescence among the many load-parallel or load-inclined tensile fractures that are generated by micro pre-existing Griffith cracks (Griffith, 1920, 1924; Bienawskie, 1964; Hoek, 1968). At the micro-scale, defects causing stress concentrations include micro-cracks, grain boundaries, pores and bedding planes, while at the macro-scale geologic fractures causing stress concentrations are referred to as joints (opening) or faults (shearing), based on their genesis (Lajtai, 1969, 1971; Rao et al., 2003). Numerous experimental and theoretical efforts have been devoted to understanding crack initiation, propagation and coalescence in brittle materials such as rocks. However, the Griffith theory in itself is not sufficient as it is restricted to only static compressive and tensile stress conditions.

Beside the Griffith theory, other well-known and internationally-used theories and rock failure criteria such as Mohr-Coulomb and Hoek-Brown also do not adequately explain the mechanism of micro-scale damage of rocks and rock strength depending on various loading conditions. The Mohr-Coulomb and Hoek-Brown criteria are concerned with failure in a continuum sense, in which the rock or rock mass undergoes permanent damage affecting its ability to sustain load. They do not consider rock as a heterogeneous/discontinuous material due to its existing natural defects, minerals, etc., and do not consider the ultimate stress of crack initiation, crack propagation or the direction of crack propagation.The effects of micro-mechanical and micro-structural parameters on rock strength have, over the last decade, been used to explain rock strength reduction and the relative damage mechanism under various loading conditions (Nasser and Deng, 1994; Zhao and Li, 2000; Xu et al., 2002; Attawel and Farmer, 1973; Haimson, 1978; Erarslan, 2011, 2012).

In geomaterial like concrete and rocks, the region near the crack tip containing micro cracked zone and ligament connections is called Fracture Process Zone (FPZ). The effect of FPZ on propagation of a tensile crack has been a subject of considerable interest over the years, and is the subject of this research (Tang and Yang, 2012, Labuz et al., 1987). The description of FPZ zone in rocks is more difficult than in metals due to complexity of the fracturing process in rock (Whittaker et al., 1992).

The full benefits of improvement in rock cutting efficiency will arise from a clear understanding of rock fracture mechanics principles. Therefore, fracture mechanics principles will be applied to the rock cutting as the nature the rock fragmentation process is based on the rock fracturing. The different types of fatigue damage mechanisms were obtained depending on the various cyclic loading conditions in literature (Ghamgoshar and Erarslan, 2014). Therefore, modelling and understanding the crack propagation behaviour depending on different amplitude and frequencies are believed very important for the dynamic rock cutting researches and rock cutting machine manufacturers.

2 EXPERIMENTAL STUDY

2.1 Mode I Fracturing and Computed Tomography (CT) Scanning Tests

The Cracked Chevron Notched Brazilian Disc (CCNBD) samples were used in both static and cyclic loading to determine the Mode I fracturing value of the selected rock types. The CCNBD specimens were preferred to use in entire test series rather than using Short Rod (SR) specimens. As far as a general comparison between the two methods is concerned, the CCNBD method definitely had advantages in terms of simplicity of sample preparation and less material required for testing. It is also unnecessary to perform pre-cracking for a CCNBD specimen because it uses a chevron notch that self-pre-cracks during testing and leads to stable crack propagation. Another remarkable advantage of the CCNBD method over the SR method in terms of accuracy is higher load capacity and

consistent results for each test. Moreover, it is believed that obtaining the FPZ zone with CCNBD geometry is more precise than obtaining with SR specimen geometry as CCNBD has an embedded chevron notch crack whereas SR specimen has edge notch crack.

The tests were carried out on Brisbane tuff, which is a host rock of Brisbane's first motorway tunnel, CLEM7, from which core samples were obtained. A series of BTS specimens were tested to evaluate the effect of cyclic loading on the tensile strength of brittle tuff rock specimens. CCNBD tests were carried out to determine the mode I fracture toughness of rocks (Fig. 1).

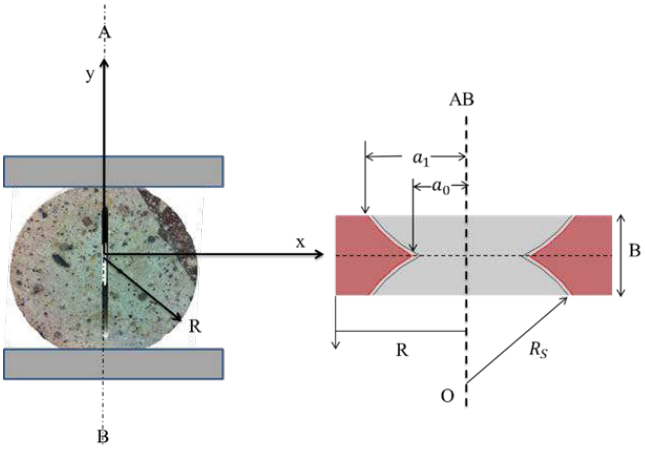

Figure 1. Prepared CCNBD sample according to the ISRM suggestions.

All geometrical dimensions were selected according to the specifications recommended by ISRM (Fowell et al., 1995). In order to achieve valid results, there are two important dimensions, that is, notched crack length α_1 and the ratio of specimen thickness to diameter α_R that must fall within the ranges outlined in ISRM suggested method (Fowell et al., 1995). In this study, the thickness of monsonite disc-shaped samples, $\mathbb{B}$, was 22.3mm, inner chevron crack notch half length, α_0, was 5.8mm, outer chevron notched crack half length, α_1, was selected 15.6mm.

An Instron loading machine with a capacity of ±150 kN (+/- 25,000 kgf, +/- 56,000 lbf) was used for static and cyclic loading tests. An Instron 2670-132 series Crack Opening Displacement (COD) gauge was used to measure the crack mouth displacement. The disc specimens were diametrically loaded parallel to the diametral compressive loading directions with a notch crack inclination angle of zero ($\beta = 0°$) to provide a mode I fracture condition. The applied load, diametral displacement, and crack mouth displacement, were continually recorded during the tests by using a computerised data logger.

Following the diametral loading tests, 3-D X-ray micro-focus CT scanning techniques was used in this study to investigate and quantify the physical properties of the damaged zone, such crack porosity (cracked volume/total volume) and crack density (number of cracks per mm^3). These samples were tested at the University of Queensland, Julius Kruttschnitt Mineral Research Centre (JKMRC). The X-ray detector is a high-resolution digital X-ray camera detector system. This detector accumulates all the energy of the transmitted photons and provides the numerical data to be used in reconstructing an image. For each head, 1500 views of the sub-sample were taken over 360° rotation. Each sample was placed vertically within the scanner so that the X-ray intersected the sample perpendicular to the longitudinal axis. Once the scans were finished, the collected raw data (the series of rotational X-ray images) were reconstructed with an ultra-high resolution noise reducing filtered back-projection. For the SkyScan 1172, the X-ray micro focus tube with 8 µm focal spot operates at 20-80 kV and 100 µA current while the source working at 20-100 kV and 0-250 µA has a 5 µm spot size. The special X-ray CCD camera is based on a 4000×2300 (10 Mp), or 1280×1024 (1.3 Mp) cooled CCD sensor with fibre optic coupling to the X-ray scintillator. For the 10Mp camera, the X-ray shadow projections are digitized as 1000 ×575 to 8000×2300 pixels with 4096 brightness gradations (12 bit). The reconstructed cross sections have a 1000×1000 to 8000×8000 pixels (floating point) format. The pixel size is isotropic and continuously variable from 0.9 µm to 35 µm. Fig. 4 represents the experimental set up for

the CT scan test and a rock sample after a fracture toughness test.

3 EXPERIMENTAL RESULTS

3.1 Mode I Fracture Toughness under Static and Cyclic Loading

Seven CCNBD samples were tested under load-control test conditions. The specimens were placed under the platens with a crack inclination angle of zero ($\beta = 0°$) to provide mode I loading conditions. The loading rate was chosen as 9 kN/s to cause failure within 20s as suggested by the ISRM (Fowell et al. 1995). The maximum recorded load and the calculated KIC values obtained from both ISRM standard tests are shown in Table 1.

Table 1 Mode I fracture toughness values of Brisbane tuff obtained by CCNBD tests.

Rock type	P_{max} (kN) CCNBD	K_{IC} (CCNBD) ($MPa\sqrt{m}$)
Brisbane tuff-1	5.2	1.3
Brisbane tuff-2	5.1	1.3
Brisbane tuff-3	4.6	1.2
Brisbane tuff-4	5.1	1.3
Brisbane tuff-5	4.1	1.1
Brisbane tuff-6	4.0	0.9
Brisbane tuff-7	3.5	0.8
Average	4.5	1.1

The series of diametral compressive increasing cyclic loading tests was performed on 12 CCNBD Brisbane tuff samples. Fracture toughness values of Brisbane tuff under static loading were calculated as 1.12–1.5 MPa√m using the ISRM suggested methods as discussed above. The fracture toughness reduction because of cyclic loading is found up to 45% by comparing with static fracture toughness values. The main purpose of this comparison is to show the clear reduction of ultimate failure load that resulted in the reduction of the mode I stress intensity factor because of rock fatigue. It is shown that crack propagation causing failure is possible with lower stress intensity values (K_I) at the crack tip than the critical stress intensity value (K_{IC}). This result goes against the classical theory, which predicts that there will be no crack growth as long as $K_I < K_{IC}$. According to the obtained results, the maximum reduction, 46% of static KIC, was obtained with the highest amplitude, 1.99 kN at 40% SUL, of cyclic loading. The mode I fracture toughness value of Brisbane tuff (NST50) was reduced from 1.12 MPa√m to 0.61 MPa√m with the highest amplitude under increasing cyclic loading. This reduction has important implications for the investigation of the effect of cyclic loading on the fracture resistance of cracks in rocks.

3.2 CT Scan Test Results

The CT scan technique was used to quantify the FPZ under different cyclic loadings. As discussed earlier, nucleation of micro-fractures is the main reason of fracturing leads to failure in brittle rocks. The CT scan tool provides a clear monitoring of micro-cracks initiation and propagation in and around FPZ zone. Dislocation of micro-fractures takes place in different ways with different rock types. In general, it was observed breaking the bonds between minerals and rock forming matrix happened due to two reasons: 1) concentration of stress at the tip of fractures and 2) formation of transcrystalline and inter-crystalline cracks. All those dislocations occurred because of the micro-fractures such as intergranular and intragranular cracks caused by the inelastic behaviour of rocks (Fig.2). This mechanical behaviour shows that decohesion and loosening start with the development of FPZ in front of the notched crack under the cyclic loading.

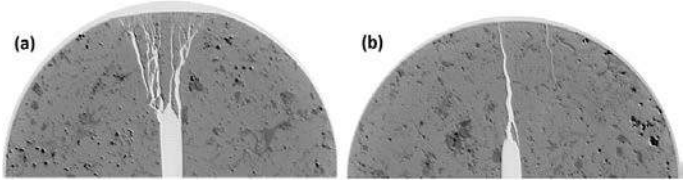

Figure 2. 5 CT-scan images of CCNBD specimens with FPZ developed under (a) cyclic and (b) static loading.

Further CT scans on CCNBD specimens showed the self-orientated stress-induced micro fractures and their interactions caused subcritical cracks and enhance energy dissipation. Static tests revealed the main crack propagation associated with the very small damage zone started from the tip of notch crack and ended at the CCNBD circumference without any fracture branches. That is why; any subcritical crack propagation before the final failure would not be expected. However, a great number of smooth and smaller cracks occurred in and around fracture process zone leads to formation of subcritical cracks under cyclic loading. Fig. 3 shows a close look in the FPZ and crack branches developed in rock matrix under the cyclic loading with increasing amplitude from 10% Static Ultimate Load (SUL) to 50% and 80% SUL.

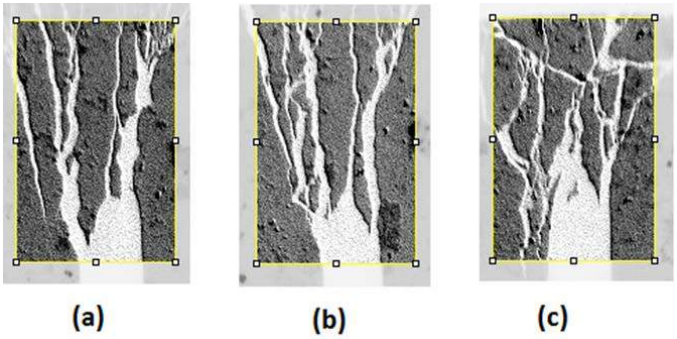

Figure 3. Different branching of the cracks in FPZ depending on the different amplitudes used with stepped cyclic loading: (a) 10%SUL, (b) 50%SUL and (c) 80% SUL.

3.3 SEM Test Results

A typical feature of rock fatigue in experimental tests can be observed by producing a progressive accumulation of permanent strain in the specimen, rather than any significant decay in the material's elastic modulus. Accumulation of plastic deformation is responsible for the fatigue damage; the magnitude and increasing trend of the irreversible deformation influences the cumulative fatigue damage.

Plots of permanent along both x and y directions show that both the CMOD and diametral axial displacement increase with increasing damage increments but at different rates.

The characteristics of the fracture surfaces were examined by means of a JEOL JMS-6460 LA SEM. The JEOL JSM-6460 LA is a tungsten low-vacuum analytical SEM. In this study, all rock fracture images were obtained under low vacuum chamber pressures, that is, 1–50 Pa (with adjustable pressure between 10 Pa and 270 Pa). This allowed certain samples to be observed uncoated and reduced damage to the specimens caused by the effects of high vacuum.

Two fatigue mechanisms were observed in the cement of Brisbane tuff: (1) grain decohesion in secondary microcrystalline quartz cement intrusions (Fig. 4) and (2) fatigue striations in primary silica cryptocrystalline cement.

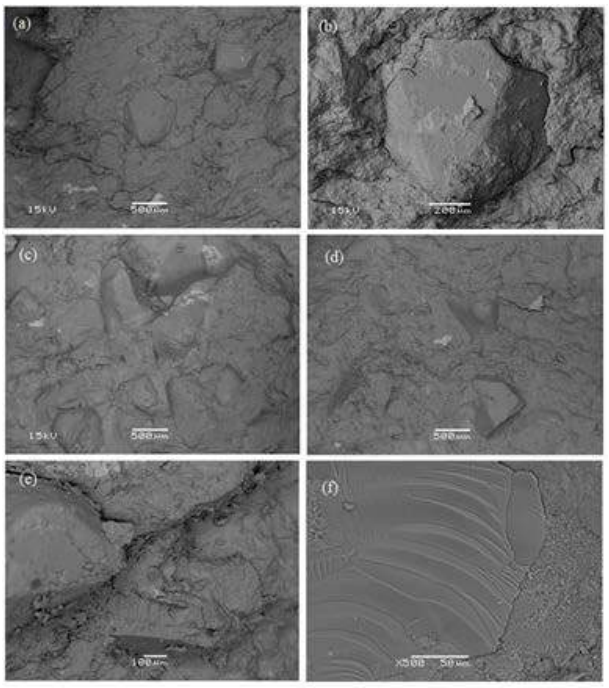

Figure 4. Grain decohesion and loosened grains (a), (b), (c), (d), (e) and fatigue striations in damaged grains under high magnification (× 500) at the surface of the fatigue crack (f).

Some microcrystalline quartz cement intrusions were seen in the primary silica cryptocrystalline cement after petrographic analyses. Similar to the fatigue damage in the cement, there were two fatigue damage mechanisms seen with grain-related damage: (1) intergranular cracks causing grain decohesion (a primary mechanism) and (2) intragranular cracks (a secondary mechanism).

4 CONCLUSIONS

This research showed the crack propagation causing failure is possible with lower stress intensity values (KI) at the crack tip under cyclic loading than the critical stress intensity value(KIC) obtained under static loading.

CT scan results indicate that FPZ obtained with the static loading is smaller than the FPZ obtained with the cyclic loading ($FPZ_{Static} < FPZ_{Cyclic}$). This finding was verified with the obtained CMOD plastic strain accumulation plots.

SEM imaging revealed that the primary fatigue damage mechanisms in front of a chevron notch crack are grain decohesion and intergranular cracks. Debris and dust are the results of fatigue damage in Brisbane tuff cement and around loosened grains. The fatigue cracks in the cement are restricted around the grains and cannot grow through the grains. Therefore, it can be deduced that those fatigue cracks are stable (subcritical) cracks that coalescence to form macroscale fatigue cracks resulting in failure. The different types of fatigue damage mechanisms were obtained with the numerical analyses depending on the various cyclic loading conditions. Therefore, modelling and understanding the crack propagation behaviour depending on different amplitude and frequencies are believed very important for the dynamic rock cutting researches and rock cutting machine manufacturers. Because the full benefits of improvement in rock cutting efficiency will arise from a clear understanding of rock fracture mechanics principles, the specific fracture mechanics principles would be applied to the rock cutting as the nature the rock fragmentation process is based on the rock fracturing.

REFERENCES

Attawel, P.B. and Farmer, I.W. 1973. Fatigue behavior of rock. *Int. J. Rock Mech. Min. Sci. Geomech. Abs.*, 10, 1–9.

Bienawskie, Z.T. 1967b. Mechanism of brittle rock fracture: Part II-Experimental studies. *Int. J. Rock Mech. Min. Sci. Geomech. Abs.*, 4(4), 407–423.

Erarslan, N. 2011. Static and cyclic laboratory testing of Brisbane rocks. PhD Thesis. The University of Queensland, Australia.

Erarslan, N. and Williams, D.J. 2012. Investigating the Effect of Cyclic Loading on the Indirect Tensile Strength of Rocks. *Rock Mechanics and Rock Engineering*, 45(3), 327-340.

Fowell, R. J., Hudson, J. A., Xu, C., Chen, J. F. & Zhao, X. 1995. Suggested method for determining mode I fracture toughness using cracked chevron notched Brazilian disc (CCNBD) specimens. International Journal of Rock Mechanics & Mining Sciences.

Ghamgosar, M & Erarslan, N. 2014. 'The Effect of Cyclic Loading Amplitude and Notch Crack Inclination Angle on the Fracture Toughness Test on Brisbane Tuff- Multiple Factorial Analyses', Eurock 2014.

Griffith, A.A., 1920. The phenomena of rupture and flow in solids. Philos. *Trans. Royal Soc. London*, 221(587), 163–198.

Griffith, A.A., 1924. The theory of rupture. *In: Proceedings of the First International Congress for Applied Mechanics*, 55-63, Biezeno, Delft. C.B., Burgers, J.M. and Waltman, J. (Eds.).

Haimson, B.C., 1978. Effect of cyclic loading on rock. *Dynamic Geotechnical testing ASTM STP*, 654, 228–245.

Hoek, E., 1968. Brittle fracture of rocks. Chapter 4 in Rock Mechanics in Engineering Practice, 99-124, London: J. Wiley.

Labuz, J., Shah, S. & Dowding C., 1987. The fracture process zone in granite: evidence and effect. International Journal of Rock Mechanics and Mining Sciences & Geomechanics Abstracts,. Elsevier, 235-246.

Lajtai, E.Z. 1971. A theoretical and experimental evaluation of the Griffith theory of brittle fracture. *Tectonophysics*, 11, 129–56.

Lajtai, E.Z., 1969. Shear strength of weakness planes in rock. *Int. J. Rock Mech. Min. Sci. Geomech. Abstr.*, 6, 299-515.

Nemat-Nasser, S. and Deng, H. 1994. Strain rate effect on brittle failure in compression. *Acta Metall. Mater.*, 42, 1013-1024.

Rao, Q., Sun, Z., Stephansson, O. and Li, C., 2003. Shear fracture (Mode II) of brittle rock. *Int. J. Rock Mech. Min. Sci.*, 40, 355–375.

Tang, C.A. and Yang Y.F., 2012. Crack branching mechanism of rock-like quasi-brittle materials under dynamic stress. Journal of Central South University, 19, 3273-3284.

Whittaker, B. N. Singh N., and Sun G., 1992. Rock fracture mechanics : principles, design, and applications /, Amsterdam ; New York, Elsevier.

Xu, S., Wu, W. and Liu, Y. 2002. Experimental study on cyclic property of rocks under uniaxial compression. *Pro. SPIE*, 4537, 261–265.

Zhao, J. and Li, H.B., 2000. Experimental determination of dynamic tensile properties of granite. *Int. J. Rock Mech. Min. Sci*., 37, 851-861.

Numerical Study of the Undrained Bearing Capacity of a Strip Footing Near a Slope

M. Baazouzi, M. Mellas A. Mabrouki, D. Benmeddour
Civil Engineering Laboratory, Biskra University, BP 145 Biskra 07000 Algeria.

ABSTRACT The bearing capacity of shallow foundation near slope has always been one of the subjects of major interest in geotechnical engineering for researchers and practical engineers. This study focuses on the numerical analysis of the undrained bearing capacity for a strip footing near a slope, and subjected to a centered vertical load, using the explicit finite difference code FLAC (Fast Lagrangian Analysis of Continua). In this study, several geometrical and mechanical parameters have been considered in order to evaluate the effect of the slope on the undrained bearing capacity. The numerical values have been compared with those available in the literature. The results show the influence on the undrained bearing capacity of the location of the footing with respect to the slope.

Keywords: Strip footing, bearing capacity, slope, shallow foundations, FLAC

1 INTRODUCTION

The bearing capacity problem of footings has been extensively studied for many decades. There is an extensive literature dealing with the bearing capacity of foundations, from both theoretical and experimental standpoints; in addition, the study of foundations requires an adequate understanding of several influenced factors such as load inclination, slope inclination, footing shape.

The bearing capacity of a shallow strip footing is generally determined by the Terzaghi method (Terzaghi, 1943). For undrained conditions the ultimate vertical bearing capacity q_u of a surface footing can be expressed by:

$$q_u = N_c c_u \quad (1)$$

where N_c is the bearing capacity factor (=2+π ; Prandtl, 1920), c_u is the undrained shear strength of the soil.

A number of engineering structures require foundation systems to be placed near an existing slope. Theoretical and experimental studies confirm that, when a strip footing is near a slope, the bearing capacity must be assessed using reduction coefficients. Meyerhof (1957) proposed design charts which are currently adopted by many design manual. Also, the bearing capacity equations of Hansen (1961) and Vesic (1975) include empirical factors for sloping ground. Giroud and Tran-Vo-Nhiem (1971) and Graham et al. (1988) provided solutions for the bearing capacity factor for a strip footing on the top of a slope in granular soil based on the method of slip-line.

Many analytical and numerical studies in bearing capacity have been conducted using different approaches. Upper bound bearing capacity solutions for strip footing on slope have been proposed by Kusakabe et al. (1981) and de Buhan and Garnier (1998). The limit equilibrium method has also been applied by several investigators to provide solutions and design charts for footing on slope (Saran et al., 1989; Castelli and Motta, 2008). Some experimental works on the bearing capacity of foundation near slope have been conducted by Shields et al. (1977) and Bauer et al. (1981). Also, Gemperline (1988) and Bakir (1993) used centrifuge tests. The finite element, upper bound plasticity and stress field methods were used by Georgiadis (2009) to investigate the influence of load inclination on the undrained bearing capacity of strip footing on or near slopes. Also, Georgiadis (2010) used the finite element analysis to investigate the influence of the distance of the foundation from the slope, the slope

height and the soil properties on bearing capacity of strip footings on or near undrained soil slopes. Shiau et al. (2011) used the finite element limit analysis method to obtain both lower and upper bound bearing capacity for strip footings placed on purely cohesive slopes.

In this study, series of numerical computation using the finite difference code FLAC (2005) are carried out to evaluate the influence of the various parameters that affect undrained bearing capacity of strip footings on or near slopes. The results of the analyses are compared to available methods.

2 NUMERICAL MODELING PROCEDURE

The finite-difference code FLAC (2005) was used to estimate the undrained bearing capacity of a strip footing on or near slopes under conditions of plane strain and subjected to a centred vertical load. FLAC (Fast Lagrangian Analysis of Continua) is a two-dimensional explicit finite-difference program for engineering mechanics computations; it simulates the behaviour of structures built of soil, rock or other materials that undergo plastic flow when their yield limits are reached. Many researchers have used the finite difference code FLAC to study the bearing capacity of strip and circular isolated footings (e.g., Frydman and Burd, 1997).

The geometry of the problem analyzed is shown in Figure 1. In the current study, we consider a rigid and rough strip footing of width B=2m on an undrained soil slope. Three slope angles β = 15°, 30° and 45°, also several slope heights H and normalized footing distances from the crest of the slope (λ = footing distance/footing width) were used in order to investigate the influence of these three parameters. The soil is modelled as a Tresca material using the Mohr–Coulomb elastic-perfectly plastic constitutive model with φ = 0. In order to make a comparison with the finite element results given by Georgiadis (2010), the model is characterized by the undrained Young's modulus E_u=30 MPa, Poisson's ratio ν = 0.49 and unit weight γ=20 kN/m^3, while the undrained shear strength was varied (c_u= 40, 100 and 200 kPa).

The footing is modelled as an elastic material with concrete Young's modulus of E_c=25 GPa and Poisson's ratio of ν = 0.4. The interface between the soil and footing is rough, it is characterized with normal stiffness K_n =10^9 Pa/m and shear stiffness K_s=10^9 Pa/m.

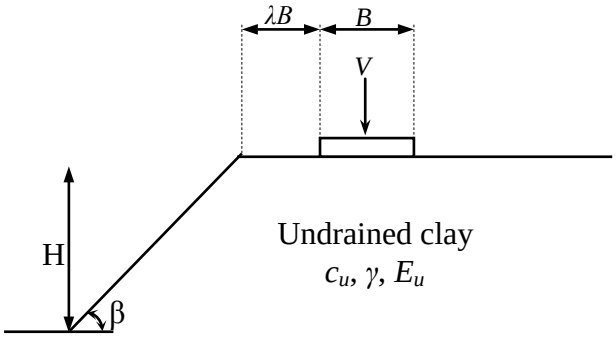

Figure 1. Problem geometry

Because of the nonsymmetrical problem, the entire model is considered in the computations. Figure 2 shows a typical finite-difference mesh, used for the case of footing located at the crest (λB=0). In all cases, the mesh is refined at the region most close to the boundaries of the foundation, under the base and near the crest of the slope. The displacement of the left and right vertical sides is constrained in the horizontal direction only. The base of the model is constrained in all directions (Fig. 2).

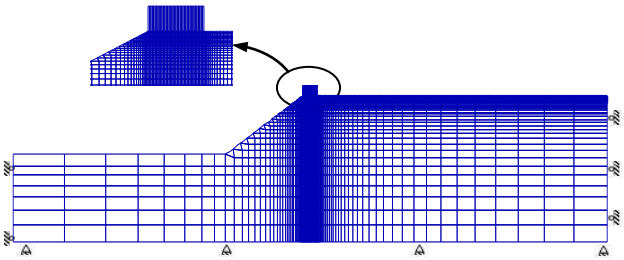

Figure 2. Finite difference mesh and boundary condition for the case λB=0.

3 RESULTS AND DISCUSSIONS

3.1 Bearing Capacity

The loading of the rigid strip footing is simulated by imposing equal vertical velocities at the area representing the footing. It is worthwhile noting that different mesh sizes with several vertical velocity values have been tested. The progressive displacement of the footing induced by the vertical velocity applied at the footing nodes is accompanied by the increase of the pressure in the soil. Finally, the pressure under the footing stabilizes for a value that indicates a limit load (Fig. 3).

The vertical bearing capacity q_u=5.225c_u was predicted in the present study for a surface footing, representing an overestimation of less than 2% from the analytical solution of q_u=5.14c_u. It means that numerical prediction obtained using FLAC, is in excellent agreement with the exact solution obtained by Prandtl (1920).

Figure 3 shows the load–displacement curves, i.e., the curves of the vertical load V versus the vertical displacement. The comparison is made for three values of slope inclination. From the results of Figure 3, it is seen that the limit load V_u decreases substantially with increasing β.

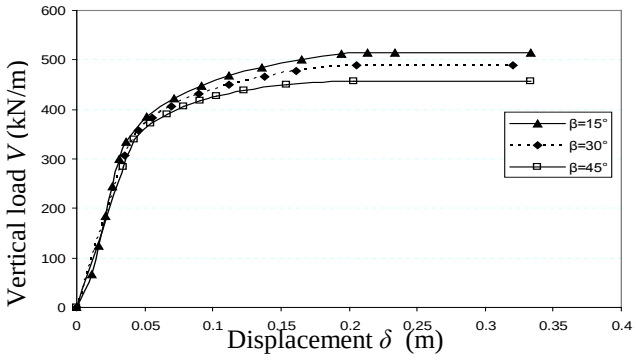

Figure 3. Load–displacement curves

3.2 Influence of the Slope Inclination

Figure 4 shows the variation of the calculated values of the undrained bearing capacity factor for a footing with the slope angle β for different $c_u/\gamma B$ ratios. The results presented in this study are compared to the solutions of Hansen (1961), Vesic (1975), Bowles (1996), Kusakabe et al. (1981) and Georgiadis (2010) for the case of a footing at the crest of a slope. The present study confirms a linear decrease of the undrained bearing capacity factor with the increase of the slope angle. Also, the finite difference results show a decrease of the value of N_c with the decrease of the ratio $c_u/\gamma B$. It is seen that the results of Bowles (1996) which gives a decrease of N_c with the decrease of $c_u/\gamma B$, is in good agreement with the finite difference results for $c_u/\gamma B$=5.

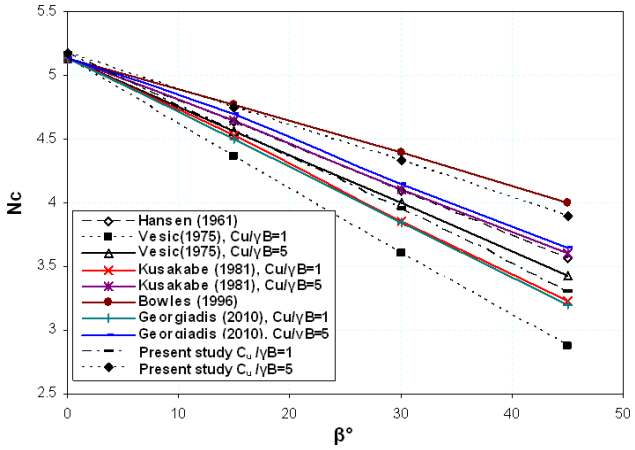

Figure 4.Variation of N_c with slope angle β for footing at crest of slope, λ =0 (Figure modified from Georgiadis, 2010)

3.3 Influence of Slope Height

The influence of slope height on the failure load for vertical loading was studied with finite element analysis by Georgiadis (2010). Figure 5 shows the variation of bearing capacity factor N_c with normalized slope height for β=30° and $c_u/\gamma B$=1. It is seen that the values of results obtained from the present study are in good agreement with the solutions presented by Georgiadis (2010). Depending on the slope height, two distinct displacement modes can be observed. The first mode shown in Figure 6 (a) is similar to the displacement mode for the case of horizontal ground surface. The second displacement mode (Fig. 6(b) involves the whole of the slope. The finite difference and finite element results give the expected initial reduction of N_c starting from the horizontal ground value, which is followed

by a horizontal section of constant N_c corresponding to bearing capacity failure and a final drop corresponding to overall slope failure.

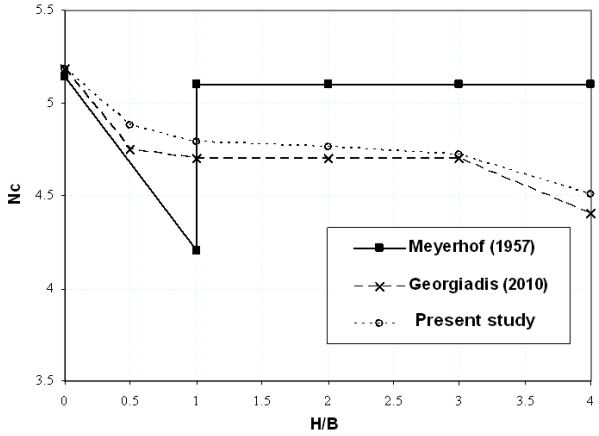

Figure 5. Variation of N_c with normalized slope height for β=30° and $c_u/\gamma B$=1 (Figure modified from Georgiadis, 2010).

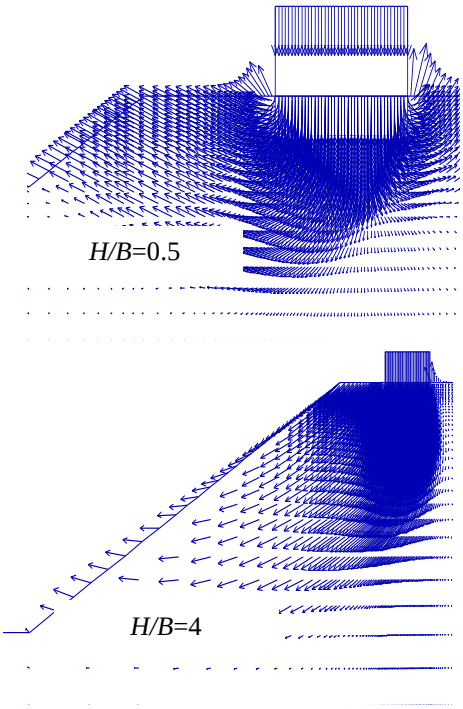

Figure 6. mode of displacement

3.4 Influence of Normalised Footing Distance

Figure 7 shows the variation of N_c with λ for slope angles 30° and 45°. Meyerhof (1957) overestimates the value of bearing capacity factor N_c. For all values of β, the increase in footing capacity tends to stop at certain values of λ. From the present study N_c reaches a constant value of 5.25 approximately at λ=1.5 for β = 30°. For β = 45° the limit value of N_c is reached at λ=2.5. The finite difference results are in good agreement with the finite element results solution proposed by Georgiadis (2010).

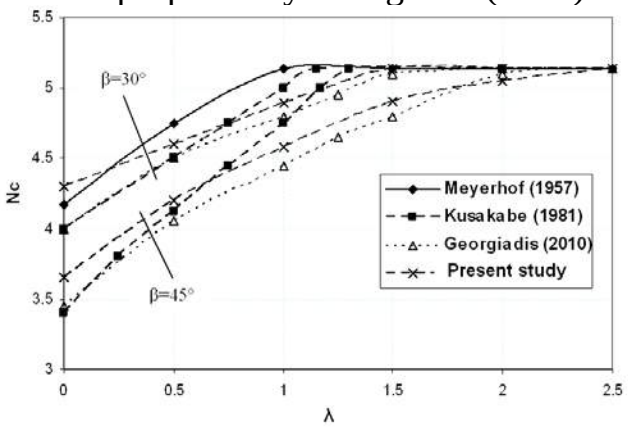

Figure 7. Variation of N_c with λ for $c_u/\gamma B$=2.5, β=30° and 45°

(Figure modified from Georgiadis, 2010)

4 CONCLUSIONS

The finite-difference code FLAC was used to study the influence on the undrained bearing capacity of strip footings on or near slopes under vertical load. Various geometries and soil properties were considered, the results of the analyses were compared to other available solutions. It was found that the bearing capacity factor N_c depends on the slope height, the distance of the footing from the slope and the slope angle. It is worth noting that most of the available methods for the evaluation of the undrained bearing capacity factor N_c do not take account of these parameters.

The increase of the distance of the footing from the slope increases the value of bearing capacity factor N_c, Also, at high values of *H/B*, overall slope failure is observed. The footing capacity decreases as the slope angle β is increased.

REFERENCES

Bakir N. (1993). Etude sur modèles centrifugés de la capacité portante de fondations superficielles. Thèse de doctorat de l'Ecole Centrale de Nantes.

Bauer G.E., Shields D.H., Scott J.D. Gruspier J.E. (1981) Bearing capacity of footings in granular

slopes. *Proc. 10th Int Conf. on soil Mech. and Found. Eng*. 2, 33-36.

Bowles, J. E. (1996). *Foundation analysis and design*, 5th Ed., McGraw-Hill, New York.

Castelli, F., and Motta, E. (2008). Bearing capacity of shallow foundations near slopes: Static analysis. *Proc., 2nd BGA Int. Conf*. on Foundations, ICOF 2008, HIS BRE Press, Watford, U.K., 1651–1660.

De Buhan P., Garnier D. (1998) Three-dimensional bearing capacity analysis of a foundation near a slope. *Soils and Foundations*, 38 (3), 153-163.

FLAC2D -Fast Lagrangian Analysis of Continua, version 5.0. (2005) ITASCA Consulting Group, Inc., Minneapolis.

Frydman S., and Burd H.J. (1997) Numerical studies of bearing capacity factor Nγ. *J. Geotech. Geoenviron. Eng*. 123 (1), 20-29.

Gemperline M.C. (1988) Centrifuge modeling of shallow foundations. *Proc. ASCE Spring Convention*.

Georgiadis K (2010). Undrained bearing capacity of strip footings on slopes. *J Geotech Geoenviron Eng*, ASCE, 136 (5), 677–685.

Georgiadis, K. (2009). The influence of load inclination on the undrained bearing capacity of strip footings on slopes. *Comput. Geotech*. 37(3), 311–322.

Giroud J.P. Tran V.N. (1971) Force portante d'une fondation sur une pente. *Annales de l'I.T.B.T.P*, Paris, n° 283-284, série théories et méthodes de calcul, n° 142, 130-179.

Graham J., Andrew M., Shields D.H. (1988) Stress characteristics for shallow footing in cohesionless slopes. *Canadian Geotechnical Journal* 25(2), 238-249.

Hansen, J.B. (1961). A general formula for bearing capacity. Bulletin 11, *Danish Geotechnical Institute*, Copenhagen, Denmark, 38–46.

Kusakabe O., Kimura T., Yamaguchi H. (1981) Bearing capacity of slopes under strip loads on the top surfaces. *Soils and Foundations*, 21(4), 29-40.

Lebègue Y. (1973) Essais de fondations superficielles sur talus. *Proc. 8th Int. Conf. on soil Mech. and Found. Eng*. 4.3, 313-315.

Meyerhof G.G. (1957) The ultimate bearing capacity of foundations on slopes. *Proc. 4th Int. Conf. on soil Mech and Found. Eng*. 1, 384-386.

Prandtl L. (1920). Uber die Harte Plastischer Korper. Nachr. Ges. Wiss. Goettingen Math. Phys. Kl., 74–85.

Saran S., Sud V.K, Handa S.C. (1989) Bearing capacity of footings adjacent to slopes. *Journal of Geotechnical Engineering*, ASCE, 115 (4), 553-573.

Shiau J. S., Merifield R. S., Lyamin A. V., Sloan S. W. (2011). Undrained Bearing Capacity of Strip Footings on Slopes. *International Journal of Geomechanics*, ASCE, 5 (11), -381–390.

Shields D.H., Scott J.D., Bauer G.E., Deschemes J.H., Barsvary, A.K. (1977) Bearing capacity of foundations near slopes. *Proc. 9th Int. Conf on Soil Mech and Found. Eng.* 1, 715-720.

Terzaghi K. (1943) *Theoretical soil mechanics*, Wiley, New York.

Vesic, A. S. (1975). Bearing capacity of shallow foundations. Foundation engineering handbook, H. F. Winterkorn and H. Y. Fang, eds., Van Nostrand Reinhold, New York.

Numerical Study of the Effect of Increasing Strength with Depth on the Undrained Bearing Capacity of Strip Footings

M. Ouahab, A. Mabrouki, M. Mellas, D. Benmeddour
Civil Engineering Laboratory, Biskra University, BP 145 Biskra 07000 Algeria

ABSTRACT The problem of the bearing capacity evaluation for a strip footing has been widely studied using theoretical and experimental approaches. This paper focuses on the bearing capacity of a strip footing on non-homogeneous clay. A series of numerical computations was carried out to evaluate the undrained bearing capacity of vertically loaded, rigid strip footing, using the finite element software PLAXIS 2D. The objective of this study is to analyse the effect of linearly increasing undrained shear strength with depth on the bearing capacity of a strip rough and smooth footing. The results of the present study are compared with those available in the literature. The values of the bearing capacity factor, obtained by the present analysis are in good agreement with the results calculated by the slip line method. It is confirmed that the correction factor is given as a function of dimensionless heterogeneity factor.

Keywords: Strip footing, bearing capacity, slip line method, PLAXIS 2D

1 INTRODUCTION

Foundations of engineering structures are designed to transfer and distribute their loading to the underlying soil. Design of shallow footings entails both settlement and bearing capacity calculations. The bearing capacity problem of footings has been extensively studied for many decades. In engineering practice, the bearing capacity of foundations (both drained and undrained) is usually estimated using well-established bearing capacity formulae (e.g. Terzaghi, 1943).

Many analytical and numerical methods can be used to estimate the vertical bearing capacity of a rigid strip footing; these methods may be classified into the following four categories:

- limit equilibrium method (e.g., Terzaghi, 1943; Meyerhof, 1951; Kumbhojkar, 1993);
- slip line method (e.g., Sokolovskii, 1960; Houlsby & Wroth, 1983 ; Martin, 2004)
- limit analysis method (e.g., Chen, 1975; Michalowski, 1997; Merifield et al., 1999);
- finite element or finite difference analyses (e.g., Griffiths, 1982; Gourvenec & Barnett, 2011; Edwards et al, 2005).

Skempton (1951) showed that for a cohesive soil (φ=0°) the value of the bearing capacity factor N_c increases with the value of the foundation depth, z. The bearing capacity of a strip footing on nonhomogeneous clay was studied by Davis & Booker (1973). By means of the theory of plasticity, their results showed that the rate of increase of cohesion with depth plays the same role as density plays in the bearing capacity of homogeneous cohesive−frictional soils. In addition, this problem has been studied previously by Houlsby & Wroth (1983) and Tani & Craig (1995). Davis & Booker's analyses have since been verified by Martin (2004) using the computer program ABC.

Griffiths (1982) used the finite element method to study the bearing capacity for both rough and smooth footing, on undrained clay whose strength varies linearly with depth and the case of two layers of different strength but within each layer the strength is constant. Ukritchon et al., (1998) used the numerical limit analyses to evaluate the undrained stability of surface footings on nonhomogeneous and layered clay deposits under the combined effects of vertical, horizontal, and moment (V, H, M) loading.

In this paper, a series of numerical computations using the finite-element code PLAXIS (2012) are carried out to determine, the bearing capacity factor N_c for rough and smooth strip footing subjected to centered vertical loads and placed on a non-homogeneous undrainded clay. The numerical results are compared with those available in the literature.

2 PROBLEM PRESENTATION

The undrained bearing capacity equation has the following form:

$$q_u = c_{uo} N_c \quad (1)$$

where N_c is a bearing capacity factor, c_{uo} is the undrained shear strength at foundation level (soil surface); if the strength parameter c_{uo} is constant, the soil is described as homogeneous; if the strength parameter vary with position, the soil is non-homogeneous; for simplicity, the shear strength is assumed to vary linearly with depth according to:

$$c_u(z) = c_{uo} + k\,z \quad (2)$$

where k is the strength gradient with depth, z. The degree of non-homogeneity for a given foundation is represented by the non-dimensional ratio kB/c_{uo}.

Davis & Booker (1973) method gives a solution of bearing capacity for a strip foundation under vertical load where c_u increases with depth. The bearing capacity can be expressed by:

$$\frac{Q}{B} = F\left[(2+\pi)\cdot c_{uo} + kB/4\right] \quad (3)$$

where Q is the total load at failure and F is a dimensionless correction factor depending only in the ratio kB/c_{uo} (for rough base footing, $F=F_R$ and $F=F_S$ for smooth base footing)

The present paper addresses the effect of increasing the strengths with depth on the bearing capacity of strip footing on clay, as shown in Figure 1.

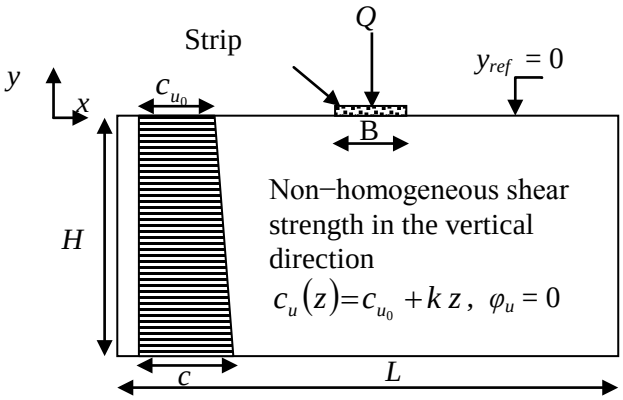

Figure 1. Problem geometry

3 NUMERICAL PROCEDURES

The two dimensional elastic-plastic finite element analysis (FEA) is conducted using PLAXIS 2D (2012) to reach the bearing capacity for strip footing.

The numerical evaluation of the bearing capacity is based on subdividing the soil into a number of elements. Because of the symmetrical nature of the problem, only half of the model is considered in the computations. The mesh adopted for all cases studied in this paper has a depth of B and $2B$ in large (B=footing width), the mesh in the footing neighborhood is refined to capture significant displacement gradients. The base of the model is constrained in all directions. The right and the left vertical sides are constrained in the horizontal direction only.

The soil was considered to be a linearly elastic-perfectly plastic material, obeying Tresca criterion. The cohesion at the soil surface c_{uo} is taken 1 kN/m^2; in the advanced settings of PLAXIS, the increase of shear strength with depth is defined by c_{incr} (k). A Poisson's ratio of υ=0.495 enforces the condition of undrained behaviour of clay. It is noted that the values of the elastic parameters had no effect on the value of bearing capacity (Edwards et al, 2005).

The strip footing was rigid, rough and smooth of width B = 1 m, subjected to a centered vertical load and located on the surface of a non-homogeneous clay. The loading of the rigid strip footing is simulated by imposing equal displacement at all nodes

representing the footing. The progressive displacement is accompanied by the increase of the pressure in the soil. Finally, the pressure under the footing stabilizes for a value that indicates a limit load; this load corresponds to the bearing capacity q_u.

4 NUMERICAL RESULTS

4.1 Bearing Capacity Factor N_c

For the case for rough strip footing on homogeneous, undrained clay (kB/c_{uo}= 0), the bearing capacity factor N_c has been obtained as N_c=2+π using the theory of plasticity (Prandtl, 1921). The numerical value of the bearing capacity factor N_c is 5.148, and the relative error is 0.15% when compared to the exact value of 5.14 kPa.

Figure 3 shows the bearing capacity factor, expressed as $N_c=q_u/c_{uo}$ versus kB/c_{uo}, where q_u is the ultimate unit bearing capacity and c_{uo} is the shear strength. As shown in Figure 3, the bearing capacity factor increases significantly with the increase of the kB/c_{uo} value.

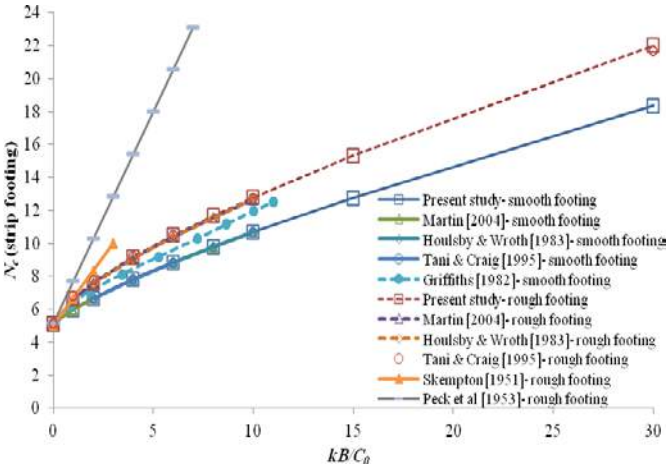

Figure 3. Comparison of obtained N_c with theoretical results for rough and smooth footing

The values of N_c obtained from the present study are in good agreement with the solutions reported by Houlsby & Wroth (1983), Tani & Craig (1995) and Martin (2004). The values of the bearing capacity factor N_c differ depending on whether smooth or rough conditions are assumed, the results for rough footing appear to be very high.

4.2 Correction Factor F_R

Figure 4 shows the bearing capacity correction factor F_R for rough strip footing. The numerical solution from the present study is compared with analytical results reported by Davis and Booker (1973) and with the numerical limit analyses by Ukritchon et al. (1998). For the homogeneous case (kB/c_{uo}=0), the obtained numerical value of F_R is 1.002, only 0.2% higher than the exact value and therefore the interface shear strength has no effect on the bearing capacity.

For non-homogeneous strength profile ($kB/c_{uo} \leq 20$), F_R increases with the increase of the rate of heterogeneity to a maximum value of 1.76, which means that the roughness increase the bearing capacity as strength heterogeneity increases. It can be seen that the numerical values of F_R obtained from this study are in good agreement with those obtained by Davis and Booker (1973) and are enclosed by the lower and upper bound solutions from Ukritchon et al. (1998) where a very good estimate of failure can be obtained by averaging the computed upper and lower bound loads Q_A=1/2(Q_L+Q_U).

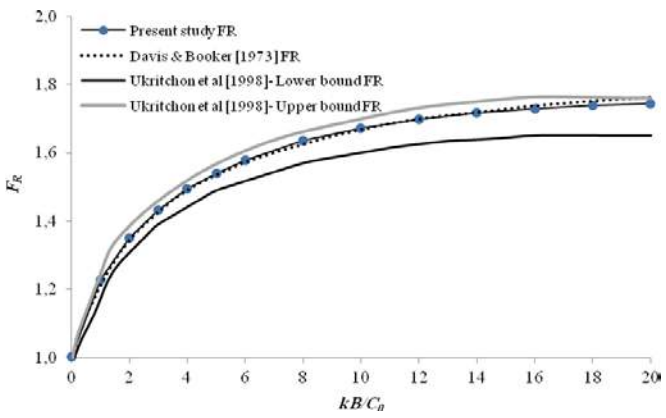

Figure 4. Correction factor for rough strip footing on a non-homogeneous soil.

4.3 Contact Stress Underneath the Footing

Curves of the normal stress σ_n acting on the smooth base of the footing loaded vertically, is plotted in Figure 5 with respect to the footing width, at different values of the ratio kB/c_{uo}. For the homogeneous case

(kB/c_{uo}=0), the analysis predicts uniform vertical contact stresses across the width of the footing. In contrast, calculations for non-homogeneous clay (kB/c_{uo}> 0) show that contact stresses increase toward the center of the footing (the results match with analytical solutions from Davis and Booker, 1973).

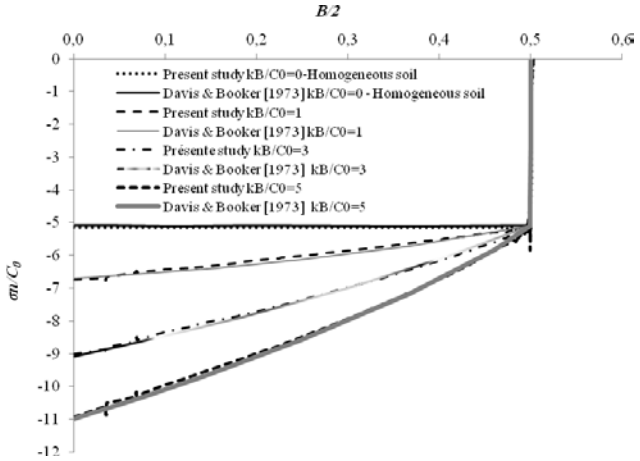

Figure 5. Distribution of normal stress underneath the smooth footing base.

5 CONCLUSIONS

The finite element software PLAXIS 2D was used to study the influence on the undrained bearing capacity of strength non-homogeneity. Results from a series of FEA have been presented and compared with data from other published studies and a good agreement has been obtained with available theoretical solutions for ultimate capacity. Various values of strength non-homogeneity ratio kB/c_{uo} from 0 to 30 have been explored for vertical loaded strip footing. The bearing capacity factor increases with the increase of the ratio kB/c_{uo}. The results show that the roughness increases the bearing capacity as strength heterogeneity increases.

REFERENCES

Chen, W.F. (1975). *Limit analysis and soil plasticity*. Elsevier, Amsterdam.

Davis, E.H. & Booker, J.R. (1973). The effect of increasing strength with depth on the bearing capacity of clays. *Géotechnique* 23(4): 551–563.

Edwards, D. H., Zdravkovic L., & Potts D. M. (2005). Depth factors for undrained bearing capacity. *Géotechnique*, Vol. 55, pp. 755-758.

Gourvenec, S. & Barnett, S. (2011). Undrained failure envelope for skirted foundations under general loading. *Géotechnique* 61, No. 3, 263–270.

Griffiths, D.V. (1982). Computation of bearing capacity on layered soils. *Proc. 4th Int. Conf.Num. Meths. Geomech*., Edmonton, Canada, (ed.Z. Eisenstein), Pub. Balkema pp.163−170.

Houlsby, G. T. & Wroth, C. P. (1983). Calculation of stresses on shallow penetrometers and footings. *Proc. Int. Union of Theoretical and Applied Mechanics (IUTAM)/International*

Kumbhojkar, A.S. (1993). Numerical evaluation of Terzaghi's N_γ. *Journal of Geotechnical Engineering*. Vol. 119, 598-607.

Martin, C.M. (2004). ABC – *Analysis of Bearing Capacity*. Software and documentation available for download from www-civil.eng.ox.ac.uk/people/cmm/software/abc.

Merifield R. S. , Sloan S. W. & Yu H. S. (1999). Rigorous plasticity solutions for the bearing capacity of two−layered clays. *Géotechnique*, 49(4), 471−490.

Meyerhof, G. G. (1951). The ultimate bearing capacity of foundations. *Géotechnique* 2, (4), 301–332.

Michalowski, R.L. (1997). An estimate of the influence of soil weight on bearing capacity using limit analysis. *Soils and Foundations*. 37, 57-64.

PLAXIS. (2012). PLAXIS 2D. Anniversary Edition.

Prandtl, L. (1920). U¨ ber die Ha¨ete plastistischer Ko¨rper. Nachr. Ges.Wissensch, Go¨ttingen, math.-[hys. Klasse, 74–85.

Skempton, A. W. (1951). The bearing capacity of clays. *Proc. Building Research Cong*. London, 1, 180–189.

Sokolovskii, V.V. (1960). *Statics of soil media* (translated from the 1942 Russian edition). London: Butterworths.

Tani, K. & Craig, W. H. (1995). Bearing capacity of circular foundations on soft clay of strength increasing with depth. Soils Found. 35(2), 37–47.

Terzaghi, K. (1943). *Theoretical soil mechanics*, Wiley, New York.

Ukritchon, B, Whittle, A.J. and Sloan, S.W. (1998), Undrained limit analysis for combined loading of strip footing on clay, J. Geot. and Geoenv. Eng. ASCE 124(3), pp. 265-276.

Open Pit Mine Waste Dump Area Design based on Stability Principles

Açık Ocak Döküm Sahasının Stabilite Esaslarına Göre Tasarımı

C.A. Öztürk, S. Erçelebi, İ.E. Önsel, M. Özkan
Istanbul Technical University, Mining Engineering Department, Istanbul

M. Zengin, D. Arslan, Y. Tuncel, Z. Baz
Asya Maden İşletmeleri, Hanönü, Kastamonu

ÖZET Bu çalışmanın amacı, Kastamonu İli Hanönü İlçesinde bulunan ve Asya Maden İşletmeleri tarafından işletilecek olan, açık ocak bakır madenindeki döküm sahasının tasarımının yapılmasıdır. Döküm sahalarının tasarlanması, tıpkı açık ocak basamak ve genel eğimlerinin dizaynında olduğu gibi, şev stabilite esaslarına dayandırılarak gerçekleştirilmelidir. Bu sebepten dolayı, öncelikle döküm malzemesinin ve dökümün yapılacağı bölgenin jeoteknik özelliklerinin tayin edilmesi gerekmektedir. Stabilite üzerinde etkisi olan, yeraltı su durumu, bölgenin depremselliği gibi konularda yine bu araştırmaların bir parçası olmalıdır. Sahada henüz döküm faaliyetleri gerçekleştirilmediği için, farklı tasarımlar gerçekleştirmek suretiyle, döküm sahasının stabilitesini etkileyen jeoteknik parametrelerin büyüklükleri, geri-analiz yöntemi ile elde edilmiştir. Bu uygulama, farklı genel eğime sahip tasarımlar için tekrarlanmıştır. Sınır – denge yöntemi esasına göre gerçekleştirilen stabilite analizleri sonucunda, her bir tasarımı stabil kılan jeoteknik parametrelerin büyüklükleri tayin edilmiştir. Bu aşamadan sonra ise, malzemelerin jeoteknik özellikleri ile döküm sahasının genel eğimi ve bağlı olarak sahanın döküm kapasitesi arasındaki ilişkiler ortaya çıkartılmıştır.

Anahtar Kelimeler: Şev stabilite analizi, döküm sahası, jeoteknik özellikler, sınır-denge yöntemi

ABSTRACT The main purpose of this study is to design waste dump area for an open pit copper mine owned by Asya Maden Inc. located in Hanonu, Kastamonu. Design studies can be carried out based on slope stability principles as per the design works of open pit bench and overall slope angle. Therefore, geotechnical properties of dump material as well as ground must be primarily determined. Hydrogeology as well as seismicity which have important effect on the stability should be also part of stability works. The values of geotechnical parameters for dump material controlled the stability of dump site determined from the back analysis method from different designs, because of the unavailability of dump material since dumping is not initiated at present. This application iterated for the other designs having different overall slope angles. As a result of the stability analyses based on limit equilibrium methods, the values of geotechnical parameters making the design stabile are determined. After this stage, relations among geotechnical properties and overall slope angle of the dump site as well as dump site capacity are presented.

Keywords: Slope stability analysis, waste dump, geotechnical properties, limit equilibrium method

1 INTRODUCTION

External waste dump area design is an important design issue of open pit mine design and planning concept. The aim of this study is to design the waste dump area for an open pit mine located in the Hanönü village of Kastamonu town. The copper mine will be operated by open-pit mining method, and the overburden material will be dumped to the site called as Corakoglu. The mine will be operated by Asya Maden Inc. Dump site area borders, digital topographical map, and information for the geology of the site were provided by the Company. Different designs were carried out to determine the relations between overall slope angle of the dump site and dump site capacity. Overall slope angle is an output of the stability analyses carried out for the dump site. Stability analyses, for this case study, were determined based on limit equilibrium methods. The required main geotechnical data for limit equilibrium stability analysis are cohesion, internal friction angle, and unit volume weight for each material at the site. During the design stage in this engineering project, it is not possible to obtain the actual values for geotechnical properties for dump material due to the unavailability of material at site. However, it needs to design the area of dump site according to the engineering point of view. In this situation, back analyses for stability investigations can be usable to understand the required values for geotechnical properties of dump material based on a certain limit of factor of safety (FoS). The details of these investigations as well as presenting a procedure for the design studies of dump site during the planning phase of a mining project are the main outputs of this research. The results proposed in this study are a part of a project completed by ITU Mining Engineering Department in 2014 (ITU Technical Report, 2014).

2 STUDY AREA AND GEOLOGY OF THE SITE

The copper mine deposit is located in northern Turkey close to the Hanönü town in the Kastamonu province (Fig.1).

Geology of the area is reported in Okay et al. (2006). A geological cross-section of the study area is given in Figure 2, while a cross-section prepared by the Asya Maden Geological Department is also given in Figure 3 to show the main geological formations in open pit mine and dump site.

3 GEOTECHNICAL PROPERTIES OF DUMP AND BASE GROUND

Material properties are one of the important input for slope stability investigations. Cohesion (c), internal friction angle (ϕ), and unit volume weight (γ) are geotechnical parameters used in limit equilibrium analyses of slope stability researches. In this case study, mainly two distinct material are defined. The first one is the dump material while the other one is called as base ground.

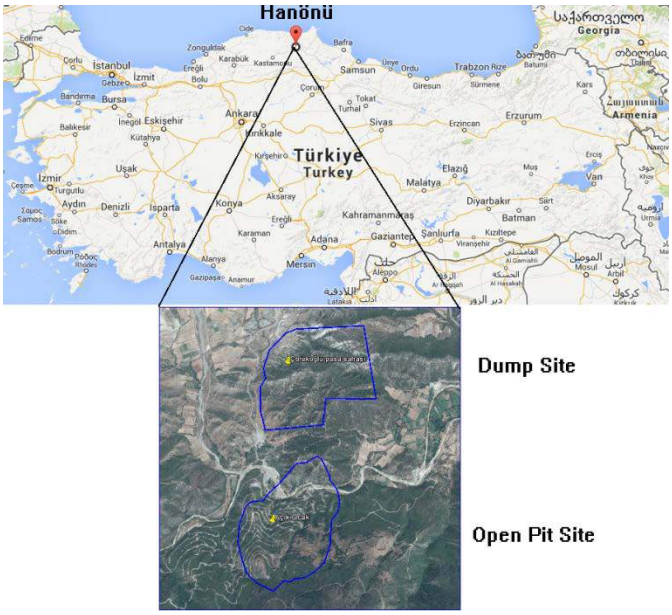

Figure 1. Location map and satellite image from Google Earth for the study area (IMC Technical Report, 2013).

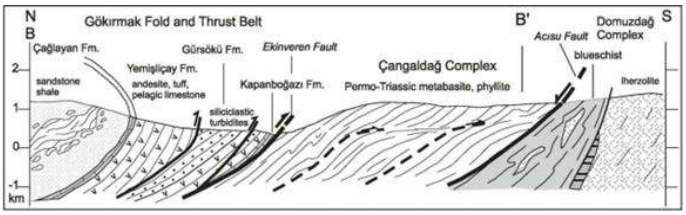

Figure 2. Cross-section for the site (Okay et.al., 2006).

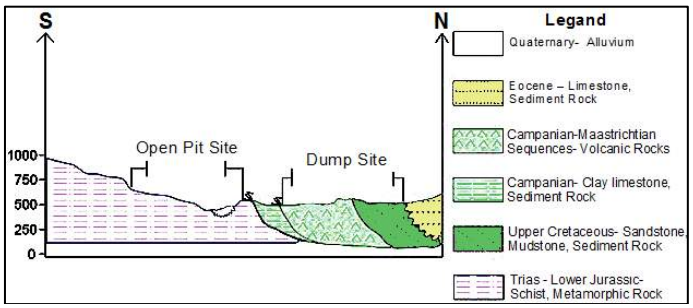

Figure 3. Geological cross-section of open pit and dump site.

3.1 Dump Material

The required geotechnical data should be determined by laboratory experiments on the samples taken from the site as well as in-situ tests. In this study, the excavation for overburden material has not been started, therefore it is not possible to obtain dump samples from the site. The unavailability of dump samples led to use the previous rock mechanics studies for open pit mine planning (ITU Technical Report, 2013). Waste dump material will be produced from the excavation of overburden material during the open pit mining activities. The original rock is mostly consist of mixed schist (MSCH), green schist (GSCH), and schist (SCH) based on the lithology of the open pit site geology. The values of geotechnical parameters for dump material are predicted from in-situ rock due to the unavailability of material at site. Triaxial compressive strength tests as well as direct shear strength tests were carried out in the existing rock mechanics project. The values of cohesion and friction angles are listed in Table 1. In order to make the most possible safe design, minimum values for geotechnical parameters are selected as design parameters which are 50 kPa for cohesion and 23.31^0 for friction angle.

Table 1. Material strength parameters for rock fill (ITU Technical Report, 2013).

Material		Stat.	Triaxial Compression Tests		Direct Shear Test - Residual	
			Cohesion (kPa)	Friction Angle (^{0})	Cohesion (kPa)	Friction Angle (^{0})
Mixed Schist	MSCH	Avg	2,270	53	220	23.31
		Min.	850	42	-	-
Green Schist	GSCH	Avg	1,750	62	50	30.67
		Min.	730	60	-	-
Schist	SCH	Avg	410	48	100	25.55
Design Parameters					**50**	**23.31**

3.2 Base Ground

Strength properties of the ground which waste will be dumped on, are also required for the stability investigations. The study carried out to determine geological and geotechnical properties for the site by DMT Corporation is used to obtain ground strength data (DMT Technical Report, 2013). The geology of the study area show that Corakoglu dump area consists of sandstone, mudstone, and sediments as well as volcanic members. Table 2 is prepared from DMT technical report to predict the strength parameters for the base ground. It should be noted that prior to dumping, the required strength tests must be carried out for the justification of the predictions for the ground geotechnical properties, as well.

Table 2. Natural ground geotechnical properties (DMT Technical Report, 2013).

Sr #	Material	Cohesion (kPa)	Friction Angle (^{0})
1	Sandstone	300-400	35-45
2	Mudstone	200-300	25-35
3	Limestone	200-300	25-35
Design Parameters		**200**	**25**

4 BENCH DESIGN

Initial study for the design of waste dump area is to decide the geometry of individual benches. A bench can be designed by selecting the value for height, width, and the slope angle (Fig. 4). First, the angle of the slope must be decided according to the type of the dump material, if there is no available site application. Common approaches can be used to decide the slope angle based on literature. Added to that, basic friction angle from site experiments or friction angle values from shear strength parameters can be also used to select the most proper slope angle.

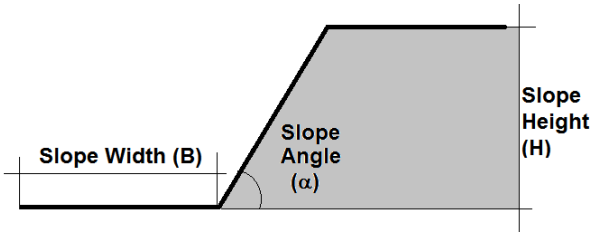

Figure 4. Slope geometry.

According to the classification proposed by Levy (2011), slope ratio between height and length can be taken as ¼:1 to ½:1 for dump material defined as mostly rock. In this study, several bench designs were considered and height is 10 m, angle is 60^0 is selected as bench design parameters for a safe and reliable design. The width of the slope is the only parameter to obtain alternative angles for overall slopes. In order to obtain different combinations of overall slope angle, different values for width are used for the design of dump site. The alternatives for slope width that make the designs for a safe overall slope angle are searched in the next section for the design of waste dump based on stability principles.

5 DUMP AREA DESIGNS

The size of the licensed area as dump site is nearly 135 hectares, while projection of the size is equal nearly 120 hectares. The elevation of the dump site ranges between 440 m and 630 m. The design of the waste dump area is carried out by considering slope stability principles. Limit equilibrium methods are used to decide the suitability of the design. Simplified Bishop multiple analyses are used during stability investigations due to the characteristic of the dump material. It is assumed that failure surface is circular.

As a result of slope stability analysis, a safety factor (FoS) value is calculated which is an indicator of stability consists of the ratio of forces resist the slippage to forces that cause slippage. When the safety factor value is 1 (FoS=1), the slope under investigation is in the limit of stable and unstable condition, and this condition is known as “Limit Equilibrium Condition”.

Back analysis is also used to determine valuable information regarding shear strength parameters such as cohesion and internal friction angle along a sliding surface as well as underground water conditions. The information of slope geometry before sliding, location of sliding surface, and underground water table level (UGWT) is important to increase the sensibility of back analysis. Unit volume weights of the material for the unstable condition shall be also known for the analyses.

There are numerous researches to define factor of safety in open pit mining as well as waste dump deposit. Huang (1983) proposed selection of safety factor in open pit mining. In this study, FoS takes as 1.30 without the effect of earthquake as the table from D’Appolonia Cons. Engnrs. Inc.

Due to the absence of the actual geotechnical data for natural ground and waste dump material, different alternatives for waste dump have been investigated based on different overall slope angle. The purpose of this study is to design the dump in a way that the amount of dumped material is not less than waste which will be excavated from open pit.

For the first design of the dump site, all waste material is considered to be dumped at the site and resulting overall slope angle is found. After determining the overall slope angle, the required strength parameters for dump material were calculated by using slope stability back analysis techniques. Back analyses can also be performed to obtain critical material strength parameters from known or assumed failure surface. Hence, it is possible to determine required cohesion and friction angle of waste dump material for the 1st design that is used to dump all waste material to the waste dump area.

Second, the reliable overall slope angle is determined where FoS is 1.30 after stability analyses. The predicted strength parameters for dump material given in Table 1 are used to for the 2nd design. Hence, it is possible to determine the slope width as well as the geometry of the waste dump. After design studies, the volume of total waste material could be dumped for the 2nd design is calculated.

When the overall slope angles for 1st and 2nd designs are determined, those are maximum and minimum values successively, 3 more designs were carried out to determine the relation between overall slope angle and total dump volume. The following figure shows the design procedures for the study.

The studies for the waste dump area design as outlined in Figure 5 were carried out by using an integrated mining and slope stability software. Micromine is used as integrated mining software to model existing topography and to draw the border of the dump. The designs numbered from 1st to 5th were also modeled by using Micromine. Cross-sections from these designs are taken from the software. Galena as a slope stability software is used to obtain the results of the stability analyses. Factor of safety for designed slopes as well as back analyses for material strength parameters determination can be handled by using Galena.

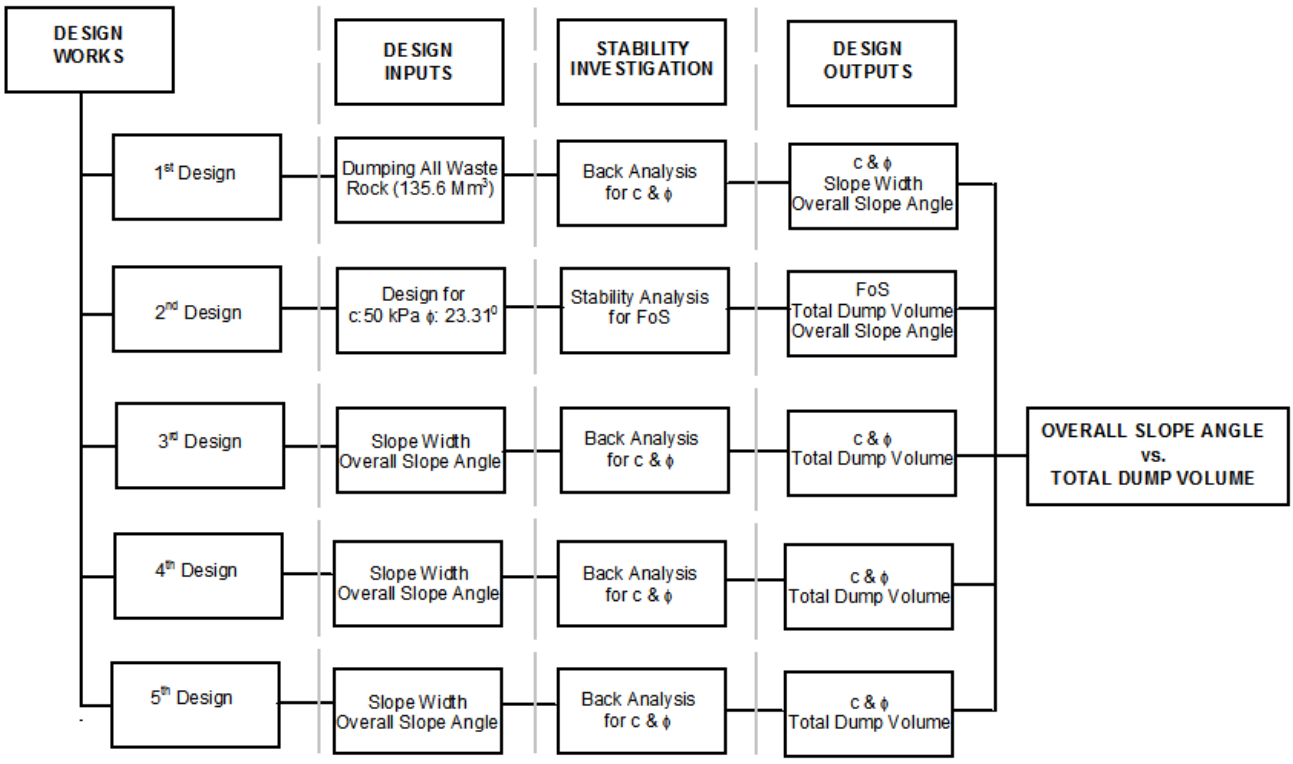

Figure 5. Design procedures based on stability principles in this project.

In order to avoid the mass presentation of figures, graphs and cross-sections used in the design studies, only 1st design outputs are presented in this study including the results of the each design in the following table.

In the 1st design, the value of bench width is selected as 5 m while the other parameters of the slope geometry is already fixed as 60^0 for slope angle and 10 m. for slope height.
The design of the dump site is given in Figure 6 as plan and views. Maximum overall slope angle is calculated as 42^0 in the 1st design with 143.5 million m^3 capacity. Cross-sections of the dump site can be seen in Figure 7.

Back analyses were carried out to find the material strength properties required for stability of this design. The output of the back analysis is given in Figure 8.

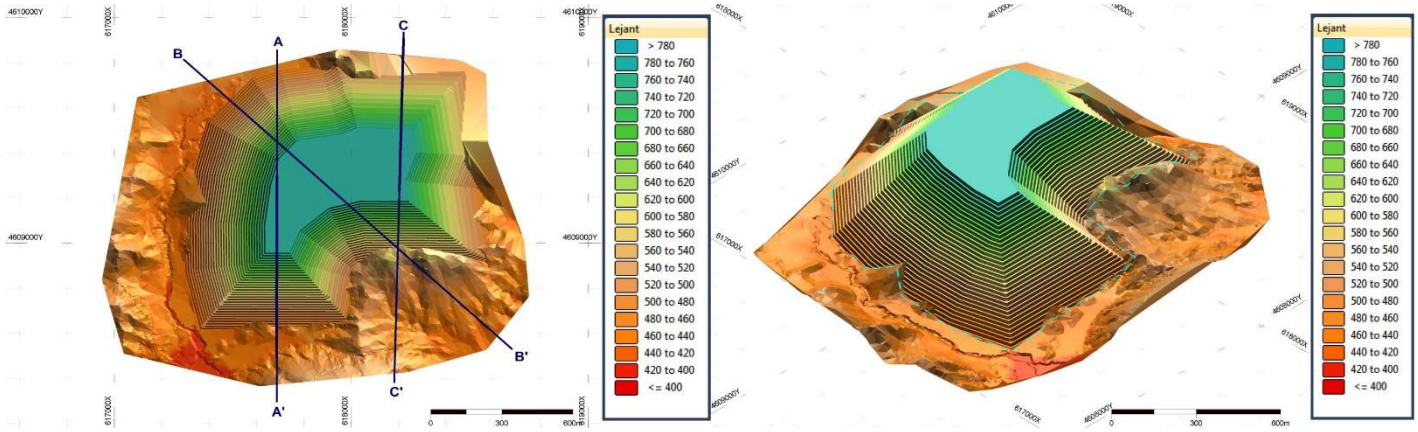

Figure 6. 1st - Design, plan and isometric view.

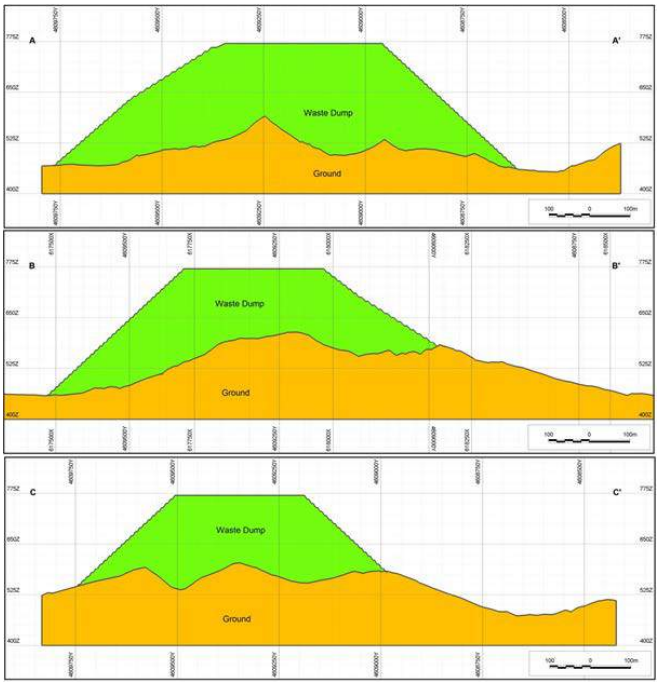

Figure 7. Cross-sections of the dump area.

The outputs of the back analyses studies are combined in a single graph given in Figure 9 for 4 designs performed as back analyses. The data obtained from this graph is used to set up a multiple linear regression model between cohesion, friction angle, and overall slope angle (OSA) for FoS=1.30. The equation determined from the multiple linear regression analysis is given below has 0.94 correlation coefficient and 1.34 standard error (Eq.1). This equation may be used to define overall slope angel after testing dump material and determining cohesion and friction angle values.

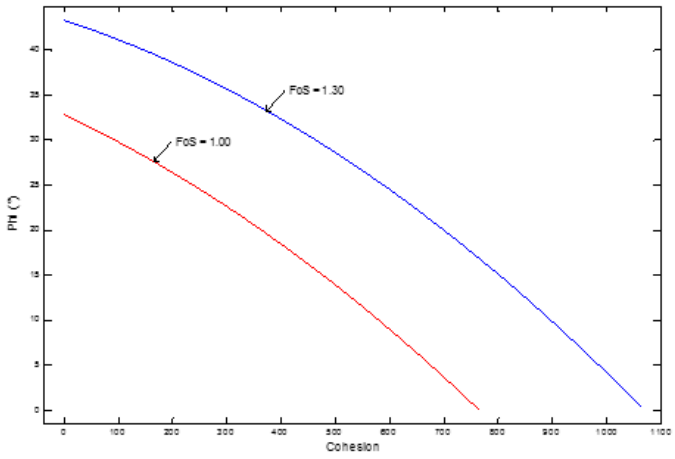

Figure 8. Back analyses results for 1st - Design.

$$OSA = 0.02xc + 0.44x\phi + 19.51 \quad (1)$$

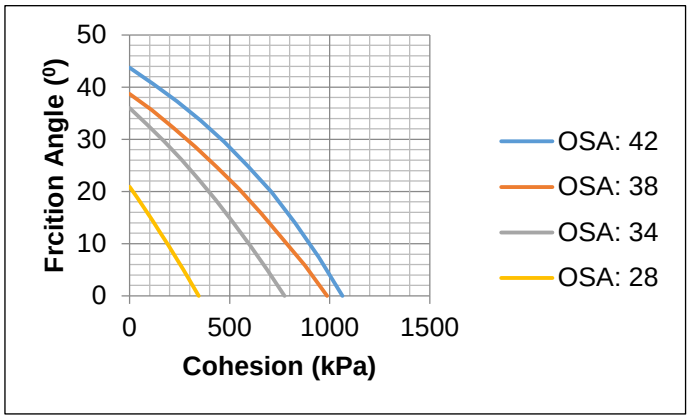

Figure 9. Results of back analyses from stability studies.

5 different designs are constructed for the dump site. The results for the geometry of dump sites as well as the individual slopes including the capacities of the damp areas are outlined in Table 3

.

Table 3. Summary of the design studies.

Sr #	Description	1st - Design	2nd - Design	3rd - Design	4th - Design	5th - Design
1	Overall Slope Angle (^{0})	42	23	28	38	34
2	Slope Angle (^{0})	60	60	60	60	60
3	Slope Height (m)	10	10	10	10	10
4	Slope Width (m)	5	17.5	13	7	9
5	Maximum Elevation (m)	890	670	730	830	780
6	Total Damp Volume (million m^3)	143.5	37.5	61.5	112.5	88.5

A relationship between overall slope angle and total dump volume that can be seen in Figure 10 is proposed as a result of these design works. The graph with a very high correlation coefficient, claims a relation between overall slope angle and dump capacity. The following arguments can be made from the graph.

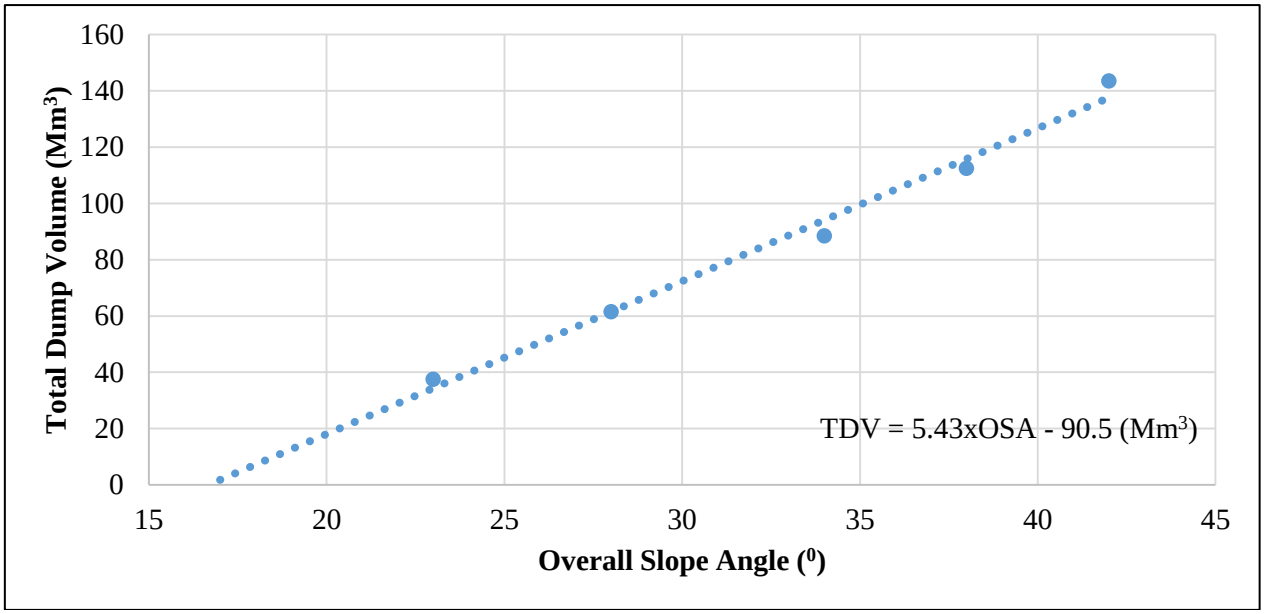

Figure 10. Correlation between OSA and total damp volume

After determining the actual material strength properties for dump material and ground, overall slope angle can be calculated from stability analyses and total dump volume will be achieved can be easily

computed from the equation in the graph based on the actual overall slop angle values.

6 HYDROGEOLOGY AND SEISMICITY

6.1 Effect of Water on Stability

The increasing level of underground water has an adverse effect on the stability of slopes. The stabilities of the designs proposed in this study were investigated under the dry condition of the slopes.

Observation well data is reported in hydrogeology report for the open pit mine prepared by Asya Maden Geological Department. According to this data, there exists an underground water table from the ground level between 3.65 m and 79 m. Average underground water table level is observed as 29.5 m from the surface (Asya Maden Technical Report, 2014).

Stability analyses by considering the underground water table level for 1st - Design is carried out to model the effect of underground water on the stability.

In the first stability analysis, underground water table elevates into the dump material. The FoS value is calculated as 1.20 which is below acceptable limit. In the second model, the rising of the UGWT into dump is prevented, and UGWT level is hold below surface. FoS value is calculated as 1.30 which is acceptable for stability.

The results of stability analyses considering water on stability show the importance of decreasing the underground water table level as well as controlling the surface water. Constructing proper drainage system to protect the dump against increasing water table level is important.

6.2 Effect of Earthquake

The effect of earthquake for the stability of dump slopes must be evaluated again by using the stability principles due to the importance of earthquake for Turkey. The scale of seismicity for Kastamonu Hanönü region is classified as 3rd degree according to the map prepared by "Turkish Republic Prime Ministry Disaster and Emergency Management Presidency, Earthquake Department Presidency"

Historical seismicity record map show that the closest earthquake bigger than magnitude of 5.0 happened in 1919, 20 km away from the Hanönü region (Özmen, 2001).

Due to the seismicity degree, magnitude of the historical earthquakes, and the distance between the biggest earthquake to the mine site, earthquake force is taken as 0.15g in this study.

In order to understand the effect of earthquake for 1st - Design and 2nd - Design, stability analyses were performed under earthquake condition. Cohesion is selected as 150 kPa while friction angle is selected as 40^0 from the result of back analyses. After applying the stability analyses, the value of FoS found as 1.03 that shows the suitability of the design under the earthquake condition for the 1st - Design. If FoS>=1.0 under earthquake condition the design is considered safe.

2nd - Design stability investigation under earthquake condition was also performed and FoS is calculated as 1.00 in this analysis that is also acceptable under stability concerns.

7 CONCLUSION

Waste dump area design is main purpose of this study. The most critical problem is having no actual material strength data for the dump material. Due to the absence of material strength properties of dump material, several different designs were performed in order to obtain a relation between overall slope angel and strength properties of dump material. Back analysis technique is used to understand value of cohesion and internal friction angle for a safe design, based on slope stability principles having factor of safety value more than 1.30.

As a result of the designs, two valid equations are determined as a main output of this research. In the 1st equation overall slope angle value can be determined from the cohesion and internal friction angle of dump material. In the 2nd equation, total dump capacity of the site can be calculated from the value of overall slope angle, so total

dump capacity of waste dump deposit area can be calculated, when the actual strength parameters of dump material are determined.

The procedure applied in this study for the design of waste dump deposit especially during the planning stage of a mining project can be applied for similar studies successfully according to the results of this study.

ACKNOWLEDGEMENTS

The Authors would like to appreciate the contributions of Ilbak Group, Asya Maden Inc. as well as the Managers and Engineers for their support to the research.

REFERENCES

Asya Maden Isletmeleri A.Ş., 2014. *Kastamonu Hanönü Bakır Madeni Açık Ocak Işletmesinde (Faz 1) Kazı Çukuruna Gelecek Suyun Hesaplanmasına Ait Rapor* (in Turkish), 31 p.

DMT Technical Report, 2013. *Technical Report - Geological and Geotechnical Mapping of Bakacak Hill Mineral Exploration Project Hanönü, Kastamonu, Turkey*.

Huang, Y.H., 1983. *Stability Analysis of Earth Slopes*. Van Nostrand Reinhold Comp, New York.

International Mining Consultants (IMC), Technical Report, 2013. *Feasibility Study Report on the Kastamonu-Hanönü-Gökirmak Copper Project, Turkey for Asya Maden Işletmeleri A.Ş.,* Report No: 20634814.

Istanbul Technical University (ITU), Faculty of Mines, Technical Report, 2014. *Kastamonu Hanönü Copper Mine Waste Dump Design* (in Turkish), 61 p.

Istanbul Technical University (ITU), Faculty of Mines, Technical Report, 2013. *Investigation the mechanical properties of rock materials for Kastamonu Hanönü Copper Mine* (in Turkish), 129 p.

Levy, S.M., 2011. *Construction Calculations Manual*. Butterworth-Heinemann Press, UK.

Okay, A.I., Tüysüz, O., Satir, M., Özkan-Altiner, S., Altiner, D., Sherlock, S., and Eren, R.H., 2006. Cretaceous and Triassic subduction-accretion, HP/LT metamorphism and continental growth in the Central Pontides, Turkey. *Geological Society of America Bulletin*, v. 118, p. 1247–1269.

Özmen, B., 2001. Kastamonu İlinin Depremselliği ve Deprem Tehlikesi (in Turkish). *54. Türkiye Jeoloji Kurultayı*. TMMOB Jeoloji Mühendisleri Odası, Ankara

Performance Evaluation of Paste Backfill in Imiter Silver Mine, Ouarzazate Region, Morocco

K. Abdelhadi, O. Latifa, B. Khadija
3GIE Laboratory, Mohammadia Engineering School, Rabat, Morocco

ABSTRACT This work is part of topic of developing Paste Backfill technology in mining operations in Morocco. The silver mine of Imiter, Ouarzazate region, was chosen as case of study because of its commitment to implement PBF practice for the remaining life of the operation. Paste Backfill (PBF) is a combination of mine processing tailings, binder (cement and additives) and water mixing with specific recipe. It's generally used to fill in underground voids improving thus rock mass strength and allowing the maximization of ore recovery. The study of PBF introduction passes through several steps. The first element to define is the function which the backfill will ensure with underground works. Thereafter, chemical and mechanical characterization is done on the different components to determine optimal formulation ensuring the required mechanical strength of hardened paste. Actually, two PBF formulations are used in Imiter mine, one for slab separation of mining levels and one for underground voids filling. In this work we present a performance evaluation of the used PBF according to defined functions. The mechanical performance of PBF was evaluated in laboratory by the uniaxial compressive strength test. The conducted tests and analysis shows that actual PBF formulations are adequate with the associated functions in the extraction sequence.

Keywords: Underground mining, paste backfill, chemical and mechanical characterization

1 INTRODUCTION

Morocco is a country with important underground mineral resources. The main underground mining activity is located in the south and concern poly-metallic and precious metal deposit.

Mining operations use different kinds of backfill depending on the extraction method. The most used backfills are mechanical backfill (only waste material) and hydraulic backfill (cemented backfill).

More than 20 years ago, concentrator treatment discharges of mining plants were wholly stored on tailings parks on surface areas. The volume and chemical characteristic of these tailings, often rich of sulfurs, generate serious problem for storage requiring spaces and mainly environmental degradation due to Acid Mine Drainage.

The environmental legislation, increasingly requiring, leads mining societies to minimize as possible, the volume of tailings stored on the surface. Morocco is one of countries which going to make the environment preservation as the first preoccupation during and at the end of mining activities.

Paste backfill (PBF) is one of ingenious solutions to minimize the quantity of tailings to store. It's a mixture of total mill tailings generated during mineral processing, Portland cement or blended cement with supplementary cementitious material (lime, pulverized fly ash, and ground granulated blast furnace slag), and water (tap water, lake water or recycled and/or treated mine process water) (Belem et al., 2008).

The first introduction step of paste backfilling practice is already in progress for the silver mine of Imiter (Ouarzazate region) in southern of Morocco. Some characterization tests are done to evaluate chemical and physical characteristics of tailings and other used aggregates materials on the paste backfill fabrication.

The purpose of this paper, in addition to show PBF advantages, is to present a performance evaluation of the paste backfill mixture used by Imiter mine. Actually, two PBF formulations are used with underground works, one for slab separation of mining panels and one for stopes filling. The mechanical performance of these two recipe was evaluated by conducting uniaxial compressive strength tests.

2 PASTE BACKFILL TECHNOLOGY

2.1 PBF Advantages

Since their introduction in 1990, PBF technology has demonstrated advantages regarding economics factors, environment, geo-mechanics and safety (De Souza et al., 2001; Benzaazoua et al., 2005).

This success of PBF is explained first by the engineered character of the product which allows high quality in comparison with old backfill methods.

Actually, the economic and environment benefits of PBF have not to be approved. Costs due to tailings management in the storage areas and closing budget can significantly be reduced.

PBF technology is suitable for most mining methods because of its versatile characteristic which has allowed the increasing of resource extraction.

In term of safety, PBF is used as local and regional ground support and also help to reduce the number and exposure time of operators by fast filling rates. The fast filling increase in addition mine productivity with shorter stop cycle times.

2.2 Influencing Parameters

As showed in figure 1, the percentage and characteristics of each PBF component (tailings, binder, and water) affect directly the mechanical strength of hardened backfill.

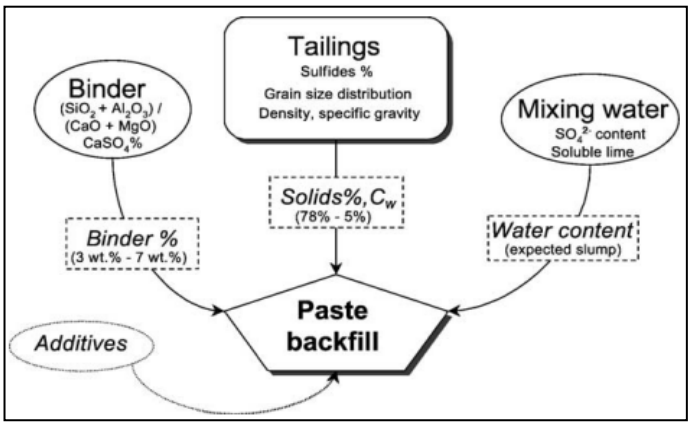

Figure1. Schematic diagram illustrating the different components of paste backfill (Benzaazoua et al., 2002).

Chemical composition of tailings: The sulfurs content is the most important parameter to verify in the chemical composition of tailings because of its direct influence on increasing the tailings density.

Morphology of grain and size distribution: Generally more spread is the grain distribution more quick is the PBF hardening. The morphology of tailings particles can also affect the quality of the final product mainly with phyllo-silicate material.

Binder and water chemistry: It's inefficient to choose paste backfill mixtures without testing first the tailings and mixing-water characteristics. The binder chemistry combined with the mixing-water chemistry affects the formation of primary and secondary hydrates during paste backfill strengthening. The cohesion of the paste backfill matrix is directly dependent on the nature of the precipitated hydrates (Benzaazoua et al., 2005).

Figure 2 shows the composition impact of each component of mixture on the backfill strength expressed with uniaxial compressive strength (UCS).

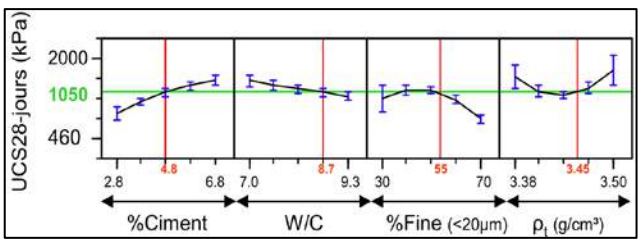

Figure 2. Example of component impact simulation curves (Fall et al., 2003).

2.3 PBF limit strength

The first step of PBF design is to calculate critical strength ensuring both stability of PBF and filled stope. The value of critical strength to reach depends on the function of the PBF in the mining method.

PBF can be used to support voids roof and then its design will be focused on rigidity and mechanical cohesion. In case where one side of PBF has to be exposed, the shear strength is the main parameter conditioning the backfill stability.

2.4 PBF Mixture Optimization

At this stage each proportion of tailings, binder (one or several cementation agents) and mixing water has to be defined in an optimized recipe.

The backfilling cost represents 2% to 20% from the total mining operation cost. Knowing that 75 % of backfilling cost corresponds to binder acquisition, it's important to optimize recipes to product backfill with a minimum cost (Belem et al., 2003).

The recipe optimization takes into consideration the mechanical and transportation exigencies thought a pertinent selection of type and binder content.

2.5 Flow Sheet Production

Generally, the PBF plant is located on the surface nearby the processing plant to facilitate the recovery of tailings at the end of the processing line.

The following present the classic procedure of PBF fabrication. Belem et al. (2003):

- Thickening of tailings slurry to about C_w = 55%. (Solid weight percentage),
- Filtration of tailings with disk filters or press filters to C_w between 70% and 82%,
- Binder addition with a proportion between 3% to 7 % from the total mass of dry tailings,
- Water addition (processing or fresh water) to generate an optimal slump comprised between 150 and 250 mm,
- Recipe mixing in a screw mixer with high power during 45 seconds to one minute.
- Underground delivery of PBF through transportation network.

2.6 Transportation

Several works were focused on the problematic of backfill transportation since their introduction (Landriault et al., 1987; Hassani et al., 1998; Li et al., 2002; Benzaazoua et al., 2004 ;…). PBF product must be delivered from surface to underground via boreholes and pipes at the highest practical density. Practically, it is not easy to have real proprieties of PBF rheology because of experimental dispositive complexity.

It makes difficult or even impossible determination or prediction of paste viscosity which depend on several factors (Benzaazoua et al., 2005).

Generally the slump test and flow-loop test are used to evaluate the paste consistence and pressures drop along the transporting network.

The prepared PBF should be pumped through pipelines reticulation network without causing any plugging. The pumpability of PBF is measured by the slump height. The fresh PBF behaves as a non-Newtonian fluid. That is, applied pressure is required to initiate flow (Belem et al., 2008).

2.7 Mechanical Behavior

Once the PBF is deposed in underground voids, it undergoes various transformations and interactions.

The PBF interactions with rock mass depend mainly on void dimension but also on pressure at the bottom and over the stope barricade.

In addition to hydration reactions which give the mechanical strength of hardened backfill, other phenomenons occur during the curing time of PBF, mainly:

- Drainage of excess water,
- Settlement and consolidation,

The strength of pastefill in the filled stope is related to the water flow which is a function of the paste properties (Belem et al.,

2001). Transformations and interactions of PBF have to be monitored in the short, middle and long term. This monitoring will show the impact of selected recipe and material characteristics on the mechanical strength of PBF. Adjustment can then be made to find the most appropriate recipe.

3 IMITER MINE OPERATION

Imiter mine is an operation located in Ouarzazate region, southern of Morocco. The exploitation concern a rich silver ore body. (Fig. 4)

3.1 Geological Overview

Imiter mine is located in NE edge of the Ouarzazate basin (Eastern Saghro, Anti-Atlas). The deposit is hosted in the volcano-sedimentary series of the Precambrian II and secondarily in volcano-clastic formations of the Precambrian III.

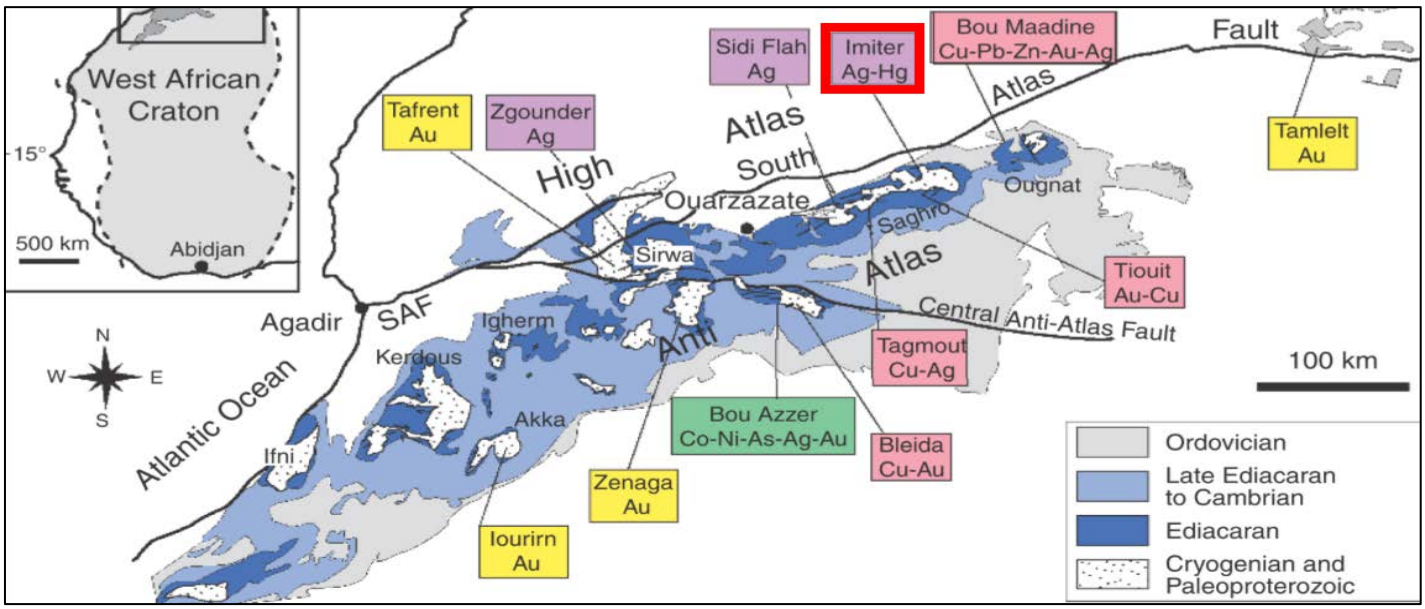

Figure 3. Location of the main ore deposits in the Anti-Atlas belt (Gasquet et al., 2005).

3.2 Ore extraction

In an old stage of the mine, the open pit was the principal extraction method. Actually the main extracted ore is coming from underground exploitation using two principal extraction methods: cut-and- fill and sublevel stopping. (Fig. 5)

Cut-and-fill method extract ore in horizontal tranches, starting from the bottom and advancing upward. Voids are backfilled with hydraulic fill or waste rock when the stope has been worked-out. Backfilling serves both to support walls and provide a working platform for equipment for the next tranche.

In sublevel stoping method ore is extracted in open stope (keep out for worker circulation). Ore body is generally large enough with an important vertical extension.

Pillars are normally shaped as vertical beams across the ore body. A specific extraction sequence is followed with primary and secondary stopes. Primary stopes are progressively filled to allow the ore extraction in secondary left ore parts.

In Imiter mine the cut-and-fill or sublevel stoping method is used depending on ore body extension and geometry. The sublevel stoping can also be longitudinal or transversal according to rock mass quality and geometry.

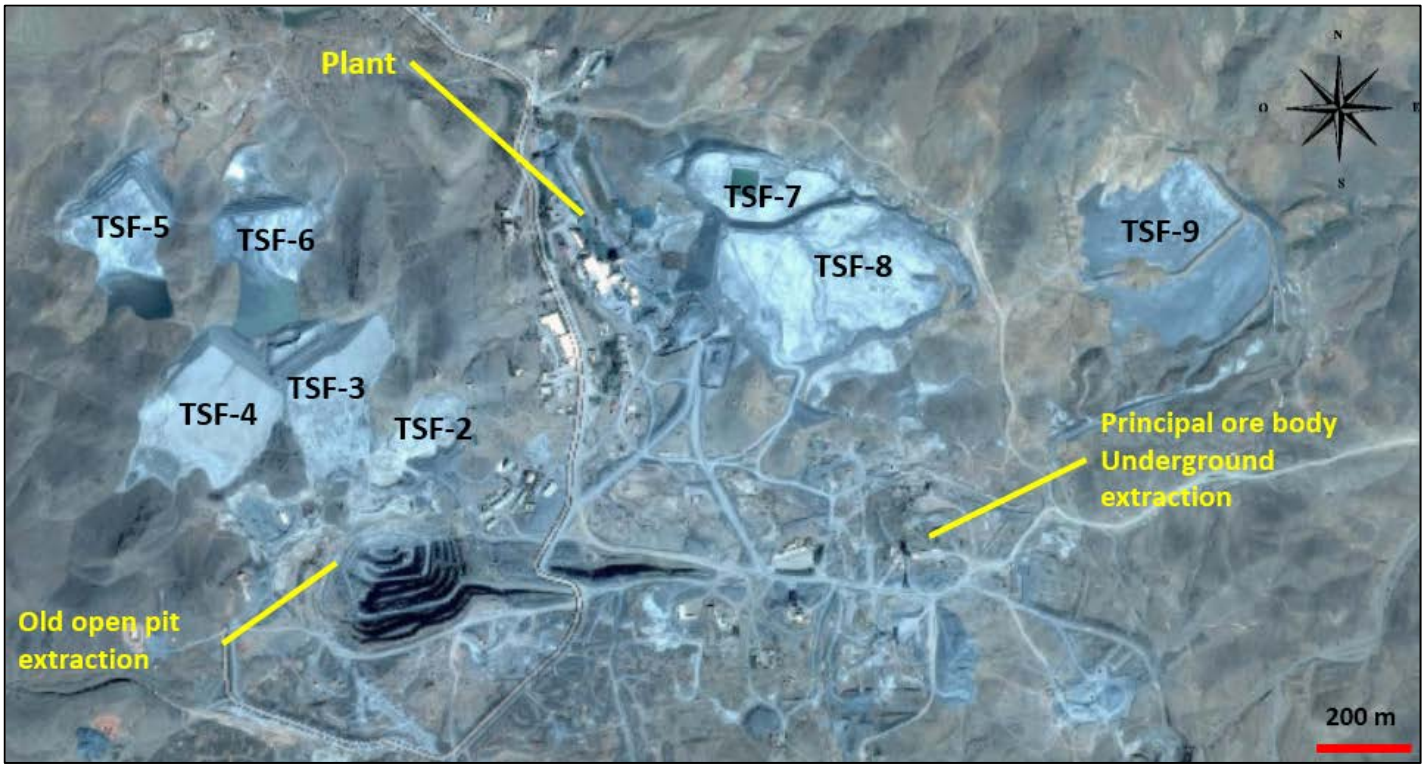

Figure 4. Satellite image showing main installation of Imiter operations area, TSF= Tailing Storage Facility (Adapted from Google maps)

4 IMITER PASTE BACKFILL

4.1 PBF Components Characteristics

Imiter operation use a PBF recipe which combine crashed waste material (Gravel and sand), tailings and cement.
Mixing water come from local drilling pumping.

The following present Imiter PBF characteristics from conducted laboratory testing.

All tests was made according to Moroccan standards (NM) or French standards (NF) in case of need.

4.1.1 Gravel and Tailings

Table 1 present results of laboratory testing generally realized for conventional concrete aggregates.
These results confirm acceptable characteristics according to Moroccan standards.

Chemical composition and particle size distribution of tailing was identified respectively by XR and sedimentation technics.

Table 2 present the obtained chemical composition and figure 5 show particle size distribution curve for gravel, sand and tailings mixture.

Table 1. Laboratory characterization of Imiter paste backfill gravel.

Laboratory testing	Flatness coefficient (%)	Superficial cleanliness (%)	Los Angeles hardness (%)	Sand equivalent (%)
Testing results	23	0.3	15	56
Standard NM10.1.27	≤ 25	≤ 3	≤ 30	≥ 60

Table 2. Chemical composition of tailings.

Chemical Elements	AL_2O_3	CaO	Fe_2O_3	K_2O	MgO	MnO	Na_2O	P_2O_5	SiO_2	TiO_2	LOI	**Total**
%	13.86	2.81	6.33	3.59	3.96	0.18	1.61	0.19	57.37	0.72	8.47	**99.12**

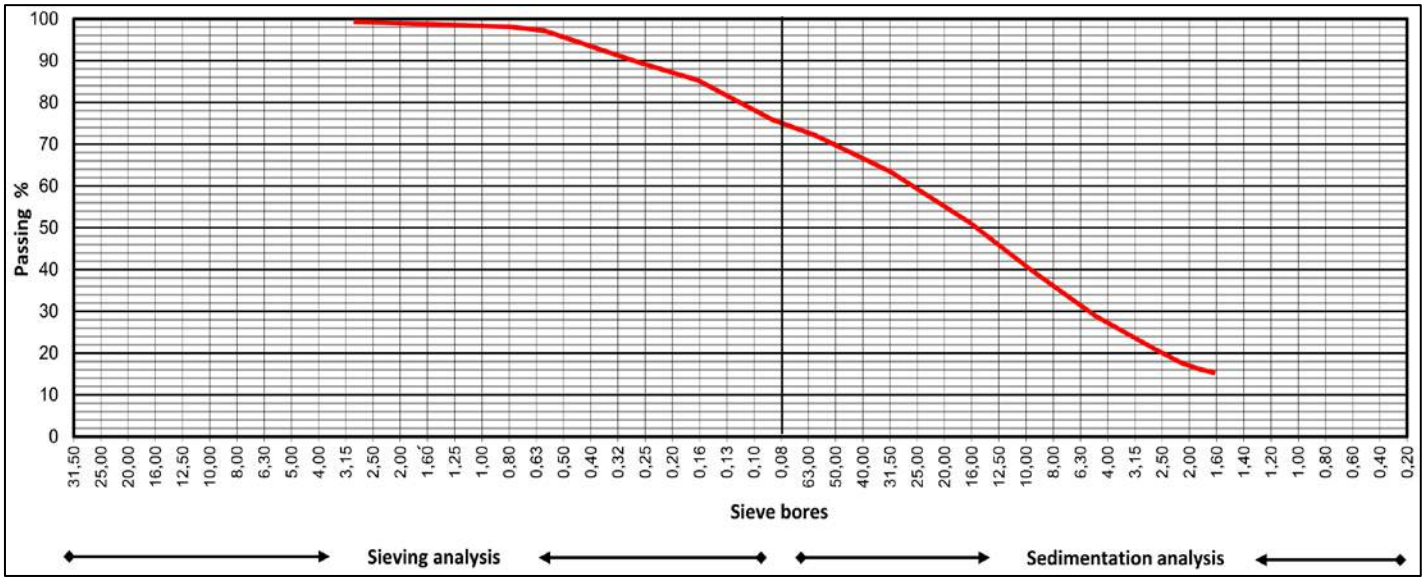

Figure 5. Imiter PBF particle size distribution

4.1.2 Binder

Table 3 and Table 4 present, respectively, physical and mechanical testing realized on cement (CPJ45 type) sampled from site stock. Results are presented in comparison with Moroccan standards NM 10-1-008 and NM 10-1-004.

Table 3. Physical testing – Cement CPJ45.

Physical parameter	Setting time	Expansion	Specific surface (BLAINE fineness)
Testing results	2h 00 min	1.7 mm	2470 cm^2/g
Standards NM 10-1-008	≥ 1h 30 min	≤ 10 mm	≥ 2200 cm^2/g

Table 4. Mechanical testing – Cement CPJ45

	Uniaxial compressive strength (MPa)		
	after 2 days	after 7 days	after 28 days
Testing results	18.7	27.3	39.5
Standards NM 10-1-004	-	≥ 20	≥ 32.5

4.1.3 Mixing water

Mixing water come from local drilling pumping. Table 5 present chemical composition obtained by laboratory analysis. Results are also presented in comparison with Moroccan standards NM 10-1-008.

Table 5. Chemical analysis of mixing water.

Chemical parameter	Ph	Material in suspension (mg/l)	Dissolved salt (mg/l)	Sulfates (mg/l)	Chlorides (mg/l)	Organic material mg/l
Testing results	6.60	0.5	617	153.60	194.70	0.00
Standards NM 10-1-008	≥ 4	≤ 2000	≤ 5000	≤ 2000	≤ 500	≤ 200

Table 6 present PBF mixtures actually used in Imiter mine and combining the above characterized materials. One formulation is for slab separation of mining levels with 7 % cement content and one for voids filling with 2 % cement content.

Table 6. Imiter PBF mixtures.

Cement %	7 %	2 %
Gravel (kg)	600	600
Sand (kg)	1000	1000
Tailings (kg)	340	340
Water (l)	500	500
Cement (kg)	160	40
Total weight (kg)	2600	2480

4.2 Prediction of PBF Strength

Typically stopes of 4 m width and 4 m height are mined with fill-and-cut instead 15 m height for sublevel stopping method.

The following present an estimation of required PBF UCS according to the assigned function.

4.2.1 PBF For Voids filling

The long term (> 90 days) UCS of filling backfill can be predicted by equation (1) whish consider a null friction angle: $\phi = 0$. (Mitchell et al., 1982).

$$\mathbf{UCS_{design}} = \mathbf{SF} * \left(\frac{\gamma_b H}{1 + \frac{H}{L}} \right) \quad (1)$$

Where FS = safety factor, γ_b = PBF bulk unit weight (KN/m^3), H = PBF height (m), and L = the stope width (m).

The required UCS was calculated for different safety factor based on Imiter ore geometry in case of each mining method. A PBF bulk unit weight of 18 KN/m3 was considered. Table 7 present the obtained results for UCS design prediction.

These results shows difference between the required UCS for each method. This difference is due to exposed PBF height face which depend on utilized method. This can be materialized by adopting two PBF recipe.

Table 7. UCS design calculation according to safety factor.

	UCS design (KPa)										
Safety factor	1.0	1.1	1.2	1.3	1.4	1.5	1.6	1.7	1.8	1.9	2.0
Cut-and fill	36.0	39.6	43.2	46.8	50.4	54.0	57.6	61.2	64.8	68.4	72.0
Sublevel stoping	56.8	62.5	68.2	73.8	79.5	85.2	90.9	96.6	102.3	108.0	113.6

4.2.2PBF For Slab Level Separation

Imiter ore body is divided into panel of 20 m height. Panel are separated by the implementation of slabs of 60 cm thick. This thickness is the minimum for verification of the non-tipping condition.

By assimilating the slag panel separation to a beam of two supports, we can use rules developed for beam calculation. By considering a non-recessed slab we can find the equation (2) giving the required thickness of the slab in terms of the admissible compressive strength σ_{ac}:

$$\mathbf{e} = \frac{\mathbf{6\,\gamma_p\,L^2} + \sqrt{\left(\left(\mathbf{6\,\gamma_p\,L^2}\right)^2 + \mathbf{32\gamma_b\,hL^2\sigma_{ac}(1-\beta)}\right)}}{\mathbf{16\,\sigma_{ac}(1-\beta)}} \quad (2)$$

Where γ_p = PBF bulk unit weight (KN/m3), L = mined tranche width (m), γ_b = backfill bulk unit weight (KN/m3), σ_{ac} = PBF admissible compressive strength (KPa), h = panel height (m), β = arbitrary coefficient $0 < \beta < 1$.

Using equation (2), we can find the admissible compressive strength of PBF considering a thickness of 0.6 m. The PBF UCS can then be calculated by equation (3).

$$\sigma_{ac} = \frac{UCS}{SF} \quad (3)$$

Where σ_{ac} = PBF admissible compressive strength (MPa), UCS: uniaxial compressive strength (MPa), SF: safety factor.

Considering a slag unit weight of 18 KN/m^3, a filling backfill unit weight of 17 KN/m^3, a height panel of 20 m and null β coefficient, we find a σ_{ac} = 1.7 MPa.

Generally a safety factor of 1.5 is associated with underground mining works, this give a required UCS of 2.55 MPa.

5 UNIAXIAL COMPRESSIVE STRENGTH RESULTS

PBF mixtures presented in chapter 4 was reconstituted in laboratory and crafted as cylindrical specimens of 10 cm diameter and 20 cm length. Mechanical performance of the analyzed PBF was evaluated by UCS testing. Tests was realized for different ages of specimens: 7, 14, 21 and 28 days after confection. UCS test is widely used as principal parameter for PBF backfilling system design because of its low cost and possibility to make correlation with other mechanical parameter.

Table 8 and 9 present respectively UCS results for PBF filling recipe (2% cement) and PBF slab recipe (7% cement).

Table 8. UCS results for PBF filling recipe (2% cement).

Age (days)	Mean unit weight (KN/m^3)	Mean UCS (MPa)
7	17.9	0.40
14	17.2	0.72
21	17.0	1.08
28	16.9	1.33

Table 9. UCS results for PBF filling recipe (7% cement).

Age (days)	Mean unit weight (KN/m^3)	Mean UCS (MPa)
7	18.5	0.49
14	18.0	1.03
21	17.9	1.59
28	17.8	2.01

6 DISCUSSION AND PROSPECTS

Table 10 present values of analytical prediction of the long term uniaxial compressive strength made in chapter 4 considering a safety factor of 1.5, and corresponding experimental laboratory testing after 28 days of curing time.

Table 10 shows that the 2% of cement recipe can be more optimized, laboratory testing give a high UCS value at 28 days of curing time compared to predicted values. This high experimental value can be explained by the mixture characteristics of Imiter PBF which combine in addition to plant tailing, crashed waste rock from mine development against an ordinary PBF combining only plant tailings, binder and mixing water.

Table 10. Predicted UCS design instead experimental values.

PBF function	Predicted UCS (KPa) Curing time > 90 days	Experimental Result (KPa) Curing time = 28 days
Void filling / Cut and fill	54	1330
Void filling / Sublevel stoping	85	1330
Slag level separation	2550	2010

For the slab recipe, experimental results gives a UCS value of 2.01 MPa against a predicted strength of 2.55 MPa. It's possible that slag PBF reach the required UCS value after a long curing time. Laboratory or in-situ testing must be done to evaluate the experimental long term strength of slag PBF.

Obtained result confirm that utilized recipes are adequate with the assigned functions of PBF. However PBF recipe for voids filling can be ameliorated to obtain an optimal mixture ensuring required mechanical strength.

The future works related to this topics will be focused on the recipe composition to find the optimal binder content ensuring required mechanical properties and evaluate the possibility to reduce or eliminate waste mine gravel from the mixture. The final objective is to determinate an optimal PBF recipe combining low possible cost and strength requirements.

REFERENCES

Belem, T., Bussière B. & Benzaazoua M., 2001 the effect of microstructural evolution on the physical properties of paste backfill. In Proceedings of Tailings and Mine Waste'01, January 16-19, Fort Collins, Colorado, A.A. Balkema, Rotterdam, pp. 372–373.

Belem, T., Benzaazoua, M., Bussière B., Dagenais A.-M., 2002, Effects of settlement and drainage on strength development within mine paste backfill. Tailings and Mine Waste02, 27-30 January, Fort Collins, Colorado, Balkema : Rotterdam, pp. 139-148.

Belem, T. & Benzaazoua M., 2003, Utilisation du remblai en pate comme support de terrain. Partie I : de Sa fabrication a sa mise en place sous terre. Après-Mines, 5-7 Février, Nancy, France.

Belem, T. & Benzaazoua M., 2008, Predictive models for prefeasibility cemented paste backfill mix design, Post-Mining, February 6-8, Nancy, France.

Benzaazoua M., Belem T., Bussière B. 2002, Chemical factors that influence the performance of mine. Cement and Concrete Research 32.

Benzaazoua, M., Fall M., Belem T., 2004, A contribution to understanding the hardening process of cemented pastefill. Minerals Engineering, pp. 17-2, 141-152.

Benzaazoua, M., Bois, D., Belem, T., Gauthier P., Ouellet S., Bussière B., Fall, M., Aubertin, M., St-Onge, J.-F., 2005, Remblais miniers: évolution des connaissances et de la pratique. 20e Colloque en contrôle de terrain de l'AMQ, 22-23 mars.

De Souza E., De Gagné D., Archibald J.F., 2001, Minefill Applications, Practices and Trends in Canadian Mines. Proceedings of the 7 th International Symposium on Mining with Backfill, Society for Mining, Metallurgy, and Exploration.

Fall, M., Benzaazoua, M., 2003, Modeling and simulation of paste backfill performance properties. Proceedings of 56 th Canadian Geotechnical Conference; September 28 to October 1, Manitoba, Canada, 2003, pp. 161-168.

Gasquet D., Levresse G., Cheilletz A., Azizi-Samir M.R., Mouttaqi A., 2005, Contribution to a geodynamic reconstruction of the Anti-Atlas (Morocco) during Pan-African times with the emphasison inversion tectonics and metallogenic activity at the Precambrian-Cambrian transition, Precambr.

Hassani, F., Archibald, J., 1998 Mine backfill, CD-ROM. Canadian Institute of Mine, Metallurgy and Petroleum.

Landriault, D., and B. Goard., 1987, Research into High Density Backfill Placement Methods by the Ontario Division of Inco Limited. CIM Bull., v. 80, No. 897, pp. 46-50.

Li M. and Moerman A., 2002, Perspectives on the scientific and engineering principles underlying flow of mineral pastes. Proc. 34th Ann. Meet. of CMP, Ottawa, Canada, pp. 35, 573-595.

Li, L., Aubertin, M., Belem, T., 2005, Formulation of a three dimensional analytical solution to evaluate stress in backfilled vertical narrow openings. Canadian Geotechnical Journal, vol. 42, no 6, p. 1705-1

Pit Slope Optimization Based on Hydrogeologic Inputs

G. Evin, F. Henriquez, V. Ugorets
SRK Consulting (U.S.), Inc., Lakewood, Colorado, USA

ABSTRACT With the variability of commodity prices and the constant increase of mining costs, it has become increasingly important to optimize pit slopes of mines, taking into consideration the complexity and the uncertainties presented by ground conditions. The variables in slope stability, geology, rock mass strength, structural defects, inherent and induced stresses, rock weathering, alterations, and groundwater, are well known, as are their impacts on slope performance. Most variables cannot be changed to optimize slopes. However, groundwater is one variable that can be managed during pit excavation, to reduce the effect of pore pressure on slope stability.

Hydrogeologists and rock mechanics engineers combine their efforts in order to quantify, simulate, and control the effect of groundwater pressures on pit slope performance. Based on comprehensive field hydrogeological data collection and interactive numerical groundwater and geotechnical modeling, it is possible to evaluate the water pore pressure effect on the pit slope, to provide an efficient depressurization strategy to meet the geotechnical engineering targets, and thus to develop cost-effective mine plans.

This paper discusses how proper management of groundwater conditions can contribute to mine planning and operations, through pit slope optimization. We show a complete approach from collection of hydrogeological data in the early stages of a project to design of an appropriate depressurization plan, taking into account the rock mass conditions, the mining plan, and the time to achieve an optimal pit slope.

Keywords: Hydrogeology, hydrogeological condition, pit slope, stability

1 INTRODUCTION

Groundwater water in open pit mines affects normal operations in many ways. Excessive water inflow into the pit can significantly impact the mine operations by reducing equipment performance and increasing loading and haulage time. Water in the pit could result in incremental increases in mining cost, reduction of mining performance, the need for special blasting products, increases in drilling time, and mechanical damage of mine equipment, etc.

A poor knowledge of the hydraulic parameters could also have a negative impact on the slope design and stability performance of the pit, which could result in an over or underestimation of the mine design; directly impacting, negatively, the net present value (NPV) of the business.

It is clear that a good understanding of groundwater conditions and their effects on the mine operation and mine design can help mining companies optimize their business.

Several authors have developed methods of data collection, interpretation and modeling of groundwater conditions to provide recommendations for pore pressure reduction and mine dewatering (Read & Stacey, 2009; Beale & Read, 2013; and others). This paper does not intend to review and comment about the current data collection and modelling technics, the objective of this paper is to discuss how the integration of the hydrogeology and geotechnical disciplines can optimize the mine operations. The paper intends to demonstrate the importance of good data collection, interpretation, and groundwater numerical modeling on slope stability as an optimization tool.

2 EFFECT OF GROUNDWATER ON SLOPE STABILITY

The literature lists different ways in which groundwater can affect open pit mine excavations, including (a) changes of effective stresses and/or (b) saturation, both contributing factors of slope stability.

2.1 Changes of Effective Stresses

In its simplest definition, the water pore pressure is the pressure of groundwater held within a soil or rock in gaps between particles (pores). Pore water pressure is used in calculating the stress state in the ground soil mechanics using Terzaghi's expression for the effective stress of a soil (below).

Soil or rock can be pictured as a frame of soil particles enclosing continuous voids containing fluids (water, air, gas etc.) as shown in Figure 1. In fully saturated soil, water is considered to be incompressible, so that a reduction in volume is possible only if some of the water can escape from the voids. In dry or partially saturated soil a reduction in volume is always possible due to the compression of air in the voids which allows the opportunity for the rearrangement of particles within the soil. In 1923, Terzaghi presented the principle of effective stress. The principle applies only to fully saturated soils and relates the following three stresses: (a) total normal stress σ_N, (b) pore water pressure (u) and effective normal stress (σ'), which represents the stress transmitted through the soil skeleton only. The Terzaghi principle is expressed by the following equation (Eq.1).

$$\sigma_N = \sigma' + u \quad (1)$$

Figure 1 shows a Normal force P applied on an area A, resisted by inter particle forces and the pressure located in the pore water. The physical model indicates that the forces at each point are in contact with the true plane XX, which can be split into two components; Normal Effective N' and tangential T forces, then the Effective Normal stress can be defined by the following equation (Eq. 2):

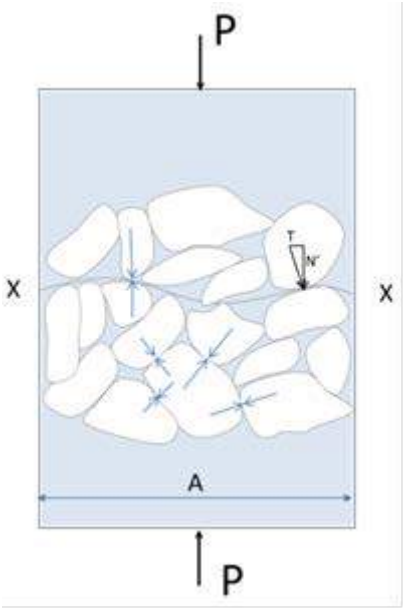

Figure 1. Interpretation of effective stresses.

$$\sigma' = \Sigma N' / A \quad (2)$$

Given the fact that the Total Normal stress is:

$$\sigma = P / A \quad (3)$$

Then the points in contact between the particles should have a total pore pressure acting on the plane (entire area A), reaching the equilibrium in direction normal to XX plane given by:

$$P = \Sigma N' + u \times A \quad (4)$$

or

$$P/A = \Sigma N' / A + u \quad (5)$$

Therefore,

$\boldsymbol{\sigma_N} = \sigma' + u$ or $\boldsymbol{\sigma'} = \sigma_N - u$

2.2 Shear Failure

In simple terms, failure occurs within the material when the shear stress becomes equal to the shear strength, expressed by Coulomb's principles (Das, Braja, 2011) in the lineal failure envelope, given in the following equation:

$$\tau = c + \sigma_N \times \tan \phi \quad (6)$$

where:

τ = shear stress;
c = material cohesion;
σ_N =normal stress; and
ϕ = internal friction angle of the material.

In other words, there are critical combinations between shear and normal stresses that produce failure. However, shearing resistance is developed by the inter-particle forces; therefore, if the effective normal stresses are zero then the shearing resistance must be zero (at least there is cementation between the particles) and the value of effective cohesion (c') would be zero.

The physical model indicates that each point in contact on the true plane XX, the Normal Effective N' and tangential T forces, will be reduced and potentially reach a critical combination of normal and shear stresses over the failure envelop establishing the failure.

2.3 Water Pore Pressure in Slope Engineering

The pore pressure in slope engineering is one of the contributing factors in slope stability. The groundwater changes, effective stresses, and increased density of the materials cause changes in hydrostatic loading (Read & Stacey, 2009). There are several different techniques to simulate water pore pressure in slope analyses; computer simulations can provide a good approach to analyze the groundwater effect on slope performance.

For saturated or partially saturated slopes, rock engineering experience establishes that a reduction of pore water pressure will improve the results of the slope performance parameters creating the opportunity to optimize slope designs. In practice, the time required to achieve the reduction of pore pressure must be considered, as well as the flexibility in the mining plan to allow enough time for getting the depressurization targets established by the pit slope engineer.

3 MINE DEWATERING AND PIT SLOPE DEPRESSURIZATION

One of first steps in pit slope stability analyses is to understand the water pore pressures in the pit slopes as the result of mining and planned dewatering. As soon as the pit floor reaches levels below the water table, natural drainage of the wall will usually occur due to seepage and with response to mining which induces relaxation of the rock mass (Beale & Read, 2013). The natural drainage in conjunction with active dewatering (if implemented) will cause a reduction of pore pressures in the rock walls. The second step is to evaluate an effect of additional pore pressure reduction on the pit slopes and the necessity of implementing a depressurization program. In some cases, the pore pressure dissipation achieved by passive and active dewatering is adequate for targeting the desired pore pressure goals. In other cases, to achieve the dewatering goals, a dedicated pit slope depressurization program is needed.

Pit dewatering is a necessary element of any mining that occurs below the water table. Pit slope depressurization is an optional method for additional reduction of pore pressure within pit walls if this is required for geotechnical reasons. Table 1 shows a comparison of general mine dewatering and pit slope depressurization.

Table 1. Comparison of mine dewatering and pit slope depressurization

Parameter	Mine Dewatering	Slope Depressurization
Material/rock	High permeability	Low permeability
Target	Lower water table	Decrease effective stress of the slope materials
Volume of water	Often high	Normally low
Area of implementation	Normally pit-wide	Often local to a specific slope sector
Most common method	By in-pit sump and vertical wells	By horizontal drain holes or gravity flowing drains in conjunction with general mine dewatering

The ability to reduce pore pressure to achieve the desired target depends on hydraulic parameters, on timing, and on the

effectiveness of dewatering and depressurization methods.

3.1 Depressurization Parameters

Major depressurization parameters and pore pressure reduction can be illustrated by a simple 1-D Flow (or Diffusivity) Equation:

$$\Delta h(x,t) = \Delta h_o erfc\left(\frac{4Kt}{S_s x^2}\right)^{-(1/2)} \quad (7)$$

where:
Δh = change in hydraulic head;
Δh_o = initial hydraulic head;
K = hydraulic conductivity;
S_s = specific storage;
t = time;
x = distance; and
erfc (α) – function which increases when α decreases and decreases when α increases.

This simple relationship (Eq. 7) indicates that slope depressurization depends on hydraulic parameters, time of dewatering, and distance from the dewatering (or depressurization) system. The hydraulic parameters need to be known. Time and distance are the only two variables which allow control of the pit slope depressurization.

Figure 2 indicates that for the given hydraulic parameters (K and S_s) the degree of depressurization increases with time and decreases with distance from the dewatering system. Figure 3 shows that more successful depressurization is potential for more permeable rock and shorter distances from the dewatering system. Equation (7) illustrates the mechanism for pore pressure reduction but it should be noted that it is based on various assumptions (linear flow, homogeneity, isotropy) that are unlikely to be met in practice, given the complex hydrogeological conditions surrounding many mine sites.

A key factor for designing a slope depressurization program in poorly-permeable materials is the time required to achieve the target pore pressure profile for the critical sector of the pit. Slopes excavated in higher-permeable rocks typically require less time for the depressurization to be effective.

In poorly-permeable weak rock environments, such as an operation with deep weathered zones or thick zones of argillic (clay) altered rock, it can take months to years to depressurize the slopes to desired targets (Beale & Read, 2013). Depending on the time available, it may be necessary to advance a general dewatering program to lower the water table and to provide additional time for drainage of less permeable pit sectors.

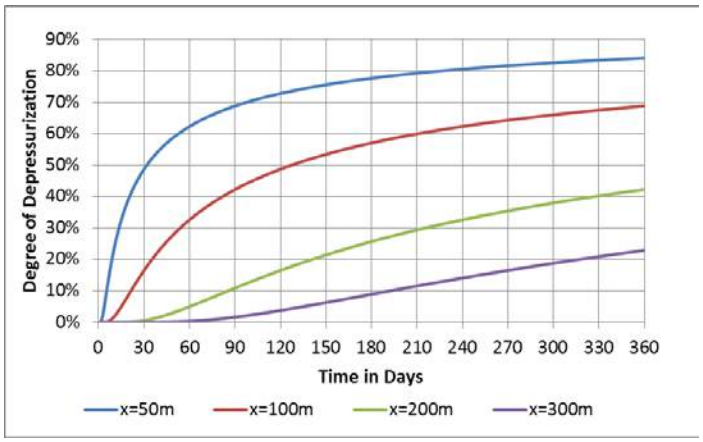

Figure 2. Pore pressure reduction vs. time and distance from dewatering (K=10^{-8} m/s, S_s=10^{-5} 1/m)

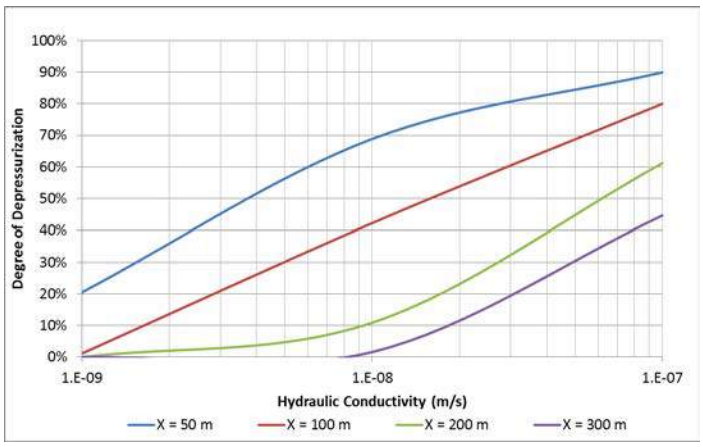

Figure 3. Pore pressure reduction as function of hydraulic conductivity and distance for 90 days of dewatering

3.2 Depressurization Methods

There are different methods of pit slope depressurization, which include:

1. Seepage from face and pumping from sumps.
2. Horizontal drain holes.
3. Gravity-flowing vertical drains.
4. Pumping wells.
5. Drainage tunnels with sub-vertical drain holes.

The first method is very common and used for passive dewatering or as part of active dewatering to intercept residual passive groundwater inflow coming to the open pit. The other methods allow for the addition of the reduction of pore pressures in the pit slopes to achieve the desired depressurization target. The choice of the best depressurization option, or a combination thereof, depends on the site specific hydrogeological, geological, structural, and geotechnical conditions which define the depressurization targets.

The use of horizontal drains or sub-horizontal drain holes (second method) is the most commonly applied method worldwide for locally reducing pore pressures behind open pit slopes. To install the drain holes, specific targets need to be identified. These targets may include:

- The water contained in low permeable material.
- Water trapped in permeable but compartmentalized fractures behind the pit slope.
- Water "dammed" behind geological structures.
- New geological units which will be encountered in pushbacks as the pit is expanded.

The effectiveness of the depressurization system from horizontal drain holes depends on the success of intersecting the defined targets and, in case of a low permeable pit slope, timing, distance between drain holes and their depth, hydraulic parameters, and the ability to discharge more water than recharged from precipitation and surface-water bodies.

3.3 Hydrogeological Characterization and Data Analysis

Hydrogeological parameters affecting pit slope stability include:

- Water levels;
- Distribution of hydraulic conductivity of rock within pit slope;
- Groundwater storage parameters; and
- Recharge from precipitation and surface-water bodies.

These parameters need to be determined during hydrogeological studies. Where it is possible, hydrogeological data should be collected during the early stages of the project and in conjunction with geotechnical studies. Table 2 summarizes content of hydrogeological studies for different stages of the project and targeted level of data confidence.

Table 2. Hydrogeological study and targeted level of data confidence

Project Stage	Hydrogeological Study	Targeted Level of Data Confidence
Conceptual	Regional groundwater survey; water level data collection in exploration holes; identification of hydrogeological units based on Geological Model	>20%
Pre-Feasibility	Mine scale airlift, pumping, packer testing and piezometer installation; initial hydrogeological parameters and groundwater flow understanding; initial hydrogeological database and conceptual model established; preliminary groundwater model and sensitivity analysis; initial assessment of dewatering and depressurization requirements	30-50%
Feasibility	Targeted pumping and airlift testing; piezometer installation; enhancement of hydrogeological database and 3D model; advancement of assessments of dewatering and depressurization requirements	40-65%
Design and Construction	Installation of dewatering wells and piezometers; refinement of hydrogeological database, 3D model, depressurization and dewatering requirements	65-75%
Operations	Ongoing management of piezometers and dewatering well network; continued refinement of hydrogeological database and 3D model	>75%

Note: Table modified by authors from Read and Stacey (2009)

4 GROUNDWATER MODELING AS A TOOL TO PREDICT PORE PRESSURES

Numerical groundwater modeling is widely used to simulate groundwater inflow to open pits for relatively complex hydrogeological conditions. The modeling process includes development of a conceptual hydrogeological model, grid discretization, assigning of hydraulic parameters and boundary conditions, model calibration, and prediction. Predictions very often include two scenarios:

- Passive inflow (or how much water will enter into the pit during its excavation without active dewatering/depressurization).
- Active dewatering to reduce residual passive inflow to the pit or active depressurization to reduce pore pressure for pit slope stability.

The active dewatering scenario is used when the rock within the pit slope is permeable and the amount of passive inflow cannot be managed safely during the mine operation. The active depressurization scenario is used when the rock within the pit slopes has low permeability, and high seepage face and pore pressures that are causing slope stability problems. The numerical groundwater models used for dewatering predictions are typically 3-D and developed at the regional scale with additional discretization around the pit both laterally and vertically. The discretization of regional dewatering models very often is not sufficient to precisely predict pore pressure distributions within the pit slopes. Therefore, 2-D cross sectional or 3-D (strip or asymmetrical) and more detailed pore pressure models are used along critical pit sections as “windows” within the regional groundwater model. These models use the hydraulic heads from the regional model to incorporate boundary conditions (sometimes variable in time) within pore pressure models. It should be noted that pore pressures in pit slopes and their changes as a result of depressurization should be predicted in time due to the fact that steady state calculations tend significantly to over predict dewatering and depressurization effects.

To evaluate the effect of depressurization parameters on pit slope stability through the calculation of the Factor of Safety (FoS), the authors developed a series of 3-D strip models. These models assume excavation of a 45 degree open pit to depths of 300m, 600m, and 1000m, in 3, 6, and 10 years (Figure 4 shows the finite-element mesh for the 1,000m pit).

Hydraulic conductivity values were varied from 10^{-9} m/s to 10^{-5} m/s (with an increase by a factor of 10; a total of 5 values were evaluated). Specific yield and specific storage were kept constant and equal to 0.05 and 10^{-6} 1/m, respectively.

The initial hydraulic heads were assumed to be 50m below the ground surface with constant-head boundary conditions at a significant distance (6km), from the center of the pit. Depending on the time and geometry of the excavations, different water levels can be predicted. Figure 4 shows the predicted water table (P=0 kPa curve) at the end of 10 years of excavation of the 1,000 m open pit, for different hydraulic conductivity values.

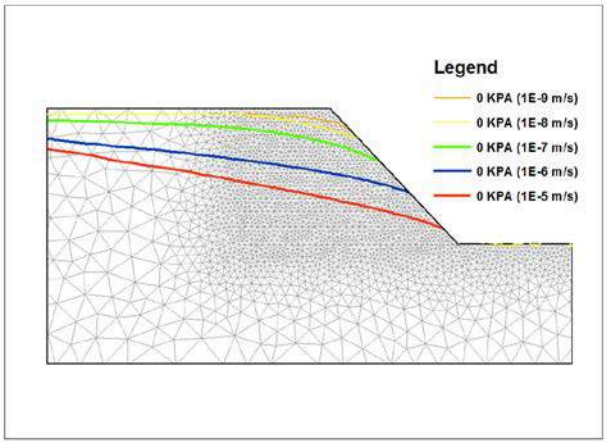

Figure 4. Predicted water table (P=0 kPa) at end of open pit excavation used for slope stability analysis

The numerical simulation provides the pore pressure distribution in the slope, which easily can be used for the slope stability analysis, as showed in Figure 5.

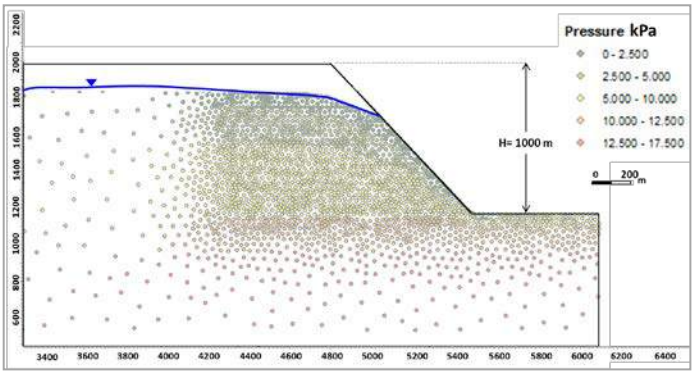

Figure 5. Pore pressure distribution at year 10 of pit excavation, K=10^{-8} m/s

Based on these models, the FoS of each pore pressure distribution was determined in order to demonstrate the effect of the hydraulic conductivity on pit slope stability. For this exercise, the simplified stability models considered the single rock mass medium to be continuous, isotropic, and lineally elastic, and assumed the lineal Mohr & Coulomb failure criteria to be valid and a good estimation of the rock mass strength.

Even though the described rock mass conditions are rarely found in the real world, this condition will be assumed valid for the purpose of this exercise.

Changes of hydraulic conductivity have a strong effect on the FoS. Figure 6 shows the FoS for 300m, 600m, and 1,000m pit slopes (excavated in 3, 6, and 10 yrs., respectively) as function of hydraulic conductivity. The geometry and the rock mass strength parameters were fixed for this example and a variable range of the hydraulic conductivity values were used to simulate the pore pressure field for each case.

This example does not intend to discuss the acceptability of the FoS given different pore pressure conditions; the chart, rather, shows the impact of the water pore pressure field, based on a large range of hydraulic conductivity, on the slope performance.

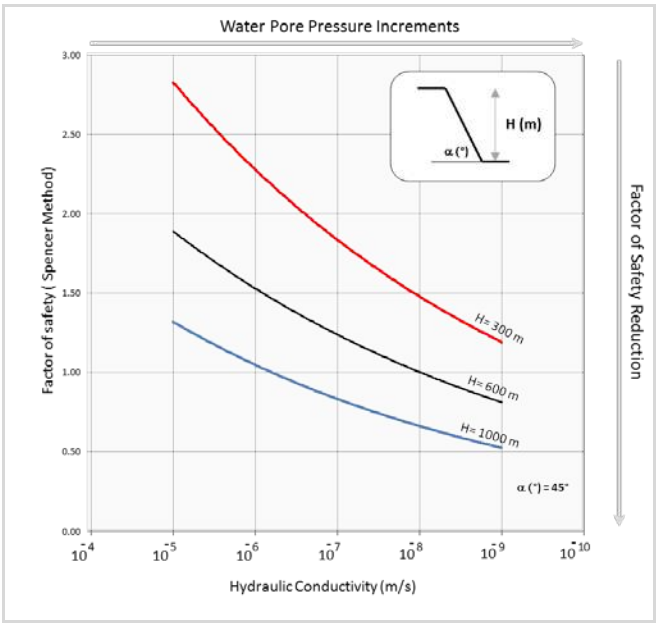

Figure 6. Relationship between FoS and hydraulic conductivity, obtained by using a test model.

The results of the test model indicate:

- Reduction of the hydraulic conductivity results in incremental increase of pore pressure within pit slopes. Therefore a reduction of the FoS is expected.
- Slopes less than 300m could be considered stable for rock with any hydraulic conductivity values, median pits (H is about 600m) requires additional depressurization for K<10^{-7} m/s, however for deep slope (1,000m) the FoS could be reduced to values below the limit of equilibrium (it should be noted that this statement is valid for only the test model used).
- In low permeable rock (*K* from 10^{-8} m/s to 10^{-9} m/s) increasing of FoS by additional pore pressure reduction could be not achievable due to required timing of depressurization and change of slope angle might be required, and should be reviewed in more detail.
- Figure 6 shows that the stability of the slope could depend upon the hydraulic conductivity at different heights. This example shows, for a medium size slope (H>600m), that a wrong assignment of the hydraulic conductivity can over or under estimates the slope angle, resulting in

extra capital cost, NPV of the project and/or safety issues, mining difficulties, negative impact on the mining plan and could jeopardize the mine reserves and the business.

5 HYDROGEOLOGICAL AND GEOTECHNICAL INTEGRATION

The success of an open pit mine design is based on quality, quantity and distribution of the geotechnical and hydrogeological data. Also, interpretation and modeling plays a "key" role in the final results. Today, mining companies have a clear understanding of the importance of data requirements, and extensive budgets are assigned to this task during different stages of the project. Unfortunately, there can be disconnection between the geotechnical and hydrogeological disciplines, affecting the final results. For example, hydrogeologists very often focus on dewatering and not on water pore-pressure modelling, placing more attention on high permeability units and not considering, in detail, the low permeable units, which might present problems for slope stability. Another example of this disconnect is reflected in the geotechnical design constraints; sometimes the geotechnical engineer's design assumes certain hydrogeological conditions, which are not achievable in reasonable time.

The disconnect between disciplines normally results in extra cost for drilling, opportunities lost for data collection, misunderstanding of the geotechnical requirements, use of non-achievable assumptions, missuses of the hydrogeological models, over or under estimation of the slope designs or excessive costs for missed selection of appropriate slope depressurization systems.

To minimize the negative impacts, it is important to recognize the need for the integration of both disciplines during each stage of the project.

Figure 7 below shows an integrated chart of geotechnical and hydrogeology processes for slope stability analysis recommended by the authors.

6 CONCLUSIONS

Integration of geotechnical and hydrogeological studies during different stages of the mining project can provide required hydrogeological input for slope stability analysis and pit optimization. At early stages of the project the Geotechnical Engineer needs to identify potential effects of pore pressure on slope stability, allowing the Hydrogeologist to characterize geotechnically important hydrogeological units. Data collected in the field need to be sufficient to develop reliable conceptual hydrogeological and numerical groundwater flow models to predict pore pressures in pit slopes during excavation and dewatering. At late stages of project development, these models should be sufficient to predict additional pit slope depressurization options (if they are necessary) and to define the required time for pore pressure reduction. These models, along with comprehensive sensitivity analysis of remaining uncertainties, should provide an input for cost-benefit analysis of implementation of pit slope depressurization. Numerical test modeling completed for this study indicates that for a medium- and high-permeable rock in a medium size slope (200 – 500 m height), there is significant impact of hydraulic conductivity on slope performance. This indicates that the accuracy of the hydrogeological inputs, and the interpretation and the modelling of the hydrogeological conditions are essential during the geotechnical investigation.

For saturated or partially saturated slopes, rock engineering experience establishes that a reduction of water pore pressure will improve the results of the slope performance parameters, creating the opportunity to optimize slope designs. Unfortunately, in some cases the slope depressurization requirements are not properly assessed due to lack of hydrogeological understanding, hydrogeological modelling objectives and, in some cases, due to miscommunication between the Hydrogeologist and rock mechanics Engineers. This disconnection between the hydrogeological and rock

mechanics teams results in a potential of over or under estimation of slope designs. In order to avoid this, it is useful to consider the following questions:

- What will pore pressures be in the ultimate pit slope and how will they change in time during planned mining/dewatering?
- What would be the effect of pore pressure reduction on slope stability?
- How much time is required to reduce pore pressure?

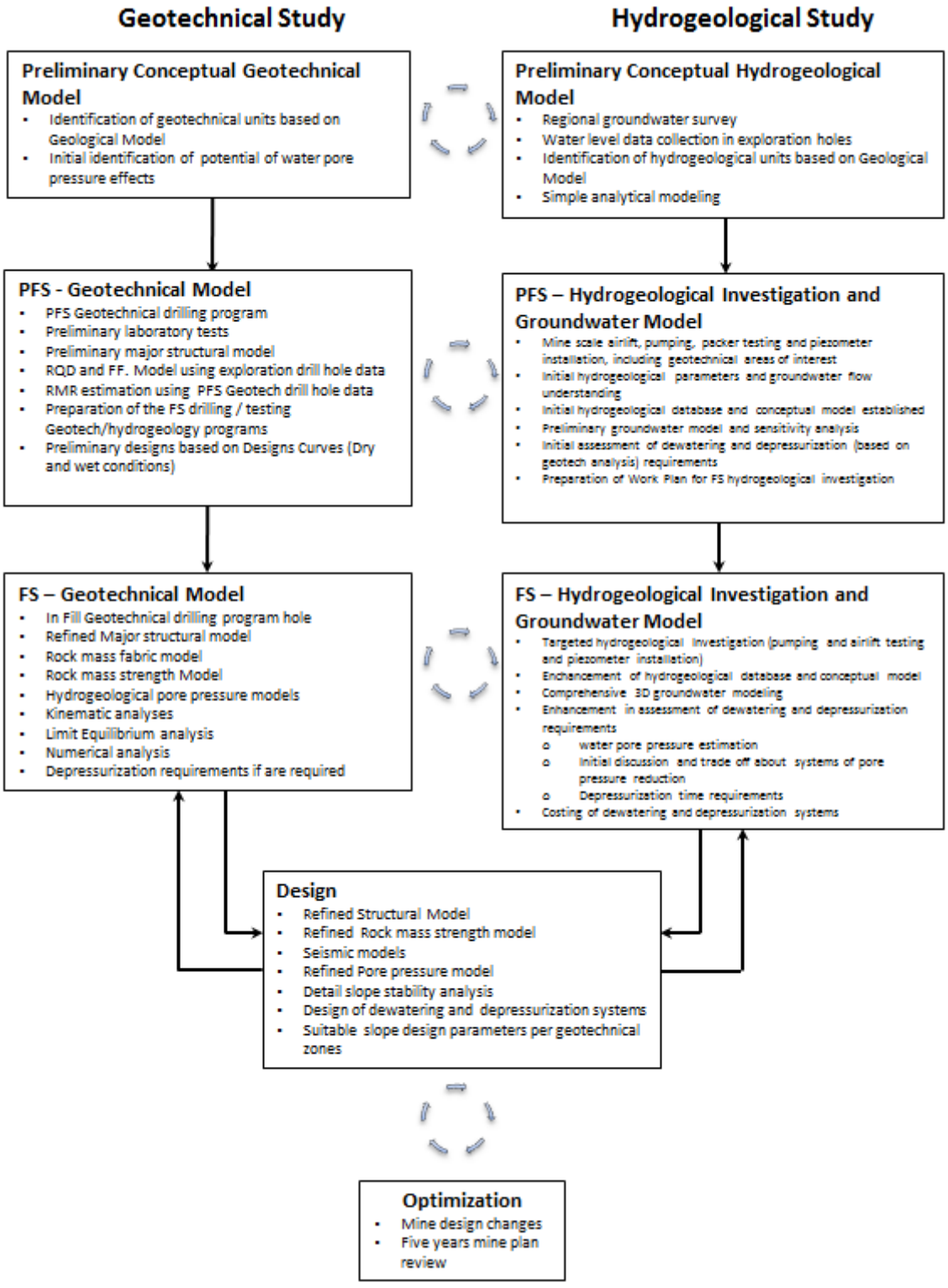

Figure 7. Integration of geotechnical and hydrogeological studies during different stages of the project (PFS: Prefeasibility Study, FS: Feasibility Study)

- Is the time required for depressurization in alignment with the mine plan and life of the mine?
- Is the knowledge regarding the hydraulic parameters sufficient for constructing a detail model to simulate the depressurization requirements?
- Does the mine plan have the flexibility to develop a proper depressurization plan?
- What depressurization method is the best for site specific hydrogeological conditions?
- What is the cost-benefit of implementation of pit slope depressurization?

These questions must be addressed in detail before moving forward to more detailed engineering.

Slope engineering is a common effort between different disciplines, and the understanding of each of the disciplines is critical in determining the final results. Also, the design process should be considered as an iterative process, where the integration between Geotech - Hydrogeology and Mine plan areas is a key in the mining cycle

REFERENCES

Das, Braja (2011). *Principles of Foundation Engineering*. Stamford, CT: Cengage Learning. ISBN 9780495668107.

Guidelines For Evaluation Of Water In Pit Slope Stability/edited by John Read and Geoff Beale, CSIRO, 2013.

Read J and Stacey P (Eds) (2009) *Guidelines for Open Pit Slope Design*. CSIRO Publishing, Melbourne.

Prediction of Open Pit Mine Slope Variation Based on Geo-Mechanical Uncertainty using Artificial Neural Network (ANN)

A.R. Kamrani, M. Osanloo, M.Minaei Mobtaker
Amirkabir University of Technology, Tehran, Iran

ABSTRACT This paper develops a model to predict open pit's slope under uncertainty condition using artificial neural network (ANN) and the defect of probabilities method is solved. Due to high cost for data collection and lack of sufficient and accurate data for ANN training, conditional random simulation is used for generating random geomechanical parameters data. Then for each group of random numbers, the stable slope angle is calculated based on specified factor of safety (FOS). In final stage, using artificial neural network, stable slope angle based on variety of geomechanical parameters is predicted. This method was applied to collected data from the great wall of Sungun copper mine in Iran. The outputs of ANN i.e. the stable slope angles, demonstrate that cohesion and internal friction angle are the most sensitive parameters respectively. It also shown that change in unit weight do not change the stable slope more than 1 degree. These results which was obtained from ANN fitted on what's conventional methods proof, completely.

Keywords: Artificial neural network, open pit slope, geomechanical uncertanity

1 INTRODUCTION

Open pit mine slope is one of the major parameter which influence on determination of ultimate pit limit. Nowadays due to metal's price increment and mineral consumption, depth of open pit mine is going to increase. On the other side, slope instability is a reason of several problems in open pit mining. Cost imposing, losing whole or some part of available ore, human safety problems and losing whole or some equipment and facilities may be forced mine to close prematurely. Consuming time to separate ore from waste and repairing the roads is another consequence of slope failure. These situations lead to additional dangerous and risk for open pit mine slope determination. So the outcome of slope failure like the huge mass of rock fall from high altitude similar to what's happen for Palabora (2003) and Bingham Canyon (2013) mines, can be divided into three principal issues: social/safety, economic and environment (Read & Stacy, 2009). Regarding to mentioned factors, studying on stable slope in open pit mines is important even during exploitation stage.

Rock's geomechanical uncertainties exist as a comprehensive system with all physical and mechanical properties changes in a non-fixed manner and dynamic process, during the project's life time (Ghanem & Spanos, 2003). In fact being randomness and uncertainty in the rock mass properties are the most important factors which affect reliability of safety factor (Peng & Jian, 2011). With respect to high sensitivity of stable slopes to geomechanical parameters, uncertainty play major role in pit slope design. Geomechanical uncertainties come from three sources: (1) lack of sufficient number of samples, (2) error on calculation of rock mass properties and (3) in most of the cases the laboratory measurement of rock property has no consistency with rock insitu condition. By decreasing 20% in strength parameters of rock mass, failure probability grows 8.4 times more than previous mode (Dianqing et al. 2011).

Pit slope influence on stripping ratio (waste/ore) and on quality of mineable reserve. Depend upon on types of ore, hanging wall and footwall material, open pit slope is ranged between 30 up to 55 degrees.

Highest pit slope will cause lower W/O and more mineable reserve exploitation. But it must be stable according to uncertainty and unreliability of the strength and mechanical rock or soil parameters. There is also some correspondence between the steepest and highest stable slopes for both natural and man-made slopes (Wyllie & Mah, 2005). In other words one of the important parameter on slope stability is height of wall or depth of mine. There are several methods have been developed during last decades to estimate pit stable slope. Probabilistic method is one way to design stable slope without uncertainty and overcome this difficulty.

Tobutt (1982) uses Monte Carlo simulation to calculate the probability of failure and Bishop simplified formula used to determine the most critical slip circle. He proposed using this method rather than conventional method for probability calculation. From that time, many researches have been carried out with Monte Carlo simulation and the stability of slopes were analyzed in probabilistic method (Griffiths & Fenton, 2004; El-Ramly & Morgenstern & Cruden, 2005; Xu & Low, 2006; Afrapoli & Osanloo, 2014). But the main disadvantage of this method is how the probabilities will change with variation of input parameters. If the system is changed, the procedure must be repeated in order to determine the effect on response statistics and probabilities (Fenton & Griffith, 2008). For that reason ANN has been applied to satisfy the need for stable slope predictability.

Application of artificial neural network (ANN) in rock mechanic as a pattern recognition or non-linear function prediction with quantity or quality parameters are vast. As an example Erzin & Cetin (2013) predicted the critical FOS for a limited slope with multiple-regression and ANN. They show that ANN have more accurate results compared to multiple-regression. Also ANN was used in probability slope stability analysis conjugated with Monte Carlo simulation (Sung, 2009). Creating qualitative index for open pit mine slope instability based on fully coupled model and various case studies from all around the world is presented by Naghadehi, et al. (2013). The author uses ANN in order to find out the relation between each couple.

2 METHODOLOGY

Figure 1 shows the algorithm of the developed model.

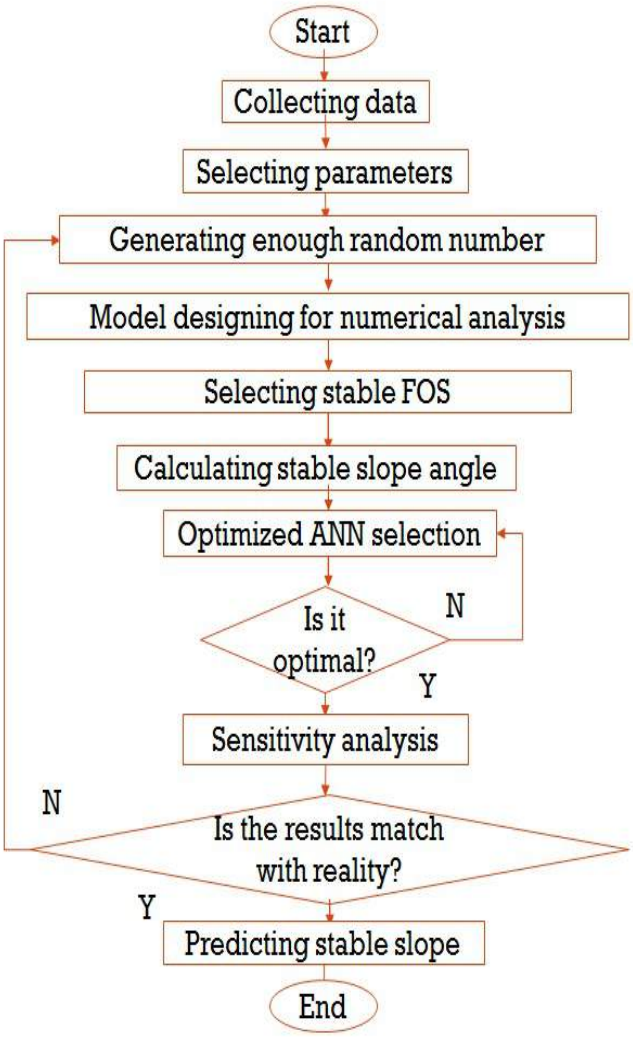

Figure 1. Algorithm of the proposed model

2.1 FOS Calculation

The first effort to provide a stable slope is measurement of resistance and disturbance forces and calculating FOS. There are several methods for FOS calculation such as limit equilibrium method or failure surface determination like Janbu and Bishop Methods or strength reduction method (SRM) which is used by numerical analysis software (e.g. FLAC, 3DEC, PHASE2). Despite of these discrepancies between methods, the logic which governing them is same: if the resisting and disturbing forces is

equal, the FOS will be 1. In this case, slope is in the state of slip and reduction in slope angle or stabilization is needed till FOS gets bigger than 1. However the amount of this growth is the biggest challenge and it depends on risk acceptance of decision makers and depth accessibility. In comparison with all FOS determination methods, Hoek suggested the SRM. Because it includes all benefits of limit equilibrium analysis and it allows the user to study slope displacements that are critical in the evaluation of open pit stability (Hoek, 2009).

The basic concept of strength reduction method (SRM) is:

1- The strength parameters of a slope are reduced by a certain factor (SRF), and the finite element/finite difference stress analysis is computed.
2- This process is repeated for different values of SRF, until the model becomes unstable (the analysis result do not coverage).
3- This determines the critical strength reduction factor (critical SRF) or safety factor of the slope (Rocscience Inc, 2010).

FLAC uses the SRM and the FOS is calculated according to 1, 2 and 3 equations:

$$C^{trial} = \frac{1}{F^{trial}} C \quad (1)$$

$$\varphi^{trial} = arc\ tan(\frac{1}{F^{trial}}\ tan\varphi) \quad (2)$$

$$\sigma_t^{trial} = \frac{1}{F^{trial}}\ \sigma_t \quad (3)$$

Which:

C is cohesion (MPa)

φ is friction angle (degree)

σ_t which is tensile strength (MPa)

By reducing C, φ and σ_t and using trial values of F_s^{trial} continuously, failure occurs. If the slope is initially unstable, C, φ and σ_t will be increased until the limiting condition is found. Note that using σ_t relation is optional, but in this study is considered.

As mentioned before, FOS is an uncertain parameter itself and this study focuses on uncertainty of geomechanical parameters so an appropriate amount of FOS should be selected and the stable slope angle evaluated.

2.2 Artificial Neural Networks

A typical structure of ANNs consists of a number of processing elements, or neuron, that are usually arranged in layers: an input layer, an output layer and one or more hidden layers (Figure 2).

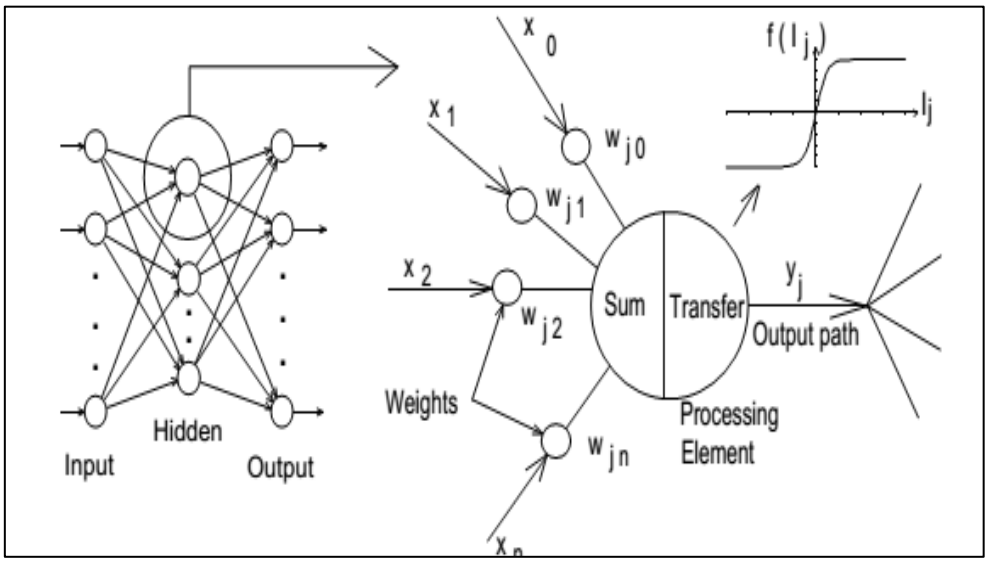

Figure 2. A typical ANN structure (Shahin, et al., 2001)

The input from each neuron in the previous layer (x_i) is multiplied by an adjustable connection weight (w_{ji}). At each neuron, the weighted input signals are summed and a threshold value which is called bias (B_j) is added. This combined input (I_j) is then passed through a non-linear

transfer function (f (.)) to produce the output of the neuron (y_j).

The output of one neuron provides the input to the neurons in the next layer. This process is summarized in Equations 4 and 5 and illustrated in Figure 2 (Shahin, et al., 2001).

$$I_j = \sum w_{ij}\, x_i + B_j \quad (4)$$

$$y_j = f(I_j) \quad (5)$$

The number of required data for ANN training should be far enough. Providing adequate data needs having enough case analysis. Otherwise to provide data, generating random numbers considering its statistical distribution will be used.

3 CASE STUDY

Sungun copper mine locates in northwest Azerbaijan province of Iran. The mine is near to the boundary of Azerbaijan and Armenia as shown in figure 3. Sungun copper mine is one of the biggest open pit mines in Iran. The history of exploitation in Sungun back to 200 years ago. Old evidence across the Sungun River shows that underground mining method was used for ore extraction.

Figure 3. Sungun copper mine location

One of the critical pit wall of Sungun copper mine is wall RS03 which is located in southwest of mine and its height is 700 meter. This wall is the biggest mine wall in Iran which is used as case study in this paper. Figure 4 shows the location of this wall in Sungun copper mine.

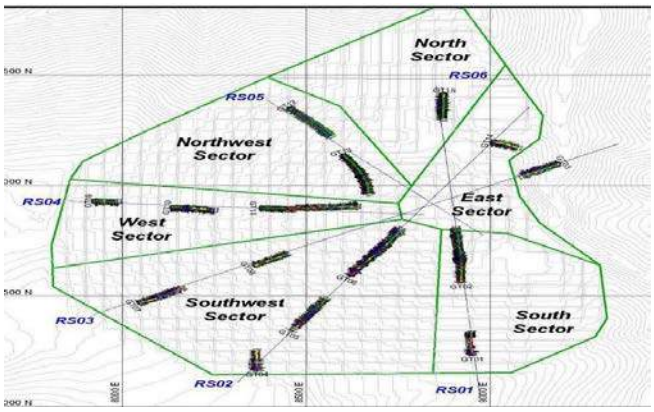

Figure 4. Location of RS03 in Sungun copper mine of Iran

4 MODEL APPLICATION

The RS03 pit wall of Sungun open pit mine was selected for application of the model. Table 1 shows the five geomechanical parameters that were tested, and their mean and standard deviation. According to the latest studies, the selected slope angle for this wall is 30 degrees and its FOS is 1.3 (srk consulting, 2008). The slope is stable only when drainage is performed.

Table 1. Mean and standard deviation of Sungun geomechanical parameters

	σ_t (MPa)	E (MPa)	phi	C (KPa)	Unit Weight (KN/m^3)
Mean	0.039	3061.167	36.285	662.142	24.466
Standard deviation	0.053	3790.032	12.592	320.790	2.059

Figure 5 shows the model which is designed by FLAC3D 5.0. Point A display where slope angle changes till the FOS of 1.3 is achieved.

In case of ANN training due to lack of experimental information, 00 group of parameters were generated randomly and for this operation conditional simulation was used.

A random field which takes on certain known values at specific points in the field is

called a conditional random field $Z_c(x)$. It takes on specific values $Z(x_a)$ at the measurement locations x_a, a = 1,2,…,n_k, where n_k is the number of measurement locations. Mathematically,

$$Z_c(x) = \{Z(x) \mid Z(x_a), a = 1,2,\ldots,n_k\}$$

To accomplish the conditional simulation, the random field will be separated into two parts spatially: (1) x_a , a = 1, 2, …, n_k, being those points at which measurements have been taken, and at which the random field takes on deterministic values $Z(x_a)$, and (2) x_η, η = 1,2,…, N-n_k , being those points at which we wish to simulate realization of their possible random values. The conditional random field is simply formed from three components in equation 6:

$$Z_c(x) = Z_u(x) + [Z_k(x) - Z_s(x)] \quad (6)$$

$Z_c(x)$ = desired conditional simulation
$Z_u(x)$ = unconditional simulation
$Z_k(x)$ = best linear unbiased estimate of field based on known (measured) values at x_a
$Z_s(x)$ = best linear unbiased estimate of field based on unconditional simulation values at x_a (Fenton & Griffith, 2008).

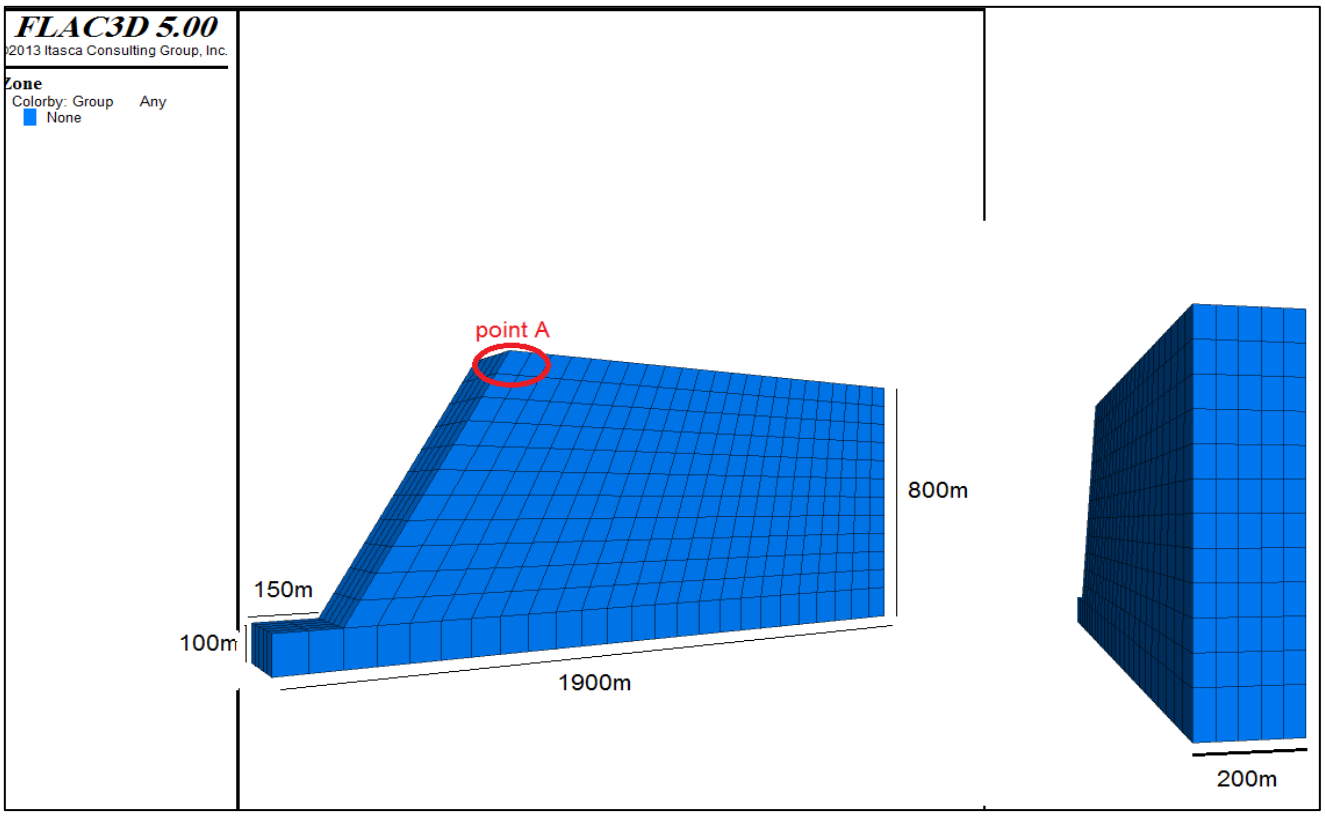

Figure 5. Slope model in FLAC

4.1 **ANN** optimization

Selection of the suitable type of network from a variety of neural networks is the first step for using ANN. Determining the application of neural networks in the problem, can be solution of this option. Back propagation error networks is capable of approximating any function with limited discontinuity points. The next step is selecting training method. Here to prevent the occurrence of over-fitting due to the low numbers of data, Bayesian framework method was used.

Bayesian framework has a simple concept. The typical performance function used for training feed forward neural networks is the Figure 6. Comparison between ANN predicted angle and FLAC calculated angle mean sum of squares of the network errors that is obtained from equation 7.

$$F = mse = \frac{1}{N}\sum_{i=1}^{N}(e_i)^2 = \frac{1}{N}\sum_{i=1}^{N}(t_i - a_i)^2 \quad (7)$$

Where **F** is error function, **mse** is sum of mean square error, **N** is the number of samples, **t** is the target value and **a** is obtained value.

It is possible to improve generalization if the performance function is modified by adding a term that consists of the mean of the sum of squares of the network weights and biases. Equation 8 shows this relation:

$$msereg = \gamma mse + (1-\gamma)msw \quad (8)$$

Where: **msereg** is modified performance function, γ is the performance ratio and **msw** is sum of mean square weights and its formulation is equation 9.

$$msw = \frac{1}{n}\sum_{j=1}^{n} w_j^2 \quad (9)$$

Where: **n** is total samples and **w** is the weight of each sample.

Bayesian framework assigns random values for the modified performance function (msereg) to find a more accurate weights and biases for the network and optimize it more efficiency.

Using this performance function causes the network to have smaller weights and biases, and this forces the network response to be smoother and less likely to over fit.

Transfer function and number of hidden layer and neurons should be selected in a way that optimized network obtained. Many researchers believe that these values can be catch only with trial and error (Zhou & Wu, 1994; Sung, 2009; Erzin & Cetin, 2013). The efficient amount of hidden layer is ranged between 2 or 3 (Zhou & Wu, 1994). So a program was written that determine the best network. Table 2 shows the optimized network which was calculated by the program. Also figure 6 shows the comparison between ANN predicted angle and FLAC calculated angle.

Table 2. The optimized ANN parameters

No.layer	**1**	**2**	**3**	**4**	**Output layer**
No.neuron	8	14	18	19	-
Transfer function	logsig	logsig	logsig	logsig	tansig

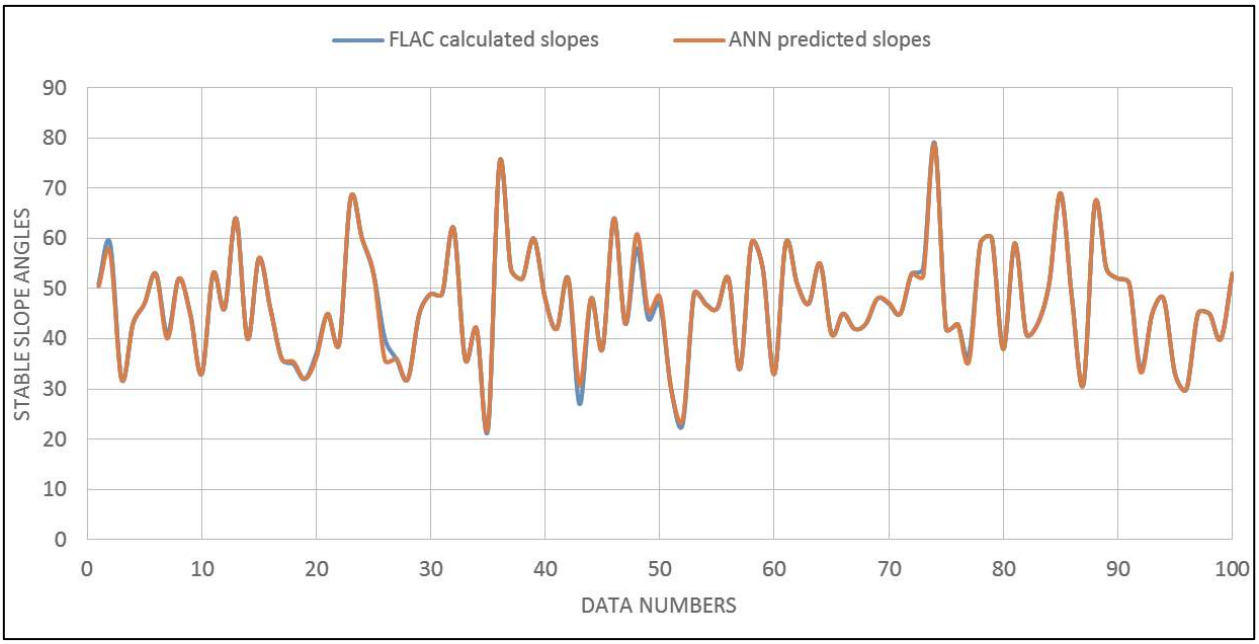

Figure 6. Comparison between ANN predicted angle and FLAC calculated angle

4.2 Sensitivity Analysis of Parameters

For training network in Bayesian framework the inputs and outputs data converted into [-1,1] range. The error of optimized network became 0.000632838. A sensitivity analysis was executed on geomechanical parameters of Dyke 1A (DK1A) lithology. With changing in parameters the predicted stable slope of different properties is compared with each other to find the most effective parameter. Table 3 shows the properties of

DK1A which was used for sensitivity analysis.

In this sensitivity analysis some of the parameters doubled (e.g. E,σ_t,C) and for some others the maximum amount were placed (e.g. φ, ρ). Table 4 shows the results of this sensitivity analysis.

Table 3. Geomechanical parameters of DK1A lithology

Lithology	E_m (MPa)	σ_t (MPa)	Phi (φ)	C (KPa)	Unit Weight (ρ) (MN/m^3)	UCS mean (MPa)
DK1A	854	0.006	34	572	0.024	50

Table 4. Sensitivity analysis results

	DK1A parameters	High unit weight	Double bulk and shear modulus	Double cohesion	High friction angle	Double tensile strength
unit weight (Kg/m^3)	2400	2640	2400	2400	2400	2400
Bulk modulus (MPa)	711.67	711.67	1423.33	711.67	711.67	711.67
shear modulus (MPa)	328.46	328.46	656.92	328.46	328.46	328.46
Cohesion (KPa)	572	572	572	1144	572	572
Internal friction angle	34	34	34	34	58	34
Tensile strength (MPa)	0.006	0.006	0.006	0.006	0.006	0.012
Slope angle (degree)	33.59	31.96	34.62	46.21	56.35	34.62

5 CONCLUSION

The objective of this study is to develop a model that uses ANN to predict stable slope and overcome to uncertainty of geomechanical parameters. Accordingly FOS calculation based on SRM was described and for compensation of lack of data in the model application, conditional simulation was used. About the ANN optimization some technique like Bayesian framework was applied. Then geomechanical parameters as an input and stable slope angles as an output were trained to an optimized ANN. The following results were obtained from sensitivity analysis

- The cohesion and friction angle (C, φ) have the greatest effect.
- The tensile strength has the lowest effect but it can't be ignore at all.
- The negative impact of unit weight with respect to height of wall was not significant and can be neglected.

Agreement of sensitivity analysis with facts shows that ANN training process performed successfully. It also indicates that the network estimates function very well. The uncertainty problem is solved with prediction capability of neural network respectively. So with the new data will be treated in two ways: 1st, the stable slope is predicted. 2nd, the new data retrain to the network to provide the network with greater precision.

REFERENCES

Afrapoli, A. M., Osanloo, M., (2014), "*Determination and stability analysis of ultimate open-pit slope under geomechanical uncertainty*", International Journal of Mining Science and Technology, 24, Elsevier, pp. 105-110.

Dianqing Li, et al, (2011), "*Stochastic response surface method for reliability analysis of rock slopes involving correlated non-normalvariables"*, Computer and Geotechnics, vol.38, No. 1, pp. 58-68.

El-Ramly H, Morgenstern NR, Cruden DM., (2005), *"Probabilistic assessment of stability of a cut slope in residual soil"*, Geotechnique ;55(1):77–84.

Erzin, Y., Cetin, T., (2013), *"The prediction of the critical factor of safety of homogeneous finite slopes using neural networks and multiple regressions"*, Computers & Geosciences, Elsevier, 51, pp. 305-313.

Fenton, G. A., Griffith, D. V., (2008), *"Risk Assessment in Geotechnical Engineering"*, John Wiley & Sons. Inc, pp. 203-238.

Ghanem, R. G., Spanos, P. D., (2003), "*Stochastic Finite Element: a Spectral Approach*", Dover Publication, New York, USA, p. 371.

Griffiths DV, Fenton GA., (2004), " *Probabilistic slope stability analysis by finite Elements"*. J Geotech Geoenviron Eng; 130(5):507–18.

Hoek, E., (2009), *"Fundamentals of Slope Design"*, Slope Stability, Santiago, Chile, pp.1-26.

Naghadehi, M. Z., et al, (2013), *"A new open-pit mine slope instability index defined using the improved rock engineering systems approach"*, International Journal of Rock Mechanics & Mining Sciences, Elsevier, 61, pp. 1-14.

Peng, W. B., Jian, Y. W., (2011), "*Rock Engineering Property of the High-Steep Open-pit Slope and its Stability"*, Journal of coal science & Engineering, Vol.16, No.1, pp. 35-40.

Read, J., Stacy, P., (2011),*"Guidelines for Open Pit Slope Design"*, CSIRO Publishing, pp. 2-20.

Rocscience Inc, (2010), Phase2 V7.0 – A two – dimensional finite element analysis program, User's Tutorials.

Shahin, M. A., et al., (2001), *"Artificial Neural Network Applicatins In Geotechnical Engineering"*, Australian Geomechanics, pp. 49-62.

srk consulting, (December 2008), "*Sungun copper project mining geotechnics and slope design studies"*, technical report.

Sung, E. C., (2009), *"Probabilistic stability analyses of slopes using the ANN-based response surface"*, Computers and Geotechnics, Elsevier, 36, pp. 787-797.

Tobutt, D. C., (1982), *"Monte Carlo simulation methods for slope stability"*, Computers & Geosciences, vol. 8, No. 2, pp. 199-208.

Wyllie, D. C., & Mah, C. W., (2005), *"Rock Slope Engineering Civil and Mining"*, Taylor & Francis Group, 4th Edition, page 4.

Xu B, Low BK., *"Probabilistic stability analyses of embankments based on finite element method"*, J Geotech Geoenviron Eng, vol. 132(11), pp. 1444–*14*54

Zhou, Y., Wu, X., (1994), "Use of neural networks in the analysis and interpretation of site investigation Data", Computers and Geotechnics, 16, pp. 105-122.

Stability Analysis and Optimized Slope Angle for the Iron Ore Open-Pit Mine

Demir Cevheri Açık Ocağı için Stabilite Analizi ve Optimize Edilen Ocak Eğim Açısı

S. Akdag, H. Basarir, C. Karpuz
Middle East Technical University, Department of Mining Engineering, Ankara

M. Ozyurt
Bilfer Mining Inc., Ankara

ABSTRACT With an increase in the overall slope height of open pit mines, stability analysis and amount of stripping waste rock becomes progressively difficult. It is necessary to optimize the overall slope angle by increasing it as much as possible with ensuring the mining safety. After comprehensive geotechnical investigation and rock mechanical laboratory tests, the combined use of limit equilibrium and numerical modeling analysis methods increases reliability and accuracy of the stability analysis. With the optimum slope design in Bizmişen iron ore mine, there will be a significant decrease in production cost and in the amount of stripping.

Keywords: Open-pit mining, rock slope stability, overall slope angle, limit equilibrium method, numerical modeling, factor of safety

ÖZET Açık ocaklarda genel ocak derinliğinin artması, stabilite analizlerini ve pasa miktarını artan bir biçimde zorlaştırmaktadır. Madencilik güvenliğini sağlayarak, genel ocak eğim açısını mümkün olduğunca büyük tutmak optimum ocak açısı tasarımı için gereklidir. Jeoteknik incelemeler ve kaya mekaniği laboratuvar testleri sonrasında, limit denge ve numerik modelleme analiz yöntemlerinin birleşik kullanımı duraylılık analizinin güvenilirliğini ve doğruluğunu arttırır. İdeal şev tasarımı ile Bizmişen demir ocağında, üretim maliyetini ve dekapaj miktarını önemli bir derecede azaltacaktır.

Anahtar kelimeler: Açık ocak madenciliği, kaya şev stabilitesi, genel ocak eğim açısı, limit denge yöntemi, numerik modelleme, güvenlik katsayısı

1 INTRODUCTION

Huge amount of minerals are exploited from the ground by open pit mining activities. With an increase in mining operations, the depth of open pit mines are getting deeper so that pit slope stability has become significant for long term sustainability. Since mining excavations are getting more difficult due to higher slope angle, stability and safety evaluations are essentially considered from the economic point of view. However, increasing overall slope angle as steep as possible is a crucial way to minimize the amount of stripped waste rock and reduce the production cost providing that the mining operations are carried out under safe conditions. Therefore, it is necessary to make optimum slope angle design for deep open pit mines. The height of final slope of a planned iron ore mine in Bizmişen region reaches its peak value of 400 m at the deepest side. The mine will be one of the deepest open pit mines in Turkey. For a large scale open pit mine which is case in point,

increasing the overall slope angle by 1° will reduce approximately 3 million m^3 of waste rock and results an economic benefit around 10 million American dollars. Hence, slope design is supposed to be optimized by increasing the economic efficiency without endangering safety conditions.

2 GEOTECHNICAL SITE CHARACTERIZATION

In the present work, overall slope angle optimization studies were carried out for the intended Bizmişen open pit mines, situates in the Eastern Turkey. To determine quality of the rock mass, geotechnical site survey around the region and geotechnical borehole core logging were conducted. Additionally, in order to determine the physico-mechanical properties of the rock materials with the help of laboratory tests, core samples from the logged drill holes and rock blocks were taken directly from the mine site.

2.1 Geotechnical Survey

In the region, according to the reserve estimation studies, multiple open pit requirement is decided to extract the orebody. Thus, field geological investigations for each planned open pits were carried out and some technical visits were conducted. Slope faces in which prior and present mining activities carried out were investigated to determine the rock mass characteristics around the site. During investigations, geological strength index (GSI) values were assigned for the dominating rock masses. The rock mass properties required for numerical analysis were assigned as suggested by Hoek *et al.* (2005).

Besides field investigations, geotechnical logging was performed with representative drillholes. To increase the accuracy and reliability as much logging study as possible was carried out and plenty of samples were taken for laboratory experiments. To designate the rock mass quality, Rock mass rating (RMR) proposed by Bieniawski (1989) and Q-system proposed by Barton *et al*., (1974) values for all dominating lithology around the region were also determined as a result of geotechnical logging. The average RMR and Q values for footwall, ore and hangingwall are presented in Table 1.

With the combined work of field observations and geotechnical logging, rock mass properties and rock quality characterization were constituted for Bizmişen region prior to stability analysis and optimization of slope angle. Regarding the characteristics of dominating rock formations, the assigned average GSI values for footwall, ore and hanging wall are given in Table 1.

Table 1. Assigned average RMR, Q and GSI values.

	RMR	**Q**	**GSI**
Footwall	60	4.28	57
Ore	55	3.22	55
Hanging wall	48	2.57	48

Additionally, since the hydrologic studies assist to gain a general comprehension of regional groundwater trends, during the technical investigations around the mine sites, hydrologic information was obtained and implemented into numerical modeling.

2.2 Laboratory Studies

For stability analysis of the slope and optimum design of the slope angle, comprehensive laboratory tests with 426 rock specimens taken from the cored exploration drillings were carried out. Based on the laboratory experiment results, rock material properties were determined. Unit weight (γ), Poisson's ratio (ν), Young's modulus (E), indirect tensile strength (σ_t), uniaxial compressive strength (σ_c), and mi constants were obtained by means of conducting the related laboratory work and the results are shown in Table 2.

Table 2. Rock material properties of slope rock masses dominating in the region

Lithology	γ (kN/m^3)	ν	E (GPa)	σ_t (MPa)	σ_c (MPa)	m_i
Footwall	26.90	0.08	36.05	13.19	123.9	37
Ore	39.48	0.10	26.68	14.30	58.3	27
Hanging wall	25.00	0.14	7.81	3.46	17.1	10

3 ROCK MASS PROPERTIES AND MODELING METHODOLOGY

Since the mine slope presents a closed-oval shape and its range is very large, the ultimate slope depth differs due to topography. The most appropriate way to carry out stability analysis is to choose the critical section including the deepest level of the open pit mine. For convenient and reliable optimum design of the slope, critical cross-section is schemed with respect to 7 various overall slope angle, between 36° and 42°.

To carry out stability analysis by using the Mohr-Coulomb failure criterion, design input parameters such as cohesion (c) and internal friction angle (Ø) were calculated as suggested by Hoek et al., (2002). Since harsh climate conditions and atmospheric actions around the region may lead to occur alteration for the shallower slopes, rock mass quality characterization was adjusted with respect to the mining depth. According to the laboratory experiment results and geotechnical site characterization studies, equivalent cohesion and friction angle (Hoek *et al*., 2002) for the hanging wall in which slope would be constructed are determined as 715 kPa and 19.6° respectively.

4 STABILITY ANALYSIS AND OPTIMUM DESIGN OF THE SLOPE

Different options are available to investigate the slope stability analysis. Limit equilibrium method is a conventional approach, it can provide information about the potential for slope failure. Numerical modeling is another one, it may assist further analysis of a more complex mechanism. Optimum design can be achieved with the combined use of limit equilibrium method and numerical modeling.

4.1 Stability Analysis by Limit Equilibrium Method

The traditional limit equilibrium method depends upon the force and moment equilibrium method. Factor of safety (FOS) value, a ratio of resisting forces to driving forces, can be determined by means of this method. As a principle, a possible failure surface is assumed and the rock mass above the surface is considered as a free body. The critical factor of safety is determined by ensuring that the rock mass can maintain the stability on the assumed possible failure surface (Read and Stacey, 2010). Although, the method provides a fast computation time, the application of the method is greatly restricted since it cannot analyze the indication of instability mechanism. Determination of displacement or deformation is not possible due to not taking into consideration the in-situ stress-state.

Several approaches based on method of slices were proposed by some researchers for limit equilibrium method. Spencer (1967), simplified Bishop (1955), and GLE/Morgenstern-Price (1965) are the most widely used techniques for stability analysis and optimum design of the slope.

Computation results of the stability analysis of optimized slope angles made by Slide v6.0 (2014) are shown in Table 3. Based on the safety requirement of the engineering, the minimum value of factor of safety is considered as 1.2 (Hoek and Bray, 1981).

It can be seen from Table 3, the factor of safety decreases as the overall slope angle increases. The results obtained using different techniques are close to each other and range from 1.106 to 1.283 depending on

the overall slope angle. As mentioned above the required FOS value is considered as 1.2 and it can only be obtained for overall slope angle of 36°.

Table 3. Factor of safety (FOS) computation results by limit equilibrium analysis for critical section with various overall slope angle

Overall slope angle	GLE/Morgenstern-Price	Bishop	Spencer
33	1.278	1.283	1.281
33	1.257	1.261	1.259
34	1.233	1.236	1.235
35	1.217	1.219	1.218
36	1.202	1.204	1.204
37	1.193	1.196	1.193
38	1.168	1.173	1.169
39	1.152	1.156	1.152
40	1.135	1.138	1.135
41	1.120	1.124	1.118
42	1.106	1.111	1.108

The relationship between factor of safety, overall slope angle and the approximate amount of stripping is given in Figure 1. The minimum suggested FOS value 1.2 is only obtained for overall slope angle of 36° or lower. On the other hand as the overall slope angle decreases, the amount of stripping material increases. Therefore for safe working conditions with minimum stripping 36° seems to be optimum overall slope angle for the Dönentaş open pit mine in Bizmişen region.

4.2 Stability Analysis by Numerical Modeling

Although limit equilibrium methods of analysis such as the method of slices are simple to use, the assessment of displacement or the development of failure surface are not possible. By considering the slopes composed of formations having complex material properties, limit equilibrium method can be found insufficient

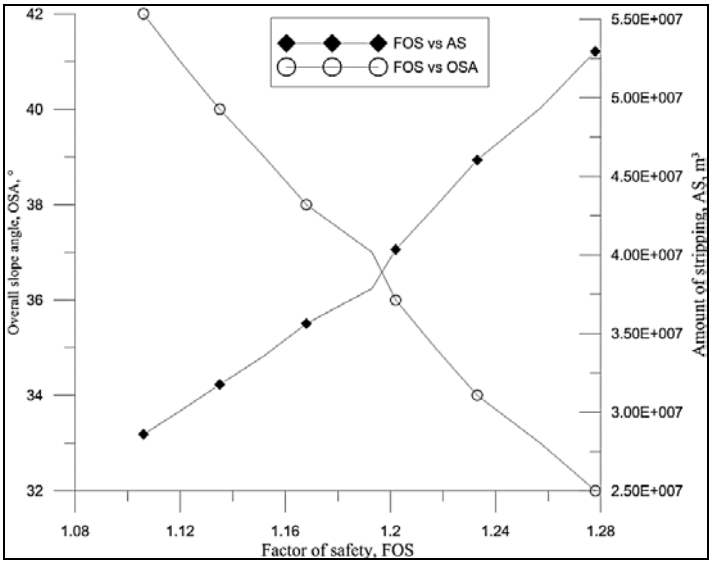

Figure 1. Overall slope angle factor of safety and amount of stripping relations.

For models with geological complexity, numerical modeling provides an insight by using the theoretical system of stress-strain relations considering the actual conditions. In order to estimate the shape of failure surface and the corresponding stability coefficient of the rock mass strength reduction method is mostly used. Strength reduction factor (SRF), which is equal or slightly less than FOS, is determined by reducing the cohesion and friction angle gradually when the non-convergence of nonlinear finite element appears, the slope is considered as unstable state and the reduction factor is determined (Zienkiewicz *et al.*, 1975). Moreover, since failure surface does not need to be assumed, the distribution of stress and deformation which has a significant influence on the initiation and growth of the failure surface can be obtained by using this method.

According to the preliminary analysis by limit equilibrium method, the ultimate slope angle is considered as 36° which meets the production requirements. Numerical modeling is carried out only for this plan, the progress of which is shown in Figure 2.

From Figure 2, it can be seen that failure surface is created automatically with the strength reduction method with respect to the stress-strain relation by using the Phase2 v9.0 (2014).

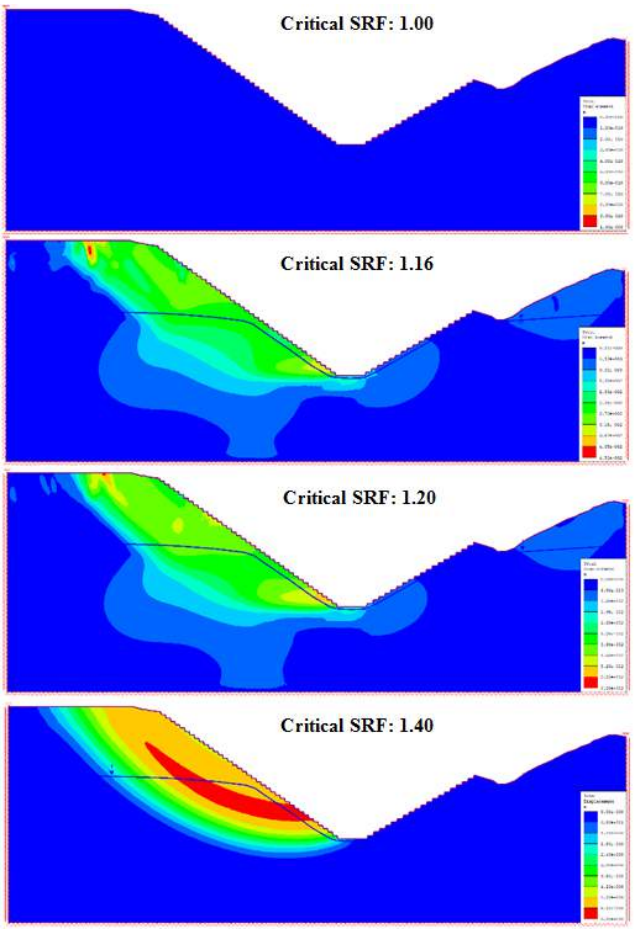

Figure 2. Progress of strength reduction method showing the SRF and related displacements.

Based on the numerical modeling computation results, strength reduction factor is determined as 1.20 with a maximum displacement of 0.287 m for the critical section. Moreover, the critical failure surface is developed with respect to the shear strain localization. Figure 3 illustrates the shear strain condition at the critical SRF and shows the plot of maximum displacement corresponding SRF.

The SSR solution procedure using model convergence as an indicator of slope stability is given in Figure 3. As the strength decreases the maximum displacement increases, at a certain point slope fails and analysis does not converge, displacement increases rapidly. The SSR value at the point is called as critical SRF.

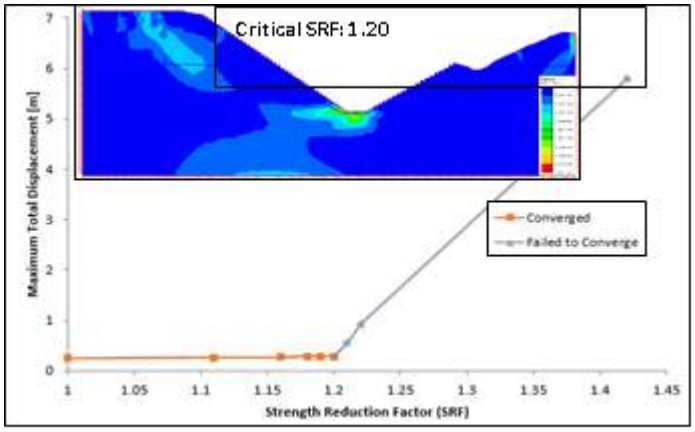

Figure 3. Maximum shear strain condition at SRF and plot of total displacement corresponding SRF

The obtained both SRF and FOS values are consistent with each other and higher than 1.2 and the result obtained from numerical modeling are coherent with the limit equilibrium results.

5 CONCLUSION

This paper presents a general description of studies conducted for stability analysis and optimum design of the open pit slope. For deep open pit mines making the overall slope angle as steep as possible can reduce the amount of stripped waste rock and diminishes the production cost under a prerequisite safety conditions.

An iron ore open pit mine in Bizmisen region, Erzincan intended to be 400 m final slope height, is the case in point for the geotechnical optimization attempt. Within this purpose, geotechnical site characterization and comprehensive laboratory studies were conducted. Rock mass and material properties were determined for stability analysis. The FOS and SRF values obtained from the limit equilibrium method and numerical modeling are higher than 1.2. This study shows that combined use of limit equilibrium and numerical modeling analysis techniques is an effective and practical way to optimize the overall slope angle by increasing the reliability and accuracy. With the optimum design, the slope angle of the iron ore mine with 400 m final slope height is proposed to

be adjusted to 36° satisfying both safety conditions and economic considerations.

ACKNOWLEDGEMENT

The authors would like to thank the staff of BİLFER Mining Inc. for their valuable supports. The company is also acknowledged for the permission to use and publish the data.

REFERENCES

Barton, N. R., Lien, R., and Lunde, J. (1974). Engineering classificiation of rock masses for the design of tunnel support. *Rock Mechanics, 6*(4), 189-239.

Bieniawski, Z. (1989). *Engineering rock mass classifications.* New York: Wiley.

Hoek, E. and Bray, J. W. (1981). *Rock Slope Engineering.* London: The Institute of Mining and Metallurgy.

Hoek, E., Carranza, T. C., and Corcum, B. (2002). Hoek-Brown criterion-2002 edition. *NARMS-TAC conference,* (pp. 267-273). Toronto.

Hoek, E., Marinos, P., and Marinos, V. (2005). The geological strength index:applications and limitations. *Bulletin of Engineering Geology and the Environment, 64*, 55-65.

Phase2 v9.0 (2014), © Rocscience Inc., Toronto, Canada.

Read, J. and Stacey, P. (2010). *Guidelines for open pit slope design.* Australia: CRS Press.

Slide v6.0 (2014), © Rocscience Inc., Toronto, Canada.

Zienkiewicz, O. C., Humpheson, C., and Lewis, R. W. (1975). Associated and non-associated visco-plasticity and plasticity in soil mechanics. *Geotechnique,* 671-689.

Study of The Bench Slope Stability By Numerical Method, Case of Ouenza Mine Algeria

R.Adil, M.L.Boukelloul
Laboratory of Mineral Resource Development and Environment -LAVAMINE- BadjiMokhtar University-Annaba

K. Talh
Laboratory of Metallurgy, Materials and Physical Properties- BadjiMokhtar University-Annaba

ABSTRACT Mine slope stability remains a key issue that arises when operating open pit deposits. Slope stability has a direct influence on work safety in the mine, technological operating principles, the total depth of mine drainage problems, etc.

Too high slope angles can lead to destabilization, landslides development and flows over the edges of the mine. These accidents cause a lot of damage to businesses and hinder the normal cycle of operations, not to mention they can be dangerous to the lives of personnel.

The definition of slope angles that ensure stable operations requires a detailed study of all geological and geotechnical factors of rock mass: lithology, tectonic conditions, physical and mechanical properties of rocks, discontinuities of the rock mass, the hydrogeological conditions, etc.

To prevent slippage in the Ouenza mine, it was proposed to study the bench slope stability by numerical method based on finite elements (implemented in PLAXIS software). To better understand the bench slope stability problem, we modelled the mine bench slope to the study of the structure in two dimensions. For the calculation of the stability, plane strain assumption is adopted. The mechanical behaviour of rocks follows the Mohr-Coulomb criteria.

Keywords: Ouenza mine, stability, slope slippage, bench

1 INTRODUCTION

Raw materials, as well as building materials metalliferous ores, are the basis for supplying and meet the various branches of the national economy. Since the independence, Algeria has initiated a broad program aimed at:

1. The exploration of new deposits of useful minerals and substances.
2. The re-opening of mines and abandoned quarries.
3. The modernization and mechanization of mining and quarrying activity.
4. The training of national personnel who will be responsible and responsibility to properly manage and according to the required standards, the production process the financial return of the equipment used and that, to meet the demand of the consumer public and / or private.

It should be noted that the operation of a given deposit must consider the characteristics of the rock mass and to wisely choose the method of slaughter rocks, the most appropriate method of operation, and mechanization of processes loading and transportation of the blasted rock.

Not to mention the evaluation of bench slope stability of the open pit or intended quarry.

In this context, it was proposed to study the stability of slopes (bench slopes) mine of Ouenza. And, to draw conclusions regarding landslides or no slope of the studied mine.

2 GEOLOGICAL AND GEOMORPHOLOGICAL OF THE OUENZA MINE

Above the shelves that extend between Oued Mellègue and the mountains of Tebessa

appear isolated reliefs, whose highlights range from 1,200 to 1.400 meters.

Jebel Ouenza belongs to this series of links located on both sides of the Algerian-Tunisian border. Consisting of Aptian limestone collapsed affecting domed cut holes, this massive contains significant iron ore deposit, whose existence has been known since antiquity.

2.1 Geographic Context

The Ouenza deposit is located in the extreme NE of Algeria near the Tunisian -Algerian border; 120 Km of El Hadjar steel complex (Annaba) which is connected by a railway line and 90 km from the capital of the Wilaya of Tebessa. It is part of the Algerian-Tunisian border, Figure 1, which are geologically known by almost exclusively sedimentary character.

2.2 Morphology and Deposit Structure

The Ouenza deposit is located in the Jebel Ouenza which is a large anticlinal direction SW- NE, Figure 2. If one moves away from the SW periclinal part that presents a spectacular field as you see the enormous mass of reef limestones of the Aptian which forms the backbone of the mountain. Chain R. (2006).

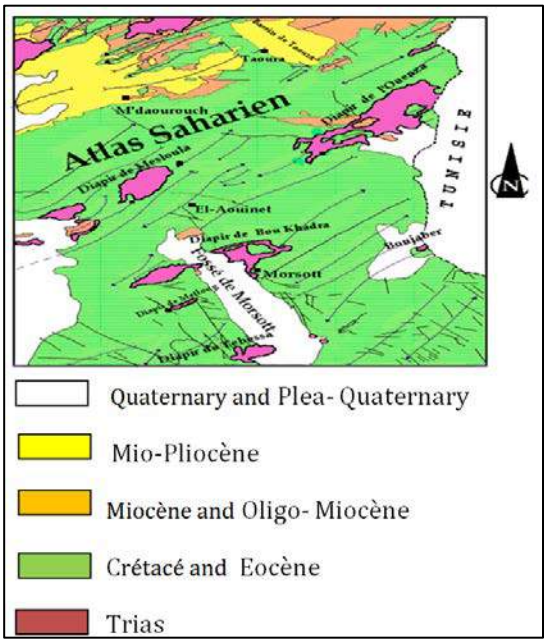

Figure 1. Structural schéma of confins algéro-tunisiens.

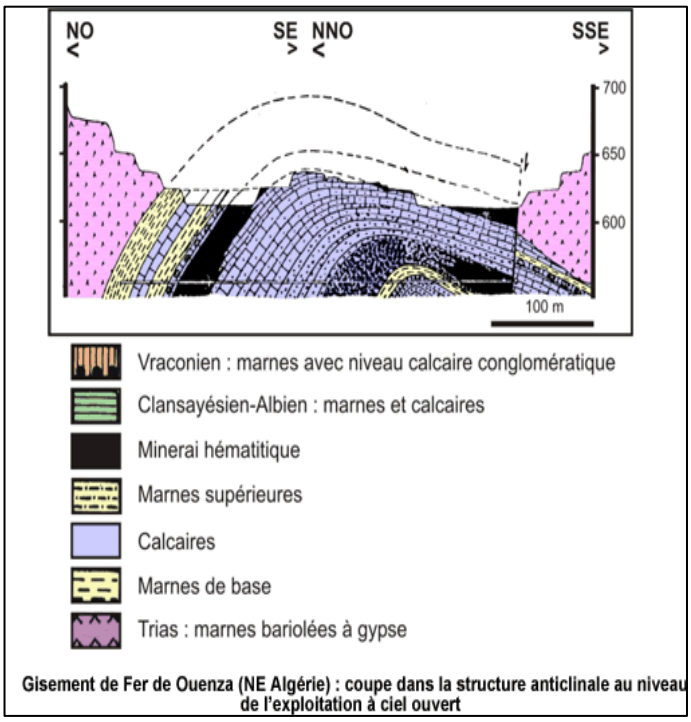

Figure 2. Structure Coupe in the Ouenza mine.

3 RESEARCH METHODOLOGY

3.1 Slope Stability of Open Pit Mines

3.1.1 Factors affecting slope stability

Analysis of the deformation process in open pits must take into account the joint influence of natural and technical factors. These can be divided into three natural factors:

- **Geographical and climatic:** Site relief, precipitation, temperature regime, specific conditions of freeze-thaw.
- **Geological:** lithology massive, tectonic setting, structural and textural characteristics of rocks and massive, mechanical properties of rocks, etc..;
- **Hydrogeological**: surface water passing through the territory of the farm or are nearby, groundwater in the massif, the presence of water in the contacts between the rocks or the tectonic discontinuities etc.

Among the technical factors include the geometry of the mine and waste rock, the slope angles of the mine and waste rock, the excavation method and slaughter of the rock, the structure of the mechanization of work, the presence near the mine underground excavations, methods and pumping parameters, etc.

From a general point of view, the rock mass can be considered as both geological objects and mechanical objects. The study of the stability of rock masses requires having knowledge of structural geology and rock mechanics.

Geologically a wide variety of rock masses based on observed:

• The nature of the rock matrix and petrographic and mechanical characteristics.
• Discontinuities at all levels and of all types, affecting the massif.
• Variability in space of the couple rock matrix / discontinuities.

3.1.2 Classifications deformations

The many classifications of natural slope movements and mining slope are very diverse and complex. Varnes D.J. (1978), NemcokA. (1972),Goulakian A.T.(1980**)** .

We can divide all the deformations in four groups based on the movement of the mechanisms:

• **Creep:** Slow movement of the masses without defining sliding surfaces
• Slip: mass movement in one or more well defined sliding surfaces
• **Slip - casting:** the dynamics of this movement is similar to that of a liquid Viscous.
• **Landslide:** sudden movement of rock masses with momentary loss of contact between the moving mass and massive.

3.1.3 Rockslide

Called rockslides moving a well-defined mass field with shear failure resistance defect following a well-identified area where the deformations are localized. Cojean R. (1985,1991). The displaced rock materials usually break and the initial slip turns into a landslide. One distinguishes rock slides with translational movement (on a stratigraphic seal a gap , a surface foliation or cleavage) , the following shifts associations discontinuities (forming dihedral, jagged surfaces, etc.) , slides with rotational movement (in highly fractured rock masses) slides with monolithic movement . Multiple combinations of different families discontinuities lead to a variety of disruptions mechanism.

For a bank, it is said that there is a risk of rupture for an association discontinuity and a given failure mechanism, if the geometric configuration formed by all elements (slope and discontinuities) supported the break. It is said that the break is cinematically possible.

Hoek E. (1981) proposed to distinguish five types of movements according to the configuration of the discontinuities and the orientation of the slope and of the kinematic motion.

• **Rupture plane simple:** the mass out is limited by a discontinuity plan; movement occurs in the direction of the dip vector of this discontinuity.
• **The dihedral out along a plane:** the mass out is bounded by two intersecting discontinuities movement occurs in the direction of the vector dip in one of two ways; there detachment without mechanical action along the other plane.
• **Breaking into true dihedral:** the mass out is bounded by two intersecting discontinuities movement occurs in the direction of the vector dip of the intersection of two planes; the mass is pressed simultaneously on both fronts during sliding.
• **The block switching by breaking:** the mass is cut out into blocks resulting from the combination of two discontinuities repeating a finite number of times, and forming, at the base, a stepped surface; the movement takes place in the direction of one of the planes; it combines the tilt of a set of upper blocks and sliding a set of lower blocks along the fracture surface.
• **Fracture on one staircase surface:** the mass out is restricted by a stepped surface resulting from the combination of two discontinuities repeating a finite number of times; the movement takes place by sliding in the direction of the dip vector of one of the two plans.

4 CASE OF STUDY

4.1 Numerical Modelling of the Stability of Benches Embankments

To better understand the bench slope stability problem, we modeled the mine bench slopes to the study of the structure in two dimensions. The bedrock is composed of layers of limestone and iron. For the calculation of the stability, plane strain assumption is adopted. The mechanical behavior of rocks follows the Mohr - Coulomb criteria. The mechanical and physical properties of rocks are determined by tests in the laboratory of Ouenza mine.

Table 1. Physical properties of rocks.

Parameters	Iron	Limestone
Permeability horizontal (K), m /s	10^{-5}	10^{-11}
Permeability vertical (K), m /s	10^{-5}	10^{-11}
Dry density (γ), g/cm^3	2.70	2.60
Saturated gravity (γ), g/cm^3	2.90	2.65

Table 2. Mechanical properties of rocks.

Parameters	Iron	Limestone
Modulus of Elasticity (E), GPa	21	19.84
Poisson's ratio (V)	0.25	0.22
Internal friction angle (ϕ),	45	50
Cohesion (C), MPa	3.20	3.50

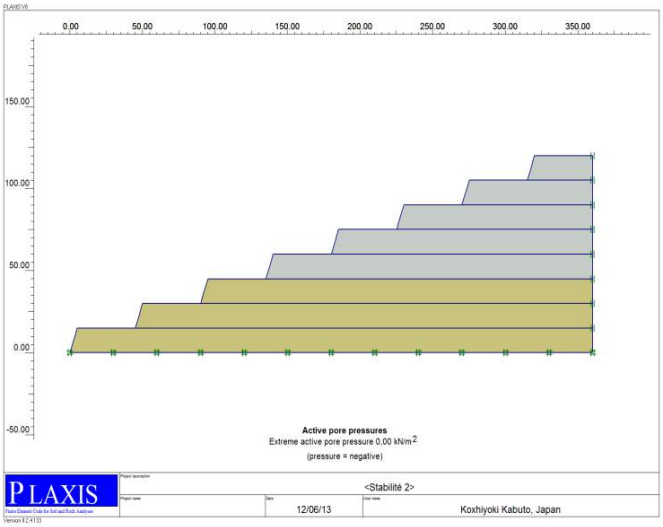

Figure 3. Geometric Model of mine slope

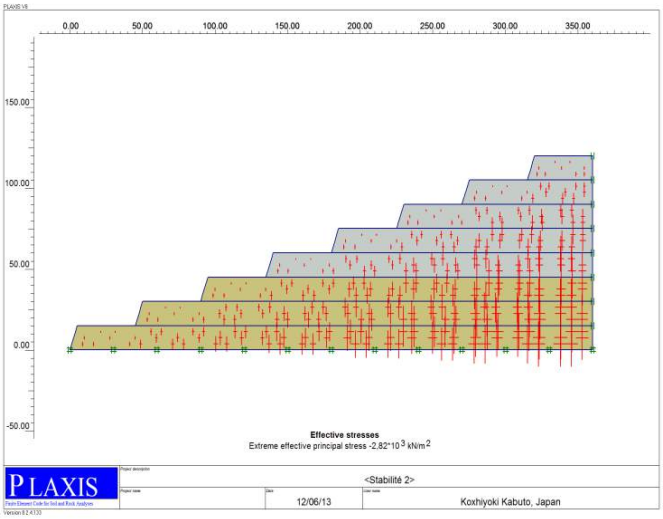

Figure 4. Maillage of mine slope

5 CONCLUSIONS

The obtained results, according to the numerical method based on finite elements and implemented in the software PLAXIS show that the movements and deformations are very low (Dh = 243.76 10^{-6} m) , which means that the bench slopes are stable.

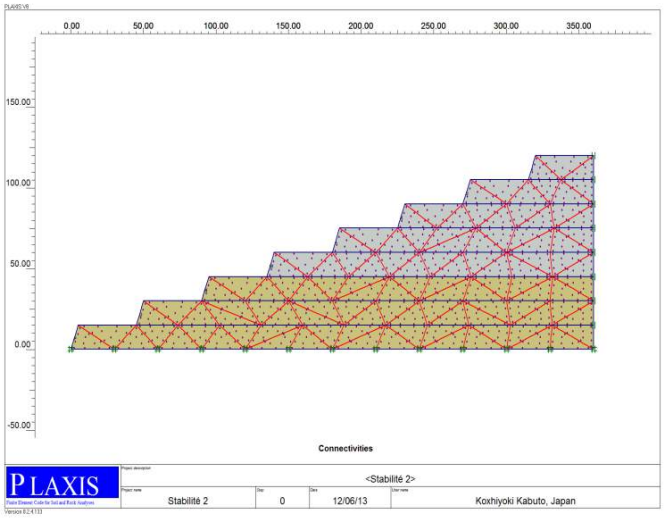

Figure 5. Zones of displacements and deformations

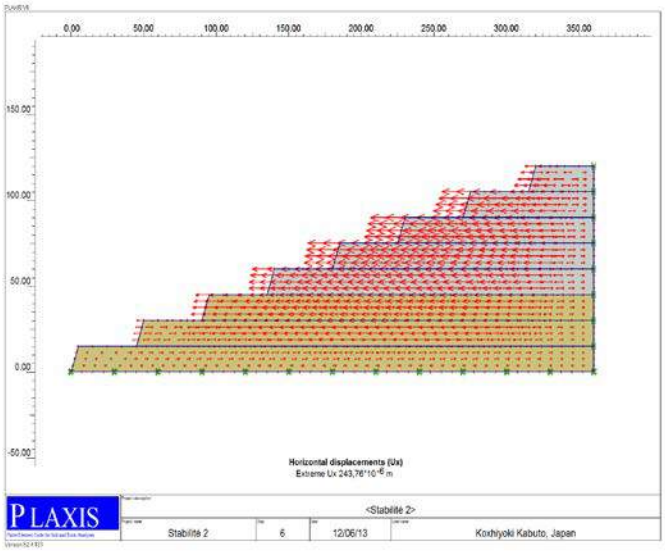

Figure 6. Horizontal displacement

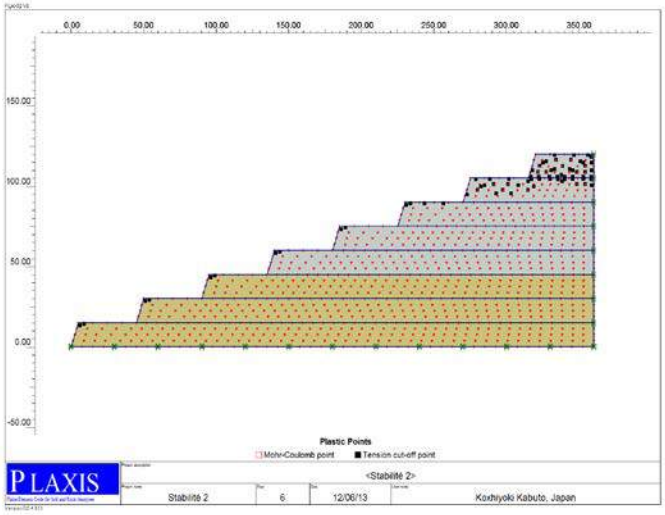

Figure7. Plasticity distribution

REFERENCES

Chain R., 2006, *Influence des travaux de forage et de tir sur la stabilité des talus et des gradins des mines à ciel ouvert (Cas: Mine de Fer de l'Ouenza).* These of doctorat, ANNABA, page interval (8-9).

Cojean R., Douiri F., 1985, *Stabilité des talus en mine à ciel ouvert.* Method of calculus, Interne rapport CGI, ENSM, Paris.

Cojean R., 1991, *Stabilité des versant et talus rocheux*, Interne rapport CGI, ENSM, Paris, page amount (e.g., 150).

Goulakian A.T., Kuntzel K.K., Postoev P.Ï., 1980, Opoiznevié processi En russe, U5 p. Ed. VSEG1NGEO. Moscou.

Hoek E., Bray. J.W., 1981. Rock slope engineering,, *3, Jl ed. Inst, of Mining,* London, page amount (e.g., 250).

NemcokA.,1972.. Slope deformation in high mountains, *Magazine24th Int. Geo Congr , London*, page interval (18-32).

Varnes D.J., 1978. *Slope movement types and process in landslides :analisis and control transBook nae*, Res. Rep. Acad. Sc, Washington.

Assessment of Engineering Behavior of Foliated Rocks Using Some Index Tests

D. Fereidooni
School of Earth Sciences, Damghan University, Damghan, Iran

G.R. Khanlari, M. Heidari, A.A. Sepahigero
Geology Department, Bu-Ali Sina University, Hamedan, Iran

ABSTRACT In this research, different experimental techniques have been used to determine the strength of five types of anisotropic foliated rocks, selected from the Hamedan Province, west of Iran. For this purpose, after sample preparation and assessment of mineralogical and physical properties, selected samples were subjected to Cylindrical Punch, Point Load and Brazilian tests and their strengths were evaluated with respect to different angles between anisotropy planes and the major loading directions. Data analyses show that the types and amounts of minerals have an influence on the physical and mechanical properties of the tested anisotropic rocks. Porosity and water absorption also have a dominant control on the mechanical indices such as cylindrical punch index (CPI), point load index ($I_{s(50)}$) and Brazilian tensile strength (BTS). On the basis of the test result, two empirical equations are proposed for calculating CPI and $I_{s(50)}$. Other empirical equations relating studied indices are also presented.

Keywords: Metamorphic rocks, anisotropy, punch test, point load test, Brazilian test

1 INTRODUCTION

The most important factors influencing the strength and deformation behaviors of intact rocks are mineral composition, crystal size, rock fabric, alteration degree, weathering and anisotropy (Saroglou et al., 2004). Some rocks of the earth's crust show well-defined fabric elements in the form of bedding, stratification, layering, foliation, fissuring or jointing. In general, these anisotropic rocks have physical, mechanical and hydraulic properties that are varied in different directions. Anisotropy can be found at different scales from intact specimen to rock masses. This property plays a significant role on the rock behavior in engineering projects. For example, in civil and mining engineering, anisotropy affects the stability of underground excavations, surface excavations, foundations, drilling, blasting and rock cutting (Chen et al., 1998).

Out of the three generic categories of rocks, metamorphic rocks usually show the highest degree of anisotropy (Ramamurthy et al., 1993). The anisotropic nature of some metamorphic rocks is mainly due to the presence of a single set of discontinuity or weakness planes such as cleavage, foliation, schistosity, joint or microfissure (Al-Harthi, 1998).

In recent years, different methods and testing techniques have been developed and implemented to determine geotechnical properties of anisotropic rocks. Standard procedures for measuring various geotechnical properties of rocks were suggested by ISRM (2007) that provides an excellent review of many available techniques in both laboratory and field environments. In laboratory testing, mechanical properties of intact anisotropic rocks are usually determined from specimens prepared at different angles with respect to the apparent planes of anisotropy. The most important laboratory static tests include uniaxial and triaxial compression, punch, point load and Brazilian tests.

Literature review shows that performing direct static laboratory tests in order to evaluate rock strength and deformation is mostly expensive and requires considerable time due to preparation of rock specimens. Therefore, different indirect testing methods were developed and used to interpret the engineering properties of anisotropic rocks. These tests are relatively easy to perform, cheap, and take short testing time (Shalabi et al., 2007). Hence, indirect index test results are often used to predict strength parameters of anisotropic rocks. For this reason, in the present research, some of the most important laboratory tests such as cylindrical punch, point load and Brazilian tests were used. Based on the results, their applications are strongly recommended for determining strength parameters of anisotropic rocks.

2 SAMPLE SELECTIONS

Suitable sampling locations of rock types were selected from the 1:250,000 scaled geological map prepared by the Geological Society of Iran (G.S.I., 1977). During field investigations, lithological characteristics of rocks were considered. Samples were obtained from quarries, road and railway cuttings and excavated foundations. Observations of hand specimens indicate that these samples are heterogeneous so that different foliation planes could be identified by their light and dark colors. The studied rock samples were selected from different parts of the Hamedan Province, west of Iran. The sampling locations include Avarzaman (AVZ), Heydareh (HDR), Malayer (MLR), Varkaneh (VRK) and Zagheh (ZGH). Five examined rock types are phyllite, sillimanite garnet hornfels, slate, andalusite garnet hornfels and staurolite andalusite schist. All selected samples are fresh rocks obtained from depths of about 5m.

3 EXPERIMENTAL STUDIES

3.1 Specimen Preparation

A total of 1050 specimens were prepared for block punch, Brazilian and point load tests (350 specimens for each test) at seven different anisotropy angles (β = 0°, 15°, 30°, 45°, 60°, 75° and 90°). Diameters of prepared specimens were about 54 mm. Specimen thickness of cylindrical punch tests (CP-test) was kept between 5-15 mm as proscribed by Ulusay et al. (2001). Length to diameter ratios of the point load test specimens and ratios to diameter of Brazilian test specimens were kept in accordance to the ISRM (2007) stipulations.

3.2 Petrographical and Mineralogical Studies

In order to identify the mineral composition and texture of the rock samples by optical microscopic observations, thin sections were prepared in two directions; parallel and perpendicular to the rock anisotropy planes. These orientations were studied by using a modern polarizing microscope as proscribed by ISRM (2007). The mineralogical studies indicated that the metamorphic rocks were commonly composed of quartz, biotite, feldspar, muscovite, garnet, sillimanite, staurolite, andalusite, graphite and other tiny cryptocrystalline matrix materials. The textures were different in the parallel and perpendicular orientations for the rock anisotropy planes. The anisotropy planes were clearly seen when the thin sections were prepared perpendicular to the rock anisotropy.

Textures of the rocks were found to be porphyroblastic and lepidoblastic. In the porphyroblastic fabric, the rock texture could be divided into two components: porphyroblasts and matrix. Andalusite, staurolite and garnet porphyroblasts were found to be dominant types of minerals with sizes of 0.2 to 1 mm (Fig. 1). The matrix was characterized by quartz, feldspar, biotite and muscovite (50-100 μm). These patterns defined a fabric characteristic of both regional and contact metamorphic rocks. Table 1 presents a summary of the average modal abundance of the minerals and the mineral compositions of the rock samples. Fig. 1 shows microscopic images of the sample of AVZ as representative sample.

Table 1 Mineral composition of tested samples

Rock mark	Rock type	Mineral content (%)									
		Qtz.	Fld.	Bt.	Mt.	Gt.	Ad.	Slt.	St.	Chl.	Other minerals
AVZ	Phyllite	20	10	40	7	-	3	-	-	12	A.(3%), T.(1%), Z.(1%), P.(3%)
HDR	Sillimanite garnet hornfels	16	9	38	5	13	4	13	1	-	T.(1%)
MLR	Slate	20	10	32	7	-	-	-	-	3	G.(12%), CM(10%), H(7%)
VRK	Andalusite garnet hornfels	20	10	41	4	10	6	-	5	-	T.(1%), Z.(1%)
ZGH	Staurolite andalusite schist	20	5	2	20	-	18	14	4	-	T.(2%), H.(15%)

Qtz.: Quartz, Fld.: Feldspar, Bt.: Biotite, Mt.: Muscovite, Gt.: Garnet, Ad.: Andalusite, Slt.: Sillimanite, St.: Staurolite, Chl.: Chlorite, G.: Graphite, A.: Apatite, T.: Tourmaline, Z.: Zircon, P.: Prehnite, H.: Hematite, CM: Clay minerals

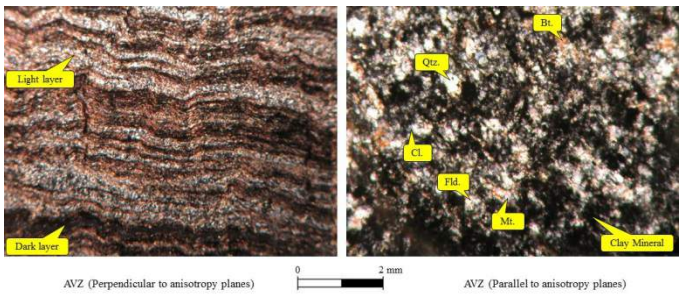

Figure 1. Photomicrographs of the sample of AVZ (The left image is perpendicular to anisotropy planes and the right image is parallel to anisotropy planes).

3.3 Physical Properties

Physical properties of different intact rocks depend on their mineral compositions and microstructures. Irfan (1996) indicated that the physical properties of the intact rocks are highly influenced by the type, texture, fabric and the minerals forming the rocks. Physical properties of the rock samples, such as dry and saturated unit weights (γ_d and γ_{sat}), specific gravity (G_s), porosity (n) and water absorption (W_a) were determined using standard testing methods suggested by ISRM (2007). For this purpose, five sets of tests were performed on the core specimens prepared in different directions of anisotropy planes (β = 0°, 15°, 30°, 45°, 60°, 75° and 90°). On each type of anisotropic rocks 35 tests were performed. Therefore, a total of 175 tests were performed for calculating physical properties. Table 2 shows the values of the parameters for the tested samples. The dry unit weight ranges between 2.55 and 2.81 gr/cm^3 with an average of 2.72. The saturated unit weight ranges between 2.64 and 2.82 gr/cm^3 with an average of 2.75. The specific gravity ranges between 2.77 and 2.84 with an average of 2.81. The porosity ranges between 1.13 and 8.99% with an average of 3.36%. The water absorption ranges between 0.40 and 3.55% with an average of 1.27%.

Table 2. Physical properties of tested samples

Rock mark	γ_d (gr/cm^3)	γ_{sat} (gr/cm^3)	G_s	n (%)	W_a (%)
AVZ	2.73	2.74	2.77	1.74	0.64
HDR	2.81	2.82	2.84	1.13	0.40
MLR	2.71	2.75	2.82	3.76	1.33
VRK	2.79	2.80	2.82	1.16	0.41
ZGH	2.55	2.64	2.80	8.99	3.55
Average	2.72	2.75	2.81	3.36	1.27

3.4 Cylindrical Punch Test

Probably, the earliest reference to the punch test is reported by Lacharite (1960). In this article, this test was used to assess the shear strength of a rock type. To this time, different researchers used the punch test to determine rock shear strength (Mishra and Basu, 2012). They placed the apparatus with a rock disc specimen in a compression machine. The compressional loading induces double shear failure planes in the specimen.

Their studies were extended in 1982 for the development of the block punch test and its index (Schrier, 1988). In his article and references, the effect of specimen size on the block punch index (BPI) was not considered. Later, a comprehensive study was carried out by Ulusay and Gokceoglu (1997) in order to investigate the specimen size effect on BPI. They proposed an empirical equation to calculate the corrected block punch index (termed as BPI_c) which considers the specimen size effect. This equation was later modified by Sulukcu and Ulusay (2001) based on additional test results. Ultimately, after considering the findings of the previous investigations, Ulusay et al. (2001) suggested a new method for the block punch test. On the basis of their suggestion, the corrected block punch index (BPI_c) can be calculated as follows:

$$BPI_C = 3499D^{-1.3926}t^{-1.1265}P \quad (1)$$

where D and t are diameter and thickness of the disc specimen in mm and P is the failure load in KN. In the case of anisotropic rocks, the BPI would change depending on the anisotropy angle. For this reason, a strength anisotropy transformation factor (K_a) was introduced for normalizing BPI of anisotropic rocks in the strongest direction (i.e. BPI_{c90}, when the loading direction is perpendicular to the weakness planes) (Ulusay et al., 2001). Based on additional test results, strength anisotropy transformation factor (K_a) was modified by Karakul et al. (2010).

In this study, instead of the block punch test (BP-test), the cylindrical punch test (CP-test) was used in order to determine the cylindrical punch index (CPI) for anisotropic rock samples. The CP-test apparatus was made in a welding laboratory from steel plates and 10×10 box profile, and the same apparatus has been used by Jafari et al. (2010). The dimensions of the CP-test apparatus used in this research are about 15×15×15 cm. This apparatus consists of an upper piece, a lower piece and a punching cylinder which are connected to each other by two connecting screws. Specimens were placed between the two pieces before the testing. This fabricated frame can be placed within a uniaxial compression or a point load machine. In order to perform this test, each specimen was placed in the apparatus, and the axial load was applied at a rate of 0.05 KN/s. Specimen loading must be axial, and each specimen must fail between 30 and 60 seconds (Ulusay et al., 2001). The process of specimen placement in the apparatus is shown in Fig. 2. Failures should be such that the traces of shear failure can be seen on both sides of specimen (Fig. 3). After performing the cylindrical punch test, cracks in specimens tend to propagate parallel to anisotropy planes. These types of failures occurred at all anisotropy angles except specimens at β=90°. For example, Figs. 4 and 5 show failures of ZGH specimens at β=0° and VRK specimens at β=90°.

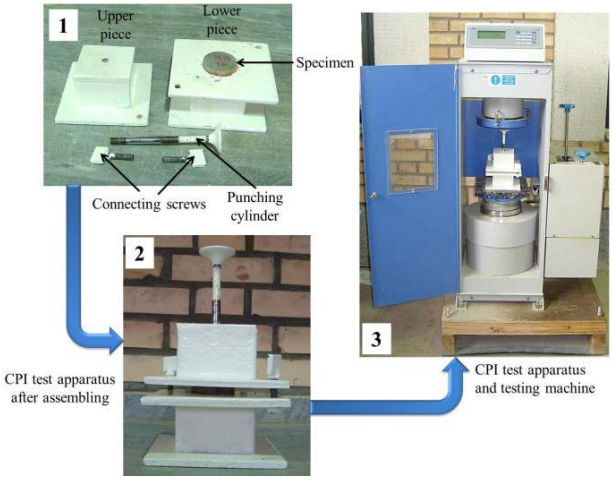

Figure 2. Cylindrical punch test apparatus and performance process of this test

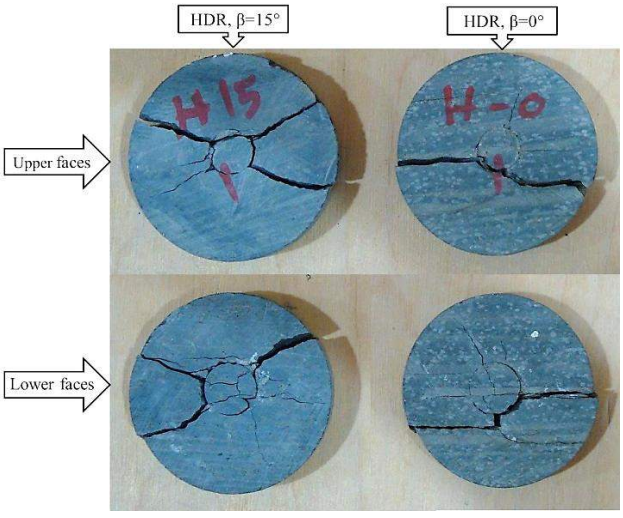

Figure 3. Trace of failure in upper and lower faces of two tested specimens

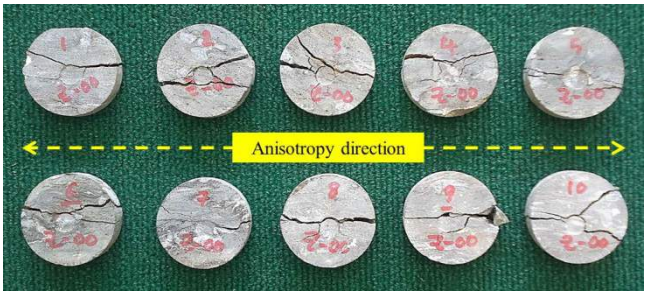

Figure 4. Crack propagation parallel to anisotropy directions at β=0°

Figure 5. Crack propagation not parallel to anisotropy directions at β=90°

On the basis of the experimental results achieved from this research, the most important advantages of cylindrical punch test (CP-test) in comparison to the block punch test (BP-test) are as follow:

1. In the CP-test, distance of the shear surface is equal from the edge of the specimen, whereas, in the BP-test the distance is not equal. These differences may affect the test results (Fig. 6).

2. Stress distribution on specimen surface in the CP-test is more uniform than in the BP-test.

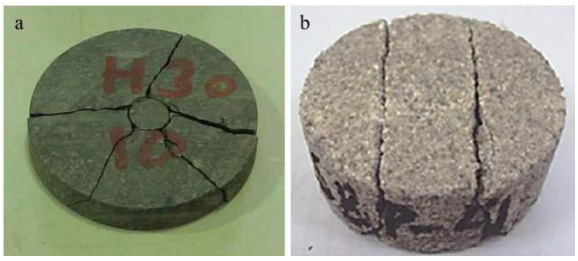

Figure 6. Comparison between failure mechanism in a) CP-test and b) BP-test(a: this research, b: Mishra and Basu, 2012)

Evaluation of CPI in MPa is possible using the following equation:

$$CPI = \frac{P}{\pi D t} \qquad (2)$$

where P is the failure load in N. D and t are the diameter and thickness of the sheared cylinder in mm.

In anisotropic rocks, the values of CPI are affected by the anisotropy angle (β). In this research, 350 disc specimens with thickness of about 10 mm were tested. Average CPI values of each sample at different β angles are presented in Table 3. For all tested samples, CPI values at β=0° are at a minimum but, at β=90° are maximum. Also, in this table the values of punch anisotropy index (PAI) were calculated from the ratio of (CPI_{90}/CPI_0).

Fig. 7 shows the correlation between CPI and β for the tested samples. The curves presented in this figure indicate a direct relationship between the parameters. In other words, with increasing anisotropy angles from 0° to 90°, the values of CPI increase. Variation rates of CPI in anisotropy angles between 0° and 15° are maximum. In other words, the slopes of the curves are maximum between β=0° and β=15°. But, with increasing anisotropy angles from 15° to 90°, variation rates of CPI decrease; especially, for the samples of AVZ and HDR (Fig. 7).

Table 3. The values of CPI and PAI for tested samples at different β

β (Deg.)	CPI (MPa)				
	AVZ	HDR	MLR	VRK	ZGH
0	13.47	18.34	9.04	27.11	11.22
15	13.99	22.16	9.35	27.94	11.83
30	14.29	23.91	9.58	28.17	12.11
45	14.50	24.30	9.71	29.60	12.90
60	14.65	25.60	10.18	30.05	13.82
75	14.75	26.46	10.20	30.04	13.63
90	15.02	26.57	10.23	30.12	14.11
PAI	1.12	1.45	1.13	1.11	1.26

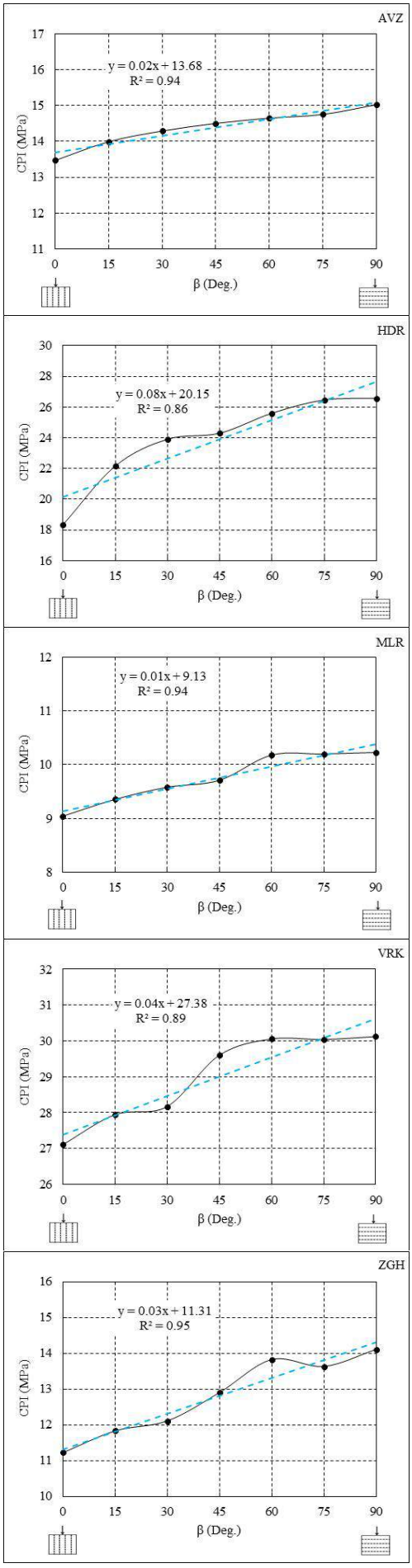

Figure 7 Correlations between CPI and anisotropy angles (β) for tested samples

After analysis of the results, Equation 3 is proposed in order to determine cylindrical punch index at different anisotropy angles ($CPI_{\beta=i}$). The importance of this equation is that by performing CP-tests only at β=90°, it is possible to determine CPI in different anisotropy angles from 0° to 90°. This equation was obtained from the trial-and-error method using the CPI data obtained at different anisotropy angles.

$$CPI_{\beta=i^\circ} = CPI_{\beta=90^\circ} - K(1-\sin\beta) \quad (3)$$

where K (difference between CPI at β=90° and in other degrees of β) is a function of β that can be achieved by Equation 4. This equation was obtained by curve-fitting between K and β.

$$K = 2.35 - (0.03 \times \beta) \quad (4)$$

where β is anisotropy angle in degrees. The calculated values of K at different anisotropy angles based on the above equation are presented in Table 4. A reverse linear relationship occurs between K and β.

Table 4. The values of K at different β

β (Deg.)	K
0	2.35
15	1.90
30	1.45
45	1.00
60	0.55
75	0.10
90	0.00

The relationship between experimented results and calculated values of CPI using Equation 3 for all tested samples at seven different β is shown in Fig. 8. For comparison of the results, the 45° line (y=x) has been plotted in this figure. It is clear that the two lines are nearly fitted to each other.

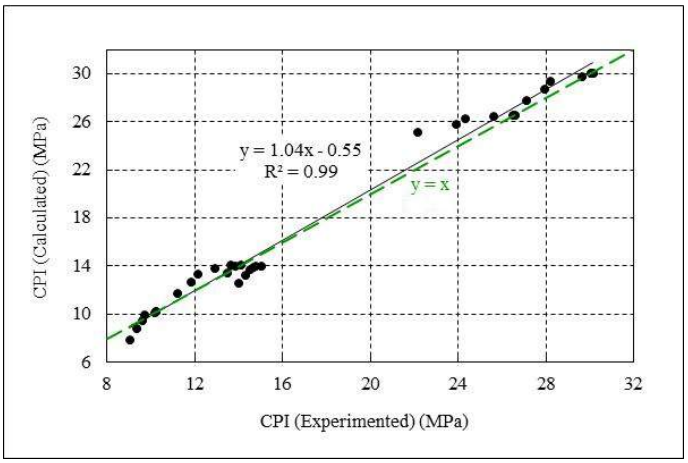

Figure 8. Correlation between experimented and calculated results of CPI for tested samples

3.5 Point Load Test

The point load test is commonly used in practice because of the ease of testing, simplicity of specimen preparation and possible field application (Kahraman and Gunaydin, 2009). The method of point load test was standardized by ISRM (2007) and ASTM (2001).

In anisotropic rocks, foliation planes are characteristics of the rocks, and it is expected that mechanical behaviors of these rocks will be controlled by these planes under a certain state of stress. If the merit of the point load test, its success, and wide use are kept in mind, the following two issues emerge to be absolutely important in rock engineering (Basu and Kamran, 2010): (1) to check feasibility of utilizing the point load test (with weakness planes at an angle with loading direction) for strength evaluation of anisotropic rocks and (2) to evaluate predictability of UCS by point load strength for these rocks.

On the basis of the literatures (Broch and Franklin 1972, Tsidzi 1990, Ajalloeian and Lashkaripour 2000), point load strength anisotropy index ($I_{a(50)}$) is reported to be a good index for anisotropic rocks. This index is defined as the ratio of $I_{s(50)}$ values measured in the strongest and weakest directions ($I_{a(50)}= I_{s(50)max}/ I_{s(50)min}$). Because the strongest and weakest directions are perpendicular and parallel to planes of foliation, respectively, the point load strength anisotropy index ($I_{a(50)}$) is close to 1.0 for quasi-isotropic rocks and are at higher values for anisotropic rocks (ISRM, 2007).
In this research, the required specimens for point load test (350 cylindrical specimens with L/D=0.3-1.0) were prepared and tested at seven anisotropy angles. On the basis of our laboratory experiments, the use of axial point load tests are easier to do and give better results than other point load tests for anisotropic rocks. A total of 10 axial point load tests were carried out in each direction of foliation planes and the mean values were calculated. The minimum and maximum values of anisotropy ratio (1.81 and 5.72) were measured for ZGH and AVZ samples, respectively (Table 5).

Table 5. The values of $I_{s(50)}$ and $I_{a(50)}$ for tested samples at different β

β (Deg.)	$I_{s(50)}$ (MPa)				
	AVZ	HDR	MLR	VRK	ZGH
0	0.64	2.80	0.69	5.46	1.01
15	0.67	4.19	0.76	4.41	1.10
30	1.50	7.15	0.89	5.53	1.25
45	1.55	5.35	1.38	6.88	1.39
60	1.33	8.68	1.56	8.08	1.72
75	2.60	9.05	1.95	9.03	1.71
90	3.66	9.80	2.51	9.51	1.83
$I_{a(50)}$	5.72	3.50	3.64	2.16	1.81

Fig. 9 shows the correlations between $I_{s(50)}$ and anisotropy angles (β) for tested samples. The curves in this figure indicate linear relationships between $I_{s(50)}$ and β with high correlation coefficients. In other words, with increasing anisotropy angles from 0° to 90°, the values of $I_{s(50)}$ increase. Therefore, the value of $I_{s(50)}$ at β=90° is maximum for all samples.

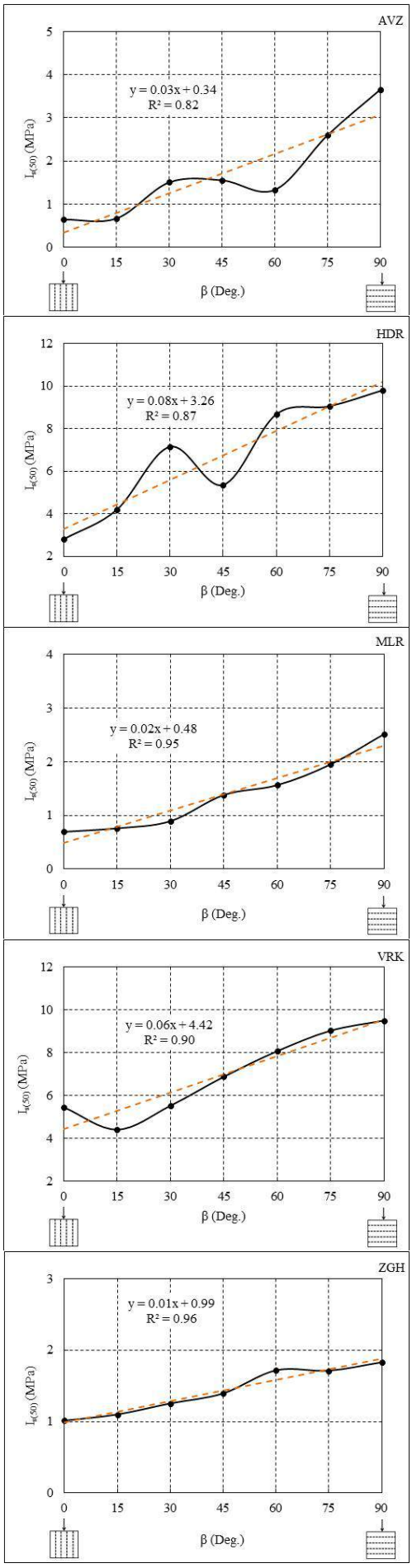

Figure 9. Correlations between $I_{s(50)}$ and anisotropy angles (β) for tested samples

Our laboratory studies show that the core preparation of anisotropic rocks can be difficult because the cores may break along their weakness planes. Therefore, in the present research a suitable method was proposed to determine point load index ($I_{s(50)}$) in different anisotropy angles (β). In our suggested method, preparation of core specimens is not necessary because it is possible to use natural specimens that that have broken along their foliation planes. By using this method and after calculation of $I_{s(50)(\beta=90°)}$, the estimation of values of $I_{s(50)}$ is possible for anisotropy angles from 0° to 90°. Estimation of the $I_{s(50)(\beta=i°)}$ is possible as follows:

$$I_{s(50)(\beta=i^\circ)} = [(0.71 \times \sin\beta) + 0.20] \times I_{s(50)(\beta=90^\circ)} \qquad (5)$$

where β is anisotropy angle in degrees. Equation 5 was obtained from the correlation between the ratio of $I_{s(50)(\beta=i°)}/ I_{s(50)(\beta=90°)}$ and β (Fig. 10).

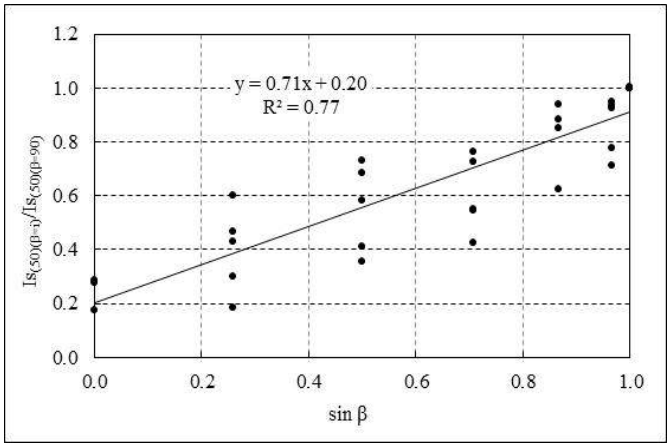

Figure 10. Relationship between $I_{s(50)(\beta=i°)}$ / $I_{s(50)(\beta=90°)}$ and β for tested samples

Relationships between experimented and calculated values of $I_{s(50)}$ using Equation 5 in seven different β are shown in Fig. 11. For comparison of the results, the 45° line (y=x) has been plotted in this figure. It is clear that the two lines are nearly fitted to each other.

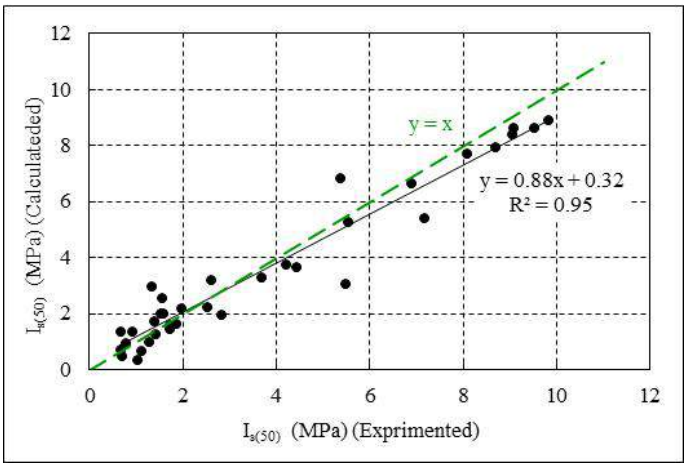

Figure 11. Correlation between experimented and calculated of $I_{s(50)}$ for tested samples

3.6 Brazilian Test

The Brazilian test is a simple indirect testing method for determining tensile strength of brittle materials such as concrete, rock, and rock-like materials (Li and Wong, 2013). This test can be carried out on rock specimens with lengths to diameter ratios from 0.5 to 0.75 according to ISRM (1978) and ASTM (2001). In this research, at least 10 tests were undertaken for each rock type. The Brazilian tensile strength (BTS) was determined by the following equation (ASTM, 2001):

$$BTS = \frac{2P}{\pi Dt} \quad (6)$$

where P is the maximum load recorded during the test. D is the diameter and *t* is the thickness of specimen.

The effect of anisotropy on indirect tensile strength determined by the Brazilian test has been investigated by many researchers such as Hobbs (1963), Barla and Innaurato (1973), Chaberlain et al. (1976) and Behrestaghi et al. (1996). In such studies, the tensile strength of anisotropic rocks was approximated by an equation based on the theory of isotropic elasticity, in spite of the anisotropic character of the rock. Brazilian tensile strengths (BTS) of anisotropic rocks increase as β increases from 0° to 90°. The tensile strengths corresponding to foliation planes oriented at other orientations are between these two values (Zhang et al., 2011).

In this research, the specimens were placed in a Brazilian test machine with different anisotropy angles of loading directions (β=0°, 15°, 30°, 45°, 60°, 75° and 90°). The correlation between Brazilian tensile strength (BTS) and anisotropy angle (β) for all tested samples are shown in Fig. 12. The resulting data are summarized in Table 6. The maximum value of BTS (21.90 MPa) was obtained for VRK sample at β=90° and the minimum value of 1.03 MPa for AVZ sample at β=45°.

The Brazilian anisotropy index (BAI) for indirect tensile strength was obtained from the ratio of tensile strength at strongest and weakest directions. The BAI varied between 1.53 and 5.59 for HDR and MLR samples, respectively.

Table 6. The values of BTS and BAI for tested samples at different β

β (Deg.)	BTS (MPa)				
	AVZ	HDR	MLR	VRK	ZGH
0	2.03	5.67	2.27	8.63	3.95
15	1.11	5.58	1.71	10.95	3.48
30	1.23	6.32	1.33	12.83	3.27
45	1.03	7.12	1.94	13.55	3.38
60	3.94	7.76	2.20	16.56	3.94
75	3.97	8.24	3.06	19.48	4.74
90	5.46	8.56	7.43	21.90	5.09
BAI	5.30	1.53	5.59	2.54	1.56

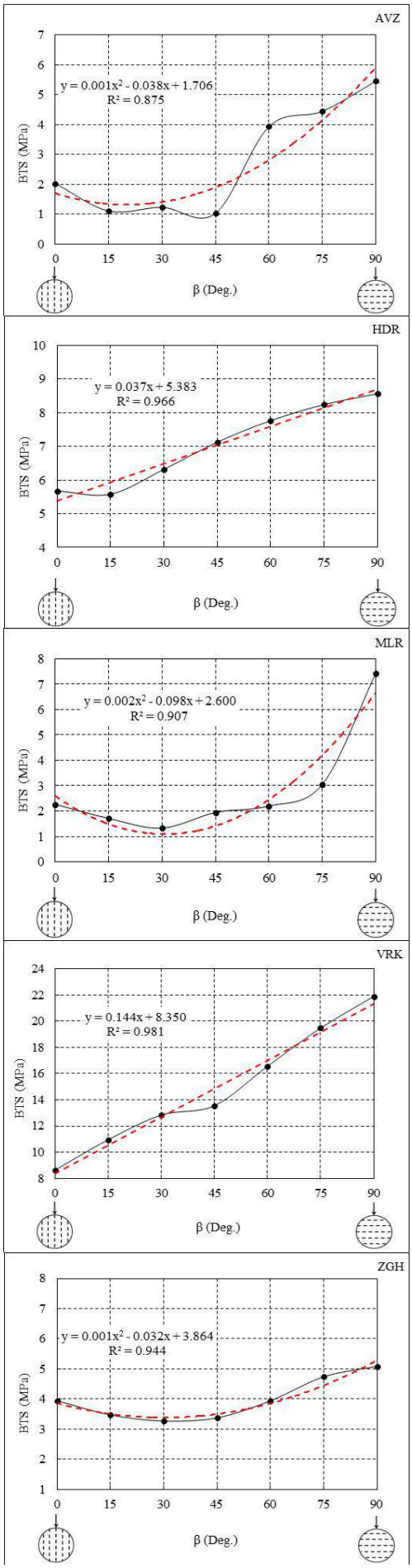

Figure 12. Relationships between BTS and anisotropy angles (β) for tested samples

Fig. 12 shows good linear correlations between the measured indirect tensile strength and angles of anisotropy (β) for the samples of HDR and VRK. A binominal-linear relationship was obtained for the samples of AVZ, MLR and ZGH. In other words, semi U-shape curves were obtained between BTS and β for these samples. These results match with those of Chen et al. (1998).

The highly foliated rocks, such as the regional metamorphic samples of AVZ, MLR and ZGH, have both weak and strong sequenced anisotropy planes in their structures (see Fig. 2). When these rocks are loaded at β=0°, the applied load is subjected to the strong anisotropy planes. This leads to increase failure load (P). Therefore, BTS at β=0° is higher than other anisotropy angles such as 15°, 30° and 45° and creates semi U-shape curves (Fig. 12). The contact metamorphic rocks, such as the samples of HDR and VRK, have been re-metamorphosed forming porphyroblasts in some places. Therefore, their textures are poorly foliated, and they do not develop semi U-shape curves. Therefore, the correlation curve between BTS and β for these rocks is linear.

4 RELATIONSHIP BETWEEN CPI, $I_{s(50)}$ AND BTS

Relationships between cylindrical punch index (CPI) and point load strength index ($I_{s(50)}$) for tested samples are presented in Fig. 13 and produce linear correlations. With performing point load test at β=90° on an anisotropic rock type, the $I_{s(50)}$ at different angles of anisotropy were obtained using Equation 5. Therefore, CPI values in different β are calculated using Equation 7:

$$CPI_i = 2.24 I_{s(50)_i} + 9.78 \qquad (7)$$

where CPI_i and $I_{s(50)i}$ are cylindrical punch index and point load strength index at different anisotropy angles (β=i°), respectively.

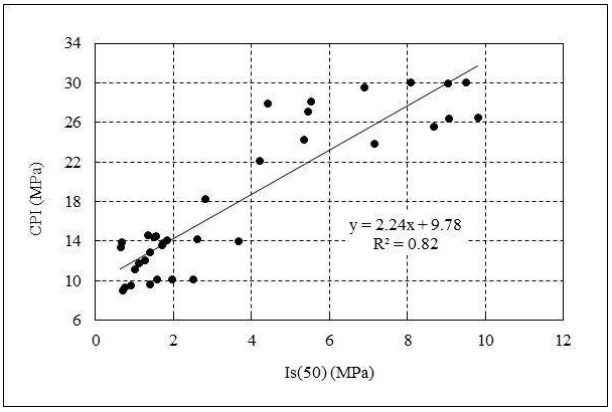

Figure 13. Relationship between CPI and $I_{s(50)}$ for tested samples

Relationships between Brazilian tensile strength (BTS) and point load strength index ($I_{s(50)}$) for tested samples are presented in Fig. 14. A power relationship exists between these two mentioned parameters. With performing point load test at β=90° on an anisotropic rock sample, the $I_{s(50)}$ in different angles of anisotropy was obtained from Equation 5. Therefore, Brazilian tensile strength for the sample can be achieved from the following equation:

$$BTS_i = 2.20 \times I_{s(50)_i}^{0.79} \quad (8)$$

where BTS_i and $I_{s(50)i}$ are Brazilian tensile strength and point load strength index in different anisotropy angles (β=i°), respectively.

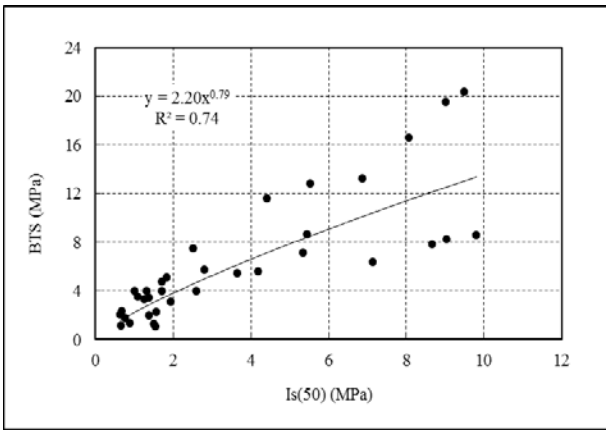

Figure 14. Relationship between BTS and $I_{s(50)}$ for tested samples

Relationships between Brazilian tensile strength (BTS) and cylindrical punch index (CPI) for tested samples are presented in Fig. 15. Here a linear relationship exists between the mentioned parameters. Therefore, Brazilian tensile strengths (BTS) in different directions of anisotropy are calculable using Equation 9:

$$BTS_i = 0.05CPI_i^2 - 1.47CPI_i + 13.06 \quad (9)$$

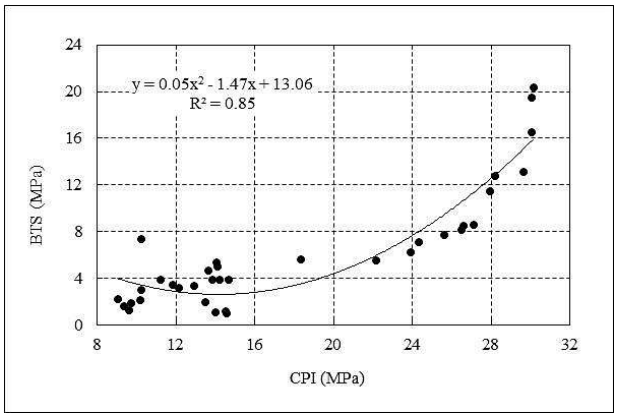

Figure 15. Relationship between BTS and CPI for tested samples

5 DISCUSSIONS AND CONCLUSIONS

The petrographic and mineralogic studies of the samples show that the HDR and VRK samples were affected by re-metamorphism. They have a high degree of metamorphism, and some contain porphyroblasts of garnet, andalusite, sillimanite and staurolite. Therefore, dry unit weight of these samples is higher than for the other samples because of their re-metamorphism, presence of dense metamorphic minerals, and decreased porosity (Table 2). The decrease of porosity causes the decrease of water absorption which increases the cylindrical punch index (CPI), point load index ($I_{s(50)}$) and Brazilian tensile strength (BTS) as can be seen in HDR and VRK samples. On the other hand, with increasing porosity and water absorption, the mechanical properties of the studied rocks decrease as can be seen in ZGH sample. The presence of metamorphic minerals in porphyroblastic texture reduces the influence of anisotropy and decreases anisotropy indexes in mechanical tests (PAI, $I_{a(50)}$ and BAI) as can be seen in HDR and VRK samples. Contrary to these observations, in the samples that the metamorphic minerals are not present as porphyroblasts but occur in lepidoblastic texture, the influence of

anisotropy is high as can be seen in microscopic images of the samples. This high influence increases the PAI, $I_{a(50)}$ and BAI as can be seen in AVZ and MLR samples. The comparison between PAI, $I_{a(50)}$ and BAI values show that these indexes have good agreement with each other in different tested rocks.

In the present research, a new empirical equation is proposed in order to calculate CPI of anisotropic rocks in different anisotropy angles (β) using CPI at β=90° (Equation 3). This equation helps to determine CPI in different anisotropy angles from 0° to 90°. Similar to CPI, a new empirical equation is proposed in order to determine the point load strength index in different anisotropy angles (β) using point load strength index at β=90° (Equation 5). This equation helps to determine $I_{s(50)}$ in different anisotropy angles.

The review of the Brazilian test results show that the maximum value of BTS is obtained at β=90° for all tested samples. On the other hand, the minimum value of BTS is obtained at β=0°, 15°, 30° and 45° in different tested samples.

In this research, the equations proposed between different parameters help to determine various index strength parameters of anisotropic rocks, such as CPI, $I_{s(50)}$ and BTS.

ACKNOWLEDGEMENTS

The authors would like to express their thanks to Prof. Lorence G. Collins for his English editing.

REFERENCES

Ajalloeian, R., Lashkaripour, G.R., 2000. **S**trength anisotropies in mudrocks. Bull. Eng. Geol. Env., 59, 195–199.

Al-Harthi, A.A., 1998. Effect of planar structures on the anisotropy of Ranyah sandstone, Saudi Arabia. Eng. Geology 50, 49–57.

ASTM, 2001. Standard method for determination of the point load strength index of rock. ASTM Standards on Disc 04.08.; Designation: D5731.

ASTM, 2001. Standard test method for splitting tensile strength of intact rock core specimens. ASTM Standards on Disc 04.08; Designation: D3967.

Barla, G., Innaurato, N., 1973. Indirect tensile strength of anisotropic rocks. Rock Mech. 5, 215–230.

Basu, A., Kamran, M., 2010. Point load test on schistose rocks and its applicability in predicting uniaxial compressive strength. Int. J. Rock Mech. Min. Sci. 47, 823–828.

Behrestaghi, M.H.N., Rao, K.S., Ramamurthy, T., 1996. Engineering geological and geotechnical responses of schistose rocks from dam project areas in India. Eng. Geology 44 (1–4), 183–201.

Broch, E, Franklin, J.A., 1972. The point load strength test. Int. J. Rock Mech. Min. Sci. 9, 669–697.

Chaberlain, P.G., Van, E., Podmieks, E.R., 1976. Four factors influencing observed rock properties. Soil Specimen Preparation Lab Test ASTM STP. 599, 21–36.

Chen, C.S., Pan, E., Amadei, B., 1998. Determination of Deformability and Tensile Strength of Anisotropic Rock Using Brazilian Tests. Int. J. Rock Mech. Min. Sci. 35(1), 43–61.

Geological Society of Iran (G.S.I.), 1977. Geological quadrangle map of Iran. No. D6, Scale 1:250000, Printed by Offset Press Inc. Tehran.

Hobbs, D.W., 1963. The tensile strength of rocks. Int. J. Rock Mech. Mining Sci. 1, 385–396.

Irfan, T.Y., 1996. Mineralogy, fabric properties and classification of weathered granites in Hong Kong. Q. J. Eng. Geology 29, 535.

ISRM, 1978. Suggested methods for determining tensile strength of rock materials. Int. J Rock Mech. Min Sci. Geomech. Abs. 15 (3), 99–103.

ISRM, 2007. The Blue Book: The complete ISRM suggested methods for rock characterization, testing and monitoring: 1974-2006. Ulusay, R., Hudson, J.A., (eds). Compilation arranged by the ISRM Turkish National Group, Ankara, Turkey. Kazan Offset Press, Ankara.

Jafari, E., Nikudel, M.R., Ahmadi, M., 2010. Evaluation of strength characteristics of rocks using cylindrical punch test results. Journal of sciences, University of Tehran, Vol. 36, Issue 1, 169–183.

Kahraman, S., Gunaydin, O., 2009. The effect of rock classes on the relation between uniaxial compressive strength and point load index. Bull. Eng. Geol. Environ. 68, 345–353.

Karakul, H., Ulusay, R., Isik, N.S., 2010. Empirical models and numerical analysis for assessing strength anisotropy based on block punch index and uniaxial compression tests. Int. J. Rock Mech. Min. Sci. 47, 657–665.

Lacharite, N., 1960. A study to correlate the shearing, bending and compression properties of rock. Fuels Min Pract Div Mines Branch, Can

Dept. Mines and Tech Surv., Ottowa, IR 60/38FMIN .17.

Li, D., Wong, L.N.Y., 2012. Point Load Test on Meta-Sedimentary Rocks and Correlation to UCS and BTS. Rock Mech. Rock Eng. DOI 10.1007/s00603-012-0299-x.

Li, D., Wong, L.N.Y., 2013. The Brazilian Disc Test for Rock Mechanics Applications: Review and New Insights. Rock Mech. Rock Eng. 46 (2), 269–287.

Mishra, D.A., Basu, A., 2012. Use of the block punch test to predict the compressive and tensile strengths of rocks. Int. J. Rock Mech. Min. Sci. 51, 119–127.

Ramamurthy, T., Rao, G.V., Singh, J., 1993. Engineering behavior of phyllites. Eng. Geology 33, 209–225.

Saroglou, H., Marinos, P., Tsiambaos, G., 2004. The anisotropic nature of selected metamorphic rocks from Greece. The Journal of the South African Institute of Mining and Metallurgy, 217–222.

Schrier van der, J.S., 1988. The block punch index test. Bull Int. Assoc. Eng. Geol. 38, 121-6.

Shalabi, F.I., Cording, E.J., Al-Hattamleh, O.H., 2007. Estimation of rock engineering properties using hardness tests Eng. Geology 90, 138–147.

Sulukcu, S., Ulusay, R., 2001. Evaluation of the block punch index test with particular reference to the size effect, failure mechanism and its effectiveness in predicting rock strength. Int. J Rock Mech. Min. Sci. 38, 1091–1111.

Tsidzi, K.E.N., 1990. The influence of foliation on point load strength anisotropy of foliated rocks. Engineering Geology, 29, 49–58.

Ulusay, R., Gokceoglu, C., 1997. The modified block punch index test. Can. Geotech. J. 34, 991-1001.

Ulusay, R., Gokceoglu, C., Sulukcu, S., 2001. Draft ISRM suggested method for determining block punch strength index (BPI). Int. J. Rock Mech. Min. Sci. 38, 1113–1119.

Zhang, X.P., Wong, L.N.Y., Wang, S.J., Han, G.Y., 2011. Engineering properties of quartz mica schist. Eng. Geology 121, 135–149.

The Relation between Uniaxial Compressive Strength and Block Punch Index for Pyroclastic Rocks

S. Kahraman
Hacettepe University, Mining Engineering Department, Ankara, Turkey

M. Sarıbıyık
Graduate School of Natural and Applied Sciences, Nigde University, Nigde, Turkey

ABSTRACT Because preparing the desired smooth specimens from pyroclastic rocks is difficult for some standard tests, the development of some equations is important for predicting the uniaxial compressive strength (UCS) of these rocks. In this study, the relation between the UCS and block punch index (BPI) for pyroclastic rocks was investigated. Twenty eight different samples of pyroclastic rocks collected from the Cappadocia Region were tested in the laboratory. The linear regression analysis shows that the UCS-BPI conversion factor for the tested rocks is 3.0. On the other hand, the correlation coefficient of power law function is higher than that of the linear function. Concluding remark is that the UCS-BPI conversion factor for the pyroclastic rocks is lower than the suggested general conversion factor of 5.5 and the UCS-BPI relation is best represented by power law function.

Keywords: Pyroclastic rocks, UCS, BPI

1 INTRODUCTION

The uniaxial compressive strength (*UCS*) of rock is commonly used in civil and mining engineering projects performed in rock environment. However, the test for determining UCS is time consuming and expensive. On the other hand, it requires well-prepared and high quality core samples. For this reason, some indirect tests such as point load, block punch index test, Schmidt hammer, and ultrasonic velocity tests have been frequently used to predict *UCS* for preliminary studies (Broch and Franklin, 1972; Gunsallus and Kulhawy, 1984; Gaviglio, 1989; Sachapazis, 1990; Katz et al., 2000; Kahraman, 2001; Ulusay et al., 2001; Yasar and Erdogan, 2004; Fener et al., 2005; Basu and Kamran, 2010; Kohno and Maeda, 2012 ; etc.). However, the core length may be too short to allow the preparation of specimens long enough even for point load testing, if rock cores are divided into small discs due to the presence of thin bedding or schistosity planes. Block punch index (BPI) test is suggested by Ulusay and Gokceoglu (1998) to solve the above problems

A wide range of rocks were tested and a linear correlation with a conversion factor of 5.1 was suggested by Ulusay et al. (2001) for the prediction of UCS from BPI. In this study, the relation between UCS and BPI was investigated for pyroclastic rocks to check whether the suggested conversion factor is valid and the relation is linear for these rocks.

2 PREVIOUS STUDIES

There are several studies on the relation between the UCS and BPI of rocks in the literature. Available studies are briefly explained and suggested regression equations are given following:

van der Schrier (1988) were tested a total of 1150 specimens pertaining to nine rock types (breccia, calcarenite, calcilutite, dunite, gneiss, limestone, marble, mudstone, and sandstone) and found a high correlation between UCS and BPI. The equation of the correlation as follows:

$$UCS = 6.1BPI - 3.3 \quad (1)$$

where UCS is uniaxial compressive strength (MPa) and BPI is block punch index (MPa).

Ulusay and Gokceoglu (1997) performed BPI and UCS tests on twenty-three different rock types including igneous, volcanic, sedimentary, and metamorphic rocks. They analyzed data by using both linear and non-linear regression method and derived following relations between UCS and BPI:

$$UCS = 5.51BPI_c \quad (2)$$

$$UCS = 5.29BPI_c^{1.01} \quad (3)$$

$$UCS = 9.82e^{-0.108BPI_c} \quad (4)$$

$$UCS = 40.48\ln BPI_c - 13.4 \quad (5)$$

where UCS is uniaxial compressive strength (MPa) and BPI_c is the size corrected block punch index (MPa).

Gokceoglu and Aksoy (2000) presented new approaches for the characterization of clay-bearing, densely jointed and weak rocks such as marl, mudstone, sandstone, and schist. They also correlated UCS with BPI and found following relation:

$$UCS = 5.25BPI_c \quad (6)$$

Sulukcu and Ulusay (2001) carried out BPI and UCS tests on twenty-three different rock types. After combining their data with the data from previous studies (Ulusay and Gokceoglu, 1997; Ulusay and Gokceoglu, 1998; Ulusay and Gokceoglu, 1999), they evaluated the data of forty one different rock types and suggested following equation:

$$UCS = 5.1BPI_c \quad (7)$$

Mishra and Basu (2012) investigated the applicability of BPI test for estimating uniaxial compressive and Brazilian tensile strengths of granite, schist and sandstone samples from India. They derived following equations:

For granites

$$UCS = 4.02BPI_c + 36.16 \quad (8)$$

For schists

$$UCS = 1.35BPI_c + 10.89 \quad (9)$$

For sandstones

$$UCS = 4.99BPI_c + 10.69 \quad (10)$$

For all tested rocks

$$UCS = 4.93BPI_c \quad (11)$$

Yesiloglu-Gultekin et al. (2013) aimed to develop some estimation models by using for the UCS of six different granitic rocks from Turkey. They used tensile strength, BPI, point load index, and P-wave velocity in their analysis and found following logarithmic relation between UCS and BPI:

$$UCS = 47.106\ln BPI_c - 17.589 \quad (12)$$

A very detailed study was carried out on a wide range of rock types and a linear relation (Eq. 7) between UCS and BPI with a conversion factor is 5.1 was suggested in 2001 (Sulukcu and Ulusay, 2001). However, recent studies (Mishra and Basu, 2012; Yesiloglu-Gultekin et al., 2013) show that the relation between UCS and BPI may differ from the suggested relation or may not be linear for individual rock types.

3 SAMPLING

The sampling area is the Cappadocian Volcanic Province (CVP) located in the central Anatolia (Fig. 1). The CVP extends as a belt in NE-SW direction with a long axis of about 300 km and is in large part situated within the Anatolide tectonic belt. The main units in the province are basement rocks, Yeşilhisar Formation, Ürgüp Formation, and Quaternary deposits.

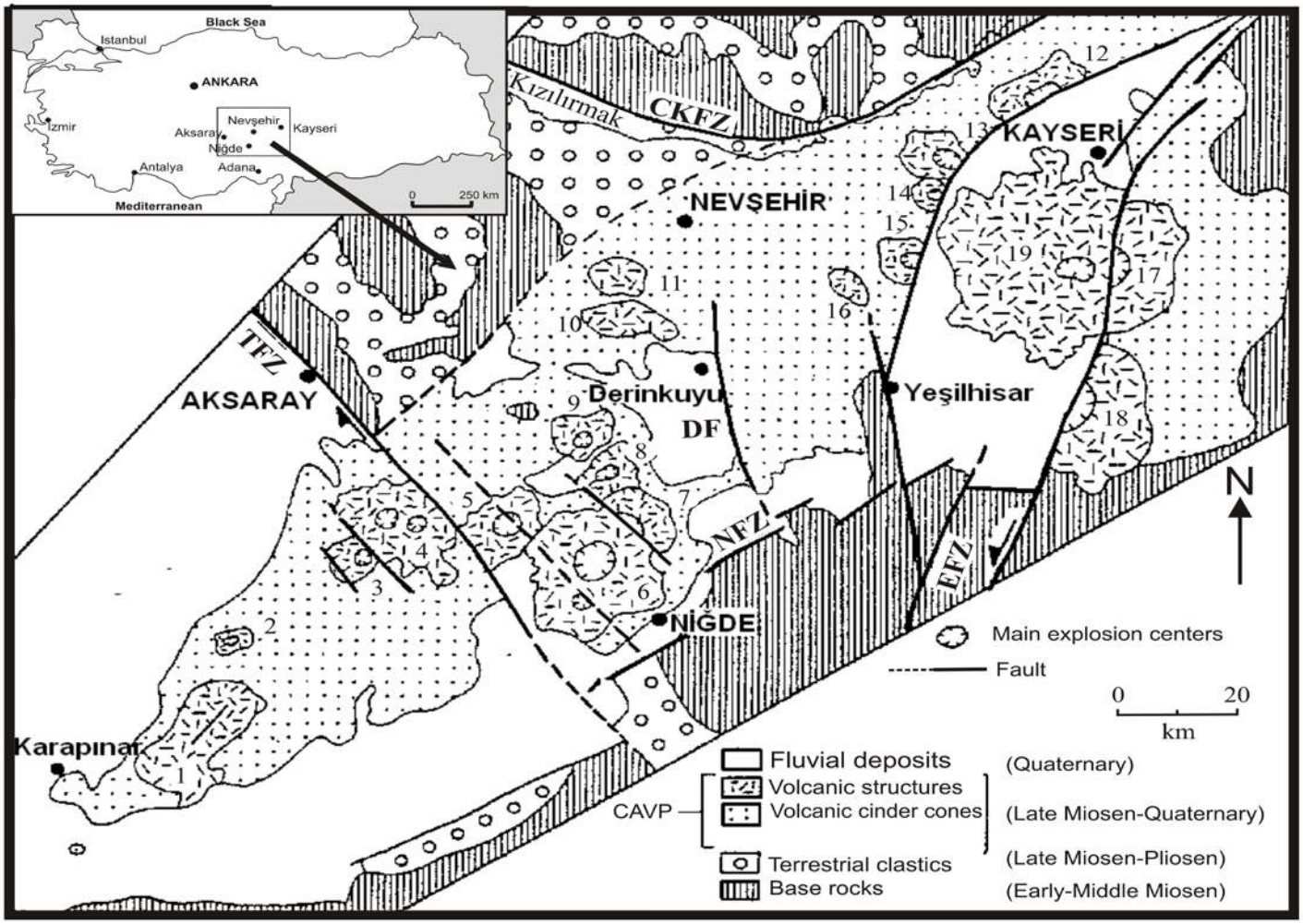

Figure 1. Simplified geological map of Cappadocian Volcanic Province (CVP). Numbers show the major volcanic complexes: 1. Karacadag volcanics, 2. Kotudag volcanics, 3. Kecikalesi volcanics, 4. Hasandag volcanics, 5. Keciboyduran volcanics, 6. Melendiz volcanics, 7. Tepekoy volcanics, 8. Cinarli volcanics, 9. Golludag volcanics, 10. Acigol volcanics, 11. Kizilcin volcanics, 12. Erkilet volcanics, 13. Hamurcu volcanics, 14. Seksenveren volcanics, 15. Tekkedag volcanics, 16. Hoduldag volcanics, 17. Kocdag volcanics, 18. Develidag volcanics, 19. Erciyes volcanics (Toprak et al. 1994).

The Ürgüp Formation corresponds to Mio-Pliocene ignimbritic volcanoclastic rocks intercalated with sediments of lacustrine and fluvial facies. It has a thickness of more than 400 m and extends throughout the CVP. It consists of seven ignimbritic members (Kavak, Zelve, Sarımaden Tepe, Cemilköy, Tahar, Gördeles and Kızılkaya), two lava flows (Damsa and Topuzdağ) intercalated with sedimentary rocks (Çökek Member).

Block samples of pyroclastic rocks were collected from the 28 different sites in the CVP. Each block sample was inspected for macroscopic defects so that it would provide test specimens free from fractures, partings or alteration zones. The sites of the samples and some properties are given in Table 1.

4 EXPERIMENTAL STUDIES

4.1 Density test

Dry and saturated densities were determined by using trimmed core samples according to ISRM (2007) standards. The specimen volumes were calculated from the average of several calliper readings. The dry and saturated mass of the specimens were determined by a balance, capable of weighing to an accuracy of 0.01g of the sample mass. The density values (ρ) were obtained from the ratio of the specimen

Table 1. Sampling areas and some properties of samples.

Rock code	Location	Colour	Dry density (g/cm^3)	Saturated density (g/cm^3)	Porosity (%)
1	Dere Mah.-1/Nigde	Grey	1.53	1.79	26.6
2	Dere Mah.-2/Nigde	Yellowish	1.43	1.72	29.4
3	Kiziloren/Nigde	Beige	1.74	1.99	24.6
4	Ozbelde/Nigde	Dark yellow	1.65	1.90	25.1
5	Aktas-1/Nigde	Grey-white	1.17	1.59	41.8
6	Aktas-2/Nigde	Black	1.45	1.55	35.1
7	Derinkuyu/Nevsehir	White	1.51	1.79	27.6
8	Karayazi/Nevsehir	Old rose	1.56	1.83	27.5
9	Akkaya/Nigde	White	1.47	1.75	20.3
10	Bahceli/Nigde	Beige-white	1.89	1.95	14.7
11	Gumusler/Nigde	Beige	1.44	1.73	28.9
12	Tomarza/Kayseri	Black	1.23	1.69	35.8
13	Avanos/Nevsehir	Pink	1.46	1.71	25.3
14	Derbent-2/Nigde	Grey	1.60	1.88	27.6
15	Gulluce/Nigde	Yellow	1.68	1.83	15.0
16	Arapli/Kayseri	Beige	1.62	1.85	23.8
17	Mustafapasa/Nevsehir	Pink-white	1.21	1.50	39.1
18	Incesu/Kayseri	Black	1.52	1.84	31.9
19	Avanos/Nevsehir	White	0.81	1.31	40.0
20	Karayazi/Nevsehir	Dark pink	1.58	1.84	25.4
21	Karayazi/Nevsehir	Light yellow	1.41	1.70	28.9
22	Karayazi/Nevsehir	White	1.42	1.68	26.1
23	Karayazi/Nevsehir	Mixed	1.39	1.66	27.6
24	Karayazi/Nevsehir	Yellow	1.40	1.70	29.3
25	Selime/Aksaray	Beige	1.65	1.91	26.2
26	Taspinar/Aksaray	Beige	1.75	1.91	16.0
27	Altunhisar/Nigde	Grey	1.85	2.04	19.0
28	Basakpinar/Kayseri	Greyish	2.05	2.17	12.2

weight to the specimen volume. At least three samples were tested for each rock type and the results were averaged (Table 1).

4.2 Porosity test

The effective porosity values were calculated by using the saturation and calliper techniques (ISRM, 2007). Pore volumes were determined from dry and saturated weights, and sample volumes were obtained from calliper readings. The porosity values (n) were obtained from the ratio of pore volumes to specimen volume. The test was repeated at least three times for each rock type and the results were averaged (Table 1).

4.3 Uniaxial compressive strength (UCS) test

UCS tests were carried out on trimmed core samples, which had a diameter of 38 mm and a length-to-diameter ratio of 2.0-2.5 (ASTM, 1986). The tests were performed on both oven-dried and saturated samples. The stress rate was applied within the limits of 0.5-1.0 MPa/s. The tests were repeated at least five times for each rock type and the average value was recorded as UCS (Table 2)

4.4 Block punch index (BPI) test

BPI tests were conducted on the discs having a diameter of 42 mm and a thickness of about 10 mm (ISRM, 2007). The tests were carried out on both oven-dried and saturated samples. The results were corrected to a

specimen diameter of 50 mm. The tests were repeated at least five times for each rock type and the average value was recorded as BPI (Table 2).

Table 2. Average values of the UCS and BPI_c values.

Rock code	Dry rock UCS (MPa)	Saturated rock UCS (MPa)	Dry rock BPI_c (MPa)	Saturated rock BPI_c (MPa)
1	8.5	3.4	3.5	2.0
2	18.5	9.7	7.8	5.9
3	27.4	17.0	7.4	4.9
4	16.5	14.3	7.5	4.1
5	5.2	3.1	2.0	1.2
6	3.9	2.3	1.9	1.1
7	8.4	4.7	4.3	2.6
8	12.7	5.2	5.5	2.5
9	21.4	14.5	8.7	6.9
10	15.8	9.0	4.8	2.7
11	9.9	4.6	3.7	2.9
12	14.1	7.4	6.2	3.9
13	15.7	8.8	4.6	2.8
14	18.3	12.5	6.8	4.7
15	41.0	28.3	12.0	8.1
16	12.4	9.0	4.8	3.6
17	7.4	1.4	2.6	0.9
18	12.4	8.3	5.5	3.8
19	2.2	1.7	1.3	0.8
20	10.3	2.7	1.7	0.7
21	9.1	3.7	2.9	1.6
22	8.5	2.6	3.0	1.7
23	7.9	2.2	1.8	1.0
24	8.8	3.6	2.8	2.1
25	25.7	12.9	5.0	4.3
26	18.8	8.0	7.0	4.9
27	23.9	16.1	6.6	4.2
28	46.7	28.0	9.8	7.0

5 EVALUATION OF THE RESULTS

As shown in Table 2, dry rock UCS values vary from 2.2 MPa for the Avanos/Nevsehir sample to 46.7 MPa for the Basakpinar/ Kayseri sample. Saturated rock UCS values vary from 1.4 MPa for the Mustafapasa/ Nevsehir sample to 28.3 MPa for the Gulluce/ Nigde sample. Dry rock BPI values vary from 1.3 MPa for the Avanos/Nevsehir sample to 12.0 MPa for the Gulluce/Nigde sample. Saturated rock BPI values vary from 0.7 MPa for the Karayazi/Nevsehir (dark pink) sample to 8.1 MPa for the Gulluce/Nigde sample.

The test results presented in Table 2 were analyzed using the method of least squares regression. Several types of relationships were investigated (e.g. linear, logarithmic, exponential, power) and the equation of the best-fit line, the 95% confidence limits, and the correlation coefficients (r) were determined for each regression.

The power law function better correlates the relation between *UCS* and BPI for both dry rocks and saturated rocks (Figs. 2 and 3). Regression analysis was repeated for the combined data of dry and saturated rock and a power law relation was found again between the two parameters (Fig. 4).

As stated above, the UCS-BPI conversion factor of 5.1 was suggested by Sulukcu and Ulusay (2001) for a wide range of rock

types. However, it was indicated in some recent studies (Mishra and Basu, 2012; Yesiloglu-Gultekin et al., 2013) that this conversion factor may not be valid for individual rock types. Similarly, pyroclastic rocks tested in this study showed a different trend with the suggested relation. As shown in Fig. 4, the UCS-BPI conversion factor is found as 3.0. This value is fairly lower than the suggested conversion factor of 5.1.

Another important result of this study is that the relation between UCS and BPI is best represented by the power law function, not by the linear function. The correlation coefficients of power law functions are higher than that of linear functions for each case such as dry, saturated and both dry and saturated rocks.

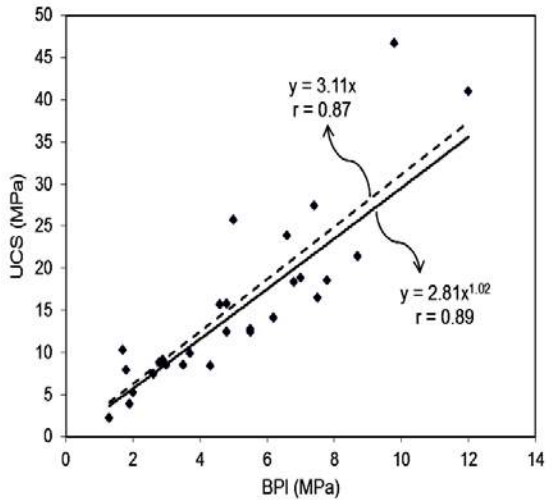

Figure. 2. The relation between UCS and BPI for dry rocks.

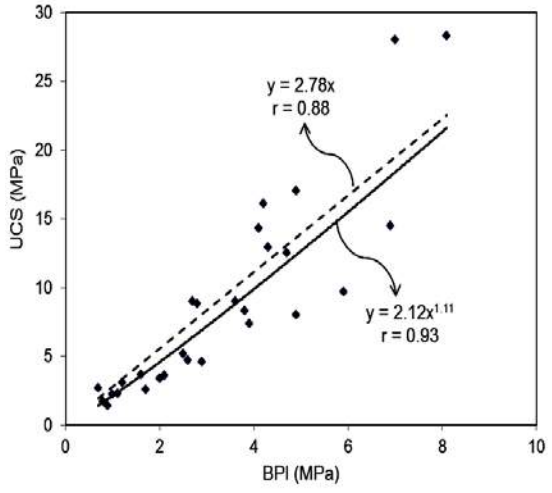

Figure 3. The relation between UCS and BPI for saturated rocks.

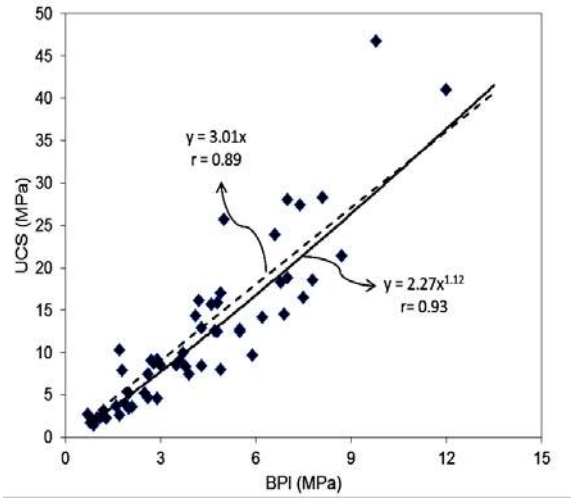

Figure 4. The relation between UCS and BPI for both dry and saturated rocks.

6 CONCLUSIONS

Twenty eight different samples of pyroclastic rocks were tested and the relation between UCS and BPI was investigated by using regression analysis. A UCS-BPI conversion factor of 3.0 was obtained by linear regression analysis for the tested rocks. This conversion factor is fairly lower than the suggested value of 5.1. The nonlinear regression analysis also indicated that the correlation coefficients of power law functions are higher than that of the linear functions for each case.

It is concluded that the UCS-BPI conversion factor is lower than the suggested general conversion factor for the evaluated pyroclastic rocks and the UCS-BPI relation is best represented by the power law function. Further research is necessary to check whether the results are valid for all types of pyroclastic and soft rocks.

ACKNOWLEDGEMENT

This study has been supported by the Turkish Academy of Sciences (TUBA), in the framework of the Young Scientist Award Program (EATUBA-GEBIP/2001-1-1).

REFERENCES

ASTM. 1986. *Standard test method of unconfined compressive strength of intact rock core specimens*. D2938.

Basu, A., Kamran, M. 2010. Point load test on schistose rocks and its applicability in predicting uniaxial compressive strength. *Int. J. Rock Mech. Min. Sci.* 47, 823–828.

Broch, E, Franklin, J.A. 1972. Point-load strength test. *Int. J. Rock Mech. Min. Sci.* 9 (6), 669-697.

Fener, M., Kahraman, s., Bilgil, A., Gunaydin, O. 2005. A comparative evaluation of indirect methods to estimate the compressive strength of rocks. *Rock Mech. Rock Eng*. 38(4), 329-343.

Gaviglio, P. 1989. Longitudinal wave propagation in a limestone: The relationship between velocity and density. *Rock Mech. Rock Eng*. 22 299-306.

Gokceoglu C, Aksoy H. 2000. New approaches to the characterization of clay-bearing densely jointed and weak rock masses. *Eng. Geol*. 58:1–23.

Gunsallus, K.L., Kulhawy, F.H. 1984. A comparative evaluation of rock strength measures. *Int. J. Rock Mech. Min. Sci.* 21, 233-248.

ISRM. 2007. *The complete ISRM suggested methods for rock characterization, testing and monitoring: 1974-2006.* Ulusay R., Hudson J.A., Editors. Ankara: Kozan Ofset Press.

Kahraman, S. 2001. Evaluation of simple methods for assessing the uniaxial compressive strength of rock. *Int. J. Rock Mech. Min. Sci.* 38, 981-994.

Katz, O., Reches, Z., Roegiers, J.C. 2000. Evaluation of mechanical rock properties using a Schmidt hammer. *Int. J. Rock Mech. Min. Sci*. 37, 723–728.

Kohno, M., Maeda, H. 2011. Estimate of uniaxial compressive strength of hydrothermally altered rocks from northeastern Hokkaido, Japan, based on axial point load strength test results. *Int. J. JCRM* 7, 17-23.

Mishra DA, Basu A. 2012. Use of the block punch test to predict the compressive and tensile strengths of rocks. *Int. J. Rock Mech. Min. Sci*. 51:119–27.

Sachapazis, C.I. 1990. Correlating Schmidt hardness with compressive strength and Young's modulus of carbonate rocks. *Bull. Int. Assoc. Eng. Geol*. 42, 75–83.

Sonmez, H. and Tunusluoglu, C. 2008. New considerations on the use of block punch index for predicting the uniaxial compressive strength of rock material. *Int. J. Rock Mech. Min. Sci*.45: 1007–1014

Sulukcu S, Ulusay R. 2001. Evaluation of the block punch index test with particular reference to the size effect, failure mechanism and its effectiveness in predicting rock strength. *Int. J. Rock Mech. Min. Sci*. 38:1091–111.

Ulusay R, Gokceoglu C, Sulukcu S. 2001. Draft ISRM suggested method for determining block punch strength index (BPI). *Int. J. Rock Mech. Min. Sci*. 38:1113–1119.

Ulusay R, Gokceoglu C. 1997. The modified block punch index test. *Can. Geotech. J.* 34: 991–1001.

Ulusay R, Gokceoglu C. 1998. An experimental study on the size effect in block punch index test. *Int. J. Rock Mech. Min. Sci*. 35(4–5): 628–629 (In: NARMS'98 ISRM International Symposium. Cancun, Mexico, Paper No. 008).

Ulusay R, Gokceoglu C. 1999. A new test procedure for the determination of the Block Punch Index and its possible uses in rock engineering. *ISRM News J*. 6 (1):50–4.

van der Schrier, J.S. 1988. The block punch index test. *Bull. Int. Assoc. Eng. Geol*. 38: 121–126.

Yasar, E., Erdogan, Y. 2004. Correlating sound velocity with density, compressive strength and Young's modulus of carbonate rocks. *Int. J. Rock Mech. Min. Sci*. 41: 871-875.

Yesiloglu-Gultekin N., Gokceoglu , C., Sezer, E.A. 2013. Prediction of uniaxial compressive strength of granitic rocks by various nonlinear tools and comparison of their performances. *Int. J. Rock Mech. Min. Sci*. 62 113–122.

Thermo-Mechanical Behaviour of Rocks from the South African Platinum Mines

G. O. Oniyide, H. Yilmaz
School of Mining Engineering, The University of the Witwatersrand, Johannesburg, South Africa

ABSTRACT This paper presents the results of the study on the impact of temperature on the behaviour of selected rocks from the South African platinum mines. These mines are influenced by increasing temperatures due to high temperature gradient. The rock samples from the platinum mines were tested under varying confinements (10 to 30 MPa) and temperatures (20 to 140 °C) using servo-controlled testing machine. The results of the laboratory tests show that increasing temperature results in reduction of yield strength and Young's modulus. Relationships between temperature and strength as well as the elastic modulus were established. These relationships would assist in the proper use of input parameters in numerical modelling exercises using the temperature option. The future design of deeper and warmer platinum mines would also hugely benefit from the knowledge of rock behaviour generated under high temperature and stresses.

Keywords: Temperature testing, rock strength, platinum mines

1 INTRODUCTION

Increasing depth of mining in underground mines brings about the challenges related to heat, in-situ stresses and logistical issues. Heat associated problems have mainly focused on the side effect of heat on workers' health (heat-stroke), increasing production costs as a result of higher cost of ventilation due to cooling and refrigeration. The effect of increasing temperature with increasing depth on the behavior of rock has not been given much consideration.

The platinum mines are in the Bushveld Igneous Complex (BIC), which is located in the northern part of South Africa. The BIC is the world's largest layered intrusion. It is about seven to nine kilometers thick and is divided into eastern, western and northern limbs. Its upper critical zone hosts the world's largest deposit of platinum group elements (PGE), (Schouwstra and Kinloch, 2000). Geological exploration information revealed the possibility of the platinum mines going for ultra-deep mining in future. Schouwstra and Kinloch (2000) stated that the Merensky Reef has been traced for 300 km around the entire outcrop of the eastern and western limbs of the BIC, and to depths of 5 km and beyond.

Gold mines in South Africa are generally deeper than the platinum mines, however, the latter has higher temperature gradient, which makes the platinum mines to be much warmer as the depth of mining increases. Biffi et al (2007) made a comparison of the geo-thermal gradient of the Witwatersrand Basin complex known by its gold mining and the BIC and reported that a virgin rock temperature of 40°C will be reached at an approximate depth of 650 m in the BIC as compared to a depth of about 1800 m in the West Witwatersrand Basin complex. The study of the effect of temperature on the rock behaviour would be beneficial to both gold and platinum mines, however the main focus of the research is on the platinum mines due to their higher temperature gradient. Donoghue (2004) stated that the virgin rock temperatures (VRT) and air temperatures increase with depth, due to the geothermal gradient and auto-compression of air column. Figure 1 shows the comparison of the VRT,

while Figure 2 shows the VRT for the mines in BIC.

Cawthorn (1999) proposed adapting the knowledge from deep mining on the gold-bearing Witwatersrand mines to platinum mines. He, however, noted that higher temperatures would be an additional factor that would influence the platinum mines as they go deeper. Therefore, in consideration of possible problems that would result from high stresses and high temperatures in deep platinum mines in the future, investigation of the influence of these parameters on the rock behaviour becomes necessary from rock engineering perspective.

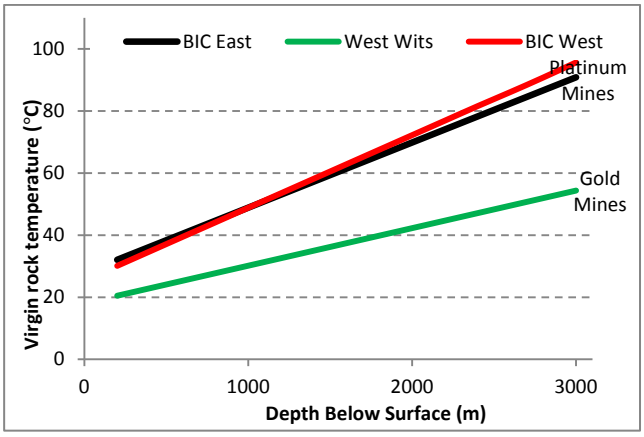

Figure 1. VRT against depth below surface (adapted from Biffi et al, 2007).

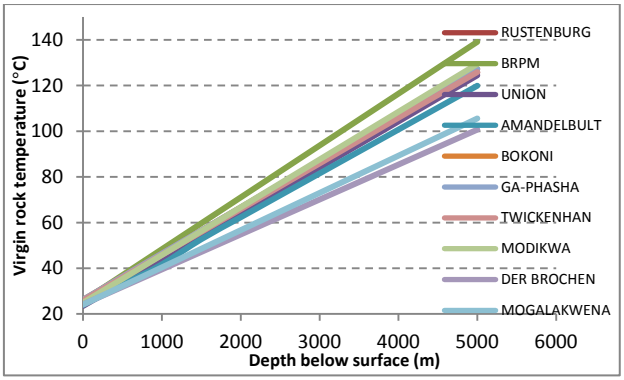

Figure 2. VRT against depth for platinum mines in BIC.

2 EXPERIMENTAL SET-UP AND ROCK TESTING

The rock samples tested were 36mm diameter cores that were obtained from Bafokeng Rasimone Platinum mine (BRPM) located in the western limb of the BIC. The samples are norite (N), leuconorite (LN), mottled anorthosite (MA), chromitite (CR), pyroxenite (PX), vari-textured anorthosite (VTA) and anorthosite-chromitite (ANCR).

MTS 793 servo-controlled testing machine, which is a stiff testing machine, was used for the triaxial compression tests at various temperatures. The MTS triaxial cell is designed for conducting tests with thermal option. The machine assembly consists of a fixed crosshead mounted on two rectangular columns which are bolted to the base, providing a high loading capacity in a stiff frame. Once the triaxial cell is inserted into the test space, the loading frame applies axial stress to the specimen inside the cell.

The load cell (Force transducer) has a maximum loading capacity of 2600 kN, which is accurate to within ±0.5% of the calibrated range. The triaxial cell has a confining pressure capacity of 140 MPa. The heating elements embedded on the cell allows tests to be done as high as 200 °C. The triaxial cell, when lowered onto the base plate forms a sealed pressure chamber for the specimen and extensometer assembly.

The tests are aimed at replicating the environment that the rocks would be exposed to in the platinum mines, where the VRT would increase as the mining depth increases. The tests are also intended to provide information on the post-peak behaviour of the rocks obtained. This information is very important in understanding the process of specimen deformation, starting from the stage of crack initiation to complete failure. The test results would provide insight into the residual strength of the in-situ rock mass.

2.1 Sample Preparation

The specimens were prepared according to ISRM (1999) standard for uniaxial and triaxial compressive strength testing with a length to diameter ratio of 2.5. The ends of the specimen were cut and ground parallel to each other and at right angle to the longitudinal axis. The disparity between the perpendicular ends of the specimen to its longitudinal axis was not more than 0.05 in

50 mm. The specimen (Figure 3) is jacketed in heat-shrink teflon material to prevent confining fluid from getting in touch with the rock specimen during heating and loading.

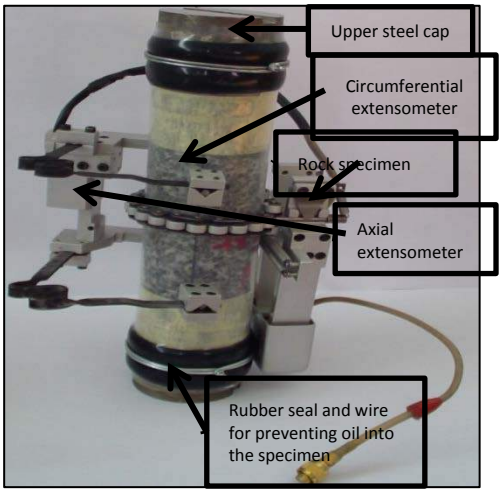

Figure 3. Prepared specimen for testing.

2.2 Temperature Control

The main objective of performing the tests was to study the response of the BIC rocks under increasing temperatures (20 °C, 50 °C, 90 °C, and 140 °C) and confinements (10 MPa, 20 MPa, and 30 MPa). The specimens were heated at the rate of 2 °C /minute until the desired temperature was reached. And then, the temperature was kept constant for one hour to allow for even distribution of heat in the triaxial cell and through the specimen.

2.3 Loading of Test Specimens

The axial stress and the confining pressure are simultaneously increased until the desired confinement is reach at rate of 0.5 MPa/minute. The control mode is then switched to axial strain control and the specimen was loaded at an axial strain rate of 0.001mm/mm/s until reaching approximately 70% of the expected peak force. Since most of the tested specimens are brittle, the axial strain control mode can only be used in the elastic region of the stress-strain curve. At 70% of peak force, the control mode was switched to circumferential strain control at a rate of 10^{-6} mm/mm/s, until the applied load dropped to 50% of peak force in the post-failure region. The control mode was then returned to axial strain control until the completion of the test.

The use of circumferential strain transducer as the feedback has been known (ISRM, 1999)) as the most sensitive means of detecting specimen failure. However, it should be noted that when a trial test was conducted with circumferential strain as the control mode at 70% of the expected peak stress, the test was terminated unsuccessfully. Then, dual compensation control, that is, using a combination of displacement and circumferential strain as the feedback mode, was used.

The machine displacement, in-built-calculated stress, temperature, confining pressure, axial and circumferential strain were continuously captured in a data file at all stages of testing. Five tests were done for each rock type. The test data were then processed to evaluate the Young's modulus at 50% of the peak strength, E_t, as the slope of tangent line of axial stress-axial strain curve.

3 RESULTS AND DISCUSSION

In this paper, the effect of temperature on the behaviour of rocks is analysed only at confining pressure of 10 MPa for ease of comparison. Table 1 shows the averages of Young's modulus of the rocks tested at 10 MPa confinement and increasing temperatures. Figure 4 shows the stress-strain behaviour of norite tested at 20°C, 50°C, 90°C, 140°C and at each temperature confining pressures of 10 MPa, 20 MPa and 30 MPa were applied.

Table 1. Average values of Young's modulus (GPa) at 10 MPa confining pressure with increasing temperature.

Rocks	Temperature			
	20 °C	50 °C	90 °C	140 °C
CR	58.5	56.2	53.8	51.7
LN	78.4	76.6	73.5	70.7
MA	87.1	84.7	82.9	79.9
N	79.6	77.7	74.3	71.1
PX	121.0	118.6	114.8	112.9

It is clearly seen in Table 1 and Figure 4 that increasing temperature results in the reduction of the Young's modulus and peak strength. The ambient temperature is approximately 20 °C at which the samples are tested initially, while 50 °C, 90 °C, and 140 °C correspond approximately to the VRT in the platinum mines at 1073 m, 2835 m and 5037 m below surface respectively. It should be noted that the test results between ambient temperature and increased levels of temperature vary considerably.

Table 2 shows the influence of temperature on the strength and Young's modulus in terms of percentage reduction in the strength and Young's modulus magnitudes as the temperature increases from 20°C to 140°C. It can be seen that 17.3% and 9.4% reductions in the strength and Young's modulus are significant. The reductions are rock type dependant with Chromitite having the highest percentage reductions. This knowledge is of particular importance since the Chromitite is the main reef body where the mining operations are concentrated. Therefore, designs based on rock engineering principals have to take the influence of temperature on rock behaviour into account, particularly in areas with high geothermal gradient .

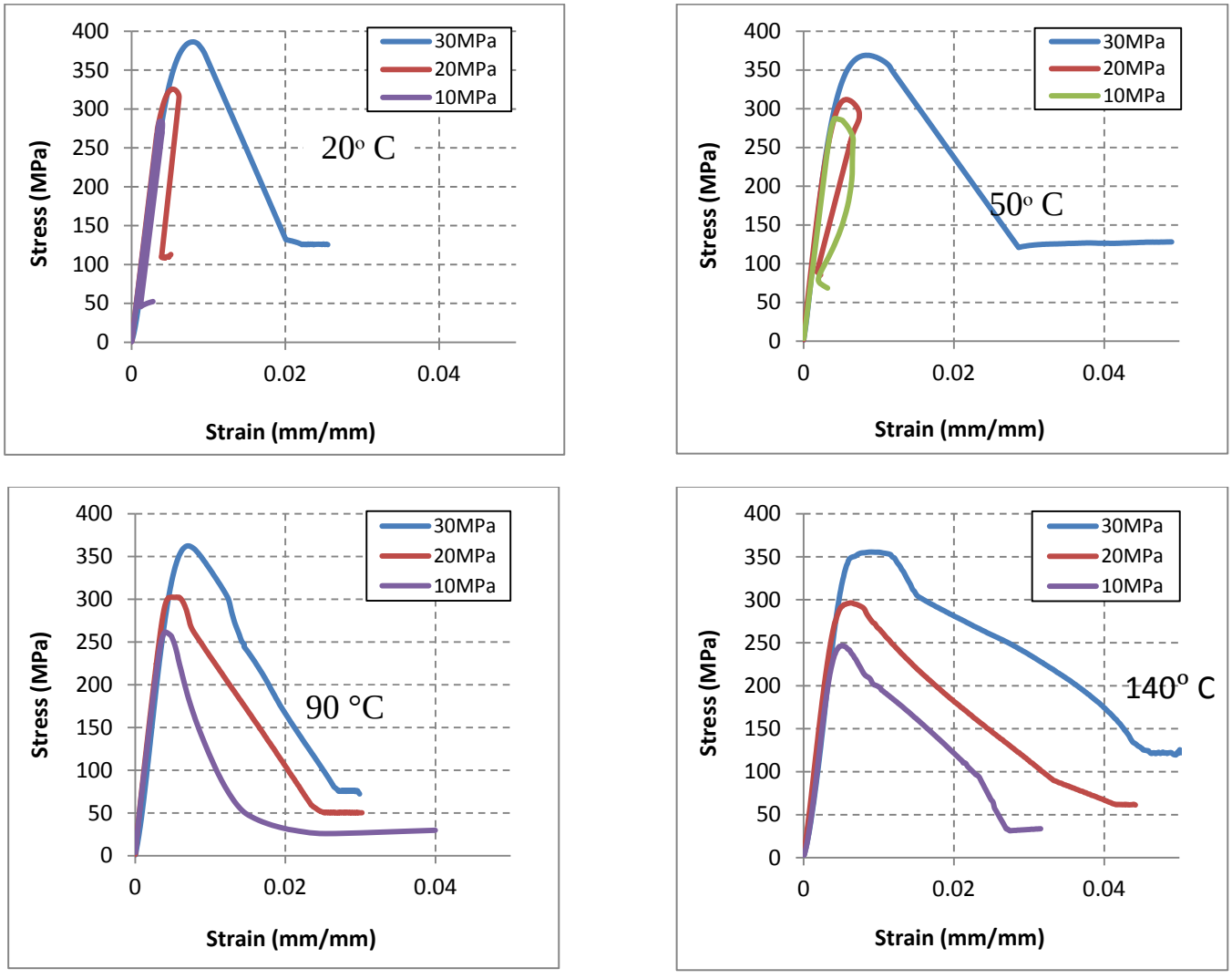

Figure 4: Influence of temperature on triaxial compressive strength and post-failure behaviour between 20°C to 140°C.

Table 2: Reduction in strength and Young's modulus of rocks due to temperature increase from 20°C to 140°C.

% REDUCTION in	CR	LN	MA	N	PX	Average
Strength	20.7	15.4	18.5	13.3	18.9	17.3
Young's modulus	11.7	9.8	8.3	10.7	6.7	9.4

3.1 Regression Analyses

Three specimens were tested per rock type per temperature at 10 MPa confining pressure and the averages of Young's modulus were used to produce the data points on the graph in Figure 4. The selected temperatures were 20 ºC, 50 ºC, 70 ºC, 90 ºC, 110 ºC, and 140 ºC. Figure 4 shows that the values of the gradient "m" range between -0.058 and -0.100. The correlation coefficients "R^2" range between 0.95 and 0.99, which means that there is strong correlation between Young's modulus and temperature.

Therefore, the data provided in Table 1 and Figure 5 is utilised to develop a simple linear regression model (y = mx + c) between temperature and Young's modulus considering that the temperature will increase as mining goes deeper. The ambient Young's modulus (E_{amb}) becomes the constant "c". The gradient "m" is evaluated for each rock type in Figure 5. Therefore, the following general equation can be written to estimate the Young's modulus for a particular rock subject to increasing temperatures:

$$E_t = -m\,(T - T_{amb}) + E_{amb} \qquad (1)$$

where ; E*t* is the temperature dependent Young's modulus (GPa)
T is any temperature between 20 ºC and 140 ºC ($T \geq T_{amb}$)
T_{amb} is the ambient temperature (in this case 20 ºC)

It should be noted that E_{amb} is the Elastic modulus taken from Table 1 at 20 ºC and not the zero intercept provided in Figure 5. The "m" value is rock type dependent. For example, norite (N) has E_{amb} magnitude of 79.6 GPa (Table 1) and m value of -0.074 (Figure 5). Further research is required to check the sensitivity of "m" value to confinements other than 10 MPa.

Although the ambient temperature used in Equation 1 is 20 ^oC, it is assumed that specimens tested at 20 ^oC ± 5 ^oC would still be accommodated. This is based on the information provided by Kruger and Shongwe (2004), who reported that the average annual temperature of South Africa for 1960 to 1990 and 1991 to 2003 as 18.18 ^oC and 18.48 ^oC respectively. This temperature given is that of outdoor. It implies that the ambient room temperature used in in equation 1 falls within acceptable range.

The comparison of the Young's modulus determined from actual laboratory testing and the one estimated using equation 1 is given in Figure 6. Only two of the rocks are provided as examples in Figure 6. The percentage difference between the laboratory determined values and the ones calculated from equation 1 is negligible as shown in Figure 6 and Table 3.

Table 3. Percentage difference between laboratory measured and calculated Young's modulus.

	50 ºC	**70 ºC**	**90 ºC**	**110 ºC**	**140 ºC**	**Absolute average**
CR	-0.97	-0.50	-1.12	-1.92	0.52	0.84
LN	0.26	-1.36	-0.44	-0.44	0.17	0.45
MA	-0.81	-0.51	-0.17	-0.39	-0.30	0.36
N	0.42	0.01	-0.19	-0.37	0.48	0.25
PX	-0.21	-0.41	-0.98	-1.12	0.52	0.54
VTA	0.76	0.42	-0.58	-0.03	0.61	0.40
ANCR	-0.37	0.73	0.11	0.04	-0.18	0.24

Note: Negative sign denotes underestimation, while positive denotes overestimation.

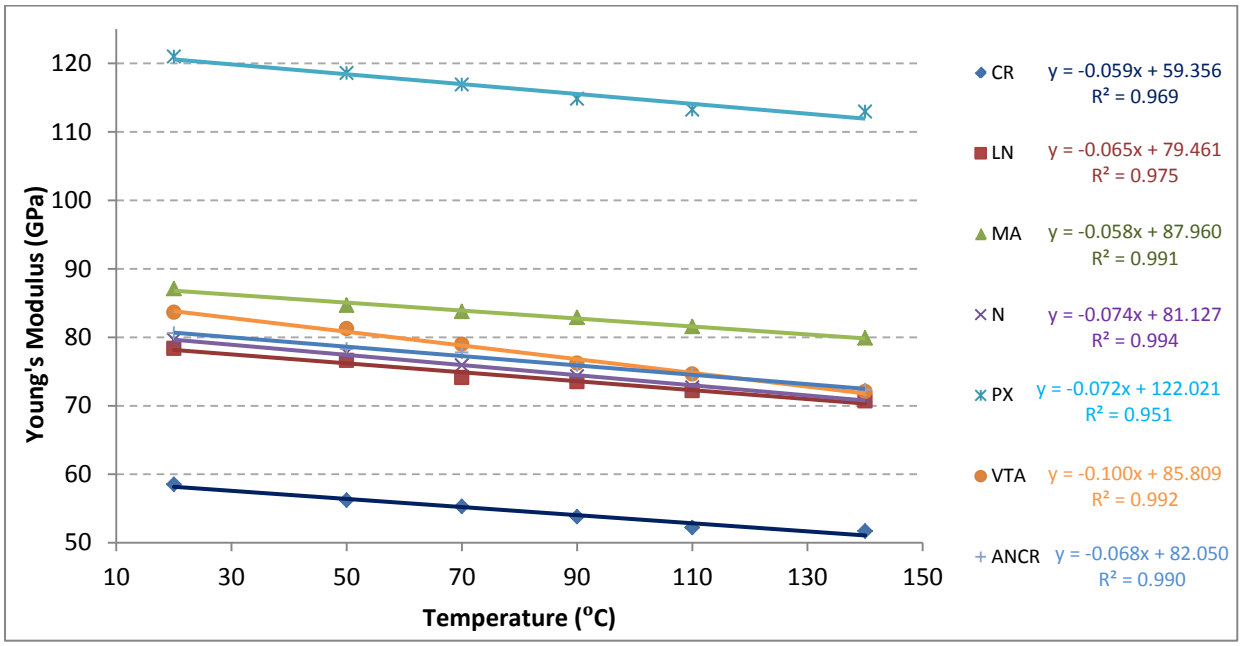

Figure 5. Young's modulus and temperature relationship for various rock types.

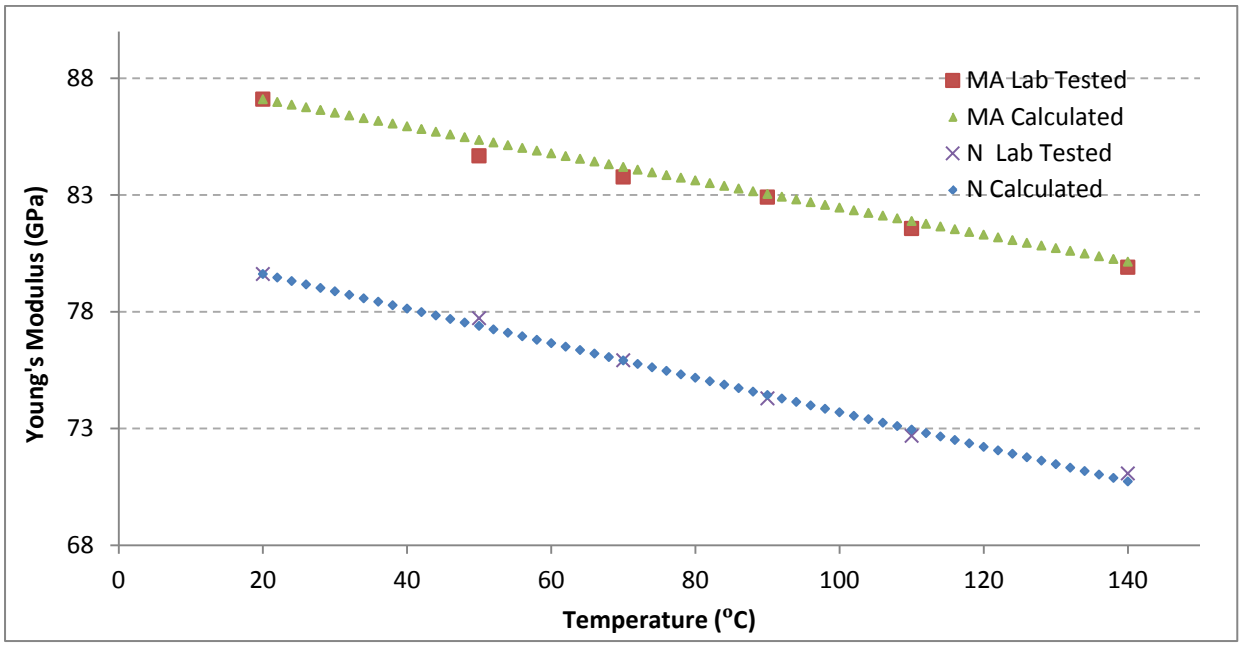

Figure 6. Comparison of Laboratory tested and calculated Young's modulus for two rocks.

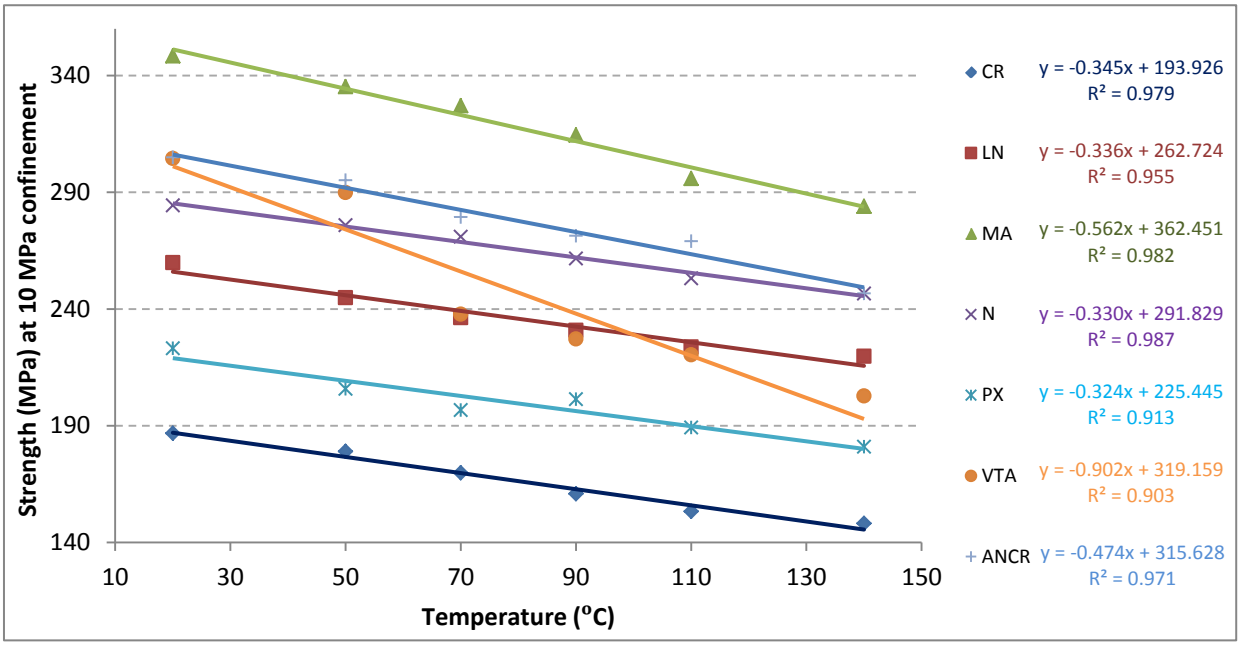

Figure 7: Strength behaviour against temperature at 10 MPa confinement.

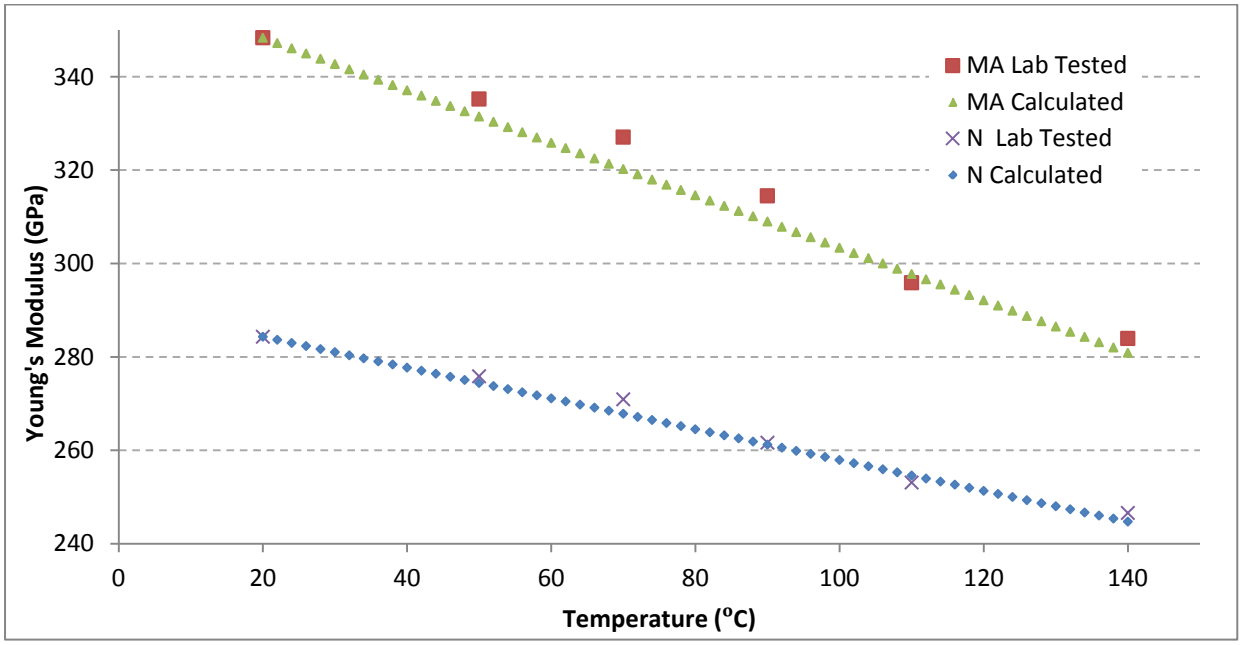

Figure 8. Comparison of Laboratory tested and calculated strength for two rocks.

The percentage difference for all rock types for the temperature range is between -1.92% and 0.76%. The highest percentage difference in absolute terms occurs with CR and the lowest is with ANCR.

Following similar steps as explained for temperature-dependent Young's modulus, a linear regression model (equation 2) was also established for temperature-dependent peak strength from the plot in Figure 7.

$$\sigma_t = -m(T - T_{amb}) + \sigma_{amb} \quad (2)$$

where; σ_t is the temperature dependent strength (MPa)
T and T_{amb} are as explained in equation 1
σ_{amb} is the strength measured at ambient temperature

The comparison of the laboratory-measured strengths and the one estimated from Equation 2 is given in Figure 8, while Table 4 shows the percentage differences. The variation between the laboratory values and the ones derived from the proposed equation 2 is again negligible, except for that of VTA. This variation could be attributed to the inconsistencies in the mineralogical composition of VTA or the presence of internalmicro-cracks.

Table 4: Percentage difference between laboratory measured and calculated strength

	50 °C	70 °C	90 °C	110 °C	140 °C	Absolute average
CR	1.48	0.19	-1.09	-1.57	1.89	1.04
LN	-2.03	-2.89	-2.39	-2.63	0.10	1.67
MA	1.12	2.09	1.75	-0.64	1.07	1.11
N	0.51	1.14	0.15	-0.60	0.75	0.53
PX	-3.68	-5.19	0.44	-2.53	-1.79	2.27
VTA	4.32	-9.01	-6.14	-1.21	3.39	4.01
ANCR	1.50	-0.66	-0.13	2.50	-0.56	0.89

It is suggested that equation 1 and 2 is used for determining the corresponding reduction in Young's modulus and strength respectively with respect to virgin rock temperature as input values for numerical modelling and for subsequent underground rock engineering design.

3 CONCLUSIONS

The South African Platinum mines are going deeper. There would be problems associated with increasing stresses, and mining cost with regards to ventilation, ore transport. An additional problem would arise due to the influence of increasing temperatures on rock behaviour. This paper, in fact, shows that the strength and Young's modulus of the rock types involved in platinum mining undergo reduction with increasing temperatures. The equations to assist the estimation Young's modulus and strength with respect to increasing virgin rock temperatures are proposed. Future rock engineering designs should bear the findings presented in this paper into account particularly when the numerical modelling and the subsequent excavation and support design is done.

REFERENCES

Biffi M., Stanton D., Rose H. and Pienaar D. (2007). Ventilation Strategies to Meet Future Needs of the South African Platinum Industry. *The Journal of The South African Institute of Mining and Metallurgy*. Vol. 107 pp. 59-66.

Cawthorn R. G. (1999). The Platinum and Palladium Resources of the Bushveld Complex. *South African Journal of Science* Vol. 95 pp. 481-489.

Donoghue A. M. (2004). Occupational Health Hazards in Mining: An Overview. *Occupational Medicine* (London). Vol. 54 pp. 283-289.

ISRM (1999). Draft ISRM suggested method for the complete stress-strain curve for intact rock in uniaxial compression. *Int J Rock Mech Min Sci* Vol. 36, No. 3, pp. 279-289.

Kruger A.C. and Shongwe S. (2004). Temperature trends in South Africa: 1960-2003, Int. *J. Climatol*. Vol. 24, pp. 1929-1945.

Schouwstra R.P., Kinloch E.D., Lee C.A. (2000). A short geological review of the Bushveld Complex. *Platinum Metals Review*, 44, pp. 33–39.

Mine Design, Modelling, and Optimization

A Prototype of Real Options Valuation Framework for Open Pit Mines Planning: A Road to Build a Dynamics Decision Making Tools

I. Inthavongsa
Department of Mining Engineering, Faculty of Engineering, National University of Laos, Vientiane, Laos,

P. Sontamino
Department of Mining and Materials Engineering, Prince of Songkla University, Thailand,

C. Drebenstedt
Institute of Mining and Special Construction Engineering, Faculty of Geosciences, Geo-Engineering and Mining, Freiberg University of Mining and Technology, Germany,

ABSTRACT There are a plenty of research have proclaimed that real options valuation (ROV) method is a promising technique for valuing the mineral resource industry in the face of uncertainties. However, it is apparently that this method is rarely used in mining company. This is due to its complexity in solving mathematical mixed integer programming problems (MIPP). Furthermore, there is no exact of existing tools which offer the ease of the quick calculations and reliable results for making flexible alternative decisions. Thus, this article presents the integration of ROV approach and system dynamics (SD) modeling method for developing the dynamics decision making tools (DDMT), for open pit mine planning projects. With the use of SD makes it possible to solve the interdependent variables as well as path-dependent activities. This paper illuminates the conceptual models as well as a roadmap towards developing better decision making tools.

Keywords: ROV, DDMT, SD

1 INTRODUCTION

1.1 Background

Mine planning is a difficult task. Even for small operations, it involves reasoning with complex variables and the practical difficulties of mining. It is also about predicting and planning the future in an unpredictable physical of economic environments. Planning affects everyone in the organization. Company executives are demanding more reliability and stability in cost and revenue forecasts from their operations. Management desires to explore ways of being more cost effective. Miners and contractors need more useful plans and realistic targets. Planners have to describe the method that will translate business into implementable plans [16]. A decision making process involves formulating options, predicting their outcomes and evaluating these against some objectives. This process is cyclically repeated until either the objectives are met or there no more time to consider more options or refine existing options.

It is undeniably that there are commercial software's for planning process, such as MineSight, Surpac, XPAC, and Vulcan, etc. Nevertheless, such software's have quite complicated functions and needed sophisticated experts to carry out the given tasks. Moreover, it is very time demanding processes and it takes many steps to generate single results, which cannot take onboard for making a strategic decision. More in actual

fact, such commercial software's do not have functions to tackle the uncertain conditions during the period of operations in life-of-mine. Martinez [10] suggests that it is of paramount importance for doing more research and development for building new tools that can account for uncertainty and risk in mine project evaluations. Ford and Sobek [4] built a product development project model that uses real options concepts to manage product design risk. Barghav and Ford [2] examined the relationship between project management quality and the value of flexible strategies. Johnson et al. [7] used an SD model to value flexibility in a large petrochemical project. These papers provide examples of how real options logic can be incorporated into SD models; yet they analyze projects with a single option and they do not focus on formalizing an algorithm to estimate the market value of projects with complex option structures using SD models.

Singh [14] proposes capacity expansion planning model for coal mining for Hunter Valley Coal Chain in Australia. The author attempts to solve the mixed integer programming (MIP) models using the commercialized software. Huh et al. [6] considers capacity planning under demand uncertainty using a network optimization based heuristic to determine the sequence and timing for purchasing and retiring machines required to manufacture different products. Sontamino and drebenstedt [15] developed decision making tools for evaluating the feasibility to open coal mines in Thailand. It is clear that there is lack of research which incorporating real options into SD methods. Particularly, there is no studies intent to develop dynamic decision making tools that can handle the uncertainty in open pit mining ventures.

The objective of this research is to develop a better decision making tool that provide user-friendly interface, quick calculations, and generate reliable results. It hopes to build tools which can advocate mine planners that under what conditions the mines should expand its capacities in order to capture the upside potential of favourable market, and at what conditions the mine should maintain, shrink, or shutdown its operations to avoid downside impact and loses. The tools will allow mine planners to input sets of data such as the target of saleable products per year, the target of total productions per year, mining capacity, milling rate, metal price, mining costs, processing costs, among others. This paper should hold an attention of those involved in helping mine operations improve outcomes from investments opportunities by managing uncertainty and risk.

The remainder of this paper is organized as follows: section 2 provides a problem formulation. Section 3 presents methods which applied in this research. In this section, the scope is outlined in order to confine the limit of studies in a certain horizon. Section 4 summarizes the key ideas and roadmap towards developing DDMT. The last section 5 is the conclusion which will provide final remark and highlight the future works of this study.

1.2 Problem Framing

There are existing tools have been used in financial decision-making such as the payback period, the discounted cash flow (DCF) and its alliance net present value (NPV), the internal rate of return (IRR) and the wealth growth rate. These tools are useful and meaningful in evaluating normal projects closely related to regular business where the number of assumptions made is usually very small and where the cost of capital is usually selected as a hurdle rate. It is arguable that in situations where a significant number of assumptions have to be made, two problems can emerge namely: (1) The risk involved is underestimated leading to a potential financial disaster; (2) A good opportunity is lost because the approach used in evaluating the project is too conservative. The reason that current techniques cannot solve the mine evaluation problems appropriately is those techniques have been developed in isolation.

The question arose afterward is that: Is the scenario analysis reflects the reality? It turns out that there are no definite answers for the above question. Johnson et al. [7] infers that

real option theory attempts to answer these questions: what are the future alternative options?; when should we choose between available options to maximize values based on the evolution of conditions?; how much is the right to take an alternative worth at any given time?. Very often in mining industry, project evaluators and decision makers will resort to previous experience and rules of thumbs in determining mining and processing capacity; rather than supporting these decisions with proper analysis. This could lead to operating inefficiencies and inaccuracies. Thus, this study will build the tools with package of the triggering conditions to support the decision makers for making a strategic decision based on best options that fit for operational and management's flexibility.

2 LITERATURE REVIEW

2.1 Real Options Valuation (ROV)

A real option is the right but not the obligation to undertake certain business initiatives, such as deferring, abandoning, expanding, staging, or contracting a capital investment project.

Brennan and Schwartz [1] and McDonald and Siegel [11] were the first economists who came up with the idea to incorporate option valuation techniques when making investment decisions. A few years before that, Myers [9] had already proposed the concept to see investment opportunities as growth options, and had attached the name real options to it. Since then a lot of studies have been published about real options and their applications in the economy. Yet, it still lacks of research conducting a study to incorporating this technique into valid tools for mine evaluation purposes. Dimitrakopoulos [3] summarize the main findings of previous work in real options applications to valuing mining investments.

- The trigger metal price for developing a mine estimated by the ROV is greater than the breakeven price determined by the conventional NPV method.
- The value of a project estimated by the ROV is greater than that estimated by the NPV method. In other words, NPV tends to undervalue mining investment.
- ROV approach is better than NPV in dealing with uncertainty and operating flexibility.
- The different between the ROV and the NPV estimates represents the value of operating or management flexibility, and different depends on the uncertainty level and the project profitability.
- The ROV and the NPV method differ fundamentally in the way the discount future cash flows and in the way they deal with managerial flexibility.

2.2 Fundamental Of System Dynamics

System dynamics (SD) is a methodology and mathematical modeling technique for framing, understanding, and discussing complex issues and problems. In the system dynamics methodology, a problem or a system is first represented as a causal loop diagram. A causal loop diagram is a simple map of a system with all its constituent components and their interactions. By capturing interactions and consequently the feedback loops, a causal loop diagram reveals the structure of a system. By understanding the structure of a system, it becomes possible to ascertain a system's behavior over a certain time period [17].

Richardson [13] reviews the core of SD methods and summarize that the system dynamics approach involves:

- Defining problems dynamically, in terms of graphs over time.
- Striving for an endogenous, behavioral view of the significant dynamics of a system, a focus inward on the characteristics of a system that themselves generate or exacerbate the perceived problem.
- Thinking of all concepts in the real system as continuous quantities interconnected in loops of information feedback and circular causality.
- Identifying independent stocks or accumulations (levels) in the system and their inflows and outflows (rates).
- Formulating a behavioral model capable of reproducing, by itself, the dynamic problem of concern. The model is usually a computer

simulation model expressed in nonlinear equations, but is occasionally left unquantified as a diagram capturing the stock-and-flow/causal feedback structure of the system.

- Deriving understandings and applicable policy insights from the resulting model.
- Implementing changes resulting from model-based understandings and insights.

3 METHODOLOGY

This research employs the SD method to allow real options techniques to unlocking the true value of managerial flexibility when applying it in valuing mineral resource investment project. Likewise, the binomial lattice will also perform alongside with Monte Carlo simulation in order to capture the upside potential and downside risk of options values. In this study, the DDMT will be developed using VensimDSS version6.0b alongside with C++ programming language. With the use of SD makes it possible to solve interdependent variable of mixed integer programming problem.

3.1 Real Options Framework

Real options are appealing to a company's management because it copes with future uncertainty and provides them flexibility.

The framework proposed in this paper is specifically devised for open pit mine planning tasks. Figure 1 depicts the framework used in this study. It is worthwhile to emphasize that real option methods can be useful tools for mining firms if they clearly understand its potentials to deal with uncertainties as superior to the traditional discounted cash flow valuation methods. Besides, the real options method should not only be known by its management level of mining ventures but it should be also engage to mining engineers as to allow them to get the idea on how to confront with the operating problems and solve it effectively. The following steps are guiding principle through the use of DDMT.

1) Base-case mine design, which is built using current mine design techniques and used to identify main cash flow drivers;
2) Determining the sources of risk and uncertainty, by incorporating geological uncertainty and metal price uncertainty into mine planning and design;
3) Using system dynamics to structure the real options valuation (ROV) model, integrating binomial lattice to visualize the options value as well as capturing upside potential and downside risk.
4) Establish financial model and run discrete event simulations using least square Monte Carlo [8]; performing sensitivity analysis to lock up the effects of uncertainty and risk.
5) Ranking the available options based on its value and the indicators of upside and downside.
6) Making final selection based on operational and managerial flexibility.

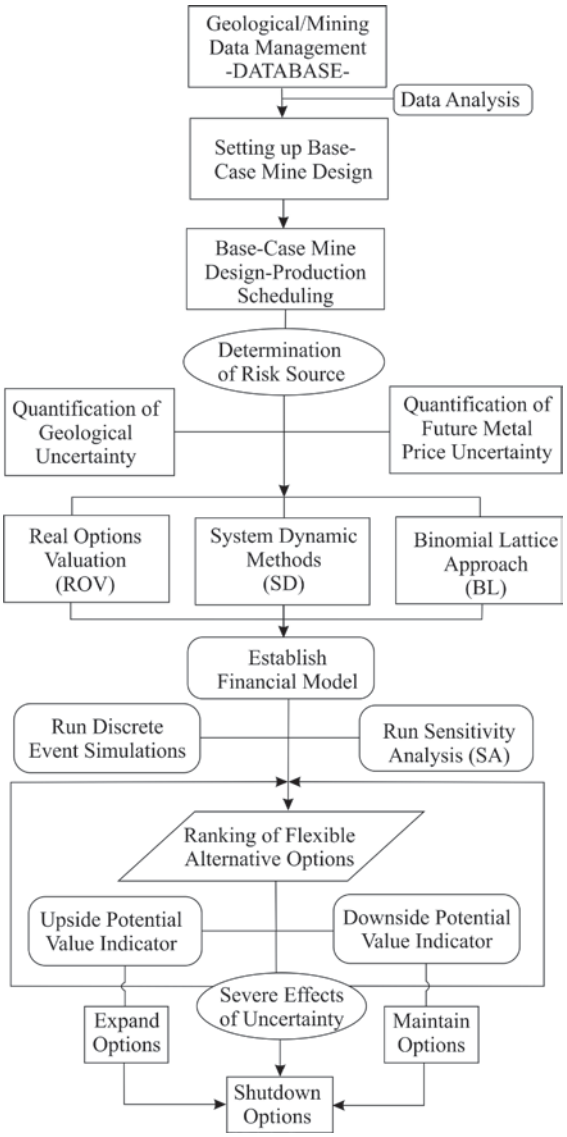

Figure 1. Schematic diagram depicting the framework for dynamics decision making tools

3.2 Prototype Of Dynamics Decision Making Tools (DDMT)

Decision-making can be regarded as the cognitive process resulting in the selection of a belief or a course of action among several alternative possibilities. Figure 2 shows the key influential variables economic feasibilities, technical measurements, and resource portions.

The DDMT model consists of major elements such as objective functions, decision variables, bounds, types, assumptions, constraints. The following passages are described for each of those elements.

- Objectives function: the objective function is to maximize the discounted NPV before tax of mining venture and minimize risk embedded in mine valuation process.
- Decision variable: the sets of inputs which resulting the highest NPV.
- Bounds: defined the upper and lower limits for the variables.
- Types: defines whether the variable is discrete or continuous types. Discrete variables are those that can only take on a finite number of values. Continuous variables that can take on an infinite number of possible values.
- Assumptions: capturing the uncertainty and risk of data inputs to model using probability distributions.
- Constraints: constraints restrict decision variables by defining their relationship among them. The major constraints refer to market conditions, operating efforts, and technical matters.

Decisions are usually triggered by internal and external conditions. In circumstance cases, decision can be made as quick as to rescue projects from the horrific impact which resulting from risk and unforeseen incidents. For example, metal price falling, pit wall sliding, concentrator in predicament, among others. This paper focuses on decisions that triggered by three main triggering conditions, namely economic, resource and technical conditions as shown in Figure 2. These decisive criteria based upon the ability of management flexibility to execute the options as well as availability of data.

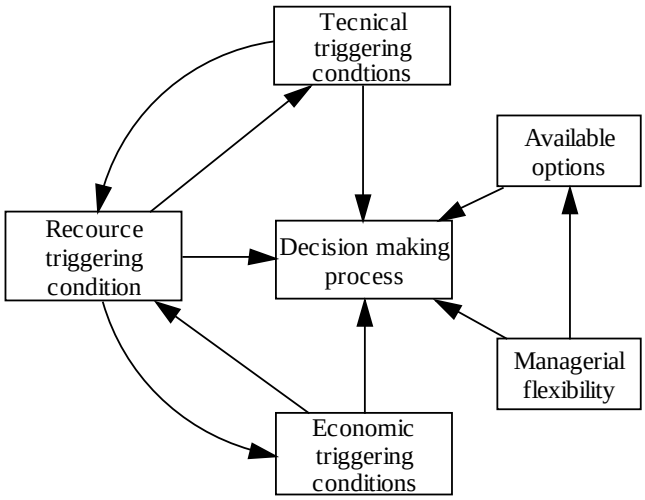

Figure 2. Decisive triggering condition for DDMT

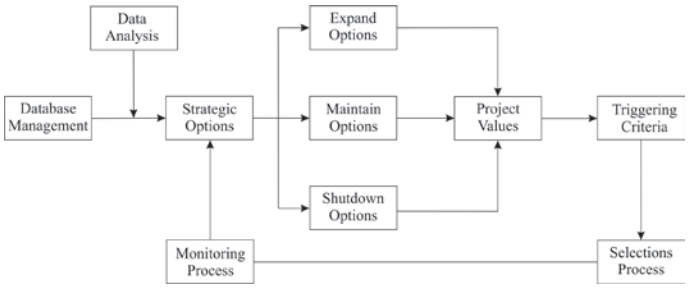

Figure 3. Decision process of options model for DDMT

Figure.3 illustrates the decision process diagram of options model for DDMT which represents the interrelationships between available options i.e., expand options, maintain options and shutdown options. These strategic options are assumed interchangeable during periods of operations. It is visibly shown in figure 3 that the strategic options will be chosen if only the calculated project value met the objective functions which defined above. It is important to note that the options must be executable against the triggering criteria. Then the selection process is performed one at a time to make a final decision on the way to take the options to action, this process will be repeated as to measure the outcome in short-term of implementation.

3.3 Conceptual Model Of DDMT

In this section, the conceptual models of dynamic decision making tools will be presented. It is very interesting to demonstrate the integration of real options valuation logics into system dynamics model. As shown in figure 4, it is apparently that options defined production capacity, putting different operating options resulting in different production capacity, and also option values.

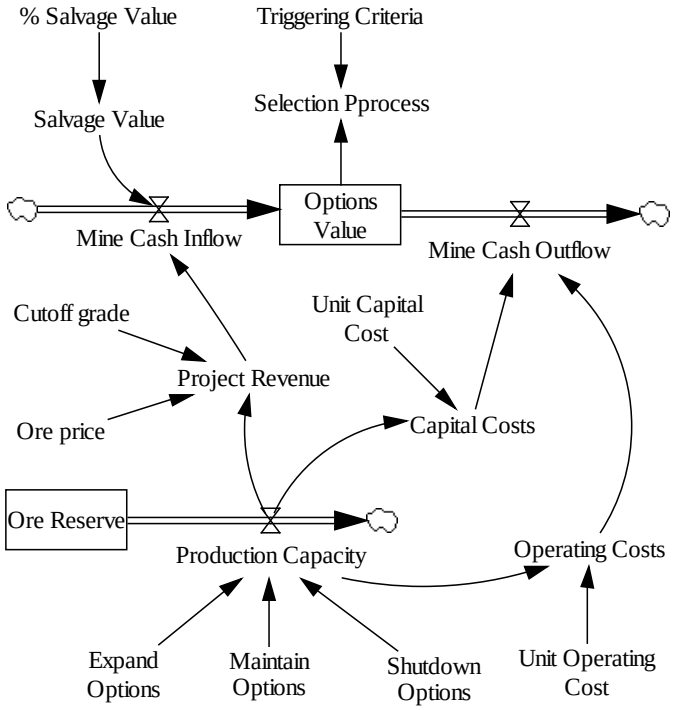

Figure 4. Prototype integration of ROV into SD model

However, switching options not only depend on its value but also rely on the ability of managerial flexibility. For example, if mining firms decide to expand its operations in times of rising metal price, the mining firm shares may be a superior to alternative physical economic investments. In other words, by executing options the mine operators are capable to yielding higher returns. In other way around, when the time of metal price falling consecutively, the mine might need to consider shutting down their operation temporarily or permanently. In this context, temporary closing is theoretically feasible but not seemingly executable for some reasons in real practice. In equilibrium market, the mining firms may possibly maintain their operating capacity, as mine operators believed that at the stability of metal price will lead them to generate higher profits than in volatile environments. In detail, the following sections provide an explanation of option models which proposed to build-in dynamic decision making tools.

3.3.1 Expansion options concept

When demand turns out to be high in line with the favourable of future market conditions, then the expansion options can be regarded as favourite choice for mining operation. Table 1 elucidates the expansion planning models which proceed in phases, where each phase is broken into stages. In doing so, we can define the marginal costs of each stages as well as marginal revenue. The idea behind is to minimize the risk which associate with infrastructure enhancements; especially in delivery of major mining and concentration equipments. The expansion capacity of both mining and processing will progressively increase as the construction of new infrastructures progresses. Table 1 tabulates the indicative stages of expansion options model. In this framework, there are three of capacity developments phases will be developed in the specified time periods, symbolize *t*, where *t* is in *T*, which represent total time of each development phase.

It is of paramount importance to note that this paper assumes there are no delays in delivery of expanded equipments, also any hindrances in construction of the support facility and infrastructures.

Table 1. Hierarchy phases of expansion options model

Stage	Timing	Description
Initial capacity development	t_0, $t \in T$; t=0,1..,T;	(a) Development of the pre-mine infrastructure and establishing the new open pit mine to deliver the target capacity of the first stage (b) Development of off-site infrastructure associated with initial mining development and concentrator plants (c) Acquiring mining equipments, i.e., shovels, trucks, concentrator and metallurgical plants, etc.
Intermediate capacity development	t_1-t_{t+1}, $t \in T$; t=0,1..,T	(a) Construct off-site facilities, concentrator plant and metallurgical plant to extract and process up to target of saleable products (b) Expansion of existing smelter to allow smelting the target concentrates (c) Develop new expanded infrastructure to support the increased capacity of the expanded of mining and metallurgical plants
Full capacity development	t_1-t_{t+1}, $t \in T$; t=0,1..,T	(a) Expansion of open pit mine, concentrator, and hydrometallurgical plants to extract and process to achieve target saleable products. (b) Fully constructed the expanded facilities to allow mining and processing achieved target saleable products

3.3.2 Maintain options concept

When market is in equilibrium state, the maintain option is reserved for a mining project. This is due to the fact that there is no gain nor loses from exercising other options. However, the producers consider that price stability can lead to higher returns than a volatile price that fluctuates in response to short-term variations in demand and supply. This is seemingly the case, since there is a strong implication between commodity price volatility and market performance, as well as mining project value. Haque et al. [5] unveils a study that when volatility increases, the risks associated with the commodity price increases and investment returns decrease, and project values typically decrease. The numerical results of his study suggest that the mine should run their project when the commodity price volatility lies either below the average or at the average volatility levels. This is probably arguable outcomes because if the mine has strategic options and the ability of management to handle uncertainty; then the mine would have gain its value and eventually profitable. In this paper, the maintain option is considered as the standby options, for when the market conditions turn out to be positive , mining firms can plan to expand their operations in order to capture the advantage from the upside potential of investments opportunity. If otherwise, the mine operators should hold their production capacity consistently.

3.3.3 Shutdown options concept

Once the triggered conditions turn out to be adverse, the abandonment option is one of the most common strategies considered in project evaluation [12]. In mining, the strategy consists of having the flexibility of closing and abandoning the open pit mining project permanently if market conditions or mineral resources decline severely. This strategy normally incurs costs for mine closure and land reclamation, while it also relies on secondary markets that are the salvage value from selling capital equipments and other assets. It is oftentimes closing a mine leads toward additional costs. For instance, reclamation costs, tailings and waste rocks treatment costs, among others. In

his conceptual model, it is evidently described that when the metal price is consecutively falling, the gross revenue generated cannot copes all the costs incurred. It is thereby causing the negative NPV. In the meantime, if the resource is radically depleting where there are no newfound ore deposits, then the mine must consider to shutdown its operation prior to the effect of erratic adversity. This kind of options would be valued if only the manager decide to execute it in advance.

4 SUMMARY

This study steps toward developing a dynamics decision making tool for open pit mine planning projects. The main idea is to build tools, which offer flexible alternative options i.e., expansion options; maintain options, and shutdown options based upon the availability of information and inputs data. It accordingly aspires to design a tools with simple features, users-friendly, quick computations, and easy-handy to setting up in operating systems of computers. Figure 5 showing a roadmap to develop DDMT(s). There are four main tasks, which linked by the connector lines, the arrow heads denote the predecessors must be done before proceed to successors. The different symbols in each connector heads represent mission of each task. The circle connector head linked between task I and task II, denote the initial stage to framing the scope and determine the constituents of tools. The rectangular connector head coupled from task II to task III indicate that thereafter finished conceptual models and its components; then proceed to design the architecture of DDMT. It includes sketch up the graphical user interface (GUI), formulate the toolkits with function guideline and the drafting the help for users. The final task is connected by the line with triangle connector head, represent methods and technologies will assemble in the DDMT.

The next stage is to synthesize those elements of four tasks (I+II+II+IV), into one package of application. The DDMT will be generating through the development process, called ‘assembling’ enactment. The final work is to testify the validation of DDMT application.

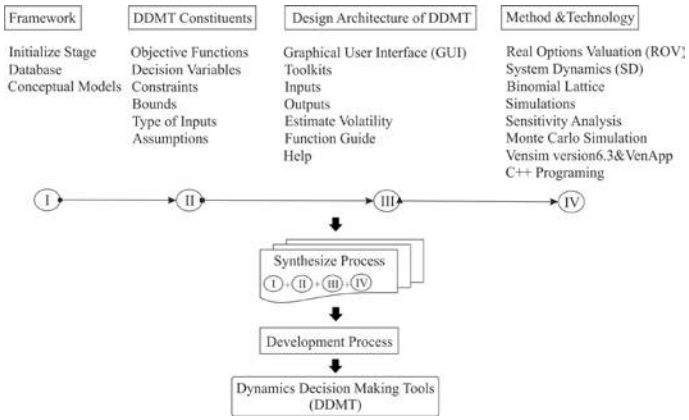

Figure 5. Diagram showing a roadmap to build DDMT

5 CONCLUSION AND FUTURE WORK

The article has presented the prototype of a dynamics decision making tools (DDMT), for open pit mining planning projects. It has pioneered an integration of real option valuation approach into system dynamics modeling methods. The tools will offer a power to mine planning engineers in valuing projects under uncertainties. The benefit of using DDMT is that it will prompt decision makers to realize the value of managerial flexibility or options premium, which can be obtained from the variation of uncertainties. It is hoping that the successfully combination of real option logics into the prototype of SD model will be extended to create a better decision making tool for solving mine evaluation problem in effective ways.

The ongoing work of this research would be continuing to shape the form of DDMT into a useful and interactive application. The future work is formulating comprehensive framework and robust triggering conditions to reinforce the decision making process. Also, considering the actual number of input variables in application is substantially important. The DDMT will be developed in the ways that it can assist mining firms to improve its management to change the way the mine runs.

ACKNOWLEDGEMENT

The author gratefully acknowledged for the financial support from German Academic Exchange Service (DAAD), granted code A/12/96777. Likewise, thanking Institute of Mining and Special Construction Engineering, TU Bergakademie Freiberg for supporting a sound environment for conducting this research.

REFERENCES

[1] Brennan, M. J., Schwart, E. S., 1985. Evaluating natural resource investments. *Journal of Business. 58(2)*, pp.135-157.

[2] Barghav,S. and Ford, D., 2006. Project management quality and the value of flexible strategies. Forthcoming of Engineering, Construction and Architectural Management, Vol.13, No.3.

[3] Dimitrakopoulos, R, Abdel Sabour, S., 2007. Evaluating mine plans under uncertainty: Can the real options make a different? Resources Policy 32 , pp.116-125.

[4] Ford, D. and Sobek, S., 2005. Adapting real options to new product development by modeling the second Toyota paradox. IEEE Transactions on Engineering Management. 52(2).

[5] Haque, Md.A, Erkan Topal, Eric Lilford, 2014. A numerical study for mining project using real options valuation under commodity price uncertainty, Resource Policy, Vol.39, pp.115-123.

[6] Huh, W., Roundy, R., Cakanyildirim, M., 2006. A general strategic capacity planning model under demand uncertainty. Naval Research Logistics 53, pp. 137-150.

[7] Johnson, S, T., Taylor, T., Ford, D., 2006. Using system dynamics to extend real options use: Insights from the oil & gas industry, System dynamics conference, pp.1-31.

[8] Longstaff, F, A., and Schwartz, E., 2001. Valuing American options by simulations: a simple least-squares approach, Review of Financial Studies, Vol.14, No.1, pp.113-147.

[9] Myers, S., 1977. Determinants of corporate borrowing, Journal Financial Economics, No.5, p. 147-175.

[10] Martinez, L, A., 2009. Why accounting for uncertainty and risk can improve final decision making in strategic open pit mine evaluation, Project Evaluation Conference, pp.113-124.

[11] McDonald, R. and Siegel, D., 1985. The value of waiting to invest, Quarterly Journal of Economics No. 101, p. 707-728.

[12] Mun, J., 2002. Real options analysis. Published by John Wiley & Sons, Inc., Hoboken, New Jersey.

[13] Richardson, G, P., Meyers, R, A, (ed), 2008. The core of system dynamics, Encyclopedia of Complexity and System Science.

[14] Singh, G. et al., 2012. A mixed integer programming model for long term capacity expansion planning: A case study from the Hunter Valley Coal Chain, European Journal of Operation Research, Vol.220, pp.210-224.

[15] Sontamino, P., Drebenstedt, C., 2013. A prototype decision making tool of coal mine planning using system dynamics model, Mine Planning and Equipment Selections Conference, pp. 1475-1484.

[16] Varenfdorff, 2003. Confidence in mine planning: The role of intelligent technologies, Conference on Mine Planning and Equipment Selection, pp.35-40.

[17] http://en.wikipedia.org/wiki/System_dynamics

Determining Refuge Chamber Location in Underground Tunnel Using 3D Computer Modelling

C. Doğruöz, M. Özdemir
Dumlupınar University, Mining Engineering Department, Turkey

A. Nieto
Penn State University, Energy and Mineral Engineering Department, USA

ABSTRACT Refuge chambers for underground mines can provide air, food, water, and supplies to miners in the event of an emergency. This paper presents an initial approach to prepare the area and install a refuge chamber located in an arched sectional underground tunnel. The proposed model was developed in order to clearly define the dimensions and safety specifications needed to properly install a refuge chamber in a given underground arched section. Rock bolt holes were designed based on simulated data to emulate roof and lateral forces created by the layers of rock above the arched section of the tunnel in question. This model can be modified based on the specific characteristics of the host rock mass and the local geology. In this study, tunnel design and refuge chamber utilization were designed in conjunction to confirm consistency of the refuge chamber geometry vs. the dimension of the tunnel section. The model was carried out using 3D computer modeling. Per our conclusions, when designing and developing a new underground mine, or opening a new underground section in already active mines, it is important to determine and define, during the early stages of the mine design, the specific location and geometry needed to deploy and install refuge chambers to comply with safety regulations and specifications.

Keywords: Refuge chamber location, refuge chamber in tunnel

ÖZET: Yeraltı madenciliğinde kullanılan yaşam odaları madencilerin kullanabilmesi için temiz hava, yiyecek, su temin etmekte ve acil durumlarda barınak olarak kullanılabilmektedir. Bu makalede yaşam odalarının konulacağı alanların önceden belirlenmesi ve yaşam odalarının kemer kesitli tünellerde konumlandırılması dizayn edilerek çalışılmıştır. Oluşturulan modelde, yaşam odalarının konumlandığı alan, iş güvenliği ve formasyon açısından yeraltında kemer kesitli tünellerde en uygun lokasyonlara konumlandırılması amaçlanmıştır. Tünellerin tavan kısımlarına açılan kaya saplamaları delikleri ile tavan kayaç katmanları belirlenerek kayaç formasyonları kemer kesitli tünellerde dizayn edilmiştir. Bu model spesifik kayaç karakteristikleri ve kayaç kütlesi ile jeolojik katmanlar belirlenerek geliştirilebilir. Bu çalışmada, yaşam odası geometrisi ile tünel boyutları arasındaki tutarlılık hedeflenerek tünel içerisinde yaşam odası dizaynı uygulanmıştır. Bu model, 3 boyutlu bilgisayar uygulaması kullanılarak oluşturulmuştur. Sonuç olarak, yeraltı madenciliğinde tünel dizaynı yapmadan önce yaşam odalarının yer tespitinin yapılması, iş güvenliği düzenlemeleri ve yaşam odalarının tüneller içerisinde önceden konumlandırılması açısından önem arz etmektedir.

Anahtar kelimeler: Yaşam odası lokasyonu, tünellerde yaşam odası

1 INTRODUCTION

After several underground mine accidents occurred around the world, the need for refuge chambers has been given markedly more attention. However, the utilization of refuge chambers alone remained inadequate. There are many safety parameters to consider for underground mines before constructing refuge chambers. Only after other safety measures are applied, should refuge chambers become a significant focus. In this study, a horseshoe sectional tunnel was designed by using a mining software program and rockbolt holes were placed based on assumptions. The main purpose of this study was to determine the proper location of refuge chambers. In addition, these refuge chambers were monitored in tunnels together with the rockbolt holes.

In underground mining, enforcement of refuge chamber laws needs to be improved and new approaches should be developed to increase the effectiveness of mine safety. Toward that goal, 3D views of underground mine planning and modelling should be a part of safety legislation. There are different scenarios of underground mine accidents and disasters such as mine explosions, mine collapses, and gas emission problems. In addition to aforementioned hazards, psychological factors of miners, escape techniques, and refuge chamber locations gain more significance for mine safety.

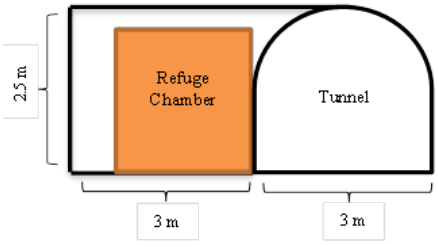

Figure 1. Cross sectional area of tunnel with refuge chamber

Within tunnels, it is important to find the most accessible location of refuge chambers for miner safety. Zhang and his colleagues have developed a model using the finite elements method. The correct dimensions for a refuge chamber are 3.2 m in length and 2.6 m in height (Zhang et al., 2014).

In this study, an underground tunnel has been designed and the rockbolt holes have been located at the roof of the tunnel. The tunnel has been developed as a horseshoe section and the roof rock layer formations have been added. The length of our tunnel section is 3 m in length, 2.5 m in height and the room in which the refuge chamber is located at 2.5 m. After modelling the tunnel, the possible refuge chamber location has been determined and designed into the tunnel. Figure 1 shows the cross sectional area of the tunnel with refuge chamber. In this study, the models and designs are defined based on possible operational scenarios. Moreover, a cross section of the horseshoe tunnel has also been studied in this article.

2. REFUGE CHAMBER UTILIZATION IN MINE ACCIDENTS

Mine explosions and mine disasters lead to new approaches to mine safety and health. After these unexpected accidents, miners psychological conditions become very significant during the escape from mines (Margolis et al. ,2011). Qunanian suggested that psychological factors for miners during emergencies such as reducing anxiety and improving morale are important considerations for using refuge chambers (Qunanian, 2007). According to Qunanion, psychological conditions regarding emergencies such as decreasing concern and increasing morale are significant parameters for using refuge chambers.

Gas and coal dust explosion has been one of the serious accidents to coal industry for many years, as in many cases miners can not have enough time to escape from high temperature and toxic gases (Brnich, M. J., Jr.(2010). In general, refuge chambers are designed to protect miners for up to 96 hours under worst conditions. (Zhang, et.al. 2014)(Safety,2008). The importance of refuge chambers is varying for each mine safety authorities to improve design and plan guidelines (Brnich and Kowalski-Trakofker, 2010).

In terms of heavy casualties are occured by underground mine accidents each year in China which are mainly due to underground miners poisining and suffocation that caused by the spread of toxic fumes in operation of accident (Mingju et. al., 2009, Keguan et.al.,2010).

In 2010, State Administration of Work Safety and State Administration of Coal Mine Safety reported the construction of a complete refuge 'six systems' and according to their notification, mine institutions must deal complete refuge system including underground monitor system, perfect positioning, underground miners, positioning system, emergency escape system, compressed air self rescue system, water supply system and communications network (Li, 2012).

According to Li (2012), emergency refuge system of refuge chamber, one of the 'six systems' of safety refuge chamber, is emergency chamber for miners to reduce damage caused by mine disasters while existing power supply is not guaranteed (Li LT,2012).

Permanent refuge chambers are fundamentally set in shaft station and near emergency exit of mining area, the distance of working face away which is based on specific situations in coal mine. In general, it is a part of emergency shelter for the complete coal mine or mining area, and it's service life time is over 10 years. Permanent refuge chambers should be determined in stable rock formations avoiding geologic tectonic zone, high temperature zone, stress anomaly locations and flooding threatened locations in order to fix that is not affected by mining operations during it's service life time (Meng et al., 2011).

Non–flammable materials should be utilized to increase the strength of roadway in 20 meters distance of is and its roof should be completed. Morever, the access route of refuge chamber safe area for the roadway does not need to be straight, and it can arrange various curve roads in order to decrease the shock wave hazard caused by gas and coal dust explosion (Hu, 2010).

The refuge chamber systems are made up by permanent refuge chamber, temporary refuge chamber and rescue capsule and they are also a refuge and transfer station to survive for the miners in disasters. A whole refuge chamber system increase the probability of being rescued for the miners in disasters, apply easy first-aid dressing for the seriously injured, and acquire self-help in reserve, decreasing loses and casualties. Thus, it is specifically significant to make safe and rational design (Meng et al, 2011).

3. REFUGE CHAMBER LOCATION IN UNDERGROUND TUNNELS

When locating a refuge chamber in an underground tunnel the walls should most definitely be smooth and rigid. Before processing continuous tunnel work, being well organized and determining the refuge chamber sight beforehand is most significant. Therefore, planning and designing the tunnel and refuge chamber simultaneously before commencing the mining operation is indispensable. Manufacturers produce the refuge chambers according to their customer's requests and demands. For that reason, each refuge chamber can be different sizes and dimensions. During the mining operations in underground, whether the tunnel coordinates, lengths and heights are well known, determining the refuge chamber location becomes easier, reliable and safer.

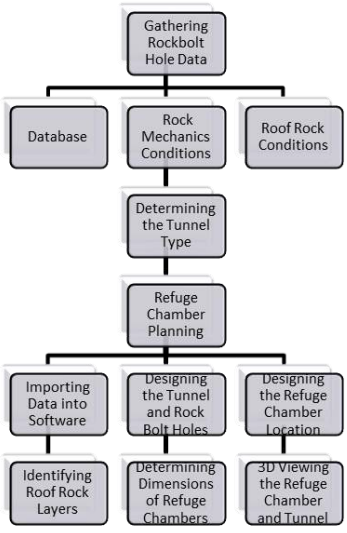

Figure 2. Flow sheet of designing and modelling tunnel and refuge chamber location in underground

As stated in the above and displayed in figure 2, planning the location design of refuge chambers most certainly needs to be well organized. In this process, there are important steps to create a 3D view of underground refuge chambers.

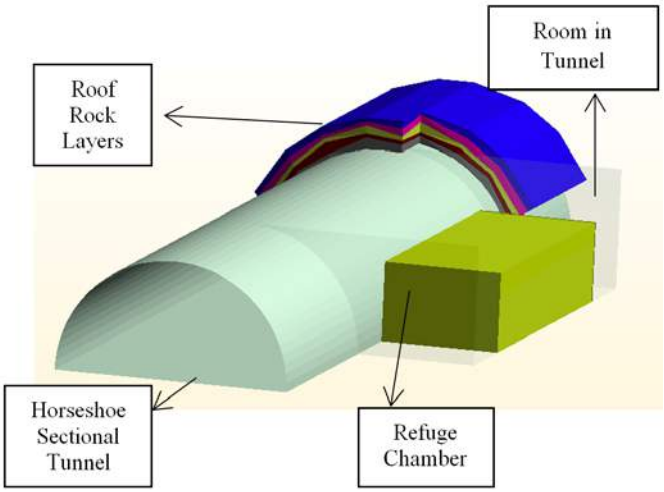

Figure 3. Model view of tunnel and roof rock characterization with refuge chamber

Each mine field show different characteristics of underground processes in terms of their depths, elevations and operational methods. Due to these reasons, placing the refuge chambers into the safest and best places depends on the refuge chambers dimensions and tunnel parameters. As shown in figure 3, the refuge chamber is positioned in the room of the tunnel.

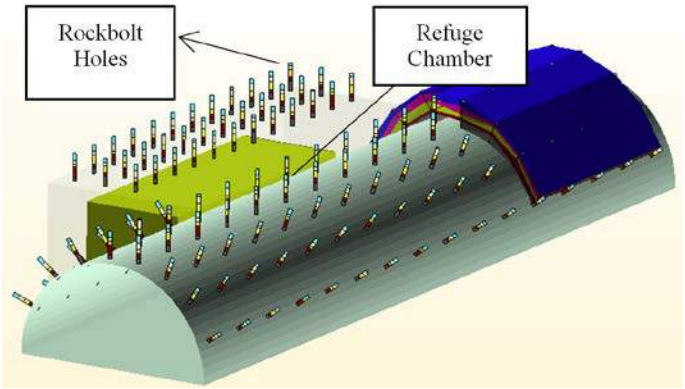

Figure 4. Refuge chamber and rockbolt holes showing roof rock layers in tunnel

Roof rock layers of tunnels give us additional information about the rock strengths or rock mechanical parameters and in knowing this information helps us find out the best place of refuge chambers in the underground. In case that the roof rock structure is weak and brittle, refuge chambers should obviously not be located in these areas.It is better to place these chambers in stronger and more durable areas. Drilling the rock bolt holes and measuring the levels of rock mass layers are the first steps of the modelling operation. After obtaining the data, rock mass properties are drawn by using mining software programmes. Figure 4 shows us the rockbolt holes and rock layers at the top of tunnel.

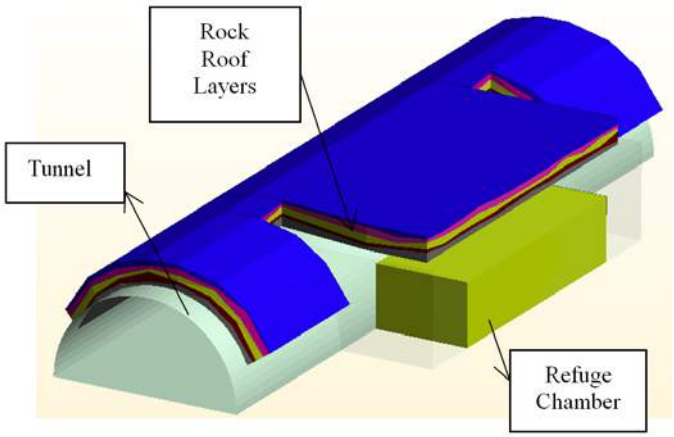

Figure 5. Refuge chamber and rock formations in underground tunneling

Through the use of cross-sectional methodology in mining software programmes, it is easier to create the rock layers and see the details of the tunnel with refuge chambers. The main purpose of this study is to view the refuge chambers in the underground. In Figure 5 it is seen that the tunnel and refuge chamber is together with the roof rock characteristics. Once the design of the tunnel and refuge chamber is completed, estimations and operations can be viewed and managed easily using the 3D view technique.

4. CONCLUSION

Refuge chamber utilization in underground mining is very significant and needs to be investigated in detail. When designing and developing a new underground mine, it is important to determine and define the specific location during the early stages of the mine design. In this study, underground tunnels and roof rock mass characteristics of

tunnels have been created. The main objective of the study is to install the refuge chambers inside the room of tunnels and forecast the next steps in operation. There are different approaches about how to find out the best place for refuge chambers and it depends on the operational method of the mines. This study presents an initial approach to prepare the area and install a refuge chamber located in an arched sectional underground tunnel. Tunnel design and refuge chamber utilization were designed in conjunction to confirm consistency of the refuge chamber geometry vs. the dimension of the tunnel section. Rock bolt holes were designed based on simulated data to emulate roof and lateral forces created by the layers. This model was designed by using computerized 3D modelling. All the coordinating data is based on possible geological assumptions. Therefore, any of the underground mining scenarios can be designed and developed using this computerized modeling. As a recommendation, the model can be developed and different underground mining types can be modified.

REFERENCES

Brnich, M.J., Kowalski-Trakofker, K.M., 2010. Underground coal mine disasters 1900-2010:events, responses, and a look to the future. NIOSH Office of Mine Safety and Health. In: Extracting the Science: a Century of Mining Research. SME Society Mining Metallurgy and Exploration. Colorado USA, 2010. pp.: 363-372

Brnich, M. J., Jr.(2010). Underground coal mine disasters 1900-2010: events, responses, and a look to the future. Extracting the Science: A century of Mining Research, 363.

Hu J., Permanent and temprary fixed refuge chamber construction in coal mining area, coal mine in Shanxi, 2010, 30(7),82,China

Keguan W., Shanyang Zhao, Xiuqing Yu, Develpoment of Refuge Chamber in Coal Mine, Mining Technology, 2010, (s1), 135-137 , China

Li LT, 2012, 'Discussion on coal mine emergency rescue based on underground refuge chamber system, Safety Environment Eng, 19(2) 110-6

Mingju L., Lei Meng, Jianping Wei, 'The statistics characteristics and preventive measures of coal and gas outburst in recent years, Mine Safety, 2009, (7) 73-76 , China

Meng L., YaoDong Jiang,Yixin Zhao, Ruyue Shan,Yimeng Song,'Probing into design of refuge chamber system in coal mine, Procedia Engineering, 2011,(26)2334-2341,China

Mejias C., Daniels Jimenes, Alejandro Munoz, Lorenzo Reyes-Bozo'Clinical response of 20 people in a mining refuge: Study and analysis of functional prameters', Safety Science 63, (2014) 204-2010

Margolis K. A., Catherine Y.Kingsley Westerman, Kathleen M.Kowalski-Trakofler, 2011, 'Underground mine refuge chamber expectations training:program development and evaluation', Safety science, elsevier, 49(2011) 522-530

Nieto, A., (2010), "Key deposit indicators (KDI) and key mining method indicators (KMI) in underground mining method selection", 2010 Transactions of the Society for Mining, Metallurgy and Engineering, Inc., Littleton, Co, vol. 328, pp. 381-396

Nieto A., (2011) SME Mining Engineering Handbook, Society of Mining Engineering, 3rd Edition. Selection Process for Underground Soft-Rock Mining, Chapter 6.4

Safety, M. (2008). Health Administration, US Department of Labor, 30 CFR Parts 7 and 75 refuge alternatives for underground coal mines; Final Rule

Qunanian, D., 2007.Refuge alternatves in underground coal mimes, Phase I Final Report, NIOSH Contract No, 200-2007-20276, July, foster-Miller, Inc., Waltham, MA

Zhang W., 2012, 'Image denoising algorithm of refuge chamber by combining wavelet transform and bilateral filtering', International journal of mining science and technology, elsevier, 23, (2013) 221-225

Zhang B., Wei Zhao, Wei Wang, Xinghua Zhang Safety,' Pressure characteristics and dynamic response of coal mine refuge chamber with underground gas explosion', Journal of Loss Pevention in the Process Industries, 30, (2014) 37-46.

Zhang, B., Zhao, W., Zhang, X., 2014, 'Pressure characteristics and dynamic response of coal mine refuge chamber with underground gas explosion', Journal of loss prevention in the process industries', elsevier, 30(2014) 37-46

Long Term Planning In Open Pit Mines In Presence Of Commodity Price Uncertainty

M. Rahmanpour, M. Osanloo
Department of mining and metallurgy, Amirkabir University, Tehran, Iran

ABSTRACT Mine planning is a multidisciplinary procedure based on which the profitability of the mining operation is guaranteed in a changing and uncertain conditions. Many factors affect the preciseness of mine plans and cause deviations in reaching the predetermined objectives. Long-term production planning in open pit mines is defined as a precedence-constraint knapsack problem. This paper deals with price uncertainty and considering different price scenarios, it determines 9 different and mutually possible mine plans. Price variations throughout the mine life are modeled using the Generalized Autoregressive Conditional Heteroskedasticity (GARCH) and Geometric Brownian Motion (GBM) methods. Finally, using the concept of value at risk, the most profitable and the less risky plan is selected as the optimum mine plan. The model is applied in a small hypothetical iron ore deposit.

Keywords: Open pit mine, commodity price uncertainty

1 INTRODUCTION

The aim of mine planning is to develop a yearly extraction plan which guides the mining operation to the highest Net Present Value (Dagdelen 2007; Yarmuch and Ortiz 2011). This plan considers the constraints such as blending requirements, block sequencing, and pit slope (Caccetta and Hill 2003). Thus, determining the extraction sequence of mining blocks through the mine life is referred to as mine planning (Johnson 1968). The mine plan affects the economy and the payback period of mining operations. Mine planning is a procedure based on which the profitability of the mining operation is guaranteed in a changing and uncertain conditions (McCarter 1992). Mine plans are normally classified into long term, medium term, and short term plans.

In a sustainable mining operation, environmental, economical and social aspects of mining and its reclamation should be considered in mine planning procedure (Osanloo 2012). The essential data required for mine planning are geological, geo-mechanical, hydrological, economic, environmental, infrastructures, and the knowledge of mining engineering. These data contribute more or less on the mine planning procedure and mine plans. The characteristics of future mining activities and also inherited uncertainty of the data (such as commodity price, ore grade, mining costs, and recoveries) highlighted the importance of mine planning under the conditions of uncertainty. These issues and mainly the price uncertainties motivate the study of the factors that affect mine planning and their management.

Open pit mine production planning is a multi period precedence-constraint knapsack problem and it normally fit into the MILP framework (Osanloo et al. 2008; Newman et al. 2010). This problem is defined on a spatial representation of the mining area called block model (Figure 1) (Hustrulid et al. 2013).

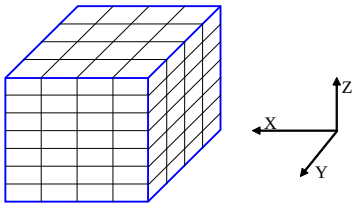

Figure 1. Simplified representation of a block model.

Considering the exploration-drilling pattern, geological condition, and the size of mining equipments to be used, the size of the blocks in a block model will be determined. After determining the block dimensions, the geological characteristics of each block are assigned using any available estimation techniques (Journel and Kyriakidis 2004). Then, considering the economic parameters such as selling price, operating costs, and overall recovery one could calculate the economic value of each block.

Using a block model, the aim of mine planning is to determine whether a given set of blocks should be mined or not, if so, at which time it should be mined, and once it is mined, then, how it should be processed to maximize the net present value of the operation (Dagdelen 2007). Once a block is mined, one could determine different destinations or processing methods for that block. Conclusively, the act of determining the time and extraction sequence of blocks through the mine life is referred to as mine production planning (Johnson 1968). The problem of production planning in open pit mines is studied by many researchers (Dowd and Onur 1992; Tolwinski and Underwood 1996; Denby and Schofield 1996; Kumral 2003; Ramazan and Dimitrakopoulos 2004; Menabde et al. 2007; Boland et al. 2008; Dimitrakopoulos and Ramazan 2008; Elkington and Durham 2009; Sattarvand 2009; Bley et al. 2010; Kumral 2010, Groeneveld and Topal 2011; Murakami et al. 2011; Gholamnejad and Moosavi 2012; Lamghari and Dimitrakopoulos 2012; Moosavi et al. 2014). These studies aimed to maximize the net present value of the operation while satisfying all the operational constraints.

There are two optimization approaches to solve the production-planning problem in open pit mines named deterministic and uncertainty based approaches (Osanloo et al. 2008). In deterministic models, all the inputs are assumed to have fixed known real values (such as Tan and Ramani 1992; Akaike and Dagdelen 1999; Zhang 2006; Elkington and Durham 2009; Cullenbine et al. 2011). However, the assumption of input's certainty is not always realistic and some data such as ore grades, future product demand, future product price, and production costs can vary throughout the mine life. Researchers (Albach 1976; Rovenscroft 1992; Smith 2001; Godoy and Dimitrakopoulos 2004; AbdelSabour et al. 2008; Abdelsabour and Dimitrakopoulos 2011 to name a few) have developed various models based on mixed integer linear programming, meta-heuristics, heuristics and simulation, chance constraint linear programming, and stochastic programming to determine the mine plan in uncertain condition.

In this paper the price uncertainty and its affect on mine planning is studied. To do so, a simple integer linear programming model is formulated to determine the production planning and mining sequence of block.

2 DESCRIPTION OF THE METHOD

Mineral price is a key factor in mine planning and it seems as the heart of any mining project. Mineral price has a volatile and changing nature. The mineral or the commodity price affects the mining cut off grade, mineable reserve, mine size, and mine life. Any long term change in commodity price will affect cutoff grade and amount of mineable reserve. For example in case of price fall, the ultimate pit limit shrinks, cutoff grade increases, low grade ore blocks will be classified as waste, amount of mineable reserve decreases, and it will change the long term and short term plans of the mine. It must be noticed that short term changes in commodity price will affect the short term plans (Tulp 1999). In these conditions, short term plans must be changed cautiously because short term gains may cause other problems in long term plans (Hall 2009-a).

This paper studies the effects of price uncertainty on mine planning and aims to minimize the risks of price changes throughout the mine life. The procedure of the study is as Figure 2.

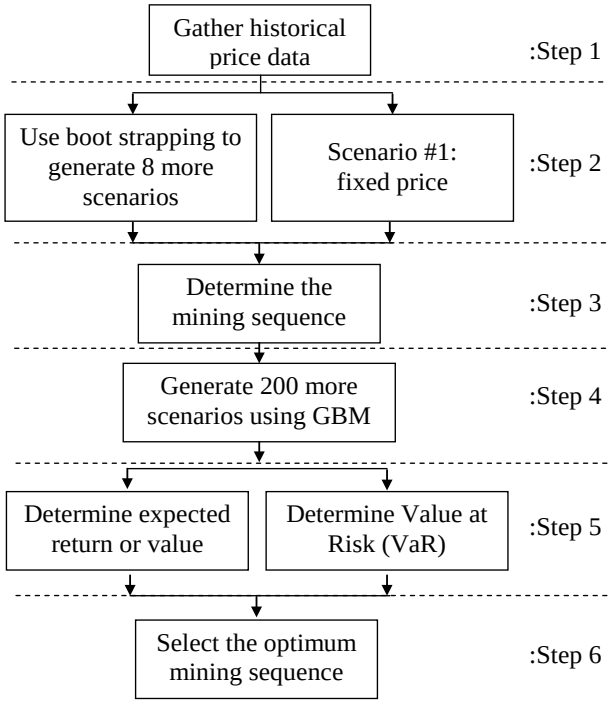

Figure 2. The procedure of determining the optimum mining sequence.

2.1 Bootstrapping

According to Figure 2, in the first step the historical changes in mineral price are collected in order to simulate the future possible price forecasts. In the 2nd step, the bootstrapping method is applied to determine 8 scenarios for future price trends and changes. Bootstrapping is a sampling method. Assuming a given data set of historical mineral prices, the yearly or monthly returns (i.e. rate of monthly/yearly price change in each period) are calculated. In order to forecast future mineral prices or to generate a new sequence of prices for a mineral, the individual returns are randomly chosen from historical returns. The main advantage of this method is that, it does not need any assumptions on the distribution of the returns and the empirical distribution of the returns is inherited in the sampling procedure. Using the method, 8 different scenarios are generated for the iron ore price (Figure 3).

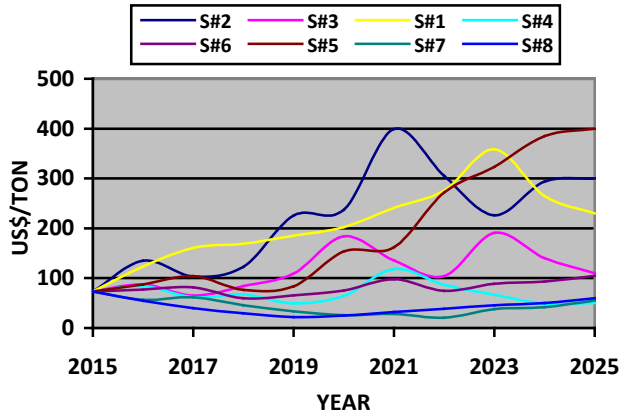

Figure 3. Simulated iron ore price using bootstrapping.

Another scenario with the assumption of fixed price throughout the mine life is made in order to have a bench mark to compare the results with the traditional approaches. Thus, at the end of the 2nd step, 9 price scenarios are determined for price changes in the next 10 year.

2.2 Mathematical Model Of Block Sequencing

In the 3rd step, the optimum block sequencing should be determined for each price scenario. An integer linear programming model of long-term production planning and block sequencing in open pit mines is formulated and it is given in equation 1. This model determines the time of extracting and processing method of each block to maximize the NPV of total operation.

Objective function:

$$\text{Max} \sum_{b\in B}\sum_{t\in T}\sum_{m\in M} c_{bmt}\, x_{bmt} \quad (1a)$$

Subject to:

$$\sum_{t\in T}\sum_{m\in M} x_{bmt} \le 1, \ \forall b \quad (1b)$$

$$MC_t \le \sum_{b\in B}\sum_{m\in M} X_b\, x_{bmt} \le \overline{MC_t}, \ \forall t \quad (1c)$$

$$PC_{mt} \le \sum_{b\in B} X_b\, x_{bmt} \le \overline{PC_{mt}}, \ \forall t,m \quad (1d)$$

$$\sum_{b\in B}(g_b - G^{t,m}_{\max})x_{bmt} \le 0, \forall t,m \quad (1e)$$

$$\sum_{b\in B}(g_b - G^{t,m}_{\min})x_{bmt} \ge 0, \forall t,m \quad (1f)$$

$$\sum_{t=1}^{t'}\sum_{b'\in P_b}(x_{bmt} - x_{b'mt}) \le 0, \ \forall b\in B, \forall t' \in \{1,...,T\} \quad (1g)$$

$$x_{bmt} = 0 \text{ or } 1, \ \forall b,t,m \quad (1h)$$

The notation of the model is as follow:

B	is the set of all blocks in the block model
P_b	is the set of blocks that overlays or precedes block b
t, t'	are the time index
T	is the mine life or number of the periods to be planned
M	is the number of possible destinations or processing alternatives
c_{bmt}	is the discounted economic value of block b mined at time t and sent to destination m
x_{bmt}	is the decision variable and it is equal to 1, if block b is mined at time t and sent to destination m and it is equal to 0, otherwise
$MC_t, \overline{MC_t}$	is the Min and Max mining rate at time t respectively
X_b	is the amount or tonnage of rock in block b
g_b	is the grade of commodity in block b (it is normally presented in percentage of the total tonnage in each block)
$G_{\min}^{t,m}, G_{\max}^{t,m}$	is the Min and Max acceptable grades at destination m at time t respectively
$PC_{mt}, \overline{PC_{mt}}$	is the Min and Max processing capacity at destination m at time t respectively

In equation 1a, the objective function of the model is defined as maximization of the discounted economic value or the NPV of the mining operation. Constraint 1b ensures that if block b is to be mined then it could only be mined once and sent to destination m at time t. Constraints 1c and 1d ensures that the total amount of rock mined and processed at time t does not exceed the prescribed lower and upper bounds on mining and processing capacities, respectively. Constraints 1e and 1f ensure that the average grade of material sent to each destination is within the prescribed lower and upper bounds. Constraint 1g is known as slope or proceeding constraint. This constraint ensures that wall slope restrictions are obeyed and block b can only be mined if all the overlaying blocks are removed beforehand. The model in equation 1 is programmed and solved using CPLEX 12.5.

According to the procedure (Figure 2), in step 2, 9 different price scenarios are generated for the mineral. The term c_{bmt} in the objective function is a function of mining time and the mineral price in that period. This term is embedded into the model using the generated scenarios.

At the end of this step, 9 different mine designs are generated for the ore deposit. The block sequencing in these plans is different from each other due to different and variable mineral prices in each period. The next step is to select the optimum block sequencing for the deposit. To do that, a simulation based approach is applied which will be described in the next subsection.

2.3 Geometric Brownian Motion

"Geometric Brownian Motion" or simply GBM is one of the most common methods for price modeling and scenario generation (Erlwein et al. 2012). In this method, the stock or the mineral price is modeled as a wiener process and it is a function of return and volatility of the mineral price (Equation 2) (Hall 2009-b).

$$S_t = S_0 \exp\left(\left(\mu - \frac{\sigma^2}{2}\right) + \sigma W_t\right) \quad (2)$$

Where, S_0 and S_t is the current mineral price and the mineral price in period t. The wiener process W_t is defined in equation 3.

$$W_t = z_t\sqrt{t},\ z_t = N(0,1) \quad (3)$$

In equation 2, μ is the return of the mineral price and it is calculated using equation 4.

$$\mu = Ln\left(\frac{S_t}{S_{t-1}}\right) \quad (4)$$

In this paper, the volatility of the mineral price in equation 2 is calculated using the Generalized Autoregressive Conditional Heteroskedasticity (GARCH) method. In this method, the volatility of the mineral price is

a function of its previous conditions and it is calculated using equation 5.

$$\sigma_t^2 = \gamma V_L + \alpha u_{t-1}^2 + \beta \sigma_{t-1}^2$$
$$\gamma + \alpha + \beta = 1 \quad (5)$$

In this equation, the term V_L is the long term variance or volatility of the mineral price. The parameters γ, α, β are defined such that they maximize the model in equation 6.

$$\sum_{i=1}^{t} \left(-\ln\left(\sigma_i^2\right) - \frac{u_i^2}{\sigma_i^2} \right) \quad (6)$$

Then, the GARCH model could be applied to estimate the future volatility of the mineral price (Equation 7).

$$E\left(\sigma_t^2\right) = V_L + \left(\alpha + \beta\right)^t \left(\sigma_0^2 - V_L\right) \quad (7)$$

Using the model in equation 6, the volatility of iron ore price in the coming years is estimated (Table 1).

Table 1. Estimated volatility of iron ore price.

Year	$E\left(\sigma_t^2\right)$
2015	0.26
2016	0.26
2017	0.27
2018	0.27
2019	0.27
2020	0.27
2021	0.27
2022	0.27
2023	0.28
2024	0.28
2025	0.28

Combining the result of Table 1 and equation 2, and using the GBM method, it is possible to simulate more scenarios for future prices. The result of 100 simulations is shown in Figure 4.

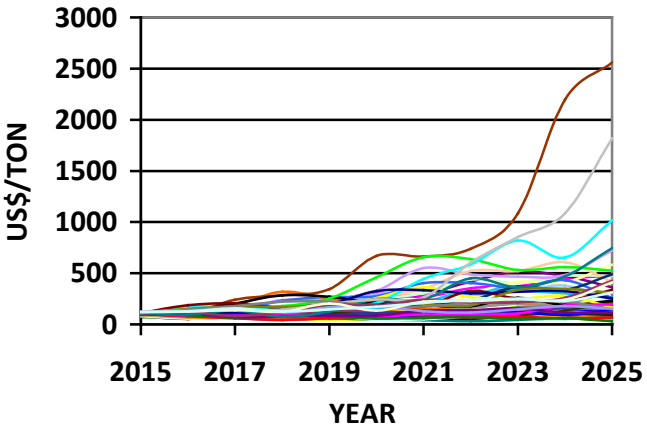

Figure 4. Simulated iron ore price using GBM.

2.4 Value At Risk And Expected Return

In the 5th step of the procedure given in Figure 2, the expected value (i.e. expected return) and the value at risk of each mine design should be determined.

In this step, the aim is to provide the answer of these questions, (1) what is the distribution of the mine value at the end of its life?, and (2) with 1 percent probability, what is the maximum loss at the end of mine life?.

Value at risk (VaR) is a measures of the worst expected loss under a normal market condition which is calculated for a specific time period at a given confidence level. VaR answers the questions like "with a probability of x%, how much can I lose over a pre-set horizon" (Benninga 2008). It means that VaR (1%) is the 1% quintile point of the probability distribution function of mine value.

3 RESULTS

The procedure described in Figure 2 is applied in a hypothetical iron ore deposit. As stated, 9 different mining plans are generated for this particular case considering the price scenarios generated via bootstrapping. After that, using the price scenarios generated by GBM method, the probability distribution of net present value of the mining operation is determined. Figure 5 represents the

cumulative probability distribution of the net present value (NPV) for plan #1.

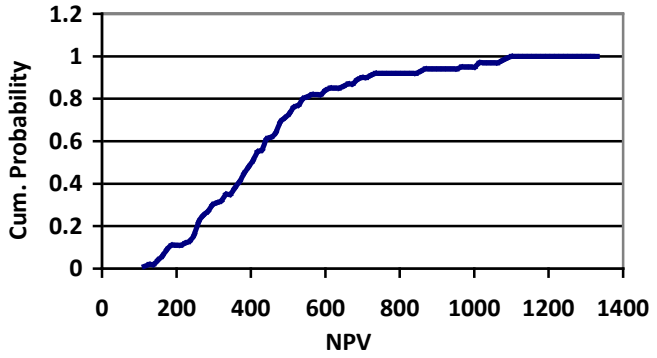

Figure 5. Probability distribution of the NPV for plan #1.

The result shows that plan#2 has the highest expected NPV compared with other plans (Figure 6). Also, considering the value at risk of each mining plan, the plan #8 has the lowest VaR (1%) among the other plans (Figure 7).

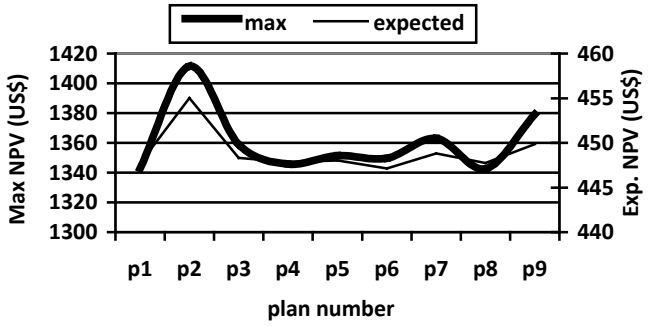

Figure 6. Maximum and expected NPV of mine plans.

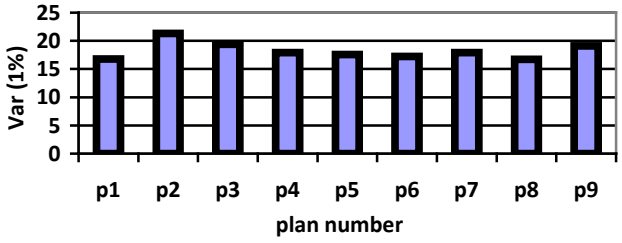

Figure 7. VaR (1%) of NPV for mine plans.

The amount of VaR in case of plan #8 is about 10.77% of the initial capital cost. The expected NPV and also the maximum possible NPV of the plan #8 is also the lowest among other plans. However, considering VaR, this plan will be comprehended as the optimum mining sequence in this example.

4 DISCUSSION

The procedure presented here is applied in a hypothetical iron ore deposit. The results should be validated using a real case data set. However, the procedure seems to be applicable in real world problems.

Following the procedure presented here, 9 different optimal mine plans were generated. These plans were analyzed in the presence of mineral price uncertainty. According to the results, the plan #8 is suggested as the optimum mining sequence in this case. Analyzing the price scenario based on which the mine plan is optimized; one could see that, in this particular scenario, the mineral price has a falling trend compared to the other scenarios. This will cause high grade ore blocks to be mined early in time in order to gain the maximum possible NPV.

The main limitation of the presented procedure is the determination of initial price trends and scenarios. The scenarios based on which the mine plans are determined are given in Figure 2. It means that there is a need to carefully determine the initial price trends. In this paper the bootstrapping method is applied to generate some price scenarios such that they are a representative sample of future price outcomes.

5 CONCLUSIONS

VaR is capable of determining the worst expected loss under a normal market condition and it helps the mine planner to determine the optimum mine plan under the uncertainty of mineral price.

The main conclusion is that, those mine plans determined based on the falling price scenarios has the lowest VaR compared with other plans.

REFERENCES

Abdelsabour, S. A., and Dimitrakopoulos, R., 2011, Incorporating geological and market uncertainties

and operational flexibility into open pit mine design, *J. of Mining Science*, 47(2), 191-201

AbdelSabour, S. A., Dimitrakopoulos, R., and Kumral, M., 2008, Mine design selection under uncertainty, *Mining Technology*, 117(2), 53-64

Akaike, A. and Dagdelen, K., 1999, A strategic production scheduling method for an open pit mine, *Proceedings of the 28th APCOM*, 729 – 738

Albach, H., 1976, Long range planning in open pit mining, *Management science*, 13(10), B549-B568

Benninga, S., 2008, *Financial modeling*, 3rd Ed., The MIT press, Cambridge, Massachusetts, London, England, 1133 pages

Bley, A., Boland, N., Fricke, C., and Froyland, G., 2010, A strengthened formulation and cutting planes for the open pit mine production scheduling problem, *Computers and Operation Research*, 37(9), 1641-1647

Boland, N., Dumitrescu, I., and Froyland, G., 2008, A multistage stochastic programming approach to open pit mine production scheduling with uncertain geology, *Optimization*, online, 33 pages, available at: http://www.optimization-online.org/DB_FILE/2008/10/ 2123.pdf

Caccetta, L., Hill, S. P., 2003, An application of branch and cut to open pit mine scheduling, *J. Global Optimization*, 27, 349–365

Cullenbine, C., Wood, R. K., and Newman, A., 2011, A sliding time window heuristic for open pit mine block sequencing, *Optim Let*, 5(3), 365-377

Dagdelen, K., 2007, Open pit optimization — strategies for improving economics of mining projects through mine planning, in Dimitrakopoulos, R., (Ed.), *Orebody modelling and stochastic mine planning*, 2nd Ed., Spectrum Series No 14, AusIMM, 145-148

Denby, B., and Schofield, D., 1996, Open pit design and scheduling by use of genetic algorithms, *Trans. Inst. Min. Metall. (Sec A: Min. Industry)*, 103, A21 –A26

Dimitrakopoulos, R., and Ramazan, S., 2008, Stochastic integer programming for optimizing long term production schedules of open pit mines, methods, application and value of stochastic solutions, *Mining Technology*, 117(4), 155-160

Dowd, P.A. and Onur, A.H., 1992, Optimizing open pit design and sequencing, in Proceedings of the *23rd International Symposium on the APCOM*, 411 – 422

Elkington, T., and Durham, R., 2009, Open pit optimization – modelling time and opportunity costs, *Mining Technology*, 118(1), 25-32

Erlwein C., Mitra G, Roman D., 2012, HMM based scenario generation for an investment optimization problem, *Ann. Oper. Res*., 193 (1), 173-192

Gholamnejad, J., and Moosavi, E., 2012, A new mathematical programming model for long-term production scheduling considering geological uncertainty, *The J. of The Southern African Ins. of Mining and Metallurgy*, Vol. 112 (2)

Godoy, M., and Dimitrakopoulos, R., 2004, Managing risk and waste mining in long-term production scheduling of open-pit mines, *SME Transactions*, 316(03), 43-50

Groeneveld, B., and Topal, E., 2011, Flexible open-pit mine design under uncertainty, *J. of Mining Science*, 47(2), 212-226

Hall, B., 2009-a, Short-term gain for long-term pain-how focusing on tactical issues can destroy long-term value, *The J. of the Southern African Ins. of Mining and Metallurgy*, March 2009 Issue, 147-156

Hall, J., 2009-b, *Options, Futures, and other derivatives*, 7th Ed., Pearson Educational Int., 814 pages

Hustrulid, W., Kuchta, M., and Martin, R., 2013, *Open pit mine planning and design*, 3rd edition, CRC Press, Taylor and Francis Group, London, UK, 245-249

Johnson, T.B., 1968, *Optimum open pit mine production scheduling*, Ph.D. Thesis, Dept. of IEOR, University of California, Berkeley, 131 pages

Journel, A., and Kyriakidis, P.C., 2004, *Evaluation of mineral reserves: a simulation approach*, Oxford University Press, 215 pages

Kumral, M., 2003, Application of chance-constrained programming based on multi-objective simulated annealing to solve a mineral blending problem, *Engineering Optimization*, 35(6), 661-673

Kumral, M., 2010, Robust stochastic mine production scheduling, *Engineering Optimization*, 42(6), 567-579

Lamghari, A., and Dimitrakopoulos, R., 2012, A diversified Tabu search approach for the open-pit mine production scheduling problem with metal uncertainty, *European J. of OR*, 222(3), 642-652

McCarter, M.K., 1992, Surface mining- deferred reclamation, in Hartman, H. L. (Editor), *SME mining engineering Handbook*, Society for Mining, Metallurgy, and Exploration (SME), 2260 pages

Menabde, M., Froyland, G., Stone, P., and Yeates, G. A., 2007, Mining schedule optimization for conditionally simulated ore bodies, in Dimitrakopoulos, R., (Ed.), *Orebody modelling and stochastic mine planning*, 2nd Ed., Spectrum Series No 14, AusIMM, 379-383

Moosavi, E., Gholamnejad,J., Ataee-Pour, M., Khorram, E., 2014, Optimal extraction sequence modeling for open pit mining operation considering the dynamic cut off grade,

Gospodarka Surowcami Mineralnymi – Mineral Resources Management, 30(2), 173-186

Murakami, S., Tamanishi, Y., Miwa, S., and Yamatomi, J., 2011, Four-dimensional network relaxation method for long-term open pit mine scheduling, In Baafi, E. Y., Kininmonth, R. J., and Porter, I., (Eds.), *35TH APCOM Symposium*, Wollongong, AusIMM, 311 -318

Newman, A. M., Rubio, E., Caro, R., Weintraub, A., and Eurek, K., 2010, A review of operations research in mine planning, *Interfaces*, 40(3), 222-245

Noble, A. C., 2011, Mineral Resource Estimation, in Darling, P. (Editor), *SME mining engineering handbook*, 3rd edition, CHAPTER 4.5, 203-217, Society for Mining, Metallurgy, and Exploration Inc. (SME)

Osanloo, M., 2012, Future challenges in mining division, Are we ready for these challenges? Do we have solid educational program?, Wroclaw, Poland, *23rd meeting of the Society Of Mining Professors*, 7 pages

Osanloo, M., Gholamnejad, J., and Karimi, B., 2008, Long-term open pit mine production planning: a review of models and algorithms, *Int. J. of Mining, Reclamation and Environment*, 22(1), 3-35

Ramazan, S., and Dimitrakopoulos, R., 2004, Traditional and new MIP models for production scheduling with in-situ grade variability, *Int. J. of mining, reclamation and environment*, 18, 85 – 98

Rovenscroft, P.J., 1992, Risk analysis for mine scheduling by conditional simulation, *Trans. Inst. Min. Metall. (Sec A: Min. Industry)*, 101, A82 – A88

Sattarvand J., 2009, *Long Term Open Pit Planning by Ant Colony Optimization*, PHD thesis, RWTH Aachen University, 1-8

Smith, M. L., 2001, Integrating conditional simulation and stochastic programming: an application in production scheduling, In Xie, L., (Eds.), *CAMI Symposium*, Swet and Zeitlinger, 203-208

Tan, S., and Ramani, R. V., 1992, Optimization model for scheduling ore and waste production in open pit mines, In Y. C. Kim (Ed.), *23rd APCOM*, Arizona, Tucson, AZ: SME, 781-792

Tolwinski, B., and Underwood, R., 1996, A scheduling algorithm for open pit mines, *J. of Mathematics Applied in Business & Industry*, 247-270

Topal, E., 2008, Early start and late start algorithms to improve the solution time for long-term underground mine production scheduling, The *J. of the Southern African Ins.e of Mining and Metallurgy*, (February), Vol. 108, pp. 99-107

Tulp, T., 1999, Economic change and pit design, AusIMM, *Optimizing with Whittle*, 151-157

Yarmuch, and Ortiz, J., 2011, A novel approach to estimate the gap between the middle- and short-term plans, In Baafi, E. Y., Kininmonth, R. J., and Porter I., (Eds.), *35TH APCOM*, Wollongong: AusIM, 419 - 425

Zhang, M., 2006, Combining genetic algorithms and topological sort to optimize open-pit mine plans, *MPES 2006*,Torino, Italy, 1234–1239

Measuring Mine Planning Software Utilisation for Decision-Making Strategies in the South African Iron Ore Mining Sector

B. Genc and C. Musingwini
University of the Witwatersrand, Johannesburg, South Africa

ABSTRACT Mine planning software has and continues to contribute to the development of the South African mining industry. As mine planning software usage continues to be more widespread, it is imperative that a methodology to evaluate mine planning software utilization for enhanced decision-making strategies in South Africa is established. This paper institutes this new methodology to measure mine planning software utilisation in the South African iron ore mining sector. An existing online database available on the website link http://db.mining.wits.ac.za was developed prior to this study in September 2012 (initial data collection date) to show the mine planning software providers, their corresponding software solutions as well as the software capabilities and information on the number of licences. The outcome of this development and implementation was published in the *Journal of the Southern African Institute of Mining and Metallurgy* in 2013. In 2014, the dataset was updated with additional and new information.

The methodology for the evaluation of utilisation of mine planning software in various commodity sectors was developed on the basis of three variables, namely, commodity, functionality, and time factor, as a key evaluation criteria. Even though the calculations can be done on any commodity in a similar manner, in this paper, calculations were only performed on one commodity, namely iron ore which is one of the most significant minerals in South Africa. The work presented in this paper is part of a Ph.D. research study in the School of Mining Engineering at the University of the Witwatersrand.

Keywords: Iron ore mining, mine planning software utilisation, database, and South African mining industry

1 INTRODUCTION

Mine planning software plays a vital role in every stage of mining operations, even before the actual mining commences. Gibbs (1994) stated that mine planning software had changed radically in the five years prior to 1994. This statement is still valid today, twenty years after it was made. The South African mining industry adopted mine planning software usage and it is imperative that a methodology to evaluate mine planning software utilization for enhanced decision-making strategies in South Africa is established. This paper outlines the development of a new methodology to define and measure mine planning software utilisation in the South African iron ore mining sector. Although the calculations can be done on any commodity, in this paper, calculations were only done on the commodity iron ore as iron ore is not only one of the most significant commodities in the South African mining industry, but also iron ore generated almost 18% of the mining income during 2013 in South Africa (Statistics South Africa, 2014).

An initial dataset showing the mine planning software providers, their corresponding software solutions as well as the software capabilities and information on the number of licences was collected and compiled in 2012 in an online database. The database development and implementation was published in the *Journal of the Southern African Institute of Mining and Metallurgy* in 2013 (Katakwa, et al., 2013). In 2014 the database attracted more software providers to be the part of the dataset and using the updated dataset, a methodology was developed to measure mine planning

software utilisation for iron ore in order to inform decision-making strategies for utilisation of the iron ore sector's software.

2 SOFTWARE UTILISATION

Utilisation is an important factor as it is often associated with the level of productivity in the South African mining industry. According to the Oxford English Dictionaries (2014), the root of the word of utilisation comes from the word "utilise", meaning "make practical and effective use of". Hence software utilisation can be defined as the effective use of mine planning software but in general, utilisation is associated with the overall equipment effectiveness which is one of the key performance-based metrics. Overall Equipment Effectiveness (OEE) is not only one of the most widely used metrics to determine performance against capability of the equipment but also it is commonly used as a key performance indicator (KPI) in Total Productive Maintenance (TPM) and Lean Manufacturing programs for measuring production efficiency (Vorne Industries, 2008). Detailed information regarding the overall equipment effectiveness was documented by Genc et al. (2014).

The fact is that OEE is designed for measuring equipment utilisation which can be defined as *hardware utilisation*, there is a need to define *software utilisation*, which can be used to establish a framework towards defining strategic mine planning software utilisation.

Some researchers tried to define software utilisation using the number of techniques available such as system-user interaction data to understand how often the software is being used as well as in which degree it is being used. (El-Ramly & Stroulia, 2004). But this approach cannot be used to measure mine planning software utilisation by considering the size of the whole South African iron ore sector and user privacy. Due to these reasons, a methodology was developed in such a way that utilisation of the various mine planning software that is used in iron ore mining sector could be measured. The next section defines this measurement framework.

3 UTILISATION FRAMEWORK

Software utilisation can be defined by associating many-to-many, one-to-many and many-to-one relationships between entity types. In this association, the relationship between software vendors, commodity, functionality and time factor were used to develop the following terminology:

$$\{C_i, F_l\} \rightarrow S_{k=\{i,\,l\}} \tag{1}$$

Where S_k is the software that performs tasks on commodity (i) and functionality (l). In the market usually there is more than one software specifically designed for commodity (i) and functionality (l). Genc et al. (2014) gave a detailed explanation about the terminology which defined utilisation: $u_{i,l}^{(m)}$ is the utilisation of the software that performs task on commodity (i) and functionality (l) by using software (m) and

$$u_{i,l}^{(m)} \in [0,1]$$

Furthermore, the utilisation formula can be extended by considering time factor (t) to the following:

$$u_{i,l}^{(m,t)} = f_{i,l}^{(m,t)}.w_{i,l}^{(m,t)}$$

where $f_{i,l}^{(m,t)}$ is a quantity factor that relates to the software that performs a specific task on commodity (i) and functionality (l) using software (m) at a specific time (t) and $w_{i,l}^{(m,t)}$ is the weighing factor, which will handle the missing data related issues and/or other factors such as market capitalisation of the companies. For instance $f_{i,l}^{(m,t)}$ can be defined as the total number of sites. For example, if the market capitalisation of the software companies X and Y are 5 million USD and 100 million USD respectively, but if both companies have a software solution having the same functionality, then the weighing factor of the small company will be higher than the other software company. Furthermore, the price of the mine planning

software as well as support availability plays an important role when considering the weighing factor.

As the software utilisation is already defined in a generic way previously, however, the software utilisation can also be defined in a specific way, i.e. the relative utilisation (*r*). Relative utilisation can be considered as a weighed software utilisation and can be formulated as:

$$r_{i,l}^{(m,t)} = u_{i,l}^{(m,t)} / \sum_{n=1}^{M} u_{i,l}^{(n,t)}$$

Calculating relative utilisation leads to weighed market impact of the software utilisation. However, calculating relative utilisation, three variables were used to generate the results, namely:

- commodity (*i*),
- functionality (*l*),
- time factor (*t*).

For example, the following results were calculated for only one commodity (*i*) namely iron ore using six different functionalities (*l*) namely (Katakwa, et al., 2013):

1. "Geological data management
2. Geological modelling and resource estimation
3. Design and layout
4. Scheduling
5. Financial valuation
6. Optimisation"

Six functionalities listed by Katakwa et al. (2013) originated from the Open Group's Business Reference Model which categorises not only the functionalities of mine planning software, but also mine value chain stages and mining methods (The Open Group, 2010). The Open Group's Business Reference Model illustrates how the various software solutions interact with each other, although this classification can be debateable. For example, Mine 2-4D software that is used in mine scheduling is often used in conjunction with the Enhanced Production Scheduler (EPS) as it cannot produce a schedule without the use of EPS. Figure 1 shows the names of available mine planning software and their functionalities along the mining value chain.

The time (*t*) factor has two timestamp indicators showing different data collection dates namely:

- September 2012, t=1
- April 2014, t=2

By using all three variables, the weighed software utilisation, hence the market impact of each participating mine planning software was calculated. The dataset were extracted from the updated database and the programming language GNU Octave was used for the data analysis and the calculation of the software utilisation per functionality for the selected iron ore commodity using two different timestamps as mentioned previously.

It is important to note that if $f_{i,l}^{(m,t)}$ is 0; it means either the subject software does not support the specific functionality or the subject software does not support the specific commodity. Furthermore, when calculating $u_{i,l}^{(m,t)}$ and $w_{i,l}^{(m,t)}$, the value is set to 1 as at this stage of calculation the weighed software utilisation did not have any impact on the calculation of the relative software utilisation. The software_id which is a unique identifier of each particular software are not named in this research work, and have been numbered randomly

.

	Geological Data Management	Geological Modelling and Resource Estimation	Design and Layout	Scheduling	Financial Valuation	Optimisation
Bentley Evaluation				■	■	
Bentley Scheduler				■		
BLOCK AGG	■			■		
CADSMine		■	■	■		
Carbon 14 Mine Scheduler				■		
Carbon Economics					■	■
Carbon Micro Scheduler				■		
Carbon Performance Manager					■	
Carbon Processing				■	■	
Carbon Risk					■	■
Carbon V						■
Chronos				■		
Dragsim				■		■
Enhanced Production Scheduler (CAE)				■		■
EPS (MineRP)				■		
EPS Viz (Visualizer)				■		
EPS-PCBC Interface				■		
EPSOT (EPS Schedule Optimization Tool)				■		■
GEMS	■	■	■			
Geological Data Management Solution	■					
HAULNET				■		
Interactive Short Term Scheduler			■	■		
LoM Economics					■	■
Maptek I-Site	■					
Maxipit					■	■
Mine 2-4D			■	■		
Mine Scenario Planning			■	■		
Mineable Layout Optimizer			■			
Mineable Reserves Optimizer (CAE)			■	■		
Mineable Shape Optimizer			■	■		■
mineCAD			■			
mineCAVE			■			
mineHAUL			■			
mineMARKUP	■					
Mineral Beneficiation					■	■
MineSched				■		
mineSERV			■			
mineSTRUCTURE		■	■			
Minex	■	■	■			
MKP (Mining Knowledge Platform)	■	■				
MRM	■	■	■	■	■	■
NPV Scheduler (CAE)				■	■	■
NPV Scheduler (MineRP)				■	■	
Open Pit Metals				■		
PCBC				■		
Pegs Lite	■					
Performance Diagnostics						■
Portfolio Modelling					■	
Qerent Modeller					■	■
Sable Data Warehouse	■					
Services and Logistics			■	■		■
Sirovision	■	■				
Strat 3D		■				
Studio 3 - Engineering			■			
Studio 3 - Geology		■				■
Studio 5D Planner			■	■		
Studio3 - Basics						■
Surpac	■	■	■			
Talpac			■			
Underground Coal				■		
Ventsim Visual (Advanced)			■			
Vulcan	■	■	■			
Whittle					■	■
Workforce Planning					■	■
Xact				■		
Xeras					■	■
Xpac				■		

Figure 1. Available mine planning software and their functionalities along the mining value chain

4 RESULTS

In this section, mine planning software utilisation for commodity (*i*) iron ore was calculated. Six functionalities (*l*) with two timestamps (*t*) were used for the calculations and the results for each functionality with two timestamps were presented as tables and figures, respectively. Accordingly, the total number of {6(*l*) x 2(*t*) = 12} tables for iron ore were created. After generating the tables, pie charts were created for each table for easy interpretation of the results. Consequently, using the functionality list, the remaining tables and figures were created in a similar manner.

The following software providers participated in this study: Geovia, MineRP Solutions, Sable, RungePincockMinarco, Maptek, Cyest Technology and CAE Mining. Note that data on CAE Mining was only made available in the April 2014 dataset. The results presented here do not cater for neither the mining methods nor the type of mine whether it is a surface or an underground operation.

4.1 Geological Data Management Software Results For Iron Ore

Table 1 shows the market impact of the individual software for commodity iron ore using the functionality, Geological Data Management, as at September, 2012 while Table 2 shows the same results using the second timestamp, i.e. April 2014. Figure 2 illustrates the graphical representation of both tables. Note that $f_{i,l}^{(m,t)}$, $w_{i,l}^{(m,t)}$, $u_{i,l}^{(m,t)}$ and $r_{i,l}^{(m,t)}$ in column headings in Tables 1 to 11 were defined in section 3.

When comparing the diagrams in Figure 2, there is a difference between the two pie charts; Although Surpac is still the leader with a 50% market impact, CAE Mining's Geological Data Management Solution software with a 31% market impact in the April 2014 chart is clearly visible.

Table 1. Geological Data Management functionality software utilisation for iron ore as of September 2012

m	software_id	$f_{i,l}^{(m,t)}$	$w_{i,l}^{(m,t)}$	$u_{i,l}^{(m,t)}$	$r_{i,l}^{(m,t)}$
1	9	2	1	2	0.1818
2	10	8	1	8	0.7273
3	13	0	1	0	0
4	38	0	1	0	0
5	68	0	1	0	0
6	72	0	1	0	0
7	83	1	1	1	0.0909
8	93	0	1	0	0
9	95	0	1	0	0
10	97	0	1	0	0
11	98	0	1	0	0
12	100	0	1	0	0
13	113	0	1	0	0

Table 2. Geological Data Management functionality software utilisation for iron ore as of April 2014

m	software_id	$f_{i,l}^{(m,t)}$	$w_{i,l}^{(m,t)}$	$u_{i,l}^{(m,t)}$	$r_{i,l}^{(m,t)}$
1	9	2	1	2	0.125
2	10	8	1	8	0.5
3	13	0	1	0	0
4	38	0	1	0	0
5	68	0	1	0	0
6	72	0	1	0	0
7	83	1	1	1	0.0625
8	93	0	1	0	0
9	95	5	1	5	0.3125
10	97	0	1	0	0
11	98	0	1	0	0
12	100	0	1	0	0
13	113	0	1	0	0

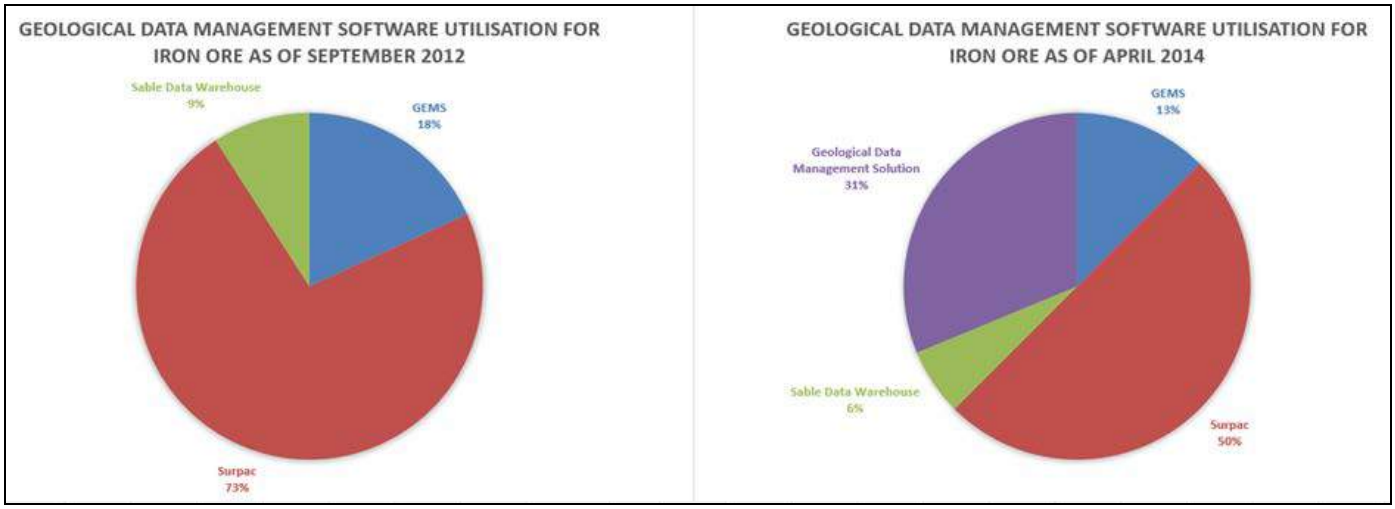

Figure 2. Geological Data Management functionality software utilisation for iron ore

4.2 Geological Modelling and Resource Estimation Software Results For Iron Ore

Table 3 shows the market impact of the individual software for the commodity iron ore using the Geological Modelling and Resource Estimation functionality as at September, 2012 while Table 4 shows the same results using the second timestamp, April 2014. Figure 4 illustrates the graphical representation of both tables.

When comparing the diagrams in Figure 3, similar to the previous results, there is a huge difference between the two pie charts; Surpac is once again the leading software with a 47% market impact in the April 2014 chart. Studio 3 - Geology have a 41% market impact in this field.

Table 3. Geological Modelling and Resource Estimation functionality software utilisation for iron ore as of September 2012

m	software_id	$f_{i,l}^{(m,t)}$	$w_{i,l}^{(m,t)}$	$u_{i,l}^{(m,t)}$	$r_{i,l}^{(m,t)}$
1	9	2	1	2	0.2
2	10	8	1	8	0.8
3	13	0	1	0	0
4	48	0	1	0	0
5	68	0	1	0	0
6	72	0	1	0	0
7	84	0	1	0	0
8	93	0	1	0	0
9	94	0	1	0	0
10	98	0	1	0	0
11	99	0	1	0	0

Table 4. Geological Modelling and Resource Estimation functionality software utilisation for iron ore as of April 2014

m	software_id	$f_{i,l}^{(m,t)}$	$w_{i,l}^{(m,t)}$	$u_{i,l}^{(m,t)}$	$r_{i,l}^{(m,t)}$
1	9	2	1	2	0.1176
2	10	8	1	8	0.4706
3	13	0	1	0	0
4	48	0	1	0	0
5	68	0	1	0	0
6	72	0	1	0	0
7	84	7	1	7	0.4118
8	93	0	1	0	0
9	94	0	1	0	0
10	98	0	1	0	0
11	99	0	1	0	0

Figure 3. Geological Modelling and Resource Estimation functionality software utilisation for iron ore

4.3 Design and Layout Software Results For Iron Ore

Table 5 shows the market impact of the individual software for the commodity iron ore using the Design and Layout functionality as at September, 2012 while Table 6 shows the same results using the second timestamp, April 2014. Figure 4 illustrates the graphical representation of both tables.

When comparing the diagrams in Figure 4, similar to the previous two results, there is a difference between the two pie charts; Surpac is still the leading software with a 44% market impact in the April 2014 chart. Studio 3 - Engineering have a 22% market impact in this field.

Table 5. Design and Layout functionality software utilisation for iron ore as of September 2012

m	software_id	$f_{i,l}^{(m,t)}$	$w_{i,l}^{(m,t)}$	$u_{i,l}^{(m,t)}$	$r_{i,l}^{(m,t)}$
1	2	1	1	1	0.0714
2	5	1	1	1	0.0714
3	9	2	1	2	0.1429
4	10	8	1	8	0.5714
5	13	0	1	0	0
6	31	0	1	0	0
7	32	0	1	0	0
8	46	0	1	0	0
9	48	0	1	0	0
10	49	0	1	0	0
11	68	0	1	0	0
12	70	2	1	2	0.1429
13	85	0	1	0	0
14	86	0	1	0	0
15	88	0	1	0	0
16	89	0	1	0	0
17	90	0	1	0	0
18	96	0	1	0	0
19	98	0	1	0	0
20	99	0	1	0	0
21	101	0	1	0	0
22	102	0	1	0	0

Table 6. Design and Layout functionality software utilisation for iron ore as of April 2014

m	software_id	$f_{i,l}^{(m,t)}$	$w_{i,l}^{(m,t)}$	$u_{i,l}^{(m,t)}$	$r_{i,l}^{(m,t)}$
1	2	1	1	1	0.0556
2	5	1	1	1	0.0556
3	9	2	1	2	0.1111
4	10	8	1	8	0.4444
5	13	0	1	0	0
6	31	0	1	0	0
7	32	0	1	0	0
8	46	0	1	0	0
9	48	0	1	0	0
10	49	0	1	0	0
11	68	0	1	0	0
12	70	2	1	2	0.1111
13	85	4	1	4	0.2222
14	86	0	1	0	0
15	88	0	1	0	0
16	89	0	1	0	0
17	90	0	1	0	0
18	96	0	1	0	0
19	98	0	1	0	0
20	99	0	1	0	0
21	101	0	1	0	0
22	102	0	1	0	0

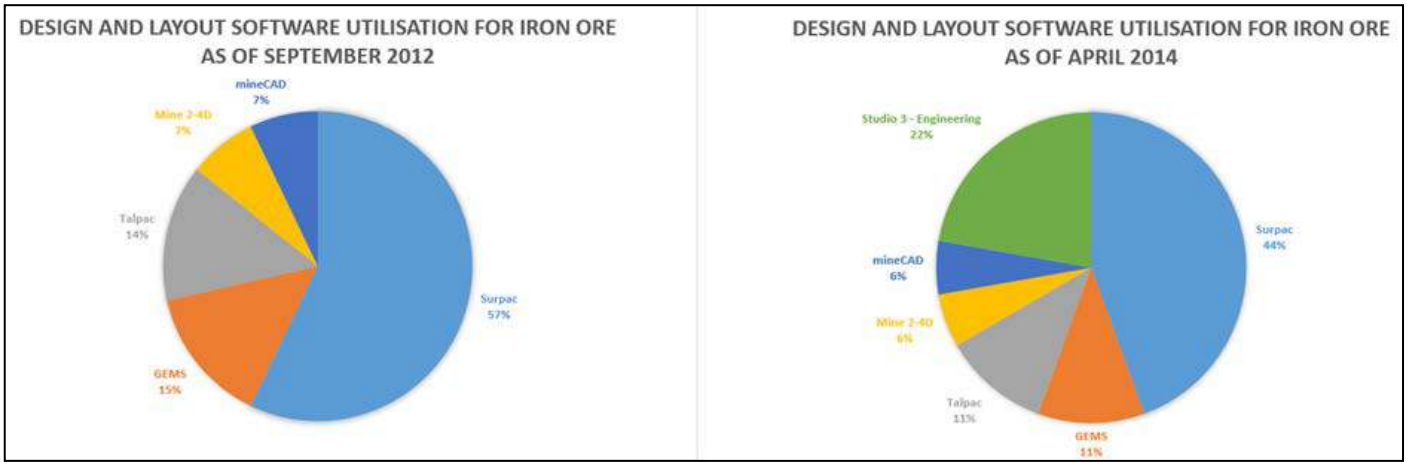

Figure 4. Design and Layout functionality software utilisation for iron ore

4.4 Scheduling Software Results For Iron Ore

Table 7 shows the market impact of the individual software for the commodity iron ore using the Scheduling functionality as at September, 2012 while Table 8 shows the same results using the second timestamp, April 2014. Figure 5 illustrates the graphical representation of both tables.

When comparing the diagrams in Figure 5, there is not much difference between the two figures; Xpac and MineSched software still has the biggest market impact with 38% and 25%, respectively in the Scheduling software field.

Table 7. Scheduling functionality software utilisation for iron ore as of September 2012

m	software_id	$f_{i,l}^{(m,t)}$	$w_{i,l}^{(m,t)}$	$u_{i,l}^{(m,t)}$	$r_{i,l}^{(m,t)}$
1	2	1	1	1	0.0455
2	4	1	1	1	0.0455
3	7	0	1	0	0
4	12	6	1	6	0.2727
5	14	2	1	2	0.0909
6	20	1	1	1	0.0455
7	21	0	1	0	0
8	33	1	1	1	0.0455
9	69	0	1	0	0
10	71	9	1	9	0.4091
11	74	0	1	0	0
12	75	1	1	1	0.0455
13	76	0	1	0	0
14	80	0	1	0	0
15	81	0	1	0	0
16	86	0	1	0	0
17	87	0	1	0	0
18	88	0	1	0	0
19	89	0	1	0	0
20	91	0	1	0	0
21	96	0	1	0	0
22	98	0	1	0	0
23	99	0	1	0	0
24	101	0	1	0	0
25	102	0	1	0	0
26	108	0	1	0	0
27	109	0	1	0	0
28	111	0	1	0	0
29	112	0	1	0	0
30	113	0	1	0	0
31	114	0	1	0	0

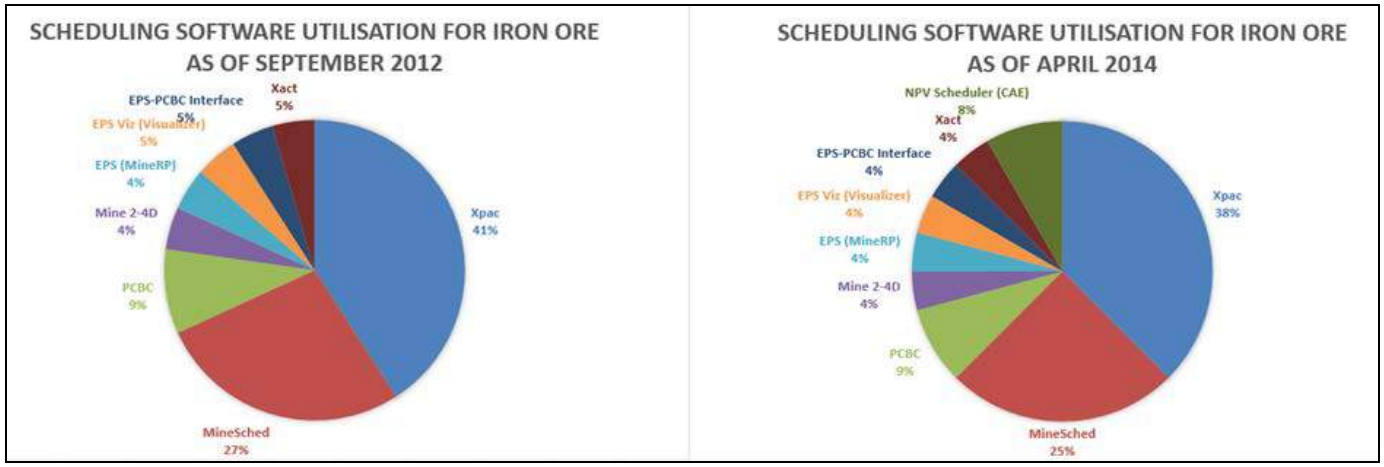

Figure 5. Scheduling functionality software utilisation for iron ore as of April 2014

Table 8. Scheduling functionality software utilisation for iron ore as of April 2014

m	software_id	$f_{i,l}^{(m,t)}$	$w_{i,l}^{(m,t)}$	$u_{i,l}^{(m,t)}$	$r_{i,l}^{(m,t)}$
1	2	1	1	1	0.0417
2	4	1	1	1	0.0417
3	7	0	1	0	0
4	12	6	1	6	0.25
5	14	2	1	2	0.0833
6	20	1	1	1	0.0417
7	21	0	1	0	0
8	33	1	1	1	0.0417
9	69	0	1	0	0
10	71	9	1	9	0.375
11	74	0	1	0	0
12	75	1	1	1	0.0417
13	76	0	1	0	0
14	80	0	1	0	0
15	81	0	1	0	0
16	86	0	1	0	0
17	87	0	1	0	0
18	88	0	1	0	0
19	89	0	1	0	0
20	91	2	1	2	0.0833
21	96	0	1	0	0
22	98	0	1	0	0
23	99	0	1	0	0
24	101	0	1	0	0
25	102	0	1	0	0
26	108	0	1	0	0
27	109	0	1	0	0
28	111	0	1	0	0
29	112	0	1	0	0
30	113	0	1	0	0
31	114	0	1	0	0

4.5 Financial Valuation Software Results For Iron Ore

Table 9 shows the market impact of the individual software for the commodity iron ore using the Financial Valuation software functionality as at September, 2012 while Table 10 shows the same results using the second timestamp, April 2014. Figure 6 illustrates the graphical representation of both tables.

Figure 6 indicates that Whittle is still the leading software with a 75% market impact in the iron ore sector when it comes to the Financial Valuation software. NPV Scheduler (CAE) is in the second place with a 25% market impact in this field.

Table 9. Financial Valuation functionality software utilisation for iron ore as of September 2012

m	software_id	$f_{i,l}^{(m,t)}$	$w_{i,l}^{(m,t)}$	$u_{i,l}^{(m,t)}$	$r_{i,l}^{(m,t)}$
1	7	0	1	0	0
2	15	6	1	6	1
3	73	0	1	0	0
4	77	0	1	0	0
5	78	0	1	0	0
6	79	0	1	0	0
7	80	0	1	0	0
8	91	0	1	0	0
9	92	0	1	0	0
10	98	0	1	0	0
11	103	0	1	0	0
12	104	0	1	0	0
13	105	0	1	0	0
14	106	0	1	0	0
15	109	0	1	0	0
16	110	0	1	0	0

Table 10. Financial Valuation functionality software utilisation for iron ore as of April 2014

m	software_id	$f_{i,l}^{(m,t)}$	$w_{i,l}^{(m,t)}$	$u_{i,l}^{(m,t)}$	$r_{i,l}^{(m,t)}$
1	7	0	1	0	0
2	15	6	1	6	0.75
3	73	0	1	0	0
4	77	0	1	0	0
5	78	0	1	0	0
6	79	0	1	0	0
7	80	0	1	0	0
8	91	2	1	2	0.25
9	92	0	1	0	0
10	98	0	1	0	0
11	103	0	1	0	0
12	104	0	1	0	0
13	105	0	1	0	0
14	106	0	1	0	0
15	109	0	1	0	0
16	110	0	1	0	0

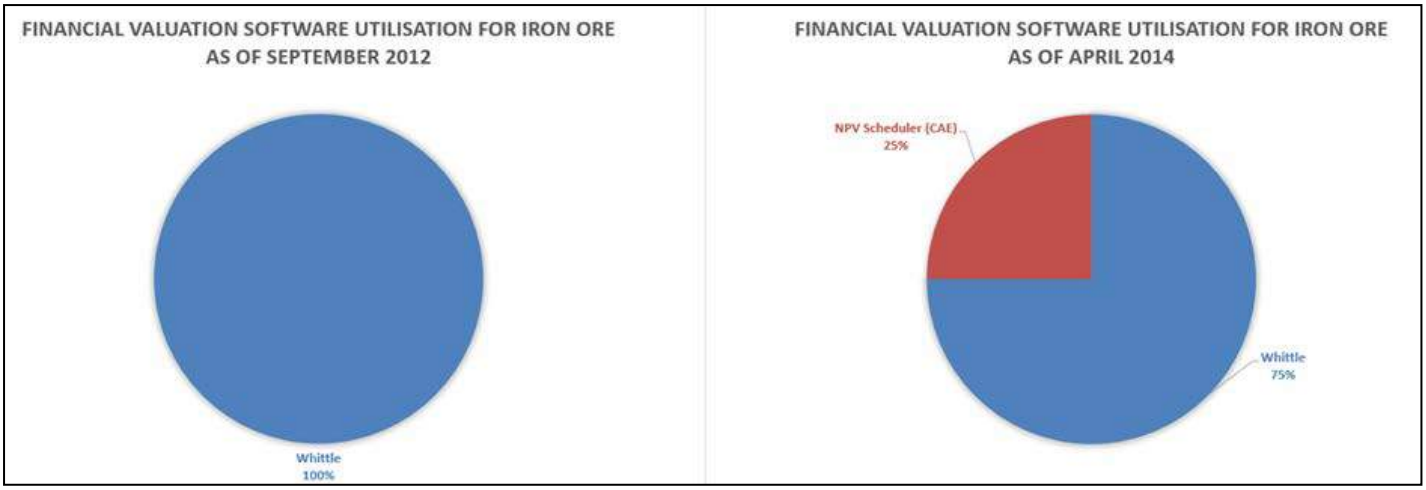

Figure 6. Financial Valuation functionality software utilisation for iron ore

4.6 Optimisation Software Results For Iron Ore

Table 11 shows the market impact of the individual software for the commodity iron ore using the Optimisation functionality as at September, 2012 while Table 12 shows the same results using the second timestamp, April 2014. Figure 7 illustrates the graphical representation of both tables, Table 11 and Table 12.

When comparing the diagrams in Figure 7, there is a noteworthy difference between the two pie charts; Studio 3 – Geology has emerged as a new leader with a 47% market impact in April 2014, which is followed by Whittle with a 40% market impact in the Optimisation software field.

Table 11. Optimisation functionality software utilisation for iron ore as of September 2012

m	software_id	$f_{i,l}^{(m,t)}$	$w_{i,l}^{(m,t)}$	$u_{i,l}^{(m,t)}$	$r_{i,l}^{(m,t)}$
1	1	0	1	0	0
2	15	6	1	6	1
3	21	0	1	0	0
4	73	0	1	0	0
5	74	0	1	0	0
6	77	0	1	0	0
7	79	0	1	0	0
8	82	0	1	0	0
9	84	0	1	0	0
10	87	0	1	0	0
11	88	0	1	0	0
12	91	0	1	0	0
13	92	0	1	0	0
14	98	0	1	0	0
15	102	0	1	0	0
16	103	0	1	0	0
17	105	0	1	0	0
18	106	0	1	0	0
19	107	0	1	0	0
20	110	0	1	0	0

Table 12. Optimisation functionality software utilisation for iron ore as of April 2014

m	software_id	$f_{i,l}^{(m,t)}$	$w_{i,l}^{(m,t)}$	$u_{i,l}^{(m,t)}$	$r_{i,l}^{(m,t)}$
1	1	0	1	0	0
2	15	6	1	6	0.4
3	21	0	1	0	0
4	73	0	1	0	0
5	74	0	1	0	0
6	77	0	1	0	0
7	79	0	1	0	0
8	82	0	1	0	0
9	84	7	1	7	0.4667
10	87	0	1	0	0
11	88	0	1	0	0
12	91	2	1	2	0.1333
13	92	0	1	0	0
14	98	0	1	0	0
15	102	0	1	0	0
16	103	0	1	0	0
17	105	0	1	0	0
18	106	0	1	0	0
19	107	0	1	0	0
20	110	0	1	0	0

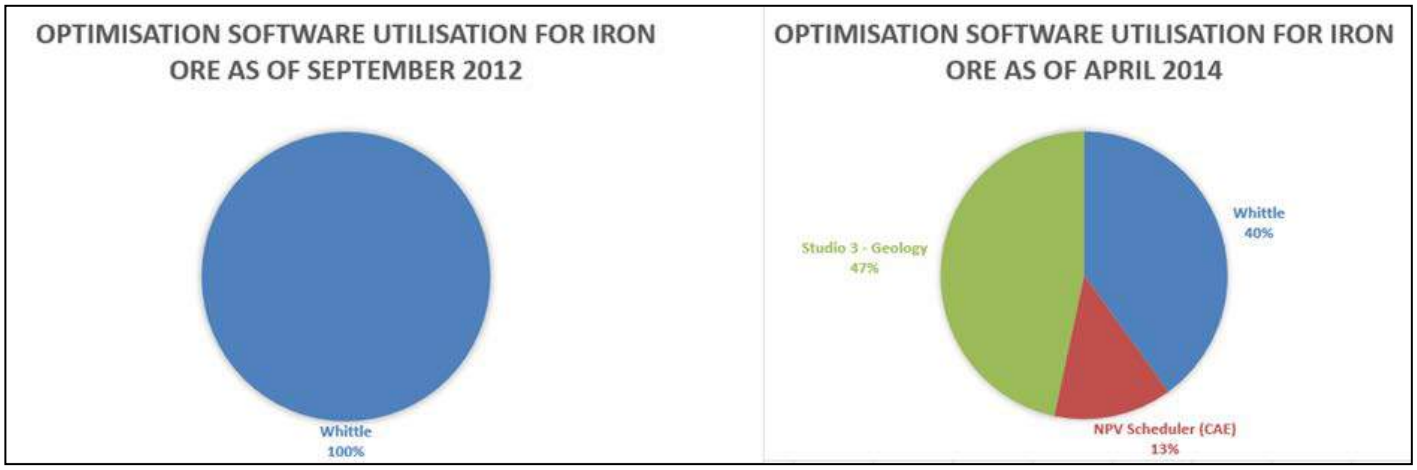

Figure 7. Optimisation functionality software utilisation for iron ore

5 CONCLUSION

The South African mining industry makes use of mine planning software in every stage of the mining operations. To gain maximum benefit from these operations, efficiency within the mining sector needs to be improved. To improve efficiency, a methodology to evaluate mine planning software utilisation for enhanced decision-making strategies was developed by calculating mine planning software utilisation with two time-stamps. Through these informed decision-making strategies, the South African mining industry is now in a position to choose the leading software solutions, which will lead to improved production efficiencies. A methodology for the evaluation of mine planning software for measuring utilisation in the South African iron ore mining sector was developed. In this framework, three variables, namely, commodity (i), functionality (l), and time factor (t) were used to calculate the results. It is important to note that data on CAE Mining was only made available in the April

2014 dataset. When comparing the results, the GEOVIA and CAE Mining market impact is visible in the iron ore sector.

This methodology provides an opportunity for all involved parties to strategically position themselves within the very highly contested mine planning software market.

REFERENCES

Genc, B., Musingwini, C. and Katakwa, P. (2014): Estimating mine planning software utilization for decision-making strategies in the South African platinum group metals mining sector. Proceedings of the Sixth International Platinum Conference: Platinum-Metal for the Future, Southern African Institute of Mining and Metallurgy, October, Sun City, South Africa. Symposium Series S81, pp. 1-10.

El-Ramly, M and Stroulia, E (2004): Mining Software Usage Data. International Workshop on Mining Software Repositories MSR 2004 W17S Workshop 26th International Conference on Software Engineering (2004), Volume: 2004, Issue: 917, pp: 64-68, 25 May 2004, Scotland, UK.

Gibbs, B. (1994): Computers – The Catalyst for Information Accessibility. SME.

Katakwa, TP, Musingwini, C and Genc, B (2013): Online database of mine planning and peripheral software used in the South African mining industry. SAIMM, Volume 113, June 2013, pp. 497-504.

Oxford Dictionaries (2014): Utilize. http://www.oxforddictionaries.com/definition/english/utilize?q=utilize. Accessed on 15th June 2014.

Statistics South Africa (2014): Publications. http://beta2.statssa.gov.za/publications/P2041/P2041January2014.pdf. Accessed on 24th July 2014.

The Open Group (2010): The exploration and mining business reference model. INTERNET https://collaboration.opengroup.org/emmmv/documents/22706/Getting_started_with_the_EM_Business_Model_v_01.00.pdf [Accessed 21 July 2014].

Vorne Industries (2008): The Fast Guide to OEE. http://www.vorne.com/pdf/fast-guide-to-oee.pdf. Accessed on 15th June 2014.

Mine Design for Silopi Üçkardeşler Asphaltite Vein
Silopi Üçkardeşler Asfaltit Filonu İşletmeTasarımı

S.G. Erçelebi, C.A. Öztürk, İ.E. Önsel, M. Özkan
Istanbul Technical University, Mining Engineering Department, Istanbul

ABSTRACT In this study, Silopi Üçkardeşler asphaltite vein is introduced and geology of the area is explained as a part of project carried out at ITU Mining Engineering Department. The experimental results for the geo-mechanical properties of the geological formations and the asphaltite itself are also presented. Silopi vein has total 39,662,238 tons of reserve with average lower calorific value of 5,216 Kcal/kg. The minable reserve for the vein by means of open pit and underground mining is calculated as to be 19,836,377 tons. Open pit and underground mine design studies are performed in order to exploit the asphaltite vein in optimum economical way. Open pit optimum depth is found to be around 885 meters which will result of 13 years of 425,000 tons yearly production. After reaching final depth of pit, a 50 m pillar is going to be left and underground production will commence. Produced asphaltite will be sent to a power plant.

Keywords: Silopi Üçkardeşler asphaltite, mine design, reserve estimation

ÖZET Bu çalışmanın amacı, Silopi Üçkardeşler asfaltit filonunu tanıtmak ve İTÜ Maden Mühendisliği Bölümünde yapılan tasarım çalışmaları hakkında bilgiler vermektir. Aynı zamanda jeolojik formasyonlar ve asfaltit numuneleri üzerinde jeo-mekanik deneyler yapılmış ve sonuçlar özetlenmiştir. Filon rezervi ortalama 5,216 Kcal/kg alt ısıl değere sahip 39,662,238 ton olarak hesaplanmıştır. Bu jeolojik rezervin 19,836,377 tonunu açık ve yeraltı işletme yöntemleri ile üretebilmek için tasarımlar yapılmıştır. Açık işletme optimum derinliği 885 m. kotu olarak 13 yıl boyunca yılda 425,000 ton cevher üretebilecek şekilde bulunmuştur. Bu derinlikten sonra işletme yer altı üretimine geçecektir. Açık işletme ve yer altı işletmesi arasında 50 metre kalınlığında bir asfaltit üretilmeden topuk olarak bırakılacaktır. Üretilecek asfaltit kurulacak termik santralde yakılarak elektrik üretilecektir.

Anahtar Kelimeler: Silopi Üçkardeşler asfaltit, maden tasarımı, rezerv tahmini

1 INTRODUCTION

Lebküchner (1969) describes asphaltic substances as all natural residues of asphaltic petroleum, disregarding whether they were found in primary or secondary deposits, associated with mineral substance or not, chemically altered or not. Lebküchner's study is one of the earliest studies among asphaltite veins occurring in South East of Turkey. Asphaltite veins (or vein-like substances) are important energy source for South-East. There are 12 economical asphaltite veins in the south of Şırnak and in Silopi. Total reserve is about 82 millions of tons (Dicle Kalkınma Ajansı 2010).

Among 12 veins, only Harbul vein which is owned by Park Elektrik Üretim Madencilik Sanayi ve Tic. A.Ş., burns asphaltite in a power plant to produce electricity. Most of the other veins already reached to open pit limit and abondened. Üçkardeşler Asphaltite vein has a high calorific value (5216 Kcal/kg) and has a potential of producing 1x135 MW electricity for 50 years or 2x135 MW electricity for 25 years.).

As now, there is no asphaltite underground mine, but known asphaltite veins go deeper and presents a great potential for underground mining. When Üçkardeşler asphaltite vein reaches its limit for open pit mining in 13 years, an underground mine will be in operation and will serve as an example to other remaining veins.

Üçkardeşler vein is investigated by General Directorate of Mineral Research and Exploration (MTA) first time between 1980-84. MTA drilled vertical and incline total 54 drills between 1980-84 and 5 inclined holes in 1985-86. 4 more holes are drilled by Şırnak Enerji A.Ş. in 2011-2012.

2 STUDY AREA AND GEOLOGY OF THE SITE

The studied area is located in the north of Gitta (Çalışkan), Besbin (Görgülü), Beşiri (Koyun Ören) villages in Silopi town in Şırnak. Silopi town covering the studied area has been neighbor to Syria (20 Km) to the southwest, Iraq (51 Km) to the southeast and Cizre town (11 Km) to the west, Şırnak city (33 Km) to the north and Uludere town (11 Km) to the northeast. E-24 highway goes through the Silopi town and reaches to Habur border. In Silopi, the way between Habur border reaches to Besbin village in the studied area. Üç Kardeşler Vein which is the main subject of the study is 2.5 km far from the Besbin village (Fig.1).

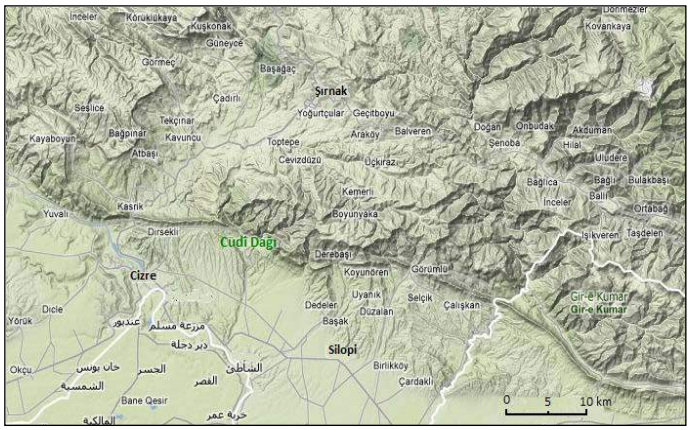

Figure 1. Location Map (Google)

A geological cross-section of the study area is given in Figure 2 to show the main geological formations in open pit mine and dump site.

Within the region, rocks deposited in the upper Paleozoic – upper cenezoic period of the time, extend roughly east-west direction. Paleozoic rocks are represented by the Permian limestone. Mesozoic rocks consist of lower-middle Triassic (Goyan Group), the upper Triassic-Jurassic-Cretaceous limestone and dolomitic limestone (the Cudi Group).

In the study area, there is the slope debris which is common and thick, affect the work of the mining. The slope debris formed coarse gravel and blocks locate near of Üçkardeşler vein.

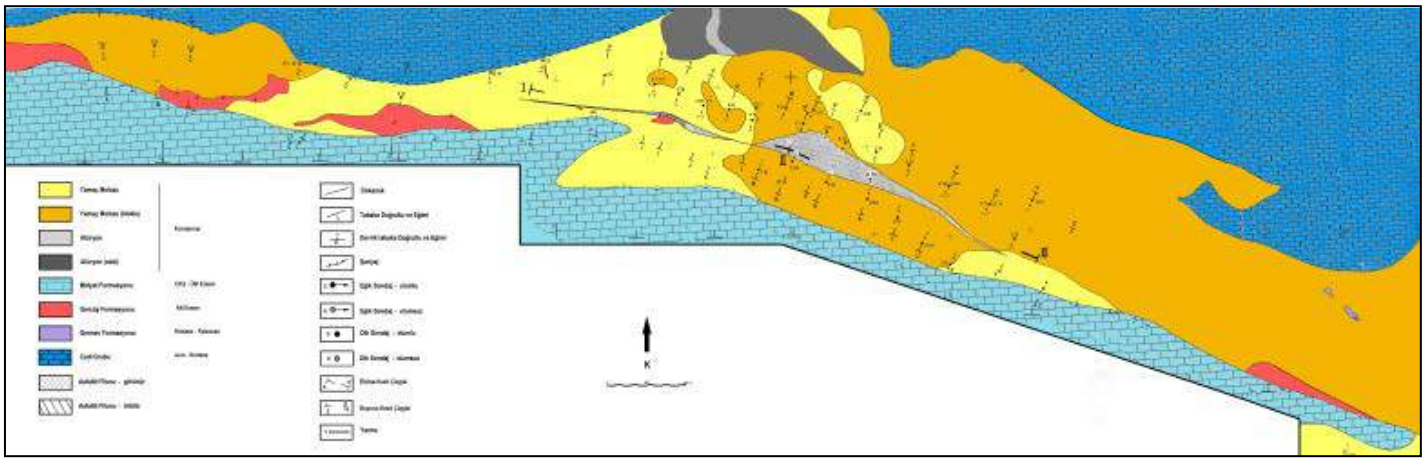

Figure 2. Geological map of the area

3 GEOTECHNICAL PROPERTIES OF FORMATIONS

Core samples for Gercüş and Midyat Formations and asphaltite were taken from Inclined boreholes drilled for the purpose of taking samples for testing. After investigation of geotechnical logs of boreholes, it was found out that sandstone, mudstone and siltstone were the main rocks of Gercüş Formation and these materials vary between themselves. Midyat formation consists of strong limestone, clay limestone and altered and clayed limestone. Material in this formation can be considered as very strong, strong and low strength. In order to determine mechanical and physical properties of rocks belonging to Gercüş and Midyat Formations and asphaltite cores are taken to rock mechanics labs of ITU Mining Engineering Department. Uniaxial compressive strength tests (σ_c), point load tests (I_s), triaxial compressive strength tests, shear strength tests were performed physical properties were determined on rocks classified. Triaxial compressive strength, uniaxial compressive strength and point load index, elasticity modulus (E_m), cohesion (c), internal friction angle (ϕ), and unit volume weight (γ) were determined after tests. Contentious tests were performed to increase reliability of results.

Average strength and density of asphaltite were found to be 17.82 MPa and 1.41 gr/ cm^3 respectively. Rock strength Parameters are given in Table 1.

Table 1. Material strength parameters (ITU Technical Report, 2012).

Rock mass	Material	σ_c (MPa)	I_s (MPa)	E_m (MPa)	c (MPa)	ϕ (^{0})	γ (kN/m^3)
Gercus formation	Gray and green sandstone containing few clay and silt	25.26	1.07	4,743.3	4.70	51.10	23.9
	Red–brown clay stone and sandstone containing sand and silt	22.97	1.05	3,529.1	5.50	45.00	25.0
	Red–brown clay stone containing silt and filled with gypsum	18.55	0.92	3,781.2	n/a	n/a	17.2
Midyat formation	Limestone	139.9	6.80	31,200	40	44.00	24.2
Uckardesler asphaltite vein	Asphaltite	17.8	0.54	599.8	4.40	37.60	14.1

4 RESERVE CALCULATIONS

In order to construct the geometry and 3 dimensional solid model of the asphaltite vein, the drill hole data obtained from MTA is used and given below. In addition 4 new holes were drilled by Şırnak Enerji. The length of Üçkardeşler vein is 1265 meters. The width of the vein is between 2 to 75 meters. Depending on the width, the vein is divided into 3 parts.

Part I (West Part)

The length of this part is 605 meters. Except the 130 meters part which is on the East of K-K' cross section, there is no overburden. On the eastern part, the vein is covered with 20-50 meters of slope rubble. The width of the vein in this section is between 2 to 40 meters. Vein is inclined 80^0-87^0 from South (1100 m) to North (900 m). Between 900 and 850 m high it becomes vertical and 85^0-80^0 inclined in lower parts. Drill holes E2B-E8, E3-E9, show that, mineralization is not continuous from one side to other. Under 950 meters, mudstone and clay wedges interfere the asphaltite.

Part II (Middle Part)

This part is 560 meters long. The width of the vein is between 5 to 75 meters. Vein is vertical until 700 m, and then 85^0-80^0 inclined to South.

Part III (East Part)

The vein is 100 meters long in this part. Vertical at the top, and 85-80 inclined to South under 850 meters. In the Eastern part there is a clay wedge. At the end of the vein clay and mudstone wedges are common.

By using all drillhole data mentioned above, 3 dimensional solid model of the vein is constructed by the help of Micromine software. Drill holes locations and solid model, with proven and probable reserves, are shown in Figure 3, 4 and 5. When calculating the proven reserve, the influence of the drill hole is taken as 100 meters, and for probable reserve calculation, influence distance is taken as 200 meters.

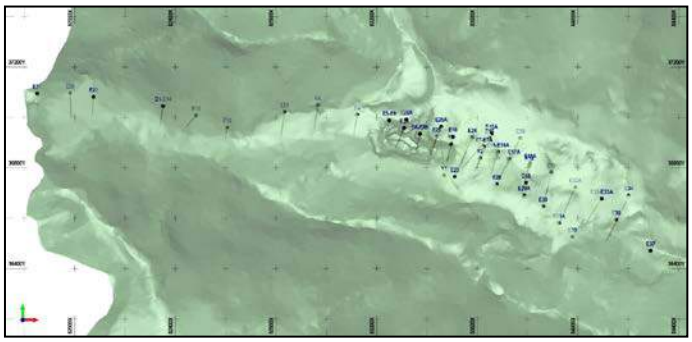

Figure 3. Topography and drillholes.

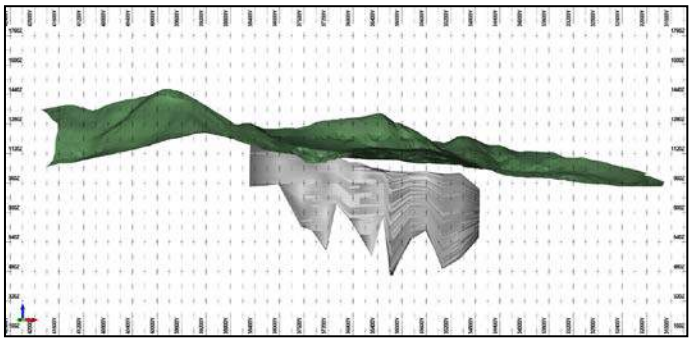

Figure 4. Proven reserve

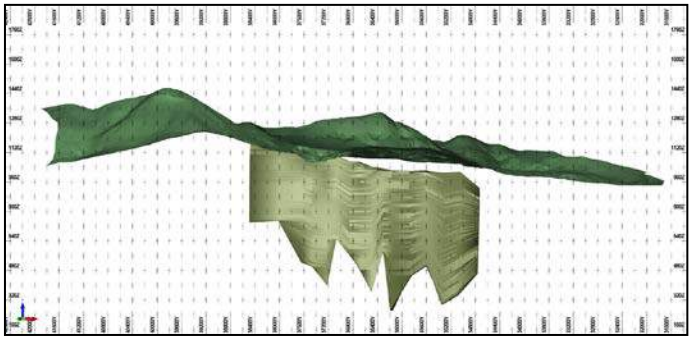

Figure 5. Proven and probable reserve

Table 2. Üçkardeşler aphaltite vein reserves.

Reserve Type	Reserve (m^3)	Reserve (Ton)
Proven Reserve	15,925,088	22,454,374
Probable Reserve	12,204,159	17,207,864
Total Reserve	28,129,247	39,662,238

Result of tests carried out to obtain the properties of the asphaltite show that the moisture content of original asphaltite is %3.52, ash content is %37.59, volatile matter is %46.66, fixed carbon is %14.10, total sculpture is %7.50, and combustible sulphure is % 7.25, low calorific value is 5,216 Kcal/Kg, and high calorific value is 5,487 Kcal/Kg.

5 OPEN PIT DESIGN AND PLANNING

5.1 Slope Stability

In this study, the minimum Factor of Safety value is taken as 1.30 for the design of open pit slopes. Factor of safety (F) has vital importance for the design of slopes that can be simply defined as the ratio of forces against sliding to driving forces. Limit equilibrium condition is defined while F=1. This is because F must be higher than 1.0 for the design of slopes against sliding.

Slide v:6.005 software was used to analyze the stability of slopes. These analyses were carried out on the cross-sections taken from the plan view of the final open pit design as given in Figure 8.1. Firstly geological information was processed to the cross-sections taken from 4 different sections of the open pit as the most vertical overall slope angle. After that, cohesion, internal friction angle, and unit volume weights of each formation were given as input parameters. Underground water table level (UGWT) was drawn as nearly close to the surface for Gercüş formation and relatively deeper for Midyat formation which is strong rock mass. Stability analyses were carried out by using Bishop multiple slipping and

Janbu multiple slipping surface analyses and the model giving the least value of F is accepted so as to be in safe side of the design.

As an example from the stability analyses Cross section 1-1' is given in Figure 6.

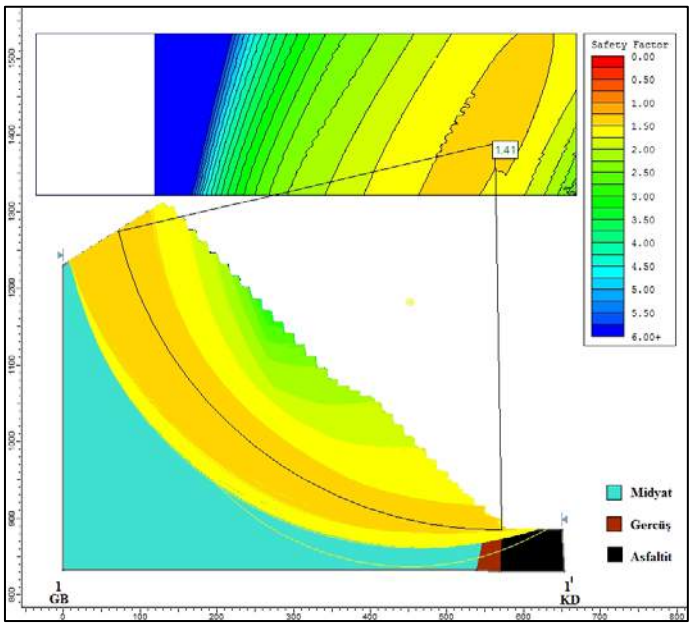

Figure 6. 1-1' Cross-section stability analysis, F=1.41; overall slope angle: 44^0

The analyses show that the overall slope angle can be designed as $37\text{-}38^0$ for Gercüş formation and 44^0 for Midyat formation both for exploitation and final overall slopes.

Bench Geometry

According to slope stability analysis results, bench heights as 15 meters, bench widths as 15 meters for production benches, 10 meters for final benches, road widths as 15 meters and road inclination as 8^0 are chosen. Bench angles are 75^0 for Midyat formation, 60^0 for Gercüş formation, 75^0 for asphaltite and 45^0 for slope debris. Overall slope angle for the pit is 36.5^0 for North slopes (Gercüş formation), 44^0 for South slopes (Midyat formation), 37^0 for East slopes and 39^0 for West slopes.

5.2 Surface Mine Design

5.2.1 Optimum pit limit

Optimum pit limit is determined by using Lersh-Grossman Algorithm implemented in Micromine software. Optimum pit depth is found to be around 885 meters. In addition, East and West end of the vein is where asphaltite becomes very thin, under 2 meters, and it is not economical to mine these parts.

5.2.2 Surface mine planning

Annual production of 425,000 tons of asphaltite of average 5216 kcal/kg is going to be used at a 1x135 MW coal firing power plant. Until reaching to the optimum pit depth it will be possible to operate open pit for 13 years. After 13^{th} year underground mine will be in operation alone.

According to slope stability analysis and the slope geometry given in previous section 5 and 10 years surface mines are planned by using Micromine software. At the end of first period (first 5 years), surface mine will be around 960 m altitude, entire asphaltite over 975 m elevation inside the economic pit, and some of the asphaltite from the 860-975m bench will be produced. The plan at the end of the first period is given in Figure 7 and 3-D shape is given in Figure 8.

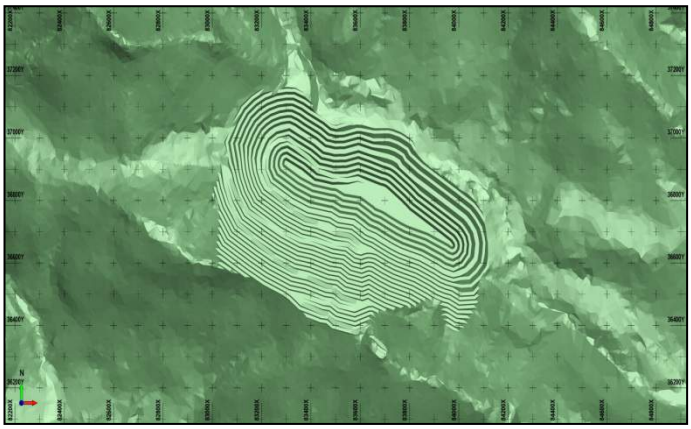

Figure 7. Surface mine plan after I^{st} period

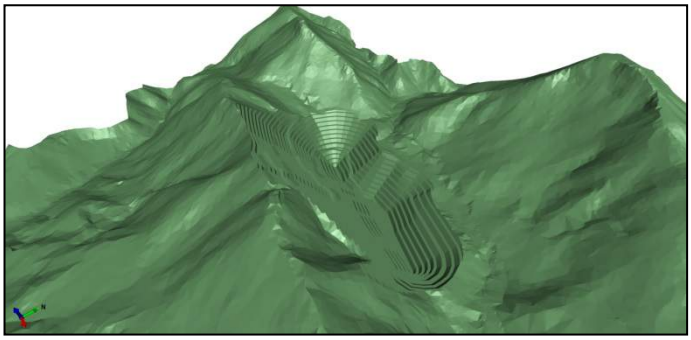

Figure 8. 3-D view of surface mine after I^{st} period (Looking from S-E direction).

Plan of the surface mine at the end of IInd Period (5-10 years) is given in Figure 9 Figure 10 shows 3-D shape. Figure 11 and 12 shows 2 period production together. Asphaltite production, overburden removal and stripping ratios for two periods are given in Table 3. For the Ist Period, stripping ratio is 16.6, for the IIth Period, it is 13.2 averaging 14.8 as total.

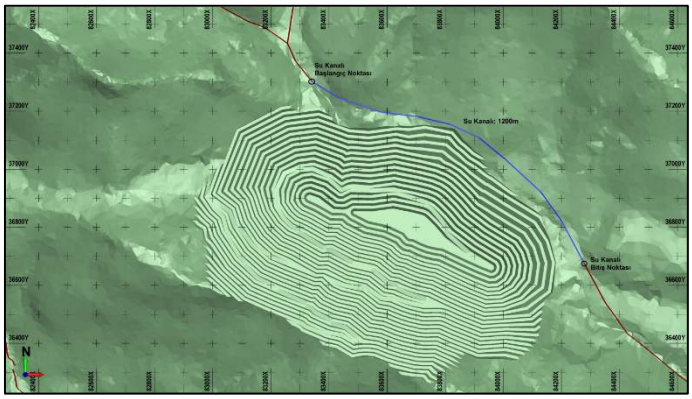

Figure 9. Surface mine plant after IInd period

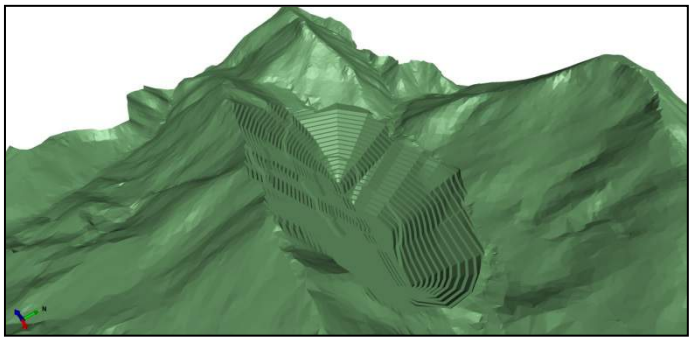

Figure 10. 3-D Surface mine after Ist period (Looking S-E).

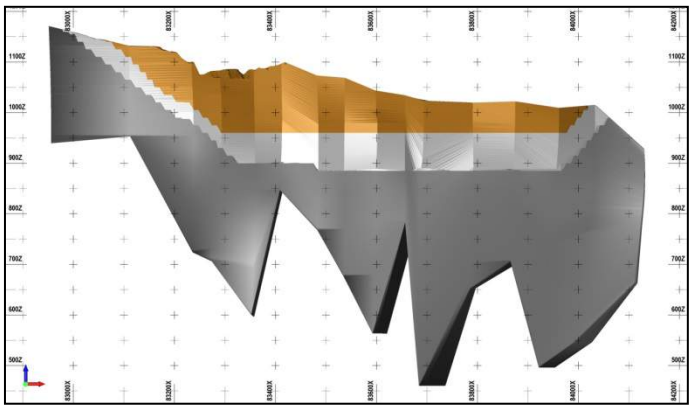

Figure 11. Surface mine example cross section showing I and IInd period

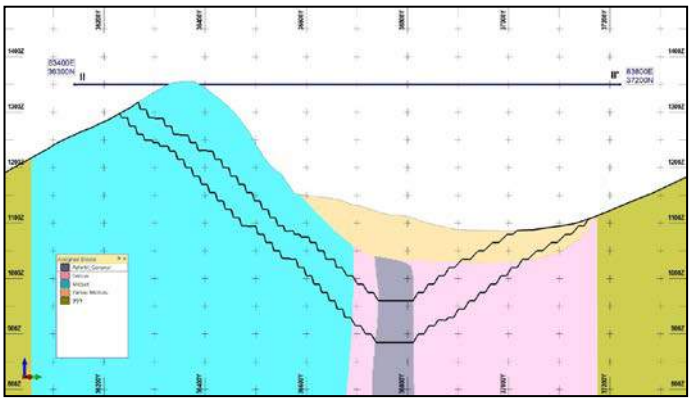

Figure 12. I and IInd period asphaltite production

Table 3. Ist and IInd period production summary of surface mine.

	Asphaltite (ton)	**Overburden (m^3)**	**Strip Ratio**
Ist Period	2,567,115	42,671,042	16.6
IInd Period	2,940,680	38,873,443	13.2
Total	**5,507,795**	**81,544,485**	**14.8**

5.2.3 Dump site

The opposite side of the Kalender Hill to the surface mine is selected as dump site. This site the most appropriate area for the dump site when considering high mountainous regional feature of the mine area. Overburden haulage will take place from a 400 meters long tunnel which will be constructed on the west of the surface mine. Another alternative is the going around Kalender hill by means of 700 meters long haulage way. Both alternatives with the local coordinates are shown in Figure 13.

It is expected that overburden material will compose 30 degree dumping slopes. In this project a slope stability study is not carried out for the dump site. Dump site slope stability study is important in terms of environmental issues and safety considerations and dump slopes should be constructed in a way that slope failures are avoided.

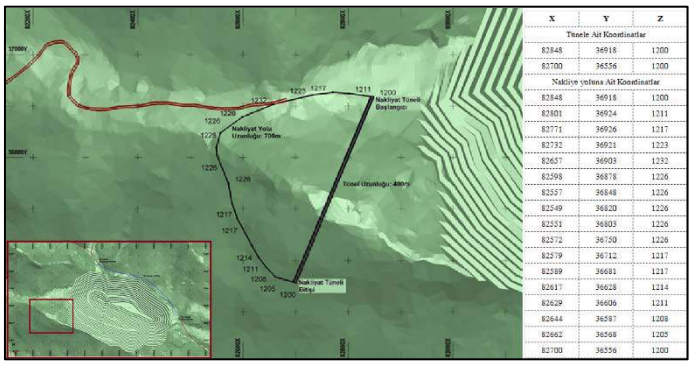

Figure 13. Surface mine to dump site haulage way alternatives

5.2.4 Open pit equipment selection

Equipment selected in open pit mine are given below with their capacity.

Equipment	Capacity	Quantity
Drill	10.16 cm(4")	3
Excavator	5 m^3	6
Truck	30 ton	28
Loader	4 m^3	1
Dozer	335 HP	3
Grader	165 HP	1
Repair equipment	10 ton	2
Sprinkler	10 ton	1
ANFO truck	10 ton	1
Equipment truck	10 ton	1
Fuel Truck	10 ton	1

6. UNDERGROUND MINE DESIGN

As can be seen from section 4, Üçkardeşler asphaltite vein has 22,454,374 ton proven reserve and proven+probable 39,662,238 ton reserve. Plan, design and cost study related to underground mine have been carried out according to proven reserve estimation.

In Section 5 amount of ore which will be produced by open pit mine is determined. To prevent the underground mine interfering the open pit mine and to prevent slides, a pillar has to be left between underground and open pit mine. The study about the height of the pillar is given in this chapter at the following part "Support of the Underground Spaces". At Table 4 ore reserves of underground, open-pit and pillar is given.

Table 4. Üçkardeşler asphaltite vein production and pillar reserves.

No	Definition	Amount (Ton)
1	Open Pit Mine Production	5,507,795
2	Underground Mine Production	14,328,582
3	Pillar	2,617,997
4	Total	22,454,374

From the table above it can be seen that proven reserve which can be produced by underground mine is 14,328,582 ton. In Figure 14 parts of the ore body which are going to produced by open pit, underground mine and pillar between them is given.

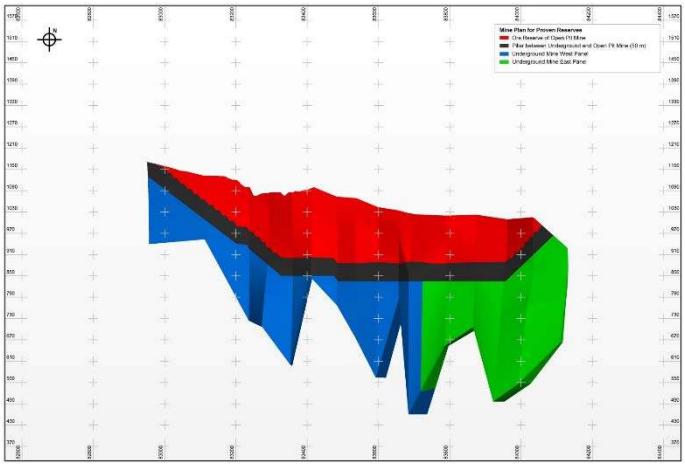

Figure 14. 3D view of Üçkardeşler asphaltite vein underground and open pit proven reserves and pillar.

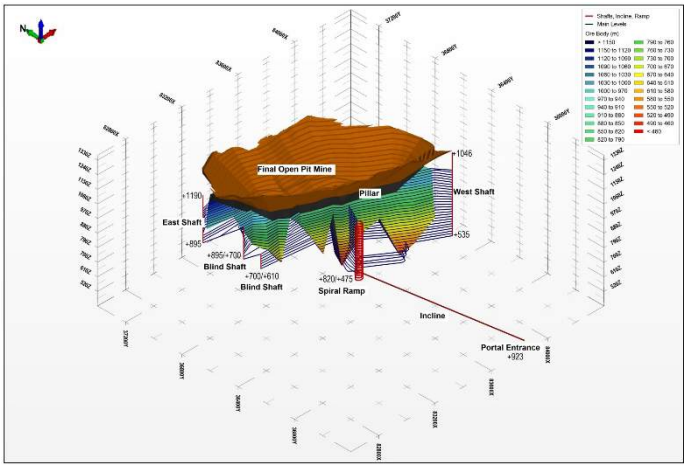

Figure 15. Underground mine development project – North East 3D view.

Details of underground mine design is given elsewhere (Ozturk, 2014) and will not be repeated here. Figure 15 shows underground mine design.

7. CONCLUSION

Asphaltite veins are only energy resources in southeastern part of Turkey. In this study, the summary of findings for Üçkardeşler asphaltite vein in Silopi region is presented. Using existing drillhole data, proved and probable reserve of the vein is calculated as 39,662,238 tons. In the study 19,836,377 tons of this reserve is estimated to be produced by means of open pit and underground mining method to feed a power plant. Open pit mine will be operated 13 years and after that underground mine will commence.

For open pit mine the slope stability analyses show that the overall slope angle should be designed as $37\text{-}38^0$ for Gercüş formation and 44^0 for Midyat formation both for exploitation and final overall slopes. Open pit mine will produce 425,000 tons of asphaltite per year to feed a 1x135 MW power plant. Also an alternative of the 2x135 MW capacity and 850,000 ton/year asphaltite production is considered. In both alternatives yearly production rate of 425,000 ton can serve the power plant in all 13 year. Underground mining operations will start after 13 years in case the 1x135 MW is used and production will be 425,000 ton/year throughout the mine life. In case 2x135 MW capacity power plant in operation underground mining operations will start in the sixth year and will serve the power plant for 20 years.

REFERENCES

Dicle Kalkınma Ajansı, 2010. *Trc3 Bölgesi (Mardin, Batman, Siirt, Şırnak) Yer Altı Ve Yer Üstü Zenginlikleri Raporu*.

Istanbul Technical University (ITU), Faculty of Mines, Technical Report, 2012. *Üçkardeşler Asphaltite Vein Prefeasibility Project*, 262 p.

Işıganer T., 1985. Mardin-Silopi-Harbul ve Üçkardeşler Asfaltit Filonlarına ait Jeoloji Raporu, *MTA Yayınları*, 7762, Ankara.

Lebkuchner, R.F., 1969. Occurrences of the Asphaltic Substances in Southeastern Turkey and Their Genesis, *MTA Bull*, No.79, Ankara.

Ozturk, C.A., 2013. Support Design of Underground Openings in an Asphaltite Mine. *Tunnelling and Underground Space Technology*. v. 38, s. 288-305.

The Future of Mega Data in Virtual Reality Environments in Mining Practice

F.T. Suorineni
UNSW Australia, Sydney, Australia

ABSTRACT At the mine feasibility stage data is collected from several sources. This data may be multi-dimensional. Space and time are examples of the multi-dimensionality of data. At the operational stages data is also collected from various sources to ensure the mine is operating optimally, economically and safely. Mines are therefore dealing with mega data from multiple sources and dimensions at any given time. Understanding mega data from multiple sources and dimensions calls for new thinking. The extreme power of computers coupled with virtual reality technology and scientific visualization provides a way for dealing with and understanding multidimensional mega data from multiple sources. The concept of Big Data has recently emerged. This paper argues Big Data application in mining should be approached cautiously and discusses the benefits and future of virtual reality and scientific visualization in dealing with multi-dimensional mega data from multiple sources in mining practice with case examples.

Keywords: Mega data, Virtual reality, Multi-dimensional data

1 INTRODUCTION

1.1 Stages in the Mining Process

The development of a mine starts from discovery of the orebody and continues through various stages to production and closure. The critical stages in the mining process are summarized in Figure 1.

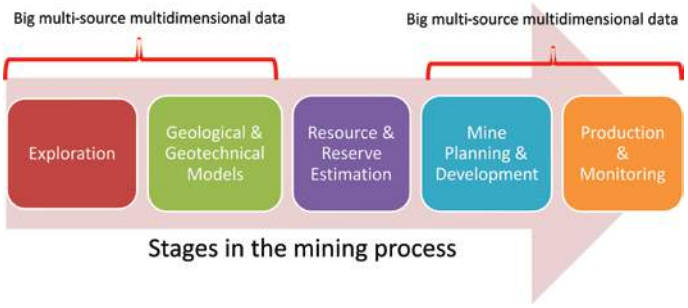

Figure 1. Stages in the mining process.

In Figure 1 the exploration stage usually involves the collection of data by multidisciplinary teams in:
– Geophysics
– Geochemistry
– Geologists
– Geotechnical, and
– Other information.

The data involved in each discipline may be several gigabytes and multidimensional – space, time and cost for example.

Several exploratory drill holes (Figure 2) would have been used to collect data from cores including grades, rock quality, structure and definition of lithologies. Geotechnical data such as rock strengths, RQD among others will also be collected at this stage.

The data from different experts from multiple sources do not sometimes correlate and are often in conflict when integrated. It is difficult resolving such data conflicts as each expert will often insists on being right.

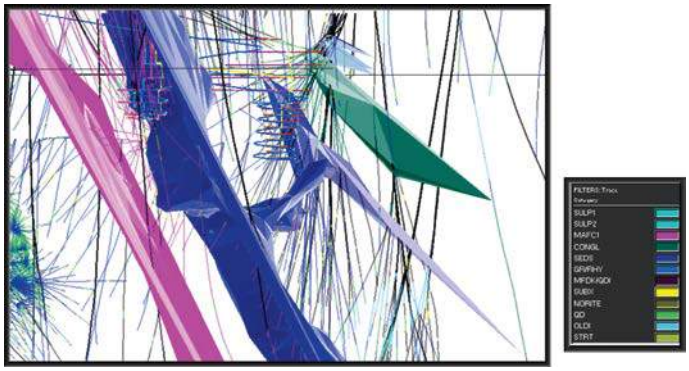

Figure 2. Several boreholes for different multi-dimensional data extraction for multiple purposes – Example of Mega Data in mining.

The next stage in the mine development process is to understand the geology of the

deposit as deciphered from Stage 1. At this stage, all data from the various sources and disciplines must be integrated to construct the geology of the deposit – the geological model. Here, the use of virtual reality and scientific visualization is critical as explained later in this paper.

Understanding the geomechanics at the exploration stage is also critical for deciding on the mining method and strategy later in the mine development. This is also achieved through integration of the various geotechbnical and geological data – the geomechanical model.

The geological model forms the basis for the ore resource and reserve estimations. Both the geotechnical and geological models provide guidelines on the mining method selection and development strategies (Fig.1).

The mining method selection stage is critical as some methods such as block caving, once selected and developed cannot be reversed. Such methods are inflexible methods as opposed to flexible ones, and must be selected with all the due care and caution necessary.

When developed, mine geometries are complex (Figure 3) and can be compared with major city infrastructures – streets, buildings, underground and above ground infrastructure – pipe and electrical networks and subways.

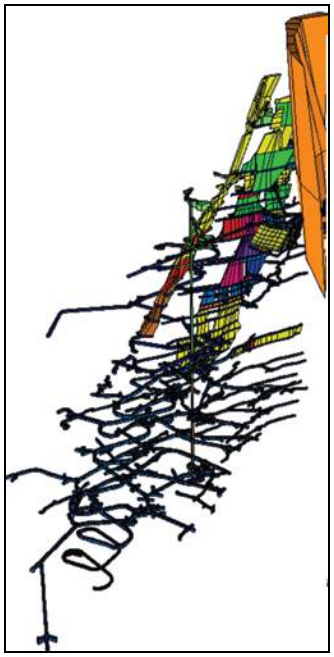

Figure 3. Complexity of underground mine infrastructure.

The complexity of a mine is more pronounced when it is in production. Optimum production and enhanced safety of workers and equipment is required at this stage. Both optimum production and enhanced safety require monitoring of various kinds.

In reality, for a producing mine large multi-dimensional datasets from multiple sources including the following:

- Geology
- Rock properties
- Different excavation types and geometries
- Monitoring data of various types and volumes such as seismicity
- Damage locations
- Support types and locations
- Production levels
- Ore grades
- Dilution levels, and
- Ventilation data and many more.

The size/volume and dimensionality of data from mines can be so overwhelming that it is difficult for the best mind to process and understand. It is not uncommon therefore, to frequently hear that mines collect so much data but never analyse that data even though understanding the data could unlock the secrets to enhanced productivity and safety.

1.2 The Big / Mega Data Phenomenon

1.2.1 Big data

The origin of the term “Big Data” may still be a matter of debate. However, it is established that the first usage of the phrase with a technical connotation to not just a lot of data, but different types of data handled in new ways in the computing context is John R Mashey in 1998 (Lohr, 2013).

Intel (www.intel.com.au/BigData) defines Big data as any collection of data sets so large and complex that it becomes difficult to process using traditional data processing applications. It lists the challenges in dealing with “Big Data” as:

– Analysis
– Capture
– Curation
– Search
– Sharing
– Storage
– Transfer
– Visualization, and
– Privacy violations.

Clearly, what is considered "Big Data" will vary from one institution / company to another depending on the capabilities of the organization and on the capabilities of the applications that are used to process and analyze the data. Big Data is also technology dependent as what is considered to be "Big" today will not be so in the future with advances in technology – Computer power.

1.2.2 Trends and challenges in big data applications

1.2.1.1 Trends

The key drivers of Big Data can be grouped into
– Business
– Technical
– Financial, and
– Intelligence / security

Businesses are using Big Data to discover new insights that drive competitive advantage from data that is increasingly everywhere and in various forms at manageable cost. Here is where “Big Data” is now a buzz word in the mining industry, where the survival of companies in finding innovative ways to reduce cost to meet low market prices is a challenge in today’s fluid mineral market prices.

According to a an article in the Generation of New Technology (GNT) (GNT, 2010) webzine, worldwide spending on hardware, software, and services for 3D visualization, simulation, and training in the defense and government segment will reach $16.5 billion in 2010 and grow to $20 billion by 2015. This foretells that the paradigm change will happen in all industries in the near future since many technological advances and innovations come from advanced defense research. The fact that we are discussing the use of this phenomenon in mining today is confirmation of this prediction coming true.

1.2.1.2 Challenges

Just as previous trendy words and phrases like “Sustainability” and “Innovation” have not resulted in their expected impacts on the mining industry, caution is required in the rush of the industry to adapt the “Big Data” phenomenon with the expectation that it will result in a paradigm shift to make it more efficient. There are challenges to overcome for the adoption of Big Data phenomenon in the mining industry to be beneficial.

The potential challenges in Big Data application include skill training and having the appropriate technologies. New skills are required for the human elements to make sense of large data and new tools are needed to help with data analysis. In the required new skills, judgment and intuition will be absolutely essential to making use of needed tools.

The technological challenges in Big Data applications are summarized in Mitchell (2014) and presented as follows:
– Big Data lakes:
– More predictive analytics
– Need for high-end data scientists
– Need for NoSQL
– Deep learning, and
– In-memory analytics

With Big Data traditional databases which require that you design the data set (Structured database) before entering any data are of little use. In place of database theory are data lakes, also called enterprise data lakes or enterprise data hubs. With data

lakes all data from all sources are dumped into a big Hadoop repository and what is required are tools for people to analyze the data, along with a high-level definition of what data exists in the lake. The challenge here is that people who use the tools to analyse data lakes in the traditional sense must be highly skilled.

With unstructured databases that suits Big Data, Structured Query Language (SQL) is of limited use and Not Only SQL (NoSQL) come into play. NoSQL tools are still in their infancy of development and until then, querying of data lakes of Big Data will remain a challenge and require skilled programmers.

An approach to overcome the SQL challenge is "Deep learning". Deep learning enables computers to recognize items of interest in large quantities of unstructured and binary data, and to deduce relationships without needing specific models or programming instructions. Like NoSQL, deep learning is also still evolving.

With Big Data, analysts have not only more data to work with, but will also require the processing power to handle the large numbers of records with many attributes. Foroohar (2013) noted that given the rise of social media, Big Data and other technical trends we should not expect boost in efficiency and productivity. This negative forecast is attributed to the declining prices of software, computers and networking technology that have potential to slow down gains in the power of technology. Simply put, slower tech-price declines and slower gains in computer power imply that pace of innovation in the short term will be sluggish. This poses a potential challenge to the benefits of Big Data in the production industries, including mining.

1.3 Virtual Reality and Scientific Visualisation

The evolution of virtual reality (VR) technology is summarized in Kaiser et al. (2005). The VR system projects dynamic stereo images onto a curved screen, providing several people with the sense of full data immersion. Subsurface excavations, infrastructure, geology, hydrology, geochemistry, geomechanics, cost and time can all be combined to provide a holistic overview of a mine property.

Inherent complexities of three-dimensional data can be viewed with a true sense of depth and spatial relationship in the VR. The scale of the screen, combined with the depth perception provides an immersion that increases the participants' overall understanding of spatially complex data relationships and accelerates data comprehension as well as transfer of experience and knowledge.

The power of VR environments lies in the illusion of being in a virtual world and individuals can see and feel their data as being part of it. The large size and extent of images combined with the depth perception in VR centres allow interpreters to see details without losing the broader perspective. In the VR, data and images can be rotated in any direction, magnified to various scales and sliced in arbitrary directions for detailed viewing, analysis and interpretation.

The human eye's ability to quickly detect and understand patterns and anomalies is unsurpassed by technology. The benefits of developing advanced visualization applications are clearly highlighted in the National Science Foundation (NSF) review of visualization technologies for science (Munzner et al., 2006). NSF notes that scientific visualisation is essentially a means of quickly identifying trends and anomalies and relies on the human's visual analysis capability as the most effective means of doing so. It is therefore a means of maximising the use of human perception and pattern recognition and thus enables better insight by all for enhanced strategic and tactical decision making.

Vasak and Suorineni (2010) differentiate between 3D modeling software visualization capabilities and scientific visualization. Proper use of VR and scientific visualization represents a fundamental paradigm shift in how we collect, store, process and interpret

multi-terabyte datasets, formerly the domain of enterprise database managers.

3D Modeling software visualization is limited to space while scientific visualization uses the geometric (easting, northing, elevation) data as a structural support for thematic (property) data. The goals between the modeling visualization and scientific visualization are also different; the former is used to create data and information, whereas the latter is used to explore datasets to find new trends and develop new knowledge. Most scientific visualization software relies on the concept of filters being applied to a dataset to extract or highlight knowledge. These filters can be connected into a visualization pipeline which, once correctly defined, can be applied to any number of datasets. This approach is particularly well suited when integrating data from multiple sources or when having to review multitudes of similar datasets.

Scientific Visualization relies more on the exploration of datasets that have been generated by simulation software whereas mining tends to rely on inferred datasets based on observational data. Examples of this type of inferred data are most exploration datasets where large volumes of space must be "defined" based on limited drill hole (or geophysical) datasets.

Another key difference lies in the use of time as a fourth dimension. While many scientific fields of study model the change in a process or object over time, the modeling of time still remains rather limited in mining. Despite these fundamental differences both disciplines require a means of quickly identifying trends and anomalies.

2 BIG / MEGA DATA AND SCIENTIFIC VISUALISATION IN MININING

2.1 Big Data in Mining

The mining industry is characterized by occasional "trendy" phrases or words to mark paradigm shifts and emphasise transformational change. Examples of these trendy words include "Sustainability" and "Innovation". Regrettably, such words end up being used so vaguely they lose meaning. The intended supposed transformational changes are now seen and the words and phrases get lost. New terms are then invented and adapted. This trend is cyclic.

Lately, the buzz phrase in the mining industry is "Big Data" that has swallowed the previous – Sustainability and Innovation. This paper cautions that to make progress with Big Data in mining we must understand what Big Data is in that industry.

Big Data in the mining industry is not the Big Data in sales business and security where the emphasis is on volume but rather on unstructured data as in Figure 4. More importantly, in the mining industry data is often deposited in hard copies, soft copies or in both forms if one is lucky. The data is also deposited not in a single repository but in different departments in individual possessions, with the risk that losing employees often imply losing critical data!

Vasak and Suorineni (2011) observed that although mining has large datasets, the lack of structure and data standards creates obstacles to integrated evaluation. It also makes it difficult to discover and establish relationships. Understanding mine data remains important for increased productivity and safety in mines.

Figure 4. The nature of Big Data in mining – Data lake, multiple sources, and different repositories: Garbage dumps.

The RAND report on the critical technologies for the mining industry

recognises that it is the knowledge management benefits of new IT technology that will provide the greatest benefit to the industry (Peterson et al., 2001). Although mine operations are generating more data, such information is rarely well utilized for reasons discussed in this paper.

The major challenge in understanding the unstructured mine data is first how to separate the important information and correct information. An often cited solution for simplifying complex data interpretation (at least currently) is the use of simple graphical interfaces that are easy to comprehend by all levels of mine personnel, since data is not as interesting as insight (Peterson et al., 2001). It is these underlying principles that form the basis for new scientific and engineering visualization techniques in mining.

2.2 Virtual Reality and Scientific Visualization In Mining

Big Data interpretation currently poses a challenge as most of the means of interpretation are still in their infancy of development. These challenges were presented in Section 1.2.1.2. The source of the challenges is defining relationships from data lakes.

Virtual reality and scientific visualization provides an alternative to defining statistical relationships / trends in Big Data data lakes and requires no expert special skills in programming. This is based on the unchallenged view that the human eye's ability to quickly detect and understand patterns and anomalies is unsurpassed by technology – "Seeing is believing".

Burgess (2012) observed that it is unlikely there will be major changes to the mechanics of mining and processing but that the use of cleverer technology and automation of equipment is an attractive alternative.

The combination of Big Data and computer power combined with virtual reality and scientific visualization will allow analysts qualitatively explore new behavioral data in real time in mines. The following sections provide case history examples of the application of virtual reality and scientific visualization in mining to understand phenomena and parameter relationships we never understood before.

The first case study is an example of application of Big/Mega Data and virtual reality scientific visualization at the exploration stage of the mineral resource while the last two are examples of the application of the technologies at the mine operation stage.

2.2.1 Case study 1: Exploration

Vasak and Suorineni (2010) noted that finding an orebody using geophysical and probing (drilling) methods is analogous to finding a tumor in a human body by using various scanning technologies and recreating a fully 3-dimensional representation that surgeons can use to operate precisely.

The exploration stage in mining was discussed in Figure 2. Figure 5 presents how the concept of "Big/Mega Data" combined with virtual reality and scientific visualization is beneficial in achieving value from data. By integrating the mapping, geophysics (surface and inversion model), drilling and the resource model, the full potential of the deposit was readily grasped using stereoscopic virtual reality. Figure 5 shows two views of the prospect property.

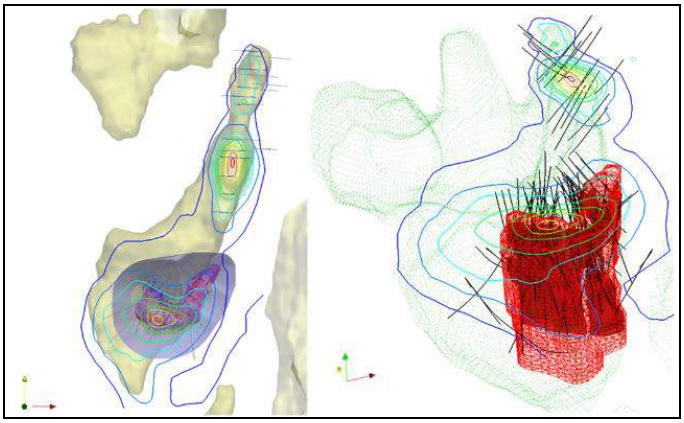

Figure 5. Example of use of Big/Mega Data in the exploration stage (Vasak and Suorineni, 2010).

Figure 6 shows the measured resource from the block model is at the highest existing drillhole concentration. To improve the bankable resource, the gaps highlighted as

inferred (yellow surface) must be strategically drilled to maximize the benefit while minimizing the drilling costs, e.g., the number of drillholes and the total footage drilled. The red drillholes are laid out in an optimized pattern that uses the exiting layout and maximizes the volume of influence (e.g., the surfaces shown on the middle four planned drillholes) to capture the largest possible volume of inferred resource.

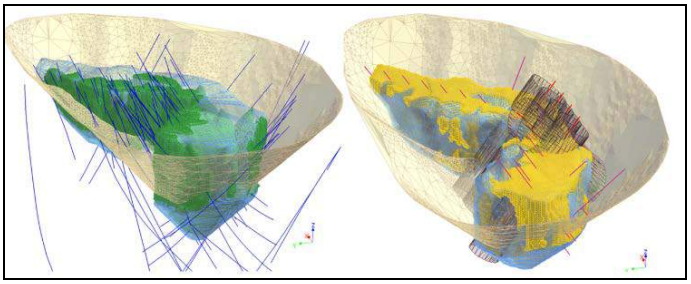

Figure 6. Benefits of Big Data and virtual reality scientific visualization at the mineral exploration stage – Optimisation of resource and reserve (Vasak and Suorineni, 2010).

2.2.2 Case study 2: Understanding rockbursts

Kaiser et al. (2005) discuss the use of VR and scientific visualization for the interpretation of seismic data that is summarized here.

Seismic and microseismic data patterns are complex, come from various sources and in large volumes from several years of seismicity monitoring, with each event involving more than a dozen measured or interpreted parameters (seismic moment, stress drop, source size, location in space and time, etc.). Seismic and microseismic data therefore have all the characteristics of "Big Data" in the mining sense (Figure 7).

Data fusion provides a "new" view of existing data and enhances the identification of hidden relationships or discovery and explanation of complex data interdependencies such as seismic and microseismic data.

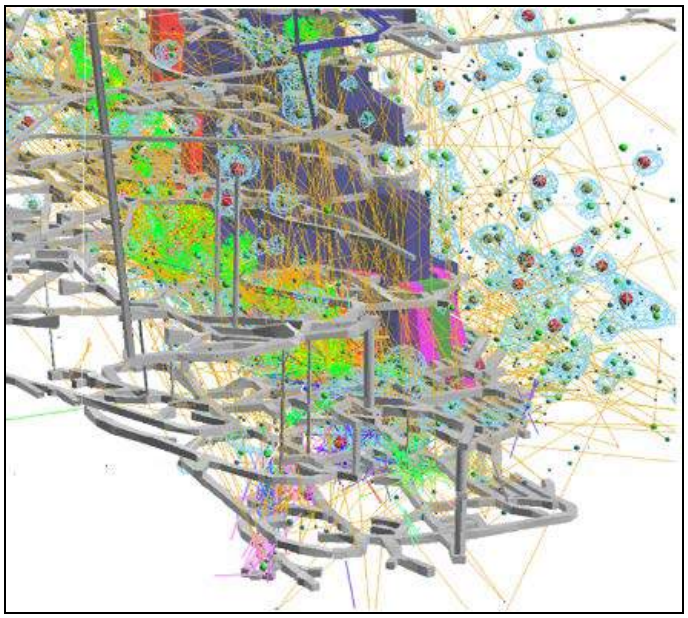

Figure 7. Use of Big/Mega Data and scientific visualization for the understanding of mine seismicity. The figure shows timelinks (lines), source parameter relationships (colour/size) and the complex mine infrastructure (Vasak and Suorineni, 2011).

The interpretation of seismic data constitutes one of the most complex forms of mining data and requires an integrated approach to data interpretation. Because of the complex nature of seismic data a multidisciplinary approach is necessary for its proper interpretation. Such an approach will bring together experts with vastly different backgrounds and expertise, including experts from seismology, geology and structural geology, geomechanics, (geo-) statistics and mining engineering.

Collaborative, immersive VR lends itself ideally for seismic data interpretation and is a good example of how Big/Mega Data combined with VR and scientific visualization is extremely vital in mining. Figure 7 is translated to a practical application (Figure 8) of in mining. In Figure 8 zones of different risk levels are identified and can help in support optimization and mine planning.

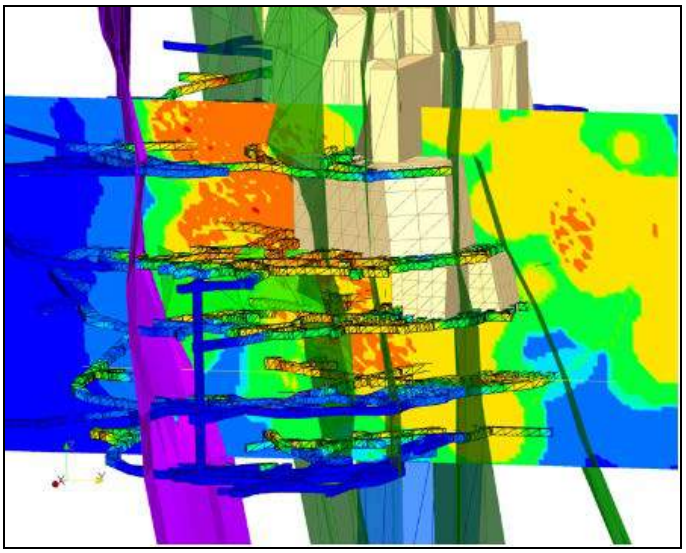

Figure 8. Seismic Excavation Hazard Map showing a section through an active region of the mine and hazard projected onto mine excavations (Vasak and Suorineni, 2011).

2.2.3 Case study 3: Understanding block caving performance

Block caving is an underground mining method which is becoming increasingly important due to its associated low operating costs. The process of block caving is extremely complex and although it is increasing in popularity because of its low operating cost, it is still the least understood of the underground mining methods.

As block caving is employed in increasingly difficult environments with; higher stresses, stronger orebodies, larger cave heights, bigger footprints and increased production rates, it is important to enhance our understanding of the geomechanics within the BCMS.

A major obstacle in the understanding of block cave mining is the lack of access to the cave. An alternative to direct access to the cave is the use of the virtual reality environment.

Block caving is a system that requires analysis as a whole, rather than looking at individual factors. Laubscher (1994) identified 25 primary factors that must be optimized for an ideal block caving mine. Independent optimization of these factors, instead optimizing them as a system, will often result in adverse offsets of others. Big Data and scientific visualization offer an opportunity for the optimisation of block caving operations as systems, as well providing virtual access to understand the in cave fragmentation process. Figure 9 is an example of this approach applied to a block caving mine.

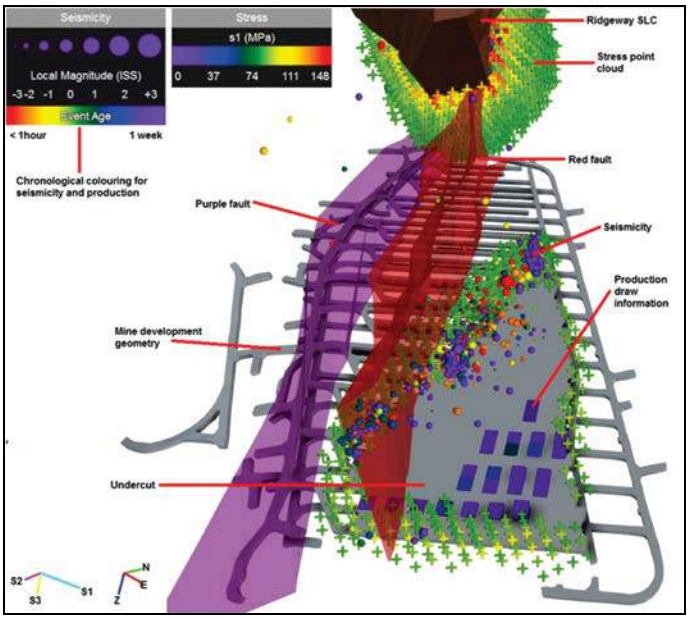

Figure 9. Use of the BCMS Visualiser for VRSV assessment of undercutting performance from a stage of development of Newcrest's Ridgeway Deeps operation. Incorporating; seismic information, stress modelling results, geological structures and production draw information along with the mine's geometrical changes, which enables a systematic investigation into undercutting performance (Tibbett et al., 2014).

3 THE FUTURE OF BIG DATA AND MNING

The ability to visualise the mining system as a whole and view the information as it occurs in real time is crucial to expanding our understanding of mining operations and in particular, block cave mining systems.

The ability to draw personnel from different backgrounds into the one environment such as a "Strategic Management Decision Making Room (SMDMR)" is a key feature of VRSV and Big Data in mining applications in the future. Collaborative assessment will form the backbone of analysing our increasingly complex mining systems in the future for

enhanced safety and productivity in the fluid economic times.

4 CONCLUSIONS AND RECOMMENDATIONS

This paper sought to examine the Big Data phenomenon in mining with particular emphasis on its future. The paper has explored what Big Data is, what it means in mining and its benefits when combined with virtual reality scientific visualisation. It then went further to explain virtual realization and scientific visualization and how by combining Big data and scientific visualization is going to be more beneficial to the mining industry.

The paper concludes that in order for Big data not to disappear like other previous trendy words/phrases that periodically captivate the industry such “Sustainability” and “Innovation” without achieving its expected transformational benefits the mining industry must first understand what Big Data means to the industry, identify potential obstacles and develop the appropriate strategies and tools to overcome such obstacles.

Ultimately, the full benefits of Big/Mega Data combined with virtual reality scientific visualization in mining will be achieved when these can be used to visualise mining processes in real time to optimize mine safety and productivity.

It is recommended that mining companies need to invest in skill training, development of tools to overcome potential obstacles in the interpretation of data in data lakes and start to develop a culture of common data repositories and continuous dialogue within and departs and inter-departments.

ACKNOWLEDGEMENTS

The author acknowledges the contributions of past colleagues and current Ph.D. students. In particular, the case examples used in this paper are derived from work with Mr. Vasak. The support of colleagues in the School of Mining Engineering at UNSW Australia is also acknowledged.

REFERENCES

Foroohar, R., 2013. Man versus Machine: Why a slowdown in tech progress is good news for jobs. *Time*, 4 February 2013, p. 12.

GNT (A Generation of New Technology), 2010. http://us.generation-nt.com/research-markets-spending-hardware-software-services-press-2183281.html

Kaiser, P.K., P. Vasak, F.T. Suorineni and Thibodeau, D., 2005. New dimensions in seismic data interpretation with 3-D virtual reality visualization in burst-prone ground. *RaSiM6*, Perth, Australia, 33-47.

Laubscher, D.H., 1994. Cave mining – the state of the art. *Journal of the South African Institute of Mining and Metallurgy*, Vol. 94(10), pp. 279–293.

Lohr, S., 2013. The Origins of ‘Big Data': An Etymological Detective Story, *The New York Times*, B4.

Mitchell, R.L., 2014. Big data technologies and practices are moving quickly. Here's what you need to know to stay ahead of the game. *Computerworld*, Oct 23, 2014.

Munzner, T., Johnson, C., Moorhead, R., Pfister, H., Rheingans, P. and Yoo, T.S., 2006. NIH-NSF Visualization Research Challenges Report Summary, IEEE Computer Graphics and Applications ,vol. 26, no. 2, pp. 20-24.

Peterson, D.J., LaTourrtette, T. and Bartis, J.T., 2001. New Forces at Work in Mining: Industry views of Critical Technologies. RAND, Science and Technology Policy Institute, Santa Monica, California: 33 – 52.

Tibbett, J., Suorineni, F.T. and Hebblewhite, B. 2014. The application of virtual reality technology and scientific visualisation to the understanding of block cave mining systems. *AusRock 2014: Third Australasian Ground Control in Mining Conference*, Sydney, Australia, pp. 195 – 200.

Vasak, P and Suorineni, F., 2010. Extracting more value from mine data using virtual reality and scientific visualization techniques. *Proceedings 1st Biennial UMaT International Mining and Mineral Conference*, Tarkwa, Ghana, 19 p.

Vasak, P and Suorineni, F., 2011. Extracting more value from mine data using virtual reality. *PositionIT*, pp. 62 – 67.

The Issue of Abandoned Mining Exploitations in Albania

G. Muka, V. Jorgji, T. Korini, R. Balla
Faculty of Geology and Mining, Tirana, Albania

ABSTRACT In cases of open stoping mining some of the key issues of abandoned mining exploitations are: identifying the impact of the exploitation area, qualitative and quantitative computation of this impact, risk quantification of the impact on the sector and taking measures to reduce damage or avoidance of mining. In Albania the use of open stoping mining is carried out mainly in deposits of chromium, copper and iron. The overall stability of openings o at these mines is assured using different variants of mining methods like cut and fill stoping (for copper deposits) or methods wherein the roof can be allowed or forced to collapse (iron deposits) or be abandoned for a delayed collapse (chrome mines).

In terms of effectiveness must be said that the mineral losses were about 15-20% in copper and chromium and about 20-30% in iron ore. In some cases these previously abandoned reserves are subject of the reactivation for exploitation, especially in chrome (the mines of Bulqiza, Krasta, Kam, Kalimash, etc.). This paper presents some of the problems associated with the design of mining exploitations in such conditions and the difficulties of the exploitation of the remaining pillars. A detailed study of all factors influencing the exploitation in such conditions is necessary for implementing rational projects and improving the mining safety.

Keywords: Abandoned mines, existing workings, designed workings, rock mass stability, abandoned pillars, tectonics and reactivation

1 ABANDONED MINING EXPLOITATIONS IN ALBANIA

The exploitation of mineral resources in Albania, with few exceptions, has started after 1945. During a period of approximately 50 years it became the main activity of the domestic economy. The request, in the framework of planned economy, was to increase the production of chrome, copper and iron-nickel minerals. The destination of this gross output, except for copper ore, up to 70's was the export. It was around the end of 70's to begin processing chrome and iron-nickel in the country with the establishment of the metallurgical plant for iron-nickel in Elbasan (1978) and the ferrochrome factory for chrome in Burrel (1979).

Under these terms, the demand for increased mining production was rapidly grown considering that gross output as well as processed minerals were the backbone of the economy. Thus, during 1985-1990, the production of chrome ore reached 1.3 million tons per year (Figs. 1, 2). It was these demands to cause intensive exploitation of mineral resources by failing to implement the opening and preparation of new exploitation fields. This intensive exploitation has evolved regardless the correct application and monitoring of the appropriate mining methods, leading to problems concerning the management of mining pressures and the recovery ratio of resources.

Taking notice of the chrome industry trend (as other minerals had even worse performance) it is concluded that mining fields were abandoned immediately after favourable geological and mining condition resources were exploited, while other less desirable resources (tiny ore body thickness, dip less than 45^0, tectonic developed sectors, etc.) were not only abandoned but further risked with the impossibility to effectively being exploited in the future. They were classified as losses at around 15-20% (Ceci

& Borici, 1986; Gurra, 2011). Under these circumstances, we can talk about abandoned exploitations, in terms of the necessity to perform an exploitation plan, ignoring the technical and technological discipline of the process (Gurra, 2011; Muka, 2013).

Another aspect relates to the thorough abandoned exploitations after 90s, when political changes conditioned economic development activities in the framework of a market economy. Since mineral resources were owned by the centralized state, weakening of it made mineral production activity fall drastically. So for chrome, (as seen in Figures 1, 2) from about 1.3 million tons, produced in 1990, production drops to about 200,000 tons in 1992. A small production increase in the period 1993-1996 (up to about 300,000 tons) is explained by the necessity to keep the miners at work, because their unemployment would lead to growing social tensions.

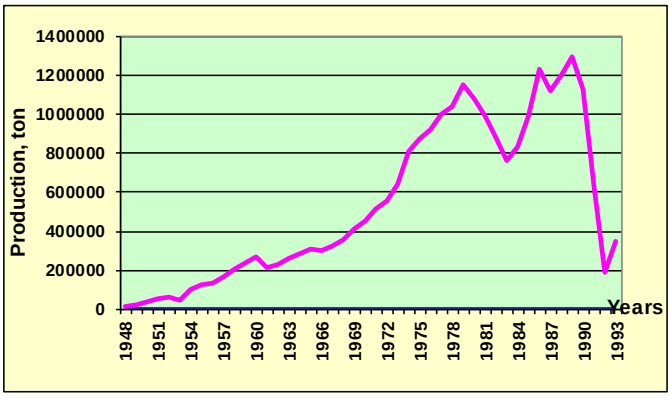

Figure 1. Chrome production during 1948-1993.

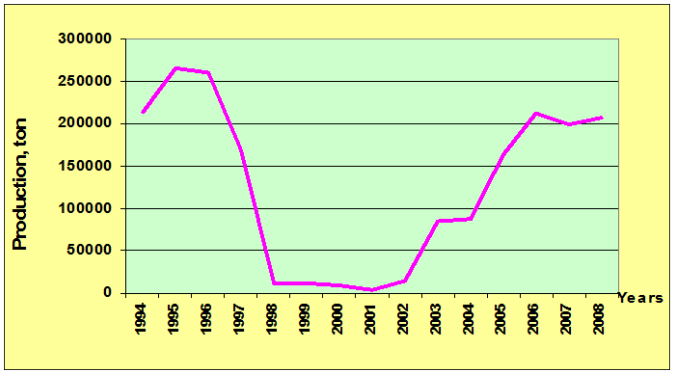

Figure 2. Chrome production rate during 1994-2008.

In 1997, Albania experienced a very difficult politico-economic period, what caused the mineral production to fall in a very low level. The consequence of this decrease, which lasted until 2003, was the creation of abandoned exploitations in all mines of the country.

Both forms of abandonment were due to "amnesia" about:

- The clear identification of the balance of mineral reserve exploitation.
- The exact presentation of opened spaces and exploitation workings.
- Technical and technological approach towards opening of preparation workings.
- Defining measures to prevent the access to the open spaces created during the old exploitations.
- The withdrawal planning of recyclable materials such as rail carriages, etc.
- Compacting and final classification of graphic documentation, etc.

2 REACTIVATION OF EXPLOITATION IN THE "ABANDONED AREAS"

In the market economy conditions the entrepreneurs' attention focuses on the market study. Even entrepreneurs in Albania, both domestic and foreign, became very active in the minerals resources market study. In this activity, they found that there was a considerable interest for minerals such as chrome, copper and iron nickel. This interest was made known to political decision-makers who were committed to create a favourable legislation for investors in the mineral exploitation sector (Goskolli 2011).

Private activity of mineral resource exploitation in Albania started in 1995, through concessions, mainly for those mines that were considered as abandoned exploitations (Goskolli, 2011).

Since the beginning, the new concessionaries faced the following problems:

- The total lack of geological and surveying documentation.
- The lack of knowledge about the current situation and the dynamics of mining pressures development.

- The inaccuracy in the balance of reserves.

Avoiding these problems required, first of all, the completion of geological and surveying documentation. For this purpose they used the archives of state entities such as "Institute of Mineral Extraction and Processing Technology " and "Albanian Geological Service". These archival materials, although not so relevant, served as the basis for fulfilling and updating the documentation.

In order to perform the ore production in abandoned exploitations, one must:

a. Define the margins of concession permits, in plan and altitude, since within a single sector, more than one permission, was granted.
b. Identify the entrances of all opening workings and inspect their situation, both in geometric and technical-mining terms.
c. Verify their stability condition and stabilize them, if necessary.
d. Check and correct the excavations' position, in plan and altitude.
e. Specify the geometry and amount of remaining reserves, to design their further exploration.
f. Fulfil the exploitation design, taking into consideration:
   - The position of remaining reserves.
   - Their geological and hydrogeological conditions.
   - Mining pressures state and their management ways.

The solution to these problems include all chromium, iron-nickel and copper permits, about 325 permits (Goskolli, 2011).

Figures 3, 4 and 5 show the distribution of chrome exploitation permits.

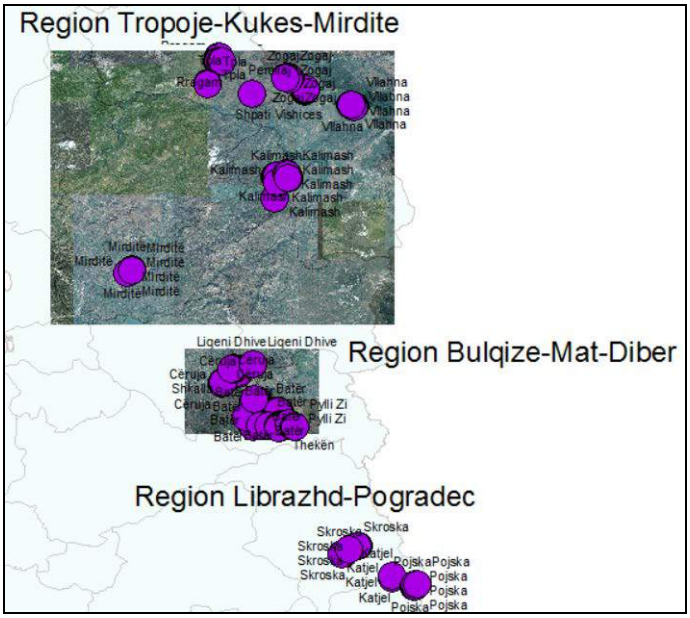

Figure 3. The distribution of chrome mining permits in Albania.

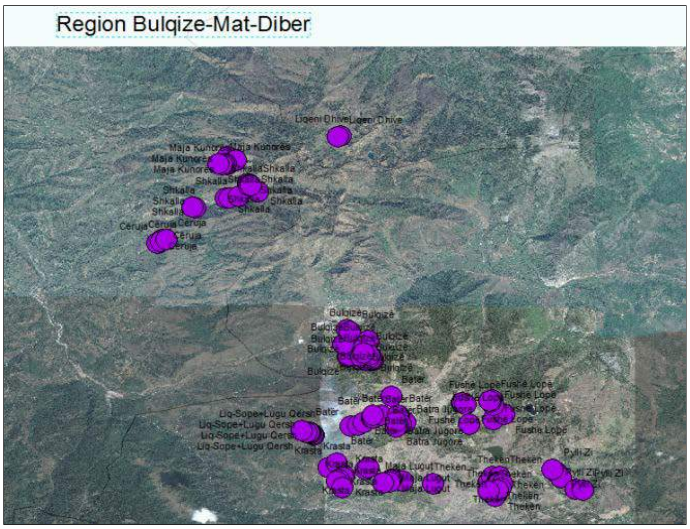

Figure 4. The distribution of chrome mining permits in Bulqizë-Mat-Dibër region.

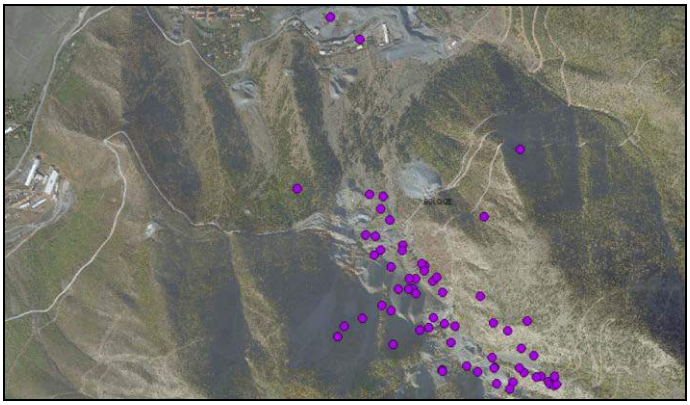

Figure 5. The distribution of chrome mining permits in Bulqiza region.

3 TECHNICAL ASPECTS OF THE REACTIVATION

Reactivation of abandoned exploitations first of all requires:

- The identification of existing opening, preparation and exploitation workings.
- Investigation of these excavations' conditions, related to the possibility of reactivation.
- Verifying the accomplishment, accuracy and clarity of geological, technical and surveying documentation.
- Recalculating the potential exploitation reserves.
- Designing a comprehensive project for the appropriate exploitation technology and safety.

Regarding Albania, focusing mainly on the chrome mines, the concession activity conduced so far is characterized by:

- The restoration of abandoned openings by "combing" the blocks (removal of potentially unstable blocks) of weak cohesion with rock mass and supporting with wooden frames, in areas evaluated as dangerous. The fill applied to realize the support cushions is also constructed with wooden materials.
- The design of exploitation excavations, outside the subsidence area. The size of influence of mining operations is calculated by adjusted models (Muka, 1989).
- Mineral extraction, both by old funnels (ore passes) unlock, as well as by exposing the miners to existing space, what has reduced the safety at work by increasing the number of fatalities and injuries (only during October 2011-August 2014, 11 miners were killed and 9 others were seriously wounded - Archival source, 2014).
- Deficiencies in proper fulfilment, according to standards, of the final exploitation documentation in order to eventually declare as abandoned the relevant exploitation zone.

4 CONCLUSIONS

a. The characteristic of abandoned exploitations in Albania, mainly for chrome, cooper and iron-nickel minerals is the necessity of their reactivation in order to exploit reserves classified as losses.
b. The lost reserves in these deposits are not created as a result of the inability of the existing technology used for exploitation, but as a result of policies to meet the needs of economic development in isolated conditions.
c. The reuse of abandoned excavations: opening, preparation and exploitation ones, provides the continuity of traditional methods of exploitation, the effectiveness of which islow, but justified by favourable market conjuncture and low cost of labour forces.
d. The perspective of further exploitation of these resources requires investments in scientific research with the main objective of increasing the safety of the mines.

REFERENCES

Ceci L., Borici, M**.** 1986**:** "Album i sistemeve të shfrytëzimit të vendburimeve të mineraleve të dobishme" (*Album of the Mining Systems*), Tiranë.

Gurra H**. (2011):** "Bulqiza – Një minierë me histori" (*Bulqiza - A Mine with History*), Tiranë.

Muka G**.** (1989) : "Parallogaritja e masës së ndikimt të shfrytëzimit për të zvogëluar e mënjanuar dëmet minerare" (*The preliminary calculation of the mining influence to reduce and avoid the mining damages*), Disertacion, Tiranë.

Muka G., etj. (2014):"Rajonizimi dhe vlerësimi i riskut mjedisor mbështetur në ndikimin e shfrytëzimeve të braktisura të lëndëve të para minerare (*Regionalization and environmental risk assessment based on the impact of utilization of abandoned mining raw materials*), Raport, Tiranë.

Goskolli E. (2011): "Aktiviteti minerar dhe burimet minerale" (*Mining activity and mineral resources*), AKBN, Tiranë.

Burim arkivor. (2014): "Regjistri i aksidenteve në miniera" (*Register of accidents in mines*), RISHM, Tiranë.

The Practicable Combination of Open Pit with Underground Mining Methods- a Decade's Experience

E. Bakhtavar
Urmia University of Technology, Urmia, Iran

ABSTRACT Among all kinds of ore deposits, there is a special form of ore deposit which starts from or near ground surface and continues to a very high depth. Open pit or underground methods separately are not practicable for the extraction of this kind of deposits; therefore, a combined mining of open pit with one of underground methods is used. In this paper, the well-known (deposits) mines with the potential of combined open pit and underground mining have been first studied. They are categorized in two simultaneous and non-simultaneous modes from the viewpoint of the extraction time in both open pit and underground parts. The non-simultaneous mode of combined mining is more acceptable because the large scale underground caving methods with high productivity and low costs can be used. In simultaneous mode, horizontal and vertical slices underhand cut & fill with cemented backfilling is more feasible to be used with open pit mining.

Keywords: Simultaneous combined mining, non-simultaneous combined mining

1 INTRODUCTION

In general, ore deposits are divided into three major categories from the extraction viewpoint. The first category includes ore deposits with outcrop or near ground surface which are most suitable to be extracted only using the surface mining methods. The second one is deep deposits that starting from a high depth and laying under a thick overburden. These deposits are most practicable for mining by underground methods. Often, surface methods are not economically feasible for extracting these kinds of the ore deposits because of raising stripping volume. Third category of the ore deposits belongs to them which start from surface or near surface and continue to a very high depth. In this case, a combination of open pit with underground mining methods are used for the extraction of the ore deposits. Open pit is used at the beginning to a level which transition from open pit to underground mining should be done because of economic reasons. In this paper, the extraction of third kind of the ore deposits using both open pit and underground methods together has been considered. In this case, the most critical problems are finding the most practicable underground alternative to be used after open pit mining and optimization of transition from open pit to underground mining, especially in non-simultaneously combined mining of two methods. Finding the best combination of underground methods with open pit is majorly focused in this paper.

2 MINES WITH OPEN PIT AND UNDERGROUND POTENTIAL

In this section, the most well-known worldwide mines using combined mining of open pit and underground methods are taken into account together with Iranian combined mines.

Grasberg is one of the mines which was planned for extracting gold and copper ores by the use of combined open pit and black caving as the most practicable underground alternative. According to the planning of the mine, open pit mining must be finished in 2015. It is located in Indonesia (Srikant et al., 2007).

Chuquicamata Copper and molybdenum mine, which is located in Chile, is another

one with the combination potential of open pit and block caving. Final open pit depth was planned to be completed in 1100 m until 2013 (Flores, 2004).

In Ernest Henry gold and copper mine located in Australia, transition from open pit to open stope mining was planned at 560-m depth (Meyers, et al., 2008).

The other one which located in Congo is Dikulushi silver and copper mine. In this mine, open pit was ceased and sublevel caving as the most feasible underground method was started in 2006 (Robinson, 2007).

Palabora mine was planned for the use of combined open pit and block caving. Final pit depth in this case is 800 m which was completed in 2003 (Brummer, 2006).

Coala north pipe had high potential for extracting using a combination of open pit and modified sublevel caving among Ekati diamond ore deposits collection located in Canada. In Coala north mine, extraction using the underground method was started in 2002 (Jakubec et al., 2004). Furthermore, there are some other cases with the combination potential in Canada, such as Diavik diamond mine.

Argyle diamond mine located in Australia is another combination of open pit and block caving. Mining by open pit was finished at the end of 2007 due to economic considerations and the underground alternative was started. It is planned that extracting by underground mining will be continued until 2018 (Hersant, 2014).

Meng-Yin diamond mine in China includes two major deposits. One of them was planned for extraction using a combination of open pit and Cut and Fill methods (Changyu, 1984).

Kiruna iron ore mine is one of the well-known case located in Sweden. Open pit was ended and was changed to sublevel caving in 1960 because of increasing in open pit mining costs.

Angouran Lead & Zinc mine is one of the biggest mine which was initially planned for open pit mining. Although Angouran ore deposit could be extracted by open pit independently but a combination with underground option (modified cut and fill) was considered because of some unpredicted purposes. The reasons are (Aminzadeh, 2014; Khani, 2014):

- Zinc selling price has been increased.
- The ore deposit with high grade was located in lower levels which could not be extracted only using open pit even until next 20 years.

Another Iranian ore deposit which was planned for mining using a combination of open pit and underground mining is Chargonbad copper deposit (Aminzadeh, 2014). The main purpose for combined mining was to increase annual extraction capacity.

Gushfil Lead & Zinc ore deposit located in Iran was planned for extraction using combined mining of open pit and cut-fill (TETE Mine Team, 2006).

Chehelkureh copper ore deposit is another combined case using open pit and underground mining (Bakhtavar, 2009).

Gol-e-Gohar Area 3 iron ore deposit with a dip of about 20-degree is other deposit located in Iran which was planned for mining by combined open pit and a different kind of Room & Pillar (Bakhtavar et al., 2010).

Chah-Gaz iron ore deposit located in Iran is one of metaliferrous ones which was planned for mining using a combination of open pit and block caving (Bakhtavar, 2013).

Mining engineers can make an appropriate decision in relation to select one / more mining method(s) only with considering all effective parameters and the special conditions of an ore deposit. Totally, after studying the ore deposits and mines with combined case of open pit and underground mining, the following notes can be deduced:

- Opposite of worldwide trend and findings, all of the mentioned ore deposits located in Iran except Chah-Gaz deposit were planned for mining simultaneously using open pit and filling underground mining options.
- In the majority of large scale mines, a combination of open pit and underground mining was planned in

feasibility study (in design stage) before development stage. Block / panel caving, which is the only competitor with open pit, was selected as the best underground alternative because of high productivity and low mining costs.

- The problems of optimizing combined mining of open pit and underground options and accordingly optimization of transition from open pit to underground mining have been taken into account in the last decades and especially in relation to solving the problem of the mentioned-above combined mines.
- Some studied mines changed their base plans by adding an underground option to open pit mining at the end of or near the mine-life when it was exploited that the ore deposit below final open pit limit continues to a higher depth.

3 PRACTICABLE COMBINATIONS OF OPEN PIT AND UNDERROUND

Generally, a combination of open pit and underground mining can be used in simultaneous and non-simultaneous forms from the exploitation time viewpoint (Bakhtavar, 2008). Based on the global trend, the non-simultaneous form is more acceptable which provides a condition to use large scale underground caving methods with high productivity and low costs. In this form, by using the caving methods such as block / panel caving there are some instabilities resulted from caving and subsidence which are transmitted to open pit limit. This restricts a simultaneous form of open pit and underground, except during 2 to 3 years before the end of open pit mine life that combined mining is simultaneously. It is notable that a higher profit can be gained using non-simultaneous form of combined mining.

The simultaneous form of combined mining is unusual but it is feasible in special conditions and purposes. For instance, if ore deposit is small in dimensions and tonnage, only small scale underground methods are practicable together with open pit from technical and economical viewpoints. In this case, in order to provide a safe working place in both open pit and underground and also to minimize the impacts of interaction between open pit and underground, small scale underground methods should be used with in-filling or artificial support system.

3.1 Simultaneous Combined Mining

In the usual combined form of open pit and underground mining, which has been highlighted in this study, underground stope is placed beneath open pit limit. Therefore, if open pit and underground operations are used simultaneously for the extraction of an ore deposit, working in underground part causes some instabilities in the benches of pit. It causes stoppage in mining operation of open pit part. In order to prevent these problems in simultaneous form, the underground methods which completely control and support stope roof and walls must be used. The simultaneous form of open pit and underground mining can be used to get the following aims:

- To supply the required feed of processing plant when the extracted ore using open pit (capacity) may decrease.
- To supply the required feed of processing plant in case of small (thin) ore deposits and correspondingly its extraction using small scale open pit.
- An increasing in the selling price of ore
- Occurring an unexpected failure in open pit mining operation. For example, happening failure and collapse in one of pit walls which cause production stoppage in that pit wall. This causes decreasing in open pit production capacity.
- Finding the high grades of an ore deposit in lower levels

Underground methods with filling working stopes such as cut & fill are the most practicable underground options for the simultaneous form of open pit and underground mining on the basis of the mentioned notes. Therefore, shrinkage, sublevel stoping, and all kinds of the caving underground methods are not feasible to be

used simultaneously with open pit mining for ore extraction.

From the viewpoint of the extraction direction, overhand and underhand extraction modes are two kinds of cut & fill underground method. As shown in Figure 1, the overhand and underhand modes are different in design and mining operation (Williams et al., 2007). Among all forms of the practical cut & fill method, the underhand form with cemented filling is more acceptable for utilization in the simultaneous combined mining. Underhand cut & fill with cemented back-filling can be divided into two modes:

- Full width horizontal slices underhand cut & fill (FWHSUCF)
- Vertical slices underhand cut & fill (VSUCF)

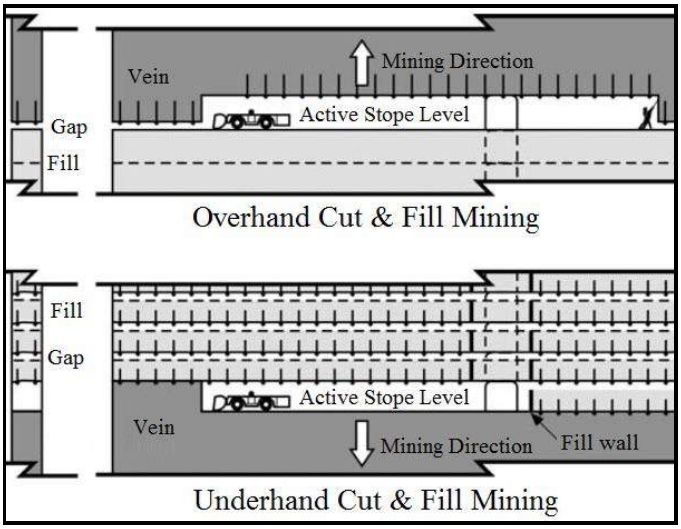

Figure 1. Overhand and underhand modes of cut & fill (Williams et al., 2007)

Often, hydraulic and pneumatic cemented-back fillings are used after the extraction of the full width ore deposits using underhand cut & fill with horizontal slices. As a rule, the thickness of each horizontal slice can be 3-4 m. In this mode of cut &fill (FWHSUCF), ore deposit is initially extracted in form of rooms with the width of 3-8 m. After extracting each room, it must be fully filled by the filling materials including a needed amount of cement. Then the remained long (barrier) pillars between each two filled rooms are extracted. After that they are filled using the materials with a less cement content in comparison to the first stage filling. The long pillars are approximately as the same width as the initial rooms.

In vertical slices underhand cut & fill (VSUCF), in order to achieve maximum mining capacity in a selective mode, the vertical slices should be perpendicular to along the direction of an ore deposit. The vertical slices of an ore deposit can be extracted successively or intermittently. In successive mode, the full width of an ore deposit should be extracted during the vertical slices. In intermittent mode, first, every other slice using the underhand cut & fill with cemented back-filling is extracted and subsequently pillars between each two extracted slices are remained. Finally, the pillars are recovered.

3.2 Non-Simultaneous Combined Mining

In contrast to the simultaneous one, non-simultaneous combination form of open pit and underground is preferred in practice because of the following reasons:

- Underground methods with high productivity and low mining costs, such as caving methods can be used.
- All kinds of underground mining methods can be used with open pit depends on an ore deposit geometrical dimensions and conditions.
- Backfilling underground methods, which impose high mining costs, do not essential for utilization.

It is notable that in non-simultaneous form, subsidence impact zone (profile) and consequently the environmental impacts are more extensive. Because large scale underground methods such as block caving are used.

Although a combination of open pit with all kinds of underground mining methods is acceptable in the non-simultaneous form but block / panel caving are more practicable.

Totally, there are three below different systems for large scale stope caving (Bakhtavar, 2009):

- Block caving: Ore deposit is divided to stopes in form of rectangular cubes. Usually, ore drawing from all draw-points is possible simultaneously.
- Panel caving: Ore deposit is divided to panels. Ore drawing from the draw-points is started from one side of the panel and gradually continues to other side.
- Mass caving: In this system, ore deposit is not divided to blocks or panels and the whole deposit is planned to be caved.

Selection of one of the caving systems mostly depends on geomechanical characteristics of an ore deposit. Block caving is most appropriate system for the extraction of the weak ore deposits which are crushed easily to small fragments. In this case, drawing rate is high. If an ore deposit is stronger and includes less discontinuities, panel caving system is more feasible. In case of a high strength massive ore deposit with low discontinuities mass caving system is preferred. In figure 2, mining direction as the main difference between block caving and panel caving is shown.

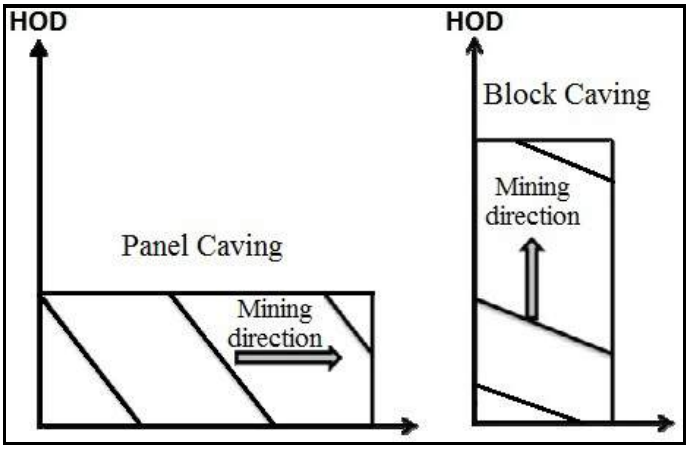

Figure 2. Mining direction in block caving and panel caving

4 CONCLUSION

When an ore deposit starts from or near ground surface and it continues to a high depth, a combination of open pit with one of underground methods is most practicable. In this case, there are two important problems to be considered correctly. First problem, which has been considered in this paper, is finding a practicable underground alternative in combining with open pit in both simultaneous and non-simultaneous extractions. Second one is optimizing transition from open pit to underground mining, especially in non-simultaneous combined of open pit and underground methods. Based on the global experience, the non-simultaneous form of combined mining is more acceptable which provides the utilization of large scale underground methods with high productivity and low costs such as block caving. In this case, there are many geotechnical challenges in interaction between open pit and caving stope. For example, instabilities from caving stopes are transmitted to open pit limit and therefore cause the slope instability of benches. This is a restriction for utilizing a simultaneous form of open pit and underground, except through 2 to 3 years of open pit mine life. Simultaneous form is strange although it is feasible in special conditions. If an ore deposit is small, only small scale underground methods are practicable from technical and economical viewpoints. Cemented backfill underground methods (such as vertical slices underhand cut & fill) are more feasible in the simultaneous mode of combined mining. In non-simultaneous mode, large scale methods with high productivity and low costs (such as block / panel caving) are more practicable. The problem of transition from open pit to underground mining, which has been regarded as a new challenge in mining engineering, is majorly related to the non-simultaneous combined mode of open pit and underground mining. The problems related to combined mining of open pit and underground methods are studied and discussed more, particularly during last decade. Now, a major portion of the mining researches belongs to the combined mining of open pit and underground mining because of its importance and desirability.

REFERENCES

Aminzadeh, A., 2014. Optimization of transition from open-pit to underground mining using computer modelling and Operations Research techniques, *MSc Thesis*, Urmia University of Technology.

Bakhtavar, E., 2009. A model for optimizing transition depth from open-pit to underground mining, *PhD Thesis*, Amirkabir University of Technology.

Bakhtavar, E., Samimi Namin, F., Shahriar, K., Oraee, K., 2010. ractical Final Pit Depth Considering the Future Underground Mining- A case study, *2010 SME Annual Meeting & Exhibit, Phoenix, AZ.*, pp. 153-156.

Bakhtavar, E., 2013. Transition from Open-Pit to Underground in the Case of Chah-Gaz Iron Ore Combined Mining, *Journal of Mining Science*, Vol. 49, No. 6, pp. 955-966.

Brummer, R. K., Li, H., Moss, A., 2006. The transition from open pit to underground mining; an usual slope failure mechanism at Palabora, *International Symposium on Stability of Rock Slopes in Open Pit Mining and Civil Engineering*, The South African Institute of Mining and Metallurgy, pp. 411-420.

Changyu, X., 1984. A study of stope parameters during changing from open pit to underground at the Meng-Yin diamond mine in China, *Journal of Mining Science and Technology*, No. 1, pp. 179-188.

Flores, G., 2004. Geotechnical challenges of the transition from open pit to underground mining at Chuquicamata Mine, *Massmin 2004*, Santiago, Chile, pp. 591-602.

Hersant, D., 2004. Mine design of the Argyle underground project, *Massmin 2004*, Santiago, Chile, pp. 610-615.

Jakubec, J., Long, L., Nowicki, T., Dyck, D., 2004. Underground geotechnical and geological investigations at Ekati Mine-Koala North: case study, *Journal of LITHOS*, No. 76, pp. 347-357.

Khani Khereshki, M., 2014. Optimization of long-term production planning of Angouran Lead and Zinc ore deposit on the basis of last updated exploration data, *MSc Thesis*, Urmia University of Technology.

Myers, P., Standing, C., Collier, P., Noppé, M., 2008. Assessing Underground Mining Potential at Ernest Henry Mine Using Conditional Simulation and Stope Optimisation, *Orebody Modelling and Strategic Mine Planning (Spectrum Series)*, Volume 14, pp. 191-200.

Robinson, S. J., 2007. Grade control in the transition from open-pit to underground sub-level caving, Dikulushi copper / silver mine, Democratic Republic of the Congo, *1st International Symposium on Block and Sub-Level Caving and Cave Mining*, The Southern African Institute of Mining and Metallurgy, pp. 173-184.

Srikant, A., Brannon, C., Flint, D. C., Casten, T., 2007. Geotechnical characterization and design for the transition from the Grasberg open pit to the Grasberg block cave mine, *Rock Mechanics Conference*, Taylor&Francis Group, London, pp. 1277-1286.

TETE Mine Team, 2006. Gushfil Underground Project, *Technical report*.

Williams, T.J., Brady, T.M., Bayer, D.C., Bren, M.J., Pakalnis, R.T., Marjerison, J.A., Langston, R.B., 2007. Underhand cut and fill mining as practiced in three deep hard rock mines in the United States, *CIM Conference and Exhibition*, The Canadian Institute of Mining, Metallurgy and Petroleum *(CIM)*, Montreal, Quebec, Canada, pp. 1-11.

A Contemporary Approach in Geotechnical Slope Stability Analysis: Lithological Implicit Modelling

A.G. Yardimci, H. Basarir
Middle East Technical University, Ankara, Turkey

ABSTRACT Open pit slope stability is a major concern in any mine prefeasibility study. Most widely used numerical and limit equilibrium methods require two inputs: rock mass mechanical parameters and bedding geometry of lithological units. Traditionally, rough geological models prepared by time consuming explicit method of manual digitization or assumptions depending on lithological drillhole logs form the basis for geometry of stability analysis models. However, the real geometry can be dramatically different. A novel method named as implicit modelling is capable of creating solid volumes for lithological units within a few minutes, free of operator bias. Also, complex geological structures like bedding and folding can be represented with high accuracy. In this paper, theoretical background of implicit modelling is covered briefly and a sample application is presented on an open pit iron mine slope stability analysis. Advantages of the geological model prepared by the new method in geotechnical studies are clearly declared.

Keywords: Implicit modelling, slope stability, geological modelling

1 INTRODUCTION

Global stability of open pit mine slopes has a vital priority due to the safety of employees and wellness of mining equipment. In any open pit mine, there are some actions need to be taken prior to and during the mining activities, so that a safe working environment can be provided. Slope monitoring is a passive, during-mining measure that is capable of predicting slope failure time. On the other hand, geotechnical slope stability analysis using numerical and limit equilibrium methods is a major topic in mine planning phase for determining safe slope design parameters. It depends on a huge knowledge base of field and laboratory studies. Rock mass mechanical properties and bedding geometry of lithological units are the main inputs. Most of the times, it is impractical and unnecessary to examine the stability in the whole mining area. Compared to the 2D alternative, 3D numerical modelling has some disadvantages. Namely, large number of input parameters, hard to generate model geometry and long computation time are some of them. Under these circumstances, 2D analysis brighten by its speed and accuracy. The well-known methodology in 2D slope stability analysis is focusing on the most critical cross-section by a plane strain assumption. The crucial subject is to generate the model geometry. Difficulty comes from identifying the bedding orientation of multiple lithological layers. Commonly, experts tend to generate a global multiple layer geometry by depending on the lithological drillhole logs. In case of considerably thick and regularly bedding layers, average thickness and simplified bedding geometry for each lithological units provide the inputs for numerical model geometry. If the geology is complex, the most common approach is to use a single lithological unit, which is the weakest one. This approach is named as pseudo isotropic medium (PIM). Although these over safe approaches have been trusted and successfully used until now, implicit modelling with some recent advances have aroused as a comfortable way of generating geological models.

Compared to the time consuming conventional method of generating solid volumes, named as explicit modelling, implicit modelling comes up with its speed and accuracy. Although it is not a new

discovery, recent optimizations in the algorithm have solved the major problem of large consumption of computer resources. Industry professionals have been publishing successful geological models prepared by implicit modelling and compare their results with the conventional explicit models. Most of them are satisfied with its speed and the solid body shape. In a technical note of SRK Consulting (2012) it was mentioned that the novel implicit modelling allows interpretation of the data without the bias of the expert and this is advantageous in terms of exploring the raw drillhole data from a different perspective. Most of the popular mine planning software providers, like Maptek Vulcan, Minesight, Geovia Surpac, Micromine, have recently included implicit modelling modules.

This paper aims to present the advantages of implicit modelling in creating geological models as an input of slope stability analyses carried out by numerical and limit equilibrium methods.

2 SOLID BODY GENERATION METHODS

2.1 Explicit Modelling

In mathematics, relationship between x and y defines curves and relationships between x, y and z defines surfaces. Three types of functions exist, which are namely explicit, implicit and parametric. In explicit functions, y is directly obtained from x values and the generic format is describes as y = f(x). Considering the circle in Figure1, it is relatively easier to generate series of values lying on the circle. The main limitation is its incapability of supporting closed lines or surfaces. To mathematically describe, a variable z defined by x and y variables return a unique z value and it is impossible to obtain different z values from the same inputs by treating the x, y pairs in different ways. This fact limits the types of shapes that the surface function can estimate (Cowan, et al., 2003). In Figure 1, it can be seen that a closed circle needs to be defined by two explicit functions.

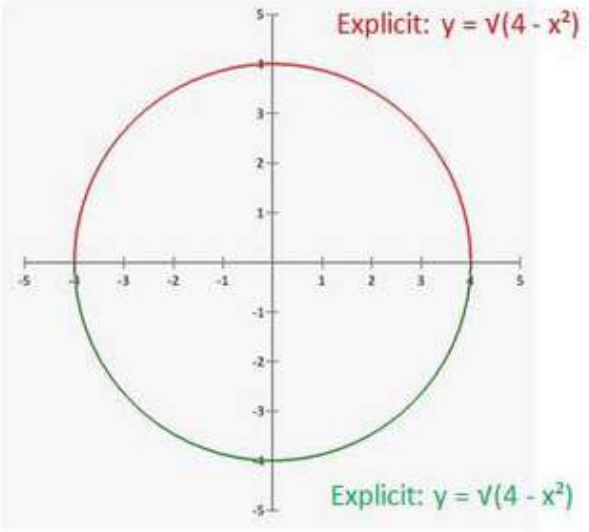

Figure 1. Mathematical representation of an explicit function *(Micromine Pty., 2014)*

Traditional explicit method of constructing geological model requires digitizing drillhole data in serial sections and joining the similar domain boundaries by polylines. In Figure *2*, illustration of this procedure using manual digitization can be seen. Black and grey sections represent two different lithologies (a) and explicitly defined border is observed in (b). The polylines generated for multiple cross-sections are joined by tie-lines to define the three dimensional relation between cross sections. Finally, each cross-section is connected to the other by triangulation and the solid model is created.

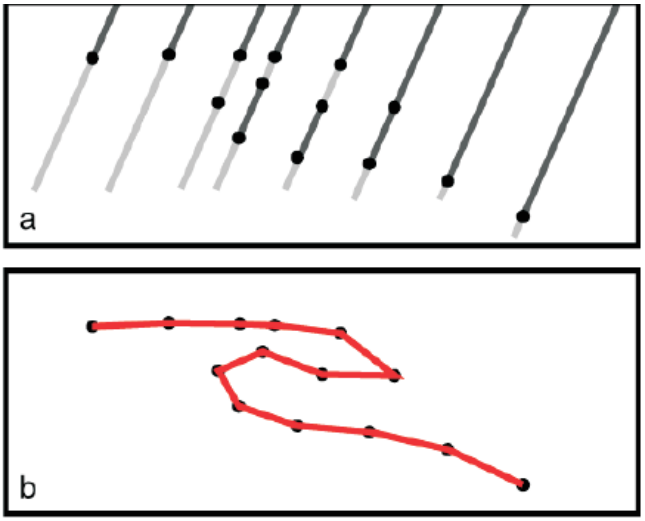

Figure 2. Cross-section view of a manually digitized domain using explicit modelling *(Cowan, et al., 2003)*

The above mentioned workflow is still the first choice of industry experts. However, it is a well-known fact that this time consuming method requires an experienced modeler and the model consists of operator bias. Cowan et al (2003) describes that each individual geologists' interpretation produces his/her unique model and the models are impossible to be replicated by others.

As it is obvious, solid model generation for multiple geological domains is a highly complex and time consuming task. Also, the generated model cannot be updated easily if new data is available. The mentioned static nature and high time dependency issues form the major drawbacks of explicit modelling

2.2 Implicit Modelling

Implicit modelling of space objects has a historical background. Field of Computer Graphics is more familiar with the subject; however, it is not well known by the Geological Society. Most of the studies on implicit modelling contain limited number of data points. This has been the limitation until now, for use in geological models in mines. A moderate mine has a drillhole database of thousands of data. To process this much data, huge amount of computer resources and time has been consumed by the algorithm, until now. Recent improvements in the algorithm and computer hardware technology made it usable in the mining industry.

Implicit functions have a general format of f(x,y)=0. Remembering the circle example (Figure 3), the function tests any random x, y couples if they lie on the circle (=0), inside the circle (<0) or out of the circle (>0). The main advantage of this method is its ability to model complex geological structures like overturned folds and enclosed surfaces such as spheres (Cowan, et al., 2003). It allows for the automation of creating solid models by using numerical data such as ore grades or even linguistic data by carrying out the conversion process explained above. Lithological implicit modelling, which is the main consideration in this paper, is just an example.

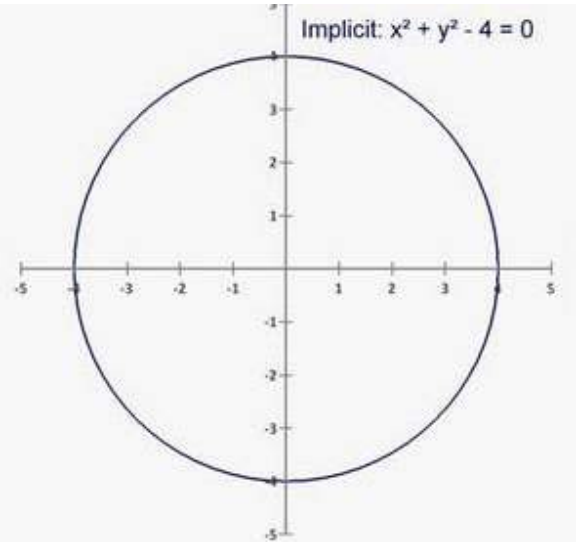

Figure 3. Mathematical representation of an implicit function *(Micromine Pty., 2014)*

In Figure 4, lithology symbolized by gray color is modeled implicitly. As can be seen in (c) lithology borders are marked by "0" because they lie on the border of the curve. Points at the upper part are marked by "+" values and the points inside the gray colored lithology are marked by "-" values. In this process, linguistic expressions are replaced by numerical values. The next step is to interpolate these values using the Radial Basis Function (RBF) in order to create a 3D (closed) surface representing the zero contour. This contour is also called as "isosurface".

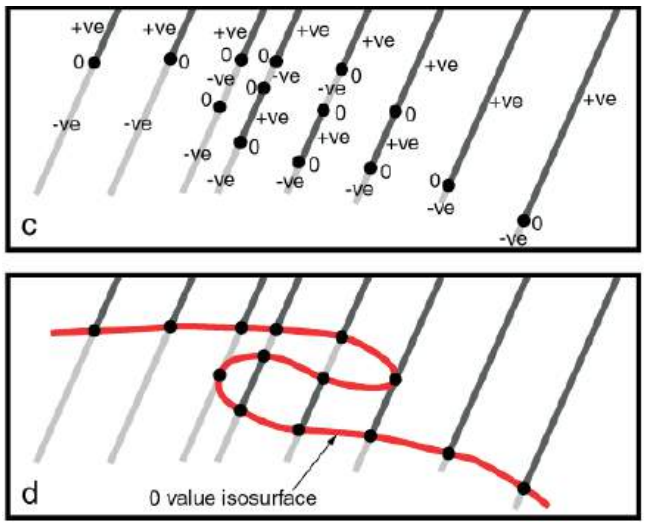

Figure 4. Cross-section view of joining a domain using implicit modelling *(Cowan, et al., 2003)*

2.2.1 Radial basis function (RBF)

In order to build up the soil volume, implicit modelling requires to have a 3D interpolation method. RBF is capable of interpolating grade and lithological data.

Cowan et. al. (2003) reported some of the drawbacks of RBF. One of them is the data storage problems in case of large data sets. Also calculation with large number of data points have been reported to be time consuming. For example, they mentioned about hours of calculation on a standard workstation of the year 2003 with 40 000 data points. These problems have been the main reason that implicit modelling has not been very popular among industry professionals. To solve this problem a fast form of RBF has been generated. The fast form avoids before mentioned problems because data matrix storage is not necessary. By this way, memory problems are avoided and the drillhole data of an entire mine can be processed within hours even on current PCs.

3 A CASE STUDY

3.1 Study Area & Rock Mass Characterizaiton

In this study, an iron mine located in Erzincan/ Bizmisen district of Turkey and owned by BILFER Mining Co. is focused on (Figure 5).

Donentas region drillhole database contains a total of 63 drillhole. 12 drillholes were selected and geotechnical logging study was carried out in terms of RMR_{89}, Q and GSI systems. 6 dominant lithological domains (including the ore) were determined. During geotechnical logging appropriate rock samples for laboratory testing were gathered and necessary rock mechanics test were done. Average rock mass and rock material properties can be seen in Table 1.

Figure 5. Erzincan/Bizmisen iron mine *(Google Earth, 2015)*

Table 1 Rock mass and rock material properties for Bizmisen dominant geological units *(Karpuz, Tutluoglu, Basarir, Yardimci, & Akdag, 2014)*

	Rock Mass Properties			Rock Material Properties				
Unit	**RMR_{89}**	**Q**	**GSI**	**γ (kN/m^3)**	**E (GPa)**	**ν**	**σ_t (MPa)**	**UCS (MPa)**
	Avg.	Avg.	Avg.					
Skarnfels	48	2.57	44	26.5	12.19	0.10	7.77	35.2
Limestone	40	1.20	35	26.2	24.54	0.16	7.10	48.8
Granodiorite	60	4.28	57	26.9	36.05	0.10	13.19	123.9
Mudstone	47	1.51	42	25.7	7.54	0.13	2.25	16.9
Serpantine	40	1.18	38	24.0	8.08	0.15	4.67	17.1

3.2 Lithological Implicit Modelling in Donentas Region

63 drillholes with a total depth of 13,051m had been logged in terms of lithological characteristics by BILFER and MTA. This study makes use of this existing database.

The database was imported into Micromine 2014 geological modelling and mine planning software. The recently established implicit modelling module of Micromine makes use of the before mentioned Radial Basis Function (RBF) to generate solid models. For the 6 dominant geological units, solid volumes were generated.

The software demands some inputs for the implicit engine. Drillhole database is the main requirement. Later, the software asks for "Include", "Exclude" and "Ignore" units. The lithology needs to be modelled should be under include box. The external units should stay in the "Exclude" box and the rock units to ignore can also be defined (Figure 7). The minimum length to be included into model should also be determined. If this value is too small, golf ball like blobs might be observed. Later, the amount of maximum points per partition is asked. Most of the times, all the points in a data set may be impractical to be included a single model. Thus, the data set is divided into overlapping regions. Each modelled separately with overlaps used to smooth out the transition from one partition to the next. It is suggested to start the analysis by 1/ 8 of the whole data and increase the number in case of observing golf ball like blobs.

If any trend exists in geological formations, anisotropic behavior can be reflected by using a search ellipsoid. The final and the most important input is the mesh size in grid units. As this value becomes smaller, the model will take more time to calculate but it will be more detailed.

In Figure 6 plan view of the Donentas can be seen on the left. On the right side, cross-section view of A-A' line is observed. The blank area between the complex geological units is the orebody. This figure is an evidence of the strong capability of implicit modelling for complex shaped volume generation. If modelled by conventional explicit way, complete modelling might take weeks and it would be very difficult for the operator. However, implicit model generated the 6 chaotic shapes just in seconds. Including the data preparation stage, whole of the process takes 15-20 minutes.

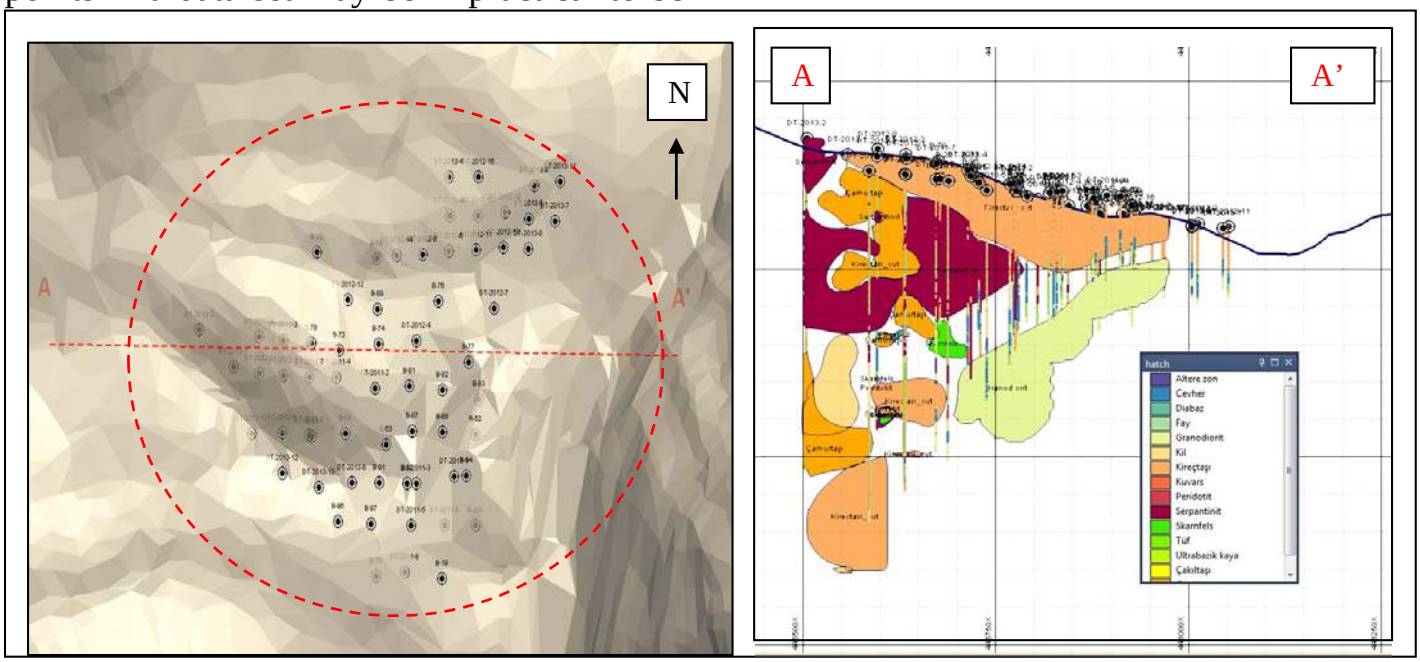

Figure 6. Plan view and section view of the lithological model of Donentas region *(Micromine Pty, 2014)*

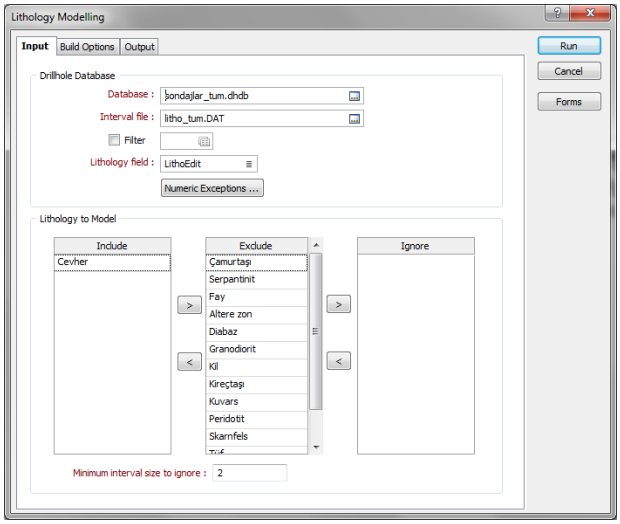

Figure 7. A screen view from implicit modelling module of Micromine 2014 *(Micromine Pty, 2014)*

3.3 Comparison of Numerical Models

In Donentas region 3D orebody model and DTM of the surface shows that topography and the orebody plunges in opposite directions. Consequence of this fact is a relatively deeper wall on the West side of the open pit.

In this study, global stability of a random production phase on the Western side of the pit will be under investigation. To describe the scenario, depth of the open pit is 180m and the overall slope angle is 41° on the West side. Numerical modelling will not be explained in detail because this paper mainly aims to show the effect of implicit geological model on numerical analysis. It is a kind of sensitivity analysis in the sense of model geometry.

Implicit lithological estimation could only be done for a limited zone in Donentas region. It is mainly the zone inside the borders of iron anomaly. The reason is that exploration drillholes only cover the iron rich zone and there is no data about the rockmass behind the open pit wall. Thus, the unknown area is defined by moderate rock properties to complete the model.

In Figure 8, cross-section of the analyzed condition can be seen. Figure 8 (a) and (b) declares the result of Shear Strength Reduction (SSR) analysis carried out by Rocscience Phase 2 software. Difference between the models lie in the geometry of dominant lithologies. In the first case the pseudo isotropic medium (PIM) approach is used. This approach relies on representing the complete host rock by the weakest rock unit. In Figure 8 (a), total displacement contours for a model with PIM approach can be seen.

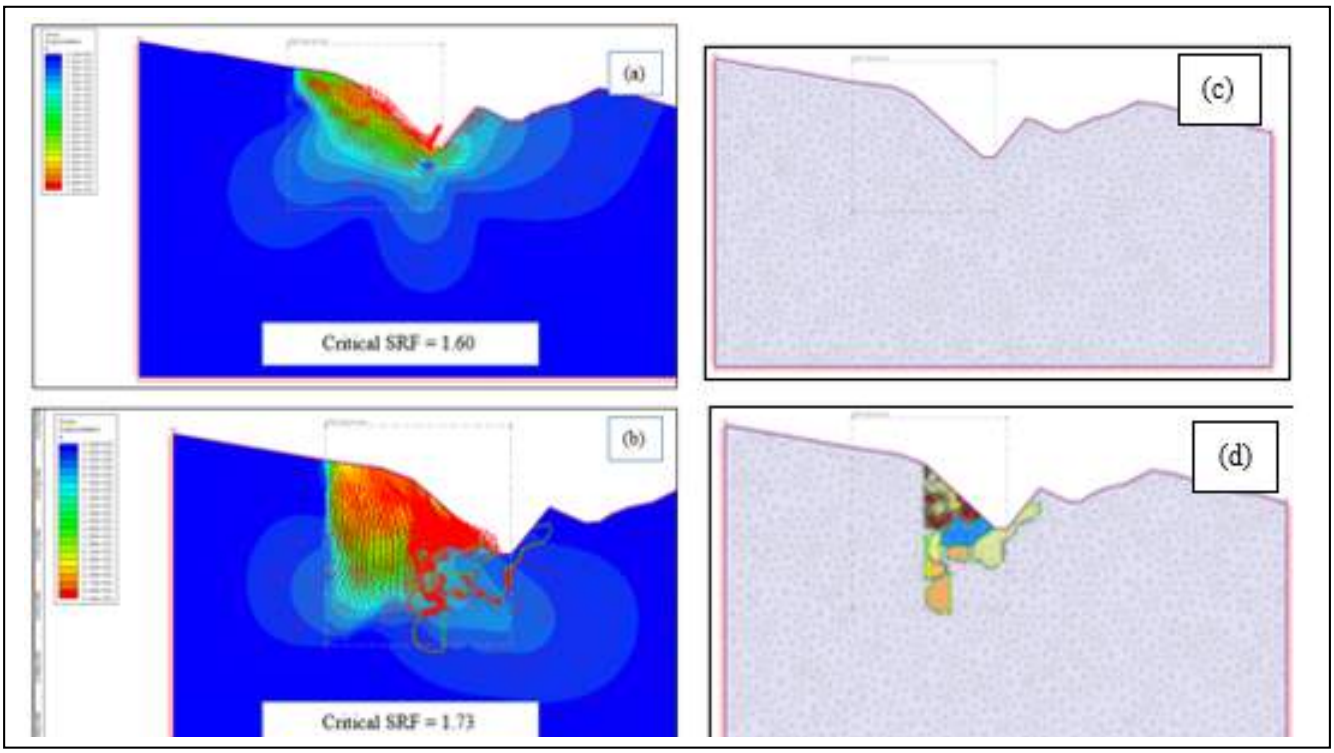

Figure 8. SSR results and total displacement contours from Rocscience Phase2 software for (a) rough model geometry, (b) lithological unit geometries determined by implicit modelling

Due to the complex geology, the assumption is plausible and in most cases provides meaningful results. The search area for SSR and the single unit domain geometry can be seen in (c). The critical SSR is found to be 1.60. In Figure 8 (d), the model geometry consisting of geological units modelled by implicit methods in detail and total displacement contours can be observed. Result of the SSR analysis can also be seen in (b) with a critical SSR of 1.73. It can be obviously seen that the first global model with PIM approach behaves more conservatively. This is mainly the consequence of assuming a weak rock unit in the whole rock mass. However, in the second model with lithologies generated by implicit model, there is a considerable increase in SSR factor. Detail geometries show a stratification in the favorable direction to the slope and this is the major reason for the increase in SSR.

4 CONCLUSION

As a proven, fast and comfortable technology, implicit modelling is a rising trend among the geological modelling society. Although geological modelling has known to be a time consuming job until now, (weeks or months especially for complex geologies), today, it can be handled within a matter of hours by the optimized algorithm of implicit modelling. This study specifically focused on its effects on the routine Geotechnical slope design. Results have shown that detailed geological modelling avoids overdesign in the studied case. SSR factor for the assumed slope geometry were 1.60 and 1.73 for PIM and implicit methods respectively. This novel modelling method also has the advantage of being free of operator bias. In complex structures, human knowledge may not be sufficient to observe some critical interrelations. The algorithm avoids human errors and theoretically provides volumes in infinite detail by using the Radial Basis Function (RBF). Implicit modelling has a high potential to be used as an auxiliary tool in geotechnical stability analysis by its speed and accuracy.

ACKNOWLEDGEMENT

The authors would like to thank the staff of BILFER Mining Inc. for their valuable supports. The company is also acknowledged for the permission to use and publish the data.

REFERENCES

Cowan, E. J., Beatson, R. K., Ross, H. J., Fright, W. R., McLennan, T. J., Evans, T. R., . . . Titley, M. (2003). The Australian Institute of Mining and Metallurgy. *5th International Mining Geology Conference* (p. 13). Bendigo: The Australian Institute of Mining and Metallurgy.

Google Earth. (2015). Erzincan Bizmişen Satellite Map. Retrieved March 04, 2015

Karpuz, C., Tutluoglu, L., Basarir, H., Yardimci, A. G., & Akdag, S. (2014). *Erzincan Bizmişen Demir Cevheri Maden İşletme Projesi.* Technical Report, METU, Ankara.

Micromine Pty. (2014). Micromine.

Micromine Pty. (2014). Micromine Help File. Perth, Australia.

Micromine Pty. (2014, November 19). *What is Implicit Modelling?* Retrieved March 04, 2015, from Micromine Blog: http://blog.micromine.com/2014/11/19/what-is-implicit-modelling/

SRK Consulting. (2012). *Implicit modelling – find more than you were looking for.* Perth: SRK.

Analysis of Sulphur Contents in Coal by Means of Henry's Beneficiation Curve Approximation

T. Niedoba, A. Surowiak
AGH University of Science and Technology, Krakow, Poland

ABSTRACT In purpose of conducting analysis of sulfur contents in selected raw hard coal its separation was performed into particle size fractions by screening. Then, such prepared material was additionally separated into particle density fractions by means of dense media analysis. Because of the fact that Henry's beneficiation curve cannot be approximated by traditional random variables distribution functions. In the paper, the approximation of function of sulfur contents versus density was done by means of application of known statistical functions. Then, using statistical distribution functions the approximation of relation between cumulated yield and density was done. The main Henry's beneficiation curve was obtained by means of determining the reverse function of cumulated yield and joining sulfur contents versus density function and reversed cumulated yield function. To evaluate the quality of approximation the mean squared error (MSE) was used. By means of obtained function the mean sulfur contents was determined in the whole material as well in individual fractions. The obtained results were then verified empirically.

Keywords: Sulphur, Henry's beneficiation curve approximation, Mean squared error (MSE)

1 INTRODUCTION

To evaluate the beneficiation ability of material being processed the Henry's beneficiation curve can be used [Drzymala, 2001], which describes the relation between any qualitative coal parameter and certain fraction yield.

From the probabilistic point of view if the change of concentration of certain component W in product is investigated and only one feature X decides about the separation then the regressive function of first type $E(W|X=x)=\lambda(x)$ determines the Henry's beneficiation curve. If the analytic form of Henry's curve is known then the mean contents of investigated component in material is given by the formula (1) [Tumidajski, 1997].

$$\alpha=\int_0^1 \lambda(\gamma)d\gamma \quad (1)$$

where γ is percentage yield of fraction; λ - contents of component in this fraction; α - mean contents of the component in whole material.

In papers [Niedoba, 2013a; 2013b; 2013c] the beneficiation processes were discussed and the approximation of Henry's curve was presented which described ash's contents in relation to fraction's yield.

In this paper the approximation of Henry's curve is done by probabilistic approach describing sulfur contents in coal dependably on the yield.

2 ANALYSIS AND CALCULATIONS

To achieve the goals described in the introduction the raw coal, type 31 (according to Polish classification of coals, which means energetic coal) was collected from one of the Hard Coal Mines located in Upper Silesia, Poland and was divided into density fractions. The experimental results are presented in Table 1.

Because of the fact that Henry's beneficiation curve cannot be approximated by traditionally used distribution functions the complex approximation was performed in the paper.

Table 1. Separation of coal into density fractions

Density ρ [g/cm^3]	Mean density ρ_{0i} [g/cm^3]	Percentage share [%]	Cumulated share γ_i [%]	Sulfur contents λ [%]
1.20-1.30	1.25	51.11	51.11	0.64
1.30-1.40	1.35	34.79	85.90	0.69
1.40-1.50	1.45	6.43	92.33	1.20
1.50-1.60	1.55	2.59	94.22	1.27
1.60-1.70	1.65	1.76	96.68	1.51
1.70-1.80	1.75	1.55	98.23	1.565
1.80-1.90	1.85	1.77	100.00	1.65

In the beginning the approximation of function $\lambda = \lambda_0(\rho)$ was performed what meant the relation between sulfur contents λ and density ρ. It was done by means of functions being applied in regression analysis.

Then, the approximation of function $\gamma = F(\rho)$ was done what showed the relation between cumulated yield γ and density ρ. This function fulfills conditions for distribution function so is possible to be approximated by means of functions being applied in probability. Function $F(\rho)$ is growing so it has its inverse function $\rho = F^{-1}(\gamma)$. Taking complexion of functions $\lambda_0(\rho)$ and $F^{-1}(\gamma)$ the function approximating Henry's beneficiation curve is obtained in the form:

$$\lambda(\gamma) = \lambda\left(F^{-1}(\gamma)\right) \tag{2}$$

The approximation of function $\lambda = \lambda_0(\rho)$ was done by means of curvilinear regression. The best one was obtained by exponential function of the formula:

$$\lambda(\rho) = 0.3731\rho^{2.6113} \tag{3}$$

To evaluate the quality of approximation the curvilinear correlation coefficient R was used, given by the general formula [Kotz et al., 2000; Sobczyk, 2001]:

$$R = \sqrt{1 - \sum_{i=1}^{k} \frac{\left(\lambda_i - \lambda_i^*\right)^2}{\left(\lambda_i - \bar{\lambda}\right)^2}} \tag{4}$$

where λ_i are experimental sulfur contents in i^{th} fraction; λ_i^* are theoretical sulfur contents in i^{th} fraction (calculated from formula (3); $\bar{\lambda}$ - mean value of sulfur contents ($\bar{\lambda} = \sum_{i=1}^{k} \lambda_i$); k – quantity of fractions.

In the analyzed example, the value of coefficient R=0.9375 what means that the fitting was acceptable. To determine function $\gamma = F(\rho)$ the logistic distribution function was applied [Niedoba, 2013; Tumidajski, 1993; 1997; Tumidajski and Saramak, 2009], presented in general form of formula (5).

$$y = \frac{1}{1 + be^{-ax}} \tag{5}$$

As the result of approximation for γ, the values of a=-6.81 and b=2522.48.

To evaluate the preciseness of approximation the curvilinear correlation coefficient was used and the value of it was R=0.9283 what meant satisfying level of fitting.

By transforming equation (5), with calculated values of a and b, the reverse function $\rho = F^{-1}(\gamma)$ is obtained and its form in this case is:

$$\rho = 1.15 + \frac{1}{6.81} \ln \frac{\gamma}{1-\gamma} \tag{6}$$

Finally, composing functions given by equations (3) and (6) the approximation function of Henry's beneficiation curve can be obtained in the form:

$$\lambda_1(\gamma) = \begin{cases} 0 & for \quad \gamma \in [0, 0.0005] \\ 0.37\left(1.15 + 0.15 \ln \frac{\gamma}{1-\gamma}\right) & for \ \gamma \in [0.0005, 0.99] \\ 1.83 & for \quad \gamma \in [0.99, 1] \end{cases} \tag{7}$$

The curvilinear correlation coefficient R is equal 0.9344 what means that the selection of the function was appropriate.

The experimental and theoretical results for functions $\lambda_0(\rho)$ and $F(\rho)$ are presented in Table 2 and on Figs 1 and 2.

Table 2. Experimental and theoretical results for functions $\lambda_0(\rho)$ and $F_0(\rho)$

Density ρ [g/cm^3]	$F_0(\rho)$ exp [%]	$F_0(\rho)$ theor [%]	$\lambda_0(\rho)$ exp [%]	$\lambda_0(\rho)$ theor [%]
1.20-1.30	51.11	58.44	0.64	0.66
1.30-1.40	85.90	79.62	0.69	0.81
1.40-1.50	92.33	91.56	1.20	0.99
1.50-1.60	94.22	93.85	1.27	1.17
1.60-1.70	96.68	96.79	1.51	1.38
1.70-1.80	98.23	98.39	1.55	1.60
1.80-1.90	100.00	99.16	\1.65	1.83

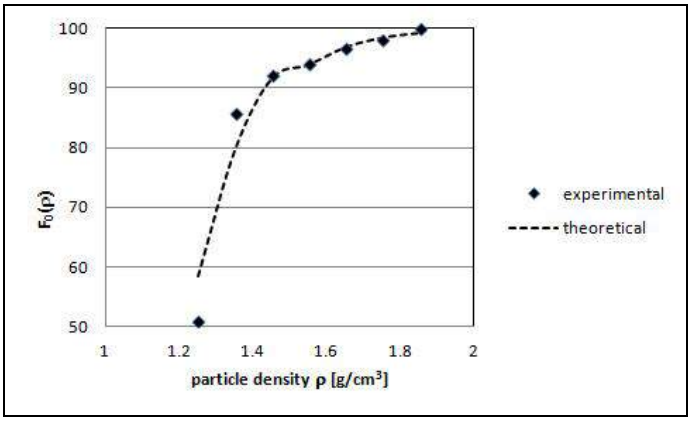

Figure 1. Experimental and theoretical results for function $F_0(\rho)$

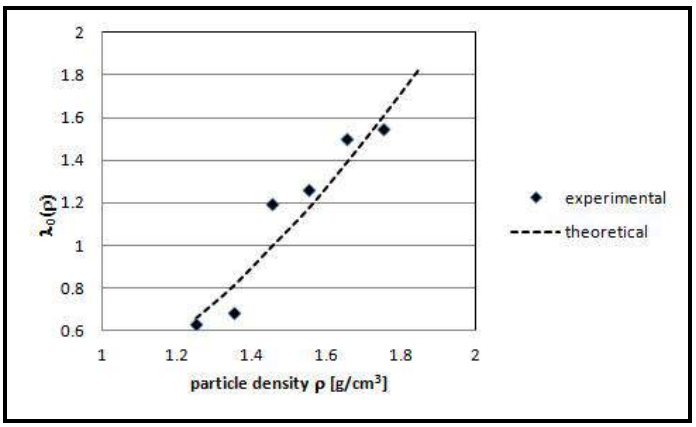

Figure 2. Experimental and theoretical results for function $\lambda_0(\rho)$

Experimental and theoretical results for Henry's curve are presented in Table 3 and on Fig. 3.

Table 3. Experimental and theoretical results for $\lambda_1(\gamma)$ curve

γ [%]	$\lambda_0(\gamma)$ exp [%]	$\lambda_1(\gamma)$ theor [%]
51.11	0.64	0.53
85.90	0.69	0.93
92.33	1.20	1.12
94.22	1.27	1.21
96.68	1.51	1.40
98.23	1.55	1.60
100.00	1.65	1.83

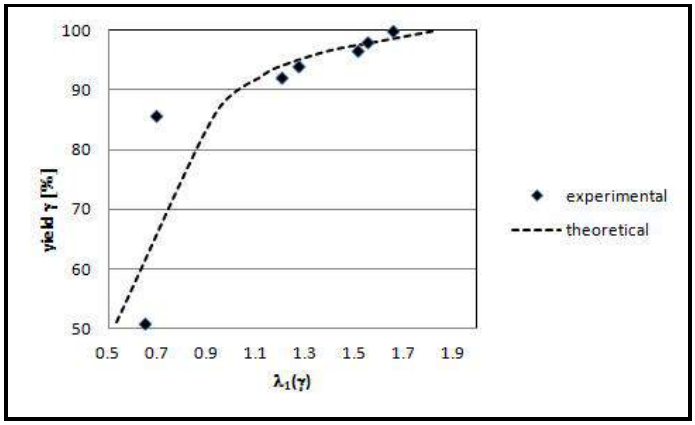

Figure 3. Experimental and theoretical results for function $\lambda_1(\gamma)$

Because the cumulated yield γ is growing function of sulfur percentage contents λ, the function $\lambda(\gamma)$ can be obtained by other method

First, the function $\gamma(\lambda)$ can be approximated by means of functions used as distribution functions in statistics and then, using the fact that function $\gamma(\lambda)$ as monotonic function is invertible function, the inverse function $\lambda(\gamma)=\gamma^{-1}(\lambda)$ can be obtained.

In this example the complexion of exponential function $y=ax^b$ with logistic function given by equation (5) was used.

The function obtained by this method is in form:

$$\gamma_1(\lambda)=\begin{cases} 8.19\lambda^{6.21} & for \lambda\in[0,0.69) \\ \dfrac{1}{1+1.47e^{-2.72\lambda}} & for\ \ \lambda\geq 0.69 \end{cases} \qquad (8)$$

Determining the inverse function to function $\gamma_1(\lambda)$ given by the equation (8) the analytical form of Henry's curve $\lambda_2(\gamma)$ is obtained.

$$\gamma_2(\lambda)=\begin{cases} 0.71\gamma^{0.16} & for\ \gamma\in[0,0.8156) \\ 0.14+0.37\ln\dfrac{\gamma}{1-\gamma} & for\ \gamma\in[0.8156,1) \\ 1.83 & for\ \ \ \gamma=1 \end{cases} \qquad (9)$$

The values of function $\lambda_2(\gamma)$ are shown in Table 4 and on Fig. 4.

Table 4. Values of function $\gamma_1(\lambda)$

γ [%]	$\lambda_0(\gamma)$ exp [%]	$\lambda_2(\gamma)$ theor [%]
51.11	0.64	0.64
85.90	0.69	0.80
93.56	1.20	1.06
94.22	1.27	1.17
96.68	1.51	1.39
98.23	1.55	1.61
100.00	1.65	1.83

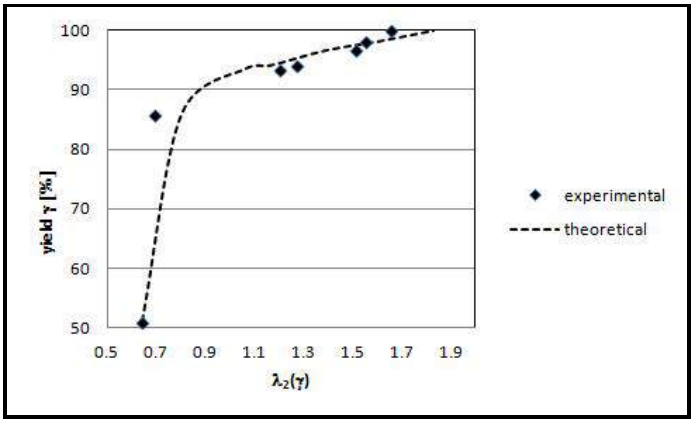

Figure 4. Experimental and theoretical results for function $\lambda_2(\gamma)$

The curvilinear correlation coefficient is equal, respectively, for function $\gamma_1(\lambda)$, R=0.99, for function $\lambda_2(\gamma)$, R=0.91.
Knowing the analytical Henry's curve form is possible to determine mean sulfur contents in the investigated material.

$$\bar{\lambda} = \int_0^1 \lambda_2(\gamma)d\gamma = \int_0^{0.8156} 0.71\gamma^{0.16}d\lambda + \lim_{\alpha\to 1^-}\int_{0.8156}^{\alpha}\left[0.14 + 0.37\ln\frac{\gamma}{1-\gamma}\right]d\gamma = \\ = \frac{0.71}{1.16}\gamma^{1.16}\Big|_0^{0.8156} + \lim_{\alpha\to 1^-}\Big[0.14\gamma + 0.37\big(\gamma\ln\gamma + (1-\gamma)\ln(1-\gamma) - 1\big)\Big]_{0.8165}^{\alpha} = 0.69 \quad (10)$$

The experimental mean value of sulfur contents in the whole material is equal to $\bar{\lambda} = \sum f_k\lambda_k = 0.75$, where f_k is percentage share of k^{th} fraction; λ_k – percentage contents of sulfur in k^{th} fraction.

Theoretical sulfur contents in individual fractions can be determined using the following formula:

$$\bar{\lambda}_k = \int_{\gamma_{k-1}}^{\gamma_k} \lambda_2(\gamma)d\gamma \quad (11)$$

where $\bar{\lambda}_k$ is mean sulfur contents in k^{th} fraction; γ_{k-1} – cumulated yield of k-1$^{\text{th}}$ fraction; γ_k – cumulated yield of k^{th} fraction.
The calculated mean contents of sulfur on the basis of formula (11) for individual fractions are shown in Table 5.

Table 5. Mean sulfur contents $\bar{\lambda}_k$

Density ρ [g/cm^3]	$\tilde{\lambda}_k = \sum_k f_k\lambda_k$ exp	$\bar{\lambda}_k$ theor
1.20-1.30	0.3271	0.3020
1.30-1.40	0.2401	0.2333
1.40-1.50	0.0772	0.0588
1.50-1.60	0.0329	0.0332
1.60-1.70	0.0266	0.3080
1.70-1.80	0.0240	0.0232
1.80-1.90	0.0292	0.0320

If the mean standard error (MSE) is applied to evaluate the fitting of theoretical sulfur contents in fractions, given by the formula (12) [Kotz et al., 2000; Sobczyk, 2001; Tumidajski, 1997; Tumidajski and Saramak, 2009].

$$MSE = \sqrt{\frac{\sum_i \left(\tilde{\lambda}_i - \bar{\lambda}_i\right)^2}{k-2}} \quad (12)$$

where $\tilde{\lambda}_i$ is mean sulfur contents in i^{th} fraction; $\bar{\lambda}_i$ - mean theoretical sulfur contents in i^{th} fraction; k – number of fractions.

3 CONCLUSIONS

Comparing the results of mean sulfur contents in the whole material (difference is equal to 0.16%) and investigating the difference between sulfur contents in individual fractions in ratio to the whole material obtained on the basis of the experimental results and results obtained by approximation (MSE=1.44%) it can be accepted that the obtained Henry's beneficiation curve describes well the course of the process.

In the paper, two methods of approximating Henry's curve were presented. Both curves are well approximated (curvilinear correlation coefficients were equal R=0.93 and R=0.91, respectively).

It can be noticed that the curve obtained by the first method is more complicated what makes difficult to apply it practically (it requires numerical integral).

The curve obtained by the second method is much simpler in form (it can be solved analytically) but to use this method for other components of researched material the assumption that cumulated yield is monotonous function of investigated component contents must be required.

REFERENCES

Drzymala, J., 2001. *Basics of Minerallurgy*, Oficyna Wyd. Politechniki Wroclawskiej, Wroclaw, [in Polish]

Kotz S., Balakrishnan N., Johnson N., 2000. *Continuous Multivariate Distributions*, John Wiley & Sons, New York.

Niedoba, T., 2013a. *Multidimensional characteristics of random variables in description of grained materials and their separation processes*, Wyd. IGSMiE, Krakow, [in Polish]

Niedoba, T., 2013b. Elements of methodology of applying two- and multidimensional distribution functions of grained materials properties to description of coal beneficiation, *Mineral Resources Management*, vol. 29(2), pp. 155-172 [in Polish].

Niedoba T. 2013c. Statistical analysis of the relationship between particle size and particle density of raw coal, *Physicochemical Problems of Mineral Processing*, vol. 49, pp. 175-188.

Sobczyk M., 2001. *Statistics*, Wyd. PWN, Warszawa, [in Polish]

Tumidajski T., 1993. *Application of statistical methods in analysis of mineral processing*, Wyd. Slask, Katowice, [in Polish]

Tumidajski T., 1997. *Stochastic analysis of grained materials properties and their separation processes*, Wyd. AGH, Krakow, [in Polish]

Tumidajski T., Saramak D., 2009. *Methods and models of mathematical statistics in mineral processing*, Wyd. AGH, Krakow, [in Polish]

Development of New Correlations to Predict Acid Fracture Conductivity Based on Rock Strength

M.R. Akbari, M.J. Ameri , S. Kharazmi, and H.A. Zafarian
Amirkabir University of Technology, Tehran, Iran

ABSTRACT One of the fundamental ways to stimulate and increase the production rate of a well completed in a carbonate reservoir is acid fracturing. Acid fracture conductivity is an important parameter for designing a fracture job. The amount of rock dissolved, fracture surface etching patterns, rock strength, and closure stress impact the resulting acid fracture conductivity. A model of acid fracturing conductivity must accurately anticipate fracture conductivity versus closure stress. The fracture conductivity is substantially influenced by rock type. A serious challenge of recent studies has been to predict behavior of different formations under various closure stresses. This study develops intelligent model to precisely predict fracture conductivity by incorporating experimental data from various formations, whereby resulting in a good match between model predictions and experimental data. The effects of rock type and treatment parameters are investigated on fracture conductivity under various closure stresses. The results show rock type plays a significant role when anticipating fracture conductivity, as various formations have behaved differently under various closure stresses.

Keywords: Acid fracture conductivity, genetic algorithm

1 INTRODUCTION

Acid fracturing is one of the preferred methods to stimulate wells in carbonate reservoirs. It consists of injecting an acid solution at high enough pressure to break down the formation and to propagate a two-wing crack away from the wellbore. The acid reacts with the carbonate formation and this causes the etching of the fracture surface (Rodrigues, 2011). In a heterogeneous formation, acid fracturing has proved to be a successful method to enhance hydrocarbon recovery. Moreover, in a tight-gas reservoir, acid fracturing becomes the most economical method to produce the gas reservoir (California Council, 2014).

Success of acid fracturing depends greatly on the created conductivity which must be retained under closure stress. Acid fracture conductivity is a measure of the capacity for fluid flow through an acidized fracture. The resulting conductivity is influenced by the amount of rock dissolved, the pattern in which the rock is dissolved, the strength of pillars that prop the fracture open, and the amount of closure stress on the fracture.

Designing acid fracturing treatments primarily aim to optimize live acid penetration distance and conductivity. Acid type and strength, acid injection volume, and injection rate are the key elements in such a design. There are many studies for live acid penetration distance. In contrast, few studies have been completed for acid fracture conductivity, and more studies are necessary to improve accuracy of conductivity predictions (Nierode and Kruk, 1973, van Domselaar et al., 1973; Coulter et al., 1974; Roberts and Guin, 1975; Anderson and Fredrickson, 1987, Beg, 1996, Ruffet & Fery, 1997, and Gong et. al., 1999). Moreover, few previous studies have considered the role of rock strength in the conductivity retained with elevated closure strength (Mou et al., 2009).

While success of the acid fracturing process depends highly on the resulting fracture conductivity, the resulting conductivity is very difficult to predict as it

inherently depends on a stochastic process and is affected by a wide range of parameters (Mou, 2009).

There have been many experimental and theoretical studies to improve understanding of acid fracture performance. There has been also extensive work on fluid flow in rough walled natural fractures. However, very few studies have concentrated on fracture conductivity, especially on developing a correlation for prediction of conductivity (Pournik, 2008).

Initially Nierode and Kruk (1973) developed an empirical correlation for fracture conductivity which is widely used in industry. The correlation is based on experimental study conducted on different formation samples acidized with HCl acid. The conductivity estimation depends on amount of rock dissolved, rock strength and closure stress.

Anderson et al. (1989) stated that formation characteristics, such as hardness, will strongly affect etched conductivities that result from fracture acidizing. For example, etched surfaces of chalk formations can be easily closed due to its natural softness (Anderson et al. 1973). Nasr-El-Din et al. (2006) suggest that the correlations developed by Nierode and Kruk (1973) were lumped together rather than separated by lithology. They recalculated the correlation by graphing and evaluating the data again both as a lumped set and as individual sets by lithology. The modified correlations kept the same form as the original ones, but made the constants different and were more precise (Gomaa & Nasr-El-Din, 2009)

The objective of this work is to develop a precise model to estimate conductivity for acid fracturing treatment based on a new approach in evaluation algorithms. Predicting conductivity is difficult because it is a function of the rock's strength, heterogeneities present in the rock, the transportation and dissolution of acid, the closure stress and other variables. The study uses a treatment parameter called dissolved rock equivalent conductivity (DREC) that stems from the total amount of rock dissolved by injected acid at zero stress. Then lets the conductivity decline as the fracture width reduces when closure stress is applied. DREC derived according to the cubic law indicates the acid dissolving power and the total volume of injected acid proportional to the geometry of the fracture created. Due to the complication of predicting acid fracture conductivity and also the capability of genetic algorithm (GA) in optimization and modelling, in this paper, a robust intelligent model based on genetic algorithm is developed to predict acid fracture conductivity accurately. The input data are considered according to rock strength to provide a better understanding of the rock type effect. Ultimately, the resulting conductivity given by GA models is compared to prior models.

2 GENETIC ALGORITHM AS AN OPTIMIZATION TOOL

Genetic algorithms are a type of optimization algorithm, meaning they are used to find the optimal solution(s) to a given computational problem that maximizes or minimizes a particular function. Genetic Algorithms are direct, parallel, stochastic method for global search and optimization which imitates the evolution of the living beings, Charles Darwin. This adaptive method may be used to solve search and optimization problems. Genetic Algorithm which is based on the genetic process of biological organisms, is used to solve both constrained and unconstrained optimization problems and could be applied to a variety of problems that are not well suited for standard optimization algorithms (especially the problems with nonlinear objective function) (Kosters et al., 1999).

Sometimes genetic algorithms are applied as a process of optimization coefficients in the engineering and mathematics. The problems are first formulated as mathematical models expressed in term of functions and then to find a solution, discover the coefficient that optimize the model or the function component that provide optimal system performance (Yeniay, 2005).

3 METHODOLOGY

In this research genetic algorithm is used to optimize coefficients of Nierode and Kruk and Nasr-El-Din's correlations. Three optimized correlation based on all input data, the data in which rock embedment strength is lower 20000 psi and the data in which rock embedment strength is higher than 20000 psi are developed. In the next step three new correlations are generated according to three data category. Absolute relative error (ARE) and regression coefficient (R) were considered as criteria to evaluate ability of proposed correlations. The quality of the fracture conductivity prediction is quantified in terms of the average absolute relative error and correlation coefficient (R^2 or R) by comparison with experimental data. Equations 1 and 2 are applied to calculate the performance criteria.

$$R = \frac{\sum_{i=0}^{n}(m_i-\bar{m})(p_i-\bar{p})}{\sqrt{\sum_{i=0}^{n}(m_i-\bar{m})^2(p_i-\bar{p})^2}} \quad (1)$$

$$ARE = \frac{WKf_P^{predicted}-WKf_P^{measured}}{WKf_P^{predicted}} \times 100 \quad (2)$$

3.1 Data Analysis

In this study, Nierode and Kruk (1973) experimental data sets are applied as input data. 116 experimental data set including dissolve rock equivalent conductivity, rock embedment strength and closer stress for specific fracture conductivity are considered as input data.. The data sets are divided into three groups; the first includes all 116 data sets to develop correlations, however all data have many different in specification of rock strength and lithology. The second group consists of 36 data sets in which rock embedment strength is lower 20000 psi. The third group includes 70 data set in which rock embedment strength is upper 20000 psi. Table 1 shows properties and ranges of all input variables in detail.

Table 1. Ranges of input data used in this study

Parameter	Min	Max	STD	Mean
DREC (md-ft)	3.E+04	1.30E+08	107826007	6.E+07
Closure Stress (Psi)	0	7000	2379.809	2939
Rock Strength (Psi)	5600	88100	1802.509	35170
Fracture Conductivity (md-ft)	1.2	7400000	1264474.65	2.E+05

3.2 Development of Acid Fracture Conductivity Correlations

Genetic algorithm begins by creating a random initial population (N chromosome). The algorithm then creates a sequence of new population. At each step, the algorithm uses the individuals in the current generation to create the next population .The algorithm creates crossover children by combining pairs of parents in the current population. At each coordinate of the child vector, the default crossover function randomly selects an entry, or gene, at the same coordinate from one of the two parents and assigns it to the child. For problems with linear constraints, the default crossover function creates the child as a random weighted average of the parents. Then GA creates mutation children by randomly changing the genes of individual parents. For unconstrained problems the algorithm adds a random vector from Gaussian distribution to the parent. For bounded or linearly constrained problems, the child remains feasible. Then the first step, the function selects parents deterministically according to the integer part of the scaled value for each individual. In the second step, the selection functions select additional parents using the fractional parts of the scaled value, as in stochastic uniform selection. If the result not suitable the code use generated population for further run of the algorithm so if the end condition is satisfied , stop and return the best solution in current population (Omid E. David, 2013).

In this study, Genetic Algorithm (GA) is used as a dominant tool. A general flow chart of GA is presented in figure 1. The parameters used to perform Genetic Algorithm are listed in Table 2. The values of these parameters are shown in table 3.

Table 2. The parameters used to set Genetic Algorithm parameters

Chromosome	A set of genes; a chromosome contains the solution in form of genes
Gene	A part of chromosome; a gene contains a part of solution. It determines the solution
Individual	Same as chromosome
Population	Number of individuals present with same length of chromosome
Fitness	The value assigned to an individual based on how far of close a individual is from the solution; greater the fitness value better the solution it contains
Fitness function	A function that assigns fitness value to the individual
Breeding	Taking two fit individuals and then intermingling there chromosome to create new two individuals
Mutation	Changing a random gene in an individual
Selection	Selecting individuals for creating the next generation

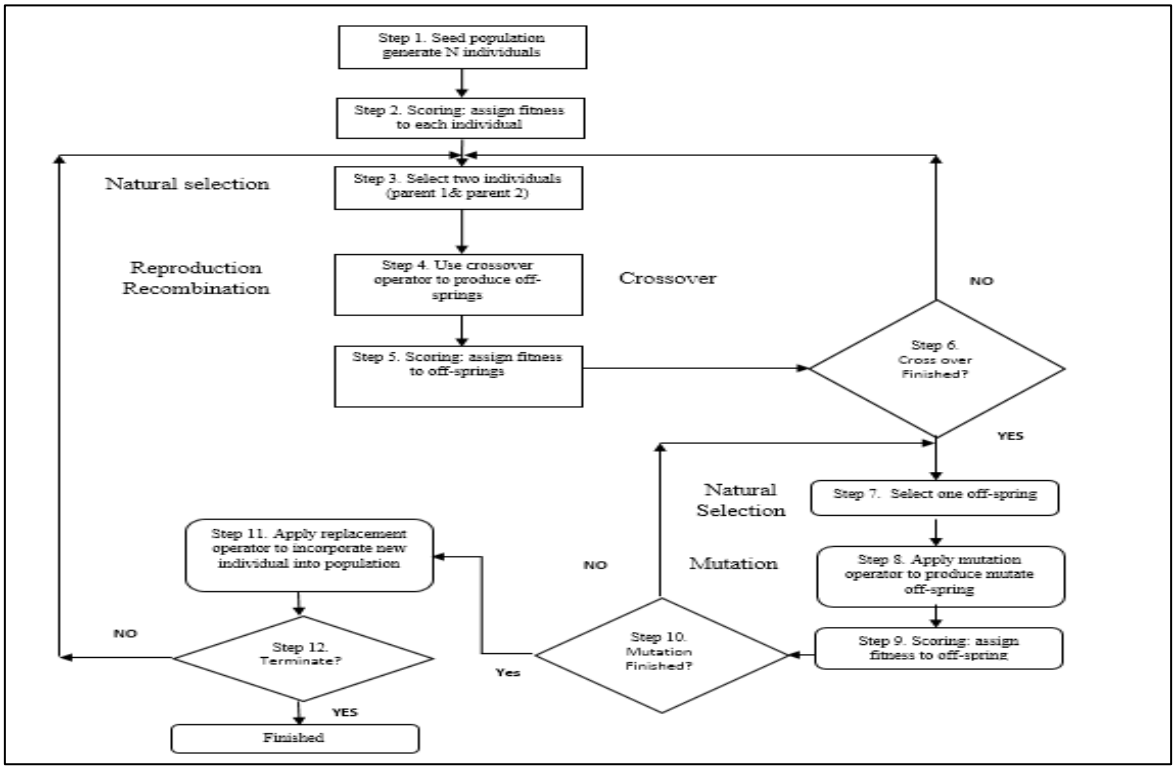

Figure 1. GA program procedure chart.

Table 3. Set GA parameters for optimized and new correlations

Input Data	**Correlation**	**N Pop**	**Pc**	**Pm**	**mu**
All Data	New Correlation	10000	0.90	0.10	0.30
	Optimized Correlation	3000	0.80	0.30	0.30
RES<20000	New Correlation	4000	0.80	0.50	0.70
	Optimized Correlation	4000	0.80	0.40	0.50
RES>20000	New Correlation	3000	0.80	0.30	0.30
	Optimized Correlation	4000	0.80	0.30	0.30

The comparison of accuracy of Nierode & Kruk, Nasr-El-Din, optimized and new correlations is shown in figure 2. As the results illustrate, the new correlation is more precise compared to other correlations at various rock strength.

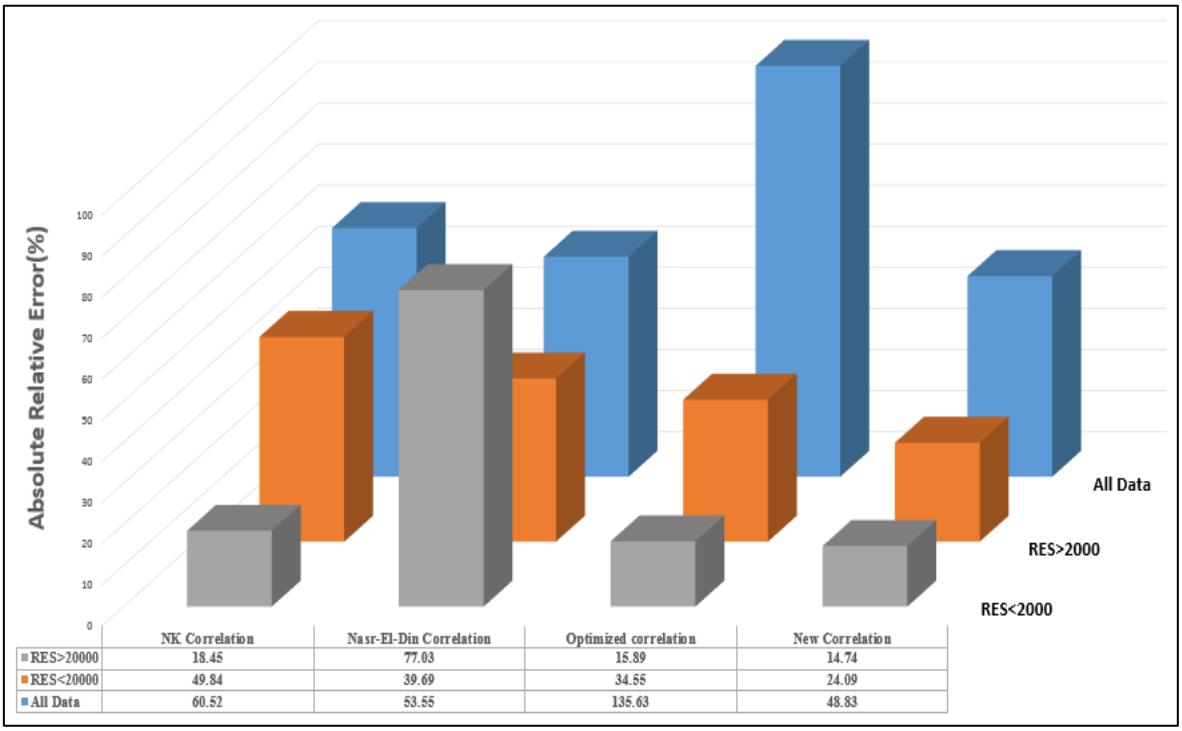

Figure 2: Average relative error of the predictive correlation

4 RESULTS AND DISCUSSION

The results show rock strength is a significant parameter to determine acid fracture conductivity. Predicted values of fracture conductivity by proposed correlations that are developed according to rock strength have good match with experimental results. Table 4 shows coefficients of optimized correlation for all input. As the results of this category was not good, new functions were used to present new correlations. Optimization algorithm were applied to find the best coefficients. Proposed correlation and their coefficients are tabulate in table 5. The correlation has 13 coefficients. Accuracy of predictive correlations to predict fracture conductivity based on all input data were compared in table 6. Although the precision of optimized correlation is very low, but the accuracy of new correlation is better than prior correlations (Nierode & Kruk and Nasr el din's correlations). Figure 3 illustrates the predicted values of conductivity by different correlations versus measured values. As shown, Nasr el din's correlation overestimates the values of conductivity. While optimized and new correlations underestimate theses values. The predicted values by Nierode & Kruk's correlation have the most deviation from experimental data

Table 4. Coefficients of optimized correlation for all input

Correlation	Coefficients
$WfK = \alpha \exp(-a_3 \beta \sigma_c)$ $\alpha = a_1 (DREC)^{a_2}$ $\beta = [a_3 - (a_4 \ln RES)] \times a_5$	a(1) 0.431 a(2) 0.742 a(3) 0.086 a(4) 0.300 a(5) 0.024 a(6) 0.547

The effect of rock strength were considered to provide a better understanding by using data of second and third categories. Table 7 shows coefficients of optimized correlation for rocks in which RES is less than 20000 Psi. The average relative error of the correlation is 34.55%. For this category new functions were used to improve accuracy of predictive correlation too.

Table 5. Proposed correlation and their coefficients to predict fracture conductivity based on all input data

Correlation	Coefficients			
$W_f K = a_1 \exp(a_2(\alpha) + (\beta)^{a13}$ $\alpha = a_3 (DREC)^{a4}$ $\beta = \gamma + \lambda$ $\gamma = a_5 + (a_6 RES) + a_7$	a(1)	0.27	a(8)	45
	a(2)	0.03	a(9)	-8
	a(3)	0.858	a(10)	0.235
	a(4)	0.268	a(11)	0.000376
	a(5)	0.854	a(12)	2
	a(6)	0.053	a(13)	-14
	a(7)	93		

Table 6. Accuracy of predictive correlations to predict fracture conductivity based on all input data

Correlation	Average Relative Error	Standard Deviation	R-Squared
NK	60.52	3.690	0.77
Nasr El Din	53.55	3.536	0.81
Optimized Correlation	135.63	3.889	0.62
New Correlation	48.83	4.10	0.72

Table 8 indicates proposed correlation and their coefficients. The correlation has 15 coefficients. The results show the new correlation is more precise compared to other correlations (Table 9). Comparison between the measured and predicted values of conductivity by predictive correlations has been depicted by figure 4

.

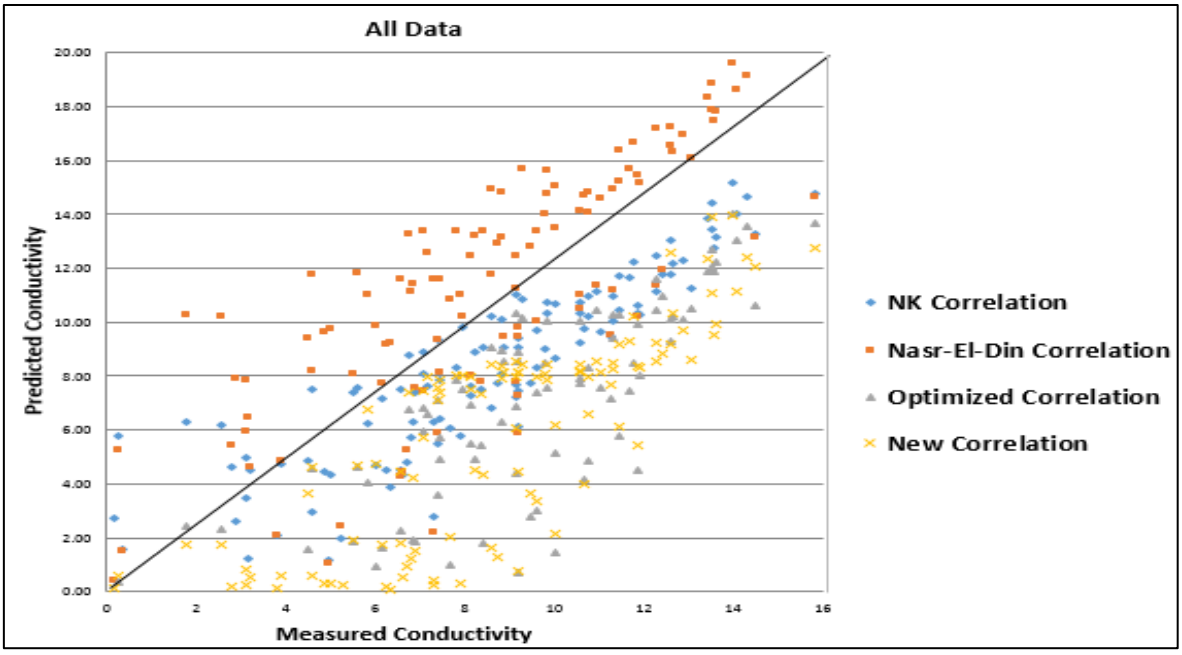

Figure 3. Comparison between the measured and predicted values of conductivity by predictive correlations for all input data

Table 10 shows coefficients of optimized correlation for rocks in which RES is higher than 20000 Psi. The average relative error of the correlation is 15.89%. Table 11 indicates proposed correlation and their coefficients. The correlation has 14 coefficients. Accuracy of predictive correlations to predict fracture conductivity for the category were compared in table 12. The Relative average error of new correlation is 14.74% that show there is a good match with experimental data. In these category, the values predicted by Nasr el din's correlation has a high error in comparison with other correlations.

Nierode & Kruk correlation but with the same parameters. Here the parameters never change. Table 9 illustrates the new correlation relative average error had shown the best result in compare with the main correlation and optimizing correlation of Nierode & Kruk with 24.09 percentages. Table 9 shows the relative average error, standard deviation and regression coefficient of different correlation that use for rock embedment lower 20000.

Table 7. Coefficients of optimized correlation for rock with RES<20000 Psi

Correlation	Coefficients	
	a(1)	100.00
$WfK = \alpha \exp(-a_3 \beta \sigma_c)$	a(2)	0.337
$\alpha = a_1 (DREC)^{a2}$	a(3)	0.91
$\beta = [a_4 - (a_5 \ln RES)] \times a_6$	a(4)	0.513
	a(5)	0.041
	a(6)	0.0135

Table 8. Proposed correlation and their coefficients to predict fracture conductivity for rocks with RES<20000 Psi

Correlation	Coefficients			
	a(1)	0.25031	a(9)	0.01
$W_f K = (a_1 * EXP(\alpha) * a_{14}) + a_{15}$	a(2)	0.4977	a(10)	-90
$\alpha = [\beta + (\lambda * \gamma * \omega)]^{a_{13}}$	a(3)	0.8778	a(11)	0.9524
$\beta = a_2 * [a_3 * (DREC)^{a_4}]$	a(4)	0.1509	a(12)	35
$\lambda = a_5 + [a_6 * (RES)^{a_7}]$				
$\gamma = (a_8 * (RES)^{a_9})^{a_{10}}$	a(5)	0.3926	a(13)	-2
$\omega = a_{11} * (E2)^{a_{12}}$	a(6)	0.344	a(14)	0.7998
	a(7)	-75	a(15)	0.0341
	a(8)	-24		

Table 9. Accuracy of predictive correlations to predict fracture conductivity for rock with RES<20000 Psi

Correlation	Relative average error	Standard deviation	R-Squared
NK	49.84	3.890	0.021
Nasr El Din	39.69	3.863	0.81
Optimized Correlation	34.55	3.691	0.68
New Correlation	24.09	3.481	0.84

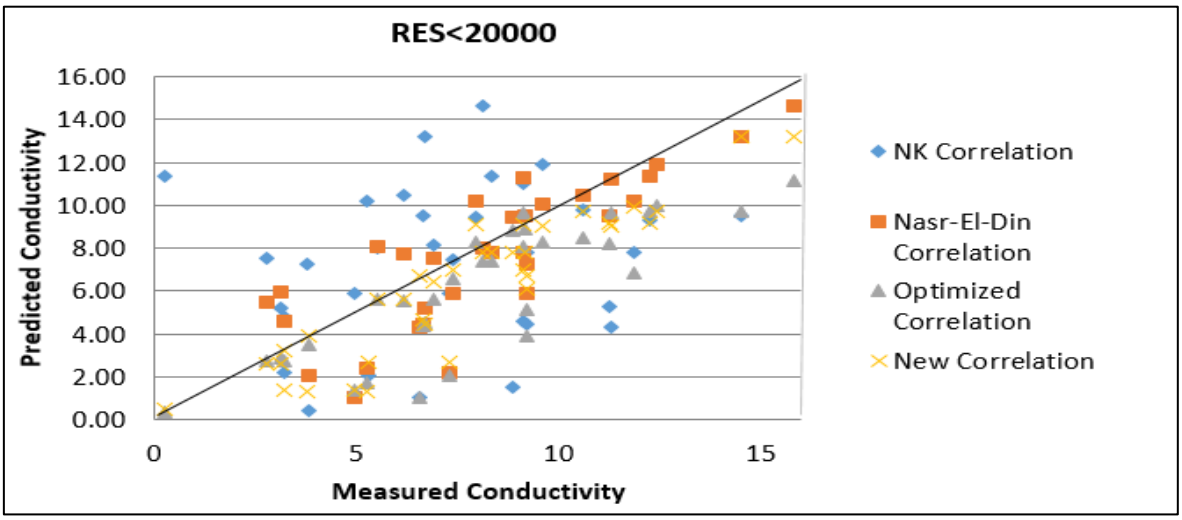

Figure 4. Comparison between the measured and predicted values of conductivity by predictive correlations for data with RES< 20000 psi.

Figure 5 illustrates the predicted values of conductivity by different correlations versus measured values. As shown, Nasr el din's correlation overestimates the values of conductivity. While optimized and new correlations underestimate theses values.

Table 10. Coefficients of optimized correlation for rock with RES>20000 Psi

Correlation	Coefficients	
$WfK = \alpha \exp(-a_3 \beta \sigma_c)$ $\alpha = a_1 (DREC)^{a_2}$ $\beta = [a_4 - (a_5 \ln RES)] \times a_6$	a(1)	0.0605
	a(2)	0.874
	a(3)	0.038751
	a(4)	-29
	a(5)	-4
	a(6)	0.0168

Table 11. Proposed correlation and their coefficients to predict fracture conductivity for rocks with RES>20000 Psi

Correlation	Coefficients			
$W_f K = a_1 * (a_2 * EXP(\alpha + (\beta * (\omega))) + a_{14}$ $\alpha = a_3 * [a_4 * (DREC)^{a_5}]$ $\beta = a_6 + [a_7 * (RES)^{a_8}] * [(a_9 * (RES) * a_{10})^{a_{11}}]$ $\omega = [a_{12} * (\sigma_c)^{a_{13}})]$	a(1)	0.413	a(8)	-52
	a(2)	5	a(9)	33
	a(3)	0.0306	a(10)	0.1478
	a(4)	74	a(11)	-4
	a(5)	0.0879	a(12)	0.752
	a(6)	0.9851	a(13)	0.9062
	a(7)	-40	a(14)	13

Table 12. Accuracy of predictive correlations to predict fracture conductivity for rock with RES>20000 Psi

Correlation	Relative average error	Standard deviation	R-Squared
NK	18.45	3.188	0.82
Nasr El Din	77.03	3.612	0.03
Optimized Correlation	15.89	3.318	0.89
New Correlation	14.74	3.143	0.88

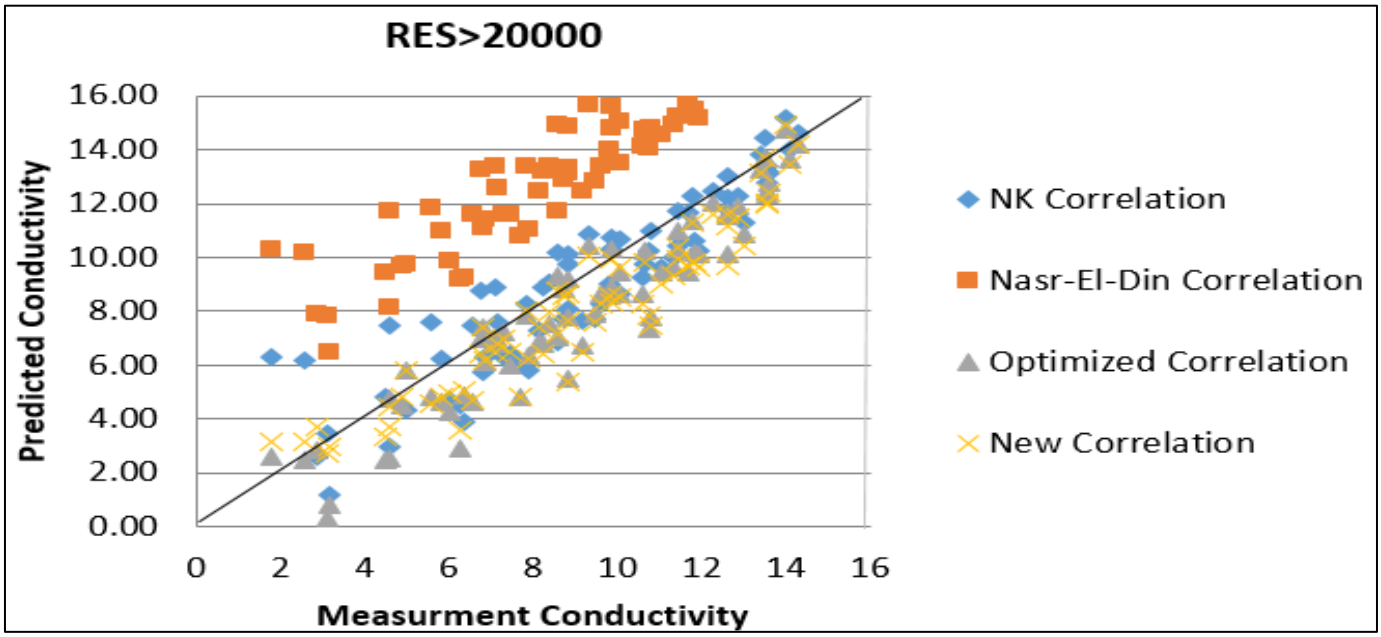

Figure 5. Comparison between the measured and predicted values of conductivity by predictive correlations for data with RES> 20000 psi.

5 CONCLUSION

1. GA is a powerful tool to precisely and rapidly predict acid fracture conductivity at different closure stresses as compared to prior well-known models. The fracture conductivity predicted by GA correlation closely matched experimental data.
2. Rock strength plays a significant role when anticipating fracture conductivity, as various formations have behaved differently under various closure stresses. Because it is not possible to present a universal precise model to predict acid fracture conductivity for all rock types, predictive models must be developed based on rock strength.
3. Although the optimized correlations show a good match with experiment data, new correlations are more precise than them. However, new correlations are more complicated. It reveal that the functionality of fracture conductivity is not necessarily exponentially.

Nomenclature

$DREC$	Dissolved rock equivalent conductivity
σ_c	Closure stress
m_i	measured data:
$\bar{m}$	mean of the measured data
n	Number of data
p_i	Predicted data
$\bar{p}$	mean of the predicted data
RES	Rock embedment strength
WK_f	Fracture conductivity

REFERENCES

Anderson, M.S., and Fredrickson, S.E. 1989. Dynamic Etching Tests Aid Fracture- Acidizing Treatment Design. *SPE Production Engineering* 4(4): 443-449. SPE-16452.

Beg, M.S., Kunak, A.O., Gong, M., Zhu, D., and Hill, A.D. 1998. A Systematic Experimental Study of Acid Fracture Conductivity. *SPEPF* 13(4): 267-271. SPE-52402.

California Council on Science and Technology Lawrence Berkeley National Laboratory Pacific Institute "Advanced Well Stimulation Technologies in California an independent Review of Scientific".

Coulter, A.W., Alderman, E.N., Cloud, J.E., and Crowe, C.W. 1974. Mathematical Model Simulates Actual Well Conditions in Fr acture Acidizing Treatment Design. Paper SPE-5004 presented at the SPE_AIME 49th Annual Fall Meeting, Houston, Texas,USA, 6-9 October 1974.

Gomaa, A.M., and Nasr-El-Din, H.A. 2009. Acid Fracturing: the Effect of Formation Strength on Fracture Conductivity. Paper SPE-119623 presented at the *2009 SPE Hydraulic Fracturing Technology Conference*, The Woodlands, Texas, USA, 19-21 January 2009.

Gong, M., Lacote, S., and Hill, A.D. 1999. New Model of Acid-Fracture Conductivity Based on Deformation of Surface Asperities. *SPEJ* 4(3): 206-214. SPE-57017.

Kosters W.A., Kok J.N. and Floreen P., Fourier analysis of Genetic Algorithms, *Theoretical Computer Science, Elsevier*, 229, 199, pp. 143-175.

Mou, J. 2009. Modeling Acid Transport and Non-Uniform Etching in a Stochastic Domain in Acid Fracturing. PhD dissertation. Texas A&M University, College Station.

Nasr-El-Din, H.A., Al-Driweesh, S.M., Metcalf, A.S., and Chesson, J.B. 2008. Fracture Acidizing: What Role Does Formation Softening Play in Production Response? *SPE Production & Operations* 23(2): 184-191. SPE-103344.

Nierode, D.E., and Kruk, K.F. 1973. An Evaluation of Acid Fluid Loss Additives, Retarded Acids, and Acidized Fracture Conductivity. *Paper SPE-4549 presented at the 48th Annual Fall Meeting of Society of Petroleum Engineering of AIME*, Las Vegas, Nevada, USA, 1973.

Özgür Yeniay Hacettepe University, Faculty of Science "Penalty Function Methods for Constrained Optimization with Genetic Algorithms "

Omid E. David, H. Jaap van den Herik, Moshe Koppel, and Nathan S. Netanyahu" Genetic Algorithms for Evolving Computer Chess Programs"

Pournik, M. 2008. Laboratory-Scale Fracture Conductivity Created by Acid Etching. PhD dissertation. Texas A&M University, College Station, Texas, USA.

Roberts, L.D., and Guin, J.A. 1975. The Effects of Surface Kinetics in Fracture Acidizing. *SPEJ* 8: 385-395. SPE-4349.

Ruffet, C.S., Fery, J.J., and Onaisi, A. 1997. Acid-Fracturing Treatment: A Surface- Topography Analysis of Acid-Etched Fractures to Determine Residual Conductivity. Paper SPE-38175 presented at the *SPE European Formation Damage Conference*, The Hague, The Netherlands, 2-3 June 1997.

Valdo F. Rodrigues, SPE, Wellington Campos, SPE, Ana C. R. Medeiros, SPE, North Fluminense State University; and Rodolfo A. Victor, Petrobras/RH/UP "Acid-Fracture Conductivity Correlations for a Specific Limestone Based on Surface Characterization"

Van Domselaar, H.R., Schols, R.S., and Visser, W. 1973. An Analysis of the Acidizing Process in Acid Fracturing. *SPEJ* 8: 239-250. SPE-3748.

Forecasting Crude Oil Price with an Artificial Neural Network model based on a Regular Pattern for Selecting of the Training and Testing Sets using Dynamic Command-Line Functions

M. H. Basiri, F. Javadnejad, and A. Saeedi
Department of Mining Engineering, Tarbiat Modares University, Tehran, Iran

ABSTRACT This paper presents a model based on a comprehensive regular pattern for selecting training and testing sets to forecast the crude oil price. The West Texas intermediate crude oil prices from 1994 to 2011 were selected for this study. The 80% of these data applied training and 20% for testing the model. Then a neural network model was designed using dynamic command-line functions to predict the monthly prices of crude oil. By examining a substantial number of tests, the influence of numbers of input neurons, the number of neurons in hidden layers, the transfer functions of layers, types of learning algorithms and a variety of fundamental economic variables (including changes in OPEC crude oil production and oil demand in industrialized countries, changes in world gold prices, changes in Dow Jones stock market index, and changes in the United States consumer price index) have been investigated. The results suggest a superior model includes two-layer back propagation network (N 8-8-1) with 2.21 in the root mean square error (RMSE), 85.71% in the directional symmetry of the model in determining the increasing or decreasing the prices and 91% in the coefficient of determination.

Keywords: West Texas Intermediate Crude Oil Price, Forecasting, Artificial Neural Network, Regular Pattern and Dynamic Command-Line Functions

1 INTRODUCTION

An uncertainty characteristic is an undesirable and inevitable property for investors in various markets including stock market and oil market. So naturally, all the investors endeavor to reduce uncertainty; hence market forecasting is one of the beneficial tools to slake the uncertainty.

Although the occurrence of the oil crises confronts the degree of reliability of these predictions with skepticism, a trustworthy prediction of world oil price can ease the process of buying and selling of oil in the world markets. It can determine the best time for performing transactions and investments.

As addressed in literature survey, there are myriad tools in forecasting discussions such as regression models, time series, and artificial intelligence approaches.

In this research we have focused on artificial neural network method based on regular pattern for selecting training and testing sets for designing a comprehensive forecasting model for West Texas Intermediates oil prices. Using dynamic command-line functions and examining a substantial number of tests, the most optimum model has been approached. In addition, we have investigated the influence of a variety of fundamental economic variables (including changes in OPEC crude oil production and oil demand in industrialized countries, changes in world gold prices, changes in Dow Jones stock market index, and changes in the United States consumer price index) on the model.

2 RELATED WORKS

Kaboudan has forecasted monthly price of crude oil by discussing the Artificial Neural Networks and compared the results with the random walk method. The data used in this study from June 1993 to December 1998 are the closure of market prices of crude oil exported to the United States. In the presented Neural Network model, it is trained using feed forward networks and only static error back propagation training algorithm. The network has one hidden layer

and the sigmoid function is used. MSE is considered as an error criterion to compare models. This researcher believe that over the time crude oil prices follow the cycle patterns which tend to greatly increase then reversed their direction and may rise again (Kaboudan, 2001). Moshiri and Foroutan to predict WTI crude oil price index suggested an artificial neural network model and compared with the results predicted by linear models and nonlinear ARMA GARCH. Results demonstrated that the neural network model has better predictive power than the ARMA model and GARCH (Moshiri et al, 2004).

Michael Ye et al have predicted short-term South Texas crude oil prices and have been reviewed the impact of market including inventory, production, imports and demand changes on monthly crude oil prices (Michael Ye et al., 2005). Zamani reviewed the performance of the international oil market in order to identify the variables required for modeling. The most important factors are the oil storage of OECD region and the affecting exchange rate of dollar. Data from the statistical viewpoint is reviewed and long-term relationships between WTI prices and other variables are estimated. Then auto regressive, error correction and auto regressive distribution models were used to predict and identify a model with minimum error (Zamani, 2005). Gori et al for examining the relationship between prices and oil consumption have studied three scenarios for oil prices. The result shows that the oil price time series is correlated with the oil consumption during 1980 to 1989. Oil prices increasing in 2003, reduced the consumption in the same year. (Gori at al., 2007).

Farjamnia et al, using two methods, ARIMA and artificial neural networks, predicted the daily world price of crude oil with 5 lags. the results show that ARIMA model is of superior to artificial neural network to predict the prices (Farjamnia et al., 2007). Bahradmehr using wavelet smoothing and artificial neural network predicted daily crude oil prices of New York and the Gulf of Mexico for 2000 to 2004. In this study, the smoothing property of wavelet transform is used to reduce noise levels and then oil prices are predicted by using the neural network and smoothed data. The results indicate that the noise reduction and data smoothing improve the performance of prediction (Bahradmehr, 2008).

Lin Yu et al have presented an empirical model decomposition (EMD) based on neural network for training trends in oil prices and predicting their future. Daily data for the modeling of oil prices from 1986 to 2007 is used. Initially, the data using transfer functions are pre-processed into limited values and then these data are trained using a feed forward three layers neural network model. This model on the West Texas and Brent oil market under using various transfer functions is used and then results of various scenarios using the neural network and ARIMA approaches have been compared based on direction symmetry criteria. The best results is obtained using empirical model decomposition in a feed forward neural network and linear transfer function with 86% accuracy in directional symmetry (Lin Yu et al., 2008).

Kullkarni and Haider in a study has forecasted the WTI crude oil price for the next three days, and concluded that a dynamic model with 13 delays to predict short-term expected crude oil spot price is suitable. Also the price prediction accuracy has been estimated 78%, 66% and 53% respectively for one, two and three days (Kullkarni at al., 2009). Azadeh used Nero-fuzzy hybrid approach to predict the price of oil annually. The amount of oil production, America's refinery capacity, oil consumption of Non-OECD the countries and excess capacity has been selected as affected indicators. Data of 1985 to 2002 for training and 2003 to 2007 to testing the model is used (Azadeh, 2011).

3 ARTIFICIAL NEURAL NETWORK

Artificial neural networks as one of the main component of computational intelligence have important properties. Learning, generalization and function approximation

ability and parallel structure are the most important properties of artificial neural networks. These properties caused their importance and application in science and engineering problems.

An artificial nerve is a model that its component directly similar to that of a real nerve. These processing elements are composed of two parts: the first part sum the weighted inputs and the second part is a linear or nonlinear smoothing called transfer function.

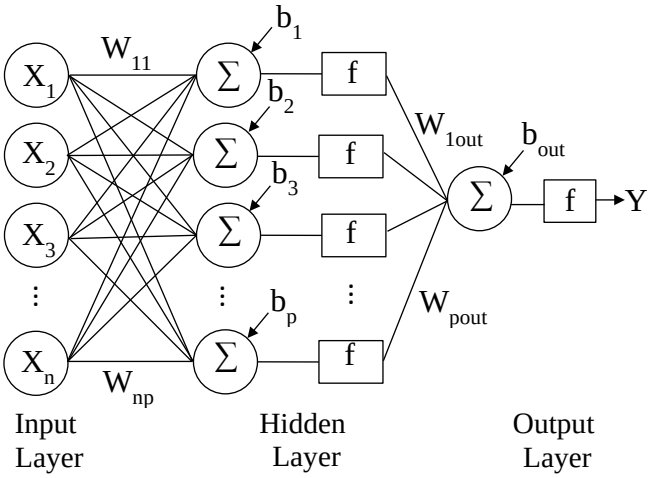

Figure 1: Mathematical model of a feed forward two layers artificial neural network.

Figure 1 shows mathematical model of a feed forward Multi-layer artificial neural network. In this model, n is the number of input layer's neurons, p is the number of hidden layer's neurons, X_1 to X_n are the input variables, W_{11} to W_{np} are neuron synaptic weights, b_1 to b_p are neuron biases, f is the neuron transfer function and Y is the output. Each input signal influenced by weights called synaptic weights. These weights can be positive or negative. W_{np} demonstrates the connection intense from nth unit to pth unit. By putting together of neural units, artificial neural networks is achieved. Obviously, by various combinations and how weights connected different types of neural networks are designed. Feed forward Multilayers networks usually called Multi-Layer Perceptron networks or MLP are considered as the most widely used type of neural networks.First in 1986 presented by Rumelhart and Mc. Holland, the algorithm of back propagation of errors is the most common learning algorithm. This algorithm is based on the error correction learning rule generalization of the least mean squares. In this method after calculating the network output, the result is compared with the desired output and the difference of them calculated. In back, the obtained error is propagated within the network and the network weights are modified so that the real answer is closer to the desired response.

Criteria	Functions
Adjusted R-Square	$\bar{R}^2 = \frac{(n-1)\sum(\hat{Y}_t - \bar{Y})^2}{(n-m)\sum(Y_t - \bar{Y})^2}$
Root Mean Square Error	$RMSE = \sqrt{\frac{\sum(Y_t - \hat{Y}_t)^2}{n}}$
Mean Absolute Error	$MAE = \frac{\sum\lvert Y_t - \hat{Y}_t\rvert}{n}$
Directional Symmetry	$DS = \frac{\sum_{i=1}^{n} di}{n} \times 100$, $di = \begin{cases} 1 & \text{if } (y_{i+1} - y_i)(\hat{y}_{i+1} - y_i) > 0 \\ 0 & \text{otherwise} \end{cases}$
Akaike Information Criterion	$AIC = \log\left(\frac{SSE}{n}\right) + \frac{2m^d}{n}$

4 EVALUATION OF NEURAL NETWORK MODEL

Different performance criteria can be considered for evaluation of a neural network model. Criteria used, depending on which issues of neural networks are in used. When using neural network to predict, the measure of prediction accuracy can be considered as the best measure for network performance. Some of these criteria are shown in Table 1. Where "Yt" is the target value, "Ŷt" is model output value, "n" is number of observations, "m" is the number of model parameters and "d" is a coefficient between 0.50 to 2.

Table 1: Some model performance evaluation criteria

5 DATA

The time series studied are data on the West Texas Intermediate crude oil prices from 1994 to October 2011. The data are on a monthly frequency and dollars per barrel. From total of 208 data categories, 80% of

which were selected for training data (of course 10% is assigned to the validation category) and 20% for testing the neural network model.

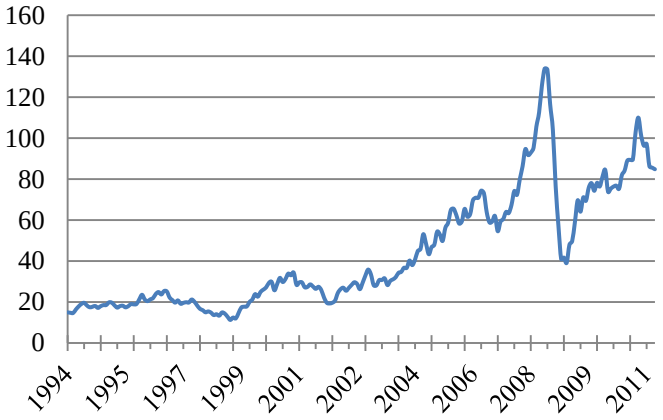

Figure 2: The time series of West Texas Intermediate crude oil prices from 1994 to 2011 -The vertical axis unite is dollars per barrel.

6 DESIGNING AN ANN MODEL BASED ON REGULAR PATTERN FOR SELECTING TRAINING AND TESTING SETS

In many researches on the field of predicting future time series, mostly the initial part of data is considered as the training set and terminal of which as the testing set. But choosing such sets make losing a large part of the data that is relevant to the terminal part of the course. This part of the data more than anything else is important and efficient to predict the future of a market because of closeness of which to the present time. In addition overlooking this part of data in such a turbulent time series of oil prices leads model to error in the test section. A model can represent a comprehensive model of a time-series data when it encompasses all parts of the model during training and testing process. In this research, testing and training sets are selected based on a regular pattern of 52 (208÷4) subsets with length 4 (proportion the training set to testing set). This regular set dividing pattern is provided the possibility of designing a superior artificial neural network model through comprehensive dynamic command-line functions.

Neural network model designing process and determining its parameters are implemented by series of trial and error process. So that a prototype model is made and then trying to change the parameters to get a better of which. During designing the model, performance criteria reflected the accuracy of the model is determined. Then by comparing these criteria together, the best model whit the best performance is chosen. For designing neural network model, delayed values of oil prices (P_{t-1}, P_{t-2}, …, P_{t-n}) and the fundamental economic variables (X_{t-1}, X_{t-2}, …, X_{t-n}, Z_{t-1}, Z_{t-2}, …, Z_{t-n}, …) are appointed as the network inputs and current prices are appointed as the outputs. Actually what the model learns is a function as follows:

$P= f (P_{t-1}, .., P_{t-n}, X_{t-1}, …, X_{t-n}, Z_{t-1}, …, Z_{t-n}, …)$

Through using the dynamic command-line functions, parameters of the model are adjustable and can be linked together. so the impact of adjusting these parameters can be investigated on the model evaluation criteria (These parameters are including the number of input neurons, the number of hidden layers and neurons of which, transfer functions, training algorithms, number of training cycles, learning rate and proportion of validation data.

In this section the process of designing the model is explained step by step. Dynamic command-line functions in MATLAB software is given at appendix.

6.1 Step 1: Definition of Input Data

Given to the research literature of oil market, the current prices are not dependent on delayed prices more than few months. The column of current Oil prices (the last column) along whit 9 columns of delayed values of which is imported into a 208×10 double workspace (named data). However after determining the optimal delayed lags, extra columns are replaced by 5 columns of past month changes of fundamental and economical parameters. Thus there are 208 data categories (observations). In command-line functions, Lag represents number of

delayed price values. This number, among 1 to 9 months, after many trials and adjustments of which, is set 3. Finally to show the input variables the columns of the extra delayed values is omitted and substituted by five columns of changes in fundamental and economic variables. As shown in table 2 we have 8 input versus 1 output.

In the command-line functions "Trainingpercentage" shows the percentage of data used as the training set. "Hiddenln" defines number of neurons of hidden layers. H1 is number of training sets, M1 is number of testing sets and L is the length of the regular pattern. Commands in lines 8 to 15 refer to designing a regular pattern to select the training and testing sets.

6.2 Step 2: Designing the Artificial Neural Network Model

After arranging the data into a regular pattern of training and testing sets, to designing an artificial neural network model we need to determine the input and target vectors in form of both training and testing sets. First "P" matrix involved the columns of input values (in table 2 the columns 1 to 8) and "T" matrix involved the column of target values (in table 2 the column 9) are arranged as training sets.

Next using similar fashion "a" matrix involved the input columns and "s" matrix involved the target column are arranged as testing sets. Other commands in this section are to define the parameters of the model (the parameters such as learning algorithm, Transfer functions, percentage of validation data set and other net training parameters.

6.3 Simulation and evaluation of model's performance

After designing the structure of network, it is time to simulate and evaluate the model. For this purpose, the network is simulated by training sets and evaluated by testing sets. Calculating almost all performance criteria, Evaluation of the model is carried out for both training and testing sets.

7 IMPROVING MODEL'S PERFORMANCE

To achieve the superior model, the structure of the model should be modified. The dynamic command-line functions provide the possibility to easily change different parts of the network structure. In the next section conducting trials and errors, network structure and parameters have been modified to improve performance.

7.1 Determination of Number of Delayed Lags

In oil turbulent market, price changes are so diverse that a significant correlation more than few months between the delayed values is not expected. In this study, using the performance criteria (especially RMSE) and trials and errors, the optimum month number for delayed values is determined three.

7.2 Determination of the Optimal Hidden Layers and Neurons

Rarely, using more than three hidden layers for prediction issues has the model shown performance improvement. In other words, more increasing number of layers, more overestimates network. To determine the optimal number of hidden layers and how many neurons in which, models in various scenarios for the numbers one to three hidden layer has been simulated. Performance criteria reflect the best scenario when the model has one hidden layer and eight neurons in that.

7.3 Determination of Optimum Transfer Functions

To determine the optimum transfer functions, using different transfer functions scenarios have been investigated. And which ones have the best performance are selected as the optimum transfer functions. the model demonstrates a better performance through using linear transfer functions in each layer. In Table 5 for instant T-P symbol used as the transfer function, illustrates hyperbolic tangent sigmoid transfer function in hidden

layer and liner transfer function in output layer.

Table 2: The influence of Delayed values on the performance of the model.

La. No	Train $\bar{R}^2_{Train}$	AIC	Test $\bar{R}^2_{Test}$	RMSE	MAE	DS
1	0.97	2.62	0.88	3.49	2.22	71.42
2	0.97	2.45	0.89	3.15	2.07	78.57
3	0.97	2.45	0.90	3.00	2.03	76.19
4	0.97	2.53	0.89	3.02	2.13	78.57
5	0.97	2.54	0.90	3.27	2.08	76.19
6	0.97	2.70	0.89	3.16	2.18	78.57
7	0.97	2.56	0.88	3.17	2.19	76.19
8	0.97	2.91	0.88	3.19	2.18	78.57
9	0.97	2.52	0.88	3.45	2.20	73.80

Table 3: Influence of number of hidden layers on the performance of the artificial neural network model.

Hidden layers No.	Train $\bar{R}^2_{Train}$	AIC	Test $\bar{R}^2_{Test}$	RMSE	MAE	DS
1 [5]	0.97	4.47	0.90	3.07	2.00	77.21
1 [10]	0.97	2.46	0.90	3.00	2.02	78.57
2[5 5]	0.97	2.45	0.90	3.20	2.07	78.57
2[1010]	0.97	4.46	0.89	3.14	2.03	78.57
2[5 10]	0.97	2.44	0.89	3.15	2.07	76.19
2[10 5]	0.97	2.45	0.88	3.20	2.07	73.80

Table 4: Influence of number of hidden layer neurons on the performance of the model

N. No	Train $\bar{R}^2_{Train}$	AIC	Test $\bar{R}^2_{Test}$	RMSE	MAE	DS
1	0.97	2.48	0.90	3.27	2.05	71.42
2	0.97	2.47	0.89	3.13	2.05	76.19
3	0.97	2.45	0.88	3.18	2.07	76.19
4	0.97	2.45	0.89	3.14	2.10	78.57
5	0.97	4.47	0.90	3.07	2.00	77.21
6	0.97	4.46	0.90	3.08	2.01	78.57
7	0.97	2.45	0.89	3.03	2.02	79.74
8	0.97	2.45	0.91	2.94	1.99	78.57
9	0.97	2.45	0.88	3.04	2.02	76.19
10	0.97	2.46	0.90	3.00	2.02	76.19

Table 5: The influence of transfer functions on the performance of the artificial neural network model. P symbol is linear transfer function, T is hyperbolic tangent sigmoid, L is log-sigmoid, S is saturating linear and R is radial basis.

Tr. Fu.	Train $\bar{R}^2_{Train}$	AIC	Test $\bar{R}^2_{Test}$	RMSE	MAE	DS
P-P	0.97	2.53	0.91	2.70	2.04	78.57
T-P	0.95	3.19	0.88	4.78	4.04	71.42
P-T	0.97	2.49	0.91	2.78	1.96	77.21
T-P	0.95	3.20	0.88	4.94	4.13	71.42
L-P	0.98	2.20	0.90	2.88	2.01	76.19
L-T	0.98	2.38	0.90	2.96	2.08	77.21
S-P	0.98	2.13	0.90	2.91	2.05	73.80
S-T	0.98	2.39	0.89	3.18	2.08	77.21
R-P	0.98	2.23	0.89	3.59	2.40	71.42

7.4 Study of Influence of the Learning Algorithms

Levenberg Marquardt (LM) learning algorithm is the common learning algorithm used in the all above models. This algorithm in scientific applications has high speed and performance. In forecasting issues besides presenting a better performance, LM is converged faster than other learning algorithms.

According to the results of Table 7, however, other learning algorithms are also used to train the model, LM shows the best performance.

Table 6: Symbols of learning algorithms.

Symbols	Descriptions
lm	Levenberg-Marquardt back propagation
bfg	BFGS quasi-Newton back propagation
br	Bayesian regularization
cgb	Powell-Beale conjugate gradient back propagation
cgf	letcher-Powell conjugate gradient back propagation
cgp	Polak-Ribiére conjugate gradient back propagation
gda	Gradient descent with adaptive learning rule back propagation
gdx	gradient descent with momentum and adaptive learning rule back propagation
oss	One step secant back propagation
rp	Resilient back propagation
scg	Scaled conjugate gradient back propagation

Table 7: The influence of using different training algorithms on the performance of the artificial neural network model.

L. A.	Train		Test			
	$\overline{R}^2_{Train}$	AIC	$\overline{R}^2_{Test}$	RMSE	MAE	DS
bfg	0.97	2.49	0.91	2.83	2.83	77.21
br	0.97	2.57	0.90	2.90	2.90	77.21
lm	0.97	2.53	0.91	2.70	2.70	78.57
cgb	0.97	2.51	0.91	2.75	2.75	76.19
cgf	0.97	2.55	0.91	2.75	2.75	76.19
cgp	0.97	2.56	0.91	2.74	2.74	78.57
gda	0.96	2.88	0.90	3.52	3.52	71.42
gdx	0.97	2.64	0.91	2.77	2.77	77.21
oss	0.97	2.48	0.92	2.77	2.77	77.21
rp	0.97	2.46	0.90	2.93	2.93	77.21
scg	0.97	2.57	0.92	2.75	2.75	76.19

7.5 The study of influence of economical and fundamental variables in the model

Factors affecting oil prices are out of financial markets and most related to current political issues in the oil producing countries and demand from major consumers such as China, Europe and the United States.

In this research on top of oil supply and demand, the influences of some key economic parameters on oil prices are examined. These parameters comprise of the oil production from OPEC, oil demand in industrialized countries (Organization for Economic Cooperation and Development member countries), the global price of gold, Dow Jons stock market index, consumer price index in the United States.

The changes in these parameters over one month ago have been added to the model. The results of adding these variables to the neural network model are shown in Table 8. The implementation of each parameter improves the network performance to forecast the prices. So that adding all of these parameters reduces the RMSE criterion to 2.21 and increase directional symmetry to 85.71 percent.

Table 8: Used input and target data for Training and Testing the artificial neural network model for forecasting crude oil price

Factors	Train`		Test			
	$\overline{R}^2_{Train}$	AIC	$\overline{R}^2_{Test}$	RMSE	MAE	DS
OPEC	0.97	3.05	0.94	2.66	2.02	80.95
OECD	0.97	3.05	0.91	2.68	2.10	83.33
Gold	0.97	3.02	0.91	2.63	1.97	83.33
DWI	0.97	3.03	0.96	2.57	2.00	80.95
CPI	0.98	2.70	0.92	2.64	2.04	83.33
all	0.98	3.63	0.91	2.21	1.17	85.71

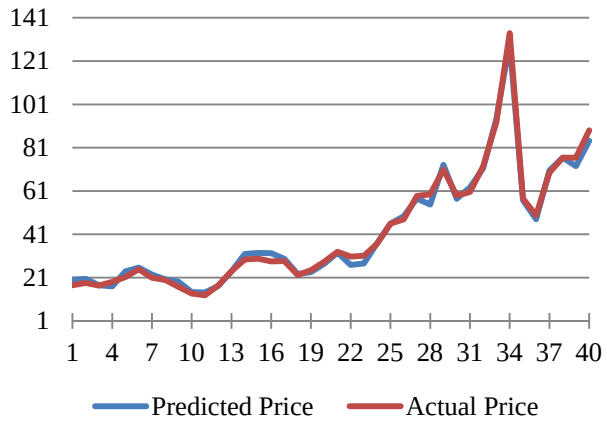

Figure 3: Comparing the predicted prices with actual values

8 PREDICTION RESULTS

Through a trials and errors process and doing plenty experiments, ultimately an optimal neural network model is presented to predict future short-term oil prices. This comprehensive model is a two-layer feed forward neural network ($N^{8\text{-}8\text{-}1}$). The structure of such a network is composed of 8 neurons in the first layer as the network's inputs (3 numbers of delayed values and 5 numbers of fundamental variables), 8 neurons in Hidden layer and 1 neuron in the last layer as a network's output. Transfer functions used in each layer are pure linear and training algorithm is Levenberg-Marquardt algorithm. This optimum model in the test section shows following results: Root mean square error (RMSE) equal to 2.21, directional symmetry in determining the increase or decrease of the prices is 85.71 percent and the adjusted-R^2 is 91 percent. In Figure 3 the predicted values are compared with actual prices.

9 CONCLUSION

In this study, the usual method of selecting the initial part of time series as training set and the terminal part as testing set in designing a model for forecasting of crude oil price has been criticized. Such set selecting in the training and testing of the models cannot provide a comprehensive model of a turbulent time series like oil market. If such models are used to predict future market, a large part data of terminal periods are excluded, while changes in these parts of data have an effective and significant role in determining the future market. Using a regular pattern for selecting training and testing sets ensures that the comprehensive proposed model includes data from all sectors of time series during the training and testing process.

In a turbulent crude oil market, the price changes are so diverse that are not expected more than few month correlations between the current prices and far delayed prices; so that in this model 3 lags are determined as the optimum and effective lags. Increasing the number of hidden layers and the neurons of which cause overestimate problems and increasing the errors of model. Using linear transfer functions, especially in the output layer, enhances the performance of the model. Among training algorithms used in the models, Levenberg-Marquardt has appropriate speed and, and converges faster than other algorithms and presents a better performance compared with other algorithms.

Adding monthly changes with one delayed in parameters included the OPEC's oil production, oil demand by industrialized countries (Organization for Economic Cooperation and Development member countries), the global price of gold, Dow Jons stock market index and consumer price index in the United States improves network performance to predict prices. So that when these parameters are implemented in the model the error criterion reduces to 2.21 and directional symmetry reaches to 85.71 percent.

REFERENCES

Bhrdad, Nafisa (1387), the crude oil price forecasting using wavelet smoothing, and artificial neural networks, Energy Economics Studies Quarterly, Year V, No. 18, pp. 98-81.

When, Mehrzad (1384), Modeling and forecasting crude oil prices for WTI, Energy Economics Studies Quarterly, Year II, No. 4, pp. 38-22.

A. Abbaspour, MR, (1381), Iran Khodro Company's stock price forecasting with neural networks, Master's thesis, Tarbiat Modarres University.

The Appeals believe Farr, N., M. and Ahmadi, Seyed Mohammad Mahdi (1386), Oil Price Forecasting with ARIMA and artificial neural networks, two methods, Iranian Economic Research Quarterly, Year IX, No. 32, pp. 183-161.

Moshiri, Saeed and humble, F., (1383), turbulence test and predict future oil prices, Quarterly Iranian Economic Research, No. 21, pp. 90-67.

Remember reading, Mohammad Bagher, (1379), Foundations of Neural Networks, AUT.

Azadeh, A., Moghadam, M., Khakzad, M., Ebrahimipour, V.,(2011), A flexible neural network-fuzzy mathematical programming algorithm for improvement of oil price estimation and forecasting, Computers & Industrial Journal.

BP Statistical Review of World Energy, (2011,June), Available online at: www.bp.com/statisticalreview, pp.6.

Emerson, S.A., (2006), When should we use strategic iol stocks?, Energy Policy, In Press.

Fieder Gori, David Ludovisi, Paulo. Cerritelli, (2007), Forecast of Oil Price and Consumption in the Short Term under Three Scenarios: Parabolic, Linear and Chaotic Behaviour, Energy, and Volume 32, pp. 491-501.

Kaboudan, M. A., (2001), "compumetric Forecasting of Crude Oil Prices", IEEE, pp.283-287.

Kastara, Iebeling and Boyd, Milton, (1996),"Designing a Neural network for forecasting financial and economic time series", Neurocomputing, 10 pp. 215-236.

Lean, Yu and Shouyang, Wang and Kin, Keung Lai, (2008)," Forecasting crude oil price with an EMD-based neural network ensemble learning paradigm", Energy Economics 2623–2635.

Micheal Ye, John Zyren, Joane Shore, (2005), A Monthly Crude Oil Spot Price Forecasting Model Using Relative Inventories, international Journal of Forecasting, Volume 21, Pages491-501.

APPENDIX

Step 1: Definition of input data

```
>> observations=209;
```

```
>>lag=8;
>> trainingpercentage=0.8;
>>Hidenl=8;
>> H1= fix(trainingpercentage*observations);
>>M1=observations-H1;
>>L=fix(H1/M1)+1;
>>datatraining(1:L , 1:lag+1)=data(1:L , 1:lag+1)
>>for i=1: fix(H1/L);
>>datatraining(i*L+1:i*L+4 , 1:lag+1)=
data(i*(L+1)+1:(i+1)*(L+1)-1 , 1:lag+1);
>>end
>>for i=1:M1-2;
>>datatesting(i:i,       1:lag+1)=data(i*(L+1):i*(L+1),
    1:lag+1);
>>end
```

Step 2- designing the artificial neural network model

```
>>P=datatraining(:, 1:lag);
>>T=datatraining(:, lag+1);
>>a=datatesting(:, 1:lag);
>>s=datatesting(:, lag+1);
PP= P'; TT= T'; aa= a'; ss= s';
>> net=newff(PP,TT,[ Hidenl], {'purelin',    'purelin',
    'purelin' },
'trainlm')
>>[trainInd,valInd,testInd]                          =
    dividerand(H1,0.90,0.1,0.0)
net.trainParam.epochs = 1000;
net.trainParam.goal = 0.01;
net.trainParam.show = 25;
net.trainParam.time = inf;
net.trainParam.min_grad = 1e-10;
net.trainParam.max_fail = 10;
net.trainParam.sigma = 5.0e-5;
net.trainParam.lambda = 5.0e-7;
net.trainParam.lr = 0.001;
>> net=train(net,PP,TT);
```

Step 3- simulation and evaluation of model's performance

```
>> Z2=sim(net,PP);
>> e2=Z2';
>> [e2 T];
>> s1=[e2-mean(T)].^2;
>> s2=[T-mean(T)].^2;
>> s3=[T-e2].^2;
>> R2train=1-(sum(s3)/sum(s2))
>>   R2TrainAdjusted=1-((1-   R2train)*(H1-1)/(H1-
    (lag+2)-1))
>> MSEtrain=mean(s3)
>> SSEtrain=sum(s3)
>> AIC1=log(SSEtrain /H1)+2*((lag+1).^2)/H1
>>                                  AIC2=log(SSEtrain
    /H1)+2*log(Hidenl*(lag+1))/H1
>> BIC= log(SSEtrain /H1)+(lag.^2)*log(H1)/ H1
>> y=sim(net,aa);
>> t=y';
>> [t s];
>> d1=[s-t].^2;
>> b1=[t-mean(s)].^2;
>> b2=[s-mean(s)].^2;
>> d2=[abs(s-t)];
>> R2test= (sum(b1)/sum(b2))
>>R2testAdjusted=1-((1-R2test)*
((observations-H1)-  1)/((observations-H1)-  (lag+2)-
    1))
>> MSEtest=mean(d1)
>> SSEtest=sum(d1)
>> MAEtest=mean(d2)
>> RMSEtest=sqrt(MSEtest)
```

```
>> MAPEtest=mean(d2./s)*100
>> MdAPEtest=median(d2./s)*100
>> ncorrectTest=0;
>> for i=1:(observations-H1-3)
>> if (s(i+1)-s(i))*(t(i+1)-t(i))>=0
ncorrectTest=ncorrectTest+1;
>>end
>>end
>> DSTest=ncorrectTest*100/(observations-H1)
```

Date	Input								Target
	price (-1) (USD)	price (-2) (USD)	price (-3) (USD)	CPI (%)	DWI (%)	Gold (%)	OECD Co. (%)	OPEC Pr. (%)	Price (USD)
1994M05	16.38	14.66	14.78	0.07	2.08	0.91	-3.67	0.49	17.88
1994M06	17.88	16.38	14.66	0.34	-3.55	1.15	4.77	0.49	19.07
1994M07	19.07	17.88	16.38	0.27	3.85	-0.07	-1.35	-0.55	19.65
.	.	.	.	.	.	.	.	.	.
.	.	.	.	.	.	.	.	.	.
.	.	.	.	.	.	.	.	.	.
2010M08	76.37	75.35	73.84	0.14	-4.31	1.46	0.53	0.47	76.82
2010M09	76.82	76.37	75.35	0.06	7.72	4.78	1.50	0.45	75.31
2010M10	75.31	76.82	76.37	0.12	3.06	5.64	-2.99	-1.37	81.90
2010M11	81.90	75.31	76.82	0.04	-1.01	2.13	2.23	0.98	84.14
2010M12	84.14	81.90	75.31	0.17	5.19	1.58	1.96	0.12	89.04
2011M01	89.04	84.14	81.90	0.48	2.72	-2.37	-4.44	1.87	89.42
2011M02	89.42	89.04	84.14	0.49	2.81	0.80	2.66	-1.36	89.58
2011M03	89.58	89.42	89.04	0.98	0.76	3.76	-1.11	-4.29	102.94
2011M04	102.94	89.58	89.42	0.64	3.98	3.63	-4.44	0.68	110.04
2011M05	110.04	102.94	89.58	0.47	-1.88	2.56	-0.88	0.40	101.33
2011M06	101.33	110.04	102.94	-0.11	-1.24	1.07	4.08	1.99	96.29
2011M07	96.29	101.33	110.04	0.09	-2.18	2.63	-0.94	0.65	97.19
2011M08	97.19	96.29	101.33	0.28	-4.36	12.18	0.48	0.26	86.33
2011M09	86.33	97.19	96.29	0.15	-6.03	1.20	-0.24	-0.13	85.61
2011M10	85.61	86.33	97.19	-0.21	9.54	-6.33	0.12	0.06	84.83

Impact the Parameter Effect of Vibration on Collision Efficiency in Flotation

K. Dedelyanova
Scientific and technical union of mining, geology and metallurgy, Sofia, Bulgaria

J. Dimitrov
University of Mining and Geology, Sofia, Bulgaria

ABSTRACT The paper presents research of mechanism for the creation of air bubbles in vibratory column flotation machine. Discussed the factors influencing increasing the duration of the bubble in the area of contact with the mineral particles.

Formulas are derived for the parameter effect of vibrations, applicable to the design of flotation machine. The collision efficiency of the bubbles in vibratory column flotation machine is determined.

Keywords: Collision efficiency, vibratory column flotation machine

1 INTRODUCTION

The increase of air bubbles flotation activity is connected with the increasing of the time of their conditioning, i.e. the interval between the formation moment and the bubble mineralization. In consequence of the column considerable height the sojourn duration of the air bubbles in it is not longer than 20 sec, i.e. a mineralization process at optimal flotation activity of the bubbles is realized (Rubinschayn, 1989).

In column apparatus under low turbulence probability of attachment and retention of large particles to the bubble is greater because under certain conditions, the use of column flotation machine can be useful for flotation of coarse material (Foot, 1986).

Dedelyanova & Metodiev (Dedelyanova & Metodiev, 2002) are presented a laboratory model of vibratory column flotation machine constructed in the Laboratory of "Vibro-acoustic Intensification of the Technological Processes" at the department of "Mineral Technologies" of the University of Mining and Geology, "St. Ivan Rilsky". It is realized on a modular principle, which provides a possibility for determination of optimal height the feeding device, infinitely – variable regulation of the pulp level and precise determination of the necessary quantity of extra water for the froth layer irrigation. The vibratory column flotation machine basic elements are sensor, vibrator, air disperser, module for creation of single gas bubbles, feeding device, machine chamber (Figure 1).

Figure 1. Photo of laboratory column flotation machine

2 EXPERIMENTAL RESEARCHES

In (Dedelyanova, 2004) is presented the study on the influence of frequency and amplitude of vibrations on the rate of sedimentation of mineral grains with different density. It is known that with the increase of the intensity of

fluctuation the rate of sedimentation decreases. However, the issue what is the influence of this effect on the diameter and the relative weight of the particles still remains open. For this purpose, a series of experiments has been carried out, during which single mineral grains with a diameter of 0.09 to 0.155 mm and density of the different grains of 2.65, 5.1 and 7.6 g/cm^3 have been used. The frequency of fluctuation changes from 20 to 70 Hz and the amplitude – from 1.5 to 3.0 mm. The average results from the tests are presented in Figure 2.

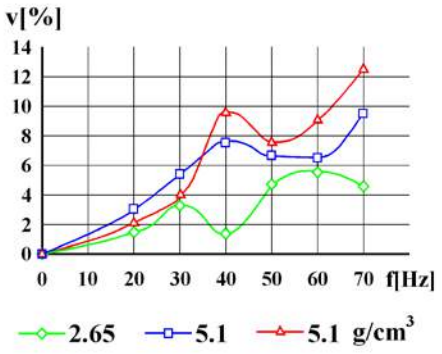

Figure 2. Reduce the speed of sedimentation depending on the vibration frequency and density of particles

In (Dedelyanova, 2004) are presented the results from the tests with vibratory column flotation machine with copper raw material (cake, taken from a control thickener). The experiments were carried out in laboratory conditions – columns flotation machine with height of 2000mm and diameter of 50 mm under vibration impact with values of Af^2 1500, 1800, 2250, 2450, 3200, 3675 and respective vibration frequency from 25 Hz to 40 Hz and amplitudes of 2.0 mm, 2.5 mm, 3.0 mm. The air dispersion is done via vibratory dispersing agent constructed for vertical vibrations. Parallel to the creation of bubbles the vertical fluctuations create vibro-acoustic field which is distributed along the height of the chamber in the flotation machine.

With values of the vibration impact Af^2 3200 ($f = 40Hz$, $A = 2.0mm$) the copper content in the concentrate reaches up to 32.23%, with copper content in the exit sample 22.76%. The copper content in the concentrate with the vibration impact increases with 3%, up to 12%. When tracking the results it was found that at value of the vibration impact of $Af^2 = 3675$ ($f = 35Hz$, $A = 3.0mm$) and content of the solid substance in the pulp 3.8%, whose value is the highest for the series of flotation experiments, the extraction is the highest – 90.68%. This coincides with the highest value of the copper content in the concentrate – 31.44%. Via this dispersion of the gas phase, the copper content in the concentrate increases with 3-3.5%, with initial content of the copper ranging from 23.31% to 27.89%.

3 IMPACT THE EFFECT OF VIBRATION ON BASIC PARAMETERS

3.1 Changing the Size of Bubble

The law of harmonious movement of the liquid is $z = A\sin(\omega t)$, where z is the vertical displacement; A - the amplitude of the harmonic movement; $\omega = 2\pi f$ and f is the frequency of vibration; t - is during the process. The speed of the fluid is determined by the relationship $v_l = A\omega\cos(\omega t)$. As a result of vibrations an affiliated part of the liquid near the bubble is subjected to harmonic effects and it causes change of the pressure p. Assume that the process of fluctuation in the volume

$$V = \frac{\pi d^3}{6} \qquad (1)$$

of the bubble is isotherm $pV = const$. In a state without of vibration on a certain level h from the surface of the liquid, the pressure in the bubble is $p_1 = p_0 + \rho_l hg$, where p_0 - atmospheric pressure; p - pressure in the bubble; ρ_l - density of liquid and g - acceleration of gravity. To this is added pressure p_2 fluctuating pressure caused by the harmonious impact on the associated mass of liquid

$$p_2 = k\rho_l \frac{\partial v_l}{\partial t} = k\rho_l A\omega^2 \sin\omega t. \qquad (2)$$

where $k << 1$ is a coefficient representing the participation of associated mass at vibrating bubble

Due to the relatively small amount of p_1 and symmetry its sign labeled with ε, does not matter. Total, the pressure in the bubble on level h is

$$p = p_0 + \rho_l hg + \rho_l kA\omega^2 \sin\omega t = \\ = p_1 + qAf^2 \sin\omega t, \quad (3)$$

where $q = 4\pi^2 k\rho_l$. By comparing the states of the bubble on level h and near surface and we obtain from the law for isothermic process

$$p_0 \frac{\pi d_b^{\,3}}{6} = p \frac{\pi d_0^{\,3}}{6}, \quad (4)$$

where d_b the diameter of the bubble; d_0 - the diameter of the bubble on the surface. Therefore

$$d_b = d_0 \sqrt[3]{\frac{p_0}{p_1 + qAf^2 \sin\omega t}} \quad (5)$$

From equation (3) can be inferred about the impact of effect of vibrations Af^2 on variation changing on the size of bubble in the process of emergence.

3.2 Determination of the Contact Angle

According to Bogdanov (Bogdanov, 1990) forces acting on the bubble and attached to him particle, accounted on the vertical axis are two types - forces acting on the particle and forces caused from the attachment of particle to the bubble. The first type forces are gravity of particle and ejection Archimedean force, as follows: gravity $P = -\pi d_p^{\,3} \rho_p g / 6$, where d_p is aligned particle diameter, ρ_p is the density of the particle and g is the gravity acceleration; ejection Archimedean force $F_A = \pi d_p^{\,3} \rho_l g / 6$, where ρ_l is the density of the fluid displaced by the particle. The second type of forces are the Laplace force F_L and capillary force F_K: Laplace pressure force that is acting on the upper wall of the particle is $F_L = -\pi d_p^{\,2} \Delta p / 4$ where $\Delta p = p_g - p_l$ is the Laplace pressure, p_g and p_l are respectively pressure in the gas and pressure in the liquid on the level of contact; capillary force $F_K = \pi d_p \sigma \sin\theta$, where σ is the surface tension recorded per unit length of contour of tangent wall of the particle and θ is the angle between the tangent wall of the particle and the surface of the bubble. As result receives equilibrium equation of bubble and attached to him particle

$$P + F_A + F_L + F_K = \frac{\pi d_p^3 \rho_p a_l}{6}, \quad (6)$$

where $a_l = A\omega^2 \sin\omega t = 4\pi^2 Af^2 \sin\omega t$ is the acceleration of the liquid, due to the harmonious movement. To determine the angle θ the equilibrium equation is expressed in the form

$$\sin\theta = \frac{d_p^2 g(\rho_p - \rho_l)}{6\sigma} + \frac{d_p \Delta p}{4\sigma} + \frac{2\pi^2 d_p^2 \rho_p Af^2 \sin\omega t}{3\sigma}. \quad (7)$$

3.3 Changing the Form Constant of Bubble

The ratio of the hydrostatic pressure on the contact side of the particle to the Laplace pressure are defined as form constant to the bubble near the particle

$$\beta = \frac{\rho_l g d_b}{\Delta p} = \frac{\rho_l g d_b^2}{4\sigma} = \frac{\rho_l g d_0^2 \left(\frac{p_0}{p_0 + 4\pi^2 qAf^2 \sin\omega t} \right)^{\frac{2}{3}}}{4\sigma}. \quad (8)$$

From the expression (8) follows that the size of the constant harmonic variation β is function of effect of vibration Af^2.

4 IMPACT THE EFFECT OF VIBRATION ON COLLISION EFFICIENCY

For obtaining an integrated evaluation of the flotation machine efficiency introduces the concepts of collision efficiency

$$E = \frac{M_0}{M}, \quad (9)$$

where M_0 is the mass of particles that meet with bubbles and M mass of all particles which are located in the level of contact at a point in time t. In (Ralston, 1999) is regarded the parameter k (called flotation rate constant) as proportional to the defined there parameter collision efficiency E. In

(Rubinschayn, 1989) the parameter E is called coefficient of grip.

4.1 Some Known Models

In (Rubinschayn, 1989) are presented multiple formulas determining the number of collisions N and collision efficiency E, divided in two groups – a relatively small group - formulas derived by accepting the model of turbulent motion of bubbles and particles; - formulas derived by analyzing the deterministic description of the bubbles and particles movement, processes of interaction and relevant forces governing these processes.

According to Derjaguin (Derjaguin et all 1960) around the bubble can define three zones:

- Zone 1 – most outside part – of hydro-static interaction;
- Zone 2 (of attachment) – area of effect of surfaces;
- Zone 3 – of stability efficiency of the bubble – particle aggregate

In order to make an analysis of the process of collision we assume that the bubble is spherical and around it we go over a rotational body with vertical axis passing through the center of the sphere. We denote with d_b the diameter of the bubble, d_p - diameter of the particles and a - diameter of

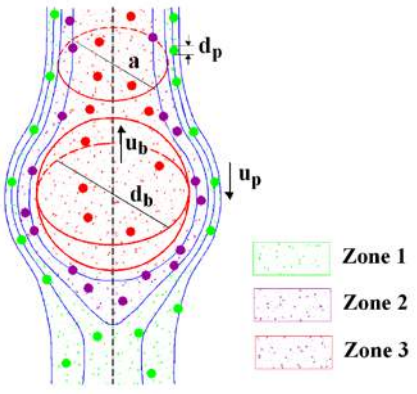

Figure 3. Scheme of collision of the particles with the bubble

the section of the cylindrical area including zones 1 and 2 prior to the level of collision (Figure 3).

In accordance with the areas of interaction in the aggregate bubble - particle (zone 1 and zone 2) the effectiveness of a collision can be represented by $E = E_{il} + E_{vl}$ where E_{il} is efficiency of laminar (gravitation) flow (ideal liquid) and E_{vl} - efficiency of viscous flow (viscous liquid). Taking into account the formulas presented in (Rubinschayn 1989). and (Bogdanov, 1990). with some approximations can accept the formulas

$$E_{il} = \frac{G}{1+G}\left(1+3\frac{d_p}{d_b}\right) \text{ and } E_{vl} = \frac{3}{2}\left(\frac{d_p}{d_b}\right)^2 f, \quad (10)$$

where $G = \frac{u_p}{u_b}$, $f \in [0.1,1]$.

Of the ways of expressing the effectiveness of conflict we can conclude that from the vibrational motion of bubbles and particles affect the effectiveness of a collision. The impact is both through variable diameters of the bubbles and by the rate of ascent of the bubbles. Given that the collision efficiency is a dimensionless quotient of ratio of the mass of the particle meeting the bubble and whole mass of flotation material, it is clear that we can not directly use formulas presented in the literature in the case of column vibration flotation machine.

4.2 Effectiveness of a Collision at Vibration Impact

To determine the increasing of effectiveness of collision in the presence of vibration will use another approach. Consider the model given by Bogdanov (Bogdanov, 1990) and will supplement it with vibrational defor-mations of the bubble. We will use and results of experimental studies of Dedelyanova (Dedelyanova, 2004).

For an analysis of the collision process we accept a bubble for sphere and and we consider a rotating body around a vertical axis, that passing through the center of the sphere. We denote by d_b is aligned bubble diameter, d_p is aligned particle diameter, and a - diameter of the cylindrical areas include zones 1 and 2 before the level of collision.

The cross section of the cylindrical region in diameter a is $S_0 = \pi a^2/4$ and at the level of collision $S_b = \pi\left(d_b + d_p\right)^2/4$. Produced for the effectiveness of conflict

$$E = \frac{S_0}{S_b} = \left(\frac{a}{d_b + d_p}\right)^2 . \quad (11)$$

According presented in Figure 3, the parameter E is ratio from the section of the straight part of the area, including areas 1 and 2 to section at the center of the bubble. Because the bubble vibrates with sound frequency f, then the mean diameter d_b is the same as without vibration. While performing a harmonic cycle of bubble volume remains the transition from sphere in rotating ellipsoid. When the bubble diameter is $d_b = 4\ mm$ and amplitude $A = 0.7\ mm$ extremes on the vertical axis of the ellipsoid are $z_{\min} = 3.3\ mm$, $z_{\max} = 4.7\ mm$ with horizontal axes, respectively $x_{\max} = y_{\max} = 4.4\ mm$ and $x_{\min} = y_{\min} = 3.69\ mm$. Due to the high velocity of the bubble oscillation at a given frequency f parameter a on Figure 5 reaches the diameter of the bubble d_b. This is confirmed by Figure 3 at value of effect of vibrations $Af^2 = 3750\ mm \cdot Hz^2$.

5 CONCLUSIONS

Experimental researches involved the conclusion that vibrating media provided additional force of resistance, applied ad to the mineral particle, which provoked decrease of the speed of falling down. This force is a function not only of the intensity of the vibrations of a complex variable vibration, but also is a function of frequency of vibration.

From the analytical study of the collision efficiency are confirmed experimentally proven facts. Enables to increase the residence time of the bubble in the zone of contact with the mineral particles. The vibrations of the hydrated layer allow for cost-effective implementation of the elementary act of flotation by providing larger relative velocities at a meeting of the bubble with the solid phase.

REFERENCES

Abramov (1984). *Flotation enrichment methods*, Moscow, Nedra

Bogdanov, O. (1990). *Theory and technology of flotation*, Moscow, Nedra

Dedelyanova Kr., M. Metodiev, (2002). Vibratory column flotation machine – vibratory – acoustic and technological researches, *Annual of UMG*, Sofia,

Dedelyanova, Kr. (2004). *Vibro-acoustic investigations in column flotation machine with vibratory air disperser* (Doctoral dissertation), University of Mining and Geology, Sofia, Bulgaria.

Derjaguin, B.V. and Dukhin, S.S. (1960). *Transactions of the Institute of Mining and Metallurgy* 70, (1960-1), p. 221

Foot, D.G., Mc. Kay, D. J., Hniatt, J.L., (1986). Column flotation of chromite and fluorite ores, *Canad. Metall Quart*, V. 25, N1, 15-21

Rubinschayn J. (1989). *Penn separation and column flotation*, Moscow, Nedra

Solvent Extraction of Palladium from Chloride Media by TBP

N. Sadeghi, E. K. Alamdari
Department of Mining and Metallurgical Engineering, Amirkabir University of Technology (Tehran Polytechnic), Tehran, Iran

N. Sadeghi
Materials Engineering Faculty, Sahand University of Technology, Tabriz, Iran

E. K. Alamdari
Research Center for Materials and Mining Industries Technology, Amirkabir University ıof Technology, Tehran, Iran

ABSTRACT In recent years, precious metals production through hydrometallurgical process has been attended; however the Low grade of metals is one of the main problems. Thus, solvent extraction method was purposed for concentration and purification of aqueous solution. In this study, Tri butyl phosphate (TBP) was used to $PdCl_3$ low concentrations of TBP could extract Pd chloride ions. The Solution containing 180 mg/l Pd was extracted by 0.05-0.25 M TBP in different HCl concentration. Increasing HCl concentration decreases Pd extraction percentage. It seems that different chloride complexes formations cause the extraction percentage to change in various HCl concentrations. The extracted macromolecule is determined $PdCl_3^-$.TBP.xH_2O. HNO_3 and NaCl has negative effect on Pd extraction.

Keywords: Solvent extraction, Palladium, TBP, Chloride media

1 INTRODUCTION

In recent years, consumption of palladium has grown; in addition, this has extensive use in jewellery, dentistry, electrical contacts, corrosion resistant apparatus, and biomedical devices. Thus there has been a renewed interest in studying new approaches for the recovery of this metal from raw and secondary resources.

As we know, PGM (Platinum Group Metals) resources are restricted. For metal recovery, palladium sources (primary or secondary) were leached in aqueous solution. But Pd concentration, basically, is low and the impurities (such as Fe, Cu, Ni, PGM and etc.) are dissolved. Concentration and purification of pregnant solution have been done in various methods. Solid/liquid (carbon active and ion exchange resin) and liquid/liquid methods were proposed for Pd ionic species transferring. Among them, solvent extraction of Pd has been applied in many cases to extract palladium from aqueous hydrochloric acid solutions (Rane and Gopal, 2006, Rovira et al., 1999, Bendekar and Dhadke, 1998).

Oximes (Shen and Xue, 2007), phosphoric acids (Bendekar and Dhadke, 1998), phosphonic acid (Bendekar and dhadke, 1998) and thiophosphinic acid (Kakio and Goto, 1994) are the popular Pd extractants from chloride media.

In the present work, extraction mechanism of palladium from chloride solutions by TBP is evaluated as well as the effect of pertinent parameters, namely as HCl, NaCl and TBP concentrations, on the extraction process that are identified. “Slope analysis” method is employed to clarify extraction mechanism of palladium with TBP diluted in kerosene.

2 MATERIAL AND METHODS

Commercial tri-n-butyl phosphate (TBP Fluka) as extractant and kerosene (Isfahan Refinery Co) as diluents were utilized. Hydrochloric acid (35%-37%vol) was

obtained from Dr. Mojallali chemical laboratories in Iran. Also, palladium ions were prepared by the standard metal chloride (PdCl, MERCK). Initially, kerosene was purified being washed by 3M HC1 solution then diluted with TBP. Palladium chloride was diluted by HCl and distilled water in different ratios. Batch experiments were carried out in a flask containing equal volumes (20 ml) of aqueous and organic solutions. The mixture was agitated at constant temperature (20 C) by a mechanical shaker at 400 rpm. Agitation was carried out for 30 min to assure equilibrium conditions then agitated samples were poured in a separating funnel for 15 min to allow complete separation of the two phases. The metal content of the aqueous phase was determined by atomic absorption spectroscopy (varian, A240) and chemical composition of the organic phase was determined by mass balance calculations.

3 RESULTS AND DISCUSSION

3.1 Effect of HCl Concentration

Figure 1 illustrates the influence of HC1concentration on palladium extraction by TBP diluted in kerosene. As shown, extractant concentration increased Pd extraction percentage but an increase in hydrochloric acid concentration leads to lower extraction percentage.

Keshavarz Alamdari and Darvishi and Haghshenas and Yousefi and Sadrnezhaad, (2011), shows that the mechanism of metallic complexes extraction by TBP involves an ion association process in which the protonation of TBP molecules by H (H_3O^+), brings the extraction ability for TBP to extract anionic species. But in this case, increasing acid concentration (or pH decreasing) leads to negative effect on Pd extraction. It seems that presence of acidic ions (H^+ or Cl^-) in solution reduces Pd extraction.

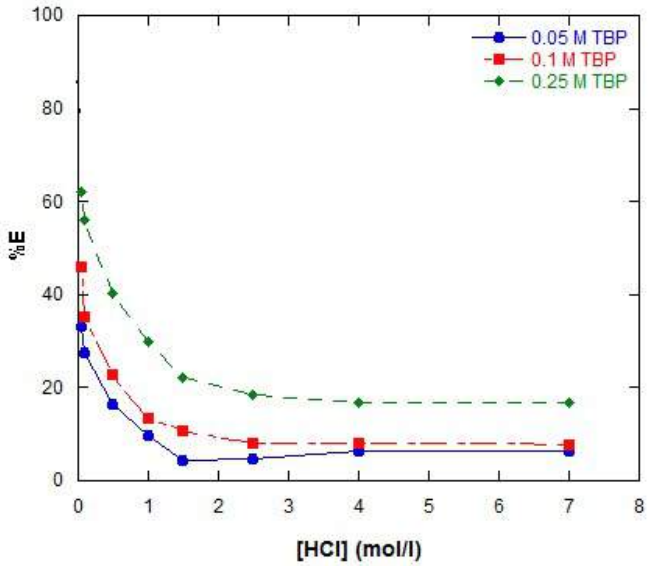

Figure 1. The influence of HCl and TBP concentrations on palladium extraction percentage.

3.2 Effect of Chloride Salts on Pd Extraction

For a closer look at the anionic chloride complexes formation, the chloride salt (NaCl) was added to solution at constant acid concentration. Increasing charged components in aqueous media may change chloride complex species and metal extraction percentage.

Fig 2 shows the results obtained from experiments carried out with organic solutions of 0.25 M TBP in kerosene and aqueous solutions which contained 0.1 M HCl and various concentrations of NaCl. It can be seen that the palladium efficiency decreases with an increasing NaCl concentration. By integrating the results of Figs 1 and 2 can be concluded that chloride ions have significant on palladium complexes formation.

3.3 Stability of Palladium Chloride Complexes in Aqueous Media

Reliable thermodynamic data on Pd-Cl system make it possible to predict palladium complexes stability. In aqueous solutions containing the Cl^- ion, Pd chloride forms complexes of the composition $[PdCl_n]^{2-n}$ (Polotnyanko and Khodakovskii, 2014).

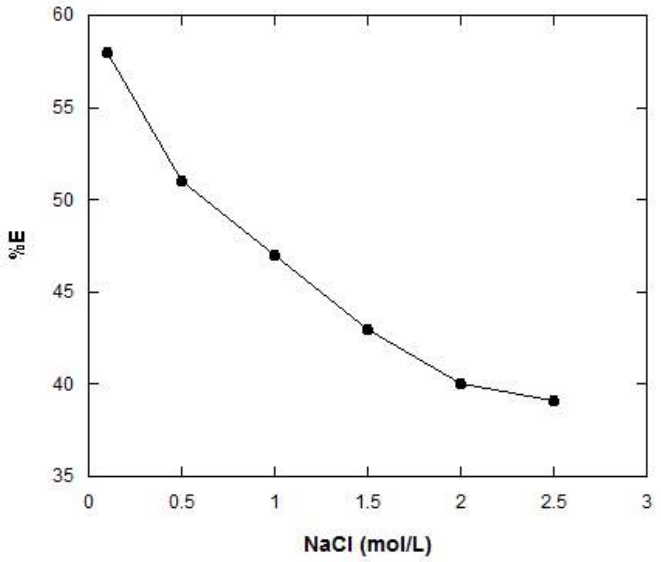

Figure 2. influence of NaCl concentration on extraction percentage by 0.25 M TBP in kerosene.

This work, mechanism of palladium chloride salt dissolution was assumed eq. 1 to eq.3:

$$PdCl_{2(s)} \rightarrow PdCl_{2(aq)} \qquad K_{sp} \cong 3 \times 10^{-12} \quad (1)$$

$$PdCl_{2(s)} + Cl^{-} \rightarrow PdCl_{3(aq)}^{-} \qquad K_{sp} \cong 0.6 \quad (2)$$

$$PdCl_{3(aq)}^{-} + Cl^{-} \rightarrow PdCl_{3(aq)}^{2-} \qquad K_{sp} \cong 36.2 \quad (3$$

As can be seen, $PdCl_2$ can't dissolve in distilled water, significantly. But palladium chloride solubility increased when low amount of hydrochloride acid was added to the system. In this case $PdCl_3^-$ is the main chloride complex. By adding further amount of acid, palladium chloride complexes are altered, again. Hence, $PdCl_3^-$ and $PdCl_4^{2-}$ are known as the main palladium chloride complexes.

UV-visible spectrophotometry can be used for palladium complexes detection. Biryukov and Shlenskaya conducted spectrophotometric studies of chloro palladate (II) at 25°C and *I* = 0.26–1.01 *m* in the UV regions. They reported UV absorption peaks occurring on 210 and 240 nm. In a later report (Elding, 1972), they were defined as $PdCl_3^-$ wave length. Boily and coworkers have carried out a comprehensive study on palladium chloride formation at different condition. They reported $PdCl_3^-$was formed in low HCl/Pd (II) ratio, but palladium complexes changes with HCl concentration increase, as UV peaks were formed at 220 280 nm. These wave lengths were known as $PdCl_4^{2-}$ Characteristic peaks.

3.4 Effect of Extractant Concentration on Pd Extraction

To make a better understanding of palladium extraction, extraction efficiency in different TBP concentration and constant HCl has been shown in Fig 3. At lower HCl concentration, TPB concentration increase leads to increasing causes to higher extraction percentage. But TBP does not effect on extraction percentage at higher HCl concentration.

$PdCl_3^-$, that forms low acid concentration, was extracted by TBP. But $PdCl_4^-$ couldn't be extracted by TBP, significantly. Hence, different extraction mechanisms should be assumed for palladium complexes.

3.5 Palladium Extraction Mechanism

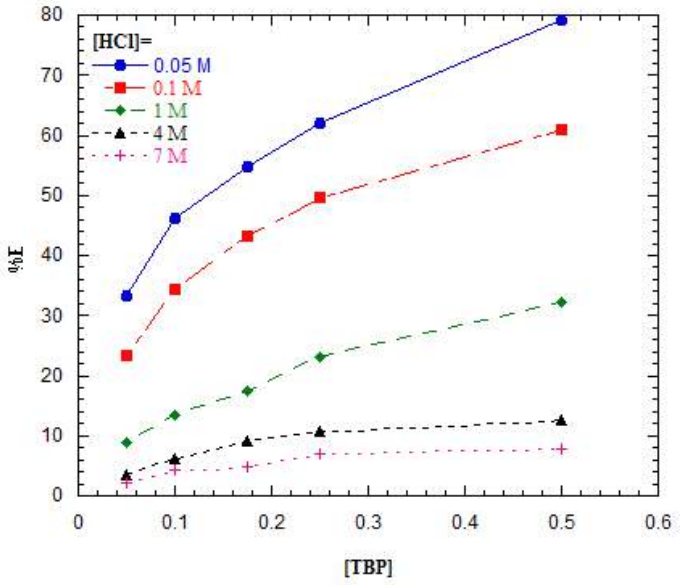

Figure 3. Effect of TBP concentration on Pd extraction percentage at constant HCl concentration and [Pd]=180 mg/l.

The extraction reaction of Pd via TBP can be represented by Eq.4:

$$[PdCl]_n^{n-2} + H^+ + H_2O + nTBP = PdCl_n^{2-n}.H.H_2OnTBP \quad (4)$$

and the corresponding equilibrium constant is:

$$K = \frac{\gamma_{HPdCl_n^{2-n}.TBP.H_2O}[HPdCl_n^m .nTBP.H_2O]_{org}}{\gamma_{H^+}[H^+]\gamma_{PdCl_n^{2-n}}[PdCl_n^m]\gamma_{TBP}^n[TBP]^n a_{H_2O}} \quad (5)$$

where brackets stand represent concentrations, and γ stands for activities coefficient. Since TBP concentration is varied in a specific range, γ_{TBP} may be considered constant. Beside, our observations indicate that pH variation in given HCl concentration is negligible, and γ_{H^+} is also constant. Furthermore, $PdCl_n^{2-n}$ is in dilute (trace) concentration, the concentrations of two palladium solutes in aqueous and organic phases are very low in which $\gamma_{PdCl_n^{2-n}}$ and $\gamma_{HPdCl_n^{2-n}.nTBP}$ can be constant (Henry behaviour). So, product of all the constant coefficients was represented as Q.

Regarding the definition of distribution coefficient ($D= [Au]_{org} / [Au]_{aq}$) as well asEq. 5, can be written as:

$$K=Q.D.[TBP]^n \quad (6)$$

Taking logarithm of Equation 6 leads to:

$$\log K=\log Q +\log D + n\log[TBP] \quad (7)$$

At constant temperature, K and Q don't change, so just logD and log TBP are variable this equation. The plot of log D *vs.* [TBP] yields a straight-line with slope ***n.*** Such plots are depicted in Fig 4; the slopes are estimated in the range 0.86 to 1. As be shown in Figure 3, an increase in HCl concentration decreases Pd extraction percentage. Hence, $PdCl_4^{2-}$ is not extracted by TBP. In the other hand, $PdCl_3^-$and TBP significantly react with each other. So, the extraction mechanism of was rewritten as eq. 7:

$$[PdCl]_3^- + H^+ + H_2O + TBP = PdCl_3^-.H.H_2O.TBP \quad (7)$$

3.6 Effect of Nitric Acid Concentration on Pd Extraction

Since the use of nitric acid in the chloride leaching of palladium bearing sources is a conventional issue, the effect of NaCl on the extraction efficiency of palladium was evaluated. As observed in Fig 5, HNO_3 have a negative effect on the extraction percentage of palladium. It seems that an increase of H^+ and NO_3^- ions solution leads to the extraction by TBP and the sit position on TBP molecules has decreased. Hence, the extraction percentage has been reduced.

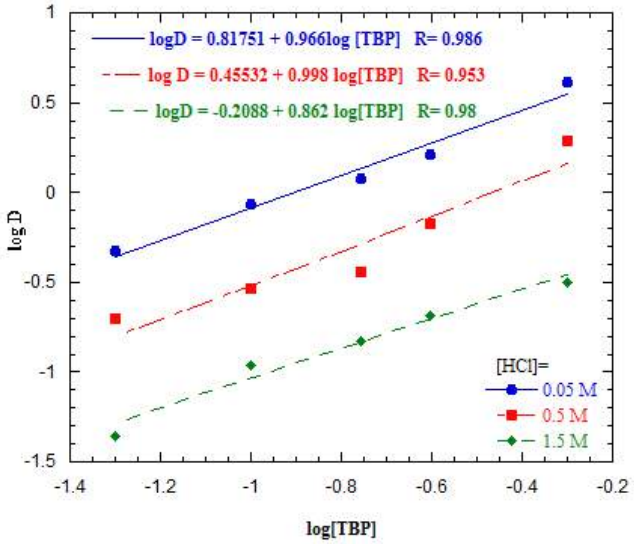

Figure 4. Variation logD of palladium vs. log[TBP] (Pd=180 mg/l).

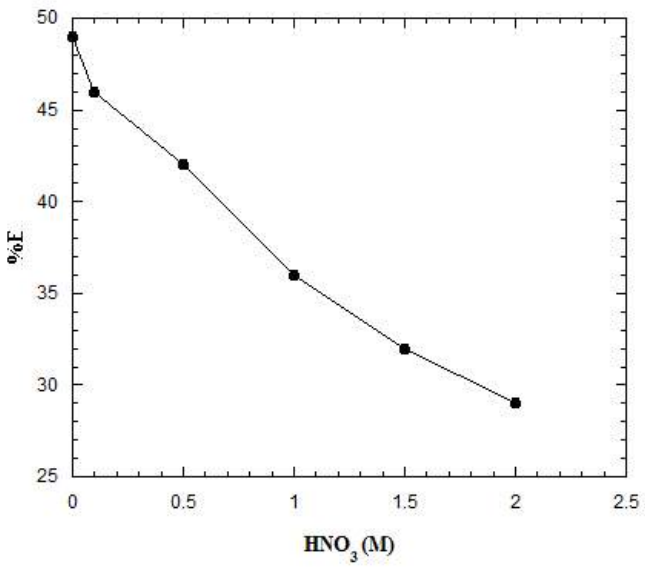

Figure 5. Effect of HNO_3concentration on Pd extraction percentage at 0.1 M HCl and [Pd]=180 mg/l.

4. CONCLUSION

1. Based on the obtained results, it was shown that the commercially available tributyl Phosphate (TBP) is an appropriate extractant for the recovery of palladium from low acidic solution.
2. Hydrochloride acid and chloride salts have negative effect on palladium extraction.

3. Presence of nitric acid decreases the Pd extraction percentage due to simultaneous extraction.
4. In the aqueous media stable complexes of palladium are $PdCl_3^-$ and $PdCl_4^{2-}$, that TBP could extract $PdCl_3^-$.
5. The organo-metallic complex of Au and TBP is proposed as $HPdC1_3L.H_2O$ where represents the extractant molecule.

REFERENCES

Bendekar, S.V., Dhadke, P.M., 1998, Solvent extraction separation of platinum(IV) and palladium(II) by 2-ethylhexyl phosphonic acid mono-2-ethylhexyl ester (PC88A), *Sep. Purif. Technol.* **13,** 129–135.

Elding L. I. (1972a) Palladium (II) halide complexes. II. Acid hydrolyses and halide anations of palladium(II) chloro and bromo aqua complexes *Inorg. Chim.Acta.***6,** 683–688

Kakio, T., Goto, M., Nakashio, F., 1994, Solvent extraction of palladium with bis (2,4,4,trimethylpentyl) dithiophosphonic acid and bis (2,4,4,-trimethylpentyl) monothiophosphonic acid, *Solvent Extr. Ion Exch.*, **12**, 541–555.

Keshavarz Alamdari, E., Darvishi, D., Haghshenas, D.F., Yousefi, N., Sadrnezhaad, S.K., 2012, Separation of Re and Mo from roasting-dust leach-liquor using solvent extraction technique by TBP, *Separation and Purification Technology*, **86**, 143–148

Polotnyanko, N. A., Khodakovskii, I. L.,□ 2014, Thermodynamic Properties of Pd Chloride Complexes and the Pd(aq) Ion in Aqueous Solutions, *Geochemistry International,* **52**, 46–56

Rane, M.V., Gopal, V.V., 2006, Study on the extraction of palladium (II) and platinum(IV)using LIX 84I, *Hydrometallurgy* **84**, 54–59.

Rovira, M., Cortina, J.L., Sastre, A.M., 1999, Selective liquid–liquid extraction of palladium(II)from hydrochloric acid media by di-(2-ethylhexyl) thiophospharic acid (DEHTPA), *Solvent Extr. Ion Exch.* **17**, 333–349.

Shen, F., Xue, W.Y., 2007, Recovery palladium, gold and platinum from hydrochloric acid solution using 2-hydroxy-4-sec-octanoyl diphenyl-ketoxime, *Sep. Purif. Technol*. **56**, 278–283.

Kinetics of Hematite Decomposition Reaction at Different Heating Rates in Air

M. Salmani, E. K. Alamdari, S. Firoozi
Department of Mining and Metallurgical engineering, Amirkabir university of Technology (Tehran Polytecgnic), Tehran, Iran

E. K. Alamdari
Research Center for Materials and Mining Industries Technology, Amirkabir University of Technology, Tehran, Iran.

M. Azizkarimi
Golgohar Iron Ore and Steel Research Institute, Sirjan, Iran

ABSTRACT The kinetics of hematite decomposition during pellet induration was studied. Decomposition reaction of hematite results in a decrease in compression strength of pellets. Thermogravimetric analysis (TGA) was used to obtain conversion values. Initially, an integral estimation method was applied and then further analysis was carried out according to ASTM standard code for model-free studies. Evidence implied the uncertainty and ambiguity of non-isothermal data. While, using isoconversional kinetic model resulted in more reliable data. Mean values for activation energy and pre-exponential factor were found to be 515 kJ and 10^{18}, respectively. So it may be assumed that chemical reaction is the controlling step in the reaction progress and thus, high temperatures in the firing zone have to be avoided.

Keywords: Hematite decomposition, Non-isothermal kinetics, Model-free kinetics, Pellet induration

1 INTRODUCTION

1.1 Pelletizing

Production of pellet as a desirable feedstock for ironmaking furnaces has exceeded 400 Mt per year in 2012, accounting for almost 23% of the iron ore processed globally (UNCTAD, 2012).

The production of iron ore pellets involves two major steps, forming the “green” pellets in rotary disks or drums, followed by heat hardening them subsequently at elevated temperatures around 1200 to 1400 °C to increase the pellet strength (Barati, 2008). The oxidation of magnetite is one of the primary physico-chemical processes associated with the heat treatment of magnetite pellets. The hematite formed on roasting pellets is a very active chemical component. Sintering of the hematite grains increases the pellet strength. The end of oxidation is associated with uniform pellet structure (Meyer, 1980).

Knowing the oxidation kinetics of iron ore pellets at high temperatures is useful in assessing the completion of indurating at any time and in optimizing the thermal conditions within the zones of the induration machine (Ru-quan et al., 2013, Yurev and Spirin, 2011).

At 1250°C, hematite begins to dissolve in the slag melt. After the firing, the iron oxides should always be present as hematite in the indurated pellets. In high temperature firing, the hematite dissociates and secondary magnetite with a high Fe_2O_3 content is formed in the maghemite stage. The equilibrium reaction

$$2Fe_3O_4 + 1/2O_2 = 3\ Fe_2O_3 \quad (1)$$

shifts to the right up to a temperature of about 1400 °C. The equilibrium again shifts to the left causing once more the formation of Fe_3O_4 and thus, an impairment of the pellet quality. This hematite dissociation starts at lower temperatures if the pellets contain basic additives (Meyer, 1980, Xiao-hui et al., 2010).

1.2 Kinetic Studies

The thermal decomposition of inorganic solids refers to reactions of the type:

$$A(s) = B(s) + C(g) \quad (2)$$

The kinetics of the thermaldecomposition of solids is heterogeneous and as such it differs fromclassical homogenous kinetics in twoaspects.One is a non-uniform distribution ofreactive sites in the reactant A(s). The other ispossible interactions between A(s) and C(g) as well as between B(s)and C(g) that can control the kinetics of the decomposition of A(s)and formation of B(s) and C(g)(Vyazovkin et al., 2014).

Considering the diversity of thereaction situations, a number of physico-geometrical reaction models, f(a), have been derived for reactions under isothermalconditions. However, it is reported that first-order rate law is completely suitable to describe this type of reactions (House, 2007). During the non-isothermal period of an isothermalexperiment, the sample undergoes some transformations that are likely to affect theresults of the following kinetic analysis. This problem especially restricts the use of high temperatures in isothermal experiments(Vyazovkin and Wight, 1998).

For non-isothermal data, one can use the Coats and Redfern equation. This method is reported to be one of the most frequently used to process non-isothermal data(House, 2007). When it comes to choosing a unique kinetic triplet, statistical methods are used in themajority of cases. These methods are based on the idea that an adequate kinetictriplet should be the best statistical description of experimental data. In other words, the adequacy of kinetic description is judged by the goodness of model fitting. However, even if the statistical analysis is performed correctly, it has one serious flawthat the capability of a mathematical model to produce meaningful information cannot be characterized by the goodness of fit(Vyazovkin and Wight, 1998).

The model-free approach to kinetic analysis rests upon the isoconversionalprinciple, according to which the reaction rate at a constant extent of conversion is only a function of temperature. This principle is the basis of so-called isoconversional methods (Vyazovkin et al., 2011, Vyazovkin and Lesnikovich, 1988). ASTM E1641 standard code provides a method to determine kinetic parameters based on isoconversional analysis. This test method covers determination of Arrhenius activation energy and pre-exponentialfactor by thermogravimetry, based on the assumption that thedecomposition obeys first-order kinetics(ASTM, 2004).

2 EXPERIMENTAL PROCEDURE

High-grade hematite powder obtained from Merck KGaA was examined by X-ray diffraction, which proved that sample met the required purity levels (Figure 1).

Since mass loss caused by the decomposition reaction is small (Gaviria et al., 2007), it is necessary to assure that samples bear no volatiles. Therefore, samples were held at 110 °Cfor three hours. Mass loss during the decomposition in air was measured using a NETZSCH 409 PC/PG simultaneous thermogravimetric analysis device under three different heating rates. Initial weight of samples, m_0, was in range of 9 to 11 mg. Conversion fraction of hematite was calculated using Equation 3 with

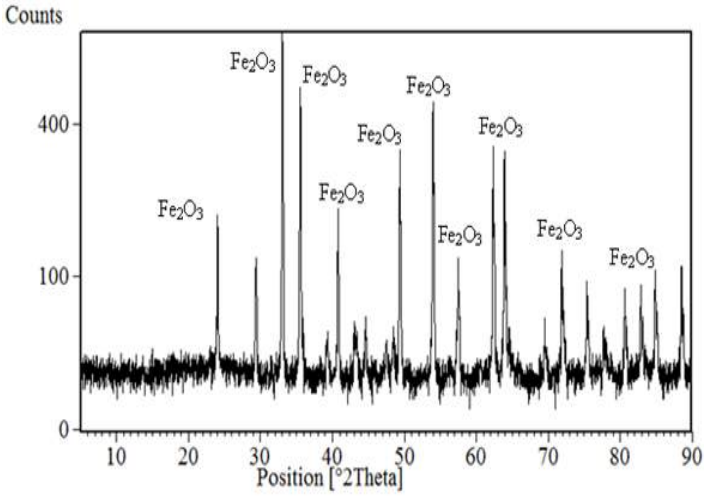

Figure1. XRD pattern of the hematite powder provided by Merck KGaA.

m_t as sample weight at time *t*, and m_∞ as the final weight (Piotrowski et al., 2007):

$$\alpha(t) = \frac{m_0 - m_t}{m_0 - m_\infty} \quad (3)$$

3 RESULTS AND DISCUSSION

The obtained results from thermogravimetry are shown in Figure 2. As it may be observed, decomposition in all tests completed before reaching 1425 °C. Using the aforementioned formula conversion fraction was calculated and illustrated in Fig. 3. Increase in heating rate that causes larger differences between sample and container temperature led to a delay in reaction progress, which is why conversion curves shifted to right.

3.1 Activation Energy

In Coats and Redfern method, higher values of n gave to larger activation energies. As it may be observed in Fig. 4, activation energy in air varies from 4000 to 8000 kJ. The obtained results imply a huge uncertainty and ambiguity to a point that is impossible to be neglected. The mean value is too high and clearly unreliable. However, isoconversional analysis resulted in much more uniform data and the mean value of activation energy was 515 kJ (Fig. 5). It seems more reasonable to take isoconversional results into account and conclude that controlling step is chemical reaction. Thereby, reaction progress is highly affected by temperature.

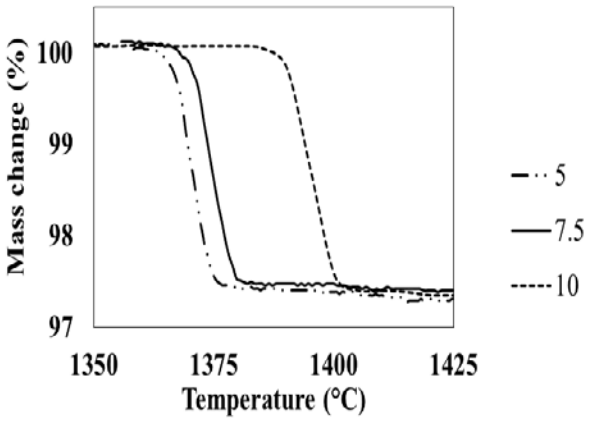

Figure 2. Loss of mass in hematite during different heating rates.

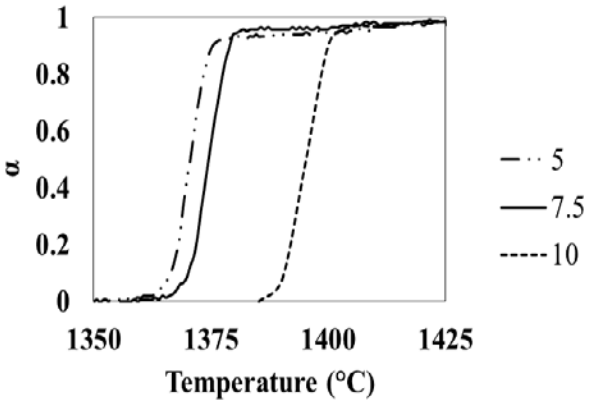

Figure 3. Conversion values recalculated by means of Equation 3.

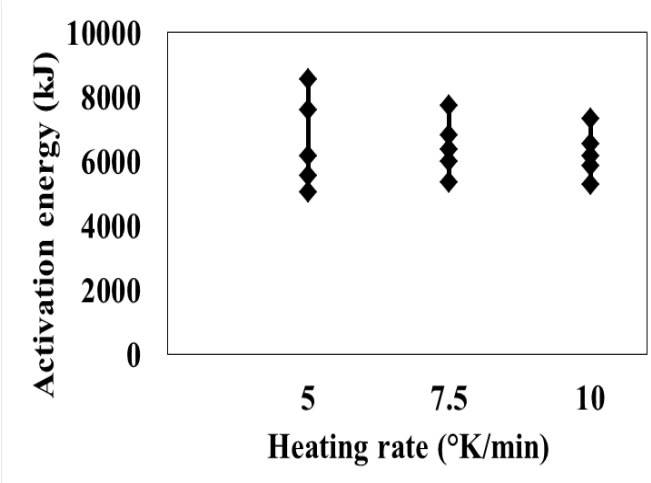

Figure 4. Obtained activation energy values using Coats and Redfern method.

3.2 Pre-Exponential Factor

Figure 6 shows that pre-exponential factor data obtained by Coats and Redfern method are ambiguous and may not be used to develop any exact explanation. Yet again, isoconversional analysis led to a uniform and acceptable results; so that, the mean value for pre-exponential factor may be considered as 10^{18} (Figure 7).

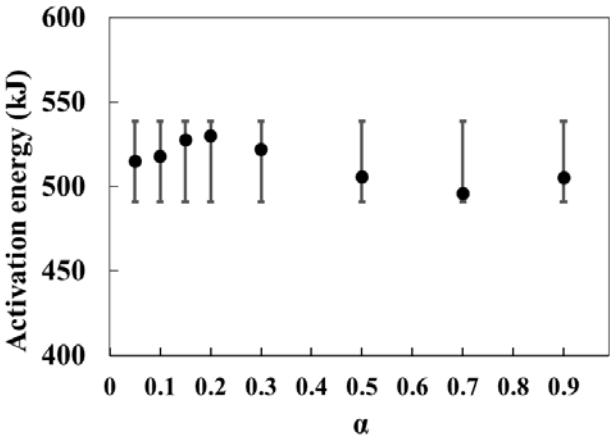

Figure 5. Obtained activation energy values using ASTM E1641.

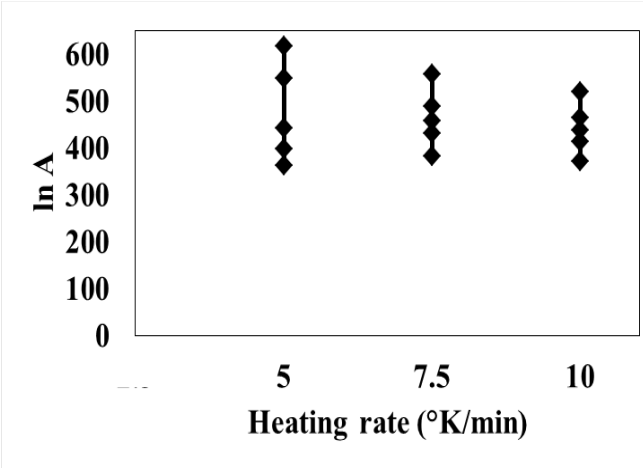

Figure 6. Obtained pre-exponential factor values using Coats and Redfern method.

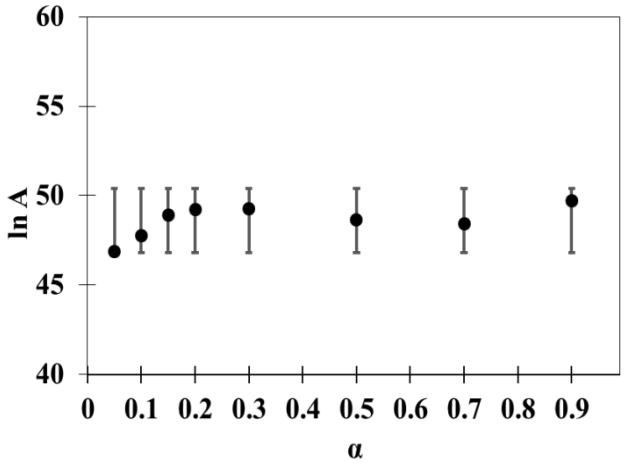

Figure 7. Obtained pre-exponential factor values using ASTM E1641.

4 CONCLUSION

In the present work, hematite decomposition in air was investigated using thermogravimetric analysis. Two different methods were applied to calculate kinetic parameters of the reaction. It was revealed that reaction temperature increased with increase in heating rates. Isoconversional method resulted in more uniform data in comparison to the Coats and Redfern method, which is a recommendedmethod for processing non-isothermal data. According to the isoconversional results, mean values for activation energy and pre-exponential factor was found to be 565 kJ and 10, respectively. Rather high value of activation energy implies on that the chemical reaction being the controlling step and thus, high temperatures must be avoided in order to prevent secondary magnetite formation.

ACKNOWLEDGEMENTS

This work was financially supported by Golgohar mining and industrial company.

REFERENCES

ASTM 2004. Decomposition Kinetics by Thermogravimetry. *E 1641*.

Barati, M. 2008. Dynamic simulation of pellet induration in straight-grate system. *International journal of minerals*, 30-39.

Gavıria, J. P., Bohe, A., Pasquevıch, A. & Pasquevich, D. M. 2007. Hematite to magnetite reduction monitored by mossbaur spectroscopy and X-ray diffraction. *Physica*, 389, 198-201.

House, J. E. 2007. *Principles of chemical kinetics,* Burlington, Academic press.

Meyer, K. 1980. *Pelletizing of iron ores,* Berlin, Springer-Verlog.

Pıotrowskı, K., Mondal, K., Wılтowskı, T., Dydo, P. & Rizeg, G. 2007. Topochemical approach of kinetics of the reduction of hematite to wustite. *Chemical engineering journal,* 131**,** 73-82.

Ru-Quan, L., Shou, Y., Fe-Sheng, Y. & Jı-Cheng, H. 2013. Kinetics of oxidation reaction for magnetite pellets. *Journal of iron and steel research, International,* 20**,** 16-20.

UNCTAD 2012. The Iron Ore Market, 2011-2013. Geneve, Switzerland.

Vyazovkın, S., Burnham, A. K., Crıado, J. M., Perez-Maqueda, L. A., Popescu, C. & Sbırrazzuolı, N. 2011. ICTAC Kinetics Committee recommendations for performing kinetic computations on thermal analysis data. *Thermochemica Acta,* 520**,** 1-19.

Vyazovkın, S., Chrıssafıs, K., Koga, N., Lorenzo, M. L. D., Pıjolet, M., Roduıt, B., Sbırrazzuolı, N. & Sunol, J. J. 2014. ICTAC Kinetics Committee recommendations for collecting experimental thermal analysis data for kinetic computations. *Thermochemica Acta,* 590**,** 1-23.

Vyazovkın, S. & Wıght, C. A. 1998. Isothermal and non-isothermal kinetics of thermally activated reactions of solids. *International reviews in physical chemistry,* 17(3)**,** 407-433.

Vyazovkın, S. V. & Lesnıkovıch, A. I. 1988. Estimation of the pre-exponential factor in the isoconversional calculation of effective kinetic parameters. *Thermochemica Acta,* 128**,** 297-300.

Xıao-Huı, F., Mın, G., Tao, J., Lı-Shung, Y. & Xu-Lıng, C. 2010. Influence of flux additives on iron ore oxidized pellets. *J. Cent. South Univ. Technol.,* 17**,** 732-737.

Yurev, B. P. & Spırın, N. A. 2011. Oxidation of iron ore pellets. *Steel in translation,* 41**,** 400-403.

Modeling and Analysis of Residence Time Distribution in Industrial Mechanical Flotation Cells

A. Hassanzadeh
Mineral Processing Department, Faculty of Mines, Istanbul Technical University, 34469 Istanbul, Turkey

E. Farhadi
Gol-E-Gohar Iron Ore and Steel Institute, Sirjan, Kerman, Iran

A. Azizi
Department of Mining, Petroleum and Geophysics, University of Shahrood, Shahrood, Iran

ABSTRACT Mean residence time (MRT) in a flotation cell is one of the most important parameters especially in terms of designing aspect and also as a key factor on recovery. The objective of determining MRT was to evaluate the effectiveness of this factor on industrial flotation cells as well as its role on 8% and 4% reduction on rougher and final flotation cells recoveries at Sarcheshmeh concentrator, respectively. Therefore, this paper was aimed to determine it by taking advantage of salt tracer. Results showed that, MRT in rougher cells at feed rate of 225 t/h and 280 t/h were 11.79 and 10.00 minutes, respectively. Also, the results indicated that the mixing condition of slurry inside the rougher cells follows N-Mixer model. RTD curves along with size-by-size copper recovery analysis of particles in different cells pointed out that, decreased residence time around 15% was the major cause of the lower recovery.

Keywords: Flotation cell, Mean residence time (MRT), N-Mixer model, copper recovery

1 INTRODUCTION

To simulate the kinetic behavior of a continuous flotation process and design a flotation cell, it is required that the mixing conditions of material be properly described (Massinaeia, 2007). Analysis of residence time distribution (RTD) offers a way to describe the mixing conditions (Lelinski, 2002). A model describing the degree of mixing of the particles in the pulp phase is essential for designing a flotation cell and this can be achieved by carrying out residence time distribution (RTD) studies using solid or liquid tracers.

Typically, RTD measurement in industrial cells involves in discharging a specific tracer inside the feed main stream and continuously monitoring the response at the outlet stream in terms of concentration or conductivity of fluid. If the tracer is injected as a pulse, then the fraction of tracer that remains in the system at any time can be described by the distribution function mathematically. The resulting patterns can be considered in connection with two ideal types: plug flow and perfect mixing (Levenspiel, 1972). Plug flow is equivalent to a batch processing system, whereas, the perfect mixing model can be considered a special case of the population balance model. But real equipment always deviates from these ideals (Kelly, 1982).

Woodburn and Loveday showed that a considerable simplification was obtained by assuming that the floatability distribution may be fitted by a Gamma function, which also represents a good approximation to describe the flotation rate constant in continuous operations (Woodburn, 1965). Measurement of RTD by the radioactive tracer technique is adaptable to different kind of equipment (Blet, 1999). A measurement was performed with the purpose of determining MRT in industrial

rougher column flotation cell by means of a liquid radioactive tracer (Massinaeia, 2007).

In this research, as flotation rougher feed rate in Sarcheshmeh copper concentration plant is increased from 225 to 280 tph in average, rougher recovery decreases in amount of 8% in comparison of criteria design. Therefore, this study is aimed to quantify the RTD in two levels, low (225 t/h) and high (280 t/h)), so that specify the role of MRT of rougher cells on 8% and 2% reducing of copper recovery of rougher cells and final copper recovery, respectively.

1.1 Sarcheshmeh Flotation Circuit

Sarcheshmeh deposit is one of the largest copper ore body in the world that it contains 1 billion tons of ore averaging 0.90% copper and 0.03% molybdenum. It is located in the southeast of Iran processing 47000 t/d of ore since 1982. The mine produces 100000 tons of copper and 2200 tons of molybdenite concentrate per year. After three stages of crushing, the ore with 80% passing size of 12.7 mm was fed to eight parallel ball mills in closed circuit with hydrocyclones to produce a product 70% finer than 75 microns. Rougher flotation cells are comprised of eight rows, divided into two sections. Each section consists of four rows of flotation cells. Each row, in turn, consists of fourteen 8.5 m^3, stepped 4-5-5 cells. Totally, a rougher bank is divided into three units of 4, 5, and 5 cells. The combined rougher flotation circuits are designed to receive ground ore at a rate of 43360 dry metric tons per day (Wunder 1979).

A schematic diagram of flotation circuit of Sarcheshmeh copper concentrator is presented in Figure 1. Rougher tailing comprises the main component of the plant final tailings. On the other side, concentrate with an average grade of 31% copper (mainly Chalcocite and Chalcopyrite minerals) obtains after cleaning and re-cleaning stages.

2 MATERIAL AND METHODS

2.1 Performance Evaluation of Rougher Cells

In flotation circuits where rougher tailing is the main tailing stream, overall recovery of the plant is mainly dependent on the rougher tailing grade. In order to prevent losses of copper values through this stream, it is essential to keep the grade of the tailings as low as possible.

Four times sampling performed from 7 different streams. A sampling period of 3 hours was chosen in which every 30 minutes, one sampling increment was taken. Before and during sampling, the circuit was checked for the steady state operation. The samples were taken from flotation circuit were dried, weighed and sieved. All samples were wet screened with a 400 mesh screen. The sub sieve analysis was carried out using the cyclosizer developed by CSIRO. Particle size distribution of each sample was determined. Then, each size fraction was assayed for copper element. Flow rates of each stream were calculated and balanced by using copper assays of the head samples. The data was mass balanced using mass balancing software (Movazen 2.1) (Yarahmadi, 1998).

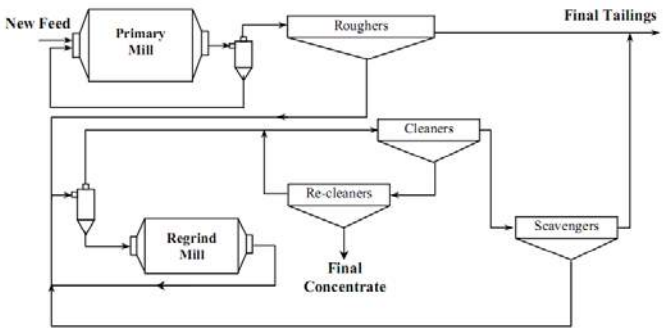

Figure 1. Sarcheshmeh copper concentration plant circuit.

2.2 Residence Time Distribution Measurement

After careful evaluation of possible tracers, sodium chloride was selected for RTD measurements in the present study. It should be noted that, each rougher cell has volume

of 8.5 m^3, which it is run in open circuit. Two sampling in practical manner were conducted on the rougher flotation cells to determine the mean residence time of slurry. In each experiment it was applied around 100 kg of sodium chloride which was dumped into the inlet stream of hydrocyclone overflow in one row of rougher circuit (row#5) almost instantaneously (within 5s) and the response was monitored in the rougher tailing at regular time intervals. Timed samples were collected manually into 500 ml plastic bottles over the duration of 60 minutes for conductivity analysis. It should be mentioned that the mill was allowed to stabilize at a feed flow rate and specific solid concentrate for about 2 hours before and during sampling time. A summary of the experimental program time is presented in Table 1. Also operating variables of rougher flotation cells during 2 series RTD measurements are listed in Table 2.

Table1. Experimental time layout for industrial sampling of rougher tailing stream.

Time (min)	10	20	30	40	50	60
Sampling interval time	0.25	0.50	1	1	2	2
Number of samples	40	20	10	10	5	5

Table 2. Operating variables of rougher floatation cells during RTD measurement.

Operational	Value	Units
Dry feed tonnages	225, 280	Metric ton/hour
Particle Size	65	%< 200 mesh
% Solids	30, 32	Wt %
pH	11.28	

After filtering, 90 samples in each MRT measurement, conductivity-meter model-712 was used for measuring conductivity of each sample. To be sure that conductivity alteration is only by the cause of added salt, various samples were collected from rougher feed and analyzed by conductivity-meter (Table. 3).

The resultant conductivity measurements of all samples were applied as inputs of RTDWEN software to model slurry mixing behaviors and determine the mean residence times according to related feed flow rates. The measured residence times were obtained from the RTD data using Eq. 1.

$$\tau = \int_0^\infty tE(t)dt \quad (1)$$

Where *E(t)* is distribution function and *t* is time (second).

The model parameters were optimized by minimizing the error between experimental tracer response data and model predictions using different software such as MATLAB, Excel and RTDWEN (Javadi, 1997). Based on the optimum values of the model parameters, eventually the mean residence time of slurry evaluated.

Table 3. Conductivity results of samples from rougher feed in different times of sampling.

Time (min)	Conductivity (ms)
0	2.92
3	2.91
5	2.86
10	2.75
20	2.80
30	2.83
40	2.92
50	2.88
60	2.78

3 RESULT AND DISCUSSION

3.1 The Importance of Mrt in Sarcheshmeh Rougher Flotation Cells

The comparison of the measured mean residence time with its expected value, as well as analysis of the shape of the RTD curve, give the most useful and valid information about the mixing properties in the cell. In a continuous flotation process and in this case the copper recovery can be described by the general Eq. 2 (Yianatos, 2006):

$$R = R_\infty \int_0^\infty \int_0^\infty (1 - e^{-kt}) F(k)E(t)dkdt \quad (2)$$

Where R_∞ represents the maximum flotation recovery at infinitive time. The

term *(1-exp (-kt))* represents copper recovery of a first order process with invariant kinetic constant *k*, as a time function. *F(k)* is the kinetic constant distribution function for mineral species with different flotation rates, and *E(t)* is the residence time distribution function for continuous processes with different mixing characteristics.

According to Eq. 2, the copper recovery depends on flotation rate of floatable minerals as well as the mixing regime in collection zone, and the actual mean residence time which is related to the effective pulp volume in flotation cell.

Based on Agar theory the rougher split should be made at the flotation time where separation efficiency is maximized (Agar 1980). At maximum separation efficiency, the grade of concentrate produced is equal to the flotation feed (Eq. 3).

$$\frac{dSE}{dt} = \frac{100m}{f(m-f)}\left[(c-f)\frac{dC}{dt} + C\frac{dc}{dt}\right] \quad (3)$$

Where *f* and *c* are grades of valuable mineral in feed and concentrate streams, respectively and *m* is the maximum grade in terms of chemical composition of that mineral. However, the big difference can be seen in our case. Whereas, four stages of sampling assay analysis show that the average copper grade of the concentrate of final unit (cells 11-14) is 3.24, while copper grade in rougher feed is 0.71. As a result of this, the reduced MRT in rougher cells can be played a significant role on copper recovery in the most of fractional sizes.

Recovery of all size fractions versus particle size depicted in Figure 2. It reveals that reducing degree of liberation and MRT for +74 microns particles caused to dramatically copper recovery diminishing in third unit of rougher flotation cells bank (cells 10-14).

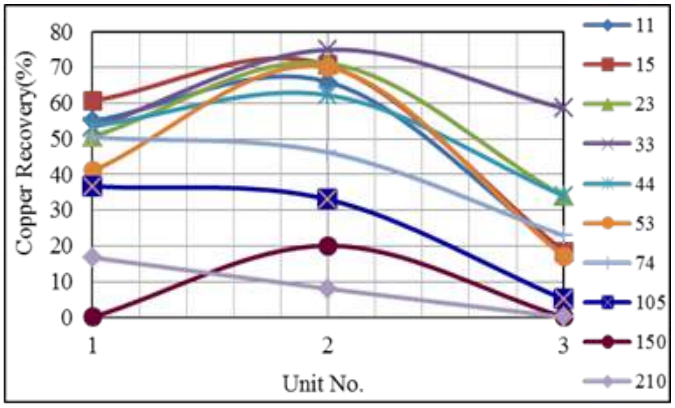

Figure 2. The size-by-size recovery at various units of the rougher bank.

3.2 Modeling of Mixing Condition in 280 Tph

The measured mean residence time is calculated from the RTD data using the following formula (Eq. 4):

$$\tau = \frac{\int_0^\infty tC_{(t)}\Delta t_i dt}{\int_0^\infty C_{(t)}\Delta t_i dt} \quad (4)$$

Where τ is the experimental mean residence time and $C_{(t)}$ and *t* are tracer intensity at time t and the measured time, respectively. In fact, to correct for background noise, the natural intensity of flotation slurry (before injection) is subtracted from the intensity measured after the injection of the tracer. Slurry RTD curves for tailing are presented in Figure 3 for N-mixer and Weller models. Data analysis and modeling are conducted using RTDWEN software (Javadi, 1997). The obtained results show that N-mixer model is the best fitted model to RTD data of tailing stream than large and small tank-in-series (Weller model). It should be noted that, Weller model consists of one plug-flow mixing cell, one large perfect mixer and two small perfect mixers. While, N-mixer model comprises of N-perfect mixers in series.

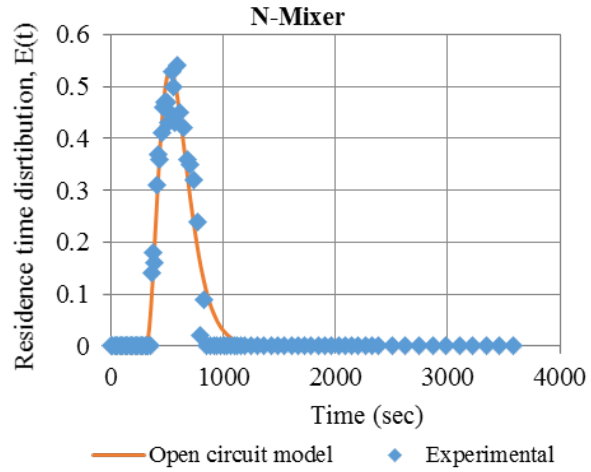

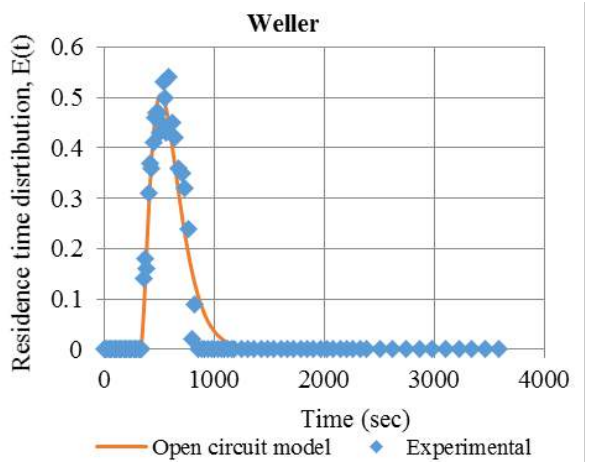

Figure 3. Residence-time distribution function for the slurry in a continuous rougher bank (14 cells) at 280 t/h by Weller model and N-Mixer model.

The comparison of measured with expected residence time, as well as analysis of the shape of RTD curves, give the most useful and valid information about the mixing properties in the cell. The quality of the fit is judged by choosing the model parameters to minimize the sum of squared errors (SSE) which is driven by the differences between the experimental and models values. Mathematically, this is expressed, as minimizing the function Z:

$$Z = \sum_{i=1}^{n} [F_m(\theta_i) - F_e(\theta_i)]^2 \qquad (5)$$

Where $F_m(\theta)$ and $F_e(\theta)$ are the model and experimental RTD results, respectively.

It can be seen that some of the tracer leaves instantaneously. Indeed, it was found that the RTD function at 280t/h can be properly represented by a model of N-perfect mixers in series with pure delay, according to the normalized distribution function. Equation 6 allows the fitting of non-integer values of N.

$$E(t) = RTD = \frac{t^{N-1}\exp(\frac{-t}{(\frac{\tau}{N})})}{(\frac{\tau}{N})^N \Gamma(N)} = (\frac{1}{\tau^N})\frac{t^{N-1}\exp(\frac{-t}{N})}{(N-1)!} \qquad (6)$$

In the case of rougher banks the best fit is obtained for an N value approximately equals to 4.

3.3 Modeling of Mixing Condition in 225 tph

The most important outcome from RTD experiments is the measured mean residence time. Figure 4 shows the RTD function in rougher bank (14 cells) at 225 t/h, where the mean residence time was 10 and 10.14 minutes by N-Mixer and Weller models, respectively. Figures 3 and 4 indicate that, there are dead volumes and short-circuiting in rougher cells. A good model should respect the parsimony principle (low number of parameters), showing a good fitting with experimental data. A number of tanks-in-series closer to 6 gave the best fitting to describe the liquid RTD in all flotation banks. Taking into consideration that the necessity of the flow through rotor, the slurry pumping rate together with the highest achievable mean residence time in a flotation cells are the best possible indication of cell performance. Figure 4 shows the residence time distribution of slurry at 225 tph.

Table 4 shows a summary of the mean residence time and other calculated parameters which are estimated from RTD measurements in the rougher flotation banks. According to SSE criteria, in two cases (225 tph and 280 tph), N-Mixer model describes the mixing condition much better than Weller model. Then, the most accurate model for rougher flotation cells in Sarcheshmeh concentrator is N-perfect mixers in series.

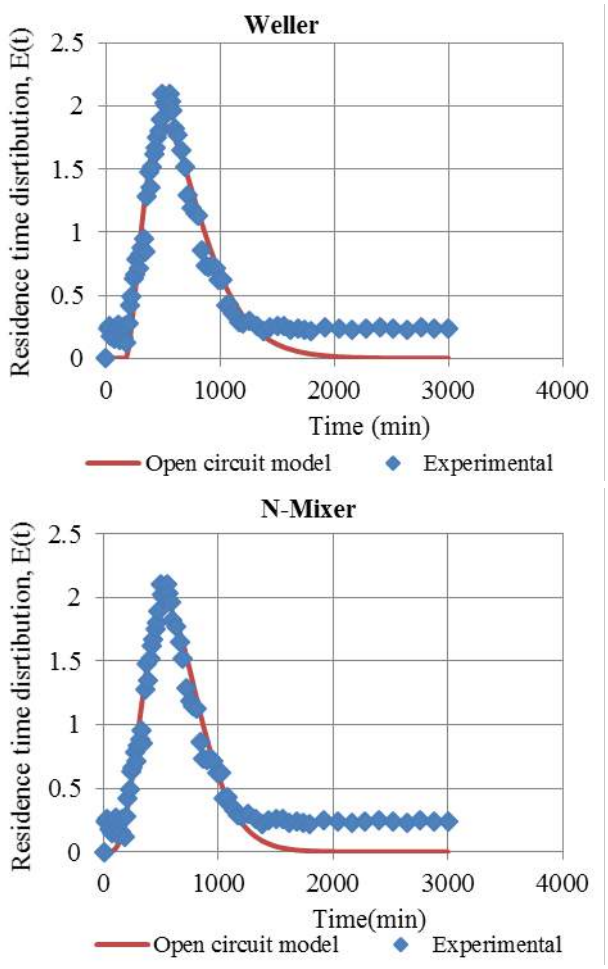

Figure 4. Residence-time distributions function for the slurry in a continuous rougher bank (14 cells) at 225t/h by Weller model and N-Mixer model.

Table 4. Statistical components in comparison of N perfect mixers model and Weller model.

Model	Term	280 tph	225 tph
N-Mixer	τ_{pf}	4.96	0.02
	τ_{av}	10	11.79
	N	4	6
	SSE	0.096	1.892
	σ_r	0.16	0.167
Weller	τ_{pf}	5.47	2.81
	τ_s	1.56	2.40
	τ_1	10.1	4.06
	τ_{av}	10.14	11.67
	SSE	0.109	2.537
	σ_r	0.071	0.206

The mean residence time of pulp in 280 t/h is 15% lower than its amount in 225t/h. The difference can be explained due to solids segregation by gravity, particularly for coarse particle sizes (>100-200 microns). Moreover, it reflects mass transfer phenomenon and the relationship between the vessel volume (V) and volumetric federate (Q). The variance (σ_r) reflects the degree of mixing which occurs within the vessel. Thereupon, for N-mixer model at 280 tph, it can be seen that relative variance is closer to perfect mixing condition compared with Weller model.

Mean residence time and relative variance are estimated from RTD data, which are calculated with three software in order to reduce error (Tab. 5).

Table 5. Software outputs in relation of MRT measurements.

Applied software	**τ_{av} (min) in 280 tph**	**τ_{av} (min) in 225 tph**
Excel	10.41	11.35
MATLAB 7.10.0	10.18	11.23
RTDWEN	10.00	11.79

4 CONCLUSION

In summary, measurement of residence time distribution in rougher flotation cells at Sarcheshmeh concentrator was performed by sodium chloride as a tracer. The results showed that the mean copper grade of third unit in rougher cells is much larger than feed. The mixing condition in industrial rougher cells using residence time data was modeled. Data analysis showed that N perfect mixer in series was the best model to present the flow pattern of liquid transferred to tailing. In addition, it is found that increase in the aeration rate resulted in a decrease in mean residence time of liquid and increase in mixing degree, which is reflected in relative variance and dispersion number. MRT in rougher cells at feed rate of 225 and 280 tph were 11.79 and 10 minutes, respectively.

ACKNOWLEDGMENT

The author would like to thanks National Iranian Copper Industries Company (N.I.C.I.Co.) for supporting this research. Special appreciation is also extended to the operating, maintenance, metallurgy and R&D personnel for their continued help.

REFERENCES

Agar, G.E., 1980, optimizing the design of flotation circuits. *CIM Bulletin*. 73, 173-182.

Blet V., Berne P., Chaussy C., Perrin S. and Schweich, D., 1999, Characterization of a packed column using radioactive tracers. *Chemical Engineering Sciences*. 54, 91-101.

Javadi, F. and Banisi, S., 1997, RTDWEN (1.1)-software for simulation of residence time distribution in open and closed circuits. *Kerman, Shahid Bahonar University of Kerman*.

Kelly, E.G., and Spottiswood, D.J., 1982, *Introduction to mineral processing.* New York, John Wiley and Sons.

Lelinski, J. Allen, L. Redden, A. Weber, 2002, Analysis of the residence time distribution in large flotation machines. *Minerals Engineering*. 15, 499–505.

Levenspiel, O., 1972, *Chemical reaction engineering.* New York, Wiley.

Massinaeia, M. K., M. Noaparast, M. Oliazadeh,M. Sahafipourb, J.A. Finch., 2007, Mixing characteristics of industrial columns in rougher circuit. *Minerals Engineering*. 20, 1360–1367.

Yarahmadi, M.R., Banisi. S., 1998, Movazen: A mass balancing software. *Fourth Chemical Engineering Congress of Iran.* Sharif University. 4, 107-115.

Yianatos, J.B., and Henriquez, F.H., 2006, Short-cut method for flotation rates modeling of industrial flotation banks. *Minerals Engineering*. 19, 1336-1340.

Woodburn, E.T. and Loveday B.K., 1965, The effect of variable residence time on the performance of a flotation system. *Journal of the South African Institute of Mining and Metallurgy*. 65, 612-628.

Wunder, G.W. 1979, Sarcheshmeh concentrator operating manual (Section 5: flotation and regrinding), Parson-Jurden International Corporation, *National Iranian Copper Industries Company*.

Optimal Mine Extraction Sequencing Using Meta-heuristics

Y. A. Sari and M. Kumral
McGill University, Department of Mining and Materials Engineering,Montreal, Canada

ABSTRACT Mine production scheduling is an interconnected decision problem of block sequencing, ore-waste destination classification and production rates. We propose to solve this problem for poly-metallic (by using equivalent grades), multiple destination plans by combining ranked positional weight algorithm and Simulated Annealing approach. The success of the proposed approach is demonstrated in a case study.

Keywords: Meta-heuristics, Mine production scheduling, Ranked positional weight algorithm, Simulated Annealing approach.

1 INTRODUCTION

Mine production scheduling consists of three sub-problems that are block sequencing, ore-waste destination classification and production rates. These decisions result in a mine plan, in which mine life is usually divided into years and each unit is called a period.

Block sequencing problem is to assign a time of extraction to each block. In other words, decisions are made in such a way that each block is assigned to a period of extraction otherwise not included in the mine plan.

Ore-waste destination classification problem, also can be called ore-waste discrimination problem in cases with only one waste destination and one process destination, is the problem of distinguishing the destinations of each block to one of the waste material destinations or process destinations.

Lastly, production rates sub-problem makes the decision of the amount of material that is sent to each destination at each period. When the production rates are known, destination capacities are adjusted accordingly thus the costs are calculated as they are influenced by economies of scale.

To solve the mine production scheduling problem, multiple approaches have been taken. These approaches can be mainly classified under three clusters; iterative approaches, ultimate pit limit based algorithms and exact methods.

Iterative approaches are heuristic methods that give an insight about the plan. Examples for these approaches include moving cone method (Carlson et al.), Korobov algorithm (David et al.), and ranked positional weight method (Gershon). Although these approaches are fast and practical, they do not yield optimal results. They are suited very well as a reference, starting point but fail to produce the most profitable plan.

Ultimate pit limit based algorithms include graph theory and maximum flow approaches. The commercial software used in mining industry is usually based on these approaches because of fast processing time and easy formulation. Notably, graph theory based Lerchs-Grossmann is the most frequently used approach in commercial software. Although these methods yield the optimal pit limit, they do not have capacity constraints thus required to be parameterized. Dagdelen and Johnson (1986) attempted to solve this problem by incorporating the Lagrangean multiplier. The selection of Lagrengean multiplier is a significant problem and the viability of sequence generated depends on this selection. This requirement of parametrization lifts the optimality of these methods.

Exact optimization methods, on the other hand, guarantee an optimal solution. However, given the number of parameters and constraints in the open pit production scheduling problem, even for the medium sized data, the problem cannot be solved via exact methods because exact optimization

methods require exponential endeavour (Rothlauf; 2011). Linear, integer, mixed integer linear Programming were proposed to solve block sequencing problem. These approaches have become popular techniques because of swiftly expanding computer and software technologies (Johnson, 1968, Gershon, 1983, Knowles, 1999, Manabe et al, 2004, Caccetta & Hill, 2003).

Roman (1973) and Dowd and Elvan (1987) used dynamic programming for various elements of mine production scheduling. Dynamic programming is a strong method for sequential decision making problem. In this approach, the block sequencing problem is divided into simpler sub-problems (are called stages). Each stage is optimized. Bellmann (1956) developed the method. Bellman's Principle of Optimality prescribes, at a certain time, the value of a decision problem depends on the pay-off initial choices and the value of the remaining decision problem. Koeninsberg (1982) used dynamic programming for three-dimensional case. Later, Wright and Weiss (1989) modified Koeninsberg algorithm.

Metaheuristics such as simulated annealing (Kumral, 2012), genetic algorithms (Denby and Schofield, 1997) and ant colonies have been also proposed to solve the problem.

In this paper, we are taking simulated annealing approach one step forward to solve poly-metallic, multiple process destinations and multiple rock types mine production scheduling problem using the equivalent grade factors.

2 METHOD

Cut-off grades for multiple destinations are calculated according to Equation 1. In multi-metallic cases, first, the cut-off grades are calculated according to the primary metal.

$$cut-off_{d} = \frac{\text{processing cost}_{d} - \text{processing cost}_{d-1}}{(\text{recovery}_{d} - \text{recovery}_{d-1}) * \text{price}} \quad (1)$$

where d is the number of destinations.

Calculation of the multi-metallic cut-off grades is done by taking the approach of Osanloo and Ataei (2003). Following this approach (1) Metal 1 is divided into a pre-set number of intervals by taking zero grade as minimum and maximum grade of Metal 1 as maximum. (2) For each metal, average grades within these intervals is calculated. (3) Separately, equivalent grade factors (F_{eq}) are calculated for each metal to metal 1 according to Equation 2. (4) A total equivalent grade of Metal 1 is obtained by adding all average grades multiplied by their F_{eq}. (5) Cut-off grades of each destination are calculated for Metal 1, following Equation 1. From the equivalent Metal 1 reference formed in Step 4, the interval the cut-off corresponds to is found and interpolation is used to determine the equivalent cut-off grade in the initial interval that is formed in Step 1. This is repeated for each destination cut-off. (6) From then on, only equivalent cut-off grades are used and other metal grades are disregarded.

$$F_{eq} = \frac{price_{i} \times recovery_{i}}{price_{1} \times recovery_{1}} \quad (2)$$

Using this factor an equivalent cut-off grade is calculated. Equivalent cut-off grade is applied to all blocks to destine blocks processing routes, which generate maximum profit. After this, a quick sub-optimal result was generated to use as an initial input to simulated annealing. Moving cones, Korobov or positional weight is ideal approaches to generated reasonable solutions in quick time.

In this model, the decision variable is not only extraction period but also block destination. In other words, ore – waste discrimination is managed by the optimization process.

$$Max \quad f(x) = \sum_{i=1}^{T} \sum_{j=1}^{N} \sum_{d=1}^{D} V_{ijd} * x_{ijd}$$

- Access constraint

$$\sum_{d=1}^{D} x_{ild} \geq \sum_{d=1}^{D} x_{ijd} \quad i = 1,...,T; \quad j = 1,...,N \text{ and } k \in L_{j}$$

- Destination capacity constraint

$$\sum_{j=1}^{N} f_j x_{ijd} - Upp_d \le 0$$

$$i = 1,...,T \quad and \quad d = 2,...,D$$

$$\sum_{j=1}^{N} f_j x_{ijd} - Low_d \ge 0$$

$$i = 1,...,T \quad and \quad d = 2,...,D$$

- Process control constraint

$$\sum_{j=1}^{N} c_j \ f_j x_{ijd} \le H_{du} \sum_{j=1}^{N} f_j x_{ijd} \quad i = 1,...,T$$

$$and \quad d = 2,...,D$$

$$\sum_{j=1}^{N} c_j \ f_j x_{ijd} \ge H_{dl} \sum_{j=1}^{N} f_j x_{ijd} \quad i = 1,...,T$$

$$and \quad d = 2,...,D$$

- Block conservation constraint

$$\sum_{i=1}^{T} \sum_{d=1}^{D} x_{ijd} \le 1 \quad j = 1,...,N$$

- Binary constraint

$$x_{ijd} \in \{0,1\} \quad i = 1,...,T, \ j = 1,...,N$$

$$and \quad d = 1,...,D$$

where D is the number of destinations that should be at least two (waste dump and one processing destination), V_{ijd} is net present value of block (NPV) j in period i in destination d, f_j is tonnage of block j and x_{ijd} is binary variable (if block j is sent to destination d in period i, the variable is 1; otherwise, it is zero).

3 CASE STUDY

A case study was carried out to evaluate performance of the proposed approach. Orebody was simulated through Sequential Gaussian co-simulation for gold and silver drill-hole data. Average values of simulations were used the input the proposed approach. In this case study, there were 5 time periods. Figure 1 provides two cross-sections of the plan generated. As can be seen from the figure, iterative approach produced a relatively small pit. However, the annealing expanded pit such that net present value of project was increased. In this case study, there are two mineral processing options: low and high grade processing. Ore prices were \$38/gr and \$0.75/gr for gold and silver, respectively.

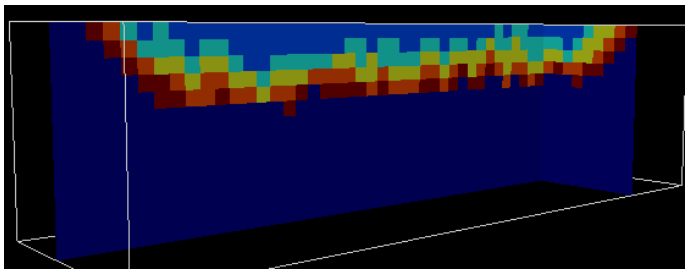

(a)

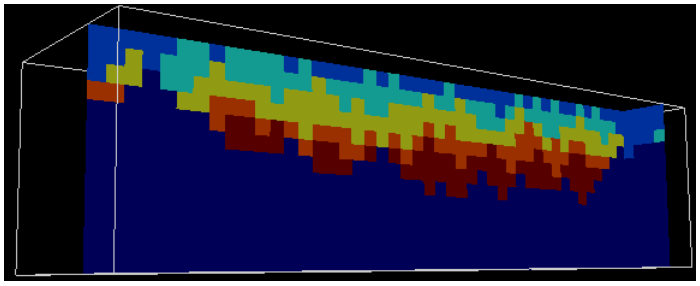

(b)

Figure 1. A cross-section of plan generated by (a) sub-optimal approach and (b) simulated annealing

Slope angles are 50^0 at all directions. Mineral processing costs are \$25/ton and \$35/ton, respectively. Mining costs are \$5 and \$10/ton for low and high grade processing, respectively. Gold recoveries are 70% and 90%, and silver recoveries 50% and 75%, respectively. Mining capacity is 350 ton/period, mineral processing capacities are 300 ton/period and 250 ton/period, respectively. The number of iteration at every temperature level was 4,000. If there are no improvement in net present value at three consecutive temperature levels, program stops and record best solution up to now as optimal result. This was stopping criterion used in the annealing approach. In terms of running time, iterative approach generated an output 30 seconds. This is very fast output that suits annealing logic. This was submitted the annealing that produces an output in 85 minutes. Given that there are a large number of decision variables and constraints, this is a quite reasonable time.

The project NPV was calculated as $1,356,309,983 for five years. For a poly-metallic mineral deposit, this is a quite profitable result.

4 CONCLUSIONS AND FUTURE WORK

In this paper a new block sequencing approach was proposed. The approach is a combination of an iterative technique and simulated annealing. Iterative approach produced a feasible result quickly and submitted to annealing module. Main problem associated with the annealing is on optimality. Even though the annealing finds optimal solution with sufficient number operations, it is difficult to find what sufficient number is. At the moment, using different random seeds, we observe the evolution of the approach in terms of the convergence to determine the number of iterations required. The case study conducted produced very promising results. In the future, the focus will be searching on optimal annealing parameters such as temperature decrement, new configuration mechanisms, optimal number of iteration at every temperature level and stopping criteria.

REFERENCES

Bellman, R. (1956). Dynamic programming and Lagrange multipliers. Proceedings of the National Academy of Sciences of the United States of America, 42(10), 767.

Caccetta, L., & Hill, S. P. (2003). An application of branch and cut to open pit mine scheduling. Journal of global optimization, 27(2-3), 349-365.

Carlson, T. R., Erickson, J. D., O'Brian, D. T., & Pana, M. T. (1966). Computer techniques in mine planning. Mining Engineering, 18(5), 53-56.

Dagdelen, K. and Johnson, T. B. (1986). Optimum open pit mine production scheduling by Lagrangian parameterization. In 19th APCOM Symposium of the society of mining engineers (AIME).

David, M., Dowd, P., and Korobov, S. (1974). Forecasting departure from planning in open pit design and grade control. In 12th Symposium on the application of computers and operations research in the mineral industries (APCOM), volume 2, pages F131-F142.

Denby, B., & Schofield, D. (1994). Open-pit design and scheduling by use of genetic algorithms. Transactions of the Institution of Mining and Metallurgy. Section A. Mining Industry, 103.

Dowd, P. A., & Elvan, L. (1987). Dynamic programming applied to grade control in sub-level open stopping. Trans. IMM, 96, A171-A178.

Gershon, M. (1987b). An open-pit production scheduler: algorithm and implementation. Min. Eng. (Littleton, Colo.); (United States), 39(8).

Knowles, T. W. (1999). Optimization models for mine planning. Computers & industrial engineering, 37(1), 469-472.

Koenigsberg, E. (1982). Twenty five years of cyclic queues and closed queue networks: A review. Journal of the Operational Research Society, 605-619.

Kumral, M. (2013). Optimizing ore–waste discrimination and block sequencing through simulated annealing. Applied Soft Computing, 13(8), 3737-3744.

Johnson, T. B. (1968). Optimum open pit mine production scheduling (No. ORC-68-11). California Univ Berkeley Operations Research Center.

Menabde, M., Froyland, G., Stone, P., Yeates G., (2004). Mining Schedule Optimisation for Conditionally Simulated Orebodies. Proceedings of Orebody Modelling and Strategic Mine Planning - Uncertainty and Risk Management, 357-342, Perth.

Osanloo, M., & Ataei, M. (2003). Using equivalent grade factors to find the optimum cut-off grades of multiple metal deposits. *Minerals Engineering*, *16*(8), 771-776

Roman, R. J. (1973). The use of dynamic programming for determining mine-mill production schedules. In Proceedings of 10. Symposium on applications of computer and operations research in the mineral industry (pp. 165-170).

Rothlauf, F. (2011). Design of modern heuristics: principles and application. Springer.

Sattarvand, J., & Niemann-Delius, C. (2008). Perspective of metaheuristic optimization methods in open pit production planning. Gospodarka Surowcami Mineralnymi, 24(4), 143-156.

Wright, E. A., & Weiss, A. (1989). Dynamic programming in open pit mining sequence planning—a case study. In Proc. Application of Computers and Operations Research in the Mineral Industry Symp., 21st, Soc. Min. Eng. of Am. Inst. Mech. Eng., Colorado (pp. 415-421).

Physical And Numerical Modeling Behavior Of Two Piles Under Horizontal Loading Cyclic

M. Akchiche, A. Rouag, K. Djedjig
University of Sciences and Technology Houari Boumediene, FGC, Algeria

ABSTRACT Piling is commonly used as foundation system in all countries. Design standards remain quite different, for school and cultural reasons, but also due to the different types of soils encountered in each country.

As part of the project of the great Mosque, numerical modeling using the CESAR-LCPC software was performed. It provided an opportunity to compare calculation results with test horizontal cyclic loading model on real stake made on construction site results. This paper presents a comparison between the three approaches in terms of accumulation of displacements

Keywords: Piling, physical modelling, numerical modelling

1 INTRODUCTION

When designing piles in cohesive soil and grained soil, one of the major concerns is the degradation of the lateral capacity under cyclic loading.

An early study on this topic was carried out by Matlock (1970), who reported two field tests on laterally loaded piles and proposed p-y curves for the pile-clay interaction under both static and cyclic loadings. The recommendations were adopted in the code of the American Petroleum Institute API (2002) and are widely applied. Other contributions in this field include the studies conducted by Hamilton & Murff (1995), Vucetic & al. (1988), Lesny, K. & Hinz, P. (2007), Peng, & al (2006), Hajialilue-Bonab & al. (2011) Ismael (2010) and Su (2012). The results of these studies indicate that the cyclic degradation of clays and the degradation of pile-clay interaction under lateral cyclic loading are progressive and that the degree of the degradation depends on factors such as the type of clay, overconsolidation ratio, number of loading cycles, loading frequency, and the cyclic displacement level or cyclic loading level.

On the other side, research testing of full-sized piles in sand under both static and cyclic loading conditions are given by "Reese & Impe" (2001) Reese & al. (1974) and O'Neill & Murchison (1983), Leblanc & al (2010)

However, Analysis of settlement is based on solutions that involve the stress-strain behavior of linear ground. However, soils behave nonlinearly. Therefore, we will evaluate in this section the results of two isolated settlement of piles, carried out in two different soil types with non-linear soil models in the absence of interface elements. Templates are created and analyzed using programs based on finite element method CESAR-LCPC. The results of the finite element model are compared with experimental results and analytical studies.

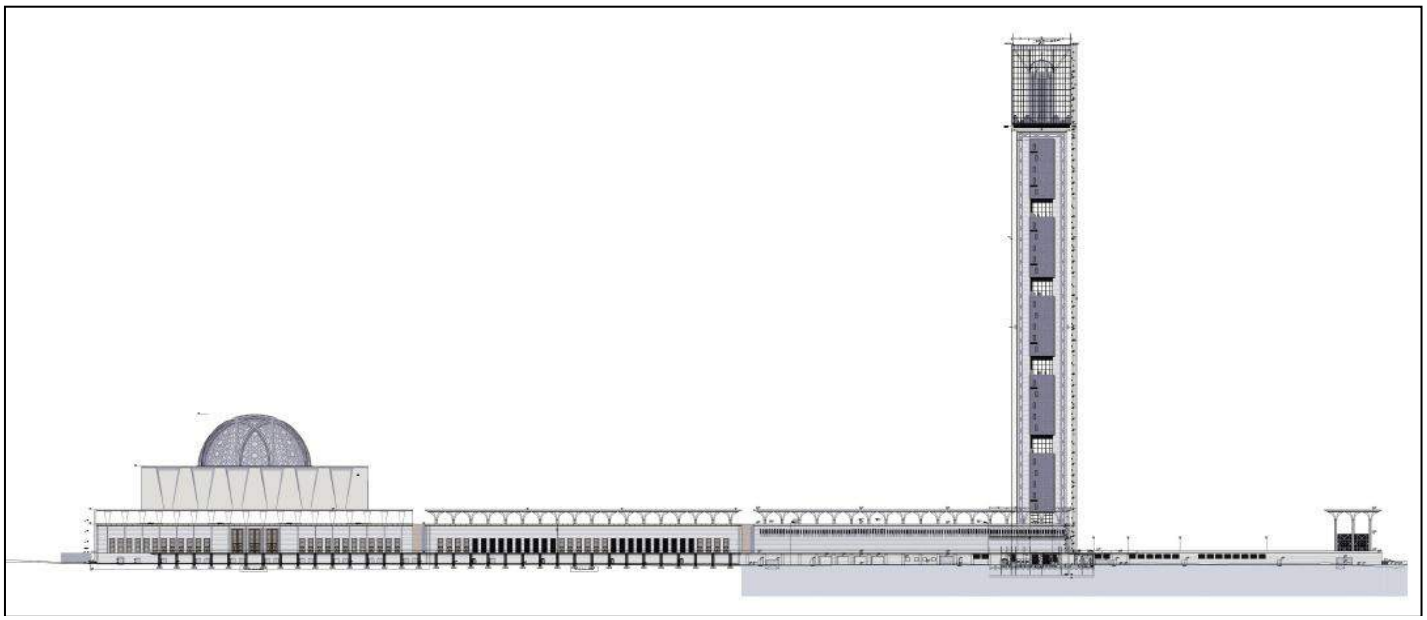

Figure 1. The Great Mosque of Algiers

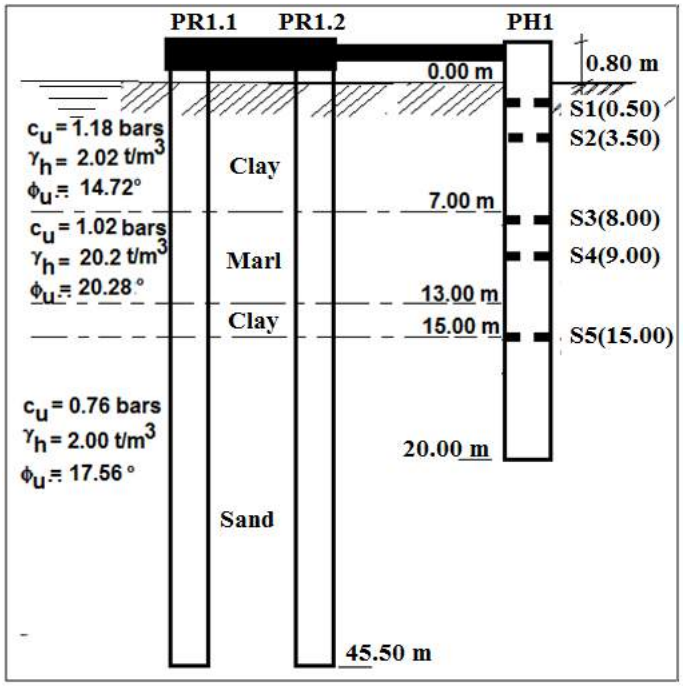

Figure 2.a. Geotechnical cut with wire strain position of sections for PH1 and PH2 piles

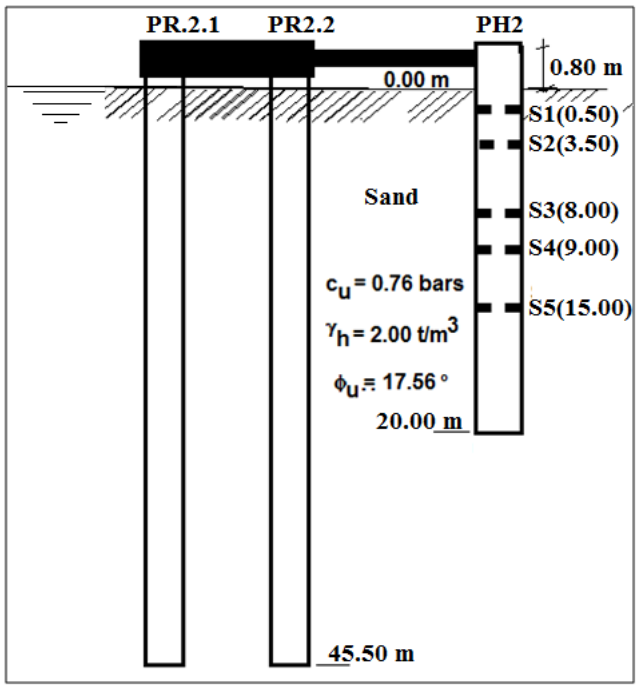

Figure 2.b. Geotechnical cut with wire strain position of sections for PH1 and PH2 piles

2 PROJECT BACKGROUND

An experimental study was carried out on the site of the great yard of the mosque in Algiers. The minaret has a total height of 264.05 m and a base of 26.86m aside and based on a system of deep foundations (Figure 1).

The horizontal static loading tests were conducted on two piles with diameters of 1 m and a test length of 20 m. These profiles across different geotechnical to PH1 it crosses the clays, marls and sands while PH2 powder crosses the sands (Figure 2). These piles were subjected to a series of horizontal axial cyclic loading. The cyclic tests were carried out to study the controlled accumulation of movement and load transfer along the pile during and after cycle strength.

3 PILE INSTALLATION AND INSTRUMENTATION

3.1 Description of the Instrumentation of the Pile

For horizontal loading tests pile driver, it was used as a reaction system a reaction piles torque. The reacti on piles (PR1-1, PR1-2 for PH-1 and PR2-1, PR2-2 for PH-2) are 45.5 m deep (figure.3 and 4). For piles of PH-1 and PH-2 trial, 20 m, the pile diameter is 1.0 m. For measuring deformations of piles testing PH1 and PH2 during the load test, it was installed on the reinforcement cages of each pile 20 strain gauges to vibrating strings arranged in sections 5 to 90 °. The test load will be applied to 50 cm above the working platform (figure 3).

The execution of the test includes several loading cycle, each with first attained the limit load calculation. During the first loading cycle, each increment will be maintained 20 minutes, in the discharge level and in all subsequent cycles loads shall be maintained for 10 minutes.

For measurements of lateral displacements are arranged two reference beams (IPE270) longitudinally with respect to the test, and the bars support eight centesimal comparators, fo ur on the pile of test and four on the reaction. Two of its comparators will report horizontal displacements of the metal plates connected to the baseboard, the other two will be positioned vertically on the front and back of the plinth to raise its head in rotation of the pile.

At the end of achieving horizontal loading tests, it was prepared:

• Pushed Equipment consists of:

- 3 hydraulic cylinders (figure. 5)
- 1 hydraulic unit

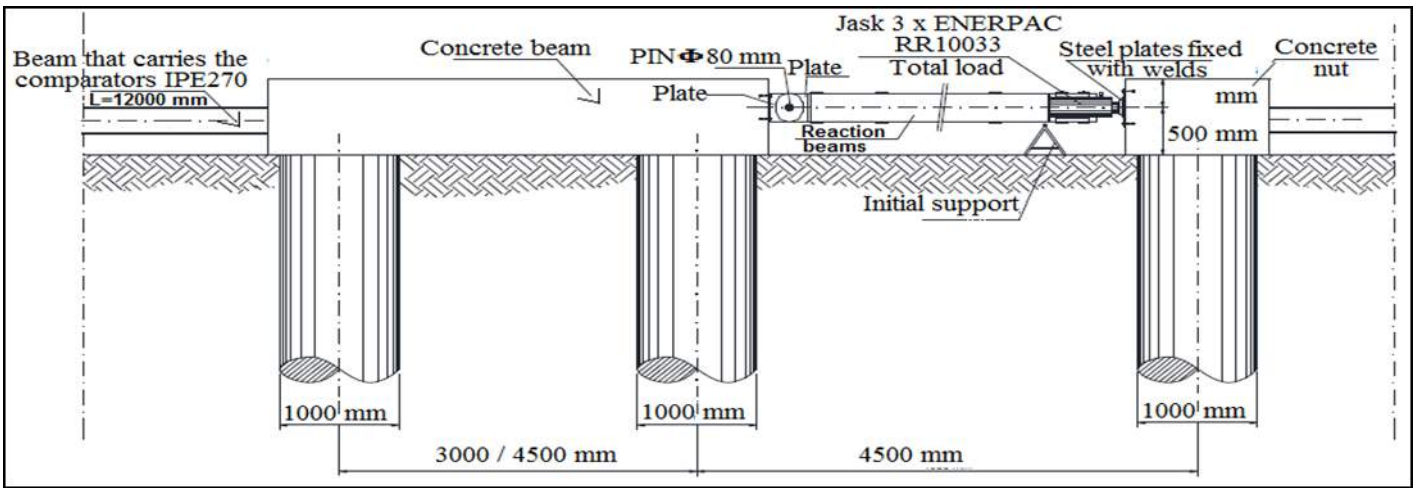

Figure 3. Device horizontal piles loading

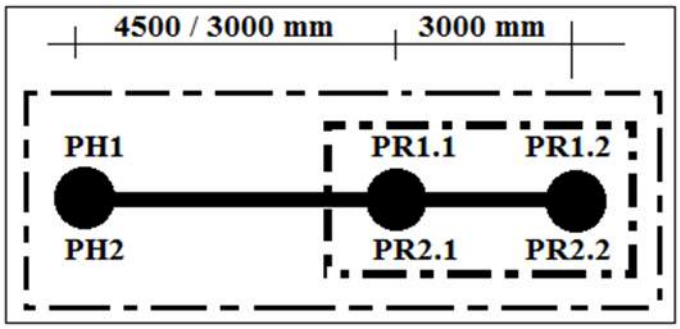

Figure 4. Reference Model for loading PH1 and PH2 piles laterally loaded

Figure 5. Load Cells and hydraulic cylinders

Table 1: loading program on the stake

Cycles	Load (kN)					Unload (kN)			
	L1	L2	L3	L4	L5	U1	U2	U3	U4
1	150	300	450	600	750	450	150	30	/
2	187.5	375	562.5	750	/	375	30	/	/
3	375	750	937.5	1125	/	750	375	30	/
4	375	750	1125	1312	1500	1125	750	375	30
5	375	750	1125	1500	/	1125	750	375	30
6	375	750	/	/	/	375	30	/	/
7	375	750	1125	/	/	750	375	30	/
8	375	750	1125	1500	/	1125	750	375	30
9	375	750	1125	1500	/	750	375	0	/

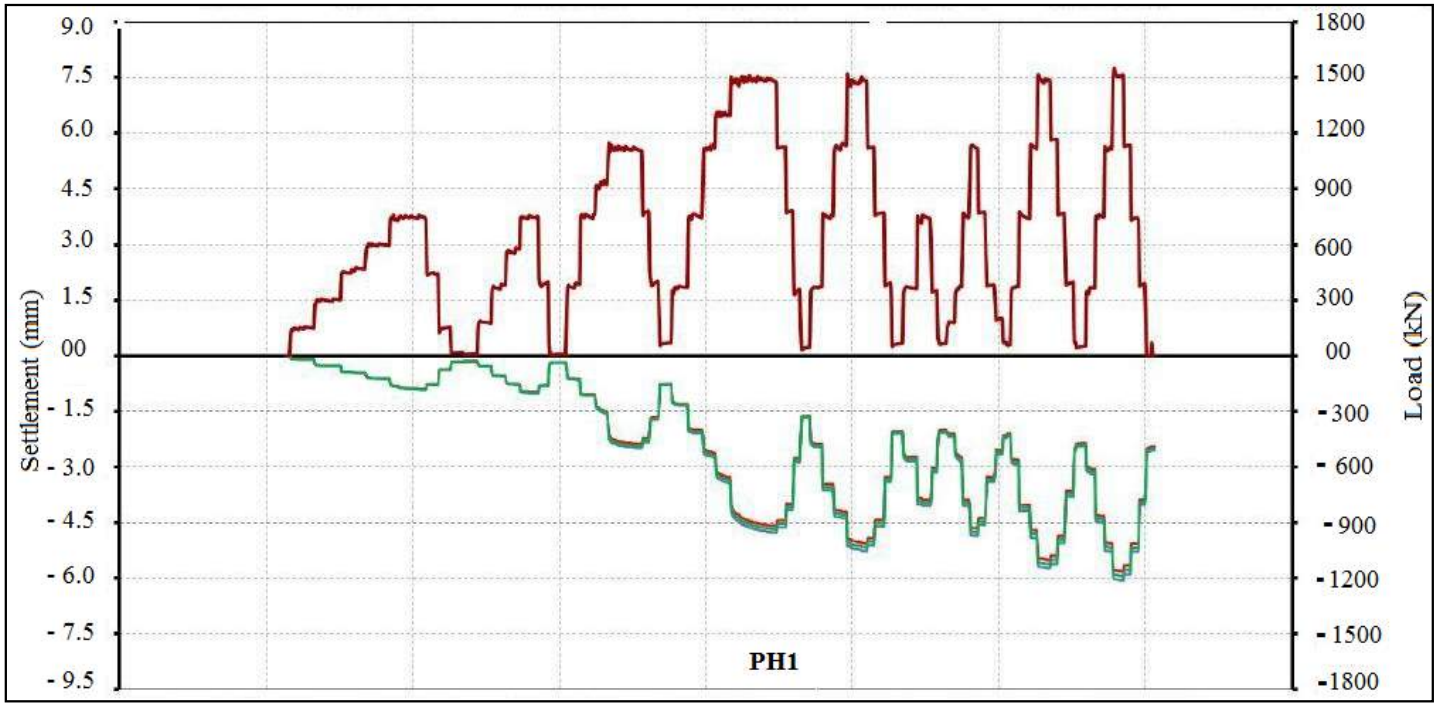

Figure 6.a. Diagrams of horizontal displacements - load PH1

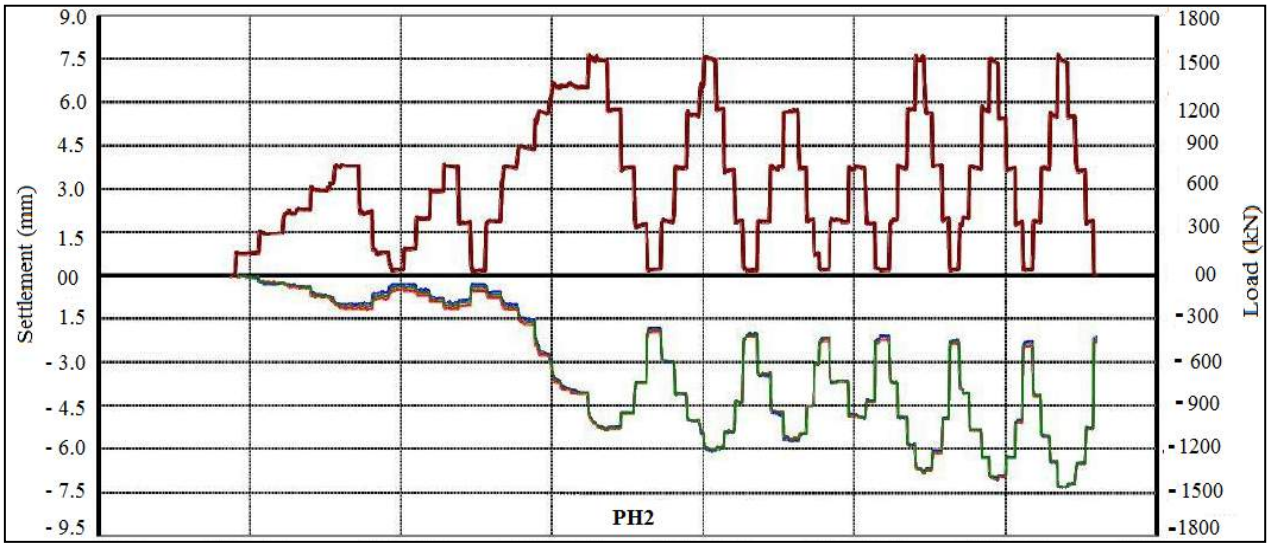

Figure 6.b. Diagrams of horizontal displacements – load PH1

• The reaction structure (figure.4) à consisting of:
- 2 piles reactions
- 1 main beam load distribution
• For the measurement of the load during the test, it was installed between the hydraulic cylinders and the nut of the head of the pile, three load cells. The cells were attached to a panel of centralization so that they can be rapidly measured during the conduct of the trial.

3.2 Load Program

For the realization of the test loading, a loading program loops and unloading was carried out and apply on several levels.

In the charging program, it has been provided first 9 loading and unloading cycles (Table 1). The load amplitude should increase by increments of 750kN to 1.500kN

For partial discharges, a minimum value of about 5% of the maximum load should not be exceeded to avoid loss of adhesion of the system elements. The charges must be brought by at least 4 equal steps. These results are shown in figures 6a, 6b, 7a and 7b.

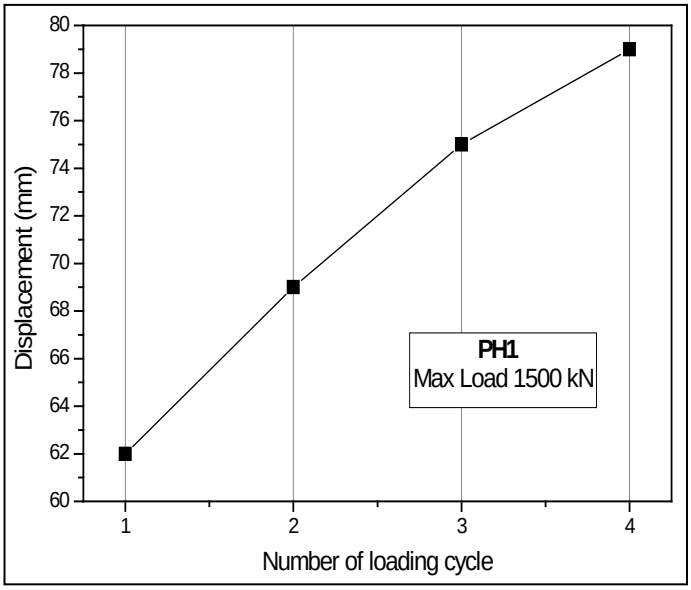

Figure 7.a. Evolution of displacement / load cycles for PH1 (load of 1500 kN).

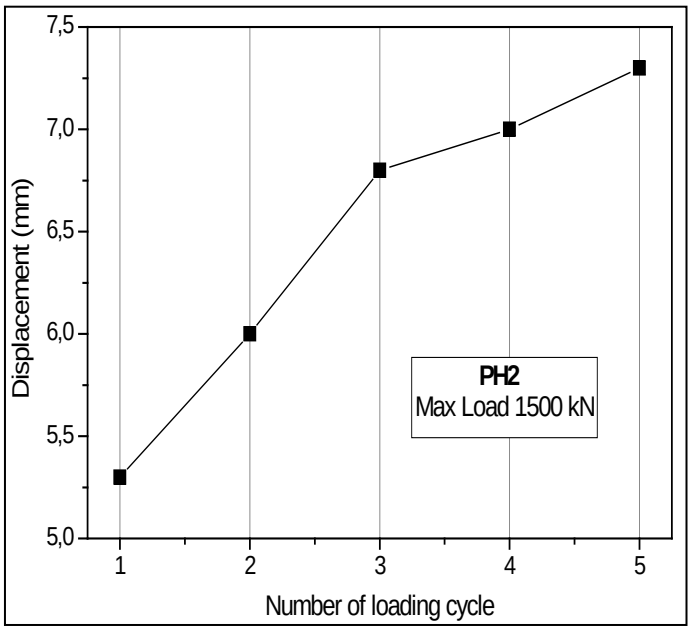

Figure 7.b. Evolution of displacement / load cycles for PH2 (load of 1500 kN).

4 ANALYTICAL CALCULATION OF PILES UNDER LATERAL LOADS

The interactions between soil and laterally loaded piles are typically accounted for by the use of p–y curves, originally introduced by Reese & Matlock (1956) and McClelland & Focht (1958). The p–y curves adopt the Winkler approach by uncoupling the response of various layers in the soil, and can therefore easily include effects of non-linearity, soil layering and other soil properties. A p–y curve defines the relationship p(y) between the soil resistance p arising from the non-uniform stress field surrounding the pile mobilized in response to the lateral pile displacement y, at any point along the pile.

We have conducted an analysis of transverse displacements of two piles testing in a lateral force in mind, this analysis was done using the method known as p–y curves method. We will compare the results with the results obtained during the lateral displacement pile load tests. p–y curves are constructed at different depths, and introduced into nonlinear FOXTA calculation software. These results are shown in the figure 8a and 8b.

5 MODELING OF PILES UNDER HORIZONTAL LOAD

The modeling of laterally loaded piles is done by the CESAR-LCPC 2D code. The different characteristics of soil layers are shown in Figure 3. The behavior of the ground is modeled by the failure criterion Mohr Coulomb by cons for the stake was modeled by a criterion of isotropic linear elastic fracture. These results deformed PH1 and PH 2 of piles are shown in the graphs figure 8a and 8b.

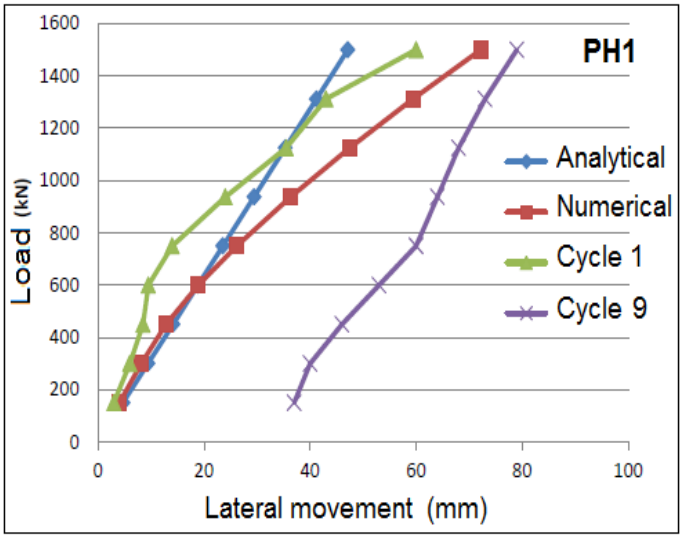

Figure 8.a. comparaison des déplacements latéraux de PH-1 en fonction des différentes méthodes de calcul

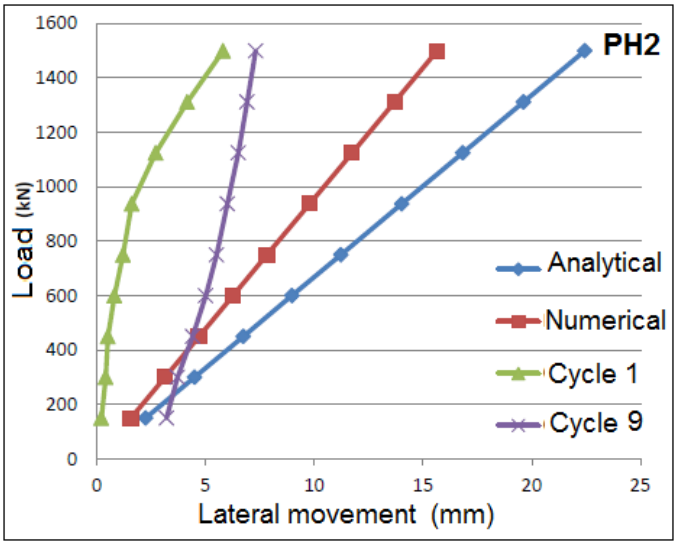

Figure 8.b. comparaison des déplacements latéraux de PH-2 en fonction des différentes méthodes de calcul

6 ANALYSIS OF THE RESULTS

In the figure 6a and 6b, Settlement of the pile "PH2" base in the final loading cycle reached the value nearly 6,3 mm for sand, corresponding to 6,3 ‰ of the pile diameter (1000 mm), But for PH1, the settlement of pile base in the final loading cycle reached the value nearly 6 mm for sand, corresponding to 6,0 ‰ of the pile diameter (1000 mm). It is observed that settlement for PH1 or PH2 are almost identical for the two soil types for the same load.

Figure 7a and 7b shows the evolution of horizontal movements based on discharge loading cycles for a load of 1500 kN for both soil types. There is a different pattern of horizontal displacements for the same load. For pile PH1 the measured value and 79 mm for the pile against PH2 is 7.3 mm. This evolution is the deformation has the effect of consolidation of clays.

Figure 8a and 8b shows the results of changes in horizontal movements of numerical modeling for both piles "PH1 and PH2". We are seeing displacements in the pile PH1 for greater load is five times greater in value to the modeling of the pile PH2 founded in sands. Horizontal movement, estimated by different methods shows a significant gap between PH-1 and PH-2. The differences in the results are due to very different soils conditions and are thus justified from a geotechnical standpoint. In Figure 8a, movements recorded during the last loading cycle are higher than the displacements of previous cycles. This variation is due to the nature of cross soils. for figure 8b, the displacements measured for the big load "pH2" does vary in a substantial way, the pile PH2 crosses sands.

Lateral displacement of the curves of piles, obtained by the numerical code CESAR-LCPC are confronted to that of the experiment, the two curves present the same appearance, the gap on displacement increases with the load level. For a maximum load of 1.5 MN displacements of the pile head was 72.20 mm for PH-1 and PH-2 to 15.65mm. By comparing the experimental values, they can be considered successful. Especially, we have not recorded lower values than the experimental values.

7 CONCLUSIONS

The calculation of lateral displacement of the two test piles realized in different soils under cyclic horizontal loads, by different methods. Allowed us to obtain results that were the subject of our analysis.

The effect of the loading on the drained response of laterally loaded piles in sand is limited. But for piles excavated in clay, we observed large horizontal displacement.

It would be of significant value to create the international database with complete static and dynamic test results of piles and the information regarding the measurements of soil resistances over the pile shaft and under the base referred to careful description of the subsoil and the in situ tests itself.

REFERENCES

API, 2002. Recommended practice for planning, designing, and constructing fixed offshore platforms: working stress design, RP2A-WSD, 20th edn. Washington, DC: American Petroleum Institute.

Hajialilue-Bonab, M., Azarnya-Shahgoli, H. and Sojoudi, Y. 2011, Soil deformation pattern around laterally loaded piles, Int. J. Phys. Model. Geotech., 11(3), 116-125.

Leblanc C. , Houlsby G. T. and Byrne B. W., 2010, Response of stiff piles in sand to long-term cyclic lateral loading . Geotechnique 60, No. 2, 79–90.

Lesny, K. & Hinz, P., 2007, Investigation of monopile behavior under cyclic lateral loading. Proc. 6th Int. Conf. on Offshore Site Investigation and Geotechnics, London, 383–390.

Hamilton J M and Murff J D., 1995, Ultimate lateral capacity of piles in clay, Proceeding of the 27th Annual Offshore Technology Conference OTC 7667.

Matlock, H., 1970, Correlations for design of laterally loaded piles in soft clay, *Proc., 2nd Annual Offshore Tech. Conf.*, Vol. 1, Society of Petroleum Engineers, Houston, 577–594.

McClelland, B. & Focht, J., 1958. Soil modulus for laterally loaded piles. Trans. ASCE 123, 1049–1086.

Ismael, N. f., 2010, behavior of step tapered bored piles in sand under static lateral loading, journal of geotechnical and geoenvironmental engineering © asce / pp.669-676.

O'Neill, M. W. & Murchison, J. M. 1983. An evaluation of p–y relationships in sands, Research Rep. No. GT-DF02-83. Department of Civil Engineering, University of Houston, TX.

Peng, J. R., Clarke, B. & Rouainia, M. 2006. A device for cyclic lateral loaded model piles. Geotech. Test. J. 29, No. 4, 1–7.

Reese.L.C and Metlock.H. 1956, Non-dimensional solutions proportional to depth, Proceedings 8th Texas conference on Soil Mechanics and Foundation Engineering, Special publication no.29, Bureau of Engineering Research, University of Texas, Austin.

Reese, L. C., and Van Impe, W. F. 2001. Single Piles and Pile Group under Lateral Loading. A. A. Balkema, Rotterdam, 463 p.

Reese, L. C., Cox, W. R., and Koop, F. D. 1974. Analysis of laterally loaded piles in sand, Proc. 6th Offshore Technology Conference, Paper 2080, Houston, Texas, 473-483.

Su D. & Yan W.M. 2013. A multidirectional *p–y* model for lateral sand–pile interactions, Soils and Foundations, Volume 53, Issue 2, Pages 199–214

Vucetic, M. and Dobry, R., 1988. Degradation of Marine Clays under Cyclic Loading, ASCE. Journal of Geotechnical Engineering, Vol. 114, No. 2, pp

Practical Considerations for Real-time Recovery Calculation Using an On-Stream Analyzer

J. Timperi, J. Loimi
Outotec, Espoo, Finland

ABSTRACT This paper discusses about different aspects that need to be considered when on-stream analyzer measurements are utilized to calculate metal recoveries of minerals processing plants in real-time. Different data reconciliation methods are described and their practical feasibility for the application is evaluated. Also a versatile recovery calculation module for a commercial on-stream analyzer system is presented.

Keywords: Metal recovery, on-stream analyzer system, recovery calculation

1 INTRODUCTION

Metal recoveries of minerals processing plants are typically calculated according to composite shift sample assays by a metallurgical on-site laboratory. These measurements give the best indication about the plant's metallurgical performance.

However, sometimes it may be useful to get a real-time indication about the plant's current recovery. For actual control purposes of the plant it is typical to use direct metal assay percentages given by the on-stream analyzer (OSA). Naturally these assays have correlation with the plants metal recovery and thus metallurgical performance. For example, when rougher tailings assay starts to climb up, it can instantly be concluded that plant's recovery is dropping.

Indication of tailings assay alone doesn't give explicit information about the plant's recovery since head grade and final concentrate grade need to be considered also. However, if the on-stream analyzer provided also the metal recovery figure in addition to individual assays, it will give plant operators more tangible indication about the current performance of the plant.

Other purposes for the use of real-time recovery figure are plant performance assessments. Rantala et al. (2014) describe a method of utilizing on-stream analyzer as a tool to evaluate changes in plant's metallurgical performance. While absolute accuracy of assays from the metallurgical laboratory is the highest, the on-stream analyzer has proven useful instrument to detect relative changes in process performance due to high sample rate of measurements and good relative accuracy.

2 RECOVERY CALCULATION

As described by Wills and Napier-Munn (2006), flotation circuit recovery can be calculated according to the "two-product" formula as follows:

$$R = 100 \times \frac{c(f-t)}{f(c-t)}\% \quad (1)$$

Where f is metal content in flotation feed, c is metal content in final concentrate and t is metal content in final tails. This formula applies to flotation circuits where there is only one metal of interest. When there are two concentrate streams containing metal a and metal b involved as illustrated in Figure 1, equations can be written to provide metal recoveries in terms of assays alone by "three-product" formulas (Taggart, 1945):

$$R_a = \frac{100c_{1a}[(f_a - c_{2a})(c_{2b} - t_b) - (f_b - c_{2b})(c_{2a} - t_a)]}{f_a[(c_{1a} - c_{2a})(c_{2b} - t_b) - (c_{1b} - c_{2b})(c_{2a} - t_a)]} \quad (2)$$

$$R_b = \frac{100c_{2b}[(c_{1a} - f_a)(f_b - t_b) - (c_{1b} - f_b)(f_a - t_a)]}{f_b[(c_{1a} - c_{2a})(c_{2b} - t_b) - (c_{1b} - c_{2b})(c_{2a} - t_a)]} \quad (3)$$

Where R_a and R_b are recoveries of metal a and b, respectively. Other variables are as follows:

f_a and f_b are metal a and b content in flotation feed

c_{1a} and c_{1b} are metal a and b content in concentrate stream 1

c_{2a} and c_{2b} are metal a and b content in concentrate stream 2

t_a and t_b are metal a and b content in final tails

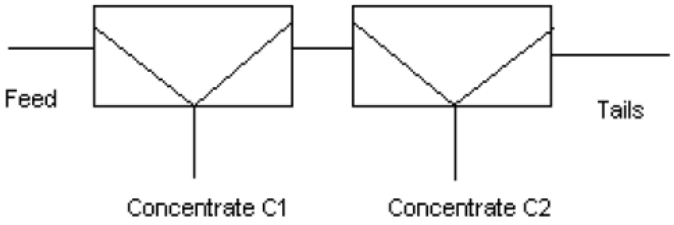

Figure 1. Flotation circuit with two concentrate streams.

When more product streams are introduced into recovery calculation, the formula becomes increasingly complicated. This is usually the case in real world applications where several concentrates are produced, for example in Cu-Zn-Pb flotation.

2.1 Accuracy of the Recovery Calculation

Saloheimo and Kongas (2001) present a method for estimating error when recovery is calculated according to the "two-product" formula.

When the equation for "two-product" formula (1) is differentiated, standard deviation for recovery can be obtained as follows:

$$\Delta R = \sqrt{\left(\frac{-t(f-t)}{f(c-t)^2}\Delta c\right)^2 + \left(\frac{ct}{f^2(c-t)}\Delta f\right)^2 + \left(\frac{-c(c-f)}{f(c-t)^2}\Delta t\right)^2} \quad (4)$$

Usually it can be assumed that c>>t, c>>f and f>>t for the produced metal, and the equation simplifies to

$$\frac{\Delta R}{R} \approx \frac{t}{f}\sqrt{\left(\frac{f}{c}\frac{\Delta c}{c}\right)^2 + \left(\frac{\Delta f}{f}\right)^2 + \left(\frac{\Delta t}{t}\right)^2} \quad (5)$$

From this formula it can be concluded that feed and tails have an equal effect to the accuracy of the calculated recovery whereas the concentrate accuracy has a smaller effect and is usually negligible in the calculation.

Because metal content in the tails stream is the lowest, this will be the most challenging stream measure accurately. When on-stream analyzer measurements are used to calculate recovery, it must be ensured that the most sensitive measurement technology is used and that the analyzer is properly calibrated. Table 1 illustrates effect of final tails measurement accuracy to error in recovery calculation.

Table 1. Accuracy of recovery calculation

	Metal content	Relative accuracy	Relative accuracy
Feed	1.50 %	3 %	3 %
Final concentrate	23 %	3 %	3 %
Final tails	0.12 %	5 %	10 %
Calculated recovery	92.5 %		
1-sigma error in recovery		0.47 %	0.84 %

Recovery calculation errors indicated in the table above serve well to emphasize the importance of the on-stream analyzer accuracy in the final tails stream. However, when practical usability of real-time recovery calculation is evaluated, the recovery figure calculated according to on-stream analyzer measurements should be compared to actual recovery figures measured by a metallurgical laboratory according to composite shift samples.

This brings out several new considerations. On-stream analyzer measures each sample point every 5…10 minutes. Composite shift sample is collected once per shift. These samples reflect averages over several hours and the composite includes also dimension of mass flow rate; changes in the process stream flow rate are relative to the amount of sample.

Spot samples measured by the on-stream analyzer every 5…10 minutes reflect momentary state of the process in each sample point. If recovery is calculated

according to these assays, delays between different sample points (e.g. phase difference between flotation feed and final tails) will have a significant effect to recovery calculation accuracy and thus these delays need to be eliminated by phase shift processing of analyzer measurements.

Figure 2 illustrates how real-time recovery calculated according to on-stream analyzer measurements corresponds to actual recovery that is calculated according to composite shift samples every 8 hours.

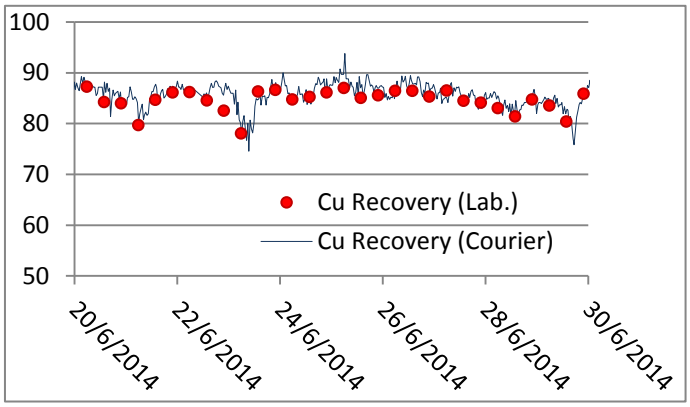

Figure 2. Recovery calculated according OSA vs. laboratory recovery (10 day period)

Generally it can be said that real-time recovery follows quite well the actual laboratory recovery during this period of 10 days. Relative error of real-time recovery compared to laboratory recovery is illustrated in Figure 3. Average relative error during this period of 10 days was 1.7% while being all the time below 6%.

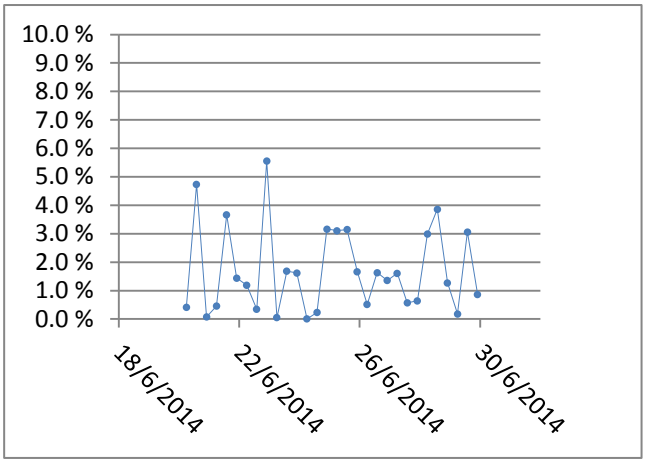

Figure 3. Relative error of OSA recovery compared to laboratory (10 day period)

However, during this period of 10 days the process was running on relatively steady feed rate and thus there was not much variation in flow rates of different streams according to which recovery was calculated. Figure 4 illustrates relative error of real-time recovery compared to laboratory recovery during a longer 3 month period which corresponds better to normal variable operating conditions. Average relative error during this 3 months period was 3.3% and from time to time error was over 10%.

It can be concluded that methods to improve real-time recovery calculation are needed in order to make a reliable to tool for plant personnel.

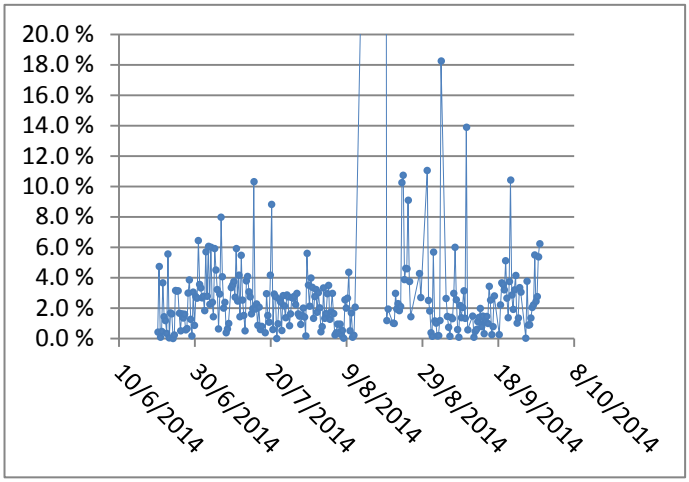

Figure 4. Relative error of OSA recovery compared to laboratory (3 months period)

3 IMPROVING REAL-TIME RECOVERY ACCURACY

Wills (1986) describes a method to improve accuracy of plant assay data by means of mass balancing. This method and its derivatives are widely used in minerals processing plants when recovery is calculated according to composite shift samples.

Calculations are relatively laborious to execute manually and thus Wills recommends use of microcomputers for these calculations. Development of information technologies has enabled several new computational technologies that were not feasible earlier. A modern on-stream analyzer for example contains enough computing power that even highly demanding calculations can be executed

locally by the analyzer CPU without auxiliary hardware.

Vasebi et al. (2012) describe several data reconciliation methods that are especially suitable for real-time execution. Bazin and Franklin (1996) describe actual implementation of real-time mass balancing application in Noranda Minerals concentrator plant in Canada.

3.1 Real-Time Data Reconciliation by Means of Steady State Mass Balancing

The real-time data reconciliation for on stream analysis results can be used to reduce the impacts of random errors. The data reconciliation improves reliability and accuracy and produces estimates that are best fits for the process model. Process model can represent the process ranging from static or steady state mass conservation constraints that calculate the process equilibrium to dynamic models that account process variation over time.

Mass balancing real time assays by steady state methods is a simple procedure for data reconciliation. The process is described by mass conservation constraints easily defined by using plant flowsheets. This solution provides good results when the inventory variations in the process are low compared to the measurement errors.

In case of process is more dynamic and the precision of the mass conservation estimates are less accurate than the measurements, the limitations of static models can be improved by handling the process inventory variation or node imbalances as random variables without increasing the model complexity.

3.2 Calculation of mass balancing adjustment components

A steady-state mass balancing process model can be developed by reducing the plant flowsheets into a series of nodes. Nodes can be either separators where input separates to two outputs or junctions where two inputs join to one output. Assuming that the process is in steady state conditions, the mass of the feed to a separating node is F and the two products C and T, and the material balance of the node is,

$$F = C + T \tag{6}$$

When each of the streams is assayed by metal content, the material balance can be written to

$$Ff = Cc + Tt \tag{7}$$

In ideal component balance where the feed F is assigned to 1 the unknown tails T can be defined by feed and concentrate.

$$F = 1 \tag{8}$$

$$T = 1 - C \tag{9}$$

The material balance is thus

$$f - Cc - (1 - C)t = 0 \tag{10}$$

But in reality there are inaccuracies in sampling and in assaying, an error e is generated in component balance.

$$f_i - Cc_i - (1 - C)t_i = e_i \tag{11}$$

$$e_i = (f_i - t_i) - C(c_i - t_i) \tag{12}$$

Where i represents a particular component. For a series of k components, the sum of errors produced is:

$$\sum_{i=1}^{k} e_i = \sum_{i=1}^{k}(f_i - t_i) - C\sum_{i=1}^{k}(c_i - t_i) \tag{13}$$

The sum of squares of the errors, SSE, is:

$$SSE = \sum_{i=1}^{k} e_i^2 \tag{14}$$

$$SSE = \sum_{i=1}^{k}(f_i - t_i)^2 + C^2\sum_{i=1}^{k}(c_i - t_i)^2 - 2C\sum_{i=1}^{k}(f_i - t_i)(c_i - t_i) \tag{15}$$

SSE cannot have zero value at any value of C but the minimum can be found by differentiating the SSE with respect to C, when:

$$\frac{\partial SSE}{\partial C} = \frac{\partial \sum e_i^2}{\partial C} = 0 \tag{16}$$

$$\frac{\partial SSE}{\partial C} = 2C\sum_{i=1}^{k}(c_i - t_i)^2 - 2\sum_{i=1}^{k}(f_i - t_i)(c_i - t_i) = 0 \tag{17}$$

The best fit value of C is then:

$$\hat{C} = \frac{\sum_{i=1}^{k}(f_i - t_i)(c_i - t_i)}{\sum_{i=1}^{k}(c_i - t_i)^2} \tag{18}$$

Where $\hat{C}$ denotes the estimate of C.

Using the method of Lagrange multipliers it is possible to define the estimates for each component subject to the equality constraints:

$$\widehat{f_i} = (f_i - f_{ia}) \quad (19)$$

$$\widehat{c_i} = (c_i - c_{ia}) \quad (20)$$

$$\widehat{t_i} = (t_i - t_{ia}) \quad (21)$$

$$\widehat{f_i} - \hat{C}\widehat{c_i} - (1 - \hat{C})\widehat{t_i} = 0 \quad (22)$$

$$(f_i - f_{ia}) - \hat{C}(c_i - c_{ia}) - (1 - \hat{C})(t_i - t_{ia}) = 0 \quad (23)$$

Where a represents the adjustment of the assayed component.

By subtracting the equation (12) from (23), the error for each component can be defined by adjustment values:

$$e_i = f_{ia} - C c_{ia} - (1 - C)t_{ia} \quad (24)$$

$$e_i - f_{ia} + \hat{C}c_{ia} + (1 - \hat{C})t_{ia} = 0 \quad (25)$$

The sum of squares for adjustment values SSE_a, can be minimized by subject to the constraint equation for e_i by finding the critical points of Lagrangian function:

$$SSE_a = \sum_{i=1}^{k}(f_{ia}^2 + c_{ia}^2 + t_{ia}^2) \quad (26)$$

$$L(f_{ia}, c_{ia}, t_{ia}, \lambda_i) = SSE_a + 2\lambda_i \sum_{1=1}^{k}(e_i - f_{ia} + \hat{C}c_{ia} + (1 - \hat{C})t_{ia}) \quad (27)$$

Where λi is the Lagrange multiplier for the component *i*. At any critical point of function *L* the partial derivates of *L* with respect to f_{ia}, c_{ia} and t_{ia} are zero:

$$\frac{\partial L}{\partial f_{ia}} = 2f_{ia} - 2\lambda_i = 0 \Rightarrow f_{ia} = \lambda_i \quad (28)$$

$$\frac{\partial L}{\partial c_{ia}} = 2c_{ia} + 2\lambda_i\hat{C} = 0 \Rightarrow c_{ia} = -\lambda_i\hat{C} \quad (29)$$

$$\frac{\partial L}{\partial t_{ia}} = 2c_{ia} + 2\lambda_i(1 - \hat{C}) = 0 \Rightarrow t_{ia} = -\lambda_i(1 - \hat{C}) \quad (30)$$

From equations (25), (28), (29) and (30) we now have for Lagrange multiplier:

$$e_i = \lambda_i\left(1 + \hat{C}^2 + (1 - \hat{C})^2\right) \Rightarrow \lambda_i = \frac{e_i}{1+\hat{C}^2+(1-\hat{C})^2} \quad (31)$$

The adjustments for each component are thus:

$$f_{ia} = \frac{e_i}{1+\hat{C}^2+(1-\hat{C})^2} \quad (32)$$

$$c_{ia} = \frac{-\hat{C}e_i}{1+\hat{C}^2+(1-\hat{C})^2} \quad (33)$$

$$t_{ia} = \frac{-(1-\hat{C})e_i}{1+\hat{C}^2+(1-\hat{C})^2} \quad (34)$$

4 REAL-TIME RECOVERY CALCULATION MODULE

In principle, real-time recovery can be calculated according to formulas (2) and (3) by applying mass balancing adjustment components as indicated in formulas (19), (20), (21), (32), (33) and (34).

This is a method that is commonly used by plant metallurgists for mass balancing of composite shift sample results. When this method is applied for real-time application, several assumptions need to be reconsidered.

Mass balancing assumes steady state conditions and that material inflows equal material outflows as per equation (6). In case of 8 hour composite samples this is typically a safe assumption. In case of on-stream analyzer samples with as high as 5 minute sample rate, effect of process dynamics need to be taken into account.

When real-time recovery calculation feature was implemented into Courier on-stream analyzer, several possibilities accommodate effect of process dynamics in recovery calculation was evaluated. During the evaluation following design parameters were considered:

- Accuracy of the recovery calculation
- Robustness of the model in variable process conditions
- Generality of the model i.e. possibility to utilize the model in various flotation circuit configurations
- Amount of configuration parameters i.e. ease of use
- Visualization of results

Target was to implement a recovery calculation module that is relatively easy to

configure for most typical flotation circuit configurations so that it would give accurate enough (1-2% rel.) recovery reading in variable process conditions.

It was concluded that for typical Cu-Zn-Pb applications, an extension up to four products was required. For polymetal applications, a reservation for more product formulas was acknowledged but these calculations were not implemented in the first version of the module.

To consider process dynamics with minimal complexity in configuration, parameters describing phase difference between different process streams were needed. Flotation residence time describes phase difference between the feed and final tails. For intermediate streams, there is a possibility to configure estimated residence times separately.

During the evaluation process, it was found that use of direct mass-flow measurements in the recovery calculation has a great potential to improve on-line recovery calculation accuracy in unstable process conditions, for example during radical change in flotation feed rate. For this reason recovery calculation module was accommodated with a possibility to utilize information from existing mass-flow measurement field instrumentation. To enable this feature, a two-way communication mechanism between the DCS and the OSA was implemented.

During the development it was acknowledged that visual reporting of the real-time recovery is essential in order to enable maximal use value for plant operators and metallurgists.

One commonly used method to visualize performance of a flotation process is to use grade-recovery curve. It was acknowledged that in addition to current on-line recovery, this chart has to visualize also historical development of the process in order to give better overall view of the situation.

One of the challenges in visualization is the sheer amount of grade-recovery data over period of time. For this reason different tones of grey color was used to indicate density on most commonly visited dots on grade-recovery chart thus giving a visualization about actual position of the grade-recovery curve itself.

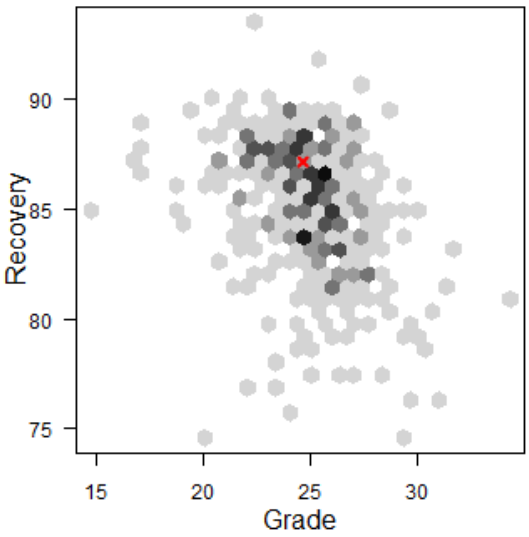

Figure 5. Grade-Recovery visualization of the real-time recovery module.

The red X describes the most recently measured grade-recovery. Grey dots indicate density of historical grade-recovery measurements.

5 RESULTS

Figure 6 illustrates the same data as in Figure 4 after the data has been reconciliated. Three assays were used from each stream for balancing the masses. The recovery was calculated using equation (2) with mass balance adjustment components (32), (33) and (34).

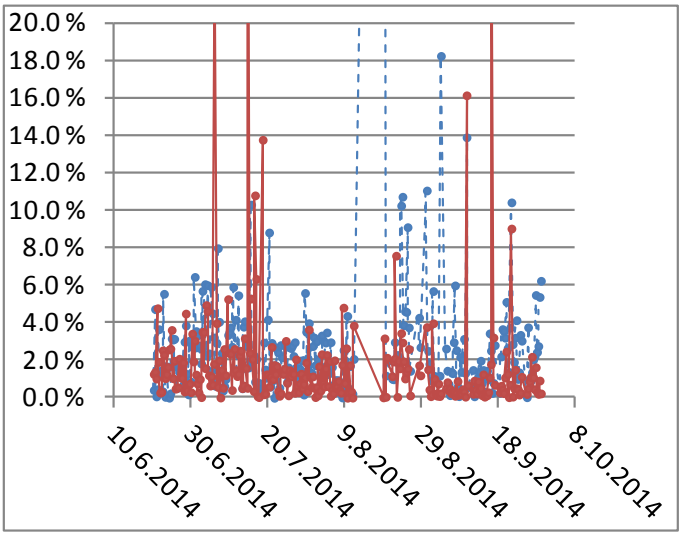

Figure 6. Relative error of OSA recovery compared to laboratory (3 months period).

Real time calculation without mass balancing in blue dotted line and recovery calculated using mass balancing data reconciliation in red line

Applying the data reconciliation methods to the data from the 3 months period the average relative error was reduced to 1.8% from 3.3%. The median error was reduced from 2.0% to 1.0%.

Table 2. Accuracy of recovery calculation with and without mass balancing

	Without mass balancing	With mass balancing
Average relative error	3.3 %	2.0 %
Median relative error	2.1 %	1.1 %

The accuracy of real-time recovery calculation can be improved by applying steady-state mass balancing methods. The reliability of the calculation could possibly be improved further by applying dynamic models for data reconciliation.

6 CONCLUSIONS

Calculation of real-time recovery based on OSA measurements brings useful information for plant operators about current state of the process. The most straight-forward way to calculate real-time recovery is to apply a "two-product" formula for OSA assay data from feed, concentrate and final tails.

Accuracy of real-time recovery calculation can be improved by utilizing a formula for three or more products. Further improvements can be achieved by utilizing data reconciliation methods based on static or dynamic process models.

However, in order to make real-time recovery calculation feasible in real world applications, configuration of calculation models must not be overly complicated.

REFERENCES

Taggart A. F., 1945, Handbook of Mineral Dressing, Ores and Industrial Minerals, *Wiley Engineering Handbook Series*, New York: John Wiley & Sons, 1945.

Rantala, A., Muzinda, I., Timperi, J., Cruickshank, C., Haavisto, O., 2014, Implementation of Advanced Flotation Control at First Quantum Minerals' Kevitsa Mine, *12th Ausimm Mill Operators' Conference*.

Wills, A, Napier-Munn, T J, 2006, An Introduction to the Practical Aspects of Ore Treatment and Mineral Recovery, *Will's Minerals Processing Technology*, 7th Edition pp 65 - 86 (Elsevier Ltd).

Kongas, M., Saloheimo, K., 2001, When is the XRF assay good enough for process control, *Preprint No. 01 - 189 of SME Annual Meeting Denver, Colorado – March 26 - 28, Denver 2001*, 5 p.

Wills, B.A., 1986, Complex Circuit Mass Balancing – A Simple, Practical Sensitivity Analysis Method, *International Journal of Mineral Processing*, 16 (1986) 245 – 262 (Elsevier Ltd).

Vasebi, A., Poulin, E., Hodouin, D., 2012, Dynamic data reconciliation in mineral and metallurgical plants, *Annual Reviews in Control* 36 (2012) 235 – 243 (Elsevier Ltd).

Bazin, C., Franklin, M., 1996. Real-time material balance for flotation plants using a least-squares recursive algorithm, *International Journal of Mineral Processing*, 46 (1996) 231 – 244 (Elsevier Ltd).

Prediction of Final Concentrate Grade Using Artificial Neural Networks from Gol-E-Gohar Iron Ore Plant

S. H. Hosseini, M. Samanipour
Islamic Azad University, Tehran South Branch, Tehran, Iran

ABSTRACT In this study, the artificial neural networks methods were used to predict the iron, phosphor, sulphur and iron oxide content of final concentrate from Gol-E-Gohar iron plant, Kerman province, Iran. The particle size (d_{80}), iron, phosphor, sulphur and iron oxide percentages of run of mine (R.O.M) were used as the inputs for the network. Feed-forward artificial neural networks (FANNs), with 5-8-7-7-4 and 5-8-8-6-4 arrangements were used to estimate the final concentrate grade in both wet and dry magnetic separation process. The outputs of the models were the iron, iron oxide, phosphor and sulphur content of the final concentrate. It was achieved quite satisfactory correlations of $R^2 = 0.98$ in training and testing stages for wet magnetic process prediction. The proposed neural network model, as an alternative to the simulation method, can be used accuratelyto determine the effects of changes in feed and concentrate grade of Gol-E-Gohar iron ore plant in dry and wet magnetic process.

Keywords: Artificial neural network, estimation of ore concentrate grade

1 INTRODUCTION

Artificial intelligence tools have been used for many years in a number of mineral processing applications. These networks have been used different applications such as modeling for particle size analysis (Maxwell et al., 1995), simulation for particle shape quantification (Oja and Nystöm, 1997), assessment of flotation experiments (van Deventer et al., 1997; Cilek, 2002; Labidi et al., 2007) and the modeling of gold liberation from diagnostic leaching data (Petersen and Lorenzen, 1997).

The Gol-E-Gohar iron ore beneficiation plant is located around 55 km southwest of Sirjan, Kerman province, Iran. This plant is situated at the center of a triangle comprising the cities of Kerman, Shiraz and Bandar Abbas in Iran and is one of the major manufacturers of iron concentrate in Iran with capacity of 3.5 million tons annually (Ghasemi, 2004). The plant feed was provided from the Gol-E-Gohar iron mine which is located in Kerman province, Iran.

The iron ore, after drilling, blasting, loading the extracted ore, are transported by mining trucks to the plant. Then the extracted ore are transferred to gyratory primary crusher. The maximum feed size to gyratory crusher is 1.5 m (d_{max}) and d_{80} of gyratory crusher product is about 20 cm. After primary crushing, the crushed ore transfers to autogenous mills. The maximum size of AG mills product is 3 mm (d_{max}) and d_{80} of product is about 550 microns. The product of AG mills transfers to dry low intensity magnetic separator (LIMS). The output of LIMS will be 3 types of products including concentrate, tailings and middlings. The middlings will be regrinded in wet ball mills in next stage and will produce the iron concentrate using wet low intensity magnetic separator. The final concentrate will be transported to tailing dam after dewatering using filters and tickeners. Finally, dry and wet concentrate will be blended together and will be ready to send to the customers. Table 1 shows the chemical properties of final iron concentrate producing by Gol-E-Gohar iron ore plant with d_{80} of 60 microns and maximum moisture of 2%.

The input-output data was obtained from the Gol-E-Gohar iron plant. In order to

obtain the most suitable ANN models which predict the final iron concentrate grade, the performances of the models in terms of mean relative error (MRE) and mean absolute error (MAE) were calculated by the following equations:

$$\text{MRE}=\frac{\sum_{i=1}^{N}\frac{X_{predicted,i}-X_{observed,i}}{X_{observed,i}}}{N}\times 100 \qquad (1)$$

$$\text{MAE}=\frac{\sum_{i=1}^{N}\left|X_{predicted,i}-X_{observed,i}\right|}{N} \qquad (2)$$

Where Xi is the grade or particle size and N is the number of data points.

The aim of the present study is the assessment of Fe, FeO, P, S % of final iron concentrate from Gol-E-Gohar iron plant, Kerman province, Iran with changing the particle size (d_{80}), Fe, FeO, P, S % of the feed from Gol-E-Gohar iron mine, and simulate the process using neural network technique.

Table 1. Chemical properties of final iron concentrate in Gol-E-Gohar iron ore plant

Element or oxide (%)	Amount
Fe	67% min.
FeO	20% min.
P	0.05% max.
S	0.5% max.
CaO	0.6% max.
SiO_2	2% max.
Al_2O_3	0.5% max.

2 RESULTS AND DISCUSSION

The used multilayer perceptron (MLP) neural networks has 3 hidden layers. Five neurons in the input layer correspond to the percentage of Fe, FeO, P, S and d_{80} of the iron ore feed, and four neurons in the output layer correspond to Fe, FeO, P and S content for the final iron concentrate.

Figures 1and 2 depict the models 1 and 3 of feed-forward network with one input layer, three hidden layers, and one output layer, which were used for the prediction of final iron concentrate grade.

Data used to test the proposed approach are taken from the Gol-E-Gohar plant chemical analysis daily database. The database consist of the percentage of Fe, FeO, P, S and (d_{80}) of the feed (iron ore) and also Fe, FeO, P, S content of the final iron concentrate. A total of 219 sets of data sets were used in the predictions by ANN; 200 data sets for training and 19 sets for testing the network were used. The training process was stopped after 200 epochs (Figure 3). In each epoch, the entire training set was presented to the network and errors are calculated and used to adjust the weights in the network using sigmoid transfer function.

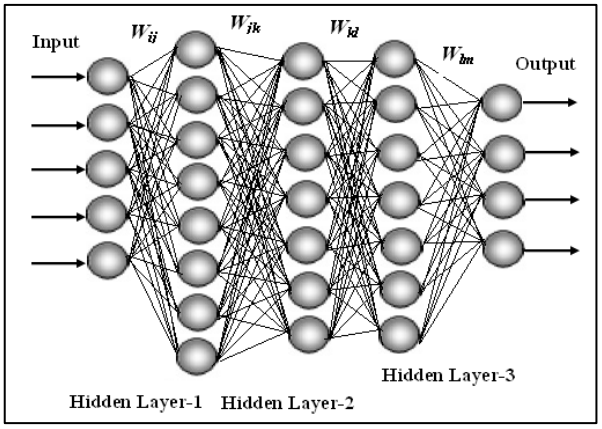

Figure 1. Multilayer perceptron neural network model 1 (5-8-7-7- 4)

Modeling was carried out in five stages according to the feed of different mills (wet or dry mills) and also the mixture of wet and dry iron concentrate. This was done in order to have a convenient comparison between the results and reliable prediction for the quality of final iron concentrate with the least error.

Table 2 shows the different stages of modeling according to the network structure and also the obtained correlation coefficients. As it can be seen, the highest correlation coefficient was observed in models of 1 and 3 for all training, testing, validating and prediction stages.The correlation coefficient value for the training set on both of models 1 and 3 were equal to 0.99. The correlation

coefficient for testing sets was 0.99 in both models of 1 and 3. The coefficient of determination value for the training set on both of models of 1 and 3 were 0.98. The test set that actually determines how good the model is shows that the models can estimate the outputs quite satisfactorily. Quite satisfactorycorrelation of 0.99 for prediction of iron concentrate grade was achieved. The quite satisfactory coefficient of determination 0.98 for prediction of iron concentrate grade was achieved. It was observed that the final concentrate grade could be predicted using the ANN model satisfactorily

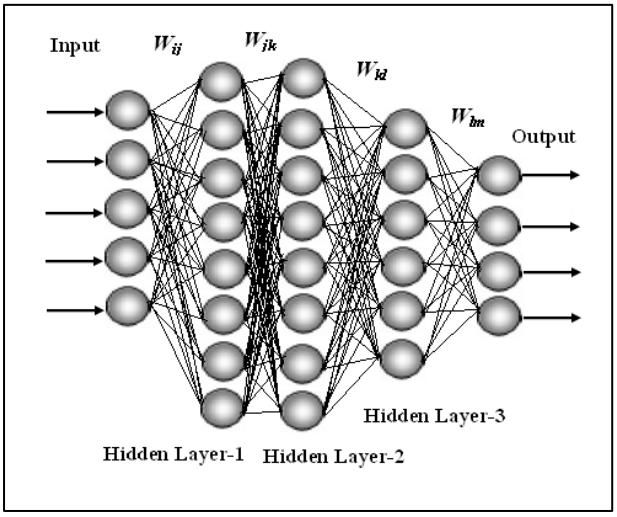

Figure 2. Multilayer perceptron neural network model 3 (5-8-8-6- 4)

Table 3 shows the prediction errors. Negative values of errors in Table 3 indicate that the prediction values and comparing with actual value. The performance of used function is the mean absolute error (MAE), the average absolute error between the network predicted outputs and the target outputs, that was 0.02, -0.23, 0, 0 for testing data in Fe, FeO, P and S % predictions for model 3, respectively. Figures 4-7 show the predicted data using FANN versus actual data in plant process. The R2 values for the testing sets were 0.96, 0.96, 0.90 and 0.94 in Fe, FeO, P and S % predictions, respectively. It was observed that the grade of final iron concentrate could be predicted using the ANN model satisfactorily.

However, the above mentioned results suggest that ANNs owing to their excellent nonlinear modeling ability are better alternative to the linear models for the prediction of final iron concentrate grade.

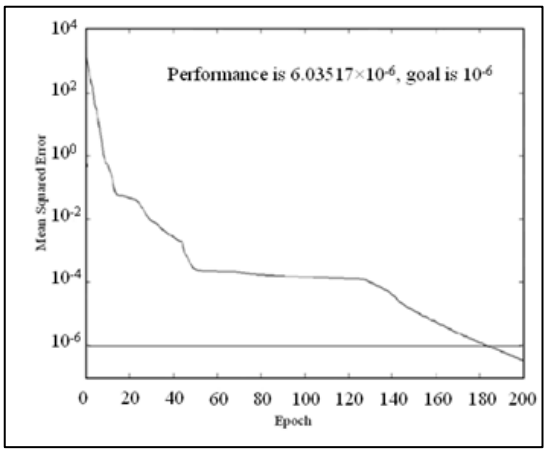

Figure 3. Parity plot for epoch and mean square error for training sets

Table 2. The different stages of modeling and obtained coefficient of determination

Model	Products	Network Structure	coefficient of determination			
			Training	Test	Validation	Prediction
1	Feed to the wet mill (wet concentrate)	5.8.7.7.4	0.99978	0.99544	0.89471	0.98121
2	Feed to the wet mill (wet tailing)	5.8.7.8.4	0.99373	0.92943	0.65774	0.88849
3	Feed to the dry mill (dry concentrate)	5.8.8.6.4	0.99990	0.99908	0.99341	0.99846
4	Feed to the dry mill (dry tailing)	5.4.5.8.4	0.98149	0.93472	0.86349	0.94411
5	Mixture of wet and dry concentrate (final concentrate)	5.10.8.9.4	0.99367	0.87127	0.86167	0.93923

Table 3. Errors Determination of the mean absolute value and mean relative error values available for five models

Model	MAE				MRE (%)			
	S	P	FeO	Fe	S	P	FeO	Fe
1	-0.0653	0.0015	1.0034	-0.3277	7.36	-3.66	-4.20	0.48
2	0.00	0.05	-0.24	-0.53	0.15	-17.42	9.40	2.22
3	0.00	0.00	-0.23	0.02	-0.38	8.04	0.99	-0.04
4	0.48	0.09	1.27	-0.48	-14.15	-40.28	-58.87	1.81
5	-0.18	0.00	-0.05	-0.34	24.21	-0.65	0.18	0.50

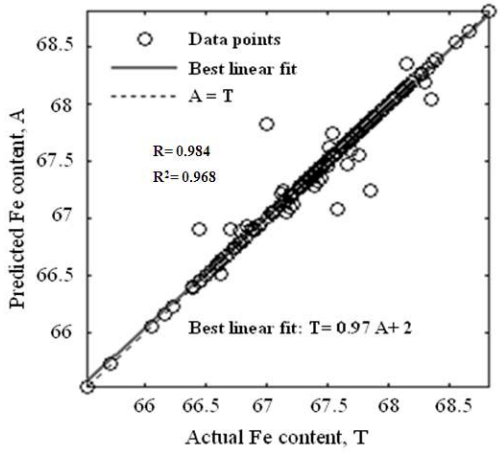

Figure 4. Linear regression predicted Fe content versus actual Fe content in final iron concentrate

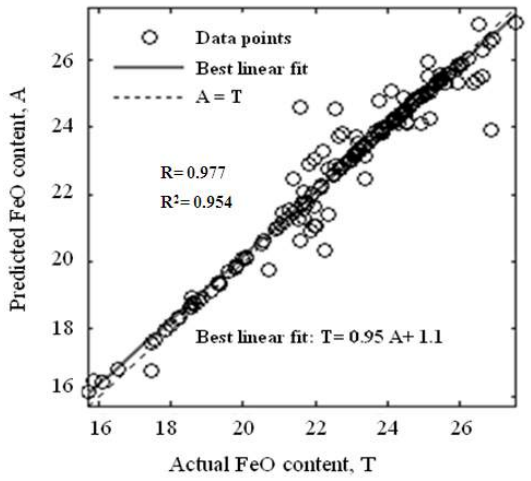

Figure 5. Linear regression predicted FeO content versus actual FeO sulphur content in final iron concentrate

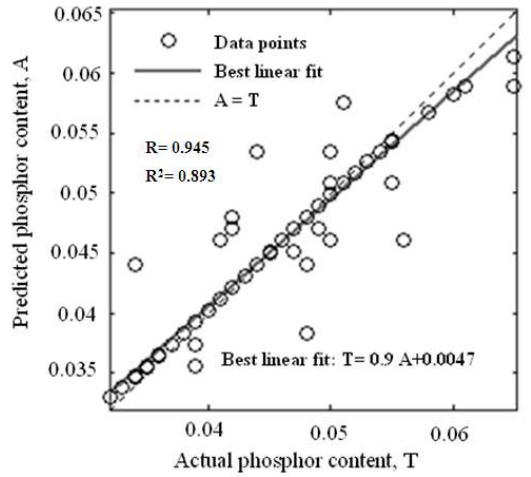

Figure 6. Linear regression predicted phosphor content versus actual phosphor content in final iron concentrate

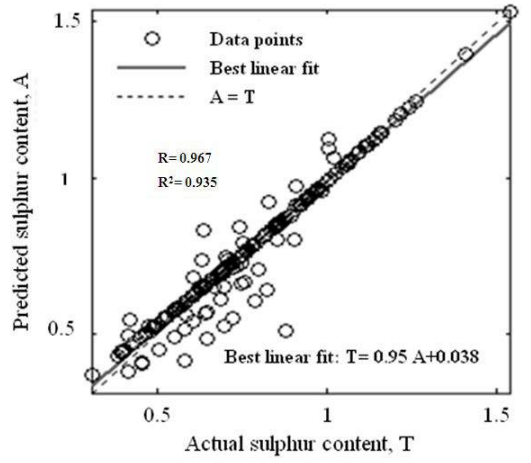

Figure 7. Linear regression predicted sulphur content versus actual sulphur content in final iron concentrate

3 CONCLUSION

(1)Based on the results from this study, the three-hidden-layer ANN model is capable of predicting the Fe, FeO, P and S % of final iron concentrate subject to different conditions.

(2) The input- output data were obtained from the Gol-E-Gohar iron ore plant, and used in the simulation by means of artificial neural network. Feed-forward artificial neural networks with 5-8-7-7-4 and 5-8-8-6-4 arrangements were used to predict the grade of final iron concentrate.

(3) In the testing process, the proposed ANN models can estimate the outputs quite satisfactorily. The correlation coefficients (R) for testing sets are 0.98, 0.98, 0.95 and 0.97 in Fe, FeO, P and S assay predictions, respectively. The coefficient of determination(R^2) for testing sets are 0.96, 0.96, 0.90 and 0.94 in Fe, FeO, P and S assay predictions, respectively.

(4)The proposed approach should be useful to geologists, mining engineers and plant engineers for predicting the grade of different iron ore types and for suggesting suitable blending of feed materials to achieve the maximum recovery.

(5)The proposed neural network model accurately reproduces all the effects in prediction of final iron concentrate grade at Gol-e-Gohar iron ore plant.

(6)These studies on forecasting the grade of final iron concentrate could be new unexamined conditions that where ANN have never been used to predict of Fe, FeO, P, S % in final iron concentrate at Gol-e-Gohar iron ore plant.

(7) In the current work the accuracy of the models were enhanced by the selection of better network structures instead of selecting a larger data set.

ACKNOWLEDGEMENTS

The authors would like to thank Islamic Azad University, South Tehran Branch, Tehran, Iran for funding this project and also Gol-e-Gohar Iron Ore Company for their assistance in collecting the required data used in this study.

REFERENCES

Cilek, E.C., 2002. Application of neural networks to predict locked cycle flotation test results. Minerals Engineering. 15, 1095–1104.

Ghasemi, karam, 2004. Dry magnetic separator performance reviews in Gol-e- Gohar Iron Ore Processing Circuit. Master Thesis, School of Mining Engineering, Amirkabir University of Technology, P. 24-28.

Labidi, J., Pelach, M.A., Turon, X., Mutje, P., 2007. Predicting flotation efficiency using neural networks. Chem. Eng. Process. 46, 314–322.

Maxwell, A.P., Denby, B., and Pitts, W., 1995. The Application of Neural Networks to Size Analysis of Minerals on Conveyors. 25th International Symposium on the Application of Computers and Operations Research in the Minerals Industries (APCOM), Brisbane, Australia.

Oja, M., and Nystöm, L., 1997. The Use of Self-Organising Maps in Particle Shape Quantification. In: Hoberg, H., and von Blottnitz, H., (eds), Proceedings of the XX International Mineral Processing Congress, Vol. 1, pp 141-150, Aachen, Germany.

Petersen, K.R.P., and Lorenzen, L., 1997. Gold Liberation Modelling Using Neural Network Analysis of Diagnostic Leaching Data, Proceedings of the XX International Mineral Processing Congress, Vol. 1, pp 391-400, Aachen, Germany.

Van Deventer, J.S.J., Bezuidenhout, M., and Moolman, D.W., 1997. On-Line Visualisation of Flotation Performance Using Neural Computer Vision of the Froth Texture, Proceedings of the XX International Mineral Processing Congress, Vol. 1, pp 315-326, Aachen, German

Production Scheduling using Augmented Lagrangian Relaxation and Genetic Algorithm Optimization

E. Moosavi
Department of Mining Engineering, Islamic Azad University, South Tehran Branch, Tehran, Iran

J. Gholamnejad
Department of Mining and Metallurgical Engineering, Yazd University, Yazd, Iran

M. Ataee-pour
Department of Mining and Metallurgical Engineering, Amirkabir University of Technology, Tehran, Iran

E. Khorram
Department of Applied Mathematical and Computer Science, Amirkabir University of Technology, Tehran, Iran

ABSTRACT To improve the quality of decision making in the mining operation, it is essential to find global optimum in problems with large dimensional scales. It is widely accepted that Long-term production scheduling (LTPS) problem is playing key role in mining projects to improve their performance by considering availability constraints while maximizing the project total profits during the period. Since production scheduling problems are NP-hard, there is need of improving scheduling methodologies to get good solution. This paper presents a hybrid model between augmented Lagrangian relaxation (ALR) and Genetic algorithm (GA) to solve the LTPS problem. We propose to apply the ALR method on the LTPS problem which to improve its performance speeding up the convergence and also, GA is used to update the Lagrangian multipliers. The results from synthetic data set show that the ALR method is effective in solving large- scale problem and generation a feasible solution then the traditional linearization method. Furthermore, the proposed hybrid strategy based on GA showed better performance in comparison to the available methods.

Keywords: Augmented Lagrangian Relaxation, Genetic Algorithm Optimization

1 INTRODUCTION

A problem that must be solved frequently by an orebodoy block model is to determine economically by what blocks will be removed to meet the forecasted processing decisions and operating constraints, over a long time horizon. The problem is commonly referred to as the Long-term production scheduling (LTPS) problem. The LTPS problem is a mixed-integer programming problem and is the class of NP-hard problems. Because of its size and NP-harness, the true optimal solution of the LTPS problem is normally difficult to obtain. Nevertheless, the high dimensionality and combinatorial nature of the LTPS problem curtail attempts to develop any rigorous mathematical optimization method capable of solving the whole problem for any real-size block model. Therefore, many research efforts have been focused on efficient LTPS algorithms for higher total production profit and computational time.

A first optimization model for this problem was proposed by Johnson [1] based on linear programming model by using Dantzig-wolf decomposition principles. Many

conventional methods were applied to solve the LTPS problem such as branch and cut method (BC) [2, 3] mixed-integer programming (MIP) [4-10], dynamic programming (DP) [11-15], classical Lagrangian relaxation (CLR) [16-20].

Aside from the above methods, there is another class of numerical techniques applied to LTPS problem. Specifically, there are Artificial intelligence (AI) [21-23], Genetic algorithm (GA) [24-27], Simulated annealing (SA) [28-29]. The GA, SA methods can search not only local but also global optimal solution. However, they are sensitive to the parameter setting and require a considerable amount of computational time for large problem size due to the large search space. Extensive surveys of different operation research techniques and modeling issues are provided by Espinoza et al. [30]. To reduce the search space in the large-scale problem, and therefore computational time, hybrid methods are much efficient than the single methods due to more production profit and faster computational time [31]. The hybrid methods are purported to incorporate more complicated constraints and are purported to have better quality solutions.

This paper proposes a hybrid method between augmented Lagrangian relaxation and Genetic algorithm (ALR-GA) to solve the open pit mines LTPS problem. ALR-GA is a combination of improved augmented Lagrangian relaxation and Genetic algorithm. The hybrid method uses the advantage of GA which can provide a near global solution combined with the advantage of ALR which can find a solution within a short time.

2 THE PROPOSED METHOD

During the past few decades, considerable attention has been focused on finding methods for solving the large-scale problems. At present, one of the potential approaches for solving proposed problems is the Lagrangian relaxation (LR) method. Within the LR method, there are two main approaches: the CLR and the ALR method [32, 33]. The basic idea of LR is to relax the complicating constraints by using Lagrangian multipliers. The relax problem is then decomposed into N subproblems. The search is an iterative algorithm that solves relaxed subproblems and updates Lagrangian multipliers according to the extent of violation of complicate constraints. The main drawback of CLR method is that there is duality gap between the solution of the Lagrangian dual problem and the solution of original problem, and often the quality of the final solution depends on the heuristic steps [34]. These difficult can be overcome by the ALR method, which is based on the linearization technique [35]. The ALR decomposition procedure is dependent on the initial estimates of the Lagrangian multipliers and on the method used to update the multipliers. On the other hand, stochastic optimization techniques such as GA start with the generation of randomly selected chromosomes as the initial population that encoded a set of possible solutions. GA can provide a near global solution but takes a long CPU time.

The ALR and GA method incorporates GA into ALR to update the Lagrangian multipliers and improve the performance of the ALR method within a reasonable CPU time. This hybrid method solves the open pit mine LTPS problem by relaxing the complicating constraints and using the dual optimization theory.

3 FORMULATION OF A LTPS PROBLEM

Long-term production scheduling model is used to predict production targets and ore material flow over several years, it is generally takes a simplified representation of the production and formulated as linear problem. The open pit mines LTPS model on the other hand is more detailed assuming that key decisions (processing decisions) have been made. To consider these two different decision-making targets, the simplest way is to formulate a full space optimization model, where in every period of the scheduling horizon, the availability

constraints are incorporated into the model. In this section, we formulate the LTPS problem as follows:

$$Maximize \quad Z = \sum_{ijk\in\Gamma}\sum_{t}^{T}\sum_{d}^{D}\frac{NV_{ijk}^{td}}{(1+r)^{t}}\cdot b_{ijk}^{td} \tag{1}$$

S.t

$$\sum_{ijk\in\Gamma}\left(\overline{\alpha}_{ijk}-L_{\overline{\alpha}}^{t}\right)\cdot Q_{ijk}^{o}\cdot b_{ijk}^{td}\geq 0 \qquad for\ all\ t,d \tag{2}$$

$$\sum_{ijk\in\Gamma}\left(Q_{ijk}^{o}\cdot b_{ijk}^{td}\right)\leq U_{o}^{t} \qquad for\ all\ t,d \tag{3}$$

$$\sum_{ijk\in\Gamma}\left(Q_{ijk}^{o}+Q_{ijk}^{w}\right)\cdot b_{ijk}^{td}\leq U_{w\&o}^{t} \qquad for\ all\ t,d \tag{4}$$

$$\sum_{t=1}^{T}\sum_{d}^{D}b_{ijk}^{td}=1 \qquad for\ all\ ijk\in\Gamma \tag{5}$$

$$b_{k}^{td}-\sum_{y}^{Y}\sum_{r=1}^{t}b_{y}^{rd}\leq 0 \qquad for\ all\ t,k,d \tag{6}$$

In the model being built, the following indications were accepted:

ijk: is the block identification number, *ijk=1,2,…,* Γ.

Γ: is the total number of blocks to be scheduled.

t: is the scheduling periods index, *t=1,2,…,T.*

T: is the total number of scheduling periods.

d: is the processing type of the block (i.e. *d*=1, 2,…, *D*)

D: is the number of processing type.

NV_{ijk}^{td}: is the net value to be generated by mining block *ijk* in period t if processed as type *d*.

r: is the discount rate in each period.

b_{ijk}^{td}: is the binary variable equal to = $\begin{cases}1 & if\ block\ n\ is\ extracted\ at\ period\ t\ as\ processing\ type\ d\\ 0 & Otherwise\end{cases}$

Q_{ijk}^{o}: is the ore tonnage in block *ijk*.

Q_{ijk}^{w}: is the waste tonnage in block *ijk*.

$\overline{\alpha}_{ijk}$: is the average grade of block *ijk*.

$L_{\overline{\alpha}}^{t}$: is the lower bound average grade of material sent to the mill in period *t*.

U_{o}^{t}: are the upper bound total tons of ore processed in period *t*.

$U_{w\&o}^{t}$: is the upper bound total amount of material (waste and ore) to be mined in period *t*.

Y: is the total number of blocks overlaying block *k*.

K: is the index of a block considered for extraction in period *t*.

y: is the counter for the *Y* overlaying blocks.

In the above model, the objective function (1) is the total profit over the scheduling horizon. Therefore, the objective function is expressed as the sum of net value of the extracting blocks taking into account discount rate. The constraints of the above can be divided into operational and physical constraints. Eqs. (2) to (5) represent the operation constraints, among them, Eq. (6) represent physical constraint.

Among the constraints of the LTPS problem, Eq. (2) limit the average grade of the material sent to the mill to a certain value. Constraints (3) ensure that the milling capacities hold. This upper bound is necessary to secure a smooth feed of ore. Constraints (4) relate the actual available equipment capacity for each period. This upper bound is total amount of material (ore and waste) to be mined in period. Constraints (5) enforce that a block is removed in one period only. Constraint (6) is the wall slope restriction on the basis of *Y* constraint for each block per period.

3.1 Decomposable Structure with Reformulation

Observing the special constraint structure of the open pit mines LTPS problem as shown in section 2, we can reformulation the problem into a decomposable structure through the processing targets. Let us refine the LTPS problem way.

$$Max\ Z=\sum_{ijk\in\Gamma}\sum_{t}^{T}\sum_{d\notin p}^{D}\frac{NV_{ijk}^{td}}{(1+r)^{t}}\cdot b_{ijk}^{td}+\sum_{ijk\in\Gamma}\sum_{t}^{T}\frac{NV_{ijk}^{tp}}{(1+r)^{t}} \tag{7}$$

$$\sum_{ijk\in\Gamma}\left(\bar{\alpha}_{ijk}-L^{t}_{\bar{\alpha}}\right)\cdot Q^{o}_{ijk}\cdot b^{tp}_{ijk}\geq 0 \qquad for\ all\ t \tag{8}$$

$$\sum_{ijk\in\Gamma}\left(Q^{o}_{ijk}\cdot b^{tp}_{ijk}\right)\leq U^{t}_{o} \qquad for\ all\ t \tag{9}$$

$$\sum_{ijk\in\Gamma}\left(Q^{o}_{ijk}+Q^{w}_{ijk}\right)\cdot b^{td}_{ijk}\leq U^{t}_{w\&o} \qquad for\ all\ t,d \tag{10}$$

$$\sum_{ijk\in\Gamma}\left(Q^{o}_{ijk}+Q^{w}_{ijk}\right)\cdot b^{tp}_{ijk}\leq U^{t}_{w\&o} \qquad for\ all\ t \tag{11}$$

$$\sum_{t=1}^{T}\sum_{d\neq p}^{D} b^{td}_{ijk}=1 \qquad for\ all\ ijk\in\Gamma \tag{12}$$

$$\sum_{t=1}^{T} b^{tp}_{ijk}=1 \qquad for\ all\ ijk\in\Gamma \tag{13}$$

$$b^{td}_{k}-\sum_{y}^{Y}\sum_{r=1}^{t} b^{rd}_{y}\leq 0 \qquad for\ all\ t,k,d \tag{14}$$

In the problem reformulation (7) we have made a compact representation of the availability constraints (2) and (3) as (8) and (9) for the sake of processing type. Also, constraints (4) and (5) are decomposed with respect to the processing type as (10) – (13). We use $p \subseteq \{1,2,\ldots,d\}$ to represent set of block indices of those blocks processed as type p. Consequently, part 1 of the objective function is used for maximizing the total discounted economic value not meeting processing targets while part 2 is used for maximizing the total expected net present value of meeting processing targets using processing type p. In this particular formulation, it is considered that there are processing capacity constraint and blending grade constraint for processing type p in each period.

4 LTPS BASED AUGMENTED LAGRANGIAN FUNCTION

The complexity of the large-scale combinatorial optimization problems motivates the use of decomposition techniques. Obviously, CLR has been widely studied for the constrained optimization problem. The major concept of CLR is to distinguish the set of complicating constraints of a general integer program and to incorporate them into the objective function in a Lagrangian fashion by adding penalty coefficients to them so to guide the search toward reducing the amount of constraints violation [33, 36]. Based on powerful duality theorem, we know that if all the constraints are convex and all the variables are continuous, the optimum of primal problem will equal the optimum of the dual problem. However, a duality gap might obtain in the presence of integer, which means that the optimal solution to the dual problem will be exactly less than the true optimum of primal problem.

Based on the above reasoning, we used an ALR technique, where can effectively generate feasible solution for the original problem; based on the augmented Lagrangian function proposed by Andreani et al. [37].

With the above reformulation, the resulted model (7) is decomposed into a wasting subproblem and a number of processing subproblems once the coupling constraints (9)-(13) are relaxed. In this work, the augmented Lagrangian method is applied to solve the open pit mines LTPS problem.

The original maximization objective is equivalent to the minimization a revised objective function. Here, we specify the objective as:

$$Min \qquad \sum_{ijk\in\Gamma}\sum_{t}^{T}\sum_{d}^{D} - Z(b) \tag{15}$$

Specifically, equality and inequality constraints (9)-(13) are relaxed and the following augmented Lagrangian relaxation problem is obtained:

$$L(b,\lambda,\mu,\upsilon,\sigma) = Min \quad \sum_{ijk\in\Gamma}\sum_{t}^{T}\sum_{d}^{D} - Z(b) +$$
$$\left[\sum_{t=1}^{T}\sum_{d}^{D}\lambda^{td}\cdot(b_{ijk}^{td}-1)+\sum_{t=1}^{T}\sum_{d\notin p}^{D}\lambda^{tp}\cdot(b_{ijk}^{tp}-1)\right]+$$
$$\sigma\cdot\left[\sum_{t=1}^{T}\sum_{d}^{D}(b_{ijk}^{td}-1)^2+\sum_{t=1}^{T}\sum_{d\notin p}^{D}(b_{ijk}^{tp}-1)^2\right]+$$
$$\left[\sum_{t=1}^{T}\sum_{d}^{D}\upsilon^{td}\cdot(Q_{ijk}^{o}+Q_{ijk}^{w})\cdot b_{ijk}^{td}+\sum_{t=1}^{T}\sum_{d\notin p}^{D}\upsilon^{tp}\cdot(Q_{ijk}^{o}+Q_{ijk}^{w})\cdot b_{ijk}^{tp}\right]+ \quad (16)$$
$$\sigma\cdot\left[\sum_{t=1}^{T}\sum_{d}^{D}\left[(Q_{ijk}^{o}+Q_{ijk}^{w})\cdot b_{ijk}^{td}\right]^2+\sum_{t=1}^{T}\sum_{d\notin p}^{D}\left[(Q_{ijk}^{o}+Q_{ijk}^{w})\cdot b_{ijk}^{tp}\right]^2\right]+$$
$$\sum_{t=1}^{T}\mu^{tp}\cdot(Q_{ijk}^{o}\cdot b_{ijk}^{tp})+\frac{\sigma}{2}\sum_{t=1}^{T}(Q_{ijk}^{o}\cdot b_{ijk}^{tp})^2$$

The objective function of the relaxed problem can be rewritten as follows:

$$L(b,\lambda,\mu,\upsilon,\sigma) = Min \quad \sum_{ijk\in\Gamma}\sum_{t}^{T}\sum_{d}^{D} - Z(b) +$$
$$\sum_{t=1}^{T}\sum_{d}^{D}\left\{\begin{array}{l}\lambda^{td}\cdot(b_{ijk}^{td}-1)+\upsilon^{td}\cdot(Q_{ijk}^{o}+Q_{ijk}^{w})\cdot b_{ijk}^{td}+\\ \sigma\cdot\left[(b_{ijk}^{td}-1)^2+[(Q_{ijk}^{o}+Q_{ijk}^{w})\cdot b_{ijk}^{td}]^2\right]\end{array}\right\}+$$
$$\sum_{t=1}^{T}\sum_{d\notin p}^{D}\left\{\begin{array}{l}\lambda^{tp}\cdot(b_{ijk}^{tp}-1)+\upsilon^{tp}\cdot(Q_{ijk}^{o}+Q_{ijk}^{w})\cdot b_{ijk}^{tp}+\\ \sigma\cdot\left[(b_{ijk}^{tp}-1)^2+[(Q_{ijk}^{o}+Q_{ijk}^{w})\cdot b_{ijk}^{tp}]^2\right]\end{array}\right\}+$$
$$\sum_{t=1}^{T}\mu^{tp}\cdot(Q_{ijk}^{o}\cdot b_{ijk}^{tp})+\frac{\sigma}{2}\sum_{t=1}^{T}(Q_{ijk}^{o}\cdot b_{ijk}^{tp})^2 \quad (17)$$

In order to minimize the Lagrangian function with respect to the Lagrangian multipliers, the adjustment of Lagrangian multipliers must be done carefully. Most references to adjust Lagrangian multipliers use a combination of subgradient method and various heuristics to achieve a rapid solution. In this paper, we use the Genetic algorithms to adjust the Lagrangian multipliers and improve the performance of Lagrangian relaxation method.

5 APPLICATION OF GA TO MULTIPLIERS UPDATING

As mentioned before, ALR is an iterative method. At each iterative, multipliers are updated, subproblems are optimally solved to obtain dual solution, and primal problem is updated by heuristics as suitable. As we know, subgradient optimization method is commonly used to solve non-differentiable problems by taking a fixed step size in direction of a subgradient [38]. Unfortunately, this method do not always provides good feasible solutions because Lagrangian relaxation is very sensitive to Lagrangian multipliers.

In this section, the Lagrangian multipliers are updated using a GA approach to overcome the convergence problems with ALR. Genetic algorithms are stochastic, parallel search algorithms based on theory of natural selection and the process of evolution [39, 40]. These algorithms start with a set of possible solutions randomly selected in the solution space as a population. Each possible solution is represented as a chromosome and evaluated for its fitness calculated using the objective function. After evaluating the fitness of each population member, a subsequent generation of population is generated by applying genetic operators, such as selection, crossover and mutation, to individual in the current population. Detailed application of the ALR-GA method is given for LTPS problem in section 5.1 to 5.2.

5.1 Generation of Random Lagrangian Multipliers

The process starts with the generation of a population of chromosome. In a genetic population, each chromosome comprises a number of genes and is encoded corresponding to a possible solution of the optimization problem. The popular methods of encoding a chromosome include binary encoding, real number encoding and integer permutation encoding. A chromosome in the ALR-GA method corresponds to an encoded normalized Lagrangian multipliers matrix, shown in Fig. 1.

$\lambda_1^1, \upsilon_1^1, \mu_1^1$	....	$\lambda_{12}^1, \upsilon_{12}^1, \mu_{12}^1$
⋮	....	⋮
$\lambda_1^T, \upsilon_1^T, \mu_1^T$	....	$\lambda_{12}^T, \upsilon_{12}^T, \mu_{12}^T$

Figure 1. The binary representation of a chromosome.

The advantage of using Lagrangian multipliers matrix as the encoded parameter is that the number of bits of chromosome will be entirely independent of the number of blocks. The more encoding bits therefore, the higher the resolution and the slower the convergence. In this paper, we use 12 bits to represent Lagrangian multipliers. The decoding of the encoded normalized Lagrangian multipliers can be expressed as:

$$\lambda_{decode}^{t} = \sum_{i=1}^{12} \lambda_i^t \cdot 2^{-i} \qquad \lambda_i^t \in \{0,1\} \tag{18}$$

$$\upsilon_{decode}^{t} = \sum_{i=1}^{12} \mu_i^t \cdot 2^{-i} \qquad \upsilon_i^t \in \{0,1\} \tag{19}$$

$$\mu_{decode}^{t} = \sum_{i=1}^{12} \eta_i^t \cdot 2^{-i} \qquad \mu_i^t \in \{0,1\} \tag{20}$$

Translating normalized, to real Lagrangian multipliers are calculated as follows:

$$\lambda^t = \lambda_{\min} + \lambda_{decode}^{t}(\lambda_{\max} - \lambda_{\min}) \tag{21}$$

$$\upsilon^t = \upsilon_{\min} + \upsilon_{decode}^{t}(\upsilon_{\max} - \upsilon_{\min}) \tag{22}$$

$$\mu^t = \mu_{\min} + \mu_{decode}^{t}(\mu_{\max} - \mu_{\min}) \tag{23}$$

Where, $\lambda_{\min}$, $\upsilon_{\min}$ and $\mu_{\min}$ are the minimum value of the input variable, $\lambda_{\max}$, $\upsilon_{\max}$ and $\mu_{\max}$ are the maximum value of the input variable.

5.2 Application of GA Operators

5.2.1 Selection

The evolution of a GA population is based on the natural selection and the survival of the fittest. In our implementation, this is achieved using the roulette wheel parent selection [39]. The chance of a chromosome to be selected for reproduction is proportional to its fitness.

5.2.2 Crossover

Crossover produces solutions by the recombination of the parent chromosomes. The operator in its classic form selects one or more crossing points in the parent chromosomes adopt a new crossover technique known as “uniform crossover” which exchange bits between the parent chromosomes to create two new offspring chromosomes by a randomly generated mask. The scheme of “uniform crossover” is shown in Fig.2. In the random mask, the “1” represent bit swapping and “0” denotes bit unchanged.

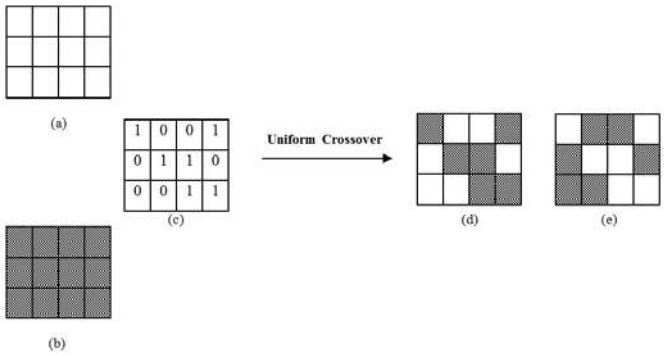

Figure 2. Uniform crossover operator: (a) is the parent chromosome1; (b) is the parent chromosome 2; (c) is the random mask; (d) is the offspring chromosome 1; (e) is the offspring chromosome 2.

5.2.3 Mutation

The mutation operation is aimed to introduce new genetic material into an existing individual. It adds diversity to the genetic characteristics of the population.

5.2.4 Fitness

Since ALR-GA method uses the relative duality gap as its basis of the convergence rule. The fitness function of the chromosome is expressed as follows:

$$FIT = \frac{1}{1 + K \cdot (\frac{F_{\max}}{F_r} - 1)} \tag{24}$$

Where:

K: is the scaling coefficient.

F_{max}= is the maximum of F_r within population.

$$F_r = \frac{1}{the\ relative\ duality\ gap} = \frac{1}{\varepsilon}$$

6 THE FRAMEWORK OF THE PROPOSED HYBRID METHODOLOGY

The proposed hybrid method is fulfilled in two stages (as shown in Fig. 3). The first stage is fulfilled, which formulate an augmented Lagrangian function proposed by Andreani et al. [37], updating the Lagrange multipliers and penalty parameters. Following this, the second stage is the constrained global maximization of the mentioned ALR function, in which a new stochastic method near to the optimal maximum is found using the GA. The framework of the proposed hybrid method can be described as in Fig. 3. The steps of methods are as follows:

Step1. Define coding type and the length of individual string.

Step2. Define Genetic algorithms operation parameters.

Step3. Generate a population of chromosomes, (Lagrangian multipliers).

Step4. Decoding individual string to get different values of multipliers.

Step5. Calculate the constrained maximum of Lagrangian function and convert it into fitness.

Step6. Perform reproduction operator according to the fitness.

Step7. Perform crossover and mutation operators to obtain a new chromosome in order to minimize Lagrangian function.

Step8. If the termination criterion has satisfied, then stop; otherwise return to step (4).

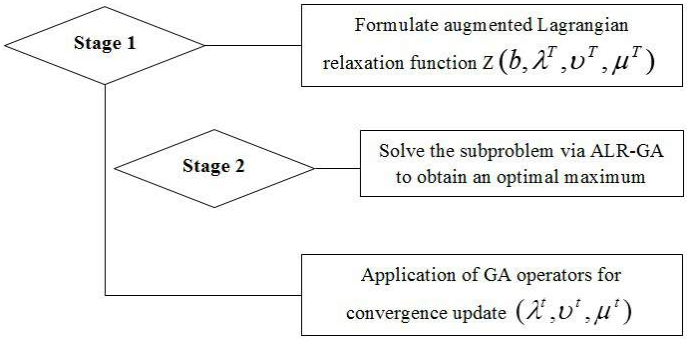

Figure 3. The framework of the proposed hybrid method.

7 CONCLUSION

To address the problem of Long-term production scheduling in open pit mines, a hybrid method between augmented Lagrangian relaxation and Genetic algorithm is proposed in this paper. Based on the special structure of the optimization model, new variables and coupling constraints for the processing decision variables are introduced, the coupling constraints are then relaxed and the resulted augmented Lagrangian relaxation problem is solved through hybrid technique. We propose a new strategy based on optimization of the Lagrangian multipliers and compare its performance with traditional approximation based subgradient method. Genetic algorithm is used to update the Lagrangian multipliers. The advantage of using normalized Lagrangian multipliers as the encoded parameter is that the number of bits of chromosome will be entirely independent of the number of blocks and only dependent of number of periods and processing type. This is particularly attractive in large scale problems.

REFERENCES

[1] Johnson, T. B., 1969. Optimum Production Scheduling, *In proceeding of the 8th international symposium on computer and operations research*.

[2] Caccetta, L., and Hill S.P., 2003. An Application of Branch and Cut to Open Pit Mine Scheduling, *Journal Global Optimization*, VOL. 27.

[3] Bley, A., Boland, N., Fricke, C., and Froyland, G., 2010. A Strengthened Formulation and Cutting Planes for the Open Pit Mine Production

Scheduling Problem, *Computer Operation Research*, VOL. 37.

[4] Gershon, M.E., 1983. Optimal Mine Production Scheduling: Evaluation of Large Scale Mathematical Programming Approaches, *International Journal of Mining Engineering*, VOL. 1.

[5] Caccetta, L., 1989. Open Pit Mine Production Scheduling, *In 3rd Regional proceeding of application computers and operation research in the mineral industry*.

[6] Ramazan, S., and Dimitrakopoulos, R., 2004. Traditional and New MIP Models for Production Scheduling with In-Situ Grade Variability, *International Journal Surface Mining Reclamation Environment*, VOL. 18.

[7] Ramazan, S., Dagdelen, K., and Johnson T.B., 2005, Fundamental Tree Algorithm in Optimizing Production Scheduling for Open Pit Mine Design, *Trans Inst Min Metall*.

[8] Boland, N., Dumitrescu, I., Froyland, G., and Gleixner, A.M., 2009. LP- based Disaggregation Approaches to Solving the Open Pit Mining Production Scheduling Problem with Block Processing Selectivity, *Computer Operation Research*, VOL. 36.

[9] Bienstock, D., and Zuckerberg, M., 2009. A New Algorithm for Precedence Constrained Production Scheduling, *Optimization Online*.

[10] Askari-Nasab, H., Pourrahimian, Y., Ben-Awuah, E., and Kalantari, S., 2011. Mixed Integer Linear Programming Formulations for Open pit Production Scheduling, *journal of mining science*, VOL. 47.

[11] Roman, R.J., 1974. The Role of Time Value of Money in Determining an Open Pit Mining Sequence and Pit Limits, *In 12th symposium on the application computers and operation research in the mineral industry*.

[12] Dowd, P.A., and Onur, A.H., 1992. Optimizing Open Pit Design and Sequencing, *In 23th symposium on the application computers and operation research in the mineral industry*.

[13] Tolwinski, B., and Underwood, R., 1996. A Scheduling Algorithm for Open Pit Mines, *IMA Journal of Mathematics Applied in Business and Industry*, VOL .7.

[14] Tolwinski., B., 1998. Scheduling Production for Open Pit Mines, *In symposium on the application computers and operation research in the mineral industry*.

[15] Wang, Q., Gu, X., and CHU, D., 2008. A Dynamic Optimization Method for Determining Cutoff Grades in Underground Mines, *Mineral Resources Management*.

[16] Dagdelen, K., and Johnson, T.B., 1986. Optimum Open Pit Mine Production Scheduling by Lagrangian Parameterization, *19th Application of Computers and Operations Research in the Mineral Industry*.

[17] Akaike, A., and Dagdelen, K.A., 1999. Strategic Production Scheduling Method for an Open Pit Mine, *In proceedings of the 28th Application of Computers and Operation Research in the Mineral Industry*.

[18] Mogi, G., Adachi, T., Akaike, A., and Yamatomi, J., 2001. Optimum Production Scale and Scheduling of Open Pit Mines Using Revised 4D Network Relaxation Method, *In proceedings of the 17th International Symposium on Mine Planning and Equipment Selection*.

[19] Gleixner, A., 2008. Solving Large-Scale Open Pit Mining Production Scheduling Problems by Integer Programming, *Master's thesis*, Technische Universität Berlin.

[20] Lambert, W.B., and Newman, A.M., 2013. Tailored Lagrangian Relaxation for the Open Pit Block Sequencing Problem, *Annals of Operation Research*.

[21] Tolwinski, B., and Underwood, R., 1992. An Algorithm to Estimate the Optimal Evolution of an Open Pit Mine, *In proceeding of the 23th international symposium on the application computers and operation research in the mineral industry*.

[22] Elevli, B., 1995. Open Pit Mine Design and Extraction Sequencing by Use of OR and AI Concept, *International Journal Surface Mining Reclamation Environment*, VOL. 9.

[23] Ibrahimov, M., Mohais, A., Schellenberg, S., and Michalewicz, Z., 2014. Scheduling in Iron Ore Open-pit Mining, *The International Journal of Advanced Manufacturing Technology*.

[24] Denby, B., and Schofield, D., 1995. The Use of Genetic Algorithms in Underground Mine Scheduling, *In proceeding of the 25th international symposium application of computers and mathematics in the mineral industry*.

[25] Denby, B., Schofield, D., and Surme, T., 1998. Genetic Algorithm for Flexible Scheduling of Open Pit Operations, *In proceeding of the international symposium application of computers and mathematics in the mineral industry*.

[26] Zhang, M., 2006. Combination Genetic Algorithms and Topological Sort to Optimize Open-pit Mine Plans, *In 15th Mine Planning and Equipment Selection, Torino, Italy*.

[27] Xiau-wei, Gu., Qing, W., Dao-zhang, C., and Bin, Z., 2010. Dynamic Optimization of Cutoff Grade in Underground Metal Mining, *Journal of Central South University*, VOL. 17.

[28] Boucher, A., and Dimitrakopoulos, R., 2012. Multivariate Block-support Simulation of the Yandi Iron Ore Deposit, *Mathematical Geosciences*, VOL. 44.

[29] Kumral, M., Dowd, P.A., 2005. A Simulated Annealing Approach to Mine Production Scheduling, *Journal of Operational Research Society*, VOL. 56.

[30] Espinoza, D., Goycoolea, M., Moreno, E., and Newman, A., 2013. MineLib: A Library of Open Pit Mining Problems, *Annals of Operations Research*, VOL. 206.

[31] Shiwei, Y., Kejun, Z., and Youn, H., 2012. A Hybrid Intelligent Optimization Method for Multiple Metal Grades Optimization, *Neural Computing and Application*, VOL. 6.

[32] Luenberger, D.G., 1984. Linear and Nonlinear Programming, 2nd Edition, *Addison-Wesley*, Reading, Massachusetts.

[33] Geoffrion, M., 1974. Lagrangian Relaxation for Integer Programming, *Mathematical Programming Studies. North Holland, Amsterdam, Netherlands*.

[34] Minoux, M., 1983. Programation Mathematique, *Dunod*, Paris, France, VOL. 1.

[35] Cohen, G., and Zhu, D., 1984. Decomposition Coordination Methods in Large Scale Optimization Problem: The Non-differentiable Case and the Use of Augmented Lagrangian, Advance in Large Scale Systems, *Theory and Application*, VOL. 1.

[36] Guignard, M., 1995. Lagrangean Relaxation: A Short Course, *Belgian Journal of Operations Research*.

[37] Andreani, R., Birgin, E.G., Martinez, J.M., and Schuverdt, M.L., 2008. On Augmented Lagrangian Methods with General Lower-level Constraints, *SIAM Journal on Optimization*, VOL. 18.

[38] Held, M., Wolfe, P., and Crowder, H., Validation of Sub-gradient Optimization, *Mathematical Programming*, 1974, VOL. 6.

[39] Holland, J.H., 1975. Adaptation of Natural and Artificial System, *the University of Michigan Press, Ann Arbor*.

[40] Goldberg, D.E., 1989. Genetic Algorithms in Search, Optimization, and Machine Learning, *Ontario, Addison,Wesley Publishing Company, Inc*.

Simulation of Thermal Profile in a Single Pellet During Drying Process with CFD Method

A. Gitiara, A. Namehi, H. Vali, H. R. Shahrokhshahi, H. Soltani, E. K. Alamdari
Department of Mining and Metallurgical engineering, Amirkabir university of Technology (Tehran Polytecgnic), Tehran, Iran

E. K. Alamdari
Research Center for Materials and Mining Industries Technology, Amirkabir University of Technology, Tehran, Iran.

A.Cheraghi
Deparment of Materials Scince and Engineering , Sharif University of Technology, Tehran, Iran

ABSTRACT Green iron oxide pellets are indurated with thermal treatment in pelletizing plant to achieve sufficient mechanical properties and to be used in iron-steel industry. In the first stage, the pellets are dried with hot air coming from the firing unit. High heat transfer makes the evaporation rate exceeding the outgoing steam rate from the pellets and as a result, increasing the inner pressure of the pellets and fragment. On the other hand, low heat transfer causes low production rate. Using the related equations and considering the pellets' moisture and porosity and applying the pellets' condition on parameters such as specific heat capacity and heat conductivity, an acceptable standard is achieved for simulation. The current work has focused on investigating the pellets' drying process to achieve the optimized condition and consequently, lowering the energy consumption and increasing the process efficiency. Simulating by ANSYS Fluent software, the velocity and temperature of the gas are studied to reach the optimized condition.

Keywords: Heat transfer, navier-stokes, pellet drying, simulation

1 INTRODUCTION

Initial load of both blast furnace and DRI (direct reduction iron) plants should have the required permeability to allow the gasses pass through them uniformly and with a high rate. Since the iron concentrates are in powder form, they make a compressed form which closes the penetration ways. By using the iron concentrate as initial load, additionally, the fine particles of ore across with gasses exit the furnace as dust. The iron concentrate powders should pass an agglomeration process in which the particles sizes grow and therefore, the load permeability and reduction rate increase and the exiting materials as dust through the furnace decrease (Eisele and Kawatra, 2003). Pelletizing provides uniformly sized and almost spherical pellets with sufficient mechanical strength in wet and dry conditions. In wet pellets, moisture content and plasticity are so important to get sufficient bed permeability. For instance, if the plasticity of wet pellets is higher than normal range, the permeability of pellet bed in drying zone on travelling grate will be affected adversely. If they are not plastic enough, they will become fragile or will not have sufficient wet pellet strength to survive on travelling grate. Therefore optimum wet strength and plasticity is important and can be controlled by changing the addition dosage of binder during wet pellet formation (Ljung et al., 2008). Thus, most pelletizing plants have been built near the iron mines.

The pellets' geometric is so that the air passes through them and consequently, the resistance on gas flow is less than briquettes (Meyer, 1980). Today pellets have been a main input of blast furnace (Ljung et al., 2011).

1.1Pelletizing Process

Low grade iron ores with impurity gangue minerals containing silica and alumina must be upgraded to an acceptable level of iron content. Concentrates, due to their fine sizes, are not suitable to be directly charged to the iron-making processes such as the blast furnace. Hence, an agglomeration technique should be applied to fine concentrate. The most commonly employed one is pelletizing in iron ore industry. In pelletizing, iron ore, water and a binder are balled in a mechanical disc or drum to produce agglomerates (Process Description of Gol–E-Gohar, Sivrikaya and Arol 2010, Sivrikaya and Arol 2012). Pelletizing of fine particles consists of a variety of stages such as drying to remove the moisture and grinding to acquire the suitable grain size. The mixed iron concentrates (with additives such as bentonite, lime and sludge) are fed in to the pelletizing discs. Then the green pellets transfer to indurate machine to indurate and to achieve the required mechanical, physical and metallurgical features for steel making plants (Figure 1).

Since the measurement and control in the machine are intricate, the process control is too complicated and a matter of debate. The indurating process generally consists of three main stages; (1) drying, (2) induration and sintering at 1200-1350 °C and (3) cooling the pellets before going to stockpile. The air passes through the steel grates within the machine. Fig. 1 depicts schematic of typical straight-grate induration system. The machine consists of seven regions; updraft drying (UDD), downdraft drying (DDD), preheating (PH), firing (F), after firing, cooling 1 (C) and cooling 2 (C2). Six fans are installed in different areas of the machine to circulate the air within the machine.

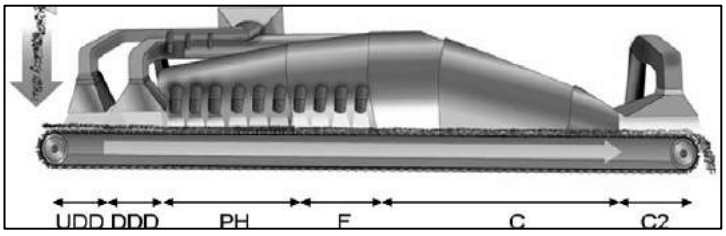

Figure 1. Schematic of assembly line of pelletizing (Ljung et al. 2011).

1.2Drying Green Pellets

In drying stage, the moisture which inhabits the green pellets' porosities evaporates by hot air (300-330 °C). Passing the air through the first layer of pellets, the air absorbs the moisture and reaches the saturation state. The drying gasses are cooled from initial state (300-330 °C) to saturation point. While passing the saturated air through the upper pellet layers which are green and cool, some of air water liquidates on the pellets. These layers will receive high moisture that leads to dropping the pellets' strength and a high plastic deformation occurs in the layers. To overcome this problem a combination of downdraft and updraft drying is applied. The down pellet layers are dried and their temperature increases in updraft drying. In the next stage, the downdraft drying carries out and the top layers are heated and dried. So, the saturated gasses flow from downer layers of hot dried pellets without cooling to saturation point. The initial drying gasses temperature is so that no thermal shock is applied on pellets. If the heating occurs very fast, the cracks appear on the pellets and pellet fragment takes place. Anyway, the pellets are places on a palette to move to different areas of indurating machine (Process Description of Gol–E-Gohar)

The current study is on modeling the heat transfer as well as fluid velocity in drying process by Computational Fluid Dynamic (CFD) method. The aim is well done and initial gasses of various temperatures and flow rates are used and modeled.

2 EXPERIMENTAL

2.1 Transport Equations

Considering the fluid's temperature, velocity, viscosity etc., the fluids are divided into two main categories; laminar and turbulent. The laminar theory is employed in this study. The Navier-Stokes equations for incompressible fluids at basic mode can assume the fluid Newtonian and extract various features. The equations, in which the modelling is done based on them, are as follow:

$$\frac{\partial \rho}{\partial t} + \nabla.(\rho u) = 0 \quad (1)$$

Equation 2 is used for momentum:

$$\rho \frac{\partial u}{\partial t} + \rho u.\nabla u = -\nabla p + \nabla.\left(\mu(\nabla u + (\nabla u)^T) - \frac{2}{3}\mu(\nabla.u)I\right) + F \quad (2)$$

The dominant equation for heat transfer in fluids is:

$$\rho C_p \frac{\partial T}{\partial t} + \rho C_p\, u.\nabla T = \nabla.(k\nabla T) + Q \quad (3)$$

and in solids:

$$\rho C_p \frac{\partial T}{\partial t} - \nabla.(k\nabla T) = Q \quad (4)$$

The relation between heat and temperature gradient is considered as:

$$q = -k\nabla T \quad (5)$$

The Reynolds equation is used to analyze the fluid flow and is as follows:

$$Re = \frac{\rho U L}{\mu} \quad (6)$$

where ρ, u, T, C_p and k are the density (kg/m^3), the velocity (m/s), the temperature (K), the specific heat at constant pressure (J/kg K) and the thermal conductivity (W/m K) of the surrounding fluid. Furthermore, Q is the energy source term (W/m^2) and μ is the dynamic viscosity (kg/m s).

Table 1 describes the used materials' properties.

2.2 Model Geometry & Boundary Conditions

ANSYS software was used to simulate the geometry and to model. Employing this software, first the model geometry is drawn. For this purpose, an 18*60 mm chamber and a semi-circular pellet with a 6 mm radius and 18 mm higher from the chamber bottom is considered. The cross section is divided in half and then rotated for convenience in calculation. The model is simulated in three-dimensional as mentioned.

Table 1. Values of pellet parameters used as the base case of simulation.

Parameter	Value
Density of magnetite	5175(Kg/m^3)
Density of water	998(Kg/m^3)
Density of air	0.633 (Kg/m^3)
porosity	25 (%)
Pellet moisture content	8 (%)
Thermal conductivity	3.75(W/m K)
Specific heat capacity of magnetite	700 (J/Kg K)
Specific heat capacity of water	4190(J/Kg K)
Specific heat capacity of air	1009(J/Kg K)

Using ANSYS facilities, the model is meshed for simulation in the next stage (Figure 2).In the last step, the boundary conditions are applied (Figure 3). The pellet's structure and the surrounding are required to build the model. The pellet is considered as a homogeneous sphere with a radius of 6 mm. The system is symmetric and using the symmetric axis, a rectangular chamber with specified dimensions is considered. It is assumed that the existing air present in this area is the effective air on the pellet's temperature. According to the defined pressure over the top and down of the chamber, the simulation condition is kept near the surrounding's real condition. It is seen that the gas velocity is used in the documents; but, in this paper, to use more precise data, the pressure difference of the chamber is calculated and used according to pressure and velocity relation (Equation 1). The simulations were carried out with the commercial software ANSYS Fluent v14.0, which is based on Finite Volume Method (FVM).

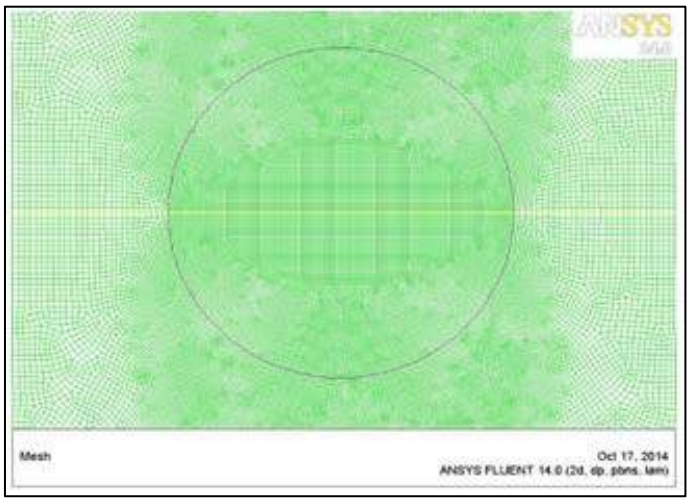

Figure 2. Mesh of the simulation around pellet with symmetry

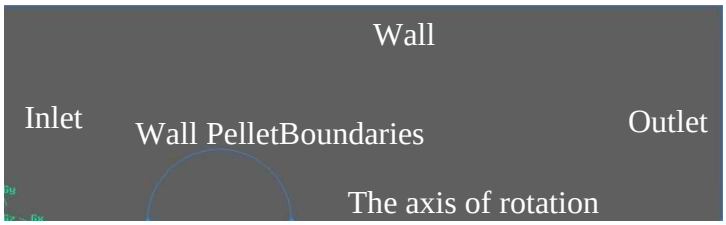

Figure 3. Model geometry with boundary conditions.

2.3 Initial and Boundary Conditions

The boundary condition is necessary to solve the equations. Different states of the system are investigated by applying various boundary conditions in this study. These data are tabulated at Table 2.

The pellets are made from magnetite ore and the initial temperature of the system is considered 70°C. The real fall in pressure is between the top and down of the pallets; however, the simulation calculations are based on a single pellet. So the real initial condition is different from the considered one.

3 RESULT AND DISCUSSION

Velocity profile is calculated for various pressure differences: 5, 10, 15, 55 and 65 Pa; and the results of the calculation for the pressure difference of 15 and 55 between two sides of chambers are reported in Figure 4-a and Figure 4-b. Due to the constant flow of gas, in areas where pellet reduces the speed of gas and lowers gas flow rate consequently, it is necessary the gas speed increases in the vicinity of pellet and the total flow rate remains constant in that case. As a result, gas velocity is increased in those areas. In other case, it is obvious that at low gas velocities, gas velocity is nearly constant in all areas of the chamber before reaching the pellet. But the velocity in these areas could vary by increasing the total velocity. As a result, pellet could change the velocity inside the chamber in a wide range. As it is obvious in Figure 4, by increasing the entrance gas velocity, the area behind the pellet, where the gas velocity is lower, becomes smaller. So it could be concluded that by increasing the entrance gas velocity, heat transfer through the back arch of the pellet can be done better. In addition, velocity of the layer near the pellet is approximately constant. As it is shown in Figure 2, by increasing the inlet and outlet pressure and the velocity as a result, the heat transfer rate gets higher and these changes are linear.

Table 2. Boundary conditions in constant pressure and temperature

Grid no.	$T_{in}(^{\circ}C)$	$\Delta P(pa)$
1	100	10
2	150	10
3	200	10
4	250	10
5	300	10
6	350	10
7	200	15
8	200	35
9	200	55

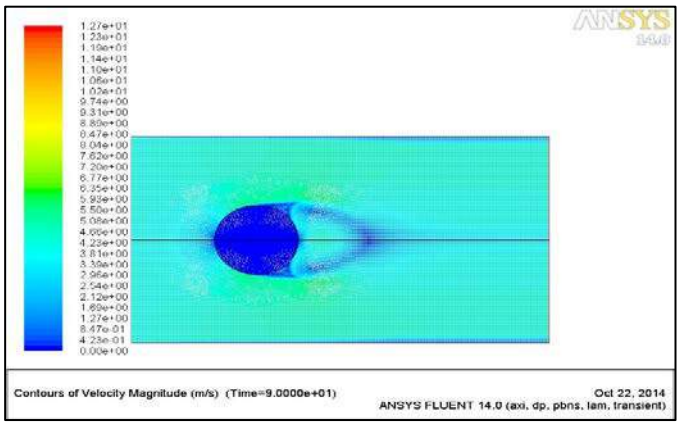

(a)

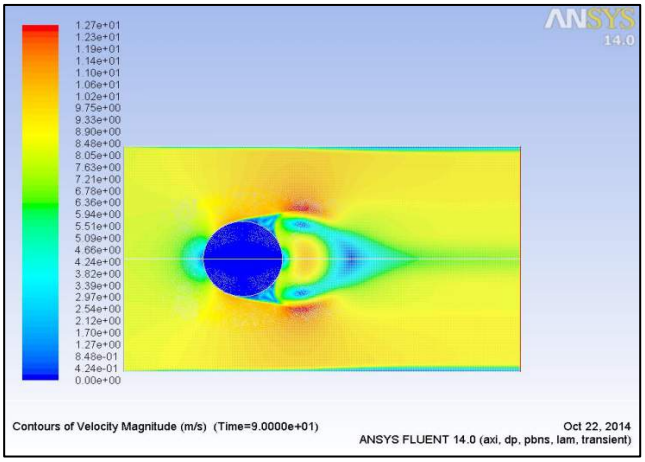

(b)

Figure 4. Velocity magnitude for flow at ΔP a) 15 Pa b) 55 Pa.

Temperature profile calculated in different temperatures is shown in Table 2. The results in which the pressure difference between two sides of the chamber is 15 Pa, initial pellet temperature is 70 °C and the entrance gas temperature is 200 °C, after 60, 120, 240 and 280 seconds are shown in figures 5-a, b, c, d. As it is obvious in Figure 5, the pellet temperature is low at first step and results in lowering the gas temperature contacts with pellet surface. This could affect the drying rate of other pellets that are placed on top layers by lowering the drying rate. Additionally, pellets' temperature is increasing up to entrance gas temperature.

Figure 6-a shows the pellet cross section of the shown temperature profile in Figure 6-b. According to temperature gradient, it is seen that the temperature variation at inside the pellet is reducing in time. All aforementioned results revealed the fact that in drying process, in order to avoid temporal stress, crack or even fragment, the first step of the drying procedure should be done very accurately. The entrance gas temperature should be low at first and could be increased gradually, so pellets would be properly prepared for next steps of the pelletizing procedure.

Moreover, other temperature profiles are calculated for different boundary conditions. The effects of gas entrance temperature and pressure difference between two sides of the chamber for single point inside the pellet with lower temperature are shown in Figures 7 and 8. As can be seen in the mentioned Figures, the results are matched properly with related equations.

As can be seen in Figure 7, the region inside the pellet where consists the lowest temperature is increased linearly with increasing the entrance gas velocity.

Figure 8 shows that the effect of entrance gas temperature is greater than entrance gas velocity which is increased linearly. In addition to, the pressure difference between 20 and 50 Pa is the range for changing the condition from layer flow to turbulence flow, which is not considered in calculations.

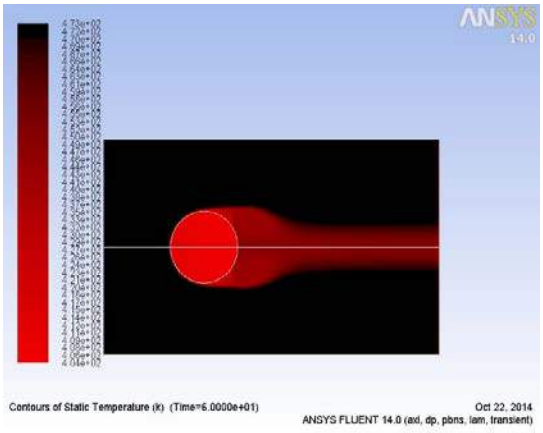

(a)

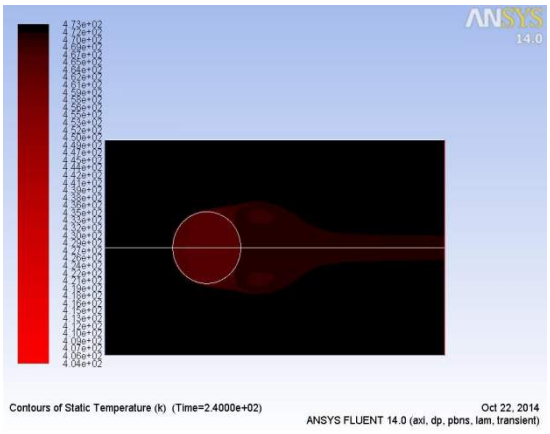

(c)

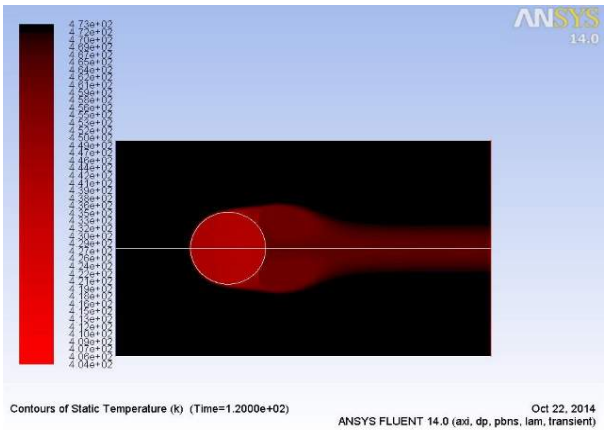

(b)

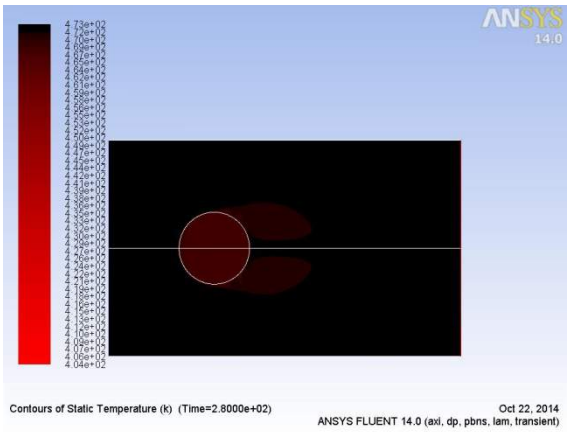

(d)

Figure 5.Temetarure profile of pellet with gauge pressure 15 Pa after a) 60 b) 120 c) 240 d) 280 seconds

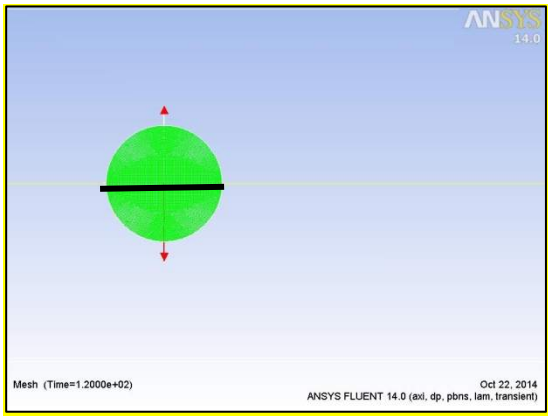

(a)

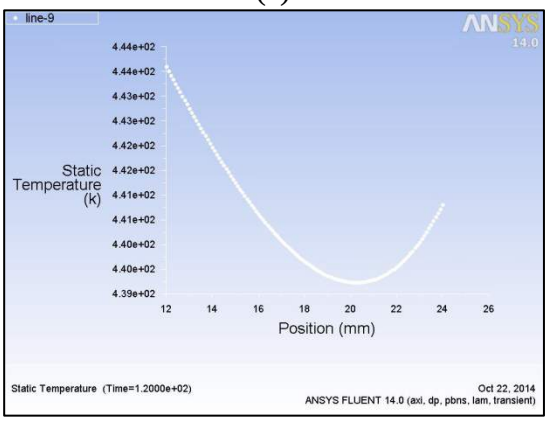

(b)

Figure 6. a) Cross section of the investigated pellet, b) Temperature profiles of pellet at 120 Sec in the diameter of pellet as shown in Fig 6a.

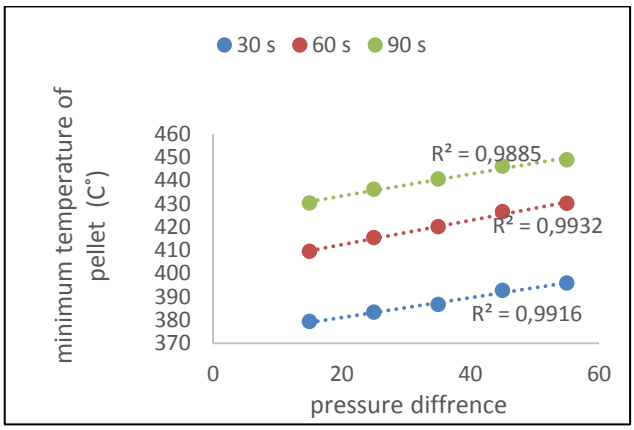

Figure 7.Effect of the gas velocity on minimum temperature of pellet at different times.

4 CONCLUSION

For a system containing a single pellet and a cylinder as the chamber, an analytical simulation is carried out to calculate fluid flow and heat transfer and the results are as follow:

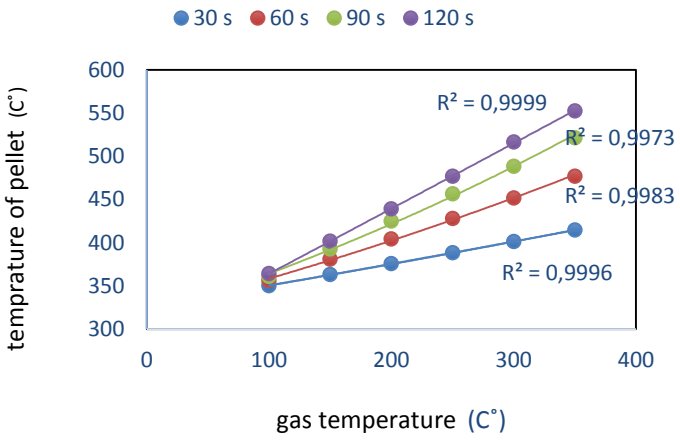

Figure 8. Effect of the gas temperature on minimum temperature of pellet at different times.

The pellet has influence on gas velocity in different areas of the chamber and as a result, affects other pellets' drying process.

- Increasing initial gas temperature increases the internal pellet temperature linearly.
- As the temperature difference inside the pellet is more at first steps of drying process and the possibility defect creation, more attention should be paid in these steps.
- The temperature effect is more considerable compared to the effect of the pressure on heat transfer inside the pellet.

ACKNOWLEDGEMENT

The authors would like to acknowledge the R&D center of Gol-E-Gohar Iron Ore Co. for contribution of the plant data for assessment of the model.

REFERENCES

Eisele T, Kawatra S., 2003, A review of binders in iron ore pelletization. *Mineral Processing and Extractive Metallurgy Review*.; 24, 1-90.

Ljung, A.L.; Lundström S.; Tano K., 2008, Fluid flow and heat transfer within and around a porous iron ore pellet placed in infinite space. *Proceedings of the 19th International Symposium on Transport Phenomena (ISTP-19)*, Reykjavik, Iceland.

Ljung A-L, Staffan Lundström T, Daniel Marjavaara B, Tano K., 2011, Convective drying of an individual iron ore pellet–Analysis with CFD. *International Journal of Heat and Mass Transfer*., 3882-90.

Meyer K., 1980, Pelletizing of iron ores: *Springer-Verlag Berlin*;.

Sivrikaya, O. and Arol, A. İ., 2010, Use of Boron Compounds as Binders in Iron Ore Pelletization, *The Open Mineral Processing Journal*, 3, 25-35

Sivrikaya, O. and Arol, A. İ., 2012, The bonding/strengthening mechanism of colemanite added organic binders in iron ore pelletization, *International Journal of Mineral Processing* 110–111, 90–100

GIS and Topography Applications

Comparative Analysis of Coordinates of Mine Traverse Points Determined on the Basis of Polygon and Tachymetric Traverse

A. Ganić, A. Milutinović
University of Belgrade – Faculty of Mining and Geology

ABSTRACT Determination of spatial coordinates of mine traverse points is to be performed on the basis of measurements of directional angles by applying gyrus method, by measuring lengths on both sides as well as differences in altitude between traverse points, with defined number of measurements repetition. Measurements, organized in this way, provide the required accuracy of points coordinates within the mine traverse in order to carry out all necessary mining works. The use of electronic instruments and the implementation of simple measurement method may provide sufficient accuracy to carry out certain mining activities to a limited extent. The paper displays comparative analysis of spatial coordinates of mine traverse points determined on the basis of measurements within polygon traverse by applying gyrus and tachymetric measurement method at the closed-down lead and zinc mine "Crveni Breg" on the Mountain Avala near Belgrade in the Republic of Serbia.

Keywords: Polygon, tachymetric, gyrus

1 INTRODUCTION

Traverses and level lines build up through underground mine chambers and structures. They consist of points that have their coordinates and altitudes within the same coordinate system, in which the points of the physical Earth's surface are located as well. In this way, underground mine chambers are geo-referenced and their spatial position can be compared with natural and artificial structures located above mining works or within the zone of their influence. Understanding of actual interactions between structures on the terrain surface and underground structures is very significant primarily in terms of safety and protection of people and structures, but also for the purpose of the development of mine pursuant to the designs (Borshch-Komponiets et al., 1989).

Coordinates and levels of traverse and bench points are not measured directly but rather indirectly, by way of calculation, on the basis of measured angles, lengths and differences in level in those traverses. Polygon traverses and level lines in underground mine chambers most often belong to the category of so called open traverses. This means that they end in points that have no known coordinates and levels, whereby this eliminates the possibility to determine actual accuracies of measured parameters within traverses, their correction and, with corrected results, calculation of the most probable values of unknown coordinates and levels of points.

In order to increase the accuracy of measurement, and thereby the accuracy of calculated coordinates and levels of points, measurements are to be repeated several times. This increases the accuracy of measurement but the time necessary to carry out those measurements increases as well.

By using modern electronic instruments, such as total station, time required to carry out measurements can be significantly reduced without significant loss of the accuracy of measurement (Schofield and Breach, 2007). To this end, experimental measurements were carried out at the closed lead and zinc mine "Crveni Breg" on the mountain Avala near Belgrade that belongs to the Faculty of Mining and Geology.

2 EXPERIMENTAL MEASURING AT THE "CRVENI BREG" MINE

The lead and zinc mine "Crveni Breg" was opened in 1886/87 by the group of Serbian capitalists. The French Association of Industry and Mining acquired rights to extract ore at this mine in 1906, when two adits, i.e. horizons were opened, on levels +247m and +195m. With periodic interruptions, ore extraction at the "Crveni Breg" mine continued till 1953, when the mine was definitely closed down.

In the meantime, four additional horizons were opened, on levels: +165m, +135m, +130m and +85m, so that at the moment of closing, there were 6 horizons, 10 inter-horizons, 2 vertical shafts connecting all horizons, several raises and chambers at the mine. Total length of all horizontal and vertical chambers is approximately 6045m. The lowest four horizons were flooded, and because of caving, the first two horizons on levels +247m and +195m are only partially passable and safe.

Furthermore, in 1953, the "Crveni Breg" mine was placed at the disposal of the Faculty of Mining and Geology in Belgrade. As a school mine, it is used for performance of field work and practice.

Experimental measurements were carried out in the so called "lower adit" on level +195m. Mine traverse (Figure 1), which is at the same time level line as well, consists of 17 points and its length is 359.83m. Average length of traverse legs is 22.49m and they range between 6.48m and 64.29m.

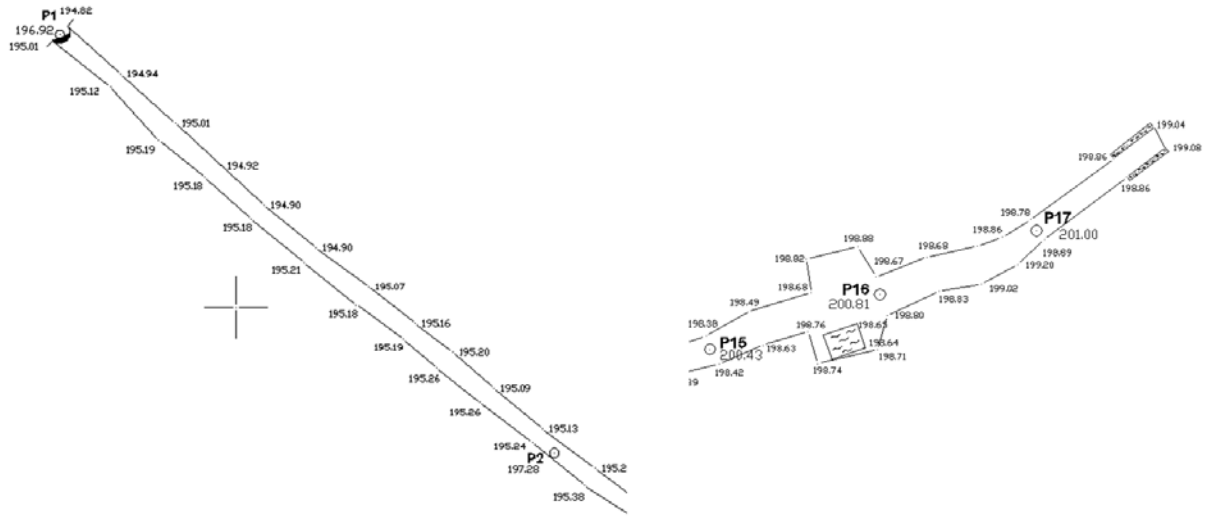

Figure 1. Beginning and the end of the mine traverse at the school mine "Crveni Breg"

During the experiment, angles and lengths within traverse and differences in level within level line were measured first. Angles were measured in two gyruses, and lengths with two repetitions "forward – backward". Differences in level were measured by geometric leveling, the method of leveling from the middle, as well as with two repetitions "forward - backward". Measurements of angles and lengths were carried out by using total station Topcon GTS-226. Specified accuracy of this instrument is ±6" for measuring directions and ±5mm+5ppm when measuring lengths. Differences in level were measured by leveling instrument Carl Zeiss NI-025 with automatic leveling. Pursuant to averaged results of measurements, coordinates and levels of points at the traverse, i.e. level line were calculated.

Thereafter, measurements were carried out at traverse, this time, though, measurements were carried out as if this was tachymetric traverse. This implied that angles (horizontal and vertical) are measured by simple method, only once and only at one position of telescope, and lengths in only one direction. On the basis of those

measurements, coordinates and levels of points in the mine traverse were recalculated. The results obtained according to both methods of measurement are shown in Table 1.

Measurements at traverses and level lines are more accurate that at tachymetric traverses. Therefore, the coordinates and levels of points obtained at traverses and level lines also have conditionally true values when compared with their values obtained by tachymetric measurements. All measured parameters are burdened with accidental errors, so that the differences of coordinates and levels of the same points have no distinctly constant trend. However, when observing spatial differences of positions of points obtained by different methods of measurement $\Delta_{N,E,H}$, it may be generally stated that there is an indicator of the increase in difference in view of accumulation of errors resulting from the lower accuracy of tachymetric measurements.

Table 1. Comparative overview of coordinates of points at the mine traverse

Point	Traverse/Leveling			Tachymetric traverse			Difference			
	N [m]	E [m]	H [m]	N [m]	E [m]	H [m]	Δ_N [cm]	Δ_E [cm]	Δ_H [cm]	$\Delta_{N,E,H}$ [cm]
P1	8922.02	835.97	196.92	8922.02	835.97	196.92	-	-	-	-
P2	8888.24	875.38	197.28	8888.24	875.39	197.29	0	+1	+1	1.4
P3	8875.77	894.76	197.62	8875.75	894.79	197.63	-2	+3	+1	3.7
P4	8881.86	908.98	198.17	8881.84	908.99	198.17	-2	+1	0	2.2
P5	8900.14	967.50	198.56	8900.11	967.52	198.57	-3	+2	+1	3.7
P6	8921.20	1028.24	199.22	8921.18	1028.28	199.21	-2	+4	-1	4.6
P7	8927.02	1042.36	199.36	8926.99	1042.38	199.36	-3	+2	0	3.6
P8	8926.69	1048.84	199.38	8926.66	1048.87	199.38	-3	+3	0	4.2
P9	8930.11	1060.97	199.60	8930.08	1061.01	199.59	-3	+4	-1	5.1
P10	8943.52	1079.17	199.89	8943.50	1079.21	199.89	-2	+4	0	4.5
P11	8950.96	1086.27	200.02	8950.92	1086.30	200.02	-4	+3	0	5.0
P12	8954.25	1095.56	200.12	8954.22	1095.58	200.12	-3	+2	0	3.6
P13	8959.91	1104.34	200.17	8959.88	1104.36	200.17	-3	+2	0	5.0
P14	8965.94	1109.54	200.24	8965.89	1109.54	200.23	-5	0	-1	5.1
P15	8968.93	1122.70	200.43	8968.89	1122.71	200.42	-4	+1	-1	4.2
P16	8972.68	1134.28	200.81	8972.63	1134.30	200.80	-5	+2	-1	5.5
P17	8977.04	1144.95	201.00	8976.99	1144.96	200.98	-5	+1	-2	5.5

When analyzing the results of measurements on angles and lengths, it was observed that the average difference of measured angles is 4.6" which corresponds to the internal accuracy of total station. At the same time, 11 angles differ from each other by less than 5", and maximum difference is 17". Average difference between the same lengths is 1.1cm, whereby seven lengths differ from each other by less than 1cm, and maximum difference is 2.6cm. The difference between the same lengths is larger than the internal accuracy of total station, so it could be concluded that the lengths are the reason for the displayed differences between the coordinates of points.

An additional analysis of spatial error of coordinates at the terminal point of the mine traverse has shown that almost entire error of the terminal point is the consequence of badly measured lengths within the traverse (Dmitrić, 2012). The reason for this is the fact that the reflector signaling could not be carried out qualitatively.

3 APPLICATION OF TACHYMETRIC TRAVERSE AT UNDERGROUND MINES

The analysis of the results obtained shows that when carrying out measurements by applying tachymetric traverse by means of electronic total station, certain tasks in field of mining surveying at mine traverses may be solved. Those are primarily measurements where high accuracy of measurement is not required, i.e. the determination of spatial coordinates is not required:

- at traverses with smaller lengths,
- executing shorter breakthroughs,
- connection of inter-horizons where there is possibility of independent checking,
- in excavation chambers,
- in temporary mine chambers etc.

Figure 2. The layout of the level +494m at the bauxite mine "Kosturi" Srebrenica

The Figure 2 shows the level layout +494m with scale 1:500 from design documentation of the underground bauxite mine "Kosturi" Srebrenica (Faculty of Mining and Geology, 2009). The designed bench passage EH-494-2 is cca 450m long and its function is to be preparation mine chamber for excavation of bauxite ore by applying the method of caving in of lateral and roof parts of the massif (Milutinović et al., 2010). Considering the length of the bench passage, its temporary character and accuracy required when constructing it, the usage of tachymetric traverse for marking directions is justified when constructing this mine chamber.

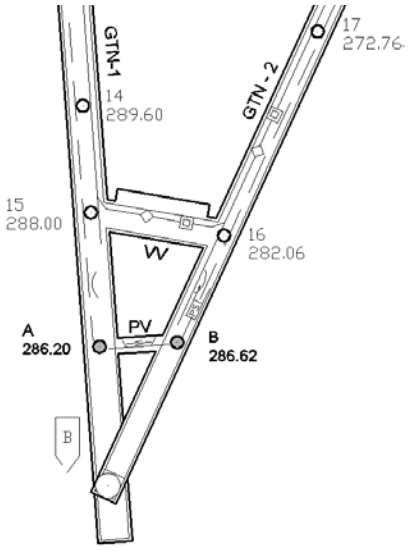

Figure 3. The detail of the layout of the brown coal mine "Soko" Soko Banja

The Figure 3 shows the detail of the design of underground brown coal mine "Soko", Soko Banja (Mining Institute Belgrade, 2002). The underground chambers (GTN-1, VV, GTN-2) shown, represent opening chambers and they are located in such working environment (limestone) where the usage of electronic measuring instruments is permitted. Considering the properties of working environment and requirements to carry out short breakthrough having the function of the transversal connection "PV" for the purposes of coal conveying (points A-B), it is constructed by marking the breakthrough direction from point "A" on the basis of data from tachymetric traverse (points 14-15-A).

4 CONCLUSION

Measurements in tachymetric traverse are carried out by applying simple method including measurements without repetition and with only one position of telescope. Therefore it is possible that such measurements are burdened with gross errors that significantly impair the results obtained. The possibility of gross errors occurrence eliminated at measurements that are being repeated. The application of tachymetric traverses, i.e. measurements in mine traverses, require therefore special attention when carried out. The usage of electronic total stations in underground traverses has the advantage over usage of classical surveying instruments because of elimination of errors occuring while reading directions and entering results. The result of this is also the quality of the directly obtained spatial coordinates of the surveyed points.

Afore-stated findings imply the need that special attention must be paid to centring the instrument and signalling the points as well as the necessity for quality sighting when carrying out those measurements. At that point the occurencies of gross errors in the results of measurements may be eliminated with large certainity, so that in cases stated in this paper or similar, tachymetric traverse may be applied as the method to determine spatial coordinates of points within the mine traverse and to solve mining and surveying tasks.

The advantages of this measurement metod are primarily the shorter time required to carry out measurements, and therefore shorter possible disruption of production causing higher economic efficiency of the production at the mine.

REFERENCES

Borshch-Komponiets, V., Navitny, A., Knysh, G., 1989. *Mine Surveying*, Mir Publishers, Moscow, 367 p.

Dmitrić, J., 2012. *Snimanje podzemnih prostorija u rudnicima metala*, Rudarsko-geološki fakultet, Beograd, 86 p.

Faculty of Mining and Geology, 2009. *The main mining project for underground mining of bauxite reserves remaining in the ″Kosturi″ deposit, Srebrenica - Republic of Srpska*, Book I, Belgrade, 127 p.

Milutinović, A., Ganić, A., Tokalić, R., Gligorić, Z., 2010. Geometrijska kontrola projekta i određivanje elemenata za obeležavanje transportnog niskopa STN-2a u rudniku boksita "Kosturi", *Podzemni radovi* (ISSN 0354-2904), No.17, pp.21-28.

Mining Institute Belgrade, 2002. *Additional mining project opening and exploitation of coal reserves affected the I horizon pit coal mine ″Soko″, Soko Banja - Republic of Serbia*, Book II-1, Belgrade, 73p.

Schofield, W., Breach, M., 2007. *Engineering Surveying*, Butterworth-Heinemann is an imprint of Elsevier, UK, 622 p

Diffusion of Geograpgic Information System at Municipalities in Istanbul

M. Çavur, M. Özturan, C. Karaduman
Boğaziçi University, Management Information System, İstanbul

A.B. İçli
Bilkent University, Electric-Electronic Engineering, Ankara

ABSTRACT This study aims to develop a better understanding of diffusion of Geographic Information Systems within municipalities and examines the infrastructure of İstanbul municipalities and whether they are ready for this technology or not. This study uses two research methods: The first one comprises interviews with the experts of GIS in Turkey. The second one comprises questionnaires conducted with Geographic Information Systems - related departments of İstanbul municipalities. Data collected online have been analyzed by using descriptive statistics, reliability tests, Anova and regression to test the hypotheses. One of the findings is that almost half of the municipalities implement Geographic Information Systems without a vision or a plan for the future. Another finding is that Geographic Information Systems is mainly used to perform registration and maintenance functions instead of supporting the decision-making process. Finally, there is an optimistic expectation of municipalities regarding the use of Geographic Information Systems in the future.

Keywords: Geograpgic Information System (GIS), Istanbul municipalities

1 INTRODUCTION AND OUTLINE OF RESEARCH

Using information technologies (IT) and information systems (IS) is a very common and compulsory issue in all sectors nowadays. Since geographic information system (GIS) is a kind of information technology which enables us visualize, question, analyze, interpret, and understand data in many ways that reveal relationships, patterns, and trends in the form of maps, globes, reports, and charts, it is being used inevitably by all sectors. Municipalities are one of the governmental organizations which use GIS mostly to collect, store, use and evaluate data related to geography.

Due to the reasons mentioned above, municipalities need a new tool or a technology to deal with those data in order to increase their efficiency. The only tool and technology to meet their requirements is GIS tool. Using such tools and techniques, municipalities reduce their work load and time spent. Also, they provide better services and make more profits. On the other hand, they have to share data and information with other governmental organizations and citizens. Therefore, they have to obey some rules and regulations enforced by the governmental organizations to bring standardization and to have high quality data and information. Also, to be more competitive, they serve those data to their citizens and in this way, they provide better services to their citizens. Because of those regulations, social requirements and special reasons, not only municipalities but also all governmental organizations, which are dealing with spatial data and information, have to use GIS technologies.

The objectives of the study are to understand the diffusion of GIS at municipalities in İstanbul, to determine failure and success factors during implementation, to find out required infrastructure for a successful GIS implementation, to understand the problems related with GIS diffusion and finally to

figure out the future expectations of İstanbul municipalities from GIS.

In the literature there are many studies about "Implementation of GIS in a Municipality" in Europe, Canada, Australia and USA, but there are only a few studies about that topic in Turkey. For this purpose, interviews with experts and surveys with municipalities were conducted to study about "The Diffusion of GIS at Municipalities in İstanbul". The interviews were held with three different groups which are academicians, employees in private sector and IT/IS managers in municipalities. The questionnaire was held online with the Metropolitan Municipality of İstanbul and 39 İstanbul districts and the data collected were analyzed through various statistical methods using SPSS 15.

2 BACKGROUND

In this section, data, information, knowledge and GIS terms are discussed in order to have a clear understanding of the study.

2.1 Data, Information and Knowledge

Data is converted into information after processing. According to Hicks (1993), information is a processed version of data which is meaningful to a decision maker. Data are meaningless without processing and interpretation. Therefore, it should be converted into a new form that is easier to be understood by the users. In this way, the user can understand and use information for their purposes and make decisions with respect to this information. Evaluating data provides a healthier decision for the decision-maker.

Longley et al. (2001) assert that information is distinct from data in terms of selection, organization and preparation for a specific purpose. Information serves some ideas which means an interpreted version of data. As can be seen from the definitions, it is clear that the words data and information have different meanings. The relation between reality, data, information and knowledge is complex (Figure 1).

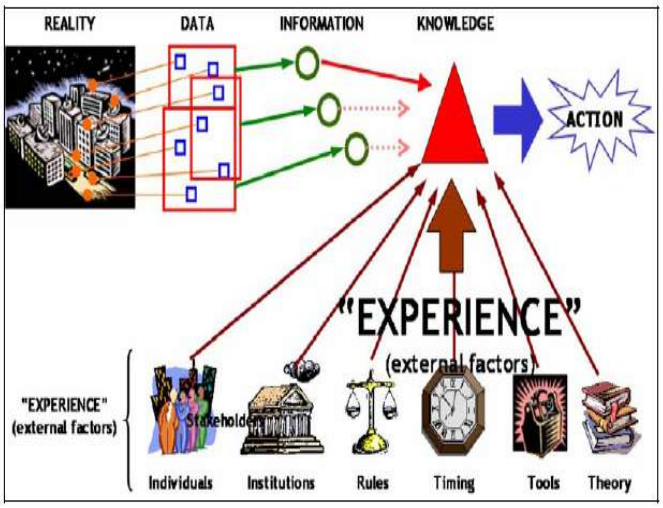

Figure 1. The relation between data, information, and knowledge. (Carrera, 2004)

2.2 Geographic Information System (GIS)

Since GIS is an interdisciplinary method of solution for different areas, there are varying types of GIS definitions with respect to different perspectives. Each profession uses a specific part of GIS extensions or modules; therefore they have different definitions for GIS.

De Man (1988) and Carter (1989) affirm that GIS are perceived as distinctive instances of information system. This is the purest definition of GIS. Indeed, it is clear that information is very important for GIS. GIS mainly consists of two different types of data which are called spatial (geographical) and non-spatial (non-geographical), and has a relational database between these two types of data and has been accepted as a remarkable information system tool.

Dangermond (1988) maintains that GIS comprise five rudimentary parts: data, hardware, software, procedure and people. One wants to use technologies mainly to benefit from them. Indeed, using GIS brings many advantages to governmental and private organizations. Time, efficiency and money are the main advantages of GIS for organizations. Carter (1989) stresses that implementation of GIS requires an organizational structure which combines technology, database, expertise and ongoing financial support. It is for certain that GIS will also bring some financial advantages in time for the organizations using GIS.

3 LITERATURE SURVEY

In the diffusion cycle, the technology is to be accepted and implementation phase is to be achieved following the satisfaction of the citizens or end users. Investing more money, time and people for a new technology brings about more success and implementation evolves into to adoption. Last stage is to develop and invest some more money for a new technology. It means that the new technology is the part of that governmental organization which has to use this technology. After this stage, the new technology not only provides intangible satisfaction for management, end users and citizens; but also provides some tangible benefits. The resources can be used more efficiently and costs of services to the organization are reduced. In accordance with the ideas of Medlin (2001) and Parisot (1995), Rogers' diffusion of innovations theory is the most suitable way of exploring the adoption of technology in higher education. There are five steps of diffusion of a new innovation (Figure 2).

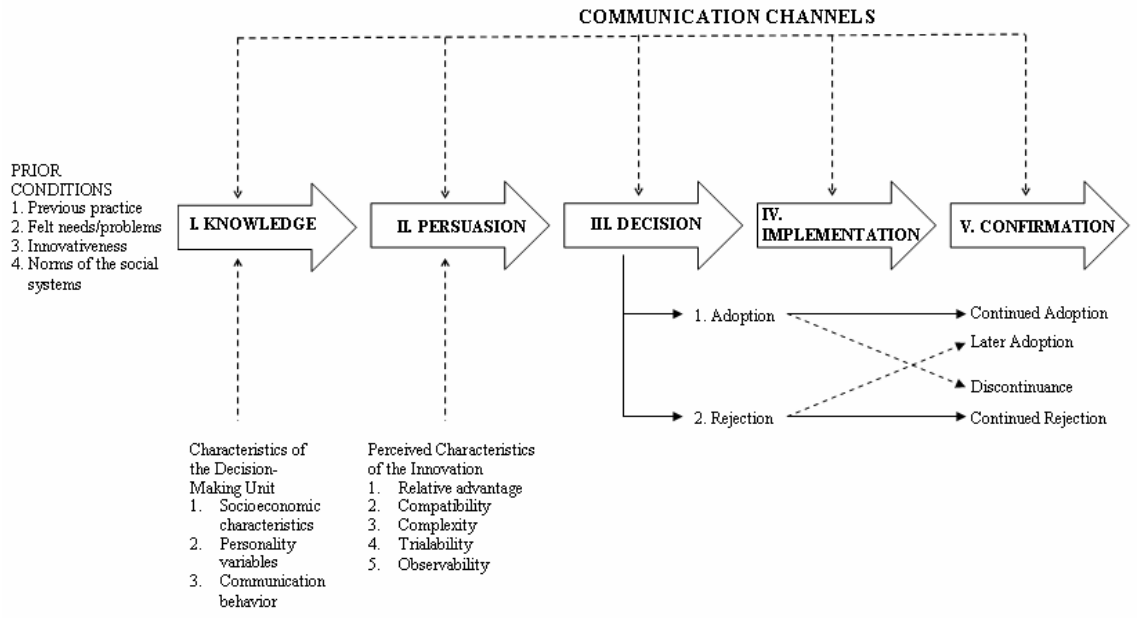

Figure 2. A Model of five stages in the innovation-decision process (Rogers, 2003)

3.1 The Diffusion of GIS at Municipalities in Istanbul

Istanbul is the largest city in Turkey. According to the address-based birth recording system of the Turkish Statistical Institute, the population of the metropolitan municipality, which corresponds to 17.98% of Turkey's population, is 13.26 million as of 2010 and this places Istanbul as the third largest city in Europe after Moscow and London. Since it is the largest and the most crowded city , management of Istanbul is a difficult task. For this reason, it had been divided into different districts throughout history. 8,156,696 people live in the European side and 4,416,867 people live in the Asian side. According to Istanbul Nufus ve Demografik Yapi [Population and Demographic Structure of Istanbul] (n.d.), there are 25 municipalities on the European side and 14 municipalities are on the Asian side.

Municipalities are the representatives of government which encounter with citizens mostly. Their main purpose is to provide better services to citizens pertaining to fresh water, electricity, real estate, tax, natural gases, sewage and more. The complexity of tasks, such as distribution and control of power, fresh water and natural gas, sewage, telephone, school and hospital networks, has been forcing municipalities to find a way to organize these tasks. Besides, some problems about these tasks that are mentioned above occur. For instance, traffic accidents, natural hazards and fire incidents all force the municipalities to come up with fastest and the most efficient solution. In

order to organize these tasks and overcome related problems, appropriate tools and techniques are needed. At this point, GIS is accepted as one of the best solutions for municipalities nowadays.

The awareness for this technology began at the beginning of 1990s; however, it was started to be used at the beginning of 2000s. Municipalities of bigger cities' with respect to their populations, such as Ankara, Bursa, Istanbul, Izmir and Konya, started to exploit the advantage of this technology firstly. However, smaller municipalities have not used it effectively due to lack of awareness and budget. Yomralioglu (2002) says that only some municipalities, such as in Istanbul, Bursa, Ankara, Izmir, Aydin and Antalya, utilize GIS more realistically than the rest.

It is clear that only 4% municipalities attempt to exploit that technology effectively. Should a further research on exploitation of this technology conducted, the percentage will surely increase.

Yomralioglu (2002) challenges the key drives of municipalities, that is awareness of thematical, topographical and administrative structure of all provinces, and adds other motives such as accomplishing health, security, population, communication and road networks, etc. In addition, municipalities actively use GIS especially in solving important local problems such as urban planning, land development, urban management, supervision, and tax collection.

4 THEORITICAL MODEL AND HYPOTHESIS

4.1 Problem Statement

Today, almost all sectors are dealing with GIS technology in one way or another. When these sectors are divided into different parts with respect to their usage level, it is found out that governmental organizations use GIS technology more heavily than private sector. If a comparison is made among governmental organizations, it is seen that municipalities use GIS tools and software mostly with respect to others. Almost all departments use GIS technologies directly or the products of GIS technologies indirectly.

Although municipalities are governmental organizations, they are independent within their internal affairs and policies in Turkey. Therefore, they can easily accept and implement new systems or projects for their use and enjoy the advantages without dealing with too much bureaucracy. There is no competition among municipalities, so they can support each other with their experiences.

4.2 Aim and Objectives

The aim of this study is to explore the usage and diffusion level of GIS at municipalities in İstanbul and opinions of their employees about the following issues:

- Development of GIS at municipalities in İstanbul
- Research about GIS implementation at municipalities in İstanbul and Turkey
- Failure and success factors during implementation of GIS at municipalities in İstanbul based on literature survey, expert opinion and survey results
- Type of infrastructure required for a successful GIS implementation at municipalities in İstanbul
- Kind of problems that may occur during GIS implementation at municipalities in İstanbul
- Anticipation of the future of GIS in the short term (5 years) and long term (10 years) at municipalities in İstanbul

4.3 Key Questions

Based on the objectives, the following research questions are prepared;

- What are the main requirements to implement GIS at municipalities successfully?
- What are the failure and success factors for municipalities during implementation of GIS?
- What kind of purposes are there for using GIS at municipalities?

- What kind of problems may occur during implementation of GIS projects at municipalities?
- Through which processes is GIS implemented at municipalities in İstanbul?
- What are the driving forces for GIS implementation in a municipality?
- What are the strategies that municipalities apply during the implementation process of GIS?
- Who are the actors and what are their roles during implementation of GIS?
- What does GIS bring to a municipality?
- What is the future of GIS at municipalities in İstanbul?

4.4 Hypothesis

Based on the aim and objectives, the following hypotheses are determined (Table 1). Each hypothesis is analyzed with different test.

Table 1. Hypotheses about Diffusion of GIS at Municipalities

NO	HYPOTHESES
H1	There is a relationship between the level of knowledge about GIS and geography- related areas with the success level of GIS diffusion.
H2	There is a relationship between the usage frequencies of GIS in municipalities' departments with the success level of GIS diffusion.
H3	There is a relationship between the levels of acceptance of GIS projects with the success level of GIS diffusion.
H4	There is a difference between municipalities with different longitude of use of GIS in terms of the success of GIS diffusion.
H5	There is a difference between municipalities with different population groups in terms of the success of GIS diffusion.
H6	There is a difference between municipalities with different numbers of employee groups in GIS departments in terms of the success of GIS diffusion.
H7	There is a difference between municipalities with different number of employee groups in municipalities that use GIS tools in terms of the success of GIS diffusion.
H8	There is a difference between municipalities with different satisfaction levels of GIS applications in terms of the success of GIS diffusion.

5 RESEARCH METHODOLOGY

The methodology of this research consists of two important stages. The first stage comprises interviews with the experts of GIS. The second stage comprises a survey focusing on local municipalities of İstanbul

5.1 Interviews

Interviews, which were held with end users, consultants, technical users, developers and managers of municipalities responsible for GIS department or projects, were conducted using face-to-face method.

5.2 Questionnaire

The research was conducted during the spring semester of 2010-2011 by means of a questionnaire which had been developed based on previous researches and theories as well as interviews with GIS experts. Municipalities in İstanbul were decided to be of concern in this study because İstanbul is considered an important research area. Although many of the municipalities use GIS technologies, some municipalities have not used GIS technologies as of the publication date of this study. The questionnaire, which covers the GIS-related departments in municipalities, includes five sections and a total of 36 questions. The questionnaire is distributed to the municipalities in İstanbul via Internet.

6 ANALYSIS AND FINDINGS

6.1 Interviews

In this part, summarized opinions of interviewees are reported under five main headings: overview of GIS, purpose and usage of GIS at municipalities in İstanbul, main problems related with GIS diffusion at municipalities in İstanbul, future of GIS for İstanbul municipalities, and criteria for a successful GIS implementation.

6.2 Purpose and Usage of GIS at Municipalities in Istanbul

- The order of priority in using GIS, in order of first priority to last, is emergency issues such as people in a difficult conditions, fire, ambulance, etc. then citizens, and finally institutions. From parcel-sale and social aid to flooding and property analysis are for what GIS is utilized.
- GIS is about spatial information but MIS is about human information. With the perfect integration of both, it provides services to

citizens with maximum performance. For example, handicapped or educated citizens can easily be followed by the integration of MIS and GIS. In this way, more accurate decisions about them can be made.

- The workload of employees of municipalities in İstanbul has been decreased with the use of GIS. Therefore, this convenience surely is reflected on the citizens. They are now enjoying faster services with higher quality. Since the number of complaints has been decreased, the management is satisfied with this new system.
- GIS is used in every task including numbers, such as road and real estate information. Briefly, it is used in everything that includes geography at municipalities in İstanbul.
- The communication between external institutions and municipalities in İstanbul has increased; so the number of mistakes has decreased. For example, determination of the rate of incomplete declaration and defective buildings is now easier thanks to the usage of GIS at municipalities in İstanbul. In this system, the problems that used to be solved in 3-5 days are dealt with one click.
- Since municipalities are not service-oriented organizations, they use CAD tools just to create maps. Therefore, they waste their time with these tools. Almost 90% of them use CAD tools instead of GIS tools.
- All matters that require the use of spatial analysis are of interest, especially the control of numeric identification, creation of a new numeric identification numbers, problem identification, detection and correction of false addresses, National Address Database System (UAVT) updates, queries of demographic data, and selection of the most appropriate site.

6.3 Main Problems Related with GIS Diffusion at Municipalities in İstanbul

In this part, the interviews are reported with respect to each problem area that has occurred during the diffusion process of GIS. The main problems are as follows:

- Management
- Bureaucratic
- Citizens
- Employee Resistance
- Time
- Budget
- Data
- Infrastructure
- Other Problems

6.4 Future of GIS for İstanbul Municipalities

In this part of study, the future of GIS for municipalities in the short term (5 years) and in the long term (10 years) is discussed.

- GIS is being developed along with the Internet technology, mobile and band communications. To this extent, developments in aerial technology, 3D, video, and cell phone processing units will have a direct impact on GIS adopted by social networks.
- Actually, the users of GIS stay away from databases. There is an increasing trend of using spatial servers, which are the center of GIS management, along with the classical database applications.
- GIS will inevitably be used not only in municipalities but also in all governmental organizations; however, they are not ready in terms of culture and the quality of employees. It is believed that GIS will be used in the daily lives of citizens and municipalities in the near future.
- The importance of local governments and the stress of European Union are increasing every day. For these two reasons, the use of GIS is inevitable for all municipalities in Turkey.

6.5 Criteria for a Successful GIS Implementation

In this part, the criteria for a successful GIS implementation are summarized as follows:

- Management Support
- Perception of Employees
- Data
- In/Out-Sourcing
- Infrastructure
- Bureaucracy

- Project Updates
- Time

6.6 Questionnaire

In this study, data are collected using online questionnaires administered to municipalities in İstanbul and analyzed by using descriptive statistics, reliability tests, linear regression analyses, and ANOVA to test the hypotheses and provide findings. In addition, some graphical representations are used to explain the use of GIS at municipalities in İstanbul.

33 participants (82%) accept that ease of CAD usage is one of the most cited advantages of GIS tools.

21 municipalities (%53) examine successful projects before GIS implementation.

17 municipalities (%43) are planning to invest more money for development of several applications in the future.

Non-user municipalities have several expectations regarding the features of GIS tools. 5 of them (%71) claim that "Reasonable Budget", "Support of Top Management" and "Availability of Useful Digital Data" are the most important reasons that force municipalities to use GIS in the future. On the other hand, only 1 of them (14%) claims that there should be more functional GIS products.

14 municipalities (%35) state that IT/IS department is responsible for GIS tools and projects.

The data indicate that 39 municipalities (%98) outsource GIS projects to consultancy firms. Also, 20 municipalities (%50) outsource GIS projects to private companies. On the contrary, 10 municipalities (%25) implement GIS projects in-house. Finally, they believe that the effect of universities and governmental organizations on municipalities' decision is worthless.

6.7 Reliability

A commonly accepted rule of thumb for describing internal consistency by using Cronbach's alpha is shown as $\alpha>0.7$. To test each hypothesis, reliability analysis is conducted. After finding Cronbach's α (alpha) value

for each piece of data, regression analysis is made for the data whose Cronbach's α value is higher than 0.7 . The Cronbach's α (alpha) value for each piece of data is above the threshold (Table 2).

Table 2. Cronbach's α (Alpha) Value for each Data

Hypothesis	Number of Item	Cronbach's α (Alpha)
Knowledge about GIS-related areas	7	0.777
Frequency of GIS usage	8	0.770
Acceptance of GIS projects	12	0.867

6.8 Linear Regression Analysis

Linear regression analysis is used for specifying the one to one relations between two or more different variables. The linear regression's dependent variable is the success in diffusion of GIS and the independent variables vary. Regression analysis is used to test Hypothesis 1, 2 and 3.

According to the F statistics significance (Sig.) values, all of the constructs are meaningful because they are below 0.05, which means that these constructs can be accepted as statistically meaningful with the confidence level of %95 and the GIS diffusion success can be explained by the related hypotheses (Table 3). The R2 values for the significant constructs show the percentage of the variance in GIS project success which is explained by the related hypotheses. B values indicate the path coefficients which mean that 1 unit change in the related independent variables will affect the GIS project success by the proportion of B values.

Hypothesis 1: Table 3 shows the result of regression analysis for Hypotheses 1. Knowledge factor about GIS-related areas explains %33 of the variance in diffusion success, and has a positive impact by the

proportion of 1.466 on GIS diffusion success.

Hypothesis 2: The result of regression analysis for Hypothesis 2 explains the frequency of GIS use by the departments of municipalities (Table 3). The significance value for this relation coefficient is less than 0.01 (Sig= 0.000); therefore, it can be concluded that there is a significant relationship between success scores and the frequency of GIS use at municipalities. Please note that the relationship is positive: as the intensity of GIS use at municipalities increases, the success in GIS diffusion increases. Therefore, our hypothesis is supported: as usage of GIS increases, so does success in the diffusion.

Hypothesis 3: For GIS diffusion to be successful, acceptance factor of GIS projects explains %54 of the variance and has a positive impact by the proportion of 0.486 on GIS diffusion success (Table 3). It is shown that there is a positive relationship between success and knowledge about GIS-related areas.

Table 3. Linear Regression Analysis of Hypotheses

Hypothesis Explanation	R^2	*Sig.*	*B*	*Hypothesis*	*Hypothesis Acceptance*
Knowledge about GIS-related areas	0.331	0.001	1.466	H1	Accepted
Frequency of GIS usage	0.619	0.000	0.624	H2	Accepted
Acceptance of GIS projects	0.535	0.000	0.486	H3	Accepted

Hypothesis 4: To test Hypothesis 4, ANOVA analysis has been conducted so that GIS diffusion success is differentiated according to their usage time. The data indicate that some municipalities have been using GIS tools and application for long time, but some other municipalities are more successful in garnering benefits from GIS projects (Table 4).

Table 4. ANOVA for Duration of Use of GIS and Success in GIS Diffusion

		Mean	**F/t Value**	**Sig.**
Hypothesis 4 (Rejected)	0-1 year	3.7326	F=0.291	0.881
	1-2 years	4.3032		
	2-5 years	3.9746		
	5-10 years	4.0500		
	10-30 years	3.8750		

It can be seen that the hypothesis is rejected since the significance value (.881) is higher than .05. Therefore, there is no difference among using various GIS tools for different durations in terms of their average success.

Hypothesis 5: To test Hypothesis 5, ANOVA analysis has been conducted so that GIS diffusion success is differentiated according to the number of inhabitants in a specific municipality. Larger municipalities in Istanbul are indeed using GIS techniques but there is no concrete relation between the size of municipalities and GIS success (Table 5). Even if they are the early adopters of GIS, it does not give rise to a successful diffusion. It can be concluded from Table 7 that the largest group of GIS users, who use GIS in several departments at least, is between 50.000 and 150.000. On the other hand, relatively smaller organizations implement GIS in GIS-related departments rather than in the entire organization.

Table 5. ANOVA for Population Groups of Municipalities and Success in GIS Diffusion

		Mean	**F/t Value**	**Sig.**
Hypothesis (Rejected)	Less than 20,000 people	3.3750	F=0.377	0.823
	20,000-50,000 people	3.6303		
	50,000-150,000 people	4.1771		
	150,000-300,000 people	3.9531		
	300,000-500,000 people	4.0021		
	More than 500,000 people	4.0010		

It can be seen that the hypothesis is rejected since the significance value (.823) is higher than .05. Therefore, there is no difference among using various GIS tools in terms of population groups living in a specific municipality.

Hypothesis 6: In addition to the size of municipalities, it is worthwhile to examine

the number of GIS users in municipalities to see whether there is an effect on success of GIS diffusion or not. To test Hypothesis 6, ANOVA analysis has been conducted so that GIS diffusion success is differentiated according to the number of employees in GIS departments of municipalities. Similar to the finding regarding direct users of GIS, the total number of GIS users, no matter if they use it directly or indirectly, have no effect on success of GIS diffusion (Table 6).

Table 6. ANOVA for Number of Employees in GIS Department and Success in GIS Diffusion

		Mean	F/t Value	Sig.
Hypothesis 6 (Rejected)	Less than 5 employees	3.9624	F=0.773	0.662
	6-10 employees	3.5122		
	11-50 employees	4.4216		
	More than 50 employees	4.5000		

It can be seen that the hypothesis is rejected since the significance value (.662) is higher than .05. Therefore, there is no difference among the number of employees working in GIS-related departments in terms of success in GIS diffusion.

Hypothesis 7: To test Hypothesis 7, ANOVA analysis has been conducted so that GIS diffusion success is differentiated according to the number of employees using GIS in a municipality.

Table 7. ANOVA for Number Employees in Municipalities and Success in GIS Diffusion

		Mean	F/t Value	Sig.
Hypothesis 7 (Rejected)	Less than 25 employees	3.5744	F=1.984	0.147
	26-50 employees	4.0751		
	51-100 employees	4.6741		
	More than 100 employees	4.3438		

The data indicate that the hypothesis is rejected since the significance value (.147) is higher than .05 (Table 7). Therefore, there is no difference among the number of employees in municipalities using GIS in terms of their success in GIS diffusion.

Hypothesis 8: To test Hypothesis 8, ANOVA analysis has been conducted so that GIS success is differentiated according to the satisfaction of GIS projects at municipalities. Satisfaction and success are strongly correlated with each other. If there is satisfaction about new tools or techniques, they will inevitably be successful at the end (Table 8).

Table 8. ANOVA for Satisfaction Levels of GIS Applications and Success in GIS Diffusion

		Mean	F/t Value	Sig.
Hypothesis 8 (Accepted)	Poor	1.6250	F=22.352	0.000
	Fair	3.9792		
	Good	3.8685		
	Very good	4.6317		

It can be seen that the hypothesis is accepted since the significance value (.000) is lower than .05. Therefore, there is a difference among satisfaction levels of municipalities with GIS in terms of their success in GIS diffusion.

7 CONCLUSION, IMPLICATIONS AND LIMITATIONS

This study intends to develop a better understanding of the nature and success of GIS diffusion at municipalities in Istanbul. An extensive survey has been conducted about GIS, diffusion process of GIS, the usage of GIS and the future of GIS. The objectives are to determine the benefits of GIS use and the barriers to adoption at municipalities in Istanbul. Success and failure factors, as well as a better understanding of development of GIS diffusion in time, were identified. Then, the interviews are held with the experts of GIS in the field. After the survey and interviews, diffusion of GIS is analyzed in detail, hypotheses are framed and a questionnaire was generated and delivered to municipalities in the online environment. At the end of data gathering process, descriptive statistics, reliability tests, regression and ANOVA analyses are performed by using SPSS 15 with data collected from 40 municipalities. Since Istanbul is the largest city in Turkey with its population of nearly 15 million people, the questionnaire is focused on municipalities in Istanbul. All

municipalities have participated in this study. Based on the research findings of analyses in previous sections, the conclusions are as follows:

- Since GIS tools have concrete superiority over CAD tools, GIS is useful and should be used in all departments by all municipalities in Turkey.
- Almost all departments of municipalities should use GIS tools for some applications.
- Awareness is a key factor for a successful implementation but education is the least important factor to affect success. Examining successful projects and successful municipalities are the most important factors which should be evaluated very carefully before implementation.
- In implementing GIS systems, some municipalities just buy a system from a supplier end introduce this into the organization.
- Budget, managerial support, useful data and number and quality of employees are key factors for non-user municipalities to use GIS in the future.
- Technical departments and GIS-related departments within a municipality take the initiative to implement GIS tools in their departments and the entire organization.
- Municipalities are not the only decision-makers.
- Live projects will be successful eventually which refers to the acceptance of that project and cultural norms at municipalities.
- Knowledge and experience exchange should be increased among municipalities.
- Because of their requirements and power, municipalities are perfect organizations to use GIS tools.
- Municipalities mainly perform registration and maintenance functions instead of support in the decision-making process.
- Another important conclusion is that half of the municipalities, which have started to implement GIS, accomplish this without a vision or a plan for the future.

An important failure factor to implement GIS is the fact that 49% of the GIS users do not have a policy.

7.1 Success and Failure Factors

The diffusion process of IT/IS technologies increases the interaction between organizations and citizens. IT/IS technologies will be accepted and diffused in a governmental organizations if its advantages are proven. Before and after implementing IT/IS technologies, the advantages and disadvantages of them should be clearly defined.

Success factors, as a summary of findings of questionnaires, are as follows:
- Determination and support of the management and the organization
- Desire to accept changes
- Examination of successful projects and municipalities
- Personnel capacity and education
- The leader who puts GIS on the agenda
- Accurate consultant selection
- Budget
- High quality of data
- Live projects

Failure factors, as a summary of findings of questionnaires, are as follows:
- Low quality and redundant data
- Time not decided upon carefully
- Not enough personnel
- Neither attention nor support of the management.
- Not enough budget
- Departmental barriers
- Changes of tasks

REFERENCES

Burrough, P.A., 1986, Principles of Geographical Information Systems for Land Resources Assessment (Oxford: Clarendon Press).

Carrara, A., M. Cardinali, F. Guzzetti, and P. Reichenbach, 1999, Use of GIS Technology in the Prediction and Monitoring of Landslide Hazard. Natural Hazards, 20(2), 117–135.

Carrera, F., 2004, City Knowledge: An Emergent Information Infrastructure for Sustainable Urban Maintenance, Management and Planning. (PhD Dissertation, MIT).

Carter, J.R., 1989, On Defining the Geographic Information System. In Ripple W.J. (Ed.), Fundamentals of Geographic Information Systems: A Compendium, Proceedings of

ASPRS/ACSM 1989, Falls Church, Virginia, November 1989, 1, 3-7.

Dangermond, J., 1987, GIS trends and comments, ARC News, Summer/Fall, 13-17.

De Man, E., 1988, Establishing E Geographical Information System in Relation to Its Use: A Process of Strategic Choice. International Journal of Geographical Information Systems, 2(2), 245-61.

DeMers, M.N., 1997, Fundamentals of Geographic Information Systems (New York : Wiley).

Demographia, Istanbul District Municipalities: Population & Density (2000), http://www.demographia.com/db-istanbul.htm

Devine, H.A. and R.C. Field, 1986, The Gist of GIS. Journal of Foresty, 84(8), 17-22.

ESRI, Municipalities and Cooperatives (n.d.), http://www.esri.com/library/brochures/pdfs/gis-for-municipalities.pdf

Service Nova Scotia and Municipal Relations, 2001, Section 5.4: GIS for Municipalities, Local Government Resource Handbook, , April 2001, http://www.gov.ns.ca/snsmr/muns/manuals/PDF/LGRH/LocalGovernmentResourceHandbook_5.4.pdf

Hicks, J., 1993, Experiences with Compiler-Directed Storage Reclamation in Proceedings of IFPCA 93 on Functional Programming Languages and Computer Architecture, New York, NY, June 1993, 1, 95-105.

Ilmavirta, A., 1995, The Use of GIS-System in Catastrophe and Emergency Management in Finnish Municipalities. Computers, Environment and Urban Systems, 19(3), 171-178.

Istanbul Nufus ve Demografik Yapi [Population and Demographic Structure of Istanbul], http://www.istanbul.net.tr/istanbul_istanbul_nufus.asp

Longley, P.A., M.F. Goodchild, and D.J. Maguire, 2001, Geographical Information Systems and Science (New York: Wiley).

Maguire, D.J., 1991, An Overview and Definition of GIS. In Maguire, D.J., M.F. Goodchild and D.W. Rhind (Eds.), Geographical Information Systems: Principles and Applications, (Harlow: Longman), 1, 9-20.

Martin, C. and P. Powell, 1992, Information Systems - A Management Perspective (Maidenhead: McGraw Hill).

Noongo, E.N., 2007, The Implementation of Geographic Information Systems in Namibia. (Finland: University of Joensuu)

Rogers, E.M., 1995, Diffusion of Innovations Theory (New York: Simon and Schuster).

Sahin, I., 2006, Detailed Review Of Rogers' Diffusion of Innovations Theory and Educational Technology-Related Studies Based on Rogers' Theory. The Turkish Online Journal of Educational Technology, 5(2), 14-23.

Samadzadegan, F., S. Saeedi, A. Alvand, and M. Hasanlou, 2008, Enterprise GIS for Municipalities – A Service Oriented Approach in Proceedings of The International Archives of the Photogrammetry, Remote Sensing and Spatial Information Sciences , Beijing , China, 37, Part B4, 1133-1136.

Van Driel, N., 1991, Geographical Information Systems for Earth Science Applications in Proceedings of IV. International Conference on Seismic Zonation, Stanford, California, Aug. 1991, 1, 469–485.

Yomralioglu, T., 2004, Developing Infrasructure Potential in Turkey with GI. GEOInformatics, 7 (April/May), 52-55.

Yomralioglu, T., 2002, GIS Activities in Turkey in International Symposium on GIS, Istanbul, Turkey, September 2002.

Rockfall Hazard Zonation based on Weights of Evidence Modeling of the Doroud –Andimeshk Railway Track, NW Iran

H. Hassani, M. Gholinezhad
Amirkabir University of Technology, Faculty of Mining and Metallurgical Engineering, Tehran, Islamic Republic of Iran

ABSTRACT A significant proportion of national and infrastructure investment is devoted to construction activities in nature. These funds must be selected with sufficient confidence to ensure survival and duration of vital interest. In this study, after collecting information including slope angle, lithology, fault length, river length, road length, rainfall, earthquake and vegetation, the packed cell map is processed in Geographical Information System (GIS). Finally, Rockfall Hazard Zonation (RHZ) in Doroud-Andimeshk railway is presented. The zonation map of the area is prepared using the Mora-Varson method and is validated using the AHP method. The slope angle is obtained from a digital elevation map of the area. The1/25000 topography map is used to obtain the digital elevation map. The lithology map is prepared using the 1/100000 geological map. The fault length, road length, river length and vegetation are obtained from the Landsat satellite map. Rainfall and earthquake data are obtained from the meteorology center and geological survey of Iran. Finally, the area with high risk zones was introduced.

Keywords:Zonation map, GIS, Slope stability, Rockfall, AHP method, Doroud Andimeshk

1 INTRODUCTION:

Rockfall zonation map is the first step in any slope stabilization program (Chacon, 2006). Nowadays the application of GIS mapping, as a quick way to achieve sensitivity maps, has become widespread. Anbalagan (1996) concluded that identifying unstable zones and helping the planner to select development locations for the construction of roads and residential areas in the early stages of planning is very useful and improves safety (Chacon, 2006). Rockfall occur for two groups of reasons as shown in figure 1.

Ahmadi et al. (2004) used the multivariable regression method and the hierarchical analysis method to investigate which parameters significantly influenced the occurrence and extent of rockfall.

In this study, 7 parameters are investigated. The hierarchical analysis method appear to be more efficient than the multivariable regression methods at identifying significant factors (Ahmadi et al.2004).

In order to classify different causes of rockfall, methods such as the Mora-Varson and Kanagava have been employed. In this study according to structural conditions, lithological conditions, topographical conditions and climatological conditions of the studied area are evaluated to estimate effective factors on instabilities. Scoring of each parameter is done using network map. After collecting different information including slope angle, lithology, fault length, rivers length, road length, rainfall, earthquake and vegetation, data are processed in a packed cell map geographical information system and eventually the rockfall zonation map of Doroud–Andimeshk railway is presented.

2 STUDY AREA

The Doroud-Andimeshk railway, with a length of 215 kilometers is located in Lorestan and Khuzestan province in south of Iran. The Lorestan province is located in western of Iran and has rough topography. This railway is a part of the route that connects Bandare-Emam in the south to Tehran the capital of Iran. It begins from the Khuzestan plain and moves onto the sidelines of Dez River from the heart of

Zagros mountains. It has very long strategic bridges such astheTelezang bridge and Absirom bridge, Shahbazan bridge, Tooh bridge, Bishe bridge and Abmamon bridge. It has over 130 tunnels, with Tunnel 22 and Tunnel 23 having lengths of over 2500 meters being the longest railway tunnels in the Middle East and covering 60 kilometers of road. About 10000 passengers travel through this route each day.

The studied area is located in the Zagros structural zone including high Zagros, folded Zagros and the Khuzestan plain. The main faults in the area are the Zagros Fault, the Main young Zagros Fault, the main young Doroud fault and the Doroud fault. The area of jungles around Dez and Sezar watershed with a railway track parallel to these rivers is about 150000 hectares. In addition to these jungles, in the study area there are 250000 hectares of pasture. The Doroud-Andimeshk district vegetation is varied.

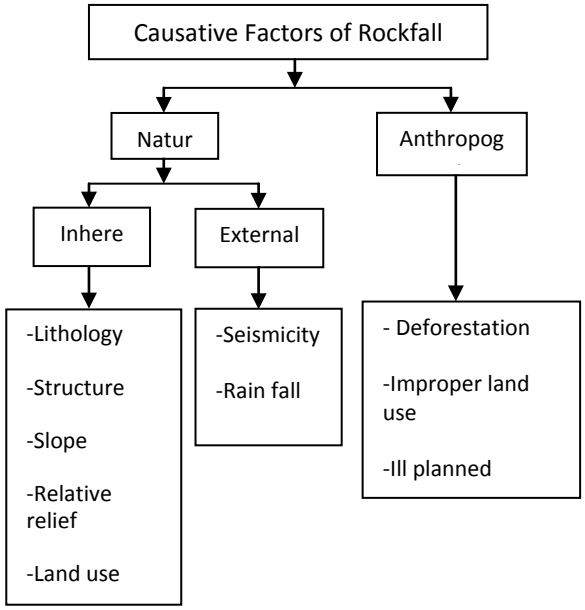

Figure 1. Flowchart showing causative factors of rockfall (Manoj and Anbalagan, 2010).

3 METHODOLOGY

3.1 Evaluation And Rating Of Affective Factors On Slope Domain Instabilities

Various factors such as topographical conditions, lithology, groundwater regime, tectonics land-use change, rainfalland vegetation may interact to cause an increase in slope instability.In this regard, the role of human activity on the slope's instability should be considered. Generally, factors that cause slope instabilityare classified into two groups, environmental and intrinsic factors. Intrinsic factors include the composition, texture and fabric of material and geometrical shape of the slope. Environmental factors include trenching, excavation, the rapid loss of water,rainfall, vegetation and weathering, freezing, vibrations and shock caused by earthquakes. In this study, all factors affecting the instability of slopes were evaluated. Seven factors are considered as significant influencesslope instability in the studied area. These factors includeslope angle, lithology, material, structural elements, rainfall and earthquakes.

3.1.1 Slope angle

The slope angle is one of the main factors influencing slope failures and can be divided into two categories: natural and artificial [4].

In order to classify slopes in the studied area, a 1:25000 topography map is used. To determine slope angle and slope strike in the studied area,the Digital Elevation Model (DEM)of the district is initially prepared from topography maps using ArcGIS. Then,the slope angle of the studied area is determined. In terms of angle,regarding slope angle, slopes are classified into five categories. Theoretically assuming all other factors being equal, the risk of rockfall in the area where slopes are greater is higher than other areas. Regarding the angle, slopes were classified into five categories.

Table 1. Effect of slope angle on instability of slopes. (F_I)

>45	36-45	26-35	16-25	5-15	**Slope angle(degree)**
Very high	**High**	**medium**	**low**	**Very low**	**Effect of instability on slopes.**
5	**4**	**3**	**2**	**1**	**coefficient**

3.1.2 Lithology

A combination of material's texture, fabricand slope materials, materials forming slopesplay an important role in stabilities and instabilities. Slopes having weak rocks with low shear strength are more likely to failure (Hassani, 2008).

Standard penetration test (SPT) is used to determine the permeability coefficient and inflation of formation. Different types of rock mechanic tests are used to determine porosity, water absorption, shear strength and compressive strength. Table 2 shows that existing materials in terms of behaviour and resistance slippage are generally classified into five groups.

Table 2. Five type of lithology in the studied area. From 1 to 5 the risk of failure is increasing

Group	Description
1	Massive limestone and thick limestone. Massive dolomite and thick dolomite. Conglomerate with silicic cement
2	sandstone and quartzitic limestone and sandstone having limestone. Siltstone and thin layers of limestone.
3	Marl limestone, clay limestone, quartzitic sandstones, piritic shales and massive limestones.
4	Shale, andesite, gipsy marl and gips.
5	Quaternary sedimentary, sand and gravel

3.1.3 River's length and Road's length

Analysing and evaluating the slope in the studied area due to limitations of ups and downs, in the road's design, excavation and trench design in the path is inevitable.Due to this operation result inthe creation of artificial slopes with a minimum dip of 45 degreesin the path.

Meteoric water is also another driving factor in creating instability of slopes. Due to the instabilities occurring in the area, the factors related to trench's length, stream's length and river's length have a decisive role. Accordingly, the density of roads and rivers have been ranked and listed in table 3.

3.1.4 Rainfall

The effect of rainfall in increasing the instability and slope's movement was investigated. The annual average rate of rainfall map of the past 40 years is used. The effect of rainfall is considered in the form of an increase of the soil's moisture due tothe rainfall increasing rate and in the form of factors causing earth movements. The effect of rainfall in slope instability is shown in table 4.

Table 3. Effect of road's length and river's length on instability**.**

>2250	1500-2250	750-1500	250-750	<750	River's length and road's length
Very high	High	Medium	Low	Very low	Effects on instability
5	4	3	2	1	(F_D)

Table 4. Effect of annual rate of rainfall in rockfall**.**

>600	500-600	400-500	300-400	<300	Rainfall(mm)
Very high	High	moderate	low	Very low	Rate of effect on instability
5	4	3	2	1	F_r

3.1.5 Earthquake

One of the driving factors increasing instability in the studied area is earthquakes. Earthquake's forces cause rupture and primary cracks in slopes. Lack of complete rupture and slip is lack of continuity of force and if the earthquake occurs for the second time, the depth and rate of the crack's opening will be increased. However, after the earthquake occurs, some other factors affect it and the weight of the mass causes completion of the earthquake effect on creating instability. Slopesaredirectly under the effect of earthquake's acceleration. The maximum horizontal acceleration that affects

the studied area is classified in table 5.

Table 5. Effect of earthquake relative risk (F_R).

Very high	high	moderate	low	Very low	Relative risk
5	4	3	2	1	F_R

3.1.6 Vegetation

Vegetation is an indirect factor on slope's stability. Barren slopes without vegetation have more potential to slide and fast erosion and instability to the forested area. In other words, meadows and forests decrease the erosion process. Roots penetrate the soil causing stability of slopes. Moisture in the soil mass is one of the important factors in reaching the mass to saturation and creation of earthquakes.The type and amount of vegetation is determined by the Landsat satellite images. Vegetation of the area was divided into five categories. The classification results are shown in table 6. Generally, by increasing the vegetation, the risk of falling rock decreases.

Table 6. Effect of vegetation (F_{Lc}).

low	Relatively low	Moderate	Relatively high	High	vegetation
5	4	3	2	1	(F_{lc})

3.2 Rockfall Hazard Zonation Map

To determine relative importance and influence of effective factors on the rockfall zonation map, the weighting method or scoring method is commonly used. In this method, based on engineering judgment and existing experience, each of the effective factors are given weight and score. During long and extensive studies on the sides of the railway in different parts of the studied area, the number of old and young rockfall were identified. The results of this part of the study were used as the calibration factor of this method in confirmation to identify factors of increasing the potential of rockfall in the studied area. Regarding the specific circumstances of the area, effective factors on instability of slopes, including lithology, slope angle, road and river,faults, rainfall, and earthquake were investigated. These factors together are in different conditions and due to the degree of relative risk of each of these factors, different influences on the instability of slopes is observed. The area was divided into a network of neat square cells with dimensions of 250*250 m^2 and on a scale of 1:25000 and using the results of classifying effective factors on instability, the instability's score for each unit was determined. Regarding the influence of the degree of each factor on slope instability, an appropriate coefficient with a rate of influence of each factor on slope instability was considered. Regarding the effective factors on slope instability, this general relationship for the studied area can be considered.

$$RHZ = (C_L \times F_L) + (C_I \times F_I) + (C_F \times F_F) + (C_D \times F_D) + (C_R \times F_R) + (C_S \times F_S) + (C_{LC} \times F_{LC}) \quad (1)$$

In the above formula, F_L=Lithology factor, F_i=slope angle factor, F_f=fault length factor F_D= road's length and river's length factor, F_{ir}=rainfall factor, F_s=earthquake relative risk, and $F_{LC=}$vegetation factor. C= coefficient that shows the importance of each factor on instability. Values obtained for C related to the each factor, shown in table 7.

Table 7. Values related to relative importance coefficient in the study area (C)

C_{lc}	C_s	C_r	C_d	C_f	C_i	C_l	coefficient
0.75	1.6	1	0.75	1.2	1	1.5	value

In exerting the coefficient in each of seven effective factors in slopes instability, value of lithology coefficient(c_l), slope angle,(ci), fault(c_f) road and river(c_d), rainfall(c_r), earthquake coefficient(c_s), and vegetation coefficient(c_{lc}) is determined and exerted in each unit.

3.3 Application Of AHP Method In Validation Of Coefficients

In the models such as linear programming, integer programming, nonlinear programming, allocation model and classical models, when decisions are analyzed based on several criterion, the results are acceptable and satisfactory. Regarding to the Multi-criterion decision models such as SAW, TOPSIS, Electere and AHP, the AHP method has been used for validation on this paper.

3.3.1 AHP method

The Analytic Hierarchy Process (AHP) is a multi-criteria decision making approach and was introduced by Saaty .The AHP has attracted the interest of many researchers mainly due to the nice mathematical properties of the method and the fact that the required input data are rather easy to obtain. The AHP is a decision support tool which can be used to solve complex decision problems. It uses a multi-level hierarchical structure of objectives, criteria, sub criteria, and alternatives. The data are derived by using a set of pair wise comparisons. These comparisons are used to obtain the weights of importance of the decision criteria, and the relative performance measures of the alternatives in terms of each individual decision criterion. If the comparisons are not perfectly consistent, then it provides a mechanism for improving consistency.

The Analytical Hierarchy Process or AHP was first developed by Professor Thomas L. Saaty in the 1970's and since that time has received wide application in a variety of areas. AHP has been applied for a vast number of areas, but it was not applied for the problem that has been taken up in this paper. Thomas L. Saaty (1980) has explained about Hierarchies, multiple objectives and Fuzzy sets . Patric T.Harker (1989) explained AHP in detail as an art of Science and Decision-making. R.Ramanathan and L.S.Ganesh (1994) used group preference aggregation methods employed in AHP by deriving members' weightages. AHP has been applied to many areas but problem chosen presently was not taken into consideration earlier in the literature.

3.3.2 AHP algorithms

It includes determining the goal, selecting important indicators, determining the options, and pair comparison matrix of indicators. Then, the paired comparisons matrix is normalized. To do this, each of the elements of the previous stage matrix is divided by the sum of the column. The matrix calculated by this method is called the normalized matrix. Then the relative weight of each index is calculated using the arithmetic average of each line of the normalized matrix. Then the paired comparisons matrix of options is determined and then the normalized matrix and relative weights are separately calculated for each index.

3.3.3 Option rating

Rating is done by multiplying the relative weight matrix of the index to the relative weight matrix of index and rating based on the number of multiplied matrix. At this stage rating is finished.

3.3.4 Calculation of incompatibility rate

Determine if there is compatibility between the paired comparisons or not.
Weight summation factor (wsv)= paired comparison matrix (D)*relative weights vector
WSV is divided by the relative weight of index to calculate compatibility vector.

3.3.5 Calculate the arithmetic mean

CV elements which are shown by:

- Incompatibility index calculation
- $II=(\lambda_{max} - n) / (n-1)$ (2)

N shows number of variables.

- Incompatibility rate calculation

$IR=II/IRI$ (3)

Which IRI is calculated from Ttable 8.

Table 8. IRI values based on number of variables

IRI	N
0	1
0	2
0.6	3
0.9	4
1.12	5
1.24	6
1.32	7
1.41	8
1.45	9
1.45	10

This operation is separately done for options and index. If IR is smaller than 0.1, then there is reasonable compatibility between the paired comparisons. In this study, the AHP method is used as rockfall and rockfall zoning in the Lorestan railway. First the relationship between parameters should be determined. Effective factors in rockfall are: B_1: lithology factor. B_2: slope angle factor, B_3: Fault length factor, B_4: Road length factor and river length factor. B_5: rainfall rate factor B_6: earthquake relative risk factor, B_7: vegetation factor.

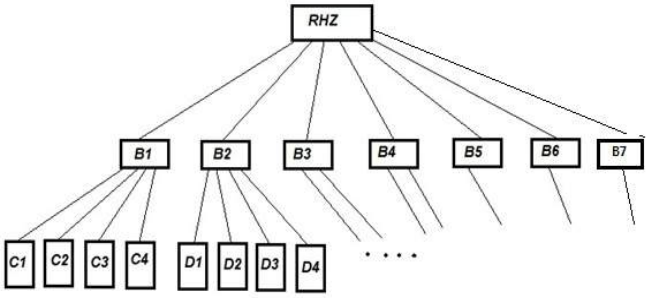

Figure 2. Flowchart of relationship between effective parameters in rockfall.

B coefficients show the importance of each effective factor on instability. Values are obtained in the studied area with regard to studies using research experiences and engineering judgments in the pattern area. In order to validate the coefficients, the stage related to the AHP method is done on the B coefficients. Results show that the AHP method confirms these coefficients.

3.3.6 Rockfall hazard zonation map (RHZ) in the Lorestan railway

In previous sections, each of the effective factors in instability and rockfall in the Lorestan railway in the packed cell map using ArcGIs is separately done. In this section, based on information and results obtained up to this stage, all information after processing with ArcGis is integrated in the packed cell map and the Rockfall hazard zonation map is obtained. Based on RHZ, the studied area is divided into five regions in terms of instability. 1- very high 2- high 3- medium 4- low 5- without risk. The number of cells in each region is shown in Figure 3.

Table 9. Risk ability rate (instability index) of slopes in the studied area.

Scores of five zones					**RHZ values**
24.42–27.15	21.69 – 24.42	18/96 – 21/69	16.23 – 18.96	13.5 – 16.23	
Very high	High	Medium	low	Without risk	Risk rate
13.06	85.625	260.75	291.43	93.54	Area (Km^2)
1.85	12.13	36.94	41.29	7.7	Cover percentage

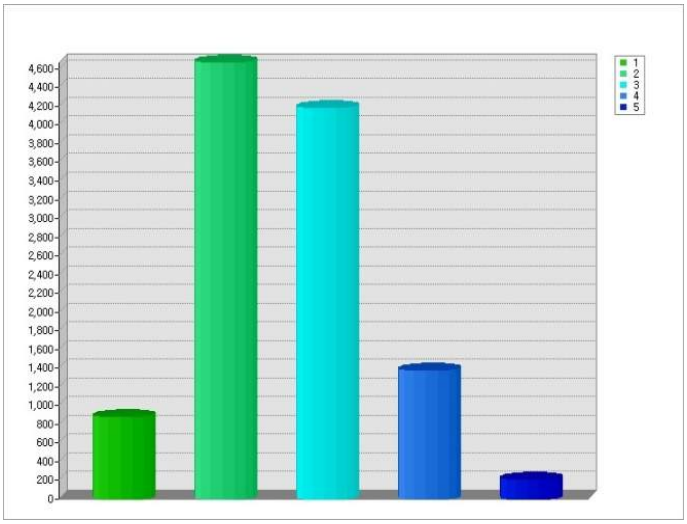

Figure 3. Graphs of cells in packed cell map of RHZ

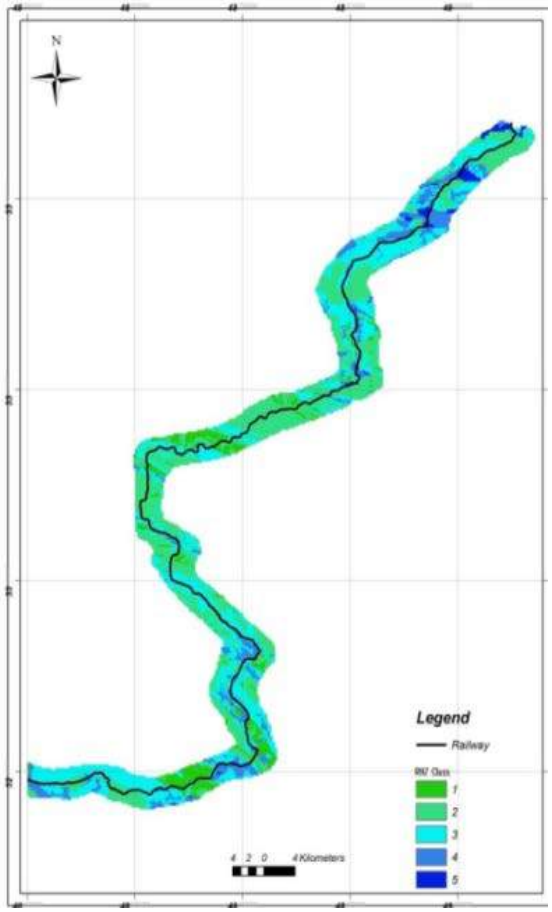

Figure 4. Rockfall zonation map in the studied area

4. CONCLUSION

The Rockfall hazard zonation map plan in Lorestan railway is an applicable developmental project, the results of which determine the regions with a potential of slope instability. Results obtained from this project can be the basis for selection of safe areas for construction of roads and railways. It is necessary that the studied area will be investigated in details and on larger scales. Rockfall is the result of a set of main and subsidiary factors and one factor can rarely cause this phenomenon alone. In forecasting and rockfall hazard zonation in a map, only the methods give good responses that have a real role on effective factors in this destructive phenomenon. In this study, with seven factors: 1- slope angle 2- lithology 3- fault's length 4- road and river length 5- Rainfal6- earthquake and 7- vegetation and using the Mora Varson's method the rockfall hazard zonation map was acquired and the map divided to 5 categories. Finally, the areas with moderate risk, high risk and critical risk were identified. After field checking and more studies, 43 risky points with moderate to critical hazard were determined and reported to Iranian railway research center.

5 ACKNOWLEDGMENT

We acknowledge those who helped us during this research, including the authority and management of the mining and metallurgy engineering faculty of Amirkabir University of Technology, and the railway research center of the Islamic Republic of Iran that helped us in collecting data and doing this research

REFERENCES

1- Aghanabati, A. 2004. Geology of Iran, Iran *Geological Survey of Iran Press*, second edition. P 586.

2- Ahmadi, A., Esmali, A. Feyznia, S. and ShariatJafari, M. 2004. Mass movement hazard zonation using multivariable regression and AHP method, *Iranian journal of natural resources*, pp 323-336.

3- Anbalagan, R. 1996. An Overview of Landslide Hazards in Himalaya – Available Knowledge base, gaps and recommendations for future research, *Himalayan Geology, Vol. 17*, pp 165-167.

4- Carusio, L. 2008. An approach for GIS-based Landslide susceptibility zonation: the case of Enna (Italy*), International Conference on Management of Landslide Hazard in the Asia-Pacific Region*, Tokyo, pp 649-660.

5- Chacon, J. 2006. Engineering Geology Maps: Landslides and Geographical Information Systems, *Bull Eng Geol Environ*, 65, pp 341-411.

6- Crosta, G. B. and Chen. H. 2006. Forecasting hazard scenarios and implications for the evaluation of countermeasure efficiency for large debris avalanches, *Engineering Geology* 83, pp 236– 253.

7- Hassani, H. 2008. New Methods of Trench Managements in Roads and Railway, *Amirkabir University Press*, first edition.

8- Moosavi, F. 2006. *Integrated remote sensing and GIS in order to explore suitable area to feed underground water, case study*, Kamestan anticline area.

9-Manoj K. Arora and Anbalagan,R. 2010, A *Report on Overview of Landslide Hazard and Risk Practices in India*, seventh

framework program.

10- Patric T. Harker. 1989. The art of Science and Decision-making: *The Analytic Hierarchy Process*, Springer Verlag,

11- Ramanathan, R. and Ganesh, L.S., 1994. Group preference aggregation methods employed in AHP: An evaluation and an intrinsic process for deriving members, weightages, *European Journal of Operational Research*, 79, 249-265.

12- Saaty, T. L. 1980. The Analytic Hierarchy Process, *Planning, Priority Setting, Resource Allocation*, McGraw Hill.

Surface Displacement Monitoring - Using Satellite Insar for Mining Operations

D. Colombo
Tele-Rilevamento Europa TRE srl, Ripa di Porta Ticinese 79, 20143 Milano, Italy

ABSTRACT InSAR (Interferometric Synthetic Aperture Radar) uses satellite radar imagery to precisely measure ground deformation. TRE developed advanced techniques, PSInSAR™ and subsequently SqueeSAR™, as a standard monitoring tools in a number of applications: natural hazards, geothermal, oil and gas, mining, urban and infrastructures monitoring.

Thanks to its capability in detecting millimeter-to-meter level displacements over long periods and large areas, SqueeSAR™ analysis can be considered complementary to conventional geological and geomorphological studies in displacement detection and monitoring, supporting also the effectiveness of landslide and subsidence inventories at regional scale.

In this presentation, we would like to present some results obtained in the mining sector; as a matter of fact these data has been widely used in open pit operations for slope instability detection and to monitor waste piles and tailing ponds.

In order to give consistency to these statements, after a brief introduction on the capabilities of the technology, a set of examples will be presented taking into account lots of different displacement phenomena.

Some examples over mining areas are presented. In the case of open pit, the greater attention would be put on the immediate surroundings of the pit and on the nearby facilities (tailing ponds and waste piles); on the other hand, surface effects of underground mining - mainly in terms of subsidence - are being measured with millimeter accuracy.

Radar imagery can detect ground displacements that could threaten the integrity and safety of road and rail infrastructure (both at grade and elevated). By identifying natural and man-made ground measurement points, and using only remote sensed data, SqueeSAR™ maps millimeter displacements along the entire length of road and rail networks, aiding risk assessments and highlighting areas that may require maintenance.

Keywords: Geographic information systems, global positioning systems and information technology, mine closure, waste management and reclamation/rehabilitation, risk assessment and management in mining, rock mechanics and geotechnical applications

1 INTRODUCTION

In the past, constant monitoring programs have been applied to small areas of current operations with the deployment of expensive ground based monitoring equipment. The cost of equipment and management of the complex data from multiple systems limited full mine site coverage. The increase in modern SAR satellites with better revisit times and ground resolutions has brought this technology to the forefront of monitoring mine site deformation on a constant basis. Advanced algorithms have brought processing times down and provide better precision. This paper addresses these advantages.

Over the last two decades, InSAR techniques progressively evolved from the use of differential interferograms (Massonnet et al., 1998; Carnec et al., 2000) to Persistent Scatterers Interferometry (Ferretti et al. 2001, Berardino et al., 2002; Werner et al. 2003; Costantini et al., 2008, Ferretti et al. 2011). PSI in fact overcomes limitations related to the atmospheric contributions affecting DInSAR standard technique and

allows to reach millimetre precision. Compared to conventional surveying methods, PSI provides higher spatial resolution at lower cost, being particularly convenient for wide areas monitoring. This is particularly true in urban and mining areas, where large number of reflecting features leads into a very dense distribution of measurement points (MP) (up to 100.000/km2).

After a brief technology overview, we present a case study over a mining site, where satellite InSAR has been used to detect and measure instabilities in the pit, over the tailings dams and the waste piles. Infrastructure monitoring is another main topic for PSI technique, both in mining areas and where tunnelling occurs; we present two case studies of metro lines tunnelling monitoring with SqueeSAR™, the first of PSI techniques, in different urban context. SqueeSAR™ has been already applied in several projects related to underground tunnelling (mainly TAV railway tunnels) and resulted to be a useful tool in all stages of a tunnelling project, from design to construction and management.

2 TECHNOLOGY OVERVIEW

InSAR Interferometric Synthetic Aperture Radar (InSAR) is a remote sensing technique that measures surface displacements. Radar sensors, mounted on dedicated SAR satellites, transmit radar signals toward the earth, some of which reflect off objects on the ground, bouncing back to the satellite. These back scattered signals are captured by the satellite's sensors and are used to compile radar images of the earth's surface. Both the amplitude and phase of the 'Back Scattered' signal are recorded.

The phase information from a pair of images is compared to detect very small changes in the surface profile. These changes relate to displacement that occurred between the acquisition dates of the pairs of images under analysis. (see Figure 1)

Advanced forms of InSAR, such as SqueeSAR™, process a large number of radar images to determine the displacement of radar targets over time. Stable targets can be naturally occurring features such as rock outcrops, or man-made objects such as buildings and artificial reflectors (referred to as Permanent or Persistent Scatterers) that maximize radar return strength and coherence (Ferretti et al., 2001, Ferretti et al., 2007). The processing of a long series of radar images (Figure 1) introduces a time factor that allows the motion history of a radar target to be observed (including non-linear motion), and increases measurement precision to millimetre level accuracy. This precision is achieved by applying advanced statistical algorithms to remove atmospheric 'noise' and orbital effects from the data. The SqueeSAR™ algorithm presents the unique feature of processing the weaker signals from spatially distributed targets covering several pixels (referred to as Distributed Scatterers), which significantly increases the density of measurement points in non-urban areas (Ferretti et al., 2010).

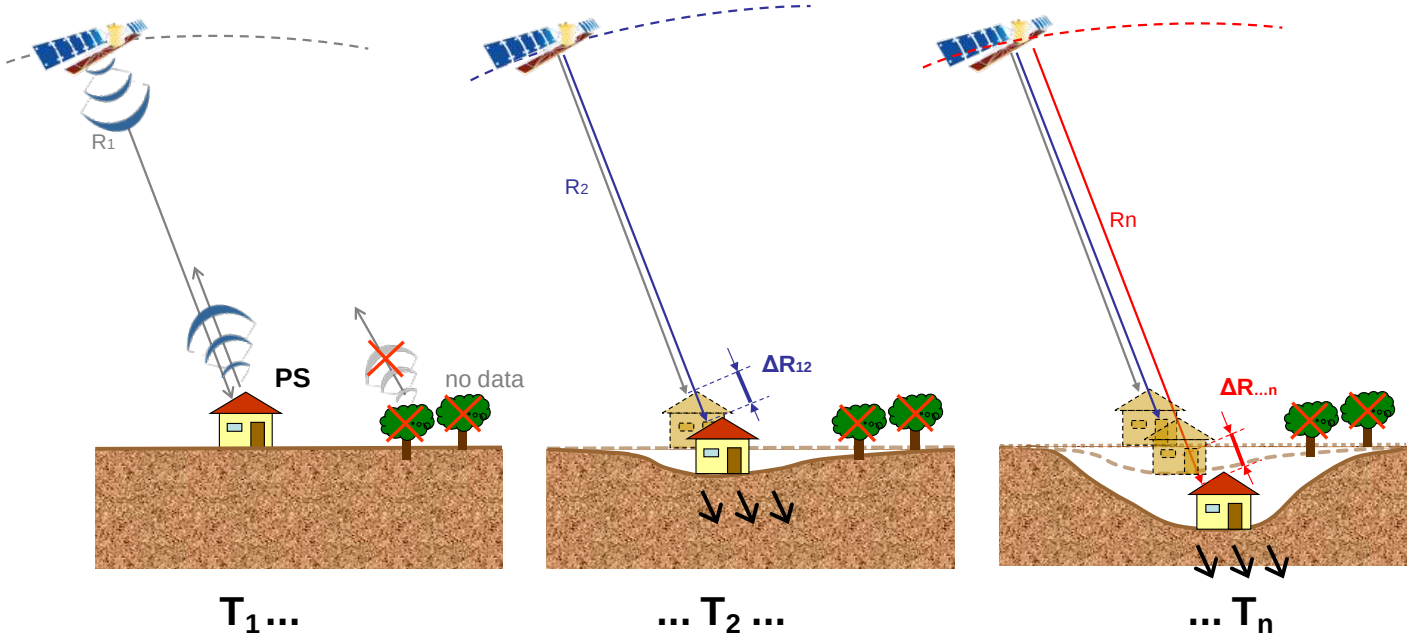

Figure 1. Basic concept of interferometric analysis: comparison between successive measurements of sensor-to-target distance, allowing ground displacement to be determined

2.1 Precision of Measurements

Error bars of SqueeSAR™ measurement are extremely complex to be estimated theoretically, before actually processing the data available (Colesanti et al. 2003). In fact, the precision of the displacement measurements depends on many different factors, such as: number of images used for analysis; spatial density of the measurement points (lower the density, higher the error bar); quality of the radar targets (signal-to-noise ratio levels); climatic conditions at the time of the acquisitions; distance between the measurement point and the reference PS; repeat cycle of the satellite (the lower, the better). An overall picture of the typical precision obtained by SqueeSAR™ analysis is provided in Table 1, which shows the values of standard deviation for average annual velocity, single measurement and positioning in terms of geographical coordinates (North, East, Height).

Table 1. Typical values of precision for a point less than 1 km from the reference point for a dataset of at least 30 scenes spanning a 2-year period

Precision (1σ)	C band satellite	X band satellite
Positioning (E-W)	7 m	4 m
Elevation (referred to ellipsoid WGS 84)	1,5 m	
Average annual velocity	<1 mm/year	
Single Measurement	< 5 mm/year	

3 MINING DEFORMATION MONITORING

Mining open pit operations require a reliable and efficient monitoring programme to assess the inevitable displacement occurring on pit walls and affecting most of the mining assets. Several geodetic tools (from Total Station to Ground based radar) are used to this purpose, and satellite InSAR proved to be a useful complement to usual survey techniques.

As an example of the information provided, a brief extract of a periodic report

is shown. In fact, together with industry standard databases, InSAR services rely on robust, custom-designed, reporting programmes; various update frequencies are available, depending on the Client needs, from weekly to semi-annual.

This monitoring example has been carried out over a very large copper (open pit) mine. The mine spreads for nearly 20.000 hectares, and it is well monitored with several in-situ sensors. This monitoring has been carried out during the first semester of 2013.

3.1 Bird's Eye View – Providing Information Over The Whole Mining Area

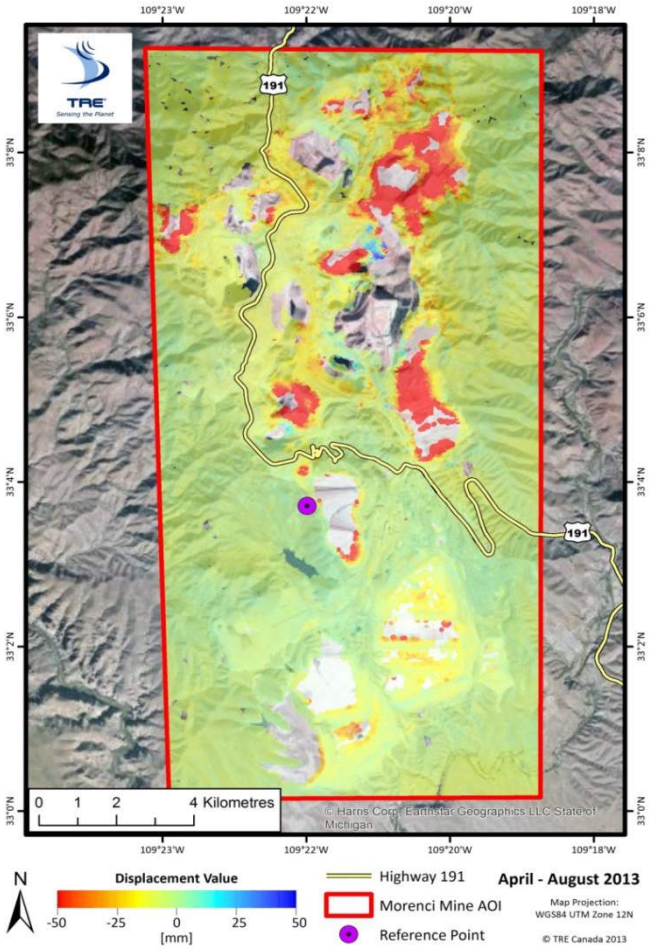

Figure 2. Cumulative displacement over the whole mining area.

Figure 2 shows the displacement occurred over the whole mining area during the accounted period (4 months).

The map has been obtained by means of the analysis of satellite images, hence without the use of any in-situ instrumentation: these set of data are then easily digested in modern GIS, allowing a convenient integration with other measurements.

This maps are produced every requested period (monthly to yearly). Among the various uses, they gained a great importance when planning for an instrumental monitoring programme.

3.2 In Pit Monitoring

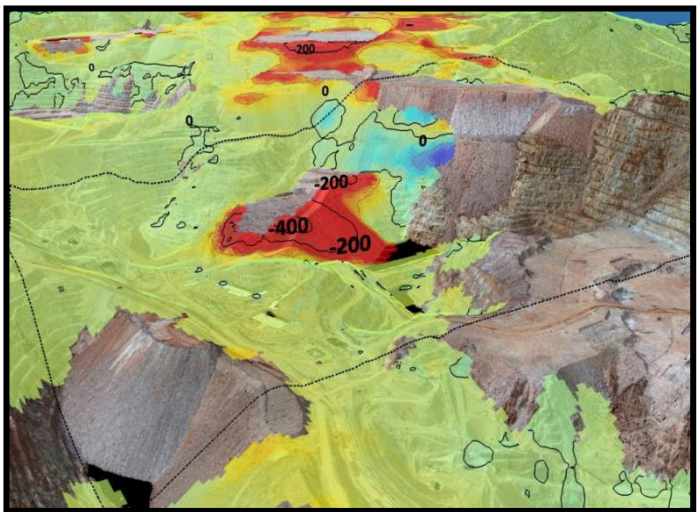

Figure 3. In pit zoomed view. Displacement unit: millimeter.

A simple zooming over the global map allows to identify and measure displacement occurring in the pit, assessing portion of the slope affected by not negligible displacement.

As these maps are not based on a material network of measurement point, an easy visualization of the displacement is achievable (Figure 3). In order to complement the displacement information, for every measurement point identified, a proper time series of displacement is provided (Figure 4).

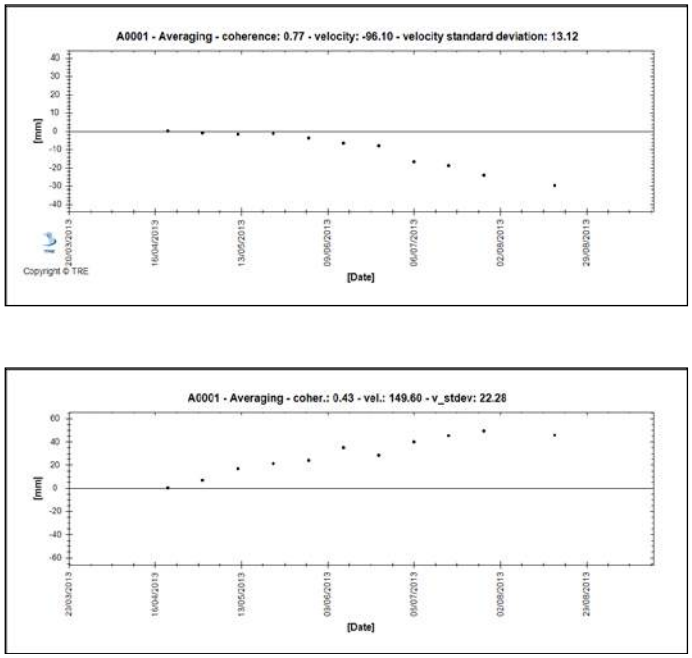

Figure 4. Time series of displacement. Examples in the pit.

3.3 Heap Leach Compaction

While the pit is usually well monitored, heap leaches and tailings dams are usually more difficult and hazardous to survey manually due to the harsh and dangerous environment. The particular structures in these areas do not fit the usual ground base instrumental monitoring strategy due to access and financial constraints.

Satellite InSAR, exploiting its unique aerial view (the line of sight is close to be vertical), provide and unprecedented tool to monitor such compaction phenomena.

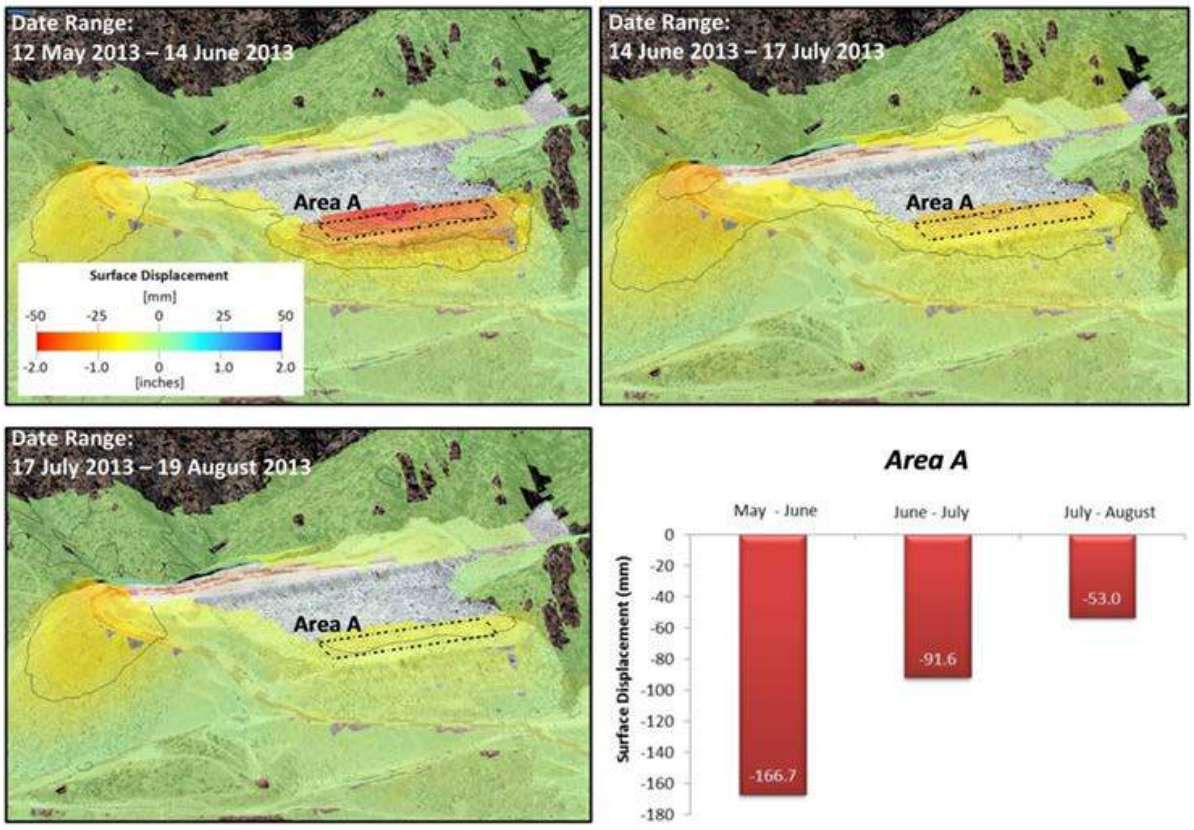

Figure 5. Compaction over heap leaches

3.4 Water Reclamation Facility: Cross-Section

Following the same approach, a dam that is in a water reclamation facility is an easy target for InSAR monitoring. In this particular case, the analysis of a cross section shows the area of displacement highlighting weak spots affecting the dam structure.

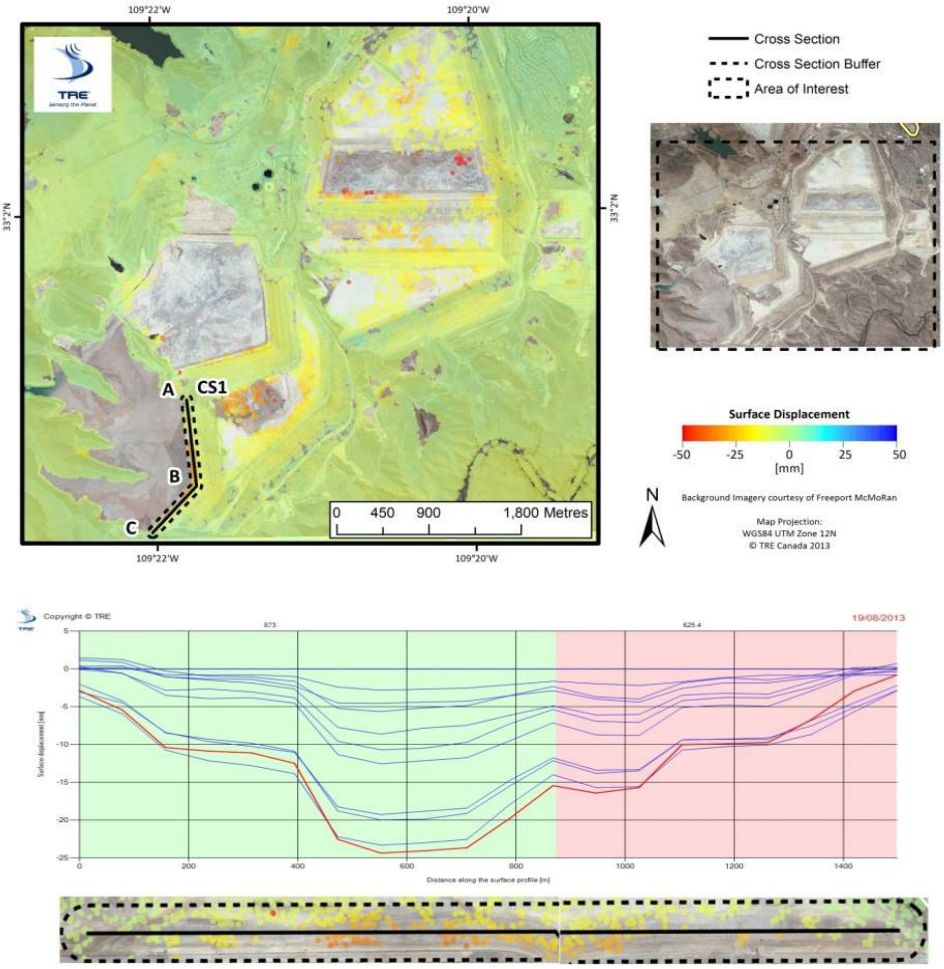

Figure 6. Water reclamation plant. Cross section of displacement over a dam

3.5 Third party Infrastructure

Mining activity may effect third party infrastructures, like railways or road, even if not directly used in the framework of upstream activity. This is the case of a major highway passing near the border of a pit, or in proximity of an instable waste pile. The first case is shown, where an evident sliding deformation affecting the mine rim triggers a deformation that spreads towards the highway (Figure 7).

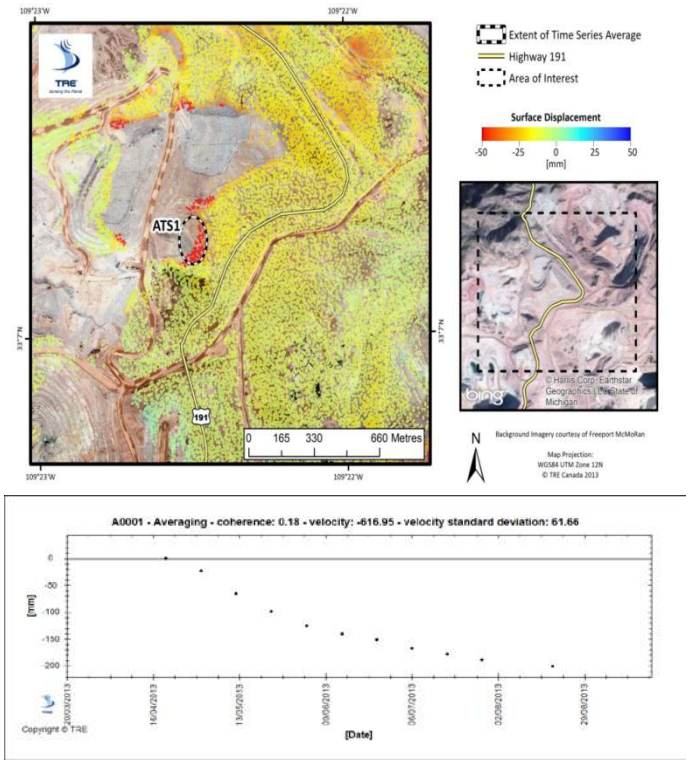

Figure 7. Third party infrastructure monitoring

4 APPLICATION IN SENSITIVE URBAN AREAS

The construction of new underground facilities inevitably interferes with existing surface buildings, even though potential ground movements have been greatly reduced thanks to the progress in the ability of tunnelling machines to cope with difficult ground conditions.

So, in urban areas, a remote monitoring systems that can detect settlements related to excavation activities can greatly assist contractors, designers and owner involved in the project.

In general it is recommended to carry out an historical analysis “ante-operam”, in order to have an overview of the area before the beginning of excavations. This is possible thanks to the availability of satellite data archives covering the last two decades (since 1992). This procedure will allows to plan a follow-up monitoring phase during the excavation and which should prolonged till the exhaustion of any long-term settlements.

4.1 Milan, Metro line 5

The M5 is a fully automatic light underground line, crossing the city of Milan (Italy) with a total length of 12.6 km.

The first stretch Bignami-Zara has been completed and is operating since February 2013. The second stretch San Siro-Garibaldi is under construction and will be operative for the Expo 2015.

In San Siro-Garibaldi stretch, a double track tunnel has been constructed using EPB machines. The tunnelling construction began in 2010 and was completed in 2013.

The SqueeSAR™ analysis of 120 high resolution radar images (TerraSAR X data) acquired from June 2008 to December 2012 identifies the TBM progress and its impact on the buildings above (Figure 8). Although the surface settlements are less than 1 cm, the precision of SqueeSAR™ data allows the detection of very small displacements without install any instrumentations on ground.

The time series (displacements over time) shown below highlight the effects of TBM progress during construction period (Figure 9).

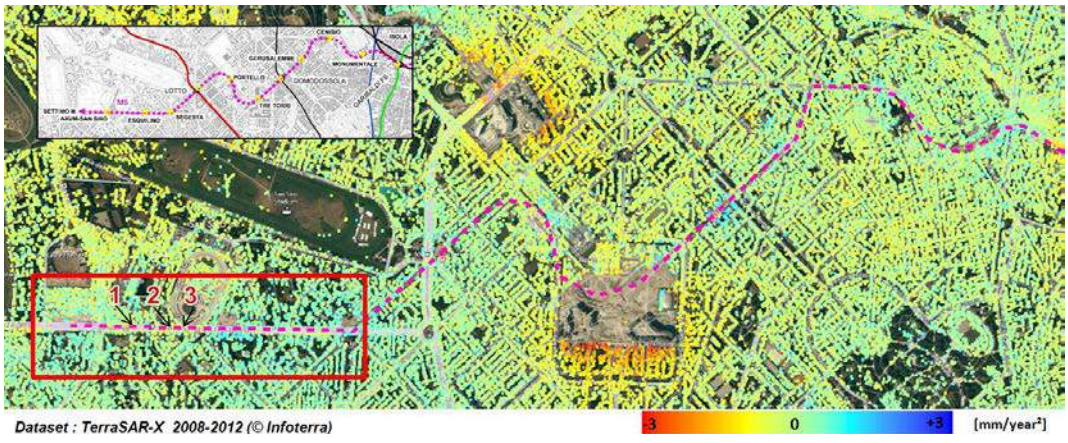

Figure 8. Milan: acceleration map [mm/year2] of measurement points identified from satellite.

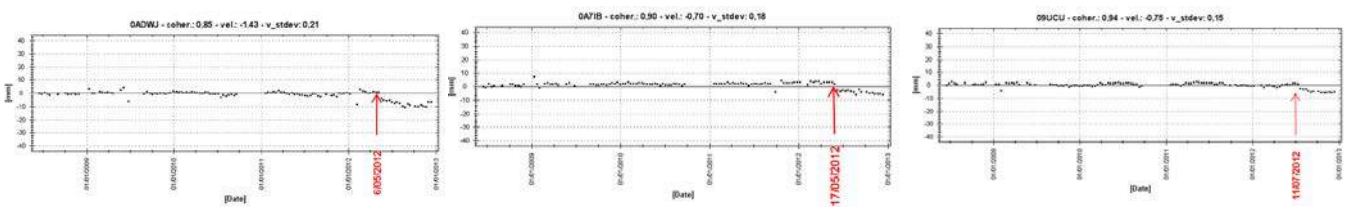

Figure 8. Time series (displacement over time) of measured points 1,2,3 respectively

4.2 Vancouver, the Canada Line

The Canada Line is a rapid transit line in the Metro Vancouver (Canada), servicing Vancouver, Richmond, and the Vancouver International Airport. The construction began in October 2005 and was completed in August 2009. Geological settings range from glacial till in the downtown area and along much of the line North of the Fraser River, to landfill along False Creek and the silt and clay deposits of the Fraser Delta in Richmond. These different conditions are likely to produce varied responses in the structures built on these terrains. The availability of archives of satellite data, provides the deformational behavior ante operam. Thereafter monitoring can be conducted during the construction phase and after the completion of the activities (long term monitoring), to follow in time the deformation. The study area was firstly analysed using 58 RADARSAT-1 images collected between 3 March 2001 and 18 June 2008, comprising ante-operam phase (2001-2005) and tunneling activities (2005-2008).

The historical analysis (Figure 10) highlights significant displacement rates in the area between the Sea Island Centre Station and the YVR-Airport Station.

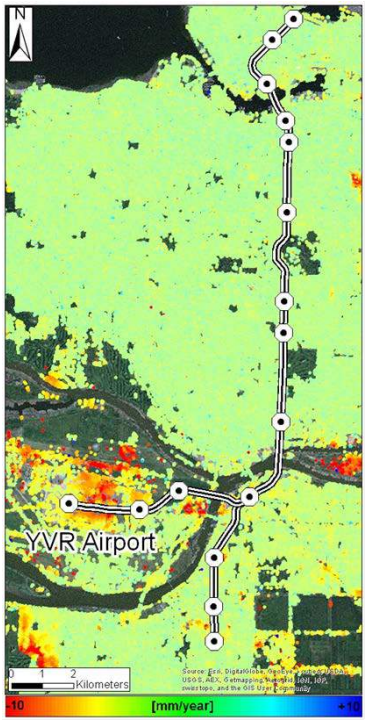

Figure 10. Canada Line: velocity map [mm/year] of measurement points identified from satellite. Monitoring time 2001-2008

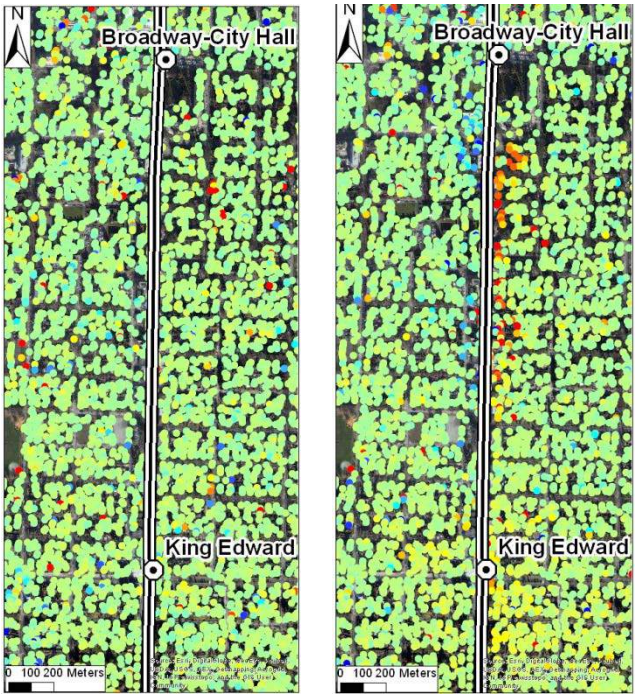

Figure 9. Average velocities map before (left) and after (right) the tunnelling activities

Nevertheless subsidence was antecedent the tunnelling activities, accelerations of about 1.5 mm/y2 have been measured during the construction. Furthermore, SqueeSAR™ data have been further analysed to detect changes in deformation trend, partitioning the time series accordingly before and after the event (in this case tunnelling). The time series analysis highlights acceleration in most of the measurement points along the Canada Line, between Broadway-City Hall and King Edward (Figure 11).

Blue and red points represent displacements toward tunnelling alignment. Differences in colours depend from satellite acquisition geometry.

Figure 12 shows that most of the measurement points in this area, reveals an acceleration in 2007, which corresponds to the year of beginning of tunnelling.

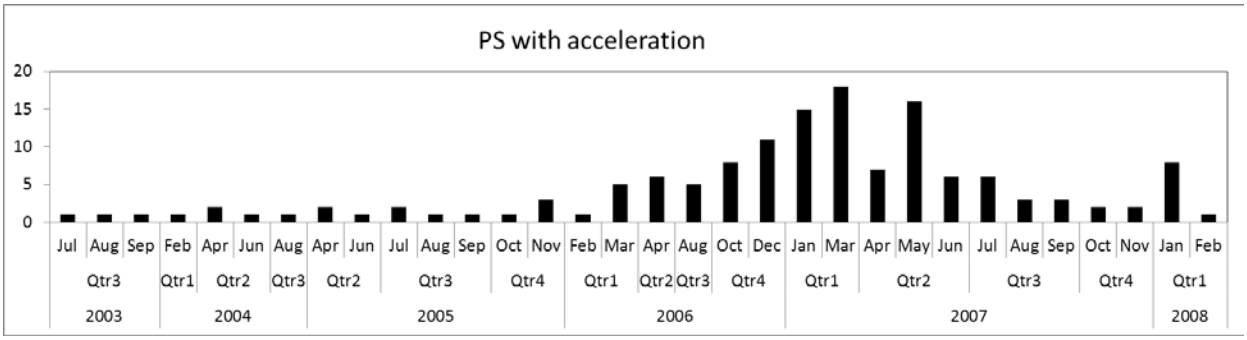

Figure 10. Histogram of measurement points between Broadway-City Hall and King Edward recording acceleration.

We observed a stable phase followed by a displacement‘s step of 2 cm in 2007, to the left and right side of the Canada Line (Figure 13) coinciding with the construction phase.

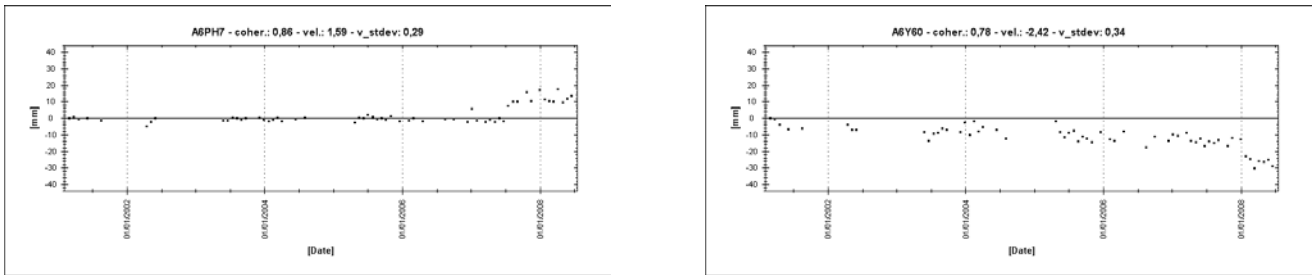

Figure 11. Time series of a Measurement Points to the left (a) and right (b) of the Canada Line

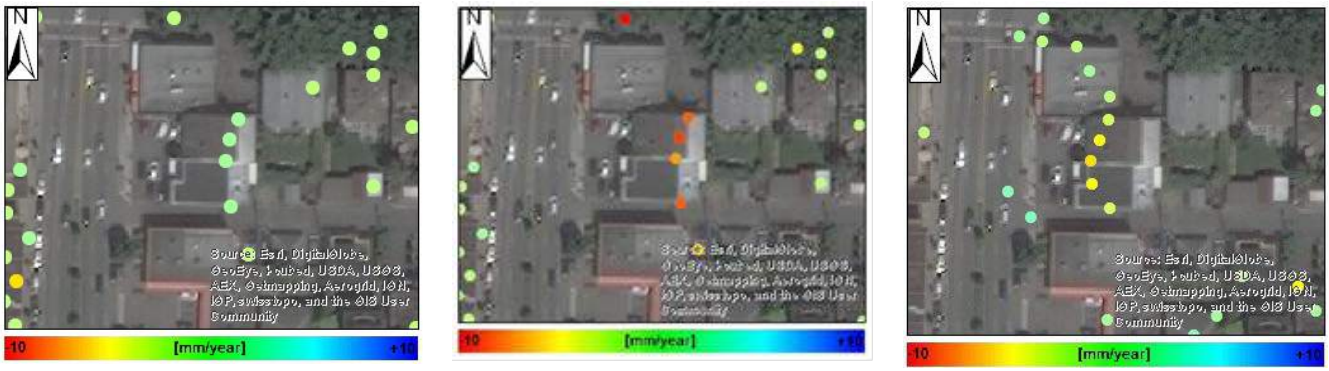

Figure 12. Velocities before the tunnelling , during, and 3 years later

Post-construction monitoring continues to verify the stability of long term displacements due to new construction near the transportation corridor. A data stack composed of 34 Radarsat-2 images, acquired from February 2009 and 11 March 2011, was processed with the SqueeSAR™ algorithm. Following this approach it was possible to assess the displacement before, during and after the construction works (Figure 14).

5 CONCLUSION

The technological advances in Satellite data specifications and InSAR processing techniques have brought deformation monitoring from space born platforms to the forefront of mine site and infrastructure applications. All mining assets can be monitored from a single sensor easing data compatibility issues across corporations and allowing a better understanding of the occurring phenomena. Moreover, the use of such measurement guide the deployment of network of sensors, both during the planning phase and the operational phase of underground and surface operations.

REFERENCES

Massonnet, D. and Feigl, K. L.: Radar interferometry and its application to changes in the Earth's surface, Rev. Geophys., 36, 441–500, 1998.

Carnec, C. and Delacourt, C., 2000. Three years of mining subsidence monitored by SAR interferometry, near Gardanne, France. Journal of Applied Geophysics, 43, pp 43–54.

Ferretti, A., Prati, C., Rocca, F. 2001. Permanent Scatterers in SAR Interferometry. IEEE Transactions on Geoscience and Remote Sensing, 39(1), January 2001, 8–20.

Ferretti, A., Fumagalli, A., Novali, F., Prati, C., Rocca, F., Rucci, A. 2011. A new algorithm for processing interferometric data-stacks: SqueeSAR™. IEEE Trans. on Geoscience and Remote Sensing, November 2010 IEEE TGRS, 49(9), 3460-3471.

Berardino, P., Fornaro, G., Lanari, R., and Sansosti, E.: A new algorithm for surface deformation monitoring based on small baseline differential interferograms, IEEE Trans. Geosci. Rem. Sens., 40, 2375–2383, 2002.

Werner, C., Wegmuller, U., Strozzi, T., and Wiesmann, A.: Interferometric point target analysis for deformation mapping, presented at Geoscience and Remote Sensing Symposium, Int. Geosci. Remote Sensing Symp. (IGARSS), Toulouse, France, 2003.

Costantini, M., Falco, S., Malvarosa, F., and Minati, F.: A new method for identification and analysis of persistent scatterers in series of SAR images, paper presented at the International Geosciences Remote Sensing Symposium, Int. Geosci. Remote Sensing Symp. (IGARSS), Boston, USA, 2008.

Colesanti, C., Ferretti, A., Locatelli, R., Novali, F., Savio, G. 2003. Permanent Scatterers: Precision Assessment and Multi-platform Analysis. IGARSS 2003, 21-25 July, Toulouse, France, 1-3.

The Application of Weight of Evidence Method for Zn Mapping in Takhte-Soleiman, Iran

M. M. Oskouei, M. Bicharanlo
Sahand University of Technology, Iran

A. R. Jafari Rad
Islamic Azad University, Iran

ABSTRACT Decision making about the importance of each data layer (weights in integration procedure) and then integrated use of them to generate a potential map is usually challenging issue in mineral exploration. Actually all data layers like, geology, geophysics, geochemistry and etc. include significant information about deposit, but a comprehensive map resulted by their combination will be more helpful for target detection. This study aims to combine data layers of lithology, geochemistry and faults of Takhte-Soleiman district with the use of weight of evidence method in a geographical information system and then find the best locations for more detail explorations. Weight of evidence method was applied using eight known zinc indices in the study area. Values of W+ and W- and contrast were calculated for all data layers. In the case of the priority indication of regions around faults, in addition to W+ and contrast, other criteria like Capture Efficiency (CE) and index number change graph were applied. The computation of weight of evidence parameters on geological and geochemical maps, lead us to recognize three amphibolite, gneiss, and limestone beside geochemical zinc anomalies and their 100m distances as optimistic locations. Finally the zinc potential map was prepared by integrating of processed layers using W+ and W- in each point.

Keywords: Weight of Evidence, Mineral Potential Map, GIS, ArcSDM

1 INTRODUCTION

Application of conventional methods in mineral deposits exploration is costly and time consuming. Integration of different data layers in GIS will however reduce exploration costs and increase reliability of the detected targets. This will able one to combine and compare information from several layers like geological, structural, geophysical, geochemical characteristics and so on [1]. The mineral potentials are identified by weighting of evidences of any available map in order to assess various methods for their combination [2].Assigned weights are depended to evaluating their relationship with known mineral resources or reserves due to the subjective judgment of experts [3].

Weight of evidence is data driven approach that employs Bayesian theory to determine the significance of evidence. The method measures the spatial dependence between the evidence maps and obtained information from the well-known indices locations [4, 5]. The Bayesian in is, fact, a method based on probabilistic structure to combine a set of data. The main parameters in the approach are prior and posterior probabilities. The technique is applied aiming to determine the importance of various evidences and to combine them [2, 6]. This study aims using all available information (geochemistry, geology, and faults data layers) to identify Zn mineralization and to generate a potential map for the region (Takhte-Soleiman). The faults were extracted from the geological map of the study area and are illustrated in figure 1 in addition to the geochemical anomalies and known Zn indices in the region.

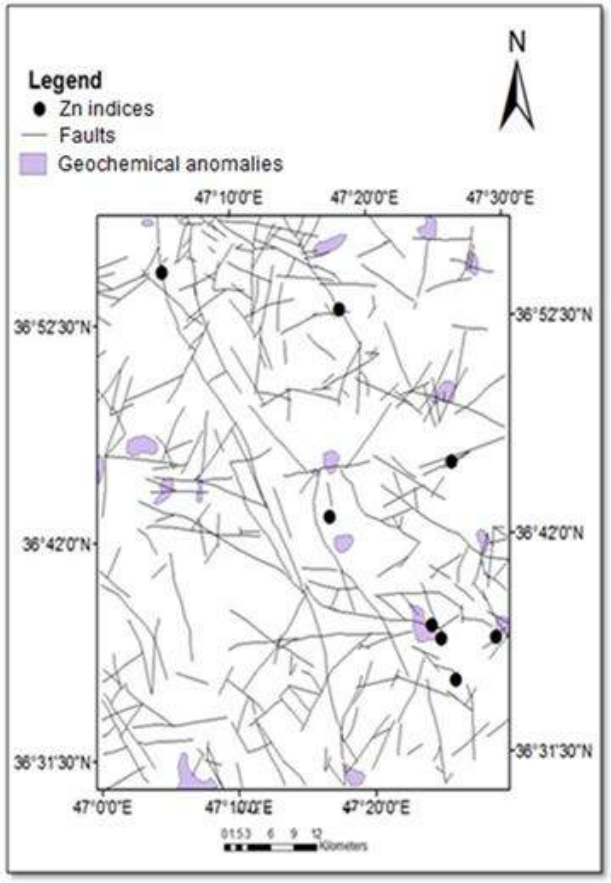

Figure 1. The map of geochemical anomalies, Zn indices, and faults in the study area

1.1 Study Area

The study area is covered by metamorphic rocks like schist, marble, gneiss and amphibolite having a North East - South West trend with a maximum altitude in the middle of the region. Generally, stratigraphy column from bottom to top consists of the Precambrian metamorphic rocks, the late Precambrian and Cambrian – Ordovician sedimentary rocks, the Palaeozoic metamorphic rocks, the Oligo-Miocene intrusive diorite, granodiorite, granite, sedimentary, and volcanic rocks, and younger Quaternary deposits. Lead and zinc mineralization were occurred in the area as a result of the returned hydrothermal fluids activities in different geological zones. These elements are appeared as sulphur-carbonate compositions in the veinlet system of marbles (Figure 2) [7].

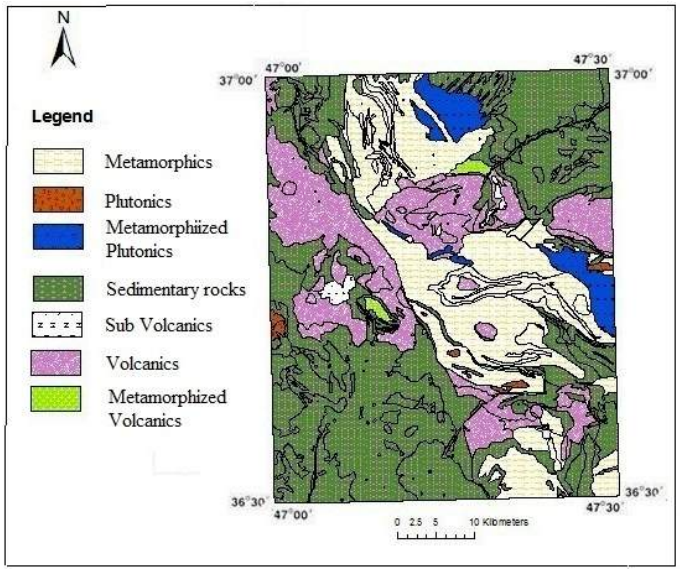

Figure 2. Geological map of the study area.

1.2 Data

All available information of the study area were used to identify optimistic locations for Zn mineralization and to generate a potential map. The geochemical, lithological, faults, and Zn recognized indices were employed to fulfil this task. The mentioned data layers were received from Geomatics division of the Geological Survey of Iran (GSI). The data driven Weight of Evidence (WofE) that is based on Bayesian probability theory was then applied using Zn indices.

2 METHODOLOGY

Agteberg (1990), Bonham Carter (1988), and Watson (1989) were among them who developed WofE for mineral potential mapping [2]. The method assigns “weights” (importance) for each data layer and to the units inside data layers using Bayesian theorem in a probability range of (0, 1) [8]. This theorem in exploration is expressed as updating the probability of a phenomenon like H in the case of E evidence to compute its posterior probability:

$$\boldsymbol{P(H \mid E)} = \frac{\boldsymbol{P(H)P(E \mid H)}}{\boldsymbol{P(E)}} \qquad (1)$$

Where $\boldsymbol{P(H \mid E)}$ is the posterior and *P(H)* is the prior probability of H before E observed evidence, and $\boldsymbol{P(E \mid H)}$ is the likelihood. The term *1/(P(E)* is independent of *H* and

considered as a normalization or scaling factor [6].

Converting the probability in the Bayesian theorem to "odds" will lead us to generate potential map using WofE. Odds is a probabilistic ratio of dividing the occurred probability *P(D)* by the not occurred probability $\boldsymbol{P(\overline{D})}$:

$$\boldsymbol{P(O(D)} = \frac{\boldsymbol{P(D)}}{\boldsymbol{P(\overline{D})}} \quad (2)$$

In the case of having more than one data layer and conditional independence of evidences, we can write:

$$\boldsymbol{O(D\ |E_1, E_2, \dots, E_n)} = \boldsymbol{O(D)} \prod_{i=1}^{n} \frac{\boldsymbol{p(E_i\ |D)}}{\boldsymbol{p(E_i\ |\overline{D})}} \quad (3)$$

Therefore:

$$\mathbf{log}_e[\boldsymbol{O(D\ |E_1, E_2, \dots, E_n)}] = \mathbf{log}_e[\boldsymbol{O(D)}] + \sum_{i=1}^{n} \mathbf{log}_e \frac{\boldsymbol{p(E_i\ |D)}}{\boldsymbol{p(E_i\ |\overline{D})}} \quad (4)$$

And according to the Agteberg modifications on the above Logit in the case of absence of the binary predicting maps:

$$\mathbf{log}_e[\boldsymbol{O(D\ |E_1, E_2, \dots, E_n)}] = \mathbf{log}_e[\boldsymbol{O(D)}] + \sum_{i=1}^{n} \mathbf{log}_e \frac{\boldsymbol{p(\overline{E_i}\ |D)}}{\boldsymbol{p(\overline{E_i}\ |\overline{D})}} \quad (5)$$

In the equations 4 and 5, the terms $\mathbf{log_e} \frac{\mathbf{p(E_i\ |D)}}{\mathbf{p(E_i\ |\overline{D})}}$ and $\mathbf{log}_e \frac{\boldsymbol{p(\overline{E_i}\ |D)}}{\boldsymbol{p(\overline{E_i}\ |\overline{D})}}$ are respectively positive and negative weights for ith prediction map remarked by W^+ and W^-. Dependence between recognized indices and the pattern of prediction of each evidence map will be calculated by contrast as

$C_i = W^+ - W^-$.

3 METHODOLOGY

Mineral Potential Mapping means detection of areas having a greater probability of mineralization for a specific element in the region [3]. Because of the need for integration of different layers for mapping, the following processes should be performed on all data layers:

a) Georeferncing of layers and verifying their same coverage

b) Preparation of the distribution of the Zn indices (8 indices shown in figure 1)

c) Deciding about the suitable cell size for converting vector to raster format

One of the most important parameters is the cell size when using GIS in raster format. The effect of cell size on the data driven methods is more than the knowledge driven algorithms [9]. The effective resolution for a map is equal to the minimum distance at which the spatial variation can be recorded. This is equal to the width of a line on a map (0.5 mm). However, a practical estimate of the cell size in meter will be achieved by multiplying of the scale denominator by 0.001 [10]. In this study, regarding to the 1:100000 scale of the maps, the cell size is 100 meter.

3.1 Faults

One of the best methods to determine the importance of surrounding areas and the relation of fault zones to intended mineralization is creating different buffers. The 100, 200 and 500 m distance buffers were then drawn to select the best distance using the weights of evidence for each one. The resultant weights and contrasts are illustrated to faults layer as an example in table 1. Finally, according to the calculated weights based on the indices locations, the 100 m buffer was selected as the best buffer. It means a distance of 100 meters buffers resolve better the study area [9, 10]. According to the graph in figure 3, the indices number increases gradually until 300m distance from faults and then sharply until 1100m, that after stays constant means no indices in the region farther 1100m. The fault map was then divided into three class as following:

1) Distances less than 300m (most favorable areas)

2) Distances between 300m and 1100m (favorable areas)

3) Distances greater than 1100m (unfavorable areas)

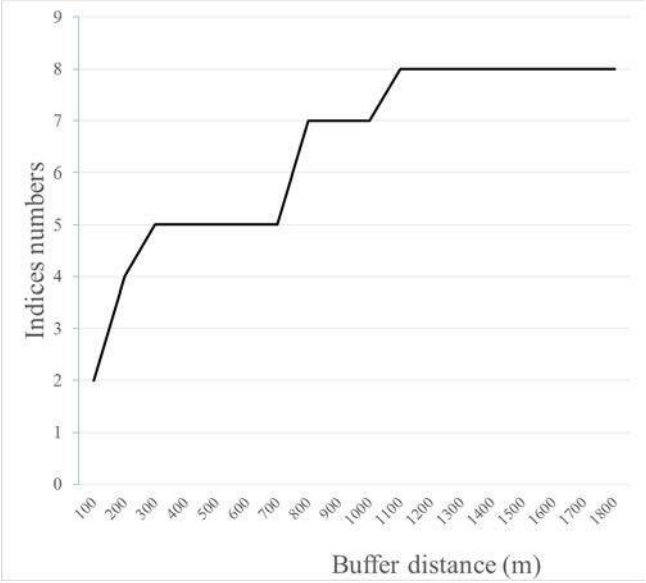

Figure 3. The number of proved indices inside different buffers.

Another indicator for optimum classification into three above mentioned classes (most favorable, favorable, and unfavorable) is *capture efficiency (CE)*. This parameter is resulted by dividing the square distance by the coverage of the related distance buffer:

$$CE = \frac{d^2}{a} \quad (6)$$

Figure 4 illustrates the calculated CE for various buffers. Regarding to the results the 1100 meter buffer has the highest value of CE. It means the 1100 meter distance of each fault is the boundary of favorable area the farther regions are not disposed for mineralization from faults systems view point.

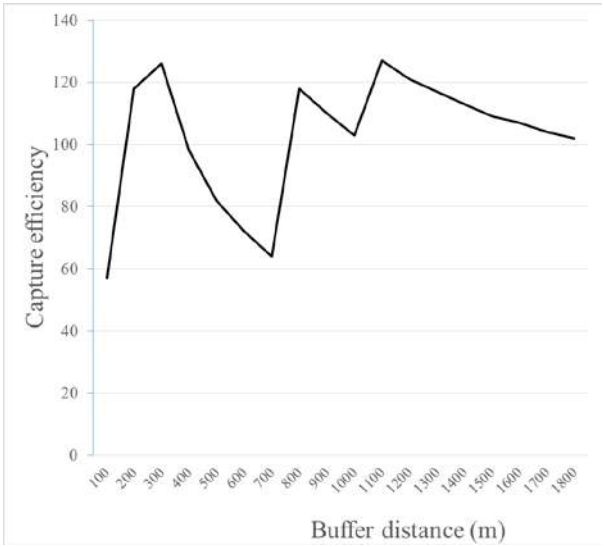

Figure 4. Calculated capture efficiency for different distances.

3.2 Geochemical Anomalies

The geochemical layer represents the Zn anomalies in the study area conducted by GSI. Each anomaly was considered as polygon and the geochemical layer was then binary encoded according to the presence or absence of the indices. The WofE weights were then calculated for the binary map. The calculation of the distance in which the positive relationship between the anomalies and indices has been increased is the next step. To this end buffers 100, 500 and 7500 meters around polygons were drawn and their weights were calculated. The results are shown in table 2.

3.3 Lithological Factor

The final objective in this part was to recognize the mineralization related rock units. The evidence weight of each unit was therefore computed and the units with positive weight and contrast were detected (amphibolite, limestone, gneiss, and an unknown unit). Different buffers (100, 200, 500, and 1000m) were then drawn for each unit. According to the calculated contrast and capture efficiency, the best buffer zone for each unit was selected as 100m for amphibolite and 0 for reminders.

Table 1. The calculated parameters for different buffers for faults layer using WofE

Buffer	Area	Indices No.	W^+	S_W^+	W^-	S_W^+
100	271.56	2	0.8055	0.7071	-0.1692	0.4083
200	524.09	4	0.8412	0.5	-0.4503	0.5
300	756.54	5	0.6972	0.4472	-0.608	0.5774
400	967.42	5	0.4513	0.4472	-0.4733	0.5774
500	1158.87	5	0.2707	0.4472	-0.3331	0.5774
600	1329.92	5	0.1331	0.4472	-0.1887	0.5774
700	1484.24	5	0.0233	0.4472	-0.0376	0.5774
800	1622.77	7	0.2705	0.378	-0.978	1.0000
900	1744.57	7	0.1981	0.378	-0.8146	1.0000
1000	1855.27	7	0.1366	0.378	-0.6386	1.0000
1100	1955.17	8	0.2165	0.3538	-5.0531	10.0000
1200	2045.3	8	0.1714	0.3538	-4.8429	10.0000
1300	2125.03	8	0.1331	0.3538	-4.6112	10.0000
1400	2197.64	8	0.0995	0.3538	-4.3399	10.0000
1500	2264.00	8	0.0698	0.3538	-4.0048	10.0000
1600	2324.31	8	0.0435	0.3538	-3.5556	10.0000
1700	2379.76	8	0.0199	0.3538	-2.819	10.0000
1800	2430.68	8	0.0013	0.3538	10.322	14.1421

Table 2. The calculated parameters for different buffers around geochemical anomalies

buffer	area(km2)	indices number	contrast
100 (most favorable)	57.56	1	2.32
500 (favorable)	116.01	3	4.68
7500 (unfavorable)	2475.76	8	-8.00

4 CONCLUSION

The integration of resulted weighted maps was performed using ArcSDM module in ArcGIS. This aims to compute posterior probability for the region and then detection of areas with higher probability for detail exploration. Determination of the layers weights was done using their W+ and W- for calculating posterior Logit and then posterior odds and finally posterior probability [2]. The resultant map of the computed posterior probability is shown in figure 5. The brighter parts of the map refer to the most favourable regions and the grey and dark parts represent favourable and unfavourable areas respectively. The known indices can be effectively used in application of WofE for mineral potential mapping. Despite the relatively low number of indices in the study area, it was able to predict high potential locations according to other conducted studies. The excessive number of indices will however result in more accurate potential map. Conditional independence between data layers reveals that an integration method is necessary for decision making.

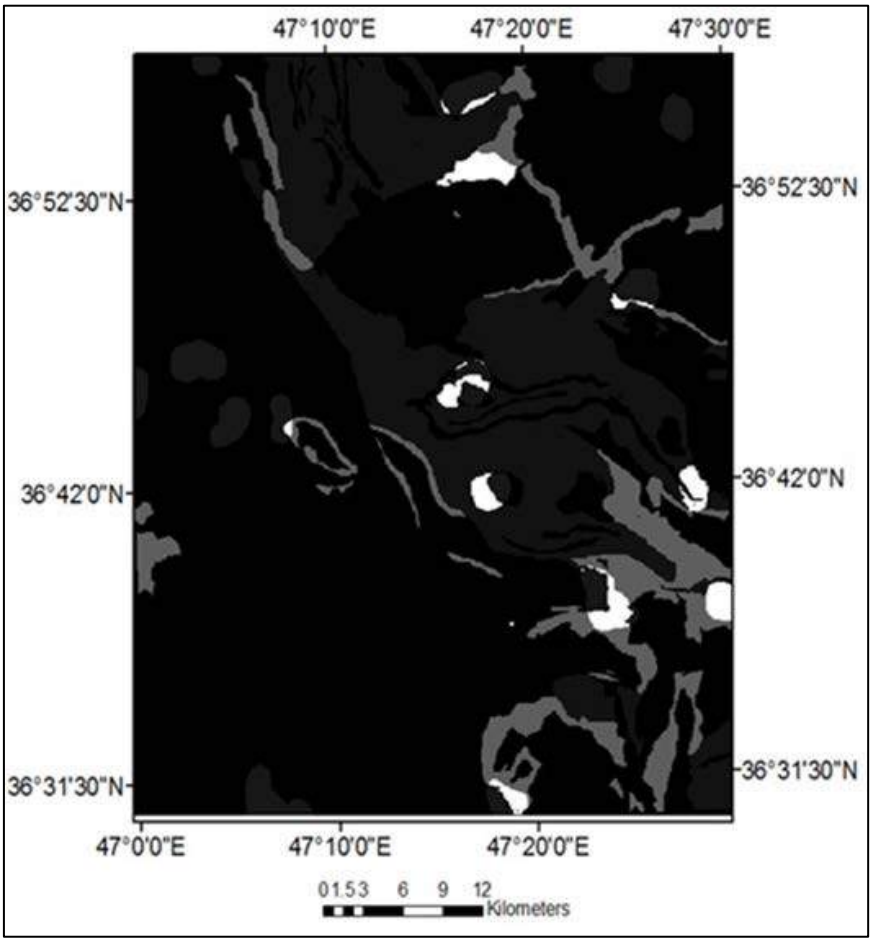

Figure 5. Potential map of the study area resulted by WofE method

REFERENCES

[1]T.B. Benomar, H. Guangdao, B.Fuling. A Predictive Gis Model for Potential Mapping of Copper,Lead,and Zinc in Langping Area. *China,Geo-Spatial Information Science.* 2006,**12**:243-250.

[2]G.F. Bonham-Carter. Geographic Information Systems for Geoscie-ntists:Modelling with GIS. *Pergamon Press, Ontario,Canada.* 1994.

[3]E.J.M. Carranza. Geochemical Anomaly and Mineral Prospectivity Mapping in GIS. Handbook in Exploration and Environmental Geochemistry. *Elsevier, UK.* 2009.

[4]R .Romero-Calcerrada and S. Luque. Habitat quality assessment using Weights-of-Evidence based GIS modelling: The case of Picoidestridactylus as species indicator of the biodiversity value of the Finnish forest. *Ecological Modelling.* 2006, 196: 62-76.

[5]G.F. Bonham-Carter,F.P. Agterberg, D.F. Wright. Weights of evidence modeling: a new approach to mapping mineral potential. In: Agterberg, F. P., and Bonham-Carter,G.F., eds., *Statistical Applications in the Earth Sciences.* 1989, **89**(9): 171–183.

[6]S.P.Rostirolla, P.C. Soares, H.K. Chang. Bayesian and multivariate methods applied to favorability quantification. In: *Reconcavo Basin and Ribeira Belt, Brazil . Nonrenewable Resources.* 1998, **7**(1): 7-24.

[7]A.R. Babakhaniand J. Ghalamghash. Geological map of Takhte-Soleiman, Geological Survey of Iran. 1991.

[8]A. Porwal., Mineral potential mapping with mathematical geological models. Ph.D. Thesis, *University of Utrecht, the Netherlands*. 2006.

[9]E.J.M. Carranza. Objective selection of suitable unit cell size in data-driven modeling of mineral prospectivity. In: *Computers and geosciences*. 2009, **10**: 2032-2046.

[10]M.J. Mihalasky and G.F. Bonham-Carter. Lithodiversity and its spatial association with metallic mineral sites, Great Basin of Nevada. *Natural Resources Research*. 2001**10**(3): 209–225.

The Porosity Estimation of Porous Basalts by Using Image Processing Methods

O. Akkoyun, S. N. Ergene,
Dicle University, Mining Engineering Department, Diyarbakir, Turkey

K. Çiftci, S. Yalvac
Dicle University, Mining Engineering Department, Undergraduate Students, Diyarbakir, Turkey

ABSTRACT In this study, the possibility of usage of image processing methods to measure porosity of porous building stones is investigated. Porosity is one of the most important parameters for evaluating and classifying natural stones, because porosity affects other properties directly or indirectly. Image processing aided porosity testing has a potential being a good nondestructive testing method. Diyarbakir basalts were selected for this investigation. The conventional porosity test method and offered image processing method were applied ad the results were presented. The correlation coefficient between conventional and offered methods is calculated as 0.66. Several valuable results for future studies to improve the study have been observed.

Keywords: Image processing, porosity estimation, porous basalt

1 INTRODUCTION

There are several tests and parameters for evaluating natural building stones such as specific gravity, uniaxial comprehensive strength, hardness, slip resistance, tensile or bending strength, water content, ultrasonic P wave velocity, and thermal conductivity. With these test results, natural building stones can be classified or evaluated from different points of view.

Porosity is also very important parameter for this aim and can be measured with different ways. As a definition porosity is the ratio of pores or micro voids to total volume. Porosity as a feature is important for natural building stones because it may affect some other features of natural stones directly or indirectly such as water content, unit weight, p-wave velocity and thermal conductivity. Therefore it is important to measure a porosity value of a building stone to obtain pre-information about its other features.

In some cases, applying conventional rock mechanics tests is not easy or forbidden (for example testing historical buildings), so that we have to use non-destructive test methods.

Image analysis and image processing techniques which are very famous in last decades have very wide range area of utilization. Basically, image processing is the realization of almost all of the performances of the human visual system by computers. These performances include color or tone detection, object and edge detection, image segmentation and rendering, and image classification and identification (Jaehne, 1997). Image processing methods involve many techniques such as the acquisition, digitization, segmentation, and enhancement, classification, recording, and re-calling of images using different numerical sub-methods (Akkoyun, 2010) and there are several studies in literature about porosity estimation by using image processing (Yetkin et.al., 2012; Zeil et.al., 2008; Grove and Jerram, 2011; Cuningham et.al., 2004) and others.

In this study, possibility of usage of image processing methods to measure porosity value of porous building stones is investigated. Diyarbakir basalts were

selected for this investigation because these basalts are the most common building stone type in Diyarbakir province for both historical and modern buildings. Almost all historical buildings were built with basalts in Diyarbakir and any of non-destructive method would be very important for investigating these buildings.

2 THE METHOD

Porosity is one the most important features for evaluating natural stones, because it affects other important features of natural stones so that it may possible to estimate other related features of stones by using its porosity value.

As the method of this study we consider taking photos of porous stone samples to apply image processing techniques. The main idea is that the porous parts have darker pixels than other parts of stones so that this color differences may let us to calculate the ratio of dark parts over total pixels.

First, the colorful pictures are turned into grayscale pictures so that the pictures have only 25 different color codes from 0 (black) to 255 (white) which mean simpler form comparing to colorful form (Fig1 and Fig2).

Figure 1. Standard Lena picture-colored

Figure 2. Standard Lena picture -grayscale

After that the pictures are scanned and some statistical data about color values are obtained such as mean value of color codes of pixels, and number of total pixels. By this way porous parts of stone have dark pixels (smaller color value), but other parts of stone have light pixels (bigger color value) comparing to porous parts.

Image processing methods involve different statistical and mathematical calculations applying into color values. One of these methods is thresholding. Thresholding is the simplest method of image processing and mainly it means turning a grayscale image (has 256 colors) into a binary image (has only 2 color) (Fig3). After thresholding, image has on two colors; 255 for black and 0 for white (Fig4).

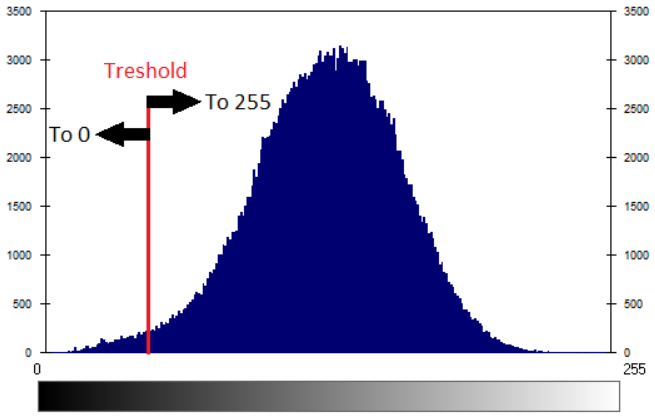

Figure 3. Color histogram and thresholding

Figure 4. Standard Lena picture -binary color

The most important point at this point is to determine the right color value to apply it as threshold point so that porous and non porous parts of stone may have different color values a 255 and 0. With this way, porous parts are represented by black pixels and finally, the last step is to calculate black pixels. The ratio of black pixels over total pixels represents ratio of porosity.

3 THE CASE STUDY

As a natural building stone, Diyarbakir basalts were selected. Diyarbakir basalts have been used for ages as natural building stone in this province and its hinterland. These basalts were used for the city walls, historical buildings, the churches and the mosques. On the other hand, basalts have been used for years in modern buildings, in walls and as pavement in city center.

The samples were obtained from porous basalts and prepared for scanning their images (Fig5).

Figure 5. The porous basalt samples

After that, the density values were calculated, then porosity values of the samples were measured. Then, in order to obtain digitized files of the samples, they were scanned by using scanner. In this step we have colorful pictures.

Following step is to turn the colorful pictures into grayscale forms. In this form, some statistical values which will be used for next step were calculated. The next step is to determine the thresholding level of the pictures so that porous parts and other parts of the pictures can be separated. After that, the pictures turned into binary files which have only black (porous) and white (other) parts (Fig6). In order to apply image processing methods, a new developed computer program (Akkoyun, 2010) was used.

Another part of the study is to measure the porosity values of the basalt samples by using conventional methods. Indirect method is used to calculate the porosity of the basalts. First, the samples were left in water for 24 hours and weights of saturated samples were measured, then after the drying step, weights of fully dried samples were measured. The differences were calculated as void volume and the ratio of this volume over total volume is calculated as porosity.

$P=Vp/Vt$

Where p is porosity,
Vp is voit volume of sample and
Vt is total volume of sample.

Figure 6(a). The original file of the sample

Figure 6(b). The grayscale form of the sample

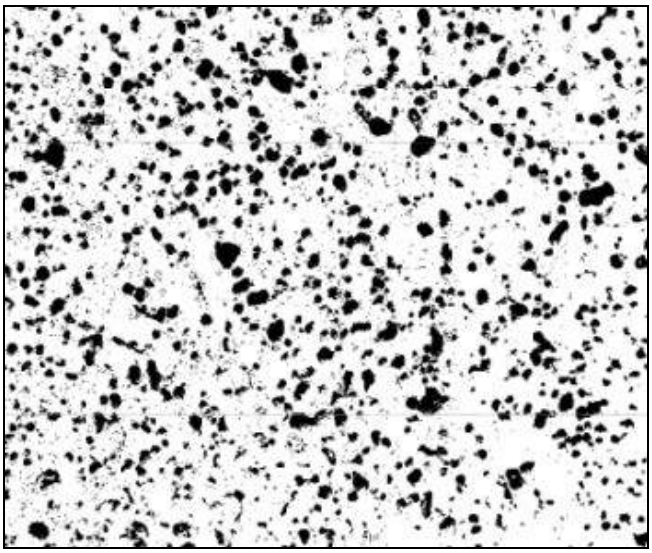

Figure 6(c). After the thresholding process

The porosity values of the samples which were calculated with both conventional and image processing method are given in Table1. The correlation between conventional and offered methods is given in Fig7.

Table1. The porosity values of the samples

Sample No	Porosity (conventional)	Porosity (image processing)
1	3.64	3.58
2	3.76	3.40
3	3.46	3.19
4	3.15	3.56
5	3.48	4.01
6	4.86	4.91

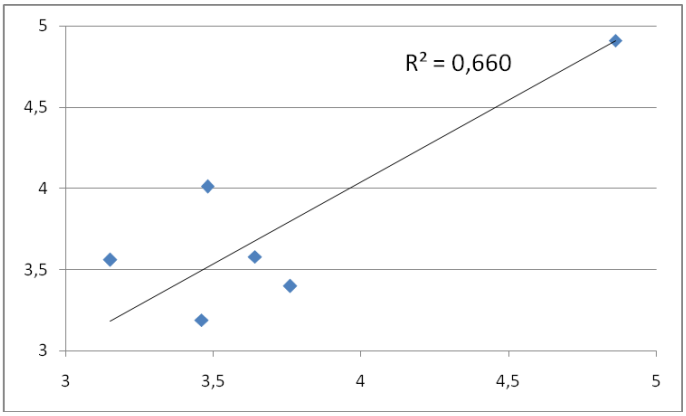

Figure 7. The correlation chart of the methods

4 THE RESULTS AND CONCLUSIONS

In this study, possibility of usage of image processing methods to measure porosity value of porous building stones is investigated. Here are the results of this study;

- Porosity is one of the most important parameters for evaluating and classifying natural stones, because porosity affects other properties directly or indirectly.
- Image processing aided porosity testing has a potential for being a good nondestructive testing method.
- Obtaining process of digital images and its conditions are crucial important as it is in every image processing study.
- The correlation coefficient between conventional and offered methods is calculated as 0.66 which is not high enough.
- Determining and selecting the threshold level is the most important part of his study and this level affects directly porosity calculations.
- One of the problems was color of the natural stone, basalt has dark colors in general and porous parts have also dark color so that it is no easy to recognize them and determine the thresholding color level. So that, relatively light stones such as travertine may have better results.
- The thickness of the samples are important, this study deals with stone's surface, but porosity is kind of

3D phenomena so that the third dimension must be considered.

- As future work, testing many samples having different thickness for one specific stone type it may possible to find a sufficient relationship between conventional and offered method.

REFERENCES

Akkoyun, O, 2010, "An evaluation of image processing methods applied to marble quality classification", International Congress on Computer and Technology Development (ICCTD-2010), Cairo, Egypt.

Grove, C., Jerram, D.A., 2011, jPOR: An ImageJ macro to quantify total optical porosity from blue-stained thin sections, Computers & Geosciences 37 (2011) 1850–1859.

Jaehne, B., 1997; "Practical handbook on image processing for scientific applications", USA :CRC Press

K. J. Cunningham, K.., Carlson, J.I., Hurley, N. F., 2004, New method for quantification of vuggy porosity from digital optical borehole images as applied to the karstic Pleistocene limestone of the Biscayne aquifer, southeastern Florida, Journal of Applied Geophysics 55 (2004) 77– 90.

Yetkin, M.E., Kahrama, B., Özfırat, MK., Şengün, B., 2012, Gözenekli Kayaçlarda Görüntü Analizi Yöntemi ile Porozite Tayini, Mersem2012, Afyon, p419-426. (in Turkish)

Zeil, R., Haus, A., Tulke, A., 2008, Quantification of the pore size distribution (porosity profiles) in microfiltration membranes by SEM, TEM and computer image analysis, Journal of Membrane Science 323 (2008) 241–246.

Drilling and Blasting, Drilling Technology, and Mechanization

Air Quality During Excavation Of Tunnels In The Rijeka Motorway Bypass

M. Klanfar, D. Vrkljan
University of Zagreb, Faculty of mining, geology and petroleum engineering, Zagreb, Croatia

ABSTRACT The main sources of dangerous and harmful gases during the excavation of tunnels are blasting operations and application of diesel equipment for loading and transport of excavated rock. Full-face driving of parallel pipes of three tunnels was conducted in the Rijeka Motorway Bypass by blasting operations and the use of diesel equipment. The quality and quantity of air was monitored in accordance with the technical conditions in the workspace of the tunnels. The concentration of harmful and hazardous gases, along with oxygen, was monitored by active continuous measuring with portable instruments. Measurements were conducted at the head of the tunnel, during blasting operations and during the process of loading and transport of the blasted rock mass. A comparative analysis of actual air loss and losses calculated in accordance with the empirical equations was conducted along the ventilation air duct, as well as the air supply requirements.

Keywords: Rijeka motorway bypass, Air quality, Tunnel excavation

1 INTRODUCTION

1.1 Tunnel Excavation Method

Most excavations of tunnels in karst are challenged with very frequent changes in geological formations and rock mass structure. For this reason, common method of excavation in karst is New Austrian Tunnelling Method or NATM, which provide great flexibility in varying formations (Chapman et.al. 2010)

Almost all tunnels in Croatia are excavated using drill and blast technique, based on NATM method, since it is found to be optimal for excavation conditions in karst (Mustapić 2012). Usual excavation phases of this method include drilling and blasting operations, ventilation, loading and haulage of blasted rock, and application of primary support.

Most profusely sources of dangerous and harmful gases during underground excavations are usage of explosives and diesel equipment for loading and haulage. If ventilation delivers insufficient quantity of fresh air at the working face of a tunnel, concentration of harmful gases can periodically rise above maximum allowable values, or even maintain high values for whole excavation phase.

Air quality measurements in three tunnels of Rijeka Motorway Bypass in Croatia were analysed in this paper, namely Škurinje I, Škurinje II and Trsat (Fig. 1).

1.2 Dangerous And Harmful Gases

Concentration of six gases regularly found during tunnel excavation were measured. They are carbon and nitrogen monoxides and dioxides, sulphur dioxide, acetaldehyde, and methane in addition.

Carbon monoxide is flammable, explosive gas, and extremely toxic. During regular underground operations it is emitted due to detonation of explosives and usage equipment powered by diesel engines. In extraordinary circumstances it occurs during fire and explosive hazards. Toxicity appears with concentrations higher then 35 ppm.

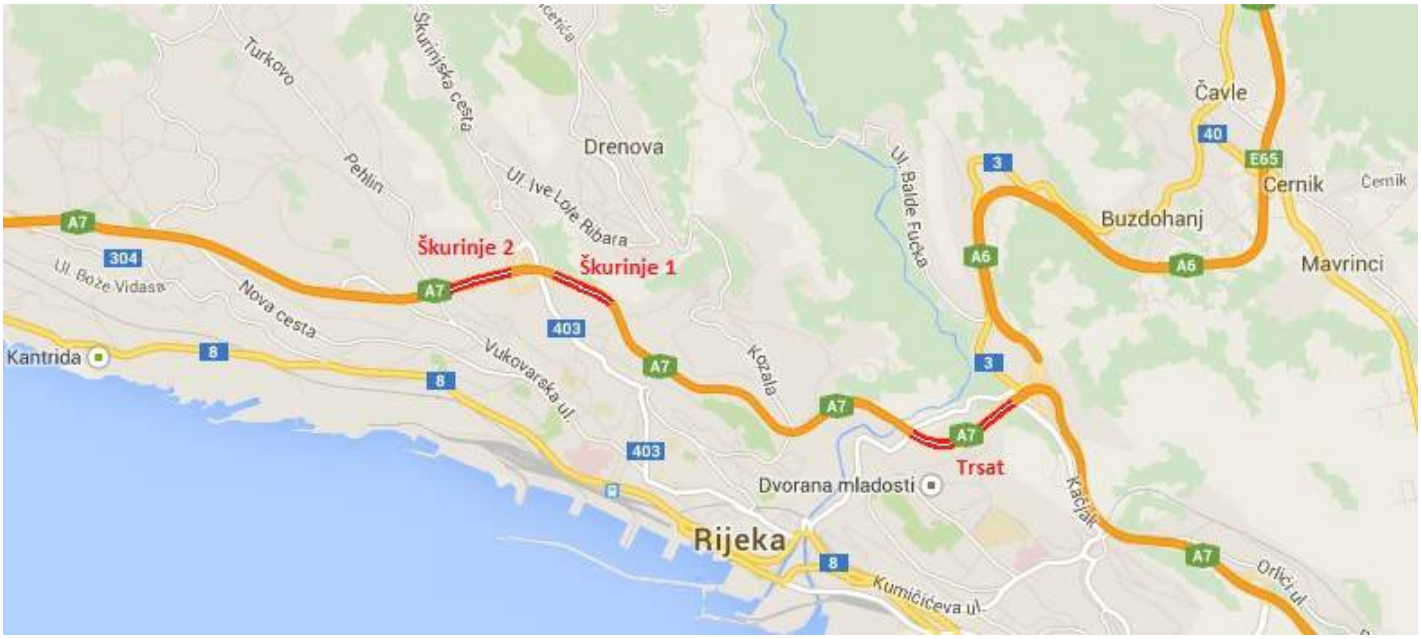

Figure 1. Tunnels locations

Carbon dioxide is normal constituent of air with concentration of 0,039%. It is not considered to be toxic, but it is an asphyxiant gas that can cause suffocation in concentration higher than 7%. Sources of this gas are same as for carbon monoxide.

Nitrogen monoxide is considered immediately harmful in concentration above 100 ppm. In air it rapidly oxidizes to nitrogen dioxide, even more toxic gas. In addition to toxicity, nitrogen oxides are readily soluble in water and thus they dissolve in tissue moisture forming acids, which can cause irritation.

Sulphur dioxide is minor component in diesel exhaust gases, and can be generated by detonation if explosives contain sulphur. It is considered to be immediately harmful in concentrations above 100 ppm.

Acetaldehyde, beside formaldehyde, is one of aldehydes that has highest portion in diesel exhaust gases. It is flammable, explosive, very toxic, and considered immediately harmful in concentrations above 2000 ppm (NOISH 1995).

2 AIR QUALITY LEGISLATION

Croatian legislation on air quality is relatively complex if we account for all application areas. However, there are several regulations of interest for this research, that deal with allowable concentrations of dangerous and harmful gases, and are applicable to the underground excavation of tunnels.

Regulation on technical standards for diesel engines in underground mining operations in non-methane mines (SL 53/90) defines maximum allowable concentrations of gases, or MDK (Tab. 1). MDK is defined as concentration that has no known harmful effects on humans, during every day eight hour work.

Regulation on occupational exposure limits and biological exposure limits for harmful substances (NN 13/09) is newer and has somewhat different approach, as it considers maximum exposure limits instead of maximum concentrations (Tab. 2). Two exposure limits are defined according to this regulation: time weighted average exposure (GVI) - exposure that has not harmful effects during every day eight hour work, and short term exposure (KGVI) - exposure that has no harmful effects during period of 15 minutes, four times daily. Both exposure limits for gases of interest here are presented in Table 2.

Other Regulations (SL 11/97, SL 24/91) deal with marginal requisites on microclimatic parameters, temperature and air quantities and velocities.

Table 1. Maximum allowable concentrations

Gas formula	MDK (ppm)
CO	50
CO_2	5000
NO	25
NO_2	5
SO_2	4
C_2H_4O	10

Table 2. Occupational exposure limits

Gas formula	GVI (ppm)	KGVI (ppm)
CO	30	200
CO_2	5000	-
NO	25	-
NO_2	3	5
SO_2	2	5
C_2H_4O	20	50

Beside maximum allowable concentrations of dangerous and harmful gases, minimum allowed concentration of oxygen at any given time is 19 %.

Required air supply at underground excavation face depends on number of factors. They can include air temperature, moisture and allowable air velocities, but two of them are essential in regular underground work operations: emissions of harmful gases and consumption of oxygen, which are in relation to the number of employees and total power of diesel equipment. It is defined that air flow should be 3-4 m^3/min per employee. In case of usage of diesel equipment air flow should be 4 m^3/min per one kilowatt of total diesel equipment power.

3 AIR QUALITY AND VENTILATION MEASUREMENTS

Concentration of aforementioned harmful gases, methane and oxygen were continuously measured during three excavation phases in sequence: drilling and blasting operations, ventilation phase, and loading and haulage of blasted rock material (Jankovic & Vrkljan 2008a, b, c).

Concentrations were measured using two gas detectors Drager Multiwarn II, which comprise infrared sensor for carbon dioxide, catalytic sensor for methane, and electrochemical sensors for all other mentioned gases.

Total, static and velocity pressures were measured along the ventilation ducts using digital manometer Airflow DM2L, with attached Pitot-Prandtl tube. Measured pressures were used to calculate pressure drop, air flow and velocity, and air loss inside the ventilation duct. In order to accurately determine air supply to the excavation face, air velocity was directly measured at the exit of ventilation duct using digital vane anemometer DA4000.

3.1 Measurement Conditions

Measurements were taken at different distances from excavation face. Distance amounts to 91 m in tunnel Škurinje I, 33 m in tunnel Škurinje II, and 100 m in tunnel Trsat.

In all three tunnels forcing (blowing) ventilation system was applied. It composes of one axial fan of 90 kW power and flexible circular polyester ducts, 1800 mm in diameter. Although mentioned parameters are the same in all three tunnels, fans and ducts have different characteristics summarised in Table 3. Blasting was done using non-electric system (NONEL) in all three tunnels, with plastic explosive charge in main and contour blastholes and gelatinous explosive charge in contour blastholes. Exception is tunnel Škurinje I, where emulsion was used in main blastholes and gelatinous explosive in contour blastholes. Total amount of explosive charges per one blast are shown in Table 4.

Loading and haulage of blasted rock material was carried out using loaders and trucks of different sizes, engine power and number of units, which is also summarised in Table 4.

Table 3. Ventilation system characteristics

Tunnel	Fan make	Nominal airflow (m^3/s)	Nominal pressure (Pa)	Nominal revolution speed (min^{-1})	Duct section length (m)	Overall duct length (m)
Škurinje I	Gia SwedVent	37	1800	1483	20	183
Škurinje II	Ekovent	40	1800	1480	30	127
Trsat	Korfman	33	3700	1480	30	370

Table 4. Explosives and diesel equipment utilized during measurements

Tunnel	Explosive charge	Loading and excavation equipment	Haulage equipment
Škurinje I	166,0 kg	Cat 966H (211 kW) Komatsu PC350 (251 kW)	Volvo A30E (251 kW)
Škurinje II	122,3 kg	Cat 966 G2 (193 kW)	MAN (294 kW) Mixer truck (278 kW)
Trsat	189,6 kg	Komatsu EX350 (192 kW) O&K L45 (177 kW)	Tatra (270 kW) Fiat hitachi (250 kW)

4 AIR QUALITY ANALYSIS

Continuous concentrations of harmful gases were compared to the MDK values according to the Regulation on technical standards for diesel engines in underground mining operations in non-methane mines (SL 53/90), as most authoritative regulation for this objective.

Peak values were noted in order to determine if concentrations rise above maximum allowable. In case they do, time of dilution below maximum allowable concentration was determined.

Typical gas concentrations versus time are presented in Figure 1. It can be seen that concentration of all detected gases raise rapidly after blasting, except oxygen. Methane was measured but was not detected, and thus it is not included in the analysis.

Ventilation system is put into operation immediately after blasting, and during period of 15 to 25 minutes harmful gases are significantly diluted. After that period, concentrations are low enough to proceed with the next tunnel excavation phase, i.e. loading and haulage of blasted rock material.

During loading and haulage phase, concentration of most gases emitted by blasting continue to fall to some extent, due to operating ventilation, but are additionally emitted by diesel equipment. After that, gases are emitted entirely by diesel equipment and remain relatively constant until the end of loading and haulage.

Peak concentration of detected gases and determined time of dilution below allowable concentration according to the Regulation (SL 53/90) are presented in Table 5.

Largest concentration can be observed for carbon dioxide in all there tunnels. Peak values range between 700 and 2800 ppm, but neither of this values is above allowable concentration of 5000 ppm, and thus dilution time is not of significance.

Concentration of carbon monoxide raises above the allowable one, in all three tunnels immediately after blasting. Extremely high concentration was recorded in Škurinje II, where peak concentration amounts to 500 ppm. Compared to most other harmful gases it takes considerable time of dilution, between 8 and 28 minutes.

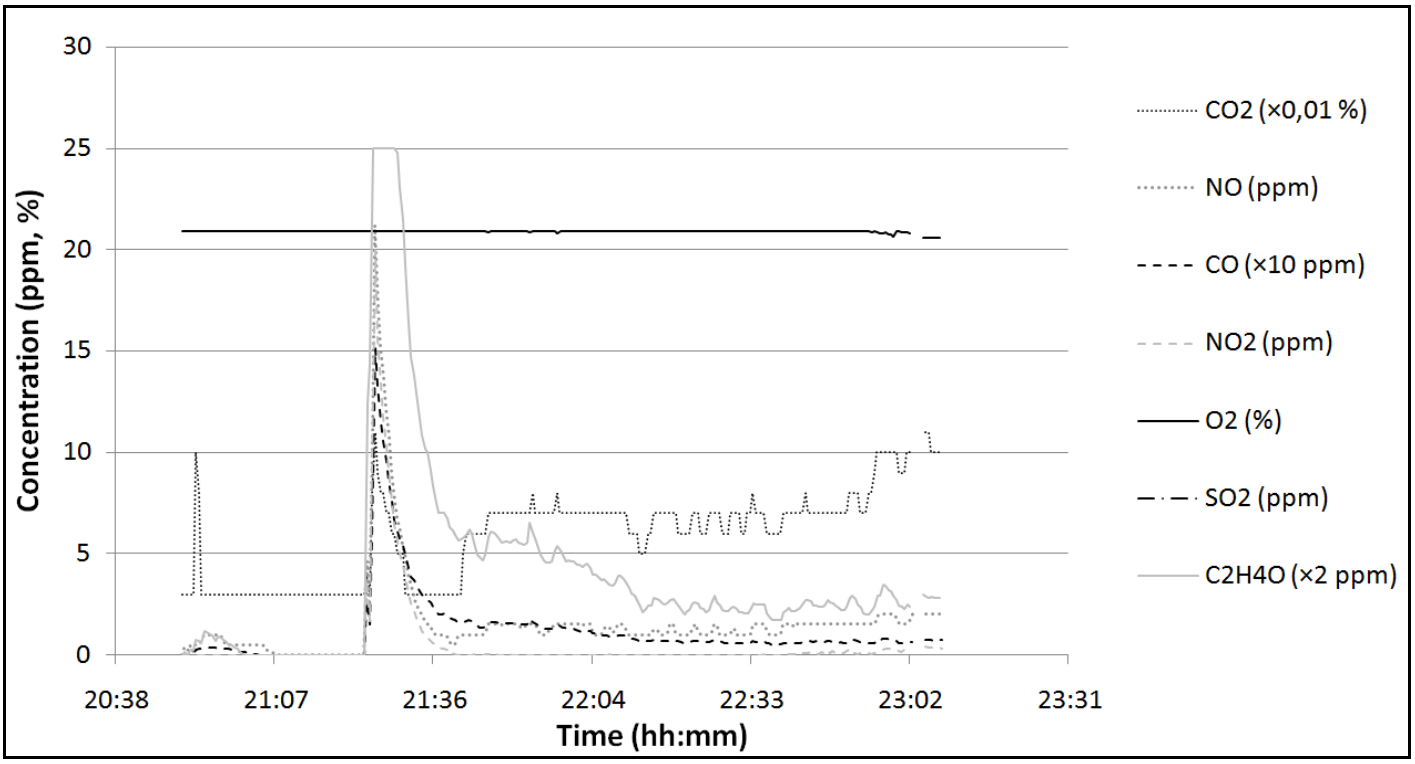

Figure 1. Typical gas concentration diagram

Nitrogen oxide is found to be higher than allowable only in tunnel Škurinje II, but for short period of 4,5 minutes. Concentration of nitrogen dioxide raises above allowable values in all three tunnels, between 3,19 and 20,00 ppm. It requires relatively small time for dilution from 3 to 6 minutes.

Sulphur dioxide was detected in two tunnels, Škurinje II and Trsat. Concentration was very small compared to other gases, with peak values significantly below allowable ones, that is from 0,02 to 0,28 ppm

Concentration of formaldehyde was considerable in all three tunnels, above 46 ppm. This value is roughly five times greater than allowable concentration of 10 ppm.. Accordingly, dilution time for formaldehyde has highest value than for other gases, with range between 19,5 and 37,00 minutes

Table 5. Peak concentrations and dilution time of harmful gases

Gas	Škurinje I	Škurinje II	Trsat
NO	21,18	50	04,95
	-	04:30	-
CO_2	1100,00	2800	700
	-	-	-
CO	151,43	500,00	55,50
	08:50	28:00	20:00
NO_2	20,00	19,15	03,19
	06:00	04:30	03:00
SO_2	00,00	0,28	0,02
	-	-	-
C_2H_4O	50,00	50,00	46,22
	35:30	37:00	19:30

00,00 – Peak concentration values (ppm)
00:00 – Time of dilution below maximum allowable concentration or MDK (mm:ss)

Oxygen concentration differed in three tunnels, but generally varied between 20,60 and 20,90 %, which satisfies minimum criteria of 19 %.

Dilution time of harmful gases mostly depends on concentration of carbon monoxide and formaldehyde, since concentration of these gases exceeds allowable values by multiple times. Actual concentration of formaldehyde in Škurinje I and II was even higher then measured 50 ppm, because this value represents measuring range of the sensor.

All other harmful gases were diluted in relatively short period of up to 6 minutes.

5 VENTILATION PARAMETERS ANALYSIS

Air velocity inside ventilation duct was calculated based on measured dynamic pressure and air density, except at the duct outlet where it was measured directly. In conjunction with duct cross section area, air flow was calculated. Given air flow for all three tunnels, with corresponding distance form tunnel portal is presented in diagrams on Figures 2-4. Total pressure, measured as difference between duct inside and outside in tunnel space, is also shown to present pressure drop as indicator of air duct resistance.

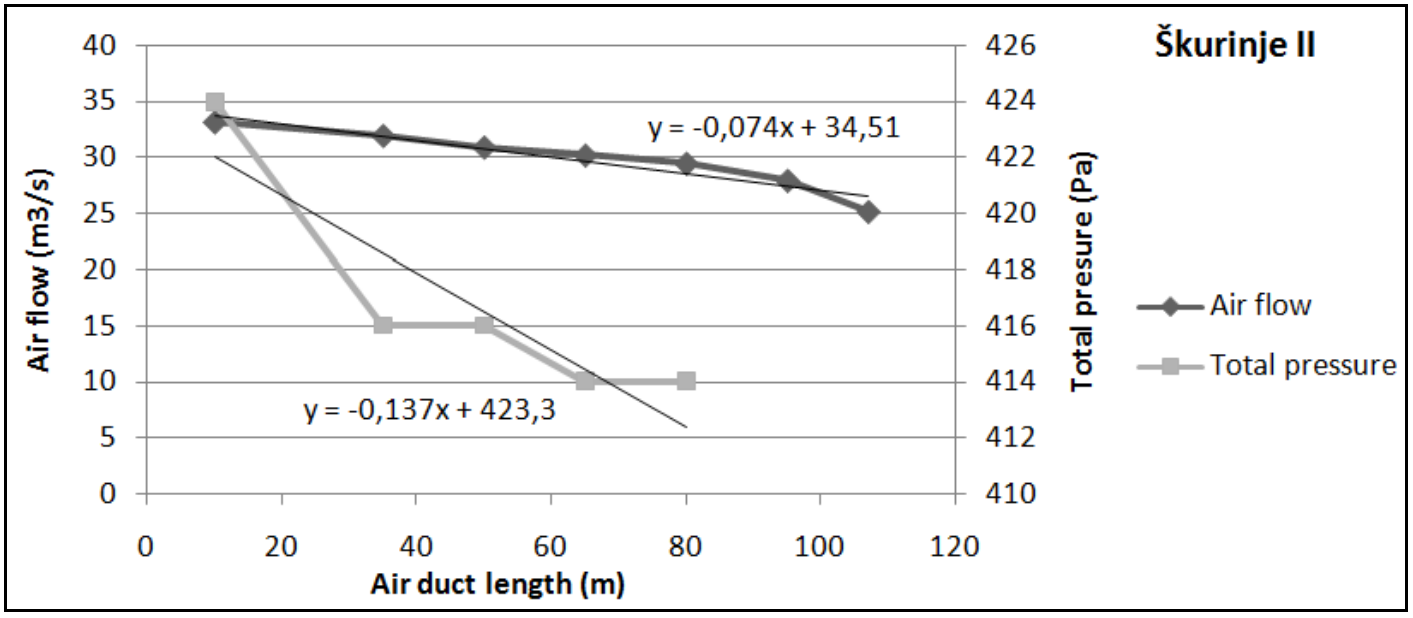

Figure 2. Air flow and pressure drop in ventilation ducts of the Škurinje II tunnel

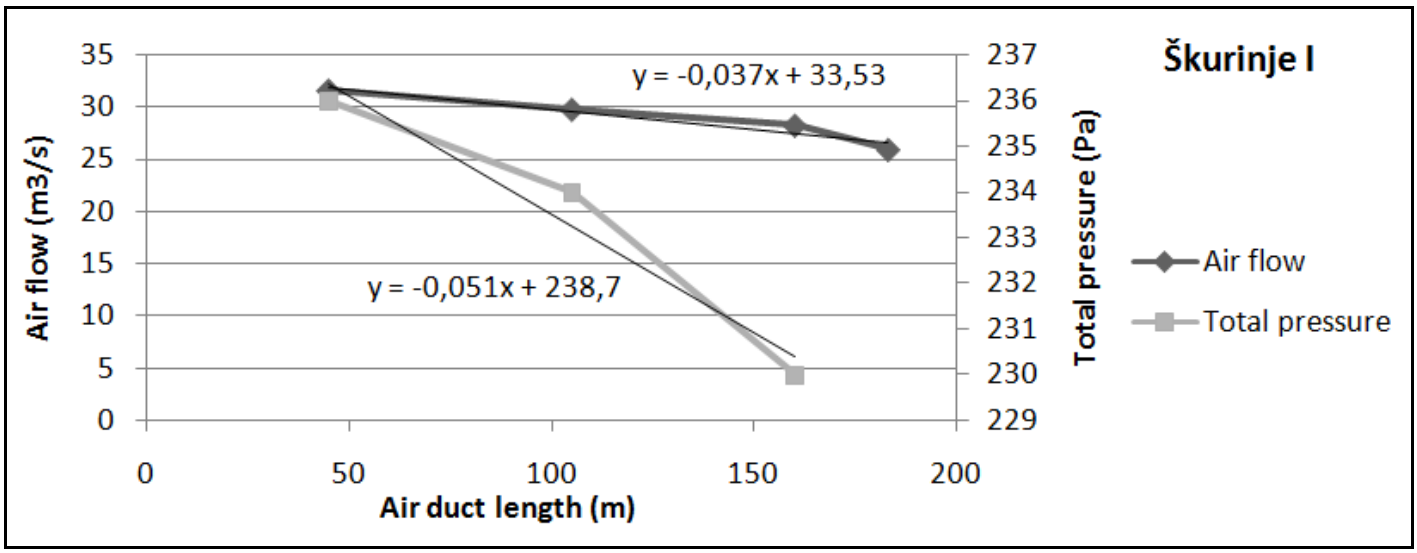

Figure 3. Air flow and pressure drop in ventilation ducts of the Škurinje I tunnel

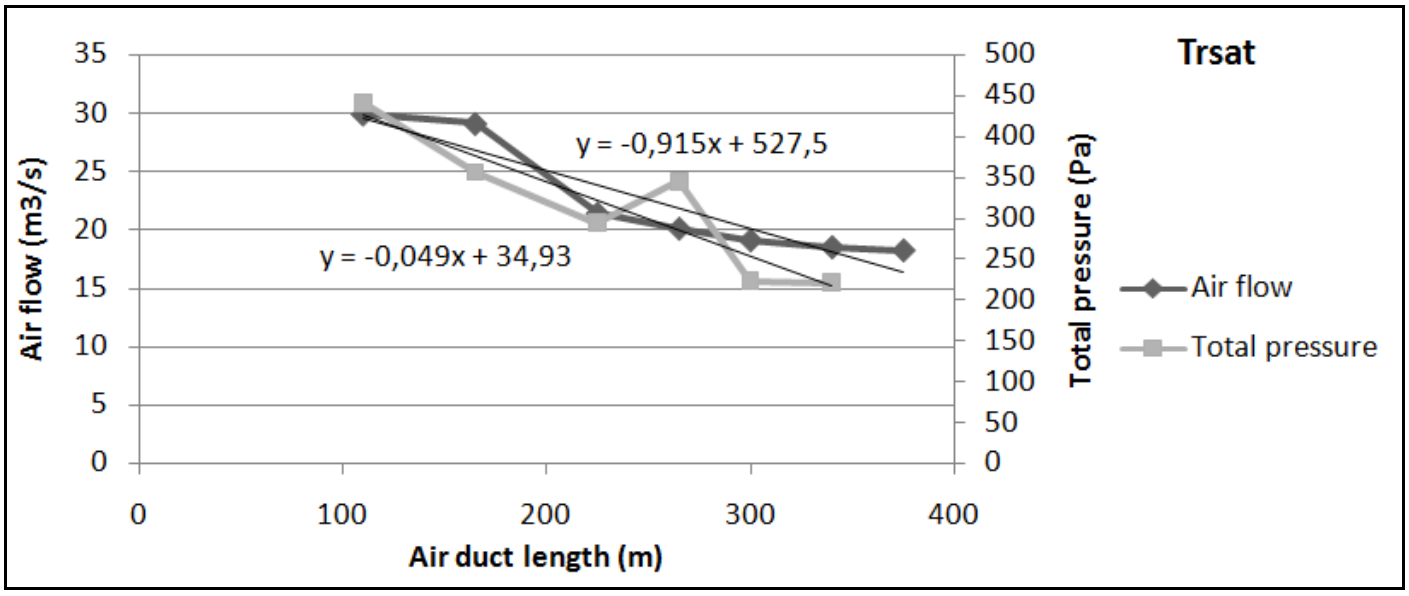

Figure 4. Air flow and pressure drop in ventilation ducts of the Trsat tunnel

Linear regression is applied to the air flow data in order to define mathematical equation of air flow and air loss, in relation to ventilation system length

It can be seen that specific air loss ranges from 0,037 to 0,074 m^3/s per meter of ventilation duct length. If we account for current excavated tunnel length, air loss amounts to 17,6 % for Škurinje I, 24,1 % for Škurinje II, and 38,9 % for Trsat tunnel. Air loss in tunnels Škurinje I and Škurinje II seems to be disproportional, because longer tunnel has lower air loss, but this could be attributed to bad jointing of duct sections or damaged duct. In accordance to its length, Trsat tunnel has largest air loss.

Overall power of diesel equipment utilised simultaneously in a tunnel can vary depending on all operations in progress at one moment. At tunnel excavation face there are usually operating one loader and one truck, due to confined workspace. According to engine powers form Table 4, combination of mentioned equipment results in overall powers from 447 kW to 487 kW, accounting for all three tunnels.

Using the rule for air demand of 4 m^3/s per kW of diesel equipment power, it can be calculated that minimum air demand at excavation face ranges from 30,8 m^3/s to 32,5 m^3/s. Accounting for measured air loss, ventilator air supply should be from 37,4 to 48,7 m^3/s, depending on the tunnel. Data for all three tunnels is presented in Table 6.

Current air flow at the outlet of ventilation duct, that is air supply to the excavation face, is lower than calculated demand in all three tunnels.

Table 6. Air loss and air demand

Tunnel	Diesel power[1] (kW)	Minimum air supply[2] (m^3/s)	Air flow[3] (m^3/s)	100m air loss (%)	Overall air loss (%)	Required air supply (m^3/s)
Škurinje I	462	30,8	26,04	12,77	17,62	37,4
Škurinje II	478	32,5	25,26	24,84	24,09	42,8
Trsat	447	29,8	18,23	14,40	38,87	48,7

[1] one loader + one truck at excavation face
[2] to the excavation face
[3] measured at ventilation duct outlet

Nevertheless, longest time of blasting gases dilution is found to be between 20 and 37 minutes, which is acceptably low, and during loading and haulage phase no gas concentration exceeds maximum allowable values.

5.1 Comparison To Air Loss According To Empirical Equations

In order to determine liability of computational assessment of air losses, results of assessment were compared to measured values. With assumption that ventilation system in good condition losses air only at duct section joints, overall air loss was calculated in accordance with empirical equations (Eq. 1-2) for air loss at ventilation duct joints (Teply 1990):

$$R_c = 0{,}81\frac{\lambda_c \rho}{D^5} l \qquad (1)$$

$$e = \left(8{,}1 \cdot k_{pt} \cdot D \cdot n \cdot \sqrt{R_c} + 1\right)^2 \qquad (2)$$

where:

- R_c duct resistance (kg/m^7)
- λ_c resistance coefficient
- ρ air density (kg/m^3)
- l duct length (m)
- D duct diameter (m)
- e air loss
- k_{pt} joint permeability coefficient
- n number of joints

Resistance and joint permeability coefficients were selected for plastic ducts in forcing ventilation system, and for diameter of 1,8 m. Given values are λ_c=0,02 and k_{pt}=0,000288. All other values were selected according to measurements or ventilation system characteristics. Input data is presented along the results in table 7.

Table 7 Air loss according to empirical equation

Tunnel	Duct length (m)	Number of joints	Air density (kg/m^3)	Duct resistance (kg/m^7)	100m air loss (%)	Overall air loss (%)	Required air supply (m^3/s)
Škurinje I	183	10	1,162	0,1823	4,43	8,1	33,29
Škurinje II	127	5	1,188	0,1293	5,19	6,6	34,65
Trsat	370	13	1,132	0,3600	8,64	32,0	39,04

6 CONCLUSIONS

Longest dilution time of blasting gases is found to be for carbon monoxide (9 to 28 min) and acetaldehyde (19 to 37 min). Dilution of other harmful gases is achieved in very short period, that amounts up 6 min. This excludes carbon and sulphur dioxide, which concentrations do not exceed maximum allowable values at all. Nitrogen oxide had concentration above allowable values only in one tunnel, and for very short period of 4 min.

After dilution of blasting gases, and during loading and haulage, concentration of all gases stays below maximum allowable values and does not rise. This means that air supply to the excavation face is sufficient in all three tunnels.

Calculated minimum air supply, accounting for overall diesel equipment power, is higher than actual air supply to the excavation face. This doesn't represent a problem, due to acceptable dilution time of concentrations below MDK. But as excavation of tunnel advances, there is certain increase in air loss and decrease in air supply, which extends time of dilution and

causes rise of gas concentrations during loading and haulage.

Comparing actual to calculated air loss, it can be seen that empirical equations do not provide reliable results, since calculated air loss is multiple times lower.

Importance of maintaining ventilation ducts and joints can be seen comparing specific air loss in all three tunnels. Škurinje II is shortest of them, but has twice as high air loss air per duct length. Other two tunnels have similar air loss, which is somewhat higher in the longer tunnel.

REFERENCES

Chapman, D., Metje, N., Stark, A., 2010. *Introduction to tunnel construction*, Spon Press, New York, 344 p.

Jankovic, B., Vrkljan, D., 2008a. V*entilation paremeters, air quality, and microclimate conditions in the workspace of tunnel Škurinje I.* Faculty of mining, geology and petroleum engineering. Zagreb. Report no. I08/03. Unpublished.

Jankovic, B., Vrkljan, D., 2008b. V*entilation paremeters, air quality, and microclimate conditions in the workspace of tunnel Škurinje II.* Faculty of mining, geology and petroleum engineering. Zagreb. Report no. I08/02. Unpublished.

Jankovic, B., Vrkljan, D., 2008c. V*entilation paremeters, air quality, and microclimate conditions in the workspace of tunnel Trsat.* Faculty of mining, geology and petroleum engineering. Zagreb. Report no. I08/01. Unpublished.

Mustapić, I., 2012. Construction of road tunnels with special emphasis on particulates during construction of the Šumbir tunnel on the A1 motorway, *Construction of traffic infrastructure*, pp. 479-512.

NN 13/09. *Regulation on occupational exposure limits and biological exposure limits for harmful substances*. Narodne novine d.d., Zagreb.

NOISH, 1995. *Chemical Listing and Documentation of Revised IDLH Values.* NOISH Publications and Products. URL: http:// www.cdc.gov/ niosh/ idlh/ intridl4.html

SL 11/67. *Regulation on technical measures and occupational safety in underground mining operations*. Službeni list SFRJ. Beograd.

SL 24/91. *Regulation on technical standards for underground exploitation of metallic and non-metallic mineral resources.* Službeni list SFRJ. Beograd.

SL 53/90. *Regulation on technical standards for diesel engines in underground mining operations in non-methane mines.* Službeni list SFRJ. Beograd.

Teply, E, 1990. *Rudnička ventilacija (Mine ventilation)*, Faculty of mining, geology and petroleum engineering, Zagreb, 355 p.

Assessment of Safe Ground Vibration Level in Sensitive Hilly Slopes Ensuring Human Response

C. Sawmliana, R.K. Singh, P.P. Roy
Blasting Department, CSIR-Central Institute of Mining & Fuel Research (CSIR-CIMFR)

ABSTRACT The paper describes the controlled blasting operations in close proximity of residential houses on hilly slopes at the road construction site of Kaladan Multi-Modal Transit Transport Project of Mizoram state of India. Human response and sensitivity were predominantly considered while fixing the safe level of ground vibration in contrary to the prescribed level suggested by the regulatory agency in India i.e. Directorate General of Mines Safety (DGMS). Experimental blasts were conducted using 32 mm drillhole diameter of 1.5 m (5 ft) depth and 25 mm diameter cartridged explosive with short-delay electric detonators. Ground vibration level of 1.85 mm/s was even found to be very severe and non-acceptable to the inhabitants. To avoid further complaints and inconvenience, controlled blast design parameters were established with limited number of holes and maximum charge per delay in a blasting round so as to confine the ground vibration level within 1 mm/s which was acceptable to the residents.

Keywords: Ground vibration, blasting, Kaladan Multi-Modal Transit Transport Project

1. INTRODUCTION

Ground vibration is one of the most perceptible side-effects of rock blasting which causes human annoyance and structural damage, although damage only occurs at levels many times higher than those that cause annoyance (Pesch and Robertson, 2007). The safe values of ground vibration generated from blasting for different surface structures have been laid down by different countries based on their respective research works. As such, the threshold values of ground vibration prescribed in a particular country may not be applicable in other countries. In India, ground vibration standards have been prescribed by three different organizations viz. Indian Standard Institution (ISI), Directorate General of Mines Safety (DGMS) and Central Mining Research Institute (CMRI). The vibration standard prescribed by ISI (IS: 6922 -1973) under 'Criteria for safety and design of structures subjected to underground blasts' is intended for the safety of normal structures constructed on/in more or less homogeneous soil or rock strata. The term 'underground blasting' had been specified as detonation of explosive in drillholes and boreholes for rock excavation and quarry blasts. Hard rocks refer to granite, basalt, quartzite, marble, crystalline schists, massive slates and other hard massive crystalline rocks whereas soft rock refers to shale, sandstone phyllites, laminated slates, mica schist, weathered hard rocks and other soft rock materials.

The CMRI (presently CSIR-CIMFR) vibration standard prescribed in the year 1993 categorized three different types of structures and formulated the threshold values of ground vibration based on dominant frequency of ground vibration. While framing the safe value of ground vibration level, CMRI vibration standard considered the ages as well as the state of condition of the structures in addition to human perceptions. This has a practical implication that the residents would never allow any blasting activity whenever the level of vibration exceeds some perception level whether it is harmful for structures or not.

The DGMS vibration standard (Technical Circular No. 7 of 1997) grouped the type of structures into two categories viz. (A) Structures not belonging to owner and (B) Structure belonging to owner. Each group is again classified based on the type of

construction, their importance and sensitivities. In such classification, dominant excitation frequency was given due importance.

In India, from practical point of view, it is difficult to follow a particular standard due to different psychological response of human being residing in the vicinity of mining areas and their consequent repercussions. Complaints of structural damages may still be raised even if the level of ground vibration falls below the prescribed threshold level of structural damage. It is normally seen that in many projects, the vibration thresholds are based on human response than on the probability of damages (Jimeno et al., 1995). The authors also experienced the similar incident while working in a road construction project wherein the blast-induced ground vibration levels were forcefully confined within the tolerable limit of the nearby populace in a sensitive hilly area of Mizoram state in India. This paper describes the controlled blasting operations executed at the road construction site of Kaladan Multi-Modal Transit Transport Project, Mizoram wherein the ground vibration level was kept at 1 mm/s as per the acceptable level of nearby inhabitants keeping aside the prescribed limits of the regulating agencies.

2. THRESHOLD VIBRATION LEVELS

The threshold values of ground vibration established by the Indian Standard Institution (ISI, 1973), CMRI (presently CSIR-CIMFR, 1993) and the DGMS vibration standards (1997) are shown in Tables-1, 2 and 3.

Table 1. After Indian Standard Institution (IS: 6922 -1973)

Soil, weathered or soft rock conditions	70 mm/s
Hard rock conditions	100 mm/s

Table 2. CMRI vibration standard (Dhar et al., 1993)

Type of structure	**Threshold value of ppv (mm/s)**	
	≤ 24 Hz	**> 24 Hz**
Domestic houses, dry wall interior, construction structures with plasters, bridge	5	10
Industrial buildings, steel or reinforced concrete structures	12.5	25
Objects of historical importance, sensitive structures, more than 50 years old construction and structures in poor state of condition	2	5

Table 3. DGMS vibration standard (Technical Circular Number 7 of 1997)

Type of structure	Dominant excitation frequency, Hz		
	< 8 Hz	8-25 Hz	> 25 Hz
(A) Buildings/structures not belonging to the owner			
1. Domestic houses or structures (Kuchcha, brick & cement)	5 mm/s	10 mm/s	15 mm/s
2.Industrial buildings	10 mm/s	20 mm/s	25 mm/s
3. Objects of historical importance and sensitive structures	2 mm/s	5 mm/s	10 mm/s
(B) Buildings belonging to owner with limited span of life			
1. Domestic houses/structures	10 mm/s	15 mm/s	25 mm/s
2. Industrial buildings	15 mm/s	25 mm/s	50 mm/s

3. INVESTIGATIONAL SITES AND THE PROBLEMS

The Kaladan Multi-Modal Transit Transport Project was initiated by the Government of India under the Look-East Policy to connect India's land-locked Northeastern states with the southern coast of Myanmar. The project will connect the seaport of Kolkata with Sittwe port in Myanmar; it will then link Sittwe to the land-locked region of Mizoram in northeastern India via inland water transport and road transport (Figure 1). The project included construction of nearly 100 km long highway starting from Lawngtlai Town, NH-54 (in Mizoram) up to Myanmar border. The initial portion of the road alignment passed through the periphery of Lawngtlai town, the capital of Lawngtlai district, Mizoram with a span of about 4 km. Residential houses were located on the hilly slope within 90 to 100 m above the road alignment. In the initial portions viz. at Ch: +400 m and Ch: +2150 m, hard rock formations were encountered during formation cutting which required drilling and blasting operations. The full cutting was required as there was no chance of widening by retaining wall at downhill side due to steep gradient. Hence, blasting operations were carried out for the construction of road in these rocky portions. However, the nearby residents alleged damages to their houses due to ground vibrations and noises generated by the blasting operations. Accordingly, the total blasting operation was stopped following the instruction given by the Deputy Commissioner (DC), Lawngtlai District, Mizoram. Hence, the formation cutting work was delayed in a small segment (about 100 m stretch only) due to the complaints raised by the nearby residents whereas the formation cutting works in other portions of the road were almost completed. In order to restart the blasting operations nearby the residential areas, the controlled blasting study was awarded to the Blasting Department of CSIR-Central Institute of Mining & Fuel Research (CSIR-CIMFR), Dhanbad.

Figure 1. An outline of Kaladan Multi-Modal Transit Transport Project

At Ch: +400 m, the unfinished rocky portion which required drilling and blasting operations for the excavation work was about 100 m length. The required excavated height using drilling and blasting varied from a few meter to 25 m with maximum width of 8.0 m (Plates 1 & 2). The top portion containing soil and softer rock formations had already been excavated using excavator. The rock formation consisted mainly of shale and shaley sandstone of softer formation. Harder sandstone formation of grey colour with thickness varying from 2 to 2.5 m was present in the top portion of the rock strata. The rock strata were dipping against the excavated slope of the highwall, favouring better slope stability. The residential houses were located above the road alignment. The nearest residential house at Ch: +400 m from the required blasting site was 90 m. One hospital was also located at a distance of less than 200 m above the required blasting site.

Plate 1. Far view of the rock formation at Ch: +400 m

Plate 2. Closer view of the rock formation at Ch: +400 m

At Ch: +2150 m, the rock strata mainly consisted of shale with heavily jointed formation. Hard sandstone formation was not found in the required excavated slope. However, the shale strata required drilling and blasting as the excavator deployed at the site could not excavate it. The length of road stretch which required blasting operation was more than 125 m. However, more than 60% had already been excavated. The residential houses were located above the required blasting site and the distance of the nearest house from the blasting site at Ch: +2150 was 89 m.

Plate 3. View of rocky portion that required blasting operation at Ch: +2150 m

4. EXPERIMENTAL BLASTS AND GROUND VIBRATION MONITORING

Before conducting the experimental blasts, an official notice was given by the Deputy Commissioner to the nearby residents of blasting sites regarding the controlled blasting programme. Since the residential houses were located within 100 m from the required blasting sites, it was decided to use 32 mm blasthole diameter, drilled with jack hammer. It was also planned to use short delay electric detonators of 25 milliseconds interval with delay series of zero to 10 numbers. However, due to remoteness of the area and difficulty in acquiring explosive and blasting accessories, only delay series of 0, 2, 5, 6, 7 & 10 numbers were available. The depth of blasthole used in all the experimental blasts was 1.5 m (5 ft). Small diameter (25 mm) cartridged explosive of 125 g weight was used.

Initially, the experimental blasts were conducted with limited number of holes. At Ch: +400 m, the first round of experimental blast was conducted with seven holes in shale strata of softer formation. The total explosive charge was 2.06 kg and maximum charge per delay was 0.624 kg. Blast induced ground vibration was monitored near the foundation as well as on the first floor of adjoining residential houses (Plates 4 & 5). In the next round of experimental blasts, the number of holes was increased in the blasting rounds. In total, eight experimental

blasts were conducted at Ch: +400 m wherein the total number of holes in a blasting round varied from 4 to 17. The explosive charge per hole varied between 0.19 and 0.31 kg. The total charge used in a blasting round varied from 1.15 to 5.31 kg and maximum charge per delay varied from 0.31 to 0.94 kg. The firing pattern of holes for experimental blasts conducted with 17 holes at Ch: +400 m is shown in figure 2. The depth of hole used in all the experimental blasts was 1.5 m (5 ft). In shale strata of softer formation, burden and spacing were 0.8 and 0.8 – 0.9 m respectively. In case of hard sandstone strata, burden and spacing were reduced to 0.7 m and 0.8 m respectively. In order to prevent flyrock, top stemming column was maintained more than 1.0 m in all the blasts.

Plate 4. View of vibration monitoring point near the foundation of an adjoining residential house at Ch: +400 m blasting location

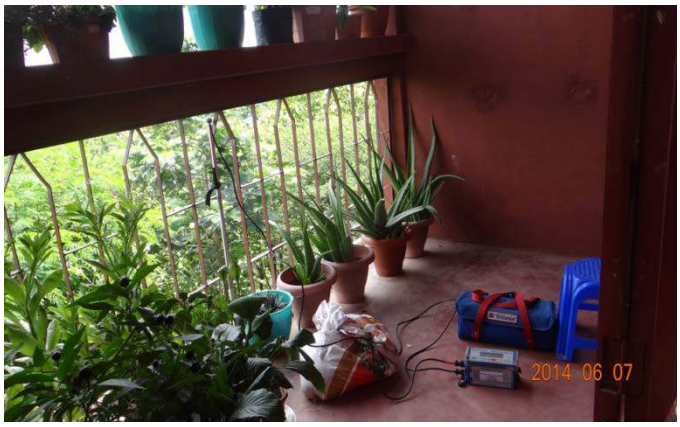

Plate 5. View of vibration monitoring point on the 1st floor of an adjoining residential house at Ch: + 400 m blasting location

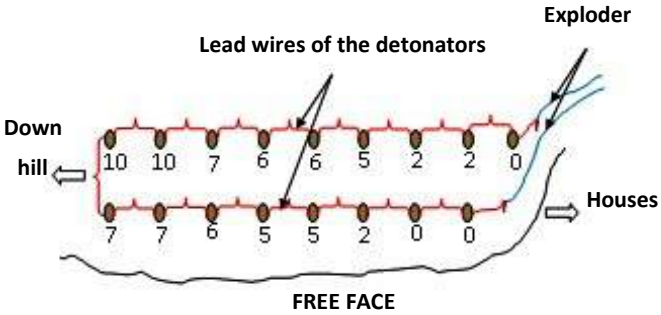

Figure 2. Firing pattern of holes in the experimental blast conducted in hard sandstone with 17 holes at Ch: +400 m (0, 2, 5, 6, 7, 10 are delay series)

At Ch: +2150 m, only shale rocks of softer formation were present. Therefore, burden and spacing were 0.8 m and 0.9 m respectively and the total number of holes varied from 11 to 23. The explosive charge per hole varied between 0.19 and 0.31 kg. The total charge in a blasting round varied from 3.44 to 6.44 kg and maximum charge per delay varied from 0.625 to 1.25 kg. The firing pattern of holes for the experimental blast conducted with 23 holes at Ch: 2250 m is given in figure 3. During the experimental blasts conducted at Ch: +2150 m, one seismograph was always fixed on the first floor of the nearest residential house and another one on the ground surface near the foundation of the house (Plate 6). The distance of vibration monitoring points from the blasting sites varied from 85 to 100 m.

5. GROUND VIBRATION RESULTS AND DISCUSSIONS

The magnitude of ground vibrations recorded during the experimental blasts at Ch: +400 m varied from 0.66 to 1.84 mm/s. The triggering levels of the seismographs were set as 0.50 mm/s. During blasting time, the people resided nearby the blasting sites were requested to stay indoors. Some were asked to sit in chairs while others to stand so that vibration could be felt differently.

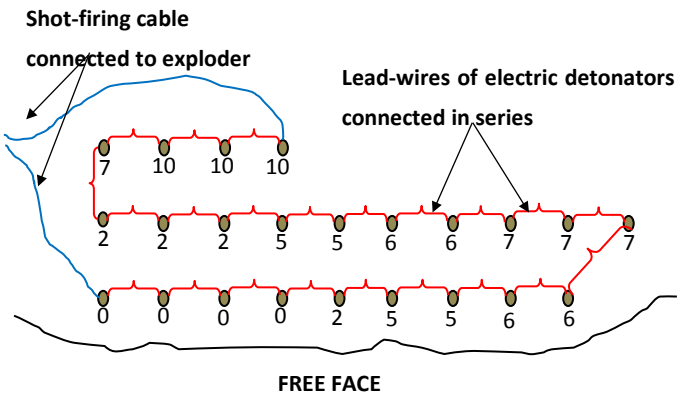

Figure 3. Firing pattern of holes in the experimental blast conducted with 23 holes at Ch: +2150 m (0, 2, 5, 6, 7, 10 are delay series)

Plate 6. View of vibration monitoring point near the house at Ch: +2150 m

When blasting was conducted in shale strata of softer formation using maximum charge per delay of 0.624 kg and total charge of 3.00 kg, ground vibration could not be recorded at adjoining residential houses. It also could not be felt by the people staying inside the house. However, when blasting was conducted in harder formation of sandstone strata, ground vibrations as well as blasting sound were higher than those conducted in shale strata. When the ground vibration value exceeded 1.25 mm/s, the nearby residents could feel the vibration and expressed their annoyance. With the ground vibration level of 1.84 mm/s, they felt frightening and said that the vibration was very severe. It was also leant that those people who were sitting on chairs could feel more vibration than those who were standing.

No vibration data could be recorded during experimental blasts at Ch: +2150 m. The ground vibration could not be felt although number of holes, total charge fired in a round of blast and maximum charge delay were higher in comparison to the experimental blast conducted at Ch: + 400 m. The nearby residents were also satisfied with the experimental blasts as they could not feel any ground vibration. The air overpressure levels recorded from the experimental blasts varied between 104.2 and 115.9 dB (L). Although the blasting sound could be heard and noticed by the nearby residents, no adverse comment was made on the blasting sound. The nearby resident were informed during blasting time and with no ground vibration to feel, they were comfortable with the air overpressure level below 116 dB (L). Maximum care was also taken to reduce the blasting sound by using electric detonators and larger top stemming column.

The Fast Fourier Transform (FFT) analyses of the vibration data showed that the dominant excitation frequency of vibration waves recorded on the ground surface (near the foundation of houses) varied between 8.0 and 15.6 Hz. However, the dominant excitation frequency measured on the first floor of the house varied between 7.25 and 7.38 Hz. Considering such dominant excitation frequency, the safe level of ground vibration for the residential houses as per the DGMS Standard comes to 10 mm/s. However, with the ground vibration level of 1.85 mm/s, the residents felt unsafe and expressed their annoyance to the blasting operation. When explained to them that the measured levels of ground vibration were much lower than the threshold values prescribed by the regulating agency, it was not convincible to them. They had claimed that the cracks had already developed in their houses due to previous blasting operations and any further ground shaking would destabilize their houses.

Plate 7. Final excavated road at Ch: +400 m

Plate 8. Final excavated road at Ch: +2150 m

Therefore, considering the sensitivity and sentiment of the nearby residents, it was decided to reduce the number of holes in a blasting round so that ground vibration level would not cross 1.0 mm/s and further complaints and any untoward incidents could be avoided. The number of holes in a blasting round was restricted to 10 in hard rock and to 15 in softer rock i.e. shale at Ch: +400 m area. Hence, the maximum charge per delay was less than 0.625 kg in case of blasting in hard rock and 0.94 kg in case of blasting in softer rock using the available short delay electric detonators. Since no hard rock strata was present in Ch: +2150 m area and no vibration data could be recorded during the experimental blasts, the total number of holes in a blasting round was restricted to 23. The excavation work using controlled blasting was finally completed without any complaint from the nearby residents. Plates 7 and 8 show the excavated road after the completion of the formation cutting work using controlled blasting.

6. CONCLUSION

When blasting operation is to be conducted nearby sensitive human habitants with hostile attitudes, human response to ground vibration cannot be ignored in deciding the safe level of ground vibration. To avoid any critical situation, it may often require reducing the permissible level of ground vibration to much below the damage threshold level prescribed by the regulatory agencies. Based on the experience stated in the paper, the vibration level of 1.85 mm/s was found to be very severe and detrimental in respect of the perception of the nearby habitants though the damage threshold level of ground vibration was 10 mm/s as per the prescribed standards. Therefore, caring the sentiment of the people and maintaining good relationships are absolutely necessary to accomplish any blasting project in sensitive environment of hilly terrain.

REFERENCES

Dhar, B. B., Pal Roy, P. and Singh, R. B., 1993. *Optimum blasting for Indian geomining conditions - suggestive standard and guidelines*, CMRI Publication, India, 40 p.

Directorate General of Mines Safety (DGMS), *Technical Circular 7, 1997.*

Indian standard, Criteria for safety and design of structures subjected to underground blast ISI. IS-6922 (1973).

Jimeno, C. L., E.L. Jimeno, and F. J. A. Carcedo. 1995. *Drilling and Blasting of Rock. Geo-mining Technological Institute of Spain*, ISBN 90 5410 1997, Pub. A. A. Balkema/Rotterdam/1995.

Pesch, R. and Robertson, A., 2007. Drilling and blasting for underground space, *Procs. EXPLO Conference, Wollongong, NSW,* 3-4 September, pp. 189-193.

Blastability Characteristics of Ewekoro Limestone Using Rock Mass Classification

B. Adebayo, P.R Adeniyi
Department of Mining Engineering, Federal University of Technology, Akure, Nigeria

S. A. Agbalajobi
Department of Mineral Resources Engineering, Kwara State Polytechnic, Ilorin

ABSTRACT This paper investigates blastability characteristics of Ewekoro limestone using rock strength properties. Rock samples were collected from three different locations at the two faces of the quarry (Ewekoro I, II and III). The rock samples were tested in the Laboratory for uniaxial compressive strength, tensile strength, using 1100 kN compression machine and point load tester respectively. Also, shear strength parameters (angle of friction and cohesion), and the rock mass parameters (tensile strength, global strength index and deformation modulus) of the deposit were determined using Roclab 1.0 from Rocscience where intact uniaxial compressive strength, material constants, disturbance factor of the rock, geological strength index and the intact modulus of the rock were used as input parameters. The results of compressive strength of the rock samples varied from 45.35-97.17 MPa and tensile strength varied from 22.68-48.80 MPa. Ewekoro II has the highest mean compressive strength of 90.0 MPa and mean tensile strength of 48.02 MPa. The friction angles obtained are 24.720, 31.860 and 28.980 for Ewekoro I, II and III respectively. The result of cohesion values are 1.928 MPa for Ewekoro I, 5.566 MPa for Ewekoro II and 2.902MPa for Ewekoro III. Finally, based on the obtained strength properties of the rock, it was discovered that Ewekoro type I has the highest blastability.

Keywords: blastability, rock mass parameters, intact modulus, angle of friction, strength

1 INTRODUCTION

Blastability can be defined as the blasting characteristics of the rock mass subjected to a specified blast design, explosive characteristics and specified legislative constraints depending on the site specifics. In other words, blastability indicates how easy to blast a rock mass under a specified condition. The blastability of rock indicates the ease with which rock mass structure could be loosen to liberate rock blocks as well as create new fractures within the intact material. Therefore any meaningful description of rock mass blastability should be a function of mechanical properties of the intact rock (such as stiffness and strength) and the rock mass structure (size of 'in-situ blocks'). Adebayo and Umeh (2007) concluded that ease of blasting is affected by strength parameters.

Several approaches have been used for estimating blastability. While some researchers tried to correlate it with the data available from laboratory and field testing of rock parameters, some others have related it with rock and blast design parameters, and yet some others have tried to estimate blastability through approaches based on the drilling rates and/or blast performances in the field. The latest improvements in computer methods have also opened up new vistas to the
researchers to use various artificial intelligence algorithms for determination of blastability. Kaushik and Phalguni (2003) found that a linear relationship exists between the compressive strength of rock (σ_c) and the amplitude of the compressive

stress wave (σ_a) propagated through the rock, which implies that σ_a α σ_c and hence, n α σ_c/σ_t and went further to name (σ_c) /(σ_t) as blasting coefficient. Atkinson *et al.* (1978) proposed that normally rock constant value (0.4 kg/m^3) might vary up to ± 25%. The objectives of the paper therefore are to determine the blastability characteristic and classified the limestone based on the blastability characteristics.

2 MATERIALS AND METHODS

2 1 Description and Location of Study Area

The study area lies within Ogun State, which is bounded in the west by Benin Republic, in the south by Lagos State, in the north by Oyo and Osun States, and in the east by Ondo State. It occupies a total area of 65.8 m^2. Ewekoro is the host to Lafarge Cement Company quarry and lies between longitude 3°05´E to 3°15´E and latitudes 6°40´N to 6°55´N as shown in Figure 1. Ewekoro formation belongs to tertiary-formed Palaeocene and Eocene; and the greater part of the depression is a potential artesian basin where ground water can be sourced. Adegoke *et al.* (1976) outlined the Albran and younger Palaeographic history of Nigeria and summarized the nature and extent of transgressive, regressive phases as well as the nature of the sediment.

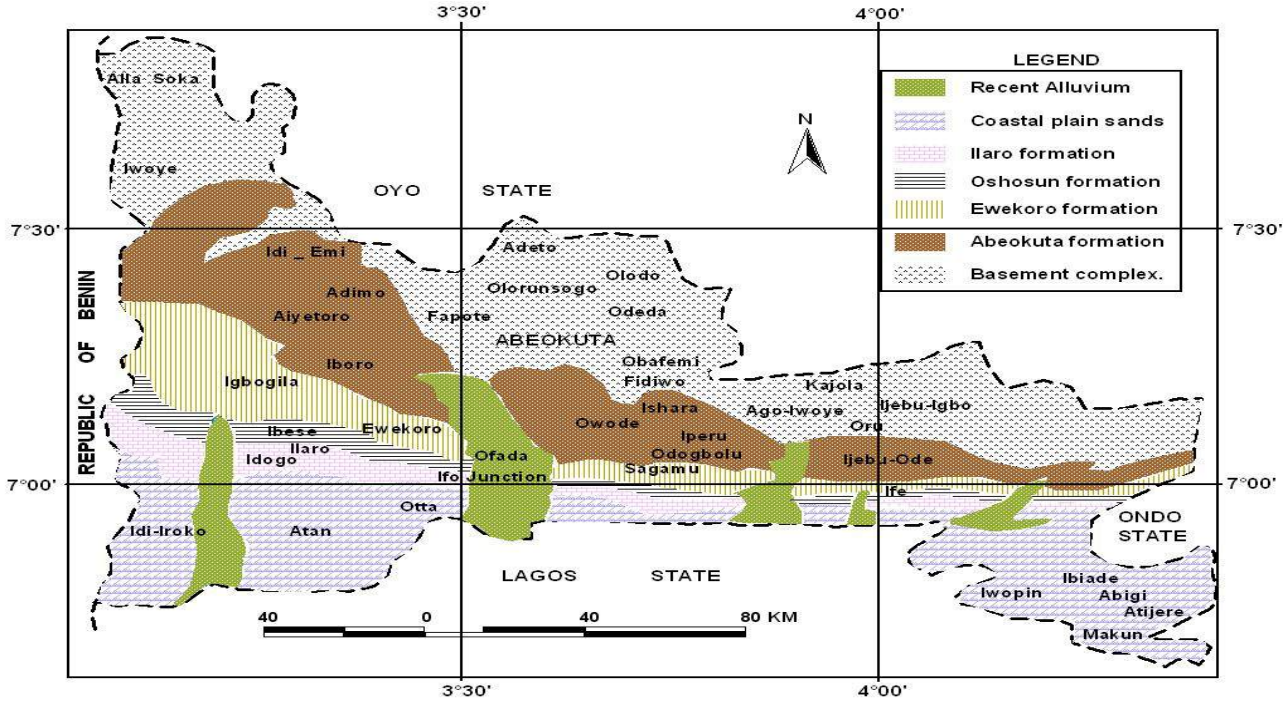

Study Area

Figure 1: Geological Map of Ogun State showing the Study Area (After Adegoke *et al.*, 1976)

2.2 Determination of Rock Hardness

The hammer was held vertically above the specimen and the plunger was placed against the specimen and depressed by pushing the plunger against the specimen (Aydin and Basu, 2005). The energy stored in the spring was automatically released and impacts a mass against the plunger. The height of rebound of the mass measured on the scale attached to the instrument and its value is taken as the specimen's hardness.

Ten samples were prepared and tests were performed on each specimen with each test point 15mm apart. The measured test values were arranged in descending order and the lower 50% were discarded. The test was performed using ISRM suggested method. The upper 50% was averaged and the rock hardness value was calculated using Equation 1.

$$H = S_aC \quad (1)$$

Where
S_a = Mean Schmidt Hammer's reading
C = Correction factor

Type N Schmidt Hammer test is mostly use for concretes while ISRM (1981) recommends the use of type L for rocks. Therefore the average values of type N obtained were converted to type L reading using Equation 2. The results are shown in Table 5.For conversion of Type N Schmidt Hammer Values to Type L Schmidt Hammer Values which is applicable to rock is expressed in Equation 2

$$R_N = 1.0646R_L + 6.3573 \quad (2)$$

2.3 Determination of Tensile Strength

Point Load Tester Model A125 was used for these tests. The machine is capable of performing the same test on three different shapes of specimen i.e. cylindrical, block and irregular shapes. The cylindrical shape can be used in two different ways – diametral and axial**.** The load frame can accommodate test samples size of up to 101.6mm in diameter and the machine has a load capacity of 55kN. The prepared specimen was loaded into the test machine and the platens were closed to make contact with the specimen along the core diameter. The point of contact of the platens was not less than half of the specimen diameter from nearest free and after longest axis has been measured as suggested by ISRM 1981. The loading diameter (D) was measured from the scale pointer and recorded. The loading rate was then increased steadily at a constant rate of 0.5 – 1.0 MPa in such a way that failure occurred within five minutes. The failure load (P) was recorded and the uncorrected tensile strength as a measure of Point Load Strength Index σ_T was calculated from Equation 3.

$$\sigma_T = \frac{P}{D^2} \quad (3)$$

P = Failure load, kN

D = Specimen diameter, m
This procedure was repeated for the replicated samples tested and the uncorrected test result is presented in Tables 9.

2.4 Determination of Uniaxial Compressive Strength

1100 kN Compressive Machine Model WF55632 with DIGICON 2 metering device capable of measuring up to ± 5% tolerance was used for this study. The machine is incorporated with DIGICON 2 metering device and has a load capacity of 1000kN. The test specimens were right circular cylinders with a slenderness ratio of 3 at a diameter of 54mm. The samples were tested at a natural water content of 0.21%. The test specimen was loaded into the machine between the upper and lower platens. A spherical seat was placed on the top end of the specimen so as to ensure that the applied load was axially and evenly distributed. The loading platen and the spherical seat were then aligned accurately to the centre of the platens. The load was applied at a constant stress rate of 0.5 – 1.0 MPa/sec such that failure occurred within 5 – 10 minutes of loading. At failure the peak stress is regarded as the maximum stress the specimen could carry when a unidirectional stress is applied in an axial direction to the end of the specimen. No end capping materials were used. This procedure was repeated for the other specimens. The compressive strength, (σ_c) was calculated from Equation 4

$$\sigma_c = \frac{P}{A} = \frac{4P}{\pi D^2} \quad (4)$$

σ_c= Uniaxial Compressive Strength, MPa
P = Peak load at failure, kN
A = Cross-sectional area of specimen, m^2

2.4.1 Density

The objective of the test is to measure the dry density of rock samples of irregular form from the three Ewekoro deposits. The Saturation and Buoyancy technique for

irregular rock sample was adopted and the procedures follow the standard suggested by ISRM (1981) and conform to ASTM (1994). The saturated volume of the sample was calculated using Equation 5.

Saturated volume of samples = V_2-V_1 (5)

Where V_1 (ml) is the initial water level and V_2 (ml) is the final water level in the cylinder after the immersion of the irregular rock sample.
The dry density of the rock samples was calculated using Equation 6. Where M (g) is the oven dried mass at a temperature of 105^0C.

Dry density of the rock samples = $\frac{M}{V2-V1}$ (6)

2.4.2 Point Load Index

The Point Load Index (IS) Values were estimated from the uniaxial compressive strength (UCS) values using Equation 7 established purely for carbonate rocks.

$$I_s = 0.047UCS - 0.328 \quad (7)$$

The IS (like the UCS) was also used for the strength classification and characterization of the intact rocks. It was further used with the Fracture Spacing Index (I_f) and the Geological Strength Index (GSI) for the assessment of the most economic excavation method which is shown with the aid of appropriate charts.

2.5 Determination of Rock Mass Strength Parameters

The rock mass strength parameters were estimated from RocLab 1.0 software. The required input data were loaded and the strength parameters were displayed.

3 RESULTS AND DISCUSSION

The result of rebounds hardness values for limestone is presented in Table 1. The rebounds hardness value varied from 29.8327 for Ewekoro type I to 40.4327 for Ewekoro type II.

Table 1. Conversion of Type N Schmidt Hammer (Rebounds Hardness Values) to Type L Values

Samples	N Values	L Values
Ewekoro I	36.2	29.8327
Ewekoro II	46.8	40.4327
Ewekoro III	39.4	33.0327

Table 2 shows the summary of uniaxial compressive and point load strength index and their classification according to ISRM (1985) standard. All the rock types tested are of ‘‘Very High Strength class” to “High Strength Class’’. Ewekoro type II deposit has the highest value which is in agreement with its high density and hardness values.

Table 2. Summary of Rock Strength Parameters and their Classification

Samples	UCS (MPa)	Is (MPa)	Rock Class
Ewekoro I	47.91	1.92	High Strength
Ewekoro II	96.00	4.18	Very High Strength
Ewekoro III	58.70	2.43	High to Very High Strength

Table 3 presents the tensile strength of the limestone. The results revealed that the value of tensile strength varied from Ewekoro I varied from 23.24 – 25.95 MPa, 47.50 – 48.80 MPa, 28.20 – 31.63 for Ewekoro I, II and III respectively.

Table 3. Tensile Strength of Ewekoro Limestone

S/N	Ewekoro I (MPa)	Ewekoro II (MPa)	Ewekoro III (MPa)
1	23.75	47.50	28.20
2	23.87	47.71	28.66
3	23.58	48.10	29.55
4	22.68	48.10	29.55
5	24.84	47.65	28.56
6	25.95	48.09	30.03
7	23.92	48.80	31.63
8	23.36	48.55	31.01
9	23.24	47.92	28.40
10	24.37	47.80	28.43

Table 4 presents the estimated rock parameters obtained from RocLab software global strength of the limestone varied from 6.021 MPa for Ewekoro I to 20. 026 MPa for Ewekoro II.

Table 4. Estimated Rock Mass Parameters for Ewekoro Limestone

	Hoek–Brown Classification			Mohr-Coulomb Fit	Rock Mass Parameters (MPa)				
	M_b	S	a	C′ (MPa)	ØDeg	Sigt	Sigc	Sigcm	E_{rm}
Ewekoro I	0.821	0.0029	0.502	1.928	24.72	0.171	2.563	6.021	1963.12
Ewekoro II	2.012	0.0155	0.501	5.566	31.86	0.740	11.908	20.026	3240.00
Ewekoro III	1.408	0.0067	0.501	2.902	28.98	0.281	4.786	9.851	2569.68

Where:
GSI = Geological Strength Index
mi ,mb, s, and a = Material Constants
C′ = Cohesion (MPa)
Ø = Friction Angle
Sigt = Tensile Strength (MPa)
Sigc = Uniaxial Compressive Strength (MPa)
Sigcm = Global Strength (MPa)
Erm= Deformation Modulus

Table 5 is a summary of the density result. The Table shows that Ewekoro II has the highest density values while Ewekoro I has the least value.

Table 5. Summary of Density for Ewekoro Limestone

Test No	Ewekoro I (t/m^3)	Ewekoro II (t/m^3)	Ewekoro III (t/m^3)
1	2.40	2.69	2.51
2	2.41	2.68	2.49
3	2.40	2.76	2.54
4	2.37	2.72	2.49
5	2.43	2.67	2.47
Average Value	2.40	2.67	2.47

4 BLASTABILITY CLASSIFICATION OF EWEKORO LIMESTONE

Considering the uniaxial compressive strength and the tensile strength of the samples obtained from three different locations on the deposit, the Ewekoro I is easy to blast having a UCS of 47.91 MPa and tensile strength value of 2.40 MPa, Ewekoro II falls under moderate class as

shown in Table 6. Ewekoro III has easy blastability property as presented in Table.

Table 6. Rockmass Parameters and Blastability for Ewekoro Limestone

FACTORS AFFECTING BLASTABILITY	DEPICTING PARAMETERS	NUMERICAL VALUE		
		Ewekoro I	Ewekoro II	Ewekoro III
1. Strength	(i) Uniaxial Compressive Strength (MPa)	47.91	96.00	58.70
	(ii) Point Load Strength Index (MPa)	1.92	4.18	2.43
2.Rock Resistance to Fracture	Density ρ (t/m^3)	2.40	2.67	2.47
3. Resistance to Dynamic Loading	Schmidt Hardness Value	36.20	46.80	39.20
4. Discontinuity Plane's Strength	(i) Cohesion C (MPa)	1.928	5.566	2.902
	(ii) Friction Angle Ø	24.72	31.86	28.98
Blastability Class		High	Low	Moderate

5 CONCLUSION

The various factors that control the rock fragment size were considered and the rock strength parameters of the Ewekoro limestone were studied. Results show that based on the rock strength parameters the first location (Ewekoro I) has the highest blastability having uniaxial compressive strength of 47.91MPa, point load strength index of 1.92 MPa, friction angle of 24.72° and cohesion of 1.98. Ewekoro III comes next with uniaxial compressive strength of 58.70 MPa, point load strength index of 2.43 MPa, friction angle of 28.98°, and 2.902 cohesion values while Ewekoro II at the second location has the lowest blastability going by its strength parameters values of 96.0 MPa for uniaxial compressive strength, 4.18 MPa point load strength index, 31.86° friction angle and 5.566 cohesion value.

REFERENCES

Adebayo, B. and Umeh, E.C (2007): Influence of Some Rock properties on Blasting Performance – A Case Study, published in *the Journal of Engineering and Applied Sciences*, Vol. 21, No.1 pp. 41-44, 2007

Adegoke, O. S., Ogbe, F. G. A., and Jan Du Chene, R. E. (1976): Excursion to the Ewekoro quarry (Paleocene-Eocene), *Geological Guide Nigerian Cretaceous-Recent Loc*., pp.1-17.

American Society for Testing Materials (ASTM), (1994): Annual Book of ASTM Standards-Construction: Soil and Rocks. *ASTM Publication,Vol.* 04.08.978, pp. 975

Atkinson, R. H., Bamford, W. E., Broch, E., Deere, D. V., Franklin, J. A., Nieble, C., Rummel, F., Tarkoy, R. J., van Duyse, H. (1978): Suggested Methods for Determining Hardness and Abrasiveness of Rocks. *International Journal of Rock Mechanics and Mining Science*, Abstr. Vol.15 No.3 pp. 89-98.

Aydin, A. and Basu, A. (2005): The Schmidt hammer in rock material characterization: *Journal of Engineering Geology*, 81 (2005), Elsivier International, pp. 1-14.

International Society for Rock Mechanics (ISRM), (1981): Rock Characterization, testing and monitoring In: Brown, E.T. (edition) *ISRM Suggested Methods.* Pergamin Press, Oxford, UK, pp. 211.

Kaushik and Phalguni (2003): Development of an Assessment System for the Blastability of Rock Masses, *International Journal of Rock Mechanics and Mining Science*, Vol. 36 pp. 41-55.

Rocscience Ltd. (2002). RocLab software for calculating Hoek –Brown Mass Strength. Toronto, Ontario, Retrieved on 20th September, 2012 from www.rocscience.com.

Charge Distribution Pattern For Different Zones In Tunnel Blasting Operations: Case Study Of The Alborz Tunnel

M. Mohammadi
General Mechanic Contracting Co., the Alborz tunnel site, Alborz, Iran

M. F. Hossaini
Faculty of Mining Engineering, Engineering University College, University of Tehran, Tehran, Iran

S. A. Taleghan, R. Bolghonabadi, N. Hajiantilaki
General Mechanic Contracting Co., the Alborz tunnel site, Alborz, Iran

ABSTRACT The most suitable type of explosive for each blasting zone amongst available explosives in the Alborz Tunnel is investigated in this paper applying concept of impedance for rock types of Tuff and anhydrite which have been tested to determine their seismic properties. For hole diameter of 57 mm, the best choice of explosive for cut and lifter holes is ANFO and for contour holes it is emulsion explosive with diameter of 27 mm. The results were the same in case of drilling holes with diameter of 45 mm. Also the results show that the coupling factor has more important role than impedance factor on the amount of transmitted energy in this particular case.

Keywords: Charge distribution, Blasting, Alborz Tunnel

1 INTRODUCTION

Tunneling as an important activity in the field of underground construction is done due to road or rail transportation, water supply and sewer, mountain caverns for industrial, recreational and storage purposes [1]. In spite of its destructive characteristic, drilling and blasting method is the most satisfactory way for excavation of rock because this method of excavation needs low capital investment and has the characteristics of high progress rate for underground excavation works [2].

Lack of adequate free surfaces toward which breakage can occur effectively, characterizes the blasts done for tunnel excavation. Creation of an opening by means of a cut and then stoping to enlarge the opening is the principle behind tunnel blasting. The different zones in tunnel blasting are shown in figure 1 [3]. Stoping holes can be compared to bench blasting though it requires powder factors four to ten times higher. Contour holes establish the final shape of the tunnel and are spaced closely [4]. While the cut and cut spreader holes due to its role in creation of free face to the other sections are of great importance, the contour holes also are important because of its impact on the final shape of the tunnel. Lifter holes also due to operating in contrast with direction of the gravity are noticeable and need maximum possible energy transmission from explosives to rock. The present paper tries to choose the most optimum charge for these sections employing the concept of impedance. It should be noted that the cut and cut spreader holes need to have most possible amount of charge to be able to create the second free face for the other holes while the contour holes need to have least possible amount of charge due to its impact on the final shape of the tunnel.

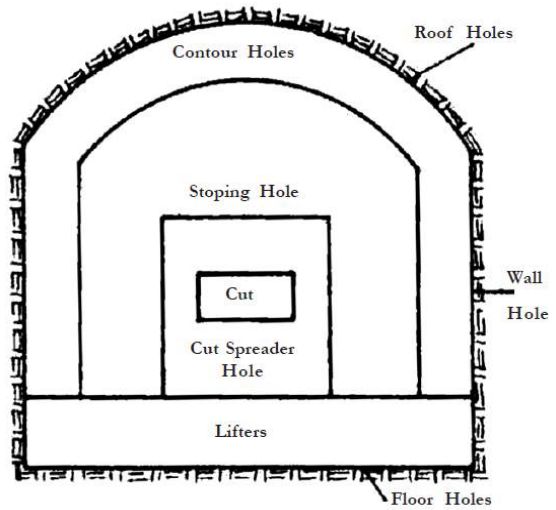

Figure 1. Zones in tunnel blasting [3]

2 CASE STUDY

The Albroz Tunnel with a length of 6400 m is one of the largest tunnels which are going to be excavated along Tehran-Shomal freeway in north of Iran. Drilling and blasting method is employed to excavate the 65 m2 face of tunnel heading where compacted clay is used as stemming material and hole diameter is 57 mm. the available explosives are emulsion explosive with diameter of 27 mm and 35 mm and ANFO. The rock type is Tuff and Anhydrite which have been tested to determine their seismic properties. Figures 2 and 3 show the location of the Alborz Tunnel and an example of blasting patterns used in this tunnel respectively.

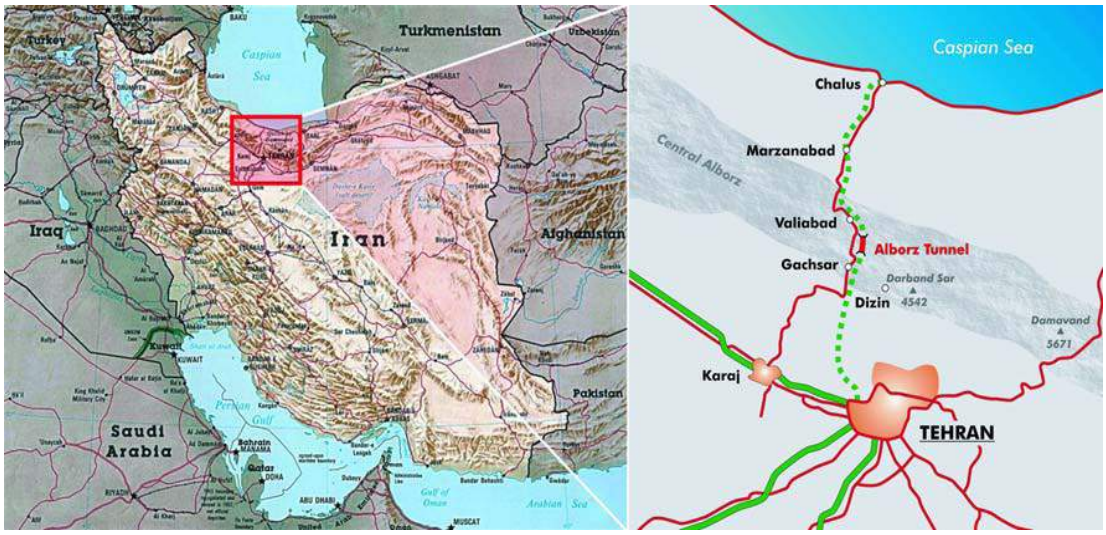

Figure 2. Location of the Alborz Tunnel [5]

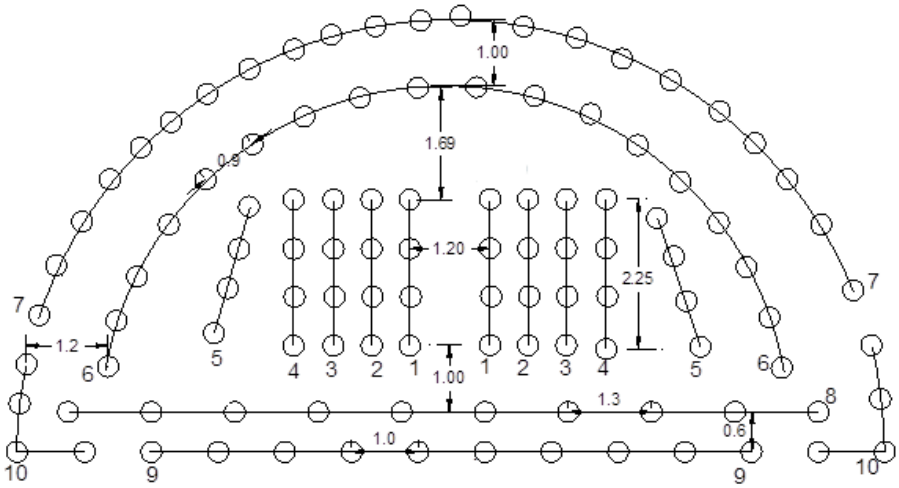

Figure 3. An example of blasting patterns used in the Alborz tunnel

3 CONCEPT OF IMPEDANCE

Energy transmission to rock mass as a result of blasting is affected by two factors [6]:

- Quality of rock mass and explosives (impedance factor)
- Coupling of charge and rock mass in holes (coupling factor)

Impedance is a factor that controls the amount of energy transmitted to rock mass from the explosives during blasting operations. The impedance of rock and explosives can be calculated from equations 1 and 2 respectively [6].

$$I_r = D_r.V \quad (1)$$

$$I_e = D_e.V_e \quad (2)$$

Where I_r and I_e are impedance of rock and explosives in kg/m^{2}sec, D_r and D_e are densities of rock and explosives in kg/m^3 respectively, v_e is velocity of detonation of explosives in m/sec and V is velocity of elastic waves in rock in m/sec.

When the impedances of the mediums are equal, a large part of the energy will be transmitted and the rest will be reflected while if the impedance of one medium is much more than the other, as for example between rock and air, almost all of energy will be reflected as a tensile wave which can be especially important in rock breakage. This is valid for the wave pressure as well as for the transmitted energy [3].

Energy transmission coefficient or impedance factor (η_1) can be calculated from the equation 3 [6].

$$\eta_1 = 1 - \frac{(I_r - I_e)^2}{(I_r + I_e)^2} \quad (3)$$

Coupling factor (η_2) can be computed using equation 4 [6].

$$\eta_2 = \frac{1}{e^{\phi_h/\phi_c} - (e-1)} \quad (4)$$

Where φ_c and φ_h are charge and hole diameter respectively.

If the total energy of explosives is shown as E_e, the energy transmitted to rock in a blasting round (E_t) can be calculated from equation 5 [6].

$$E_t = \eta_1.\eta_2.E_e \quad (5)$$

In this paper, using the aforementioned concepts, the most suitable charge for cut, contour and lifter holes will be selected bearing in mind that the cut and lifter holes need maximum transmittable energy while the contour holes should have the least possible transmission of energy from which the final shape of the tunnel could be established with minimum percent of overbreak and underbreak.

4 SELECTION OF CHARGE FOR DIFFERENT ZONES

The available explosives in the Alborz Tunnel are emulsion explosive with diameter of 27 and 35 mm along with ANFO which are referred as explosive type a, b and c respectively from this point forward. The diameter of drill holes is 57 mm and there is two rock types namely Tuff and Anhydrite. The wave velocity test on rock specimens was carried out with OYO Sonic viewer–SX version 1.20E testing equipment. The results of the test along with rock densities and computed impedance for each type are shown in table 1.

Table 1. Wave test results along with rock densities and calculated impedance of rock types.

Rock type	Density (kg/m^3)	P-wave velocity (m/sec)	Impedance (kg/m^{2}sec)
Tuff	2660	5467	$14.54*10^6$
Anhydrite	2830	6462	$18.29*10^6$

The properties of explosives along with calculated values of impedance are shown in table 2.

Table 2. properties of available explosives along with calculated impedance of explosives.

Explosive type	Density (kg/m^3)	Velocity of detonation (m/sec)	Impedance (kg/m^2sec)
a	1400	6000	$8.4*10^6$
b	1500	5000	$7.5*10^6$
c	900	4500	$4.05*10^6$

As the energy content of emulsion explosive is 80 to 104 percent of ANFO[7] the calculations of transmitted energy are done based on energy content of ANFO, where the energy content of explosives a and b is regarded as 90 and 95 percent of ANFO respectively. For example the total amount of transmitted energy to Tuff in case of using explosive a will be as follows:

$$\eta_1 = 1 - \frac{(14.54 * 10^6 - 8.4 * 10^6)^2}{(14.54 * 10^6 + 8.4 * 10^6)^2} = 0.93$$

$$\eta_2 = \frac{1}{e^{57/27} - (e-1)} = 0.15$$

$$E_t = 0.9*0.93*0.15*E_{ANFO} = 0.13E_{ANFO}$$

Therefore, the transmitted energy to Tuff in case of using Explosive a will be 13 percent of energy content of ANFO. The rest of the calculations of transmitted energy in case of using each explosive type in each rock type are given in table 3. It should be noted that the diameter of charge in case of using ANFO is regarded as 54 mm as it is charged with compressed air. As it is obvious, the amount of transmitted energy in both rock types is the highest in case of using explosive c or ANFO and it is the lowest in case of using explosive a or emulsion explosive with diameter of 27mm. Therefore in both rock masses, using ANFO in cut and cut spreader sections in order to attain maximum possible fragmentation and emulsion explosive with diameter of 27 in contour holes to establish the final shape of the tunnel with minimum possible percent of overbreak is recommended.

Though the impedance of explosives a and b is nearer to impedance of both rock types, the amount of transmitted energy is higher in case of using explosive c and that's because of the impact of coupling factor which is more higher in explosive c. regarding the concept of energy transmission and the fact that lifter holes operate in contrast with the direction of gravity, the best choice of explosive for this section would be explosive c (ANFO) but the fact that these holes have water inside, forces the selection of other explosives due to negative impact of water on ANFO. Therefore the second best choice, namely explosive b (emulsion explosive with diameter of 35 mm) was used in lifter holes showing that the effect of ground condition can be of crucial importance.

Table 3. Energy transmission to each rock type in case of using different explosives for holes with diameter of 57mm.

Rock type	Explosive a	Explosive b	Explosive c
Tuff	$0.13E_{ANFO}$	$0.25E_{ANFO}$	$0.59E_{ANFO}$
Anhydrite	$0.12E_{ANFO}$	$0.23E_{ANFO}$	$0.51E_{ANFO}$

5 EFFECT OF DIAMETER OF HOLES

In this section the effect of diameter of holes on energy transmission is investigated. The available bits in the Alborz Tunnel allow drilling of 45 mm holes in addition to 57 mm. Therefore, the amount of energy transmission is calculated for 45 mm holes. The results are given in table 4. In this case, the diameter of charge in case of using explosive c (ANFO) is regarded as 42.75 mm which is 95 percent of diameter of hole like the previous section.

Table 4. Energy transmission to each rock type in case of using different explosives for holes with diameter of 45mm

Rock type	Explosive a	Explosive b	Explosive c
Tuff	$0.23E_{ANFO}$	$0.45E_{ANFO}$	$0.59E_{ANFO}$
Anhydrite	$0.22E_{ANFO}$	$0.41E_{ANFO}$	$0.52E_{ANFO}$

In this case, the results are the same as the previous section. Comparing tables 3 and 4 in both rock types for explosives a and b, the values of transmitted energy have increased noticeably. This is due to increase of coupling factor because of decrease in diameter of holes. In case of using explosive type c (ANFO) the values of transmitted energy have remained the same as previous section which was due to constancy of coupling factor in this case. Therefore the importance of coupling factor can be concluded in this particular case where the efficiency of blasting operations can be affected by this factor.

6 CONCLUSIONS

In this research, employing concept of impedance, the most suitable charge for each section of tunnel blasting was selected. The obtained results are as followings:

- The amount of transmitted energy in both rock types is the highest in case of using explosive c or ANFO and the lowest in case of using explosive a or emulsion explosive with diameter of 27mm.
- In both rock types, using ANFO in cut and cut spreader sections in order to attain maximum possible fragmentation is recommended.
- In both rock types, using emulsion explosive with diameter of 27 mm in order to establish the final shape of the tunnel with minimum possible overbreak is recommended.
- Though the impedance of explosives a and b is nearer than the impedance of explosive c to impedance of both rock types, the amount of transmitted energy is higher in case of using explosive c and that's because of the impact of coupling factor which is more higher in case of using explosive c.
- The best choice of explosive for lifter holes is explosive c (ANFO) but the fact that these holes have water inside, forces the selection of other explosives due to negative impact of water on ANFO. Therefore the second best choice, namely explosive b (emulsion explosive with diameter of 35 mm) was used in lifter holes showing that the effect of ground condition can be of crucial importance.
- Decreasing the diameter of holes from 57 mm to 45 mm has no effect on changing the explosive type for each section but the amount of transmitted energy in both rock types has noticeably increased in case of using explosive types a and b. this is because of the increase in coupling factor due to decrease in hole diameter. The coupling factor in case of using explosive c has been remained constant due to which the amount of transmitted energy has not changed.
- The coupling factor has more effect than the impedance factor in the amount of transmitted energy in this particular case.

REFERENCES

[1] Murthy V. M. S. R., Dey K., Chimankar R. R., 2006. Tunnel Blast Design Using Artificial Neural Network - a Case Study, IE(I) Journal−MN, Vol. 86.

[2] Mandal S., Singh M., 2009. Evaluating extent and causes of overbreak in tunnels, Tunneling and Underground Space Technology, 24(1): 22-36.

[3] Jimeno C. L., Jimeno E. L., Carcedo F. J. A., 1995. Drilling and Blasting of Rocks, A. A. Balkema Publishers, Rotterdam, 391 P.

[4] Gustafson R., 1997. Swedish blasting technique, SPI, p 23.

[5] Wenner D., and Wannenmacher H, 2009. Alborz Service Tunnel in Iran: TBM Tunneling in Difficult Ground Conditions and its Solutions, 1st Regional and 8th Iranian Tunneling Conference, Tehran, Iran.
[6] Ostovar R., 2008. Blasting in mines: blasting theories, bench blasting and tunneling, volume 2, third edition, publication of JIHAD Amirkabir University, Tehran, 388 p. (in Farsi).
[7] Ostovar R., 2008. Blasting in mines: explosives, drilling, loading, explosives in Iran, volume 1, third edition, publication of JIHAD Amirkabir University, Tehran, 326 p. (in Farsi).

Improving Drilling and Blasting Programs At Al-Jazi Limestone Quarry-Lafarge-Jordan

M. Amaireh
Tafila technical university, Natural Resources and Chemical Engineering Department/ Mining Engineering Tafila Jordan

ABSTRACT A 60 meters thickness outcropped medium-hard limestone is being extracted for the use in Alrashadiyah cement plant-Lafarge-Jordan. Several benches each of 10 m. high have been designed for this purpose. Thin layers of clay and shale interact with limestone beds. The company has to drill and blast the limestone beds for subsequent operations.

In this modest study, we are going to shed light on quarry drilling and blasting practices of the company, analyzing the important factors affecting the operation, and give suggestions about improving the overall efficiency of the whole operation.

Keywords: Limestone, Lafarge Cement Company, Tafila, clay, shale

1 INTRODUCTION

1.1 Drill Performance

In evaluating drill performance, four parameters are measured or estimated most frequently:

1-process energy and power consumption
2-penetration rate
3-bit wear (life)
4-cost (ownership + operating = overall)

Energy and power affect operating cost, but they are more important as determinates of penetration rate. Both penetration rate and bit wear are major criteria of importance, with wear critical in deep holes and hard rock. Cost is the ultimate measure of performance; a drill can have excellent performance, but if it is not cost effective, then an alternative system should be sought. It is well to understand, however, that a goal of mining is the minimization of all rock breakage costs and that drilling does not stand alone. Overall breakage costs include costs for blasting and also for crushing and grinding if mineral processing occurs.

1.2 Blast Performance

It has been observed in many case studies that power consumption of loading machineries and crushers operating on the site and of primary crusher operating on the plant depends on the ratio of desired fragmentation obtained from the blast. On the other side, a lower ratio of fragmentation decreases the primary blasting costs.

Poor fragmentation results lead to:

1-increased secondary blasting
2-increasing loading cycle time.
3-increased difficulty in transport
4-increased energy consumption at crushing or milling
5-low crusher or mill performances

On the other hand, when operating on fragmentation results in order to reduce secondary blast or other kind of secondary fragmentation before crushing, primary blast costs and drilling costs increase, making the efficiency of the mine site workings decrease.

When secondary blasting is avoided or reduced to its minimum in order to increase mine site working efficiency, the amount of cost related to the reduction of dimension of blocks is transferred to crushing or milling, reducing its efficiency and increasing its costs.

Loading, hauling and crushing costs decreased with increasing rock fragmentation while drilling and blasting

costs increased with increasing rock fragmentation.

2 COMPANY PRACTICE

2.1 Limestone Properties

The study area (Aljazi limestone quarry) consists of a successive benches of limestone beds as shown in Figure 1.

Figure 1. Pit benches

Figure 2. Bench layers

Figure 2. shows us the interacting layers of clay, marl, and shale.

2.1.1 Weight characteristics

Limestone has the following weight characteristics:
1-Bank weight (2610 kg/m^3)
2-Swell percent (69%)
3-Swell factor (0.59)
4-Loose weight (1540 kg/m^3)
5-Specific gravity (2.65 g/cc)

2.1.2 Limestone physical properties

Limestone physical properties are:
1-Hardness 3 to 4 on Mohr's Scale.
2-Compressive Strength1800-2100 Kg/cm^2.
3-Water Absorption Less than 1%.
4-Porosity Quite low.
5-Weather Impact Resistant.

2.1.3 Limestone chemical properties

Limestone chemical properties are:
1-Lime CaO (38-42)%
2-Silica SiO_2 (20-25)%
3-Alumina Al_2O_3 (2-4)%
4-Other oxides (1.5-2.5)%

2.2 Drilling Equipments and Tools

The company uses the following drilling equipments and tools:

2.2.1 DI 300 Titon DTH drill rig

1-Model Titon 300,Figure 3.
2-Hole Range (89-127) mm
3-Drill Pipe Diameter (76-89)mm
4-Drill Tube Length (4000)mm
5-Compressor (14 m3/min/17 bar)
6-Weight (40749) kg

Figure 3. Drill Rig

2.2.2 DTH hammer

1-Model (Mission 40).Figure 4.
2-Bit Range (115-152)mm, (4.5-6.0) inch.
3-Outside Diameter (98)mm, (3.86) inch.
4-Hammer Length (914)mm, (36) inch.

2.2.3 DTH drill bits

1-Model (Mission 40 Bits).Figure 5.
2-Bit Diameter (115-121)mm, (4.50-4.75) inch.

Figure 4. Hammer

Figure 5. Bit

2.3 Blasting Materials

The company experience the following blasting materials

2.3.1 ANFO prill

A dry blasting agent blend of Ammonium Nitrate and Fuel. ANFO PRILL is an efficient, economical and easy to use explosive. It comes in (25 kg) plastic bags of specific gravity (0.85), it's local price (JD 671 /tonne).

2.3.2 Watergel explosives

Slurry explosives are energy efficient, waterproof, that can be used for mining, quarry and construction blasting. Detonator sensitive PETRABOOST (cap-sensitive), packaged in carton packs (20±1 kg) of 4 polyethylene cartridges of 125mm diameter, 7 pieces of 83mm diameter, and 10 pieces of 70mm diameters. Specific gravity (1.1). Price (JD 1.7/kg). all cartridges are (50 cm) length.

2.3.3 Electric detonators

Electric detonators: designed to provide precise control that is necessary consistent blasting results in variety of blasting applications. Price (JD 2.72/detonator).

2.4 Company Blasting Design

The company blasting design is based on the following assumptions:

1. average bench height = 10.0 m
2. burden distance = 3.5 m
3. spacing distance = 3.5 m
4. subdrilling = 0.6 m
5. stemming depth = (hole depth)/3
6. bit diameter = 114.3 mm
7. main explosive:
   a. ANFO
   b. sp.gr.(0.8)
   c. loading density (7 kg/m)
   d. price (JD 671/tonne)
8. initiating explosive:
   a. Petra Boost
   b. sp.gr. (1.1)
   c. loading density (8% of ANFO)
   d. price (JD 1.7/kg)
9. detonator:
   a. electric delay detonator
   b. price (JD 2.72/piece)

2.5 Company Calculations

According to the company records, we can summarize it's drilling and blasting practice as follows:

Table 1. Blasting design parameters

Blasting design parameters	Shot No. 1 (20 holes)	Shot No. 2 (15 holes)	Shot No. 3 (20 holes)
Burden, m	3.5	3.5	3.5
Spacing, m	3.5	3.5	3.5
Planned hole depth, m	10	11	8
Avg. actual hole depth, m	6.9	11	6.9
Avg. stemming depth, m	2.3	3.7	2.3
Avg. powder column length, m	4.6	7.3	4.6

Table 2. Explosives consumption

Explosive consumption	Shot No. 1 (20 holes)	Shot No. 2 (15 holes)	Shot No. 3 (20 holes)
ANFO/shot (kg)	641.67	770.00	640.73
Boost/shot (kg)	64.17	61.60	51.26
Total (ANFO+ Boost) /shot (kg)	705.84	831.60	691.99

Table 3. Powder factor calculations

Powder factor calculations	Shot No. 1 (20 holes)	Shot No. 2 (15 holes)	Shot No. 3 (20 holes)
Total rock volume blasted / shot, m^3	1690	2021	1690
Total (ANFO + Boost) / shot (kg)	705.84	831.60	691.99
Average powder factor (Kg/m^3)	0.40	0.41	0.41

Table 4. Explosives cost calculations

Explosive cost calculations	Shot No.		
	1 20 holes	2 15 holes	3 20 holes
Total ANFO/shot (kg)	641.67	770.00	640.73
Total Boost/shot (kg)	64.17	61.60	51.26
ANFO cost @ JD0.671/kg	430.56	516.67	429.93
Boost cost @ JD1.70/kg	109.09	104.72	87.14
Detonator price JD2.72 / piece	54.40	40.80	54.40
Total explosive cost per shot (JD)	594.05	662.19	571.47

Table 5. Rock cost calculations

Rock blasted cost	Shot No.		
	1 20 holes	2 15 holes	3 20 holes
Total rock volume blasted per shot, m^3	1690	2021	1690
Total explosive cost per shot (JD)	594.05	662.19	571.47
Blasted rock cost JD/m^3	0.35	0.33	0.34

We could say that (according to the company practice), the average cost of unit volume of limestone rock produced by blasting in Aljazi limestone quarry is (JD0.34/m^3).

3 STUDY PRACTICE

3.1 Blast Design Parameters

The more important parameter in the blast design is how to choose the burden distance, because nearly all the other parameters depend on it. But to achieve a good shot we should have a stiffness ratio of at least (3). The average bench height (L) is 10 meters which is approximately (33 ft).

$$SR(Stiffness\ Ratio)=\frac{L}{B}\Rightarrow B=\frac{L}{SR}=\frac{33}{3}=11\ ft=3.35\,m$$

This value of burden distance should be the field distance or the corrected distance. The correction comes from the rock conditions such as deposition and structure. The conditions of limestone rock in the quarry are as follows:

1-deposition (bedding dipping into face), we should adopt a (0.95) value for K_d

2-structure (heavily cracked, frequent weak joints, weakly cemented layers), we should adopt a (1.30) value for K_s .

So, the calculated value of burden can be predicted as follows:

$$B_{corrected}=B\times K_d\times K_s$$

$$\Rightarrow 11=B\times 0.95\times 1.3$$

$$\Rightarrow B=\frac{11}{0.95\times 1.3}=8.9\ ft$$

The general formula for calculating the burden distance is:

$$B(ft)=\left(\frac{2SG_e}{SG_r}+1.5\right)D_e(in),$$

so we can use it to find the suitable exp*losive diameter as folows*

$$\Rightarrow 8.9=\left(\frac{2\times 0.8}{2.65}+1.5\right)\times D_e$$

$$\Rightarrow D_e=\frac{8.9}{\left(\frac{2\times 0.8}{2.65}+1.5\right)}=4.24\approx 4.25\,inch\,(108mm)$$

As ANFO is the main explosive, and it takes the shape of the hole; the suitable bit diameter will be (4.25 inch.).

We can now predict the blast design parameters assuming the burden distance(11ft).

Stemming depth

$$T=0.7\times B=0.7\times 11=7.7\approx 8\ ft\,(2.5\,m)$$

subdrilling depth

$$J=0.3\times B=0.3\times 11=3.3\approx 3\ ft\,(1.0\,m)$$

spacing; delayed initiation: 1 < SR < 4

$$\Rightarrow S\ \frac{L+7B}{8}=\frac{10+7(3.35)}{8}=4.2\,m$$

Spacing in the field should be within plus or minus 15% of the calculated value.

$$4.2-(15\%\times 4.2)\langle\ S\ \langle\ 4.2+(15\%\times 4.2)$$

$$\Rightarrow 3.6\,m\langle S\langle 4.8\,m$$

so, values of S should be within this range.

Blasthole depth (*H*)= bench height + subdrilling=33+3=36 ft (11 m)

Powder column (*PC*) = blasthole depth – stemming=36-8=28 ft (8.5 m)

We could summarize our work as follows:

Table 6. Suggested blast design parameters

Suggested blast design parameters	
Burden, (m)	3.5
subdrilling, (m)	1.0
Stemming, (m)	2.5
Spacing, (m)	4.5
Bench height, (m)	10
Hole depth, (m)	11
Powder column, (m)	8.5

3.2 Explosive Loading

1. loading density of ANFO at (0.8) specific gravity and (4.25) inch diameter is (4.94lb/ft) (7.36kg/m).
2. loading density of Boost at (1.1) specific gravity and (3.25) inch diameter is (3.98lb/ft) (5.93 kg/m).
3. loading density of boost as a percentage of ANFO varies according to several factors, such as
   a. rock structure, which is here heavily cracked, frequent weak joints, weakly cemented layers.
   b. blasthole diameter, 4.25 inch. is considered medium size hole.
   c. powder column length, 8.5 m is not considered a deep hole.

Loading density of Boost could reach (10% of ANFO) in the tough conditions, but in our case we may use (5% of ANFO), which may be suitable.

A powder column of 8.5m may need one full length cartridge of PETRA Boost of 83 mm diameter and 50cm length, which is equal to (2.9 kg). So, the remaining 8 meters of the column powder could be filled with ANFO.

3.3 Explosive Calculations

So, the explosives calculations could be as follows:

$$\begin{aligned}&Amount\ of\ ANFO\ /\ hole\\&= loading\ density \times column\ powder\ length\ of\ ANFO\\&= 7.36 \times 8.0 = 58.9\ kg\ /\ hole\end{aligned}$$

$$\begin{aligned}&Cost\ of\ ANFO\ /\ hole\\&= 58.9\ kg\ /\ hole \times JD\ 0.671/\ kg\\&= JD\ 39.52\ /\ hole\end{aligned}$$

$$\begin{aligned}&Amount\ of\ Boost\ /\ hole\\&= 5\% \times amount\ of\ ANFO\ /\ hole\\&= 0.05 \times 58.9 = 2.9\ kg\ /\ hole\end{aligned}$$

$$\begin{aligned}&Cost\ of\ Boost\ /\ hole\\&= 2.9\ kg\ /\ hole \times JD\ 1.7\ /\ kg\\&= JD\ 4.93\ /\ hole\end{aligned}$$

$$\begin{aligned}&Total\ \cos t\ of\ \exp losives\ /\ hole\\&= 39.52 + 4.93 + 2.72\\&= JD\ 47.17\ /\ hole\end{aligned}$$

$$\begin{aligned}&Total\ amount\ of\ \exp losives\ /\ hole\\&= 58.9 + 2.9\\&= 61.8\ kg\ /\ hole\end{aligned}$$

$$\begin{aligned}&Amount\ of\ rock\ blasted\ (m^3\ /\ hole)\\&= Pattern\ Area\ (m^2) \times Bench\ Height\ (m)\\&We\ may\ choose\ a\ pattern\ of\ (3.5\,m \times 4.5\,m)\\&Amount\ of\ rock\ blasted = 3.5 \times 4.5 \times 10\\&= 157.5\,m^3\ /\ hole)\end{aligned}$$

$$\begin{aligned}&Powder\ Factor\ (PF)\\&= \frac{Amount\ of\ Explosives\ /\ hole}{Amount\ of\ Rock\ Blasted\ /\ hole}\\&= \frac{61.8\,kg\ /\ hole}{157.5\,m^3\ /\ hole} = 0.39\,kg\ /\ m^3\end{aligned}$$

$$\begin{aligned}&Total\ Cost\ /\ Rock\ Blasted\\&= \frac{Total\ \cos t\ of\ Explosives\ /\ hole}{Amount\ of\ Rock\ Blasted\ /\ hole}\\&= \frac{JD\ 47.17\ /\ hole}{157.5\,m^3\ /\ hole} = JD\ 0.30\ /\ m^3\end{aligned}$$

Summarizing our work a follows:

Table 7. Explosives cost.

Item.	Cost (JD)
ANFO cost JD/hole	39.52
Boost cost JD/hole	4.93
Detonator cost JD/piece	2.72
Total explosives cost JD/hole	47.17
Rock blasted / hole m^3	157.5
Rock blasted cost JD/m^3	0.30

4 CONCLUSIONS

According to the company practice of drilling and blasting operations in Aljazi limestone quarry, and our detailed study of the case mentioned, we can conclude the following matters:

First: by comparing the blast design parameters for both we arrive at these results:

Table 8. Comparison of blast design parameters.

Blast design parameters	Company practice	Study practice
Bench height, (m)	10	10
Burden, (m)	3.5	3.5
Spacing, (m)	3.5	4.5
Subdrilling, (m)	0.6	1.0
Stemming, (m)	2.3	2.5
Actual hole depth, (m)	6.9	11
Powder column, (m)	4.6	8.5

Second: by comparing the explosives calculations for both we arrive at these results:

Table 9. Comparison of explosives cost.

Explosive calculations comparisons		Company practice	Study practice
Amount of explosives /hole (kg / hole)	ANFO	32.1	58.9
	Boost	3.2	2.9
Cost of explosives / hole (JD / hole)	ANFO	21.53	39.52
	Boost	5.45	4.93
Cost of detonator / hole (JD/piece)		2.72	2.72
Total cost of explosives / hole (JD/hole)		29.7	47.17

Third: by comparing the rock blasted cost calculations for both we arrive at these results:

Table 10. Comparison of blasted rock calculations.

Item.	Company practice	Study practice
Total rock volume blasted / hole, m^3	84.5	157.5
Total explosive cost / hole JD	29.7	47.17
Blasted rock cost JD/m^3	0.35	0.30

It can be seen that the blasted rock cost (JD / m^3) calculated by the study team is better than the one practiced by the company.

So, we could suggest the followings:

1. Try to use (4.25) inch. bit instead of (4.5) inch.
2. You may expand the spacing distance from (3.5)m to (4.5)m because of the rock conditions.
3. Use (5%) instead of (8%) as a percentage of ANFO quantity for calculating the suitable amount of Boost.

REFERENCES

[1] "Applied Drilling Engineering". Adam T. Bourgoyne Jr. Society of Petroleum Engineers. 1991.
[2] " Blasting Principles for Open Pit Mining". W.A. Hustrulid. Taylor & Francis. 1999.
[3] " Drilling and Blasting of Rocks". Carlos Lopes. Taylor & Francis. 2006.
[4] " Excavation Handbook". Horace K. Church. McGraw-Hill Book Company. N.Y. 1981.
[5] " Construction Planning, Equipments and Methods". R.L. Peurifoy. Mc-Graw Hill. 1990.

Numerical Study of the Behaviour of Jointed Tunnel Lining

M. Barzegar, S. Gharehdash
University of Amirkabir Technology, Department of Mining Engineering, Tehran, Iran

M. Sharifzadeh
Curtin University, Department of Mining Engineering, Perth, Western Australia

ABSTRACT This paper presents the results of a numerical study that has been performed to investigate the factors affecting the maximum bending moment induced in a jointed tunnel lining. The effects of joint number and orientation have been studied in detail. Observations of the results demonstrate that increasing joint number reduces the maximum bending moment induced in the lining. However, the effects of joint number and orientation on the maximum bending moment induced in the tunnel lining become insignificant once the critical joint number has been exceeded. In addition, the sensitivity of the joint number to various ground conditions, tunnel depths and lining flexibility are also highlighted. From the parametric studies, a simple design methodology is proposed to facilitate the determination of maximum bending moment induced in a jointed tunnel lining without incorporating joints in the analysis.

Keywords: Jointed tunnel, bending, lining

1 INTRODUCTION

The design of the precast segmental lining is based upon the proposed tunnel alignment and the expected geological condition at the tunnel level. The geometrical arrangement of the segment type might vary along the tunnel route, dependent on the tunnel boring machine steering alignment. This in turn affects the orientation of joints within each segmental ring. Furthermore, the possible mode of joint orientation is governed by the joint number. The combination of these two factors might influence the stresses induced in the tunnel lining. Subsequently, both the cost and planning purposes might be affected. Hence, it is the main purpose of the present research to investigate the various factors affecting the maximum bending moment induced in a jointed tunnel lining. These factors include joint number and orientation for a given range of ground condition, tunnel depth and lining flexibility. Based on the results obtained, a simple design methodology to determine the maximum bending moment induce in the jointed lining without incorporating joints in the analysis are prepared and presented.

2 FINITE ELEMENT MODELLING

Figure 1 illustrates the most favourable and critical orientation of joints adopted in this numerical investigation. The study was performed using a two-dimensional finite element method program, PLAXIS. Typical lining parameters of Singapore Mass Rapid Transit (MRT) Tunnel were adopted in the modelling and were summarized in Table 1. The main analysis focused on tunnel of 6m in diameter (D) with a depth-to-diameter ratio (H/D) of 2. The ground is considered elastic with properties as suggested by Copsey and Doran (1987) for the Bukit Timah Residual Soil, as shown in Table 2. These properties have been varied during the parametric studies. The modelling procedures involved a full-face excavation of a tunnel with segmental lining supporting the tunnel immediately after the excavation. The lining segments were modelled by applying a number of joints within the lining with their orientations shown in Figure 1. A

reference joint is defined as a joint that is located closest to the tunnel crown, in clockwise direction from the tunnel crown. The location of the reference joint was measured by an angle "Θ". An angle $\Theta = 0^o$ represents a reference joint being positioned at the tunnel crown, while an angle $\Theta = 45^o$ represents a reference joint located at the tunnel shoulder.

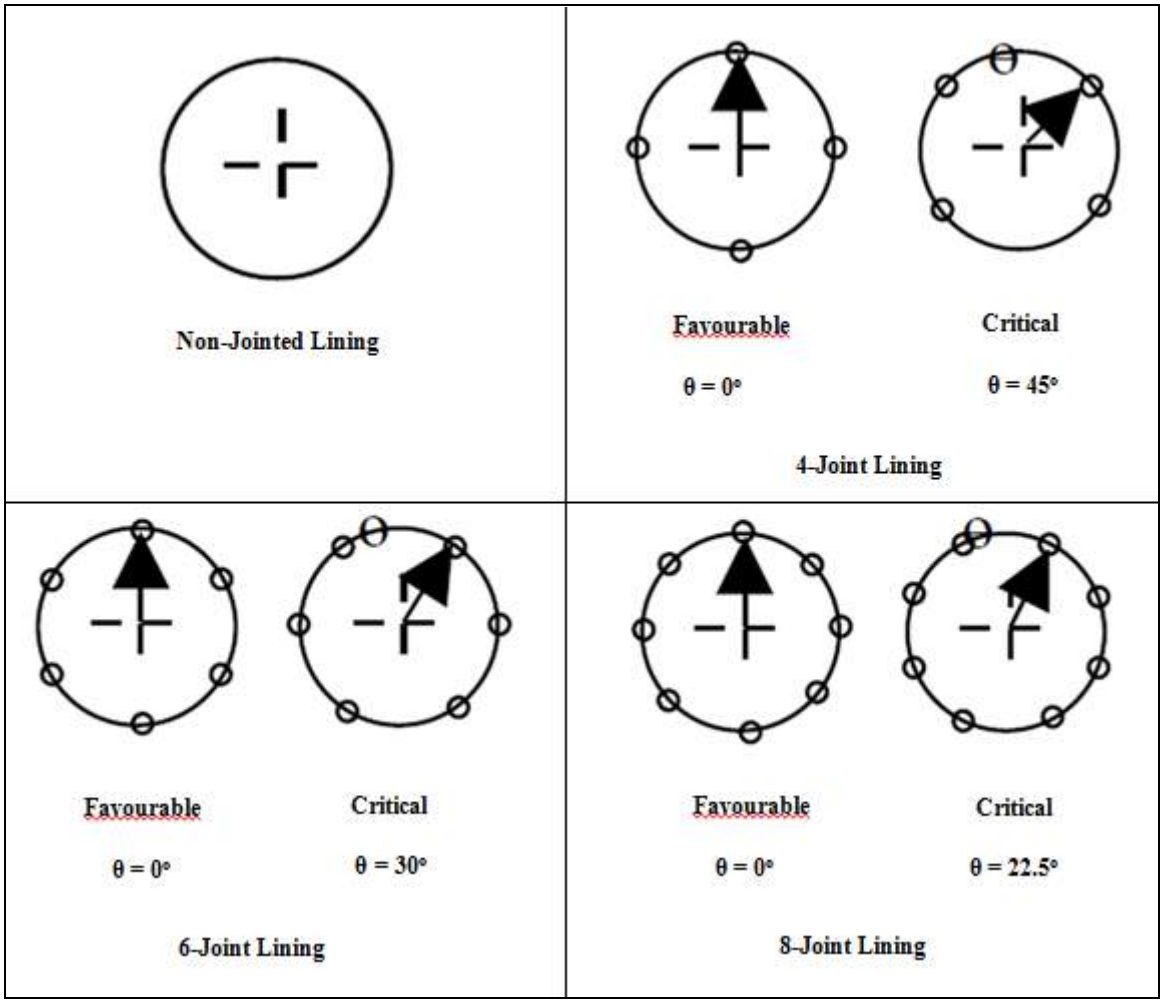

Figure 1. Illustrations of Jointed Tunnel Lining

Table 1. Properties of Elastic Tunnel Lining

Parameter	Symbol	Value	Unit
Young's modulus	E_1	32000	MN/m^2
Poisson's ratio	υ_1	0.2	-
Lining thickness	t	0.275	m

Table 2. Properties of Bukit Timah Residual Soil (after Copsey and Doran, 1987)

Parameter	Symbol	Value	Unit
Unit weight	γ_S	18	kN/m^3
Young's modulus	E_S	8250	kN/m^2
Poisson's ratio	υ_S	0.495	-
Coefficient of earth pressure at rest	K_0	0.5	-

3 PARAMETRIC STUDIES

A series of parametric studies was conducted to investigate the effects of joint number and orientation on the maximum bending moment induced in the tunnel lining. Furthermore, additional analyses focused on 6-joint, 8-joint and non-jointed tunnel lining were also being performed for a given range of coefficient of earth pressure at rest, tunnel depth and lining flexibility. Both 6-joint and 8-joint were chosen to represent the typically joint numbers encountered in segmental tunnel ring.

3.1 Effect of Number and Orientation of Joints

The influence of number and orientation of joints on the maximum bending moment induced in the tunnel lining was studied. The results of the largest and lowest maximum bending moment, correspond to the most critical and favourable joint orientation for each joint number, are plotted in Figure 2a.

Figure 2(a) shows that increasing joint number reduces the maximum bending moment induced in the lining. This is attributed to the fact that the span of the beam is shorter with more number of joints, in turn, induced lower bending moment in the lining. The maximum bending moment induced in the lining becomes negligible small when the joint number exceeds 8-joint. In addition, it should be noted that the most favourable orientation of 4-joint induced much lower maximum bending moment as compared to 5-joint and 6-joint. This indicates that the joint orientation significantly influence the maximum bending moment induced in the lining. However, the maximum bending moment for cases involved a minimum of 8-joint is about similar in magnitude, regardless of the joint orientations. This could be explained by the fact that for tunnel ring with greater segment number, the span of each beam becomes shorter. Hence, the average loading acting on each beam becomes almost similar in magnitude, despite joint orientations. As a result, the variation of maximum bending moment with joint orientations becomes insignificant for cases involved greater joint number. In addition, a comparative study was carried out for 4-joint, 6-joint and 8-joint tunnel lining and the results are presented in Figure 2(b). The 4-joint lining was adopted as a reference case in the investigation as it shows the most significant variation of maximum bending moment with joint orientation, as indicated in Figure 2(a). Both 6-joint and 8-joint lining were chosen as they represent the typical joint numbers encountered in most segmental tunnel ring. The results in Figure 2(b) show that the maximum bending moment induced in the jointed lining is the lowest for reference joint at $\Theta = 0^o$, i.e. when the reference joint is located at tunnel crown. However, the maximum bending moment induced in the lining is the largest when the reference joint is located in between the angle of $\Theta = 0^o$ and the largest possible Θ value for each case of joint number. For instance, the largest maximum bending moment for 4-joint, 6-joint and 8-joint tunnel lining occurred at $\Theta = 45^o$, 30^o and 22.5^o respectively, as illustrated in Figures 1 and 2(b). These observations are of practically important in the design of segmental tunnel ring due to the fact that the location of the reference joint for each segmental tunnel ring varies along the tunnel alignment. Hence, the stresses induced in each segmental tunnel ring of different joint orientation are different, for the same ground condition and tunnel depth.

3.2 Effect of Coefficient of Earth Pressure at Rest

The effect of K_o-value was studied in this section. The K_o-value of 0.5 and 1.0 were adopted to represent normally consolidated ground while K_o-value of 2.0 for overconsolidated ground. The results of the study are presented in Figure 3 (a . as shown in Figure 3(a), the largest maximum bending moment occurred when $K_o = 2.0$ and the lowest was observed for $K_o = 1.0$ (approximately zero moment), with $K_o = 0.5$ in between.

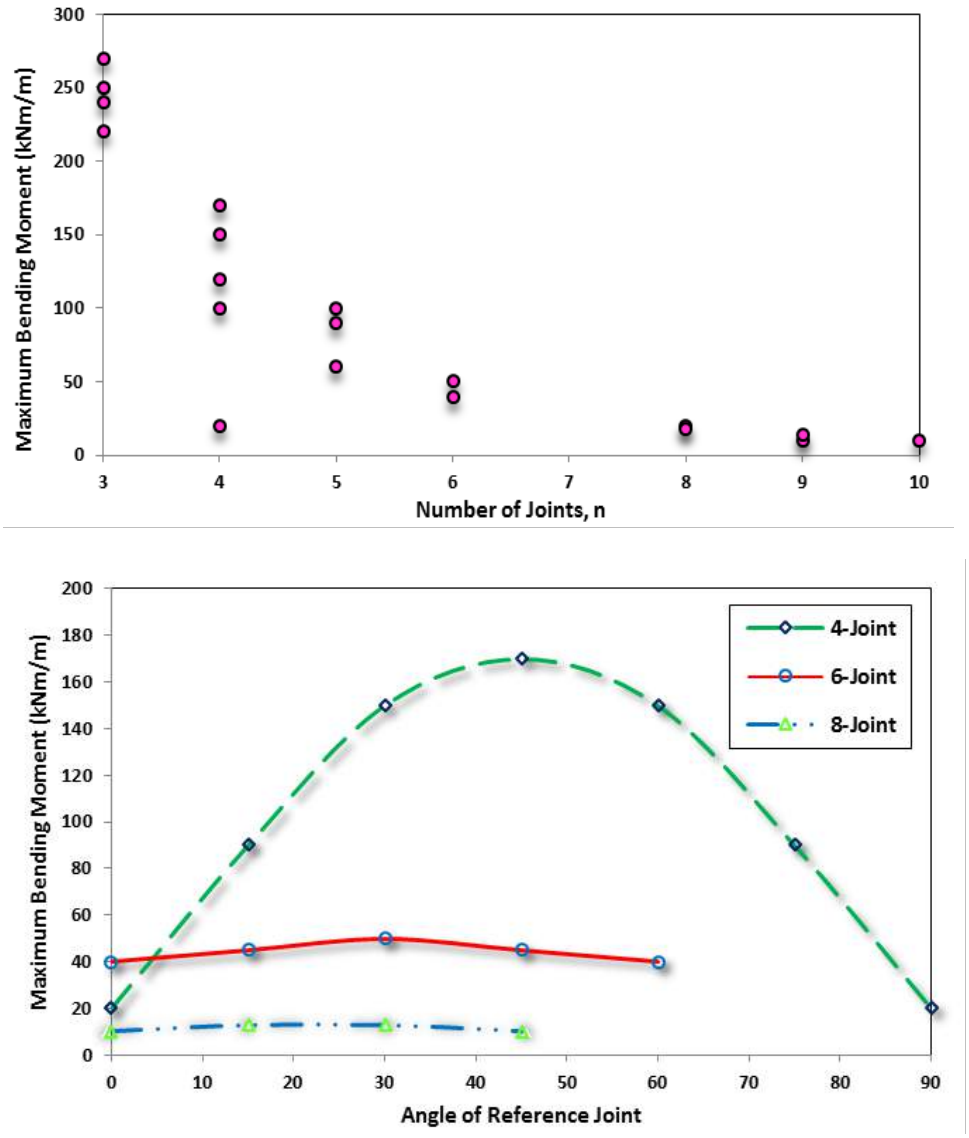

Figure 2. Variation of Maximum Bending Moment with (a) Number; and (b) Orientation of Joints

As expected, this is attributed to the larger difference between the vertical and horizontal loading acting on the lining for K_o = 2.0, as compared to K_o = 0.5 and 1.0. For the given range of K_o-value, the maximum bending moment induced in the lining with a maximum of 3-joint is greater than nonjointed lining. However, a lower maximum bending moment was observed for lining with a minimum of 5-joint, as compared to the non-jointed lining. In addition, it should be noted that the maximum bending moment induced in the 4-joint lining is about similar in magnitude as the non-jointed lining, for the given range of K_o-value. These observations are in line with the statement made by Muir Wood (1975) that the effect of joints would only influence the rigidity of the lining if the number of lining segments is greater than 4.

3.3 Effect of Tunnel Depth

The influence of tunnel depth on the maximum bending moment induced in the jointed tunnel lining was studied. Analyses were performed for a range of depth-to-diameter ratios, i.e. H/D ranging from about 1.0 to 3.5, for shallow and deep tunnel case. Results of the variation of maximum bending moment with depth of burial are presented in Figure 3(b.(Figure 3(b) shows the maximum bending moment induced in the lining increases with tunnel depth. This is due to the increase in the overburden pressure acting on the lining as the depth

increases. At shallower depth of burial, e.g. H/D of about 1.0, the maximum bending moment induced in both 6-joint and 8-joint lining is about similar. However, the difference becomes increasingly significant at greater tunnel depth. This indicates the influence of joint number is much more significant for deep tunnel case as compared to shallow tunnel. In addition, it should be noted that the maximum bending moment induced in the non-jointed lining at shallower depth of burial is significantly larger than cases involved 6 and 8-joint. Furthermore, a relatively steeper slope shown in Figure 3(b) for non-jointed lining as compared to 6-joint and 8-joint indicates that the incremental maximum bending moment with depth of burial for non-jointed lining is much more significant than jointed lining.

3.4 Effect of Lining Flexibility

The influence of lining flexibility on the maximum bending moment induced in the jointed tunnel lining was examined based on the flexibility ratio, F, defined by Peck (1972) in Equation 1. Increasing lining flexibility increases flexibility ratio. Hence, the lining behaves more flexible. However, it should be pointed out that the flexibility ratio proposed by Peck (1972) assumed a continuous tunnel lining and therefore does not take into consideration of joint factor. Figure 3(c) shows that for jointed tunnel with stiff lining, the maximum bending moment induced in the lining is significantly influenced by the number of joints. For instance, increasing joint number from 6 to 8-joint for very stiff lining case with flexibility ratio of about 0.05 reduces nearly 70% of the maximum bending moment in the lining. However, the influence of joint number becomes gradually insignificant with increasing lining flexibility, particularly for cases involved lining with flexibility ratio of greater than 15. It is important to emphasize that similar lining thickness was adopted for both jointed and nonjointed tunnel lining, for a given flexibility ratio defined by Peck (1972). The results shown in Figure 3c) indicate that increasing joint number for jointed lining is tantamount to increasing lining flexibility which in turn, flexibility ratio of non-jointed lining. This is attributed to the fact that the maximum bending moment induced in both jointed and non-jointed lining show a similar descending trend with increasing joint number and lining flexibility respectively. In addition, observations of the results also reveal that the application of flexibility ratio proposed by Peck (1972) in the interpretation of lining flexibility for cases involved jointed lining might not be as efficient as for continuous lining. For the same lining thickness, the lining flexibility of jointed lining is higher than the non-jointed lining, resulted from the joint effect. Thus, the necessity of considering a new effective second moment of inertia to replace the existing second moment of inertia, as defined in Equation 1, is established to facilitate the determination of effective flexibility ratio for jointed lining. Furthermore, this finding also opens up the possibility of estimating the maximum bending moment induced in the jointed lining without incorporating joints in the analysis and subsequently, simplifying the design procedures of the jointed lining. The detail illustrations are presented in the following section.

$$F = (E_s/(1+\upsilon_s))/(6E_lI_l/(1-\upsilon_1^2)R^3) \quad (1)$$

where I_l is the second moment of inertia for continuous tunnel lining; and R is the tunnel radius.

4 SIMPLIFIED DESIGN METHODOLOGY

From the parametric studies, a simplified design methodology was proposed to facilitate the determination of maximum bending moment induced in a jointed tunnel lining without incorporating joints in the analysis. The design chart shown in Figure 4 gives the maximum and minimum effective second moment of inertia for the non-jointed lining that is of equivalent to the jointed lining. It can be noted from the design chart that increasing number of joints reduces the effective second moment of inertia, I_e, of the lining which in turn, equivalent to a reduction in the lining thickness of the nonjointed lining.

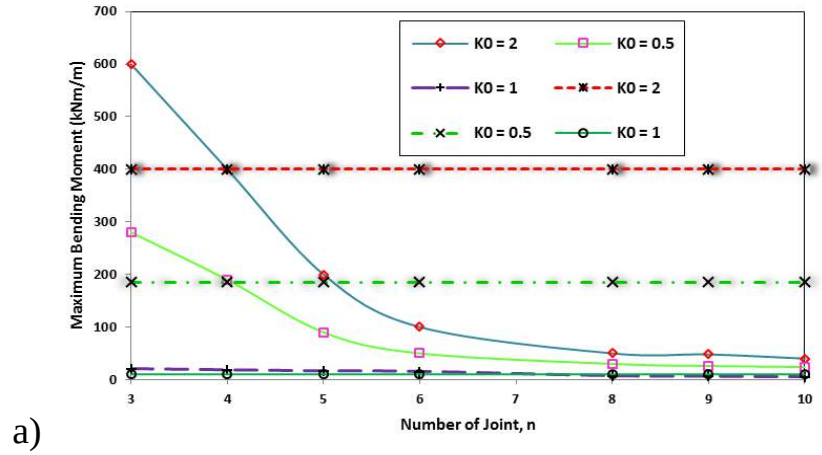

a)

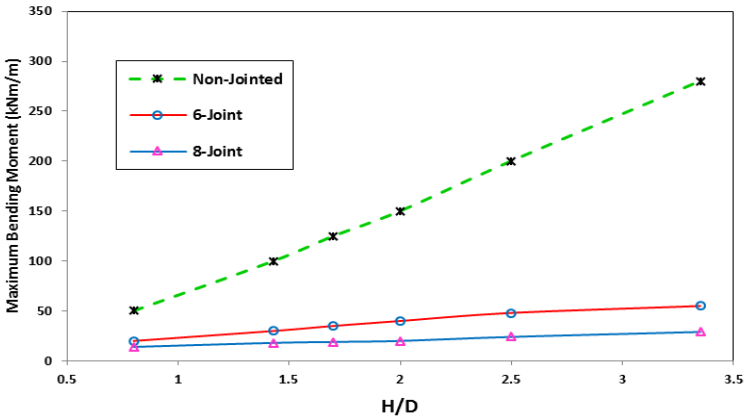

b)

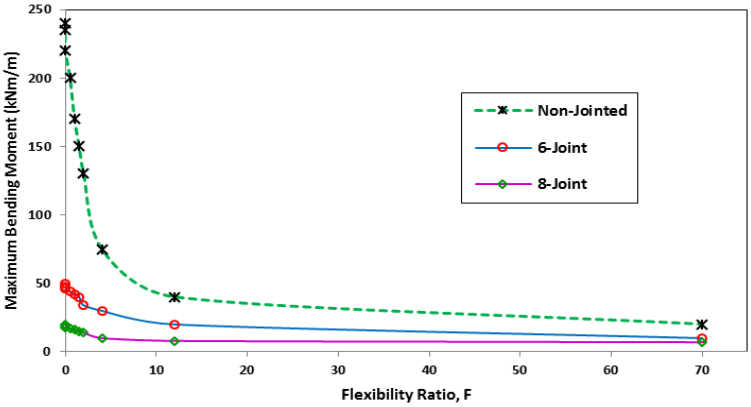

c)

Figure 3. Variation of Maximum Bending Moment (most critical joint orientation) with (a) K_o-Value (b) Tunnel Depth; and (c) Flexibility Ratio (as defined in Equation 1)

The design chart, together with Equations 2 and 3, facilitate the determination of both $I_{e,max}$ and $I_{e,min}$. The $I_{e,max}$ correspond to the effective second moment of inertia for the most critical orientation of joints while $I_{e,min}$ represents the effective second moment of inertia for the most favourable orientation of joints. The substitution of I_l in Equation 1 with $I_{e,max}$ and Ie,min enables the effective flexibility ratios of the non-jointed lining to be computed, which correspond to the most critical and favourable orientation of joints for the jointed lining. These effective flexibility ratios allow the moment coefficients, and subsequently maximum bending moments induced in the jointed lining to be estimated from Figure 5 and Equation 4 respectively. The design of the jointed tunnel lining could therefore be carried out based on the relatively lower

maximum bending moment estimated using this approach, as compared to the conventional design methodology assuming continuous tunnel lining, for cost and planning purposes.

$$I_{e,min}/I = 429/n^{4.} \quad (2)$$

$$I_{e,max}/I = 159.2/n^{4.3} \quad (3)$$

$$M_p = M_{max}/\gamma HR^2 \quad (4)$$

Where M_p is the moment coefficient; M_{max} is the maximum bending moment; and n is the joint number.

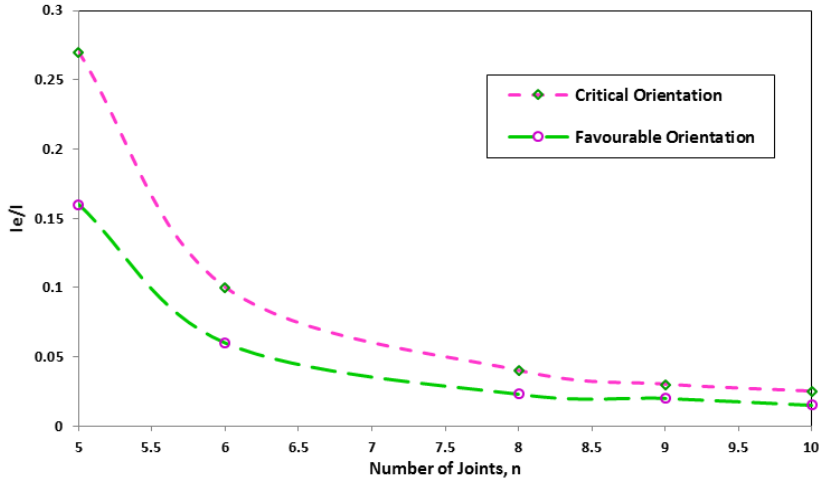

Figure 4. Variation of I_e/I with Number of Joints

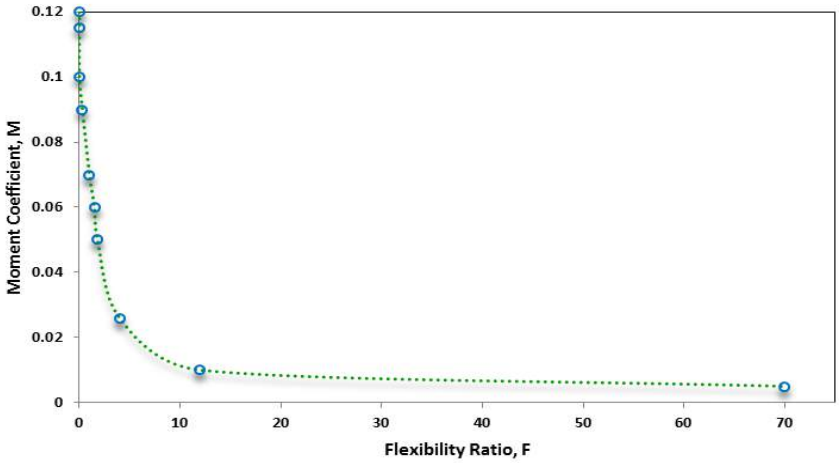

Figure 5. Variation of Moment Coefficient with Flexibility Ratio

5 CONCLUSIONS

A numerical study to investigate the factors affecting the maximum bending moment induced in a jointed tunnel lining has been performed. The influence of number and orientation of joints, ground condition, tunnel depth and lining flexibility have been studied in detail. The finite element method program PLAXIS was adopted in the investigation. Observations of the results demonstrate that the number and orientation of joints have significant influence on the maximum bending moment induced in the jointed lining, for a given range of ground condition, tunnel depth and lining flexibility. The lowest maximum bending moment (most favourable joint orientation) induced in the lining when the reference joint is located at tunnel crown ($\Theta = 0^o$). However, the largest maximum bending moment (most critical joint orientation) induced in the

lining when the reference joint is located at an angle between $\Theta = 0^o$ and the largest possible Θ value for each case of joint number. For segmental tunnel ring of less than 4-joint, with the most critical joint orientation, the maximum bending moment induced in the lining is greater than the non-jointed case. However, the opposite trend was observed for segmental tunnel ring of more than 4-joint. The maximum bending moment induced in 4-joint segmental tunnel ring is about similar to non-jointed case. For cases of K_o-value of lesser or greater than unity, the influence of joint number on the maximum bending moment induced in the lining is significant. The largest maximum bending moment induced in the lining for K_o = 2.0, as compared to K_o = 0.5. The influence of joints on the maximum bending moment induced in the lining increases with tunnel depth. However, the maximum bending moment for the non-jointed lining increases more significantly with tunnel depth as compared to jointed lining. The influence of joint number on the maximum bending moment induced in the lining is significant for stiff lining case of small flexibility ratio. A simplified design methodology has been proposed to facilitate the determination of the maximum bending moment induced in a jointed tunnel lining without incorporating joints in the analysis. The results of the parametric studies, together with the proposed design methodology are believed to be useful for the preliminary design of jointed tunnel lining.

REFERENCES

Copsey, J.P, Doran, S.R, 1987. Mass Rapid Transit Systems. *Proc.of the Singapore Mass Rapid Transit Conference*, (pp. 225-235).

Lee, K.M, Ge, X.W, 2001. The equivalence of a jointed shield-driven tunnel lining to a continuous ring structure. *Canadian Geotechnical Journal*, 38(3), (pp. 461-483).

Muir Wood, A.M, 1975. The circular tunnel in elastic ground. *Géotechnique*, 25(1), (pp. 115-127).

Peck, R.B, Hendron, A.J, Mohraz, B, 1972. State of the art of soft ground tunneling. *Proc. 1st Rapid Excavation and Tunneling Conference, AIME*, (1), (pp. 259-286).

Evaluation of Blast Induced Ground Vibrations at Ozarslan Quarry

Özarslan Taşocağında Patlatma Kaynaklı Yer Sarsıntılarının Değerlendirilmesi

M.C. Ozyurt, U. Kalayci, A. Karadogan, U. Ozer
Istanbul University, Mining Engineering Department, Istanbul, Turkey

ÖZET Bu çalışmada, Kırklareli ili Vize yöresinde bulunan Özarslan Taşocağında yapılan patlatma kaynaklı titreşim ve yersarsıntıları incelenmiştir. Çalışma kapsamında, 13 atıma ait 48 olay, titreşim ölçer cihazlar ile kaydedilmiştir.

Elde edilen veriler, dört bantlı filtrelemeye tabi tutularak gerçek titreşim ve frekans verilerinin elde edilmesi amaçlanmıştır. Kaydedilen maksimum parçaçacık hızı ile ölçekli mesafe arasındaki ilişki statik analiz ve anlamlılık testi ile değerlendirilmiştir. Değerlendirme sonucunda söz konusu ilişkinin anlamlı olduğu ortaya konmuştur.

Anahtar kelimeler: Yer sarsıntısı, titreşim analizi

ABSTRACT This paper presents blast induced vibration analysis on blasting at Ozarslan Quarry located in Vize district in Kırklareli province in Turkey. During the study, 13 shots were monitored at different times and 48 events were recorded by vibration monitors.

A four layered band filter applied to vibration data in order to obtain actual vibration signal and frequency data. The recorded peak particle velocities and scaled distances were subjected to statictical analysis and variance analysis. After the evaluation, site specific attenuation formula is obtained and found as significant.

Keywords: Ground vibration, vibration analysis

1 INTRODUCTION

After the detonation of explosive, the immediate vicinity of the blast hole that may extent as the diameter of the blast hole is called as shock zone. In this zone, the rock behaves mechanically as viscous solid and the rock is crushed or extensively cracked. The domain immediately outside the shock zone is called as the transition zone. In this zone, the rock behaves as non-linear elastic solid and new fractures are initiated and propagated in the radially compressive stress field. The outside of transition zone is called as seismic zone. In seismic zone the rock behaves linearly elastic (Brady and Brown 1985).

For damage levels which occurs in seismic zone, the carried energy level of vibrations is not only responsible (Kalaycı, 2011). The following parameters are using for determination of the energy level of vibrations; particle displacement (mm), particle velocity (mm/sec), particle acceleration (mm/sec2), wave frequency (Hz).

Features and characteristics of ground vibration are effected by blasting design and parameters; especially the amount of explosives detonated at the same time, firing sequence (time delay) and the direction of the firing, in the close fields of shot point. However, far from shot point, ground and rock mass characteristics, which carries the seismic waves, effects the vibration feature and specialty. Besides, land coefficients and the frequency of vibrations are important and decisive factors for damage mechanism (Karadoğan, 2008; Özer et all, 2011).

Blast induced damage criteria developed by various researchers, until today have been applied with varying degrees of success. Frequency is one of the basic damage criteria according to many researchers. Frequency based damage approaches; Rockwell's (1934) energy formula based on frequency and amplitude; Crandell's (1949) energy ratio approach which based on acceleration and frequency; the chart of Langefors and Kıhlström (1973); Medearis's (1976) damage estimation based on particle velocity and dominant frequency; United States Bureau of Mine's (1980) Criteria Based on particle velocity, frequency, construction and building type; German DIN 4150 standards (1984), which based on particle velocity, frequency and structural characteristics; Indian CMRI standards (1987), which based on particle velocity, frequency and structural characteristics; United States Office of Surface Mining's (OSM), peak particle velocity limit, scaled distance and frequency based approach (Karadogan, 2008).

Frequency and particle velocity components are the most effective parameters on blast induced damage. Several methods are using for determining of the rock mass frequency by seismic waves. These methods are zero crossing frequency and Fourier frequency methods. Zero crossing frequency, calculates the event waveform's frequency at the largest peak by using 1/period formula. The zero crossing calculation is limited because it assumes a single predominant frequency at the peak, typically represented by sinusoidal waveforms. In practice the peak may be the result of two or more major frequency components representing compound waveforms (Kalaycı et al, 2014).

The most trustable method to determine the frequency is the Fourier transform method which is the mathematical tool that deconstruct the waveform into its sinusoidal components. Thus, it transforms the time based function to frequency based function. The Fourier algorithm is used for digital filtering to extract the cosine and sine parts of the fundamental frequency component. These components are functions of time and have the same frequency as the fundamental harmonic of the signal (Kalaycı et al, 2014).

2 TEST SITE DECSCRIPTIONS

The research program was carried out in order to eliminate environmental problems and to optimize blasting conditions during the blasting excavations at Ozarslan Const. and Mining Industry.and Trade's Quarry located in Vize district in Kırklareli provincein Turkey. The location of this site is shown in Figure 1.

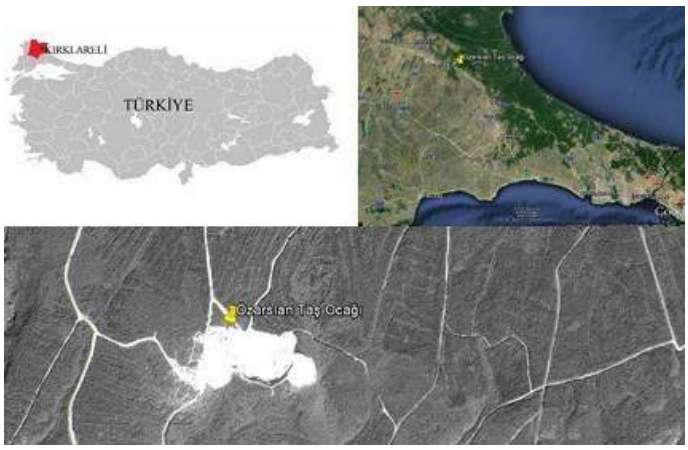

Figure 1. The Location of Ozarslan Quarry

2.1 Geology

Kırklareli Limestone (The Sogucak Formation), the most common shallow marine unite in Thrace, consists mainly of limestones deposited in a variety of depositional settings ranging from reef to back-reef and to fore-reef environments The unit in most cases directly overlies the metamorphic rocks and upper Palaeozoic siliciclastics in the nothern and eastern part of Thrace.

The Soğucak Formation is either overlain by continental beds of the Pınarhisar Formation or by deep marine (partly shallow marine as in Karaburun) beds of the Ceylan Formation, which is widely distributed in the southern part of Thrace. The Pınarhisar Formation comprises continental sandstones/conglomerates and Congeria-rich limestones considered to be Oligocene in age based on fish remains, ostracods and molluscs (Less et all, 2011).

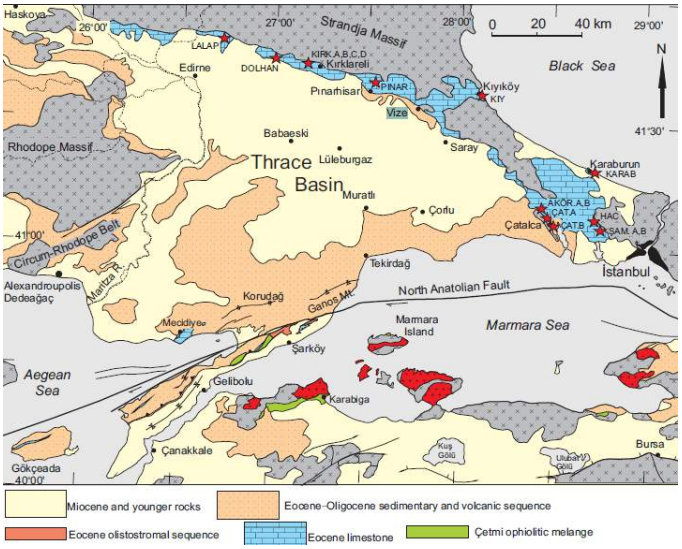

Figure 2. Tectonic map of the Th race and Marmara region with the location of stratigraphic sections and samples (red stars) (Less et all, 2011)

Figure 3. The Kirklareli formation's reef environment

2.2 Physico-Mechanical Parameters of Rock

According to recent studies in Ozarslan Quarry, the physico-mechanical parameters of rock are presented in Table 1.

Table 1. Physico-Mechanical Parameters of Rock (Ozer, et all, 2013).

PARAMETERS	VALUE
Density	2,34 g/cm^3
Ultrasonic Sound Transmission	5147 m/sn
Toughness Strength	1,26 Mpa.m^1/2
Uniaxial Compressive Strength	93,94 MPa
Uniaxial Tensile Strength	5,3 MPa

According to the physico-mechanical parameters of rock, it was understood that the blasting operations were inevitable for excavation in Ozarslan Quarry.

3 TEST PROCEDURE

In this study, the blast design and procedures were observed. During this observation, no changes were made to the blasting patterns that are systematically applied by company engineers.

During the field study, 13 shots were monitored, and 48 events were recorded by 9 vibration monitors (four of them are 4 channels, 5 of them are 8 channels). Most of these monitors were located along and both sides of the Fault that cuts the field in the direction of N-S. The coordinates of monitor stations and shot points were determined by GPS and blasting patterns were recorded for each shot.

After the measurements, the obtained data were analyzed by taking Particle velocities, frequencies, distances, charge amounts, the fault plane and rock unit changes along the fault plane into consideration. At the analysis stage, scaled distance were estimated by the SD equation which extensively suggested in literature

$$(SD = R / W^{0.5})$$

Where, SD, scaled distance; R, distance; W, maximum charge per delay.

After the measurements, the obtained data were analyzed by taking Particle velocities, frequencies, distances, charge amounts, the fault plane and rock unit changes along the fault plane into consideration.

To calculate the frequency values, Fast Fourier Transform algorithm is used via Matlab program. The fast Fourier transform (FFT) is a discrete Fourier transform algorithm which reduces the number of computations (Matlab, 2014).

The functions Y = fft(x) implement the transform and inverse transform pair given for vectors of length N by

$$X(k) = \sum_{j=1}^{N} x(j)\omega_N^{(j-1)(k-1)}$$

$$x(j) = (1/N)\sum_{k=1}^{N} X(k)\omega_N^{-(j-1)(k-1)}$$

Where $\omega_N = e^{(-2\pi i)/N}$ is an Nth rooth of unity.

4 MEASUREMENT RESULTS

The coordinates of shot and station points are given in Table 2 and 3, respectively.

Table 2. The Coordinates of Shot Points

Shot No	Coordinates		
	Y	X	Z
1	559902	4607354	350
2	559675	4607263	344
3	560002	4607507	348
4	559953	4607448	335
5	560002	4607432	338
6	559958	4607478	340
7	559971	4607420	339
8	559764	4607529	335
9	559926	4607440	340
10	559952	4607453	327
11	559840	4607493	333
12	559959	4607400	314
13	559866	4607496	322

Table 3. The Coordinates of Vibration Monitoring Device Station Points

Station No	Coordinates		
	Y	X	Z
1	559546	4607210	340
2	559663	4607105	336
3	559556	4607464	333
4	559545	4607496	335
5	559661	4607300	341
6	559740	4607350	334
7	559538	4607415	325
8	559593	4607483	342
9	559690	4607330	341
10	559540	4607435	341
11	559536	4607520	334
12	559547	4607432	332
13	559615	4607273	325
14	559617	4607274	322
15	559553	4607434	330
16	559529	4607157	311
17	559999	4607439	332
18	559978	4607407	327
19	559964	4607384	322
20	560032	4607424	330
21	560009	4607384	329
22	559991	4607361	325
23	560001	4607360	340
24	559990	4607344	337
25	559991	4607361	325
26	560001	4607360	340
27	559990	4607344	337
28	559681	4607320	335
29	559641	4607300	334
30	559571	4607410	338
31	559586	4607484	336
32	559589	4607483	331
33	559613	4607388	334
34	559683	4607313	327
35	559614	4607273	321
36	559542	4607439	330

Some of the results of ground vibration measurements, vibration monitor models are given in Table 4

Table 4. Some of the Results of the Ground Vibration Measurements

Shot No	Vibration Monitor Serial Number	PPV (mm/sn)	Z-C Frequency (Hz)	FFT Frequency (Hz)	Air Shock (dB)	Station
1	BE10773	0,51	22,3	21,5	109,2	2
2	BE10771	5,46	64	45,3	135,9	1
3	BE10771	0,76	42,7	27	106	4
4	BE10707	1,02	39,4	10,5	69,5	6
5	BE10771	0,51	21,3	11,3	34	5
	BE10707	0,51	19,7	21	75,8	6
6	BE10688	1,02	28,4	32,9	114,8	8
	BE10707	1,52	28,4	34,8	116,6	9
7	BE10707	1,52	42,7	17,8	129,2	11
	BE10708	0,89	13,8	18,3	128,7	12
8	BE10707	1,65	51,2	62,5	115,2	11
	BE10708	1,9	26,9	16,3	113,5	12
9	BE10688	0,64	21,3	17,8	104,2	14
	BE10708	0,64	34,1	21	100	16
10	BE10773	25	56,9	69,3	*	22
	BE10708	11,8	64	88,9	*	24
11	BE10688	2,03	22,3	19,6	*	17
	BE10687	1,65	23,3	20,3	*	23
12	BE10688	1,65	32	16,9	123,7	28
	BE10772	0,89	24,4	17,1	*	29
13	BE10709	3,56	85,2	68,4	88	35
	BE5724	1,27	15,1	14,8	88	36

5 EVALUATION OF THE RESULTS

During the Ozarslan Quarry blasting operations, vibration monitors were used for investigation of frequency and particle velocity levels around the fault plane. The stations of vibration monitors were located in boundaries of field, and also along and both sides of the fault plane. 48 events were recorded for 13 shots.

To estimate particle velocity, the relationship between particle velocty and scaled distance, derived by considering charge per delay and distance between shot location and vibration monitors' stations is investigated. The relationship between particle velocity and scaled distance is shown in Figure 4.

As a result of the regression analysis by considering distance between shot location and vibration monitors' stations, charge per delay and peak particle velocity, the formula that contains the constants of the study area,

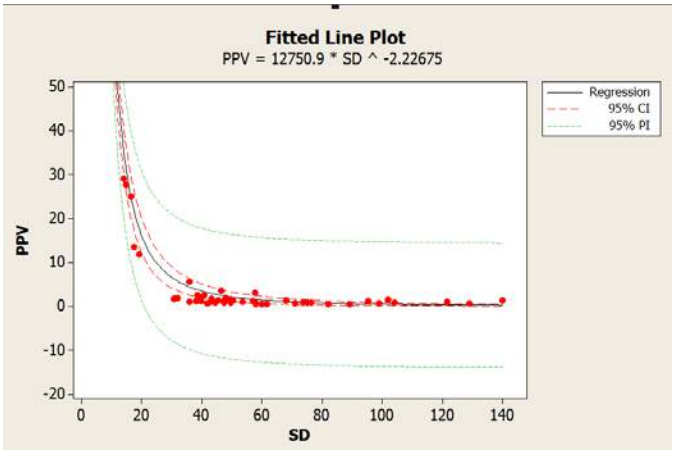

Figure 4. The Relationship Between Particle Velocity And Scaled Distance

recommended for use in blasting operations to estimate particle velocity. The formula is given in Equation 1.

$$PPV = 12750 \times SD^{-2,227} \quad (r=0,866) \qquad (1)$$

To validate that if SD variation is affected the PPV values, hypothesis test is performed. Hypotheses are as follows; H_0 (Null) hypothesis: PPV values are not affected by SD variation; H_1 hypothesis: PPV values are affected by SD variation.

All hypothesis tests use a P-value to weigh the strength of the evidence. The p-value is a number between 0 and 1 and interpreted in the following way:

•A small p-value (typically ≤ 0.05) indicates strong evidence against the null hypothesis, null hypothesis should be rejected.

•A large p-value (> 0.05) indicates weak evidence against the null hypothesis. That means unsuccessful to reject the null hypothesis.

•P-values very close to the designated limit (0.05) must considered to be marginal (Rumsey, 2011).

Analysis of variance results (Anova) is given in Table 5.

Table 5. Analysis of variance results

Source	Sum of Squares	Degree of Freedom	Mean Squares	P Value
Regression	7976.90	99	79.7786	0.002
Residual	0.97	1	0.9661	
Uncorrected Total	7977.86	100		

Due to the P value lower than 0.05, null hypothesis is rejected. In other words, in this data set the peak particle values are affected by variation of scaled distance values at %5 significance level.

The noises prevent the existence of dominant frequency in vibration analysis. For this reason, 4-band filter has been applied to vibration datas. Band filter coefficients and flow chart are given in Figure 5.

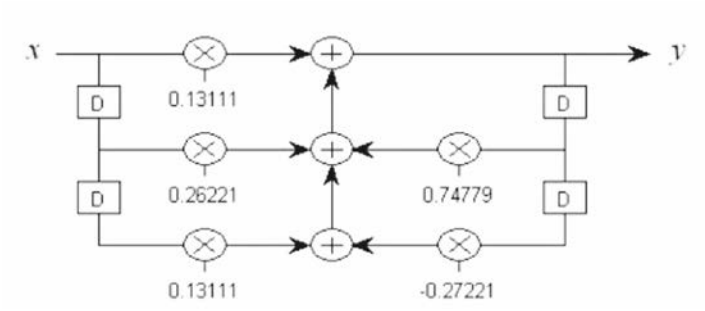

Figure 5. Band Filter Coefficients And Flow Chart

Filtered L component of vibration caused by Shot No. 5 is shown in Figure 6. This process is performed to each shots' all vibration components.

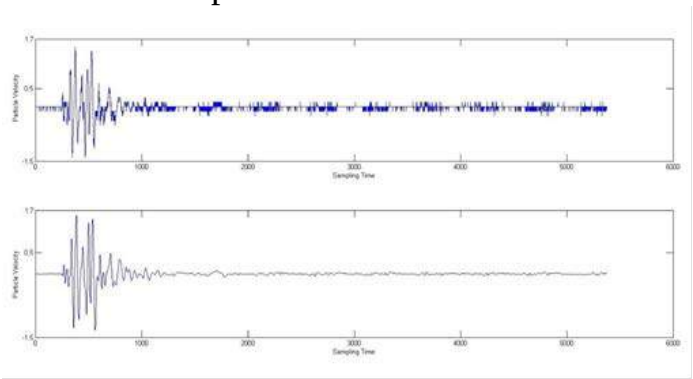

Figure 6. Filtered L Component of Vibration Caused by Shot No. 5

When the change in frequency values recorded are closely examined, 3 different frequency groups are spotted.

The frequency range spectrum, which calculated with Fourier Transform method and its filtered view, also given for each region in Figure 7.

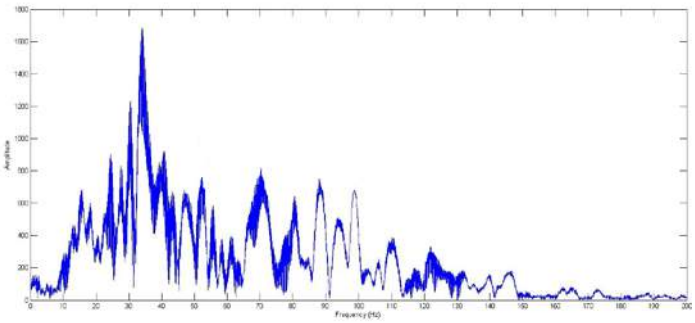

Figure 7. Frequency Oscillation Of Region I

As a result of filtering process, frequencies that given maximum amplitude, are about 30 Hz.

6 EVALUATION OF THE RESULTS

During the study, 48 events for 13 shots were recorded. As result of investigation of these events, some suggestions were presented.

It was understood that the blasting operations were inevitable for excavation in Ozarslan Quarry, the physico-mechanical parameters of rock.

In order to monitored vibration and air shock caused by blasting, vibration monitor devices were placed around the quarry. The recorded peak particle velocities and scaled distances were subjected to statictical analysis. The results are written below.

Filtering process outputs a dominant frequency. As a result of this, filtering process must be done. The noise affects the measured data. Therefore, it shouldn't be used in calculations.

The variance analysis on the measured data is performed, relationship and significance of datas are tested. As result of the test, the relationship between PPV and SD is proved to be significant.

As a result of filtering process, frequencies that given maximum amplitude, are about 30 hz.

Vibrations propagation equation for Ozarslan Quarry is found in the %95 confidence interval, by nonlinear analysis.

Before analyzing the frequency data, 4 layered band filter is applied to vibration data to prevent noises. While analyzing the frequency data both zero crossing and Fourier transform methods were used. According to results, Fourier transform method was decided because of reliability and utilization extensity.

REFERENCES

Brady, B.H.G, and Brown E.T., 1985, Rock Mechanics for Unfergrounde Mining, Chapman Hall. 517 pages.

Crandell, F.J., 1949; Ground Vibration Due to Blasting and Its Effect Upon Structures, Reprinted from Journal of Boston Society of Civil Engineers.

Dowding CH (1985) Blast Vibration Monitoring and Control. Prentice-Hall, Inc., Englewood Cliffs, NJ, pp. 119-126.

Kalayci Ü, Karadoğan A, Özer Ü, Güçlücan Z, Akgül M (2011) "Beykoz Atık Su Tüneli Kazı Çalışmaları Sırasında Patlatma Kaynaklı Titreşim Analizi" The Symposium of Mining and Environment, İzmir, Turkey, 2-3 January, Vol.1, pp.133-142.

Kalaycı, U., Ozer, U., Karadogan, A., Ozyurt, M.C., Investigation of Dominant Frequency by Vibration Monitors, V. Globalstone congress, Antalya/Turkey.

Kalayci Ü, Özer Ü, Karadoğan A (2012) "Patlatmada Harcanan Faydalı Enerji Ile Patlatma Verimi Arasındaki İlişkinin Araştırılması", The Journal of Mining, vol.5, pp.14-18.

Kalayci Ü (2011) The Investigation Of Relationship Between Spending Useful Energy in Blasting with The Efficiency Of Blasting, İstanbul University, Institute of Sciences, Master Thesis.

Karadogan, A., 2008, Patlatmadan Kaynaklanan Titreşimler İçin Ulusal Yapı Hasar Kritlerleri Oluşturulabililiğinin Araştırılması, İstanbul Üniversitesi, Fen Bilimleri Enstitüsü, Doktora Tezi

Langefors, U, Khilström, B., 1973, Rock Blasting, John Wiley and Sons, New York.

Less, G., Özcan E., Aral I. Okay, 2011, Straigraphy and Larger Formanifera of Middle Eocene to Lower Oligoscene Shallow-Marine Units in the Northern and Eastern Parts of the Th race Basin, NW Turkey, Turkish Journal of Earth sciences, TÜBİTAK

Matlab, 2014, Users Manual.

Medearis, K., 1976, Structural response to nuclear detonation ground motions, Proceedings of the ASCE Engineering Mechanics Division Specialty Conference on the Dynamic Response of Structures, March.

Ozer U, Karadogan A, Kalayci, U, Aksoy M, Keti, Z, Effects to The Motion of Vibrations Waves of Fault Planes, ISEE Symposium, 2011, Tennesee, USA.

Ozer, U., Karadogan, A., Aksoy, M., 2013, Açık Ocaklarda Patlatma Enerji Bileşenleri Dağılımının Belirlenmesi ve Bu Dağılımdan Hareketle Patlatma Tasarım Optimizasyonu Yapılabilirliğinin Araştırılması, Tübitak Project, Project No: 110M555

Rumsey DJ (2011) Statistics For Dummies, ISBN: 978-0-470-91108-2, 384 pages.

Uzler, H.M., Dalgiç, S., Uzer, U., Vize (Kirklareli) 200703840 Ruhsat Numarali II.Grup Taşocağında Gerçekleştirilen Patlatmalı Madencilik Faaliyetlerinin Jeolojik, Hidrojeolojik ve Madencilik Açısından Değerlendirilmesi, İstanbul Üniversitesi Çevre ve Yerbilimleri Uygulama ve Araştırma Merkezi, İstanbul, 2011.

Plaster Stemming Application at a Basalt Quarry: a Case Study
Bir Bazalt Ocağında Alçı Sıkılama Uygulaması

H. Cevizci, H. Yavuz
Suleyman Demirel University, Mining Engineering Department, Isparta

Ş. Caran
Suleyman Demirel University Geology Engineering Department, Isparta

Y. Tosun
Şırnak University, Mining Engineering Department, Şırnak

ABSTRACT In this study, plaster stemming application at a basalt quarry was investigated. For comparison of two stemming method, test blasts were carried out in the same quarry bench. For unit volume rock, plaster stemming provided lower cost than drill cuttings stemming. Because, burden and spacing distances were increased at plaster stemming round. Although length of charge column was increased, the cost of unit volume rock was lower for plaster stemming round. Rock piles fragmentation of plaster stemming round and drill cuttings stemming round were similar.

Keywords: Plaster stemming, blasting, stemming, fragmentation, vibration

ÖZET Bu çalışmada, bir bazalt ocağında alçı sıkılama uygulaması incelenmiştir. İki sıkılama yönteminin karşılaştırılması için aynı basamakta test atımları yapılmıştır. Birim hacimdeki kayaç için, alçı sıkılama daha düşük maliyet sağlamıştır. Çünkü, alçı sıkılama atımında, dilim kalınlığı ve delikler arası mesafe artırılmıştır. Bunun yanında, sarj kolonu boyu artmasına rağmen, birim hacim kaya maliyeti, alçı sıkılama yönteminde daha düşük olmuştur. Her iki atımın parça boyut dağılımı birbirine yakın gerçekleşmiştir.

Anahtar Kelimeler: Alçı sıkılama, patlatma, sıkılama, parçalanma boyutu, titreşim

1 INTRODUCTION

The stemming of blast hole collars in surface mines with an inert material redirects blasting energy to the rock more efficiently, thus the energy is utilized more effectively in breaking rock. In this procedure, high efficiency of blockage is important since the blast gases should not be allowed to escape due to loose stemming material. More efficient stemming with better confinement therefore increases the generation of fines. In addition, better rock breakage can be obtained. On the other hand, scatter distance is increased; giving rise to a looser muck pile that can be more easily loaded and transported (Ozkahraman, 2006).

Drill cuttings are the most common stemming material used in open pits and quarries, since they are most readily available at blast sites and are cheap. However, dry drill cuttings eject very easily from blast holes without offering much resistance to the explosion of blast energy is wasted and lost to the atmosphere (Cevizci, 2013).

Apart from the work of Cevizci (2012), there is no previous work found in the literature citing the usage of this material. Blasting tests were carried out in quarries using both the suggested new stemming method and classical stemming material, and

performance measurements carried out by image analysis of fragmented rock piles.

The new method employs a plaster prepared as a thick paste, which hardens in less than 25–30 minutes after application. The hardened plaster creates a very strong plug, therefore the stemming column length can be reduced and the explosive column length increased. This increased explosive column results in better rock breakage than similar holes stemmed with dry drill cuttings. Also, this increased utilization of hole length reduces specific drilling costs due to increased burden and spacing distances. Blast hole drilling constitutes a major cost in blasting operations. Another advantage of the new method is better fragmentation, with more induced cracking in the rock mass.

In one series of blast tests, blasting costs per unit volume of rock were reduced to 16 % by increasing burden and spacing distances (Cevizci 2012). Also, better fragmentation was obtained by using the plaster stemming method. Blast trials showed that plaster stemming produced finer material. In the same blast tests, +30 cm size fragments reduced to 5.4 % of the total, compared to 37.7 % in the conventional method of drill cuttings stemming. With this method of stemming, vibration and air shock values increased slightly due to more blast energy being available for rock breakage, but these increased values were small and under the permitted limit for blast damage criteria (Cevizci 2012)

2 METHOD

The study was carried out at Asagi Caglayan basalt quarry of Bazalt Company. The quarry is located at south-west of Eskisehir city. Both fast-setting moulding plaster and drill cuttings were used as stemming material at different lengths in similar blast holes on the same quarry bench. A thick milky moulding plaster was prepared by mixing ten units of plaster powder and seven units of water in a barrel, and charged into the blast holes as shown in Figure 1. This wet paste hardens in 25–30 minutes. The design of the stemming, using the tests at Asagi Caglayan basalt quarry is shown in Figure 2.

Figure 1. Application of plaster paste to hole collar

Wet plaster should not be placed in contact with ANFO, which is water-sensitive, thus 25 cm of drill cuttings were placed between the explosive and the plaster paste. Plaster column length was 40 cm. The top 45 cm of the drill hole should not be filled with plaster, since this section of the hole collar is deformed and cracked during drilling.

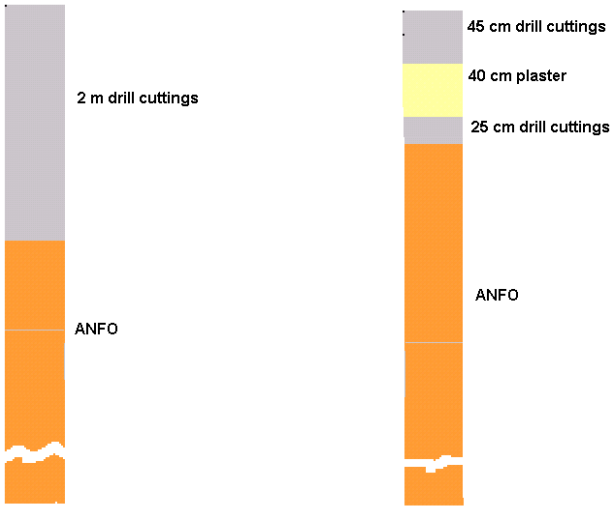

(a)Drill cuttings St.(b) Stemming with plaster

Figure 2. Blast hole stemming at Asagi Caglayan Basalt quarry

No benefit is expected from filling this section with plaster, and therefore it was filled with dry drill cuttings after the plaster had hardened instead of leaving it empty. This had the advantage of protecting the hole from loose stones dropping in.

3 BLAST TRIALS AND RESULTS AT ASAGI CAGLAYAN BASALT QUARRY

Two blast rounds fifteen meters apart were carried out with the plaster stemming and with the classic conventional drill cuttings stemming, each consisting of one row of six holes. First round was carried out by using plaster stemming. Second round was carried out by drill cuttings stemming. Both two rounds all 89 mm diameter holes were drilled with Gemsa drillers. Compared to blasting with drill cuttings stemming, burden and spacing distances were approximately 15 % farther at plaster stemming method (Table 1). Nobelex TG dynamites were used as primer at the bottom of holes. Only one primer initiated with Nonel cap in each hole which was considered enough for detonation. The firing was started with detonation cord. At the surface 25 ms and at hole bottom 500 ms Nonel millisecond caps were used. Bench height was approximately 10 m.

Drill cutting stemming method is generally used globally in open pits and quarries. Therefore, the stemming blast holes with drill cutting procedure was a standard procedure and details of this procedure is not given in the paper instead the new and more efficient plaster stemming method is more emphasized. For comparison of two stemming procedure, test blasts were carried out in the same location. Therefore, the rock structure and strength were similar. In both rounds ANFO, with one primer containing of 500 g dynamite was used. A quick hardening moulding plaster was used for plaster stemming.

3.1 The Evaluation Of Blast Trials

The blasting results of two stemming methods were compared. Muck pile fragmentation was evaluated using Split Desktop image-analysis software and verified standard ‘‘compare photo’’ method. The rock piles from the blasting tests at Asagi Caglayan Basalt quarry are shown in Figure 3 and Figure 4. The cumulative percentage of retained size at the Asagi Caglayan Basalt quarry blasting tests is given in Table 2.

Figure 3. Rock pile from blast round with drill cuttings stemming at Asagi Caglayan Basalt quarry

The first round was carried out using drill cuttings stemming with six holes. The length of the stemming was 2 m. The second round was carried out by plaster stemming with six holes. The length of the stemming was 1.1 m. Each blast hole was filled with 46.2 kg ANFO initiated with one primer with 0.5 kg in weight in the case of the drill cuttings stemming method. For the plaster stemming method, the quantity of ANFO was 51 kg per blast hole. The total length of ANFO column in the plaster stemming method was 90 cm greater than for the conventional method of drill cuttings stemming.

Table 1. Summary of properties of materials at blast sites, blast patterns and measurements of blast tests

Blast Tests	Dip direction/ angle of dip /angle of blast direction relative to dip direction of discontinuity	Block size index (cm)	RQD (%)	Stem. Leng. (m)	Bench Height (m)	Aver. Burd. (m)	Aver. Spac. (m)	+ 70 cm Size Fraction (%)	Delay (surface/ Bott.) (ms)	Spec. charge (kg/ m^3)	Specific drilling (m/m^3)
Aşağı Çağlayan (drill cut. stem.)	30/65/0	44	60	2	10	2	2.1	55	25/ 500	1.14	0.29
Aşağı Çağlayan (Plaster stem.)	30/65/0	44	60	1,1	10	2.35	2.5	50	25/ 500	0.95	0.22

Figure 4. Rock pile from blast round with plaster stemming at Asagi Caglayan Basalt quarry

Table 2. Comparison of cumulative percentage of retained size (oversize) from blast trials with plaster stemming and drill cuttings stemming

Fragment size (cm)	Asagi Caglayan Basalt quarry	
	Drill cuttings stemming (%)	Plaster stemming (%)
200	11.0	3.4
150	21.4	11.0
100	39.5	30.1
70	55.2	49.5
50	67.7	65.4
40	74.4	73.8
30	81.4	82.1
20	88.3	89.8
15	91.7	93.3
10	94.9	96.3
5	97.8	98.7

The blasted area was 29.2 m^2 for the plaster stemming trial, and blasted volume was 292 m^3 in situ. The specific charge was found to be 0.95 kg/m^3 and the specific drilling was 0.22 m/m^3. The blasted area was 22.1 m^2 for the drill cuttings stemming blast trial and yielding the blasted volume was 221 m^3 in situ. The specific charge was 1.14 kg/m^3 and the specific drilling was 0.29 m/m^3.

The total length of holes for the plaster stemming trial at Asagi Caglayan Basalt quarry was 20.8 m less than for the drill cuttings stemming round. This resulted in 24 % less drilling per unit volume rock. The cost saving for drilling calculated was $208 (20.8mx10$/m). At this site, specific drilling and specific charge decreased because a larger burden and spacing were applied with the plaster stemming method. In order to fragment the same volume of rock as for the plaster stemming round, an additional hole length of 20.8 m should be drilled for the drill cuttings stemming round. The profit per unit volume was $0.94 and total profit by using plaster stemming was $ 277.4 (Table 3).Therefore, the plaster stemming trial was found to be more economic, as well as giving similar fragmentation.

4 ENVIRONMENTAL EFFECTS AT ASAGI CAGLAYAN BASALT QUARRY

With this method of stemming, vibration and air shock values increased slightly due to more blast energy being available for rock breakage, but these increased values were small and under the permitted limit for blast damage criteria (Cevizci, 2012).

Because of too close measuring distance (22 m), all values were over the permitted level (Figure 5 and 6). But if measuring distance is enough, there will be no problem (Cevizci, 2012).

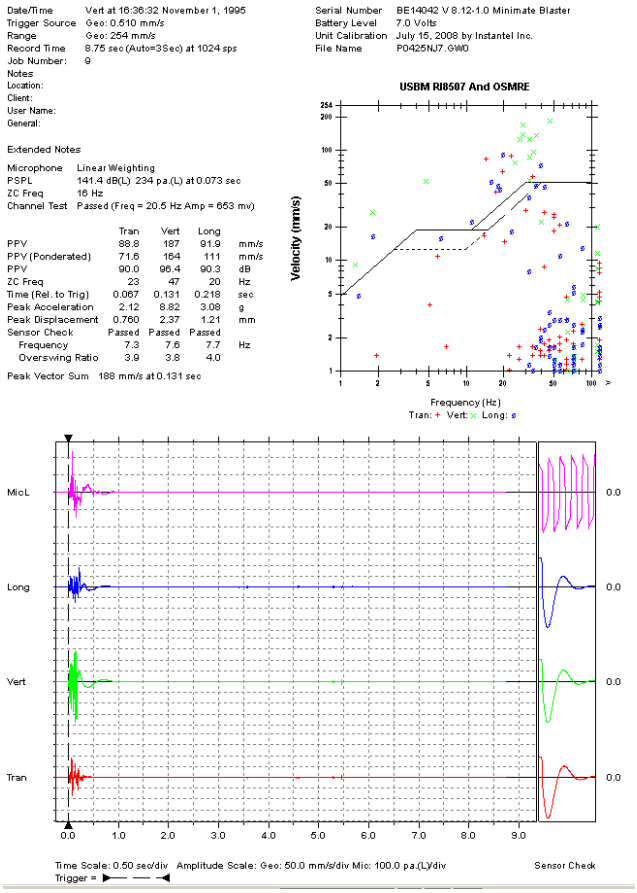

Figure 5. Measured vibration and noise levels in the dill cuttings stemming test

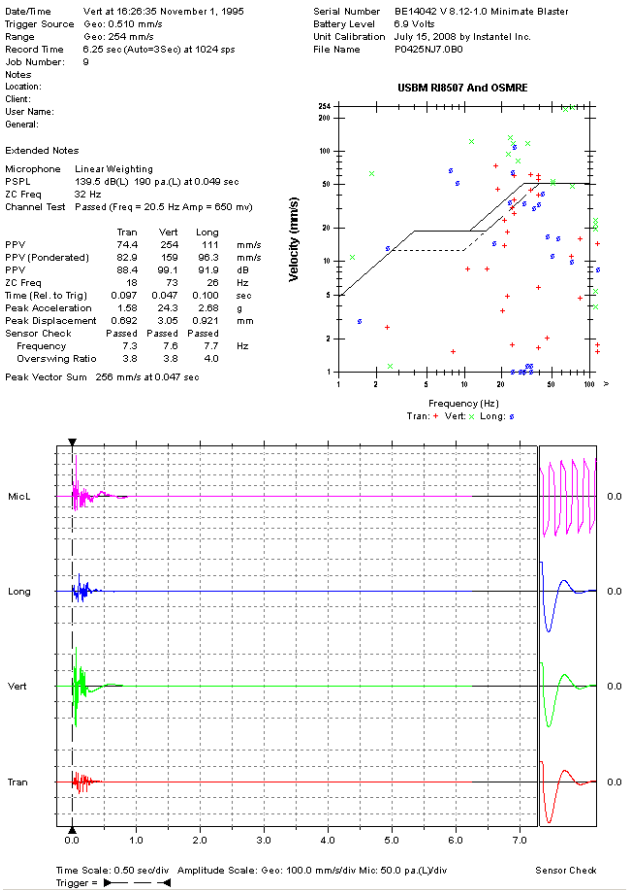

Figure 6. Measured vibration and noise levels in the plaster stemming test

Table 3. Comparison of blasting cost of plaster stemming versus drill cuttings stemming

Cost item	Asagi Caglayan Bas. quarry	
	Plaster stemming ($)	Drill cuttings stemming ($)
ANFO	302.9	274.8
Nonel caps	32	32
Initiating el. cap	0.5	0.5
Dynamite	51	51
Plaster and labor	20	-
Drilling cost	648	648
Total Cost	1054.44	1006.3
Fragmented rock(m^3)	292	221
Unit cost ($/$m^3$)	3.61	4.55
Specificc.(kg/m^3)	0.95	1.14
Specificdrill.(m/m^3)	0.22	0.29

4 CONCLUSION

In the method presented in this study, the inefficiency of the drill cuttings method of stemming is overcome by using plaster stemming. With the old method of stemming, loosely placed drill cuttings do not effectively confine the high-pressure stress produced by blasting. The study clearly shows how gases escaping from the drill hole, without efficient confinement, waste blasting energy. With the plaster stemming method, the pressure of the explosive is used successfully due to the more efficient confinement of the blast because better fragmentation was obtained.

Stemming heights were 0.9 m greater in the old drill cuttings stemming method than with the plaster stemming method. These long stemming columns caused problems in blasting, since the upper collar region was not broken properly, creating large boulders (Cevizci & Ozkahraman, 2012). This region, called the hard cap rock region, is not effectively broken with the classic drill cuttings stemming method. Generally, as the stemming column increases in length, more boulders are produced, which are dangerous and costly to move.

Additionally, the new method offers a more profitable solution. The cost of drilling for one meter of hole length is almost $10.8.

With plaster stemming, more of the hole length is better utilized by increasing the loaded length of the hole, resulting in better breakage at the hole collar. The increased length of loading in the hard cap rock region improves the cap rock breakage, thus reducing the creation of oversized boulders and increasing both efficiency and profit. It was observed that a plaster stemming column 0.40 m in length provided a more robust sealing than 2 m of drill cuttings used in the classical method.

ACKNOWLEDGEMENT

Author thank to Saddam Sir and Bazalt Company for his encouragement and help.

REFERENCES

Cevizci, H. *A Newly Developed Plaster Stemming Method For Blasting*. The J. of The South African Inst. of Min. and Metall., December. p. 1071- 1078, 2012.

Cevizci, H., Özkahraman, H.T. *The Effect Of Blast Hole Stemming Length To Rockpile Fragmentation At Limestone Quarries.* International Journal of Rock Mechanics and Mining Sciences, v. 53, p. 32-35, 2012.

Cevizci,H. *A New Stemming Application For Blasting: A Case Study*, Rem: Rev. Esc. Minas vol.66 no.4 pp.513-519 Ouro Preto Oct./Dec. 2013

OZKAHRAMAN, H.T. *Fragmentation Assessment And Design Of Blast Pattern At Goltas Limestone Quarry*, Turkey. International Journal of Rock Mechanics& Mining Sciences 43, p.628-633. 2006.

Analysis of Impacts of Ground Condition on Performance of a Hard Rock TBM in Alborz Service Tunnel Project

M. Hedayatzadeh
Mining Engineering Department, University of Politecnico Di Torino, ITALY

C. Doğruöz
Mining Engineering Department, Dumlupınar University, Kütahya, TURKEY

J. Rostami
Department of Energy and Mineral Engineering, the Pennsylvania State University, USA

J. K. Hamidi
Mining Engineering Department, Tarbiat Modares University, IRAN

ABSTRACT Predicting rate of penetration (ROP) of tunnel boring machine (TBM) ground conditions has been a crucial issue in the mechanized tunneling. TBM penetration rate and machine performance in a given project is a function of various rock mass properties such as RMR or GSI rock mass classification, orientation of joints or plane of weakness relative to tunnel axis, intact rock properties including rock strength, as well as machine specification including net thrust or cutterload. Influence of these parameters on machine performance was investigated along the Alborz service tunnel constructed by an open or gripper type TBM. Statistical analysis was performed on the data collected from the site to seek relationship between above noted parameters and the penetration rate (PR) of TBM. The results showed that each of the three different parameters has strongly affected the penetration rate of TBM. Multi variable regression analysis was performed to examine the combined effects of these parameters on the observed penetration rate of TBM. A site specific empirical formula is introduced to predict TBM rate of penetration based on the rock, rock mass, and machine operating parameters with reasonably good coefficient of correlation.

Keywords: TBM penetration rate, rate of penetration, rock mass properties, TBM operational parameters

1 INTRODUCTION

Over the years, a number of rock mass classification systems have been introduced in mining and civil engineering for different purposes including rock mass characterization, stability analysis, and support design. In fact, when Terzaghi (1946) introduced his rock load idea, followed by Lauffer's (1958) stand-up time concept and Deere's (1963) RQD index, these empirical design approaches were directed towards the selection of rock support system for conventional tunnel construction by drill and blast. Even the subsequent "modern" rock mass classifications, proposed in the 1970s, by Wickham at al. (1972), Bieniawski (1973) and Barton et al. (1974) were predominantly directed to drill and blast tunnels and not based on TBM bored tunnels. These models were developed based on special weighting system for each rating factor for use in ground support design and not geared towards measuring or quantifying the influence of rock mass features on TBM performance. This is perhaps the main reason for suggested modifications by the proposers of the two main rock mass classification systems, namely Q and RMR in recent years when introducing Q_{TBM} and RME (Barton, 2000; Bieniawski et. al.,

2006) to overcome shortcoming of these systems in predicting TBM field performance in various rock mass conditions.

Due to the simplicity and worldwide acceptance of the classification systems in general engineering practices, they have been long utilized in TBM performance prediction. However, as was illustrated by Khademi Hamidi et al. (2010), use of such rating based classification systems in their present scheme has many practical limitations. There has also been some attempts to modify the RMR classification system for use in performance prediction of hard rock TBM. This study will focus on modification and use of GSI classification system (Hoek and Brown, 1997) in predicting TBM penetration rate.

2 PROJECT DESCRIPTION AND GEOLOGY OF THE STUDY AREA

Alborz service tunnel is the longest tunnel (6.5 km) along Tehran-Shomal Freeway, situated in the high elevation portions of Alborz Mountain Range in Iran, connecting the capital city of Tehran to the Caspian Sea in the North. This service tunnel with diameter of 5.20 m was excavated by an open gripper TBM in advance of two main tunnel tubes to be excavated by conventional methods. The purpose of the service tunnel is site investigation, drainage of the rock mass, providing access for main tunnel excavations and for service, ventilation and drainage during operation of the complete tunnel system which will be used as road tunnel. Site investigation for the service tunnel included geological surface mapping, geophysical investigation along the alignment from the surface and some index laboratory tests on rock samples. The results of geotechnical site investigations show that the main lithological units through in which the tunnel will be driven consist of sandstone, tuff, gypsum, shale, and limestone layers (Figure. 1).

3 FACTORS INFLUENCING TBM RATE OF PENETRATION

Predicting rate of penetration of TBM (ROP) is one of the most important issues to estimate the advance rate of TBM. Performance of a TBM in a given project depends on many factors including rock material, rock mass parameters, machine characteristics, and operational parameters. Some of the factors influencing the TBM performance are discussed in following sections.

3.1 Intact Rock Characteristics

Some of the rock characteristics and properties that influence TBM performance are:

- Intact rock strength (e.g. uniaxial compressive strength “UCS”, Brazilian tensile strength “BTS”, Point load index “Is (50)”),
- Toughness (as represented by Punch penetration index, Fracture toughness index),
- Hardness and drillability (Siever’s J-value, Total & Taber hardness index, Schmidt hammer hardness),
- Brittleness (Swedish brittleness number “S20”, brittleness indices; $B_1 = \sigma_c / \sigma_t$ and $B_2 = [(\sigma_c - \sigma_t) / (\sigma_c + \sigma_t)]$), where σ_c and σ_t are uniaxial compressive and tensile strength of intact rock, respectively,
- Abrasiveness (often measured by Cerchar Abrasivity Index, Abrasion Value “AV”),
- Poisson ratio “ν”, modulus of Elasticity “E”, Internal friction angle “φ”, Porosity, Grain size etc.

3.2 Rock Mass Properties

Rock mass properties are defined as rock structure (or block size) and joint conditions. They could be listed as:

- GSI rock mass classification system indicates combined effect of jointing and weathering as rock mass properties,
- RMR rock mass rating classification system, based on intact rock strength, RQD, discontinuity spacing, joint

conditions ground water conditions, and adjustment for joint orientation.

- NGI or Q rock mass classification system, Q = (RQD/Jn).(Jr/Ja).(Jw/SRF) that is based on RQD, joint number, joint roughness, joint surface alteration, groundwater, and stress conditions.
- RMi classification system, RMi = σci * JP. where Jp is related to volumetric joint count (Jv) through the block volume (Vb), the mean block diameter (L), spacing of joints within a set (S) and the joint conditions rating (jC).

3.3 Ground Conditions

There are other rock mass properties that may not be accounted for in the rock mass classifications but can impact TBM performance such as:

- Joint orientation relative to the tunnel axis
- Stress condition (i.e. SRF that represents stress reduction factor in Q system), in-situ stress conditions (σv and σh),
- Ground water conditions that is included in some classifications and not the others

3.4 Machine Specification and Operational Parameters

The main machine specifications that are pertinent to rate of penetration can be summarized as follows:

- Disc cutter Geometry (e.g. diameter, tip width, angle of tip), maximum allowable velocity
- Cutters spacing and number of on the cutter head
- Applied cutter load
- Machine thrust (representing cutter load),
- Cutterhead rotational speed (RPM),
- Cutterhead torque,
- Cutterhead power,

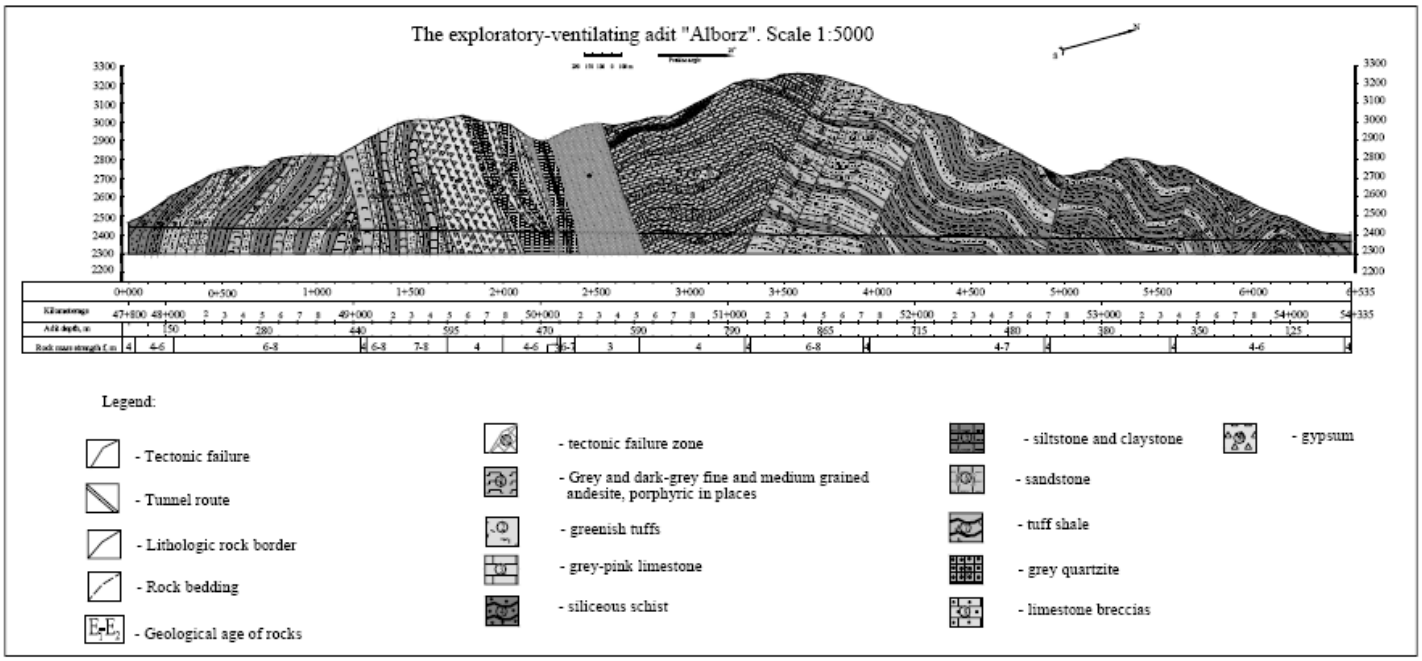

Figure 1. Longitudinal geological profile of the Alborz tunnel

One should keep in mind that developing a predictive model which can take into consideration all these parameters together has been always a problem. This is why over three decades after its inception, no single universal model has been proposed for TBM performance prediction. In this study, an attempt is made to consider some of these parameters for predicting TBM penetration rate. Among the rock material characteristics, UCS was selected for developing a model due to simplicity and commonality of the test for representing intact rock strength properties. Also, cutter load was selected as the machine parameter in the model.

As mentioned by Shahriar et al. (2010), rock mass properties can be extracted from

part of the Q, RMR, RMi and GSI classification systems. In this study GSI rock mass classification was selected to reflect the rock mass properties for TBM tunneling.

Three distinct parameters were taken into account for constructing the model as discussed before and they are:

- F_{GSI} = GSI, representing rock mass properties
- $F_f = (F_N.K_a.K_d)/UCS$, to reflect intact rock properties and machine specifications, and
- F_α = log ArcSin (Sin α_f * Sin ($\alpha_t - \alpha_s$)), joint orientation.

F_{GSI} is the fabric index of GSI system. F_N is cutter load, K_a and K_d are the correction factors for cutter spacing and diameter in NTNU TBM prognosis model (Bruland, 1998), and α is the angle between tunnel axis with planes of discontinuities.

4 PROPOSED SITE SPECIFIC MODEL FOR PREDICTING TBM PERFORMANCE

In order to develop a model for predicting TBM performance 33 data sets were compiled from 34 tunnel sections along the 6.5 km of bored Alborz service tunnel. The database consists of 34 records including input parameters of the GSI classification system, uniaxial compressive strength of rock material (UCS), the angle between tunnel axis and the joint sets (alpha), the TBM thrust and the measured TBM rate of penetration (ROP). In this study, the modified thrust per cutter normalized by UCS was used to reflect intact rock strength and cutter load. Descriptive statistical distribution of variables in the database and input parameters for development of the model are summarized in Table 1.

Table 1. Descriptive statistics of input parameters in the TBM field performance database

Variables	N	Min.	Max.	Mean	Variance
GSI	33	36	55	46.5	22.5
$(F_N.K_a.K_d)/UCS$ (Ton/MPa)	33	2.02	5.95	2.81	0.754
F_{alpha}(degree)	33	8.00	83.0	39.41	39.381
ROP (m/h)	33	2.85	5.30	3.93	0.535

The proposed TBM performance prediction model has been developed by performing multiple linear regression analysis on the data sets from Alborz Service tunnel project. Relationship between independent variables and actual measured ROP are illustrated in Figures 2 to 4.

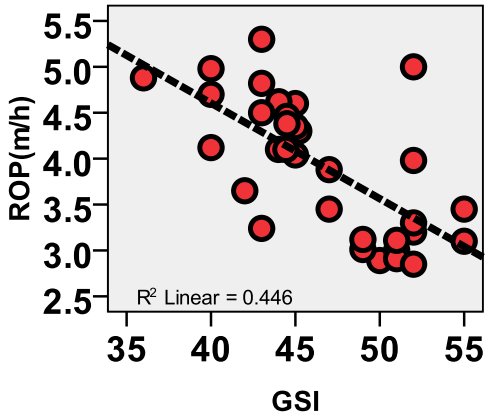

Figure 2. Relation between measured ROP and GSI

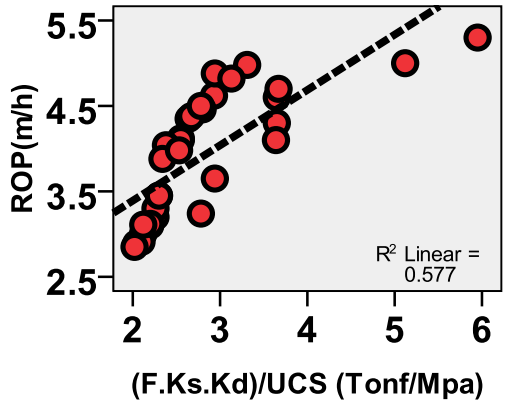

Figure 3. Relation between measurd ROP and F_{fmod}

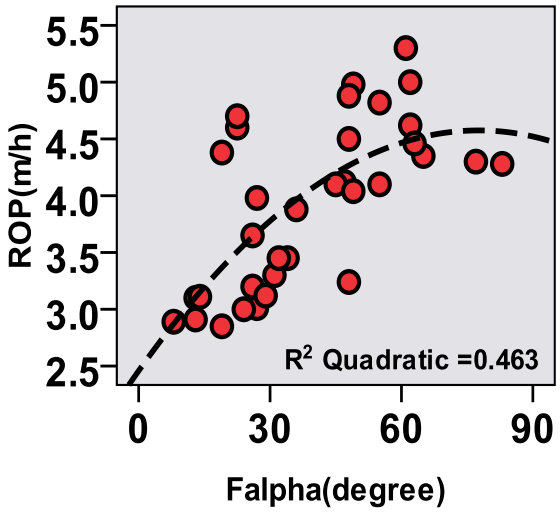

Figure 4. Relation between measured ROP and F_α

The figures also contain the correlation factors (R^2) which denote the degree of correlation between the two parameters. For the given data set, Fig.3 (relating ROP with UCS and cutterload) shows the highest R^2 value, (0.58). The R^2 value decreases for relationship between ROP and F_{alpha} (R^2 = 0.46) or GSI (R^2 = 0.45). The results indicate that the modified thrust per cutter normalized by the uniaxial compressive strength of rock material and F_{alpha} is the most significant variable controlling the rate of penetration of TBM.

As shown in the Fig. 2, increasing GSI will result in decreased ROP, since decreased the number of joint sets leads to stronger rock mass and more difficult boring process, thus decreasing penetration rate. Similarly, the increase in GSI due to better joint condition leads to lower boreability. Uniaxial compressive strength of intact rock (UCS) has a crucial influence on penetration rate in such a way that penetration rate will decrease with increased UCS as expected. The effect of TBM thrust on ROP has been also studied by many researchers. In this study, cutter thrust, modified by two parameters including K_a and K_d representing machine specification, is normalized by UCS and used in the statistical analysis. The normalized value of UCS by cutter load is expected to show improved result due to incorporation of the effect of machine thrust in the model using this composite index. As illustrated in Fig. 3, with the increase in F_f ($F.K_d.K_a/UCS$) that could be by higher cutter load or lower rock strength, penetration rate will increase. The angle α, represent-ting orientation of discontinuities relative to the axis of the tunnel, have been measured in the field by measuring strike and dip of the joints mapped at the face. The α in degrees, can be calculated using the equation suggested by Bruland (1998):

$$\alpha = \text{ArcSin}\,(\text{Sin}\,\alpha_f * \text{Sin}\,(\alpha_t - \alpha_s)) \qquad (1)$$

Where, α_f and α_s are dip and strike of planes of discontinuities in rock mass, and α_t is the direction of the tunnel axis in degrees.

The relationship between ROP and α angle illustrated in Fig. 4, is consistent with findings of the field studies by Bruland (1998), Yagiz (2008) and Khademi Hamidi at al. (2010).

In order to develop a linear equation, all the parameters for setting up the model including objective and independent variables should have a reasonable normal distribution. For checking the validity of the proposed model by statistical analysis, is necessary to check for any type of co-linearity between the parameters used in the regression model. Co-linearity occurs when two or more independent variables are highly correlated. The *variance inflation factor* (VIF) analysis performed on independent variables shows that there is no inter-correlation between independent parameters. Hence, the TBM performance model based on three independent variables of GSI, F_f, and Fα with good correlation coefficient with ROP can be considered valid for prediction of performance of the given machine of the same diameter in similar geologies.

A model has been developed by using standard statistical analysis software package (SPSS). The model has P factor of less than 0.05 which is an indicator of validity of the model based on the statistical analysis of input data. This model with high correlation coefficient is recommended as the main model for performance estimation of open type TBM of the same size and

general specification as Alborz tunnel TBM. The proposed multiple linear regression model is as follow:

$$ROP = 4.304 - 0.057*GSI – 0.435*F.k_a.k_d/UCS + 0.693*\log \alpha \quad (2)$$

A comparison between the measured and estimated ROP of the model is illustrated in Fig. 5. As seen in the Fig. 5, the predicted data shows strong correlation with the measured values of TBM ROP in database with a good correlation coefficient of nearly 79%.

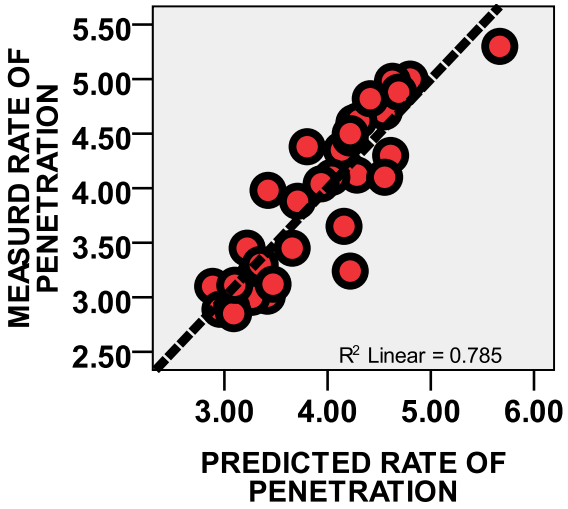

Figure 5. Comparison between measured and predicted ROP in Alborz Service Tunnel

5 CONCLUSIONS

A site specific model for estimation of rate of penetration of hard rock TBM is proposed by using multiple regression analysis on field data collected from 6.5 km of Alborz service tunnel. The model is based on use of GSI for rock mass classification, cutter load, UCS, and the angle between the dominant joints and tunnel axis (alpha). Multi-variable linear regression was employed to develop a correlation between the measured ROP and three input parameters with correlation coefficient of about $R^2 = 0.79$. The proposed model showed meaningful correlations with the observed ROP. The statistical significance and validity of the obtained models was checked by using standard statistical tests, which proved that the obtained relationship is reliable for the given database of TBM field performance and can be considered for estimation of ROP for a machine with similar specifications in similar geological units.

REFERENCES

Terzaghi, K., 1946. Rock defects and loads on tunnel supports. In Rock tunneling with steel supports, Youngstown, Ohio, 15-99.

Lauffer, H., 1958. Classification for tunnel construction (in German). Geologie und Bauwesen, 24(1),46-51.

Deere, D.U., 1963. Technical description of rock cores for engineering purposes. Rock Mech. Eng. Geol., 1(1), 17-22.

Wickham, G.E., Tiedemann, H.R., Skinner, E.H., 1972. Support determination based on geologic predictions. In: Proc. RETC, AIME, New York, 43-64.

Bieniawski, Z.T.,1973. Engineering classification of jointed rock masses. Trans. S. Afr. Inst. Civil Engrs. 15, 335–344.

Barton, N., Lien, R., Lunde, J., 1974. Engineering classification of rock masses for the design of rock support. Rock Mech. 6, 189-236.

Barton, N., 2000. TBM tunnelling in jointed and faulted rock. Rotterdam: Balkema, Brookfield, p. 173.

Bieniawski, Z.T., Tamames, B.C., Fernandez, J.M.G., Hernandez, M.A., 2006. Rock Mass Excavability (RME) Indicator: new way to selecting the optimum tunnel construction method, ITA-AITES World Tunnel Congress & 32nd ITA General Assembly, Seoul.

Khademi Hamidi, J., Shahriar, K., Rezai, B., Rostami, J., 2010. Performance prediction of hard rock TBM using Rock Mass Rating (RMR) system. Tunnell. Undergr. Space Technol. 25(4), 333-45.

Hoek, E., Brown, E.T. 1997. Practical estimates of rock mass strength. Int J Rock Mech Min Sci 34(8):1165-86

Shahriar, K., Sargheini, J., Hedayatzadeh, M., Khademi Hamidi, J. 2010. *Performance prediction of hard rock TBM using rock mass classification*, Eurock 2010, Lausanne, Switzerland.

Bruland, A., 1998. Hard rock tunnel boring. PhD Thesis, Norwegian University of Science and Technology, Trondheim.

Yagiz, S., 2008. Utilizing rock mass properties for predicting TBM performance in hard rock condition. Tunnell. Undergr. Space Technol. 23(3), 326-39.

Availability Analysis of Drum Shearer Machine; a Case Study

S. H. Hoseinie, B. Ghodrati

Division of Operation & Maintenance Engineering, Lulea University of Technology, Lulea, Sweden

A. Hosseini

Tabas Parvadeh Coal Company, Iran Minerals Production & Supply Co., Tabas, Iran

ABSTRACT Drum shearer plays an important role in the face production in longwall coal mines. Therefore, monitoring of this machine can lead the whole extraction operation to high level of productivity and safety. Availability is one of the most important measures for evaluation of the mining machineries. High availability of equipment can be helpful in satisfying the desired production goals. In this article the availability of drum shearer in an Iranian coal mine has been studied. For this purpose, the failure and maintenance data for a period of two years have been used. After data sorting and analysis, the inherent availability, achieved and operational availability of this machine have been calculated. The results show that the studied shearer machine performs in high level of availability. Nevertheless, the logistics delay time and administrative delays with the share of 25% of whole downtimes are so important influencing factors which should be controlled and planned to minimize it.

Keywords: Drum shearer, availability analysis, longwall

NOTATIONS

A_a:	Achieved Availability
A_i:	Inherent Availability
A_o:	Operational Availability
MDT:	Maintenance delay time
MPMT:	Mean preventive maintenance time
MTBF:	Mean time between failures
MTBM:	Mean time between maintenance
MTR:	Mean time to restore
$\overline{M'}$:	Mean system downtime with delays
$\overline{M}$:	Mean system downtime
$m(t_d)$:	Cumulative average number of failures over the t_d
SDT:	Support delay time
TR:	Time to restore
t_d:	Design Life
T_{pm}:	Preventive maintenance interval

1 INTRODUCTION

Nowadays, all of the elements of modern, high production longwall systems are provided in an integrated manner for maximum productivity gains and lowest cost per ton.

A longwall production chain consists of several subsystems and machines which their operational conditions affect the total availability, and reliability performance of the production face. Due to continuance production system in longwall mines especially face-to-surface ore hauling system, availability of each machinery is very critical for system continuity and production.

Shearer is the most critical part of longwall production process. That's why high-performance longwall operations demand shearers that deliver the highest productivity, availability and reliability (Caterpillar, 2011).

High reliability and maintainability of the shearer lead operation to high availability. High availability itself ensures the maximum return on investment for longwall operation.

Reliability of the longwall systems have been studied by several researchers so far, nevertheless, few studies have been done on availability of these systems (Furuly et al., 2014, Hoseinie et al., 2014). In this article, operational and downtime hours of drum

shearer in an Iranian coal mine in have been analyzed and a comprehensive availability analysis has been done on this machine. It has been tried to answer the following questions:

1) What is the mean time between failures and mean time to restore of whole drum shearer machine
2) How much are the availability related parameters of shearer
3) How much are the inherent availability, achieved and operational availability of studied machine

2 AVAILABILITY ANALYSIS

2.1 Background and Definitions

Availability is the probability that a system or component is performing its required function at a given point/over a stated of time period when operated and maintained in a prescribed manner (Ebeling, 2009). In other words, availability is the ability of an item to be in a state to perform a required function under given conditions at a given instant of time or over a given time interval, assuming that the required external resources are provided (IEC, 1990, CEN, 2010).

Like reliability, availability is a probability. Consider a system (device) which can be in one of two states, namely 'up (on)' and 'down (off)'. By 'up' it is meant that the system is still functioning and by 'down' it is meant that that the system is not functioning. In the latter case the system is being repaired or replaced, depend on whether it is repairable or not (Barabady, 2005). Availability depends on the combined aspects of reliability, maintainability and maintenance supportability (IEC, 1990, CEN, 2010).

System reliability and availability analysis is a mature field and there is abundance of analysis techniques including methods such as reliability block diagrams, fault tree analysis, failure mode and effects analysis, Markov processes and Bayesian analysis (Høyland and Rausand, 1994, Närman et al., 2014). There are three common measures that widely are used in practice and can be found in both standards and books (Ebeling, 2009, Stenström, 2014); inherent availability, achieved and operational availability. The mathematical definitions and detailed components of these measures are presented in following.

2.2 Availability Measures

2.2.1 Inherent availability

Inherent availability is the steady state availability when considering only the corrective downtime of the system (Ebeling, 2009). It is defined as the expected level of availability for the performance of corrective maintenance only. Inherent availability is determined purely by the design of the equipment. It assumes that spare parts and manpower are 100 percent available with no delays. It excludes logistics time, waiting or administrative downtime, and preventive maintenance downtime. It includes corrective maintenance downtime. Inherent availability is generally derived from analysis of an engineering design. Inherent availability fulfills the need to distinguish expected performance between planned shutdowns (Katukoori, 2006). Inherent availability is expressed as Equation (1).

$$A_i = \underset{t\to\infty}{Lim} A(t) = \frac{MTBF}{MTBF + MTTR} \quad (1)$$

Inherent availability is based solely on the failure distribution and repair-time distribution. It can therefore be viewed as an equipment design parameter, and reliability-maintainability trade-off can be based on this interpretation (Ebeling, 1997).

2.2.2 Achieved availability

The probability that an item will operate satisfactorily at a given point in time when used under stated conditions in an ideal support environment (i.e., that personnel, tools, spares, etc. are instantaneously available) (Katukoori, 2006, Ebeling, 2009). Achieved availability is defined as the achieved level of availability for the

performance of corrective and preventive maintenance. It is determined by the hard design of the equipment and the facility. It excludes logistics time and waiting or administrative downtime. It includes active preventive and corrective maintenance downtime. Achieved availability also assumes that spare parts and manpower are 100% available with no delays.

This measure is very similar to inherent availability with the exception that preventive maintenance downtimes are also included. It can be computed by looking at the MTBM and $\overline{M}$ by using Equation (2).

$$A_a = \frac{MTBM}{MTBM + \overline{M}} \tag{2}$$

Where, MTBM and $\overline{M}$ are calculated by Equation (3) and (4) (Ebeling, 2009).

$$MTBM = \frac{t_d}{m(t_d) + t_d / T_{pm}} \tag{3}$$

$$\overline{M} = \frac{m(t_d)MTTR + (t_d / T_{pm})MPMT}{m(t_d) + t_d / T_{pm}} \tag{4}$$

2.2.3 Operational availability

Operational availability is a measure of the average availability over a period of time and it includes all experienced sources of downtime, such as administrative downtime, logistic downtime, etc. It is the probability that an item will operate satisfactorily at a given point in time when used in an actual or realistic operating and support environment (Ebeling, 2009). It includes logistics time, ready time, and waiting or administrative downtime, and both preventive and corrective maintenance downtime. Finally, the operational availability is the availability that the customer actually experiences and is expressed as Equation (5) (Ebeling, 2009).

$$A_o = \frac{MTBM}{MTBM + \overline{M}'} \tag{5}$$

Where, $\overline{M'}$ is determined by replacing the MTTR with MTR= MTTR + SDT + MDT as shown in Equation (6) (Ebeling, 2009).

$$\overline{M}' = \frac{m(t_d)(\mathrm{MTTR} + \mathrm{SDT} + \mathrm{MDT}) + (t_d / T_{pm})MPMT}{m(t_d) + t_d / T_{pm}} \tag{6}$$

Above definition includes all supply and maintenance delays as a part of the unscheduled downtime.

The calculation of A_o can vary somewhat depending on the definitions of uptime and downtime. The inclusion of certain ‘‘operational states’’ can be legitimately expressed as either uptime or downtime; and as long as the definition is clear there can be various ‘‘correct’’ interpretations (methodology).

3 CASE STUDY

The case study of this research was done in an Iranian coal mine. The annual production of the mine is 1.5 million ton raw coal and it is planned to be in operation for 30 years lifetime. The most suitable seam for mining has 1.8m thicknesses and is extracted by retreat longwall method using a double-drum shearer machine. The length of studied longwall face is 215m and panel length is 1200m.

3.1 Data collection and classification

In this paper, for availability analysis of the drum shearer, failure, maintenance, operation and workshop data from archived records along with direct observations collected from October 2007 to October 2009 was used.

According to available data, the first panel in studied mine has been extracted during the 960 working shifts. Each shift is seven hours and one hour is considered for shift changing and employees transfer (totally equal to 8 hours).

It total, 139 failures have been happened during the data collection period and

machine has done 2606 hours cutting operation. The histogram of TBFs and TRs of the recorded failures are presented in Figure 1 and Figure 2 respectively.

The Figure 1 shows that TBFs of drum shearer machine vary from few minutes to more than 100 hours. However, more than 90% of the failures have been happened in a period less than 50 hours.

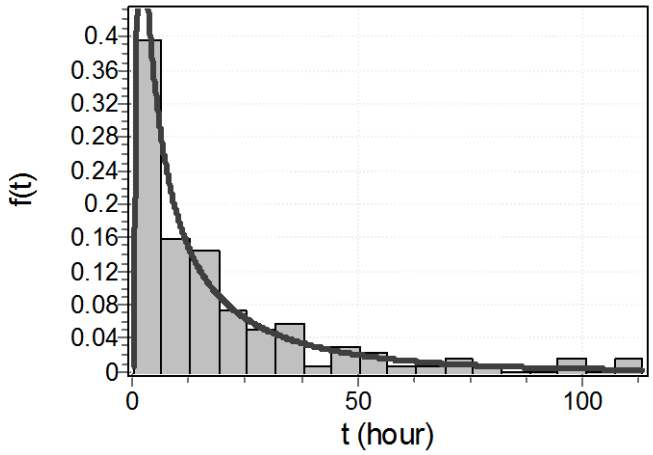

Figure 1. Probability density function of TBFs

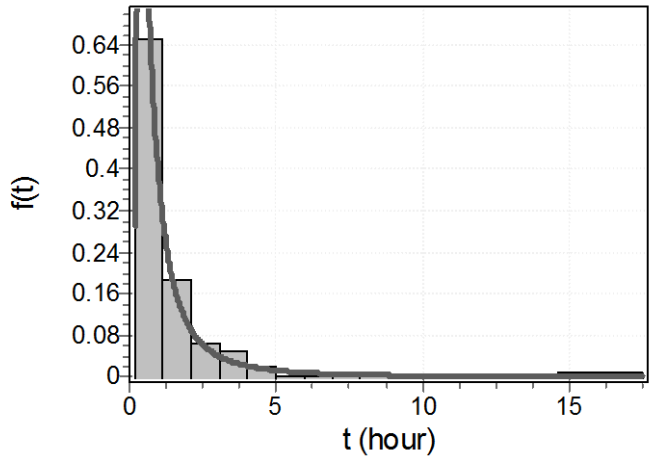

Figure 2. Probability density function of TRs

The Figure 2 shows that the drum shearer has had a wide range of time to restore. However, more than 65% of failures has been maintained in less than one hour.

The calculations show that MTR for studied drum shearer is 1.47 hour (88.5 minutes) which includes the maintenance operation, support and logistic, testing and re-running the machine.

3.2 Calculation of input parameters

Using the collected data, and considering the current preventive maintenance and service plan in mine, the input parameters for calculating the availability measures have been calculated and presented in Table 1.

Table 1. Calculated input parameters based on collected data

Parameter	Value
MTBF	18.42 hour
MTTR	1.1 hour (66 minute)
t_d	2606 hours
T_{pm}	80 hours
$m(t_d)$	139
MPMT	0.83 hours (50 minute)
SDT + MDT	0.37 hour (23 minute)

3.3 Calculation of Availability Measures

3.3.1 Inherent availability

As it was discussed before, the inherent availability is the simplest availability measure which is calculated by Equation (1). Regarding the available data in Table 1, inherent availability of studied drum shearer is 94.3%. It means that in ideal condition without any delay in maintenance support and logistics, machine will be available in 94.3% of its active lifetime.

3.3.2 Achieved availability

Regarding the Equation (2) to (4), for calculating the achieved availability, MTBM and $\overline{M}$ most be calculated. Using the presented parameters in Table 1, MTBM is equal to 13.95 hours and also $\overline{M}$ =1.05 hour. Therefore, achieved reliability for the current operation and maintenance plan in studied mine is equal to 93%.

3.3.3 Operational availability

As it was discussed, the operational availability is the measure that customer actually experiences and it directly affects the mine production rate. Therefore, its proper calculation is critical and very important. In this measure, MDT and SDT are included in calculations. Based on the field data, the detailed information on these

delay times was missed. However, the time to restore and its mean value were clearly available. Thus, the difference between the TR and TTR was assumed as a delay times in total (SDT+MDT) which is equal to 23 minutes in average. Thus, MTR (=MTTR+SDT+MDT) is equal to 1.47 hour.

Regarding the Equations (6) and the calculated input parameters, $\overline{M'}$ is equal to 1.35 hour. Therefore, using Equation (5), the operational availability is 91.2%.

3.1 Discussion

According to the achieved results from data analysis and availability modeling, the values of three availability measures are presented in Figure 3.

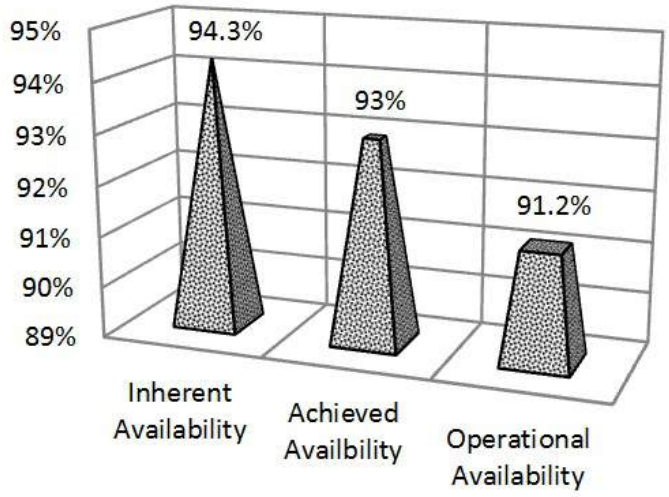

Figure 3. Calculated availability measures for studied shearer machine

As shown in Figure 3, inherent availability of studied drum shearer is the highest value among the three measures. The less value of achieved availability in comparison with the inherent one reveals that in this mine, preventive maintenance reduces the machine availability due to more stoppages. However, 1.3% is really negligible difference in availability, nevertheless, the positive effects of preventive maintenance in reliability of this machine is very impressive (Hoseinie et al, 2012).

The comparison between the achieved and operational availability shows that the maintenance and support delays are responsible for 2.8% in availability of the whole machine. 2.8% reduction in availability is not so much change in operation condition but the important point is that the 25% of TR is belongs to delays. It means that by improving the maintenance logistic is value of reduction is removable.

4 CONCLUSION

In this article, availability of drum shearer machine was analyzed using three common measures; inherent, achieved and operational availability. The results show that, TBFs and TR of this machine in very variable and changes from few minutes to several hours.

The calculations reveal that in total, the studied drum shearer performs in a very good level of availability. However, the logistics and support delays during the maintenance operation reduces the availability from 94.3% in inherent level to 91.2% in operational level, it is more or less acceptable. Because, in longwall mining in which the whole operation is located in underground, the operation logistics is very complicated and costly. In this view, machine and operation are in a very good condition.

As calculation show, the current preventive maintenance plan with intervals of 80 hours sounds good view point of machine availability. Because, it doesn't reduce the machine's availability in considerable level.

REFERENCES

Barabady, J., 2005. *Improvement of system availability using reliability and maintainability analysis*, Licentiate Thesis, Lulea University of Technology, Lulea, Sweden.

Blanchard, B.S., Fabrycky, W.J., (3rd ed.), 1998. *System Engineering and Analysis*, Prentice Hall, New Jersey.

Caterpillar, 2011. Longwall Shearers Catalog Booklet. (www.cat.com)

CEN, 2010. EN 13306: Maintenance terminology. Technical report, European Committee for Standardization (CEN).

Ebeling, C.E., (2nd ed.), 2009. *An Introduction to Reliability and Maintainability Engineering*, Waveland Press Inc., Illinois, USA, p. 550.

Furuly, S., Barabady, J., Barabadi, A., 2014. Availability analysis of the main conveyor in the Svea Coal Mine in Norway, *International Journal of Mining Science and Technology* Vol. 24 (2014), pp. 587–591.

Hoseinie, S. H., Ataei, M., Khalokakaie, R., Ghodrati, B., Kumar, U., 2012. Reliability analysis of drum shearer machine at mechanized longwall mines, *Journal of Quality in Maintenance Engineering.* Vol.18, No.1, pp. 98–119.

Hoseinie, S. H., Ghodrati, B., Kumar, U., 2014. Assessment of Reliability-Related Measures for Drum Shearer Machine, a Case Study, *Sixth International Symposium High Performance Mining (AIMS 2014)*, 11-12 June 2014, Aachen, Germany.

Høyland, A., Rausand, M., 1994. *System reliability theory: models and statistical methods*. John Wiley & Sons, New York, 636 p.

IEC, 1990, IEC 60050-191: International Electrotechnical Vocabulary: Chapter 191: Dependability and quality of service. Technical report, International Electrotechnical Commission (IEC).

Katukoori, V.K., 2006. Standardizing Availability Definition, Naval Architecture and Marine Engineering, University of New Orlean, USA, 22 p.

Närman, P., Franke, U., König, J., Buschle, M., Ekstedt M., 2014, Enterprise architecture availability analysis using fault trees and stakeholder interviews, *Enterprise Information Systems*, Vol. 8, No. 1, pp. 1-25.

Pryor, G.A., 2008. Methodology for Estimation of Operational Availability as Applied to Military Systems, International Test and Evaluation Association (ITEA) Journal Vo. 29 (2008), pp. 420–428.

Stenström, C., 2014. *Operation and Maintenance Performance of Rail Infrastructure; Model and Methods*, PhD Thesis, Lulea University of Technology, Lulea, Sweden.

Determination of Optimum Drum Shearer for Tabas Mine Using Decision Making Process

E. Bakhtavar
Urmia University of Technology, Urmia, Iran

ABSTRACT Mechanization and the proper decision in relation to choice the most appropriate shearer machine for longwall mines lead to maximum productivity with minimum energy consumption. In this paper, a mechanized shearer loader system has been selected among four alternatives for Tabas Parvadeh1 coal mine by integrating the results from an analytical procedure and a multi-criteria decision making system. During the decision making process, the analytical procedure was initially used to find effective criteria. Then most important criteria were considered on the basis of the mechanical properties of coal seam and the important characteristics of shearer loader, especially from technical viewpoints. Finally, a two drums shearer system was selected to be applicable in Tabas Parvadeh1 mine. The results of using the MCDM system are completely in accordance with the results of the analytical procedure.

Keywords: Tabas Mine, drum shearer, VICOR, decision making

1 INTRODUCTION

Generally, mechanized coal extraction can provides better production, productivity and safety (Singh, 1999). Performance of the mechanical machines (such as road headers, continuous miners, and shearers) is one of the most important factors affecting the production rates in coal mining engineering projects.

In order to obtain the maximum possible productivity and minimum energy consumption in coaling selection of the most suitable shearer loader is of at most important together with the most fitness picks and a good arrangement on cutter head. Selection of the most appropriate shearer directly depends on physical and mechanical characteristics of a coal seam which directly control mechanical characteristics of shearer machine.

There is a study of detailed investigation for the Iranian coal seams (Shahriar et al., 2009). The study represents some simple field and laboratory tests carried out to visualize the nature and variation extent of mechanical properties across C1 coal seam in Parvade1 mine.

.

A research in form of an analytical procedure was presented by Bakhtavar and Shahriar (2013) in order to select a shearer loader machine to be most appropriate for coal extraction in Tabas Parvadeh1 longwall mine. In this research, the mechanical properties of C1 coal seam were focused during designing and selecting the components of a shearer such as pick, drum, and vanes. The laboratory and in-situ tests were also reviewed and their suitability to aid machine design and selection was discussed.

In the present study, with considering the results obtained from the analytical procedure by Bakhtavar and Shahriar (2013) and using VIKOR decision making system the most appropriate shearer loader machine has been selected for Parvadeh1 longwall mine located in east of Iran. In this case, the most crucial mechanical properties of C1 coal seam together with the critical physical characteristics of shearer loader system have been focused during the decision process

2 TABAS PARVADEH1 COAL REGION

The main coal horizons in Tabas Parvadeh1 region (located in east of Iran as shown in Figure 1) are seams B1, B2, and C1 that occurred within 50 m of strata. Other seams C2, D and possibly E will affect mining principally because of their methane content. Parvadeh1 coalfield is a basin between two major North-South trending fault systems, the Kalmard Fault and the Hidden Fault to the West and the Nayband Fault to the East. The covered rocks are mostly mudstone with prominent coarsening up siltstone and sandstone sequences. The seam thickness of C1 varies from approximately 2.2 m in the northeast to 1.5 m in the South West.

Figure 1. Location of Tabas Parvadeh1 coal field

There is a very general indication of an increase in sulphur content from the North to the South in this seam. In the initial mining area sulphur content varies from 1.75 to 2.0% (IRITEC, 2003).

According to Russian classification of coal seams, the C1 coal seam of Tabas Parvadeh1 is taken in the class of Low Volatile Coking Coal or Low Volatile Bituminous Coal, and due to National Coal Board (NCB) classification, its class is 301, additionally based on American Society for Testing Materials (ASTM) classification, it is taken place in class1 of Bituminous Coals (Shahriar et al., 2009).

The detailed engineering of the mine infrastructure ensures that it is adequate so that the longwall can operate based upon the information provided by the supplier in the tender and appended to the order (IRITEC, 2003).

3 MOST APPROPRIATE SHEARER

3.1 A Summary on the Results of the Analytical Procedure

The results obtained from the analytical procedure adopted by Bakhtavar and Shahriar (2013) have been used together with the results of a MCDM system in order to find the most appropriate shearer loader for mechanization of Tabas Parvadeh1 coal faces.

The mechanical characteristics of C1 coal seam in Tabas Parvadeh1 mine which resulted from a number of in-situ and

laboratory tests are summarized in Table 1 (Bakhtavar and Shahriar, 2013). As given in Table 1, the compressive strength of C1 coal seam is low and also there are three joint sets in Tabas Parvadeh1 longwall mine. The data given in Table 1 are essential for the suitable judgments by experts during the decision process, especially using MCDM systems.

Four alternatives of shearers were considered for selection during the analytical procedure (research by Bakhtavar and Shahriar (2013)) as given in Table 2. Besides, the most important technical characteristics of the shearer alternatives resulted during the analytical procedure are summarized in Table 2. According to the results obtained during the analytical procedure, especially with emphasis on the required shearer cutting power of 886.4 KW (nearly 93%), among the four shearer alternatives, "double ended ranging drum shearer (DERDS)" model EL600 is most appropriate for selection.

Table 1. Mechanical characteristics of C1 coal seam (Bakhtavar and Shahriar, 2013)

Parameter	Meaning (Unit)	Value
σ_c	Uniaxial compressive strength (MPa)	6.66
σ_t	Tensile strength (MPa)	0.39
δ	Shear strength (MPa)	0.53

Table 2. Shearer characteristics made by DBT Company (Bakhtavar and Shahriar, 2013)

Electra Range	EL3000	EL2000	EL1000	EL600
Seam range (m)	2.2-6.0	1.5-3.5	1.8-5.0	1-3.5
Typical machine length (m)	14.6	12.2	11.8	11.9
Typical installed power (KW)	1940	1940	1380	869
Available cutting power (KW)	2×850; 2×650	2×500	2×600	2×450; 2×375; 2×285
Cutting drum diameter (m)	1.9-3.0	1.2-2.2	1.4-2.5	1.1-2.2
Machine weight (tons)	100	55	75	50

3.2 VIKOR for Decision Making on the Most Appropriate Shearer

VIKOR (Vlse Kriterijumska Optimizacija I Kompromisno Resenje in Serbian) was introduced as a compromise ranking method which categorized in Multi-Criteria Decision Making (MCDM) system. VIKOR system focuses on ranking and selecting from a set of alternatives, and it also can find compromise solutions for a problem with conflicting criteria (Opricovic and Tzeng, 2004 and 2007). This system is capable to optimize aggregation of different criteria scores of various alternatives simultaneously.

In this research, decision is made for selection of the most appropriate shearer among the four alternatives considered in the analytical research. In this case, the main characteristics of shearer loaders those influenced by the coal seam physical and mechanical properties are emphasized. They are assigned as technical criteria. It is notable that the authors assumed that the capital investments of the shearers are not critical and the most important limitations are technical considerations in Tabas Parvadeh1 mine. It means that no economical criteria are considered during the selection process. The technical criteria which considered for the decision process are as given in Table 2.

All criteria scores and weights during the shearer selection process can majorly assign from the ideas of related experts using questionnaires. Significance of the criteria for the shearer decision process was specified according to the judgments of a number of experts by the means of a scoring range 0-100.

In first step, decision matrix should be organized as the following:

$$A=\begin{bmatrix} a_{11} & a_{12} & \cdots & a_{1J} \\ a_{21} & a_{22} & \cdots & a_{2J} \\ \vdots & \vdots & \ddots & \vdots \\ a_{I1} & a_{I2} & \cdots & a_{IJ} \end{bmatrix} \quad (1)$$

$$N=\begin{bmatrix} n_{11} & n_{12} & \cdots & n_{1J} \\ n_{21} & n_{22} & \cdots & n_{2J} \\ \vdots & \vdots & \ddots & \vdots \\ n_{I1} & n_{I2} & \cdots & n_{IJ} \end{bmatrix} \quad (2)$$

where,

A: Decision matrix

I: Number of alternatives *i*

J: Number of criteria *j*

a_{ij}: Performance score of alternative *i* with respect to criterion *j*

The decision matrix of the shearer selection problem according is given in Table 3. The matrix includes the weights and performance scores based on Equation 1.

Then the scores are normalized using Equations 2 to 4.

$$n_{ij}=\frac{a_{ij}}{\sqrt{\sum_{i=1}^{I}(a_{ij})^2}};\ j=(1,2,...,J) \quad (3)$$

$$n_{ij}=\frac{\frac{1}{a_{ij}}}{\sqrt{\sum_{i=1}^{I}(\frac{1}{a_{ij}})^2}};\ j=(1,2,...,J) \quad (4)$$

Table 3. Decision matrix during the shearer selection

Criteria	Shearer alternatives				Mean scores	Weight
	EL3000	EL2000	EL1000	EL600		
Seam thickness range (m)	2.2-6.0	1.5-3.5	1.8-5.0	1-3.5	78	0.22
Typical machine length (m)	14.6	12.2	11.8	11.9	31	0.09
Typical installed power (KW)	1940	1940	1380	869	89	0.25
Available cutting power (KW)	2×850; 2×650	2×500	2×600	2×450; 2×375; 2×285	37	0.11
Cutting drum diameter (m)	1.9-3.0	1.2-2.2	1.4-2.5	1.1-2.2	56	0.16
Machine weight (tons)	100	55	75	50	61	0.17

Table 4 shows the normalized decision matrix (*N*) based on Equation 2. The normalized values (n_{ij}) can be calculated for benefit and cost related criteria using Equations 3 and 4, respectively.

In this step, the ideal (Z*) and non-ideal (Z−) solutions are determined through Equations 5 and 6. For the shearer selection process the results from the ideal and non-ideal solutions are given in Table 5.

$$Z^*=\left\{\max_i n_{ij} \mid j=1,2,...,J\right\}=\left\{n_1^*,n_2^*,...,n_J^*\right\} \quad (5)$$

$$Z^-=\left\{\min_i n_{ij} \mid j=1,2,...,J\right\}=\left\{n_1^-,n_2^-,...,n_J^-\right\} \quad (6)$$

Table 4. Normalized decision matrix during the shearer selection

Criteria	Shearer alternatives				Weight
	EL3000	EL2000	EL1000	EL600	
Seam thickness range	0.09	0.55	0.37	0.74	0.22
Typical machine length	0.21	0.42	0.63	0.63	0.09
Typical installed power	0.11	0.11	0.21	0.96	0.25
Available cutting power	0.26	0.52	0.26	0.77	0.11
Cutting drum diameter	0.1	0.59	0.4	0.69	0.16
Machine weight	0.11	0.63	0.21	0.74	0.17

Table 5. Ideal and non-ideal solutions

Criteria	Ideal solution	Non-ideal solution	Weight
Seam thickness range	0.74	0.09	0.22
Typical machine length	0.63	0.21	0.09
Typical installed power	0.96	0.11	0.25
Available cutting power	0.77	0.26	0.11
Cutting drum diameter	0.69	0.1	0.16
Machine weight	0.74	0.11	0.17

Equation 7 is given to find a consensual set of criteria weights according to the mean scores of the experts.

$$W_j = \prod_{k=1}^{K} (W_j^k)^{W_k} \tag{7}$$

where,

W_j: Weight of the jth criterion

W_j^k: Weight of the jth criterion according to expert k's judgment

W_k: Normalized weight by expert k

K: Number of experts

In the last step, after calculating utility and regret measures through Equations 8 and 9 VIKOR index should be calculated.

$$U_i = \sum_{j=1}^{J} \frac{W_j (n_j^* - n_{ij})}{(n_j^* - n_j^-)} \tag{8}$$

$$R_i = \max_j \left[\frac{W_j (n_j^* - n_{ij})}{(n_j^* - n_j^-)} \right] \tag{9}$$

where,

U_i: Utility measure

R_i: Regret measure

Q value as VIKOR index should be calculated using Equation 10. The shearer alternatives are sorted by the values U_i, R_i, *and* Q_i.

$$Q_i = \nu \left[\frac{U_i - \min_i U_i}{\max_i U_i - \min_i U_i} \right] + (1-\nu) \left[\frac{R_i - \min_i R_i}{\max_i R_i - \min_i R_i} \right] \tag{10}$$

Where,

ν: Weight of the maximum group utility (or weight of the strategy of "the majority of criteria") which is usually set to 0.5 (Tong et al., 2007)

Table 6 shows the results including all utility and regret measures and VIKOR index for the shearer alternatives.

The alternative which includes minimum VIKOR index is determined as the best compromise solution. Therefore, the shearer loader model EL 600 is the best choice among four alternatives considered in this research from the technical point of view according to the results summarized in Table 6.

Table 6. VIKOR index for the shearer selection

Parameters	Shearer alternatives			
	EL3000	EL2000	EL1000	EL600
Utility measure	1	0.47	0.68	0
Regret measure	0.25	0.25	0.22	0
VIKOR index	1	0.73	0.78	0

3.3 Final Results and Discussion

According to the analytical procedure, characteristics of the four shearer alternatives were considered to be adjusted to the mechanical properties of the coal seam located in Tabas Parvadeh1 longwall mine. In this case, the physical parameters of shearer such as pick, drum and vanes were designed and consequently the most useful kind of drag pick was selected among point-attack and conical ones. The diameter and width of shearer were respectively estimated 1.5 m and 0.8 m on the basis of the thickness, strength, and hardness of the coal seam. Based on all important points, "double ended ranging drum shearer" model EL600 was selected as the most appropriate one to be practicable for Parvadeh1 longwall mine. The mentioned technical viewpoints and most crucial parameters were also considered during the application of the MCDM system, in order to select a most suitable shearer loader system for Parvadeh1 mine. Accordingly using the MCDM system, EL 600 shearer loader was also selected among the four alternatives from the technical viewpoints. It means that the results of the MCDM system are completely in accordance with the results of the analytical procedure.

4 CONCLUSION

The integrated results obtained from the analytical procedure proposed by Bakhtavar and Shahriar (2013) and VIKOR multi-criteria decision making system were used in order to decide on the most appropriate shearer loader system for application in Tabas Parvadeh1 longwall mine. During the decision making process, the analytical procedure was initially used to find effective criteria. The most crucial criteria were found from the analytical procedure and then considered during the MCDM system on the basis of the mechanical properties of C1 coal seam together with the critical characteristics of shearer loader. Both analytical procedure and the MCDM system indicated that EL 600 two drums shearer system can be appropriately applicable among the four considered alternatives from the technical viewpoints.

REFERENCES

Singh, R., 1999. Mining methods to overcome geo-technical problems during underground working of thick coal seams- case studies, *Transactions of the Institution of Mining and Metallurgy (Section A Mining Industry)*, Vol. 18, pp. A121-A131.

Shahriar, K., Bakhtavar, E., Moeinzadeh, A., 2009. Some experiments in-situ and in laboratory to determine the physico-mechanical properties of coal, *Gospodarka Surowcami Mineralnymi (Mineral Resources Management) Journal*, Vol. 45, pp. 51-62.

IRITEC (Iran International Engineering Company), 2003. Tabas Coal Mine Project. *Detailed Design Report*, Vol. 1, Underground Mine Revision B., pp. 19-22.

Opricovic, S., Tzeng, G.H., 2004. The Compromise solution by MCDM methods: A comparative analysis of VIKOR and TOPSIS, *European Journal of Operational Research*, Vol. 156, No. 2, pp. 445-455.

Opricovic, S., Tzeng, G.H., 2007. Extended VIKOR method in comparison with outranking methods, *European Journal of Operational Research*, Vol. 178, pp. 514-529.

Tong, L.I., Chen, C.C., Wang, C.H., 2007. Optimization of multi-response processes using the VIKOR method, *International Journal of Advanced Manufacturing Technology*, Vol. 31, pp. 1049-1057.

Bakhtavar, E., Shahriar, K., 2013. Selection of a practicable shearer loader based on mechanical properties of coal for Parvadeh1 mine, *Journal of Archives of Mining Sciences*, Vol. 58, No. 1, pp. 145-157.

Review of Graphical Methods Utilized in System Reliability Assessment

Sistem Güvenilirliği Değerlendirilmesinde Kullanılan Grafiksel Yöntemlerin İncelenmesi

D. Tuncay, N. Demirel
Middle East Technical University, Mining Engineering Department, Ankara

ABSTRACT In modern mining activities, mine productivity highly relies on the availability of high capacity machines. Reliability assessment of these machines has significant impact on understanding the failure behaviors, thus determining maintenance policies accordingly. Reliability analysis of complex systems, such as mining machinery, requires knowledge about failure behavior of their components for more accurate results. In order to combine the failure information of system components to analyze system reliability, there are various methods that can be utilized. Reliability block diagrams (RBD) and fault tree analysis (FTA) are two of the commonly used graphical methods in system reliability analysis. In this paper, general information on RBD and FTA is presented and reliability analysis of a sample system is conducted, utilizing both methods.

Keywords: Fault tree analysis, **r**eliability assessment, reliability block diagram

ÖZET Modern madencilikte, madenin verimliliği, büyük ölçüde yüksek kapasiteli maden makinalarının kullanılabilirliğine dayanmaktadır. Bu makinaların güvenilirlik değerlendirmeleri, arıza davranışlarının anlaşılmasında ve bu sayede bakım onarım politikalarının uygun şekilde belirlenmesine yardımcı olur. Maden makinaları gibi karmaşık sistemlerin güvenilirlik analizlerinin daha gerçek sonuçlar vermesi için, bu sistemleri oluşturan bileşenlerin arıza davranışları hakkında bilgiye sahip olunmalıdır. Bu arıza bilgilerinin birleştirilip sistem güvenilirliğinin belirlenmesi için kullanılan çeşitli yöntemler mevcuttur. Güvenilirlik blok diagramları (GBD) ve hata ağacı analizi (HAA) sistem güvenilirlik analizinde yaygın olarak kullanılan iki grafiksel analiz yöntemidir. Bu bildiri GBD ve HAA hakkında genel bilgileri içermektedir ve örnek bir sistem için, her iki yöntem kullanılarak güvenilirlik analizi yapılmıştır.

Anahtar Kelimeler: Hata ağacı analizi, güvenilirlik değerlendirmesi, güvenilirlik blok diagramı

1 INTRODUCTION

Reliability is commonly defined as the probability of a product not to fail under a certain condition during a defined duration. Reliability analysis is the calculation and evaluation of the reliability of a system, sub-units of a system or the critical parts of a system (Uzgören and Elevli, 2010).

The purpose of a reliability engineer is to examine the relation between the system operation and failure by studying:

- The reasons for system failure,
- The ways to develop reliable systems,
- The ways to measure and test reliability in design, operation and management, and
- The ways to maintain reliable systems by maintenance, fault diagnosis and prognosis.

The problems of a reliability engineer to solve are: representation and modeling of the system, quantification of the model and representation, propagation and

quantification of the system behavior uncertainties. (Zio, 2009).

The reliability of a system depends on the analysis of the failure times, times between failures and number of failures of a system during a given time. The main goal in reliability analysis is to define a statistical model which fits these data best.

After determining the probability distributions of component failures, these distributions are used for system reliability analysis. There are various methods for determining system reliability. Two of the graphical methods that will be mentioned are: reliability block diagram (RBD) and fault tree analysis (FTA). Both methods can be used alternatively to demonstrate the relations of system components, their effects on system reliability and quantify the system reliability, utilizing the failure probabilities of individual components.

2 RELIABILITY BLOCK DIAGRAMS

A system is a network of components connected in series, parallel or other combinations. Reliability block diagram is a schematic and logical representation of a system that helps investigating the stated connections among components and estimating the overall system success (Kumar *et al*., 2006).

Most systems in RBD are in series or in parallel configurations. A network in series indicates that the system success can only occur if all components are in working condition. The reliability of a series system (Figure 1) can be calculated as given in Equation [1].

$$R_s=R_1.R_2.R_3...R_k \quad [1]$$

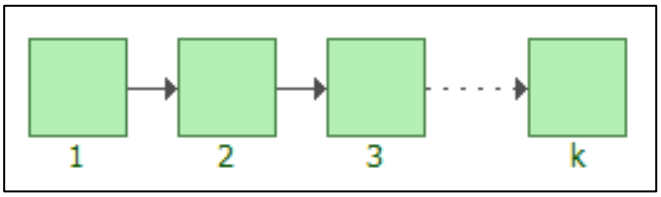

Figure 1. A series system

In parallel systems, the system continues to operate until every component fails. This indicates, the components cannot stop system operation individually. The equation used to calculate reliability for parallel systems (Figure 2) is given in Equation [2]

$$R_p=1-(1-R_1)(1-R_2)...(1-R_k) \quad [2]$$

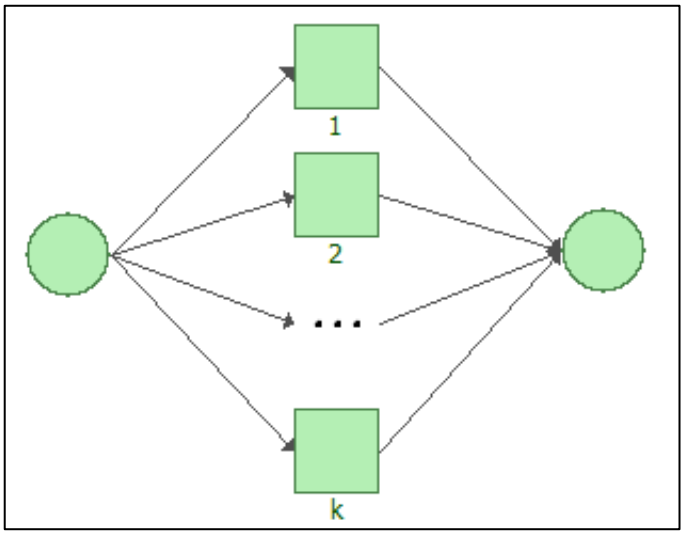

Figure 2. A parallel system

Another special configuration is the k-out-of-n system that indicates system operation when at least k components out of n components stay operational i.e. failure in (n-k) components can be tolerated. The reliability of the k-out-of-n system (Figure 3) can be expressed using Equation [3].

$$R_{k/n} = \sum_{i=k}^{n} \binom{n}{i} R^i (1-R)^{n-i} \quad [3]$$

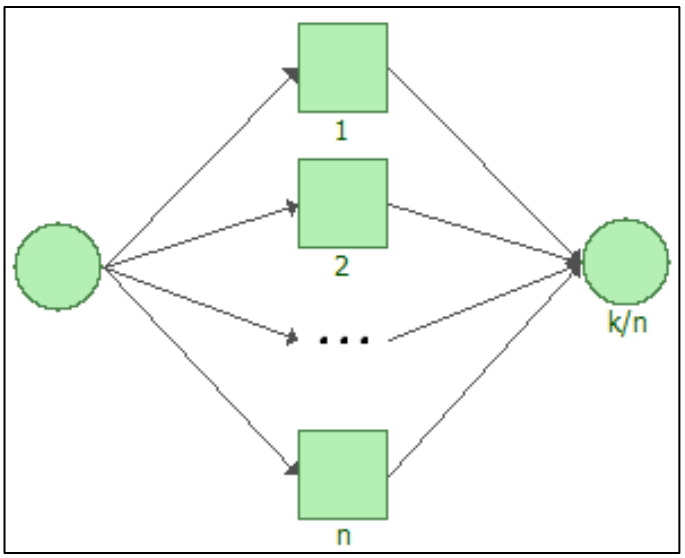

Figure 3. k-out-of-n system

3 FAULT TREE ANALYSIS

Fault tree analysis (FTA) is an analytical technique used to analyze a system to determine all the credible ways in which a single undesired event (top event) can occur. FTA is a top to down, failure oriented symbolic logic model used to determine the probability of the top event by identifying failure paths leading to it (Ericson II, 1997).

FTA is firstly applied to the Minuteman Launch Control System in 1961 by H. Watson in the Bell Labs together with U.S Air Force (Lee *et al*., 1985). Then, Boeing Company used it for complete quantitative safety analysis of the Minuteman weapon system. The Boeing Company enhanced the technique, developed the first FT computer codes and used it for many other products. Then the FTA was discovered by nuclear power industry and enhanced and refined further (Ericson II, 1999).

FTA consists of the generation of the fault tree, determination of the failure probabilities of each event, determining probability of the top event by propagating failure probabilities and determining cut sets and path sets. The cut set is any set of events where if they all occur, the top event occurs. The path set is a group of sets which guarantees that the top event cannot occur if none of them occurs.

Fault tree analysis can be used for different purposes: to understand the logical path leading to the top event, to determine the prior contributors to the top event, to anticipate actions to prevent the top event, to monitor the performance of the system, to optimize resources, to help with the system design, to determine the cause of the top event and determine a solution. FTA can be used throughout the life cycle of the system. FTA has a wide variety of uses in decision making as seen above from design process through system implementation and improvement (Stamatelatos and Vesely, 2002).

The terminology in fault tree analysis is of great importance for defining the problem. There are some standard definitions and mechanics provided to define the problem completely. Some of these standard definitions are as follows (Ericson II, 1997):

- Tree: A fault tree composed of all events and logic connections which lead to the occurrence of the undesired incidence, i.e. top event.
- Top Event: The ultimate undesired event that is being investigated. A fault tree can only have one top event.
- Branch: A section of the fault tree with events and logic gates.
- Module: An independent branch with a sub-top event that does not occur anywhere else.
- Node: A general term used to define every event on the tree; failure, gate, condition etc.
- Basic Event: A node that represents a failure event that failure probability is given as input.
- Gate: A logical Boolean operator with a specific function that combines input events (AND, OR, Inhibit, Priority AND and Exclusive OR gates).
- MOE (Multiple Occurring Event): An event that occurs in multiple places in the fault tree causing branch dependencies.
- Cut Set: A set of events that’s occurrence cause the top event to occur (failure path).
- Minimum Cut Set: A cut set with the minimum number of events that still cause the top event to occur.
- Critical Path: A cut set with the highest probability which consequently has the biggest effect on the probability of the top event. Improvements in this path results in most dramatic system improvements.

The logic operators (Gates) are the main components in FTA and indicate the relations between events (component failures) and top event (system failure). Logic operators used in fault tree analysis are defined as (Ericson II, 1997):

- OR Gate: Occurrence of at least one input is enough for the output to occur (Series Configuration).
- AND Gate: All input events must occur for the output event to occur (Parallel Configuration).
- Inhibit Gate: Inputs must occur and a condition should be satisfied for the output event to occur.

- Exclusive OR Gate: Only one input should occur for the output event to occur.
- Priority AND Gate: All input events must occur in a specific sequence for the output to occur.

The symbols assigned to these operators are shown in Figure 4.

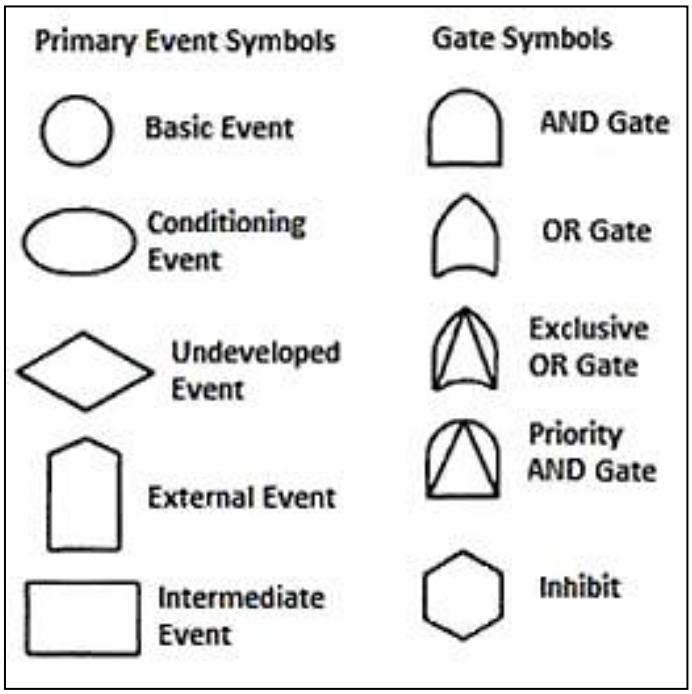

Figure 4. Operator symbols in fault tree analysis (Vesely *et al.*, 1981)

The graphical representation of the most common gates (AND, OR, VOTING), and their probability relations are explained in Table 1.

Table 1. The graphical representation of the gates and the probability relations (modified from Samanta *et al*., 2002)

Logic gate	Logic symbol	Probability relation
OR		$P(y) = P(\bar{x}_1 + \bar{x}_2 + \bar{x}_3)$ $= P(\bar{x}_1) + P(\bar{x}_2) + P(\bar{x}_3) - P(\bar{x}_1)P(\bar{x}_2) - P(\bar{x}_1)P(\bar{x}_3) - P(\bar{x}_2)P(\bar{x}_3) + P(\bar{x}_1)P(\bar{x}_2)P(\bar{x}_3)$
AND		$P(x_1x_2x_3) = P(\bar{x}_1)P(\bar{x}_2)P(\bar{x}_3)$
Voting gate		$P\{\bar{x}_1\bar{x}_2 + \bar{x}_1\bar{x}_3 + \bar{x}_2\bar{x}_3\}$ $= P(\bar{x}_1\bar{x}_2) + P(\bar{x}_1\bar{x}_3) + P(\bar{x}_2\bar{x}_3) - P(\bar{x}_1\bar{x}_2)(P(\bar{x}_1\bar{x}_3) - P(\bar{x}_1\bar{x}_2)(P(\bar{x}_2\bar{x}_3) - P(\bar{x}_1\bar{x}_3)(P(\bar{x}_2\bar{x}_3) + P(\bar{x}_1\bar{x}_2)P(\bar{x}_1\bar{x}_3)P(\bar{x}_2\bar{x}_3)$

For these probability relations to be valid, the events should be independent since the assumption, $P(x_1,x_2) = P(x_1)P(x_2)$ is valid for independent variables.

Since the fault tree analysis is highly dependent on the knowledge and expertise of the analyst, it is difficult to make a clear definition on how to construct a fault tree. Fault tree requires detailed analysis and may require comprehensive assumptions, but other than those, the main steps to be followed are as follows (Öktem, 2006):

- Determining the Top Event: The undesired event to be analyzed is chosen.
- Combining the Known Causes: Existing faulty states and failure events are determined with the available knowledge. Even though the failure list can be lacking, it is important for the fault tree construction.
- Construction of Fault Tree: Independent events that may cause the top event are determined. These events are connected with an OR gate and the construction continues from top to bottom trying to find other failure causes.
- Revision, Addition, and Testing: Fault tree construction is a trial and error process no failure causes should be overlooked.
- Evaluation of the Results: The completed fault tree is evaluated according to the purpose of the analysis. The evaluation can include various stages: listing minimum cut sets, grading minimum cut sets, and calculation of probabilities etc.

4 SAMPLE CASE STUDY

4.1 Determining Appropriate Probability Density Functions for Components

Assume there is a system composed of 5 components namely: A, B, C, D, and E and these components have individual failure data. The failure data are randomly generated by Monte Carlo simulation. First failure probability density functions should be determined for each component's generated failure data. From the failure data of 5 components, following failure probability distributions are obtained (Table 2).

Table 2. Component failure distributions

Components	Distribution	Distribution Constants	
A	Weibull-2P	β	1.17
		η	546.25
B	Weibull-2P	β	0.84
		η	941.83
C	Weibull-2P	β	1.73
		η	264.32
D	Exponential	λ	9.4E-3
E	Exponential	λ	2.20E-3

Weibull distribution is widely used for failure data and can be with 2 or 3 parameters. 2 parameter Weibull distributions have scale and shape parameters that determine the life characteristics (Reliasoft 2014). β is the shape parameter and η is the scale parameter. Lower shape parameters ($\beta < 1$) suggest that the failure frequency is high at start and decreases continuously which is similar to an exponential distribution which occurs when β equals to one. Shape parameters, greater than one, suggest that the failure frequency increases to maximum and then decreases with time. The scale parameter is an estimate of the mean and gives the time when the failure probability is 63.2%.

Exponential distribution suggests a failure behavior starting with high failure frequency and decreasing continuously. The exponential distribution has one parameter which is the failure rate (λ) which is the inverse of mean (Reliasoft, 2014).

There can also be a location parameter (γ) for both Weibull and exponential distributions, that indicates the distance from origin of the distribution start point. Positive location parameter suggests no failure occurs before a certain time, called as failure free time.

4.2 Determining System Configuration

Configuring the system requires a good understanding of the system and the relations between components. There can be series and parallel configuration in the system. Series configuration means failure in one component results in failure of the system or the sub-system. In a parallel configuration, for the system to fail, all components in the configuration should fail. In some cases, there can be a type of configuration where system failure occurs if a given number of components fail. For the sample case; failure of component A causes system failure. Failure of component B combined with failure of C or failure of 3 out of 5 D components also causes system failure. Another way for the system to fail is either two of the E components should fail or one E combined with a subsystem composed of a D and an E component with parallel configuration should fail.

4.3 Constructing the Reliability Block Diagram

According to the defined system network configuration, the reliability block diagram is constructed as seen in Figure 5.

Extra starting and ending blocks are placed on two sides of the diagram. These blocks are assigned as “cannot fail” and do not affect the reliability calculations. Similarly, the extra node connecting D* and E* is also assigned as “cannot fail”.

D* and E* components have the same failure distributions of D and E respectively but to be able to distinguish those components during analysis, different names were assigned.

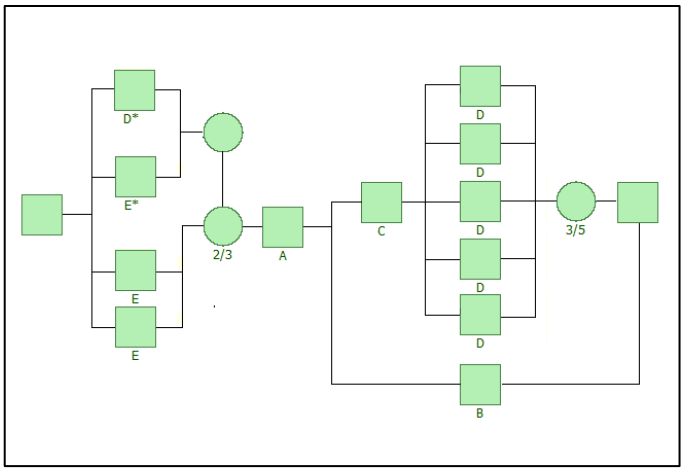

Figure 5. Constructed reliability block diagram of the system

4.4 Constructing the Fault Tree and Reliability Analysis

Considering the defined relations between components, by utilizing logic gates, the following fault tree is constructed (Figure 6).

VT gates are voting gates where the gate connecting five D components have a vote number of 3 and the other voting gate has 2. The top event is defined as the system failure.

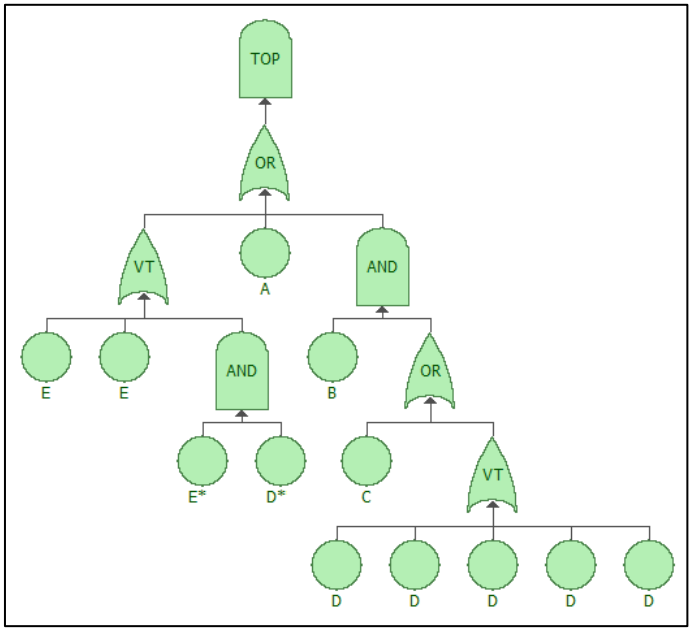

Figure 6. Constructed fault tree of the system

The reliability calculations are carried out following the equations assigned for different gates and they are the same for both RBD and FTA. Weibull++7 (2011) and Blocksim 7 (2011) software were utilized for the analysis of the sample system. The obtained reliability vs. time plot can be seen in Figure 7.

It can be seen from Figure 7 that around 160 hours, the system reliability drops down to 50%. The mean life time of the system is estimated as 207 hours.

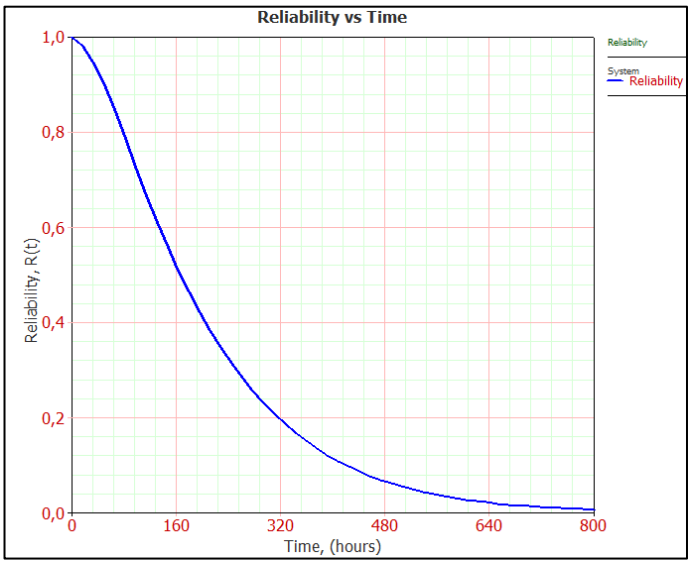

Figure 7. System reliability change with respect to time

Another practical data obtained from fault tree analysis are “Reliability Importance Values” (RI). RI values are calculated considering the reliability of the component, reliability of the system and the component’s location in the fault tree configuration. RI values are calculated for a given time and can be helpful when determining a maintenance policy. The RI values of the components at the system’s estimated lifetime (207 hours) can be seen in Figure 8.

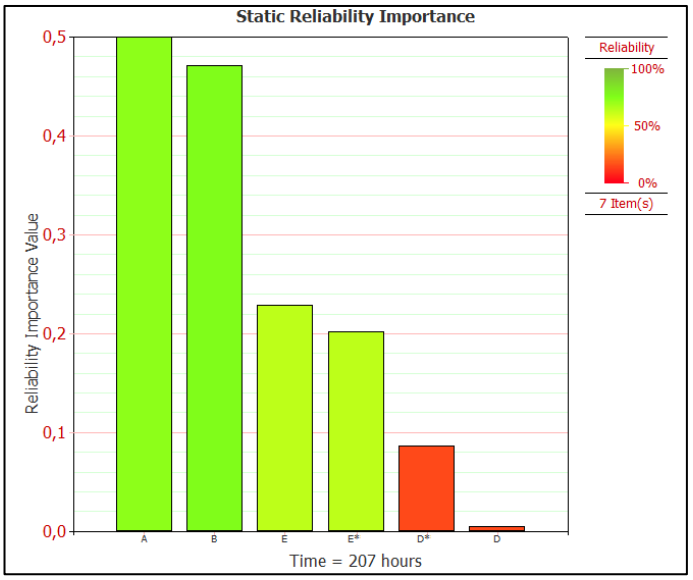

Figure 8. RI values of components at 207 hours

The higher RI values indicate that an improvement on that components reliability will be more significant for system reliability compared to other components. It can be

seen that even though component D has a low reliability, its RI value is smaller compared to component A which has the highest RI value despite its high reliability. This is due to their location in the system configuration and their effect on system reliability. Component A has direct effect on system reliability since its failure result in system failure. This can be easily seen in the sample system but in more complex systems, it may not be so obvious.

For different time intervals, RI values must be checked since different components may have a higher importance for different times. RI vs. time plots can also be obtained to see if any component gains importance over another component.

For example, as seen in Figure 9, for around 85 hours component C has higher RI value compared to D*, but after 85 hours, D* has a higher RI value due to its failure distribution.

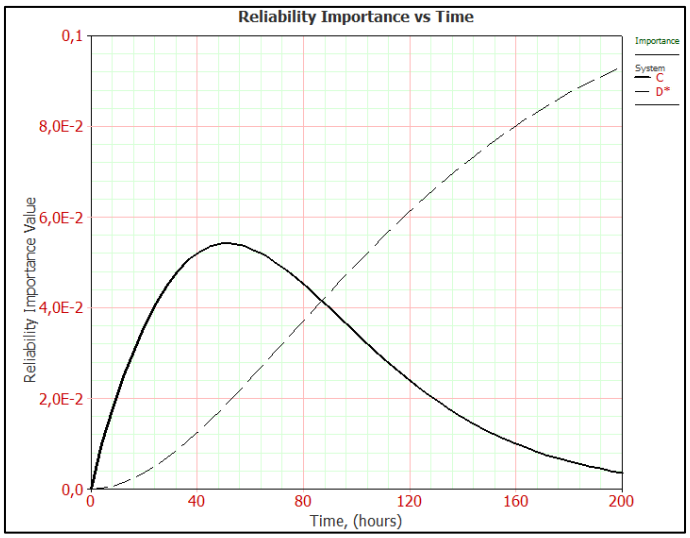

Figure 9. RI changes with respect to time for components C and D*

5 CONCLUSIONS AND RECOMMENDATIONS

Reliability analysis of mining machines is important for determining failure behavior of the machines and consequently predicting possible failures beforehand. For complex systems, there are different methods that can be utilized for system reliability assessment. Reliability block diagram and fault tree analysis are two of the graphical methods which are useful tools for demonstrating component configurations within the system and determining system reliability considering those relations.

The sample study was used to illustrate the use of these methods and to show the possible outcomes of the analyses that can be beneficial for preparing maintenance plans thus improving machine availability.

The main conclusions derived from this paper can be listed as:

- Reliability block diagrams and fault tree analysis are effective tools in determining complex system reliability.
- Reliability Importance (RI) factor can be utilized effectively to detect the critical elements in varying operation periods.
- At different times, different components have higher importance values meaning those components may require special attention to prevent failure.
- Having a good understanding of the system at hand and proper classification of failure data accordingly are important for reliability analysis.

The items that can be recommended for the future studies can be listed as follows:

- Results of reliability analyses should be utilized to prepare a maintenance plan considering the critical components. Preparing an appropriate maintenance plan considering the component reliabilities will increase the machines availability, thus decreasing the direct and indirect costs caused by unplanned down times of the machinery.
- Optimum preventive or corrective maintenance intervals should be decided considering maintenance costs, repair efficiencies and losses in revenue due to breakdowns.
- There can be units that take time to be repaired in case of failure and may require detailed scheduled maintenance considering the repair and maintenance times.
- Maintenance personnel should be specially trained to keep failure logs precisely in order to prevent inaccurate data. If possible, a practical and detailed maintenance data sheet should be prepared to acquire more information about machine lifetime behavior.

REFERENCES

Blocksim 7 (2011), software, ReliaSoft Office 7, ReliaSoft Corporation Tucson.

Ericson II, C. (1997). FTAB - A New Generation Computer Code for Fault Tree Analysis. *15th International System Safety Conference*, (pp. 437-447).

Ericson II, C. (1999). Fault Tree Analysis – A History. *Proceedings of The 17th International System Safety Conference.* Orlando.

Kumar, E., Crocker, J., Chitra, T., and Saranga, H. (2006). *Reliability and Six Sigma.* Springer Science+Business Media Inc.

Lee, W. S., Grosh, D. L., Tillman, F. A., and Lie, C. H. (1985). Fault Tree Analysis, Methods, and Applications - A Review. *IEEE Transactions on Reliability*, 194-203.

Öktem, R. (2006). Hata Ağacı Analizi. In L. H. Ringdahl, *Safety Analysis Principles and Practice in Occupational Safety*. Türk Tabipler Birliği.

Reliasoft. (2014). Life Data Analysis Reference. ReliaSoft. Retrieved 02 2014, from reliawiki.org

Samanta, B., Sarkar, B., and Mukherjee, S. (2002). Reliability assessment of hydraulic shovel system using fault trees. *Mining Technology*, 129-135.

Stamatelatos, M., and Vesely, W. (2002). *Fault Tree Handbook with Aerospae Applications.* Washington: NASA.

Uzgören, N. and Elevli, S. (2010). Homojen olmayan Poisson Süreci: Bir Maden Makinasının Güvenilirlik Analizi. *Gazi Üniversitesi Mühendislik ve Mimarlık Fakultesi Dergisi, 25*(4), 827-837.

Vesely, W., Goldberg, F., Roberts, N., and Haasl, D. (1981). *Fault Tree Handbook.* Washington, D.C.: U.S. Government Printing Office.

Weibull ++7 (2011), software, ReliaSoft Office 7, ReliaSoft Corporation Tucson.

Zio, E. (2009). Reliability Engineering: Old Problems and New Challenges. *Reliability Engineering and System Safety, 94*, 125-141.

Review of Trend Tests for Detection of Wear-Out Period for Mining Machineries

Maden Makinalarının Aşınma Periyodunun Tespit Edilmesinde Kullanılan Eğilim Testlerinin İncelenmesi

O. Gölbaşı, N. Demirel

Middle East Technical University, Department of Mining Engineering, Ankara

ABSTRACT Machinery systems are extensively utilized in all mining stages from beginning to end of ore production. They are capital-intensive systems and substantial amount of money is spent annually to keep their functionalities in desired levels. Therefore, implementation of effective maintenance strategy has a vital importance to prevent unexpected breakdowns due to failures and to minimize operational cost. These maintenance strategies can be constituted effectively regarding functional and structural dependencies between system components and forecasting their expected lifetimes and deterioration rates over time. However, forecasting of expected failures can fail due to aging trend in system components. This paper summarizes qualitative and quantitative trend tests in detection of wear-out period where system starts to age. In the paper, two separate graphical methods are investigated in qualitative analysis of data trend behavior where hypothesis testing techniques such as Crow/AMSAA, Laplace, Lewis-Robinson, and Reversal Arrangement and indirect trend test using imperfect maintenance concept are examined as quantitative tests. Implementation of all test are supported via their theoretical backgrounds and numerical examples.

Keywords: Wear-out period, qualitative and quantitative lifetime trend tests, imperfect maintenance

ÖZET Makina sistemleri, cevher üretiminin başından sonuna kadar tüm madencilik aşamalarında yaygın olarak kullanılmaktadır. Bu makinalar sermaye-yoğun sistemler olup, makinaların işlevlerini yeterli seviyede tutmak için her yıl önemli bir miktar para harcanmaktadır. Bu sebepten dolayı, etkili bakım onarım stratejileri uygulanışı, arızalardan kaynaklı beklenmedik duraksamaların önlenmesi ve operasyonel masrafların en aza indirgenmesinde kritik bir öneme sahiptir. Bu bakım-onarım stratejileri, sistem bileşenleri arasındaki fonksiyonel ve yapısal bağımlılıkların göz önüne alınarak ve bu bileşenlerin beklenen yaşam süreleri ve kötüleşme hızlarına yönelik tahminlerle etkili şekilde oluşturulabilir. Fakat, muhtemel arızalara dair tahminler, sistem bileşenlerindeki yaşlanma eğilimden dolayı başarısız olabilir. Bu bildiri, sistemin yaşlanmaya başladığı yıpranma periyodunun tespitinde kullanılan nitel ve nicel eğilim testlerine yönelik bir özet sunmaktadır. Bildiride, iki adet grafik yöntemi veri eğilim davranışının nitel analizinde incelenirken; Crow/AMSAA, Laplace, Lewis-Robinson, Reversal Arrrangement gibi hipotez testleri ve noksan onarım konsepti kullanılarak yapılan dolaylı eğilim testi de nicel testler olarak incelenmiştir. Bütün testlerin uygulanışları, teorik arka planları ve sayısal örneklerle desteklenmiştir.

Anahtar Kelimeler: Aşınma periyodu, nicel ve nitel yaşam eğilim testleri, kusurlu bakım-onarım

1 INTRODUCTION

Mining is a capital-intensive sector where substantial amount of money is spent in maintenance and purchase of machineries for sustainability of mining operations in order to supply raw material to various industries. Performance and reliability of machineries have a major effect on production since any lack of functionality in these systems can cause production losses and delays in planned production schedule.

In their operational life, machines are exposed to breakdowns in several times due to failure of components and they are recovered via corrective maintenance. Occurrences of failures are ordinary and expected events. However, failure rate can change due to operational age of machines. Variations in expected number of failure for unit time can cause disappearance of randomness. In the lack of randomness, it becomes hard to forecast failure arrival time and constitute a fixed maintenance policy. Majority of systems, even human body, generally follows a failure rate path called as bathtub curve. This curve can be divided into three parts as infant mortality, useful period, and wear-out period (Figure 1).

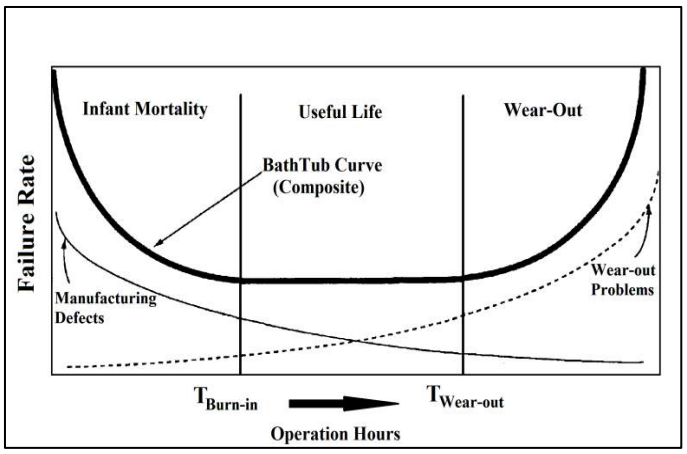

Figure 1. Sample Bath Tub Curve

In early times of systems, failure rate is high at the beginnings and falls dramatically at the following operational hours. This period is also called infant mortality or burn-in period. Failures are expected to appear in high frequency since there can be errors due to design, operational, installation or redundant-maintenance conditions. After stabilization of system functionality and accommodating to production, failure rate gets smaller and reach to an almost-constant level. In the sequel, failure rate remain constant for a long time and it is called as useful life, i.e. normal life. Failures occur randomly during this interval. Following this period, system enters a period with increasing failure rate due to wear-out conditions of system components. In the latest stage of this period, randomness of system failures highly disappears. In this period, implementation of only corrective maintenance after failure without any preventive action can cause long-term breakdowns. Therefore, maintenance actions such as, preventive replacements and condition monitoring, become crucial to detect oncoming failures.

Detection of wear-out start is important to re-arrange maintenance strategy for systems. There are various qualitative and quantitative techniques to be utilized in decision of system failure trends. In this sense, Section 2 will discuss how to assess trend condition of failure rate using graphical method quickly where Section 3 will mention about quantitative trend detection methods.

2 QUALITATIVE TREND TESTS

Qualitative methods offer quick way of detecting changes in failure rate. If the failure rate is nearly constant in a specified time period, time between failures (TBF) data is called as non-trend data or vice versa. Occurrence of data trend can be verified using graphs by plotting cumulative failure numbers (CFN) versus cumulative time-between-failure (CTBF) and failure times versus cumulative mean-time-between-failures (MTBF) in log-log scale (Duane graph). Using datasets of two sample systems, these two graphical methods are illustrated in Figure 2 and Figure 3, respectively.

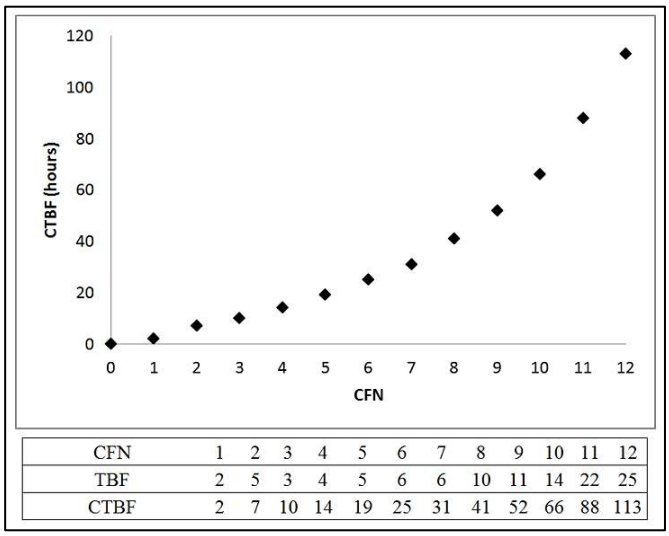

CFN	1	2	3	4	5	6	7	8	9	10	11	12
TBF	2	5	3	4	5	6	6	10	11	14	22	25
CTBF	2	7	10	14	19	25	31	41	52	66	88	113

Figure 2. Qualitative Trend Test using CTBF versus CFN Plot

Figure 2 shows that CTBF, i.e. system time, follow a curvilinear path with upward trend. It can be evidence of that failure rate is falling over time with rising time between failure values and system is in the early life period in bathtub curve. Therefore, this system is far away from wear-out period. In the case of non-trend condition, graph line is expected to straight.

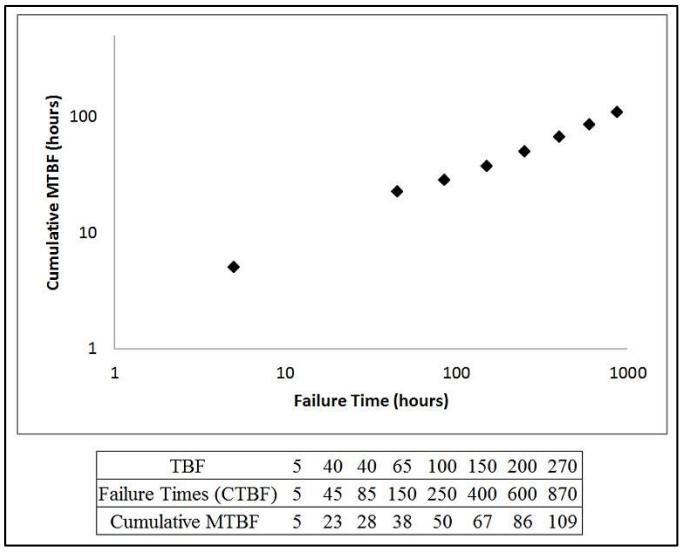

TBF	5	40	40	65	100	150	200	270
Failure Times (CTBF)	5	45	85	150	250	400	600	870
Cumulative MTBF	5	23	28	38	50	67	86	109

Figure 3. Qualitative Trend Test using Failure Time versus Cumulative MTBF Plot

Figure 3 illustrates Duane plot for another system. Failure times in the plot are the points in time horizon where failures take place. It neglects repair times and it is the same as CTBF in Figure 2. Cumulative MTBF is time-based mean survival time. For instance, third failure appears at 85th operation hour. Therefore, Cumulative MTBF is 28 hour as division of 85 to 3. This graph is plotted in the log-log scale and expected to be straight if there is no data trend. Figure 3 is an example of system with non-trend failure behavior.

Although these graphs offer easy and effective way in trend analysis, they are generally interpreted subjectively. They sometimes need to be validated quantitatively, especially for large data sets and complex systems. Section 3 will discuss background of the hypothesis testing methods and imperfect maintenance approaches in interpretation of data trend in quantitative way.

3 QUANTITATIVE TREND TESTS

3.1 Hypothesis Testing Methods

Hypothesis testing methods can be utilized to verify the results of qualitative techniques. Crow/AMSAA, reversal arrangement test, Laplace test, and Lewis-Robinson test are generally used in observation of data trend for repairable systems. These methods test validity of various stochastic processes to discuss presence of data trend. For instance, Crow/AMSAA and Laplace methods test whether the data can be fitted in homogenous Poisson process (HPP) or not where reversal arrangement test and Lewis-Robinson methods check suitability of data for renewal process (RP). Validity of HPP or RP in these tests is good evidence of non-trend behavior. It is why these methods test stochastic processes to find out trend behavior. Otherwise, data show trend behavior and it can be treated using non-homogenous Poisson process (NHPP). Detailed expressions of the tests can be investigated from Kobbacy and Murthy (2008), Stephens (2011), Wang and Coit (2005), and Bendat and Piersol (2010). In all tests, X_i, T_i, and N notate ith time between failure (TBF_i), cumulative time between failures up to ith failure ($\sum_1^i TBF_i$), and total number of failures, respectively.

Crow/AMSAA test, i.e. military test, investigates whether the data can be fitted in HPP or NHPP, analyzing value of parameter β. Best estimate of β using maximum

likelihood estimation is given in Equation 1 (Wang and Coit, 2005).

$$\hat{\beta} = \frac{N}{\sum_{i=1}^{N-1} \ln\left(\frac{T_N}{T_i}\right)} \quad (1)$$

According to the test, null hypothesis which agrees on non-trend data behavior is rejected if $2N/\hat{\beta} < \chi^2_{2N,1-\alpha/2}$ or $2N/\hat{\beta} > \chi^2_{2N,\alpha/2}$, where χ^2 is the score of chi-squared distribution for given confidence interval and degree of freedom.

Reversal arrangement test checks whether the data can be modelled using renewal process or not. Presence of renewal process (null hypothesis) is rejected if $U_{RA} > z_{\alpha/2}$ or $U_{RA} < -z_{\alpha/2}$. U_{RA} can be evaluated using Equation 2 (Wang and Coit, 2005). In the formula, U is the total number of counts for the condition $X_j > X_i$ for each X_i where $j > i$.

$$U_{RA} = \frac{U - N(N-1)/4}{\sqrt{\frac{(2N+5)(N-1)N}{72}}} \quad (2)$$

Laplace test examines whether data is well fitted in HPP or NHPP, as in Crow/AMSAA test. Acceptability of HPP (null hypothesis) is rejected if $U_L > z_{\alpha/2}$ or $U_L < -z_{\alpha/2}$. Test statistics, U_L, is stated in Equation 3 (Wang and Coit, 2005)..

$$U_L = \frac{\sum_1^{N-1} T_i - (N-1)\frac{T_N}{2}}{T_N\sqrt{\frac{N-1}{12}}} \quad (3)$$

Finally, Lewis-Robinson test analyze whether data is fitted in renewal process or not. Division of Laplace test statistics, U_p, to coefficient of variance is the hypothesis test statistic as given in Equation 4 (Wang and Coit, 2005). Coefficient of variance can be expressed as $\sqrt{Var[X]}/\bar{X}$ where X is TBF dataset. Again, null hypothesis rejected if $U_{LR} > z_{\alpha/2}$ or $U_{LR} < -z_{\alpha/2}$.

$$U_{LR} = \frac{U_L}{CV[X]} \quad (4)$$

As discussed at the beginning of Section 3.1, these tests utilize HPP, NHPP, and renewal process to reveal potential data trend behavior. It should be remind that renewal process assumes that system is recovered in to as good as new condition after maintenance activities. Any distribution can be fitted in renewal function. HPP is special version of renewal process where time between failure values is good fitted in exponential distribution. On the other hand, NHPP assumes that maintenance recovers the system to as bad as old condition and failure rate is allowed to rise. Therefore, trend behavior of data is good explained using NHPP. Although mathematical background of the processes is out of scope for this paper, reader can utilize Rausand and Hoyland (2004) for detailed investigation.

Numerical Example

Trend testing methods discussed in Section 3.1 will be evaluated using sample failure statistics given in Table 1.

Table 1. Time between Failures Data

#	Time between Failures (hours)	Cumulative Time between Failures (hours)
1	15	15
2	8	23
3	25	48
4	14	62
5	18	80
6	21	101
7	25	126
8	23	149
9	20	169
10	32	201
11	9	210
12	15	225
13	45	270
14	47	317
15	33	350
16	24	374
17	27	401
18	31	432
19	19	451
20	22	473

Trend behavior of the data in Table 1 is initially assessed with Crow/AMSAA test. Parameters to be utilized in Equation 1 are calculated as in Table 2. Best estimate of $\hat{\beta}$ is found to be 0.9 and rejection criterion, $2N/\hat{\beta}$, is between the interval specified by the scores of chi-squared distribution. Therefore, null hypothesis of the test is accepted, agrees on non-trend behavior of the data set.

Table 2. The Test Values of Crow/AMSAA

Test Parameters	Parameter Values
N	20
T_N	22
$\sum_{i=1}^{N-1} ln(\frac{T_N}{T_i})$	21.8
$\widehat{\beta}$	0.9
$2N/\widehat{\beta}$	43.7
$\chi^2_{40,0.025}$	24.4
$\chi^2_{40,0.975}$	59.3
Decision:	Accept H_0

The data was also evaluated using reversal arrangements test with Equation 2. In the formula, U is the total number of reversal. For instance, $X_{10} = 32$ is given in Table 1. Number of reversals for X_{10} is found as 3, which is the total counts for $X_j > X_{10}$ for $j > 10$. This is repeated for each X_i and the reversals are summed to find out U parameter. U is found as 123, given in Table 3. Test statistic of the method, U_p, is then calculated as 1.82 and it is between standard normal distribution scores, ± 1.95. Therefore, the test accepts null hypothesis and rejects presence of data trend.

Table 3. The Test Values of Reversal Arrangements

Test Parameters	Parameter Values
N	20
U	123
U_p	1.82
$\pm z_{0.025}$	± 1.95
Decision:	Accept H_0

Failure behavior of the system is also evaluated with Laplace test. The test fails to reject null hypothesis and defense non-trend behavior of the data set since test parameter U_L is between ± 1.95, as shown in Table 4.

Table 4. The Test Values of Laplace Method

Test Parameters	Parameter Values
N	20
T_N	22
$\sum_{i=1}^{N-1} T_i$	4004
U_L	-0.82
$z_{0.025}$	1.95
Decision:	Accept H_0

Last interpretation method for the data is Lewis-Robinson test. It is simply division of U_L parameter found in Laplace test to coefficient of variance of the time between failures values. Non-trend behavior of the system is also validated with this test since the test parameter U_{LR} is in the range of $\pm z_{0.025}$ score (Table 5).

Table 5. The Test Values of Lewis-Robinson

Test Parameters	Parameter Values
U_L	-0.82
$CV[X]$	0.43
U_{LR}	-1.89
$z_{0.025}$	1.95
Decision:	Accept H_0

It is seen that all hypothesis testing methods prove non-existence of trend for the given data set. It is important that Crow/AMSAA and Laplace methods test whether data is fitted to HPP. HPP is a special type of renewal process where data is distributed exponentially. These methods can fail to find trend behavior of a system if its data is non-exponentially distributed, even though data follow non-trend behavior. Therefore, if Crow/AMSAA and Laplace methods defense trend behavior rigorously

where other tests reject the condition, distributional characteristics of data set should be checked. If the distribution is strictly different from exponential distribution, it can be better to choose Crow/AMSAA and Laplace after double checking with the graphical trend test.

3.2 Trend Detection Using Imperfect Maintenance

As mentioned in Section 3.1, HPP and renewal processes assume that system is in as good as new condition after repairing activities where NHPP supposes that system is only back to the condition just prior to failure after maintenance, i.e. as bad as old condition. These conditions are called as perfect and minimal repairs, respectively. In many maintenance activities, system is recovered to a level between as good as new and as bad as old conditions. It is called as imperfect repair. Effect of these repair types on failure rate can be viewed in Figure 4.

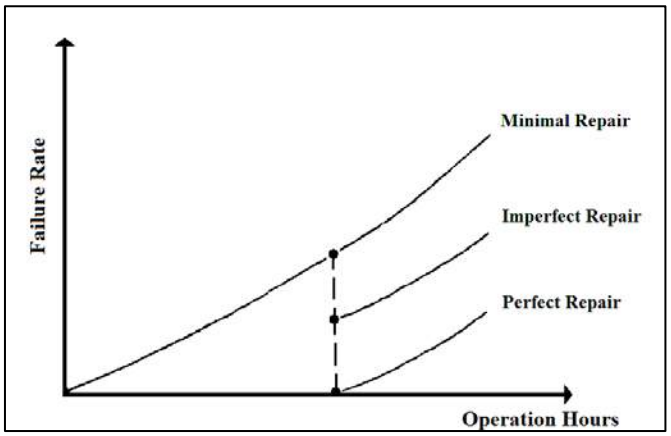

Figure 4. Failure Rate Change after Repair Types (Modified after Blischke and Murthy, 2000)

Determination of imperfect repair effect on system can be beneficial to detect whether system is in deterioration period or not. Imperfect maintenance can be modelled using various models. One of the common model is virtual age method by Kijima *et al.* (1988). The proposed method is expressed using two type models: i) Maintenance activity eliminate damage between only n^{th} and $(n-1)^{th}$ repairs, ii) maintenance activity eliminate cumulative damage, not only a period. Mathematical expressions of the models are given in Equation 4-5, respectively. V_n is virtual age of system before n^{th} repair, A_n is degree of repair and X_n is n^{th} time between failure. If A_n is exact 0 or 1, imperfect repair is turned to perfect or imperfect repair, respectively.

$$V_n = V_{n-1} + A_n X_n \quad (5)$$

$$V_n = A_n(V_{n-1} + X_n) \quad (6)$$

Imperfect repair phenomenon is adapted to renewal process and called as general renewal process (Jacopino *et al.*, 2004). This process allows analyzing of system reliability with introducing restoration factor ($RF=1-A_n$).

In order to validate trend results in Section 3.1, dataset given in Table 1 was analyzed using general renewal process via Reliasoft Weibull software. Instantaneous failure rate of the system was found as in Figure 5. Parameters β and η are reliability characteristics of the system, also called as Weibull process. Restoration factor, ($RF = 1-A_n=1$), refers perfect repair. Moreover, failure rate in the figure exhibit nearly constant behavior. It can be concluded that system is recovered effectively after maintenance activities and trend for time between failure data isn't observed.

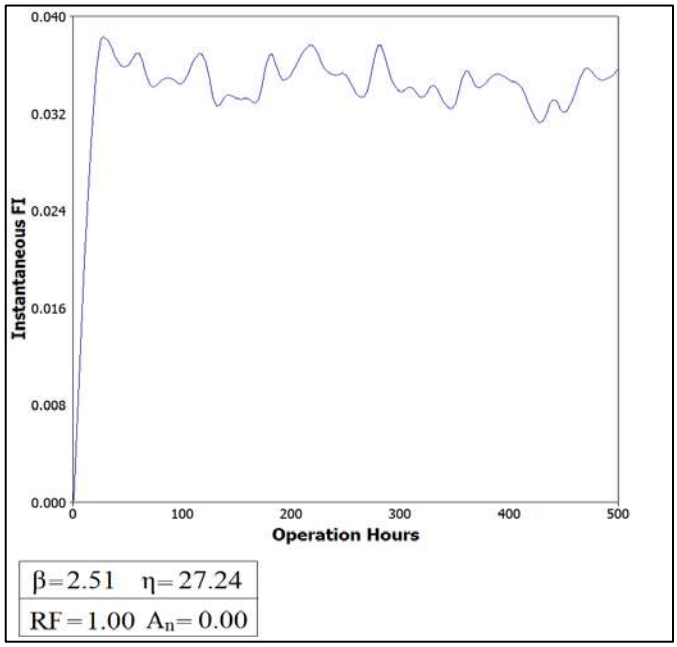

Figure 5. Instantaneous Failure Rate using General Renewal Process

This section considers only general renewal process using Kijima'a virtual age model. For detailed analyzing of various imperfect repair type, Pham and Wang (1996) and Wang and Pham (2006) can be investigated.

4. CONCLUSIONS

Failure data offer beneficial statistics to forecast number of breakdowns in a time interval. It is generally easy to implement forecasting methods for system in useful life with a constant failure rate. In degradation period, machine exhibit lower performance with unexpected failures. Detection of machinery behavior is critical for constitution of effective maintenance strategies. This paper briefly summarizes qualitative and quantitative methods utilized to examine changes in failure intensities and potential data trend.

REFERENCES

Bendat, J. S. and Piersol, A. G. (2010). *Random Data: Analysis and Measurement Procedures.* John Wiley and Son Inc.

Blischke, W. R. and Murthy, D. P. (2000). *Reliability Modeling, Prediction, and Optimization.* John Wiley and Son Inc.

Jacopino, A., Groen, F., and Mosleh, A. (2004). Behavioural Study of the General Renewal Process. *Proceedings Book of IEEE Reliability and Maintainability Symposium*, (pp. 237-242).

Kijima, M., Morimura, H., and Suzuki, Y. (1988). Periodical Replacement Problem Without Assuming the Minimal Repair. *European Journal of Operational Research, 37*, 194-203.

Kobbacy, K. A. and Murthy, D. P. (2008). *Complex System Maintenance Handbook.* Springer.

Pham, H. and Wang, H. (1996). Imperfect Maintenance. *European Journal of Operational Research, 94*, 425-438.

Rausand, M. and Hoyland, A. (2004). *Sytem Reliability Theory: Models, Statistical Methods and Application.* John Wiley and Son Inc.

Stephens, K. S. (2011). *Reliability Data Analysis with Excel and Minitab.* American Society for Quality.

Wang, H. and Pham, H. (2006). *Reliability and Optimal Maintenance.* Springer.

Wang, P. and Coit, D. W. (2005). Repairable Systems Reliability Trend Tests and Evaluation. *Proceedings Book of IEEE Reliability and Maintainability Symposium*, 416-421.

Tool Wear Estimation in Erath Pressure Balance (EPB) Machine Tunneling

M. Hedayatzadeh
Politecnico di Torino university

D. Peila
Politecnico di Torino university

ABSTRACT: The use of mechanized excavation especially tunnel boring machines (TBMs), has grown more and more in tunnel projects. One of the advantages of TMB compared to conventional method is that these machines can be used in several geological conditions. In the recent years, The Earth Pressure Balance (EPB) shield method was successfully used in urban areas and its application is developed. One of the decisive issues for successful EPB tunneling using conditioning agent is the wear estimation and the assessment of the effects of abrasive ground on the costs and schedule of a project. The estimation of primary wear as well as secondary wear is important for performing a successful project. Among the parameters that can be affected on wear, the soil conditioning is very important. Soil conditioning has been increasingly used to improve the performance of tunnelling process adding foaming agent. It can reduce the wear of machine cutter head face plate and tools, and all wear parts of the muck removal system. In order to assess the impact of the soil conditioning on tool wear, this paper introduces a new test apparatus with new propeller built to measure soil abrasion. Moreover, a specific test procedure has been designed and several sets of tests was conducted in the "Tunnelling and Underground Space Center" of Polytechnic university of Turin, in collaboration with UTT Mapei S.P.A. The primary examination shows that utilizing soil conditioning can reduce the wear of tool. More tests are underway to evaluate the effect of soil conditioning as well as other parameters on wear tool that lead to introduce the model and index for predicting the wear in soft ground tunnelling.

Keywords: Soil conditioning, tool wear, Shield tunneling, soil abrasivity

1. INTRODUCTION

In the last few years, one of most significant issue in soft ground tunneling has been the abrasiveness of soil influencing EPB tool life. In technical references there are a large number of methods to determine the abrasivity of hard rock. This fact arises from long tradition of predicting e.g. TBM performance rates and tool wear (Nilsen, Dahl, Holzhäuser & Raleigh; 2006, pp:36-38). In soil and soft ground tunneling very few methods are defined. Nilsen et al and Jakobsen and Dahl converted NTNU/SINTEF´ existing abrasivity measurement technique for hard rock and made it applicable for measuring soil abrasivity (Thewes & Budach; 2010). Thuro et al converted the LCPC abrasive-meter to measure soil abrasivity (Ozdemir & Nilsen; 1999; pp:21-35). Gharahbagh and Rostami and Rostami et al developed a new soil abrasivity measuring technique that takes into account in situ soil properties (Nilsen, Dahl, Holzhäuser & Raleigh; 2006, pp:43-45). In soft ground tunneling excavated by EPB shields, soil conditioning play significant role in satisfied fulfillment of tunneling process. Furthermore the presence of the conditioning agent changes the mechanical behavior of the soil that enters in the buck chamber and is extracted through the screw conveyor (Report 1B-98; 1998; pp168; NW.U.of.Sci&Tech) and (Gharahbagh,Rostami & Gilbert; 2010). The study of the effect of soil conditioning on tool wear has been limited to few

applications carried out by Peila et al and Rostami (Peila, Oggeri & Vinai; 2007; pp.1622–1625) and (Peila, Oggeri & Vinai; 2009).

2. TOOL WEAR

Modern researches have established that there are four main types of wear besides a few processes that can be considered (Gharahbagh,Rostami & Palomino; 2011). Adhesive wear occurs when two smooth bodies slide over each other, and fragments are pulled off one surface and adhere to the other. Later these fragments are pulled off one surface and adhere to the other. Later this fragment may come off the surface on which they are formed and be transferred back to the original surface, or else form loose wear particles. Adhesive wear arises from the strong adhesive forced set up whenever atoms come into intimate contact with similar patches on one of the surface, and there is a probability, small but finite, that when this contact is broken the break will occur not at the original interface, but within one of the material. In consequence a transferred fragment will be formed. Abrasive wear occurs when a rough hard surface or a soft surface containing hard particles, slides on a softer surface and plush a series of grooves in it. The material from the grooves is displaced in the form of wear particles, generally loose one. Corrosive wear occurs when sliding take place in a corrosive environment. In the absent of sliding, the corrosion will form a film on the surface. This film tends to slow down or even arrest the corrosion. However the sliding action wears the film away, so the corrosive attack continues. Surface fatigue wear is observed during repeated sliding or rolling over a track the repeated loading and unloading cycles to which the materials are expected may induce the formation of surface or subsurface cracks, which eventually will result in the breakup of the surface as form of where It shown by brittle materials, which break up in the form of large fragments. In both surface fatigue wear and surface fracture where the amount of damage is augmented if the slides of the forward-backward nature.

In addition to these wear mode, erosion should be taken into account in soft ground tunneling that is the special type of abrasive wear. Erosive wear is a process in which a particle carried in a fluid medium hits a solid surface and remove materials from it. Two types of erosion are mainly encountered, low speed and high speed erosion. Among these types of wear, the main phenomenon in soft ground tunneling is abrasion wear. The lubricant and foam of conditioning can play a significant role in wear reduction.

3. SOIL CONDITIONING

In soft ground tunneling, the tool replacement is very expensive. As already discussed the wearing of tools must be considered with great care. Soil abrasiveness is influenced by many characteristic of soil such as soil features (homogeneity, density, porosity), sedimentary features (mineralogical composition and grain shape) and the grains mechanical characteristics (uni-axial compressive strength and abrasiveness) moreover the average life of tools is strictly related with the percentage of hard minerals in the soil. To determine a wear index of a soil, different laboratory tests have been proposed by various researches mainly based on tools rotating inside the soil. A good discussion of the available tests can be found in Gharahabagh et al. (Peila, Oggeri & Vinai; 2007; pp.1622–1625) and Nilsen (Ozdemir & Nilsen; 1999; pp:21-35). It should be highlighted that these researches did not analyze the influence of soil conditioning used in EPB tunneling. On the other hand the correct design of soil conditioning for the management of an EPB machine is of key importance for achieving good result in the tunneling process. Furthermore the presence of the conditioning agents changes the mechanical behavior of the soil that enters in the buck chamber and is extracted though the screw conveyor (Gharahbagh,Rostami & Gilbert; 2010). Soil conditioning is usually obtained by adding foam to the soil to change its properties. The

foam bubbles are inserted between the soil grains thus changing the properties of this new materials . This change has also great influence on the wear and therefore is necessary to study it.

4. WEAR TEST EXPERIMENTAL APPARATUS

The experimental apparatus was designed to examine weight and torque reduction both on natural and conditioned soils with different conditioning sets. The test is conducted by a metal disc which rotates with a constant speed rate around its axis into a tank filled with the soil. During the test the torque applied to the disc by an electric engine is recorded. A rotation rate of 320 rpm was chosen. This value is different from the cutter head or the screw conveyor rotation rate but it is a compromise between the duration of the test (that should be less than 15 min to guarantee that the bubbles are maintained and are “alive” inside the soil) and the time needed for a reasonable wear of the disc. Based on the above, easily wearing material was chosen for the disc. After some tests an aluminum disc was chosen (a tensile strength of the material: 440MPa; elastic modulus: 3.3 GPa). After each test, the weight loss of material can be measured. In figures 1 and 2 the most important geometrical features of the experimental apparatus are reported.

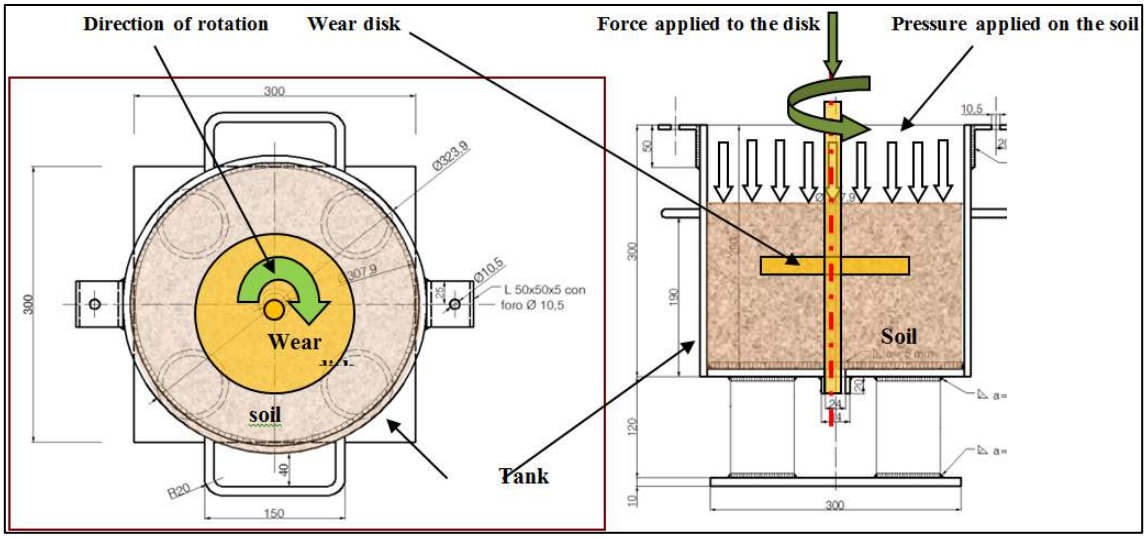

Figure 1. Scheme of the proposed test

Figure 2. Global views of the test device assembled in the laboratory

In order to evaluate weight loss of simple disk, some tests were conducted on different granular soil with different grain size curves represented in figure 3 and with the relevant parameters summarized in Table 1. The soils were conditioned to their optimal level as defined following the procedure presented by Peila et al using the slump test [6]. The conditioning agent is the commercial product Polyfoamer. As a whole 30 test was conducted by three conditions including dry, wet (with different values of water content) and conditioned. Results are summarized in Figure 4 where it is possible to see the great effect of the conditioning agent with significant reduction of wear and torque

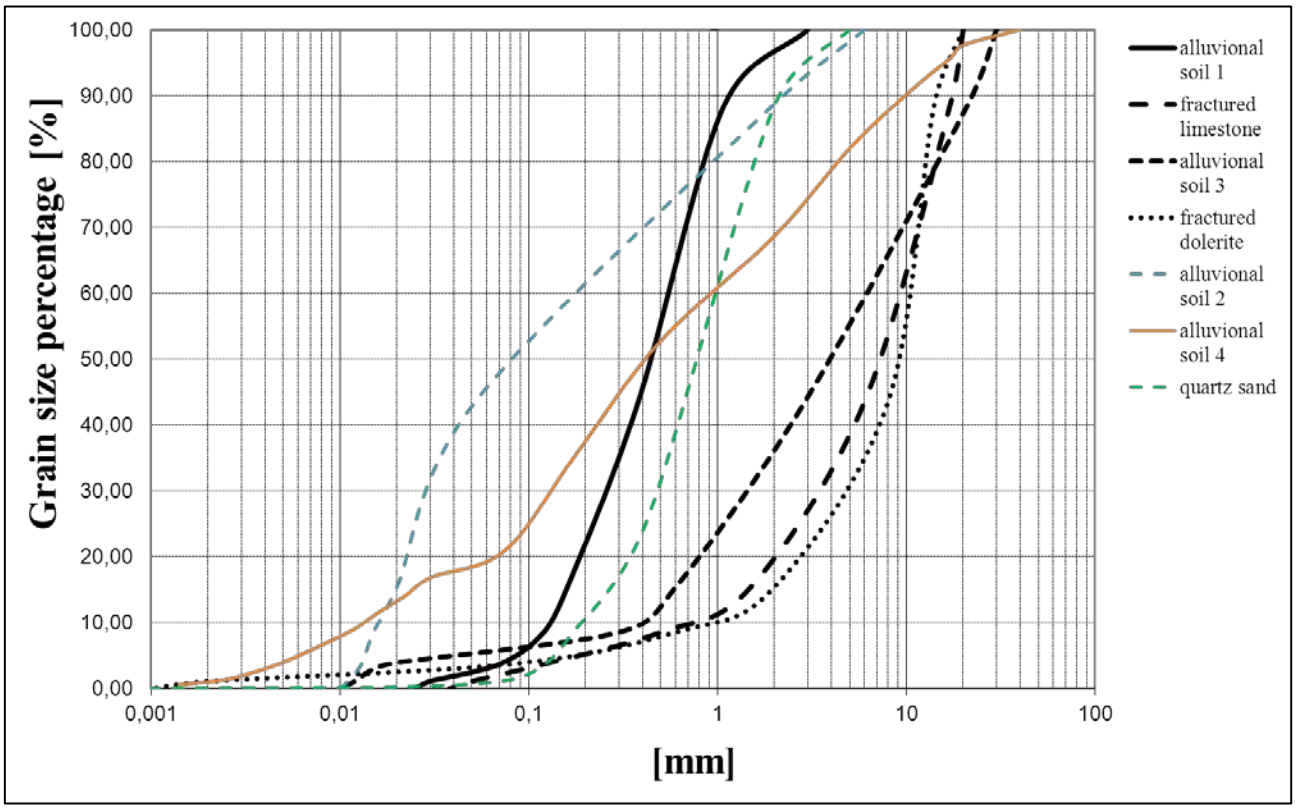

Figure 3. Granumetrical curve of soils

Table 1. Studied soils data

Soils	*D10*	*D60*	*U*	*Notes*	*Test of optimal conditioning*
Fractured limestone	0.70	9.00	12.80	Fractured rock mass, with sharp grains of Limestone.	FIR[%]=50, FER[%]=15 WATER[%]=3
Alluvional soil - 1	0.13	0.55	4.20	Alluvional soil, with rounded grains. Quartz content 20-25%	FIR[%]=80, FER[%]=15 WATER[%]=15
Alluvional soil – 2	0.017	0.18	14.80	Alluvional soil, with rounded grains. Quartz content 50-60%	FIR[%]=40, FER[%]=10 WATER[%]=0
Alluvional soil – 3	0.40	6.00	15.00	Alluvional soil with rounded grains. Quartz content 30-35%	FIR[%]=40, FER[%]=15 WATER[%]=8
Alluvional soil – 4	0.014	0.90	64.30	Alluvional soil with rounded grains. Quartz content 30-35%	FIR[%]=60, FER[%]=12.5 WATER[%]=3
Fractured dolerite	1.00	10.00	10.00	100% of hard minerals	FIR[%]=50, FER[%]=11 WATER[%]=18
Quartz sand	0.20	10.00	50.00	Quartz content of 95-100%	FIR[%]=40, FER[%]=13 WATER[%]=5

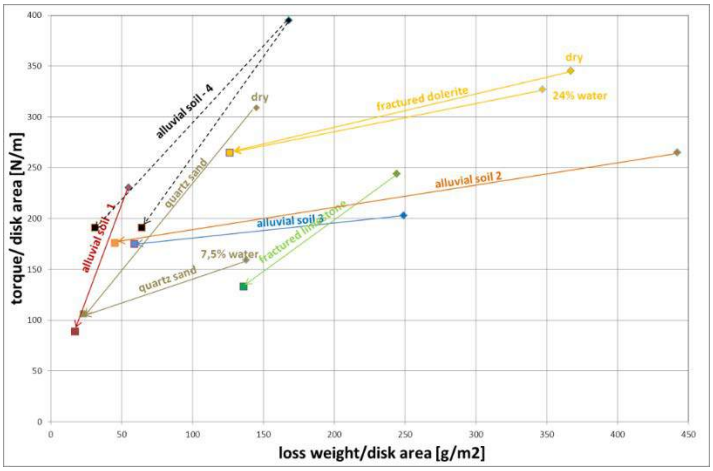

Figure 4. Results achieved with the carried out tests. The obtained results are presented to compare the values obtained with the natural soils and the conditioned ones [6].

In the second step of the research, in order to find the impact of various sets of conditioning on wear and torque four tests was conducted on granular soil with D_{10} = 0.11, D_{60} = 2 and Quarts content in about 50% (characteristics of soil , granumetrical curve and microscopic picture of soils are shown in figure 5 by changing the conditioning set . The four test conditions are listed below:

1. Test (1Gs): Dry granular soil.

2. Test (2Gs): Conditioning agents: Polyfomer(FP), FER = 15, FIR = 30%, w = 5%.

3. Test (3Gs): Conditioning agents: Polyfomer(FP), FER = 15, FIR = 20%, w = 2%.

4. Test (4Gs): Conditioning agents: Polyfomer(FP), FER = 15, FIR = 50%, w = 10%.

Figures 6, 7 and table 2 show the obtained results

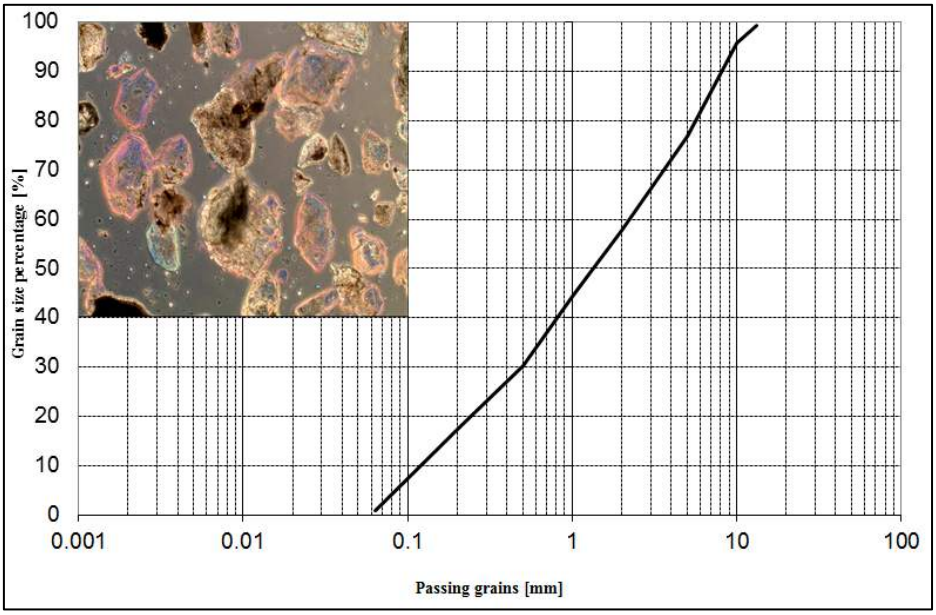

Figure 5. Granumetrical curve of granular soil and Microscopic picture of the soil of the granular soil. The blue color grains are those of quartz.

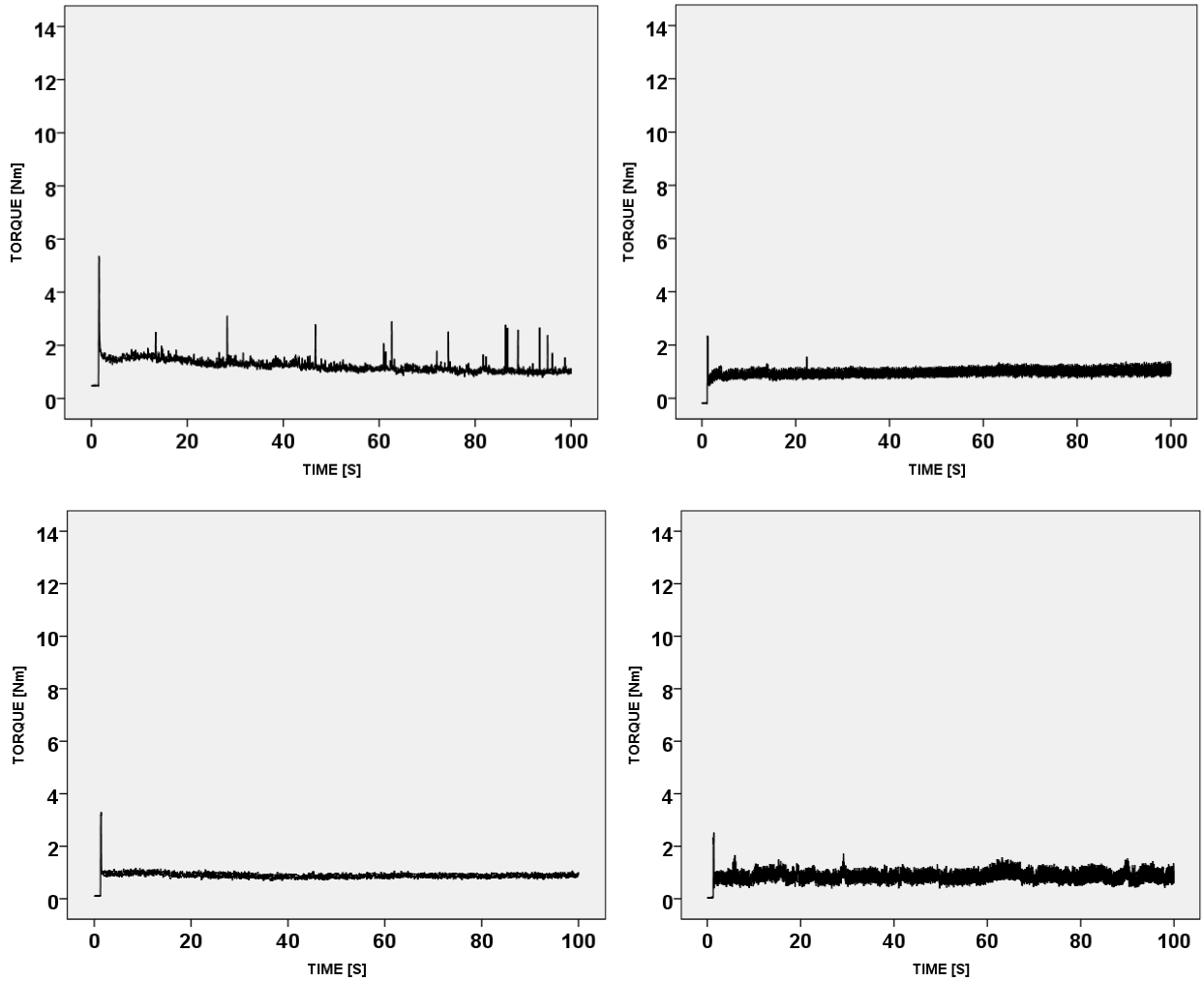

Figure 6. Correlations between torque and time in four condition of granular soil

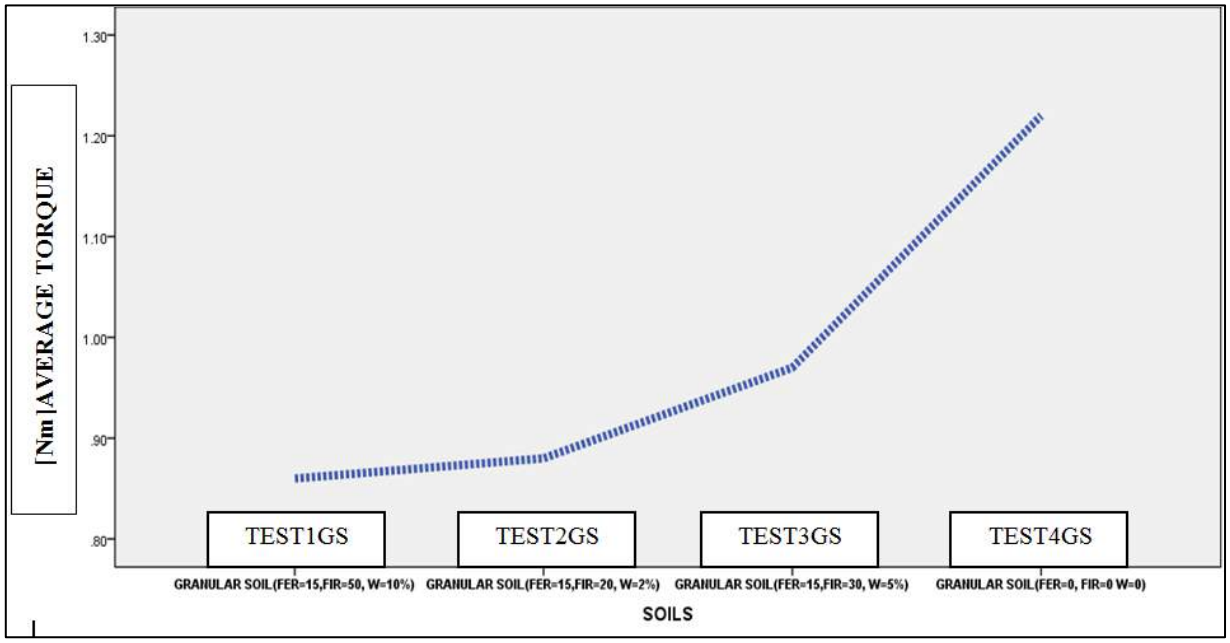

Figure 7. Correlation between torque and all type of soil

As can be seen in the figure 7, the conditioning reduces the torque and wear. This is due to the fact that with conditioning the angle of internal friction deceases. The reason for reduction of the angle of internal friction is due to the presence of bubbles that interact between the grains that facilitate their movements.

Table 2. Results of the carried out tests

Torque	Minimum value of torque [N.m]	Maximum value of torque [N.m]	Average with initial traction of torque [N.m]	Average without initial traction of torque [N.m]	Reduction of weight [g]
Test (1Gs)	0.470	5.34	1.22	1.17	1.01
Test (2Gs)	0.190	2.35	0.97	0.90	0.59
Test (3Gs)	0.097	3.29	0.88	0.78	0.80
Test (4Gs)	0.031	2.51	0.86	0.80	0.001

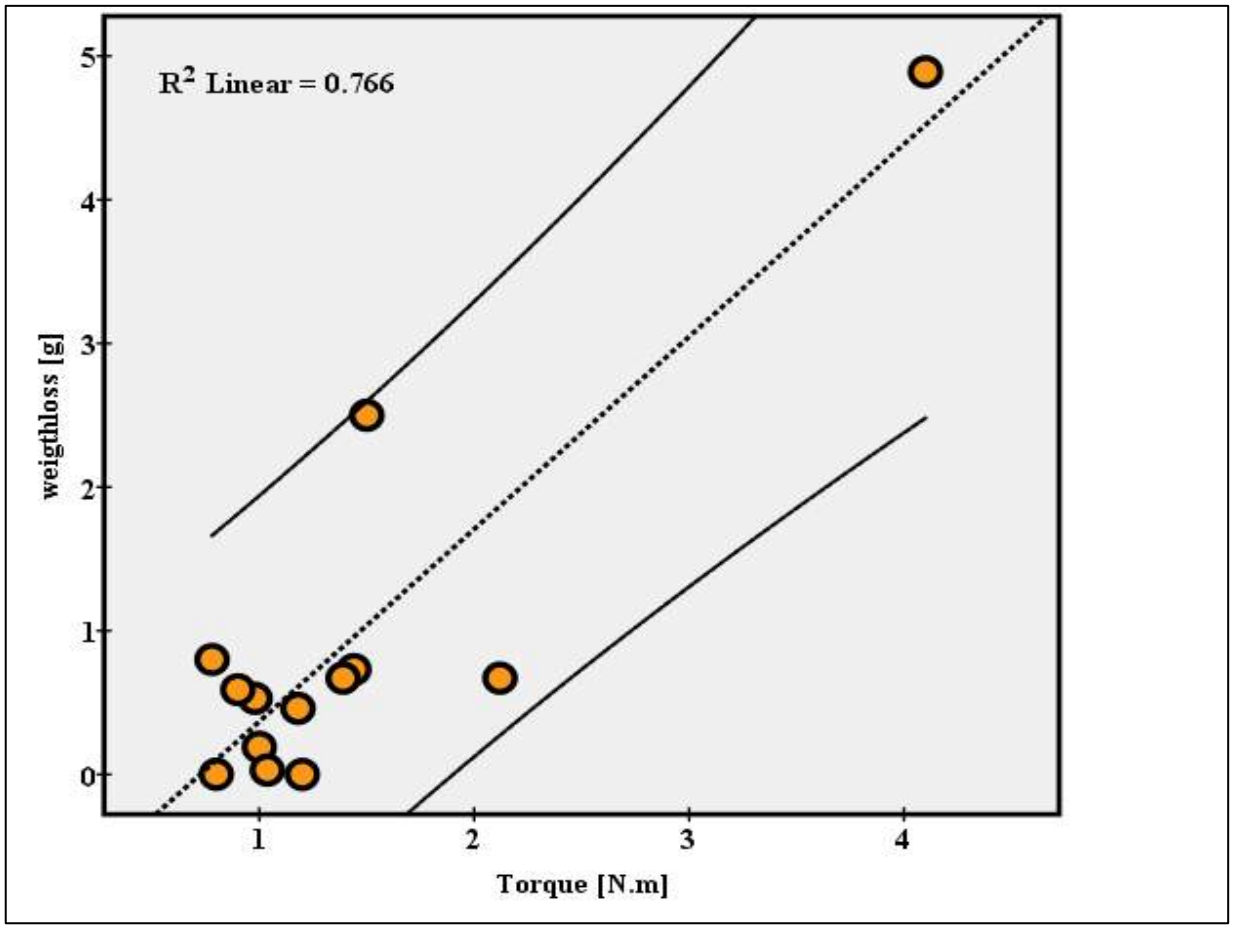

Figure 8. Relationship between torque and weight loss in conditioned soil

As illustrated in figure 8 there is a good relationship between torque and weight loss because increasing in torque means that the internal friction is high so the amount of weight loss will increase.

In order to simulate what exactly is happening for cutter head in EPB tunneling the new propeller was constructed to consider surface and lateral force that can be affected on disk cutter in EPB machines. This new propeller (figure 10) has some advantage in comparison with old one:

1. Changeable blade (flexibility to choose the different type of materials of the blades).
2. Possibility of study on both surface and lateral wear.

With new propeller some tests were conducted on the quartzite sand with D10 = 0.2, D60 = 10 and quartz content of 95-100%. The photo of grains and geometrical curve of studied soil are illustrated in figure 9.

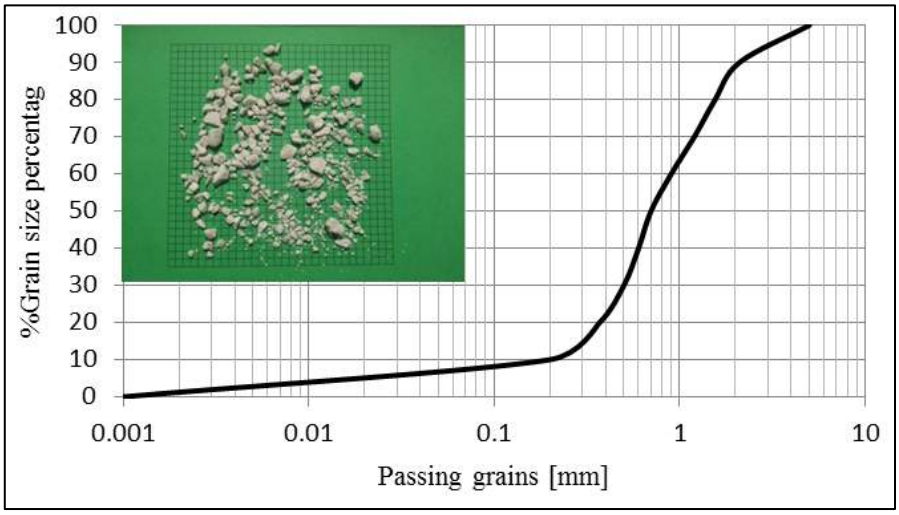

Figure 9. Photo of quartzite grains and its granumetrical curve

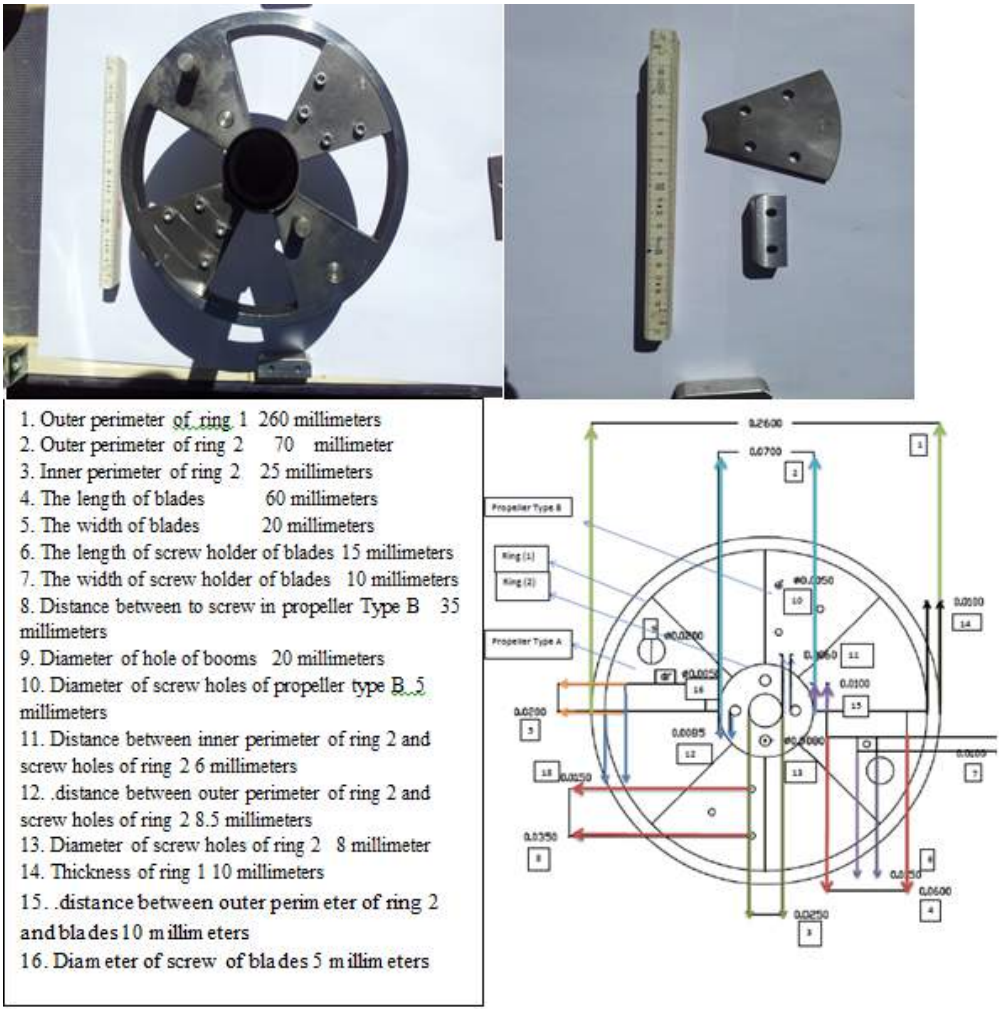

Figure 10. Photographs and drawing of improved propeller

Table 4. Result of three number test with new propeller conducted on quartzite

Number of tests	Weight loss [g]	Test duration [min]	Water[%]	Conditioning
1	0.22	15	0	No
2	0.13	15	5	No
3	0.07	15	5	FIR=30, FER=13%

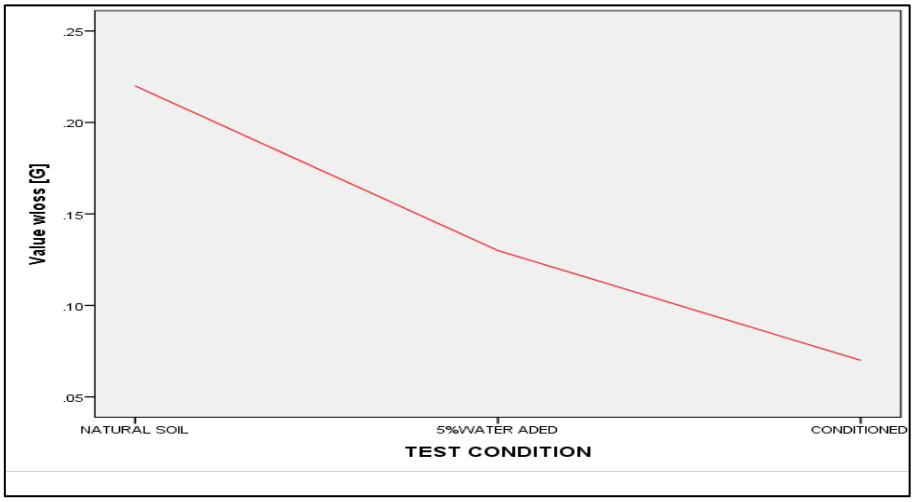

Figure 11. Relationship between weight loss and test condition

As can be extracted from figure 11 there is a reduction in weight loss from dry to conditioned soil. The primary results gained from new propeller shows that the test can be used for further test, hence the more test is under way.

5 CONCLUSION

The proposed wear test device with full disk and the newly improved propeller and test methodology have observed to be a feasible tool to measure the wear reduction that can be achieved by conditioning cohesionless soil for EPB tunneling.

The results obtained are quite consistent with the properties of the soil and the expected results show that the addition of water is generally not enough to reduce the tool wears and the torque. On the other hand when foam is added with the correct conditioning parameters (which are previously found out with slump tests following already established procedures and methodologies), wears and torque are greatly reduced. This effect is positive since facilitates the EPB operations from a technical and economical points of view.

REFERENCES

Nilsen, B., Dahl, F., Holzhäuser, J., Raleigh, P., "Abrasivity of soils in TBM tunneling",. Tunnels & Tunnelling International, pp. 36–38, March 2006.

Thewes M., Budach C., "Soil conditioning with foam during EPB tunneling", *Geomechanics and Tunnelling, Vol. 3,* No. 3, pp. 256–267, 2010.

Ozdemir, L., Nilsen B., "Recommended laboratory rock testing for TBM projects", AUA news, Vol, 14, No. 2, pp. 21-35, 1999.

Nilsen, B., Dahl, F., Holzhäuser, J., Raleigh, P., "SAT: NTNU's new soil abrasion test*", Tunnels & Tunneling International*, pp. 43–45, May 2006.

NTNU, "Hard Rock Tunnel Boring", Norwegian University of Science and Technology, *Dept. of Building and Construction Engineering, Report* 1B-98, 164 p. 1998.

Gharahbagh, E.A., Rostami, J., Gilbert M, "Tool wear issue in soft ground tunnelling. *Developing a reliable soil Abrasivity Index", North American Tunnelling Conference*, Portland, 2010.

Peila D., Oggeri C., Vinai R.,. "Screw conveyor device for laboratory tests on conditioned soils for EPB tunneling operations", *Journal of Geotechnical and Geoenvironmental Engineering*, ASCE, Vol. 133, pp.1622–1625. 2007.

Peila D., Schulkins R., "Soil conditioning and backfill grout, ITA/AITES – Training Course ", Tunnel Engineering, Budapest, 2009.

Gharahbagh, E.A., Rostami, J., Palomino A.M., "New soil abrasion testing for soft ground tunneling applications", *Tunnelling and Underground Space Tecnology, Vol. 26*, pp. 604-613, 2011.

Nilsen, B., Dahl, F., Holzhäuser, J., Raleigh, P., "Abrasivity testing for rock and soils", *Tunnels & Tunneling International*, pp. 47–49, April 2006.

Sensitivity Analysis of the Underground Mining Machines Based on Power Generating System

Yeraltı Maden Makinalarının Güç Üretim Sistemlerine Göre Duyarlılık Analizi

C. Doğruöz
Dumlupınar University, Mining Engineering Department, Kütahya, Turkey

A. Nieto
Penn State University, Mining Engineering Department, USA

R. Schatz, S. Lvov
Penn State University, Electro-Chemistry Department, USA

ABSTRACT There is a variety of equipment used in the mining industry for a long time in underground mines all around the world. Some machines require substantial amounts of power and need direct connections to external generators in underground, while others can be powered via diesel engine. Some of the most significant underground mining equipment was analyzed and sensitivity analysis was figured out in this study to determine whether it is feasible to incorporate current battery technology into these machines. Currently, diesel engines are the standard power source for light duty mining equipment however they are not a perfect solution. They are a source of ignition, noisy, and emit fine particulates as well as carbon dioxide into the mine. For that reason, current battery technology is being explored as a safer alternative in the mining machines. In this study, underground mining methods and tethered electric powered machines were the focus of the investigation and the sensitivity analysis. The most common of these methods, room and pillar and longwall were reviewed and mining vehicles were selected based on their significance in each method. Because of their tasks, dimensions and energy requirements, locomotives and load-haul-dump (LHD) vehicles are the most important equipment as they are used for each of the mining methods. The main objective of this study is to compare battery powered equipment to tethered electric and diesel vehicles in order to assign sensitivity analysis of LHD and locomotives in underground mining.

Keywords: LHD sensitivity analysis, tethered electric powered vehicles, underground mining vehicles

ÖZET Dünya'da maden endüstrisinde birçok yeraltı maden işletmesinde uzun zamandır çeşitli madencilik ekipmanları kullanılmaktadır. Bu anlamda yeraltı madenciliğinde, bazı maden makinaları dizel motorlu güç kaynağı kullanırken diğer maden makinaları ve harici jeneratörler ise önemli derecede güç kaynağına ihtiyaç duymaktadır. Bu çalışmada, yeraltı madenlerinde çok önemli bir yere sahip olan bazı maden makinalarının ekonomik analizleri yapılmış ve günümüzde mevcut batarya teknolojilerinin bu makinalara uygulanabilirliği konusunda duyarlılık analizleri çalışılmıştır. Günümüzde hafif iş makinalarında standart olarak dizel güç kaynaklı motorlar kullanılmaktadır fakat bu ekipmanlar en uygun çözüm olmamaktadır. Aksine bu ekipmanlar gürültülü, ateşli ve karbondioksit emisyonu açısından madenlerde kullanımı sıkıntılı güç kaynaklarıdır. Bu sebeple, mevcut batarya teknolojisinin maden makinalarında kullanımı araştırılmaktadır. Bu çalışmada, yeraltı madencilik yöntemleri

ve kablolu elektrik güç kaynaklı maden iş makinaları araştırmanın ve duyarlılık analizinin odak noktası olmaktadır. En çok kullanılan yeraltı işletme yöntemlerinden oda topuk ve uzun ayak yöntemleri gözden geçirilmiş ve her bir işletme yöntemi için en uygun maden araçları seçilmiştir. Her bir maden yöntemi için yeraltındaki işlevleri, ebatları ve enerji ihtiyaçları göz önüne alındığında, lokomotifler ve LHD maden makinaları en önemli maden ekipmanlarındandır. Bu çalışmanın temel unsuru batarya kaynaklı ekipmanların kablolu elektrik güç kaynaklı ve dizel araçlara kıyasla yeraltında çalışan LHD ve lokomotifler için duyarlılık analizlerinin hesaplanmasıdır.

Anahtar kelimeler: LHD, duyarlılık analizi, batarya kaynaklı elektrikli makinalar, yeraltı maden makinaları

1. INTRODUCTION

Soft rocks usually are part of the sedimentary minerals classification. This is further categorized into three subdivisions; clastic, organic, and chemical. Coal, shales, potash, salt, and trona encompass the majority of soft-rock ores. The most common geographical layout for these ores consists of laterally extensive beds in a nearly horizontal inclination but with, at most, a shallow dip angle (Nieto, 2011). In underground mining, especially for coal mining, mining equipment has a significant role in industry. The best equipment combination should be employed to ensure efficient mining. Furthermore, the more efficient the machines are at extraction, the higher the profit margin will be. Therefore, the ability to use a greater number of battery powered than diesel powered machinery in the same area of the mine is of significant interest.

Current mining methods are so diverse that any ore type can be extracted by adapting existing extraction methods. Underground methods require an extensive evaluation of the geological variables (Hartman, Mutmansky, 2012). Underground mining methods are classified into three groups: unsupported, supported and caving. Unsupported methods include room-and-pillar, stope-and-pillar, shrinkage stoping, sublevel stoping and vertical crater retreat; the supported group includes cut-and-fill and the caving category includes longwall, sublevel caving (Nieto, 2011).

Every mining method has benefits and risks that must be understood when determining the technique to be used for a given set of variables (Hustrulid, 1982). This is especially important when determining duration of mine operation, operating costs and required capital as an uninformed decision can result in significant loss of profit. Room and pillar and longwall are among the most utilized in coal mining and are expanded upon below. Using battery powered mining vehicles in underground soft rock methods can be more economic and is a safer technology for underground mining methods.

The room and pillar mining method is popular for tabular and lenticular deposits and is frequently applied in soft-rock mines. The most important parameters for this method are the position of the ore-body, elevation of the mining horizon, slope of the ore and depth of the deposit. This method is used if there is no need to drill or blast which is usually the case in soft rock mining. Continuous miners are the preferred equipment for this method. This type of autonomous miner uses a large rotating drum to break the material in front of the platform. After that an internal part loads the broken ore onto the onboard conveyor. The material is then sent to a separate haulage system which carries the material to the surface, usually consisting of a shuttle car and locomotive or a belt conveyor (Nieto, 2011). For the room and pillar underground mining method, using the battery powered mining vehicles can be more efficient due to the relatively larger space in the underground rooms. LHDs will have enough space to easily maneuver even with the large battery packs at the rear of the vehicle. High maneuverability allows for greater ease in

charging the vehicles or the maintenance of the equipment.

The longwall mining method is generally combined with the room-and-pillar technique to generate the most efficient and highest-producing underground coal mines. Initially the main entries follow the conventional room and pillar techniques and are created using continuous miners. In this method, a series of panels, branching perpendicular from the main entries, are bounded by a two-to-three entry room-and-pillar border, leaving a huge solid block of coal within it (Buchan, 1998). A longwall shearer, armored face conveyor and shield wall are moved to the end of the panel before longwall mining commences. The shearer moves back and forth across the coal block, excavating only the ore, causing the material to fall onto the conveyor and be transported away to the main belt conveyor system. The shields advance along with the shearer to hold up the roof directly above the equipment. The excavated area behind the shields is allowed to collapse. Mining progresses as continuous miners develop additional longwall panels and the shearers are moved from one to the next throughout the course of the mine life (Nieto,2011). Though longwall equipment requires too much power, LHDs and locomotives are irreplaceable and possess power requirements within the range to be considered for conversion to battery power (Schatz et. al., 2014).

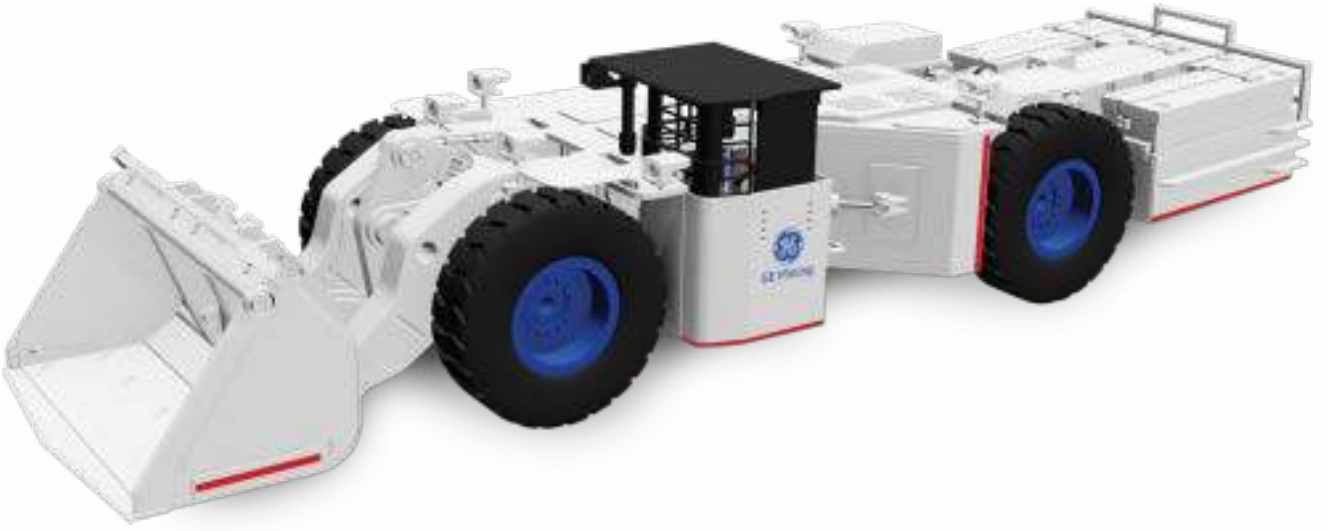

Figure 1. Load-Haul-Dump vehicle © General Electric Co. 2014

2. UNDERGROUND MINING VEHICLES

In underground coal mining, the most common vehicles are locomotives, load-haul-dump vehicles (LHDs), continuous miners, and longwall equipment. As mentioned before, continuous miners, and longwall equipment require too much energy to make battery conversion feasible. The locomotives and LHDs are most commonly powered by diesel engine. Several companies, however, have shown a large interest in powering these vehicles solely from battery power. According to the mining methods and all other parameters such as material strength, ore type, rock mass etc, it is very important to choose the best suited vehicles and power systems.

Transportation of miners and materials underground is one of the most significant operations in the mining sector. For this reason, locomotives are mainly used in underground mines due to their capabilities. There are different types of locomotives such as diesel powered, battery powered and trolley locomotives. Locomotives have been used for many years in underground mining and because of their reliability and are preferred as an easy, economical transportation vehicle (Hartman, 2004, Konietzky, Schlegel, 2007).

Load-haul-dump mining vehicles, Figure 1, are used to haul waste rock and ore from the production face in underground mines to haulage trucks, crushing stations, and ore dumping points (Bhattacherya et. al., 2006).

LHDs are a specialized loading machine manufactured solely for the underground mining industry. They are also known as a scoop tram as they are used to scoop extracted ore, such as coal, with a bucket and load it into the car. The ore is then dumped in the bottom of the mine to undergo primary crushing before being hoisted to the surface out of the mine.

Most LHDs are diesel powered because they require a large amount of energy and move around a lot. If the vehicle were to be powered by an electrical cable, it would pose a constant trip/entanglement hazard. This could be avoided, however, by replacing the diesel engine with a battery pack. Below in Table 1, battery pack specifications for a 112 kW LHD vehicle for the three types of cell chemistries namely lead acid, lithium ion and sodium metal halide are estimated. They are compared on an isometric basis of 5000 L (Table 1).This was approximated by finding the engine compartment volume for a Caterpillar CL115 LHD vehicle, which would be vacant if the diesel engine were to be replaced.

Table 1. Estimated parameters for alternate cell chemistries for 112kW LHD

Parameters	**VRLA**	**NaMx(Na-$NiCl_2$)**	**Li-ion (LFP)**
Run Time (h)	4	8.5	17
Volume (L)	5000	5000	5000
Weight (kg)	14,310	8,200	13,490
Battery Cost (USD)	64,500	274,050	665,000
Capacity (kWh)	430	945	1,900

The NaMx cells would provide enough energy to last one 8-hour shift and would be the lightest of the three packs at just over 8,000 kg. An LFP pack would last more than two shifts but costs 60% more than the NaMx battery pack. Since a VRLA pack would only last 4 hours, requiring the operator to replace the battery during the shift. However, the battery is significantly cheaper than the other two and may make up for the inefficiency of lasting only half a shift.

In underground soft rock mines, mostly coal mines, the mining equipment most commonly used, besides extraction equipment, are haulers, loaders, and locomotives. As mentioned above, these vehicles may also be used in hard rock underground mining operations. In underground hard rock mining other light duty vehicles are used include low profile haulers or load haul dump (LHD), and drilling jumbos. Haulers are mainly used to muck and haul material to dump points over relatively short distances. Drilling jumbos are mainly used in hard rock mining for drilling holes for either installing bolts or blasting. Transportation of miners and materials in underground mining is a key operational task. Locomotives are mainly used in underground mines to accomplish this task. There are different types of locomotives such as diesel powered, battery powered and trolley locomotives. Locomotives have been used for many years in underground mining and because of their reliability they are preferred as a simple and economical solution for material and personnel transportation purposes (Miller, 2002).

Figure 2. Underground mining locomotive adapted to be fuel cell powered (4 ton -7.2 kW).

3. SENSITIVITY ANALYSIS OF MINING VEHICLES

In general, as it is known, sensitivity analysis is used to determine how different values of an independent variable will impact a particular dependent variable under a given set of assumptions. In this study, sensitivity analysis is a process which helps us to understand what will happen to the value of economical analysis in underground mining vehicles if any of our key inputs or assumptions were to change. The main process for conducting a sensitivity analysis includes changing each input variable one at a time, and specifying the effect that has on the total project value. It is usually investigated at the effect on the net present value (NPV), but it could be equally looked at the internal rate of return (IRR) or the payback period as a measure. In sensitivity analysis, the key point is that only one variable is changed at a time in the financial model, leaving all other variables constant. This allows us to see what effect each different assumption would have if it proves to be incorrect. For this method, we usually pick four to six particular values which we will use to do sensitivity cases.

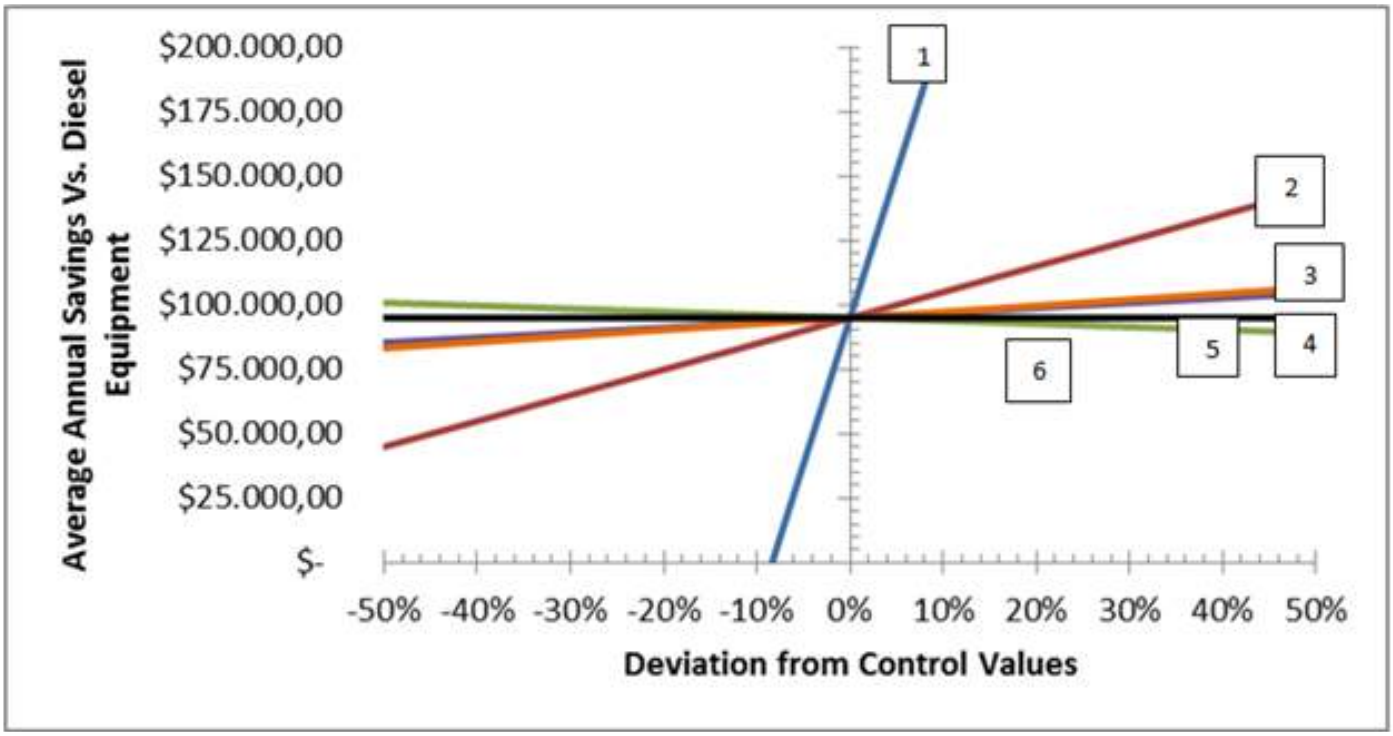

Figure 3. Battery Vs Diesel-Adjustment of tons moved(blue as no.1), ore density(red as no.2), electricity price(green as no.6), battery equipment capital(purple as no.4), and Diesel maintenance cost(Orange as no.3)| reference line (black as no.5)

The sensitivity analysis for costs took many of the parameters that are very volatile during the operation of the mine. These costs include energy prices, both electric and diesel, equipment capital and maintenance costs. It was found that there were several different methods of calculating cost variation. Maintenance costs for example could be calculated as keeping one cost fixed and adjusting the other, adjusting the ratio, seen in Figure 3. It could also be varied by adjusting one cost and keeping the other at a fixed ratio , seen in Figure 3(orange as no.3). It was found that the two methods had significantly different impacts on costs.

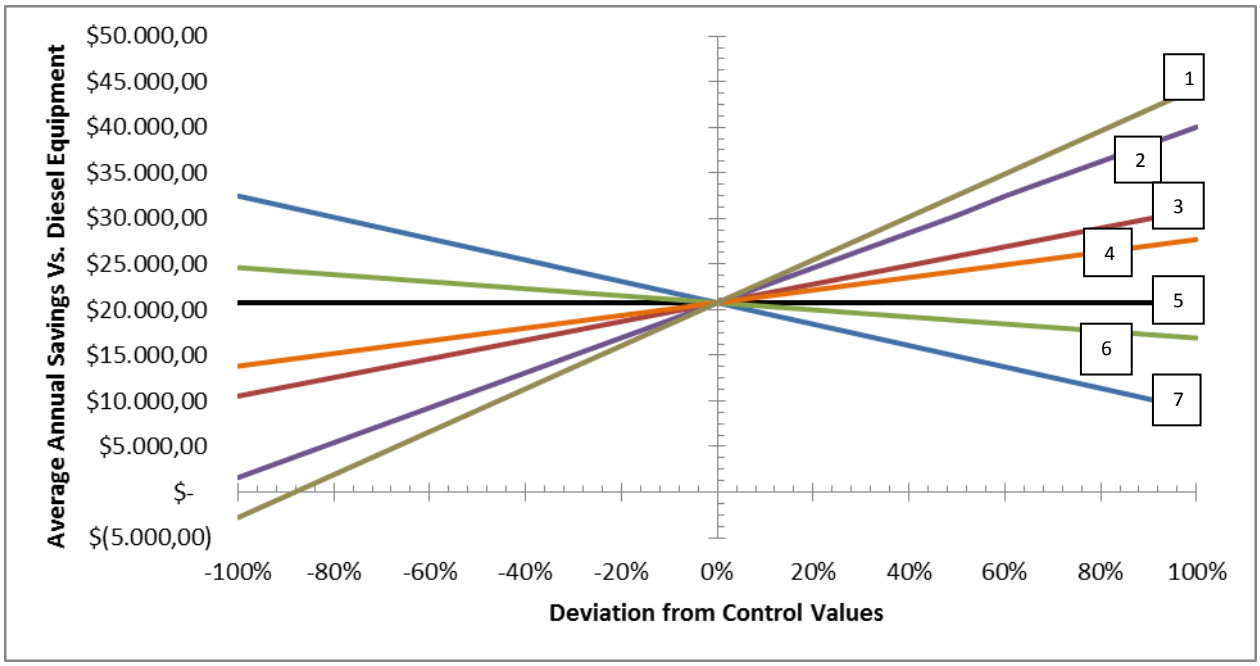

Figure 4. Adjustment of electricity cost(blue as no.7), cost of fuel(red as no.3), cost of battery pack(green as no.6), Equipment capitol (battery equipment costing 5% more than diesel)(purple as no.2), cost of maintenance (ratio of diesel to battery constant)(orange as no.4), and cost of Diesel Maintenance(tan as no.1), reference line (black as no.5)|.

Another, interesting comparison was the energy costs with respect to electricity price(blue as no.7) and diesel price(red as no.3) in figure 4. Figure 4 also shows that cost difference is more sensitive to electricity prices than to diesel fuel fluctuations. The cost differentiation for adjusting capital cost was used fixing the cost of battery equipment to 5% higher than diesel costs, however, this ratio is not a guarantee.

4.CONCLUSION

The energy costs with respect to electricity price and diesel price show that the cost difference is more sensitive to electricity prices than to diesel fuel fluctuations. It should be noted that in the future the price of diesel is expected to rise significantly while increases in electrical costs may be mitigated by alternative forms of generation such as advances in solar or wind energy technology. Comparing the effect of capital cost on cost savings, varying the price increase from 5% to 25%, showed significant impact on the average annual cost savings. It was also found that in order for battery equipment to remain less costly, they must provide at least extra one year of service than diesel equipment.

Taking revenue into account only improved the value of battery equipment due to increased uptime and productivity. The revenue was found to be especially sensitive to the amount of tons each vehicle hauls. Decreasing the amount of battery haulage by 5% or 0.2 tons per hour amounts to a $40k loss of profit per year.

REFERENCES

Nieto, A. *SME Mining Engineering Handbook*. 389–396, 2011

Hartman, H. L. & Mutmansky, J. M. *Intoductory Mining Engineering*. 570 (2002).

Nieto, A. Key deposit indicators (KDI) and key mining method indicators (KMI) in underground mining method selection. *Trans. Soc. Mining, Metall. Eng.* 328, 381–396 (2011).

Hustrulid, W. A. *Underground Mining Methods Handbook*. (1982).

Buchan, G. Long panels for longwall mining at Cyprus twentymile Coal. *Min. Eng.* 50, 21–27 (1998).

Bhattacherya, I., Dunn, P. & Eger, T. Development of a new operator visibility assessment technique for mobile equipment. *JOURNAL-SOUTH AFRICAN …* 87–92 (2006). at

Schatz,R., Nieto,A., Dogruoz,C. and Lvov,S.N. 'Using Modern Battery Systems in Light Duty Mining Vehicles', International Journal of Mining, Reclamation and Environment, Taylor and Francis, November 10,2013

Konietzky, H., Schlegel, R., ,Using Sensitivity Analysis and Optimization for Civil Engineering and Geotechnical Applications', 4th Weimar optimization and stochastic days, 2007

Miller, A. & Barnes, D. Advanced underground vehicle power and control fuelcell mine locomotive. *Proceeding 2002 US DOE Hydrog.* … 1–7 (2002). at

Hartman, J.C., Schafrick I.C., The relevant internal rate of return, The Engineering Economist, 139-158, (2004)

Role of geophysical technique to validate the subsurface strata conditions due to blasting in underground coalmines

K.K.K. Singh, P. K. Singh and *M. P. Roy
CSIR-Central Institute of Mining and Fuel Research, Dhanbad 826015, Jharkhand, India

ABSTRACT Production from underground coal mining in India has been decreasing since last two decades. Presently, greater emphases are given on opencast mining to meet the energy demand of the country but the future requirement of coal would be met by underground mining as the coal will be available at greater depth which will not be economically viable to exploit by open-pit mining methods. Blasting-off-the-solid (BOS), in Indian underground mines, has been a widely practised method for winning coal while developing mine galleries in Bord & Pillar system. The blast holes are drilled in solid coal without free face in BOS method of mining and are blasted with permitted type of explosives and delay detonators. The coal reserves are being exploited very fast and mine owner cannot ignore to take the coal beneath the structures/houses. Although, the use of explosives in underground mines are not too much, but it causes annoyance to the inhabitants residing over the underground mines. Ground vibrations from blasting have been a continual problem for the mining and construction industries, the public living near the mining activities and the regulatory agencies responsible for setting safety and environmental standards. Questions frequently arise about blast vibration effects and specifically about whether vibrations can or could have caused cracking and other damages in homes and other structures. The general growth of mining activities in India, the presence of underground mines beneath the populated areas and the greater awareness have all necessitated an in-depth study for investigation into the causes of alleged damages to the houses. In this paper, Geophysical Resistivity Imaging technique has been used to document the change of subsurface structures/features between the surface and underground face, where blasting is carried out to extract the coal in underground coalmines. Resistivity Imaging survey conducted at three mining sites revealed that there was no significant change in sub-surface strata conducted during pre and post blasting conditions. The slight change in resistivity values up to 35 ohm.m up to a few meters peripheral area of the blasting face in the mine may be either due to the effect of blast vibration and/or same void created by blasting or increase in porosity of overlying sub-surface strata.

Keywords: BOS; Bord & Pillar; Resistivity Imaging; underground mines; Blast vibration

1 INTRODUCTION

Production from underground coal mining in India has been decreasing since last three decades. Presently, around 91% of the coal production comes from opencast mining and only 9% of coal production is from underground mines. It is reported that opencast production will reach to its maximum level within next 15-20 years and there will be no option except to go for underground mining with mass production technology to sustain production and productivity level for coping up with the energy demand of the country. To meet the enhanced requirement of coal in future at greater depths, the Indian mining industry has to adopt in a big way the mechanised underground mining methods.

Blasting-off-the-solid (BOS), in Indian underground mines, has been a widely practised method for winning coal while developing mine galleries in Bord & Pillar system (Room & Pillar system). The blast holes are drilled in solid coal without free face in BOS method of mining and are blasted with permitted type of explosives and delay detonators. The permitted explosives are classified based on the classification of

gassiness of the underground mine. Keeping in view the dangers associated in such blasting operations, the mine regulatory agency has also restricted the explosive weight in a shot hole in accordance with the degree of gassiness of the mine.

In future, also, blasting-off-solid will play an important role in underground coal production. The mines which were planned earlier to be away from residential areas are now approaching to those areas. The coal reserves are being exploited very fast and mine owner cannot ignore to take the coal beneath the structures/houses. Although, the consumption of explosives in underground mines are not much, but it causes annoyance to the inhabitants residing over the underground mines. A few court cases have been lodged in the recent past by the villagers for compensation of the alleged damages to their houses due to underground mining.

Ground vibrations from blasting have been a continual problem for the mining and construction industries, the public living near the mining activities and the regulatory agencies responsible for setting safety and environmental standards. Questions frequently arise about blast vibration effects and specifically about whether vibrations can or could have caused cracking and other damages in homes and other structures. The answer depends primarily on vibration levels and frequencies and to a lesser degree on site and structure specific factors.

The residents may feel blast vibrations produced by the underground blasting beneath the residential or industrial structures and there may be apprehensions of likely damages to their houses/structures. The residents of the villages residing over the underground mines may ask the mine owners to stop the mining operations beneath their houses because, in every population, there are always some persons who will react no matter how low the vibration is. But the sheer apprehensions of damages should not stop the mining of the precious mineral.

The general growth of mining activities in India, the presence of underground mines beneath the populated areas and the greater awareness have all necessitated an in-depth study for investigation into the causes of alleged damages to the houses. In this paper, Geophysical Resistivity Imaging technique has been used to know the change of subsurface structures/features between the surface and underground face, where blasting is being carried out to extract the coal in underground coalmines.

2 STUDY SITES

Under this programme of study, three underground mines were selected as experimental sites. The selected mines were Kalidaspur and Narsmunda mines of Eastern Coalfields Limited (ECL) and Orient Mine no.3 of Mahanadi Coalfields Limited (MCL). The impacts of 129 blasts conducted at the aforesaid mines were monitored at the structures and 391 blast vibrations data were recorded on or near the structures. Resistivity multi-electrode (Electrical imaging) system (an advanced version of DC resistivity four electrodes) was used to know the change of subsurface inhomogeneities like solid strata, cavities, fractures, caves etc due to underground blasting in proposed three coalmines of different regions of India.

3 METHODOLOGY

The Resistivity Imaging (RI) is a geophysical method that measures subsurface resistivity distribution from the ground surface. These measurements are normally made by passing electric current into the ground through two metallic electrodes and measuring the resulting voltage difference at two potential electrodes. From these measurements, the true resistivity of the subsurface can be estimated. The ground resistivity is related to various geologic parameters such as the mineral and fluid content, porosity, degree of fracturing, the percentage of the fractures filled with groundwater, and the degree of water saturation in the rock. Surveys using multi-electrode arrays are usually carried out using 48 or more electrodes in a series connected to a multi-core cable. A program on a laptop computer and an electrode-

switching unit automatically select the relevant four electrodes for each measurement. Apparent resistivity measurements are recorded sequentially. High definition pseudo-sections with dense sampling of apparent resistivity variations at shallow depths (10–150 m) are obtained in a short time which allows detailed interpretation of the 2D resistivity distribution in the ground. This survey used a resistivity meter (SYSCAL Junior Switch) with 48 electrodes deployed in three different arrays like Pole-Pole (PP), Wenner-Schlumberger (WS) and Wenner (W) in this proposed study.

Despite some limitations, this technique is very useful in delineating subsurface geology. The use of 2D and 3D electrical surveys are now practical commercial techniques with the relatively recent development of multi-electrode resistivity surveying instruments (Griffiths et al., 1990) and fast computer inversion software (Loke, 1994). The resistivity measurements are normally made by injecting current into the ground through two current electrodes and measuring the resulting voltage difference at two potential electrodes. From the current (*I*) and voltage (*V*) values, an apparent resistivity value is calculated (shown in Fig.1). The calculated resistivity value is not the true resistivity of the subsurface

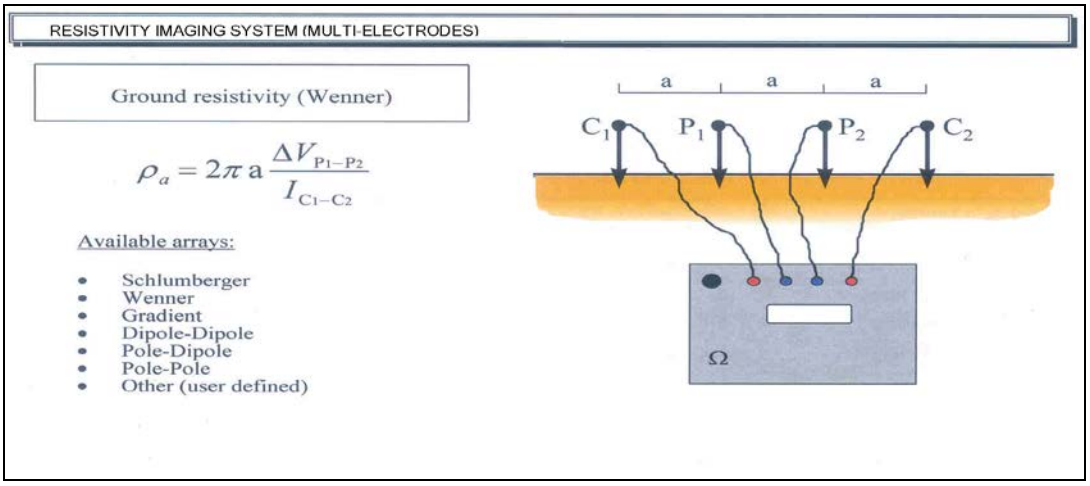

Figure 1: Principle of Resistivity Imaging Survey

To determine the true subsurface resistivity, an inversion of the measured apparent resistivity values using a computer program must be carried out (Loke, 1999). To interpret the data from a 2D imaging survey, a 2D model for the subsurface, which consists of a large number of rectangular blocks, is used. A computer program is then used to determine the resistivity of the individual blocks so that the calculated apparent resistivity values agree with the measured values from the survey.

The computer program RES2DINV.EXE (Loke, 2000) was used in this survey to determine the appropriate resistivity values. The Syscal Junior made by IRIS Instruments was used for the present study. It is a high-powered, fully automatic resistivity meter for DC electrical surveys applied to groundwater exploration, environmental studies, civil engineering, and structural geology investigations. A newly developed hybrid array utilizing Wenner & Schlumberger arrays (Pazdirec and Blaha, 1996) has been used for surveying.

The purpose of selecting multiple layers was to distinguish the different lithological units and to convert the resistivity values into a geologically reasonable picture. Table 1 gives the resistivity values of common rocks (Keller and Frischknecht, 1966; Daniels and Alberty, 1966), which are typically encountered at the sounding sites.

Table 1 - Resistivities of some common rocks

Rock type	Resistivity in Ω-m
Granite	$5 \times 10^3 – 10^6$
Basalt	$10^3 – 10^6$
Slate	$600 – 4 \times 10^7$
Quartzite	$100 – 2 \times 10^8$
Sandstone	$8 – 4 \times 10^3$
Shale	$20 - 2 \times 10^3$
Clay	1 – 100
Alluvium	10 – 800
Groundwater (fresh)	10 – 100

4 RESULTS AND DISCUSSION

4.1 Kalidaspur Project

Six experimental blasts were conducted at below ground working of Kalidaspur project. The maximum vibration recorded was 5.73 mm/s with dominant peak frequency of 61 Hz at the vertically above point of the blasting face (36EL/12R face). The total explosive weight used and explosive weight per delay was 4.995 kg.

Wenner-Schlumberger (WS) resistivity imaging surveys were also carried out the same day at same location. The study of Inverse Model Resistivity Section shows that resistivity values in pre-blasting condition ranges from 2.94 ohm.m (minimum) to 101 ohm.m (maximum), while it ranges from 2.93 ohm.m (minimum) to 101 ohm.m (maximum) in post blasting condition. The underground depth coverage by WS arrays at the site was 45.6 m, while the actual depth of working face (developed) was approximately at 77.40 m just vertically below the central point of the resistivity section. The observed apparent resistivity sections along with an inversion model are presented in Figure 2. The recorded images of resistivity survey indicate that there is no apparent change in the resistivity values after blasting from those of before blasting. The interpretation of layered wise resistivity values of different underground strata at surface position of 120 m deciphered that there was no recognisable change in overlying strata condition.

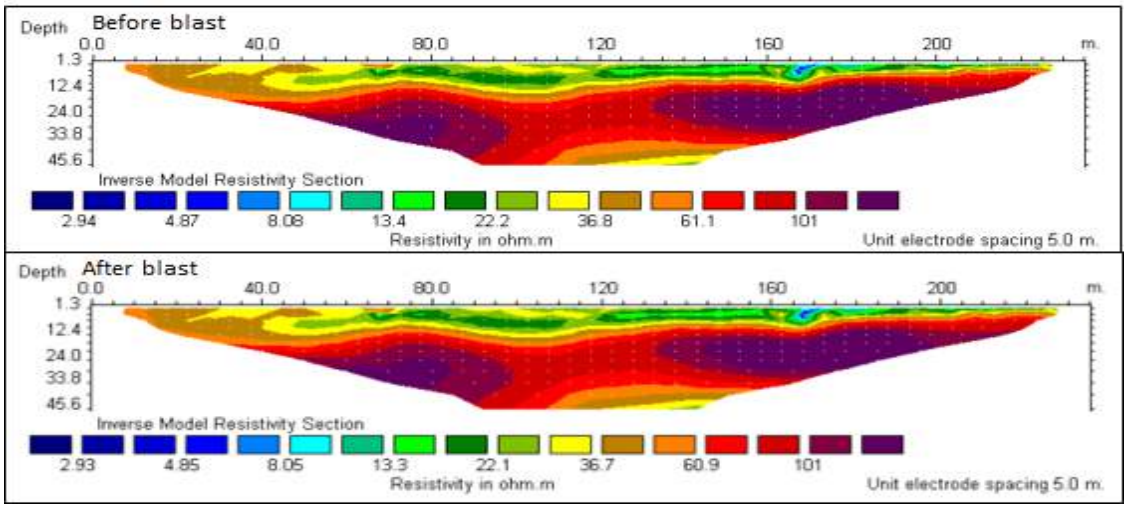

Figure 2: Resistivity image section recorded before and after blasting at Kalidaspur project on 12.04.2005.

Five experimental blasts were conducted at below ground working of Kalidaspur project. The maximum vibration recorded was 10 mm/s with dominant peak frequency of 3.5 Hz at the vertically above point of the blasting face (19L/12-13D-Roof). The

interpretation of the Wenner-Schlumberger (WS) resistivity imaging surveys conducted on the same day shows that the underground depth coverage of WS arrays at the site is 45.6 m, while the actual depth of working face (depillared from the mine plan) was approximately 72.90 m just vertically below the central point of the resistivity section. Figure 3 shows that resistivity values in pre-blasting condition ranges from 15.70 ohm.m (minimum) to 79.5 ohm.m (maximum), while it ranges from 15.8 ohm.m (minimum) to 78.9 ohm.m (maximum) in post blasting condition. Recorded resistivity images show the negligible changes in the resistivity values after blasting. The interpretation of layered wise resistivity values of different underground strata at surface position of 120 m deciphered that there was no recognizable change in overlying strata condition.

Two experimental blasts were conducted at below ground working of Kalidaspur project. The maximum vibration recorded was 1.22 mm/s with associated dominant peak frequency of 20.9 Hz at 25 m horizontally away from the vertically above point of the blasting face ($7^1/_2$LS/9R). The total explosive weight and explosive weight per delay was 4.625 kg. The depth of cover in this blast was 70 m.

Wenner-Schlumberger (WS) resistivity imaging surveys was conducted for shallow depth cover (up to 50 m). As the depth of cover in this blast was 70 m, therefore the Pole-Pole (PP) resistivity imaging survey was conducted on the same day. The underground depth coverage of PP arrays at this location was 66.20 m. Interpretations of results obtained from resistivity imaging survey indicates change in resistivity values after blasting as compared to before blasting. The study of Inverse Model Resistivity Section shows that resistivity values in pre-blasting condition ranges from 4.39 ohm.m (minimum) to 57.90 ohm.m (maximum) to 2.82 ohm.m (minimum) to 55.40 ohm.m (maximum) in post blasting, which is presented in Figure 4.

It is observed that the resistivity values were slightly of lower range after blasting indicating some minor change in compactness of the rock formation. The interpretation of layered wise resistivity values of different underground strata at surface position of 120 m deciphered that there was no recognizable change in overlying strata condition, except slight change in resistivity values. Changes were observed only up to a few meters peripheral area of the blasting face in underground mine. It is either due to effect of blast vibration or due to increase of porosity in overlying sub-surface strata.

.

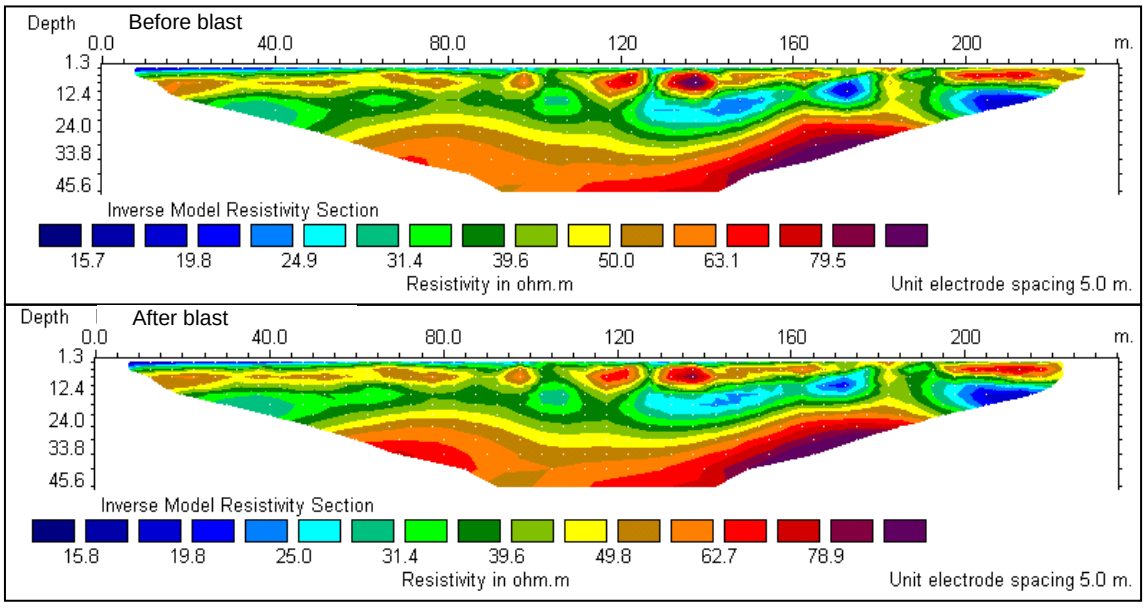

Figure 3: Resistivity image section recorded before and after blasting at Kalidaspur project on 14.04.2005

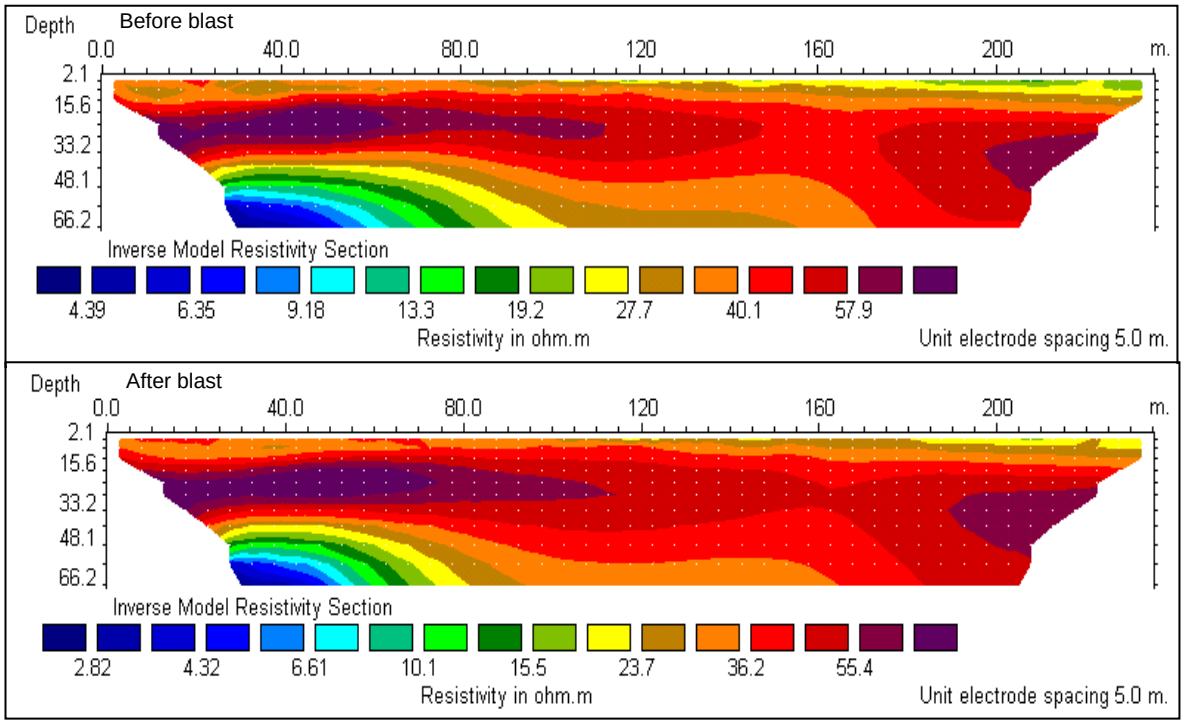

Figure 4: Resistivity image section recorded before and after blasting at Kalidaspur project on 28.03.2006

Two experimental blasts were conducted at below ground working of Kalidaspur project. The maximum vibration recorded was 3.21 mm/s with dominant peak frequency of 41.3 Hz at vertically above point of the blasting face ($20^{1}/_{2}$E/8R). The total explosive weight and explosive weight per delay was 6.29 kg. The depth of cover in this blast was 71.5 m.

Pole-Pole (PP) configuration inverted resistivity survey was conducted for deeper depth of cover (more than 50 m). The underground depth coverage of PP arrays at this site was 72.7 m and depth of working face (depillared) was approximately 71.50 m just vertically below the central point of the resistivity section. Interpretations of results obtained from resistivity imaging survey indicates change in resistivity values after blasting as compared to those of before blasting. The study of Inverse Model Resistivity Section of Kalidaspur project shows that resistivity values in pre-blasting condition ranges from 2.50 ohm.m (minimum) to 178 ohm.m (maximum), while it ranges from 2.37 ohm.m (minimum) to 174 ohm.m (maximum) in post blasting condition, which is presented in Figure 5.

It is observed that the resistivity values were slightly lower range after blasting. The interpretation of layered wise resistivity values of different underground strata at surface position of 120 m deciphered that there was no recognisable change in overlying strata condition, except slight change in resistivity values. Changes observed were only up to a few meters peripheral area of the blasting face in underground mine. It is either due to effect of blast vibration or due to increase of porosity in overlying sub-surface strata. The change of resistivity value for all the experiments conducted at Kalidaspur Project is presented in Figure 6.

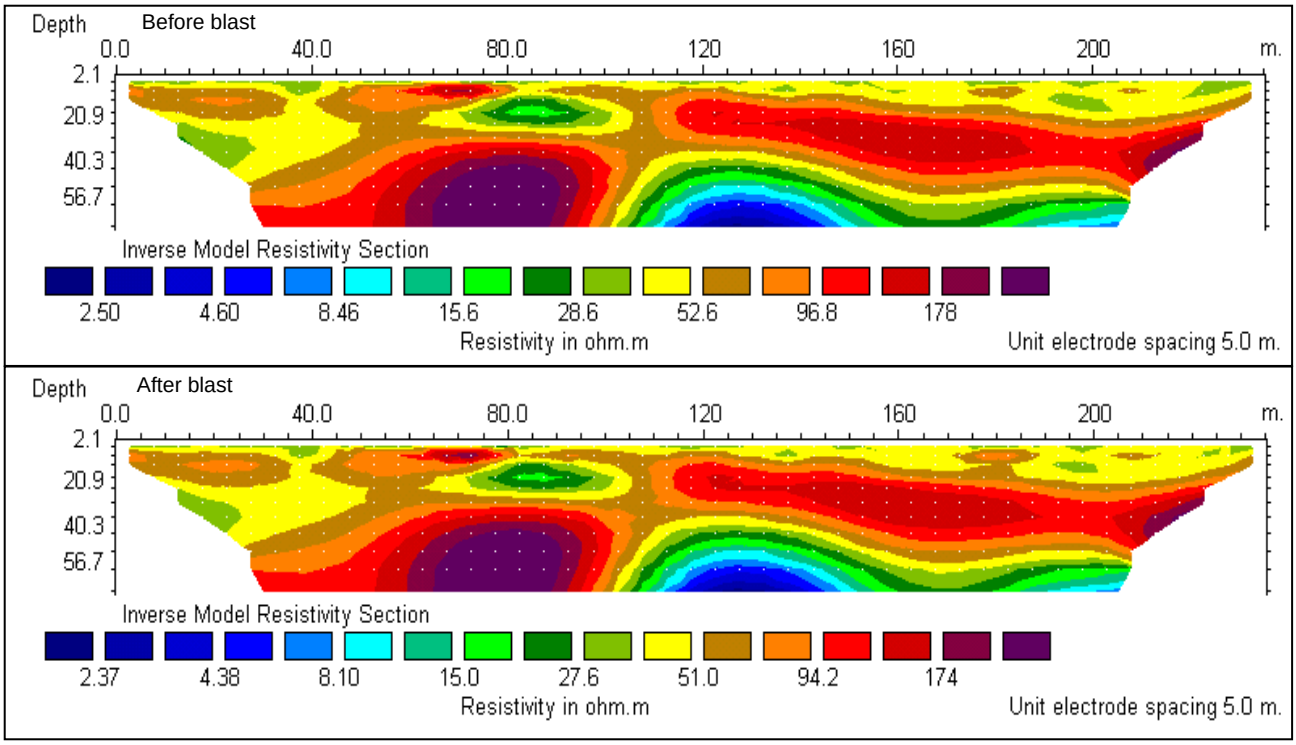

Figure 5: Resistivity image section recorded before and after blasting at Kalidaspur project 19.05.2006

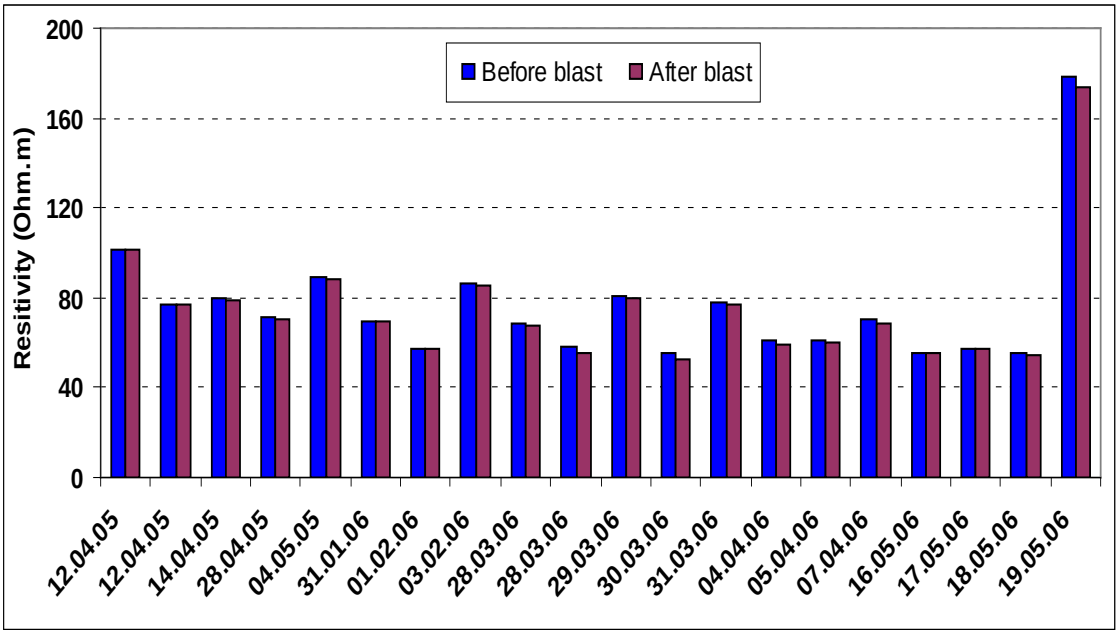

Figure 6: Change in resistivity recorded before and after blasting for all the experiments conducted at Kalidaspur project

4.2 Narsamuda colliery

Three experimental blasts were conducted at below ground working of Narsamunda colliery. The maximum level of vibration recorded was 4.06 mm/s with dominant peak frequency of 53 Hz at the vertically above point of the blasting face. The total explosive weight and explosive weight per delay were 5.55 kg and 1.85 kg respectively in this blast. The depth of cover was 50 m.

Wenner-Schlumberger (WS) resistivity imaging surveys were carried out on the same day of experimental blast for shallow depth (less than 50 m). The underground depth coverage of WS arrays at this site was 39.4 m and depth of working face (developed) was approximately 50 m just

vertically below the central point of the resistivity section. The study of Inverse Model Resistivity Section of Narsamuda colliery shows that resistivity values in pre-blasting condition ranges from 15.7 ohm.m (minimum) to 114 ohm.m (maximum) (Figure 7), while it ranges from 16.7 ohm.m (minimum) to 96.8 ohm.m (maximum) in post blasting condition (Figure 7). It was observed that the resistivity values were slightly of lower range after blasting. The interpretation of layered wise resistivity values of different underground strata at surface position of 120 m deciphered that there was change of maximum 17.2 ohm.m. Changes observed were only up to a few meters peripheral area of the blasting face in the mine. It is either due to effect of blast vibration or some void created by blasting.

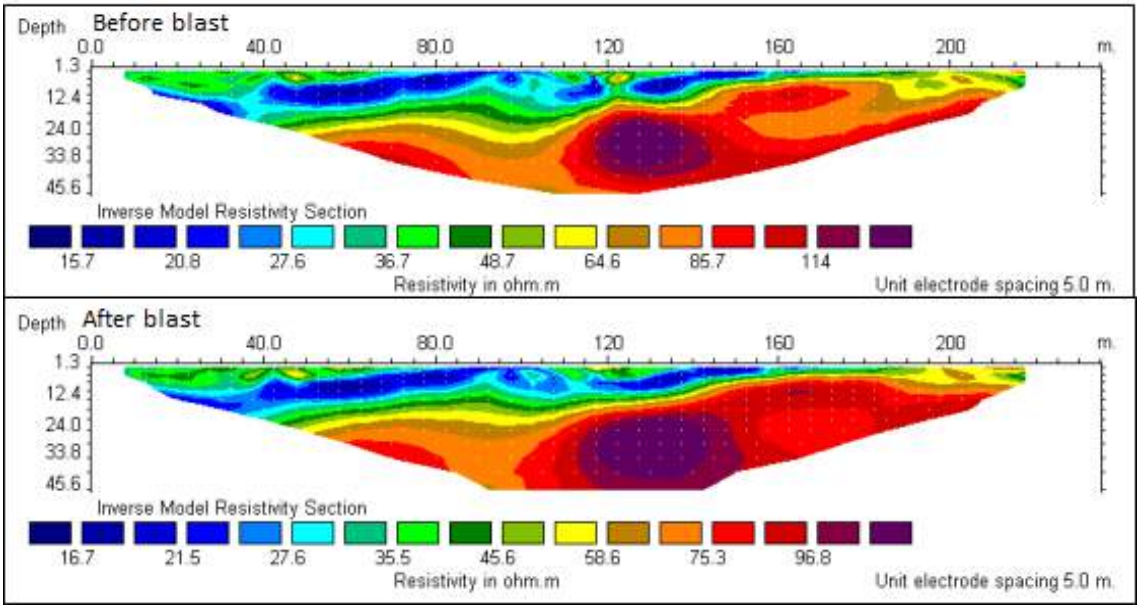

Figure 7: Resistivity image section recorded before and after blasting at Narsamunda colliery 02.03.2005

Further, two more experimental blasts were conducted and the maximum level of vibration recorded was 5.23 mm/s with dominant peak frequency of 47 Hz at the vertically above point of the blasting face (3-cross cut deep of 11 level). The total explosive weight and explosive weight per delay were 5.55 kg and 1.85 kg respectively.

Wenner-Schlumberger (WS) resistivity imaging surveys were also carried out on same day at same location. The study of Inverse Model Resistivity Section shows that resistivity values in pre-blasting condition ranges from 12.1 ohm.m (minimum) to 160 ohm.m (maximum), while it ranges from 13.4 ohm.m (minimum) to 125 ohm.m (maximum) in post blasting condition (Figure 8). The underground depth coverage of WS arrays at the site is 45.6 m, while the actual depth of working face (developed) was approximately 41 m just vertically below the central point of the resistivity section. The change in resistivity values was recorded up to 35 ohm.m. Changes observed were only up to a few meters peripheral area of the blasting face in the mine. It is either due to effect of blast vibration or some void created by blasting. The change in resistivity value (before and after blasting) for all the experiments conducted at Narsamunda colliery is presented in Figure 9.

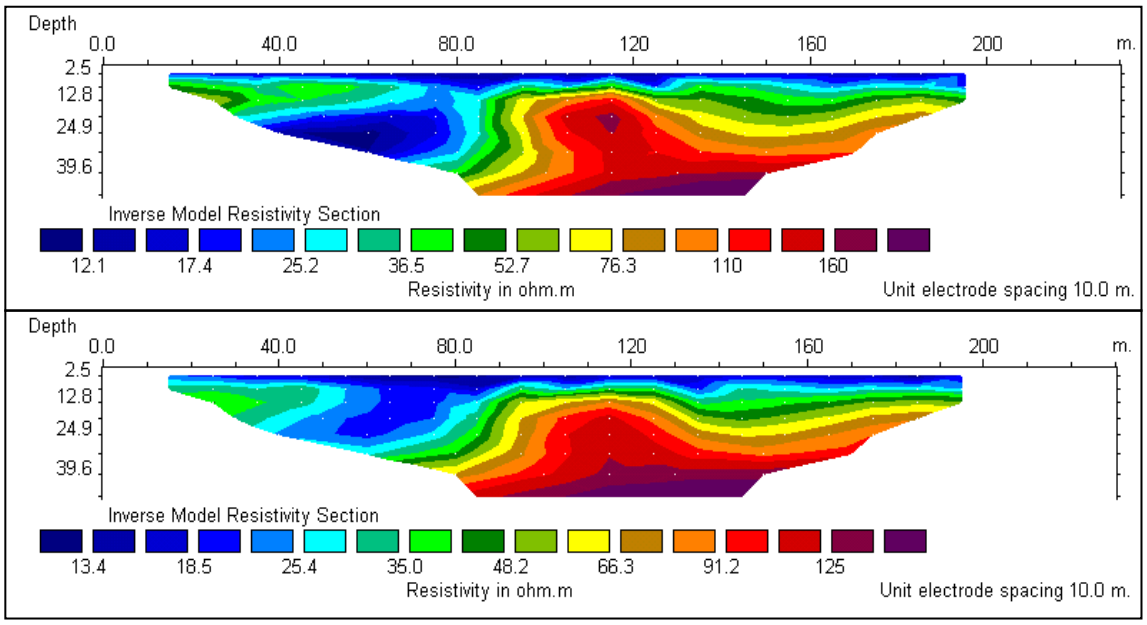

Figure 8: Resistivity image section recorded before and after blasting at Narsamunda colliery 14.02.2006

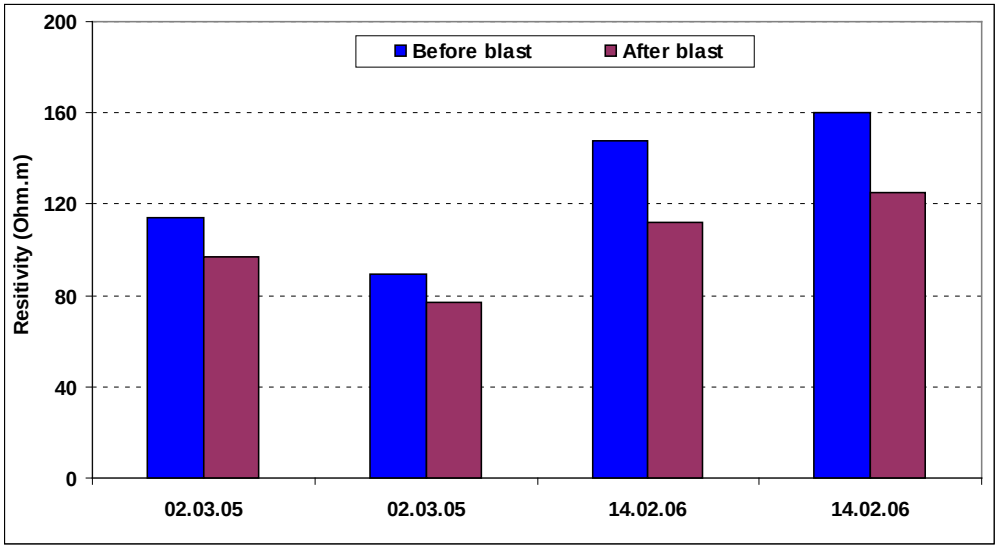

Figure 9: Change in resistivity value recorded before and after blasting at Narsamunda colliery.

4.3 Orient Mine No. 3

An experimental blast was conducted at below ground working of Orient Mine No. 3. The maximum level of vibration recorded was 0.716 mm/s with dominant peak frequency of 145 Hz at the vertically above point of the blasting face (10R/30LN). The total explosive weight and explosive weight per delay were 5.55 kg and 2.22 kg respectively. The depth of cover was 146 m.

Pole-Pole (PP) configuration inverted resistivity survey was conducted for deeper depth of cover (more than 50 m). The underground depth coverage of PP arrays at this site was 146 m and depth of working face (depillared) was approximately 150 m just vertically below the central point of the resistivity section. Interpretations of results obtained from resistivity imaging survey indicates changed in resistivity values of post blasting as compared to those of pre-blasting.

The study of Inverse Model Resistivity Section of Orient mine no. 3 shows that resistivity values in pre-blasting condition ranges from 0.598 ohm.m (minimum) to 1734 ohm.m (maximum), while it ranges

from 0.598 ohm.m (minimum) to 1708 ohm.m (maximum) in post-blasting condition (Figure 10). It is observed that the resistivity values were slightly of lower range after blasting. The interpretation of layered wise resistivity values of different underground strata at surface position 120 m deciphered that there was no recognizable change in overlying strata condition, except slight change in resistivity values. Changes observed were only up to a few meters peripheral area of the blasting face in the mine. It is either due to effect of blast vibration or due to increase of porosity in overlying sub-surface strata. The change in resistivity value (pre and post blasting) at Orient mine no. 3 is presented in Figure 11

.

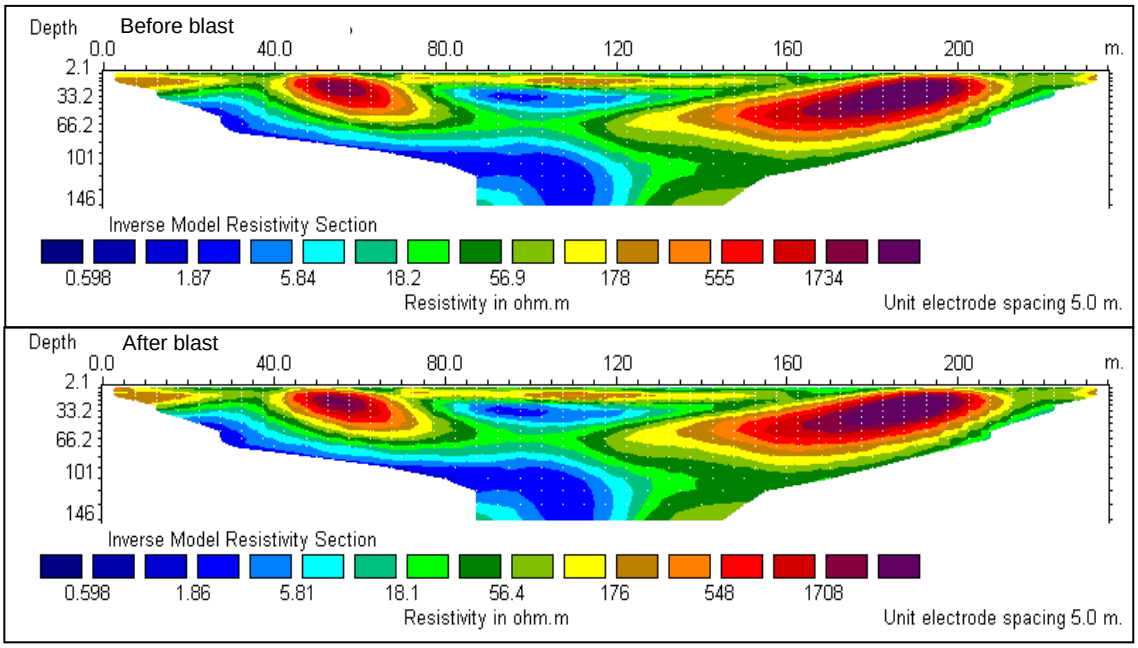

Figure 10: Resistivity image sections recorded before and after blasting at Orient mine no. 3 on 14.09.2006.

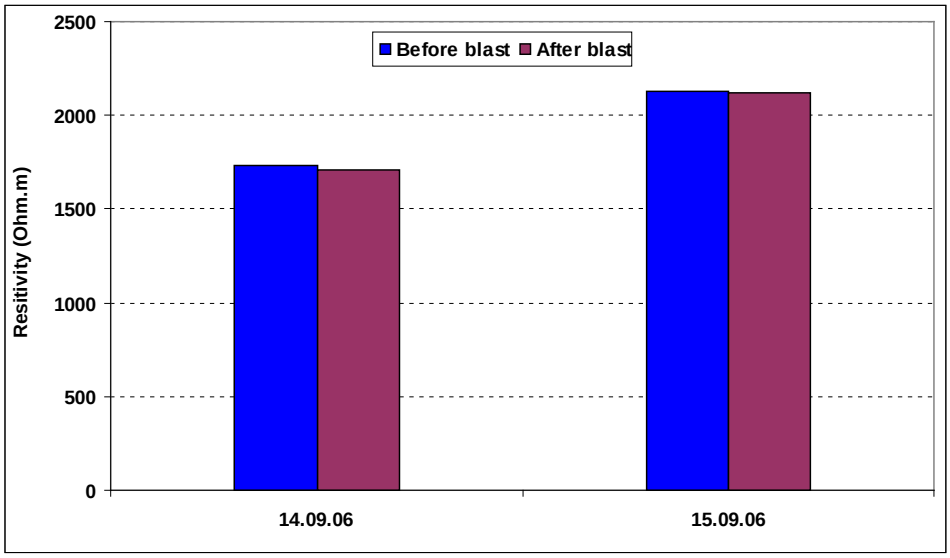

Figure 11: Change in resistivity recorded before and after blasting at Orient Mine No. 3 of MCL.

5 RESISTIVITY IMAGING DATA VERIFICATION USING BLASTING DATA

In addition to geophysical Resistivity Imaging survey, monitoring of vibrations was carried out at the surface above the underground workings of Kalidaspur project and Narsamunda colliery of Eastern Coalfields Limit and Orient Mine No. 3 colliery of Mahanadi Coalfields Limited. Altogether 391 blast vibration data were recorded from 129 blasts. Vibrations were recorded in terms of peak particle velocity (PPV) in mm/s and frequency in Hz. The maximum explosive weight in a blasting round varied between 1.11 kg and 10.175 kg whereas the depth of cover varied between 41 m and 137 m. In few blasts all the holes were fired instantaneously maintaining charge per delay of 10.175 kg. The maximum vibration recorded was 10 mm/s at the vertically above point of the blasting face (19L/12-13D-roof) of Kalidaspur project. The dominant peak frequency was 73.5 Hz. This was recorded when 10.175 kg of explosive was detonated instantaneously in a blasting round. Thus, the charge weight per delay was 10.175 kg. The depth of cover was 73 m. The recorded PPV of all the experimental sites are presented in Figure 12

.

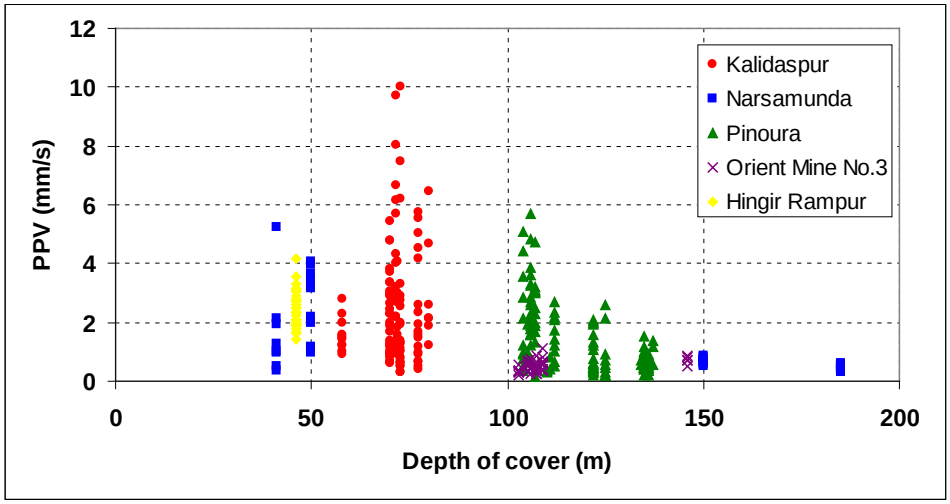

Figure 12: Plot of peak particle velocities recorded at different depth of cover at all the experimental sites.

The dominant peak frequencies of all the vibrations recorded were in the range of 20.3-219 Hz. A representative plot of peak particle velocities with their associated frequencies is depicted in Figure 13. The result confirms the earlier study conducted by Singh et al. (1999, 2007) at different mines in which the dominant peak frequencies of the waves propagating due to underground blasting to ground surface varied from 27 Hz to 156 Hz.

Wenner-Schlumberger, Wenner and Pole-Pole arrays of Resistivity Imaging survey were conducted with a view to determining the change in sub-surface strata conditions during blasting (before and after) in underground coalmine workings of Kalidaspur colliery, Narsamuda colliery and Orient mine No. 3 at various depths. The recorded change in the resistivity values for the aforesaid collieries is presented in Table 2.

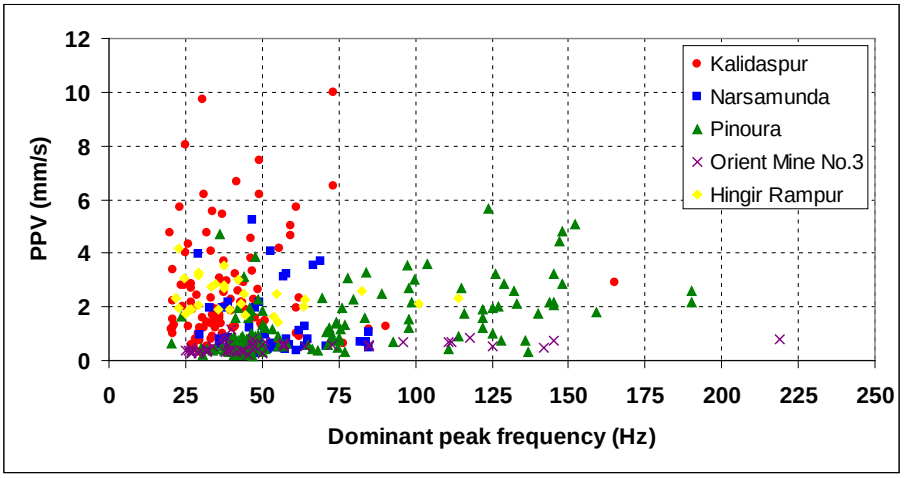

Figure 13: Plot of dominant peak frequencies recorded on ground surface at various locations.

Table 2: Resistivity recorded before and after blast with the depth coverage by the WS/W/PP arrays at Kalidaspur project, Narsamunda colliery and Orient Mine No. 3.

S. No./date	Depth coverage of WS /W/PP arrays (m)	Depth of coal working face (m)	Resistivity value	
			Before blasting (ohm.m)	After blasting (ohm.m)
Kalidaspur Project, ECL				
1/12.04.2005	WS-45.6	77.4	2.94-101	2.93-101
2/12.04.2005	WS-19.8	77.4	4.82-76.7	4.8-76.6
3/14.04.2005	WS-45.6	72.9	15.7-79.5	15.8-78.9
4/28.04.2005	WS-45.6	58.3	11.3-71.8	11.3-70.6
5/04.05.2005	PP-101	80.4	0.0525 -89.40	0.0458-88.5
6/31.01.2006	WS-45.6	72	10.9-69.3	10.9-69.1
7/01.02.2006	PP-72.7	72	12.2-57	12.2-56.9
8/03.02.2006	WS-45.6	72	12.3-86.8	12.3-85.2
9/28.03.2006	WS-45.6	70	13.9-68.7	15.7-67.5
10/28.03.2006	PP-66.2	70	4.39-57.9	2.82-55.4
11/29.03.2006	PP-66.2	70	15.5-81.2	15.7-80.0
12/30.03.2006	PP-66.2	70	1.99- 55	2.77-52.6
13/31.03.2006	PP-66.2	70	12.6-78.3	12.6-77.1
14/04.04.2006	PP-72.7	70	12.3-60.6	12.4-59.3
15/05.04.2006	PP-72.7	70	14.88-61	14.3-60.0
16/07.04.2006	PP-72.7	70	2.73-70	2.79-68.3
17/16.05.2006	PP-72.7	71.5	1.3-55.7	1.32-55.5
18/17.05.2006	PP-72.7	71.5	7.01-57.7	7.06-57.4
19/18.05.2006	PP-72.7	71.5	5.45-55.7	5.45-54.2
20/19.05.2006	PP-72.7	71.5	2.5-178	2.37-174
Narsamunda Colliery				
21/02.03.2005	WS-39.4	50	15.7-114	16.7-96.8
22/02.03.2005	W-39.4	50	18.6-89.2	18.6-77.1
23/14.02.2006	WS-45.6	41	6.79-148	7.47-112
24/14.02.2006	WS-47.1	41	12.1-160	13.4-125
Orient Mine No. 3				
25/14.09.2006	PP-146	150	0.598-1734	0.598-1708
26/15.09.2006	PP-146	150	0.919-2132	0.902-2118

6 CONCLUSIONS

Resistivity Imaging survey carried out at three mining sites led the following conclusions:

- The resistivity imaging survey conducted with the help of Wenner-Schlumberger (WS) Wenner (W) & Pole-Pole (PP) arrays revealed that there was no significant change in sub-surface strata conducted during pre and post blasting conditions.
- The slight change in resistivity values up to 35 ohm.m up to a few meters peripheral area of the blasting face in the mine may be either due to the effect of blast vibration and/or same void created by blasting or increase in porosity of overlying sub- surface strata.

Altogether, 391 blast vibration waveforms were recorded on the surface from 129 blasts conducted at three underground mines. The ground vibrations recorded were of very short duration (less than one second) with low magnitude. Higher frequencies of vibrations were observed in each and every blast irrespective of depth of covers and geo-mining conditions. On the other hand, there was mismatch between the ground vibration frequency and the natural frequency of the houses/buildings, very little energy was transmitted into the structure and hence the reduction in vibration level in the houses/buildings.

There are number of causes other than blasting to create cracks in the houses. A few of them may be due to universal existence of natural, cultural stresses, thermal cycles, humidity-produced changes, material curing and shrinking affecting houses and developing cracks. The non-blasting sources also produce significant vibration levels such as movement of heavy vehicles, trains etc. Environmental changes and human activities produce strains equivalent to 12-15 mm/s and even higher in some cases.

The study clearly demonstrates that there is no chance of damage to surface structures due to blasting being carried out at 50 m and beyond in underground workings. The fear of damage of the structures of the villagers is only an apprehension and not the real cause.

ACKNOWLEDGEMENTS

The authors are thankful to Director, CSIR-Central Institute of Mining and Fuel Research, Dhanbad for the permission to publish this paper. The co-operations extended by the Kalidaspur, Narsamunda and Orient Mine no.3 Collieries managements during field investigations are thankfully acknowledged.

REFERENCES

Daniels, F. and Alberty, R. A., 1966. *Physical chemistry*. John Wiley and Sons, Inc.

Griffiths, D. H, Turnbull, J. And Olayinka, A.I., 1990. *Two dimensional resistivity mapping with computer controlled array*, First break 8, pp 121-129.

Keller, G. V. and Frischknecht, F. C., 1966. *Electrical methods in geophysical prospecting*, Pergamon Press Inc., Oxford.

Loke, M. H., 1994. *The inversion of two dimensional resistivity data*, Unpublished Ph.D. thesis, University of Birmingham.

Loke, M. H., 1999. Time- lapse resistivity imaging inversion. *Proceedings of the 5th Meeting of the Environmental and Engineering Geophysical Society European Section*, Eml.

Loke, M. H., 2000. *Electrical imaging surveys for environmental and engineering studies*. A practical guide for 2D and 3D surveys. Copy right of M. H. Loke.

Pazdirek, O. and Blaha, V., 1996. Examples of resistivity imaging using ME-100 resistivity field acquisition system. *EAGE 58th Conference and Technical Exhibition Extended Abstracts*, Amsterdam.

Singh, P. K., Singh, R. B. and Singh, T. N., 1999. A study on surface damage characterization due to underground blasting. 9th *International Society for Rock Mechanics Congress*, Paris (G. Vouille & P. Berest), pp1203-1207

Singh, P. K. & Roy, M. P., 2007. *Damage to surface structures due to underground coal mine blasting: apprehension or real cause?* Published on line on 18.03.2007 by Environmental Geology, Germany, Publisher Springer.

Mine Ventilation, Methane, and Shale Gas

An Initial Investigation of Room and Pillar Ventilation Using CFD to Investigate the Effects of Last Through Road Velocity

T. Feroze, H.R. Phillips
University of the Witwatersrand, Johannesburg, South Africa

ABSTRACT Computational Fluid Dynamics (CFD) has often been used to analyze the air flows in underground mines. In this paper the results of a base-line investigation conducted using a three dimensional CFD analysis to find the depth of air flow in empty headings without any auxiliary devices are presented. The model dimensions are kept constant and air penetration into the heading for four last through road (LTR) velocities is compared. Determination of penetration of air is based on the maximum axial velocity and flow rates are calculated using absolute axial velocity at different depth planes. The results have been compared with experimental results of another researcher published 25 years ago, Meyer (1989).

Further research is continuing to determine the effects of different auxiliary ventilation devices using this CFD methodology, as well as obtaining empirical data in an experimental tunnel established at the University of the Witwatersrand.

Keywords: Ventilation, room and pillar, Computational Fluid Dynamics (CFD), Last Through Road (LTR) Velocity

1 INTRODUCTION

Underground coal mines are always subject to the inherent risks of methane explosions, coal dust explosions and lung diseases if they are not properly ventilated. Generally the out-bye ventilation is well planned by competent and experienced ventilation personnel, often using simulation packages to meet the requirements set by legislation and Codes of Practice. This area is also routinely monitored by production supervisors as well as ventilation officials and in most cases underground instrumentation reports to a surface control room.

Room and Pillar mining is based on creating blind headings until through ventilation is established by holing through when the pillar is formed. Even when longwall mining is the preferred method the access roadways (gate roads) are created by room and pillar mining. This all leads to the development of many blind headings which require ventilation both when being mined and when standing. Localised ventilation may be planned and be the subject of mine standards but implementation on a day to day basis is usually left to the first level of supervisory staff.

Although modeling of ventilation systems for room and pillar has been undertaken for many years, the current study using Computational Fluid Dynamics (CFD) and the ANSYS software package is looking at the effects of correct and incorrect use of line brattices and fans (with and without ducts). This paper describes a base-line study of short blind headings (20 m) where the only ventilation is produced by the air in the last through road (LTR). The variation of penetration depths and distribution of air inside the headings for different velocities of air in the last through road (LTR) is investigated using four different LTR velocities. The results are compared with the field results of the experiments conducted in 1989 in an actual mine, Meyer (1989).

Network design software applications are normally used for the design and planning of primary ventilation but computational fluid dynamics analysis is used for the working face areas, Wu and Gillies (2005). A

number of studies using CFD have been conducted for underground coal mines, some to predict the design and installation of line brattices, Aminossadi and Hooman (2008). In some studies methane behavior in a road way has been studied using CFD, Torano (2009). Heerden and Sullivan (1993) used CFD to simulate the ventilation of both continuous miners and road headers in working areas. A number of CFD studies pertaining to the ventilation of underground mines have been conducted by Wala - notably a CFD simulation of face area ventilation with a blowing curtain (2007) and the effect of machine-mounted dust scrubbers on the performance of face ventilation systems using extended-cut mining with a blowing curtain (2008). Phrushotham and Bandopadhyay (2010) simulated the shock-loss phenomenon of different configurations of air-crossings. Diego (2011) simulated the air loss calculation throughout an installation using CFD. Yuan (2009) simulated the spontaneous heating of coals in gob areas. Meyer and Vanzyle (1999) showed why the U type of flow produced by a jet fan is preferred for better dust and methane control in mines.

2 GOVERNING EQUATIONS

Fluid flows are governed by the Bernoulli's equation or a set of Partial Differential Equations (PDE's) i.e. the conservation of mass, the conservation of momentum (Navier Stokes Equations) and the energy equations. Numerical solvers along with additional equations of the selected turbulence model for turbulent flows are designed to solve these PDE's for fluid dynamics problems. The governing equations are coupled equations, which are nonlinear and are very difficult to solve analytically, necessitating the use of numerical methods. Such a system of equations is converted into algebraic equations which are subsequently solved numerically, using different explicit and implicit numerical techniques. The governing equations used for this simulation are the conservation of mass; equation 1 and conservation of momentum; equations 2 to 4.

2.1 Conservation of Mass

$$\nabla \cdot (\rho \vec{v}) = -\frac{\partial \rho}{\partial t} \quad (1)$$

where,

ρ = Density (kg/m^3), v = Velocity (m/s)

$$\nabla \equiv i\frac{\partial}{\partial x} + j\frac{\partial}{\partial y} + k\frac{\partial}{\partial z}$$

$$\nabla.(\rho \vec{v}) \equiv \frac{\partial(\rho u)}{\partial x} + \frac{\partial(\rho v)}{\partial y} + \frac{\partial(\rho w)}{\partial z}$$

u, v, w are velocity components in x, y, z direction

2.2 Conservation of Momentum

$$\rho\frac{Du}{Dt} = \frac{\partial(\rho u)}{\partial t} + \nabla \cdot (\rho u \vec{v}) = -\frac{\partial p}{\partial x} + \frac{\partial \tau_{xx}}{\partial x} + \frac{\partial \tau_{yx}}{\partial y} + \frac{\partial \tau_{zx}}{\partial z} + \rho f_x \quad (2)$$

$$\rho\frac{Dv}{Dt} = \frac{\partial(\rho v)}{\partial t} + \nabla \cdot (\rho v \vec{v}) = -\frac{\partial p}{\partial y} + \frac{\partial \tau_{xy}}{\partial x} + \frac{\partial \tau_{yy}}{\partial y} + \frac{\partial \tau_{zy}}{\partial z} + \rho f_y \quad (3)$$

$$\rho\frac{Dw}{Dt} = \frac{\partial(\rho w)}{\partial t} + \nabla \cdot (\rho w \vec{v}) = -\frac{\partial p}{\partial z} + \frac{\partial \tau_{xz}}{\partial x} + \frac{\partial \tau_{yz}}{\partial y} + \frac{\partial \tau_{zz}}{\partial z} + \rho fz \quad (4)$$

Where,

$\tau_{xx}, \tau_{yy}, \tau_{zz}$ = Normal Stress in x,y,z direction respectively (Pa).

τ_{ij} = Shear Stress in j direction exerted on a plane perpendicular to the i axis (Pa).

u, v, w are the velocity components in the x,y, and z direction (m/s).

$\frac{D}{Dt}$ = Substantial Derivative

$\frac{\partial}{\partial t}$ = Local Derivative

f_x, f_y, f_z are the body forces in the x,y, and z directions respectively (N)

P = Pressure (Pa)

3 MODEL GEOMETRY AND MESHING

The three dimensional model as shown in Figure 1 was generated in the Ansys Design Modeler software. The width chosen for the LTR and the heading is 6.6 m, while both are 3 m high. The length of the LTR modeled on both the upstream and downstream side of the heading is 10 m and the length of the heading is 20 m. A hexahedral mesh with a size of 0.05 m was created using the Ansys Mesher as shown in Figure 2. A finer mesh of 0.0009 m was created in the near wall region. A total of 10 boundary layers are used in this fine mesh using a growth rate of 1.2 to accurately resolve the boundary layer and to allow a smooth transition between the boundary mesh and the main mesh. The fine mesh at the boundary/walls of the domain kept the y^+ value (calculated using equation 5) at all the walls below 5. The total number of nodes and cells are 11152149, 10960320 respectively.

$$y^+ = \frac{yu_T}{\nu} \qquad (5)$$

Where,

u_T is the frictional velocity $= \frac{\tau_w}{\rho} = (m/s)$

v is the kinematic viscosity (m^2/s)

y = Distance to wall

τ_w is the wall shear stress (Pa)

ρ = Density (kg/m^3)

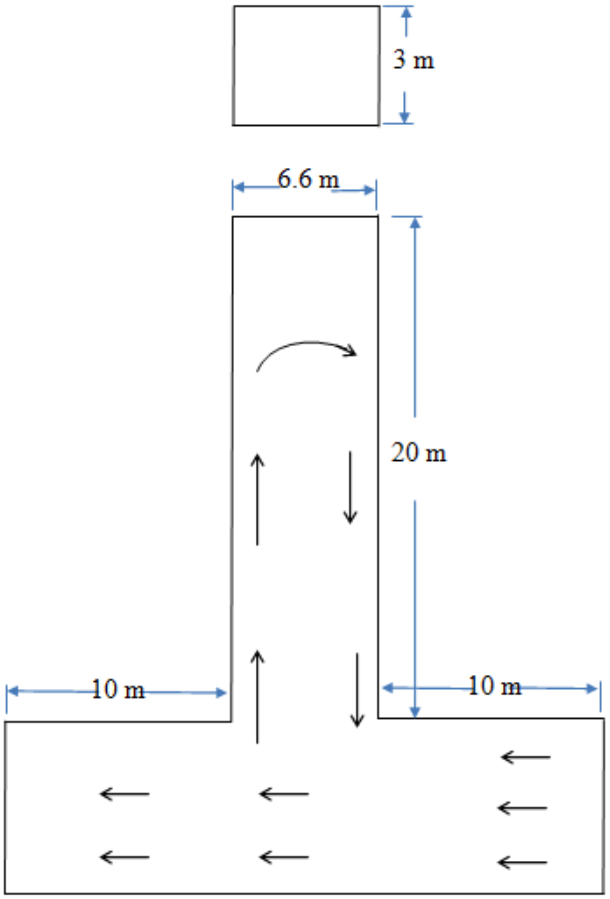

Figure 1. Three dimensional model.

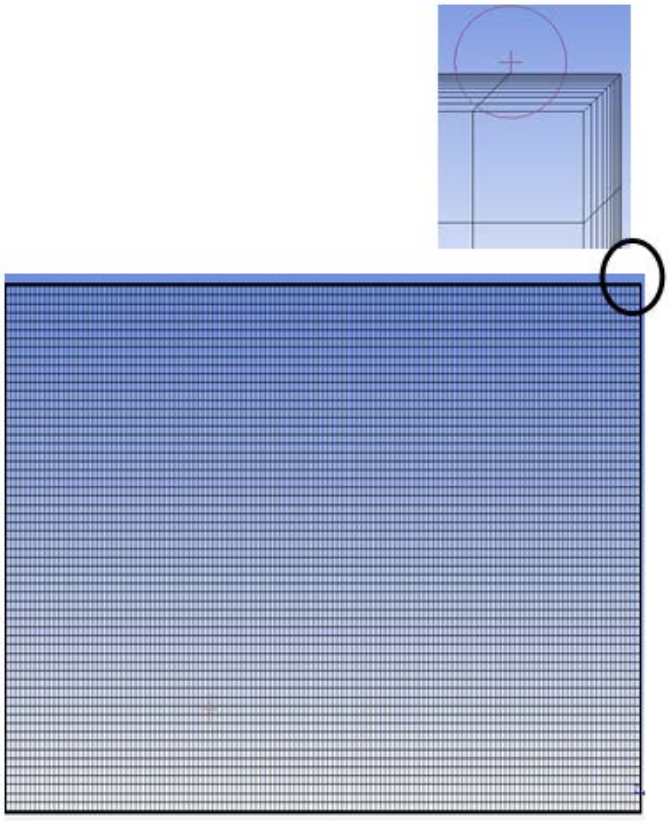

Figure 2. Hexahedral mesh with boundary layers (Inset detailed view of mesh boundary).

4 BOUNDARY CONDITIONS AND NUMERICAL DETAILS

"Velocity Inlet" and "Outflow" boundary conditions were used at the inlet and outlet of the LTR. Since it was intended to validate the CFD results with experimental results obtained in a coal mine located near Johannesburg, the properties of air at 20°C were used. Reynolds numbers for the four LTR velocities (0.78 m / s, 1 m / s, 1.35 m / s, 1.9 m / s) were calculated to be 1.74 x 10^5, 2.23 x 10^5, 3.01 x 10^5, 4.24 x 10^5 respectively. The Reynolds number was calculated using equation 6.

$$\mathrm{Re} = \frac{\rho u D}{\mu} \qquad (6)$$

where,

ρ = Density (Kg / m^3), μ = Viscosity($Pa.s$)

D = Hydraluc Diameter (m), u = m / s

The K-e model is the mostly widely used model for similar problems, involving turbulent flows due to the accuracy of results. This model is a two equation model and solves two additional transport equations besides the governing equations of flow (continuity, pressure and energy) to solve the turbulent flows. K represents the kinetic energy, and, e, represents the turbulence dispersion rate, Ansys Fluent Theory Guide (2014). Therefore, the two equation K-e realizable turbulent model with enhanced wall treatment was used for this study. The iterative process used for the calculation of results was set to run until five orders of residual reduction was achieved (convergence criteria of 10^{-5}) with second order accuracy. At the velocity inlet, turbulent intensity and hydraulic diameter were used as the turbulent quantities.

5 RESULTS AND DISCUSSION

Table 1 shows the maximum axial velocities (velocity component along the direction of the heading) on planes inside the heading, located at depths of 1 m, 5 m, 12 m, 15 m, and 16 m. These velocities have been compiled for each LTR velocity i.e. 0.78 m / s, 1 m / s, 1.35 m / s, 1.9 m / s. If we assume 0.05 m / s as the minimum measurable limit of velocity, the penetration depth with 1.35 m / s and 1 m / s LTR velocities are the maximum i.e. 15 m.

Table 1. Maximum Axial Velocity at Specified Planes.

Planes at Depth (m)	**LTR Velocities (m / s)**			
	0.78	**1**	**1.35**	**1.9**
	Maximum Axial Velocity at Specified Planes (m / s)			
1	0.32411	0.38731	0.59680	0.83610
5	0.23650	0.28110	0.41279	0.70290
12	0.08455	0.17340	0.27185	0.52830
15	**0.02694**	**0.06061**	**0.08572**	**0.02423**
16	0.03304	0.04098	0.04308	0.01561

Figure 3 shows the variation of maximum axial velocities on the specified planes. The velocities are decreasing with the depth of the heading. The maximum decrease rate can be seen for 1.9 m / s LTR velocity.

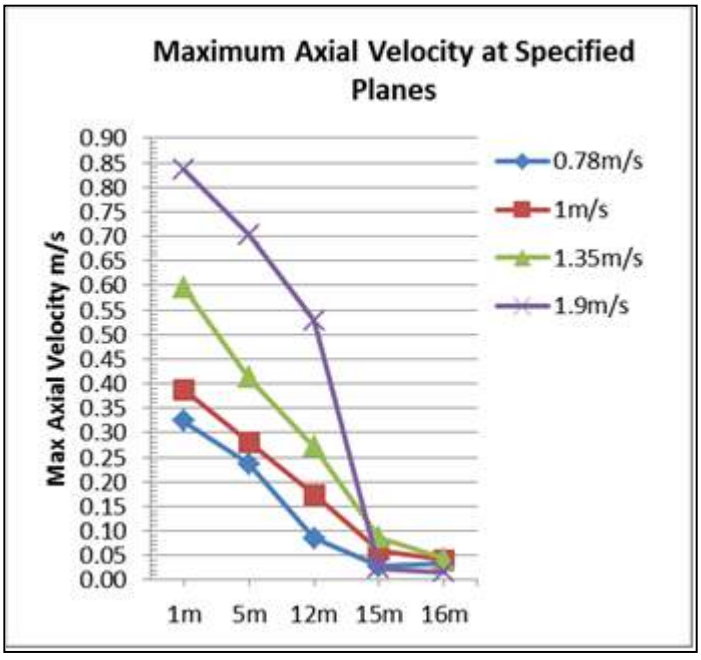

Figure 3. Maximum Axial Velocity at Specified Planes.

Figures 4-7 shows the detailed variation of axial velocity contours on a plane located at 15m depth for each LTR velocity. The

contours have been divided into five regions; showing different velocity ranges. The velocity ranges for these regions are shown with the contours. Positive velocities indicate inflows and the negative flows are the return air flows. The return axial velocity for the case of 1.35 m / s LTR is again the maximum i.e. 0.04294 m / s.

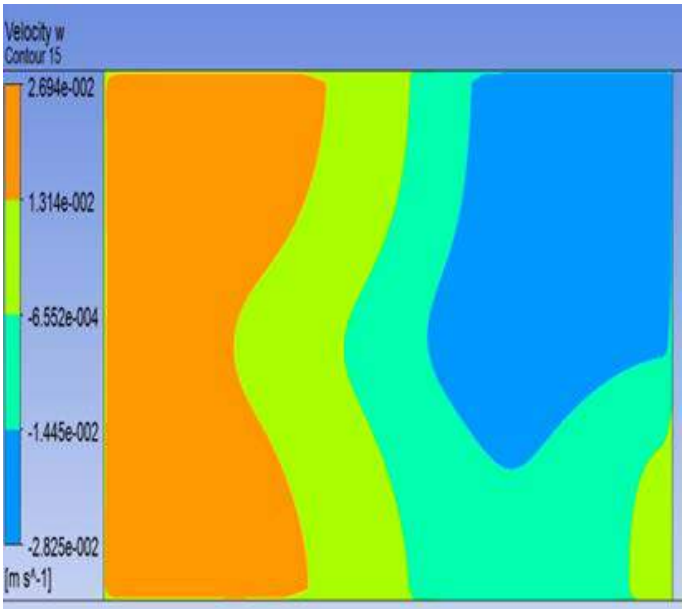

Figure 4. Axial Velocity Contours at 15m plane in the heading for 0.78 m / s LTR Velocity.

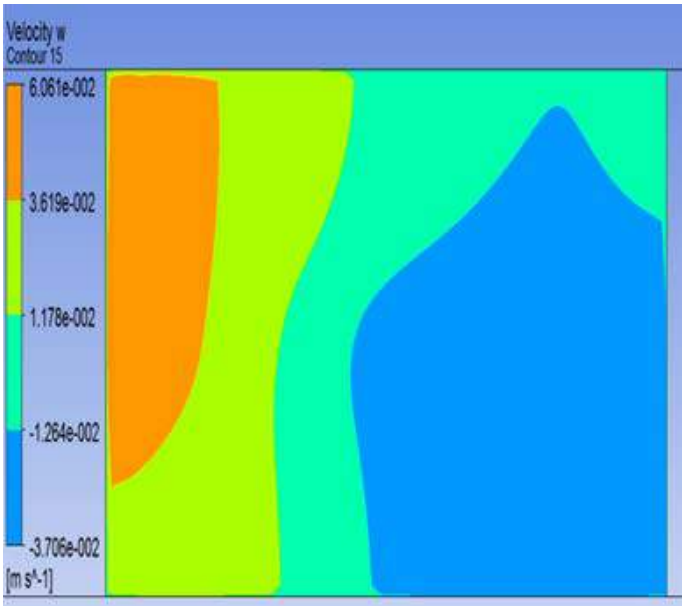

Figure 5. Axial Velocity Contours at 15m plane in the heading for 1 m / s LTR Velocity.

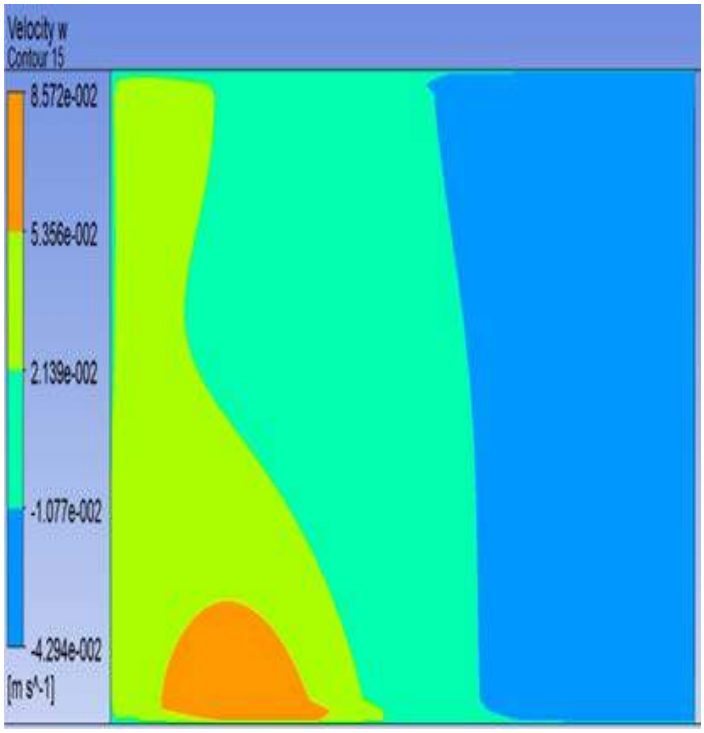

Figure 6. Axial Velocity Contours at 15m plane in the heading for 1.35 m / s LTR Velocity.

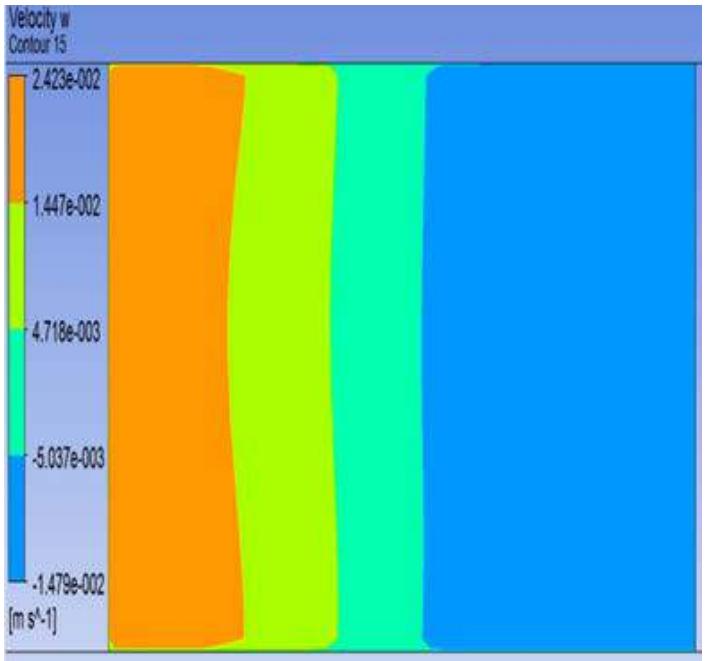

Figure 7. Axial Velocity Contours at 15m plane in the heading for 1.9 m / s LTR Velocity.

Table 2 and Figure 8 illustrate the average positive “flow in” of air through planes set at the specified depths of 1,5,12, and 15 m inside the heading. The air flow rates decrease considerably after the depth of 12 m for all the LTR velocities.

Table 2. Average Positive Flow Inwards at Specified Planes.

Planes at Depth (m)	LTR Velocities (m / s)			
	0.78	1	1.35	1.9
	Average Positive Flow Inwards at Specified Planes (m / s / m^2)			
1	0.44641	0.52216	0.73248	1.09781
5	0.74364	0.87828	1.29108	2.88777
12	**0.21092**	**0.43951**	**0.76674**	**0.21202**
15	0.15206	0.23408	0.22431	0.11558

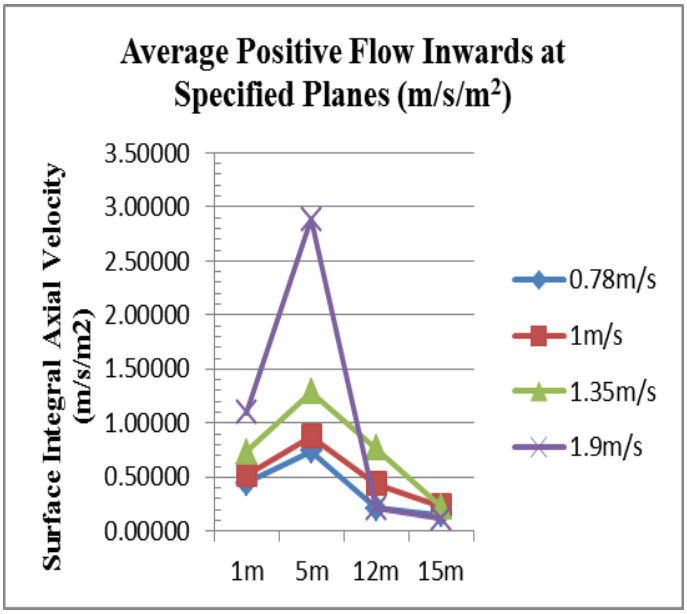

Figure 8. Average Positive Flow In at Specified Planes.

Figure 9-12 shows the velocity contours on a horizontal plane at a height of 1.5 m. It can be seen from these contours that air enters from the downstream side and the flow rate decreases very considerably after the 12 m depth for all the LTR velocities. At a depth of 12 m maximum flow rate is observed for LTR velocity of 1.35 m / s. For LTR velocity of 1.9 m / s, most of the air continues to flow in the last through road and does not ventilate the heading beyond the 12 m depth.

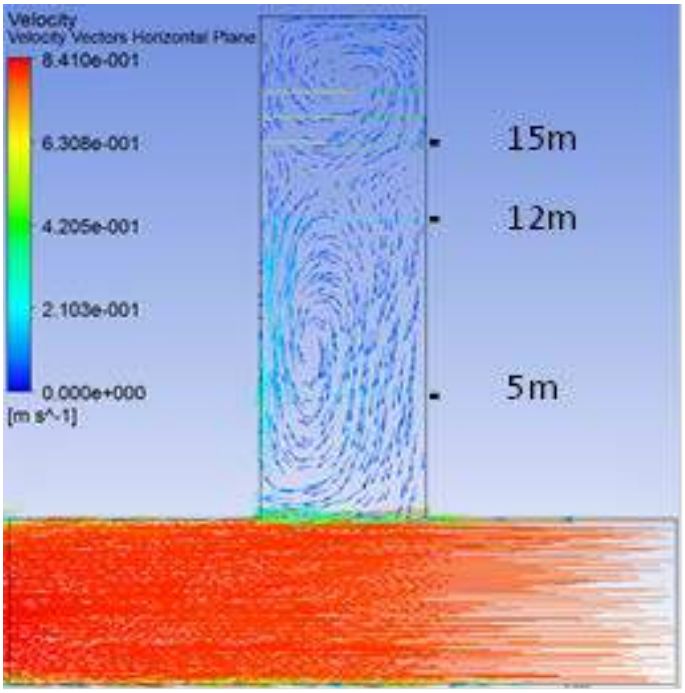

Figure 9. Velocity Vectors on 1.5 m Horizontal Plane for 0.78 m / s LTR Velocity.

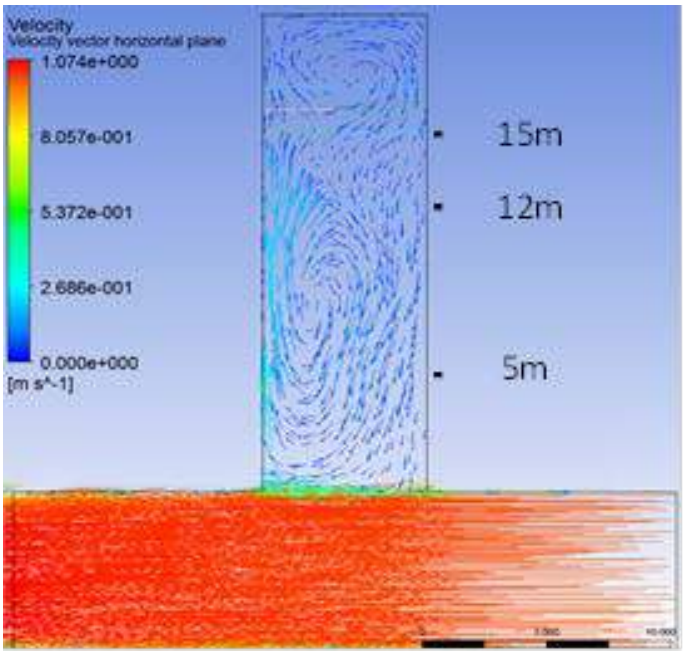

Figure 10. Velocity Vectors on 1.5 m Horizontal Plane for 1 m / s LTR Velocity.

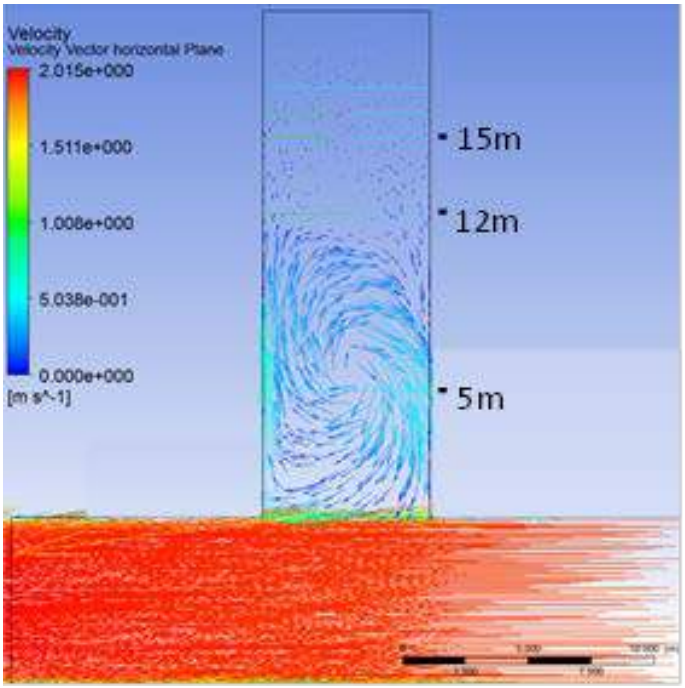

Figure 11. Velocity Vectors on 1.5 m Horizontal Plane for 1.35 m / s LTR Velocity.

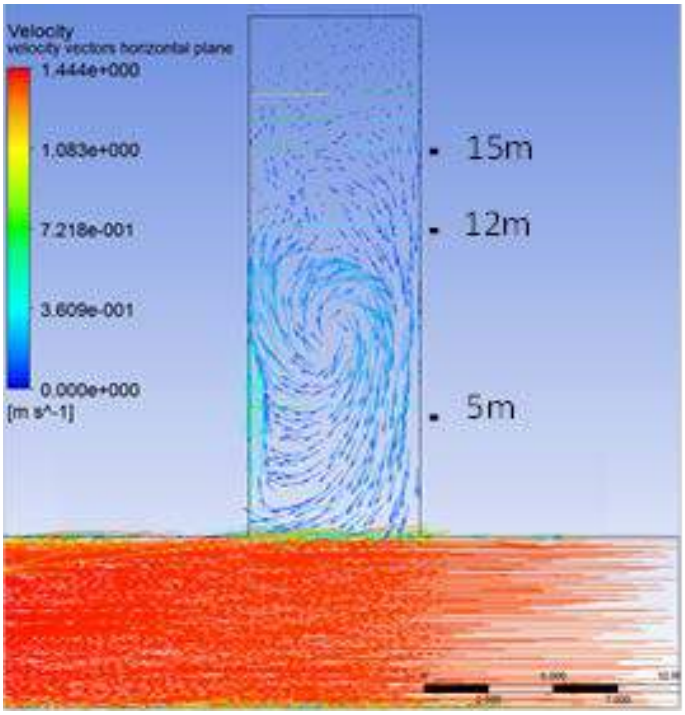

Figure 12. Velocity Vectors on 1.5 m Horizontal Plane for 1.9 m / s LTR Velocity.

6 VALIDATION

In 1989 Meyer conducted a study of the ventilation in Bord and Pillar headings of a coal mine. He selected the headings which were not ventilated by any auxiliary means and, using regulators, varied the LTR velocity to see its effect on the airflow patterns and penetration distance inside the headings (Meyer, 1989). He used smoke generating chemical tubes to visualize the airflow patterns and to measure the penetration distances. Table 3 shows the results of his experiments in a heading with dimensions of 6.6 x 3 x 20 m (the same size that was chosen for the present study). The maximum penetration depth for each LTR velocity was determined and the results of the field trial showed that the maximum penetration depth is achieved with a LTR velocity of approximately 1.35 m / s.

Table 3. Measured Experimental Results of Maximum Penetration Depths for each LTR Velocity, Meyer (1989).

Experimental Results	
LTR Velocity (m / s)	Penetration Depth (m)
0.78	12.2
1	15.8
1.35	16.8
1.9	12.4

A comparison of the present CFD simulation results with those of Meyer (shown in Tab. 3) shows a strong correlation between the two results. The maximum penetration depth is achieved by a LTR velocity of 1.35 m / s.

A 68 m long, well instrumented experimental tunnel, as shown in Figure 13, has been established at the School of Mining Engineering, University of the Witwatersrand to study ventilation aspects using auxiliary ventilation equipment. The experimental data will be used to validate the results obtained from simulations. It is anticipated that the simulations and results from the tunnel will identify shortfalls in face ventilation practice. This should lead to a better understanding of how to provide effective ventilation of working and standing faces in room and pillar mining using a variety of auxiliary ventilation devices.

Figure 13. Tunnel at the School of Mining Engineering, University of the Witwatersrand.

7 CONCLUSION

CFD ANSYS' k-e realizable model with enhanced wall treatment has shown acceptably accurate results when compared with experimental results. A LTR velocity of 1.35 m / s has achieved the maximum penetration depths and a maximum flow rate at 12 m depth, whereas, a LTR velocity of 1.9 m / s gives a maximum flow rate at shallower depths of well below 12 m. Therefore, increasing the LTR velocity beyond a particular level will not do any good as far as the penetration depth is concerned. The validation of the CFD results against the experimental work conducted underground by another researcher 25 years ago is of sufficient promise that work will continue using CFD, scale models, the experimental tunnel and finally a section of a local coal mine. The results of this research will not only define the effects of LTR velocity and the efficacy of auxiliary ventilation devices but can be developed into a training aid to ensure production personnel at the coalface have a better understanding of the impact of their actions on the proper ventilation of working areas of a coal mine.

REFERENCES

Aminossadati, S.M., and Hooman, K, 2008. Numerical simulation of ventilation air flow in underground mine workings, 12th U.S. North American Mine Ventilation Symposium, Reno, USA, (pp.253-259).

ANSYS® Academic Research, 2014, Release 15.0, Help System, Fluent Theory Guide, ANSYS, Inc.(section 4.3.1.1).

Diego, I., Torno, S., Toraño, J., Menéndez, M., and Gent, M, 2011. A practical use of CFD for ventilation of underground works. Journal of Tunneling and Underground Space Technology, Volume 26, Issue 1, (pp.189-200).

Meyer, C.F, 1989. The effect of last through road air velocities on unventilated headings, Project CC8E10, COMRO (15 p). Available on www.cmsafety.org.za.

Meyer, C. F., and Van Zyle, F. J, 1999. Reduce explosive risks and improve safety and health conditions by better ventilation practices in mechanical miner headings. SIMRAC Project COL205, CSIR, Miningtek.

Purushotham, T., and Bandopadhyay, S, 2010. Analyzing shock losses at air-crossings in a mine ventilation network using CFD simulations, 13th U.S. North American Mine Ventilation Symposium, Sudbury, Ontario, Canada, (pp.463-468).

Van Heerden, J., and Sullivan, P, 1993. The application of CFD for evaluation of dust suppression and auxiliary ventilating systems used with continuous miners. Sixth US Mine Ventilation Symposium, Univeristy of Utah Salt Lake City, Utah, (pp.293-297).

Wala, A.M., Vytla, S., Taylor, C.D., and Huang, G, 2007. Mine face ventilation: a comparison of CFD results against benchmark experiments for the CFD code validation. Mining Engineering, Volume 59, Issue 10, (pp.49–55).

Wala, A.M., Vytla, S., Huang G. and Taylor C.D, 2008. Study on the effects of scrubber operation on the face ventilation. 12th U.S. North American Mine Ventilation Symposium, Reno, USA, (pp.281-286).

Wu, H.W., and Gillies. A.D.S, 2005. Real-time airflow monitoring and control within the mine production system. Eighth International Mine Ventilation Congress, Melbourne, (pp.383-389).

Toraño, J., Torno, S., Menendez, M., Gent, M., and Velasco, J, 2009. Models of methane behaviour in auxiliary ventilation of underground coal mining, International Journal of Coal Geology, Volume 80, Issue 1, (pp.35-43).

Yuan, L., and Smith A.C., 2008. Numerical study on effects of coal properties on spontaneous heating in longwall gob areas. Fuel, Volume 87, Issue 15, (pp.3409-3419).

Underground Environment Management System

M. B. Massanés
Iberpotash Chair in Sustainable Mining, Polytechnic University of Catalonia, Manresa, Spain

Ll. S. Pera, J. O. Moncunill
Department of Mining and Natural Resources, Polytechnic University of Catalonia, Manresa, Spain

ABSTRACT Efficiency and safety issues are highly related to the management of the ventilation system in underground mining. This paper presents the design of a geographical information system –also known as GIS– able to store, manipulate and administrate underground environmental data in a long term.

Two important conditions have been taken into account to create the database: the location where the measures have been taken and the fact that the evolution of the underground workings can change the layout of the ventilation system.

The geographic information system has given insight into the working conditions and where are the most critical places concerning the gas concentrations, temperatures and airflow in a case study. Determining the impact of the airflow recirculation in the different working faces.

Keywords: Underground environment, airflow recirculation, GIS

1 INTRODUCTION

Efficiency, safety and health issues are crucial in the underground ventilation system, but sometimes they are overlooked. Currently, more than 60% of mining operation costs are related to ventilation (Reddy, 2009) and there is a direct relationship among hygienic conditions such as gas concentrations and temperature with occupational accidents and worker's efficiency (García et al. 2012).

The usage of a geographic information system, also known as GIS, in mining is quite frequent due to being able to manage any sort of information with spatial components (Bahuguna and Kumar, 2006; Cheng and S. Yang, 2012; Düzgün et al., 2011; Likar and Čadež, 2000). However, the connection of safety and efficiency is hardly considered, despite the GIS is able to insight the real situation inside the mine (Saleh and Cummings, 2011) so procedures can be implemented to ensure the occupational health and safety objectives (Akcil, 2006) and connect it with the efficiency issue through a database of the underground environment features such as airflow, gases concentration or air pressure drop.

The software gathers all the necessary characteristics to manage the information of the ventilation system due to its user friendliness and capability of managing huge quantity of interconnected spatially referenced information, being able to visualize and query historic data and how the ventilation system would react after introducing any change. This fits perfectly with what is demanded for a place like an underground mine, which is evolving and spreading out every day.

2 CASE STUDY: MINE DESCRIPTION

This paper focuses on a mine exploiting potassium from the Catalan basin. The resource is exploited by means of a room and pillar system 500 meters below the surface. The connection between the underground tunnels and the surface is done through a shaft and a ramp, using the shaft for the intake and the ramp for the return.

The main fan is placed at the beginning of the ventilation circuit, leading the airflow by temporary stoppings, curtains and doors. An exhausting system is used in the working faces to supply clean air. Figure 1 shows a scheme of the mine described above and concerning the configurations created by means of the GIS.

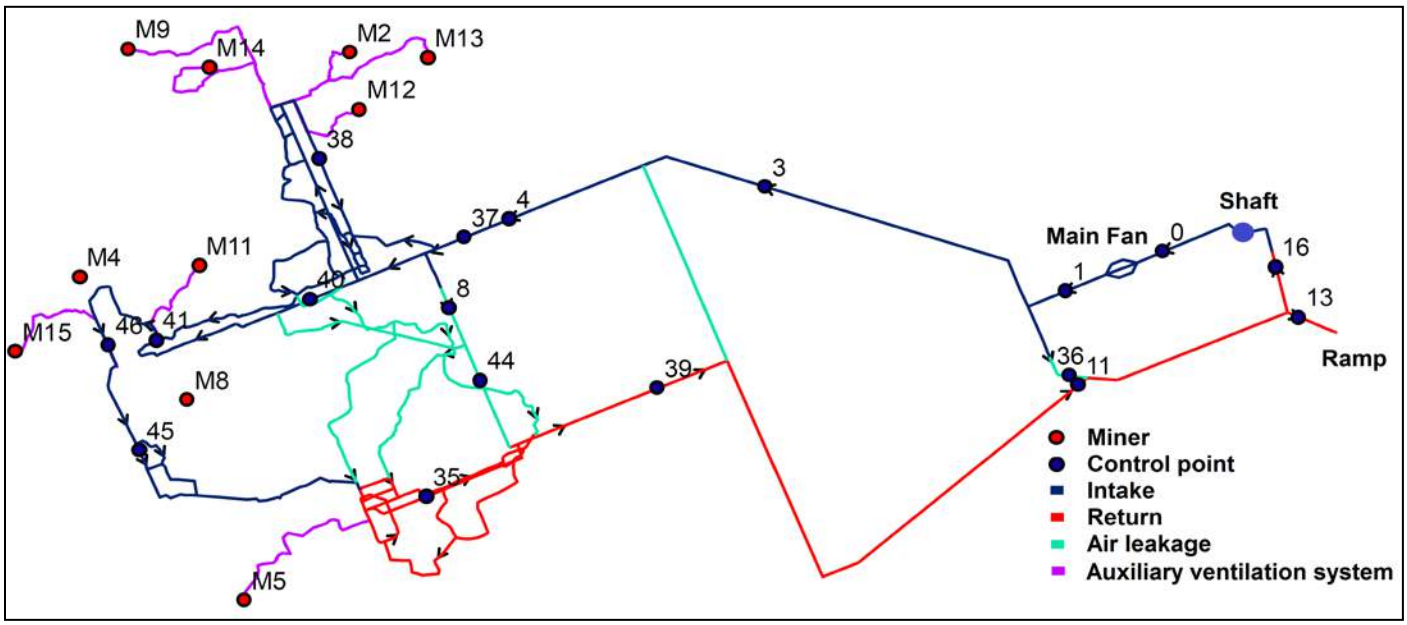

Figure. 1. Scheme of the mine and the ventilation circuit.

3 METHODOLOGY AND DATA

3.1 Data Collection

The data have been taken in situ, using manual methods (sling psychrometer, rotating vane anemometer, gas detector and a laser distance measurer) every month during two consecutive days, one day for the principal ventilation system and the other one for the working faces. In order to obtain reliable measures, the equipment is calibrated regularly (Cook et al., 1990; Lipsey, 1990). Any abnormal value obtained is taken twice.

3.2 Database Design and Management

Initially, the information available consisted in several maps of the ventilation layout in CAD format and the data collected in an excel file. Both types have been merged and transformed to a shape file by means of ArcGis software, using UTM coordinates and taking into account 3 aspects in order to store the information:

- Principal ventilation measure points
- Auxiliary ventilation measure points
- Ventilation layout

This division of the information has been done because it allows an easier management and a better understanding and data analysis. Figure 2 shows the configurations created. Each configuration is a different layout of the ventilation system. The principal ventilation layer includes the intake, the return, the leakages and the points where the measures have been taken. Meanwhile, the auxiliary contains the position of the continuous miner and the pipeline that provides airflow to the working faces. In addition, the mine workings layer stand for all the galleries exploited so far and it helps to get a better understanding of the mine. The principal and auxiliary ventilation layers within each configuration contain the information detailed in Table 1.

Figure 2. Design of the GIS.

Table 1. Ventilation parameters within the GIS.

Principal ventilation	**Auxiliary ventilation**
- Point identification number - Point coordinates (UTM) - Date of the measure - Air velocity (m/s) - Section (m^2) - Airflow (m^3/s) - Dry, wet and effective temperature (ºC) - Gases: CO, CO_2, NO, NO_2 (ppm) and O_2 (%)	- Miner identification number - Continuous miner state - Miner coordinates (UTM) - Date of the measure - Air velocity (m/s) - Section of the pipeline (m^2) - Airflow (m^3/s) - Dry, wet and effective temperature (ºC) - Distance working face – pipeline (m) - Type of fan - Other information - Gases: CO, CO_2, NO, NO_2 (ppm) and O_2 (%)

According to the Spanish law (RGNBSM, itc 04.7.02) the values of NO and NO_2 have to be summarized to know the threshold limit value. In addition the temperature analysis have to be done by means of the effective temperature which can be calculated with the following expression: $te = 0{,}9 \cdot tw + 0{,}1 \cdot td$. Where te is the effective temperature, tw the wet temperature and td the dry temperature.

The data stored has been divided in columns, where each one is a representative parameter of the ventilation system as it can be seen in Table 2. Meanwhile, Figure 3 summarizes the steps followed to create a geographic information system able to manage the underground environment.

Table 2. Part of the data from one of the configurations of the GIS.

Point	X (m)	Y (m)	Velocity (m/s)	Section (m^2)	Cabal (m^3/s)	Td (ºC)	Tw (ºC)
0	406645	4632795	4,71	41,02	193,20	6	3
1	406299	4632650	5,33	33,75	179,89	16	9
2	406313	4632339	0,90	32,18	28,96	25	15
3	405240	4633032	4,92	30,55	150,31	19	12
4	404338	4632914	6,32	23,89	150,98	26	15
5	404049	4632822	0,82	29,92	24,53	28	17
6	402927	4632448	3,00	36,16	108,48	38	25
7	403029	4632063	2,75	30,93	85,06	40	26
8	404125	4632587	0,53	30,41	16,12	34	21
9	403601	4633172	2,19	27,86	61,01	29	17
10	404044	4631897	4,68	29,60	138,53	42	29
12	406344	4632305	7,34	20,98	153,99	38	26
13	407123	4632553	4,98	35,44	176,49	36	24

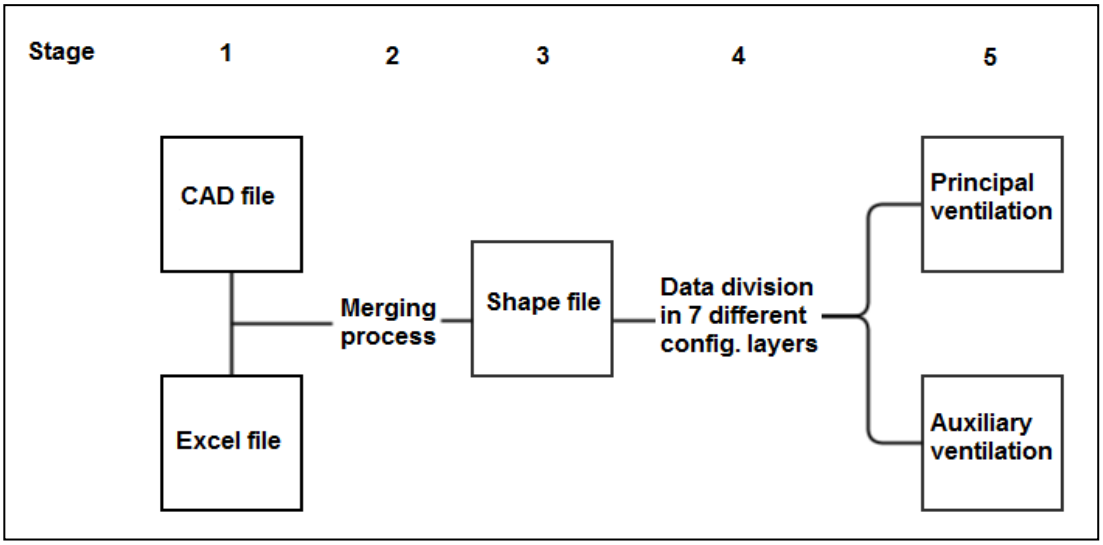

Figure 3. Scheme of the process followed to create the GIS file.

4 RESULTS AND DISCUSSION

The usefulness of a geographic information system in underground environments can be very extensive. The following paragraphs detail some of the possible outcomes.

4.1 Effective Temperature

Table 3 comprise a selection, using the GIS tools, of the measures in the working faces that have been over 30 ºC during 2012, while Figure 4 displays the location of the miners where the measures were taken and the ventilation layout. Combining the graphical information and the data, it can be analyzed the current situation of the mine globally and identify potential future adverse working zones in term of temperatures. This information could be useful for mine planning decisions, efficiency measures or taking safety actions.

Table 3. Selection of the measures over 30ºC during 2012.

Miner	X	Y	Month	Day	Effective temp. ºC
M5	403584	4631491	February	21	34,40
M5	403501	4631512	April	21	32,10
M11	403192	4632604	April	21	31,00
M15	402635	4632536	April	21	30,20
M7	403423	4631908	May	23	30,00
M11	403198	4632596	May	23	31,00
M14	403016	4633352	October	19	30,80
M2	404010	4633606	October	19	32,00
M12	403802	4633316	October	19	32,50
M6	404061	4631677	October	19	31,80
M5	403500	4631509	October	19	33,80
M7	403521	4631717	October	19	30,00
M5	403403	4631515	November	22	30,00
M11	403243	4632742	November	22	31,10

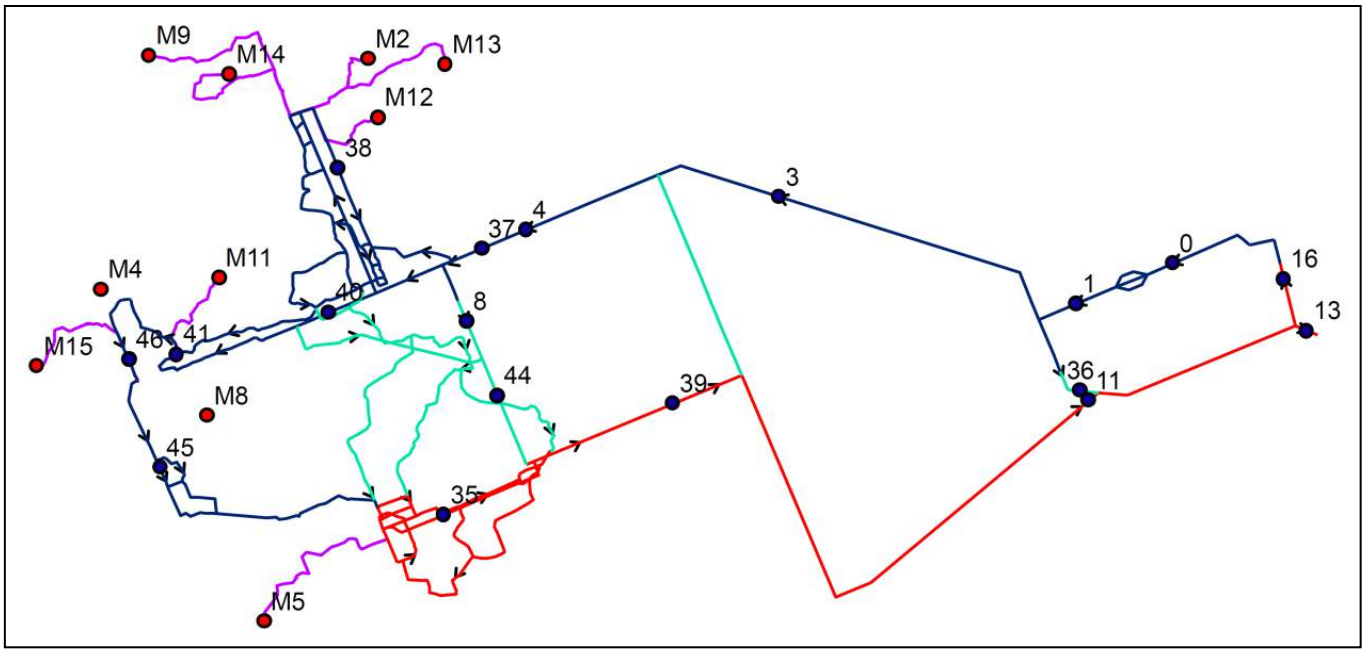

Figure 4. Principal and auxiliary ventilation layout belonging to the configuration 7.

4.2 Environmental conditions in the working faces

Analyzing the different ventilation layouts created by means of the GIS, 3 different zones in terms of airflow recirculation have been identified. In the first zone the miners are provided with clear airflow, in the second one with partially recirculated airflow and in the last one almost all the air is recirculated. Table 4 shows the mean values of 245 measures taken from April 2009 to December 2012 in the different working faces of the mine. The data have been split regarding the 3 zones using the combination of visual information and data of the geographical information system to identify the position of the miners and the data linked to them.

Table 4. Mean values of each zones.

	Airflow (m^3/s)	Effective temperature (ºC)	CO (ppm)	CO_2 (ppm)	NO_x (ppm)
Zone 1	10,59	27,99	6,18	1819,27	7,974
Zone 2	10,03	28,17	5,81	1641,62	8,28
Zone 3	11,32	29,19	8,43	1883,53	9,306

Table 5. Percentage change using the first group as reference.

	Airflow (%)	Effective temperature (%)	CO (%)	CO_2 (%)	NO_x (%)
Zone 1	0,00	0,00	0,00	0,00	0,00
Zone 2	-5,29	0,64	-5,99	-9,76	3,84
Zone 3	6,89	4,29	36,41	3,53	16,70

5 CONCLUSIONS

The GIS created has been confirmed as a powerful tool to provide a safer and healthier work environment as well as improving the efficiency of the ventilation circuit.

The system allows enquiring and analyzing data in a long term, which is totally compatible and complementary with short term environmental control options, such as monitoring and manual systems. Besides, the possibility of improving and complementing the GIS with any other software gives an enormous flexibility to control and assess an evolving environment.

The results have permitted to locate the most sensitive parts of the mine in terms of gases, temperature and airflow, obtaining an environmental pattern based on the mine ventilation conditions, which could be useful to take corrective measures and monitoring their evolution in a long term.

ACKNOWLEDGEMENTS

The authors would like to thank the staff from Iberpotash S.A. for their willingness and high commitment to improve the safety of the mine.

REFERENCES

Akcil, A. (2006) Managing cyanide: health, safety and risk management practices at Turkey's Ovacik gold–silver mine. *Journal of Cleaner Production*, 14(8), 727–735.

Bahuguna, P.P., Kumar, D. (2006) Application of Geographical Information System (GIS) for opencast coal mines. *Proceedings of the Indian Conference on Mine Surveying*, 125-132.

Cheng, J., Yang, S. (2012) Data mining applications in evaluating mine ventilation system. *Safety Science*, 50(4), 918–922.

Cook, T.D., Campbell, D.T., Peracchio L. (1990) Quasi experimentation. In: Dunnette, J.D., Hough, L.M. (Eds.), *Handbook of Industrial and Organizational Psychology*. Palo Alto, California: Consulting Psychologists Press, 491-576.

Düzgün, Ş., Künzer, C., Özgen Karacan, C. (2011) Applications of remote sensing and GIS for monitoring of coal fires, mine subsidence, environmental impacts of coal-mine closure and reclamation. *International Journal of Coal Geology*, 86(1), 1–2.

Garcia-Herrero, S., Mariscal M.A., García-Rodríguez J., Ritzel D. O. (2012) Working conditions psychological physical symptoms and occupational accidents. Bayesian network models. *Safety Science*, 50, 1760-1774.

Likar, J., Čadež, J. (2000) Ventilation Design of Enclosed Underground Structures. *Tunnelling and Underground Space Technology*, 15(4), 477–480.

Lipsey, M.W. (1990) *Design Sensitivity*. Newbury Park, California: Sage Publications.

Reddy, A.C. (2009) *Development of a Coal Reserve GIS Model and Estimation of the Recoverability and Extraction Costs*. West Virginia University: Master of Science Thesis, Department of Mining Engineering.

Saleh, J. H., Cummings, A. M. (2011) Safety in the mining industry and the unfinished legacy of mining accidents: Safety levers and defense-in-depth for addressing mining hazards. *Safety Science*, 49(6), 764–777.

Numerical Study on the Fire Protection System in The Galaje Tunnel

B. Niknam, K. Shahriar, H. Madani
Amirkabiruniversity, Tehran, Iran

ABSTRACT In this work, a numerical 3D simulation of ventilation and sprinkler systems in the Galaje Tunnel, a two-lane, 2250 m long road tunnel in Iran, are developed to evaluate the effects of different designs and of emergency systems, and to assess the performance of safety measures over a wide range of fire scenarios. According to simulation result, sprinkler droplets are too light to penetrate the fire plume and are simply swept away. Simulation results suggested that the longitudinal ventilation system was very effective for blowing all smoke and hot gases in the downstream direction, which could be generally deemed empty, so immediately creating upstream the fire a safe route for evacuation and rescue

Keywords: tunnel, Galaje,fire, ventilation, sprinkler, simulation

1 INTRODUCTION

Fires in road tunnels are extremely hazardous for induced drivers and rescue teams. Recent disasters, like crashes in the Mont Blanc tunnel or San Gottardo [1,2], have shown the need for better integral actions in the case of fire incidents. In particular, the minimum delay time required for starting the jet fans, or the evolution of the smoke patterns inside the tunnel are critical issues when rescue plans are designed. Since major interest is placed on developing systems that minimize both material and personal damages, the design of ventilation systems must be focused on the life protection, while the evacuation of the tunnel is completed. Therefore, these ventilation systems must incorporate an integral operating manual in which the airflow necessary to control the smoke or the direction and schedule of fresh-air supply should be clearly specified. Unfortunately, there is not just one simple procedure to estimate these operating conditions because of the inherent complexity of the problem: a non-linear convection of multispecies mixture of gases inside one particular tunnel geometry, function of heat and energy sources (fire characteristics) and weather conditions (variable boundary conditions).

Three deferent methodologies can be cited as basic tools to study the smoke propagation in case of fire: pseudo thermal scale models, full scale tests and numerical models. In the first case, significant contributions using the pseudo-thermal method can be found in the bibliography though their results are difficult to extrapolate to different operating conditions and are quite limited to low temperature applications. The second method (full scale tests) is really expensive and only few of them have been conducted recently: the EUREKA Project , the Memorial Tunnel Fire Ventilation Test Program and Runehamer fire test. Because they require of large experimental facilities, they are difficult to operate and maintain in order to obtain good results. The last method (numerical modeling), now under development, consists of customizing CFD codes to analyze the fire evolution when the ventilation system operates inside meshed tunnel geometries. However, in order to be completely reliable, these codes must be calibrated and verified through comparison with experimental data .In this paper we use numerical method to study fire characteristic and fire control approach in Galaje tunnel.

2 GALAJE TUNNEL

Galaje tunnel (figure1) is 2,250 m long, 10.6 m wide, and 8.35 m high, with the cross section of 72 m2; of rocky type and is situated on route to Ilam_kermanshah road. The tunnel has a lane in each direction. The road traffic is heavy, many accidents occurred in the road that may be cause to fire in the tunnel

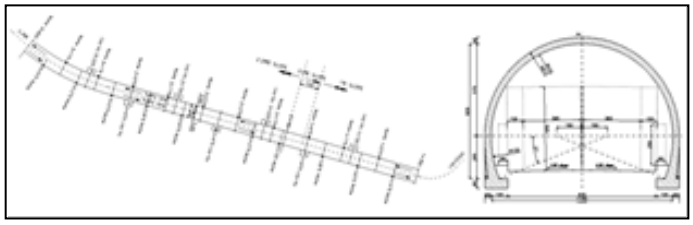

Figure1.Galaje tunnel rout and cross section

3 PROBLEM DESCRIPTION

The ventilation system is used for controlling smoke, hot and toxic combustion gases during a fire emergency, in order to allow safe evacuation and rescue. Ventilation may be provided by natural means (Fig. 2), or by mechanical equipment (longitudinal, semi-transverse or full transverse ventilation systems,(Fig. 4).

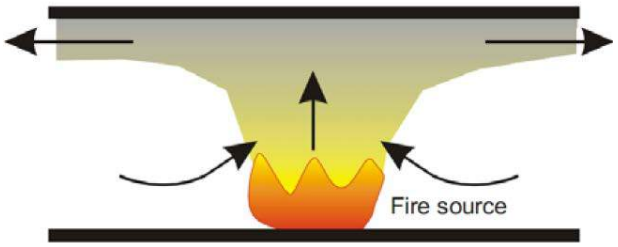

Figure2. Natural fire

With no air current in the fire zone, the smoke progresses in a symmetrical way on both sides of the fire. The smoke remains stratified until it cools down due to the combined effects of the convective heat exchange with the walls and the mixing between the smoke and the fresh air layer, . A natural ventilation system depends on the pressure differential that is created by atmospheric conditions and differences in elevation (Fig. 3).

The longitudinal ventilation system (Fig. 4) creates a longitudinal flow along the roadway tunnel by introducing or removing air from the tunnel at a number of points. Longitudinal flow is provided by jet fans. The ventilation system would be operated to force the smoke and hot gases in the direction of the empty tunnel to provide a clear and safe environment behind the fire for evacuees and fire fighters. If the ventilation capacity is sufficient (Fig. 5b and Fig. 5c), all of the heated air and smoke will flow in the downstream direction. If the ventilation is weak (Fig. 5a), the upper layer of heated air and smoke may flow in the opposite direction causing back layering, .

The occurrence of back layering depends on many factors including the intensity of fire, the grade and geometry of the tunnel, and the velocity of the ventilating air approaching the fire.

The ability of the longitudinal ventilation system to prevent back layering is the current industry standard to measure the adequacy of the system for smoke control (Fig. 6).

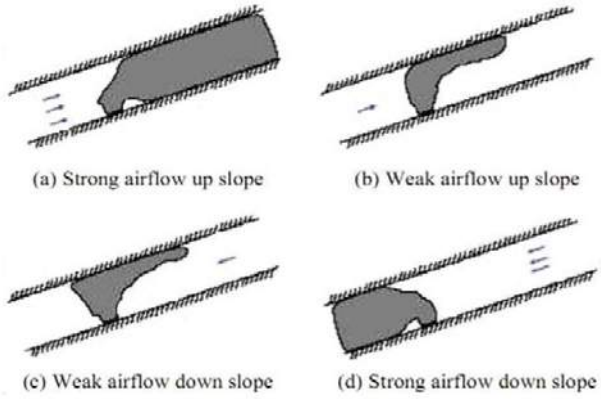

Figure3. Smoke behavior in a sloping tunnel

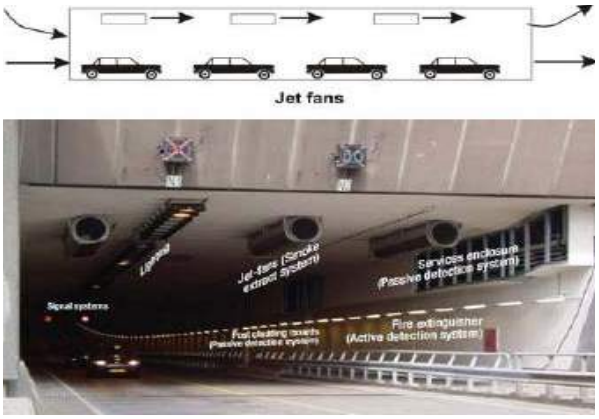

Figure 4. Longitudinal ventilation system

The simultaneous solution of Eqn. (1) and Eqn. (2), by iteration, determines the critical

velocity. The critical velocity, Vc, is the minimum steady-state velocity of the ventilation air moving toward a fire that is necessary to prevent back layering, .

The simultaneous solution of Eqn. (1) and Eqn. (2), by iteration, determines the critical velocity. The critical velocity, Vc, is the minimum steady -state velocity of the ventilation air moving toward a fire that is necessary to prevent back layering, .

$$V_C = k_1 k_g \left(\frac{gQH_t}{C_p T_f \rho_0 A} \right)^{\frac{1}{3}} \quad (1)$$

$$T_f = \left(\frac{Q}{C_p \rho_0 A V_C} \right) + T \quad (2)$$

Where:

A - Area perpendicular to the flow [(m2)]
Cp - Specific heat of air [(kJ/kg K)]
g - Acceleration caused by gravity [(m/sec2)]
H - Height of duct or tunnel at the fire site [(m)]
K1 - 0.606
Kg - Grade factor (see Fig. 7)
Q - Heat fire is adding directly to air at the fire site [(MW)]
T - Temperature of the approach air [(K)]
Tf - Average temperature of the fire site gases [(K)]
Vc - Critical velocity [(m/sec)]
ρ - Average density of the upstream air [(kg/m3)]

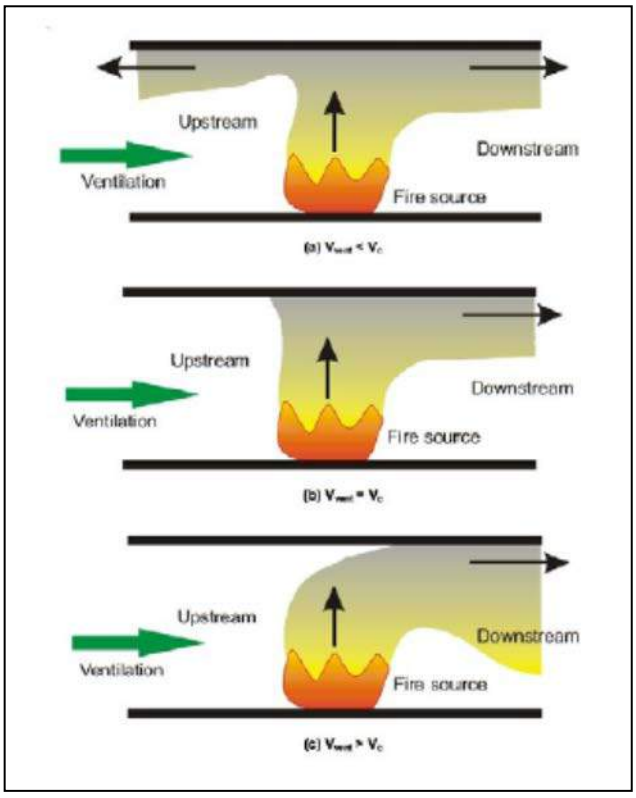

Figure 5. Influence of longitudinal air velocity (Vvent) on smoke progress in the fire zone (Vc= critical velocity)

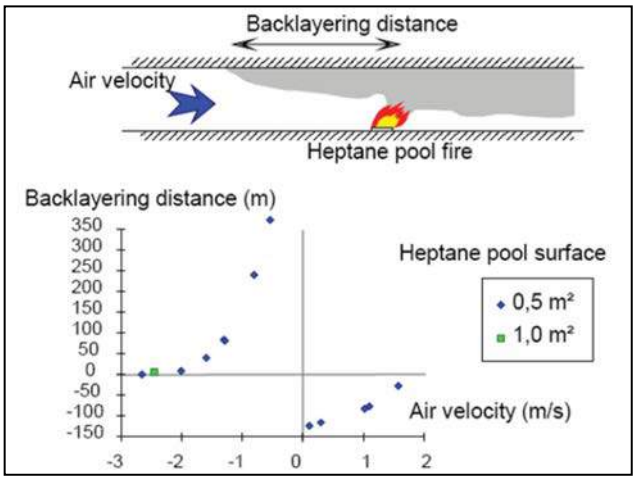

Figure 6. Backlayering distance vs. longitudinal air velocity for two heptane pool surfaces

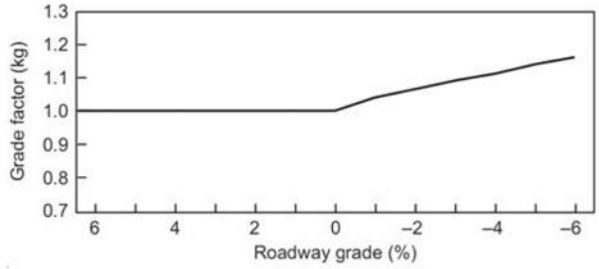

Figure 7. Grade factor for determining critical velocity

For large tunnel fires critical velocity can be taken as dependent of the HRR (Fig. 8).

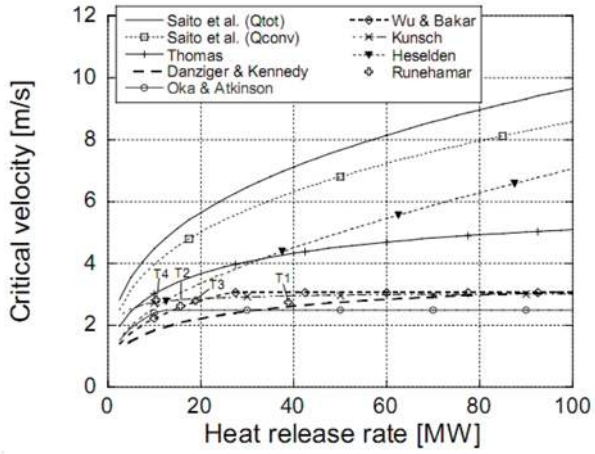

Figure 8. Critical velocities as function of total HRR according to four different relations

Fire Data for Typical Vehicles, according NFPA 502Standard for Road Tunnels, Bridges and Other Limited-Access Highways are shown in the Table 1, .

Table 1. Fire Data for Typical Vehicles

Type of vehicle	**HRR(MW)**
Car	5-10
Multi passenger cars (2-4vehiles)	10-20
Bus	20-30
Heavy goods vehicles	70-200
Tanker	200-300

In Figure 9 the five fire temperature curves are presented graphically (the first two hours), .

In Japan and Australia water extinguishment systems are widely used in tunnels. In Europe, however, there has been a reluctance to use sprinkler in tunnels. According NFPA 502 Standard the major concerns expressed by tunnel authorities regarding fire sprinkler use and effectiveness include the following, :

(a) Typical fires usually occur under vehicles or inside passenger or engine compartments that are designed to be waterproof from above; therefore, overhead sprinklers have no extinguishing effect.

(b) With any delay between ignition and sprinkler activation, a thin water spray on a very hot fire produces large quantities of superheated steam without suppressing the fire. Such steamhas the potential to be more damaging than smoke.

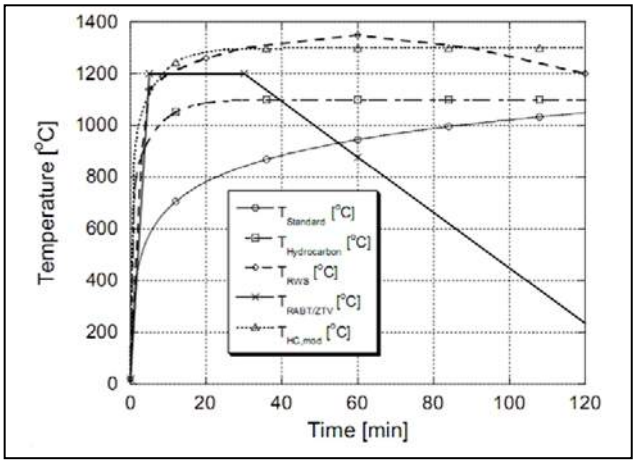

Figure 9. Specific temperature curves of hydrocarbon firesin tunnels

(c) Tunnels are long and narrow, often sloped laterally and longitudinally, usually ventilated, and never subdivided, so heat normally is not localized over afire.

(d) Because of stratification of the hot gases plume along the tunnel ceiling, a number of activated sprinklers are unlikely to be located over the fire. A large number of activated sprinklers are likely to be located at a distance from the fire scene, producing cooling effect that tends to draw the stratified layer of smoke down toward the roadway level.

(e)Even a light spray from sprinklers can catch motorists unaware and can exceed that which windshield wipers could clear. Sprinkler discharge can also cause the roadway to become dangerously slippery.

(f)Water that sprays from the ceiling of a subaqueous tunnel suggests tunnel failure and can induce panic in motorists.

(g)The use of sprinklers can cause the delamination of the smoke layer and induce turbulence and mixing of the air and smoke, thus threatening the safety of motorists in the tunnel.

(h)Periodic testing of a fire sprinkler system to determine its state of readiness is impractical and costly.

4 NUMERICAL SIMULATION

The CFD software package NIST Fire Dynamics Simulator version 5 (FDS5) was used to calculate temperature and smoke concentration fields formed in case of fire with in the Galaje tunnel space . For the calculation of flow and temperature fields of the air formed within the tunnel, large eddy simulation turbulent model was used. Because of certain identical segments of the tunnel and the high length of the entire tunnel (Fig 10), in simulation used segment dimension was: 1200 m x 11.3m x 8.3m (length, wide, high, respectively).The FDS5 domain was divided into cells of dimension 0.5 m × 0.2 m × 0. 2 m. The tunnel is built at grade in concrete. The fire source in the simulation was represented by burning of a flammable liquid in a pool with dimensions 3 x 10 m. The maximum heat release rate per unit area (HRRPUA) of the fire was 6733 kW and the total heat release rate (HRR) was 200 MW same as tanker fire. The initial air temperature in the whole tunnel was set to 15 °C. This calculation determined that the ventilation of tunnel is to be carried out by 22×2 pairs of regularly arranged jet fans and three parallel lines of sprinklers K-11 type. Distance between sprinklers is 3.05 m, according NFPA 13 Standard, . The maximum volumetric flow of fresh air through these jet fans should be 28.55 and 57.1 m3/s.

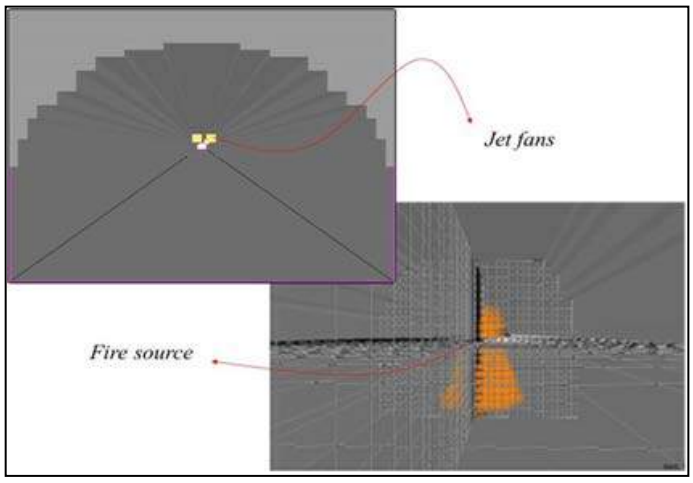

Figure 10. The computational domain for the tunnel fireSimulations

5 RESULT OF SIMULATION

5.1 Heat Release Rate

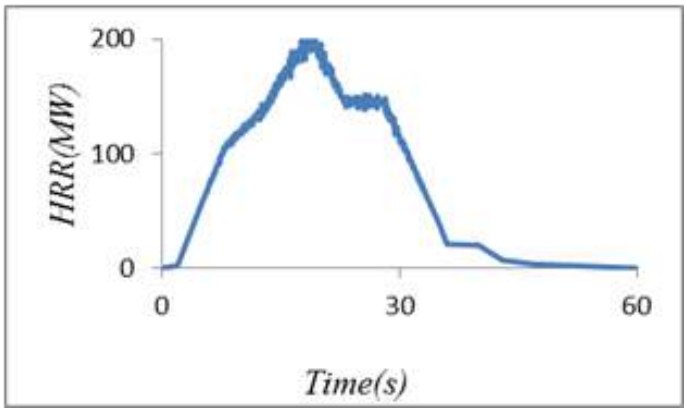

Figure 11. Heat Release rate from fire

5.2 Smoke propagation in tunnel

a) Natural ventilation

b) Forced ventilation (28.55m3/s) back layering

c) Forced ventilation (57.1m3/s)

Figure 12. Spread of smoke in a tunnel

5.3 Temperature

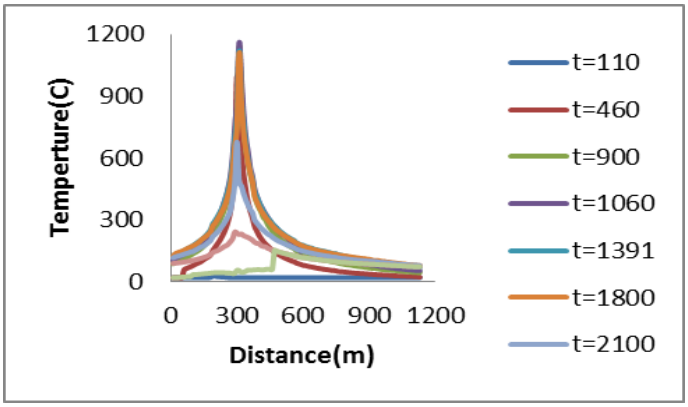

a) Forced ventilation (28.55m3/s)

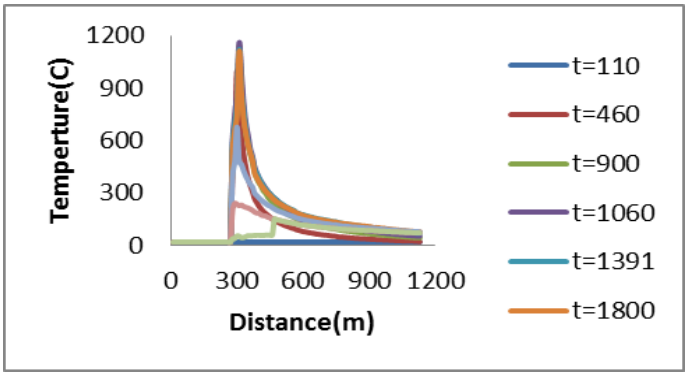

b) Forced ventilation (57.1m3/s)

Figure 12. Temperature profile along the centerline vertical plane

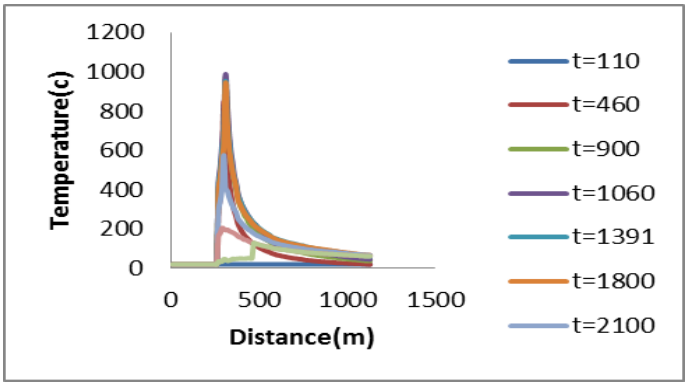

Figure 13. Temperature schedule along the centreline vertical plane with activated sprinklers

5.4 Sprinklers activation

a) Without sprinklers activation

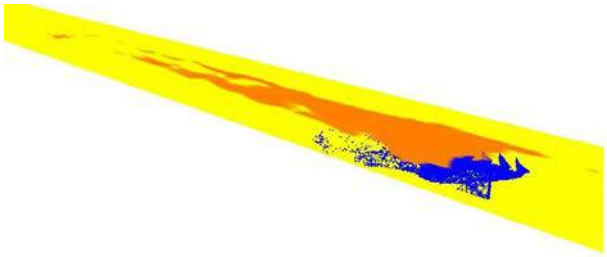

b) Sprinklers activated

Figure 14. Spread of smoke in a tunnel without and with activated sprinklers

6 CONCLUSION

The heat release rate of fire is a critical factor in the determination of fire intensity. This factor is in direct relationship with some factors like temperature, smoke distribution, air flow speed, and flame length and fire development. According to figure 11, the heat release rate in Galaje tunnel consists of six phases: ignition, initial, growth, fully-developed, decay and extinguish. The ignition phase begins from time zero and lasts up to 174 seconds. During this phase, fire intensified with liner growth rate As time passes, the fuel temperature reaches its ignition point so that within 174sec<t<260sec, flames appeared , stabilized and fire growth with quadratic rate. With the lapse of time, hot fuel-controlled fire is generated where the fire spread rate depends on the consumption of the substance. As time passes, the entire surface of the substances are engaged with fire and a rapid transfer from the growth phase to a fully-developed phase occurs .In the fully-developed phase, the heat and energy released from the fire will be at a maximum. Oxygen accessibility limits the development of fire during this phase. Thus, this phase is called ventilation-controlled fire . Within 260sec<t<1160sec, Galaje fire begins its fully-developed phase and growth exponentially. Finally, the heat release rate is decreased due to lack of fuel source in the decay phase in which the fire changes from

ventilation-controlled mode to the fuel-controlled modeIn the event of a fire in Galaje tunnel with natural Ventilation (fans turn off-Fig12a), due to difference in densities, hot combustion products rise above the fire and entrain the surrounding cold air forming a plume. The rising plume reaches the ceiling and forms two smoke streams flowing in opposite directions along the ceiling. In tunnels with longitudinal ventilation systems (Fig. 12b and Fig. 12c), the symmetry of the rising plume and the ceiling smoke streams is broken.The rising plume bends and the length of the ceiling layer flowing against the ventilation current is reduced. The reversal of the flow of the plume is referred to as back layering(Fig. 12b). If ventilation system operates only half at the maximum flow rate designed for the ventilation of the tunnel (28.55m3/s) come to a back layering effect. If ventilation system operates only at the maximum flow rate designed for the ventilation of the tunnel (Fig.12c), no will be back layering effect. In fire simulation with sprinklers, sprinklers activation come to destroying the smoke stratification (Fig. 14b) and thereby decreasing the visibility, spreading liquid fuel over a larger area and there by spreading the fire, the risk for explosion, the production of steam affecting the people inside the tunnel. The maximum predicted gas temperature near the ceiling was 1200 °C (Fig. 12), in simulations with activated sprinklers1000°C (Fig. 13). Also, the sprinkler system was not able to reduce temperature directly above the fire in the unshielded simulation. Apparently, sprinkler droplets are too light to penetrate the fire plume and are simply swept away. Simulation results suggested that the longitudinal ventilation system was very effective for blowing all smoke and hot gases in the downstream direction, which could be generally deemed empty, so immediately creating upstream the fire a safe route for evacuation and rescue

REFERENCES

Leitner, A., 2001. The fire catastrophe in the Tauern tunnel: experienceand conclusions for the Austrian guidelines. Tunn. Undergr. Sp. Tech.16 (3), 217–223.

Vuilleumier, F., Weatherill, A., Crausaz, B., 2002. Safety aspects ofrailway and road tunnel: example of the Lotschberg railway tunneland Mont-Blanc road tunnel. Tunn. Undergr. Sp. Tech. 17 (2), 153–158.

Vantelon, J.P., Guelzim, A., Quach, D., Son, D.K., Gabay, D., Dallest,D., 1991. Investigation of fire-induced smoke movement in tunnels and stations: an application to the Paris metro. In: Third International Symposium on Fire Science, IAFSS

EUREKA-Project EU 499: Firetun, 1995. Fires in Transport Tunnels: Report on Full-Scale Tests. Studiengesellschaft Stahlanwendung e.V., Du¨ sseldorf.

Bechtel/Parsons Brinckerhoff, 1995. Memorial Tunnel Fire Ventilation Test Program, Comprehensive Test Report. Massachusetts Highway Department.

Ingason H, Lo¨ nnermark ,2003,A. Large-scale fire tests in the Runehamar tunnel—heat release rate (HRR).In: Ingason H, editor. International Symposium on Catastrophic Tunnel Fires(CTF). Bora˚ s, Sweden:SP Swedish National Testing and Research Institute.

Hu, L.H., Huo, R., Peng, W., Chow, W.K., Yang, R.X., 2005. On the maximum smoke temperature under the ceiling in tunnel fires .Tunneling and Underground Space Technology 21.

.Galaje tunnel report, ministry of road and transportation, Tehran, Iran

Kashef,A . Bénichou ,N, G. Lougheed: “Numerical modeling and behavior of smoke produced from fires in the Ville-Marie and L.H.-Laontaine Tunnels”, literature review, NRCC Report IRC-RR-141, 2003

NFPA 502: “Standard for Road Tunnels, Bridges, and other Limited Access Highways”, 2004 ed., National Fire Protection Association, 2004.

NFPA 13: “Standard for the Installation of Sprinkler Systems”, 1999 ed., National Fire Protection Association, 1999.

Possibilities to Priorly Establish the Structure of Ventilation Networks Affected by Underground Explosions

D. Cioclea, G.A. Găman, I. Gherghe, F. Rădoi, C. Boantă, V.M. Păsculescu
National Institute for Research and Development in Mine Safety and Protection to Explosion – INSEMEX, Petroşani, Romania

ABSTRACT The explosion type phenomenon is an extremely complex physical – chemical process which leads to the physical change of objects and objectives encountered over the propagation pathway and to the chemical change of underground atmosphere from the area of influence.

During the development of the explosion type phenomenon, due to the energy of the dynamic wave, there occur significant mechanical effects at the level of affected mining works and at the level of ventilation constructions. In addition, due to intense burning reactions at high temperatures, there occur major effects concerning the composition and concentration of the underground atmosphere from the area of influence. Changes, respectively perturbations occurred after the event at the level of underground mining works of coal faces, endanger staff and may lead to the occurrence of similar events.

An explosion has direct effect upon the ventilation network by modifying the operational parameters of main ventilation fans. This determines different natural post event reparation of air flows at branch level. At the same time, there is modified the underground atmosphere at coal face level, leading to the increase of a potential risk of occurrence of new underground explosions, respectively to major difficulties related to the retreat of affected working staff or special intervention teams.

Prior establishment of work environment after an event is conducted through simulations over a ventilation network using the Australian software Ventsim Visual Advanced.

Keywords: Ventilation network, underground explosion, Ventsim

1 WORK ENVIRONMENT CHANGES ESTABLISHMENT

In normal conditions of hard coal exploitation, in the underground work environment occur a variety of gases of various concentrations.

The most representative and at the same time the most hazardous ones for working staff are methane, carbon monoxide and carbon dioxide.

Highest gas quantities are usually released from active coal faces during technological processes and during the coal's spontaneous combustion processes.

1.1 Gas Concentration Establishment Before the Event

In order to establish gas concentrations at the level of a coal face, there shall be performed specific measurements during a one week time period. The maximum concentration is recorded during actual exploitation works, and the minimum values are recorded during the resting periods from the end of the week.

After the occurrence of an explosion type phenomenon, the level of concentrations in air is very close or even identical to the one recorded in the resting days.

1.2 Gas Concentration Establishment After the Event

There is considered the air flow circulated at the level of the coal face Q_1

$$Q_1 = \frac{q_a \cdot 100}{c_1} \text{ (m}^3\text{/min)}$$

in which: q_a – absolute gas flow (methane or carbon dioxide) (Cioclea, 2008; Cioclea et al., 2008; Cioclea et al., 2013; Matei et al.,

2003; Matei et al., 2004) specific for the coal face (m^3/min);
c_1 – average methane or carbon dioxide concentration during the resting days from the end of a week (%);

After the event, the circulated air flow at the level of the coal face is Q_2, which is obtained by simulation using VENTSIM VISUAL ADVANCED software (m^3/min).

$$Q_2 = \frac{q_a \cdot 100}{c_x} \quad (m^3/min)$$

in which: q_a - absolute gas flow (methane or carbon dioxide) specific to the coal face (m3/min);
c_x – average concentration of methane or carbon dioxide after the event (%);

The following equation may be written:

$$c_x = c_1 \cdot \frac{Q_1}{Q_2} \quad (\%)$$

2 ESTABLISHING THE CHANGES OF THE WORK ENVIRONMENT AFTER THE OCCURRENCE OF AN UNDERGROUND EXPLOSION

Significant for establishing the work environment after the occurrence of an explosion are the information related to the changes of gas concentrations (CO_2, CH_4, CO) and of air flow (Băltăreţu and Teodorescu, 1971; Cioclea, 2006; Crăciunescu, 1984; Gherghe, 2004; Patterson, 1992; Teodorescu et al., 1980).

In this regard, for establishing environmental conditions after the occurrence of an explosion, several steps are required to be performed:

- Simulation of explosive and or toxic gas dispersion, in normal exploitation conditions;
- Establishing the structure of the ventilation network after the occurrence of an explosion;
- Simulation of explosive or toxic gas dispersion after the occurrence of an explosion.

2.1 Simulation of Explosive and / or Toxic Gas Dispersion in Normal Exploitation Conditions

In order to perform the simulations a ventilation network has to be selected, in this case Vulcan mining unit ventilation network, network which is modelled and solved using a specialized software such as VENTSIM Visual Advanced (Figure 1).

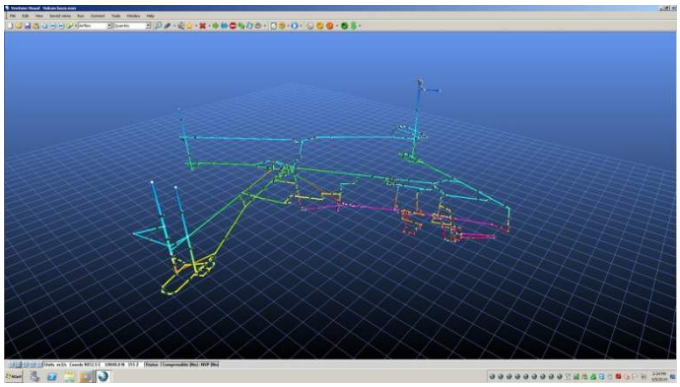

Figure 1. Ventilation network of Vulcan mine

For conducting the simulations in order to establish explosive or toxic gas dispersions (User Guide, 2012) the following steps have to be performed:

- Simulation of CH_4 dispersion at the level of the ventilation network;
- Simulation of CO_2 dispersion at the level of the ventilation network;
- Simulation of CO dispersion at the level of the ventilation network.

2.1.1 Simulation of gas dispersion at ventilation network level

For conducting the required simulations there has been used VENTSIM Visual Advanced software Figure 2, Figure 3 and Figure 4. The results of methane, carbon dioxide and carbon monoxide dispersion in normal exploitation conditions are the following:

- CH_4 is present in coal faces and has an average concentration of 0.3% vol.;
- CO_2 is present in coal faces and has an average concentration of 0.2 – 0.6 % vol.;
- CO is present in one coal face and has an average concentration of 220 ppm.

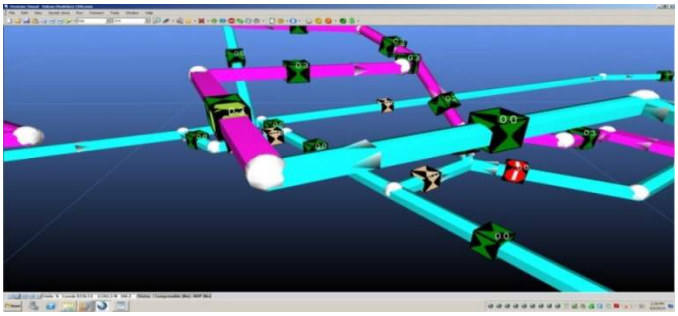

Figure 2. Simulation of CH_4 dispersion at the level of the ventilation network

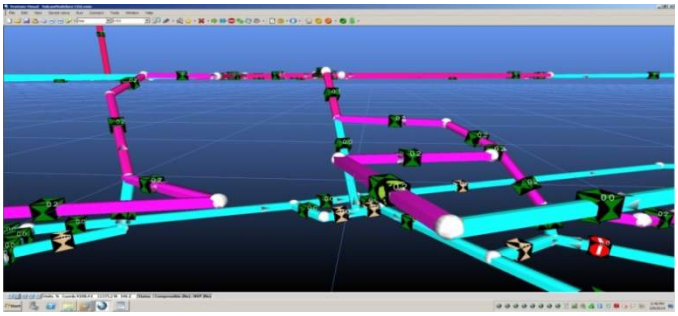

Figure 3. Simulation of CO_2 dispersion at the level of the ventilation network

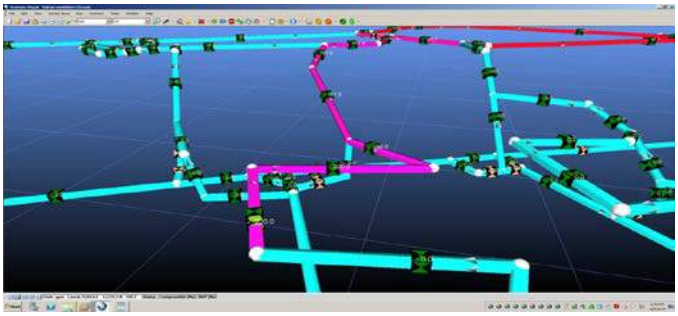

Figure 4. Simulation of CO dispersion at the level of the ventilation network

2.2 Establishing the Structure of the Ventilation Network After the Occurrence of an Explosion

In order to establish the structure of the ventilation network after the occurrence of an explosion (Bana, 1985; Bardocz, 1973; Barthnecht, 1981; Freytag, 1965; Hîndoreanu, 1972; Plasche, 1955) the following steps shall be performed:

- Establishing the influence of the explosion type phenomenon upon the ventilation network;
- Solving the ventilation network by taking into account the changes generated by the explosion

2.2.1 Establishing the influence of a high intensity explosion type phenomenon upon the ventilation network

In order to identify the effects of a high intensity explosion there shall be firstly established the following:

- The ventilation network on which the simulation is performed is the one of Vulcan mine;
- The chosen area for simulating the explosion is the coal face with undermined coal bed no. 1/3/VII;
- Length of the coal face: 54 m;
- Volume of the explosive mixture:375 m^3.
- Length of the face over which the methane accumulation occurs: 40 m;
- Section of the face: 9.375 m^2;
- Air-methane concentration 10 % vol.;
- Ignition source– spontaneous combustion phenomenon degenerated into an endogenous fire;
- Approximate explosion pressure: 10 bar.

2.2.1.1 Rate of pressure rise

The rate of the explosion pressure rise dP/dt_{max} is given by (Cleuet and Gros, 1994) the cubical law:

$$\frac{dP}{dt}\ \text{max} = K_g V^{-1/3} \quad \text{(bar/s)}$$

in which:

V – volume of the enclosure m^3;

K_g – gas characteristic constant, for turbulent mixture, having a value of 460;

$\frac{dP}{dt}$ max = 63,79 bar/s

2.2.1.2 Determination of the explosion pressure loss gradient

Taking into account the specialized literature and the experimental data developed in tunnels with relatively reduced lengths of 100 m, respectively 896 m ,(Bana, 1985; Bardocz, 1973; Cîrloganu, 1986; Hîndoreanu, 1972; Lei et al., 2012; Sochet, 2010; Zheng and Li, 2012) compared to the length of the mining works from within an underground mine which may add up to tens of km, with a high complexity degree from the structural point of view, there is

considered the maximum pressure loss gradient of dP/dx = 0.35 bar / 100 m.

Taking into account the explosion pressure of 10 bar, respectively the values of 0.07 bar and 0.15 bar for which ventilation doors, respectively insulation constructions structurally collapse (Technical expertise, 2014), it results that the dynamic wave generated by the explosion destroys the following ventilation doors belonging to the uniquely identified branches: 52; 63; 70; 103; 137; 147; 170; 171; 187; 197; 200; 202; 216; 258; 278; 286; 276; 285; 309 and 310, respectively the insulation constructions belonging to the uniquely identified branches: 226; 230.

3 SOLVING THE VENTILATION NETWORK WITH REGARD TO CHANGES GENERATED BY THE EXPLOSION

Figure 5 presents the spatial ventilation network of Vulcan mining unit in 3D solid format, modified with regard to the structural changes generated by the explosion (User Guide, 2012).

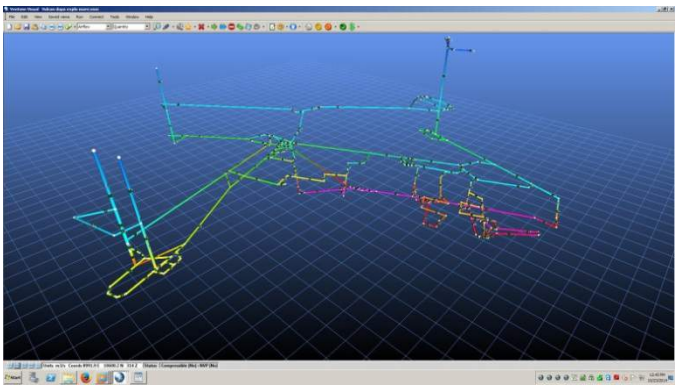

Figure 5. Vulcan mine ventilation network after the occurrence of the explosion

3.1 Simulation of Explosive or Toxic Gas Dispersion After the Occurrence of an Explosion

For conducting the simulation in order to establish the dispersion of explosive and or toxic gases after the occurrence of an explosion type phenomenon (Sochet, 2010), the following steps shall be performed:

- Simulation of CH_4 dispersion at the level of the ventilation network;
- Simulation of CO_2 dispersion at the level of the ventilation network;
- Simulation of CO dispersion at the level of the ventilation network.

Changes of the ventilation network's structure bring along the change of airflows at branch level and there occur major changes of gas concentrations in areas of influence.

3.1.1 Simulation of CH_4 dispersion at ventilation network level

Figure 6 provides the simulation of methane dispersion at the level of the ventilation network, representing the area of the active coal face no. 2/3/VI, no. 1/3/VII.

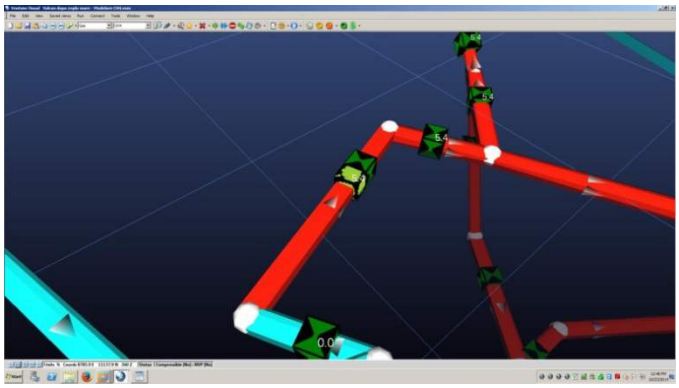

Figure 6. CH_4 dispersion in the undermined coal bed no. 2, layer no. 3, block VI

Following the simulation of methane dispersion at the level of the ventilation network, the following results have been obtained:

- CH_4 concentration at the level of the coal face with undermined coal bed no. 2, layer no. 3 bl. VI with unique no. 55, has a value of 5.4 % vol.;
- CH_4 concentration at the level of the face with undermined coal bed no. 1, layer no. 3 bl. VII with unique no. 191, has a value of 10.8 % vol.;
- CH_4 concentration at the level of the face with undermined coal bed no. 1, layer no. 3 bl. VIII with unique no. 214, has a value of 17.4 % vol.;
- CH_4 concentration at the level of the faces no. 1 – no. 4, layer no. 3 bl. VIII

with unique no. 223, has a value of 17.4 % vol.;
- On the ventilation shaft, branch with unique no. 274, CH_4 concentration is 0 % vol.

3.1.2 Simulation of CO_2 dispersion at ventilation network level

Figure 7 provides the simulation of carbon dioxide dispersion at the level of the ventilation network, representing the area of the active coal face no. 1/3/VIII.

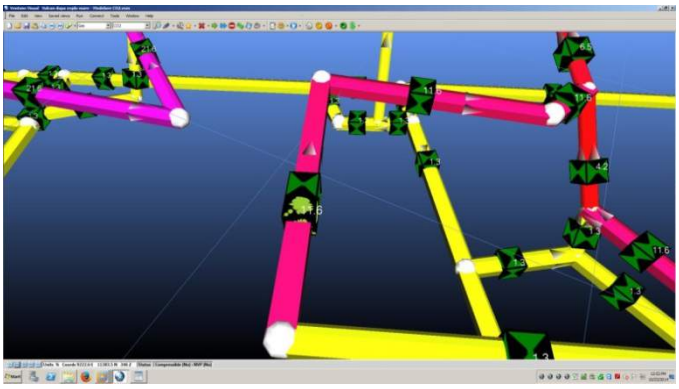

Figure 7. CO_2 dispersion in the undermined coal bed no. 1, layer no. 3, block VIII

Following the simulation of carbon dioxide dispersion at the level of the ventilation network, the following results have been obtained:
- CO_2 concentration at the level of the face with undermined coal bed no. 2, layer no. 3 bl. VI with unique no. 55, has a value of 3.6 % vol.;
- CO_2 concentration at the level of the face with undermined coal bed no. 1, layer no. 3 bl. VII with unique no. 191, has a value of 21.6 % vol.;
- CO_2 concentration at the level of the face with undermined coal bed no. 1, layer no. 3 bl. VIII with unique no. 214, has a value of 11.6 % vol.;
- CO_2 concentration at the level of the faces no. 1 – no. 4, layer no. 3 bl. VIII with unique no. 223, has a value of 11.6 % vol.;
- On the ventilation shaft, branch with unique no. 274, CO_2 concentration has a value of 1.5 % vol.
- At the level of the main ventilation station, branch no. 304, CO_2 concentration has a value of 0.1 % vol.

3.1.3 Simulation of CO dispersion at ventilation network level

Figure 8 presents a detail of the carbon oxide dispersion the level of Vulcan mine unit ventilation network, representing the area of the active coal face no. 1/3/VIII.

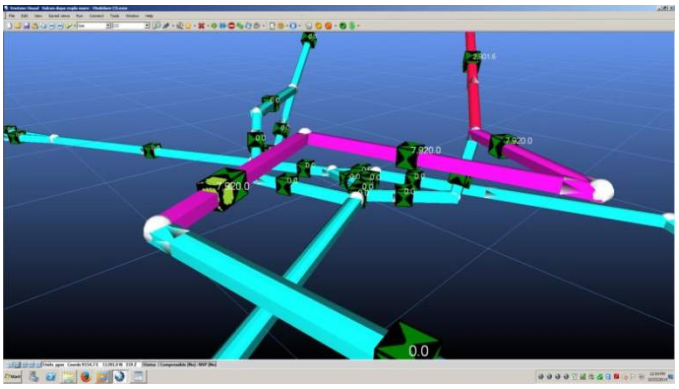

Figure 8. CO dispersion in the undermined coal bed no. 1, layer no. 3, block VII

Following the simulation of carbon oxide dispersion at the level of the ventilation network, the following results have been obtained:
- CO concentration at the level of the face with undermined coal bed no. 1, layer no. 3 bl. VII with unique no. 191, has a value of 7920.0 ppm;
- On the ventilation shaft, branch with unique no. 274, CO concentration has a value of 252.7 ppm;
- At the level of the main ventilation station, branch no. 304, CO concentration has a value of 5.7 ppm.

4 CONCLUSIONS

- Methane releases in areas of front faces is a complex phenomenon which depends in value and intensity on a series of natural-geological and technological factors.
- For establishing the methane, carbon dioxide and carbon monoxide concentration after the event there has been used the absolute gas flow method.

- Identifying environmental conditions after the occurrence of an explosion consists of the following phases:
- Simulation of explosive or toxic gases dispersion in normal exploitation conditions;
- Establishing the structure of the ventilation network after the occurrence of an explosion;
- Simulation of explosive or toxic gas dispersion after the occurrence of an explosion;
- Establishing explosive or toxic gas dispersion before and after the occurrence of an explosion, involves the following simulations at the level of Vulcan mine unit ventilation network:
  - CH_4 dispersion simulation;
  - CO_2 dispersion simulation;
  - CO dispersion simulation.
- Results on the dispersion of methane, carbon dioxide and carbon oxide after the occurrence of a high intensity explosion are the following:
  - CH_4 is present in coal faces and has concentrations of 5.4-1.4 % vol.;
  - CO_2 is present in coal faces and has concentrations of 3.6 – 21.6 % vol.;
  - CO is present only in one coal face and has a concentration of 7920.0 ppm.

REFERENCES

Bana, F., 1985. *Study on the explosion mechanism of flammable atmosphere constituted of methane and/or coal dust in mixture with air, in order to establish the characteristic effects*, (in Romanian), C.C.S.M. Study, Petrosani, Romania.

Bardocz, V., 1973. *Establishing the characteristic effects of mining faults generated by the ignition or explosion of a flammable environment, in order to reproduce the conditions in which it occurred*, (in Romanian), S.C.S.M. Study, Petrosani, Romania.

Barthnecht, W., 1981. *Explosionen*, Springer Verlag, Berlin.

Băltăreţu, R., Teodorescu, C., 1971. *Ventilation and Occupational Safety in Mines* (in Romanian), Didactical and Pedagogical Publishing House, Bucharest, Romania.

Cîrloganu, C., 1986. *Rapid combustions*, (in Romanian), Technical Publishing House Bucharest, Romania.

Cioclea, D., 2006, *Ventilation network solving based on pressure measurements in order to establish air flows, depressions, aerodynamic resistances overt the workplaces, in order to put into operation the new VOD 2.1 fans station from shaft no. 10- Valea arsului,* Research Study, National Institute for Research and development in Mine Safety and Protection to Explosion INSEMEX, Petrosani, Romania.

Cleuet, A., Gros, P., 1994. Les melanges explosifs, *INRS Bulletin,* Marseille, France.

Cioclea, D., 2008. *Methods and manners for preventing and fighting against spontaneous combustions when applying the undermined coal bed exploitation method*, (in Romanian), INSEMEX Publishing House, Petrosani, Romania.

Cioclea, D., Toth, I., Lupu, C., Jurca, L., Gligor, C., 2008, *Coal susceptibility to spontaneous combustion*, (in Romanian), INSEMEX Publishing house, Petrosani, Romania.

Cioclea, D., Lupu, C., Jurca, L. Gherghe, I., 2013. *Guide for dimensioning industrial ventilation installations*, (in Romanian), INSEMEX Publishing house, petrosani, Romania.

Crăciunescu, I., 1984. *Establishing the methane balance in mechanized coal faces and development of technical solutions for preventing and fighting against methane accumulations*, (in Romanian), CCSM Petrosani research study, Romania.

Freytag, H.H., 1965. *Raumexplosionen*, Heraugeber Chemie Gmbh Weinheim.

Gherghe, I., 2004. *Rationalization of ventilation networks in mines from Jiu Valley in terms of their restructuring and following the closure of inactive areas*, Research Study, National Institute for Research and development in Mine Safety and Protection to Explosion INSEMEX, Petrosani, Romania.

Hîndoreanu, E., 1972. *Establishing the characteristic effects of mining faults generated by the ignition or explosion of a flammable environment, in order to reproduce the conditions in which it occurred*, (in Romanian), S.C.S.M Study, Petrosani, Romania.

Lei, P., Jialei, T., Yabo, X., 2012. Hazard characteristics from gas explosion in underground constructions, *International Symposium ISSSE*, China.

Matei, I., Toth, I., Cioclea, D., Purcaru, I. S., Vochiţoiu, H., 2003. *Spontaneous combustions in coal mines*, (in Romanian), PRINT-EVEREST Publishing house, Deva, Romania.

Matei, I., Cioclea, D., Toth, I., Gligor, C., Voinoiu, N., Purcaru, I. S., 2004. *Spontaneous combustion prevention in coal exploitation using the undermined coal bed method*, (in Romanian), Agora Publishing house, Calarasi, Romania.

Patterson, A.M., 1992. *The Mine Ventilation Practitioner's DATA BOOK*, M.V.S. of South Africa.

Plasche, F., 1955. *Wetterlehre und brandbekampfung im bergbau,* Fachbuchverlag Leipzig.

Sochet, I., 2010. Blast effect of external explosions, *8th International Symposium on Hazards, Prevention, and Mitigation of Industrial Explosions*, Yokohama, Japan.

Teodorescu, C., Gontean, Z., Neag, I., 1980. *Mining Ventilation* (in Romanian), Technical Publishing House, Bucharest, Romania.

Zheng, Z., Li, J., 2012. Surface pressure of the mine refuge shelter in underground gas explosion, *International Conference MEMS.*

*** User Guide, 2012. Ventsim Visual Advanced.

*** Technical expertise, 2014. Technical expertise on the event dated December 15th 2013 in block A38 located in Calarasi, Bucuresti street, no 139, Calarasi county, (in Romanian), National Institute for Research and Development in Mine Safety and Protection to Explosion – INSEMEX Petrosani, Romania.

Provenance of Organic Matter Preserved in the Chattanooga Shale at Hurricane Bridge, Tennessee, as Indicated by Organic Carbon Isotope

M. Musa and A. Swadan
Almergab University, Mesellata, Libya

J. Puckette
Oklahoma State University, Stillwater, Oklahoma, USA

ABSTRACT Stable isotopes of the organic carbon (δ13Corg) and organic carbon concentration in samples from the Upper Devonian -Chattanooga Shale were used to investigate sources of organic matter. Marine organic matter source that is characterized by more depleted δ13Corg is dominated in the Chattanooga Shale. Terrestrial organic matter was significantly contributed in the upper Dowelltown as indicated by some positive excursion of δ13Corg. These terrestrial spikes relatively have lower organic carbon contents. Most marine organic source (more negative organic δ13C) reflects good preservations of the organic carbon. A positive shift of δ13Corg at the base of the lower Gassaway member associated with high organic carbon contents (the highest in the entire formation) may reflect the global signature of the δ13Corg across the Frasnian-Famennian boundary. Variation in organic carbon content within the same level of marine organic source (same level of δ13Corg) may indicate variation in the intensity of organic matter productivity and or preservation conditions.

Keywords: Organic carbon, Chattanooga Shale, organic matter

1 INTRODUCTION

Organic carbon isotopes (δ13Corg) is reflected in the geologic timescales a reason that δ13Corg is used as a primary processes proxy (Philip, 1994). δ13Corg uses to distinguish between different sources of organic matter as a result of different CO2 sources using in their metabolisms (Alt-Epping et al., 2007; Lamb et al., 2006; Peters-Kottig et al., 2006; Philip, 1994, 2003; Tue et al., 2011). Phytoplankton favors utilizing lighter carbon isotope as a kinetics fractionation preferentially (Murphy et al., 2000). The fractionation of the δ13C is controlled by the rate of phytoplankton growth and the amount of dissolved CO2 (Bidigare et al., 1997; Laws et al., 1995). If the rate of growth increases or the reservoir of dissolved CO2 decreases, δ13C increases as a result of decreasing isotope fractionation between dissolved CO2 and photosynthesis (Murphy et al., 2000). In contrast decreasing the rate of growth or increasing in CO2 reservoir leads to increase carbon isotope fractionation resulting in depletion of δ13C (Murphy et al., 2000). Land plants are not largely influenced by surrounding CO2 as the phytoplanktons do because land plants use stomata to control CO2 diffusion (O'Leary, 1981). Consequently, carbon isotopes of land plants are not influenced by changes in the surrounding CO2 (gas) (Murphy et al., 2000).

Marine phytoplankton had tended to utilized lighter carbon isotopes compared to land plant during periods when the atmospheric CO2 was high compared to modern world (Arthur et al., 1988; Wenger et al., 1988). For instance, CO2 of the atmosphere was estimated as grater as six times from the present day at the end of Upper Devonian (McGhee, 2005). Consequentially, the concentrations of dissolved CO2 increased resulting high

isotope fractionation in marine organic matter that produced lighter (more negative) δ13Corg than land plants (Arthur et al., 1988). This pattern is opposite to what is observed in today marine and land organisms (Philip, 1994, 2003). (Maynard, 1981) illustrated that δ13Corg is strongly related to siliciclastic dispersal forms in the Catskill Delta of the Devonian Appellation Basin. These patterns show that the heavier δ13Corg is abundant at the shoreline area where coarse grain sediments (sandstone and siltstone) are dominated, while the lighter carbon isotope concentrates at the basin area that is characterized by mudstones rich (Maynard, 1981). This heavy and light δ13Corg distribution is opposite to what is observed in the present day shoreline and basin trends (e.g., (Kennicutt et al., 1987). Marine sources that are characterized by lighter δ13Corg than land plants have been observed in different locations and geological times. For instance, it is observed in Cretaceous rocks (Arthur et al., 1985; Dean et al., 1986), Devonian-Mississippian shales of Anadarko Basin (Sullivan, 1983) and Appalachian Basin (Maynard, 1981; Zielinski, 1977), and Jurassic shale in Germany (Küspert, 1982). The end-members of marine and land plant sources determined from Devonian Appalachian Basin have contributions of approximate -31‰ for marine plankton and -26‰ for land plants (Murphy et al., 2000). Contributions for marine and terrestrial sources were also estimated as -30.5 ‰ and -25 ‰ respectively (Maynard, 1981) in the upper Devonian at eastern United States. Therefore, the positive shifts of δ13Corg to the direction of -26 ‰ indicates increasing land plant influence, while a negative excursion to the direction of -31 ‰ indicates an increased influence in marine organic matter contributions.

The Chattanooga Shale formed from sediments deposited in the southwestern part of the Appalachian Basin (Figure 1), and is one of the a black shales that formed on the North America Craton during the Upper Devonian (de Witt et al., 1993). Economically, the Chatta=nooga Shale is considered an important hydrocarbon source rock (Charpentier et al., 1993; Comer and Hinch, 1987; Conant and Swanson, 1961; de Witt et al., 1993; Roen and Kepferle, 1993). The Chattanooga Shale was deposited in epicontinental shallow marine setting with low sedimentation rate on a low-relief shelf area (Breger and Brown, 1962; Conant and Swanson, 1961; Lobza and Schieber, 1999; Schieber, 1998b, 2001; Schieber and Riciputi, 2004). Sediments were carried from the east side of the basin and the perennial streams were dominate (Woodrow et al., 1988). Such environments may provide a significant amount of both terrestrial and marine organic matter. The mixing of land plant and marine organic matter in the Chattanooga Shale was remarked as indicated by kerogen analysis (Breger and Brown, 1962) and field observations (Conant and Swanson, 1961; Swanson et al., 1962). These studies were lacking to evaluate the variation of organic matter sources as they contribute in the entire Chattanooga Shale section. The objective of this study is to evaluate the contributions of marine and terrestrial organic matter sources in the Chattanooga Shale by using δ13Corg technique. Shale samples were collected from the Hurricane Bridge outcrop, DeKalb County, Tennessee, where the outcrop represents the reference section of the Chattanooga Shale (Kepferle and Roen, 1981).

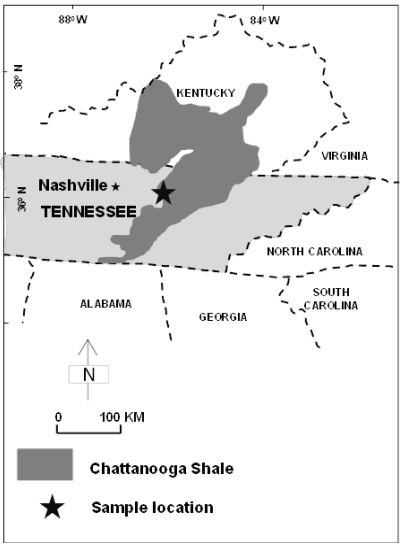

Figure 1. Sample location and geographic extent of the Chattanooga Shale [modify after de Witt, et al (1989).

2 THE EFFECT OF DIAGENESIS AND THERMAL MATURITY ON Δ13CORG IN THE STUDY SITE

Isotopic composition of organic matter could be affected by late diagenesis and metamorphic processes (Hoefs and Frey, 1976; Monin et al., 1981). The changing in the isotopes composition is estimated at about 1‰ as indicated by experiment carried out at 180 oC for several months (Schleser et al., 1999). Also the change recorded on wood material showed an increases by 0.5‰ at up to150 oC then decreasing about 1‰ up to 600 oC (Jones and Chaloner, 1991). With respect to δ13Corg alteration, no significant correlation between vitrinite reflectance and δ13Corg was observed (Strauss and Peters-Kottig, 2003). Other studies suggested that there is no systematic increase in carbon isotope concentration at temperatures below 250 oC or even approximate 350 oC (Schwarzkopf and Schoell, 1985; Watanabe et al., 1997; Whiticar, 1996). Generally, most studies suggest a common change of less than 1‰ (Peters-Kottig et al., 2006). Records show that δ13Corg keeps their original values even during organic matter transformation processes that include diagenesis, catagenesis, and metagenesis unless organic carbon and carbonate mineral isotopes exchange occur at high level of metamorphic processes (Schidlowski et al., 1983). It has been suggested that δ13Corg increases due to loss of lighter isotopes such as CH4 during organic matter transformation (Des Marais, 1992; Hayes, 1994; Hayes et al., 1983; Strauss et al., 1992). (Lewan, 1986) found that there is no significant changes in the carbon isotopes of the organic carbon in the Woodford Shale, the equivalent for the Chattanooga Shale, at different stages of thermal maturity a case that they could be used as a geochemical biomarker.

The estimated vitrinite reflectance of the Chattanooga Shale at the Hurricane Bridge outcrop and adjacent outcrops is less than 0.5% (Roberts, 1987). This low value (< 0.5%) is classified as immature source rock (Peters and Cassa, 1994; Wallace, 1977). Immature source organic rich shale has been affected by diagenesis processes without a significant influence of high temperature that is estimated between 60-80 oC (Peters and Cassa, 1994). As a result, the stable isotopes of the organic carbon in the Chattanooga Shale at the Hurricane Bridge outcrop should exhibit the original signature.starts immediately after a heading or a gap.

3 CHATTANOOGA SHALE GEOLOGY

The Upper Devonian-Chattanooga Shale was deposited in the Appalachian Basin as a part of hydrocarbon rich shales deposited in North America (de Witt et al., 1993). The name of the Chattanooga Shale was given by Hayes (1891) (Hayes, 1891). The thickness of the shale is approximately 10 m and thins westward. It represents deposition in a shallow marine setting with low sedimentation rate on a low-relief shelf area (Conant and Swanson, 1961; Schieber, 2001; Schieber and Riciputi, 2004). The study section of the Chattanooga Shale is located at the Hurricane Bridge outcrop, DeKalb County, Tennessee (Figure 1) where it is considered as a reference section of the Chattanooga Shale (Kepferle and Roen, 1981). The thickness of the Chattanooga shale in the Hurricane Bridge outcrop is approximately 10 m (Over, 2007; Schieber, 1998a; Schieber, 2001). The age of the Chattanooga Shale is Upper Devonian (Frasnian-Famennian) (Hass, 1956; Over, 2007). The shale is in regional disconformity with the underlying carbonate of the Liepers Formation and is subjacent to the Lower Carboniferous, Maury Formation, at the study section (Figure 2) (Conant and Swanson, 1961; Hass, 1956). The Chattanooga Shale is divided into three members; Hardian Sandstone (lower), Dowelltown (middle), and Gassaway (upper) (Conant and Swanson, 1961). The lowermost part (Hardian Sandstone) is only found in the southwestern Tennessee and it does not occur in the study area (Schieber, 1998a). The Dowelltown started at age of middle Frasnian as indicated by conodont biostratigraphy (Over, 2007) and it is divided further into lower and upper parts (Figure 2) (Conant and Swanson, 1961; Over, 2007;

Schieber, 1994a; Schieber, 1998a). The lower Dowelltown is about 2 m thick and consists of more resistant black shale interbeded with bioturbated gray shale (Conant and Swanson, 1961; Over, 2007; Schieber, 1994a; Schieber, 1998a). The upper Dowelltown is characterized by less resistant, more biotubated gray shale interbedded with black shale with a thickness of approximately 3 m (Conant and Swanson, 1961; Over, 2007; Schieber, 1994a; Schieber, 1998a). The Gassaway Member, Famennian (Ettensohn et al., 1989; Hass, 1956; Over, 2007) is also divided further into three parts (Figure 2) (Conant and Swanson, 1961; Over, 2007; Schieber, 1994a; Schieber, 1998a). The lower Gassaway is about 1.7 m and it consists of resistant dense black shale. The middle part of the Gassaway member consists of less resistant dark and light bioturbated gray shales with thickness about 1 m. The upper Gassaway member is about 2.5 m and it consists of black shales with interbedded lighter gray shale. The Frasnian-Famennian boundary in Chattanooga Shale is located at the base of the lower Gassaway Member as suggested by conodont stratigraphic study of the Chattanooga shale on different locations including the study site location (Over, 2002, 2007).

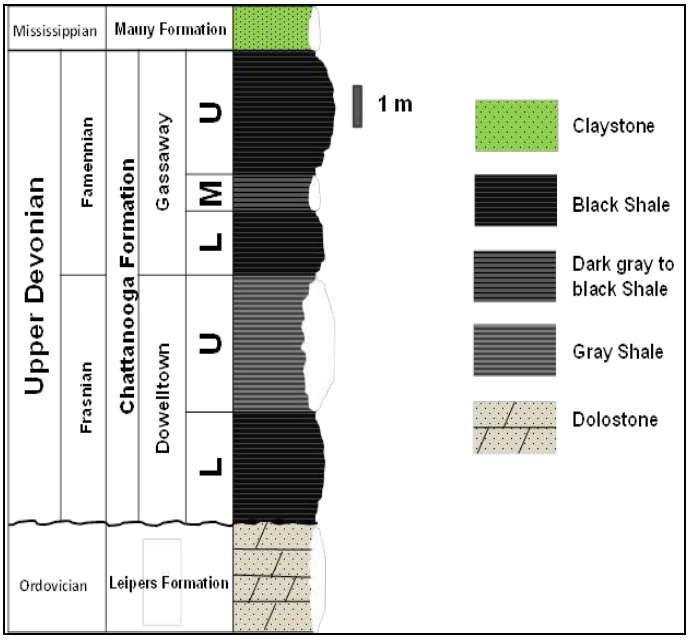

Figure 2. The stratigraphic profile of the Chattanooga Shale in the study area.

4 SAMPLING AND METHODS

Prior to collecting samples from the outcrop, weathered material was scraped away to access fresh, unweathered rock. Thirty three samples were collected at approximately 30 cm intervals from the Upper Devonian Chattanooga Shale at the Hurricane Bridge outcrop, TN. Samples were stored in plastic bags and labeled. Samples were powdered using a SPEX 8000 ball mill with alumina ceramic vial sets. Powdered samples were stored in labeled vials for further analyses. For stable isotopes of the organic carbon analysis, samples were acidified by applying 50 ml of hydrochloric acid (25%) to about 250 mg of powdered sample in centrifuge tubes for about 24 hours. All acid was removed by centrifuging the spent liquid first and then by adding ultrapure water three times and centrifuging. The residual samples were dried in an oven (60oC for 48 h) and stored in glass vials.

The concentrations of inorganic carbon (TIC) and total carbon (TC) were achieved by measuring the carbon through acidification with 2 N HCl and combustion at 950 oC under oxygen respectively. The mass for samples used in each run is about 50 mg. Pure calcite standards were reduplicate in both sides to calibrate the sample results. Finally, total organic carbon (TOC) for each sample was calculated by subtracting TIC from TC.

The concentrations of the δ13Corg in the samples were determined by processing acidified samples using a costech ECS 4010 combustion elemental analyzer that is connected to Thermo Finnigan Deltaplus XL mass spectrometer. Samples were folded in silver capsules in amounts ranges from 3 - 50 mg. the mass of samples was estimated based on a mass test done on different TOCs to give similar δ13C peak to that of the PDB. The USGS 40 (0.4 - 0.6 mg) and graphite (0.4 - 0.6 mg) standards were run after 10 sample sets to calibrate the results.

5 RESULTS AND DISCUSSION

The δ13Corg values varies across the Chattanooga Shale and it ranges from -28.4 ± 75 ‰ to -31.2 ± 0.75 ‰ with an average value of -30 ± 0.75 ‰ (Table 1; Figure 3). δ13Corg gradually decreases from the base of lower Dowelltown with a value of -29.35 ± 0.75 ‰ up to about half meter above the base of the Upper Dowelltown with value approximate -31.19 ± 0.75 ‰. Organic carbon content (TOC) in this interval increases from the base of the formation with value about 3 ± 5.7 wt. % until the middle of the lower Dowelltown at a height of 1 m where TOC is about 16 ± 5.7 wt. % then it gradually decreases to the base of the upper Gassaway with values of about 5 ± 5.7 wt. %. δ13Corg shows positive shift at the base of the upper Dowelltown from value about -31 ± 0.75 ‰ to about -28.5 ± 0.75 ‰. In the upper Dowelltown, δ13C generally shows enrichment/depletion fluctuations mostly with opposite directions to TOC (Table 1; Figure 3). For instance, at a height of 3.6 m δ13C is about -28.38 ± 0.75 ‰ and TOC is about 0.15 ± 5.7 wt. %, while at 4.6 m these values are about -30.8 ± 0.75 ‰ and 9.3 ± 5.7 wt. % respectively. A decreases in δ13Corg to values around -30 ‰ in the Devonian Appalachian Basin is interpreted as an increases in marine organic matter contributions, while increase around -26 ‰ indicates an increase in terrestrial organic matter sources (Maynard, 1981; Murphy et al., 2000; Zielinski, 1977). This depleted values in marine δ13Corg compared to land plants is related to the high fractionation between marine planktons and dissolved CO2 during periods when the atmospheric CO2 was high (Murphy et al., 2000). In the lower Dowelltown, decrease δ13Corg may indicate an increase in marine organic matter contributions that may lead to enhance organic matter preservation in this section especially in the lower part of the lower Dowelltown. A decline in TOC in the upper part of the lower Dowelltown may reflect a variation in organic matter productivity and/or preservation issues. Decrease δ13Corg to values of about -29 ‰ and less was interpreted as increasing marine organic matter sources (Strapoc et al., 2010). Strapoc et al (2010) showed that there is a strong relationship between more negative δ13C of the organic carbon (less than -29 ‰) and organic petrographic observations in the Upper Devonian-New Albany Shale. In contrast, an increase in δ13Corg in the upper Dwelltown may indicate increase in the contribution of the terrestrial organic matter. This may reflect that the area was in or very close to the shoreline that may have led to an increase in the oxygen concentrations that prohibited organic carbon preservation. This is consistent with the low TOC values that are associated with relative increase δ13Corg in the upper Dowelltown. Terrestrial organic source as indicated by δ13Corg is used as an indicator for the direction of the shoreline in Devonian shale at the Appellation Basin (Maynard, 1981) and in present day sediments (Kennicutt et al., 1987) by assuming that there is more terrestrial input near the shoreline than offshore. Sedimentology and stratigraphic studies have been done on the Chattanooga Shale at the same study section (Hurricane Bridge outcrop, TN) suggested that the dominate of the bioturbation gray shale and erosion surfaces in the upper Dowelltown represents periods where the water was more shallower than the interpreted black shale that was deposited in a more reduced environment (Schieber, 1994a; Schieber, 1998a).

At the base of the lower Gassaway Member, there is a sharp increase of δ13Corg from about -30.5 ± 0.75 ‰ at the top of the upper Dowelltown to -28.7 ± 0.75 ‰ at the base of the lower Gassaway. This is clearly indicting a positive excursion of δ13C in this interval that is also characterized by increasing TOC concentrations to about 20.7 ± 5.7 wt. % (Table 1; Figure 3). δ13Corg then gradually decreases throughout the top of the lower Gassaway. At the middle upper Gassaway δ13Corg remains semi constant with an average of -30 ± 0.1 ‰. In the upper Gassaway, δ13Corg is generally low with an approximate average of -30 ± 0.4 ‰ and it is slightly higher compared to the middle Gassaway. The organic carbon concentration in the lower, middle, and upper

Gassaway is generally high with averages of approximately 17 ± 2 wt. %, 8 ± 1 wt. %, and 15 ± 2 wt. % respectively. (Riquier et al., 2005)

A positive excursion at the base of the Gassaway Member is described by (Joachimski et al., 2002) as an unexpected shift through the Frasnian-Famennian boundary. This boundary is located at the study site (the Chattanooga Shale at Hurricane Bridge outcrop) at the base of the Gassaway member (Over, 2002, 2007). The shift in δ13Corg throughout Frasnian-Famennian boundary is interpreted as decreasing concentration of the dissolved CO2 that results in lower fractionation of carbon isotope during photosynthesis (Joachimski et al., 2002). The δ13Corg of marine algal biomarkers also exhibited identical trends to that of bulk organic carbon (Joachimski et al., 2002). Therefore, this positive shift of the δ13Corg may not reflect a change in the organic matter sources. We suggest that the marine organic matter may be dominate resulting high organic matter content due to increasing the sea level in that time that the depositional environment became more basinal areal. A major transgression during the begging of the Fammenian time when the Gassaway Member was deposited, was indicated by constraining the sea level curve (Johnson et al., 1985).

The relative decrease in δ13Corg through the top of the upper Gassaway to the end of the Gassaway Member may indicate an increase marine organic carbon contribution. May be some of the terrestrial organic matter sources caused the relative increase of δ13Corg at the top of the upper Gassaway. Increasing marine organic matter was interpreted as a shift from shoreline to more basinal environment (Kennicutt et al., 1987; Maynard, 1981). Thus, the dominance of marine organic sources in the Gassaway Member may indicate a shift of depositional environment from shoreline at upper Dowelltown to more basinal environment. This is consistent with the high organic carbon content in the Gassaway Member relative to the upper Dowelltown. Although the organic carbon concentrations are high in the Gassaway Member, the relative variation between member parts (e.g. TOC relatively low in middle Gassaway, Table 1; Figure 3) may indicate different organic matter productivity or preservation levels.

Table 1. δ13Corg and TOC concentrations for the Chattanooga Formation.

Height (m)	TOC wt. %	$\delta^{13}C$ ‰	Height (m)	TOC wt. %	$\delta^{13}C$ ‰
5.3	5.63	-30.48	10.6	14.17	-29.26
5	0.97	-29.87	10.3	16.69	-29.24
4.6	9.34	-30.87	10	17.12	-29.26
4.3	0.81	-29.8	9.6	17.65	-29.55
4	3.86	-30.52	9.3	16.67	-29.57
3.6	0.15	-28.38	9	15.23	-29.8
3.3	4.64	-28.52	8.6	12.99	-29.84
3	8.91	-31.19	8.3	12.33	-30.16
2.6	4.59	-31.13	8	9.37	-30.26
2.3	6.59	-30.96	7.6	9.65	-30.42
2	8.46	-30.92	7.3	7.58	-30.23
1.6	10.4	-31.04	7	15.92	-29.98
1.3	13.55	-30.74	6.6	16.02	-29.42
1	15.93	-30.61	6.3	16.76	-29.99
0.6	16.42	-30.74	6	17.37	-29.38
0.3	10.98	-29.98	5.6	20.69	-28.73
0	3.36	-29.35			

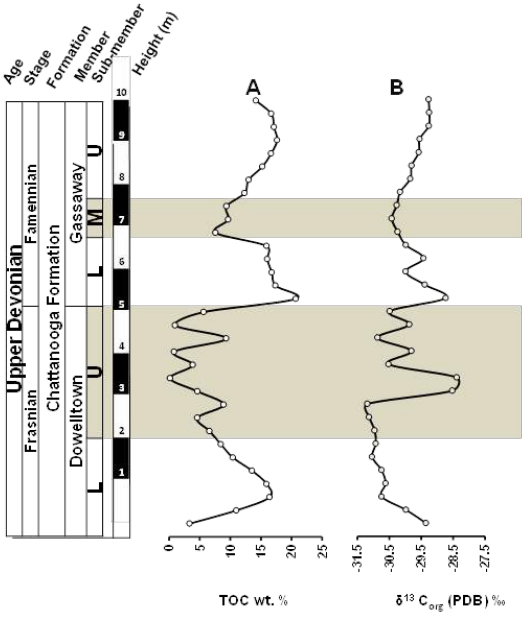

Figure 3. Total organic carbon (TOC) concentrations (A) and stable isotope of the organic carbon (δ13C) (B) in the Chattanooga Shale, Hurricane Bridge, Tennessee.

6 CONCLUSIONS

Organic matter preserved in the Chattanooga Shale appears to be mostly of marine origin, except where there was significant contribution of terrestrial origin in the upper Dowelltown. Marine and terrestrial organic matter resulted in different δ13Corg values where marine δ13Corg was more depleted than the terrestrial organic carbon. Marine organic matter in the most parts reflects high organic matter contents as indicated by organic carbon concentration (TOC). Variation in organic carbon content within levels of marine organic origin may reflect difference organic matter productivity/preservation levels. Most positive excursion reflects lower organic carbon contents, except the one at the base of the Gassaway member which may represent the unexpected spike of the Frasnian-Famennian boundary.

REFERENCES

Alt-Epping, U., Mil-Homens, M., Hebbeln, D., Abrantes, F., and Schneider, R.R., 2007, Provenance of organic matter and nutrient conditions on a river- and upwelling influenced shelf: A case study from the Portuguese Margin: Marine Geology, v. 243, p. 169-179.

Arthur, M.A., Dean, W.E., and Claypool, G.E., 1985, Anomalous 13C enrichment in modern marine organic carbon: Nature, v. 315, p. 216-218.

Arthur, M.A., Dean, W.E., and Pratt, L.M., 1988, Geochemical and climatic effects of increased marine organic carbon burial at the Cenomanian/Turonian boundary: Nature, v. 335, p. 714-717.

Bidigare, R.R., Fluegge, A., Freeman, K.H., Hanson, K.L., Hayes, J.M., Hollander, D., Jasper, J.P., King, L.L., Laws, E.A., Milder, J., Millero, F.J., Pancost, R., Popp, B.N., Steinberg, P.A., and Wakeham, S.G., 1997, Consistent fractionation of 13C in nature and in the laboratory: Growth-rate effects in some haptophyte algae: Global Biogeochem. Cycles, v. 11, p. 279-292.

Breger, I.A., and Brown, A., 1962, Kerogen in the Chattanooga Shale: Science, v. 137, p. 221-224.

Charpentier, R.R., deWitt, W., Claypool, G.E., Harris, D., Mast, R.F., Megeath, J.D., Roen, J.B., and Schmoker, J.W., 1993, Estimates of unconventional natural gas resources of the Devonian Shales of the Appalachian Basin: US Geol. Surv. Bulletin 1909: N1-N20.

Comer, J.B., and Hinch, H.H., 1987, Recognizing and quantifying expulsion of oil from the Woodford Formation and age-equivalent rocks in Oklahoma and Arkansas: AAPG Bulletin, v. 71, p. 844-858.

Conant, L.C., and Swanson, V.E., 1961, Chattanooga Shale and related rocks of central Tennessee and nearby areas: Journal Name: Geological Survey Professional Paper; Journal Volume: Vol: 357; Other Information: Orig. Receipt Date: 31-DEC-62, p. Medium: X; Size: Pages: 97.

de Witt, W., Roen, J., and Wallace, L.G., 1993, Stratigraphy of Devonian black shales and associated rocks in the Appalachian Basin: United States Geological Survey Bulletin v. 1909B, p. 1-57.

Dean, W.E., Arthur, M.A., and Claypool, G.E., 1986, Depletion of 13C in Cretaceous marine organic matter: Source, diagenetic, or environmental sigal?: Marine Geology, v. 70, p. 119-157.

Des Marais, D.J., 1992, Palaeogeogr. Palaeoclim. Palaeoecol., v. 97, p. 93-96.

Ettensohn, F.R., Goodman, P., Norby, R., and Shaw, T., 1989, Stratigraphy and biostratigraphy of the Devonian-Mississippian black shales in west-central Kentucky and adjacent parts of Indiana and Tennessee Proceedings Vume: Eastern Oil Shale Symposium, p. 237-245.

Hass, W.H., 1956, Age and correlation of the Chattanooga shale and the Maury formation, Professional paper (Geological Survey (U.S.)) ;: U.S. Govt. Print. Off., Washington.

Hayes, C.W., 1891, The overthrust faults of the southern Appalachians: Geological Society of America Bulletin, v. 2, p. 141-154.

Hayes, J.M., 1994, Global methanotrophy at the Archean-Proterozoic transition.: In Early Life on Earth, Nobel Symposium No. 84. (ed. S. Bengtson), pp. 220-236. Columbia Uniw Press.

Hayes, J.M., Kaplan, I.R., and Wedeking, K.M., 1983, Precambrian organic geochemistry, Preservation of the record.: In Earth's Earliest Biosphere: lts Origin and EvolUtion (ed. J. W. Schopf), Chap. 5, pp. 93-135. Princeton Univ. Press.

Hoefs, J., and Frey, M., 1976, The isotopic composition of carbonaceous matter in a metamorphic profile from the Swiss Alps: Geochimica et Cosmochimica Acta, v. 40, p. 945-951.

Joachimski, M.M., Pancost, R.D., Freeman, K.H., Ostertag-Henning, C., and Buggisch, W., 2002, Carbon isotope geochemistry of the Frasnian–Famennian transition: Palaeogeography, Palaeoclimatology, Palaeoecology, v. 181, p. 91-109.

Johnson, J.G., Klapper, G., and Sandberg, C.A., 1985, Devonian eustatic fluctuations in Euramerica: Geological Society of America Bulletin, v. 96, p. 567-587.

Jones, T.P., and Chaloner, W.G., 1991, Fossil charcoal, its recognition and palaeoatmospheric significance: Palaeogeography, Palaeoclimatology, Palaeoecology, v. 97, p. 39-50.

Kennicutt, M.C., Barker, C., Brooks, J.M., DeFreitas, D.A., and Zhu, G.H., 1987, Selected organic matter source indicators in the Orinoco, Nile and Changjiang deltas: Organic Geochemistry, v. 11, p. 41-51.

Kepferle, R.C., and Roen, J.B., 1981, Chattanooga and Ohio shales of the southern Appalachian Basin (Field Trip No. 3), p. 259–362. In T. G. Roberts (ed.), GSA Cincinnati '81 Guidebooks. Volume II. Economic Geology, Structure. American Geological Institute.

Küspert, W., 1982, Environmental changes during oil shale deposition as deduced from stable isotope ratios: In Cyclic and Event Stratification (Edited by Einsele G. and Seilacher A.), pp. 482-501. Springer, Berlin.

Lamb, A.L., Wilson, G.P., and Leng, M.J., 2006, A review of coastal palaeoclimate and relative sea-level reconstructions using δ13C and C/N ratios in organic material: Earth-Science Reviews, v. 75, p. 29-57.

Laws, E.A., Popp, B.N., Bidigare, R.R., Kennicutt, M.C., and Macko, S.A., 1995, Dependence of phytoplankton carbon isotopic composition on growth rate and [CO2)aq: Theoretical considerations and experimental results: Geochimica et Cosmochimica Acta, v. 59, p. 1131-1138.

Lewan, M.D., 1986, Stable carbon isotopes of amorphous kerogens from Phanerozoic sedimentary rocks: Geochimica et Cosmochimica Acta, v. 50, p. 1583-1591.

Lobza, V., and Schieber, J., 1999, Biogenic sedimentary structures produced by worms in soupy, soft muds; observations from the Chattanooga Shale (Upper Devonian) and experiments: Journal of Sedimentary Research, v. 69, p. 1041-1049.

Maynard, J.B., 1981, Carbon isotopes as indicators of dispersal patterns in Devonian-Mississippian shales of the Appalachian Basin: Geology, v. 9, p. 262-265.

McGhee, G.R., 2005, Modelling late devonian extinction hypotheses, in D.J. Over, J.R.M., and Wignall, P.B., eds., Developments in Palaeontology and Stratigraphy, Volume Volume 20, Elsevier, p. 37-50.

Monin, J.C., Boudou, J.P., Durand, B., and Oudin, J.L., 1981, Example of the enrichment of carbon-13 in coals in the process of coalification: Fuel, v. 60, p. 957-960.

Murphy, A.E., Sageman, B.B., Hollander, D.J., Lyons, T.W., and Brett, C.E., 2000, Black Shale Deposition and Faunal Overturn in the Devonian Appalachian Basin: Clastic Starvation, Seasonal Water-Column Mixing, and Efficient Biolimiting Nutrient Recycling: Paleoceanography, v. 15, p. 280-291.

O'Leary, M., 1981, Carbon isotope fractionation in plants: Phytochemistry, v. 20, p. 553-567.

Over, D.J., 2002, The Frasnian/Famennian boundary in central and eastern United States: Palaeogeography, Palaeoclimatology, Palaeoecology, v. 181, p. 153-169.

Over, D.J., 2007, Conodont biostratigraphy of the Chattanooga Shale, Middle and Upper Devonian, southern Appa;avhian Basin, eastern United States: Journal of Paleontology, v. 81, p. 1194-1217.

Peters-Kottig, W., Strauss, H., and Kerp, H., 2006, The land plant δ13C record and plant evolution in the Late Palaeozoic: Palaeogeography, Palaeoclimatology, Palaeoecology, v. 240, p. 237-252.

Peters, K.E., and Cassa, M.R., 1994, Applied source rock geochemistry: in L. B. Magoon and W. G. Dow, eds., The petroleum system—from source rock to trap: AAPG Memoir 60, p. 93–120.

Philip, A.M., 1994, Preservation of elemental and isotopic source identification of sedimentary organic matter: Chemical Geology, v. 114, p. 289-302.

Philip, A.M., 2003, Applications of organic geochemistry to paleolimnological reconstructions: a summary of examples from the Laurentian Great Lakes: Organic Geochemistry, v. 34, p. 261-289.

Riquier, L., Tribovillard, N., Averbuch, O., Joachimski, M.M., Racki, G., Devleeschouwer, X., El albani, A., and Riboulleau, A., 2005, Chapter 8Productivity and bottom water redox conditions at the Frasnian-Famennian boundary on both sides of the Eovariscan Belt: constraints from trace-element geochemistry, in D.J. Over, J.R.M., and Wignall, P.B., eds., Developments in Palaeontology and Stratigraphy, Volume Volume 20, Elsevier, p. 199-224.

Roberts, L., 1987, Organic Geochemistry Of The Devonian-Mississippian Chattanooga Shale And Cumberland Plateau Oils In Tennessee: A Source To Oil Correlation Study [M.S. thesis]: United States -- Texas, The University of Texas at Arlington.

Roen, J.B., and Kepferle, R.C., 1993, Petroleum geology of the Devonian and Mississippian black shale of eastern North America: US Geol. Surv. Bulletin 1909.

Schidlowski, M., Hayes, M., and Kaplan, I., 1983, Isotopic inferences of ancient biochemistries - Carbon, sulfur, hydrogen, and nitrogen: Earths Earliest Biosphere, Princeton University Press, Princeton, New Jersey, p. 149-186.

Schieber, J., 1994a, Evidence for high-energy events and shallow-water deposition in the Chattanooga Shale, Devonian, central Tennessee, USA: Sedimentary Geology, v. 93, p. 193-208.

Schieber, J., 1998a, Developing a Sequence Stratigraphic Framework for the Late Devonian Chattanooga Shale of the southeastern US: Relevance for the Bakken Shales, in Christopher,: J.E., Gilboy, C.F., Paterson, D.F., and Bend, S.L., eds., Eighth International Williston Basin Symposium: Saskatchewan Geological Society, Special Publication, v. 13, p. 58-68.

Schieber, J., 1998b, Sedimentary features indicating erosion, condensation, and hiatuses in the Chattanooga Shale of Central Tennessee : Relevance for sedimentary and stratigraphic evolution: in Schieber, J., et al., eds., Shales and mudstones, Volume 1: Stuttgart, Schweizerbart'sche Verlagsbuchhandlung, p. 187–215.

Schieber, J., 2001, A role for organic petrology in integrated studies of mudrocks: examples from Devonian black shales of the eastern US: International Journal of Coal Geology, v. 47, p. 171-187.

Schieber, J., and Riciputi, L., 2004, Pyrite ooids in Devonian black shales record intermittent sea-level drop and shallow-water conditions: Geology, v. 32, p. 305-308.

Schleser, G.H., Frielingsdorf, J., and Blair, A., 1999, Carbon isotope behaviour in wood and cellulose during artificial aging: Chemical Geology, v. 158, p. 121-130.

Schwarzkopf, T., and Schoell, M., 1985, Die Variation der C-und HIsotopenverhältnisse in Kohlen und deren Abhängigkeit von Maceralzusammensetzung und Inkohlungsgrad: Fortschritte in der Geologie von Rheinland und Westfalen 33, p. 161–168.

Strapoc, D., Mastalerz, M., Schimmelmann, A., Drobniak, A., and Hasenmueller, N., 2010, Geochemical constraints on the origin and volume of gas in the New Albany Shale (DevonianMississippian), eastern Illinois Basin: AAPG Bulletin, v. 94, p. 17131740.

Strauss, H., Des Marais, D.J., Hayes, J.M., and Summons, R.E., 1992, The carbon-isotope record: In Proterozoic Biosphere: A multidisciplinary study (ed. J. W. Schopf and C. Klein), pp. 117- 127. Princeton Univ. Press.

Strauss, H., and Peters-Kottig, W., 2003, The Paleozoic to Mesozoic carbon cycle revisited: The carbon isotopic composition of terrestrial organic matter: Geochem. Geophys. Geosyst., v. 4, p. 1083.

Sullivan, K.L., 1983, Organic facies variation of the Woodford Shale, in western Oklahoma [EP15024 thesis]: United States -- Oklahoma, The University of Oklahoma.

Swanson, V.E., Landis, E.R.j.a., and Geological, S., 1962, Geology of a uranium-bearing black shale of Late Devonian age in north-central Arkansas: Arkansas. Geological and Conservation Commission. Information circular no. 22: [Little Rock], Arkansas Geological and Conservation Commission, p. v, 16 p.

Tue, N., Hamaoka, H., Sogabe, A., Quy, T., Nhuan, M., and Omori, K., 2011, The application of δ¹³C and C/N ratios as indicators of organic carbon sources and paleoenvironmental change of the mangrove ecosystem from Ba Lat Estuary, Red River, Vietnam: Environmental Earth Sciences, v. 64, p. 1475-1486.

Wallace, G.D., 1977, Kerogen studies and geological interpretations: Journal of Geochemical Exploration, v. 7, p. 79-99.

Watanabe, Y., Naraoka, H., Wronkiewicz, D.J., Condie, K.C., and Ohmoto, H., 1997, Carbon, nitrogen, and sulfur geochemistry of Archean and Proterozoic shales from the Kaapvaal Craton, South Africa: Geochimica et Cosmochimica Acta, v. 61, p. 3441-3459.

Wenger, L.M., Baker, D.R., Chung, H.M., and McCulloh, T.H., 1988, Environmental control of carbon isotope variations in Pennsylvania black-shale sequences, Midcontinent, U.S.A: Organic Geochemistry, v. 13, p. 765-771.

Whiticar, M.J., 1996, Stable isotope geochemistry of coals, humic kerogens and related natural gases: International Journal of Coal Geology, v. 32, p. 191-215.

Woodrow, D.L., Dennison, J.M., Ettensohn, F.R., and Kirchgasser, W.T., 1988, Middle and Upper Devonian stratigraphy and paleogeography of the central and southern Appalachians and eastern Midcontinent, U.S.A: In Devonian of the world, N.J. McMillan, A.F. Embry & D.J. Glass., v. 1, p. 277-301.

Zielinski, R.E., 1977, Geochemical characterization of Devonian gas shale: In Proc. U.S.D.O.E. Eastern Gas Shales Symp. ERC/SP-77/5, EGS-35.

Estimation of Coal Gas Content Using Geostatistical Methods in GIS Environment: A Case Study From Tabas Coal Mine

V. Vaziri, J. Khademi Hamidi, A.R. Sayadi
Tarbiat Modares University, Tehran, Iran

ABSTRACT Coal gas content is one of the most effective parameters in safety and productivity of mechanized mining system. This gas can be explosive when it reaches a certain percentage of the mine air, i.e. lower explosive limit (LEL). Hence, knowledge about the coal gas content before exploitation operation is so necessary. This study uses geostatistical estimator to predict gas content of coal seams. First in this study, core data from 33 exploration boreholes in Tabas coal mine were gathered. Having preprocessed the quality of data and the absence of isotropy, Universal Kriging method was chosen as the best estimation method. Using estimation evaluation criteria, the best model among exponential, spherical and Gaussian model was selected. The map of gas content was plotted using of ArcGIS. Results showed that approximately 4% of total study area has the gas content less than 5 m^3/ton, and 7% between 5 and 10 m^3/ton. Meanwhile, in about 57% of total area, gas content more than 15 m^3/ton was predicted.

Keywords: Coal mining, Gas content, Geostatistical methods, ArcGIS

1 INTRODUCTION

Due to numerous advantages, such as coking and use in steel industry, coal has become a common energy carrier. However, coal mining, especially in underground mines, is one of the most dangerous industrial activities in each country. For example, according to the annual report of Social Security Organization (SSO) of Turkey in 2005, the coal industry in this country is in top of occupational diseases and disabilities, and also third and fifth places of fatal injuries and occupational injuries, respectively (US Bureau of Labor Statistics News, 2007). This type of disaster has been recognized worldwide as a potentially fatal and major hazard during the mining of gassy coal seams (Wold et al., 2008; Cao et al., 2001). Therefore, the most important task before coal extraction is to create a safe work environment. Hence, estimation of coal gas content before starting extraction in underground coal mines has a significant impact on safety and productivity.

There are various estimation methods for gas content among which Kriging is the most common. Almost half a century ago, kriging technique was used by Krig to estimate the distribution pattern of gold in South Africa mines. In this method, for choosing neighborhood radius, it is necessary to consider the maximum distance for which the data are spatially correlated. This work in kriging is done based on semivariogram, which is not involved in any other estimation techniques. In addition, data anisotropy detection and estimation error calculation and distribution are performed by using the same tool.

Geostatistical estimations have been widely used in mining engineering. Two dimensional kriging and co-kriging cross validation grade estimation results of the sample points were compared by using the data taken from Küre copper mine in Turkey and noted that the co-kriging technique estimates the variable with lower variance than the ordinary kriging. Moreover, the co-kriging estimation variance decreases as the block dimension increases (Yalcin, 2001). Kriging method was used to interpolate the content of feldspar in the entire granite deposit in order to characterize the saleable feldspar in a granite deposit, and they used

the same method to calculate the quantity of feldspar (Taboada, 2002).

A combination of geostatistical and GIS models has been used to estimate the amount of residual sulfur in coal beds (Watson et al., 2001). An example of integrated kriging technique and GIS is found in the work done by Diodato and Ceccarelli (2004). They used multivariate geostatistical technique of indicator kriging to detect and classify macro zones according to their tendency to soil degradation. Ahmed et al. (2007) used GIS to delineate the areas suited to soil degradation maps. A critical review of literature shows that integrated geostatistical and GIS have a good capability for estimation of quantitative parameters.

Because of long delays and significant down times across the extraction of w_1 panel in Tabas mechanized coal mine (i.e. due to high existing gas content of coal seam), the operation efficiency has been drastically decreased. It is expected that in deeper panels, due to high gas content gradient, the problems will be more than past. Hence, in this study, because of the ability of GIS in collecting, storing, analyzing spatial data, managing database, overlaying input parameters, validating output and providing the final model as a map, geostatistical estimation in GIS environment for estimating the gas content of coal seam in Tabas mine is used.

2 TABAS COAL MINE

Parvadeh-I is an underground coal mine located 85 kilometers south-east of Tabas city, southwest Khorasan province in east of Iran (Fig. 1). The total coal reserve is estimated 98 million ton (SKANSKA, IRASCO and IRITEC, 2002). The Tabas coal deposit includes five seams namely; C_1, B_1, B_2, C_2 and D. Currently, the seam C_1 is workable seam using mechanized longwall system. Within the mine, production started in 2007 using retreat system. The thickness and dip of seam mostly vary from 1.8 to 2 m and from 11 to 26°, respectively. The depth below surface changes between 100 and 680 m. Six main geological units including coal, mudstone, siltstone, sandy- siltstone and overburden are present in the mine area. A generalized stratigraphic column is shown in Fig. 2. Intermittently low strength sandstone and siltstone layers form the hanging wall of the coal seam. The footwall is formed by siltstone and mudstone seams, alternately. Totally, 27 longwall panels were planned for extraction by means of fully mechanized face. Up to date of this study, only three panels have been fully extracted. Panels' layout in Parvadeh-I of Tabas coal mine is shown in Fig. 1.

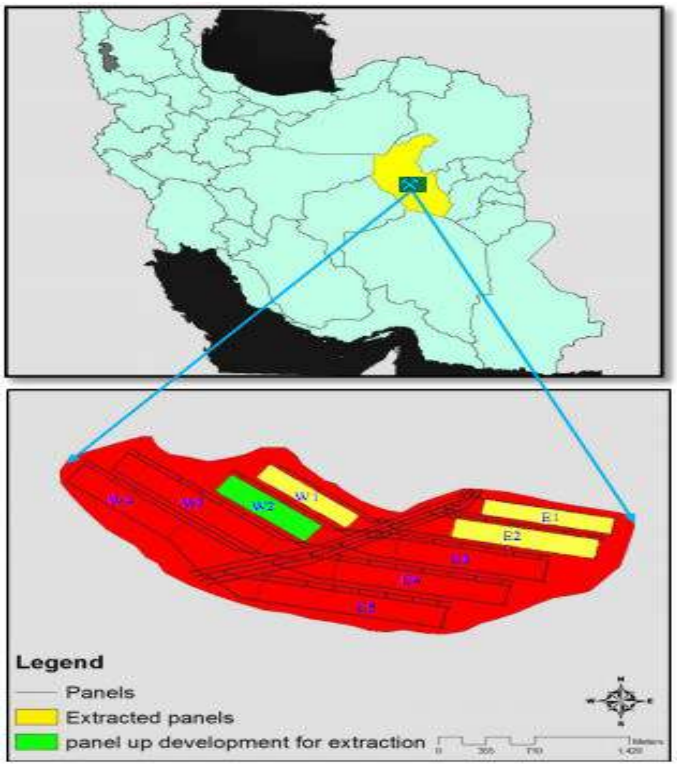

Figure 1. Tabas coal mine, location and panels' layout

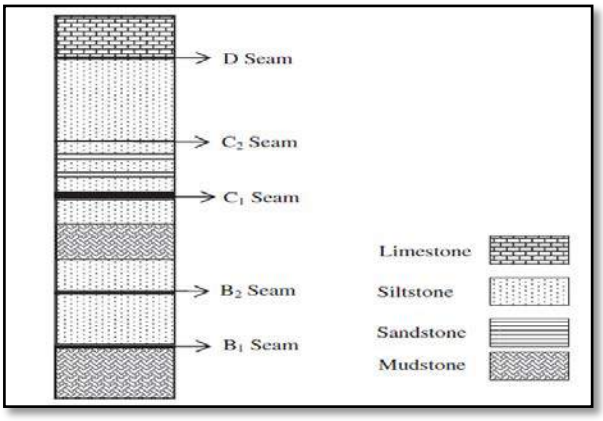

Figure 2. A generalized stratigraphic column for the Parvadeh coalfield

3 METHODOLOGY

Core data from 33 exploration boreholes in Tabas coal mine were gathered. Because of practical limitation and not being able to cover sampling in an area for gas content determination, interpolation method is utilized as a tool for analyzing and defining the amount of gas content in points where sampling was not performed. Therefore, Kriging technique is used for estimation of gas content of coal seam. The equation of Kriging is as following (Margaret, Carignan, 1997):

$$z^*(x_i) = \sum_{i=1}^{n} l_i z(x_i) \quad (1)$$

where; z^* is the estimated variable at x_i, l_i is the weight of i^{th} sample, $z(x_i)$ is the sample measured value and n is the number of samples. First, using histogram and QQ plot the normality of gas content data is evaluated. Having evaluated the normality in data distribution using histogram and semivariogram cloud, presence of global and local obvious outliers is studied. Meanwhile, using Statistical Package for the Social Sciences (SPSS) and ArcGIS, presence or absence of trend is determined. Finally, kriging method for gas content estimation was used. Considering the anisotropy in different steps, Semivariogram is plotted. Error evaluation criteria including MPE, RMSSPE, ASE and RMSPE are determined, accordingly the best model among exponential, spherical and Gaussian model is selected. Cross validation method to ensure the accuracy of estimation is used. Skochinsky & Komarov (1996) classification for classifying the amount of gas content of coal seam is presented. Finally, the map of gas content in Tabas coal mine is plotted. The proposed methodology is given as a flowchart in Fig.3.

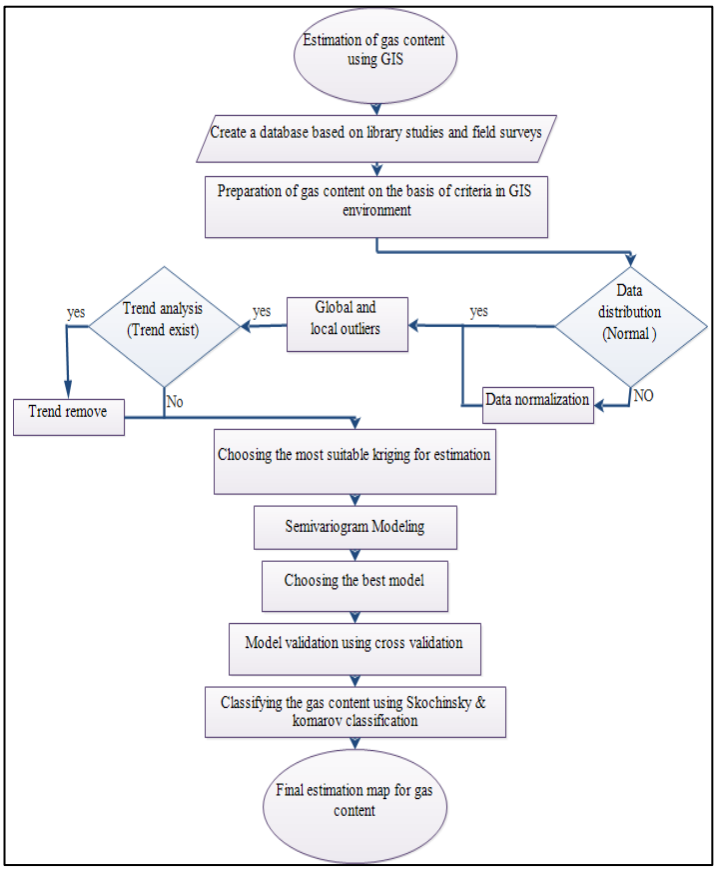

Figure 3. Flowchart of gas content estimation

4 EVALUATION OF GAS CONTENT CONDITION

4.1 Distribution of gas content data

Generally, the important features of the distribution are its central value, spread, and symmetry. (Johnston, K., et al., 2003). For normally distributed data, the mean and median should be similar, the skewness should be near zero, and the kurtosis should be near 3. If the data is highly skewed, then linear, box-cox or logarithmic techniques should be used to make a normal data distribution (Kamble and Aggrawal, 2011). Gas content data normalization survey was assessed with histogram and normal QQ plot. The results indicate that gas content data is not symmetric and don't have a normal distribution. So, the data redistribution is carried out by using logarithm method.

4.2 Global and local outliers

It is important to identify gas content outliers for two reasons: they may be real abnormalities in the phenomenon, or the value might have been measured or recorded

incorrectly. Global and local outliers were evaluated using histogram and semivariogram cloud. The analysis results reveal that there are neither global nor local outliers in gas content data in this study.

4.3 Trend analysis

Trend analysis for gas content data was performed using SPSS and ArcGIS as shown in Fig. 4. The points are projected onto the perpendicular planes, an east–west and a north–south plane. A best-fit line (a polynomial) is drawn through the projected points, which model trends in specific directions. If the line were flat, this would indicate that there would be no trend (Johnston, K., et al., 2003). As can be followed from Figs. 4a and 4b, the data seem to exhibit a strong trend in the north – south direction caused by increasing the depth (Z axis) and a weaker one in the east – west direction. So, before estimation, the trend of data was remedied.

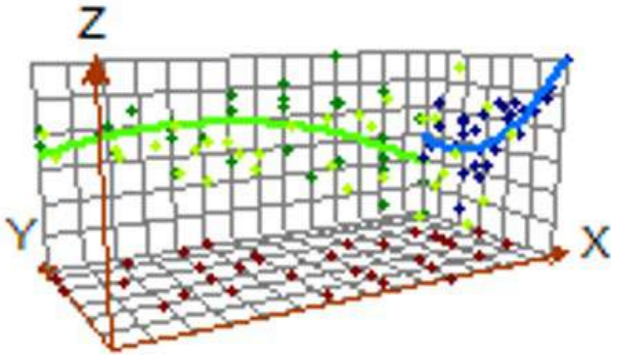

a)

			x	y	z	gas
Spearman's rho	x	Correlation Coefficient	1.000	-.370*	.308	-.321
		Sig. (2-tailed)	.	.034	.081	.069
		N	33	33	33	33
	y	Correlation Coefficient	-.370*	1.000	.720**	-.683**
		Sig. (2-tailed)	.034	.	.000	.000
		N	33	33	33	33
	z	Correlation Coefficient	.308	.720**	1.000	-.893**
		Sig. (2-tailed)	.081	.000	.	.000
		N	33	33	33	33
	gas	Correlation Coefficient	-.321	-.683**	-.893**	1.000
		Sig. (2-tailed)	.069	.000	.000	.
		N	33	33	33	33

*. Correlation is significant at the 0.05 level (2-tailed).

**. Correlation is significant at the 0.01 level (2-tailed).

b)

Figure 4. Trend Analysis of gas content data; a) ArcGIS, b) SPSS.

4.4 Choosing the most appropriate kriging type for estimation

Because of trend existence in gas content data, universal kriging is used for estimation purpose. Once the trend is removed, the statistical analysis will be performed on the residuals or the short-range variation component of the surface. The trend will automatically be added back before the final surface is created so that the predictions produce meaningful results. By removing the trend, the analysis that is to follow will not be influenced by the trend, and once it is added back to the gas content, a more accurate surface will be produced. The semivariogram cloud allows one to examine the spatial autocorrelation between the measured sample points. In spatial autocorrelation, it is assumed that things that are close to one another are more alike (Johnston, K., et al., 2003). Variogram is calculated by the following equation (Margaret, Carignan, 1997):

$$\hat{\gamma}(h) = \frac{1}{2N(h)} \sum_{i=1}^{N(h)} \left[Z(x_i) - Z(x_i + h) \right]^2 \qquad (2)$$

where $Z(x_i)$ is the value of the examined variable at the position x_i, $Z(x_i+h)$ is the value of the examined variable at the position x_i+h and N is the number of pairs of sample points separated by distance h, called lag. To actually account for the directional influences on the semivariogram model, it is necessary to evaluate the anisotropy in different directions. Variography analyses of gas content in different directions show the maximum and minimum autocorrelation in 70° and 160° to the north direction, respectively. The semivariogram increases slowly in the north east – south west direction which represent the lowest violet line in the variography curve. Also, the semivariogram increases rapidly in south east - north west direction which is shown by the uppermost violet line in variography curve Fig.5.

So, the results show there is anisotropy in data and also, the major axis of the anisotropy ellipse is in NE-SW direction.

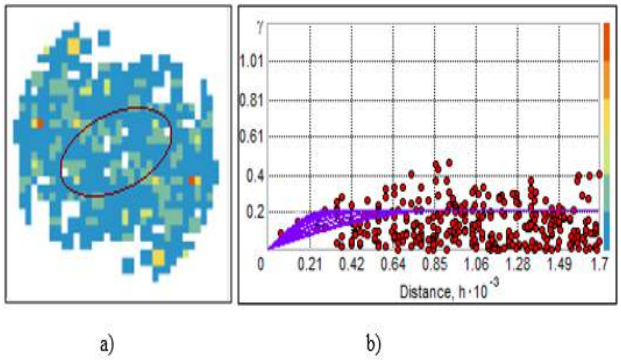

Fig.5. Gas content data evaluation; a) using semivariogram surface; b) using semivariogram plot.

4.4.1 Choosing the most appropriate model

ArcGIS have optimization functions to determine the best-fit parameters for a given variogram model. So, in cross validation, four statistics were evaluated for verification of the model outcomes. These statistics are standardized mean, root mean squared (RMS), root mean squared standardized (RMSS), average standard error and standardized mean. The most suitable model should have a standardized mean closest to 0, a smallest RMS value, an average standardized error that is close to the RMS prediction error and a RMS standardized value close to 1. Models that produce a RMS that is close to the average standard error is preferred more than the model that has a lower average standard error and a lower RMS (Burke, et al., 2013). Therefore, in this study, variography by Gaussian, spherical, and exponential models was performed. Based on these statistics, universal kriging seems to be the most suitable model as it has the smallest RMS value, a RMS standardized error close to 1 and an average standardized error that is close to the root mean square (Table. 1).

The values of other parameters showed in Table.2. The spherical semivariogram model fitted to gas content data is shown in Fig.6.

Table. 1. Calculated statistics of the cross validation

Model	Spherical	Exponential	Gaussian
MPE	0.0044	-0.0023	0.0015
RMSPE	0.4516	0.4478	0.4492
ASE	0.4737	0.4738	0.5071
MSPE	0.0044	-0.0054	-0.0013
RMSSPE	0.9525	0.9447	0.8871

Table2. Parameters of variography for gas content data estimation (spherical model)

Parameters	Value
Major range	490
Minor range	190
Max. number of points	5
Min. number of points	3
Nugget effect (C0)	0.01
Sill (C)	0.21
Lag size	100
Number of Lags	17

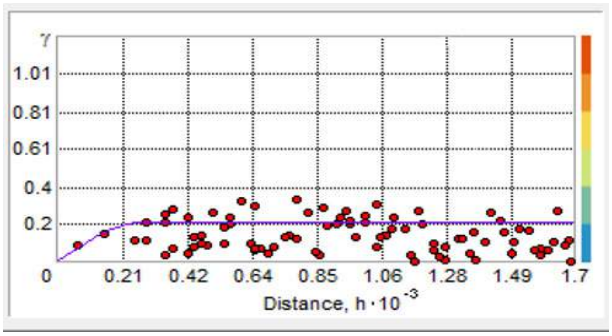

Fig.6. Spherical model of semivariogram for gas content data

4.4.2 Cross - validation

To check the suitability of model, cross validation is used. Cross-validation gives an idea of how well the model predicts the unknown values. For all points, cross validation sequentially omits a point, predicts its value using the rest of the data, and then

compares the measured with predicted values (Ahmed, et al., 2007). Results of cross validation for spherical model is shown in Fig.7. As seen in this figure, spherical model has an acceptable estimation accuracy.

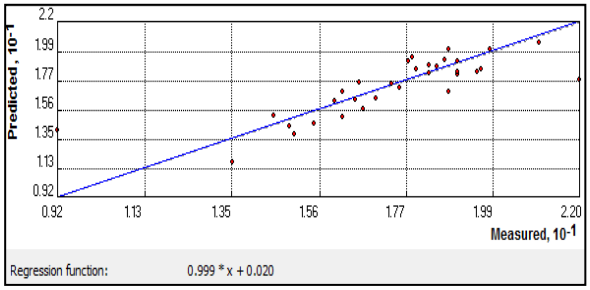

Fig.7. Cross – validation plot between predicted and measured data.

The term "prediction error" is used to check the difference between predicted and measured values of each borehole's gas content. The less the difference, the more accurate the model is. The measured and predicted values of seven boreholes along with prediction errors are given in Fig. 8. As seen in the figure, prediction error of each borehole is low, indicating the accuracy of the outcomes.

Source ID	Included	Measured	Predicted	Error
30	Yes	17.9	18.523	0.62301
0	Yes	18.6	18.139	-0.46061
21	Yes	18	18.227	0.22721
11	Yes	18.6	18.467	-0.13259
28	Yes	17.05	17.355	0.30468
27	Yes	19.27	18.532	-0.73751
12	Yes	18.3	18.276	-0.024278
32	Yes	17.6	17.414	-0.18595

Fig.8. Typical comparison between predicted and measured values of each borehole

4.4.3 Gas content estimation map

With accurate geostatistical analysis on gas content data using classification showed in Table.3, the final prediction map of gas content using ArcGIS in Tabas coal mine was built. Areas with gas content of lower than 5 m^3/ton is shown with yellow color (first class), between 5-10 m^3/ton with yellow-brown (second class), between 10-15 m^3/ton with light brown and gas content of more than 15 m^3/ton is shown with dark brown.

Table.4. Coal gas content classification **(**Skochinsky and Komarov, 1996)

Gas content level (m^3/ton)	Definition	Color on map
0 - 5	First class	
5-10	Second class	
10 -15	Third class	
15 <	Over class	

Results of geostatistical analysis and gas content map in ArcGIS show that approximately 4% of total area has the gas content less than 5 m^3/ton and 7% between 5 and 10 m^3/ton. While, about 57% of total area has the gas content more than 15 m^3/ton which it seems a high gradient compared to world standards in similar depths. Hence, the risk of exploitation in this panels is very high (Fig.9).

The results of estimation map show high gas content for coal seams in Tabas coal mine. Experiences obtained during production in E_1, E_2 and W_1 panels show that the gas content is high.

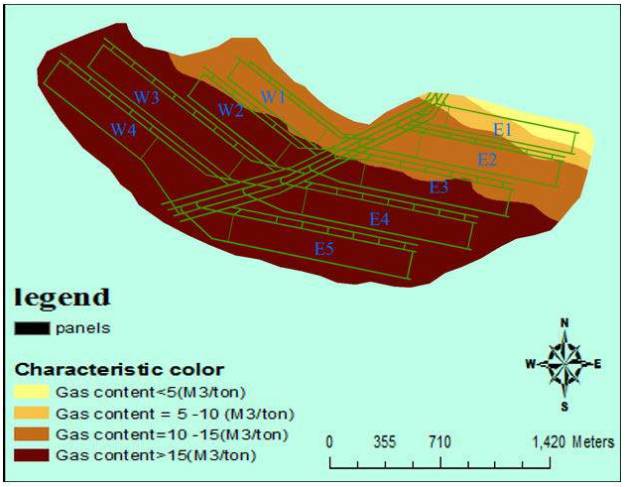

Fig.9. Gas content estimation map of Tabas mechanized coal mine

In Tabas coal mine, two methane gas detection systems are used: portable gas detector and fixed monitors. Portable detectors are designed to be hand-carried, so measurements can be made at any location. Fixed gas monitors are mounted at the ceiling, usually at the T-junction of tailgate and headgate and operate continuously.

The gas monitoring system includes a design that prevents the mining equipment from operating unless the gas monitoring system is functioning, an automatically controlling means that shut off power to the equipment when the gas concentration is 1.25 volume percent. This will provide a chance for mine crew to apply some emergency reactions such as adjustment of ventilation system or mine evacuation.

In Fig. 10, methane gas measurement for a period of one month (i.e. 21/04/2014 to 17/05/2014) during mining of panel W_1 is shown. The data were recorded by gas sensor installed in the tailgate. As seen in the figure, the methane gas concentration is generally high.

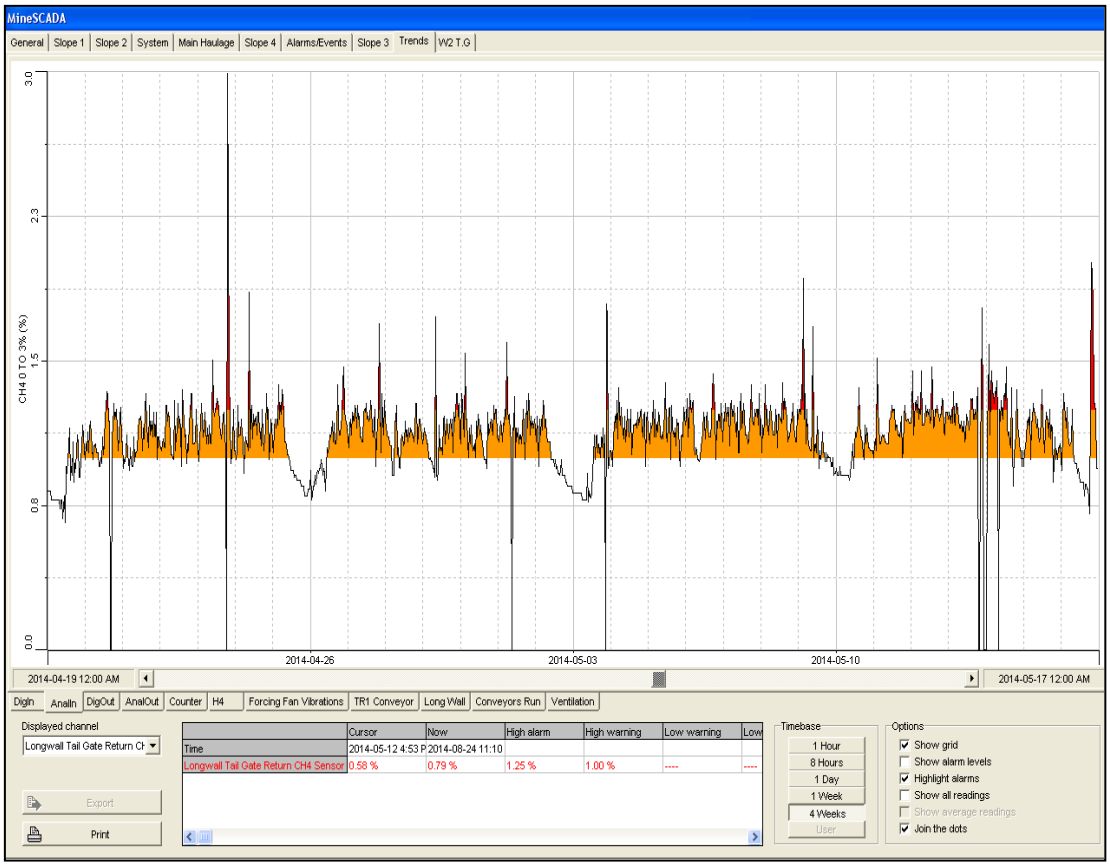

Fig.10. Methane gas concentration in W1 panel for the date; 21/04/14 to 17/05/14

Also, the gas concentration reached the maximum permissible value, i.e. 1.25%, several times a month, as shown in red colored areas in the figure. Meanwhile, the delays associated with the high gas concentration in W_1 panel for the same time period are given in Fig. 11. As can be followed from the figure, high gas concentration caused delays in mining operation, sometimes more than ten hours a day, which equals to more than a working shift.

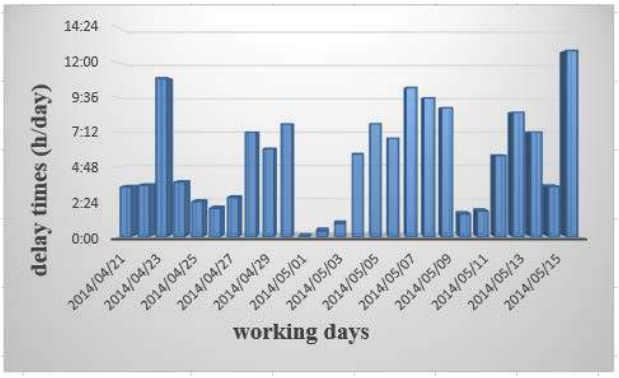

Fig.11. Delays associated with high gas concentration in W_1 panel for the date; 21/04/14 to 17/05/14

Figures 10 and 11 show that the coal gas content is generally high and expected to increase with the depth of coal seam, as

predicted and illustrated in ArcGIS map (Fig. 9). So, preventing or controlling the gas content of coal seam using methane gas drainage techniques is suggested for the panels that are under development or going to be worked in future in Tabas mechanized coal mine.

6 CONCLUSION

In this study, the gas content map of C_1 coal seam in Tabas coal mine was developed by using GIS. Having analyzed the normality distribution, global and local outliers and trend, the most appropriate method for estimation was selected. Due to existence of trend in gas content data, global kriging for interpolation was used. Accordingly, the variography was carried out on coal gas content data. Obtained results showed the anisotropy exists in data. The spherical semivariogram model was selected as offering the best fit to the estimated semivariance values. In order to check the estimation accuracy, cross validation was used. Totally, the results of estimation maps show high gas content of coal seams in Tabas coal mine. They show a high gas content even at shallow depths for which the gas content increases at 2 m^3/ton for every 100m in depth. This is a high gas gradient compared to World norms and standards. Also, estimation map shows that about 57% of total area has the gas content more than 15 cubic meter per ton of coal pertaining to over-class coal seams.

REFERENCES

US Bureau of Labor Statistics News, 2007. *National Census of Fatal Occupational Injuries in 2006*, USDL 07-1202.

Wold, M.B., Connell, L.D., Choi, S.K., 2008. The role of spatial variability in coal seam parameters on gas outburst behaviour during coal mining, *International Journal of Coal Geology*, 75 (1), 1–14.

Yalcin, E., 2001. Co-Kriging and its effect on the estimation quality, *7th International Conference on Mining, Petroleum and Metallurgical Engineering (MPM)*, Vol. 1, pp. 72-79.

Taboada, J., Vaamonde, A., Saavedra, A., and Ordóñez, C., 2002. Geostatistical study of the feldspar content and quality of a granite deposit, *Engineering Geology*, 65, pp. 285–292.

Watson, W. D., Ruppert, L. F., Bragg, L. J., and Tewalt, S. J., 2001. A geostatistical approach to predicting sulfur content in the Pittsburgh coal bed, *International Journal of Coal Geology*, Vol. 48, pp. 1–22.

Diodato, N., and Ceccarelli, M., 2004. Multivariate indicator Kriging approach using a GIS to classify soil degradation for Mediterranean agricultural lands, *Ecological Indicators*, 4, pp. 177–187.

Ahmed, S. S., Eltahlawi, M. R., Rashad, M. Z., Saleem, H. A., 2007. Kriging techniques and GIS for management of phosphate extraction at Hagaria district, Egypt, *Journal of Engineering Sciences*, Vol. 35, No. 6, pp. 1559-1574.

SKANSKA, IRASCO and IRITEC, 2002. Tabas coal mine project detailed design report- mining, Tabas, Iran.

Margaret, A., Carignan, J., 1997. *Geostatistique linear application au domain miner*, Presses de IEcole des Mines de Paris.

Johnston, K., Jay M., Hoef, V., Krivoruchko, K., Lucas, N., 2003. Using ArcGIS Geostatistical Analyst, *Enivironmental System Research Institute* – USA.

Kamble, K. H., Aggrawal, P., 2011. Geostatistical Analyst for Deciding Optimal Interpolation Strategies for Delineating Compact Zones, *International Journal of Geosciences*, PP. 585-596.

Burke, S., Chu, G., Heyer, J., Lee, J., Tang, X., Tran, T., Zhang, L., 2013. Mass Quantification of PCE in Los Angeles Groundwater from the GeoTracker Database, *UCLA Institute of the Environment and Sustainability Senior Practicum*.

Skochinsky, A., Komarov, V., 1996. *Mine ventilation*, Mir publishers – Moscow.

Cheng, Y.-P., Wang, L., Zhang, X.-L., 2011. Environmental impact of coal mine methane emissions and responding strategies in China, *Int. J. Greenhouse Gas Control*, 5, PP. 157-166.

Gatnar, K., Tor, A., 2003. Drainage and economic utilization of methane from coal seams in the Jastrzebie mining-field, *Appl. Energy*, 74, PP.331-341.

Yang, M., 2009, *Climate change and energy policies, coal and coalmine methane in China*, Energy Policy 37, PP. 2858-2869.

Cheng, Y., Yu, Q., 2007, *Development of regional gas control technology for Chinese coalmines*, J. Min. Saf. Eng. 24, PP.383-390.

Creedy, D., Tilley, H., 2003, *Coalbed methane extraction and utilization*, Proc. Inst. Mech. Eng. Part A J. Power Energy 217, PP.19-25.

Europe, U.N.E.C.f., Partnership, M.t.M., 2010. Best Practice Guidance for Effective Methane

Drainage and Use in Coal Mines. United Nations Publications.

Whittles, D.N., Lowndes, I.S., Kingman, S.W., Yates, C., Jobling, S., 2006, “Influence of geotechnical factors on gas flow experienced in a UK longwall coal mine panel”, International Journal of Rock Mechanics and Mining Sciences, PP. 369–387.

Uncertainty and Variability in Gas Desorption Measurements from Coal

J. Pope, A. Dutton & C. Nelson
CRL Energy Ltd, 97 Nazareth Ave, Christchurch, New Zealand.

ABSTRACT Total desorbed gas content of coal is used to estimate economic potential of coal bed methane resources and to identify hazards for underground mine operations. Total desorbed gas analysis of coal samples have several sources of uncertainty related to different approaches to sample collection, analysis equipment, data processing and calculation methods. The largest uncertainties that arise could cause up to about 25% variation in the measured total desorbed gas content when using methods that are compliant with published analytical standards.
Methods to minimize the uncertainties are well established, however are not always applied to data collection and analysis. In addition to analytical uncertainty, the total desorbed gas content of coal is variable between samples that are adjacent, even when robust and identical analytical methodologies are applied.
We present data on the scale of analytical uncertainties related to different aspects of data collection for total desorbed gas content of coal from data collected throughout New Zealand over the last 15 years.

Keywords: Gas desorption measurement, uncertainty minimization methods, variability

1 INTRODUCTION

Coal is a high surface area, micro-porous substrate that can store substantial quantities of gas as an adsorbed phase. Typically CH_4 and CO_2 are the most abundant gases adsorbed to *in-situ* coal and these are emplaced in coal either during coalification through thermogenic processes or after coal formation through biogenic processes (Butland and Moore, 2008). Gas content measurement of coal is commonly completed by desorption analysis and has two main applications;

1) to determine the size of coal bed methane resources for economic assessment,

2) to quantify gas that will be released when coal is disturbed by underground mining for hazard management.

In both of these applications the objective of gas content measurement is to determine the *in-situ* amount of gas stored in the coal recognizing that this value is often less than the total amount of gas that could be stored in the coal. The *in-situ* gas content of coal is dependent on many geological, geochemical, hydrogeological and biological processes.

The theory and approach to desorption analysis for both applications are identical and the same analytical standards apply. However the standard reference methods (ASTM, 2010) allow for quite variable, analysis methodologies, equipment, and data processing. The variability of results delivered by different methods is difficult to reconcile because duplicate samples cannot be collected and there is no standard reference material currently available for inter-laboratory comparison. In addition, there are uncertainties associated with quantification of gas in coal that are large and cannot easily be avoided.

As well as analytical uncertainty, coal is an inherently heterogeneous material and therefore has variable gas storage reservoir properties. There can be substantial variability in gas content spatially and stratigraphically in a coal deposit and also within samples from a single seam in a single drill hole.

We present examples of analytical uncertainty and variability from desorption data collected by CRL Energy Ltd over 15

years of service provision for coal bed methane exploration and coal mine methane gas measurement in New Zealand, Vietnam, Indonesia, China and Turkey. The method and data processing adopted by CRL evolved from a method developed by the US Bureau of Mines (Diamond and Levine, 1981) and currently operates within requirements of international standard reference methods (ASTM, 2010).

2 METHODS

Gas content measurement methods commonly measure or calculate three components of gas that can be desorbed from a coal core sample.

1) Gas that is desorbed between the time the sample is removed from its *in-situ* position by drilling operations and the time the sample is placed in a sealed vessel, commonly referred to as Lost Gas or Q1.
2) Gas that is desorbed from intact coal core in a sealed vessel, commonly referred to as Measured Gas or Q2.
3) Gas that is released by crushing coal, commonly referred to as Residual Gas or Q3.

In Australasia two approaches to gas content determination in coal have been applied and these are referred to as fast desorption and slow desorption (Australian Standard 1999). The difference in these approaches relates to the length of time that coal samples are stored in a sealed vessel while desorbed gas volumes are measured; this influences the ratio of the desorbed gas that is reported as Measured Gas (Q2) vs Residual Gas (Q3).

2.1 Lost Gas (Q1)

Lost Gas is calculated by extrapolation of data collected after the sample is sealed in the sample vessel. There are two main sources of uncertainty associated with lost gas calculations and these relate to assumptions regarding the point of time at which desorption of gas from the samples begins (time 0) and the method of extrapolation of measured data back to time 0.

We present a sensitivity analysis of the effect of assumptions related to time 0 and the use of different extrapolation methods for calculation of lost gas (Q1).

2.2 Measured Gas (Q2)

Measured gas is typically determined by either a falling head manometer or zero head manometer coupled to the air tight sample vessel (Figure 1). Gas volume measurements are accompanied by synchronous measurements of canister temperature and ambient pressure and all measured volumes are corrected to standard temperature and pressure (STP) conditions. Typically coal is desorbed at reservoir temperature with samples placed in a water bath or temperature controlled room to maintain constant temperature.

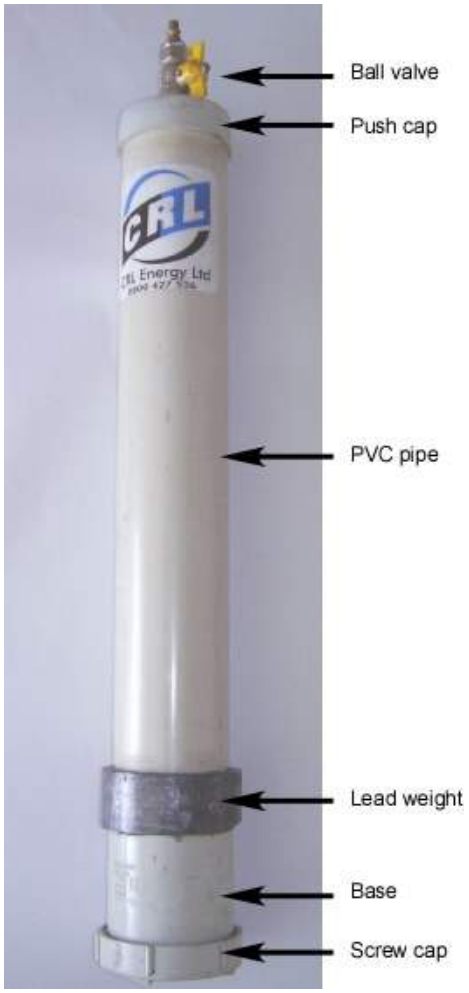

Figure 1. Sealed sample vessel for collection of measured gas. PVC construction is used for slow desorption only, similar stainless steel canisters are used for fast or slow desorption.

During data collection for slow desorption methods, gas volume measurements are commonly made until desorption diminishes to about 10mL/week for a ~1kg core sample. Volume measurements are made at regular intervals to ensure that the desorption rate from the coal is not influenced by pressure build up in the sample vessel.

During data collection for fast desorption gas volume measurements are made for between 1 and several days until the sample can be transported to a laboratory for Residual Gas determination.

There are several sources of uncertainty in Measured Gas data collection. These include operator bias, sensitivity differences between alternative equipment (including canisters with different headspace volumes and different types of manometer), gas solubility, partial pressure effects on gas desorption, oxidation of coal and differences in data processing.

In general, uncertainties related to Measured Gas are lower than those related to either Lost or Residual Gas. We present data that demonstrate oxygen depletion in headspace gas during desorption which increase analytical uncertainty if it is not corrected, and the influence of STP corrections on measured gas volumes.

2.3 Residual Gas (Q3)

Residual Gas analysis is completed by crushing one or more subsamples of core and use of similar manometer equipment to measure gas released during and immediately after the crush.

Uncertainty for Residual Gas analysis is mostly related to selection of representative subsample(s) and the number of subsamples that are analysed. In addition, there are differing crushing procedures and the potential for either re-adsorption of headspace gas by reactive surfaces exposed during crushing or overestimation of gas release due to heating of the sample and crushing apparatus.

Uncertainty related to Residual Gas calculation impacts fast desorption methods more than slow desorption methods because the proportion of residual gas compared to measured gas is higher in fast desorption samples. We present data showing the impact of subsample variability and crushing procedures on residual gas analysis.

3 RESULTS

Lost, Measured and Residual Gas are presented for samples collected from different coal fields in New Zealand using fast and slow desorption. Uncertainties associated with calculation of total gas are demonstrated through assessing the sensitivity of gas content to alternative interpretations related to desorption or alternative approaches to data processing.

3.1 Uncertainties Related to Lost Gas

The largest potential source of uncertainty for lost gas analysis is poor interpretation or mistakes relating to selection of the onset of desorption (time 0). When coal samples are collected from surface drilling via wireline methods, the point at which desorption commences is the time at which drilling operations cause a reduction in pressure on the sample compared to the *in-situ* condition. For a sample where groundwater is saturated from topographic surface (or close to) the pressure reduction that initiates desorption occurs immediately the sample is removed from *in situ* during core retrieval. At this point in time, the pressure on the sample is not atmospheric pressure, instead the pressure reduces as the sample is winched upward by wireline. The most common approach in these circumstances is to assume time 0 is when the sample is at half of the *in situ* pressure when it is half way up the wireline and (and therefore has approximately half of the *in situ* groundwater head on it). This approach to identification of time 0 can be corrected for the density of drilling fluids if data is available (ASTM, 2010).

For samples that are collected from underground workings via inseam drilling, the onset of desorption is likely to be during the drilling operation when the low pressure

drilling fluid is in contact with the sample. Therefore it could be assumed that desorption starts during drilling of the sample. In these circumstances time 0 could be estimated as half way through the drilling process.

Inappropriate selection of time 0 strongly influences the lost gas calculations (Figure 2). Using exactly the same measured gas data from bituminous coal of the Greymouth Coalfield in New Zealand, lost gas varies between 0.43 and 1.12m^3/t by selecting time 0 during sample retrieval (appropriate for samples collected by surface sampling) or during drilling (for underground sampling).

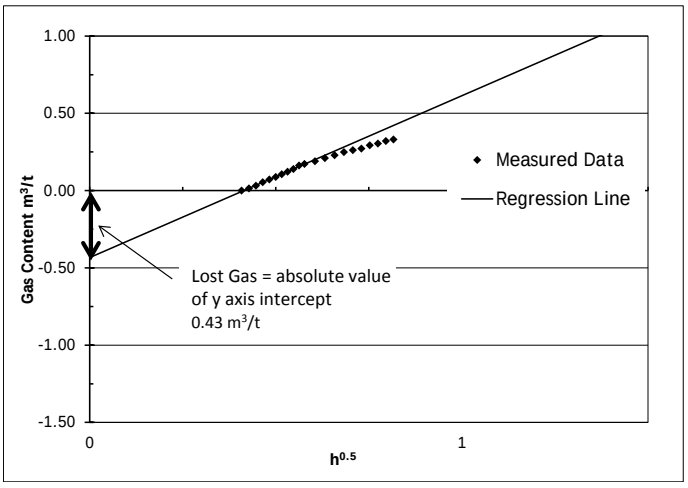

(a)

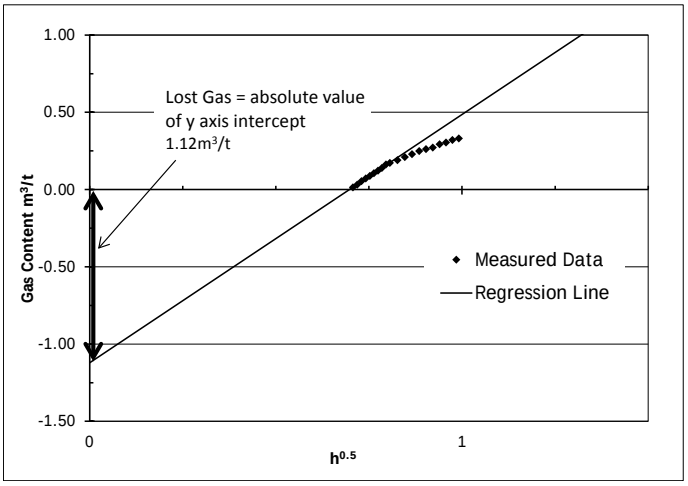

(b)

Figure 2. a) Lost Gas extrapolation when time 0 is assumed to be half way through core retrieval by wireline. b) Lost Gas extrapolation when time 0 is assumed to be half way through coring of sample.

A second source of uncertainty for Lost Gas analysis arises from different approaches to extrapolating Measured Gas desorption data to time 0. The most common approach is to assume that early desorption data (less than 20 % of total desorbed gas) is released from the coal in a linear manner with respect to the square root of time (Bertard et al., 1970; Diamond and Schatzel, 1998) and to calculate lost gas from a linear regression. However, there are alternative interpretations and approaches to extrapolation of measured gas back to time 0 including a logarithmic approach (Chase, 1979) and an curve fit approach (Yee et al., 1993).

Differing approaches to correlation cause different values to be calculated for Lost Gas. Lost Gas varies between 0.25 and 0.35m^3/t using linear regression and a curve fit method respectively for identical measured gas data collected from sub-bituminous coal in the Huntly Coalfield in New Zealand (Figure 3).

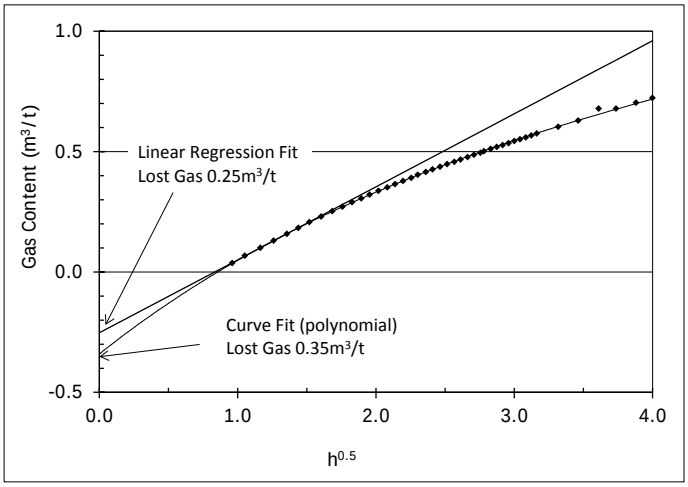

Figure 3. Lost Gas values calculated by linear regression compared to lost gas calculated by curve fit.

3.2 Uncertainties Related to Measured Gas

The main potential for uncertainty related to Measured Gas is caused by oxygen consumption in sample vessel headspace and corrections related to ambient pressure and temperature.

Gas composition analysis (Table 1) from air filled canister headspace using samples of sub-bituminous coal in New Zealand indicates that oxygen is consumed with time. Therefore the desorbed gas volumes that are measured are a mixture of gas released from the coal minus oxygen that is removed from the headspace volume by oxidation of coal (Jin et al., 2010). Inert gas (typically He or Ar) purging of headspace is commonly used to prevent oxidation especially for low rank coal. An alternative approach could be to complete multiple gas analyses of headspace gas over time and calculate a corrected desorbed volume that allows for oxygen consumption and dilution by desorbed gas.

Table 1: Example analyses gas samples showing O depletion. Methane has diluted the headspace by almost half of the total gas volume and the oxygen concentration had reduced by >75% indicating oxygen consumption as well as dilution.

Sample	CH_4	CO_2	N	O
Air	0	0.03	78	20.9
Gas from vessel	46.8	1.7	46.8	4.7

Correction of measured desorbed gas volumes for ambient pressure and temperature conditions at the time of measurement to STP (standard temperature and pressure) is critical for accurate analyses especially for long desorption datasets where many measurements are made over time with variable ambient conditions.

The Measured Gas from a sample of bituminous coal from the Pike River Coalfield in changes from 6.40 to 6.14m^3/t (Figure 4) if ambient pressures at the time of desorption are used instead of STP corrections, and from 6.40 to 6.52m^3/t if all volumes are assumed to be at STP during measurement (Figure 5).

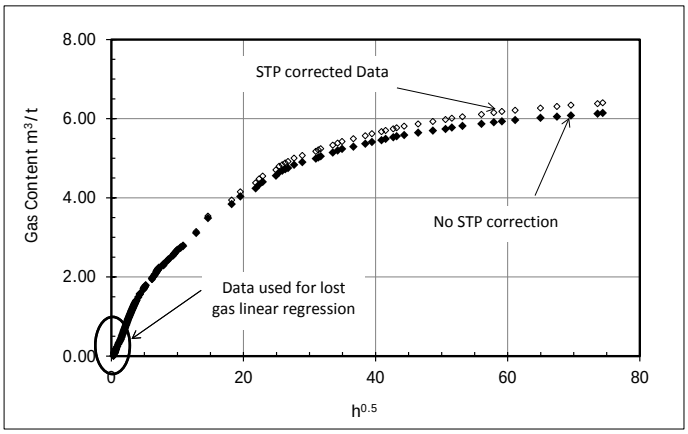

Figure 4. Example of the effect of STP correction to measured gas volumes. The size of this the difference between corrected data and non corrected data is proportional to the difference between measurement/ambient conditions and STP.

3.3 Uncertainties Related to Residual Gas

Subsample variability is the largest source of uncertainty related to Residual Gas measurement. This variability does not only reflect analytical uncertainty but indicates the heterogeneity of coal, which is variable at many different scales from microscopic to basin wide stratigraphy. Gas content varies with ash yield, coal type, maceral content (Masterlez et al., 2008; Moore et al., 2001) within the size of subsamples that can be collected for crushing.

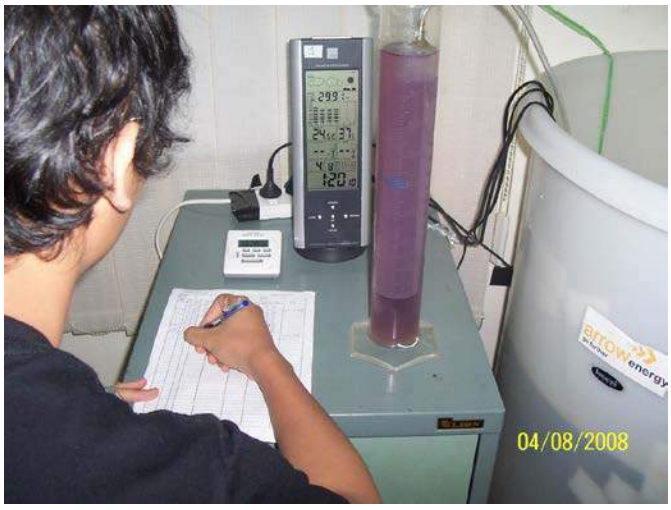

Figure 5. Collection of gas volume data using zero head manometer (nested measuring cylinders with pink die), ambient temperature and pressure measured with digital weather station and samples kept in water bath – (right hand side)

Residual gas content of samples of bituminous coal collected from the Greymouth Coalfield commonly vary by 30% and up to about 40% (Figure 6).

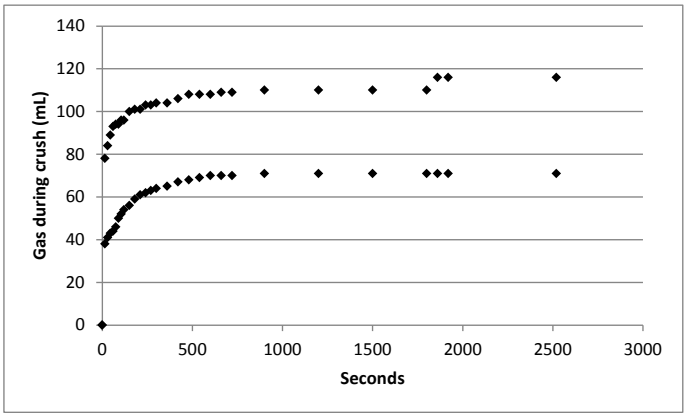

Figure 6. Gas released by different 100g residual gas sub-samples from bituminous coal samples collected in the Greymouth Coalfield. One sub-sample released 71mL and the other 116mL.

Crushing procedures also influence the residual gas content. Crushing requires 95% of the material passes through a 212µm sieve to ensure that all gas is removed from coal micro-pore spaces (ASTM, 2010). However, crushing for an extended period can cause the mill apparatus and sample to heat up and gas volumes can increase due to thermal expansion particularly in coals that is difficult to crush.

In addition, crushing procedures can lead to rapid oxidation of coal or readsorption of headspace gas causing the volume measured to be a mix gas released from pores and gas/oxygen depletion of the mill headspace. Argon purging of mill headspace prevents rapid oxidation or re-adsorption (Figure 7). In samples of lignite from the Mataura coalfield in New Zealand, up to half of the residual gas volume is lost by oxidation/re-adsorption if the mill is not purged with Ar.

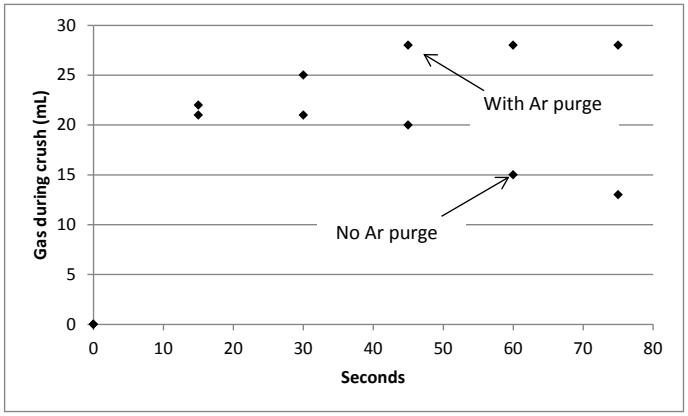

Figure 7. Residual Gas content during crushing of subsamples of lignite with and without Ar purge.

3.4 Gas Content Variability

Adjacent samples collected from the same seam and using identical desorption methodologies can be variable (Table 2). Samples collected from sub-bituminous coal in the Ohai Coalfield in New Zealand have greater than 25% variation over about 2m of continuous sampling. Adjustment of desorption data to a dry ash free basis can reduce variability of gas content, however variability of gas content commonly remains higher than variability of other analytical properties of coal.

Table 2. Selected slow desorption data from adjacent samples in the same drill hole. From and To depths in m and gas volumes in m^3/t (as received basis)

From	To	Lost	Measured	Residual	Total
464.2	464.7	0.39	5.54	0.26	6.19
464.7	465.2	0.39	5.24	0.26	5.89
465.2	465.6	0.15	5.16	0.26	5.57
465.6	466.0	0.21	4.3	0.26	4.78

Variability of desorption and adsorption analyses for coal seams have been researched (Mares et al., 2009) and in general multiple samples (at least 5) are required to obtain a robust value for gas content for a seam.

4 DISCUSSION

Uncertainties within gas content measurement can be large because of different approaches, assumptions and methodologies that are compliant with standardized methodologies.

Uncertainty related to lost gas can be significant if time 0 selection is inappropriate. The Lost Gas values derived can vary by more than 100% if this selection is inaccurate. Commonly, lost gas is 5 to 20% of the total desorbed gas content and therefore this uncertainty can cause up to about 20% variation in the total desorbed gas content. Smaller uncertainty in Lost Gas values also arise from selection of the correlation method used to extrapolate measured gas data to time 0.

Uncertainty related to Measured Gas content is generally low. However, variations in the application of STP correction could cause an uncertainty of up to about 5% of total desorbed gas. Oxygen consumption within sample vessel headspace can be measured especially in sub-bituminous coal and lignite and could be corrected with gas composition analysis if available. More commonly, inert gas purging of sample vessel headspace is used to prevent this uncertainty.

Sub sample selection for Residual Gas analysis can cause a 30-40% variation in the gas released on crushing. Where quick crush analytical methods are employed and Residual Gas can account for 50-70% of the total desorbed gas, this uncertainty can cause an analytical uncertainty of more than 25% of the total desorbed gas.

Natural variability in gas content is high with adjacent samples commonly varying by greater than 10% when analysed by the same method and assumptions. Statistical analysis of variability indicates multiple samples are required to adequately quantify the gas content of coal seams.

4.1 Minimizing Uncertainties

The uncertainties and variabilities in analysis methods for total desorbed gas content of a coal sample are large but they can be minimized. Uncertainties related to Lost Gas can be minimized by ensuring that Lost Gas is kept to a minimum as a proportion of total desorbed gas. This means that samples must be placed in sample desorption vessels as quickly as practical for collection of Measured Gas data. In addition, the assumptions related to time 0 for samples should be examined by a technical expert to ensure they are appropriate.

Uncertainties related to Measured Gas content are minimized by good data collection of ambient pressure and temperature and correction to STP conditions. Typically oxidation or re-adsorption headspace gas is minimized by inert gas purging of sample vessel headspace. However, in older datasets before publication of current standards (ASTM, 2010) oxidation or gas readsorption might remain an issue, especially for sub-bituminous coal or lignite.

Uncertainty related to Lost Gas analysis can be minimised by completing replicate analysis on 2 or 3 subsamples from each desorption sample. In addition, proximate analysis on the sub samples compared to the whole desorption sample could be used ensure that representative sub samples are collected. Uncertainty related to crushing is reduced if curves of Residual Gas release during crush are plotted (Figures 4 & 5) so that readsorption or thermal effects on the crushing apparatus are identified.

5 SUMMMARY AND CONCLUSION

Desorbed gas content of coal seams is commonly measured to examine the economic potential of coal bed methane or identify gas hazards for underground mining. We present data on several sources of uncertainty for the measurement of total desorbed gas content. These uncertainties can be large, causing up to about 25% uncertainty in the total measured gas content using analysis techniques that are compliant with standardized methods.

These uncertainties can be minimized by good analytical practice including:

- Robust assessment of time 0 by a technical specialist
- Purging desorption equipment with inert gas
- Sub-sample repetition for Residual Gas analysis with supporting proximate analysis

With the analytical uncertainties minimized the gas content of coal is spatially variable, even within adjacent samples in the same coal seam. Therefore, most accurate assessment of desorbed gas content of coal horizon requires assessment of multiple samples.

ACKNOWLEDGEMENTS

Data collected for this study is related to coal seam gas exploration and mining projects in New Zealand. We acknowledge the contribution of the anonymous New Zealand mining and exploration companies to collection of this data. Dr Jane Shearer (Resoultionz) provided robust review of this paper.

REFERENCES

ASTM, 2010, Standard Practice for Determination of Gas Content of Coal-Direct Desorption Method, D7569-10, p. 1-12.

Australian Standard 1999, Guide to the determination of gas content of coal--Direct desorption method. , Volume AS3980-1999, p. 1-33.

Bertard, C., Bruyet, B., and Gunther, J., 1970, Determination of desorbable gas concentration of coal (Direct Methd): International Journal of Rock Mechanic & Mining Science, v. 7, p. 43-65.

Butland, C. I., and Moore, T. A., 2008, Secondary biogenic coal seam gas reservoirs in New Zealand: A preliminary assessment of gas contents: International Journal of Coal Geology, v. 76, p. 151-165.

Chase, B. S., 1979, A comparison of methods used for determining the natural gas content of coalbeds from exploratory cores: US Department fo Energy.

Diamond, W. P., and Levine, J., R., 1981, Direct Method Determination of the Gas Content of Coal: Procedures and Results: United States Department of the Interior, Bureau of Mines, RI 8515.

Diamond, W. P., and Schatzel, S. J., 1998, Measuring the gas content of coal: A review: International Journal of Coal Geology, v. 35, p. 311-331.

Jin, H., Schimmelmann, A., Mastalerz, M., Pope, J., and Moore, T., 2010, Coalbed gas desorption in canisters: Consumption of trapped atmospheric oxygen and implications for measured gas quality: International Journal of Coal Geology, v. 81, p. 67-72.

Mares, T. E., Moore, T. A., and Moore, C. R., 2009, Uncertainty of gas saturation estimates in a subbituminous coal seam: International Journal of Coal Geology, v. 77, p. 320-327.

Masterlez, M., Drobniak, A., Strapoc, D., Acosta, W. S., and Rupp, J., 2008, Variations in pore characteristics in high volatile bituminous coals: Implications for coal bed gas content: International Journal of Coal Geology, v. 76, p. 205-215.

Moore, T., R., F., Stanton, R., and Stricker, G., 2001, The role of macroscopic texture in determining the variability of coal bed methane in the Anderson-Wyodac coal seam, Powder River Basin, Wyoming, EIghteenth Annual Meeting of the Society of Organic Petrologists: Houston, p. 85-88.

Yee, D., Seidle, J. P., and Hansen, W. B., 1993, Gas sorption on coal and measurement of gas content., *in* Law, B. E., and Rice, D. D., eds., Hydrocarbons from Coal: Tulsa, American Association of Petroleum Geologists, p. 159-184.

Study of Porosity and Permeability of Coal and Coal Measure Rocks from Raniganj Coalfield of India

B. K. Prusty, S. K. Pal, J. H. Kumar
Indian Institute of Technology, Kharagpur, India-721302.

ABSTRACT Porosity and permeability are critical reservoir properties that affect the flow behavior of methane in coal and coal measure rocks. The field-scale permeability is significantly different than the value determined in the laboratory. However, permeability is usually determined in the laboratory since it is less expensive. Porosity and permeability measurements were carried out in the laboratory using coal and coal measure rocks such as sandstone and shales from the Raniganj coalfields of India. The gas permeability was measured using the inert gas argon. Permeability of shale, coal and sandstone were found to be 0.022, 1.97, and 32.38 mD respectively. Porosity of the rocks was measured using the buoyancy method. Effective porosity values for coal, shale and sandstone were found to be 1.8, 12.38 and 17.31 % respectively. It was observed that the flow of gas deviated from the Darcy's law. An exponential relation between permeability and porosity was observed for coal and sandstone.

Keywords: Coal, coal measure rocks, porosity, permeability

1 INTRODUCTION

Permeability and porosity are the most important reservoir parameters which control the flow of fluid in porous rocks. Porosity is the measure of voids in the rock and is calculated as the ratio of volume of voids to the total rock volume. Porosity is generally measured in percentage. Effective porosity is the inter-connected voids in the rock that contributes to fluid flow. Permeability is the measure of the inter connectivity among the pores and is a measure of ease of flow of fluid in the porous medium through the connected pores. Permeability plays an important role incontrolling the economic viability of coal bed methane (CBM) reservoir. Permeability is a dynamic property and changes through the active life of reservoir.

Coal consists of cleats and fractures which contributes to the permeability of the CBM reservoir. The cleats are of two types, namely, face cleats which are continuous and butt cleats which are discontinuous; butt cleats terminate against face cleats. In general, face cleats contribute more to the permeability than the butt cleats. In addition to face cleats and butt cleats, there may be fractures and fissures present in the coal contributing to the permeability of the coal reservoir. The study of permeability and porosity of the coal and coal measure rocks are very important to quantify methane emissions in the mine as well as recovery of coal mine methane (CMM).

2 THEORETICAL BACKGROUND

In general, coal reservoirs are in equilibrium until some external processes like CBM recovery or enhanced CBM recovery are initiated. To recover CBM, the reservoir is depressurized by pumping off large volumes of formation water which leads to desorption of methane from the coal pores (Puri and Yee, 1990). Primary recovery method usually yields not more than 50% of gas in-place reserves (Murray, 1996). CBM recovery is enhanced by injecting a second gas such as CO_2into the coal. The recovery can go up to 90% of gas in-place while simultaneously a large quantity of CO_2can be sequestered (Stevens et al, 1999). Study

of porosity and permeability is very important both from the recovery of CBM and also to ascertain the CO_2 sequestration potential of the CBM reservoir.

When primary recovery starts, the fluid pressure starts to decrease and subsequently the effective stress increases. The increase in effective stress results incompaction of cleat/fracture leading to decrease in permeability (Gray, 1987). With lowering of fluid pressure below the equivalent sorption pressure, methane starts desorbing from the coal and this results in 'shrinkage' of coal matrix. The shrinkage associated with desorption opens up the cleats, and results in an increase in the permeability of coal. The increase of permeability depends on the initial in situ stress conditions and the shrinkage characteristics of the coal. The shrinkage of coal matrix with desorption may not only widen the cleats, but also reduce the effective horizontal stress. In fact, a very large shrinkage may even lead to a complete loss of horizontal stress. Overall, matrix shrinkage can have a significant impact on long-term gas production from coalbed methane reservoirs (Gray, 1987). Somerton et al (1975) conducted a series of permeability experiments on bituminous coals by flowing methane gas axially through a cylindrical coal specimen under specific stress conditions, and observed that the permeability is highly stress dependent. Hence, for CO_2 sequestration and enhanced coal bed methane recovery, it is very important to understand the impact of injection of CO_2 on the microstructure of coal and the resultant change in porosity and permeability.

The mechanisms of storage and transport of gas and water in coal differ from that of conventional gas reservoirs. Figure 1 illustrates the mechanism of transportation of gas in coal, which occurs in two steps: flow in cleat and fractures, and flow in coal matrix. Flow in the cleat system is pressure-driven and is described using Darcy's law, whereas flow through the matrix is by diffusion. The basic law governing the flow of fluids through the fractures and cleats is the Darcy's law which is given below.

$$q \propto \frac{\Delta P}{L} \tag{1}$$

The proportionality constant is found to be dependent on the viscosity property of the flowing fluid and Equation 1 can be re-written as;

$$q = \frac{Q}{A} = k\frac{(P_1 - P_2)}{\mu L} \tag{2}$$

q = flux rate or pore velocity m/s.
Q = Total discharge rate, m^3/s.
A = Cross sectional area to the flow, m^2.
k = Permeability of the rock, milliDarcy.
P_1, P_2= Pressures across the fluid flow in a porous medium, N/m^2.
μ = Viscosity of the fluid, kg/m.s
L =Length of the sample, m.

Darcy's law does not hold good for flow of compressible fluids like gas at higher pressures and has been modified as below:

$$Q = k_c \frac{A\{P_1^{(1+m_1)} - P_2^{(1+m_1)}\}}{(1+m_1)P_2^{m_1}} \tag{3}$$

where k_c is the permeability coefficient for compressible fluid.

m_1 = constant determined by thermodynamic character of flow (m_1=1 for isothermal flow).

$$Q = k_c \frac{A\,(P_1^2 - P_2^2)}{2\mu L P_2} \tag{4}$$

$$k_c = \frac{Q\mu L P_2}{A P_m (P_1 - P_2)} \tag{5}$$

Where $P_m$is the mean pressure across the sample and may be assumed to be the average of P_1 and P_2.The Equation 4 may be re-written as:

$$k_c = \frac{2Q\mu L}{A}\frac{P_2}{P_1^2 - P_2^2} \quad \text{(in Darcy)} \tag{6}$$

$$k_c = \frac{2000Q\mu L}{A}\frac{P_2}{P_1^2 - P_2^2} \quad \text{(in milliDarcy)} \tag{7}$$

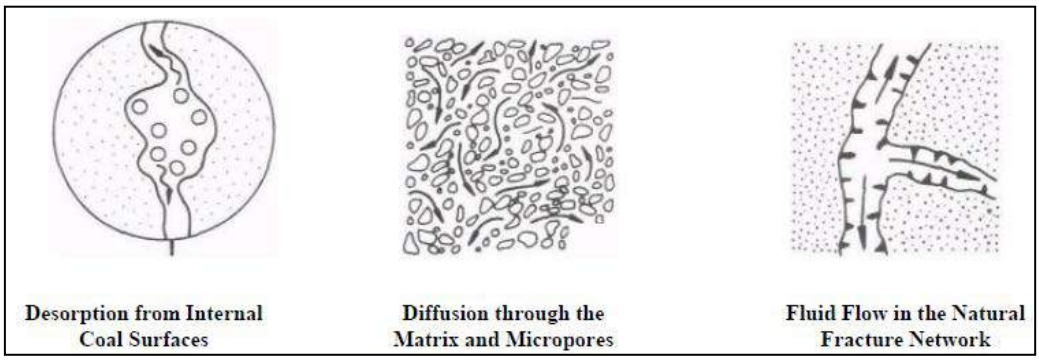

Figure 1. Methane transport mechanism in coal (Law and Rice, 1993).

2.1 Klinkenberg Effect

It has been observed that there is deviation from Darcy's law for flow of gas in porous medium. The permeability of rocks for gas is different from that for water. Permeability of porous rocks to gases is approximately a linear function of pressure under steady state and laminar flow. Klinkenberg observed that the permeability of air (gas) is more than the water (liquid) in porous medium. Liquid (water) generally possess zero velocity at the sand grain surface and gases possess some finite velocity. This is due to the gas slippage or the Klinkenberg effect. (Jones and Owens, 1980). The amount of slippage is directly proportional to the frequency of molecular collisions or the mean free path of the flowing gas. The Klinkenberg effect is more in rocks of low permeability. Considering the Klinkenberg effect, the coefficient of gas permeability is given by Ohle (1951) as:

$$k_g = -\frac{Q_m \mu L}{A(P_1 - P_2)} + \frac{4C}{P_m r_{av}} \quad (8)$$

where, P_m=mean pressure
Q_m= mean flow rate
k_g = coefficient of gas permeability
C= ratio of mean free path to the reciprocal of mean pressure
P_1=gas inlet pressure
P_2 =gas outlet pressure
r_{av}= average capillary radius for slip correction

2.2 Permeability and Pore Structure

Permeability of any porous medium is dependent upon whether the pores are interconnected or not and on the size of pores. Porosity of rocks is of two types: total porosity and effective porosity. In most rocks, many pores are blind at one end and these pores do not allow any flow across them. Thus rocks having same porosity may have different permeability depending upon the degree of interconnection between pores in the direction of flow. Further, the size of the pores has effect on the permeability. For example, shales usually have large porosity; however most of the pores of shales are of very small size of the order of nanometer and many of the pores are closed pores. These small pores offer high resistance to flow resulting in very less permeability of shales. For the flow of gas in rocks, the effective porosity is more important rather than the total porosity.

3 LITERATURE SURVEY

Gensterblum et al. (2014) studied the interaction between the coupling of slip-flow of gases and the cleat volume compressibility of coals using two Australian samples from Surat Basin, Queensland. Permeability measurements were performed using inert(helium and argon) and sorbing gases (nitrogen, methane and carbon dioxide) as the permeating fluid and at varying effective stress. Apparent permeability coefficients decreased in the order: helium >argon>nitrogen > methane>carbon dioxide. It was suggested that the Darcy equation, which is derived using the ideal gas law has a reduced validity for non-ideal gases like N_2, CH_4 and CO_2.

Adeboye and Bustin (2013) investigated the flow properties (permeability and diffusivity) of sub-bituminous to high

volatile bituminous coals from the Horseshoe Canyon and Mannville formations of the Western Canada Sedimentary Basin using both solid coal plugs and crushed samples (20–30mesh). Permeability of crushed coal ranged from 1.46E−5 mD to 7.6E−3 mDand that for coal plug ranged between 0.01 to 0.38 mD. This difference of up to four orders of magnitude between crushed and coal plug permeability is attributed to different stress conditions during sample testing and the influence of cleats and fractures on coal plug permeability. Increasing effective stress, with all other factors kept constant, leads to a decrease in coal plug permeability. Coal plug permeability declines exponentially with increasing effective stress which is attributed to the closure of permeability pathways due to compaction of coal at high effective stress levels. Probe gas type influences plug permeability. Helium permeability measurements are higher than permeability measured with methane or nitrogen. Permeability difference with probe gas is attributed to a combination of different probe gas molecule size, relative swelling effects of probe gas on coal and associated changes at in-situ stress during tests.

Letham (2011) studied the matrix permeability of low permeable gas shale. At pressures less than 4 MPa, matrix permeability of gas shales show a strong dependence upon the pore pressure. In case of gas flow in porous media in the low pressure regime, the Darcy's Law breaks down and gas slippage dominates. In gas shales, the range of pore pressures where gas slippage is recognizable is larger than in conventional reservoir rocks. This is due to smaller pore sizes in the gas shales. The molecular size of the probing/permeating gas will also influence the matrix permeability. Thus, matrix permeability determined using helium as a probing gas will be different than when methane is used.

Cui et al. (2009) measured permeability in gas shales, coal, and tight gas sands using gases with larger adsorption potentials than He, such as N_2. This study measured permeability using the pulse-decay measurement technique and considering the effect of gas adsorption. They explained that this new approach of permeability measurement is more reliable and theoretically accurate.

4 MATERIALS AND METHODS

4.1 Sample Description

Coal, sandstone and shale blocks from Raniganj coalfields were collected to study porosity and permeability. For porosity measurement, cylindrical core samples of 22 mm diameter and nearly 25 mm long are used. For gas permeability measurement core samples of 54 mm diameter and 57-59 mm in length are cut using the Bosch2000 model rotary drill in the laboratory. The two ends of the cylindrical core sample are smoothened to remove irregularities. Care is taken to ensure that the two circular ends of the core are perpendicular to the axis of the cylindrical specimen.

4.2 Experimental Setup to Measure Porosity

The effective porosity of the rock samples are measured using a setup based on the buoyancy method. The schematic of the setup is shown in Figure 2. The experimental setup consists of a vacuum pump connected to a vacuum desiccator containing samples through two 3-way stop cocks A and B. One end of stop cock A is connected to a vacuum gauge having minimum graduation of 1 torr and one end of the stop cock B is connected to a bottle filled with deaerated water. All connections are made permanent and leak-proof using araldite. The total system is checked for leakage. Stop cocks A and B are turned such that vacuum pump is directly connected to the vacuum desiccator and the pump is switched on to evacuate the desiccator. The pump continues to evacuate till the vacuum gauge shows 5 torr. At a vacuum gauge reading of 5 torr, the stop cock A is turned to connect the desiccator and the vacuum gauge, thereby isolating the pump from the system. Now the system is kept in vacuum for 24 hours. Then the stop cock B is turned slowly to connect vacuum

desiccator and the water bottle. Water is sucked into the desiccator and when the samples are completely submerged under water, stop cock B is turned off to stop further water inflow. Another 24 hours are allowed for samples to be submerged under water at normal atmospheric pressure. Samples are then transferred to a beaker containing deaerated water. Each sample is tied to a string and hung from the hook of a balance and weighed while the sample is still immersed in the water. Then the sample is removed from water and string is untied and surface-water is quickly absorbed on a blotting paper and the weight of the saturated sample in air is measured. The sample is then dried for 24 hours at 110 °C in an oven and transferred to a desiccator. After cooling, the sample is weighed again. The step-wise experimental and computational procedures are given as below:

1. Clean and dry the rock.
2. Fully saturate the rock in de-aerated water as explained above.
3. Weigh the saturated sample suspended in the water bath to give its submerged weight, W_{sub} as shown in Figure 3.
4. Remove the surface water from the sample by mopping with a blotting paper and measure the weight of the saturated sample in air (W_{sat}).
5. Dry the sample in the oven for 24 hours at 110 °C in a hot-air oven and take the dry weight (W_{dry}).
6. The effective porosity($\emptyset_e$) is calculated using the formulae:

$$\emptyset_e = \frac{W_{sat}-W_{dry}}{W_{sat}-W_{sub}} * 100 \text{ (in \%)} \qquad (9)$$

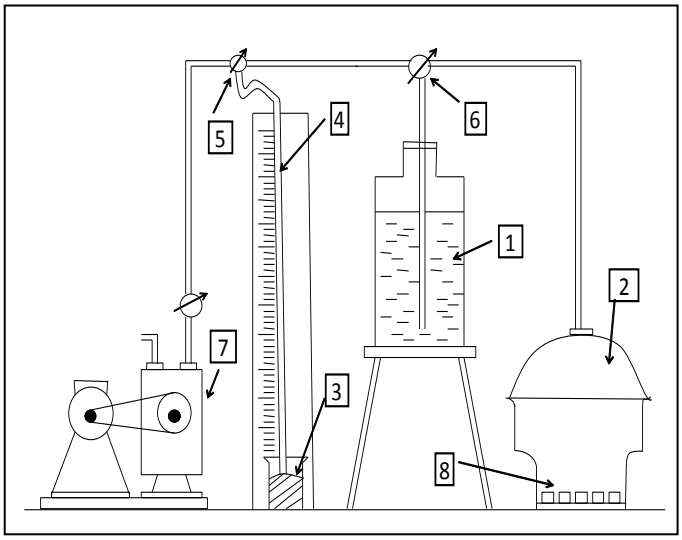

1.Container with deaerated water 2. Vacuum desiccators 3. Beaker filled with mercury 4. Capillary tube 5. Stop Cock A 6. Stop Cock B 7.Vacuum Pump 8. Rock samples

Figure 2.Setup to measure effective porosity.

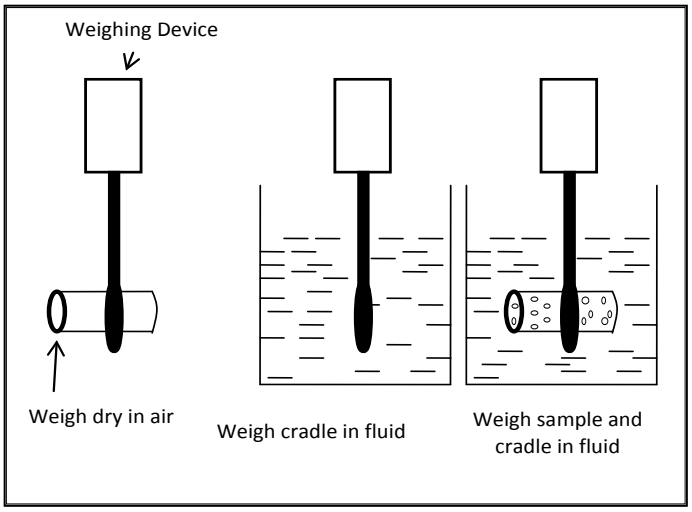

Figure 3.Different type of weight used in porosity measurement.

4.3 Experimental Setup and Procedure to Measure Permeability

The setup used to measure permeability is shown in Figure 4. It consists of rock sample holder, leveling bottle, burette, pressure transducer and transparent water bath. The sample holder contains stainless steel sleeve in which the sample core is cast using araldite. The steel sleeve is held at the center of the sample holder by two flanges on either side. A pressure transducer is connected to the 3-way inlet valve and a digital display shows the inlet pressure. The setup is first

tested for leakage under the highest working pressure. Permeability of the core sample is measured by flowing a fluid of known viscosity while maintaining a set pressure difference across the core. The fluid used is usually an inert gas. In this study, Argon gas has been used. The Argon gas cylinder is connected to one end of the sample holder by high pressure tubes. The other end of the sample holder is connected to a graduated 50 cm^3 glass burette through a flexible polyethylene tube. One end of the burette is fitted with a 3-way stop cock which allows bleeding of the gas when the measurements are not taken. The other end of the burette is connected to a leveling bottle through a flexible polyethylene tube for measuring gas flow rate under atmospheric pressure condition. The barometric pressure and room temperature are recorded while conducting the experiment. The following steps are performed sequentially to determine permeability.

1. The core sample is kept in the steel casing and araldite is applied. It is ensured that there is no gas leakage along the walls of the casing.
2. The two ends of the rock sample are smoothened to remove the irregularities.
3. The core casing is placed in the setup and the bolts are tightened.
4. After connecting the inlet and outlet valves, the setup is again checked for leakage.
5. The inlet pressure is set to the desired constant value.
6. Under the set pressure difference, the time required for 25 ml of gas to flow through the sample is measured by a stop watch.
7. The atmospheric pressure and temperature are noted.
8. The above procedure is repeated for different set pressure differences.

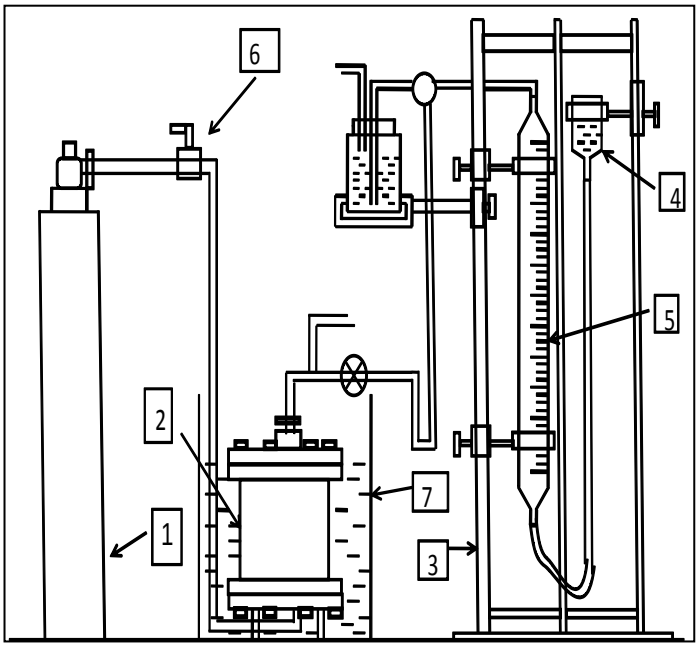

1. Gas cylinder 2. Rocksample holder
3.Burette stand 4. Levelingbottle
5.Burette6.Pressure transducer 7. Water bath

Figure 4.Setup to measure permeability.

5 RESULTS AND DISCUSSIONS

The permeability and effective porosity values of the studied samples are shown in Table 1.It can be seen that sandstone sample-2 has high effective porosity and permeability of 17.31% and 32.38 mD respectively. Shale has 12.38% of effective porosity and very low permeability value of 0.022 mD respectively.

Table 1. Effective porosity and permeability of the coal measure rocks.

Sl. No.	Sample	Effective Porosity (%)	Permeability (mD)
1	Coal	1.825	1.975
2	Sandstone-1	6.34	1.632
3	Sandstone-2	17.31	32.38
5	Shale	12.38	0.022

The relationship between the applied pressure gradient, $(\Delta P/L)$, and the resulting flow rate per unit cross-sectional area of gas through different rock and coal samples are plotted in Figures 5-7.

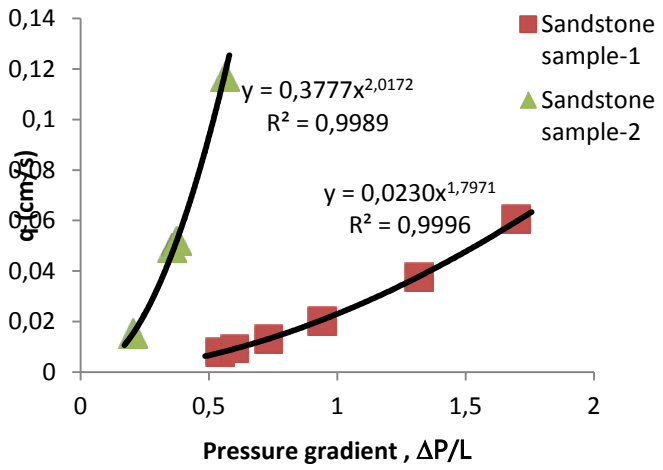

Figure 5. Flux rate versus pressure gradient for sandstone samples.

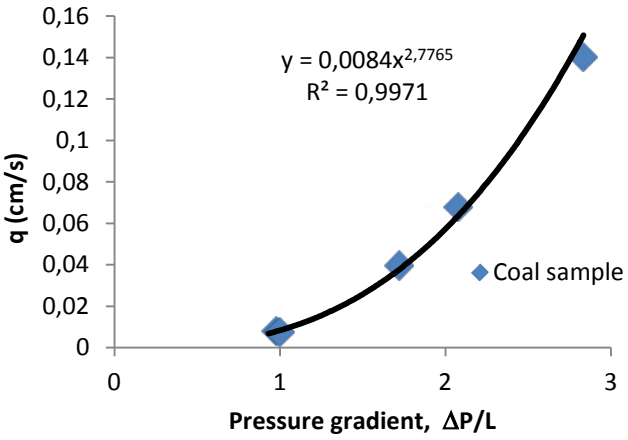

Figure 6. Flux rate versus pressure gradient for coal sample.

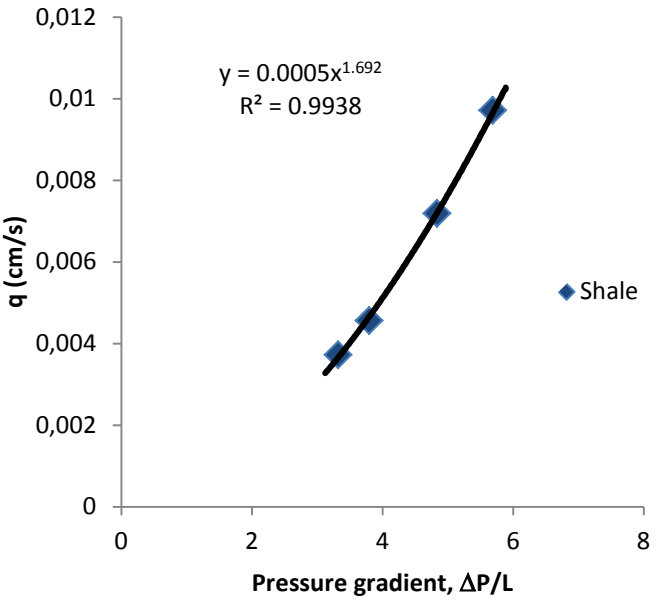

Figure 7. Flux rate versus pressure gradient for shale sample.

The relationship between the flow rate and pressure gradient has been observed in the form of Equation 10.

$$q = a\left(\frac{\Delta P}{L}\right)^{m} \quad (10)$$

Where a and m are constants. The values of a, m and the coefficient of correlation (R^2) values are given in Table 2.

Table 2. a, m and R^2 for the flow equation.

Sl. No.	Sample	a	m	R^2
1	Coal	0.0084	2.776	0.99
2	Sandstone-1	0.023	1.797	0.99
3	Sandstone-2	0.377	2.017	0.99
5	Shale	0.0005	1.692	0.99

The above data indicate that the gas flow equation is non-Darcy. The value of index m is greater than one, and it suggests that a large increase in flow rate corresponds to a small increment in pressure rise. This is possible when the total cross-sectional area of flow increases with increase in inlet pressure. The increase in cross-sectional area of inter-connected pores can occur due to elastic compression of isolated pores in rocks owing to higher static fluid pressure acting normal to the pore-walls. In the experiment, enlargement of inter-connected pores occur during continued step-wise pressure increment of the flowing gas, through gradual compression of isolated pores. The rock samples are capable of accommodating this temporary elastic deformation of the pores. The gas permeability co-efficient is calculated from Equation 6 and are presented in Table 3.

Table 3.Gas permeability experimental results.

Sl. No.	Sample Name	Inlet Pressure (P_1), in bar	Outlet Pressure (P_2), in bar	Flow rate (Q), cm^3/s	Gas Permeability(K_c), in mD	Mean K_c, in mD
1	Coal	6.2	1.013	0.216	0.536	0.901
		6.3	1.013	0.204	0.490	
		10.1	1.013	1.046	0.962	
		12	1.013	1.793	1.165	
		16	1.013	3.703	1.349	
2	Sandstone-1	3.9	1.021	0.206	1.363	1.429
		4.2	1.021	0.245	1.386	
		4.9	1.021	0.345	1.408	
		6	1.021	0.531	1.424	
		8	1.021	0.994	1.480	
		10	1.021	1.601	1.515	
3	Sandstone-2	2.1	1.016	0.401	11.071	15.670
		2.9	1.016	1.295	16.364	
		3	1.016	1.369	16.024	
		4	1.016	3.086	19.219	
4	Shale	18.6	1.018	0.098	0.0265	0.025
		21.1	1.018	0.120	0.0253	
		26.6	1.018	0.189	0.0250	
		31.1	1.018	0.256	0.0248	

The Equation 6 can be re-written as:

$$\frac{1000QP_2}{P_1-P_2} = k_c \frac{AP_m}{\mu L} \quad (11)$$

The *permeability plot*, i.e., plot between $\frac{1000QP_2}{P_1-P_2}$ and $\frac{AP_m}{\mu L}$, should be a straight line passing through the origin. The permeability plots are shown in Figures 8-10. It can be seen that the plots are linear but not passing through the origin. The plots not passing through the origin may be due to:

1. The thermodynamic character of flow may not be isothermal where index m_1 is considered as one.
2. Elastic expansion of inter-connected flow path at higher pressures.
3. The molecular effect due to slip flow of gas. This effect is important in the case of pore diameter compared to or less than the mean free path of the flowing gas.
4. The wall effect in sample holder of the permeability set-up.

The phenomenon of slip flow in coal is very important from the CBM recovery point of view. The occurrence of slip-flow in coals, may lead to a significant increase in productivity of coalbed methane reservoirs near the abandonment pressure.

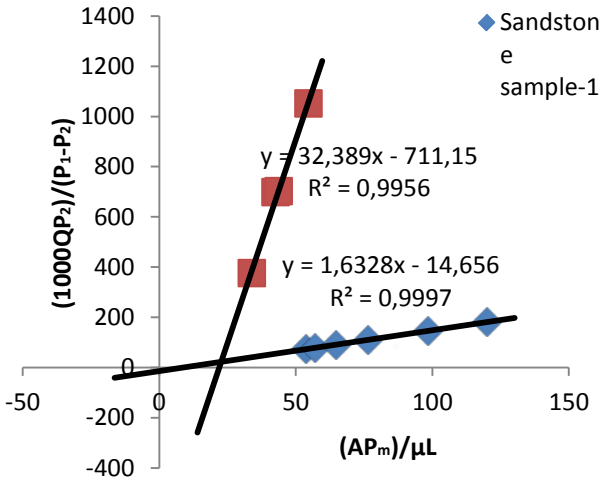

Figure 8.Permeability plot for sandstone samples.

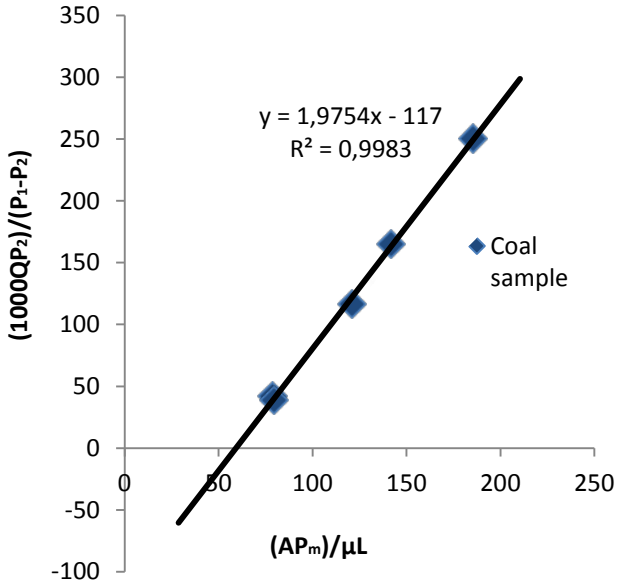

Figure 9.Permeability plot for coal sample.

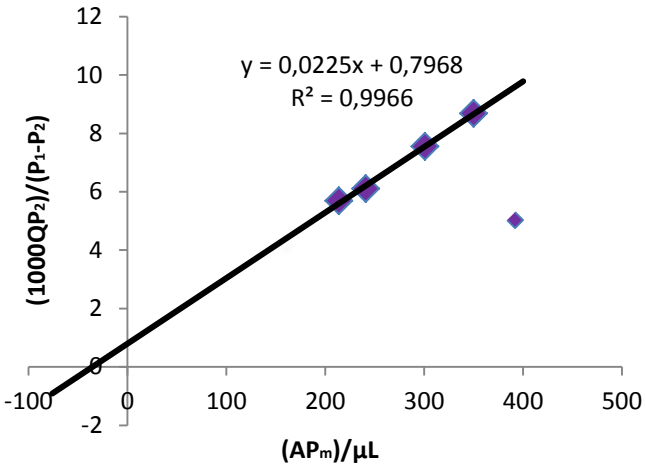

Figure 10.Permeability plot for shale.

The relation between$\emptyset_e$and k_c depends on the pore space configuration. As per Aschenbrenner and Chillingar (1960), for rocks with $\emptyset_e < 12\%$, k_c is given as:

$$k_c = 2.0\, e^{0.316\emptyset_e} \qquad (mD) \qquad (12)$$

The relation between permeability and effective porosity for the studied four samples are plotted in Figure 10. It can be seen that for coal and two sandstone samples, the relation is exponential as given by Equation 13. However, the same equation is not holding good for the shale sample. This may be due to the fact that shale has very fine grain sizes and have different pore space configuration. For the coal and sandstone samples, the permeability and effective porosity are related as:

$$k_c = 0.878\, e^{0.197\emptyset_e} \qquad mD \qquad (13)$$

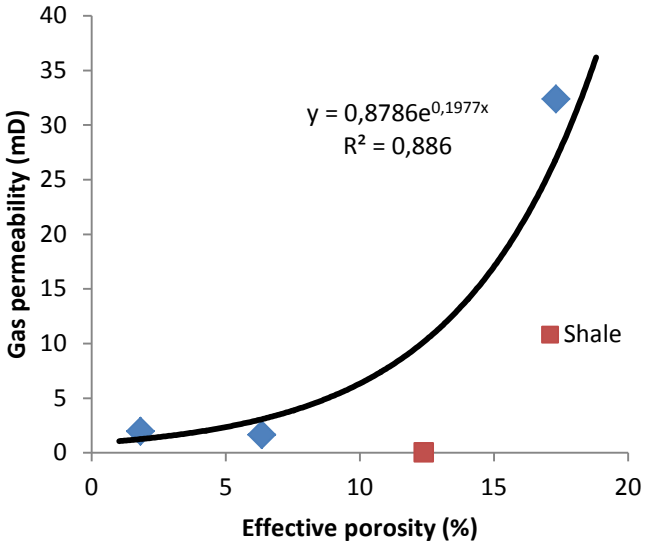

Figure 11.Relation between effective porosity and permeability.

6 SUMMARY

1. The pressure gradient $\frac{\Delta P}{L}$ and flow rate per unit cross-sectional area 'q'are related as$q = a\left(\frac{\Delta P}{L}\right)^m$. The value of a varies from 0.0005 to 0.377 and m varies from 1.692 to 2.776.
2. The value of m more than unity indicates that there is greater increase in flow rate against a smaller increase in pressure gradient. It may be due to increase in flow path area on account

of higher static pressure on walls of inter-connected pores.

3. The permeability co-efficient of coal sample is 1.018 mD, and for sandstone it varied from 1.499 mD to 21.27mD. The fine grained shale sample has the lowest permeability of 0.017 mD because of its extremely small size pores.
4. All samples exhibit deviation from the Darcy's Law. Deviations are attributed to: (a) Non-isothermal gas flow condition, (b) Expansion of flow path area at higher pressures, (c) Molecular effect arising from slip flow and (d) Wall effect during permeability measurement.
5. The relationship between gas permeability co-efficient and effective porosity for the coal and coal measure rocks under study except shale is given by: $k_c = 0.878\, e^{0.197\emptyset_e}$ (mD)

REFERENCES

Adeboye, O O, and Bustin, R M, (2013), Variation of gas flow properties in coal with probe gas, composition and fabric: Examples from western Canadian sedimentary basin, *International Journal of Coal Geology*, 108, (pp. 47–52).

Aschenbrenner, B C, Chilingar, G V, (1960), Teodorvich's method for determining permeability from pore space characteristics of carbonate rocks. *Bulletin of American Association of Petroleum Geologists*, 44(8), (pp. 1421-1424).

Cui, X, Bustin, M M, and Bustin, R M, (2009), Measurements of gas permeability and diffusivity of tight reservoir rocks: different approaches and their applications, *Geofluids*, 9, (pp. 208–223).

Gensterblum, Y, Ghanizadeh, A, and Krooss, B M, (2014), Gas permeability measurements on Australian subbituminous coals: Fluid dynamic and poroelastic aspects, *Journal of Natural Gas Science and Engineering*, 19, (pp. 202 -214).

Gray, I, (1987), Reservoir Engineering in Coal Seams: Part 1. The Physical Process of Gas Storage and Movement in Coal Seams, *SPE Reservoir Engineering*, 2, (pp. 28-34).

Jones, F O, and Owens, W W, (1980), A laboratory study of low permeability gas sands, *Journal of Petroleum Technology*, 32, (pp.1631–1640).

Law, B E, and Rice, D D, (1993), Hydrocarbons from Coal, *The American Association of Petroleum Geologists*.

Letham, E A, (2011), Matrix Permeability Measurements of Gas Shales: Gas Slippage and Adsorption as Sources of Systematic Error, *B. S. Thesis*, University of British Columbia, Vancouver.

Murray, D K, (1996), Coalbed Methane in the USA: Analogues for Worldwide Development, in Gayer, R. and Harris I. (ed), *Coalbed Methane and Coal Geology*, (pp. 1-12).

Ohle, E L, (1951), Influence of permeability on ore distribution in limestone and dolomite, *Economic Geology*, 46 (7), (pp. 667-674).

Puri, R, and Yee, D, (1990), Enhanced Coalbed Methane Recovery, *65th Annual Technical Conference and Exhibition of the Society of Petroleum Engineers New Orleans, Louisiana*, (pp. 193-202).

Somerton, W H, Soylemezoglu, I M, and Dudley, R C, (1975), Effect of Stress on Permeability oCoal, *International Journal of Rock Mechanics Mining Science and Geological Abstracts*,12, (pp. 129-145).

Stevens, S H, Spector, D and Riemer, P, (1998), Enhanced Coalbed Methane Recovery by Use of CO_2 Injection: Worldwide Resources and CO_2 Sequestration Potential, *SPE International Conference and Exhibition, Beijing, China*, (pp. 489-501).

Gas Content and Spontaneous Combustion Investigations for Uckardesler Asphaltite Vein

Üçkardeşler Asfaltit Filonunun Gaz İçeriğinin ve Kendiliğinden Yanma Eğiliminin Tayini

A. Fisne, S.C. Özer, O. Esen, C.A. Öztürk, S. Erçelebi
Istanbul Technical University, Mining Engineering Department, Istanbul

ABSTRACT Asphaltite with its high calorific value is important raw material for energy and thermal power plant. Southern eastern part of Turkey is also a good deposit for asphaltite. The increasing amount of demand from energy sector will cause in the production of asphaltite from deeper levels. Therefore, production of asphaltite from underground mining methods will be interested in mining sector. Gas content and risk classification of spontaneous combustion are the important factors to understand the applicability of underground mining methods for asphaltite. These investigations are used to select the underground mining method not only for economic reasons but also for safety concerns. This study contains the results of these investigations specified for Uckardesler asphaltite vein located in Silopi, Sirnak, Turkey. The results of this study shall be discussed among designers and planners specialized in mining for the possibility of underground mining applications for asphaltite production.

Keywords: Uckardesler Asphaltite Vein, gas content, spontaneous combustion

ÖZET Yüksek kalori değeri ile asfaltit önemli bir enerji ve termik santral hammaddesidir. Türkiye'nin güneydoğusu ise iyi bir asfaltit maden yatağıdır. Enerji sektöründeki artan talep, asfaltitin daha derin seviyelerden üretilmesine sebebiyet verecektir. Bu durumun bir sonucu olarak, asfaltitin yeraltı üretim teknikleri üretilmesi, maden sektörünün ilgi alanları içerine girecektir. Asfaltitte, gaz içeriği ve kendiliğinden yanma risk sınıflaması, yeraltı üretim yöntemlerinin uygulanabilirliklerinin anlaşılması için önemli faktörlerdendir. Bu araştırmalar yeraltı üretim yönteminin seçiminde sadece ekonomik değil iş güvenliği ile ilgili sebeplerden dolayı da yapılır. Bu çalışma, Silopi İli Şırnak İlçesinde bulunan Üçkardeşler asfaltit filonu özelinde yapılan araştırmaların sonuçlarını içermektedir. Bu çalışma, madencilik alanında çalışan tasarım ve planlamacıların, asfaltitin yeraltı madencilik uygulamaları ile üretilebilme ihtimallerini tartışabileceği sonuçları içermektedir.

Anahtar Kelimeler: Üçkardeşler asfaltit filonu, gaz içeriği, kendiliğinden yanma

1 INTRODUCTION

Asphaltite is a hard and black solid fuel formed in geological time by oxidation of crude oil and losing volatile matter with influence of bacteria and temperature. Although it is an oil-based, it is used a solid fuel like coal and is included to coal group in assessments (Ünalan, 2010).

The coalification process is defined as the transformation of plant material to anthracite and graphite passing through the stages of peat, lignite and bituminous coals (Gürdal, 1998). It is well known that large amount of gas is formed during the coalification process and significant amount of this gas is stored in coal and rock. The storage gas in coal contain a mixture of gases in which methane makes up 90-95 % Minor amounts of carbon dioxide, nitrogen, hydrogen sulphide, and sulphur dioxide make up the other

components of storage gas in coal (Flores, 1998).

A large part of the gas in coal is stored as free and adsorbed gas with equilibrium pressure in coal seams and layers. Due to disturbed of pressure equilibrium by mining methods, methane gas storage in coal fractures and pores is released in various ways resulting from bursting, firing and strangulation. Furthermore in some underground mines, the storage gas in coal seams under pressure is spontaneously exceeding the strength of face that results high amounts of gas is emitted. It can be defined as a sudden outburst of gas and coal and is the most important problem of the underground mining safety (Ökten, 1983).

In underground coal mines, the management of methane is controlled by "Ventilation and Methane Drainage". In working places, methane emission should be estimated previously. There are various techniques developed for methane emission prediction. The gas contents of coal seams are the more important parameter for methane emission prediction (Noack, 1998).

The amount of carbon monoxide gas which is formed in coalification process decreases with time due to the solution in water. A large part of methane gas is released to atmosphere when the coal seams are closer to the surface. The gas is commonly stored in pores when the coal seams is bedded at deep and covered with compact rocks.

The methane gas exists in coal and rock as free and adsorbed gas (Figure 1). The amount of free gas found in fractures, micro fractures and pores of coal and rock is very low than adsorbed gas in micro fractures and pores of coals. The ratio of free gas in total gas is given by 5-10% (Didari ve Ökten, 1994).

On the other hand, spontaneous combustion is described as the event that starts with adsorption of oxygen with connection between air and coal and continues with oxidation, and then it can be converted to open fire by the storage of the heat which is occurred in the working place, (Ramlu, 1991; Banerjee, 1985; McPherson, 1993; Durucan and Guyaguler, 1987).

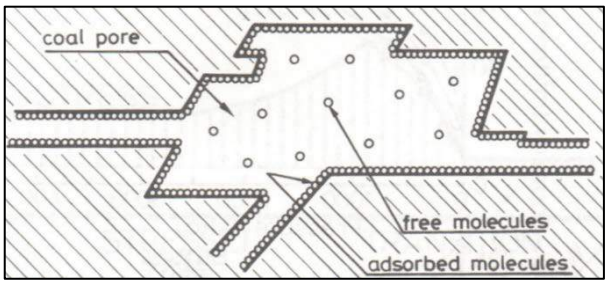

Figure 1. Existence of gas molecules in coal pores (Didari ve Ökten, 1994)

Oxidation is an exothermic reaction. In normal circumstances, the heat which is a result of reaction is transported with air flow and the event continues without causing dangerous heating. However in some cases, produced heat never leaves the medium and then temperature starts increasing. If this continuous reaction isn't prevented, the spontaneous combustion is converted to open fire when the heat reaches the ignition temperature. Because of this, the ramble openings, gobs, fractured pillars, fault zones, silos etc. are suitable for spontaneous combustion (Ayvazoglu, 1984).

Each coal has spontaneous combustion risk in appropriate environmental conditions. In addition each coal type reacts different because of different structural features even they exist in same environmental conditions. For the spontaneous combustion of coal, the following three important conditions must be occurred:

- A coal source able to oxidize in normal conditions,
- Sufficient oxygen source for oxidation,
- A storage feature of heat (unreleased from working place).

The oxygen is adsorbed by coal when contacts with oxygen because of its structure even in low degrees. This adsorption process increases the temperature of the environment by turning to an exothermic reaction at temperatures over 40°C. If this temperature couldn't be reduced, the CO and CO_2 gas concentrates become increasing after the temperatures approximately 70°C or higher and the water steam (H_2O) is occurred at 125°C. When the increased temperature of the working place reaches the ignition degree, coal starts to ignite. The first level of

the coal oxidation is adsorbing of the oxygen to coal by physical ways. As the result of chemical reaction, generated by this physical adsorption, the coal-oxygen complexes are occurred and then this complexes are decomposed to CO, CO_2 and H_2O (Ramlu, 1991; Banerjee, 1985).

The aim of this study is to investigate gas content as well as spontaneous combustion of an asphaltite vein called as Uckardesler located in Silopi. The results are participated in this study for design and planning studies especially for the research of underground mining production of asphaltite.

2 STUDY AREA INFORMATION

Study area is located in the City of Sirnak, Silopi region where is in the southern eastern part of Turkey,

Uckardesler asphaltite vein with its approximately 22.5 million ton reserve capacity is an important energy raw material for a thermal power plant planned to construct in this region.

The vein is formed in between Gercus and Midyat formations that are consists of mostly clay stone and limestone, respectively. A geological cross-section is given in Figure 2 to show a brief geological aspect of the study area. A study of Karpuz et.al. (1986) was the first application for the site.

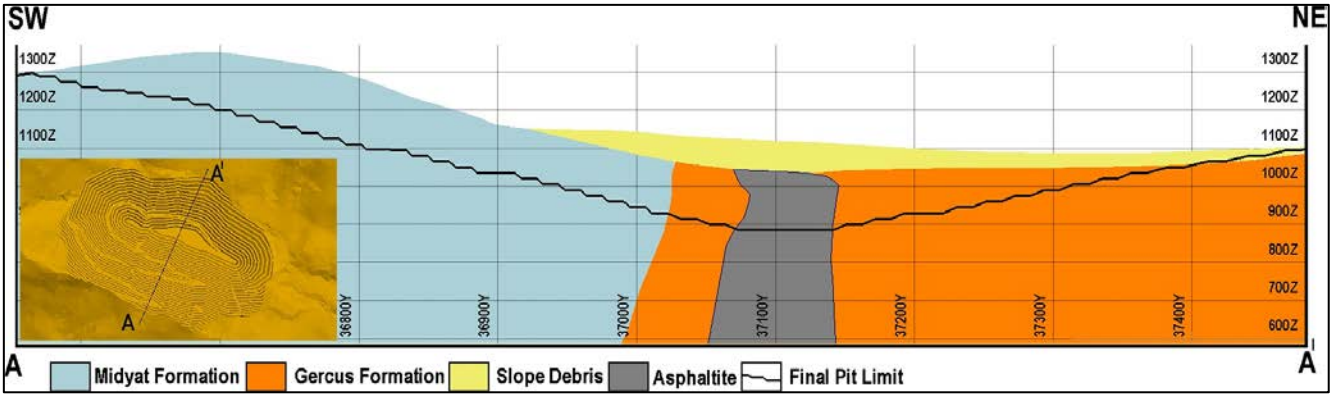

Figure 2. Geological cross-section of Uckardesler asphaltite vein (Ozturk, 2013)

3 GAS CONTENT DETERMINATION OF ASPHALTITE SAMPLES

The gas content of the coal seams is required to know in the designing of preventive measures for the gas emissions during the coal production in underground coal mines. The measurement of gas content of the coal seams can be determined by direct or indirect methods. In addition it can be calculated by empirical methods which were developed by different researcher (Diamond ve Schatzel, 1998).

There are a lot of direct methods to determine the gas content of the coal. The most commonly used gas content determination methods subdivide the total gas content of a coal sample into three parts: lost, desorbed and residual gas. Each of these parts is generally measured or estimated by a different procedure, and then combined to yield the total gas content of the sample. The US Bureau of Mines direct method (USBM) was used to measure the gas content of Uckardesler asphaltite vein. The schematic view of gas content measurement apparatus is given in Figure 3.

In the direct methods, immediately after drilling, the sample is collected. It is sealed in a specially designed canister, which allows measuring the volume of gas with high accuracy. The actual release (desorption) of the total volume of gas is determined in three stages: measurement of desorbed gas, determination of residual gas and estimation of lost gas. For the first few hours, the volume of desorbed gas released from the sample is regularly measured at short intervals. This data is later used to estimate the lost gas released during retrieval and handling at the surface. The volume of released gas is measured over increasingly longer intervals until the volume decreases to 0.05 ml/g/day for several days.

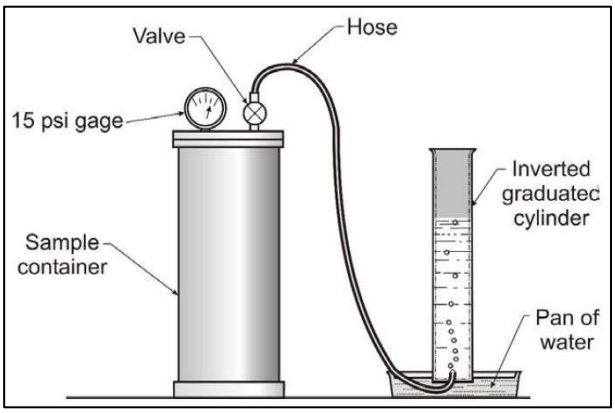

Figure 3. Gas content measurement apparatus (Kissell, 2006)

Once the sample effectively stops releasing gas, weighs and prepare the sample for the determination of residual gas. Core samples are crushed and the volume of residual gas measured through water displacement. Finally, the volume of lost gas is calculated graphically. Data for a number of variables including drilling medium, drilling times, times for reaching the surface and time sealed in the canister are applied to reach an accurate volume of lost gas. The actual gas content of the sample is calculated by adding the volumes of desorbed gas, residual gas and lost gas.

3.1 Site Study and Results

Measuring the gas content of Uckardesler asphaltite vein, a vertical drilling was made by The Company "Sirnak Enerji Inc". This drilling was cut the seam at least 80 m from the surface and the samples were taken the depths from 97, 143, 180 and 340 meters.

USBM method was used to determine the gas content of samples which are taken on the Uckardesler asphaltite vein. During the drilling, samples were taken in the canisters. In order to determine the lost gas, the time was measured during since the bits cut the seam and the samples were taken in the canisters. The desorbed gas was measured till the end of releasing of gas in canister using the apparatus given in Figure 3. The lost gas was determined by a graphical technique. The desorbed gas data are plotted on a graph of cumulative desorbed gas versus the square root of desorption time. The residual gas is determined with grinding of the samples in laboratory.

The lost gas is that portion of the total gas that escapes from the sample during its collection and retrieval prior to being sealed into an airtight desorption canister. Lost gas volumes cannot be directly measured and therefore must be estimated from the subsequently measured gas volume data. Since the lost gas is an estimated quantity, it is generally considered to be the least reliable component of the total gas content. Desorption gas volume data of the Uckardesler asphaltite vein and the estimation of their lost gas data are given in Figure 4, 5,6 and 7.

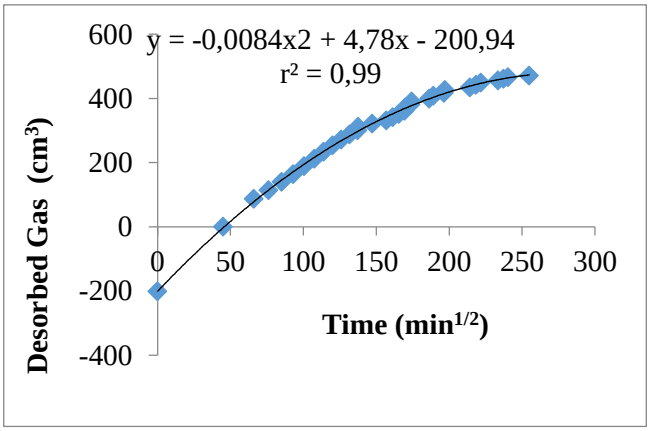

Figure 4. The desorbed and lost gas of the first sample (97 m)

The results of the determined gas content of the Uckardesler asphaltite vein was given in the Table 1. The gas content of the samples varied from 1.34 m^3/ton and 2.33 m^3/ton.

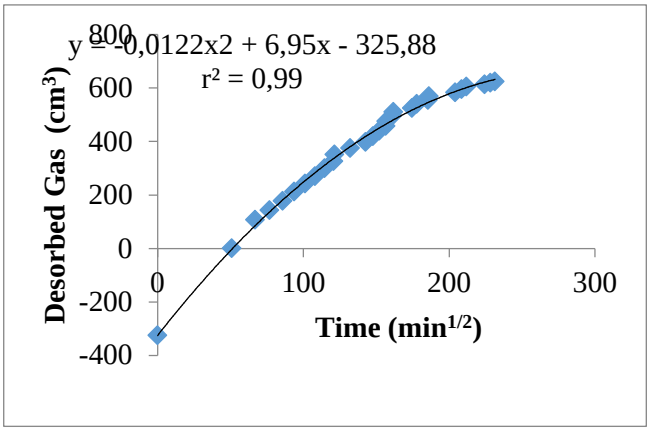

Figure 5. The desorbed and lost gas of the first sample (143 m).

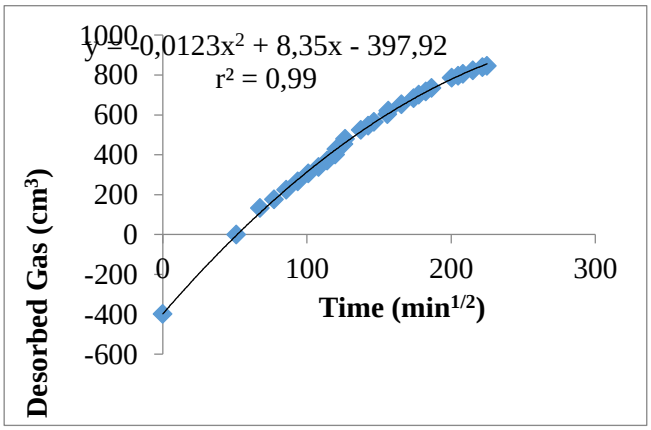

Figure 6. The desorbed and lost gas of the first sample (180 m).

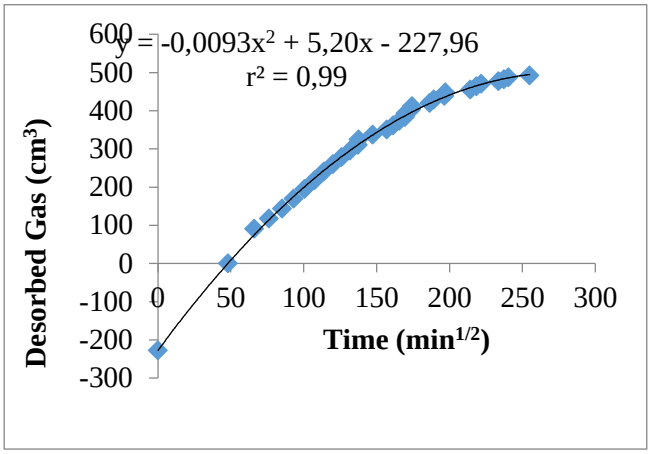

Figure 7. The desorbed and lost gas of the first sample (340 m).

It can be seen from the results that the gas content of Uckardesler asphaltite vein determined with direct method increase with the increasing of depth. The gas content of the Uckardesler asphaltite vein are lower than the gas content of coal seams.

Table 1. Gas content of samples from Uckardesler asphaltite vein.

Depth (m)	Gas Emission (m³/ton)			Gas Content (m³/ton)
	Desorbed	Lost	Residual	
97	0.84	0.36	0.14	1.34
143	1.06	0.56	0.20	1.82
180	1.33	0.63	0.16	2.12
340	1.41	0.65	0.27	2.33

4 LIABILITY INDEX FOR SPONTANEOUS COMBUSTION RISK CLASSIFICATION

The aim of this section's study is the determination of liability index for spontaneous combustion of Uckardesler asphaltite vein which will be mined by Sirnak Enerji Inc. with underground mining methods.

Table 2 is prepared to explain the important factors called as inner and outer effecting spontaneous combustion.

The structure of coal and geological features are defined as inner factors because they are unchangeable; changeable features like mining applications are defined as outer factors.

Further information can be determined from the studies of Banerjee, 1985; Ramlu, 1991; McPherson, 1993; Ayvazoglu, 1984; Durcan ve Guyaguler, 1987.

4.1 Liability Index for Spontaneous Combustion

Two different methods are used for determination of Liability Index of Spontaneous Combustion and they called "Laboratory Techniques" and "Practical Methods" (Kaymakcı, 1998). Practical methods are based on the classifications that acquired experiences, environmental conditions and frequency of heating events. Laboratory techniques are depended on observing the changes on coal as a result of airflow passing over coal

Table 2. The Factors influencing the spontaneous combustion (Kaymakcı, 1998).

Inner (Natural) Factors		Outer Factors
Coal		Environmental
Structure of Coal	Geological Factors	Structure of Coal
Coalification (Rank)	Seam Thickness	Coalification (Rank)
Petrography	Seam Dip	Petrography
Grain Size	Roof Collapsing Skills	Grain Size
Dry Content	Faults and Joints	Dry Content
Pyrite Content	Depth of Coal Bed	Pyrite Content
Physical Features	Geothermic Gradient	Physical Features
Ash Content	Seismic Movings	Ash Content
Volatile Matter	Roof-Hanging Conditions	Volatile Matter Content
Content	Gassiness of Coal Seam	Oxygen Content
Oxygen Content	Layered Seams	
	Methane Emissions	

The basis of the intersection point method is; passing the air over coal sample in a reactor placed in a directly heated furnace and monitoring the time - temperature relations. The heats of both the furnace and the sample are recorded and the point that sample's heat reaches the furnace's heat or intersects is called the "intersection point" (Kaymakcı ve Didari, 1992). The coals which have high liability index have lower intersection temperature points (Didari et.al., 1993). A typical intersection point graph is given in Figure 8 (Kaymakcı,1998).

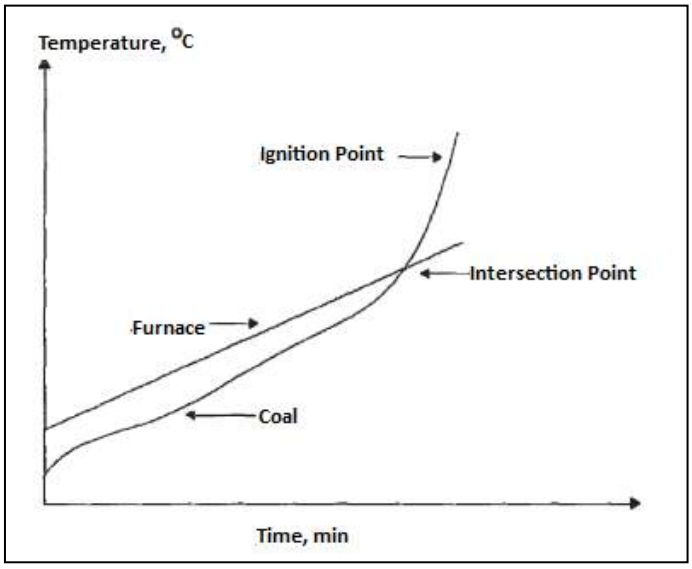

Figure 8. A typical intersection point graph.

In the experiments based on intersection point are made by Feng et.al. (1973), 100 grams of coal samples are placed into a reactor, and it placed into a furnace which has temperature increasing linearly 0.5 °C/min of acceleration. Also 40 ml/min air are passed over coal samples and make them oxidized. Coal temperature which is lower than furnace temperature in the beginning becomes higher with the effect of oxidation and starts passing it. The point that sample temperature surpasses the furnace temperature 1°C is accepted as the intersection point.

"FCC (Feng, Chakravorty, Cochrane) index" is used for determining the liability index of coal as given in Equation 1, which is developed by Feng et.al. (1973).

$$FCC\ (\text{min}^{-1}) = \frac{\text{Average temperature increase (°C/min)}}{\text{temperature of igniton point (°C)}}\ x\ 1000 \quad [1]$$

When the Heating Risk Index is found from the Formula above, this value is compared with the data in Table 3 and the risk classification is made for the coal.

Table 3. The liability to heating according to FCC Index.

FCC Value (min^{-1})	Prone to Spontaneous Combustion
0 - 5	Low
5 -10	Medium
> 10	High

Under these circumstances, high heating rate and low combustion temperature of coals would be more obvious liable to spontaneous combustion.

4.2 Experimental Studies

Experimental test were carried out in Bulent Ecevit University, Mining Engineering Department Laboratory. The Intersection Point Method is used to determine the "Spontaneous Combustion Risk Index" of Uckardesler Asphaltite vein. In this method, passing the air over asphaltite sample in a reactor placed in a directly heated furnace and therefore asphaltite is oxidized. During the experiment the furnace and the sample's temperature are recorded at regular ranges. The experiment equipment is shown at Figure 9.

Figure 9. The intersection point method's experiment equipment.

The representative asphaltite are taken from core samples and they are crushed in conic and jaw crushers. Finally, the samples are grinded and the grain sizes of samples are decreased under 200 mesh. Two samples are packed about 35 grams as they would be used in spontaneous combustion.

The conditions for spontaneous combustion experiments are given below.

Amount of sample: 35±0.1 g
Air flow : 100±0.5 ml/min
Furnace temperature: 0.5°C/min
Getting data frequency: 1 min

The results for spontaneous combustion experiment are given in Figure 10.

The temperature of the sample was increased 30°C in 1 hour, during 313 minute in heating bed, it was heated to the ignition temperature and above this degree. The reaction between oxygen and asphaltite was accelerated with increasing of the temperature and after 277 minute in 165°C the sample was reached and went beyond the degree of the heating bed temperature (Figure 10).

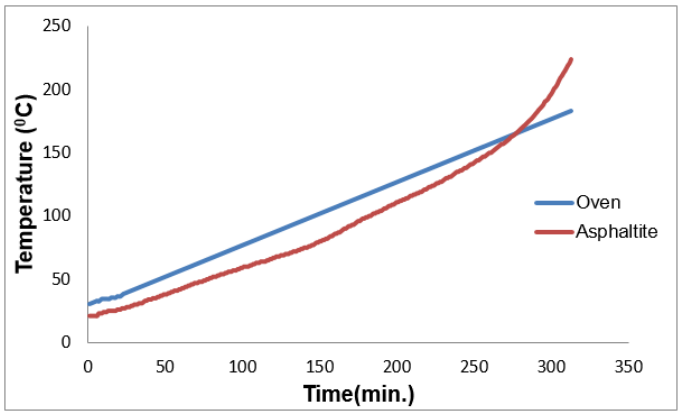

Figure 10. The temperature-time graph for the results of spontaneous combustion test.

The average increased temperature and the FCC Index value which is calculated by intersection point and the ignition degrees according to the spontaneous combustion test data are given in Table 4.

According to FCC index value (5.96 min^{-1}) as it is shown in Table 4; the liability index of Uckardesler asphaltite sample is determined as "Medium".

Table 4. The spontaneous risk classification of Uckardesler Asphaltite.

Asphaltite Vein	Intersection Point Temp. (°C)	Igniton Point Temp. (°C)	Average Increased Temp. (°C/min)	FCC index (min^{-1})	Risk
Uckardesler	164.9	165.9	0.98	5.96	MEDIUM

5 CONCLUSION

Gas content and spontaneous combustion risk classification is investigated in this study for Uckardesler asphaltite vein located in Silopi, Turkey. The results are especially important for the use of planning and design studies carried out for underground mine production project.

Gas content investigations were carried out at site, and measurements were initiated in the drill studies including laboratory investigations. Average gas content of the vein is 1.90 m^3/ton while the content increases with depth. 2.33 m^3/ton gas content is the maximum determined from the laboratory investigations however the amount should be more for deeper depth.

The vein is classified as medium for the risk of spontaneous combustion based on the outcomes determined from laboratory works.

ACKNOWLEDGEMENTS

This paper contains some of the outputs from the project titled as “Uckardesler Asphaltite Vein Prefeasibility Project” completed by Istanbul Technical University Mining Engineering Department. The Authors would like to appreciate the contributions of Sirnak Enerji Inc. for their support to the research.

REFERENCES

Ayvazoğlu, E., 1984. *Madenlerde Havalandırma ve Emniyet (in Turkish).* İTÜ Maden Fakültesi, İstanbul.

Banerjee, S.C., 1985. *Spontaneous Combustion of Coal and Mine Fires*. AA Balkema, Rotherdam.

Diamond, W. P., & Schatzel, S. J. (1998). Measuring the gas content of coal: a review. *International Journal of Coal Geology*, 35(1), 311-331.

Didari, V., Kaymakçı, E., Toroglu, 1993. Kendiliginden yanmanın arastırılmasında kullanılabilecek bir laboratuar deney düzenegi (in Turkish). *Turkey 13th Mining Congress*, p. 69–78.

Didari, V., Ökten, G., 1994. *Methane, the Coalbed Gas.* In Coal, resources, properties, utilization, pollution, Eds. Kural, O., 1994. Turkey. 139 – 151.

Durucan, Ş., Güyagüler, T., 1987. *Yeraltı Kömür Madenciliğinde Çevre Sorunları ve Kontrol Yöntemleri (in Turkish).* Ankara.

Feng, K.K., Chakravorty, R.N., and Cochrane, T.S., 1973. Spontaneous combustion – a coal mining hazard. *CIM Bulletin,* October, 75-82.

Flores, R., 1998. Coalbed methane: From hazard to resource. *International Journal of Coal Geology* v. 35, p. 3–26.

Gürdal, G. (1998). *Kömürde Gaz Depolanmasını Kontrol Eden Parametreler (Doktora).* İstanbul Teknik Ünivesitesi, İstanbul.

Karpuz, C., Bölükbaşı, N., Paşamehmetoğlu, A., Gürhan, A., 1986. GAL Silopi asfaltitlerinin gaz içeriği, kendiliğinden yanma riski ve kesilebilirliğinin araştırılması (in Turkish). *Turkey 5th Coal Congress*, 379-391.

Kaymakçı, E., 1998. *Zonguldak havzası kömür damarlarına uygulanabilecek bir kendiliginden yanmaya dogal yatkınlıgı degerlendirme tekniginin gelistirilmesi (in Turkish).* PhD Thesis, Zonguldak Karaelmas University.

Kaymakçı, E., Didari, V., 1992. Kömürün kendiliginden yanmaya yatkınlıgının belirlenmesinde kullanılan indeksler (in Turkish). *Turkey 8th Coal Congress*, p.129-140.

Kissell, F.N., 2006. Handbook for Methane Control in Mining National Institute for Occupational Safety and Health Information Circular No. 9486, Pittsburgh, PA.

Noack, K., 1998. Control of gas emissions in underground coal mines. *International Journal of Coal Geology*, v. 35, p. 57–82.

Ökten, G. (1983). Zonguldak Taşkömür Havzasındaki Ani Gaz ve Kömür Püskürmesi Olaylarının İncelenmesi ve Olaya Eğilimli Zonların Belirlenebilirliğinin Araştırılması. (Doktora), İstanbul Teknik Ünivesitesi, İstanbul.

Ozturk, C.A., 2013. Support Design of Underground Openings in an Asphaltite Mine. *Tunnelling and Underground Space Technology*. v. 38, s. 288-305.

Ramlu, M.A., 1991. *Mine Disasters and Mine Rescue*. AA Balkema, Rotherdam.

McPherson, M.J., 1993. *Subsurface Ventilation and Environmental Engineering*. Chapman and Hall, London.

Ünalan, G., 2010. *Kömür Jeolojisi (in Turkish).* MTA Eğitim Serisi-41, Ankara.

Coal and Coal Technology

Geology and Mineralogy Investigation of Pb-Zn Mineralization in El Abed Deposit, Algeria.

H. Chaa, A .Boutaleb
LMMA-FSTGAT-USTHB, Algiers, Algeria

ABSTRACT The Aaleno-Bajocien formation of El Abed deposit is situated in northwestern of Algeria, hosted the most important Mississippi Valley Type (MVT) of Pb, Zn mineralization. This area is characterized by horst and graben system. The bodies of ore include: (i) Stratabound" epigenetic mineralization is hosted dolomie.(ii) Mineralization hosted in dissolution cavities (karsts) filling. Such the karst was control most economic bodies of zinc ores.

The mineralization that related to karst cavity is dominantly detritic (DIS: Detrital Internal Sediment), formed by the galena, sphalerite, pyrite, organic matter, dolomie, clay (kaolinite), and the silica.

The ore have mechanical and chemical reworked redesigning in the cavities of dolomites, caused by the action of hot acid and reducing fluids.

Keywords: El Abed, karst, lead and zinc mineralization, detritic, reworked, mechanical, chemical.

1 INTRODUCTION

The Touissit, Bou Beker, El Abed metallogenic province of eastern Morocco and western Algeria is the most important Mississippi Valley Type (MVT) district of Northern Africa, extending from the Oued Mekta deposit eastward to Bou Beker (Morocco) and to El Abed in Algeria (Fig. 1). In all deposits of economic interest, the stratiformand and karst sulfide-bearing ore bodies are found exclusively within a dolomitic Aaleno-Bajocien condensed series.

This sedimentary cover overlies unconformably a Paleozoic basement made up of igneous rocks (granodiorite and rhyodacite) and low-grade schists (Makhoukhi, 2003).

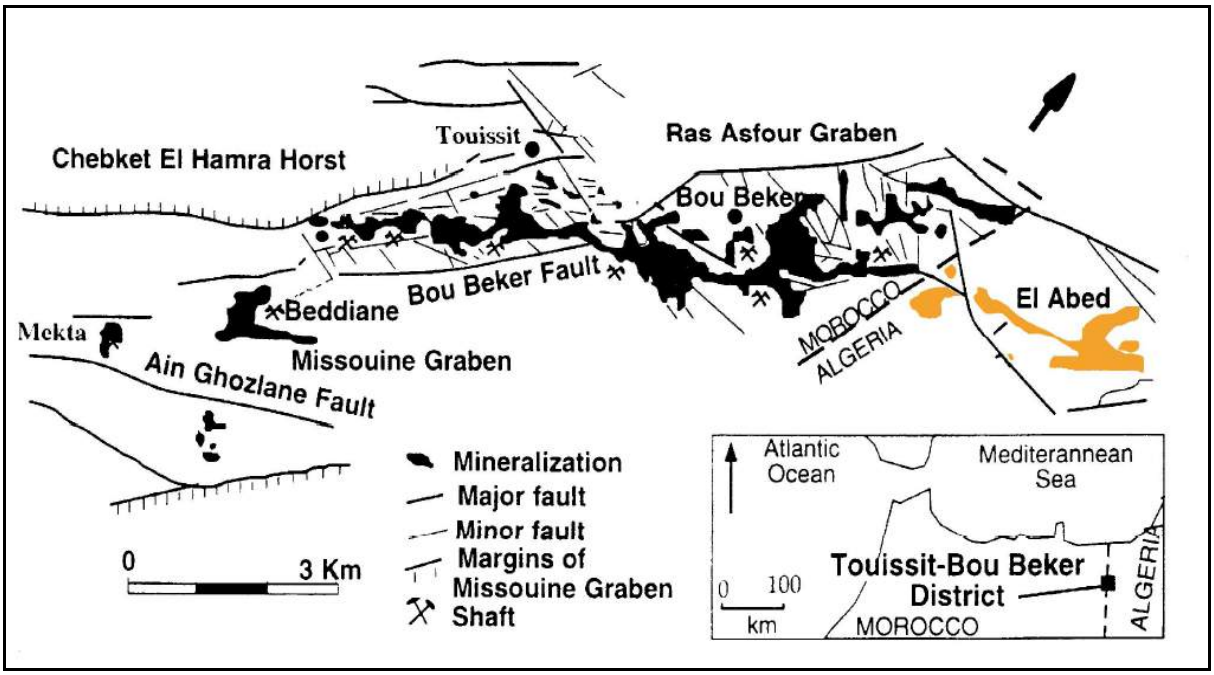

Figure 1. Structural map of Touissit, Bou Beker, El Abed (Boutaleb,1996)

2 GEOLOGICAL SETTING

In the El Abed deposits, mineralization are essentially lead –zinc bearing, rarely with copper. They form stratiform and karst ore bodies in the upper part of dolomitic series and are overlain by a thick sedimentary cover. They form a small number of steeply dipping veins along tensional faults (Touahri, 1987; Makhoukhi, 1994). Two main types of ore bodies have been distinguished in the El Abed deposit. Type I correspond to powdery and reworked mineralization with a karst formation. The ascending fluids were chemically aggressive to the dolomitic host rock which has been strongly dissolved. Type II corresponds to stratiform ore bodies where mineralization has almost replaced the carbonate host rock without destroying sedimentary structures.

3 PETROGRAPHY SETTING

Karst products are rich in organic matter (Fig.2) and sulfide ore, silica, clays and carbonates (Fig.3). Mineralization consists essentially of pyrite, sphalerite (Fig.4) and galena; incidentally; barite, kaolinite and chalcopyrite. Petrographic study show that the mineralization related to karst level is detrital dominant (clastic internal sediments), originated from the mobilization and transformation of mineralization hosted in stratabound dolomies.

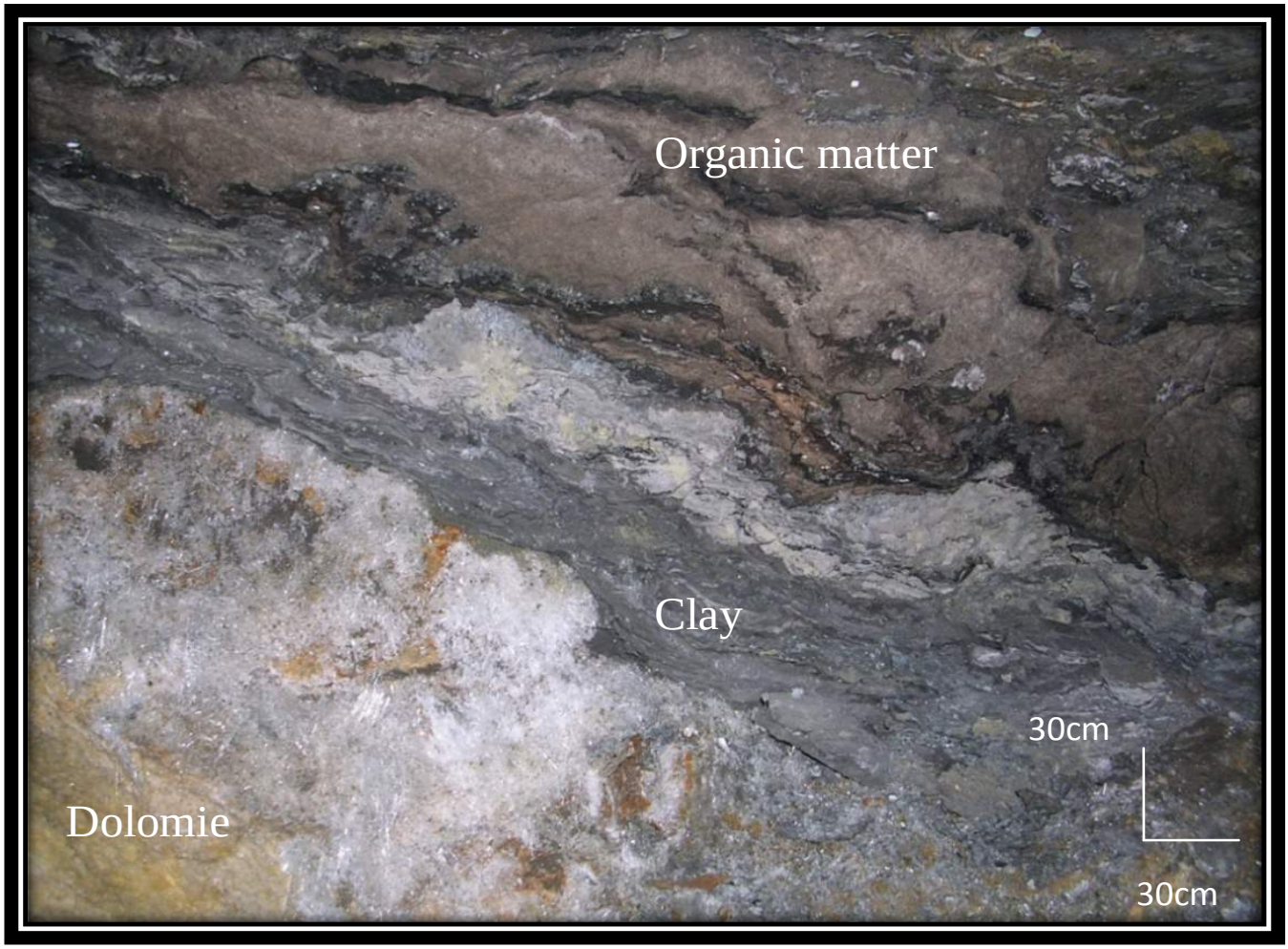

Figure 2. Photograph show detritic karst morphology

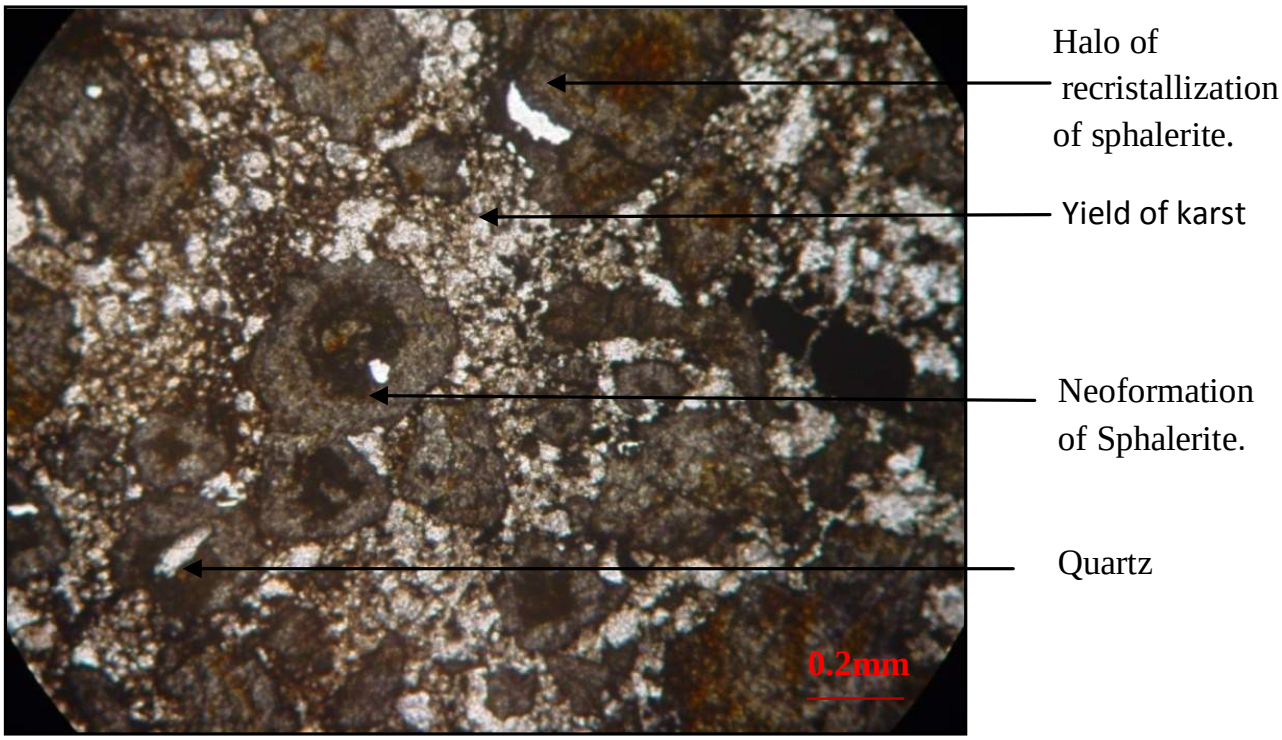

Figure 3. Microphotograph of karst product (Reflected light, crossed polars) (Gx5).

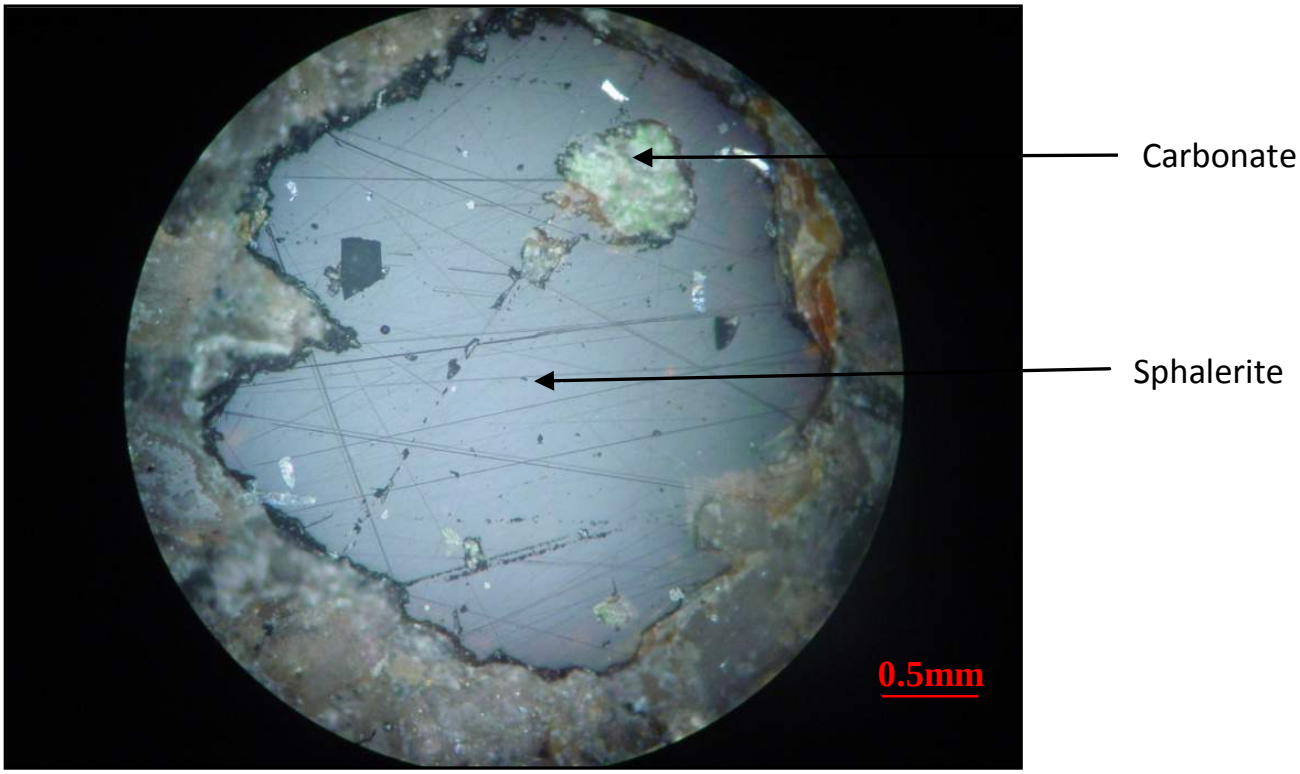

Figure 4. Sphalerite with carbonate inclusion (Reflected light, crossed polars) (Gx10).

4 CONCLUSION:

From the metallogenic study of karst and with the comparison to the stratabound mineralization, we can reconstruct the chronological sequence of events that have prevailed in this deposit as follows:

In Eocene movements, there is the expulsion of hot and salty fluids from subsidence areas to paleohorst (Bouabdellah, 1996 Boutaleb, 2003) giving the stratabound mineralization.

Later; another hot fluid, acid reducer and "sterile" karstified dolomites, reworked

mechanically and chemically, transported over short distances and redeposited clastic products in karst cavities.

REFERENCES

Bouabdellah, M(1993). Métallogenése d'un district de type MississippiValley, cas de Beddiane, district de Touissit-bouBeker, Maroc. Thèse PhD, Ecole polytechnique de Montreal, Montreal,Canada.

Boutaleb, A(1993). Métallogénie des gites à Pb-Zn-Ba du Setifien-Hodna-Aurés. In: proceeding of workshop MVT. Mississippi valley type deposits in Europe and North Africa, comparison with North American deposits, constraints on modeling paleo-circulation. Pp.203.210.

Makhoukhi S, Marignac C, Pironon J, Schmitt J.M., Marrakchi C, Bouabdelli M, Bastoul A (2003). Aqueous and hydrocarbon inclusions in dolomite from Touissit-BouBeker district, Eastern Morocco: a Jurassic carbonate hosted Pb-Zn (Cu) deposit, Journal of Geochemical Exploration 78 - 79: 545-551.

Makhoukhi-Marrakchi, S(1993). Le gisement de plomb de Beddiane (Maroc Oriental): Gitologie et éléments de modé1isation d'une minéralisation de type Mississippi Valley. Thèse de l'Ecole des Mines de Paris, Mémoires des Sciences de la Terre (1994). 141 pp.

Touahri, B(1987). Géochimie et métallogénie des minéralisations plomb et zinc du nord de l'Algérie. Thèse de doctorat d'état des Sciences Naturelles, Université Paris VI. 380 pp.

Chemical Inhibitors – Scope for Using Control and Combating Surface Mine Fire as Clean Coal Technology

R. V. K. Singh
Mine Fire Division, CSIR-Central Institute of Mining & Fuel Research, Dhanbad, 826015, Jharkhand, India

ABSTRACT The problem of spontaneous heating/mine fire not only endangers the lives of men in mines, but also causes considerable economic losses to the nation and damage the environment. Surface fire in coal mines directly affects the atmosphere with respect to clean coal technology. Due to fire in coal mines, huge quantity of CO, CO_2 and methane, noxious gases are liberated and evolved to the atmosphere. Presently, In Indian coal mines about 70 to 75 % coal is being extracted by surface mines. Besides this, most of the fires in different coalfields originated from many decades ago in collapsed workings of thick seams, at shallow depth. Where the workings were at shallow depths and the extracted seam thickness were high subsidence cracks appeared on the surface providing a path of the air flow to the fire zone. In this way many underground fires turned to surface fires at a later stage. The problem of spontaneous heating/fire in coal mines is very serious and needs immediate attention. There are two important aspects of mine fire- one is prevention and other is control and combat. Presently only water is being used for control of fire in coal mines, but it is not properly suitable for fire of high intensity (temperature). Previously identified chemical inhibitors are mainly suitable for preventing spontaneous heating in coal mines. Presently, there is urgent need for identification and application of chemical inhibitors for controlling and combating surface coal mine fire of high intensity (blazing fire). After carrying out literature survey work, some of the different chemical inhibitors have been identified and analysed in Differential Scanning Calorimeter (DSC) equipment and other techniques for development of suitable composition for use in surface coal mines to control and combat spontaneous heating/fire. This objective of the paper is to describe the scope for use of chemical inhibitors for controlling and combating surface coal mine fire as clean coal technology.

Keywords: Mine fires, clean coal technology

1 INTRODUCTION

Searching for the suitable chemical inhibitors for control and combating surface fires in coal mines is the dream of researchers. Some of the inhibitors have been identified to prevent spontaneous fires by hindering the process of oxidative heating of coal, perhaps by blocking the formation of free radicals, or otherwise. Besides this, work is being continued to develop suitable chemical inhibitors/additives for control and combating high intensity fire in coal mines.

Coal can interact with oxygen in the air at ambient temperature liberating heat. If the heat is allowed to accumulate the interaction rate increases and may ultimately lead to fires – known as spontaneous fires. The exact mechanism of the reaction of oxygen with coal is not completely understood as the chemical nature of coal is not yet fully established. But most of the workers agree that the reaction of oxygen with coal is a surface phenomena and proceeds through a loosely bound coal-oxygen-water complex with subsequent steps being breakdown of the complex to simpler molecules such as

CO, CO_2 and H_2O etc. Most popular hypothesis is that the overall reaction proceeds through a chain mechanism with moisture facilitating the formation of free radicals that act as chain carrier.

2 LITERATURE SURVEY

Tarpagosova (1) tested the oxidation inhibiting action of various reagents over coal and found petroleum products and theiremulsions to be fairly effective, while fatty acids and a few other agents showed only minor improvements. Nakano and Yamski claimed to have obtained encourasing result by applying a thick coat of asphalt emulsion over the coal surface (2).

Banerjee et al (3) corroborated the observation of Nakano and Yamski running a trial with a coat of tar and burnt mobile emulsion, in the ratio 1:3 over a quarry bench wall in Jhingurda seam MP, India). They claimed to have increased the incubation period considerably. But the chief drawback of such agents is that they induce greater risk from contact fire (exogenous fire) and cannot be used in a hot spot/fire nereby. These agents have however been improved upon making them fire resistant, which offers good promise as a protective agent (4).

Accordingly, Singh et al of Central Institute of Mining & Fuel Research, Dhanbad, India developed a cationic bitumen emulsion based fire protective coating material (under S&T project, funded by Ministry of Coal, Govt. of India) for preventing spontaneous heating in coal mines. It would, therefore help not only in saving a huge amount of coal lost every year due to fire in coal mines but also in minimising environmental pollution.

The efficacy of the coating has been well proved by rigorous laboratory scale studies as well as field trials in coal benches at Karkatta opencast project, Dakra (CCL), Jagannath opencast project, Talcher (MCL) and Jhingurdah opencast project, Singrauli (NCL) having coal of high susceptibility of spontaneous heating. These studies have confirmed that a fire protective coating material has following advantages : (i) offers good fire resistance (ii) prevents air permeation and (iii) does not washed down by water/rain (iv) it forms no cracks, remains intact for a long period of time (more than one year) and does not create the problem of scaling-off the material. Moreover, it is easy to spray and is very much compatible with coal. A patent application has been filed for the fire protective coating and the technology has been commercialised to M/s Signum Fire Protection (India) Pvt. Ltd., Nagpur, India for manufacturing and marketing. The said firm is manufacturing & marketing this product under the trade name SIGNUM-CMRI Fire Protective Coating/Sealant (5).

Polish workers claim to have achieved encourasing results using plastic/PVC sheet layering over vulnerable patches and hot spots on coal stacks, thereby preventing ingress of fire. Among the two groups, CaCl2 used by Enterbrink and Lewer (6) and NH3 suggested by Kroger and Beier (7) have showed promise as oxidation heating inhibitors. Chinese workers claim to have achieved good results by infusing inhibiting agent such as 10-15% CaCl2/MgCl2.6H2O in the goaf (8). Czechoslovakian and Hungarian researchers have confirmed 10% calcium chloride to be suitable for reducing the incidence of spontaneous combustion in pits. Australian researchers have suggested use of ammonium hydrogen tetraborate for preventing spontaneous heating. In Japan Diapon T (Na-N methyl-N olieltuarte) is claimed to be surface active agent (9).

The search for suitable Chemical inhibitors to spontaneous heating is in progress in many countries, but a foolproof solution has not yet to be achieved. There are two important aspects of mine fire- one is prevention and other is control and combat. Presently only water is being used for control of fire in coal mines, but it is not properly suitable for fire of high intensity (temperature). Previously identified chemical inhibitors are mainly suitable for preventing

spontaneous heating in coal mines. Presently, there is urgent need for identification and application of chemical inhibitors for controlling and combating surface coal mine fire of high intensity (blazing fire). This objective of the paper is to describe the scope for use of chemical inhibitors for controlling and combating surface coal mine fire as clean coal technology.

3 CHEMICAL INHIBITORS

The endothermic characteristics of chemicals have been determined for prevention & control of coal mine fire using Differential Scanning Calorimeter (DSC) equipment. Chemical inhibitors like NH_4Cl, $CaCl_2$ and NaCl – when mixed with coal show varied degree of endothermicity on heating at Different temperature regions. NH_4Cl shows pronounced endothermicity at 250^0C; $CaCl_2$ indicates minor endothermicity at 50^0C and $150\text{-}170^0C$; and NaCl shows at around 400 to 450^0C. NH_4Cl may find use for preventing goaf fires because of liberation of NH_3 as its endothermic effect at the onset of heating.

3. 1 Differential Scanning Calorimeter (DSC)

Differential Scanning calorimeter (DSC) is a technique in which the difference in energy inputs into a substance and reference materials is measured as a function of temperature while the substance and reference materials are subjected to a controlled temperature programme.

In Differential Thermal Analysis (DTA) equipment, a thermogram of coal can be divided into three segments or stages. In the initial stage of heating (stage I), the endothermic reaction predominates, probably due to the release of inherent moisture in coal. In the second stage (stage II), the exothermic reaction becomes significant but the rate of heat release is not steady all through, as it changes with temperature. A steep rise in heat evolution is observed in the third stage (stage III).

But in the DSC technique, the ordinate value of an output curve at any given temperature is directly proportional to the differential heat flow between a sample and reference material in which the area under the measured curve is directly proportional to the total differential calorific input. By this technique, coal samples can be studied under experimental conditions that simulate spontaneous heating process of materials (10). Author used DSC equipment named METTLER TOLEDO DSC 821^e and LINSEIS L 62 H 1550. The temperature range of the METTLER TOLEDO DSC 821^e equipment is 0 (room temperature) to 600^0C and LINSEIS L 62 H 1550 is 0 to 1450^0C.

In Mettler Toledo $STAR^e$ system, the DSC 821e module is designed in modular concept (basic module with the facility of later extension. The basic module consists of:

- DSC 821e measuring cell with ceramic sensor,
- Module electronics
- Manual furnace lid
- Operating status indicator
- Air cooling (cooling at room temperature by ventilator).

The DSC measurement in the instrument is based on the heat flux principle. It can only be operated in conjuction with the personal computer. LINSEIS DSC equipment comprising a programme for higher temperature range data evaluation to display a large amount of data in a very short time on a screen. Any energy difference in the independent supplies to the sample and the reference is then recorded against the programme temperature. Thermal events in the sample in DSC equipment shows endothermic or exothermic direction (downward and upward peak), depending upon whether more or less energy has to be supplied to the sample relative to the reference material. Downward peak represent the endothermic and upward peak represent the exothermic behavior of the chemical inhibitors. Presently, we are

analyzing the chemical inhibitors using High temperature Differential scanning calorimeter DSC 404F3A01 Pegasus equipment supplied by NETZSCH Geratebau GmbH, Germany.

3.2 Analysis of Results from DSC Thermogram

The thermogram represents the various reactions occurring during oxidation process. It was followed by endothermic and exothermic reaction took place in the sample during analysis. Particularly in the coal sample, the temperature of initiation of exothermic reaction can be considered as an indicator of spontaneous heating susceptibility of coal sample, which is known as the onset temperature. The onset temperature obtained from differential scanning calorimetry may be the better indication for determining spontaneous heating susceptibility. Similarly, different composition of identified chemical inhibitors has been analysed in the DSC equipment. The degree of endothermicity represents the absorbing capacity of the chemical inhibitor at different temperature. After that some of the composition has been identified and selected after laboratory scale study and applied successfully in the field application for controlling and combating fire. The results of the field application are excellent.

4 FIELD APPLICATION

Author is presenting a case studies of fire at Giddi colliery, Argada Area, CCL. The project Giddi 'A' is accessible from Ramgarh Ranchi Road and Patratu railway station which lies on the National Highway No. 33. The project was started in June 1958 for operation of both underground mine and mechanised opencast mine. Mining activities were started in both underground and opencast mines in Argada, Argada-A, Sirka, Bansgarha, Hatidari and Semana seam. Underground mine working was stopped by March 1984 whereas coal production is limited to opencast mine only. Fire was noticed in the year 1997 near Giddi workshop and surface was subsided from the quarry side. The colliery authority tried to control the fire using overburden material. But after some time, filled up overburden material was also heated and fire reached very near to Workshop and Sub-station (11).

4.1 Location

The Karanpura coalfields in Jharkhand forms the western most patch of the lower Gondwana of the Damoder Valley situated within latitude $23^0$28' and $23^0$56' North and longitude $84^0$46' and $85^0$28' east. This coalfield is extended over an area of 550 sq. miles (1424.50 Km^2). An elongated patch of the Lower Gondwana rocks, covering an area of 75 sq. miles (194.25 Km^2). Giddi-A block comprising almost a rectangular patch 1.75 sq. miles (4.50 Km^2) situated in the district Hazaribagh, Jharkhand. The Damoder River which forms the western and southern block boundaries takes 'Z' blende here. The southern margin is also marked by the confluence of Damoder River and Nakri Nallah. In the north east the mine is bounded by the mining lease of Religara colliery (Giddi- B block). To the north lies "Kurkutta Block", on the west the sub leases of Khas Karanpura & the Associated Karanpura collieries are situated. To the south west and south Sounda block-B and working mines of Bhurkunda collieries of CCL are lying.

4.2 Geology of the Seam

The coal seam occurring in Giddi – A block belongs to Barakar formation. Thirty two coal seams have been proved varying in thickness from 0.76M to 24.28M. Out of 32 seams the Sirka, Argada, Argada-A and Argada –B is considered as working seams due to their thickness and persistence. Argada seam varies from 15.85m to 24.28m. Parting between Sirka seam and Argada seam varies from 43.28m to 62.33m. Argada –A seam varies in thickness 7.92 to 13.89m

and parting between Argada and Argada –A seam varies from 18.6m to 45.90m. The seam wise thickness, gradient, grade and present status are given below.

Particulars	**Name of Seam**			
	Sirka	**Argada**	**Argada-A**	**Argada- B**
Average Thickness (m)	12.0	18.0-20.0	10.0	6.0
Gradient	1:3.54	1:2.96	1:2.75	1:2.75
Direction	$N70^0$29'W	$N82^0$40'W	$S85^0$30'W	$S80^0$15'W
Grade	B	C-D	C-D	C-D
Present status	Standing on Pillar	Standing on Pillar	Standing on Pillar	Virgin
Estimated reserve below Washery (million ton)	Nil	1.600	1.320	0.125

5 SCIENTIFIC INVESTIGATION

Fire site of Giddi-A colliery near by Giddi workhop, sub-station and Giddi Washery was visited and it was observed that Argada and Argada –A seam are developed on pillar lying below the Giddi workshop whereas Argada A seam lying below Giddi washery and sub-station also. Both the seam partially quarried by opencast mining method. Argada - B seam is virgin and lying below the Giddi workshop and Giddi Sub-station at a depth of 54m. Argada seam quarried before March, 1986 whereas Argada-A seam quarried before 1976. Fire observed in September 1997 near Giddi workshop from the quarry mouth edge due to the presence of loose coal (Fig. 1). The area is subsided near road and workshop which is creating several cracks and passage for ingress of oxygen leads to spontaneous heating/fire. The blazing flame is coming out through the mouth due to further progress of spontaneous heating and chemical chain reaction. Mine authorities tried to control the fire by filling the overburden material but it was not controlled, the problem became more serious when filling material was heated near the Mining Workshop.

Temperature was measured with the help of Heat Spy Infra-red Thermometer at different locations near the Giddi workshop, sub-station, washery, mine road and the quarry edge (Figure 2). The maximum temperature was observed as 492^0C near washery boundry and road side. Fire fighting chemicals/inhibitors, have been applied which reduced the flame and extract the heat near mining workshop. Different chemical inhibitors were mixed with water in different proportion and applied on blazing flame as per intensity of the fire and site specific condition. Continuous fire fighting operation was carried out for five to six months and after that the combated portion was covered with binding material and top soil (Figure 3).

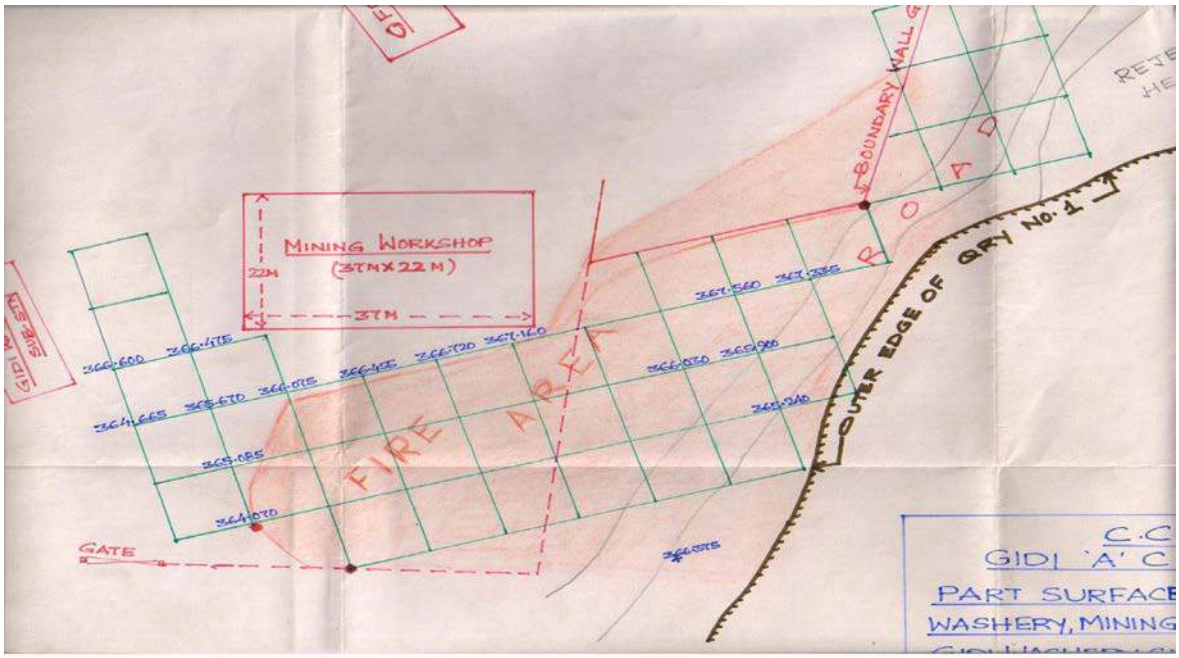

Figure 1. An overview of fire area near substation workshop and Giddi Washery, CCL.

Figure 2. Thermal investigation using Heat spy Infra-red Thermometer near Giddi Sub-station and Mining workshop, CCL.

Figure 3. Fire combated portion treated with binding material with top soil near Mining workshop and Giddi power sub- station, CCL.

6 RESULTS AND DISCUSSION

During thermal investigation, it was found that fire was present in most of the portion near by area of roadways, sub-station and fire was under blazing condition near Giddi workshop. Temperature was in the range of 265 to 307^{0}C at workshop and 492^{0}C observed near the washery boundry towards road side (Fig. 4). After application of fire fighting Chemical inhibitors/additives temperature reduced to 35 to 46^{0}C (Fig. 5). Then combated fire surface was treated with different binding material and finally to minimise the ingress of air an area of 3750 sq.m was sealed on surface using 7250m^3

topsoil. Detailed thermal profile was marked on surface lay out before application of fire fighting chemicals to the final surface sealing operation as per requirement. Finally, temperature was found near about ambient after surface sealing. Mine authorities were trained for application of fire fighting chemicals. Suggestion was also given for making two benches using top soil in quarry side for checking the penetration of air from the mouth of gallery and blanketed area should be compacted time to time. Early implementation of the control and combating technology has given successful result for control of fire near Giddi workshop and sub-station. After control of fire, the valuable national property like Giddi Sub-station and washery have been saved and environment was also protected from the release of noxious gases (11).

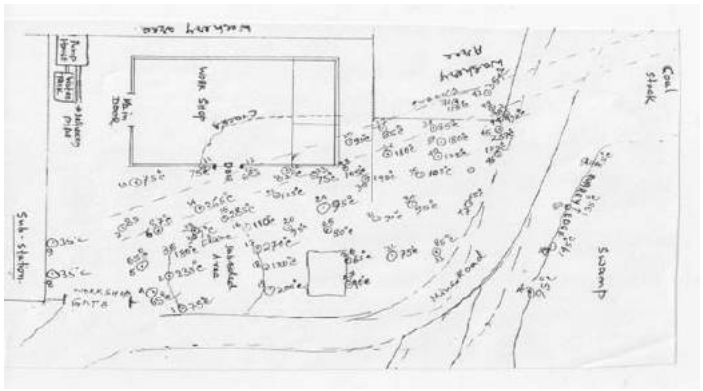

Figure 4. Thermal mapping using Infra red-Gun nearby fire affected area at Giddi Sub-station and Washery, CCL (Not to scale).

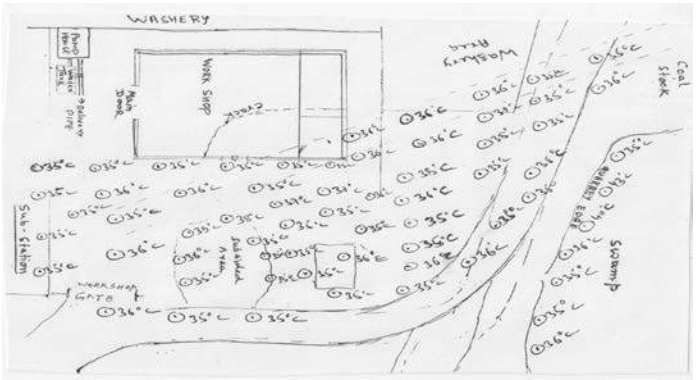

Figure 5. Thermal mapping after application of combating and preventive measures nearby fire affected area at Giddi Sub-station and Washery, CCL (Not to scale).

7 SUGGESTIONS

As per the studies carried out during the project work and site specific fire condition, the following preventive and control measures are suggested: -

1. Thermal monitoring should be carried out using Heat spy Infra red thermometer regularly for detection of fire, so that immediate control measures can be planned as per site situation.
2. Fire should be combated by application of fire fighting chemical inhibitors for suppressing the fire and extracting the heat and it should be continued till the temperature reduces to ambient level.
3. Dozing/compaction is very much essential in the compacted area after some interval to minimise the air ingress.
4. Minimum two benches should be formed from bottom to top using top soil in quarry side for checking the ingress of air from the mouth of gallery to save the mine roadways, washery and sub-station.

8 CONCLUSIONS

After carrying out scientific investigation for control of fire near Mining workshop and sub-station, it is concluded that speedy implementation of the control and combating technology has given successful result. After control of fire, the valuable national property has been saved. Environment was also protected from the release of noxious gases. Under these circumstances, direct application of fire fighting chemical inhibitors will be much effective for suppression of flame, extraction of heat and cooling the hot mass. Author has taken a new R&D Project under 12th Five Year plan from Planning Commission, Government of India for development of suitable chemical Inhibitor for control and combating high intensity surface fire in coal mines under Clean Coal Technology. Research work of this project is being continued and rigorous laboratory work is going on.

ACKNOWLEDGMENTS

Author is grateful to Dr. A. Sinha, Director, CSIR-Central Institute of Mining & Fuel Research, Dhanbad for giving permission to present the paper. Author is also grateful to the management and officials of Giddi–A colliery for providing all facilities and full co-operation for carrying out the project work. Thanks are due to the staff of Mine Fire Division of CSIR-CIMFR for their assistance in various stages during laboratory & field work. Views expressed in this paper are of author and not necessarily of CIMFR.

REFERENCES

1. Tarpagosova, EA, Inhibitors of low temperature oxidation of coal,izv, Akad, Nauk, USSR, OTn, 1954, 147 (Translated from Russians).
2. In Dortmund, GH, Exchange of Information on Mine Fire Hazards at the 10th International conference on safety in Mines, Research Establishment, Glauckauf, March 1961, pp.260-264.
3. Banerjee, S.C., Singh, R. G. and Bagchi, S., Surface Coal Fires, Seminar on Surface Fires at CMPDIL, Ranchi, 20th May, 1976.
4. Banerjee, S. C., Singh, R. G., Acharya, A. K., Ghosh, S. K. and Singh, B., Advancement in Fire combat design, Minetech, vol. 13, No. 5, sept-Oct. 1992, pp.16-22.
5. Singh, R. V. K., Ghosh, S. K. and Dhar, B. B., Development of coating material for preventing spontaneous heating in the benches of opencast coal mines, Minetech, Vol.17, No.2&3, March-June 1996, P.20-24.
6. Enterbrink, W and Lewer, H, Reducing the danger of spontaneous combustion of coal by means of calcium chloride of Montan type, Glaukauf 107 (17), 1971, pp.652-53.
7. Kroger, C., and Beier, E. Die verwettering Von Steinkohlen, Brennstoff chemie, 43, 1962,pp. 328.
8. Banerjee, S. C., Spontaneous combustion of coal and Mine Fires, Oxford and IBH Publisher Co. 1985, p.1-9.
9. Lukasvewski, G. M., Natural oxidation and reaction of ANFO explosive in mineral sulphides at Mr. Isa Mines, Australia, 9th Commonwealth Mining and Met. Conf., 1969, London, p. 33.
10. Mahajan, O. P., Tomita, A and Walker, P.L., 1976, Differential Scanning calorimetry studies on coal, 1. pyrolysis in an inert atmosphere , Fuel, vol. 55, January, pp.63-69.
11. CSIR-Central Institute of Mining & Fuel research **(**CIMFR) unpublished Project report, 2009. Scientific investigation for control of fire nearby Giddi A workshop, Giddi washery plant and advice thereof, CCL Project No. GC/MS/156/2007-08.

Effective Approaches for the Fast Liquidation of Locked Up Coal in Standing Pillars in Indian Underground Coal Mines

A. Kushwaha, R. Bhattacharjee, S. Tewari and A. Sinha
CSIR-Central Institute of Mining and Fuel Research, Dhanbad, India

ABSTRACT Ensuring energy security for the growing population with rising per-capita energy demand has emerged as one of the greatest challenges before India. The developing nation like India will continue to rely heavily on thermal power plants for meeting energy demands against restricted access to nuclear technology and mixed success of non-conventional energy sources. Since inception of mining industry till now, Bord and Pillar (Room and Pillar) method of mining is still the predominant method of working in India. In most cases only the development workings have been done due to various complex mining conditions. As a result, huge amount of coal reserves are locked as Standing on Pillar (SOP) in these mines. Therefore, the adoption of effective mining technologies for the fast liquidation of these standing pillars is the need of the time to meet energy demands of India up to some extent. This paper presents a brief review and successes of different mass production technologies like continuous miner technology, shortwall mining and blasting gallery method of mining adopted for fast liquidation of SOP reserves in some of the Indian coal mines.

Keywords: Fast liquidation, coal, Indian coal mines

1 INTRODUCTION

Ensuring energy security for the growing population with rising per-capita energy demand has emerged as one of the greatest challenges before India. The developing nation like India will continue to rely heavily on thermal power plants for meeting energy demands against restricted access to nuclear technology and mixed success of non-conventional energy sources. Since inception of mining industry till now, Bord and Pillar (Room and Pillar) method of mining is still the predominant method of working in India. In most cases only the development workings have been done due to various complex mining conditions. As a result, huge amount of coal reserves are locked as Standing on Pillar (SOP) in these mines. Conventional depillaring using SDL's/LHD's of these standing pillars is slow and uneconomical. With widening gap in production and demand of coal, production has to be ramped up from existing mines to keep the shortfall within limit. Hence, the coal pillars in underground need to be rightly exploited to meet the country's present coal requirement. Under such circumstances, the only option is to innovate and improve the available technological scenario. Therefore, the adoption of effective mining technologies for the fast liquidation of these standing pillars is the need of the time to meet energy demands of India up to some extent.

This paper presents a brief review and successes of different mass production technologies like continuous miner technology, shortwall mining and blasting gallery method of mining adopted for fast liquidation of SOP reserves in some of the Indian coal mines. The paper deals with basic design parameters, support assessment, strata monitoring, safety issues, improving methods of operation, reducing machine downtime, manpower effectiveness and others covering macro and micro level management for planning and execution of pillar extraction/depillaring. Adoption of these technologies in other mines will ensure higher production, improved productivity and enhanced safety standard.

2 MASS PRODUCTION TECHNOLGY FOR UNDERGROUND DEVELOPED COAL PILLARS

Underground production has remained stagnant over the decade in Indian coal mining industry in spite of large area of the coal seam has been developed and standing on coal pillars. The main reason is that there is a lack of suitable underground fast liquidation mining technology for these developed pillars, although the overall coal production has considerably increased. The increase in overall production contributed mainly due to opencast mines. The coal production in India during 2013-14 was 565.64 Million tonnes as published in Annual Report 2013-2014from Ministry of Coal, Govt. of India. Out of which only 9% of the coal produced was from the underground mines.

Due to increasing demand of coal world-wide and the fast depletion of open castable reserves at shallow depth cover, the mining of coal by underground methods in mass scale is inevitable. The main bottleneck in this endeavour is that the adoptability of the mass production technology for developed coal pillars from underground in Indian coal mining sector is very slow. Fortunately, Coal India Limited (CIL) and Singareni Collieries Company Limited (SCCL) both are now realizing to adopt mass production technology in their underground coal mines at large scale to cope up with coal demand and future necessity. To initiate in this direction, the following mass production technologies are being introduced in some of the Indian coal mines:

1. Continuous Miner Technology
2. Short Wall Mining Technology
3. Blasting Gallery Method of Mining

3 BASIC PARAMETERS OF ROOF ROCK STRATA REQUIRED FOR SUCCESS OF THE MASS PRODUCTION TECHNOLOGY

All the above described technology are new to India and is vastly different from other mechanized Bord & Pillar mining methods, mainly due to extraction of developed pillars at high rate. This resulted quick variation in stress re-distribution pattern at the face and in surrounding rocks in the working areas. For achieving successful implementation of these technologies in any mining field, the following strata characteristics, have to be studied properly:

3.1 Cavability Characteristics of the Roof Rock Strata

CSIR-CIMFR Dhanbad has developed its own method for assessing the cavability of roof rocks strata. The following empirical relationship expresses the relation between caving index ‘I’ (Sarkar, S.K. and Singh, B., 1985) with the influencing factors as mentioned below:

$$I = \sigma_c \frac{t^{0.5}}{5} L^n \qquad (1)$$

where, I = Cavability index; σ_c = Intact rock compressive strength(kg/cm^2); t =Bed thickness(m); L= Average core length(cm); n=1.0 for RQD<80 and 1.2 for RQD > 80.

For estimating the Cavability Index of the roof rock strata of any seam, rock samples of at least two bore hole sections of the proposed area have to be studied properly in the laboratory. The measuring parameters are length of the core samples, its thickness and RQD. Putting these values in above Eq. 1, cavability index of the roof rock strata can be estimated. Based on field observations and caving behaviour, the roof rock has been categorized as given in below Table 1.

Table 1. CSIR-CIMFR Characterization of Roof Rock Strata

Sl. No.	Category of the roof	Range of Cavability Index	Roof Rock Strata Characteristics
1	Category – I	Up to 2000	Easily cavable
2	Category – II	2000 to 5000	Moderate cavable roof
3	Category – III	5000 to 10000	Roof strata cavable with difficulties
4	Category – IV	10000 to 14000	Cavable with substantial difficulty
5	Category – V	>14000	Cavable with extreme difficulty

3.2 Possibility of Air Blast During Caving

The chances of air blast during extraction of any seam are dependent on roof rock strata characteristics. If the cavability index of the majority of the roof rock strata is less than 5000, chances of air blast will be minimal and the roof rock failure in the goaf will be in periodic manner. If this index is between 5000-10000, the roof rock failure in the goaf will delay, but there is a little chance of air blast at the face. In case of Cavability Index more than 10,000, chances of air blast at the face will always be there if area of exposure will increase more than a certain limit. CSIR-CIMFR Dhanbad has developed a correlation between the equivalent face advances or ultimate stable span a_{eq} with RQD as given below:

$$a_{eq} = 0.59\ RQD + 5.2m \quad (2)$$

Expected area of main fall

$$= (1.55 \times a_{eq})^2\ m^2 \quad (3)$$

In case of depillaring of developed pillars from any mine, if the area of expected main fall increased more than the calculated value using above Eq. 2 & 3, the chances of the air blast cannot be ruled out. Under such condition, blasting of hard overhanging strata at the goaf edge can be one of the alternatives to avoid air blasts. In this technique it is by no means intended to bring down the entire overhanging strata. It is only meant to cause a blockage with broken rock so that air cannot escape outbye in the event of an air blast. It can also be used as a regular measure during extraction. The method is more amenable to application in those mines where long hole rock drills (Jumbo drills) are available.

3.3 Design of Method of Extraction and Support System

To design a suitable method of extraction and support system in and around the face a well established numerical modelling technique has to be used to assess the stability of the surrounding rock strata and required support density at the face. For the modelling purposes, the following rock properties (Floor rock, Coal and Roof rock) have to be estimated in the laboratory as per ISRM Standard given below:
(1)Young's Modulus, (2)Poisson's Ratio, (3)Compressive strength, (4)Tensile Strength and (5)Rock Density.

Rock mass ratings (RMR) of the roof rock strata along with RQD of the borehole rock samples are also needed at the time of designing of method of extraction, support system and induced caving pattern to achieve successful extraction of developed pillars with high production and productivity with Mass Production Technology.

4 CASE STUDIES

4.1 Continuous Miner Technology: VK7 Incline, SCCL Mine (India)

This is a case study of VK7 Incline of Singareni Colliery Company Limited (SCCL), where CM technology (with a combination of Continuous Miner i.e. Coal Cutting machine + Quad bolter i.e. Bolting machine + Shuttle car i.e. Coal Loading machine) was deployed for the extraction of 6.5m thick King Seam. This seam has already been developed with a height of about 3m along the roof, almost 20 years back. CSIR-CIMFR Dhanbad has conducted

detailed scientific study for its first two caving panels such as CMP-5A and 5B to design the extraction pattern. The cavability index of the proposed seam was determined which came to category I & II of the Table 1. Therefore, chances of air blast during extraction of King seam with caving is very less as the overlying strata are not very difficult to cave. However, it has been tried to quantify the extent of the area of roof exposure after which the induced blasting is required to initiate the roof fall in the goaf areas of King seam using CIMFR formula Eq. (2) & (3). The average RQD up to 23m for the immediate roof was found to be 72. Putting this value into above equation (2), the ultimate stable span can be calculated as: $\mathbf{a_{eq}}$ = 0.59 x 72 + 5.2m = 48m approximately and the expected first main fall will be around = $(1.55 \times 48)^2 = (74.4)^2$ = 5535 sq.m

Considering the maximum 3 pillars wide extraction at VK-7 incline, this area will be achieved just within 1st row of pillar extraction. Regular controlled caving of overlying roof rocks of King Seam will obviate the risk of air-blast, stress abutments in working areas and goaf encroachment. Therefore, seeing the characteristics of roof rock strata of King seam, it has been decided that the proposed panel CMP-5 (Fig. 1) can be extracted with CM Technology with full caving using "Split & Slices" method of mining as described below:

Geometrical parameters of the development workings of CMP-5 Panel at VK-7 Incline were as follows:

Pillars size:	45m x 45m (centre to centre)
Development roadways:	4m along the roof
Roadway height:	2.8m to 3.0m
Depth of cover:	325m to 425m

To minimize the effect of adjacent worked out panel on this new panel, two rows of barrier pillars between this panel CMP-5 and already extracted panels were left. In the first step, all the developed roadways have been widened up to 6.5m from both sides of the pillars and height was left 3m only, so that shuttle car can move smoothly. Total widened roadways had been supported with resin encapsulated rock bolts of length 1.8m at an interval of 1.5m. For depillaring of these pillars, a single split of 6.5m wide and 3m height had been driven along level in such a way that it divided pillar in two stooks with dimension of one stook was 38.5m x 18.5m and of other stook was 38.5m x 13.5m. Similarly, one more experiment was done with double split of 5.5m over a pillar so that three stooks of size 38.5m x 9m can be formed. To estimate load coming over the stooks in both the cases, 3D numerical modelling using FLAC^{3D} software (Itasca Consulting Group Inc, FLAC3D, 1997) was performed against the goaf. Isometric view of model is shown in Fig. 2.

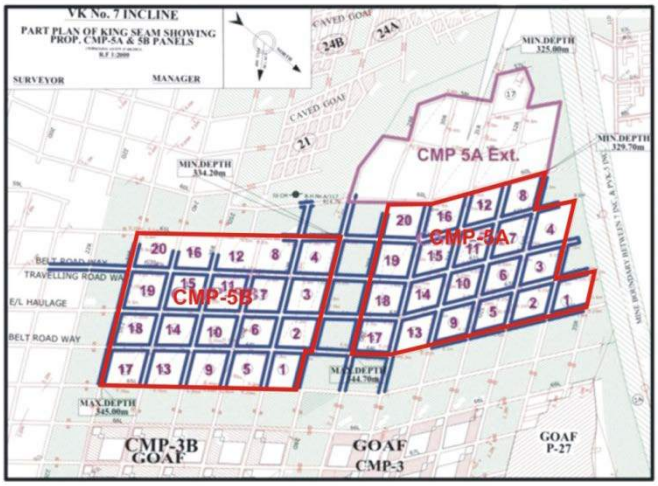

Figure 1. Part plan of CMP-5A and 5B panels with sequence of extraction of pillars

The safety factor of stook with single split was found to be 1.35 and 1.04 for 18.5m wide and 13.5m wide stooks respectively. With double split it was 0.84. This study concludes that the safety factor of the stook with double split was less than 1, therefore; single split option with stook width of 18.5m and 13.5m was followed in panel CMP-5 during depillaring at VK-7 Incline Mine of SCCL during application of CM Technology.

4.1.1 Support system used in CMP-5

For supporting the widened roadways and split level, resin encapsulated rock bolt of 1.8m length and 22mm dia was used as shown in Fig.3a. These support patterns

have been designed based on the modelling results. For side support, wire mesh with cuttable GRP bolts has been used to check the spalling of the pillar during depillaring process as shown in Fig. 3a. In case of slips and fault intersecting the roadways, 2.4m long resin encapsulated rock bolts was used as shown in Fig. 3b.

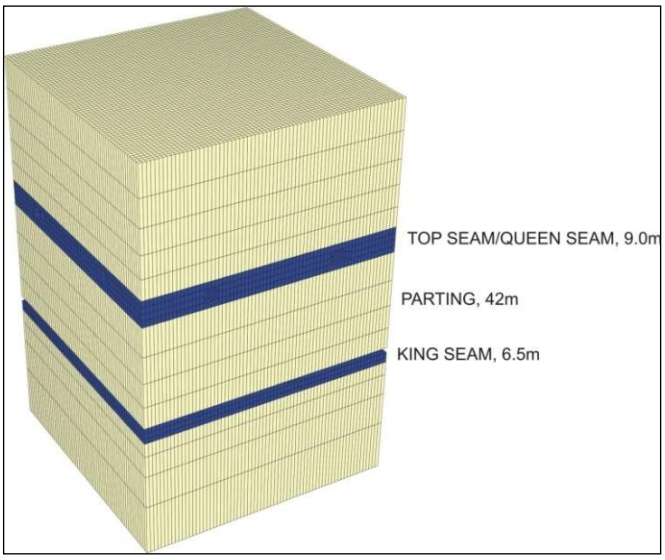

Figure 2. Isometric view of the model showing grid pattern used

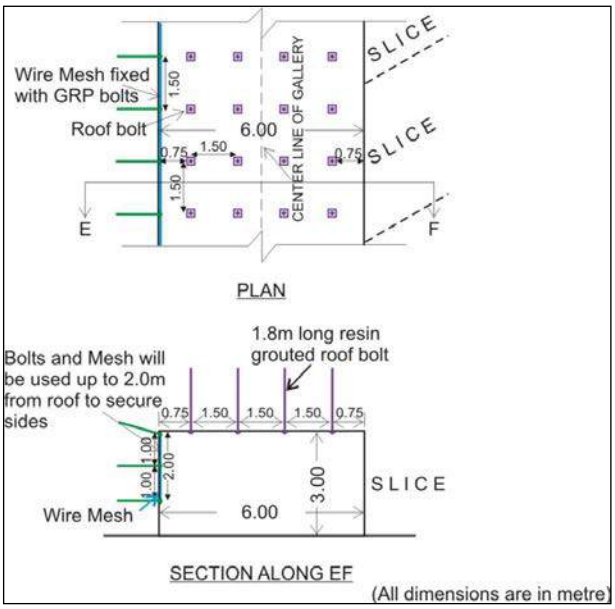

Figure 3a. Support design for widened galleries and level splits

Figure 3b. Support design for the area intersected with slips and faults

Figure 3b. Support design for the area intersected with slips and faults

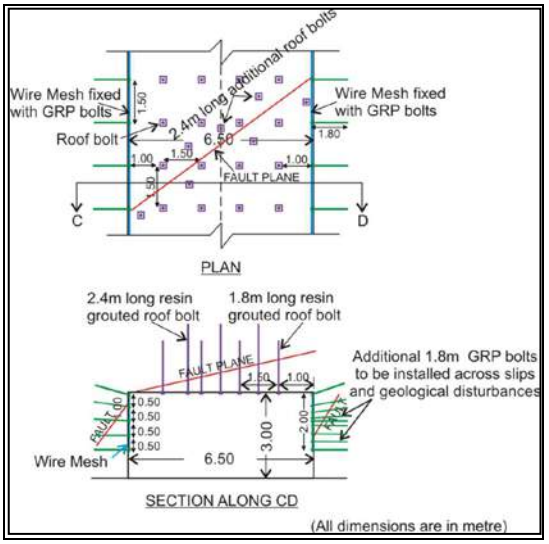

Figure 3b. Support design for the area intersected with slips and faults

4.1.2 Pattern of extraction of pillars with CM technology in CMP-5

In CM Technology during pillar splitting, two pillars are attacked at a time as shown in Fig. 4. The sequence of splitting and slicing of a pillar with CM technology in CMP-5 panel of VK-7 Incline was as follows:

- Two dip-rise pillars were splitted simultaneously by driving level split galleries of 3.0m height along the roof and 6.5m wide, from stages 1 to 6 (Fig. 4) forming two stooks in respective pillars of the dimension 38.5m x13.5m (1/3rd, dip side Fender-A) and 38.5m x 18.5 (2/3rd, rise side Fender-B).
- Roof bolting with resin grouted rock bolts, side supports with wire meshing and GRP bolts were completed in splits along with the installation of breaker lines as shown in Fig. 4.
- A ramp of 1 in 7 gradient was made along dip gallery from the rise side junction of the same pillar as shown in Fig. 4 (stage 7D) and deepened to 4.6m height by floor dinting.
- The split of first pillar was deepened up to 4.6m by dinting (stage 8D).
- Slicing operation from no. 9 to 11 by slicing 5m in upper side (upper stook) and 13.5m in lower stook (Fender-A) (Fig. 4); up to 4.6m height was completed leaving 3m thick ribs after each slicing till it reaches against last snook.

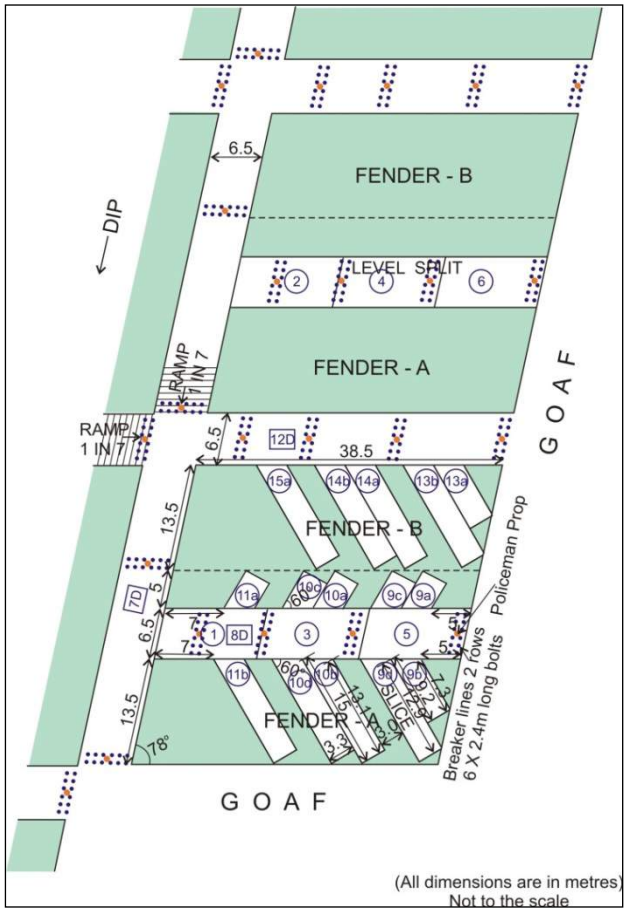

Figure 4. Extraction sequence during splitting, slicing and dinting for CMP-5 panel along with breaker line supports

- The dimension of the last snook was kept 7m x 13.5m x 15m x 14m. The estimated safety factor of this snook was 0.27, which can stand for few hours to withdraw the men and machine from face.
- Sometimes, this snook was not crushing, in that condition one slice of 3.3m was taken from this snook to weaken this snook, so that it fails and it allows the roof to come down.
- Lastly, level gallery (between pillar first and second) shown as 12D was dinted and slicing stages from number 13 to15 were completed with full height of 4.6m leaving 3m ribs in between. A snook of size 7m x 13.5m (Fig. 4) was left against four way junction for judicious extraction.
- If the caving in the goaf got delayed, goaf-edge induced blasting at the roof of the level junction was adopted. Before going for induced blasting over the junction of splits and level galleries after extraction of each fender, the snooks/ribs were further reduced or knocked down to facilitate the roof caving in the extracted area.

4.1.3 Findings

Average production with CM technology in CMP-5 panel at VK-7 incline was around 2000 tpd and coal recovery within the panel was around 72%. Due to this technology, VK-7 Incline underground mine was running in profit.

4.2 Shortwall Mining

The shortwall mining technology is the method of extraction suitable for developed bord and pillar workings is similar to longwall mining but with shorter face lengths, ranging between 40 and 90m, with the aim of controlling the caving nature of the overlying upper strata, the load on support and the overall operation of the supports applied at the face. In shortwall mining technology, face is generally inclined 9^0 to 11^0 from pillar edge so that stability problem at the face can be maintained (Fig. 5). This technology was firstly introduced in Balrampur Mine of SECL (Kushwaha, A. and Banerjee, G., 2005) with following mining geometry:

Depth of cover : 50m;
Developed pillar size : 20m x 20m
Roadway width : 4.2m
Seam Thickness : 2.4m
Development height : 2.4m

4.2.1 Mining pattern in shortwall mining

Orientation of the short longwall face was kept as oblique to avoid the formation of a thin long rib which could collapse suddenly. To overcome this problem, obliquity of the face minimized the exposed area and provides easier access to cross the advance gallery, from one end of the face to the other. Obliquity for Balrampur mine was kept as 9^0 to cross one advance gallery at a time.

With an oblique face crossing the advance gallery, a triangular rib was formed at last in every junction of the extracted pillar. In order to estimate the safety factor of the

triangular rib, its strength was estimated using CIMFR strength formula and the load by using FLAC 3D numerical models. Factor of safety of ribs was ≥ 0.6 which stand stable for few days. Therefore, two travelling power support of 4.5m length was used in the advance gallery against rib which travelled from one end to other as the face progressed.

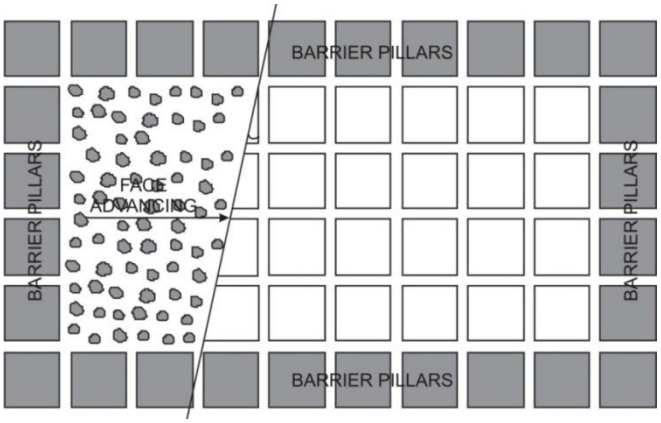

Figure 5. Face Obliquity during Short Wall mining

4.2.2 Support Requirement at the Face and in the Advance Gallery

The similar equipment used in Longwall is utilized here too and open galleries ahead the face are well supported with longer roof bolts and cable bolts. Additionally, breaker line supports which are of normal power supports set in the open galleries with remote operation. Self advancing, crawler mounted supports are also used as breaker line supports. Numerical models using FLAC 2D software was used for estimation of support requirement at the face and in the advance gallery. Support resistance on the powered support applied at the face was adequate to prevent failure of the immediate roof as the face approaches the advance gallery. This support system was designed with the safety factor more than 2.0.

4.2.3 Findings

Average production with shortwall mining technology at Balrampur Mine of SCCL was around 1500 tpd and coal recovery within the panel was around 95%. With Shortwall mining technology, about 8 developed panels of was extracted successfully.

4.3 Blasting Gallery (BG) Method of Mining

Extraction of seams thicker than 4.8 meters has always been a technical problem for the mining industry. The problem is further aggravated by the presence of already developed pillars that are estimated to be of several million tons. Several methods had been tried in India for the extraction of thick coal seam but Blasting Gallery method of mining is considered to be the only economical and viable technology for thick seam extraction and it can be treated as Mass production Technology.

At Vakilpalli Mine of RG-II area of Singareni Collieries Company Limited (SCCL), there are four seams viz., seam 1, 2, 3 and 4 in descending order which are dipping at an average gradient of 1 in 8.5. The upper most Seam 1 at a parting of 92m above 3 Seam was already extracted with longwall caving method and Seam 2 was not workable due to poor quality of the coal. Keeping in view of low gradient and seam thickness more than 9m of seam 3, Blasting Gallery method of mining was adopted in the south side property at Vakilpalli Mine. Parting between Seam 3 and Seam 4 is 8m. 4 Seam was being worked by depillaring with sand stowing underneath the BG panels. During extraction of Seam 4 and Seam 3; number of experimentation with mining sequences was done in the field to minimize the strata control problem. It was found that when 4 Seam is being worked first by depillaring with sand stowing followed by BG in 3 Seam with a lag of around 30–60m, the results were encouraging with significant improvement in roof rock strata condition.

4.3.1 Extraction Pattern in BG Method at Vakilpalli Mine, SCCL

The basic principle of Blasting Gallery Method as adopted in Seam 3 at Vakilpalli Mine of SCCL was to recover coal from 9.6m thick seam by drilling and blasting the

coal roof and sides of 4.2m wide and 2.7m height galleries developed along the floor of the seam at regular intervals. Ring holes up to 5-7m long are drilled in the roof and sides of galleries at regular distances varying between one to two meters by means of a Crawler mounted Jumbo drill (Fig. 6). Blasting is done with explosive cartridges separated by inert spacers and detonating fuses so that the explosive is distributed uniformly. Special custom-made Permitted Explosive (P-3) is used for Ring Blasting. Loading is carried out by Load Haul Dumpers fitted with remote control system, which enables the operator to stand under the supported roof and operate the LHD to load the blasted coal from the goaf. The LHD bring coal from the faces and discharge onto armoured chain conveyor from there to belt conveyor network, which transport coal to the surface Fig. 7.

It has been observed that caving of the immediate strata in the goaf was taking place regularly; as a result abutment pressure at the face was nominal which caused low convergence of the gallery roof with face advancement. Geologically disturbed areas containing slips and fault planes, shown very high convergence values before goaf formation in comparison to other areas.

4.3.2 Design of Support System for BG Method in Seam 3

For the design of suitable support system at the face and in the advance galleries, maximum required support load density at the face (obtained from the numerical models) has been taken into consideration, which came to 19.45 t/m^2. If two 40T capacity OC hydraulic props are used as support system with 150 x 150 mm^2 cross sectional roof bars (girders) of 3.8–4m length, in a row at an interval of 1.0m between two consecutive rows all along the original and split level galleries along with four number of 2.4m long full column cement grouted bolts in a row and at an interval of 1m between two consecutive rows, then applied load was estimated using the equation 4 as given below:

$$\textit{Applied Support Load} = \frac{n1\ x\ Hp + n2\ x\ G}{B\ x\ Sp1} + \frac{n3\ x\ C}{B\ x\ Sp2}$$

where, n1 is the number of hydraulic props in a row, 2; n2 is the number of girder in each row, 1; Hp is the bearing capacity of hydraulic props, 40T; G is the bearing capacity of girder, 4T; B is the gallery width, 4.2m; Sp1 is the spacing between two consecutive rows of the H.P, 1m; n3 is the number of bolts in a row, 4; C is the capacity of full column cement grouted bolts, 8T; and Sp2 is the spacing between two consecutive rows of the bolts, 1m.

Putting all the above values in equation 6, the applied support load density will be = 27.62 t/m^2. Therefore, safety factor of each support with single split of the pillars will be = 27.62/19.45 = 1.42 > 1.0. A longitudinal sectional view of the original or split level galleries supported with the recommended support system for both the cases is shown in Fig. 7.

In case of geological anomalies like slips/faults found in the roof, it can be supported by using additional cable bolts as shown in Fig. 8.

4.3.3Findings

Average production with BG Method of mining at Vakilpalli Mine of SCCL was around 1200 tpd and coal recovery within the panel was around 70%. Since the seam thickness was 9.6m, therefore, 70% recovery with indigenous support system was a very good achievement. This underground mine was also running in profit.

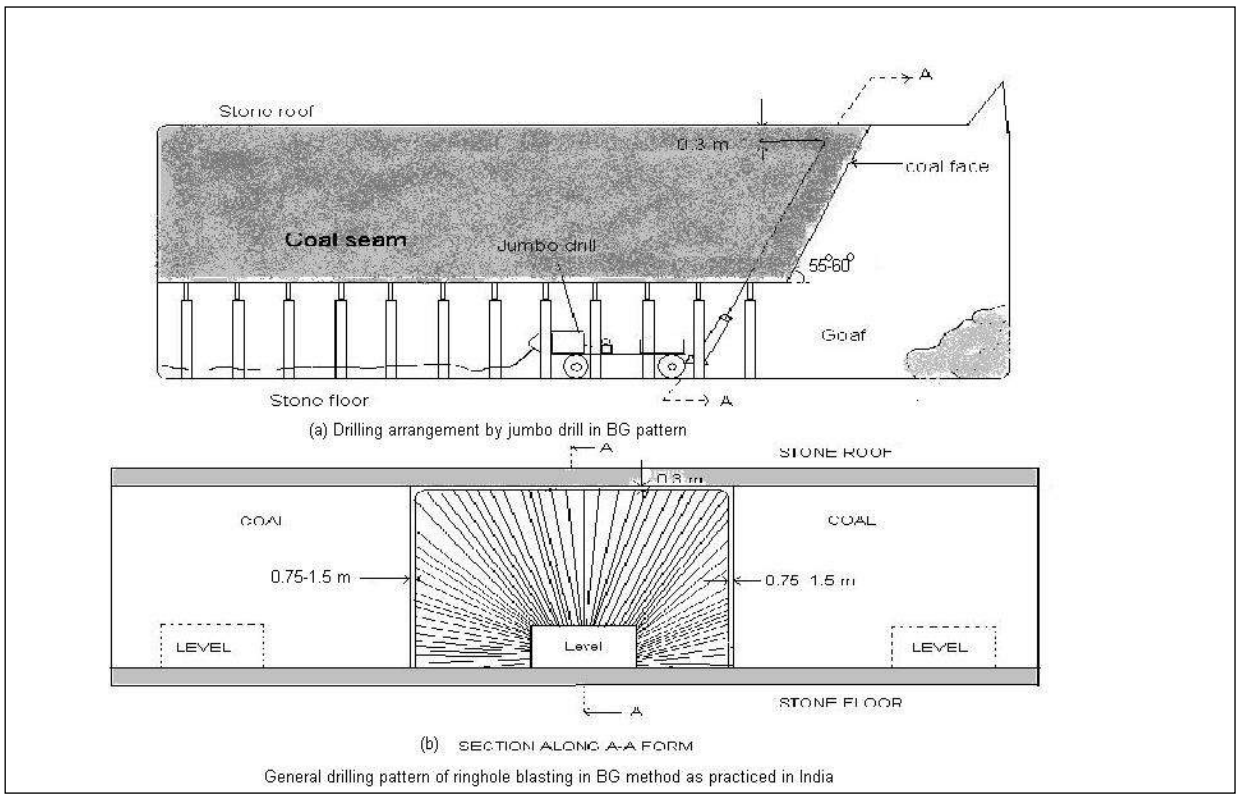

Figure 6 a & b. Crawler mounted electro-hydraulic Jumbo drill machine used for drilling

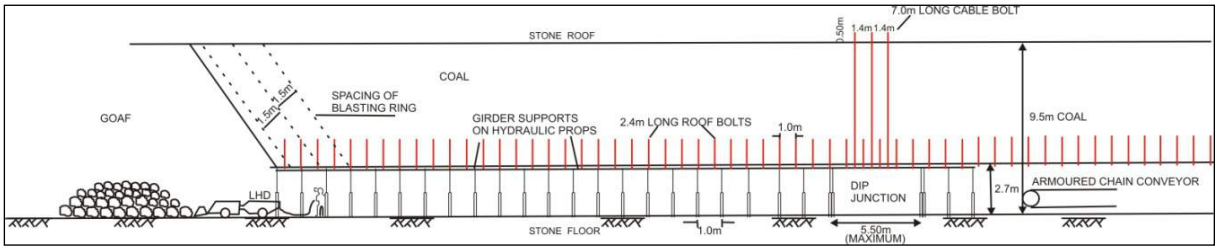

Figure 7. A longitudinal section of the roadway/split level with the recommended support system

5 CONCLUSION

India is upgrading technology and the prospect of mass production technologies in the country is very bright which will contribute considerably in ramping up underground coal production. Case studies described in the paper reflect the efforts of mechanization for underground coal production enhancement in the recent years by introducing mass production technologies in Indian coal mines. These technologies are safe, fast, flexible and highly productive with limited capital investments. For its successful application, scientific studies need to be carried out carefully before its introduction in particular mines. The design of extraction methodology may be modified as per the requirement of the underground mining conditions.

REFERENCES

Itasca Consulting Group Inc, FLAC3D (Fast Lagrangian Analysis of Continua in 3 dimensions). Version 2.0. Minneapolis, MN, 1997.

Kushwaha, A. and Banerjee, G. (2005). Exploitation of developed mine pillars by shortwall mining – a case example. *Int. J. Rock Mech. Min. Sci*. 42, pp.127-136.

Sarkar, S.K. and Singh, B. (1985). Longwall Mining in India. Sunanda Sarkar, Dhanbad

R&D in Coal Sector in India

A. K. Debnath, V. K. Sinha, B. Prasad
CMPDIL, a subsidiary of Coal India Limited, Ranchi, India

ABSTRACT: There was a very little R&D in the Indian coal industry before independence. Recognizing the need for coordinated and sustained R&D work in coal sector, **s**oon after nationalization of the coal industry in early 70's the Government of India initiated Coal S&T Grant in 1975 and in-house R&D by Coal India Limited in 1997 to intensify research work for indigenous development of technologies suitable for the Indian coal industry and to meet the rising energy demand of the country. Since then a large number of research projects have been carried out which have yielded considerable benefits, resulting in operational improvement, safer working conditions, better resource recovery and protection of environment.

This paper gives a brief on R&D set up in coal sector in India, notable achievements of R&D efforts and also the need for enhancing quantum of R&D work needed to address the complexity of operations of coal industry.

Keywords: Coal, R&D, India

1 INTRODUCTION

India is the third largest producer in the world with present production of around 566Mt (2013-14) and, with a total coal resource inventory of about 302 Billion tons (Bt) as on 01.04.2014. Coal is one of the important abundant source of energy in the country, accounting over 50 percent share in commercial energy, is indispensable for economic growth and so are the research and development activities in Indian coal sector.

Since the start of organized research in coal sector in 1975, quite a good number of research projects were completed; and research projects, with outlay of 2.02 Billion INR are under implementation by various academic and research institutes in association with coal and lignite producing companies. While some of these completed projects, admittedly, did not produce the desired results, there have been many which have contributed significantly towards all round growth of the industry.

2 R&D SET UP IN COAL SECTOR

The S&T Grant is administered by the Standing Scientific Research Committee (SSRC) of the Ministry of Coal (MoC) and research funding of Coal India Limited (CIL) is administered through CIL R&D Board. Substantial funds are being earmarked annually by MoC and CIL R&D Board to carry out research work for improvement in production, productivity and safety in coal mines, coal beneficiation & utilization and, protection of environment and ecology. In addition inter sectorial research proposals are considered through Technology Information, Forecasting and Assessment Council (TIFAC) under the Department of Science and Technology (DST).

Central Mine Planning and Design Institute (CMPDI), a subsidiary company of CIL which carries out planning, design and exploration work for coal sector is the nodal agency to coordinate and monitor the R&D activities funded by MoC and CIL. CMPDI, besides being the nodal agency, a number of research projects were executed/are being implemented by CMPDI alone or in association with other organizations.

3 SALIENT ACHIEVEMENTS OF R&D EFFORTS

As mentioned above, many of these projects yielded considerable benefits in operational improvement, safer working conditions, and resource recovery and environment protection. While some research projects produced tangible impact on industry directly, there are others which strengthened mine planning, design and technical services required by mines/projects. Design tools developed specially for Indian geo mining conditions are now available for a variety of mining problems. Small selection of these is outlined below:

3.1 Rock Mass Rating

Rock Mass Rating (RMR) developed for quantifying roof strata through R&D efforts is now routinely being used for support design in underground mines. So far, over 800 underground workings in over 200 mines have been covered.

3.2 Blasting Gallery Method

Blasting Gallery was introduced through R&D funding with technical collaboration from CdF, France, in thick seams of CIL and Singareni Collieries Company Limited (SCCL). The system as adopted in India involves blasting of a series of holes drilled into the sides and roof of galleries in ring hole pattern. Remote controlled LHDs are employed for loading of the blasted coal and transporting to conveyors. The coal recovery is found to be about 70% in the panels, which is substantially higher than what is possible through conventional means.

3.3 Mining by Cable Bolts

A new mining method commonly referred to as Thick Seam Mining by Cable Bolts, was developed through research funding mainly for extraction of thick seams with developed pillars. The method was successfully tried in 6m thick seam at Chirimiri Colliery of South Eastern Coal Fields (SECL). Wire ropes of 19 to 22mm diameter and 6 to 8m length with safe bearing load of over 20 tons under tension were grouted into the roof to avoid roof coal from sagging and bed separation. A part of these cables so grouted went into the immediate roof strata up to a height of about 1.5m above the coal seam and provided support even after blasting of roof coal, which allowed coal loading under the supported strata. The coal recovery improved significantly (up to 75%) along with improvement in underground mine productivity.

3.4 Shortwall Mining

Shortwall Mining was successfully introduced at Ballrampur underground project of SECL with output of over 1000 tons per day. This is one of the future mining methods for liquidation of standing pillars with powered supports, and enhances production from underground mines which is stagnant from decades.

3.5 Controlled Blasting Technique

Controlled Blasting Technique developed through R&D is now being used for excavation in opencast mines near surface structures without endangering safety of inhabitants. This has enabled relaxation in the statutory provision of maintaining 300m distance from surface structures by the Directorate General of Mines Safety (DGMS), India.

Figure 1. Blasting near structures.

Regular production blasts are now being allowed up to 100m and in some cases even up to 50m away from structures by this technique. Consequently, over 150 Mt coal

was extracted in over 100 mines which otherwise would have remained sterilized.

3.6 Ground Penetrating Radar

For mine safety, a significant progress through R&D work has been made by introducing a modern technique, Ground Penetrating Radar for detection of old unapproachable water logged workings in underground mines.

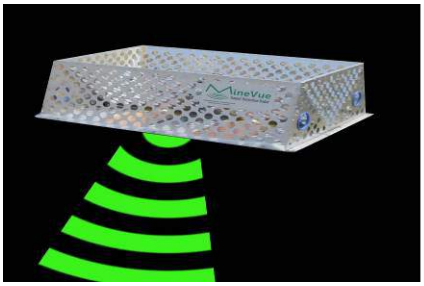

Figure 2. Ground Penetrating Radar.

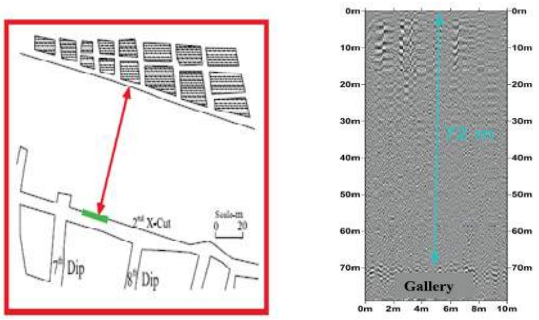

Figure 3. GPR Traverse & Data Obtained.

The developed GPR is capable of delineating barrier thickness of 60m or so towards blind water logged heading with an accuracy of ± 10%. After obtaining permission from DGMS, the GPR is now being used for detection of water logged workings in underground mines. This new technology provides a major tool for enhancing safety in underground mines close to water logged workings.

3.7 Coal Bed Methane

In India, reserve of *Coal Bed Methane (CBM)*, a clean energy source**,** is around 3.4 trillion cubic meters. A demonstration project on recovery of CBM and its utilisation, was successfully implemented through research funding at Moonidih project, Bharat Coking Coal Limited (BCCL).

Figure 4. CBM Rig & Gas Generators.

The recovered gas is almost 98% pure methane which is now being utilized to run 2x250kWh gas based generators and the electricity generated is being supplied to the Moonidih residential colony.

3.8 ALTM and TLS

A new technique - use of Airborne Laser Terrain Mapper (ALTM) and ground based Terrestrial Laser Scanner (TLS) have been introduced through research efforts for rapid volumetric analysis of excavated in situ overburden in CIL mines. Use of TLS measurement reduces 75% time and 50% manpower with respect to conventional survey.

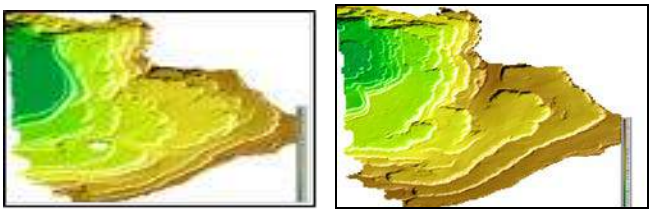

(a) Dec 2008 (b) Dec 2007

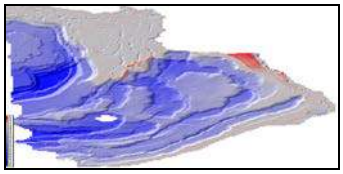

(c) Volume calculation

Figure 5. Digital Terrain Model (DTM) based on ALTM data.

The methodology developed is being used in routine manner for OB measurement in the opencast mines of CIL and also

Singareni Company Coalfields Limited (SCCL) mines.

3.9 Development of Chock Shield

4X800T Chock Shield, with support density of around 140T/m^2, has indigenously been developed at a lower cost (about 50%) than what it would have cost coal companies to import similar equipment.

Figure 6. 4x800T Chock Shield.

3.10 Goaf Edge Supports

Self-Advancing (Mobile) Goaf Edge Supports (SAGES) have been developed indigenously for depillaring operations in underground coal mines to avoid the labor intensive and time consuming process in erecting wooden chocks and props at goaf edges for protection of roof during depillaring operations.

Figure 7. Goaf Edge Supports.

The supports were successfully tested at Bastacola underground mine, BCCL. These self propelled mobile supports of medium duty (2x220T) has closed and extended height range of 1.85 to 3.4 m and can offer support resistance of 71 T/m^2.

3.11 Two Way Communication Systems

Through-The-Earth (TTE) one way messaging system and two way voice communication and tracking system has been developed through research funding. The integrated system is now being used with digital wireless telephones in Bhurkunda mine of Central Coalfields Limited (CCL).

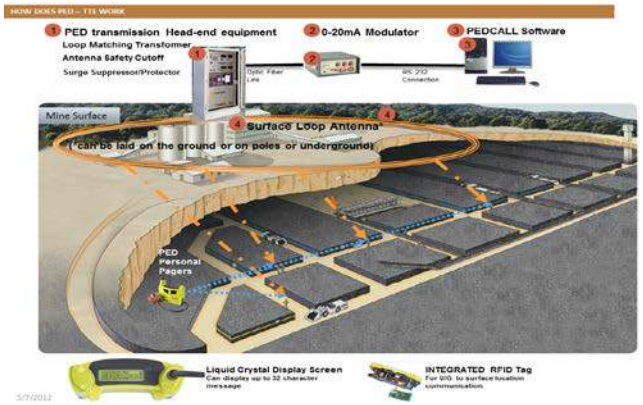

Figure 8. Two way communication system.

Now one can make and receive a voice call from anywhere to underground personnel. The another interesting aspect of the system is to send the text messages through TTE to the mine personnel working in underground mine through rocks right from the surface to below ground on all weather conditions across the entire length and breadth of the mine area and is not dependent on any underground infrastructure.

3.12 Dumper Collision Avoidance System

Indigenous Integrated Dumper Collision Avoidance System (DCAS) has been developed for safety in operating a large feet of heavy dump trucks in opencast mines in India. The system consists of anti collision devices to avoid head to tail collision between dump trucks and proximity warning system to avoid collision between dumpers and blind objects and also reverse safety system to prevent the dumpers from toppling down from the overburden (OB) dumps while unloading. The anti collision devices provide three layers of safety to detect objects on three sides within 10m range, provides directional and distance information of the other dumpers present in the vicinity of 100m and positional information of the dumpers through GPRS by sending SMS. The system is now

working successfully in one of the opencast mine of CIL.

Figure 9. Sensors fitted with Trucks.

3.13 Random Sampling and Testing of Explosives

An indigenous tool (AccuTime Instrument) for carrying out the job of random sampling and testing of explosives and accessories has been developed through R&D. The AccuTime Instrument is capable of measuring the unconfined VoD of various types of explosive products and precise delay time in nanoseconds instead of milliseconds for accessories like electronic detonators, nonelectronic detonators etc.

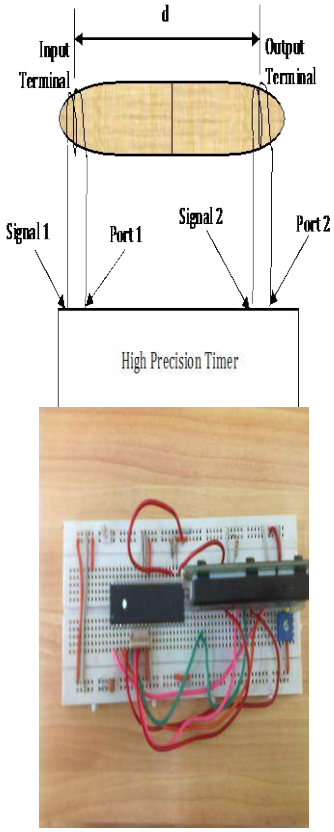

Figure 10. VoD measurement instrument & Microcontroller High Precision Timer.

Figure 11. AccuTime Instrument.

3.14 Use of Fly Ash

A number of research projects have been taken up in the area of environment and ecology to integrate coal mining activities with ecological conservation and to minimize air and noise pollution, land degradation and other environmental hazards due to mining. The findings of these research projects have made a significant impact on the industry resulting in the adoption of proper environmental control measures. Notable trials have also been made for re vegetation of mined out areas, use of fly ash and production of humic acid from lignite for use as fertilizer etc.

3.14.1 Utilization of lignite fly ash in agriculture

It was demonstrated that application of lignite fly ash maximum 200tons @20t/ha/year has found to increase the yield of groundnut and maize by 30% to 40%. Based on the outcome of field trials, fly ash is now being used by nearby villagers at Neyveli, Tamil Nadu through Krishi Vigyan Kendras.

Figure 12. Fly Ash treated Maize and Groundnut crops.

3.14.2 Application of lignite humic acid on crops

Application of humic acid extracted from Neyveli lignite has shown 35% increase in the yield in capsicum and tomato crops and substantial growth in other crops like onion, flower plants, Rose, Jasmine, Zinnia etc. Humic acid is now being used by the farmers in the states of Tamil Nadu, Karnataka, Andhra Pradesh and Kerala.

(a) (b)

Figure 13. Application of Humic Acid on Crops (a) Tomato, Cabbage and (b) Capsicum.

3.14.3 Lignite fly ash based pesticides

Lignite fly ash based bio pesticides developed under research study found to be highly effective against the immature stages of mosquitoes, which serve as vectors for malaria, filariasis, dengue, Japanese encephalitis, chikungunya etc.

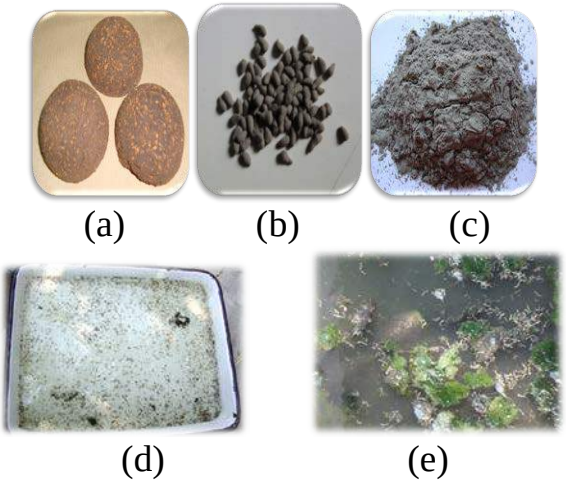

(a) (b) (c) (d) (e)

Figure14. (a) Water Dispersible Powder (b) Granules (c) Briquettes (d) Live Mosquito Larvae and (e) Dead Mosquito Larvae

Figure15. Field Trials of Fly Ash Based Pesticides.

They can be used for the control of these disease vectors and ultimately control of the diseases transmitted by them. A single treatment with 1.5 to 2 g/m^2 was able to provide 100% mortality for up to 3 months.

3.15 Coal Beneficiation

With depletion in availability of good quality power coal and large scale mechanized opencast mining, the ash content in raw coal supplies to power sector has increased over the years. Ministry of Environment and Forest, Government of India has made it mandatory through a gazette notification that power stations located beyond 1000km, in critical, sensitive and urban areas will have to use washed coal with ash not exceeding 34%. A number of research projects have been carried out to tackle some of important issues related to coal beneficiation, especially for high ash Indian coals.

4 MAJOR RESEARCH PROJECTS UNDER IMPLEMENTATION

Application of robotics for online continuous monitoring of various mine parameters related to underground mine environment and roof strata, coal bed methane recovery and utilization, assessment of shale gas potentiality, indigenous development of catalysts for conversion of coal to liquid, greenhouse gas emissions in mine fire areas, dry coal beneficiation systems, development of integrated dumper collision avoidance systems, projects related to explosives use

in mines, solar photovoltaic powered micro grids for mining areas etc., are some at different stages of implementation.

5 SOME OF THE AREAS FOR FUTURE RESEARCH

5.1 Extraction Technology For Thick Coal Seams

In India, we have several thick coal seams. Also, there are large numbers of seams closely held together with varying partings of as little as 3m. Mining in multi flat/moderately inclined seam scenarios have a variety of difficulties such as stability of workings during mining in the immediate top and bottom seams, time delay between extraction of different seams, sequence of extraction, strata control problems, etc. A suitable method of extraction is required to be developed so that coal from these thick seams shall be extracted fully to avoid spontaneous combustion and other hazards.

5.2 Mining Methods for Extraction of Thick and Steep Coal Seams

The coal seams of North Eastern Coalfields (NEC), Assam are characterized by very steep gradient varying from 28 to 90 degrees, friable coal and weak roof and floor. Very high degree of gassiness and proneness to spontaneous combustion of the coal seams, high sulfur content of the coal and acidic mine water compound the problems of coal mining in the region. Various underground mining methods have been tried in NEC mines since nationalization, including various types of Russian Shield Mining Methods with Russian collaboration. Huge requirement of wood and metallic wire netting in these methods have resulted in high cost of production. A suitable mining method is required for extracting coal from these seams to improve substantially the present production level from these coalfields.

5.3 Water Jet Cutting Technology for Coal Seams on Fire

Huge reserves of good quality coal are blocked in seams on fire in Indian coalfields. A study is required to explore possibility of application of water jet cutting technology to extract these seams safely and economically. The technology which would be developed should include recovery of broken coal up to a dispatch terminal and arrangement of recycling of water.

5.4 Longwall Mining with Stowing

In India, a considerable amount of high grade coal is lying in moderate to steep gradient seams and these coals are not being extracted due to non availability of appropriate technology or due to surface constraints.

In the past, conventional longwall with stowing was tried with limited success.

Although, powered support longwall with stowing is an established technology and is being implemented successfully in China, Poland, New Zealand and other countries, but in India it was not tried either with powered supports or with continuous miner technology. A research study is required to adopt the available technologies with stowing in Indian geo mining conditions.

5.5 Hard Roof Management

Hydro fracturing or blasting in roof strata has been resorted to induce caving in several countries. In India, blasting from surface through bore holes has been tried in South Eastern Coalfields Limited (SECL) mines to avoid large overhangs. But it was found that it is not cost effective and is also associated with many difficulties in blasting. Further research on this important aspect may be required to explore various other alternatives like use of slow acting expansion cement / chemicals for application in drill holes into the roof strata to induce fractures to manage with hard

5.6 Warning Device to Indicate Impending Roof Failure

A reliable and a portable warning device is required to be developed which can provide early indication of roof falls. The device needs to be such that it can be operated on a regular basis during depillaring operations including for monitoring of roof condition at junctions.

5.7 Development of Portable Drilling Machine

At present, manually operated electric drills which are slow and insufficient and do not keep up pace with the drivage advance in mechanized developmental heads are being used for drilling the holes required for the bolting operations. There is a need to develop a light weight portable hydraulic drilling machine through R&D funding which would find application in all types of mine workings including in hard roof strata conditions.

5.8 Underground Coal Gasification

Earlier, some research work was carried out on Underground Coal Gasification(UCG) but unsuccessful by one or more reasons such as fear of pollution ground water, complex hydrogeology of the seams and also lack of continuous technical support. A pilot scale study may be undertaken through research funding to demonstrate techno economic viability of UCG technology for deep seated Indian deposits which cannot be mined through present mining technologies.

5.9 Liquefaction of Coal

Some limited research work on the subject was carried out in India in the past, the technology for conversion of coal to oil suitable for Indian coals for maximum yield at least possible cost is yet to be established.

As India has huge coal reserves and relatively small oil reserves, further studies are required to come out with a concrete result on feasibility of liquefaction of Indian coals to oil.

5.10 Shale Gas Assessment, Recovery and Utilisation

Although some research studies are being carried out through R&D funding, still there is a need to continue these efforts involving international expertise for developing methodology for shale gas assessment, recovery technologies and its utilization aspects.

5.11 Biological Debris Detection of Buried Body under Overburden Dumps

A Biological Debris Detector is required to detect burial of a dead body in case of dump failure in opencast mines. The device should be based on bio functions of a human body for predicting the orientation of the body buried under the OB dumps in opencast mines.

There are other areas like, fly ash based paste fill for void stowing in underground mines, capturing of ventilation air methane and its utilization, coal slurry transport where international expertise is required to take up research projects/or another other area of interest which would benefit coal industry either in financial terms or mine safety.

6. CONCLUSION

India has seen a lot of change in the forms of research work, especially over the last 35 years. Each of the approaches to research activity has had both merits and demerits from time to time. Some of the R&D efforts have translated into immediate gains for improvement in mine production, safety and conservation. Others are more indirect and long term gains.

There is also an increased impetus on development of renewable and other energy sources including coal based non conventional resources like Coalbed Methane, Coal Mine Methane, Underground Coal Gasification and new

energy sources like Shale Gas etc., are under focus.

Continuous efforts are being made to enhance R&D base in coal sector in India through wider participation of national and international scientific and academic organizations with adequate infrastructure and expertise to address the complexity of mine operations in Indian coal industry.

ACKNOWLEDGEMENTS

Acknowledgement is clearly due both to the research teams, their organizations and the research funding providers who have enabled this work to take place. The views expressed in the paper are those of authors and not necessarily of the organisation to which they belong.

REFERENCES

Study reports of various research and academic organizations involved in coal research under the funding of Ministry of Coal and Coal India Limited.

Selection of Recovery Sieve Size in Oil Agglomeration of Coal

E. Sahinoglu, T. Uslu
Karadeniz Technical University, Department of Mining Engineering, Trabzon-TURKEY

ABSTRACT The present study was undertaken to determine the effect of recovery sieve size on the performance of oil agglomeration of coal. An oxidized fine coal sample was subjected to oil agglomeration process. Combustible recoveries and ash-sulphur rejections were investigated. 72.90% of ash, 90.90% of pyritic sulphur, and 87.75% of sulphate sulphur was removed from the coal with combustible recovery of 76.53%. While increase in recovery sieve size had positive effect on rejections of ash and sulphur, it reduced combustible recovery sharply. It was concluded that use of recovery sieve whose size is higher than top feed size was not feasible at applied test conditions.

Keywords: Oil agglomeration, coal

1 INTRODUCTION

Mechanised mining has been resulting in production of large quantities of fine coals (Mehrotra et al., 1983; Cebeci et al., 2002; Sahinoglu and Uslu, 2013a). New environmental regulations as well as loss of valuable combustible matter with fine coal do not allow the current practice of discarding the coal fines with refuse. The finer the coal, the less efficient and more expensive are the conventional techniques of coal cleaning (Mehrotra et al., 1983; Capes, 1991). Therefore, flotation, selective flocculation, and oil agglomeration methods have gained importance to clean fine particles. Among these methods, flotation is most commonly used one. However, compared to flotation, oil agglomeration has important benefits, such as, quality of product in terms of pyrite, easy handling and transportation of the product, high recovery, suitability to oxidized coals and coals with clay slimes, simplicity and cheapness of dewatering stage (Mehrotra et al., 1983; Cebeci et al., 2002; Sahinoglu and Uslu, 2013a).

As with flotation, oil agglomeration of coal relies on the differences in the surface properties of hydrophobic coal particles and hydrophilic inorganic gangue (Laskowski and Yu, 2000). When a small amount of oil is introduced into an agitated suspension of coal particles, hydrophobic coal particles become oil coated and stick together to form agglomerates while the hydrophilic mineral water particles remain unaffected. The agglomerated particles can be separated from the other materials by a single screening operation or alternatively by floating and skimming. Performance of selective oil agglomeration depends on a great extent of the surface properties of solid particles (Gurses et al., 1997; Sahinoglu and Uslu, 2008; Sahinoglu and Uslu, 2013b). Hydrophobicity of coal surfaces, hydrophilicity of mineral matter surface and liberation of mineral matter from coal are required for efficient rejection of mineral matter in coal by this technique (Sahinoglu and Uslu, 2008).

Performance of the agglomeration process is affected by various parameters. One or more of the these parameters including, solid content, oil dossage, oil type, agglomeration time, agitation speed, coal particle size, pH of the medium, have been investigated by several authors (Aktas, 2002; Cebeci and Sonmez, 2006; Valdes and Garcia, 2006; Sahinoglu and Uslu, 2008; Aslan and Unal, 2011; Chary and Dastidar, 2012; Shaobin et al., 2012; Chary and Dastidar, 2013; Aslan, 2013; Sahinoglu and Uslu, 2014; Kumar et al., 2015).

Although recovery sieve size has vital importance for performance of the oil agglomeration process, very limited number of study has been reported relating to its effect on combustible recovery and ash-sulphur rejections. Therefore, another work is required to investigate the relationship between recovery sieve size and agglomeration performance in term of combustible recovery and ash-sulphur rejections. Coal sample used in this study differs from many coals used in agglomeration studies in that it shows typical characteristics of an oxidized coal with its brittle nature, high specific gravity, and high sulfate sulfur content. Waste sunflower oil was used as agglomerant. Moreover, pyritic and sulphate sulphur rejections of the process was investigated unlike the most of the previous coal agglomeration studies which have been contented with ash rejections.

2 MATERIALS AND METHODS

2.1 Materials

A coal sample from Muzret (Artvin-Turkey) coal deposit was used in this study. Proximate analysis of the sample shows that Muzret coal has high ash and pyritic sulfur content (Table 1). XRD analysis of the sample revealed that clay minerals (kaolinite, illite, montmorillonite), calcite, gypsum, quartz are present in the coal as mineral matters. Coal sample was dry ground to size fractions of -0.5 mm, -0.25 mm and -0.125 mm for oil agglomeration tests. The waste sunflower oil was used in the experiments.

Table 1. Proximate, sulphur and calorific value analyses of the coal sample.

Proximate Analysis	Air Dried	Dried
Moisture (%)	2.25	-
Ash (%)	34.85	35.65
Volatile Matter (%)	10.73	10.98
Fixed Carbon (%)	52.17	53.37
Sulphur Analysis	**Air Dried**	**Dried**
Sulphate Sulphur (%)	0.99	1.01
Pyritic Sulphur (%)	5.44	5.57
Organic Sulphur (%)	1.3	1.33
Total Sulphur (%)	7.73	7.91
Calorific Value Analysis	**Air Dried**	**Dried**
Calorific Value (kcal/kg)	4970	5084

2.2 Methods

Cylindrical glass vessel (11.7 cm in diameter) with four removable baffles of 1.1 cm in width was used for the tests. The agitation of vessel contents was performed using RZR 2021 type overhead stirrer equipped with a 45°-pitched blade turbine (four blade, 50 mm in diameter). Distilled water was used in the tests. Coal samples with different particle sizes (-0.125, -0.250 and -0.500 mm) were mixed with water (solid ratio: 10%). Coal-water mixtures were conditioned at 1000 rpm for 5 min. in order to achieve complete wetting of coal particles. Waste sunflower oil (10% of coal) was then added as bridging oil and coal-water-oil mixture was further agitated at 1400 rpm for 10 min. The tests were carried out at the natural pH of the coal-water-oil mixture. After agglomeration, the suspension was transferred to a recovery sieve to separate the agglomerates from water and tailings. Size of the recovery sieve changed in the range of 0.125-0.5 mm, 0.25-0.6 mm, and 0.5-1 mm for feed size of -0.125, -0.250 and -0.500 mm, respectively. In order to remove the entrained mineral matter, agglomerates were carefully washed with 1.5

L water. The agglomerates rejected from the sieve were vacuum filtered and de-oiled by washing with acetone. Oil-free agglomerates were dried at 105±5 °C. After drying, agglomerates were weighed and stored for analyses. Finally, agglomerates were analyzed for ash, pyritic sulphur and sulphate sulphur contents by using standard analyses methods. The combustible recovery, ash rejection, pyritic sulphur rejection, sulphate sulphur rejection were determined.

3 RESULTS AND DISCUSSION

As seen from the Figures 1-3, increasing of recovery sieve size had adverse effect on combustible recovery.

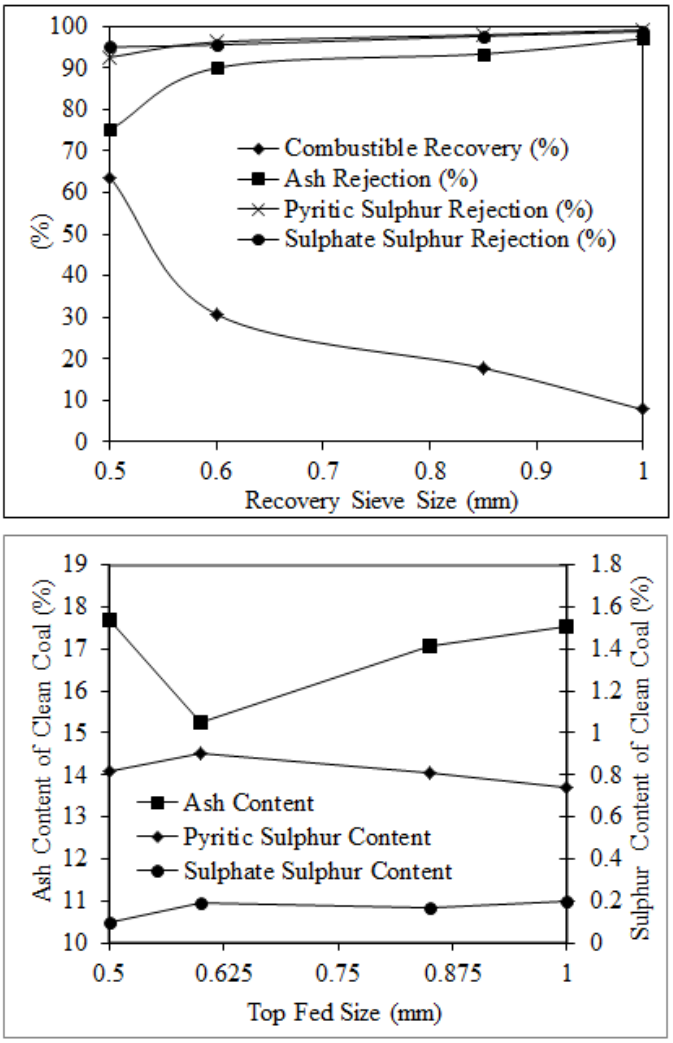

Figure 1. Effect of recovery sieve size on the performance of the oil agglomeration (feed size: -0.5 mm).

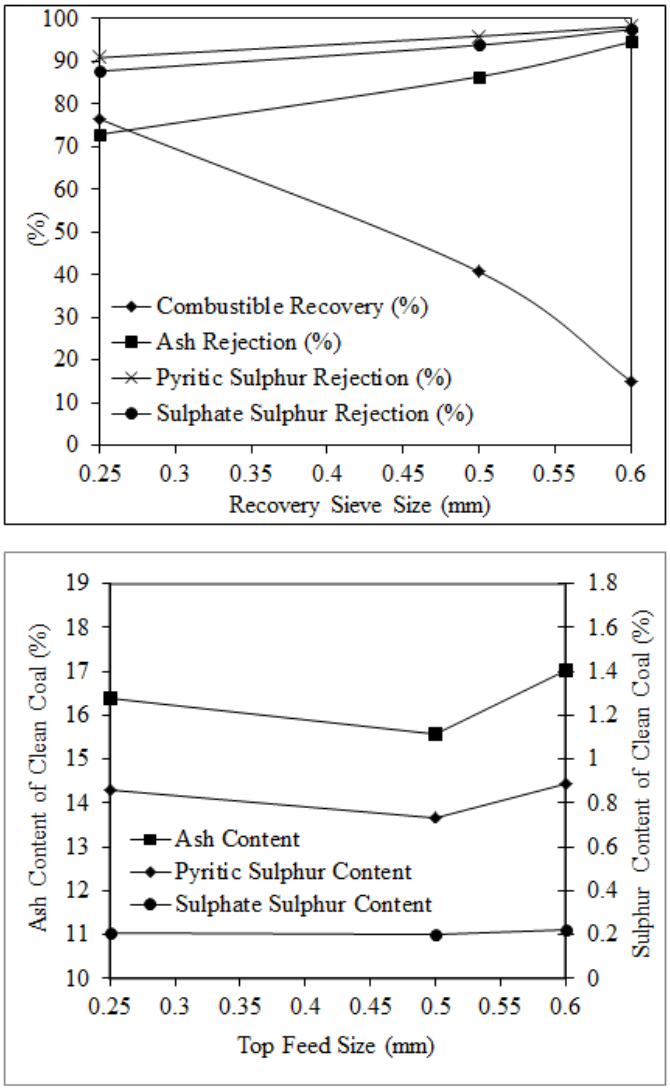

Figure 2. Effect of recovery sieve size on the performance of the oil agglomeration (feed size: -0.25 mm).

Because, small sized agglomerates could not retain on the sieve whose aperture size is over the top feed size and passed through the sieve apertures during agglomerate recovery and washing. Combustible recoveries obtained by using a sieve whose size is equal to top feed size are 55.54%, 76.53% and 63.62 % for feed size of -0.125, -0.250, and -0.5 mm, respectively. Adverse effect of increasing size of recovery sieve was observed. For the feed size of -0.5 mm, combustible recovery decreased by 87.69% as a result of doubling the recovery sieve size from 0.5 mm to 1mm.

For the feed size of 0.25 mm and 0.125 mm, reduction in combustible recoveries resulted from doubling of recovery sieve size whose size equals to top feed size were 46.80% and 79.36%, respectively.

Higher ash and sulphur rejections obtained at greater recovery sieve size shows that agglomeration process is more selective at higher sieve sizes. This can be attributed to easier passage of nonagglomerating and entrained mineral matter from higher sieve holes during agglomerate recovery and washing. Ash rejections, pyritic sulphur rejections and sulphate sulphur rejections achieved at the tests changed in the range of 72.90-97.56%, 89.04-99.23%, 87.75-98.79%, respectively. However, optimum values can be recorded as 72.90%, 90.90%, and 87.75%, respectively.

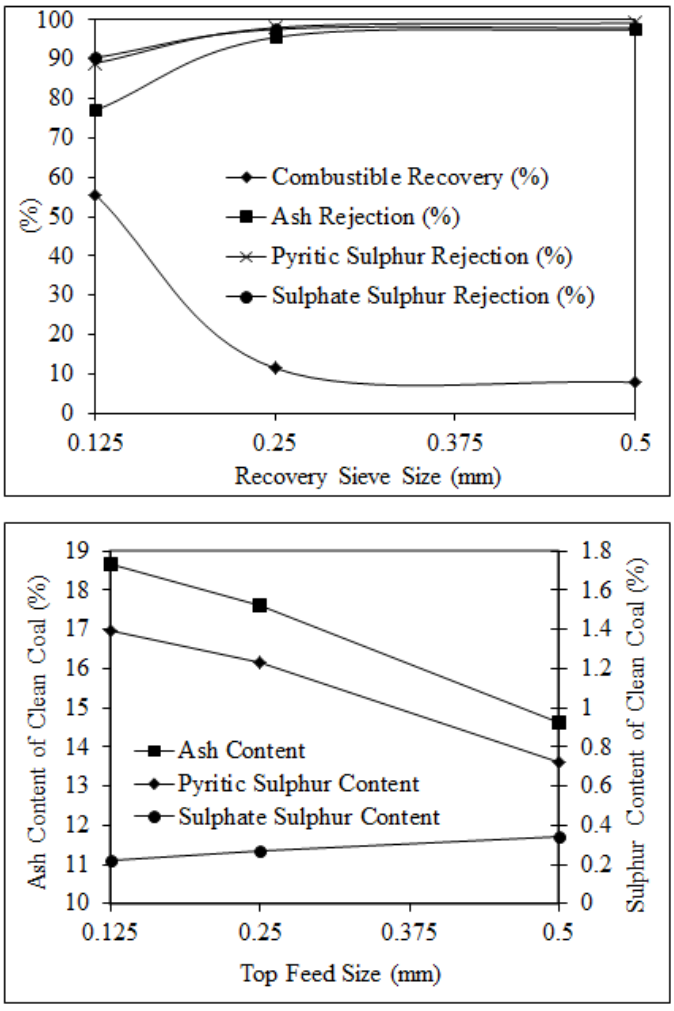

Figure 3. Effect of recovery sieve size on the performance of the oil agglomeration (feed size: -0.125 mm).

4 CONCLUSIONS

Although increasing recovery sieve sizes enhanced ash and sulphur rejection from coal, it had adverse effect on the combustible recovery. While cleaner agglomerates are produced, combustible matter reduces sharply as a result of increase in recovery sieve size. Further studies should investigate the relation between the agglomeration performance and recovery sieve size at higher oil dosages due to importance of oil dosage on growths and strength of agglomerates. Optimally, 72.90% of ash and and 90.90% of the pyritic sulphur and 87.75% of sulphate sulphur was removed from the coal at combustible recovery of 76.53%.

REFERENCES

Aktas, Z., 2002. Some factors affecting spherical oil agglomeration performance of coal fines, International Journal of Mineral Processing 65, pp. 177-190.

Aslan, N., 2013. Use of the grey analysis to determine optimal oil agglomeration with multiple performance characteristics, Fuel 109, pp. 373-378.

Aslan, N., Unal, I., 2011. Multi-response optimization of oil agglomeration with multiple performance characteristics, Fuel Processing Technology 92, pp. 1157-1163.

Capes, C.E., 1991. Oil agglomeration process principles and commercial application for fine coal cleaning. In: 5th ed., Coal preparation, Littleton, CO: Society for Mining, Metallurgy, and Exploration Part 4, pp. 1020–1041.

Cebeci, Y., Sonmez, I., 2006. Application of the box-wilson experimental design method for the spherical oil agglomeration of coal, Fuel 85, pp. 289-297.

Cebeci,Y., Ulusoy, U., Simsek, S., 2002. Investigation of the effect of agglomeration time, pH and various salts on the cleaning of Zonguldak bituminous coal by oil agglomeration, Fuel 81, pp. 1131-1137.

Chary, G.H.V.C., Dastidar, M.G., 2012. Investigation of conditions in coal-oil agglomeration using Taguchi experimental design, Fuel 98, pp. 259-264.

Chary, G.H.V.C., Dastidar, M.G., 2013. Comprehensive study of process parameters affecting oil agglomeration using vegetable oils, Fuel 106, pp. 285-292.

Gurses, A., Doymus, K., Bayrakceken S., 1997. Evaluation of response of brown coal to selective oil agglomeration by zeta potential measurements of the agglomerates, Fuel 76, pp. 1439–1444.

Kumar, S., Chary, G.H.V.C., Dastidar, M.G., 2015. Optimization studies on coal–oil agglomeration using Taguchi (L16) experimental design, Fuel 141, pp. 9–16.

Laskowski, J.S., Yu, Z., 2000. Oil agglomeration and its effect on beneficiation and filtration of low-rank/oxidized coals, International Journal of Mineral Processing 58, pp. 237–252.

Mehrotra, V.P., Sastry, K.V.S., Morey, B.W., 1983. Review of oil agglomeration techniques for processing of fine coals, International Journal of Mineral Processing 11, pp. 175-201.

Sahinoglu, E., Uslu, T., 2008. Amenability of Muzret bituminous coal to oil agglomeration, Energy Conversion and Management 49, pp. 3684–3690.

Sahinoglu, E., Uslu, T., 2013a. Use of ultrasonic emulsification in oil agglomeration for coal cleaning, Fuel 113, pp. 719-725.

Sahinoglu, E., Uslu, T., 2013b. Increasing coal quality by oil agglomeration after ultrasonic treatment, Fuel Processing Technology 116, pp. 332–338.

Sahinoglu, E., Uslu, T., 2014. Effect of particle size on cleaning of high-sulphur fine colal by oil agglomeration, Fuel Processing Technology 128, pp. 211-219 .

Shaobin, L., Bo, C., Wenrong, C., Wenhua, L., Sheng, W., 2012. Study on clean coal technology with oil agglomeration in Fujian Province, Procedia Engineering 45, pp. 986-992.

Valdes, A.F., Garcia, A.B., 2006. On the utilization of waste vegetable oils (WVO) as agglomerants to recover coal from coal fines cleaning wastes (CFCW), Fuel 85, pp. 607-614.

An Assessment of Turkish Lignite Fields for Underground Coal Gasification

Türk Linyitlerinin Yeraltı Kömür Gazlaştırma Yöntemi için Değerlendirilmesi

K. Het, Ş.Yürek
General Directorate of Turkish Coal Enterprises

D. W. Camp, J. L. Wagoner
Lawrence Livermore National Laboratory

ABSTRACT Underground Coal Gasification (UCG) is a way to convert *in-situ* coal into an energy-rich gas (synthesis gas). Like surface gasification, a combination of air, oxygen, and/or steam is reacted with the coal to produce a mixture of CH_4, H_2, CO, CO_2, H_2O, and lesser amounts of H_2S, NH_3, and assorted organics. UCG eliminates mining, transporting, pulverizing, cleaning, and handling the coal and most of its ash residue by doing the gasification in the coal seam in situ.

In this study, fourteen Turkish lignite fields were evaluated for their suitability to produce energy by UCG by Lawrence Livermore National Laboratory (LLNL) in the United States, together with Turkish Coal Enterprises (TKI) in Turkey. LLNL uses software during preliminary site assessments called UCG-ZEE (Underground Coal Gasification- Zonal Energy Estimator). This was one tool used to estimate the potential for UCG in coal fields in Turkey. By using the above-mentioned software, four important UCG parameters for each defined coal zone were calculated. These are: 1) the zone thickness, 2) the mass-average lower calorific value (CV) of the mixture of coal and rock layers within coal zone, 3) the maximum areal gas energy (MAGE) value for the zone, and 4) a figure of merit that combines CV and MAGE.

Keywords: Lignite, gasification , UCG-ZEE , MAGE

ÖZET Yeraltı Kömür Gazlaştırması (YKG), kömürü yerinde enerjice zengin bir gaza (sentez gazı) dönüştürmek için kullanılan bir yöntemdir. Aynen yüzey gazlaştırma işleminde olduğu gibi hava, oksijen ve/ve ya buhar kömür ile reaksiyona sokularak CH_4, H_2, CO, CO_2, H_2O ve az miktarda H_2S, NH_3 gazları ile çeşitli organikler üretilebilmektedir. YKG yöntemi, kömür gazlaştırma işlemini kömür damarının içinde gerçekleştirerek madencilik, nakliye, pulverizasyon (öğütme), yıkama ve kömürün kullanımı aşamalarını ortadan kaldırmakla birlikte, kömürün gazlaştırılması sonucundan oluşan kül artığının da kömür damarının içinde kalmasını sağlar.

Bu çalışmada, Türkiye'de bulunan on dört linyit sahasının YKG yöntemi ile enerji üretimine uygunlukları Amerika Birleşik Devletleri'nden Lawrence Livermore Ulusal Laboratuarı ve Türkiye'den Türkiye Kömür İşletmeleri tarafından değerlendirilmiştir. LLNL ön saha değerlendirme aşamasında UCG-ZEE (Yer altı Kömür Gazlaştırma-Bölgesel Enerji Değerlendirici) adlı yazılımı kullanmaktadır. Bu yazılım ile Türkiye'deki linyit sahalarının YKG potansiyelleri tespit edilmeye çalışılmıştır. Söz konusu yazılım kullanılarak tanımlanan her bir linyit bölgesine yönelik dört önemli YKG özelliği hesaplanmıştır. Bunlar: 1) Bölge kalınlığı, 2) Kaya ve linyit karışımına ait Kütle-Ortalama Alt Isıl Değeri (AID) 3) Maksimum alansal gaz enerji değeri (MAGE) 4) AID ve MAGE değerlerini birbirine bağlayan değer katsayısı.

Anahtar Kelimeler: Linyit , gazlaştırma, UCG-ZEE , MAGE

1 INTRODUCTION

Underground Coal Gasification (UCG) is a way to convert in-situ coal into an energy-rich gas called synthesis gas. Like surface gasification, a combination of air, oxygen, and/or steam is reacted with the coal to produce a mixture of CH_4, H_2, CO, CO_2, H_2O, and lesser amounts of H_2S, NH_3 and assorted organics. UCG eliminates mining, transporting, pulverizing, cleaning, and handling the coal and most of its ash residue by doing the gasification in the coal seam *in-situ*.

This is accomplished by drilling and completing wells into a coal seam; these wells are used for injecting the air/oxygen/steam and for the eventual recovery of the product gas. Modern UCG generally targets coal seams deeper than 200 meters. Similar to surface gasification, the product gas can be burned to make electricity or converted to one of many products such as methane (synthetic natural gas), methanol, liquid fuels, ammonia, and fertilizers. Moreover, CO_2 in the product gas can efficiently be separated for sequestration or other uses.

Over the past 80 years, a hundred or so experimental, pilot, and demonstration UCG operations worldwide have shown UCG to be technically feasible and the technology has continued to improve. A large effort to improve and commercialize UCG in the United States in the 1970's and 1980's hit a commercial dead end with the drop in energy prices in the 1980's. Significant modern efforts toward commercial-scale development are found in many parts of the world today, including Australia, South Africa, China, Canada and Eastern Europe.

UCG avoids the safety and environmental issues associated with mining, transport and processing of the coal and most of the ash. UCG has a similar potential for subsidence and subsurface structural changes as underground mining. UCG produces some contaminants and some small fraction of these contaminants is left underground. Proper site selection, design and operation practices have been demonstrated to manage this issue but it is still important to recognize, UCG should be done at depths and locations where a significant geological barrier can be assured between it and fresh groundwater aquifers.

Generally, UCG is best deployed where:

- Coal fields are technically well-suited for UCG,
- Energy (especially electricity and natural gas) costs are high and/or variable,
- Energy (especially natural gas) supply is not secure,
- There is an infrastructure to support UCG development,
- There is nearby use/demand/market/infrastructure for UCG product gas,
- Deep level underground coal mining is expensive or challenging.

In this study, fourteen Turkish lignite fields, listed in Table 1, were evaluated for their suitability to produce energy by UCG. At this stage of assessment, the purpose was not to produce quantitative predictions of performance and cost, but rather to guide the assessment of feasibility.

Table 1. List of Turkish lignite fields evaluated for UCG

Name of Lignite Field
Soma-Eynez
Soma-Evciler
Tunçbilek-Domaniç
Tunçbilek-Demirbilek
Muğla-Turgut
Bursa-Keles-Davutlar
Konya-Beyşehir
Adana-Tufanbeyli
Thrace Basin-Çerkezköy 1-2
Thrace Basin-Vize
Thrace Basin-Edirköy
Thrace Basin-Küçükyoncalı
Thrace Basin-Safaalanı

2 APPROACH TO UCG ASSESSMENT

2.1 Preliminary Screening

A preliminary screening of the lignite fields was performed to identify the most promising sites and those that might be suitable for additional analysis. Preliminary screening focused on easily available technical factors including depth of the coal zone, thickness of individual coal seam and rock layers and zones, and the coal heating values of those layers. Qualitative geographical factors were also considered, such as economic land use within the local area. The most important of the many technical factors considered in preliminary screening are summarized below in Table 2 according to their importance.

Table 2. Summary and approximate ranking of the most important technical criteria required for site selection

Ranking	Criteria
Most Important	Average as-received calorific value of coal zone
	Maximum areal gas energy (MAGE)
	Roof rock resistance to cavity growth/collapse
	Coal and rock geomechanical properties
	Depth of coal seam
Very Important	Coal and rock hydrological properties
	Fault distribution and characteristics
Important	Thickness of coal zone including partings
	Dip angle of coal seam
	Lateral continuity of coal seam
	Roof rock spalling propensity
	Proximate analysis
	Ultimate analysis
	Coal rank (avoid swelling bituminous)
	Decomposition of overburden rock minerals

2.2 UCG-ZEE Analysis

LLNL has developed a tool for preliminary site assessment called "UCG Zonal Energy Estimator" or UCG-ZEE. UCG-ZEE is a tool for assessing borehole data consisting of many layers of rock and coal having different heating values within a coal zone. The user defines or picks the boundaries of the zone, with the bottom and top layers being coal. The bottom layer is where the user estimates the lowest place where reactants can readily transport (the location of the injection well in horizontal "Controlled Retraction and Injection Point" or CRIP construct). The top layer is below where the user estimates that roof rock will hold well enough that next coal layer will not be involved. The model allows for three alternative picks of zone top and bottom to be chosen and evaluated. Once a zone is defined, the model calculates four metrics for that zone: the zone thickness; the mass-average lower calorific value (CV) of the mixture of coal and rock layers within it; the maximum areal gas energy (MAGE) value for the zone; and a figure of merit that combines CV and MAGE.

The maximum areal gas energy (MAGE) is the chemical energy per square meter of land surface area that would be embodied in the gas product if the zone were completely gasified using pure oxygen and the ideal amount of steam. MAGE assumes no heat losses but incorporates reasonable estimates for the final temperature of the hot remaining ash and for the temperature of UCG product gas. MAGE is the expected product gas chemical energy if the UCG operation on the zone in question underwent no heat losses to the surroundings, no roof spalling or collapse and no inward groundwater permeation.

In general, the greater the MAGE values and the greater the CV values for a seam, the higher value the seam has for UCG potential. But both parameters are important. For instance, a very thin layer of rich coal may have a high CV but an unacceptably low MAGE. A very thick zone with more rock than coal may have a high MAGE but an unacceptably low CV. At this point, "Figure of Merit" is a function of CV and MAGE

that is intended to correlate with expected UCG technical and economic performance.

For the purposes of screening of fields and of areas within fields, areas were divided into four categories (Favorable, Promising, Possible and Challenging) depicted in Table 3. The numerical thresholds for each quadrant were set by integrating LLNL's proprietary material and energy calculation results for Turkish lignites, knowledge of results from past UCG field tests and operations, knowledge of currently operating UCG projects around the world, and knowledge of many planned UCG operations around the world.

Table 3. Classification of the suitability coal zones for UCG based on UCG-ZEE screening

		MAGE		
		>80k	40k-80k	<40k
CV	>3500	Favorable	Promising	Challenging
	2500 - 3500	Promising	Possible	Challenging
	<2500	Challenging	Challenging	Challenging

Based on UCG-ZEE screening, regions in the Favorable quadrant of Table 3 are suitable for UCG deployment in terms of the parameters modeled. Of course, many other factors are important in the overall determination of UCG suitability. It is also possible that successful UCG may be conducted at regions in the Promising and Possible quadrants, depending on the outcome of detailed analyses, testing, and development. On the other hand, by using current state of knowledge, experience, and technology, UCG is unlikely to be successful and economic at regions in the Challenging quadrant.

2.3 Geological 3D Models and Visualization of UCG-ZEE Results

A second tool used in this study is Earthvision 3D geological modeling software. This software is extensively used for building and visualizing 3D geological models to characterize and better understand the subsurface geology. In this study, 3D geological models were only generated for four most promising UCG sites. The results from the UCG-ZEE analyses were incorporated into each local Earthvision models. These colored contour plots of CV, MAGE and Figure of Merit were draped over the 3D model and used to identify areas within the field that met defined criteria for being favorable, promising, possible and poor. These areas were then integrated for the calculation of total area.

In this study, 3D geological models were developed for the most promising coal fields by using Earthvision geological modeling software. Also colored plan view contour pilots including the UCG-ZEE results were constructed for the most promising coal fields. The 3D geologic model for the Tunçbilek-Domaniç region is illustrated in Figure 1.

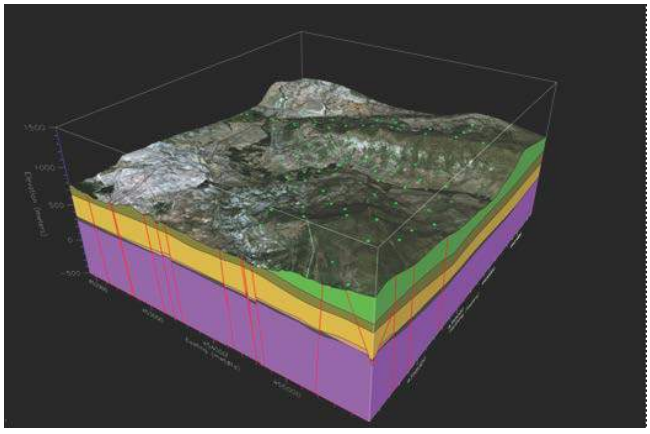

Figure 1. Earthvision 3D Geomodel for Tunçbilek-Domaniç region. Borehole collar locations are shown as green symbols. The stratigraphic units are (lowest to highest): Basement rock (purple), Coal (beige), Marl (yellow), Limestone (Light Green). The dipping faults intersecting the side of the model are shown as red lines.

3 SUMMARY OF ASSESSMENT OF ALL FIELDS

A high-level summary of many important characteristics of the fourteen fields is presented in this section. The fields were grouped as four best, three possible and six unfavorable. The four best fields were investigated in greater detail than the other ten fields.

3.1 Four Best Fields

Table 4 summarizes results for the following four best fields: Soma-Eynez, Tunçbilek-Domaniç, Muğla-Turgut and Soma-Evciler lignite fields. The scale for CV is relative to lignites, which tend to be lower than sub-bituminous coals. These fields have a combination of geographic, technical and energy economic characteristics that make them very well suited for both pilot and demonstration projects, and are leading candidates for commercial-scale energy production by UCG. In comparison to UCG projects being advanced around the world, two of these fields, Soma-Eynez and Tunçbilek-Domaniç appear to be at a similar or better level of favorability according to the factors considered. In addition, Turgut and Soma-Evciler have some advantages in certain important attributes.

Table 4. Summary results for the four best fields assessed in this study

Properties	Soma-Eynez	Tunçbilek-Domaniç	Soma-Evciler	Muğla Turgut
Average CV of entire zone coal + partings	Great	Very good	Good - Fair	Good - Fair
Zone MAGE (net energy in zone)	Great	Very good	Good-Fair	Good-Fair
Figure of Merit	Great	Very good	Good-Fair	Good-Fair
Depth	Good (Deep)	Good (Deep)	Most Good	Much Good
Over-burden	Massive Marl, Very Good	Mostly Marl, Probably Good	Marl, Probably Good	Weak
Summary	Probably Excellent	Probably Very Good	Probably Very Good to Marginal	Probably Good to Ok

3.1.1 Soma-Eynez lignite field

The Soma-Eynez Lignite field is the most promising lignite field in Turkey for UCG. Both technical factors and infrastructure/environment factors appear promising. The Soma-Eynez Lignite field may be amongst the better ones in the world for UCG based on the factors considered. The coal zone has outstanding CV and MAGE values everywhere and the area and the volume of this resource is very large. The coal characteristics and depth from the surface appear excellent for UCG. The marl overburden is massive and appears to be strong, at least at moderate temperatures; it also has a low porosity and water content. One factor that creates technical uncertainity for UCG at Soma-Eynez is the uncertainity of how the marl will behave surrounding a hot UCG operation. A combination of lab testing and a UCG pilot will be needed to quantify marl thermochemical behavior and the extent of its effect on the UCG operation. After this uncertainity is eliminated, Other factors such as environmental hydrology were not considered at this point in the evaluation. Pending results from further, more detailed and wider-scoped investigation, Soma-Eynez has the potential to be an internationally top-level opportunity for UCG.

3.1.2 Tunçbilek-Domaniç lignite field

Considering its technical and infrastructure/environmental factors, Tunçbilek-Domaniç is a very promising field for commercial UCG. The coal zone has very good CV and MAGE. The area and volume of good coal and MAGE is large but less than at the Soma-Eynez Lignite Field. The properties and depth of the coal are expected to be excellent for UCG. The overburden at the Tunçbilek-Domaniç field is somewhat variable and/or uncertain containing a number of lithologies including both marl and clastic rocks. In addition, underground mines in that area have had some problems with flooding, perhaps from intersecting faults. It is very likely that UCG can be run successfully in this field, at least at the pilot

and small demonstration scale, but the factors noted above suggest that a detailed characterization and a series of pilot and demonstration operations and design work are needed to accurately determine the exact performance and economics that would be expected from a commercial operation here.

3.1.3 Soma-Evciler lignite field

The Soma-Evciler lignite field appears to have stronger overburden than Muğla-Turgut lignite field but not as good coal and potentially more challenging geological structure; it is possible that UCG could successfully perform there. Commercial prospects at Soma-Evciler are uncertain because the energy content and the richness of its coal zones at the optimal depths are less than ideal, the area and volume of candidate coal zones for UCG are limited, and the geological structure is more complex. The overburden rock at Soma-Evciler is predominantly marl. This may be as strong and massive as at Soma-Eynez but the limited data and observations available suggest that it may be more heterogeneous have more fractures and lower rock mass strength value than Soma-Eynez. There are UCG design and operation approaches that can minimize these disadvantages and at this stage it cannot be judged whether a commercial operation there would be good, medium or poor. It would need a more detailed site characterization and preliminary design estimates followed by a pilot and better design calculations to know how economical a commercial operation could be there.

3.1.4 Muğla-Turgut lignite field

The Muğla-Turgut lignite field appears to be very good for at least a UCG pilot, and possibly for a commercial operation. Muğla-Turgut warrants additional characterization and design to determine feasibility. The coal zone has more ash, water and rock partings than Soma-Eynez but its CV and MAGE values are such that UCG appears possible. In particular, large-scale and commercial prospects at Muğla-Turgut are uncertain due to weak overburden. This issue could be managed by narrow UCG cavities to minimize the roof collapse. Such an approach is expected to produce good technical performance but economic performance will not be as good as at a field with strong overburden. The costs may be acceptable and energy can be produced by UCG from this lignite field. What is needed next for Muğla-Turgut lignite field is a more detailed site characterization. Once better understood, preliminary design estimates for Muğla-Turgut lignite field would be created, followed by a pilot and better design calculations to determine the best approach to this field.

3.2 Three Possibly Feasible Lignite Fields

Three fields (Bursa-Keles-Davutlar, Thrace Basin Çerkezköy 1 and Thrace Basin Çerkezköy 2) may possibly be feasible for UCG. Bursa-Keles-Davutlar has good coal zones locally but the field is shallower than general good UCG practice would employ in commercial operations. Thrace Basin Çerkezköy 1 and Thrace Basin Çerkezköy 2 are deep lignite fields but have coal zone energy characteristics that are marginal for UCG. It is possible that UCG could work there but technical and economic performance would probably be less than the four best sites noted above. Table 5 summarizes results for the three possibly feasible lignite fields.

Table 5. Summary of the results for the three possibly feasible lignite fields

Properties	Bursa-Keles-Davutlar	Thrace Basin Çerkezköy 1	Thrace Basin Çerkezköy 2
Average CV of entire zone coal + partings	Some Good CV	Medium-Low CV	Medium-Low CV
Zone MAGE (net energy in zone)	Some Good MAGE	Medium-Low MAGE	Medium-Low MAGE
Figure of Merit (FOM)	Some Good FOM	Medium-Low FOM	Medium-Low FOM
Depth	Shallow coal >120 m	Deep Coal	Deep Coal
Summary	Possible	Possible	Possible

3.3 Seven Unpromising Lignite Fields

Unless new information appears or UCG technology changes dramatically, the following seven fields do not appear suitable for commercial UCG deployment: Tunçbilek-Demirbilek, Adana-Tufanbeyli, Thrace Basin-Edirköy, Thrace Basin-Küçükyoncalı, Thrace Basin-Safaalanı, Thrace Basin-Vize, Konya-Beyşehir. Some of the boreholes in some of these fields show possibility of supporting small pilot tests for the purpose of training or research investigation. For example in two or three boreholes in Demirbilek, rich coal zones can be found that are thick enough to potentially support underground coal gasification technically, but the economics would be poor.

4 PLOTS OF MAGE AND CV RATINGS FOR THE FOUR BEST FIELDS

For the four best fields, a UCG-ZEE analysis was done for two or three zone picks for each different coal zone in each borehole. For each borehole the most favorable coal zone pick was identified, mainly on the basis of the UCG-ZEE figure of merit. Each of these best picks has a MAGE and a CV value. Given a MAGE and a CV value, Table 3 was used to assign a relative UCG suitability rank of "promising", "possible" or "challenging". These descriptors are in a commercial context. Pilot tests could be run successfully in "possible" areas.

Figures 2 to 5 show color contour plots of these suitability rankings from the Earthvision models. It is important to remember that these plots only consider MAGE, CV and depth and not the many other important factors.

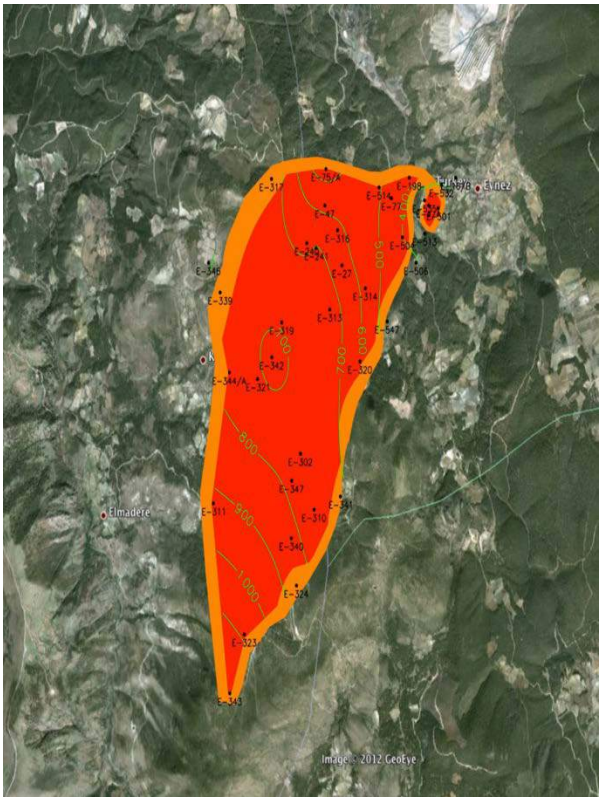

Figure 2. Coal zone suitability for the Soma-Eynez Lignite Field. Red=Favorable; Brown=Promising; Yellow=Possible; Uncolored areas with boreholes=Challenging. Green contours are depth to coal seam.

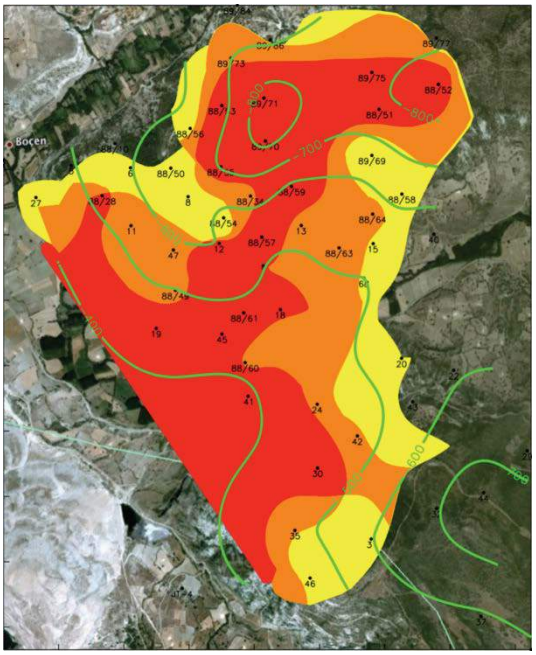

Figure 3. Coal zone suitability for the Tunçbilek-Domaniç Lignite Field. Red=Favorable; Brown=Promising; Yellow=Possible; Uncolored areas with boreholes=Challenging. Green contours are depth to coal seam.

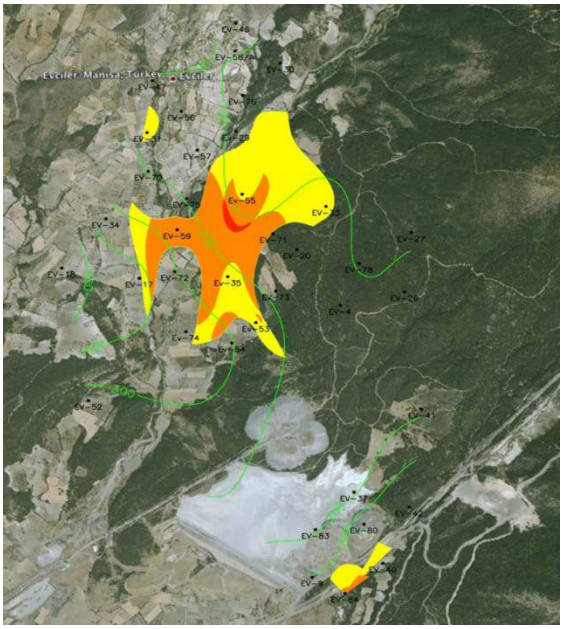

Figure 4. Coal zone suitability for the Soma-Evciler Lignite Field. Red=Favorable; Brown=Promising; Yellow=Possible; Uncolored areas with boreholes=Challenging. Green contours are depth to coal seam.

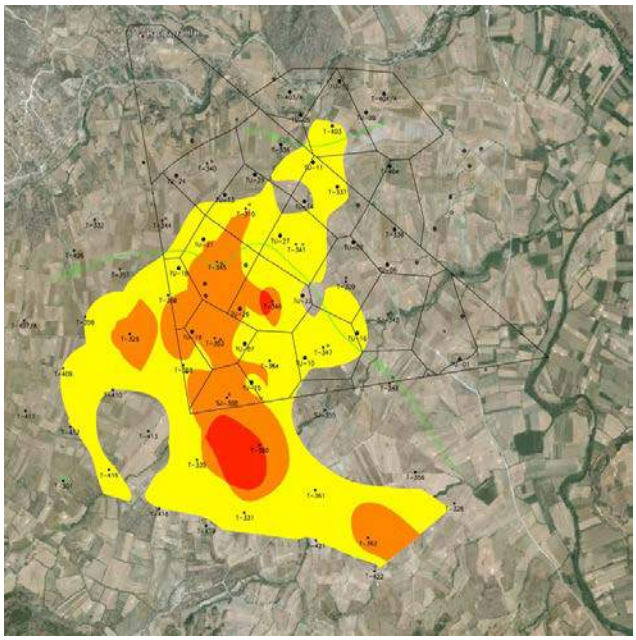

Figure 5. Coal zone suitability for the Muğla-Turgut Lignite Field. Red=Favorable; Brown=Promising; Yellow=Possible; Uncolored areas with boreholes=Challenging. Green contours are depth to coal seam.

Table 6 gives the approximate number of square kilometers for each of the four best sites that are favorable, promising, or possible in terms of their MAGE and CV values for the best some pick of each borehole. No other factors are considered here.

Table 6. Approximate number of km^2 in each category for the best fields

	Favorable	Promising	Possible
Soma-Eynez	9.2	0.3	0
Tunçbilek-Domaniç	3.8	1.3	0.8
Soma-Evciler	0.01	0.4	0.4
Muğla-Turgut	0.1	0.6	3.0

5 CONCLUSIONS

Underground coal gasification in selected Turkish lignite fields can enable the use of Turkey's indigenous low-rank coal resource to increase useful energy production in a safe and environmentally responsible way. This would enhance Turkey's energy security, and the economics may be favorable. Turkey's

energy, political and economic situation is very well suited for UCG.

- High and variable gas and oil prices from foreign suppliers,
- Growing demand for electricity, gas fuels and liquid fuels,
- Infrastructure for expanding and building electrical generation and distribution and industrial conversion plants,
- Strong science and engineering educational and research institutions capable of staffing and leading new technology projects.

Turkey has several lignite fields that are technically well suited to UCG. These fields are in locations that can provide the workforce and infrastructure and energy market (electrical production and distribution) to support UCG. The following conclusions are based on this study and current knowledge.

- Soma-Eynez lignite field is an outstanding target for UCG commercial deployment. Early and focused attention is needed to confirm that the behavior of the marl overburden is good under UCG conditions, and that the hydrology is favorable.
- Tunçbilek-Domaniç lignite field may be a very attractive target for UCG commercial development. Early and focused attention is needed to assess the behavior of the various overburden materials under UCG conditions and to characterize and design for fault-related hydrologic aspects.
- Muğla-Turgut lignite field is a good place for a pilot program and may prove to be good for commercial development. UCG module construction and operation will need to be tailored to manage the weak overburden strata.
- Soma-Evciler lignite field is a good place for a pilot program and may prove to be good for commercial development. In addition to confirming marl overburden behavior, a commercial mine plan would need to be designed to accommodate faults and dips.
- Bursa-Keles-Davutlar and Thrace Basin Çerkezköy 1 and Çerkezköy 2 lignite fields would be acceptable locations for a pilot program and/or have some potential for commerical development.

UCG projects are being advanced at locations around the world that have worse combinations of energy situation and coal resource. Turkey is unfortunate in having a challenging situation with expensive unreliable gas and oil imports. Turkey is fortunate to have domestic lignite resources that are very good for UCG that can help solve this problem. UCG can provide a secure Turkish energy supply from Turkish coal resources with production costs that should not fluctuate as much as natural gas or oil prices.

REFERENCES

Camp, D. W. and Wagoner, J. L. (2012). *Assessment of Turkish Lignite Fields for Underground Coal Gasification* (OUO). LLNL-TR-579618, 43pp.

Industrial Raw Materials and Precious Metals

Gravity Concentration and Sensor-Based Sorting to Value Recycled Aggregates

R.S. Paranhos and R.O. Neto
Federal University of Pampa (UNIPAMPA). Mining, Planning and Mineral Processing Laboratory (LATRAM), Brazil

B.G. Cazacliu and F. Huchet
The French Institute of Science and Technology for Transport, Developments and Networks (IFSTTAR), France

C.H. Sampaio and C.O. Petter
Federal University of Rio Grande do Sul (UFRGS). Mineral Processing Laboratory (LAPROM), Brazil

ABSTRACT
The proposition of this paper is to propose a sorting platform aiming to increase quality on recycled aggregates by supplementary use of mineral processing techniques and more sorting. The difficulty of liberation is discussed and the methodology currently used in mineral processing is proposed. Jigs, hydrocyclones and sensor-based sorting are equipments considered as having good performances to sort adequately recycled aggregates.

The new perspectives of sorting and liberation for recycling aggregates are discussed. Based on current process in recycling platforms, the new process with supplementary sorting of the concrete recycled is presented. The gain in density and the reduction in water absorption were studied. The relation between the water content and the density of aggregates is analysed for three quality levels of recycled aggregates.

The gain in density and the reduction in water absorption were linked with rates of replaced aggregates. In our study, replacing a lower quality aggregate by another with medium quality leads an expected gain in density about 4%. On the other hand, if replaced by superior quality, the expected gain will be 8.4%. As consequence, 34% on reduction in water absorption could be obtained too.

Keywords: Gravity concentration, sensor-based sorting, aggregate recycling

1 INTRODUCTION

The construction industry is a major solid waste generator around the world (Ulsen, 2013). Construction and demolition waste (CDW) is generated through the construction, renovation, and demolition processes of residential or commercial buildings, roads, bridges, etc. The CDW material usually is not (re)used and becomes an important environmental problem (Raoa et al., 2007). They can be stock in landfields, or the inert part is traditionally in roads, dams, etc.

In order to facilitate recycling, automatic optical sorting were developed in mining industry to process different ores. Gülsoy et al. (2012) studied optical sorting with CCD cameras in coal beneficiation. The technique was used to improve coal beneficiation for coals with high near-gravity materials. Optical sorting was tested with positive results for materials having significant colour differences. Ergün et al. (2012) used optical sorting to treat iron and chromium ores. For iron ores, samples were taken from a magnetite processing plant. The purpose of the study was to concentrate hematite that

was mixed with silicates. Optical sorting depends of many factors, such as, particle size, surface conditions, light source, feed rate, etc.

Dehler et al. (2012) conducted two tests with borates treatment, by the use of near-infrared sorting. CCD cameras were used as sorting sensors, which have opened new possibilities for sorting in the mining industry. The difference is based on the wavelength of response spectrum.

In urban and metropolitan areas, the building materials recycling industry has used stationary plants to process concrete and masonry demolition waste. A relatively pure, high quality granulates are produced with recycling requirements. Considering these environmental context, the aim of this paper is to make more attractive the sorting systems, i.e. less energy consumption and less emissions. They can produce different flows with more homogeneous composition and provide a specific reuse or a recycling. The process detailed in this paper is based on the use of gravity concentration and sensor-based sorting.

2 MINERAL PROCESSING APPLIED IN CDW

2.1 Difficulty of Liberation

Several studies about recycled concrete have been published in the last years (Gomez-Soberon, 2002; Oikonomou, 2005; Akbarnezhad, 2010; Marie et al., 2012). Recycled concrete is produced by reducing the size of concrete debris through multiple crushing stages. According Akbarnezhad (2010), depending on the size, the crushed concrete particles can present middlings, which contains particles of natural aggregates mixed with mortars (Figure 1).

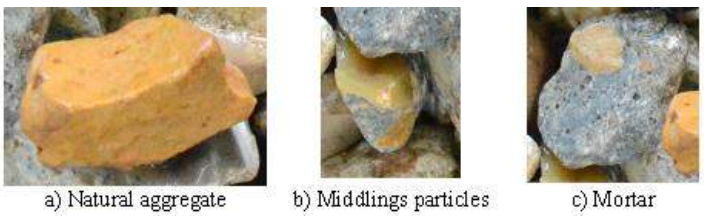

Figure 1 - Recycled aggregate (6-10 mm) (Source: PN Recybéton project, 2011.

After comminution, a mineral can be totally or partially liberated. The particles liberation depends on the mineralogical origin, the quality of the concrete, the angularity of the original aggregates, the comminution process, size, etc. In order to increase liberation, a preparation circuit should be used, to allow more intensive use of the recycled materials. With the beneficiation of recycled concrete material, more liberated particles can be achieved. In this sense, the use of innovative separation techniques in quarries, as sensor-based sorting or/and gravity concentration, will increase the quality of the products generated, as well as the price that they can be sold. These mining techniques, which are common in mining industry, could ensure a more efficient sorting in quarries.

2.2 Use Of Mineral Processing Techniques With Recycled Concrete

Gravity concentration is defined as the process whereby particles of different sizes, shapes and densities are separated from each other by gravity or by centrifugal forces. It is called gravity concentration once the separation is performed mainly based on the density (specific gravity) (Sampaio, 2005). Gravity concentration processes show high mass throughput and low investment and operational costs. Moreover, there is no limit for the maximum particle size and can be used for particles with wide size ranges. Furthermore, reagents are not used and this contributes significantly for low operational costs as well as for low environmental impacts.

Jigging is a separation process which consists of repeated expansion (dilatation) and contraction (compression) of a vertical bed of particles by a pulsating movement of water or air (Agricola, 1950)(Lyman, 1992). The result is the stratification of the bed. The particles are deposited in layers with increasing densities from the top to the bottom. Jigs were and still are widely used mainly due to their costs. They present low operational costs, are robust, have high capacity, are easy to operate and can treat

ores with a wide particle size range. They are also capable of working with large fluctuations of ore contents, feed rate and solids amount. For this reason, they are largely used in the treatment of alluvial ores.

Water-Only Cyclone (WOC) is a hydrocyclone in which the density is the major separation property. The shape of the hydrocyclone was changed to improve the influence of the particle density and to diminish the influence of the particle size and shape (O'Brien, 1976) (Weyher, 1969). There are several different names used in the industry to name WOC, such as wide-angle cyclone, circulating bad-concentrator (CBC), autogenous hydrocyclone, etc.

The use of optical sorting devices are increasing each year in the mining industry (Nienhauss et al., 2014) (Raulf et al., 2012). There are several reasons for the ever increasing use of this kind of sorting: ability to automate the sorting process, possibility of separation (quantity and accuracy), add an economic value to the final products in relation to the traditional separation process, etc. In recycling, Angulo (2013) performed experiments on optical separation of bricks from CDW in Brazil. The main difficulty faced was the non-homogenous Brazilian waste. Angulo identified significant variations in their characteristics such as density and water absorption. The origin of these fluctuations, such as porosity, is due to red tiles, bricks and mortars. Density and water absorption are related to the porosity. The higher is absorption of water, the higher is porosity. That is the main problem of mixed particles in aggregates; porosity has an important impact on the quality of concrete.

3 NEW PERSPECTIVES OF SORTING AND LIBERATION FOR RECYCLING AGGREGATES

Despite techniques for sensor-based sorting, as well as for gravity concentration processes, are widely used in material recycling and in ore treatment (Sampaio, 2005; Wills, 2006), the choice of concentration equipment to be installed depends, besides the desired cut precision, on the physical properties of the material to be beneficiated. Therefore, an extensive characterization before the mineral processing is indispensable. The main characteristics to be studied are porosity, water absorption and density distribution because they are associated with liberation. Many different techniques of separation or concentration may be used, alone or associated with others. Gravity concentration processes, as for instance jigs and cyclones, has many positive characteristics suggesting that they can be used to treat CDW.

3.1 Current Advanced Process

Many studies show that RCA with different replacement rate provides concrete building of quality. The recent standards provides for the possibility of introducing recycled aggregates in structural concrete, limiting the rate of substitution. In the quarries, the material can be processed by stages: a first stage of sorting by many techniques as manual sorting and/or screening; in a second stage, a sensor-based sorting and/or a gravity concentration is used. In addition, sand fraction had a relative importance in this context. If quarries produce a significant amount of fine particles during the process, on the other hand, recycling plants need to produce all size fractions from recycled aggregates, including sands.

Nowadays, there are the pre-sieving and segregation of ferrous scrap by overhead magnetic separators. The use of picking belts enables separation of large disturbing substances, before material with a particle size of > 45 mm is transformed into granulates, mainly by impact crushers. After repeated segregation of separated ferrous scrap, follow a fractional sieving and separation of light substances by air classifiers. This technique allows the production of well qualified, close size fraction granulate mixtures. Products being processed in this way are of high quality and can be assigned as recycling materials (RCA1). In many countries, this material is currently used on roads and terracing. They

rarely are used on concrete structures. In general, the aggregate for these applications are obtained from well mastered sources (specific demolition sites, producing a large amount of not contaminated concrete).

3.2 Process With Supplementary Sorting Of The Concrete Recycled (First Improved Process)

Aiming to increase the recycling rate on concrete formulation, the use of high quality recycled aggregates during recycling off-site or on-site is suggested. In this stage of recycling, gravity concentration by jigs and sensor-based sorting are used to separate different particles (2/20 mm) as bricks, tiles, gypsum and glass, previously concentrated. The aim is to have high quality particles and more liberated particles. These particles have similar colours and could not be separated by conventional optical sorting by colour. Impurities here are can represent around 14% of total waste according Coelho (2013) and Ulsen (2013).

These recycled aggregates, before concentrating, still contain a significant amount of adhered mortar. Firstly, the jig will treat the coarser particles of recycled aggregates in two different density fractions. The fraction with density > 2.1 g/cm^3, that represent 90% according Sampaio (Sampaio, 2005), is sent to an optical sorting to generate a concentrate called Recycled Concrete Aggregate (RCA2). The impurities from sensor-based sorting that represent at least 11% considering jig efficiency, and the fraction with density < 2.1 g/cm^3 from jig are called Light Recycled Aggregate lower quality and they sent to next stage.

3.3 Process With Supplementary Production With High Quality Recycled (Second Improved Process)

This process aims at further increase recycling rates, perhaps beyond 100% substitution of gravel. A priori, this process is developed for recycling or reuses the on-site materials to minimize the production of waste leaving the site. In addition, the lower density recycled sand may have applications in the manufacture of new cements or on public works applications with better binding properties, for instance, their use as an addition (after re-grinding) during production concrete on site. We limit ourselves in this work to study how to sort recycled aggregates and the advantage of increasing the degree of substitution of aggregates at the site.

This stage of sorting receives Light Recycled Aggregate with low quality (density < 2.1 g/cm^3) and impurities of jig and sensor-based sorting. All granulates are crushed at size < 4 mm in order to liberate mortar that is adhered to the sand fraction (0/4 mm). Gyratory crusher has high efficiency to release aggregates but another type of crusher can be used (PN Recybéton, 2011). Then WOC beneficiate the fines particles of RCA lower quality in two different density fractions. The first fraction with density > 2.1 g/cm^3 is sent to Concrete Aggregate High Quality (RCA3). The second fraction with density < 2.1 g/cm^3 from WOC is sent to improve terracing (Figure 2).

This last stage is yet dedicated to increase the quality of the products considered inferior, aiming at the production of top-sands for high quality concrete and earthworks. The advantages are a best concrete, or more extended use of recycled material or less cement consumption, or maybe better road aggregates. The reduction of sorting in the current process can save costs. It means reduction of gypsum still present in the mixture, by the replacement of picking belts. The disadvantages are the costs that will be discussed later.

The efficiency of air jigs are lower than the same type of process using water (water jigs). Air jigs have larger feeding rate as a function of the equipment size, due to the fact that the particles settle in air faster than in water (Sampaio, 2005). It makes the investment and operational costs lower. The jig can be used primarily for the removal of part of the light particles (density < 2.1 g/cm³), as a rougher stage. The pre-concentrate (density > 2.1 g/cm³) will be treated in the sensor-based sorting. In this

way, many of the low density particles will be removed in the jig and the final concentrate will be quite pure. A major disadvantage of using air jigs for fine particles treatment is its low efficiency. Particles below 2 or 3 mm are treated with very low efficiency in air jigs. In these sizes, wet processes are always recommended.

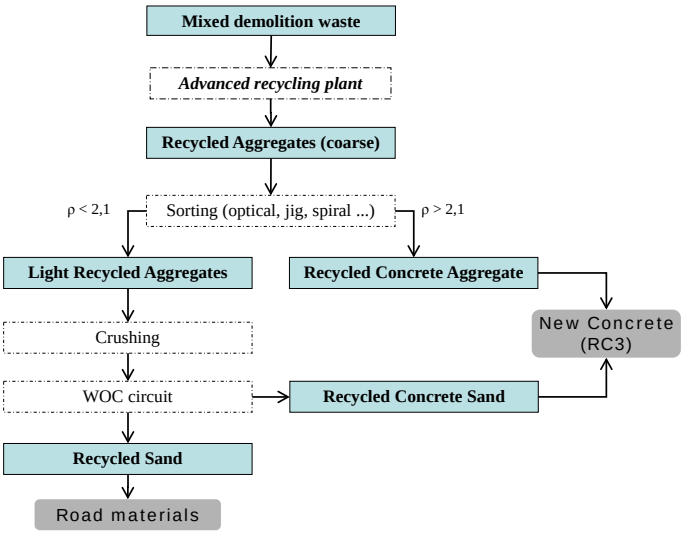

Figure 2 – Scheme of recycling production of high quality recycled concrete production (Paranhos et al, 2015).

All the particles will be comminuted under 4 mm (size of sands). In this last stage, a circuit of water-only cyclones was chosen, due to, besides the size of the particles to be treated, its versatility in gravity concentration. Investment costs of a WOC circuit are very low. When they are used in series of 2 or 3 equipment, they present quite good cut efficiencies.

4 METHOD OF COMPARISON

4.1 Method to Fix the Substitution Rate For a Given Concrete Application

A standard formula is proposed (for example: Aggregates = 1000 kg, Sand = 900 kg, Cement = 280 kg and Water = 180 kg), without recycled aggregate, to allow an identical result at the product RCA3. The products are based on a typical concrete formulation and the density of a mix concrete can be calculated according its proportions and densities in the mixture:

$$D = \frac{FA}{100} \times \left(\frac{subst_{FRA} \times d_{FRA} + (100 - subst_{FRA}) \times d_{FNA}}{100} \right) + \frac{CA}{100} \times \left(\frac{subst_{CRA} \times d_{CRA} + (100 - subst_{CRA}) \times d_{CNA}}{100} \right)$$

Where:
D – Weighed density of concrete mixture;
FA – Percentage or fine aggregates used in the mixture;
CA - Percentage or coarse aggregates used in the mixture;
substFRA – Replacement level (%) of fine natural aggregates with fine recycled aggregates;
substCRA – Replacement level (%) of coarse natural aggregates with coarse recycled aggregates;
dFRA – density of fine recycled aggregates;
dFNA – density of fine natural aggregates;
dCRA – density of coarse recycled aggregates;
dCNA – density of coarse natural aggregates.

To solve the above equation, it is necessary to know the water absorption of gravel and sand recycled. These values are determined taking into account the average density of the aggregates.

4.2 Price of Transportation and Taxes

It is important to determine transportation costs of aggregates or recycled materials mainly of the construction and demolition works. The price of transportation Pr can be calculated in function of distance, as indicated:

$$\Pr = \left(VC \times d + FC \times \frac{(\frac{d}{s} + t)}{10} \right) \times (1 + m) / w$$

Where:
Pr = price per tonnes (€/tons)
VC = variable costs (€/tons)
FC = fixed costs (€/day)
d = distance (Km)
w = weight per truck (tons) = 20 tons fixed
t = time to charge and discharge (h)
s = speed (Km/h)
m = profit margin

The transport costs by trucks can be related with the transport of virgin aggregates to construction sites or with the transport of CDW to recycling plants. They always have linearity with distance travelled. These results were obtained considering truck speed of 63 km/h, time to charge and discharge of 2 h, fixed costs of 156.01 €/day, variable costs of 0.43 €/km and business's margin of 0.33.

5 RESULTS AND DISCUSSIONS

5.1 Optimal Substitution Rate

The estimation of water absorption of the recycled aggregates from sorting plants, according to the rate of replaced aggregates is presented in Figure 3. The average absorption and density of natural aggregates were considered as 0.8% and 2650 kg/m³, respectively. This figure shows clearly that the treatment improves a lot of quality on recycled aggregates changing water absorption (and densities) of the products easily. According to the plant described (Figure 2), the water absorption of RCA1 was 11.7%, 7.0% of RCA2 and 3.6% of RCA3. Densities were 1900 kg/m^3, 2085 kg/m^3, 2210 kg/m^3 and 2650 kg/m^3, respectively.

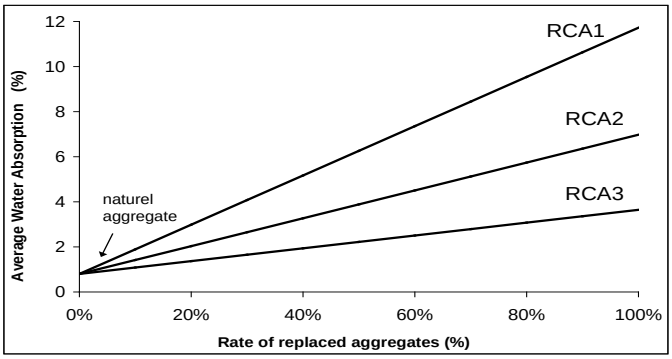

Figure 3 – Estimation of water absorption of recycled aggregates RCA1, RCA2 and RCA3 obtained from treatment according the rate of replaced aggregates

5.2 Gain in Density and Reduction in Water Absorption

Figure 4 shows the possibility of quality increasing of recycled aggregates by the use of a recycling plant. The probable gain on density or reduction on water absorption is linked with the percentages of replaced aggregates. If 50% of RCA1 were replaced by RCA2, the expected gain in density will be 4% (Figure 4a). On the other hand, if RCA1 were replaced by RCA3, the expected gain will be 8.4%. The same situation concerning reduction on water absorption is showed in Figure 4b. The levels of quality described in this analysis (i.e. levels of density and water absorption) can be assured by fine adjustment of gravity concentration equipment mainly changing the cut-off grade. The mass balance and the metallurgical balance should be carried out after any adjustments.

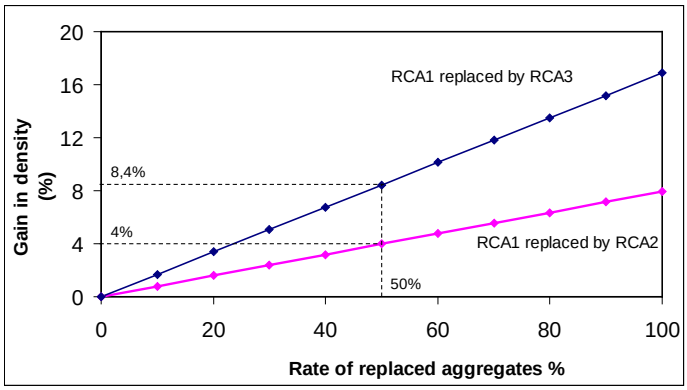

a) Gain in density

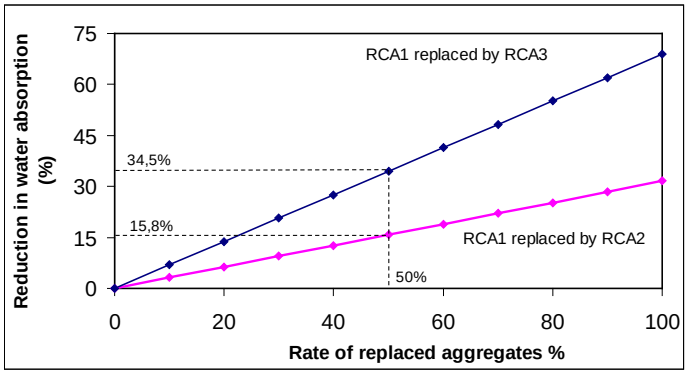

b) Reduction in water absorption

Figure 4 – The potential gain in density and the reduction in water absorption, linked with rates of replaced aggregates.

By the methodology proposed, the real possibility of gain in quality can be measured by the economic advantages obtained using the processing plant. In this context, the choice of improve or not improve sorting is related with the costs balance including transport, distances and indirect costs.

6 CONCLUSIONS AND PERSPECTIVES

The improvement of recycled concrete is the main subject of this paper. As an alternative to the heat treatment, the proposition is increase quality on recycled aggregates by supplementary use of mineral processing techniques.

A sorting plant is proposed. Fine and coarse aggregates are treated by gravity concentration processes, which are widely used in mineral processing. During all stages of sorting process, it is possible to adjust the quality of recycled aggregates, i.e. density and water absorption. An approximate graphic method has been used to estimate mixed aggregates proportion.

The main advantages of recycling plants are the superior quality of the materials. It is possible to increase the rate of recycling in concrete and save costs. The main disadvantages are the investments in sorting equipment. Their maintenance was not evaluated in this work. However, the gain in density and the reduction in water absorption were studied.

In the study, replacing a lower quality aggregate by another with medium quality, for instance RCA1 replaced by RCA2, leads an expected gain in density about 4%. On the other hand, if RCA1 is replaced by RCA3 (superior quality), the expected gain will reach 8.4%. As consequence, there are 34% reductions in water absorption.

ACKNOWLEDGEMENTS

The Coordination for the Improvement of Higher Education Personnel (CAPES) and the CNPq from Brazil, Federal University of Pampa (UNIPAMPA), Federal University of Rio Grande do Sul State (UFRGS) and the French Institute of Science and Technology for Transport, Development and Networks (IFSTTAR) are acknowledged.

REFERENCES

A. Akbarnezhad, K.C.G. Ong, M.H. Zhang, C.T. Tam, T.W.J. Foo. Microwave-assisted beneficiation of recycled concrete aggregates, 2010. Construction and Building Materials 25, 3469–3479.

Agricola, G., 1556. De Re Metallica, (Translated by H.C. Hoover e L.H. Hoover), Dover Publications (1950).

Ângulo, S.C., John, V.M., Carrijo, P. M., Figueiredo, A. D. and Chaves A. P., V. On the classification of mixed construction and demolition waste aggregate by porosity and its impact on the mechanical performance of concrete. Materials and Structures (2010) 43:519–528. DOI 10.1617/s11527-009-9508-9.

Ângulo, S.C., John, V.M., Ulsen, C., Kahn, H., Mueller, A., 2013. Separação óptica do material cerâmico dos agregados mistos de residuos de construção e demolição. Revista Ambiente construido, Porto Alegre, ISSN 1678-8621.

Cazacliu, B., Sampaio, C.H., Miltzarek, G., Petter, C., Le Guen, L., Paranhos, R., Huchet, F. And Kirchheim, A.P., 2013. The potential of using air jigging to sort recycled aggregates. Journal of Cleaner Production 66, 46-53.

Coelho, A. and de Brito, J., 2013. Economic viability analysis of a construction and demolition recycling plant in Portugal – part 1: location, materials, technology and economic analysis. Journal of Cleaner Production 39, 338-352.

Colas, S., Louis, H., Moreau, J. and Pasquier, J.L., 2013. La production de granulats par département. Datar – Observatoire des territoires, Ministère du développement durable, France.

Dehler, M., Robben, M., 2012. NIR versus Color Sorting of Industrial Minerals. Sensor Based Sorting 2012, Aachen, Germany.

Ergün, L.Ş., Gülsoy, Ö.Y., Gülcan, E., 2012. Optical Sorting of Iron and Chromite Ores. Sensor Based Sorting 2012, Aachen, Germany.

European Committee for Standardization, February 2011. Aggregates for concrete. Final Draft Fr EN 12.620.

European Committee for Standardization, September 19, 2011. Use of Aggregates in Concrete. TC104-SC1-TG19, Sixth Draft Text for EN 206.2011.

French Law n° 2010-788, 2010. National engagement for environnemental (Grenelle de l'environnement). Ministère de l'écologie, du développement durable, des transports et du logement.

Gomez-Soberon, J.M.V. Porosity of recycled concrete with substitution of recycled concrete aggregate. An experimental study, 2002. Cement and concrete research 32, 1301– 1311.

Gülsoy, Ö.Y., Ergün, L.Ş., Gülcan, E., 2012. Optical Sorting of Low Rank Coals – a Subsidiary Study. Sensor Based Sorting 2012, Aachen, Germany.

Kohler, G., and H. Kurkowski. Optimising the use of RCA. Sustainable construction: use of recycled concrete aggregate – proceedings of International Symposium. Department of Trade and Industry

Conference Centre, London, UK, 11-12 Nov. 1998. http://trid.trb.org/view.aspx?id=709927.

Lyman, G.J., 1992. Review of jigging principles and control, Coal Preparation, vol. 11, pp. 145-165.

Marie, I., Quiasrawi, H. Closed-loop recycling of recycled concrete aggregates 2012. Journal of Cleaner Production 37, 243-248.

Miller, F.G., De Mull, T.J., Matoney, J.P., 1985. Centrifugal specific gravity separator, In: SME Mineral Processing Handbook (N.L. Weiss, ed.), SME, Littleton.

Muigai, R., M. G. Alexander, and P. Moyo. "Cradle-to-Gate Environmental Impacts of the Concrete Industry in South Africa." Journal of the South African Institution of Civil Engineering 55, no. 2 (January 2013): 02–07.

Mulder, E., Tako P. R. J., and Lourens F. "Closed Cycle Construction: An Integrated Process for the Separation and Reuse of C&D Waste." Waste Management, Wascon, 2006. 6th International Conference: Developments in the re-use of mineral waste, 27, no. 10.

Nagataki S, Gokce A, Saeki T, Hisada M. 2004. Assessment of recycling process induced damage sensitivity of recycled concrete aggregates. Cem Concr Res; 34:965–71.

Nienhaus, K., Pretz, T., Wotruba, H., 2014. Sensor technologies: Impulses for the raw materials Industry. Shaker Verlag GmbH, Aachen, 2014. ISBN 978-3-8440-2563-7.

O'Brien, E.J., 1976. Water-only cyclones: their functions and performance, Coal Age, January, pp.110-114.

Oikonomou, N.D. Recycled concrete aggregates, 2005. Cement & Concrete composites 27, 315–318.

Paranhos, R.S., Cazacliu, B.G., Sampaio, C.H., Petter, C.O., Neto, R.O., Huchet, F. A new methodoogy to value recycled concrete, 2015. Journal of cleaner production.

PN Recybéton. May 2011. Complete Recycling of Concrete. Feasibility Report. PN Recybéton, France (in French).

Raoa, A., Jhab, K., Misraa, S., 2007. Use of aggregates from recycled construction and demolition waste in concrete. Resources, Conservation and Recycling 50, 71 – 81.

Raulf, K., Pretz, T., Wotruba, H., 2012. Potential of Sensor Technologies in the Raw Materials of Industry. Sensor Based Sorting 2012, Aachen, Germany.

Sampaio, C.H, Tavares, L.M.M., 2005. Beneficiamento gravimétrico. Uma introdução aos processos de concentração mineral e reciclagem de materiais por densidade. Editora da Ufrgs.

Silva, R.V., Brito, J. and Dhir, R.K. Properties and composition of recycled aggregates from construction and demolition waste suitable for concrete production. Construction and Building Materials 65 (2014) 201-217.

Tam, V.W.I. and Tam, C.M. Evaluations of existing waste recycling methods: A Hong Kong study. Building and Environment 41 (2006) 1649–1660.

Tromp, K.F., 1937. New methods of computing the washabilities of coals, Glükauf, vol. 37, pp. 125-156.

Ulsen, C., Kahn, H., Hawlitschek, G., Masini, E. et Angulo, S., 2013. Separability studies of construction and demolition waste recycled sand. Waste Management 33, 656-662.

Visman, J., 1962. Die Sortierung abriebempfindlicher Kohle im Hydrozyklon, proceedings, IV International Coal Preparation Congress, Harrogate, UK, pp.161-170.

Weyher, L.H.E., Lovell, H.L., 1969. Hydrocyclone washing of fine coal, Transactions AIME, vol. 244, pp. 191-203.

Wills, B.A., Napier Munn, T., 2006. Mineral Processing Technology. An Introduction to the Practical Aspects of Ore Treatment and Mineral. Elsevier Science & Technology Books.

Influence of Cutting Wire Tension on Travertine Cutting Rate

S.N. Almasi, R. Bagherpour
Department of Mining Engineering, Isfahan University of Technology, Isfahan, Iran

R. Mikaeil
Department of Mining and Metallurgical Engineering, Urmia University of Technology, Urmia, Iran

A. Khademian
Department of Mining Engineering, Isfahan University of Technology, Isfahan, Iran

ABSTRACT One of the affecting parameters on production rate of dimension stone quarries is the tension in diamond cutting wire which itself can change the cutting rate. Achievement to an optimum cutting rate could be an effective step toward increasing production and reduction of costs. So, this study aims to determine the optimum cutting wire tension for different block dimensions. For this purpose, 30 cutting surface with various dimensions and under different thrust forces have been evaluated in Targh travertine quarry. These surfaces were divided into groups based on their area which varied from 50 to 100 m^2 and then each group were cut with 6 different wire tension values ranging from 45 to 65 A and eventually all of observed data were recorded. Results showed that in order to achieve the optimum cutting rate, the cutting wire tension should be high for small blocks and low for large blocks.

Keywords: Diamond wire cutting, travertine, cutting wire tension, cutting rate

1 INTRODUCTION

Nowadays diamond wire saw is widely used for cutting and shaping dimension stones in quarries, which is considered as a costly operation in these quarries. Since any increase in productivity of cutting wire leads to a reduction in total cost of stone mining, stone industry researchers always have been working on identifying the affecting factors on cutting process and improving the cutting tools efficiency.

Generally based on Mikaeil et al. (2011) opinion, affecting factors in stone cutting process are classified into three major class, including: a) stone characteristics b) cutting characteristics and c) management characteristics. Cutting characteristics and management characteristics are among controllable parameters which are influencing in efficiency, cutting capacity and cutting process. There have been many researches on how each of these parameters can affect cutting process.

In a series of researches on disk cutting process, Ertingshausen (1985) found that in shallow cuts, up-cutting mode exhibit less power consumption compared to down-cutting mode. Luo & Liao (1995) showed that while the diamond particles in segment structure have the same hardness, by reducing the diamond particles size, their chipping capacity will be reduced and as a result, more energy is required for cutting the unit surface. Kahraman et al. (2004) showed that increasing the disk diameter leads to reduction in cutting rate. Özçelik (2007) demonstrated that in cutting process of carbonate rocks, increasing the particles size cause a decrease in wear rate of beads. By investigating 6 type of granite stones, Buyuksagis (2007) found that the specific energy amount in downward cutting mode is lower compared to upward cutting mode.

Mikaeil et al. (2012) examined 7 carbonate and travertine rock samples to achieve an empirical relation for predicting the electricity power consumption for

different rocks. In the resulted relation, all of major operational parameters including disk peripheral speed, feed rate, cutting depth and rock sawability index, which represents all of rock characteristics in practice, are involved. Sengun & Altindag (2013) showed that rock strength, hardness and porosity have stronger effects on specific energy than other rock characteristics.

Unlike other researches in these field which investigate hard and soft rocks separately, Mikaeil et al. (2013) by examining 17 different rock types showed that there is an empirical relation between B3 brittleness index and production rate of granite, marble and travertine rocks with a high correlation. Mikaeil et al. (2014) in a recent study obtained some valuable relations between system vibration and operational characteristics and brittleness indexes.

There have been less investigation concerning diamond cutting wire than cutting disk, however the history of their usage are almost the same. Investigating different diamond beads, Tönshoff & Warnecke (1982) found that in high production rate condition, diamond particles density on segment should be high but their size have to be medium, and in low production rate condition, both particle size and their density should be low.

Ozcelik et al. (2004) by characterization of rock texture found a significant relationship between texture coefficient and unit wear and cutting rate of carbonate rocks so that any increase in texture coefficient, increases the unit wear of diamond particles and decreases the cutting rate.

Cai et al. (2007) conducted a research on the effects of cutting wire entrance angel and concluded that increasing the cutting angel will increase the cutting rate and this effect intensifies in higher speeds. Besides, they found that for a constant cutting area, any increment in cutting speed leads to a decline in cutting wire lifetime. In other hand, they believe that by reducing the cutting speed with the aim of increasing the lifetime of the cutting wire, the energy consumption will increase.

Ataei et al. (2011) by examining 14 carbonate rocks in 14 different quarries, found some logical empirical relations between cutting rate and rock characteristics. Ghaysari et al. (2012) by cutting 7 type of carbonate rocks with diamond wire saw, found a relation between rock textural characteristics and the cutting rate. Yarmohamadi & Yarahmadi (2012) presented a classification system named DSRMR for dimension stones at first, and then they showed that with the increase of this index, stone cutting rate increases. It is remarkable that they neglected the presence of discontinuities in the classification system, because the data validation showed that removal of this parameter strengthens the validity of the results.

The number of diamond beads in unit length is another affecting operational parameter. Bagherpour et al. (2014) recorded the cutting rate in different faces of a working travertine quarry and concluded that the optimum beads number in unit length equals to 31.

One of the main operational parameters in diamond wire saw method is the thrust force or the pull-back force. Despite great importance of this parameter, there is no research in this field among previous studies. This study, by using performed experiments in a travertine quarry, investigates the effects of thrust force on the cutting efficiency. For this purpose, cutting of 30 surfaces with various dimensions and by different thrust forces have been evaluated. The area of these studied surfaces varied between 50 to 100 m^2 while the pull-back force range was between 45 to 65 amp. Using the recorded cutting performance parameters during these cutting and then analyzing and processing them, some results have been concluded which demonstrate the optimum state of this operational parameter.

Required data for this study have been recorded on some active working faces of Targh quarry, which is one of the largest travertine quarry of Iran. This quarry is located about 3 kilometers away of Targh village, which is located in Natanz county in Isfahan province. The experiments and field

studies of this research took benefit of the great extent and presence of various working faces in this quarry.

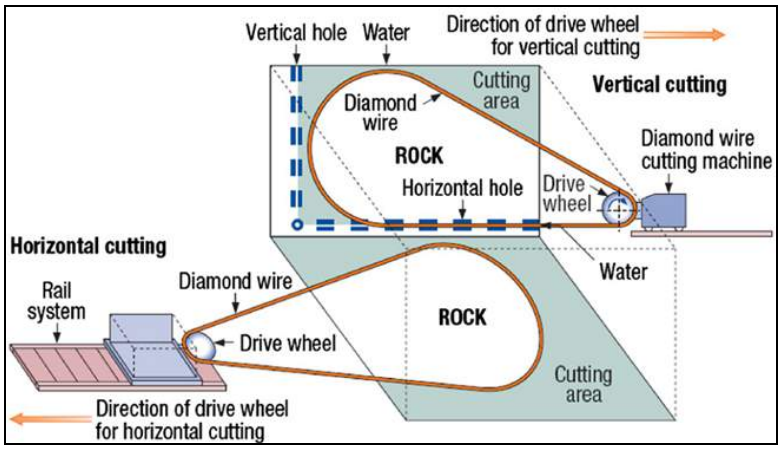

Figure 1. Diamond wire saw method in dimension stone quarrying (Ozcelik & Yilmazkaya, 2011)

2 DIAMOND WIRE SAW METHOD AND CUTTING PROCESS

Diamond wire saw method is the most common method of dimension stone mining in most countries, which has been illustrated in Figure 1. This method is widely using in dimension stone quarries and have been passed multiple developmental stages already.

Diamond cutting wire consists of some cutting beads that some springs set them apart and all of them are mounted on a steel cable formed by several strands of metal wire twisted into a helix (wire rope). Every bead is simply a steal cylindrical ring, which is equipped with some abrasive material by sintering or electroplating techniques.

Stone cutting by these beads takes place by abrasion of rock forming particle of the stone by some abrasive diamond grits. Depending on the position of beads in relation to the cutting face, various amounts of forces apply to the cutting face. Molfino & Zoppi (2012) Believe that the maximum force applied to the cutting surface occurs when the bead is about to leave the cutting surface and at this point, the chipping process will be accomplished. This process occurs for all of beads and in this way, the cutting process of the stone happens.

3 AFFECTING PARAMETERS ON CUTTING CAPACITY IN DIAMOND WIRE SAW METHOD

As can be seen in table 1, all of affecting parameters on the cutting process are divided into two categories of controllable and uncontrollable. The uncontrollable parameters are constant in all cutting methods including disk cutting, sawing, and wire cutting, while controllable parameters differ from a method to another and one can optimize them to achieve a higher production rate.

Table 1 is a developed version of what other researchers including Ozcelik (2010), Ataei (2012) and Mikaeil (2011) have used in their published researches.

During performance evaluation of a system in order to achieve optimal conditions, there are different criterion that considering each of them is important. In diamond wire saw method, the electricity power consumption, cutting rate, cutting wire cost, cutting wire efficiency of lifetime, diamond bead wear rate and cutting specific energy are the most important criterions. Achievement to any correlation between these criterions and the parameters listed in Table 1 can be effective in planning and optimization of cutting process. However, during investigation the correlation of a variant, it is so important to keep all of other parameters invariant, which is impossible in many cases and brings some uncertainty into the results. As previously

mentioned, this study intends to investigate the correlation between pull-back force and the production rate. In order to achieve reliable results, it is necessary to perform all of cuttings with the same machine and tools. Table 2 summarizes operational parameters of cutting machine, which maintained constant during all of field studies.

Table 1. Effective parameters of diamond wire saw method

Uncontrollable parameters	Controllable parameters	
Rock characteristics	**Cutting characteristics**	**Management characteristics**
❖ **Physical properties**	❖ **Tool Properties**	Skilled manpower
Density	Main Motor power	Machine vibration
Porosity	Machine required voltage	Environmental conditions
Texture	Pulley diameter	
Particles size and shape	Bead type (sintered or electroplated)	
Cementation type and degree	Bead Matrix structure	
Quartz content	Diamond grits size, type and density	
Water absorbtion coefficient	❖ **Operational properties**	
Water content	Cutting wire linear speed	
Waves conductivity	Pull-back force	
❖ **Mechanical properties**	Cutting wire entrance angel	
Strength properties	Block dimensions	
Hardness	Wire length	
Abrasiveness	Cutting type (vertical or horizontal)	
Brittleness	Wire geometry during cutting	
Elasticity	Distance between machine and face	
❖ **Structural properties**	Number of beads per meter	
Discontinuities	Orientation and quantity of Water used	

Table 2. Operational parameters of cutting machine

Parameter	Description
No. of beads per meter	30-32
Power of machine (Main motor)	37 KW
Wire peripheral speed	30-35 m/s
Voltage	380 V
Wire length	60-75 m
Pulley diameter	800 mm
Diamond beads (sintered)	0.63 carats/bead

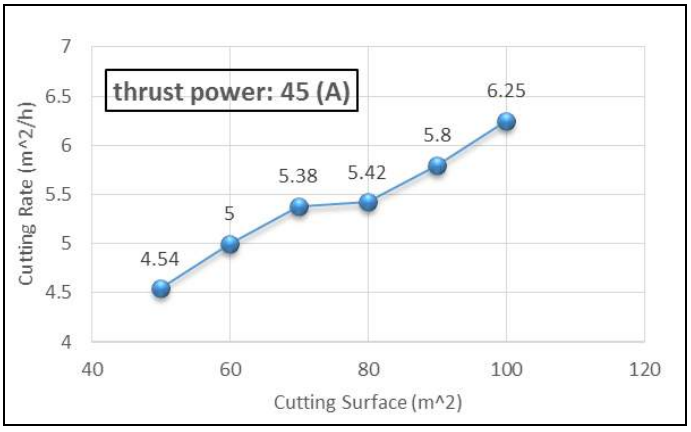

Figure 2. Cutting efficiency against cutting surface

4 CORRELATION OF THRUST FORCE AND CUTTING EFFICIENCY

The pull-back (thrust) force is typically set on 45 to 65 amp for cutting travertine stones. As table 3 shows, by fixing the thrust force on 45 amp, it can be seen that as the cutting surface decreases, the cutting rate decreases also. In other words, the highest cutting efficiency occurs with cutting surface of 100 m^2 while the lowest cutting efficiency happens with cutting surface of 50 m^2. Figure 2 demonstrates the trend of these variations.

Table 3.Cutting efficiency for thrust 45 A

Cutting dimensions (m)	Cutting surface (m^2)	Cutting time (hour)	Cutting efficiency (m^2/h)
10×10	100	16	6.25
10×9	90	15.5	5.80
10×8	80	14.75	5.42
10×7	70	13	5.38
10×6	60	12	5
10×5	50	11	4.54

It is wondering that how the thrust force can affect the cutting efficiency. In order to answer such questions, by changing the thrust force, the efficiency values of cutting blocks with various dimension are recorded. Tables 4–7 report the cutting efficiency for different thrust cases including 50, 55, 60 and 65 amp.

Table 4. Cutting efficiency for thrust 50 A

Cutting dimensions (m)	Cutting surface (m^2)	Cutting time (hour)	Cutting efficiency (m^2/h)
10×10	100	18	5.55
10×9	90	16	5.62
10×8	80	15	5.33
10×7	70	13.5	5.18
10×6	60	11	5.45
10×5	50	10	5

Table 5. Cutting efficiency for thrust 55 A

Cutting dimensions (m)	Cutting surface (m^2)	Cutting time (hour)	Cutting efficiency (m^2/h)
10×10	100	19	5.26
10×9	90	16	5.62
10×8	80	14	5.71
10×7	70	12	5.83
10×6	60	10.75	5.58
10×5	50	9.25	5.40

Table 6. Cutting efficiency for thrust 60 A

Cutting dimensions (m)	Cutting surface (m^2)	Cutting time (hour)	Cutting efficiency (m^2/h)
10×10	100	20	5
10×9	90	17	5.29
10×8	80	14	5.71
10×7	70	11	6.36
10×6	60	10	6
10×5	50	8	6.25

Table 7. Cutting efficiency for thrust 65 A

Cutting dimensions (m)	Cutting surface (m^2)	Cutting time (hour)	Cutting efficiency (m^2/h)
10×10	100	20	5
10×9	90	17	5.29
10×8	80	14	5.71
10×7	70	11	6.36
10×6	60	10	6
10×5	50	8	6.25

As can be seen in table 4, thrust force of 50 brings the highest cutting efficiency for blocks with cutting surface of 90 m^2, while the efficiency decrease with any increase or decrease in cutting dimensions. Table 5 shows that in thrust force of 55, the highest efficiency is achieved with the cutting dimensions of 70 m^2. According to table 6, the highest efficiency with thrust force of 60, belongs to cutting surface of 70. Table 7 which reports the cutting parameters for the highest thrust force, shows that the highest thrust force in this case occurs with cutting surface of 50 m^2.

5 DISCUSSION

It can be concluded from previously mentioned tables that it is better to use lower levels of thrust force when the block dimensions are high, and as the cutting surface decreases, it is better to increase the thrust force. Besides, as it can be seen in figure 2, which is based on table 3 and table 6, for thrust forces of 45 and 65 the cutting rate shows a totally reverse correlations. In other words, for thrust force of 45 A increasing the dimensions will lead to increased cutting efficiency while for thrust force of 65 A as the dimensions increases, the cutting efficiency reduces.

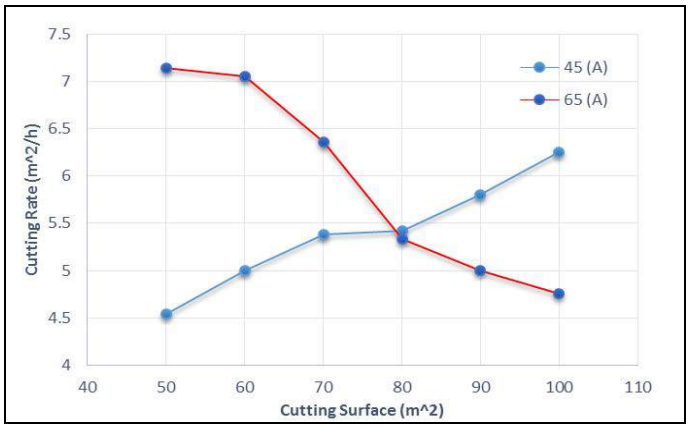

Figure 3. Cutting efficiency against Cutting rate

Of course, this fact cannot be ignored that excessive increase in pull-back force, rises the wire tension consequently and increases the likelihood of wire rupture. Wire rupture reduces the safety level of working place and

induces some financial and time loss to the quarry.

There is not any analysis on cutting surface of 80 m^2 in above discussions. So it seem that in order to achieve a more comprehensive analysis it is required to summarize tables 3 to 7 in a single table. Therefore, table 8 summarizes the cutting efficiency of cutting operations for all values of thrust forces.

Table 8. Cutting efficiency values for various thrust forces

Block Dimensions (m^2)	Cutting efficiency				
	Thrust: 45	Thrust: 50	Thrust: 55	Thrust: 60	Thrust: 65
100	6.25	5.55	5.26	5	4.76
90	5.80	5.62	5.62	5.29	5
80	5.42	5.33	5.71	5.71	5.33
70	5.38	5.18	5.83	6.36	6.36
60	5	5.45	5.58	6	7.05
50	4.54	5	5.40	6.25	7.14

The following results can be conclude from table 8:

1. For the cutting operations with cutting surface of 90 m^2, both thrust forces of 50 and 55 produces the same cutting efficiency, so in order to enhance the safety condition of working place it is suggested to use the thrust force of 50 A.
2. In case of cutting surface of 80 m^2, both thrust forces of 55 and 60 produces the same highest efficiency, so one must choose the thrust force of 55 because of the same reason mentioned previously.
3. for the cutting operations with cutting surfaces of 70 m^2, however the thrust force of 65 A produces the same efficiency, the thrust force of 60 A is suggested.
4. For cutting surface of 60 m^2 and below, the maximum thrust of 65 A is suggested.

It must be noted that practical experiences in quarries will examine the validity of these results. Besides, in higher thrust forces there should be more consideration about the cutting machine power.

6 CONCLUSION

- In order to achieve the optimum efficiency, it is better to lower the pull-back force as the cutting surface area increases.
- In case of lowest thrust force, an increase in block dimension associates with increasing the cutting rate, while the reverse is true for the highest thrust force.
- For cuttings that have cutting surface below 60 m^2, the highest efficiency achieves with higher thrusts, so if the machine can afford the required power, the highest thrust should be chosen for the cutting operation.
- While the cutting efficiency is the same for two different thrust values, it is better to operate with the lower thrust due to safety reasons.
- All results of this study appertains to travertine rocks, which can be generalized for all carbonate rocks. But for granite and other hard rocks some further studies should be performed.
- Data uncertainty arises from two source in this study: a) measurement of values in a workshop environment, which is totally affected by human errors b) effects of other operational parameters on cutting efficiency. Therefore, in order to perform a more detailed and precise evaluation, the investigation should be done in a more controllable condition in a standard laboratory. These kind of studies are following up at Isfahan University of Technology.

ACKNOWLEDGEMENT

Authors would like to express their high appreciate to Ahrar-e-Sepahan Company especially Mr. Majid Alaei, the head of their exploration department.

REFERENCES

Ataei, M., Mikaeil, R., Hoseinie, S. H., & Hosseini, S. M., 2012. Fuzzy analytical hierarchy process approach for ranking the sawability of carbonate rock. International Journal of Rock Mechanics and Mining Sciences, 50, 83-93.

Ataei, M., Mikaiel, R., Sereshki, F., & Ghaysari, N., 2011. Predicting the production rate of diamond wire saw using statistical analysis. Arabian Journal of Geosciences, 5(6), 1289-1295.

Bagherpour, R., Khademian, A., Almasi, S., & Aalaei, M., 2014. Optimum cutting wire assembly in dimension stone quarries. Journal of Mining and Metallurgy, Section A: Mining, 50.

Buyuksagis, I., 2007. Effect of cutting mode on the sawability of granites using segmented circular diamond sawblade. Journal of Materials Processing Technology, 183(2), 399-406.

Cai, O., Careddu, N., Mereu, M., & Mulas, I., 2007. The influence of operating parameters on the total productivity of diamond wire in cutting granite. IDR. Industrial diamond review (3).

Ertingshausen, W., 1985. Wear processes in sauring hard stone. IDR. Industrial diamond review, 45(510), 254-258.

Ghaysari, N., Ataei, M., Sereshki, F., & Mikaiel, R., 2012. Prediction of Performance of Diamond Wire Saw with Respect to Texture Characteristics of Rock/Prognozowanie Wydajności Pracy Strunowej Piły Diamentowej W Odniesieniu Do Charakterystyki Tekstury Skał. Archives of Mining Sciences, 57(4), 887-900.

Kahraman, S., Fener, M., & Gunaydin, O., 2004. Predicting the sawability of carbonate rocks using multiple curvilinear regression analysis. International journal of rock mechanics and mining sciences, 41(7), 1123-1131.

Luo, S., & Liao, Y., 1995. Study of the behaviour of diamond saw-blades in stone processing. Journal of materials processing technology, 51(1), 296-308.

Mikaeil, R., Ataei, M., Ghadernejad, S., & Sadegheslam, G., 2014. Predicting the Relationship Between System Vibration with Rock Brittleness Indexes in Rock Sawing Process. Archives of Mining Sciences, 59(1), 139-153.

Mikaeil, R., Ataei, M., & Yousefi, R., 2011. Application of a fuzzy analytical hierarchy process to the prediction of vibration during rock sawing. Mining Science and Technology (China), 21(5), 611-619.

Mikaeil, R., Ataei, M., & Yousefi, R., 2012. Evaluating the Power Consumption in Carbonate Rock Sawing Process by Using FDAHP and TOPSIS Techniques. Efficient Decision Support Systems: Practice and Challenges-From Current to Future/Book, 2, 478.

Mikaeil, R., Ataei, M., & Yousefi, R., 2013. Correlation of production rate of ornamental stone with rock brittleness indexes. Arabian Journal of Geosciences, 6(1), 115-121.

Molfino, R. M., & Zoppi, M., 2012. A robotic system for underwater eco-sustainable wire-cutting. Automation in Construction, 24, 213-223.

Özçelik, Y., 2007. The effect of marble textural characteristics on the sawing efficiency of diamond segmented frame saws. IDR. Industrial diamond review (2).

Ozcelik, Y., Polat, E., Bayram, F., & Ay, A., 2004. Investigation of the effects of textural properties on marble cutting with diamond wire. International Journal of Rock Mechanics and Mining Sciences, 41, 228-234.

Ozcelik, Y., & Yilmazkaya, E., 2010. Performance analysis of a diamond bead in its lifetime by using single bead test machine. Paper presented at the Proceedings of the Global Stone Congress, Alicante, Spain.

Ozcelik, Y., & Yilmazkaya, E., 2011. The effect of the rock anisotropy on the efficiency of diamond wire cutting machines. International Journal of Rock Mechanics and Mining Sciences, 48(4), 626-636.

Sengun, N., & Altindag, R., 2013. Prediction of specific energy of carbonate rock in industrial stones cutting process. Arabian Journal of Geosciences, 6(4), 1183-1190.

Tönshoff, & Warnecke, G., 1982. Research on stone sawing. Advances in Ultrahard Materials Applications Technology, 1, 36-49.

Yarmohamadi, H., & Yarahmadi, A. R., 2012. Prediction of the sawing quality of Marmarit stones using the capability of artificial neural network. International Journal for Numerical and Analytical Methods in Geomechanics, 36(7), 881-891.

Optimum Distance Between Cutting Machine And Working Face In Travertine Exploitation With Diamond Wire Cutting Method

A. Khademian, R. Bagherpour, S.N. Almasi
Department of Mining Engineering, Isfahan University of Technology, Isfahan, Iran

M. Aalaei
Ahrar Sepahan Co, Ahrar building, Baborrahme Ave, Isfahan, Iran

ABSTRACT Production process in dimension stone quarries, which are exploiting with diamond wire cutting method, has a close relationship with cutting machine properties. Cutting wire length is among these affecting properties which this study intends to find out the governing relationship between this parameter and cutting efficiency according to empirical findings in Targh travertine quarry. For this purpose, the cutting wire length has been changed by changing the cutting machine track position relative to the face entry. To do so, in 3 different mode of cutting height of 7, 10 and 12 m and with various cutting length, distance between the track position and the face has been changed. Evaluation of cutting rate during these cuttings specified the optimum condition in each mode of height. Results showed that increasing the cutting height from 7 to 12 m, leads to increasing the optimal cutting machine distance from 3 to 4.5 meters.

Keywords: Diamond wire cutting, Travertine, Optimization, Machine-Face distance

1 INTRODUCTION

Selection of mining method in exploitation of dimension stone is usually based on parameters such as physical, mechanical, textural and geological characteristics of rocks, blocks exploitability and production capacity. Nowadays, nearly all of travertine quarries are being exploited by diamond wire cutting method. Since the costs of cutting wire constitute a big portion in exploitation costs, its optimization can lead to great improvements in mining economy. So, in order to minimize the operational costs, some investigations about the optimum cutting parameters are essential.

The important point on efficient usage of diamond wire cutting is to produce blocks at minimum cost by adjusting the effective cutting parameters adequately (Ozcelik et al. 2004). These parameters can be divided in two groups; controllable and uncontrollable. Uncontrollable parameters consist of physical and mechanical properties, geology and texture of rocks and the climate conditions. Controllable parameters are mainly in relation to heavy machineries (such as cutting and boring machine) performance. One can change the controllable parameters by changing the designs and decision, but uncontrollable parameters cannot be changed by human being. Parameters that can affect cutting efficiency are given in Table 1 (Ozcelik 1999).

After determination of uncontrollable parameters, one can achieve a suitable cutting process with modifying controllable parameters. There have been some studies in order to reply how each of these parameters can affect cutting process. Burgess correlated sawability to hardness, abrasion resistance, grain size and mineralogical composition (Burgess & Birle 1978). Moreover, Sengun and Altindag conducted some researches in order to find some relations between specific energy of cutting process and some strength

Table 1. Effective parameters of diamond wire saw exploitation performance (Ozcelik 1999)

Uncontrollable parameters	Controllable parameters	
Rock properties	Cutting machine properties	Operating conditions
• Hardness	• Machine power	• Technical personnel
• Strength	• Machine position	• Vibration of machine
• Water content	• Number of beads per meter	
• Degree of alteration	• Cutting angel between wire and horizontal level	
• Discontinuities	• Amount of cutting area relative to angel variation	
• Mineralogical properties	• Wire speed	
• Textural characteristics	• Amount of water used	
	• Bead structure	

properties of 12 carbonates rocks (Sengun & Altindag 2013). Regression analysis showed that high correlations exist between specific energy and uniaxial compressive strength, Shore and Schmidt hardness, bulk density, apparent porosity, and flexural strength. However, Bayram believes that Cone indenter hardness, Shore hardness, and brittleness are the dominant properties for prediction of sawing performance in marbles (Bayram 2013). Ertingshausen studied on the power consumption during granite cutting in up-cutting and down-cutting modes (Ertingshausen 1985). Jennings and Wright carried out a general evaluation on affecting parameters on sawing performance. They concluded that small diamond grains must be used in hard rock cutting (Wright & Jennings 1989). Ozcelik completed extensive researches on diamond wire saw method. Ozcelik and Kulaksiz studied the relationship between cutting angle and wear of beads in diamond wire method (Ozçelik et al. 2000). He also investigated the wear of diamond beads in cutting process for different rock types with ridge regression (Ozçelik et al. 2002). Ozcelik worked on the optimum working conditions of cutting machines for marble rocks (Ozçelik 2005). Also, he studied on the relation between textural characteristics of rocks and their sawability with diamond-mounted saws (Ozçelik 2007). Ataei used a statistical analysis to develop a prediction model for production rate of diamond wire saw method (Ataei et al. 2011). Mikaeil et al. found a mathematical relation between production rate and rock brittleness indexes for stone sawing in rock processing plants (Mikaeil et al. 2013).

The cutting wire length is one of the controllable parameters which is associated with the cutting machine position. There is no considerable research on this parameter in previous studies, so this study intends to investigate the effect of cutting wire length on the cutting efficiency by using some experiments carried out in a real operational scale. For this purpose, the cutting efficiency has been evaluated in three different cutting height state of 7, 10 and 12 meters. In order to determine the optimum length of cutting wire in each mentioned states, by changing the distance between the cutting machine and the working face, different cuttings with various length have been performed and then the cutting efficiency of all of these cuttings have been recorded. Using the resultant data and processing them, concluded with some diagrams for selection the optimum conditions.

Field studies of this research performed in an active travertine quarry located in Isfahan province near Natanz city belonging to Ahrar-e-Sepahan Company. The quarry has geographical coordinate of 39 S 572979 3692785 in (WGS 84) UTM system and it lies near Natanz road, after YahiaAbad and Targh villages. These travertine rocks are a part of Urmia-Dokhtar (northwest- southeast) zone and have 1 or 2 km distance from some active faults. According to these faults, the main formation factor of the deposits is the local tensions in overlapped sheet of faults (Momenzade & Heydari 1988).

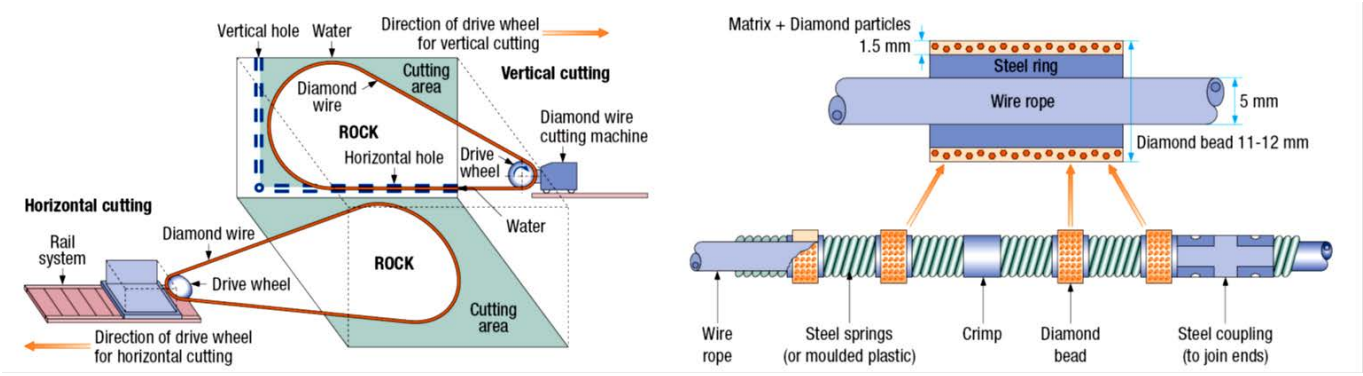

Figure 1. Schematic view of diamond wire saw method and the cutting wire (Ataei et al. 2011)

2 EXPLOITING BY DIAMOND WIRE SAW

Diamond wire cutting machines have been used in marble industry since 1985 and have affected the production rate and efficiency considerably (Ozcelik 2005). Today, they are widely used in more than 90% of the natural stone quarries (Momenzade & Heydari 1988). In diamond wire cutting machines, cutting process takes place through some abrasive diamond wires. The diamond wire is simply a steel cable on which small beads, bonded with diamond abrasive, are mounted at regular intervals with spacing material placed between the beads (Ozcelik 1999; (Özçelik et al. 2000). The diameter of diamond wire saw and steel cable are 10-12 mm and 5 mm respectively. Number of beads varies between 30 and 35 in one meter of the wire that makes intervals between 25 and 32 mm. Controlling of cutting machine parameters such as rotation, tension force and speed is performed through an automatic control panel. An electrical engine supplies the force of cutting machine and makes a drive wheel to rotate the diamond wire. Whole of cutting machine is mounted on a rail, which enables the machine to move back and forward. Figure 1 illustrates a schematic view of diamond wire cutting method and cutting wire.

3 CALCULATION OF CUTTING EFFICIENCY IN VARIOUS SITUATIONS

The amount of rock surface cut in a unit time interval (typically one hour) is called cutting efficiency which depends on physical and mechanical characteristics of rock, cutting tool characteristics and operator skills. In order to assess this parameter and optimize the cutting process through changing the cutting wire length, data are collected during a period of 10 month of travertine quarrying. During all stages of this experimental study, a single type of cutting machines with the same operating parameters has been used. The operational characteristics of this cutting machine are reported in Table 2. Also, all of investigation carried out on the same rock with the same mechanical characteristics. In other words, all of the affecting parameters were remained constant except the targeted parameter.

Table 2. Cutting machine operational parameters

Parameter	Description
No. of beads per meter	30-32
Power of machine (Main motor)	37 KW
Wire peripheral speed	30-35 m/s
Voltage	380 V
Wire length	60-75 m
Pulley diameter	800 mm
Diamond beads (sintered)	0.63 carats/bead

Figure 2 shows a schematic view of cutting geometry in a typical quarry. This figure illustrates geometrical parameters of stone cutting including cutting height, cutting length, cutting machine distance from the face and the cutting wire length. In an individual cutting operation, cutting machine travels on a rail, which changes the distance of cutting machine from the face. So in this

study the meaning of cutting machines distance from the face simply refers to the distance between the rail beginning and the face or in other words the distance between the cutting machine and the face when the cutting process begins (the minimum distance between cutting machine and face).

During the field experiments, the required data of quarrying 60 blocks have been collected and recorded. As previously mentioned, all of field experiments are divided into three categories based on their cutting height including 7, 10 and 12 meters. The research procedure in each cutting height case, in 4 different cutting length, the cutting operation performs in 5 various distance of cutting machine from the face. Therefore, for any cutting height case, 20 distinct cutting operation performed and their associated data are recorded. Each of these cutting scenarios is analyzed individually in the following sections.

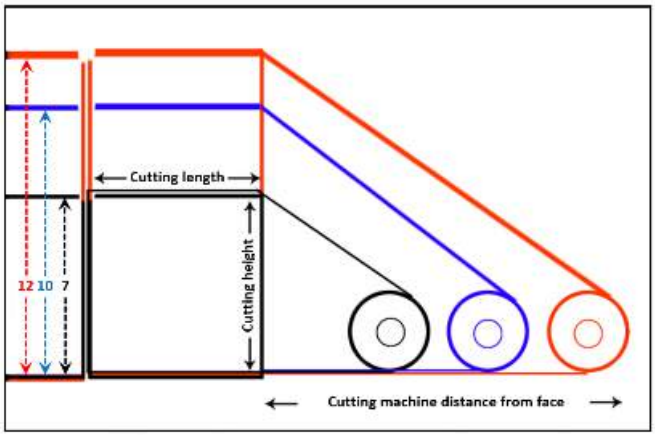

Figure 2. Cutting geometry of diamond wire cutting

3.1 Cutting Height 7 m

In this scenario, all of cuttings perform with the smallest cutting height, which equals to 7 m. Nevertheless, these cutting operations are done with 4 different cutting lengths of 5, 6, 7 and 8 meters. Also, in each of these cutting length situations, distance between cutting machine and working face varies in five modes of 1.5, 2.5, 3, 4 and 5 meters. For each cutting operation in addition to cutting dimensions and distance of cutting machine from face, some other cutting parameters such as wire length and cutting time are also recorded. Two parameters of cutting surface and cutting time are required in order to calculate the cutting efficiency. The cutting surface is simply obtained by multiplying the cutting length by the height and then by dividing it by the recorded cutting time (in hour), the cutting efficiency would be resulted. Based on this procedure, by using all of obtained data during cutting of blocks with heights of 7 m, the cutting efficiency of every individual cutting operation has been calculated. Table 3 shows the detailed summary of the data and results values. This table has been divided into 4 sections based on the length of cutting surface.

By summarizing all the 20 initial cuttings, a diagram can be obtained which has been shown in Figure 3. In this diagram, the cutting efficiency is plotted against the cutting machine distance to face individually for each cutting length. This diagram shows that for all different cutting length, an increase in cutting machine distance, increases the cutting efficiency at first and then decreases it. The maximum cutting efficiency, which is the optimum value, occurs in distance of 3 meters for all 4 cases. Therefore, it can be concluded that while the cutting height is 7 meters, the optimum distance of cutting machine from the working face equals to 3 m.

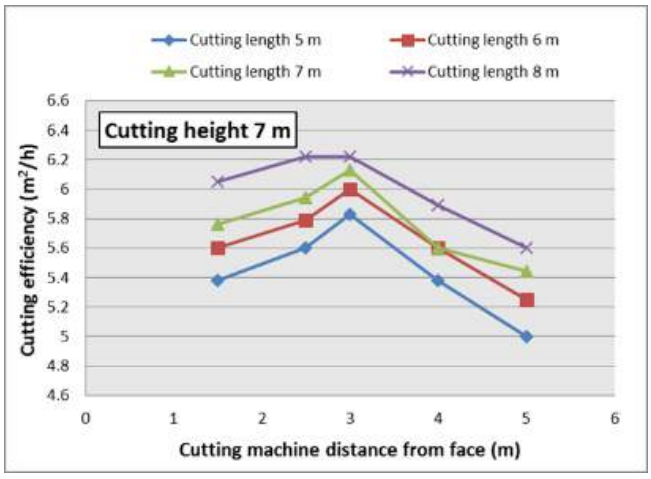

Figure 3. Cutting efficiency for cutting height 7 m

3.2 Cutting Height 10 m

In this scenario, all of cuttings are performed with the cutting height of 10 m. This second 20 cutting are divided into 4 groups based on the cutting length which are equal to 7, 8, 9

and 10 meters. Besides, for each cutting length case, the cutting machine distance changed between 1.5, 2.5, 3.5, 4.5 and 5 m. Similar to previous scenario, the required cutting data are recorded during the cutting process and then, by using these data, the cutting efficiency of each cutting operation can be calculated. Based on this procedure, all recorded data as well as the cutting efficiency of all cutting processes with the cutting height of 10 m are summarized in Table 4. This table has been divided into 4 sections based on the length of cutting surface.

Table 3. Cutting parameters for cutting height of 7 m

No.	Wire length (m)	Cutting dimensions		Machine distance to face (m)	Cutting time (hour)	Cutting efficiency (m^2/h)
		height	length			
1	28	7	5	1.5	6.5	5.38
2	29	7	5	2.5	6.25	5.6
3	30	7	5	3	6	5.83
4	31	7	5	4	6.5	5.38
5	32	7	5	5	7	5
6	30	7	6	1.5	7.5	5.6
7	31	7	6	2.5	7.25	5.79
8	32	7	6	3	7	6
9	33	7	6	4	7.5	5.6
10	34	7	6	5	8	5.25
11	32	7	7	1.5	8.5	5.76
12	33	7	7	2.5	8.25	5.94
13	34	7	7	3	8	6.13
14	35	7	7	4	8.75	5.6
15	36	7	7	5	9	5.44
16	34	7	8	1.5	9.25	6.05
17	35	7	8	2.5	9	6.22
18	36	7	8	3	9	6.22
19	37	7	8	4	9.5	5.89
20	38	7	8	5	10	5.6

Table 4. Cutting parameters for cutting height of 10 m

No.	Wire length (m)	Cutting dimensions		Machine distance to face (m)	Cutting time (hour)	Cutting efficiency (m^2/h)
		height	length			
21	38	10	7	1.5	11	6.36
22	39	10	7	2.5	10.75	6.51
23	40	10	7	3.5	10.5	6.66
24	41	10	7	4.5	11	6.36
25	42	10	7	5	11.5	6.09
26	40	10	8	1.5	12.25	6.53
27	41	10	8	2.5	12	6.66
28	42	10	8	3.5	11.75	6.81
29	43	10	8	4.5	12.5	6.4
30	44	10	8	5	13	6.15
31	42	10	9	1.5	14	6.43
32	43	10	9	2.5	13.5	6.66
33	44	10	9	3.5	13	6.92
34	45	10	9	4.5	13.25	6.79
35	46	10	9	5	14.5	6.21
36	45	10	10	1.5	14.75	6.78
37	46	10	10	2.5	14.5	6.9
38	47	10	10	3.5	14	7.14
39	48	10	10	4.5	14.25	7.02
40	49	10	10	5	15.5	6.45

Cutting efficiency behaviors against the cutting machine distance from the face for cutting height of 10 m is plotted as a diagram in Figure 4. In this figure, the associated information of the second 20 cuttings are separated based on the cutting length. This diagram indicates that, as the previous scenario, with increasing the cutting machine distance, the cutting efficiency initially increases and then decreases. However, the optimum value, which is the maximum efficiency, occurs with the machine distance of 3.5 m for all 4 cases. The other concluding fact of this diagram is that for nearly all of specified machine distances, any increase in cutting length leads to increasing the cutting efficiency. Eventually, it can be concluded that while the cutting height is 10 meters, the optimum distance between cutting machine and the working face equals to 3.5 meters.

3.3 Cutting Height 12 m

In this scenario, similar to the two previous scenarios, 20 unique cutting operations are performed with cutting height of 12 m. The cutting length changes between four states of 7, 8, 9 and 10 m and for each of these cutting length states, the cutting machine distance from face differs in five different distances of 2, 3, 4, 4.5 and 5.5 m. During all of these 20 cuttings, all of required data for calculation of cutting efficiency are recorded. With these information (cutting time and cutting surface area), the efficiency of each individual cutting have been calculated. All of recorded data as well as the cutting efficiency values are reported in Table 5. This table has been divided into 4 sections based on the length of cutting surface.

Based on provided information in Table 5, one can plot the diagram of cutting efficiency against the cutting machine distance. This diagram is presented in Figure 5. Data trends in this diagram show that with increasing distance from the face, the efficiency increases at first and then decreases. However the optimum efficiency occurs in distance of 4.5 meters for all kinds of cutting length. On the other hand, the diagram shows that for all distances, an increase in cutting length increase the cutting efficiency. As a result, these researches turned out that while the cutting height equals to 12 m, the optimum distance between cutting machine and the working face equals to 4.5 meters.

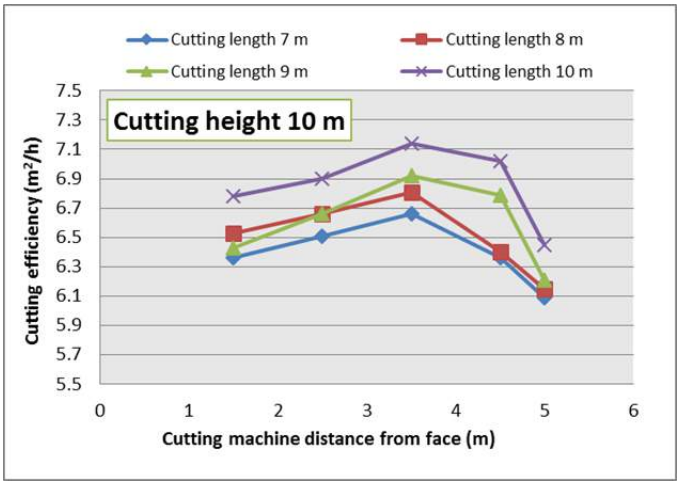

Figure 4. Cutting efficiency for cutting height 10 m

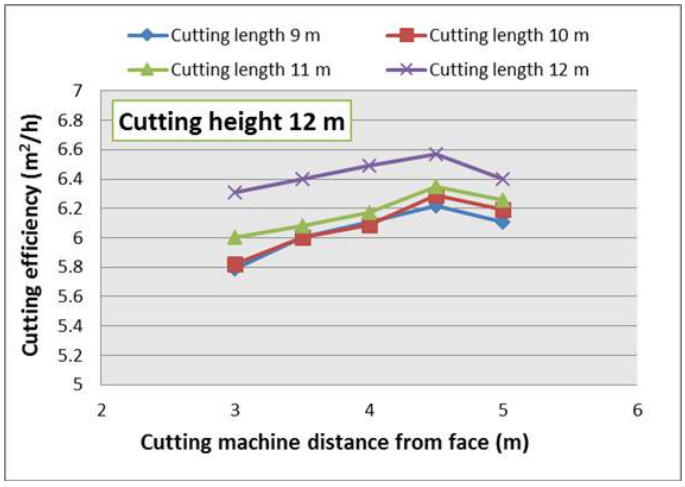

Figure 5. Cutting efficiency for cutting height 12 m

Table 5. Cutting parameters for cutting height of 12 m

No.	Wire length (m)	Cutting dimensions		Machine distance to face (m)	Cutting time (hour)	Cutting efficiency (m^2/h)
		height	length			
41	43	12	7	2	14.5	5.79
42	44	12	7	3	14	6
43	45	12	7	4	13.75	6.11
44	46	12	7	4.5	13.5	6.22
45	47	12	7	5.5	13.75	6.11
46	46	12	8	2	16.5	5.82
47	47	12	8	3	16	6
48	48	12	8	4	15.75	6.09
49	49	12	8	4.5	15.25	6.29
50	50	12	8	5.5	15.5	6.19
51	47	12	9	2	18	6
52	47.5	12	9	3	17.75	6.08
53	48	12	9	4	17.5	6.17
54	49	12	9	4.5	17	6.35
55	49.5	12	9	5.5	17.25	6.26
56	49	12	10	2	19	6.31
57	50	12	10	3	18.75	6.4
58	51	12	10	4	18.5	6.49
59	52	12	10	4.5	18.25	6.57
60	53	12	10	5.5	18.75	6.4

4 CONCLUSION

This study investigated the governing relationships between cutting machine distance from the face and the cutting efficiency by using empirical finding at Targh travertine quarry. For this purpose, in three cutting height scenarios of 7, 10 and 12 meters with various cutting surfaces, the distance between the cutting machine and the working face has been changed. Evaluation of cutting efficiency during each of these cutting operations determined the optimum conditions for each of cutting height scenarios. The results showed that for cutting height scenarios of 7, 10 and 12 meters, the optimum cutting machine distance equals to 3, 3.5 and 4.5 meters respectively. Moreover, for all of cutting situations and for all of machine distances, increasing the cutting length led to increasing the cutting efficiency. Besides, among the different cuttings with different cutting height, the maximum cutting efficiency belonged to blocks with cutting height of 10 meters. The results of this study came up from observation on travertine rock and might be generalized for all kind of carbonate rocks. Further researches are required for igneous and metamorphic rocks.

ACKNOWLEDGEMENT

Authors would like to thank Ahrar -e-Sepahan Company for their great cooperation during this study.

REFERENCES

Ataei, M., Mikaiel, R., Sereshki, F., & Ghaysari, N., 2011. Predicting the production rate of diamond wire saw using statistical analysis. Arabian Journal of Geosciences, 5(6), 1289-1295.

Bayram, F., 2013. Prediction of sawing performance based on index properties of rocks. Arabian Journal of Geosciences, 6(11), 4357-4362.

Burgess, R., & Birle, J., 1978. Circular sawing granite with diamond saw blades. Paper presented at the Proceedings of the fifth industrial diamond seminar.

Ertingshausen, W., 1985. Wear processes in sauring hard stone. IDR. Industrial diamond review, 45(510), 254-258.

Mikaeil, R., Ataei, M., & Yousefi, R., 2013. Correlation of production rate of ornamental stone with rock brittleness indexes. Arabian Journal of Geosciences, 6(1), 115-121.

Momenzade, M., & Heydari, E., 1988. Geographical-stratigraphical extension of Iran's

Dimensional and ornamental stones. Paper presented at the 1th Iranian semianr of ornamental stones.

Ozcelik, Y., 1999. *Investigation of the working conditions of diamond wire cutting machines in marble industry.* Ph. D. thesis, Hacettepe University, Ankara, Turkey, 242 pp.(In Turkish).

Ozcelik, Y., 2005. Optimum working conditions of diamond wire cutting machines in the marble industry. IDR. Industrial diamond review (1), 58-64.

Ozcelik, Y., 2007. The effect of marble textural characteristics on the sawing efficiency of diamond segmented frame saws. IDR. Industrial diamond review (2).

Ozcelik, Y., Kulaksız, S., & Çetin, M., 2002. Assessment of the wear of diamond beads in the cutting of different rock types by the ridge regression. Journal of Materials Processing Technology, 127(3), 392-400.

Ozcelik, Y., Kulaksız, S., Panagiotou, G., & Michalakopoulos, T., 2000. Investigation of the relationship between cutting angles and wear on beads in diamond wire cutting method. Paper presented at the Mine Planning and Equipment Selection Symposium, Athens, Greece.

Ozcelik, Y., Polat, E., Bayram, F., & Ay, A., 2004. Investigation of the effects of textural properties on marble cutting with diamond wire. International Journal of Rock Mechanics and Mining Sciences, 41, 228-234.

Sengun, N., & Altindag, R., 2013. Prediction of specific energy of carbonate rock in industrial stones cutting process. Arabian Journal of Geosciences, 6(4), 1183-1190.

Wright, D., & Jennings, M., 1989. Guidelines for sawing stone. Ind Diam Rev, 2, 70-75.

Numerical Modelling of the Influence of Coefficient of Utilization on the Exploitation Profitability of Dimension Stone Deposit

I. Galić
Mining, Geology and Petroleum Engineering Faculty, Pierottijeva 6, 10000 Zagreb, Croatia

D. Vidić
Ministry of Economy, Ulica grada Vukovara 78, 10000 Zagreb, Croatia

B. Farkaš
Mining, Geology and Petroleum Engineering Faculty, Pierottijeva 6, 10000 Zagreb, Croatia

ABSTRACT The coefficient of utilization of rock directly affects the profitability of the dimension stone deposit exploitation. Dimension stone is a highly valuable raw mineral material per unit of product. Past experience and literature show that for a certain amount of commercial dimension stone blocks, a significantly larger volume of raw rock mass should be dug up. Mineral residue as a result of the extraction of the commercial dimension stone blocks is usually the material of less or even minor value per product unit. Profitability of the exploitation of dimension stone in a reservoir is directly dependent on the rock coefficient of utilization. It is therefore a priority task and a challenge to improve the efficiency of dimension stone deposit and to reduce the accumulation of mineral residue that would ultimately increase profits. Numerical models can clearly demonstrate the influence of the coefficient of utilization on the exploitation profitability of the dimension stone deposit, which is presented in this paper. From the analysis of the real "in situ" performance and numerical models, the coefficient of utilization can be determined whereby the exploitation of dimension stone deposit is on the edge of profitability.

Keywords: Numerical modelling, utilization coefficient, dimension stone, exploitation profitability

1 INTRODUCTION

Dimension stone is highly valuable raw mineral materials per unit of product and it is mostly used in the final stages of construction and less to produce supporting structures. Market value of dimension stone is several times greater than the value of other types of non-metallic minerals (Vidić, D., 2012.).

Profitability of the exploitation of dimension stone in a deposit directly depends on coefficient of utilization of that deposit, and any activity that can improve the exploitation of deposits of dimension stone may have a decisive impact on the economy of operations of the company which is engaged in the exploitation of dimension stone.

From the literature and practice it is well known that for a certain quantity of commercial blocks of dimension stone a significantly larger volume of rock mass, in natural condition, needs to be dug up (cut) (Galić, I., 2003).

Importance of ratio of the usable quantities of commercial dimension stone blocks and the total quantity of excavated rock is most vividly displayed in the case studies and models.

This paper will analyse the impact of coefficient of utilization on profitability of dimension stone exploitation, in other words the sensitivity of mining project of dimension stone exploitation regarding the coefficient of utilization.

2 MODELLING OF DIMENSION STONE RESERVES CALCULATION

In expert literature, there is some controversy and disagreement about the definition of concepts and calculation degree of utilization of dimension stone deposits. Recently, the degree of utilization of dimension stone deposits is defined by coefficient of utilization, exploitation losses and correctional coefficient.

2.1 Model 1 – Calculation of the reserves from the total quantity of rock

Correctional coefficient (k_p) is the loss of rock mass through the surface waste (unless separately calculated), rock mass in fragmented areas, and non-commercial pieces of stone. The correctional coefficient expresses the loss of rock mass of dimension stone caused by the conditions prevailing in the deposit, and it is used in calculating the balance reserves, according to the expression:

$$Q_{bil} = Q_u \cdot k_p, m^3 k_i = \frac{O_{kb}}{O_u} \quad (1)$$

Where is:
Q_{bil} – balance reserve (m^3)
O_u – total volume of cut rock mass (m^3)
k_p – correctional coefficient

For a large number of dimension stone deposits in the Republic of Croatia, waste rock located on top of exploitation reserves of rock mass is not separately calculated and is shown trough correctional coefficient. Usually this is the case in the deposits with no surface waste rock in the classical meaning of the word (humus, clay, earth, etc.) but it is the karst surface area that is not clearly separated from the exploitation rock parts (Archives, 2011).

When large quantities of waste rock are located on top of exploitation rock mass, the waste rock is usually calculated separately.

The correctional coefficient is directly dependent on geological conditions of deposit in which the exploitation of dimension stone is performed, and primarily on thickness of waste rock, structural-tectonic set of deposit, the size of rocks that have commercial value, etc.

The correctional coefficient is different for every dimension stone deposit, and in the Republic of Croatia, it is usually in the range between 0.18 and 0.22, extremely up to 0.54 (deposit "Kanfanar" in Istria).

Exploitation loss (E_g) is loss of rock mass mainly caused by destruction of rock mass by various tools (chain saw, diamond wire saw, etc.) and it can be exactly calculated or obtained by statistical analysis of data. Substituting exploitation loss in expression (1) we get the equation for calculating the exploitation reserves;

$$Q_{eks} = Q_{bil} \cdot E_g, m^3 \quad (2)$$

Where is:
E_g – exploitation loss (m^3)

Quantity of exploitation losses, in contrast to correctional coefficient, is not dependent on deposit's geological conditions in which the dimension stone exploitation is preformed but primarily on the thickness of cutting elements of chain saw and diamond wire saw, and ranges from 8 to 10% of the balanced reserves. Exploitation loss is calculated by the expression:

$$E_g = Q_{bil} \cdot p, m^3 \quad (3)$$

Where is:
p – share of exploitation loss, %.

Coefficient of utilization (k_i) is, in general, the ratio of usable substances of raw mineral materials and the total quantity of excavated rock. In the case of dimension stone, the coefficient of utilization is the ratio of the volume of commercial blocks and the

total volume of the rock mass that needs to be cut out for a commercial blocks to be formed (Galić et al, 2011; Dragičević et al, 2009). The volume of commercial blocks is actually a volume of extraction reserves in a deposit. The coefficient of utilization is obtained by calculation from expression:

$$k_i = \frac{O_{kb}}{O_u} \quad (4)$$

Where is:
O_{kb} – volume of commercial blocks (m^3)

In conclusion, it can be determined that the coefficient of utilization integrates the correctional coefficient and exploitation losses.

2.2 Model 2: Calculating the total quantity of rock according to the planned quantity of blocks

In the introductory section the expressions and the process of calculating the exploitation reserves for any raw mineral material, including dimension stone, are clearly defined. However, when it comes to calculating capacity or planned production, the procedure is completely inversed.

In the Model 2 the assumed yearly dimension stone production is 1 000 m^3, the correctional coefficient k_p = 0.18 and exploitation loss p = 10%. The main task is to determine the total volume of the rock mass that needs to be cut out annually in order to obtain 1 000 m^3 of commercial dimension stone blocks.

Since the planned annual production is actually an annual exploitation reserves in the quantity of 1 000 m^3, it is therefore necessary to add that the exploitation losses and the annual balance reserves will be calculated by the following expression:

$$Q_{bil} = Q_{kb} \cdot \frac{100}{100-p}, m^3 \quad (5)$$

It follows that the annual balance reserves are:

$$Q_{bil} = 1\,000 \cdot \frac{100}{100-10} \cong 1\,111, m^3$$

From that exploitation losses are:

$$E_g = 1\,111 - 1\,000 = 11\ m^3$$

To calculate the total annual quantity of the rock mass that needs to be cut (dug) out it is necessary to predict the loss of rock mass through correctional coefficient in the form of surface waste rock, rock mass in fragmented areas. Therefore the total quantity of excavated rock mass will be:

$$Q_u = \frac{Q_{bil}}{k_p}, m^3 \quad (6)$$

It follows that the total annual quantity is:

$$Q_u = \frac{1\,111}{0{,}18} \cong 6\,172\ m^3$$

Of which the stone waste is:

$$Q_{k.o.} = Q_u - Q_{bil} = 6\,172 - 1\,111 = 5\,061\ m^3$$

Coefficient of utilization in the Model 2 is:

$$k_i = \frac{O_{kb}}{O_u} \quad (7)$$

$$k_i = \frac{1\,000}{6\,172} \cong 0{,}162$$

3 INFLUENCE OF COEFFICIENT OF UTILIZATION ON DIMENSION STONE DEPOSIT EXPLOITATION

The utilization coefficient has the crucial influence on profitability and investment return and operation of company which carries out exploitation of dimension stone in the deposit.

Coefficient of utilization is different for every deposit, and in the deposits in the Republic of Croatia it is usually in the range between 0.14 and 0.20, and exceptionally more.

Following the previously stated report, further analysis of dependence of investment profitability on the coefficient of utilization shows the economic sensibility of mining operation when the coefficient of utilization ranges from 0.14 to 0.20.

3.1 Model 3: The input parameters of the test model

For the most realistic analysis a specific example from existing deposit will serve as test model and the data from Mining project of dimension and technical building stone exploitation on deposit field "Dolit" (Živković, S. A., 2005).

The basic input data taken from test model design, on which the analysis of the dependence of investment profitability on the correctional coefficient was done, are as follows:

- planned production of all categories of commercial blocks is 1 560 m^3;
- average market price of all categories of commercial blocks is 367 \$/m^3;
- total annual revenue from the block sale is 572 000 \$;
- initial investment is 1 440 000 \$;
- annual cost of exploitation for gaining 1 560 m^3 of commercial blocks is 505 523 \$;
- correctional coefficient kp= 0.20;
- exploitation losses E_g = 10%;
- coefficient of utilization ki = 0.18.

3.2 Model 4: Output parameters for the test model

Based on the input parameters of the test model the total volume of rock mass is calculated which should be cut out in order to get the planned 1 560 m^3 of commercial blocks. Based on the exploitation loss p = 10% and correctional coefficient k_p = 0.20, it was calculated that 8 667 m^3 should be cut out. With these parameters coefficient of utilization k_i = 0.180.

Table 1 - Output parameters of the test model

Gross valume O_u (m^3)	Exploitation losses E_g (%)	Correctional coefficient k_p	Coefficient of utilization k_i	Volume of commercial blocks O_{kb} (m^3)	Total cost of cutting blocks (\$)	Block production price (\$/m^3)	Block market price (\$/m^3)	Total revenue UP (\$)	Profit (\$)
8 667	10	0.23	0.207	1 794	505 523	282	367	658 398	152 875
8 667	10	0.22	0.198	1 716	505 523	295	367	629 772	124 249
8 667	10	0.21	0.189	1638	505 523	309	367	601 146	95 623
8 667	10	0.20	0.180	1 560	505 523	324	367	572 520	66 997
8 667	10	0.19	0.171	1 482	505 523	341	367	543 894	38 371
8 667	10	0.18	0.162	1 404	505 523	360	367	515 268	9 745
8 667	10	0.17	0.153	1 326	505 523	381	367	486 642	-18 881
8 667	10	0.16	0.144	1 248	505 523	405	367	458 016	-47 507

Analysis in Table 1 is created under the assumption that employees, machinery and equipment per year could cut out up to 8 667 m^3 gross volume of the rock mass and that the selling price of 1 m^3 block of all categories is fixed to the amount of 367 \$/ m^3.

Table 1 shows profitable threshold of mining company, under the given conditions, when coefficient of utilization is in the range from 0.162 to 0.153.

It is significant to notice that the increase of coefficient of utilization from k_i = 0.180 to k_i = 0.207 the annual gross profit of the mining company is increasing from 66 997 \$ to 152 875 \$, that is more than double.

Should the coefficient of utilization decrease from k_i= 0.180 to k_i= 0.162, when utilization of rock mass is decreased by less than 2%, the annual profit of the mining company would decrease to 9 745 \$, that is about eight times.

4 BUSINESS PROFITABILITY DEPENDING ON THE COEFFICIENT OF UTILIZATION

Profitability is defined as an indicator of economic operating performance and is

commonly based on loss and profit data. The most commonly used formula is:

$$E = \frac{UP}{UT} \quad (8)$$

Where is:
UP – total income ($),
UT – total costs ($).

Obtained result indicates:
$E > 1$ – profitable business,
$E = 1$ – business at the border of profitability,
$E < 1$ – business is not profitable.

4.1 Model 5: Determining the profitability threshold by computation

Determining profitability threshold of dimension stone deposit in which the gross volume of rock mass could be cut out is 8 667 m^3 with the selling price of all commercial block of all the categories is 367 $/$m^3$, could be done by computation or graphically.

For a profitability threshold to be determined by calculation, first the smallest quantity of commercial blocks should be calculated that will ensure profitable business. In other words, we need to calculate the minimum quantity of blocks whose exploitation costs will be equal to revenue from their sale.

Following the stated, we set this relationship:

$$Q_{min} = \frac{UT}{CT} \quad (9)$$

Where is:
Q_{min} – minimal quantity of blocks for company to be profitable (m^3)
UT – total exploitation costs ($/$m^3$)
CT – average sale value of 1 m^3 block ($/$m^3$)

Substituting the output values obtained from the test model we obtain:

$$Q_{min} = \frac{505\,523}{367} = 1\,379\ m^3$$

Therefore, the minimum quantity of blocks that must be cut out from total volume of 8 667 m^3 and the average sale price of 367 $/$m^3$, for a business to be profitable, is 1 379 m^3.

By setting the relationship between minimum quantities of blocks that need to be obtained from the total volume so the business is profitable (Q_{min}) and the total volume (Q_{uk}) from which the minimum quantity of blocks was obtained, gives us marginal coefficient of utilization with which the business will be marginally profitable.

$$k_{igr} = \frac{Q_{min}}{Q_{uk}} \quad (10)$$

$$k_{igr} = \frac{1\,379}{8\,667} = 0{,}159$$

Thus, marginal coefficient of utilization – profitability threshold, at the fixed volume of 8 667 m^3 and fixed price of 367 $/$m^3$, the k_i = 0.159.

Marginal correctional coefficient of the coefficient of utilization ki = 0,159 and exploitation loss E_g = 10% is:

$$k_{pgr} = \frac{Q_{min} \cdot \left(\frac{100}{100-Eg}\right)}{Q_{uk}} \quad (11)$$

$$k_{pgr} = \frac{1\,379 \cdot \left(\frac{100}{100-10}\right)}{8\,667} = 0{,}177$$

Reducing the coefficient of utilization under 0.159 or correctional coefficient under 0.177 the mining company would operate with a loss.

4.2 Model 6: Determining the profitability threshold graphically

Figure 1 shows the success of the mining company operations during dimension stone exploitation considering the coefficient of utilization.

It is noticeable that when the coefficient of utilization ki = 0.162 the minimal annual income will be 9 745 $, and when ki = 0.153 mining company will create year loss of 18 881 $.

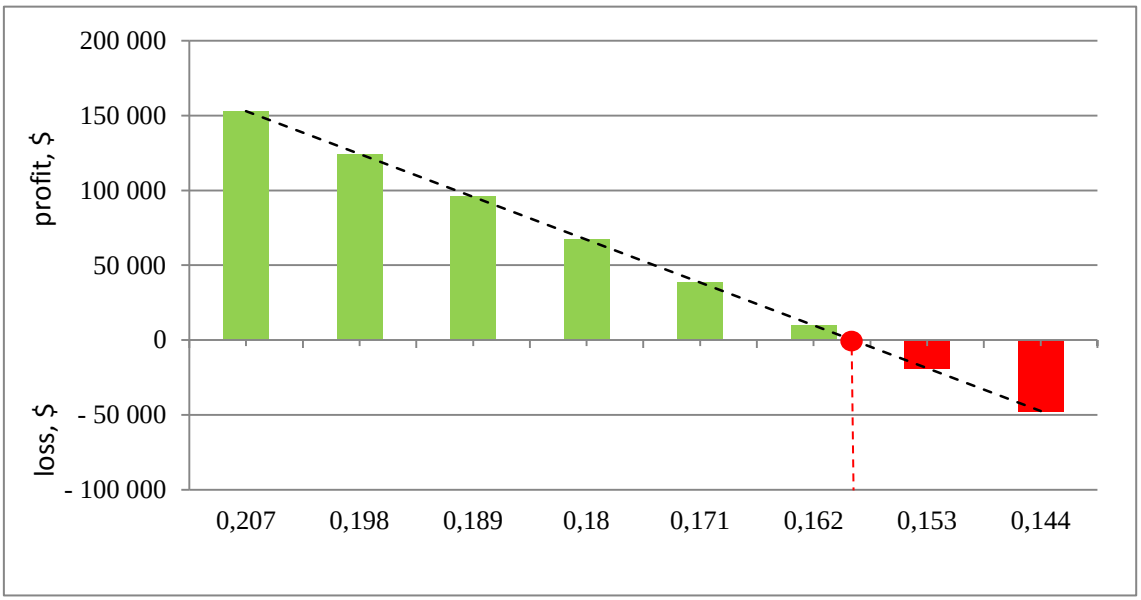

Figure 1. Diagram of business success depending on the coefficient of utilization

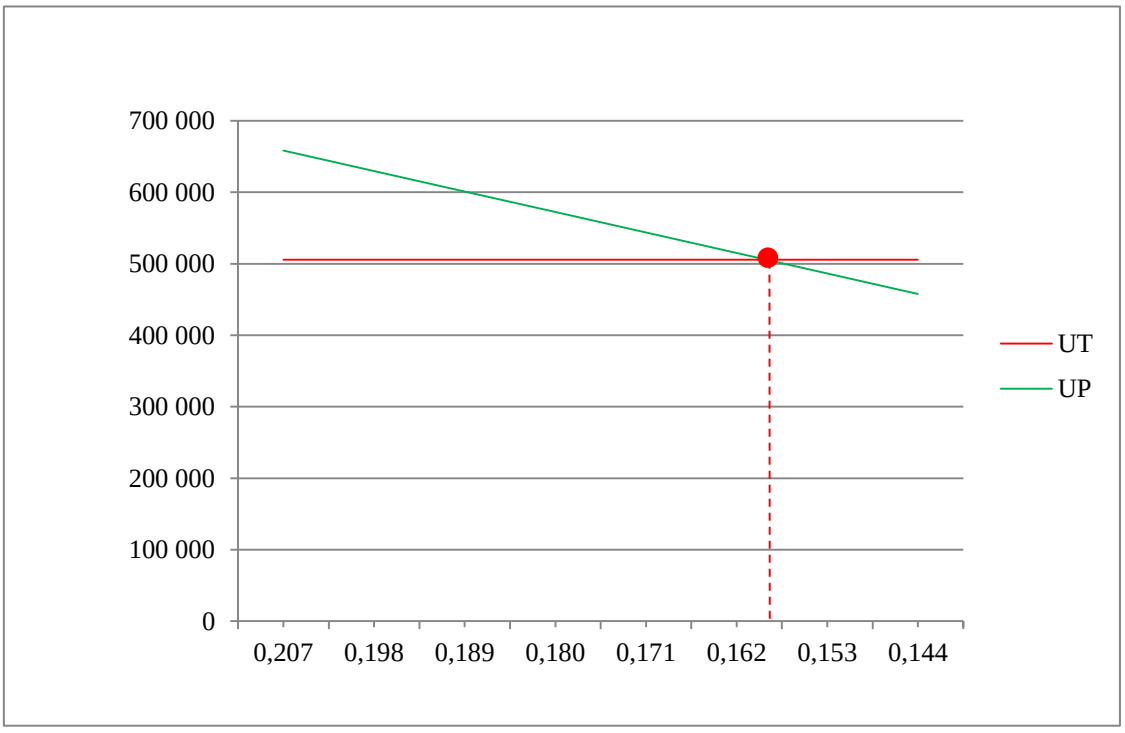

Figure 2. Diagram of profitability threshold

Intersection of lines that show total annual costs (UT) and total annual revenue (UP) represents the mining company's business profitability. Figure 2 clearly shows that total annual costs are fixed (505 523 $), and total annual revenue is reduced according to the reduction of coefficient of utilization.

Figure 3 shows the direct dependence of the production cost ($/m^3) on the amount of coefficient of utilization where the gross cut-out mass is limited to 8 667 m^3 due to the capacity of the available machinery.

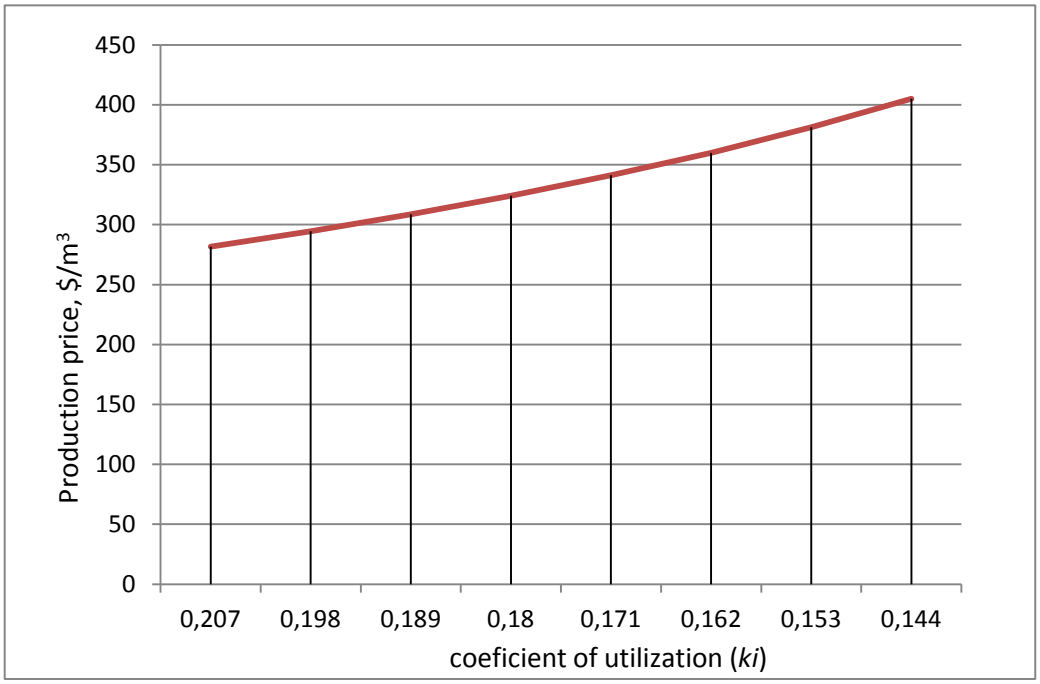

Figure 3. Coefficient of utilization dependence on exploitation cost

It is evident, from Figure 3, that with a fixed annual production, production price increases almost in proportion to the reduction of the rock mass coefficient of utilization.

With coefficient of utilization k_i = 0.207, production price is approximately 280 \$/m^3, while with coefficient of utilization k_i = 0.144 production price is approximately 405 \$/m^3.

5 CONCLUSION

In numerical models the correctional coefficient and exploitation losses of dimension stone deposit exploitation were analysed and in the end summarized in the coefficient of utilization.

This analysis showed a very large dependence of mining operation of dimension stone exploitation on the coefficient of utilization. This dependence is so large that it is recommended to express the coefficient of utilization with three decimal digits.

A real example from practise was taken as the test model, with planned annual exploitation of 1 560 m^3 of commercial blocks of all types and average market price of commercial blocks of all types in the amount of 367 \$/m^3. The planned coefficient of utilization of the deposit is k_i= 0.18 (correctional coefficient k_p = 0.20, exploitation loss E_g = 10%). Based on the design solutions total gross cut-out volume of the rock mass is 8 667 m^3.

Based on the analysed data, from the test model, the obtained results can serve as reference data for making the final decision on economic justification of dimension stone deposit exploitation, but also for the optimization of investment, designed capacity and necessary equipment.

All the above shows the necessity of extremely cautious and detailed planning of the dimension stone exploitation in the deposit.

Particular attention should be paid to dimension stone deposits research data interpretation, determination of rock structural set, space orientation of discontinuities and other data that influence the coefficient of utilization.

Therefore, before exploitation, it is necessary to explore and learn about the planned deposit, in other words to determine the coefficient of utilization as accurately as possible.

Mining engineers and geologist, who are engaged in exploration and exploitation of dimension stone, are the only ones capable and authorized to precisely determine the

coefficient of utilization in the new dimension stone deposit, by using the existing and recognized methods (e.g. method of linear and spatial integrity), but also new scientific methods.

REFERENCES

Dragičević, I., Galić, I., Vranjković, A., Galić, M., (2009): Elaborate of the reserves of dimension stone exploitation field "Kusačko brdo" in Široki Brijeg.

Dunda, S., Kujundžić, T., (2003): Digital textbook: The exploitation of dimension stone, *Faculty of mining, geology and petroleum engineering* Zagreb.

Galić, I., Vidić D., Jembrich, Ž., (2011): The influence of The coefficient of utilization of reservoir feasibility of dimension stone production and improvement opportunities, *Mining and Geology Bulletin*, vol. 15; 117-130.

Galić, I. (2003): Supplementary mining project of exploitation of dimension and technical-building stone in the exploitation field "Pučišća", deposits "Punta-Barbakan", "Sivac-Sivac jug" and "Kupinovo-Kupinovo istok". *Jadrankamen d.d.*, Pučišća.

Galić, I. (2003): The main mining project of dimension stone exploitation in the exploitation field "Kusačko brdo". *Proin 21 ltd.*, Široki Brijeg.

Archives: Collection of documents, studies and projects of the *Ministry of Economy, Labour and Entrepreneurship*, Zagreb.

Tomašić, I. Kršinić, A. (2010): Some important fact for estimation of natural stone deposits during the exploration. *Stone masonry and construction*, Vol.3-4, pp.5-15, Pučišća.

Tomašić, I. (1994): The influence of discontinuity fabric and other factors on optimum exploitation of dimension stone, *Mining, Geology and Petroleum Bulletin*, Vol.6, pp.101-105, Zagreb.

Tomašić, I. Jakić, V. (1990): Optimal excavation front position in relation to the structural set (Graphical method using a computer), *Mining, Geology and Petroleum Bulletin*, Vol.2, pp.41-46, Zagreb.

Vidić, D., Galić, I. & B. Farkaš (2012): The profitability of dimension stone deposit exploitation in relation to the coefficient of utilization, *Mining, Geology and Petroleum Bulletin*, Vol. 24, Zagreb.

Živković, S. A. (2005): Supplementary mining project of exploitation of dimension and technical-building stone in the exploitation field "Dolit", *Jadrankamen d.d.*, Pučišća.

Design of Mineral Processing Plants and Beneficiation Methods

A Technology for Force Field Separation in Vibrofluidized Layers of Granular Materials

L.A. Vaisberg, K.S. Ivanov, S.V. Dmitriev, A.O. Mezenin
REC "Mekhanobr-tekhnika", St. Petersburg, Russia

ABSTRACT The work presents a technology for electrostatic and magnetic separation of vibrofluidized granular materials. This approach allows extended adjustability of the process rate and extraction through control of vibration excitation parameters. This feature guarantees more flexibility and better adaptation of the process for particular materials in comparison with traditional technologies. This approach also allows avoiding the use of water as a dispersion phase. The technology was tested on apatite rocks, sphene concentrate, and Fly ashes.

Keywords: Vibrofluidized granular materials, electrostatic separation, magnetic separation

1 INTRODUCTION

Over one billion tons of solid minerals are mined annually in the Russian Federation, forty percent of which are further enriched with the use of water as the process fluid. The water is used to ensure transportation and subsequent separation of rock mass components after disintegration. Water consumption in mineral processing reaches 3 to 10 cubic meters per ton of ore, resulting in an overall rate of more than two billion cubic meters of water per annum.

Even today, the water is already becoming a scarce commodity. The use of water in mineral processing fuels both environmental problems (due to the negative impact on the environment by flooded tailings) and technical and economic problems (due to the high costs of pumping of process water and suspensions, dehydration of concentrate and safe storage of tailings). Moreover, it is not always possible to use the full water cycle in mineral processing.

Against this background, finding ways to reduce the amount of water consumed in mineral processing is becoming crucial.

Dry methods of ore processing for grain sizes of over 5 mm are well known, while the creation of dry processing methods for crushed ore with grain sizes of 0 to 5 mm is of particular interest and enables the extensive use of the vibration technology.

In particular, due to the fact that most minerals are hydrophilic, water often acts as a dispersion medium, leveling autohesive mineral particle interactions and thereby smoothing the production processes. However, a similar anti-autohesion effect may be ensured by means of vibrational fluidization, a well-known effect of intensification of processes occurring in a gas/solid system [1].

When under vibration, polydisperse powders may reach various dynamic states of total or partial destruction of contacts between the particles, which are, in a way (within the mathematical description), similar to the aggregation states of substances. In the semi-liquid state, material particles are displaced relative to each other with partial contact losses. In the state as a granular gas, particles are detached from each other and subject to vigorous mixing.

2 PRACTICAL APPLICATIONS

2.1 Separation by Magnetic Properties

Iron ore processing is one of the most high-scale industries, which, in particular, mainly uses magnetic separation.

Dry magnetic separation processes are hindered by dry friction type forces emerging between the particles. The presence of dry friction forces reduces the

efficiency of separation of the magnetic concentrate from non-magnetic products, which makes it advisable to apply the granular gas effect. It may be expected that this type of extraction of magnetic particles from the layer would result in the recovery of magnetic particles from the entire bed thickness and not only from its surface.

In its relevant research, Mekhanobr-Tekhnika Research and Engineering Corporation has developed the EVS-15/5 separator [2] (Fig. 1). The device is distinguished by the fact that, when transferring the material processed, its vibratory feed tray ensures the creation of a granular gas effect.

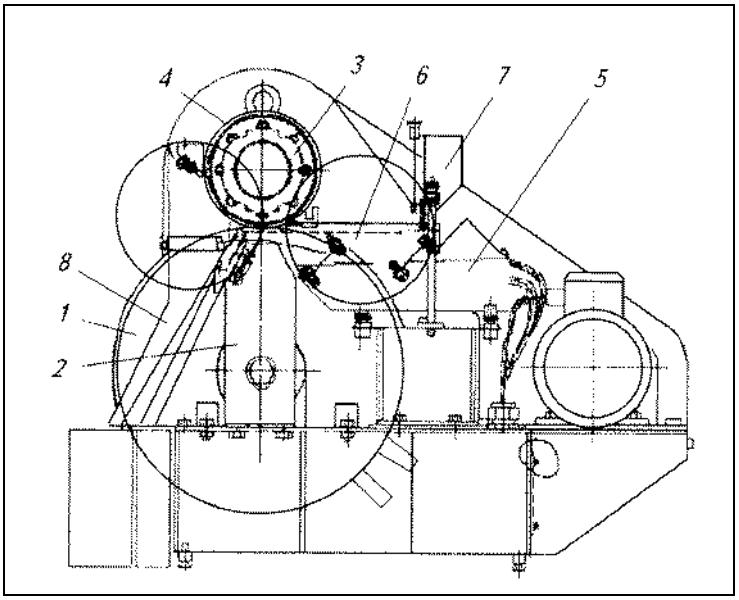

Figure 1. EVS–15/5 Separator Design

Theoretical estimates and experimental results [3, 4, 5] demonstrate that increased electromagnetic separation efficiency may be expected for the values of overload factor of $w \geq 2.5$. Moreover, the average velocity of the material may be adjusted in accordance with the process requirements by changing the vibration frequency and amplitude using the functions included in the EVS-15/5 separator.

A hematite ore sample for the technological research was prepared as follows.

The original material sample was screened to separate grains of 0 to 2 mm and +2 mm. The content of grains of 0 to 2 mm was 57.1%, and those of +2 mm was 42.9%. The grains of +2 mm were dry crushed to the grain size of -2+0 mm.

The resulting two products were combined and used as the source feed for the magnetic separation in EVS-15/5.

In accordance with the requirements of metallurgy, iron content in the magnetic concentrate must be within 61% to 63.5%, and the content of Al_2O_3 must amount to 1.8% to 3%.

In order to study the influence of the granular gas effect on magnetic separation process parameters, experiments were conducted in conditions of material transportation via the vibratory tray in the form of a fluidized bed and in conditions of regular conveying (Fig. 2).

An analysis of the resulting figures suggests the following conclusions:

– the feeding of non-dedusted material particles of -2+0 mm in the form of a fluidized bed ensures a higher iron content in the magnetic concentrate (60.2% versus 59.2%) as compared to regular conveying with a 1.5-fold yield (7.2 kg/h against 4.9 kg/h), but with lower iron yield (71.3% vs. 80%).
– dedusted material particles of -2+0.16 mm demonstrates doubled processing yield with similar indicators of iron content in the magnetic concentrate for a fluidized bed and regular conveying (of 61.0% vs.

61.6%), but with a higher iron yield (79.4% vs. 72.9%);
- the content of Al_2O_3 in the magnetic concentrate is within the allowable range of 3% even at the iron content of 59% or more, which suggests that at the standard iron content of 61% the content of Al_2O_3 will automatically satisfy the requirements set.
- The research covered two different process flow sheets:
- magnetic separation of non-dedusted material particles of -2+0 mm (Figure 6, Option 1);
- magnetic separation of dedusted material particles of -2+0.16 mm (Figure 6, Option 2).

The main process parameters are shown in the Table 1.

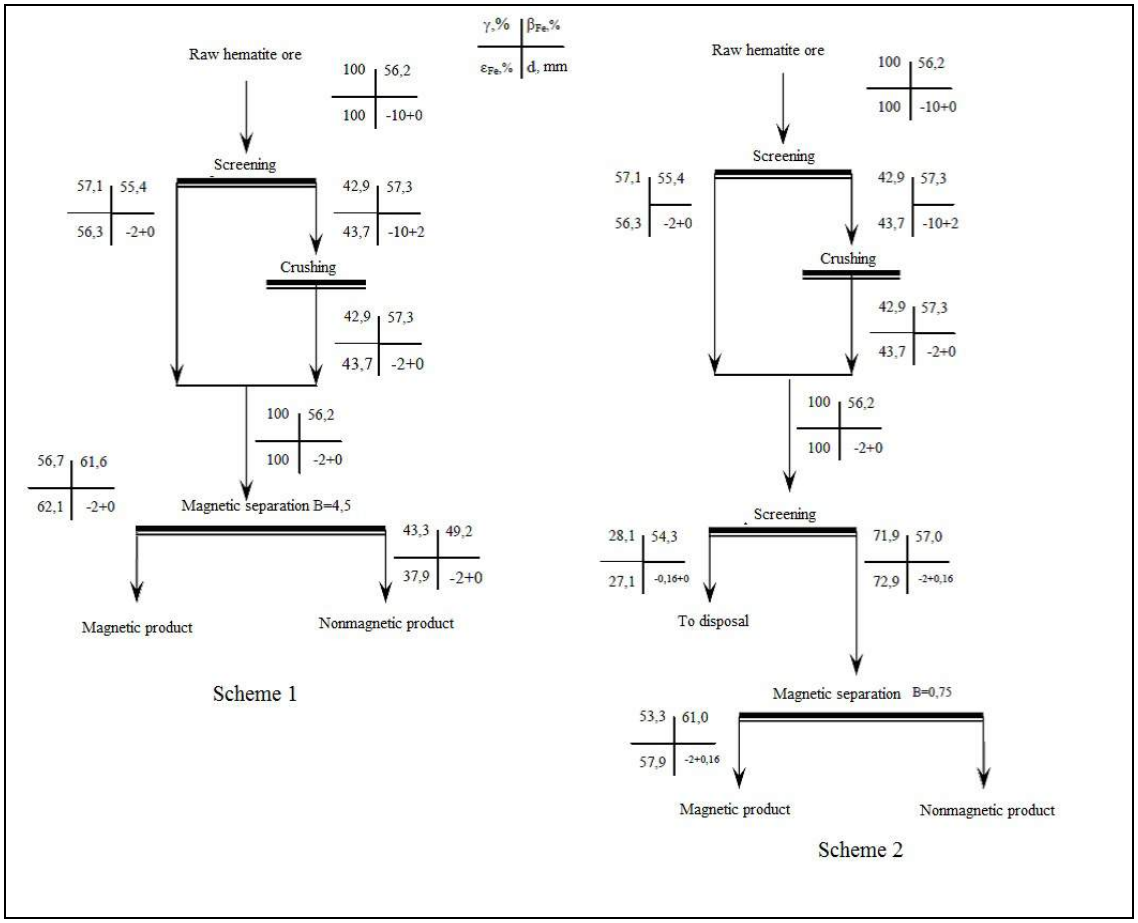

Figue 2. Magnetic Separation Flow Sheets

Table 1. Comparison of Process Parameters of Hematite Ore Magnetic Separation

Scheme	Process Flow Sheet 1	2
Magnetic Concentrate Yield, %	56.7	53.3
Iron Content, %	61.6	61.0
Iron Yield, %	62.1	57.9

A comparison of the indicators listed in Table 1 demonstrates that Option 1 ensures higher process parameters of iron content (61.6% vs. 61.0%) and iron yield (62.1% vs. 57.9%).

When the iron content in the magnetic concentrate is 59% or more, the standard content of Al_2O_3 does not exceed 3%.

A fluidized bed is effective in magnetic separation of non-dedusted material particles of -2+0 mm, while for dedusted material particles of -2+0.16 mm the influence of the fluidized bed is barely noticeable.

Therefore, the developed and manufactured modified design of a laboratory separator for processing weakly oxidized iron ores eliminates the use of

water as a dispersion medium and improves the separation efficiency.

2.2 Separation by Electrical Properties

Fly ash of coal-based thermal power plants is formed by mechanical treatment of waste flue gases and contains a significant amount of unburnt carbon, thus complicating the re-use of this type of waste.

It was suggested to remove the unburnt carbon using the flotation process; however, upon interaction with water, the mineral fraction of fly ash loses its binding properties, greatly reducing its value for the building industry where it is otherwise in the highest demand.

Given that fly ash has a grain size of less than 0.5 mm and is prone to aggregation in dry form and that its components (carbon and mineral fractions) have different electrical conductivity, the approach was applied that is used for dry magnetic separation of iron ore, implying conversion of the powder into a state of a granular gas with subsequent separation in an electrostatic field.

The schematic diagram of an electrostatic separator is shown in Figure 3.

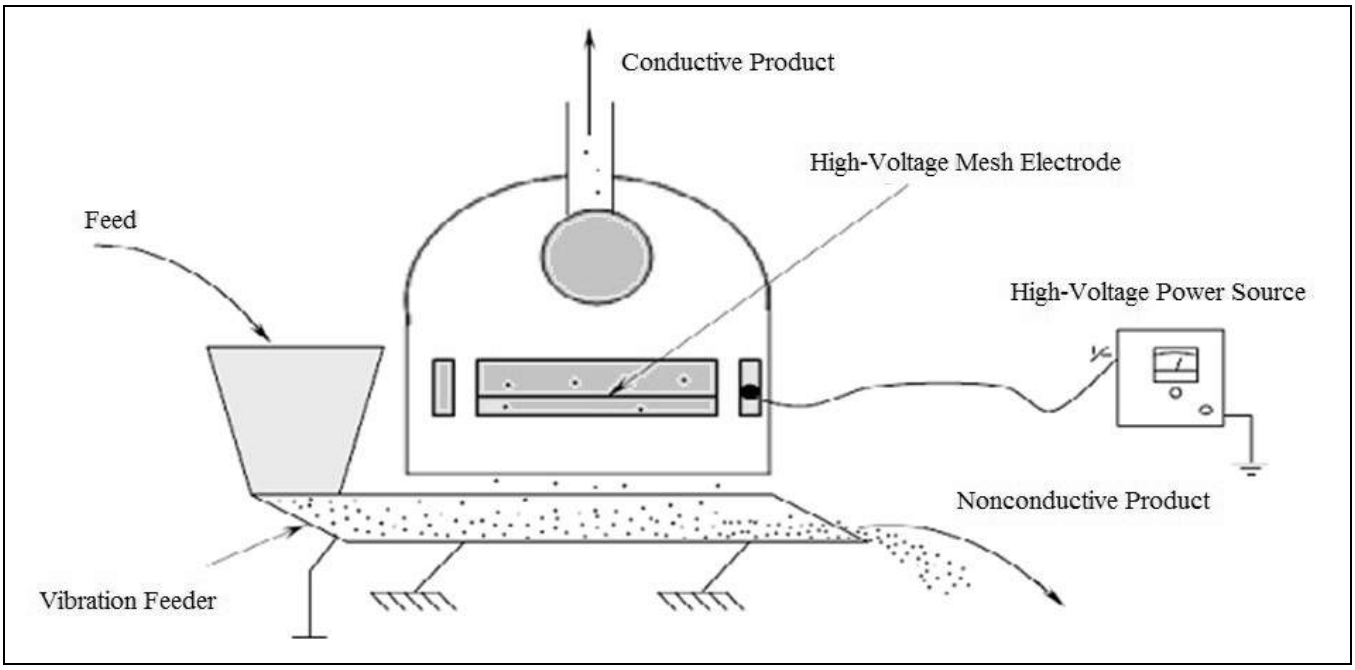

Figure 3. Schematic Diagram of an Electrostatic Separator with Fluidization

Initial dry fly ash is screened to 40 microns. The resulting particles of +40 microns are transferred for dry magnetic separation yielding magnetic and non-magnetic products. The non-magnetic product is fed for electric separation, with prior material fluidization, and is then separated in an electrostatic field into conductive and non-conductive products. As a result, the initial ash with the carbon content of 6.2% is transformed into a commercial product with the content of the carbon component of not more than 4.0% at a yield of 88.5%. The respective flow sheet is shown in Figure 4.

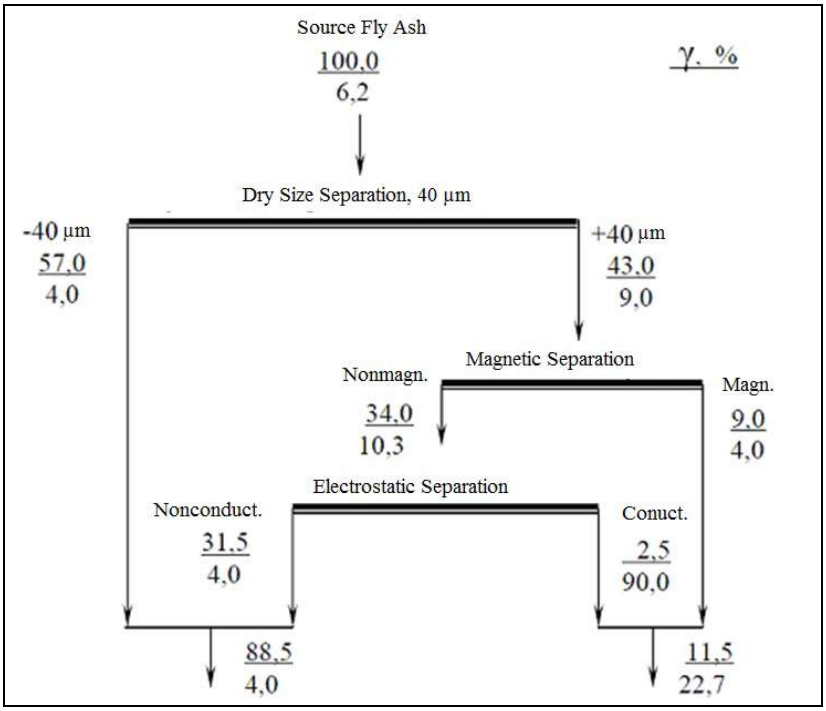

Figure 4. TPP Fly Ash Separation Flow Sheet

The application of vibratory impacts, therefore, enables efficient separation of fine mineral particles in an electric field with sufficient capacity to replace the flotation technology.

3 CONCLUSIONS

The use of vibrational technology, particularly in the processing of granular materials in the state of a granular gas, allows minimizing or totally eliminating the use of water in mineral processing, which not only expands the range of process tools available to engineers, but may provide significant economic benefits.

ACKNOWLEDGEMENT

The research was supported by the Russian Ministry of Education, grant No.14.579.21.0023.

REFERENCES

[1] Uriev N.B. 1988, Physico-Chemical Bases of Dispersed Systems and Materials Technology, Khimiya, Moscow, 250 p.

[2] Mezenin, A.O., Dmitriev S.V. et al, 2012, Study on Dry Magnetic Separation of Hematite Ore using the Vibrational Fluidization Effect, Obogoschenie Rud, 2012 , No. 2, p.21-24.

[3] Ogawa S. 1978, Multitemperature theory of granular materials, Proceedings of the US - Japan Seminar on Contin-Mechanical and Statistical Approaches Mechanical Granular Material (Gukujustu Bunken Fukyakai, Tokyo, p. 208

[4] Brilliantov N.V., Poschel T., 2004, Kinetic Theory of Granular Gases, Oxford University Press.

[5] Golovanevskiy V.A., Arsentyev V.A., Blekhman I.I., Vasilkov V.B., Azbel Y.I., Yakimova K.S., 2011, Vibration-induced phenomena in bulk granular materials, International Journal of Mineral Processing. № 100 (2011), PP. 79–85. http://dx.doi.org/10.1016/j.minpro.2011.05.001

Comminution: Technology, Energy Efficiency and Innovation

B. Klein
University of British Columbia, NBK Institute of Mining Engineering, Vancouver, BC, Canada

N. E. Altun
Middle East Technical University, Mining Engineering Department, Ankara, Turkey

M. J. Scoble
University of British Columbia, NBK Institute of Mining Engineering, Vancouver, BC, Canada

ABSTRACT With pressures to improve energy efficiency in mining, reducing energy usage in comminution has become the focus of innovation. Several advances have been made however the uptake of innovations and technologies is slow. A Technology Readiness Level guide has been developed for other industries that may be a useful tool for the mining industry. Examination of selected successful energy efficient technologies provides some insights and lessons that may provide direction for advancing new technologies. This paper presents the present state and future opportunities for innovation to reduce energy usage for comminution. The main focus will be in relation to pathways to shorten the timelines to advance technologies through stages of readiness for commercialization for the risk averse mining industry.

Keywords: Comminution, energy, efficiency, innovation, technology readiness level

1 BACKGROUND

1.1 Energy Usage in Mining and the Role of Technology

Mining is an energy intensive activity and as such is vulnerable to risks associated with fluctuating energy costs as well as costs associated with government regulations aimed at reducing environmental impacts such as greenhouse gas (GHG) emissions. As a consequence the mining sector is motivated to become proactive in approaches to improve energy efficiency. Initiatives such as the Towards Sustainable Mining (TSM) implemented by the Mining Association of Canada (MAC) have identified Energy and GHG as one of three main areas of focus to improve the sustainability of mining. To support improvements, the MAC has generated several tools for industry including management guidelines that promote Research and Development and Technology Demonstration.

The Mining Energy Value Chain starts at the face and extends to smelting and refining of the metal product. The main energy consumption results from material transport and for underground mines ventilation, but in general the greatest energy consumer is comminution. More energy efficient technologies in each of these areas will result in significant reductions in overall energy usage. The Coalition for Energy Efficient Comminution (http://www.ceecthefuture.org) state that comminution accounts for 53% of all energy used in the mining industry.

Defining energy efficiency as the energy required for breakage divided by the energy used by the mechanical system, the energy efficiency for comminution is reported to range from 0.1% to 2% (Fuesrstenau and Abouzeid, 2002; Tromans and Meech, 2002). Based on fundamentals of fracture

mechanics, Tromans (2008) hypothesized that there is a maximum limiting energy efficiency for comminution of between 5% and 10%.

Figure 1 presents the main technology types responsible for comminution along the energy value chain. The main energy consumers are blasting, crushing and grinding. Also presented in the figure are technologies that can contribute to reduced energy usage including continuous mining technologies, ore sorting, rock weakening and improved size classification. Systems engineering approaches of the integration of mining and processing activities have led to concepts of Mine to Mill and Geometallurgy that result in strategies for optimization of energy use.

Comminution at Face | Coarse Comminution | Fine Comminution

Particle Weakening | Size Classification

Sensing and Sorting

Mine to Mill

Lithology | *Mineralogy* | *Geometallurgy*

Figure 1. Comminution Energy Value Chain

1.2 Technology Readiness Level

One approach to advancing technologies for commercialization is the Technology Readiness Level that was developed for the aerospace industry (http://www.esto.nasa.gov/files/TRL_definitions.pdf, 2015). The approach is the basis for a roadmap that can be followed during research and development to validate concepts, scale-up and adapt the technology to the industrial environment. Table 1 presents the nine technology readiness levels that have been used. Researchers are very effective at developing technologies from TRLs of 1 to 3. To achieve TRLs 7 to 8, end users need to be active participants in the process. Key to the success of commercialization is advancing the technology through TRLs of 4 to 7 referred to as the “valley of death”. It is at these TRLs that many innovations become stalled.

2 ENERGY EFFICIENT TECHNOLOGIES

2.1 Recent Innovations

Over the past 20 years several novel technologies that greatly reduce energy usage have been developed. However, new technology is perceived as a risk to the mining sector and as such the acceptance and implementation of these technologies have been slow. The conservative mining culture reflects on the need for greater efforts to focus on technology development through efforts such as demonstration to shorten the timeline for acceptance.

Mine to mill and geometallurgical concepts were introduced to the mining industry over 30 years ago. Despite knowledge of the benefits of these concepts, they are not used by all operations. High Pressure Grinding Rolls and High Speed Stirred Mills represent step changes in energy efficiency, yet both technologies are only considered for niche applications. Looking forward, innovations in particle weakening through technologies such as

electric pulse and microwave treatment offer benefits related to energy usage as well as improved mineral separation through enhanced liberation. Sensing and sorting technologies for rock rejection or bulk separation improves our abilities to discriminate between ore and waste and thereby allow us to avoid grinding waste resulting in direct energy savings. Technology areas that require innovation include increasing the level of automation and new developments in specific areas such as size classification.

Over the past 25 years several process technologies have been introduced to the mining industry that impact comminution energy usage. Of note were the introduction of Mine to Mill concepts and technologies such as High Pressure Grinding Rolls (HPGR) and High Speed Stirred Mills (HSSM). Each has significant energy benefits plus several other advantages related to operating costs and metallurgical performance. While the technologies have been applied at the industrial scale, their application is still somewhat tenuous.

Table 1. List of Technology Readiness Levels(www.esto.nasa.gov/files/TRL_definitions.pdf, 2015)

TRL	Description
1	Basic principles observed and reported
2	Technology concept and/or application formulated
3	Analytical and experimental critical function and/or characteristic proof-of- concept
4	Component/subsystem validation in laboratory environment
5	System/subsystem/component validation in relevant environment
6	System/subsystem model or prototyping demonstration in a relevant end-to-end environment
7	System prototyping demonstration in an operational environment
8	Actual system completed and "ready for implementation in mining operation" through test and demonstration in an operational environment
9	Actual system through successful application at mining operations

2.1.1 Mine to mill

The Mine to Mill concept integrates information about lithology, mineralogy and mining systems to identify synergies that would benefit downstream processing. The greatest focus has been to promote particle fragmentation by blasting in order to reduce energy usage or increase throughout in downstream grinding. Several case studies have demonstrated energy savings of up to 20%, which translates into comparable increases in throughput for existing operations (McKee et al, 1995, Dance et al, 2011). Environmental benefits resulting from waste and tailings reduction are also significant. Since the development of Mine to Mill approaches, about one hundred mines globally have applied Mine to Mill to improve either production rates or energy efficiency (Dance, 2015). In relative terms, Mine to Mill concepts were commercialized quickly because they were developed by operators at operations resulting in almost immediate application following the development of the concepts. This approach accelerated the concept up the readiness level scale. Concepts were developed and accelerated through the TRLs such that trials at operations advanced the concept through TLR's 7, 8 and 9. The involvement of operations willing to apply the concept was critical to commercialization. Despite proven benefits of Mine to Mill, the uptake has not been fast which may be attributed to a lack of incentives to motivate implementation.

2.1.2 High pressure grinding rolls

Based on fundamental work on fracture physics, Professor Klaus Schoenert (1979) concluded that increased energy efficiency could be achieved by breaking particles in compressive beds. He applied the concept to the development of High Pressure Grinding Rolls in which material is choke fed between two counter rotating rollers, one of which is fixed and the other is floating in connection with a hydraulic cylinder. The material forms a compressive bed between the two rollers resulting in interparticle breakage (Schoenert, 1988). Energy savings of

between 15 and 30 % over SAG Mill Circuits have been reported (Rosario, 2010; Rosario et al., 2011). Energy benefits relate to improved energy efficiency from compression breakage but also result from micro-fractures that lower the Bond Work Index by about 10% for subsequent grinding (Drozdiak, 2011).

In the early 1990s, the HPGR found applications for the breakage of soft materials such as clinker (Patzelt, 1992) and kimberlites. For diamond ores, the ability of the HPGR to break kimberlite host rocks without breaking diamonds added significant value motivating the implementation (Anguelov et al., 2008). The first hard rock application was in 1995 at Cyprus Sierrita in Arizona, which demonstrated that wear issues needed to be overcome (Thompsen et al., 1996; Morley, 2008). The introduction of studded liners that trapped particles at the roll surface and thereby created an autogenous layer greatly improved wear life and led to the successful installation of the HPGR at the Cerro Verde copper mine in Peru in 2007.

Since then, the HPGR technology has been used at a number of operations although it is still primarily considered only for niche applications such as for very hard ores. Perceptions are related to dust issues, extensive material handling systems. Specific criticisms relate to the complexity of material handling in environments that can freeze, causing operational problems and the inability to operate at high moisture levels in high rainfall areas. Despite these challenges, HPGR circuits result in energy savings for comminution that range from 10 to 30%. When considering that up to 70% of all electrical power in large open pit mines is consumed by semi-autogenous-ball milling-crushing (SABC) circuits, the advantages of the HPGR are substantial. There are presently six manufacturers of the HPGR namely Polysius, Koeppern, KHD, Metso, FLSmidth and Citic. While the HPGR is perceived to be the comminution technology of the future, it still has not received full acceptance by a technical community who are most comfortable with SABC circuits. However the technology is receiving considerable interest and its application is expected to increase. An indication of the strong interest is reflected by the number of technical publications on the subject. For the upcoming SAG 2015 Conference, the HPGR is considered to be a competing technology to SAG milling and as many as 25% of all presentations will focus on this topic. As a result, the conference title has been changed to International Conference on Semi-Autgenous Grinding and High Pressure Grinding Rolls (SAG 2015, http://sagconference.com).

In terms of the Technology Readiness; Level, the concept was developed in 1979 and 46 years later (2015) there is good industry acceptance of the technology. Over this period barriers to commercialization included a range of technical issues that were addressed. However equally important is that the perception of low TRL and low incentives for change (such as low energy prices) likely slowed the development. The Cerro Verde Mine (http://www.fcx.com/operations/Peru_Arequipa.htm) that installed the HPGR in 2007 was key to acceptance of the technology.

2.1.3 High speed stirred mills

Mount Isa Mines were the first to apply high speed stirred milling as a means of liberating fine grained polymetallic ores. The scale-up of the Netzsch Mill, that had been applied to pigments and other specialized industrial mineral products, to a size that could be applied for metal mining led to the development of the ISA Mill (Gao et al., 1999). The technology represented a breakthrough because it could reduce particle size to below 10 microns with relatively low energy input as compared to regrind tower mills or ball mills. For fine regrinding applications, energy savings of 50% were demonstrated over Verti-Mills at target size of 80% passing 18 microns. For grinding below 10 microns energy savings were even greater.

Mount Isa maintained exclusive use of the technology until the late 1990’s when they

marketed the technology under Xstrata Technology. The development of the technology was led by a mining company, which was key to the advancement through the TRLs and commercialization in a relatively short period of time.

Within a decade of developing the concept to scale-up the Netzsch mill to meet the demands for large scale ultrafine grinding, several operations around the world had applied the technology. With respect to technology readiness level, the ISA Mill technology advanced quickly. This likely relates to development of the technology by a mining operation to prove and demonstrate the concept in an industrial environment to help it attain industry acceptance.

More recently, efforts have been put towards adapting the technology to applications requiring a coarser grind where it has also demonstrated energy benefits over tower mills and ball mills. It is now over twenty years since the ISA Mill was first developed and while it has gained significant market access, it is still considered primarily for ultrafine regrind applications. There are presently four manufacturers of high speed stirred mills (Outotec, FLSmidth, Metso, Xstrata Technology).

2.2 Energy Savings

A number of studies have been conducted to quantify the energy savings that can result from combining Mine to Mill, HPGRs and High Speed Stirred Mills. Using process simulation, Valery and Jankovic (2002) determined that a novel system involving high intensity blasting, HPGR and Verti Mills required about 45% less energy than a conventional SAG Mill – Ball Mill Circuit. Based on pilot scale studies, Drozdiak et al. (2011) compared a conventional cone crusher-ball mill circuit to a novel HPGR-ISA Mill circuit that reduced comminution energy requirements from 17.8 kWh/t to 14.8 kWh/t, which is about a 17% reduction in energy usage. Plant operating energy usage for an SABC circuit was compared to a novel two stage HPGR circuit – ISA mill circuit and demonstrated 30% energy savings (Wang 2013; Wang et al, 2013). There is sufficient information to show that each technology represents a step change in energy efficiency and that by combining the technologies in innovative processes, energy usage can be greatly reduced.

3 EMERGING AND FUTURE TECHNOLOGIES

Several technologies have been developed at the conceptual stages that if developed through to commercialization would represent a significant breakthrough. Continuous mining equipment has been developed for soft ores and efforts have been made to evolve these technologies to hard rock mining. Hydrofracking has been investigated for breaking coal and the technology has been considered for block caving to improve control of the caving process. There is ongoing work to improve blast control evolving intensive blasting to reduce energy usage in downstream comminution. A significant breakthrough has been made using microwaves that fragment or weaken rock. The application of microwaves induces differential thermal expansion of minerals of different composition that weakens the rock and promotes breakage along grain boundaries reducing the energy input needed for downstream breakage from crushing and grinding and potentially improving mineral liberation (Charikinya and Bradshaw, 2014). Similarly high voltage pulse technology has been developed that weakens rocks by inducing electrical explosions causing shockwaves (Cabri et al, 2008, Zou et al, 2014; van der Wielen et al., 2014). The weakening results in lower grinding energy and breakage is reported to be preferential along grain boundaries enhancing liberation. One area that requires innovation is high capacity size classification in particle size ranges where screening rates become slow and above sizes where classifying with hydrocyclones can be applied. Another emerging technology area is sensor based sorting, which rejects barren rock ahead of

downstream comminution resulting in energy savings that are directly proportional to the amount of rock rejected.

3.1 Sensing and Sorting Systems

Sorting has been applied for some time to mining such as the case of radiometric sorting of uranium ores in Canada in the 1960s. X-ray sorters have been a standard separation technology in the diamond industry since the 1980s when they introduced in the Argyle diamond mines in Australia. With the development of recycling technologies in Europe, several manufacturers developed sorting technologies that are commercially available with a range of sensor technologies. These companies have applied the sorting technologies to mining applications. Despite several benefits related to energy and material handling, particle sorters have found only niche applications in the mining industry. The two main barriers to broader application relate to sensors that can discriminate barren rock particles from valuable ore particles and the limited capacity of industrial machines (Wotruba, 2006; Klein et al., 2011).

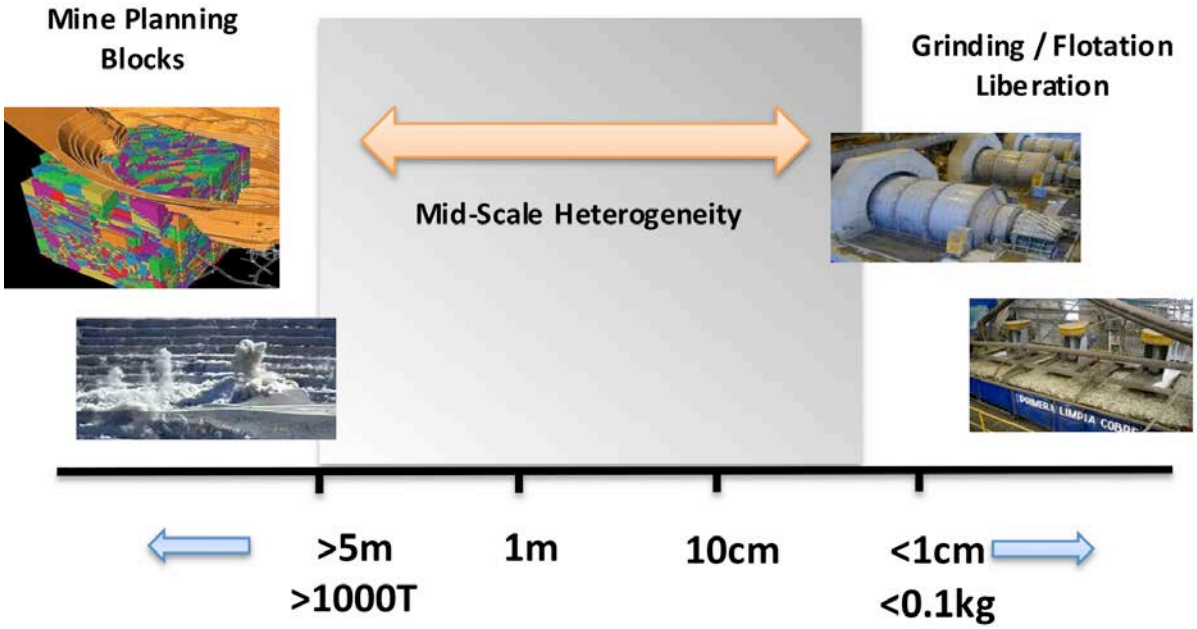

Figure 2. Schematic Illustrating Midscale Heterogeneity (courtesy of MineSense Technologies Ltd. 2014)

3.2 Heterogeneity and Sensing Systems

There are several potential benefits to ore sorting including reduced material handling costs, lower operational costs associated with energy consumption particularly for comminution, more consistent feed grades and higher grade of ore reporting to the concentrator, and it also enables the application of lower cost bulk mining methods over more selective mining potentially allowing a lowering of the mined cut-off grade. A key to successful sorting is the heterogeneity of the ore that will be exploited. In mining systems, heterogeneity is exploited at the bulk ore body scale to distinguish between ore and waste rock as well as at the mineral separation stage where liberation determines separation. Sorting focuses on exploiting heterogeneity in sizes intermediate to these two extremes. The scale of heterogeneity can vary considerably as presented in Figure 2.

One approach to quantifying heterogeneity was proposed by Pierre Gy (Pitard, 1993) and is referred to as Constitution Heterogeneity (CH). For a “lot” of particulate materials (such as a stockpile), CH is the difference between the composition of various units in the lot (such

as the particles that make up the units) and not between the individual units themselves; for example the grade of each rock compared to the other rocks and average grade of the lot (Gy, 1992).

$$CH_L = s^2(h_i) = \frac{1}{N_F}\sum_i h_i^2 = N_F \sum_i \frac{(a_i - a_L)^2}{a_L^2}.\frac{M_i^2}{M_L^2} \quad (1)$$

where α_i and α_L are the grades of the fragment *i* and the lot, respectively, while M_i and M_L are the masses of fragment *i* and the lot. If the fragments are part of a much larger lot, N_F in equation (1) should be substituted by N_F*-1*.

When it comes to assessing sorting of a specific ore deposit, two approaches are available: Sorting either targets the metal of interest, such as copper or gold; or focus is on rejection of waste, such as silica. In some cases it could be beneficial to sense and reject gangue rather than attempt to recover metal.

Early stage assessment of amenability to sorting should focus on characterization of heterogeneity. To exploit heterogeneity, a range of sensors can be applied. Approaches include measurement of sensor responses and calibrating against rock assays. In addition to the individual sensor signals, methods that should be considered include:

1. Analysis of sensor response signatures rather than relying on a single threshold level.
2. Combining sensor responses to improve discrimination.
3. Analysis of proxies for target metals.
4. Assessing heterogeneity of gangue phases for rock rejection.
5. Applying regression analysis to sensor signals.
6. Assessing rock size heterogeneity.

While work is required to improve the resolution and speed of sensors, the above methods need to be applied in order to assess the potential for sorting. Present studies evaluate sorting on the basis of sorting machines that are commercially available. In some cases the ability to apply the commercially available sorters is the basis for classifying the ore as sortable or not sortable. As a consequence ores are prematurely considered not sortable based on a general misconception that "if our machine cannot sort the material then it is not sortable". Research and development that relies on better sensors and applies innovative approaches that relate geology and mineralogy are needed to improve the resolution of sensing. As such sensing systems presently available will have a technology readiness level of 9, but much work is still needed to be conducted at the conceptual TRLs of 1 to 3 to enable broader application of sorting.

3.3 Throughput Limitations – Rock vs. Bulk Sorting

In order to address capacity challenges, efforts are being directed towards bulk and/or semi-bulk sorting. Platforms exist for rock sorting that requires screening of feed into narrow size fractions and then feeding the sorter with a mono layer of particles that can be sensed and subsequently accepted or rejected using pneumatic or mechanical particle ejectors. While these technologies have a proven track record for selected ores, their application is limited by the throughputs that are achievable. The case for sorting can be made for low tonnage operations, however, rock sorters cannot be applied to low grade deposits that utilize less selective mining methods and operate at high production rates.

The approaches aimed at increasing through focus on semi-bulk or bulk sorting. Sensors along the material handling system can be applied to discriminate between ore and waste. Conservative strategies aimed at waste rejection reduce the risk of sending ore to waste dumps. MineSense Technologies are developing systems that incorporate sensors in the material handling equipment such as shovels and on conveyor belts (http://minesense.com). For example, sensors in a shovel loading waste can inform the operator that the shovel contains ore.

Similarly, the sensors can inform the operator that the shovel contains waste. Conveyor sensors can trigger deflection of ore from waste at head pulleys. Keys to these systems are sensors that are calibrated to properties of the ore and the waste. Also, while considerable heterogeneity may exist when the material is being excavated at the face, through material handling and stockpiling, the ore flows through stages of mixing and blending reducing the level of heterogeneity. Therefore, the opportunity for bulk sorting is best closest to the face.

The technology readiness level of rock sorting has been demonstrated for selected applications. Bulk or semi-bulk sorting has been applied in niche applications such as for high phosphate versus low phosphate iron ores (Kiruna). There are similar opportunities for other ores but the technology is at a lower state of readiness. The application of bulk sorting needs to be developed for ore types such as porphyry, laterites or iron ore and then refined for individual deposits. Potential applications to large tonnage ores such as nickel laterites, copper porphyrys and iron ores will greatly impact resource utilization and profitability.

4 CONCLUSIONS

Several advances have been made that reduce energy usage in comminution. Individual technologies such as intensive blasting, HPGRs and high speed stirred mills represent a step change in energy efficiency. Combining these technologies in innovative flowsheet designs amplifies the amounts of energy savings. The key to technology acceptance was the participation of mining operations in the development process. Early stage participation accelerated the advancement of the concepts from TRL 3 through the “Valley of Death” to TRL 9. Emerging technologies should engage mining operations as soon as possible which will reveal technological barriers and demonstrate the opportunity to the implementers of the technologies. Sensor based sorters for rock separation are commercially available, however they have found only niche application. Improved sensor systems along with the development of higher capacity sorters that rely on semi-bulk and/or bulk sensing systems will support broader application. The key to advancing the technology through to commercialization requires participation between researchers, manufactures and end users.

REFERENCES

Anguelov, R., Alexander, J., Ghaffari, H, 2008. High pressure grinding rolls (HPGR) an alternative technology versus SAG milling, MEI Comminution’08 Conference, Falmouth, Cornwall, UK.

Cabri, L.J., Rudashevsky, N.S., Rudashensky, V.N., Oberthür, T., 2008. Electric-Pulse Disaggregation (Epd), Hydrosearation (Hs) and Their Use in Combination for Mineral Processing and Advanced Characterization of Ores, Proceedings of the 40th Annual Canadian Mineral Processors Conference, Ottawa, Ontario, Canada, pp.211-235.

Charikinya, E., Bradshaw, S., 2014. Use of X-ray computed tomography to investigate microwave induced cracks in sphalerite ore particles. International Mineral Processing Congress, Santiago, Chile.

Dance, A., 2015. Personal Communication on Application of Mine to Mill.

Dance, A., Mwansa, S., Valery, W., Amonoo, G., Bisiaux, B., 2011. Improvements in SAG Mill Throughput From Feiner Feed Size at the Newmont Ahafo Operation, SAG 2011, Paper #011.

Drozdiak, J.A., 2011. A Pilot-Scale Examination of a Novel High Pressure Grinding Roll / Stirred Mill Comminution Circuit for Hard-Rock Mining Applications, MASc Thesis, University of British Columbia, Vancouver, BC, Canada, 228p.

Drozdiak, J., Nadolski, S., Bamber, A., Klein, B., Wilson, S., 2010. A Comparison of the Energy Requirements of an HPGR / Stirred Mill Circuit and Conventional Grinding Circuits for the Comminution of Mesaba Ore, 42nd Annual Meeting of the Canadian Mineral Processors, Ottawa, Ontario, Canada.

Fuerstenau, D.W., Abouzeid, A.M., 2002. The energy efficiency of ball milling in comminution, International Journal of Mineral Processing, 67(1-4), pp.161-185.

Gao, M., Weller, K.R., Allum, P., 1999. Scaling-up Horizontal Stirred Mills froma 4-litre Test Mill to a 4000-litre “IsaMill”, Powder Technology

Symposium, Pennsylvania State University, PA, USA.
Gy, P.M. 1992. Sampling of Heterogeneous and Dynamic Material Systems. Theories of heterogeneity, Sampling and Homogenising, Elsevier, Amsterdam.
Klein, B., Bamber, A., Altun, N.E., Scoble, M. 2011. Towards tomorrow's 'smart mine' – Embedded sensor telemetry and sensor based sorting, Proceedings Second International Future Mining Conference 2011, AUSIMM, Melbourne, pp.59-68.
McKee, D.J., Chitombo, G.P., Morrell, S., 1995. The Relationship Between Fragmentation in Mining and Comminution Circuit Throughput, Minerals Engineering, 8(11), pp.1265-1274.
MineSense Technolgies Ltd, 2015. http://minesense.com
Morley, C., 2008. HPGR – FAQ, MEI Comminution'08 Conference, Falmouth, Cornwall, UK.
Parry, J., 2006. Ultrafine Grinding for Improved Liberation in Flotation Concentrate, MASc Thesis, University of British Columbia, Vancouver, BC, Canada.
Patzelt, N., 1992. High-pressure grinding rolls, a survey of experience, Cement Industry Technical Conference, IEEE, pp.149-181.
Pitard, F.F., 1993. Pierre Gy's Sampling Theory and Sampling Practice, 2nd Ed. CRC Press, USA, 516p.
Rosario, P., 2010. Comminution Circuit Design and Simulation for the Development of a Novel High Pressure Grinding Roll Circuit, PhD Thesis, University of British Columbia, Vancouver, BC, Canada.
Rosario, P., Hall. R., Grundy, M., Klein, B., 2011. A Preliminary Investigation into the Feasibility of a Novel HPGR-based Circuit for Hard, Weathered Ores Containing Clayish Material, Minerals Engineering, 24 (3-4), pp.290-302.
Schoenert, K., 1979. Aspects of the physics of breakage relevant to comminution, Tewksbury 4th Symposium on Fracture: Fracture at Work, Melbourne Australia.
Schoenert, K., 1988. First survey of grinding with high-compression roller mills, International Journal of Mineral Processing, 22(1-4), pp.401-412.
Thompsen, L., Patzelt, N., Knecht, J., 1996. High-pressure grinding for copper at cyprus sierrita, Mining Engineering, 48 (9), pp.23-26.
Tromans, D., Meech, J.A., 2002. Fracture toughness and surface energies of covalent minerals: Theoretical estimates for oxides, sulphides, silicates and halides, Minerals Engineering, 15(12), pp.1027-1041.
Tromans, D., 2008. Mineral comminution: Energy efficiency considerations, Minerals Engineering, 21(8), pp.613-620.
Valery, W., Jankovic, A., 2002. The Future of Comminution, 34th IOC on Mining and Metallurgy, Sept 30-Oct 3, 2002, Bor Lake, Yugoslavia.
van der Wielen, K., Weh, A., Giese, H., Käppeler, J., 2014. High voltage breakage: A review of theory and applications, International Mineral Processing Congress, Santiago, Chile.
Wang, C., 2013. Comparison of HPGR – Ball Mill and HPGR – Stirred Mill Circuits to the Existing AG/SAG Mill – Ball Mill Circuits, MASc Thesis, University of British Columbia, Vancouver, BC, Canada, 169p.
Wang, C.T., Nadolski, S., Mejia, O., Drozdiak, J., Klein, B., 2013. Energy and Cost Comparisons with the SABC Circuit Installed at the Huckleberry Mine, 45th Annual Canadian Mineral Processors Operators Conference, January 22-24, Ottawa, ON, Canada, pp.121-135.
Wotruba, H., 2006. Sensor Sorting Technology – is the minerals industry missing a chance?, XXIII International Mineral Processing Congress, Istanbul, Turkey, pp.21-30.
Zou, W., Shi, F., Manlapig, E., 2014. The effect of metalliferous grains on electrical comminution of ore, International Mineral Processing Congress, Santiago, Chile.

APPENDIX

Definition of Technology Readiness Levels

TRL 1 Basic principles observed and reported: Transition from scientific research to applied research. Essential characteristics and behaviors of systems and architectures. Descriptive tools are mathematical formulations or algorithms.

TRL 2 Technology concept and/or application formulated: Applied research. Theory and scientific principles are focused on specific application area to define the concept. Characteristics of the application are described. Analytical tools are developed for simulation or analysis of the application.

TRL 3 Analytical and experimental critical function and/or characteristic proof-of- concept: Proof of concept validation. Active Research and Development (R&D) is initiated with analytical and laboratory studies. Demonstration of technical feasibility using breadboard or brass board implementations that are exercised with representative data.

TRL 4 Component/subsystem validation in laboratory environment: Standalone prototyping implementation and test. Integration of technology elements. Experiments with full-scale problems or data sets.

TRL 5 System/subsystem/component validation in relevant environment: Thorough testing of prototyping in representative environment. Basic technology elements integrated with reasonably realistic supporting elements. Prototyping implementations conform to target environment and interfaces.

TRL 6 System/subsystem model or prototyping demonstration in a relevant end-to-end environment (mining operation): Prototyping implementations on full-scale realistic problems. Partially integrated with existing systems. Limited documentation available. Engineering feasibility fully demonstrated in actual system application.

TRL 7 System prototyping demonstration in an operational environment (mining operation): System prototyping demonstration in operational environment. System is at or near scale of the operational system, with most functions available for demonstration and test. Well integrated with collateral and ancillary systems. Limited documentation available.

TRL 8 Actual system completed and "ready for implementation in mining operation " through test and demonstration in an operational environment (mining operation): End of system development. Fully integrated with operational hardware and software systems. Most user documentation, training documentation, and maintenance documentation completed. All functionality tested in simulated and operational scenarios. Verification and Validation (V&V) completed.

TRL 9 Actual system "operations proven" through successful implementation at a mining operation): Fully integrated with operational hardware/software systems. Actual system has been thoroughly demonstrated and tested in its operational environment. All documentation completed. Successful operational experience. Sustaining engineering support in place.

Comparative Study of Mineral Processing Applied To The Local Feldspar's Assessment

R.Akkal, M.Ouldhamou
National Polytechnic School of Algeria, Alger's, Algeria

ABSTRACT In the field of ceramics and glassware, feldspars are extensively used worldwide as cooking or melting additives. Feldspars act as a flux to melt the silica into a liquid glass. This is caused by the high amounts of Potassium in the pot ash feldspar, Sodium in the Soda ash Feldspars and Lithium in Spodumene. The amount of coloring iron substances must be low. The main objective of this study is focused on the mechanical preparation of Algerian crude feldspar with a view to extract the information about the comminution and the coloring iron rate distribution, on the one hand, and to remove the oxides of iron, on the other hand, main impurities of crude feldspar by magnetic separation, flotation and more particularly by chemical bleaching (leaching). The bleaching chemical used is the nitric acid reducing medium to replace sulfuric acid and dithionite as reducing agent, the application tests have yielded negative results.

Keywords: Feldspar, Ain Barbar, chemical purification

1 INTRODUCTION

Feldspars are essential constituents of igneous rocks, plutonic or extrusive (59.5% of the minerals of magmatic rocks). Their chemical composition varies with the nature of the rocks : acidic rocks contain alkali feldspar, intermediate rocks of alkali feldspar and plagioclase means, basic rocks calcic plagioclase. Feldspars belong to the family tectosilicates.

Analysis of feldspars allows them as more or less homogeneous mixtures of three basic components : KAlSi3O8 : Orthose (Or) (Sanidine ou microcline), NaAlSi3O8 : Albite (Ab) et CaAl2Si2O8 : Anorthite [1–3]. They generally occur together with quartz, mica, iron oxides, rutile and hornblende. Basically, the two properties which make feldspars useful for downstream industries are their alkali and alumina content. Feldspars play an im- portant role as fluxing agents in ceramics and glass applications, and are also used as functional fillers in the paint, plastic, rubber and adhesive industries [4–8].

Presence of iron in feldspar is not desirable as it imparts color to the final product, and therefore, iron content has to be kept below a certain value, 0.10% for glass making and 0.07-0.08% for ceramics [5, 9]. Several conventional enrichment techniques, such as hand sorting, comminution, magnetic separation and flotation, are employed to remove coloring impurities including iron bearing minerals from feldspar. These techniques are used for the treatment of particles larger than 40 microns. Other technics are applied for the ultra-fine particles treatment(slimes) , less than 40 micron such as flocculation [10]. The mechanical properties
of feldspathic rock have a direct impact on eight yields different size fractions for purification and marketing ; therefore they affect the selection and sizing of comminution and screening equipment. Any method of treating an ore often requires that it be reduced or broken at a dimension that allows the release of its ingredients (minerals and gangue products) making the separation of the latter accessible. As part of this work, which was to achieve optimal locate a chemical purification feldspar of Ain barbar conditions using nitric acid in the presence of ammonium bifluoride as the reducing, we prefer to review all the results of all characterization and optimization tests

achieved in the past. This allowed us to compare a number of results and extricate useful conclusions to any project development.

1.1 Materials and Methods

A representative sample of the Ain Barbar deposit located in the east of Algeria received in the ENP laboratory, whose Mineralogical composition and chemical analysis are presented in table 1 and 3. The sample was previously crushed in a jaw crusher followed by grinding in an impact mill of Ain Barbar unit. In this work, we aim to produce the size fraction [-0.8+0.1] mm for the glass. In view of the glass market application, we screened the sample E0 in [0.8 mm] size, were extracted by sieving the fines [-0.1 mm] to avoid over-grinding. Grinding and sieving are carried out as shown in the following schematic.

The desired results are the production of three fractions sizes [-0.8+0.4], [-0.4+0.25] and [-0.250] mm taken as the basis for subsequent recovery treatments as shown on the Figure 1.

Table 1. Grain size distribution of sample

Size fraction (mm)	RP (%)	Fe2O3 (%)
[+0.8]	3.30	0.45
[-0.8+0.6]	19.23	0.46
[-0.6+0.250]	19.58	0.49
[-0.250+0.1]	23.35	0.56
[-0.1+0.04]	7.92	0.63
[-0.04]	28.42	0.77

Grain size distribution of sample is shown in table below Table2.

Table 2. Mineralogical composition of sample

Element	Percentage
Orthose	52.66
Quartz	37.42
Pyllites	7.02
Albite	1.70
Anorthite	0.58
Fe_2O_3	0.53
Apatite	0.38

In a second step, we conducted the high magnetic intensity separation trials of iron oxides content in feldspars. Slices prepared underwent magnetic separation into two passages on magnetic separator intensive CARPCO brand. The next step is to treat the treated particles by magnetic separation will be treated by flotation; the other party will be processed by leaching. The requirements for effective flotation: the first condition to obtain good flotation is to achieve a grinding of the maximum releasing minerals from each other; and a suitable release of the particles to float. In some cases, it is necessary to desliming pulp before the float and to avoid that the recovery of the mineral particles surfaces.

In our cases, dry milling was performed in a ball mill ceramic to avoid contamination with iron, the milling time and the grinding mass are determined on the basis of tests. For this work, the grinding time is estimated about 8min, with a mass gain of 300 g. After grinding, we conducted a screening to remove particulates, which are smaller than -0.04 mm dimensions. The purpose of the grinding is to achieve the size less than 0.250 mm, to release the most of the mixed iron oxide particles, whose operation is controlled with a sieve whose opening is smaller -0.250 mm. At the end of the operation desliming refusals and passersby were dried and weighed.

A pulp containing between 5 and 50% solids mixture with water, the pulp is stirred in a conditioning tank to ensure the homogeneity of the medium. In a first time, dispersants AP 801 and AP 840 are added to avoid any kind of agglomeration before floating the concentrate (feldspar), then the collector Dodycelamine agent and hydrofluoric acid are added to modify the surface feldspar particles to be driven to the surface by the air bubbles. This process is repeated every time before flotation concentrate. In this work, the flotation operation is repeated 3 times. After flotation, we washed, dried filtered and concentrated and the discharges.

Table 3. Chemical analysis of sample

Element	Pourcentage
SiO2	75
Al_2O_3	12.45
Fe_2O_3	0.57
TiO_2	<0.05
CaO	0.30
MgO	0.20
Na_2O	0.30
K2O	<0.20
MnO	<0.20
P.F	0.70
P_2O_5	0.20

2 RESULTS AND DISCUSSION

Feldspar fragments having a maximum dimension of [150] mm are first crushed with a mass to be able to place in a laboratory jaw crusher, whose maximum aperture is [50] mm adjustable. A sample of forty pounds is inserted into the jaw crusher for a first step. The crushed product is recycled again after reducing the outlet opening of the crusher without sieving. Refusal to [0.8] are ground mm [0.8] mm in a FORPLEX grinder to reduce to [0.8] mm, the [+0.8] mm go over 3 times in FORPLEX mill.

We have taken after thorough mixing three samples we screened separately. The results are shown in the following schematic. A granular-chemical analysis was performed for all three screening. The level of the fine [-0.04] mm from the power decreases with the increase in recycling, this finding can be explained by the fact that the fragile particles crumble at the first passage on the crusher and mill, the hardest produce fewer fines remaining. [+ 0.25 -0.4] mm slice is produced with a rate that varies little regardless of the number of recycles, this rate varies between 10 and 12%, this is due to the fact that all comers has a good degree of homogeneity of hardness and perspective structure. The pattern of grinding applied in this study responds to market demand. Knowledge of the physical properties of size fractions required by customers, help in choosing based on the results of this study the quality and types of equipment that would be most suitable for the production unit projected. Knowing the results of weight crushing / screening assessment is used to size the facilities of a production unit based on size fractions required and demand.

2.1 High Intensity Magnetic Separator of Iron Oxides

Size fractions prepared underwent two passages on a laboratory magnetic separator intensive (mark CARPCO). Initially, we vary the magnetic field keeping the other factors fixed. The results obtained are shown in the following figure. The magnetic purification reduces the iron oxide content of feldspar to the value of 0.34% to 99.62% by performance weight relative to food, treating the size fractions [-0.8+0.1], [-0.6+0.1], [-0.6+0.250] and [-0.250+0.1] mm separately, except size fraction [-0.8 +0.1] mm which the iron oxide content is reduced from 0.50 to 0.39%. For a better release of iron oxides generated by a finer grinding, there is a better treatment for size fractions greater than 0.1 [mm]. For particle size fractions [-0.1] mm, removal of iron oxides is needless, caused by the ultra-fine particles that the magnetic field strength is no longer able to attracted and retain them on the drum machine Figure 2. These ferrous dust mixed with those of finely ground feldspar, which cover the receivable oxides, they reduce the driving forces generated by the magnetic field on these oxides, however favorable to their extraction feldspar dimensions [11–13]. Purification of the particle size range [-0.8 +0.1] mm by high gradient or high intensity magnetic field resulted in only a iron residual of 0.34 and 0.39 % values very close who do not justify the high investment in the use of high gradient separator. For products used in the ceramic industry, the high intensity magnetic purification gives contents oxide iron 0.34

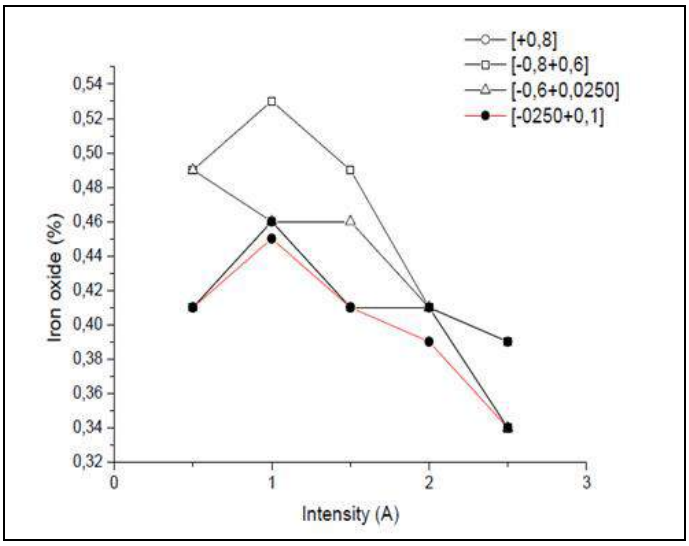

Figure 2. iron oxides (%) vs high intensity magnetic values

0.31% for size fractions [-0.2+ 0.080] ; [-0.25+0.1] mm. It is best to treat several size fractions separately and then mix them to reconstruct the portion that meets the required criteria for use.

2.2 Flotation Purification

A part of the size fractions treated by magnetic separation will be processed by flotation, followed by leaching, the other part will be treated by leaching. Dry grinding was carried out in a ball mill ceramic to avoid contamination with iron, the milling time and the grinding mass are determined on the basis of tests. In our case the grinding time is 8minutes to slice 0.1-0.8 mm and 6 minutes for the portion 0.1-0.6m.

2.2.1 The feldspars preparation scheme for flotation

After grinding, we conducted a screening to remove particles whose dimensions are less than [-0.04] mm using sieve whose opening is [-4mm].

The purpose of the grinding is to achieve fractions sizes less than [0.250] mm, to release the most of the iron oxide particles mixed, so the operation is always controlled with a sieve whose opening is less than [-0250] mm. The ore is desliming in [-0.04] mm with an opening sieve of [0.04] mm. At the end of the operation desliming refusals and passersby were dried and weighed to calculate the yield weight [14]. The weight average yield is 60.49 % for the group [-0.8 + 0.1] mm, that for [-0.6 + 0.1] mm is 64.80 %, these results are very close to those of the BRGM study. The schematic process of flotation is given in the following figure Figure 3.

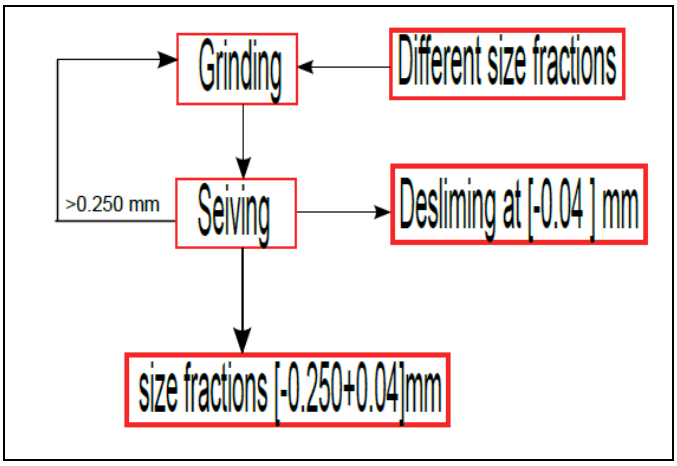

Figure 3. Grinding feldspar scheme for flotation application

Whatever the size fractions treated by magnetic separation, purification limited stops at
0.34% iron oxide, value already encountered in the BRGM study, who recoveries exceed 99%. Flotation applied for the size fractions treated with high intensity magnetic separation improves the purification by lowering content of Fe2O3 for about a third collector consumption 3ml, 4 ml or 5 ml and 0.05 kg/t, and 0.1 0,200Kg/t respectively. Fine particles were removed upper size fractions [-0.8 + 0.1] mm and [-0.6 + 0.1] mm, where more concentrated iron oxides, so they are less rich in oxides.

The contents of these oxides in the rough particles are released by grinding at [0.250] mm and removed by flotation. The final content of the concentrates is lower than in the case of thinner fractions sizes flotation ([-0.6 +0.25] mm [-0.25 + 0.1] mm [0.04 +- 0.1] mm). The results that we can reasonably extricate from these flotation tests carried out under the specified conditions, show that the decrease in content of the samples removed iron by magnetic purification, reached a rate of 40% to 50%.

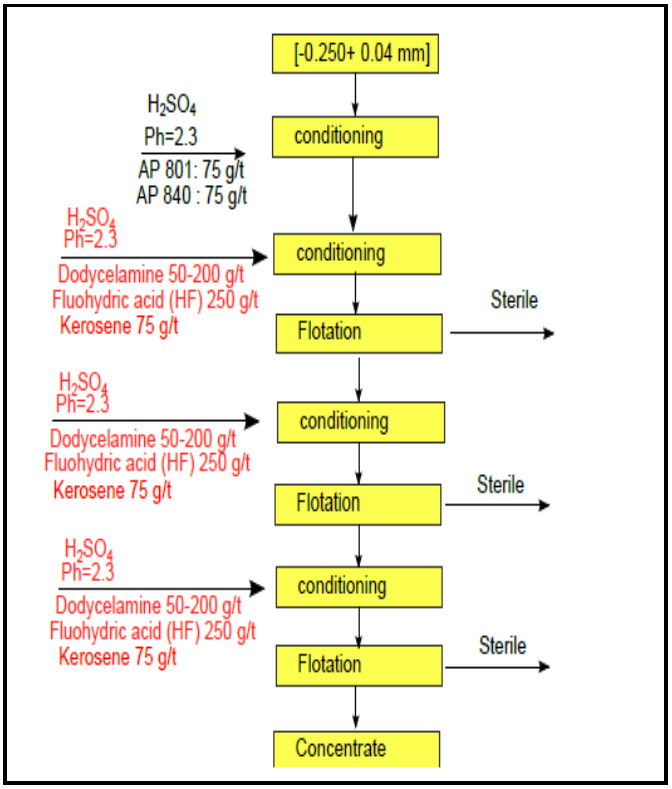

Figure 4. Flotation flowheet for feldspar purification

The final content of feldspar removed iron by magnetic purification and floated into the optimal conditions will be : Feldspar grinding to [0.8]mm where the fractions less than [-0.1] mm is extracted we have 54.85% yield weight with 0.23% a content of iron oxide.

For the size fractions [-0.6 + 0.1] mm subtracted from all comers crushed to [0.8] mm, we have 38.56% yield weight with iron oxide content of 0.20%, a decrease of 40% to 50%. The uncrushed size fractions to [0.25] mm and purified by magnetic separation, flotation gave weight yields very similar to those given in the two previous cases with iron oxides content ranging between 0.31 and 0.34%. The lower level of this impurity is only 0.18%. This result is explained by the fact that the non-grinding does not release encrusted oxides (mixed grains) in the grains of feldspar. For other thinner size fractions, the final content of iron oxide after flotation does not go lower than 30% with a drop that is around 11% for [-0.6 + 0.25] mm and [-0.25 +0.1] mm fractions and 50% for [-0.1 + 0.04] mm fractions. We note that the content of iron oxide is the least important in the upper size fractions, the more we go down to the fine, the content more increases ; this is due to the oxides physical characteristics, in particular oxides friability and connection nature which is associated with mineral feldspar, where it is finely disseminated. The size fraction [-0.6+ 0.1] mm contains more fines than [-0.6 0250]mm, hence the explanation that the Fe2O3 content of [-0.6 + 0.1] mm is higher (0.51%) than [-0.6 0250] mm (0.49%), which got rid of the fine [-0250 +0.1] mm richer in Fe2O3. The levels between 0.2% and 0.23% Fe2O3 with respective weight yields of 38.56% and 54.85% is commercial feldspar for ceramics for high consumption Figure 5.

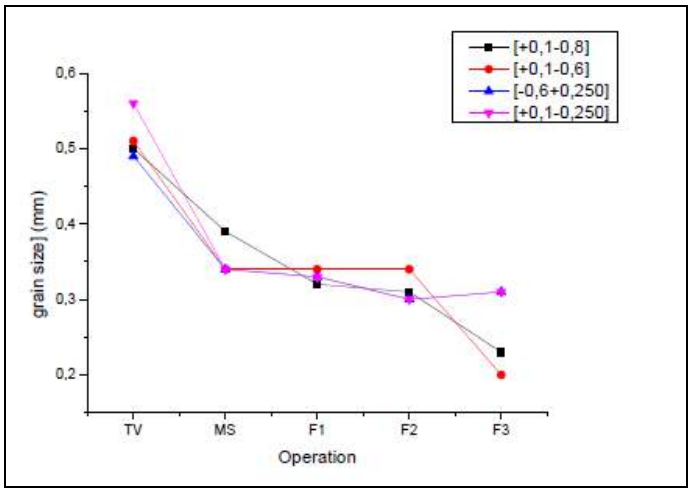

Figure 5. Flotation purification results compared with MS and TV

Table 4. Iron oxide composition for different sizes before and after grinding

Size fraction	Initial weight (g)	Fe2O3 (%)	Concentrate weight (g)	Fe2O3 (%)	Rp (%)
[-0.8+0.1]	300	0.39	149.2	0.32	49.73
[-0.8+0.1]*			276.9	0.23	92.30
[-0.6+0.1]	300	0.34	281.3	0.34	92.30
[-0.6+0.1]*			288.3	0.20	93.07
[0.1-0.250]	300	0.34	283.5	0.33	96.10
			267.0	0.30	94.50
[-0.14+0.04]	300	0.36	245.9	0.30	81.97
			285.6	0.30	89.83
[-0.6+0.250]	300	0.34	284.4	0.31	95.20
				0.30	94.80

2.3 Leaching Purification

In what follows, a hydrometallurgical process is applied. It consists of the selective dissolution of the metals present in the feldspar ore by a suitable reagent in aqueous solution. In our case, ferric iron oxides are reduced to ferrous iron. The experimental protocol consists of a beaker equipped with a heatproof cover and limiting the evaporation of the etching solution. The lid is provided with three ports, one to inject the acid, the second port is to fix a thermometer for measuring the pulp temperature and the third port serve as a location for refrigerant tube of the cooling gas which evaporates due to etching solution evaporation. The stirring and heating the mixture of the etching solution and ore are made using magnetic bars and a hot plate Figure 6.

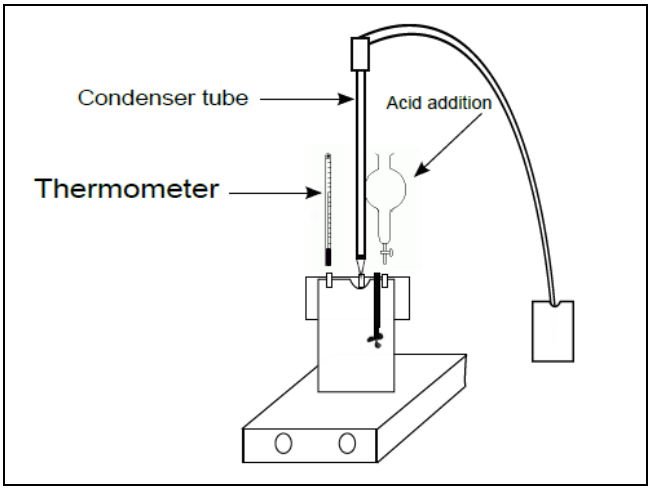

Figure 6. Leaching purification scheme for feldspar ore

To get some results for orientation, we performed some preliminary tests based on the three parameters influence with respect to the iron oxide recovery. Theses parameters are: consumption of nitric acid and ammonium bifluoride, the temperature with magnetic stirring bar and liquid/solid ratio. Initially, we vary the quantity of nitric acid, we noticed that for a quantity of 280 kg/ton of nitric acid, coloring and feldspar is remarkable that the iron oxide was reduced rate 0.06%. In a second step, we varied the ammonium bifluoride in consumption, the rate of iron oxide is reduced to 0.04%. This result shows already good feldspar that does not require to further purification except for special cases such as enameling high quality or manufacture of glassware. To achieve a concentration of 0.06% iron oxide, it will be necessary to use 40 kg/ton and ammonium bifluoride and 280 Kg/ton of nitric acid without prior purification. For a feldspar processed by high intensity magnetic separation to achieve iron oxide residual content equivalent to (0.06%), the consumption of the same reagents are reduced up to 100 kg/ton of acid and 20kg /ton of ammonium bifluoride. The optimum treatment conditions found above are applied to the different size fractions previously treated by magnetic separation at high intensity. Subsequently, we applied the same conditions to the same size fractions purified by magnetic separation followed by flotation. We noticed that the effect of flotation resulted in a gain of the iron oxide content down 0.05%.

3 CONCLUSION

As part of this work, to achieve the optimal conditions of ain barbar feldspar chemical purification requirements, using nitric acid in the presence of ammonium bifluoride as the reducing, we preferred to review the all tests results for characterization and recovery achieved in the past. This allowed us to compare a number of results and extricate conclusions for the development of the project. All chemical analyzes on all-comers or size fractions represent a panoply of iron oxides content, they give of a certain homogeneity in the sense that the majority are between 0.6- .7%. The origin of the iron oxide pollution comes largely from surface oxidation and water seeping into cracks veins. Feldspar is very homogeneous in terms alkaline oxide, silica and free silica. In conclusion, mainly potassium feldspar with 9% of K2O and 0.25% of Na2O, 12% Al2O3, 75% SiO2 and 0.59 to 0.7% Fe2O3, is part of very average feldspars. Improved quality requires high intensity magnetic epuration and free silica reduction achieved only by flotation. Purification of size fractions [-0.6 + 0.1] mm [-0.6 + 0.250] mm

[-0250 + 0.1] mm by high intensity magnetic separation, lowers the amount of iron oxide Fe2O3 until 0.34% with weight yields compared to all comers respectively 41.26%, 19.30% and 23.06%. As against the size fraction [-0.8 + 0.1] mm used by the glass industry, the rate of reduced iron is 0.39% with a weight of 60.89% yield. This purification yielded unsatisfactory results, the use of flotation purification of these same size fractions decreased the rate of iron oxides from 0.39% to 0.23 for [-0.8+ 0.1] mm and 0.34 to 0.20% for [-0.6 + 0.1] mm with a weight of 54.63% 38.40% yield respectively compared to all comers. These levels 0.20% and 0.23% iron oxide are appreciated by the glass and ceramics industry. For size fractions [- 0.6 + 0.250] mm, [-0250 +0.1] mm and [-0.1] mm, purification by flotation, pushes downward the iron oxide content of 0.34% to 0.30% only, does not meet the requirements of consumers. The application of hydrometallurgical process, excluding the effect of pressure in an autoclave and using sulfuric acid yielded poor results in the experimental conditions. The process using nitric acid in a reducing medium (HFNH4F) is effective and pushes the degree of removal of

Fe2O3 around 0.01%. This process applied to the glass-blower size fractions [-0.8 + 0.1] mm previously ironed by High Intensity a magnetic field reduces iron levels up to 0.054% with a weight of 58.32% compared to those all comers.

REFERENCES

[1] B. Anselmi and H. Harbeck. Multicolor optical sorting : A large scale application in a feldspar treatment plant in sardinia-italy. In Paolo Massacci, editor, Oral Session Proceedings of the XXI International Mineral Processing Congress, volume 13 of Developments in Mineral Processing, pages C11–9 – C11–16. Elsevier, 2000. doi: http://dx.doi.org/10.1016/S0167-4528(00)80086-1. URL:ttp://www.sciencedirect.com/science/article/pii/S0167452800800861. 1

[2] Ewa Slaby, Jens Götze, Gerhard Wörner, Klaus Simon, Roman Wrzalik, and MichalC Smigielski K-feldspar phenocrysts in microgranular magmatic enclaves : A cathodoluminescence and geochemical study of crystal growth as a marker of magma mingling dynamics. Lithos, 105 :85 – 97, 2008. ISSN 0024-4937. doi: http://dx.doi.org/10.1016/j.lithos.2008.02.006.URL:http://www.sciencedirect.com/science/article/pii/S0024493708000376. 1

[3] Ilaria Adamo, Valeria Diella, Alessandro Pavese, Pietro Vignola, and Fernando Francescon Nafeldspar(f) and kaolinite (k) system at high temperature : Resulting phase composition, microstructural features and mullite-glass gibbs energy of formation, as a function of f/k ratio and kaolinite crystallinity. Journal of the European Ceramic Society:3387 – 3395, 2013. ISSN 0955-2219. Doi http://dx.doi.org/10.1016/j.jeurceramsoc.2013.06.003.
URL :http://www.sciencedirect.com/science/article/pii/S0955221913002872. 1

[4] O. Kangala and A. Guneya. Beneficiation of low-grade feldspars using free jet flotation. Mineral Processing and Extractive Metallurgy, 23 :129–140, 2002. 2

[5] I. Dogu and A.I. Arol. Separation of dark-colored minerals from feldspar by selective flocculation using starch. Powder Technology, 139(3) :258 – 263, 2004. ISSN 0032-5910. doi : http://dx.doi.org/10.1016/j.powtec.2003.11.009. URL :http://www.sciencedirect.com/science/article/pii/S0032591003003735. 2

[6] E. Bernardo, J. Doyle, and S. Hampshire. Sintered feldspar glass-ceramics and glass-ceramicmatrix composites. Ceramics International, 34(8) :2037 – 2042, 2008. ISSN 0272-8842. doi : http://dx.doi.org/10.1016/j.ceramint.2007.07.027. URL http://www.sciencedirect.com/science/article/pii/S0272884207002106. 2

[7] Aisha S.G. Stumpf, Carlos P. Bergmann, Juliane Vicenzi, Rebecca Fetter, and Karina S. Mundstock. Mechanical behavior of alumina and alumina-feldspar based ceramics in an acetic acid (4 Materials & Design, 30(10) :4348 – 4359, 2009. ISSN 0261-3069,doi: http: //dx.doi.org/10.1016/j.matdes.2009.04.009. URL http://www.sciencedirect.com/science/article/pii/S0261306909001587. 2

[8] Xiaosu Cheng, Shanjun Ke, Qianghong Wang, Hui Wang, Anze Shui, and Pingan Liu. Fabricationand characterization of anorthite-based ceramic using mineral raw materials. Ceramics International, 38(4) :3227 – 3235, 2012. ISSN 0272-8842. doi : http://dx.doi.org/10.1016/j.ceramint.2011.12.028. URL:http://www.sciencedirect.com/science/article/pii/S0272884211010959. 2

[9] L.O. Filippov, V.V. Severov, and I.V. Filippova. An overview of the beneficiation of iron ores via reverse cationic flotation. International Journal of Mineral Processing, 127(0) :62 – 69, 2014. ISSN 0301-7516.doi: http://dx.doi.org/10.1016/j.minpro.2014.01.002. URL:http://www.sciencedirect.com/science/article/pii/S0301751614000155. 2

[10] Cengiz Karaguzel. Selective separation of fine albite from feldspathic slime containing colored minerals (fe-min) by batch scale dissolved air flotation (daf). Minerals Engineering, 23(1):17 – 24, 2010. ISSN 0892-6875. doi: http://dx.doi.org/10.1016/j.mineng.2009.09.002. URL:http://www.sciencedirect.com/science/article/pii/S0892687509002271. 2

[11] M.A.Amarante, A. Botelho de Sousa, and M.Machado Leite. Beneficiation of a feldspar ore for application in the ceramic industry. The Journal of The South African Institute of Mining and Metallurgy, page 4, JULY/AUGUST 1997. 6

[12] J. Svoboda. Magnetic Techniques for the Treatment of Materials. Advances in Global Change Research Series. Kluwer Academic Publishers, 2004. ISBN 9781402020384.
URL:http://books.google.dz/books?id=WFBpOXSe8kQC. 6

[13] Mousa Gougazeh. Evaluation and beneficiation of feldspar from arkosic sandstone in south Jordan for application in the ceramic industry. American Journal of Applied Sciences, Volume 3, Issue 1 :1655–1661, 2006. 6

[14] Burat.F, Kokkilic.O, Kangal.O, Gurkan.V, and Celik.M.S. QuartzUfeldspar separation for the glass and ceramics industries. Miner. Metal. Process, 24 :75U80, 2007. 7

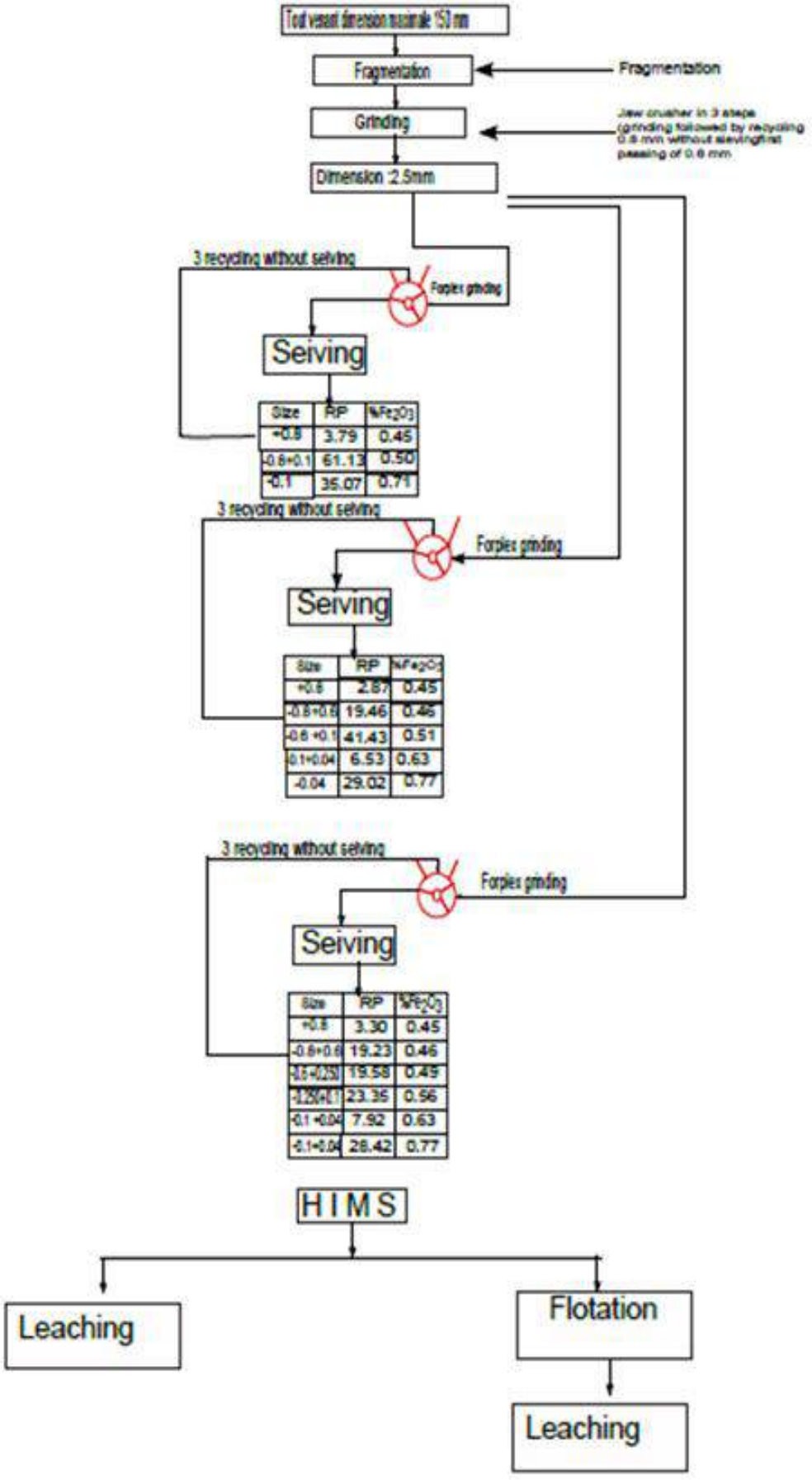

Figure 7. Grinding scheme

Effect of Calcination on the Grindability of Concentrated Phosphate of Djebel Onk Algeria

A. Bouzenzana
Laboratory of Mining, University of Tébessa. Faculty of Science and Technology, Department of Mining Engineering

ABSTRACT Grinding is a process essential for the preparation, is subjected to phosphate during treatment and especially their transformation. This is a very expensive operation because of its high energy consumption which is characterized by the grindability index « index Hardgrove and Bond »

The purpose of this study was to characterize different types of concentrated phosphate and determine their behavior during grinding (calculating indices Hardgrove and Bond) and compare them with other phosphates across the world

Keywords: concentrated phosphate, calcination, Grindability, Hardgove and Bond Indexes

1 INTRODUCTION:

The Djebel-Onk deposit is located in North-West of Algerian Sahara specifically in the East of mountains of Nememcha, 20 km from the Algerian-Tunisian boundaries.

The deposit belongs to Tahitian formation, which characterized by the appearance of the first substantial deposit of phosphate but it is highly clay strata succeed to its black marl and main phosphate deposition which is approximately 30 m deep with carbonated natural formation.

The total geological reserves of ore at our deposit are 317 Mt (P_2O_5 = 26.53% and MgO=2.16%). (FERPHOS)

The actually flow-sheet of Djebel-Onk is argued by the following two properties:

-*Texture (1st property):* The phosphate is formed by ooliths (grains) adjacent to 0.5 mm. Chemical analyzes of different tranches show that our phosphate is rich between 0.08 and 0.8 mm, the fragmentation and classification of this tranche with dry process gives us a concentrated phosphate (62% in TPL) approximately 28.5% of P_2O_5.

-*Structure (2nd property):* Phosphate contains a carbonate gangue. A simple calcination at 900 to 950 °C reduces dolomite, magnesite, calcite and lime. The latter can be eliminated from the rich ore hydrometallurgical treatment after extinguishing in water, by this way and according to the demand of costumers, we can obtain two types of concentrated phosphate; (69 -72%in TPL and 73-75% TPL. (FERPHOS DOCUMENT)

1.2 Utilization of Phosphates

The fertilizer industry consumes about 90 % of phosphates world production (sulfuric acid, simple superphosphate (SSP), phosphoric acid, triple superphosphate (TSP), ammonium phosphate and NPK). Phosphate is also used in the fine industrial, to produce the animal feed supplements and foodstuffs.

Another important use is the production of elemental phosphorous and its derivatives particularly sodium tripolyphosphate, and the important component of the bleaching strong detergents.

For their transformations and their commercialization, phosphates must be a high content in P_2O_5 and have a low cost to their grinding (energy consumption)

The Grindability testes on different samples by different methods, show that if the phosphate is rich in P_2O_5, energy consumption of grinding will be high , this consumption shows that if the enrichment method by calcination gives a very rich ore

nevertheless energy consumption is very high

For the transformation of phosphates into phosphoric acid we use the pushed grinding until the complete liberation of constituent.

The grinding costs represent a big expense for the treatment process [2]; they can reach more than 50% of treatment energizing costs. [THE CEMENT GRINDING OFFICE]

1.3 Production Process of Phosphoric Acid

The production process of phosphoric acid is obtained by the direct attack of phosphate with utilization of sulphuric acid.

The three main phases include:

- *Grinding*

Grinding of raw phosphate is designed to increase the attack surface of the mineral by sulfuric acid.

- *The attack filtration*

Grinded phosphate is attacked by concentrated sulphuric acid 98.5% and medium phosphoric acid (18-22% P_2O_5) in aqueous milieus, this mixture gives porridge.

The filtration of this porridge (goop) consists to separate phosphoric acid 29% in P_2O_5 of phosphogypsum via a rotary filter. The product is stored in decanting ferries.

- *Concentration*

The concentration objective of acid phosphoric is to allow the water evaporation to obtain an acid pulling 54% in P_2O_5.

1.4 Grinding Operation

Grinding of phosphate is one of the decisive steps in the process of acid phosphoric production, because in this level the consumption of energy reaches its maximum. Grinding of phosphate is one of the decisive stages of the manufacturing process of phosphoric acid because this energy reaches its maximum consumption level.

Grinding objective is to increase the attack surface of ore, the chemical reaction is especially easy than the surface offered the reactive is large; for this reason, the grinding is an operation that presents a particular importance in fact:

- An insufficient grinding, driven to a very difficult attack, a very elevated reaction time, and a lower efficiency.

- An over grinded of phosphate driven in contrary to the elevated decomposition degree, which drives to increase the temperature and to obtain a stable semi-hydrated phosphate.

The grinding could be optimized by good acquaintance of the spatial distribution of the phosphates Hardgrove.

In order, to increase the energizing efficiency and to avoid the over-grinding, we eliminates since the grinder's exit the sufficient fineness of grains. [BOUCHAIS S]

1.5 Balls Grinder

The grinder's choice to cannonballs must authorize to reach fineness in the order of millimeters to a few score of micrometers.

The balls grinder choice must authorize to reach fineness in the order of a few millimeters to some tens of micrometers. The grinder represents a very heavy investment; his operative cost is very elevated, either by the usury of its pieces or by its consumption in energy.

1.6 Grinding Energy Law

The performances of grinding installation depend between physical and mechanical characteristics of the product to grind. The determination of some physical properties of materials to grind permits a judicious choice of fragmentation devices and gives us an idea on the energizing consumption and the costs of the grinding operation for a given substance.

These properties are characterized by the fragility (friability) of Grindability Index and Bond energy Index

1.6.1 Bond energizing index

➢ Bond energizing Index: or grinding Index, Wi of material is defined as the consumed energy in kwh/t to obtain the total reduction of this material, since a theoretically infinite

initial dimension, until 80% passing through a sieve of 100 µm

- It may be calculated from any wet grinding by the relation:

$$W = Wi\ (10/\sqrt{P} - 10/\sqrt{F})$$

Where:

W: net energy consumption in kWh/t
Wi: Bond Index (in imperial or metric units of measure)
P: the passing size of 80% of the product grinds in µm.
F: the passing size of 80% of the diet in µm.

This test is a Hardgrove test performed in a standard ball grinder. It can be performed at the openings of meshes ranging from 28 to 40 meshes. The normal finish size is 100 meshes.

Table 1. Multiplier Coefficient of W for special cases

Coefficient multiplier of w for particular cases		
General case of Formula application	Particular case	Multiplier Coefficient
Wet grinding	Dry Grinding	1.3
Ø of grinder ≈ 2.45 m	Ø of grinder ≠ 2.45 m	$(2.45/\ Ø)^{0.2}$
Fragmentation report I= da/dp ≥ 4	i≤4	$\frac{i - 1,2}{i - 1.35}$
Closed circuit	Open circuit with passing through a sieve of 100 µm	
	50 %	1.035
	60 %	1.05
	70 %.	1.10
	80 %	1.20
	90 %	1.40
	95 %.	1.57
	98 %	1.70

1.6.2 Friability grindability index

This measure is based on the Rittinger law, which expresses an evaluation of the necessary energy E for grinding can be obtained by writing that the value of this energy is proportional to the difference between the specific surfaces of the grains before and after grinding.

$$E = K(S_f - S_i)$$

With;
S_f and S_i: initial and final specific grain surfaces
K: Constant energy that must be spends to make appear a new surface unit which depends on the nature of the material and the mode of fragmentation.

The objective of this method was to measure empirically the relative difficulty of coal to get the grain-size requisite for a complete combustion inside a home of furnace to pulverized coal. Thereafter, the use of Hargrove Grindability test (Index) (HGI) has been extended to other materials.

1.6.2.1 Procedure

A sample of 50 g was introduced into a ball grinder with fixed vertical grinding track.

Eight balls are placed above the material and the ring that the united pressure of a rotating shaft is disposed above the balls .the grinder makes 60 rotations.

The grinded material is sifted through a cell of 0.074 mm (200 meshes), the mass of passing (m) in grams, permit to determine Hardgrove Grindability Index (HGI) by the equation:

$$HGI = 13 + 6.93\ m$$

m: mass of the product passing through the sieve 0.074 mm (g).
For the transformation of the HGI Index into Bond Index we use the following formulas;

$$Wi = \frac{88}{HGI^{0,5}}$$ (Proposed by Bond, 1951)

$$Wi = \frac{435}{HGI^{0,91}}$$ (Modified by Bond, 1961)

In 1971, the Hardgrove Grindability Index was calculated with the ASTM norm using a linear equation. It has been prepared using quarter's standard samples of coal imported form the company in which the respective Index of Hardgrove (HGI) are: 43, 61, 80 and 103,

The weight Determination of passers at 74 microns after grinding, allows calibrating the experimented material with ASTM norms. [THE CEMENT GRINDING OFFICE,]

Table 2. HGI Values

Grindability Index (HGI)	Passing weight (m) at 74μm
43	4.89
61	7.04
80	9.52
103	13.05

- Linear equation:

HGI = f(P) is HGI = 8.13+ 7.35m

1.6.2.2 The used Grinder

- Type of grinder: ball grinder
- Rotation speed: 70 tr/min
- Engine power: 1.5 Kw / 380 V
- Ø of balls: (≈ 50 mm)
- Ø of Drum: 200 mm

2 EXPERIMENTAL PART

(Characterization of concentrated phosphate)

2.1 Grain-Sizes Analysis of Concentrated Phosphate Before Grinding (Tab 3)

2.2 Grain-Sizes Analysis of Concentrated Phosphate After Grinding (Tab 4)

Table 3. Grain-sizes analysis (before grinding)

d mm	66-68 % TPL				69-72 % TPL				73 -75 % TPL			
	P(g)	γ%	Σγ%	Σγ%	P(g)	γ%	Σγ%	Σγ%	P(g)	γ%	Σγ%	Σγ%
- 1.56 +1.25	4.57	4.86	4.86	100	5.47	5.76	5.76	100	5.1	5.53	5.53	100
- 1.25 + 1.0	7.95	8.45	13.31	95.14	8.52	8.97	14.73	94.24	7.78	8.44	13.97	94.47
- 1.0 + 0.8	18.36	19.52	32.83	86.69	19.56	20.59	35.32	85.27	19.53	21.2	35.17	86.03
- 0.8 + 0.63	18.51	19.67	52.5	67.17	22.01	23.16	58.49	64.68	20.04	21.76	56.93	64.83
- 0.63 + 0.5	44.69	47.5	100	47.5	39.45	41.52	100	41.52	39.68	43.07	100	43.07
- 0.5 + 0.315	-	-			-	-			-	-		
- 0.315 + 0.2	-	-			-	-			-	-		
-0.2 +0.125	-	-			-	-			-	-		
Total	94.08	100	-	-	95.01	100	-	-	92.13	100	-	-

Table 4. Grain-sizes Analysis (After grinding)

d mm	66-68 % TPL				69-72 % TPL				73 -75 % TPL			
	P(g)	γ%	Σγ%	Σγ%	P(g)	γ%	Σγ%	Σγ%	P(g)	γ%	Σγ%	Σγ%
- 1.56 +1.25	0.70	0.75	0.75	100	0.30	0.32	0.32	100	1.90	2.30	2.30	100
- 1.25 + 1.0	1.33	1.42	2.16	99.15	0.72	0.77	1.09	99.68	2.49	3.02	5.32	97.70
- 1.0 + 0.8	6.82	7.26	9.42	97.83	3.62	3.85	4.94	98.91	6.16	7.47	12.79	94.68
- 0.8 + 0.63	12.86	13.69	23.11	90.57	7.93	8.43	13.37	95.06	9.66	11.72	24.51	87.21
- 0.63 + 0.5	20.77	22.11	45.22	76.88	23.49	24.96	38.33	86.63	24.47	29.68	54.19	75.49
- 0.5 +0.315	10.18	10.84	56.06	54.77	10.99	11.68	50.01	61.67	10.32	12.52	66.71	45.81
- 0.315 + 0.2	3.68	3.92	59.98	43.93	23.10	24.55	74.56	49.99	1.45	1.76	68.47	33.29
-0.2 +0.125	20.27	21.58	81.56	40.01	5.83	6.20	80.76	25.44	0.98	1.19	69.66	31.53
-0.125 +0.00	17.31	18.43	100	18.43	18.11	19.24	100	19.24	25.02	30.34	100	30.34
Total	93.92	100	-	-	94.09	100	-	-	82.45	100	-	-

2.3 Grains-Sizes Characteristics of the Three Concentrated Phosphate

The grains- sizes characteristics are represented in figure 1, 2 and 3:

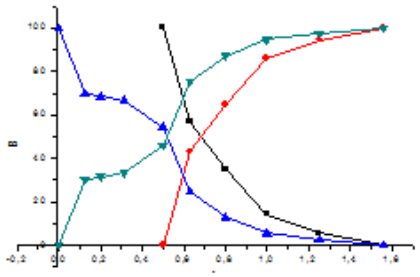

Figure 1.Grains- size characteristics of concentrated phosphate at 66-69% in TPL

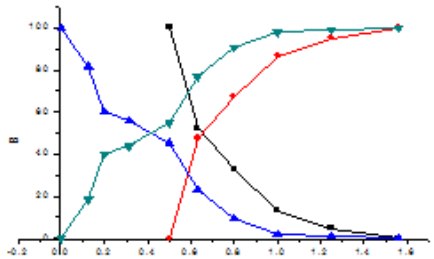

Figure 2.Grains -size characteristics of concentrated phosphate at 69-72% in TPL

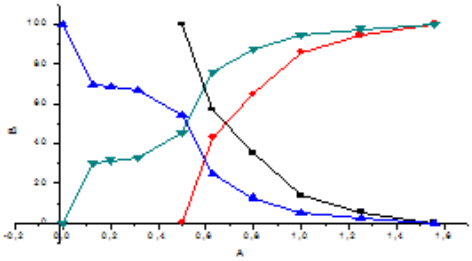

Figure 3.Grain-size characteristics of concentrated phosphate at 73-75% in TPL

Σγ↓% prior to grinding
Σγ↑% after to grinding
Σγ↑%
Σγ↑%

2.4XRD Analysis of Concentrated Phosphate

The XRD Analysis of concentrated phosphate is presented in figure 4, 5 and 6.

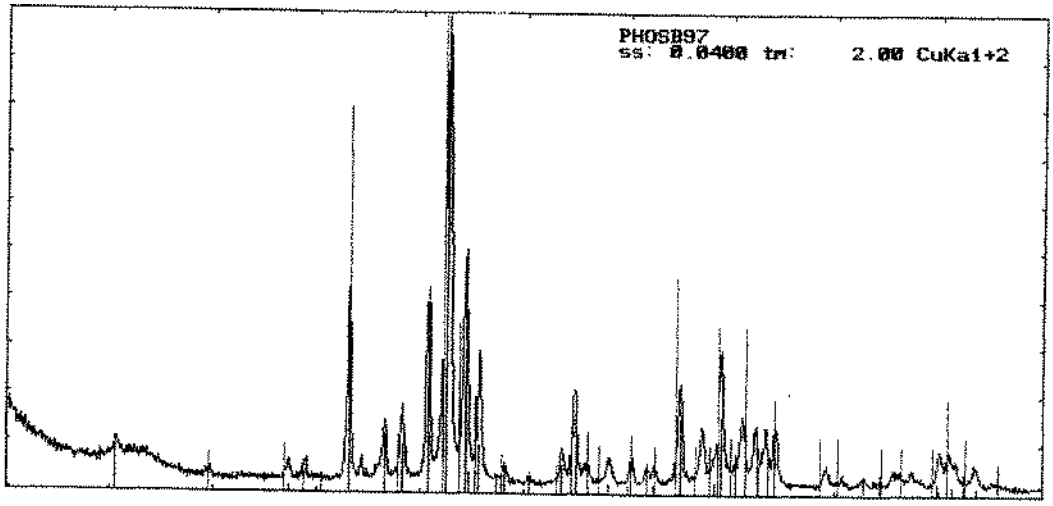

Figure 4. XRD of concentrated phosphate at 66-68% in TPL

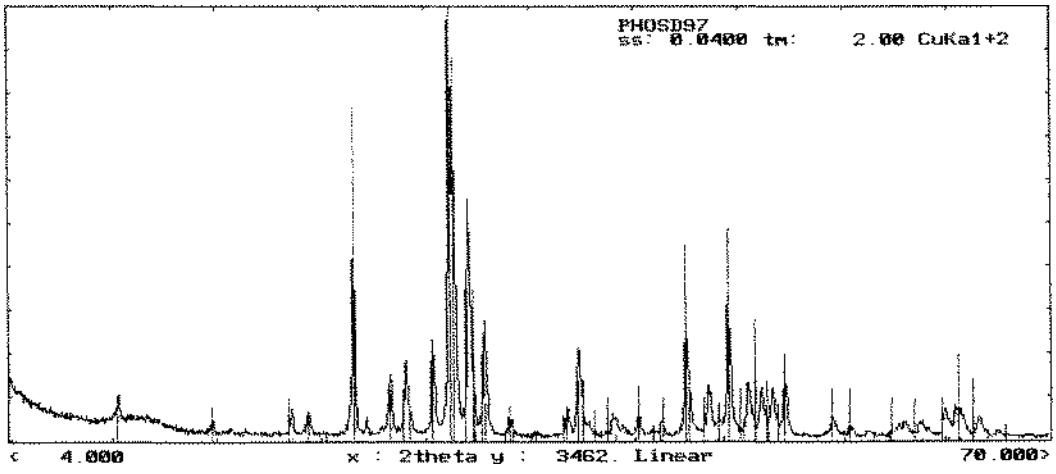

Figure 5. XRD of concentrated phosphate at 69 - 72% in TPL.

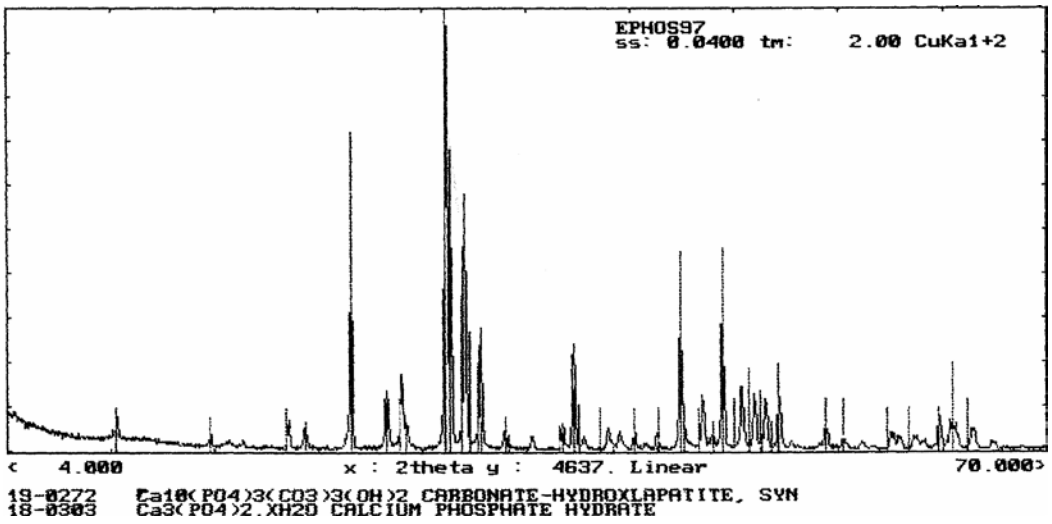

Figure 6. XRD of concentrated phosphate at 73 - 75% in TPL.

According to the peaks and the corresponding wavelengths in XRD patterns, we see that for phosphates:

- Concentrated at 66-68% and 69-72% in TPL Contain:
  - Magnesium carbonates (dolomite): Ca Mg $(CO_3)_2$.
  - Hydrated calcium phosphate: $Ca_3 (PO_4)_2$.
  - Carbonated hydroxyapatite: $Ca_{10} (PO_4)_3 (CO_3) 3 (OH)_2$.
- Concentrated at 73-75 % in TPL
-
  - Absence of magnesium carbonates: The absence of dolomite is due to the calcination and washing causing;
  - Enrichment of phosphates with increase of the content in TPL
  - The thermal destruction of carbonates (dolomite, calcite and magnesite), according to the reactions;

$$Ca\ Mg\ (CO_3)_2 \longrightarrow CaCO_3 + Mg\ CO_3$$
$$CaCO_3 \longrightarrow CaO + CO_2$$
$$Mg\ CO_3 \longrightarrow MgO + CO_2$$

After washing, we obtain:

$$MgO + H_2O \longrightarrow Mg\ (OH)_2$$
$$CaO + H_2O \longrightarrow Ca\ (OH)_2$$

2.5 Chemical Analysis of the Three Concentrated Phosphate Depending on the Ratio Of TPL (Tab 5)

Table 5. Chemical analysis of concentrated phosphate

Elements in %	66 - 68 % in TPL	69 - 72 % in TPL	73 - 75 % in TPL
Humidity (H_2O)	0.8 à 1.0	0.8 à 1.0	0.8 à 1.0
P_2O_5	29.5 à 30.0	30.2 à 30.5	32.0 32.8
CO_2	6.5 à 7.5	6.0 à 6.3	6.0 à 6.3
CaO	49.0 à 50.0	50.0 à 51.0	50.5 à 52.0
MgO	1.0 à 0.8	0.7 à 0.9	0.5 à 0.6
Fe_2O_3	0.30 à 0.40	0.30 à 0.40	0.30 à 0.40
Al_2O_3	0.30 à 0.40	0.25 à 0.35	0.25 à 0.35
Na_2O	1.1à 1.3	1.1 à 1.3	1.1 à 1.3
K_2O	0.1 à 0.2	0.1 à 0.2	0.1 à 0.2
SO_3	2.5 à 3.0	2.5 à 3.0	2.5 à 3.0
SiO_2	2.0 à 3.0	2.0 à 2.5	2.0 à 2.5
LOI (CO_2Deducted)	2.0 à 3.0	2.0 à 2.8	2.0 à 2.8
F	3.5 à 4.0	3.5 à 4.0	3.5 à 4.0
Cl (ppm)	300 à 400	250 à 350	220 à 300
Organiccarbon	0,15 à 0,20	0.10 à 0.15	0.7 à 0.11

2.5 Weight of Passing Stitch At 0.074 Mm (200 Meshes)

Table 6: Results of passing stitch at 0.074 mm

Concentrated	66-68 % in TPL	69-72 % in TPL	73-75 % in TPL
Weight of passing at 0.074 mm (g)	10.02	8.68	5.24

3 CALCULATION

3.1 Calculation Formula

- ❖ Friability Grindability Index HGI = 8.13 + 7.35 m
- ❖ Bond Index $Wi = \frac{435}{HGI^{0,91}}$
- ❖ Multiplier of w for special cases
- Open Circuit: 80% passing (multiplier = 1.2)
- Ø of drum: 200 mm ($(2.45/ Ø)^{0.2}$ = 1.65)
- Dry Grinding (multiplier = 1)

Table 7. Values of HGI and Wi

Concentrated	Weight of passing at 74 µm(g)	HGI Index	Wi (KWh/t)	Wi (corrected) (KWh/t)
66 - 68 % in TPL	10.02	81.78	7.90	20.33
69 - 72 % in TPL	8.68	71.93	8.88	22.85
73 - 75 % in TPL	5.24	46.64	13.18	33.91

3.2 HGI Index Comparison Of Concentrated Phosphate With Other Indexes Around The World

Table 8. Values of HGI and Wi of phosphates around the world

Concentrated phosphate	HGI	Wi
Florida USA	49	12.6
Youssoufia (66/68% in TPL) Morocco	49	12.6
Phosphate of Togo	80	8.1
KalaaDjardaTunisie	81	8
Khouribga 75 Marocco	92	7.1
MoularesRedeyefTunisie	96	6.9
M'DillaTunisia	96	6.9
Khouribga 72 Morocco	100	6.6
M'Rata Tunisia	113	5.6

3.3 Usual HGI Values of Some Materials

Table 9. Values of HGI of some materials [4]

Materials	HGI
Clay	97
Clinker	30-50
Anthracite	30-50
Bituminous coal	45-85
Feldspar	45
Iron ore	38
Sand (Quartz)	25-55
Lime	105
Calcite	54 - 78
Iron oxide	57
Manganese	45-65

4 CONCLUSION

According to the results obtained we remark that more phosphate is richer, the grinding resistance is increased.

The phosphates of Djebel-Onk are composed of apatite that represents the useful mineral with gangue constituted mainly of carbonate (Calcite, dolomite, Quartz...etc.). All these materials cause a heavy resistance to the grinding according to the table 9 such as the quartz, that is very hard and the clays that promote the agglomeration of phosphate ooliths.

We remark that our phosphates which has been calcined at high temperature (concentrated 73-75% in TPL)show the Grindability more increased than that those of which the calcination temperature is lower (concentrated 69-72% in TPL) or cleaned phosphate (concentrated 66 - 68% in TPL).

The Grindability tests show that if phosphate has a high content in P_2O_5, the energy consumption of grinding will be big.

This observation shows that if the calcination permits to give a very rich phosphate, she participates at the same time to make the grinding more difficult.

From the results obtained after that we see for the Algerians concentrated energitiques and grindability index have average values compared to other concentrates around the world

The values types of induced HGI are consisted between 30 (increased resistance to

the pulverization) and 100 (pulverized more easily).

REFERENCES

Bouchais S., Characterization and spatial modeling of rock masses Hardgrove: Troilus mine, University of Laval, 2007;

Bouzenzana A., Complex enrichment of phosphate ore "Djebel-Onk» Algeria, University of Annaba, Algeria, 2007;

Ferphos Document Technical specifications for the Algerian phosphate Documentation company Ferphos Algeria

The Cement Grinding Office « Hardgrove and Grindability tests », 2014;

Predicting Size Distribution of Jaw Crusher Product by Using Discrete Element Modelling (DEM)

H. Es-haghi, B. Rezai
Department of Mining and Metallurgy Engineering, AmirKabir University of Technology, Tehran, Iran

A. Refahi
Department of Mining Engineering, Zanjan University, Zanjan, Iran

ABSTRACT Material comminution by crushers and mills is an essential stage in mineral processing. Because of low energy consuming in crushers in competition with mills, it is better to crush materials by crushers as far as possible. Particle size distribution in any stages of comminution is one of the most important issues, but takes a lot of time and cost. Therefore, numerical simulating for predicting of product particle size distribution can be useful. PFC3D that is a three-dimensional particle flow code software that models the movement and interaction of particles by the discrete element method (DEM) techniques was employed to simulate the particle movement and to product size distribution of jaw crusher.

In this paper, single spherical and cubic shape specimens were simulated in crushing process between two rigid jaws, after simulating jaw crusher, the sieving process was simulated and particle size distribution of product was predicted. For validating the results of simulation, they were compared with the experimental sieving tests. Particle size distribution plots of both approaches had fairly good accordance.

Keywords: Particle size distribution, jaw crusher, discrete element modelling

1 INTRODUCTION

The size reduction of brittle materials is the most essential mechanical operation within the raw material processing, i.e. mining, industry. The size reduction performs in crushing and grinding stages. Crushing is usually a dry process, and is performed in several stages, Particle size distribution in any stages is one of the most important issues, but takes a lot of time and cost. Therefore, numerical simulating for predicting of product particle size distribution can be useful.

Many researches have been done for predicting of product particle size distribution. In previous works size distribution often was determined for mill product and they used numerical methods for this purpose. The discrete element method (DEM) has been adopted by many researchers as a tool for simulating and understanding comminution devices and was employed in the present work to study the particle breakage within the jaw crushers.

The DEM has been used to model many industrial applications over the past decade and was first proposed by Cundall and Strack (1979) to model the behavior of soil particles subject to dynamic loading conditions. Mishra (1991) pioneered the application of DEM in mineral processing and modelled grinding mills.

Mishra (1991) by using the 2Dmill code predicted the size distribution of mill product from the knowledge of energy distribution inside the charge, breakage behavior of the particles, and the transport properties of the charge. Djordjevic et al (2003) modelled two types of impact crushers: the vertical- and horizontal-shaft impact crusher. They calculated the distribution of collision energies was then converted into a product size distribution for a particular ore type using JKMRC impact

breakage test data. Moreover other methods has been used, Donovan (2003) used fracture toughness and develops models for the prediction of power consumption, breakage function/product size, and volumetric capacity have been developed based on fracture toughness experimental result.

Refahi et al (2007, 2009) Used rock mechanical properties to predict the Bond crushing index and compared bond crushing energy and fracture energy. Refahi et al (2010) was applied DEM to model the fracture behavior of a single spherical and cubic rock in a laboratory jaw crusher. In this study we used that model of jaw crusher.

This article presents a numerical model based on the discrete element method to describe crushing and sieving process. Because of the discontinuous nature of rocks, a distinct element code, PFC, developed by Itasca Consulting Group, Inc. was used for this purpose. PFC3D represents a model as an assemblage of spheres bonded together by parallel bonds. In this paper, the modelling steps will be described first. Then the numerical Results of product size distribution will be compared to the experimental measurements. The goal of this research is to use both numerical modelling and laboratory product size distribution to compare and show if numerical modelling can be used for predicting product size distribution.

2 MATERIALS AND METHODS

In this work, crushing and sieving process for two rock types with different mechanical properties, limestone and granite, were simulated, and the results were verified by comparison with the experimental data. Rock blocks were obtained from mine transmitted to the laboratory and where samples prepared by coring and cylindrical cores were prepared at the laboratory. Uniaxial compressive tests were conducted on cylindrical samples. The mechanical properties (elasticity modulus, uniaxial compressive strength) were experimentally evaluated. For this purpose a standard compression test was carried out on ten cylindrical specimens with 54 mm in diameter and 135 mm in height. To measure the modulus of elasticity, five strain gauges were used in the compression test. The dry density of the limestone and granite was estimated by the saturation and caliper technique, which was defined by the International Society for Rock Mechanics (ISRM). The obtained mechanical properties of the rocks studied are shown in Table 1.

Table 1. Mechanical properties of the rocks

Rocks	**Uniaxial compressive strength (MPa)**	**Elasticity modulus (GPa)**	**Density (tonne/m3)**
granite	49	104	2.52
limestone	30	35	2.40

From Table 1 it is seen that the strength and the elasticity modulus of limestone, which were determined from the simulated uniaxial compression test, are 30 MPa and 35 GPa, respectively and for granite are 49 MPa and 104 GPa, respectively.

Single cubic specimen with 5 cm in length and single spherical specimen with 6 cm diameter of limestone and granite were prepared. A laboratory jaw crusher was then used to crush the specimens. After sieving the jaw crusher product, Size distribution curves of the products emerging out of the crusher are determined that are shown in Figure 1

The curves demonstrate that the size distribution of the material in the product is independent of the size distribution in the feed and is primarily a function of the setting of the crusher and to a lesser extent of the nature of the material that is crushed (king, 2000). From Figure 1 the d_{80} is seen to be approximately 16.5 mm.

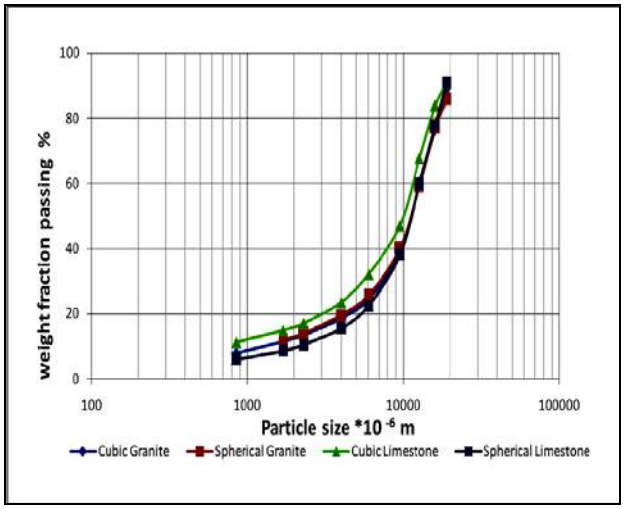

Figure 1. Size distribution of crushed products coming out of the jaw crusher for limestone and granite specimens

3 THE MODELLING STEPS

PFC3D Version 3.00 in which the particles are spheres was used to simulate these tests in the computer. The simulation process for predicting size distribution of jaw crusher product has been developed in several steps, each step being described in the following sections.

3.1 Conversion of Macro to Micro Properties

The input properties (such as modulus and strength) can be derived directly from measurements performed on laboratory specimens. PFC synthesizes macro-scale material behavior from the interactions of micro scale components, the input properties of the microscopic constituents are usually not known. In this case, we must first determine the relevant behaviors (and response set that best characterizes these behaviors) of our intended physical material, and then choose the appropriate microproperties by means of a calibration process in which the responses of the synthetic material are compared directly with the relevant measured responses of the intended material. On the other hand an inverse modelling method is used to determine the correct micro-mechanical properties of the numerical models from the macro-mechanical properties of the rock obtained during laboratory testing. This was performed by comparing simulated uniaxial compression test by PFC3D and laboratory tests. The Young's modulus, peak load and the fracture mode were matched to that obtained in the laboratory using the micro-mechanical modeling. (Itasca 1999) Also according to the properties of parallel and contact bonds, the parallel bond could completely nominate the feature of rock materials. The strength and the elasticity modulus of limestone and granite, which were determined from the simulated uniaxial compression test, are shown in Table 2.

Table 2. Mechanical properties of the rocks obtained from PFC3D model.

Rocks	Uniaxial compressive strength (MPa)	Elasticity modulus (GPa)
granite	106.60	49.20
limestone	30.20	35.10

Table 3 gives the micromechanical properties and bond strengths of limestone and granite, which are determined by simulating the uniaxial compaction test.

Table 3. Micromechanical properties of particles and bond strengths used for modelling studied rocks (determined from simulated uniaxial compression test by PFC3D

Micromechanical properties	granite	limestone
Ball density (kg/m3)	2520	2400
Ball-ball contact modulus (GPa)	65	44
Ball stiffness ratio	2	2.525
Parallel-bond modulus (GPa)	65	44
Parallel-bond stiffness ratio	0.65	0.70
Ball friction coefficient	2	2.525
Parallel-bond normal strength (MPa)	135	48
Parallel-bond shear strength(MPa)	135	48

3.2 Modelling of Rock

To achieve the cubic and spherical specimen each of limestone and granite such as ones used in laboratory test were modelled. For the purpose of modelling, a cubic specimen of 5 cm in height and a spherical specimen of 6 cm in diameter were prepared from two rock types that were studied. The model is made up of approximately 3000–4000 randomly placed particles ranging in size from 1.5 to 3 mm (see Figure 2).

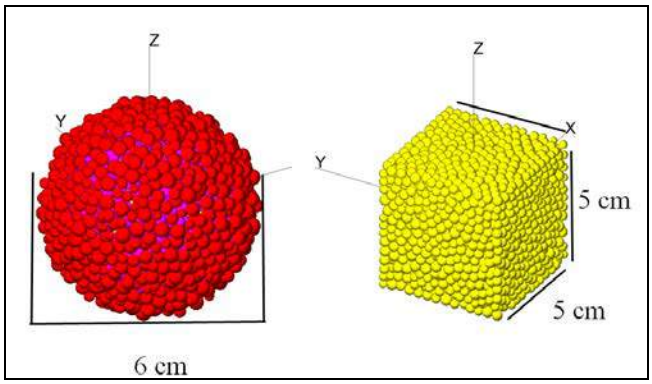

Figure 2. Models of spherical and cubic rocks studied displayed by PFC3D software

3.3 Modelling of Jaw Crusher

A laboratory jaw crusher was modelled using the PFC3D (Refahi et al, 2009). This model is based on single macroparticle simulation in a crusher, and multi-body interactions are ignored. The crushing process for a single cubic and/or a single spherical specimen in the jaw crusher is simulated using the PFC3D model. The jaw crusher has two plates (jaws), one of them is fixed and the other, swinging open and closed, trapping and crushing material between the two surfaces. The feeding entrance is 10 cm wide, and its maximum discharge aperture is 2.5 cm (open status). The minimum open space between the jaws during the crushing cycle is 17 mm (closed status). The rotational speed of the moving jaw is almost 300 rpm. The jaw surface is corrugated; the height and width of a corrugation is 0.5 cm (see Figure 3).

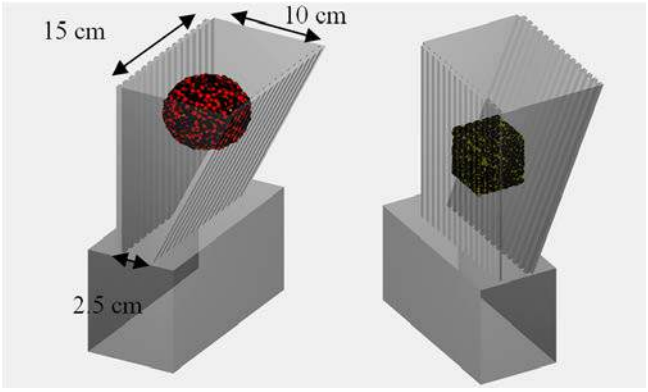

Figure 3. PFC3D model of a) a cubic and b) a spherical specimen between two rigid jaws (the black spots show parallel bonds).

3.4 Modelling of Sieving Process

In PFC3D by using walls and balls, materials and other shapes can be built. In order to build sieve using wall, one should use four coordinates and stiffness properties of walls. Table 4 show comparison between Geometrical parameters of sieves used in laboratory and simulation.

Table 4.comparison between Geometrical parameters of sieves used in laboratory and simulation

Rocks	**cross Section**	**Height (cm)**	**area (cm^2)**	**Diameter (or length) Of cross Section (cm)**
laboratory	Spherical	5	176.7	15
simulated	Cubic	5	170	13

As in Table 4 the sieves simulated are square and the sieves used in lab are gyrate, as the shape of sieves has a little effect on the result and also modelling of square sieves is easier it is acceptable to use square section sieves in instead of gyrate ones for modeling purpose. In order to model the wires of sieves one should be used perpendicular walls with different thickness. The diameter of wires was selected according to ASTM standards. When the shapes of sieves are ready then they should be vibrated. In order to vibrate the sieves define a velocity in special directives (x and

z direction).The sieves is oscillated upwards and to two side(x and z direction) with a frequency of 2 Hz, a amplitude of 10 mm, and a sideways amplitude of 8 mm. As sieves moves upwards, smaller particles move freely through the holes. The total number of sieves is 9. It should be noted that the smallest ball radius is 1.5 mm, so sieves with openings smaller than 3 mm is avoided. The sieve with openings equal to 2.8 mm acts as a pan (see Figure 4).

3.5 Calculation of the Cumulative Percentage of Material Passing

After the screening of crushed material (the material was crushed using jaw crusher). It is essential to measure the weight of materials on each fraction, first the volume of balls should be calculated (material is modelling using balls with different radius) and sum of these volumes is the total volume of crushed material in each fraction. It should be noted that the density of balls is equal, so by using volumes of ball in each fraction and total volumes of balls be calculated. After this by using the cumulative percentage of material passing, d_{80} can be calculated.

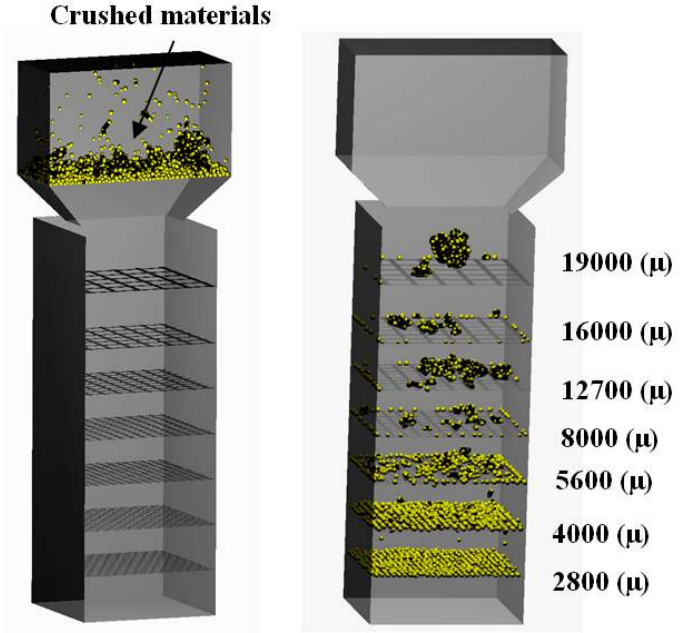

Figure 4.PFC3D model of sieving process a) before sieving b) after sieving

4 RESULTS AND DISCUSSION

Simulations are conducted for granite and limestone specimens and Figure 5 & Figure 6 show the distribution curves obtained from experiment and simulation for the two rock types studied in two modes (spherical, cube). The results of the simulation match the experimental results acceptably, especially for spherical shaped. d_{80} for both experimental and modelling results were almost similar(see Table 5). It is necessary to noted that because of limits of computers capability the radius of particles cannot be decreased. As the number of particles increases, the resolution, which is defined as the number of particles across the model diameter will be greater. Thus, greater the number of particles, the better the resolution and hence better results are expected to be obtained. However, with the Increase in the number of particles, there is increase in the computation time. (Mitra, 2006)

Table 5. Comparison between d_{80} result from DEM and laboratory

Specimen	Spherical granite	Cubic granite	Spherical limestone	Cubic limestone
d_{80} simulation(µ)	16900	16800	16700	16400
d_{80} laboratory(µ)	16700	15900	16400	15700

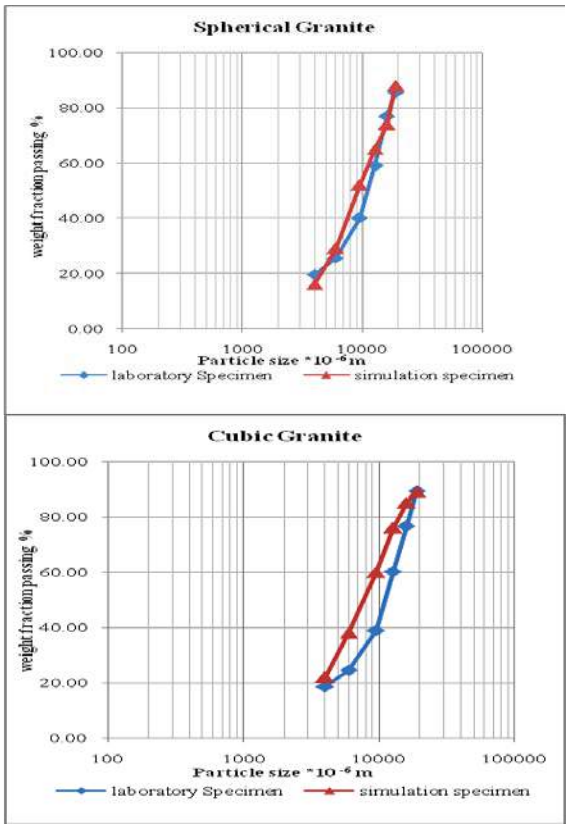

Figure 5.Comparison between Size distributions of crushed products coming out of the jaw crusher and simulation for granite specimens

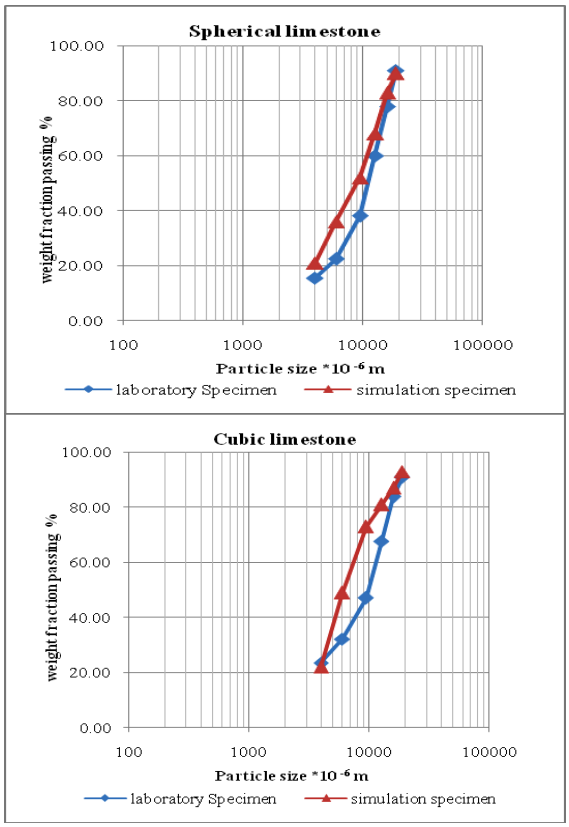

Figure 6.Comparison between Size distributions of crushed products coming out of the jaw crusher and simulation for limestone specimens

5 CONCLUSION

A PFC3D model within the framework of the discrete element method has used to simulate sieving process of jaw crusher product. In order to confirm the modelling results, Laboratory test has performed. Particle size distribution of crushed products coming out of the jaw crusher for granites and limestone specimens in laboratory showed that product size distribution of jaw crusher is independent from shape of feeds and the nature of material is lesser effect on particle size distribution. Comparing the results of simulating and the experimental sieving tests showed the particle size distribution plots of both approaches have good accordance, especially for spherical shape specimens. The increase in computer power can enable the creation specimens with greater the number of particles and make the use of discontinue models to simulate rock behavior more feasible. The ability of DEM to simulate sieves demonstrates this method has potential for use as a design tool for such equipment in mineral processing.

REFERENCES

Cundall, P.A, Strack, O.D.L., 1979. A discrete model for granular materials, Geotechnique Vol. 1, pp. 47–65.

Djordjevic ,N., Shi , F.N and Morrison,R.D.,2003., Applying discrete element modelling to vertical and horizontal shaft impact crushers., Minerals Engineering 16 ,P 983–991

Donovan, J.G., 2003. Fracture toughness based models for the prediction of power consumption, product size, and capacity of jaw crushers, Ph.D. Thesis, the Virginia Polytechnic Institute and State University, USA., 220 pp.

King, R.P., 2001. Modeling and Simulation of Mineral Processing Systems, Elsevier, USA, 412 pp.

Mishra, B.K., 1991. Study Of Media Mechanics In Tumbling Mills By The Discrete Element Method., Ph.D. Thesis, University of Utah, USA., 150 pp.

Mitra, r., 2006. Imaging Of Stress In Rock Samples Using Numerical Modeling And Laboratory tomography, Ph.D. Thesis, the Virginia Polytechnic Institute and State University, USA., 189 pp.

PFC3D Particle Flow code in 3 Dimensions ., 1999. Itasca Consulting Group, Inc. Minneapolis, MN, USA.

Refahi, A., Rezai, B and Aghazadeh, J., 2007. Use of rock mechanical properties to predict the Bond crushing index, Miner. Eng. Vol.20, PP. 662–669.

Refahi, A., Rezai, B and Aghazadeh, J., 2010. Discrete element modelling for predicting breakage behavior and fracture energy of a single particle in a jaw crusher, International Journal of Mineral Processing. Vol.94 , PP. 83–91

Refahi, A., Aghazadeh, J.A., and Rezai, B., 2009. Comparison between bond crushing energy and fracture energy of rocks in a jaw crusher using numerical simulation, The Journal of The Southern African Institute of Mining and Metallurgy., Vol. 109, PP. 709–719

Examination of Albanian Chromite Ores In Terms of Liberation Size and Ratio Problem

Arnavutluk Krom Cevherlerinin Tane Serbestleşmesi ve Rasyo Sorunu Acısından İncelenmesi

H. Bastürkcü, B. Aydin, M. Özer, A.E. Yüce
Istanbul Teknik Üniversitesi Cevher Hazirlama Mühendisligi Bölümü

ÖZET Krom cevherlerinin gravite yöntemleriyle zenginleştirilmesinde temel yaklaşım, olabildiğince iri boyutlarda konsantre ürünler alabilmektir. Bazı cevher türleri iri boyutlarda zenginleştirilebilirken bazı cevherlerde çok ince boyutlara kadar öğütme gerekli olabilmektedir. Diğer yandan elde edilen krom konsantrelerinin rasyo değerleri de satış koşulları için önemli bir parametredir. Bu araştırma kapsamında Arnavutluk'tan ayrı bölgelerden alınan iki cevher numunesinin zenginleştirilme özellikleri incelenmiştir. KJM kodlu cevherde, iri boyutlarda (-25+1 mm) jig ile; ince boyutlarda ise (-1 mm) sarsıntılı masa ile satılabilir nitelikli konsantrelerin elde edilebileceği belirlenmiştir. Bu cevherlerden elde edilen konsantrelerin rasyo değeri ise 2,5 civarındandır. KM kodlu cevher ancak 0,6 mm'nin altında yeterli serbestleşme derecesine ulaşabilmektedir. Bu nedenle iri boyutlarda bir konsantre üretimi mümkün olmamıştır. Bu cevherlerden elde edilen konsantrelerin rasyo değerleri ise 2,18-2,41 arasında değişmektedir. Yapılan incelemelerde, çok ince boyutlara kadar öğütülmüş olmasına ragmen kromit tanelerinin yapısında çok ince dağılımlı manyetit bulunmuştur. Bu araştırma kapsamında; elde edilen sonuçlara göre her iki cevhere ait en uygun zenginleştirme koşulları belirlenerek proses akım şemaları oluşturulmuştur.

Anahtar Kelimeler: Rasyo sorunu, serbestleşme, kromit, akım şeması

ABSTRACT In beneficiation of chromite ores using gravity methods, the basic approach is to obtain concentrates with coarse sizes as long as possible. While some type of ores respond to this approach, some type of the ores needs very fine grinding. On the other hand, ratio values have importance in determining the quality of the marketable product. In this study, beneficiation properties and ratio values of two different chromite ores taken from Albania were investigated. On the KJM coded sample, jig tests (-25+1 mm) and shaking table tests (-1 mm) were performed. The ratio of the concentrate was determined as nearly 2.5. Besides, the liberation of the other sample – coded as KM – was provided below 0.6 mm. The concentrates of this sample had ratios varying from 2.18 to 2.41, since finely disseminated magnetite particles existed in chromite particles. In addition, magnetic separation tests were conducted in order to reduce the iron content. According to the optimized test results, appropriate process flow-sheets were established for both of the chromite samples.

Keywords: Ratio problem, liberation size, chromite, flow chart

1 INTRODUCTION

Chromium is one of the indispensable element and a raw material for steel industry. Different grades of ferrochrome are produced from the chromite ores by using metallurgical methods. While 90% of the chromite reserves is evaluated in ferrochrome production, 80% of ferrochrome is consumed in stainless steel industry (Murthy et al., 2011).

Depending on the deposit differences, different amounts of iron, aluminum, magnesium, and chromium exist in the

spinel structure of the mineral. During the formation of the mineralogical structure, iron is replaced by magnesium and aluminum resulting in higher Cr:Fe ratios in chromite. On the other hand, major gangue minerals can be pronounced as talc, quartz, hematite, goethite, limonite, gabbro, serpentine, anorthosite, dunite, and pyroxinite (Murthy et al., 2011).

Chromite ore is generally beneficiated using several methods, owing to the ore source and the end use requirements. Coarse clean ore is hand sorted, while the fine clean ore is subjected to gravity separation. Lumpy ore associated with host rock may require heavy medium separation. If chromite minerals occur in fine grains, then crushing, gravity separation and magnetic separation may be used (Papp, 1994).

It is difficult to obtain pure chromium, since it is contaminated by many other elements. Therefore, efforts have been made to produce cleaner chromite concentrates (Atalay and Ozbayoglu, 1992; Guney et al., 1992, 1994, 2009; Gul et al., 1995; Cicek et al., 2000; Yüce et al., 2003; Mohan et al., 2006; Önal et al., 2009).

Since a comparison cannot be made based on the effect of operating conditions alone, Pascoe et al. (2007) showed that it is possible to make a sensible selection of gravity separation in terms of the data obtained from particle size and the mineralogy of the ore.

In this study, beneficiation properties and ratio values of two different chromite ores taken from Albania were investigated. According to the optimum test results, appropriate process flow-sheets were established for both of the chromite samples

2 MATERIAL AND METHODS

The tests were performed on two different chromite samples taken from Albania. The disseminated chromite sample, which was suitable for shaking table tests, was coded as “KM”. While the other sample was coded as “KJM”, jig and shaking table tests were conducted on it.

The chemical analyses of both of the samples are given in Table 1. After the beneficiation tests, the concentrates were evaluated in mineralogical aspects.

Table 1. The Chemical Analyses of the Samples

Analyze	KJM, %	KM, %
Cr_2O_3	28.32	22.71
Fe	8.77	8.30
SiO_2	18.53	24.43
Al_2O_3	10.28	8.33
MgO	27.6	28.4
P	0.027	0.039
S	0.039	0.007
Ratio	2.21	1.87

3 RESULTS

3.1 Beneficiation Tests with KJM

3.1.1 Jig tests

The particle size of the sample was reduced below 25 mm and classified into size fractions such as (-25+19 mm, -19+13 mm, -13+9 mm, -9+6 mm, -6+3.36 mm, -3.36+1 mm) for the jig tests. Results obtained from different size fractions are given in Table 2, while combined and distributed results are shown in Table 3 and 4.

The jig tests provided a marketable concentrate containing 40.62% Cr_2O_3 with 53% of metal recovery. The next step was grinding the middling and tailings below 1 mm. The ground sample was combined with the -1 mm sample, which was classified before jig tests. The obtained sample was subjected to the shaking table tests.

3.1.2 Shaking table tests

The sample, which was obtained as middlings and -1 mm fraction from jigging process, ground and sized such as (-1+0.5 mm), (-0.5+0.212 mm), (-0.212+0.106 mm), and (-0.106 mm) and introduced to shaking table tests. Table 5 shows the results of shaking table tests in detail, while the combined and distributed test results are given in Table 6 and Table 7 respectively.

The results show that the particle liberation could be provided below 1 mm. In this way, a concentrate containing 48.58% Cr_2O_3 was obtained with 88% recovery.

Table 2. Jig Test Results

Size fraction, mm	Products	Weight, %	Cr_2O_3, %	Rec., %
-25+19	Conc.	10.7	40.56	15.1
	Middling	9.0	24.11	7.6
	Tailings	3.7	7.58	1.0
	Feed	23.4	29.00	23.7
-19+13	Conc.	15.9	38.68	21.5
	Middling	12.8	28.14	12.5
	Tailings	6.8	11.03	2.6
	Feed	35.5	29.57	36.6
-13+9	Conc.	5.3	44.75	8.4
	Middling	5.0	27.53	4.8
	Tailings	5.8	13.29	2.6
	Feed	16.1	28.19	15.8
-9+6	Conc.	2.4	44.05	3.7
	Middling	2.3	25.94	2.1
	Tailings	2.2	10.55	0.8
	Feed	6.9	27.29	6.6
-6+3.36	Conc.	1.6	42.19	2.3
	Middling	2.2	28.76	2.2
	Tailings	1.6	12.44	0.7
	Feed	5.4	27.76	5.2
-3.36+1	Conc.	1.3	39.97	1.8
	Middling	2.3	26.95	2.2
	Tailings	2.0	16.99	1.2
	Bottom of screen	0.3	39.19	0.3
	Feed	5.9	26.92	5.5
-1 mm		6.8	27.99	6.6
Total		100.0	28.74	100.0

Table 3. Combined Jig Test Results

Products	Weight, %	Cr_2O_3, %	Rec., %
Concentrate	37.4	40.62	53.0
Middling	33.7	26.89	31.6
Tailings	22.1	11.43	8.8
-1 mm	6.8	27.99	6.6
Feed	100.0	28.68	100.0

Table 4. Distributed Jig Test Results

Products	Weight, %	Cr_2O_3, %	Rec., %
Jig Conc.	37.4	40.62	53.0
- 1 mm	62.6	21.55	47.0
Total	100.0	28.69	100.0

Table 5. Shaking Table Test Results

Size fraction, mm	Products	Weight, %	Cr_2O_3, %	Rec., %
-1+0.5	Conc.1	4.4	47.32	9.2
	Conc.2	4.1	39.39	7.3
	Conc.3	5.1	30.38	7.0
	Middling	6.3	20.21	5.8
	Tail. 4	5.1	15.00	3.4
	Tail. 3	4.4	7.61	1.5
	Tail.2	4.1	6.30	1.2
	Tail.1	4.3	4.79	0.9
	Feed	37.8	21.40	36.3
-0.5 +0.212	Conc.1	5.4	51.78	12.6
	Conc.2	1.9	49.88	4.2
	Conc.3	0.8	46.85	1.6
	Conc.4	0.9	45.35	1.8
	Middling	5.4	30.84	7.5
	Tail.3	3.5	9.01	1.4
	Tail.2	3.8	5.18	0.9
	Tail.1	5.1	2.25	0.4
	Feed	26.8	25.32	30.4
-0.212 +0.106	Conc.1	6.4	51.70	14.9
	Conc.2	1.1	46.15	2.3
	Middling	5.0	13.02	2.9
	Tail.2	3.4	1.37	0.2
	Tail.1	3.0	1.01	0.2
	Feed	19.0	24.10	20.5
-0.106	Conc.1	2.1	53.12	5.0
	Conc.2	0.5	50.56	1.2
	Middling	3.8	13.09	2.2
	Tailings	1.7	4.66	0.4
	Slime	8.3	10.73	4.0
	Feed	16.4	17.33	12.8
Total		100.0	22.29	100.0

Table 6. Combined Shaking Table Test Results

Products	Weight, %	Cr_2O_3, %	Rec., %
Concentrate	27.6	48.58	60.1
Middling	42.8	17.12	31.9
Tailings	21.4	3.16	3.0
Slime	8.3	10.73	4.0
Feed	100.0	22.29	100.0

Table 7. Distributed Shaking Table Test Results

Products	Weight, %	Cr_2O_3, %	Recv., %
Concentrate	40.8	48.58	88.8
Tailings	50.9	3.16	7.2
Slime	8.3	10.73	4.0
Feed	100.0	22.29	100.0

When an evaluation in terms of a combined gravity separation processes including jig+shaking table, it was understood that final concentrate contents of 40.61% Cr_2O_3 and 48.58% Cr_2O_3 were achieved by using jig and shaking table, respectively. Besides, the chromite remained in the tailings was determined as 3.16%.

Table 8. Combined Test Results

Products	Weight, %	Cr_2O_3, %	Recv., %
Jig Conc.	37.4	40.61	52.1
ST Conc.	17.3	48.58	28.8
Middling	26.8	17.12	15.8
Tailings	13.3	3.16	1.4
Slime	5.2	10.73	1.9
Feed	100.0	29.15	100.0

Table 9. Distributed Test Results

Products	Weight, %	Cr_2O_3, %	Recv., %
Jig Conc.	37.4	40.61	52.1
ST. Conc.	25.5	48.58	42.5
Tailings	31.9	3.16	3.5
Slime	5.2	10.73	1.9
Feed	100.0	29.15	100.0

After application of the combined beneficiation process, 94.6% total efficiency was obtained as sum of 52.1% (using jig) and 42.5% (using shaking table). On the other hand, another important issue was considered as Cr:Fe ratio. Fe analyses were performed on the concentrates obtained from jigging and shaking table tests. The ratio values were determined as 2.67 and 2.59 respectively.

3.2 Beneficiation Tests with KM

3.2.1 Shaking Table Tests

The sample was prepared as -1 mm and classified into the size fractions of (-1+0.5 mm), (-0.5+0.212 mm), (-0.212+0.106 mm), and (-0.106 mm) for the tests. As it is possible to see the results in Table 10, the combined results are available in Table 11.

Table 10. Shaking Table Test Results

Size fraction, mm	Products	Weight, %	Cr_2O_3, %	Recv., %
-1+0.5	Conc.1	1.4	45.02	2.7
	Conc.2	1.3	42.10	2.4
	Conc.3	0.9	39.06	1.5
	Middling	3.7	31.39	5.0
	Tail. 6	6.9	26.49	7.7
	Tail. 5	3.6	19.28	2.9
	Tail. 4	3.9	16.65	2.8
	Tail. 3	3.2	13.38	1.8
	Tail. 2	3.6	10.58	1.6
	Tail. 1	3.5	7.90	1.2
	Feed	32.0	21.77	29.6
-0.5 +0.212	Conc.1	3.8	52.86	8.4
	Conc.2	2.6	49.75	5.5
	Conc.3	3.8	43.72	7.0
	Conc.4	1.1	41.81	1.9
	Middling	5.4	25.97	6.0
	Tail. 4	2.0	24.72	2.1
	Tail. 3	3.8	10.86	1.8
	Tail. 2	2.3	5.53	0.6
	Tail. 1	3.9	3.63	0.6
	Feed	28.7	27.76	33.9
-0.212 +0.106	Conc.1	6.5	53.12	14.7
	Conc.2	2.4	49.09	4.9
	Conc.3	1.0	41.07	1.8
	Middling	3.9	12.27	2.0
	Tail. 3	3.8	2.41	0.4
	Tail. 2	2.6	2.38	0.3
	Tail. 1	1.3	2.62	0.1
	Feed	21.5	26.41	24.1
-0.106	Conc.1	2.0	52.866	4.6
	Conc.2	0.6	50.72	1.2
	Middling	2.0	12.63	1.1
	Tail. 2	1.2	8.74	0.4
	Tail. 1	1.5	2.93	0.2
	Slime	10.5	10.93	4.9
	Feed	17.8	16.37	12.4
Total		100.0	23.53	100.0

According to the chemical analyses, a concentrate containing 48.97% Cr_2O_3 was obtained as 26.4% by weight. However,

when the contents of middling and tailings were considered, it can be concluded that particle liberation could not be provided with a particle size fraction at minus -1 mm. Therefore, it was decided to reduce the size fraction to -0.6 mm. The tests were carried out with the size fractions of (-0.600+0.300 mm), (-0.300+0.150 mm), and (-0.150 mm). The results of this group test were given in Table 12, 13 and 14

Table 11. Combined Shaking Table Test Results

Products	Weight, %	Cr_2O_3, %	Recv., %
Concentrate	26.4	49.97	55.1
Middling	44.1	19.60	36.7
Tailings	19.0	4.10	3.3
Slime	10.5	10.93	4.9
Feed	100.0	23.52	100.0

As result after distributing middling product, since it can be recycled in an operating plant, a concentrate of containing 48.90% Cr_2O_3 was obtained with 88.6% efficiency.

It was determined that the particle liberation was provided below 0.6 mm with the KM sample. When -0.6 mm sample was subjected to shaking table tests, marketable concentrate could be produced. In order to increase the efficiency of the process, as it was performed with the KJM sample, the middling could be recycled to the hydraulic classifier and beneficiated with shaking table in closed circuit.

Table 12. Shaking Table Test Results

Size fraction, mm	Products	Weight, %	Cr_2O_3, %	Recv., %
-0.600 +0.300	Conc.1	2.8	51.41	6.1
	Conc.2	3.1	47.69	6.3
	Conc.3	2.8	44.42	5.3
	Conc.4	2.7	39.36	4.6
	Middling	9.8	24.01	10.0
	Tail. 3	2.7	11.50	1.3
	Tail. 2	4.3	8.78	1.6
	Tail. 1	6.1	5.38	1.4
	Feed	34.4	25.09	36.5
-0.300 +0.150	Conc.1	3.8	53.63	8.7
	Conc.2	3.4	52.43	7.6
	Conc.3	3.7	50.13	7.9
	Conc.4	1.8	49.33	3.7
	Conc.5	2.4	44.61	4.5
	Middling	4.9	25.38	5.2
	Tail. 4	2.6	12.63	1.4
	Tail. 3	3.4	6.54	0.9
	Tail. 2	3.8	3.37	0.5
	Tail. 1	5.3	2.15	0.5
	Feed	35.1	27.57	40.9
-0.150	Conc.1	2.9	53.61	6.7
	Conc.2	1.9	52.13	4.2
	Conc.3	1.1	50.55	2.3
	Conc.4	0.5	45.83	1.0
	Conc.5	0.7	34.52	1.0
	Middling	2.3	6.64	0.7
	Tail. 2	2.9	3.21	0.4
	Tail. 1	3.2	2.21	0.3
	Slime	15.0	9.46	6.0
	Feed	30.5	17.50	22.6
Total		100.0	23.57	100.0

Table 13. Combined Shaking Table Test Results

Products	Weight, %	Cr_2O_3, %	Recv., %
Concentrate	33.8	48.90	70.1
Middling	30.0	16.59	21.1
Tailings	21.2	3.12	2.8
Slime	15.0	9.46	6.0
Feed	100.0	23.57	100.0

Table 14. Distributed Shaking Table Test Results

Products	Weight, %	Cr_2O_3, %	Recv., %
Concentrate	42.6	48.90	88.4
Tailings	42.4	3.12	5.6
Slime	15.0	9.46	6.0
Feed	100.0	23.57	100.0

3.3 Investigation of Magnetite Content and Ratio on the Concentrates and Middlings of the KM Sample

Some concentrates of the sample, whose particle size was reduced below 0.6 mm, was selected to determine their Fe content. In Table 15, Cr_2O_3, Fe and ratio values can be seen.

Table 15. Ratio Values of -0.6 mm Products

Size Fraction, mm	Product	Cr_2O_3, %	Fe, %	Ratio
-0.6+0.3	Conc. 1	51.41	14.62	2.41
	Conc. 3	44.42	13.43	2.26
-0.3+0.15	Conc. 1	53.63	15.39	2.38
	Conc. 4	49.33	14.73	2.29
	Conc. 5	44.61	13.99	2.18
-0.150	Conc. 3	50.55	15.88	2.18
	Conc. 5	34.52	12.81	1.84

Although the content of the concentrates reached up to 53% Cr_2O_3, ratio was found to be less than 2.38. Besides, it can be concluded that as Cr_2O_3 content increased, Fe content increased, too. These determinations can be explained in two ways:

- When the chromite concentrate content increased, the liberated magnetite particles existed in the mineralogical structure of the ore had a similar move in the chromite band.
- Even the sample was milled below 0.6 mm, it can be claimed that the liberation of chromite-magnetite could not be provided yet.

In order to determine which of these indications were true, the “Concentrate 1” of -0.150 size fraction with 53.61% Cr_2O_3 content was milled below 38 µm and fed to Davis Tube. Since this device can separate magnetite particles, it could be easy to understand the structure. As seen from Table 16, different ratios were obtained. After Davis Tube test, it can be indicated that the magnetite particles were associated with chromite particles.

Table 16. Davis Tube Test Results

Products	Weight, %	Cr_2O_3, %	Fe,%	Ratio
Non magnetic	86.4	53.95	15.0	2.46
Magnetic	13.6	48.08	21.8	1.51
Feed	100.0	53.15	15.93	2.33

Since the magnetite and chromite particles were thought to be associated together, then, it was decided to perform mineralogical analyses on these products.

3.4 Mineralogical Examinations

Basically, chromite and magnetite were found as expected. But olivine, serpentine minerals and less amounts of pyroxene could be counted as the gangue minerals. The related pictures were illustrated in Figure 1, 2, 3 and 4.

Chromite was found as an anhedral and fragmented structure. Only the sample demonstrated in Figure 4 had angled chromite particles. Also, the chromite and magnetite crystals showed fragmented morphology with twiggy and needle-shaped structure in the sample demonstrated in Figure 3.

According to the examinations, as long as the particle size decreased, the liberation of magnetite particles increased. Especially some part of magnetite was found in the fractures of chromite, which led to a decrease in ratio. This can be traced from Figure 1 and 2.

Magnetite particles had a disintegrative character and a part of it started to transform

to hematite. The size of the micro fractures the magnetite existed was nearly 30 µm. Besides, it was probable that the magnetite was formed as an alteration product of chromite.

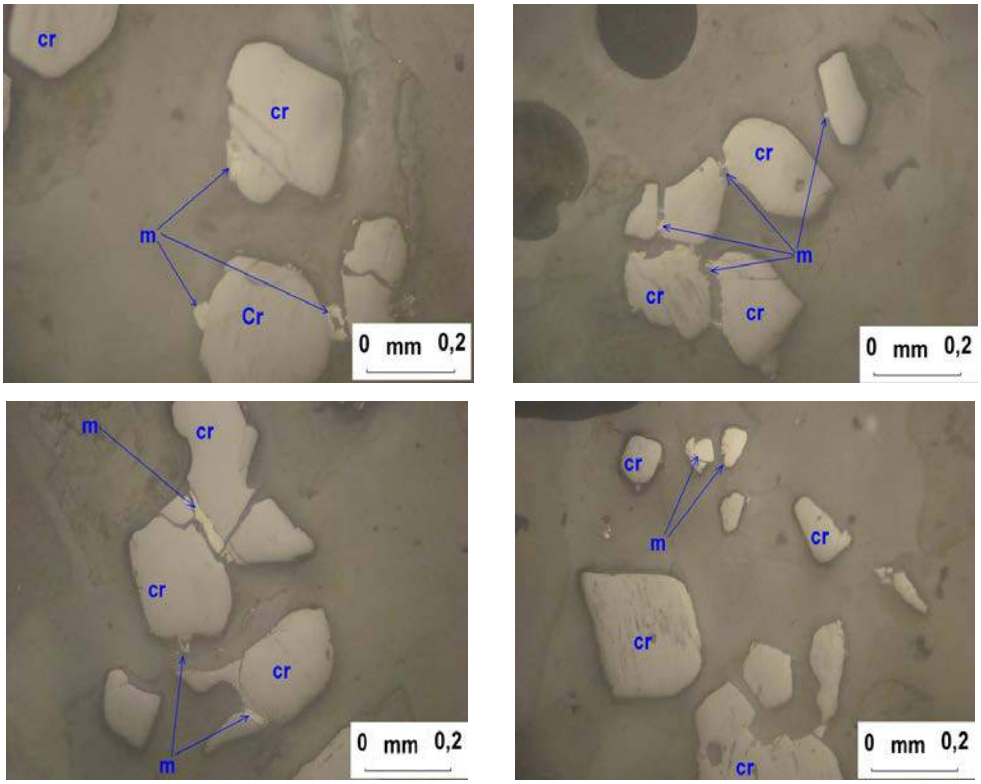

Figure 1. Chromite and magnetite crystals. Particles are euhedral and has clean surfaces. Magnetite is observed in the sides and fractures of chromite particles.

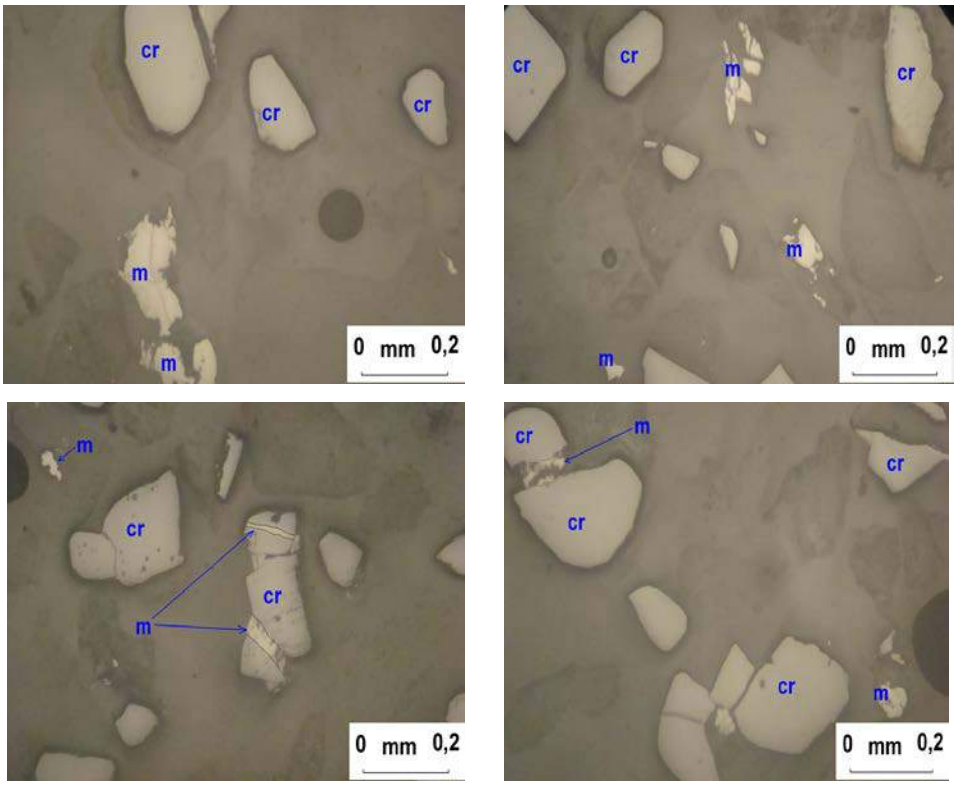

Figure 2. Euhedral and disseminated chromite particles. Fine grained magnetite exists in the fractures of chromite.

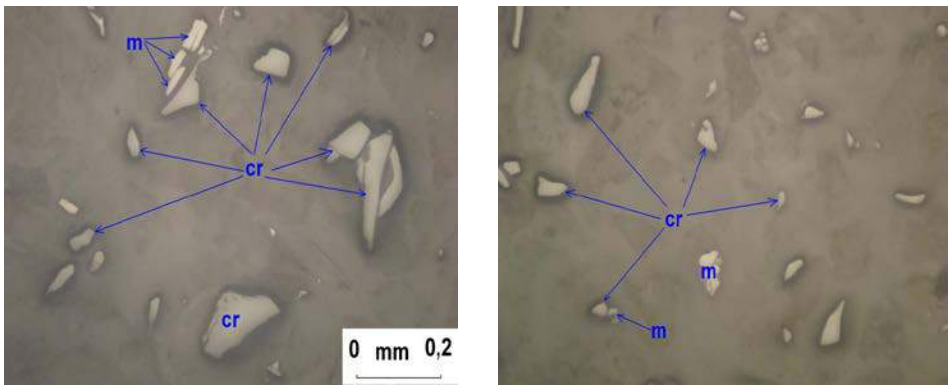

Figure 3. Fine grained and liberated chrmoite and magnetite crystals. Rarely associated. Mostly anhedral and fractured. Fine grained magnetites exist in the crystal matrix of silicates.

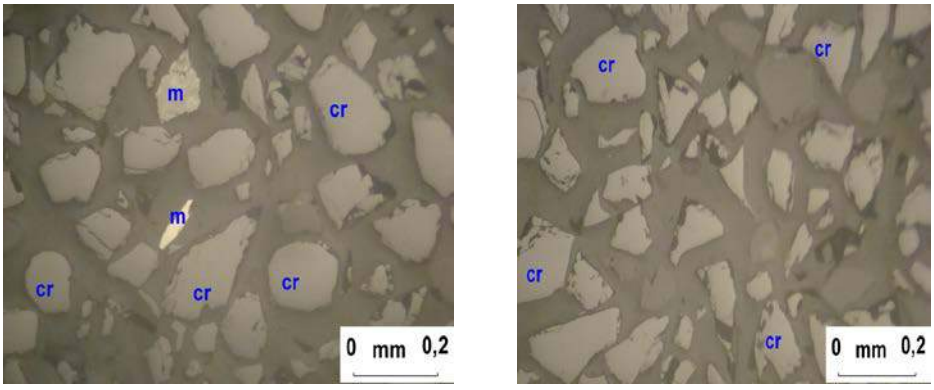

Figure 4. Relatively equidimensional, anhedral, locally needle shaped chromite and magnetite crystals. Not associated with silicates. Only a few magnetite particles exist.

4 RESULTS

In this study, examination of two different chromite samples taken from Albania in terms of particle liberation and ratio problem was investigated. With the KJM coded sample it was found that:

- Chromite concentrates containing nearly 40% Cr_2O_3 were possible with the size fraction of -25+1 mm using jig.
- When middling and residues of jig tests were milled below 1 mm, they could be subjected to shaking table tests resulted in 48.58% Cr_2O_3 content in concentrate.
- In a combined process of using jigging+shaking table, 80.9% of total metal recoveries were able to be achieved.
- If the middling of shaking table was recycled into the beneficiation system, then, it was seem to be possible to increase the efficiency.
- According to the chemical analyses, the ratio of the concentrates varied from 2.59 to 2.67.

With the KM coded sample it was found that:

- The particle liberation was provided below 0.6 mm.
- While the concentrate was obtained with 48.9% Cr_2O_3 content, the efficiency was calculated as 70.1%. However, the middling was obtained as 30% by weight, which could be recycled to the beneficiation unit in an operating plant. By applying this step, it was thought that 10-12% efficiency increases might be gained.
- The ratio values of these concentrates were found in a range of 2.29-2.41.
- Although Davis Tube tests were carried out, it was not found sufficient to

remove iron content. The reason for that situation was investigated utilizing mineralogical analyses.

- It was determined that the magnetite particles were associated with chromite particles.

REFERENCES

Abubakre, O.K., Muriana, R.A., Nwokike, P.N., 2007. Characterization and beneficiation of Anka chromite ore using magnetic separation process. Journal of Minerals & Materials Characterization & Engineering 6 (2), 143–150.

Atalay, U., Ozbayoglu, G., 1992. Beneficiation and agglomeration of chromite–its application in Turkey. Mineral Processing and Extractive Metallurgy Review 9, 185–194.

Cicek, T., Cocen, I., Birlik, M., 2000. Applicability of multi-gravity separation to kop chromite concentration plant. In: Mineral Processing on the Verge of the 21th Century, Balkema, Rotterdam. Proceedings of 8th International Mineral Processing Symposium, Antalya, pp. 87–92.

Gul, A., Yuce, E., Guney, A., Gurkan, V., Arslan, F., Onal, G., 1995. Evaluation of low grade chromite ores from Adana-Karsanti region. In: The 14th Turkish Mining Congress, Chamber of Mining Engineers of Turkey.

Guney, A., et al., 1992. Concentration of chromite gravity tailings by free jet type and column flotation system. In: Proceedings of the First International Conference on Modem Process Mineralogy and Mineral Processing. Beijing, China.

Guney, A. et al., 1994. Flotation of fine chromite tailings using novel techniques. In: Demirel, H., Ersayin, S. (Eds.), Progress in Mineral Processing Technology. Balkema, Rotterdam, The Netherlands, pp. 473–477.

Güney, A., Yüce, A.E., Kangal, M.O., Burat, F., Kökkılıç, O., Gürkan, V. 2009, "*Beneficiation and process flow sheet development of chromite ores*", XIII. Balkan Mineral Processing Congress, Edts: S.Krausz, L.Ciobanu, N.Cristea, V. Ciocan, G.Cristea, ISBN:978-973-677-159-0, Vol:1, pp:401-408, 14-17 June, Bucharest, Romania.

Mohan Rao, S., Chandrakala, K., Gajanan, K., Nath, G., Rao, N.D., 2006. Recovery of Chromite Values from Chrome Ore Beneficiation Plant Tailings. Tata Search, Tata Steel Limited, pp. 59–64.

Murthy, Ch.V.G.K., Sripriya, R., Rao, P.V.T., 1994. Enrichment of Cr/Fe ratio in chromite concentrate produced in chromite beneficiation plant at Tata Steel. Transactions of the Indian Institute of Metals 47 (6), 413–416.

Murthy, Y.R., Tripathy, S.K., Raghukumar, C., 2011. Chrome ore beneficiation challenges & opportunities—a review. Miner. Eng. 24, 375–380.

Önal, G., Güney, A.**,** Yüce, A.E., 2003, "*The beneficiation of chromite tailings by Multi-gravity separator*", Proceeding of the International Seminar on Mineral processing Technology MPT-2003, ISBN:81-7764-405-x, pp. 203-207, February, 6-8, Goa, India.

Papp, J. 1994. "Chromite" in Industrial Minerals and Rocks. 6th Edition Society for Mining, Metallurgy and Exploration. P. 210.

Pascoe, R.D., Power, M.R., Simpson, B., 2007. QEMSCAN Analysis As a Tool for Improved Understanding of Gravity Separator Performance. Minerals Engineering 20, 487–49520.

Yüce, A. E., Güney,A., Önal, G., Girgin, Ş., Kangal, O., 1998, "*Final Tailings Disposal After Beneficiation of Chromite Fines Using New-age Seperator*", Proceedings of the Fifth International Symposium on Environmental Issues and Waste Management in Energy and Mineral Production - SWEMP 98, ISBN:90-5410-956-4, pp: 469-472, 18-20 May, Ankara-Turkey.

Beneficiation of Dry Magnetic Separator Tailings Using Dense Medium Cyclones: A Simulation Study

A. Aghlmandi Harzanagh, Ş. L. Ergün
Hacettepe University, Department of Mining Engineering, 06800 Ankara, Turkey

ABSTRACT The aim of this research is to investigate the possibility of beneficiation of dry low intensity magnetic separator tailings of an iron ore concentration plant located in Malatya region of Turkey by using dense medium cyclones. After three stages of low intensity dry magnetic separation, there is a moderately high amount of iron (near 30% Fe) because of remaining hematite and goethite.

After taking samples from the tailings, size distribution analysis was performed. Then, the sample was divided into size fractions and sink-float tests were performed for each fractions. Using the size distributions and heavy liquid test results, simulation studies were performed to predict the performance of dense medium cyclone to recover iron minerals. The results showed that an iron ore concentrate containing 60.45% Fe with a 80% recovery could be obtained from the tailings using dense medium cyclones.

Keywords: Dense medium cyclones, Dry magnetic separator tailings, Tailing beneficiation

1 INTRODUCTION

Dense medium cyclones (DMCs) have been extensively used in coal preparation. Dense medium cyclone had been installed in over 25% of the coal preparation plants worldwide Reeves (2002). About 93% of 58 coal preparation plants in South Africa employes dense medium cyclones de Korte (2014). Large tonnages of iron ore and diamonds are also processed by dense medium cyclones Burt (1984). Dense medium cyclones (DMC) has several advantages such as ability to make sharp separations, ability to maintain controllable separation density, ability to handle a wide range of feed size, ability to remove products continuously, ability to change specific gravity of separation to meet varying market requirements and high capacity, comparing with other gravity separation methods (Aplan, 1985). Amenability of dense medium separation is usually evaluated by heavy liquid analysis. For the densities higher densities require organic liquids which are highly toxic.

Aqueous solutions of sodium polytungstate (SPT) or lithium polytungstate have certain safety advantages over organic liquids for the densities up to 3.1 g/cm^3. Koroznikova et al (2007) have developed a technique using finely ground tungsten carbide (TC) suspension in SPT to obtain densities upto 4 g/cm3.

Due to the relative simplicity of heavy liquid testing for coal and later development of density tracers, modelling and simulation studies have started earlier and matured to use reliable predictions for design and optimization of coal preparation plants Davis (1987). These have been applied to high density separations like diamond and lead-zinc Scott (1988).

Although a few earlier applications in chromite and magnesite, currently application of dense medium cyclones is limited to coal washing in Turkey, although its application would be beneficial for some problematic ores Aghlmandi Harzanagh (2014).

The aim of this paper is to investigate the possibility of using dense medium cyclone for the tailings of low intensity magnetic separator by using simulation as a tool.

2 EXPERIMENTAL STUDIES

2.1 Material and Method Used

The sample is the tailing of three stages of dry low intensity magnetic separation. The size of the sample is 100% passing 9.5mm. Figure 1 shows the size distribution of the sample.

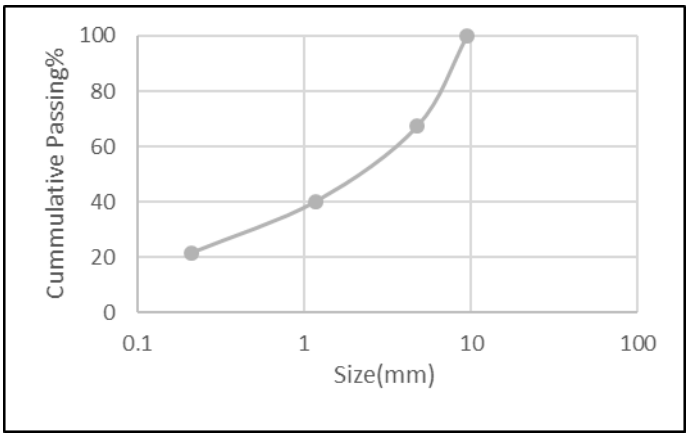

Figure 1. Size distribution of iron ore sample

Chemical analysis showed that Fe content of the sample is 31.9% and according to the results of the XRD analysis, Fe element mostly related to Hematite (Fe2O3) with specific gravity of 5.26 and Goethite (FeO (OH)) with specific gravity of 3.3-4.3. Also Specific gravity of the sample was measured as 3.18. After size distribution analysis of the sample, the sample was divided to -9.5+4.75 mm, 4.75+1.18mm, -1.18+0.212mm and -0.212mm size fractions for sink-float tests (Figure 2).

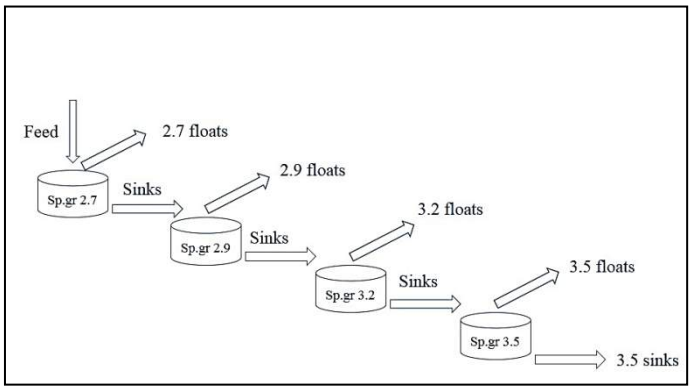

Figure 2. Schematic illustration of sink-float test

In this study, tetrabromoethane and acetone combination were used for preparing heavy liquids with specific gravies of 2.7 and 2.9 and suspensions of SPT and TC were used for preparing heavy suspensions with specific gravities of 3.2 and 3.5.

Preparing heavy suspension of SPT and TC consists of four steps:

- Preparation of SPT solution with 2.5 g/ml density (by this way the viscosity will not be high to separate fine particles).
- Pouring 20-30% of SPT solution into a separate container on a magnetic stirrer.
- Slow addition of the TC powder to form a homogenous suspension.
- Addition of this suspension to the SPT solution and stirring it very slowly until the desired density is obtained.

Then, sink-float tests were performed for all of the samples. In the case of coarse samples (+1mm) a normal beaker was used for fine size fraction (-1mm) special funnel (Figure 3) was used.

Figure 3. Modified separation funnel

2.2 Results

Figure 4-6 show the results of the sink-float tests for different size fractions of the sample.

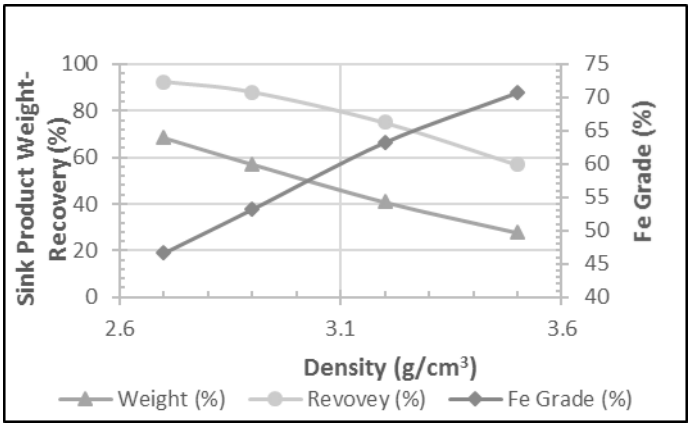

Figure 4. Heavy liquid density vs Fe grade (%), Fe recovery (%) and weight of the sink products (%) for -9.5mm+4.75mm size fraction

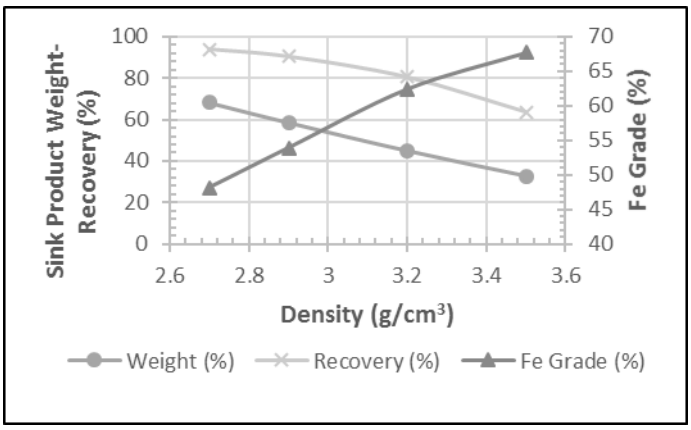

Figure 5. Heavy liquid density vs Fe grade (%), Fe recovery (%) and weight of the sink products (%) for -4.75mm+1.18mm size fraction

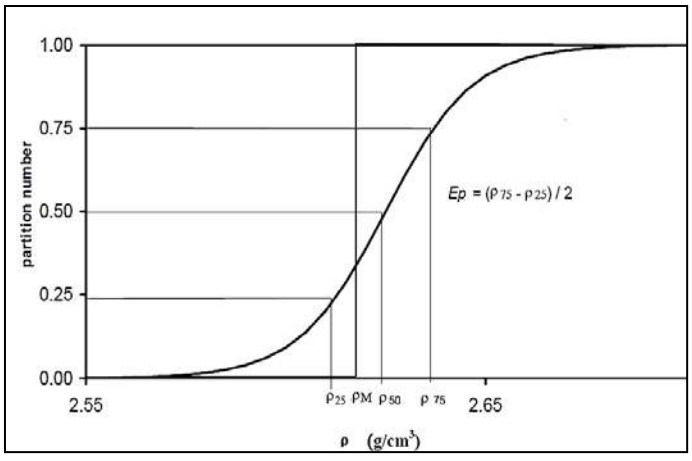

Figure 6. Heavy liquid density vs Fe grade (%), Fe recovery (%) and weight of the sink products (%) for -1.18mm+0.212mm size fraction

3 SIMULATION STUDIES

Any sink and float process can be described by a partition curve. Partition curve reports the amount (weight fraction) reported to the sinks versus solid density. If α is the partition coefficient, (1-α) is the amount of material reported to the floats.

The partition curve depends on: Feed properties (particle size distribution and density weight distribution), employed device and settings and dense medium stability and viscosity. In Figure 7 a typical partition curve is reported. The main important parameters describing the partition curve are Bevilacqua and Zanin (2002) :

- efficiency of separation (Ep): gives a measure of the curve slope
- Cut density (ρ50): is the density of the solids reported 50 % to the sinks and 50 % to the floats
- Offset: is the density difference between cut density and medium density (ρ50 – ρm).

Better separation occurs in low Ep values. Ideal separation has Ep = 0 and offset = 0. Ep and offset values depend on both feed and operational conditions like cyclone geometry, head pressure, separation density, medium stability and viscosity and flow rate. Coarser particles have smaller Ep and offset values than fine particles.

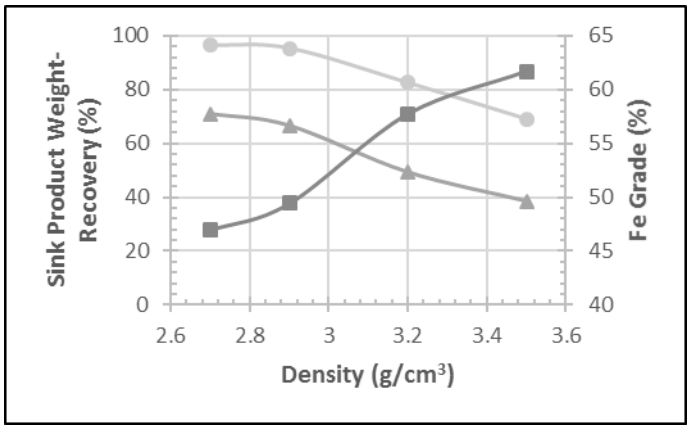

Figure 7. Partition curve and main parameters

According to Scott (1988), one of the simplest empirical efficiency curve expressions, Equation 3.1 is attributable to Whiten (1966) and has been used extensively by other workers. Where the partition number (Yj) is defined as the weight fraction

of density species (ρj) in the feed which reports to the underflow, (ρ50) is separation density and (∝) is a measure of the reduced efficiency curve slope.

Scott (1988) reported that Equation (3.1) could be presented by equation (3.2) and in case of high density separation, Ep value could be calculated by the following equations:

$$Y_{j=}\frac{exp\left(\propto\frac{\rho_j}{\rho_{50}}\right)-1}{\exp\left(\propto\frac{\rho_j}{\rho_{50}}\right)+\exp(\alpha)-2} \quad (3.1)$$

$$Y_j=\frac{1}{1+\exp\left[\frac{1.099(\rho_{50}-\rho_j)}{Ep}\right]} \quad (3.2)$$

$$Ep=Z+K.d^n \quad (3.3)$$

$$Z=19.6+0.16\Delta\rho-6.3Vmo \quad (3.4)$$

$$\ln(k)=6.87+0.59\ln(\mu)+0.30\ln(D_c) \quad (3.5)$$

Where, $\Delta\rho$ is the density differential in the cyclone, Vmo is the volumetric medium to ore ratio, μ is heavy medium viscosity and D_c is cyclone diameter. It is apparent from the equation that Ep value increases with all this parameters and high Ep values represent inefficient separation.

Because of similarity between the density and size distribution used in this study and diamond ore, the values of Z and K which was calculated for 400mm dense medium cyclone in Argyle diamond plant was used to predict Ep values in different size fractions Scott (1988).

$$Z=4+52d^{-1} \quad (3.6)$$

Lave 1.0 program was used to simulate the performance of the HMC plant. This computer program has been developed at the Department of Mining Engineering of Hacettepe University by Orhan, Gülsoy, and Ergün (2010) and it uses JKMRC model based on Whiten equation (Equation 3.2).

Lave 1.0 is able to run with minimal information that listed below:

- Particle size distribution of feed
- Heavy liquid analysis on each size range
- Separation density
- Ecart probable of separation (Ep)

As mentioned above, separation Ep changes for different size fractions of the feed so we have to calculate it for each size fraction then import them to the simulator program. Equation (3.6) was used to calculate Ep values for different size fractions. Figure 8 shows the principle of working with Lave 1.0 simulator.

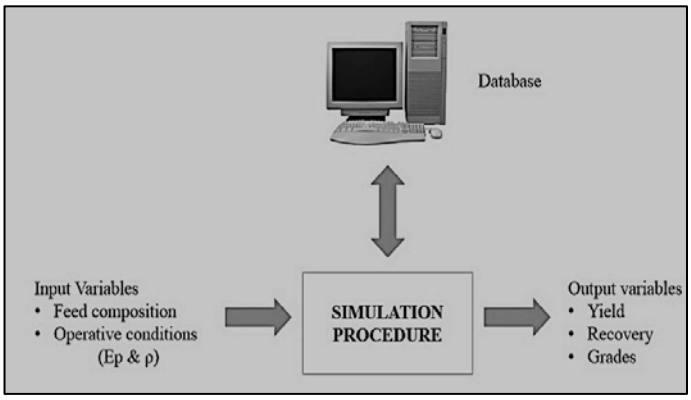

Figure 8. Principle of working with Lave 1.0 separator

For simulations the performance of HMC a simple circuit, including one screen and one HMC was considered. Using equation (3.6), Ep values were calculated for different size fractions and then these values were inputted to Lave 1.0 simulator. As a second variable pulp densities from 2.5 gr/cm3 to 3.5 gr/cm3 were entered to the simulator and simulation outputs were listed to select the best separation density (saleable concentrate grade with maximum recovery). Table 1 shows the calculated Ep values for different size fractions of ores and Figure 9 shows the grade and recovery changes according to separation density for iron ore sample. Figure 10 also shows grade-recovery curve.

Table 1. Calculated Ep values for different size fractions

Size fractions (mm)	Mean Size (mm)	Calculated Ep
-9.5+4.75	7.12	0.011
-4.75+1.18	2.96	0.021
-1.18+0.212	0.70	0.091

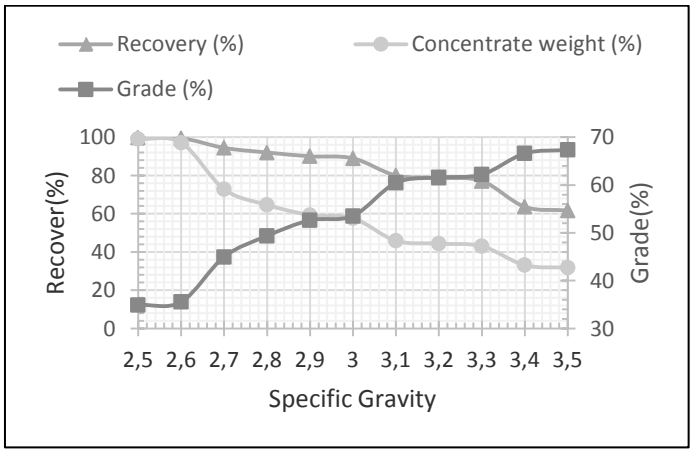

Figure 9. Grade, recovery and concentrate weight for different separation densities (based on simulation results)

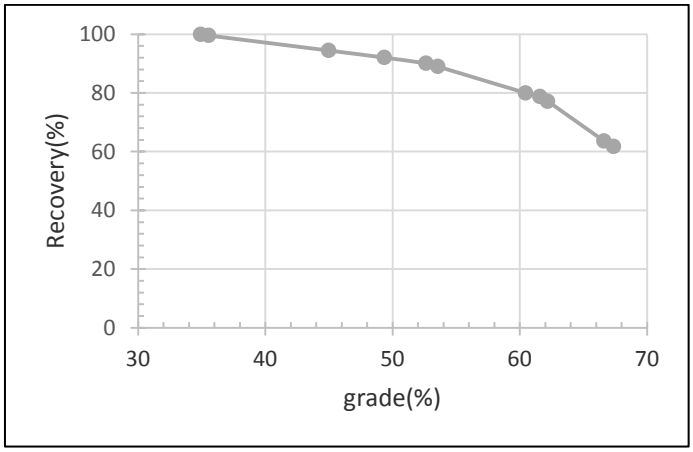

Figure 10. Grade-recovery relationship for iron ore sample based on simulation results

4 RESULTS AND DISCUSSIONS

According to the results of the simulations, Separation density of 3.1 gr/cm^3 is the most favorable density for the İron ore circuit. In this separation density it is possible to obtain concentrate with 60.45% Fe grade and 80% Fe recovery. Figure 11 shows the simulated flowsheet for iron ore with 100 t/h feed capacity and separation density of 3.1 gr/cm3.

The difficulty in gravity concentration processes can be evaluated using heavy liquid test results. according to Wills and Napier-Munn (2006) when the amount of near gravity particles is higher than 10%, it is really hard to obtain good results with jigs, tables, spirals and other gravity methods and the only efficient gravity method is dense medium separation. Table 2 shows the amount of near gravity particles for difference size fractions which calculated based on sink-float test results.

Table 2. Amount of near gravity materials for different size fractions

Size Fraction (mm)	Cum. Sinks Weight (%)		Difference
	- 0.1 of Separation Density	+0.1 of Separation Density	
-9.5+4.75	51.5	40.78	10.63
-4.75+1.18	54	45	9
-1.18+0.21	61	49.36	11.64

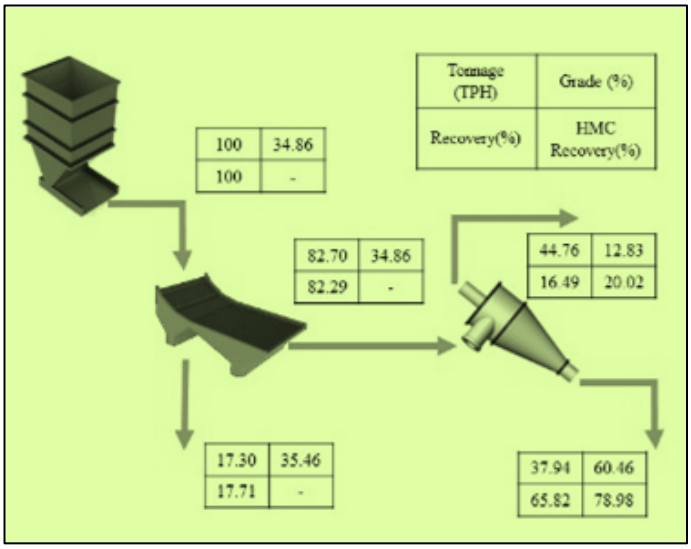

Figure 11. Schematic flowsheet of HMC plant for iron ore in separation density of 3.1 gr/cm^3

It is apparent from the Table 2 that, the amount of near gravity particles in most of size fractions are more than 10%. Therefore, this ore can not be beneficiated with the other gravity methods efficiently and using of dense medium cyclone is inevitable for this application.

5 CONCLUSIONS

Mineralogical analysis showed that hematite and goethite are the major iron minerals in the ore. Following sink-float tests, simulation results showed that obtaining a concentrate with up to 60.45% Fe grade and about 80% Fe recovery is possible for a dense medium cyclone plant with 3.1 g/cm^3 separation density, -9.5mm +0.5mm feed size.

6 ACKNOWLEDGEMENT

The authors would like to thank Dr. E.Caner ORHAN from the Department of Mining Engineering of Hacettepe University for the valuable discussions.

REFERENCES

Aghlmandi Harzanagh, A, 2014. Simulation Aided Investigations On Non-Coal Applications Of Heavy Medium Cyclone. *Master of Science Degree Thesis*, Department of Mining Engineering, Hacettepe University.

Aplan, F, 1985. Heavy Media Separations. In *SME Mineral Processing Handbook* Volume 1 (pp. 1–16).

Bevilacqua, P., and Zanin, M, 2002. A Simulation Procedure For The Design Of Dense Medium Separation Circuits. In *The Eighth Samancor Symposium on Dense Media* (pp. 1–13). Port Douglas.

Burt, R, 1984. *Gravity Concentration Technology*, Elsevier, Amesterdam-Oxford-New York-Tokyo

Davis, J, 1987. A Study of coal washing dense medium cyclones. *PhD Thesis*, Department Of Mining And Metallurgical Engineering, Queensland University

De Korte, J, 2014. Index Of South African Coal Preperation Plants. Retrieved February 25, 2014, from *http://www.sacoalprep.co.za/information.htm*

Koroznikova, L, Klutke, C, Knight, S, and Hall, S, 2007. The Use Of Low-Toxic Heavy Suspensions In Mineral Sands Evaluation And Zircon Fractionation, In *The 6th International Heavy Minerals Conference 'Back to Basics', The Southern African Institute of Mining and Metallurgy*, 1996, 21–30.

Orhan, E, Gülsoy, Ö and Ergün, Ş, 2010. Lave v1. Coal Washing Plant Simulator, *Hacettepe University, Depertment of Mining Engineering . Ankara,Turkey*

Reeves, R, 2002. Types And Characteristics Of Heavy-Media Separators And Flowsheets. In *Mineral Processing Plant Design, Practice, and Control Proceedings* (pp. 962–977). New York.

Scott, I, 1988. A Dense Medium Cyclone Model Based On The Pivot Phenomenon. *PhD Thesis*, Department Of Mining And Metallurgical Engineering, Queensland University

Whiten, W, 1966. Winter School On Mineral Processing, *Course Notes*. Department of mining and metallurgical engineering Queenslan University.for

Wills, B, and Napier-Munn, T, 2006. Mineral Processing Technology. *Elsevier Science & Technology Books*.

Flotation Circuit Efficiency Enhancement Regarding Increase of Rougher Cells Throughput

A. Hassanzadeh
Mineral Processing Department, Faculty of Mines, Istanbul Technical University, 34469 Istanbul, Turkey

A. Azizi
Department of Mining, Petroleum and Geophysics, University of Shahrood, Shahrood, Iran

ABSTRACT Rougher flotation cells of Sarcheshmeh copper concentrator are expected to produce a concentrate assaying 7.6% with 96% recovery. Due to some reasons its recovery was decreased to 90 % during last year. Moreover, its recovery is of great significant because 80% of the final tailings is disposed from this section. In this work, mineralogical surveying, size by size copper recovery analysis, reagents stage addition and dosage were investigated. It is shown that, in the +75 μm size fractions in rougher tailings most of the free particles were chalcopyrite and pyrite minerals. The maximum recovery of copper was observed in 25-75 μm fractions, while the major copper loss was in +105 μm size fractions. It was found that, stage addition of collector (75, 13, 12) could improve the rougher recovery up to 2 percent.

Keywords: Flotation, circuit efficiency, rougher cell, copper

1 INTRODUCTION

The industrial practice of froth flotation is widely recognized to be a complex and highly self-compensating system (Klimpel, 1993).

Sarcheshmeh deposit which is one of the largest copper ore body in the world contains 1 billion tonnes of ore averaging 0.90% copper and 0.03% molybdenum. It is located in the southeast of Iran processing 47000 t/d of ore since 1982. The mine produces 100000 tonnes of copper and 2200 tonnes of molybdenite concentrate per year (Wunder, 1979). The rougher flotation in Sarcheshmeh copper complex is comprised of two sections which consisting of four rows of fourteen 8.5 m^3, stepped 4-5-5, cells (Fig. 1).

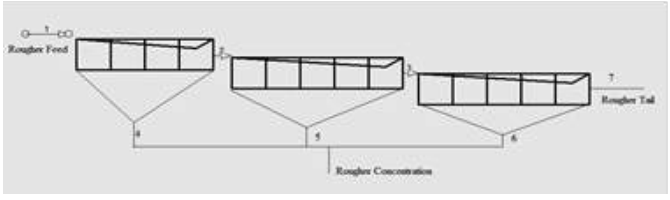

Figure 1. One of the selected rows of rougher cells and sampling points.

The relationship between particle size and flotation recovery has been the subject of several studies and it was shown that, the behaviour of fine and coarse particles in flotation follows different trends (Gaudin, Groh, 1931). In addition, the effect of reagent dosage and particle size on metallurgical performance has also been studied in detail (Shannon, 1986). Clearly, coarse and extremely fine particles are more difficult to be recovered by froth flotation compared to intermediate size particles (Gaudin, 1931). Also, mineral liberation plays an important role in flotation processes as demonstrated by studies on detachment of particles from bubbles during coalescence, or by comparing flotation kinetic constants of liberated and locked particles (Trahar, 1981).

In Sarcheshmeh concentrator, Banisi et al. showed that, 17% of copper was lost in tailings and the lowest copper recovery was corresponding with the particles coarser than 105 microns, while only one of the eight identical flotation banks was sampled (Banisi & Kargar, 2001). Furthermore,

focusing on mineralogical composition it was found that, 91.2% recovery could be obtained, while there was a reduction of 15% in the amount of free valuable minerals in the tailings stream, with chalcocite in the -38 microns size fraction having the highest contribution (Banisi & Iranmanesh, 2002). Since 80 percent of the final tailings was rejected from the rougher section the overall recovery was mainly dependent on the grade of rougher tailings (Banisi & Sarvi, 2003).

In this work, firstly the recorded performances of the past 6 month of the plant operations were compared with the design criteria. It was found that the final recovery was reduced to 86 from 90 percent, while the rougher recovery was decreased 8 percent. Increased throughput from 225 up to 280 and even 300 tph to each one of the 8 ball mills in circuit and consequently a coarser grind size and a shorter residence time in the cells, mineralogical variations due to the increased depth of the mine, major changes in the regime of reagent addition, could be responsible for the decrease in recovery. Thus, it was essential to investigate into the responsible factors to compensate for the loss of recovery.

2 METHODOLOGY

2.1 Determination of the performance of rougher cells

The rougher bank in Sarcheshmeh is divided into three units of 4, 5, and 5 cells. To analyze the flotation circuit, a section consisting of four of the rougher rows were selected for sampling and sampled at 7 points (Fig. 1). In a 3 hour period when the plant operation was in steady state six incremental samples were collected from each of the sampling points. Wet screenings of the samples were performed, while a -400 mesh fractions were classified by using the CSIRO cyclosizer. Eighty percent passing size of the feed to the flotation circuit was determined 62 µm in normal operation. Each size fraction was assayed for copper content. Flow rate of each stream was calculated and balanced by copper grade of the head samples using mass balancing software (Movazen 2.1) (Yarahmadi & Banisi, 1998).

It was determined that rougher and final recoveries are highly correlated (Fig. 2).

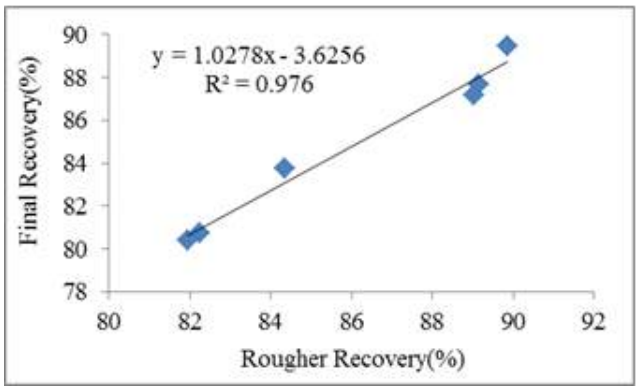

Figure 2. The correlation of final and rougher recoveries.

2.2 Mineralogical analysis

During a six-month period, the composite samples of each month of the feed and tailings streams of the flotation circuit were prepared. At first, polished samples were provided and the mineral counting procedures were executed through a detailed study. Liberation degrees and type of locking valuable minerals in both streams were determined. Grain sizes were measured manually and associate minerals for locked particles were also recorded routinely.

3 RESULTS AND DISCUSSION

3.1 Performance Monitoring

A six months survey of the flotation circuit revealed that the metallurgical objectives declined dramatically. According to design criteria, rougher and final recoveries must be 96 and 90%, respectively, while dropped to 88 and 86%, respectively. It was observed that, increased rate of throughput up to 280 led to the coarser grind size, 62% passing 74 µm (Table 1). Whereas, the average copper grade of rougher feed and rougher tailings streams were 0.83 and 0.10 during the period.

Reagent schemes used for the treatment of porphyry copper and copper-molybdenum ores are relatively simple and usually involve lime as a modifier, xanthate as the

primary collector and a secondary collector (Bulatovic, 2007). In practice, with a relatively coarser grind size, 62% passing 74 µm, an appropriate combination of collectors must be selected for flotation of coarse and middling particles.

Table 1. The results of monitoring rougher flotation circuit for 6 months

Month	rougher recovery, %	final recovery, %	rougher feed particle size, %	Cu%, rougher feed	Cu%, roughr tailings
Oct.	90	88	66	0.87	0.08
Nov.	88	86	63	0.82	0.10
Dec.	91	88	65	0.82	0.09
Jan.	88	85	61	0.81	0.10
Feb.	85	84	60	0.78	0.11
Mar.	87	85	62	0.86	0.10

The presence of valuable minerals in tailings and a subsequent decrease in recovery can be attributed to a deficient reagent regime in the circuit. Table 2 indicates a comparison between designed and operated condition of the type and dosages of collectors and frothres which were being consumed in the circuit. The average dosage of Z11 was 8.49 g/t which was very lower than the design criteria. Z11 is a strong collector that can improve the recovery of coarse particles. A low dosage of Z11 can contribute to a decrease in the recovery of coarse particles in the final cells of the bank. Table 2 shows a comparison between the layout values with operating dosage and type of surfactants in the concentrator plant.

Table 2. Designed and consumed reagents

Design layout			Current	
Reagent type		Dosage (g/t)	Reagent type	Dosage (g/t)
Collectors	Z11	56	Z11	9
	R404	18	Nascol-1451	20
	Z200	13	FlominC-4132	13
Frothers	MIBC	13	MIBC	15
	Fuel Oil	13	Fuel Oil	7
	Dowfroth250	13	A65	15

The degree of liberation is a determinant factor in mineral separation processes and can be used to estimate the selectivity of grinding and the sharpness of separation. Increasing throughout from 225 to 280 tph caused a decrease in the average residence time of material in primary ball mills. Consequently, the degree of liberation of the valuable minerals in rougher feed reached 72%. The result of residence time distribution (RTD) measurement with 280 tph throughput, showed that, MRT was about 5.75 min by the use of N-Mixers model, while according to the design criteria it should be 8 min.

Based on Agar theory the rougher split should be made at the flotation time where separation efficiency is maximized. At maximum separation efficiency, the grade of concentrate produced is equal to the flotation feed. Four stages of sampling were performed from the feed and products of different units of rougher flotation banks. The average copper grade of the concentrate of final unit copper concentration grade (cells 11-14) was 3.24, while copper grade in rougher feed was 0.71 (Figure 3).

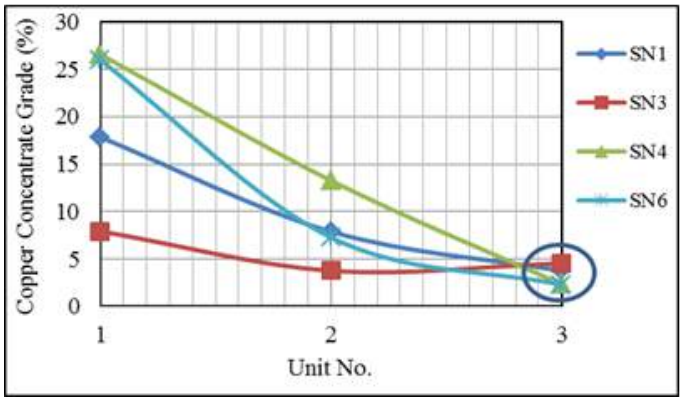

Figure 3. Copper grade in rougher cells in four sampling series vs. unit No. at a selected bank.

The observed results showed that, the mean residence time with 280 tph throughput was relatively 15% lower than with 225 tph.

3.2 Performance Evaluation of Rougher Cells by Size-by-Size Analysis

The recoveries of rougher cells in 10 size fractions were determined and are shown in Figure 4. As can be seen, the recoveries of +150 microns fractions in the last unit are zero that can be attributed to the deficiency and single stage addition of collectors. The

maximum and minimum recoveries in 3 units are corresponding to (15, 150), (33, 210) and (33, +150) microns, respectively.

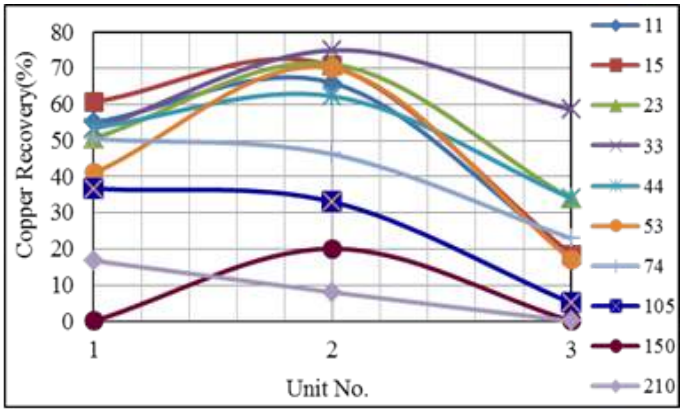

Figure 4. The size-by-size recovery at various units of the rougher bank.

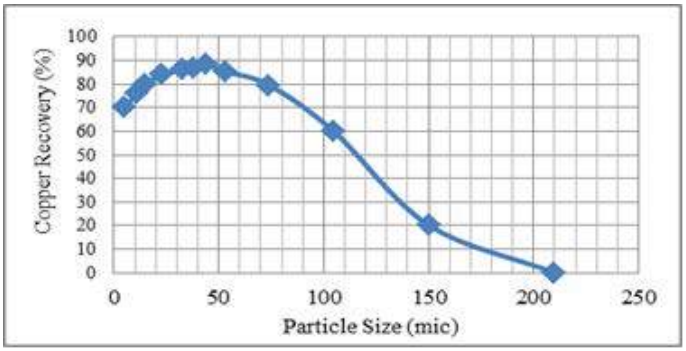

Figure 5. Copper recovery in different size fractions from rougher cells.

Copper losses from rougher cells were mostly related to the coarser particles (+105 μm). It can be seen from Figure 5 that, flotation recovery drops rapidly for the extremely fine fractions (<25 μm), and copper recovery also declines gradually for coarse particle size ranges (>105 μm). The maximum recovery was obtained for particles in the size range between about 25 to 75 μm, for which according to mineralogical study of the samples, the liberation of copper bearing minerals was maximized (>95%). This implies that, the lower recovery from out of this fraction size was mainly due to the locking of copper minerals and gangue.

3.3 Stage Addition of Z11 Into Rougher Cells

For small particles which have a larger specific surface area than coarse particles the dosage of collector required to render a given degree of particle coverage per unit mass is much higher than for coarse particles (Tucker, 1984). Since in the flotation circuit at Sarcheshmeh collector was merely added at the top of the bank (100-0-0), it would mostly be consumed by fine particles which in fact needed a little coverage to be efficiently floated. Thus, there would not be sufficient collector available to produce the hydrophobic coverage required to float the coarse particles, particularly, in the third unit (cell number of 10 to 14). Where, the d_{80} of concentrate and tailings were very higher than the first and second units (Fig. 6) Implying that coarse particles had not been floated in primary cells. For example cumulative percent finer than 200 mesh for RC1, RC2 and RC3 were 76, 65 and 53, respectively.

To avoid loss of valuable minerals as coarse particles in rougher tailings, stage addition of Z11 was implemented in different units of rougher cells. It was revealed that, the copper grade of rougher tailings was around 0.1. From figure 7 it can be observed that, more than 80% of the particles in rougher tailings were coarser than 105 μm. Therefore, stage addition of Z11 was examined. Results indicated that, with stage addition of the collector at heads of the three units (75-13-12) of the rougher cells the copper grade of rougher tailings was decreased about 30% (Fig. 7). Furthermore, an enhancement of 2 percent in the recovery of the rougher section was observed.

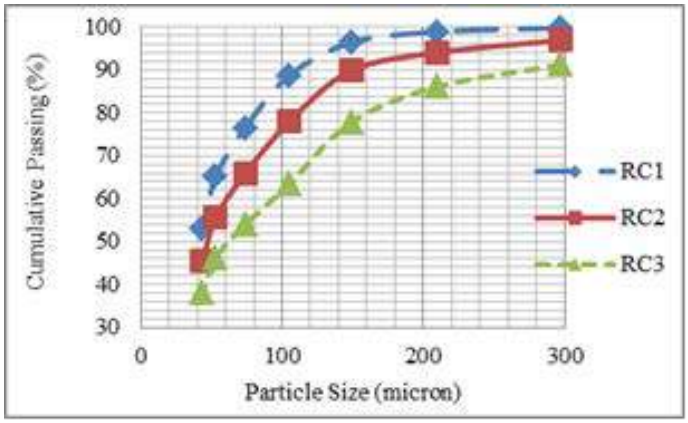

Figure 6. The size distribution of concentrates of the three rougher units.

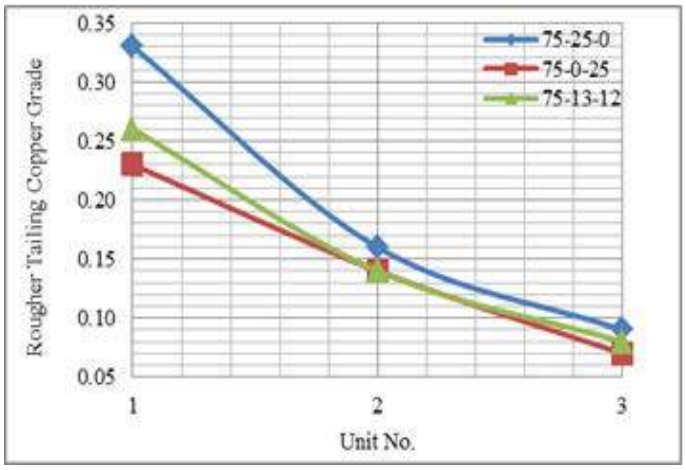

Figure 7. The effect of three methods of stage addition of Z11on the copper grade of rougher tailings.

4 CONCLUSION

Increased throughput into the concentration plant at Sarcheshmeh copper complex had led to a decrease in rougher cells recovery. The reduction in recovery was found to be due to the loss of coarse particles. Decreased MRT of 15 percent in rougher cells with increasing the throughput into each rougher row from 225 to 280 t/h was detected to be one of the major factors affecting the results. This was confirmed by lower separation efficiency in the last rougher cells (unit 3).

Results indicated that, the maximum recovery of rougher cells was achieved in the range of 25-75 μm size fractions. Stage addition of Z11 at heads of the three units (75-13-12) of the rougher cells contributed to about 30% decrease in copper grade in rougher tailings. In addition, the copper recovery of rougher cells was improved up to 2%.

ACKNOWLEDGEMENTS

The author gratefully acknowledge the support of National Iranian Copper Industries Company (N.I.C.I.Co.). The author also appreciate Mr. Yarahmadi, Mr. Fazeli, and Mr. Jabbari for their valuable comments and continuous help.

REFERENCES

Banisi, S., Sarvi, M., Hamidi, D. and Fazeli, A. 2003, Flotation circuit improvements at Sarcheshmeh copper mine, *Mineral processing and extractive metallurgy*, Vol 112, PP. 198-205.

Banisi, S., Kargar, A., Pourkani, M., Sarvi, M., Hamidi, D., 2001, Recent changes at the Sarcheshmeh copper mine flotation circuits. *Proceedings of 33rd Annual Meeting of the Canadian Mineral Processors*, PP. 471-488.

Banisi, S., Iranmanesh, H., Shayestehfar, M. R., Shekarchian, H., 2002, Mineralogical Tracing of Mineralogical results. The Sarcheshmeh Copper Mine Case, *35th Annual Meeting of the Canadian Mineral Processing*. Ottawa, Canada.

Bulatovic, S. M., 2007, *Handbook of Flotation Reagents*, Elsevier Science & Technology Books.

Gaudin, A.M., Groh, J.O., Henderson, H.B., 1931, Effect of particle size on flotation, Technical Publication. *American Institute of Mining and Metallurgical Engineering*, PP. 3-23.

Klimpel, R. 1993, The interaction of grind size, collector dosage, and frother type in industrial chalcopyrite rougher flotation, *society for mining, metallurgy, and exploration*, pp.80-93.

Shannon, L.K., Trahar W.J., 1986, The role of collector in sulfide ore flotation, *Advances in Mineral Processing, SME, Littleton, Colorado*, PP. 408-425.

Trahar, W.J., 1981, A rational interpretation of the role of particle size in flotation, *International Journal of Mineral Processing*, Vol.8, No.4, PP. 289-329.

Tucker, R. J., Meech J.A., 1984 ,Collector consumption heads or tails', *17th Conference of Canadian Mineral Processing*, CMP, Ottawa, PP.419-454.

Wunder, G.W., 1979, Sarcheshmeh Concentrator Operating Manual (Section5: Flotation and Regrinding) *Parson-Jurden International Corporation*, National Iranian Copper Industries.

Yarahmadi, M.R. and Banisi, S., 1998, Movazen: A mass balancing software, *Fourth Chemical Engineering Congress of Iran*, Sharif University, 4, PP. 107-115.

Granulometric Separation in Laminar Flow

I. Grigorova, I. Nishkov
University of Mining and Geology "St. Ivan Rislki", Department of Mineral Processing and Recycling, 1700 Sofia, Bulgaria

ABSTRACT Research and development program was undertaken to develop a new generation of hydraulic separators which are more efficient and less costly to operate and maintain. Two methods of granulometric separation of fine particles in laminar flow have been tested. A method of hydraulic airlift size classification has been developed. For the laboratory experimental studies glass microspheres have been used. It has been shown that fine particles are dragged into the boundary layers of the rising bubbles and have been separated as an overflow (fines stream) product. The hydraulic Airlift separator has been tested in quartz-kaolin industry for recovery kaolin from technological waste. A method of particle size classification in a fluidized bed containing parallel inclined plates has been developed. The ballotini glass beads have been used in the laboratory experiments. The Reflux classifier has been tested for recovery of fine kaolin from technological waste. The data obtained from industrial tests illustrate the potential application of granulometric separation in laminar flow using AirLift and Reflux separators.

Keywords Granulometric separation, laminar flow

1 INTRODUCTION

In a variety of applications involving suspensions of small particles in fluids, it is desirable to classify or separate the particles based on differences in physical characteristics such size, shape and density. Common commercial equipment capable of effecting particle classification includes hydrocyclones, elutriators, centrifuges, cone classifiers, spiral classifiers and screens.

Particle classification may also be accomplished by hydrodynamic chromatography, field-flow fractionation, inertial deposition, filtration, and electrophoretic or magnetic mobility. An especially desirable classification method is the exploitation of differences in particle settling velocities undue the action of gravity. Gravitational classifiers are both simple in design and exert very little shear on the particles.

However, gravitational sedimentation may be quite slow, especially if the particles are very small.

Hydraulic classification is commonly used for particle size classification and gravity concentration of minerals and coal. Hydraulic separators are frequently used in mineral processing industry to classify fine particles according to size or density (Wills & Tim Napier-Munn 2006). Unfortunately, the efficiency of these processes can be quite low due to poor equipment design and variations in feed consistency. To help alleviate these problems, a research and development program was undertaken to develop a new generation of hydraulic separators which are more efficient and less costly to operate and maintain. Two methods of granulometric separation of fine particles in laminar flow have been tested in Bulgarian kaolin industry.

2 EXPERIMENTAL

2.1 Hydraulic Airlift Classification Laboratory Tests

It is known from the flotation theory and practice that although slime particles are hindered to form three-phase contact, due to thermodynamic (Scheludko, Toshev &

Bojadjiev 1976) and hydro dynamic (Derjaguin, Roulev & Dukhin 1977, Derjaguin & Dukhin 1959) barriers, they are nevertheless drawn into the froth product. The capture of fine particles in the froth is attributed to their small size and bears no relation to their surface properties. As a result the froth product is contaminated by fine particles of the non-floatable mineral. Gaudin (1957) has found that the amount of fine hydrophilic particles captured in the lower layers of the froth is linearly proportional to their concentration in the pulp.

The occurrence of this unwanted in the classical froth flotation secondary process of capture of fine particles has lead us to the idea of using it for separation by size of hydrophilic materials. Thus a method of hydraulic airlift size classification has been developed. The major goal of the method is to extract the finer fractions of a single mineral or the extraction of a mineral, the particles of which are known to be of smaller size than those of the other mineral components in the suspension.

The regime of motion of the gas bubbles corresponds to $Re_b \approx 1\text{-}150$. According to the theory at such values of Re_b the hydrodynamic field around the rising bubbles may be separated into two characteristic regions (Levich 1962): a boundary layer with an effective thickness δ_0 situated immediately at the bubble surface and potential flow extending from the boundary layer inside the liquid.

The hydrophilic mineral particles, which are not subjected to the "winnowing" effect of the flow, are dragged into the boundary layers around the floating air bubbles. The residence time of these particles in the boundary layer is different for various sizes and it is the determinant factor for their extraction into the upper layer. The residence time of the fine particles is much longer than that of the larger ones. This allows the fine particles drawn into the boundary layers to reach the upper layer and to form a separate upper product. The large particles remain in the bulk of the cell as a bottom product. The qualitative estimation of the forces acting on the particles shows that the main classifying effect is their radial migration in the boundary layer in a direction normal to the bubble surface.

The laboratory experiments were conducted in a glass cell with a porous bottom for dispersion of the gas phase. The cell volume was 150 cm^3. Glass micro spheres of radii: 1; 2; 5; 10; 25 and 50 μm products of Duke Scientific Co, were used. Weak inner circulation of the suspension in the bottom of the cell was generated by means of a magnetic stirrer.

The experiments were carried out under the following conditions: content of solid phase in the suspension – 2 g/dm^3; duration of the experiment - 20 min; consumption of gas phase (nitrogen) – 50 cm^3/min.

2.2 Steady-state Particle Classification Laboratory Tests

The work of Davis et al. (1982) suggests that lamella settlers may be used to classify particles according to differences in their settling velocities. This possibility for a single inclined settling channel is shown in Figure 1. A feed suspension containing a distribution of particle sizes is introduced into the channel. By use of the basic principle that larger particles settle more quickly than do smaller ones of the same density and shape, this feed suspension is classified into a coarse fraction (underflow) and a fine fraction (overflow). If the hold-up time in the inclined settler is larger than the required sedimentation time for a given particle size, then particles of that cutoff size and larger will settle onto the lower wall of the channel (and subsequently slide down it to the underflow) and will not be carried into the overflow. Thus, the overflow will be essentially devoid of particles larger than a certain cutoff size, which may be controlled by adjustment of the vessel geometry or the flow rate through the vessel. As a consequence, the underflow will be enriched in the faster settling, larger particles.

Several experiments were carried out in a single-channel inclined settler. The vessel has the dimensions L = 60 cm, b = 2.5 cm,

and w = 3.5 cm. Glass micro spheres of diameter from 0 to 60 μm products of Duke Scientific Co were used. The suspending fluid was water at room temperature. The reservoir volume was 4.0 L. Dry particles were weighed and added to the water so that the particle concentration was less than 1% by volume. The angle of inclination of the settler from the vertical was aired, although the value θ = 45° was used in all of the experiments. This choice was made because it allowed both for high settling rates and for the sediment to easily flow down the lower wall of the channel.

For the steady-state experiments, feed suspension was pumped from the magnetically stirred reservoir up through the bottom of the settler, as shown in Figure 1.

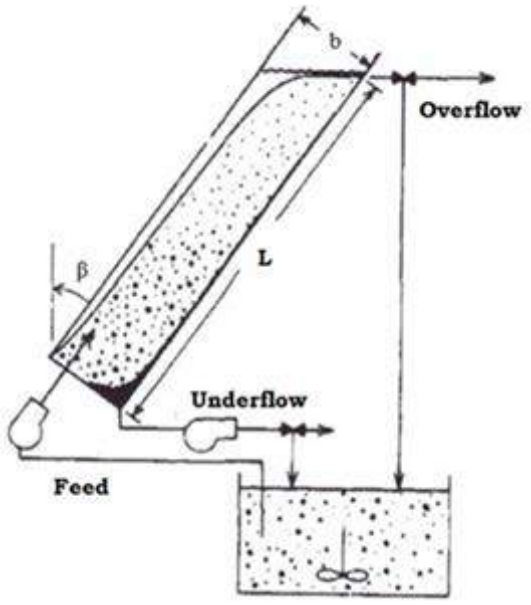

Figure 1. Continuous inclined settler for steady-state particle classification.

Concentrated sediment was withdrawn from the lowest corner of the settler and recycled to the reservoir. The bottom of the settler contained a machined insert with a splitter plate designed to separate the feed stream from the sediment and to prevent remixing of the sediment with the suspension. Both the feed rate and underflow rate were controlled with variable-speed peristaltic tubing pumps. The overflow rate was subject to level control and is simply the difference between the feed and underflow rates. The overflow was also recycled to the reservoir. A total of 20 steady-state experiments were performed by systematically varying the feed and underflow pump settings. For each experiment, approximately 1 h was required for steady state to be reached, with the slow step being the equilibrium formation of the thin layer of sediment deposit on the lower wall of the channel. Samples for later analysis were then taken from the feed, reservoir and from the underflow and overflow streams.

2.3 Technological Tails Characterization

A number of samplings in one mouth duration in Vetovo processing plant of Kaolin AD were performed. Sampling and performance evaluation was applied to final technological tails at two different feed capacities – 100 and 150 t/h. The samples were collected from each stream every one hour and were combined in a shift every time. The following characteristics of the sampling products were determined: particle size distribution and chemical composition. Particle size distribution of samples was determined by wet sieving: fraction "+45 μm" using vibratory sieve shaker Analysete 3, FRITSCH and fraction "- 45 μm" using SediGraph 5100. The chemical composition was determined using AES-ICP.

2.4. Pilot Plant Trial

Based on technological kaolin tails characterization and the hydraulic airlift classification experiments a hydraulic Airlift separator was developed. A schematic representation of the hydraulic Airlift separator is shown in Figure 2. The technological waste and additional water are introduced into classifier. Air flowed up through a distributor plate in the volume of the vessel, dispersing the gas phase into fine air bubbles. The fine particles are dragged into the boundary layers of the rising bubbles and have been separated as an overflow product. The large particles remain in the bulk of the Airlift separator as a chamber product and were separated as an underflow – final waste.

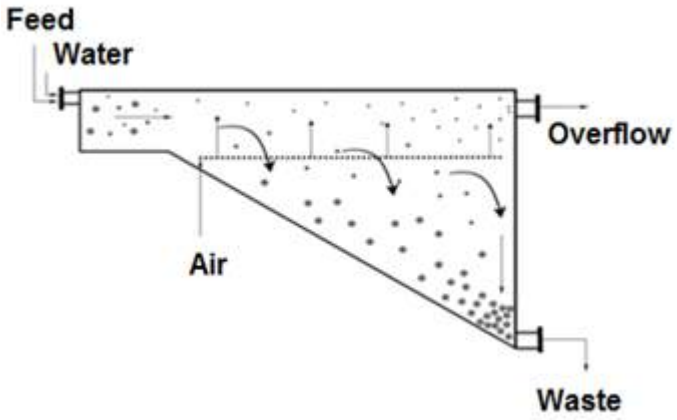

Figure 2. Schematic representation of the hydraulic Airlift separator.

Based on laboratory tests using a single-channel inclined settler a Reflux classifier was developed. A schematic representation of the Reflux classifier is shown in Figure 3. The feed slurry was delivered through the side of the vessel. Fluidization water flowed up through a distributor plate at the base of the vessel, suspending the particles within the vessel. Fluidized suspension passes up through the inclined channels, with the slower settling fine particles continuing on through to the overflow. Faster settling large particles segregate onto the inclined plates and slide back down as concentrated sediment to the fluidized zone below. A “reflux” action develops which in turn produces a sharper separation.

The both full scale units were trialed in Vetovo processing plant for recovery kaolin from technological waste. The technological waste treatment flowsheet is presented in Figure 4.

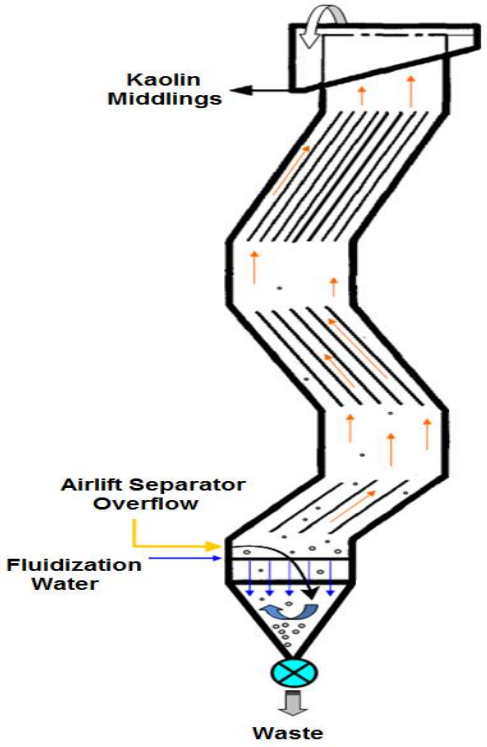

Figure 3. Schematic representation of the Reflux classifier

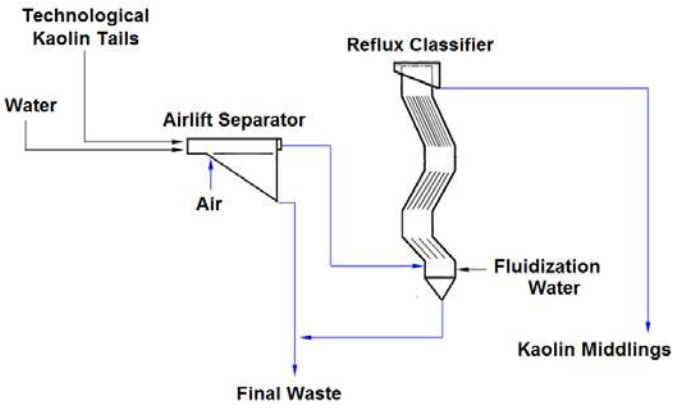

Figure 4. Two stages granulometric separation flowsheet.

The final tails are introduced into a hydraulic Airlift separator. The fine particles are dragged into the boundary layers of the rising air bubbles and have been separated as an independent product – overflow. This product is fed to the Reflux classifier where the fine particles are extracted as an overflow – kaolin middlings. The both underflows from Airlift separator and Reflux classifier were combined as final technological waste.

The pilot plant tests were carried out under the following conditions:

- Tailings slurry capacity – 21.15 m^3/h;
- Solids Mass Flow – 3.79 t/h;

The influence of the following variables is studied:

- Pressure air, bar;
- Ratio Overflow: Underflow of Airlift separator, %;
- Fluidization water, m^3/h;
- Ratio Overflow: Underflow of Reflux classifier, %.

3 RESULTS AND DISCUSSION

3.1 Hydraulic Airlift Classification Laboratory Tests

The results obtained in the laboratory experiments with glass micro spheres are presented in Figure 5. The dependence of recovery (mass yield of upper layer product) on particle size shows that mainly particles finer than 5 μm are extracted.

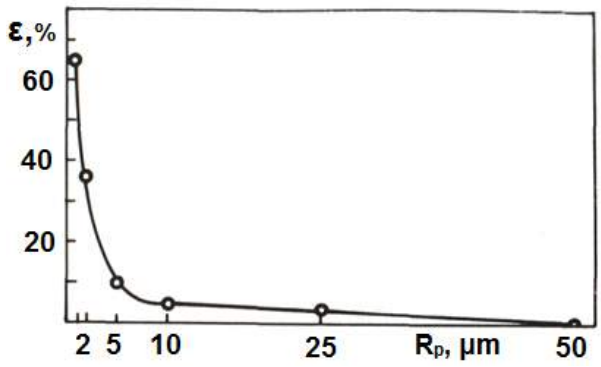

Figure 5. Dependence of recovery on particle size.

The theoretically calculated residence times for particles of various sizes in the boundary layer of a bubble of radius P_b = 250 μm are in good agreement with the experimental results (Grigorova & Nishkov 2008). Fine particles of sizes below *5* μm are mainly extracted in the upper layer product because their residence times are much greater than those for larger particles.

3.2 Steady-state Particle Classification Laboratory Tests

The results obtained in the laboratory experiments with single-channel inclined settler are presented in Figure 6. The cumulative size distributions of the particles in the feed, underflow and overflow streams for steady-state particle classification experiment are shown.

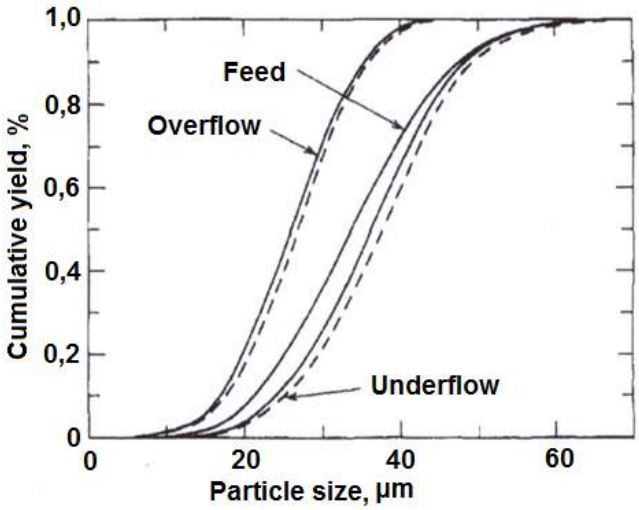

Figure 6. Cumulative size distribution of particles in the feed, underflow, and overflow steams for steady-state particle classification.

It is clear that a classification of particles by size was achieved; the overflow distribution is devoid of the larger particles, whereas the underflow distribution has a significantly reduced fraction of smaller particles.

3.3 Technological Kaolin Tails Characterization

The data from particle size distribution and chemical composition of final technological tails are presented in Table 1.

The performed analyses clearly demonstrate that the final kaolin tails is fine product – fewer than 56 μm. There are some losses of kaolin in final tails. The content of Al_2O_3 is in the frame of 6 - 9 %.

Table 1. Tails characterization data.

Parameters	Feed capacity, (100 t/h)			Feed capacity, (150 t/h)		
	Fraction under 100 µm, 96.47 %	Fraction under 45 µm, 60.58 %	Fraction under 25 µm, 45.01 %	Fraction under 100 µm, 96.61 %	Fraction under 45 µm, 67.92 %	Fraction under 25 µm, 52.88 %
Chemical composition, %						
SiO_2	89.40	81.18	77.54	85.50	80.56	76.50
Al_2O_3	6.70	12.52	14.80	9.49	13.03	15.43
Fe_2O_3	0.39	0.56	0.63	0.57	0.66	0.80
TiO_2	0.25	0.30	0.31	0.26	0.30	0.32
CaO	0.12	0.20	0.20	0.13	0.16	0.20
MgO	0.12	0.14	0.18	0.13	0.16	0.19
K_2O	0.47	0.58	0.66	0.56	0.60	0.69
Na_2O	0.076	0.081	0.090	0.087	0.092	0.10
L.o.i	2.45	4.15	5.24	3.23	4.42	5.54
Particle size distribution, %						
< 100 µm	100.0			100.0		
< 63 µm	93.3			96.9		
< 56 µm	88.5	100.0		94.0		
< 45 µm	77.8	99.9		86.7	100.0	
< 32 µm	60.1	91.3	98.7	71.6	92.7	99.3
< 25 µm	48.5	78.9	93.4	60.4	81.4	95.1
< 20 µm	39.5	66.5	82.9	50.4	68.7	85.3
< 10 µm	20.1	34.7	44.8	25.8	35.6	47.5
< 7 µm	15.8	27.6	35.0	19.8	28.2	36.7
< 5 µm	13.3	23.9	30.4	16.8	23.9	31.4
< 2 µm	10.4	17.2	21.4	12.3	16.9	21.6
< 1 µm	8.6	13.4	16.8	10.5	13.1	17.0
< 0.5 µm	5.5	10.2	12.2	7.7	10.2	11.8

3.4 Pilot Plant Trial

The results obtained in the pilot plant experiments with two stages granulometric separation are presented on Table 2 and 3.

The data clearly demonstrate that a classification of particles by size in laminar flow is achieved. The content of Al_2O_3 in overflow of Reflux classifier increases more than 2.3 times.

Table 2. Pilot plant trial data.

Airlift separator				
Pressure air, bar	Feed	Underflow	Overflow	Ratio Overflow: Underflow, (%)
	Al_2O_3, (%)	Al_2O_3, (%)	Al_2O_3, (%)	
0.30	6.34	5.38	7.63	35:65
0.50	8.32	7.99	8.60	70:30
0.50	6.88	6.53	7.43	60:40
0.50	6.86	6.17	7.54	40:60
0.50	5.96	5.24	6.91	40:60
0.50	7.37	7.00	8.69	30:70
0.50	5.43	4.90	6.00	70:30
0.30	7.70	7.08	9.54	35:65
0.30	5.93	5.21	8.89	40:60
0.30	6.67	4.97	8.79	40:60
0.30	7.43	7.06	9.67	40:60
0.20	8.56	5.95	12.65	40:60
0.20	8.93	7.59	11.61	30:70
0.20	7.76	6.13	11.72	30:70
0.20	7.52	6.76	10.77	30:70
0.20	7.87	5.66	10.76	30:70
0.20	7.37	6.19	10.02	20:80
0.20	6.98	4.88	10.17	20:80
0.20	6.85	5.34	10.82	20:80
0.20	6.18	4.81	9.89	40:60
0.05	9.92	8.18	15.19	15:85
0.05	9.98	8.98	14.77	15:85
0.05	9.75	6.85	14.98	15:85
0.05	8.51	5.71	12.90	30:70
0.05	8.77	6.09	12.98	20:80
0.05	9.12	5.47	14.49	15:85
0.05	8.10	5.12	13.77	15:85

Table 3. Pilot plant trial data

Reflux Classifier				
Fluidization water, (m^3/h)	Feed - Overflow Airlift separator	Underflow	Kaolin middlings	Ratio Overflow: Underflow, (%)
	Al_2O_3, (%)	Al_2O_3, (%)	Al_2O_3, (%)	
2.00	7.63	5.11	13.50	40:60
3.00	8.60	7.88	9.32	60:40
3.00	7.43	6.23	8.40	60:40
3.00	7.54	6.80	7.90	60:40
3.00	6.91	6.12	7.00	70:30
3.00	8.69	6.34	12.64	40:60
3.00	6.45	6.23	6.60	50:50
2.00	9.54	7.06	12.50	45:55
2.00	8.89	6.13	14.87	40:60
2.00	8.79	6.31	14.30	40:60
2.00	9.67	6.76	15.48	30:70
1.00	12.65	10.17	17.86	30:70
1.00	11.61	8.24	18.60	20:80
1.00	11.72	8.08	17.58	30:70
1.00	10.77	7.53	16.55	30:70
1.00	10.76	7.49	16.99	30:70
1.00	10.02	7.11	16.77	20:80
1.00	10.17	7.32	17.06	20:80
1.00	10.82	6.95	17.31	20:80
1.00	9.89	7.77	16.03	20:80
0	15.19	13.88	18.30	30:70
0	14.77	9.60	18.61	30:70
0.30	14.98	9.43	21.44	15:85
0.20	12.90	8.21	19.34	15:85
0.20	12.98	8.13	19.06	20:80
0.30	14.49	10.14	21.55	15:85
0.30	13.77	9.50	19.24	15:85

4 CONCLUSIONS

The two stages granulometric separation with Airlift separator and Reflux classifier is a new approach on recovery of kaolin from technological waste. The content of Al_2O_3 increases from 6 – 9 % in technological waste to over 21 % in the final product – kaolin middlings.

REFERENCES

Derjaguin, B, Roulev, N, Dukhin, S, 1977. Vlyanie razmera tshastiz na heterokoagulyatzia v elementarnom act flotation, *Kolloidn. Jour.*, XXXIX (4), (pp. 680-691).

Derjaguin, B, Dukhin S, 1959. Teoria dvigenija mineralnih tshastiz vblizi bsplivaushevo puzirka v primeneaii k flotazii, *Izvestia Academy Science Russian*, 1, (pp. 82-83).

Gaudin, A, 1957. *Flotation*, McGraw-Hill, New York.

Grigorova, I, Nishkov, I, 2008. Granulametric separation of fine hydrophilic particles by suspension foaming. Proc. of XXI International Serbian Symposium on Mineral Processing, Serbia, (pp. 108-113).

Levich, V, 1962. *Physicochemical Hydrodynamics*, Chapt B, Engelwood Cliffs, Prentice-Hall.

Scheludko, A, Toshev, B, Bojadjiev, B, 1976. Attachment of particles to a liquid surface, *Jour. Chem. Soc*., Faraday Trans, 72 (I), (pp. 2815-28).

Wills, B, Tim Napier-Munn, 2006. *Mineral Processing Technology. An Introduction to the Practical Aspects of Ore Treatment and Mineral Recovery*. Elcevier Science & Technology Books.

Evaluation of Spiral Chromite Tailings of South Africa
Güney Afrika Spiral Kromit Artıklarının Değerlendirilmesi

Ş. B. Aydın, M. Özer, A.E. Yüce
Mineral Processing Engineering Department, Faculty of Mines, Istanbul Technical University, Istanbul, Turkey

ABSTRACT In this study, beneficiation of the spiral chromite tailings taken from South Africa, which contains 22.5% Cr_2O_3, were investigated by using combination of gravity units. Shaking table tests were carried out at size fractions such as -0.841+0.355 mm; -0.355+0.212 mm; -0.212+0.074 mm and Mozley table was used for -0.074 mm, however, appropriate results were not obtained in terms of acceptable concentrate and tailing grade. Therefore, original material was ground under 0.355 mm in size, fractioned and subjected to gravity separation tests. Gravity separation tests were carried out at size fraction between -0.355+0,150 mm, -0.150+0.074 mm by using shaking table and at -0.074 mm using Mozley table. According to the overall gravity concentration test results under 0.355 mm; 34.6 % of feeding material can be obtained as a chromite concentrate having 41.52% Cr_2O_3 grade with 62.0% metal recovery. Final tailings having 6.24% Cr_2O_3 content can be separated with a 7.8% metal losses. Since Cr_2O_3 concentrate content of 40-42% is found sufficient in line with company's demand, 41.52% of Cr_2O_3 content is determined as the optimum value.

Keywords: Chromite, tailing, evaluation

ÖZET Bu çalışmada, Güney Afrika'dan alınan % 22.5 Cr_2O_3 içerikli spiral devresinden elde edilen kromit artıklarının gravite cihazlarının kullanımı ile zenginleştirilmesi incelenmiştir. -0.841+0.355 mm, -0.355+0.212 mm ve -0.212+0.074 mm boyut gruplarında sarsıntılı masa, -0.074 mm boyut grubunda ise Mozley masası kullanılmıştır. Ancak kabul edilebilir konsantre ve artık tenörleri açısından uygun sonuçlar elde edilmemiştir. Bu sebeple, orijinal numune 0.355 mm boyut altına öğütülmüş, boyut gruplarına ayrılmış ve gravite ile ayırma deneylerine tabi tutulmuştur. Gravite ile ayırma deneyleri -0.355+0.150 mm, -0.150+0.074 mm boyut gruplarında sarsıntılı masa, -0.074 mm boyut grubunda ise using Mozley masası kullanılarak gerçekleştirilmiştir. 0.355 mm altı malzeme ile yapılan gravite deneylerine göre, beslenen malzemenin %34.6'sı, % 41.52 Cr_2O_3 içeriğine ve %62'lik metal kazanımına sahip bir kromit konsantresi olarak elde edilmiştir. 6.24% Cr_2O_3 içerikli artık, %7.8' lik metal kaybı ile ayrılabilmiştir. Firmanın talebi doğrultusunda, konsantrede %40-42 Cr_2O_3 içeriği yeterli bulunduğundan dolayı, %41.52 Cr_2O_3 içerikli konsantre optimum değer olarak belirlenmiştir.

Anahtar kelimeler: Kromit, atık, değerlendirme

1. INTRODUCTION

Chromite is found in peridotite from the Earth's mantle. It also occurs in layered mafic and ultramafic intrusive rocks which contain olivine, pyroxenes and plagioclase.

Chromite varies widely in composition according to the chemical formula (Mg, Fe^{+2}) (Cr, Al, Fe^{+3})$_2O_4$. Chromium occurs as chromium spinel, a complex mineral containing magnesium, iron, aluminium and chromium in varying proportions depending upon the deposit (Rama et al., 2011).

Chromite is an important mineral due to its usage as alloying materials such as ferrochromium, ferrosilicochromium, and chromium compounds in the metallurgical industry. However, ferrochromium, which is used in making stainless steel, is the most

significant usage area of chromite (Kogel et al., 2006).

Chromite ores are usually concentrated by gravity concentration techniques such as shaking table, jig, spiral, and Reichert cone based on differences in specific gravity between chromite and the common associating gangue minerals and rocks such as serpentine and olivine (Yuce et al., 1998; Cicek, 2002; Onal et al., 2003) Another reason for selection gravity concentration techniques is their simplicity, low operating cost and easy to operate. Therefore, after crushing and grinding, the shaking tables and spirals generally are the basic separation units at chromite plants (Guney et al., 2009)

South Africa, with 80% of world chrome reserves having about 3.1 billion tonnes and a further estimated resource of 5.5 billion tonnes, is one of the major producers of ferrochrome. South Africa produces 75% of the world's ferrochrome for the local and export markets. (Xiaowei, 2013; SSI Holdings, 2014).

In South Africa, chromite concentrating plants generally use gravity separation. For gravity separation, mainly spiral concentrators are preferred, although shaking tables are used in few instances.

In this study, the gravity concentrator tests were carried out using shaking table (Wilfley) and Mozley table in order to evaluate spiral chromite tailings of South Africa. According to the tests results, process flow sheet including material balance was established.

2. MATERIAL AND METHODS

The chromite tailings samples below 2 mm (particle size passing of 80%) used in this study were obtained from the spiral concentrator plant of South Africa. According to the chemical analysis, the sample contains 22.5% Cr_2O_3.

The gravity tests were performed for enrichment of chromite by using gravitational units such as shaking table and mozley table. Due to company's request, it is aimed that final concentrate grades are acceptable between 40-42% Cr_2O_3.

2.1 Gravity Tests with -0.841 mm in Size Material

Original material was ground to below 0.841 mm and size fractions such as -0.841+0.355 mm; -0.355+0.212 mm; -0.212+0.074 mm and -0.074 mm were subjected to the gravity separation tests.

Wilfley and Mozley table tests were carried out for the each particle size fraction. The combined test results are given on Table 1.

Table 1. The combined result of tests carried out below 0.841 mm in size

Product	Weight, %	Cr_2O_3, %	Recovery,%
Concentrate	29.3	41.62	53.9
Middlings	48.6	18.81	40.4
Tailings	22.2	5.73	5.6
Total	100.0	22.59	100.0

According to the overall gravity concentration test results below 0.841 mm; 29.3 % of feeding material can be obtained as a chromite concentrate having 41.62% Cr_2O_3 grade and 53.9 % metal recovery.

As a result of tests at minus 0.841 mm in size, it is seen that the chromite concentrate recoveries are not acceptable. Also, it is understood that the liberation size is not adequate due to the fact that the significant amount of chromite remains in middling. Therefore it was decided to ground the sample to minus 0.355 mm in order to obtain the optimum particle liberation and so increase chromite recovery.

2.2 Gravity Tests with -0.355 mm in Size Material

According to the gravity concentration test results, it was evaluated that the reason for lower concentrate grades are obviously related with liberation of the materials at that size fraction. Therefore, original material was ground to minus 0.355 mm in size,

fractioned and subjected to gravity based concentration tests.

Gravity concentration tests were carried out at size fraction between -0.355+0.150 mm, -0.150+0.074 mm by using shaking table and at -0.074 mm in size by using Mozley table.

Wilfley and Mozley table tests with the different size fraction were performed. The combined test results are given in Table 2.

Table 2. The combined results of tests carried out below 0.355 mm in size

Products	Weight %	Cr_2O_3 %	Recovery %	Cr/Fe ratio
Concentrate	34.7	41.52	62.0	1.347/1
Middlings	36.2	19.27	30.2	1.012/1
Tailing	29.1	6.24	7.8	0.628/1
Total	100.0	23.18	100.0	

It can be seen in Table 2 that 34.6 % of feeding material can be obtained as a chromite concentrate having 41.52% Cr_2O_3 grade and 62.0% metal recovery. Final tailings having 6.24% Cr_2O_3 content can be separated with a 7.8% metal losses.

As a result of tests at minus 0.355 mm, final chromite concentrate grades could not be increased more than 43% of Cr_2O_3 content. According to preliminary estimates; Cr/Fe ratio for chromite concentrates could not be increased more than 1.347/1 due to possible high iron content of concentrates.

2.3. Magnetic Separation Test

In order to investigate the reason of lower ratio of chromite concentrates, belt type high intensity dry magnetic separation test was conducted on concentrate (42.64% Cr_2O_3) obtained from -0.150+0.074 mm size fraction.

In magnetic separation tests; four different magnetic field magnitutes were installed between 0.5 amper (6000 gauss) and 3.5 amper (11.500 gauss). Test result is presented in Table 3.As can be seen from Table 3, there is no significant change for both chromite grades and ratios.

Table 3. Magnetic separation test results on chromite concentrate

Product	Weight, %	Cr_2O_3, %	Cr/Fe ratio
MP1 (0.5 A)	5.2	42.54	1.30/1
MP.2 (1.0A)	16.3	43.47	1.35/1
MP.3 (2.5A)	7.6	43.38	1.36/1
MP.4 (3.5A)	33.7	43.21	1.35/1
NMP (3.5A)	37.2	41.78	1.36/1
Total	100.0	42.70	

MP: Magnetic product; NMP: Non magnetic product

2.4. Development of Process Flow Sheet

According to final test results on ground material below 0.355 mm, process flow sheet including material balance was developed and given in Figure 1.

3. CONCLUSION

The beneficiation of spiral chromite tailings taken from South Africa which contains 22.5% Cr_2O_3, were investigated using combination of gravity units. Gravity concentration tests were conducted on ground samples below 0.841 mm and 0.355 mm separately. At minus 0.841 mm in size, 29.3 % of feeding material can be obtained as a chromite concentrate having 41.62% Cr_2O_3 content and 53.9% metal recovery while 22.2% of feeds can be separated as a tailings containing 5.73% Cr_2O_3. As a result of tests, quite high amount of middlings with a high grade chromite values shows that the ore need adequate liberation and further beneficiation. In order to increase of chromite content and to decresase of middling amount, second group gravity tests on minus 0.355 mm ground material were carried out. According to test results, 34.6% of feeding material can be obtained as a chromite concentrate having 41.52% Cr_2O_3 grade and 62.0% metal recovery. Final tailings having 6.24% Cr_2O_3 content can be separated with a 7.8% metal losses. In that point, it is seen that appropriate liberation size of chromites are still lesser than 0.3 mm in size.

According to preliminary estimates, Cr/Fe ratio for chromite concentrates could not be

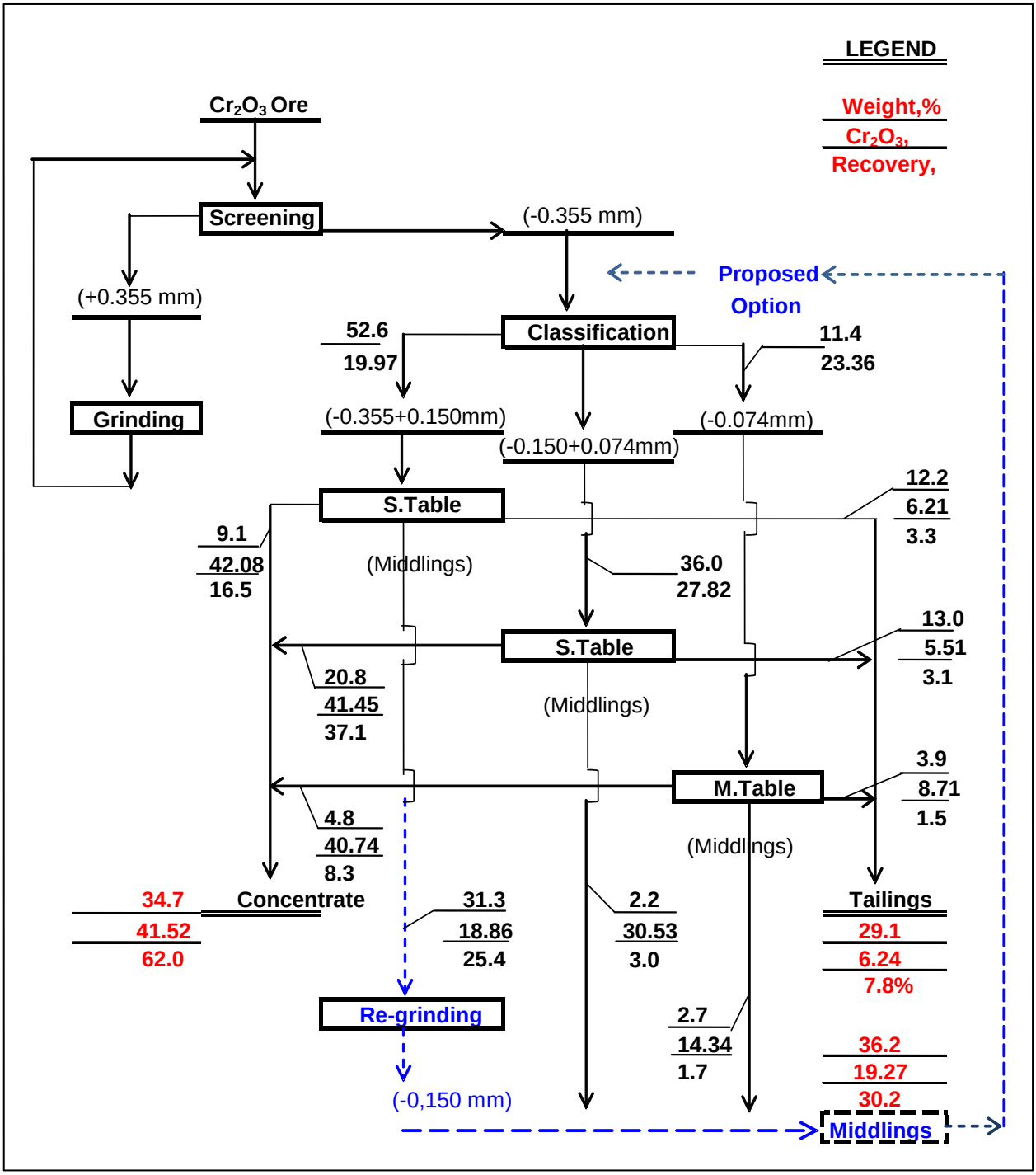

Figure 1. Process flow sheet for -0.355 mm

increased more than 1.347/1 due to possible high iron content of concentrates. Although the high intensity dry magnetic separation test is performed in order to investigate the reasons of lower Cr/Fe ratio, there are no significant changing both chromite grades and ratios.

REFERENCES

Cicek, T., Cöcen, I., 2002. Applicability of Mozley multigravity separator (MGS) fine chromite tailings of Turkish chromite concentrating plants. *Minerals Engineering*, Vol. 15, pp. 91-93.

Güney, A., Yüce A.E., Kangal M.O., Burat, F., Yüce, A. E., Güney,A., Önal, G., Girgin, Ş., Kangal, O., (1998), "*Final Tailings Disposal After Beneficiation of Chromite Fines Using New-age Seperator*", Proceedings of the Fifth International Symposium on Environmental Issues and Waste Management in Energy and Mineral Production - SWEMP 98, ISBN:90-5410-956-4, pp: 469-472, 18-20 May, Ankara-Turkey.

Kogel J.E, Trivedi N.C., Barker J.M., Krukoswki S.T.,2006. Industrial Minerals & Rocks, 7th

edition, Society for Mining, Metallurgy and Exploration, Littleton, Colorado

Kökkılıç, O., Gürkan, V., (2009), "*Beneficiation and process flow sheet development of chromite ores*", XIII. Balkan Mineral Processing Congress, Edts: S.Krausz, L.Ciobanu, N.Cristea, V. Ciocan, G.Cristea, ISBN: 978-973-677-159-0, Vol:1, pp:401-408, 14-17 June, Bucharest, Romania.

Önal, G., Güney, A.**,** Yüce, A.E., (2003), "*The beneficiation of chromite tailings by Multi-gravity separator*", Proceeding of the International Seminar on Mineral processing Technology MPT-2003, ISBN:81-7764-405-x, pp. 203-207, February, 6-8, Goa, India.

Rama Murthy Y., Kumar Tripathy S., Raghu Kumar C.,2011. Chrome ore beneficiation challenges & opportunities – A review, *Minerals Engineering*, 24, pp. 375-380.

SSI Holdings (Pty) Ltd, 2014. The South Africa Chrome Industry a Position Paper.

Xiaowei, P, 2013. Effect of South Africa Chrome Ores on Ferrochrome Production, *International Conference on Mining, Mineral Processing and Metallurgical Engineering*, pp.106-110, Johannesburg (South Africa).

Recovery of Silver From an Arsenical Silver Ore by Knelson Concentrator and Cyanide Leaching

O. Celep, P. Altınkaya, E.Y. Yazici, and H. Deveci
Hydromet B&PM Research Group, Department of Mining Engineering, Karadeniz Technical University, 61080, Trabzon

ABSTRACT In this study, the recovery of silver from an arsenical silver ore was investigated using a laboratory type Knelson Concentrator and cyanide leaching. Silver was found to be as acanthite, which occurs both as free grains and closely associated with other mineral phases such as quartz, barite, mica and the group of clay minerals. Gravity tests have demonstrated that the silver recovery tends to increase with increasing the rotation speed of bowl or decreasing the fluidizing water velocity. About 30% of the silver was recovered into a concentrate assaying 275 g/t Ag. Cyanide leaching tests have revealed that the silver extraction substantially improved from 60% up to 85% in cyanidation after ultra-fine grinding of the ore to <8 μm (d_{80}). These findings indicate that the ore is not particularly amenable to centrifugal gravity separation. It can be also deduced from cyanide leaching tests that the refractoriness of the ore is essentially physical in character apparently due to the physical encapsulation of silver phases.

Keywords: Arsenical silver, cyanide leaching, silver recovery

1 INTRODUCTION

Extraction of gold and silver from ores can be traditionally achieved using cyanidation method while gravity separation can be also used to recover free and coarse gold/silver particles (La Brooy et al., 1994; Marsden and House, 2006). Gravity separation can be utilized as an option with the possibility of maximizing the net smelter return and improving the overall precious metal recovery. Centrifugal gravity separators have been recently developed to recover even fine gold particles in the gold milling practice (Huang and Mejiab, 2005; Laplante and Nickoletopoulos, 2005).

In centrifugal separators, the application of centrifugal force allows effective capture of fine heavy minerals/metals. The centrifugal force acting on a particle can be equal to or even higher than 50 times the force of gravity. The size of particles that can be recovered becomes finer as the intensity of centrifugal forces generated is increased (Liu et al., 2006). The centrifugal force (Fc) in a centrifugal concentrator can be expressed as (Celep et al., 2006; Alp et al., 2008):

$$Fc = \left(\frac{\pi}{6}\right)(d_p)^3.(\delta_s - \delta_l).\vec{r}.\omega^2$$

Where ‘r’ is the displacement of the moving particle from the rotation axis to its present position, ‘dp’ is the diameter of the particle, ‘δ_s’ is density of the particle, ‘δ_l’is the density of the medium and ‘ω’ is the angular velocity of the particle (Huang, 1996).

The Knelson Concentrator is considered as essentially a hindered settling device with the application of a centrifugal force on particles instead of gravity force. Concentrator consists mainly of a rotating ribbed cone (bowl) and retention zones between the ribs where heavy concentrate is retained (Figure 1). Ore slurry is fed through a central feeding tube to the bottom of the cone and is dispersed outwards by the action of centrifugal force. Heavy (or large) particles are trapped in the retention zone between the ribs while the light particles (or fine particles) are washed away upward into the

tailings stream. Injection of water through small holes located in the retention zones leads to formation of a fluidized and penetrable concentrate bed consisting of heavier particles (Figure 1). The Knelson Concentrator has been successfully applied in the recovery of gold, platinum silver, mercury and native copper (http://www.flsmidth.com) (Figure 2).

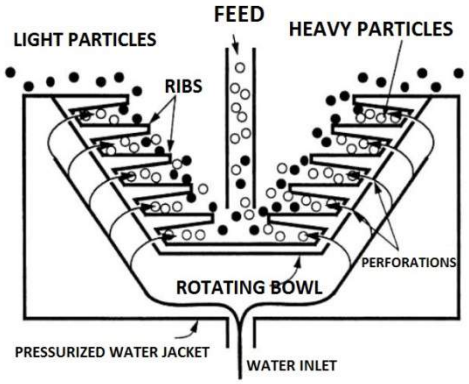

Figure 1. Schematic illustration of a Knelson Concentrator (Kawatra and Eisele, 2001)

In this study, the recovery of silver from an arsenical silver ore was investigated using a laboratory batch type Knelson Concentrator (KC-MD3). In experiments, the effects of fluidizing water pressure and rotation speed was investigated on silver recovery. Furthermore, cyanide leaching of the ore was also studied and effect of fine grinding on silver recovery in cyanide leaching was demonstrated.

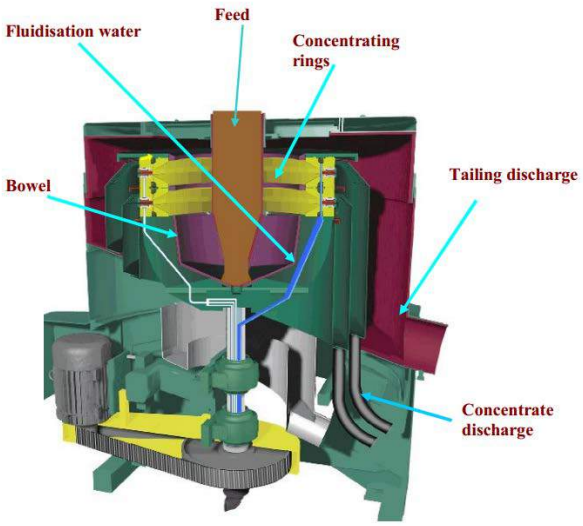

Figure 2. View of Continuous Knelson Concentrator (http://www.flsmidth.com).

2 MATERIAL AND METHOD

In this study, an arsenical silver ore (Turkey) were used. The ore sample was prepared for the experiments by crushing in a jaw crusher (-4 mm) and ground down to 106 µm in a rod mill at 50% pulp density (Figure 3). The chemical composition of the ore sample (Table 1) was determined using ICP-ES (Inductively Coupled Plasma-Emission Spectroscopy) after four acid digestion, fire assay fusion and X-ray fluoressans (XRF). Silver content of the ore was determined by fire assay method with a gravimetric finish. The ore contains 63.7% SiO_2, 11.7% Al_2O_3, 1.31% As and 127 g/t Ag.

Detailed mineralogical characterization of the ore sample with particular reference to the mode and occurrence of silver was also performed. The ground ore sample was split using a Quantachrome Mini-riffler to obtain representative sub-samples, which were used to prepare a number of resin mounts. Polished mounts were examined for MLA using an FEI Quanta 600F scanning electron microscope (SEM).

Table 1. Chemical composition of the ore sample used in the study

Compound	Content (%)	Element	Content (g/t)
SiO_2	63.7	Ag	127
Al_2O_3	11.7	As	1.31%
$BaSO_4$	5.5	Zn	7182
Fe_2O_3	5.19	Pb	7252
CaO	0.73	Sr	491
MgO	0.69	Sb	699
Na_2O	0.2	Ni	245
K_2O	4.14	V	86
TiO_2	0.47	Zr	148
P_2O_5	0.16	U	8
MnO	0.2	Cd	103
Cr_2O_3	0.068	Ga	13
Tot. S	0.99	Tot. C	0.21
LOI	7		

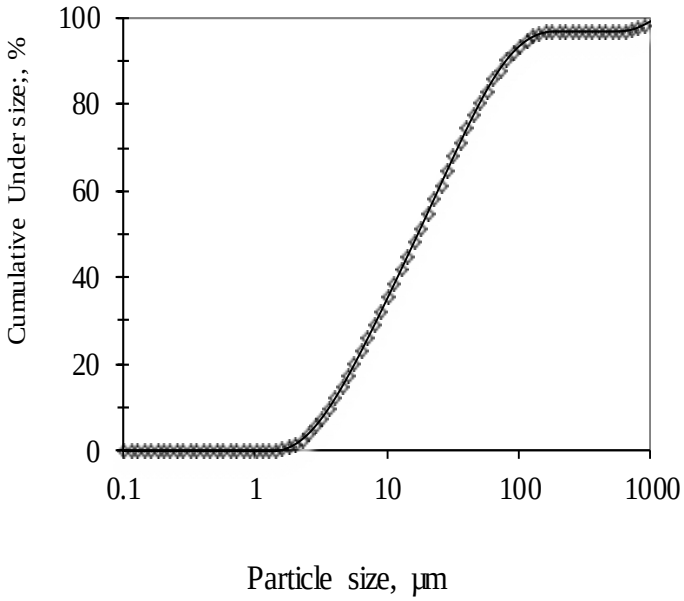

Figure 3. Particle size distribution of the ore sample used in gravity tests and in ultra-fine grinding

Ultra-fine grinding of the ore before cyanide leaching was conducted using 2 mm ceramic ball in a laboratory scale pin-type vertical stirred at 26%w/w solid-liquid ratio and 600 rpm stirring rate. The particle size analysis of sample was performed using the laser diffraction method by Malvern Mastersizer 2000 MU.

The ground ore samples (-106 µm) were subjected to Knelson gravity separation. The experiments were carried out using a laboratory batch type Knelson Concentrator (KC-MD3) (Figure 4). The operating conditions of Knelson Concentrator for the recovery of silver from the ore are presented at Table 2.

Table 2. Experimental conditions

Parameters	Unit	Value
Pulp density	%	6
Water flowrate	L/min.	1-3-5
Rotation Speed	rpm	500-1250-2000
Particle size	µm	106

Bowl rotation speed [500 rpm (11.2 G-force), 1200 rpm (28 G-force), 1500 rpm (100 G-force) and 2000 rpm (179 G-force)] and fluidizing water velocity (1 L/min., 3 L/min. and 5 L/min.) were investigated as parameters. Feed pulp was prepared at ≈6% solids by weight in volume of 500 mL. Agitation of pulp was performed using IKA RW-20 type overhead stirrer equipped with a 45° pitched blade turbine (four blade, 50 mm in diameter) for 15 min. The dispersed slurry was fed to the Knelson Concentrator at a rate of 15 g/min. Overflow (tailings) was collected in a bucket while concentrate remained in the bowl. The bowl content (i.e. the concentrate) and tailings were washed into beakers. After dewatering, the products were dried and weighed. Products were digested with aqua regia and analyzed for silver using Atomic Absorption Spectrometer (Perkin Elmer-AAS 400).

Figure 4. A photograph of Knelson Concentrator used in experiments

The cyanide leaching tests (1.5 g/L NaCN, 0.3 L/min air) were conducted in overhead-stirred glass reactors over a period of 24 h. The concentration of NaCN in solution was monitored by silver nitrate titration (0.02 mol/L $AgNO_3$) using p–dimethylamino–benzal–rhodanine (0.02% w/w in acetone) as the indicator. Sodium cyanide was added, if

required, to maintain the concentration of titratable NaCN at the predetermined level (1.5 g/L) over the leaching period. The consumption of cyanide was determined. pH was controlled at ≅10.5 by the addition of 1 M NaOH. Pulp (25% w/w) was stirred at 450 rpm.

3 RESULTS AND DISCUSSION

3.1 Mineralogical characterization

The mineralogical analysis indicated that the ore is composed of mainly quartz, barite, mica and the group of clay minerals. Silver (127 g/t) was found to be present mainly as acanthite, which occurs both as free grains (57 wt %) and closely associated with and/or encapsulated in other mineral phases that can restrict the contact of cyanide with silver (Figure 5).

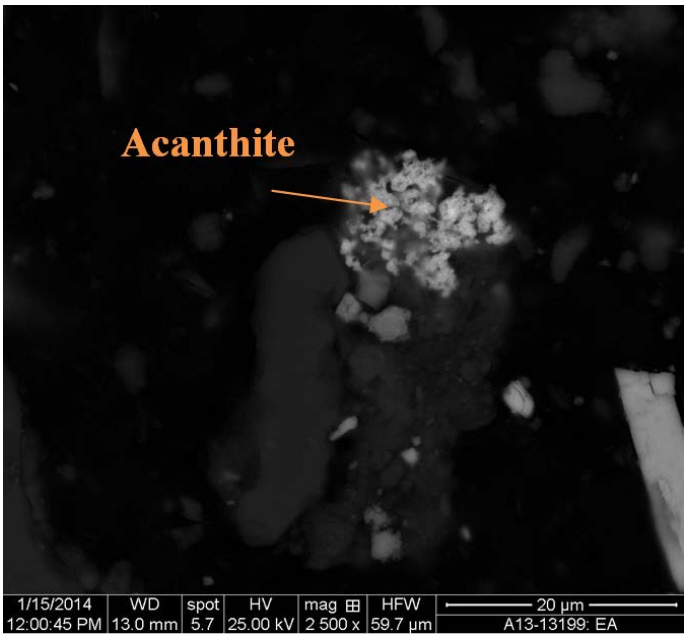

Figure 5. An acanthite grain in a particle that is composed of quartz, K-feldspar, Pb-Fe illite and muscovite

3.2 Gravity Recovery of Silver From Ore using a Knelson Concentrator

The silver recovery appears to increase with increasing the rotational speed of bowl or decreasing the fluidizing water velocity (Figure 6). Silver recovery was determined to be 30% into a concentrate that assayed 275 g/t Ag at 500 rpm rotation speed and 3L/min. fluidizing water velocity(Figures 6 and 7). Increasing bowl speed and flowrate of fluidization water improved silver recovery at the expense of reduced separation efficiency (e.g. 58.4% recovery, 150.6 g/t Ag grade and 10.1% mass yield at 2000 rpm bowl speed and 5 L/min fluidized water). High bowl speeds allows the recovery of even fine heavy particles. Increasing the flowrate of fluidizing water leads to the cleaning of concentrate in the retention zone.

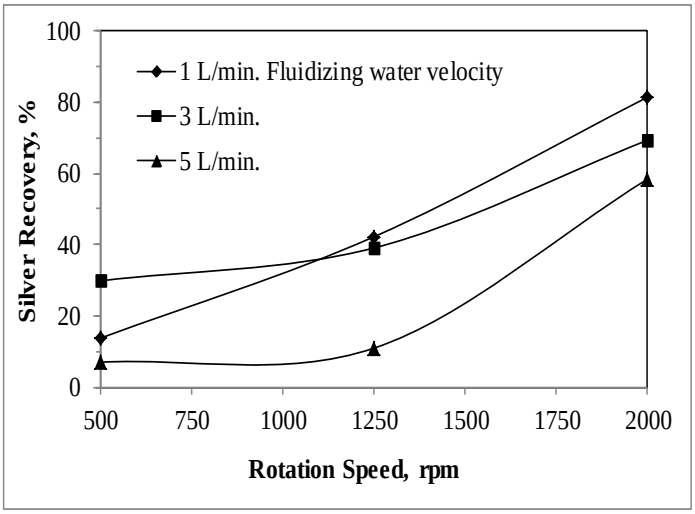

Figure 6. Effects of rotation speed and fluidizing water velocity on silver recovery

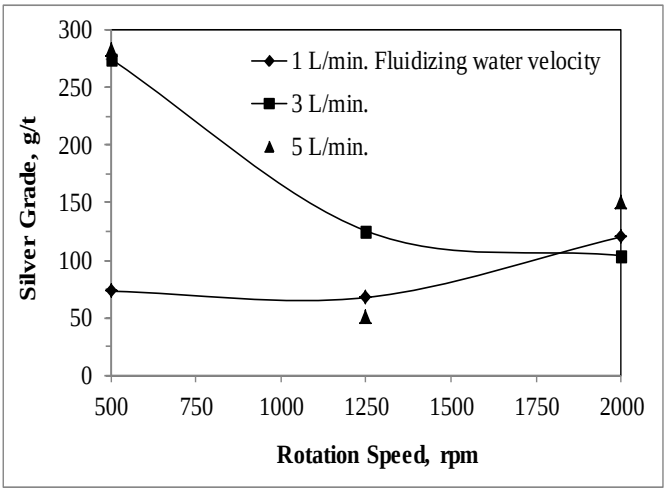

Figure 7. Effects of rotation speed and fluidizing water velocity on silver grade

3.3 Cyanidation of the ore

Effect of fineness of grind on silver extractions is shown in Figure 8. Silver extraction was observed to improve from 60% to 71% when the particle size was

decreased from 200 µm to 50 µm (d80) by conventional grinding. Similarly, silver extraction increased up to 85% after ultra-fine grinding of the ore down to 8 µm (d80) in the stirred mill. This enhancement in the level of silver extraction was attributed to the increased availability of silver for cyanide leaching. These findings also suggest that ultra–fine grinding is an appropriate pre–treatment method for the ore ahead of cyanide leaching. It can be also deduced that the refractoriness of the ore to cyanide leaching is partially physical in nature.

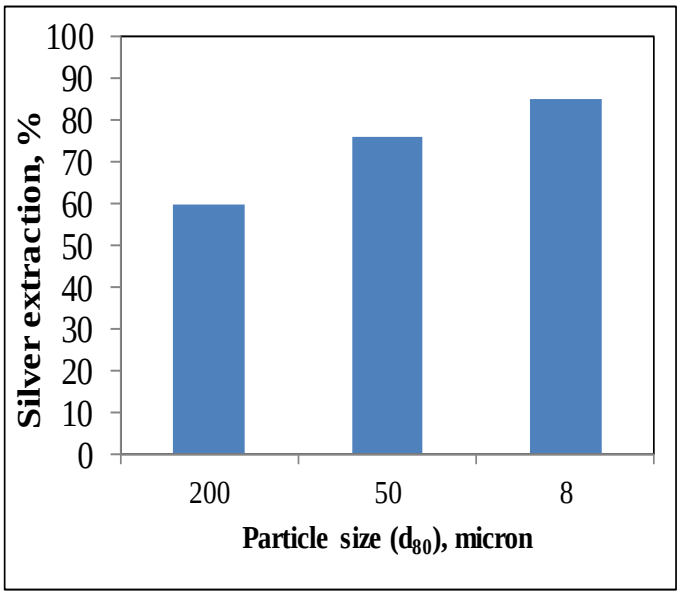

Figure 8. Extraction of silver from direct cyanidation of the ground ore (d_{80}: 50 µm and 200 µm) and after ultra-fine grinding (d_{80}: 8 µm)

4 CONCLUSIONS

In this study, the amenability of an arsenical silver ore to centrifugal gravity separation and cyanide leaching was demonstrated. Acanthite appears to be the main silver phase and occurs both as free grains and closely associated with and/or encapsulated in other mineral phases such as quartz, barite, mica and the group of clay minerals. Gravity separation tests have shown that bowl speed and fluidizing water flowrate are significant parameters affecting the recovery and grade. However, the findings suggest that the ore is not amenable to the gravity separation as indicated by low separation efficiency. Cyanide leaching tests have also revealed that silver extraction improves with decreasing the particle size of the ore apparently due to the increased availability of silver phases for cyanide. This indicates physical nature of refractoriness of the ore.

ACKNOWLEDGEMENTS

The authors would like to express their sincere thanks and appreciation to the Research Foundation of Karadeniz Technical University (Project No: 9200) and TUBITAK (Project No: 213M539) for the financial support and to Yıldızlar Holding for kindly providing the samples.

REFERENCES

Alp, İ., Celep, O., Deveci, H., Vıcıl, M., 2008. Recovery of gold from a free-milling ore by centrifugal gravity separator, Iranian Journal of Science & Technology, Transaction B, Engineering, 32, B1, 67–71.

Celep, O., Alp, İ., Deveci, H., Vıcıl, M., Yılmaz, T., 2006. Gold Recovery From Mastra (Gümüşhane) Ore Using Knelson Centrifugal Separator), İstanbul University Earth-Sciences Journal, 19, 2, 175–182. (in Turkish)

Huang, L., 1996. Upgrading of gold gravity concentrates a study of the Knelson Concentrator, PhD., Department of Mining and Metallurgical Engineering, McGill University, Montreal.

Huang, L., Mejiab N., 2005. Characterizing gravity recoverable pgms and gold in grinding circuit, Iranian Journal of Science & Technology, Transaction B, 29, B6, 587-596.

Kawatra, S.K., Eisele, T.C. 2001. Coal Desulphurization, High-Efficiency Preparation Methods, First ed., Tylor&Francis Inc., New York.

La Brooy, S.R, Linge, H.G, Walker, G.S., 1994. Review of gold extraction from ores, Minerals Engineering, 10, 1213-1241.

Laplante, A.R., Nickoletopoulos, N., 1996. Validation of a Falcon model with a syntetic ore, Canadian Metallurgical Quarterly, 36, 7-13.

Liu Q, Cui Z, Etsell T H., 2006. Pre-concentration and residual bitumen removal from athabasca oilsand froth treatment tailings by a Falcon centrifugal concentrator, International Journal of Mineral Processing, 78, 220-230.

URL: http://www.flsmidth.com

Effect of Hot Water Absorption on the Flexural Properties of Jute Mat Fiber Reinforced Polymer Matrix Composites

E. A. Elbadry
Mining and Metallurgical Engineering Department, Faculty of Engineering, Assiut University, Assiut 71515, Egypt

ABSTRACT Recycled needle punched natural jute fiber mats with 32 % by vol. fiber volume content were used as reinforcement for unsaturated polyester matrix composites. This study intended to study the durability of jute mat composites by investigating the flexural properties of jute mat composites including flexural strength and modulus under the effect of hot water absorption at 100oC for 96, 192, 384 h immersion times compared to the virgin specimens. The results showed that as the immersion time of the composites increases, the water absorbed by the composites increases and so the thickness swelling increases. As a result of that, the flexural strength and modulus of jute mats composites decrease compared to the virgin specimens. On the other hand, when the immersed specimens are dried for 6 hours, the flexural strength and modulus of the composites was recovered compared to the immersed specimens due to the decrease in the absorbed water content.

Keywords: Jute mat composites; Flexural properties; Water absorption; Swelling; Interface.

1 INTRODUCTION

Natural fiber composites are nowadays widely used instead of synthetic fibers due to their advantages like biodegradability, low weight, low cost and high specific mechanical properties, however the incompatibility with the hydrophobic polymer matrices and poor resistance to moisture absorption reduce significantly the mechanical properties of the natural fibers reinforced composite materials [1-5].

However, because of the hydrophilic nature of the fiber, the use of natural fiber reinforced composites requires to know their behavior in a wet environment including water and other chemical solutions. Research investigations showed that the exposure of vegetal fiber composites in a wet environment leads to a decrease of the mechanical properties when subjected to wet environment. Studies of the water absorption on the different mechanical properties of some natural fibers such as jute, palm, bamboo, flax, kenaf, and hemp composites have been reported in the literature [6–12].

Natural fiber composites can be used in indoor and outdoor applications and as a result of those natural fiber composites may be subjected to water, therefore the study of the effect of water on the mechanical properties of the composites became very urgent. In this work, the flexural properties of jute mat composites including flexural strength and modulus will be investigated in terms of hot water absorption and thickness swelling of the composites.

2 EXPERIMENTAL ROCEDURE

2.1 Materials

Jute fiber mats consisting of 50% jute slivers and 50% recycled jute were prepared by Yano Co.LTD, Japan with three jute mats layers with 32 % by vol. fiber volume content. Unsaturated polyester, RigoracTM was obtained from Showa Denko K.K., Japan and the curing agent is Methyl ethyl ketone peroxide (PERMEK® N) obtained from NOF Corporation, Japan.

2.2 Preparation of the Composites

Jute mats were dried for 6 h at 1000^{o} C and were completely submerged in unsaturated

polyester resin. The next step which differentiates the modified technique over the conventional technique is that the jute mats were degassed in a vacuum for 20 minutes at room temperature to remove the entrapped air bubbles and the details were mentioned in [13]. Sheets were prepared with 32 % by vol. fiber volume content and the specimens of required dimensions were cut from the sheets and used for testing.

2.3 Mechanical Characterization

2.3.1 Hot water absorption of the composites

Hot water absorption test of the composites was carried out by immersing the test sample in hot water in boiler at 100°C for 0, 96, 192, and 384 hours. After immersion, the specimens were taken out from the water and all surface water was removed with a clean dry cloth. The specimens were reweighed by sensitive digital balance. The moisture absorption was calculated by the weight difference. The percentage weight gain of the samples was measured at different time intervals and the moisture content and the weight excess versus the time was plotted. Six samples were selected for each time interval and three specimens were dried in a drying oven at 100°C and the other three specimens were lifted without drying. These specimens with and without drying were then tested under three point bending test for each case.

2.3.2 Three point bending test of the composites

Three-point bending test was also done using the same machine according to ASTM D 790-03 at a crosshead speed of 1mm/min. with sample dimensions of 140×18×6 mm and the span to depth ratio was 16:1 and three testing specimens were prepared for different cases and for the virgin specimens.

3 EXPERIMENTAL PROCEDURE

3.1 Hot Water Absorption Of The Composite

Water absorption of the composites after immersion in hot water at a specific time can be calculated by the following equation:

$$\Delta W(t) = \frac{w_t - w_o}{w_o} \times 100 \qquad (1)$$

Where $\Delta W(t)$ is the water absorption of the composites and w_t, w_o are the weight of the samples after immersion in hot water at time t and before immersion, respectively.

In order to show the water diffusion in jute mat composites, water absorption of the composites in terms of weight gain versus square root of soaking time is illustrated in Fig. 1. It can be observed that the weight of the composites increases as the time of immersion increases due to the increase of the water absorbed by the composites as shown in Fig. 1. Moreover, water sorption behavior of jute mat composites at 100oC displayed a pseudo-fickian behavior where a saturated moisture level had not been attained at the end of the 16 days aging period and initial uptake is rapid and characterized by linear dependency on square root of immersion time ($t^{1/2}$) followed by a slow approach to final true equilibrium, as shown in Fig. 1.

On the other hand, when the immersed specimens are dried for 6 h, the water absorbed by the composites was significantly decreased compared to the immersed specimens without drying as was shown in Fig. 1.

A plausible cause is that internal degradation of jute fiber and jute fiber-matrix interface continues to occur with soaking time. As the immersion time of the composites in hot water increases, the water absorbed by the composites increases and therefore this will have a high significant effect on internal degradation of jute fiber and jute fiber-matrix interface.

The resistance to absorb the water by these jute mat-unsaturated polyester composites is higher compared to that of hemp-unsaturated

polyester composites of the same nearly volume fraction prepared by [7] which hemp-unsaturated polyester composites reaches the same water absorption faster than jute mat-unsaturated polyester composites.

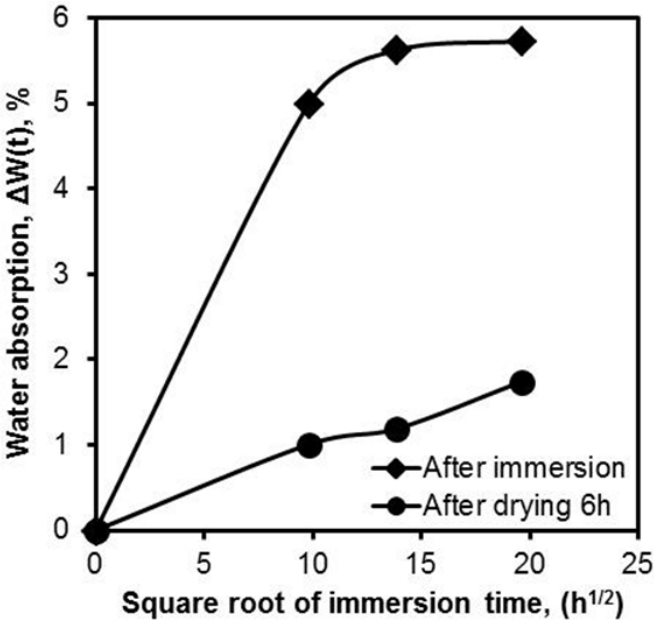

Figure 1. Water absorption at 100°C of jute fiber mats composites.

3.2 Changes Of Flexural Properties By Aging

$$\sigma_f = \frac{3PL}{2bd^2} \quad (2)$$

Where P is the load (N), L is the length of support span (mm), b is the specimen width (mm), and d is the specimen thickness (mm). The flexural modulus (E_f) was calculated using:

$$E_f = \frac{L^3 m}{4bd^3} \quad (3)$$

Where m is the slope of the initial straight line portion of the load-deflection curve.

According to Eldadry et al. [13] the flexural strength and modulus of Jute mat composites was improved at 32 % by vol. As a result of that the test of hot water absorption was carried out for the jute mat composites at 32 % by vol. to determine the mechanical efficiency of these composites when subjecting to hot water.

Stress-displacement curves of jute mat composites after immersion in hot water for different time of immersion compared to those of virgin composites are shown in Fig. 2.

It can be observed that all composites at different times of immersion exhibit the linear response and as the time of immersion increases, the flexural strength and modulus decrease compared to the virgin specimen are shown in Figure 2.

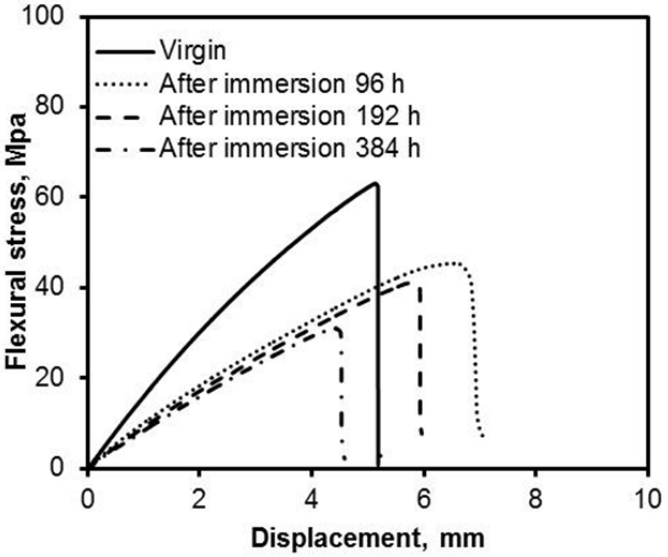

Figure 2. Stress-displacement curves of jute mats fiber composites after immersion for different immersion times.

On the other hand, Stress-displacement curves of immersed jute mat composites after drying for 6 hours compared to virgin composites are shown in Fig. 3. It can be observed that the same behavior as immersed specimens but the flexural strength and modulus were enhanced compared to those of immersed specimens as shown in Figure 3 compared to Figure 2.

Degradation of mechanical properties of jute mat composites depend on the amount of water uptake, soaking time, and temperature at which aging is carried out. The effect of immersion time on the flexural strength and modulus of jute mat composites compared to virgin specimen is displayed in Fig. 4 and 5, respectively. It can be observed that flexural properties decrease after water immersion which can be related to the weak fiber–matrix interface due to water absorption.

It can also be observed that the strength of the composites decreases when the composites were immersed in hot water for different immersion times compared to that of the virgin specimen as shown in Fig. 4. On the other hand, when the immersed specimens are dried for 6 hours, the strength of the composites was slightly recovered compared to the immersed specimens due to the decrease in the absorbed water content as was shown in Figure 1.

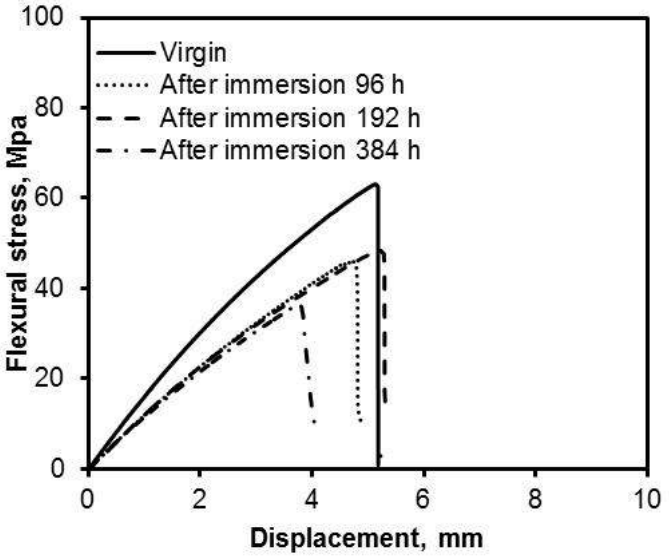

Figure 3. Stress-Displacement Curves Of The Immersed Jute Mats Fiber Composites After Drying For 6 H At 100^{o}c.

The effect of immersion time on the flexural modulus of jute mat composites compared to virgin specimen is displayed in Figure 5. It can be observed that the flexural modulus of the composites decreases compared to that of the virgin specimen when the composites were immersed in hot water for different immersion times as shown in Figure 5.

Moreover, as the time of immersion increases, the modulus of the composites has significantly decreased due to the higher absorption of hot water by the composites with longer immersion times as was shown in Figure 1. On the other hand, when the immersed specimens are dried for 6 hour, the modulus of the composites was recovered compared to the immersed specimens due to the decrease in the absorbed water content as was shown in Figure 5.

The thickness swelling of the composites after immersion in hot water at a specific time can be calculated by the following equations:

$$\Delta S(t) = \frac{s_t - s_o}{s_o} \times 100 \qquad (4)$$

Where ΔS(t) is the thickness swelling of the composites and s_t, s_o are the thickness of the samples after immersion in hot water at time t and before immersion, respectively.

The swelling of the composites as a result of hot water absorption versus square root of soaking time is illustrated in Figure 6. It can be observed that the swelling of the composites increases as the time of immersion increases due to the increase of the water absorbed by the composites.

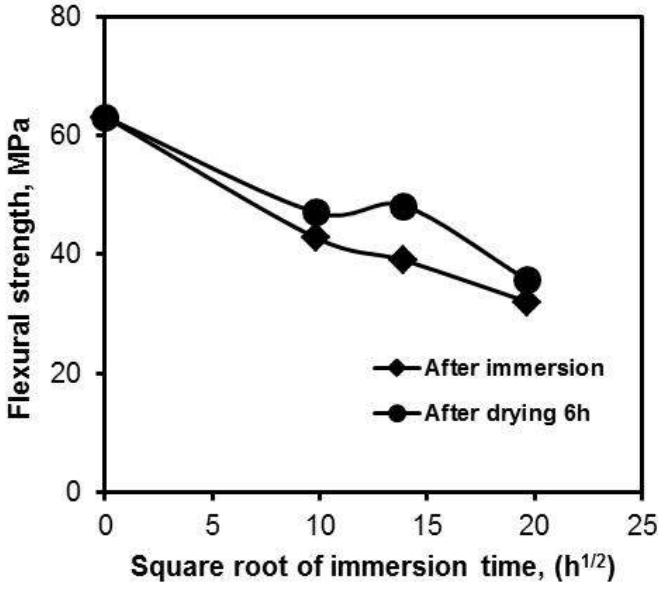

Figure 4. The effect of the immersion time on the flexural strength of jute fiber mats composites.

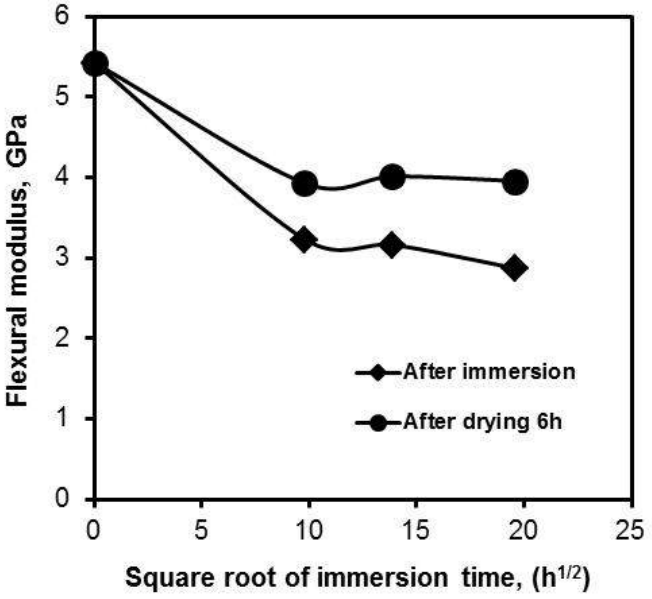

Figure 5. The effect of the immersion time on the flexural modulus of jute fiber mats composites.

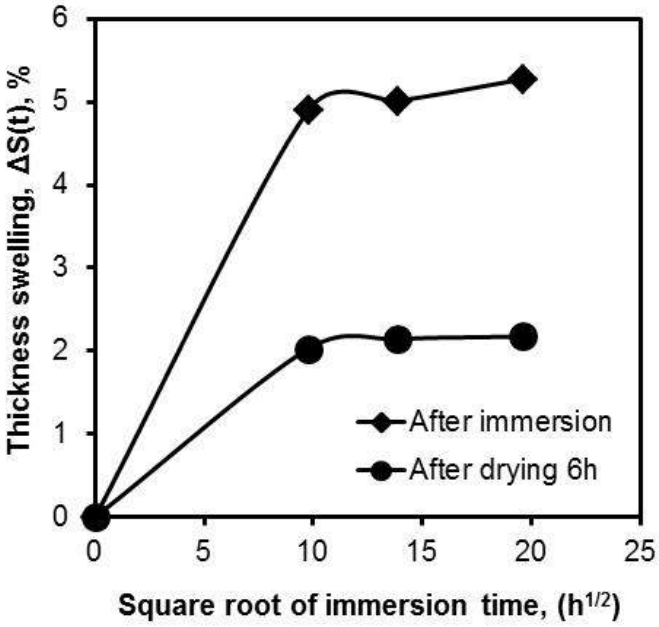

Figure 6. Thickness swelling of jute fiber mats composites.

The composite swelling of these jute mat reinforced polyester composites is lower than as that of jute and palm reinforced epoxy composites as reported by [9]. On the other hand, when the immersed specimens are dried for 6 h, the swelling of the composites was significantly decreased from around 2% to about 5% compared to the immersed specimens due to the decrease in the absorbed water content as was shown in Fig. 6.

The way in which the material absorbs water depends on many parameters, such as hygrometric rate, temperature, fiber fraction, fiber nature, porosity fraction, reinforcement geometry, matrix type. The transport of water can be facilitated by its diffusion inside the resin, by the presence of defects within the matrix, formed during the compounding process (micro-space, pores or cracks) or by capillarity along interfaces which present some defects between the fibers and the resin [14]. As the composite cracks and gets damaged, capillarity and transport via micro cracks become active. The capillarity mechanism involves the flow of water molecules along fiber–matrix interfaces and a process of diffusion through the bulk matrix. The water molecules are actively attack the interface, resulting in debonding of the fiber and the matrix [8].

The high cellulose content in jute fiber further contributes to absorb high amount of water and therefore, more water penetrating into the interface and the high water temperature enhance the dissolution of jute components which leads to a weak interfacial bonding between the fiber and the matrix and so this will lead to degradation of the flexural properties. Moreover, Differences in both thermal and moisture expansion coefficients of fibers and matrix also contribute to progressive debonding and therefore this will contribute in the weakening of the composites.

To understand deeply the detrimental effects of water on mechanical properties of the composite, the future work study may be concerned to study the effect on the constituents of the composites, the fiber, the matrix, and the fiber/matrix interphase region through microstructure examination at different immersion times.

4 CONCLUSIONS

The results showed that as the immersion time of the composites increases, the water absorbed by the composites increases and so the thickness swelling increases and therefore, the flexural strength and modulus of the composites decrease compared to the

virgin specimens. On the other hand, when the immersed specimens are dried for 6 hours, the flexural strength and modulus of the composites was recovered compared to the immersed specimens due to the decrease in the absorbed water content.

REFERENCES

[1] Azwa Z.N., Yousif B.F., Manalo A.C., Karunasena W., 2013. A review on the degradability of polymeric composites based on natural fibres. Materials and Design, vol. 47, pp. 424–442

[2] Akil H.M., Omar M.F., Mazuki A.A.M., Safiee S., Ishak Z.A.M., Abu Bakar A., 2011.Kenaf fiber reinforced composites: A review. Materials and Design, vol. 32, pp. 4107–4121.

[3] Azwa Z.N., Yousif B.F., 2013. Characteristics of kenaf fibre/epoxy composites subjected to thermal. Polymer Degradation and Stability, 98, pp. 2752-2759.

[4] K.L. Pickering, 2008 "Properties and performance of natural-fibre composites," CRC Press LLC: Washington, DC, New York, 541 p.

[5] Bismarck A, et al., 2002. Surface characterization of flax, hemp and cellulose fibres; surface properties and the water uptake behaviour. Polymer Composites, vol. 23, pp. 872–94.

[6] Salleh Z., Taib Y. M., Hyie K.M., Mihat M., Berhan M.N., Ghani M.A.A., 2012. Fracture toughness investigation on long kenaf/woven glass hybrid composite due to water absorption effect. Procedia Engineering, vol. 41, pp. 1667 – 1673.

[7] Thwee MM, Liao K., 2003. Durability of bamboo-glass fiber reinforced polymer matrix hybrid composites. Composites Science and Technology, vol. 63, pp. 375-387.

[8] Dhakal H.N., et al., 2007. Effect of water absorption on the mechanical properties of hemp fibre reinforced unsaturated polyester composites. Composites Science and Technology, vol. 67 pp. 1674–1683.

[9] Jawaid M., et al., 2011. Hybrid Composites Made from Oil Palm Empty Fruit Bunches/ Jute Fibres: Water Absorption, Thickness Swelling and Density Behaviours. Journal of Polymers and Environment, vol. 19 (1), pp. 106-109.

[10] Phani K. K., Bose N. R., 1987. Hydrothermal ageing of jute-glass fibre hybrid composites - an acousto-ultrasonic study. Journal of Materials Science, vol. 22, pp. 1929-1933.

[11] Singh B., Gupta M., Verma A., 2000. The durability of jute fibre-reinforced phenolic composites. Composites Science and Technology, vol. 60, pp. 581-589.

[12] Tajvidi M, Takemura A., 2009. Effect of fiber content and type, compatibilizer, and heating rate on thermogravimetric properties of natural fiber high density polyethylene composites. Polymer Composites, vol. 30 (9), pp. 1226–1233.

[13] Elbadry E. A., Aly-Hassan M.S. and Hamada H., 2012. Mechanical Properties Natural Jute Fabric/Jute Mat Fiber Reinforced Polymer Matrix Hybrid Composites. Advances in Mechanical Engineering, vol. 2012, doi:10.1155/2012/354547.

[14] Scida D., Assarar M., Poilâne C., Ayad R., 2013. Influence of hygrothermal ageing on the damage mechanisms of flax-fibre reinforced epoxy composite. Composites: Part B, vol. 48, pp. 51–58.

Influence of the Impurities on the Quality of Kaolin Collected From the Field of DjebelDebbagh, Algeria

M. Laraba
University of Tébessa, Tébessa city, Algeria

A. Roula
University of Jijel, Jijel city, Algeria

ABSTRACT Kaolin is a common clay mineral with general formula: Al2(OH)4Si2O5, discovered at the origin in China. Kaolin is characterized by high reflectivity, inertness, fine particle size and low fluid viscosity. Because of these properties, it has many industrial uses and applications: paper filling and coating, in the production of ceramics and porcelain as well as in fiberglass, paint and plastic industry.

The aim of this study was to determine the influence of the kaolins impurities on their quality. For this reason, we took 2 kaolins samples from the mine of DjebelDebbagh (DD2 and DD3), situated in the East of Algeria.

The chemical analysis with XRF, show the DD2 sample is a kaolin alumina-silicate of the first order, and very low (traces) impurities like Fe_2O_3 and TiO_2, and the whiteness is very high which places it among the kaolin most sought by various industries. The presence of MnO in DD3, gives a gray color to the kaolin.

The mineralogical analysis with XRD, show that the most peaks of DD2 present as kaolinite phases and there is no impurities, which is nearly in conformity with the structure of a halloysite. The sample DD3 contains as impurities phases; manganese and organic matters, therefore a valorization is necessary to eliminate these impurities.

Keywords: kaolin, impurities, chemical analysis, mineralogical analysis.

1 INTRODUCTION

Kaolinitic clay is a versatile industrial mineral. The oldest known use of the clay is as a ceramic raw material. Presently, the clay also finds application as a coating and filler pigment for paper, as a filler for paint, rubber, insecticide, formulation of medicine, cosmetics, etc. The main characteristic, which determines the utility of the clay for various applications, is its purity. Pure kaolinite ($Al_2O_3.2SiO_2.2H_2O$) is white in color and its chemical composition is 46.54% SiO2, 39.50% Al2O3 and 13.96% H2O (Grimshaw, 1971).

Presence of impurities, particularly iron- and titanium-bearing materials, imparts color to kaolin. The mined kaolin is usually associated with various impurities like quartz, anatase, rutile, pyrite, siderite, feldspar, etc., depending on the origin and depositional environment (Grimshaw, 1971). These impurities impair the characteristics of kaolin and affect its utility for various end applications.

Kaolin generally presents different features in the same deposit. This deposit has a hydrothermal formation and is close to the repute thermal sources (Lalmi Khier, 2008).

The quality of this kaolin change with the lodes of extractions, some lodes give an appearance very white, on the other hand, the others are characterized by a color, which varied between gray and blackish color.

The treatment method used for this kaolin is the manual sorting, where the workers select the good quality of kaolins and they leave the bad quality.

Kaolin marketed, satisfied generally the following conditions:

- To remain white after burning to 1400°C;
- To present a maximum diameter of the grains (generally 20µm), doesn't exceed 50 - 63µm;
- To contain at least 80% in weight of kaolinite (BelamriZehira, 2008).

Kaolin minerals depend on the amount and nature of the mineral impurities associated to it. Although these methods are quite useful in removing impurities, they are, at the same time, costly, complicated and environmentally hazardous (Rawlings D.E., 2004).

In this study we took 2 kaolin samples from Djebel Debbagh mine (DD2 and DD3), situated in the East of Algeria. To characterize these samples, XRF and XRD techniques have been used and then to study the influences of the impurities on the quality of our kaolin. .

1.1 Geographic Situation

The DjebelDebbagh mine is situated at 35 km to the Northwest of Guelma city and at 7 km in the N-NE of the thermal sources of HammamDebbagh (ex Meskhoutine) (Figure 1).

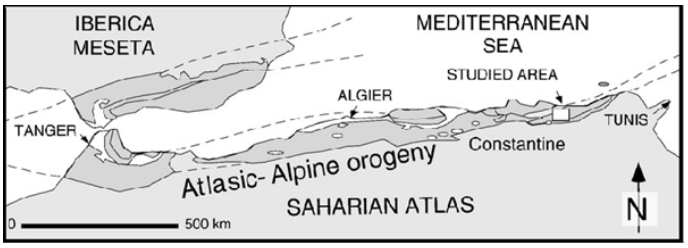

Figure 1.Geographic Situationof DjebelDebbagh(C. Renac et al, 2009)

This massif belongs to the most important chalky chains of the Constantinois neritic mole (marine sedimentation); it's lengthened on meadows of 10 km from east-west and large of 3 km from the North to the South(ENOF, 2004).

The Djebel Debbagh layer is located in the karstics cavities. Currently 74 karstics cavities exist on the whole layer (ENOF, 2008). He presents two parallel crest lines oriented East-west, His altitude varies from 700m to 1060 m (Soalka SPA, 2012).

2 MATERIALS AND METHODS

Two kaolins samples (labeled DD2 and DD3) have been collected from Djebel Debbagh mine, following criterion of different color, as raw materials, were accordingly characterized. These samples are presented in the below figures.

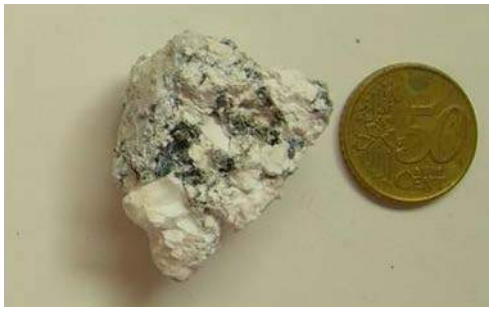

Figure 2. White-Gray kaolin D2

Figure 3. Blackish kaolin KDD3

We can see in the two figures that the colors are different between DD2 witches is white-gray and DD3 witches is blackish.

2.1 Characterization of Kaolin DD2 and DD3

Our kaolin has been characterized in order to have the necessary information for this research.

2.1.1 DRX Analysis

The nature of the present phases has been subtracted from the diagrams of diffraction X-rays (XRD) gotten in 30 min. of acquisition

The XRD diagrams of the different kaolin are presented in the figure 4 and 5.

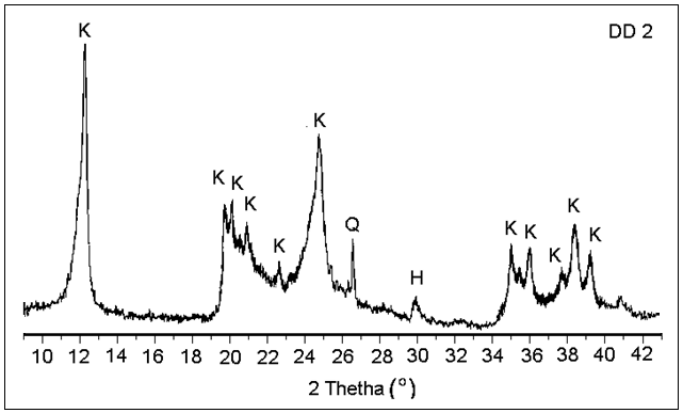

Figure 4. XRD Diagram of DD2; (K): Kaolinite, (Q): Quartz, (H): Henritermierite.

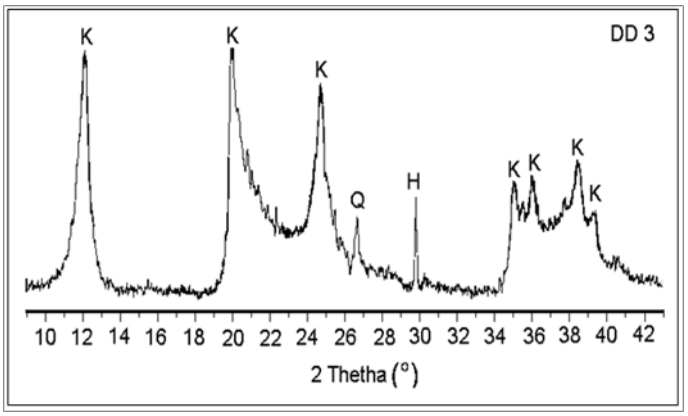

Figure 5. XRD Diagram of DD3; (K): Kaolinite, (Q): Quartz, (H): Henritermierite.

In the two cases, the most intense stripes are to 2θ = 12.30°, 19.85° and 24.85°, characteristics at a time of the kaolinite and the halloysite.

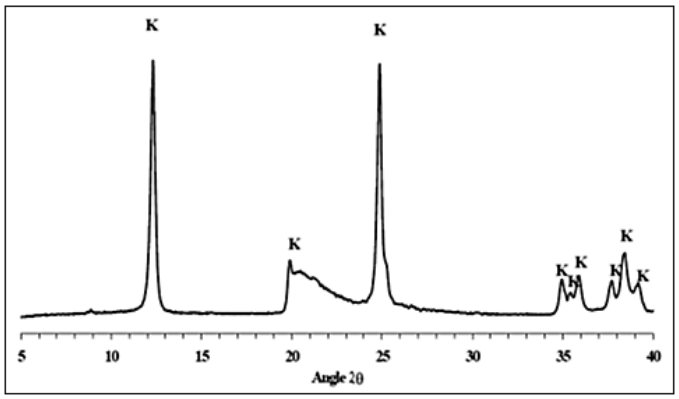

Figure 6. X RD Diagram of KGa-2 (K : Kaolinite)

2.2 Comparison of Kaolin DD2 and DD3 with Kga-2

2.2.1 Kaolin Cristallinity

The clayey minerals generally include crystalline default. For example, in the nature, the kaolinites exists under shape going very well of the crystallized to very disorganized. (D. N. Hinckley, 1962)

The XRD powder diagrams indicate the influence of crystalline state on the form of the diffraction stripes feature of kaolinite: some intense and fine stripes (peaks) become diffuse, and badly determined, with increasing of the structural disorder and stacking default of the kaolinite leaflets.

The physico-chemical properties of kaolinites are strongly dependent on the nature and the quantity of defaults.

Numerous empiric relations have been established in order to estimate this crystalline disorder. They are based on the intensity, the height and the form of diffraction peaks strips (hk0).

When the crystalline disorder increases in the plan (a, b), the corresponding stripes become larger and their intensities decrease. They can even constitute some wholes without distinct peaks.

The most used cristallinity indices is the one described by Hinckley (W. D. Kingery et al, 1076), sensitive to the defaults set presents in the plan (a, b), he is defined from the strips peaks (02*l*) and (11*l*) (figureII-2) while using the relation:

$$HI = \left(\frac{A+B}{At} \right)$$

Where

- A and B are respectively, the heights of strips (02*l*) et (11*l*)
- At : is the height of pic (110) measured from the continuous bottom existing in the outside of these strips.

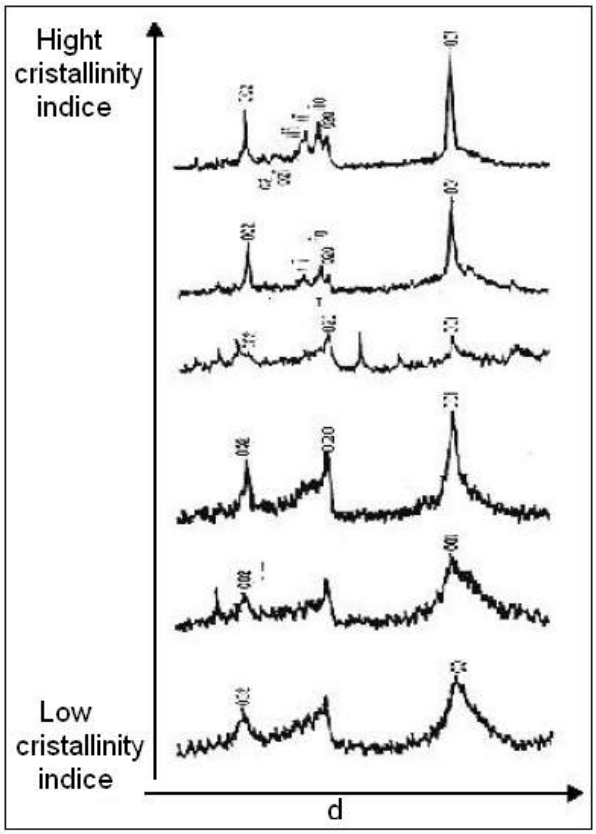

Figure 7. Variation form of stripes (001) and (002) of kaolinite with stacking defaults (J. M. Amigo, 1994)

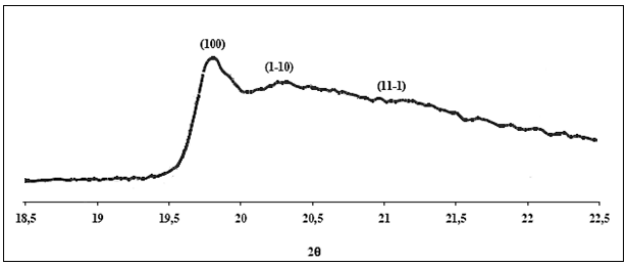

Figure 7. Strip (02) and (11) of XRD specter kaolin (KGa-2)

2.2.2 Chemical composition

Table 1 gives the contents of the different oxides present in the tow kaolins. We compared DD2 and DD3 with reference kaolin KGa-2, relatively pure, coming from the state of Georgia (USA). This kaolin was already the subject of many studies (B. Tchoubar, et al 1982), (Jean-Paul Legros, 2007), (N. S. Soro, 2003), its chemical composition has been determined by ICP (B. Tchoubar, et al 1982)..

Table 1: chemical composition of DD2, DD3 and the reference of KGa-2, (%).

Elements	KGa-2	DD2	DD3
SiO_2	43.90	43,58	42,57
Al_2O_3	38.5	38,14	37,84
TiO_2	2.02	--	--
Fe_2O_3	1.13	0.09	0, 14
K_2O	0.0065	--	--
Na_2O	0.005	--	--
MnO	0, 00	0, 59	1, 49
MgO	0, 03	0, 32	0, 11
CaO	--	0, 05	0, 21
LOI	13, 72	16, 18	16, 80
Whiteness /color	> 85%	withe-Gray	Blackish

The KGa-2 kaolin show that the Al2O3/SiO2 report is equal to 0.88, that the contents in TiO_2 and Fe_2O_3 are relatively important and that the loss in ignition is 13, 72%. While comparing these results with the results gotten for the DD2 and DD3, we remark that the Al_2O_3/SiO_2 reports are near; on the other hand the loss in ignition of the order of 16% are superior to those gotten with the KGa-2 kaolin.

2.2.2 Mineralogical composition

Table 2 presents the mineralogical composition of DD2, DD3 and the reference KGa-2

The research of minerals composing DD2 and DD3 kaolin is led by X-rays diffraction. The indexing of the peaks watches that three main crystalline phases constitute DD2 and DD3 kaolin, the first is represented by the kaolinite that is extensively present. The second phase is the Al $(OH)_3$ gibbsite, carrier of alumina, and Finally a third phase that is carrier of the manganese with elevated ratio in DD3.

We don't discover the presence of quartz, certainly; this kaolin is very little soiled by the free silica. Some peaks remain unidentifiable.

Table 2: Mineralogical composition of DD2, DD3 and the reference KGa-2 in (%)

Sample	Kaolinite	Illite	Quartz	Anatase	Organic matters
DD2	85	---	14	---	<1
DD3	60	---	35	---	<5
KGa-2	97	---	<1	< 2	---

The richest kaolin in kaolinite is DD2 (85%) compared with the DD3 kaolin (60%), at the same time the DD2 kaolin is close to the composition of KGa-2 kaolin.

The mineralogy of KGa-2 kaolin studied by the XRD, show that kaolin is essentially constituted of the kaolinite (97%).

3 RÉSULTS AND DISCUSSION

The silica and alumina are the majority constituent oxides in our sample.

The SiO_2/Al_2O_3 reports of DD2 is 1.14 instead of 1.1 for the pure kaolin, This gap suggests the presence of free silica (quartz), on the other hand for the DD3 is equal to 1.12 which also confirms the presence of the free silica. , these values indicate that the quality of our kaolins is varied, the DD2 characterized by a middle quality, the second DD3 characterized by a weak quality.

We remark that the percentage in impurities is not elevated in relation with kaolins used in the industry; however a small presence of the manganese oxide in DD3 made the difference compared with other kaolins, because this one gives a gray color to ores.

The calculations of Hinckleys indices values that calculated from these strips are: 0.409 and 0.214 for DD2 and DD3 respectively, and are different from the value Hinkley indices references of KGa-2 that equals to: 0.37 (B. Tchoubar, et al 1982), which confirms that our samples of kaolin are badly crystallized.

It is proved that a relation exists between the evolution of the Hinckley indices of the kaolinite and the increase of the number of structural defaults from the moment all diagrams are recorded on the same device and in the same conditions (O. Castelein, 2000)

The rates of the iron oxide are very low (0,09% for DD2 and 0,14% for DD3), in relation with the kaolin used in the industries of ceramics 0.6–1% , Paper coating and Paper filler 0,5 to 1 %.(Siddiqui et al., 2005).

As we know, the iron oxide is a harmful element for the kaolin and can give reddish, brown and brunette for kaolin.

We remark that the impurities percentage is not heighten, however a small presence of the manganese oxide made a compared difference with other kaolins, because this one gives a gray and blackish color to the kaolins.

The loss on ignition (LOI) for DD2 and DD3 is superior to 16%, in relation with KGa-2 kaolin, that due to the existence of structural water.

4 CONCLUSION

Our different kaolins are characterized by several aspects.

According to the chemical and mineralogical analysis, the essential mineral is always hydrated silica-alumina, under kaolinite or haloysite form; it is come accompanied except in DD2, by several impurities: micas and feldspars bring potassium.DD3 contains the manganese and the organic matters; DD2 is nearly in conformity with halloysite.

The SiO_2/Al_2O_3 reports of DD2 and DD3 are 1.14 and 1.12 respectively instead of 1.1 for the pure kaolin, This gap suggests and confirms the presence of free silica (quartz), these values indicate also that the quality of our kaolin is varied the middle quality to the second poor quality.

It is noted that DD3 contains non negligible contents in Fe2O3, K2O, CaO and MnO. These impurities present with traces in DD2, It is coherent with the white-gray color DD2, and the blackish color of DD3.

After comparison with the KGa-2 kaolin, it is appears that the DD2 and DD3 are not kaolinites ($2SiO_2,Al_2O_3,2H_2O$) but rather a

hydrated form that approaching to the halloysite ($2SiO_2,Al_2O_3,4H_2O$).

ACKNOWLEDGEMENT

The authors hereby acknowledge the help and facilities extended by SOALKA society in Jijel, Algeria.

REFERENCES

BAKHAREV, T., 2005. Geopolymericmaterials prepared using Class F fly ash and elevated temperature curing. Cement and Concrete Research 35, 1224–1232.

BelamriZehira, 2008, Elaboration et caractérisation des matériaux polycristallins à base de kaolin DD et KT2.p 9.

B. Tchoubar, A. Plançon, J. B. Brahim, C. Clinard and C. Sow, Bull Mineral., 105, 477- 491 (1982).

C. Renac and F. Assassi, Sedimentary Geology 217, P 140–153, (2009).

D. N. Hinckley, Proc. 11th Nat. Conf. on clays and clay miner., Ottawa, P 229-235, (1962).

ENOF, 2004, Entreprise Nationale Des Produits Miniers Non Ferreux Et Des Substances Utiles, Alger, Algérie

Grimshaw, R.W., 1971. Physics and Chemistry of Clay, 4th ed. Ernest Benn, London, ISBN: 0510-47701-7.

J. M. Amigo, J. Bastida, A. Sanz, M. Signes and J. Serrano, Appl. Clay Sci., Vol 9, P 51- 69, (1994).

Jean-Paul Legros, ‘‘Les grands soles des monde”, première edition ISBN-Presses Polythechniques et Universitaires Romandes, P. 372 (2007).

LalmiKhier, 2008, Mémoire De Magister En Physique, Etude Par Diffraction Des Rx De Matériaux A Base De Kaolin De KT2 Et DD.

N. S. Soro, Ph.D. Thesis, Universite´ de Limoges, France, (2003).

O. Castelein, Thèse de Doctorat d’Etat, Univ. Limoges, (2000)

Rawlings, D.E., 2004. Microbially assisted dissolution of minerals and its use in the mining industry

Siddiqui, M.A., Ahmed, Z., Saleemi, A.A., 2005. Evaluation of Swat kaolin deposits of Pakistan for industrial uses. Applied Clay Science 29, 57–72.

SOALKA, SPA, 2012. Société Algériennes Des Kaolins

W. D. Kingery, H. K. Bowen, D. R. Uhlmann, « Introduction to ceramics », 2nd Ed., J. Wiley and Sons, (1976)

Microstructural Evolution of Consolidated and Unconsolidated Cemented Paste Backfills by SEM-EDS Analysis

E. Yilmaz
University of Quebec in Abitibi-Témiscamingue (UQAT), Department of Applied Sciences, 445 Boul. de l'Université, Rouyn-Noranda (Québec) J9X 5E4 Canada

ABSTRACT This paper investigates the microstructural characterization of consolidated and unconsolidated cemented paste backfill (CPB) by scanning electron microscopy coupled with energy dispersive X-ray spectroscopy (SEM/EDS). The two different pressure application during curing (i.e., unconsolidated samples cured under 0 kPa and consolidated samples cured under the pressure up to 400 kPa) were tested in the experiments. Samples were prepared with 100wt% general use Portland cement and subjected to unconfined compression tests after curing time of 28 days. Results show that the strengths of consolidated backfills are always higher than those obtained from unconsolidated ones because of removal of excess free water and an efficient curing process leading to a high grain density. SEM micrographs of polished and fractured sections have also revealed that consolidated backfills give more solid matrix than unconsolidated ones. This is due to hydration products filling up the interstitial space within CPB cured under pressure and create a stronger bridge between particles.

Keywords: Cemented paste backfill, scanning electron microscopy, energy dispersive x-ray spectroscopy

1 INTRODUCTION

Cemented paste backfill (CPB) is a relatively high density, low strength material, which consists of mill tailings (typically with more than 70% solids), hydraulic binder (typically 3-7% binder to total solids ratio), and mixing water (typically reflects a slump consistency of 15-25 cm (Bernier et al., 1999; Kesimal et al., 2003, 2004; Potvin et al., 2005; Tariq and Nehdi, 2007; Yilmaz, 2011). Mine fills may be delivered to underground stopes in several ways: either by truck, by pumping or gravity or paste by boreholes and pipelines (Belem and Benzaazoua, 2008; Ercikdi et al., 2010). CPBs are often used for backfilling stopes in underground mines. This may allow a safer management of potentially acid generating tailings, while at the same time offer ground support to the surrounding rock mass (Fall et al., 2004, Kesimal et al., 2005; Landriault, 2006; Bussiere, 2007; Yilmaz, 2010; Coussy et al., 2012; Wu et al., 2013).

In comparison with concrete and/or mortar mixtures (having typically a water-to-cement w/c ratio of <0.5), CPB reflects a very high w/c ratio of >2.5) which has a harmful effect on its micro-structure. Paste backfills mixed with high water contents cannot make higher strengths, slowing down cement hydration (Benzazoua et al., 2004; Ercikdi et al., 2008, 2013; Cihangir et al., 2011, 2014; Ghirian and Fall, 2014; Yilmaz et al., 2015a,b).

Investigators have published some works on CPB microstructure by scanning electron microscopy equipped with energy dispersive spectroscopy (Ouellet et al, 1998, 2004,2006, 2007, 2008; Belem et al., 2001; Benzaazoua et al., 1999, 2002, 2004; Mohamed et al., 2003; Ramlochan et al., 2004; El Aatar et al., 2007; Cihangir et al., 2008; Deschamps et al., 2008; Ercikdi et al., 2009). These works were done on fractured or polished samples and gave precious info. Using the polished sections also permitted quantitative analyses.

Although the microstructure of concretes or mortars is relatively well known (Poon et al., 1997; Diamond and Kjellsen, 2008; Choi et al., 2009; Thomas et al, 2013; Abd El Aleem et al., 2014; Grilo et al., 2014; Heikal et al., 2014; Hu, 2014; Huang et al., 2014; Manfroi et al., 2014; Vaitkevicius et al.,

2014), the micro-structural behavior of CPB thus needs to be further understood. It has been well documented that curing cemented materials under effective stress increases the strength gain, depending on cement type and ratio (Belem et al., 2007; Yilmaz et al., 2009, 2011, 2012, 2013, 2014a,b). It should be however noted that the time of application of stress plays a key role on the CPB strength. Fourie et al. (2006) showed that if effective stress is applied immediately before the start of curing, samples gain more strength than when the effective stress is applied after the hydration is complete. This is attributable to the cement bonds that form during hydration (Revell, 2004; Fall and Samb, 2009; Yilmaz, 2010). If CPB is subjected to curing stress after a couple of days, then the cement bonds that are forming may break down, therefore reducing the material's stiffness.

Consequently, the complete information of these aspects is needed to evaluate the micro-structural behaviour of CPB. The principal purpose of this paper is to present the results of the experimental testing undertaken for assessing the microstructure of consolidated and unconsolidated paste backfills. The two different pressure sequences were applied to backfills during curing. The unconsolidated samples were cured under zero pressure (0 kPa) while the consolidated samples were cured under a pressure sequence up to 400 kPa. The consolidation effect on the CPB microstructure was assessed after unconfined compression testing. CPB samples contained 100wt% general use Portland cement and tested for their microstructural analyses after curing time of 28 days alone.

The key interest of the present paper stems in part from the fact that this is one of the very original attempts, to the authors' best knowledge, to investigate the microstructural behaviour of CPB samples being cured under time-dependent consolidation loadings.

2 MATERIALS AND METHODS

2.1 Materials

Paste tailings were sampled as representative of the tailings streams from the paste plant of the LaRonde mine, located in the Abitibi region of northwestern Quebec, Canada. The samples were received in plastic containers and subjected to the material characterization tests. Based on American Society of Testing Materials standards testing procedures, lab experiments were done in triplicate and their average values are reported. Further details on paste tailings material characteristics can be found in Yilmaz (2010).

2.1.1 Physical Tests

The paste material used was analyzed using a Mastersizer (Malvern Instruments) laser diffraction particle size analyzer. The test procedure consists simply of mixing 0.2-0.4 g of powder in a dispersant contained in an ultrasonic bath operated until the grain size distribution curve stabilizes. The laboratory analysis results show that the tailings sample has an average water content w of 23.4 wt%, a specific gravity G_s of 3.7, a specific surface S_s of 2.2 m^2/g, a relative compaction R_c of 91 wt%, a liquid limit w_L of 23 wt%, a plastic limit w_P of 18 wt%, a liquidity index LI of 1 wt%, a plastic index PI of 5 wt%, and a clay activity A (simply defined as the PI divided by the percent of clay-sized particles present, < 2 µm) of 1. The Atterberg limit results showed that the paste tailings studied would be designated as ML.

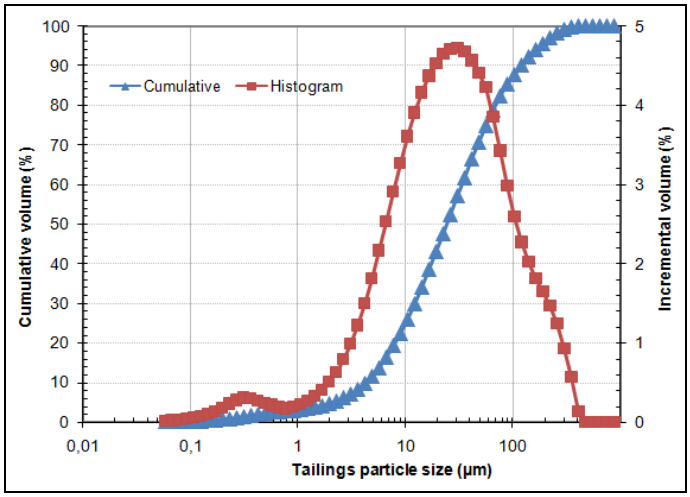

Figure 1. Cumulative and incremental GSD curves of paste tailings

2.1.2 Chemical Tests

X-ray diffraction (XRD) analysis and ICP-AES analysis show the results of the tailings

sample studied. It can be concluded from XRD analysis that the sample contains a high proportion of pyrite (47 wt%), mainly responsible for the high G_s of tailings (3.7). The other major minerals are quartz (31.6 wt%), chlorite (8.9 wt%), paragonite (7.3 wt%) and muscovite (4.6 wt%). The ICP-AES analysis also indicates iron Fe (27.4 wt%) and sulphur S (24.9 wt%) are the most abundant elements identified within tailings.

The binder used for CPB preparation was 100 wt% of general use ordinary Portland cement (GU). Chemical composition was listed in Table 1. Physical characterization shows that specific surface area and specific gravity are 1.6 m^2/g and 3.1, respectively.

Table 1. Physical and chemical properties of the cement used.

Parameter	Value
Specific gravity G_s	3.1
Specific surface area S_s (m^2/g)	1.6
Al_2O_3 (%)	4.9
CaO (%)	65.8
Fe_2O_3 (%)	2.5
MgO (%)	2.2
Na_2O (%)	2.1
SO_3 (%)	3.7
SiO_2 (%)	19.5
Hydraulic modulus	2.3

The mixing water used in the tests is very highly aggressive regarding sulphate content (4883 ppm) but also contains calcium Ca of 559 ppm because of addition of lime during milling. Tap water used within CPB contains a calcium concentration of 40.9 ppm and a magnesium concentration of 2.27 ppm.

2.1.3 Sample Preparation and Curing

The amounts of paste backfill ingredients such as mine tailings, cement and water were prepared in a Hobart mixer. The total mixing time for CPB materials was 12 minutes. Each CPB mixture has a solid concentration of 78 wt% and 4.5 wt% cement (corresponding to a water-to-cement ratio of 6.5).

Consolidated CPB samples were obtained by a transparent cylinder within the CUAPS apparatus while unconsolidated CPB samples were obtained by plastic moulds. Paste mixes were cast into both cylinders and moulds in one-third increments. After the cylinders or moulds were filled, the paste was rammed in 25 blows using a small steel rod to eliminate any large trapped air bubbles within sample. After sealing, the moulds were stored in a foggy room set at 80% humidity and 25 °C temperature over a curing time of 28 days. Please note that after the paste was poured into cylinders within the CUAPS apparatus, the top porous stone, the loading piston and platen connected with a pneumatic pressure line were placed in order to simulate in situ backfill conditions. Figure 2 illustrates the different test conditions of CPB samples.

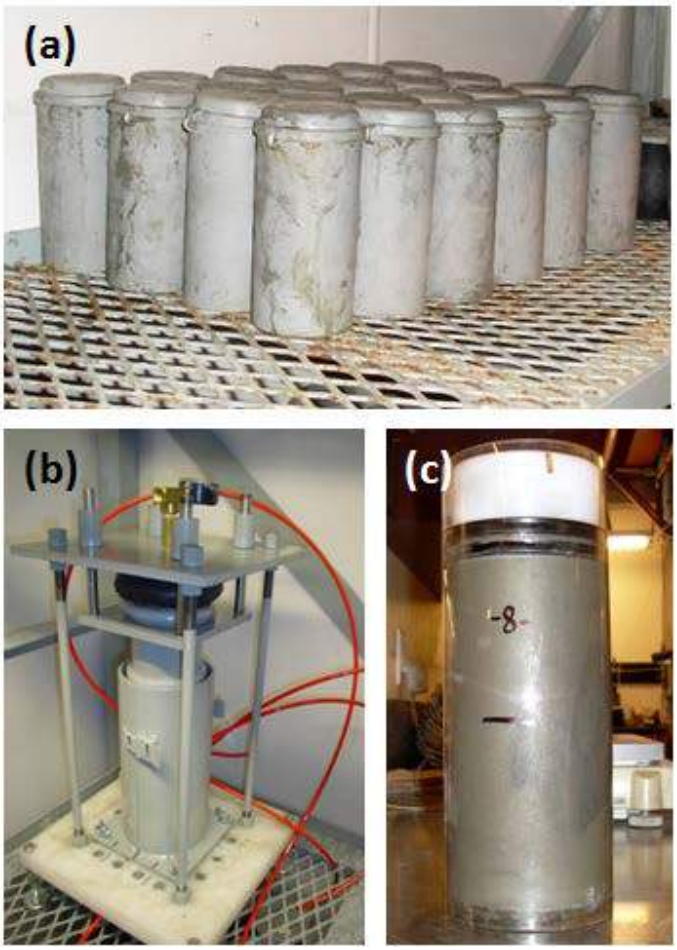

Figure 2. Photos illustrating the different test conditions: a) conventional moulds stored in the humidity room, b) the CUAPS apparatus allowing simulate field backfill conditions, and c) CUAPS cylinder filled with CPB.

2.2 Methods

2.2.1 Curing Under Applied Pressure Tests

These tests were run to simulate the strength behaviour of in situ paste backfill samples

and compare it to of paste backfill samples in standard laboratory conditions. The CUAPS setups were filled with freshly prepared paste backfill material. For the first half an hour, no pressure was applied to the CPB sample, with pressure gradually increased thereafter up to 400 kPa for a total duration of 35 h. Average compression rate was 11.4 kPa per hour, for a filling rate of 0.5 m per hour. A final pressure or stress application of 400 kPa corresponds to an equivalent overburden of 20 m in height of CPB in an underground stope. Each sample was left to cure under the final pressure of 400 kPa for a curing time of 28 days, chosen arbitrarily.

2.2.2 Unconfined Compression Tests

At the predetermined curing period (28-day), CPB samples were subjected to unconfined compression tests in order to determine their strength properties. Unconfined compressive strength (UCS) test was used because of its simplicity and reliability. A mechanical press (MTS 10/GL) with a normal loading capacity of 50 kN was used. The samples' two ends were first planed to get their surfaces normal to the plates of the mechanical press prior to the tests. Figure 3 shows a typical UCS test.

Figure 3. Photos of (a) MTS Sintech 10/GL mechanical press, (b) a sample rectification with typical results, and (c) the CPB sample under compression testing.

2.2.3 SEM-EDS Characterization Tests

The microstructure and texture of samples were characterized using a Hitachi 3500-N scanning electron microscopy with energy dispersive X-ray spectroscopy (Fig. 4).

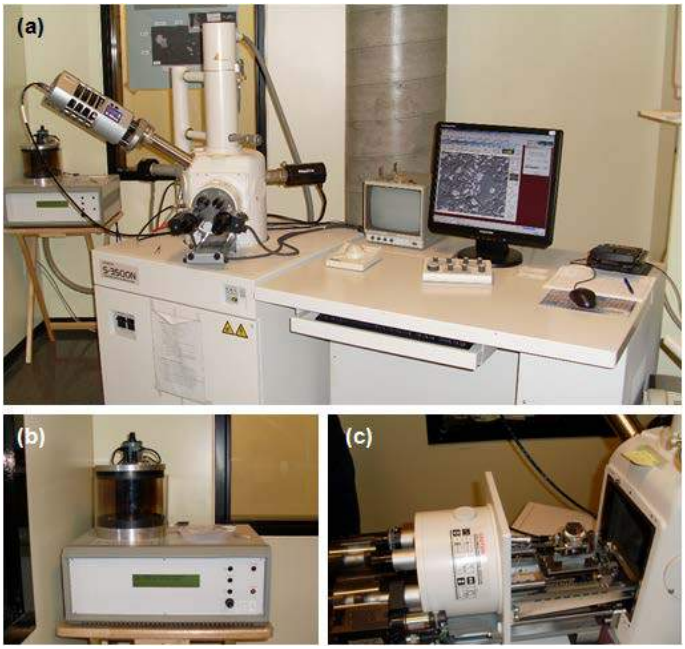

Figure 4. Photos of (a) the SEM-EDS tool, (b) impregnation unit and (c) internal section of sample placement in SEM equipment.

To examine both oxidized and unoxidized sections, a piece of sample was extracted gently from CPB and cut transversally. Once the sample was dried, vacuum impregnated with low viscosity epoxy, polished and gold coated, SEM observations were performed in the secondary electron mode at high vacuum (<0.1 Pa), using a primary voltage of 20 keV and a working distance of 15 mm. Figure 5 shows polished and fractured CPB samples.

Figure 5. Photos of polished and fractured paste backfill samples.

3 RESULTS AND DISCUSSION

To assess the variation in the conditions of the CPB placed in an underground mined out

stope, the two extreme points of the stope were simulated by choosing 0 kPa (reflects the top of the stope, Case I) and 400 kPa (reflects the bottom of the stope, Case II).

Case I allows us to better understand the information of CPB material close to the top of the stope, which is initially subjected to no consolidation, and thus represents a loose material). Case II allows us to better realize the information of CPB material close to the bottom of the stope, which is subjected heavily to self-weight and/or time-dependent consolidation, and thus represents a dense backfill. Please note that the stope height simulated is site-specific and limited to max stope height to 20 m.

3.1 Consolidation Effect on Strength Behaviour of CPB Samples

Figure 6 shows that consolidated backfills always provide higher mechanical strengths those obtained from unconsolidated samples. The stiffness of the samples cured under a stress of 400 kPa increases with increased cement hydration rate. When compared to the undrained backfills cured under 0 kPa, consolidated backfills provided a strength increase of 33%, 31%, and 26% after curing times of 7, 14, and 28 days at 4.5wt% binder, respectively.

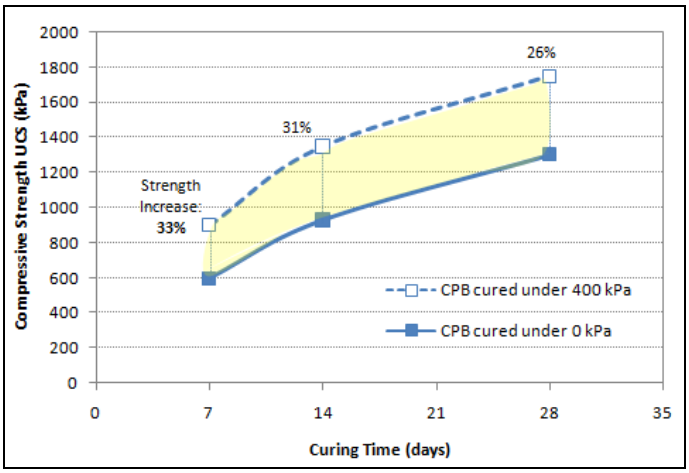

Figure 6. Change in the compressive strength with curing time for both consolidated (cured under 400 kPa) and unconsolidated (cured under 0 kPa) CPB samples.

Results indicate that consolidation process plays a key role in the strength development of CPB samples. The consolidated backfills display smaller degree of saturation than the unconsolidated ones because of the reduced pore size distribution in paste backfill being cured under stress. During cement hydration, the capillary voids present in the sample due to consolidation will be filled with hydrated products, thus increasing internal cohesion. This observation was confirmed by a variety of microstructure tests (MIP, SEM, etc) done on consolidated and undrained CPB samples (El Aatar et al., 2007; Yilmaz, 2010).

3.2 Scanning Electron Microscopy (SEM) Investigation of 'Polished' Samples

The polished section samples provide us the central information on quantitative chemical elemental analyses of CPB samples through SEM-EDS, based on the Ca/Si ratio. Please note that the polished section analyses might have some errors because the microstructure of the paste backfill samples is altered during sample preparation. There is not anything to recover this fact because it is based on the technique studied. On the other hand, it is a good analysis so that the information on the void ratio changes can be obtained.

Figure 7 demonstrates scanning electron microscopy (SEM) micrographs of polished section of paste tailings without cement. It is apparent that the void ratio of paste tailings (grey zone) is too much and need to be filled with the hydrated products when the cement is added to tailings. The microstructure of tailings was comprised of particles varying between 15 µm and 35 µm. The interstitial space between larger particles was loosely filled up with much smaller particles varying between 1 µm and 5 µm. The majority of the space present within paste tailings was empty and unrelated with one another. The image analysis of paste tailings confirmed that there were more than 50% void space within the material tested. This is in a good agreement with bulk measurements of the total porosity of similar uncemented paste tailings samples, which are obtained using mercury intrusion porosimetry (MIP) tests.

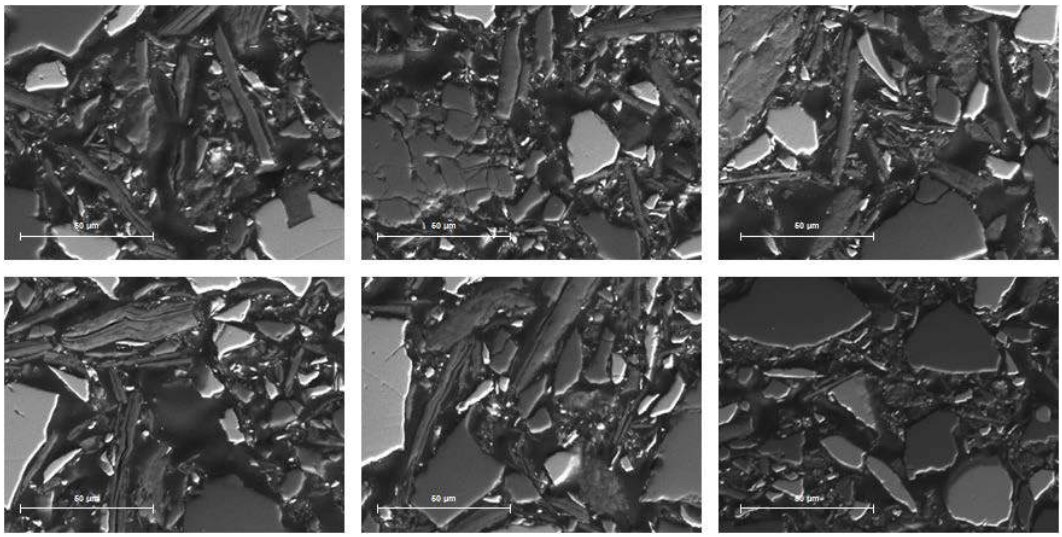

Figure 7. SEM micrographs of the polished section of uncemented mine tailings.

3.2.1 Effect of Curing Without Stress

Figure 8 shows the SEM micrographs of the polished section of unconsolidated backfill samples cured under 0 kPa. The structure of CPB samples consisted of a combination of fine particles and hydrated cement products. Even though the cemented material studied appeared very porous, the hydrated products could get in touch with the tailings particles, as expected. Due to the fact that there is no drainage from unconsolidated CPB samples (no holes perforated at the bottom of mould), there exists much more free water within the sample. This causes a sober delay of cement hydration, thereby resulting in larger voids.

Unlike mortars or concretes, there was no observation about a cementitious formation between tailings particles. It is well known that the application of pressure to the backfill during curing leads to a significant increase in the compressive strength of CPB samples. From Figure 8, it can be also inferred that the interstitial space between tailings particles was much greater than the space occupied by the hydrated products. This also confirmed that it was not created a bridge between the tailings particles in consequence of calcium silicate hydrate products. The microstructure of unconsolidated backfills is less dense than the one of consolidated ones.

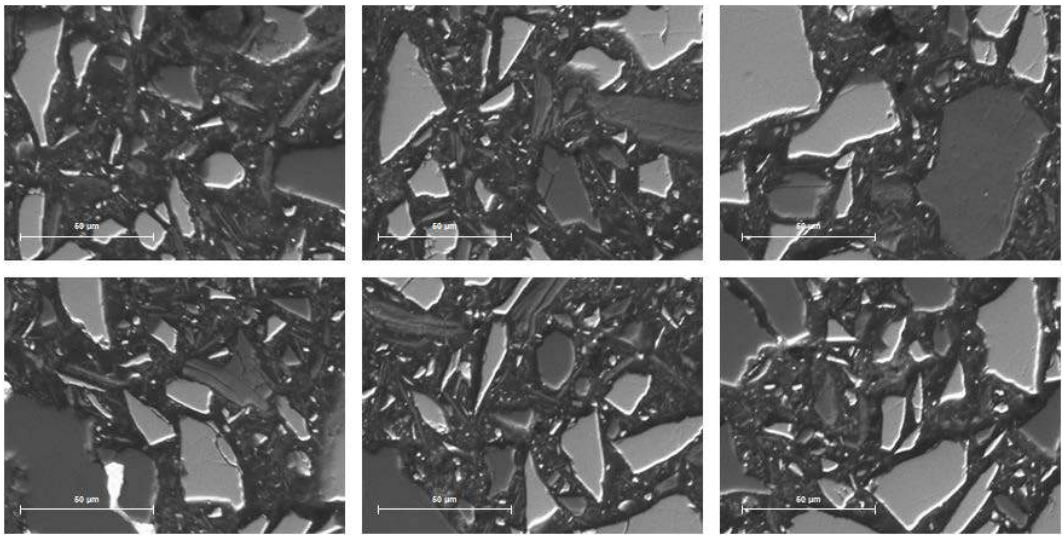

Figure 8. SEM micrographs of the polished section of unconsolidated CPB samples prepared with GU@100 wt% and cured under no applied pressure during curing. Samples contain a binder content of 4.5 wt% and show a curing time of 28 days.

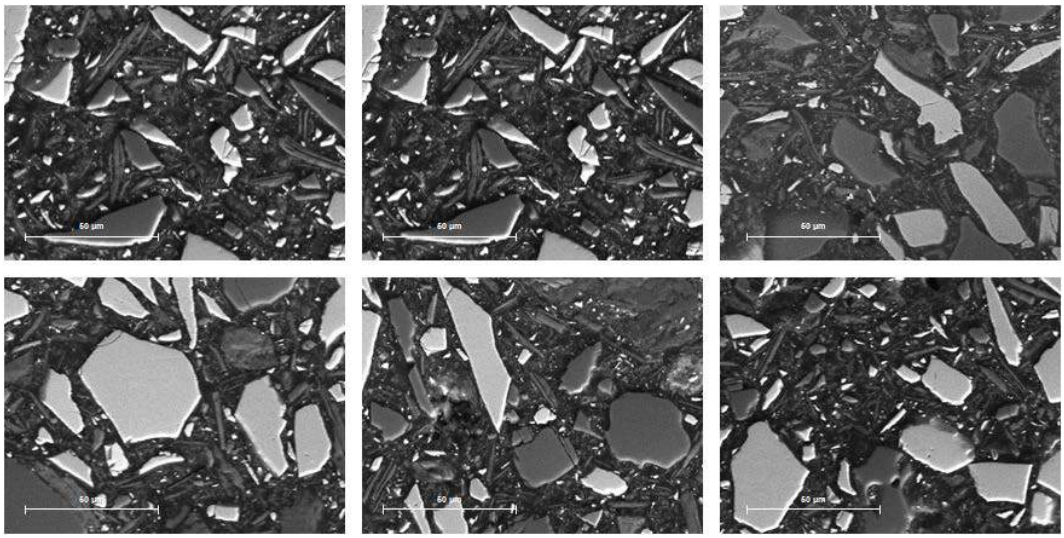

Figure 9. SEM micrographs of the polished section of consolidated CPB samples prepared with GU@100 wt% and cured under an applied pressure of 400 kPa during curing. Samples contain a binder content of 4.5 wt% and show a curing time of 28 days.

3.2.2 Effect of Curing Stress (400 kPa)

Figure 9 shows the SEM micrographs of the polished section of the consolidated backfill samples cured under a pressure of 400 kPa. The studied backfills appeared to embrace a larger proportion of fine-grained tailings than the unconsolidated backfills. As a result of the removal of free water within the backfill cured under the applied pressure (named as consolidation), the number of micro-cracks in the backfill sample reduces due to the fact that the tailings particles are pulled together under capillary forces. This may result in an increase of the CPB's rigidity, accelerating cement hydration and therefore, generating higher unconfined compressive strengths.

The amount of hydrated products within the consolidated CPB samples found infilling void spaces (Fig. 9). The microstructure also shows that precipitated secondary minerals contribute to the cohesion of paste backfill matrix by filling the granular voids. From the SEM micrographs, one can notice that the microtexture of consolidated CPB matrix is denser than the one of unconsolidated CPB samples (with void spaces).

The lab curing conditions (with or without stress during curing) seems to have an effect on the microstructure of CPB as we can see as comparing the images corresponding to paste fill samples with similar binder content at similar curing days.

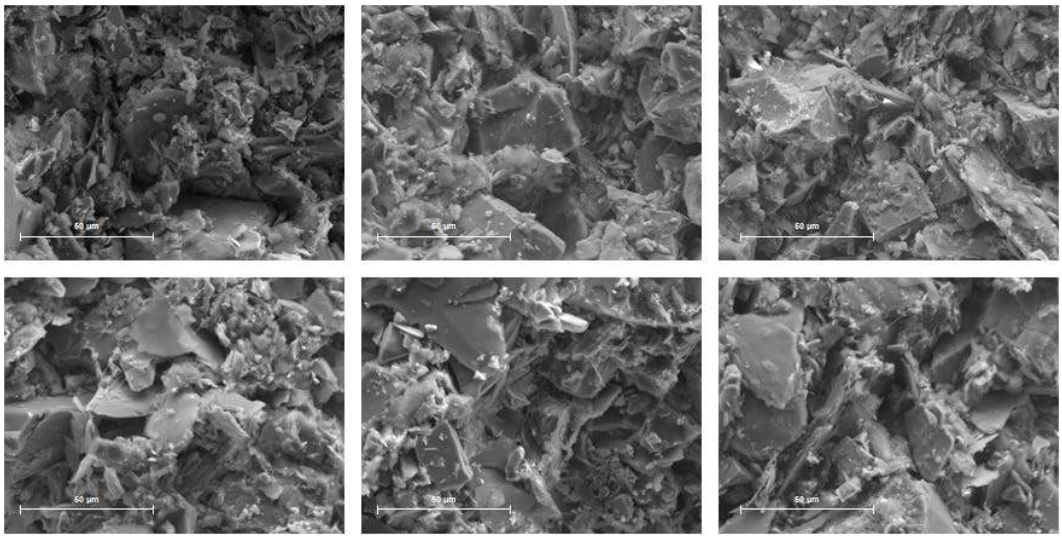

Figure 10. SEM micrographs of the freshly-fractured surface of uncemented mine tailings.

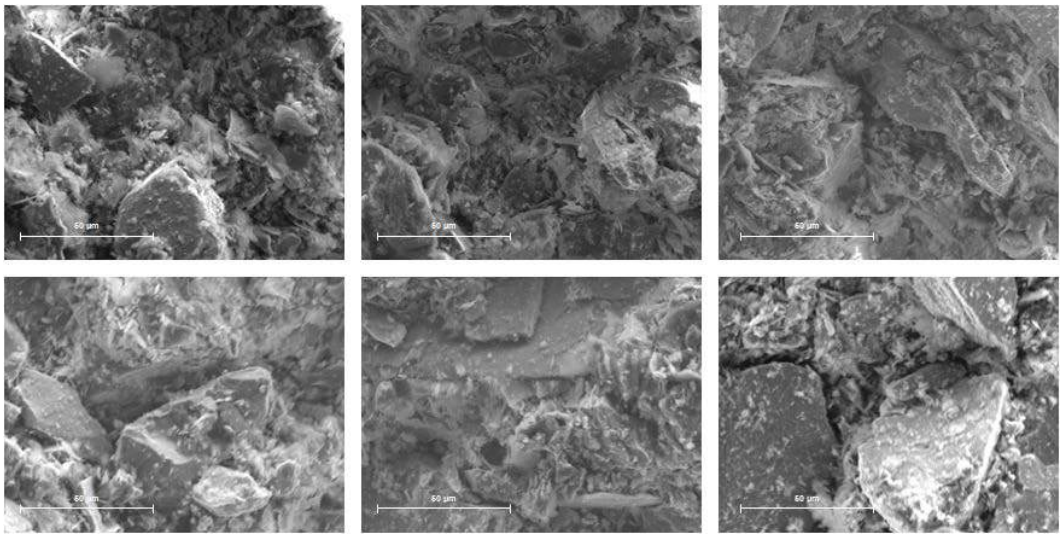

Figure 11. SEM micrographs of the freshly-fractured surface of unconsolidated CPB samples prepared with GU@100 wt% and cured under no applied pressure during curing. Samples contain a binder content of 4.5 wt% and show a curing time of 28 days.

3.3 Scanning Electron Microscopy (SEM) Investigation of 'Fractured' Samples

The fractured section analyses provide us the important information of cement hydration products such as C-S-H and general sample morphology. Due to the fact that samples are not disturbed and freshly cut (non-altered surfaces are necessary to do these analyses), the SEM-EDS analyses give us the better microstructure characterization information. After completing these works, it will be able to make clear interpretation on two extreme experimental conditions.

Figure 10 shows the SEM micrographs of the freshly-fractured surface of paste tailings without cement. The high amount of meso- and macro-pores observed in the tailings may be attributed mainly to a heterogeneous mix containing micro-cracks and irregular grain dispersion pattern. The void spaces between the coarser and angular particles are filled up mostly with ultra-fine particles. However, it is good to point out that there are still some unfilled parts in tailings which reveal gaps. The high water-to-cement ratio also affects negatively the micro-structure of tailings.

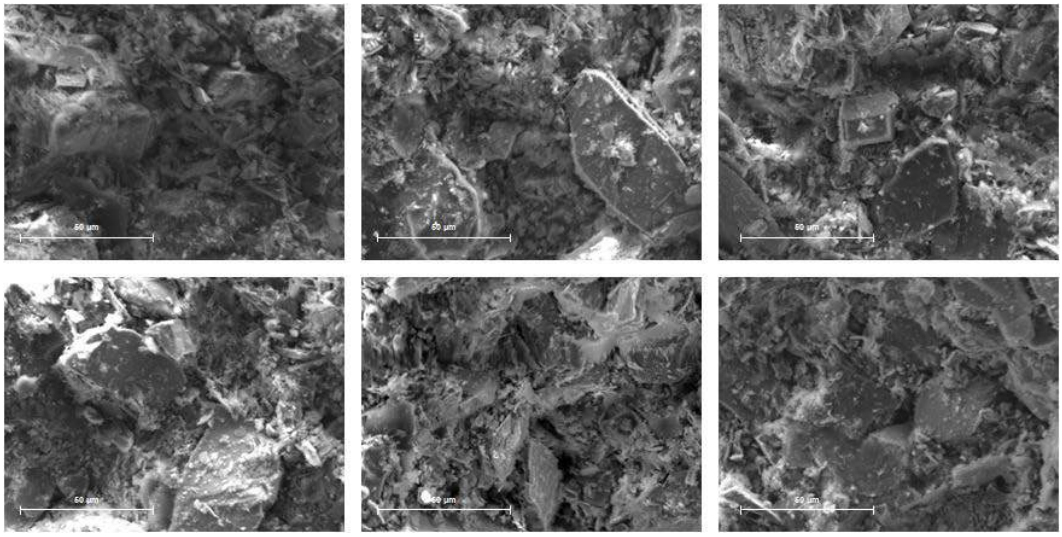

Figure 12. SEM micrographs of the freshly-fractured surface of consolidated CPB samples prepared with GU@100 wt% and cured under an applied pressure of 400 kPa during curing. Samples contain a binder content of 4.5 wt% and show a curing time of 28 days.

3.3.1 Effect of Curing Without Stress

Figure 11 shows the SEM micrographs of the fractured CPBs cured under zero pressure.
It is clear that tailings particles are not well connected to each other because there is no applied pressure during curing. Observation was made by SEM analyses that there are still some unfilled gaps within samples even though hydration products appear clearly.
It is apparent that there are no clear cement bonds around the particles as a consequence of excess free water still available in sample. Since there is no a superior testing procedure or equipments which allow samples to drain out free water from CPB during curing, the cement bonds cannot be observed within the samples studied.

One can also speak that, although empty spaces are partially filled up with the C-S-H gels, there are still some voids between the interlayer of tailings particles. This might be explained simply by the fact that there is no consolidation during curing and thus no grain rearrangement which leads to an increase in the packing density of samples (the reduction of the porosity of the material).

3.3.2 Effect of Curing Stress (400 kPa)

Figure 12 shows the SEM micrographs of the fractured CPB samples cured under 400 kPa. Results show the effect of consolidation. It is interpreted that time-dependent consolidation provides compaction during curing due to pressure application and thus the consequent porosity reduces principally due to cement hydration products. Even with a naked eye, it is seen that sample is compacted and there are no empty voids between interlayer zones, therefore porosity is fairly low compared to the samples cured no pressure. That analysis for samples cured under a pressure of 400 kPa proves why consolidated samples always produce higher strengths than unconsolidated and samples. This may be well explained by a strong bridge among the particles. Some secondary minerals like sulphate also help decreasing the porosity, precipitating during curing. Sulphate ions precipitation as well as cement hydration products, both of them, are reducing significantly the resulting porosity or void ratio of the material tested.

3.4 Energy Dispersive X-ray Spectroscopy (EDS) Analysis of 'Fractured' Samples

Figure 13 shows the results of quantitative elemental analyses through the SEM coupled with energy dispersive X-ray spectroscopy EDS analyses. To characterize the hydration performance, it is common to use the Ca/Si ratio for concretes or mortars as the most abundant hydration products are C-S-H gels. Shortly, the Ca/Si ratio allows to quantify the amount of C-S-H formed during hydration process. In this regard, the fractured backfill samples cured with 0 kPa gives the highest Ca/Si ratios (45%) when compared to others (41% for consolidated backfill samples cured with 400 kPa and 4% for tailings alone).

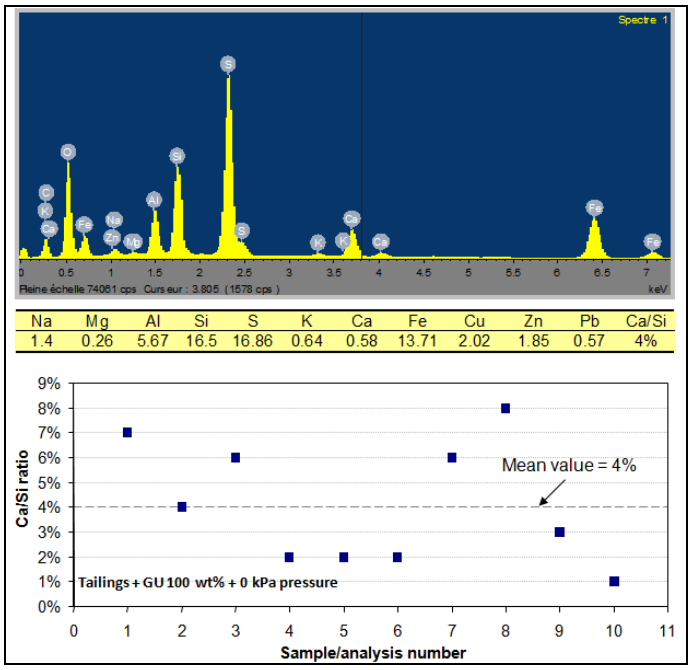

Figure 13. The EDS analysis and Ca/Si ratio curve of the freshly-fractured surface of the uncemented mine tailings.

For tailings, the lowest Ca/Si ratio (4%) is common since there is no cement hydration reaction (Fig. 13). It was also logical Ca/Si ratio for the samples cured with minimum (0 kPa) and maximum (400 kPA) pressures. Due to the fact that the higher pressure make samples more compact and denser than the sample cured with zero pressure, this sample covers lower voids to be filled completely by

hydrated produces and consequently gives lower Ca/Si ratio (41%, Figure 14).

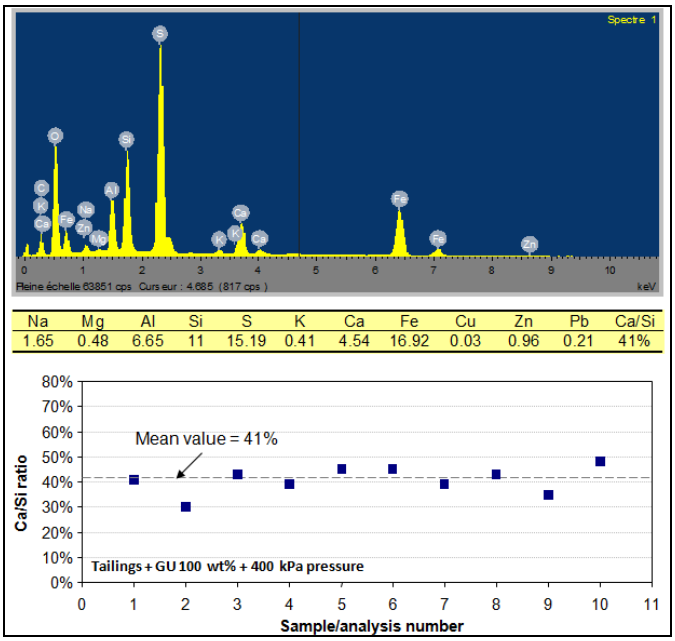

Figure 14. The EDS analysis and Ca/Si ratio curve of fractured surface of consolidated CPB prepared with GU@100wt%.

Besides, unconsolidated backfills where no pressure is applied to the samples during curing keeps larger voids to be filled fairly by cement hydration products and so gives higher Ca/Si ratio (45%, Figure 15). These analyses have shown that curing with stress does help to keep the sample denser at early stages of compaction or consolidation.

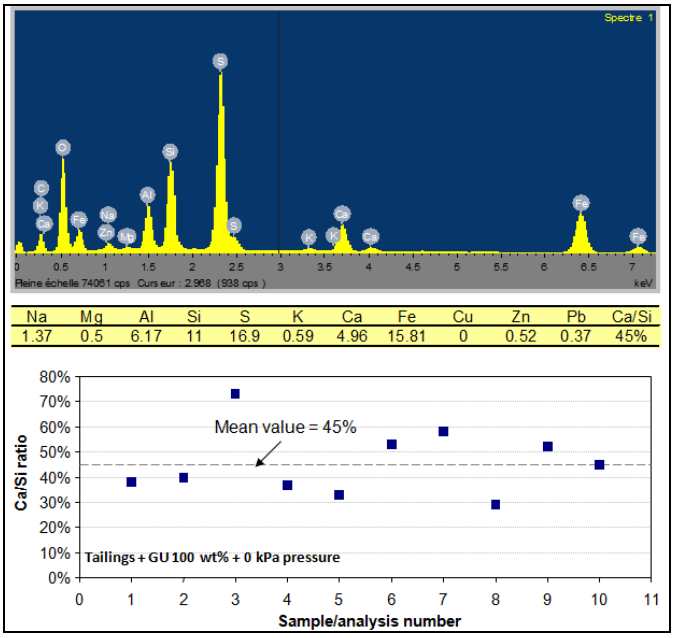

Figure 15. The EDS analysis and Ca/Si ratio curve of fractured surface of unconsolidated CPB prepared with GU@100wt%.

As a result, samples cured under pressure become denser and consequently, there does remain no space to be filled by hydration products. On the other hand, samples cured under no pressure become loose and have lots of free space which need to fill up with hydration products. Hence, the Ca/Si ratio of the latter becomes higher than the former, as we measured in the current paper.

4 CONCLUSIONS

This study presented the results of SEM-EDS analysis that were used to assess the micro-structural evolution of CPB samples. Two different curing conditions (samples cured under no pressure (0 kPa: unconsolidated) and with pressure (400 kPa: consolidated) were applied to the samples prepared using 4.5wt% cement. After 28-day curing, CPBs were first subjected to strength tests and then SEM-EDS analyses. The results have shown that curing under stress has a major effect on the CPB's microstructure. It was confirmed that consolidation greatly affects the void spaces within CPB and create sample denser and well connected between tailings particles and hydration products. SEM analyses have also confirmed that there were visible cement bonds within the consolidated samples. This work brings new light on influence of curing conditions on micro-structural evolution of CPB that can donate to better optimization of paste backfill mixes at modern mines.

ACKNOWLEDGEMENTS

The author gratefully acknowledges a number of project funds as follows: Canada Research Chair on Integrated Management of Sulphidic Mine Wastes using Mine Backfill Technology. Special thanks are Nil Gaudet, Mélinda Gervais, David Bouchard, Yvan Poirier, Mélanie Bélager, Alain Perreault and Hassan Bouzahzah of the URSTM Laboratory for their technical help in conducting a variety of physical, chemical, mechanical and microstructural tests. Finally, the author wishes to express his sincere thanks and appreciation to Professors Tikou Belem, Bruno Bussière and Mostafa

Benzaazoua for their technical and financial support during this project work.

REFERENCES

Abd.El.Aleem, S., Heikal, M., Morsi, W.M., 2014. Hydration characteristic, thermal expansion and microstructure of cement containing nano-silica. *Constr. Building Materials,* Vol. 59, pp. 151-160.

Belem, T., Benzaazoua, M., 2008. Design and application of underground mine paste backfill technology. *Geotechnical and Geological Engineering,* Vol. 26, No. 2, pp. 147-174.

Belem, T., Bussière, B., Benzaazoua, M., 2001. The effect of microstructural evolution on the physical properties of cemented tailings paste backfill. In: *Proceedings of the 8th International Conference on Tailings and Mine Waste.* Fort Collins, Colorado, USA, January 16-19, pp. 365-374.

Belem, T., El Aatar, O., Benzaazoua, M., Bussière, B., Yilmaz, E., 2007. Hydrogeotechnical and chemical characterization of column consolidated cemented paste backfill. In: *The 9th International Symposium in Mining with Backfill,* Montreal, Québec, Canada, April 29-May 2, pp. 162-171.

Benzaazoua, M., Belem, T., Bussière, B., 2002. Chemical factors that influence the performance of mine sulphidic paste backfill. *Cement and Concrete Res.*, Vol. 32, No. 7, pp. 1133-1144.

Benzaazoua, M., Belem, T., Yilmaz, E., 2006. Novel laboratory tool for paste backfill. *Canadian Mining Journal,* Vol. 127, No. 3, pp. 31-32.

Benzaazoua, M., Fall, M., Belem, T., 2004. A contibution to understanding the hardening process of cemented pastefill. *Minerals Engineering,* Vol. 17, pp. 141-152.

Benzaazoua, M., Ouellet, J., Servant, S., Newman, P., Verburg, R., 1999. Cementitious backfill with high sulfur content: physical, chemical and mineralogical characterization. *Cement and Concrete Research,* Vol. 29, No. 5, pp. 719-725.

Bernier, R.L., Lee, M.G., Moerman, A., 1999. Effects of tailings and binder geochemistry on the physical strength of paste fill. In: *The 2nd Int. Symposium on Mining and the Environment,* Sudbury, Ontario, Canada, pp. 1113-1122.

Bussière, B., 2007. Colloquium 2004: Hydrogeo-technical properties of hard rock tailings from metal mines and emerging geoenvironmental disposal approaches. *Canadian Geotechnical Journal,* Vol. 44, No. 9, pp. 1019-1052.

Choi, Y.W., Kim, Y.J., Choi, O., Lee, K.M., Lachemi, M., 2009. Utilization of tailings from tungsten mine waste as a substitution material for cement. *Constr. Building Materials,* Vol. 23, No. 7, pp. 2481-2486.

Cihangir, F., Ercikdi, B., Kesimal, A., Deveci H., Akyol, Y., Ocak, S., Kurtuluş, M., 2014. The effect of binder type on porous structure development of paste backfill. In: *Proceedings of the 11th Regional Rock Mechanics Symposium,* Afyon, Turkey, pp. 205-212.

Cihangir, F., Ercikdi, B., Turan, A., Kesimal, A., Deveci, H., Yazıcı, M., Karaoğlu, K., 2011. Utilisation of sodium silicate activated blast furnace slag as an alternative binder in paste backfill of high-sulphidic tailings. In: *The 14th International Seminar on Paste and Thickened Tailings,* Perth, Australia, pp. 465-475.

Cihangir, F., Yilmaz, E., Ercikdi, B., Kesimal, A., 2008. The effect of tailings particle size on the strength and microstructure of paste backfill. In: *The 9th Regional Rock Mechanics Symposium,* Izmir, Turkey, October 30-31, pp. 108-115.

Coussy, S., Benzaazoua, M., Blanc, D., Mozkowicz, P., Bussière, B., 2012. Assessment of arsenic immobilization in synthetically prepared cemented paste backfill specimens. *Journal of Environmental Management,* Vol. 93, pp. 10-21.

Deschamps, T., Benzaazoua, M., Bussière, B., Aubertin, M., Belem T., 2008. Microstructural and geochemical evolution of paste tailings in surface storage. *Minerals Engineering,* Vol. 21, No. 4, pp. 341-353.

Diamond, S., Kjellsen, K.O., 2008. Scanning electron microscopic investigations of fresh mortars: Well-defined water-filled layers adjacent to sand grains. *Cement and Concrete Research,* Vol. 38, pp. 530-537.

El Aatar, O., Belem, T., Bussiere, B., Benzaazoua, M., Yilmaz, E., 2007. Microstructural properties of column consolidated paste fill. In: *Proceedings of the 60th Canadian Geotechnical Conference,* Ottawa, Ontario, October 21-24, pp. 45-52.

Ercikdi, B., Baki, H., Izki, M., 2013. Effect of desliming of sulphide-rich mill tailings on the long-term strength of cemented paste backfill. *J. Environmental Management,* Vol. 115, pp. 5-13.

Ercikdi, B., Cihangir, F., Kesimal, A., Deveci, H. and Alp, I., 2008. Effect of drainage conditions on the strength of paste backfill. *Turkish Mining Journal,* Vol. 47, No. 2, pp. 15-24.

Ercikdi, B., Cihangir, F., Kesimal, A., Deveci, H. and Alp, İ., 2010. Effect of natural pozzolans as mineral admixture on performance of cemented paste backfill of sulphide-rich tailings. *Waste Management and Research,* Vol. 28, pp. 430-435.

Ercikdi, B., Cihangir, F., Kesimal, A., Deveci, H., Alp, I., 2009. Utilization of industrial waste products as pozzolanic material in cemented paste backfill of high sulphide tailings. *J. Hazardous Materials,* Vol. 168, No. 2-3, pp. 848-856.

Fall, M., Benzazoua, M., Ouellet, S., 2004. Experimental characterisation of the influence of mill tailings fineness and density on the quality of cemented paste backfill. *Minerals Engineering,* Vol. 18, pp. 41-44.

Fall, M., Samb, S., 2009. Effect of high temperature on strength and microstructural properties of cemented paste backfill. *Fire Safety Journal*, Vol. 44, No. 4, pp. 642-651.

Fourie, A.B., Fahey, H., Helinski, M., 2007. Using effective stress theory to characterize the behaviour of backfill. *CIM Bulletin*, Vol. 100, No. 1103, pp. 1-9.

Ghirian, A., Fall, M., 2014. Coupled thermo-hydro-mechanical-chemical behaviour of cemented paste backfill in column experiments. Part II: mechanical, chemical and microstructural processes and characteristics. *Engineering Geol.*, Vol. 170, pp. 11-23.

Grilo, J., Faria, P., Veiga, R., Santos Silva, A., Silva, V., Velosa, A., 2014. New natural hydraulic lime mortars: Physical and microstructural properties in different curing conditions. *Constr. Build. Mat.*, 54, 378-384.

Heikal, M., Nassar, M.Y., El-Sayed, G., Ibrahim, S., 2014. Physico-chemical, mechanical, micro-structure and durability characteristics of alkali activated Egyptian slag. *Construction and Building Materials*, Vol. 69, pp. 60-72

Hu, C., 2014. Microstructure and mechanical properties of fly ash blended cement pastes. *Constr. Building Materials*, Vol. 73, pp. 618-625.

Huang, X.Q., Hou, H.B., Zhou, M., Wang, X.W., 2014. Mechanical properties and microstructure analysis of copper tailings solidifying with different cementitious materials. *Advanced Materials Research*, Vol. 878, pp. 171-176.

Kesimal, A., Ercikdi, B., Yilmaz, E., 2003. The effect of desliming by sedimentation on paste backfill performance. *Miner. Eng.*, Vol. 16, pp. 1009-1011.

Kesimal, A, Yilmaz, E, Ercikdi, B, 2004. Evaluation of paste backfill mixtures consisting of sulphide-rich mill tailings and varying cement contents. *Cem. Concr. Res.*, Vol. 34, pp. 1817-1822.

Kesimal, A., Yilmaz, E., Ercikdi, B., Alp, I., Deveci, H., 2005. Effect of properties of tailings and binder on the short and long terms strength and stability of cemented paste backfill. *Materials Letters*, Vol. 59, No. 28, pp. 3703-3709.

Landriault, D., 2006. They said "It will never work"-25 years of paste backfill 1981-2006. In: *The 9th International Seminar on Paste and Thickened Tailings*, Limerick, Ireland, pp. 277-292.

Manfroi, E.P., Cheriaf, M., Rocha, J.C., 2014. Micro-structure, mineralogy and environmental evaluation of cementitious composites produced with red mud waste. *Constr. Building Materials*, Vol. 67, pp. 29-36.

Mohamed, A.M.O., Hossein, M., Hassani, F. P., 2003. Role of fly ash and aluminum addition on ettringite formation in lime-remediated mine tailings. *Cem. Concr. Aggr.*, Vol. 25, pp. 1-10.

Ouellet, J., Benzaazoua, M., Servant, S., 1998. Mechanical, mineralogical and chemical characterization of paste backfill. In: *The 4th International Conference on Tailings and Mine Waste*, Vail, Colorado, USA, pp. 139-146.

Ouellet, S., Bussière, B., Aubertin, M., Benzaazoua, M., 2008. Characterization of cemented paste backfill pore structure using SEM and IA analysis. *Bulletin of Engineering Geology and the Environment*, Vol. 67, No. 2, pp. 139-152.

Ouellet, S., Bussiere, B., Benzaazoua, M. Aubertin, M., 2007. SEM-XMAP: scanning electron microscopy and X-ray dot-mapping applied to cemented paste backfill. In: *The 9th International Symposium in Mining with Backfill*, Montreal, Québec, Canada, April 29-May 2, pp. 1-10.

Ouellet, S., Bussière, B., Benzaazoua, M., Aubertin, M., Belem, T., 2004. Effect of binder type and mixing water chemistry on microstructural evolution of cemented paste backfill. In: *The 57th Annual Canadian Geotechnical Conference*, Quebec city, Canada, October 23-27, pp. 1-8.

Ouellet, S., Bussière, B., Monimpa, M., Benzaazoua, M., Aubertin, M., 2006. Reactivity of an underground mine sulphidic cemented paste backfill. *Miner. Eng*, Vol. 19, No. 5, pp. 407-419.

Poon, C.S., Wong, Y.L., Lam, L., 1997. The influence of different curing conditions on the pore structure and related properties of fly-ash cement pastes and mortars. *Construction and Buildings Materials*, Vol. 11, pp. 383-393.

Potvin, Y., Thomas, E.H., Fourie, A.B., 2005. Handbook on Mine Fill. *Australian Centre for Geomechanics*, Perth, Australia.

Ramlochan, T., Grabinsky, M.W., Hooton, D.H., 2004. Microstructural and chemical investigations of cemented paste fills. In: *the 11th International Conference on Tailings and Mine Waste.* Vail, Colorado, US, October 10–13, pp. 293-304.

Revell, M., 2004. Paste: how strong is it? In: *The 8th International Symposium in Mining with Backfill*, Beijing, China, pp. 286-294.

Tarig, A., Nehdi,M., 2007. Developing durable paste backfill from sulphidic tailings. *Waste Resources Management*, Vol. 160, No. 4, pp. 155-166.

Thomas, S., Damare, A., Gupta, C., 2013. Strength and durability characteristics of copper tailing concrete. *Con. Buil. Mat.*, Vol. 48, pp. 894-900.

Vaitkevicius, V., Serelis, E., Hilbig, H., 2014. The effect of glass powder on the microstructure of ultra high performance concrete. *Construction and Building Materials*, Vol. 68, pp. 102-109.

Wu, D., Fall, M., Cai, S., 2013. Coupling temperature, cement hydration and rheological behaviour of fresh cemented paste backfill. *Minerals Engineering*, Vol.42, pp. 76-87.

Yilmaz, E., Belem, T., Benzaazoua, M., 2012. One-dimensional consolidation parameters of

cemented paste backfills. *Mineral Resources Management*, Vol. 28, No. 4, pp. 29-45.

Yilmaz, E., Belem, T., Benzaazoua, M., 2013. Study of physico-chemical and mechanical properties of consolidated and unconsolidated cemented paste backfills. *Min. Res. Man.* Vol. 29, pp. 81-100.

Yilmaz, E., Belem, T., Benzaazoua, M., 2014a. Effects of curing and stress conditions on hydromechanical, geotechnical and geochemical properties of cemented paste fill. *Engineering Geology*, Vol. 168, pp. 23-37.

Yilmaz, E., Belem, T., Benzaazoua, M., 2015b. Specimen size effect on strength behaviour of cemented paste backfill subjected to different placement conditions. *Eng. Geol.*, (accepted).

Yilmaz, E., Belem, T., Bussière, B., Benzaazoua, M., 2011. Relationships between porosity, microstructure and compressive strength of consolidated and unconsolidated cement paste backfills. *Cement and Concrete Composites*, Vol. 33, No. 6, pp. 702-715.

Yilmaz, E., 2010. Investigating the hydrogeo-technical and microstructural properties of cemented paste backfills by the versatile CUAPS apparatus. In: *Ph.D. Thesis*, UQAT, Canada (http://depositum.uqat.ca/34/1/erolyilmaz.pdf).

Yilmaz, E., 2011. Advances in reducing large volumes of environmentally harmful mine waste rocks and tailings. Mineral Resources Manag., Vol. 27, No. 2, 89-112.

Yilmaz, E., Belem, T., Bussière, B., Mbonimpa, M., Benzaazoua, M., 2015a. Curing time effect on consolidation behaviour of cemented paste backfill containing different cement types and contents. *Construction and Buildings Materials*, Vol. 75, pp. 99-111.

Yilmaz, E., Benzaazoua, M., Belem, T., Bussière, B., 2009. Effect of curing under pressure on compressive strength development of cemented paste backfill. *Minerals Engineering*, Vol. 22, No. 9-10, pp. 772-785.

Yilmaz, T., Ercikdi, B., Karaman, K., Kulekci, G., 2014b. Assessment of strength properties of cemented paste fill by ultrasonic pulse velocity test. *International Journal of Ultrasonics*, Vol. 54, No. 5, pp. 1386-1394.

Evaluation of Grout Curtain Efficiency of Kalu-Ganga Dam

A. Aalianvari
Department of mining engineering,Faculty of engineering, University of Kashan, Kashan, I. R. Iran

ABSTRACT The main objective of this work was to study the design rationale for the optimum grout curtain of Kaluganga dam. One of the important points in the study stages and along the performance works for the earth dams construction is seepage analysis through foundation and dam body, which is a serious problem for dam designers. So calculation of seepage amount from foundation and dam body and evaluation of control or decrease methods for this problem is essential. This study was based on a combination of geotechnical investigations, geological investigations, and numerical modeling. The dam is located in the volcani rocks such as Garnet granulitic gneiss and calcareous gneiss.This paper presents finite element model for prediction of water seepages from dam to determine optimum depth of grout curtain. Results show without grout curtain around 0.7 m3/s water seepages from dam and with the 70 m grout curtain depth, reduces to the 0.185 lit/sec.

Keywords: Grout curtain efficiency, geological and geotechnical investigation, numerical modelling

1 INTRODUCTION

Kalu Ganga Main Dam and Saddle Dam are located in about 24 km upstream of Moragahakanda Dam. The project also includes water transfer system (tunnel + canal) conveying water from Kalu Ganga Dam Reservoir to the reservoir of Moragahakanda Dam. The transfer canal and tunnel are about 7 km and 3.5 km long respectively.

The bedrock of dam consists of 3 different types of gneisses can be clearly differentiated at the main dam area garnet granulitic gneiss, calcareous gneiss and charnockitic gneiss. Figure 1 show the geological section along the dam axis.

Based on the engineering judgments and water pressure test results in exploratory boreholes the average permeability for each abutment and foundation has been estimated.

At the left abutments maximum permeability in these boreholes (DH25, DP05, DH26, DH27, and DP03) is around 20 to 30 Lu. And minimum permeability is less 1 Lu. Therefore average permeability in these boreholes has been estimated around 10 Lu.

At the right abutments maximum permeability in these boreholes (DH21, DH23, DH22, DH02, DH09, and DH17) is around 30 to 50 Lu. And minimum permeability is less 1 Lu. Therefore average permeability in these boreholes has been estimated around 4 Lu.

In the foundation of dam (riverbed area) maximum permeability in these boreholes (KT14, KT12, DH05, DH15, and DH04) is around 5 to 10 Lu. And minimum permeability is less 1 Lu. Therefore average of permeability in these holes as around 4Lu.

According to ASTM D6032-96 (table 3) at the drilled boreholes in dam site the rock quality in left bank(based on boreholes: DH25,DH10,DH26,DH27,DH28) is Medium (R.Q.D=72%), in right bank(based on boreholes: DH21, DH23, DH22, DH02, DH18, DH09, DH17) is Poor (R.Q.D=36%) and the foundation or riverbed (based on boreholes: DH20, DH19, DH05, DH15) is good (R.Q.D=84%).

In this paper, a numerical finite element model using SEEP/W software (Geo-Slope International Ltd, 2006) and analytical equations to predict water flow seepage from

dam in different conditions and according to their results the optimum grout curtain depth pit has been selected.

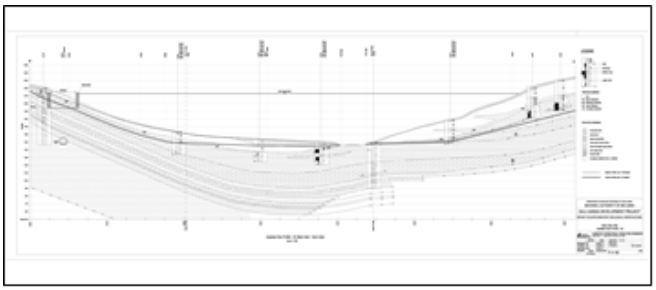

Figure 1. Geological section along the dam axis

2 SEEPAGE ANALYSIS OF KALU GANGA DAM

All earth dams are subject to seepage through the embankment, foundation, and abutments. Seepage control is necessary to prevent excessive uplift pressures, sloughing of the downstream slope, piping through the embankment and foundation, and erosion of material by loss into open joints in the foundation and abutments.

The purposes of the seepage analysis are includes:

1- Estimation of water seepage through the foundation and abutments
2- Determination of lateral extension and depth of grout curtains
3- Prediction of grout curtain efficiency

Estimation of water seepages from the Kalu Ganga dam has been done at 2-D steady state status with Geostudio package and Seep/w software.

Normal water level of reservoir, Tail water level and rock mass permeability are the major parameters regulating water seepage from dams. In this project Normal water level is 210 m.a.s.l and Tail water level is the river elevation (152 m.a.s.l) but the major parameter that affects the water flow is rock mass permeability.

Estimation of rock mass permeability is very important, so before modeling the water seepage from dam, different alternation of permeability has been studied and analyzed.

2.1 Rock Mass Permeability

The water permeabilities of most rock materials lie in the range 10-10to 10-15ms-1 (Louis, 1969), which means that from an engineering point of view an unfractured rock mass is effectively impermeable to water. All rocks, particularly those near to the ground surface, contain discontinuities which can provide major conducting pathways for migrating fluids. Natural processes such as mineralisation and aquifer recharge, together with manmade processes such as water, oil and gas recovery rely upon the contribution made to mass permeability by discontinuity networks.

Major discontinuities such as faults, bedding and geometrical properties of joints have been controlled the rock mass permeability, so to accurate estimation of seepage from dam 3 modes have been studied for rock mass permeability of dam.

- Rock mass permeability based on the average of the water pressure tests in boreholes at new axis dam.
- Rock mass permeability based on the maximum lugeons of the water pressure tests in boreholes at new axis dam.
- Sensitivity analysis for various permeability based on the geological conditions, engineering judgment and water test results

2.1.1 Permeability based on the average of lugeon tests on boreholes

Based on the engineering judgments and water pressure test results in exploratory boreholes the average permeability for each abutment and foundation has been estimated.

At the left abutments 7 exploratory boreholes have been drilled (DH21, DH26, DH27, DP03, DP04, DP05, DH10). Results show that average permeability in these boreholes is around 10 Lu.

At the right abutments 8 exploratory boreholes have been drilled (DH21, DH22 ,DH23,DH02,DH18,DH09,DH17,DP09). Results show that average permeability in these boreholes is around 20 Lu.

At the foundation of dam 8 exploratory boreholes, DH05, DH19, DH20,

DH05,KT14,KT12,DH04 DH14 and KT10 have been drilled and water pressure test has been done in these holes. The average of permeability in these holes as around 4Lu.

2.1.2 Maximum permeability in exploratory boreholes

When the number of water pressure tests in the exploratory holes is not sufficient, maximum lugeon in the holes can be considered as the basis of water seepage. Therefore at the left abutment, 30 lugeon has been considered as the equivalent permeability that this value taken from DH25 borehole.

At the right abutment due to the limestones, the 50 lugeon was the maximum value in the tests (DH21) and the foundation 11 lugeon has been considered as the highest value in the holes (DH05)

2.1.3 Sensitivity analysis for various permeability based on the geological conditions and water test results

Water pressure test results in exploratory boreholes show that in a few sections the lugeon value higher than 50 has been obtained so based on the geological conditions, engineering judgment and water pressure test results and to sensitivity analysis, numerical modeling of seepage done with 3 alternative, 100, 200 and 500 lugeons.

2.2 Seepage Analysis

There are different ways to calculate water seepage from the reservoir, such as analytical and numerical methods. In this project, water seepage from the KaluGanga dam was estimated using a finite element method.

A finite element method (FEM) is a numerical technique for finding approximate solutions to boundary value problems for differential equations. It uses variation methods (the calculus of variations) to minimize an error function and produce a stable solution FEM.

In this project, a numerical finite element model implemented in the SEEP/W software package (Geo-Slope International Ltd. 2006) is presented. It is capable of predicting the water seepage from dam.

The SEEP/W model is able to analyze different flow conditions such as saturated/unsaturated flow and a confined/unconfined aquifer in a two-dimensional situation. To calculate the amount of water seepage, different geological sections were prepared. Figure 2 show the location of geotechnical sections in the geological map.

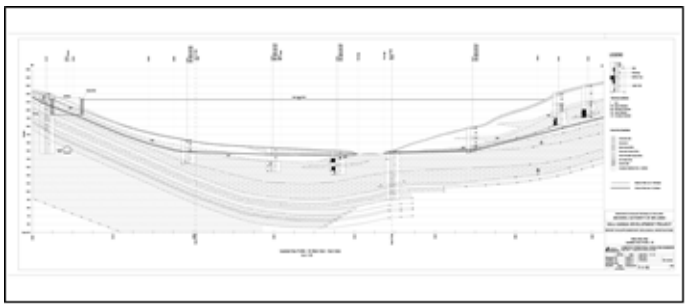

Figure 2. Location of seepage sections

The seepage model of geological sections at abutments and foundations has been generated with Seep/w software.

To determine the optimum depth of grout curtain at the abutments and foundation, seepage models have been done in 2 cases, with grout curtain at different depth and without grout curtain. Figures 2,3 and 4 show the seepage sections.

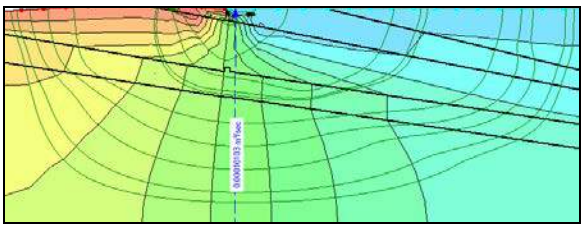

Figure 3. Seepage section along dam foundation(without grout curtain)

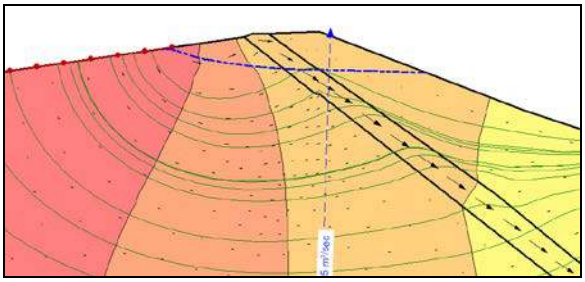

Figure 4. Seepage section at left abutment(without grout curtain)

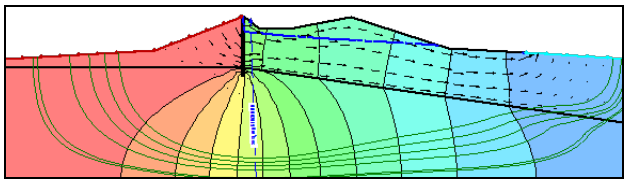

Figure 5. seepage section at right abutment(with grout curtain)

3 RESULTS AND DISCUSSION

According to results, without grout curtain about 0.7m3/Sec water seepage from dam , so this amount of water is very dangerous for construction and it is very important to design optimum drainage systems to prevent the water flow.Table 1 shows the results of numerical modeling for the seepage sections at the case of without grout curtain and various permeability.

Table 1. Seep/w results for the sections (without grout curtain and various permeability) (Lit/Sec)

Case	Right Abutment	Foundation	Left Abutment	Total
Average Permeability	9	5	4	18
Max Permeability	15	13	11	39
100 Lu	29	100	22	151
200Lu	56	194	40	290
500 Lu	138	484	96	718

To determination of optimum depth of grout curtain, seepage sections at various depth (40 m, 50 m, 60m and 70m) was modeled and results show in the table 2. The grout curtain extends to the impermeable area beneath dam foundation. The design of grout curtain mainly is depended on hydrogeological conditions and water column height on the dam foundation and condition of calcareous gneiss. Table 2 shows the results of analysis for different depth of grout curtain in whole of KaluGanga dam site.

Table 2. Seep/w results for the different depth of grout curtain (Lit/Sec)

Case	Grout curtain with 40 m depth	Grout curtain with 50 m depth	Grout curtain with 60 m depth	Grout curtain with 70 m depth
Average Permeability	17.9	17.8	17.7	17.6
Max Permeability	38	37	36	35.8
100 Lu	104	99	83.5	83
200Lu	202	190	175	122
500 Lu	447	396	188	185

Efficiency of grout curtain for right abutment, left abutment and foundation are shown on the below figures.

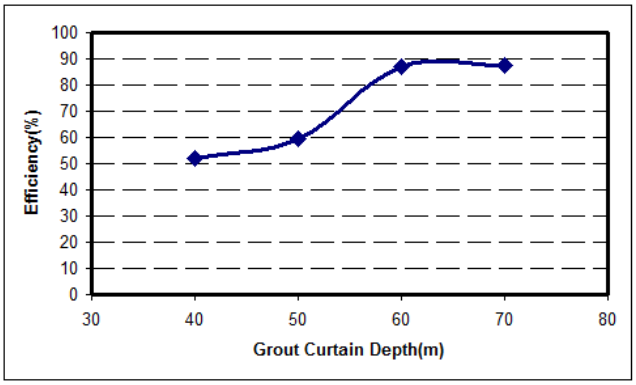

Figure 6. Grout curtain efficiency for dam foundation

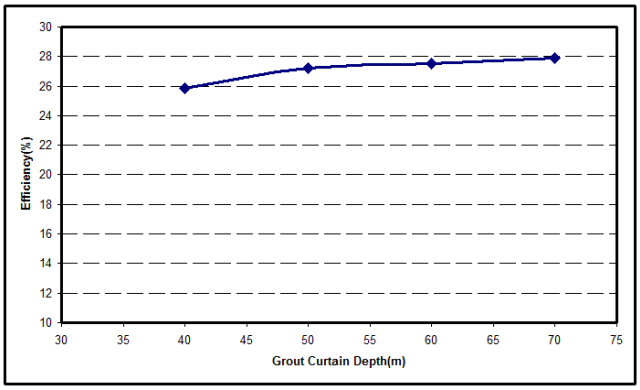

Figure 7. Grout curtain efficiency for left abutment

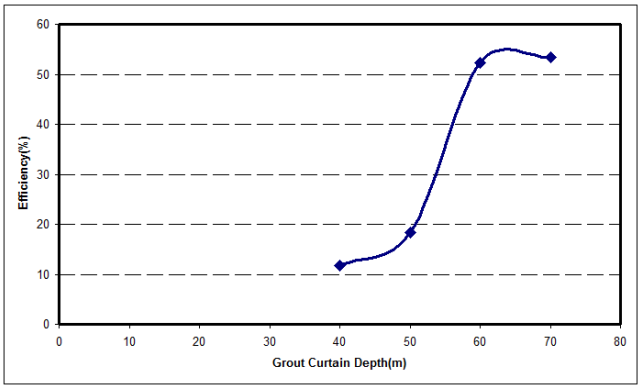

Figure 8. Grout curtain efficiency for right abutment

4 CONCOLUSION

The grout curtain extends to the impermeable area beneath dam foundation. The design of grout curtain mainly is depended on hydrogeological conditions and water column height on the dam foundation and condition of calcareous gneiss.

Based on the geological conditions for each abutment and numerical results:

- Due to the presence of calcareous gneiss with high permeability at right abutment and Seep/w results, 75 to 90 m is the optimum depth of grout curtain for the right abutment. In this case, the grout curtain efficiency is around 70%.
- The optimum depth of grout curtain for the dam foundation is around 55 m with about 60% efficiency.
- For the left abutment, due to the nearest of calcareous gneiss unit to the surface, the 25 m depth of grout curtain is an optimum depth.
- Due to the importance of accurate permeability, it is recommended to surveying the geometrical properties of discontinuities such as joint spacing, joint aperture.

REFERENCES

Aalianvari A, Katibeh H, Sharifzadeh M (2010) A new approach for computing permeability of fault zones case study: the upper reservoir of Azad pumped-storage power station in Iran. Arch Min Sci 55(3):605–621

Aalianvari A, (2014) Optimum depth of grout curtain around pumped storage power cavern based on geological conditions. Bull Eng Geol Environ (2014) 73:775–780

Aalianvari A, Malekitehrani,M. Soltanimohammadi, s. (2014), Estimation of Water Flow from Upper Reservoir of Azad Pumped Storage Power Plant, Using Geostatistical Methods, Journal geological society of india, Vol.83, January 2014, pp.76-82

Atkinson, L.C.,T.M.Hanna, and I.W.Anthony.1989. "Investigation and implementation of mine dewatering systems"World Gold' 89 Conferences.Sigapore.

Bear, J.1979.Hydraulics of groundwater.New York:McGraw-Hill Inc.

Esteban Hormazabalz, 2005, "Estimation flow and pore pressures in open pit mines", M.Sc thesis, Dept of Geology and Geophysics, Boston college.

Freeze R.A., Cherry J.A. 1979. Groundwater. Prentice-Hall, Inc, Englewood Cliffs, NJ, 604 p.

Goodman, R.E., D.G.Moye, A. Van Schalkwyk and I.Javandel.1965. Groundwater inflows during tunnel driving. Engineering Geology,39-56

Hanns,T.M.,A. A. Elfadil, and L.C.Atkinson 1994. Use of analytical soloution for preliminary estimates of groundwater inflow to pit. Minin Engineering 46, no. 2: 149-152

Hotckkiss, J.S. Downey, E.D. Gutentag and J.E. Moore (Eds.), American Institute of Hydrology, 162-177.

Kruseman G.P., De Ridder N.A. (1979). Analysis and evaluation of pumping test data. Bulletin 11, International Institute for Land Reclamation and Improvement, The Netherlands, 200 p.

Marinelli F., Niccoli W.L. (2000). Simple analytical equations for estimating ground water inflow to a mine pit. Ground Water 38 (2), 311-314.

Selection of Chromite Processing Plant Site Using The Fuzzy TOPSIS Approach

H. Bejari
Department of Mining Engineering, University of Sistan and Baluchestan, Zahedan, Iran

A. Daya
Department of Mining Engineering, University of Sistan and Baluchestan, Zahedan, Iran

ABSTRACT One of the large province of Iran is the Sistan and Baluchestan that is a rich region based on ore deposit. From the major metal mines of Sistan and Baluchestan, it can be mentioned to the chromite mines. According to the existence of chromite deposits in the province and also various applications of chromite in different industries, it's expected that the establishment of chromite processing plant is needed in the erelong. This paper presents an application fuzzy TOPSIS which is used to select an appropriate site for chromite processing plant in Sistan and Baluchestan province. For this purpose, based on concentration of chromite deposits in different regions of the province, four feasible alternatives, including Zahedan, Khash, Iranshahr and Nikshahr cities, were selected for the chromite processing plant. Quantitative and qualitative criteria such as access to raw materials, availability of labor, education, water and weather, environmental effects, export market and domestic demand and security are used to compare the feasible alternatives. Finally, the alternatives are ranked and convenient location are recommended for the construction of chromite processing plant.

Keywords: Fuzzy, plan site, TOPSIS, chromite

1 INTRODUCTION

Localization is one of the spatial analyses that have great effect on reducing the costs of creating and construction of various activities. Today, finding a suitable place or places for the creation of an activity in a specific geographical area is an important step especially at the macro and national projects. Final possible sites must meet all provisions of these terms and constraints and lack of evaluation of such projects will lead to many undesirable results. Suitable location selection for construction of processing plant will create jobs and increase production of chromite mines. Also the demand for raw materials in Sistan and Baluchistan province and various industries such as metallurgical, chemical and pharmaceutical industries will be supplied. With proper selection of plant location, energy consumption, environmental impact and costs are significantly reduced. Site selection is a critical decision which requires considering a number of factors and evaluates several alternatives. In most cases, all the factors involved in site selection have not been taken into consideration and optimum alternative cannot be chosen. The goal of site selection is to find the best location with desired conditions that satisfy predefined criteria. Site selection for mineral processing plant needs to evaluate several alternatives with regard to a number of criteria. Therefore, this issue can be considered as a decision making process, which involves to find the best option among the feasible alternatives or to rank them. Over the past decades, many methods such as simple additive weighting (Hwang and Yoon 1981), the technique for order preference by similarity to ideal solution (Hwang and Yoon 1981), analytical hierarchy process (Saaty 1980), data envelopment analysis (Cooper et al. 2000), and so on have been developed to deal with a multiple decision making problem. in this

paper, fuzzy Analytic Hierarchy Process (Fuzzy-AHP) method is used for determining the importance weights of evaluation criteria, and fuzzy technique for order performance by similarity to ideal solution (Fuzzy TOPSIS) is used to obtain the performance ratings of the feasible alternatives in linguistic values parameterized with triangular fuzzy numbers (TFNs) (Zadeh, 1975).

2 FUZZY ANALYTIC HIERARCHY PROCESS (F-AHP)

Analytic hierarchy process (AHP) has been developed by Saaty (1990). The AHP structures the decision problem in levels which correspond to one understands of the situation: goals, criterion, sub-criterion, and alternatives. By breaking the problem into levels, the decision-maker can focus on smaller sets of decisions. In AHP technique the elements of each level compared to its related element in upper level inform by pair-wise comparison method.

It must be noted that, in pair comparison of criterion if the priority of element i compared to element j is equal to w_{ij} , then the priority of element j compared to element i is equal to $1/w_{ij}$. The priority of element compared to it is equal to one.

Inability of AHP to deal with the imprecision and subjectiveness in the pair-wise comparison process has been improved in fuzzy AHP. Instead of a crisp value, fuzzy AHP uses a range of value to incorporate the decision maker's uncertainty (Kuswandari 2004).

Fuzzy AHP method is applied in this research for criteria weighting. So, A fuzzy judgment matrix ($\tilde{J}$) is generated using fuzzy pairwise comparison index ($\tilde{j}_{ij}$). A relative importance of the pairwise comparison is assigned using a scale of 1–9 (Saaty 1977, 1988), which are fuzzified to capture vagueness in perception and meaning (Table 1). For n number of comparison items, the fuzzy judgment matrix $\tilde{J}$ is:

$$\tilde{J} = \begin{bmatrix} \tilde{j}_{11} & \tilde{j}_{12} & \cdots & \tilde{j}_{1n} \\ \tilde{j}_{21} & \ddots & & \tilde{j}_{2n} \\ \vdots & & \ddots & \vdots \\ \tilde{j}_{n1} & \tilde{j}_{n2} & \cdots & \tilde{j}_{nn} \end{bmatrix} \quad (1)$$

Table 1. Fuzzy scales for pairwise comparisons

Relative importance	Fuzzy scale
$\bar{1}$	(1, 1, 1)
$\bar{x}$	(x-1, x, x+1) for x= 2, 3, 4, 5, 6, 7, 8
$\bar{9}$	(8, 9, 9)
$1/\bar{1}$	(1/2, 1, 1)
$1/\bar{9}$	(1/9, 1/9, 1/8)

It is important to ensure that there is consistency in the pairwise comparisons (Saaty 2005). In order to measure the degree of consistency, one can calculate the Consistency Index (CI). Consistency index therefore, indicates whether a decision maker provides consistent values (comparisons) in a set of evaluation. The CI is calculated as:

$$CI = (\lambda_{max} - n)/(n-1) \quad (2)$$

The final inconsistency in the pairwise comparisons is solved using consistency ratio $CR = CI/RI$ where RI is the random index, which is obtained by averaging the CI of a randomly generated reciprocal matrix (Saaty 1980). The values of RI are tabulated in Table 2. In this paper, though the pairwise comparison indices of the judgment matrix are TFNs, however, the CI is evaluated for the most likely value.

As the next step fuzzy weights are calculated. Various techniques are used to compute the final fuzzy weights, such as, computation of the eigenvector, arithmetic mean, geometric mean, etc. In this study, for the ease of implementation the geometric mean is adopted to estimate the weights. Fuzzy arithmetic operations are utilized over matrix $\tilde{J}$ to compute the fuzzy weights. The geometric mean is computed for each row $\tilde{J}_i$. Given $\tilde{J}$ from Equation 1, the corresponding fuzzy weights are computed as:

$$\tilde{J}_i = (\tilde{j}_{i1} \otimes \cdots \otimes \tilde{j}_{in})^{\frac{1}{n}} \quad (3)$$

$$\tilde{w}_i = \tilde{J}_i \otimes (\tilde{J}_1 \oplus \cdots \oplus \tilde{J}_n)^{-1} \quad (4)$$

Where $\tilde{w}_i$ is the fuzzy weight (where i =1 to n).

Table 2. Random inconsistency indices (RI)

No. of criteria	1-2	3	4	5	6	7	8
RI	0	0.58	0.9	1.12	1.24	1.32	1.41

3 FUZZY TOPSIS

The TOPSIS method (Technique for Order Preference by Similarity to Ideal Solution) is a linear weighting technique which was first proposed in its crisp version by Chen and Hwang (1992). The ideal solution (also called the positive ideal solution) is a solution that maximizes the benefit criteria/attributes and minimizes the cost criteria/attributes, whereas the negative ideal solution (also called the anti-ideal solution) maximizes the cost criteria/attributes and minimizes the benefit criteria/attributes. The so-called benefit criteria/attributes are those for maximization, while the cost criteria/attributes are those for minimization. The best alternative is the one that is closest to the ideal solution and farthest from the negative ideal solution. The use of fuzzy theory allows us to incorporate unquantifiable information, incomplete information, non-obtainable information, and partial facts into the decision model. Therefore, in this paper, the concept of the approach used for solving the processing plant site selection problem will be based on the fuzzy technique for order preference by similarity to ideal solution (Fuzzy TOPSIS). This is because four advantages are addressed: (1) a sound logic that represents the rationale of human choice, (2) a scalar value that accounts for both the best and worst alternatives simultaneously, (3) a simple computation process that can be easily programmed, and (4) the performance measures of all alternatives on attributes can be visualized as a polyhedron, at least for any two dimensions. In the following section the fuzzy TOPSIS method is detailed in steps:

Step 1: Calculate the decision matrix (D) as equation 5:

$$\tilde{D} = \begin{array}{c} \\ A_1 \\ A_2 \\ A_3 \\ \vdots \\ A_m \end{array} \begin{array}{c} \begin{array}{ccccc} C_1 & C_2 & C_3 & \cdots & C_n \end{array} \\ \begin{bmatrix} \tilde{x}_{11} & \tilde{x}_{12} & \tilde{x}_{13} & \cdots & \tilde{x}_{1n} \\ \tilde{x}_{21} & \tilde{x}_{22} & \tilde{x}_{23} & \cdots & \tilde{x}_{2n} \\ \tilde{x}_{31} & \tilde{x}_{32} & \tilde{x}_{33} & \cdots & \tilde{x}_{3n} \\ \vdots & \vdots & \vdots & \ddots & \vdots \\ \tilde{x}_{m1} & x_{m22} & \tilde{x}_{m3} & \cdots & \tilde{x}_{mn} \end{bmatrix} \end{array} \quad (5)$$

Where $\tilde{x}_{ij}$ (i=1, 2… m, j= 1, 2… n) are the linguistic values for alternatives with respect to criteria. The fuzzy linguistic rating the property $\tilde{x}_{ij}$ preserves that the ranges of normalized triangular fuzzy numbers belong to [0, 1]; thus, there is no need for normalization.

Step 2: Calculate the criteria weighted matrix as equation 6 (fuzzy weights for criteria in this section calculate based on Fuzzy-AHP):

$$\tilde{W} = \begin{bmatrix} \tilde{w}_1 & \cdots & 0 \\ \vdots & \cdots & \vdots \\ 0 & \cdots & \tilde{w}_n \end{bmatrix} \quad (6)$$

Where $\tilde{W}j, J = (1,2,...,n)$ are fuzzy numbers and represents the weight of the jth attribute, Cj.

Step 3: Calculate the weighted normalized decision matrix. The weighted normalized value $\tilde{v}_{ij}$ is calculated as:

$$\tilde{v}_{ij} = \tilde{w}_j \times \tilde{x}_{ij} = \tilde{W} \times \tilde{D} \quad (j = 1,2,...,n \text{ and } i = 1,2,...,m) \quad (7)$$

Step 4: Determine the positive ideal and negative ideal solutions, A^*, A^- respectively. The fuzzy positive-ideal solution (FPIS, A^*) and the fuzzy negative-ideal solution (FNIS, A^-) are shown as Equations 8 and 9:

$$A^* = (\tilde{v}_1^*, \tilde{v}_2^*, ..., \tilde{v}_n^*) = \left\{ \left(\max_j v_{ij} \middle| i \in K \right), \left(\min_j v_{ij} \middle| i \in L \right) \right\} \quad (8)$$

$$A^- = (\tilde{v}_1^-, \tilde{v}_2^-, ..., \tilde{v}_n^-) = \left\{ \begin{array}{l} \left(\min_j v_{ij} \,|\, i \in K \right), \\ \left(\max_j v_{ij} \,|\, i \in L \right) \end{array} \right\} \quad (9)$$

Where K is associated with benefit criteria, and L is associated with cost criteria.

Step 5: Calculate the separation measures, using the n-dimensional Euclidean distance. The distance of each alternative from the ideal solution (A^*) and the distance from the negative ideal solution (A^-) are given as equations 10 and 11 respectively:

$$D_i^* = \sum_{j=1}^{n} d(\tilde{v}_{ij}, \tilde{v}_j^*), i = 1,2,...,m \quad (10)$$

$$D_i^- = \sum_{j=1}^{n} d(\tilde{v}_{ij}, \tilde{v}_j^-), i = 1,2,...,m \quad (11)$$

Step 6: Calculate similarities to ideal solution. The relative closeness of the alternative Ai with respect to A^* is defined by equation 12:

$$RC_i = \frac{D_i^-}{D_i^* + D_i^-} \quad (12)$$

Step 7: Rank the alternatives according to the relative closeness to the ideal solution (RC_i)

The higher value of RC_i indicates that an alternative is closer to the positive ideal solution and farther from the negative ideal solution simultaneously. A value of 1 (or 100 per cent) for an alternative indicates that the alternative is equal to the positive ideal solution and a value of 0 (or 0 per cent) is equal to the negative ideal solution. The best alternative is the one with the greatest relative closeness to the positive ideal solution.

The proposed model for selection of chromite processing plant site, composed of fuzzy AHP and fuzzy TOPSIS methods, consists of two basic stages: (1) identify the criteria to be used in the model and Assigning criteria weights via Fuzzy-AHP (2) evaluation of alternatives with Fuzzy-TOPSIS and determination of the final rank.

In the first stage, criteria used in processing plant site selection are assigned weights using Fuzzy-AHP. In this phase, pairwise comparison matrix is formed to determine the criteria weights. The values of the elements of pairwise comparison matrices determine using the scale provided in Table 1. As the next step fuzzy weights are calculated using the geometric mean technique.

Alternatives ranks are determined by using fuzzy TOPSIS method in the second stage. Linguistic values are used for evaluation of alternatives in this stage. the linguistic variables divided to five-levels, fuzzy linguistic values ‘very bad, ‘bad’, ‘medium’, ‘good’ and ‘very good. In next step, linguistic values are converted to fuzzy numbers with transformation of fuzzy membership functions, as are shown at Table 3.

Table 3. Linguistic values for the ratings

Linguistic values	Fuzzy numbers
Very bad (VB)	(0, 1, 3)
Bad (B)	(1, 3, 5)
Medium (M)	(3, 5, 7)
Good (G)	(5, 7, 9)
Very Good (VG)	(7, 9, 10)

4 APPLICATION OF PROPOSED MODEL TO CHROMITE PROCESSING PLANT SITE SELECTION IN SISTAN AND BALUCHESTAN PROVINCE

Sistan and Baluchestan province is one of the largest and richest areas of mineral deposits in southeast of Iran. One of the important metallic mineral deposits is chromite one that can be found in various parts of the province. Distribution of chromite deposits in the province illustrated in Figure 1. The red spots in this figure represent the chromite deposits. It can be clearly seen that chromite mines are concentrated around Zahedan, Khash, Nikshahr and Iranshahr.

The first step in the process of site selection is collecting and evaluating the required information. The selection of an

appropriate site for mineral processing plant involves considering many criteria. The large number of criteria leads to a computational difficulty, a time consuming process and an unrealistic outcome.

The criteria of decision-making for chromite processing plant site selection in Sistan and Baluchestan province including access to raw materials (C1), availability of labor (C2), education (Access and promotion of labor) (C3), water and weather (temperature , humidity, precipitation, number of dusty days per year and …) (C4), environmental effects (C5), export market and domestic demand (C6) and security (C7). Also with evaluating distribution map of chromite deposits in Sistan and Baluchistan province, feasible alternatives are those locations that chromite deposits are more concentrated. Selected locations are Zahedan (A1), Khash (A2), Iranshahr (A3) and Nikshahr (A4). Each alternative is evaluated with relevant criteria based on the technical and experimental experiences and also by asking the decision makers and experts.

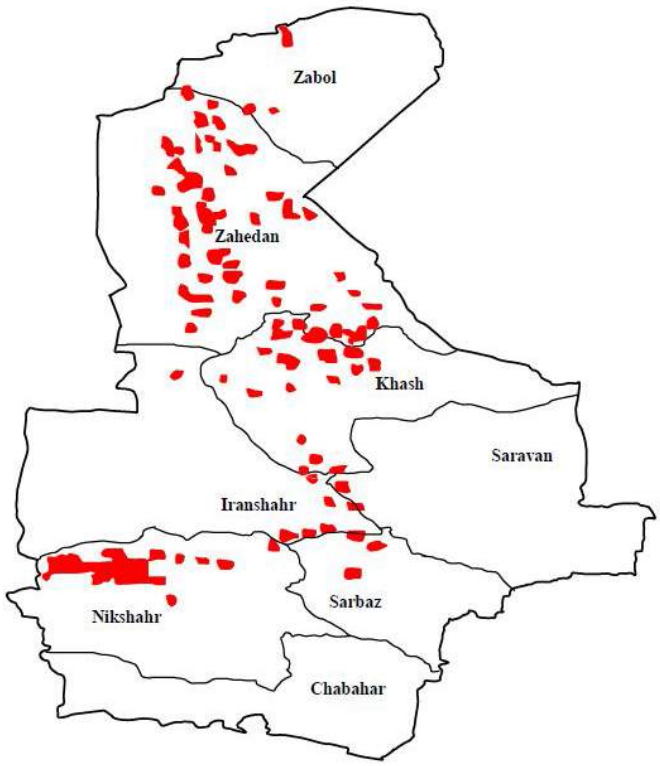

Figure 1. Distribution of chromite deposits in Sistan and Baluchestan province (the red spots represent the chromite deposits)

After determination of the criteria, the weights of the criteria to be used in evaluation process are calculated by using fuzzy AHP method. In this phase, the experts in the expert team are given the task of forming individual pairwise comparison matrix by using the scale given in Table 1. Geometric means of these values are found to obtain the pairwise comparison matrix on which there is a consensus (Table 4). The results obtained from the computations based on the pairwise comparison matrix are presented in Table 4. Consistency ratio of the pairwise comparison matrix is calculated as $0.056 < 0.1$. So the weights are shown to be consistent and they are used in the selection process.

In next step, the decision matrix establish by comparing alternatives under each of the criteria separately. Fuzzy evaluation matrix established by the evaluation of alternative rifles by linguistic variables in Table 3, is presented in Table 5. The table is composed of the triangular fuzzy numbers which are equivalent of linguistic variables. As the decision matrix should be normalized, the corresponding matrix is presented in Table 6.

After the fuzzy evaluation matrix was determined, the next step is to obtain a fuzzy weighted decision table. Using the criteria weights calculated by fuzzy AHP (Table 4), the Weighted Evaluation Matrix is established with equation 7. The resulting fuzzy weighted decision matrix is shown in Table 7.

In next step, we define the fuzzy positive-ideal solution (FPIS, A^*) and the fuzzy negative-ideal solution (FNIS, A^-). Therefore, the distance of each alternative from A^* and A^- can be currently calculated using equations 10 and 11. The final step solves the similarities to an ideal solution by equation 12. The resulting fuzzy TOPSIS analyses are summarized in Table 8. Based on RC_i values, the ranking of the alternatives in descending order are A2, A1, A3 and A4. Proposed model results indicate that A2 (Khash see Fig.1) is the best alternative with RC_i value of 0.465.

Table 4 A weighting scheme for criteria via Fuzzy-AHP

	C1	C2	C3	C4	C5	C6	C7	$\tilde{w}_i$
C1	1	5	7	2	3	7	3	(0.1893, 0.3270, 0.5313)
C2	1/5	1	3	1/5	1/5	3	1/5	(0.0334, 0.0538, 0.0879)
C3	1/7	1/3	1	1/7	1/5	3	1/5	(0.0229, 0.0357, 0.0582)
C4	1/2	5	7	1	2	7	2	(0.1327, 0.2389, 0.4183)
C5	1/3	5	5	1/2	1	7	1/2	(0.0878, 0.1446, 0.2656)
C6	1/7	1/3	1/3	1/7	1/7	1	1/7	(0.0157, 0.0237, 0.0385)
C7	1/3	5	5	1/2	2	7	1	(0.1028, 0.1763, 0.3108)

Table 5 Fuzzy decision matrix using triangular fuzzy numbers

	C1	C2	C3	C4	C5	C6	C7
A1	(7, 9, 10)	(7, 9, 10)	(7, 9, 10)	(1, 3, 5)	(3, 5, 7)	(7, 9, 10)	(5, 7, 9)
A2	(5, 7, 9)	(5, 7, 9)	(5, 7, 9)	(5, 7, 9)	(3, 5, 7)	(5, 7, 9)	(3, 5, 7)
A3	(3, 5, 7)	(3, 5, 7)	(5, 7, 9)	(5, 7, 9)	(3, 5, 7)	(3, 5, 7)	(3, 5, 7)
A4	(3, 5, 7)	(3, 5, 7)	(3, 5, 7)	(3, 5, 7)	(1, 3, 5)	(3, 5, 7)	(3, 5, 7)

Table 6 Normalized fuzzy decision matrix

	A1	A2	A3	A4
C1	(0.7, 0.9, 1)	(0.5, 0.7, 0.9)	(0.3, 0.5, 0.7)	(0.3, 0.5, 0.7)
C2	(0.7, 0.9, 1)	(0.5, 0.7, 0.9)	(0.3, 0.5, 0.7)	(0.3, 0.5, 0.7)
C3	(0.7, 0.9, 1)	(0.5, 0.7, 0.9)	(0.5, 0.7, 0.9)	(0.3, 0.5, 0.7)
C4	(0.1, 0.3, 0.5)	(0.5, 0.7, 0.9)	(0.5, 0.7, 0.9)	(0.3, 0.5, 0.7)
C5	(0.3, 0.5, 0.7)	(0.3, 0.5, 0.7)	(0.3, 0.5, 0.7)	(0.1, 0.3, 0.5)
C6	(0.7, 0.9, 1)	(0.5, 0.7, 0.9)	(0.3, 0.5, 0.7)	(0.3, 0.5, 0.7)
C7	(0.5, 0.7, 0.9)	(0.3, 0.5, 0.7)	(0.3, 0.5, 0.7)	(0.3, 0.5, 0.7)

Table 7 fuzzy weighted decision matrix

	A1	A2	A3	A4
C1	(0.133, 0.294, 0.531)	(0.095, 0.229, 0.478)	(0.057, 0.164, 0.372)	(0.057, 0.164, 0.372)
C2	(0.023, 0.048, 0.088)	(0.017, 0.038, 0.079)	(0.010, 0.027, 0.062)	(0.010, 0.027, 0.062)
C3	(0.016, 0.032, 0.058)	(0.011, 0.025, 0.052)	(0.011, 0.025, 0.052)	(0.007, 0.018, 0.041)
C4	(0.013, 0.072, 0.209)	(0.066, 0.167, 0.376)	(0.066, 0.167, 0.376)	(0.040, 0.119, 0.293)
C5	(0.026, 0.072, 0.186)	(0.026, 0.072, 0.186)	(0.026, 0.072, 0.186)	(0.009, 0.043, 0.133)
C6	(0.011, 0.021, 0.038)	(0.0078, 0.017, 0.035)	(0.0047, 0.012, 0.027)	(0.0047, 0.012, 0.027)
C7	(0.051, 0.1234, 0.28)	(0.031, 0.0881, 0.218)	(0.031, 0.0881, 0.218)	(0.031, 0.0881, 0.218)

Table 8 Fuzzy TOPSIS results and ranking of alternatives

	D_i^*	D_i^-	RC_i	Ranking of Alternative
A1	0.922	0.797	0.464	2
A2	0.928	0.806	0.465	1
A3	0.991	0.717	0.420	3
A4	1.051	0.618	0.370	4

5 CONCLUSIONS

In this study, a decision model is proposed for the selection of chromite processing plant site in Sistan and Baluchestan province of Iran. The proposed model is based on the comparisons of alternatives according to identified criteria. AHP and TOPSIS in a fuzzy environment compound decision-making method have been used in the proposed model. Fuzzy AHP is used to assign weights to the criteria to be used in processing plant site selection, while fuzzy TOPSIS is employed to determine the priorities of the alternatives. Empirical results showed that the proposed model can be a suitable tool to select the processing plant site.

REFERENCES

Chen, S.J., Hwang, C.L., Hwang, F.P, 1992. Fuzzy Multiple Attribute Decision Making, Springer-Verlag, Berlin.

Cooper W.W, Sieford L.M, Tone K, 2000. Data Envelopment Analysis: A Comprehensive Text with Models, Applications, References and DEA Solver Software, Kluwer Academic Publishers.

Hwang CL, Yoon K, 1981. Multiple attribute decision making. Springer- Verlag, Berlin.

Kuswandari, R, 2004. Assesment of different methods for measuring the sustainability of forest management, International Institute for Geo-Information Science and Earth Observation Enschede, Netherlands.

Saaty, T.L, 1977. A scaling method for priorities in hierarchical structure. J. Math. Psychol. (15), pp.234–281.

Saaty, T.L, 1980. The Analytic Hierarchy Process, McGraw Hill Company, New York.

Saaty, T.L, 1990. The Analytic Hierarchy Process", McGraw Hill. New York.

Saaty, T.L, 2005. Theory and applications of the analytical network process: decision-making with benefits, opportunities, costs, and risk. RWS Publications, University of Pittsburgh.

Zadeh LA, 1975. The concept of linguistic variable and its application to approximate reasoning. Info Sci 8(1), pp.199–249.

Effect of Different Depressants on Galena Flotation

Farklı Bastırıcıların Galen Flotasyonuna Etkisi

Ü. Yenial, A. Gül
Istanbul Technical University, Faculty of Mines, Mineral Processing Engineering, 34469 Maslak/Istanbul, Turkey

Ü. Yılmaz
ETİ Bakır Küre Plant, 37900 Küre/Kastamonu, Turkey

ABSTRACT Selective separation of sulphide minerals such as galena, chalcopyrite, sphalerite, pyrite etc., can be achieved with various collectors, depressants and modifiers. The aim of this study is to investigate different depressants for depression of galena. On this basis, the effect of Na_2S, H_2O_2 and S7260 were investigated on galena flotation. Pure galena was used as ore sample and experiments were conducted with Denver flotation cell using 3418A as a collector and MIBC as a frother. The effects of depressant amount and different pH were examined. Flotation recovery of galena approached the highest value at pH 7 and decreased at pH 11 without any depressant. As a result of experiments it is found that depressing effect of these depressants was related to their amount and pH. The depressing effect of all depressants reached highest value at pH 11. It is found that S7260 was the most effective depressant among them.

Keywords: Flotation, depressant, Na_2S, H_2O_2, S7260

ÖZET: Galen, kalkopirit, sfalerit ve pirit gibi sülfürlü minerallerin birbirlerinden seçimli olarak ayrılmasında çeşitli kollektörler, bastırıcılar ve düzenleyiciler kullanılmaktadır. Bu çalışmanın amacı farklı bastıcıların galen flotasyonuna etkisini incelemektir. Bu amaçla Na_2S, H_2O_2 ve S7260'ın bastırıcı etkileri araştırılmıştır. Saf galen numunesiyle Denver flotasyon hücresinde 3418A kollektörü ve MIBC köpürtücüsü ile flotasyon yapılmıştır. Bastırıcıların etkileri farklı miktarlarda ve çeşitli pH'larda incelenmiştir. Herhangi bir bastırıcı kullanmaksızın galenin flotasyon verimi pH 7'de en iyi değere ulaşmış, pH 11'de düşmüştür. Deneylerin sonucunda bastırıcıların etkisinin pH'ya bağlı olduğu görülmüştür ve tüm bastırıcıların etkisi pH 11'de en yüksek değere ulaşmıştır. S7260 içlerinde en etkili bastırıcı olarak bulunmuştur.

Anahtar kelimeler: Flotasyon, bastırıcı, Na_2S, H_2O_2, S7260

1 INTRODUCTION

Flotation is an important step for separation of Cu-Pb-Zn minerals from gangue minerals and pyrite. The treatment processes of selective separation Cu-Pb-Zn minerals are generally complex. Effective selective separation depends on a variety of collectors and modifiers to adjust surface properties. In practice, when treating complex sulphide ores, the use of two or more depressants are common, especially when a selectivity problem is present or separation of several valuable minerals are required (Bulatovic and Wyslouzil, 1995).

The methods used in the processing of copper-lead-zinc ore could be classified as follows (Bulatovic, 2007):

a) Sequential copper, lead, zinc flotation method

b) Bulk flotation of copper and lead followed by zinc flotation from the bulk tailings. The copper–lead separation is performed on the upgraded bulk concentrate. This is the most

commonly used method in the treatment of copper, lead-zinc ores

c) Bulk flotation of copper-lead-zinc minerals followed by a selective flotation of copper, lead and zinc from the bulk concentrate

The bulk copper–lead flotation method is the most common method. In this method, the copper–lead bulk concentrate is floated, followed by Cu–Pb separation. Usually, in the Cu–Pb separation, tailing is the final lead or copper concentrate depending on the separation method used (Bulatovic, 2007).

In general, there are two basic copper–lead separation methods commonly used during the treatment of copper–lead–zinc ores:

a) In copper depression and lead flotation generally cyanide treatment is used.

b) In lead depression and copper flotation, the methods below are preferred:

(i) Use of oxidizing reagents (i.e. bichromates, hypochlorites, etc.)

(ii) Use of sulfoxy compounds with or without oxidants, or with starch derivatives (Gül, 2007; Gül et al., 2008)

(iii) Use of SO_2 /starch with or without heating (i.e. thermal treatment)

Generally in the copper-galena selective flotation, the copper minerals are floated while galena is depressed (Houot and Duhamet, 1992).

In the literature, there are several inorganic and organic compounds used in depression of galena. These are sodium sulfide, sodium chromate, polysaccharides such as carboxy methyl cellulose, dextrin and caustic starch. Sodium sulfite and SO_2 were used for depression of galena and sphalerite between 250-2000 g/t amount. Sodium dichromate was another chemical which was used for galena depressant in Cu/Pb separation.

The aim of this study is to investigate different depressants for selective depression of galena. On this basis the effect of Na_2S, H_2O_2 and S7260 were investigated on galena flotation.

2 MATERIAL AND METHOD

The galena sample used in this study was supplied from Esan Balya Lead and Zinc plant in Turkey. The impurities were elected by handsorting. The chemical composition of galena was 85.69% Pb, 13.35% S and 0.8% SiO_2. The sample is almost 99% purity. The collector used in flotation experiments was 3418A (Cytec), and methyl isobuthyl carbinol (MIBC) from Aldrich was employed as a frother. 3418A is a sodium-diisobutyl dithiophosphinate (DTPINa) type collector. Na_2S (Merck), H_2O_2 (Merck) and S7260 (Cytec) were used in the experiments to investigate effect of these depressants on flotation recovery of galena. S7260 is a polymeric depressant and contains between 30 to 60% polymer in an aqueous solution with up to 10% isopropanol and 10% sodium metabisulphite. H_2SO_4 and lime were used as pH regulators. The pure galena sample was ground dry with agate mortar freshly for each experiment. According to sieve analysis the d_{80} and d_{50} size of the galena was found as 0.046 mm and 0.015 mm, respectively. The experiments were conducted with 50 g of sample using 1L cell with Denver machine, the impeller speed was at 1200 rpm. The results were shown as flotation recovery and calculated through the mass balance of the floated and remained products. The experimental conditions were given in Table 1.

Table 1: Experimental Conditions

Collector: 3418A	*100 g/t*
Frother: MIBC	*300 g/t*
Conditioning Time with depressant	*10 min*
Conditioning Time with collector	*3 min*
Flotation Time	*5 min*

3 RESULTS

3.1 Effect of pH

A series of experiments were conducted to investigate effect of pH at experimental conditions given in Table 1. The results were given in Figure 1 and Table 2. It was found that galena could float in every pH with high recovery however the highest recovery was obtained between pH 7-9. Above and below this pH the recoveries slightly decreased and the lowest recovery was obtained at pH 11.

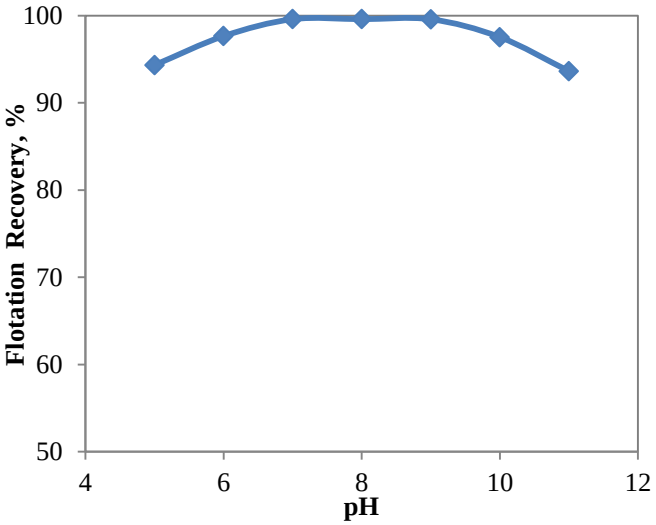

Figure 1. Effect of pH on galena flotation

Table 2: Effect of pH on galena flotation

pH	*Recovery, %*
5.0	94.34
6.0	97.66
7.0	99.60
8.0	99.60
9.0	99.59
10.0	97.54
11.0	93.64

3.2 Effect of Depressants

In order to investigate the effect of depressants on galena flotation, H_2O_2 Na_2S, and S7260 were used. The amount of H_2O_2 was changed between 500-10000 g/t at different pH values. The results were shown in Figure 2. It was found that increasing H_2O_2 amount did not affect the recovery of galena at pH 7. However a decline could be seen at other pH values. It is worth to note that very low H_2O_2 amount decreased the flotation recovery of galena at pH 11. As a result, increasing H_2O_2 amount from 500 g/t to 10000 g/t decreased the flotation recovery from 93.6% to 15.1%.

Na_2S was used as another depressant in this study. The amount of Na_2S was changed between 500-10000 g/t at different pH values. The results were shown in Figure 3. According to experiments it was found that increasing Na_2S amount decreased the flotation recovery from 99.4% to 67.4% at pH 7. Besides, increasing Na_2S amount was more effective than H_2O_2 on the flotation recovery above pH 7. The lowest recovery was obtained as 10% at pH 9 and 11 using 10000 g/t Na_2S.

The third depressant used in this study was S7260. The amount of S7260 was changed between 200-2000 g/t at different pH's and the results were depicted in Figure 4. The most efficient depressant was found to be S7260 even in very low amounts. When 2000 g/t S7260 amount was used the flotation recovery was decreased to 10% at pH 7. In other pH values, 10% recoveries were obtained even at lower amounts. The highest influence of S7260 amount occurred again at pH 11.

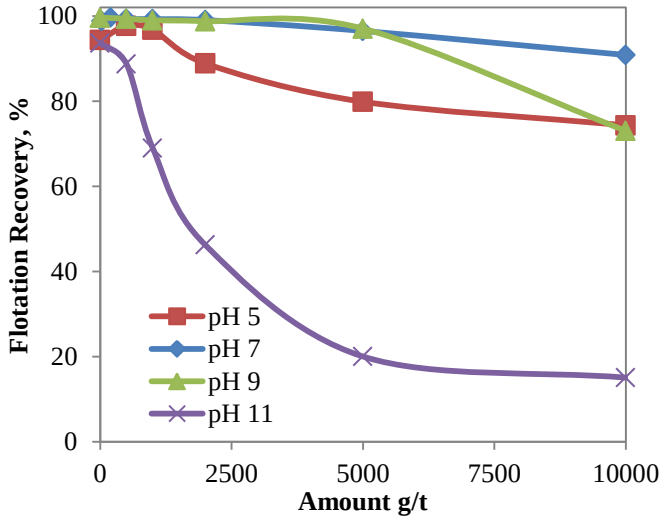

Figure 2. Effect of H_2O_2 amount on galena flotation

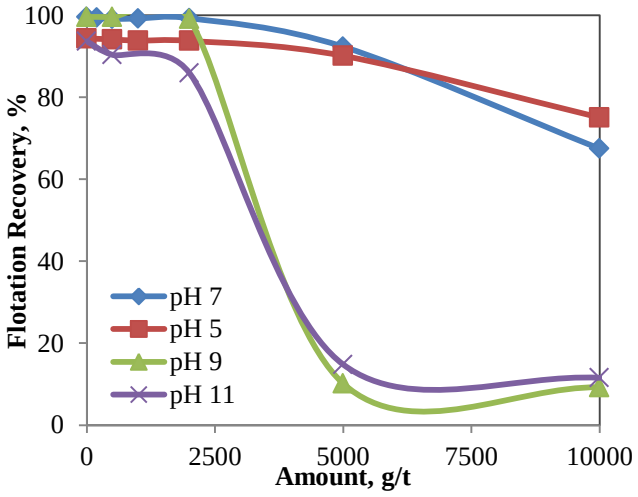

Figure 3. Effect of Na_2S amount on galena flotation

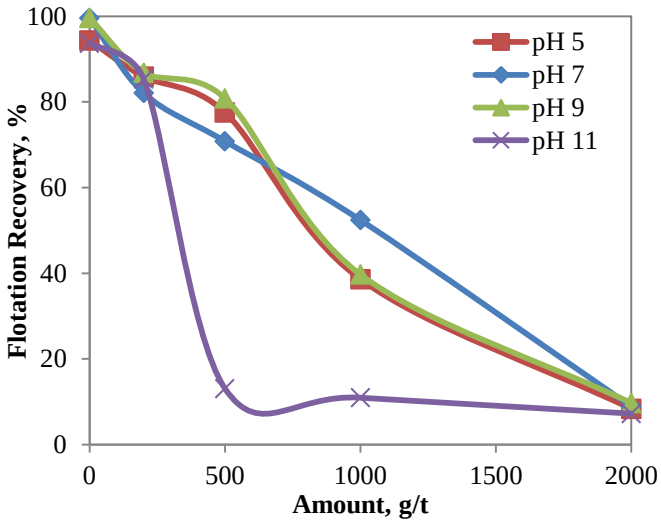

Figure 4. Effect of S7260 amount on galena flotation

4 DISCUSSION

In this study, the effects of different depressants were investigated using pure galena. The purity of galena sample was 99%. The collector used in the experiments is 3418A, which is an anionic sodium-diisobutyl dithiophosphinate collector and mainly adsorbs on galena at every pH. The collector 3418A adsorbs onto the surface of galena regardless of its negative charge, thus suggesting the contribution of a chemisorption mechanism (Pecina-Trevino et al., 2003).

First of all, the effect of pH was investigated without the use of any depressant. It was found that the flotation recovery of galena was highest between pH 7-9 and decreased above and below these pHs. The lowest recovery was found as 93.6% at pH 11. However in another study (Barsakçı, 2008) the flotation recovery was found as 66% at pH 11 using pure galena sample at same experimental conditions. The tendency of the flotation recovery was found similar while the recoveries were not due to different origin of the galena samples. In the literature it has been noted that complete flotation of galena can occur from pH 2 to 10 (Weiss, 1985). Flotation of galena in acid solutions is explained by increased hydrophobicity with oxidation due to formations of sulphur on the surface by Kocabağ et al. (1990). Passing from acidic to neutral and alkaline solutions oxidation of galena takes place forming $Pb(OH)_2$ on the surface in addition to S^0, which decreases the hydrophobicity due to the formation of $Pb(OH)_2$ or metal-sulpoxy compounds (Kocabağ et al., 1990).

In the second stage, the effect of H_2O_2 was investigated, in 500-10000 g/t amount range. It was found that, 500 and 1000 g/t H_2O_2 addition increased the flotation recovery of galena at pH 5, above this amount it was decreased and 73.4% galena recovery was obtained at 10000g/t H_2O_2 amount. The same tendency was observed at pH 9. At pH 7 flotation recovery was slightly decreased even at 10000 g/t H_2O_2 amount. H_2O_2 is a strong oxidant which causes non selective oxidation of sulphide minerals. It was also reported that galena flotation decreases and completely get depressed if the concentration of H_2O_2 exceeds 10^{-3}M (Wang, 1992). The similar findings were observed by Hu et al., (2010) who stated that the flotation recovery of galena decreased at pH 9.5 when H_2O_2 concentration was above 10^{-3}M but the chalcopyrite remained floatable and suggesting these conditions were applicable to selective separation of chalcopyrite and galena.

In the third stage, the effect of Na_2S was investigated in 500-10000 g/t amount range and different pHs. It was found that increasing the amount of Na_2S had not a significant depressing effect on galena at pH 5 and 7. However increasing amount of Na_2S depressed the galena flotation and the recovery of galena was found to be 10% at pH 9 and 11 with 10000 Na_2S. The concentration of Na_2S is very critical, low dosages of Na_2S can be used as an activator while high dosages can prevent mineral-reagent reaction so it can be used as a depressant (Bulatovic, 2007). Lead sulfide is a very insoluble compound so that additions of sodium sulfide will result in the formation of lead sulfide rather than lead-collector if two chemicals are present at the same time (Fuerstenau et al., 1985).

In the last stage, S7260 was used as a depressant between 200 and 2000 g/t amount. The results at pH 5, 7 and 9 showed

similar tendency and flotation recoveries were decreased to 9% at 2000 g/t amount. Like other depressants, the highest depressing effect was observed at pH 11, the recovery of galena decreased to 13% using 500 g/t amount of S7260. The increasing amount decreased the recovery of galena to 7%. S7260 is generally known as an iron sulphide depressant, which requires low dosages (Cytec, 2010). S7260 was previously used by Gül et al., (2013) for the selective separation of Cu and Pb . Very low amounts (25 g/t) of S7260 were used for selective depression of pyrite and Cu minerals. In addition, Baştürkcü et al., (2012) used S7260 for pyrite rejection in rougher Pb-Cu circuit. It is necessary to note that the amount of S7260 is very critical for Pb flotation; low amounts depress the other sulphide minerals and increase selectivity whereas high amounts may cause Pb depression as shown in this study.

5 CONCLUSION

According to this study, the highest recovery of pure galena found at pH 7 and lowest recovery was obtained at pH 11. Among used depressants in this study such as H_2O_2, Na_2S and S7260, S7260 was found as the most efficient in all pH ranges. H_2O_2 was found inefficient at pH 5, 7 and 9 and efficient at pH 11 at high dosages. Na_2S was found to be effective at pH 9-11 at high dosages. These depressants can be used for depression of Pb minerals.

REFERENCES

Barsakçı, B., 2008. *Investigation of different deppresants on galena flotation*. Bachelor Thesis, İstanbul Technical University, İstanbul Turkey.

Baştürkcü H, Yenial Ü, Kökkılıç O, Yüce A.E, Erdoğan E.B, 2012. Beneficiation of Copper, Lead and Zinc Concentrates From Complex Ore By Using Environmentally Friend Reagents. *Proceedings of XIIIth International Mineral Processing Symposium* 10-12 October, Bodrum Turkey. 349-355

Bulatovic S. M., 2007, *Handbook of Flotation Reagents: Chemistry, Theory and Practice: Volume 1: Flotation of Sulfide Ores,* 2007. Elsevier, 163

Bulatovic S, Wyslouzil D.M, 1995, Selection and evaluation of different depressants systems for flotation of complex sulphide ores, *Minerals Engineering*, 8, 1–2, 63.

Cytec 2010. Mining Chemical Handbook.

Gül A., 2007. The role of $Na_2S_2O_5$ and activated carbon on the selective flotation of chalcopyrite from a copper ore usıng a dithiophosphine –type collector, *Mineral Processing. Extractive Metal.Rev*., 28, 235-245.

Gül A., Yüce A.E., Sirkeci A.A.., Özer M., 2008, Use of non-toxic depressants in the selective flotation of copper lead-zinc ores, *Canadian Metallurgical Quarterly*, 47, 2, 111-118.

Gül A, Bulut G, Sirkeci A.A., 2013. Beneficiation of Arsenic Bearing Complex Sulphide Ore By Flotation, *Physicochem. Probl. Miner. Process*. 49(1), 203−212

Hu Y, Sun W, Wang D, 2010. Electrochemistry of Flotation of Sulphide Minerals, *Springer Science & Business Media*, 124

Hout, R, Duhamet, D., 1992. The Use of Sodium Sulphite to Improve the Flotation Selectivity Between Chalcopyrite and Galena in a Complex Sulphide Ore, *International Journal of Mineral Processing*, 5, 343-355

Kocabağ D, Kelsall G.H., Shergold H.L, 1990. Natural Olephicity/Hydrophobicity of Sulphide Minerals I. Galena, *International Journal of Mineral Processing*, 29, 195-210

Pecina-Treviño E.T, Uribe-Salas A, Nava-Alonso F, Pérez-Garibay R, 2003. On the sodium-diisobutyl dithiophosphinate (Aerophine 3418A) interaction with activated and unactivated galena and pyrite, *International Journal of Mineral Processing* 71, 201–217

Wang D., 1992. Potential adjustment of sulfide mineral and collectorless flotation. *In: New Development of Flotation Theory.* Beijing: Science Press, 79–143.

Weiss N.L., 1985. *Mineral Processing Handbook*, SME, New York, 1

Fuerstenau M.C; Miller J.D. 1985. Kuhn M.C. *Chemistry of Froth Flotation*, Society of Mining Engineers, New York.

Matematical Modeling of Elementary Act of Flotation in Vibratory Column Machine

J. Dimitrov
University of Mining and Geology, Sofia, Bulgaria

Kr. Dedelyanova
Scientific and Technical Union of Mining, Geology and Metallurgy, Sofia, Bulgaria

ABSTRACT The paper presents research on hydrodynamic processes occurring at the elementary act of flotation. Discussed existing models to determine the effectiveness of conflict of bubbles with particles in vibration column flotation machine

It is proposed an analytic description of the mathematical model representing the mechanism of attachment of the particles to the bubble.

Keywords: Flotation, vibratory column machine, mathematical model, bubble attachment

1 INTRODUCTION

The wide practical introduction of column flotation machine is a great achievement in during the last decade in the field of flotation concentration. The advantages of the column flotation machine in comparison with the mechanical and pneumo - mechanical are following: increased productivity improved hydrodynamics, of concentrate with the required quality at minimal quantity purifying and control operations, production area decrease and economy of electric power.

Work efficiency in flotation machines depends on the terms of the dispersion of air. Aerators should provide maximum gas content in optimum average particle size of the bubbles. For aerators put the following requirements: ensuring that size of the bubbles, which provide buoyancy the flotation complex and minimal macro-circulation of the pulp chamber (Finch, 1990).

At vibration flotation machine has additional factors influencing the increase of the duration of bubble's existence in the contact zone with the mineral particles was discussed. In Dedelyanova & Dimitrov (2013) the mechanism for attachment of the particles to the bubbles in the vibratory column flotation machine was studied. The effectiveness of the collision of the bubbles in the vibratory column flotation machine were defined.

This paper will focus on an improved model of the elementary act of flotation in the vibratory column flotation machine.

2 MODEL OF BUBBLE OSCILLATION

In order to make an analysis of the process of collision we assume that the bubble is spherical and around it we go over a rotational body with vertical axis passing through the center of the sphere. We denote with d_b the diameter of the bubble, d_p - diameter of the particles and a - diameter of the section of the cylindrical area including area involved in collision from particle and bubble.

Consider the model given by Bogdanov (Bogdanov, 1990). The section of the cylindrical area of the fluid before the collision at a diameter a is $S_0 = \pi a^2/4$ and at the level of collision - $S_b = \pi\left(d_b+d_p\right)^2/4$.

For the effectiveness of collision we obtain

$$E = \frac{S_0}{S_b} = \left(\frac{a}{d_b + d_p}\right)^2. \quad (1)$$

Then the parameter E is the ratio of the section of the narrow part of the area before

collision and the section through the center of the bubble.

As the bubble vibrates with acoustic frequency f, its mean diameter d_b is the same as without vibrations. While making one harmonic cycle, the volume of the bubble is preserved as it changes its form from sphere to rotational ellipsoid. A bubble with a spherical form and a diameter d_b has a volume

$$V_b^s = \frac{\pi}{6} \cdot d_b^3. \tag{2}$$

During each harmonic cycle the bubble changes from sphere to rotational ellipsoid with axis (diameter) in horizontal direction d_{xy} and axis in vertical direction $d_z \neq d_{xy}$. The volume of the ellipsoid is:

$$V_b^e = \frac{\pi}{6} \cdot d_{xy}^2 d_z. \tag{3}$$

If we disregard the change of the typical size d_b of the bubble, then we can assume that at a moment close in time the following equation is satisfied $V_b^s = V_b^e$ and hence it follows that:

$$d_{xy}^2 d_z = d_b^3. \tag{4}$$

During the experiments made in Dedelyanova (Dedelyanova, 2004), the average size of the bubbles was $d_b = 4\ mm$ and the amplitude A was from 1.5 to 3.0 mm. A significant condition for the models which we apply is the inequality $d_b > A$ executed during these experiments. In one harmonic cycle of the bubble at a given time, it has the form of a rotational ellipsoid with a larger horizontal diameter $d_{xy} = d_{xy\max}$. At another time the horizontal diameter is the smallest possible $d_{xy} = d_{xy\min}$. In these extreme conditions the respective sizes of the vertical diameter are:

$$\begin{aligned} d_{z\max} &= d_b + A \\ d_{z\min} &= d_b - A \end{aligned}. \tag{5}$$

The next equations follow from formula (4):

$$\begin{aligned} d_{xy\max} &= \sqrt{\frac{d_b^3}{d_{z\min}}} \\ d_{xy\min} &= \sqrt{\frac{d_b^3}{d_{z\max}}} \end{aligned}. \tag{6}$$

Variation changing on the size of bubble in the process of emergence is given by the formula.

$$d_b = d_0 \sqrt[3]{\frac{p_0}{p_1 + qAf^2 \sin \omega t}} \tag{7}$$

where d_b the diameter of the bubble; d_0 - the diameter of the bubble on the surface; $p_1 = p_0 + \rho_l hg$, where p_0 - atmospheric pressure; ρ_l - density of liquid; h - level from the surface of the liquid and g - acceleration of gravity.

3 EXPERIMENTAL RESEARCHES

For determination the essential parameters of the flotation process is used stereology analysis. Figure 1 represents a photograph of a part of the column machine camera.

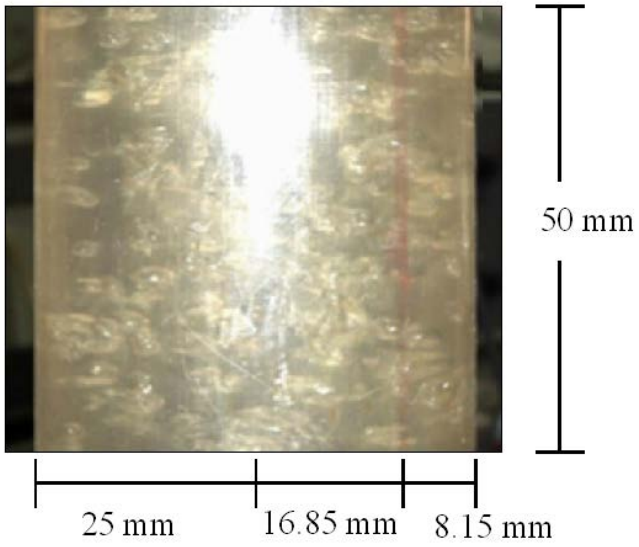

Figure 1. Photograph of a part of the camera in column machine and a scheme for stereological analysis

On the photo is applied marker with a red line. In Figure 1 are shown and dimensions with the aid of which it can calculate the geometric parameters of the cylinder representing the photographed part of the camera. The marker, represented by a red line, sets the vertically planar section of a

cylinder, which has a certain volume - sector of the cylinder. From the photographic image we can obtain the number of bubbles in the sector and the number of those of them that cross the section marked with the red line.

Section of the cylinder is a rectangle with height $50\,mm$ and width that after the corresponding calculation shall be determined on $39.94\,mm$. The surface of the section is $S = 50 \times 39.94 = 1997\ mm^2 = 19.97\ cm^2$.

The volume of sector compartments with a red line is $V_1 = 182.26 \times 50 = 9113\ mm^3 = 9.1\ cm^3$

From the photographic image in Figure 3 are counted about 30 bubbles per limited by the red line sector. Then

$$N = \frac{30}{9.1} = 3.29\ mm^{-3}. \quad (8)$$

is the number of bubbles by volume

From Figure 1 can be determined and the number of bubbles that are in contact with the section limited by the red line. This number is 26. We receive number of bubbles per unit area from section -

$$n = \frac{26}{19.97} = 1.3\ cm^{-2}. \quad (9)$$

For the determination of average diameter of the bubbles is used stereological equation (Saltykov, 1976, Weibel, 1980):

$$d_b = \frac{n}{N} = 0.395\ cm = 3.95\ mm. \quad (10)$$

In Dedelyanova (Dedelyanova, 2004) made studies on the rate of ascent of the bubble at different frequencies of vibration and without vibration. The average speed of ascent is $25\,cm/s$. Is obtained a decrease of 13-14% in the rate of ascent in vibration.

4 IMPROVEMENT OF ELEMENTARY ACT OF FLOTATION

There are two forces acting on the forming bubble during the vibration of the dispersing agent: lifting force of the fluid displaced by the bubble and the resistance force caused by the flow-around of the bubble by the flow of fluid which moves along the inclined wall of the dispersing agent. While the lifting force is always targeted upwards, the resistance force from the flow-around is dependent on the phase of fluctuations. The lifting force increases with the increase of the diameter of the forming bubble, the resistance force also increases with the increase of the diameter of the bubble but it changes also according to a sinusoidal law.

4.1 Schematic Presentation of the Harmonic Cycle of Bubble

Figure 2 shows schematically several harmonic cycles of the bubble. The harmonic cycle includes five characteristic states:

ST1 – the state in which $d_{xy} = d_{xy\max}$. In this state the bubble is with a small diameter along axis z;

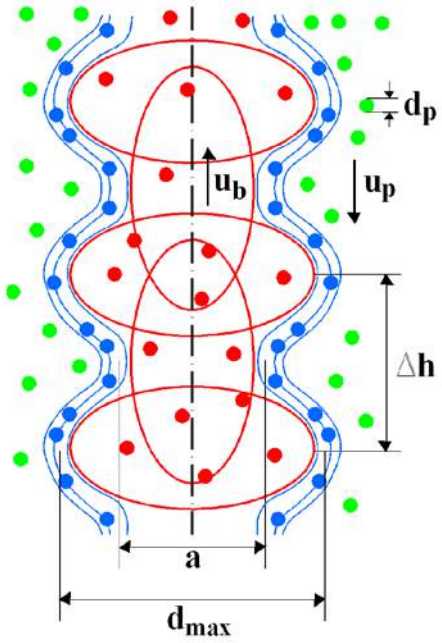

Figure 2. Scheme of several harmonic cycles of the bubble

ST2–the state following in time after ST1, in which $d_{xy} = d_z = d_b$ is the characteristic size of the bubble with the form of sphere;

ST3–state after ST2, in which $d_{xy} = d_{xy\min}$;

ST4–state after ST3, in which $d_{xy} = d_z = d_b$. We have a sphere as in state ST2;

ST5–state following ST4 and the beginning of the next harmonic cycle – it

coincides with ST1 of the next harmonic cycle.

On Fig. 3 the parameter a is the radius of the section S_0 and $d_{\max} = d_{xy\max} + d_p$ - radius of S_b. Δh designates the step in one harmonic cycle of the bubble during its movement in relation to the particles with rate $u = u_b + u_p$. It is fulfilled

$$u = \Delta h \cdot f \,. \tag{11}$$

The radius a is different for the different frequencies f of vibration. We can discern three different cases:

1. The frequency $f < f_0$ is high enough and respectively Δh - low enough, so that $a < d_{xy\min} + d_p$;

2. Case $f = f_0$, in which $a = d_{xy\min} + d_p$ and

3. Case $f > f_0$. Then $a > d_{xy\min} + d_p$.

4.2 Presentation of the Collision Efficiency

We assume that the bubble has the shape of a rotating ellipsoid with axis Oz. Denote by r_{xy} the horizontal radius of the ellipsoid and by r_z - the vertical radius (Figure 3).

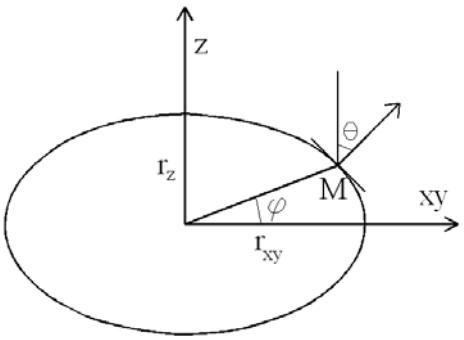

Figure 3. Schematic of contact between a particle and bubble

It is true that

$$r_{xy}^2 r_z = r_b^3 , \tag{12}$$

where r_b is the characteristic radius of the bubble when it takes the shape of a sphere.

Figure 2 schematically shows a vertical section of the ellipsoid:

θ - angle between the trajectory of the falling particle (axis Oz) and the normal to the ellipsoid at the point of contact M;

φ - polar angle of the point of contact M.

$$\theta \in [0, \theta]_{\max} \tag{13}$$

where $\theta_{\max}$ is the maximum angle at which the particles will be retained on the wall of the bubble.

Is fulfilled

$$\theta_{\max} \in \left(\frac{\pi}{4}, \frac{\pi}{2}\right), \quad \theta_{\max} = const \,. \tag{14}$$

On this position M of the point of contact corresponds abscissa a - radius of the cylindrical part of the fluid containing the particles stick to the bubble. This cylindrical portion of the fluid is in contact with the bubble and its projection on the wall of the bubble is the area of contact.

After the appropriate calculations is obtained:

$$a = \frac{r_{xy}^2 \sin\theta_{\max}}{\sqrt{r_z^2 \cos^2\theta_{\max} + r_{xy}^2 \sin^2\theta_{\max}}} \tag{15}$$

Let $\varphi_{\min}$ is the polar angle of the point of contact M, when it is in the boundary of the area of contact. Then $a = r_{xy}\cos\varphi_{\max}$ and

$$tg\varphi_{\min} = \frac{r_z}{r_{xy}} tg\left(\frac{\pi}{2} - \theta_{\max}\right) \tag{16}$$

The surface of the area of contact is

$$S(r_{xy}, r_z) = \frac{\pi r_{xy}^4 \sin^2\theta_{\max}}{r_z^2 \cos^2\theta_{\max} + r_{xy}^2 \sin^2\theta_{\max}} \,. \tag{17}$$

The shape of the ellipsoid varies periodically as the vertical radius can be represented

$$r_z = a\sin wt + r_b \,, \tag{18}$$

where $w = 2\pi f$,

f - vibration frequency.

$T = \frac{2\pi}{w} = \frac{1}{f}$ - period.

As defined, the effectiveness of a collision at the time when the bubble is in the shape of a sphere is

$$E_0 = \frac{S_0}{\pi\left(r_b + r_p\right)^2}, \quad (19)$$

where r_b - a characteristic bubble radius;

r_p - characteristic radius of the particle.

$$S_0 = \pi r_b^2 \sin^2 \theta_{\max} \quad (20)$$

is the face of the area of contact.

If we ignore the size of the particle, we can accept that

$$E_0 = \sin^2 \theta_{\max}. \quad (21)$$

Effectiveness of conflict have changed over time, together with a change in shape of the bubble. The instantaneous efficiency of conflict is represented by the formula

$$E(t) = E_0 \frac{S\left(r_{xy}, r_z\right)}{S_0}. \quad (22)$$

Effectiveness of conflict for a period of vibration T is given by the formula

$$E = \frac{1}{T}\int_0^T E(t)dt = \frac{E_0}{T}\int_0^T \frac{S\left(r_{xy}, r_z\right)}{S_0}dt \quad (23)$$

Due to the high frequency of vibration in relation to the velocity $u = u_b + u_p$ of the contact and the relatively large inertia of the particles, the radius of the cylindrical region of the fluid which is in contact with the bubble, is determined by the state of the bubble at the largest horizontal radius.

$$r_{xy} = r_{xy\max} = r_b + \frac{A}{2}$$

and $r_z = r_{z\min} = r_b - \frac{A}{2}$

In this case we have

$$\frac{S\left(r_{xy}, r_z\right)}{S_0} = \frac{r_b^2 + r_b\frac{A}{2}}{r_b^2 + r_b\left(\frac{A}{2}\right)^2 \cos 2\theta_{\max} - 2\frac{A}{2}r_b \cos^2 \theta_{\max}} \quad (24)$$

because of $\cos 2\theta_{\max} < 0$ we receive

$$\frac{S\left(r_{xy}, r_z\right)}{S_0} > 1 \quad (25)$$

which shows that the effectiveness of collision at vibration is greater than without the vibration

$$E > E_0. \quad (26)$$

5 CONCLUSIONS

In paper is presented a improved model of the elementary act of flotation.

It includes:

- model of bubble oscillation on a given level on camera of column machine;
- stereological analysis for obtaining the basic parameters of the flotation process;
- schematic presentation of the harmonic cycle of bubble and
- analytical method for the expressing of the average of the collision efficiency.

Facts which were proved through experiments are confirmed by the analytical study of the effectiveness of collision E.

The vibrations make possible the increase in the time of stay of the bubble in the contact zone with the mineral particles and the more cost-effective implementation of the elementary act of flotation by ensuring higher rates of the collision of the bubble with the solid phase.

The analytical expressions for the effectiveness of collision E can be used during the design of vibratory column flotation machines.

REFERENCES

Bogdanov O. (1990). *Theory and technology of flotation*, Moscow, Nedra

Dedelyanova, Kr. (2004). *Vibro-acoustic investigations in column flotation machine with vibratory air disperser* (Doctoral dissertation), University of Mining and Geology, Sofia, Bulgaria.

Dedelyanova Kr., J.Dimitrov, (2013). Investigation on the effectiveness of air bubbles collision in vibratory column flotation machine, 23rd World Mining Congress, Montreal, Canada, p. 286-294

Finch, J. A., Dobby, G. S. (1990). Column flotation. Pergamon Press Canada Ltd., 29.

Saltykov, S.A. (1976). Stereometric Metallography, Moscow, "Metallurgy"

Weibel, E.R.(1980). Stereological Methods, New York: Academic Press

Optimization of Physico-Chemical Parameters of Pyrite Flotation

M. Chettibi
Annaba University, BP12- Algeria, Faculty of Earth Sciences, Mining Department, Annaba 23000, Algeria

A. Boutrid
Annaba University, BP12- Algeria, Faculty of Earth Sciences, Mining Department, Annaba 23000, Algeria

A.A. Abramov
Moscow State Mining University, Leninskii pr. 6, 117049 Moscow, Russia

ABSTRACT Tailings issued from polymetallic ore flotation of Chaabat el-Hamra mine contain sulfides such as Galena (PbS), Pyrite (FeS_2) and Chalcopyrite ($CuFeS_2$). They present environmental threats such as the acid mine drainage. Chemical analysis showed that the major element of these tailings is Pyrite. The processing of the latter eliminates much of the sulfur.

The flotation is based on the difference of the minerals surface properties such as hydrophobicity, hydrophility, addition of appropriate reagents and their adhesion to bubbles.

In this work, we propose to use the method of thermodynamic analysis in view of studying and identifying the main physico-chemical parameters of flotation, such as the thermodynamic potential and pH, which play a main role in collector adsorption on the mineral surface.

The obtained results show that the optimal pH value is 7, in this condition; we can get an optimal adsorption and maximum recovery of Pyrite up to 90%.

Keywords: Pyrite, flotation, surface properties.

1 INTRODUCTION

The sulphuric minerals, having an economic value, are mainly recovered by flotation. The precious sulphides, however, are mainly found in complex ores form associated with the gangue. They can present similar surface properties. In the case of Chaabat El Hamra deposit, the Pyrite is a gangue of which surface properties are similar to Chalcopyrite, Galena and Sphalerite.

This similarity, relative to the surface properties of the above-mentioned sulphuric minerals, presents some difficulties during minerals separation by selective flotation [Hiçyilmaz, 2009].

The study of the surface properties plays a significant role in the frame of the floatability and the efficiency of minerals separation. The chemistry of sulphides surface is more complicated than that of other metals and oxides [Gonçalves, 2003]. During crushing, a galvanic contact occurs between sulphuric minerals and the liquid phase of pulp, which generates an electric field provoking the reactions of oxydo-reduction on mineral surfaces, due to the various values of the pulp potential.

The phenomena, which occur at the time of the contact of mineral surfaces with the pulp liquid phase, define the electrochemical variation of the surface properties [Chettibi, 2003]. These last directly influence on the effectiveness of the sulfurs flotation.

The relevance of the electrochemical phenomena, during the flotation of sulphuric minerals, was highlighted in the Thirties of last century. By the Sixties, this obviousness was reinforced through many applications. At the present time, it is necessary to establish a correlation between the

performance of the flotation reagents and the electrochemical properties of pulp [Junia et al., 2009].

The sulphides float for three different reasons: the presence of the element of free sulphur, the connection metal-xanthate and formation of the dexanthogen layer on mineral surface. These reactions are of electrochemical nature [Puonala et al., 1997]. So, the control of the state of mineral surfaces oxidation must be recommended during the process in order to maximize the technical and economic indices of enrichment.

The electrochemical nature of the interaction (mineral-collector) also means that the phenomena leading to the hydrophobicity of minerals can present a subject of research by using electrochemical techniques. This is important not only because it allows establishing the chemical reactions which may occur in the flotation systems, but also, such study is essential if effective potential methods of control are to be introduced in practice [Buckley et al., 1997].

Actually, it is established that, the surface state and the floatability of sulphides, are defined with high accuracy by exploiting the following parameters: the potential redox(Eh), potential of electrode and pH of pulp [Heifetz et al;, 1959].

The purpose of this work is to determine the conditions and the optimal parameters of pyrite flotation, resulting from the treatment of factory rejections, by using the thermodynamic method of analysis and chemical calculation of the mineral surface state. In terms of pH optimal values we ensure a complete pyrite flotation according to the potential minimal charge.

2 METHODOLOGY

The method of the thermodynamic analysis for a longtime is largely applied for the study of the chemical, geochemical and hydrometallurgic processes. It is also used in mineral processing and particularly in flotation [Abramov, 1993]. This method permits to define the composition of the connections representing mineral surface, to realize physicochemical models for the processes of interaction of mineral surface with the reagents, and to carry out a chemical calculation of the ionic components state of the pulp liquid phase. The latter method is based on the following equations [Chettibi, 2003]:

- Equation of the equilibrium constant:

$$K = \frac{[C]^c.[D]^d}{[A]^a.[B]^b}\ ; \qquad (1)$$

- Equation of the relation between the reaction free standard energy and the equilibrium constant:

$$\Delta F_r^0 = \sum \Delta F^0_{final.} - \sum \Delta F^0_{init.} = R.T.\ln K; \qquad (2)$$

Or, at 25 0 C:

$$\Delta F^0_r = -1{,}364.\lg K$$

- Equation of the relation between the reaction free standard energy and the potential of standard electrode:

$$\Delta F^0_r = E^0.n.f = 23{,}06.n.E^0 \qquad (3)$$

- Equation of the relation between the reactions measured potential, the standard potential and the reaction equilibrium constant:

$$E = E^0 +. \frac{R.T}{n.F} \ln \frac{[C]^c.[D]^d}{[A]^a.[B]^b} \qquad (4)$$

Or at temperature 25 ^{0} C:

$$E = E^0 + \frac{0{,}059}{n} \log \frac{[C]^c.[D]^d}{[A]^a.[B]^b} \qquad (5)$$

The possibility of estimating the surface state of mineral salts, based on thermodynamic calculation, was theoretically and experimentally confirmed in different Abramov's works [Abramov, 1993, 1978, 1977]. The point of this method is to create a system of basic reactions of dissociation and hydrolysis of minerals in solution, and to

settle the equations obtained on the basis of these reactions. Added to that, the elaborated system must be completed by the equations of balance and the electro-neutrality.

While modeling, the standard free energies (Gibbs energies) of species and compounds were used (in Kcal/mol): according to [Latimer, 1952]FeS_2 -38,29; Fe^{2+} -20,30; $Fe(OH)_2$ -115,57;$Fe(OH)^+$ -65,20; $FeCO_3$ -161,06; Fe^{3+} -2,53; $Fe(OH)^{2+}$ -55,91; $Fe(OH)_2^+$ -106,2; $Fe(OH)_3$ -166,06; Fe_2O_3 -177,1; Fe_3O_4 -242,1; FeOOH -117,2; $HFeO_2^-$ -90,6; S^{2-} +22,1, HS^- +3,01; H_2S -6,54; SO_3^{2-} -116,10; SO_4^{2-} -177,34; CO_3^{2-} -126,22; HCO_3^- -140,31; H_2CO_3 -149,0; OH^- -37,595; H_2O -56,69; H_2SO_4 -177,34; and according to [Garrels, et al., 1964] $S_2O_3^{2-}$ -127,20.

3 RESULTS AND DISCUSSION

3.1 Influence of pH on the Surface State of Pyrite

The thermodynamic analysis of the pyrite surface quality shows that oxidation of pyrite and sulphur presents many compounds derived from iron and sulphur, mainly the following: Fe_2O_3, FeO, Fe_3O_4, $Fe(OH)_2$, FeO(OH), $Fe(OH)^{2+}$, $Fe(OH)_2^+$, $Fe(OH)_3$, $HFeO_2$, FeO_2^{2-}, FeO_4^{2-}, $FeCO_3$, $FeSO_4$, SO_4^{2-}, HSO_4^-, SO_3^{2-}, $S_2O_3^{2-}$, S^0, S^{2-}, HS^-, H_2S. The most probable products of pyrite oxidation (at any oxidation variant of the minerals sulphur) are: $Fe_2O_3$and Fe_3O_4.Moreover, Garrels R. M. indicates in his works that, during the precipitation of iron salts, we could obtain also $Fe(OH)_2$and $Fe(OH)_3$, presenting a great sensitivity to the change of pH and Eh values of the medium [Garrels et al., 1964]. Thus, we can present the pyrite oxidation to $FeCO_3$, $Fe(OH)_2$ and $Fe(OH)_3$ with the release of SO_4^{2-} and HSO_4^-.

Table 1 recapitulates the various reactions of pyrite surface oxidation in the presence of water, oxygen and also according to the pH values. These reactions can occur simultaneously, in various places of the surface, depending on the reactivity induced by the crystallinity. These kinds of reactions have thermodynamic and kinetic characteristics which play a very significant role in the case of sulphides flotation presenting difficulties for their beneficiation such as pyrite [Abramov, 1978].

Results of iron ionic components activity: $[Fe^{3+}]$, $[Fe(OH)^{2+}]$, $[Fe(OH)_2^+]$, $[Fe^{2+}]$, $[Fe(OH)^+]$ and $[HFeO_2^-]$, equilibrated with FeS_2, $Fe(OH)_2$, $Fe(OH)_3$ and $FeCO_3$, show that, in all cases the principal ion resulting from the pyrite oxidation is (Fe^{2+}).

The results of thermodynamic analysis allow establishing the variations of pyrite state surface according to different pH and thermodynamic potential values of the solution (Figure. 1).

From this, it results that for:

• The highly positive values of the Redox potential of the solution, the principal product of oxidation is presented by $Fe(OH)_3$;

• In The case of less positive (or negative) values of the Redox potential of the solution, there can be a formation of $FeCO_3$ (at pH< 8,6) or a formation of $Fe(OH)_2$(at pH> 8,6). If the medium is opened, in that case, $Fe(OH)_2$ will be replaced by $FeCO_3$.

Table1. Thermodynamic characteristics (ΔF^0, E^0) reactions and equations

N°	Reactions	ΔF^0 reactions, Kcal/mol	E^0, V.
1	$FeS_2 + 10H_2O \Leftrightarrow Fe(OH)_2 + 2SO_4^{2-} + 18H^+ + 14e$	+134,94	+0,41
2	$FeS_2 + 10H_2O \Leftrightarrow Fe(OH)_2 + 2HSO_4^- + 16H^+ + 14e$	+129,74	+0,40
3	$FeS_2 + 11H_2O \Leftrightarrow Fe(OH)_3 + 2SO_4^{2-} + 19H^+ + 15e$	+141,20	+0,40
4	$FeS_2 + 11H_2O \Leftrightarrow Fe(OH)_3 + 2HSO_4^- + 17H^+ + 15e$	+136,00	+0,39
5	$FeS_2 + CO_3^{2-} + 8H_2O \Leftrightarrow FeCO_3 + 2SO_4^{2-} + 16H^+ + 14e$	+102,29	+0,31
6	$FeS_2 + CO_3^{2-} + 8H_2O \Leftrightarrow FeCO_3 + 2HSO_4^- + 14H^+ + 14e$	+97,09	+0,30
7	$Fe(OH)_2 + H_2O \Leftrightarrow Fe(OH)_3 + H^+ + e$	+6,26	+0,27
8	$FeCO_3 + 3H_2O \Leftrightarrow Fe(OH)_3 + CO_3^{2-} + 3H^+ + e$	+38,91	+1,68
9	$Fe(OH)_2 \Leftrightarrow Fe^{2+} + 2OH^-$	+20,08	
10	$FeCO_3 \Leftrightarrow Fe^{2+} + CO_3^{2-}$	+14,54	

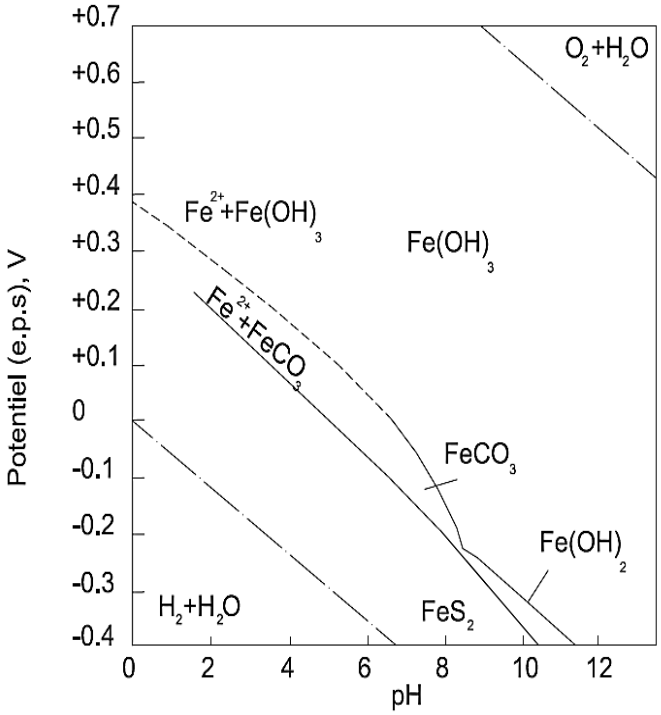

Figure 1. pH and Eh values influence on the pyrite surface state [Abramov, 1978].

3.2 Influence of the Surface State on Pyrite Hydrophobicity and Floatability, and its Equilibrium pH Determination

The surface of the pyrite in solution is not homogeneous; it presents many compounds derived from iron. According to solution conditions' (pH and Eh), we can find the sulfates:$Fe_2(SO_4)_3$, $FeSO_4Fe_2(SO_4)_3$,$9H_2O$and the oxides and hydroxides as well: $Fe(OH)_3$, FeOOH, Fe_2O_3, FeO^{2-}, FeS_2 and FeS. Each product possesses its own thermodynamic properties.

The existence of these surface species involves such heterogeneity of surface (fig. 1) due to their non-uniform distribution on pyrite surfaces. The distribution of the surface species is done according to specific zones of oxidation, created by crystallographic defects, impurities or little variations of stoichiometry of the crystal lattice [Mermillod-Cableway, 2005].

For a considered chemical species, the determination of equilibrium pH value with water is carried out by using various reactions of dissociation and hydrolysis (Table 2), which are directly or indirectly related to the considered species[Abramov, 1978].

Table 2.Thermodynamic characteristics (K, ΔF^0, E^0) reactions and equations

N°	Reactions et Equations	K	$\Delta F^0_{React.}$, Kcal./mol	E^0, V
11	$Fe(OH)_3 \Leftrightarrow Fe^{3+} + 3OH^-$	$6,93.10^{-38}$	50,69	
12	$Fe(OH)_2 \Leftrightarrow Fe^{2+} + 2OH^-$	$1,89.10^{-15}$	20,08	
13	$FeCO_3 \Leftrightarrow Fe^{2+} + CO_3^{2-}$	$2,19.10^{-11}$	14,54	
14	$Fe(OH)_2^+ \Leftrightarrow Fe(OH)^{2+} + OH^-$	$4,95.10^{-10}$	12,695	
15	$Fe(OH)^{2+} \Leftrightarrow Fe^{3+} + OH^-$	$2,68.10^{-12}$	15,79	
16	$Fe(OH)^+ \Leftrightarrow Fe^{2+} + OH^-$	$4,41.10^{-6}$	7,31	
17	$H_2CO_3 \Leftrightarrow HCO_3^- + H^+$	$4,26.10^{-7}$	8,69	
18	$HCO_3^- \Leftrightarrow H^+ + CO_3^{2-}$	$4,677.10^{-11}$	14,09	
19	$H_2O \Leftrightarrow H^+ + OH^-$	$.10^{-14}$	19,095	
20	$[Fe^{2+}]+[Fe(OH)^+]=[H_2CO_3]+[HCO_3^-]+[CO_3^{2-}]$			
21	$3\,Fe^{3+} + Fe(OH)_2^+ + 2\,Fe(OH)^{2+} + H^+ = OH^-$			
22	$2Fe^{2+} + Fe(OH)^+ + H^+ = OH^-$			
23	$2Fe^{2+} + Fe(OH)^+ + H^+ = HCO_3^- + 2CO_3^{2-} + OH^-$			
24	$Fe + 3OH^- \Leftrightarrow Fe(OH)_3 + 3e$		-53,22	-0,769
25	$Fe + 2OH^- \Leftrightarrow Fe(OH)_2 + 2e$		-80,38	-1,743
26	$Fe + CO_3^{2-} \Leftrightarrow FeCO_3 + 2e$		-34,84	-0,755
27	$E = +0,057 + 0,059pH$			
28	$E = -0,917 + 0,059pH$			
29	$E = -0,755 - 0,059.lg.[CO_3^{2-}]$			

The calculation steps depend on one another, they consist in determining successively:

- The free energy ($\Delta F°_{reaction}$) of each considered reaction of dissociation and hydrolysis;
- The equilibrium constant (K) of each reaction;
- The concentration (C) of each ion resulting from the reactions of dissociation and hydrolysis according to K and $[H^+]$.
- Afterwards, these concentrations (C) are represented graphically according to the pH values by using the following function: log(c) = f (pH).
- The equilibrium pH value is the intersection point of the highest curves [Abramov, 1978].

3.2.1 Equilibrium pH value of [Fe(OH)₃-water] system

For the determination of equilibrium pH value of [$Fe(OH)_3$- water] system, we used the equations (11), (14), (15) and (19) see Table 2. The obtained results of chemical computing are illustrated in figure 2. They show that the value of equilibrium pH of [$Fe(OH)_3$ - water] system is equal to 7,8.

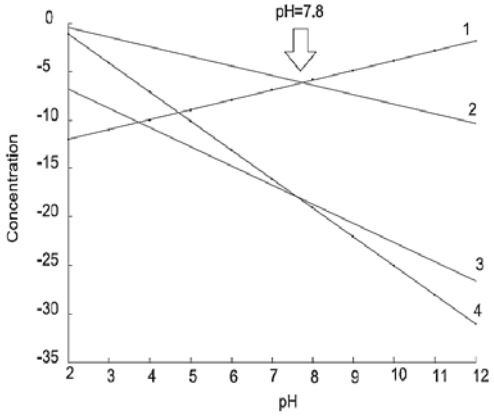

Figure 2. pH influence on the ions concentration [OH^- (1),$Fe(OH)^{2+}$(2),$Fe(OH)^{2+}$(3),Fe^{3+} (4)]

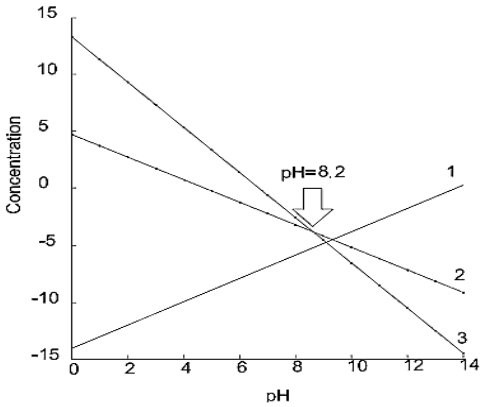

Figure 4. pH influence on the ions concentration [OH^-(1), $Fe(OH)^-$ (2), Fe^{2+} (3)]

3.2.2 Equilibrium pH value of [$FeCO_3$ - water] system

For the determination of equilibrium pH value of [$FeCO_3$-water] system, we used the following equations (13), (17), (18) and (19) of Table 2. The obtained results of chemical computing are illustrated in figure 3. They show that the value of equilibrium pH of [$FeCO_3$ - water] system is equal to10,3.

3.2.3 Equilibrium pH value of[$Fe(OH)_2$ - water]system

In order to determine the equilibrium pH value of [$Fe(OH)_2$-water] system, we used the equations (12), (16) and (19) of Table 2. The results of the carried out chemical calculation are illustrated in figure 4. It is evident that equilibrium pH value of [$Fe(OH)_2$ - water] system is equal to 8,2.

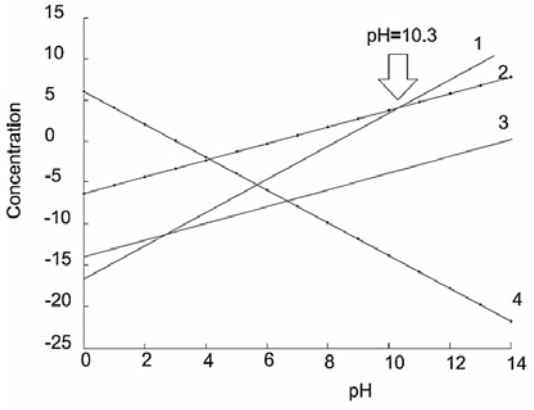

Figure 3. pH influence on the ions concentration [CO_3^{2+} (1), HCO_3^- (2), OH^- (3), Fe^{2+} (4)].

3.3 Determination of optimal pH value and thermodynamic potentials of various pyrite surface oxidation products

The studying of thermodynamic potential helps to define the major components that could be created in the equilibrium conditions [product -water] and also to know the types of chemical reactions occurring at the given moment. The standard potential values were computed by using the equations (I, II, III, IV, V).

Table 2 recapitulates the reactions which are considered for the determination of the various thermodynamic potentials, with the defined thermodynamic constants values, as well as the free energies of the various reactions.

The optimal pH value of pyrite flotation is determined from the graphic (figure 5) of the cumulated thermodynamic potentials of the considered pyrite oxidation products.

It is noticed that $Fe(OH)_3$ is located in the interval [3- 8,6], $FeCO_3$ in [8,6- 10,2] and $Fe(OH)_2$in the interval [10,2-12].

So, the line obtained represents the ΔE of each oxidation products. The optimal pH value necessary for pyrite flotation corresponding to the point of zero charge, in our case, is about 7,0, see figure 5.

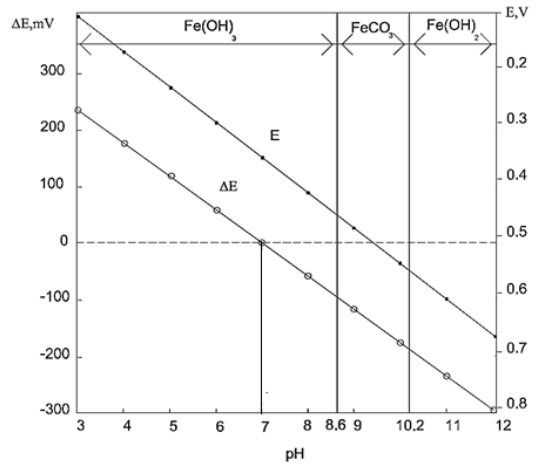

Figure 5.Variation of thermodynamic potential E and its differences ΔE of the pyrite surface oxidation products, according to the pH values.

3.4 Experimental Results and Discussion

The Results obtained by the method of thermodynamic analysis are confirmed by the experimental data in terms of initial potassium butyl xanthate concentration 10 mg/l (figures 6, 7, 8).

These last respectively present the influence of pH values on:

a/ The cumulated values of pyrite surface potential (1) and physical adsorption of dixanthogen (2);

b/ The floatability of pyrite before and after moving away the dixanthogen molecules adsorbed on pyrite surface(2, 1);

c/ The xanthate chemical adsorption before and after moving away the molecules of dixanthogen on mineral surface (2, 1).

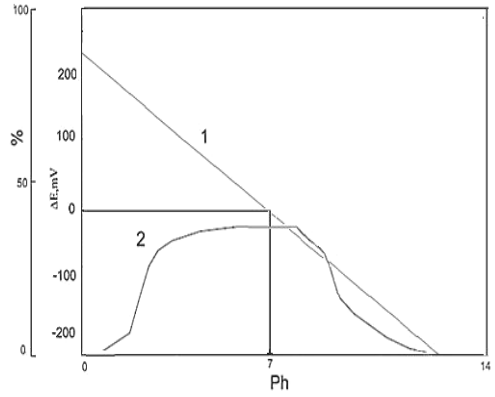

Figure 6. pH influence on dixanthogen physical adsorption on mineral surface(2) and the potential differences of pyrite oxidized surface (1).

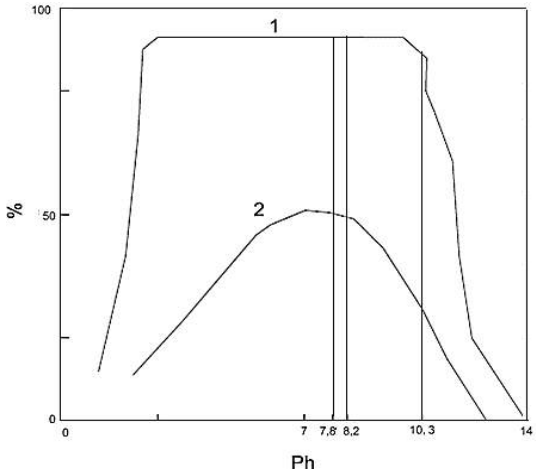

Figure 7. pH influence on the floatability of pyrite before and after moving away the dixanthogen molecules adsorbed on pyrite surface(2, 1);

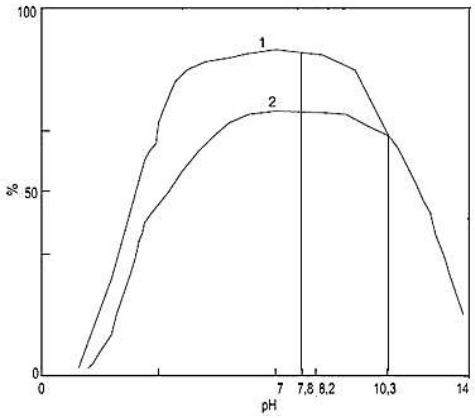

Figure 8.pH influence on the xanthate chemical adsorption before and after moving away the molecules of dixanthogen on mineral surface (2, 1).

The analysis of the results of pH influence on dixanthogen physical adsorption on pyrite surface (figure 6), shows that the maximum adsorption of dixanthogen is located in pH = 7,8 corresponding to equilibrium pH values.

The floatability variation of pyrite according to the pH values before and after dixanthogen adsorption is presented by the curves (1, 2) of figure 7. The latter presents three parts, the first one shows an increase in floatability up to an optimal value. In the second part, a regular floatability is observed. Finally we remark that pyrite extraction decreases in the third part.

In addition, the variation of xanthate chemical adoption on pyrite surface, according to the pH values before and after

the dixanthogen desorption from mineral surface, is illustrated in figure 8. For a pH value equal to 7,0, a maximum adsorption before and after taking away the collector was obtained. It is Also noticed that chemical adsorption decreases at pH equal to 10,3.

So, at pH equal 7,0, we can obtain:

•Maximum physical adsorption (40%);
•Maximum chemical adsorption (90%);
•Maximum degree of extraction (floatability) nearly 90%.

Since the equilibrium state of the system answers to the maximum value of xanthate adsorption on mineral surface and of pyrite floatability, the obtained pH values of equilibrium systems are those of zero charge potential of oxidation products surfaces and correspond to the oxidized pyrite surfaces stability.

4 CONCLUSION

From the results of thermodynamic analysis of pyrite-water system, flotation and adsorption test at various pH and initial potassium butyl xanthate concentration 10 mg/l., it has been established:

- Highlighting of thermodynamic method of analysis characterizing the chemical nature of the elements present on the oxidized pyrite surface. By using their thermodynamic potential, the optimal pH value which is the most significant parameter of the separation medium, it was computed.

- Equilibrium pH value corresponding to minimum charge potential of pyrite oxidized surface, presenting the most important condition of maximum hydrophobicity, dexanthogen adsorption and mineral floatability. The given pH value makes: in the case of $Fe(OH)_3$ 7,8; $FeCO_3$ 10,3; and $Fe(OH)_2$ 8,2.

- Optimal pH values for pyrite flotation answers the surface potential of minimal charge, and guarantees the formation of collector optimum adsorption coverings structure.

- Optimal pH value equal to 7,0 is considered valid owing to the fact that it was experimentally confirmed. It is mentioned that the critical pH flotation of pyrite starts from 6,3, beyond pH equal to 10,3 the pyrite is depressed.

REFERENCES

Abramov A. A., 1993. *Mineral processing by usingflotation methods*. Nedra, Moscow.

Abramov A. A., 1978. *Theoretical Principles of Optimization of sulphide ores by selective flotation*. Moscow, Nedra.

Abramov A. A. 1977. *Physico-chemical modelling of flotation systems*, Moscow, ed."MISIS", p. 110, Russia.

Buckley A. N.,Woods R., 1997. Chemio-sorption of the thermodynamically favored process in the interaction of thiol collectors with sulphide minerals. *Int.J To mine. Process*. 51, pp. 15-26.

Chettibi Mr., 2002.*Optimization of Sulfide Mineral (PbS, ZnS) flotation*. PhD Thesis;Moscow Mining University. Russia.

Garrels R. M., Christ CL, 1964. *Solutions, Minerals and Equilibria.Freeman*, San Francisco,California, the USA.

Gonçalves K L C, 2003. *Surface oxidation effect on Salobo's copper and gold ore*. M. SC. Thesis, Curso de po's – graduaçaoemEngenheriametalurgica e de mines. Escola de engenheria da UFMG, Belohorezonte. 136 p. (in Portuguese).

Heifetz V L, Krasikov B S., 1959.Influence of surface active substances on kinetics of certain cations discharge. *Scientific notes of LGU*. 262, p.3-30.

Hiçyilmaz C, 2009.Electrochemical behavior of pyrite in the absence and presence of DTPI at acidic and alkaline conditions, *Proceeding Of 21st International Mining Congress And Exhibition Of Turkey,* May 6-8, 2009, Antalya, Turkey. V. 1, pp. 609-615.

Junia S. A., and al., 2009.Eh effect on a Lead-Zinc Sulphide flotation. // *Proceeding Of 21st International Mining Congress And Exhibition Of Turkey,* May 6-8, 2009, Antalya, Turkey. V. 1, pp. 257-259.

Puonala Mr., Heimala S.,Jounela S., 1997. Different aspects of using electrochemical potential measurements in mineral processing. *Int. J. Miner. Process. 51*, pp. 97-110.

Raichur A. M., Wang X H., Perekh BK, 2001. Estimate of surface free energy of pyrites by contact anglemeasurements, Ores Engineering,

Mermillod-Cableway R., 2005.*Influence Surface Properties Of The Pyrite On The Retention Of*

The Sulphur Organic Molecules: *Application To The Desulphurization Of Themining Residues*, Thesis of doctorate, University of Montreal.

Wang X H., 1989. *The Chemistry Of Flotation, Activation And Depression Of Iron-Containing Sulphides*, Thesis of doctorate, LuleaUniversity of Technology, p. 507.

Woods R., Richardson P. E,1986. The flotation of solid minerals-electrochemical aspects, *Proceeding Of The Advances In Mineral Processing Symposium*, 1986.

Selection of Flotation Reagents in Order to Improve Metal Recovery from Ores via Computer-Aided Approach

P.M. Solozhenkin

Federal state budgetary scientific establishment of Russian Academy of Sciences Research Institute of Comprehensive Exploitation of Mineral Resources of the Russian Academy of Science (IPKON the RASci) , Moscow, Russia

O.I. Ibragimova

University of Dodoma, Dodoma, Tanzania

ABSTRACT Molecular modeling has experienced constant and considerable development over the past ten years in India, China, Turkey, Russia and Finland. In the present study computational modeling of minerals and reagents was performed using Chem Bio 3D and ChemOffice2005 by CambridgeSoft with optimization by MM2. The semi empirical calculations were provided by MOPAC. Molecular structures of antimony clusters were created. DTF approach was used to determine energies such as HOMO, LUMO and SOMO. Absolute hardness η and chemical potential χ by Pearson and Parr have been calculated. The strategy of prognosis of collector activity evaluation (PCAE) has been proposed as a consistent approach to estimate the interaction between a collector and a mineral cluster as a difference of total energy and sum of cluster energy and collector energy. The lower PCAE the stronger the ability of the collector to interact with the mineral cluster. Although PCAE cannot play the role as an indicating physico-chemical parameter for the particle floated but allows to make some significant conclusions. To improve the separation of minerals the method of complex formation between collectors and mineral clusters was harnessed. The main physico-chemical parameters have been determined. The probable increasing collecting ability of sulfhydril collectors for stibnite follows the order as : butyl xanthic acid (BXA), dimethyldithiocarbamic acid (DMDTCA), piperidine dithiocarbamic acid (PDTCA),mixture of butyl xanthic acid and dithiocarbamic acid (BXA+DTCA), Bis(2-(dibutylamino)ethyl)dithiophosphonic acid (DBAEDTPA) and diethyl aminoethylxanthic acid (DEAEXA). Dialkylamino sulfhydril collectors may be considered to be prospective reagents for sulfide ore flotation. The results obtained were confirmed by experimental data in ore flotation.

Keywords: flotation, mineral clusters, molecular modeling, chemical programs, program MOPAC, collector activity evaluation, metal recovery

1 INTRODUCTION

Several millions organic compounds with various structure have been synthesized over the past 20 years. Several thousands of chemicals were either tested or suggested as flotation reagents. Nowadays there are only a few hundred of these reagents that are extensively used in flotation. Sulfur-containing reagents are widespread collectors for sulfide minerals recovering. The representation of sulfhydryl collectors that has been extensively studied, are xanthates, dithiophosphates and dithiocarbamates, although their derivatives are equally important (Bulatovic, 2007). Xanthates as powerful collectors are commonly used for flotation of sulfide minerals such as chalcopyrite, galena, sphalerite, stibnite and etc. Dithiophosphates are weaker but more selective then xanthates (Ackerman et al, 1987; Bulatovic,2007; Valli et al,1994; Güler et al,2006; Grano et

al,1997; Nagaraj and Ravishankar,2007).Dithiocarbamates have a high specificity for antimony minerals (Bulatovic,2007,Solozhenkin,1994).

Although all of these compounds contain sulfur, the structure of molecules is rather different. This is the connection between the spatial structure of molecules and chemical activity of the compounds. The flotation performance of these collectors have been investigated related on their functional groups. Moreover each compound has its special physico-chemical properties. Therefore the most troublesome question for researchers remains the estimation of quantitative structure-property relationship. The knowledge generated in these studies is extremely helpful in quick selection of collectors with desired properties as well as in designing of new reagents schemes. The correlation established can allow to determine the direction of synthesis of new compounds which could play the key role as collectors for sulfide flotation.

There are a fairly large number of approaches to choose the flotation reagents with definite properties (Soloviev M.E.,Soloviev M.M.,2005).The approach for reagent selection is based on the consideration of more than just the chemistry of one reagent in isolation or more than just one type of reagent for a given mineralogy. In fact, all the chemical and operational factors are considered simultaneously. The preference of using of chemical programs and computer technologies appears to be at the significant value (Khel`l`e,2013, Solozhenkin P.,2013).

Stereochemical representations of mineral and reagent molecules play the significant role in explanation of their behavior in flotation. Modern computational methods allow to find the way of visualizing a three-dimensional model of the molecule and to understand the connection between the spatial structure of the molecule and physical properties of the substance as well as its chemical activity (Soloviev M.,2005,Roshupkin S,2004) .

First principle density functional theory (DFT) method offers an effective tool in the calculation of the properties and energies of the various collectors (Porento and Hirva, 2002, 2004; Yekeler and Yekeler, 2004, 2006; Liu et al, 2008b, 2010, 2011). DFT study is used to determine the optimal molecular structure and calculate atomic charge values, the compositions and energies of HOMO and LUMO of sulfhydryl collectors. The theoretical methodology established and results obtained provide an atomic level understanding on interactions and bond formation mechanisms between collector molecules and sulfide mineral surfaces(Liu, 2012).

2 METHODS AND OBJECTIVES

2.1 Computational Methods

In the present study computational modeling of minerals and reagents was performed using Chem Bio 3D and ChemOffice2005 by Cambridge Soft with optimization by MM2. The semi empirical calculations were provided by MOPAC.

2.2 Docking Method

Complex formation have been established with the aid of computational docking technique. The docking method is a search algorithm and a scoring function that predicts the preferable orientation of one molecule to a second to form a stable complex and estimate collecting activity of reagents. The approach has proved useful in identifying relevant candidates for several flotation applications (Solozhenkin P, 2006).

2.3 Objectives

The objectives of the present study are antimony minerals and thiol collectors which are used in practice for stibnite flotation from Sb-Hg,Sb-As ores at Djijicrut deposit (Tadjikistan) and Sarilah Mineral Processing Plant (Yakutia, Russia) . These collectors have been established as standard reagents for estimation the effectiveness of organic compounds studied. The strategy of evaluation has been proposed as an approach to make a choice of organic compounds as a

prospective collectors in stibnite flotation. Possessing the high chemical activity the organic compounds studied can show the stronger complexing properties comparing to the other collectors because of the presence of the functional group of thione and thiol sulfur atoms having donor properties. The characteristics of flotation reagents and organic compounds studied are provided in Table 1.

Table 1. Samples characteristics

Sample No	Chemical formula	Molecular weight(g)	Elemental analysis
1	$C_5H_{10}OS_2$	150	C40.0;H6.67;
			O10.67;S42.66
2	$C_3H_7NS_2$	121	C29.75;H5.78;
			N11.57;S52,90
3	$C_7H_{15}NOS_2$	193	C43.49;H7.82;
			N7.24;O8.28;S33.17
4	$C_6H_{11}NS_2$	161	C44.68;H6.87;
			N8.68;S39.76
5	$C_{20}H_{45}N_2PS_2$	408	C58.78;H11.10;
			N6.85;P7.58;S15.69
6	C_9H_7NS	161	C67.08;H4.35;
			N8.69;S19.88
7	$C_7H_6N_4S$	178	C47.19;H3.37;
			N31.46;S17.98
8	$C_{10}H_{23}O_2PS_3$	302	C39.71;H7.66;
			O10,58;P10.24;S42,66

Table 1 contains the information about chemical formulas, molecular weights and chemical analysis data for various organic compounds where 1-Butyl xanthic acid(BXA); 2-Dimethyldithiocarbamic acid(DMDTCA); 3-Diethylaminethylxanthic acid(DEAEXA); 4-Piperidinedithiocarbamic acid(PDTCA); 5-Bis(2-(dibutylamino) ethyl) dithiophosphonicacid (DBAEDTPA); 6-Quinolinethiol (QT); 7-Tetrasol;8-O,O dibutylS-(2-mercaptoethyl) hosphorodithioate (DBMEDTPA).The stibnite cluster activated has been presented as a formula $PbSb_2S_4$ (PbS Sb_2S_3) based on the special studies. Molecular structures of mineral-collector clusters were created. DTF approach was used to determine energies such as HOMO, LUMO and SOMO. Absolute hardness η **and** chemical potential χ **by** Pearson and Parr have been calculated.

3 RESULTS AND DISCUSSION

3.1 Molecular Models of Mineral Clusters

The strategy of prognosis of collector activity evaluation (PCAE) has been proposed as a consistent approach to estimate the interaction between a collector and a mineral cluster as a difference of total energy and sum of cluster energy and collector energy.

The chemical reaction between a thiol collector and a sulfide mineral is a frontier-controlled reaction (Liu, 2008b, 2010; Klopman, 1968; Wang et al,1996), i.e. a thiol collector transfers its HOMO electrons to a metal atom on the sulfide mineral surface to form a normal covalent bond. Additionally, if a metal atom on the sulfide mineral surface has richly d-orbital electrons and a thiol

collector has the electron-accepting ability, the metal atom can transfer some of its d-orbital electrons to the LUMO of the thiol collector to form back donation covalent bonds.

The complex of the stibnite cluster with three molecules of butyl xanthate attached to antimony atom is shown in Figure 1. In case of stibnite the atom of antimony has oxidation number equal to three therefore Figure 1 indicates the collector attached using three arrows. Figure 2 represents the similar complex but for stibnite activated by Pb^{2+} cations. As arrows indicate lead cation is attached to two molecules of butyl xanthate.

Additionally, the complex of stibnite cluster activate by Pb^{2+} with dimethyldithio carbamate and its optimized geometrical structure are shown in Figure 3 a and respectively.

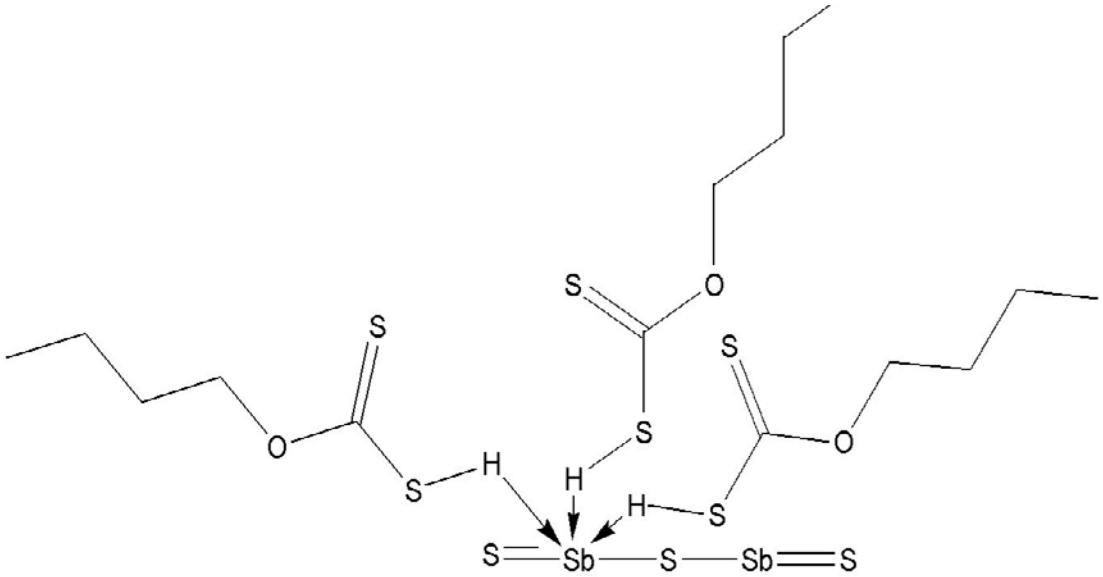

Figure 1. Complex of stibnite cluster with 3 molecules of butyl xanthate attaching to antimony atom.

.

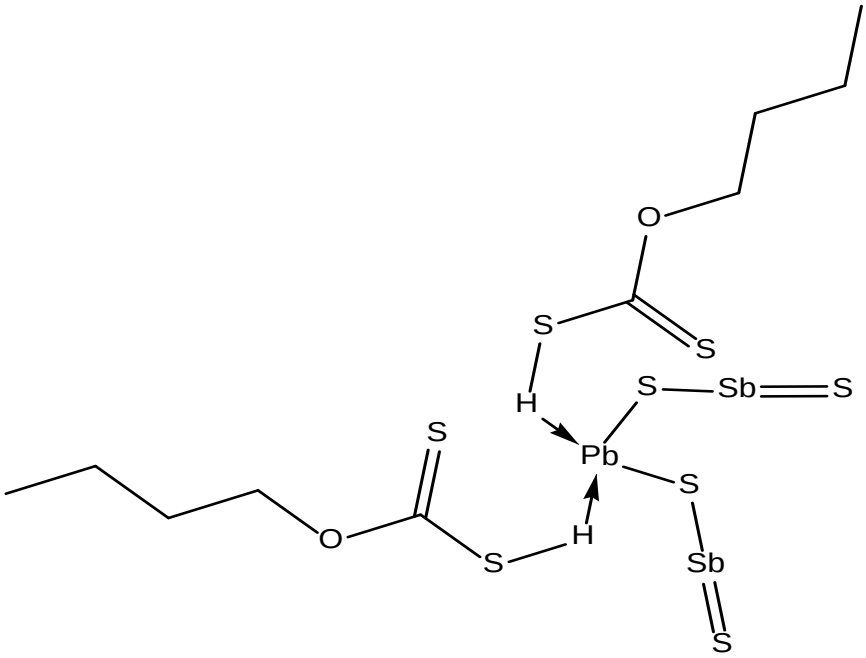

Figure 2. Complex of stibnite cluster with 2 molecules of butyl xanthate attaching to lead atom.

a

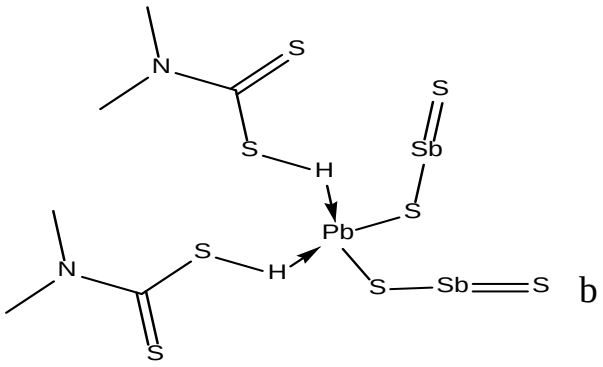

b

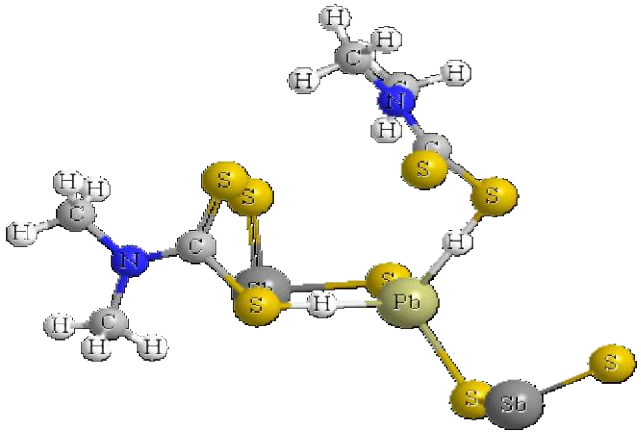

Figure 3. Complex of stibnite cluster with 2 molecules of DMDTC attaching to lead atom (a) and its optimized geometrical structure (b).

The optimized geometrical model of activated stibnite cluster with the combination of butyl xanthate and dimetyldithiocarbamate was created. This model represents the real flotation process with the mixture of collectors such as BX and DMDTC. Figure 4 shows the complex of activated stibnite attaching to three molecules of BX by antimony atom and to two molecules of DMDTC by lead atom.

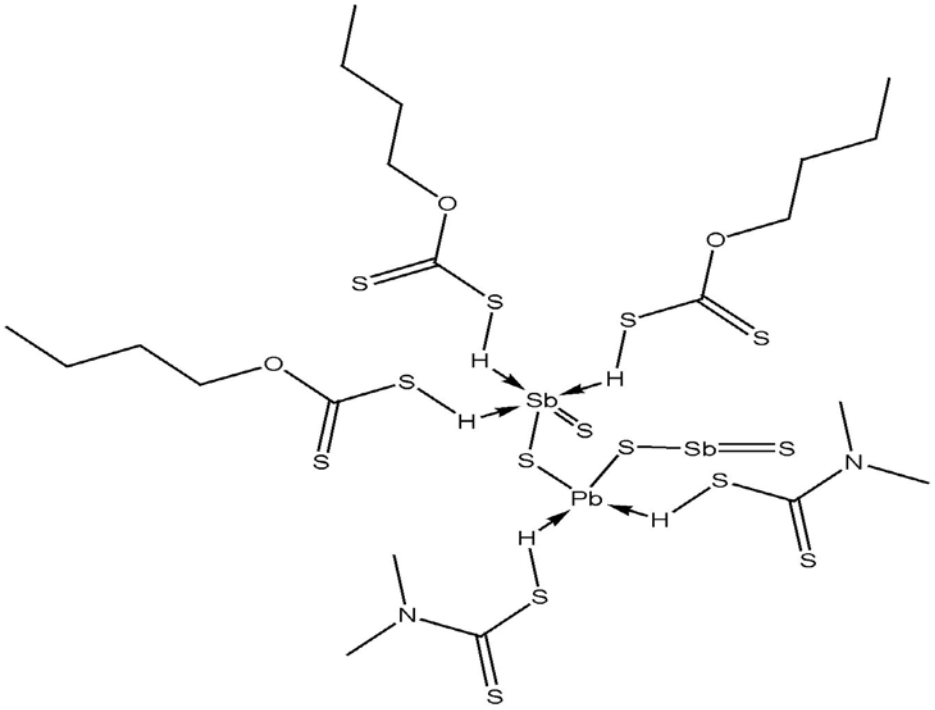

Figure 4. Complex of activated stibnite attaching to three molecules of BX by antimony atom and to two molecules of DMDTC by lead atom.

3.2 Prognosis of Collector Activity Evaluation (PCAE)

Models given in Figure 1-4 have been taken into account to calculate the physico-chemical constants for collectors.

The strategy of collector activity evaluation has been proposed as a consistent approach to estimate the interaction between a collector and a mineral cluster as a difference of total energy and sum of

cluster energy and collector energy (Solozhenkin 2012a, 2012b, 2012c).

E = E complex - (E cluster + E collector), eV(1)

The lower PCAE the stronger the ability of the collector to interact with the mineral cluster. The calculated PCAE for various mineral clusters and collectors such as BXA, DMDTCA and the mixture of them are given in Table 2.

Table 2. Calculated PCAE (eV)

Mineral cluster	PCAE ,eV BXA	DMDTCA	BXA+DMDTCA
Sb_2S_3	-0.5491	-0.6871	
$PbSb_2S_4$	-1.1517	-1.6756	-1.8463

According to Table 2 the decrease of prognosis of collector activity evaluation (PCAE) for stibnite activated is in the following order: BXA (-1,1517), DMDTCA (-1,6756), BXA+DMDTCA(-1,8463). From the relevant studies conducting on flotation it can concluded that floatability of stibnite is changing in reverse order to PCAE. Based on this order the stibnite floatability is increasing from the individual collector up to the mixture. As a matter of fact, the lower PCAE the higher floatability of stibnite. The lowest magnitude of PCAE obtained for the mixture of BXA and DMDTCA is related to the maximum recovery of stibnite.

The theoretical knowledge obtained from research on PCAE provided a basis for the industrial flotation testing of stibnite by the combination of BX and DMDTC from Sb-Hg, Sb-As sulfide ores on Sarilah Mineral Processing Plant (Yakutia, Russia). The antimony ore with the grade of 15,6-14,91% Sb and 0,33-0,21% As was processed in differential flotation circuit in which antimony is recovered to a concentrate at a grade of 62,39-59,20% Sb, 0,43-0,36% As, leading tailings containing 1,73-1,13% Sb and 0,33-0,21% As.

Furthermore on the base of computer modeling it was suggested the range of organic compounds which properties as proposal collectors were predicted. Table 3 contains a PCAE data for stibnite clusters and various reagents with amino group

Table 3. Calculated PCAE (eV)

Reagents	Mineral cluster	PCAE,eV
Tetrasol	$PbSb_2S_4$	-1.1846
DBMEDTPA	$PbSb_2S_4$	-1.0846
QT	$PbSb_2S_4$	-1.5104
PDTCA	PbSb2S4	-1.7696
DBAEDTPA	PbSb2S4	-8.0223
DEAEXA	$PbSb_2S_4$	-602.3262

The results indicate that the difference in PCAE for some derivatives and BXA does not have the significant value while the complex of stibnite with DEAEXA has PCAE of - 602,3262 eV . Comparing this with the PCAE data for stibnite activated and BXA, a significant decrease in PCAE for DEAEXA from – 1,1517 (BXA) to – 602,3262 can be seen and from the previous discussion it is evident that this reagent can be considered as the most perspective collector for stibnite flotation. The complex of DEAEXA with stibnite activated is shown in Figure 5 and its optimized geometrical structure presents in Figure 6

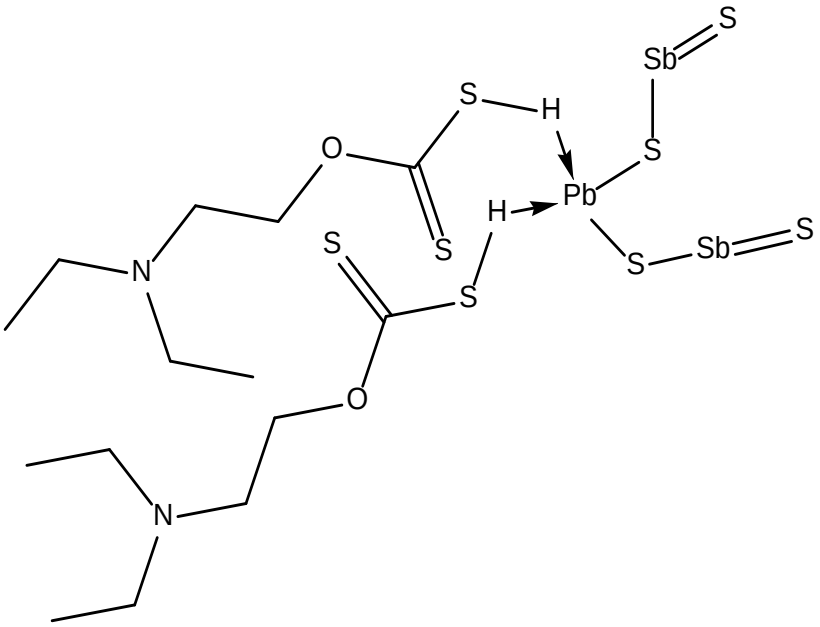

Figure 5. The complex of DEAEXA with stibnite activated Pb^{2+}

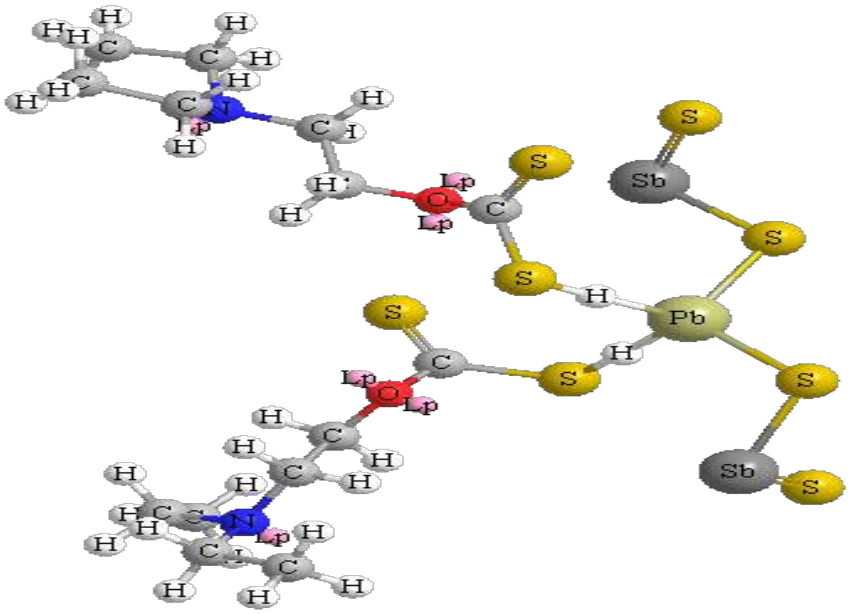

Figure 6. Optimized geometrical structure of the complex of DEAEXA with stibnite activated.

CONCLUSIONS

1. The computative method can be directly applied as a tool in investigation of surface-collector interaction.

2. The theoretical knowledge obtained from research on mineral-collector clusters provided a basis for the stibnite flotation from Sb-Hg and Sb-As ores with the combination of BX and DMDTC.

3. The values of PCAE for stibnite clusters with sulfhydril collectors have been calculated.
4. It has been established that PCAE was decreased in order of: butyl xanthic acid (BXA), dimethyldithiocarbamic acid (DMDTCA), piperidine dithiocarbamic acid (PDTCA), mixture of butyl xanthic acid and dithiocarbamic acid (BXA+DTCA), Bis(2-(dibutylamino)ethyl) dithiophosphonic acid (DBAEDTPA) and diethyl aminoethylxanthic acid (DEAEXA). The flotability of stibnite is changing in reverse order comparing to PCAE.
5. There is a strengthening effect of amino group in collectors on flotability of stibnite therefore dialkylamino sulfhydril collectors can be considered to be prospective reagents for sulfide antimony ore flotation.

REFERENCES

Ackerman, P K, Harris, G H, Klimpel, R R, Aplan, F F, 1987. Evaluation of flotation collectors for copper sulfides and pyrite: I. Common sulfhydril collectors, *International Journal of Mineral. Processing*, Vol 21, pp 105-127.

Bulatovic, S M, 2007. *Handbook of flotation reagents: chemistry, theory and practice*, volume 1: flotation of sulfide ores (Elsevier B.V., Amsterdam).

Grano, S R, Cnossen, H, Skinner, W, Prestidge C A, Ralston J, 1997. Surface modifications in the chalcopyrite- sulphite ion system, II. Dithiophosphate collector adsorption study, *International Journal of Mineral Processing*, Vol 50, pp 27-45.

Güler, T, Hiçyilmaz, C, Gökağaç, G, Ekmeçi, Z, 2006. Adsorption of dithiophosphate and dithiophosphinate on chalcopyrite, *Minerals Engineering*, Vol 19, pp 62-71.

Khel`t`e el at. *Molecular Modeling: Theory and Practice* .Moscow; Binom. Laboratory of Knowledge,2013,319 p

Klopman, G, 1968. Chemical reactivity and paths, *Journal of American Chemical Society*, Vol 90, pp 223-230.

Liu, G Y, Zhong, H, Dai, T G, Xia, L Y, 2008b. Investigation of the effect of N-substituents on performance of thionocarbamates as selective collectors for copper sulfides by ab initio calculations, *Mineral Engineering*, Vol 21, pp 1050-1054.

Liu, G Y, Zhong, H, Xia, L Y, Wang, S, Dai T G, 2010. Effect of N-substituents on performance of thiourea collectors by density functional theory calculations, Transactions of *Nonferrous Metals Society of China*, Vol 20, No 4, pp 695-701.

Liu, G Y, Zhong, H, Xia, L Y, Wang, S, Xu, Z H, 2011. Improving copper flotation recovery from a refractory copper porphyry ore by using ethoxycarbonyl thiourea as a collector, *Minerals Engineering*, Vol 24, pp 817-824.

Nagaraj, D R, Ravishankar, S A, 2007. Flotation reagents a critical overview from an industry perspective, *In Froth Flotation: A Centuary of Innovation*(Editors: Fuerstenau M, C, Jameson G, Yoon R, H, Society for Mining, Metallurgy, and Exploration Littleton, Colorado), pp 375-424.

Porento M. & Hirva P. (2000) Theoretical studies on the interaction of anionic collectors with Cu^{+}, Cu^{2+}, Zn^{2+} and Pb^{2+} ions, *Theor. Chem. Acc.* 107,pp. 200–205.

Porento M. & Hirva P. (2004) A theoretical study on the interaction of sulfhydryl surfactants with a covellite (001) surface., *Surf. Sci.* 2004, 555,pp. 75–82.

Roshupkin S.I. Space modeling of molecular compounds.Chemistry: methods of teaching.2004.№1.pp.46-58

Soloviev M.E.,Soloviev M.M. *Computational chemistry*. SOLON Press.2005,536p.

Solozhenkin P.M.,Ivanova N.K.,Ibragimova O.I.,Stoyanov A.F. Optimization of antimony ore flotation technology.*Non-Ferrous Met*.J.,1994.№ 7,pp.63-66.

Solozhenkin P.M.2006,Ecological problems-new tendency of rational usage of gold-antimony ores and concentrates.VINITI .*Scientific and technical acpects of environmental protection.*Survey.M,№2,pp1-120

Solozhenkin P.M. (2012a) Quantum–chemical and molecular-dynamic aspects of forecasting of properties of collectors of metals from productive solutions of nonferrous metals, Works of the international scientific symposium «Week of the miner 2012», *The collection of articles, Separate release of the mountain-information analytical bulletin (scientific and technical magazine)* M: Publishing house «Mountain book» , NOR1-632 . pp.431-455.

Solozhenkin P. M**.** **(**2012b) Research of interaction of prototypes of minerals with solutions of reagents quantum - chemical method, *Proceeding 16-th Conference on Environment and Mineral Processing*, 7–9 June, 2012, VSB-TU OSTRAVA, Czech Republic. Part II.pp.207–212.

Solozhenkin P. M, Solozhenkin O. I. & Krausz S. **(**2012c) Prediction of Efficiency of Flotation Collectors Based on Quantum Chemical Computations. *Books of Abstracts. XXVI*

International Mineral Processing Congress, 2012. New Delhi, India, September 24-28, vol. 2, p. 638

Wang, D, Z, Lin, Q, Jiang, Y R, 1996. *Molecular design of reagents for mineral and metallurgical processing* (Changsha: Central South University of Technology Publishers), pp 88-110.

Yekeler M. & Yekeler H. (2004) Reactivities of some thiol collectors and their interactions with Ag^{+} ion by molecular modeling, *Appl. Surf. Sci*. 236,pp. 435–443.

Yekeler M. & Yekeler H.(2006) A density functional study on the efficiencies of 2-mercaptobenzoxazole and its derivatives as chelating agents in flotation processes, Colloids Surf. A: *Physicochem. Eng. Aspects* .2006, 286, pp.121–125.

Mechanical Properties of Feldspars and Their Influence on the Choice of Method of Comminution.

R.Akkal, M.Ouldhamou, S.A.Hadj-Sadok
National Polytechnic School of Algeria, Alger's, Algeria

ABSTRACT The mechanical properties of feldspathic rock have a direct impact on weight yields of different particle size fractions for purification and marketing. Therefore they affect the selection and sizing of size reduction and screening equipment.

Our analysis provides the basis for assessing the degree of homogeneity from the hardness and energy consumption standpoints. The energy consumption is evaluated by the Bond Index, which is the number of KWh consumed per ton of milled ore.

Given the demand from users of feldspars with its various particle size, the operating cost (crushing and screening) increases with the fineness of the fractions. It is very useful to determine the effect of a comminution provided with a number of recycling of refuse screenings. This provides sufficient data to optimize the production according to the demand, taking into account the level of fines and the losses caused by the selected process.

Keywords: Comminution, feldspar, purification, screening

1 INTRODUCTION

Grinding is the essential step in a processing plant for the production of a desired mesh for subsequent unit operations such as leaching, flotation. For this purpose, various types of equipment can be used according to the requirements of a processing system which directly affects the efficiency of a given process. [1]

In mineral processing, milling represents almost 80% of the energy consumed in the plant. The grinding efficiency depend not only on the high production rates, but also on conventional grinding systems used and the quality and type of ore undergoing such operations. Particularly, feldspars are a mixture of two or more minerals which differ in their chemical and physical properties, the use of a grinding pattern can lead to a significant effect on the production rate. The constituent minerals feldspar ore are of different forms and from different regions, so are heterogeneous. The grinding of such minerals requires a good understanding of the various components forming the ore. [2,3]

Crushing a large tonnage of heterogeneous run of mine ore, understanding of how the different components behave individually and in mixtures and how they interact with each other is a high priority in the proposal of a scheme final treatment. The mechanical properties of feldspathic rock have a direct impact on weight yields of different size fractions for the purification and commercialization, therefore they influence the choice and design of comminution and screening equipment, once the planned industrial capacities arrested on the basis of a study.

Any method of an ore treatment often requires fragmentation to a size that allows the release of its ingredients, minerals and gangue products thus making the separation of the latter accessible to use by following the physical, chemical or physico-chemical processes applied to the separation of minerals from a mineralized rock. These techniques are used individually or combined depending on the complexity of the mineralization and the cost of treatment.

In our present work this analysis provides the evaluation components of the degree of homogeneity of the hardness point of view and therefore the energy consumption standpoint. This is calculated according to the performance of a normative test called

Index Bond, giving the number of KWH consumed per tonne of ore milled.

Given customer demand users of feldspars in its various forms of particle size, the operating cost of crushing, grinding and screening increases with the fineness of market size slices and the economic consideration related to the losses caused by the process set up. It is very useful to determine the effects of a controlled comminution with a number of recycles screening refusal corresponding to the size determined by the choice of the operator after having extracted before each recycling, allowing to provide sufficient data to modulate the production according to demand knowing the level of fines <40 µm caused by the process.

The supported study in this work focuses on mechanical preparation of crude feldspar, to maximize comminution data and energy consumption.

1.1 Materials and Methods

A sample from the site of Ain Barbar east of Algeria was crushed to a size of 1 mm in three stages in a jaw crusher. The maximum initial size was [250mm]. This sample is undergone crushing operations in a jaw crusher, followed by grinding in an impact mill of Ain Barbar unit. The particle size obtained is in the order of [6.3mm]. All coming obtained was sieved down to [0.8 mm] in view of the application of the glass market. Fines [-0.1mm] was extracted by sieving to avoid over-grinding. These grinding / sieving are carried out as shown in Figure 1. The desired outcomes are the production of the three size fractions [-0.8 + 0.4mm], [-0.4 + 0.250mm] and [-0250 mm] taken for further processing enhancement. Sufficient amounts were treated to extrapolate the results to a scale up. Concerned size fractions were extracted in each grinding (Fig.1).

2 RESULTS AND DISCUSSION

Initially, the E1 sample is ground and sieved at [0.8mm] with recycling [+ 0.8mm] from the sieving E0 at [0.8mm] and reduced to [-0.8mm]. The results obtained are given in the following Table 1:

Table 1: Total production of different size fractions obtained from the sample E1 after crushing/screening 0.8 mm and recycling +0.8 mm size fraction.

Size fraction (mm)	W(g)	Rw(%)	Rw(%)/W0
[-0.8+0.4]	7834.75	32.65	15.21
[-0.4+0.250]	2441.60	**10.18**	4.74
[-0.250]	13717.25	57.17	26.63
Total	23993.59	100	46.58

W0: in the initial weight

The total production of different particle size from [-0.8mm] of the sample E2 obtained from the sieving of the sample E0 is given in the following Table 2:

Table 2: Total production of different size fractions obtained from - 0.8 mm from the sample E0.

Size fraction (mm)	W(g)	Rw(%)	Rw(%)/W0
[-0.8+0.4]	7814.14	28.56	15.17
[-0.4+0.250]	3358.48	**12.27**	6.52
[-0.250]	16184.75	59.16	31.43
Total	27357.37	99.99	53.11

In a second step, all size fractions [-0.250mm] obtained in all cases grinding/sieving, were screened. The results obtained are given in the following Table 3:

Table 3: Screening of all slices [-0.250 mm] obtained in all cases grinding / sieving.

Size fraction (mm)	W(g)	Rw(%)	Rw(%)/W0
[-0.250+0106]	5041.51	17.12	9.79
[-0.106+0.04]	12787.93	43.41	24.83
[-0.04]	11627.00	39.47	22.57
Total	29456.44	100	57.19

Through the results, we note that the grinding of all spared from reduced [-250 + 200 mm] to [0.8mm] gave 13.15% (Fig.1) for the portion [-0.04mm] obtained on the

basis of the screening of the sample E0 ground to [6.3mm], while the resulting crushing / screening of [+ 0.8mm] is 9.42% (22.57%- 13.15%) (see Tab3 and Fig1). An run of mine ore crushed at [0.8mm] give a class production rate of 51.43% from E0 sample. The particle size [-0.1 + 0.04 mm] represents 24.83%, while fine [-0.04 mm] represent 22.57% of the sample E0.

The fraction for the glass is provided by the process described above (Fig.1), it would give an output of 51% of run of mine ore. The production of fine [-0.04] mm is 22.57% will be used in the very ordinary ceramic (floor tiles) which his treatment after dishelming to [0.020mm] is very expensive, the rest [-0.1 + 0.04 mm] will be for ceramics of lower quality products. It is refined by the wet high field gradient for a satisfactory result.

In the following, the particle size [-0.8 + 0.4 mm] was ground to [-0.4 mm] in two stages comprising a grinding / sieving, the results obtained are given in the following table to give the total weight of each slice obtained by grinding / sieving [-0.8 + 0.4 mm] reduced to [-0.4mm] (Tab.4):

Table 4: Total production of slices obtained by crushing / screening of [-0.8+0.4] mm reduced to [0.4 mm].

Size	W(g)	Rw(%)	Rw/W0	Ex/W0
[-0.8+0.4]	376.02	2.41	0.26	0.73
[-0.4+0.250]	1014.76	6.50	0.70	1.97
[-0.250+0.106]	1529.86	9.80	1.06	2.97
[-0.106+0.04]	8154.11	52.21	5.66	15.83
[-0.04]	4543.23	29.09	3.16	8.82
Total	1567.98	100	10.85	30.32

Ex/w0: extrapolation versus the initial weight (w0)

In turn, the particle size [-0.4 + 0.250] was ground / sieved to [0.25 mm] and the results obtained are given in the following Table 5:

Table 5: Total production of grinding / sieving slice [-0.4 + 0.25 mm] to [0.25 mm]

Size fraction (mm)	W(g)	Rw(%)	Rw/W0	Ex/W0
[-0.4+0.250]	294.79	4.34	0.18	0.57
[-0.250+0.106]	2872.64	42.30	1.72	5.57
[-0.106+0.04]	1763.89	25.97	1.05	3.42
[-0.04]	1859.11	27.37	1.11	3.60
Total	6790.43	99.98	4.06	13.16

Through these results, the fine rate [-0.04mm] relative to feed down with increasing recycling. This finding can be explained by the fact that the fragile particles crumble at the first passage on the crusher or mill, the more remaining hard produce fewer fines. The particle size [-0.4 + 0.250 mm] is produced with a rate that varies little regardless of the number of recycling, this rate varies between 10 and 12% (Tab1 and Tab2). This is explained by the fact that the all-comers present a good homogeneity degree from the point of view hardness and structure.

Knowledge of results in weight crushing / screening report is used to size the unit of production equipment according to the required size fractions and demand. According to the results of the fine rate is of the order of 35.72% to reduce the size of [6.3mm] to [0.250mm] rate lower than that obtained in the treatment scheme proposed by BRGM (Bureau de recherche geologic et minière) (44.45%) including a screening of the [-4mm] to [1 mm], a classification of [-1mm] to give two fractions [-1 + 0.2 mm] and [-0.2mm], a grinding cone crusher of [-4 + 1mm] to [-0.2mm], a grinding mill cone of [-4mm] to [0.2mm]. The -0.2mm particles were subjected to attrition and classification wet to give 0.02mm and -0.2 + 0.020 mm fractions respectively. Product -1 +0.2 mm is ground in a ball mill (wet) to 0.2mm to 0.02mm and deslamming then mixed with the fraction A to be classified to [0.04mm] to give slices [-0.02 +0.04 mm] and [- 0.04 + 0.02mm] fractions respectively. The fine production of [-0.04mm] is of the order of 44.45%

Examination of the graphs relating to the mechanical tests and particle size analyzes of

the sample including the recycling of the refusal of each grinding / sieving [0.8mm] shows that the intersection of the graphs (corresponding to the 50% passing 50% refusal) moves well regularly to fine particles (Fig 2).

To better highlight the evolution of the different results, we have compiled the following table showing the cut 50% of refusal and passing cumulative in function of the grinding level. According to the results, cuts 50% refusal cumulative (CR) and 50% passing cumulative (PC) down with decreasing level grinding (Tab 6).

Table 6: Grade for 50% RC and 50% PC in function of grinding level

Experiment N°	Grinding level	Grade 50% RC et 50% PC
I	[250 mm] reduces to [6.3mm]	0.65
II	[250 mm reduces to [0.8mm]	0.27
II	[150 mm reduces to [0.8mm]	0.2
IV	[150 mm reduces to [0.63mm]	0.2
V	[0.8 mm reduces to [0.4mm]	0.065
VI	[0.4 mm] reduces to [0.25mm]	0.055

Production of [-0.40 mm] and [-0.250 mm]

The results of the production of two size fractions [-0.40 mm] [-0.250 mm] in function of the grinding level are given in the Table 7 :

Through the results, it should be noted that the production of the two size fractions increase with the grinding level. The reduction of run of mine ore from [250 mm] and [150 mm] in order to obtain [0.8 mm] and [0.4 mm] give almost the same rate of production of the grain size range, explained by that the feldspar treated with a high degree of homogeneity. Jumping production of [-0.4mm] is more important in the grinding of feldspar at [0.8mm].

Table 7: Size fractions [-0.40 mm] and [-0.250 mm] in function of grinding level

Experiment N°	Level grinding of run of mine	Production of [-0.40 mm]	Production of [-0.250 mm]
I	[250 mm] reduces to [6.3mm]	37.95	31.43
II	[250 mm] reduces to [0.8mm]	68.48	57.19
II	[150 mm] reduces to [0.8mm]	67.2	84.81
IV	[250 mm] reduces to [0.4mm]	98.07	84.81
V	[250 mm] reduces to [0.25mm]	----------	97.39

Fines production [-0.04mm]

As part of the study of the production of fine [-0.04mm], we performed several tests at different grinding levels. The results obtained are given in Tab 8:

Table 8: Size fractions of [-0.040 mm] production as a function of grinding level

Experiment N°	Grinding level	Fines production [-0.04 mm]
I	[250mm] reduces to [6.3mm]	13.15
II	[200mm] reduces to [4mm] (VS)	5.4
III	[200mm] reduces to [4mm] (VH)	14.53
IV	[250mm] reduces to [0.8mm] (BM)	22.57
V	[150mm] reduces to[0.8mm] (BNM)	27.42
VI	[250mm] reduces to [0.4 mm]	31.39
VII	[250mm] reduces to [0.250 mm]	34.47
VIII	[200mm] reduces to [0.2 mm]	45

Through the results, we note that the fine rate increases with increasing grinding level. Run of mine ore from [200 mm] size is reduced to the same size [4 mm], with two

different ways. It was found that, the wet path give a greater rate of fines (14.53%) which could be explained by the washing with the water generating further fine particles.

It should also be noted that the reduction of run of mine ore size of [150 mm] and [250 mm] respectively, with and without extraction of the desired slice [0.8mm] to each recycling mill have generate a fine rate of 22.57% and 27.42% respectively.

Overall production of the various tranches

The production of different particle size ranges [-0.8mm] [-0.4mm] and [-0.250mm] are given in the following table 9:

Table 9: Size fractions [-0.8mm], [-0.40mm], [-0.250mm] mm production as a function of grinding level

Comunition	Production of [-0.8mm]	Production of [-0.4mm]	Production of [-0.250mm]
Grinding	32.35	21.15	18.03
1st recycling	12.72	9.19	7.65
2nd recycling	1.51	1.02	0.93

Based on the results, we note that the production of different size fractions decreases with the number of recycling achieved on the grinder. Production of the size fraction of [-0.8mm] is more important as compared to the other two size fractions which are [-0.4mm] and [-0.250mm] whatever the number of recycling.

3 CONCLUSION

As part of this work, it was aimed to study the grindability of Ain Barbar fledspar ore and maximize results on the various size destined to the industries glassware and ceramics. We preferred to review by all the results obtained in the past. This allowed us to compare a number of results and draw useful conclusions to any development project. From the point of view, we enjoy the rather homogeneous nature physical property, in particular regarding the hardness and the results of comminution related to energy consumption; it is in the range of 8.5-10 kWh/t.

The rate of fines generated by a crushing / grinding system, for access to a given size fraction, is an important factor, because it is a by-product of poor quality, which is accessible at a prohibitive price. It becomes necessary to assess the fine production rates and seek to reduce it by spared grinding. We compared the results of a crushing / grinding / sieving of run of mine ore without extracting the main particle size [-0.8 + 0.1] mm by sieving or cyclone. Recycling of [+ 0.8mm] was achieved with those of the same operation but with extracting the desired slice to each recycling [+ 0.8mm]. It is shown that the second method produces less fines [-0.04mm], the over-grinding is avoided. The presented results provide a forecast of production rates of particle size which may be required by some customers and could make it more effective in the later applied purification processes.

Nomenclature:

W0: Initial weight for the sample E0 [g]
Ext: Extrapolation against run of mine ore
Rw: performance weight [%]
W: Weight [g]
E0: Initial sample

REFERENCES

[1]Deniz Altun, Carsten Gerold, Hakan Benzer, Okay A ltun, and Namk Aydogan. Copper ore grinding in a m obile vertical roller mill pilot plant.International Jour nal of Mineral Processing, 2014, url="http://www.sciencedirect.com/science/article/ pii/S0301751614001537

[2]D.W.Fuerstenau, P.B.Phatak, P.C.Kapur, and A.Z. M.Abouzeid. Simulation of the grinding of coarse/fi ne (heterogeneous) systems in a ballmill. Internationa l Journal of Mineral Processing, 99(1-4):32 – 38, 2011.

[3]Abdel-Zaher M. Abouzeid and Douglas W. Fuerstenau. Grin ding of mineral mixtures in high-pressure grinding rolls. International Journal ofMiner al Processing, 93(1):59 – 65, 2009.

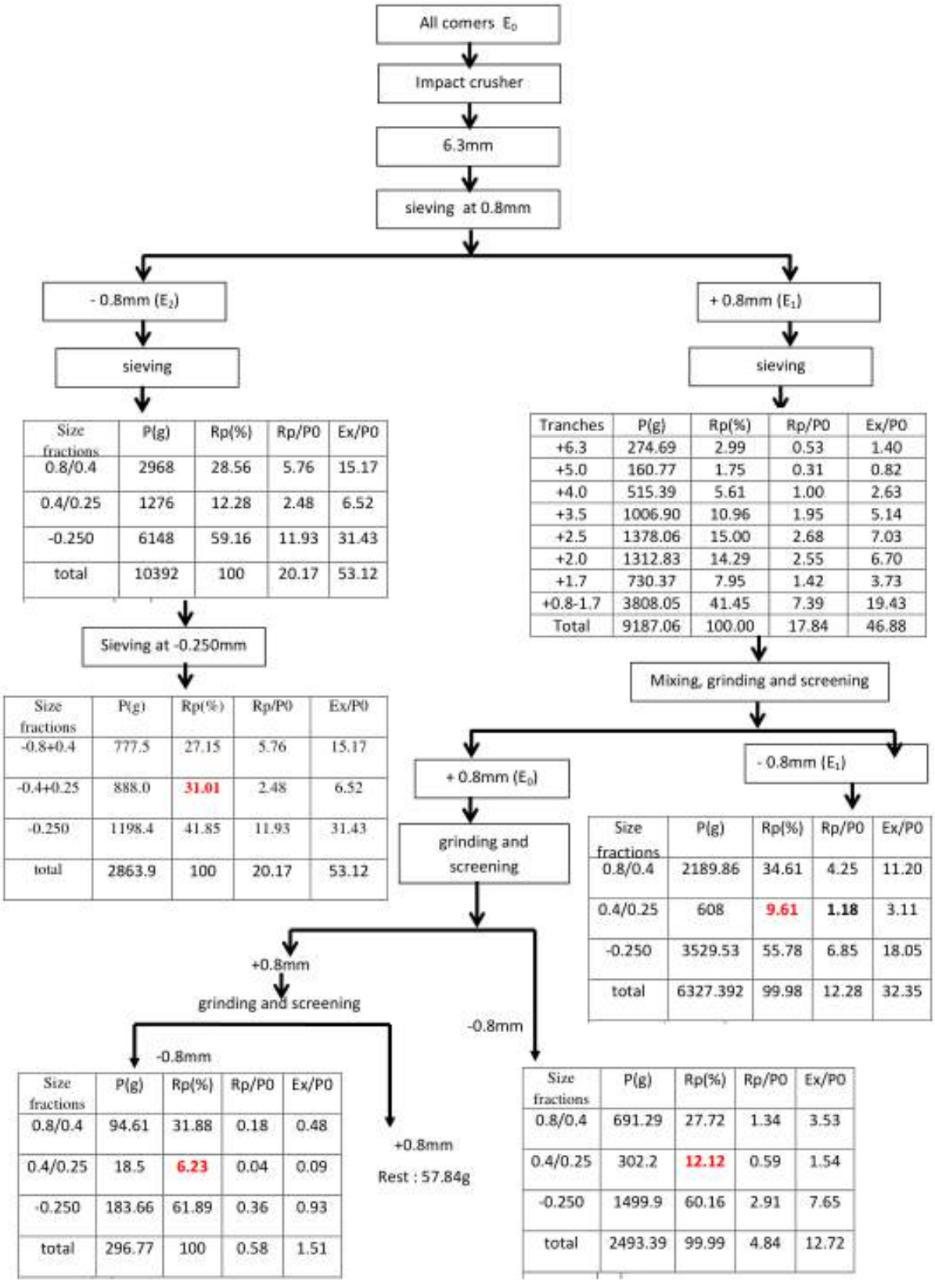

Size fractions	P(g)	Rp(%)	Rp/P0	Ex/P0
0.8/0.4	2968	28.56	5.76	15.17
0.4/0.25	1276	12.28	2.48	6.52
-0.250	6148	59.16	11.93	31.43
total	10392	100	20.17	53.12

Tranches	P(g)	Rp(%)	Rp/P0	Ex/P0
+6.3	274.69	2.99	0.53	1.40
+5.0	160.77	1.75	0.31	0.82
+4.0	515.39	5.61	1.00	2.63
+3.5	1006.90	10.96	1.95	5.14
+2.5	1378.06	15.00	2.68	7.03
+2.0	1312.83	14.29	2.55	6.70
+1.7	730.37	7.95	1.42	3.73
+0.8-1.7	3808.05	41.45	7.39	19.43
Total	9187.06	100.00	17.84	46.88

Size fractions	P(g)	Rp(%)	Rp/P0	Ex/P0
-0.8+0.4	777.5	27.15	5.76	15.17
-0.4+0.25	888.0	**31.01**	2.48	6.52
-0.250	1198.4	41.85	11.93	31.43
total	2863.9	100	20.17	53.12

Size fractions	P(g)	Rp(%)	Rp/P0	Ex/P0
0.8/0.4	2189.86	34.61	4.25	11.20
0.4/0.25	608	**9.61**	**1.18**	3.11
-0.250	3529.53	55.78	6.85	18.05
total	6327.392	99.98	12.28	32.35

Size fractions	P(g)	Rp(%)	Rp/P0	Ex/P0
0.8/0.4	94.61	31.88	0.18	0.48
0.4/0.25	18.5	**6.23**	0.04	0.09
-0.250	183.66	61.89	0.36	0.93
total	296.77	100	0.58	1.51

Size fractions	P(g)	Rp(%)	Rp/P0	Ex/P0
0.8/0.4	691.29	27.72	1.34	3.53
0.4/0.25	302.2	**12.12**	0.59	1.54
-0.250	1499.9	60.16	2.91	7.65
total	2493.39	99.99	4.84	12.72

Figure 1: Material balance of fragmentation and classification operations

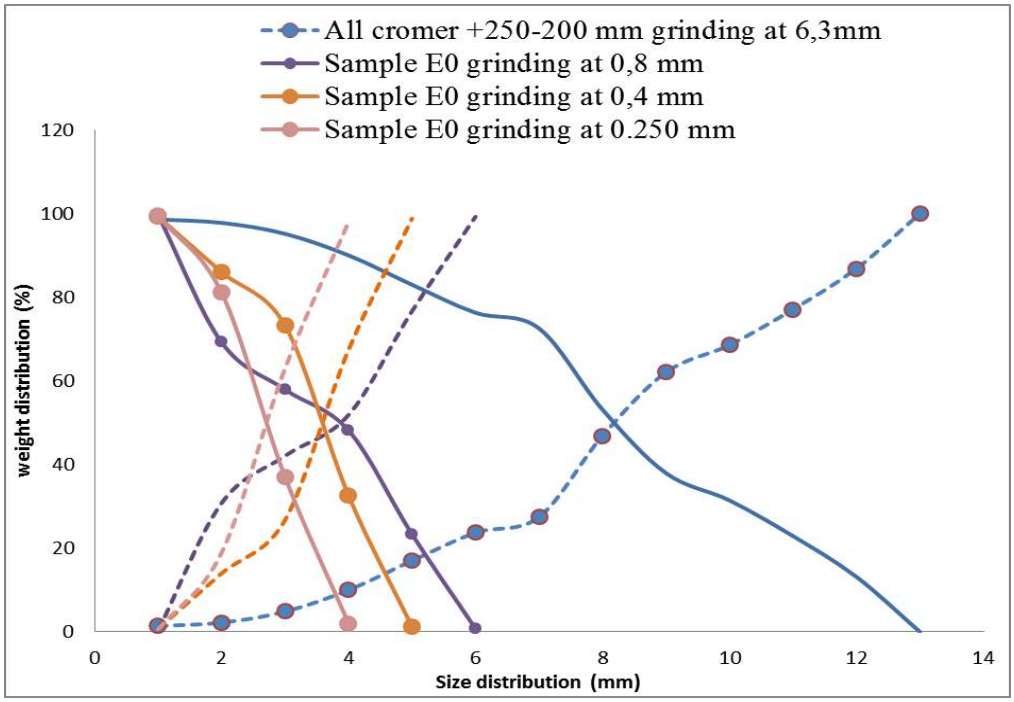

Figure 2: Weight distribution in% of refusal RC) and passing cumulative (PC)

Hydrometallurgy and Biohydrometallurgy

Extraction of Gold and Silver from Bolkar Gold Plant Tailings

Bolkar Altın Madeni Artıklarından Altın ve Gümüş Kazanımı

H. Bastürkcü, F. Burat, M. Özer, A. Gül, A. A. Sirkeci
Istanbul Teknik Üniversitesi Cevher Hazirlama Mühendisligi Bölümü

ABSTRACT This scientific study aims to investigate the extraction of gold and silver using agitation leaching method from tailings of Bolkar gold plant. The tailings contain 1.01 ppm Au and 41.8 ppm Ag. The effect of leaching duration, mechanical activation, pre-aeration and water quality were investigated. During the leaching tests, 40% solid ratio and 0.5 g/L NaCN concentration were kept constant, in order to provide an industrial application. After 2 hours of mechanical activation, d_{90} size of the sample was determined as 38 µm. When this sample was leached for 48h, 64.10% Au and 48.42% Ag extractions were able to be achieved. Although pre-aeration had a positive effect on extractions, in the case that was tested with the activated sample, only 1% Au increase was obtained with the same Ag extraction. On the other hand, if plants' recycle water was used in the leaching tests, the gold and silver extractions decreased 5% and 12%, respectively.

Keywords: Gold, silver, pre-treatment, cyanide leaching

ÖZET Bu çalışmada Bolkar Altın Tesisi liç artığından altın ve gümüşün kazanımı araştırılmıştır. Artık numunesi 1,01 ppm Au ve 41,8 ppm Ag içermektedir. Siyanürlü karıştırma liçi deneylerinde liç süresi, mekanik aktivasyon, ön havalandırma ve su kalitesi parametrelerinin etkileri incelenmiştir. Deneyler boyunca, endüstriyel uygulama göz önünde bulundurularak, %40 pülpte katı oranı ve 0,5 g/L NaCN konsantrasyonu sabit tutulmuştur. 2 saat mekanik aktivasyon sonunda d_{90} tane boyutu 38 µm olarak belirlenmiştir. Aktive olmuş bu ürün 48 saat liç işlemine tâbi tutulduğunda %64,10 Au ve %48,42 Ag çözündürme verimlerine ulaşılmıştır. Her ne kadar ön havalandırmanın çözündürme verimleri üzerinde olumlu etkisi görülmüşse de, mekanik olarak aktive edilmiş numune üzerinde uygulandığında altın çözünmesinde sadece %1'lik artış gözlenmiştir. Gümüş çözünme veriminde ise herhangi bir artış sağlamamıştır. Ayrıca tesiste kullanılan geri dönüşüm suyu ile liç testleri yapıldığında, altın ve gümüş çözünme verimlerinde sırasıyla %5 ve %12'lik düşüşler gözlenmiştir.

Anahtar kelimeler: Altın, gümüş, siyanür liçi

1 INTRODUCTION

The cyanidation process has been the most preferred process in the extraction of gold for the past 100 years. In 1888, MacArthur and his friends patented the process, in which gold dissolves in aerated cyanide solutions to produce the gold cyanide complex (Jeffrey and Breuer, 2000). The chemical reaction occurs is known as the Elsner (1846) equation.

Due to the environmental concerns, great effort has been made to find alternative gold lixiviants (De Andrade Lima and Hodouin, 2005; Ficeriová et al., 2005; Çelik, 2004; Broadhurst and Du Preez, 1993). Although some of the scientific studies gave promising results, today, cyanide protects its indispensable position in industrial applications.

Depending on the mineralogical structure of the gold ore, different amounts of cyanide concentrations can be used. Usually, a range of 0.15-0.50 g/L of cyanide concentration is utilized in industrial applications. However, when the gold ore contains cyanide

consuming minerals and/or high silver content (i.e.>20 g/t), then higher cyanide concentrations varying from 2 to10 g/L NaCN could be needed (Marsden and House 2006). On the other hand, in terms of solids ratios used in industrial applications of gold leaching, usually 35% to 50% ratios are used. By applying these standard criteria, above 90% gold extraction is obtained in many operating gold plants for leaching durations of 24 to 36 hours.

But in some situations, certain processes are performed before leaching, in order to expose gold particles, which increases the chance of contact with cyanide. When sulfide or carbonaceous minerals exist in the gold ore body, different pretreatment processes are practiced. With the data from Sinadinovic et al., (1999), Iglesias and Carranza, (1994) and Celep et al., (2009), these methods can be counted as roasting, pressure oxidation, biooxidation, ultrafine grinding, and modified cyanidation.

In this study, extraction of gold and silver from Bolkar Gold Plant tailings was investigated by testing the effect of mechanical activation, pre-aeration, and water quality.

2 MATERIALS AND METHOD

2.1 Material Characterization

The gold ore sample used in the present study was obtained from Bolkar Gold Plant tailings, which contained 1.01 ppm Au and 41.8 ppm. According to the mineralogical analyses performed on the polished section samples, gold particles could not be determined clearly, however, the liberated silver particles were found with a particle size up to 45 µm. Differently from liberated particles, silver was observed as associated with quartz, iron minerals, and calcite (Figure 1 and 2).

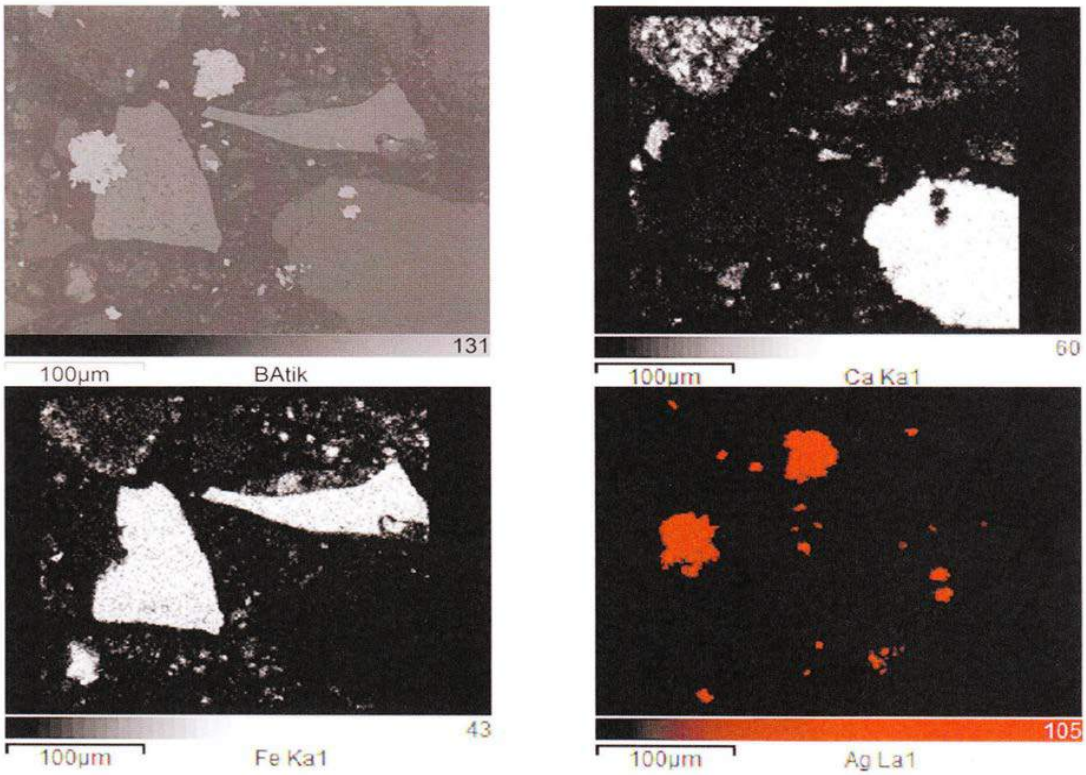

Figure 1. X-Ray Elemental Map of the Sample

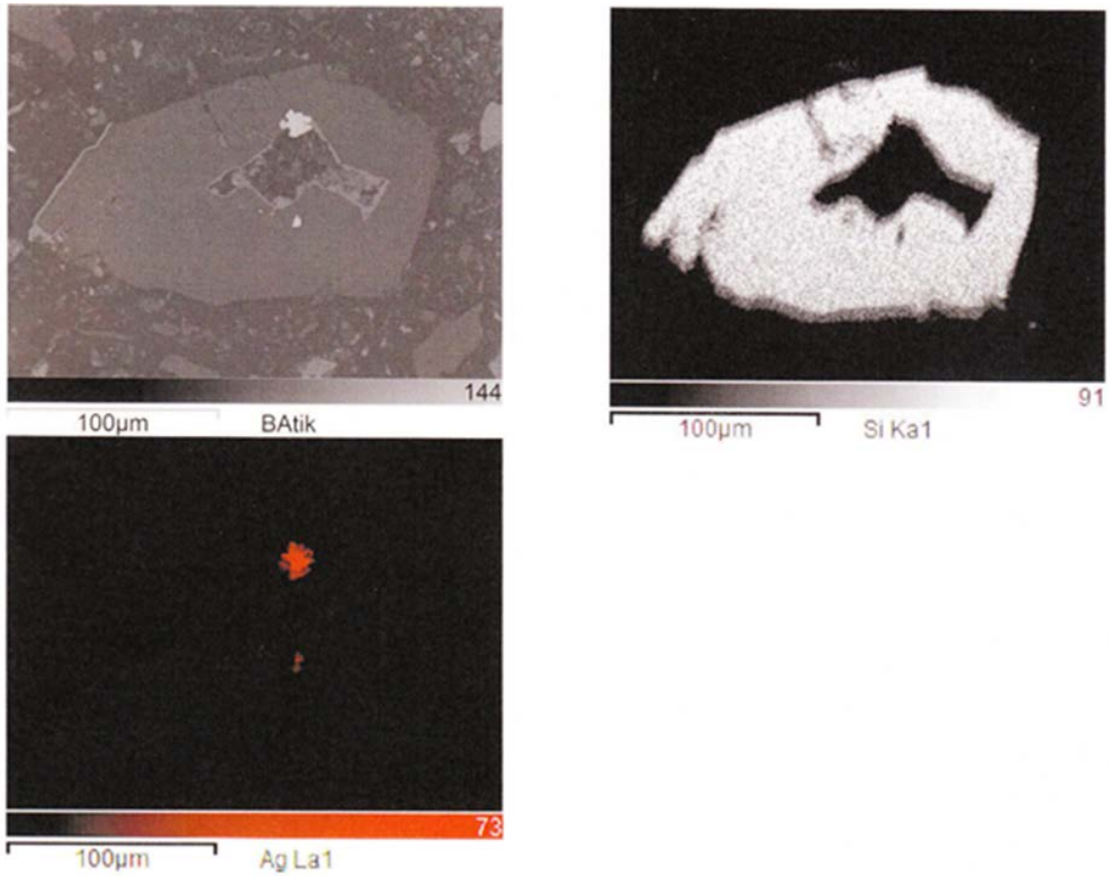

Figure 2. X-Ray Elemental Map of the Sample

The particle size of the associated silver was varying from 5 to 45 µm. Also, galena (~ 50 µm), dolomite (~ 125 µm), psilomelane (~ 75 µm), and plagioclase (~ 60 µm) were determined in the mineralogical structure of the ore sample.

2.2 Methods

The leaching tests were conducted using IKA RW 20 model mechanical stirrer, which had teflon coated impellers. During the tests, pH value was adjusted with lime and measured by WTW 3401 pH meter. After the leaching process, Buchner funnel was used in separation of solid-liquid phases. The Au and Ag contents of the dried leach cakes were analyzed by fire assay method.

In the leaching tests, the plant operating conditions of 40% solid ratio and 0.5 g/L NaCN concentration were kept constant. The effect of mechanical activation, pre-aeration, and water quality were investigated.

3 RESULTS

3.1 The Effect of Mechanical Activation

In this group of experiments, 1, 2, and 4 hours of mechanical activation durations were tested using a vibrating mill. The activated samples were then leached for 48 hours with 0.5 g/L NaCN at 40% solid ratio.

According to the results given in Table 1 and Figure 3, 2 hours of mechanical activation was seemed to be optimum, since it provided the highest gold and silver extractions of 64.2% and 48.4%, respectively. The particle sizes of the mechanically activated samples are shown in Table 2. As the particle size decreased, the extraction values increased. Particles tend to be agglomerated for longer mechanical activation durations than 2 hours.

Table 1. The Leaching Results of the Activated Samples

Mechanical Activation	Extractions, %	
	Au %	Ag
0	52.0	29.5
1	57.9	40.8
2	64.1	48.4
4	58.8	33.7

Table 2. Results of the Particle Size Measurements

Mechanical Activation	Particle Size (d_{90}), µm
0	64
1	46
2	38
4	43

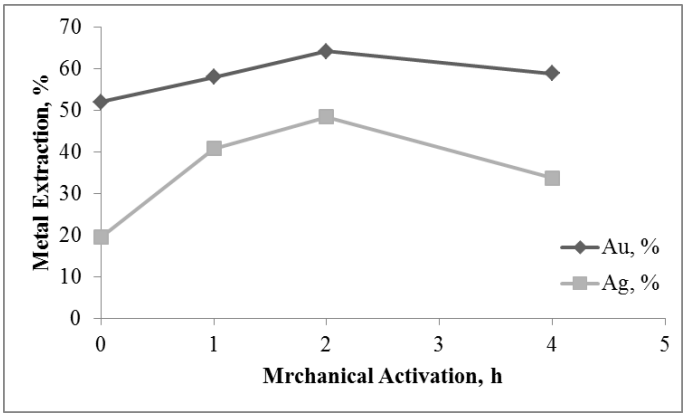

Figure 3. The Leaching Results of the Activated Samples

3.2 The Effect of Pre-Aeration with Different Leaching Durations

In this part of the study, 4 hours of pre-aeration was applied using an air pump with a 6 L/min capacity before leaching of the ore sample. Then 24 and 48 hours of leaching tests were conducted. It was expected to provide a reduction in the leaching duration required for gold extraction.

According to the results given in Table 3, better extractions were obtained with 48 hours of leaching duration.

Table 3. The Leaching Results of 4 Hours Pre-Aeration

Leaching Duration	Extractions, %	
	Au %	Ag
24	49.9	23.2
48	55.2	29.4

3.3 The Effect of Water Quality

Up to this part of the study, it was found that mechanical activation and pre-aeration showed positive effects to some extent on gold and silver extractions. Therefore, the ore sample was mechanically activated for 2 hours and pre-aerated for 4 hours. Later, 48 h of leaching was performed using two different type of water: tap water and plant recycle water.

As is seen from Table 4, application of mechanical activation and pre-aeration did not provide significant enhancements in gold and silver extractions. Only 1% of increase was obtained in Au extraction.

On the other hand, when plant recycle water is used in the leaching tests, siginificant reductions in Au and Ag recoveries were observed (5% for Au ve 12% for Ag). The reason for this result was thought to be the existence of the ionic impurities in the plant water.

Table 4. The Leaching Results of Water Quality Tests

Water Type	Extractions, %	
	Au %	Ag
Tap	65.1	48.4
Plant	60.1	36.4

CONCLUSION

- The gold ore sample used in the tests contains 1.01 ppm Au and 41.8 ppm Ag.
- It was nearly impossible to determine gold particles in the polished section samples.

- The particle size of liberated silver particles were up to 45 µm. Also, silver was associated with quartz, iron minerals and calcite.

- The positive effect of the mechanical activation was observed. However, for longer activation durations than 2 hours, the sample became agglomerated, which prevented gold and silver extractions.
- Preaeration tests showed that 3% Au increase could be obtained.
- When mechanical activation and preaeration was applied in a row before leaching, only 1% Au increase was observed. This result shows that the highest gold extraction could be reached already.
- Considering usage of the plant recycle water, the negative effect was observed depending on the ionic impurities existed in the plant water.

REFERENCES

Broadhurst, J.L., Du Preez, J.G.H., 1993. A thermodynamic study of the dissolution of gold in an acidic aqueous thiocyanate medium using iron (III) sulfate as an oxidant. *Hydrometallurgy* 32, 317–344.

Celep, O., Alp, I., Deveci, H., Vicil, M., 2009. Characterization of refractory behaviour of complex gold/silver ore by diagnostic leaching. *Transactions of Nonferrous Metals Society of China* 19, 707–713.

Çelik, H., 2004. Extraction of gold and silver from a Turkish gold ore through thiourea leaching. Miner. *Metall. Process*. 21, 144–148.

De Andrade Lima, L.R.P.,Hodouin,D., 2005. A lumped kineticmodel for gold ore cyanidation. Hydrometallurgy 79, 121–137.

Ficeriová, J.P., Baláž, P., Villachica, C.L., 2005. Thiosulfate leaching of silver, gold and bismuth from a complex sulfide concentrate. *Hydrometallurgy* 77, 35–39.

Iglesias, N., Carranza, F., 1994. Refractory gold-bearing ore: a review of treatment methods and recent advances in biotechnological techniques. *Hydrometallurgy* 34, 383–395.

Jeffrey, M.I and Breuer,P.L. 2000**. "**The Cyanide Leaching of Gold in Solutions Containing Sulfide". *Minerals Engmeering,* Vol. 13, No. 10-11, pp. 1097-1106.

Marsden, J.O. and House, I.C., 2006, The Chemistry of Gold Extraction. *Published by the SME Inc., 2nd Edition.*

Sinadinovic, D., Kamberovic, Z., Vakanjac, B., 1999. Refractory gold ores, characteristics and methods of their procession. *Proceedings of 8th Balkan Mineral Processing Conference*, Belgrade, Yugoslavia, pp. 411–418.

Determination of Leaching Cutoff Grade Using Economical Evaluation in Sarcheshmeh Copper Mine

S. N. Almasi, R. Bagherpour, A. Khademian, R. Yarahmadi
Department of Mining Engineering, Isfahan University of Technology, Isfahan, Iran

ABSTRACT There is an economical challenging question in this respect: Which portion of the deposit should be sent to leaching unit? Dispatching the trucks, which haul deposit to mineral processing plants or heap leaching unit, is subject to accurate economic computations. The issue addressed in this article is the analysis of the fundamental economic concepts in achieving optimal cutoff grade. This leaching cutoff grade sorts the ores in two sections: the high-grade, to be processed in the mineral processing plant and the low grade, to be processed in the leaching plant. The second group processing can be done in a mineral processing plant also, but it would have more profitable at the leaching plant surely. The data used in this investigation was adapted from Sarcheshmeh copper mine. According to the computation at this mine, the leaching cutoff grade equals to 0.354%, which means ores with grades between 0.15% and 0.354% should be transferred to the heap leaching unit.

Keywords: Leaching, optimal cutoff grade, Sarcheshmeh

1 INTRODUCTION

One of the most important aspects of mine design is determining the optimum cutoff grade. The extracted materials are sent to different processing units based on their cutoff grade. Optimization of cutoff grade in this industry is an accepted procedure for open pit mine planning (Osanloo and Ataei, 2003).

The cutoff grade strategy, in fact, is a decision making process about what materials have to be mined, processed and leached and which must be considered as waste, or where is the limit between mineral processing and heap leaching. The optimal cutoff grade strategy requires basic knowledge in some fields, including economics, mining production planning, mining operations, mineral processing, production restrictions and grade distribution of deposit, all of which have significant influence on annual working capital (Bascetin and Nieto, 2007). In this respect the geologic and mining restrictions in addition to the mine planning and design are the main contributing aspects focusing on an economic justification of all which is considered above (Camus, 2002). The most common approach used for obtaining the optimal cutoff grade is maximizing the net present value (NPV) which takes the unstable status of the economy into account. This approach is applicable to any type of mining operation. This concept implies that: the sum of all future cash flows discounted by an appropriate interest rate should be at least equal to the capital costs of the project (Minnitt, 2004). Of course, in this respect some researchers believe that the real NPV maximization would be actualized when the environmental costs become minimized through proper management (Osanloo et al., 2008). That is, maximizing NPV must be eliminated from the ore-based exclusivity and full control of environmental issues throughout the life of the mine should be considered in order to guarantee the optimality of the mining process (Rashidinejad et al., 2008). Now it is revealed that a special complexity has engulfed the NPV issue, so that despite the high concern on the issue, the obtained results are still uncertain (Azimi et al., 2013).

Increasing the number of variables in problems makes their solving more difficult, even impossible, especially in multi-metal

deposits. Lwambiyi et al., (2009) evaluated the effect of some by products like cobalt, manganese and quartz gangue on the heap leaching process of the Disele copper deposit in South Africa and found that they increase the complexity of problem solving significantly. This problem made the researchers to adopt some management and statistical techniques. Applying the equivalent grade factor for finding the optimal cutoff grade is one of the tactics. Here, the objective function of the multi-metal deposits is defined and the objective function is changed into variable function through the equivalent grade factors. The optimal cutoff grade of the main metal can be obtained through optimization techniques like, Lane algorithm and elimination methods. At the final stage, the optimal cutoff grade is determined by applying the grade interpolation together with tonnage distribution (Osanloo and Ataei, 2003).

Combining genetic algorithms (GA) and artificial neural networks (ANN) is the other method proposed to solve this problem. The advantage of this technique is to achieve the optimal cutoff grade instantly, so that once the general data enters, the program proposes the optimal cutoff grade. The confidence level here is influenced by the same confidence level obtained through the combined GA and ANN techniques (He et al., 2009).

This article can shed more light on the issue of determining optimal cutoff grade, which has been neglected somewhat by previous investigations. The data used in this investigation was adapted from Sarcheshmeh copper mine, which is located 160 km south-west of Kerman region (Figure.1). Sarcheshmeh is a large open cast copper mine in the Kerman Province of Iran, considered to be the second largest copper deposit worldwide. Also containing substantial amounts of molybdenum, gold and other rare metals. Geologically in a vertical section, it is divided into three zones. Named oxide, supergene, and hypogene. In recent years, copper in addition to the mineral processing has been recovered by hydrometallurgical methods (Shayestehfar et al., 2008).

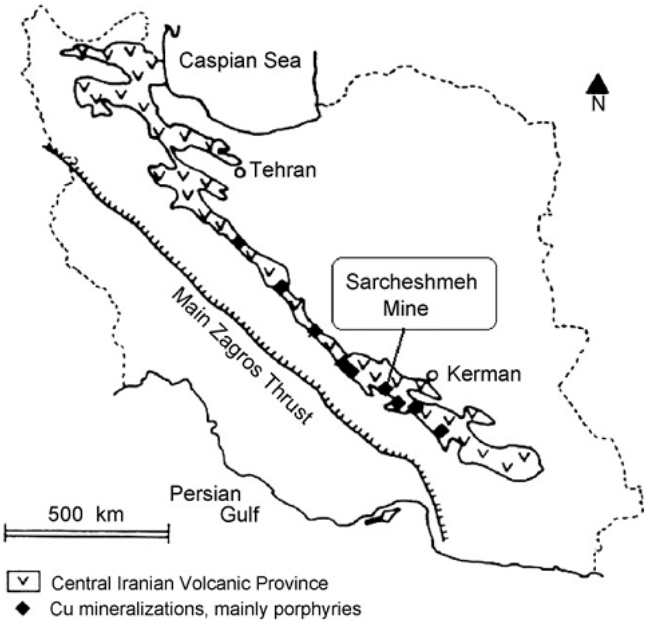

Figure 1. Location of Sarcheshmeh copper mine at the porphyry copper mineralization zone (Shayestehfar et al., 2008)

2 HEAP LEACHING

In the leaching process, the ores containing soluble metallic minerals become dissolved in aqueous solutions, containing chemical agents like sulfuric acid. The active solvent elements are some ions that due to gravity pass through the pores in the ore heap and then get separated. Complete separation may take years. The drainage layer of sand and the half-cracked polyethylene pipes are the two main features in the heap leaching drainage structure.

The metallic ion containing liquid is guided towards the half cracked polyethylene pipes through the drainage layer of sand. In this process, the Pregnant Leached Solvent (PLS) is transferred to solvent extraction electro-wining (SX-EW) plant (Majdi et al., 2009). This method in metal extraction takes the aspects of technical and the economical (providing maximum profit) production of clean and quality product into account. Of course, the factors like providing feed, mineralogical analysis and the accuracy of the analyzing apparatus should not be overlooked.

Dhawan et al. (2012) consider X-ray examination as one of the essential tools in analysis and detailed understanding of heap leaching process. Close follow up of the liquid path in the material heap and its optimization has a significant effect on heap leaching costs. Applying the available science and technologies like the X-ray and radioactive material can provide efficient data from the drainage system. Applying analytical methods which are generally based on Bernoulli Eq. as well as considering the materials particle size distribution can contribute to better explanation regarding the drainage process (Mellado et al., 2009).

At the Sarcheshmeh copper mine, copper oxide and low grade sulfide rocks are kept in the leaching dump and are exposed to a gradual flow of dilute sulfuric acid. In this process, the copper dissolves in the acid and the solution produced is collected from this section. Cathodic copper is deposited after a special electrolytic process. This method is preferred to a pyrometallurgical one on both economic and environmental grounds. The exploitation of copper oxide ores and low grade sulfide ores was not economical in the past, but heap leaching now has the advantages of low investment, better working conditions, and lower energy consumption. This process is continuously being developed to improve the removal of copper from a wide variety of ores.

3 OPTIMAL CUTOFF GRADE

In every mine where leaching process is an available choice, the grading is defined in at least two ways that has been illustrated in Figure.2. In this Figureure the horizontal bars are marked with G1 and G2 as the grades where;

G1, indicates the limit between waste and the ore and G2, indicates the limits of metal extraction method selection in a mineral processing or heap leaching method, named leaching cutoff grade.

Of course, the heap leaching technology is not specific to low grade material and it is a possible choice for some special mineralogical combinations. As in case of Sarcheshmeh copper mines, the oxidized deposits which are not capable to be processed by pyro-metallurgy methods or if so, are not economically affordable are transferred to heap leaching dump (Shayestehfar et al., 2008).

In choosing the materials destination, especially in multi-metal deposits, multiple parameters can be involved, for example, in copper mines the sulfurous or oxidized nature of the deposit or even having sulfuric materials in the primary or secondary genesis effect the processing quality and the related costs.

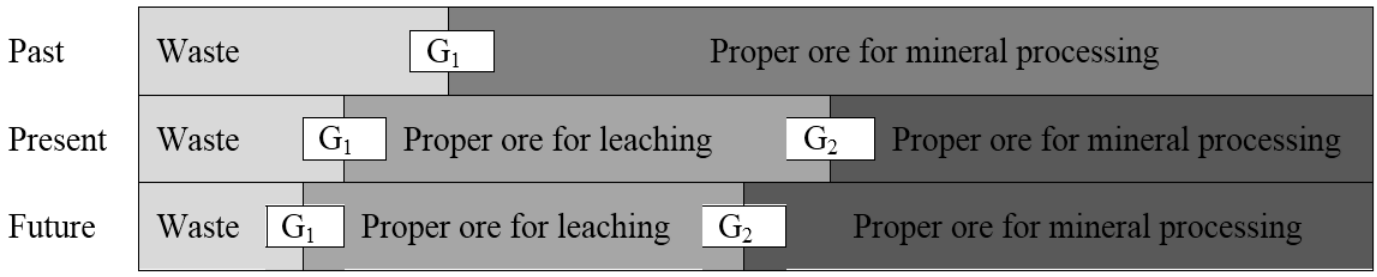

Figure 2. The changes in cutoff grade based on technology in the Past, Present and Future

This issue is more evident in oxidized minerals, so that these minerals, even with a high cutoff grade are not suitable for mineral processing and it is better to apply heap leaching technique. The availability or lack of essential elements like gold, silver and molybdenum changes the cutoff grade for both G1 and G2. In order to have an accurate and efficient assessment, it is necessary to conduct separate economic computations for each area (G1 and G2) based on the type of the mineral's main genesis and the percentage of essential elements content which would lead to determining the most

beneficial optimal cutoff grade and the best practical approach in extracting the metal.

4 THE METHODS AND PROCESS

When the metal content in a mineral is lower than a standard limit, no recovery is expected in practice. In the case of copper, the grade limit known as waste limit is 0.15%; therefore, the lowest grade limit in this study of this method is considered as 0.15%, upon which the deposit destination would be decided. The upper cutoff grade is a grade above which the minerals are sent to processing plant while minerals with lower grade are sent to the heap leaching unit.

To determine this grade, the net value should be calculated for the mineral processing and heap leaching unit in order to find the breakeven point (Hustrulid et al., 2013). To calculate the net value (NV) of one ton of mineral with a specific grade, the total costs (Ct) and the income (I) generated from metal extraction must be computed. The difference between the income and the costs is the NV (NV=I-Ct); the assessment pattern of this process is presented in a flowchart in Figure.3.

5 COMPUTATION OF NV FOR MINERAL PROCESSING METHOD

As mentioned, to calculate the net value it is required to have the incomes and costs per unit weight of mineral. In this article, the economical analysis is performed based on US dollar unit and the weight unit for ore and involved product is explained by short ton and pound.

The required costs of copper extraction at a mineral processing unit consists of:

A. Operational, 5.9 $/Ton: at this stage the copper grade increases by about 20%

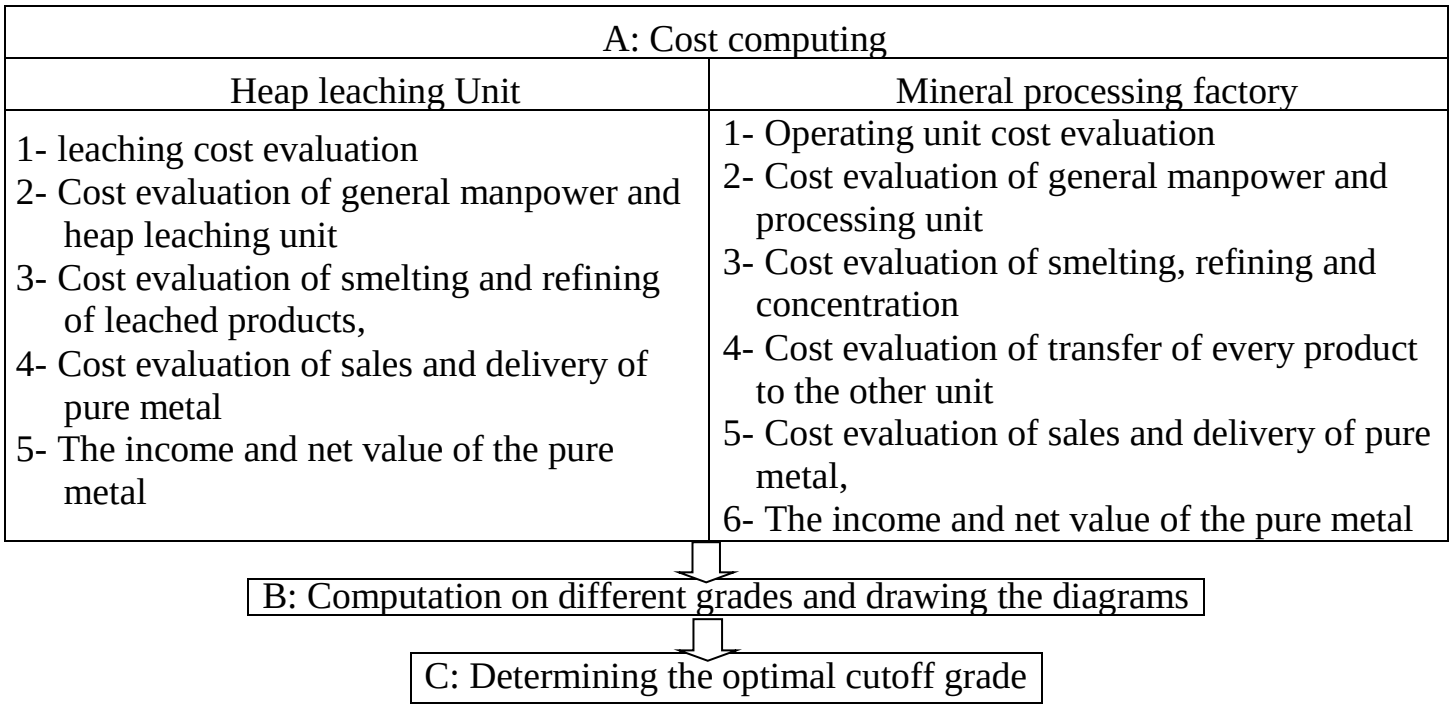

Figure 3. The leaching cutoff grade analysis and computation flow chart

B. Transferring of concentrated material to the smelting plant, 3.60 $/Ton of concentrates

C. Smelting, 100.00 $/Ton of concentrates

D. Transferring from smelting to refining plant, 210.00 $/Ton of non-refined metal

E. Refining, 260.00 $/ Ton of non-refined metal

F. The sales and delivery, and general plant at 0.16 $/Pound of pure metal

Having the detailed costs associated for each stage makes the computation of extraction costs easy. The recovery

percentage differs in each section: it is 80% at mineral processing, it increases up to %97.5 at smelting unit and the same is true as it reaches the refining unit, that is, 99.8% (Hustrulid et al., 2013).

Since the ore entering the plant releases its metal and by changing into the concentrate material exits the plant in a few days, no discount is ascribed to it. In heap leaching plant due to durability of metal extraction from the ore, such discounting is involved in the financial computations.

5.1 Describing the Method in the Copper Mineral Processing Plant

Here, it is assumed that one Ton of copper ore with metal content of 0.4% is subjected to mineral processing in the plant. The attempt is made to compute the NV after going through the full process cycle. According to Table 1, the NV/Ton for this example would be $7.81. The same computations are also made for grades ranging from 0.3% to 0.6% by 0.05 gradual steps. Details of these computations have been summarized in table 2. The diagram reflecting Table 2 is illustrated in Figure.4.

6 COMPUTATION OF NV FOR HEAP LEACHING PROCESS

At this phase, the cost and income of leaching process are computed first and the difference of these two represents the NV of product. The difference here is the time factor that was not an effective element in mineral processing, but sine the heap leaching process is time consuming, it has a direct effect on costs and naturally on the income.

Table 1. The NV of copper ore with metal content of 0.4% subject to mineral processing

Row	costs	Unit	Volume	Unit/$	Total/$	Notes
1	Operational	Ton of ore	1	5.9	5.9	--------
2	General and Administrative	Ton of ore	1	0.885	0.89	%15 of 1
3	Transporting concentrated material to smelting plant	Ton of concentrated	0.02	3.6	0.06	%80 recovery, concentrated grade %20
4	Smelting	Ton of concentrated	0.02	100	1.6	
5	Transporting from smelting to refinery plant	Ton of non-refined metal	0.0031	210	0.66	
6	Refining	Ton of non-refined metal	0.0031	260	0.41	Recovery at this stage is 97.5%
7	Miscellaneous	lb of Pure metal	6.2	0.16	0.99	--------
Total costs					10.91	--------
Metal extraction income		lb of Pure metal	6.2	1	18.72	--------
NV ($/Ton)					7.81	--------

To have a rational comparison between the two methods the NV here should be assessed in present time as described in the following sections.

Table 2. The NV calculation for different grades of copper

Grade (%)	Income ($/ton)	Cost ($/ton)	NV ($/ton)
0.30	14.4	9.88	4.16
0.35	16.38	10.39	5.99
0.40	18.72	10.91	7.81
0.45	21.06	11.42	9.64
0.50	23.4	11.94	11.46
0.55	25.74	12.45	13.29
0.60	28.08	12.97	15.11

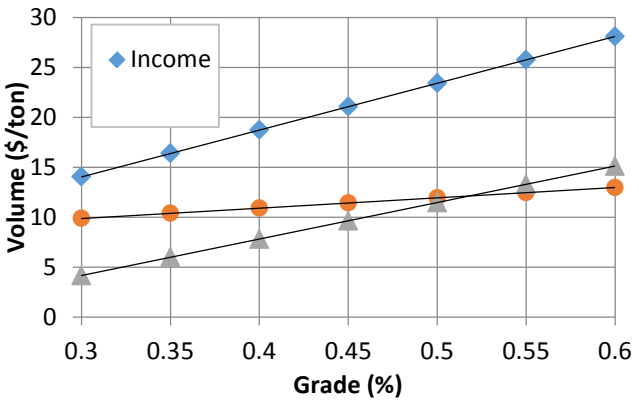

Figure 4. The NV diagram for different grades of copper in mineral processing unit

The required costs of copper extraction at a heap leaching plant consist of:

A. Leach, 0.35 $/ pound of Pure metal
B. Smelting and producing copper slabs, 90.00 $/Ton of leached material
C. Transporting from smelting to refining, 120.00 $/ Ton of non-refined metal
D. Refining, 230.00 $/ Ton of non-refined metal
E. Sales, delivery and general, 0.16 $/ pound of Pure metal

The recovery percentage at smelting and refining plants and the amount of produced metal and its sales value should be computed. Having in mind that extracted ore has to go through a period (usually few years); the generated income is subject to a discount rate. The recovery coefficient as a function of year in this process is presented in Table 3.

Table 3. The recovery coefficient as a function of year for heap leaching system

Year	Recovery Coefficient
1st	0.4
2nd	0.3
3rd	0.14
4th	0.1
5th	0.06

To compute the recovery percentage of the materials with low grade Eqn.1 is applied:

$$R\ \% = \frac{FG - FWG}{FG} \times 100 \qquad (1)$$

Where: R= Recovery, FG= Feed Grade and FWG= Fixed Waste Grade.

As for copper, the fixed wastes grade is 0.15%. Thus, for materials with a grade less than or equal to 0.4%, recovery rate is calculated using Eq.1 and for the materials with a grade above 0.4%, recovery rate over a period of five years will not surpass 50%. For example, if the heap leaching unit feed grade is 0.55%, the copper content rate will be 11 lb/Ton of ore. Since the recovery rate is 50%, it is expected to have 5.5 lb recovery in a 5 year period.

The net value is the difference between costs and incomes. Therefore, based upon aforementioned concepts, it is necessary to calculate the costs and revenues in order to determine the net present value. The calculated net value should be discounted to present time. Eq. 2 can calculate the present value of any cash flow in each year:

$$PV_n = \frac{FW_n}{(1+i)^n} \qquad (2)$$

where, PV_n is the present value of the n^{th} year of metal recovery, FW_n is the recovered metal value of the n^{th} year, i is the capital return rate and n is the designated or given year. In computing FW_n of a given year Eqn.3 must be applied:

$$FW_n = \alpha_n \times M \times P \qquad (3)$$

where, α_n is the recovery coefficient, extracted from table 3, M is the total salable metal in lb, P is metal prices in terms of $/lb.

6.1 Describing the Method by a Numerical Example in Heap Leaching Plant

Using the same procedure implemented in sections 4 and 5, economical calculations including costs, incomes and NV computations have been done for grade of 0.4 %. Table 4 expresses all of these findings.

These computations have been repeated for different grades varying from 0.3 to 0.6 and all of results are summarized in table 5 and have been illustrated in Figure.5.

The Summary of costs and incomes computations for different grades between 0.3% and 0.6% by 0.05 gradual steps are presented in Table 5.

7 DISCUSSION

Provided information in tables 1, 2, 4 and 5 leads to significant results, which all have been summarized in table 6. Also, calculated NV for both metal processing methods at grades 0.3-0.6% are illustrated as a diagram in Figure.6. As it can be observed table 6, at grade 0.354% the NV is 6.07$ per ton of deposit for both methods which indicates the breakeven point.

Above this grade, the mineral processing method reveals a higher NV and hence for lower grade ores the heap leaching method is more appropriate.

Table 5. The summation of the costs and incomes at heap leaching unit

Grade (%)	Income ($/ton)	Cost ($/ton)	NV ($/ton)
0.30	6.94	2.19	4.74
0.35	9.25	2.93	6.32
0.40	11.56	3.66	7.90
0.45	10.40	3.29	7.11
0.50	11.56	3.66	7.90
0.55	12.71	4.02	8.69
0.60	13.87	4.39	9.48

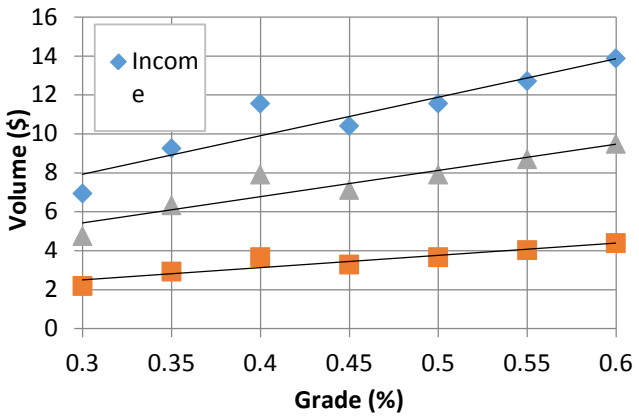

Figure 5. The NV diagram for different copper grades in heap leaching unit

Accordingly, the grade of 0.354% is considered as the breakeven point for dispatching truck to either of the plants; while, grades above this would be routed to mineral processing plant and grades below this would be routed to the heap leaching plant.

Table 4. Computing the NV of copper ore at 0.4% grade subject to heap leaching

Row	Description	Unit	Volume	Price/$	Total/$
1	leaching costs	Pound of Recovered metal	5	0.35	1.75
2	Smelting costs	Ton of leached material	0.0029	90	0.26
3	Transferring cost from smelting to refining unit	Ton of Non refined material	0.0025	120	0.295
4	Refining costs	Ton of Refined material	0.0025	230	0.565
5	Miscellaneous costs	pound of pour metal	4.09	0.164	0.78
	Total costs $/Ton of ore				3.66
	Income from metal extraction $/Ton of ore				11.56
	NV $/Ton of ore				7.90

Table 6. The NV per ton of ore for different grades and metal extraction methods

Ore grade (%)	NV ($/Ton of ore)	
	Mineral processing unit	Heap leaching unit
0.30	4.16	4.74
0.35	5.99	6.32
0.354	6.07	6.07
0.40	7.81	7.90
0.45	9.64	7.11
0.50	11.46	7.90
0.55	13.29	8.69
0.60	15.11	9.48

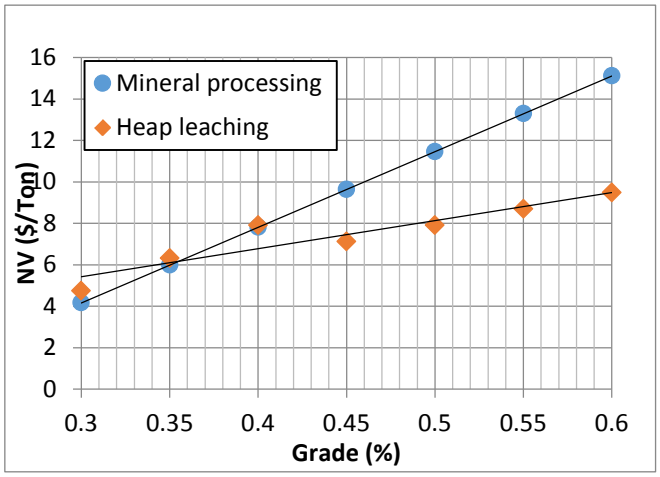

Figure 6. The breakeven point of both the methods

If in the diagram of Figure 5, X represents the grade, Y_1 represents the NV in mineral processing unit and Y_2 represents the NV in heap leaching method, the resulted trends of the parameters will be in accordance with the following:

A: For Mineral processing method

$$Y_1 = 36.5X - 6.97 \qquad R^2 = 1 \qquad (4)$$

B: For Heap leaching method

$$Y_2 = 13.5X + 1.35 \qquad R^2 = 0.87 \qquad (5)$$

8 CONCLUSIONS

The findings here are presented through the following points:

- According to the computation for sarcheshmeh copper mine, the 0.354% is the leaching cutoff grade, which means ores with grades between 0.15% and 0.354% should be transferred to the heap leaching unit.
- In the heap leaching process, due to the absence of material transfer to smelting unit and the low sedimentation cost, metal extraction from low grade minerals is justified economically. This fact is true for the oxidized copper ore as well.
- In multi metal deposits with different genesis, determining the main metal grade is a complicated task. To make this task less complicated, adopting statistical and managerial methods based on expert opinion in the field of optimal cutoff grade is of essence.
- In multi metal and multi genesis deposits the mine zoning and hauling route assignment per zone will contribute to the accurate transport of the material to the proper destination.

ACKNOWLEDGMENTS

The authors would like to thank Ali Sadjadi & Shahin Ghasemnezhad in Sarcheshmeh complex for their cooperation during the present investigation. The authors also appreciate Amin Nouri for their helpful comments.

REFERENCES

Azimi, Y., M. Osanloo, et al. (2013). "An uncertainty based multi-criteria ranking system for open pit mining cut-off grade strategy selection." *Resources Policy* 38(2): 212-223.

Bascetin, A. and A. Nieto (2007). "Determination of optimal cut-off grade policy to optimize NPV using a new approach with optimization factor." *Journal-South African Institute Of Mining And Metallurgy* 107(2): 87.

Camus, J. P. (2002). Management of mineral resources, *SME*.

Dhawan, N., M. S. Safarzadeh, et al. (2012). "Recent advances in the application of X-ray computed tomography in the analysis of heap leaching systems." *Minerals Engineering* 35: 75-86.

He, Y., K. Zhu, et al. (2009). "Theory and method of genetic-neural optimizing cut-off grade and grade of crude ore." *Expert Systems with Applications* 36(4): 7617-7623.

Hustrulid, W. A., M. Kuchta, et al. (2013). Open Pit Mine Planning and Design, Two Volume Set & *CD-ROM Pack, CRC Press*.

Lwambiyi, M., K. Maweja, et al. (2009). "Investigation into the heap leaching of copper ore from the Disele deposit." *Hydrometallurgy* 98(1): 177-180.

Majdi, A., M. Amini, et al. (2009). "An investigation on mechanism of acid drain in heap leaching structures." *Journal of hazardous materials* 165(1): 1098-1108.

Mellado, M. E., L. A. Cisternas, et al. (2009). "An analytical model approach to heap leaching." *Hydrometallurgy* 95(1): 33-38.

Minnitt, R. (2004). "Cut-off grade determination for the maximum value of a small Wits-type gold mining operation." Journal-South African Institute Of *Mining And Metallurgy* 104: 277-284.

Osanloo, M. and M. Ataei (2003). "Using equivalent grade factors to find the optimum cut-off grades of multiple metal deposits." *Minerals Engineering* 16(8): 771-776.

Osanloo, M., F. Rashidinejad, et al. (2008). "Incorporating environmental issues into optimum cut-off grades modeling at porphyry copper deposits." *Resources Policy* 33(4): 222-229.

Rashidinejad, F., M. Osanloo, et al. (2008). "cutoff grades optimization with environmental management; a case study: sungun copper project." iust *International Journal of Engineering Science* 19(5-1): 1-13.

Shayestehfar, M., S. K. Nasab, et al. (2008). "Mineralogy, petrology, and chemistry studies to evaluate oxide copper ores for heap leaching in Sarcheshmeh copper mine, Kerman, Iran." *Journal of hazardous materials* 154(1): 602-612.

Evaluation of Phase Transformation During Mechanochemical Leaching of Zinc from Zinc Plants Residues in Alkaline Medium

P. Ashtari, P. Pourghahramani
Mining Engineering Faculty, Sahand University of Technology, Tabriz, Iran

ABSTRACT In Iranian zinc plants, hot filtercake (HFC) is an important waste which contains valuable metal like zinc, manganese, calcium and cobalt. Commonly, HFC is processed by selective mechanochemical alkaline leaching to zinc extraction. In this paper, the phase transformation during mechanochemical alkaline leaching of HFC was studied using an attritor. XRD patterns of leaching residues in milling time of 3, 15, 26, 37 and 48 revealed that a progressive phase transformation occurred. Sulfate form of calcium ($CaSO_4.2H_2O$) and oxidic form of manganese (Mn_2O_3) transform to a mixed hydroxide form of calcium and manganese. This finding is very important to disclose the zinc leaching mechanism.

Keywords: Leaching, Zinc, phase transformation, alkaline medium

1 INTRODUCTION

In Iranian zinc plants, to eliminate cobalt from zinc sulfate solution manganese permanganate is used. Hot filtercake (HFC) or cobalt filtercake is generated during this step which contains 0.5-3% cobalt, 6-16% manganese and 8-20% zinc. Thus, HFC appears to be a promising source for further processing. Hydrometallurgical processes are usually preferred for processing of valuable metals from various residues because of their advantages (Gupta and Mukherjee, 1990). According to Arzu Özverdİ and Mehmet Erdem studies, concentration of the contaminant released from zinc plants residues (ZPRs) is higher than the threshold values which cause HFC to be classified as a hazardous waste (Özverdİ and Erdem, 2010). Therefore, HFC should be inevitably retreated for Zn, Mn and Co recycling.

Acidic leaching commonly dissolve Co, Mn and Zn collectively with low selectivity. However, alkaline leaching could be utilized to leach zinc selectively. Then, zinc powder can be obtained by electrowinning (Dutra et al., 2006; Gürmen and Emre, 2003; Lee and Piron, 1995; Li et al., 2012; LIU et al., 2005; Orhan, 2005; Zhang et al., 2014; Zhao et al., 2009). Zinc extraction from HFC facilitates the following processes of cobalt and manganese extraction. Therefore, alkaline leaching can promote cobalt and manganese extraction steps. As seen in literature, zinc is not usually dissolved in alkaline medium completely.

Mechanochemical treatment enhances the reactivity of material through a wide structural changes occurring during the extensive milling. Structural changes like lattice strain, bonds breakages, X-ray amorphization degree, decreasing in crystallinity, phase transformation, increasing in dislocation density and surface area and so on are responsible for the reactivity improvement (Balaz, 2008; Boldyrev, 2006; Zdujić et al., 1992; Zhang et al., 1997).

During mechanochemical leaching, namely combination of the leaching and mechanical activation process into a single step, the performance of leaching could be promoted, remarkably (Baláž and Achimovičová, 2006; Chenglong and Youcai, 2009). Consequently, it would be expected that high amount of zinc from HFC could be recovered by mechanochemical alkaline leaching (MCAL).

The objective of this study is to investigate

the phase transformation of crystalline phases present in HFC which was treated by mechanochemical alkaline leaching method to zinc selective dissolution. The main aim was to evaluate the effect of various milling conditions on phase transformation which occurred during zinc dissolution. In addition, the performance of zinc dissolution was related to the crystalline phase.

2 MATERIALS AND METHOD

A representative hot filtercake (HFC) sample was collected from ALVAN zinc plant, Zanjan, Iran. In order to remove the soluble salts, the as-received wet HFC was first washed with distilled water several times. The pre-treated HFC (PHFC) was dried in an oven at 95 °C for 24 h. The mechanochemical alkaline leaching (MCAL) experiments were performed in a vertical stirred ball mill (attritor) with a stainless steel chamber using a 9 M NaOH solution. Milling time (leaching time) of 3, 15, 26, 37 and 48 min as well as milling speed of 0, 420 and 670 rpm was parameters and their levels that considered to zinc leaching from PHFC with MCAL method. Milling conditions were as given in Table 1. Pure NaOH from Merck was used in leaching experiments.

Table 1. Milling conditions.

Balls to powder weight ratio	50
Mill speed (rpm)	420-670
Mill Volume (cm^3)	470
Void volume of media (cm^3)	187
Filling ratio of ball volume (%)	80
Number of balls	750
Ball weight (g)	1500
Ball diameter (mm)	7.8
Media type	Tempered steel
Media corrosion	negligible
Media density (g/cm^3)	7.8

3 RESULTS AND DISCUSSION

3.1 PHFC characterization

Chemical composition of PHFC is presented in Table 2. The average particle size of the initial PHFC sample was 6.5 µm which is very fine.

Table 2. Chemical composition of PHFC.

Element	Zn	Mn	Co	Ca	Ni	Cd	Cu	other
wt. %	10.46	15.43	2.2	7.5	0.08	0.30	0.075	trace

The XRD pattern of HFC is shown in Fig. 1. As shown, different kinds of hydrous calcium sulfate like gypsum ($CaSO_4 \cdot 2H2O$) and plaster of pairs ($2CaSO_4 \cdot ½H_2O$) were the major crystalline phases in PHFC. Other phases included manganese oxide (MnO_2), zincite (ZnO), quartz (SiO_2) and cobalt oxide (Co_3O_4). But, intricate composition of PHFC, likewise very fine particles and low degree of crystallinity made phase assessment more difficult.

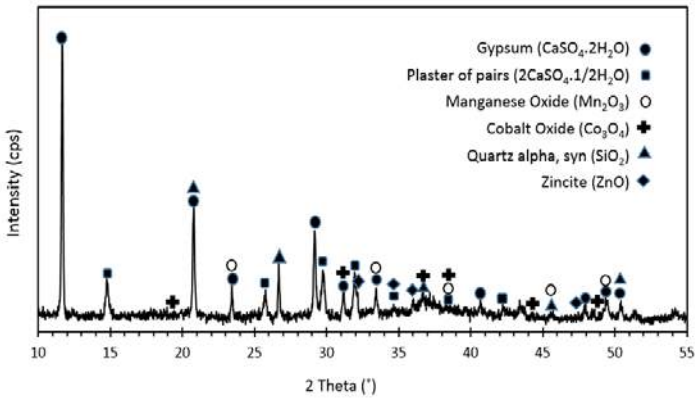

Figure 1. XRD pattern of the PHFC sample.

SEM-EDS analysis was used to find more information. As shown in Figure 2a, the only crystalline particles which have relatively large grains (compared to other particles) viz. EDS1, EDS3 and EDS5 points contain Ca and S, confirming the presence of calcium sulfate phases. Zn, Mn and Co could be observed instantly on the some fine particles with varying ratios of zinc, manganese, cobalt, calcium and oxygen. High-resolution image of fine surface morphology is also shown in Figure 2b.

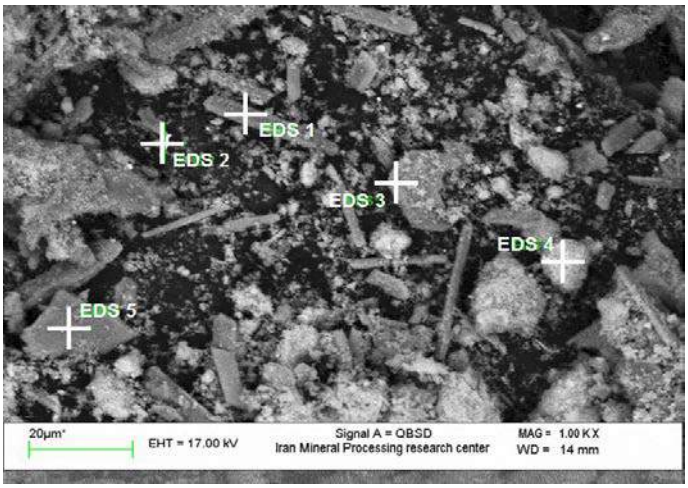

(a) Backscattered electron mode

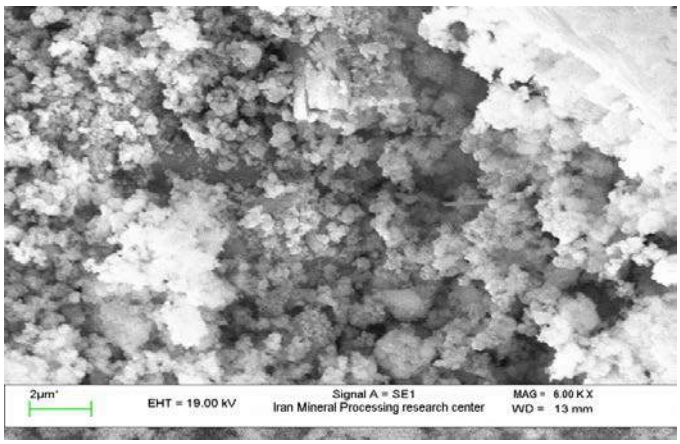

(b) Secondary electron mode

Figure 2. SEM micrograph of HFC.

It was concluded that most of the particles are in sub-micron sizes and fine particles aggregate on surface of larger crystalline particles.

3.2 Zinc dissolution with MCAL method

Based on XRD analysis of PHFC sample, the main zinc bearing phase is zincite (ZnO). Among the all phases presents in PHFC, ZnO was the only phase could be dissolved in alkaline medium. Our preliminary experiments showed that lead and cadmium have not leached, remarkably. So, the leaching process could be completely selective for zinc. It is thought that Zincite dissolves in alkaline medium according to the reaction below:

$$ZnO_{(s,\ in\ PHFC)} + 2NaOH_{(aq)} + H_2O \rightarrow Na_2Zn(OH)_{4(aq)}$$

The results of all experiments as well as their operational condition are summarized in Table 3 and graphically shows in Fig. 3. It can be seen that when leaching time progressed, there were three different behaviors for zinc alkaline leaching: 1.Through CAL method (conventional alkaline leaching or MCAL with R=0 rpm), the recovery of zinc remains approximately at a constant value; 2. In MCAL method, a slight increase in the recovery of zinc can be observed by applying low milling speed (R=420 rpm); 3. By spending more energy in milling (R=670 rpm), a noticeable increase in zinc recovery can be obtained during MCAL. Based on the results, in CAL method, the maximum recovery was 82.4%. However, in MCAL zinc recovery of 99.9% can be achieved with 9 M NaOH concentration, 670 milling revolution and 15 min of milling. During MCAL, zinc leaching readily increases while the milling speed and leaching time increase. At a given leaching time, with increasing of milling speed from 420 to 670, leaching recovery will be promoted. It means that more energy applied in milling leads to more zinc dissolution.

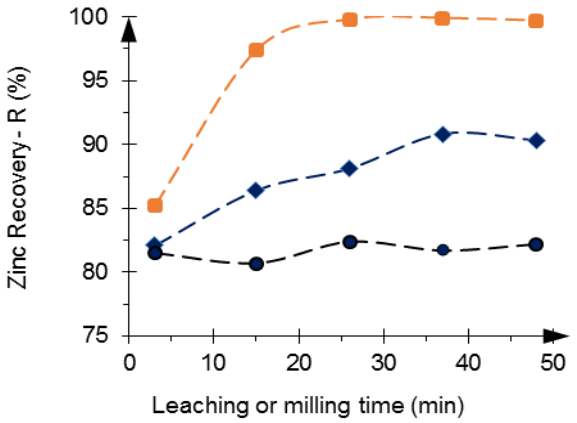

Figure 3. Effect of milling speed on zinc alkaline leaching recovery from PHFC at C_{NaOH}= 9 M, liquid to solid ratio= 6/1 (V/W), mass ratio of ball to HFC= 50/1 (W/W) and temperature= 25±2 ˚C [(●), (◆) and (■) stand for mixing in CAL, R=420 and R=670 in MCAL, respectively].

Table 3. Operating parameters of zinc alkaline leaching and results.

Leaching method	Milling speed (rpm)	Zinc alkaline leaching recovery (%)				
		Leaching time (min)				
		3	15	26	37	48
Conventional alkaline leaching (CAL)	0 (mixing)	81.5	80.7	82.4	81.7	82.2
Mechanochemical alkaline leaching (MCAL)	420	82.1	86.4	88.1	90.8	90.3
	670	85.2	97.4	99.8	99.9	99.7

* Mixing was used to denote mechanical mixing of solution in CAL method.

** the values of the other parameters including temperature, liquid to solid ratio (L/S) and mass ratio of ball to PHFC (B/P) were kept constant at 25±2 ˚C, 6/1 (V/W) and 50/1 (W/W), respectively.

As seen, in alkaline leaching of zinc from PHFC using CAL method, an unusual rapid increasing in zinc recovery was observed during the first seconds of leaching. But, the first stage followed by the second step with constant recovery. With high probability, during the leaching process an insoluble layer was progressively formed on the surface of the dissolving particles to prevent leaching of unreacted core. This insoluble layer is very stable in alkaline medium and it was expected to be in hydroxide form.

3.3 Phase transformation of crystalline phases presents in PHFC during MCAL process

In this section phase transformation of main crystalline phase of PHFC during MCAL process was studied. As given in Fig. 5, Pattern (a) shows the main crystalline phases presented at PHFC. To simplify the figure, minor phases hasn't been shown.

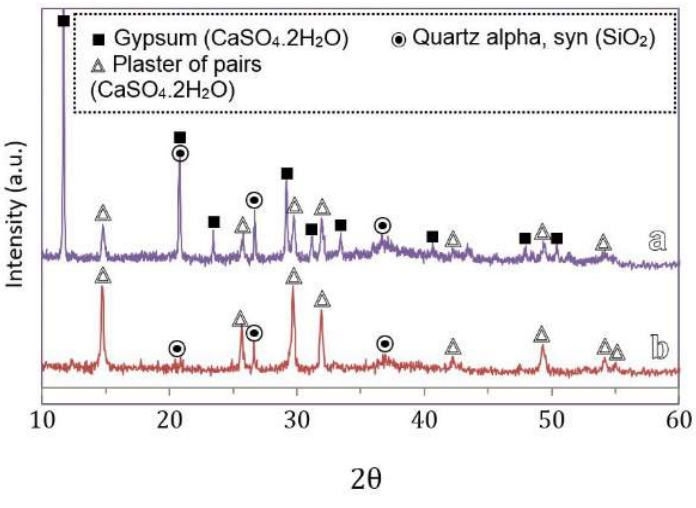

Figure 4. Effect of MCAL on phase transformation of crystalline phases presents in PHFC during wet milling (C_{NaOH}= 0 M, liquid to solid ratio= 6/1 (V/W), mass ratio of ball to HFC= 50/1 (W/W), temperature= 25±2 ˚C and milling speed= 670 rpm).

Pattern (b) at Fig. 5 shows wet mechanical activation of PHFC after 48 min with milling speed of 670 rpm [The values of the other parameters are mentioned at the caption]. As a result, gypsum peaks disappeared, while compare to pattern (a) plaster of pairs peaks became more intense. For this reason, it could be concluded that in wet mechanical activation of PHFC gypsum phase converts to plaster of pair.

Fig. 5 shows the effect of time on the XRD patterns of the residues of PHFC leaching during MCAL method. Pattern (a) shows PHFC and patterns (b), (c), (d), (e) and (f) related to leaching residue for 3, 15, 26, 37 and 48, respectively. As it is obvious, even after a few minute, all peaks of gypsum and plaster of pairs was disappeared and just quartz peaks remained unchanged. On the other hand, after a while, some other new peaks grew up. All new peaks belong to a certain phase named calcium manganese hydroxide. After beginning of reaction and progressing of time, amount of calcium manganese hydroxide increases since almost at t=26 min becomes detectable with X-ray diffractometer. This trend continued till 37 and 48 min that we can see sharp peaks with high intensity. As expected, quartz peaks are same at the all patterns.

Therefore, additional to abrasion, the most part of transferred energy during attrition process in MCAL method, expends to crystal growth of new phase. Based on low broadening of this new phase peaks, no amorphization occurred. Another important point is that the mentioned insoluble layer probably is composed of identified calcium manganese hydroxide.

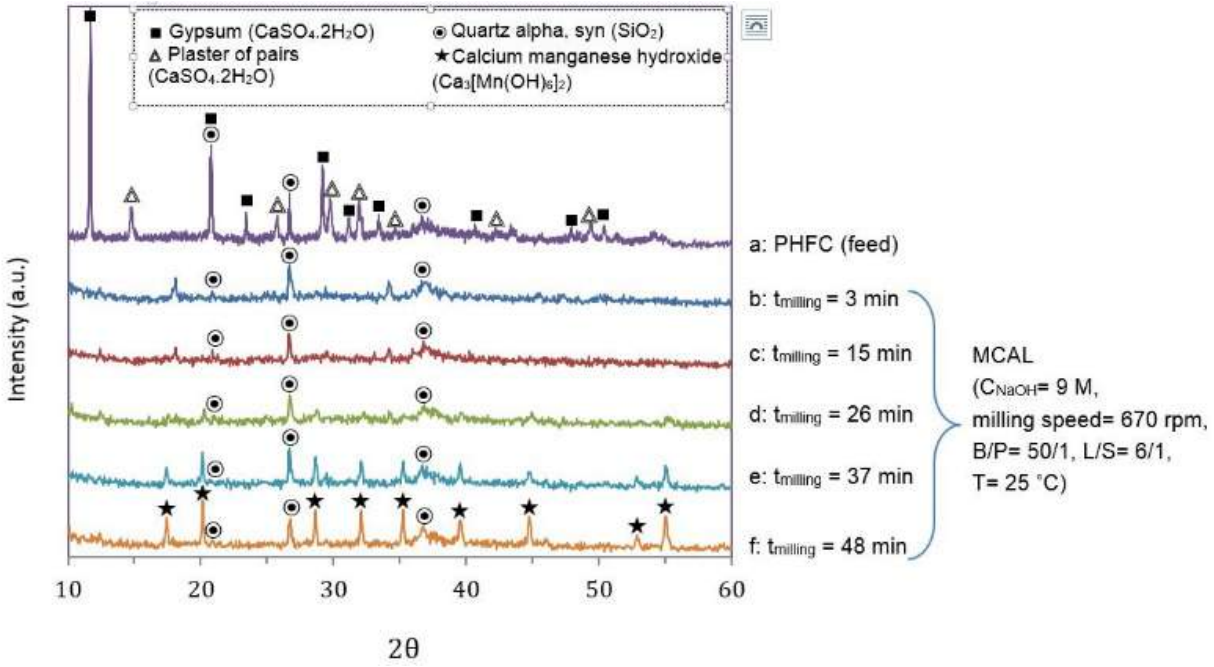

Figure 5. Effect of milling time on phase transformation and XRD patterns of zinc alkaline leaching from PHFC using MCAL method at C_{NaOH}= 9 M, liquid to solid ratio= 6/1 (V/W), mass ratio of ball to HFC= 50/1 (W/W), temperature= 25±2 ˚C and milling speed of 670 rpm.

4 CONCLUSION

In this work, phase transformation of crystalline phase presented in PHFC was considered to study during MCAL. It was found that during wet mechanical activation of HPFC for 48 min and at milling speed of 670 with ball to powder ratio of 50/1 (W/W), gypsum transformed to plaster of pairs. But, at the same condition and in the alkaline medium, all gypsum and plaster of pairs in addition to manganese bearing phase during MCAL of PHFC transformed to a new calcium manganese hydroxide phase. Therefore, it could be concluded that some of transferred energy during MCAL process expends to crystal growth of new phase.

REFERENCES

Balaz, P., 2008. Mechanochemistry in nanoscience and minerals engineering. Springer.

Baláž, P., Achimovičová, M., 2006. Mechano-chemical leaching in hydrometallurgy of complex sulphides. Hydrometallurgy 84, 60-68.

Boldyrev, V.V., 2006. Mechanochemistry and mechanical activation of solids. Russian Chemical Reviews 75, 177.

Chenglong, Z., Youcai, Z., 2009. Mechanochemical leaching of sphalerite in an alkaline solution containing lead carbonate. Hydrometallurgy 100, 56-59.

Dutra, A., Paiva, P., Tavares, L., 2006. Alkaline leaching of zinc from electric arc furnace steel dust. Minerals Engineering 19, 478-485.

Gupta, C.K., Mukherjee, T., 1990. Hydrometallurgy in extraction processes. CRC Press.

Gürmen, S., Emre, M., 2003. A laboratory-scale investigation of alkaline zinc electrowinning. Minerals Engineering 16, 559-562.

Lee, H., Piron, D., 1995. Kinetics of alkaline leaching of pure zinc oxide. Chemical Engineering Communications 138, 127-143.

Li, Q., Zhao, Y., Jiang, J., Zhang, C., 2012. Optimized Hydrometallurgical Route to Produce Ultrafine Zinc Powder from Industrial Wastes in Alkaline Medium. Procedia Environmental Sciences 16, 674-682.

LIU, S.-j., OU, L.-m., FENG, Q.-m., ZHANG, G.-f., LU, Y.-p., 2005. Alkaline Leaching of Zn from Zinc Oxide Ore. Hydrometallurgy of China 1, 006.

Orhan, G., 2005. Leaching and cementation of heavy metals from electric arc furnace dust in alkaline medium. Hydrometallurgy 78, 236-245.

Özverdİ, A., Erdem, M., 2010. Environmental risk assessment and stabilization/solidification of

zinc extraction residue: I. Environmental risk assessment. Hydrometallurgy 100, 103-109.

Zdujić, M., Milošević, O., Karanović, L.Č., 1992. Mechanochemical treatment of ZnO and Al_2O_3 powders by ball milling. Materials Letters 13, 125-129.

Zhang, Q., Sugiyama, K., Saito, F., 1997. Enhancement of acid extraction of magnesium and silicon from serpentine by mechanochemical treatment. Hydrometallurgy 45, 323-331.

Zhang, Y., Deng, J., Chen, J., Yu, R., Xing, X., 2014. The electrowinning of zinc from sodium hydroxide solutions. Hydrometallurgy 146, 59-63.

Zhao, Z., Long, S., Chen, A., Huo, G., Li, H., Jia, X., Chen, X., 2009. Mechanochemical leaching of refractory zinc silicate (hemimorphite) in alkaline solution. Hydrometallurgy 99, 255-258.

Galvanic Leaching of Chalcopyrite Using Manganese Oxides in Spent Carbon-Zinc Batteries

H. Nakazawa and W. Hareyama
Faculty of Engineering, Iwate University, Morioka 020-8551, Japan

ABSTRACT It is well known that galvanic interaction between sulfide minerals and manganese oxides in manganese nodules accelerates the leaching of sulfide minerals. Carbon ï zinc batteries contain a moist paste (hereafter, black paste) of manganese oxides and graphite powder as cathode mix. In Japan spent carbon-zinc batteries are collected and treated by incineration and landfill. We have investigated the feasibility of galvanic leaching of chalcopyrite concentrate using chemical reagent MnO_2 and black paste. Addition of MnO_2 enhanced the leaching of chalcopyrite concentrate in sulfuric acid solution with pH1.0 and Mn concentration also increased remarkably. Extraction yields of Cu and Mn were 42% and 20% respectively at a MnO_2 to chalcopyrite mass ratio of 4 in 14 days. In the presence of black paste the kinetics of chalcopyrite leaching was accelerated dramatically and 83% of Cu in the concentrate was extracted in 40 hours. The graphite powder contained in black paste could play an important role in the galvanic leaching of chalcopyrite in the presence of MnO_2.

Keywords: Galvanic leaching, chalcopyrite, manganese oxides, spent carbon-zinc batteries.

1 INTRODUCTION

Galvanic interactions among different minerals are well-known phenomena. Paramguru and Nayak (1994) investigated galvanic interaction between sphalerite and manganese dioxide in sulfuric acid solution and found a substantial increase in leaching of both the minerals. Galvanic leaching of manganese nodule and cobalt-rich crust has been investigated using sulfide minerals. Nakazawa et al (2010) showed that the dissolution of manganese in cobalt-rich crust was accelerated in the presence of pyrite. Since manganese dioxide was nobler than pyrite, manganese dioxide acts as a cathode to be reduced resulting into release of manganese from the crust in the contact with pyrite. On the other hand, pyrite acts as an anode to be oxidized.

Gantayat et al (2000) investigated galvanic interaction between chalcopyrite and manganese dioxide in sulfuric acid medium using compact disc electrodes of both minerals. They reported that chalcopyrite and MnO_2 form a galvanic corrosion couple where the former acts as anode and the latter as cathode leading to strong interaction between the minerals. Devi etal (2001) studied the dissolution in the presence of manganese dioxide in hydrochloric acid medium. They found that chalcopyrite didnœt dissolved independently but underwent oxidative dissolution with manganese dioxide by (i)galvanic interaction (ii) cyclic action of F^{3+} /Fe^{2+} redox couple and (iii) chlorine gas by MnO_2 dissolution. The last one was observed to be most effective. But so far, no study is reproted on galvanic leaching of chalcopyrite using manganese dioxide in sulfuric acid solution.

Spent carbon-zinc batteries and alkaline batteries are mostly collected as incombustible waste by municipal authorities and are buried in landfill sites without recycling them in Japan. These batteries contain variable materials such as manganese, zinc and iron. Carbon-zinc batteries consist of a carbon rod cathode with a moist paste (hereafter, black paste) of MnO_2 and NH_4Cl mixed with graphite powder to improve conductivity and retain moisture in the acid electrolyte (McComsey,2001). During discharging of carbon-zinc batteries, chemical reactions between the anode and cathode could occur

to give ZnO, and Mn_2O_3 (McComsey, 2001)

.

$$Zn + 2MnO_2 \rightarrow Mn_2O_3 + ZnO \quad (1)$$

Mn_2O_3 dissolves to form MnO_2 in sulfuric acid solutions according to equations (2)

$$Mn_2O_3 + H_2SO_4 \rightarrow MnO_2 + MnSO_4 + H_2O \quad (2)$$

In this study, we have examined the feasibility of the galvanic leaching of chalcopyrite using black paste obtained from spent carbon-zinc batteries and chemical analysis reagent MnO_2 in sulfuric acid solution.

2 SAMPLES AND EXPERIMENTAL PROCEDURE

Chalcopyrite concentrate (-100μm) used in this study was provided by Atakama mining in Chile. XRD analysis of the sample shows only the peaks of chalcopyrite. The chemical compositions are as follow; Cu: 28.9%, Fe:28.9%.

Chemical analytical grade MnO_2 was provided by Kanto chemical Co.Ltd. Black paste was collected from the dismantled spent carbon-zinc batteries and dried at 80 ^oC for 24 h followed by grinding with a porcelain mortar and a pestle. In order to remove the zinc from the black paste, the original black paste was washed with 1N sulfuric acid solution at 1/10 solid/liquid ratio by mixing at 200rpm for 1h with a magnetic stirrer. The washed black paste was dried and ground in the way as described above. Table 1 shows the chemical compositions of MnO_2 and black paste. XRD patterns of MnO_2 and black paste are shown in Figure 1. The counts are low and broad peaks are observed for black paste. XRD analysis of the black paste indicates the presence of graphite that is used as conductive material in carbon-zinc batteries.

Table 1. chemical composition of black paste samples

Sample	Mn	Zn
MnO_2	54.6%	ND
Black paste	40.8%	0.4%

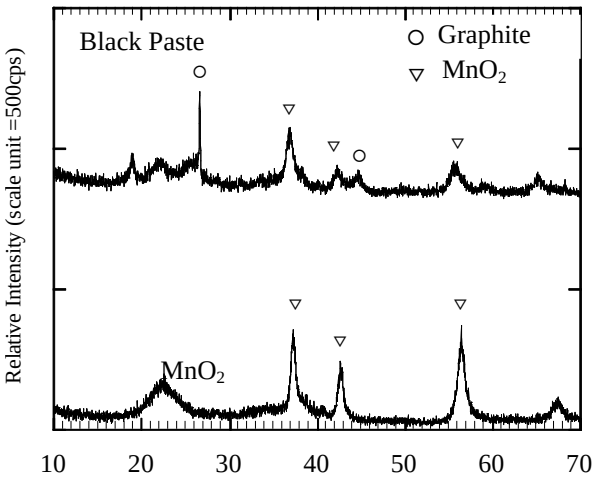

Figure 1. XRD patterns of MnO_2 and Black paste

Leaching experiments were carried out in 300mL elementary flask with 200mL sulfuric acid solution. Samples were added into the flask and stirred on magnetic stirrer at 200rpm. At desired interval the pH and the redox potential of the leaching solution were measured. The redox potentials were measured using Pt electrode with Ag-AgCl (3.3N KCl) reference electrode and it was converted to a value against NHE. Then an aliquot was withdrawn and centrifuged (10000rpm, 10min). The supernatant was analyzed for Mn, Cu, total Fe and ferrous irons (Fe(II)). Cu, Mn and total Fe(Fe(II)+Fe(III)) concentration were measured with an atomic absorption spectrophotometer (Hitachi Z-5000).

At the end of the leaching experiment the leachate was filtered and the residue was recovered with filtration and dried at 60 ^oC and RDX analysis was conducted. The surface studies of the residues were also investigated by scanning electron microscopy (SEM) equipped with an energy dispersive X-ray spectrometry (EDS).

Rest potential was measured using MnO_2 and chalcopyrite electrodes prepared by mounting granular MnO_2 (chemical grade,Kanto chemical Co.Ltd.) and chalcopyrite obtained from a mine in Indiana state, USA in 6.25mm ID Lucite tubing as described by Adam et al (1984). Electrical contact was made using a few drops of mercury to contact to a platinum wire. Before each measurement, the electrode

surfaces were cleaned by polishing with 400 and 600 grit abrasive papers and then on a metallurgical polishing wheel with 0.5μm diamond powder as the abrasive.

3 RESULTS

3.1 Rest Potential of MnO_2 and Chalcopyrite

The steady-state rest potentials of MnO_2 in chemical grade and chalcopyrite after one hour in pH0.8 sulfuric acid solution were 965mV and 321 mV (NHE), respectively. These materials are expected to form galvanic couple in contact with each other. MnO_2 can act as a cathode while chalcopyrite serves as an anode, suggesting that chalcopyrite could be oxidized to dissolve.

3.2 Effect of MnO_2 on the Kinetic of Chalcopyrite Leaching

Fig.2 (A)-(D) show the effect of the MnO_2 on the chalcopyrite leaching. The leaching rate of chalcopyrite increased in the presence of MnO_2. The extraction yield of copper was 52% in 24 days while that was17% in the absence of MnO_2. MnO_2 dissolution was accelerated in the presence of chalcopyrite and the extraction yield was 22%. Chalcopyrite and MnO_2 could be leached through galvanic interaction between them according to equation (3) and (4).

$$CuFeS_2 \rightarrow Cu^{2+} + Fe^{2+} + 2S^o + 4e^- \quad (3)$$

$$MnO_2 + 4H^+ + 2e^- \rightarrow Mn^{2+} + 2H_2O \quad (4)$$

Iron ions occurred as ferrous ions in the absence of MnO_2 whereas ferric ions existed in the presence of MnO_2. Ferrous ions dissolved from chalcopyrite were oxidized to ferric ions by MnO_2 according to the reaction (5):

$$2Fe^{2+} + MnO_2 + 4H^+ \rightarrow 2Fe^{3+} + Mn^{2+} + 2H_2O \quad (5)$$

Overall reaction between chalcopyrite and MnO_2 is described as follow:

$$2CuFeS_2 + 5MnO_2 + 20H^+ \rightarrow 2Cu^{2+} + 2Fe^{3+} + 5Mn^{2+} + 4S^o + 10H_2O \quad (6)$$

The molar ratio of dissolved Mn ions to Cu ions was 3.9 at the experiment.

The redox potential in the presence of MnO_2 remained over 900mV during the experiments whereas it was about 600mV without MnO_2.

MnO_2 accelerates the kinetics of chalcopyrite leaching, but leaching rate of chalcopyrite was not so adequate that it would require a lot of time to complete the leaching.

3.3 Effect of Black Paste on the Leaching of Chalcopyrite

The leaching experiments were carried out using black paste. The results are shown in Figure 3. The kinetics of chalcopyrite leaching was enhanced dramatically in the presence of black paste. The extraction yields of copper in the presence of 2g black paste was 60% in 16h while that was 4.6% in the absence of black paste. 83% of copper in the concentrate dissolved in 40h, but extraction yield of copper leveled off after then. Extraction yield of Mn increased remarkably and were 53%.

The pH increased with time in the presence of the black paste while pH didn't change in the absence of the black paste. Eh also increased up to over 900mV in the presence of the black paste while it decreased without the addition of black paste because of increase in ferrous concentration. Iron ions occurred as ferrous ions in the absence of black paste whereas ferric ions existed in the presence of black paste. Ferrous ions were oxidized by MnO2 in the black paste according to the reaction (1). Figure 4 shows SEM microphotograph of the residue. Unleached chalcopyrite and graphite powder are observed.

Following experiments were carried out using the black paste

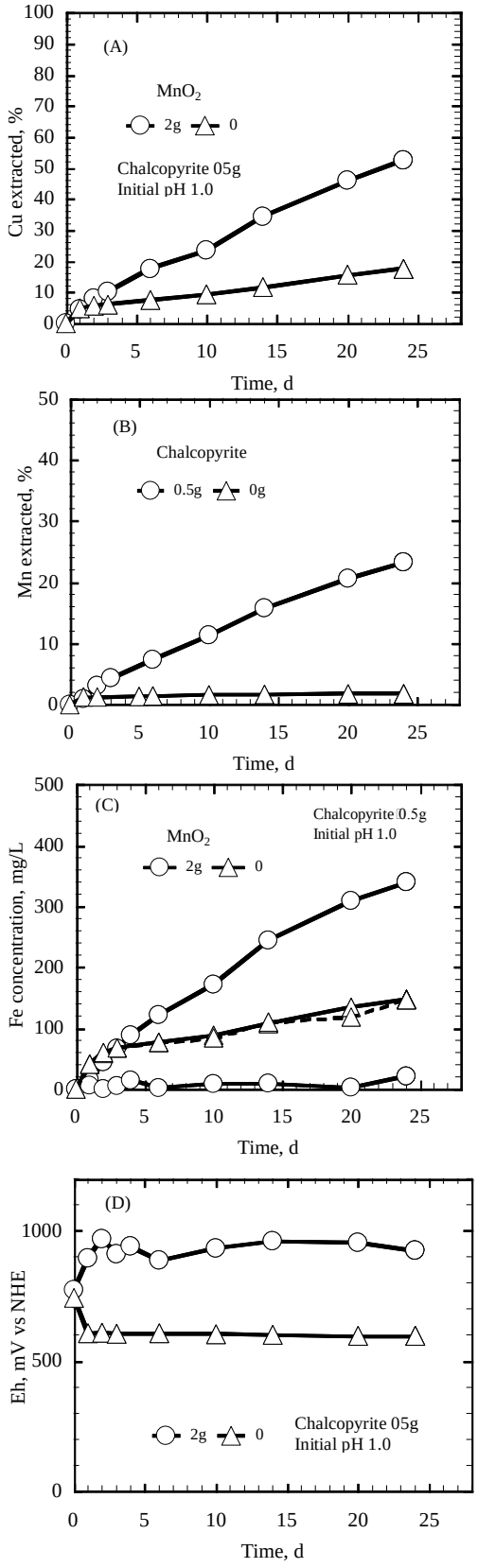

Figure 2. Effect of MnO_2 on the chalcopyrite leaching

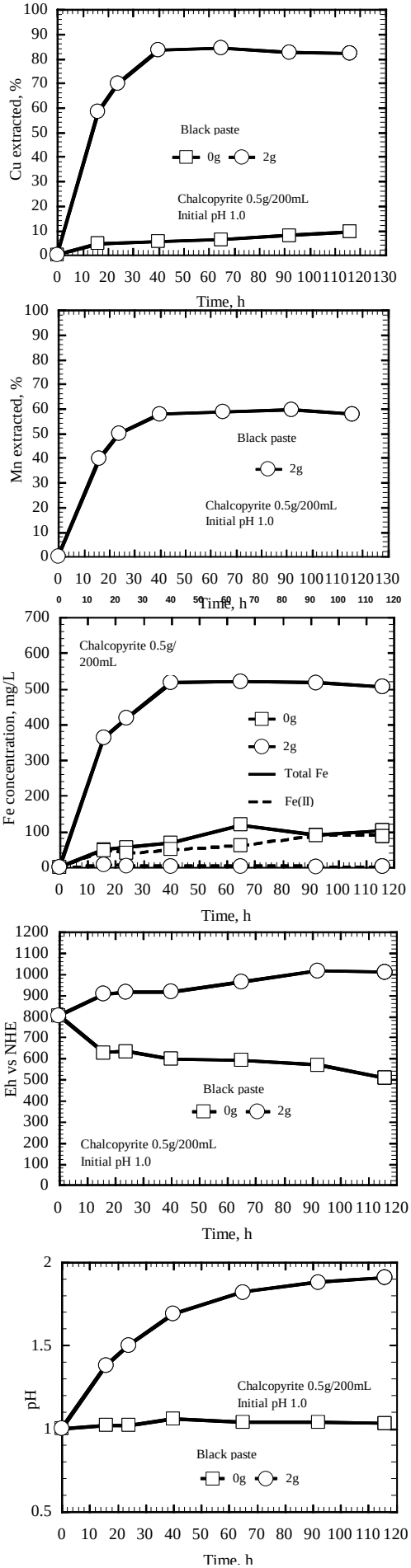

Figure 3. Effect of black paste on the chalcopyrite leaching

3.4 Effect pf Initial pH on the Kinetics of Chalcopyrite in the Presence of Black Paste

In order to investigate the effect of initial pH, leaching experiments were carried out at initial pH 0.8 and 1.2. The results are shown at Figure 5. There are no so much differences in the copper extraction rate between them. For initial pH 1.2, pH raised to 2.4 in 116h.

3.5 Effect of Temperature on the Kinetics of Chalcopyrite in the Presence of Black Paste

In order to study the effect of temperature on the leaching of chalcopyrite, leaching experiments were conducted at 50°C and ambient temperature. The results are shown at Figure 6. Elevating temperature increased extraction rate at the middle stage of the experiment, but the extraction yield of copper was the same as that at the ambient temperature in 50h. Total iron concentration deceased after 20h at higher temperature. Ferric ions could precipitate as jarosite because jarosite tend to form with increase in temperature.

3.6 Effect of the Graphite Powder in the Black Paste on the Chalcopyrite Leaching in the Presence of MnO_2

Black paste contains graphite powder to increase the electric conductivity. Effect of graphite powder was examined on the leaching in the presence of MnO_2. The graphite powder in black paste was collected in the way described below:

0.2g black paste was digested with aqua regia

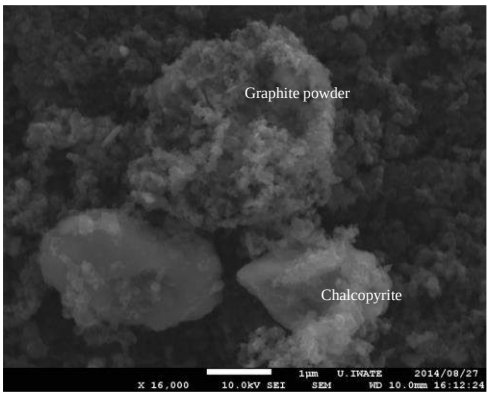

Figure 4. SEM microphotograph of the residue

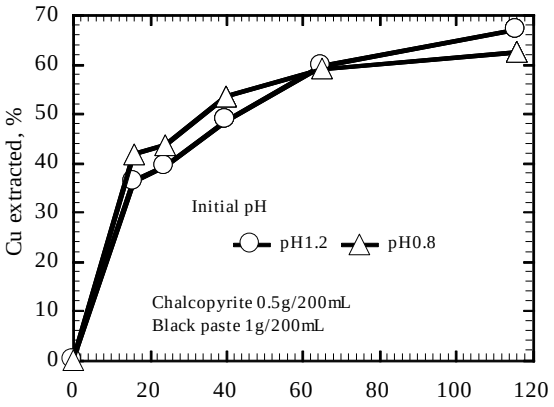

Figure 5. Effect of initial pH on the chalcopyrite leaching in the presence of black paste

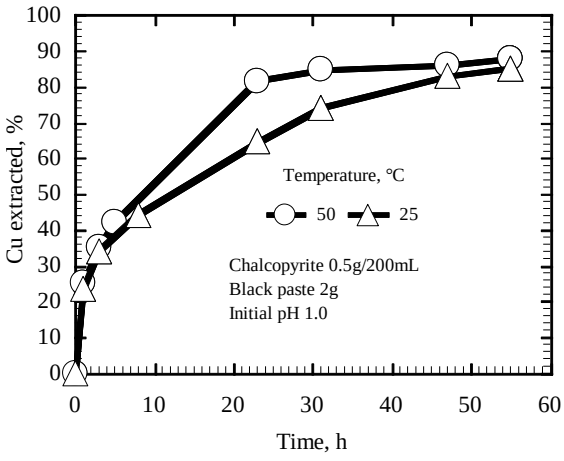

Figure 6. Effect of temperature on the chalcopyrite leaching in the presence of black paste

mL of HNO_3:HCl=1:3) by gentle boiling on a hot plate for 6h. The sample was filtered and the residue on the filter paper was rinsed with distilled water until the electrical conductivity of the filtrate remained constant and dried at the 40°C for 24h. Leaching experiment was conducted by adding 0.03g graphite powder to the leaching solution with 0.5g chalcopyrite and 2g MnO_2. The results are shown in Figure 7. The kinetics of chalcopyrite leaching rate was accelerated extremely in the presence of graphite powder and extraction yield of copper was 78% in 5days in. The leaching rate of MnO_2 was also increased significantly and 37% of MnO_2 was dissolved in 5days.

4 DISCUSSION

Since MnO_2 is noble than chalcopyrite, chalcopyrite and MnO_2 form a galvanic corrosion couple in sulfuric acid solution where the former acts as anode and the latter as cathode leading to simultaneous dissolution of both materials.

In the presence of MnO_2 the kinetics of chalcopyrite leaching was enhanced, but the leaching rate was not so adequate that it would require a lot of time to complete the leaching. Adding the black paste increased the rate and extent of chalcopyrite leaching significantly. Carbon-zinc batteries contain manganese dioxide and graphite powder. The graphite powder obtained from black paste enhanced the kinetics of chalcopyrite leaching in the presence of MnO_2, indicating that graphite powder play important role in the galvanic interaction between chalcopyrite and MnO_2.

It is widely accepted that on the chalcopyrite leaching in the ferric sulfate solution sulfur layers of extremely low electrical conductivity form on the surface of chalcopyrite by the oxidation of ferric ions. Graphite powder is used to increase the electrical conductivity of the black paste in the carbon-zinc batteries. The graphite powder could improve electron transfer from chalcopyrite to MnO_2, which accelerates the galvanic interaction between them resulting into increasing the kinetics of chalcopyrite leaching.

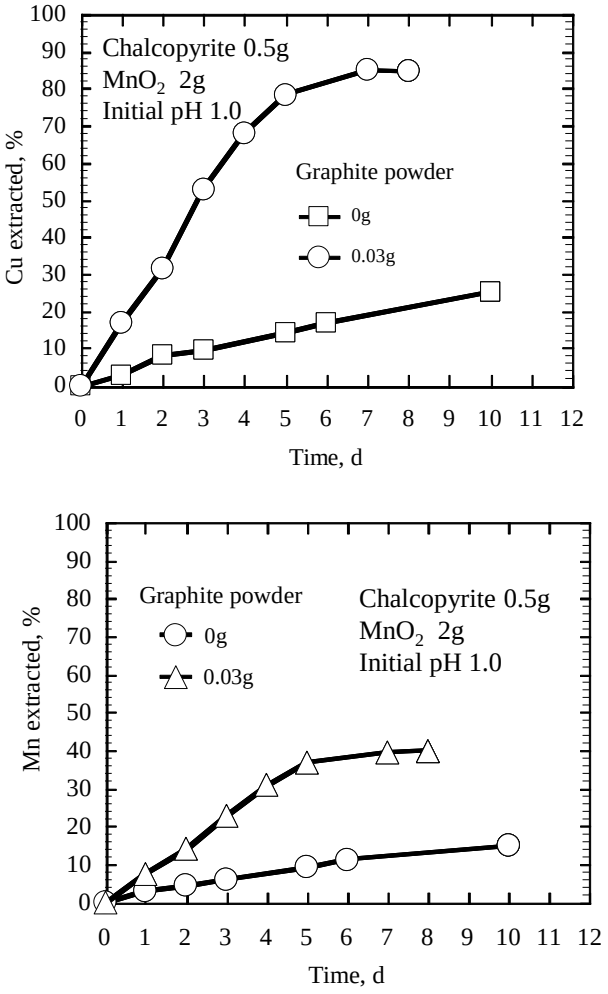

Figure 7. Effect of graphite powder e on the chalcopyrite leaching in the presence

5 CONCLUSIONS

The feasibility of galvanic leaching of chalcopyrite was examined using MnO_2 and black paste collected from spent carbon-zinc batteries. Black paste accelerated the kinetics of chalcopyrite leaching dramatically. The graphite powder contained in the black paste could smoothen electron transfer between the chalcopyrite and MnO_2 resulting into acceleration of the galvanic leaching of chalcopyrite.

REFERENCES

Adam,K., Natarajan,K.A., and Iwasaki,I., 1984, Griding media water and its effect on the flotation of sulfide minerals, Inter. Journal. of Mineral processing, Vol.12, pp.39-54

Devi, N.B., Madhuchhanda M., Rath, P.CS.,M., Srinivasa Rao, K., , Paramguru, R.K., 1999. Dissolution of metal values from deep-sea manganese nodule in HCl medium in presence of chalcopyrite. Annual Technical Meeting, Indian Institute of Metals, 15–16, Nov. Paper PB-14.

Gantayat B.P., Rath P.C., Paramguru R.K. and Rao S.B., 2000, Galvanic interaction between chalcopyrite and manganese dioxide in sulfuric acid medium, B, Metall. Trans. B, 31B, pp.55-61

McComsey, D.W., 2001, (Linden,D.), Handbook of Batteries, Chapter 8, pp. 193–237(2001)

Nakazawa H., Tazawa K. and Hareyama W., 2010, Galvanic leaching cobalt-rich ferromanganese in the presence of pyrite, Jurnal of MMIJ,Vol126,pp.679-682

Rath P.C. and Paramguru R.K., 1994, Galvanic interaction between manganese dioxide and sphalerite, Met. Mater. Processes, 1994, vol. 6(1),pp.27-30

Improvements the Performance of the Sungon Secondary Flotation Circuit

P. Pourghahramani
Mining Engineering Department, Sahand University of Technology, Tabriz, Iran

A.Bagherian
Sungon Copper Mine Complex, Tabriz, Iran

ABSTRACT In this paper the performance of the secondary flotation circuit at Sungon plant was evaluated using several systematic sampling surveys from the plant. The evaluation of cleaner performance indicated that the recovery of molybdenite never exceed of 24.29%. The copper recovery varies from 23.27 to 90.9%. Troubleshooting investigations revealed that the formation of dry and strong froth in cleaner cells is responsible for decreasing dramatically the copper and molybdenum recoveries. By changing operational conditions, the copper and molybdenum recoveries increased by 86.04% and 60.8% which show considerable improvements. Changes in re-cleaner operating conditions increased the recovery of molybdenum from zero to more than 99.4% and molybdenum contents increased from 0.21% to 1.031%. The operation in scavenger was found to be normal and satisfactory at the current state.

Keywords: Secondary flotation, Sungon plant, copper

1 INTRODUCTION

The secondary flotation circuit in the Sungon plant consists of cleaner, re-cleaner and scavenger units for up grading of the rougher concentrate. Recently, a decision was made for molybdenum upgrading because of operating molybdenum plant. Initially, it was planned to produce a copper concentrate with 30% Cu in the secondary flotation circuit [1]. However, due to wide changes in ore properties and operation conditions, the final concentrate grade was declined and in addition the recovery of molybdenum was not satisfied and upgrading molybdenum in newly operated plant faces with difficulties. The objective of this paper is to investigate the performance of the secondary flotation units to achieve to the nominal copper and molybdenum recovery and grade at secondary flotation circuit. For the investigation, several sampling surveys were planned for systematic investigation. In addition, improvements were made to improve the circuit performance.

2 THE SUNGON REGRINDING AND SECONDARY FLOTATION CIRCUIT

The Sungon copper complex is located at the East Aazarbaijan province, in the north-west of Iran. The Sungon mine is an open pit mine of the porphyry copper deposit which is the second largest copper mine in Iran. At this plant, a 3.962x5.791 m regrinding tumbling ball mill with an overflow discharge is used to grind and subsequently liberate locked valuable minerals from an entering feed ground to-300µm using primary and secondary milling processes in a circuit closed with cyclones. The discharge of the regrinding mill is mixed with the rougher and scavenger concentrates and then sent to the secondary cyclones. The discharge of the regrinding mill is named as the regrinding product through the manuscript. The underflow of the secondary cyclones is the regrinding mill feed (Fig. 1). The secondary flotation circuit includes cleaners with two column cells, re-cleaner with one column cell and scavenger with 4 RCS50 cells. The load circulation is shown in Fig.1, wherein cyclones overflow forms

the secondary flotation feed. Cleaners concentrate is upgraded once more by re-cleaner unit and re-cleaner-tail is circulated as cleaner feed for further upgrading. The cleaner tail is also upgraded by scavenger unit and its tail passes into final tail dam and scavenger concentrate is classified, regrinds by regrinding mill and classification units and then is sent to the secondary flotation circuit.

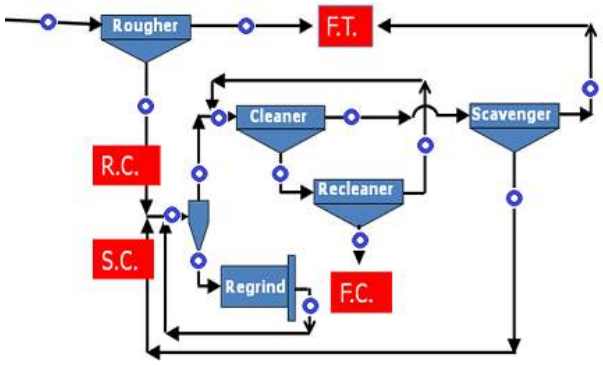

Figure 1. Re-grinding and secondary flotation circuit, Open circles are sampling stations [2].

3 EXPERIMENTAL

The ability to access the complete evaluation of the flotation circuit performance mainly depends on the quality and nature of the collected information from the flotation circuit. To collect a valid and reliable data, flotation circuit was initially investigated to find appropriate stations for sampling.

To get insight into the performance, it was planned to take samples from the streams of cyclone, regrinding mill, rougher, cleaner, re-cleaner as shown in Fig.1 with circles. At the next step, proper sampling cutters were designed and constructed by considering the available geometry in the flotation circuit cutters as shown in Fig. 2.

The sampling duration from the circuit was around 3h in each survey. The gross samples obtained by mixing of increments collected in an equal time intervals. During each sampling survey, 8-10 increments from each sampling station were collected. Dry mass of the samples were determined for each survey and then the percent solid was evaluated. The five sampling surveys were made at various date depending on pending feed into circuit. At each survey, available operation parameters of fresh feed rate (t/h), air flow rate (m^3/h) in flotation cells, pH value in cells,… were collected. Once the representative samples were collected, a number of the samples were dried and weighed for size analysis. The size distribution of the sample was determined using the sieve analysis to-37µm. The size analysis was repeated to insure the measurement reliability.

Figure 2. Sampling cutters for collecting samples from the secondary flotation circuit

4 RESULTS AND DISCUSSION

In the following sections, the performance of three upgrading units in the secondary flotation circuit are explained and discussed.

4.1 The Performance of the Cleaners Units

To evaluate the performance of cleaner unit, five sampling surveys from cleaner streams including its feed, concentrate and tail were taken. Three surveys were made without any changes in circuit operating conditions and the two other surveys were made by changing some operational variables in order to improve its performance. The cleaner feed size distribution is shown in Fig. 3. It is seen that the cleaner feed was finest and coarsest during surveys 5 and 1, respectively. In addition, the fraction -37µm

increases steadily from surveys 1 to 5. In other words, surveys 5 have more slime and fines amount.

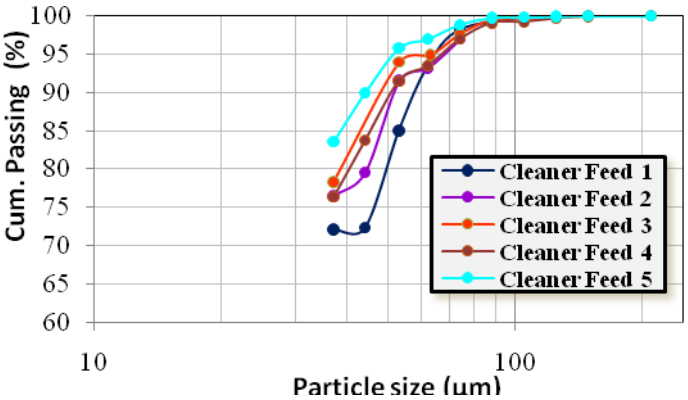

Figure 3. Particle size distribution of cleaner feeds during surveying periods

The operating conditions of cleaners unit are given in Table1. It is obvious that feed solid in survey 1 math the initial design value but during surveys 2 and 3, which is higher than the initial design value. The observation during surveys revealed the formation of dry and strong froth during surveys 2 and 3 as shown in Fig. 4. In these cases, the recovery of froth to concentrate is hindered and the newly floated particles cannot be reached on froth surface. As a result, molybdenite and copper particles losses considerably and passes into tail stream. The situation in surveys 3 was stronger than survey 2.

Table 1. Operating conditions of cleaner during surveys

Operating factor	Initial	S. 1	S. 2	S. 3	S. 4	S. 5
feed rate (t/h)	900	851	929	932	792	855
Feed solid (%)	22.2	22.87	27.41	27.13	23.08	13.7
Tail solid (%)	16.2	15.2	20.76	25.43	20.8	-
Air flow (m^3/h)	180	2*175	2*180	2*181	2*200	2*225
K_{80} of Feed (µm)	40	49.4	44.3	38.4	40.4	34
K_{80} of Tail(µm)	--	55.7	41.8	40.2	--	--

The evaluation of cleaner performance during three initial surveys indicated that the recovery of molybdenite never exceed of 24.29% which approaches zero in survey3 (Table 2). The copper recovery varies from 23.27 to 90.9% wherein the minimum values are attained in surveys 3. Higher performance in surveys 1 could be related to larger size of feed avoiding entrainment, proper percent solid and higher feed grade as a results of re-circulated higher tailing grade. However, by the formation of dry and strong froth during surveys 2 and 3, the copper and molybdenum recoveries decreased dramatically. As expected, the concentrate 1 has higher grade. Higher copper and molybdenum in the tail of surveys 2 and 3 implies the tailing of valuable minerals because of strong and dry froth (Fig. 4). This is while using low flow rate and the formation of higher froth depth in columns.

Figure 4. The formation of dry and strong froth during surveys 2 and 3

To improve the cleaner performance, the air flow increased from 180 to 200 m^3/h and solid in feed declined to the designed value approximately. In addition, fuel oil with 0.25L/min rate was added to cleaner feed tank. As results, the copper and molybdenum recoveries increased to 76.74% and 51.64%, respectively. In addition, the molybdenum content was increased 2.5-4.1 folds compared with previous surveys. Slight increase in copper recovery should be related to the competition between copper and molybdenum mineral particles during attachment step to air bubbles. In addition, being finer feed could be another reason for decreasing concentrate grade. After the initial changes in circuit, the obtained results are satisfying in comparison with the initial design, wherein the production of a copper concentrate with 18.33% Cu content and recovery of 76.91% from a feed with 6.36% Cu is target.

To improve further the circuit performance in survey 5, the air flow rate

was increased to 225 m^3/h and feed solid decreased to 13.7%. In addition, the amount of fuel oil was kept constant similar to survey 4 and A70 frother with 0.05 L/min rate was added in cleaner feed tank. Once the operation stabilized, the sampling was made and the obtained results are summarized in Table 2. The copper concentrate grade increased to 22.02% Cu in spite of finer feed. The copper and molybdenum recoveries calculated by 86.04% and 60.8% implying considerable improvements in comparison with survey 4. Generally, the results proved that the recovery of molybdenum increases as feed solid decreases. This could be probably related to the decrease in pulp viscosity and subsequently increasing local distribution which affect the hydrodynamic behavior of flaky molybdenum particles.

Table 2.The evaluation of cleaner performance through 5 sampling surveys

NO	St	Cu %	Mo%	C/F%	R_{Cu}%	R_{Mo} %
1	F	13.4	0.261	53.5	90.9	18.1
	T	2.6	0.243			
	C	22.7	0.392			
2	F	9.0	0.389	32.5	73.28	24.39
	T	3.6	0.38			
	C	20.4	0.42			
3	F	10.2	0.269	12.8	23.3	--
	T	8.9	0.485			
	C	18.5	0.259			
4	F	5.7	0.396	22.5	76.7	51.6
	T	1.7	0.237			
	C	19.5	1.065			
5	F	8.3	0.446	32.5	86.0	60.9
	T	1.7	0.237			
	C	22.0	1.029			

In general, the imperfection in cleaner units can be ascribed to much more fine feed, the formation of strong and dry froth which hinders the recovery from froth zone to concentrate stream and subsequently the newly floated valuable minerals cannot reach to froth zone surface. In addition, the formation of dry and strong froth on cleaner cell avoids entrainment process and caused to the concentrate grade declines as a result of entering gangue particles into froth zone.

4.2 The Performance of the Re-Cleaner Units

According to the initial plant design, the re-cleaner unit operation with a grade of 18.66% Cu must result in a concentrate having 30% Cu with a recovery of 81.26% and a tail having 7.07% Cu.

The particle size distributions of re-cleaner feed for five sampling surveys are shown in Fig. 5. It is clear that about 76 – 86% of feed is finer than 37 µm depending on surveying time and date. d_{80} of feeds are almost the same, accounting for 37-40 µm and the differences enhanced in fine fractions. Also, the results verify that 96-95% of feeds are finer than 74µm. it is expected that with the mentioned feeds including much more fine fractions, upgrading could not be satisfied because of much more fines particles entrainment.

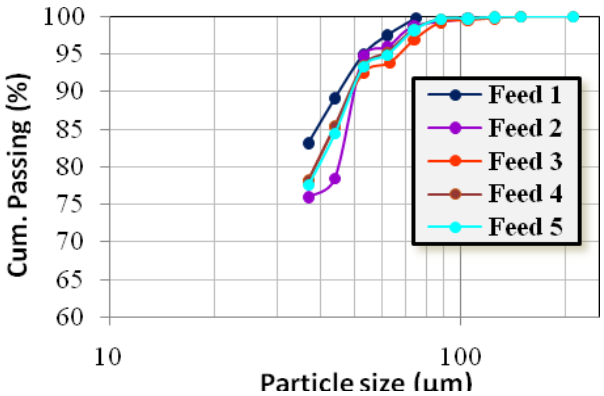

Figure 5. The particle size distributions of re-cleaner feeds

For investigation of re-cleaner performance, the sampling was made simultaneously with cleaner surveys. During three initial surveys, no changes were made in operating conditions. In surveys 4 and 5, only the air flow rate was changed to 180 and 225 m^3/h, respectively. The operating conditions for re-cleaner unit are given in Table 3.

Table 3. Operating conditions of re-cleaner during surveys

Operating factor	Initial	S.1	S. 2	S. 3	S.4	S. 5
Feed rate (t/h)	900	851	929	932	792	855
Air flow rate (m^3/h)	180	167	165	158	180	225
Feed solid (%)	28.6	12.14	17.29	22.8	17.2	19.5
Tail solid (%)	15	7.89	8.58	12.5	9.79	7.42
K_{80} of Feed (µm)	40	37	40.9	38.8	38.7	39.4
K_{80} of Tail(µm)	--	K90=37	K93=37	--	--	--

The obtained results are summarized in Table 4. It is seen that the weight recovery increased significantly by 50.55% which could not be due to the increase of feed grade. No dramatic changes can be observed in concentrates grade as a result of tailing of valuable minerals in tail and entrainment as the tail grade is always higher than the initial design value. The comparison of feed size distribution with tails grade reveals that with increasing feed fineness, the grade in tail stream would be increased. On the other hand, molybdenum recoveries in the three initial surveys approaches to zero but copper recovery is satisfied. It can be concluded that the fine particles spilt into tails and concentrate and flotation is not selective and lowering concentrate grade.

The changes through surveys 3 and 4 improved dramatically the re-cleaner performance especially for molybdenum. Although, the copper grade in concentrate was not increased considerably, the recovery of molybdenum has increased dramatically. As molybdenum recovery increases from zero to more than 99.4% and molybdenum contents increased to 1.23 and 1.031% during surveys 4 and 5, respectively. Increasing molybdenum in final concentrate will certainly improve the processing scheme in subsequent molybdenum beneficiation plant.

Table 4. The evaluation of re-cleaner performance through 5 sampling surveys

NO	St	Cu%	Mo%	C/F%	R_{Cu}%	R_{Mo}%
1	F	22.7	0.39	77.42	84.55	--
	T	15.5	0.42			
	C	24.8	0.46			
2	F	20.4	0.42	63.83	80.07	--
	T	11.2	0.714			
	C	25.5	0.325			
3	F	18.5	0.259	55.38	67.43	--
	T	13.5	0.423			
	C	22.5	0.21			
4	F	19.5	1.065	79.41	91.04	72.37
	T	8.5	0.788			
	C	22.3	1.23			
5	F	22.0	1.029	98.7	99.3	99.49
	T	11.4	0.744			
	C	22.2	1.031			

4.3 The Performance of the Scavenger Units

Scavenger circuit consists of 4 cells designed for processing of the cleaner tail as feed. The scavenger concentrate sent to regrinding circuits for further grinding and classification and the scavenger tail passes into final tail dam. Based on the initial plant design, for a feed with 1.99% Cu, a concentrate with 7% Cu and a recovery of 87.15% in scavenger should be obtained. Then, the copper lose in tail will be maximum 0.34% Cu content.

For evaluation of scavenger performance, four sampling surveys were made.33.3% of total fuel oil is added in scavenger unit. Fig. 6 represents scavenger feed size distribution during 4 samplings. As seen, Feed 1 is coarser than the other feeds and the finest feed was processed in survey 3. The most difference in size distribution is in fine fractions of feeds. In Survey 3, about 85% of feed is smaller than 37µm which shows an increase of 15% compared to the feed in suvey1.

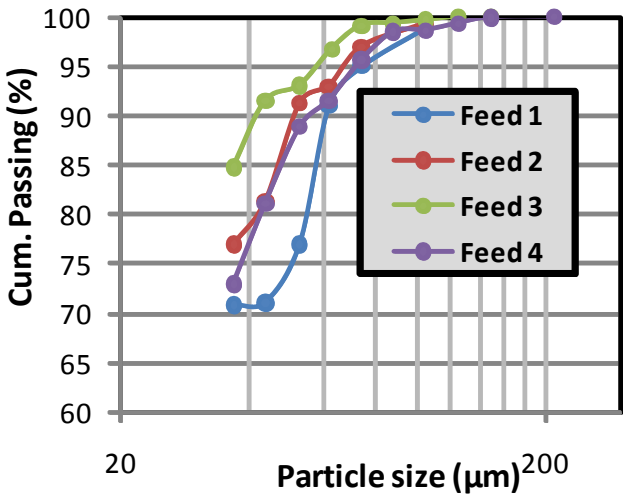

Figure 6. The particle size distributions of Scavenger feeds

The operating conditions during 4 surveys are summerized in Table 5 where the solid in feeds 2 and 4 are more than the others. d80 of feed varies between 35 and 55 µm depending on surveying dates.

Table 5. The operational conditions in scavenger unit in 4 survey

Operating factor	Initial	S.1	S. 2	S. 3	S. 4
Circuit feed rate (t/h)	900	851	929	932	792
Feed solid (%)	16.2	15.2	20.76	25.43	20.8
Tail solid (%)	15.2	14.8	18.25	15.54	19.7
K_{80} of Feed (µm)	40	54.9	41.8	35.4	43
K_{80} of Tail(µm)	--	59.9	45.9	44.5	--
fuel oil (g/t)	--	6.96	7.5	3.46	7.8

The obtained results for scavenger unit are summarized in Table 6. With a first glance, it can be seen that the performance of scavenger unit is satisfied comparing with cleaner and re-cleaner units as the copper recovery varies from 93.13% to 97.05%. The concentrate grade is even higher than the value of initial plant design. A close look on the results indicates that copper grade in scavenger tail 3 is higher than the others. The reason may be related to feed size distribution, higher feed grade and fuel oil consumption wherein more than 85% of feed is finer than 37 µm and the minimum amount of fuel oil is used during this survey. Unexpected increase in weight recovery may be related to much more fine size of feed. On the other hand, the recovery of molybdenum varies between 91% and 92.8% through surveys of 1-3 and the results are much more appreciated. Decreasing molybdenum recovery in survey 4 could be due to low grade feed because of much more recovery of molybdenum in cleaner and re-cleaner units. As a whole, it could be concluded that the scavenger performance is satisfactory and higher losses of valuable minerals in scavenger should be related to much more fines presence in feed. In the situation molybdenum recovery increases, while the copper recovery declines. It is recommended that an increase in air flow rate or using some oily frother in scavenger unit would result higher recovery.

Table 6. The evaluation of scavenger performance through 4 sampling surveys

NO	St	Cu%	Mo%	C/F%	R_{Cu}%	R_{Mo}%
1	F	2.62	0.143	38.61	93.67	91.05
	T	0.27	0.019			
	C	6.35	0.399			
2	F	3.59	0.38	29.55	97.05	91.85
	T	0.15	0.037			
	C	11.79	2.14			
3	F	8.98	0.485	62.10	96.96	92.86
	T	0.72	0.078			
	C	14.02	0.81			
4	F	1.72	0.237	19.23	95.3	77.46
	T	0.1	0.064			
	C	8.52	1.11			

5 IMPROVEMENT IN THE PERFORMANCE OF THE SECONDARY FLOTATION CIRCUIT

The secondary flotation circuit could be summarized as given in Fig. 7. The recovery each unit is given into parentheses with appropriate synonyms.

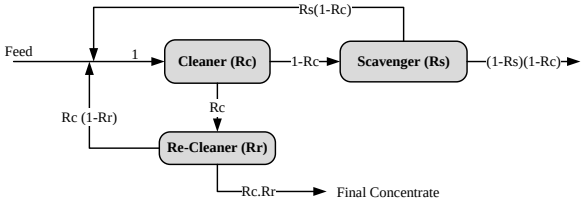

Figure 7.Summarized scheme of the secondary flotation circuit

The total recovery of secondary flotation circuit can be calculated from the equation:

$$R_2 = \frac{Rc \times Rr}{1-[Rc(1-Rr)+Rs(1-Rc)]} \quad (1)$$

Using the above mentioned equation, the total recovery of the secondary flotation circuit was calculated as given in Tables 7 and 8.

Table 7. Overall recovery of copper in the secondary flotation circuit (%)

NO	Rc	Rr	Rs	R2
initial	77	81	87	95
1	91	84	93	99
2	73	80	97	98
3	23	67	96	87
4	77.4	91	95	98
5	86	99	95	99

Table 8. Overall recovery of molybdenum in the secondary flotation circuit (%)

No	Rc	Rr	Rs	R2
1	18	0	91	0
2	24	0	92	0
3	0	0	92	0
4	51	72	77	77
5	61	99	77	87

The results show that the copper recovery is always higher than the initial design value but the final concentrate grade is always lower than the initial design value. The improvement in the secondary flotation circuit performance will be certainly enhanced the overall flotation circuit performance.

6 CONCLUSIONS

It was found that the performance of scavenger unit is satisfied comparing with cleaner and re-cleaner units as the copper recovery varied from 93.13% to 97.05%. The concentrate grade was even higher than the value of initial plant design. The evaluation of cleaner performance indicated that the recovery of molybdenite never exceed of 24.29%. The copper recovery changed from 23.27 to 90.9%. It was found that the formation of dry and strong froth in cleaner cells was responsible for decreasing dramatically the copper and molybdenum recoveries. By changing operational conditions, the copper and molybdenum recoveries calculated by 86.04% and 60.8% which show even considerable improvements. Changes in re-cleaner operating conditions increased the recovery of molybdenum from zero to more than 99.4% and molybdenum contents increased to 1.031%. The operation in scavenger was found to be normal and satisfactory. Generally, by improvement the copper and molybdenum recoveries at the secondary flotation circuit increased to more than 99.4% and 87.29% respectively.

ACKNOWLEDGEMENTS

The authors would like to thank National Iranian Copper Industries Company (N.I.C.I.Co.) and Azarbayjan copper Co. for supporting this research and permission to publish this article. Special Thanks is also extended to the metallurgy and R&D personnel for their continued assistance.

REFERENCES

A. Bagherian, 2007, Copper Upgrading process in Sungon plant, Sungon Libraray internal report.

P. Pourghahramani, H. Dehghani and A. Sam., 2013, A new approach for evaluating the performance of industrial regrinding tumbling ball mills based on grindability and floatability, Minerals Engineering 49 (116-120).

Microstructural Characterization of Pyrite during Mechanical Activation by Using Rietveld and XRD Line Profile Analysis

B.N. Akhgar, P. Pourghahramani
Mining Engineering Faculty, Sahand University of Technology, Tabriz, Iran

ABSTRACT The X-ray diffraction analysis was used for the characterization of structural changes in mechanically activated pyrite. Applying the Rietveld and XRD line profile analysis, comprehensive investigations were carried out to separate the crystallite size and microstrain contributions in peak broadening. The results indicated that no phase transformation occurred in pyrite during mechanical activation. In addition, crystallite size and microstrain decreased and increased, respectively. Also, the lattice parameter of mechanically activated pyrite increased as a function of milling time, implying that pyrite lattice volumes were expanded probably due to vacancy formation. Regarding to shape parameter study, the crystallite size broadening portion is more than the strain broadening portion on the broadened peaks. This may ascribed to the pyrite structure which refined mainly by decreasing crystallite size rather than lattice strain increases. The X-ray amorphization degree increases to about 67% after 100 min intensive milling, reflecting the refractory nature of pyrite.

Keywords: Microstructural characterization, Pyrite, Rietveld and XRD line profile analysis

1 INTRODUCTION

Mechanical activation is a branch of mechanochemistry science with a wide range of potential applications. It has been proved that mechanical activation of minerals can accelerate reactivity of activated minerals in subsequent process such as leaching and adsorption (Akhgar, et al., 2012, Pourghahramani and Akhgar, 2014). These advantages are related to changes in mineral structures such as formation of amorphous phase, grain refinement and lattice strain (Pourghahramani et al., 2008). The mentioned changes are responsible for the reactivity improvement of mechanically activated pyrite.

The mechanical activation pretreatment was employed to improve hydrometallurgical processing of minerals. The obtained results demonstrate that the mechanical activation pretreatment brings about the enhanced dissolution of the minerals due to crystalline disorders and new surface formation (Balaz, 2003; Akhgar et al., 2012). The measurement of crystallite size, lattice strain, amorphization degree and lattice parameter can provide detailed information for behavior prediction of mechanically activated minerals in different process related to its reactivity variations.

Pyrite (FeS_2) as a most common gangue sulfide mineral is associated with valuable minerals in ore deposits. Pyrite hydrometallurgical processing has been studied because of its importance in cyanidation of gold ores (Hu et al., 2002). Regarding to refractory nature of pyrite (Lehmann et al., 2000), improvement of the sulfide mineral reactivity during the hydrometallurgical processing can be a matter of interest. Therefore, mechanical activation would be a promising treatment for the improvement of pyrite reactivity due to extreme structural changes (Hu et al., 2003, 2004, 2007). Also, the used techniques for reactivity promotion of pyrite can give some insight into hydrometallurgical treatments of other sulfide minerals.

The X-ray diffraction (XRD) analysis as an indirect and non-destructive method can provide valuable information about structural changes in mechanically activated

minerals. The microstructural analysis is based on XRD peak broadening reflecting imperfections in the crystal structure. The peak broadening subdivided into crystallite size and microstrain portions after the removal of instrumental effects. In present paper, we made an attempt to investigate the structural changes of mechanically activated pyrite using the XRD analysis. Different approaches such as the Rietveld, Williamson-Hall and Warren-Averbach methods were employed for the assessment of the structural characters of mechanically activated pyrite.

2 EXPERIMENTAL

A high purity concentrate was prepared through conventional beneficiation methods. The XRD analysis of the concentrate showed only pyrite reflections corresponding with JCPDS No. 1-1295 (Figure 1).

The XRD analysis was applied for the examination of pyrite, milled samples and the standard sample, LaB6 SRM660a, used for the elimination of instrumental effects (Figures 1 & 2). The X-ray diffraction test was performed by Bruker Axs D8 advanced instrument by applying Cu Kα radiation (λ = 1.5406 Å) at 50 kV and 250 mA in the two theta range of 25–70°. All records were performed using a step size of 0.02 and a counting time of 3 s per step.

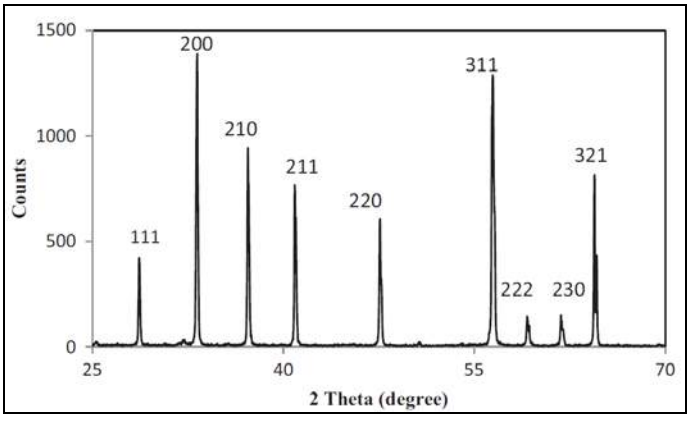

Figure 1. XRD pattern of initial pyrite.

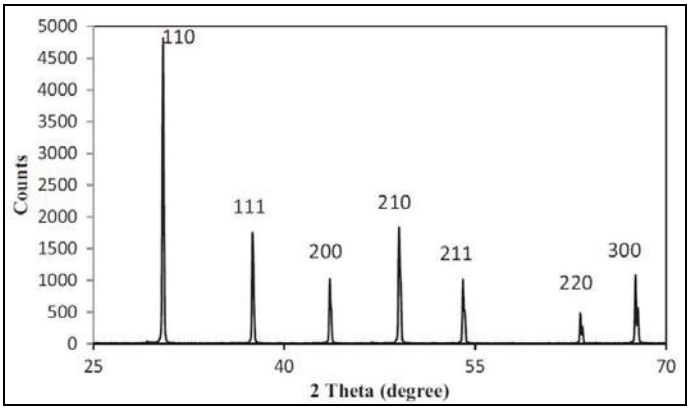

Figure 2. XRD pattern of standard LaB_6 (SRM660a).

The mechanical activation of pyrite was conducted in a planetary ball mill (Pulverisette 6, FRITSCH, Germany) with a 250 ml cup volume and rotation speed of 400 rpm under argon atmosphere to prevent possible chemical reaction. 15 stainless steel balls with a diameter of 20 mm were used for milling by a ball to powder weight ratio of 20:1. The samples were mechanically activated for 20, 50 and 100 min. The obtained powders were kept in sealed condition in a freezer. According to the XRD patterns, no major oxidation phase occurred during sample preparation and mechanical activation (Figure 3).

The Rietveld and Warren-Averbach methods was performed by the X'pert high score plus and Winfit software, respectively.

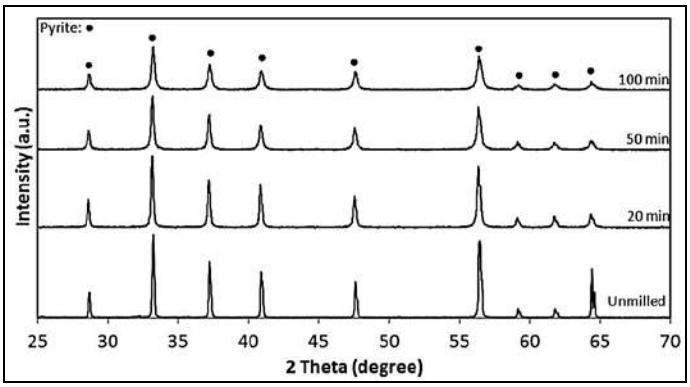

Figure 3. XRD patterns of the initial pyrite and mechanically activated pyrites.

3 RESULT

3.1 X-Ray Diffraction Analysis

The XRD patterns of the initial pyrite and mechanically activated pyrites were matched with the standard XRD pattern of FeS_2 (JCPDS No. 1 -1295) in simple crystallographic arrangement (face-centered cubic, FCC). Additionally, diffraction peak positions shifted toward lower peak positions indicating that the unit cell measures in mechanically activated pyrites were increased.

The lattice parameters of mechanically activated pyrites were calculated by using UnitCell software. The lattice parameter and consequently unit cell volume of pyrite expanded during mechanical activation with increasing milling time (Figure 4). The expansion can be ascribed to the elemental sulfur release during mechanical activation (Hu et al., 2004) forming point defects (vacancies) in pyrite structure. In general, the unit cell volume of pyrite would be larger with more release of elemental sulfur.

Regarding to the XRD patterns of pyrite and milled powders, the broadening increased and the intensity of reflection peaks decreased with milling time (Figure 3). The production of amorphous phase during the mechanical activation can result in the weakening of the intensity of peaks. The X-ray amorphization degree (A) of milled samples was calculated using the four most intensive reflection peaks as defined before (Ohlberg and Strickler, 1962).

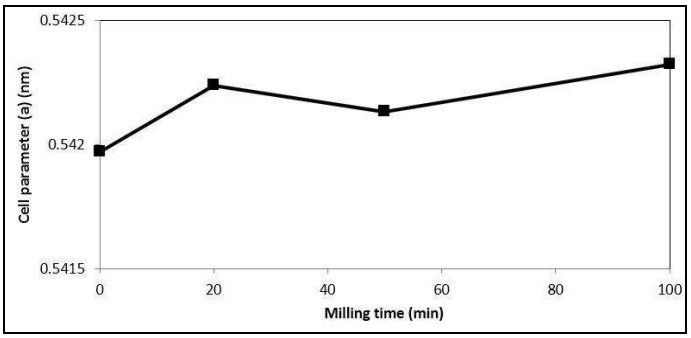

Figure 4. Changes in the lattice parameter of milled pyrite powders.

The X-ray amorphization degree increased more rapidly in the initial stage of mechanical activation and peaked about 67% after 100 min milling (Figure 5). The endurance of crystalline structure of pyrite (more than 30%), even in intensive milling conditions, proved that pyrite has the resistant and refractory structure.

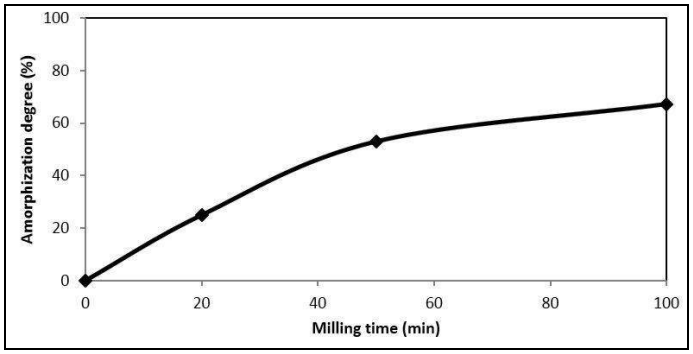

Figure 5. X-ray amorphization degree variations during the mechanical activation of pyrite.

3.2 Microstructure Characterization

The methods of Rietveld, Williamson-Hall and Warren-Averbach were applied to investigate microstructural changes of pyrite during mechanical activation. The Williamson-Hall plot was used to deconvolute the broadening component of crystallite size from microstrain. The results of Williamson-Hall method are summarized in Table 1. The volume weighted crystallite size decreased and microstrain increased with milling time. The obtained results are in line with previous reports (Hu et al., 2004; Li et al., 2008).

The Williamson-Hall curves were obtained by the regression method and all diffraction peaks were involved. The volume weighted crystallite size and microstrain were attained from intercept and slope of Williamson-Hall plots.

Table. 1 The volume weighted crystallite size and microstrain values obtained by using Williamson-Hall method

	Milling time (min)	D_v (nm)	(%)
P1	0	316	0.05
P2	20	182	0.1
P3	50	100	0.141
P4	100	57.73	0.224

The Warren-Averbach method was conducted by the Winfit software and the surface weighted crystallite size and the root mean square strain (RMSS) were computed after profile fitting and removal of instrumental effect (Table 2). The changes observed in surface weighted crystallite size and RMSS using the Warren-Averbach method were the same as the Williamson-Hall method. The surface weighted crystallite size decreased and RMSS increased with the milling time.

Also, regarding to the results, it can be claimed that the surface weighted crystallite size would be smaller than volume weighted crystallite size.

Table 2. The surface weighted crystallite size and RMSS values obtained by using Warren-Averbach method

	Milling time (min)	Ds (nm)	RMSS (%)
P1	0	103.6	0.04
P2	20	53.8	0.085
P3	50	27	0.105
P4	100	25.1	0.117

The obtained crystallite size and microstrain by using Rietveld method are presented in Table 3. It is clear that the parameters variation are similar to the previous results obtained by Williamson- hall and warren-Averbach methods, when crystallite size decreases and microstrain increased in mechanically activated pyrites. The crystallite size gradually decreases to 74 nm in mechanically activated pyrite for P4(100min).

Table 3. The volume weighted crystallite size and microstrain values obtained by using Rietveld method

	Milling time (min)	Dv (nm)	ε (%)
P1	0	763	0.06
P2	20	132	0.08
P3	50	77	0.09
P4	100	74	0.183

Comparison of the crystallite size and strain values obtained from Williamson-Hall and Warren-Averbach methods (Tables 1&2) indicated that the smallest crystallite size and strain were obtained by the Warren-Averbach method. The results clarified that with increasing milling time and the peak broadening, the separation of crystallite size and strain by Williamson-Hall and Warren-Averbach methods would be more different. The comparison also verified that Williamson-Hall method devotes more broadening portion to strain rather than crystallite size in comparison with the Warren-Averbach method.

Shape parameter value were used to determine the broadening portions of crystallite size and microstrain by using a Voigt function with predominant Lorentzian and Gaussian character, respectively (Clearield et al., 2008). An increasing influence of crystallite size portion on the microstructural changes and consequently on the peak broadening results in the shape variations of the fitting profiles from the Gaussian character (shape parameter = 0) to the Lorentzian character (shape parameter = 1). The two most intensive diffraction peaks of (200) and (311) were selected and the mean value of their shape factors was presented (Figure 6). This result clarified that the shape parameter was about zero in the initial pyrite when the crystallite size was not small enough to have a significant influence on peak broadening. The shape parameter increased to about 0.74 in 20 min milled pyrite powders and then peaked at 0.94 after 50 min milling indicating the crystallite size had a more important role than microstrain in the peak broadening of milled pyrite. The shape parameter decreased to 0.77 in 100 min milled pyrite demonstrating that the strain broadening portion increased in comparison to the 50 min milled pyrite. The shape parameter measurements indicated that the strain broadening had less influence on peak broadening and crystallite size portion remained the predominant broadening component during mechanical activation of pyrite.

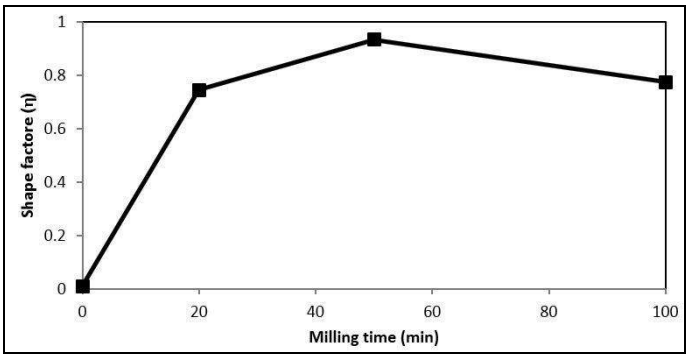

Figure 6. Variations of shape parameter during mechanical activation of pyrite.

As mentioned before, the Williamson-Hall devoted more broadening to strain than crystallite size in comparison with Warren-Averbach. Regarding to obtained shape factors and mentioned fact, the results obtained by Rietveld method which share properly peak broadening to the crystallite size and microstrain can be more reliable than other methods.

4 CONCLUSION

The XRD line profile analysis of the Williamson-Hall and Warren-Averbach methods and Rietveld method were applied to extract microstructural characteristics of mechanically activated pyrite. The conclusions can be as follows;

1. The primary XRD studies confirm that pyrite concentrate has the FCC crystallographic arrangement. The investigation of obtained XRD patterns proved that due to the intensive milling of pyrite, the intensity of diffraction peaks was reduced and the amorphization phenomena occurred. The refractory nature of pyrite was reconfirmed when the XRD amorphization degree of mechanically activated pyrite was 68% after 100 min intensive milling.

2. As expected and all methods proved, the crystallite size decreased and microstrain increased with milling time. The comparison of the obtained result by the methods also proved that Williamson-Hall and Rietveld methods devote more broadening portion to strain rather than crystallite size in comparison with the Warren-Averbach method.

3. Rietveld method which share moderately peak broadening to the crystallite size and microstrain can be more reliable than other methods.

REFERENCES

Akhgar B.N., Pazouki M., Ranjbar M., Hosseinnia A. and Salarian R., 2012. Application of Taguchi method for optimization of synthetic rutile nano powder preparation from ilmenite concentrate, *Chem. Eng. Res. Des.* 90 (220–228).

Balaz P., 2003. Mechanical activation in hydrometallurgy, *Int. J. Miner. Process.* 72 (341–354).

Clearield A., Riebenspies J. and Bhuvanesh N., 1st (ed.), 2008. *Principle and Application of Powder Diffraction*, Wiley-Blackwell (400).

Hu H., Chen Q., Yin Z., Zhang P., Zou J. and Che H., 2002. Study on the kinetics of thermal decomposition of mechanically activated pyrites, *Thermochem. Acta* 389 (79–83).

Hu H., Chen Q., Yin Z. and Zhang P., 2003. Thermal behaviours of mechanically activated pyrites by thermogravimetry (TG), *Thermochem. Acta* 398 (233–240).

Hu H., Chen Q., Yin Z., Zhang P. and Wang G., 2004. Effect of grinding atmosphere on the leaching of mechanically activated pyrite and Sphalerite,*Hydrometallurgy* 72 (79–86).

Hu H., Chen Q. and Yin Z., 2007.Mechanism of mechanical activation of sulfide ores,*Trans. Nonferrous Met. Soc.* 17 (205–213).

Lehmann M.N., Leary S.O. and Dunn J.G., 2000. An evaluation of pretreatments to increase gold recovery from a refractory ore containing arsenopyrite and pyrrhotite, *Miner. Eng.* 13 (1–18).

Li C., Liang B. and Wang H., 2008. Preparation of synthetic rutile by hydrochloric acid leaching of mechanically activated Panzhihua ilmenite,*Hydrometallurgy* 91 (121–129).

Ohlberg, S.M. and Strickler D.W., 1962. Determination of Percent Crystallinity of Partly Devitrified Glass by X-Ray Diffraction, *J. Am. Ceram. Soc.* 45 (170-171).

Pourghahramani P. and Akhgar B.N., 2014, Influence of Mechanical Activation on the Reactivity of Natural Pyrite in Lead (II) Removal from Aqueous Solutions, *J. Ind. Eng. Chem.* In prees.

Pourghahramani P., Altin E., Madhusudhan R.M., Peukert W. and Forssberg E., 2008. Microstructural characterization of hematite during wet and dry millings using Rietveld and XRD line profile analyses, *Powder Technol.* 186 (9–21).

Preparation of Nano Zero-Valent Iron (NZVI) From Mechanochemically Treated Pyrite

B.N. Akhgar, P. Pourghahramani
Mining Engineering Faculty, Sahand University of Technology, Tabriz, Iran

ABSTRACT A new procedure has been proposed to prepare nano zero-valent iron (NZVI) form the sulfide mineral of pyrite by using mechanochemical pretreatment. The XRD analysis indicated that pyrite and iron phases remained after 50 min co-milling of pyrite and iron during mechanochemical treatment and new phase of troilite was formed. The microstructural changes of mechanochemically treated pyrite were investigated by Rietveld method. The mechanochemical treatment reduced crystallite sizes and microstrain measures. Total iron extraction increased from 1% in initial pyrite to 87% in 50 min mechanochemically treated pyrite after leaching by 1M sulfuric acid at ambient temperature. Finally, the NZVI particles were synthesized from the obtained leach liquor through precipitation method by titration of sodium borohydride. The FE-SEM and XRD results indicated that the NZVI was prepared with particles less than 100 nm which are protected by an iron oxide shield.

Keywords: Nano zero-valent iron (NZVI), Mechanochemical pretreatment, Pyrite

1 INTRODUCTION

Nano zero-valent Iron (NZVI) preparation is classified in nanoscale environmental technology due to appreciable capability of NZVI for removing of various contaminants such as chlorinated organic solvent, organochlorine pesticides, organic dyes, various inorganic compounds and metal ions such as Pb (II), As(III), Cu(II) (Yuang-Pang et al., 2006).

Various methods have been used for preparation of nano zero valent iron. In general, most of the methods are based on reduction of ferric or ferrous iron from related aqueous solutions. Among the methods, preparation of NZVI by using sodium borohydride has been described as simplest method wherein titration of sodium borohydride into iron aqueous solutions brought about the reduction of ferric or ferrous ions to zero-valent iron (Zhang, 2003; Karlsson et al., 2005).

There are lots of minerals containing noticeable amount of iron and during hydrometallurgical processing of them, ferrous sulfate solution was produced raising serious environmental concerns (Habashi, 1999). Preparation of NZVI form the iron ferrous sulfate solutions can be interesting matter which has the advantages such as preparation of advanced nano powders of NZVI and provision a solution for disposal problems of the iron sulfate solutions.

The hydrometallurgical treatment of pyrite has been studied for various reasons. The iron sulfate solutions can be obtained during pyrite concentrate leaching and the solutions produced from the gangue mineral of pyrite will be cost-effective. In addition, the leaching of pyrite as refractory mineral can provide more information to improve leaching of other sulfide minerals such as chalcopyrite.

The hydrometallurgical treatment of pyrite is technologically difficult operation for extreme reaction conditions required. The new method of mechanochemical pretreatment is proposed to overcome the problems. The aim of this paper is to prepare zero-valent iron nanoparticles from the leach liquors obtained during pyrite leaching. Also, an attempt was made to increase iron extraction from pyrite during its leaching with sulfuric acid at ambient temperature and pressure by using high-energy ball milling pretreatment.

2 EXPERIMENTAL

2.1 Materials

A high purity concentrate was provided using conventional beneficiation methods. An ore bearing high amount of pyrite mineral as raw sample was crushed and milled manually to a particle size of -100 μm. For the preparation of pyrite concentrate from the mentioned raw sample in laboratory scale, the flotation tests were performed in three steps of rougher, cleaner and recleaner. Then, pyrite concentrate was passed through a wet magnetic separator for further upgrading. Finally, the probable contaminations trapped between pyrite particles were removed by washing. The XRD analysis of pyrite concentrate proved that pyrite reflections corresponded with JCPDS No. 1-1295 (Figure 1).

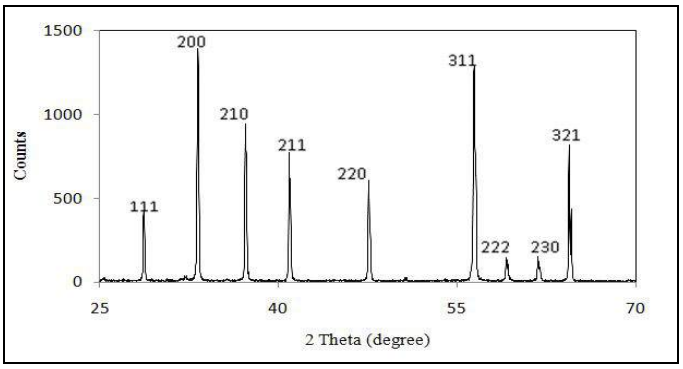

Figure 1.XRD pattern of the initial pyrite.

2.2 Mechanochemical treatment

To reduce disadvantageous impact of high-energy ball milling processes on energy consumption and industrial capacity, the mechanochemical treatment was performed in a short period, less than one hour. Mechanochemical treatment was conducted by a planetary ball mill (Pulverisette 6, FRITSCH, Germany) for 50 min with a rotation speed of 400 rpm under argon atmosphere to prevent probable chemical reactions. 15 stainless steel balls with a diameter of 20 mm were used for milling by a ball to powder weight ratio of 20:1. As initial feed for the planetary ball mill, a mixture of pyrite and iron powder (Merck 3800.1000) was prepared by the stoichiometry ratio presented in following reaction.

$$FeS_2 + Fe \rightarrow 2FeS \quad (1)$$

2.3 Leaching tests

The leaching experiments were carried out in a 500 ml baker reactor by 1M H_2SO_4 solution. According to experimental details (Table 2), the initial feeds of leaching experiments were the natural pyrite and mechanochemically treated pyrite (MCTP) for 50 min. The experiments started with addition of the initial feed and an agitator with 475 rpm stirring speed was used for mechanical agitation. The leaching experiments were performed for 5 h and then the leach liquors were separated from the leach residues.

The final concentrations of extracted iron in the obtained leach liquors were measured by UV spectophotometr (specord 200 plus, analytikjena, Germany).

Obtained leach liquors from 50 min mechanochemically treated pyrite was used for preparation of nano zero-valent iron (NZVI). NZVI can be prepared through reduction of ferric or ferrous iron from their aqueous solutions by using sodium borohydride (Dickinson and Scott, 2010). The preparation of iron nanoparticles was performed by titration of sodium borohydride (Merck, 8.06373.0100) in a flask reactor equipped with a mechanical agitator (500 rpm), as described in previous investigations (Dickinson and Scott, 2010). Then, the precipitated powder was dehydrated using freeze drier for XRD analysis. Figure 2 shows a schematic route of the used techniques for preparation of NZVI from natural pyrite.

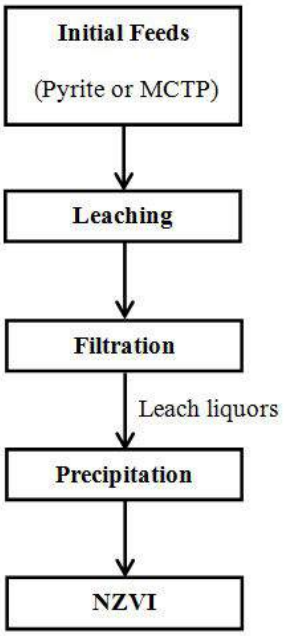

Figure 2. A schematic flow sheet of techniques used.

2.4 Characterization

The X-ray diffraction patterns were collected with Bruker Axs D8 advanced instrument (Germany), applying Cu Kα radiation (λ= 1.5406 Å) at 50 KV and 250 mA in the two theta ranges of 25-70º. The patterns were recorded using a step size of 0.02 and a counting time of 3s per step. Also, investigation of field emission scanning electron microscopy (FE-SEM) was carried out by using a Hitachi S4160 (Japan) instrument.

3 RESULT AND DISCUSSION

3.1 Microstructural changes during mechanochemical treatment

The XRD patterns of mechanochemically treated pyrite are illustrated in in Figures 3 & 4. As seen in Figure 3, the intensity of iron peaks (JCPDS No. 6-0696) decrease by increasing the milling time. The pyrite and Fe peaks remain after 50 min milling and do not disappear. The result reveals that the induced mechanical energy to the mixture of pyrite and iron during mechanochemical treatment cannot provide the sufficient energy for complete reaction between them- even after 50 min intensive milling.

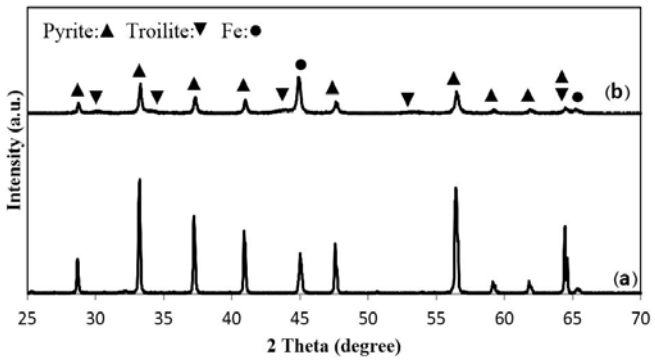

Figure 3. XRD patterns of a) the initial pyrite and b) mechanochemically treated pyrite for 50

According to the Bragg equation (Eq. 2) and lattice parameter equation of cubic systems (Eq. 3), (Suryanarayana and Norton, 1998), the unit cell parameter of the added Fe increases during mechanochemical treatment.

$$n\lambda = 2d\sin\theta \tag{2}$$

$$\frac{1}{a^2} = \frac{h^2 + k^2 + l^2}{d^2} \tag{3}$$

where d is the interplanar spacing, n is known as the order of reflection (n=1, 2, 3 and…) and (h,k,l) are Miller indices of diffracting plan. λ and θ are wavelength and Bragg angle of a defined reflection, respectively and (a) is referred to the unit cell parameter in cubic form. The anchor scan data of XRD patterns reveals that the anchor of iron most intensive peak changes from 45.02 in initial feed (iron and pyrite mixture) to 44.92 in 50 min mechanochemically treated pyrite. The shift of the main peak position toward lower angles during mechanochemical treatment verified that Fe unit cell parameter increased. Point defects created by Fe atoms lost during mechanochemical treatment are responsible for the increase. For more explain, the Point defects can be formed during incomplete mechanochemical reaction between iron and pyrite where the iron atoms leave their position in Fe structure empty to form troilite (FeS- JCPDS No.1-1247) during a mechanochemical treatment with pyrite (Figure 4).

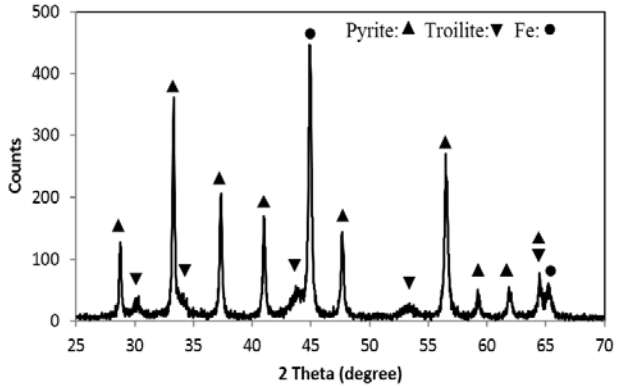

Figure 4.XRD pattern of mechanochemically treated pyrite for 50 min

To begin the structural changes study of mechanochemically treated pyrite, amorphization degree (A) calculated for obtained XRD pattern after 50 min milling as described before (Ohlberg and Strickler, 1962). According to the results (Table 1), the amorphization degree of mechanochemically treated pyrite rises to 83% after 50 min milling. Regarding to the fact that amorphization phenomena is the main reason for the enhancement of pyrite reactivity, mechanochemical treatment can tremendously affect the leachability of pyrite.

Table 1. Microstructural parameters of pyrite and mechanochemically treated pyrite (MCTP).

	pyrite	MCTP
A (%)	0	83
Unit cell volume (Å3)	159.2315	159.5515
Microstrain (%)	0.06	0.052
Crystallite size (nm)	763	57

The unit cell volume of the face-centred cubic pyrite increased by milling time during mechanochemical treatment (Table 1). The results reveal that the unit cell of pyrite expanded during intensive milling. Similar to added iron powder, vacancies were forming in pyrite structure when elemental sulfur was releasing during mechanochemical treatment. The release of elemental sulfur during high-energy milling of pyrite was reported in previous investigations (Hu et al., 2004). Due to the phenomena and the mentioned mechanochemical reaction, the point defects (vacancies) were formed in pyrite structure increasing pyrite unit cell volume.

The mechanochemical treatment effects on crystallite size and microstrain are presented in Table 1. It is clear that crystallite size and microstrain decrease in mechanochemically treated pyrite. The crystallite size decreases from 763 nm in initial pyrite to 57 nm in mechanochemically treated pyrite for 50 min. The results indicated that the structural changes has completely different influences on the pyrite reactivity. The microstrain reduction has a hindering effect on the pyrite reactivity promotion, but the variations of crystallite size and amorphization degree have positive influences on pyrite reactivity improvement.

3.2 Leaching tests

There is no doubt that the most advantageous aspect of high-energy milling of minerals can be reduction of reaction temperature and rise of metal extraction. As mentioned before, the mechanochemical treatment induced structural changes in pyrite with discrepant effects on the reactivity of pyrite by microstrain reduction.

The leaching tests was conducted on pyrite at ambient temperature by 1M sulfuric acid, according to the technique illustrated in Figure 2. Also, the result of leaching tests provide information to evaluate influence of the microstructural reduction during mechanochemical treatment on leachability of pyrite. The results are summarized in Table 2. As expected, the maximum iron extraction was attained by the leaching of mechanochemically treated pyrite for 50 min when 87% of total iron was extracted. It is notable that by consideration of complete digestion of iron powder, the iron extraction from pyrite is about 74% which is much more than 1% in initial pyrite leaching.

The leaching tests confirm that the amorphization degree rise and crystallite size reduction promote iron extraction by reactivity enhancement of mechanochemically treated pyrite and the

microstrain reduction cannot hinder the pyrite reactivity improvement.

Table 2. Iron extraction percentage in leaching of pyrite and mechanochemically treated (MCTP) pyrite

Feeds in leaching tests	Iron extraction (%)
pyrite	1
Pyrite with iron	57
MCTP	87

The results proved that iron addition during mechanochemical treatment has main role in the enhancement of pyrite leachability. The iron addition can impose microstructural changes to pyrite as amorphization degree increases and crystallite size reduces during mechanochemical treatment accelerating pyrite reactivity. In atomic scale, the iron atoms (belong to iron powder) can affect the strength of existed bonds among Fe and S atoms in pyrite structure and make them more weakened. Also, the iron addition can completely destroyed some atomic bonds between constituent elements of pyrite by formation of new troilite phase during mechanochemical treatment. Thus, iron addition and troilite formation during the incomplete mechanochemical reaction are responsible for promoting reactivity of mechanochemically treated pyrite.

3.3 Preparation of nano zero-valent iron (NZI)

As mentioned before, the titration of sodium borohydride technique was used for precipitation of NZVI form obtained leach liquors. For the nano zero-valent iron characterization, images of iron nanoparticles were recorded with FE-SEM and phase identification was conducted using XRD analysis. Figure 5 illustrates the FE-SEM image of the iron nanoparticles in which the representative iron particles size is around 50 nm (x:41, y:53 nm). The image verifies that the most of the particles are less than 100 nm.

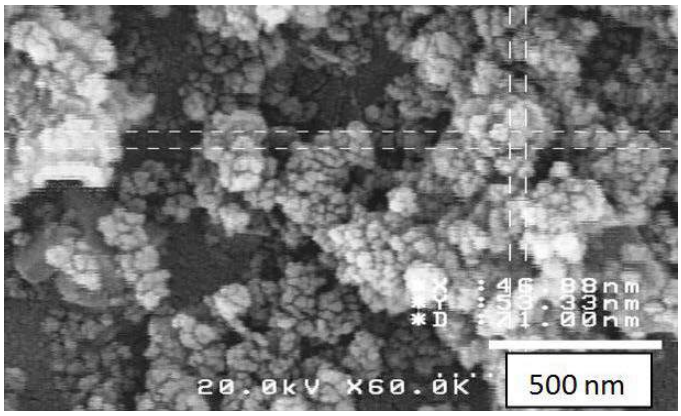

Figure 5. FE-SEM image of aggregations of the zero-valent iron particles nanoparticles

The XRD pattern of the nanosized iron particles is shown in Figure 6. The phase analysis indicates that both iron (JCPDS No. 6-696) and iron oxide (JCPDS No. 25-1402) phases are detectable in the final product. The detected phase of iron oxide can be ascribed to the preparation and maintenance conditions where oxygen was not removed completely. The iron oxide can be considered as a protective shield for the zero-valent iron particles improving their performance (Yuang-Pang et al., 2006). The aim of our paper is far from comprehensive characterization of the iron nanoparticles.

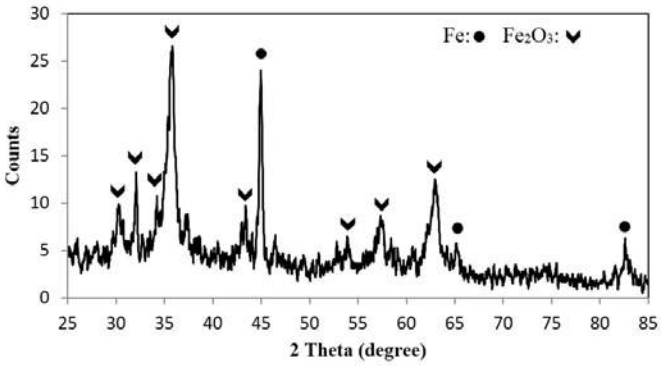

Figure 6.XRD pattern of the zero-valent iron nanoparticles

4 CONCLUSION

The main achievements of this paper are as follow. The mechanochemical treatment can improve reactivity of pyrite during leaching test with 1M sulfuric acid at ambient temperature. The NZVI is prepared from leach liquors produced during hydrometallurgical processing of pyrite.

Also, the following conclusions can be concluded from the obtained results.

1- XRD patterns indicated that during mechanochemical treatment, new phase of troilite is detected along with previous phases of iron and pyrite.

2- Unit cell volume of pyrite and added Fe increased during mechanochemical treatment by formation of vacancies.

3- It was also proved that the crystallite size reduced and amorphization degree increased during mechanochemical treatment of pyrite in favor of reactivity promotion.

4- The iron extraction from pyrite was about 1 % after 5 h leaching at ambient temperature by 1M sulfuric acid. By using mechanochemical pretreatment, the iron extraction increased to 87 %.

5- Finally, NZVI particles were prepared from obtained leach liquors. According to FE-SEM image, the particle size of the NZVI was less than 100 nm. Also, the XRD analysis proved that the NZVI powders were protected by an iron oxide shield.

REFERENCES

Dickinson, M., Scott, T.B., 2010. The application of zero-valent iron nanoparticles for the remediation of a uranium-contaminated waste effluent, *J. of Hazardous Materials*, 178 (171-179).

Habashi F., Second edition 1999. *A Textbook of Hydrometallurgy*, Métallurgie Extractive Québec, Québec City, Canada.

Hu, H., Chen, Q., Yin, Z., Zhang, P., Wang, G., 2004. Effect of grinding atmosphere on the leaching of mechanically activated pyrite and sphalerite, *Hydrometallurgy*, 72, (79-86).

Karlsson A, Deppert K, Wacaser A, Karlsson S, Malm O., 2005. Size-controlled nanoparticles by thermal cracking of iron pentacarbonyl, *Appl Phys A Mater A*80 (1579- 1583).

Ohlberg, S.M., Strickler, D.W., (1962). Determination of Percent Crystallinity of Partly Devitrified Glass by X-Ray Diffraction, *J. Am. Ceram. Soc*. 45 (170-171).

Suryanarayana, C., Grant Norton, M., 1998. *X-Ray Diffraction: A Practical Approach*, Plenume Press, New ypork.

Yuang-Pang Sun, Xiao-qin Li, Jiasheng Cao, Wei-xian Zhang, H. Paul Wang., 2006. characterization of zero-valent iron nanoparticles, *advances in colloid and interface science* 120 (47-56).

Zhang W. J., 2003. Nanoscale iron particles for environmental remediation: An overview. *J. Nanopart. Res.* 5 (323-332).

Recovery of Indium From Zinc Oxide Flue Dust

Wei Liu, Honglin Luo, Wenqing Qin, Yongxing Zheng, Kang Yang, Junwei Han
School of Minerals Processing and Bioengineering, Central South University, Changsha, Hunan, China

ABSTRACT The main purpose of this study was to extract indium from the zinc oxide flue dust (ZOFD), which contained 753 g/t indium. Two-stage leaching process to recover indium from the ZOFD was investigated. The conditions for neutral leaching were optimized at 60 °C for a leaching duration of 30 min with sulfuric acid concentration of 0.16 M and a liquid/ solid ratio of 10 mL/g. In the neutral leaching, zinc (> 95%) was selectively leached into the solution and indium (> 95%) was concentrated in the residue, which indicated the successful selective separation of zinc and indium. The dissolution rate of indium was more than 88% under the leaching conditions: temperature of 80 °C, sulfuric acid concentration of 0.8 M, liquid/solid ratio of 6 mL/g and reaction time of 2 h. The conditions in extraction of indium by di(2-ethylhexly)-phosphoric acid (D2EHPA) were optimized that organic phase: 20% D2EHPA and 80% kerosene, aqueous phase/oil phase ratio (A/O): 4 and initial acid concentration of the aqueous solution: 1-1.5 M, the fraction of extracted indium from solution was more than 95%, which is a significantly increase compared with less than 70% in traditional process. This work would contribute to provide a novel cleaning and efficiently process to separate and recover zinc and indium from zinc oxide flue dust, and prevent heavy metal pollution.

Keywords: Indium, zinc oxide flue dust, leaching, solvent extraction

1 INTRODUCTION

Indium is a rare and valuable metal, which is used mainly as indium tin oxide-films (84% in 2007) in liquid crystal displays (LCDs) (Alfantazi and Moskalyk, 2003; He et al., 2014; Kang et al., 2011; Virolainen et al., 2011). These indium tin oxide (ITO) films are composed of 90% of In_2O_3 and 10% of SnO_2. New types of solar panels containing indium are being developed and they may become an important application sector for indium in the future potentially increasing the demand for indium. However, indium represents a very minor percentage of the earth's crust, which is about 0.1 part per million, and does not occur in the native state. Sphalerite is the main mineral source for the zinc and indium production (Alfantazi and Moskalyk, 2003; Koleini et al., 2010; Lu et al., 2014; Zhang et al., 2010). So indium has to be recovered as a byproduct from other metallurgical processes, especially for the Zn-bearing byproduct, or from secondary raw materials.The typically traditional process for extracting indium from In-Zn concentrates includes the following steps (Alfantazi and Moskalyk, 2003; Koleini et al., 2010; Li et al., 2010; Zhang et al., 2010). Firstly, ferric is removed by the method of jarosite, and indium goes into jarosite. In order to recovery indium, jarosite residue is dissolved using hot sulfuric acid solution. In this method, indium is directly extracted from leach solution by di-(2-ethylhexyl) phosphoric acid (D2EHPA)(Batchu et al., 2014; Darvishi et al., 2007; Haghshenas Fatmehsari et al., 2009; Kang et al., 2011; Virolainen et al., 2011). Generally, in this method the leach solution to solvent extraction process is contained relatively high concentrations of indium. The

recovery ratio of indium is low in this method, and serious pollutions are produced, such as low concentrate of sulfur dioxide and large quantity of ferric oxide residues.

Therefore, the purpose of the present study was to explore the new process (Fig.1) for recovering indium from zinc oxide flue dust. In this two stages leaching process, it was tried to firstly enrich indium by pre-leaching zinc and acidic leaching indium and then use solvent extraction with D2EHPA as an extractant to separate and concentrate indium from its acidic solutions.

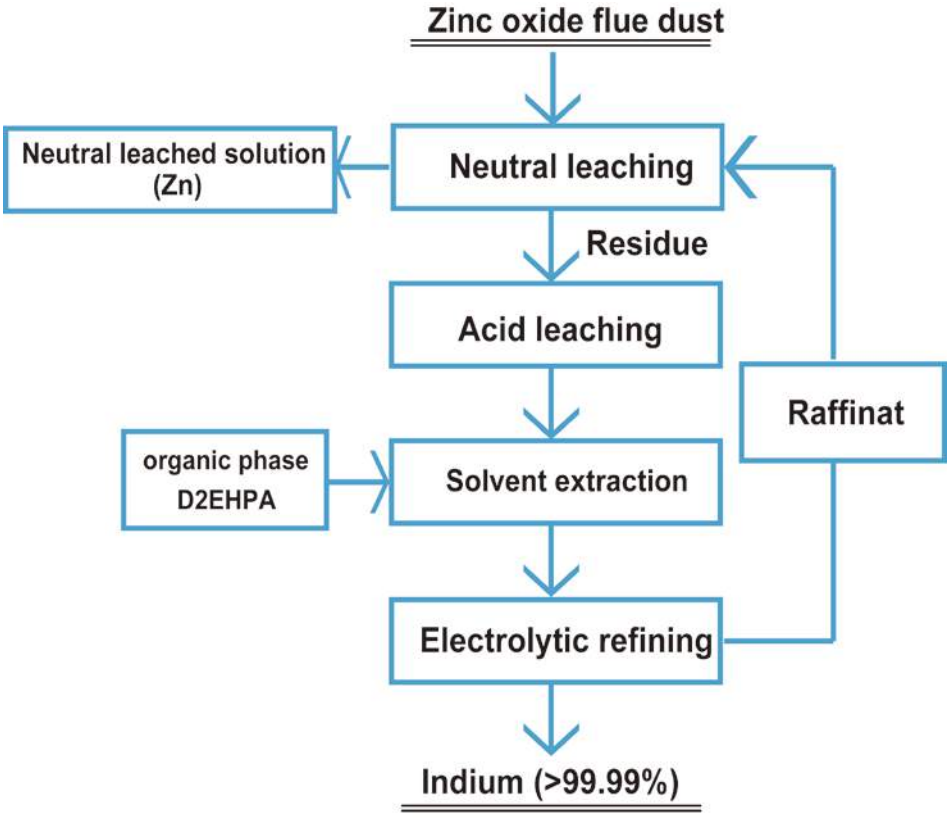

Figure 1. Schematic two-stages leaching flow diagram to recover indium.

2 MATERIALS AND METHODS

2.1 Materials

The zinc oxide flue dust used in the research was produced at the lead smelting Co.'s (Henan, China). The main metals in the flue dust are lead and zinc with some cadmium and indium (Table 1).The commercial D2EHPA (Henan, China) and the diluents, kerosene (Hunan, China), were used in the solvent extraction experiments. Analytical grade sulfuric acid and sodium hydroxide (Hunan, China) were employed in the leaching and solvent extraction

Table 1. Chemical compositions of zinc oxide flue dust (mass fraction,%)

F	Na	S	Cl	K	Fe	Cu	Zn	Cd	In/g·t^{-1}	Sn	Pb	Bi
0.603	5.159	5.095	34.029	7.948	0.648	0.058	15.596	0.349	753.408	0.41	20.255	0.392

2.2 Analytical Techniques

The X-Ray Diffraction (XRD) and Scanning Electron Microscope (SEM) of the flue dust are shown in Fig. 2, and Fig.3, respectively. These analyses indicate that the raw material was primarily zinc and lead compounds, such as ZnO, PbS and ZnS, and have a small particle size. The metals (Fe, Zn, Cd and In) concentrations in solid samples were analysed by means of the oxidation-reduction titration with EDTA and aqueous samples were determined by Inductively Coupled Plasma-Atomic Emission Spectrometry (ICP-AES).

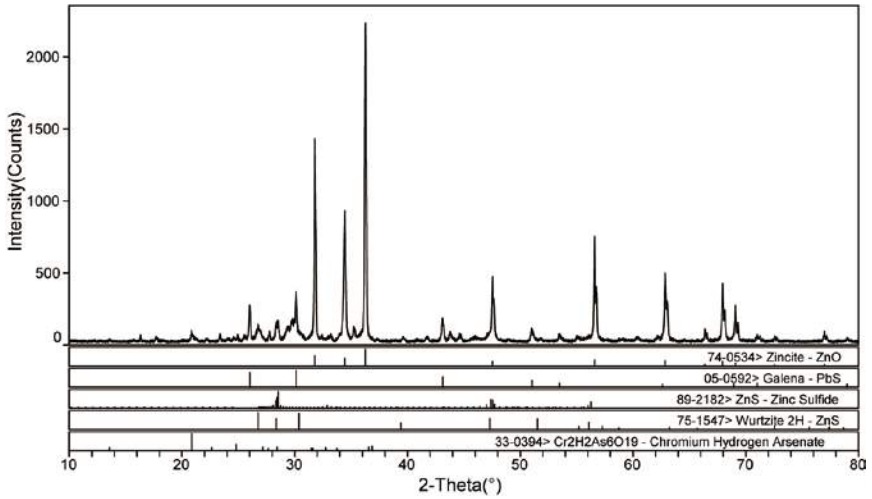

Figure 2. XRD of zinc flue dust

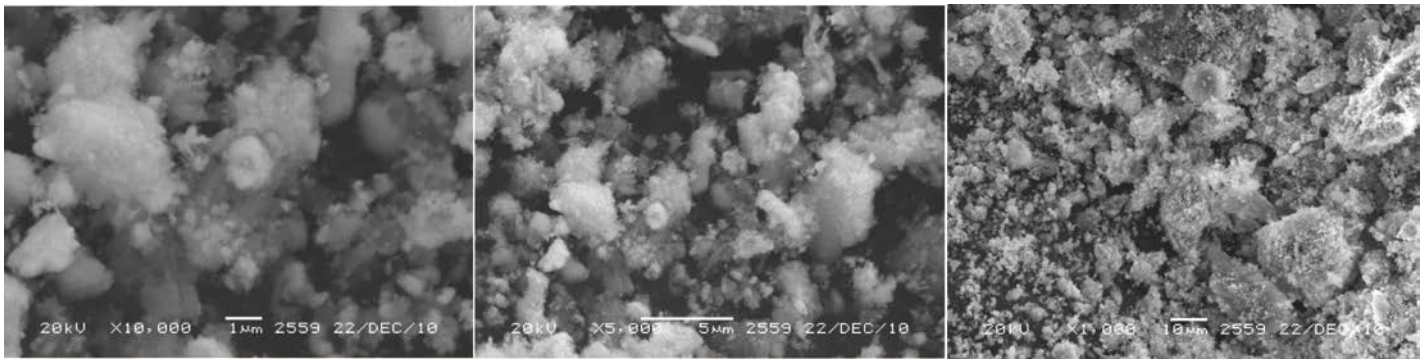

Figure 3 SEM micrographs of zinc oxide flue dust.

2.3.Leaching and Dissolution

For the study of the leaching of zinc oxide flue dust, the dissolution experiments were carried out in a 1 L glass flask reactor in thermostatically controlled water bath, equipped with mechanical stirrer and thermometer. The temperature could be controlled within ±0.1°C. Deionized water and sulfuric acid or sodium hydroxide were used to prepare the leach solutions when the temperature reached the pre-set value. Experiments were carried out at stirring speeds of 500 rpm. The leached residues were withdrawn after various times. In these experiments, the effects of reaction temperature, liquid/solid ratio, sulfuric acid concentration and reaction time were considered. The second leaching stage feed was the neutral leached residue.

The fractions of leaching extraction E_L is defined as follows:

E_L=

where

c_0=initial concentration of the metal in zinc oxide flue dust, %

W_0=initial weight of the zinc oxide flue dust added of the leach solution, g

c=concentration of the metal in the leached residue, %

W=weight of the leached residue, g

2.4. Solvent Extraction

A batch of experiments was carried out in a flask containing equal volumes (100 ml) of aqueous and organic solutions. The mixture was agitated at a constant temperature with a mechanical shaker for 10 min. Samples were then retained in the flask for 2 hours to allow complete separation of the phases through a separation funnel.

The effects of organic phase composition, aqueous phase/oil phase ratio (A/O), and the initial acid concentration of the aqueous solution were considered.

The fraction of solvent extraction E_E is defined as follows:

E_E=

where

c_0=initial concentration of the metal in aqueous phase, mg/L.

c_{aq}=equilibrium concentration of the metal in aqueous phase, mg/L.

3 RESULTS AND DISCUSSION

3.1. Leaching and Dissolution

3.1.1. Neutral leaching

3.1.1.1. Effect of temperature

The effect of reaction temperature from 30 to 80 °C on the extraction rate was studied while other conditions were constant. The extraction rate of zinc was partly dependent on temperature (Fig.4). Notably, the leaching efficiencies of zinc were higher compared with indium. At above 60 °C, 90% of zinc was leached into the solution. In the following neutral leaching experiments, the solution temperature was chosen to be 60 °C.

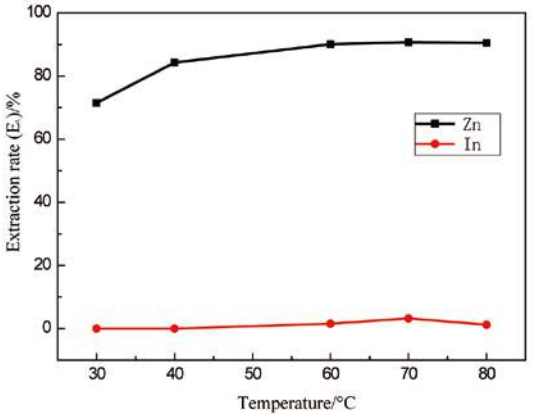

Figure 4. Effect of temperature on zinc extraction and indium extraction in neutral leaching (0.16 M H_2SO_4; liquid/solid ratio: 10mL/ g; reaction time: 2h).

3.1.1.2. Effect of liquid/solid ratio

The effect of the liquid/solid ratio from 5 to 15 mL/g on the extraction rate was studied when other conditions were constant. The extraction rate of zinc was strongly dependent on the liquid/solid ratio (Fig.5). At the ratio of 5 mL/g, about 45% of zinc was extracted, and 90% was extracted at 10 mL/g. At above 10 mL/g, the extraction rate of zinc was slightly higher, but that of indium notably increased, probably because the leaching efficiencies of zinc and indium were improved as the liquid/solid ratio increased. The optimal result was obtained at the liquid/solid ratio of 10 mL/g.

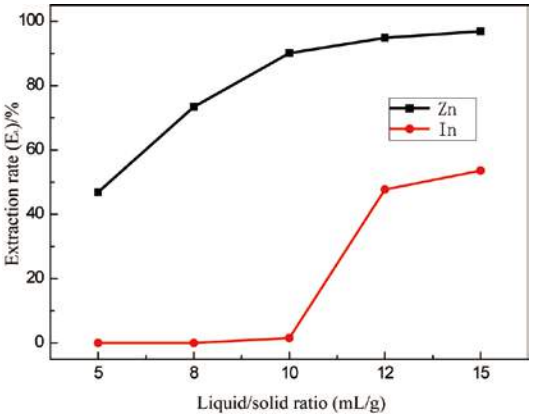

Figure 5. Effect of liquid/solid ratio on zinc extraction and indium extraction in neutral leaching (0.16 M H_2SO_4; 60 °C; reaction time: 2h).

3.1.1.3. Effect of sulfuric acid concentration

The effect of H_2SO_4 concentration (0.1, 0.13, 0.16, 0.19, and 0.22 M) on the dissolution of ZOFD was investigated. The H_2SO_4 concentration strongly affected the leaching rate (Fig.6). The leaching efficiencies of zinc and indium were improved as the H_2SO_4 concentration increased. The zinc extraction increased to 90%, when the concentration of H_2SO_4 was 0.16 M. However, the indium extraction was promoted with the increased concentration of H_2SO_4.

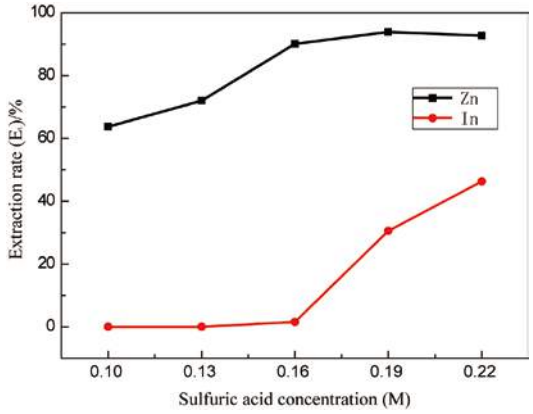

Figure 7.a Effect of the sulfuric acid concentration on zinc extraction and indium extraction in neutral leaching (60 °C; reaction time: 2 h; liquid/solid ratio: 10 mL/g).

3.1.1.4. Effect of reaction time

The effect of reaction time (0.5, 1, 1.5, 2, 2.5 and 3 h) on the dissolution of ZOFD was studied. The zinc extraction was slightly improved with time, and the indium extraction was nearly 0 when the reaction time was 3 h (Fig.7), indicating that the leaching efficiencies of zinc were high and the indium was not leached in these conditions. Considering the economy, the optimal result was obtained at the reaction time of 30 min. Under the optimal condition, the concentrations of zinc and indium were 75.05 g/L and 12 mg/L in the solution, respectively. In the industrial process, such solution can recover zinc through synthesis of zinc carbonate ($ZnCO_3$).

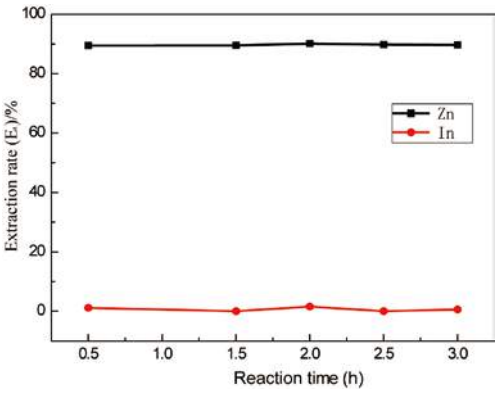

Figure 7.b Effect of the reaction time on zinc extraction and indium extraction in neutral leaching (60 °C; 0.16 M sulfuric acid; liquid/solid ratio of 10 mL/g).

3.1.2. Acid leaching

The acid leaching materials were the residue from the first leaching stage. Table 2 shows the chemical compositions. In the first leaching stage, zinc was selectively leached into the solution and indium was concentrated in the residue.

Table 2. Chemical composition of the residue from the first leaching stage (mass fraction, %)

S	Fe	Zn	In/g·t^{-1}	Pb
7.21	4.32	1.36	1254	32.51

3.1.2.1. Effect of temperature

The effect of reaction temperature from 30 to 90 °C on the extraction rate was studied while other conditions were constant. Notably, the leaching extractions of zinc and indium were high within this temperature range (Fig.8). At 80 °C, about 80% of indium was leached into the solution. In the following acid leaching experiments, the solution temperature was chosen to be 80 °C.

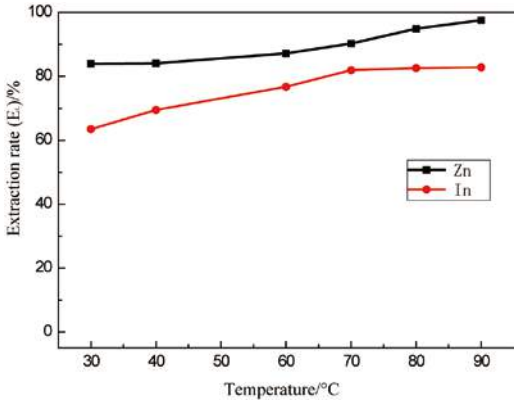

Figure 8. Effect of temperature on zinc extraction and indium extraction in acid leaching (0.7 M H_2SO_4; liquid/solid ratio: 4mL/ g; reaction time: 2h).

3.1.2.2. Effect of liquid/solid ratio

The effect of the liquid/solid ratio from 3 to 7 mL/g on the extraction rate was studied while other conditions were constant. The extraction rate of indium was improved with the increased liquid/solid ratio (Fig.9). At the ratio of 3 mL/g, only 60% of indium was extracted into the solution, but it was promoted to 80% at 6 mL/g. Above 6 mL/g, the extraction rate of indium was slightly higher. The optimal result was obtained at the liquid/solid ratio of 6 mL/g

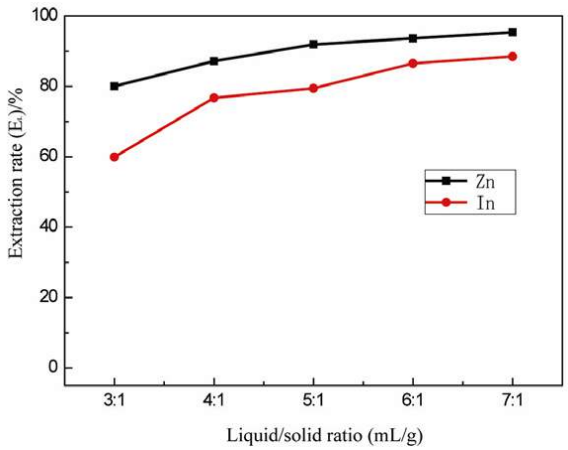

Figure 9. Effect of liquid/solid ratio on zinc extraction and indium extraction in acid leaching (0.7 M H_2SO_4; reaction temperature: 80 °C; reaction time: 2h).

3.1.2.3. Effect of sulfuric acid concentration

To investigate the influence of H_2SO_4 concentration on the dissolution of neutral leached residue, the experiments were carried out using solutions containing different initial H_2SO_4 concentrations (0.5, 0.6, 0.7, 0.8, and 0.9 M). The H_2SO_4 concentration strongly affected the indium extraction (Fig.10). The indium extraction was 80% for 0.8 M H_2SO_4.

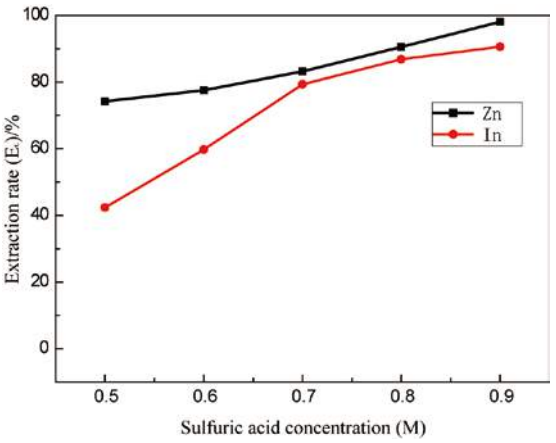

Figure 10. Effect of the sulfuric acid concentration on zinc extraction and indium extraction in acid leaching (80 °C; reaction time: 2 h; liquid/solid ratio: 6 mL/g).

3.1.2.4. Effect of reaction time

The effect of reaction time (0.5, 1, 1.5, 2, and 2.5 h) on the dissolution of neutral leached residue studied was studied. The indium extraction was improved with the extension of time (Fig. 11). After 2 h of agitated leaching,
88.65% of indium was extracted into the solution, and the solution contained 0.3 M H_2SO_4, 560 mg/L indium, 3.55 g/L zinc and 12.21 g/L iron, and the acid leached residue contained 191 g/t indium.

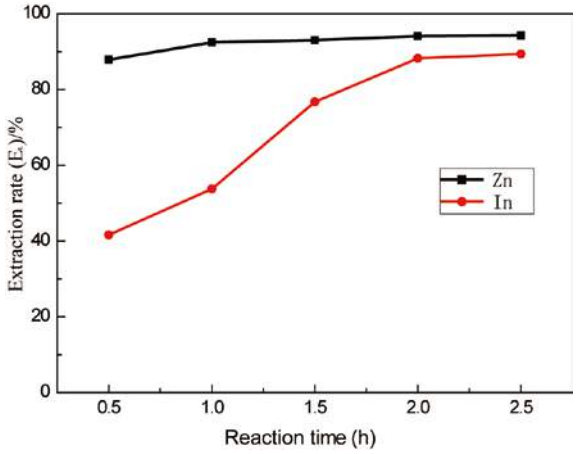

Figure 11. Effect of reaction time on zinc extraction and indium extraction in acid leaching (80 °C; 0.8 M sulfuric acid concentration; liquid/solid ratio 6 mL/g).

3.2 Solvent Extraction

The solution from the acid leaching extracted indium through solvent extraction with D2EHPA, and the selective extraction of indium was much higher at high acid concentration. The divalent heavy metal ions, such as Zn^{2+}, Cd^{2+} and Fe^{2+}, extracted by D2EHPA should be at a low acid concentration. However, the solvent extraction behavior of impurity ion, Fe^{3+} was the same as indium ion when D2EHPA was used. The aqueous solution was first purified to remove Fe^{3+} by addition of iron power, and Fe^{3+} was detected using potassium rhodanide.

3.2.1 Effect of the component of organic phase

In the D2EHPA-kerosene system, the D2EHPA concentration varied from 5 to 30 vol.% in the organic phase. The extraction percentage of indium was improved with the increased D2EHPA concentration (Fig.12). The extraction percentage was improved from 85% at 5% D2EHPA to more than 93% at 20% D2EHPA. However, the density of organic phase was intensified with the increased D2EHPA concentration, and the phases could not be separated within short time. Considering the economy and efficiency, the optimal result was obtained for the components of organic phase: 20% D2EHPA and 80% kerosene.

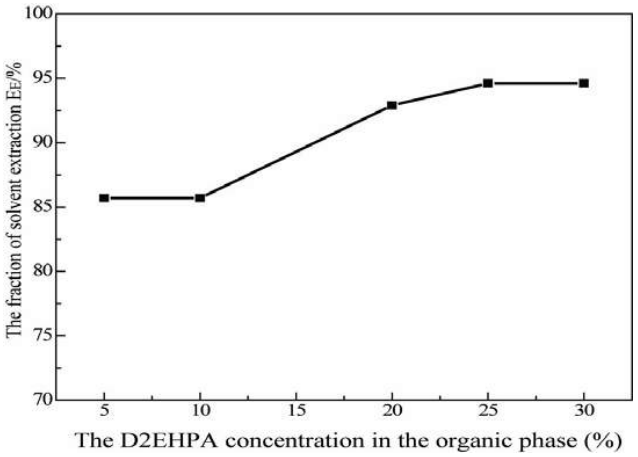

Figure 12. Effect of the D2EHPA concentration in the organic phase on indium solvent extraction (A/O:6; initial concentration of acid in aqueous phase: 1.2 M).

3.2.2 Effect of the volume phase

The effect of A/O (2, 4, 6 and 8) at the same condition was studied. The extraction percentage of indium was improved along with the increased A/O (Fig. 13). At A/O=8, about 80% of indium was extracted into the organic phase, and the extraction percentage was improved to more than 95% at A/O=2 or 4. However, the concentration of indium in the organic phase was low, and phase separation time was long when A/O=2. The following solvent extraction experiments were carried at A/O=4.

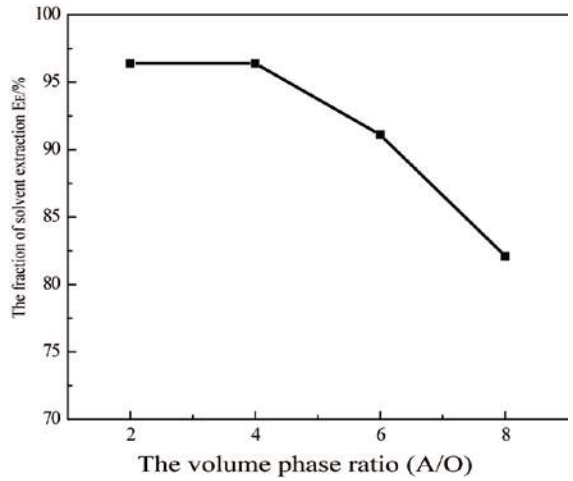

Figure 13. Effect of the volume phase ratio on indium solvent extraction (organic phase: 20% D2EHPA and 80% kerosene; initial concentration of acid in aqueous phase: 1.2 M).

3.2.3 Effect of the initial acid concentration

The effect of the initial acid concentration in the aqueous solution to the indium extraction was studied. The indium solvent extraction mechanism can be simplified as:

$$In^{3+}+3[H_2A_2]_0 \rightarrow [InA_3 \cdot 3HA]_0+3H^+$$

(where A is D2EHPA)

H^+ was released from the indium solvent extraction with D2EHPA. The decreased initial acid concentration in the aqueous solution could improve the extraction process. However, the impurity ions were hydrolyzed when the acid concentration decreased to a certain degree, which made the solution emulsifiable and the phases inseparable.

The extraction percentage of indium decreased along with the increased initial acid concentration (Fig.14). With 0.5 mol/L acid, the solution experienced slight emulsion and no obvious delamination. The extraction percentages sharply decreased when the acid concentration increased to more than 2 mol/L. The initial acid concentration should be controlled within the range 1 to 1.5 mol/L in the aqueous phase. Under these optimal conditions, the extraction percentage of indium was 94.6%; the raffinate at pH 2 contained 30 mg/L indium, and it could be used as an acid adjustment in neutral leaching to reduce the discharge of waste water quantity and sulfuric acid amount.

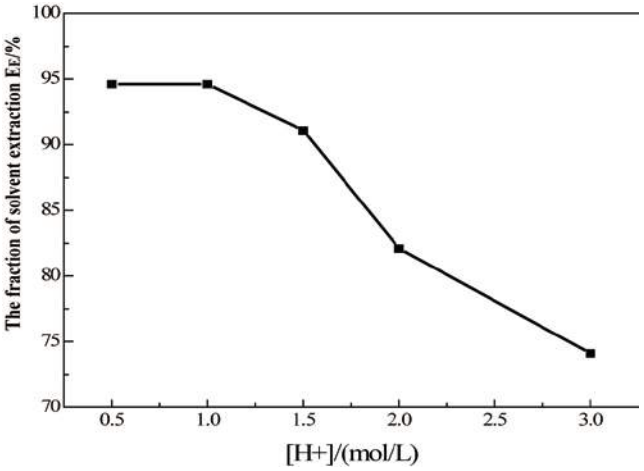

Figure 14. Effect of the initial concentration of acid in the aqueous phase on indium solvent extraction (organic phase: 20% D2EHPA and 80% kerosene; A/O:4).

4. CONCLUSIONS

The zinc oxide flue dust was leached by two stages. In the neutral leaching, zinc was selectively leached into the solution and indium was concentrated in the residue, indicating that the selective separation of zinc and indium was realized. In the acid leaching, indium in the neutral leached residue was efficiently leached into the solution. The dissolution rate of indium was more than 88%. The recovery of indium from the aqueous solution by solvent extraction was investigated, considering the effects of organic phase composition, aqueous phase/oil phase ratio (A/O), and the initial acid concentration of the aqueous solution. The fraction of extracted indium was more than 95%, which is a significantly increase compared with less than 70% in traditional process.

ACKNOWLEDGEMENTS

The authors would like to acknowledge the National Natural Science Foundation of China (No. 51204210), the National High Technology Research and Development

Program of China (No. 2011AA061001), and the National "Twelfth Five-Year" Plan for Science & Technology (No. 2012BAC12B04) for financial support.

REFERENCES

Alfantazi, A. M., R. R. Moskalyk, 2003. Processing of indium: a review. Minerals Engineering 16: 687-694.

Batchu, N. K., C. H. Sonu, M. S. Lee, 2014. Solvent extraction equilibrium and modeling studies of manganese from sulfate solutions by a mixture of Cyanex 301 and TBP. Hydrometallurgy 144-145: 1-6.

Darvishi, D., D. F. Haghshenas, S. Etemadi, E. K. Alamdari, S. K. Sadrnezhaad, 2007. Water adsorption in the organic phase for the D2EHPA–kerosene/water and aqueous Zn2+, Co2+, Ni2+ sulphate systems. Hydrometallurgy 88: 92-97.

Haghshenas Fatmehsari, D., D. Darvishi, S. Etemadi, A. R. Eivazi Hollagh, E. Keshavarz Alamdari, A. A. Salardini, 2009. Interaction between TBP and D2EHPA during Zn, Cd, Mn, Cu, Co and Ni solvent extraction: A thermodynamic and empirical approach. Hydrometallurgy 98: 143-147.

He, Y., E. Ma, Z. Xu, 2014. Recycling indium from waste liquid crystal display panel by vacuum carbon-reduction. J Hazard Mater 268: 185-190.

Kang, H. N., J.-Y. Lee, J.-Y. Kim, 2011. Recovery of indium from etching waste by solvent extraction and electrolytic refining. Hydrometallurgy 110: 120-127.

Koleini, S. M. J., H. Mehrpouya, K. Saberyan, M. Abdolahi, 2010. Extraction of indium from zinc plant residues. Minerals Engineering 23: 51-53.

Li, X.-h., Y.-j. Zhang, Q.-l. Qin, J. Yang, Y.-s. Wei, 2010. Indium recovery from zinc oxide flue dust by oxidative pressure leaching. Transactions of the Nonferrous Metals Society of China 20: 141-145.

Lu, D., Z. Jin, L. Shi, G. Tu, F. Xie, E. Asselin, 2014. A novel separation process for detoxifying cadmium-containing residues from zinc purification plants. Minerals Engineering 64: 1-6.

Virolainen, S., D. Ibana, E. Paatero, 2011. Recovery of indium from indium tin oxide by solvent extraction. Hydrometallurgy 107: 56-61.

Zhang, Y., X. Li, L. Pan, X. Liang, X. Li, 2010. Studies on the kinetics of zinc and indium extraction from indium-bearing zinc ferrite. Hydrometallurgy 100: 172-176.

Recovery of Valuable Metals from E-Waste, Part (I): Use of Central Composite Design for evaluation of Copper Recovery from Electronic Waste Leaching

Y. Nosratzad, M. Kavousi, An. Sattari, E. K. Alamdari, D. Haghshenas
Department of Mining and Metallurgical engineering, Amirkabir university of Technology (Tehran Polytecgnic), Tehran, Iran

E. K. Alamdari
Research Center for Materials and Mining Industries Technology, Amirkabir University of Technology, Tehran, Iran.

D. Darvishi, A. K. Alamdari, A. B. K. Rafsanjani
Rare Metals Production Corporation, Rafsanjan, Iran.
Non-Ferrous Metals Recovery Corporations, Rafsanjan, Iran

ABSTRACT Electronic wastes are the mixture of various metals such as Cu, Sn, and Pb as well as platinum group metals (Au, Ag, and Pt). The recovering of electronic waste is an important subject not only due to the waste treatment but also for recycling of valuable materials. In the present work, leaching process of Cu, Sn and Pb from electronic wastes was carried out using Fluoroboric acid as the leaching agent. Several factors including concentration of acid, temperature, liquid-solid ratio, and concentration of H_2O_2 as oxidizing agent were statistically studied. The obtained experimental results, showed the optimal condition of the process.

Keywords: Electronic waste; Leaching; Fluoroboric acid, Hydrogen Peroxide

1 INTRODUCTION

Nowadays, electrical/electronic waste reach its alarming growth rate (Ongondo et al., 2011). Currently, the major treatments on such waste are the reuse, remanufacturing, and recycling of them (Cui and Zhang, 2008). Electronic wastes are composed of valuable metals, particularly copper as well as aluminum and gold (Ongondo et al., 2011). Hydrometallurgical process can facilitate the recovery of precious metals from E-wastes (Agrawal et al, 2010). Leaching is the process for extracting soluble constituents from a solid with a solvent in the first step of hydrometallurgical processes (Cui and Zhang, 2008). Various leachants such as nitric acid (Oishi, 2007), hydrochloric acid (Lu and Dreisinger, 2013) and sulfuric acid (Vagili et al, 2003) have been used for the leaching of metallic sources. In the case of copper recovered from nitric and sulphuric acid leaching solution, a significant amount of copper deposit as Cu_2O. Furthermore, in the case of hydrochloric and sulphuric acid solution it was found that $PbCl_2$ Precipitate is formed (Masavetas et al, 2009). Additionally there are some impurities such as silver in chloride solution (Lu and Dreisinger, 2013). A process for E-wastes recovery by leaching and solvent extraction is explored in the present study. This investigation was carried out by using Fluoroboric acid as a leaching agent. The influence of temperature, and solid to liquid were examined with the help of CCD.

2 MATERIALS AND METHODS

2.1. Reagents And Analytical Methods

All chemicals in this experiment were of analytical reagent grade. Water was double

distilled. Hydrogen peroxide, used in this study was purchased from MERCK Company. HBF4 utilized as a leaching agent which was supplied by MERCK Company. Atomic adsorption spectroscopy (Varian, type AA240) for analyzing the concentration of Cu(II) ions was used in the experiments.

3 RESULTS AND DISCUSSION

3.1 Model Fitting

Table 1 lists the values of copper dissolution percentage after 180 minutes of leaching at each of the 28 combination of factor levels generated by the principles of RSM with the values ranging from as low as 0.29 to as high as 0.96. The results of the ANOVA are presented in Table 2; the low P- values for the regression ($P<0.001$) and the fact that the lack of fit of the model was not significant ($P>0.05$) indicates the suitability of the model the value of the regression coefficients are presented in Table 3. Based on regression coefficients calculated for the response (Table 3) a polynomial regression model equation that fitted 90% of the variation in the data was proposed as:

$$\text{Cu recovery} = 66.13 + 4.70\ L/S - 1.57\ T + 6.306\ HBF_4 - 7.31\ (L/S)^2 + 0.07\ T^2 - 9.313\ (HBF_4)^2 + 0.679\ L/S \times T \quad (1)$$

2.2. METHOD

Physical pretreatment was performed by crushing printed circuit boards (PCB) with the aim of changing the wastes to the size less than 1mm. The received solid from crushing treatment was mixed with a certain amount of HBF4 in a stirring reactor accompanied by injection of hydrogen peroxide with known concentration and constant mass flow for 3 hours. Then the solution was sent to the filtering system for solid/liquid separation.

Response surface methodology (RSM) was employed to survey of Temperature, L/S and H_2O_2 volume on copper recovery. A central composite design (CCD) was adopted in this work to study four factors at three levels. Ten experimental runs consisting of 4 star points (star distance is 0) and 2 center points were generated with 4 factors and 3 levels by the principle of RSM using MINITAB Release 15. The CCD matrix conducted which includes the levels employed for the different factors, is presented in Table 1.

Table 1. Central composite design arrangement and response (Cu dissolution).

Test No.	L/S	T (^OC)	H_2O_2 (SR)	HBF_4 (SR)	Cu Recovery %
1	15	52.5	1.5	1.5	58
2	20	75	11	1	64
3	10	75	1	1	16
4	15	52.5	1.5	2	55
5	10	52.5	1.5	1.5	40
6	15	52.5	1.5	1.5	60
7	20	30	2	2	50
8	15	52.5	1.5	1	44
9	10	75	2	2	51
10	20	75	1	2	47
11	10	75	2	1	24
12	15	52.5	1.5	1.5	55
13	20	30	2	1	32
14	10	30	1	1	36
15	15	30	1.5	1.5	68
16	15	52.5	1	1.5	44
17	10	30	1	2	30
18	20	75	2	1	61
19	20	52.5	1.5	1.5	63
20	15	52.5	1.5	1.5	57
21	10	30	2	2	67
22	10	75	1	2	15
23	15	52.5	2	1.5	63
24	15	75	1.5	1.5	67
25	20	30	1	1	57
26	10	30	2	1	28
27	20	30	1	2	57
28	20	75	2	2	84

Table 2. ANOVA table.

	Degree of freedom	Sum of square	Mean squares	F-values	P-values
Total	27	7722.74			
Regression	14	7387.88	527.706	20.49	0.000
Residual error	13	334.86	25.758		
Lack of fit	10	321.86	32.186	7.43	0.063
Pure error	3	13.00	4.333		
R^2	90				

Table3. Values of regression coefficient calculated for the Cu dissolution.

Independent factor	Regression coefficient	Standard error	T - value	P – value
Constant	66.129	3.373	19.603	0.000
L/S	4.704	1.708	2.753	0.016
T (^{O}C)	-1.566	0.587	-2.666	0.019
HBF_4	6.306	1.708	3.691	0.003
$(L/S)^2$	-7.313	3.160	-2.314	0.038
T^2	0.0781	0.0284	2.749	0.017
$(HBF_4)^2$	-9.313	3.160	-2.974	0.011
L/S × T	0.679	0.120	5.640	0.000

3.2 Effects of Parameters: Analysis of Response Surfaces

According to equation (1), an increase in L/S values and temperature results in an increase in the Cu recovery at the end of 180 minutes of leaching. In the cases where interaction between factors is statistically significant, surface plots give more complete information regarding the effect of a factor on the response. The curvature of the surface presented in Fig. 1 suggests that L/S × T have interaction with each other in the leaching process. This is further confirmed by the results presented in Table 3.

As it can be seen in Figure 1, the effect of L/S on the Cu dissolution is more significant at high temperature. It was also observed that the excessive accretion of L/S ratio do not have a considerable effect on copper dissolution, after reaching to the optimum point

As it can be seen in Figure 2, the effect of L/S and HBF_4 has an optimum value on the Cu dissolution. An increasing on of L/S and

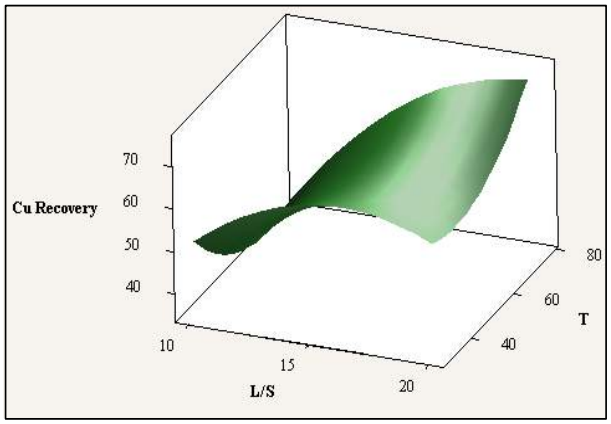

Figure 1. Surface plots for Cu recovery with respect to L/S and T.

HBF_4 increases the copper recovery at the first step and after optimum condition decreases the copper recovery. The surface plot of the effect of temperature and HBF_4 on copper recovery is shown at Fig 3. As seen as in Fig 3, the effect of temperature and HBF_4 on copper recovery show a saddle curve and by increasing of temperature, the copper recovery decreases to obtain a minimum value and then increases by increasing of temperature.

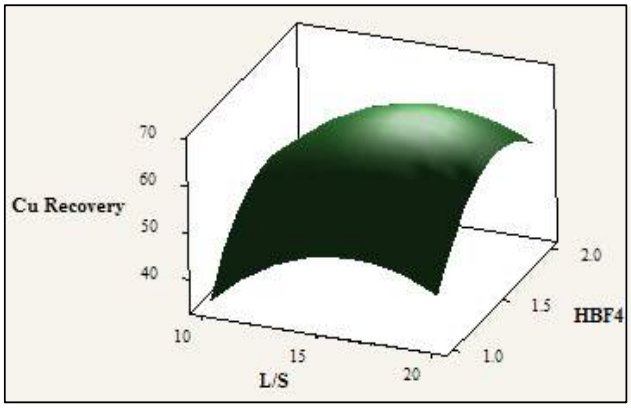

Figure 2. Surface plots for Cu recovery with respect to L/S and HBF_4.

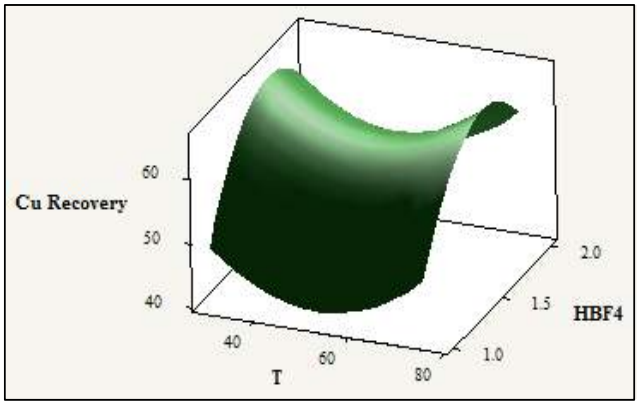

Figure 3. Surface plots for Cu recovery with respect to $HBF_4$and HBF_4.

4 CONLUSION

In this paper, CCD coupled with RSM was used to study the interaction between factors in Cu dissolution process from E-waste leaching by using HBF_4 with the following results:

- According to the statistically developed model, an increase in L/S and T, results in an increase in the Cu dissolution. In addition, it was found that L/S and T have interaction with each other in the E-waste leaching process.
- The effect of L/S on the Cu dissolution is more significant at high Temperature.
- The effect of temperature and HBF_4 on copper recovery shows a saddle behavior.
- -The maximum recovery of Cu that can be achieved after 180 minutes of leaching of WEEE, in a 3 L reactor running at 210 rpm is 0.75 under the following conditions: L/s: 20, Temperature: 70 ^{O}C and HBF_4: 1.62 SR.

REFERENCES

Agrawal, A., Perween, M., 2010. Recovery of copper from PCB leach solution by solvent extraction, Mineral Processing Technology, pp. 1189 -1194.

Cui, J., and Zhang, L., 2008, Metallurgical recovery of metals from electronic wastes: A review, *Journal of Hazardous materials*, (158), pp. 228-256.

I. Masavetas et al, 2009. Production of copper powder from printed circuit boards by electro deposition, Global NEST Journal, vol11, No 2, pp 241-247.

Lu, J., Dresinger, D., 2013. Solvent extraction of copper from chloride solution 1: Extraction Isotherms, Journal of Hydrometallurgy, pp 309-6350.

Oishi, T., Koyama, K., Alam, S., Tanaka, M., and Lee, J-C., 2007, Hydrometallurgy, 89, p. 82.

Ongondo, F.O., Williams, I.D., Cherrett, T.J., 2011, How are WEEE doing, A global review of the management of electrical and electronic wastes, *Waste Managemnet*, (31), pp. 714-730.

Vagili, F et al, 2003, Recovery of valuable metals from electronic and galvanic inductrial wastes by leaching and electrowinning, Journal of Waste Management, pp 245-252.

Recovery of Valuable Metals from E-Waste, Part (II): Selective Solvent Extraction of copper

M. Kavousi, A. Sattari, E. K. Alamdari, S. Firoozi
Department of Mining and Metallurgical engineering, Amirkabir university of Technology (Tehran Polytecgnic), Tehran, Iran

E. K. Alamdari
Research Center for Materials and Mining Industries Technology, Amirkabir University of Technology, Tehran, Iran.

D. Darvishi, A. K. Alamdari, A. B. K. Rafsanjani
Rare Metals Production Corporation, Rafsanjan, Iran.
Non-Ferrous Metals Recovery Corporations, Rafsanjan, Iran

ABSTRACT The electronic waste (E-Waste) contains such precious metals as gold, silver, and platinum. In addition to the Platinum group metals, large amounts of copper, tin and lead are present in E-Waste. For an effective recovery of precious metals, it is essential to recover these metals. It is also important from an economic perspective. In this paper, separation of copper from tin and lead by solvent extraction is studied. Fluoroboric acid and LIX984N was used as leachant and organic solvent, respectively. Effective factors such as the concentration of organic solvent, pH, temperature and concentration of copper on the extraction of copper were investigated. Combined and separate extraction curves for Cu, Sn and Pb were plotted using pure reagents. Finally, the optimal condition for the purification was determined**.**

Keywords: Electronic waste, Solvent extraction, LIX984N, Fluoroboric acid

1 INTRODUCTION

Wastes from electrical and electronic equipment (WEEE) are a waste category that is growing rapidly (Jha and Lee, 2006). This fact requires efficient WEEE recycling strategies (Bertram et al., 2002). Furthermore, WEES contains metals with high commercial value, as well as other hazardous or toxic elements. WEEE is regarded as an important source for recovery of valuable metals (Lee et al., 2004). Because of the complex composition of the e-waste, recovery treatment for all metals may not be possible, however precious and valuable metals such as gold, silver, copper, lead, zinc, and tin can be recovered by the hydrometallurgical route (Agrawal et al., 2010). Copper is the major metallic component in the E-wastes; hence a process for selective recovery of copper by leaching and solvent extraction is explored in the present investigation. Several commercially available solvents such as LIX 64, LIX 84, LIX 6022, LIX 860, and LIX 984N is capable of recovering copper by solvent extraction. However, for extraction of copper from chloride solution LIX 984 N shows more promise (Lu and Dreisinger, 2013).

Present study focuses on the recovery of copper from E-waste concentrate by Fluoroboric acid dissolution and selective extraction of copper from leach solution by using LIX 984N as a solvent diluted in the kerosene.

2 MATERIALS AND METHODS

2.1 Reagents and Materials

All chemicals in this experiment were of analytical reagent grade. Water was double distilled. Commercial LIX 984N was provided by Recovery of nonferrous Metals

Company, which was diluted in industrial kerosene after treatment with Sulfuric acid. HBF_4 and ammonia solution 25%, (extra pure, Mojallali chemicals) were used for adjusting the pH value.

2.2 Instruments and Analytical Method

Mettler Toledo precision pH meters, and the atomic adsorption spectroscopy (Varian, type AA240) for analyzing the concentration of Cu (II) ions were used in the experiments.

2.3 Method

Batch experiments were carried out in a flask containing equal volumes (20 mL) of aqueous and organic solutions. Then, the produced mixture was transferred to a 250 mL separation funnel. The two layers were allowed to settle and separate. pH of aqueous layer was measured and the concentration of Cu(II) in an aqueous solution was determined by atomic adsorption spectroscopy.

Agitation was carried out for 30 min to assure equilibrium conditions, even though equilibrium could have been achieved in less than 10 min (Kim & Lee & Jung & Kim & Kim, 2005).

Organic solutions were prepared by diluting different percentages of LIX 984N (10%, 20%, and 30%) in kerosene.

3 RESULTS AND DISCUSSION

3.1 Effect of pH on Extraction of Cu (II)

The extraction was carried out with an aqueous solution of 2g/l Cu(II) and the organic phase containing 20% (v/v) LIX 984N diluted in kerosene at 25ºC. The effect of pH on the extraction of these metals was investigated in the pH range 0.8 – 2.5 using the O/A phase ratio of 1:1. pH and concentration of Cu ions in an aqueous phase was determined.

Figure 1 represents the extraction percent of copper in different pH values. It is evident that the percentage of extraction was increased for extraction of copper with increase in the equilibrium pH, and maximum extraction (~99%) was obtained at equilibrium pH 3.

3.2 Effect of LIX 984N Concentration in the Organic Phase on Extraction of Cu (II)

In this study, for evaluating the effect of the extractant concentration on extraction of copper from the leach liquor at O/A phases ratio 1:1, experiments were conducted with 10%, 20%, and 30% (v/v) LIX 984N in kerosene at 25℃ (Figure 2).

It was observed that the percentage extraction of copper increased at higher LIX values. Consideration high costs and consumption of the organic phase, a 20% (v/v) LIX 984N concentration in kerosene was chosen for all experiments.

3.3 Effect of Temperature

To determine the effect of temperature on the extraction of copper, experiments were performed at three different temperatures (10, 25 and 60 ℃). Figure 3 shows the copper extraction versus pH. As can be seen from Figure 3, the percentage of extraction curve shifted to the left with increasing temperature. It can be concluded that the copper extraction was endothermic process; however extraction rate increases with increasing temperature.

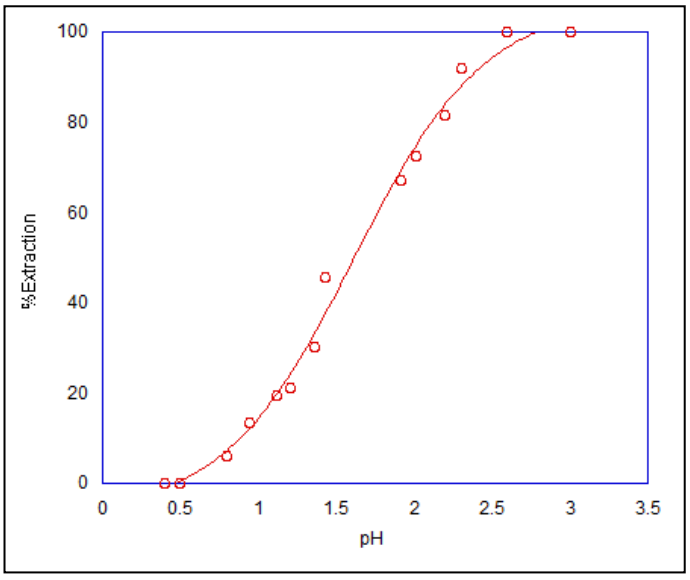

Figure 1. Effect of pH of the HBF_4 on extraction of Cu from leach solution using LIX 20% at 25ºC.

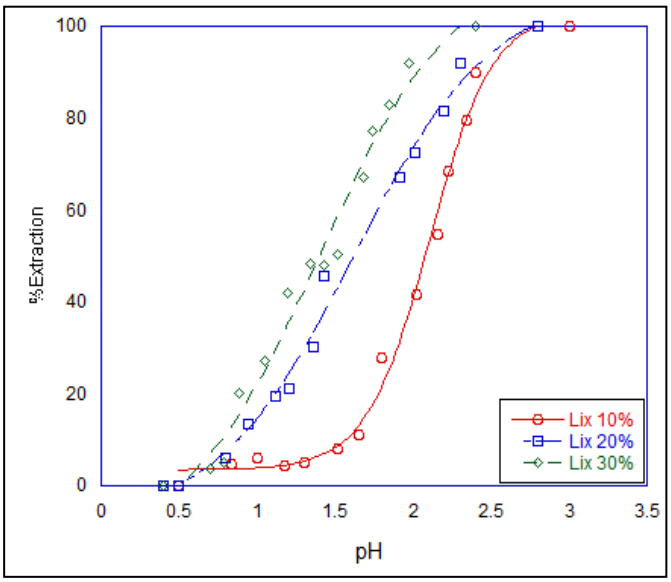

Figure 2. Percentage of extraction of copper from HBF_4 leach solution versus pH in different LIX concentration.

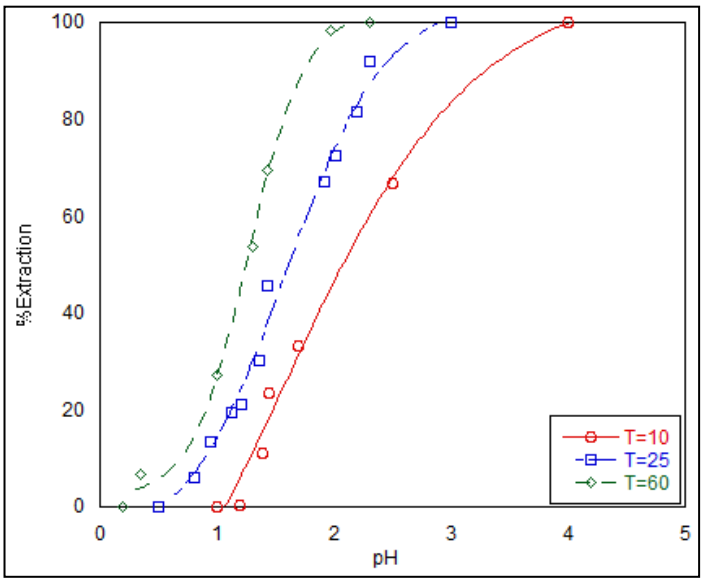

Figure 3. Percentage of extraction of copper from HBF_4 leach solution versus pH in different Temperatures.

4 CONCLUSION

In this paper, different parameters were studied for extraction of copper from an acid medium, such as pH, concentration of the organic phase and temperature. In consideration of cost and overall efficiency, it was shown that the extraction of copper is preferable to be carried out with an organic solution containing 20% (v/v) LIX 984N which was diluted in kerosene, in ambient temperature. The pH-%E curves of extraction showed that the percentage extraction of copper increased with increasing equilibrium pH and extractant concentration**.**

REFERENCES

Agrawal, A., Perween, M. et al, 2010. Recovery of copper from PCB leach solution by solvent extraction, pp. 1189 -1194.

Bertram, M., Graedel, T. E., Rechberger, H., Spatari, S., 2002. The contemporary European copper cycle: waste management subsystem, Ecology and Economics. 42, 43-57.

Jha, M. K., Lee, J. C., 2006. A review on the status of WEEE recycling in Korea. J. Met. Mater Sci. 48(3), 117-128.

Kim, M. S., Lee, J. C., Jung, J. K., Kim, B. S., Kim, E. Y., 2005. Leaching of copper from waste printed circuit boards using electrogenerated chlorine in hydrochloric acid. J. Korean Inst. Resour. Recycl. 14(5), 45-53.

Lee, C. H., Chang, C. T., Fan, K. S., Chang, T. C., 2004. An overview of recycling and treatment of scrao computers. J. Hazard. Mater. 114B, 93-100.

Lu, J., Dreisinger, D., 2013. Solvent extraction of copper from chloride solution 1: Extraction Isotherms, Journal of Hydrometallurgy, pp 309-6350.

Selective Zinc Recovery From a Valuable Iranian Zinc Plants Residue Using a Facile Selective Alkaline Leaching Method

P. Ashtari, P. Pourghahramani
Mining Engineering Faculty, Sahand University of Technology, Tabriz, Iran

ABSTRACT Large amounts of three different kinds of zinc plants residues are annually generated in Iran. Hot filtercake (known as HFC) is one of them which could be used as a promising secondary resource of zinc, cobalt and manganese. Unfortunately, despite its valuable elements, HFC isn't treated and the most of its hazardous constituents are easily exposed to the environment. For the first time, in this paper, zinc was selectively leached from HFC employing alkaline leaching. Secondly, it was tried to optimize leaching through L16 taguchi experiments design to obtain the maximum recovery of zinc. In addition, the effect of each affecting parameter was studied.

Keywords: Selective zinc recovery, Zinc plant residue, Selective alkaline leaching

1 INTRODUCTION

Zinc is mainly extracted from primary resources. A part of zinc is also obtained from different secondary. Waste materials could be used to recover valuable elements or it may be stock piled. But, stringent environmental regulations concerning waste disposal cause to impose expensive disposing costs. During metallurgical processes, a large amount of several solid wastes including flotation tailings, slags, slimes, filtercakes (filtering residuals), etc. are produced. Nowadays, a proper process is strongly required for zinc production from secondary recourses, especially wastes (Huhtala, 1997; Jha et al., 2001).

In the Iranian hydrometallurgical zinc plants (leach-electrolysis process), a great amount of wastes are often produced. One of them contains Zn, Mn, Ca and Co which known as hot filtercake (HFC). Due to its heavy metals, HFC could harm humans, animals, and plants. Evaluating the impacts of releasing of toxic heavy metals from such waste materials to surface and ground water shows that they can be one of the reasons for particular concern (Altundogan et al., 1998). High metal content in secondary resources could be considered as a good source for supplying Zn, Mn and Co. In this purpose, if a proper process could be developed, the HFC also can be considered as a very important resource for production of such elements (Altundogan et al., 1998).

Metal extraction from metallurgical wastes often requires hydrometallurgical treatment (Rao, 2011). Alkaline leaching has some advantages compared to acidic leaching. Alkaline leaching is usually used to extract valuable metals selectively from secondary resources. Aluminum, zinc and some other amphoteric metals can selectively dissolve in alkaline solution; however, acidic leaching commonly results to collective dissolution with low selectivity. Even though, in some cases, by manipulating the effective parameters, the recovery of undesirable elements in acidic leaching could be controlled, but, solution impurities usually increase (because of high metal content in secondary resources) and purification processes have to be done, inevitably (Gupta and Mukherjee, 1990). A relatively clean and impurity-free leach solution can be obtained by alkaline leaching and the complex purification and impurities removal

processes are avoided. Because of the insolubility of iron, calcium, manganese and cobalt compounds in sodium hydroxide solutions, the main advantage of sodium hydroxide leaching is its good selectivity between those compounds and zinc. Consequently, NaOH leaching could be a suitable leaching procedure for leaching of amphoteric hydroxides or oxides.

The previous studies have implied that the solubility of some specific amphoteric elements in strong caustic alkaline solution decreases in the following sequence Zn > Pb > Al > Cr (III) > Cu. Cr (III), Cu and Cd dissolve negligibly in the presence of zinc and lead. The solubility of lead is decreased provided that the zinc concentration in caustic pregnant solution is almost high (Stafanova and Aromaa, 2012).

So far, many researches have been reported zinc extraction form various secondary resources using acidic leaching (Ahmed et al., 2012; Dvořák and Jandova, 2005; El-Nadi et al., 2007; Ognyanova et al., 2009; Ruşen et al., 2008; Safarzadeh et al., 2009; Sayilgan et al., 2009) and alkaline leaching (Dutra et al., 2006; Moradkhani et al., 2012; Nagib and Inoue, 2000; Shin et al., 2009; Xia and Picklesi, 2000). However, few papers have been devoted for zinc recovery from HFC.

The objective of this study is to investigate the selective leaching of zinc from HFC in the alkaline medium. The main aim was to evaluate the effects of various leaching affecting parameters on zinc dissolution from HFC. Optimization process of the leaching study was conducted according to L16 taguchi experimental design to determine the optimum leaching condition for zinc extraction.

2 MATERIALS AND METHOD

2.1 Materials

The initial hot filtercake (HFC) sample was obtained from ALVAN zinc plant, Zanjan, Iran. In order to remove the trapped pregnant solution resulted in deficient filtering and separate the soluble salts, the as-received wet HFC was first washed with distilled water several times. The pre-treated HFC was dried in the oven at 95 °C 24 h. For leaching experiments, pure NaOH from merck was used.

2.2 Experimental Procedure

The leaching experiments were conducted in a two neck glass reactor of 250 ml volume equipped with a condenser and mechanical stirrer having a digital controller unit and a thermostat which controlled the temperature of the reaction medium within ±0.5 ˚C. Seventy five milliliters NaOH solution at a given concentration was decanted into the reactor. When the desired temperature of the reactor content was reached, a predetermined amount of HFC was added into the solution while the content of the vessel was being stirred at a certain speed. After 30 minutes, the content of the vessel was filtered and the filtered liquor was then analyzed by atomic absorption spectroscopy for Zn, Pb and cadmium (and some other impurities). Experimental parameters and their levels determined in the light of preliminary tests are given in Table 1.

Table 1. Experimental parameters and their levels.

Process parameter	Designation	Level 1	Level 2	Level 3	Level 4
Temperature (°C)	A, T	50	70	90	105
NaOH concentration (M)	B, C_{NaOH}	3	5	7	9
solid to liquid ratio (g/cc)	C, S/L	1/5= 0.2	1/10= 0.1		
stirring speed (rpm)	D, R	500	800		

Based on L16 ($4^2\times2^2$) taguchi fractional orthogonal array (OA) four process factors are considered to determine their best levels in order to optimize the zinc extraction from HFC (ZnE[1]). Two parameters (C_{NaOH} (NaOH concentration) and T (temperature)) in four levels and two parameters (S/L (solid

[1] ZnE is abbreviated form of zinc extraction (%)

weight/solution volume) and R (stirring speed)) in two levels applied in this study are listed in Table 1. For analysis the data obtained, Minitab® 16 Statistical Software was used.

3 RESULTS AND DISCUSSION

3.1 PHFC Characterization

Chemical composition of PHFC is presented in Table 2. Size analysis revealed that the HFC particles are -150 µm.

Table 2. Chemical composition of PHFC.

Element	Zn	Mn	Co	Ca	Pb	Cd	Fe	other
wt. %	10.5	15.4	2.2	7.5	1.4	0.3	2.5	trace

The XRD pattern of PHFC is shown in Fig. 1. As shown, different kinds of hydrous calcium sulfate like gypsum (CaSO4·2H2O) and plaster of pairs (2CaSO4·½H2O) were the major crystalline phases in HFC. Other phases included manganese oxide (MnO2), zincite (ZnO), quartz (SiO2) and cobalt oxide (Co3O4). But, intricate composition of HFC, likewise very fine particles and low degree of crystallinity made phase assessment more difficult.

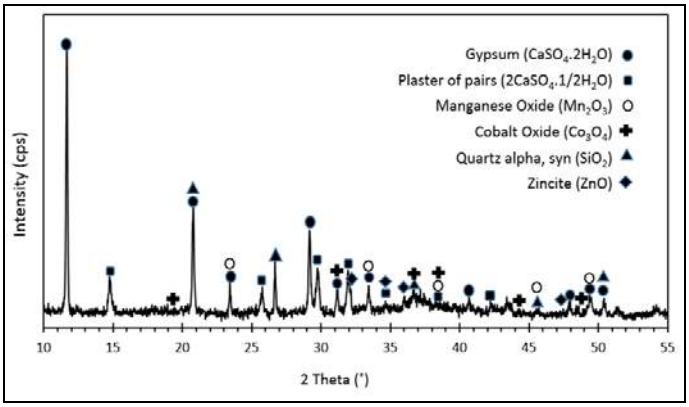

Figure 1. XRD pattern of the HFC sample.

SEM-EDS analysis was used to find more information. As shown in Figure 2a, the only crystalline particles which have relatively large grains (compared to other particles) viz. EDS1, EDS3 and EDS5 points contain Ca and S, confirming the presence of calcium sulfate phases. Zn, Mn and Co could be observed instantly on the some fine particles with varying ratios of zinc, manganese, cobalt, calcium and oxygen. High-resolution image of fine surface morphology is also shown in Figure 2b. It was concluded that most of the particles are in sub-micron sizes and fine particles aggregate on surface of larger crystalline particles.

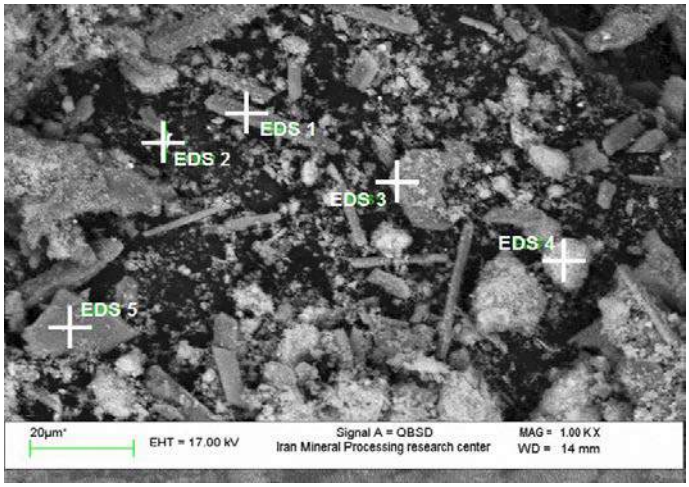

(a) Backscattered electron mode

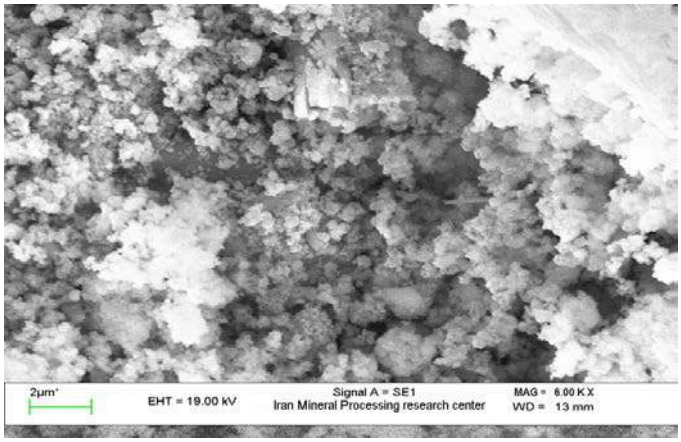

(b) Secondary electron mode

Figure 2. SEM micrograph of PHFC.

3.2 Zinc dissolution from HFC with alkaline medium

Based on the XRD analysis of PHFC sample, the main zinc bearing phase is zincite (ZnO). Among the all phases presents in HFC, ZnO was the only phase could be dissolved in alkaline medium. Our preliminary experiments showed that lead and cadmium have not leached, remarkably. So, the leaching process could be completely selective for zinc. It is thought that zincite dissolves in alkaline medium according to the reaction below:

$$ZnO_{(s,\ in\ HFC)} + 2NaOH_{(aq)} + H_2O \rightarrow Na_2Zn(OH)_{4(aq)} \quad (1)$$

Preliminary experiments showed that reaction time has no significant effect on the

leaching recovery and it seems that 30 minutes could be enough to get equilibrium. For the evaluation of the effect of other parameters on the zinc dissolution from HFC, the collected data were analyzed by using Minitab®16 Statistical Software. The results of all experiments as well as their operational condition are summarized in Table 3.

The intensity of the effects of parameters on the zinc dissolution are given at Figure 3. The principal intention was to maximize the response parameter ZnE to the greatest extent. Accordingly, as seen at Figure 3 "*A*4 (T = 105 °C), *B*4 (C_{NaOH}= 9 M), *C*1 (S/L = 0.1 g/cc) *and D*2 (R = 800 rpm)" combination resulted to the most outstanding zinc extraction recovery. This could be concluded based on the mean of process response. At the suggested optimum level of parameters, the confirmation test revealed that 83.4 % of the zinc could be extracted. This value is higher than all our observed values in Table 3.

Table 3. Taguchi L16 (42×22) results for zinc extraction (ZnE).

Experiment no.	A T (°C)	B C_{NaOH} (M)	C S/L (g/cc)	D R (rpm)	ZnE (%)
1	50	3	0.2	500	13.1
2	50	5	0.2	500	54
3	50	7	0.1	800	71.9
4	50	9	0.1	800	71.4
5	70	3	0.2	800	20.9
6	70	5	0.2	800	52.1
7	70	7	0.1	500	70.5
8	70	9	0.1	500	72
9	90	3	0.1	500	48
10	90	5	0.1	500	62.8
11	90	7	0.2	800	58.4
12	90	9	0.2	800	67.4
13	105	3	0.1	800	65.1
14	105	5	0.1	800	63.1
15	105	7	0.2	500	61.9
16	105	9	0.2	500	69.2

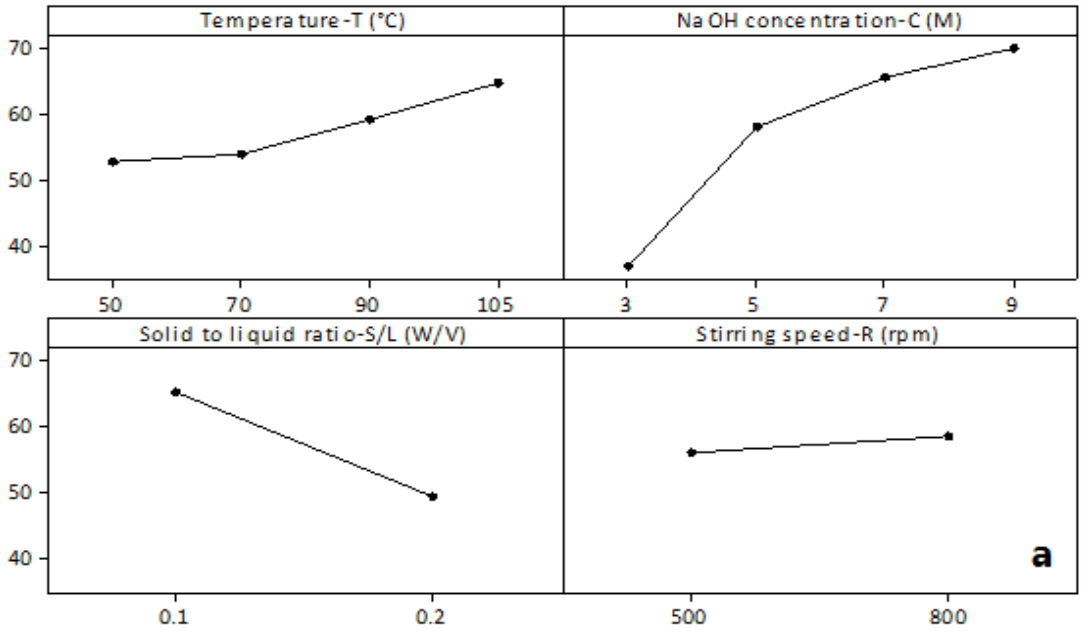

Figure 3. Main effects plots of each parameter for means of the zinc extraction (ZnE).

3.3 Response Plots For Various Affecting Parameters On Zinc Leaching Recovery From HFC

To show the simultaneous effects of parameters on zinc recovery, response plots was used. Figure 4a shows the relationship between NaOH concentration and solid to liquid ratio at a temperature of 55 ˚C and 500 rpm stirring speed. The presented arrow shows the maximum direction of variation (highest gradient) of zinc recovery. As seen, the arrow is more inclined to NaOH concentration axis. It means that with comparison to solid to liquid ratio, zinc

dissolution was more influenced by NaOH concentration. As before mentioned, this result was proved with taguchi method, previously. At the other hand, as it is obvious at Figure 4a, zinc recovery could be increased by decreasing solid to liquid ratio as same as increasing NaOH concentration.

Figure 4b shows the relationship between NaOH concentration and temperature at a solid to liquid of 1/10= 0.1 (W/V) and 500 rpm stirring speed. As seen, at low temperature (T < 65 ˚C), temperature has no significant effect on zinc recovery. In this region, NaOH concentration affects zinc recovery, lonely. But, at high temperature (T > 65 ˚C), the effect of temperature increased and the direction of arrow was more inclined to temperature axis. Thus, it must be considered that at temperature above 65 ˚C, the effect of temperature on zinc dissolution is significant as well as NaOH concentration.

4 CONCLUSION

In the present study, L16 Taguchi method was employed for design of experiment to determine the effective parameters on zinc extraction from HFC. Based on the experimental results and given analysis, at the optimum operating condition (T = 105 °C, C_{NaOH}= 9 M, S/L = 0.1 g/cc and R = 800 rpm), approximately 83.4 % of zinc was leached selectively in NaOH solution. The most important parameter in the zinc alkaline leaching is NaOH concentration. Zinc extraction due to alkaline dissolution of HFC also increase when solid to liquid ratio decreases and temperature increases. Stirring speed has no reasonable effect. It was shown that the alkaline leaching of HFC is an efficient method to recover zinc selectively. High amount of HFC zinc content could be extracted with alkaline leaching.

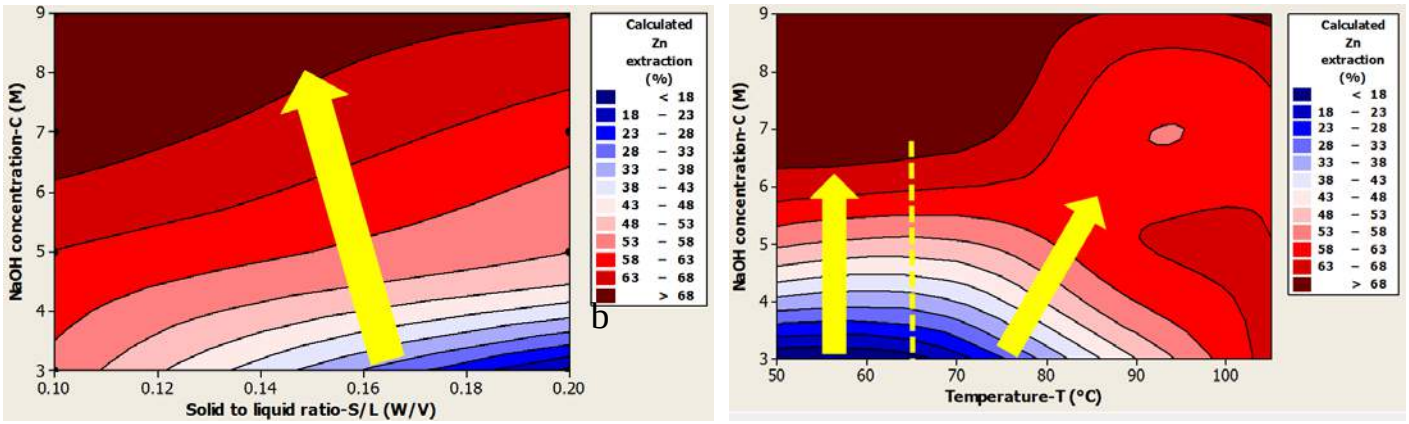

Figure 4. Contour plots of the interactive effect for zinc recovery: (a) effect of NaOH concentration and solid to liquid ratio at constant temperature 55 ˚C and stirring speed 500 rpm and (b) effect of NaOH concentration and temperature at constant solid to liquid ratio 1/10 (W/V) and stirring speed 500 rpm.

Taguchi method can successfully be applied to optimize the zinc alkaline dissolution from HFC.

REFERENCES

Ahmed, I., Nayl, A., Daoud, J., 2012. Leaching and Recovery of Zinc and Copper from Brass Slag by Sulfuric Acid. Journal of Saudi Chemical Society.

Altundogan, H.S., Erdem, M., Orhan, R., Ozer, A., Turnen, F., 1998. Heavy metal pollution potential of zinc leach residues discarded in Çinkur plant. Tr. J. Eng. Environ. Sci 22, 167-177.

Dutra, A., Paiva, P., Tavares, L., 2006. Alkaline leaching of zinc from electric arc furnace steel dust. Minerals Engineering 19, 478-485.

Dvořák, P., Jandova, J., 2005. Hydrometallurgical recovery of zinc from hot dip galvanizing ash. Hydrometallurgy 77, 29-33.

El-Nadi, Y., Daoud, J., Aly, H., 2007. Leaching and separation of zinc from the black paste of spent MnO_2/Zn dry cell batteries. Journal of hazardous materials 143, 328-334.

Gupta, C., Mukherjee, T., 1990. Hydrometallurgy in extraction processes. CRC Press.

Huhtala, A., 1997. A post-consumer waste management model for determining optimal

levels of recycling and landfilling. Environmental and Resource Economics 10, 301-314.
Jha, M.K., Kumar, V., Singh, R., 2001. Review of hydrometallurgical recovery of zinc from industrial wastes. Resources, Conservation and Recycling 33, 1-22.
Moradkhani, D., Rasouli, M., Behnian, D., Arjmandfar, H., Ashtari, P., 2012. Selective zinc alkaline leaching optimization and cadmium sponge recovery by electrowinning from cold filter cake (CFC) residue. Hydrometallurgy 115, 84-92.
Nagib, S., Inoue, K., 2000. Recovery of lead and zinc from fly ash generated from municipal incineration plants by means of acid and/or alkaline leaching. Hydrometallurgy 56, 269-292.
Ognyanova, A., Ozturk, A., De Michelis, I., Ferella, F., Taglieri, G., Akcil, A., Vegliò, F., 2009. Metal extraction from spent sulfuric acid catalyst through alkaline and acidic leaching. Hydrometallurgy 100, 20-28.
Rao, S.R., 2011. Resource recovery and recycling from metallurgical wastes. Access Online via Elsevier.
Ruşen, A., Sunkar, A., Topkaya, Y., 2008. Zinc and lead extraction from Çinkur leach residues by using hydrometallurgical method. Hydrometallurgy 93, 45-50.
Safarzadeh, M.S., Moradkhani, D., Ashtari, P., 2009. Recovery of zinc from Cd–Ni zinc plant residues. Hydrometallurgy 97, 67-72.
Sayilgan, E., Kukrer, T., Civelekoglu, G., Ferella, F., Akcil, A., Veglio, F., Kitis, M., 2009. A review of technologies for the recovery of metals from spent alkaline and zinc–carbon batteries. Hydrometallurgy 97, 158-166.
Shin, S.M., Senanayake, G., Sohn, J.-s., Kang, J.-g., Yang, D.-h., Kim, T.-h., 2009. Separation of zinc from spent zinc-carbon batteries by selective leaching with sodium hydroxide. Hydrometallurgy 96, 349-353.
Stafanova, A., Aromaa, J., 2012. Alkaline leaching of iron and steelmaking dust.
Xia, D., Picklesi, C., 2000. Microwave caustic leaching of electric arc furnace dust. Minerals Engineering 13, 79-94.

Simulation of Fluid Flow in the Settler of Copper Solvent Extraction

D. Mansourian, S. Parvizi, O. Kazemi, E. K. Alemdari
Department of Mining and Metallurgical engineering, Amirkabir university of Technology (Tehran Polytecgnic), Tehran, Iran

E. K. Alamdari
Research Center for Materials and Mining Industries Technology, Amirkabir University of Technology, Tehran, Iran.

ABSTRACT Mixer settler equipment is widely used for solvent extraction process. The aim of this project is betterment of settler performance that leads to clean phase separation, minimizing the loss of reagents and declining surface area of the settlers. Computational fluid dynamics provides a convenient way to achieve exact details about fluid flow through solving differential equations by numerical methods. Settler of Sarcheshmeh copper complex in Iran is selected for this survey. Geometry of settler is designed in Gambit software and then computational fluid dynamics simulation based on Euler-Euler two-phase method applied to study aqueous-organic dispersion. Experimental measurements have been used to validate accuracy of simulation results. Flow simulation, separation of phases and the effect of ratio of phases on separation pattern have been investigated. By analyzing the mentioned parameters, the optimized ones are achieved.

Keywords: CFD, Settler, Solvent extraction

1 INTRODUCTION

Solvent extraction process is widely used in many fields such as petrochemical and pharmaceutical industries as well as hydrometallurgy of copper, cobalt, nickel and zinc. Liquid-liquid extraction is a process for separating components in solution distributing them between two immiscible liquids. This technique is used for treatment of complex ores and recovery of non-ferrous metals (Ying and Mikiya, 2009). Using Mixer settler equipment is a convenient method for operating solvent extraction processes in hydrometallurgy industry. The main advantages of this equipment are: strong operational loads, easy operation and maintenance and simple start-up (Shabani and Mazahert, 2012). The function of the mixer is to provide an adequate combination of mixing and dispersion for the desired degree of extraction (Shabani and Mazahert, 2012). After complete mixing, the homogenous combination of phases enters the settler to be separated by gravity force. Figure 1 shows a schematic of mixer-settler equipment. Stanbridge and Sullivan (1999) showed that feed arrangement distribution has a great effect on settler performance (Stanbridge and Sullivan, 1999). In their results, optimum conditions of flow in the settler can be obtained by uniform feed distribution along the width of the settler. Miller (2006) reported that performance of a settler can increase up to 30–50% by improving the feed distribution and coalescence systems (Miller, 2006). These systems also increase settler performance when an emulsion band is not present due to fast breaking emulsions. In order to control the flow entrance to settler, vertical plates called “picket fence” are used. Any improvement in understanding of hydrodynamics and flow pattern within a mixer-settler unit would enable effective design of the mixer-settler equipment and this is provided by using CFD simulation. By CFD simulation, not only the experimental

tests are not required to be done to find out optimum conditions of mixer-settlers but also it leads to a decrease in operation costs.

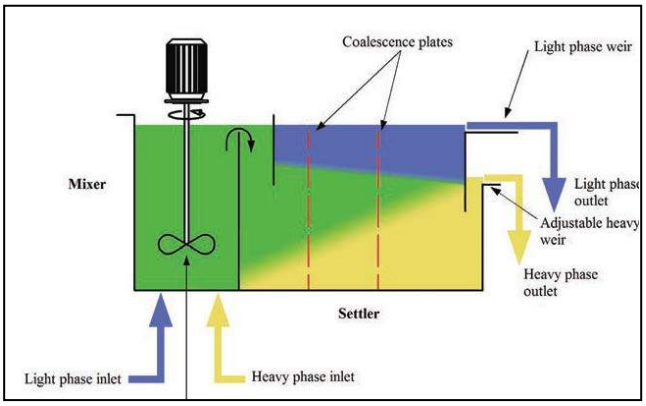

Figure 1. Schematic of mixer settler equipment.

A CFD model of a mixer-settler requires these to be selected, amongst others, an appropriate grid resolution, discretization scheme, impeller rotation model and turbulence model. The selection of these, largely numerical considerations, can have a dramatic influence on both the accuracy of the CFD simulation and the associated computational expenses. This is particularly important when performing CFD simulations of large industrial vessels (engineering studies) as the number of control volumes in the grid increases enormously with increasing the size of mixer-settler (Miller, 2006; Sadeghi et al., 2011). The aims of the present work are as follows: Flow simulation, separation of phases and investigating the effect of ratio of phases on separation patterns.

2 MATERIAL AND METHODS

2.1 Governing Equations

The equations are solved through Finite volume method in ANSYS CFX 14.5. The CFD simulation involves the continuity equation for incompressible flow and time averaged navier-stocks equations. Droplet coalescence and break up model is implemented in the ANSYS CFX.

2.1.1 Continuity equations

The continuity equations for continuous (c) and dispersed (d) phases are as follows (Versteeg, and Malasekara, 2007; White, 1991):

$$\nabla(\rho_c \alpha_c U_c) = 0 \quad (1)$$

$$\nabla(\rho_d \alpha_d U_d) = 0 \quad (2)$$

Where ρ, α, and U are density, volume fraction and mean velocity vector respectively.

2.1.2 Momentum equations

The time averaged governing equation for a steady, incompressible, turbulent flow form as (Versteeg, and Malasekara, 2007; White, 1991):

$$\rho_c[\nabla(\alpha_c U_c U_c)] = -\alpha_c \nabla P + (\mu_c + \mu_t)\nabla^2(\alpha_c U_c) + S_{M.} \quad (3)$$

$$\rho_d[\nabla(\alpha_d U_d U_d)] = -\alpha_d \nabla P + (\mu_d + \mu_t)\nabla^2(\alpha_d U_d) + S_{M.d} \quad (4)$$

Here μ, μ_t, P and S_M are dynamic viscosity, turbulent viscosity, pressure and source term respectively. U_c and U_d are the time averaged mean vectorial velocities.

2.1.3 Other equations

The k-ε turbulent model has been used to calculate the turbulent viscosity. Where k and ε are turbulent kinetic energy and turbulent dissipation rate respectively (Sadeghi, et al., 2011; Ansys Cfx 14.5 Users' Guide, 2013).

Fluid flow field calculation has been carried out through standard K- ε turbulence model. K- ε is one of most established turbulence model which is successfully used by the other researchers, for simulating similar cases. The turbulence model includes buoyancy, drag, lift and turbulent dispersion force (Sadeghi, et al., 2011; Ansys Cfx 14.5 Users' Guide, 2013). Buoyancy, drag and lift effect are considered respectively as follows:

$$F^{buo} = (\rho - \rho_\circ)g \quad (4)$$

$$F^{drag} = \frac{1}{2}|U_{rel}|U_{rel}A_p C_D. \quad (5)$$

$$F_d^{lift} = \alpha_d \rho_c C_L (U_c - U_d) \times \nabla U_c. \quad (6)$$

2.2 Calculation Process

In order to analyze the flow pattern in settler, a case study has been selected for verifying the simulation results with experimental data; so the settler of Sarcheshmeh copper complex was chosen for this task.

Settler tank was designed and meshed by Gambit software as shown in figure 2. Settler is rectangular with one entrance for fluid. Type of mesh and distance between the nodes hugely influence the time of mixing equations and the reliability of the results. Considering the cubic shape of the tank, Hex dominant mesh was selected. In curved or near picket fence areas, nodes with less distance were used with 400000 cells, according to Sadeghi et al. Research for settler tank, 500000 and 600000 cells were examined and concluded that with 600000 cells, results of simulation are not dependent on the number and shape of the cells. Flow pattern was investigated in settler tank and finally the results were validated by Sadeghi et al. data (Sadeghi, et al., 2011; Sadeghi, et al., 2011).

For investigating the interaction of two fluids, two phase Euler-Euler model was used because of its good results in condition that volume ratio of disperse is not negligible. Hydrostatic pressure by atmosphere is considered in the volume of settler tank. Entering volumetric rate of flow according to the operating condition was considered 1100 m^3/hr. Stationary situation applied on the walls.

By a camera which is connected to a computer, minimum and maximum sizes of droplets were calculated 100 and 2000 micrometers respectively.

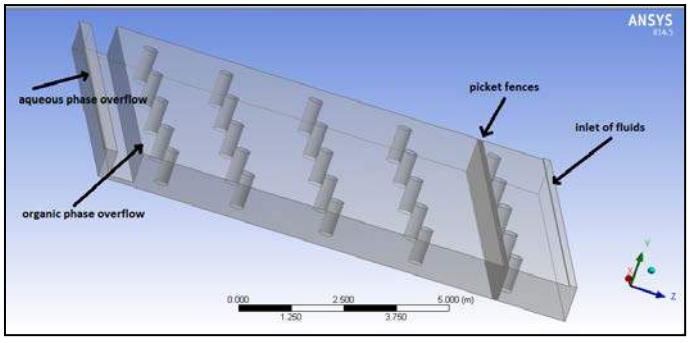

Figure 2. Schematic of settling tank.

Settler equipment of Sarcheshmeh includes two separated outlets for aqueous and organic phases in which the exhausting condition of tank is considered as pressure outlet in atmosphere constant pressure. In inlet valve, ratio of flow rate of phases according to the operational condition was set by 0.95.

For assessing the flow pattern, it was supposed that inlet fluid consists only of water by 1100 m^3/hr flow rate. Continuity and momentum balance equations were modeled. At first, the tank was empty so for studying the way of filling it by fluid was done by two phases; air and water.

According to the Sadeghi et al. research data for these dimensions, 500000 cells are appropriate and are correspondent with experimental data. After meshing, the geometry was referred to Ansys Fluent software. Velocity of inlet was set 1100 m^3/hr and volume ratio of organic to aqueous phase was considered 0.95.

Since the phases are isotherm and there is no heat transformation in volume of settler, solving heat transformation equations was ignored. Time-transient type of simulation was selected and time steps size for calculation and reserving the results was applied by 0.01 Sec. Total time of calculations according to inlet fluid, inlet area and total volume of tank, was adjusted by 200 second. In modeling at the start point, the volume fraction of water was 0 and the total volume consisted of air and at the entrance it was 1. For converging the results, sum of squared residuals method was used by 10^{-4} criteria.

There are some spaces in settler which eddy currents occur. These currents not only reduce the efficiency of fluid distribution in settler, but also aggravate the separation of phases, Hence, diminishing these areas results in decreasing the costs and performing the gravity separating reactors.

This simulation was done in three dimentional, unsteady state, turbulent flow, incompressible and without transformation of heat and mass conditions. Reynolds numbers based on hydraulic diameter in launder and settling tank were 93000 and 11000 respectively. For this reason turbulent

flows were considered in this simulation.

3 RESULTS AND DISCUSSION

3.1 Simulation of Flow and Investigating Separation of Phases

One of the significant factors of flow pattern is volumetric rate of flow. Figure 3 shows the volume ratio of organic phase at different height of settler. Desirable separation is obtained when the separation layer is less and organic phase is thick. Figure 4 and 5 show the distribution of phases in 2 views.

Volumetric rate of inlet influences the collision of droplets and separation of phases. For analyzing this parameter at different inlet volumetric rate by 375, 550, 1000, 1500, 1200, 2200 and 3600 m^3/hr were examined. The approach of separation of phases shown in figure 6 to 10. As these figures indicate, by choosing inlet volumetric rate near to 1000 m^3/hr, the separation improved among other velocities. Figure 11 shows organic volumetric ratio at different inlet volumetric rate.

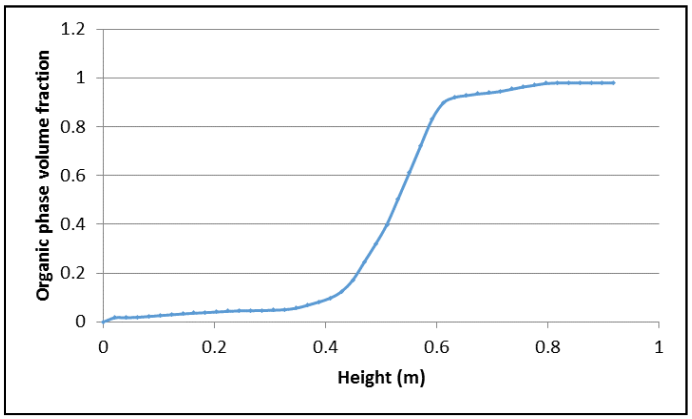

Figure 3. Organic phase volume fraction in different heights of the settler.

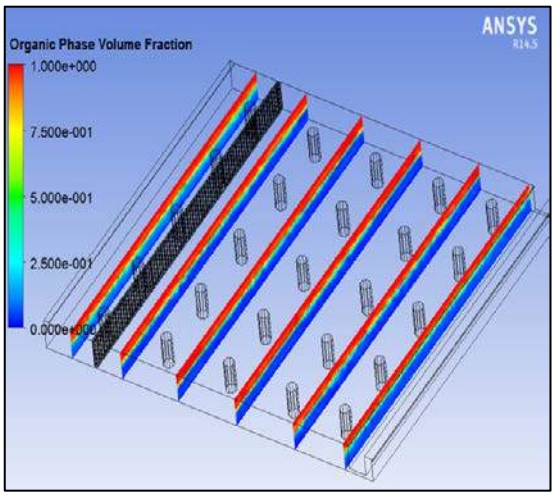

Figure 4. Side view pattern of distribution of phases.

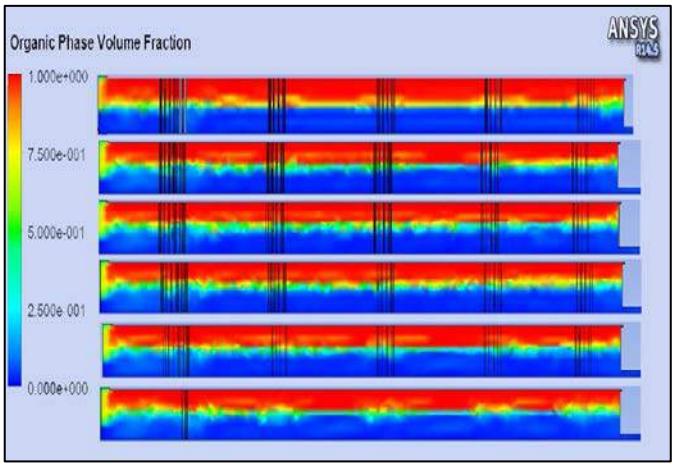

Figure 5. Front view pattern of distribution of phases.

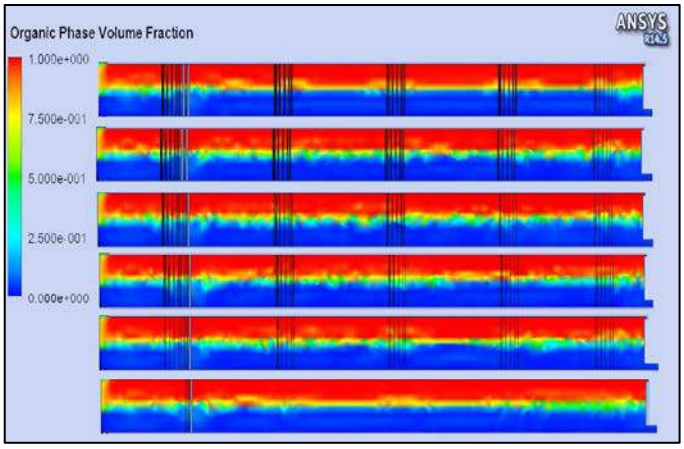

Figure 6. Pattern of separation in 375 m3/hr inlet volumetric rate.

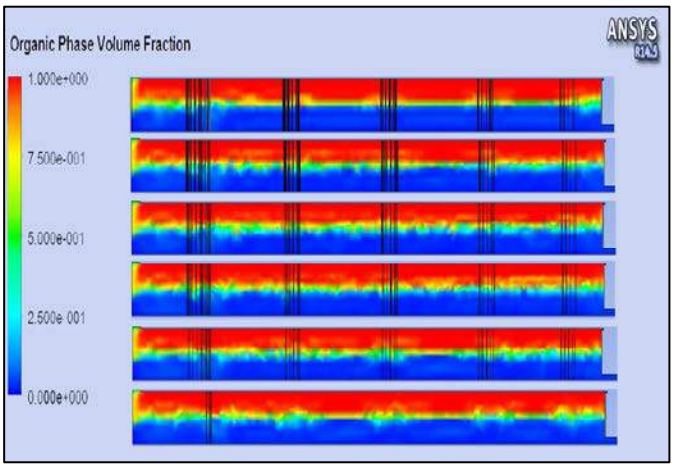

Figure 7. Pattern of separation in 575 m3/hr inlet volumetric rate.

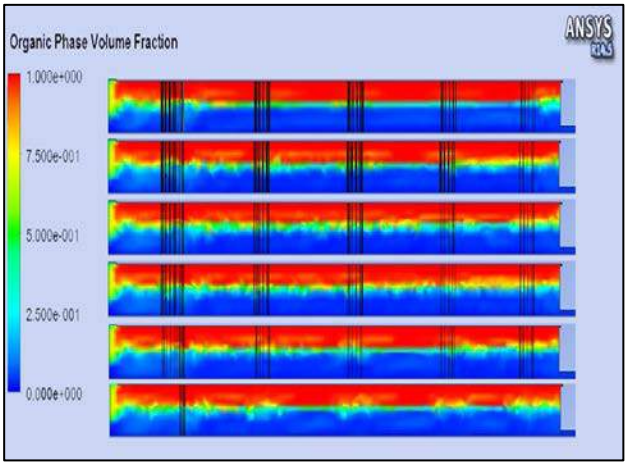

Figure 8. Pattern of separation in 1000 m3/hr inlet volumetric rate.

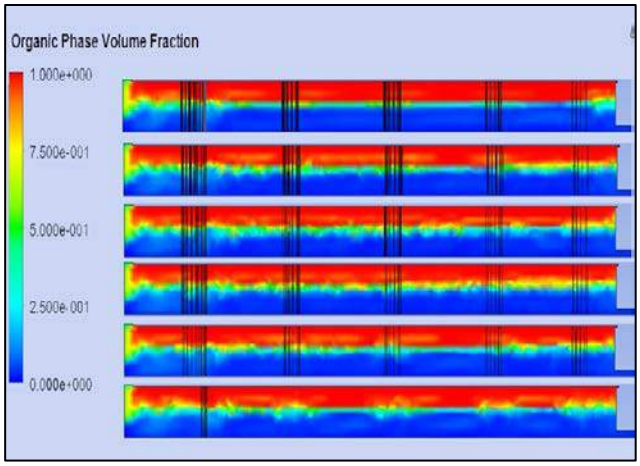

Figure 9. Pattern of separation in 1200 m3/hr inlet volumetric rate.

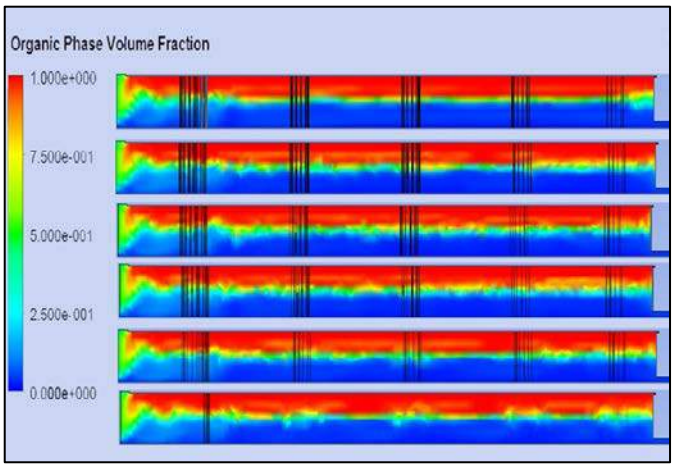

Figure 10. Pattern of separation in 1500 m3/hr inlet volumetric rate.

3.2 Studying Ratio of Phases on Separation Pattern

Volumetric ratio of organic phase to aqueous phase was set 0.95 in all simulations. One of the effective parameter affecting on separation could be volumetric ratio. For analyzing effect of this factor, different volumetric ratios with optimum volumetric rate of flow were examined. These ratios were equal to 0.5, 0.25, 0.1, 2, 4 and 10. Results were compared with ratio of 0.95 as shown in figures 12 to 17.

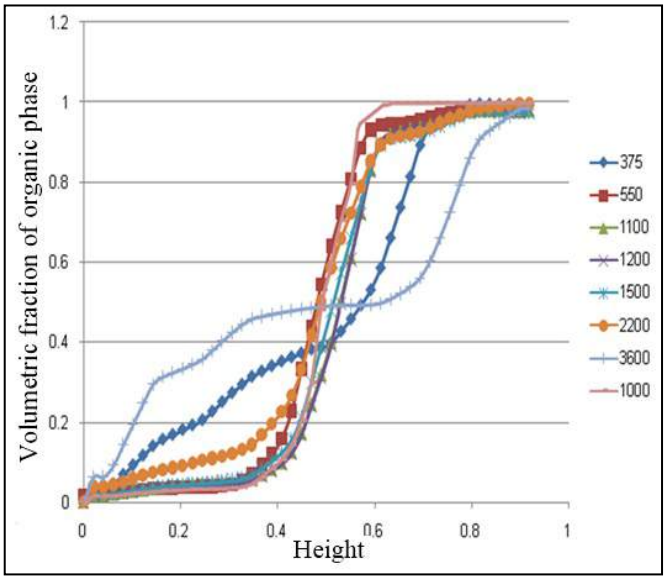

Figure 11. Organic phase volume fraction in different heights (m) of settler and in the presence of different inlet flow rates.

Simulation results of separation pattern in settler volume show that by changing volumetric ratio of organic to aqueous phase

in input valve, the separation pattern becomes distorted, and the separation layer increases. So, ratio equal to 0.95 was considered as optimum ratio. Figure 18 shows volumetric ratio of organic phase in 0.6 m height from the bottom of the settler.

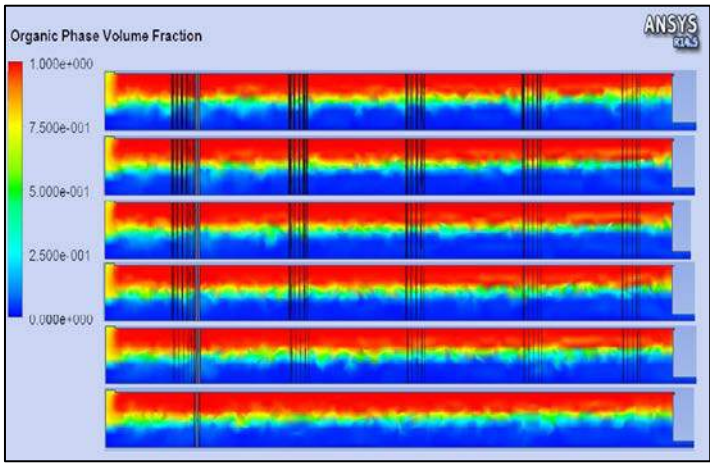

Figure 12. Separation pattern in volumetric ratio 0.5.

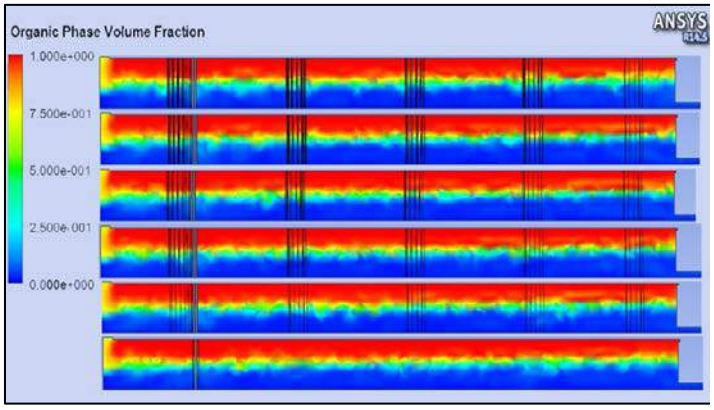

Figure 13. Separation pattern in volume ratio 0.25.

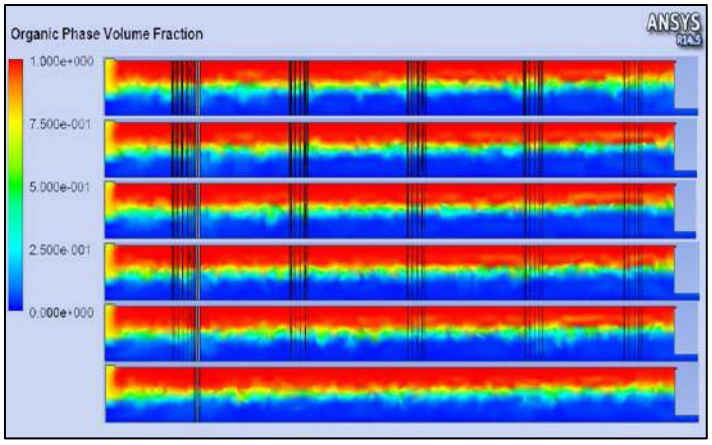

Figure 14. Separation pattern in volume ratio 0.1.

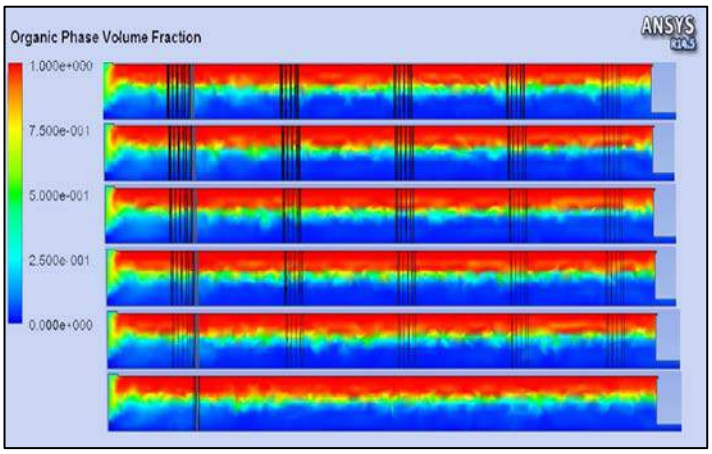

Figure 15. Separation pattern in volume ratio 2.

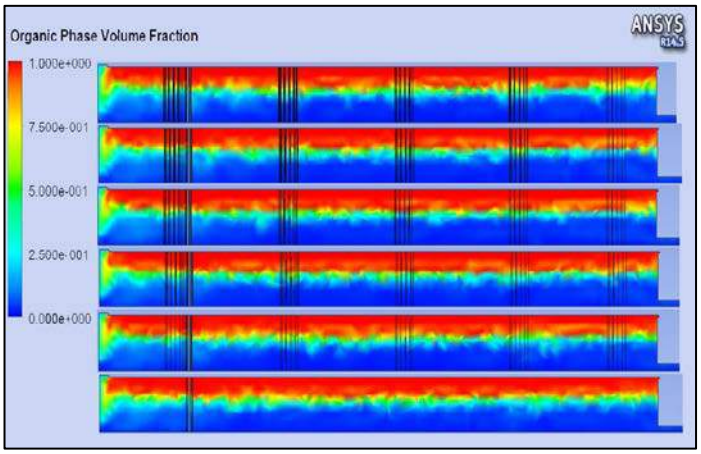

Figure 16. Separation pattern in volume ratio 4.

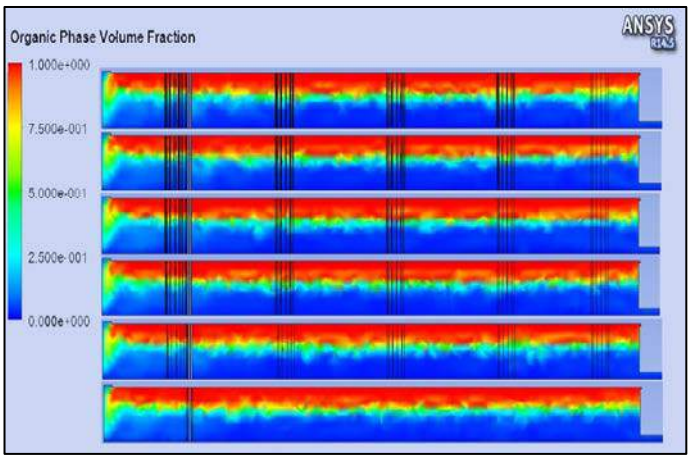

Figure 17. Separation pattern in volume ratio 10.

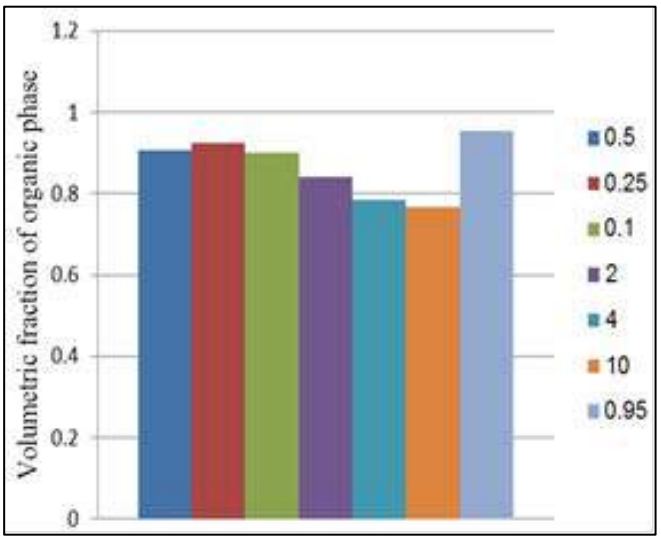

Figure 18. Volumetric fraction of organic phase in 0.6 meter height in different volumetric ratio.

4 CONCLUSIONS

Demanded separation is obtained when the separation layer is less and organic phase is thick. Different inlet volumetric rates by 375, 550, 1000, 1500, 1200, 2200 and 3600 m^3/hr were simulated and it was concluded that by decreasing inlet volumetric rate to 1000 m^3/hr, the separation improved among other velocities. For analyzing the effect of ratio of phases, different volumetric ratios in presence of picket fence with optimum volumetric rate of flow were examined. These ratios were equal to 0.5, 0.25, 0.1, 2, 4 and 10. By changing volumetric ratio of organic to aqueous phase in input valve, the separation pattern became distorted, and the separation layer increased. So, ratio equal to 0.95 was considered as optimum ratio.

REFERENCES

[1] Huang Ying, Tanaka Mikiya, 2009. Analysis of continuous solvent extraction of nickel from spent electroless nickel plating baths by a mixer-settler, *Journal of Hazardous Materials*, 164, pp. 1228–1235.

[2] Shabani M.O., Mazahert A., 2012. Computational fluid dynamics (CFD) simulation of liquid-liquid mixing in mixer settler, Archive of materials and metallurgy engineering, 57.

[3] Stanbridge, D., & Sullivan, J. (1999). One Example of How Offshore Oil & Gas Industry Technology Can Be of Benefit to Hydrometallurgy. In second international conference on CFD in the minerals and process industries, CSIRO, Melbourne, December

[4] Miller G., 2006. Design of Mixer–settlers to Maximize Performance, Proceedings ALTA Copper 10. Alta Metallurgical Services, Melbourne.

[5] Sadeghi, R., Mohebbi, A., Sarrafi, A., Soltani, A., Salmanzadeh, M., & Daneshpojooh, S. (2011). CFD simulation and optimization of the settler of an industrial copper solvent extraction plant: A case study. *Hydrometallurgy*, *106*(3), 148-158.

[6] Mandar T., Lane G., 2009, CFD simulation of a solvent extraction pump mixer unit: evaluating large eddy simulation and rans based models, 7th International Conference on CFD in the Minerals and Process Industries, Melborn, Australia.

[7] Versteeg, H.K and Malasekara, W. ”an introduction to computational fluid dynamics, the finite element volume method”, Longman Group Ltd, 2007, New York, 257 p.

[8] White, F.M, “Viscous fluid flow”, Second edition, Mcgraw-Hill, Inc., 1991, Singapore, 641 p.

[9] Sadeghi, R., Mohebbi, A., & Baniasadi, M. (2011). CFD modeling of the launder of settler of an industrial copper solvent extraction plant: A case study on Sarcheshmeh copper complex, Iran. *International Journal of Mineral Processing*, *98*(1), 55-65.

[10] ANSYS CFX 14.5 Users' Guide, 2013.

Solvent Extraction of Selenium in Hydrochloric Acid Media by Using Triisobutyl Phosphate/Dodecaol Mixture

A. Sattari, M. Kavousi, E. K. Alamdari
Department of Mining and Metallurgical engineering, Amirkabir university of Technology (Tehran Polytechnic), Tehran, Iran

E. K. Alamdari
Research Center for Materials and Mining Industries Technology, Amirkabir University of Technology, Tehran, Iran.

D. Darvishi, A. K. Alamdari, A. B. K. Rafsanjani
Rare Metals Production Corporation, Rafsanjan, Iran.
Non-Ferrous Metals Recovery Corporations, Rafsanjan, Iran

ABSTRACT Selenium is well known for both an essential and toxic role in lives of human beings and animals. Actually, very few extraction methods have been available for selenium (IV) so far. In the present study, the mechanism of selenium extraction in hydrochloric media by solvent extraction was carried out in two steps. First, extraction of selenium by triisobutyl phosphate was employed and then in the next step, Dodecanol was used as a modifier. The effect of concentration of acid, concentration of TIBP in the organic phase, pH, temperature, contact time, aqueous to organic volume ratio, and Dodecanol as a modifier on the extraction of selenium (IV) was studied.

Keywords: Solvent extraction; Selenium (IV); Triisobutyl phosphate; Dodecanol

1 INTRODUCTION

It is well known that selenium is both an essential and toxic trace element for man and animals with an upper intake limit of 400 μg/day (Sarger, et al., 2011). Selenium has many applications in electronic and metal alloy industries, and the largest use of it is in glass and ceramic manufacturing, it is also used in chemical industry, rubber industry and pharmaceuticals (Chowdhury and Sanyal 1993; Sarger, et al., 2011; Swapnil, et al., 2013). Solvent extraction is commercially used for recovery of precious metals, such as gold, silver, selenium, tellurium and etc. from copper electrorefining anode slimes (Abdollahy and Shafaei 2004, Gupta 2009). Very few extraction methods of selenium (IV) are available in the literature (Sarger, et al.,2011). The extraction and back extraction of selenium (IV) with N503 was studied by (Li, et al., 2012). This investigation proved that the extraction efficiency of Se (IV) is 100% by two times of extraction. (Aeungmaitrepirom, et al., 2001) studied the solvent extraction of Se (IV) by diaminocalix[4]arene. They came to the conclusion that Selenium (IV) was extracted into chloroform as (LH_2^{2+}, Cl^-, $HSeO_4^-$) and [$(LH_2^{2+})_2$, $2Cl^-$, SeO_4^{2-}] species at pH 2.6. While the extraction of Se (VI) was severely decreased as pH increased. (Chowdhury & Sanyal 1993) used tributyl phosphate (TBP) as an extractant for investigating the solvent extraction of selenium (IV), and this study was followed by studying the separation of selenium (IV) and tellurium(IV) using 1.1M TBP in kerosene as an extractant. N-n-octylaniline was also used by (Sargar, B.M., Anuse 2001) for the extraction of Se (IV) from dilute hydrochloric acid media. This method offered sequential separation of selenium (IV) from tellurium (IV). This paper surveyed the affecting parameters such

as the concentration of TIBP, pH, acid concentration, and modifier on extraction of selenium (IV) systematically, and estimated the thermodynamics of the overall extraction process.

2 MATERIALS AND METHODS

2.1 Reagents and Materials

All chemicals in this experiment were of analytical reagent grade. Water was double distilled. The Se (IV) solution was prepared by Selenium dioxide which was purchased from Merck Company. The triisobutyl phosphate (TIBP) was provided by Recovery of nonferrous Metals Company was diluted in kerosene after treatment with Sulphuric acid. Dodecanol was purchased from MP Biomedical Netherland Company which was used as a modifier. Ammonia solution 25% extra pure was employed for adjusting the pH of the system which was purchased from Mojallali Company.

2.2 Main Instruments and Analytical Method

Mettler Toledo precision pH meters, EUTECH instruments ORP meter (Oxidation Reduction Power meter) for measuring voltage of solutions, and the atomic adsorption spectroscopy (Varian, type AA240) for analyzing the concentration of Se (IV) ions were used in the experiments.

2.3 Method

Aqueous solution of Se (IV) of 0.05 Mwas made by dissolving appropriate mass of Selenium dioxide, in the stoichiometric value of hydrochloric acid and diluted to volume with double distilled water. Organic solutions were prepared by diluting different percentages of TIBP (10%, 20%, and 30%) in kerosene. In the second step of experiments organic phase containing 20% (v/v) Dodecanol as a modifier and 20% (v/v) TIBP was prepared which was diluted in kerosene. Aqueous solution and organic solution were shaken for 30 minutes in the mechanical shaker then the produced mixture was transferred to 250 mL separatory funnel. The two layers were allowed to settle and separate. pH of aqueous layer was measured by pH meter, and the concentration of Se (IV) in aqueous solution was determined by atomic adsorption spectroscopy.

3 RESULTS AND DISCUSSION

3.1 Choice of Diluent

Considering the important role of diluents in solvent extraction, due to their influence on the efficiency of process, the choice of diluent is one of the consequential steps in solvent extraction process. On the basis of (Chowdhury and Sanyal, 1993) investigations, distribution coefficient of nonpolar diluents is higher than polar diluents in TBP system. The results of their studies illustrated that kerosene and hexane are the best diluents in the mentioned system. In this investigation kerosene was chosen because of its low cost, minimum toxicity, and availability.

3.2 Effect of pH on Extraction of Se (IV)

The extraction was carried out with an aqueous solution of 0.05 M Se (IV) and organic phase containing 20% (v/v) TIBP diluted in kerosene at 25℃. pH and concentration of selenium ions in aqueous phase was determined. Figure 1 represents the extraction percent of selenium in different pH values. As it is shown in the figure, there are some irregular changes in comparison with usual sigmoid graphs of pH-%E for solvent extraction processes.

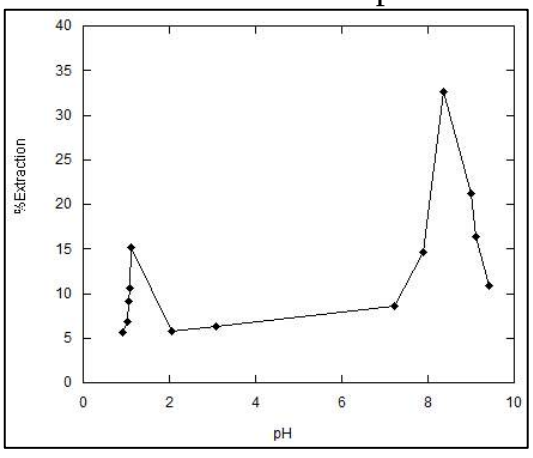

Figure 1. Effect of pH on extraction of selenium.

The considerable difference in represented graph is the sudden and severe accretion in the percent of extraction at the pH of 8.5. To find out the reason of the difference, the Pourbex graph of selenium in the hydrochloricmedia and ORP graph (Figure 2) of aqueous solutions in different pH values was taken into consideration. Evaluation of two graphs came into considerable and reliable results that can justify the unusual pH-%E curve of selenium.

Results illuminated that Se occurred in two complex forms, as SeO_3^{2-} and SeO_4^{2-}before and after the pH of 8.5, respectively. So that selenium could be in its tetravalent state before and after the mentioned pH, and in its hexavalent state at the pH of 8.5. Therefore, it can be denoted that selenium has its maximum extraction at TIBP system in its hexavalent state.

3.3 Effect of TIBP Concentration in the Organic Phase on Extraction of Se (IV)

In this study, the effect of the concentration of extractant TIBP was also examined with 5%, 10%, 20%, 30% and 40% (v/v) TIBP in kerosene at 25℃. Figure 3 shows an increase in Se extraction with an increase in TIBP concentration, but as it is clear, there is no significant enhancement in extraction of selenium by increasing the concentration of TIBP in organic phase. Figure 3 also illustrates that there is a severe accretion at the pH of 8.5 in all considered TIBP concentrations. Thus, in regards to the acquired pH-%E, and taking cost and consumption of the organic phase into account, a 20% (v/v) TIBP concentration in kerosene was chosen for all experiments, even though the higher TIBP concentrations showed a little higher extraction efficiency.

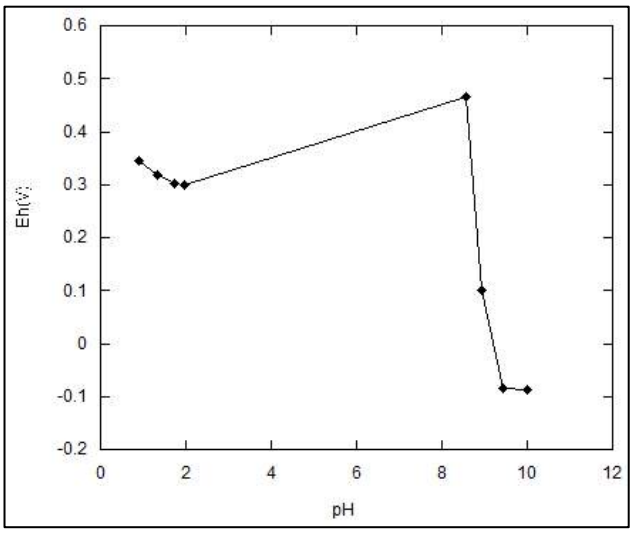

Figure 2. ORP graph of selenium extraction with 20% (v/v) TIBP.

3.4 Effect of Acid Concentration on Extraction of Se (IV)

The extraction was carried out with an aqueous solution of 0.05M Se (IV) and an organic solution containing 20% (v/v) TIBP in kerosene. The results presented in figure 4 imply that the extraction of Selenium (IV) does not have a considerable accretion by increasing the concentration of acid in the aqueous solution.

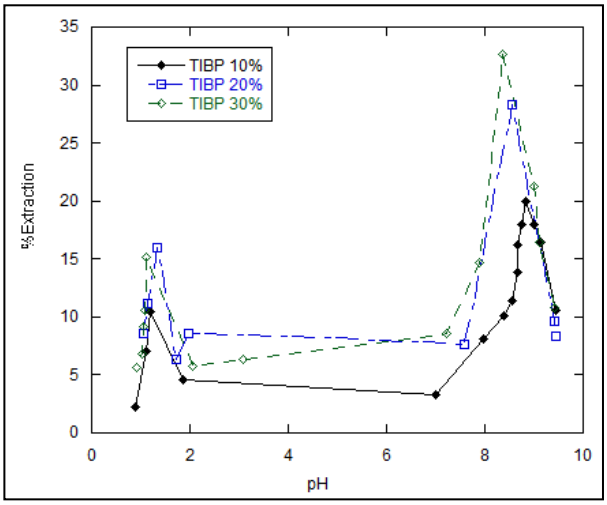

Figure 3. Effect of TIBP concentration on extraction of selenium.

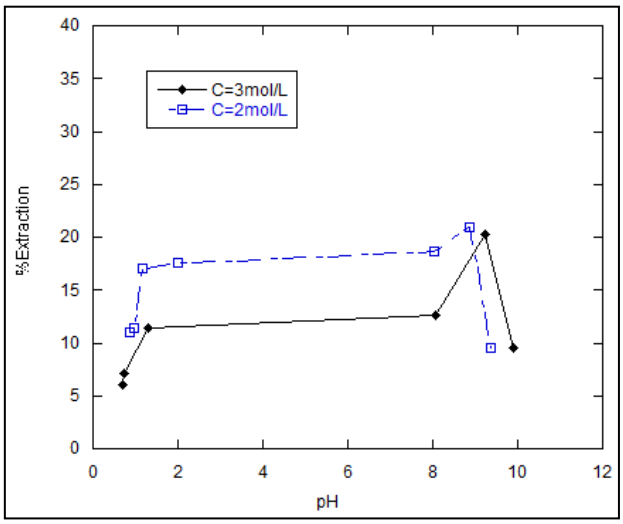

Figure 4. Effect of acid concentration on Se (IV) extraction at 25℃ and 20% (v/v) TIBP.

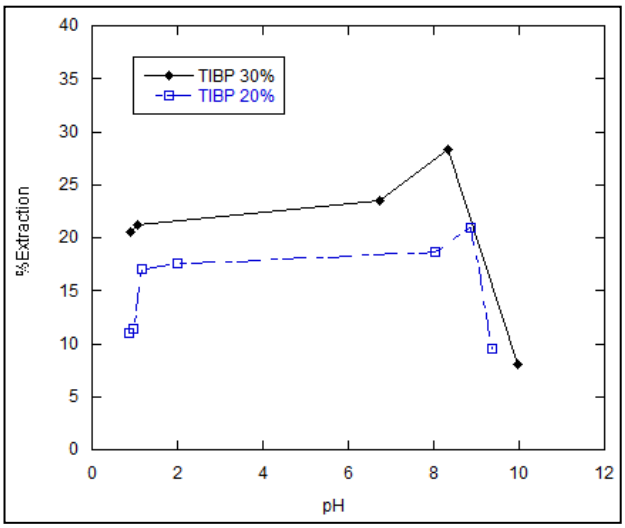

Figure 5. Effect of acid concentration on selenium extraction at 25℃and acid concentration of 2 mol/lit.

But it is shown in the figure 5 that by increasing acid concentration in aqueous solution and TIBP concentration in the organic solution from 20% (v/v) TIBP and to 30% (v/v) TIBP simultaneously, the maximum amount of extraction percentage is enhanced from almost 20% to 30% which can be considered as a useful parameter for improving selenium extraction efficiency.

3.5 Effect of Dodecanol as Modifier on Extraction of Se (IV)

In the second step of this study, Dodecanol was used as modifier for extraction of selenium in order to enhance the extraction percentage of Se (IV). The process was carried out with 20% (v/v) versus pH in the presence of Dodecanol and Dodecanol and 20% (v/v) TIBP in kerosene at 25℃. Figure 6 shows extraction percentTIBP in the organic phase. As it is clear in the figure, the extraction percent increased intensely at pH less than 1, whereas at pHs close to zero the extraction percent can be increased up to 99%. It can be concluded that the modifier's effect on extraction of Se (IV) is positive at lower pH and negative at higher pH.

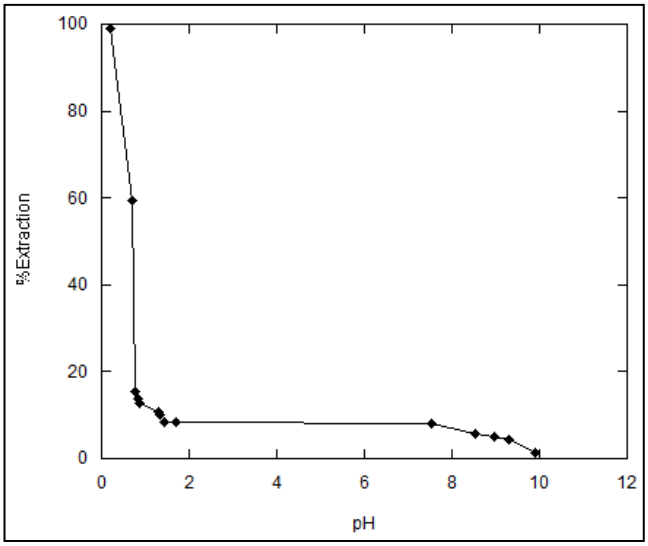

Figure 6. Effect of Dodecanol on etraction of selenium by TIBP at 25℃.

4 CONLUSION

In this paper, different parameters were studied for extraction of selenium species from an acid medium, such as pH, concentration of organic phase, and modifier. Considering cost and overall efficiency, it was shown that the extraction of selenium is better to be carried out with an organic solution containing 20% (v/v) TIBP diluted in kerosene, and ambient temperature. The pH-%E curves of extraction of selenium (IV) showed different behavior in the considered system. There was a severe accretion in extraction percentage in the pH of 8.5 which occurred as a result of the species of

selenium's alteration at the mentioned pH. Changing of different parameters did not have a considerable impact on enhancement of selenium extraction in TIBP system while using Dodecanol as a modifier has a significant effect on extraction of selenium by using Dodecanol, the extraction of selenium has a severe increase, specifically, at the pHs less than 1. Thus, the effect of modifier is positive at lower pH and negative at higher pH.

REFERENCES

Abdollahy, M., Shafaei, S.Z. 2004, Optimized Leaching Conditions for Selenium from Sar-Cheshme Copper Anode Slimes, *Iranian Journal of Chemistry and Chemical Engineering*, 23, 101-106.

Aeungmaitrepirom, W., Hagege, A., Asfari, Z., Vicens, J., and Leroy, M., 2001, Solvent Extraction of Selenate and Chromate Using a Diaminocalix[4]arene, *Journal of inclusion phenomena and macrocyclic chemistry*, 40, 225-229.

Chowdhury, M. and Sanyal, S., 1993, Separation by Solvent extraction of Tellurium (IV) with tri-n butyl phosphate: some mechanistic aspects, *Hydrometallurgy*, 32(2). 189-200.

Gupta, P., 2009, Deportment of Copper, Silver, Bismuth and Selenium during solvent extraction of gold, *A Master Thesis, Department of Metallurgical Engineering, University of Utah*.

Li, Q., Zhang, B., Min. X., Shen W., 2012, Leaching process of selenium residue, *Journal of Central South University* 19(9), 2440-2446

Sargar, B.M., Anuse, M.A., 2001, Liquid–liquid extraction study of tellurium(IV) with N-n-octylaniline in halide medium and its separation fromreal samples, *Talanta* 55, 469–478

Sarger, B.M., Mahamuni, S.V., Anuse, A., 2011, Sequential separation of selenium (IV) from tellurium(IV) by solvent extraction, *Journal of Suadi Chemical Society*, 15(2), 177-185

Swapnil, P.J., Sanjay, S.K., Sung, H.H., Mansing, A.A., 2013, Liquid-liquid Extraction of Selenium (IV) and Tellurium(IV) by N-*n*-octylcyclohexylamine followed by their Spectrophotometric Determination, *Research Journal of Chemical Sciences*, 3(1), 72-81.

Study of the Zircon Processing Aiming the Recovery of Zirconium and Silica

C.A. Ferreira, T.S. Formiga, C.A. Morais
Centro de Desenvolvimento da Tecnologia Nuclear – CDTN/CNEN Belo Horizonte, Minas Gerais - Brazil

ABSTRACT The zircon ($ZrSiO_4$) is the most abundant mineral of zirconium and the main source for the production of metallic zirconium, its compounds and alloys. The alkaline fusion with sodium hydroxide is the most widely used process in the chemical opening of zircon to obtain the metal zirconium. The present work describes the influence of the process variables in the alkaline fusion, zirconium dissolution from fusion product and in silica recovery steps. In the study of silica and zirconium dissolution two routes were investigated: the traditional alkaline an acid leaching and a new route in which just the acid leaching was used. In the alkaline fusion step, results showed that with a reaction time of 45 min, a NaOH/sample ratio of 1.3 is sufficient to achieve a complete fusion reaction. The leaching experiments showed that the direct acid leaching (new route) was able to obtain a good zirconium and silica separation. From a molten mass of zircon containing 31.8% ZrO_2, 14.1% SiO_2, 47.8% Na_2O and 5 % humidity, in the alkaline leaching a dissolution of approximately 73% of silica, a liquor containing about 20 g/L silica and a residue with 85% ZrO_2 and 10 % SiO_2 was obtained. In the direct acid leaching of the molten mass using HNO_3 as leaching agent, a dissolution of approximately 97% ZrO_2 and a residue containing 92% SiO_2 were obtained, with a mass reduction of approximately 80%.

Keywords: Zircon, silica and zirconium dissolution, leaching

1 INTRODUCTION

The zircon (ZrSiO4) is the most abundant mineral of zirconium and the main source for the production of metallic zirconium, its compounds and alloys. Zircon is a tetragonal zirconium orthosilicate and the chemical composition of the mineral mass contains approximately 65% of ZrO_2, 32% of SiO_2, and other elements at low concentrations, such as Hf, Fe and Ti (Habashi, 1997; Manhique et al, 2003; Bertolino et al, 2008). Due to high thermal and chemical stability, the decomposition of zircon requires drastic conditions. Different methods are used for the mineral decomposition, such as thermal or chemical decomposition at high temperatures. The alkaline fusion with sodium hydroxide is the most widely used process in the chemical opening of zircon to obtain the metal zirconium. This fusion occurs at temperatures between 550-700 °C. During the alkaline fusion, zirconium silicate ($ZrSiO_4$) is converted into sodium zirconate and sodium silicate. Also, the decomposition of zircon generates large ammounts of sodium silicate, along with zirconium oxide, according to Equation 1 (Abdel-Rehim, 2005).

$$ZrSiO4 + 4NaOH \rightarrow Na2ZrO3 + Na2SiO3 + H2O \quad (1)$$

The variables that affect the characteristics of the product of the fusion are: mass ratio, temperature and reaction time (ABDEL-Rehim, 2005; ZOLFONOUN et al 2010). According to BISWAS et al, 2010, considering the reaction presented in Equation 1, it is possible to form other products, besides zirconate and sodium silicate, such as Na_4SiO_4, $Na_2Si_2O_6$, $Na_6Si_2O_7$, $Na_4ZrSi_3O_{12}$.

Silica recovery from zircon is an alternative concerning the environmental and economic issue, since silica is an inorganic

material that can be widely used in a variety of applications such as resins, molecular sieves, catalyst carriers, as raw material in the glass, and electronic industry, amongst other applications. This removal is generally accomplished by alkaline leaching using water as a leaching agent. In this step there is a very high consumption of water and a highly pollutant effluent having a high content of silica is produced. An alternative method evaluated in this work was the leaching of sodium zirconate, keeping the silica insoluble. This new route can reduce the cost of the process with satisfactory results.

In this work, the influence of the following variables were investigated:

- alkaline fusion step: NaOH/sample ratio, temperature and reaction time;
- alkaline leaching: solid percentage, temperature and reaction time;
- acid leaching: acid concentration, temperature and reaction time.

In the study of silica and zirconium dissolution, two routes were investigated: the traditional alkaline an acid leaching and a new route in which just the acid leaching was used.

2 METHODOLOGY

2.1 Reagents

The sample of zircon concentrate used in this work was provided by the Nuclear Industries of Brazil - INB. Prior to this study, the decomposition of the zircon concentrate by alkaline fusion with sodium hydroxide was performed. In the study of the separation of Zr/Si; 100 kg of zircon concentrate was melted, generating approximately 200 kg of molten mass (alkaline melt product). The sample was homogenized and reduced to fractions of different masses in order to enable the laboratory experiments and the chemical characterization. The sodium hydroxide used was of commercial grade (99% w/w) and the nitric acid (HNO_3) was of analytical grade. Distilled water was used for alkaline leaching as well as for solutions preparation.

2.2 Experiments Methodology

The zircon fusion experiments were carried out by using iron crucible in a furnace at the specified temperature and time. The alkaline fusion efficiency was investigated through X-ray diffraction, where the unreacted zircon and fusion products phases were identified.

The leaching studies were performed in a 250 ml beaker using mechanical agitation at controlled temperature. After the reaction time stated, the pulp was vacuum filtered using buchner funnil and kitasato. After filtration, the solid was transferred for drying in an oven at 110°C. Then the residue was weighted and the volume of the filtrate was measured and sent to chemical analysis. The metals present in the residue and in the leaching liquor were analyzed by Energy Dispersive X-ray Fluorescence Spectrometry - EDXRF - using an X-ray spectrometer of dispersive energy brand SHIMADZU, model EDX-720. The nitrate content in the liquor was determined by molecular absorption spectrophotometry in the ultraviolet region (302nm) using an UV – visible spectrometer, brand VARIAN model Cary 50 conc.

The new route experiments were conducted similarly to previous experiments. Experimental conditions are shown in Table 1. Experiments 1 to 3 were carried out in order to precipitate the solubilized silica and experiments from 4 to 6 were the continued leaching of the waste generated in the previous experiments. The experiment number 7 was similar to previous experiments, but without drying the residue after the first leaching. In experiment 8 was conducted a sequential leaching without the separation of the first reaction residue, as follow: in a beaker was added 40 ml of HNO_3 3.0 mol/L, left under stirring for a period of 4 hours and then added 85 mL of HNO_3 3.0 mol/L to complete the zirconium dissolution.

Table 1. Experimental conditions of direct acid leaching

Test	H_2O (ml)	Sample mass (g)	HNO_3 3mol/l (ml)
Zrlac-T1	10	10,0	25
Zrlac-T2	20	20,0	44
Zrlac-T3	30	30,0	58
Zrlac-T4	10	4,7	45
Zrlac-T5	10	9,4	85
Zrlac-T6	10	16,1	144
Zrlac-T7	40	20,0	40+85
Zrlac-T8	40	20,0	40+85

3 RESULTS AND DISCUSSION

3.1 Chemical Characterization

The chemical composition of the main components of the zircon concentrate and of the molten mass (fusion product) of zircon used in the experiments of recovery of silica is shown in Table 2 below.

Table 2. Chemical composition of zircon before and after the alkaline fusion

Species	Sample/Content (%)	
	Zircon	**Fusion Product**
ZrO_2	65.0	31.8
SiO_2	29.0	14.1
HfO_2	1.33	0.57
Na_2O	-	47.8
H_2O	-	5.70
Er_2O_2	0.58	-
Y_2O_3	0.18	-
Al_2O_3	2.22	-
TiO_2	0.94	-
Fe_2O_3	0.53	-
BaO	0.58	-

3.2 Alkaline Leaching

The chemical opening of zircon performed through fusion with sodium hydroxide produces a strongly alkaline molten mass. This allows to use water as the leaching agent for the dissolution of the sodium silicate formed during melting. In the study of silica dissolution with water (alkaline leaching) the following process parameters were investigated: solids percentage (sample/water ratio) temperature and reaction time.

Variation of the solids percentage and the temperature

The influence of the solids percentage and temperature on the sodium silicate dissolution was investigated for percentages of 10%, 15%, 20% and 30% at temperatures of 25°C and 70°C with a reaction time of two hours. The results are presented below in Table 3.

Table 3. Effect of the percentage of solids in the dissolution of sodium silicate generated in the alkaline fusion of zircon

Percentage of Solids	Temperature (°C)	Dissolution (%)
10	25	73
10	70	76
15	25	75
15	70	73
20	25	72
20	70	72
30	25	71
30	70	72

As can be seen in Table 3, the influence of the percentage of solids and the temperature on the dissolution of sodium silicate was not significant. However, one can observe a slight tendency towards higher dissolution in solids percentages between 10 and 15%. In the intervals investigated, the dissolution of the silicate ranged from 71 to 76%,

considering an experimental error of about 4%, it can be said that the dissolution of the silicate present in the fusion product is not influenced by temperature.

Reaction time

The reaction time was investigated ranging from 1 to 6 hours, within a percentage of solids of 10% and at room temperature. The results showed that there was only a slight variation in the percentage of the silicate dissolution – 73 to 76%. Considering the small difference in the silicate dissolution obtained in this step of the study, the reaction may be conducted with 1 hour of stirring at room temperature.

Final products of the alkaline leaching

At the end of the experiments presented in this paper, an alkaline liquor containing approximately 15 g/L of Si and a residue containing 89% of ZrO_2 and 6.7% of SiO_2 was obtained. The silicon present in the liquor was precipitated through acidification with hydrochloric acid 5.0 mol/L up to pH 1.0. The chemical composition of the alkaline solution, the residue of leaching and silica obtained in the neutralization liquor is given in Table 4. The mass reduction in the alkaline leaching was approximately 45%. The dissolution of the residue of the alkaline leaching with HNO_3 generated a liquor containing around 50g/L Zr, 2.5 g/L Si, 3.5 g/L Na, 1.0 g/L Hf and 0.2 g/L Fe. The yield of the dissolution of Zr and Hf from the residue of the alkaline leaching was 97%.

Table 4 – Chemical characterization of the products of the alkaline leaching

Species	Sample/Content (%)		
	Alkaline Liquor (g/L)	**Residue of leaching (%)**	**Silica (%)**
SiO_2	31.1	6.73	95.3
ZrO_2	0.09	89.4	2.30
HfO_2	0.002	0.96	0.09
Na_2O	67.1	0.98	0.57
Fe_2O_3	-	1.14	0.04
TiO_2	-	0.54	-
CaO	0.08	0.26	0.20

3.3 Acid Leaching

As shown in Table 3, the residue of the alkaline leaching had a SiO_2 content of 6.7%, which is not desirable in the process. Therefore, another process route was investigated; the dissolution of Zr without previously removing the silicon. The dissolution of Zr was made by leaching with HNO_3 in a beaker using mechanical stirring at controlled temperature. The process variables investigated were: acid concentration, temperature and reaction time.

Variation of the concentration of HNO3 and temperature

The influence of the concentration of HNO_3 in the dissolution of zirconium from the fusion product was investigated at the range of 4 mol/L to 12 mol/L at three different temperatures: 25°C, 50°C and 70°C. The experiments were performed in triplicates and the results are shown in Figure 1. As seen in Figure 1, there is an increased dissolution of Zr as the temperature increases. The influence of temperature is more significant for lower concentrations of HNO_3 (4.0 mol/L). The dissolution of silica was below 2% for all the concentrations of HNO_3 investigated. The subsequent experiments were carried out in acidity of 12 mol/L. The high acidity of HNO_3 is justified by the fact that in the next stage of the study, which comprises the separation of Zr/Hf by solvent extraction, is performed at high acidity. The behavior of Hf was similar to that of Zr and therefore was not reported in Figure 1.

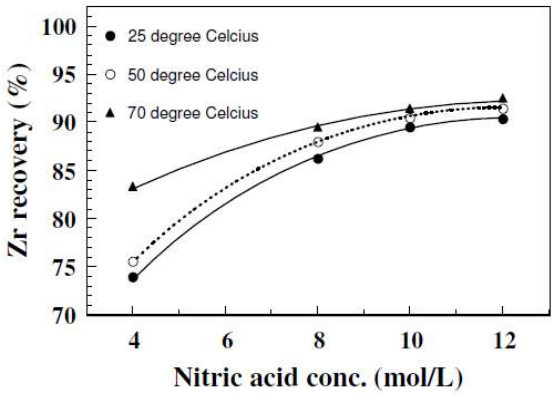

Figure 1 Influence of temperature and HNO_3 concentration in the dissolution of zirconium.

Reaction time

The reaction time was varied from 0.5 to 4 h, using a HNO_3 concentration of 12.0 mol/L (ratio acid/water of 3:1) at a temperature of 70°C and using a percentage of solids of 10%.

The experiments indicated a progressive increase in the dissolution of the zirconium with an increase of time, however negligible. For the reaction time of 30 min. (0.5 h), the dissolution of Zr was approximately 89% and 95% for the time of 4 hours. The results are shown in Table 4 below. The dissolution of Si was lower than 2% in all experiments.

Table 4 Effect of reaction time on the SiO_2 and Zr dissolution

Time (h)	Zr Dissolution (%)	Hf Dissolution (%)	Si Purity (%)
0,5	88,7	85,6	84,2
1,0	91,5	89,4	85,5
1,5	92,0	91,2	86,5
2,0	92,7	92,7	86,7
2,5	94,0	92,0	88,7
3,0	92,9	91,6	87,0
4,0	94,9	93,5	89,3

New Route (direct acid leaching)

The new route is presented as a great option for the dissolution of zirconium present in the material. This methodology reduced one step in the process, and did not need the prior dissolution of silica by alkaline leaching neither the zirconium precipitation with ammonium sulfate.

In preliminary studies (experiments 1 to 3), a low zirconium dissolution was observed, because the amount of added acid was not sufficient for a complete zirconium dissolution. This low zirconium dissolution can also be noted for experiments 4 to 6 due to the low solubility of the second leaching step residue, observed by the sample mass (first leaching residue) and the residue mass obtained in these experiments.

From a molten mass of zircon containing 31.8% ZrO_2, 14.1% SiO_2, 47.8% Na_2O and 5 % humidity, in the alkaline leaching a dissolution of approximately 73% of silica, a liquor containing about 20 g/L silica and a residue with 85% ZrO_2 and 10 % SiO_2 was obtained.

After optimization of the direct acid leaching of the molten mass using HNO_3 as leaching agent, a dissolution of approximately 97% ZrO_2 and a residue containing 92% SiO_2 were obtained, with a mass reduction of approximately 80%.

4 CONCLUSION

The previous dissolution of the sodium silicate by acid leaching before the dissolution of the zirconium, is already being used industrially, however the drawback of this route is the high water consumption, as water plays an important role in the sustainability of the environment. The route of zirconium leaching without the prior leaching of sodium silicate has the advantage of demanding lower water consumption besides saving one step in the purification of zirconium.

The leaching experiments showed that the direct acid leaching (new route) was able to obtain a good zirconium and silica separation. As shown in these results, the zirconium dissolution increased considerably when compared with previous experiments.

ACKNOWLEDGEMENTS

The Authors are grateful to FAPEMIG, FINEP, CNPq and CAPES for the financial support and also would like to thank CDTN's technicians involved in this study, mainly Luiz C. da Silva and Liliane P. Tavares.

REFERENCES

Abdel-rehim, A.M. (2005). 'A new technique for extracting zirconium from Egyptian zircon concentrate', *International Journal of Mineral Processing*, Elsevier, pp. 234–243.

Banda R., Young Lee, H., Seung Lee, M. Separation of Zr from Hf in Hydrochloric Acid Solution Using Amine- Based Extractants. American Chemical Society. Ind. Eng. Chem. Res. v. 51, p. 9652−9660, 2012.

Bertolino, L.C.; Palermo, N.; Sampaio, J.A.; França, S.C.A. (2009) *Zirconita, Rochas & Minerais*

Industriais: Usos e especificações, *Cetem/MCT*, pp. 917–930.

Biswas, R.K.; Habib, M.A.; Karmakar, A.K.; Islam, M.R. (2010) 'A novel method for processing of Bangladeshi zircon: Part I: Baking and fusion with NaOH.', *Hydrometallurgy*, Elsevier, vol. 103, pp. 124–129.

Brown, A.E.P., Wain, A.G. Separation of zirconium from hafnium in nitric acid solutions by solvent extraction using dibutyl butylphosphonate - part 2. Mixer-settler runs. Hydrometallurgy, v. 3, Amsterdam, p. 275-282, 1978.

Habashi, F. (1997) *Handbook of Extractive Metallurgy*, Wiley-VCH, vol. 3, pp. 1649–1684.

Manique, A.; Kwela, S.; Focke, W.W. (2003) 'The wet process for the beneficiation of zircon: optimization of alkali fusion step.', *Industrial & Engineering Chemistry Research.*, American Chemical Society, vol. 42, pp. 777– 783.

Zolfonoun, E.; Monji, A. B.; Taghizadeh, M.; Ahmadi, S. J. (2010) 'Selective and direct sorption of zirconium from acidic leach liquor of zircon concentrate by rice bran.', *Minerals Engineering, Elsevier*, vol. 23, pp 755–756.

Sulfation Roasting and Water Leaching of Lepidolite

T.T. Hien-Dinh, R. Gieré
Earth and Environmental Sciences, Albert-Ludwigs University, Albertstr. 23b, D-79104 Freiburg, Germany.

V.T. Luong, T. Tran
Department of Energy and Resources Engineering, Chonnam National University, 300 Yongbong-Dong, Buk-Gu, Gwangju 500-757, South Korea.

ABSTRACT Lithium extraction from a lepidolite concentrate was studied by roasting in the presence of the additives S+CaO or FeS+CaO and subsequent leaching by water. Thermodynamic models were used to forecast the dependence of the roasting process on various parameters (e.g., temperature, molar ratios of S/Li and Ca/F). Simulations and preliminary experimental results showed that various Li-compounds (e.g., $LiKSO_4$, Li_2SO_4) were formed and that SO_2 and SO_3 played a significant role in lithium liberation. Moreover, addition of Fe seems to greatly benefit lithium extraction: roasting in the presence of S+CaO and FeS+CaO resulted in extraction of up to 23.1% and 75.4% Li, respectively. The absence of Fe during roasting appears to cause formation of spodumene ($LiAlSi_2O_6$) and eucryptite ($LiAlSiO_4$), which could hinder formation of other, water-soluble lithium compounds. Addition of CaO led to a decrease in the liberation of HF gas.

Keywords: Lepidolite, lithium, roasting, leaching

1 INTRODUCTION

Lithium, the lightest metal, is used for many industrial applications, such as electric vehicles, batteries, ceramics, glass, lubricating greases, air treatment, metallurgy, polymers, pharmaceuticals, and primary aluminum production. The global total demand of lithium in industries has been increasing every year. The world total of mine production in 2011 was 34100 million tons, increasing to 37000 million tons in 2012 (USGS 2013).

Lepidolite sulfation during the roasting process has the purpose to form new Li compounds, which dissolve in water. Prior experimental work confirmed the efficiency of this method by using lepidolite in combination with various compounds: Na_2SO_4, K_2SO_4 and CaO (Yan et al 2012b), Na_2SO_4 and CaO (Luong et al 2013); $FeSO_4.7H_2O$ and CaO (Luong et al 2014), and Na_2SO_4 + $CaCl_2$ (Yan et al 2012a).

The present study investigates the effects of using S and FeS with CaO as the additives for roasting lepidolite and reports preliminary results.

2 EXPERIMENTAL

2.1 Material

The lepidolite (1.55 wt. % Li) used in this study was collected in the La Vi area, Quang Ngai province, Vietnam, where it occurs a major component of an albite granite. Chemical and mineral compositions of the lepidolite concentrate are shown in Table 1 and Figure 1.

2.2 Equipment and Chemicals

Major components of the concentrate and leach liquors were determined by X-Ray Fluorescence (XRF) and atomic absorption spectroscopy (AAS), respectively.

Table 1. Chemical composition of lepidolite (wt. %)

SiO_2	Al_2O_3	Fe	Mn	Mg	Ca	Na	K	Cs	Rb	Li	P	F
54.67	25.10	0.25	0.39	0.6	0.71	1.16	6.82	0.063	0.8	1.55	0.12	2.91

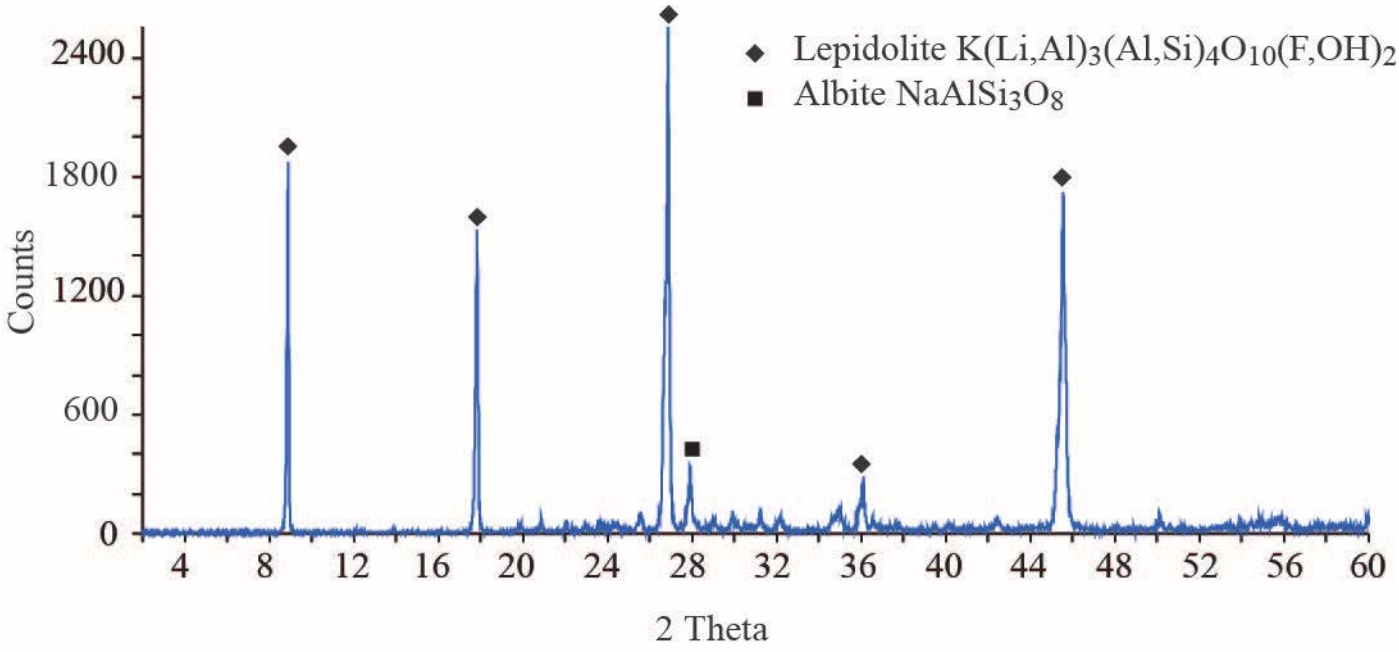

Figure 1. XRD pattern of lepidolite

Minerals contained in the lepidolite concentrate were identified by X-ray diffraction (XRD), followed by Rietveld refinement using the BRUKER Topas 4.2 software.

Roasting tests were carried out in a tube furnace with a gas supply system, whereas leaching was conducted by using hot plates with magnetic stirring bars.

All chemicals used were of analytical grade and were purchased from Merck and Alfa Aesar.

2.3 Experimental Techniques

The lepidolite and the additives were first mixed at specified molar ratios of S/Li and Ca/F. The mixtures were then placed in the furnace for roasting at various temperatures and durations. Calcines obtained after roasting were cooled down to ambient temperature, followed by being finely ground. The pulverised calcines were subsequently leached in distilled water at different temperatures, mass ratios of water/calcine and time. The flowchart of the process is illustrated in Figure 2

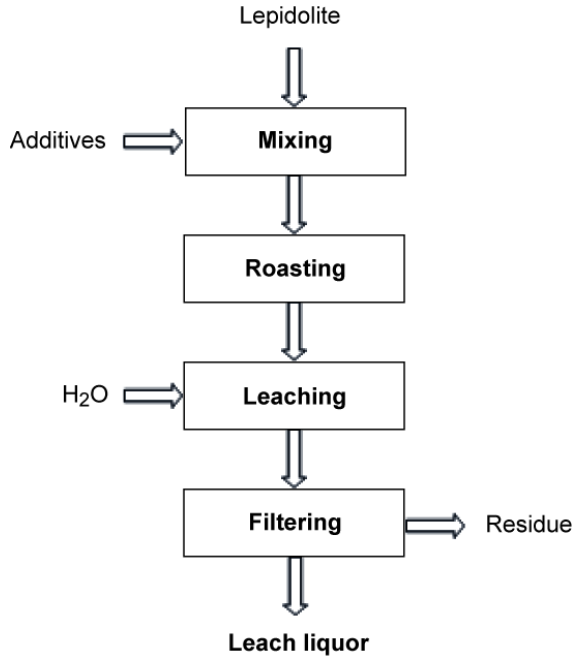

Figure 2. Flowchart of lepidolite processing.

3 RESULTS AND DISSCUSSION

3.1 HSC Modelling

The outcome models of roasting lepidolite and the additives simulated by the HSC software (Outotec 2011) were shown in Figure 3. Roasting lepidolite with the mixture of S and CaO resulted in $LiKSO_4$ and Li_2SO_4 as major solid compounds with a minor amount of $LiAlSiO_4$. A similar result was also indicated when FeS was used, but in addition other compounds of Fe including Fe_2O_3, Fe_2O_3(G), $LiFeO_2$ were created. In both cases, high quantities of SO_2 and SO_3 were liberated in parallel with the presence of HF and LiF gases. Luong et al 2014 suggested that SO_2/SO_3 formed during the decomposition of $FeSO_4.7H_2O$ played a key role in the extraction of lithium from lepidolite based on HSC modelling and LOI (loss on ignition) obtained from experiments. Similarly, roasting lepidolite with S or FeS would also create SO_2/SO_3 gases generated through oxidation as observed in Figure 3. A gas-solid interaction of the gases with lepidolite was therefore also believed to be a factor controlling the extraction of Li in the form of $LiKSO_4$ and Li_2SO_4 in this study.

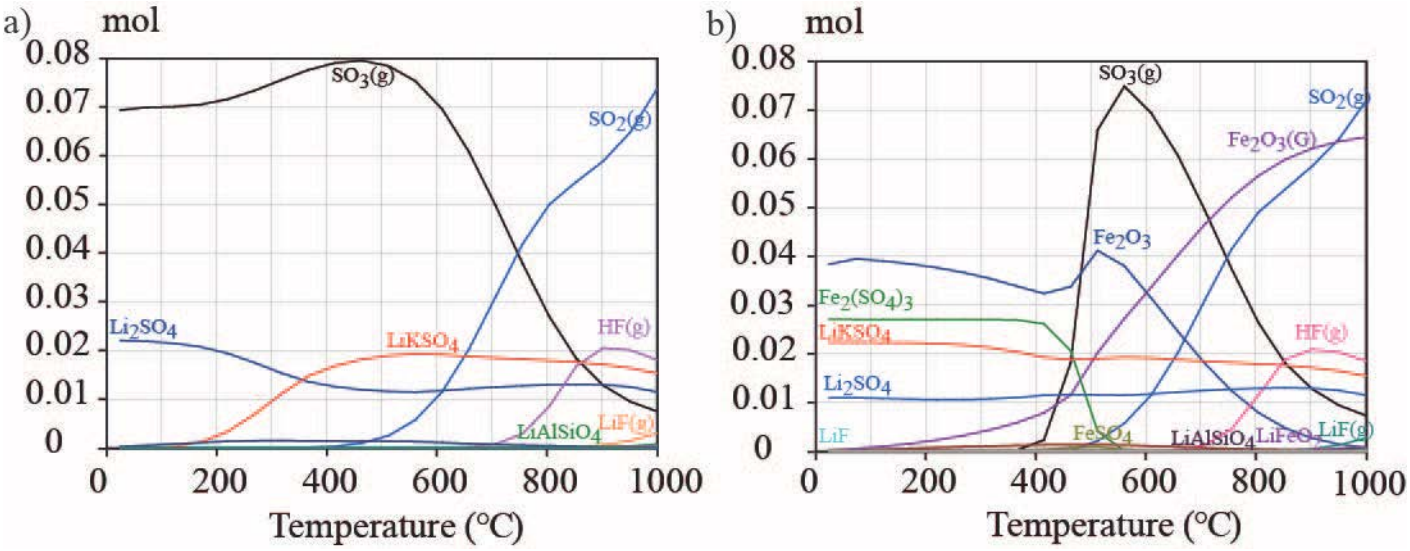

Figure 3. HSC models for roasting of a) lepidolite and S, b) lepidolite and FeS at S/Li molar ratio of 3/1. *Abbreviation*: G = gamma, g = gas.

3.2 Extraction of Lithium from Lepidolite

To investigate the role of SO_2/SO_3 gases on the extraction of lithium, both open and closed roasting systems were performed as described in Luong et al 2014. An S/Li molar ratio of 3/1 was applied for mixtures of the concentrate with S or FeS. There was an indication that roasting in the closed system at 800°C-950 °C resulted in ~5-16 % Li extraction when S was used as the additive. The recovery of lithium was sharply increased when S was replaced by FeS, in which case ~57 % of Li was extracted at 850-900 °C. However, using the open system for roasting of lepidolite and the additives could greatly enhance the amount of soluble lithium compounds created as well as reduce the amount of thermal energy required for the optimal extraction of lithium. As shown in Figure 4, a maximal Li recovery of ~75.4 % was attained at temperature of 750 °C after 1.5 h roasting using mixtures of lepidolite and FeS. Meanwhile, the improvement in Li extraction from lepidolite-S mixtures seemed to be negligible.

The effect of roasting manners on Li extraction seemed to be incompatible with that obtained from Luong et al 2014, in which roasting in the closed system yielded higher extractions of Li. However, the behaviour of S and FeS is different from $FeSO_4.7H_2O$ indeed. Heating of $FeSO_4.7H_2O$ could directly liberate SO_2 during its decomposition, which

subsequently interacts with lepidolite to release Li. In contrast, S and FeS first needed to be oxidised to form SO_2/SO_3 that required ventilation for a supply of oxygen.

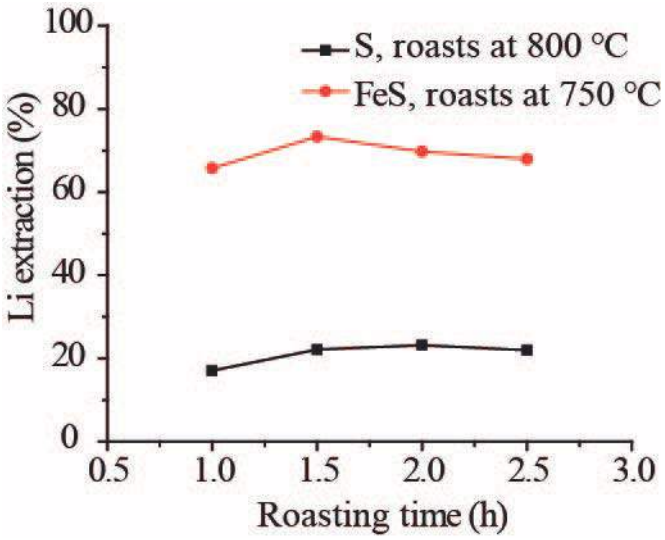

Figure 4. Effect of roasting time on Li extraction from lepidolite-S and lepidolite-FeS mixtures at S/Li molar ratio of 3/1. Leaching at 85 °C for 2h, using water/calcine mass ratio of 5/1.

On the other hand, the gases created could be rapidly lost before reacting with lepidolite if no cap was used to cover crucibles. As a result, the maximal extraction of Li, as obtained by Luong et al 2014 when iron sulphate was utilised, could not be achieved. Finally, roasting in the open system was more suitable for mixtures of lepidolite and either S or FeS.

The use of CaO as secondary additive during sulfation roasting of lepidolite lowers the amount of HF gas liberated due to the formation of CaF_2, as also reported by Luong et al 2014 and Yan et al 2012b. A Ca/F molar ratio of 1/1 was found to effectively decrease the liberation of HF gas with an insignificant influence on the lithium extraction in this study.

Microscopy and electron probe microanalysis (EPMA) were used to observe the external morphology of calcines obtained from roasting. Lepidolite seemed to be slightly decomposed when being roasted with S. Only the rim of lepidolite particles was metamorphosed during roasting while their surfaces were contaminated by the additives (Fig. 5a). In contrast, lepidolite was obviously affected by FeS, causing a conversion to new compounds as shown in Figure 5b.

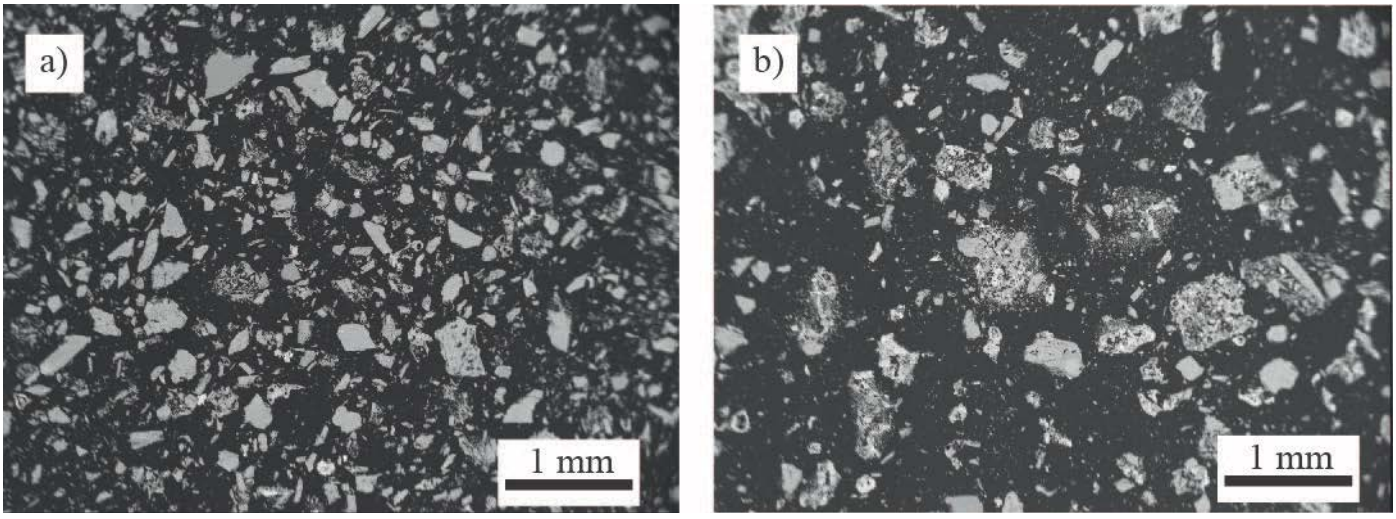

Figure 5. BSE images of calcines roasted at S/Li molar ratio of 5/1 and a) at 800 °C for 2h using S, b) at 750 °C for 1.5h using FeS.

XRD patterns of calcines obtained from roasting of lepidolite and the additives using the optimal conditions are shown in Figure 6. It was noticeable that lepidolite was still present in the calcine after roasting with S as seen by its clear peaks (Fig. 6b). Other compounds such as CaF_2 and $CaSO_4$ were formed due to the addition of CaO.

Meanwhile, lepidolite seemed to have completely disappeared when FeS was utilised, resulting the dominance of Fe_2O_3 peaks (Fig. 6c). The existence of Li_2SO_4 and $LiKSO_4$ in the calcines was also found, but these phases exhibit poor crystallinity. Thus, the effectiveness of FeS compared to S on the extraction of lithium from lepidolite was evident.

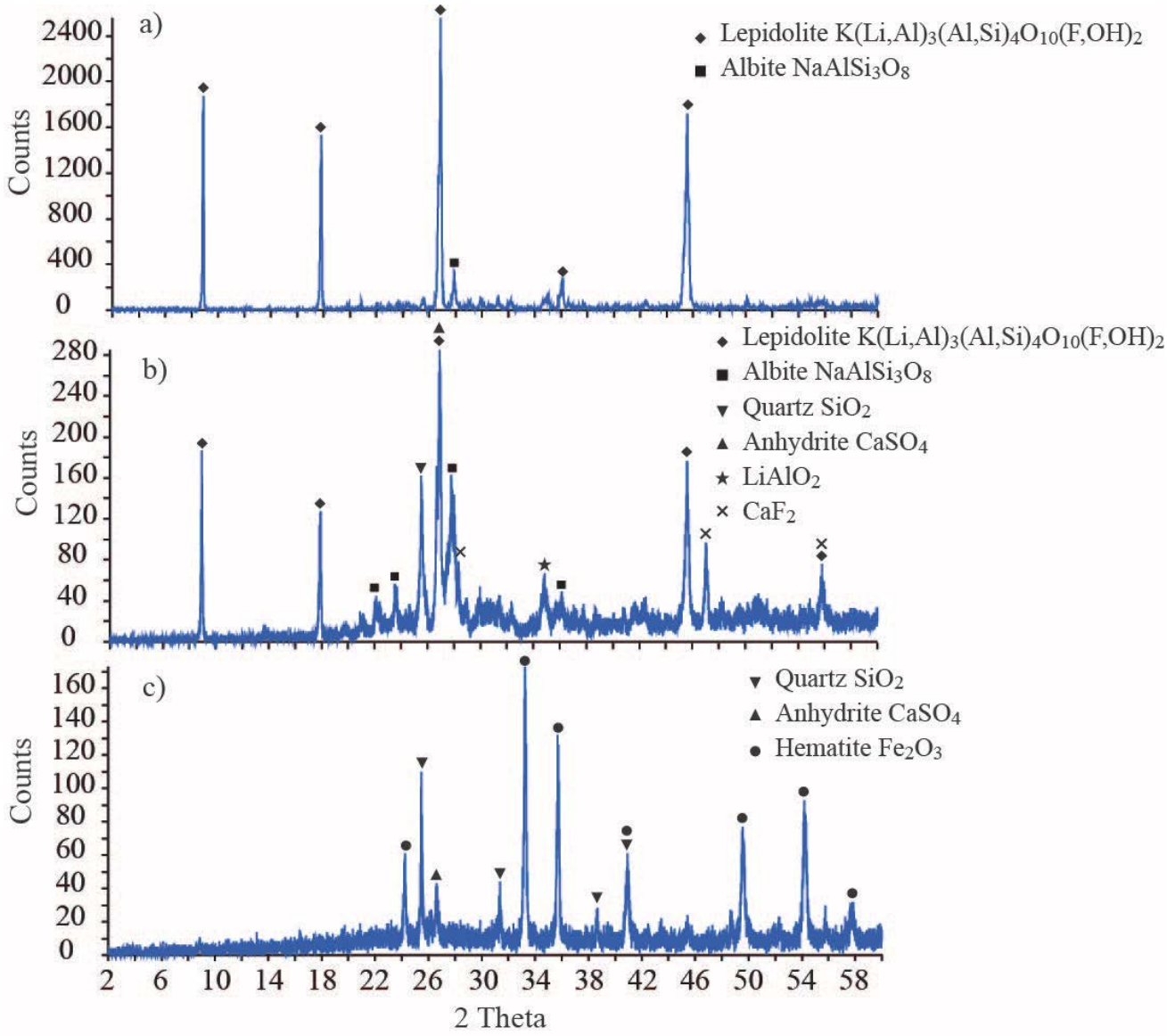

Figure 6. XRD patterns of a) lepidolite, b) calcine at 800 °C for 2h using S, c) calcine at 750 °C for 1.5h using FeS. Roast using S/Li molar ratio 5/1.

4 CONCLUSIONS

The extraction of lithium from lepidolite via sulfation roasting and water leaching was experimentally performed based on HSC thermodynamic models. It was found that using FeS as the additive could extract a maximum of ~75 % Li from lepidolite in the open roasting system. Sulphur (S) was found to be an unsuitable additive for the recovery of Li due to a low extraction obtained (~23 %). The usefulness of FeS compared to S was confirmed by EPMA and XRD. The role of CaO in lowering the formation of HF gas was also tested.

5 ACKNOWLEDGEMENTS

We like thank Dr. Hiltrud Müller-Sigmund, Isolde Schmidt, Sigrid Hirth-Walther for laboratory assistance. This study is the part of the PhD work of the first author and is

financial supported by scholarship of Vietnamese Government (project 322) and German Academic Exchange Program (DAAD).

REFERENCES

Luong V.T. et al, 2014. Iron sulphate roasting for extraction of lithium from lepidolite. Hydrometallurgy. 141, 8–16.

Luong V.T. et al, 2013. Factors affecting the extraction of lithium from lepidolite. Hydrometallurgy. 134–135, 54–61.

Outotec, 2011. HSC chemistry software, version 7.1.

USGS-US Geological survey, 2013. Minerals Commodity Summareis-lithium. USGS, Virginia. ISBN 978–1–4113–3548–6, 94-95.

Yan Q. et al, 2012a. Extraction of valuable metals from lepidolite. Hydrometallurgy. 117–118, 116–118.

Yan Q. et al, 2012b. Extraction of lithium from lepidolite by sulfation roasting and water leaching. International Journal of Mineral Processing, 110–111, 1–5.

Recycling

Comparison of Two Consolidation Methods of Waste Fill in Longhole Open Stoping

S.B. Avcı, İ. Erdem
Eldorado Gold, Efemcukuru Gold Mine, İzmir, Turkey

ABSTRACT: Longhole Open Stoping and Drift & Fill are commonly utilized mining methods in underground metal mines in Turkey. Both of these methods are employed at Efemcukuru Gold Mine. The primary mining method of Efemcukuru Gold Mine is drift and fill due to being appropriate for selective mining. As a secondary mining method, longhole open stoping is used because of its high production rate, low dilution and low operating costs. In this method, standard drilling-blasting and material handling operations are utilized as indicated in the technical methodology. Also the backfilling stage can be changed according to the stope conditions. Generally paste fill is used in backfilling operation at Efemcukuru Gold Mine. However for longhole open stoping, the backfilling operation is generally done by waste fill material in order to disposal of development waste.

The purpose of this paper is regarding the usage of waste fill material in the longhole open stoping method. Subsequently this requires a suitable consolidation method of the waste material in order to produce from the next stope.

Keywords: Longhole open stoping, drift and fill, Efemcukuru Gold Mine

1 INTRODUCTION

Efemcukuru Gold Mine is located approximately 20 km southwest of İzmir/Turkey as one of the ongoing operations of Eldorado Gold Corporation (Fig. 1). Efemçukuru is an intermediate sulfidation epithermal gold deposit hosted within Upper Cretaceous phyllite and schist at the western end of the Izmir-Ankara Suture Zone in SW Turkey.

Figure 1. Location of Efemcukuru Gold Mine.

The orebody is crosscut by hornfels, phyllites and rhyolite dikes. The primary vein is the Kestane Beleni which is the focus of ore production in the first step of the mine life. The secondary vein is known as Kokarpinar that outcrops approximately 450m northeast of the Kestane Beleni Vein (Fig.2). There are three types of orebody generated inside the Kestane Beleni vein, which are South Ore Shoot (SOS), Middle Ore Shoot (MOS) and North Ore Shoot (NOS).

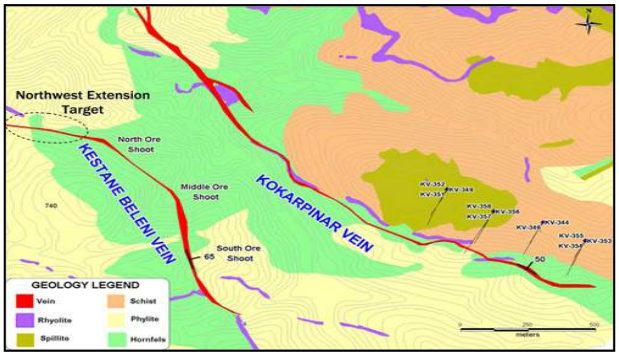

Figure 2. Geological Map of Efemcukuru Site.

2 MINING METHODS

There are mainly two underground mining methods based on 100% extraction with minimum or no dilution. These are the drift & fill and the longitudinal longhole open stoping mining methods. The Drift & Fill mining method is used as the primary mining method since it enables selective mining. As a secondary mining method, longitudinal longhole stoping is used where suitable ore and host rock properties are available. Important factors for selecting the mining method can be listed as below;

- Orebody characteristics; size, shape, dip angle, strike
- Host rock conditions; RQD, ground support requirements, structures
- Grade of ore, mining dilution and recovery

Level by level these factors are analyzed to determine the appropriate mining method. The decision of the mining method for a level is carried out by the long term mine planning engineer and designs are kept up-to-date annually as part of the life of mine process.

2.1 Drift & Fill Mining Method

The Efemcukuru Gold mine employed drift-and-fill mining method as the primary ore production method. The Kestane Beleni vein is the current working orebody and has varying thickness throughout its strike. Drift and fill is a cost intensive method of mining that is done in areas where rock conditions are challenging (Fig. 3). Rather than opening a large excavation in soft rock conditions which may be difficult to hold, ore is taken out by a number of stopes that are mined along the ore strike and then filled with paste fill at the closure phase of the stop.

The orebody is accessed from three ramp systems from the footwall. The main levels are at 80 m vertical intervals with sublevels at 20 m. Footwall drifts are driven from the level accesses across to the orebody and crosscuts are driven from the footwall drives as lifts (C1, C2, C3, and C4) with approximately 45 m length and inclination of %17. The production stopes are driven approximately 5 m height and 4.5 m width. The shape of a stope generally follows the shape of the orebody, from which the side walls can be 55 to 60 degrees, angled according to the hanging wall inclination. The length of the sill drifts depend on the thickness of the orebody and its grade.

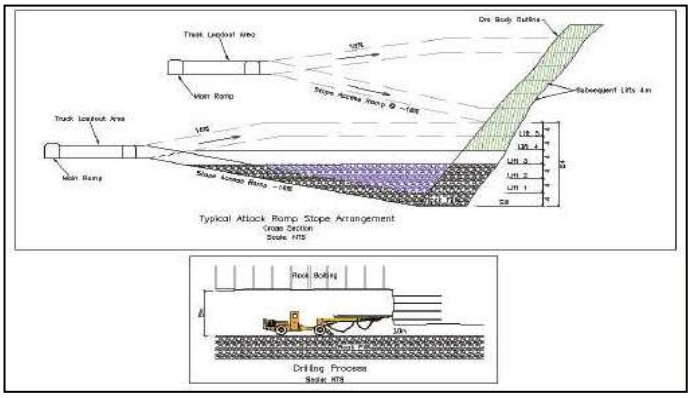

Figure 3. Sample Scheme for Drift & Fill Mining Method.

The average length of the production stopes is approximately 75 m from the crosscut to the left and right sides of the orebody, which indicates the interval between the crosscuts entrances from footwall drives. In the drift & fill mining method, the backfilling material is paste fill at all C1, C2, C3 and C4 lifts.

2.2 Longhole Open Stoping Method

The secondary mining method utilized at the Efemcukuru Gold Mine is longhole open stoping. The longhole open stoping method can be applied in stable footwall and hanging wall conditions, suitable vein dip and thickness. Vertical stope production comprises of the extraction of a 15 m height between two drifts.

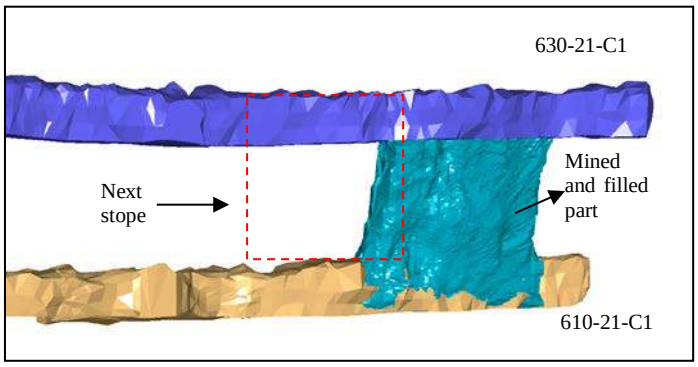

Figure 4. Longhole Open Stoping between 630-610 levels and the next stope to produce.

The minimum ore production width is 0.75 m and a maximum width of 6.5 m. In this mining method; first sill (C1) of the lower level and first sill (C1) of upper level are mined (Fig. 4). Then blast holes are drilled from C1 lower level to the upper level and blasted to create an initial opening named "slot". The slot is often the most difficult, and costly component of mining. After blasting the stope, the rest of the orebody is blasted towards to the slot void. Then, remote control LHDs muck the blasted material from the lower level. After the drilling-blasting and mucking operations, the filling takes place before commencing the initial stage of the adjacent stope. At Efemcukuru Gold Mine, the longhole stopes are generally filled with waste material for disposal of development waste.

Consolidation of the filled void is critical to provide a stable area and to prevent dilution when producing from the next stope.

3 FILLING AND CONSOLIDATION OPERATION OF MINED LONGHOLE STOPES

As the final step of the longhole open stoping method, waste fill is used as backfill material in the stope void. Waste fill is a loose rock material (generally from capital development) and has the potential to dilute future stopes. In order to consolidate the waste material to prevent dilution, two methods have been applied; (i) cement grouting with self-drilling bolts and (ii) consolidation of waste material by shock blasting.

3.1 Consolidation with Grouting Bolts

In Figure 4, the waste filled stope is indicated as the blue color and prior to commencing the ring blasting of the next stage, the filling material of the previous void must be consolidated. This process is undertaken by self-drilling bolts which are named "IBO Bolts". These bolts have sacrificial 51mm bits that enable grouting while drilling (Figure 5).

Self-drilling bolts are used for consolidation or reinforcement of loose material.

Figure 5. IBO Bolts Used in Consolidation Process.

The main applications of self-drilling anchors are slope stabilization, foundations with micropiles, and tunneling. In this operation, 2 m R32 bolts are used with couplings to extend the bolts to the lower level. The drilling length is varied, from 12 - 21 meters, therefore bolt usage also varies from hole to hole.

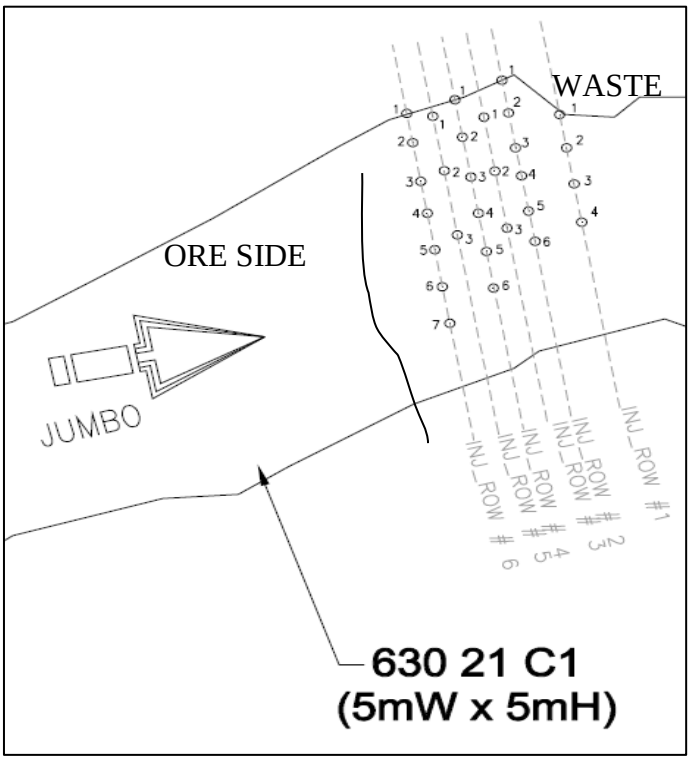

Figure 6. Upper Level Injection Row Plan.

The consolidation operation is designed with six rows of injection holes on the waste fill material (Figure 6). These rows are designed by slicing the solids of the upper and lower levels, and the solids of the cavity measurement (CMS) of the produced stope.

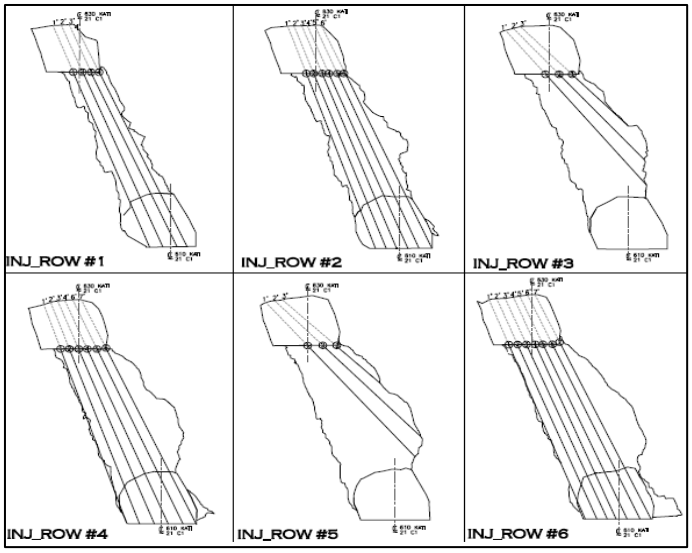

Figure 7. Row Designs, Section View

Injection rows commence from one meter behind the waste fill boundary at the waste side and with the exception of the first row, the interval between rows are designed as 0.5 m (Figure 7).

Self-drilling bolts are applied with jumbo, drilling and grouting is undertaken simultaneously with the use of an adapter attached to the jumbo drill rig and connected to a grouting pump (Figure 8).

Figure 8. Adapter attached to jumbo drill and connected to a grouting pump that sends grout into bolts while drilling.

Cement, self-drilling bolts, sacrificial bits and couplings were used as main consumables of the operation. For grouting; 720 liters of water and 1,000 kg of cement mixture is used for each hole.

Firstly, the jumbo drills the injection hole and simultaneously the grouting mix is pumped inside the hole. After each bolt, a coupling is placed and a bolt is attached to the coupling and the drilling-grouting operation resumes. While drilling continues, only rotation is applied due to working in loose ground. Bolts are inserted into the waste by grouting a row of injection holes, making a consolidated wall at the boundary of the waste fill/ore face.

Each hole is calculated to consume approximately 1,500 kg of cement to attain the required strength for a stable wall. In the first trial of this method, completing the injection drilling task took 14 shifts. In addition, at least four laborers were required to carry out the operation.

Figure 9. Finished consolidation work.

In figure 9, the completed view of the consolidation work is shown. In the figure, the solid wall contact is observed after the first blasting of the adjacent stope. In this operation, the consolidation of the waste fill material reduced the dilution percentage of blasted waste material.

3.1.1 Cost calculation

The cost of the operation is calculated and shown at Table I below (excluding labor).

Table 1. Cost Calculation of Grouting Bolts Method.

	Number of Holes	Number of Bolts	Coupling ea.	Bits ea.	Cement (ton)
Row1	4	40	36	4	6
Row2	6	60	54	6	9
Row3	3	18	10	3	3
Row4	6	60	54	6	9
Row5	3	18	10	3	3
Row6	7	70	63	7	10
TOTAL	29	226	227	29	40
Total IBO Bolt Set Cost			$		4,750
Total Cement Cost			$		5,700
TOTAL COST			***$***		***10,450***

3.2 Consolidation with Shock Blasting

The second method for consolidation of waste fill is the shock blasting method. In this method, only one row of holes is blasted to create shock on waste fill. This method designed to utilize elasticity of the waste fill structure. Before dumping the waste to the stope void, the method needs two different stoppers at the lower sill (Figure 10).

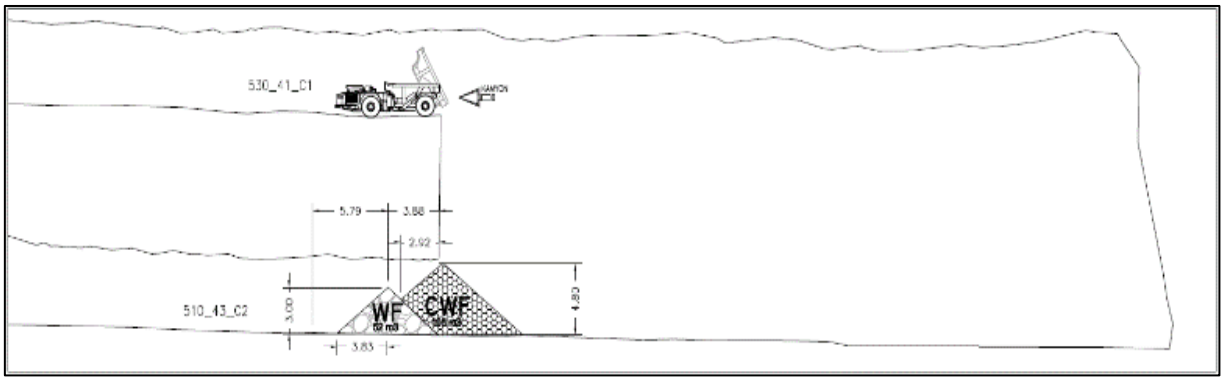

Figure 10. Providing stoppers.

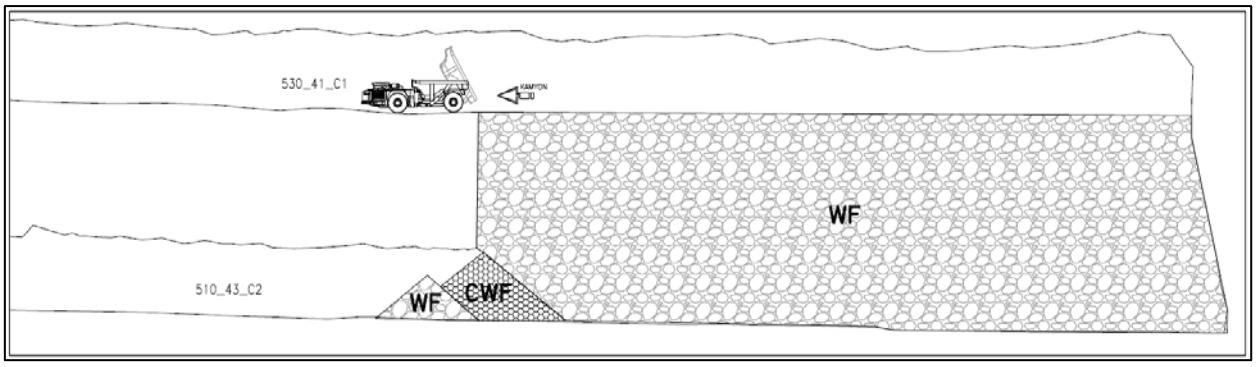

Figure 11. Filling with waste material.

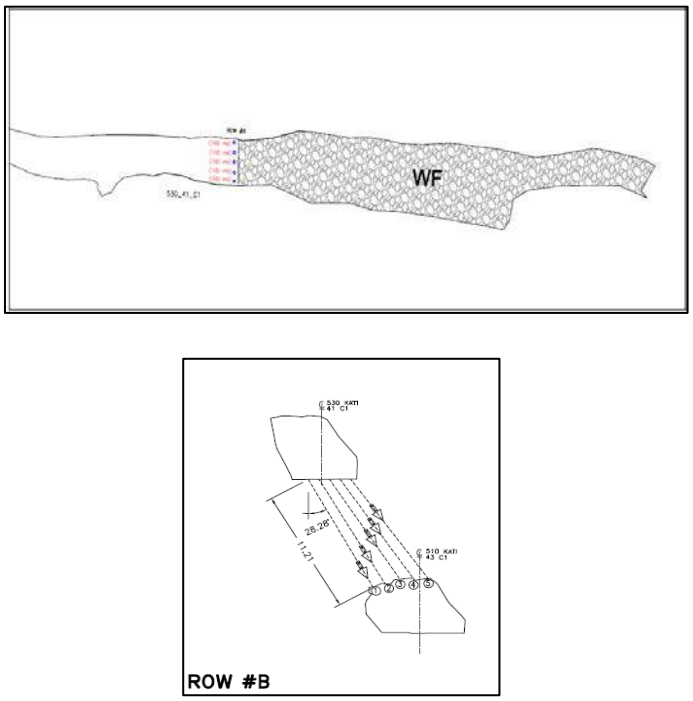

Figure 12. Blast hole design.

Illustrated at Figure 10, approximately 50 tons of 8% cemented waste fill (CWF) is pushed to the drawpoint of the stope void by remote control loader. Then a 3 m height of waste is dumped near the cemented waste fill. These two stoppers will prevent waste fill contamination at the lower level when blasting takes place.

Waste fill dumping starts from the upper level when the stopper construction is completed (Figure 11). Blast holes are drilled with an 86 mm diameter within 50 cm from the boundary of the ore and waste fill. The drill holes are drilled on the ore side.

Similar to the consolidation with grouting drill holes method, one blasting ring is designed by slicing the solids from the upper level, lower level and the solid of the orebody (Figure 12).

Drilling takes place over 2 shifts with the assistance of two laborers. Following the drilling, each hole must be stemmed with sand approximately 30 cm from the bottom and the top. Then the rest of the hole will be filled with ANFO after inserting the primer. In addition, each hole must blast at the same detonation sequence to break 50 cm thickness of ore and create an efficient shock effect towards the waste material.

After blasting the ring, an opened free slot surface must be covered with 20cm. thick shotcrete with the use of a SprayMec nozzle (Fig. 13).

In Figure 14, the completed view of consolidation work is shown. In the figure, the solid wall contact is observed after the shock blasting.

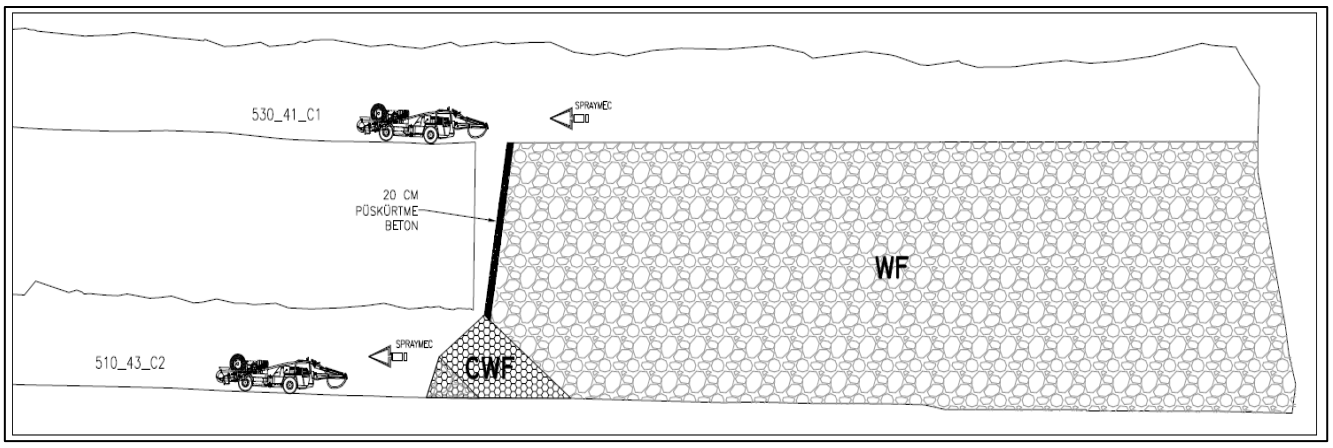

Figure 13. After blasting opened free surface must be cover with shotcrete.

3.2.1 Cost calculation

The cost of the operation is calculated and shown at Table II below (excluding labor).

Table 2. Cost Calculation of the Shock Blasting Method.

	Number of Holes	ANFO (KG)	Cement (ton)
RowB	5	225	3
Total ANFO Cost			$ 190
Total Cement Cost			$ 450
TOTAL COST			$ 640

Figure 14. Finished consolidation work.

4 CONCLUSIONS

Both of the consolidation methods were successful at their first trials. All of them give a stable working area in waste filled long hole stopes. As it is shown in the cost tables; the cement grouting method is timely, costly and more labor intensive job compared to the shock blasting method.

The shock blasting method is more cost effective, however it has the disadvantage of increased dilution to the ore at the initial blast.

ACKNOWLEDGEMENT

The author wishes to thank management of Efemcukuru Gold Mine for their support in presenting this work.

Optimization of Copper Recovery from Copper Converted Slag. Part I: Pyrometallurgical Aspects

B. Aghelnejad, R. Golmohammadzadeh, E. K. Alamdari, S. Firozi, D. Haghshenas
Department of Mining and Metallurgical engineering, Amirkabir university of Technology (Tehran Polytecgnic), Tehran, Iran

E. K. Alamdari
Research Center for Materials and Mining Industries Technology, Amirkabir University of Technology, Tehran, Iran.

D. Darvishi, A. K. Alamdari, A. B. K. Rafsanjani
Rare Metals Production Corporation, Rafsanjan, Iran.

Non-Ferrous Metals Recovery Corporations, Rafsanjan, Iran

ABSTRACT In this study, roasting and leaching of copper converter slag was carried out and the effects of their significant parameters were investigated. Minitab programing was put to use in design and analysis of these experiments. In roasting experiments the results show that roasting temperature has the greatest influence on solubility of Copper, while roasting time and grain size are in second and third place. Roasting slag with 237μ average grain size in 600 ° C with duration of 90 minutes was the best case of roasting. It resulted in 75.3% Copper recovery after leaching. Then in second stage, for obtaining optimum leaching parameters, all samples were prepared under previously mentioned roasting parameters and then went through leaching as its parameters were being manipulated. Best case was achieved when leached in boiling 150 gr/L acid, with L/S=10 and leaching time of 45 minutes which leads to Copper recovery of 92.2%.

Keywords: Roasting of copper, leaching of copper, optimization

1 INTRODUCTION

Copper is one of the earliest metals extracted by humans. As the time went by, it became more strategic and significant and today it has a wide spectrum of usage from simple ones like tools to the more complicated ones in the electrical and technological industries. The conventional method to extract Copper from sulfide ores using pyro-metallurgy have been used for decades and there are various furnaces with different percentages of copper in their products available for this mean. Slags from Inco Flash smelting contains <1% Cu, convertor slag 5% Cu, Noranda continuous submerged-tuyere converting 10% Cu, Mitsubishi top blown converting 14% and Outokumpu flash converting 20% Cu(W.G. Davenport, M. King, M.Schlesinger, A.K Biswas).

Nowadays, world faces lack of copper resources and even the remaining ones have very little amount of Copper (Less than 2%) while there are many secondary sources (copper slags) which were remained from pyrometallurgy furnaces mentioned above.
Recycling copper converter slag back to the flash furnace has been practiced in some plants and it leads to an increase in the matte grade (Antonioniet al., 1982). Dissolution behavior of Co, Cu, Fe, Ni, and Zn from smelter slag in aqueous sulfur dioxide has also been studied (Ahmed et al., 2000). Ausemelt top entry submerged lance technology is also used to recover Cu, Ni, and Co from slags (Hughes, 2000; Vernon and Burks, 1997). In some plants, flash smelting furnace slag (1.6–2% Cu) and converter slag (5–7% Cu) are cleaned in an

electric arc furnace, where coke is used as reductant and copper content of waste slag decreases to 0.5-0.8% (Kim, 1982, Suziki et al., 1982).

The purpose of this project was investigating of optimum parameters of roasting and leaching for slags from convertor of Non-Ferrous Metals Recycling Company of Rafsanjan (RFNR.CO). At first these slags were roasted and then were leached in Sulphuric acid solution. The effects of important parameters such as grain size, roasting time, roasting temperature, leaching time, leaching temperature, acid concentration and the liquid to solid ratio (L/S) on the copper recovery was determined by use of Minitab statistical computer program.

2 EXPERIMENTAL

2.1 Material

The slag sample used in this investigation came from convertor of Non-Ferrous Metals Recycling Company of Rafsanjan (RFNR.CO), which its important consisting elements are shown in Table 1 and Table 2 with two different micron average sizes.

As it can be seen, the mentioned slag has considerable amount of Cu and even Re which is a very valuable and expensive element as a rare metal.

2.2 Crushing and Grading

The crushing of slag was performed many times with three different crushers includes jaw crusher, cone crusher and roll crusher, and then was graded in to 8 categories.

Table 1. Important elements from XRF analysis for micron average size 237.

Element	Weight Percentage
Re	0.082
Al_2O_3	14
ZnO	2.25
NiO	0.28
Co_3O_4	0.032
CaO	11.1
SiO_2	34
MgO	8.7
Fe_2O_3	16.9
CuO	5.7

Table 2. Important elements from XRF analysis for micron average size 547.

Element	Weight Percentage
Re	0.091
Al_2O_3	14.1
ZnO	2.15
NiO	0.27
Co_3O_4	0.029
CaO	11.4
SiO_2	35
MgO	8
Fe_2O_3	16.7
CuO	5.4

2.3 Roasting of the Slag

Three different average grain sizes and four various roasting temperatures were given to Minitab statistical computer program as input. The result was 12 unique tests. Time of roasting was also considered as another parameter, so every mentioned test of Minitab result carried out in 9 various times, consequently, the total tests raised up to 108. For every test 20 gr of slag with a specific grain size average was poured into a stainless steel 316 container put into furnace with desired temperature and favorable time duration.

2.4 Leaching of the Slag

Leaching tests were designed to investigate the effect of acid concentration, liquid to solid ratio (L/S), leaching time and leaching temperature on the Copper recovery. By using the existing relation equations in the solution making, the required volume of solution (mixture of H2SO4 and distilled water) with specified concentration was poured into a beaker. The beaker was put on a hitter- stirrer so that its solution reaches to the desired temperature. Then the roasted slag and a magnet were added to solution and this time was considered zero time. Aluminum foil was also used to prevent vaporization. The leach liquor has been smoothed completely afterwards. In the end the final smooth solution was analyzed for Cu by titration and Fe by Atomic Absorption Spectroscopy (AAS).

3 RESULTS AND DISCUSSION

3.1 Effects of Roasting Parameters and Grain Size

The roasting process was conducted with slags included average grain sizes of 237, 392 and 547 µ. They each were roasted under temperatures 150, 300, 450 and 600 ° C with durations of 5, 10, 15, 20, 30, 45, 60, 90 and 120 min. 10 gr of each batch were leached under the same condition, 100 mL of Sulfuric acid solution with concentration of 100 gr/L.

It needs to be pointed out that solubility of Fe was very high (60- 97%) and also irregular, so, it was eliminated in consideration for optimizing the parameters. In conclusion, only the solubility of Cu is being considered as an important factor. Percentage of Copper solubility was calculated not according to the whole amount of Cu in the slag but based on dissolved Cu in the observer solutions. These amounts can be observed in table 3.

All leach specimens were analyzed and the results were compared for optimization of roasting parameters and grain size by use of Minitab software. Fig 1 shows the effect of grain size, roasting temperature and roasting time on solution of copper.

Generally, increasing of the temperature caused in enhancement of copper solubility. Usually roasting time increased copper solubility as well but recovery reached its peak at 90 and not 120 min. In most cases increasing grain size at first decreased and then increased solubility percentage of copper so effect of grain size is periodic and minimal. In conclusion it can be said that effect of temperature was more sensible and important than two other parameters.

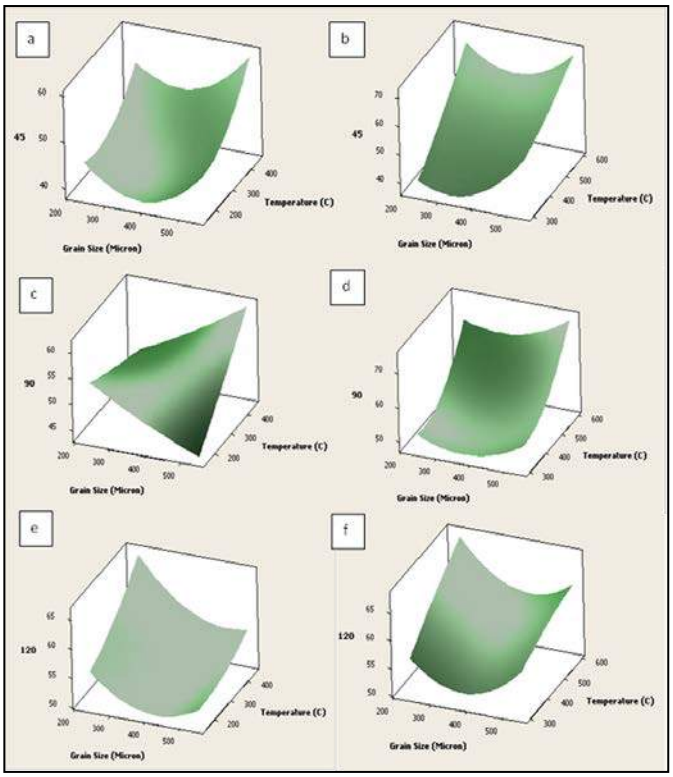

Figure 1. Effect of grain size, roasting time and temperature on solution of Cu:
a) 150 to 450 ° C and 45 min
b) 300 to 600 ° C and 45 min
c) 150 to 450 ° C and 90 min
d) 300 to 600 ° C and 90 min
e) 150 to 450 ° C and 120 min
f) 300 to 600 ° C and 120 min

With all considerations, the best copper recovery was obtained when roasting slag was performed with 237 µ average grain size in 600 ° C with time duration of 90 minutes which was equal to 75.3%. It is worth mentioning that the same average grain size of slag with the same condition of leaching, just without roasting, resulted into 45% copper recovery which obviously shows the importance of roasting process.

Table3. Amount of total Cu and soluble Cu in slags with various grain sizes.

Average Grain Size (µ)	Total Cu in slag (%)	Total Soluble Cu in slag (%)
237	5.7	4.9
392	-	5.2
547	5.4	4.7

3.2 Leaching in High Acid Concentrations

The optimum condition of roasting was considered for the rest of the experiments. As mentioned the slag with average grain size of 237 µ that was roasted in 600 ° C furnace as long as 90 minutes was selected and a set of experiments was designed for investigation of the leaching parameters.

Slag samples were leached in acids with 120, 150 and 180 gr/L concentration with liquid to solid ratios of 4, 7 and 10 which initially made 9 tests. Also time of leaching parameter was added by pulling out an approximately homogenous (same initial ratio of liquid to solid) leach liquor from the beaker with a syringe at times of 1, 5, 10, 15, 30, 45 and 60 min. The final 63 samples were analyzed for Fe and Cu and were compared together in order to optimizing leaching parameters.

Some of the samples in those 63 cases were observed in gelatinous state. This could be because of excessive leaching time and acid concentration which activated slag's consisting silica and solution of silica was the reason of the mentioned problem in 63 cases. In the end sample derived from leaching batch of 150 gr/L acid concentration, L/S=10 and leaching time of 45 min had highest copper recovery of 92.2%.

4 CONCLUSIONS

Primary lab-scale results show that an intensive Pyro metallurgical slag treatment before hydrometallurgical process leads to a further cleaning rate of the copper in copper slags.

This study has surveyed the effect of several parameters such as time of roasting, grain size, roasting temperature, acid concentration, ratio of liquid to solid and leaching time by use of MiniTab statistical computer program.

In conclusion, it was found that changes in grain size had no clear trend, and had staggering effect on copper recovery. With increasing in acid concentration and leaching time to the time which do not form silica gels in solution, usually copper recovery increased that was equal to 92.2%.

REFERENCES

Ahmed, I.B., Gbor, P.K., Ji, C.Q., 2000. Aqueous sulfur dioxide leaching of Cu, Ni, Co, Zn, and Fe from smelter slag in the absence of oxygen. *Canadian Journal of Chemical Engineering* 78 (4), 694– 703.

Antonioni, T.N., Diaz, C.M., Garvern, H.C., Landolt, C.A., 1981. Control of the Inco oxygen flash smelting process. In: George,D.B., Taylor, J.C. (Eds.), Copper Smelting—An Update. AIME, New York, pp. 17–31.

Kim, T.J., 1981. Flash smelting in Korea. In: George, D.B., Taylor, J.C. (Eds.), Copper Smelting—An Update. AIME, New York, pp. 33– 39.

W.G. Davenport, M. King, M.Schlesinger, A.K Biswas: Extractive Metallurgy Of Copper.

Optimization of Copper Recovery from Copper Converted Slag. Part II: Hydrometallurgical Aspects

R. Golohammadzadeh, B. Aghelnejad, E. K. Alamdari, S. Firozi, D. Haghshenas
Department of Mining and Metallurgical engineering, Amirkabir university of Technology (Tehran Polytecgnic), Tehran, Iran

E. K. Alamdari
Research Center for Materials and Mining Industries Technology, Amirkabir University of Technology, Tehran, Iran.

D. Darvishi, A. K. Alamdari, A. B. K. Rafsanjani
Rare Metals Production Corporation, Rafsanjan, Iran.
Non-Ferrous Metals Recovery Corporations, Rafsanjan, Iran

ABSTRACT In this investigation, the extraction of copper from converter slag via a pyro-hydro metallurgy process was statistically evaluated during a two-step roasting -leaching process. The optimum conditions for roasting including the average particle size, time and temperature, were determined and employed for all slag samples; then a leaching plan with low acid concentration with aim of the lowest level of iron and relatively high copper level, was examined. Optimum leaching parameters were also proposed as: liquid to solid ration (L/S) of 8, acid concentration of 45 g/L and temperature of 30°C. Under these conditions the recovery of copper was ~41%.

Keywords: Copper slag, leaching, acid concentration, L/S, Minitab, RSM.

1 INTRODUCTION

Steady depletion of the world's primary copper sources has led to secondary copper processing.

One of the most important secondary sources of copper is smelter slags. There are some hydrometallurgical methods presented in the literature for the treatment of slags, such as leaching in nitrate, perchloride, chlorate and sulfuric acid, ferric chloride, cyanide, ferric sulfate, and ammonia solutions (Lindblad & Dufresne 1974). Dissolution behavior of Co, Cu, Fe, Ni, and Zn from smelter slag in aqueous sulfur dioxide was also studied (Ahmed & Gbor & Ji 2000). Due to the amorphous structure of smelter slags, they cannot be efficiently leached with sulfuric acid and the formation of silica gel leads to difficulties for pulp filtration and crud formation during solvent extraction. However, this problematic issue could be overcome by the addition of hydrogen peroxide into the system (Banza & Gock & Kongolo 2002).

Acid roasting of slags followed by hot water leaching was also carried out to bring the metal values into solution (Arslan & Arslan 2002).

Roasting of the slag with sulphuric acid (Arslan & Arslan 2002, Sukla & Panda & Jean 1986), ammonium sulphate (Sukla & Panda & Jean 1986), ferric sulphate (Altundogan & Tümen 1997) or under reducing conditions prior to acid leaching (Anand & Das & Jena 1981) roasting of the slag under reductive conditions to produce Cu–Co–Fe–Pb alloy, electrolytic dissolution of the alloy in an ammonia-ammonium chloride solution, ammoniacal leaching of the slime and selective copper and Cobalt electrowinning (Rudnik & Burzyn´ ska & Gumowska 2002) was also reported in the literature.

In the present research, the slag obtained from the converter of Non-Ferrous Metals Recycling Company of Rafsanjan (RFNR.CO) was used. First the optimum parameters for particle size, roasting time and temperature were evaluated. Then tests were designed with low acid concentrations to minimize the solution of iron and give the best result in recovery of copper. Then the effect of L/S, temperature and acid concentrations was analyzed by use of Minitab statistical program.

2 EXPERIMENTAL

2.1 Material

The slag used in this study was obtained from convertor of Non-Ferrous Metals Recycling Company of Rafsanjan (RFNRCO). XRF analysis (Table 1) shows that mentioned slags have significant amount of CuO. The crushing of slag were carried out with three different crushers (jaw crusher, cone crusher, roll crusher) and then were graded in to 8 classes.

2.2 Roasting of the Slag

For this reason, 108 tests were designed by use of Minitab 15 using three different average particle size (237µm, 392µm and 547µm) at four roasting temperatures(150°C, 300°C, 450°C and 600°C), and different roasting times (5, 10, 15, 20, 30, 45, 60, 90 and 120 min). These tests were performed in a stainless steel 316 container.

Table1. Result of XRF analysis.

Sample no	Particle size	CuO (Wt%)
1	237 µm	5.70%
2	547 µm	5.40%

2.3 Leaching in High and Low Acid Concentrations

To evaluate the effect of acid concentration, liquid to solid ratio (L/S) and leaching temperature on copper recovery, 63 tests at high acid concentrations were designed. For this purpose, a mixture of H_2SO_4 and distilled water at the desired acid concentration was poured into a 100 ml beaker. To achieve the desired temperature, the beaker was put on a heater- stirrer and then the roasted slag was put into the beaker and a magnet was used for stirring. For low acid concentrations 18 tests were carried out with three factors at three levels by the principle of RSM using MiniTab 15 (Table 2.). Mechanical stirrer was used instead of magnetic stirrer. A stopwatch was used to measure the time of leaching. For prevention of vaporization, top of the beaker was covered with aluminum foil and distilled water was added periodically. After the completion of leaching, leach liquor was filtered.

2.5 Measurements and Analysis

The concentration of Cu and Fe was determined by Atomic Absorption Spectroscopy (AAS). It should be noted that due to the large number of tests, some of the Cu analysis were done by titration method using sodium thiosulfate.

3. RESULTS AND DISCUSSION

3.1 Effects of Roasting Parameters and Particle Size

According to the results obtained and their analysis by use of Minitab statistical computer program, as the temperature increase, copper recovery improves, and also the particle size has little impact on recovery of Cu. Best time for roasting of slag achieved at 90 minutes. Totally the effect of temperature in recovery of copper was greater in compare with particle size and time of roasting.

Table 2. Central composite design arrangement and responses (Cu and Fe dissolution concentration and recovery).

Sample no.	Central composite design arrangement			response (Cu and Fe concentration)		response (Cu and Fe recovery)	
	L:S	T	Acid	Cu (g/L)	Fe (g/L)	Cu Recovery %	Fe Recovery %
1	4	30	5	0.0	0.1	0.8	7.3
2	8	30	5	0.1	0.2	4.5	20.0
3	4	90	5	0.0	-	0.0	0.0
4	8	90	5	0.0	-	3.0	0.0
5	4	30	45	0.7	0.3	26.7	13.6
6	8	30	45	0.5	0.3	41.0	26.0
7	4	90	45	0.1	0.1	2.5	6.0
8	8	90	45	0.5	0.2	38.5	16.9
9	4	60	25	0.1	0.1	2.3	4.5
10	8	60	25	0.0	0.1	3.4	12.0
11	6	30	25	0.4	0.1	28.5	10.0
12	6	90	25	0.5	0.1	25.6	4.2
13	6	60	5	0.1	0.0	4.2	2.4
14	6	60	45	0.7	0.2	35.6	13.3
15	6	60	25	0.0	0.1	16.2	7.5
16	6	60	25	0.4	0.1	23.8	6.6
17	6	60	25	0.1	0.1	16.2	8.2
18	6	60	25	0.4	0.1	23.0	6.2

The average particle size of 237 µm, temperature of 600°C and time duration of 90 minutes were selected as the best condition for roasting.

The copper recovery after leaching, for 237 µm fraction was 75.3% which has about 30.3% increase in comparison with the sample without roasting that this shows the importance of roasting in these experiments.

3.2 Effects of Leaching Parameters

Slag used in this stage, was first roasted under optimum conditions acquired from the last stage (237 µm, 600 ° C, 90 minutes). Then two processes were designed for investigating the leaching parameters, one with high and the other with low acid concentrations.

3.2.1. Leaching in high and low acid concentrations

In this part, the effect of acid concentration, temperature, leaching time and L/S parameters for leaching experiments in recovery of copper was examined. At first, roasted samples were leached in 120, 150 and 180 g/L acid solutions at L/S ratios of 4, 7 and 10.

The results have shown that under the conditions of 150 g/L acid concentration, L/S of 10 and leaching time of 45 min the highest copper recovery of 92.2% was obtained.

Some tests were done with low acid concentrations too. For this purpose 18 tests were modeled by use of Minitab release 15 at three different temperatures: 30, 60 and 90°C; acid concentrations of 5, 25 and 45 g/L and also three levels of L/S: 4, 6 and 8.

In this study we tried to examine the Cu extraction, since the dissolution of Fe was significant, so the amount of both Cu and Fe were analyzed and Table 2 lists the values of solution of Cu and Fe after leaching.

Results illustrated that maximum recovery with 41% Cu in the 6th test as sample number is given in Table 2 (T=30°C, L/S=8, Acid Concentration=45 g/L). All of the results were analyzed with Minitab 15 and the following Figures obtained as output.

The values of the regression coefficients and P-values for Cu extraction are presented in

Table 3. It should be mentioned that the significance level employed in the analysis was 5%, so variables with P-values more than 5% are not statistically significant. Furthermore, the quadratic forms of the variables would not be statistically significant too. All of the linear and quadratic variables for Cu are statistically significant except T and its quadratic variables which mean that temperature has no effect on the extraction of Cu. On the other hand the extraction of Cu is affected by the L/S and acid concentration and their interaction.

Table 3. P values for Cu extraction.

Term	**Coef**	**P**
Constant	20.4	0.000
L/S	5.8	0.007
[Acid]	13.2	0.000
$(L/S)^2$	-12.1	0.001
$[Acid]^2$	5.0	0.584
L/S × [Acid]	5.5	0.018

P-values and regression coefficients for Fe dissolution are presented in Table 4. According to P-values shown in Table 4 all of the linear terms are statistically significant and on the other hand all of the quadratic variables except [Acid]*[Acid] are not statistically significant, which means that Fe dissolution is affected by temperature, L/S and acid concentration so its value varies with changes in the value of this variables.

The statistical analysis of the interaction terms for Cu dissolution show that, at 5% significant level, there is significant interaction between [Acid] and L/S and as a result, for finding an optimum condition for [Acid], L/S is involved and vice versa. On the other hand, temperature and L/S have no significant interaction same as temperature and [Acid].

Table 4. P values for Fe dissolution.

Term	Coef	P
Constant	9.2	0.000
L/S	4.4	0.000
T (°C)	-5.0	0.000
[Acid]	4.6	0.000
L/S × T (°C)	-1.8	0.040

The statistical analysis of the interaction terms for Fe show that, at 5% significant level, L/S and temperature have significant interaction that means an optimum level of L/S depends on the temperature and vice versa. On the other hand, the interaction of [Acid] with temperature and L/S is insignificant due to a P value higher than 5%. The P-values for Cu and Fe are less than 5% and lack of fit values for Cu and Fe are more than 5%, so as a result the model is statistically significant (Table 5 and Table 6).

According to regression coefficient resulted from calculations (Table 3 and Table 4) a polynomial regression model equation for Cu and Fe were propound as follows:

$$Cu\ (g/L) = 20.4 + 5.8\ L/S + 13.2\ [Acid] - 12.1\ (L/S)^2 + 5\ [Acid]^2 + 5.5\ L/S \times [Acid] \qquad R^2 = 72.73\% \quad (1)$$

$$Fe\ (g/L) = 9.2 + 4.4\ L/S - 5\ T + 4.6\ [Acid] - 1.8\ L/S \times T \qquad R^2 = 91.07\% \quad (2)$$

Table 5. ANOVA table for Cu.

Source	DF	Seq SS	Adj SS	Adj MS	F	P
Regression	9	3227.98	3227.98	358.66	13.38	0.001
Linear	3	2177.03	2177.03	725.68	27.06	0.000
Suare	3	683.79	683.79	227.93	8.50	0.007
Interacion	3	367.16	367.16	122.39	4.56	0.038
Residual Error	8	214.51	214.51	26.81		
Lack-Of-Fit	5	162.35	162.35	32.47	1.87	0.322
Pure Error	3	52.16	52.16	17.39		
Total	17					

Table 6. ANOVA table for Fe.

Source	DF	Seq SS	Adj SS	Adj MS	F	P
Regression	9	765.326	765.326	85.036	20.3	0.000
Linear	3	649.750	649.750	216.58	51.6	0.000
Suare	3	62.281	62.281	20.760	4.95	0.031
Interacion	3	53.295	53.295	17.765	4.23	0.046
Residual Error	8	33.559	33.559	4.195		
Lack-Of-Fit	5	31.132	31.132	6.226	7.69	0.062
Pure Error	3	2.427	2.427	0.809		
Total	17	798.885				

Based on regression coefficients (Equations 1 and 2), acid concentration has the most significant effect on the values of Cu and Fe concentrations. However, the effect of acid concentration on the Cu extraction is higher than that of Fe extraction.

The main effect plot for Cu (Figure 1) indicates that, the effect of acid concentration is more significant than L/S, and temperature has negligible effect on extraction of Cu. The main effect plot for Fe (Figure 2) demonstrates that increase in the level of L/S and acid concentration and decrease in the level of temperature have significant effect on the extraction of Fe.

Surface plots are produced to show and identify clearly interactions between significant terms.

The curvature of the surface presented in Figure 3a indicates that there is a significant interaction between L/S and acid concentration in the Cu extraction; i.e. at a constant level of acid, increasing in the level of S/L, up to ~1/6, leads to higher extraction percentage of Cu. However, when the S/L is higher than 1/6, the same increasing in the level of acid results in a decrease in the Cu extraction percentage. Thus, the optimum range for dissolution of Cu is 6< L/S <8 at an acid concentration of 45g/L.

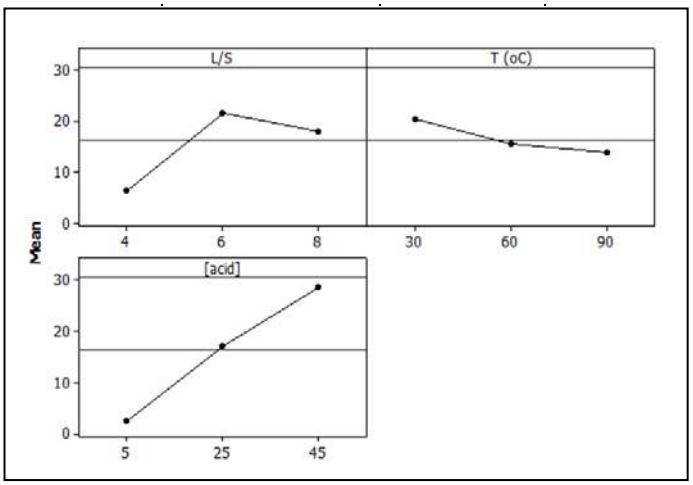

Figure 1. Effect of temperature, L/S and acid concentration on solubility of Cu.

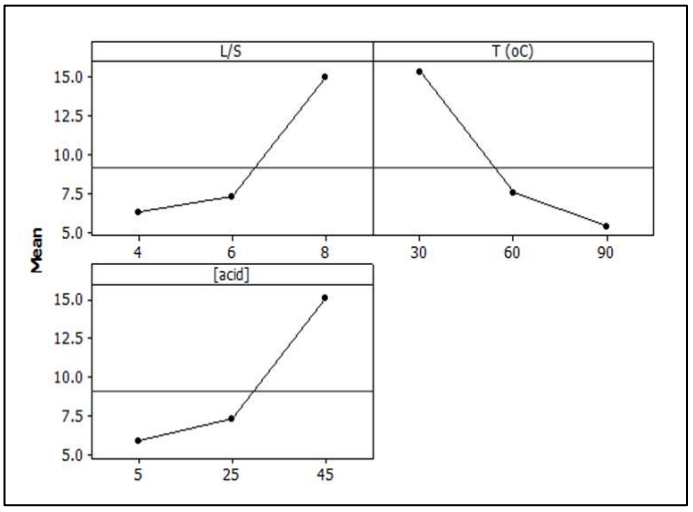

Figure 2. Effect of temperature, L/S and acid concentration on solubility of Fe.

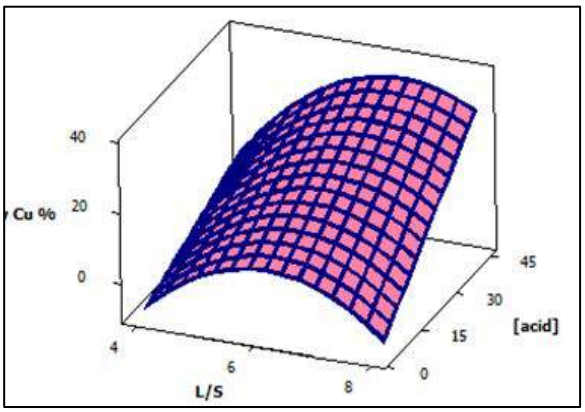

(a)

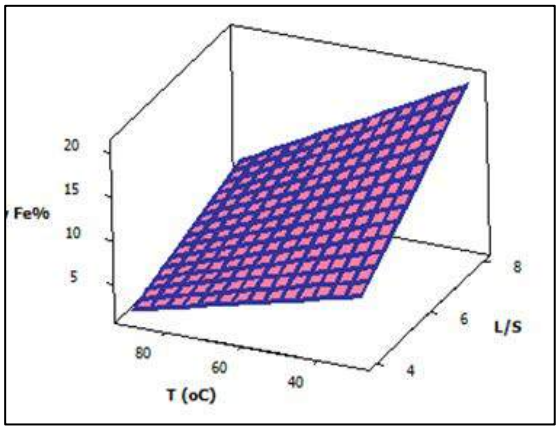

(b)

Figure 3. Surface plot for a) Cu, b) Fe.

The surface plot presented in Figure 3 shows that reducing in L/S from 8 to 4 and increasing the temperature from 30° C to 90° C adversely affect the dissolution of Fe. The counter plot presented in Figure 4. Indicates that the lowest recovery of Fe is obtained when L/S is less than 6 and temperature is higher than 60°C.

4 CONCLUSIONS

In this article, leaching parameters were studied in detail to evaluate the optimum conditions for leaching of copper slag. The most reliable approach for finding the best parameter was optimizing the leaching parameters. This study revealed that a recovery of 92.2% Cu was achieved after 45 minutes of leaching at an acid concentration of 150g/L and liquid to solid ratio of 10. Furthermore, the optimized leaching parameters in low acid concentrations was obtained at a L/S>6 and acid concentration>40g/L. As a result, the sample with liquid to solid ratio of 8, acid concentration of 45g/L and temperature of 30°C had the highest recovery of 41%.

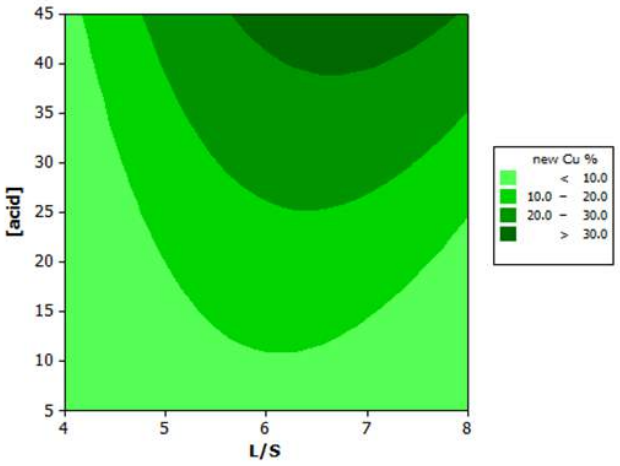

(a)

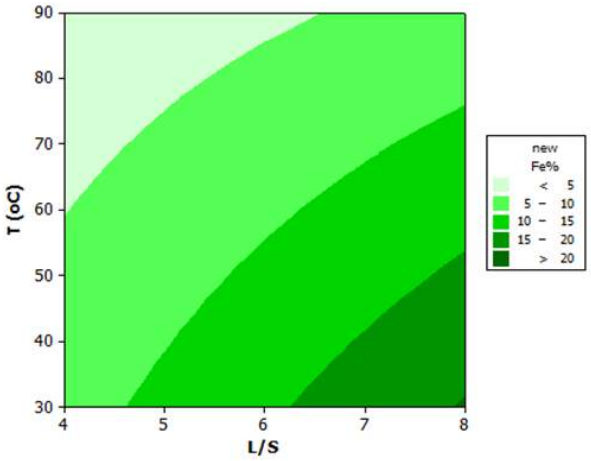

(b)

Figure 4. Recovery Range for a) Cu, b) Fe

REFERENCES

Ahmed, I.B., Gbor, P.K., Ji, C.Q., 2000. Aqueous sulfur dioxide leaching of Cu, Ni, Co, Zn, and Fe from smelter slag in the absence of oxygen. *Canadian Journal of Chemical Engineering,* 78 (4), 694– 703.

Altundogan, H.S., Tümen, F., 1997. Metal recovery from copper converter slag by roasting with ferric sulphate, *Hydrometallurgy*, 44, 261–267.

Anand, S., Das, R.P., Jena, P.K., 1981. Reduction-roasting and ferric chloride leaching of copper converter slag for extracting copper, nickel and cobalt values, *Hydrometallurgy*, 7, 243–252.

Arslan, Cuneyt., Arslan, Fatma., 2002. Recovery of copper, cobalt, and zinc from copper smelter and converter slags, *Hydrometallurgy*, 67, (2002) 1 – 7.

Banza, A.N., Gock, E., Kongolo, K., 2002. Base metals recovery from copper smelter slag by oxidizing leaching and solvent extraction, *Hydrometallurgy*, 67, (2002), 63–69.

Lindblad, K.O., Dufresne, R.E., 1974. Acid leach of copper reverberatory slag, *a new approach. Journal of Metals*, 29– 31.

Rudnik, Ewa., Burzyn´ ska, Lidia., Gumowskaz, Wanda., 2009, Hydrometallurgical recovery of copper and cobalt from reduction-roasted copper converter slag, *Minerals Engineering*, 22, (2009) 88–95.

Sukla, L.B., Panda, S.C., Jean, P.K., 1986., Recovery of cobalt, nickel, and copper from converter slag through roasting with ammonium sulphate and sulfuric acid, *Hydrometallurgy*, (16), 153– 165.

Recovery of Nanoparticles from Flue Gas using Dielectrophoresis

A. Neculae, A. Lungu, N. Strambeanu, M. Lungu
Faculty of Physics, West University of Timisoara, Bd. V. Parvan 4, Timisoara, Romania

ABSTRACT The industrial burning processes are responsible for the emission of a significant amount of nanoparticles. As the presence in the environment of nanoparticles with size ranging from 50nm to 150 nm was proved to have a profound impact on human health, the filtration of nanoparticles suspended in flue gas became an important technological challenge. In this context, the nanoparticle manipulation using strongly non-uniform electric fields, and especially dielectrophoresis (DEP), proved to be an extremely efficient tool.

This paper presents an experimental DEP-based micro-system used for the selective retaining of nanoparticles suspended in a gaseous environment. The particles deposited on the electrodes are analyzed using a reflection metallographic microscope with CCD camera and a data analysis system. The experimental results highlight the deposition of nanoparticles on electrodes and the fact that the concentration of captured particles diminishes as one depart from the input region, in concordance with our simulation results.

Keywords: Flue gas, recovery, dielectrophoresis, nanoparticles, numerical simulation

1 INTRODUCTION

Filtration of nanoparticles suspended in flue gas is an important technological challenge, as in urban environment the burning processes including waste incinerators or diesel emissions are responsible for the emission of a significant amount of nanoparticles (Sbrizzaia et al., 2005). The presence in the environment of nanoparticles with size ranging from 50nm to 150 nm has a profound impact on human health. Once inhaled, due to their tendency to remain trapped in the inner respiratory ways, infiltrate into the blood and cannot be eliminated, because the macrophage cells cannot identify them. Inhaled nanoparticles may generate free radicals, affect the DNA and alter the genes, being responsible for mutagens and carcinogenic effects or causing a variety of lung-disease typologies (Gatti and Montenari 2014). From a public health standpoint, the size of a particle is as important as its composition, recent research showing that although raw materials may not be dangerous, they can become toxic under the form of nanoparticles (Rickerby and Morrison, 2007, Minutolo et al., 2010, Shegokar 2014). Although the nanoparticles have smaller masses than microparticles, their number is at least four orders of magnitude higher than the number of all other particles found in the flue gas. Sources of polluting emissions are generally equipped with various filters that capture the micron particles, but permit nanoparticles to escape in atmosphere (Chang and Huang, 2001, Lungu et al., 2010).

The traditional methods (retention and separation) have not been successful when were applied for nanoparticles manipulation. In a typical particle-capture device, only a small fraction of them is collected, and the method is successful only when the nanoparticles are attached to larger ones. Mechanical devices used for filtering the post combustion gases resulted in waste incinerators (cyclones, bag filters, sedimentation chambers) are less effective at this scale because of the nanoparticles' low weight, while Corona electrostatic filters have high micrometric particle retention efficiencies (93-99%), yet most nanoparticles still remain undetected

(Sbrizzaia et al., 2005, Rickerby and Morrison, 2007).

The most promising technique for nanoparticle trapping and controlled spatial separation is a method based on dielectrophoresis (DEP), phenomenon in which a spatially non-uniform AC or DC electric field induces a dipole moment in a dielectric particle. Hence, the particle undergoes a DEP motion under the resulting translational force. This force does not require electrically charged particles; the strength of the force depends on the medium and particle's electrical properties, particle's shape and size, and on the applied electric field amplitude and frequency (Pethig, 2010, Neculae et al., 2012). Due to its ability to manipulate particles based solely on their dielectric properties and size, DEP is used for a wide variety of applications such as separation of particles, simultaneous capturing of multiple groups of nanoparticles, etc. (Green et al., 2002, Barbaros and Dongquing, 2011).

This paper presents a study regarding the filtering process by the entrapment of nanoparticles dispersed in flue gas in a microfluidic device using positive dielectrophoresis. The first part of the study presents a set of results obtained by numerical simulations describing the behavior of nanoparticles with size ranging from 50 to 150 nm in a 3D DEP-based microsystem, which consists in a microchannel-working unit of a particulate trap. The concentration profile of nanoparticle suspension inside the microfluidic separation device is calculated using input parameters previously determined experimentally, and the performance of the device is analyzed in terms of a new specific quantity of separation process, called *Filtration rate*. In the second part of the study, the experimental microfluidics device for dielectrophoretic manipulation of nanoparticles from flue gas is presented, together with some preliminary but relevant experimental results highlighting the capability of the device to capture the nanoparticles. The analysis system of the images is described as well. Combining of numerical analysis with experimental investigation, lead to the improvement of the mathematical model and the determination of the optimal parameters of the experimental device.

2 THEORETICAL BACKGROUND

The time averaged DEP force acting on a spherical particle situated in an AC electric field can be written as (Green et al., 2002):

$$\left\langle \mathbf{F}_{DEP} \right\rangle = 2\pi a^3 \varepsilon_m K_R(\omega) \nabla \left(\left| \nabla V_R \right|^2 + \left| \nabla V_I \right|^2 \right) \quad (1)$$

where we denoted by a the particle radius, ω the angular field frequency, and V_R, respectively V_I the real and imaginary part of the electric potential phasor, $\tilde{V} = V_R + jV_I$, with $j = \sqrt{-1}$. For a homogeneous medium, the electric potential satisfy the Laplace equation $\nabla^2 \tilde{V} = 0$.

$K_R(\omega)$ is the real part of the complex quantity $\tilde{K}(\omega) = \left(\tilde{\varepsilon}_p - \tilde{\varepsilon}_m \right) / \left(\tilde{\varepsilon}_p + 2\tilde{\varepsilon}_m \right)$, called the Clausius–Mossotti (CM) factor, which is a measure of the effective polarizability of the particle. $\tilde{\varepsilon}_p$ and $\tilde{\varepsilon}_m$ are the complex dielectric permittivities of particle and medium. The complex permittivity is defined as $\tilde{\varepsilon} = \varepsilon - j\left(\sigma/\omega\right)$, where σ is the electrical conductivity. Consequently, the CM factor can be expressed as:

$$\tilde{K}(\omega) = \frac{\left(\varepsilon_p - \varepsilon_m \right) + j/\omega \cdot \left(\sigma_p - \sigma_m \right)}{\left(\varepsilon_p + 2\varepsilon_m \right) + j/\omega \cdot \left(\sigma_p + 2\sigma_m \right)}. \quad (2)$$

The CM factor depends on the dielectric properties of the particle and medium and on the frequency of the applied field; at low frequencies the sign is determined by the electrical conductivities of the particle and of the medium and at higher frequencies by the corresponding permittivities. The variation in this factor results in a frequency-dependent dielectrophoretic force that is unique for a particular type of particle. Therefore, DEP is an effective tool for separating particles, based solely on their

dielectric properties and size. When the sign of K_R is positive, the particle is attracted to the locations of electric field intensity maxima and repelled from the minima, phenomenon known as positive dielectrophoresis (pDEP). The opposite occurs when K_R is negative, situation referred to as negative dielectrophoresis (nDEP).

A typical DEP-based separation device has parallel interdigitated bar electrodes placed on the bottom surface, as illustrated in Figure 1.

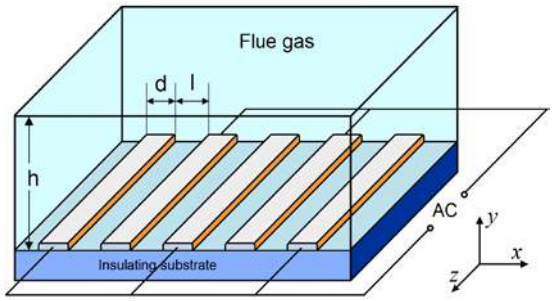

Figure 1. Schematic representation of experimental device used for DEP separation.

In most of the reported models, due to the symmetry of the geometry and considering the electrodes much longer than their width, the problem is treated in two dimensions and the electrodes' height is neglected. In our study, in order to have a more realistic description of the experimental device, a 3D geometry and a detailed description of the electrodes' shape are used. Anyway, taking into account the periodic distribution of the electrodes, the numerical calculations of the DEP force and the concentration field can be performed considering as computational domain only a so called "basic unit cell", which fully describes the entire system, except the vicinity of the device walls. The geometry of the computational domain, together with the associated boundary conditions necessary to solve the Laplace equation for electric potentials, V_R and V_I, are presented in Figure 2.

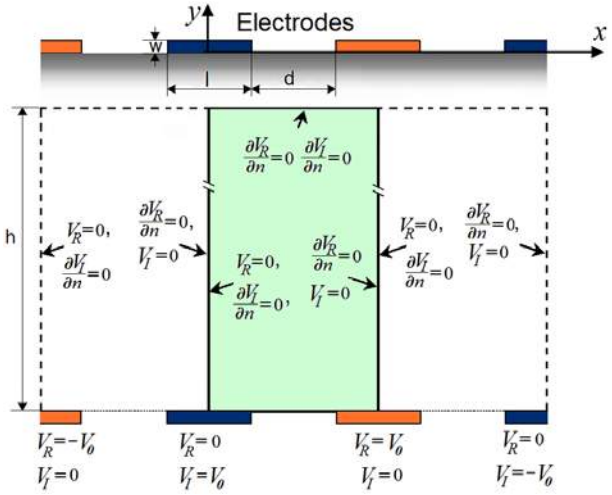

Figure 2. The geometry of the computational domain and the associated boundary conditions for the electric potentials. The solid lines indicate the basic unit cell.

The macroscopic behavior of a suspension of spherical particles of radius a in a fluid of viscosity η is modeled by considering the mechanical equilibrium between an external force **F** (DEP force in this case) and the Stokes drag force. For small particles (i.e. nanoparticles), the dynamics of the system is governed by the following system of equations (Neculae et al., 2012):

$$\mathbf{v} = \mathbf{u} + \frac{2a^2}{9\eta}\mathbf{F}, \qquad (3a)$$

$$\frac{\partial C}{\partial t} + \nabla \cdot \mathbf{j} = 0, \text{ where } \mathbf{j} = C\mathbf{v} - D\nabla C. \qquad (3b)$$

Here **u** and **v** are the fluid and particle velocities, t is the time, **j** the particle flux, D the diffusion coefficient of the particles, and C is the particle volumic concentration.

The fluid flow field inside the separation device, **u,** is calculated by solving the classical Navier-Stokes equation in the compressible case, together with the corresponding boundary conditions. For the obtained DEP-force and fluid flow field, the particle concentration is evaluated by numerically integrating equations (3a) and (3b). This calculated particle concentration field gives information at a local scale, showing how the particles are attracted on the margins of electrodes and the influence of the main parameters of the problem on this process. For the analysis of the filtration

process we define the novel quantity named *Filtration rate* (*F*), which describes the process in terms of nanoparticles entrapment at the electrodes, related to the concentration distribution:

$$F = \frac{C_{input} - C_{output}}{C_{input}} = 1 - C_{output} / C_{input} \quad [\%] \qquad (4)$$

where C_{input} and C_{output} are the mean concentrations of the suspended nanoparticles at the input and the output surfaces of the device, respectively, as schematically sketched in Figure 3.

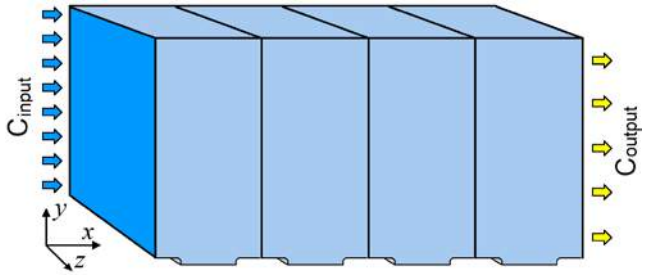

Figure 3. Schematic representation of the separation device revealing the parameters used for defining the *Filtration rate.*

This proposed quantity gives the global information on the filtration process, and can be used in order to evaluate the efficiency of the filtration process.

3 NUMERICAL RESULTS

After we compute the pDEP force distribution inside a typical DEP device we move to the problem of determining the distribution profile of nanoparticles under the influence of dielectrophoresis. We analyze and discuss the obtained numerical results in terms of *Filtration rate*, a global quantity correlated with the concentration field, which offers a more suggestive characterization of the capabilities of the device regarding the separation process of nanoparticles from flue gas. All the numerical simulations were performed using the *COMSOL Multiphysics* program.

For the computation of the pDEP force, we first solved the Laplace equation for the real and imaginary components of the electric potential, together with the associated boundary conditions presented in Figure 2. The computational domain consists of a unit cell described by the following set of geometric parameters: $d=l=100\ \mu m$, $h=500\ \mu m$ and $w=2\ \mu m$. The simulations were performed for a suspension of particles with characteristic sizes a=50nm, a=100nm and a=200nm respectively, in air. The dielectric response of the particles is characterized by the real part of the CM factor $K_R = 1$ and we considered the amplitude of the electric potential applied on the electrodes in the range $V_0 = 12 \div 24V$.

The efficiency of the filtration process can be evaluated by calculating the *Filtration rate* given by relation (4) for different values of problem's parameters. The computation is performed using an iterative procedure: the output concentration in one unit cell is considered to be the input concentration for the next unit cell, in order to describe the cumulative effect of the filtration inside the microfluidic device. This type of analysis allows an estimation of the necessary number of cells (or electrodes) in order to obtain a certain desired filtration rate, when the other parameters of the problem are fixed. The results presented in Figure 4a show that, for example, in the case of particle having size of 100nm, a desired filtration rate of 90% can be obtained by using about 30 electrodes when applying a voltage of 24 V, about 60 electrodes for 18 V, and nearly 200 electrodes for an applied voltage of 12 V.

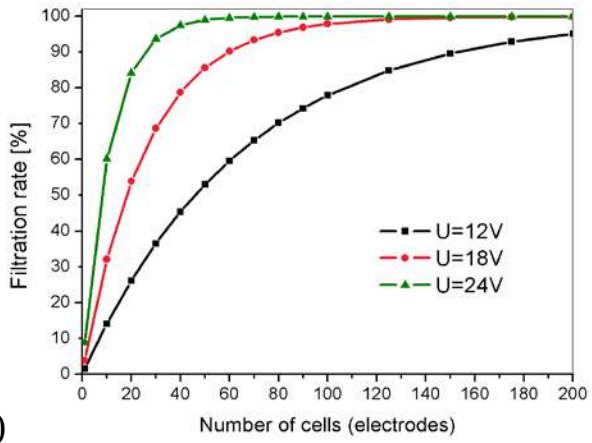

a)

b)

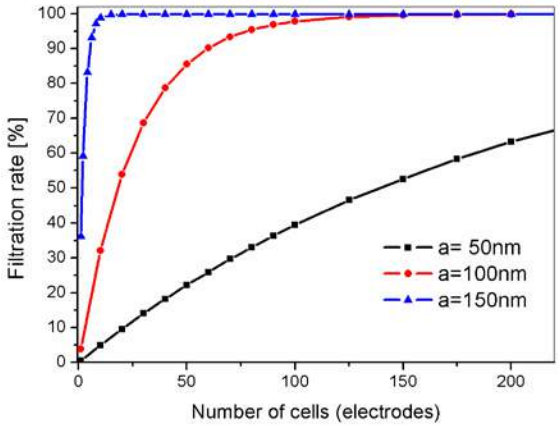

Figure 4. Calculated filtration rate versus cell numbers for a) particles with a=100nm at three different applied voltages and b) particles with three different radii at a fixed applied voltage of $V_0 = 18\text{V}$ ($d = l = 100$ μm).

When we analyze the effect of particle radii on the filtration capacity, the results presented in Figure 4b predict that, for example, when the applied voltage is 18 V, particles of 150 nm are completely captured after 10 electrodes, for particles of 100 nm we need about 150 electrodes for the complete capture, while the particles of 50 nm are captured less than 60% even if one use devices with 250 electrodes.

In conclusion, the simulations performed in the frame of the presented mathematical model allow an estimation of the performances of the filtration as a function of the geometric and physical parameters of the problem.

4 MATERIALS AND METHODS

Based on the results obtained from the mathematical model and numerical simulations, it was realized and tested a laboratory microfluidic device for retaining nanometric particles in non-uniform electric field by positive dielectrophoresis (pDEP). Practical tests were conducted on an emission source represented by a pilot plant for incineration of different waste categories. The main active parts of the device consist of the deposition plates, made by PCB (Printed Circuit Board) technique (Figure 5), with electrode width and gap between electrodes $d = l = 100$μm.

a)

b)

Figure 5. Deposition plate made by PCB technique, a), detail of intedigitated electrodes, b).

We performed experiments for nanoparticle trapping from flue gas, by fumigation at the bottom of the experimental device. The outline of the laboratory experimental device is presented in figure 6a, and a detail with experimental device under work conditions (with flue gas fumigation at the bottom), is shown in figure 6b.

a)

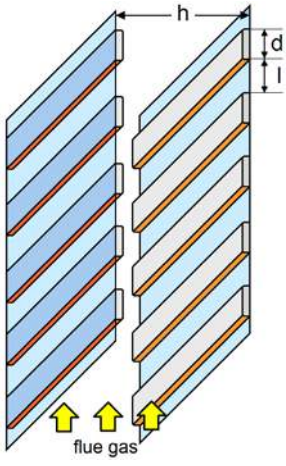

b)

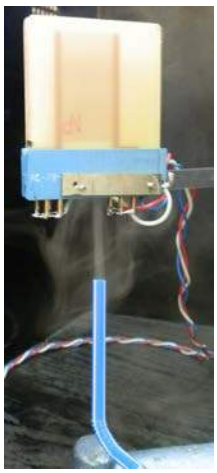

Figure 6. The outline of the laboratory experimental device, a), device at work with flue gas at the bottom, b).

Figure 7 presents the installation for the analysis of the deposition plates (consisting in a reflection metallographic microscope with CCD camera and the related computer), during analyze of a deposition plate before fumigation, in the absence of the applied voltage. On screen it appears a snapshot with a detail of the deposition plate obtained at a 100x magnitude. The vertical light stripes on the display are the electrodes, while the dark stripes are the gaps.

Figure 7. The installation for the analysis of the deposition plates, on screen appears a snapshot of a detail of the deposition plate obtained at 100x.

The tests performed with a DEP-based separation device having $l=d$=100µm and h=2mm reveal that in the absence of the applied voltage the particles are not at all attracted to the electrodes, while once applied an AC voltage, the dielectrophoretic effect appears. In the absence of applied voltage on the electrodes, the nanoparticles that exist in the flue gases are not attracted to them and, therefore, will not be deposed on the plates. By applying an AC voltage, the deposition phenomenon occurs due to positive dielectrophoresis. Figure 8 shows successive video frames (snapshots) representing the deposition of nanoparticle on the collection plates by pDEP of the smoke resulted from the incineration of wastes in the pilot plant. On the electrodes were applied AC signals. Snapshots were performed at different distances from the top of the plate, where obtained a minimum density of the collected material versus the bottom, where the density of deposited nanoparticle is the greatest. The figure shows a decreasing in the concentration of captured nanoparticles, vertically from the entrance toward the exit area. As the smoke "climbs" the device, particles in suspension are lost by their accession to the collection plate, the result being in accordance with numerical simulations.

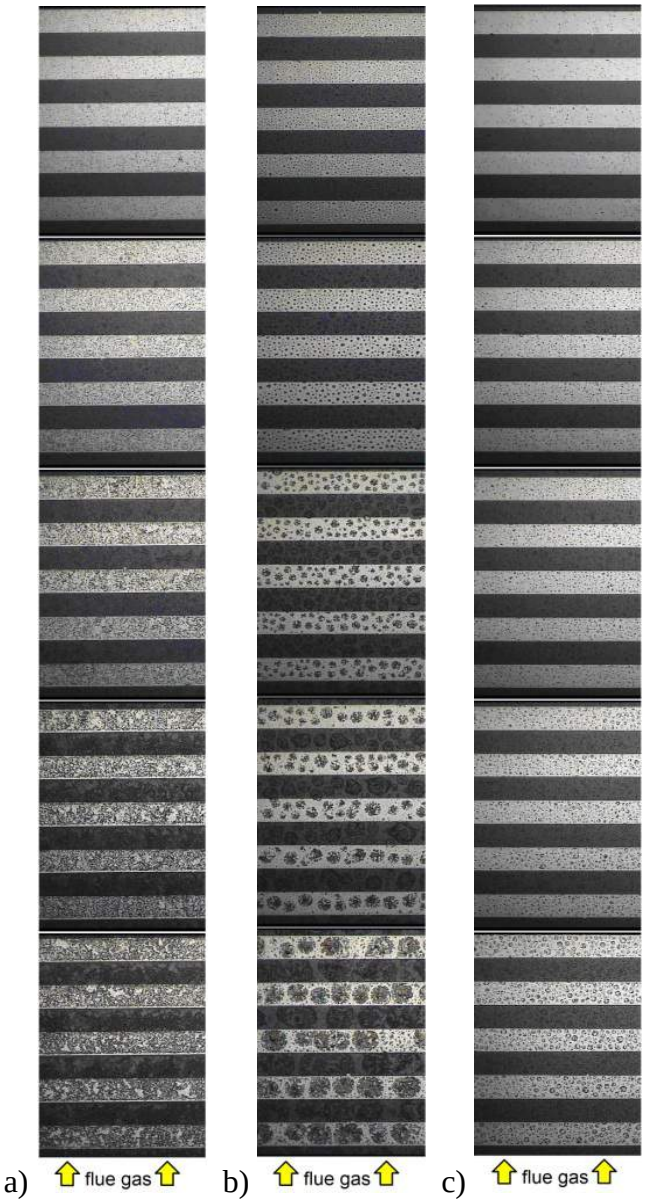

Figure 8. Successive snapshots revealing the results obtained after fumigation with the DEP-based separation device with $l=d$=100µm, h=2 mm, at: U=37V, AC sinusoidal signal, f=50Hz, time of fumigation t=30s, a); U=12V, AC rectangular signal, f=100Hz, time of fumigation t=30s, b); and U=12V, AC rectangular signal, f=100Hz, time of fumigation t=30s, c). A decreasing in the concentration of captured nanoparticles, vertically from the entrance toward the exit area is observed.

5 CONCLUSIONS

This contribution presents the study of a DEP-based microsystem for the selective manipulation of nanoparticles using dielectrophoresis. We applied a theoretical model and build-up of an experimental

device for retaining the nanoparticles from combustion gases in non-uniform electric fields based on the simulations of a physically realistic problem, and then we performed experiments on nanoparticle trapping from flue gases.

The numerical study focuses on the effectiveness of filtering nanoparticle from combustion gases in a microfluidic device designed to improve the filtering process of nanoparticle suspended in flue gas using positive dielectrophoresis. This type of analysis allowed the estimation of the number of cells (or electrodes) required to achieve a given filtration rate when other parameters of the proposed model are established.

Based on the results obtained from mathematical modeling and numerical simulations, it was designed, developed and tested a laboratory microfluidic device for retaining in nonuniform electric field by positive dielectrophoresis of nanometric particles from the emissions of a pilot plant incinerator. The experiments performed with this device highlight the deposition of nanoparticles on electrodes and the fact that the concentration of captured particles decreases as we move away from the entrance area of the smoke resulted from the combustion of different wastes, the results being in good agreement with the numerical simulations.

ACKNOWLEDGMENTS

This work was supported by a grant of the Romanian National Authority for Scientific Research, CNCS – UEFISCDI, project number PN-II-ID-PCE-2011-3-0762.

REFERENCES

Barbaros, C and Dongqing L, 2011. Review – Dielectrophoresis in microfluidics technology, *Electrophoresis*, 32, pp. 2410 – 2427.

Chang, M and Huang, C, 2001. Characteristics of Energy Flow in Municipal Solid Waste Incinerator, *J. of Environ. Eng.*, 127, pp.78–81.

Gatti, A and Montenari, S, Nanopathology: The nano-bio-interaction of Nanoparticles Inside the Human Body, 2014. *Nanoparticles' Promises and Risks*, Springer Cham Heidelberg, New York, Dordrecht, London, 355 p.

Green, NG, Ramos, A and Morgan, H, 2002. Numerical solution of the dielectrophoretic and travelling wave forces for interdigitated electrode arrays using the finite element method, *J. of Electrostatics*, 56, pp.235-254.

Lungu, M, Neculae, A and Bunoiu, M, 2010. Some considerations on the dielectrophoretic manipulation of nanoparticles in fluid media, *J. of Optoelectronics and Advanced Materials*, 12, pp.2423-2426.

Minutolo, P, Sgro, L, Costagliola, M, Prati, M, Sirignano, M and D'Anna, A, 2010 Ultrafine particle emission from combustion devices burning natural gas, *Chem. Eng. Trans.*, 22, pp.239-244.

Neculae, A, Biris, C, Bunoiu, M and Lungu, M, 2012. Numerical analysis of nanoparticles behavior in a microfluidic channel under dielectrophoresis, *J. Nanopart. Res.*, 14, pp.1-12.

Pethig, R, 2010. Review Article—Dielectrophoresis: Status of the theory, technology, and applications, *Biomicrofluidics*, 4, pp.022811-1 – 02281-34.

Rickerby, D and Morrison, M, 2007. *Report from the Workshop on Nanotechnologies for Environmental Remediation*, JRC Ispra, http://www.nanowerk.com/nanotechnology/reports/reportpdf/report101.pdf.

Sbrizzaia, F, Faraldib, P, Soldatia, A, 2005. Appraisal of three-dimensional numerical simulation for sub-micron particle deposition in a micro-porous ceramic filter, *Chem. Eng. Sci.*, 60, pp. 6551 – 6563.

Shegokar, S, Nanotoxicity: Must Consider Aspect of Nanoparticle Development, 2014. *Nanoparticles' Promises and Risks*, Springer Cham Heidelberg, New York, Dordrecht, London, 355 p.

Recycling Mixed Plastic Waste and its Blend with Sawdust as Reductant in Ironmaking

J.R. Dankwah
Minerals Engineering Department, University of Mines and Technology, Post Office Box 237, Tarkwa, Ghana

E. Baawuah
Metallurgical Department, Golden Star Resources Limited, Post Office Box 11, Bogoso, Ghana

J. Dankwah
Chemical Engineering Department, Kwame Nkrumah University of Science and Technology, Kumasi, Ghana

P. Koshy
School of Materials Science and Engineering, University of New South Wales, Sydney, NSW 2052, Australia

ABSTRACT One of the major obstacles to the implementation of an appropriate plastics recycling scheme is the inhomogeneity of many plastics waste. Accordingly, most of the existing recycling schemes require a feedstock that is reasonably pure and contains only items made from a single polymer type. This often requires sorting into different polymer fractions, a process that is both cumbersome and expensive. This work therefore investigates the reduction of two sources of iron oxide by mixed plastic waste (MPW) and its blend with sawdust (SD) through experiments conducted in a laboratory scale horizontal tube furnace. Composite pellets of EAF slag (47.1% FeO) with a blend of MPW and SD were rapidly heated at 1520 °C under high purity argon gas and the off gas was continuously analysed for CO, and CO2 using an online infrared gas analyser (IR). The extent of reduction after fifteen minutes was determined for each carbonaceous reductant. The results show that iron oxide can be effectively reduced to produce metallic iron using MPW and its blend with SD as reductant. An improvement in extent of reduction was observed over conventional metallurgical coke and the individual polymers when the blend (MPW+ SD) was used as reductant. This eliminates the need to sort out individual plastics from municipal solid waste for their effective utilisation as reductants, carburisers and desulphurisers in iron making.

Keywords: Reduction, metallurgical coke, mixed plastics waste, sawdust, extent of reduction, carburization, desulphurisation

1 INTRODUCTION

One of the major obstacles to the implementation of an appropriate plastics recycling scheme is the inhomogeneity of many plastics waste. Accordingly, most of the existing recycling schemes require a feedstock that is reasonably pure and contains only items made from a single polymer type. In the metallurgical industry, particularly in iron and steelmaking technologies, the use of postconsumer plastics is currently gaining the attention of various researchers. However, most of the existing research in this area involves the use of a single plastic [1-4] and/or its blends with metallurgical coke or graphite [5-12] or with biomass as reductants [13, 14]. In reality, most postconsumer wastes contain a mixture of plastic types, and are often contaminated

with non-plastic items. Little or no information exists in the literature on the use of MPW and blends of MPW with biomass as reductants in the metallurgical industry as reductants. The potential feasibility of utilising MPW and its blend with biomass as reductant in iron oxide reduction is thus the motivation of this research project.

2 EXPERIMENTAL

2.1 Sample Selection

The MPW used in this investigation was comprised of 40 wt % HDPE, 30 wt % PP, 10 wt % LLDPE, 10 wt% PET and 10 wt % SD. The chemical composition (wt %) of the carbonaceous samples and the ash analysis (of Met Coke and SD) are given in Tables 1and 2, respectively. No ash analysis was performed on the plastics because of the negligible amounts of ash produced An EAF slag with 47.1 % FeO and basicity (B3) of 1.66 was provided by OneSteel Sydney Steel mill, which was further analysed by XRF and its composition after removal of free metallic iron by a magnet is given in Table 3..

Table 1: Compositions of the carbonaceous materials utilised in this investigation

Component	Met Coke	HDPE	PP	LLDPE	PET	SD
Moisture	4.6	0	0.01	0	0.18	1.90
Ash	18.3	0.3	0.45	0.3	0.04	10.30
VM	3.00	99.7	98.8	99.7	88.42	80.20
Fixed Carbon	71.36	0	0.74	0	11.35	7.60
Total Carbon	78.7	85.5	83.8	85.5	62.5	50.30
Sulphur	0.32	0.30	0.092	0.20	0.00	0.04
Hydrogen	0	14.2	13.9	14.3	4.2	5.78
Oxygen	0	0	0	0	33.3	43.64

Table 2: Ash analysis of Met Coke and SD used in current study*

Component (wt %)	SiO_2	Fe_2O_3	Al_2O_3	TiO_2	P_2O_5	CaO	MgO	Na_2O	K_2O	SO_3	SrO
Met Coke	50.7	4.8	36.0	1.4	1.6	3.3	0.94	0.39	0.53	0.39	-
SD	32.5	0.64	1.6	0.09	2.2	27.9	13.1	0.92	13.5	3.2	0.21

(*-analysis conducted at Amdel laboratories, Newcastle, Australia)

Table 3: Composition of EAF slag used for the investigation*

Component	CaO	FeO	Al_2O_3	SiO_2	MgO	MnO	Basicity B3 = %CaO/(%SiO_2 + %Al_2O_3)
Composition (wt %)	24.1	47.1	4.9	9.6	10.2	4.8	1.66

(*-analysis conducted at Analytical Centre, UNSW-Sydney, Australia)

2.2 Sample Preperation

Samples of SD were ground and sieved to particle size in the range of -470 +450 µm while samples of granulated HDPE, PP, PET and LLDPE were crushed to smaller sizes by using a cutting mill “Pulverisette 15” (Fritsch GmbH, Idar-Oberstein, Germany), Fig. 1. By means of a sieve insert with 0.5 mm trapezoidal perforations in the cutting mill a particle size -470 +450µm, similar to that of metallurgical coke was obtained. The slag was subsequently mixed with the carbonaceous blends and compacted in a die to produce cylindrical pellets (11.6-12.0 mm thick and 14 mm diameter) (Fig. 2), by applying a load of 7.5 tonnes for 1 minute in a hydraulic press.

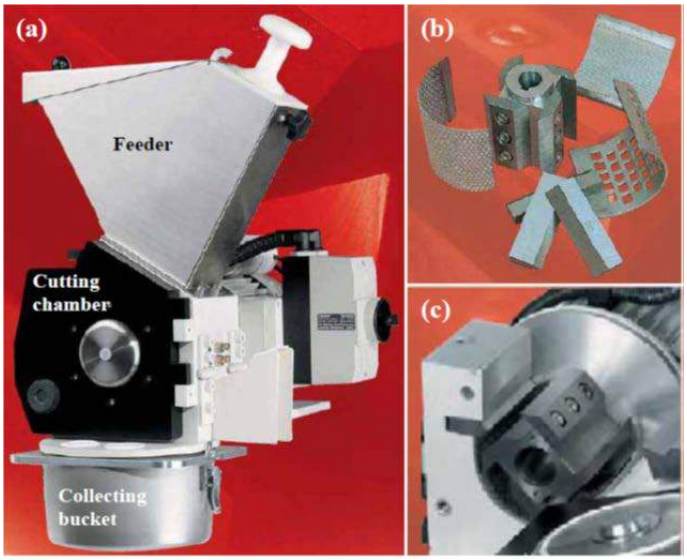

Figure 1. (a) Cutting Mill Pulverisette 15, (b) Cutting rotor and sieve inserts and (c) Grinding Chamber. [6]

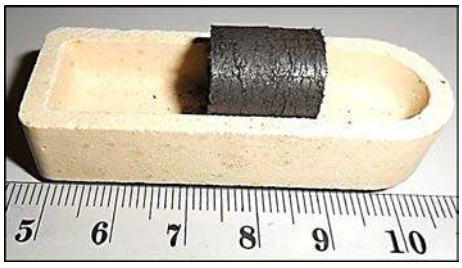

Figure. 2: Cylindrical pellet (slag + carbonaceous material) placed in the LECO crucible prior to the experiments

2.3 Experimental Procedure

The experimental procedure involved three parts: the reactions in a custom-made horizontal resistance heated furnace (Fig. 3), visual observation using a CCD camera and off-gas analysis using a gas chromatographic analyser (SRI 8610C Chromatograph Multiple Gas #3 GC configuration equipped with a thermal conductivity conductor (TCD)) and a continuous infrared gas analyser, to monitor off- gases produced by the reduction reaction.

The results (gas analyses and visual imaging) were recorded in a data-logging computer. The sample assembly was inserted in the furnace, which was purged continuously with argon (of 99.995 % purity and flowing at1L/min) to ensure inert conditions in the furnace. After the furnace had attained the desired hot zone temperature (1520 °C), the sample was pushed into the reaction hot zone and the reactions were monitored for 30 minutes.

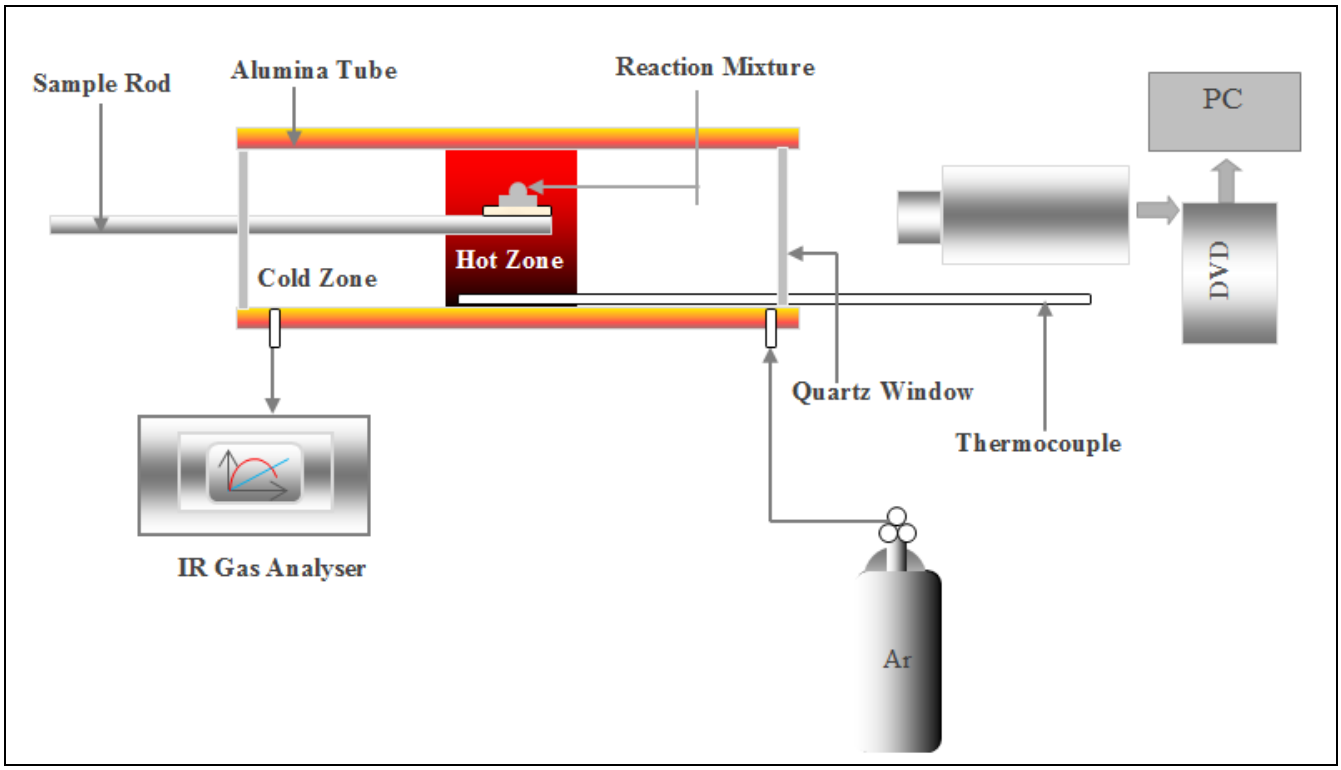

Figure 3. Schematic of the horizontal tube furnace and IR gas analyser system

This time was selected since initial trials showed that the reactions ceased and thus there were no further changes in gas composition or degree of reduction beyond this time. The reacted carbonaceous material/slag samples were quenched by rapidly withdrawing the tray from the hot reaction zone into the cold zone of the furnace.

2.4 Results and Discussions

Particles of reduced iron metal, which were clearly visible to the naked eye (Fig. 4), were removed magnetically and analysed.

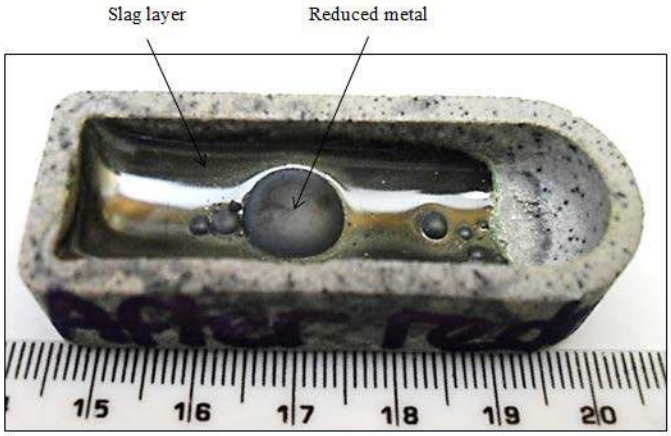

Figure 4. Nature of metal produced from reduction of slag-MPW composite at 1520 °C

2.4.1 Gas generation rates (IR Analyser)

The contents of CO and CO2 in the off-gas were measured continuously by an infrared (IR) gas analyser and the amounts of CO and CO2 removed from the slag were calculated using the off-gas data for each blend. The results are shown in Figs. 5 and 6 for MPW-SD and coke, respectively.

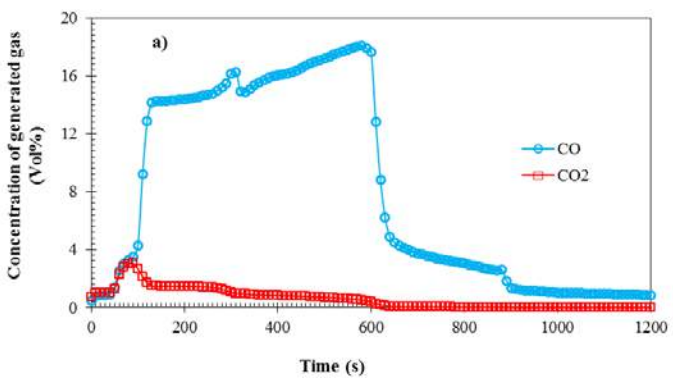

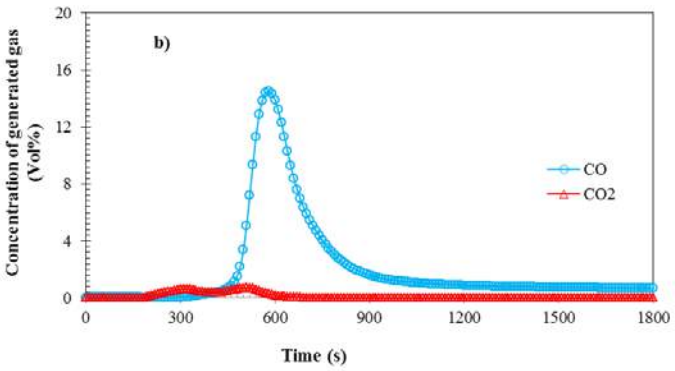

Figure 6. Concentration of generated gas as a function of time during the reduction of FeO in slag by a) MPW + SD and b) Coke 1520 °C

The relatively lower values recorded for CO_2 compared to CO may be an indication of direct reduction of FeO by C (equation 1) or a dominant Boudouard reaction (equation 2) or carbon gasification reaction (equation 3).

$$(FeO) + C = Fe + CO \quad (1)$$

$$CO_2 + C = 2CO \quad (2)$$

$$H_2O + C = CO + H_2 \quad (3)$$

Another possible reaction is the direct reduction of FeO by CH4, which was the predominant hydrocarbon detected in the off-gas above 1500 °C.

$$CH_4 + FeO = Fe + 2H_2 + CO \quad (4)$$

2.4.2 Extent of reduction

After reduction the reduced metal, was removed magnetically and weighed and the content of oxygen was determined using a LECO Nitrogen/Oxygen analyser (model TC-436 DR 602-500-600, LECO Corporation, Michigan, USA). The extent of reduction was determined from the oxygen values, bearing in mind that the initial concentration of removable oxygen from the reducible component of the slag (FeO) is about 22.27%. The result is illustrated in Fig 5.

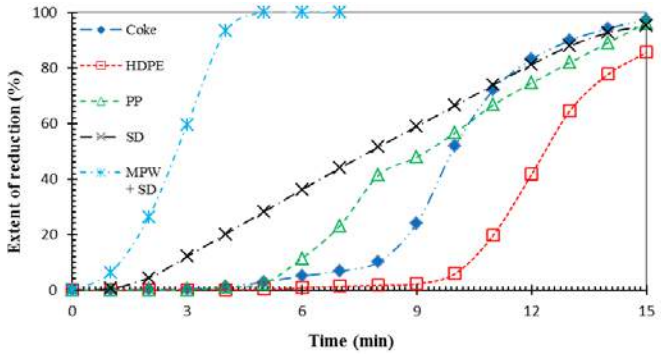

Figure 5 Observed extent of reduction for each carbonaceous reductant during the reaction of FeO in slag by various reductants

From Fig 5, each of the polymers shows a slightly lower extent of reduction than that by coke after 15 min, with the measured extent of reduction being 85.9, 95.2, 96.2 and 97.3 % for HDPE, SD, PP and coke respectively. However, blending the mixed plastics with SD the polymer (MPW + SD) resulted in a significant improvement in the extent of reduction, with the reaction essentially going to completion after about five minutes. This improvement in reduction is attributed to the extra reducing gases H2 and CH4 made available in the system through the thermal decomposition of the mixed polymers along with the fixed carbon from SD. The beneficial effect of H2 on the reduction of iron oxide by coke was elucidated in earlier investigation [5,6, 13-19].

The observed improvement in extent of reduction in the presence of a polymer is consistent with previous observations by Rahman et al. (sessile drop approach) [6], Dankwah et al. (crucible reduction approach) [5,7] and Kongkarat (sessile drop approach) [8].

3 CONCLUSIONS

The reduction of FeO from EAF slags by MPW-SD has been investigated in a horizontal tube furnace at 1520 °C. Extent of reduction of FeO from EAF slag by MPW-SD was compared with those by the individual polymers and metallurgical coke. It was observed that:

- MPW-SD is an effective reductant for iron oxide reduction.
- Significant improvements in the extent of reduction were observed for MPW-SD over the individual polymers and coke.
- Iron oxide reduction therefore offers and effective route for recycling waste plastics without the need to sort out individual plastics.

ACKNOWLEDGEMENTS

Part of this investigation was carried out at the School of Materials Science and Engineering, UNSW, Sydney, Australia. The authors are grateful to Prof Veena Sahajwalla for fruitful discussions.

REFERENCES

[1] K. Nishioka, T. Taniguchi, Y. Ueki, K. Ohno, T. Maeda, and M. Shimizu, (2007): ISIJ Int., 47(4), 602-607

[2] T. Matsuda, M. Takekawa, M. Hasegawa, Y. Ikemura, K. Wakimoto, T. Ariyama, and M. Iwase, (2006): Steel Research International, 77, 774-778

[3] T. Matsuda, M. Hasegawa, A. Ikemura, K. Wakimoto and M. Iwase, (2008): ISIJ Int., 48 (9), 1186-1196

[4] Y. Ueki, R. Mii, K. Ohno, T. Maeda, K. Nishioka, and M. Shimizu: ISIJ Int., 48 (2008), 1670-1675

[5] J.R. Dankwah, P. Koshy, N.M. Saha-Chaudhury, P. O'Kane, C. Skidmore, D. Knights, and V. Sahajwalla, (2011): ISIJ Int., 51(3), 498-507

[6] M. Rahman, (2010): PhD Thesis, UNSW-Sydney, Australia

[7] J.R. Dankwah, P. Koshy, P. O'Kane, and V. Sahajwalla, (2012): Steel Research International, 83(8), pp. 766-774

[8] S. Kongkarat, R. Khanna, P. Koshy, P. O'Kane, and V. Sahajwalla, (2011): Steel Research International, 82(10), 1228-1239

[9] V. Sahajwalla, M. Zaharia, A. Anthony, J. Lee, S. Darma, R. Khanna, N. Saha-Chaudhury, D. Knights, P. O'Kane and E. Pretorius: Proceedings of AISTech07, (2007), CD.-I

[10] J.R. Dankwah, (2012): PhD. Thesis, UNSW-Sydney, Australia

[11] T. Murakami, T. Akiyama, and E. Kasai, (2009): ISIJ Int., 49(6), 809-814
[12] T. Murakami, and E. Kasai, (2011): ISIJ Int., 51(1), 9-13
[13] J.R. Dankwah, (2014): International Journal of Scientific and Technology Research, Vol. 3, Issue 1, pp. 40-46
[14] J.R. Dankwah, (2013): International Journal of Engineering Science and Technology, Vol. 5, No. 12, pp. 1967-1976
[15] El-Geassy, A.A. and Rajakumar, R., (1985): Trans. Iron Steel Inst. Jpn., 25, 449-458
[16] I. Sohn and R.J. Fruehan: Met. Mat. Tras. B, 36B (2005), 605-612
[17] H. Ono-Nakazato, T. Yonezawa and T. Usui: ISIJ Int., 43 (2003), 1502-1511
[18] E. Donskoi, D.L.S. McElwain, and L.J. Wibberly: Met. Mat. Tras. B, 34B (2003), 255-266
[19] J.Y. Shi, E. Donskoi, D.L.S. McElwain, and L.J. Wibberly: Ironmaking and Steelmaking, 35 (2008), 3-13

The Dissolution of Vanadium in Silica Sand with Organic and Inorganic Acids

Silis Kumundaki Vanadyumun Organik ve İnorganik Asitlerle Çözünmesi

H. Hacıfazlıoğlu, İ. Kurşun, T.D. Tombal, M. Terzi
İstanbul Üniversitesi, Maden Mühendisliği Bölümü, İstanbul

ABSTRACT Being one of the important rare elements, vanadium is mainly used for the production of certain alloys. Various methods have been adopted so far for the recovery of vanadium. New methods are also being tried together with the developing technology and such methods have been included in the literature. The sample of the silica sand used within the scope of this study was taken from the silica sand beneficiation facility of a private mining company operating in Sile, Istanbul. In such facility, raw silica sand was filtered through a scrubber first and then sized with the help of a hydrocyclone and a hydrosizer and taken to the beneficiation facility. Several characterization tests and leaching tests with organic and inorganic acids were conducted for the recovery of vanadium from the sample and the dissolution conditions of vanadium with the best grade and efficiency were investigated. Following such leaching tests, the best result for vanadium dissolution was obtained with hydrofluoric acid. As a result of 2-hours leaching process performed with 800 kg/tons hydrofluoric acid amount under 40 ^{o}C, the dissolution efficiency of vanadium was found as 76%.

Keywords: Vanadium, silica sand, dissolution

ÖZET Önemli nadir elementlerden biri olan vanadyum, ağırlıklı olarak, belirli alaşımlar üretmek için kullanılmaktadır. Vanadyumun kazanımı için geçmişten günümüze çeşitli yöntemler uygulanmıştır. Gelişen teknolojiyle birlikte de yeni yöntemler denenmekte ve literatüre alınmaktadır. Bu çalışma kapsamında kullanılan silis kumu numunesi İstanbul Şile' de faaliyet gösteren özel bir madencilik şirketine ait silis kumu zenginleştirme tesisinden alınmıştır. Söz konusu tesiste, tüvenan silis kumu önce pervaneli yıkayıcıdan (scrubber) geçirilmekte, daha sonra hidrosiklon ve hidrosizer ile boyutlandırılarak zenginleştirme tesisine girmektedir. Numuneden vanadyum kazanılması için bir dizi karakterizasyon testi ve organik asitlerle liç deneyleri yapılarak en yüksek tenör ve verimde vanadyumun çözünme koşulları incelenmiştir. Liç deneyleri sonrasında vanadyum çözünme verimi için en iyi sonuçlar hidroflorik asitle elde edilmiştir. 800 kg/ ton hidroflorik asit miktarı ile 40^{o}C' de yapılan 2 saatlik liç işlemi sonunda vanadyum çözünme verimi % 76 bulunmuştur.

Anahtar Kelimeler: Vanadyum, silis kumu, çözünme

1 INTRODUCTION

The existence of vanadium was discovered for the first time by Spanish mineralogist Manuel Del Rio in 1801 in Mexico as a result of the studies performed on lead vanadate ore (Oztürk, 2008; Lagerkvist and Oskarsson, 2007). Vanadium is a relatively abundant trace element found on the crust of the earth and constitutes in many minerals and mineral beds. It does not constitute as a natural metal in the nature; however, it always co-exists with other elements.

Vanadium minerals are classified into seven classes which are namely oxides, phosphates, silicates, sulphates, sulphurs, titanates and vanadates (Gharehbagheri et al., 2013). The minerals containing vanadium consist of carnotite, mottramite, patronite, roscoelite and vanadinite (Ozturk, 2008; Moskalyk and Alfantazi, 2003). China is the world's market leader in terms of production and reserves of vanadium with a production of 40000 tons and reserves of 5 million tons, followed by Russia and USA respectively (USGS, 2013)

Vanadium is almost sole significant by-product which is used in iron or iron free alloys thanks to its physical properties such as high tensile strength, hardness and fracture strength. Vanadium is used in a wide range of combination with iron, titanium, nickel, aluminium, chrome and other metals for various commercial applications from railroads, steel tools and catalytic to aviation. Global supply of vanadium includes such primary resources as feedstock, concentrates, metallurgic slag and petroleum wastes. Furthermore, some mining wastes and waste ashes have a significant economical potential as they contain high amounts of vanadium and nickel (Moskalyk and Alfantazi, 2003; Yang et al., 2013).

Various methods are made use of for the recovery of vanadium which are namely hydrometallurgic and pyro + hydrometallurgic. The most applied methods among these are direct acid leach, direct alkali leach, post-roasting acid leach, post-roasting alkali leach and post-roasting water leach. Generally the alkali leach method is benefited from for the selective recovery of vanadium in comparison with iron. However, this method causes the dissolution of some amount of silica as well together with vanadium. Moreover, it is known as a costly and expensive method due to the used reagents. The dissolution of silica in sulphuric acid leach is relatively limited; but selective recovery is not possible for the co-recovery of nickel and vanadium. This method, on the other hand, is known to be a cost-effective and efficient method (Ozturk, 2008).

Li et al., (2010) performed some tests for vanadium production out of black shale through acid leach. Within the scope of this study, feasibility of the vanadium recovery was investigated with the use of sulphuric acid and hydrochloric acid solutions. According to the E-pH diagram for V-H_2O under 25 ° C, it was observed that the dissolved vanadium in an aqueous solution was in the form of VO^{2+} and VO_2^{+} at high potential and low pH value. The obtained optimum parameters are 87.5 g/L sulphuric acid concentration within 6-hours reaction time, 15 g/L hydrofluoric acid concentration, 1 g/L sodium hypochloride concentration (added after a reaction time of 3 hours), 95 °C leach temperature and 4 mL/g solid/liquid rate. Under these conditions, 86% vanadium was recovered to the utmost. Li et al., (2011) performed some tests for vanadium production through oxidization process out of a low grade vanadium slag in the existence of Na_2CO_3. In this study, the oxidization conditions of a low grade vanadium slag were investigated with the techniques of XRD, SEM / EDS and TG-DSC. The results obtained showed that vanadium slag was oxidized in the temperature range of 273 °C and 700 °C. Aarabi-Karasgani et al., (2010) also conducted some tests for vanadium production through the sulphuric acid leach method from Linz–Donawitz (LD) converter slag. In this study, an alkali roasting-acid leach study was performed for the sake of vanadium recovery out of LD converter slag in a steel production facility and the effect of different parameters on vanadium dissolution kinetics was determined. Optimum leach conditions were reached under 70 °C, 3 M acid concentration and 150 minutes leaching period and approximately 95% maximum vanadium recovery was obtained. Fan et al., (2013) performed both bulk and column tests for the purpose of vanadium decomposition from chrome with the use of D314 which is a mild base resin for the sake of vanadium recovery from the chromate solutions containing vanadium.

In China, various other studies were conducted for the recovery of vanadium out of hard coal (Min-Zhang et al., 2011). Wang et al., (2013) performed some studies as well for vanadium recovery from the hard coal through floatation. Final vanadium concentrate slime-floatation process was obtained with 1.88% V_2O_5 and 76.58% recovery rate and 72.51% of the raw ore was discarded as a waste.

2 EXPERIMENTAL STUDIES

2.1 Materials

The sample of the silica sand used in the experimental studies was taken from the silica sand beneficiation facility of a private mining company operating in Sile, Istanbul. In such facility, raw silica sand was filtered through the scrubber first and then sized with the help of a hydrocyclone and a hydrosizer and transferred to the beneficiation facility. The sample of the silica sand which subjected to the experimental studies was taken from the slime removal exit and brought to the Mineral Processing Laboratory of the Mining Engineering Department of the Engineering Faculty of Istanbul University in sealed containers. Within the scope of experimental studies, chemical content, particle size distribution and mineralogical analyses were performed first for the performance of sample characterization in terms of leach tests. The chemical analyses results of the sample which were conducted with the methods of XRF and ICP are given in Table 1; the particle size distribution graph obtained as a result of the particle size distribution analysis conducted with the wet sieving method is given in Figure 1 and the optical and scanning electron microscope photos are respectively given in Figure 2 and Figure 3.

Table 1. Chemical analysis results of the sample

Content	Assay Value
SiO_2 (%)	81,63
Al_2O_3 (%)	15,66
TiO_2 (%)	1,15
Fe_2O_3 (%)	0,54
K_2O (%)	0,37
ZrO_2 (%)	0,17
CaO(%)	0,12
MgO(%)	0,07
Cr_2O_3 (%)	0,07
P_2O_5 (%)	0,07
SO_3 (%)	0,05
BaO(%)	0,05
Na_2O (%)	0,04
V (ppm)	50,00
Other (%)	0,01
Total	100,00

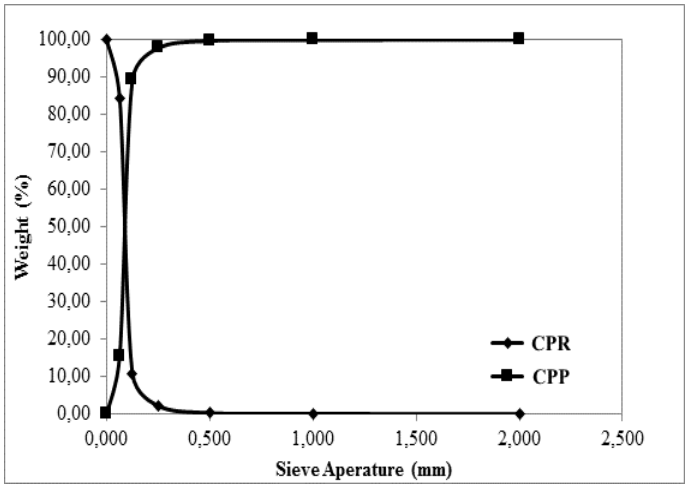

Figure 1. Particle size distribution graph of the sample

It was understood from the particle size distribution graph that the d_{50} and d_{80} sizes of the sample were respectively 0.08 mm and 0.12 mm. Following the optic and scanning electron microscope examinations performed within the scope of mineralogical analyses, on the other hand, it was identified that the sample contained hematite, ilmenite, magnetite and rutile minerals in addition to quartz. It is thought that vanadium likely exists depending on the magnetite content in the sample.


+1,000 mm
10x Magnification

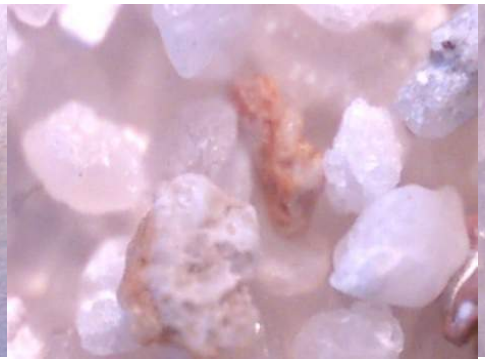
-1,000+0,500 mm
60x Magnification

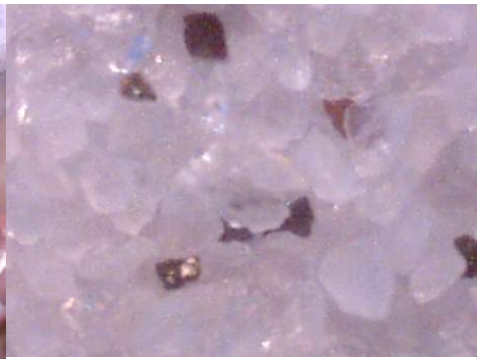
-0,125+0,063 mm
200x Magnification


-0,500+0,250 mm
60x Magnification


-0,250+0,125 mm
60x Magnification

Figure 2. Optical microscope images of the particle size fractions

According to SEM analysis of the sample, silica particles are while preserved their overall euhedral structures and they showed roundness in several areas of the general distribution.

Particles that containing iron are distributed in silica particle sand they also preserving their euhedral crystal structures.

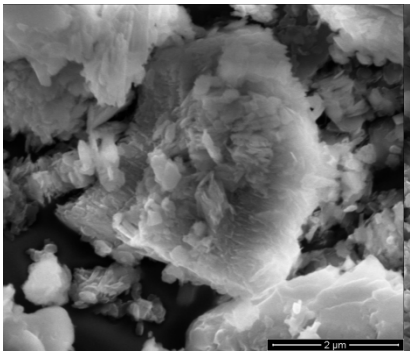

40000x Magnification

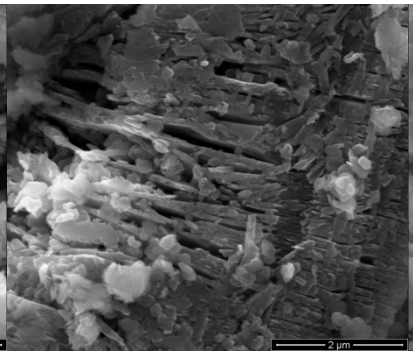

40000x Magnification

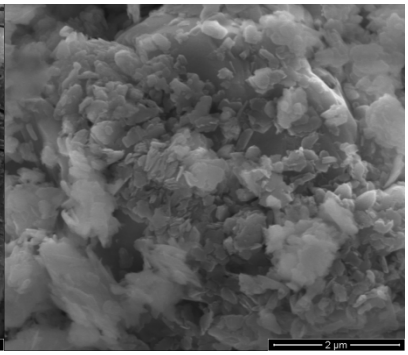

40000x Magnification

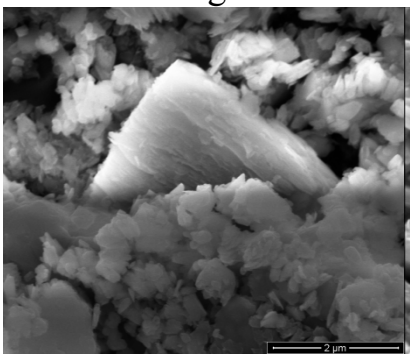

40000x Magnification

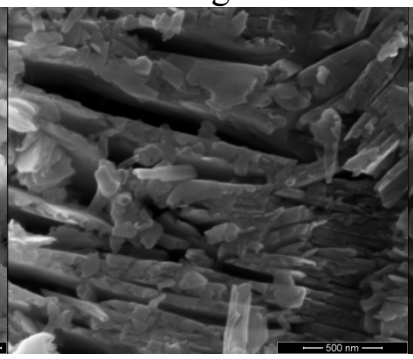

100000x Magnification

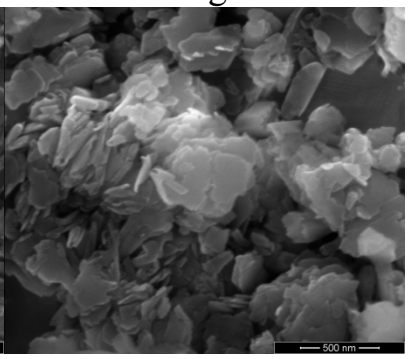

100000x Magnification

Figure 3. Scanning electron microscope images of the silica sand sample

2.2 Methodology

Leaching tests were conducted with the use of different organic and inorganic acids for the purpose of dissolution of the vanadium in the silica sand within the scope of this study. The organic acids used were citric, tartaric and oxalic acids whereas the inorganic acids were sulphuric (H_2SO_4), hydrochloric (HCl) and hydrofluoric (HF) acids. The vanadium dissolution efficiencies obtained as a result of the leaching tests performed with each of the abovementioned acids were calculated and the obtained results were interpreted. The silica sand was subjected to the leaching process for 2 hours under an average leaching temperature (40 ^{o}C) at different acid amounts (100, 200, 400, 600, 800 and 1000 kg/t) with the separate use of the abovementioned organic and inorganic acids. The leaching tests in question were performed in 250 cc of conical flasks in shaking water bath. The shaking rate of the shaking water bath was selected to be 250 rpm. Solid-liquid separation was also performed through a filtration process following the leaching procedure. The filter cake obtained as a result of solid-liquid separation process was dried in a drying stove and the vanadium content was analyzed through the ICP method. The vanadium dissolution efficiency was calculated through the following formula:

$$\text{V dissolution efficiency (\%)} = \frac{\left[\underset{\text{(ppm)}}{\text{V in the feed}} - \underset{\text{(ppm)}}{\text{V in the filter cake}}\right]}{\text{V in the feed(ppm)}} * 100 \quad (1)$$

3 RESULTS

The effects of different organic and inorganic acids on vanadium dissolution efficiency were respectively displayed in Figure 4 and Figure 5 in a graphical manner.

A regular increase was observed up to the acid quantity of 800 kg/tons in the vanadium dissolution efficiency within the scope of the tests performed with citric acid. The vanadium dissolution efficiency was found to be 36% in 800 kg/ton citric acid quantity and 4% decrease took place in terms of the efficiency in 1000 kg/ton acid quantity tried after this point. In the leaching tests performed with the use of tartaric acid, on the other hand, despite the fact that an efficiency increase of 200 kg/ton acid quantity, no significant change took place after this value. Consequently, the best results for vanadium dissolution efficiency in the leach tests performed with the use of organic acids were obtained with oxalic acid. The vanadium dissolution efficiency was found to be 50% as a result of the 2-hours leaching process performed under 40^{o}C with 200 kg/ton oxalic acid quantity.

No significant change was observed in terms of vanadium dissolution efficiency up to the acid quantity of 600 kg/ton within the scope of the leaching tests performed with the use of sulphuric acid. Vanadium dissolution efficiency showed an increase after this point up to the point of 800 kg/ton and it reduced to 46% with a decrease of 14% in the acid quantity of 1000 kg/ton. An efficiency increase was observed up to 400 kg/ton acid amount where 62% vanadium dissolution efficiency was obtained in the tests performed with hydrofluoric acid. After this point, on the other hand, vanadium dissolution efficiency showed a decrease tendency. In the leach tests performed with the use of inorganic acids, the best results for vanadium dissolution efficiency were obtained with hydrofluoric acid. A dramatic efficiency increase of 20% took place in 200 kg/ton acid quantity in comparison with 100 kg/ton acid quantity in the tests performed with hydrofluoric acid. The efficiency increase tendency sustained up to the point of 800 kg/ton depending on the acid quantity but it was less than the increase between the first two quantities tried. 76% vanadium dissolution efficiency was obtained in 800 kg/ton hydrofluoric acid quantity where the best result was obtained. Figure 6 shows the concentrate and the impurities in it that was obtained as a result of the leaching process performed with hydrofluoric and oxalic acids. As can be seen from the microscopic images, hydrofluoric acid was more efficient than oxalic acid, which is an organic acid, in terms of the dissolution of V bearing impurities.

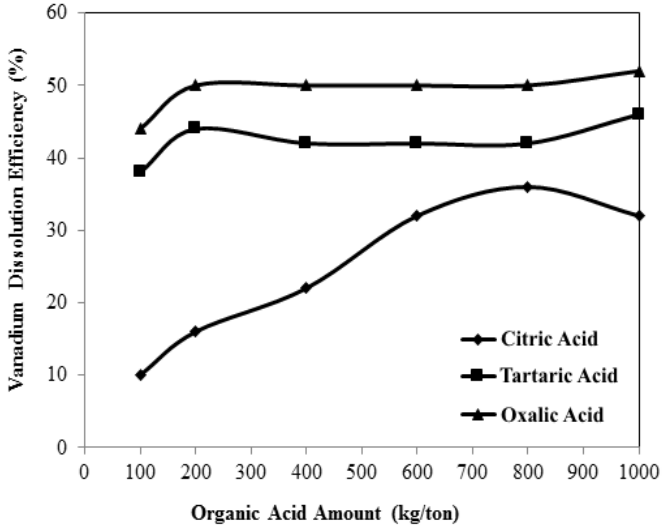

Figure 4. The effect of different organic acids on vanadium dissolution efficiency

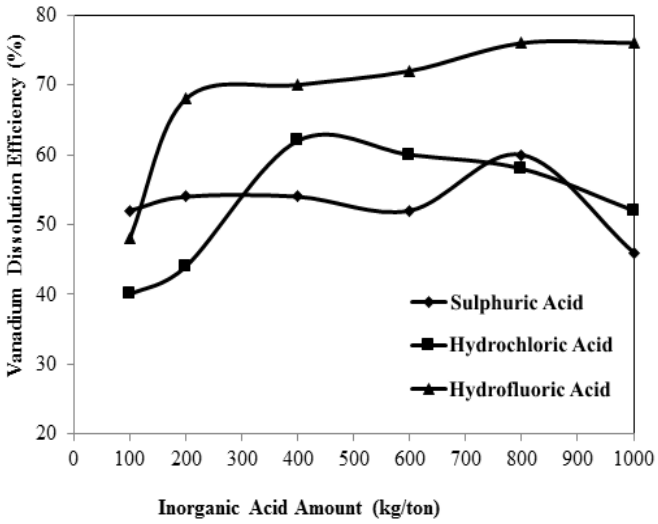

Figure 5. The effect of different inorganic acids on vanadium dissolution efficiency

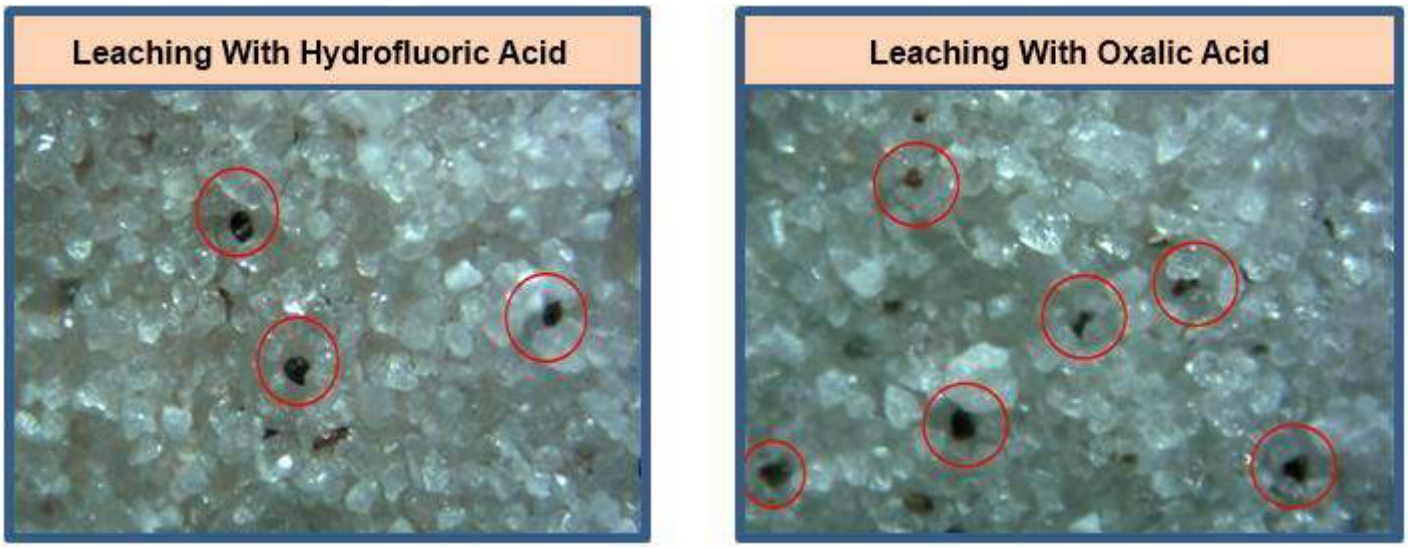

Figure 6. Images of concentrates obtained as a result of the leaching tests

4 DISCUSSION AND CONCLUSION

The best results for vanadium dissolution efficiency were obtained with oxalic acid in leaching tests conducted with the use of organic acids. Vanadium dissolution efficiency was found to be 50% as a result of the 2-hours of leach test conductedwith 200 kg/ton oxalic acid under 40 ^{o}C.

The best results for vanadium dissolution efficiency were obtained with hydrofluoric acid in leaching tests conducted with the use of inorganic acids. Vanadium dissolution efficiency was found to be 76% as a result of the 2-hours of leaching test performed with 800 kg/ton hydrofluoric acid under 40 ^{o}C.

REFERENCES

Ozturk, A.T., 2008. *Acquisition of Vanadium and Nickel out of Waste Ashes and Used Industrial Catalytic*, Suleyman Demirel University, MSc. Thesis, Isparta.

Aarabi-Karasgani, M., Raschi, F., Mostoufi, N., Vahidi, E., 2010. Leaching of vanadium from LD converter slag using sulphuric acid, *Hydrometallurgy*, 102, p.14–21.

Min-Zhang, Y., Bao, S., Liu, T., Chen, T., Huang, J., 2011. The technology of extracting vanadium from stone coal in China: History, current status and future prospects, *Hydrometallurgy*, 109, p.116–124.

Li, M., Wei, C., Fan, G., Wu, H., Li, C., Li, X., 2010. Acid leaching of black shale for the extraction of vanadium, *International Journal of Mineral Processing*, 95, p.62–67.

Li, X., Xie, B., Wang, G., Li, X., 2011. Oxidation process of low-grade vanadium slag in presence

of Na_2CO_3, *Trans. Nonferrous Met. Soc. China*, 21, p.1860-1867.

Gharehbagheri, H., Safdari, J., Roostaazad, R., Rashidi, A., 2013. Two-stage fungal leaching of vanadium from uranium ore residue of the leaching stage using statistical experimental design, *Annals of Nuclear Energy*, 56, p.48–52.

Moskalyk, R.R., Alfantazi, A.M., 2003. Processing of vanadium: a review, *Minerals Engineering,* 16, p.793–805.

Yang, J., Tang, Y., Yang, K., Rouff, A.A., Elzinga E.J., Huang, J., 2013. Leaching characteristics of vanadium in mine tailings and soils near avanadium titanomagnetite mining site, *Journal of Hazardous Materials*, 264, p.498– 504.

Lagerkvist, B., Oskarsson, A., 2007. *Handbook on the Toxicology of Metals*, Chapter 46, p.905-923.

USGS, 2013, U.S. Geological Survey, Mineral Commodity Summaries, February 2014, Vanadium.

Fan, Y., Wang, X., Wang, M., 2013. Separation and recovery of chromium and vanadium from vanadium-containing chromate solution by ion exchange, *Hydrometallurgy*, 136, p.31–35.

Wang, L., Sun, W., Liu, R., Gu, X., 2013. Flotation recovery of vanadium from low-grade stone coal, *Trans. Nonferrous Met. Soc. China*, 24, p.1145−1151.

Mining and Environment

Forestry Biological Reclamation of Damaged Mining Terrains

I. Grigorova, I. Nishkov
University of Mining and Geology "St. Ivan Rislki", Department of Mineral Processing and Recycling, 1700 Sofia, Bulgaria

ABSTRACT Subject to reclamation are all damaged terrains as well as the adjacent land lots which have partly or completely lost their productivity as a result of the negative impact upon them from the mining activities and the damaged terrains. A similar problem exists in Kaolin AD, Bulgaria. The main raw material mined in the company's open pits is quartz-kaolin sands. The overburden dumps are formed as a result of the accumulation earth material extracted with open pit mining. These earth formations have no purposeful economic use and damaged mining terrains is need of reclamation. Chemical modified zeolite, organo-zeolite compost and bio-zeolitic ameliorants for forestry biological reclamation were studied. The basic mineral ameliorant is Bulgarian natural zeolites. The pot experiments were performed. Different tree types were shown in the studied substrate mixtures and the plant growth is investigated.

Keywords: Biological reclamation, damaged terrains, the pot experiment

1 INTRODUCTION

The technology for creating forest cultivars on the damaged by the mining industry terrains differs considerably from the ones applied in the creation of plantings upon non damaged terrains and depends mainly on the forestry growing conditions which at the damaged terrains (dumping grounds and quarries) are quite specific and extremely unfavorable. The ameliorative activities should follow the objectives of an accelerated forestry biological effect through decreasing the acidity of the substrata, increasing the fertility of the dumps, creating appropriate conditions for growth of the vegetation characteristic for the natural for the region ecosystems. Tree types used for reclamation should be appropriate for the geographical climatic and forestry area, to be non exigent towards the edaphic conditions and more specially to be resistant to acidity and with high anti erosion potential.

The patterns for reforestation should be specific and should ensure a good anti erosion effect as well as to be able to quickly establish a sustainable forestry ecosystem.

Subject to reclamation are all damaged terrains as well as the adjacent land lots which have partly or completely lost their productivity as a result of the negative impact upon them from the mining activities and the damaged terrains. A similar problem exists in Kaolin AD, Bulgaria. The main raw material mined in the company's open pits is quartz-kaolin sands. The overburden dumps are formed as a result of the accumulation earth material extracted with open pit mining. These earth formations have no purposeful economic use and damaged mining terrains is need of reclamation. Numerous soil samples were taken from overburden dump and agrophysical and agrochemical properties of anthropogenic soil are determined (Prokopiev et al 2012; Ming et al 1993; Chapman 1965).

Research and development program is started to develop new ameliorants for amending the agrochemical and physicochemical properties of anthropogenic soil. The program has undertaken restoring the function of damaged lands and the creation of balanced ecological systems.

This paper describes some results on an experimental work in the frame of the research program for forestry biological reclamation of damaged mining terrains.

2 EXPERIMENTAL

2.1. Methods and Materials

For amending of agrochemical and physicochemical properties of anthropogenic soil new ameliorants for forestry biological reclamation are developed. The basic mineral ameliorant is Bulgarian natural zeolites. Three different mineral ameliorants were studied:

- Chemical modified zeolite (CMZ). This product is a slow-acting mineral ameliorant enriched of nitrogen, phosphorus, potassium and microelements.
- Organo-zeolitic fertilizer (OZF). This ameliorant is a mechanical mixture of organo-matter and chemical modified zeolite which is enriched additionally with humus (Filcheva et al 1988; Chakalov et al 2002).
- Biozeolite ameliorant (BZM). This product is chemical modified zeolite enriched of biological enzymes.

Agro-chemical parameters of new ameliorants were determined. The phosphorus and potassium in aqueous extract of ameliorants were determined by method of Egner-Riim (Chakalov et al 2002). The exchange nitrogen is determined using 1 % solution of KCl and the digestible forms and microelements - using Morgan extract solution at pH = 4.8.

One year pot experiments were performed. The substrates including studied overburden dump soil and different mineral ameliorants were produced. The ameliorant contents in the substrate mi*xt*ures are 5 and 10 vol. %, respectively. Six different substrates were studied:

- K-1 (Control): Anthropogenic soil;
- K-2 (Control): Mechanical mixture of anthropogenic soil with Nitrogen – phosphorus - potassium (NPK) fertilizer (40 g/100 kg substrate);
- B-1: Mechanical mixture of anthropogenic soil with 5 % chemical modified zeolite;
- B-2: Mechanical mixture of anthropogenic soil with 10 % chemical modified zeolite;
- B-3: Mechanical mixture of anthropogenic soil with 5 % chemical modified zeolite and 5 % organo-zeolitic fertilizer;
- B-4: Mechanical mixture of anthropogenic soil with 5 % organo-zeolitic fertilizer and 5 % biozeolite ameliorant.

Numerous pot experiments were conducted. Different plants were sown in the substrate mixtures and the process of annual growth was investigated. The following forest cultivars were studied: *Paulownia tomentosa; Paulownia elongate; Lycium barbarum; Robinia pseudoacacia L.*

The biometric measurements of annual plants were performed. The diameter of the tree trunk, tree height, number of leaves, leaf surface, number of fruits, fruit weight, average fruit weight and number of offshoots are determined. After annual plants growth the chemico-biological measurements of substrate mixtures were performed. Additionally the leaf diagnosis of annual trees was performed.

3 RESULTS AND DISCUSSION

The agro-chemical parameters of chemical modified zeolite, organo-zeolic fertilizer and biozeolite ameliorant are presented in Table 1.

The data show that all three ameliorants have slightly acidic pH and high electrical conductivity. This will be beneficial in preparation of substrate mixtures including overburden dump soil and ameliorant in relevant ratio.

Table 1. Agro-chemical parameters of new ameliorants.

Agro-chemical parameters	Chemical modified zeolite	Organo-zeolitic fertilizer	Biozeolite ameliorant
Aqueous extract			
pH	4.44	4.65	5.71
Electrical conductivity, (μS)	7260	7596	8411
P_2O_5, (mg/100 g)	772.50	772.50	653.94
K_2O, (mg/100 g)	42.76	42.76	49.69
Exchange N, (mg/100 g)	551.43	551.43	615.06
Digestible forms			
P_2O_5, (mg/100 g)	560.25	560.25	613.13
K_2O, (mg/100 g)	106.00	106.00	128.29
CaO, (mg/100 g)	757.28	757.28	1094.93
MgO, (mg/100 g)	65.84	65.84	107.24
Fe, (mg/1000 g)	-	300	300
Mn, (mg/1000 g)	-	250	250
Cu, (mg/1000 g)	-	150	150
Zn, (mg/1000 g)	-	150	150
Mo, (mg/1000 g)	-	5	5
B, (mg/1000 g)	-	5	5

The data presented on Table 2 show the annual growth of *Paulownia tomentosa* in condition of pot experiments for biological reclamation of anthropogenic soil.

The anthropogenic soils fertilized with Nitrogen – phosphorus – potassium (NPK) fertilizer (40 g/100 kg substrate) providing nutrients to the middle of the second month after planting. Subsequent to initial good plants development growth retardation occurs. Similar treatment effects of the substrates with biozelite ameliorant since the initial growth stimulation are depleted nutrients and the plants cease growth.

Upon soil improvement with 5 и 10 % chemical modified zeolite and organo-zeolitic fertilizer very strong growth was established. The diameter of the tree trunk exceeds over two times that seen in the control. Tree heights are over three times greater than that of the control. The leaf surface is much larger - up to 15 times greater than the control.

The results of annual growth of *Paulownia elongate* in condition of pot experiments are presented on Table 3.

In this plant sorts the differences in the annual growth are crisper. The treatment with 10% chemical modified zeolite increased the tree trunk diameter two and a half times and the tree height up to twice. The number of the leaves increased from six to seven times compared with the control with NPK fertilizer.

The statistical analysis indicates that both two types *Paulownia* reared and treated with 5 and 10 % chemical modified zeolite and organo-zeolitic fertilizer have well-proven differences compared with control tests К-1 и К-2. These alternative solutions have no proven significant differences in plant development and can be concluded that the variant with chemical modified zeolite 5 % chemical modified zeolite probably will be economically preferred.

The biometric measurements of *Lycium barbarum* are presented on Table 4.

Table 2. Biometric measurements of *Paulownia tomentosa.*

Substrate type	Tree trunk diameter, (mm)	Tree height, (cm)	Number of leaves	Leaf surface, (cm^2)
К - 1	5.25	16.00	6.00	452.5
К - 2	6.24	22.75	9.00	1068.84
В - 1	11.30	51.50	11.67	4897.83
В - 2	13.55	55.20	12.60	7227.50
В - 3	11.82	53.67	13.17	6586.42
В - 4	8.52	24.80	7.80	1154.17

Table 3. Biometric measurements of *Paulownia elongate.*

Substrate type	Tree trunk diameter, (mm)	Tree height, (cm)	Number of leaves	Leaf surface, (cm^2)
К - 1	5.86	10.20	10.40	228.62
К - 2	9.72	44.80	11.20	2410.02
В - 1	13.38	86.20	18.40	10559.27
В - 2	12.94	92.60	16.40	9117.17
В - 3	15.18	77.80	14.40	7999.46
В - 4	6.98	23.80	9.20	1528.36

Table 4. Biometric measurements of *Lycium barbarum.*

Substrate type	Tree height, (cm)	Number of fruits	Fruit weight, (g)	Average fruit weight
К - 1	20.40	0	0	0
К - 2	88.60	0	0	0
В - 1	154.80	54.60	13.27	0.24
В - 2	145.60	158.40	52.53	0.34
В - 3	141.00	41.60	18.91	0.36
В - 4	62.60	14.60	4.55	0.31

Table 5. Biometric measurements of *Robinia pseudoacacia L.*

Substrate type	Tree trunk diameter, (mm)	Tree height, (cm)	Average number of offshoots
К - 1	8.14	66.60	1.00
К - 2	8.26	61.00	2.60
В - 1	9.04	62.60	2.20
В - 2	8.44	73.40	2.00
В - 3	8.30	69.00	2.20
В - 4	9.34	79.80	2.00

The treatment of anthropogenic soil with mineral ameliorants stimulates rapid growth and development of this plant sort. Once again confirms that the treatment with biozeolite does not provide prolonged normally mineral nutrition of plants.

The plants reared with 5 и 10 % chemical modified zeolite and organo-zeolitic fertilizer has doubled the height of the shrub. All mineral ameliorants supporting the first growing season to plants fruitage. In both controls fruitfulness plants do not realize. The substrate comfortable mineral nutrition treating with 10 % chemical modified zeolite providing larger fruits and nearly three times higher yield compared with those in 5% of treatment with chemical modified zeolite.

The data presented on Table 5 show the annual growth of *Robinia pseudoacacia L.* in condition of pot experiments for biological reclamation of anthropogenic soil.

Proven difference has not been established at none of biometric measurements in condition of pot experiments with *Robinia pseudoacacia L.* By visual observation was found that the best plants grow reared in anthropogenic soil with biozeolite ameliorant. Probably due to the root system initial stimulation and the organic nitrogen subsequent accumulation in the rhizosphere of these plants.

The data presented on Table 6 show the influence of mineral ameliorants on the mobile forms of macro-elements in pot experiment conditions.

The results obtained from pot experiments with *Paulownia tomentosa* indicate that N-NH_4 content increases from 22 to 102%, the N-NO_3 content - from 58 to 91%. The mobile forms of P_2O_5 increases from three to four times and a K_2O average twice times. At pot experiments with *Paulownia elongata* due to a rapid growth of the species significantly faster depletion of accessible nitrogen was found. Obviously this sort is less demanding to phosphorus and treatment with 5 and 10% chemical modified zeolite in the substrate has a good availability of phosphorous and potassium. There is enhanced nitrification activity and in some variants the nitrate nitrogen is up to 15 times higher than the control. The mobile forms of P_2O_5 are increased 6 to 14 times and potassium - from 37 to 87%.

The ameliorants have slight influence on the medium active reaction. A slight tendency to decrease the medium alkaline reaction was established. Positive effects on agrochemical characteristics are found. The positive effects on the agrochemical characteristics of the treated substrates affect plants mineral nutrition.

The macro-elements content in *Paulownia tomentosa* leaves is presented on Table 7.

The results show that *Paulownia tomentosa* grown in treated with zeolite substrates, the plants absorbed to three times much nitrogen. The phosphorus is comparable to control content and potassium is up to twice over in the plants leaves reared under ameliorated with zeolite products anthropogenic soils. The plants assimilate in large amounts of magnesium.

The leaf diagnosis of *Paulownia elongate* is shown on Table 8.

The results shows that *Paulownia elongate* grown by treated with zeolite substrates, the plants contain from 21% up to twice nitrogen in the control. This means that powerful vegetative growth which was established saplings accumulate several times over nitrogen than control plants. The phosphorus content is comparable to the control, but the content of potassium is 32 to 85% more than the control. Zeolite soil conditioners control the absorption of calcium and magnesium and significantly reduce their content in leaves.

The data presented on Table 9 show the influence of mineral ameliorants on the mobile forms of macro-elements in pot experiment conditions with *Lycium barbarum.*

Table 6. Agrochemical characteristics of studied substrates in *Paulownia* pot experiments.

Substrate type	pH	EC, (µS/cm)	Total N	N NH_4	N NO_3	P_2O_5	K_2O
			(mg/100 g)				
Paulownia tomentosa							
K - 2	7.94	161.00	58.17	2.52	0.84	1.70	15.66
B - 1	7.97	176.00	62.80	3.08	1.61	4.70	30.12
B - 2	8.00	189.00	70.51	4.97	1.33	7.30	44.09
B - 3	7.90	225.00	80.52	5.11	1.33	6.15	31.32
Paulownia elongate							
K - 2	8.10	163.00	51.81	2.52	1.40	1.60	19.27
B - 1	7.90	195.00	60.18	1.12	3.36	9.50	26.50
B - 2	7.80	395.00	69.73	0.70	15.68	22.35	36.12
B - 3	7.90	238.00	75.39	2.66	3.57	12.50	26.50

Table 7. Leaf diagnosis – Macro-elements content in *Paulownia tomentosa* leaves.

Substrate type	N	P_2O_5	K	Ca	Mg
			(mg/100 g)		
K - 1	1.36	0.44	1.00	180	0.58
K - 2	1.15	0.31	1.52	1.57	0.39
B - 1	3.12	0.40	1.74	1.68	0.56
B - 2	3.45	0.48	2.04	1.58	0.50
B - 3	3.24	0.46	2.04	1.65	0.50
B - 4	1.63	0.41	2.17	2.00	0.49

Table 8. Leaf diagnosis – Macro elements content in *Paulownia elongate* leaves.

Substrate type	N	P_2O_5	K	Ca	Mg
			(mg/100 g)		
K - 1	1.71	0.49	1.34	1.96	0.83
K - 2	1.72	0.38	1.91	1.33	0.64
B - 1	1.72	0.38	1.91	1.33	0.62
B - 2	3.60	0.53	1.77	1.25	0.73
B - 3	3.40	0.56	2.39	1.51	0.83
B - 4	2.07	0.44	2.49	1.61	0.74

Table 9. Agrochemical characteristics of studied substrates in *Lycium barbarum* pot experiments.

Substrate type	pH	EC, (µS/cm)	Total N	N NH_4	N NO_3	P_2O_5	K_2O
			(mg/100 g)				
K - 2	7.90	192	68.77	4.76	2.45	2.55	16.86
B - 1	8.00	194	64.40	1.05	3.15	6.05	26.12
B – 2	8.00	304	80.17	3.08	8.89	16.90	45.77
B - 3	7.80	202	92.82	2.10	1.68	10.22	27.11

The results obtained from pot experiments with *Lycium barbarum* confirm the trends that were established in experiments with *Paulownia*. The active medium reaction slightly influenced by meliorants. Using 10% zeolite ameliorant salt concentration of the aqueous extract and the total nitrogen increases. Ammonia nitrogen content reduce due to its absorption by plants and nitrification activity of represented the rising microflora. The content of available nitrogen and phosphorous in the middle of the vegetation of *Lycium barbarum* is sufficient for plant growth at a dose of 10% in this pot experiment. All substrates are well stocked with absorbable potassium.

4 CONCLUSIONS

The experimental results show that anthropogenic substrates from Vetovo region improving with zeolite meliorants increase their productivity 2.5 times in terms of pot experiments. This is due of the improved mobility of macronutrients and their enhanced absorption by the plants.

ACKNOWLEDGEMENTS

Financial support for this study and permission to publish this paper from KAOLIN AD is gratefully acknowledged.

REFERENCES

Chapman, D, 1965. Cation-exchange capacity. Methods of Soil Analysis – Chemical and Microbiological Properties, *The Agronomy Proceedings*, (pp. 891-901).

Chakalov, K, Popova, T, Filcheva, E, 2002. Soil fertility management with zeolite amendments. Zeolite effect on maintaining the soil, CRC – Press LLC: Boston, *Proceeding of International Symposium Agriculture Practices and Policies for Carbon Sequestration in soil*, (pp. 229- 235).

Filcheva, E, Chakalov, K, Popova, T, (ed. J Balcan), 1988. Model approach to improve soil quality using organo-zeolite compost, *The Ecology Proceedings*, 1-1, (pp. 72 -78).

Ming, D, W, Allen, E, R, Galindo, C, Jr, Henninger, D, L, (ed. G, R, Fuentes, J, A, Gonzales), 1993. Methods for determining cation exchange capacities and compositions of native cations for clinoptilolite, in *Proceeding of the 3rd International Conference on the Occurrence, Properties and Utilization of Natural Zeolites*, (pp. 31-35).

Prokopiev, A, Popov, N, Chakalov, K, Popova, T, Grigorova, I, Nishkov, I, Mineral and Organic-Mineral Ameliorants for Biological Mining Terrains Reclamation, *Proc. of XXVI International Mineral Processing Congress*, New Delhi, India, September 2012, (pp. 03871-03881).

.

Effect of Crack Width, Length, and Depth on Surface Disposal of Sulphidic Paste Tailings

E. Yilmaz
University of Quebec in Abitibi-Témiscamingue (UQAT), Department of Applied Sciences, 445 Boul. de l'Université, Rouyn-Noranda (Québec) J9X 5E4 Canada

ABSTRACT A field study was initiated to assess the effect of crack with, length and depth on the performance and quality of sulphide-rich paste tailings. This investigation included the construction of two experimental cells covered by special disposal configurations (categorized as cemented cell CC and uncemented cell UC). Each cover was instrumented by a number of sensors to monitor its geotechnical behavior. Results show that the width and depth of cracks in the UC is bigger than those of the CC. The formation of cracks occurred in layers is reliant on the time interval and configuration of deposition. The longer the deposition process, the deeper and wider the formation of crack causes. The drainage of upper layer is accelerated after the deposition of tailings on a dry surface layer. This is due to the suction which creates a fast movement of water towards the bottom and may lead to a fast crack occurrence.

Keywords: Surface tailing disposal, Crack width, Crack length, Crack depth

1 INTRODUCTION

Mine tailings require careful management to certify the storage stability, and to avoid land contamination. The unsuitable management of mine tailings creates the unwanted events, such as acid rock drainage (Verburg, 2002; Bussière et al., 2004; Aubertin et al., 2006; Blight, 2010; Fourie, 2012). Technological advances have resulted in significant changes in the tailings management practices over the last decade. As a result of alternative tailings deposition methods, mine tailings are now better managed than they have been in the past (Slotte, 2004; Dixon-Hardy and Engels, 2007; Hudson-Edwards et al., 2011; Yilmaz, 2011; Lotermoser, 2011; Edraki et al., 2014). One of these ways is surface paste disposal (SPD), where each layer of paste tailings is deposited and allowed to dry before the next layer is put in place. Paste (70-85% solids) is made in the specialised paste thickeners or high-density thickeners and transported with the pumps into underground stopes.

Paste disposal has been effectively used as underground backfill for many years (Fall et al., 2009; Benzaazoua et al., 2008; Potvin et al., 2005; Kesimal et al., 2006; Cihangir et al., 2012; Belem et al, 2013; Ercikdi et al., 2014). Evolved from the technology used for backfilling of underground voids, SPD is new and its application is relatively limited (Robinsky, 2000; Landriault et al., 2001; Bussière, 2007; Deschamps et al., 2008; Yilmaz, 2010). Transporting and producing paste is costly due to the high capital and operating cost of thickeners and pumps. Compared to other methods, SPD becomes an attractive option since it allows for a smaller footprint area, an improved water recovery capability and lower environmental impacts (Sofra and Boger, 2002; Grabinsky et al., 2002; Crowder et al., 2002; Cadden et al., 2003; Benzazoua et al,, 2004; Deschamps et al., 2007, 2011; Bryan et al., 2010; Tariq and Yanful, 2013; Yilmaz et al., 2014). A lot of investigations have been done on quality and behaviour of SPD at laboratory and field environments. These consist of rheological behaviour for an advanced tailings delivery system, disposal behaviour for minimizing the environmental impact, and environmental behaviour for the improved geotechnical properties of tailings (Theron et al., 2005; Verburg et al., 2006; Simms et al., 2007; Martin et al., 2010; Mizani et al., 2013).

The Bulyanhulu mine (Tanzania) was the first gold mine to adopt the technology of SPD for tailings management (Shuttleworth et al., 2005). Paste tailings do not contain any binder when they are used for surface disposal. Tailings have a slump consistency of 250 mm (Theriault et al., 2003). One of the most challenging tasks to be considered for SPD is to eliminate the tailings' potential reactivity. It is well known that sulphide-rich paste tailings may oxidize in the presence of water and oxygen, and generate sulphuric acid (Benzaazoua et al., 2004). The SPD's behaviour has also been examined using lab-scale physical models, which could replicate the in situ conditions of surface disposal in terms of climatic conditions, consolidation, volume change, evaporation, surface cracks, and geometry (Landriault et al., 2001; Kwak et al., 2005; Oxenford and Lord, 2006; Henriquez and Simms, 2009; Deschamps et al., 2011; Yilmaz et al., 2011, 2013). These studies have well confirmed that field testing is vital to realize the SPD's behaviour.

Consequently, a complete understanding of these aspects is needed to evaluate in situ depositional behaviour of tailings at Laronde Mine (Canada). This paper deals the two field cells undertaken to study the effect of crack width, length, and depth on surface disposal of tailings. The goals of this work are; *i)* to assess the effect of two different disposal conditions (cemented cell – CC and uncemented cell – UC) on surface paste disposal; and *ii)* to characterize the behaviour of sulphidic paste tailings. The key interest of the present paper stems in part from the fact that this is one of the very first attempts, to the authors' knowledge, to investigate in situ behaviour of tailings under accurately simulated surface disposal conditions. The key contribution of this paper is related to the assessment of SPD's crack behaviour.

2 LARONDE MINE

LaRonde is Agnico-Eagle's flagship mine, located in the Abitibi region of northwestern Quebec, 45 km from the town of Rouyn-Noranda and 650 km in the direction North West of the city of Montreal. Since 1988, LaRonde has produced more than 4.3 million ounces of gold. With proven and probable gold reserves of 4.7 million ounces (33 million tons grading 4.4 g/t gold), LaRonde has one of the largest gold reserves of any mine operating in Canada. In 2006, LaRonde began to construct a deep extension of the mine to access higher-grade ore to a depth of about 3.1 km and extend the life of the operating mine. The 7,200-ton-per-day mine and plant are expected to average about 320,000 ounces of gold production annually, over a mine life lasting through to 2023.

2.1 Tailings Management

Mine tailings not recycled underground in paste backfill, are stored in tailings ponds covering an area of approximately 119 hectares and waste rock is stored in two waste rock piles with a combined volume of approximately 1.43 million cubic meters. The Company holds mining claims to the north-east, to the east and to the south-east of the mine tailings ponds that would allow expansion of the tailings ponds and the establishment of additional waste disposal areas. Figure 1 shows an aerial view of the tailings pond sites.

Figure 1. Laronde's tailings impoundments sites, including mine tailings discharged by spigotting off dykes

2.2 Paste Backfill Plant

The mine uses paste backfill as a means of supporting underground excavations and to return a large percentage (30-50%) of mill tailings. Paste backfill is made up of total tailings, mine recycled water for mixing and a binding agent (a blend of ordinary Portland

cement and high sulphate resistant hydraulic cement with a ratio of 50:50) at a binder content of 5 wt% (by the solid mass of dry tailings). Figure 2 shows a typical flow chart of the LaRonde paste backfill plant.

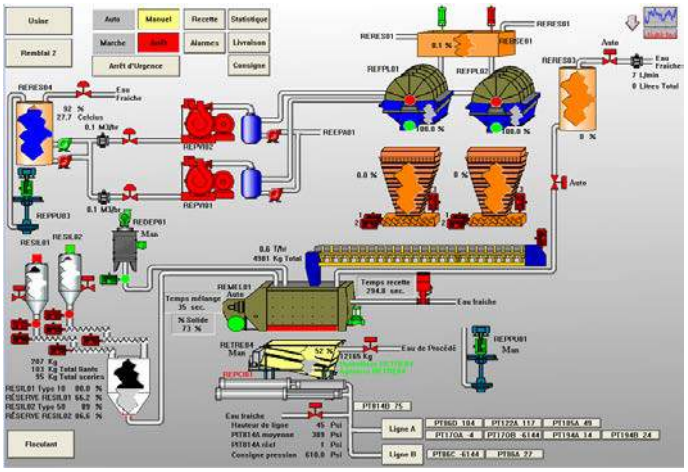

Figure 2. Laronde's paste plant flowsheet

Tailings are first fed into a high capacity conventional thickener of 20 m diameter to increase the solid concentration to 60 wt%. The thickened tailings are then pumped from the thickener to a high capacity holding tank (900 tonnes). From the high-density storage tank, the thickened paste tailings are fed to two disc filters operating in parallel to make filter cake with a solid concentration of 70-85 wt%. The filter cake is then discharged onto a reversible belt conveyor and fed to a feeder for weighing. Finally, the filter cake batches are mixed in a high intensity mixer (5 m^3) with binder and water added for about 45 sec to make a paste with a consistency of approximately 267 mm. The paste material prepared is transported underground through a piping system using pump and gravity. The underground stopes to be filled by tailings with cement are characterized by a fractured rock which allows a well drainage conditions during the gravity-driven consolidation.

3 MATERIALS AND METHODS

3.1 Materials

Tailings were sampled as representative of the tailings streams from the paste plant of the LaRonde mine. Portions of the samples were air dried to conduct a set of lab tests needed for the material characterization. The following tests were conducted according to ASTM standards testing procedures. Further details on material properties can be found Yilmaz (2010), and Yilmaz et al. (2011).

3.1.1 Paste tailings characteristics

The representative paste tailings were sized using a Malvern Mastersizer® laser particle size analyser under wet conditions. Based on unified soil classification system (McCarthy, 2007), the tailings tested can be classified as low plastic silt. The fine content (minus 20 μm) within paste tailings was 41 wt%. Table 1 lists a summary of the tailings' physical properties. The effective grain diameter D_{10} in the tailings was 5.04 μm.

Table 1. Physical properties of tailings

Parameter	Value
Gravimetric water content w (%)	24.3
Solids specific gravity G_s	3.37
Clay-sized particles (< 2 μm, %)	3.5
Silt-sized particles (2-50 μm, %)	67.0
Sand-sized particles (50-2000 μm, %)	29.5
Coefficient of uniformity C_u	6.90
Coefficient of curvature C_c	1.03

3.1.2 Hydraulic cement characteristics

For the cemented cell CC, the first layer was cemented paste tailings. The binder used for the mixture preparation is Portland cement or type (PCI). Only 2wt% of binder was chosen to evaluate the influence of barrier cover as cemented material on surface paste disposal. Proportion was calculated on basis of weight, relative to total dry tailings. The chemical analyses and physical property tests show that PCI has a specific gravity of 3.15, a specific surface area of 1.58 m^2/g, a Al_2O_3 content of 4.86 wt%, a CaO content of 65.76 wt%, a Fe_2O_3 content of 2.44, and a SiO_2 content of 19.51 wt%.

3.1.3 Pore water characteristics

ICP-AES (Perkin Elmer Optima 3100RL) system was used to analyze the chemistry of initial tailings pore water. Results show that sulphate content was high at 3295 ppm due to cyanide destruction by SO_2/Air method.

The calcium content was high at 505 mg/L, due to the addition of lime for pH control during milling. Given that the acidification potential AP of 897.2 kg $CaCO_3/t$ (AP = $31.3 \times S_{sulphide}$), tailings are acid generating.

3.1.4 Paste tailings mineralogy

The mineralogy of tailings was evaluated by X-ray diffraction tests. The diffractograms used to assess the detectable mineral phases of paste tailings were evaluated by Rietveld fitting method using the TOPAS software. Results revealed that tailings were dominated by quartz (53%) and pyrite (29%). Minor quantities of alumino-silicate minerals which mainly include paragonite (6.7%), muscovite (4.9%), chlorite (4.7%), and gypsum (2.1%) were detected.

3.1.5 In-situ porosity determination

The porosity measurement of in-place paste tailings is made by using a volume-known and end open cup ($D \times H$ =6.7 cm × 3.2 cm), based on a specific gravity and dry mass of the tailings (Fig. 3). Results exhibit that for all the layers, cemented cell CC provides a porosity of 48% while uncemented cell UC provides a porosity of 49%.

Figure 3. In-situ porosity determination

3.2 Methods

3.2.1 Field experimental cells

The testing site selected for construction of two field cells is near the existing tailings pond at LaRonde mine. A significant amount of tailings is currently discharged as slurry from mill to this pond via pumping. The cells are installed at old tailings pond. This area was chosen together with mine operators, taking consideration several factors, such as capacity, topography, and accessibility. Due to the fact that site elevation is about 3 m below the tailings pond, tailings are pumped easily to the cells. The site is roughly 100 m long by 25 m wide, ensuring the enough space so as to handle cells and construction equipment. A space of at least 5 m is also left between the cells for machinery.

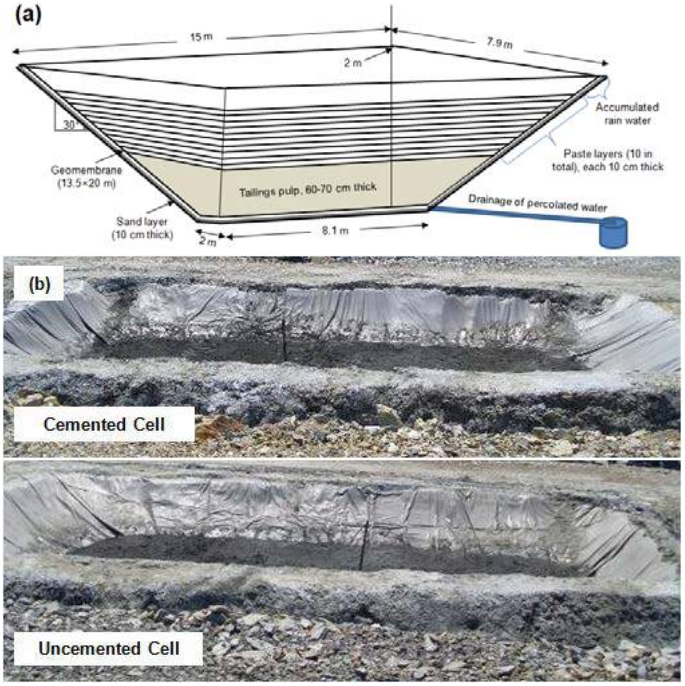

Figure 4. A schematic view (a) and photos (b) of field experimental cells

The two mini field experimental cells were designed at the surface depositional area of the LaRonde mine (Fig. 4). The first cell is designed by filling partially with the tailings containing a low cement content of 2 wt% and termed as Cemented Cell – CC while the second cell is designed by filling completely with tailings without cement and termed as Uncemented Cell – UC. This latter is also regarded as control cell.

3.2.2 Different disposal configurations

Disposal configurations refer to the layering patterns of the different layers of paste with our without cement addition. The deposition frequency was set at about one layer every

one week or three weeks, depending on paste plant and tailings availability. Underground mine operations required more paste to back-fill the mined-out openings. Figure 5 shows the photos of two field experimental cells designed in two configurations.

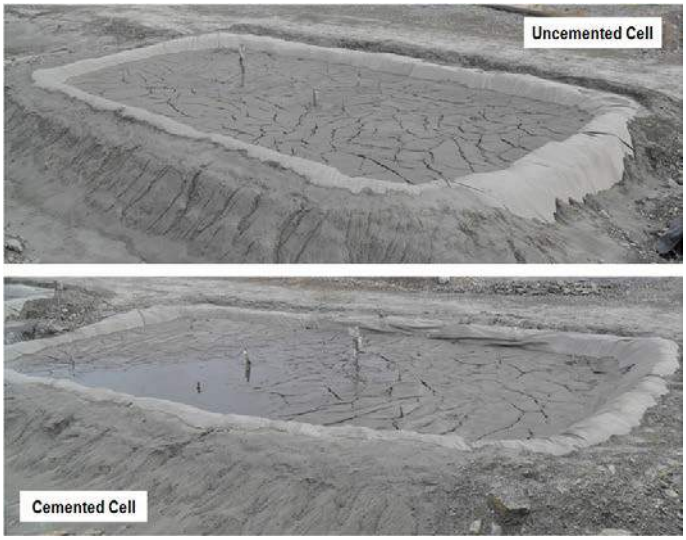

Figure 5. Photos of a successfully-completed layer of paste tailings into field cells

Each disposal configuration was made of 10 paste layers, each about 10 cm. The main reason behind this thin layer deposition is to let the paste material attain faster strength gains through desiccation since thick layers do not permit adequate desiccation to stop flows as the stack rises in height. To get a flat layer of the tailings, a Topcon® RL-H3C Rotating Laser is used across the cell. Only first layer is kept cemented in order to show the cementation effect as a barrier layer on mitigation or prevention of acid rock/mine drainage or tailings oxidation. The binder content used was only 2% by dry weight of tailings. The selected binder was ordinary Portland cement. Following the deposition of each layer, the deposited angle of layer is monitored and adjusted to 5° to ensure good drainage water. Between each layer disposal, some photos are taken to better characterize the phenomenon of desiccation.

3.2.3 Surface crack measurements

At the end of the drying period that followed the deposition of each layer, a number of crack measurements were taken using 5 m plastic tape meter rule (Fig. 6). Please note that the measurements taken will help better understanding the effect of cementation layer on overall surface disposal of paste tailings. In normal conditions, it is expected that the width, length, and depth of surface cracks in the uncemented cell is relatively larger than the ones in the cemented cell.

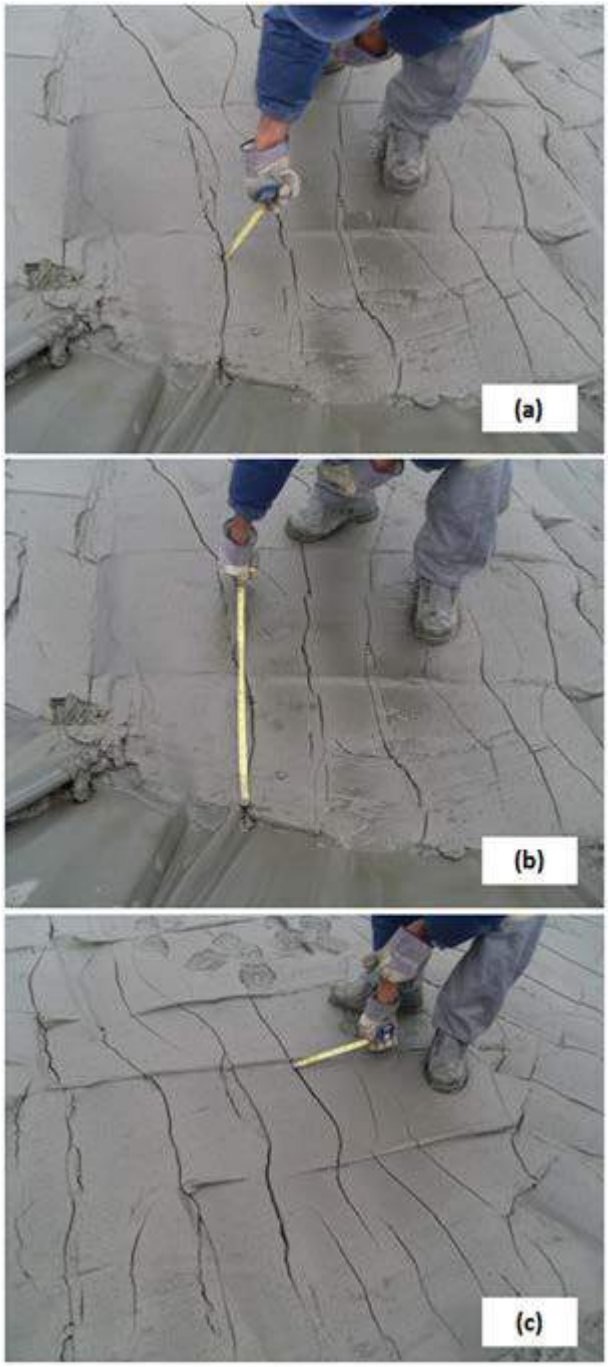

Figure 6. Photos of top surface crack depth (a), length (b) and width (c) of paste tailings in the field experimental cells

4 RESULTS AND DISCUSSION

Figures7-8 presents the raw and processed images of the top surface cracks (Layers 1 to 10) of deposited paste tailings in the CC and

UC configurations. The processing of the selected top images was performed using the Adobe Photoshop version 7.0 software. Once the cracked top surface of paste tailings layer is photographed, the cracks appear darker than the intact zones in the matrix; this clear different in contrast makes possible a good analysis. To give a consistency, the images taken are processed at similar configurations: balance = 1; black = 1; and white = 5.

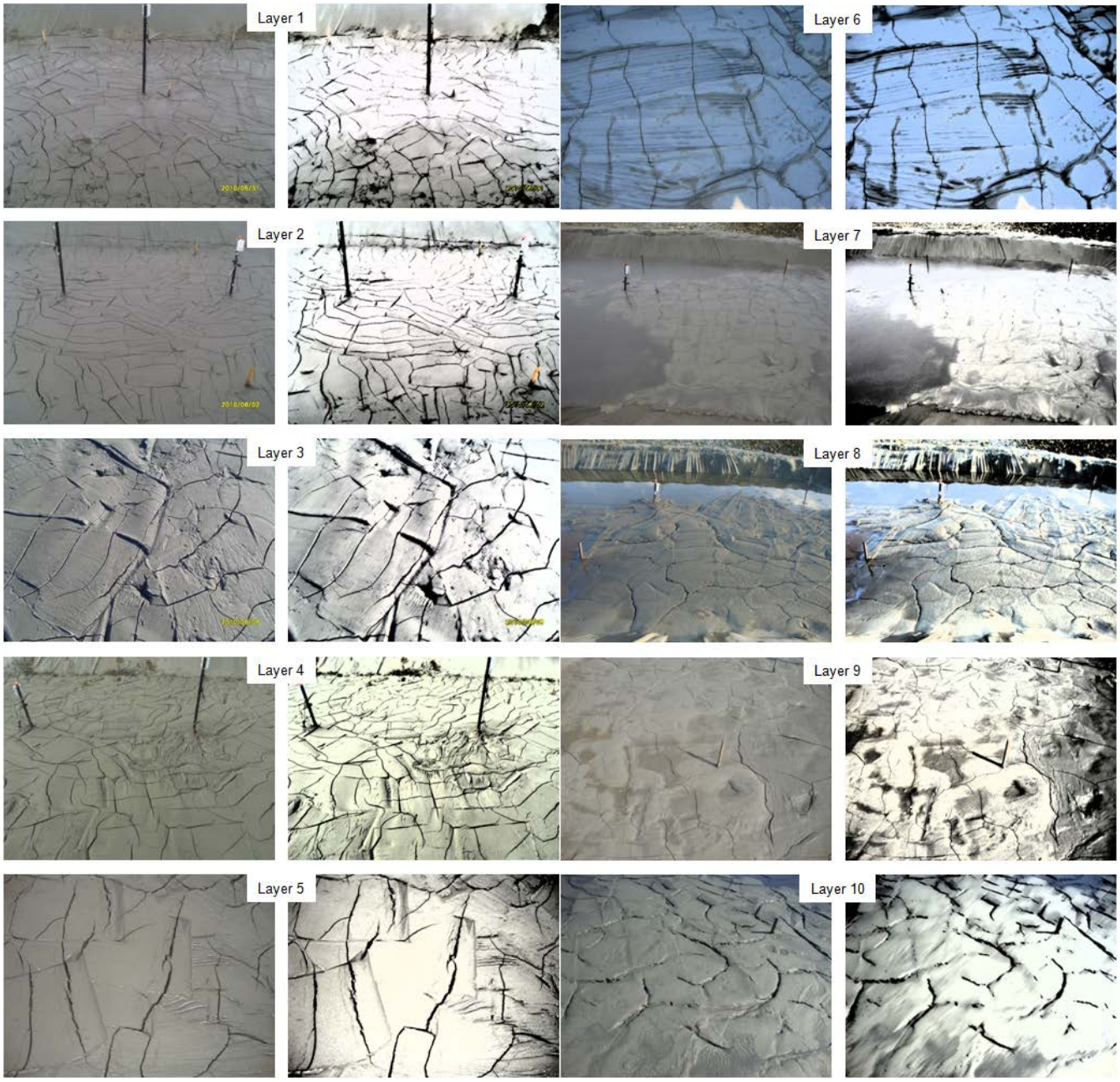

Figure 7. The raw (left) and processed (right) images of the top surface cracks (Layers 1-10) of paste tailings within the cemented cell (CC) disposal configuration

One can observe clearly that, irrespective of the layer, the first five layers shows more cracks than the remaining five layers due to the climate condition where evaporation is higher than precipitation, and the deposition time. Overall, the width, length and depth of cracks occurred in the UC is relatively bigger than the ones gained by the CC. This may be explained by continuous water consumption or retention (reflects increased saturation) of the cemented layer by the fresh-placed paste addition and self-desiccation processes.

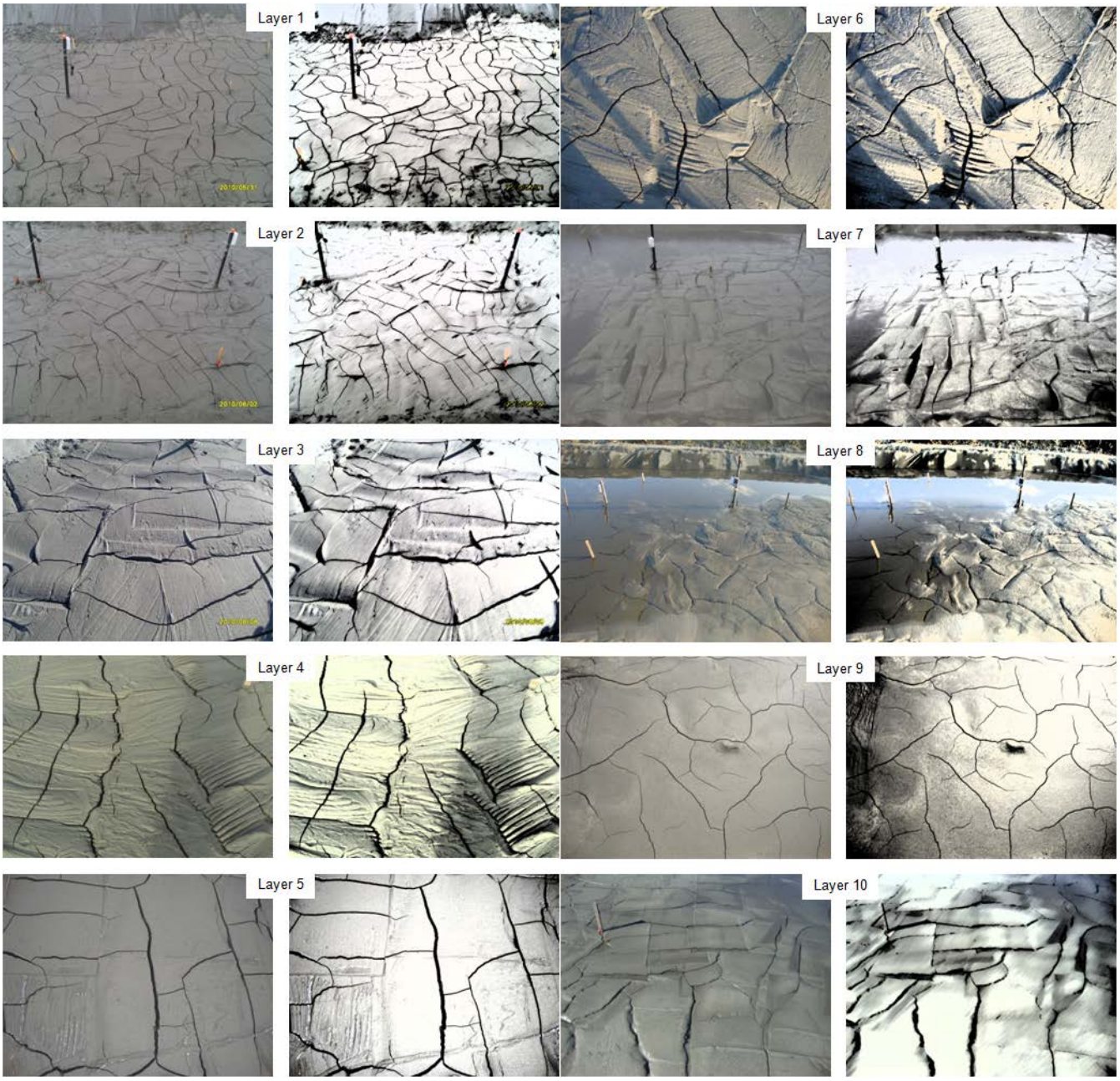

Figure 8. The raw (left) and processed (right) images of the top surface cracks (Layers 1-10) of paste tailings within the uncemented cell (UC) disposal configuration

It may also be interpreted that the total number of cracks decreases notably with the increasing number of deposited paste layers, but the width and depth of these cracks are getting fatter and bigger since they seem to reopen within previously-occurred cracks at similar locations in the cells. Figure 9 shows the plots of top surface crack measurements in terms of width, length and depth for paste tailings in the CC and UC configurations. One can speak that the crack width reduces or the surface crack depth increases when the number of the layers is increased. The range of crack width is reduced from 18.5 mm to 15 mm for the CC, and reduced from 21.5 mm to 20 mm for the UC while the crack depth is increased from 57 mm to 68.5 mm, and from 65 mm to 80 mm for the CC and UC, respectively. It must be noted that the formation of cracks occurred in the surface layers is dependent on the time interval and disposal configuration. The longer the paste storage process, the deeper and wider the formation of crack causes. The drainage of upper paste layer is accelerated right after the deposition of fresh tailings on a dry surface layer. This is due to the suction developed by layer below. This suction creates a fast

movement of water towards the bottom and might lead to a fast crack occurrence. This phenomenon is observed in the first layers where the crack occurred within three to four hours after the placement of paste.

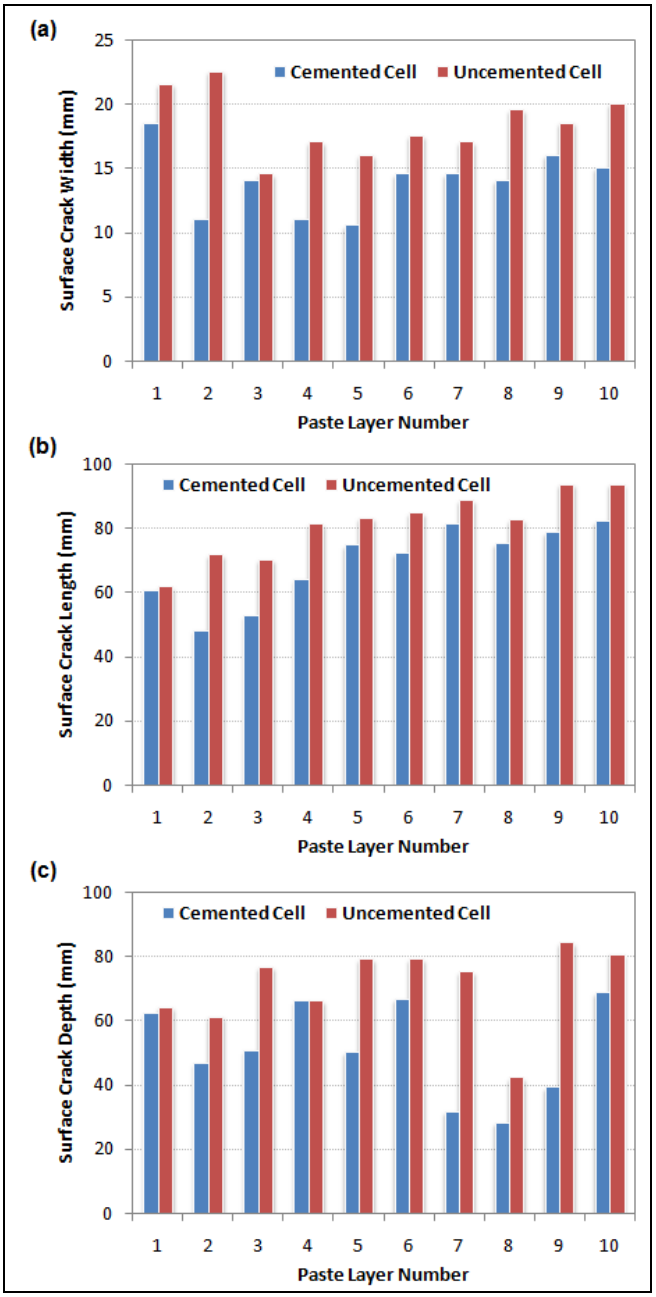

Figure 9. The plots of surface crack width (a), length (b), and depth (c) measurements of paste tailings in the CC and UC conditions

Please note that thinly-deposited tailings layers up to 30 cm are affected by the daily circle of the sun and may let excess water drain and therefore strength gains up to 20 kPa which allow for foot access within 1-2 days. The deposited paste layer in the UC was found to be more resistant than the ones deposited in the CC. This may be a part due to formation of cracks occurred depending on cemented layer and evaporation.

5 CONCLUSIONS

A field experimental study was carried out at the LaRonde Mine (Quebec, Canada) to investigate a possible application for surface disposal of paste tailings in the cemented cell CC and uncemented cell UC configurations. Paste tailings are prepared in the paste plant, transported by a read-mix truck to the mine site, and then deposited in the experimental cells layer by layer. A slump consistency of at least 10 inches (250 cm) for all the paste tailings is used prior to their placement. All the paste layers were made up of uncemented paste tailings, except layer 1 in the CC where 2 wt% of cement is added to paste tailings. This cement addition was chosen to assess the leachate reduction/ removal potential by the release of the contaminated metals and to prevent tailings oxidation by making layers saturated. Thus, this eliminates the diffusion of oxygen between layers. The top surface crack measurements show that the width, length and depth of cracks increase with the increasing number of the accumulated layers. This is due to the reappearance of already-occurred cracks in prior layers by the effects of evaporation and settlement. As a result, it is strongly believed that the results of these field works will bring a new light to tailings planners and operators and modern mines will shift their current tailings management systems to paste technology.

ACKNOWLEDGEMENTS

The author wishes to state his sincere gratitude to Mostafa Benzaazoua and Bruno Bussière for their financial support during this investigation. Special thanks are extended to Denis Bois, the principal of the UQAT-URSTM Laboratory, for experimental facilities, and to the professional people of URSTM Laboratory for their technical assistance. The Agnico-Eagle's LaRonde Mine and the Industrial NSERC-Polytechnic-UQAT Chair in Environment and Waste Management and the Canada Research Chair in the Integrated Management of Sulphidic Tailings are gratefully acknowledged for funding this project. A special

thank also goes out to Sandra Pouliot and Martin Bernard of the LaRonde Mine for their technical assistance during the project.

REFERENCES

Aubertin, M., Bussière, B., Bernier, L., 2002. *Environnement et gestion des résidus miniers*. Presses Internationales Polytechnique, Canada.

Belem, T., Benzaazoua M., El Aatar, O., Yilmaz, E., 2013. Effect of drainage and pore water pressure dissipation on backfilling sequencing. In: *23rd World Mining Congress, Canada,* pp. 1-10.

Benzaazoua, M., Bussière, B., Demers, I., Aubertin, M., Fried, É., Blier, A., 2008. Integrated mine tailings management by combining environmental desulphurization and cemented paste backfill: Application to Doyon, Quebec, Canada. *Min. Eng.*, Vol. 21, pp. 330-340.

Benzaazoua, M., Perez, P., Belem, T., Fall, M., 2004. A laboratory study of the behaviour of surface paste disposal. In: *The 8th International Symposium on Mining with Backfill*, Beijing, China, pp. 180-192.

Blight, G., 2010. *Geotechnical engineering for mine waste storage facilities*, Taylor & Francis, UK.

Bryan, R., Simms, P., Verburg, R., 2010. Coupling oxidation to transient drying during multilayer deposition of thickened gold tailings, *Minerals Engineering*, Vol. 23, No. 14, pp. 1101-1112.

Bussière, B., 2007. Colloquium 2004: Hydrogeo-technical properties of hard rock tailings from metal mines and emerging geoenvironmental disposal approaches, *Canadian Geotechnical Journal*, Vol. 44, No. 9, pp. 1019-1052.

Bussière, B., Benzaazoua, M., Aubertin, M., Mbonimpa, M., 2004. A laboratory study of covers made of low-sulphide tailings to prevent acid mine drainage, *Environmental Geology*, Vol. 45, No. 5, pp. 609-622.

Cadden, A., Newman, P., Fordham, M., 2003. New developments in surface paste disposal of mine wastes, *Disposal of Mineral Industry Wastes*, Falmouth, Cornval, UK, pp. 1-17.

Cihangir, F., Ercikdi, B., Kesimal, A., Turan, A., Deveci, H., 2012. Utilisation of alkali-activated blast furnace slag in paste backfill of high-sulphide tailings: Effect of binder type and dosage. *Miner. Eng.*, Vol. 30, pp.33-43.

Crowder, J., Grabinsky, M., Klein, K., 2002. Laboratory characterization of tailings paste for surface disposal. In: *The 55th Canadian Geotechnical Conference*, Canada, pp. 401-409.

Deschamps, T., Benzaazoua, M., Bussière, B., Aubertin, M., 2011. Laboratory study of surface paste disposal for sulphidic tailings: Physical model testing, *Minerals Engineering*, Vol. 24, No. 8, pp. 794-806.

Deschamps, T., Benzazoua, M., Bussière, B., Belem, T., 2007. The effect of disposal configuration on the environmental behaviour of paste tailings, *Proceedings of the 9th International Conference on Mining with Backfill*, Canada, pp. 1-8.

Deschamps, T., Benzaazoua, M., Bussière, B., Aubertin, M., Belem T., 2008. Microstructural and geochemical evolution of tailings in surface storage, *Miner. Eng.*, Vol. 21, pp. 341-353.

Dixon-Hardy, D.W., Engels, J.M., 2007. Methods for the disposal and storage of mine tailings. *Land Contamination and Reclamation*, Vol. 15, No. 3, pp. 301-317.

Edraki, M., Baumgartl, T., Manlapig, E., Bradshaw, D., Franks, D.M., Moran, C.J., 2014. Designing mine tailings for better environmental, social and economic outcomes: a review of alternative approaches. *Journal of Cleaner Production*, Vol. 84, pp. 411-420.

Ercikdi, B., Yilmaz, T., Kulekci, G., 2014. Strength and ultrasonic properties of cemented paste backfill. *Ultrasonics*, Vol. 54, No. 1, pp. 195-204

Fall, M., Célestin, J.C., Han, F.S., 2009. Suitability of bentonite- paste tailings mixes as engineering barrier material for mine waste containment facilities. *Miner. Eng.*, Vol. 22, pp. 840-848.

Fourie, A., 2012. Perceived and realized benefits of paste and thickened talings for surface deposition. *The Journal of The Southern African Institute of Mining and Metallurgy*, Vol. 112, pp. 919-926.

Grabinsky, M.W., Theriault, J., Welch, D., 2002. An overview of paste and thickened tailings disposal on surface, *Proceedings of the First Symposium on Mine Waste and Environment*, pp. 5-12, Rouyn-Noranda, Quebec, Canada.

Henriquez, J., Simms, P., 2009. Dynamic imaging and modelling of multilayer deposition of gold paste tailings. *Minerals Engineering*, Vol. 22, No. 2, pp. 128-139.

Hudson-Edwards, K., Jamieson, H. Lottermoser, B., 2011. Mine wastes: past, present, future. *Elements*, Vol. 7, pp. 375-380.

Kesimal, A., Yilmaz, E., Ercikdi, B., Alp, I., Deveci, H., 2005. Effect of properties of tailings and binder on the short and long terms strength and stability of cemented paste backfill. *Materials Letters*, Vol. 59, No. 28, pp. 3703-3709.

Kwak, M., James, D., Klein, K., 2005. Flow behaviour of tailings paste for surface disposal, *International Journal of Mineral Processing*, Vol. 77, No. 3, pp. 139-153.

Landriault, D.A., Welch, D., Frostiak, J., Evans, D., 2001. Bulyanhulu Mine: Blended paste backfill and surface paste deposition: the state of the art in paste technology. In: *The 7th Int. Symposium on Mining with Backfill*, Seattle, USA, pp. 1-14.

Lottermoser, B.G., 2011. Recycling, reuse and rehabilitation of mine wastes. *Elements*, Vol. 7, pp. 405-410.

Martin, V., Aubertin, M., Benzaazoua, M., Zhan, G., 2010. Investigation of near-surface exchange processes in reactive paste tailings. In: *The 13th International Seminar on Paste and Thickened Tailings,* Canada, pp. 265-278.

Mizani, S., He, X., Simms, P., 2013. Application of lubrication theory to modeling stack geometry of high density mine tailings. *J. Non-Newtonian Fluid Mechanics,* Vol. 198, pp. 59-70.

Oxenford, J., Lord, E.R., 2006. Canadian Experience in the application of paste and thickened tailings for surface disposal. In: *Paste and Thickened Tailings,* Limerick, Ireland, pp. 93-105.

Potvin, Y., Thomas, E., Fourie, A., 2005. Handbook on mine fill. ACG, Australia, pp.1-220.

Robinsky, E.I., 2000. Sustainable development in disposal of tailings. In: *Tailings and Mine Waste 00.* Colorado, USA, A.A. Balkema, pp. 39-48.

Shuttleworth, J., Thomson, B.J., Wates, J.A., 2005. Surface paste disposal at Bulyanhulu – practical lessons learned. In: *The 8th Int. Seminar on Paste and Thickened Tailings,* Chilli, pp. 207-218.

Simms, P., Grabisky, M., Zhan, G., 2007. Modelling evaporation of paste tailings from the Bulyanhulu mine. *Can. Geotech. J.,* Vol. 44, pp. 1417-1432.

Slottee, J.S., 2004. Update on the application of paste thickeners for tailings disposal - mine paste backfill. In: *International Seminar on Paste and Thickened Tailings,* South Africa, pp. 1-7.

Sofra, F., Boger, D., 2002. Environmental rheology for waste minimisation in the minerals industry. *Chemical Eng. J.*, Vol. 86, pp. 319-330.

Tariq, A., Yanful, E.K., 2013. A review of binders used in cemented paste tailings for underground and surface disposal practices. *J. Environ. Manag.,* Vol. 131, pp. 138-149.

Theriault, J., Frostiak, J., Welch, D., 2003. Surface disposal of paste tailings at the Bulyanhulu mine, *In: The 2nd Mining Environment Conference,* Sudbury, Canada, pp. 1-8.

Theron, M., Addis, P.C., Wates, J.A., Martin, V., 2005. Bulyanhulu mine (Tanzania) paste tailings facility: relating unsaturated properties of gold tailings to rate of rise. In: *The 8th International Seminar on Paste and Thickened Tailings,* Santiago, Chilli, pp. 219-230.

Verburg, R., Newman, P., Fordham, M., 2006. Surface paste disposal of high-sulphide tailings-field cell monitoring and pilot plant testing. In: *International Conference on Acid Rock Drainage,* St. Louis, Missouri, USA, pp. 2170-2187.

Verburg, R.B.M., 2002. Paste technology for disposal of acid-generating tailings. *Mining Environmental Management,* Vol. 13, pp. 14-18.

Yilmaz, E., 2010. A field investigation of the behaviour of fine-grained, sulphide-rich paste tailings under a surface disposal condition. *Post-Doc Project,* UQAT, Canada**,** pp. 1-126.

Yilmaz, E., 2011. Advances in reducing large volumes of environmentally harmful mine waste rocks and tailings. *Miner. Resour. Manag.,* Vol. 27, No. 2, pp. 89-112.

Yilmaz, E., Benzaazoua, M., Bussière, B., Pouliot, S., 2011. Field experimental cells to investigate the hydrogeotechnical behaviour of surface paste disposal: design, implementation, and preliminary results, *Sustainability for Resource Conservation and Recycling,* Falmouth, Cornval, UK, pp. 1-20.

Yilmaz, E., Benzaazoua, M., Bussière, B., Pouliot, S., Bernard, M., 2013. Hydrogeotechnical and geochemical characterization of surface paste disposal, In: *The 23rd Int. Mining Congress and Exhibition of Turkey,* Kemer, Antalya, Turkey, April 16-19, pp. 1815-1828.

Yilmaz, E., Benzaazoua, M., Bussière, B., Pouliot, S., 2014. Influence of disposal configurations on hydrogeological behaviour of sulphidic paste tailings: A field experimental study. *Int. J. Miner. Proces.,* Vol. 131, pp. 12-25.

Possibilities for Reclamation by Using Suitable Geological and Waste Materials

P. Pavlov
University of Mining and Geology "S. Ivan Rilski", Sofia, Bulgaria

M. Banov, P. Ivanov
N. Poushkarov Institute of Soil Science, Agrotechnologies and Plant Protection, Sofia, Bulgaria

ABSTRACT Present paper discusses the problems related to accumulation of waste (pyrite cinder) on the territory of chemical plant "Neochim" Joint Stock Company, Dimitrovgrad, Bulgaria. Based on detailed study of affected areas is recommended technology for restoration of disturbed areas. The technology includes: neutralization of adverse pH activity; construction of surface layer of appropriate materials for technical and biological reclamation (fly ash from thermal power plants, soil and geological materials); selection of suitable plant species; organic-mineral fertilization with appropriate rates.

Keywords: pyrite cinder, reclamation, waste dumps

1 INTRODUCTION

Most of the production processes in different sectors of industry are connected with parallel creation of waste products. Some of these secondary materials have characteristics that allow their use for improving of properties and quality of soils, influenced somewhat by natural or anthropogenic degradation as well as for reclamation of technogenically constructed areas (Banov et al., 2009 a, b).

In other cases, composition and properties of industrial waste products pose a risk of ecological damage on the pedosphere. Often such wastes are associated with the chemical industry, which provides materials and reagents for subsequent use in various industries and mining activities. As an example can be mentioned, applied to 1994 geotechnological method for extraction of uranium using sulfuric acid solutions (Banov et al., 2010).

In present paper, based on preliminary studies, we present detailed characteristics of the area of chemical plant "Neochim" JSC, Dimitrovgrad and adjacent waste dumps for reclamation purposes.

2 MATERIAL AND METHODS

The "Neochim" JSC plant for production of sulfuric acid has operated until 1993. So far, the process of production of sulfur dioxide – SO_2 (semi product for production of sulfuric acid) was connected with accumulation of so-called pyrite cinder (waste from combustion of the pyrite concentrate). Deposition of waste products was carried out at two sites bordering the ash pond of thermoelectric power plant "Maritsa 3".

Preliminary studies were carried out in the area of pyrite cinder waste dumps, in order to identify the specific characteristics of the region and to prepare climate, geomorphological, geological, hydrological, and soil characteristics of the surrounding area. The soil types were correlated with the World Reference Base for Soil Resources (IUSS Working Group WRB, 2006).

Different materials from the area were studied to establish their suitability for possible use in technical and biological reclamation of waste dumps. The studies include geological materials from the area of mine "Marbas", fly ash from ash pond of thermoelectric power plant "Maritsa 3" and soil materials stored along the Maritsa River.

For complete characterization of appropriate geological materials, additional sampling was performed. The collected samples from all types of materials were analyzed for the following parameters:

- Mechanical composition – Kachynski (1958);
- Carbonates content – by the method of Sheibler (Vilenskiy, 1945; Nikolaev, 1962);
- Content of organic carbon – by the modified method of Tyurin (Kononova, 1963);
- pH (H2O) – potentiometric (Arinushkina, 1962);
- Content of available nitrogen (mg/kg) (Bremner, 1965);
- Content of available phosphorous (mg/100g) (Ivanov, 1984);
- Content of available potassium (mg/100g) (Ivanov, 1984;
- Content of heavy metals – ISO 114 66: 1995;

3 RESULTS AND DISCUSSION

Field study was carried out in the area for establishment of soil types. In addition with published data (Koynov et al., 1968; Dimitrov et al., 1992), it was found that soil groups in the area are the following:

- Vertisols (Pellic);
- Rendzic Leptosols;
- Fluvisols;

Impact of chemical plant on the soils in the area has been described by many authors. Dimitrov et al., (1992) found changes in soil pH values in surface horizons with up to 1 unit compared with the values found during the mapping carried out by the Institute of Soil Science "N. Poushkarov". Studies of other authors (Chuldzhiyan et al., 1995) indicate that emissions from the plant affect soils in two ways:

1. There is a fertilizer effect of nitrogen deposition;
2. Soil acidification due to nitrification;

On one hand, fertilizer effect is beneficial within certain limits, but on the other hand, acidification reduces buffer capacity of soils and lead to disturbance of their agronomic properties.

The studies show that there is soil contamination with heavy metals (lead and zinc) and sulfur in the periphery of the plant at a distance of 1,5 – 2,5 km. At a distance of 2,8 – 3,0 km east and south of the plant pollution is weak, but there are soil profiles where the content of cadmium, lead and zinc in depth is over limited permissible concentrations (BSECEEP and POVVIK-CAB Ltd., 2000; BSECEEP, 2000). That can be explained by the influence of airflows – established less contamination on the southeastern area around the plant corresponds to the prevailing west winds.

Studies of geological materials from the area for establishment of their suitability for technical and biological reclamation show that materials from "New mines" are suitable for technical reclamation of pyrite cinder waste dumps (Tables 1, 2).

As a result of studies on mechanical composition (Table 1) and average values of particles, the waste (fly ash), soil and geological materials have sandy loam texture. This creates prerequisites for creation of favorable water-air status and nutrient enrichment.

Table 1 Mechanical fractions in waste, soil and geological materials from studied region (%)

Sample	Particle size (mm)							
	>1	1,00 0,25	0,25 0,05	0,05 0,01	0,01 0,005	0,005 0,001	sum <0,001	sum < 0,01
1. fly ash	0,0	7,2	52,1	30,1	5,5	4,0	1,1	10,6
2. fly ash	0,0	8,2	37,8	38,9	10,2	2,4	2,7	15,3
3. fly ash	0,0	6,8	49,5	31,2	7,5	3,2	1,8	12,5
4. fly ash	0,0	8.5	41.3	35.5	8.2	4.3	2.2	14.7
5. soil materials	0,0	1,6	43,7	31,4	12,3	4,7	6,3	23,3
6. soil materials	0,0	3,2	61,3	19,4	9,2	2,1	4,8	16,1

Table 1. (cont'd) Mechanical fractions in waste, soil and geological materials from studied region (%)

7. soil materials	0,0	2,8	57,6	12,0	14,4	6,3	6,9	27,6
8. soil materials	0.0	2,5	49,3	25,3	13,7	4,1	5,1	22,9
9. geological materials	sandy loam							
10. geological materials	sandy loam							
11. geological materials	sandy loam							
12. geological materials	sandy loam							

Agrochemical studies show that soil and waste materials are alkaline. The geologic materials are characterized by neutral values of pH (Table 2).

Availability of phosphorus and potassium in fly ash and soil materials is good, while the content of these elements in geological materials is low. All studied materials have low nitrogen content (Table 2).

Carbon content, which is the basis for determination of humus content, defines low preservation of soil materials. In fly ash, the carbon quantities are result of presence of coal admixtures and do not give us a reason for interpretation of data in terms of humus content. Similarly is explained the high carbon content in geological materials from "New mines". In fact, in this case the values are also a result of presence of coal admixtures in collected samples (Table 2).

Table 2. Agrochemical characteristics of waste, soil and geological materials from studied region

Sample	pH		P_2O_5	K_2O	NH_4	NO_3	C
	H_2O	KCl	mg/100 g		mg/kg		%
1. fly ash	9,0	8,8	18,1	35,0	2,00	2,31	2,33
2. fly ash	8,9	8,7	16,8	29,7	2,40	4,06	2,78
3. fly ash	8,8	8,7	17,4	32,6	2,30	3,82	2,54
4. fly ash	9,0	8,8	18,5	30,5	2,40	4,26	2,18
5. soil materials	8,5	7,8	14,0	67,7	9,08	11,10	1,05
6. soil materials	8,5	7,9	8,3	42,6	6,20	9,08	1,73
7. soil materials	8,4	7,8	10,5	59,6	10,30	12,45	1,28
8. soil materials	8,5	7,9	11,6	70,23	8,70	9,94	1,53
9. geological materials	7,1	6,1	7,2	-	5,94	7,34	4,72
10. geological materials	7,3	6,5	8,3	-	6,12	8,52	6,55
11. geological materials	7,5	6,2	6,5	-	7,45	8,76	4,35
12. geological materials	7,5	7,2	7,6	-	6,57	7,84	3,17

The heavy metals content in studied materials (Table 3) was evaluated according to the requirements of Ordinance 3 on the admissible content of harmful substances in soils and Ordinance on supplementing Ordinance 3. According to the pH values (Table 2), which is limiting factor in terms of maximum admissible concentrations (MAC) of heavy metals, it is established that the fly ash, soil and geological materials do not contain heavy metals above the MAC.

Table 3. Heavy metals content in waste, soil and geological materials from studied region (mg/kg)

Sample №	Pb	Cu	Ni	Mn	Fe	Zn
1. fly ash	33,3	73,0	53,0	760	38000	93,5
2. fly ash	28,8	74,0	55,0	636	34200	105,0
3. fly ash	30,1	72,0	51,0	810	31000	87,5
4. fly ash	27,6	69,0	49,0	685	37500	108,0
5. soil materials	40,5	66,0	38,0	725	26250	99,0
6. soil materials	36,0	36,0	26,5	520	23060	75,0
7. soil materials	42,4	47,0	35,5	490	21300	65,0
8. soil materials	39,2	52,6	27,0	685	29650	82,0
9. geological materials	61,2	54,2	41,5	840	34200	145,0
10. geological materials	55,4	45,7	34,2	720	26400	160,5
11. geological materials	65,6	61,3	37,3	650	31500	157,0
12. geological materials	60,7	57,2	44,6	810	29450	162,5

4 CONCLUSION

As a result of the studies and additional research it can be concluded that the waste (fly ash), soil and geological materials are suitable for technical and biological reclamation of waste dumps for pyrite cinder. Essential for the success of reclamation is proper planning of: activities in different stages; the quantitative ratios between different groups of materials; the choice of appropriate plant species. First of all, it is necessary to be carried out neutralization of the adverse pH value in the terrains. The sandy loam texture of the studied soil and geological substrates will facilitate development of plant species, especially in the initial post reclamation period. Neutral and alkaline pH value of studied materials will have an additional positive effect on unfavorable acidity. The low content of available nitrogen may be offset by fertilization with appropriate rates. The lack of heavy metals in fly ash, soil and geological materials in quantities above the MAC exclude the possible negative impact on the environment.

REFERENCES

Arinushkina, E. V., 1962. *Guidelines for chemical analysis of soils*. Publishing House of Moscow University. Moscow. p. 490 (Ru).

Banov, M., N. Dinev, P. Ivanov. 2009 a. *Reclamation of coal dump from the region "Kaltinska mera" – Gorna Oriahovitsa*. In: L. Totev and P. Pavlov (Eds.). Proceedings – International Scientific Conference – "Mining Science and Geotechnics – European Challenge". 1 – 3. 10. 2009. University of Mining and Geology "St. Ivan Rilski". Sofia, Mining Academy, Germany, MGGU, Russia, Technical High School Rein – Westphalia, Mining University, Leoben, Austria. ISSN 1314-0469. Lux Print, Sofia, 71-77. (Bg).

Banov, M., N. Dinev, P. Ivanov, V. Tsolova. 2009 b. *Examination on waste materials as a resource for acid soils amelioration.* In: L. Totev and P. Pavlov (Eds.). Proceedings – International Scientific Conference – "Mining Science and Geotechnics – European Challenge". 1 – 3. 10. 2009. University of Mining and Geology "St. Ivan Rilski". Sofia, Mining Academy, Germany, MGGU, Russia, Technical High School Rein – Westphalia, Mining University, Leoben, Austria. ISSN 1314-0469. Lux Print, Sofia, 113-120. (Bg).

Banov, M., V. Tsolova, P. Ivanov, M. Hristova. 2010. *Anthropogenically Disturbed Soils and Methods for Their Reclamation*. Agricultural Science and Technology, vol. 2, No 1, 33-39.

Bremner, J. M., (1965). *Inorganic Forms of Nitrogen*. In: C. A. Black et al., (Eds.). Methods of Soil Analyses. Part 2: Chemical and Microbiological Properties. № 9, Agronomy. American Society of Agronomy Inc. Madison, Wisconsin, USA. p. 1179-1237.

BSECEEP**,** 2000. *Final EIA report on "Neochim" JSC*, Dimitrovgrad. (Bg).

BSECEEP and POVVIK-CAB Ltd., 2000. *Independent evaluation of past pollution in the region of "Neochim" JSC*, Dimitrovgrad. (Bg).

Chuldzhiyan, H. et al. 1995. *EIA report for the site: "Plants for production of nitric acid and ammonium nitrate – old" in "Neochim" JSC*, Dimitrovgrad, Sofia. (Bg).

Climatic Reference Book of Bulgaria, 1982. Vol. 4, Wind. Kyuchukova, M. (Eds), General Directorate Meteorology and Hydrology,

Bulgarian Academy of Sciences, Institute of Hydrology and Meteorology, Science and Technology, Sofia, p. 382 (Bg).

Climatic Reference Book of Bulgaria, 1983. Vol. 3, Air temperature, soil temperature, frost. Kyuchukova, M. (Eds.), General Directorate of Meteorology and Hydrology, Bulgarian Academy of Sciences, Institute of Hydrology and Meteorology, Science and Technology, Sofia, p. 440 (Bg).

Dimitrov, D. et al. 1992. *Environmental assessment of agricultural lands in village Chernogorovo*. N. Poushkarov Institute of Soil Science, Sofia. (Bg).

ISO 114 66: 1995. *Extraction of trace elements soluble in aqua regia*.

IUSS Working Group WRB. 2006. *World reference base for soil resources 2006*. 2nd edition. World Soil Resources Reports No. 103. FAO, Rome. p. 128.

Ivanov, P., 1984. *New acetate-lactate method for determining of available forms of phosphorus and potassium in the soil*. Soil Science and Agrochemistry 4: 88-98. (Bg).

Kachynski, N.A., 1958. *Mechanical and micro-soil composition, methods of its study*. Publisher Academy of Sciences of the USSR. Moscow. p. 191 (Ru).

Koleva, E., R. Peneva, 1990. *Climate reference book. Rainfall in Bulgaria*. Institute of Meteorology and Hydrology, BAS, Sofia, p. 169 (Bg).

Kononova, M., 1963. *Soil organic matter. Its nature, properties and methods of study*. Academy of Sciences of the USSR. Moscow. p. 314. (Ru).

Koynov, V., et al., 1968. *Soil map of Bulgaria*, M 1:400 000. General Directorate of Geodesy and Cartography, Kartproekt, Sofia. (Bg).

Nikolaev, A.V., 1962. *Rational method for determination of soil microaggregate composition*. Agriculture of Tajikistan. (Ru).

Ordinance № 3 on the Admissible Content of Harmful Substances in the Soil. State Journal, 36, 1979. (Bg).

Ordinance supplementing the Ordinance № 3 of 1979 on the admissible content of harmful substances in the soil. State Journal, 54, 1997. (Bg).

Vilensky, D.G., 1945. *Aggregation of soil, its territory and practical application*. (Ru).

Restoration of Land Damaged in Mining Activities

M. Banov
N. Poushkarov Institute of Soil Science, Agrotechnologies and Plant Protection, Sofia

P. Pavlov
University of Mining and Geology "S. Ivan Rilski", Sofia

M. Blagiev
Blagiev engineering LtD, Sofia

ABSTRACT The present paper deals with possibilities for technical and biological reclamation of damaged areas in the region of Chiprovtci, Chiprovtci Municipality.

The physical and chemical characteristics of soil varieties from the territory of Chiprovtci region, disturbed during ore excavation were determined. The soil differences in the area and the climatic characteristics are described. Traditional scientific and analytical methods for soil analyses are used.

Different materials from the area were studied in order to establish their suitability for possible use in technical and biological reclamation of waste dumps.

A technological scheme for the implementation of technical and biological reclamation of damaged areas is proposed. Technology includes: filling of soil materials, fertilization, grassing and reforestation.

Keywords: Soil differences, Geological materials, Reclamation, Grassing, afforestation.

1 INTRODUCTION

The extraction of ore minerals is accompanied by extreme violations of the environmental components – mainly soil. The violations result from excavation and mining operations, the accumulation and distribution of the sterile geological materials, the construction of industrial zones of the mine, the building of subsidiary roads and others. Additionally, soils in neighboring area are subject to contamination with heavy metals and anthropogenic acidification. In conclusion, soils are mostly completely destroyed, as in most cases the changes even affect the landscape of the site.

According to the requirements of the European regulations (Directive 2004/35/ of the European Parliament and the Council on environmental liability regarding the prevention and remedying of environmental damage; the Thematic Strategy for Soil Protection; the Proposal for a Directive of the European Parliament and of the Council; the Establishing Framework for the Protection of Soil and amending Directive 2004/35/EC/) and the Bulgarian legislation (Ordinance 26 for Land Restoration, Improvement of Low Fertility Lands, Removal and Utilization of the Humus Layer) damaged and contaminated sites are subject to restoration and fertilization – reclamation.

This process is linked to the execution of a number of events that are directly dependent on the specific terms /condition of the terrain, the weather conditions, the presence of vegetation, etc. / on-site and in the adjacent areas.

2 MATERIAL AND METHODS

The subject of this study are the damaged and contaminated sites due to the activities of mine "Martinovo", where ferrous ore is extracted.

Mine “Martinovo” is located about 8 km west of the town of Chiprovtzi. The production activity of the mine was suspended in 1999.

As a result of the mining and processing activities in the area of mine "Martinovo" a technogenic (industrial) landscape has formed.

The established damaging of the natural landscape and the effect of the negative impact on the environment components can be prevented through the application of appropriate reclamation measures.

Preliminary studies were carried out in the investigated area in order to identify the specific characteristics of the region and to prepare climate, geological, hydrological, vegetation and soil characteristics of the surrounding area.

Different materials from the area were studied to establish their suitability for possible use in technical and biological reclamation of waste dumps. For complete characterization of appropriate geological materials, additional sampling was performed. The collected samples from all types of materials were analyzed for the following parameters:

- Mechanical composition – Kachynski (1958);
- Carbonates content – using the method of Sheibler, 1945; Nikolaev, 1962);
- Content of organic carbon – using the modified method of Tyurin (Kononova, 1963);
- pH (H_2O) – potentiometric (Arinushkina, 1962);
- Content of available nitrogen (mg/kg) (Bremner, 1965);
- Content of available phosphorous (mg/100g) (Ivanov, 1984);
- Content of available potassium (mg/100g) (Ivanov, 1984).

3 RESULTS AND DISCUSSION

3.1 Climatic Characteristics on Site

The climate of the studied area is temperate continental, with significantly greater precipitation during the spring and summer seasons.

Warm weather starts in April and lasts until the end of October - 210 days. The highest monthly temperatures are in July and August.

In winter, the average monthly temperature ranges from 0,4 ^{o}C to –1,8 ^{o}C. The coldest winter months are January and February, during which the average monthly temperature is below 0 °C /Table 1/. If there is insufficiently thick snow cover in winter, it is possible for the winter crops to freeze.

In the spring and summer winds blow strongly and continuously from northwest, they prevail during this period and act by restraining the rapid development of agricultural crops.

Where crops with a long growing period are concerned, the negative climatic factors should be taken into account - frost, long northwesterly winds and cold weather in winter, in order to reduce their negative impact to a minimum.

Table 1 Average monthly and yearly air temperature

Stations Berkovitza and Belogradchik

Months												Average Year Temperature (^{0}C)
I	II	III	IV	V	VI	VII	VIII	IX	X	XI	XII	
-1,8	-0,5	4,7	11,0	15,6	19,0	21,6	17,5	11,3	7,2	5,4	0,4	10,5
-1,4	-0,5	4,6	10,8	15,4	19,0	21,6	17,7	11,0	6,9	4,9	-0,1	10,4

The distribution of rainfall during the year has a decisive influence on the development and yield of crops /Table 2/.

The average annual rainfall for Chiprovtzi station is 776 mm, and for station Berkovitza - 953 mm. The first rainy maximum covers the period from April to August, and the second - the months of October and November. The lowest rainfalls in winter are from December to February. There is low monthly rainfall in September too.

The data for rainfalls presented in Table 2 show that their yearly movement is characterized by a marked spring-summer maximum. A second maximum could be established in the months of May and June.

Table 2 Average monthly and yearly precipitation in mm

Stations Chiprovtzi, Berkovitza, Montana, G.Genovo

Months												Average yearly sum
I	II	III	IV	V	VI	VII	VIII	IX	X	XI	XII	
39	39	51	70	107	100	68	72	50	69	58	53	776
46	53	62	93	116	132	94	80	71	83	75	61	953
42	25	34	48	80	82	55	61	41	52	46	38	586
36	30	37	57	76	77	54	42	40	59	50	41	599

3.2 Geological and hydrological characteristics of the region

The studied region occupies part of Western Stara Planina and Predbalkana, due to which the relief is varied. Predbalkan here is hilly and significantly truncated with ravines and gullies. Bedrocks show quite a wide variety of non-carbonate eruptive, metamorphic and sedimentary rocks. Weathering material from these rocks has formed different thickness weathering crust that has leaked soil forming processes.

The area of the site has a rich hydrographic network. The main river artery is river Chiprovska Ogosta. It collects the waters of river Martinovska and river Androvitsa in the town of Chiprovtzi.

3.3 Vegetation

The area of mine "Martinovo" falls in the lower and middle forest vegetation belt of Trakia area, also called the Beech Belt.

Forest vegetation is mainly deciduous and is represented by oak, beech, hornbeam, willow, hawthorn, drain, rosehip and others. There are plantations of pine, acacia and others. Due to the mountainous nature of the terrain, the terrain is occupied mainly by forests and pastures.

The effect of the forests as a soil making factor is huge, but a large portion of them have been cut. Deforestation in sloping terrain has contributed to increasing the erosion in the area.

3.4 Soil characteristics

A study was conducted in order to establish the soil diversity in the area of the site. On the basis of the conducted study and the used literature data it was found that the prevailing common soil types in the area of the site are as follows:

- Brown forest soils, shallow, heavily eroded, slightly sandy clay;
- Shallow, undeveloped soils and rocks.

The identified soil types are characterized by the following physical, physico-chemical, chemical and other indicators and properties:

3.4.1 Brown forest soils, shallow, heavily eroded, slightly sandy clay

They are formed on sandy clay non-carbonate materials with the participation of erosion. Their profile is represented mainly by the humus layer with a capacity of 18 to 20 cm, compact, with a small grain structure. The surface horizon of these soils is formed at the expense of lower iluvial horizon and part of base rock. Due to strong erosion and adjacent base rock the soils have deteriorated water and physical properties.

Mechanical composition: soils are slightly sandy clay. The content of physical clay in the surface horizon is 28,6%, and the content of fraction under 0,001 mm is 10,5%. The predominant fraction in the mechanical composition are particles from 0,05 to 0,01 mm, as their content in the surface horizon is 25% (Table 3).

The content of organic matter (humus), characterizes studied soils as poor humus. The content of humus in the surface horizon is 1,90% (Table 2).

The availability of total nitrogen is low – 0,098%, and the availability of total phosphorus is average - from 0,122% to 0,096 (Table 4).

Carbonates have not been established. The soil reaction is moderately acid (Table 4).

Table 3 Mechanical Composition

Horizon and depth of the sample	Particles size in mm							
/cm/	sum >1	1 - 0,25	0,25 - 0,05	0,05 - 0,01	0,01 - 0,005	0,005 - 0,001	<0,001	sum <0,01
A/C_1								
0 - 20	14,0	17,7	12,3	25,0	10,5	7,6	10,5	28,6
C_2								
35 – 45	10,1	9,6	13,8	24,7	13,5	11,3	14,9	35,7
C_3								
80 - 90	4,4	14,5	11,5	27,2	13,6	10,5	16,1	40,2

Table 4 Chemical Properties

Horizon and depth of the sample /cm/	Humus /%/	pH in KCl	Carbonates /%/	Total nitrogen /%/	Total phosphorus /%/
A/C_1 0 - 20	1,90	4,8	no	0,098	0,112
C_2 30 – 40	no	4,7	no	no	0,096
C_3 80 - 90	no	4,6	no	no	no

3.4.2 Shallow, underdeveloped soils and rocks

Underdeveloped shallow soils and rocks are found mostly on the steepest terrain. They are very shallow - from 0,0 to 15 cm and are located directly on the solid rock.

Conducted field and analytical studies have shown that the soil in the area of the site and adjacent lands are destroyed, damaged and very dirty. Since the humus and soil materials have not been previously collected and disposed they are practically lost. Underlying soil analyses show high levels of arsenic and cyanide, which makes impossible the direct cultivation of energy crops without amelioration of damaged and contaminated areas.

Figure 1. Disturbed Area From Martinovo Mine

The established violation of the natural landscape, its transformation into an industrial and the effects of the negative impact on the environmental components can be prevented through the application of appropriate reclamation measures.

The purpose of reclamation is not rapid economic effect, which leads to immediate and rapid recovery of the investment. In this case, the aim is environmental performance that is of greater public importance, because in the long run, its economic impact is greater than the rapid payback of the cost of reclamation.

The effect of timely and quality reclamation is expressed in several ways:

1. Ecological effect.

a) Suspension and removal of heavy metal contamination on site.

b) Improving the adjacent areas due to eliminating the adverse effects of reclaimed areas.

c) Protection of reclaimed territory from erosion or swamping

d) Complete Landscape restoration of damaged areas.

2. Social impact.

a) Elimination of the risk of harmful effects on the population and the related health problems.

b) Increase in the number of jobs and increased employment during the execution of the reclamation activities.

Remediation of contaminated and violated sites takes place in two stages – technical reclamation and biological reclamation. During the technical stage a preparation of the land is made by preparation for restoration of damaged areas and improvement of the landscape of the area.

In the next stage (biological), on the technically prepared areas specific crops are grown under specific technological schemes.

For a full and qualitative implementation of the reclamation activities and optimal recovery of damaged areas and natural landscape a number of events are needed, the most important of which are the following:

1. Cleaning the field from the construction and other waste and its leveling.
2. Filling of soil and geological materials with suitable physicochemical characteristics for full alignment and enhancing the landscape of anthropogenic areas.
3. Submission of sludge from waste water treatment plant in order to improve the quality of reclamation substrate and provide medium for plants
4. Plant species - Grass and tree.

Figure 2. Filling Of Soil And Geological Materials

Figure 4. Sowing and planting certain plant species

Figure 3. Submission of sludge from waste water treatment plant

Figure 5. Sowing and planting certain plant species

Sludge from wastewater treatment plants is a biomass rich in macro- and micronutrients and organic reserve that can be used to maintain the fertility of the reclamation substrates. Mechanical composition sediments are sandy clay. Dominant is the fraction of fine sand which has high hygroscopic humidity. In sediments, there are high microbial densities of soil microorganisms, lower respiratory capacity, large amount of microbial carbon, high potential nitrogen-fixing activity and immobilization of nitrogen. C/N ratio shows great heterogeneity of the studied sediments and evidence of smoldering process of transformation and the initial phase of humifitsirane. Research conducted by the Institute of Soil Science, Agrotechnologies and Plant Protection "Nikola Poushkarov" in the area of Chiprovtzi - Martinovo mine show that sediments improve the physical properties of soils and can be used with success for reclamation of disturbed lands, without the risk of environmental pollution.

The use of sludge will optimize the diet of plants and reduce the utmost application of organo-mineral fertilization.

In this case, a suitable source of sediments, corresponding to the soil and climatic conditions and physico-chemical composition of geological materials used in the process of reclamation in the area of mine "Martinovo" is the wastewater treatment plant - Sofia.

4. CONCLUSION

As a result of the studies a technological scheme for the implementation of technical and biological reclamation of damaged areas is proposed. The technology includes:

1. Cleaning the field from construction and other waste and its leveling.
2. Filling of soil and geological materials with suitable physicochemical characteristics for full alignment and enhancing the landscape of anthropogenic areas.
3. Submission of sludge from waste water treatment plant in order to improve the quality of reclamation substrate and provide medium for plants.

REFERENCES

Arinushkina, E. V., 1962. *Guidelines for chemical analysis of soils*. Publishing House of Moscow University. Moscow. p. 490 (Ru).

Bremner, J. M., (1965). *Inorganic Forms of Nitrogen*. In: C. A. Black et al., (Eds.). Methods of Soil Analyses. Part 2: Chemical and Microbiological Properties. № 9, Agronomy. American Society of Agronomy Inc. Madison, Wisconsin, USA. p. 1179-1237.

Ivanov, P., 1984. *New acetate-lactate method for determining of available forms of phosphorus and potassium in the soil*. Soil Science and Agrochemistry 4: 88-98. (Bg).

Kachynski, N.A., 1958. *Mechanical and micro-soil composition, methods of its study*. Publisher Academy of Sciences of the USSR. Moscow. p. 191 (Ru).

Kononova, M., 1963. *Soil organic matter. Its nature, properties and methods of study*. Academy of Sciences of the USSR. Moscow. p. 314. (Ru).

Nikolaev, A.V., 1962. *Rational method for determination of soil microaggregate composition*. Agriculture of Tajikistan. (Ru).

Vilensky, D.G., 1945. *Aggregation of soil, its territory and practical application*. (Ru).

A Review of Acid Mine Drainage in Turkey
Türkiye'deki Asit Maden Drenajının İncelenmesi

S. Yerel Kandemir
Bilecik Şeyh Edebali Üniversitesi, Mühendislik Fakültesi , Bilecik

H. Ankara
Eskişehir Osmangazi Üniversitesi, Mühendislik Fakültesi , Eskişehir

ABSTRACT Natural transformations and environmental changes are very complex in the world. Mineral, water and soil interactions are important topic influencing environmental changes. The interaction generates a large quantity of mine waste. Acid mine drainage is a key concern of mining industry due to its impact of water and soils.

Turkey is one of the developed countries in the world. Mining activities have been going on in several parts of Turkey and acid mine drainage are affected issue in Turkey. In this study, acid mining drainage and mine wastes in Turkey are reviewed.

Keywords: Acid mine drainage, mine waste

ÖZET Dünyamızdaki doğal dönüşümler ve çevresel değişiklikler çok karmaşık bir yapı sunmaktadır. Maden, su ve toprak etkileşimleri çevresel değişiklikleri etkileyen önemli bir konudur. Bu etkileşimler büyük miktarda maden atıkları üretmektedir. Bu atıklar nedeniyle asit maden drenajının meydana gelmesi ve su ve toprakların etkilenmesi madencilik sektörünün önemli bir husustur.

Türkiye, dünyanın gelişmiş ülkelerinden biridir. Madencilik faaliyetleri Türkiye'de artarak devam etmekte ve madenlerin bulunduğu çeşitli yerlerde asit maden drenajı görülmektedir. Bu çalışmada, Türkiye'deki maden atıkları ve asit maden drenajı meydana gelen sahalar incelenmiştir.

Anahtar Kelimeler: Asit maden drenajı, maden atıkları

1 INTRODUCTION

The mining of certain minerals, including gold, copper, and nickel, is associated with acid drainage problems that can cause long-term impairment to waterways and biodiversity. Furthermore, some effluents generated by the metals mining industry contain large quantities of toxic substances, such as cyanides and heavy metals, which have serious human health and ecological implications (Azapagic, 2004; Akcil and Koldas, 2006). Of all chemical pollutants of the environment, heavy elements are considered to be of a special ecological significance because excessive concentrations of them may be toxic to living organisms and affect the quality of surface water and groundwater (Kabata-Pendias et al., 1992; Loredo et al., 2005).

Mining activity compose a large quantity of mine waste. Acid mine drainage causes environmental pollution that affects many countries having historic or current mining industries (Johnson and Hallberg, 2005).

The potential hazard of mine waste depends on the host mineral. The tendency of mine waste to produce acid mine drainage containing potentially toxic metals depends on the amounts of sulfide, carbonate minerals, and trace-element concentrations found in ore deposits (Yucel and Baba, 2013).

For example, massive sulfide deposits and resultant mine wastes can affect the environment through several pathways. Oxidative weathering of pyrite can generate highly acidic conditions, which in turn enhances the solubility of metals from other sulfide minerals and from gangue silicate and carbonate minerals. The acid and metals collectively affect surface and groundwater quality and the associated aquatic ecosystems and drinking water supply (Gunduz et al. 2007; Gunduz and Baba 2008; Seal et al. 2008; Baba and Gunduz 2010).

Acid mine drainage has been widely recognized as one of the major environmental problems caused by mining worldwide, as evidenced by numerous studies (Pozo-Antonio et al., 2014). In this paper, firstly overviewed of acid mine drainage. After, provides a case studies of acid mine drainage in Turkey.

2 OVERVIEW OF ACID MINE DRAINAGE

Acid mine drainage is produced when sulfide-bearing material is exposed to oxygen and water (Akcil and Koldas 2006). Rivers affected by this kind of contamination are characterized by their acidity and also by the high sulfate and heavy metal content in their waters and metal content in their sediments (Nebel and Wright 1999). The pollutant effluent from acid mines is complex and is characterized by elevated concentrations of iron and sulfate, low pH, and elevated concentrations of a wide variety of metals (Gray 1998 in Achterberg et al. 2003; Grande et al., 2010).

Both sulfate and conductivity are useful indicators of acid mine drainage contamination. Unlike pH, they are both extremely sensitive to acid mine drainage even where large dilutions have occurred. The advantage of using sulfate to trace acid mine drainage is that conductivity is especially sensitive to sulfate ions (Gray 1996).

Acid mine drainage sources is showed in Table 1.

Table 1. Acid Mine Drainage Sources (Akcil and Koldas, 2006)

Primary sources
- Mine rock dumps
- Tailings impoundment
- Underground and open pit mine workings
- Pumped/nature discharged underground water
- Diffuse seeps from replaced overburden in rehabilitated areas
- Construction rock used in roads, dams, etc.
Secondary sources
- Treatment sludge pounds
- Rock cuts
- Concentrated load-out
- Stockpiles
- Concentrate spills along roads
- Emergency ponds

3 PREVENTIVE AND CORRECTIVE TECHNIQUES OF ACID MINE DRAINAGE

Acid mine drainage is a well-known international environmental problem related with both working and abandoned mining operations (Candeias et al., 2014). Preventive techniques and corrective techniques about acid mine drainage is given below.

3.1 Preventive Techniques

Acid mine drainage preventive techniques are classified of five class. This techniques are given below.

- Control of water migration
- Separation and blending

- Dry covers, soil covers and liners
- Water cover "sub-aqueous disposal"
- In-pit disposal (Kuyucak, 2012)

3.2 Corrective Techniques

Acid mine drainage corrective techniques are classified of five class. This techniques are given below.
- Chemical neutralization plants
- “In-line system” plants
- Treatment plants by ion exchange
- Neutralization plants by reverse osmosis
- Natural neutralization with river waters. "Synergistic" solutions (Pozo-Antonio et al., 2014).

4 ACID MINE DRAINAGE IN TURKEY

4.1 Acid Mine Drainage in Can Region, Canakkale

Can region (Canakkale) is very important in coal reserve and contains numerous mines that were operated by private companies and later abandoned without any remediation. Abandoned open pit mines typically fill with water from runoff and groundwater discharge, producing artificial lakes. Acid drainage waters have resulted in the degradation of surface water quality in Can region.

The results show that the concentration of most elements, such as Fe and Al, exceed national and international water quality standards (Yucel and Baba, 2013).

4.2 Mercury Mine, Alasehir

Mine waters are dominantly acidic with pH values and are sulfate rich. Acidity is caused mainly by the oxidation of sulfide minerals. Pyrite is the main acid producing mineral in the Alasehir.

Mine waters have showed As, Fe, Mn, Ni, and Al with concentrations higher than drinking water standards. The stream sediments derived from the mining area with the surface waters are potentially hazardous to the abandoned Hg mine and the mine is needed of remediation (Gemici, 2007).

4.3 Simav Plain, Kutahya

Simav Plain (Kutahya), were conducted to determine the source of high arsenic levels in the surficial aquifer. Rock and sediment samples supported the fact that local metamorphic rocks contained important ratios of sulfur minerals where arsenic-containing lenses are present inside. Another potential arsenic source in the study area was the geothermal fluid. Thus, the natural sources and anthropogenic influences of arsenic were found to create high concentrations in local water reserves of the area and influence human health (Gunduz et al., 2010).

4.4 Mining Activity of Koyulhisar, Sivas

The study area has active Pb–Zn–Cu mining. It is thought that the sulfide minerals in the region generally contribute to the acidification of groundwater. Mining wastes have affected concentrations of trace elements in the water. These values exceed the Turkish drinking water standard (Keskin and Toptas, 2012).

4.5 Emet Stream Basin, Kutahya

Emet Stream (Kutahya) is one of the most important branches of Uluabat Lake and also one of Turkey’s most important river systems. According to data obtained, statistically significance differences were identified between Kinik and Emet Streams according to Cr and Ni accumulations in water and sediment. Chromium levels of Kinik Stream were extremely higher an average of 153 times for water and 10 times for sediment than uncontaminated stations (Tokatli et al., 2014).

4.6. Halikoy Mercury Mine, Western Turkey

The acid drainage and the mine wastes create environmental problems around the mine. Surface and ground water samples were collected and analyzed to evaluated Hg and other heavy metals. Finally, this paper show

that the main sources of pollutants are derived from calcines and adit discharge (Gemici, 2004).

5 CONCULUSION

The present study reviewed the mine waste and acid mine drainage such as Can region (Canakkale), mercury mine (Alasehir), Simav Plain (Kutahya), Koyulhisar (Sivas), Emet Stream (Kutahya) and Halikoy Mercury Mine (Western Turkey) in Turkey. This study illustrated that mine wastes and mine acid drainage is affected surface and underground water. Thus, preventive and corrections techniques are urgently performed and developed in new techniques about to reduce acid mine drainage.

REFERENCES

Azapagic A., 2004, Developing a framework for sustainable development indicators for the mining and minerals industry. *Journal of Cleaner Production*, 12(6), 639-662.

Akcil, A. and Koldas, S. 2006. Acid Mine Drainage (AMD): causes, treatment and case studies, *Journal of Cleaner Production*, 14, 1139-1145.

Gemici, U., 2004, Impact of Acid Mine Drainage from the Abondoned Halikoy Mercury Mine (Western Turkey) on Surface and Groundwater, *Bull. Environ. Contam. Toxicol*, 72, 482-489.

Candeias, C., Ávila, P. F., Silva, E. F., Ferreira, A., Salgueiro, A. R. and Teixeira, J. P., 2014, Acid mine drainage from the Panasqueira mine and its influence on Zêzere river (Central Portugal), *Journal of African Earth Sciences*, 99, 705–712.

Yucel, D. S. and Baba, A., 2013. Geochemical Characterization of Acid Mine Lakes in Northwest Turkey and Their Effect on the Environment, *Arch Environ Contam Toxicol*, 64, 357–376.

Gunduz, O. and Baba, A., 2008. Fate of acidic mining lakes in Can Lignite District, Turkey. In Proceedings of the XXXVI IAH congress integrating groundwater science and human well-being, Proceedings CD-ROM, 26 October–1 November 2009, Toyoma, Japan.

Gunduz, O., Okumusoglu, D., Baba, A., 2007. Acidic mining lakes and their influence on water quality: a case study from Can (Canakkale)-Turkey. In: Trefry MG (ed) Proceedings of the 6th groundwater quality conference (GW07: securing groundwater quality in urban and industrial environments), Fremantle, Western Australia

Seal, R. R., Hammarstrom, J. M., Johnson, A. N., Piatak, N. M. and Wandless, G. A., 2008. Environmental geochemistry of a kuroko-type massive sulfide deposit at the abandoned Valzinco mine, Virginia, USA. *App Geochem*, 23, 320–342

Baba, A. and Gunduz, O., 2010, Effect of alteration zones on water quality: a case study from Biga Peninsula, Turkey, *Arch Environ Contam Toxicol*, 58, 499–513.

Johnson, D. B. and Hallberg, K. B., 2005. Acid mine drainage remediation options: a review, *Science of the Total Environment* 338: 3 – 14.

Pozo-Antonio, S., Puente-Luna, I., Lagüela-López, S., Veiga-Ríos, M., 2014. Techniques to correct and prevent acid mine drainage: A review, *Dyna*, 81 (186): 73-80.

Kuyucak, N., 2012, Acid mine drainage prevention and control options, IMWA Proceeding 1999, Sevilla Spain, 599-606.

Grande, J. A., Jiménez, A., Borrego, J., Torre, M. L. and Gómez, T., 2010. Relationships Between Conductivity and pH in Channels Exposed to Acid Mine Drainage Processes: Study of a Large Mass of Data Using Classical Statistics, *Water Resour Manage*, 24:4579–4587.

Kabata-Pendias, A. and Pendias, H., 1992. *Trace elements in soils and plants* (2nd ed.), CRC Press, Boca Raton (FL), 315 pp.

Loredo, J. Alvarez, R. and Ordonez, A., 2005, Release of toxic metals and metalloids from los rueldos mercury mine (asturias, spain), science of the total Environment, 340 (1-3): 247–260.

Gemici, U., 2007, Evaluation of the water quality related to the acid mine drainage of an abandoned mercury mine (Alaşehir, Turkey), Environ Monit Assess (2008) 147:93–106.

Gunduz, O., Simsek, C. and Hasozbek, A., 2010, Arsenic Pollution in the Groundwater of Simav Plain, Turkey: Its Impact on Water Quality and Human Health, *Water Air Soil Pollut*, 205:43–62.

Keskin, T.E. and Toptas, S., 2012, Heavy metal pollution in the surrounding ore deposits and mining activity: a case study from Koyulhisar (Sivas-Turkey), *Environ Earth Sci*, 67:859–866.

Tokatli, C., Cicek, A., Emiroglu, O., Arslan, N., Kose, E. and Dayioglu, H., 2014. Statistical approaches to evaluate the aquatic ecosystem qualities of a significant mining area: Emet stream basin (Turkey), *Environ Earth Sci*, 71: 2185–2197.

Gas Monitoring in the Environment, Following a Fire in an Underground Touristic Facility

M. Kovacs, G. A. Găman, A. Calamar, L. Toth, S. Simion
INCD INSEMEX, str. G-ral. Vasile Milea nr. 32-34, jud. Hunedoara, Petroşani, România,

ABSTRACT: The therapeutic effect of salt mines, in medical terms, were found only in the last decades of the twentieth century. In course of time, Speleotherapy's beneficial effects have been proven, namely: high degree of air purity (sterility, relatively high air humidity (vapor content), vapor condensation favorite content, constant air temperature, low air flow rate, high content of carbon dioxide in the air, high negative ionization (high number of micro ions).

For some events, INCD-INSEMEX Petrosani as specialized institute and national authority is empowered to carry out technical valuations under GD. 1461 / 18.10.2006, Annex no. 1 "development of methods for technical valuation of events caused by explosive atmospheres and / or toxic and / or explosive materials."

The current paper presents the monitoring of environmental factors parameters preceding a fire that took place the fresh air inlet circuit of a treatment saline, as well as measures taken for reopening the tourist area of the underground salt mine.

Keywords: Gas monitoring, INCD-INSEMEX Petrosani, treatment saline, fresh air inlet circuit

1 GENERAL MEDICAL ASPECTS REGARDING SPELEO THERAPEUTICAL TREATMENT

The therapeutic effect of caves and underground excavations (galleries and abandoned operating rooms), has been known for centuries. In scientific and medical terms, the effects on the respiratory system were determined only in the last decades of the twentieth century. In the cave "Klutert" of Westphalia (near the town of Ennepetal) during the Second World War, a bombproof shelter was set up. Among the refugees there were some that were ill, suffering from asthmatic disorders. After a certain period of staying in the cave, the patients showed some signs of improvement in respiratory disease.

The salt mines of Ukraine, at "Solotvino" ("Aknaszlatina"), the practice of speleotherapy treatment for respiratory diseases is ongoing since 1968. Patients are placed in abandoned operating rooms, corresponding to hospital rooms with 2-3 beds at a depth of 206 m, attending four-week treatment cycles.

According to doctors who looked into speleotherapy is not about particular medical factors, but about a set of manifesting physical, chemical and biological conditions, causing complex effects on the human body. Based on research conducted the following factors, which contribute to the specific of speleotherapy, may be numerated:

a. The high degree of air purity (sterility). The characteristic specificity of caves and abandoned mine rooms microclimate is the lack allergenic and irritant effects on the airways. In the polluted air of large cities, floating particles (number of germs) exceeds 1000 particles / cm^3, and in the air of caves and cavities, the number is less than 100 particles / cm^3.

b. The relatively high air humidity (vapor content). Under these conditions, microscopic particles (aerosols) dust, germs, pollen and fungal spores (Mycromicetes) are precipitated on the walls of the rooms, and under the action of moist air, an aqueous film is formed that increases the diameter of particles. Therefore, the inhaled air, rich in

these particles, is deposited on the airway mucosa (nasal mucosa, pharynx and trachea). With inspiration, the air is warmed, the relative humidity decreases, and again it can be again saturated with water vapor and by exhaling the vapor-saturated air eliminated from the lungs, causes the dilution of adherent tracheal secretion.

c. Favorable vapor condensation content. After research conducted in the air of mines and caves, the vapor condensation seems to have a relatively high presence of calcium ions, which has an anti-inflammatory effect, when inhaled. Inhaling air with high content of NaCl, draws tissue secretions from the walls of the bronchia system, through the osmotic effect. In addition to the osmotic effect, the stimulating action of the hypertonic mucous secretion on the bronchia mucous enhances secretion development and contributes to its elimination. In addition to Ca^{2+} ions, dominant in the saline air there can also be found other aerosols rich in sulphates, nitrates, ammonium, Mg, K, Na, I and Br, floating through microscopic droplets of water, thus completing the therapeutic effect of Ca and Na particles.

d. Constant air temperature. Usually, in underground cavities (natural or artificial) at a larger distance from the entrance, air temperature is stable with a few tenths of a degree difference.

e. Secondary effect of relatively low temperature. Relatively cool air from the saline galleries and chambers, similar to cold aerosols, has a stimulating effect on the "cough receptors" in the human body.

f. Low speed air currents. Operating room section varies between 240-250 m^2 so, because these dimensions, humans do not perceive air currents, not feeling the cold.

g. High content of carbon dioxide in the air. The active mines and caves, the highest CO_2 values recorded vary between 0, 1-0, 3 %, which stimulates the breathing center, thus increases lung aeration.

h. High negative ionization (high number of micro ions). After the results of recent measurements in some underground cavities negative air ionization is very high (compared to surface measurements). In the saline the main component of radioactivity is isotope Ra 222. The decomposition of the isotope forms beta and gamma radiations and air ionization increases. The increased share of natural negative ions decreases the intensity and number of asthma attacks also increases the rate of bacteria and allergens elimination from the airways.

i. Reduced quantity of ozone in the air. From the medical point of view, the lack of ozone (O^{3+}) in the saline air means a high purity and reduces smooth muscle convulsions. The low concentration of the reducing material is in inverse proportion with the degree of air purity.

j. Air pH is low (acidic character). The low pH of the saline air contributes to the air disinfection and reduces bacterial flora.

k. High oxygen partial pressure. Usually, in underground cavities air pressure is higher (about 12-15 m / m Hg), and because of this oxygen partial pressure is 2.07% higher than at the surface. It is understood that when inhaling saline air, body supplying with oxygen is increased by 2%.

2 SHORT HYSTORY OF THE ANALYSED TOURISTIC AND SPELEO THERAPEUTICAL TREATMENT FACILITY

Based on the positive therapeutic results obtained in the salt mines abroad, at the analyzed mine, speleo therapeutic treatment began in 1960, in one of the chambers of the old exploitation. Salt extracting was performed at the same level with the treatment rooms, at an appropriate distance.

Many events and exhibitions ensured the influx of visitors, especially the influx of patients. In these abandoned operating rooms painting and sculpture competitions and camps were organized, who's works even these days, adorn as drawings and bass relief the saline's walls.

Based on data collected from the patients treated, began to develop the scientific basis for speleo therapy and climatic treatments.

Subsequent the treatment base moved from the underground to a higher mine level, located at 120 m depth from the surface in a drier chamber system, where it functions even today.

Currently, treatment rooms and annexes are electrically illuminated and have continuous general ventilation. They are also equipped with playgrounds, chairs and sun loungers, pool tables, ping-pong tables, internet club, historical museum, coffee terrace and souvenir shop, an ecumenical chapel and bathroom facility, all to make the mandatory minimum 4 hours of underground treatment daily more bearable and more varied.

For the future they intend to expand this base on a new level (at the bottom of the current one), thus creating an underground complex for tourism and treatment.

We mention that currently they are still exploiting the salt deposits on four lower levels, using the "method of operation with small chambers and rectangular pillars (Canadian method)". Operating room size is 20-275x20x12 m and pillar size is 95-100x20x12 m. The thickness of the plateau between levels is 8 m.

3 CHARACTERISTICS OF THE ANALYSED TOURISTIC FACILITY'S AMBIENT AIR

The physical, chemical and biological characteristics of the tourist attraction ambient air are:

- low concentration of allergens and pathogens, the number of germs varies between 180-270 germs / cm^3, thus observing the condition of fresh air. There are present certain fungal strains (Mycromicetes) some of which may have the same effects as antibiotics (eg. type Penicillium),
- relative vapor content is 45-50%, which is maintained in all seasons, ensuring a constant hidric environment, regardless of outside conditions,
- 50% of microscopic particles of salt (NaCl) in ambient air are under 5 microns in size,
- During the cold season air temperature is 16.4 - 17.40C and 20.80C during summer,
- Salt rock temperature covers the range between 15.4 to 16.4° C,
- Air velocity is 0.1-0.2 m / sec, independent of outside weather conditions,
- CO_2 content varies between 387-775 mg / m^3,
- Ionization level varies between 413-580 ion / m^3, the share of negative ions being higher during summer,
- Natural radioactivity in air expressed as Ra 222 varies between 1.5-1.9 x 10-13 Curie / liter, 2-3 times less than that of the outside atmosphere,
- The low value of air pH varies between 6.5 ÷ 6.9,
- Atmospheric pressure varies between 734 mm Hg in October, and 726 mm Hg in June, directly related to the variation of atmospheric pressure on the surface.

From the statistics stated, resulted that in recent years in the case of the patients present for treatment 3-4 times / year, the number and intensity of asthma attacks decreased, convulsion cough was improved, quantity of eliminated secretion and it's viscosity decreased and the body's respiratory capacity increased. Results show that underground speleo treatment and climatic therapy are simple and effective natural methods that contribute to rapid improvement of the condition of patients suffering from respiratory diseases, maintaining and restoring mental balance and neurovegetative system's tonus.

3.1 The Results of Monitoring Gases from Underground Treatment Tourism Objective's Air after a Fire

On 07.30.2013 at the mining unit from which belongs the tourist and treatment objective, in an abandoned gallery located at 190 m surface (two floors down to that objective) a fire broke out. Through this gallery, was ensured the fresh air supply to the mine, including the treatment area.

The unit immediately triggered a general alarm, following which hundreds of people, tourists, patients and workers were evacuated after gases and odors were infiltrated in the objective area. Fire outbreak manifested in an area of 30 square meters of wood and beams abandoned gallery.

To extinguish the fire the area was flooded by rescue teams However, the management of the mine ordered intensive ventilation in tourism objective and the control of air quality so that they can be reopened only after the gas will be below the limits permitted by the rules of protection of public health.

INCD INSEMEX – Petroşani made a technical expertise to this fire, setting the occurrence of the event (fire) due to a short circuit produced at the power cord from the underground ventilation system, from which were lit wooden beams.

In order to check the air quality INCD INSEMEX Petrosani was asked for monitoring residual gas remaining after the fire till their placing below the permissible standards.

Since the fire occurred on 07/30/2013 and fire-rescuers intervention and ventilation of the objective lasted several days, measurements were performed in two stages during 02 ÷ 04.08.2013 and 19 ÷ 20/08/2013.

The results carried out in two steps close to fire are given in Table 1.

The analysis results show the following:

- CO concentrations (190 mg / m^3) determined on 08.02.2013 in the fire and at 100 m from the fire scene (180 mg / m3) exceeded the limit of 10 mg / m3 established by Law 104/2011 on air quality ambient 18-19 times,
- CO concentration determined on 20.08.2013 in the fire was reduced to 31 times on 02.08.2013, thereby falling into admissible concentration of 10 mg / m^3,
- SO_2 concentration determined on 08/02/2013 at fire exceeded the maximum permissible concentration (MPC) of 350 mg / m^3 established by Law 104/2011, 1.1 times. At the determination made on 8/20/2013 the concentration decreased to 320 mg / m3, falling within the permissible limit,
- for NO_2 and CH4 were identified only traces,
- O_2 and CO_2 were enrolled in normal atmospheric air.

From Fig. 1 can see how the CO concentration decreases over time below the maximum permissible limit specified in Law 104/2011 (on 08.19.2014). During 07 ÷ 19/08/2013 determinations were not made because the ventilation was increased

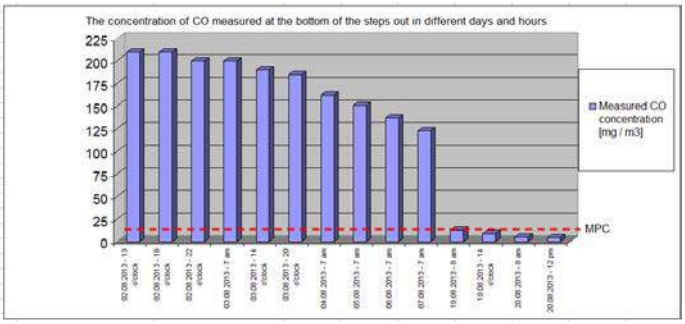

Figure 1. Concentration of CO due to the different time intervals and the at different tours.

The determination results are shown in Table no.2.

Table 1.

Gas sampling location	Gas analyzed	UM	Maximum permissible concentration (MPC) according to Law 104/2011	Gas concentration determined on 02.08.2013, after the fire of 7.30.2013	Gas concentration determined on 20.08.2013, after the fire of 30.07.2013	Decreasing the concentration of gas in 20.08.2013 to 02/08/2013 Col 4 / col 5 [times]	Comments
0	1	2	3	4	5	6	7
The area of the fire incident, lower floor gallery	SO_2	$\mu g/m^3$	350	**400**	320		
	NO_2	$\mu g/m^3$	200	traces	traces		traces
	CO	mg/m^3	**10**	**190**	6	↙ 31	6 < MPC
	O_2	%		20,2	20,1		
	CH_4	%LEL		traces	traces		traces
	CO_2	%		0,02	0,01		
At 100 m from the fire place, to the area exhaust air from the lower floor gallery	SO_2	$\mu g/m^3$	350	**380**	330		
	NO_2	$\mu g/m^3$	200	traces	traces		traces
	CO	mg/m^3	**10**	**180**	5	↙ 36	5< MPC
	O_2	%		20	20,1		
	CH_4	%LEL		traces	traces		traces
	CO_2	%		0,03	0,02		

Table 2.

Gas sampling location	Gas Analysis / climate conditions, T, Wr	UM	Maximum permissible concentration (MPC) according to Law 104/2011	The concentration of gases and climate conditions determined on 02-04.08.2013, after the fire incident of 07.30.2013		The concentration of gases and climate conditions determined on 08.20.2013, after the fire incident of 30.07.2013	Decreasing the concentration of gas in 20.08.2013 to 02.08.2013 Col 5/col 7 [times]	Comments
				02-03.08.2013/ time	04.08.2013 7.00 am			
1	2	3	4	5	6	7	8	9
Entry into recreational basis. Waiting Room (pt. M1)	SO_2	$\mu g/m^3$	350	330	280	260		
	NO_2	$\mu g/m^3$	200	traces	traces	traces		traces
	CO	mg/m^3	**10**	**140** - 02.08.2013- 13 o'clock	**120**	4,0	↙35	4,0 < MPC
	O_2	%		20,2	20,1	20,3		
	CH_4	%LEL		traces	traces	traces		traces
	CO_2	%		0,02	0,01	0,04		
	T	ºC		17,2	24	23,3		
	W_r	%		39,1	38,4	35,6		
Playground, before passage (pct.M2)	SO_2	$\mu g/m^3$	350	190	160	150		
	NO_2	$\mu g/m^3$	200	traces	traces	traces		traces
	CO	mg/m^3	**10**	**190** - 02.08.2013- 13 o'clock	**175**	4,5	↙42,2	3,5 < MPC
	O_2	%		20,1	20	20,3		
	CH_4	%LEL		traces	traces	traces		traces
	CO_2	%		0,02	0,03	0,06		
	T	ºC		18,1	20,6	20,7		
	W_r	%		41,1	46	47		

The gymnastics area (pct.M3)	SO_2	$\mu g/m^3$	350	300	340	200		
	NO_2	$\mu g/m^3$	200	traces	traces	traces		traces
	CO	mg/m^3	**10**	**160** - 02.08.2013- 13 o'clock	**145**	3,5	↙ 45,7	3,5 < MPC
	O_2	%		20,1	20,2	20,3		
	CH_4	%LEL		traces	traces	traces		traces
	CO_2	%		0,02	0,05	0,09		
	T	^oC		18,7	24,3	20,6		
	W_r	%		43,2	45	47		
At the bottom of the exit stairs (pct.M4)	SO_2	$\mu g/m^3$	**350**	340	320	320		
	NO_2	$\mu g/m^3$	200	traces	traces	traces		traces
	CO	mg/m^3	**10**	**210** - 02.08.2013- 13 o'clock **210** - 02.08.2013-hour 18 pm **200** - 02.08.2013-hour 20 pm **200** - 03.08.2013 – 7 o'clock **190** - 03.08.2013-hour 14 pm **185** - 03.08.2013-hour 20 pm	**180**	4,5	↙ 46,6	4,5 < MPC
	O_2	%		20,1	20,3	20,3		
	CH_4	%LEL		traces	traces	traces		traces
	CO_2	%		0,001	0,009	0,08		
	T	^oC		19,9		21,5		
	W_r	%		45,3		47		

Note:
T- air temperature [^oC]
W_r - relative humidity, [%]

We chose four target locations analyzed as follows:

- Pt. M1. Waiting room,
- Pt. M2 the playground before passage,
- Pt. M3- Flatbed Gymnastics,
- Pt. M4- At the bottom of the stairs out.

From Table 2 shows the following:

- CO concentrations determined on 08/02/2013 at 1 PM in four locations M1, M2, M3, M4 were 140, 190, 160 and 210 mg/m^3, exceeding the limit of 10 mg / m^3 14, 19, 21, or 16, times
- CO concentrations determined on 04/08/2013 at 7.00 AM in four locations M1, M2, M3, M4 were 120, 175, 145, 180 mg/m^3, exceeding the limit of 10 mg / m^3, 12; 17.5; 14.5 and 18 times,
- CO concentrations determined on 20.08.2013 in four locations had values of 4; 4.5; 3.5; 4,5, reducing 35; 42.2; 45.7 respectively 46.6 times the concentrations determined on 02.08.2013 at 1 PM
- SO_2 concentrations determined in 02 and 08.04.2013 in four locations M1, M2, M3, M4, did not exceed the limit of 350 mg / m^3 established by Law 104/2011,
- for NO_2 and CH_4 were only traces identified in the four locations M1, M2, M3, M4,
- O_2 and CO_2 were scored within the normal range of air in four locations M1, M2, M3, M4,
- Temperature (T) in four locations M1, M2, M3, M4 had values between 17.2 and 19.9 ° C,
- Relative humidity (Wr) ranged between 39.1 and 47% specific of dry air.

4 CONCLUSIONS

• Research by doctors who were occupied with speleotherapy have demonstrated the beneficial effect of physical factors, chemical and biological from underground

excavations on human respiratory tract.
In Romania there are several underground facilities, where due to the air quality were designed to treat patients with respiratory diseases.

• On 07.30.2013 at the mining unit from which belongs the tourist and treatment objective, in an abandoned gallery located at 190 m surface (two floors down to that objective) a fire broke out. Through this gallery, was ensured the fresh air supply to the mine, including the treatment area.

Because of fire hundreds of people, tourists, patients and workers were evacuated after gases and odors were infiltrated in the objective area.
To extinguish the fire the area was flooded by rescue teams However, the management of the mine ordered intensive ventilation in tourism objective and the control of air quality so that they can be reopened only after the gas will be below the limits permitted by the rules of protection of public health.

• In order to check the air quality INCD INSEMEX Petrosani was called for monitoring residual gas remaining after the fire till their placing below the permissible standards.

Since the fire occurred on 07/30/2013 and fire-rescuers intervention and ventilation of the objective lasted several days, measurements were performed in two stages during 02÷04.08.2013 and 19 ÷ 20/08/2013.

• Measurements of SO_2, NO_2, CO, O_2, CH_4, CO_2 conducted between 08.20.2014 and 02÷04.08.2013 close to fire showed that only CO exceeded the limit. Thus CO concentrations determined on 08.02.2013 in the fire and at 100 m from the place of fire exceeded the limit of 10 mg / m^3 established by Law 104/2011 on ambient air quality, 19 and 18 times.

Determinations dated 08.20.2013 in the fire area showed that CO was reduced by 31 times from the date 02.08.2013 and at 100 m from its the area of 36 times, falling under admissible concentration of 10 mg / m^3 .

For NO_2 and CH_4 were only traces identified and O_2 and CO_2 were enrolled in normal atmospheric air.

• Measurements of SO_2, NO_2, CO, O_2, CH_4, CO_2 conducted between 08.20.2014 02-04.08.2013 in four locations M1, M2, M3, M4 showed that only CO exceeded the limit upheld.

Thus the concentration of CO due on 08/02/2013 exceeded limit of 10 mg / m^3 determined by the Law 104/2011 14, 19, or 16, respectively, 21 times

CO concentrations determined on 20.08.2013 in the four locations M1, M2, M3, M4 decreased to values of 4; 4.5; 3.5; 4,5, reducing 35; 42.2; 45.7 respectively 46.6 times from the concentrations determined on 08/02/2013 at 1 PM falling below the limit of 10 mg/m^3.

For NO_2 and CH_4 were only traces identified and O_2 and CO_2 were enrolled in normal atmospheric air.

Temperatures in four locations M1, M2, M3, M4 had values between 17.9 and 19.9° C and relative humidity between 39.1 and 47% specific of dry air.

• Based on the report of mine air parameters monitoring conducted by INCD INSEMEX - Petrosani, by reducing the concentration of CO under the the limit of 10 mg/m^3, the management ordered the reopening of the treatment area.

REFERENCES

A X-a Conferință națională de balneologie cu participare internațională. Sovata, 10-12 mai 2012, Editura balneară, Volum de rezumate.

Constantin Atudorei, Emil Bocanete, Pavel Miclea, Editura Tehnică, Bucureşti, 1971 - Cercetarea, exploatarea şi valorificarea sării,

Coriolan Stoica, Ion Gherasie, Editura Tehnică, Bucureşti, 1981 - Sarea şi sărurile de potasiu şi magneziu din România,

Horvath Istvan - Istoricul mineritului de sare-2012

Legea 104/ 2011 privind calitatea aerului înconjurător

Ovidiu Drâmba vol. I. Editura Ştiinţifică şi Enciclopedică, Bucureşti, 1985 - Istoria culturii şi civilizaţiei,

Impacts of Mechanical Preparation and Agglomeration of Iron Ore on Environment. Case: Arcelormittal Annaba (Algeria)

Z. Mekti, A. Boutemdjet, M. Bounouala, M. Boukeloul, and A. Idres
Laboratory Natural Resources and Management, Mining Department, Faculty Earth Science, Badji Mokhtar University of Annaba, Algeria

ABSTRACT Among the industries involving exposure to silicogenic risk, the metallurgy occupies, unfortunately, a significant part, this present article highlights the extent of the dust issues in ArcelorMittal stell manufacturer in Annaba, thus a reality of pollution of the region. For this purpose, a methodology for dusts characterization was developed to aim:

- The assessment of the impact of metallic dusts collected at the steel complex,
- Avoid, prevent or reduce harmful effects of these substances on human health, animals, fauna & flora and materials.

The present article, which the main purpose is the identification of dust risk in the sector of Preparation of Raw materials and Addition "PMA" of ArcelorMittal, was conducted during the period of September and November 2012. It is based on the measurement of concentrations of dust, and the determination of levels of their main chemical constituents. These measurements, conducted within acceptable technical conditions, allowed realizing the importance of this nuisance.

Keywords: Iron ore, mechanical preparation, agglomeration, environmental impact

1 INTRODUCTION

Although unavoidable in many materials processing operations, the particle emission of dust into the atmosphere is undesirable; the chemical composition of the solid particles identified two dangerous factors, iron and silicon dioxide in the form of quartz.

These two elements are present in average rates for iron 34.27%, and low for silicon dioxide 6.16%. On the other hand, the quantities of dust are very high and exceed the allowable threshold values; this is particularly alarming because the greater proportion of the particles (62%) have a size less than 5µm and can penetrate inside the human alveoli.

2 RESEARCH METHODOLOGY

Guided by this work, a current medical study try to establish the causal relationship between the air pollution by dust in the workplace and the incidence of respiratory disease. Confrontation and interpretation of these results will allow the development of a specific prevention program for dust related risks.

Since the allowable limit for the human body of neutral dust in a workshop is 10 mg/m^3, it will be necessary to:

- If the dust contains 10% of silica, the maximum permissible concentration must be lowered to 4 mg/m^3.
- If the dust contains 10 to 70% of silica, the maximum allowable concentration should be reduced to 2 mg/m^3.
- If the dust contains more than 70% of silica, it should be reduced to 1 mg/m^3.

3 CASE STUDY

The steel complex of El Hajar ArcelorMitall, is located in the North East side of the country, in the industrial zone of Annaba, 15 km south of the city. It occupies an area of 800 hectares including:

- 300 hectares occupied by the production workshops.
- 300 ha for storage.

- 200 ha for utilities.

Inside, there are more than 60km of rails used for the circulation of raw materials and nearly 100 km of roads for the movement of vehicles (buses, trucks, light vehicle).

4 EXPERIMENTAL PART

4.1 Introduction

The present article is based on the measurement of dust concentrations and the determination of levels attained in an acceptable technical conditions. This allowed us to realize the importance of this nuisance. Thus we can make the following observations:

- The dust concentrations measured were far exceeding the health limits; 1.2 to 7 times the international standards.
- The least polluted area is the coke preparation workshop “PMC”.
- The most polluted area is the ore preparation workshop “PM2”.
- In the mixer building (agglomeration) the situation is critical, because the values found are 10 times the USSR standards and 40 times the US standards. This building looks like a metric source that pollutes the surrounding environment,
- The contents of silicon dioxide in the dust are 5.53% to 7.30%.

The causes of this increase in air pollution are summarized in Table No. 1.

Table 1. Dust concentration in the air of workplace.

Sector	Workshop	Machines	Concentration			Limit values	Observations	
			Posts		Workshop			
			Total	Respirable				
PMC	T1	TRO-302	9.1	4.6	4.6	1.3 mg/m^3	Conditions Atmospheric	wind : low Soil: humid Temperature : 18-20°C
	Crushing Post	BRO-301	16.2	8.3	8.1			
		CRI-301	15.5	7.9				
	T2	DEP-308	13.6	6.9	6.9			
	T3	TRO-333	15.8	8.0	8.0			
	T4	EXT-313	12.6	6.4	6.4			
	Crushing Post	BRO-304	10.2	5.2	7.0			
		BRO-305	17.3	8.8				
	Screening Post	CRI-309	9.7	4.9	6.8			
		CRI-310	28.2	8.8				
PM2	Mineral discharge	EXT-206	18.2	21.2	21.2	4 mg/m^3		wind : variable Soil : dry Temperature : 20-22°C
	T5	TRO-206	33.9	25.4	25.4			
	Screening Post	TRO-222	40.1	30.0	28.3			
		TRO-220	35.5	26.6				
	Crushing Post	BRO-204	58.0	43.5	29.6			
		BRO-218	20.9	15.7				
AG2	Mixer	SIL 26-27	77.4	46.5	46.5	1 mg/m^3		wind : low Soil : slightly dry Temperature : 19-21°C
	Agglomeration	EXT-2	11.1	6.6	12.4			
		BAA-1	23.6	14.1				
		SIL-25	23.8	14.3				
		DOS-6	24.2	14.5				

4.2 Particle Diameter

The particles with size higher than 5 µm are stopped in the air see above (Table 2). Those having diameters of less than 4µm penetrate to the alveoli and are retained by the lungs. The percentage of lung penetration depending on the particle size is as follows.

Table 2. Diameters of particles

Particle size (µm)	Percent penetration (%)
2	90
2.5	75
3.5	50
5	25

4.3 Chemical Nature of Dust

It is the silicon dioxide (SiO_2) or free silica which is implicated in the occurrence of silicosis. Free silica may exist under : An amorphous, non-pathogenic; and another crystallized pathogen which is in the form of compounds:

- Quartz = Hexagonal Crystal.
- Cristobalite = cubic Crystal.
- Tridymite = hexagonal crystal.
- Coesite = hexagonal crystal.

4.4 Limit Values of Dust

A formula proposed by American hygienists, sets a limit value valid for dust particles smaller than 5 µm;

$$\frac{10}{Quartz + 2} \ (\mathrm{mg/m^3})$$

This maximum allowable concentration reflects the SiO_2 content. When it comes to tridymite or cristobalite, the value of this crystallization is divided by two. Therefore, our work method was as follows:

- Determining the average dust concentration from 6 samples of 15 minutes each. The device used is the type Gravicon Sariorius;
- Determination of the chemical composition of the dust. The analysis was focused on the research of four basic elements such as iron, silicon dioxide SiO_2, CaO Calcium oxide, aluminum oxide Al_2O_3.
- Determination of the particle size characteristics using the optical microscope.
- Establishment of the map of studied dust.

4.5 Description of the Industrial Process

The PMA field is a part of the First raw materials and cast iron. The raw materials; coke, ore, adding: limestone, sand, dolomite, quartzite are handled, prepared (screening, grinding, homogenization) before being sent to towns and blast furnaces for the production of chipboard and then cast iron.

The main workshops are:

- The ore iron circuit, ore iron processing.
- Coke circuit, coke processing and additions.
- Agglomeration areas 1 and 2 provide agglomerate for blast furnaces.

The product consists of agglomerated ore (-10mm) fine coke, thin back and additions in the proportions according to Figures 1.

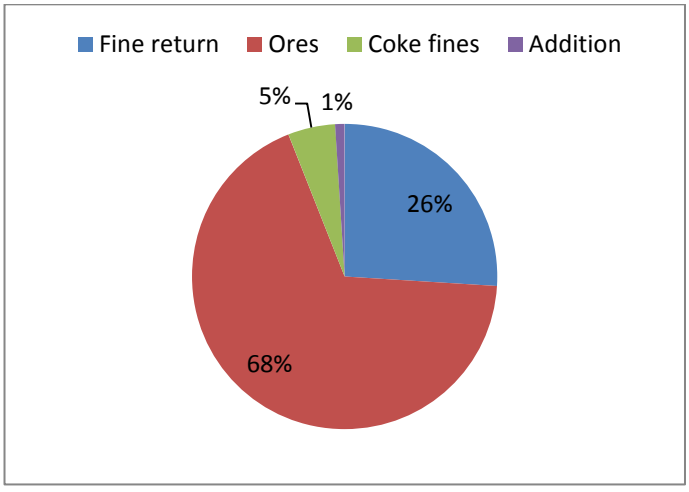

Figure 1. Component of agglomerate

Table 3. Chemical analysis of contents

Substances %	Matières premières						agglomère
	Coke	Minerai	Castine	Sable	Dolomie	Quartz	
Fe	-	50-55	<2	<3	<1	<1	55 ± 2
CaO	<2	4 ± 1	53 ± 2	4± 1	35 ± 3	2 ± 1	8 ± 1
MgO	-	-	-	-	13 ± 3	-	-
SiO_2	5 ± 1	5 ± 1	<0.5	80 ± 5	< 2	<2	7 ± 1
Al_2O_3	<6	<2	-	1 – 2	-	-	-
MnO	-	2-3	-	-	-	-	-
S	<1	<2	-	-	-	-	-
P	<0.002	0.02	-	-	-	-	-
H_2S	-	5-6	-	-	-	-	-
FeO	-	-	-	-	-	-	10 ± 3

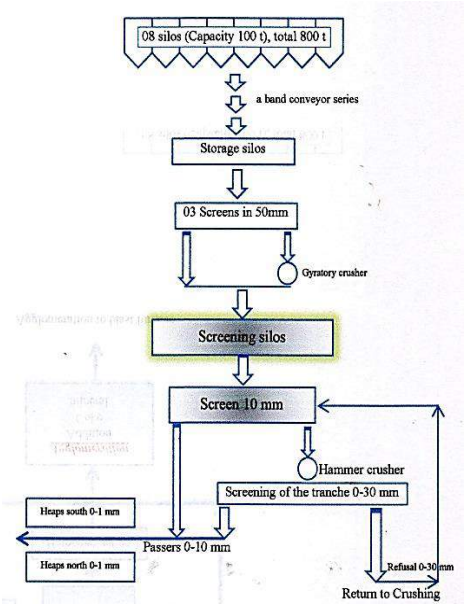

Figure 2. Technological scheme of ore sector

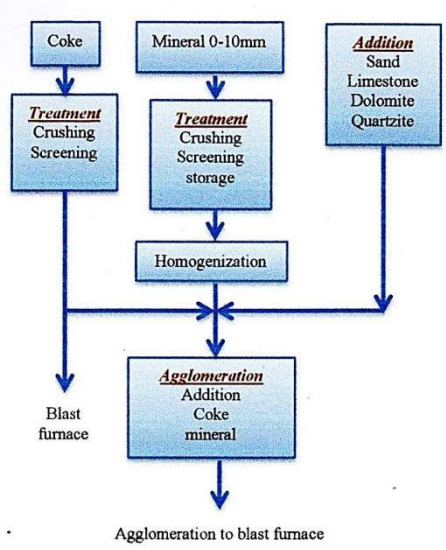

Figure 3. Routing of raw materials

Dust concentrations and the results of grain size analyzes are shown in tables and figures below:

Case the dust of the workshop mechanical preparation of coke (PMC)

The chemical analysis of the substances is; Fe : 1.16%, CaO : 0.8%, SiO_2 5.67% and Al_2O_3 : 2.5%, with a density of 2.02 g/cm^3.

The measurement results are recapitulated in Figure 4 and Table 5.

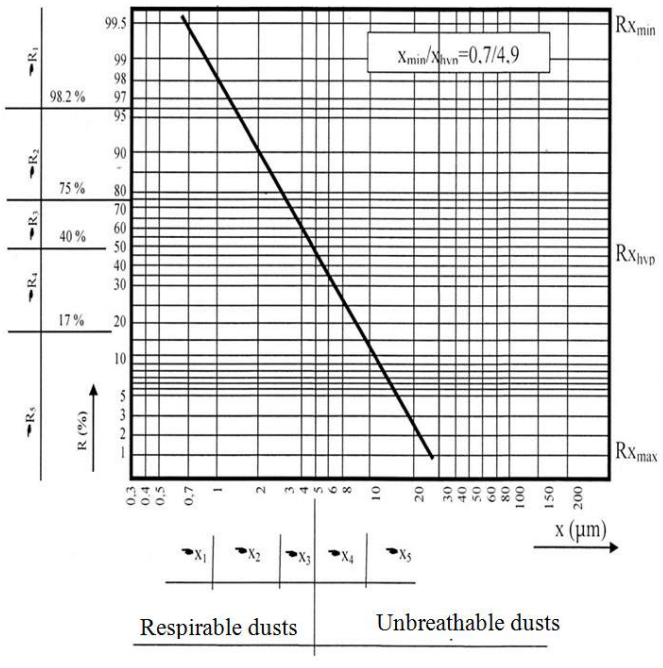

Figure 4. Granulometric characterization dust of PMC

Table 5. Dust particle size analysis (PMC)

Particle size X (µm)	frequencies R(%)	Observation
$X_1 <$ 1	R_1 = 1,3	Particle inferior than à 5µm 75%
X_2 = 1-3	R_2 = 23,0	
X_3 = 3 - 5	R_3 = 26,0	
X_4 = 5 - 10	R_4 = 32,0	Particle superior than à 5µrn 25 %
X_5 > 10	R_5 = 17,0	

Case the dust of the workshop mechanical preparation of ores (PM2)

The chemical analysis of the substances is; Fe: 52.52%, CaO: 4.29%, SiO_2 5.53% and Al_2O_3: 2.34%, with a density of 4.28 g/cm^3.

The measurement results are recapitulated in Figure 5 and Table 6.

Table 6. Dust particle size analysis (PM2)

Particle size X (µm)	frequencies R(%)	Observation
X_1= < 1	R_1= 3,5	Particle inferior than 5µm 75%
X_2 = 1 - 3	R_2 = 41,5	
X_3 = 3 - 5	R_3 = 30,0	
X_4 = 5 - 10	R_4 = 21,5	Particle superior than 5µm 25 %
X_5 > 10	R_5 = 3,5	

Case the dust of the workshop mechanical preparation of ores (AG2)

The chemical analysis of the substances is; Fe: 49.14%, CaO: 6.87%, SiO_2 7.30% and MnO_3:3.30%, with a density of 5.33 g / cm^3.

The measurement results are recapitulated in Figure 6 and Table 7.

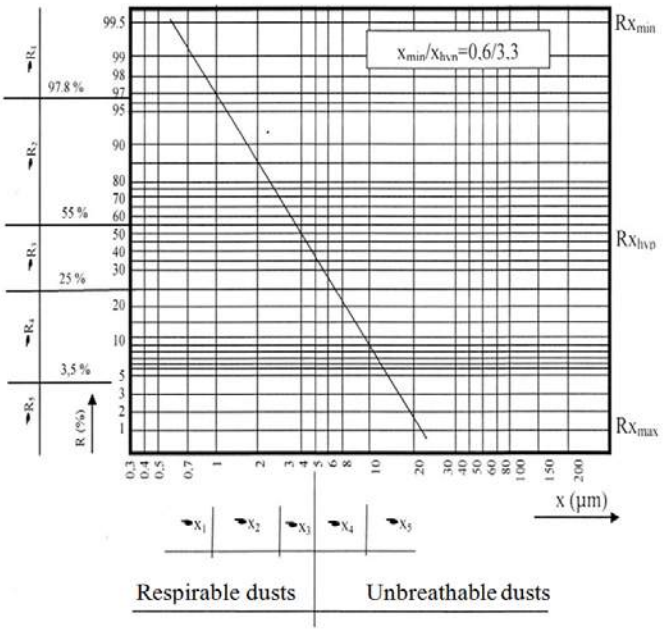

Figure 5. Granulometric characterization dust of PM2

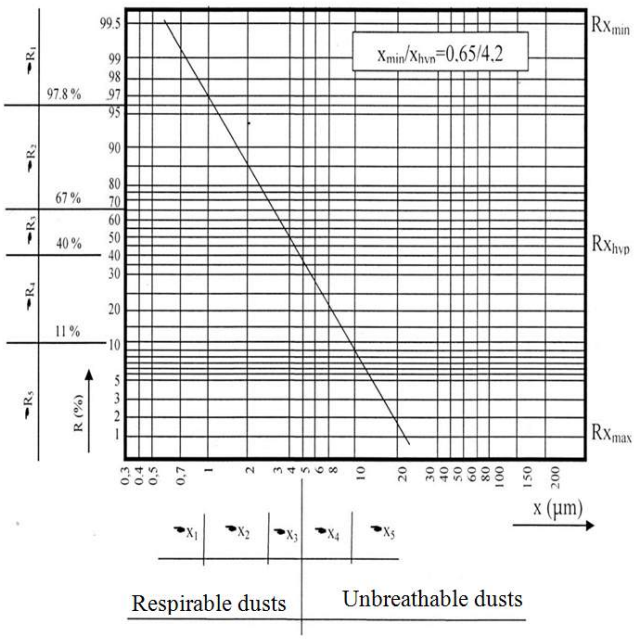

Figure 6. Granulometric characterization dust of AG2

Table 7. Dust particle size analysis (AG2)

Particle size X (Fm)	frequencies R (%)	Observation
$X_1 < 1$	R_1=2,2	Particle inferior than 5µm 60 %
$X_2 = 3 – 1$	$R_2 = 30,8$	
$X_3 = 3 – 5$	$R_3 = 27,0$	
$X_4 = 5 - 10$	$R_4 = 29,0$	Particle superior than 5µm 40 %
$X_5 > 10$	$R_5 = 11,0$	

5 GENERAL CONCLUSION AND RECOMMENDATIONS

A general study of pollution by dust in the air was carried out at the PMA. After comparing these measures with international standards advocated for coal, mineral dust and respirable quartz, it appears that the dust levels well beyond tolerable limits in the three areas of preparation materials and Surroundings (PMC, PM2, AG2). These rates vary from 4.6 to 46.5 mg / m3.

The proportion of dust respirables fluctuates between 51% and 75%; these dusts are less than 5 µm and can attack the respiratory tract.

Chemical analysis of the dust reveals the following average composition:

- Fe 42-50%.
- CaO 4-8%.
- SiO_2 5-8%.

One particular point should be stressed: the website of the mixture of raw materials or dust concentrations reached alarming values, or 10 to 40 times higher than the permissible level. The presence of a considerable amount of dust in the air can also cause danger to the facilities (wear parts, disruption of machinery ...). We will not dwell on the discomfort produced in workers operating the equipment periodically. This site is similar to a transmitting source that pollutes the environment unnecessarily.

All the conditions exist to promote bronchopulmonary aggression characteristic of the dustiness plus the emanation standards of toxic gases and vapors and microclimate conditions of the workshops. The daily inhalation of charged particles of iron and silica involves Sidero-silicosis risk. While taking account of this dust for the effect of high temperatures. In this case, the activated silica is extremely dangerous because it may precipitate the occurrence of silicosis, this formidable assignment characterized by the destruction of the normal structure of the lung parenchyma and its inexorable move towards the aggravation. An important dustiness can cause material damage, yield loss of equipment or a disruption in production.

REFERENCES

T. Bachtarzi, approche méthodologique pour la surveillance de la qualité de l’air dans l’environnement et dans les locaux de travail. Communication présentée aux XIII^{éme} journées Médicales de constantine, Algerie le 25-26 Avril 1984.

S. Serege, la verification de la pollution de l’air, le 2^{éme} conférence national pour protection de l’air, Budabest, 1974.

J. Normandeau, les silicoses Association pour l’hygiéne industrielle au Quebec, Volume 4 N°3, Septembre-Octobre 1982.

T. Nezzal, D. Tourab, T. Bachtarzi, S. Serge, Détermination des poussières dans les lieux de travail au niveau de la PMA/PMC Sider d’El-Hadjar, Université Badji Mokhtar Annaba, Unité de recherche Travail-Santé-Développement.

P. Sadoul, G. Manel, B. Petit, B. Poncelet, Les silicoses de la métallurgie et des industries annexes. Archives des maladies professionnelles, T-40, Janvier – Février 1979.

Investigation of Environmental Pollution Caused by Waste Dump of Takab Gold Mine in West-Azarbaijan of Iran

E. Moosavi, A. Vameghi
Department of Mining Engineering, Islamic Azad University, South Tehran Branch, Tehran, Iran

R. Javani
Department of Basic Sciences, Faculty of Plant Physiology, Arak University, Arak, Iran

ABSTRACT Waste rocks aggregated by grinding, gritting and grading up of ores extracted from North West of Takab gold mine, naturally contains significant amounts of arsenic and sulfide compounds, leading to extended pollution of soil and ground water. Additionally, wet waste rocks removed from flotation and leaching processes in mineral processing are discarded in the same place as dry waste dump of the mine. Waste dump contains a great percentage of chemical materials and increase the pollution of ground water in the area. Various factors including atmospheric rainfall causes chemical compounds to permeate to depth along with water, broadening and accelerating the contamination. Rocks samples taken from different areas of waste dump indicate that pollution is chemical type and consist of sulfate, carbonate and nitrate compounds. Altogether have basic of acidic effect compounds; the amount of which is higher in the western part of waste dump. Chemical dissolving by original cations and anions of water samples showed the intensity and location of pollution of ground water; so that polluted areas were separated from unpolluted ones.

Keywords: Environmental pollution, gold mine, waste dump

1 INTRODUCTION

Mining is one of the earliest activities of human, which has been necessary for developing and continuing civilization. Dependency of human on minerals has been constantly increasing and modern civilization is unable to continue without products of mining. However, the best miner is the one who is also responsive to environmental issues, as to be able to change the mined areas into its original state as much as possible or take some measures to impose minimum damage to physical environment of the mined areas. The effect of extraction of minerals on an environment depends on some factors such as mining methods, materials and types of the rocks, hydrologic and climatic conditions of an area, size of mining operation, topography and many related factors [2]. As Iran is a developing country and it needs to develop mines for its development, environmental aspects of mines and mineral industries should be identified and studied for sustainable development of country's mine industry with respect to its different climatic zones.

As far as local divisions are concerned, the area under study is located extreme southeastern of West Azarbaijan province. The area includes north, northwest, and west regions of Takab city. It is about 700 km2 between longitudes of 46 º, 55' and 47º, 15' E and latitudes of 36º, 25' and 36º, 45' N. North region of Takab is a mountainous and relatively impassable area. It has cold and dry winters covered with snow and temperate summers. The highest point in extreme northwestern region is called Garadagh mount, which is 2955 m above sea level. The lowest height is located southwest of Yahrlī village in extreme southwest of the area under study. It is 1785 m above sea level. It has a mountainous climate.

Farmlands are in foothills region usually with steep slopes. the slopes are steeper at the elevations higher than 1900 meters, but the slopes gradually become less steep, as they reach about 2-3 percent.

As the region is mountainous with high mountains, most rainfalls are as snow and its surface currents flow into the rivers around and finally the Saruq main river through the primary and secondary branches. Saruq river flows into the Zarriné-Rūd river, 58 km southeast of the area under study. Permanent rivers (armlets) of the area include the Zarshoran, Ahamd Abad, Agh Darreh, Ghizghapan, Nabi Kandi, and Gogerdchi rivers. With respect to the mines and mineral potentials in the upstream sections of the rivers, the Zarshoran and Agh Darreh rivers are environmentally more important. Means of rainfall in Takab were measured by Alasghol station and Takab Synoptic Station as 400.3 and 399.10 ml, respectively. The approximate total distance between Takab and Agh Darreh mine is 38 km. Figure 1 shows the access road to the area under study.

2 CONTAMINATION OF AGH DARREH MINERAL AREA

The area under study consists of watershed of the Agh Darreh river and downstream environment of confluence of the Agh Darreh river and the Saruq river in northwest of Takab in West Azarbaijan province. The Agh Darreh river at upstream sections is made up of a primary and a secondary branches. Water and bed sediments of the primary branch are clean and without specific contamination, whereas water and sediments of the secondary branch of the Agh Darreh river has a very high contamination of potentially toxic elements of mercury, antimony and arsenic. This way, after flowing water of the secondary branch into the primary branch in the downstream area, water of Agh Darreh river is contaminated. In the downstream, contamination rate increases by flowing runoff into the mined sections of Agh Darreh gold mine to the Agh Darreh river. As per the results, positions of the primary and secondary branches of the Agh Darreh river, geographical position and topography of the mined sections, and the place of waste dumps of Agh Darreh gold mine, it is necessary to conduct some studies on layout and improvement of substructure of waste dump.

Generally, in order to study the contamination formed in mining waste dumps, it is necessary to recognize source(s) of contamination, types, areas or contamination extents, contamination control geologic and hydrologic factors, and the way contamination is spread. Agh Darreh gold mine in Takab region is detached at different stages and dumped in a place. It contaminates soil and rock layers above groundwater table and finally groundwater table of the region. This article discusses underground contamination due to these waste dumps in Takab region. Figure 1 shows access road of the area under study. The second paragraph is written 5 mm inside the left.

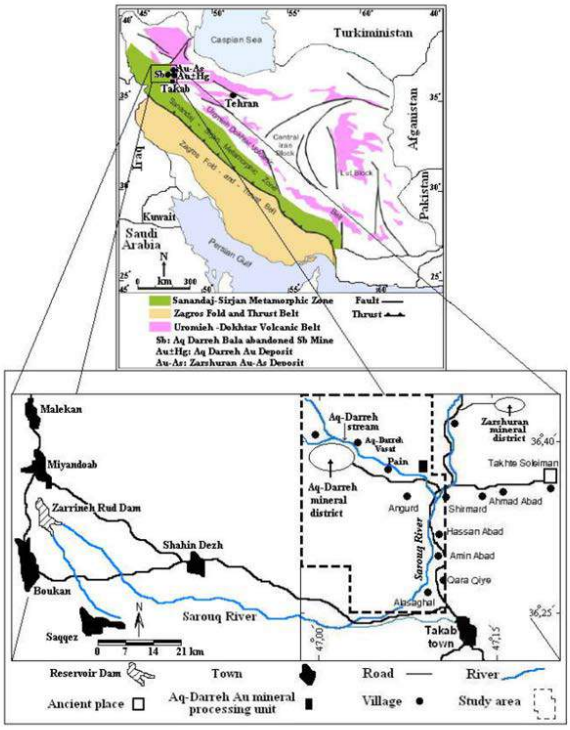

Figure 1. Access road of the area under study.

3 METHODS TO EXAMINE CONTAMINATION IN AGH DARREH WASTE DUMP

Collection of samples from mining waste dump aims at finding a small portion for examining and conducting research. Before any sampling, a sampling project should be designed for supervising research objectives or plan. The sampling project includes specific information concerning sampling place and positions, methods and techniques, number of samples, types of samples, sampling times, samples storage duration, types of preservatives, and numbers and types of standard samples for quality control and quality assurance. Sampling operation may be time-consuming and costly. Factors that should be considered in selection and sampling methods are:

1) *Accuracy of sampling*
2) *Cost of sampling methods*

Sampling of different rock units within the area was made of dry and wet waste dumps of Agh Darreh mine in a specific period. Surface water resources (rivers) and ground water resources (springs) of the area were contaminated by arsenic and antimony. Riverbed sediment, runoff sediment, surface and arable soils, and the vegetation of some parts of the area were contaminated by arsenic, antimony, and mercury. Therefore, only the main phase and environmentally significant minerals of the three elements in the area were studied.

4 SAMPLING AND STUDYING SAMPLES IN WET AND DRY WASTE DUMP

In the first stage, sampling of different parts of the accumulated wastes was performed to study contamination of the region. Generally, many waste samples were collected, but necessary studies and experiments were conducted on a few of them. Among numerous samples taken from different northern and southern parts of the waste dumps (with respect to area slope and its rivers), only five samples were analyzed chemically. Figures 2 and 3 show some images of the northern and southern waste dumps, respectively.

Figure 2. View of the waste dump from the Agh Dareeh mine- Northern region [2].

Figure 3. View of the waste dump from the Agh Dareeh mine- Southern region [2].

The results of chemical analyses indicate that some samples of the area are also contaminated; they contain high concentrations of potentially toxic elements of mercury, antimony, and arsenic. The sampling positions show that most of the contaminated samples include fixed samples formed by source rocks (gold mineralization host rocks and their elements) with a high concentration of these elements or they are carried surface rocks formed in the downstream of source rocks. The chemical analyses indicate that most samples are contaminated by arsenic and antimony. In contrast, samples of the area are less

contaminated by mercury. Tables 1 and 2 show chemical analysis results of the wet and dry waste samples taken from Agh Darreh region, respectively.

Table 1. Chemical analysis results of the dry waste samples.

Percentage	Element	Environment
73.18	As	Waste dump Southern region
81.18	Sb	
36.42	Hg	
79.45	As	Waste dump Northern region
63.06	Sb	
49.86	Hg	

Table 2. Chemical analysis results of the wet waste samples.

Percentage	Element	Environment
89.04	As	Waste dump Southern region
93.53	Sb	
45.37	Hg	
84.67	As	Waste dump Northern region
77.75	Sb	
57.19	Hg	

5 CONCLUSION

The wastes extracted from the ores of Agh Darreh mine in Takab region in northwest of Iran are separated during different mining stages and dumped in the region. Naturally, they contain considerable amount of mercury, arsenic, and antimony compositions; they caused widespread contamination of soil and groundwater. Moreover, wet wastes of a processing and acid treating factory are discarded where dry wastes are dumped. They contain considerable amount of toxic elements and increase contamination intensity in the region. Different factors - such as rainfalls - lead to further influence of chemical substances with water into the underground levels. They intensify, accelerate, and spread contamination of neighboring rivers. Interpretation and chemical analysis of the samples of the mineral wastes dump, which were selected with respect to the region slope and adjacency of streams, represent toxic elements of arsenic, antimony, and mercury. Therefore, severe rainfalls in the region during rain seasons and active streams in the region have environmentally potential threats.

To prevent any consequences caused by mining activities in the region, it seems necessary to use waste dams with geosynthetic infrastructure. Concrete barriers can be used to control sewage of different mined sections of Agh Darreh mine. It seems necessary to conduct several environmental studies on groundwater, agriculture and fertile soil of the region in order to complete its environmental process.

REFERENCES

[1] National database of Geosciences, Land Bank Iran Medical, 2008.

[2] Vameghi, A, 2014. Environmental Geochemistry of Mineral Dere-tekab, find out the source of contaminant elements arsenic, antimony and mercury, and to assess the impact of mining activities, *Dissertation for Master*, Islamic Azad University, South Tehran Branch, Tehran, Iran, (e.g., pp.252).

[3] Flakenmark, M, and Suprato, R.A, 1999. *Population-landscape intractions in development: A water perpective to environmental sustainability*, Ambio, 21, (e.g., pp.31-36).

[4] Brundland, G.H, 1987. *Our common future*, Report of the world commission on environment and development, Oxford university press.

[5] Bell, F.G, De Bruyn, I.A, and Stacey, T.R, 2002. *Some examples of impact of mettaliferous mining on the environment: a South African perspective*, Bulletin of Engineering Geology and Environment, 61, (e.g., pp.1-20).

[6] Keller, E.A, 1999. *Introduction to environmental geology*, Prentice Hall, New Jersey, (e.g., pp.383).

Studies on Gravity Backfilling Method for Blind Backfilling of Abandoned Coal Mines

S. K Pal, S. Panda
IIT Kharagpur, Kharagpur, INDIA

A. K Tripathi
NIT Surathkal, Mangaluru, INDIA

ABSTRACT In this paper a new, simple and low cost gravity backfilling method for stabilization of ground above abandoned underground mines is proposed. Laboratory investigations carried out on this simple gravity hydraulic blind backfilling method to fill up a fully transparent model of a section of a bord and pillar mine, have indicated that deposition of the filling material surrounding the inlet hole occurs in a regular shape with full packing up to the roof. Some empirical relationships on maximum volume of sand throughput and spread of sand around the inlet hole have been developed with a view to help the practicing engineers. In the field trial the spread of sand in different directions has been witnessed using an ROV camera fitted with a sonar imaging system. The shape and nature of deposited sand bed surrounding the feeder hole in field and laboratory studies are alike. The empirical relationships developed under field conditions have also been found to be similar to those of laboratory model.

Keywords: Gravity backfilling, blind backfilling, coal mines

1 INTRODUCTION

In earlier days many coal mines in India have been worked under shallow cover and were practically extracted using Bord and Pillar system of working. Depillaring with regular stowing provides adequate support of the voids and reduces the risk of accidents arising out of pillar spalling and premature collapse of large areas. But depillaring with stowing could not be always followed due to various constraints. Therefore, the coal mines which have been worked without stowing of void spaces became either fully or partially waterlogged and are now unapproachable. Blind hydraulic backfilling is a commonly used technique for subsidence control of the strata over unapproachable waterlogged underground excavations.

2 BLIND BACKFILLING METHODS

There exists number of differences between backfilling methods in active mines and those used in blind backfilling of abandoned mines. The main difference is the lack of access to the abandoned mine voids. The backfilling operation in active mines can be directly observed. The backfilling operation in abandoned mines can only be monitored by special techniques. In abandoned mines due to lack of access, all the work must be done from the surface in remotely controlled manner.

According to placement mechanism, the blind backfilling can be classified into:
(a) Pneumatic method, and
(b) Hydraulic method.

2.1 Pneumatic Blind Backfilling Method

The pneumatic backfilling refers to a special form of pneumatic conveying in which the backfill material is transported through a blind borehole into the mine and thrown all around the inlet zone with the help of compressed air. This method can only be used in dry mines. With suitable design good packing of fill material may be achieved

around one small inlet hole (Sand et al, 1990).

2.2 Hydraulic Blind Backfilling Method

In hydraulic blind backfilling method filling material is mixed with water to form slurry and the mixture is injected from surface into the mine through a feeder borehole. This technique is used to fill up a relatively larger area from the inlet feeder borehole. Walker (1993) had described the state-of-the-art techniques for backfilling the abandoned mine voids by hydraulic flushing from single or multiple boreholes. Thill et al. (1983) described the process of backfilling the flooded mines using sand or crushed mine refuse. The following section describes two important variants of this method that are practiced widely.

2.2.1 Air assisted hydraulic backfilling

This method which is also known as hydro-pneumatic backfilling technique is developed and practiced in India. In this system, solid-water mixture is sent to fill underground voids through a larger diameter hole and compressed air is sent through a smaller diameter pipe placed inside the larger diameter hole. The solids used for filling may be sand, fly ash, small size gravel, crushed stone or washery rejects. Detailed research work in this area in the form of model studies had been conducted at CMRI and at I.I.T. Kharagpur, India (Saxena, 1984, Pal et al, 2001 and 2011). Saxena et al. (1989) presented a field trial carried out at 'Jogta Fire Project' for stabilizing ground over unapproachable workings, which were underneath a jore. Ghosh et al. (1988) described the hydropneumatic method on a field trial in Ramjivanpur colliery.

2.2.2 Pumped slurry injection

In pumped slurry injection method sand-water slurry is pumped down a well under pressure. With this approach, increased spread of the fill material within the mine can be achieved due to the increased velocity at which the slurry is injected. Solid particles settle out near the borehole when the slurry is first delivered and the velocity of the injected slurry drops as it enters in the mine workings. As more material is injected, the fluid velocity increases in the mine workings and the solid materials are transported further away from the borehole (Colaizzi et al. 1981).

Various types of material, such as, crushed stones, mine refuse, and fly ash, can be used for pumping them into the mine with water. The fill material is transported into the mine as slurry and deposited in the void until the void is completely filled. But most of the time filling has to be abandoned due to choking or jamming of flow path inside the mine. The slurry pumping technique includes two methods:

A) High-volume Pumping
B) Low-volume pumping

In high-volume and low-volume pumping methods the granular material is blended with water in a large mixing tank at a processing plant and is then pumped to a series of injection bore holes through pipe lines. The energy provided from the pump and the static head of water in the borehole gives the back fill material the required velocity to keep them in suspension and governs the size of the packing area surrounding the injection borehole.

2.2.2.1 High volume pumping

The high-volume pumping is normally used on very large mine areas that are known to be open and have few obstructions. The high volume of water and its velocity at the injection point ensure wider spread of material than in any of the other methods since the energy of the slurry is much greater. The advantages of high-volume pumping are that a large amount of material can be placed in a short period of time, at low cost, and locally available backfill material can be used. The disadvantages of the system are the costs of establishing central slurry mixing plant, setting pipeline network, and a high volume water supply.

2.2.2.2 Low volume pumping

In low volume pumping water requirements are about 10 times lower than that of high volume pumping. The advantages of the system are that the small, portable, construction-type pumping equipment causes little or no congestion within the working area. The disadvantages of the system are longer material placement time and need for additional boreholes because the material spreads over a limited distance from the injection point.

2.3 Drawbacks of Existing Methods

In air-assisted gravity backfilling process the injected air, if not released completely from the rise side holes, may cause troubles by way of creating cracks and potholes on the surface. The pumped-slurry technique has exhibited filling up of relatively larger areas at a faster rate, especially when high-volume, low-pressure method was selected. This method requires high initial investment on pumps and mixing arrangements. This also requires frequent maintenance and replacement of components on account of excessive wear and tear. Thus, development of a low cost and safer method to stabilize areas over old and abandoned mines has become extremely important under the present context because some regions in Raniganj coalfield have experienced sudden collapse due to subsidence without any prior warning thereby causing loss of property and lives.

In the present study a simple gravity blind backfilling method is proposed where backfill material and water mixed in the form of low concentration slurry, is fed into the mine through a borehole without the assistance of compressed air or pump pressure, till the time the inlet hole will not accept any additional backfill material. The effectiveness of the proposed simple gravity blind backfilling depends on several parameters like slurry flow rate and sand concentration, inclination of the seam and depth of water table from surface.

3 LABORATORY EXPERIMENTS

In this study, laboratory investigation on simple gravity hydraulic blind backfilling has been carried out in a fully transparent scaled model of underground coal mine worked by bord and pillar method. It has 72 pillars of two different sizes representing 45% and 75% extractions. Figure 1 shows a schematic diagram of the experimental set up. A variable-speed bucket elevator is used to transport sand from the storage bunker to the mixing funnel. The sand flow rate from the conveyor is calibrated with the rpm of the conveyor. The volumetric sand flow rate, Q_S in litres per minute, is related to rpm of bucket elevator as

$$Q_S = 0.1389 * (\text{rpm}) \quad (1)$$

The recirculating water feeding arrangement has a small capacity centrifugal pump which delivers water through a turbine type flow meter into the mixing funnel. A manually operated throttle valve is used to vary the volumetric flow rate of water.

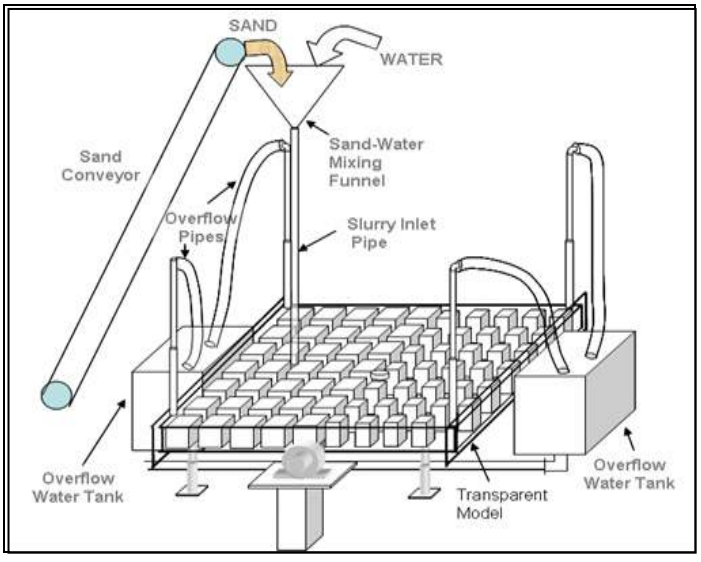

Figure 1. Experimental arrangement in laboratory.

The sand water slurry of given concentration from the mixing funnel gravitates down and enters the model through a transparent inlet pipe. The volumetric flow rates of sand and water as well as the inlet pressure of slurry are recorded in the computer using a continuous data acquisition system. The experiments are continued till flow jamming

occurs, and no further amount sand could be injected. From the stored data the cumulative volume of sand injected may be calculated.

3.1 The Filling Process

When the slurry first gravitates down to the open void of the model through the inlet tube, its velocity decreases rapidly and solid particles drop down from the slurry towards the bottom of the model and form a conical-shaped heap on the floor (Fig. 2). As the height of the heap approaches the roof, the narrowing of the gap between the roof and the fill material causes an increase in the velocity of the slurry. The impact of the input slurry forms a crater at the top of the conical heap just under the bottom of inlet hole. The turbulence created by the water helps the sand particles to be in suspension and transports them through the narrowed gap between the top of the truncated conical heap and the underside of the top cover of the model and finally the particles get deposited along the slope of the conical heap. In this way, the slanted surface of the conical heap advances almost equally in all the directions from the inlet pipe.

The channel flow configuration started after the deposited sand mound grows further in the form of a top-truncated conical heap with a central crater. It was observed that at the beginning four to eight small channels existed, but ultimately after some time, only one, two or at most three channels continued. When sand-transport along the routed channels continued for some time, the pressure within the channel increases sufficiently to cause a puncture a new flow route to deposit sand in a new area of the model. As the new channel starts the old channel gets plugged with sand. This meandering nature of the channels continued through a sequence of depositions and breakthroughs. Finally, a diamond-shaped sand deposit is built up extending almost equally along both left and right strike directions and slightly more in the rise direction. This phenomenon of transport of sand is more similar to the sediment transport phenomenon in open channels or rivers.

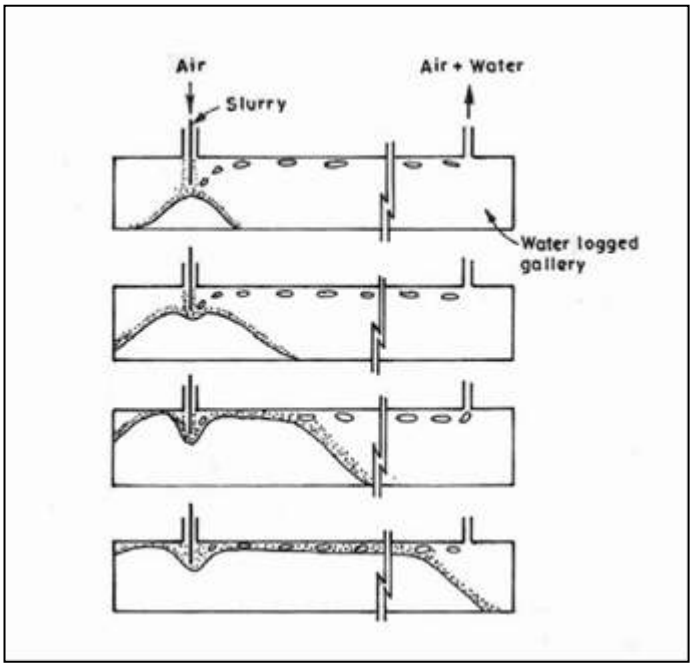

Figure 2. The filling process.

3.2 Effect of Slurry Flow Rate and Sand Concentration on Volume Throughput

Different experiments, with varying slurry flow rates were conducted when the inlet pipe located towards the bottom-end of the model. Figure 3 depicts the maximum volume throughput from a single inlet pipe for a given flow rate at varying concentrations. It may be seen that with increase in sand concentration in the slurry, the maximum sand throughput V_S decreases exponentially for all flow rates of slurry following a general relationship as

$$V_S = K * e^{-n*C} \quad (2)$$

where K ranges from 228 to 604 and n from 0.0822 to 0.1232

Again, for a fixed sand concentration, the maximum sand throughput V_S increases nearly linearly with increase in slurry flow rates.

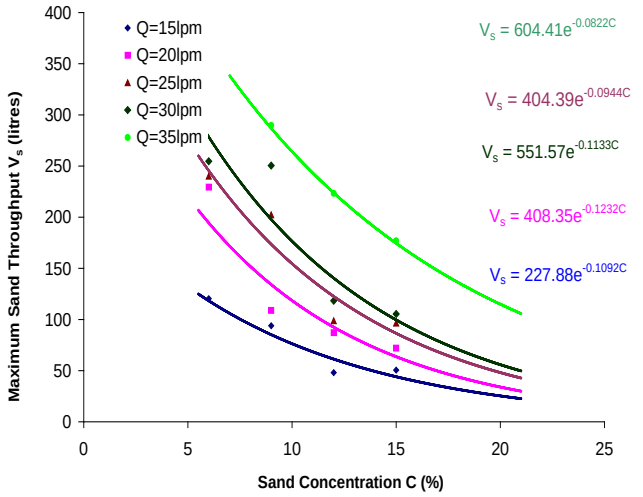

Figure 3. Variation of V_S with C in laboratory experiments at fixed flow

The maximum volume of solid throughput V_S may also be related to both slurry flow rate Q and sand concentration C by using multiple regression as

$$V_S = 0.224 * h * Q^{1.294} * C^{-0.8}, \quad (3)$$

where h is the height of fill.

3.3 Shape of the Filled-up Area

The filled-up area by the sand may be approximated as pentagonal shape in the initial stages of filling, as shown in the Figure 4, and the size of pentagon grows along the strike directions as well as towards the rise direction till the side walls of the model in the strike direction is touched.

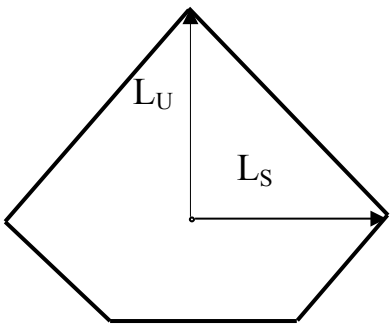

Figure 4. An approximation of the shape of sand-filled area.

Until this stage of filling, the spread along strike and rise directions, L_S and L_U, are measured from the inlet pipe. The volume of the deposited sand, V_S, is then correlated with L_U and L_S through multiple regression technique. The general relationship obtained is

$$V_S = 1.062 * k * h * L_U^{0.378} * L_S^{1.149} \ldots \quad (4)$$

where, k is extraction coefficient and h is height of fill. The inter relationship between L_U and L_S are shown in Figure 5.

If k and h are known, the spread of sand along strike and rise direction may be determined for any given volume of sand pushed into the mine void. This information is useful to the practicing engineers to locate the position of the next inlet hole at the time of filling a large area using multiple inlet holes.

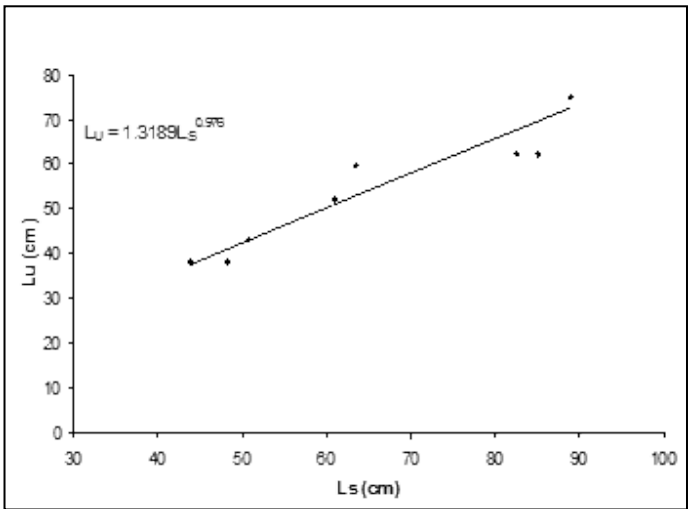

Figure 5. Relationship between L_U and L_S.

The results obtained from Section 3 indicate that with simple gravity blind backfilling method, a large area can be filled up from a single inlet hole by suitably controlling the slurry rate and the solid concentration.

4 FIELD INVESTIGATION

In the light of encouraging results obtained from the laboratory investigations, field implementation of the proposed simple gravity blind backfilling technique has been tried in an abandoned coal mine so as to observe the effectiveness of the suggested method under real field conditions. The relative spread of sand in different directions is measured using a remotely operated vehicle-mounted (ROV) camera. This endeavor is taken up for the first time in the world.

4.1 Drilling of Boreholes

As the mine is abandoned, water-logged and unapproachable, it has been a very difficult task to locate the surface position of the boreholes for successful connections to the underground workings. For this purpose surface control points are selected from the combined surface and underground map of the mine, and locations for drilling three holes are initially marked on the surface. After drilling of these three boreholes at their respective locations, it has been found that only one out of three could connect the underground workings. This failure has given rise to reconsideration of the survey procedure for marking the surface points of future boreholes. A complete survey two surface permanent stations, buildings, roads etc. is conducted to find out the correctness of the surface features of the available map with respect to the two shaft-mouths of the abandoned mine. After adjusting for a small error in location of surface features in the available mine map, the surface points of the further boreholes are positioned and marked in the field. A total of 45 holes are drilled with more than 80 percent success in connecting the galleries boreholes to underground mine. Different types of boreholes of varied sizes are drilled to serve different purposes. The Figure 6 shows the position of different types of boreholes in the mine map. Twenty four air holes are drilled mainly at the rise-most locations covering the entire top part of the filling zone. The purpose of these holes is to release the trapped air which often enters the mine along with the feed of the sand-water slurry through the inlet feeder hole. About 10 large diameter boreholes have been drilled with inside steel casings of 355 mm for insertion of underwater ROV Camera to observe and plot the spread of sand-bed along different directions. Two medium sized boreholes of 250 mm diameter are drilled for installation of submersible pumps which are used to supply water from the water-logged mine into the mixing vat for preparation of sand-water slurry. Water in slurry when fed through mother borehole flows back to the mine, thereby creates a closed-circuit flow of mine water. Six mother boreholes are used for feeding sand-water slurry into the mine to fill-up a section of the mine.

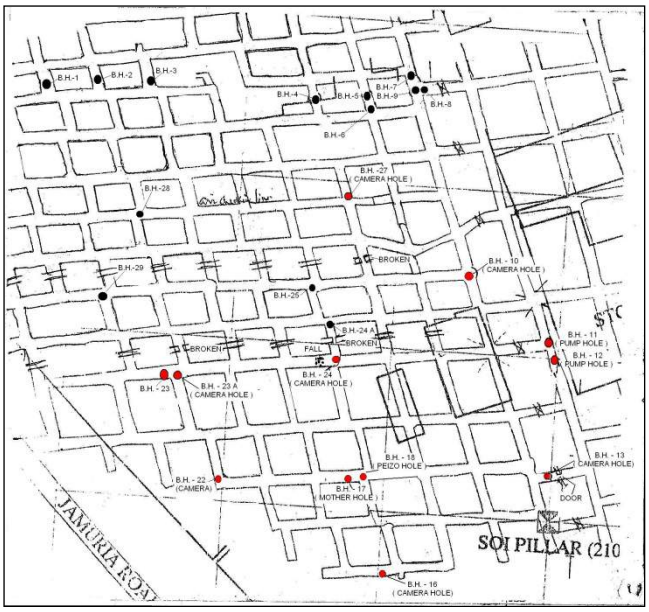

Figure 6. Map of a section of mine showing positions of different types of boreholes.

4.2 Surface Arrangements

Surface arrangements are made to mix measured proportions of sand and water in a mixing vat and send the homogeneous mixture to water-logged abandoned mine by gravity through a mother or feeder borehole.

4.2.1 Water pumping

Two 22 kW power and 2.3 m^3/min capacity, each, submersible pumps are installed at a depth of 40 m below the surface inside Borehole Nos. 11 and 12 connected to two dip-rise crossings of the underground mine. (Fig. 7)

The pumps can be operated either from the pump house or from the movable filling laboratory via wireless antennas. This wireless operation for starting and stoppings of the pumps has been designed for convenience of re-connection of the pumping units after shifting the movable laboratory to a new location for filling through the next feeder borehole.

Figure 7. Pump house for two submersible pumps.

As there has been shortage of storage space on the surface, the sand is procured in stages of about 300 to 500 m^3 and filling is continued in phases.

4.2.2 Sand flow control and measurement

A Payloader is used to load sand on to a small bunker near the movable laboratory, from where a measured amount of sand is fed into the mixing vat through a bucket elevator (Fig. 8).

Figure 8. Sand feeding arrangements.

The sand feed rate by the bucket elevator is calibrated with the speed of the driving sprocket of the sand conveyor. An electrical vibrator motor is fitted at the lower side of the sand bunker for permitting continuous flow of wet sand from the bunker, which otherwise gets stuck at the mouth of sand bunker causing jamming of sand flow from the bunker to the bucket elevator. A proximity switch type rpm indicator is fixed to measure the rotary speed of the driving sprocket of bucket elevator. Two electro-magnetic valves are fitted on the two water inlet pipelines to indicate the water flow rates delivered by the individual submersible pumps. Suitable 4 to 20 mA signals are sent to the data logger for recording of the pumping data during continuous filling operation.

4.2.3 Slurry mixing and feed monitoring

Figure 9 shows the picture of a movable backfilling laboratory was designed and fabricated in the form of a caravan, which is positioned exactly above the mouth of mother borehole.

Figure 9. Caravan with the overhead tank.

Water from pumps and sand from bucket elevator is mixed together in a mixing vat constructed inside the caravan and the slurry is then allowed to flow down into the mine by gravity through the mother borehole. As a safety measure, an overhead water tank of $5m^3$ capacity is placed over the top of the caravan so as to release the water from the tank through a motorized valve to the mixing vat in case of sudden power failure. This additional flushing water will keep the flow channels open and prevent accidental jamming in the case an accidental power cut.

The backfilling laboratory is fitted with a control panel (Fig. 10), where different displays or indicators for different parameters like, individual pump flow rates, the total water flow rate, conveyor RPM, laser water level and piezometer based slurry head, are mounted. A high capacity UPS is also placed at the control panel for uninterrupted monitoring of various parameters in the case of sudden power tripping.

An eight-channel continuous data recording system is installed in the caravan for recording of water flow rates from pumps, sand conveyor RPM, fluctuations in laser water level as well as piezometer water level during filling operations. Figure 11 shows the front view of the continuous data recording system, in which fluctuations in the piezometer water level is indicated in the form of a graph with respect to time.

Figure 10. The control panel inside caravan.

Instantaneous rise and fall of water levels indicated by both laser distance meter and piezometer are also shown symbolically by the rise and fall of levels in two vertical bar-type indicators in the right-hand side of data logger window. Continuous fluctuation of the water level in the data logger window can provide a quick indication about an imminent jamming tendency.

Figure 11. View of data logger in control panel

4.3 Field Experimentation

Since filling from dip-most side has been found to be more effective in the laboratory experiment, the Borehole No.17, which is located towards the dip-most zone of the proposed filling area, is chosen to be the first mother borehole. The diameter of the mother borehole is kept at 200 mm so that the inlet velocity of the slurry becomes nearly 3 m/s. In the beginning of the filling work through the first mother borehole, sand concentration in the slurry has been kept at 15 percent and the slurry level in the mother borehole continuously fluctuates as witnessed in the data logger window. After sufficient progress of filling the flow path length increases, thereby increasing the flow path resistance. This in turn increases the slurry level in the mother borehole, which can be noted from the vertical red bar showing slurry head in the data logger window. When slurry level reaches within 2 m from the surface, the sand conveyor is stopped and plain water flushing of the borehole is allowed to continue for some time so that flow stabilizes and slurry level returns to normal range. Then the sand conveyor is restarted. In this way filling at 15 percent concentration is continued for some more time and then it is reduced to 12 percent concentration when the slurry level in the mother hole reaches within 2 m from the surface very frequently. In the same manner, the concentration gradually reduced to 9 percent as the filling progresses.

During downward movement of slurry through the borehole air bubbles get trapped and enters the mine, which are then released intermittently from other boreholes located on the rise side. Figure 12 shows the gushing release of air and water from Borehole No. 24 located in the rise side of the feeder borehole.

Figure 12. Effusive release of air bubbles

Filling through the first borehole continued with gradual reduction in volumetric concentration of sand from 15% to 9%. Finally the first mother borehole is jammed after injecting 6689 m^3 of sand. Next, the caravan or movable backfilling laboratory is shifted to Borehole No. 23 and re-connection of water pipelines from pumps and power line from nearest power pole are completed. The sand bunker is relocated at the new site. Then filling is started at Borehole No. 23. Due to presence of series of stoppings on the rise side of this mother borehole, filling through this could not be progress beyond 1427 m^3 of sand injection. In the same way filling has been continued in Borehole Nos. 28, 29 and 27 in sequence. The Borehole No. 29, being located in between the two series of stoppings, could not intake sufficient amount of sand and is jammed with a total sand throughput of 1544 m^3. Lastly the filling has been continuing in Borehole No. 3 with 1357 m^3 of sand being sent into the mine and the project was terminated in December 15, 2011. In this way, a total of 21,476 m^3 of sand has been sent into the mine. Table 1 displays the quantities of sand deposited through the respective boreholes.

Table 1. Details of sand filling

Sl. No.	Borehole No.	Sand Deposited (m^3)	Remarks
1.	17	6689	Unhindered filling
2.	23	1427	Hindered filling due to stoppings
3.	28	6236	Unhindered filling
4.	29	1544	Hindered filling due to stoppings
5.	27	4223	Unhindered filling
6.	3	1357	Incomplete filling (project terminated)

5 BACKFILL MONITORING

For the first time in the world the condition of the sand-bed in the underground gallery of a blind backfilling operation could be viewed using special underwater remotely operated vehicle-mounted (ROV) camera. The sonar-head mounted on the ROV camera is used to produce a map of the required part of the abandoned mine to show gradual progress of sand bed along different directions.

5.1 The Underwater ROV Camera

The main components of the Underwater ROV camera (Fig. 13) system are:

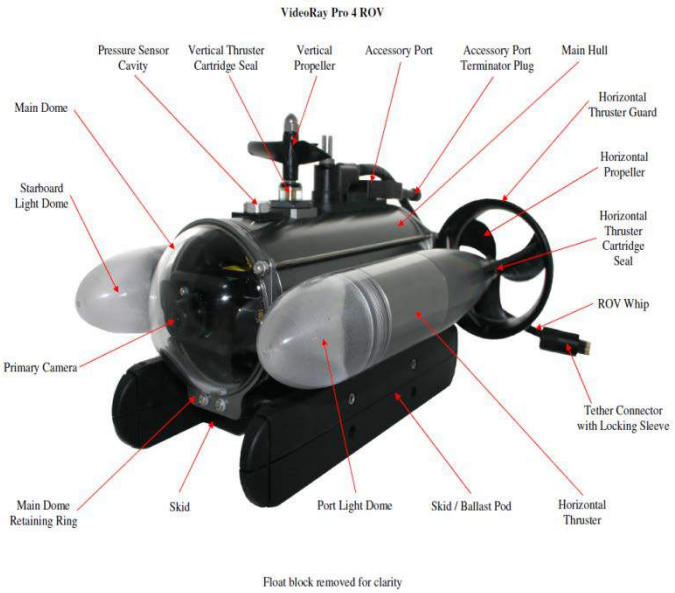

Figure 13. ROV camera

(i) Remotely Operated Vehicle
(ii) Front and back cameras
(iii) control panel
(iv) handheld remote operating device
(v) tether cable

The Remotely Operated Vehicle, or ROV, carries the cameras, lights and sensors or accessories to the underwater places to be observed. Thrusters in the remotely operated vehicle provide mobility and are controlled from the surface. The control panel includes the system's power and communications modules, computer and hand controller, and serves as the operator's console and video display. The handheld remote operating device or controller is used to control the operation of ROV camera system underwater and mainly consists of joystick, depth control knob, bright and dim buttons for lights, and camera tilt up and down buttons. The joystick controls the forward, backward, left and right movement of the ROV. The depth control knob controls the rate of ascent and descent of the ROV. When centered, the vertical thruster is idle. The lights buttons control the intensity of the lights. The camera tilt buttons control the up and down tilt of the front camera. The tether connects the ROV to the control panel and delivers power and control signals to the ROV, and returns video and sensor data (optional) from the ROV to the surface.

5.2 Mapping of the Filled-up Area

Filling work has been executed through six boreholes, out of which the first five boreholes are filled up to the final limit till jamming takes place. Filling from the sixth borehole has been continuing when the project term ended. Monitoring during filling in each borehole is performed from surrounding camera boreholes using ROV mounted camera.

The ROV camera is inserted into the mine through the 14″ diameter camera borehole using remote operating device for the camera system. On entering the mine gallery the camera is slowly moved towards the direction of mother borehole getting guided by the indicated azimuth from the built-in compass as well as from the sonar image. Different screenshots (Fig. 14) of sonar image were used to build a map of the path travelled by the camera. The orientations of camera during successive the screenshots were also noted and this information was used while superimposing the screenshots with one another. At least three well identified common points in the two successive screenshots were also utilized for their superimposition for construction of the mine map.

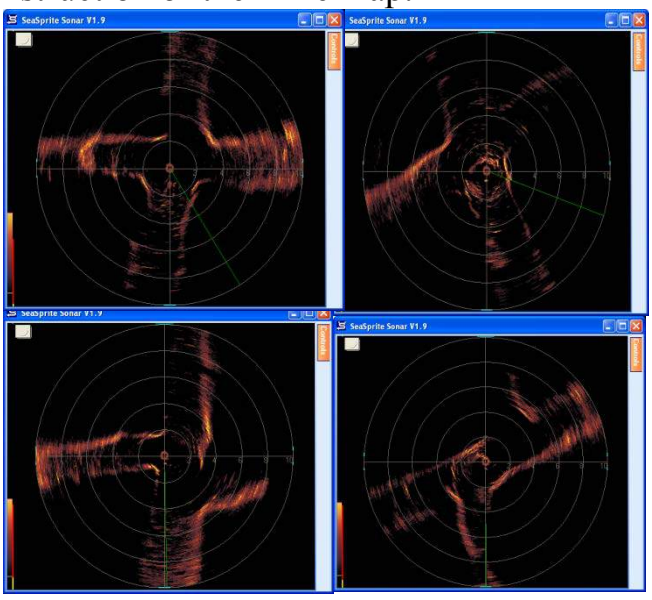

Figure 14. Four successive sonar screenshots

Normally water in underground mine galleries become very turbid during filling and visibility becomes very poor. Therefore filling is done in stages. After input of 400 to

500 m^3 of sand in each stage, filling is stopped for two days for allowing sand and dust particles to settle so that water in underground roadways become clear. Then the ROV camera is inserted from surrounding camera holes in a sequence and transported close to the deposited sand bed from different directions. Then, photographs of sand bed were taken and simultaneously sonar imaging of the underground gallery was done to obtain the exact position of the deposited sand bed with respect of the mine void. Figures 15 and 16 show the spread of sand after 7^{th} and 15^{th} stages of filling.

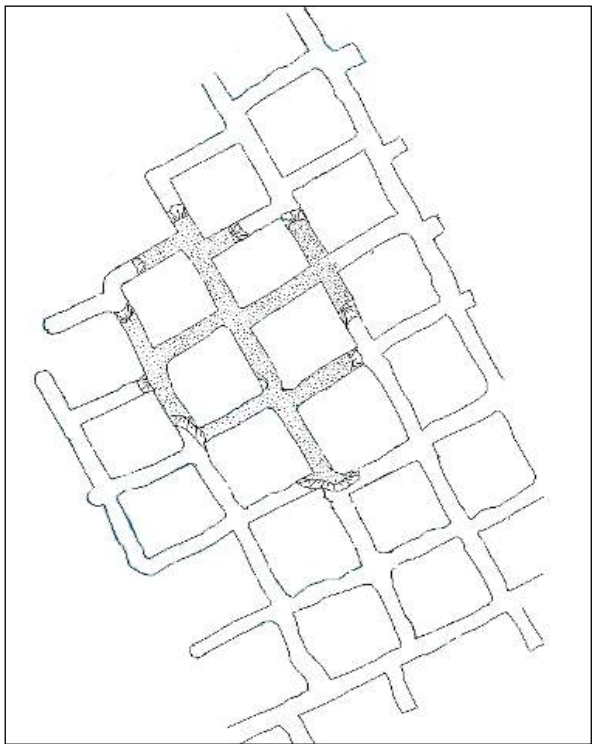

Figure 15. Spread of sand after 7^{th} stage.

The underwater photographs of the sand bed by the ROV camera when it is taken close to the sand bed from different directions showed that the height of deposited sand bed equals the height of the mine gallery, which means that there is no gap left between the sand bed and the mine roof. In normal backfilling or stowing of active underground mine a gap between the mine roof and the deposited sand bed always exists. So, in this method of backfilling yields 100 percent filling. This fact has also been verified in the laboratory study in the transparent model.

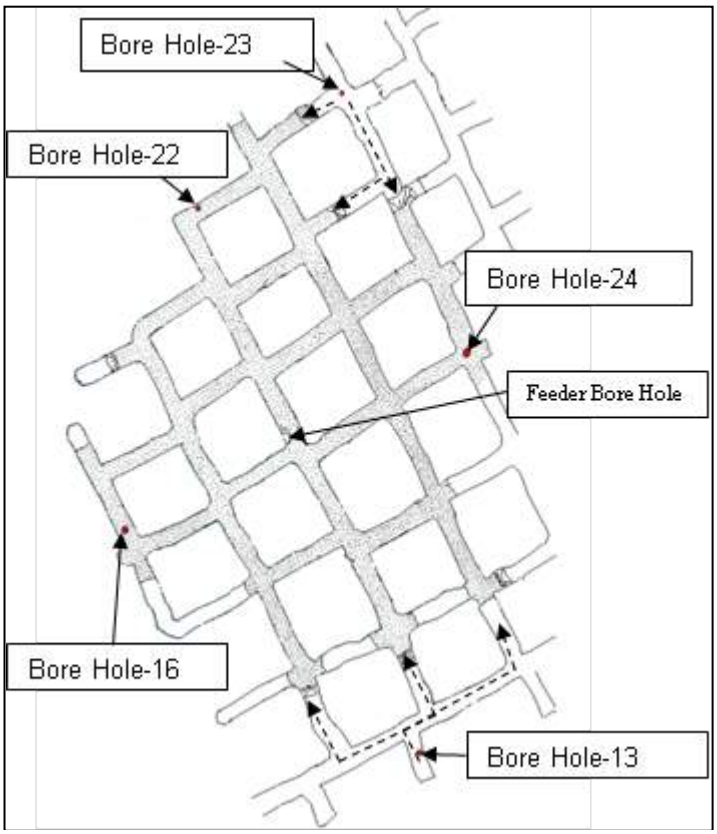

Figure 16. Spread of sand after 15^{th} stage.

Figure 17 shows a typical close view of the deposited sand bed taken by the ROV camera when moved very near to it.

Figure 17. Close view of deposited sand bed.

5.3 Empirical Relationships

During the model study experiments with flow rates varying from 15 lpm to 30 lpm, the nature variation of maximum sand throughput (V_S) with sand concentration (C)

has been observed in the form as given by the Equation (2), where the values of K ranges from 228 and 604, and n from 0.0822 to 0.1232. In the field experiment, a similar nature of variation between maximum sand throughput (V_S) and sand concentration (C) has been detected for the fixed water flow rate of 4.5 m^3/min, but in the field relationship of $V_S = Ke^{-nC}$, the K value becomes as high as 48089 and n becomes 0.227. The above relationship may readily be observed from Figure 18.

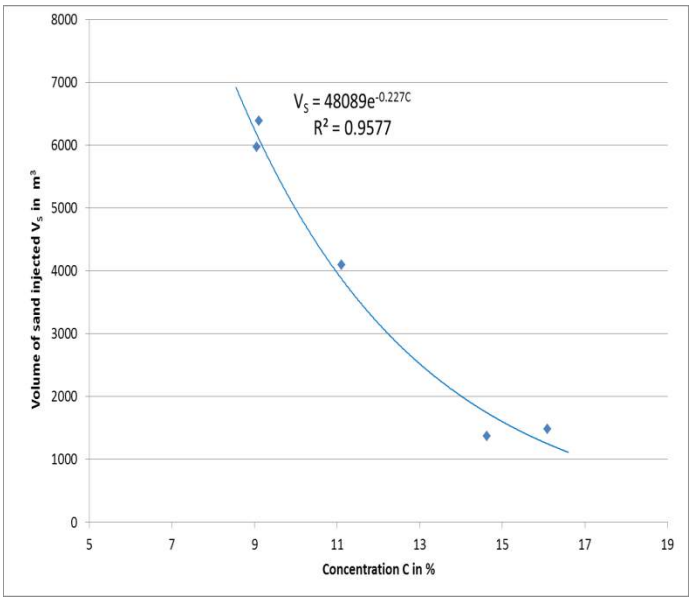

Figure 18. Plot of V_S against C for the

The maximum volume of sand deposited, V_S, has been found to be related with the slurry flow rate Q and sand concentration C in the form

$$V_S = 1.041 * h * Q^{1.313} / C^2 \quad (5)$$

This is similar to Equation (3) of model study. The spread of sand along rise, L_U, and along strike, L_S, are related to maximum volume of sand deposited as:

$$A = 10.55 * k * h * L_U^{0.509} * L_S^{0.764} \quad (6)$$

This is also similar to Equation (4) of model study. Unlike Figure 5 the relationship between L_U and L_S has been found to be non-linear for the case of field study and is given by the Equation (7).

$$L_U = 0.015 * L_S^{2} \quad (7)$$

6 CONCLUSION

From the study of simple gravity blind backfilling in the laboratory model study and in field trials, the following conclusions may be drawn:

I. The process of backfilling in the field study is perceived to be similar to that witnessed in the transparent model study in the laboratory. The process of blind backfilling has been found to be more similar to sediment transportation on river beds rather than slurry transport through pipe lines. The sequence of filling can be observed from Figure 2.

II. It has been observed in the laboratory from transparent model study that filling from rise side towards dip direction suffers from the difficulty of lower maximum sand throughput owing to counter-movement of the downwardly moving sand-water slurry against upwardly moving trapped air bubbles that enters the mine while feeding through vertical inlet borehole. Therefore it is inferred that it is always better to stat the filling operation from the dip-most area of the mine void.

III. The jamming phenomenon, especially the pre-mature jamming incidents are very sudden and arrive without any precursor. In such cases a system for continuous monitoring of the slurry level is helpful for sensing the imminent jamming tendency, and a timely appropriate action may be initiated to dodge any pre-mature jamming.

IV. In order to make the simple gravity backfilling process more efficient, the filling should start with high sand concentration of 15%, and then it should gradually be reduced to 9% or less. This will ensure maximum filling from single borehole at a quicker rate. In this manner up to 6000 m^3 of sand can be filled into the mine from a single mother borehole.

V. During progressive filling work successful monitoring of sand spread along different directions in the abandoned, water-logged underground mine, has been performed using a ROV

mounted underwater camera fitted with real-time sonar imaging system (Figs. 14, 15 and 16). This attempt of remote mapping of the deposited sand-beds in an unapproachable, water-logged underground mine has been made for the first time in the world and completed successfully.

VI. As monitored by the ROV camera the deposited sand bed in the underground mine gallery is packed tightly up to the roof (Fig. 17), thereby ensuring 100% filling by this technique.

VII. For field implementation of this method, empirical relationship for spread of sand along rise (L_U) and strike directions (L_S) with maximum volume of sand throughput (V_S) has been established to assist engineers to locate the position of the subsequent boreholes once the currently running borehole approaches its maximum limit (V_S).

VIII. Empirical relationships between maximum amount of sand throughput (V_S) and slurry flow rate (Q) as well as sand concentration (C) have been found to be similar for model study and field trial, except that these have different values of constants or co-efficients.

With suitable modification of sand concentration and flow rate, the life of the filling process from a single borehole can be extended to fill up considerably large area surrounding the inlet hole. Since sand-water slurry is fed into the mine by gravity and does not involve costly imported equipment, which requires frequent maintenance and replacement of wearable components. This makes it a simple and cost effective method that may be easily adopted by a developing country like India.

REFERENCES

Colaizzi, G. H., Whaite, R. H., Donner, D. L., 1981, Pumped-slurry backfilling of abandoned coal mine working for subsidence control at Rock Springs; Wyo., *IC 8846, United states Department of Interior, Bureau of Mines, USA*, (11-20).

Ghosh, H. B., Dugar, M. L., Gautam, N. N. and Saxena, N. C., 1988, Pilot Trial of Hydropneumatic System of Blind Backfilling at Ramjeevanpur Colliery of E.C.L., *Transactions Journal of MGMI*, Vol. 85 No. 1.

Pal S. K., Ray S. C. and Barve S. D., 2001, System optimization of air-assisted backfilling of inaccessible water-logged mine workings – a model study approach, *Transactions of Mining, Geological and Metallurgical Institute of India*, v 97, n 1, October, (105-113).

Pal Samir K., Mukhopadhyay Subir. K., Tripathi Anup K., 2011, Laboratory studies on stabilization of old, abandoned and waterlogged underground workings, *Journal of Mines, Metals & Fuels*, Vol. 59, Nos. 5 & 6, May-June, (150-154).

Sands, P. F., Boldt, C. M. K., and Ruff, T. M,. 1990. Blind Pneumatic Stowing in Voids in Abandoned Mines, *U.S. Bureau of Mines, Information Circular 9268, Spokane Research Center, Spokane, WA.*

Saxena, N. C., Parti, S. K., Kumar, B. and Singh, B., 1984, Blind Backfilling of Unapproachable Workings Underneath Surface Properties, *Transactions Journal of MGMI*, Vol. 81 No. 2, (47-59).

Saxena, N. C., Roychoudhury, S. K., and Singh B., 1989, Stabilization of unapproachable underground working in coal mining areas, *Proceedings of the Int. Symp. on land subsidence, Dhanbad, India*, (660-670).

Thill, R. E., Hulk, P. J., and Stegman, B. G., 1983, Monitoring Blind Backfilling in Abandoned Mines, *Mining Engineering*, Dec.,(1625-1630).

Walker, R. H., 1993, State-of-the-art techniques for backfilling of abandoned mine voids, *U. S. Bureau of Mines, IC, Pittsburg, P.A., USA.*

Whaite, R. H. and Allen, A. S., 1975, Pumped-slurry backfilling of inaccessible mine workings for subsidence control, *IC U. S. Bureau of Mines, Washington D. C., USA.*

Mathematical Analysis Of Spontaneous Fire In Coal Mines For Designing More Efficient Fire Control Techniques

D. D. Tripathi, A. Sinha
Central Institute of Mining & Fuel Research, Dhanbad–826015

ABSTRACT Energy security is now prime issue to uphold GDP in India. Presently, coal is playing vital role in fulfilling the primary energy need of the country.But, thetendency of self heating of coal is playing a significant hazardinmining the coal. In fact, coal having molecular formula $C_{10}H_7O$; attains thermodynamic equilibrium over the years, but a little added oxygen tilts the thermal stability and leads to spontaneous heating or fire, hence the mechanism of spontaneous heating has been evaluated. The most effective way to investigate the dependency of spontaneous heating on various factors is mathematical modeling. Coal ignites spontaneously when temperature reaches above the critical temperature; at which the oxidizing process becomes irreversible thermo active -

$$\boldsymbol{T = \frac{E}{R} / ln(k_0/\mu)}$$

Where E is activation energy of burning reaction/mole: R=8.3144J/(mole^{0}K);universal gas constant, k_0 frequency factor, 1/sec; and gas constant, μ oxidation reaction rate constant for mechanically activated carbon. The critical temperature of coal self ignition can be loweredby decreasing activation energy in the fields of mechanical stresses.

Once a fire broke-up in the mines huge resources are required to combat, sometimes it's unnecessarily costly due to overuse or underuse of resources. Indeed, a cost effective fire combat techniques cannot be made without mathematical understandingof incubation period, quantitative analysis of fire risk potentials,the state and extent of fire,its direction of progress andair feeding to the seat of fire etc.

This paper summarizes the R&D carried out in CIMFR (Central Institute of Mining and Fuel Research, India) using mathematical approach for prevention and control of spontaneous fire has been summarized. Few successes storiesin realistic field have also discussed.

Keywords: Oxidative spontaneity, incubation period, mathematical simulation, fire fighting

1 INTRODUCTION

Coal mining in Indiahasstarted in August, 1774in Dishergarh seam at Aitura (Ethora),Chinakuri Colliery of Raniganj Coalfield; since those days, extraction is progressively continued. At present nearly 265BT coal reserve is available for mining and new resources get added years on years. Due to spontaneous nature of coal, mining industry is suffering from large extent of endogenous fires in their underground mines, open pit mines (virgin coal seam and developed galleries), stockpiles, discard dumps and moreover during transportationof coal through trains, trucks and ships [1].

Hazards of spontaneous fire have long been a problem in the wining of coal. At present, 87% coal is produced by open pit mines, but most of big open pit mines are facingthe large extent of active fires.Besidethis, only 15% geological reserves are amenable by open pit mining within economical depth (300 m). Difficulties in obtaining forest land and environmental clearances, high stripping ratio of coal seams and limited scope of large scale mechanizations;mining stalwarts are telling at every opportunity that greater attention should be paid to underground mining thus occurrences of spontaneous fire will increase in future.

2. MATHEMATICAL SIMULATION OF OCCURENCES OF SPONTANEOUS FIRES

Coal implicates energy therefore we have to save it from self-heating; but themeasures are not adequate for defeating the very purpose of it. The problems commonly met are, infrared thermometer and other temperature detecting devices can't outline the temperature profile of isolated area of the mines and composition analyses of fire gases are unable to locate the seat of fire. Nevertheless, numerical models give adequate and feasible results

2.1 Perceptives of Heating due to Aerial Oxidation

Oxidative spontaneity in coal is too common therefore, prior to designing long term mining plan it is indispensable to understand occurrences of spontaneous fire. Coal interacts with atmospheric oxygen at ambient temperature with varying rate of oxidation 2000-10 ml/kg/hr; depending on the extent of weathering of coal [2].

$$C + O_2 = CO_2 + \Delta H \quad (1)$$

The process is exothermic, evolves heat (25-0.3 J/ml O2 absorbed) which raises the temperature of coal.

$$dQ/dt = Cp(T)/H\ dT/dt \ \ ml/kg/hr \quad (2)$$

Where Q, amount of oxygen consumed per unit weight of coal, dT/dt, rate of temperature rise; H is heat of reaction; Cp (T), specific heat capacity of coal.Rate oxidation of coalbecomes double for every 10^0C rise in coal temperature.

2.2 Spontaneous Heating Predictive Models

Energy Conservation equation (3)

Heat accumulation at a point = [Heat produced due to exothermic oxidation of coal – Conductive heat transfer - Convective heat transfer - Heat to drying or wetting]

$$C_{ps}\,P_s\,\frac{\partial T}{\partial t} = H_0\{D_0 \in \frac{\partial^2 \rho_0}{\partial x^2} - V_g\,\frac{\partial \rho_o}{\partial x}\} \quad - \left\{-k\frac{\partial^2 T}{\partial x^2}\right\} - C_{pg}\,\rho_g\,V_g\,\frac{\partial T}{\partial x} - H_w\left\{-D_w \in \frac{\partial^2 \rho_w}{\partial x^2} - V_{wd}\,\frac{\partial \rho_0}{\partial x}\right\} \quad [3]$$

Oxygen mass conservation equation

Oxygen accumulation = {Diffusion of O_2 - Convective transfer of O_2}

$$r_0 = D_0 \in \frac{\partial^2 \rho_0}{\partial x^2} - \ V_g\,\frac{\partial \rho_o}{\partial x} \quad (4)$$

Moisture mass conservation equation

Rate of drying = {Diffusion of water vapor– Convective transfer of water vapor}

$$r_w \ = -D_w \in \frac{\partial^2 \rho_w}{\partial x^2} - V_{wd}\,\frac{\partial \rho_0}{\partial x} \quad (5)$$

Symbols have their usual meaning.

One dimensional transient pseudo (local mass accumulation is negligible compared with mass transfer) steady state model equations, in which mass transfer of both oxygen and moisture occurs by diffusion and convection, are used - to avoid the complexity in finding the exact solution.

2.3 Simulation Of Spontaneous Fire

Heating of coal corresponds to the third stage in which the moisture present in pores is dried out and at any instant increase in surface oxidation of coal becomes over. Mass transfer of oxygen and moisture both occurs through convection. Implementing the conditions - energy balance equation transform into-

$$k\frac{\partial^2 T}{\partial x^2} - H_0 V_g\,\frac{\partial \rho_o}{\partial x} \ - C_{pg}\,\rho_g\,V_g\,\frac{\partial T}{\partial x} - H_w V_{gd}\,\frac{\partial \rho_{wd}}{\partial x}\} \ = 0 \quad (6)$$

with boundary conditions-

at x = 0 ; $\quad k\frac{\partial T}{\partial x} = C_{pg}\,\rho_g\,V_g\,(T_i - \ T_a)$

$\rho_0 \ = \rho_{0,i} \ = \rho_{0,a}$; $\quad \rho_{wd} \ = \rho_{wd,i} \ =$

$\rho_{wd,,a}$ (7)

at x=1; $k\frac{\partial T}{\partial x} = \frac{\partial \rho_o}{\partial x} = \frac{\partial \rho_{w,d}}{\partial x} = 0$

Integrating equation (4) and substituting the boundary conditions -

$$\Delta Tmax = \frac{H_0}{C_{pg}\,\rho_g}(\rho_{0,a} - \rho_0) + \frac{H_w}{C_{pg}\,\rho_g}(\rho_{w,d,a} - \rho_{w,a}) \quad (8)$$

The equilibrium temperature rises up to $\approx 90^0$C. As a result, the occurrences of spontaneous combustion of coal in an underground mine panel i.e. in realistic mining conditions can be controlled by both reduction in oxygen concentration and reducing the relative humidity in gas stream.Moreover the rate of mass of coal can spontaneously ignite only when it reaches some temperature T^0 C above critical.

T > TCr **(**9)

The process of transition of spontaneous heating to spontaneous ignition depends on partial pressure of oxygen and heat exchange in the coal mass and surroundings and described with equation -

$$dT/dt = H/Cp\,(T)\,A \exp[-E/RT - bQm]\,(Po_2 / 0.21)^n \quad (10)$$

Where Q, amount of oxygen consumed per unit weight of coal, dT/dt, rate of temperature rise; H is heat of reaction; Cp (T), specific heat capacity of coal. A, pre-exponential factor; E, activation energy; R, universal gas constant; b and m are constants, T, absolute temperature; P_{02}, partial pressure of oxygen and n, the order of reaction belonging to the range of 0.5-1.0; for freshly to wreathed coal.

Numerical simulation of equation (10)provides estimated time in which spontaneous heating may setup inspecific panel or place.

3. SIMULATION AND ANALYSIS OF PROPAGATION OF FIRE

3.1 Propagation of Surface and Subsurface Fires

Spontaneous heating generally starts at a single point or several independent points at a time and heat transferoccurs through conduction, the equation, rate = driving force/resistance, can be applied directly. The driving force is the temperature difference per unit length of heat-transfer path, also known as the temperature gradient. Instead of resistance to heat flow, its reciprocal called the conductance is used. The rate of heat transfer=driving force x conductance,i.e. [4]

$$\delta T/\delta t = \alpha \delta^2 T/\delta x^2 \quad (11)$$

$$T = Ts \text{ at } x = 0;\ T = f(x) \text{ at } t = 0 \quad (12)$$

α, thermal diffusivity. Using boundary conditions, equation (1) transformed into probability integral as-

$$T_f - T_0 / T_s - T_0 = \phi(\gamma\eta) = 2/\pi^{1/2} \pi e^{-\beta^2 d}\beta \quad (13)$$

Where $\phi = \frac{1}{2}\,\alpha^{1/2}$ t, t is time to attain the temperature T_f at a distance x from heat source.

The moment thermodynamic equilibrium is reached, cellular convection setup-

$$q/k\rho c = 1/(\pi t)^{1/2}(T_f - T_0) \quad (14)$$

Where, q is heat flux at the surface of the solid (W/m^2), k is thermal conductivity, ρ is density and c is specific heat capacity.

Since, intervening strata of coal seam comprises different formations like shale bands nevertheless sandstone bands as intricate part of the seam, then heat absorbed by their respective boundaries are-

$$q_1 / k_1\rho_1 c_1 = q_2/ k_2\rho_2 c_2 = q_3/ k_3\rho_3 c_3 = \ldots = q/ k_i\rho_i c_i \quad (15)$$

Where scripts 1, 2, 3, ---- i are the boundary element of enclosures. Moreover total heat absorbed per unit area by its constituent boundaries are-

$$1/(k\rho c)^{1/2} f_0^{\pi} q\,dt \quad (16)$$

Where, π is the length of the solid exposed to sense the convective heat flow. Shale and sand stone in the solid form are more risky in propagating the fire.

4.RAPID COOLING OF STRATA HEATED BY FIRES

4.1 Cooling of Hot strata by Water percolation –model approach

Water is one of the most useful and cost effective in all available fire extinguishers. Under pressure and controllable-discharge, water infiltrate and knockout deep-seated fires. The general model of infiltration of water from surface ponds to a fire area is based on Darcy law or its modifications [5]-

$$V = -(\kappa/\mu)\Delta P/L \quad (17)$$

V, average fluid velocity through the pores with pressure drop ΔP measured across the system,κ, permeability, μ, viscosity, L length in flow direction.

The rate of water percolation from surface ponds, into a fire area depends on permeability of soil that gives passage to flow through it's inter connecting voids. The effect of inertia, on the flow, through porous media is characterized by Forchheimer equation i.e. modified Darcy Law [6],

$$-\Delta P/L = \alpha\mu V + \beta\rho V^2 \quad (18)$$

α, reciprocal of permeability, β inertial parameter. Bothα andβ depend on porosity of the material. Equation (18) can be derived by Navier Stroke equations for one-dimensional, steady, incompressible, laminar flow of a Newtonian fluid in rigid porous medium -

$$f = 1/Re' + 1 \quad (19)$$

Where $f = -\Delta P/L\beta\rho V^2$ and $Re' = \beta\rho V/\alpha\mu$. We obtain a frictional factor - Reynolds number type correlation, which is successfully used to correlate large variety of porous materials and broad range of flow conditions.

5.FIRES IN JHARIA COALFIELD (JCF)

Jharia Coalfield (JCF) is worldwide famous for coal fires; and lie within latitude 23^{03}9'N - 23^{04}8'N and longitude 86^{01}1'E-$86^{0\ 2}$7'E in Damodar river basin. The mining activity in JCF was started in 1894 and occurrence of fire was noticed in 1916 at XIV/XIII seam of Bhawra colliery and causing devastation since last 100 years or so. Coalfield having 18 regular coal seams (XVIII-I, top to bottom) and 46 coal horizons. Several seams are consists of discontinuous splits namely top-bottom, upper-lower and local seam with nomenclature (0, A, B, -- --; etc.) with varying thickness of 0.5-55M and gradient 5-40^0 up to a maximum depth of 1200m. Area is geo-spatially disturbed with dyke, sills, igneous intrusions, extensive folding and more than 250 faults. Indeed, coal seams existing at shallow depth have been mined out unscientifically in the beginning; caused spontaneous fire in due course. Initially, these fires are inadequately sealed and monitored, so, gradually; they had grown up to the surface and spread over a long region as shown in Figure 1.

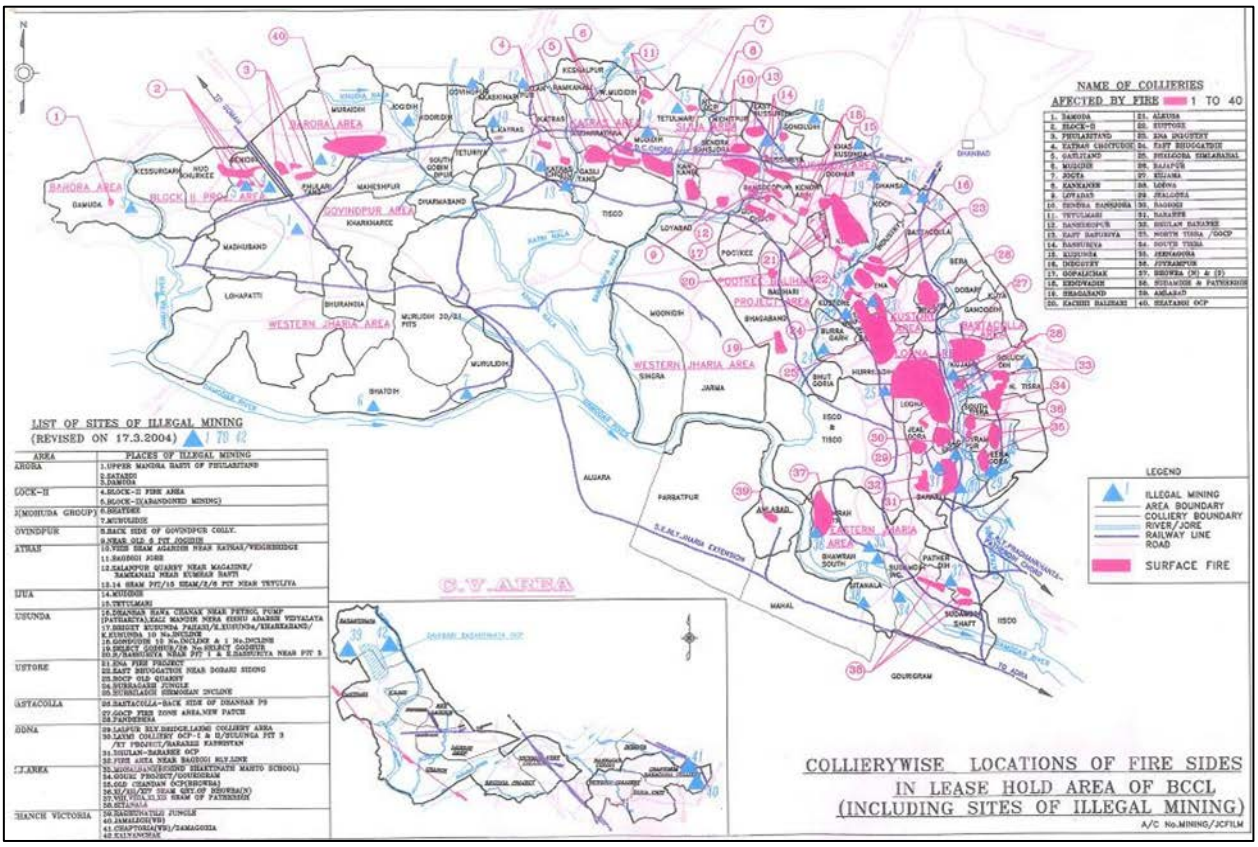

Figure 1. Fires in different collieries of Bharat Coking Coal Limited in Jharia coalfields

5.1 Impacts of Coal Fires

Emission of greenhouse gases—carbon dioxide (CO_2), methane (CH_4), carbon monoxide (CO), nitrogen oxides, sulfur dioxide and other toxic organic substances into the atmosphere is major environmental concern of open coal fires. Although, contribution of CO_2 and CH_4 into global atmospheric pool is nothing from small fire but can't be overlooked.

Fires affects air water, and land; smoke, from these fires contains poisonous gases that causes lung and skin diseases. Fires also pollute water by contamination of sulpher that is present in coal. In Jharia coalfield shallow depth underground fires had come up to the surface at many places and threatening the life of habitant.

5.2 Simulation of Firefighting

a. Inertization

The most important feature of dealing subsurface fires is oxygen depletion; whether, by sealing or inertization using inert gases CO_2 or N_2. Simultaneously to check the success of firefighting operation the knowledge of varying oxygen concentration at any point is quit important. There expression for changing O_2 concentration at time t has been given-

$$t = V/ CO_2 \, 1n \, Oc/ Ocrt \qquad (20)$$

Where, V is volume of the sealed of fire area; CO2 is flow rates into sealed off fire area m^3 /min; C_o initial oxygen concentration at t=0, C_t , concentration of oxygen after time t min.

In a perfectly sealed of area of volume V, the quantity of inert gas Q, necessary to reduce the O_2 concentration from 21% to 2 % will be Q = 2.3 V. Ratio, Q/V must be kept considerably higher than 2.3 in actual field condition owing to inherent air leakage.

5.3 Rapid Cooling Of Strata Heated By Subsurface Fires

Two water pods of dimension 504mX66mX2m and 540mX70mX2m were made in the fire.Insitu temperature was reported as360^0C (maximum). Then, ponds

were filled with water up to a height of 2m. Boreholes C_1, C_2, C_3, C_4 andC_5 exist in the vicinity of pods. Then, duration of lowering the water level in the ponds, temperature, gases and effectiveness of cooling by water percolation has been monitored weekly for one year. The inferences drawn are given below.

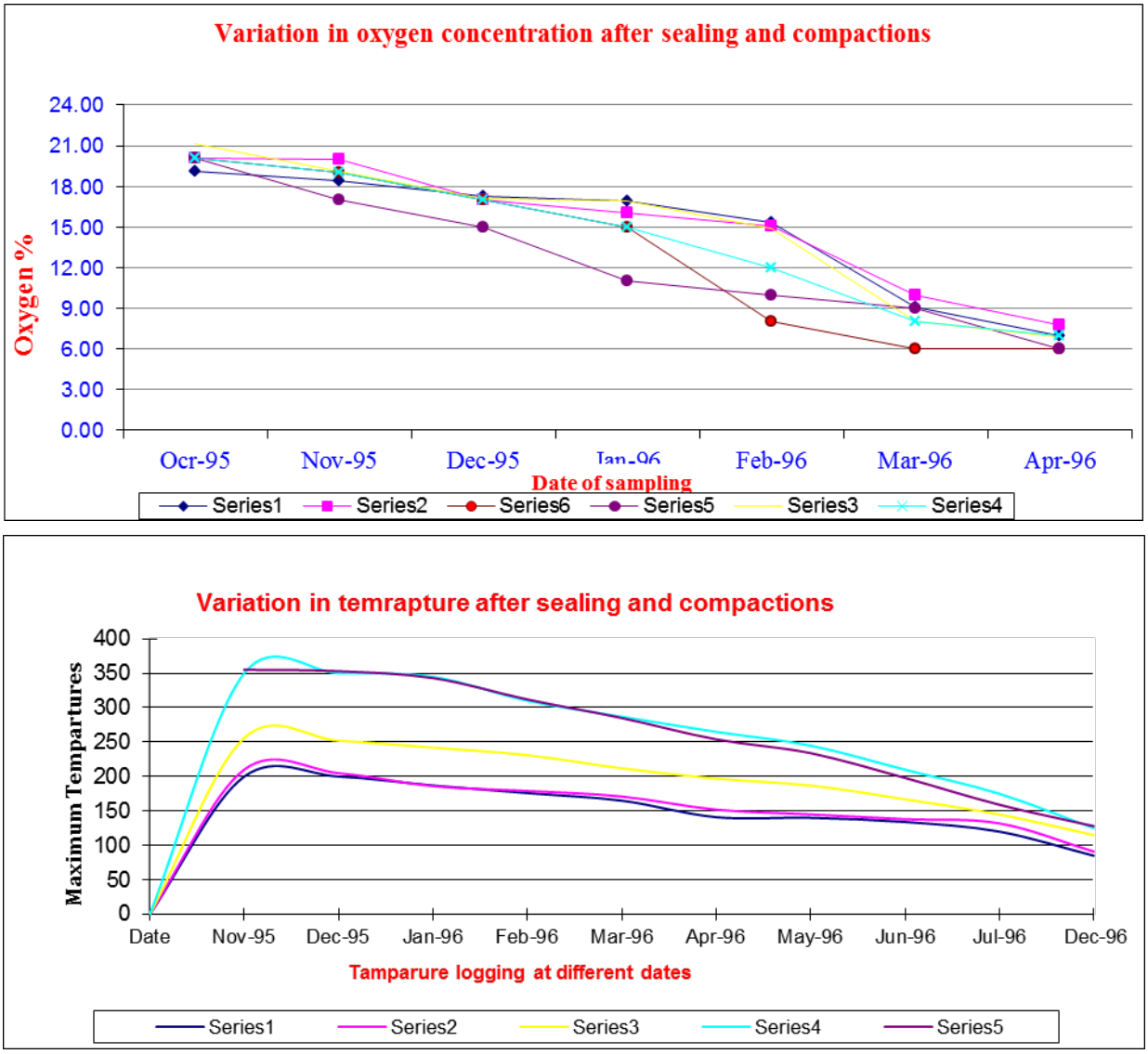

Figure 2. Above figures are showing the oxygen concentration and temperature variation after sealing the fire area and cooling through water ponds on surface.

5.4 Direct Dealing Of Fire With Water Mix Additives

In western quarry of Chasnalla Colliery (SAIL-ISP) most of the exposed coalfaces were under blazing fires. Examining the situation, e.g. location, depth, size and intensity of the fire; dealing of fire started primarily with-flame suppression and rapid cooling of hot strata.

Due to high heat capacity (4.2J/g0K) and latent heat of vaporization (2442J/g), water is most commonly used to deal the fires. Water expands 1700 times while it changes to vapor. This diluted the oxygen concentration and subsequently creates an oxygen exclusion barrier near the seat of fire; and smothering the fire.

Due to risk of water gas explosion water alone can't be recommend for flame suppression and dealing the glowing fires. Surface tension of water does not allow it to penetrate, in flaming fire, water droplets blow away before reaching the flaming zone. Additives mixed water significantly improved the effectiveness of fires fighting operations - by means of rapid cooling, retarding surface oxidations and minimizing the possibilities of re-ignition. Concentration

of solution varies from 0.01% to 0.1% according to intensity of fire. Spray volume discharged from a nozzle, spray angle and penetration distance is very much useful and determined by the formula-

$V = \frac{1}{3}\pi \{\tan\frac{\theta}{2}\}^2$

Where θ is the spray angle.

Table 1. Spray volume with spray angle and penetration distance.

Spray angle (o)	30^0	60^0	90^0
Spray volume (m3) (2 m of penetration)	0.3	1.39	4.18
Spray volume (m3) (3 m of penetration)	0.676	3.14	9.42

The spray volume with a spray angle of 90^o is approximately14 times larger than that with a spray angle of 30^o.

In theory, small droplets are more efficient in cooling and diluting the gases than large droplets, because of the larger total surface area available for evaporation and heat extraction. As shown below in table 2, when the droplet diameter is reduced from 1000 μm to 100 μm, the total surface area increases 10 times from 6 m^2 to 60 m^2 for 1 liter of water.

Table 2.Droplet size (μm), droplet number and surface area (m^2).

Droplet size (μm)	1000	100	10
Total number of droplet	1.91×10^6	1.91×10^9	1.91×10^{12}
Total surface area (m^2)	6	60	600

These analytical results are consistent with experimental results and more effective in cooling hot gases than traditional straight or narrow angle attack due to the fine droplets and wide spray angle. However, water fog technique is that excess steam may be generated as large amounts of fine droplets are discharged. This can reduce visibility and cause comfort problems to the firefighters [7].

Figure 3. A synoptic views of firefighting operations using different modus operandi in western quarry of Chasnalla Colliery.

ACKNOWLEDGEMENTS

Authors are thankful to mine authorities for assigning the project under which data has been developed. Opinions expressed in the article are of the authors not necessarily of theCSIR-CIMFR.

REFERENCES

1. Banerjee, S. C., 1985. Spontaneous Combustion of Coal Mine Fires; A.A. Balkema/Rotterdam.
2. Tripathi, D. D. and Sen, S. K. (1996); Prediction of fire status - A new approach to an old problem, Coal International, May, p 118
3. Stott, J. B. (1971): Ph.D. Thesis in the University of Canterbury, New Zealand.
4. Tripathi, D. D., Jayanthu, S. 1996. Numerical techniques to improve fire control measures during thick-seam mining. Journal of Mine Metals and Fuels, pp163-166.
5. Carslaw, H .S. and Jaeger J.C. (1959) Conduction of Heat in solids Oxford press P. 77
6. Tripathi, D. D. et.al. (1997); Rapid Cooling of strata heated by fires at South Tisra Fire Area of BCCL. CMRI Project Report, GAP-V/33.
7. Tripathi, D. D.;2011. Scientific investigation & advice for control of fire IN XIII/XIV (combined) seam in Western quarry of Chasnalla colliery, SAIL-ISP. Project no. CNP/2381/09-10.

Modeling of Turkey's CO_2 Emissions Using Economic and Demographic Variables

I. Karakurt, G. Aydin, S. Kaya
Karadeniz Technical University, Mining Engineering Department, Trabzon, Turkey

ABSTRACT: In this paper, regression analysis (RA) was applied for modeling the CO_2 emissions of Turkey. Real gross domestic product (GDP), total and urban populations and energy consumption were considered as economic and demographic variables. The developed model was tested using a test data set which were not utilized during building of the model. Additionally, the developed regression model was verified using various statistical approaches. The result of regression analysis was also used to determine the significant variables affecting the CO_2 emissions. Furthermore, the performance of derived model was measured for showing the accuracy levels in predicting the CO_2 emissions.

Keywords: CO_2 emission, economy, demography, regression analysis

1 INTRODUCTION

The world depends heavily on fossil fuels to meet its energy requirements. It seems that they will remain the dominant energy source for the next 30–50 years as well (Garg and Shukla, 2009; Panwar et al., 2011). However, fossil fuels are inflicting enormous impacts on the environment. The increasing use of fossil fuels causes a significant increase in greenhouse gases (GHGs), especially carbon dioxide (CO_2) emissions (Karakurt and Aydin, 2013). Among several GHGs, CO_2 has solely a rate of 74% in total anthropogenic GHG emissions and the rest follows CO_2 (Fig.1) (Aydin et al., 2010). Globally, 35094.4 million tons CO_2 were released to atmosphere in 2013. The six largest emitting countries and/or regions in the world are China (28%), United States (16%), European Union (11%), Indian (6.8%), Japan, (6.2%) and Russian Federation (5.1%) respectively.

Turkey is a rapidly growing country whose income level is moving towards that of the rest of the OECD area. This growing trend has been followed by a rapid growth of greenhouse gas (GHG) emissions, most notably carbon dioxide (CO_2) emissions. Turkey's total CO_2 emissions amounted to 328.8 million tones in 2013. That means, 0.9% of CO_2 emissions of world total comes from Turkey. Emissions grew by 53% compared to 2000 levels and by just over 130% compared to 1990 levels (BP, 2014). All energy consumption sectors (power, industrial, residential, and transportation) contribute to this increased CO_2 emissions. Although the country has a relatively low level of CO_2 emissions, rapid economic growth could significantly increase the emissions in the coming years. Hence, great efforts are required to deal with the adverse impact of the CO_2 emissions. Therefore, research on emissions should be conducted in adjusting related policies. Modeling and forecasting of CO_2 emissions are one of the best efforts to provide alerts, mitigation, adaptation, financial and sustainability policy options. Hence, this paper presents a modeling study based on the socio-economic and demographic variables of Turkey using regression technique.

2 REGRESSION ANALYSIS

Regression analysis (RA) is a branch of statistical methodology concerned with relating a response y to a set of independent, or predictor, variables $x_1, x_2, \ldots, x_k$. It aims at building a good model, a prediction

equation relating *y* to the independent variables (Gorucu and Gumrah, 2004).

2.1 Simple Linear RA

Simple linear RA builds models to explain the relationship between the dependent variable as a linear function of one independent variable. The general equation of the simple linear regression model is given below.

$$y = (\beta_0) + (\beta_1)x \quad (1)$$

where β_0 donates the regression line intercept, the y axis, and β_1 is the regression coefficient representing the slope of the regression line (Yerel and Ersen, 2013).

2.2 Multiple Linear RA

Multiple linear RA builds models for explaining the relations between the more than one independent variable and dependent variable. The mathematical form of the multiple linear regression is given by Eq. (2).

$$y = (\beta_0) + (\beta_1)x_1 + (\beta_2)x_2 + ... + (\beta_n)x_n \quad (2)$$

where *y* is the dependent variable, x_1; x_2;... x_n are the independent variables, *n* is the number of independent variables, β_0 is the intercept, and the regression coefficient of descriptors is β_n (Yerel and Ersen, 2013).

3 DATA AND METHODOLOGY

To build regression model, real gross domestic product (GDP), total and urban population (TP, UP) and energy consumption (EC) are considered as independent variables while CO_2 emissions (E) are considered as dependent variables. Both the independent and dependent variables have been collected from BP (British Petroleum) Statistical Review of World Energy as a period of 1965-2012 (BP, 2014). The data was divided into two groups. First group (between 1965-2006) was used for building the model and second group (between 2007-2012) was used for testing the model. The used data are presented graphically in Figure 2.

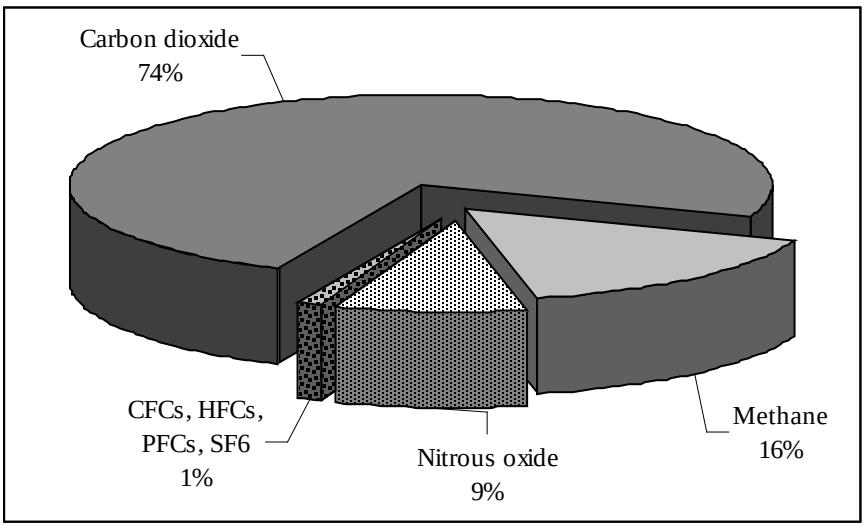

Figure 1. Anthropogenic GHG emissions (Aydin et al., 2010).

After preparation of the data belonging to the independent and dependent variables, the regression model was build. The model building was carried out using a statistical package program called SPSS 21. Following the building model, the confirmation and statistical significance of the estimated variables were done by considering the determination coefficient (R^2), F-and t-tests for both overall fit and individual variables respectively. The residual plots of the error are also studied to determine the appropriateness of the model.

4 MODELING RESULTS

The developed regression model for Turkey's CO_2 emissions is given in Eq.(4). As it is seen, the R^2 value for the developed model is 0.998 indicating a high degree of relationship between the UP, EC and CO_2 emissions. The coefficient of determination also indicates that 0.002% of the variation in the CO_2 emissions is due to all causes other than the predictors. From the weighs of coefficients, energy consumption (EC) was determined as the most significant variable affecting the CO_2 emissions.

$$E = (-0.2943) + (0.9515) * (\mathrm{UP}) + (2.2993) * (\mathrm{EC}) \quad (4)$$

where, E is the CO_2 emissions (Mtoe), UP is the urban population (million) and EC is the energy consumption (Mtoe).

4.1 Validation of the Developed Model

The statistical results of the developed model (Eq.4) is presented in Table 1. As seen, the tabulated F (3.13) is much smaller than the calculated F value. Therefore, it can be concluded that Eq. (4) is significant at the 95% confidence level. The t-test results for the coefficients are higher than the tabulated t-values (1.729). That is, the coefficients in Eq. (4) are significant in their use in the final model. The plots of the residuals against the predicted CO_2 emissions for the model case are also shown in Fig.3(a). The figure indicates that the residuals appear to be randomly scattered about the line, confirming the accuracy of the model.

4.2 Performance Measure

To measure the model performance, there are several methods in the literature such as mean absolute percentage error (MAPE), root mean scored error (RMSE) and mean absolute error (MAE). The accuracy of prediction is evaluated based on the estimation of error, thus the smaller the value of MAPE, RMSE and MAE, the better the prediction is. Among them, the criterion of MAPE whose equation given below (Eq.3) is the decisive factor since it is expressed in easy generic percentage term (Aydin et al., 2014). Table 2 shows the criteria of MAPE for model evaluation.

$$MAPE = \frac{1}{n}\sum_{i=1}^{n}\left|\frac{e_i}{Y_i}\right| * 100 \quad (3)$$

where n is the total number of measurements, e_i is the differences between actual and predicted values and y_i is the actual values.

Table 2. MAPE for model evaluation (Lewis, 1982).

MAPE (%)	Evaluation
>50	Weak and inaccurate prediction
20-50	Reasonable prediction
10-20	Good prediction
<10	Highly accurate prediction

The MAPE value was determined as 2.39% for the developed model. This result has shown that the derived model can give adequate prediction for Turkey's CO_2 emissions. The model can be also classified as a high accuracy prediction model because its MAPE is in the ranges of 10% (see Table 2). Moreover, it can be deduced from Fig. 3(b) that the predicted CO_2 emissions are close to the actual CO_2 emissions.

5 CONCLUSIONS

Recently, anthropogenic GHG emissions and global warming have become the most important research topics in the fields of both science and politics. The existing studies indicated that CO_2 has solely a rate of 74% in total anthropogenic GHG emissions and the rest follows CO_2. Hence, modeling and predicting the CO_2 emissions are of critical importance in adjusting policies in countries all over the world. In this paper, Turkey's CO_2 emissions was modeled by considering economic and demographic variables using regression technique. The modeling results showed that the developed regression model can successfully be used as a tool for predicting the CO_2 emissions of Turkey. Additionally,

energy consumption was determined as the most significant variable affecting the CO_2 emissions. As the modeling approaches are useful for policy makers and scientists to examine the future scenarios on the CO_2 emissions, different modeling techniques should be applied and the results should be compared with RA in order to select the best ones in future studies.

Table 1. Statistical results of the developed regression model.

Independent Variables	**Coefficient**	**Standard error**	**Standard error of estimate**	**t-value**	**F-value**
Constant	-0.2943	1.8010	2.4601	-0.1633	15704.46
UP (Million)	0.9515	0.1944		4.8932	
EC (Mtoe)	2.2993	0.0894		25.6932	
Tabulated t-value	1.729	**Tabulated F-value**	3.13	**R^2**	0.998

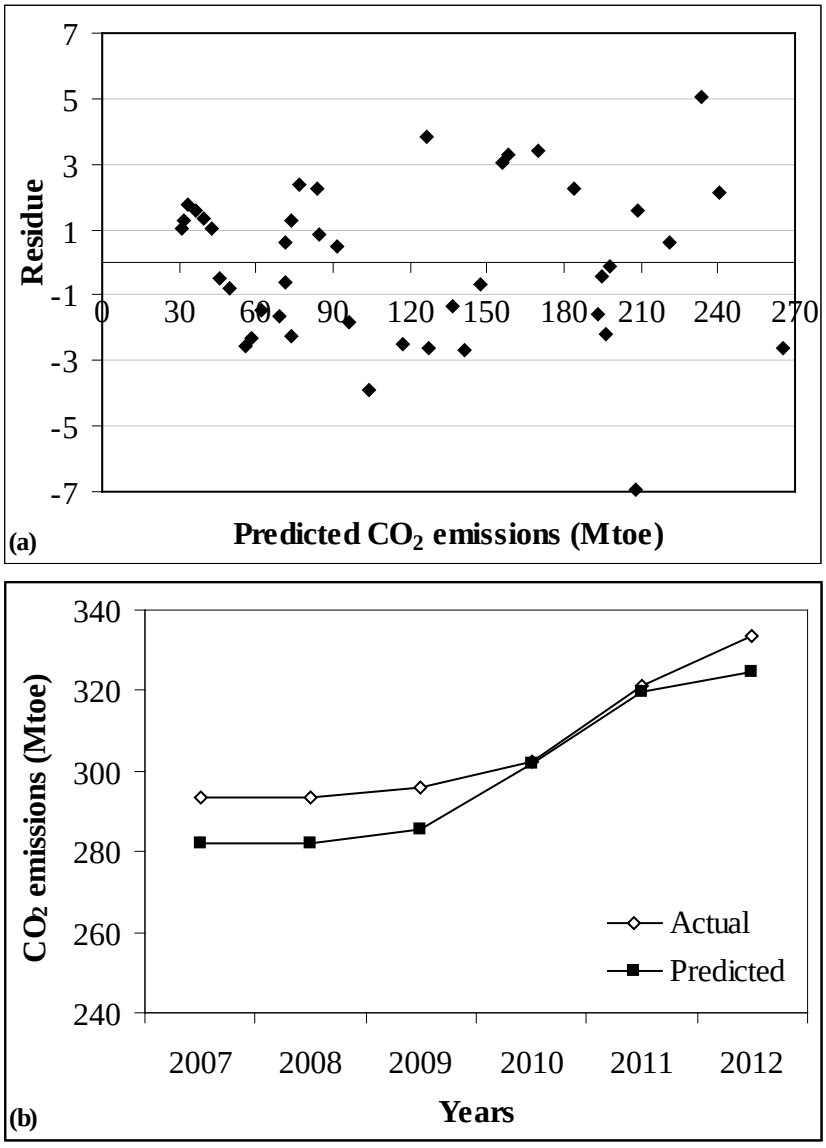

Figure3. **(a)** Residues vs predicted CO_2 emissions, **(b)** Actual vs predicted CO_2 emissions

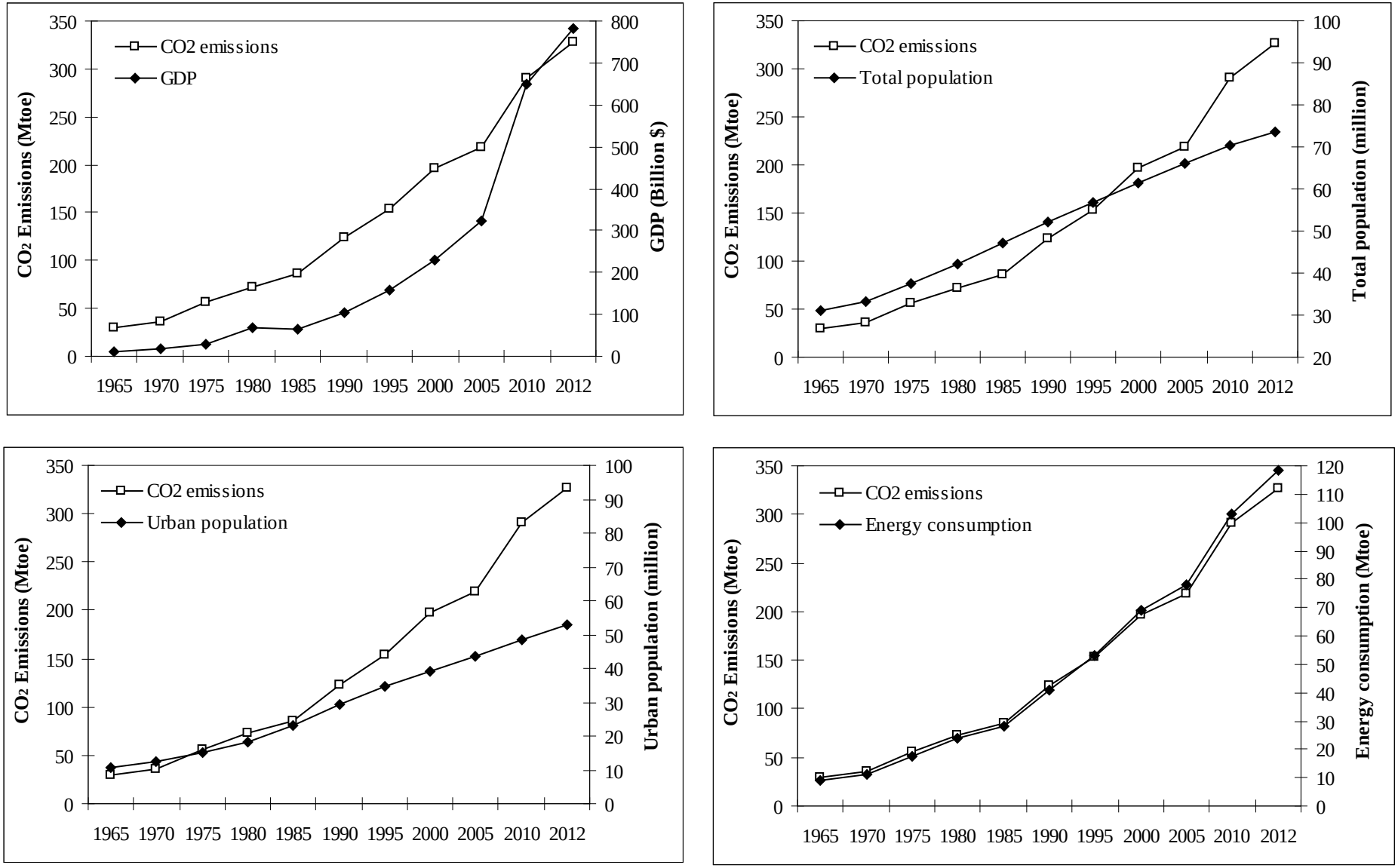

Figure 2. Relations between CO_2 emission and socio-economic and demographic variables in Turkey (Data source: BP, 2014).

REFERENCES

Aydin, G., Karakurt, I., Aydiner, K., 2010. Evaluation of geologic storage options of CO_2 : Applicability, cost, storage capacity and safety. Energy Policy 38(9): 5072-5080.

Aydin, G., Karakurt, I., Hamzacebi, C. 2014. Artificial neural network and regression models for performance prediction of abrasive waterjet in rock cutting. The International Journal of Advanced Manufacturing Technology 75(9-12): 1321–1330.

BP., 2014. Statistical review of World energy full report by British Petroleum, available at http://www.bp.com/en/global/corporate/about-bp/energy-economics/statistical-review-of-world-energy.html., accessed on 1 November 2014.

Garg, A., Shukla, R.P., 2009. Coal and energy security for India: Role of carbon dioxide (CO_2) capture and storage (CCS). Energy 34, 1032-1041.

Gorucu, F.B., Gumrah, F., 2004. Evaluation and forecasting of gas consumption by statistical analysis. Energy Sources 26: 267–276.

Karakurt, I., Aydin, G., 2013. Fossil fuel use and related carbon dioxide emissions: A global perspective. 23rd International Mining Congress and Exhibition of Turkey, pp. 2137-2141, Antalya-Turkey.

Lewis, C.D., 1982. International and business forecasting methods. London, Butterworths.

Panwar, L.N., Kaushik, C.S., Kothari, S., 2011. Role of renewable energy sources in environmental protection: A review. Renewable and Sustainable Energy Reviews 15, 1513-1524.

Yerel, S., Ersen, T., 2013. Prediction of the calorific value of coal deposit using linear regression analysis. Energy Sources, Part A: Recovery, Utilization, and Environmental Effects 35: 976--980.

Opportunities for Environmental Impact Assessment of the Geothermal Area Beiuş

R. Călburean
Faculty of Economics and Business Administration, Babeş-Bolyai University, 58-60 Teodor Mihali Str., RO-400591, Cluj-Napoca, Romania

V. A. Codrea, O. Barbu
Faculty of Biology and Geology, Department of Geology, Babeş-Bolyai University, 1, Kogălniceanu Str., RO-400084, Cluj-Napoca, Romania

ABSTRACT The specific objectives of this paper are to formulate answers to the following questions: a. which is the accurate possibility of assessing environmental impact for geothermal waters, what are its stages? b. can we develop the types of impact assessment? c. what are the prospects for our research, what are the limits of research in this case? Our subject is inciting through the timeliness and importance in the present context of a globalized economic environment, further less the challenge for the European and national authorities to build a proper correlation between the environmental policy and a renewable resource of energy. We chose the geothermal area Beiuş (north-western Romania), while being a leading example for investments in geothermal heating system with available geothermal primary source through its main characteristic: it stands for the benefit of citizens by way of keeping a clean environment.

Keywords: Environmental impact assessment, Beiuş, Geothermal heating system

1 INTRODUCTION

Europe 2020 Strategy, launched by EU leaders in 2010, highlights the need to modernise the economy, to focus on economic growth and employment by addressing the challenges of globalisation and demographic changes and to support economic, social and environmental objectives.

Our subject is related to the present context of a globalized economic environment through the reach of the European and national authorities to build a proper correlation between the environmental policy and a renewable resource of energy (Speth 2002, 2003).

We performed the Life Cycle Assessment (abbreviated, LCA) of geothermal water by following steps such as: purpose and objectives, life cycle inventory, life cycle impact assessment and interpretation of results of life cycle assessment. In this case, the boundary research is the lack of defining and analysing the impact categories, because they are the subject of a long and thorough study and the interpretation of the data is performed by dedicated software (Preiss *et al.*, 2008).

2 EUROPE 2020

Europe 2020 Strategy, launched by EU leaders in 2010, highlights the need to modernise the economy, to focus on economic growth and employment by addressing the challenges of globalisation and demographic changes and to support economic, social and environmental objectives. The Strategy aims to address the shortcomings of the European growth model and to create the conditions for three mutually reinforcing priorities smart growth (developing an economy based on knowledge and innovation), sustainable growth (promoting a more resource efficient, greener and more competitive economy) and inclusive growth (fostering a high-

employment economy delivering social and territorial cohesion).

A number of five headline targets are interrelated and critical to the overall success for the European Union by 2020. These cover (EC 2005, EC JRC 2010):

– employment: 75 % of the population 20-64 year-olds to be employed;
– research and development: 3% of the EU's GDP to be invested in R&D;
– climate/energy: The "20/20/20" climate/energy targets should be met (including an increase to 30% of emissions reduction if the conditions are right) – greenhouse gas emissions 20% (or even 30%, if the conditions are right) lower than 1990, 20% of energy from renewables and 20% increase in energy efficiency;
– education: The share of early school leavers should be below 10% and at least 40% of the 30-34–year-olds should have a third level education;
– social inclusion and poverty reduction: at least 20 million fewer people in or at risk of poverty and social exclusion.

The targets are illustrative for the three priorities of smart, sustainable and inclusive growth, but they are not far-reaching: a comprehensive range of actions at national, international and EU levels will be necessary to reinforce them.

Therefore, seven flagship initiatives were put forward to catalyse progress under each priority theme (EC JRC 2010):

– Smart growth: "Innovation Union", "Youth on the move" and "A digital agenda for Europe";
– Sustainable growth: "Resource efficient Europe" (to help decouple economic growth from the use of resources, support the shift towards a low carbon economy, increase the use of renewable energy sources, modernise our transport sector and promote energy efficiency) and "An industrial policy for the globalisation era";
– Inclusive growth: "An agenda for new skills and jobs" and "European platform against poverty".

Thus, we focused one the most appropriate way of evaluating the impact on the environment, as well as on the economy, of a natural resource, by giving answers to the research questions listed above. We came to the consensus of doing that through the life cycle assessment methodology.

Therefore, we focused on the geothermal resource situated in the north-western side of Romania, Beiuş area.

3 GEOLOGICAL SETTING

From geological viewpoint, this geothermal area is an easternmost part of the regional thermal anomaly located under the Pannonian basin and the Neogene sedimentary basins splitting the western margin of the Apuseni Mountains. The geothermal water is collected into the sole of the Neogene Beiuş basin, with Triassic dolomites and limestone belonging to the Inner Dacides (Codru Nappe System; Bleahu *et al.*, 1981, 1994). Some drillings crossed these rocks, allowing the recovery and exploitation of the geothermal water in Beiuş town (Codrea & Călburean, 2013).

Apart the older three hypotheses concerning the evolution of the Pannonian Basin exposed by Meissner & Stegena (1988) - i.e.: gabbro-eclogite phase transition, lithospheric stretching and mantle diapirism -, another structural pattern belongs to Ren *et al.* (2012) with a molten astenosphere sandwiched between the crust and deeper former sunken cold slabs.

4 LIFE CYCLE ASSESSMENT

The use of the LCA technique goes back to the 1960s (Curran 1996, Owens 1997, Ekvall *et al.* 2005). The Society of Environmental Toxicology and Chemistry (SETAC) was the first international body to work on the development of LCA methodology, with its initial participation starting in 1989 (Guinée, 2002). SETAC put out a science-based platform for development of LCA, and they formalized the LCA methodology by outlining the terms to describe LCA as well as laying down the initial framework (Curran, 1996).

The development of the code of practice by SETAC (Consoli *et al.*, 1993) was an important step towards standardization of LCA as the code acted as the forerunner to the activities of the International Organization for Standardization (Guinée, 2002). The International Organization for Standardization (ISO) started working on standards relating to LCA in 1994. The first of the ISO 14040 series of standards (Environmental management – Life Cycle Assessment), which laid down the procedure for performing LCA, was first released in 1997 (Baumann & Tillman, 2004).

The United Nations Environmental Programme (UNEP) is another important international player in LCA, having taken on the role of stimulating global use of LCA (Guinée, 2002). Their work mainly centres on encouraging the application of LCA, particularly in developing nations. In 1996 the UNEP published a user-friendly guide to LCA, as part of their effort to encourage wide application of LCA (Guinée, 2002).

As shown in Fig. 1 (after ISO 14040 2006, modified), a LCA is carried out in four distinct phases (SETAC 1997):

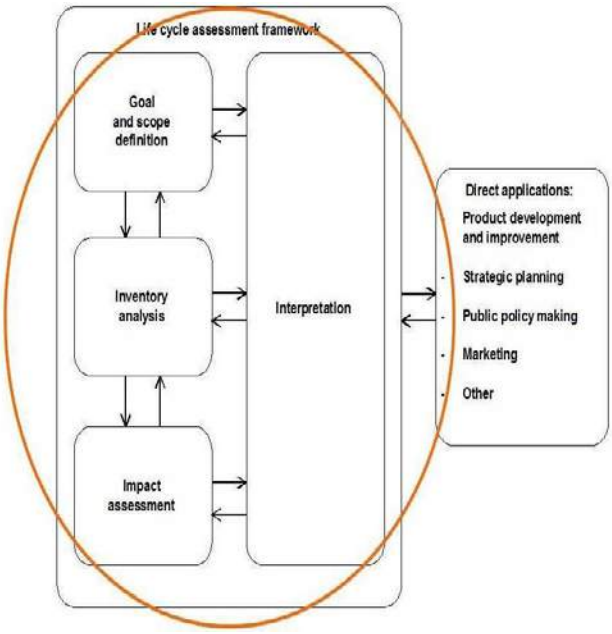

– Step 1: Goal definition and scoping. Identify the LCA's purpose, the products of the study, and determine the boundaries. (what is and is not included in the study);
– Step 2: Life-cycle inventory. Quantify the energy and raw material inputs and environmental releases associated with each life cycle phase;
– Step 3: Impact analysis. Assess the impacts on human health and the environment;
– Step 4: Report results. Evaluate opportunities to reduce energy, material inputs, or environmental impacts at each stage of the product life-cycle.

In the context of the environmental impact of geothermal waters, we have chosen the most appropriate instrument in order to make an accurate analysis that takes into account mainly the environmental component. Furthermore, we shall discuss briefly the LCA methodology applied to the geothermal waters in Beiuş area. Each of the four distinct phases can easily be the topic of other papers while having a comprehensive character.

4.1 Purpose and Objectives

We studied in Beiuş the stages of the economic product geothermal waters regarding its life cycle, and we listed them as follows: the extraction of geothermal water out of the exploitation well, the transport of geothermal water to the heating unit, the production of heat (thermal energy is distributed to final consumers) and the transportation of the waste geothermal to the discharge system: sewerage and injection well. Once the water exits the heating plant during the life cycle, the geothermal water is considered a residue (Mangena & Brent 2006, Reich 2005). Therefore, we speak of a "cradle-to-grave" assessment: the product is recovered after the exhaustion of its useful life. It is recovered in both cases: after extracting thermal energy it is recovered and transported to discharge into surface emissaries or to the injection well where it enters its natural cycle.

Geothermal water is in Beiuş area is capitalized through two ways: in form of cubic meters of geothermal water, for consumers who own heating units, and in form of thermal energy, the local investor has its own heating plants for preparing heat,

which is for heating and hot water consumption.

In Beiuș, two wells serve for the exploitation of geothermal waters (3001H, 3003H) while the other one (3004H) serves to the re-injection of the used thermal water. Until now, the outputs are around 40 l/s, while the temperatures recorded at the well heads are 70 0C at well 3003H and 84 0C at 3001H (Codrea & Călburean, 2013). The production level of the year 2013 was 828.323 m^3: a volume of 417.736 m^3 has been extracted from 3001H and a volume of 410.587 m^3 out of 3003H (Tab. 1).

4.2 LCI – Life Cycle Inventory

During a year time, 828.323 m^3 of geothermal water were extracted out of the Beiuş perimeter. From 436.226 m^3, a quantity of 15.081,53 Gcal were prepared as thermal energy, while the difference of 392.097 m^3 was sold as m^3 (Tab. 1).

Table 1. Total extracted geothermal water in Beiuş, year 2013

	Thermal energy	m^3 equivalent for thermal energy preparation	Capitalization under form of m^3	Total used geothermal water
3001H well	7125.1	171002	246734	417736
3003H well	7956.73	265224	145363	410587
	15081.83	436226	392097	828323

In this aspect, a volume of 329.312 m^3 was discharged in the sewerage. The difference of 106.915 m^3 between the extracted geothermal water (436.226 m^3) and the one discharged in the sewerage (329.312 m^3) was injected in 3004H well (Tab. 2).

Table 2. Volume of discharged geothermal water Beiuş, year 2013

Well	m^3 discharged
3001H	64087.03
3003H	265224.47
Total Beiuş	329311.5

4.3 LCIA – Life Cycle Impact Assessment

Given the context of the injection of all the waste geothermal water, we wouldn't be speaking of an impact on the environment, while the geothermal water would have been circulating in a closed system – from the production to the injection well.

Under the assumption that can be practiced in Beiuş, namely partial injection and discharge of geothermal water into the sewerage, environmental impact in form of thermal pollution may appear only if problems occurred at the heating plant. We cannot speak of pollution from chemical point of view, given that studies showed that the mineralization of geothermal water is lower than that of surface water that supplies drinking water for the inhabitants of Beiuş.

4.4 LCIA – Life Cycle Impact Assessment

Our studies showed that discharge temperatures didn't exceed 35 °C. The national environmental law stipulates a temperature above 40 °C for waste geothermal water being transformed into a pollutant while entering the surface emissaries.

Although the ideal solutions would be the injection into the geothermal deposit, the thermal conditions don't take place, as: there isn't a collecting pipe for waste geothermal water that collects it from all consumers (only the geothermal water used by the local investor in thermal energy production modules is collected), and the responsiveness of the injection well is below the flow extracted by the two production wells, which gives her a limited character.

5 CONCLUSIONS

While being the European's Union ten-year strategy, Europe 2020 is more than just overcoming the crises from which the economies are recovering; it is also about creating the conditions of a smart, sustainable and inclusive growth.

That is the case of a globalized economic environment through the establishment of a proper correlation between the

environmental policy and a renewable resource of energy. Geothermal energy stands for a leading example in this matter – it stands for the benefit of citizens by way of keeping a clean environment.

Therefore, we performed the life cycle assessment (LCA) of geothermal water, a technique to assess environmental impacts associated with all the stages of a product's life cycle. LCA compiles an inventory of relevant energy and material inputs and environmental releases, evaluates the potential impacts associated with identified inputs and releases and brings us to the interpretation of the proper results.

Given the context of the geothermal area Beiuş, LCA was performed by following steps such as: purpose and objectives, life cycle inventory, life cycle impact assessment and interpretation of results of life cycle assessment.

REFERENCES

Baumann, H., Tillman, A., 2004, *The Hitch Hiker's Guide to LCA: An orientation in Life Cycle Assessment Methodology and Application*, Student litteratur, Lund, 543 pp.

Bleahu, M., Lupu, M., Patrulius, D., Bordea, S., Ștefan, A., Panin, S., 1981. The Structure of the Apuseni Mountains. *Guide to Excursion B3. Institute of Geology and Geophysics*, Geological Institute of Romania, Bucharest, 103 pp.

Bleahu M., Haas J., Kovács S., Péró Cs., Mantea Gh., Bordea S., Panin Ş., Bérczi-Makk A., Ştefănescu M., Konrád G., Nagy E., Rálisch-Felgenhauer R., Sikić K., Török Á., 1994. Triassic facies types, evolution and paleogeographic relations of the Tisza Megaunit. *Acta Geologica Hungarica*, 37/3, 4, pp. 187-234

Codrea, V., Călburean, R., 2013, Geothermal Energy in Western Apuseni Mountains (Romania) for Economic and Sustainable Purposes. *Proceedings of 23rd International Mining Congress and Exhibition of Turkey*, Antalya, pp. 1707-1712.

Consoli, F., Allen, D., Boustead, I., Fava, J., Franklin, W., Jensen, A.A., de Oude, N., Parrish, R., Perriman, R., Postlethwaite, D., Quay, B., Sie´guin, J., Vigon, B., 1993, *Guidelines for Life Cycle Assessment. A Code of Practice*, SETAC Press, Pensacola, 79 pp.

Curran, M. A., 1996, The History of LCA, *Environmental Lifecycle Assessment*, McGraw-Hill, New York, 1-9 pp.

EC JRC, 2010, *Our Thinking Life Cycle Thinking*, European Commission Join Research Center - Institute for Environment and Sustainability, Institute for Environment and Sustainability website at http://lct.jrc.ec.europa.eu/index_jrc

EC, 2005, *ExternE - Externalities of Energy – Methodology 2005 Update*, Office for Official Publications of the European Communities, Luxenbourg, 270 pp.

Ekvall, T., Tillman, A.-M., Molander, S., 2005, Normative Ethics and Methodology for Life Cycle Assessment, *Journal of Cleaner Production*, 13, pp. 1225-1234

Guinée, J.B., 2002, *Handbook on Life Cycle Assessment: Operational Guide to ISO Standards*, Kluwer Academic Publishers, Dordrecht, 692 pp.

ISO 14040, 2006, *Environmental management – Life cycle assessment – Principles and framework*, European Committee for Standardisation, Brussels, 20 pp.

Mangena, S.J., Brent, A.C., 2006, Application of a Life Cycle Impact Assessment framework to evaluate and compare environmental performances with economic values of supplied coal products, *Journal of Cleaner Production*, 14, pp. 1071-1084

Meissner R., Stegena, L., 1988. *Lithosphere and Evolution of the Pannonian Basin*. In: AAPG Memoir 45, The Pannonian Basin, A Study In Basin Evolution in: L.H. Royden, F. Horváth (eds.), pp. 147-152

Owens, J. W., 1997, Life-Cycle Assessment in Relation to Risk Assessment: An Evolving Perspective. *Risk Analysis an International Journal*, 17, 3, pp. 359-365

Preiss, P., Friedrich, R., Klotz, V., 2008, Report on the procedure and data to generate averaged/aggregated data, *NEEDS Project: deliverable No. 1.1 - RS 3a IER*, Institute of Studies for the Integration of Systems University of Stuttgart, 95 pp. + annex 57 pp.

Reich, M.C., 2005, Economic Assessment of Municipal Waste Management Systems – Case Studies Using a Combination of Life Cycle Assessment (LCA) and Life Cycle Costing (LCC), *Journal of Cleaner Production*, 13, pp. 253–263

Ren, Y., Stuart, G.W., Houseman G.A., Dando, B., Ionescu, C., Hegedus, E., Radovanovic, S., Shen, Y., South Carpathian Project Working Group, 2012, Upper mantle structures beneath the Carpathian–Pannonian region: Implications for the geodynamics of continental collision. *Earth and Planetary Science Letters*, 349-350, pp. 139-152

SETAC, 1997, *Ecological Risk Assessment: SETACTIP Technical Issue Paper*, Society of Environmental Toxicology and Chemistry website at http://www.setac.org/node/99

Speth, J.G., 2002, The Global Environmental Agenda: Origins and Prospects in Global Environmental Governance Options & Opportunities, in: Esty, D.C , Ivanova, M.H. (eds.), *Global Environmental Governance: Options and Opportunities*, Island Press, Yale School of Forestry and Environmental Studies, 20 pp.

Speth, J. G., 2003, Two Perspectives on Globalization and the Environment, in: Speth J.G. (ed.) *Worlds Apart: Globalization and the Environment*, Island Press, Yale, pp. 1-18

Overview of Zone Monitoring of Flotation Tailing Dump "Veliki Krivelj",Serbia

M. Mikić, M. Ljubojev, D. Kržanović, I. Jovanović, D. Urošević
Institute of Mining and Metallurgy Bor, Zeleni Bulevar 35 19210 Bor, Serbia

ABSTRACT The flotation tailing dump Veliki Krivelj,Serbia, is the tailing dump of valley type and occupies the area in a former river bed of the Krivelj River. Flotation tailing is divided into the first field (the old tailings), field 2 (new tailings), which is located downstream of the field 1 and field 3. The concrete collector, total length 2075 m, was built in the Field 2 to remove the Krivelj River outside the boundaries of the tailing dump.

Overview of zone monitoring is presetned in this paper which includes monitoring period of 12 months, between january 2013 till january 2014. Monitoring covered water quality and air pollution at the site of flotation tailings „Veliki Krivelj“.

Keywords: Monitoring, collector of the Krivelj river, flotation tailing dump, Veliki Krivelj

1 INTRODUCTION

Near the open pit Veliki Krivelj, near Bor,in Serbia, is the Flotation tailing dump Veliki Krivelj, which has been in operation since the beginning of exploitation at the open pit. Flotation tailing dump Veliki Krivelj is a tailing dump of a valley type and occupies space in the former bed of the Krivelj River (Miomir Mikić,et.al., 2011). Downstream of the tailing dump is the village Oštrelj and upstream the belt conveyor system to waste transport from the open pit Veliki Kriveljs to the Old open pit in Bor and open pit Veliki Krivelj (Daniel Kržanović,et.al., 2011).

Since the beginning of its work in 1982 until 1989, the Flotation plant Veliki Krivelj has dumped tailings in the old tailing dump - Field 1. Field 1 is formed by closing the valley of the Krivelj River by two dividing sand dams, an upstream dam 1 and downstream dam 2. For water evacuation of the Krivelj River, a tunnel was built through the rock massif with the route from the left bank of the original watercourse. The tunnel has diameter of 3 m, and its length is 1414 m.

In 1990, the Flotation tailing dump Veliki Krivelj was extended downstream taking an additional space in the bed of the Krivelj River. Thus was formed a new tailing dump, which was called the Field 2. Construction of only one dam – Dam 3 was enough for contouring the new tailing dump. For drainage the Krivelj River water, a collector, diameter of 3 m and 2075 m in length, which is a continuation of the existing tunnel, was constructed at the bottom of the Krivelj River.

Considering that the current state of the collector is threatened, as it is shown in this work, and that overflow effects of the dam and collector destabilization are the ecological disasters of great proportions, a constant monitoring is necessary for the Flotation tailing dump dams and collector (Miomir Mikić,et.al., 2012).

The importance of such monitoring is enormous, both for the local population of the Bor municipality and population of neighboring countries in the Danube Basin, in which the Krivelj River flows (Miomir Mikić,et.al., 2012).

2 STATE OF THE EXISTING COLLECTOR

Program of monitoring the existing collector includes the monitoring of collector state by visual observation and measurements along the entire route of the collector. Visual observation monitors any changes on

collector. Measuring monitors the temperature, flow rate of air, oxygen amount and concrete brand. Monitoring program performed between January 2013 and January 2014.

2.1 Auscultation of the collector chainage

The complete collector is divided into chainages, which were repaired depending on the rehabilitation phase: with the phase of restoration: a stable outlet of the collector from chainage 0+0.00 to the chainage 0+200, rehabilitated part of the collector from chainage 0+200 to the chainage 0+903, from chainage 0+903 to the chainage 1+457 is the collector zone in which the first phase of rehabilitation was carried out by chainages 1+012 to 1+097 and 1+160 to 1+172, and chainage from 1+320 to 1+457, and the other parts to 2+026 is a zone which requires rehabilitation.

The starting chainage of the Veliki Krivelj collector is below the dam Veliki Krivelj 3A, where the zero chainage is defined, Figure 1.

Figure 1. Start of the collector route below the Flotation dam 3A and Flotation tailing dump of the Field 2

Damages were observed along the entire route of collector. These damages are manifested in the form of: breaking up of concrete to the reinforcement and large cracks, Figure 2, concrete cracks in larger number of places, where the aggressive flotation water comes out under pressure.

Figure 2. The appearance of concrete damages to the reinforcement in the side part of calotte

Figure 2b, chemism that occurs as the effect of aggressive flotation water and concrete.

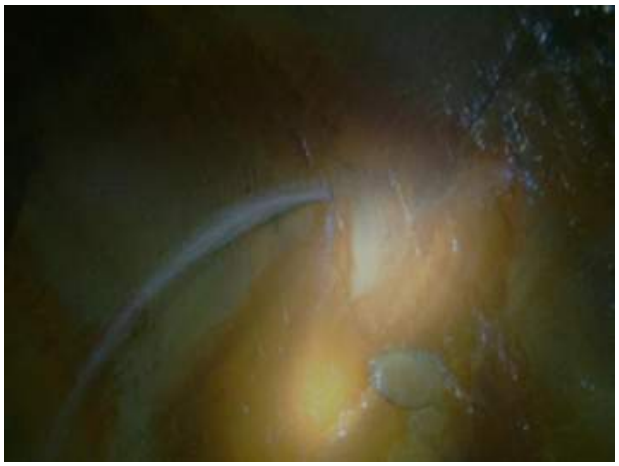

Figure 3. A set of cracks on the left side of campade through which water comes out under pressure

Figure 4 shows large number of cracks through which, in addition to the water outflow under pressure, the chemism of this water occurs that sprays onto concrete.

According to the visual observation of collector concrete, there are large number of aggressive water penetrations from the Flotation tailings, as well as chemism of aggressive water and concrete. Based on the measured concrete brand by sclerometre, it can be concluded that the concrete construction of collector is stable and secure in terms of functionality.

Figure 4. Chemism of concrete and aggressive water

Winter period was characterized by high rainfall. This has affected the level of water in the collector is high. Due to this, all measuring and recording the collector in this period was difficult.

These weather conditions have caused a significant drop in air temperature in the collector (Table 1).

Based on recordings and measurements observed a significant increase in the level of water and also the Krivelj 's water clearing appear despite turbulent motion.

State of the atmosphere in the observed part of the collector is satisfactory, there is the toxic gases that would have a negative impact on human health.

Due to the rapid melting of snow in the spring there was a massive influx of water at the entrance portal. This situation has caused damage in the form of pulling and major damage to metal cladding panels.

Analyzing the results, we can see that there has been no significant damage other than loss calotte tin lining. Significant damage to the concrete does not exist, and therefore the concrete structure is stable and safe in terms of functionality.

Table 1. The measureed values on the collector in the observed period

Year	Month	Flow rate of air, m/s	Oxygen amount O_2 %	Temperature C	Concrete brand MB Mpa
2013	January february march	*1,4*	*21*	*-0,025*	*30/35*
	april may	1,16	20,5	17	30
	june July August	1,78	21,77	16,3	30
	September October November December	-	-	-	-

3 MONITORING PROGRAM OF THE QUALITY OF WATER AND AIR

Monitoring program of the quality of water and air is carried out for twelve months from January 2013 to January 2014.

3.1 Program for Monitoring Water Quality

The water quality monitoring program includes weekly and monthly monitoring of groundwater and surface water. Monitoring of surface water quality was performed at 8 measuring points, as follows: Waters of Saraka stream (MP[1] * -1), Krivelj river before flows into the Saraka stream (MP-2), Krivelj river after empties into Saraka stream (MP-3), Bor river below the dam 1 (before entering the collector) (MP-4), Krivelj river below the dam 3 of flotation tailings Veliki Krivelj (MP-5), Bor River before joining the Krivelj river (MP-6), Krivelj river before flows into the Bor river (MP-7), the waters after the mergering of Bor river and Krivelj river and mine waters (MP-8).

Measuring the concentration of metals in the water was used standard SRPS EN ISO 11885.

[1] Measurung point

3.1.1 The results of water quality monitoring

Results of monitoring water quality are presented in Table 2-4.

Table 2. Results of monitoring water quality for period january-march 2013

Mesauring places	Parameters			
	Cu	**Cd**	**Fe**	sus. solids
MP1	18,42	<0,020	3,6	142,3
MP2	0,35	<0,020	1,48	426,3
MP3	0,88	<0,020	1,6	318,6
MP4	3,9	<0,020	10,4	63,3
MP5	1,49	<0,020	3,8	268,0
MP6	27,30	<0,020	40,1	256,0
MP7	0,77	<0,020	0,5	351,7
MP8	5,15	<0,020	3,6	330,0

Table 3. Results of monitoring water quality for period april-august 2013

Mesauring places	Parameters			
	Cu	**Cd**	**Fe**	sus. solids
MP1	2,59	<0,020	0,06	123,5
MP2	0,28	<0,020	0,12	29,0
MP3	0,47	<0,020	0,04	52,5
MP4	1,29	<0,020	0,15	63,5
MP5	3,59	<0,020	0,03	141
MP6	7,08	<0,020	3,48	428
MP7	8,73	<0,020	2,60	148,5
MP8	8,90	<0,020	1,88	233,5

Table 4. Results of monitoring water quality for period september 2013-january 2014

Mesauring places	Parameters			
	Cu	**Cd**	**Fe**	sus. solids
MP1	152,1	0,022	5,2	357,0
MP2	0,12	<0,02	0,28	802,0
MP3	17,4	<0,02	0,37	674,0
MP4	0,022	<0,02	0,14	12,0
MP5	20,8	<0,02	0,30	250,0
MP6	24,1	0,13	3,2	329,0
MP7	15,2	<0,02	1,2	224,0
MP8	19,4	0,091	3,6	284,0

The quality of surface water at eight mesurng points, for analysis, chemical parameters were taken – the pollutants - heavy metals.

Analasys of quality water is compered acording the new regulations of Repubic Serbia which defines the limit values for substances, levels of emissions to surface water quality assessment annually.

Acordinglly, increased content of copper and iron is characteristic for almost all the water at this location, and ranges up to 152,1 mg / L for copper and up to 5,2 mg / L of iron.

3.2 Program for Monitoring Air Quality

Air quality monitoring program includes daily air temperature, humidity, precipitation, atmospheric pressure, wind speed. Monitoring of air quality (particulate matter) is performed on six measuring points: Above Saraka landfills, above field 2 of flotation tailings Veliki Krivelj, abowe the dam 3 (village Ostrelj), Below the dam 3 (Manastirište), LC Sloga and village Slatina.

3.2.1 The results of air quality monitoring

During summer, the average monthly temperature values have ranged from 11,6 °C to 26,5 °C. The values of relative humidity were in the range of 35% to 80%. Atmospheric pressure ranged from 964,2 to 982,2 mbar. The total amount of precipitation was on average about 19 mm / m^2. The prevailing wind direction was from the WNW. Mean wind speed ranged from 0 m/s to 2,9 m/s.

In the winter, average monthly temperature values have ranged from -4.3 °C to 19.5 °C. The values of relative humidity were in the range of 34% to 100%. Atmospheric pressure ranged from 949,7 to 990,8 mbar. The total amount of precipitation was on average about 20 mm/m^2. The prevailing wind direction was from the WNW. Mean wind speed ranged from 0 m / s to 2,6 m/s.

Period- winter

Particulate matter

liquid phase

The average monthly pH value is constant and ranged from 3,8 to 7,1.

Mean values of sulphate ranged from 0,3 mg/m^2/d to 13,9 mg/m^2/d.

Mean values of soluble substances ranged from 1,3 mg/m^2/d to 112 mg/m^2/d.

Solid phase

Mean monthly values of insoluble matter ranged from 8,3 mg/m^2/d to 158 mg/m^2/d.

Mean values of combustible materials ranged from 0,5 mg/m^2/d to 61,8 mg/m^2/d.

Mean values of ash ranged from 3,1 mg/m^2/d to 144 mg/m^2/d.

Ash analysis was established that:

- Lead, cadmium, and nickel were below the lower limit of determination.
- Arsenic ranged from <0,3 to 34,3 μg/m^2/d,

Total particulate matter

Mean monthly values of sedimentary matter are ranged from 39,7 mg/m^2/d to 201 mg/m^2/d. Pursuant to the Decree on conditions and requirements for monitoring air quality („Sl.Glasnik RS No.11/2010, 75/2010, 63/2013) increased values were not reported.

Period - summer

Particulate matter

liquid phase

The average monthly pH value is constant and ranged from 5,7 to 7,6.

Mean values of sulphate ranged from 7,2 mg/m^2/d to 27,9 mg/m^2/d.

Mean values of soluble substances ranged from 20,1mg/m^2/d to 72,1 mg/m^2/d.

Solid phase

Mean monthly values of insoluble matter ranged from 21,3 mg/m^2/d to 179 mg/m^2/d.

Mean values of combustible materials ranged from 0,8 mg/m^2/d to 54,5 mg/m^2/d.

Mean values of ash ranged from 12,4 mg/m^2/d to 87,7 mg/m^2/d.

Ash analysis was established that:

- Lead, cadmium, and nickel were below the lower limit of determination.
- Arsenic ranged from <0,4 to 64,6 μg/m^2/d.

Total particulate matter

Mean monthly values of sedimentary matter are ranged from 38,7 mg/m^2/d to 407 mg/m^2/d. Pursuant to the Decree on conditions and requirements for monitoring air quality („Sl.Glasnik RS No.11/2010, 75/2010, 63/2013) increased values were not reported.

4 CONCLUSION

Flotation tailing dumps present a constant threat to the ecological environmental factors both theu are in operation, or after termination of dumping and filling the landfill space. The causes of accidents in the flotation tailing dumps are technical defects and natural catastrophic disasters (Miomir Mikić,et.al., 2012).

Chemical haful materials which can get to living environment at damages, can cause endangering of ecological factors (soils, water, air) and through them the whole ecosystem of the area.

From the results obtained it can be inferred that surface waters contain increased concentrations of heavy metals regarding III and IV class water standards (Table 2-4).

Samples collected from surface waters, where the tailing dump has increased water pollution systematic analyses willbe needed.

From the results obtained for air quality it can be inferred that increased values for particulate matter were not reported.

This paper presents the auscultation of dams of the Flotation tailing dump Veliki Krivelj, near Bor, Serbia and chainages of collector. Based on the presented situation and measuring results, it can be concluded that there is a problem of preservation the Flotation tailing dump in operation.

ACKNOWLEDGEMENT

This work has resulted from the Project No. TR33021, funded by the Ministry of Science and Technological Development of the Republic of Serbia.

REFERENCES

Miomir Mikić, Daniel Kržanović, Milenko Ljubojev: Auscultation and zone monitoring of current collector of the Krivelj river below flotation tailing dump "Veliki Krivelj", Serbia. 12th Scientific Geoconference SGEM 2012, proceedings volume I, Geology Exploration and Mining. Proceedings,17-23th June, Albena Bulgaria. pp.465-472

Miomir Mikić, Daniel Kržanović, Milenko Ljubojev: Overview of zone monitoring of current collector of the Krivelj River below flotation tailing dump "VELIKI KRIVELJ", SERBIA. XV Balkan mineral procesing congress, proceedings, 12-16th June, Sozopol Bulgaria.

M. Ljubojev, D. Ignjatović, L. Djurdjevac Ignjatović, V. Ljubojev, Preparations for Investigation the Tunnel Route and Field Surveying, Mining Engineering Journal, No. 1, 2011, pp. 135-166.

S.Krstić, M.Ljubojev, M.Mikić, V.Ljubojev: „Methods of geotechnical investigations for rehabilitation and remediation the flotation tailing dump Veliki Krivelj (Serbia)''. XIV Balkan mineral processing congress, proceedings, Jun,2011, Tuzla, BIH (851-853).

Slađana Krstić, Miomir Mikić, Milenko Ljubojev, Omer Musić, Vesna Ljubojev:*„Conditions of drainage of flotaion tailing of "Veliki Krivelj*''. 43rd International october conference on mining and metallurgy, proceedings, Octobar 2011, Kladovo, Srbija. (221-238).

Miomir Mikić, Daniel Kržanović, Slađana Krstić: **„**Overview of the current situation of major facilities of the flotation tailing dump Veliki Krivelj near Bor with special review to the collector of the Krivelj River''. 43rd International october conference on mining and metallurgy, proceedings, Octobar 2011, Kladovo, Srbija. (303-306).

Daniel Kržanović, Miomir Mikić, M.Ljubojev:„Analysis the spatial position of mining facilities of the Veliki Krivelj mine to the proposed tunnel route for relocation the Krivelj River. Mining engineering 3/2011, 2011. (95-100).

Daniel Kržanović, Miomir Mikić, M.Ljubojev: „ Analysis of development effects of the Veliki Krivelj mine on construction the new facilities for deviation the Krivelj River''. Mining engineering 4/2011, 2011. (57-65).

S.Krstić, R.Lekovski, M.Mikić: „ Environmental protection from dust from flotation tailings Veliki Krivelj''. Air protection 2011, proceedings, Zrenjanin Hotel Vojvodina 7.-9.11. 2011. (200-206)

Predicting the Levels of Noise from Quarry Operations

K. J. Bansah
Mining & Nuclear Engineering Department Missouri University Science and Technology Rolla-Missouri, USA

E. Assan, C. Bosompem
Safety & Environmental Research Consultancy Limited Tarkwa, Ghana

ABSTRACT Mining activities impact on surrounding environments. Notable among these impacts is noise emission from sources such as machinery, drilling, blasting, dumping and crushing. It is important therefore, to determine the levels of noise to be generated by mining, and its impacts on surrounding communities so that potential impact(s) could be averted. A 24-hour noise monitoring was conducted for 25 days at a proposed quarry site and five surrounding settlements to obtain baseline noise levels. The noise to be generated by the proposed machinery on the quarry site were obtained and used to predict the noise levels at various receptor locations. Activities during the day at the quarry site were found to have the potential of altering noise levels in the surrounding settlements by 2 dB(A) to 10 dB(A), though the composite noise levels in these settlements compared well with permissible limits. Moreover, it was deduced that the quarry will not impact on night noise levels in the surrounding settlements. A few recommendations were given to further reduce the noise levels from the quarry site.

Keywords Mining, Quarry, permissible limit, receptor location, impact, health implication

1 INTRODUCTION

Noise is most often defined as “unwanted or objectionable sound”. Noise pollution adversely affects the lives of people (Anon, 2011). Problems related to noise include stress related illnesses, high blood pressure, speech interference, hearing loss, sleep disruption, and loss of productivity. Research has shown that exposure to constant or high levels of noise can cause countless adverse health effects (Anon, 2011). Quarrying mainly generates noise from overburden excavation, blasting, loading, hauling, dumping and crushing. Noise levels however, must be controlled to allow nearby land holders to relax or sleep during evening hours, reduce noise burdens, and also protect the hearing of employees.

A medium scale quarry company acquired roughly 16.50 acres granite rock concession in the Western Region of Ghana to undertake medium scale quarry projects. The quarry concession is however, surrounded by five major settlements anonymously referred to as Site 1, Site 2, Site 3, Site 4 and Site 5. The locations of these settlements are such as to be affected by noise emission from the quarry operations. It is therefore, necessary to predict the levels of noise that may be propagated from the quarry site and determine the potential impact on inhabitants of the surrounding settlements.

2 BRIEF INFORMATION ABOUT THE STUDY AREA

The Quarry site, Sites 1, 2, 3, 4 and 5 are all located in the Shama District of the Western Region of Ghana. The topography of these areas is generally undulating with elevations ranging from 32 to 95 m above mean sea level. The landscape is located within the moist semi-deciduous vegetation. However, the original vegetation structure has been altered due to intense farming activities by the inhabitants of the settlements.

The minimum and maximum temperatures of the area are respectively, 23 °C and 27 °C, with a mean annual temperature of 26 °C. Average rainfall is around 12 mm, with peaks in the months of June and July. These periods are generally characterized by high rainfall values in Ghana. Average wind speed is 0.5 m/s, with predominant direction of West (Anon, 2013).

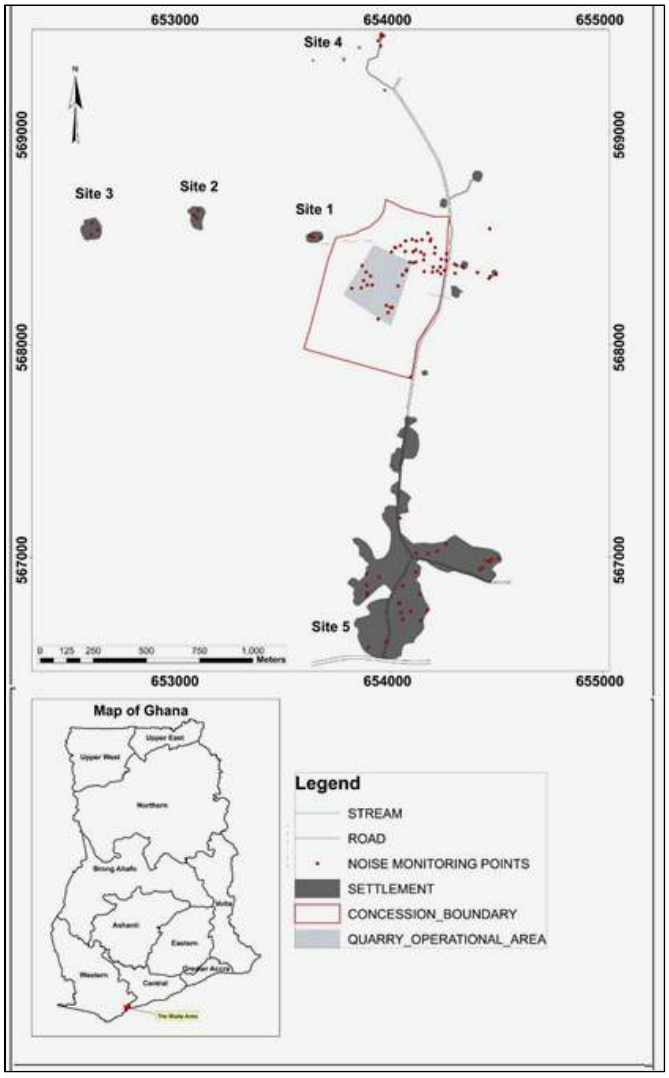

Figure 1. Map of Study Area

Site 5, the largest settlement (over 400 building structures) in the area, is located to the south of the quarry concession. The closest structure in this settlement is about 500 m from the boundary of the quarry's operational area. Site1, with nine building structures, is located 245 m to the North-West of the quarry operational area. Sites 2 and 3 are also located to the North-West of the quarry concession. While Site 2 has total number of 24 building structures and is 754 m from the quarry operational area, Site 3 has 13 building structures and is 1200 m from the edge of the concession. Site 4 is however, to the North of the concession, with 14 structures at 900 m from the periphery of the operational area. Figure 1 shows the quarry concession and the locations of the surrounding settlements.

3 DATA COLLECTION, RESULTS AND DISCUSSIONS

The following sections summarize the data collection procedure; the results obtained and the discussions of the various results.

3.1 Noise Monitoring

Noise monitoring was carried out with sound level meters at the quarry site and surrounding communities. The monitoring activity was categorized into two parts: "Day" and "Night", in accordance with the Environmental Protection Agency of Ghana (EPA) criteria. "Day" monitoring went from 6:00am to 10:00pm, while "Night" monitoring was carried out between 10:00pm and 6:00am. The monitoring locations fall within Zones "A" and "B2" of the EPA criteria as shown in Table 1. It must be noted however, that the quarry site becomes a heavy industrial area and therefore have permissible noise levels of 70 dB(A) when operations commence. The noise levels obtained from the monitoring activities were summarised and presented in Figure 2.

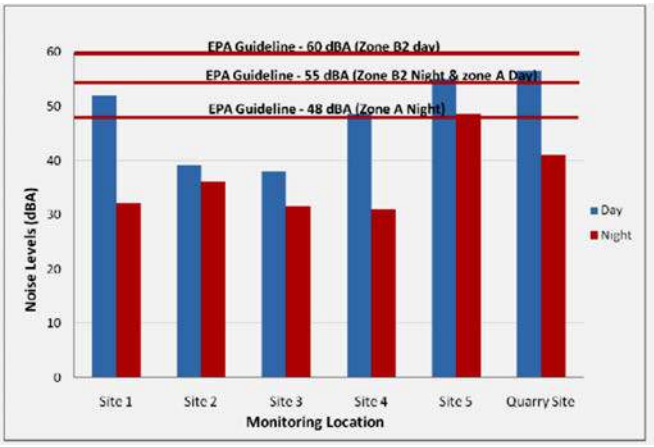

Figure 2. Mean Noise Levels at Monitoring Locations

Table 1. Description of Monitoring Locations According to EPA Criteria

Monitoring Location	Description of Area of Noise Reception	Zone	Permissible Noise Level dB(A)	
			Day (0600-2200)	Night (2200-0600)
Quarry site	Area with some commercial or light industry	B2	60	55
Site 1	Residential area with negligible or infrequent transportation	A	55	48
Site 2	Residential area with negligible or infrequent transportation	A	55	48
Site 3	Residential area with negligible or infrequent transportation	A	55	48
Site 5	Residential area with negligible or infrequent transportation	A	55	48
Site 4	Residential area with negligible or infrequent transportation	A	55	48

The mean noise levels at the monitoring locations generally compared well with permissible limits. Mean noise levels at all the monitoring locations were lower compared to their respective recommended levels, except “Day” noise levels at Site 5, which exceeded the threshold limit by about 1 dBA. On the average, “Night” noise levels at Site 5 were the highest; this is due to pronounced domestic activities. Site 5 is likely to experience population increase due to migration of persons in search of jobs and related businesses at the Quarry. This may lead to increased domestic and other activities, which may cause higher noise levels than the baseline. It is also observed that the noise level at the Quarry site is lower than permissible by 3 dBA for “Day” and far lower at “Night”. The high noise level at “Day” could be due to usage of heavy earthmoving machinery and trucks during day time at the Quarry site. Nonetheless, the “Day” noise levels at the Quarry will be far lower compared to permissible limit (70 dB(A)) of a heavy industrial area. Since there were virtually no activities at the Quarry site at night, noise levels were generally lower. Sources of noise at Site 5 may include vehicular movements and domestic activities, while that of Site 1, 2, 3 and 4 were purely of domestic origin.

3.2 Sound Pressure Level Modelling

Sound pressure level (SPL) modelling was conducted to predict noise levels that may propagate from the Quarry site to residents of Site 1, 2, 3, 4 and 5. The major source of noise expected at the Quarry site is heavy machinery provided by the Quarry management and shown in Table 2.

Table 2. Types and Number of Machinery provided by Quarry Management

Plant	Number	Noise Level (dBA)
CAT 336D Wheel Loaders	4	105
CAT972H Wheel Loaders	5	111
CAT950H Wheel Loaders	5	111
CATD735 Articulated Dump Truck	6	79
Toyota Hilux	7	73
Terex Pegson Prim./Sec. Crusher	1	116

Anon (2013a) suggests that the noise level measured from Cat D735 articulated dump-truck is 79 dB(A). While noise levels generated by both Cat 950H and Cat 972H wheel loaders are respectively, 111 dB(A) (Anon, 2013b), noise level from Cat 336D is 105 dB(A) (Anon, 2013c). Also, according to Anon (2013d), Toyota High-Lux DC generates 73 dB(A) while noise emitted by Terex Pegson primary/secondary crusher is 116 dB(A) (Anon, 2013e). Given the number of each of these machinery, and assuming that the machinery operate simultaneously, the noise levels were composited together with the highest baseline noise (67 dBA) measured at the Quarry site at "Day" to obtain a total of 122 dB(A). The sound pressure level Lp_2 at a distance r_2 from the source (Quarry site) was then estimated using equation 1 (Amegbey, 2011).

$$Lp_2 = \mathrm{Lp}_1 - 20\log\frac{r_2}{r_1} - Ae_{1,2} \quad (1)$$

Where Lp_1 is the sound pressure level measured at location 1 (Quarry site), $Ae_{1,2}$ is attenuation along path r_2 - r_1 between location 1 and 2, and represents factors affecting sound propagation. Such factors include atmospheric absorption, ground attenuation, wind or temperature gradient, trees, barriers or buildings (Anon, 2002). As a rule of thumb SPL is reduced by 6 dB(A) when the distance from the source is doubled in free field conditions. As a conservative estimate, a value of 5 dB(A) to 5.5 dB(A) is used to account for ground reflections. Assuming 6 dB(A) for each of the remaining attenuation parameters, $Ae_{1,2}$= 13 dB(A) and using Equation 1, noise levels that may be propagated from the Quarry site were estimated and shown in Table 3.

The predicted noise levels at "Day" compared well with permissible limits of noise for an "area with some commercial or light industry (Zone B2)", but higher than that of "residential area with negligible or infrequent transportation (Zone A)" within a distance of 500 m.

Table 3. Predicted Noise Levels

Distance (m)	Predicted Noise Levels (dBA)	
	Day	Night
100	67	30
300	57	20
500	53	16
700	50	13
900	48	11
1100	46	9
1300	45	8
1500	43	6
1700	42	5
1900	41	4

It must however, be noted that noise levels at day exceeded the Zone B2 guideline by 7 dB(A) within a distance of 100 m of the periphery. Beyond 500 m, the noise levels fell within permissible limits of Zone A. This suggests that inhabitants beyond 500 m may not be affected by noise generated at the quarry. Predicted noise levels at "Night" appear to be very low because of virtually no activity during the night at the quarry site. From the predicted noise levels (Table 3), only building structures that fall within a distance of 500 m from the operational area will receive higher than permissible noise levels.

To determine the composite noise levels in the settlements, the predicted noise levels were added to the mean baseline noise levels. Table 4 is a summary of the composite noise levels at the various settlements.

From Table 4, it can be observed that the total noise levels at Site 5 for "Day" exceeded the permissible limit by 2 dB(A). "Night" noise level at Site 5 was exactly equal to the threshold limit. Site 1 at night had total noise level of 58 dB(A), exceeding the recommended levels by 3 dB(A). Site 1 has the highest total noise level due to its closeness (245 m) to the quarry operational area. Site 2, Site 3 and Site 4, all had noise levels lower than permissible. It can be deduced that activities at the quarry site do not impact on night noise levels at the specified settlements.

Table 4. Composite Noise Levels in the Settlements

Settlement	Baseline Noise Level (dBA)		Baseline + Predicted Noise Level (dBA)	
	Day	Night	Day	Night
Site 1	52	32	52+57=58	32+20=32
Site 2	39	37	39+48=49	37+11=37
Site 3	38	31	38+45=46	31+9=31
Site 4	49	31	49+48=52	31+11=31
Site 5	55	48	55+53=57	48+16=48

4 CONCLUSIONS

This work studied the potential impact of noise to be emitted by quarry operations on five surrounding settlements. Firstly, noise monitoring was conducted at the quarry site and the surrounding settlements to obtain baseline noise levels. Secondly, noise levels that may be propagated from the quarry operations were predicted and added to the mean baseline noise levels in the settlements to obtain composite noise levels. After compilation of data, it was deduced that activities at the quarry site have the potential of altering background noise levels at day, in the surrounding settlements by 2-10 dB(A). It is however, worthy to note that the composite noise levels generally compared well with the permissible limit, though that of Site 1 and some parts of Site 5 exceeded the permissible limit by 3 dB(A) and 2 dB(A), respectively. While the noise levels at Site 1 may be due to activities at the quarry site that of Site 5 is purely of domestic origin. Nonetheless, Site 1 falls within the Minerals Commission of Ghana regulatory buffer (500 m from the quarry operational zone), and is therefore likely to be resettled. It can also be concluded that the quarry will not impact on night noise levels in the surrounding settlements. Continuous ambient noise monitoring however, should be conducted at the quarry site and surrounding communities to ensure that noise levels are kept below acceptable limits. Also, management of the quarry should ensure the quietest equipment available is used at the quarry site to further reduce noise levels.

ACKNOWLEDGEMENTS

The contribution of every individual who made the study a success is acknowledged.

REFERENCES

Amegbey, N. (2011), "Environmental Management", *MSc. Lecture Material*, University of Mines and Technology, Tarkwa, 100 pp.

Anon, (2013), "Blast, Air, Noise & Water Quality Assessment at West Africa Quarries Limited (Beposo) & Surrounding Settlements", Technical Report, Safety and Environmental Research Consultancy Limited, Tarkwa, Ghana, pp. 74.

Anon, (2013a), "Caterpillar D735 Articulated Dump-truck", *www.cat.com*, Accessed: July 15, 2013.

Anon, (2013b), "Caterpillar 950H Wheel Loader," *www.catmms.com*, Accessed: July 15, 2013.

Anon, (2013d), "Toyota High-Lux DC", *www.buyacar.co.uk*, Accessed: July 16, 2013.

Anon, (2013c), "Caterpillar 336D Hydraulic Excavator", *www.witraktor.lt*, Accessed: July 16, 2013.

Anon, (2013e), "Terex Pegson Primary Crusher Screens", *idox.monmouthshire.gov.uk* Accessed: July 16, 2013.

Anon, (2002), "Sound Attenuation by Silex", 16pp.

Protection of Cultural Heritage from the Area of Future Open Cast Mine Radljevo

N. Drljevic, G. Tomic
EPI Serbia, Mining Basin Kolubara, Serbia

ABSTRACT From the coal in lignite mines in Kolubara coal basin, more than 52% of Serbian electricity has been obtained. To maintain this ratio, it is very important to continue corresponding development of the new coal deposits.

Within spatial boundaries of the Kolubara basin there is a great number of existing settlements. Geographical position of coal basin and the fact that it runs through valley of river Kolubara and its numerous tributaries, indicates to centuries-old continuity in human settling in this significant area.

One of the human merits is a need to build object for everyday life, for cultural, religious or some other purposes. A great number of these buildings still exist at this space.

Inside defined boundaries for the new open cast mine Radljevo there are significant number of objects of cultural heritage and assets inscribed in appropriate registers.

Because of that, it is important to determine and establish extent and level of protection for each of them. Accordingly, the negative influence from the open cast mine on the population that dwells in this area will be reduced.

Keywords: coal mine, development, population, protection, cultural heritage and assets

1 OPEN CAST MINE "RADLJEVO"

Future open cast mine Radljevo is situated at western part of Kolubara coal basin, along with the active open cast mines Tamnava-West field and Veliki Crljeni.

Based to extensive exploration and other calculations a "Preliminary design of coal exploatation" has been made, where all elements, which are necessary for working, were defined for the purposes of coal exploatation.

Area, which future mine "Radljevo" covers, is with slightly wavy and flat terrain from alluvium of river Kladnica and streamlet Stublenica. These water-bodies are permanent, along with their tributaries: Negica stream, Orlovac stream and Stojkovac stream. A torrential flow characterizes all water occurrences in this area. The land is mainly for agricultural purposes. There are also parts under woods mostly in valleys of rivers and streams.

1.1 Territorial distribution

Settlements that exist in forest-highland of river Kolubara and its tributaries and which are within the area of future open cast Radljevo, are very rich in archaeological sites and objects of cultural heritage. First communities at these areas were formed in period of Vinca's culture (6000. b.c.), and they had a continuity during time throughout all periods of human and society development.

Open cast mine "Radljevo" is located at area of municipalities Ub (cca. 95%) and Lajkovac (cca. 5%). Settlements that belong to municipality Ub, and also are in area of future mine, respectively in zone of mine's influence, are: Kalenic, Brgule, Radljevo, Sarbane, Stublenica and Paljuvi. To the municipality of Lajkovac belongs settlement Jabucje.

1.2 Opening and further development of open cast mine

Inside the projected boundaries of future mine "Radljevo" calculated reserves of coal

are about 340 mill.of tons. Based to the technical documentation, it has been predicted that coal exploatation will start in year 2018-2019. Development was planned in two phases:

1) first phase-fulfillment of planned annual production of coal up to 7 million tons per year,

2) second phase-up to achievement of projected production of 13 million tons per year and until the end of the exploitation.

Prior to coal exploatation is overburden excavation, meaning overburden work will begin in 2017-2018 year. At figure 1 is a view of mining advancement at future open cast “Radljevo” during years.

Figure 1. Development of mining work

1.3 Aspects of the impact during mining

Development goal in Kolubara coal basin is efficient, rational and organized usage of natural resources in socio-economic, spatial and ecological view. All of this implies detailed planning and creation of conditions for efficient coal exploitation on new fields, development of energy facilities, rational connection between settlement’s net, reconstruction and improvement of existing systems, construction of the new objects, harmonization of social development and improving the quality of life of local population, rational use of water resources, environment object’s control etc.

Beside the importance from the opening of new mine ”Radljevo” for continuity in lignite production, negative impacts of mining activities at nearby environment will be evident, and the most significant are:

- partial and complete relocation of the settlements and population with all existing objects,
- impact on the water resources important for water supply of settlements in area of mine’s influence and nearby surrounding, and decreasing of water-flows potential along with underground water level with direct impact to the draining of agriculture land,
- relocation of roads-public roads of II order and local roads
- degradation of natural ecosystems because of the occupation of large areas under agricultural and forest land,
- devastation of relief, population, settlements, cultural goods,
- social and socio-economic influences

All of these influences must be analyzed in details in order to define appropriate activities through planning processes, projecting, preparations for work, performing of the work, supervision, financing, legislation, expropriation etc.

2 CURRENT STATUS OF CULTURAL HERITAGE AT THE AREA OF FUTURE MINE “RADLJEVO”

Continuity of human settlement in the area since the period of the Vinca culture until recent history has been confirmed with previous archaeological researches and findings.

These finding are supported with the existence of the immovable objects of cultural goods, archeological sites, buildings of architectural heritage, monumental landmarks, cemetery etc.

2.1 Object of cultural heritage

According to the “Study of preservation and revitalization of the immovable cultural heritage for the purposes of development of Urban Plan for Radljevo”, as well as conducted archeological and monumental research, along with field reconnaissance, a large number of various objects of cultural heritage on the area of future mine Radljevo has been recorded.

All of these objects were divided into groups according to characteristics:

1. Group of the immovable cultural heritage includes:

- church Shroud of the Holy Mother of God in Radljevo,
- church house (parish house) in Radljevo,
- tombstones with monumental values at village's cemetery in Radljevo, Sarbane and Kalenic,
- cemetery in u Sarbane, Kalenic, Radljevo and Brgule,

2. Group of archaeological findings includes:

- site "Popovica imanje", from the period of Late Antiquity and the Iron Age, in Brgule and Radljevo,
- site "Crkvine", Middle Age, Ottoman period - Radljevo,
- site "Makvine", Bronze and Iron Age - Radljevo,
- site "Stare kuce", Late Antique - Kalenic.

3. Group of valuable buildings of architectural heritage includes:

- primary school's building in Radljevo,
- primary school's building in Sarbanu,
- house of Nade Tesic, former village tavern,
- house of Velje Milicic in Radljevo,
- house of Milovana Matijasevic in vilage Sarbane.

On figure 2. is spatial distribution of all of these objects on area covered by future open cast mine Radljevo.

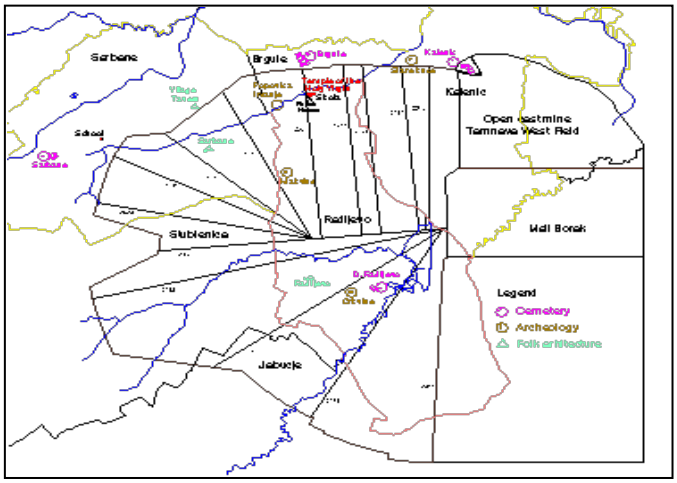

Figure 2. Objects of cultural heritage

2.2 Limitations and conveniences for cultural heritage protection

Primary limitations concerning protection of cultural heritage are reflected in direct physical endangering to the cultural monuments and archeological sites which are under development of open cast mine. Also there is an inefficient and untimely investment in protection of cultural heritage, and accordingly there is a great devastation of buildings with architectural heritage in villages under influence of future mine Radljevo.

But, beside these limitations there are certain benefits for heritage protection, and they are manifested through:

- existence of institutions responsible for the protection,
- legal obligations for harmonization between mining work's development and the needs to protect cultural heritage,
- the possibility of finding the new archaeological sites and presentations of findings in museums or other suitable places,
- the possibility of preservation some of the endangered objects by moving them at new location or by making of new technical documentation for purposes of data preservation.
- raising of the awareness about the importance of cultural heritage preservation.

3 PLAN SOLUTIONS FOR THE PROTECTION OF CULTURAL HERITAGE

Significance of cultural goods and objects that exist in the area of the future mine Radljevo implies a detail overview of their current state and definition of the methods of protection that will be conducted. The overall protection plan predicts activities that will enable permanent preservation of these objects, and thus continuance of their importance to the historical definition for all structures that exist in this area. With the conservation, restoration and revitalization of objects, the conditions for further preservation will be obtained. This allows continuity in historical testimony of identity

of area itself and civilization's cultural range from the settlers.

3.1 Activities for the protection

Concerning to the analysis from the archaeological site's aspects and from the objects of cultural heritage, in order to protect cultural goods, it is necessary to conduct:

- for all evidenced archeological sites, a protection of archeological excavations must be provided, and for so far registered cultural goods certain spatial-plan measures for their protection should be carry out,
- intensify research work on the project area in accordance with the dynamics of the mine's development,
- if at observed area new significant objects emerges, it is necessary to do their previous conservation,
- provide conditions for mining mechanization's work that will disable damages of objects and other belongings of cultural goods,
- all users from this area are obliged to communicate between themselves as well as competent institutions, and accordingly to the international convention saying "monument is inseparable from history which he is witness and from environment where he's placed",
- keeping adequate record of objects and archeological findings belonging to the cultural heritage with the provision of technical expertise,
- provide continuous care for the monuments and objects protection at observed area,
- during rebuilding of new or reconstruction of existing objects, all elements of traditional folk architectures should be used, and the area for their placement must be protect from degradation and improper use,
- to amend the classification and registry of cultural - historical heritage.

3.2 Concept for the protection

For the purposes of protection for the cultural heritage in the area that is affected by mining operations of the future mine Radljevo, following activities must be anticipated:

- for all evidenced immovable cultural goods that won't be relocated, it is necessary to make detailed technical documentation (project of current state, and photo documentation), and to plan new location for their construction. For the objects which will be relocated, it is important to define spatial units, on which they will be relocated,
- continuity in exploration of archeological sites according to developed Plan for the archeological researches protection, that was done by competent institutions.

3.2.1Church "Shroud of the holy mother of God" and parish house in radljevo

Church was built in 1873. at position of former log-house church from 1826. Building style belongs to Baroque and Neoclassical, typical for the churches in Vojvodina in 18. and 19. century. Church is single-nave edifice elongated shape, with narthex, nave and altar. On western part there is high belfry with the dome decorated in Baroque style. Inside, the church is decorated, and especially valued is iconostas with icons which are made with oil paints on canvas.

In churchyard is Parish House with two units and hall built in 1939. House is single-storey building with elongated base and central entrance, and with covered porch containing four massive stone pillars, and two sidewise entrances. The roof is complex, in more directions and covered with pepper tiles. This object is typical example of Modern style in Serbian architecture between two wars.

Both of these objects, (figure 3.) along with the others built later, are unmovable objects foreseen for demolition. This means that detailed technical and photo documentation will be done prior to demolition. After that, with the agreement of

local population and church authorities, new church and additional objects will start to be built. This location will be defined according to the demands of local population, which will be relocated from the mine's area and which will use the church.

Figure 3. Church and parish house

3.2.2Cemeteries in villages

Inside the area, which will be endangered by mining work, there are local cemeteries in villages Sarbane, Kalenic, Radljevo and Brgule. All of these objects belong to movable cultural goods and they are predicted for relocation to new places defined between all subjects (local population, municipalities, scorch organs, Mining Company, etc.). Also, on these cemeteries there are a large number of monuments with historical values from further and closer past, and they are very important for preservation of national identity and history.

Activities for the preservation of these objects means development of appropriate time-plan which will define conditions for suspension of burial on existing cemeteries, area and conditions of location for new cemetery, refinement of rights for the graves trustees, exhumation, equipment, transfer and burial of the remains in accordance with the legislation. Last, there are activities in order to bring area to it's purposes, respectively excavation of land after cemeteries relocation and sanitation.

Considering the importance of these objects and sensitivity and connection of local population with them, it is crucial to solve this conflict carefully and precisely with the presence of all involved sides.

On figures 4. and 5. are images of cemeteries in some of the villages.

Figure 4. Kalenic cemetery

Figure 5. Radljevo cemetery

3.2.3 Objects with the attributes of folk architecture

In the villages belonging to the future planed mining area there is a large number of objects of folk architectures (village schools and residential houses) which will be endangered by mining works from the future open cast mine Radljevo. Relocation of these building to the new locations has been planned.

Schools in Radljevo and Sarbane, foreseen for demolition, technical and photo documentation will be done previously in order to preserve information about their characteristics and importance for local population.

For the residential houses under the protection of State, a documentation that shows current state will be done, along with photo documentation. Information from these documents will be exposed on appropriate locations (planned ethno parks), with the possibility to apply traditional elements of folk architectures during reconstruction or building of new similar objects on the area under the influence of mine's work.

Figure 6. School in Radljevo

Figure 7. Family house of M. Matijasevic-Sarbane

3.2.4Archeological localities

For the all listed localities at observed area (see.2.1, figure 8.), findings and movable exhibits are foreseen to be relocated to the new locations which will be previously defined. Before that it is necessary to obtain detailed reconnaissance of the terrain, exploration and excavation, marking and restoration, protection of all moving parts and objects, and then their packing and transportation to new site.

Considering that the zone of future mining works is situated within two municipalities, a place for the relocation of archeological exhibits from all localities will be determined, whether it is museum or ethno-park with special assignment according to the age of the archeological findings, probability for reconstruction of some of the excavated objects etc.

Figure 8. Archeological site "Crkvine" in Radljevo

4 CONCLUSION

Electric production from coal combustion in power plants, and significance of it doesn't necessarily means that all objects under the influence of mining work should be demolished and devastated. The importance of objects that suggests continuity of settling in this region shows existence of the good geographical and other conditions, and that enables cultural and nation's development and shows important historical facts significant for region itself.

Thus, all necessary activities for the purposes of protection of these objects of cultural heritage must be done for the sake of existing and future population which will be connected with this area and for the preservation of national consciousness and history in general.

REFERENCES

Vatenfall Europe Mining Consulting & Mining University Belgrade, 2010, *"Preliminary design of coal exploitation at open cast mine Radljevo"*, Belgrade, Serbia, pp 147,

Institute of Architecture and Urban&Spatial planning of Serbia, 2010, *"General regulation plan for the zone of impact from open cast mine Radljevo"*, Belgrade, Serbia, pp 287-314,

Institute for Protection of Cultural Monuments Valjevo, 2010, *"Terms of protection and revitalization of cultural heritage for the development of the General Regulation Plan"*, Valjevo, Serbia, pp 58-60;

The Life of Tires on Wheeled Heavy Duty Mining Vehicles from Point View of the Environmental Apprehension

I. Celik
Dumlupinar University, Mechanical Engineering Department, Kutahya, Turkey

C. Sensogut
Dumlupinar University, Mining Engineering Department, Kutahya, Turkey

ABSTRACT The tires are important elements of a wheeled vehicle as they carry the weight and the load of the vehicles. While they realize this work, they are worn out on rough ground conditions accounting for significant spare parts and repair work costs as well as environmental impacts. Discarded tires have been a disposal problem in the past and continue to accumulate throughout the world today. In the present work, the wears of tires on heavy duty vehicles operating at Western Lignite Corporation (WLC) in Turkey have been investigated. The main purpose of the current research in general was to investigate the reasons for leaving scrap of tires and the wear conditions according to their location on the vehicle.

The main outcome of the work in concern is that cut-out brought about by sharp stones on mining area is the primary cause for disposal of tires. Additionally, the deterioration of the tires changes depending on the location of tire on the vehicle.

Keywords: Tire life; mining; rubber; truck

1 INTRODUCTION

The tires mainly carry the weight of load and vehicle. The torque formed by the engine and traction force is transferred onto road by means of them. Shocks coming from road and the motion of the vehicle are also absorbed by them. The break effect is transferred onto road while the vehicle is decelerating; the lateral forces are carried while the vehicle is turning the bend by means of tires.

Tire accounts for the most important cost following fuel for the heavy duty vehicles therefore the life of tire is desired to be as long as possible. In addition, discarding is always an important problem from the view of environmental care. If the factors affecting the life of tire are investigated, surface of the road is seen to be one of the most important factors. If tire always works on the stony ground, its life is reduced by 80% compared to smooth asphalt road. The wear of tires which are on the drive axle is higher than other tires of non - driving axle. Besides, the wear of tire is directly affected by wheel alignments varying for each vehicle (caster, camber, toe - in angles). If the tire overheats, strength of the rubber may decrease causing the life of tire to decrease too. In order to avoid this situation in hot weather, the tire pressure can slightly be increased by the value of the catalogue. If the vehicle works for a long period, tires simply heat up. However, in case the vehicle stopped for a while, the heating of the tire can be prevented. Another important factor which affects the life of tire is the speed of the vehicle. The overspeed causes the overheat of tires resulting in the wear resistance to decrease. Therefore, maximum load and speed limits prescribed at the tire sidewall must not be exceeded. Otherwise, the life of tire decreases and the safety of driving is jeopardized. If the load decreases, the life of tires increases. In order to get the optimum performance, maximum load and speed limits must not be exceeded.

Rubber is a viscoelastic material and its friction behaviour is governed by

viscoelastic material properties. Additionally, rubber friction force depends on the operating speed and temperature. Further, viscoelastic losses and dependence on frequency can also affect the tribological behavior of rubber (Baek and Khonsari, 2005).

Some of the works conducted regarding the life of tires, its environmental effects and precautions to be taken are emphasized below:

Lower tire pressure not only leads to decreased fuel economy, but also causes many unnecessary injuries and loss of lives. Under inflated tires can increase the stopping distance of a vehicle, particularly on wet or slippery surfaces. In addition, when tires are under inflated, their sidewalls flex increasing the temperature more and resulting in failure (Pearce and Hanlon, 2007). At works of Kocsis et al (2008), it was noted that if carbon black (CB) increase, specific wear rate also increases (Kocsis et al., 2008).

US drivers do not adequately monitor the tire pressures in their vehicles. The study of Joshua et al (2007) indicates that substantial benefits would accrue if vehicle-care facilities offered complimentary tire pressure checks with oil changes to systematically regulate tire pressure including: increased safety, reduced fuel consumption, increased customer discretionary spending that could be recouped in retail/auto stores, reduced pollution and emissions and enhanced national security (Pearce and Hanlon, 2007).

Discarded tires have been a disposal problem in the past and continue to accumulate throughout the world today. Recent figures from the US Environmental Protection Agency show that over 279 million discarded tires are being added to an estimated 2~3 billion tires currently stockpiled around the U.S. (Jang et al., 1998). The discarded tires can present both health and environmental hazards (EPA, 1989). The rubber coating life is related to running conditions, i.e. the load, the velocity and the displacement amplitude (Baek and Khonsari, 2005).

There are currently more than 1900 facilities in the U.S. and Canada. However, the number is shrinking nowadays due to the decreased markets for passenger retreats. The decline is primarily because of low prices of new tires. Truck tires are often re-treaded three times before being discarded and the truck tire re-treading business is, therefore increasing. Most of the good truck tire casings are being re-treaded owing to the high cost of new truck tires (Jang et al., 1998).

Wik and Dave (2009) summarized the existing knowledge on the occurrence of tire wear particles in the environment, and their eco-toxicological effects. They suggested that management should be directed towards the development and production of more eco-friendly tires and improved road runoff treatment (Wik and Dave, 2009).

The average passenger car tire lasts for 40000 km before it is worn out, and during its lifetime about thirty percent of its tread rubber is eroded away off and emitted into the environment (Dannis, 1974).

For tire and brake wear emissions, average wear rates and heavy metal contents of different materials were utilized to develop emission factors for tire and brake wear. Road transport is the cause for heavy metal emissions like arsenic, cadmium, chrome, lead and nickel that emerge from the abrasion of tire tread and brake linings. Although their amount is highly uncertain, the conclusion can be drawn that activities from this sector are contributing to some extend to the total anthropogenic heavy metal emissions. A comparison with other anthropogenic sectors like the production of industrial goods or small combustion installations shows that this contribution can reach up to 13% for lead in the business as usual scenario. As transport activities will continue to increase in the future, this will also gain more importance (Kummera et al., 2009).

Higgins et al (2008) were formed a friction map to determine friction regimes in the range of velocities 0.005 ms^{-1} to 2.6 ms^{-1} and temperatures -33 °C to -0.5 °C. The values of μ in the map range over two orders of magnitude from 0.01 to 1.14. Low friction is observed at high velocities. A maximum in

friction was measured for low velocities at 0.005 ms^{-1} around -25 °C (Higgins et al., 2008).

The tire companies support the re-grooving (re-treading) operation to extend tire life. In this process, the teeth on the worn tires can be re-opened without damaging the tire casing with the re-grooving machine and the lives of tires can be extended for a while (Michelin, 2011).

Celik et al (2007) have expressed the importance of tire pressure. They examined the tires of wheeled heavy duty machines and stated that if the tire pressure is checked daily according to the catalogue value, an extension of tire life can be made possible for a longer period.

In this study, the tires of heavy duty vehicles used at the opencast mining area were investigated in detail. The discarded tires for various reasons were evaluated between the years 2007-2012. The purpose of the present research in general was to investigate the reasons for leaving scrap of tires and the wear conditions according to their location on the vehicle.

According to the results obtained from, some suggestions were made in order to increase life of tires. There are a large number of heavy duty vehicles utilized in opencast mining areas such as wheel and track-type loaders, trucks, road roller, bulldozer, angledozer, grader, excavator, driller, etc. The cost of an average tire is about $ 7000 - $ 7500 for trucks which have a capacity of 77-85 tons. In addition, a single tire cost of truck with a capacity of 156 tons can reach up to $ 19000. Prolonged life of the tire is essential from the point of economics and environmental reasons.

2 MATERIALS AND METHODS

In this study, the tires of heavy duty vehicles have been investigated at Western Lignite Corporation (WLC) between the years 2007-2012. During this period, a total of 770 tires were examined to find out the main reasons for them to be left to the scrap. According to the result of the present research, five main events have been determined taking place at discarded of tires which are;

a- the blowout (Fig. 1),
b- the wear of the teeth (Fig. 2),
c- the tread separation (Fig. 3),
d- the stone cutting (Fig. 4),
e- the damage of the toe (Fig. 5).

Figure 1. The blowout

Figure 2. The tire wear

Figure 3. The tread separation

Figure 4. The stone cutting

Figure 5. The toe damage

The reasons for disposal of tires were shown in Table 1 and Fig. 6. When Table 1 and Fig. 1 are assessed, it can be seen that the most important reason for disposal for tires is the stone cutting. Later, the reasons for the damage of tires are the wear, the tread separation, the blowout and the toe damage, respectively.

Table 1. The disposal reasons of tires for heavy duty vehicles (between 2007-2012 years)

Cause of Damage	Number of Tires
Blowout	25
Wear	232
Tread Seperation	36
Stone Cutting	468
Toe Damage	9
Total	**770 pieces**

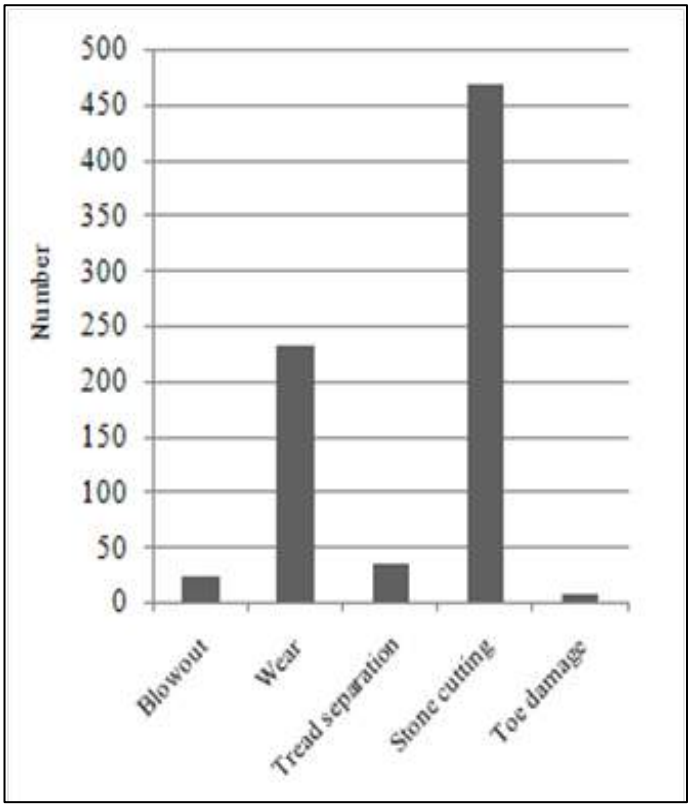

Figure 6. The main reasons for the disposal of the tires

It is desired that the tires are only discarded with the wearing. However, it is not possible in practice. Especially, the stone cutting is more than double exceedance the wear. Nevertheless, it is possible to reduce this damage by taking a number of measures. The hard and sharp objects such as stones, rocks,

metal parts, trees etc. mainly cause the stone cutting. If the truck is overloaded, the stones, the rocks and the mineral particles are eventually poured onto the roads. If the bucket of the loader and the excavator is overfilled during the trucks loading, the stones, the rocks and the mineral particles are also poured onto the working area. Therefore, the vehicles like loader, excavator, trucks etc. should not be charged more than their load capacity. In addition, the hard and sharp materials on the roads and the working areas should be frequently cleaned away. In addition to these precautions, the production chains should be attached to the tires of loaders and excavators during the working on hard ground conditions.

The hard and sharp materials scattered around on the ground can also cause the blowout of tires. Other causes of the blowout (sudden explosion) are the overloading of vehicles and high inflation pressures of tires. Several works carried out indicate, and the consensus among tire manufacturers is that under inflation in tires is also a major contributor to the tire failure (Federal Motor Vehicle Standards, 2001; Aguirre, 1986).

3 RESULTS AND DISCUSSIONS

In addition to the above described general tire damages, the six-wheeled truck tires were also examined. The situation of 311 pieces of the truck tires and the wear conditions were evaluated according to their locations on the truck. In this study, the tire numbering was used for each tire according to their locations on the truck. The tires were fitted at the same shaft location even if they were changed. Fig. 7 shows the numbering and the positions of the tires on the vehicle.

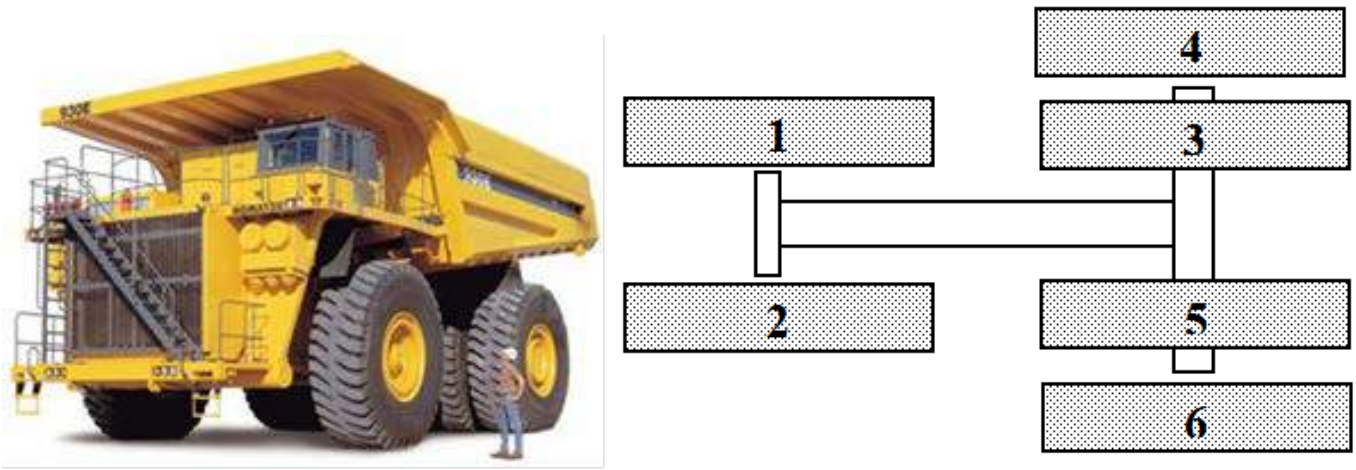

Figure 7. The truck and its the numbered tires

Table 2 shows the life of the tires mounted on trucks between years 2007-2012. The working hours of trucks were also recorded when both the tires were mounted as original on the truck and then the tires were discarded at the end of their application lives. In this way, the average lives of tires were studied according to their location on the truck. In this study, only the tires discarded due to wearing have been evaluated. The disposed tires owing to the stone cutting, the blowout, the tread separation and the toe damage have not been evaluated. The examined tires are the new and the original products. The coated tires have also not been taken into evaluation. The tires having been in the same location on the trucks were paid attention during the studying period. The tires were fitted at the same shaft location even if the trucks were changed.

As shown in Table 2, 43 tires were used at the 1st numbering location on the trucks while 47 tires were used at the 2nd numbering location. However 45, 53, 58 and 65 tires were utilized at the 3rd, 4th, 5th and 6th numbering locations respectively. The

working hours (lives of tires) were recorded for each tire as well. The values at A columns in Table 2 are original values which are not statistically assessed. The values at B columns in Table 2 are the regulated ones. This regulation will be described below.

The statistical evaluations are shown in Table 3 for the group of every tire. The values at the column A in the Table 3 are the average lives and standard deviations for tires calculated from the column A of the Table 2.

However, in the column A of the Table 2, some values shown in bold are outside the range of their standard deviations for group of every tire. The values which are outside the standard deviations were deleted and the column B of Table 2 was generated. For example, for the 1st tire life, 2898 value (in the column A of Table 2) is outside the standard deviation which is 6277 (7779-1502) in the column A of Table 3. Therefore, this value was deleted. In this way, 11 values were not shown in the column B of Table 2 considering standard deviation values in the column A of Table 3.

The column B of Table 2 contains the regulated values for the group of every tire. The column B of Table 3 show statistical values which are the average life of tires and the standard deviations from the column B of Table 2. The tire lives were determined according to the column B of Table 3 for the six wheeled trucks.

Graphically, the average lives of tires based on the data in the column B of Table 3, are shown in the Fig. 8.

When the column B of Table 3 and Fig. 8 are examined, it is seen that the longest-lived tires are the 1st numbered ones which are working on the right-front axle. The life of these tires is about 8018 hours. Then, the 2nd numbered tires have the life of 7223 hours. The 2nd numbered tires are the front tires of the trucks too. The front tires are not at the driving (traction) axle. As the front tires are not at the driving axle, they are less worn out. However, the 2nd numbered tires are worn out more than the 1st numbered tires. These left-front tires have been worn out 9.92% more when compared with the right-front tires. The reason of this situation is that left-front tires are working on the harder ground. The traffic flow is on the right hand side at the working area. Therefore, the left tires are in contact with the harder ground.

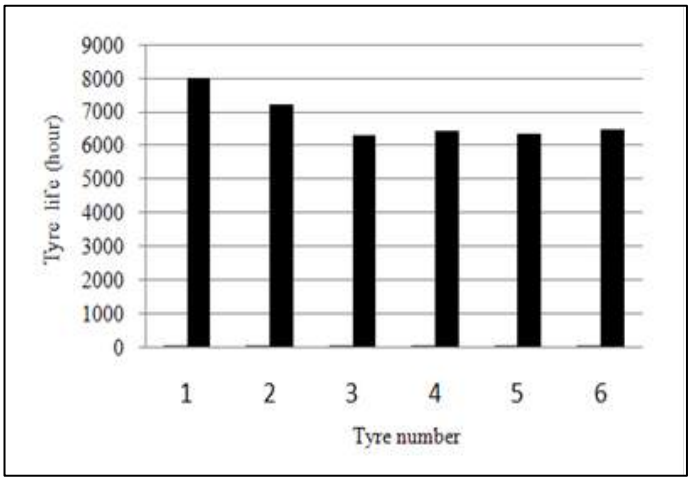

Figure 8. The life of tires on the heavy duty trucks

The shortest-lived ones are the 3rd numbered tires (6322 hours) and the numbered 5th (6356 hours) tires which are working on the rear axle. The rear axle is the driving axle and the numbered 3rd and 5th tires are on the inner side along the rear shaft. The weight of the truck and the load carried is handled by the the rear-in tires more. Fig. 9 shows the geometric dimensions and the mass center of the trucks utilized.

For these trucks, the weight distribution is as follows: empty front axle is 47%, empty rear axle is 53% and loaded front axle is %32, loaded rear axle is %68 (Komatsu, 2011). The numbered 3rd and 5th tires are more worn out due to the effects of the weight and the traction. On average, the rear-in tires have shorter life 16.82% by compared to the front tires in this calculation, the average life of the two front tires is 7621 hours, the average life of two rear-in tires is 6339 hours.

The numbered 4th and 6th tires which are on the outside along the rear traction shaft have 6431 and 6490 hours life respectively.

The average life of the numbered 4th and 6th tires is 6460.5. These tires have a longer life by 1.92 % with a comparison of the numbered 3rd and 5th tires which are the inner side on the same axle.

Table 2. The lives (hour) of tires on heavy duty trucks

Number	1st tire Life		2nd tire life		3rd tire life		4th tire life		5th tire life		6th tire tife	
	A	B	A	B	A	B	A	B	A	B	A	B
1	2898	6408	3935	5973	3315	7489	5466	5466	6155	6155	9148	8013
2	6408	7704	5973	6947	7489	4157	5466	5466	8013	6408	9148	7489
3	4157	7027	6947	7724	2898	6392	5466	5466	6408	5466	3315	5048
4	7704	6480	7724	5849	4157	6392	6155	6155	5466	5466	8013	6408
5	7027	6939	3704	6030	6392	5973	5048	5048	5466	5466	7489	6480
6	6480	8457	5045	8359	6392	6947	4157	5895	5466	4987	5048	6239
7	6939	6353	5849	9148	2935	7724	2686	6432	4987	6266	2898	6127
8	6127	8359	6030	9007	5973	5849	5895	6353	6266	6366	6408	6353
9	8457	8759	9394	8901	6947	6030	6432	7489	6366	5933	4157	6146
10	6353	8759	8359	8742	7724	5767	2704	4794	3878	6146	2704	8265
11	8359	8359	9148	5135	3704	4490	3760	5767	4462	7489	4027	4656
12	6146	7489	9007	7548	2045	5123	3704	6901	2081	6909	6480	7038
13	8759	8063	8901	5895	5849	6891	6353	6242	4457	7904	6239	7904
14	8759	6909	8742	6432	6030	7643	7489	6242	8287	3517	6127	6901
15	8359	7490	5135	8518	5767	7647	4794	7726	5933	6176	4457	5518
16	6146	7904	4205	5704	4490	7669	5767	7726	3663	6176	6353	5468
17	7489	7989	7548	5704	2910	4603	8265	5064	8359	7643	8359	5468
18	8063	8759	2686	8881	7904	7141	4490	4774	6146	7904	6146	6505
19	6909	8759	5895	5468	3989	6040	4514	6155	7489	5358	8265	4603
20	5767	8063	6432	5468	5123	7725	8095	6155	8063	5973	4656	6597
21	7490	8221	8518	5442	6891	7225	9007	5547	6909	5809	4514	6597
22	5910	7141	9394	6463	9394	4303	6901	5809	7904	5693	7038	5547
23	7904	8359	5704	8400	7959	5520	6242	7458	3517	5693	7904	7082
24	7989	9148	3760	7416	3561	7416	6242	7384	6176	8343	6901	7465
25	8759	9007	5704	7458	3144	7458	7726	7669	6176	6536	5518	8221
26	8759	8901	8881	8063	7643	5135	7726	6990	10275	5901	9394	5291
27	10275	8742	5468	7200	7647	7210	5064	7082	4603	7458	10275	5901
28	8063	7904	5468	6622	7669	5947	4774	7082	7643	7458	8881	5204
29	8221	8701	5442	8762	4603	5442	6155	7082	7904	5752	5468	5135
30	7141	8518	6463	7959	8221		6155	7173	5358	6812	5468	6480
31	9394	8881	3806	7489	7141		4223	7173	5973	4882	6505	6646
32	8359		8400	8435	6040		5547	7049	5809	7458	9202	7481
33	9148		7416		7725		5809	5834	3846	5135	4603	7200
34	9007		7458		7225		7458	7458	3846	7548	6597	6622
35	8901		13275		8506		8435	8063	5693	7711	6597	7562
36	8742		8063		4303		8499	6327	5693	6622	4223	7562
37	9842		7200		3263		7384	5442	8343	6622	5547	7562
38	7904		6622		5520		7669		4354	6622	8435	7562
39	8701		8762		8400		6990		6536	6505	8435	6622
40	8518		9562		7416		7082		5901	6252	7082	5718
41	9394		9394		7458		7082		7458	6463	8499	5442
42	9894		7959		5135		7082		7458	5979	7465	6463
43	8881		7489		7210		7173		5752		8221	
44			9894		8063		7173		6812		5291	
45			10173		5442		7049		4882		8759	
46			10173				5834		7458		8759	
47			8435				7458		5135		3263	
48							10173		4205		5901	
49							10173		7548		5204	
50							4206		7711		5135	
51							8063		6622		6480	
52							6327		6622		6646	
53							5442		6622		7481	
54									6505		7200	
55									8063		6622	
56									6252		7562	
57									6463		7562	
58									5979		7562	
59											7562	
60											6622	
61											2898	
62											5718	
63											5442	
64											6463	
65											2306	

Table 3. Average life and standard deviation of heavy duty truck tires (from Table 2)

	1st Tire Life (hour)		2nd Tire Life (hour)		3rd Tire Life(hour)		4th Tire Life(hour)		5th Tire Life(hour)		6th Tire Life(hour)	
	A	B	A	B	A	B	A	B	A	B	A	B
Average Life	7779	**8018**	7724	**7223**	5947	**6322**	6321	**6431**	6162	**6356**	7779	**6490**
Standard Deviation	1502	823	2154	1288	1918	1138	1663	919	1518	983	1844	965

At the same time, 4th and 6th tires are less worn out by 15.32% with a comparison of two front tires.

Moreover, the base of road is convex in cross-section. The middle part of road is a little higher than the edges in general. It means that the rear iner tire is more in contact with the ground. All these events are causing the more wear on the rear in tires.

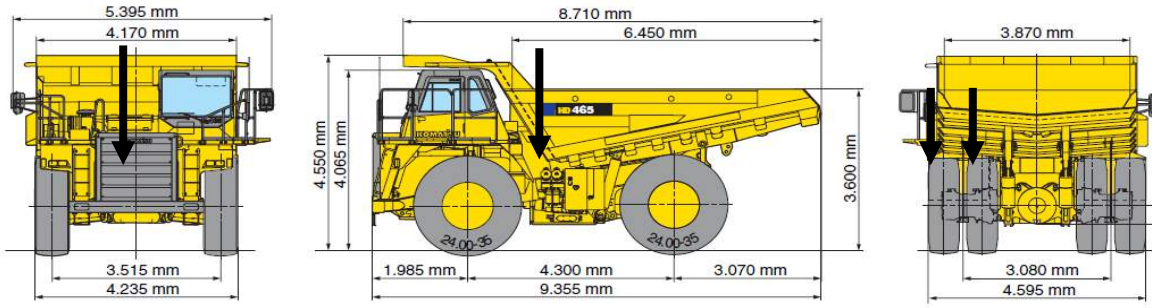

Figure 9. Geometrical dimensions and the mass center of the trucks

4 CONCLUSIONS

Between the years 2007-2012, 770 pieces of tires were examined in an opencast mining area at WLC. At the end of this experimental research work, it can be said that the most important reason for the disposal of tires is the stone cutting. Later, the wear, the tread separation and the blowout are ranked, respectively while the toe damage is the least damage. The cost of tires comes second after fuel consumption for a mining company. However the damages of the tires can be decreased out of the natural wear by taking same measures. The falling and scattered parts which are hard and sharp rock materials on the working area and the roads should be cleaned frequently. The carrying capacities of the vehicles must not be exceeded. The overloading should not be permitted at all. Tire inflation pressure should also be kept in the range of normal values.

In addition, at the same working area, 311 pieces of tires of the heavy duty truck with six tires were examined according to their location on the trucks. The results obtained from this study can be explained as follows: the most worn out tires are on the rear traction inner side. The outer tires on the rear traction shaft were less worn out compared with the inner tires on the same shaft. The longest-lived tires are the front tires on the truck as there is not the traction effect at these tires. Moreover, the tires which are at the front-right are less worn out. The reasons for the different tire wears are the load distribution on the truck, irregular distribution of hardness on the road from the edge to the middle and traction effect on the tires. While the inner tires which are on the rear traction shaft most worn out, the right-front tires are the least worn out ones. As a result of the present work, for the trucks, it is recommended that the rotation can be made between the rear in side tires - the front tires on the same line (not cross) for a homogeneous wear.

ACKNOWLEDGEMENT

The authors thank to the management of Western Lignite Corporation in Kutahya/Turkey for their valuable support and permission to this study.

REFERENCES

Aguirre, R.G., 1986. Tire maintenance program helps prevent tire failure, World Waste, 29, pp.33-34.

Celik, I., Koc, O. and Mandal, E.Z., 2007. Extension the life of the tires on wheeled heavy duty mining machinery, 1st Mining Machinery Symposium Proceedings. pp.365-372.

Baek, A.K. and Khonsari, M.M., 2005. Friction and wear of a rubber coating in fretting, Wear. 258, pp.898-905.

Dannis, M.L., 1974. Rubber dust from the normal wear of tires, Rubber Chemistry and Technology, 47, pp.1011–1037.

EPA/530-SW-89-019, 1989. The Solid Waste Dilemma: An Agenda for Action, US Environmental Protection Agency Office of Solid Waste.

Federal Motor Vehicle Safety Standards, 2001. Tire Pressure Monitoring Systems, Controls and Displays, Department of Transportation (DOT), National Highway Traffic Safety Administration 49 CFR Part 571 [Docket No. NHTSA 2000-8572] RIN 2127-AI33]. 45-46.

Higgins, D.D., Brett, A., Marmo, B.A., Jeffree, C.E., Koutsos, V. & Blackford, J.R., 2008. Morphology of ice wear from rubber–ice friction tests and its dependence on temperature and sliding velocity, Wear, 265, pp.634-644.

Jang, J.W., Yoo, T.S., Oh, J.H. and Iwasaki, I., 1998. Discarded tire recycling practices in the United States, Japan and Korea. Resources, Conservation and Recycling, 22, pp.1-14.

Kocsis, J.K, Mousa, A., Major, Z. and Bekesi, N. 2008. Dry friction and sliding wear of EPDM rubbers against steel as a function of carbon black content, Wear. 264, pp.359-367.

Kummera, U., Pacyna, J., Pacyna, E. and Friedrich, E., 2009. Assessment of heavy metal releases from the use phase of road transporting Europe, Atmospheric Environment. 43, pp.640-647.

http://www.komatsu.com/ce/products/pdfs/HD465-7_.pdf . (2011). p.9.

http://www.michelintransport.com/ple/front/affich.jsp?codeRubrique=20071106105640&lang=EN (2011)

Pearce, J.M. and Hanlon, J.T., 2007. Energy conservation from systematic tire pressure regulation, Energy Policy. 35, pp.2673-2677.

Wik, A. and Dave, G., 2009. Occurrence and effects of tire wear particles in the environment - A critical review and an initial risk assessment, Environmental Pollution, 157, pp.1-11.

The Study of Risk Movements of Land Related to Underground Mining Work and Environmental Impact Of Soil and Basement (Case of Boukhadra Iron Ore Mine-Algeria).

M.L. Boukelloul, K. Talhi, R. Adil, M. Bounouala, A. Idres, and A. Boutrid
Laboratory of Mineral Processing Resources and Environment, University Badji Mokhtar, BP 12, 23000, Annaba, Algeria.

ABSTRACT The underground mine workings induce instability risks in the surface that can cause subsidence and collapse. These risks can occur as well during and long term operation phase after abandonment of the work. The magnitude of these risks depends on the mechanical and physical characteristics of the rock mass, the geometric dimensions of ore bodies, their spatial arrangement, the overlay protective pillars and the state of the exploited space. In the case of preventive measures of security and technology are not taken into account for this purpose, the environment will be affected.

The main objective of this work is to assess these risks by scientific, analytical and numerical methods based on geological, hydrogeological and Geotechnical characteristics of Boukhadra rock mass possibly to put into place the preventive measures.

The obtained results have allowed us to get an acceptable safety factor and to quantify subsidence base into 2D with Plaxis 8.2 software.

Keywords: Abandoned underground mining openings, stability risk, 2D analysis

1. INTRODUCTION

In underground mining, the phenomenon of instability of surface land is quite common in the case of the exploitation of vein deposits and erecting by the methods of empty rooms as shown in Figure 1. These instabilities can cause severe damage to structures, fatal accidents, blockage of transportation routes, stopping production, negative impact on the environment, etc...

Many factors affect the stability of underground mines. A quote from global geological, hydrogeological, Geotechnical and technology.

The mine stability condition can be evaluated using analytical and / or numerical. These methods determine the safety factor which is the ratio of the resistance of protective pillars and mono axial stress of overlying rocks.

In this work, we take Boukhadra mine Algeria as case of study. The two approaches used in this work are the analytical method and numerical modelling using a computer code by finite elements, application of Plaxis2D version 8.2 software.

The main objective of this paper is to design crown pillar and operated space, to ensure the stability for the short and / or long term with an optimal extraction rate for ore with an acceptable safety factor.

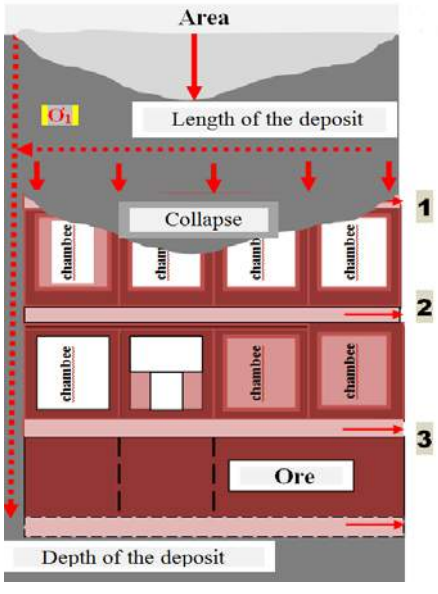

Figure 1. Presenting the collapse of the crown pillar. (If the operation of erecting deposit)

Nomenclature

Empty room (used), (Stage 1)

Rooms in the operational phase, (Stage 2)

Rooms in the phase of preparation, (Stage 3)

1 Adit ventilation, first floor

2 Adit haulage, first floor

3 Adit haulage, second floor

2. RESEARCH OF METHODOLOGY

The problem of the rock mass instability caused by underground mining has been supported by many investigators around the world such as: Deck O. (2002), DRS-05-55102 / R02. (2005) Gadri et al. (2012), Laouafa F. (2004) Pastarus & Toomik (2000), Hutchinson, DJ Phillips. (2002) and others, because it is the one of the priorities of their research. The exploited voids can be the cause of the appearance in the short and / or long-term the subsidence and the collapses after D. Hantz.(2012), as shown in the Figures 2-3-4. These phenomena are very dangerous and can ruin all structures on the surface. To overcome this problem, numerical, analytical and empirical methods have been developed by scientists. Numerical methods yield to significant results because they are very reliable and adapt to different conditions and Oraee Hosseini (2007) Oraee et al (2008). Numerical methods such as finite elements, distinct elements, finite difference and boundary elements are optimal only in special situations (Oraee , al. 2009).

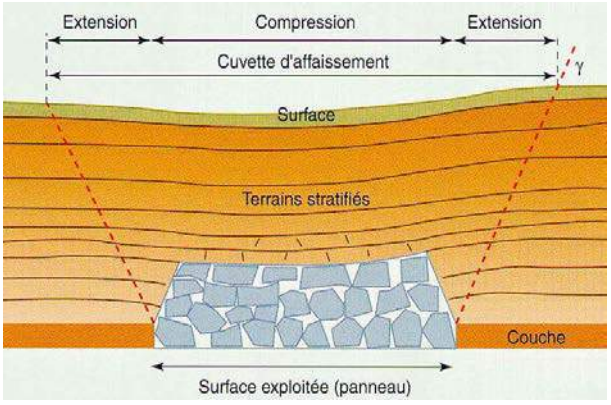

Figure 2. Collapse of a mine (According to INERIS paper)

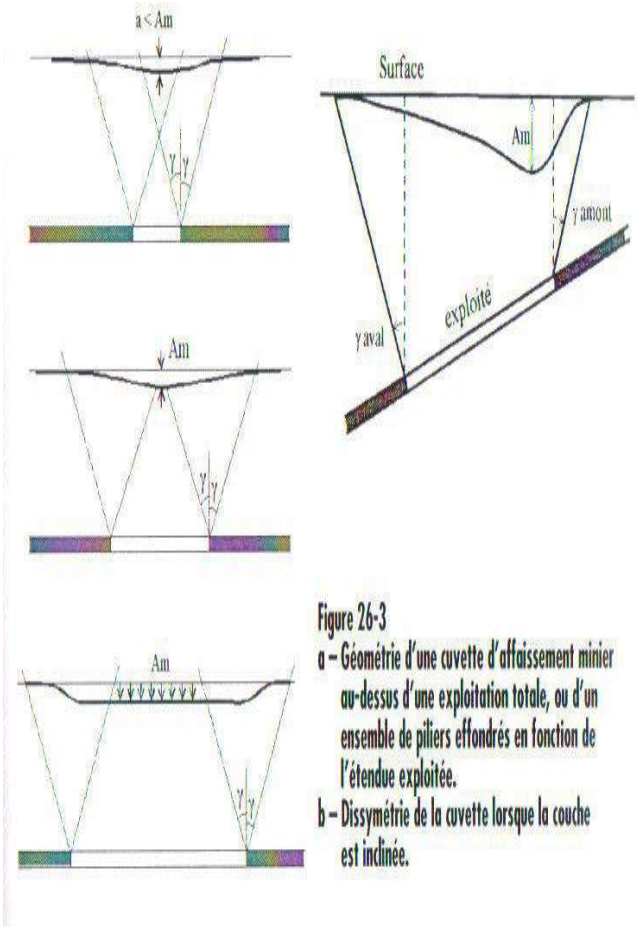

Figure 3. Subsidence: Case of the Deposits aligning and horizontal

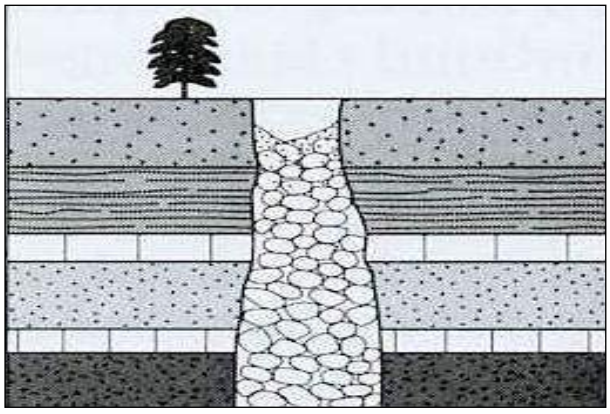

Figure 4. Sudden and localized collapse

Modeling of the exploitation of salt deposits has been the object of the study by Laouafa F, (2004).This work led to important results as shown in figures 5, 6. The validity of the results are only for the case of flat deposits.

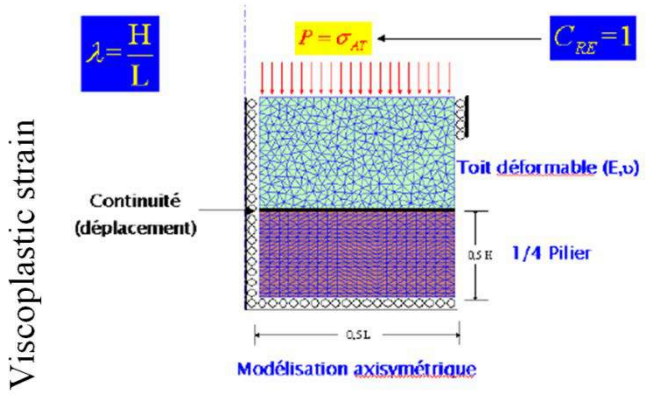

Figure 5. Basic model for the determination of the coefficient of correction

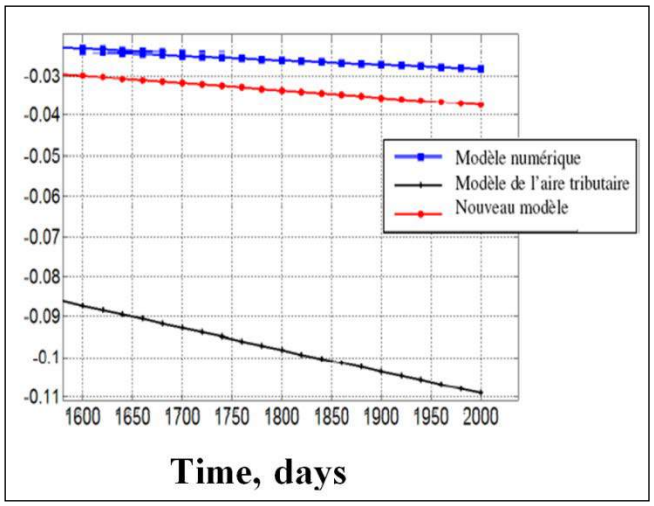

Figure 6. Evolution of the viscoplastic deformation versus time

In the report DRS-05-55102 / R02 (2005), the researchers have supported the case of disorders observed at the surface resulting from the operation slope deposits and flat. They highlighted the characteristics associated with failure mechanisms and stress distributions with high dip of the deposit. The obtained results of their research have categorized the surface phenomena in several disorders including:
A. Localized collapse associated with a breakage protection of the stot (crown pillar) when the operation has reached close to the surface 6.
B. Localized collapse due to the rupture of an underground stop a barrier and
stripping of fillers to deeper empty;
C. Localized collapse due to a rupture of the roof room (fragility of the walls);
D. Subsidence asymmetrical.

In the same report, the authors defined the main criteria to be considered in an assessment of hazards in slope deposits and / or vein which are:

• The geometry of the work (width exploited panels);
• The opening of the underground workings;
• The method of operation (presence of residual voids, backfilled stopes, reclaim rate, etc.);
• The dip of the layers;
• The depth of the panels;
• The thickness of the stot surface protection;

• The nature and characteristics, including mechanical recovery of rock mass, the presence of faults, surface topography, etc…
In their analysis, the authors explain that the concept of pillar "crown" is different from the traditional notion of pillars in the case of the abandoned room and pillar method.
This term refers to the field in place slab between the surface and the shallow adit (Crown pillar: pillar closest to the surface, Figure 7. Hutchinson, Phillips and Cascante [2002]).

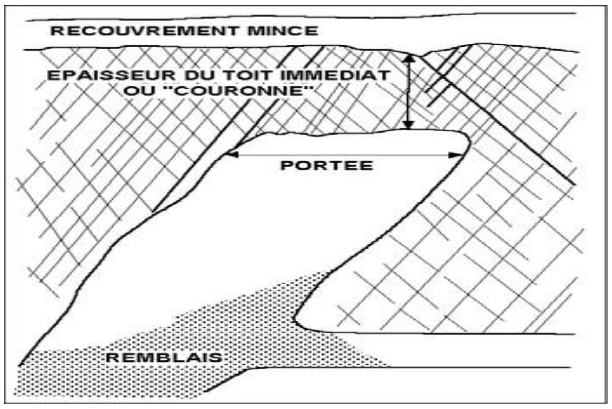

Figure 7. General scheme of a "crown" (according to Hutchinson, Phillips and Cascante [2002]).

The method proposed by the author can be applied for viscoplastic materials. The analytical method developed by the conditional height Talve (1978), Pastarus & Toomik (2000) has given significant results in the Estonia mines stability. The types of model showed in the figure 8 which allowed them to assess long-term stability of the mine of the basis conditional height. The formulas

1, 2, below have crowned their work:

$$C = \frac{\text{H.Sr}}{\text{Sp}} \quad (1)$$

$$Ccrit = \frac{Ha.L^2}{\sum Spi}, m \quad (2)$$

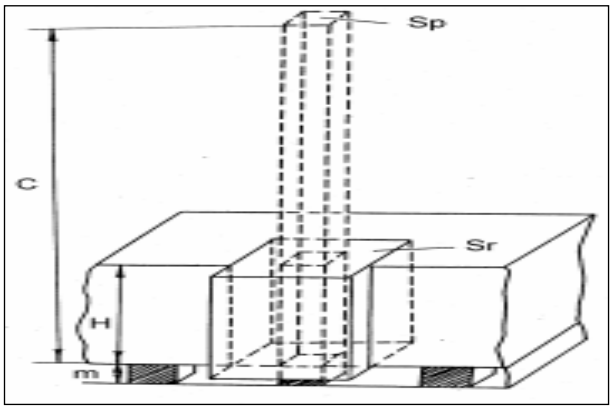

Figure 8. Geometrical interpretation of conditional thickness

Where:
C- The width of the critical operation panel
Cc - conditional thickness of the critical area, m;
Ha - average thickness of waste rock in the critical zone, m;
Spi - sectional area of the II pillar in the critical area, m.

In his study, D. Hantz. (2012) developed a methodology for calculating the average load on the pillars by the following formulas:

- Force exerted on the entire area

$$F = \gamma \, h \, S \text{ totale} = \sigma p \, S \text{ pillars}, \quad (3)$$

- The average stress in the pillars

$$\sigma p = \gamma \, h \, S \text{ totale} / S \text{ pillars}, \quad (4)$$

The methodology proposed by the author can only be applied for the exploitation of deposit flats.

Conclusion:
After analysis of the literature review, it appears that a significant number of influential factors directly implicated on the stability of underground mines are as follows:

- The geology of the deposit, particularly its lithological and structural aspect;
- The state of the rock mass;
- The spatial arrangement of the deposit;
- The physical and mechanical properties of the rock mass;
- The geometry of the deposit, the parameters of the method of operation and the empty space.

The different scientific methods used in their research have shown instabilities related to the solutions or preventive character which is highlighted to address the problems posed.

3 CASE OF STUDY

3.1 Presentation of the Boukhadra Mining Site

The Djebel Boukhadra is located in eastern Algeria, 45 Km north of Tébessa city, 13Km from the Algerian-Tunisian border (figure 9).

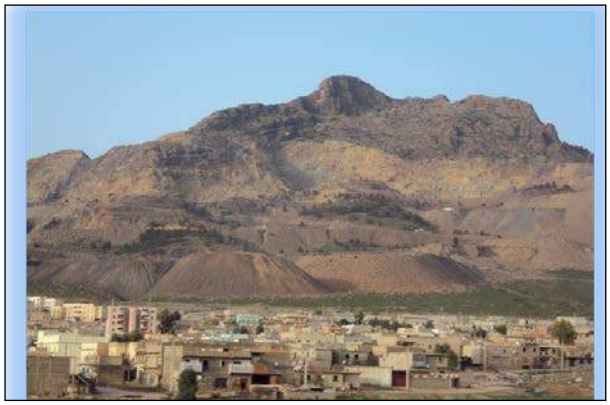

Figure 9. Mine in Boukhadra

3.2 Geological and Hydrogeological Approach.

Stratigraphy of Mount Boukhadra to show that these layers with subvertical orientation (N0 0E) which can accelerate the landslide phenomenon rocks.

Tectonics of Jebel Boukhadra to show that it is hit by a diapirisme causing an upheaval of all existing layers. This is endorsed by the existence of diaclase and internal fragmentation of the different layers also by the existence of

the Triassic formations. The discontinuity present in the solid leads to their quantifications (geometry, and geology) . The water table is below the mineralization that does not affect the mine workings so the water problem does not arise in the conditions of the mine.

The visual field geological study has enabled us to achieve a schematic section of existing training and their dimensions (Figure 10).

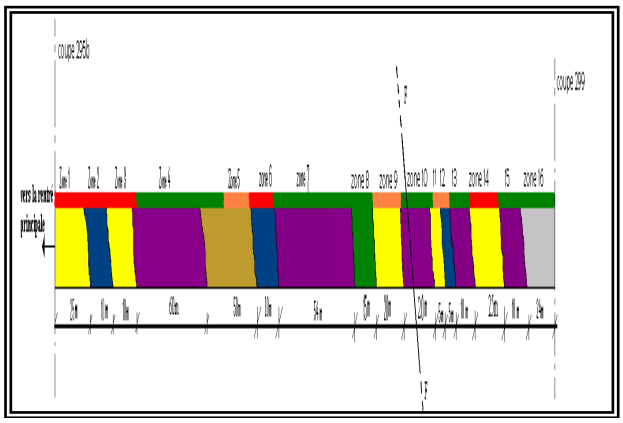

Figure 10 . Schematic section of existing training

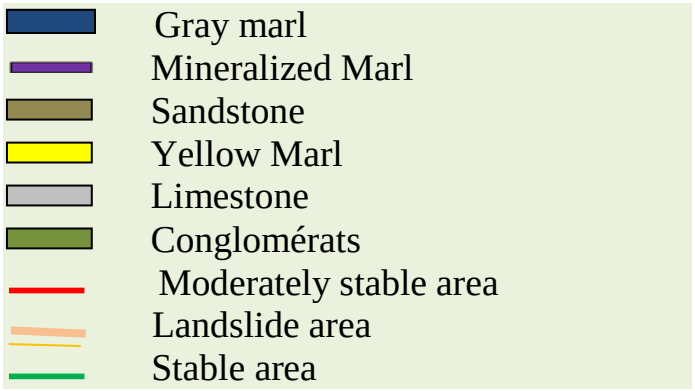

In the mining work, the deposit studied is operated by the method of sub levels slaughtered as part of the methods of empty rooms (figure 11).

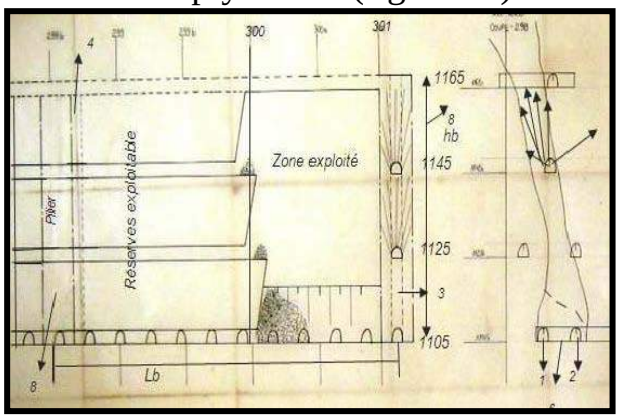

Figure 11. Method in slaughtered levels

The geometric parameters of the deposit are presented in Table 1

Table 1: Geometrical Parameters

	Dimensions
Length of the field, m	500m
Height of the operating block, m	60m
Deposit thickness, m	5m à 50m
Dip angle of the deposit, in degrees	50° à 70°
Length of the operating block, m	40m
The thickness of the crown pillar, m	10m
Width of the barrier pillar between the blocks, m	10m
The thickness of the basic block pillar, m	10m
Distance between recoupes loads, m	7,5 m à 10m

Conclusion

The geological and hydrogeological conditions are determining the degree of difficulty and cost of realization of any underground work and also they have a great influence on the choice of the excavation methods and supporting system. Gadri .L & all (2012).

Other parameters such as degree of weathering, strength of intact rock and water flow are also important in the process of the design rock support system. The knowledge of the former conditions has been of a great help in the identification of potential problems and the suggestion of appropriate solutions, i.e. special supporting system, drainage system, and/or treatments of the encountered problems.

4 NUMERICAL MODELING

To better understand the problem, we modelled two-dimensional structures in the room and pillar (square pillars) in the case of the mine study. The Boukhadra mine rock mass is composed of layers

of Gray marl, Mineralized Marne, Sandstone, Yellow Marl, Limestone And Conglomerates.

For the stability calculation, the assumption of plane strain is adopted. The mechanical behaviour of materials follows the Mohr-Coulomb criterion. The mechanical and physical properties of the materials were determined from laboratory tests at the University of Tebessa Gadri & all (2012),

The mean values of the results are presented in Table 2.

Numerical modelling is performed on the basis of a parametric study, which includes four cases with the variation of the geometric parameters of the real signs of the mine table 1. These cases were calculated analytically by the analytical method which is validated by the modelling method.

Table 2. Physicals and mechanical characteristics of Boukhadra rock mass.

Rocks	**E [GPa**	**ɣ h [g/ cm3]**	**ɣ sat [g/ cm3]**		**C [Bars]**	**α [°]**	Hardness	Rc [Mpa]
yellow marl	4.47	0.33	2.2	2.6	0.33	23	3	20
mineralized marl	4.47	0.3	2.4	2.5	2.6	40	-	20
conglomerate	4.47	0.35	2.2	2.4	0.33	26	4	20
sandstone	4.47	0.35	2.3	2.7	2.7	35	4	20
limestone	19.84	0.22	2.6	2.65	3.5	50	7	70
multicolored marl	3.35	0.38	1.95	2.2	0.3	19	-	20
iron ore	21	0.25	2.7	2.9	3.2	45	**5**	78.4

4.1 Presentation of the Geometrical Model

Since the Boukhadra deposit is erecting the model was presented by its thickness, to better understanding when modelling the total displacements and deformations of the pillars levels (Figures 12ab).

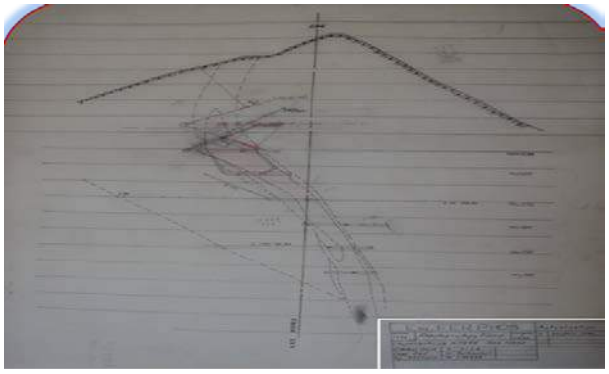

Figure 12a. Vertical section of the northern axis.

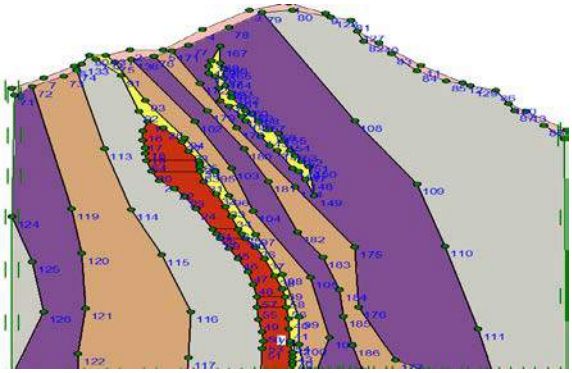

Figure 12b. Overview of the geometric model.

The pattern boundaries are fixed horizontally and vertically at the lower end and equally are fixed horizontally at the terminal sides. The model consists of triangular
elements, each element of 15 nodes and stres s points. The boundary conditions and mesh study are present in the Figure 13.

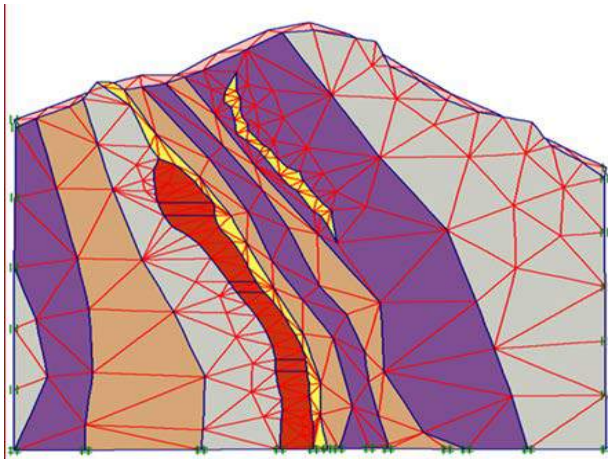

Figure 13. Boundary conditions and mesh of the study.

4.2 General Information About the Model

Our model consists of 426 triangular elements, 3501 nodes with 15 nodes for each element of 5112 points of tension and 15,27m of medium-sized items

4.3 Results of Numerical Analysis with Finite Element Method

Phase after operating

The results obtained allowed us to have the values of total travel (vertical and horizontal), the relation: point of charge – total displacements and distribution of plasticity see Figures 14-15-16.

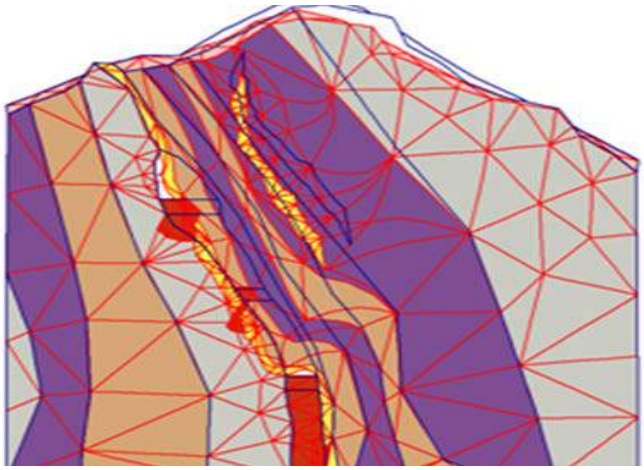

Figure 14. Average total displacement **Utotaux** = 31, 3.10^{-3} m

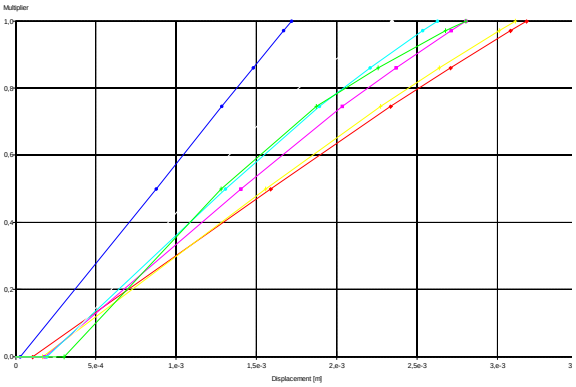

Figure 15. Relation: Point of charge –total displacements

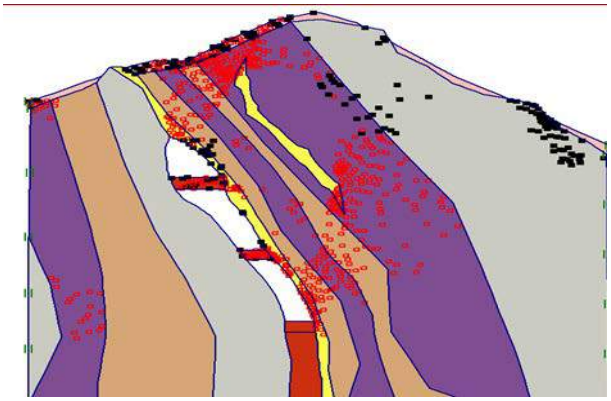

Figure 16. distribution of plasticity

5 CONCLUSION AND OUTLOOK

The study undertaken as part of this research has allowed us to draw the following conclusion:

One of the main objectives of the underground mining is to ensure the stability above all which is an important parameter for the safety of minors.

The geological study of Boukhadra deposit is generally a very complex structure (heterogeneity of the rock mass and the presence of significant discontinuities). (Gadri et al 2012). This complexity results in the short and long-term instability of the mine.

In analytical methods used by different scientists in their studies, the factor of time has not been the subject of extensive study, while this parameter is important for the stability of the mines.

The obtained results of numerical modeling for the case of Boukhadra mine showed

large displacements of the order of $31.3.10^{-3}$ m, and high plasticity distribution at the crown of pillars in the form of a localized collapse. (D. Hantz. (2012).

In order to remedy to the problems, we recommend:

1. The application of a paste backfill system, including in areas of the past mining works and tablecloths.
2. A systematic control of stops rocks. Using the convergence-confinement method.

REFERECES

Bieniawski Z. T, (1968). The effect of specimen size on the compressive strength of coal, Int J Rock Mech Min Sci., 5 (1968), pp. 325-335

Deck .O, Verdel.T,Salmon .R, (2005) . Vulnerability assessment for mining subsidence hazard.Colloque International Post-mining 2005, 16-18 novembre, Nancy. CD ROM.

Gadri.L, Boumazbeur.A , Nouioua.I, Boukeloul. M-L, (2012). The Classification Systems as a Tool to Estimate the Stability of Discontinuous Rock Mass—A Numerical Approach: The iron mine of Boukhadra (Algeria) as a case study. ejge, Vol. 17 [2012], Bund. D

Hantz, D, (2012). Stability of underground cavities.

Laouafa .F, (2004). Modélisation des exploitations de sel. Rapport INERIS DRS-04-56168/R01

Navid. H, (2007). Modelling of pillars in longwall method using advanced numerical techniques, M.Sc Thesis, Islamic Azad University, South of Tehran branch.

Nikitin.O. (2001), Monitoring and analysis of room-and-pillar mining with continuous miner in Estonian oil shale mines. 3 International Conference “Environment. Technology. Resources.” Rezekne, Latvia, P.116-121.

Oraee .K. Hosseini N, H. Yasipur, (2008), Using chain pillars in longwall mining, Polytechnic University Bolur J., 22 pp. 22-25

Pastarus & Toomik ,(2000). Methods of mining block stability analysis for room-and-pillar mining with continuous miner in estonian oil shale mines

Renaud.V,(2004). Contribution à l’analyse des conditionsd’effondrement des gisements pentés des bassins ferrifères de Soumont, May-sur-Orne et Segré(Calvados, 14 et Maine-et-Loire, 49)INERIS DRS-04-50864/RN01

Valorization and Recycling of Quarries Waste as an Addition in Cement

S. Berdoudi
National Polytechnic School of Algiers, Alegria

H. Hebhoub, M. Belachia, R. Djebien
Department of Civil Engineering ; University of Skikda, Alegria.

ABSTRACT: The recycling of quarries waste may offer interesting advantages and solutions in order to preserve the environment and should be considered as a supplementary source of construction materials.

The main objective of this study is to technically show the possibility to recuperate the dust of the marble wastes as a substituted addition in the cement and mortar.

The basis of this study is the effect of marble waste fillers substitution in the cement and mortar paste (0, 5, 10, 15 and 20%) with a fineness lower than that of the cement, to compare the results obtained through control samples of cement paste properties in the fresh condition and the mechanical performances of mortar in the hardened condition.

The obtained results show that the marble wastes fillers can be technically used as an addition in cement.

Keywords: Waste, valorization, fillers, marble, substitution, cement, mortar

1 INTRODUCTION

In this study, we recovered the wastes of white marble from the quarry of FILFILA (the deposit is located at 25 km at the eastern side of Skikda City, Algeria) in the manufacturing of cement.

2 CHARACTERIZATIONS OF THE USED MATERIALS

The used materials for this period are:

- Cement CEM I class 42.5 coming from the cement works of HADAJ SOUD
- The additions of marble wastes are obtained by crushing the mass rejects in a crusher, then a grinding in a grinder with a standard nut.
- The mortars are prepared with a standard sand CEN according to the norm EN 196-1, this natural siliceous sand with an apparent voluminal mass of 1.63 g/Cm3 and an absolute voluminal mass of 2.5g/Cm3, this sand is inert from a chemical point of view with fineness module of 2.33

Results of Characterizations Tests are shown in the Table 1:

Table 1. Characteristics of Used Materials

Sample	CEM I 42.5	Marble Wastes Fillers	Sample	CEM I 42.5	Marble Wastes Fillers
Mvabs g/cm^3	3,33	2,79	R . Insoluble	0,85	0,035
SSb Cm^2/g	4457	2997	Free CaO	0,4	--
CaO	61,31	55,29	MS	2,52	--
Al_2O_3	5,45	0 ,14	MAF	1,54	--
Fe_2O_3	3,54	0,09	LSF	0,88	--
SiO_2	22,73	0,53	MH	1,93	--
MgO	0,48	0,2	C3S	28,14	--
Na_2O	0,19	0,00	C2S	38,71	--
K_2O	0,63	0,01	C3A	8,45	--
Cl^-	0,035	0,025	C4AF	10,76	--
SO_3	2,44	0,04	$CaCO_3$	--	98,67
PF	2,45	43,40			

3 EXPERIMENTAL PROGRAM

In the experimental program, we study the substitution of a cement part by the marble wastes additions, through varying the substitutions rate (0%, 5%, 10%, 15%, 20%).

Campaign 1: manufacturing starting from cement CEMI and marble wastes fillers of cement pastes with substitutions rates (0%, 5%, 10%, 15%, 20%).

Campaign 2: manufacturing starting from cement CEMI and marble wastes fillers of mortars with substitutions rates (0%, 5%, 10%, 15%, 20%).

The parameters and tests made for the Campaign 1 are shown in the table 2:

Table 2. Parameters and tests made for the Campaign 1

Scoring	Type of Cement Paste
Witness (0%)	Cement paste made of CEM I
FM2 (5%)	Cement paste made of 95% of CEM I and 5% of marble wastes fillers
FM2 (10%)	Cement paste made of 90% of CEM I and 10% of marble wastes fillers
FM2 (15%)	Cement paste made of 85% of CEM I and 15% of marble wastes fillers
FM2 (20%)	Cement paste made of 80% of CEM I and 20% of marble wastes fillers
Constant Parameters	W/C = 0.27
Variable Parameters	Substitution Rate
Tests Made	Consistency Setting Steadiness

The parameters and tests made for the Campaign 2 are shown in the table 3:

Table 3. Parameters and tests made for the Campaign 2

Scoring	Type of Mortar
Mot (0%)	Normal Mortar made of CEM I
Mo2(5%)	Normal mortar made of 95% of CEM I and 5% of marble wastes fillers
Mo2(10%)	Normal mortar made of 90% of CEM I and 10% of marble wastes fillers
Mo2(15%)	Normal mortar made of 85% of CEM I and 15% of marble wastes fillers
Mo2(20%)	Normal mortar made of 80% of CEM I and 20% of marble wastes fillers
Constant Parameters	W/C = 0.5 Sand
Variable Parameters	Substitution Rate
Tests Made	Compressive strength in 2, 7, 28, and 90 days. flexural strength in 2, 7, 28, and 90 days.

4 EFFECT OF RECYCLED FILLERS ON THE CEMENT PASTE CHARACTERISTICS

4.1 Consistency

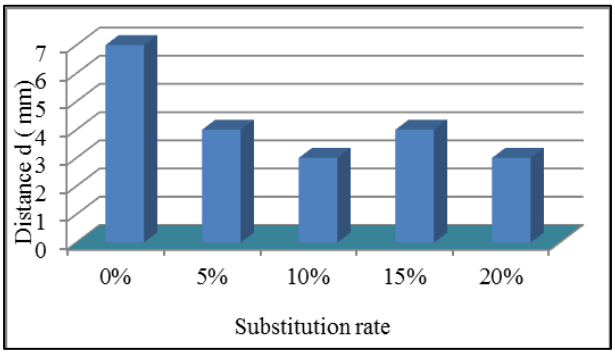

Figure 1. Variation of Consistency according to the substitution rate

For SSb Marble wastes fillers inferior to SSb Cement (Figure 1), we obtain a decreasing variation until a substitution rate of 10%, beyond 10%, we notice a light decrease of the cement paste consistency, correlated with the results obtained with A. Messan (2006).

Generally, and according to S. Caré and al (2002), the addition of marble wastes fillers leads to ameliorate the consistency according to the decrease of SSb and the substitution rate until 10%.

4.2 Start and End of Setting

For a lower SSb (Figure 2) there is an increase in the time of end of setting up to 10% or the effect reverses. Beyond 10%, the variation between the start of setting and the end of setting is very close. Plus the SSb is lower and the substitution rate is important (Superior to 10%) more the time between the start and the end of setting is shorter (M. Benia 2011).

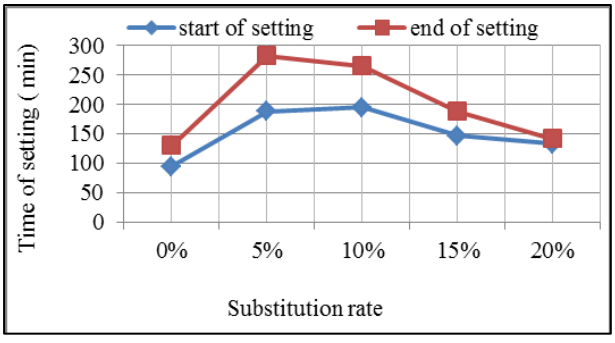

Figure 2. Variation of time of start and end of setting according to the substitution rate

4.3 Steadiness

Steadiness varies from a rate to another, this variation remains below 10mm. The steadiness decreases according to the decrease of SSb.

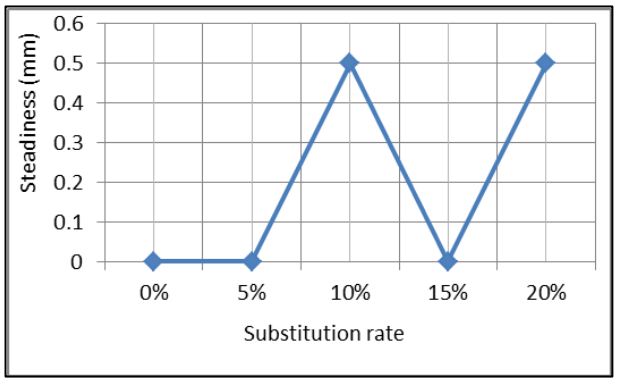

Figure 3. Variation of Steadiness according to the substitution rate

5 EFFECT OF RECYCLED FILLERS ON THE MORTAR CHARACTERISTICS

5.1 Compressive Strength

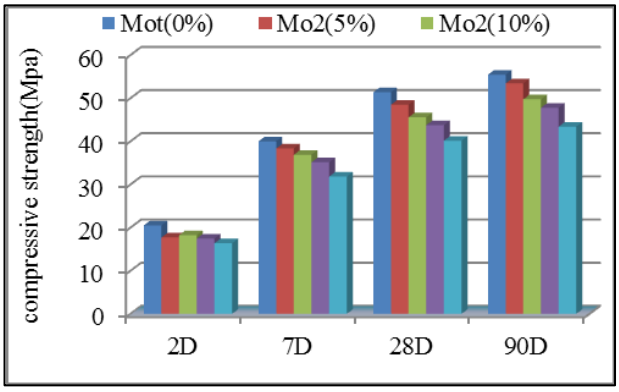

Figure 4. Influence of Substitution rate on the Compressive strength

For bigger marble wastes fillers particles (SSb lower), the best performances are obtained through the witness mortars, more the SSb is lower , more we obtain a fall of resistance for all the mixtures.

At the short term (2Days) more the SSb is lower, more the chemical reaction of hydration is disturbed by the introduction of the marble wastes fillers. The witness cement gives the best performances; this is due to the raised quantity of CaO which gives a higher resistance at the court term. At long term, the raised SiO2 gives lot of C2S because it reacts

with all the CaO and the cement hardens slowly, in accordance with (S. Caré 2002**,** M Benia. 2011, Ch. Amouri. 2009) and this explains the maximal resistance at the middle and long terms.

5.2. Study of the Influence of Age on the Variation of the Compressive strength According to the Substitution Rate

For a lower SSb, we notice a fall of initial resistance at the short term, and the pace of curves is a decreasing function with the raise of Substitution rate.

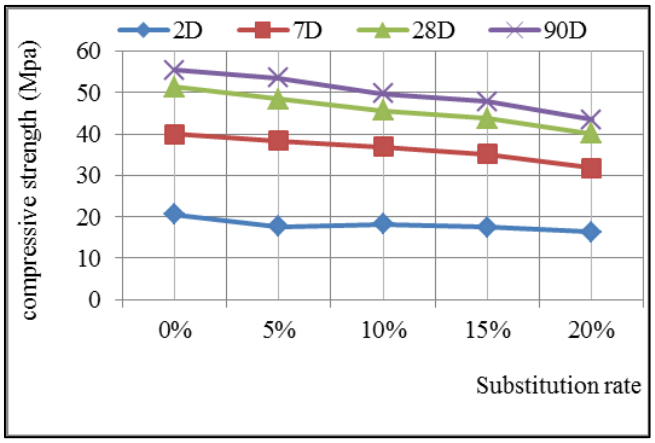

Figure 5. Influence of Age on the Variation of the Compressive strength According to the Substitution Rate

5.3. Flexural strength

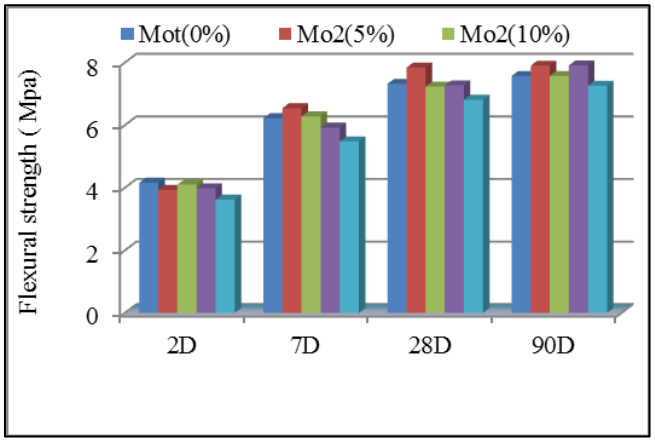

Figure 6. Influence of Substitution rate on the flexural strength

For lower SSb, we notice a decrease in the resistance for all ages.

5.4. Study of the Influence of Age on the Variation of the Flexural Strength According to the Substitution Rate

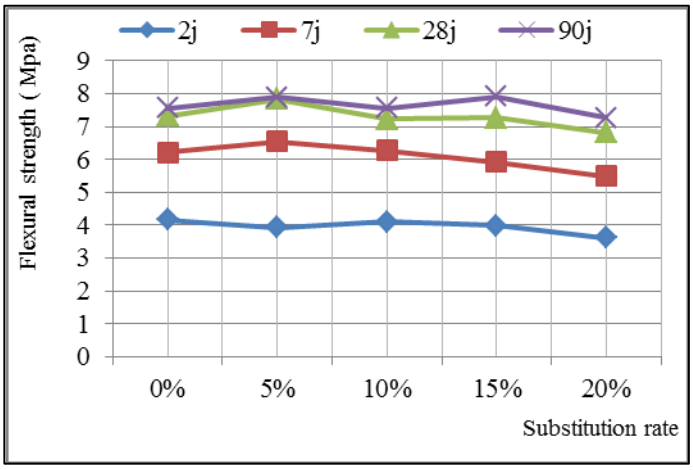

Figure 7. Influence of Age on the Variation of the flexural strength According to the Substitution Rate.

For bigger fillers particles, the curves at long term are very close and show the same pace.

6. CONCLUSION

This work carries on the study of the possibility to recover the marble wastes as an addition in the cement, the study shows that:
-The addition of marble wastes filers leads to ameliorate the consistence of cement paste, they cause a decrease of the C3A quantity.
-For lower SSb (SSb marble wastes fillers inferior to SSb cement CEM1), there is a raise of time of the end of setting.
-Introducing marble wastes fillers leads to increase the cohesion.
-The mechanical resistances decrease with the increase of the substitution rate of recycled fillers for a very weak fineness.

REFERENCES

A.Messan: Contribution to the study of thin structure out of mortar behavior at very early age. Doctoral thesis, Montpellier, 2006.

Ch.Amouri: Contribution to the study of the influence of different additions on the properties of cement matrices, doctoral thesis, Constantine university , algeria,2009.

M. Benia: Influence of specific surface cements with mineral additives on the mechanical behavior of mortar and concrete using local materials, Magister memoy, Msila university. (2011).

S.Caré, R linder, V Baroghel Bouny, F De Larrard, Y Charonnat: Effect of mineral admixtures on concrete use properties. Experience plan and Static Analysis, LCPC, 2002.

UCTEA The Chamber of Mining Engineers of Turkey
ISBN: 978-605-01-0705-0